

PROCEEDINGS

OF THE

PHYSICAL SOCIETY

JANUARY TO JUNE 1961

VOLUME 77



Published by
THE INSTITUTE OF PHYSICS AND THE PHYSICAL SOCIETY
1 Lowther Gardens, Prince Consort Road,
London S.W. 7

OFFICERS AND MEMBERS OF THE FIRST COUNCIL

PRESIDENT

Sir JOHN COCKCROFT, O.M., K.C.B., C.B.E., M.A., D.Sc., F.Inst.P., F.R.S.

IMMEDIATE PAST PRESIDENTS OF THE INSTITUTE AND OF THE SOCIETY

Sir GEORGE THOMSON, M.A., LL.D., Sc.D., Hon.F.Inst.P., F.R.S.

J. A. RATCLIFFE, C.B.E., M.A., F.R.S.

VICE-PRESIDENTS

Prof. R. W. DITCHBURN, B.Sc., M.A., Ph.D., F.Inst.P.

A. J. PHILPOT, C.B.E., B.Sc., M.A., F.Inst.P.

W. H. TAYLOR, M.A., D.Sc., F.Inst.P.

J. TOPPING, M.Sc., Ph.D., F.Inst.P.

HONORARY TREASURER

J. TAYLOR, M.B.E., D.Sc., F.R.I.C., F.Inst.P.

HONORARY SECRETARY

C. G. WYNNE, B.A., Ph.D., F.Inst.P.

ORDINARY MEMBERS OF THE COUNCIL

Prof. B. BLEANEY, M.A., D.Phil., F.R.S.

E. R. DAVIES, O.B.E., B.Sc., F.Inst.P.

Prof. B. H. FLOWERS, M.A., D.Sc.

J. M. A. LENIHAN, M.Sc., Ph.D., A.M.I.E.E., F.Inst.P.

G. R. NOAKES, M.A., F.Inst.P.

Prof. C. F. POWELL, M.A., Sc.D., F.R.S.

F. A. VICK, O.B.E., Ph.D., A.M.I.E.E., F.Inst.P.

Prof. D. A. WRIGHT, D.Sc., F.R.A.S., F.Inst.P.

REPRESENTING BRANCHES

M. R. HOPKINS, M.Sc., Ph.D., F.Inst.P.

Prof. H. LIPSON, M.A., D.Sc., F.Inst.P., F.R.S.

EXECUTIVE OFFICERS

Secretary:

H. R. LANG, B.Sc., Ph.D., A.R.C.S., F.Inst.P.

Deputy Secretary:

N. CLARKE, B.Sc., F.Inst.P.

Editor and Deputy Secretary:

A. C. STICKLAND, M.Sc., Ph.D.

W. G. BOWMAN

CONTENTS

Part 1

January 1961

	PAGE
Prof. F. HOYLE. 44th Guthrie Lecture: Observational tests in cosmology	1
Mr. J. S. WILCZYNSKI. Some properties of photographic image recording	17
Prof. E. R. ANDREW, Dr. K. M. SWANSON and Dr. B. R. WILLIAMS. Angular dependence of nuclear spin-lattice relaxation time for several alkali halide crystals	36
Dr. P. G. BURKE and Dr. W. LASKAR. Four nucleon reactions with central forces	49
Prof. D. R. BATES. Excitation of the 1s-2p transition of atomic hydrogen by proton and alpha particle impact	59
Dr. F. H. READ and Dr. J. M. CALVERT. Pick-up reactions on a ^9Be Target	65
Mr. D. P. JONES, Dr. P. G. MURPHY, Mr. P. L. O'NEILL and Dr. J. R. WORMALD. Redetermination of the Panofsky ratio for negative pions stopped in hydrogen.	77
Dr. J. DA PROVIDENCIA. Perturbation theory in finite nuclei	81
Dr. D. ECCLESHALL and Mr. M. J. L. YATES. The 0^+ , $T=1$ level in ^{18}F	93
Mr. D. I. PORAT and Dr. K. RAMAVATARAM. Rate of energy loss and ranges of carbon and oxygen ions in solids	97
Prof. B. BLEANEY and Mr. R. S. RUBINS. Explanation of some 'forbidden' transitions in paramagnetic resonance	103
Prof. B. BLEANEY. Quadrupole-quadrupole interaction in the rare earths.	113
Dr. A. DANIELIAN and Prof. K. W. H. STEVENS. The estimation of antiferromagnetic exchange interactions	116
Dr. A. DANIELIAN and Prof. K. W. H. STEVENS. Exchange interactions in the polymorphic forms of MnS	124
Dr. A. J. F. BOYLE, Dr. St. P. BUNBURY, Mr. C. EDWARDS and Dr. H. E. HALL. The Mössbauer effect in tin from 120°K to the melting point	129
Dr. G. L. SEWELL. Diamagnetism of many-fermion systems	136
Dr. H. MOHAN and Dr. K. MAJUMDAR. Absorption spectrum of tellurium monosulphide in the ultra-violet region	147
Mr. J. E. CAFFYN and Dr. B. K. RIDLEY. Z-centres in sodium chloride containing calcium	153
Mr. M. COHEN and Dr. A. DALGARNO. The Hartree energies of the helium sequence	165
Mr. I. M. THORSON and Prof. L. KATZ. Fine structure in the $^{12}\text{C}(\gamma, n)^{11}\text{C}$ activation curve	166
Dr. M. J. SEATON. Strong coupling in optically allowed atomic transitions produced by electron impact	174
Dr. M. J. SEATON. The evaluation of partial wave integrals in the Born approximation.	184
Mrs. J. LAWSON, Mr. W. LAWSON and Dr. M. J. SEATON. The calculation of Born partial wave integrals for some transitions in H produced by electron impact.	192
Mrs. V. M. BURKE and Dr. M. J. SEATON. The calculation of electron-hydrogen collision cross sections using the Born approximation for the reactance matrix	199

Letters to the Editor:

Mr. D. GRIFFITHS and Dr. B. R. COLES. Antiferromagnetic behaviour of GdB_6	213
Mr. S. J. FRAY, Dr. F. A. JOHNSON, Mr. J. E. QUARRINGTON and Mr. N. WILLIAMS. The optical absorption of gallium arsenide in the reststrahlen band	215
Dr. N. M. WOLCOTT. The calculation of Debye characteristic temperatures	218
Reviews of Books	219

Part 2

February 1961

Mr. J. E. KNOWLES. A further explanation of the shape of the hysteresis loop of 'square loop' ferrites	225
Dr. G. PARRY, Mr. H. D. SCOTT and Mr. S. SWIERSZCZEWSKI. The elastic scattering of ^3He by C, Mg, Al and Cu	230
Mr. J. V. ALLABY, Dr. A. ASHMORE, Dr. A. N. DIDDENS, Mr. J. EADES, Mr. G. B. HUXTABLE and Dr. K. SKARSVÄG. Spin correlation measurements in p-p scattering at 382 and 320 mev	234
Mr. J. H. PACE, Mr. D. F. SAMPSON and Dr. J. S. THORP. Spin-lattice relaxation times in sapphire and chromium-doped rutile at 34.6 Gc/s	257
Mr. C. B. P. FINN, Dr. R. ORBACH and Dr. W. P. WOLF. Spin-lattice relaxation in cerium magnesium nitrate at liquid helium temperature: a new process	261
Dr. J. B. HASTED. The energy transferred in inelastic ion-atom collisions	269
Dr. J. G. POWLES and Mr. A. HARTLAND. The measurement of indirect (J) coupling between nuclei and liquids in magnetic resonance by the transient method	273
Dr. G. R. ALLCOCK and Mr. A. N. KAMAL. The S-wave pion-pion interaction	278
Dr. P. V. MARCH and Mr. T. G. WALKER. The photoproduction reaction $^{60}\text{Ni}(\gamma, \pi^-)^{60}\text{Cu}$	293
Dr. P. G. HARPER. The quasi-particle approximation in superconductivity	299
Dr. B. DAYAL and Mr. B. B. TRIPATHI. A revision of Kellermann's calculations of the specific heats of sodium chloride	303
Dr. B. H. BRIGGS. Diffraction by an irregular screen of limited extent	305
Dr. R. P. MERCIER. Diffraction by finite irregular objects	318
Dr. P. HARIHARAN and Dr. D. SEN. The separation of symmetrical and asymmetrical wave-front aberrations in the Twyman interferometer	328
Mr. M. J. P. MUSGRAVE and Mr. M. F. MARKHAM. Features of the elastic wave surface for a zinc crystal	335
Mr. I. N. CAPON. The application of ray tracing methods to radio signals from satellites	337
Dr. J. R. COOK. Internal conversion of ^{141}Ce	346
Dr. D. C. CHAMPENEY and Prof. P. B. MOON. Absence of Doppler shift for gamma ray source and detector on same circular orbit	350
Mr. C. T. CHUDLEY and Dr. R. J. ELLIOTT. Neutron scattering from a liquid on a jump diffusion model	353
Mlle. N. GILBERT. Gamma rays corresponding to a dipole or a high quadrupole excitation of carbon 12 by 150 mev protons	362
Dr. J. C. BARTON and Dr. E. G. MICHAELIS. Multiple Geiger counter coincidences due to gamma radiation	377
Mr. A. N. PRASAD and Prof. J. D. CRAGGS. Measurement of Townsend's ionization coefficients and attachment coefficients in oxygen	385

	PAGE
Dr. J. H. TOWLE and Mr. B. E. F. MACEFIELD. A study of the reactions $^{12}\text{C}(^3\text{He}, n)^{14}\text{O}$ and $^{16}\text{O}(^3\text{He}, n)^{18}\text{Ne}$.	399
Dr. J. H. CARVER. The reaction $^{51}\text{V}(\gamma, \alpha)^{47}\text{Sc}$ and some remarks on (γ, α) reactions	417
Prof. SYDNEY CHAPMAN. Scale times and scale lengths of variables: with geomagnetic and ionospheric illustrations	424
Dr. S. F. EDWARDS and Mr. M. A. NAQVI. Integrable many body wave functions for a system of Bose particles	433
Dr. A. L. STEWART. An approximate method for the calculation of multipole polarizabilities of atoms	447
Dr. D. M. BURLEY. A lattice model of a classical hard sphere gas: II	451
Mr. W. DUNSTAN. Variation of photovoltaic response with magnetic field for a germanium p-n junction	459
Dr. A. DALGARNO and Dr. A. L. STEWART. A perturbation-variation calculation of eigenvalues	467
Prof. M. BLACKMAN and Dr. I. H. KHAN. The polymorphism of thallium and other halides at low temperatures	471
Dr. J. R. M. COULTER, Mr. N. H. K. ARMSTRONG and Prof. K. G. EMELEUS. Moving striations and anode spots in neon	476
Dr. E. H. ANDREWS. Stresses at a crack in an elastomer	483
Mr. A. G. GREGORY and Dr. P. B. TREACY. Polarization of protons from low resonances in $^{12}\text{C}(d, p)^{13}\text{C}$	499
Mr. S. K. MUKHERJEE, Mr. A. K. GANGULY and Mr. N. K. MAJUMDER. Activation cross sections with 14 mev neutrons	508
Prof. K. W. H. STEVENS. The Hamiltonian formalism of damping in a tuned circuit	515
Mr. R. F. COLEMAN, Mr. D. N. HERBERT and Dr. J. L. PERKIN. Upper limits for the radiative capture cross sections of ^{27}Al and ^{31}P for ^{16}O ions	526
Dr. F. J. PEARSON. Some notes on theories of helium	531
Letters to the Editor:	
Dr. R. LACROIX. Cubic crystal field splitting of the Gd^{3+} ion	550
Mr. B. G. SKINNER. On the validity of two conjectures relating to resonance collisions	551
Reviews of Books	554

Part 3

March 1961

Dr. G. S. BOGLE, Mr. H. F. SYMMONS, Mr. V. R. BURGESS and Mr. J. V. SIERINS. Paramagnetic resonance spectrometry at zero magnetic field	561
Prof. L. F. BATES and Mr. A. J. PACEY. The thermomagnetic behaviour of cobalt ferrite	567
Mr. J. E. KNOWLES. The irreversible change of magnetization produced in 'square loop' ferrite by pulsed magnetic fields	576
Dr. F. ASHTON. The range-energy relation for high energy μ -mesons	587
Dr. V. LAKSHMINARAYANA and Prof. S. JNANANANDA. Scattering cross sections of gamma radiation	593
Dr. W. M. FAIRBAIRN. The isobaric triplets in the nuclear 2p-shell and the charge independence of nuclear forces	599
Dr. W. D. HAMILTON. The lifetime of the 364 kev level in ^{131}Xe .	610

	PAGE
Mr. A. SALMONA and Dr. M. J. SEATON. Electron collisions with Na atoms . . .	617
Dr. H. N. V. TEMPERLEY. Improvements in the lattice model of a liquid . . .	630
Dr. M. G. HAINES. The effect of electrodes in a linear pinched discharge . . .	643
Dr. L. SALGUEIRO, Dr. J. G. FERREIRA, Dr. J. J. H. PARK and Dr. M. A. S. ROSS. Fluorescence and other yields of the L_{II} shell in Pu . . .	657
Dr. M. B. K. SARMA. Selective pressure broadening of Si and F spectral lines . . .	665
Dr. J. N. DODD. A 'level crossing' experiment in mercury . . .	669
Dr. A. DALGARNO and Mr. J. M. McNAMEE. The Hartree perturbation method for helium . . .	673
Dr. B. N. SRIVASTAVA and Mr. A. K. BARUA. Rotational-translational relaxation time in H_2 calculated from thermal conductivity . . .	677
Dr. A. W. DALTON, Dr. G. PARRY, Mr. H. D. SCOTT and Mr. S. SWIERSZCZEWSKI. The $^{58}Ni(d, p)^{59}Ni$ and $^{60}Ni(d, p)^{61}Ni$ reactions . . .	682
Prof. L. F. BATES and Dr. R. D. BARNARD. The electrical resistivities and magnetic susceptibilities of some stable and metastable uranium-molybdenum alloys . . .	691
Dr. J. C. WOOLLEY, Dr. C. M. GILLET and Mr. J. A. EVANS. Electrical and optical properties of GaAs-InAs alloys . . .	700
Mr. R. E. BORLAND. One-dimensional chains with random spacing between atoms . . .	705
Dr. M. L. CANUT and Prof. J. L. AMORÓS. On the inversion temperature function of the first-order (one phonon) scattering and the determination of Debye characteristic temperatures . . .	712
Dr. B. L. MOISEWITSCH. Elastic scattering of slow electrons by helium atoms . . .	721
Dr. A. E. KINGSTON and Mr. B. G. SKINNER. The elastic scattering of electrons and positrons by hydrogen atoms . . .	724
Dr. J. G. POWLES and Mr. M. H. MOSLEY. A thermal motion effect in the electron spin resonance of a free radical in solution . . .	729
Dr. J. G. POWLES and Mr. D. J. NEALE. Molecular motion in liquid toluene by proton magnetic resonance relaxation . . .	737
Mr. M. COHEN and Dr. A. DALGARNO. Stationary properties of the Hartree-Fock approximation . . .	748
Mr. J. C. ROBERTSON and Mr. J. G. LYNCH. The luminescent decay of various crystals for particles of different ionization density . . .	751
Mr. A. E. CARTE. Air bubbles in ice . . .	757
Dr. D. K. AITKEN, Dr. F. F. HEYMANN, Dr. R. E. JENNINGS and Dr. P. I. P. KALMUS The design and construction of a 29 mev microtron . . .	769
Dr. A. P. STONE. Nuclear and relativistic effects in atomic spectra . . .	786
Dr. K. CODLING. Ultra-violet extensions of the arc spectra of the alkaline earths: the absorption spectrum of magnesium vapour . . .	797
Dr. A. A. WARE and Dr. J. A. WESSON. The ohmic heating of positive ions in an impure plasma . . .	801
Dr. J. M. TITMAN. The heat capacities of some copper-manganese alloys . . .	807
Prof. Sir HARRIE MASSEY and Mr. A. H. MOUSSA. Positronium formation in helium . . .	811

Letters to the Editor:

Dr. N. L. SINGH and Mr. D. C. JAIN. Relative intensities in the triplet system of CO bands . . .	817
---	-----

Reviews of Books . . .	818
------------------------	-----

	PAGE
Dr. R. ORBACH. On the theory of spin-lattice relaxation in paramagnetic salts .	821
Mrs. H. E. SARAPH. Application of the Schwinger variational method to zero-energy electron-hydrogen scattering	827
Dr. D. HOARE, Dr. A. B. ROBBINS and Dr. G. W. GREENLEES. Polarization of 9 mev protons elastically scattered from C and Al	830
Dr. J. S. LILLEY. The emission of charged particles from the bombardment of silver with nitrogen ions	833
Dr. W. S. WHITLOCK and Mr. J. E. BOUNDEN. Negative oxygen ions from a glow discharge source	845
Dr. F. DE S. BARROS, Dr. P. D. FORSYTH, Dr. A. A. JAFFE and Dr. I. J. TAYLOR. An investigation of some (t, d) reactions in light nuclei at 5.5 mev	853
Dr. G. S. HIGGINSON and Dr. L. W. KERR. The 2^3S excitation in helium	866
Mr. J. C. MALE. Luminescence excitation spectrum of diamond near the fundamental absorption edge	869
Mr. N. L. SVENSSON. The variation of the fracture energy of brittle plastics with temperature	876
Dr. M. A. JASWON and Mr. B. J. SHAW. A note on non-equilibrium elastic constants	885
Dr. I. J. ZUCKER. The reduced equation of state of the inert gas solids at the absolute zero	889
Dr. K. G. BIRCH. A scanning instrument for the measurement of optical frequency response	901
Dr. D. M. S. BAGGULEY and Mr. M. HEATH. Ferromagnetic resonance in nickel-copper alloys	913
Mr. A. N. KAMAL. P-wave pion-pion resonance	917
Dr. C. P. FLYNN and Dr. E. F. W. SEYMOUR. Diffusion narrowing of nuclear magnetic resonance in aluminium and copper	922
Dr. T. B. GRIMLEY. Stereospecific polymers and Markoff chains	931
Reviews of Books	937

The Late Dr. S. P. F. HUMPHREYS-OWEN. Comparison of reflection methods for measuring optical constants without polarimetric analysis, and proposal for new methods based on the Brewster angle	949
Prof. B. RAMACHANDRA RAO and Dr. J. SATYANARAYANA MURTY. Diffraction of light by very high frequency ultrasonic waves	958
Mr. N. J. PHILLIPS. Plasma diffusion in systems with particle losses	965
Mr. N. ANDERSON. Oscillations of a plasma in a static magnetic field	971
Mr. Z. HORÁK. On the identification of the K_{α} satellites. I: LS region	980
Mr. R. HERDAN and Mr. T. P. HUGHES. (d-d) reaction product velocities in SCEPTRE III according to a two-group model	987
Dr. P. E. HODGSON. Optical model analysis of the elastic scattering of 5.5 mev ^3He by carbon, magnesium, aluminium and copper	997
Dr. J. GRINDLAY. The hole theory of liquids	1001
Dr. G. V. CHESTER and Prof. A. THELLUNG. The law of Wiedemann and Franz	1005
Dr. W. LASKAR, Dr. C. TATE, Mr. B. PARDOE and Dr. P. G. BURKE. Two channel five nucleon reactions with central forces	1014

Dr. G. PARRY, Mr. H. D. SCOTT and Dr. S. SWIERSZCZEWSKI. The angular distributions of alpha particle groups from the reaction $^{24}\text{Mg}(^3\text{He}, \alpha)^{23}\text{Mg}$	1024
Miss G. RAUMANN and Dr. D. W. SAUNDERS. The anisotropy of Young's modulus in drawn polyethylene	1028
Dr. J. M. BAKER, Mr. J. A. J. LOURENS and Dr. R. W. H. STEVENSON. Antiferromagnetism of mixed crystals of zinc and manganese fluoride	1038
Dr. M. SUFFCZYNSKI. Faraday effect for direct magneto-optical transitions in germanium	1042
Mr. P. E. BEST and Mr. J. L. ROBINS. An x-ray absorption process in ionic crystals	1046
Mr. B. E. F. MACEFIELD, Dr. J. H. TOWLE and Mr. W. B. GILBOY. A study of the reaction $^{40}\text{Ca}(d, n)^{41}\text{Sc}$	1050
Dr. A. J. F. BOYLE, Dr. D. St. P. BUNBURY and Mr. C. EDWARDS. The nuclear Zeeman effect, and quadrupole splitting in ^{119}Sn	1062
Mr. G. N. HARDING, Mr. M. F. KIMMITT, Mr. J. H. LUDLOW, Mr. P. PORTEOUS, Mr. A. C. PRIOR and Mr. V. ROBERTS. Emission of sub-millimetre electromagnetic radiation from hot plasma in ZETA	1069
Dr. A. F. B. WOOD. On the indication of vibration nodes by fine powders	1076
Dr. J. B. BIRKS and Dr. K. N. KUCHELA. Energy transfer in organic systems. II: Solute-solute transfer in liquid solutions	1083
Letters to the Editor:	
Dr. J. B. BIRKS, Dr. K. N. KUCHELA and Mr. F. H. READ. Energy transfer in organic systems. III: Spectral effects in liquid solutions	1095
Dr. T. J. GOODING. Kinetic energy effects in the thermal neutron fission of ^{235}U	1097
Dr. A. W. DALTON, Dr. G. PARRY and Mr. H. D. SCOTT. Gross structure in the proton spectra from the $^{51}\text{V}(d, p)^{52}\text{V}$ reaction	1098
Dr. B. H. CLAUSSEN. Modulation of light by means of an electric field	1100
Dr. B. V. ROLLIN. Detection of millimetre and sub-millimetre wave radiation by free carrier absorption in a semiconductor	1102
Reviews of Books	1104

Part 6

June 1961

Mr. S. K. MAJUMDAR. Radiation by charged particles passing through an electron plasma in an external magnetic field	1109
Mr. A. C. PRIOR. Some theoretical considerations on the longitudinal magnetic field induced oscillations in semiconductors (the oscillistor) and a tentative explanation	1121
Dr. P. R. J. BURCH. Gamma-ray spectra in large organic scintillators	1125
Dr. M. ASLAM KHAN. MgH and MgD bands at 2819 Å and 2702 Å	1133
Dr. W. N. FOX and Dr. G. W. SERIES. Hyperfine structure of the level $5^2\text{P}_{1/2}$ of potassium 39.	1141
Mr. K. G. HAMBLETON, Dr. C. HILSUM and Mr. B. R. HOLEMAN. Determination of the effective ionic charge of gallium arsenide from direct measurements of the dielectric constant.	1147
Dr. C. F. BARNABY. The energy loss of singly charged heavy relativistic particles in an organic material	1149
Mr. H. P. D. LANYON and Dr. W. E. SPEAR. Space charge limited current flow and deep trapping in selenium.	1157

	PAGE
Mr. E. THORNTON. Viscosity and thermal conductivity of binary gas mixtures: krypton-argon, krypton-neon, and krypton-helium	1166
Dr. A. SUDDABY and Mr. J. R. N. MILES. A correction to the Smoluchowski equation in the molecular theory of liquids	1170
Dr. D. J. THOULESS and Mr. D. R. TILLEY. Collective modes in the theory of superconductivity	1175
Mr. T. GASKELL. The collective treatment of a Fermi gas: II	1182
Dr. W. R. HINDMARSH and Dr. K. A. THOMAS. Collision broadening in the argon spectrum	1193
Dr. W. M. DEUCHARS and Mr. D. DANDY. Angular correlations in the reactions $^{18}\text{O}(\alpha, n\gamma)^{21}\text{Ne}$ and $^{22}\text{Ne}(\alpha, n\gamma)^{25}\text{Mg}$	1197
Mr. B. R. JOSHI. Orbital electron capture ratio and beta spectrum of ^{204}Tl	1205
Letters to the Editor:	
Dr. S. HINDS, Dr. R. MIDDLETON, and Dr. A. E. LITHERLAND. An energy level of ^{24}Mg at 6.44 mev excitation	1210
Dr. C. BROUDE and Dr. H. E. GOVE. The spin of a new level in ^{24}Mg	1211
Dr. T. E. PEACOCK. The effective number of electrons in the π band of graphite	1214
Mr. BAL KRISHNA AGRAWAL and Dr. G. S. VERMA. Dislocation relaxation in zinc at low temperatures	1216
Dr. J. H. TOWLE and Mr. B. E. F. MACEFIELD. The threshold of the $^{12}\text{C}(^3\text{He}, n)^{14}\text{O}$ reaction	1217
Dr. T. DOBROWOLSKI and Dr. J. YOUNG. The determination of the half-life of RaC'	1219
Mr. R. PETERKOP (with a note by Dr. S. Geltman). Consideration of exchange in ionization	1220
Prof. H. FRÖHLICH. New heavy bosons	1223
Corrigendum:	
Mr. C. B. P. FINN, Dr. R. ORBACH and Dr. W. P. WOLF. Spin-lattice relaxation in cerium magnesium nitrate at liquid helium temperatures: A new process	1223
Obituary Notices:	
Professor F. J. M. Stratton	1224
Robert Kenworthy Schofield, M.A., Ph.D.	1225
Harry Moore	1226
Abram Feodorovich Ioffe	1227
S. P. F. Humphreys-Owen	1228
George William Osborn Howe	1229
Sir Arthur Fleming	1230
Maurice, Duc de Broglie	1232
Thomas Yeomans Baker	1232
Charles Vickery Drysdale	1235
Subject Index, Vol. 77	1237
Index to Authors (with Titles), Vol. 77	1244
Index to Reviews of Books, Vol. 77	1254



Digitized by the Internet Archive
in 2024

PROCEEDINGS OF THE PHYSICAL SOCIETY

VOL. 77, PART 1

1 January 1961

No. 493

44th GUTHRIE LECTURE

Observational Tests in Cosmology

By F. HOYLE

Lecture delivered before the Physical Society, on 21st March, 1960

Abstract. Cosmologies separate sharply into those which predict that a definite origin of the whole universe occurred a precise finite time ago, and those which require no such origin to have taken place. Observational methods exist for arriving at a decision between these two forms of theory. In particular, these are:

(i) *Geometrical tests*

Proposed differences between the present state of the universe (determined by the observer's immediate locality) and the past condition of the universe (determined by observation of very distant objects) are investigated under this heading.

(ii) *Local evolutionary tests*

The past history of the universe must have been such as to lead to the present state. When applied to the formation of galaxies, the ages of galaxies, to the generation of cosmic rays and cosmic radio waves, this simple condition turns out to have far-reaching implications.

The current status of tests under these headings will be reviewed.

NORMALLY in science we are concerned with isolated systems, systems that we visualise as contained inside a box—perhaps a large box. In cosmology, however, we are concerned with the whole universe, so that any idea of a localized containment must be abandoned. Even simple everyday concepts can then become quite difficult. Suppose space is infinite, as indeed it is in many systems of cosmology. How then do we formulate the conservation of energy? This is a part of two wider questions: how far do the laws of physics, determined from local observation, possess a universal validity? how far do our ideas on the distribution of matter, determined from local observation, possess a universal validity?

According to modern physics, the answer to the first question is confidently affirmative. The laws are of a field type, which means that if one knows the situation completely for an infinitesimal volume of space time one knows the situation for the whole universe. It is important that the situation for the infinitesimal volume be formulated with full generality however. Only too often we are content to accept a formulation in terms of special cases, provided the special cases are the ones we normally encounter. The closed box formulation of the conservation of energy is an example. The general statement of the conservation of energy should be obtained not from the box concept but from the zero divergence of the energy-momentum tensor. It is this latter formulation that possesses universal validity.

In the second question, by local observation is meant not an infinitesimal volume, as in the case of the physical laws, but the reliable range of our telescopes. The distribution of galaxies becomes so nearly uniform at a distance of only about $1/10$ of the range of the largest telescopes that the following uniformity postulate has been introduced into cosmology, by way of answering this second question.

A division of space-time can be made such that at any time the galaxies are distributed uniformly throughout space, provided by this we imply that averages are taken over spatial volumes with dimensions of order 100 megaparsecs, i.e. about $1/10$ of the range of the largest telescopes.

In other words, an observer who ignores the detailed forms and distribution of the nearest galaxies cannot distinguish his position in space. The observer is not restricted to one moment of time. He is allowed to compare his observations at different times, and he is still unable to distinguish his own position from that of any other observer who uses the same space-time coordinates. The answer to our second question is therefore again affirmative. Uniformity not only implies that our observer is unable to distinguish his position, he is also unable to distinguish any preferred directions in space; the properties of the objects he sees in any one part of the sky will appear similar to those which he finds in any other part of the sky. It is again implicit here that he ignores the nearest objects, such as the stars of his own galaxy.

It has sometimes been asked: how can we know that a space-time coordinate system really does exist with this uniformity property? Perhaps beyond the range of our largest telescopes the distribution of galaxies becomes markedly non-uniform. Perhaps the observed uniformity is more or less accidental?

There are two answers to this objection, one a surprisingly practical answer and the other an answer of principle. In science we are not concerned to prove the truth of hypotheses, but only the converse. When observation and theory disagree at least one of the hypotheses on which the theory is based must be rejected. Science makes progress by a process of rejection, not by a process of proof. Our aim then must be to compare the consequences of the uniformity postulate with observation. If there is agreement the situation rests, for no scientific theory can do better than explain all the facts! But if there is disagreement we shall know that one or other of our affirmative answers to the original two questions was wrong. And, except in the unlikely event that we are quite mistaken in our understanding of the nature of physics, the fault would lie with the uniformity postulate. We should then be in a position to assert that there is no system of coordinates in which the general spatial distribution of the galaxies is uniform. This would be a profound conclusion.

It follows that our uniformity postulate should be followed up, if possible, to the stage where observation and theory can be closely compared. A persistent critic would argue that since the uniformity postulate is based on observation, how can observation do anything else but confirm it? Is the procedure not tautological? A similar criticism could of course be made in every branch of science. It is answered by the circumstance that theoretical hypotheses are formulated in practice from observational data that are more restricted than the data used to test the consequences of the theory. The uniformity postulate was arrived at (in historical fact) by counting the numbers of galaxies

in different directions and at different distances. Only the most gross features of the galaxies themselves were considered, such as their overall structural forms. But having thus arrived at the uniformity hypothesis we can refine the observational data. We can consider properties that depend on individual stars. Particularly, we can consider properties that depend on the evolution of stars. This leads to a startling broadening of the data, as will now be seen.

Distances of the order of 500 to 1000 megaparsecs were involved in the original observations. The evolution of stars introduces the operation of physical processes over time intervals greater than 10^{10} years, perhaps as great as 2×10^{10} years. Such time intervals can be converted into distances by multiplying by the velocity of light—we are then comparing absolute distances in the sense of the theory of relativity. The resulting values are of order 5000 megaparsecs. Hence, by introducing the astrophysics of stellar evolution into the problem we bring in time-like distances that exceed the original space-like distances by a factor of order 10. The situation is that when we are concerned with the astrophysics of stars, even of purely local stars, we bring events into the problem that happened at space-time points far more remote from us than are the events we observe in the faintest galaxies visible in the largest telescopes! This explains in principle why the introduction of astrophysical observations into cosmology has provided a fruitful and far-reaching extension of the original data. Instead of the data being restricted to a comparatively small part of the light cone, we possess information (by no means complete, it is true) about events in a more or less cylindrical volume of space-time, the spatial radius of the cylinder being about 1000 megaparsecs and the time-like length being about 5000 megaparsecs.

The uniformity postulate has far-reaching implications, particularly in simplifying the mathematics of cosmology—as was shown first by Lemaître, and then independently by Robertson and Walker. The main effect of the postulate can readily be stated in words. In the particular space-time coordinate system in which uniformity holds, consider one particular time. Take a set of galaxies. Thinking of the galaxies as mass points, the set determines a lattice of points. The same galaxies also determine a lattice at later values of the time. All such lattices are the same except for a scale factor $R(t)$ say, where t is the time. The lattice simply expands or contracts according as $R(t)$ increases or decreases with t . In this connection, we take t to be increasing in the sense that light travels. (We choose the sign of t to be such that, if a light signal leaves P_1 at time t_1 and reaches P_2 at t_2 , then $t_2 > t_1$. Also we must think of the sides of a present-day lattice as being of order 100 megaparsecs, otherwise the uniformity concept is not applicable. Lattices with significantly smaller sides could change with time in a more general way.)

The central problem of cosmology is to determine the dependence of $R(t)$ on t . The field equations of Einstein's general theory of relativity provide the appropriate mathematical tool. The theory of relativity gives equations that are formal in one important respect. The energy-momentum tensor appears in the equations. This tensor must be constructed from physical knowledge that lies outside the theory of relativity itself. Each physical field makes a contribution; there is a gravitational term, an electromagnetic term, a nuclear term, ...

Proceeding with the form of the energy-momentum tensor given by normal present-day physics it turns out that one static solution is possible— R independent of t . This solution was discovered by Einstein at the time the theory of relativity was announced. At first it was thought to represent the universe. But with the observational discovery of the red-shift of the spectrum of the light from distant galaxies it was realized that this could not be the case. To obtain a red-shift it is necessary that R should increase with t . Solutions of the equations with this behaviour can indeed be found. They all have the remarkable property that R possesses a zero for t finite. That is to say, if we follow time backwards we arrive at a finite time ago at $R=0$; in words, the points of our lattice become jammed together, and the density of matter tends to infinity.

After solving for $R(t)$, two constants of integration appear. In addition to these, there is also the possibility that Einstein's equation should contain a term involving a cosmical constant, λ say, in which case R depends on λ . Since R determines the red-shift of the spectrum of distant galaxies it is in principle possible to determine all these constants from observation, i.e. by observing galaxies at different distances and by comparing their red-shifts. Unfortunately, difficulties of observational selection (this will be discussed later) have so far prevented this procedure from being carried through in a satisfactory way. Yet some progress can be made.

Consider the case $\lambda=0$. Write $t=0$ at $R=0$, i.e. set the zero of time at the singular state mentioned above. What is the present-day value of t ? According to the best available data t cannot be appreciably greater than 10^{10} years. But we have already seen that evidence concerning past times of this order can be obtained from astrophysical considerations. Is there any indication of a singular state of the universe? The answer is negative. The oldest stars of our own galaxy appear to have an age of about 1.5×10^{10} years. Such an age already extends back beyond the singular state, yielding an immediate contradiction.

The contradiction can be avoided if $\lambda \neq 0$. But then a further astrophysical test arises in this case. It can be shown that only at one phase of the expansion of the universe can galaxies have condensed from an intergalactic gaseous medium. This phase is now past. Hence this cosmology can be disproved if it can be demonstrated that new galaxies are indeed forming at the present epoch.

The indications here are uncertain. Some astronomers believe they have obtained fairly clear-cut evidence in favour of the formation of new galaxies. Others deny this. The nature of the evidence will be discussed below at a more convenient moment.

The condition $R \rightarrow 0$ is so remarkable that it is natural to ask whether it is quite certain that the universe originated in such a singular state. Could our uniformity postulate really be responsible for an unwarranted conclusion?

It has recently been shown by Heckmann and Schücking that $R \rightarrow 0$ can be prevented if we dispense with spatial isotropy, but still adhere to spatial homogeneity. That is to say our observer still fails to distinguish his position in space, but he can distinguish preferred directions in space. This relaxation from the uniformity postulate permits the universe to possess absolute rotation. Extra terms now enter the field equations. These terms prevent the lattice scale-factor R from tending strictly to zero.

Heckmann and Schücking favour a model of the universe in which R oscillates periodically between finite values R_1 and R_2 . (An alternative possibility is that the universe started in an infinitely dispersed state. Contraction occurred over an infinite time scale until R reached a minimum value R_1 . Thereafter R began to increase, and R will go on increasing until it tends to infinity again.) Possibilities for testing the Heckmann-Schücking theory will also be discussed at a later stage.

THE STEADY STATE THEORY

If we continue to adhere to the strict uniformity postulate, and if we wish to prevent R tending to zero, our only recourse is to modify the energy-momentum tensor. We ask first: do fields at present unknown to physics exist? No definite answer can of course be given, but the probability is in favour of the existence of such fields. New fields are constantly being added to physics. It is accordingly improbable that the last of them has been discovered. The next question is more uncertain: is it possible that a new field might make an important contribution to the energy-momentum tensor? The possibility of producing an important cosmological modification depends on an affirmative answer to this question.

It is worth noticing in this connection that although it is in principle possible to discover the laws of physics by observations made only in a very small space-time volume—for example observations in a terrestrial laboratory—it may prove a very difficult matter to do so. If the existence of gravitation had not been forced on our attention by large-scale phenomena outside the laboratory its discovery would have been subtle and difficult. Ironically, gravitation makes a far more important contribution to the cosmological problem than the more easily discovered fields do. Could there be another field, still more difficult of discovery in the laboratory, that also has an important influence on the cosmological problem?

The first work on this question some twelve years ago (Hoyle 1948) showed that a field could be postulated that would alter the structure of Einstein's field equations in a remarkable way, preventing R tending to zero at any finite value of t . The solution for R was $R = \exp(Ht)$, with H a constant related to the coupling constant of the new field. Thus $R \rightarrow 0$ only at $t \rightarrow -\infty$. A similar result was obtained a year or two later by McCrea (1951).

At the time of my own work and at the time of McCrea's the number of possibilities for introducing a new field of the required type seemed rather depressingly large. But more recently a formulation of the problem in terms of an action principle by M. H. L. Pryce shows that, so long as one keeps to fields of a simple type, the available freedom is very much less than was formerly supposed. Indeed, the formulation of a scalar theory is unique, apart from the value of a coupling constant. Provided only that the coupling constant is non-zero, one has the remarkable result already stated, $R = \exp(Ht)$. The universe must possess the geometry discovered some forty years ago by de Sitter.

Although R is still to be regarded as a lattice scale-factor, some caution is necessary in interpreting R at past times. We visualise galaxies as forming mass points in the lattice. But galaxies belonging to a present-day lattice did not necessarily exist in the past, for as we go backwards in time galaxies drop one

by one out of the lattice. Thus $R \rightarrow 0$ as $t \rightarrow -\infty$ does not require the mass density to tend to infinity. In fact the equations require the average mass density to remain constant at all times; this arises because the new field causes matter to be created continuously. The constancy of the mass density is derived from the zero divergence of the energy momentum tensor (which now includes a contribution from the new field) and is therefore an expression of the conservation of energy.

Already existing galaxies expand apart in accordance with the increasing scale-factor, $R = \exp(Ht)$. But new galaxies can condense from the newly created material. Such new condensations tend to increase the spatial density of galaxies, whereas expansion tends to decrease it. The state of affairs at any particular moment is a compromise between these opposing effects, and, provided new condensations form at a steady rate, the compromise between condensation and expansion will be steadily maintained. That the universe preserves such a steady-state condition is the basic postulate of Bondi and Gold (1948). Their postulate is an extension of the uniformity hypothesis. Instead of merely asserting that an observer cannot determine his spatial position, Bondi and Gold postulate that no set of observations that concern only averages over large volumes (100 megaparsecs dimension) can determine the epoch—there is no large scale evolution of the universe to serve the observer as a clock. The relation of this point of view to the field theory method is indicated by the above remarks.

Creation is to be visualized as taking place in the simplest manner, as elementary particles created throughout space. There is no question of organized structures, such as galaxies, being created directly. Organized structures must be formed by explicit astrophysical processes, and there is the crucial requirement that all such structures must be formed continuously by explicit processes, otherwise the expansion of the lattice factor over an infinite time scale would by now have reduced their spatial density to zero. Hence in the steady-state theory all observed structures must be in a state of continuous regeneration. This requirement exposes the theory to severe observational tests. The opportunities offered to the observer to negate the theory are thus far more explicit and varied than they are in other forms of cosmology.

THE OBSERVATIONS

Having now described the different cosmologies, we pass on to the main topic of this lecture—the exposure of the different cosmologies to observational test.

Time Scale and Age Problems

The ages of the oldest stars in our own galaxy appear to be at least 1.5×10^{10} years, and may indeed be as high as 2×10^{10} years. If we accept the present-day distance estimates of the galaxies, the certain requirement that our galaxy be younger than the whole universe rules out normal cosmologies with $\lambda = 0$. It also rules out the oscillating model of Heckmann and Schücking. Only Lemaître's cosmology with $\lambda \neq 0$, and the steady-state theory, survive this test.

The possibility does arise, however, that the present distance scale of the universe is in error. The distance scale is usually expressed as a rate of increase with distance of the red-shift velocity, defined as $-c\Delta\nu/\nu$, where c is the velocity

of light and $-\Delta\nu$ is the measured red-shift in frequency of light of initial frequency ν . The present estimate of the rate of increase of $-c\Delta\nu/\nu$ is $75\text{--}100\text{ km sec}^{-1}\text{ megaparsec}^{-1}$. For radial distances r , not so great as to require non-Euclidean considerations, we can write

$$-c\Delta\nu/\nu = Hr.$$

With r measured in megaparsecs and c in km sec^{-1} , the Hubble constant H is the quantity just mentioned, viz. $75\text{--}100\text{ km sec}^{-1}\text{ megaparsec}^{-1}$. This is the same quantity as that which appears in the steady-state theory, $R = \exp(Ht)$. The Hubble constant has dimensions (time^{-1}), and in c.g.s. units $H^{-1} = 3 \times 10^{17}\text{ sec}$, i.e. about 10^{10} years.

In normal cosmologies with $\lambda = 0$, H^{-1} gives an upper limit to the age of the universe, and in an oscillating cosmology, such as that of Heckmann and Schücking, the time elapsed since the last minimum phase is less than $\frac{2}{3}H^{-1}$, i.e. less than about 7×10^9 years. Since it is necessary, for a reason to be explained in a moment, that the ages of the galaxies be less than the time elapsed since the last minimum phase, an age discrepancy by a factor of order 3 arises in such a case.

To save these cosmologies it is necessary to double or even treble the value of H^{-1} . Since $\Delta\nu/r$ is an accurately measured quantity such a reassessment of H^{-1} requires the distance estimates r to be increased by a corresponding factor. In recent years the estimates of r have indeed increased considerably. Hence it might be suggested that a further increase by a factor 3 is by no means impossible. There is one important consideration that tends to discourage this point of view, however. The apparent angular size θ of a galaxy seen face on is related to its physical diameter d and to its distance r by $\theta = d/r$, provided again that r is not so large as to involve non-Euclidean considerations. Since θ can be measured with fair accuracy, an estimate for r implies an estimate for d . Now with the present-day scale of distances for r , the diameters d of galaxies possessing similar structural forms to our own galaxy turn out to be similar to the independently known diameters of our own galaxy and of nearby galaxies, such as M31 and M81. If the values of r for the distant galaxies were systematically revised upwards by a factor of 3 this agreement would evidently be destroyed. The independently measured nearby galaxies would then become anomalously small.

Referring back to the oscillating case, it may be wondered why all galaxies must have condensed at epochs later than the last minimum phase. This again brings in an astrophysical argument. Hydrogen is converted into helium inside stars. Plainly then, the universe cannot have passed through an infinite series of oscillations without all its hydrogen becoming burned up inside stars unless there is some reverse process in which helium is returned to hydrogen. Such a reverse process demands a high-density, high-temperature condition, in which the whole of the matter of the universe is densely packed together. Hence there can be no separate galaxies at the minimum phase. All the galaxies we now observe must therefore have originated as organized structures at epochs later than the last minimum phase.

It is worth adding that even granted a high-density, high-temperature condition for the whole of the matter in the universe it is not clear whether the helium really can be returned to hydrogen. It may well be that considerations

of nuclear physics can be used to exclude all oscillating models of the universe. This remains open for investigation.

If we accept the present evidence only two cosmologies survive the age criterion, the steady-state theory and Lemaître's cosmology with $\lambda \neq 0$. The situation is quite different in these two cases, however. In Lemaître's cosmology the galaxies all condensed at one particular epoch—at the time when the expansion rate R passed through a minimum value. Thus all galaxies possess ages comparable with our own, say 1.5×10^{10} years. A very different situation arises in the steady-state theory.

Remembering that R is a scale-factor, it is clear that the spatial density, Q say, of already existing galaxies decreases at a rate $3Q\dot{R}/R$. For $R = \exp(Ht)$ this is just $3HQ$. To maintain a steady-state situation new galaxies must evidently be born at this same rate, viz. $3HQ$ per unit volume per unit time. Next, writing $q(t)dt$ for the density of galaxies with ages between t and $t + dt$, we have

$$Q = \int_0^\infty q(t)dt,$$

and

$$q(t + dt) = q(t) - 3q(t)\frac{\dot{R}}{R}dt,$$

giving

$$\dot{q} = -3q\frac{\dot{R}}{R} = -3Hq,$$

from which it is easily seen that q decreases with t proportionately to $\exp(-3Ht)$. Inserting this proportionality into the above integral for Q we obtain

$$q = 3HQ \exp(-3Ht).$$

Hence we expect galaxies of all ages to exist, ranging from newly born galaxies up to galaxies with $t \rightarrow \infty$. But since the spatial density declines rapidly as t exceeds H^{-1} , we shall not expect to observe more than at most one galaxy with $t \gg H^{-1}$.

The mean age of all galaxies is

$$Q^{-1} \int_0^\infty tq(t)dt.$$

This is readily found to be $(3H)^{-1}$. With the present-day estimate of H the mean age is therefore no more than 4×10^9 years. Hence in the steady-state theory the great majority of galaxies must be far younger than the age of our own galaxy.

Before we consider the implications of these simple conclusions it is worth noting that a similar argument applies to any type of object that possesses permanence after it is formed. Objects that are evanescent in themselves—for example radio sources—decline in density at a rate faster than $3Q\dot{R}/R$. Thus to maintain a steady-state situation such objects must be born at a rate faster than $3HQ$. When the evanescence takes place in a time very much less than $(3H)^{-1}$ the birth rate is essentially controlled by the natural decay of the objects themselves, not by the expansion of the universe.

Returning to the case of galaxies, there is no difficulty in understanding what is meant by the birth of galaxies, *provided we deal with all galaxies taken together.*

New galaxies must be born out of gas distributed throughout the intergalactic medium—the gas that is constantly resupplied by the creation process.

The problem can be much more awkward, however, if we consider only galaxies of a particular structural type. It is true that if one makes the assumption that each type of galaxy is a separate species of animal—that one type never changes into another—then an exactly similar interpretation of the birth of each type must be made. Each type must be born separately from the intergalactic medium. Without, I think, realising that an assumption was involved in his argument, Baade (1958) stated that his failure to observe E-type galaxies newly condensed from the intergalactic medium proved the steady-state theory to be incorrect. Baade's argument has recently been repeated by Bok, without critical discussion of the problem being given.

If an object of type A changes to type B through a process of astrophysical evolution, then the astrophysical evolution itself produces the birth of objects of type B. Thus if galaxies undergo evolution in the sense

$$A \rightarrow B \rightarrow C \rightarrow D \rightarrow E$$

there need be no direct condensation of E-type galaxies from the intergalactic medium at all.

The nature of the stages A, B, C, and D was purposely left unspecified in the preceding paragraph since the precise identification of these stages is not important to the logical situation. The work of Morgan (1958) suggests, however, that we make the tentative identification $B = Sc$, $C = Sb$, $D = Sa$. The stage A then represents an initially small primitive galactic condensation.

It is still true in this astrophysically evolutionary picture that the average age of the E-type galaxies must be $(3H)^{-1} \approx 4 \times 10^9$ years. But this is not the age of the oldest stars, for the oldest stars belong to stage A. Taking each stage as occupying a time $(3H)^{-1}$, and accepting the tentative identifications, we have the following situation:

Type of galaxy	Primitive forms	Sc	Sb	Sa	E
Age of the oldest stars (10^9 years) in the average galaxy	4	8	12	16	20

In a particular case the ages of the oldest stars could of course be greater than the values given in the present table. This appears to be so for our own galaxy, although the discrepancy is not very great. The ages of the oldest stars in the galaxy could be no more than 15×10^9 years. Only a slight change of H would then be needed to bring the values into concordance. (This could be done without raising the difficulty mentioned above that a marked increase of H^{-1} would lead to our galaxy, and other nearby galaxies, becoming abnormally small in their linear dimensions.)

To avoid possible misunderstandings, it should be mentioned that the elliptical galaxies considered here are the so-called giant ellipticals, not small objects such as the companions of M31.

Morgan's arguments in favour of an evolutionary scheme of the above type are based on the integrated spectra of the galaxies. A similar argument can be obtained from the integrated colours. The stars of the nuclei of Sb and Sa spirals seem to be similar in character to those of the E-galaxies, but the integrated colours become increasingly red along the sequence Sb, Sa, E. According to

recent theoretical work (Crampin and Hoyle 1961), the colour of a star group does indeed become increasingly red with increasing age, so that the observations are qualitatively in accord with the age sequence of our table. Furthermore, preliminary quantitative values derived from the colours agree very well with the age values given in the table. It would be wrong, however, to overemphasize conclusions that are still tentative. The colours of the nuclei of the spirals may possibly turn out to be affected by halos of the blue globular cluster-type stars. Until such effects have been allowed for it would be premature to attach great weight to considerations of colour.

Perhaps the strongest evidence in favour of the existence of comparatively young galaxies has been obtained by E. M. Burbidge and G. R. Burbidge from their dynamical study of a cluster of predominantly spiral galaxies in the constellation of Hercules (Burbidge and Burbidge 1959). The cluster possesses the general shape of a capital V, which shape must of necessity be short-lived. Measurements of the speeds of motion of the separate galaxies show indeed that the cluster must be in a state of dissolution, unless the galaxies themselves are of improbably large individual masses or unless the cluster contains an improbably large mass of diffuse gas; and if the cluster is in a state of dissolution the whole structure must be young.

There are other factors that also point in the same direction. The giant elliptical galaxies are systematically more massive and more luminous than are the spirals, as if there were a continuous process of growth along our sequence. It is moreover a common feature of the general galactic field that spiral galaxies are found in small groups that seem to be dominated by one, or perhaps two, giant ellipticals. The implication seems to be that the spirals in such groups have condensed from the intergalactic medium through the agency of the dominating elliptical. A possible mechanism for this has recently been considered by Burbidge and Hoyle (1961).

To conclude the present discussion of the formation of new galaxies, we ask: is there evidence of the formation in large numbers of primitive galaxies, possibly galaxies of quite small mass? Recently Vorontsov-Velyaminov (1958) has published a catalogue of strange objects to be found in the Palomar sky survey. A surprising feature of the catalogue is that the proportion of such objects comes out to be unexpectedly large: down to about the 15th magnitude the fraction seems to amount to three or four percent of the total number of more or less normal galaxies. When we consider that the lifetime of these strange objects cannot in most cases be longer than about 10^8 years, it follows that the number of queer objects that arise in a time interval of 4×10^9 years must be at least of the order of the total number of galaxies.

Nothing is so far known about the absolute magnitudes and distances of these objects, but the probability is that the objects are not giant systems. They are probably faint and comparatively close by. If this is so the spatial density of queer objects arising in a time interval of 4×10^9 years must be very high indeed. A proportion of these could very well prove to be the primitive galaxies of type A required by the steady-state theory.

Geometrical Tests in Cosmology

So far we have only considered distances from the observer that are small enough for Euclidean geometry to yield adequate accuracy. If we increase the

distance non-Euclidean considerations become important, however, and these effects differ from one cosmology to another. Hence, observations that reveal the character of the non-Euclidean effects will serve to decide the correct cosmology, or at any rate many of the features of the correct cosmology.

The relation between distance and red-shift is a case in point. Non-Euclidean geometry introduces a second-order term. Written in terms of the wavelength λ instead of the frequency,

$$c\Delta\lambda/\lambda = Hr + Kr^2$$

except in the case of the steady-state theory where $K = 0$. Can it be demonstrated that K is not zero?

In practice, astronomers do not measure r of course. They measure the magnitude M of a galaxy, M being related to r by

$$M = 2.5 \log L - 2 \log r - 2 \log \left(1 + \frac{\Delta\lambda}{\lambda} \right) + \text{const.},$$

where L is the intrinsic energy emission of radiation by the galaxy (for example, measured in terms of the solar luminosity). The constant in this equation simply determines the zero-point of the magnitude scale.

Now provided we are concerned only with galaxies possessing the same value of L , these equations can be solved to give M in terms of $\Delta\lambda/\lambda$. The resulting relation is given in Fig. 1, both for the steady-state theory and for the well-known cosmology of Einstein and de Sitter (this is a critical member of the set of cosmologies in which the cosmical constant is put equal to zero). The curve appropriate for Lemaitre's cosmology falls close to the steady-state case, so that the present criterion is not a suitable one for separating these two latter theories.

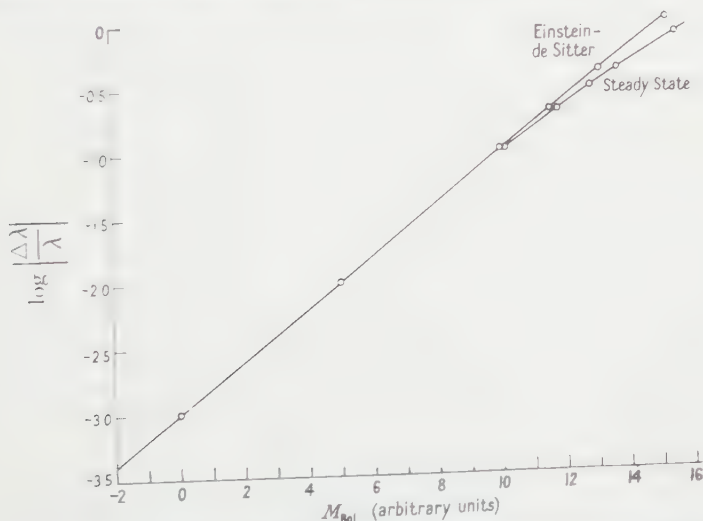


Fig. 1. Apparent magnitude as a function of red-shift for a source of standard intensity.

Both M and $\Delta\lambda/\lambda$ are measured quantities. Hence we have here a critical test that will serve to separate the Einstein-de Sitter cosmology from the Lemaitre cosmology and from the steady-state theory, *provided we can be sure that L really is the same for all the galaxies that are observed*. It is here that a difficulty arises. Galaxies differ widely in their values of L . The observation

of comparatively close-by galaxies suggests, however, that L tends to saturate at an upper limit close to 10^{44} erg sec $^{-1}$. If there were indeed a strict upper limit, and if we were to work always with galaxies at the upper limit, then L would indeed be constant. This is the hypothesis on which first Hubble, and then Sandage, based their work.

But almost certainly the upper limit is not strict. There is moreover a selection effect as $|\Delta\lambda/\lambda|$ increases in favour of choosing galaxies with larger and larger values of L . To measure $\Delta\lambda/\lambda$ a spectrum must be obtained, and for this it is desirable to have as much light as possible admitted to the spectrograph. This naturally biases the observer in favour of the brightest galaxies he can find, and since the sample of galaxies increases rapidly with distance, intrinsically brighter specimens are likely to be found the larger the sample becomes, i.e. the greater $|\Delta\lambda/\lambda|$ becomes.

This effect biases the observed curve. The important question is to what degree? If the bias out to $|\Delta\lambda/\lambda|=0.4$ is appreciably less than one magnitude (one unit in M) then the results so far obtained would contradict both the steady-state theory and Lemaitre's cosmology. They would favour a cosmology of the Einstein-de Sitter type (zero cosmical constant), but since we cannot be sure of this the position is really one of stalemate.

To make effective progress along these lines it is clearly necessary to choose galaxies by a criterion free from selection effect. Suggestions have been made as to how this might be done. None based entirely on optical astronomy is really satisfactory. A possibility involving collaboration with the radio-astronomer offers much better hope, however.

The most powerful known radio source is a peculiar object in the constellation of Cygnus, thought by many astronomers to be a pair of galaxies in collision. Very hot gases are present in the object that emit strong bright spectrum lines, in particular the line 3727 of OII. A similar object situated at much greater distance would be detectable as a radio source. It might well also be possible to measure $\Delta\lambda/\lambda$, because this is easier to do in the case of bright line emission than it is for a normal galaxy.

Such a programme has recently been carried out by Bolton and Minkowski. The radio source is No. 295 of the Cambridge 3C catalogue. The measured wavelength of one observed bright line gives $|\Delta\lambda/\lambda|=0.4614$, if the line is interpreted as the 3727 line of OII.

It would of course be unsafe to assume that such peculiar objects possess a standard value of L . But by good fortune 295 3C appears to be associated with a cluster of galaxies, and the mean value of L for, say the ten brightest of these cluster galaxies, can be taken as equal to the mean L for the ten brightest galaxies in other clusters.

What is being done here is to use the radio source as a criterion for choosing the cluster, thereby avoiding the difficulties of optical selection effects. The radio source also assists in the measurement of $\Delta\lambda/\lambda$ because of the strong concentration of light in one or more bright lines.

The difficulty with this method is to obtain an adequate number of cases. This is necessary in order to eliminate the normal statistical scatter that exists in the values of L for cluster galaxies. If about a dozen similar cases could be found much of the statistical scatter could be removed and the test contained in Fig. 1 could be made. To obtain anything like a dozen cases it will probably

be necessary to consider radio sources that are considerably fainter than 295 3C. Precise position measurement, without which the relevant optical identifications cannot be made, then becomes very difficult. Thus it appears rather unlikely that many similar cases will come to light in the immediate future. The difficulty of selection seems therefore as if it will be replaced by a difficulty of statistics.

Turning now to a different type of geometrical test, our uniformity postulate, taken together with a knowledge of the precise non-Euclidean properties of a cosmology, allows number counts to be worked out either as a function of $\Delta\lambda/\lambda$ or as a function of M . Results for the steady-state theory and for the Einstein-de Sitter theory are shown in Fig. 2 (numbers against M). The two theories coincide up to the distances where non-Euclidean properties become important.

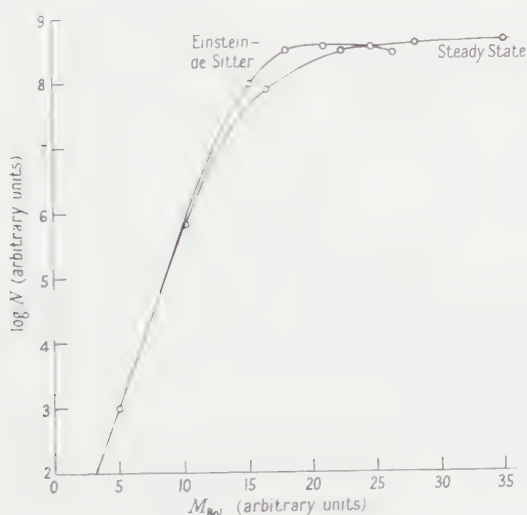


Fig. 2. Number of objects per unit magnitude range plotted against apparent magnitude.

So far as the steady-state theory is concerned these considerations can be applied unambiguously to any type of object, galaxy or radio-source, provided only that the object is of sufficiently frequent occurrence (the mean spatial density should not be much less than one object in a cube with side 100 megaparsecs). But an assumption is involved in the case of the Einstein de Sitter theory, namely that the ratio of the spatial density of objects to the total spatial mass density remains the same at all times. This would not be correct if the number of objects were to change with the square of the spatial mass density—as it might in the case of radio-sources, if indeed radio-sources arise mainly in collision between galaxies.

The classic attempt to apply a number count test to galaxies was made by Hubble. Unfortunately the results were disappointingly inconclusive. Since Hubble's work astronomers have been generally unwilling to undertake the immense labour involved in this test, for the probability is that any new programme will also end in uncertainty.

The situation is better in the case of radio-sources since the number of sources to be counted is very much less than it is in the case of galaxies. Complications arise, however, in the radio case from the fact that the radio-astronomer cannot deal with each source separately—sources tend to overlap in the radio beam. This prevents the curves of Fig. 2 from being applied directly to the radio observations. What the radio-astronomer must do is to take the curves of Fig. 2 and to decide how such a distribution of numbers would affect his particular form of equipment. After this he can compare his theoretical deductions, based on different cosmologies, with the actual observations.

The most extensive observations so far reported along these lines are due to Ryle and his collaborators. The latest results reported by Ryle and Scheuer (1960) give counts of some 2000 sources at a wavelength of 1.9 metres. The results are consistent with Euclidean geometry. There is a rather large fluctuation of numbers among the brightest sources. Whether this is due to a combination of instrumental and statistical reasons, or whether it represents a genuine physical deficiency of nearby sources, is still uncertain.

The implication is that the counts have not yet penetrated to sufficiently great distances for the required effects to show themselves. Work now proceeding at Cambridge may eventually turn out to reveal these elusive non-Euclidean effects.

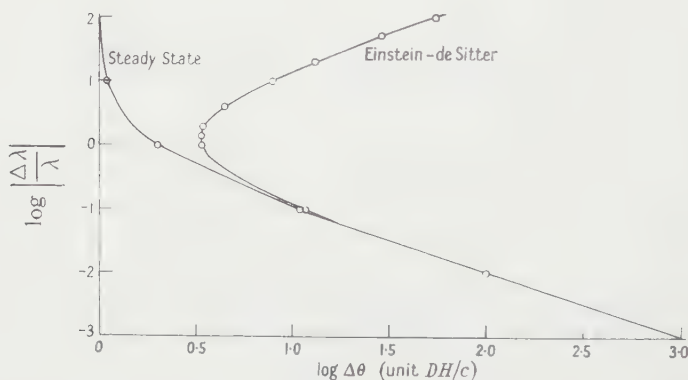


Fig. 3. Apparent diameter $\Delta\theta$ of a source of absolute diameter D plotted against red-shift.

Perhaps the most remarkable geometrical difference between the steady-state theory and that of Einstein-de Sitter theory lies in the measurement of the apparent angular diameters, $\Delta\theta$ say, at different $\Delta\lambda/\lambda$, of sources of fixed physical dimensions (say spheres of fixed diameter D). Results are given in Fig. 3. The existence of a minimum value for the Einstein-de Sitter case is very remarkable. This minimum is some three times greater than the limiting value in the steady-state case. If radio sources of fixed diameter turn out to exist, the present property might well provide a method for separating the theories since the actual numerical values of $\Delta\theta$ are just within the range of what might be measured. For sources with the diameter of the Cygnus source, the minimum value of $\Delta\theta$ in the Einstein-de Sitter case is about $15''$.

Further Astrophysical Tests

The situation concerning the condensation of galaxies under purely gravitational forces in the different cosmologies is given in the following table:

Cosmology	Growth of small density fluctuation under purely gravitational forces
Oscillatory models	Condensation at all times
Einstein-de Sitter theory	Condensation at all times
Other cosmologies with zero cosmical constant	No condensation at any time
Lemaître's cosmology with non-zero cosmical constant	Condensation at a particular epoch (that of minimum rate of expansion)
Steady-state theory	No condensation at any time

It seems then that non-gravitational forces must be introduced if the steady-state theory is to survive the requirement that galaxies must form. If the intergalactic gas were hot a local cooling of the gas could produce condensation through the pressure exercised by hotter surrounding regions. After compression, once higher densities have been reached, gravitation could of course become the dominating force.

It is possible for the intergalactic gas to be very hot in the steady-state theory, but not in other cosmologies. In the latter, the universe has expanded from a high density phase in which the kinetic temperature T_k and the radiation temperature T_r must have been equal, since at high density there is a strong coupling between radiation and matter. Now it can readily be shown that as a consequence of the expansion of the universe T_k decreases at a rate that is greater than or equal to the rate of decline of T_r (equal to if the particle motions are highly relativistic, otherwise greater than). Hence we expect $T_k < T_r$, and since T_r cannot exceed about 10^4 K it follows that no appreciable value of T_k can have survived from the early high density phase of the universe. (It is true that T_k might be lifted locally through heating by stars, but the values of T_k that can arise in this way are only of the order of a few thousand degrees. This is quite inadequate for the purposes of the present discussion. The temperatures of interest here exceed 10^6 deg K.)

The heating in the steady-state case can arise from the nature of the created material. If these are neutrons then some 3×10^{17} erg g⁻¹ of heat is supplied by the decay of the neutrons, and this is adequate to lift T_k to a value near 10^9 deg K.

An attractive feature of the cooling argument is that a natural scale is fixed for the size of the condensations. By inserting the velocity of sound, V_s say, into the red-shift relation,

$$V_s = H r_c$$

we obtain a value of r_c which represents this natural scale. Since $V_s \propto T_k^{1/2}$ it follows that $r_c \propto T_k^{1/2}$. With $T_k = 10^9$ deg K, $H^{-1} = 3 \times 10^{17}$ sec, $r_c = 30$ megaparsecs. Thus the heat of neutron decay would introduce irregularities into the distribution of matter in the universe, the maximum scale of the irregularities being about 30 megaparsecs.

This value agrees very well with observation. We saw at the outset that in order to obtain average uniformity it is necessary to consider the spatial

distribution of matter on a scale of about 100 megaparsecs. This agrees with 30 megaparsecs for the maximum scale of the irregularities.

In contrast to this, it is an unsatisfactory feature of a purely gravitational condensation process that it does not yield a condensation scale. The condensations formed gravitationally in other cosmologies could be of any size.

All this can be related to observation. If there is gas in space, and if the gas possesses a very high kinetic temperature, there will be a weak emission of comparatively hard x-rays. For $T_k = 10^9 \text{ deg K}$ the x-ray quanta possess energies of order 50 kv, and these should pass freely through our own galaxy. Hence a faint glow of x-rays should be visible in the sky. The calculated energy flux is in the range 10^{-7} to $10^{-8} \text{ erg cm}^{-2} \text{ sec}^{-1}$. This is not outside the intensity levels that are susceptible to observation.

It could be of course that T_k is lower. A value of 10^7 deg K would be adequate to give condensations on the scale of individual galaxies. The quanta in this case would be in the 500 ev region, and these would tend to be absorbed in the interstellar gas. The problem of detection would then not be so clear-cut.

All this is part of a general point of view. If matter is created continuously then it may well be created in a form that yields high energy quanta. If matter and anti-matter were both created some annihilation γ -rays would be expected, for example. The observation of high energy quanta, whether x-rays or γ -rays, would provide a strong confirmation of the steady-state theory since their presence would be very difficult to explain in other cosmologies. The opposite situation holds. If no high energy manifestations of the creation process can be found, then doubt would be cast on the steady-state theory. In particular, it would then be difficult to explain the formation of galaxies.

In some degree one can argue that the existence of cosmic rays, and of the relativistic electrons that give rise to the cosmic radio sources, already give indications of the presence of just such a high energy world. The question here is whether this world exists outside the galaxies as well as inside them. Here we run into a new class of problems: can the whole of the cosmic rays be produced inside the galaxies? Can they be confined inside the galaxies? Why do all radio sources possess nearly the same frequency spectrum? A consideration of these questions would take us much too far from the main topic of this lecture. Suffice it to say that if these high energy manifestations should turn out to be intergalactic, rather than interstellar, their significance to cosmology will be profound. A whole new range of observational experience will then be added to our subject.

REFERENCES

- BAADE, W., 1958, *11th Solvay Conf.*, p. 303.
 BONDI, H., and GOLD, T., 1948, *Mon. Not. R. Astr. Soc.*, **108**, 252.
 BURBIDGE, E. M., and BURBIDGE, G. R., 1959, *Astrophys. J.*, **130**, 629.
 BURBIDGE, G. R., and HOYLE, F., 1961, *Astrophys. J.*, in the press.
 CRAMPIN, J., and HOYLE, F., 1961, *Mon. Not. R. Astr. Soc.*, in the press.
 HOYLE, F., 1948, *Mon. Not. R. Astr. Soc.*, **108**, 372.
 MCCREA, W. H., 1951, *Proc. Roy. Soc. A*, **206**, 562.
 MORGAN, W. W., 1958, *11th Solvay Conf.*, p. 297.
 RYLE, M., and SCHEUER, P. A. G., 1960, *Session of the International Statistical Institute, Brussels*.

Some Properties of Photographic Image Recording†

By J. S. WILCZYNSKI‡

Department of Physics, Imperial College, London

Communicated by H. H. Hopkins; MS. received 16th May 1960

Abstract. An investigation of both the linear and non-linear parts of the photographic process has been carried out using the concept of optical frequency response for the description of the contrast degradation resulting from diffusion of light in the emulsion which is the linear part of the process. An analogy between the operation of a low-pass passive filter and valve and photographic image recording is established and a simple theory for calculating the resulting opacity in a photographic image is described. This latter introduces the idea of harmonic distortion to describe the non-linear part of the process. The experimental results obtained by means of an optical Fourier analyser for transparencies were found to be in good agreement with the theory. A description of the instrument is given in the first part of the paper. Some other applications of the theory are considered.

§ 1. INTRODUCTION

DURING the last few years frequency response techniques have begun to play a very important role in the evaluation of the quality of optical images. Numerous papers have appeared describing measurements of the optical frequency response of lenses and of photographic emulsions, but very few have considered directly the frequency spectra of the distributions of intensity or transparency corresponding to photographic scenes and images respectively. The frequency response method can be used successfully only if the system to which it is applied is linear. This restriction gives rise to some difficulties in its application to the photographic process. To overcome the difficulty of non-linearity Frieser (1935) showed that the whole photographic process could be considered in two stages. The first consists of the actual exposure of the photographic emulsion to light together with a linear scattering of this light in the emulsion. In this way the original 'printed-on' exposure results in a different distribution of light in the emulsion, which has been called the 'effective exposure'. In the case of a sine-wave test object the illumination in the effective exposure will be similar to that in the printed-on sine wave but will have smaller amplitude. Under normal conditions no phase shift occurs. The effective exposure then gives rise to a density distribution which depends on the development conditions. In this second stage there is a non-linear relationship between the effective exposure and the resulting density. Frieser obtained

† The contents of this paper form part of the subject matter of a thesis submitted to the University of London for the Ph.D. degree.

‡ On leave of absence from: Katedra Fizyki, Politechnika Krakowska, Krakow, Poland.

the form of the effective exposures from the measured density distributions in the photographic images of sine-wave test objects using the H & D macro-characteristic curve to relate them, provided no pronounced neighbourhood† effect was present. In this way a density distribution, which contains in fact both the fundamental spatial frequency and its harmonics, leads to an effective exposure of sinusoidal form. Frieser has further shown that the effective exposure of a sine-wave has the same mean value as the printed-on exposure, but that it is of reduced amplitude of variation, that is, of lower contrast. Frieser denoted the ratio of the amplitude of the effective exposure to that of the printed-on exposure by 'Verkleinerungsfaktor', and this contrast reduction was shown to be a function of the spatial frequency of the test object.

In the present work an automatically operating optical Fourier analyser was constructed for the measurement of the Fourier spectra of the distributions of opacity in photographic images. It was considered desirable to undertake initially a study of the relationship between printed-on sine-wave exposures and the resulting opacity distributions in photographic emulsions. In order to examine this problem in detail a method of calculating the output of the instrument to allow comparison with measured results was established. Also discussed is a method by which the frequency response of a photographic emulsion may be derived from the harmonic composition of the output signal of the instrument, whose operation depends directly on light fluxes and not on densitometric measurements.

A useful analogy may be established between the operation of a triode valve and the recording of an image on a photographic emulsion. If sine-wave signals of large amplitude are applied to the grid of a valve then non-linearity occurs between the anode current and the grid voltage. A complete analogy exists if for the anode current we substitute opacity and for the grid voltage the effective exposure. To simulate the contrast transfer function a low-pass filter which attenuates higher frequencies is placed in the grid circuit of the valve. The input signal (printed-on exposure) is attenuated by the filter depending on its frequency (frequency response), and this attenuated signal (effective exposure) modulates the anode current (opacity) in a non-linear manner which depends on working conditions (exposure, development). As a result one may speak, as will be shown later, of spatial harmonic distortion, mean opacity and shift of mean opacity owing to the presence of even harmonics, similar to the concepts of electrical harmonic distortion, mean anode current and the rectifying effect found in the operation of a valve. The well-known Espley (1933) five- or seven-point method of analysis may be used to relate the final opacity distribution to the effective exposure. Measurements made with the instrument were found to be in good agreement with the values computed using the method outlined above.

A study of the Fourier spectrum of a distribution of transparency may be done in several ways. The simple method in principle is to scan the transparency with a microphotometer and then analyse the trace numerically. Another method which uses the Fraunhofer diffraction pattern has been described by Mlle du Marache (1952). Several other devices have been constructed which

† The term neighbourhood effect is commonly used to describe the increased density that can arise at the edge of an exposed region of a photographic plate. The effect is generally ascribed to the greater concentration of developer relative to development products in the neighbourhood of an unexposed portion of the photographic plate.

measure the squared modulus of the Fourier spectrum in terms of the auto-correlation function measured using two identical transparencies. In this category may be mentioned the instruments of Kovaszny and Arman (1957) and of Fellgett (1953). A further possibility is to analyse the transparency by illuminating it with a two-beam interference pattern and recording the variation in total transmitted light flux as a function of fringe spacing. This latter method (Viénot 1958) has been improved and adopted for the present work.

§ 2. PRINCIPLE OF THE METHOD

In the photographic image the density usually varies in two dimensions, so that a function of two variables has to be used to represent the distribution of transparency. Consider an extended distribution of transparency $B_0(\xi_0, \eta_0)$ referred to a rectangular coordinate (ξ_0, η_0) on a photographic plate. The function $B(\xi_0, \eta_0)$ will have a two-dimensional Fourier transform given by

$$b_0(s_0, t_0) = \iint B_0(\xi_0, \eta_0) \exp \{-i2\pi(\xi_0 s_0 + \eta_0 t_0)\} d\xi_0 d\eta_0$$

which after a rotation of the axes (ξ_0, η_0) through an angle $\psi = \tan^{-1}(t_0/s_0)$ and putting $R = (s_0^2 + t_0^2)^{1/2}$ may be written

$$b_0(s_0, t_0) = \int \left\{ \int B(\xi, \eta) d\eta \right\} \exp \{-i2\pi\xi R\} d\xi.$$

$B(\xi, \eta)$ is simply the transparency function referred to the new axes and R is the spatial frequency. If the integrated transparency along the η axis is denoted by

$$B(\xi) = \int B(\xi, \eta) d\eta$$

the two-dimensional transform $b_0(s_0, t_0)$ may be seen to be obtainable from the one-dimensional transform

$$b(R) = \int B(\xi) \exp(-i2\pi\xi R) d\xi$$

when this is known as a function of R for different azimuths ψ , since

$$b(R) = b_0(R \cos \psi, R \sin \psi).$$

This interpretation shows that any object may be considered as a superposition of cosinusoidal line gratings of different wavelength, frequency and orientation.

It is possible to measure $b(R)$ by illuminating the transparency with a light distribution varying cosinusoidally along the ξ axis with a spatial frequency R and measuring the maxima and minima of the light flux as the relative positions of the transparency and the cosinusoidal light distribution are varied along the direction of ξ .

Two-beam fringes formed by an interferometer may be used to provide a cosine-wave pattern of illumination. Let $P(\xi)$ be the distribution of intensity in such fringes, having frequency R lines mm, and let α be the mean intensity and β the amplitude of variation. The ratio β/α is then the Michelson visibility of the fringe pattern as shown in Fig. 1, and

$$P(\xi) = \alpha + \beta \cos 2\pi R\xi.$$

Provided that the transparency function is taken to be zero outside the region to be analysed the total light flux transmitted through a photographic plate

illuminated by the fringes is given by

$$F(\xi_0; R) = \int B(\xi) \{ \alpha + \beta \cos [2\pi R(\xi - \xi_0)] \} d\xi$$

where $B(\xi)$ is the integrated transparency as defined above, ξ_0 being the displacement of the fringe system along the ξ axis. Alternatively the total light flux may be written in terms of the spectrum $b(R)$ as follows:

$$b(R) = |b(R)| e^{i\theta(R)}$$

and then

$$F(\xi_0; R) = b(0) \left[\alpha + \beta \frac{|b(R)|}{|b(0)|} \cos [2\pi R\xi_0 - \theta(R)] \right].$$

This equation indicates that as ξ_0 is made to vary, the total light flux has a constant component proportional to α and a variable component related to the frequency R and of amplitude $\beta|b(R)|$. If the phase of the variable component is measured it will give the lateral phase shift $\theta(R)$. The modulus of $b(R)$ gives the spectrum density for the frequency R in the transparency. To obtain the normalized frequency density $T(R)$ it is necessary to use the ratio $|b(R)|/|b(0)|$, so that $T(0) = 1$.

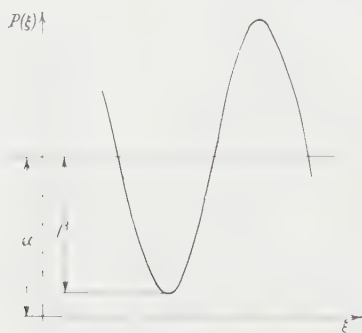


Fig. 1.

An automatic device constructed to measure the frequency spectrum of a transparency should therefore be capable of continuously and independently changing the spatial frequency R and linearly displacing the fringe position ξ_0 . Then provided the Michelson fringe visibility β/α remains constant the mean value of the variation in $F(\xi_0; R)$ will be directly proportional to $b(R)$.

The apparatus described below and shown schematically in Fig. 2 is designed to satisfy the above conditions and to measure automatically the value $T(R)$. It consists of three main parts: (i) a Michelson interferometer, (ii) optical mechanical devices for changing the spatial frequency and for shifting the fringes, and (iii) an electronic and recording unit.

§ 3. THE INTERFEROMETER

The light source L (Fig. 2), a medium pressure mercury lamp supplied from batteries, illuminates the collimator slit SL_1 through a green Wratten 77A filter F and condenser CO_1 . The Michelson interferometer consists of the two mirrors M_1 , M_2 , a dielectric beam-splitter and a coated compensator plate, all mounted on a heavy cast-iron base plate which in turn lies on a 6-inch thick layer of foam rubber, the latter being to insulate the interferometer against vibrations.

The objective O images the mirrors M_1 and M_2 on the transparency TR , through a limiting stop S_2 . This diaphragm prevents most of the stray and ghost image light in the instrument from reaching the transparency, with a consequent improvement in the fringe visibility.

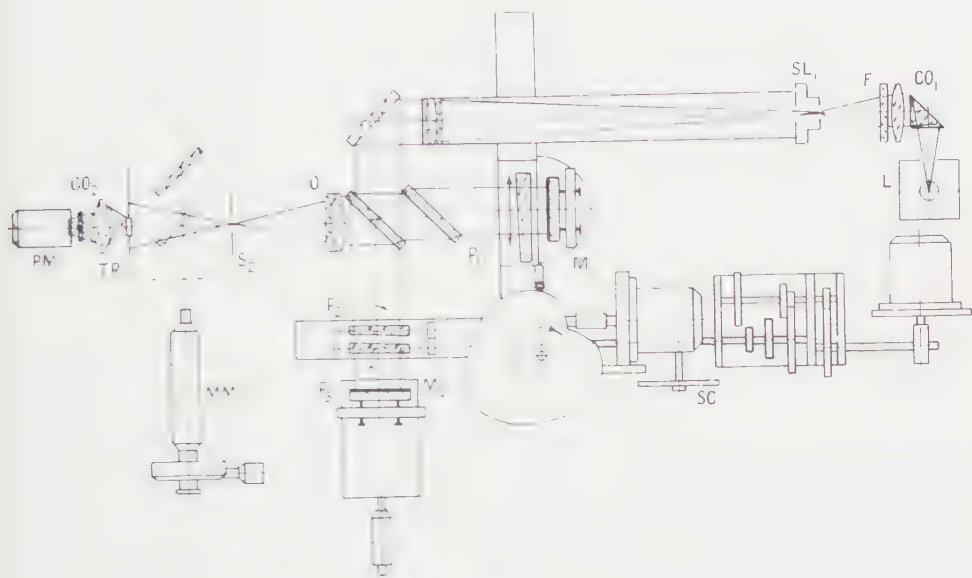


Fig. 2. Schematic diagram of the apparatus.

To keep the instrument compact the light is directed from the light source along the collimator axis by a prism and similarly a mirror is used to reflect the light into the interferometer. The two interferometer mirrors may be easily adjusted for coincidence of the images formed along the two arms of the interferometer. Mirror M_2 is mounted on a kinematic slide and may be moved by a micrometer screw to adjust for zero path difference, or alternatively to change the fringe visibility by introducing a suitably large path difference. Mirror M_1 can be tilted around a vertical axis by means of another micrometer screw. Relative tilt between the two emergent wave fronts is obtained by means of a pair of identical rotating prisms P_2 , P_3 placed in one arm of the interferometer which together are equivalent to a variable angle prism. The resulting spatial frequency of the fringes obtained is given by the formula

$$R = \frac{4(n-1) \sin \alpha \sin \phi}{\lambda}$$

where α is the angle of prisms P_2 , P_3 and ϕ the angle of rotation of the prisms in a direction away from the position in which $R=0$.

Two pairs of prisms are used, one pair with $\alpha=1$ to obtain the spatial frequencies up to 66 lines mm, and the other pair with $\alpha=2$ to obtain spatial frequencies up to 132 lines mm. These prisms are built into a double worm gear, having a reduction of 100:1, which serves to rotate the prisms in opposite directions. This unit is mounted in ball bearings and great care was needed to secure the precision necessary to ensure that the fringe pattern remains vertical. This unit is driven through a six-speed gearbox which enables the measuring

time, corresponding to a half rotation of the prisms, to be changed over a range from 40 seconds to 12 minutes. A synchronous motor running at 1500 rev/min into a 50:1 reduction is used to operate the gearbox.

The spatial frequency is indicated on the scale SC and a measuring microscope MM may be used to check both adjustment and spatial frequency.

The prism P_1 is used to shift the fringes across the photographic plate. When this prism is reciprocated linearly with time along a direction perpendicular to the light passing through arm 1 of the interferometer, the light travels through a linearly varying thickness of glass, so that a similar linear variation in path difference is introduced. The movement of the prism is provided by an Archimedian cam, and results in a frequency of variation of the total light flux to be measured which is independent of the spatial frequency of the fringe pattern. The frequency of the resulting electrical signal in the photomultiplier is given by

$$f \simeq \frac{4(\mu - 1)l\alpha m}{\lambda}$$

where l is the stroke length, α the prism angle, m the number of cam revolutions per second and λ the wavelength of light used (5461 Å for mercury green line). For $l=1.5$ in. (38.1 mm), $\alpha=7$ min and $m=0.25$ sec⁻¹, the frequency f is equivalent to 67.5 c/s. This arrangement simplifies the electronic units by providing an output of frequency which is kept constant, independent of the spatial frequency examined, merely by giving a constant speed of rotation to the cam.

All three prisms with their mechanical attachments are mounted on a bridge which is quite independent of the interferometer. Similarly the two synchronous motors are screwed to a heavy cast-iron bridge and all connections between these two units are made by universal couplings. This prevents vibrations from the mechanical arrangements passing into the fringe generating system.

The thickness of the prisms P_2, P_3 is chosen to compensate the path difference introduced by the prism P_1 , otherwise a considerable loss of fringe visibility is experienced.

The photomultiplier cathode is illuminated by the condensor CO_2 whose diameter should be large enough to gather all the light passing through the transparency assuming that it acts as a grating of the frequency R_{\max} . Further, a diffusing screen is placed close to the photomultiplier cathode to obtain equal illumination over its surface. In some experiments, namely when the dimensions of the transparency were small as compared with those of the photomultiplier cathode or when gratings were analysed, the photomultiplier was placed directly behind the transparency.

The focal length of the objective O should be as short as possible since it limits the pupil diameter and the useful transparency size or the maximum spatial frequency R which may be examined. In the apparatus described a doublet of 4 in. focal length was used.

§ 4. ELECTRONIC AND RECORDING SYSTEM

The photomultiplier output signal is fed to a cathode follower input utilizing one half of an ECC 82 valve. The value of the grid resistor used depends to some extent on the amount of light available and high values up to 10 MΩ have been tried in some circumstances. The cathode follower stage is followed by a

voltage amplifier built on an EF 86 with volume control and negative feedback. Then follow two stagger tuned stages of cascade selective amplification. The circuit described by Fleisher (1948) is used with several modifications. The band-pass of the selective stages of the amplifier must be sufficient to accept the frequency range 60–75 c/s in order to accommodate variation of the output frequency arising from small variation in the velocity of the prism. The complete pre-amplifier power supply is provided by batteries to avoid mains hum and interference at very low input signal levels.

The output of the pre-amplifier is then fed through a high fidelity audio-frequency amplifier to a 20 v a.c. pen recorder.

With this circuit the output meter readings are directly proportional to the mean light flux variation at the frequency of approximately 67.5 c/s and hence to the frequency density in the analysed transparency.

§ 5. ADJUSTMENT OF THE INSTRUMENT

The prisms P_2 , P_3 are adjusted by rotation in their mounts until only a horizontal shift of the entrance slit image is observed when contra-rotating them as a pair. The prisms are then rotated through an angle so that they give together exactly the same deflection of the light beam as the prism P_1 . This is necessary to reduce the influence of any possible vibrations which may affect the interferometer. The mirrors M_1 and M_2 are now adjusted to give two parallel wave fronts with no path difference between them. The prism system is then placed in the instrument and final adjustment of the mirrors M_1 , M_2 is made without rotating the frequency changing prisms and with the prism P_1 at half its stroke. The path difference is now compensated by shifting mirror M_2 on its kinematic slide and zero frequency is set by rotating the mirror M_1 about a vertical axis.

An EMI 6094 photomultiplier is used to detect the light flux passing through the transparency, and good signal-to-noise ratio is obtained using 90v per stage between the dynodes. For the zero spatial frequency the pen recorder is made to give full scale deflection either by altering the gain of the amplifiers or by changing the collimator slit width.

The fringes of maximum contrast, corresponding to zero path difference, move across the transparency as the path difference is varied by the prism P_1 . Thus even when the fringe spacing is kept constant the sinusoidally varying component of the light flux passing through the transparency varies slightly with a frequency equal to twice that of the cam rotation. During the operation of the instrument this effect shows itself as a series of small kinks in the curve traced by the pen recorder.

It was found in practice that the medium pressure mercury lamp used gave a sufficiently narrow spectral line provided the operating current did not exceed 0.75A and the collimator entrance slit could then be set to give sufficient light. The amplitude of the a.c. output signal varies with the Michelson fringe visibility and it was found that a better signal-to-noise ratio was obtained for a contrast of about 82% with a consequently larger amount of light than when the fringe visibility was made to exceed 95% but with much less light available.

The instrument was tested by automatically recording the Fourier transform of a number of slits of different width. An accuracy to ± 0.01 in $T(0)$ was achieved up to 40 lines/mm for the first three maxima of the $\sin X/X$ function representing the Fourier transform of a slit.

§ 6. GENERAL CONSIDERATIONS

The instrument described above lends itself to a fundamental study of the photographic process. This study was undertaken in terms of Frieser's analysis of the photographic process supplemented by the concept of harmonic distortion and shift of the level of mean opacity as described above in the introduction. Because the instrument described has a linear response to light flux, and not to photographic density, these studies were made directly in terms of distribution of opacity. In each experiment a sine-wave distribution of intensity was used for the 'printed-on' exposure, and simultaneously a density step wedge was exposed, for the purpose of deriving the H & D curve for the given emulsion and development conditions.

If the H & D macro-characteristic curve is measured it is possible to calculate from it the amplitudes of the fundamental spatial frequency and its harmonics for any given mean intensity and contrast of the fringe pattern to which the emulsion is exposed. An advantage of the present apparatus is that such a fringe pattern is immediately available as the test object, and after development the resultant transparency may be replaced in the instrument and the amplitudes of the fundamental and harmonics measured directly, using the same fringe pattern. This may be done with good accuracy, and a test of the theory is thereby made available.

The simplest method of determining the amplitudes of harmonics present in the photographic image of a sine-wave pattern after exposure and development would be to assume that the photographic recording takes place on an assumed straight portion of the characteristic curve. Harmonics are present even under these conditions unless $\gamma = 1$. A study of the second harmonic in connection with variable density voice recording was carried out by Miller (1936). His investigations were also extended to higher harmonics. The calculated ratios of both the second and third harmonics to the fundamental are plotted in Fig. 3 for different values of γ and object contrast. Satisfactory agreement with measurement is only obtained for low contrast, for low values of γ and for development giving a very short toe to the characteristic curve.

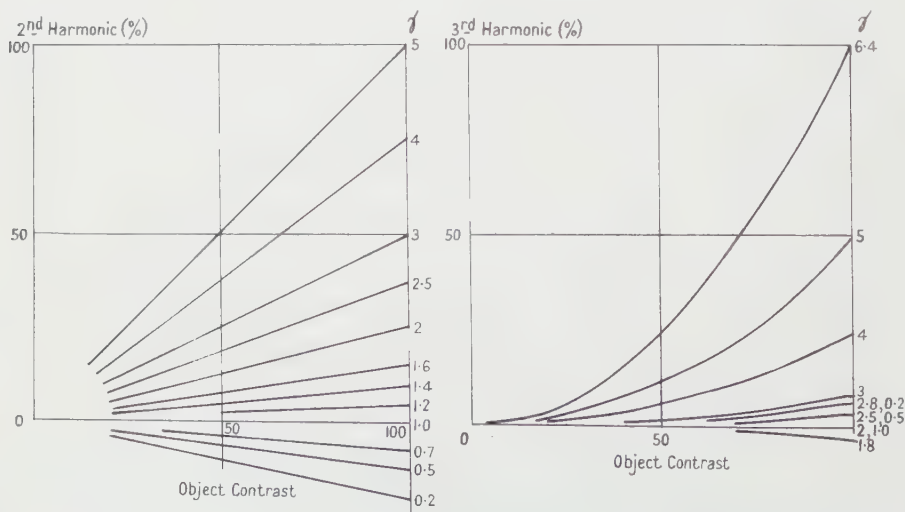


Fig. 3. Calculated percentage ratios of second and third harmonic to fundamental on the straight portion of the H & D curve for different γ and object contrast values.

The very restricted validity of this treatment may be explained as follows. The H & D curve is usually plotted on a logarithmic scale, for which an increase of density from 0 to 1 corresponds to an increase in opacity from 1 to 90. Similarly, an increase of density from 1 to 2 gives a smaller increase in opacity, from 90 to 99 for a given intensity distribution in the printed-on exposure. For these reasons the opacity variation, corresponding to a printed-on exposure, may be called the output signal of a photographic emulsion and will always have its maximum variation in the region of densities lower than one. Normally the approximately straight portion of the characteristic curve begins at a density between 0.2 and 1.0, depending on the type of emulsion and development conditions. If the straight portion begins at a higher density then the corresponding opacity variation is very small and thus the amplitude of the recorded sine wave is also small. It may also be noted that it is for these larger densities that the neighbourhood effect is of greater importance. If it is negligible then the toe portion is rather long.

Because of the very restricted validity of the above procedure a fuller investigation of the problem was undertaken. The well-known Espley (1933) five- and seven-point methods, used commonly in electronic amplifier design, may be used to calculate the frequency spectrum of the opacity distribution from the H & D curve for any given exposure of a sine wave, and this was found to provide results giving satisfactory agreement with measurements.

Assume that the equation of the H & D curve, using the opacity z and the exposure E as coordinates, may be represented by the power series

$$z = f(E) \simeq f(\alpha) + a_1(E - \alpha) + a_2(E - \alpha)^2 + a_3(E - \alpha)^3 + a_4(E - \alpha)^4 \quad \dots\dots (1)$$

where α is the mean exposure. Higher terms are neglected. If the effective exposure as defined above varies sinusoidally it may be written

$$E = \alpha + \beta \sin 2\pi R\xi \quad \dots\dots (2)$$

and substituting $2\pi R\xi = \Omega$ (1) may be rewritten in the form

$$\begin{aligned} z \simeq f(\alpha) + a_1\beta \sin \Omega + a_2\beta^2 \left[\frac{1}{2} - \frac{1}{2} \cos 2\Omega \right] \\ + a_3\beta^3 \left[\frac{3}{4} \sin \Omega - \frac{1}{4} \sin 3\Omega \right] + a_4\beta^4 \left[\frac{3}{8} - \frac{1}{2} \cos 2\Omega + \frac{1}{8} \cos 4\Omega \right]. \end{aligned} \quad \dots\dots (3)$$

Collecting coefficients of the different harmonics we obtain

$$\begin{aligned} z \simeq f(\alpha) + \frac{1}{2}a_2\beta^2 + \frac{3}{8}a_4\beta^4 + (a_1\beta + \frac{3}{4}a_3\beta^3) \sin \Omega - \frac{1}{2}(a_2\beta^2 + a_4\beta^4) \cos 2\Omega \\ - \frac{1}{4}a_3\beta^3 \sin 3\Omega + \frac{1}{8}a_4\beta^4 \cos 4\Omega. \end{aligned} \quad \dots\dots (4)$$

Eqn (4) may be regarded as describing the output signal of the photographic emulsion for a sine-wave illumination within the approximation implied by Eqn (1).

If five points having the equally spaced values of E shown in Fig. 4 are selected on the sine wave five values of z , denoted by z_{\max} , z_2 , z_0 , z_1 , z_{\min} , are obtained. The five equations resulting from inserting these values in (4) may be inverted to give

$$\begin{aligned} f(\alpha) &= z_0 \\ a_1 &= -\frac{1}{6}\beta^{-1}(z_{\max} - 8z_2 + 8z_1 - z_{\min}) \\ a_2 &= -\frac{1}{6}\beta^{-2}(z_{\max} - 16z_2 + 30z_0 - 16z_1 + z_{\min}) \quad \dots\dots (5) \\ a_3 &= \frac{2}{3}\beta^{-3}(z_{\max} - 2z_2 + 2z_1 - z_{\min}) \\ a_4 &= \frac{2}{3}\beta^{-4}(z_{\max} - 4z_2 + 6z_0 - 4z_1 + z_{\min}) \end{aligned}$$

so that the equation for the H & D curve may be obtained in terms of the power series (1) given a knowledge of these five values of z .

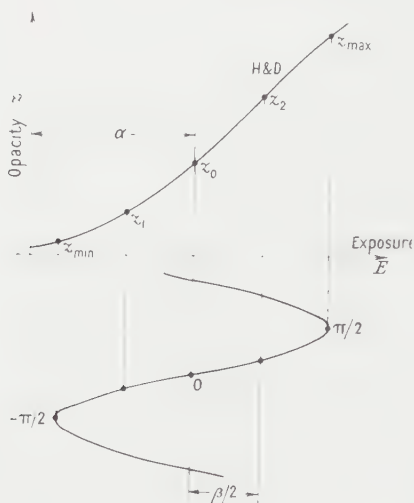


Fig. 4.

The coefficients in (4) give the mean opacity and the amplitude of the fundamental and harmonics terms. For this reason it is useful to introduce the following notation:

$$\begin{aligned}
 \text{mean opacity} &= \bar{Z}_0 = z_0 + \frac{1}{2}a_2\beta^2 + \frac{3}{4}a_4\beta^4 \\
 \text{amplitude of fundamental} &= \bar{Z}_1 = a_1\beta + \frac{3}{4}a_3\beta^3 \\
 \text{amplitude of second harmonic}^\dagger &= \bar{Z}_2 = \frac{1}{2}(a_2\beta^2 + a_4\beta^4) \quad \dots\dots (6) \\
 \text{amplitude of third harmonic} &= \bar{Z}_3 = \frac{1}{4}a_3\beta^3 \\
 \text{amplitude of fourth harmonic} &= \bar{Z}_4 = \frac{1}{8}a_4\beta^4.
 \end{aligned}$$

Substituting the values of the coefficients from (5) in (6) gives for the five values of these quantities

$$\begin{aligned}
 \bar{Z}_0 &= (z_{\max} + 2z_2 + 2z_1 + z_{\min})/6 \\
 \bar{Z}_1 &= (z_{\max} + z_2 - z_1 - z_{\min})/3 \\
 \bar{Z}_2 &= (z_{\max} - 2z_0 + z_{\min})/4 \\
 \bar{Z}_3 &= (z_{\max} - 2z_2 + 2z_1 - z_{\min})/6 \\
 \bar{Z}_4 &= (z_{\max} - 4z_2 + 6z_0 - 4z_1 + z_{\min})/12.
 \end{aligned} \quad \dots\dots (7)$$

If the coefficients α and β of the effective exposure (2) are known the relations (7) permit calculation of the resulting mean opacity and the amplitude of the fundamental and harmonic terms. Consequently, if these latter quantities are determined by measurement the values of opacity at the five reference points are given, by inverting (7), as

$$\begin{aligned}
 z_{\max} &= \bar{Z}_0 + \bar{Z}_1 + \bar{Z}_2 + \bar{Z}_3 + \bar{Z}_4 \\
 z_2 &= \bar{Z}_0 + \frac{1}{2}\bar{Z}_1 - \frac{1}{2}\bar{Z}_2 - \bar{Z}_3 - \frac{1}{2}\bar{Z}_4 \\
 z_0 &= \bar{Z}_0 + 0 - \bar{Z}_2 + 0 + \bar{Z}_4 \\
 z_1 &= \bar{Z}_0 - \frac{1}{2}\bar{Z}_1 - \frac{1}{2}\bar{Z}_2 + \bar{Z}_3 - \frac{1}{2}\bar{Z}_4 \\
 z_{\min} &= \bar{Z}_0 - \bar{Z}_1 + \bar{Z}_2 - \bar{Z}_3 + \bar{Z}_4.
 \end{aligned} \quad \dots\dots (8)$$

[†] By second harmonic is meant here the first harmonic above the fundamental.

These five points suffice to determine the H & D curve in the neighbourhood of the mean exposure α .

The above treatment may be extended to include the 5th and 6th harmonics, and amounts to the so-called seven equal-space method of analysis (Espley 1933).

In terms of the analogy between the response of an emulsion and a valve operating under class A conditions, it may be recalled that the opacity corresponds to the anode current, the mean opacity to the d.c. component of the anode current, the amplitude of the effective exposure to that of a sine-wave grid input signal, the shift in the mean opacity due to the presence of even harmonics to the rectifying effect and the linear (as opposed to logarithmic) H & D curve to the static characteristic curve of the valve.

§ 7. EXPERIMENTAL RESULTS FOR LOW SPATIAL FREQUENCY

A study of test objects of low spatial frequency is of particular value because the frequency response of the emulsion is then high and has negligible influence on the developed image. As a result the macroscopic H & D curve should be the primary factor influencing the final image.

7.1. Harmonic Distortion for Low and High Contrast Test Object: Influence of Exposure and Development Conditions

Ilford Chromatic Plate was chosen as the material, this being suitable since it may be developed to any value of γ between one and five using dish development in I D-2. The experimental procedure was as follows. The emulsion was exposed to a sinusoidally varying light distribution (two-beam fringes of spatial frequency 2 lines/mm). Twelve neutral density filters were placed in turn in front of the collimator slit to vary the exposure by steps through a range of logarithmic units. Four plates were exposed in this way using a fringe visibility of first 42% and then 82.5%, giving each plate 24 recorded sine-wave patterns. A density wedge of 16 steps was also exposed at the middle of each plate. The same exposure time of 15 seconds was used, with the green mercury line ($\lambda = 5461 \text{ \AA}$) as the light source. The four plates were developed for different times, namely, 1 min 15 sec, 2 min 15 sec, 4 min, and 6 min respectively. The resulting characteristic curves were obtained from the step wedge images and are shown in Fig. 5.

The continuous curves of Figs 6 and 7 show the mean opacity, fundamental, second, third and fourth harmonic amplitudes as calculated from these characteristic curves by means of Eqn (7) for the lower and higher contrast fringes

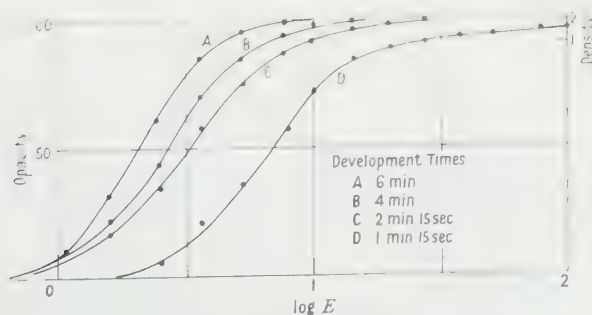


Fig. 5. The measured H & D curves for Ilford Chromatic plates.

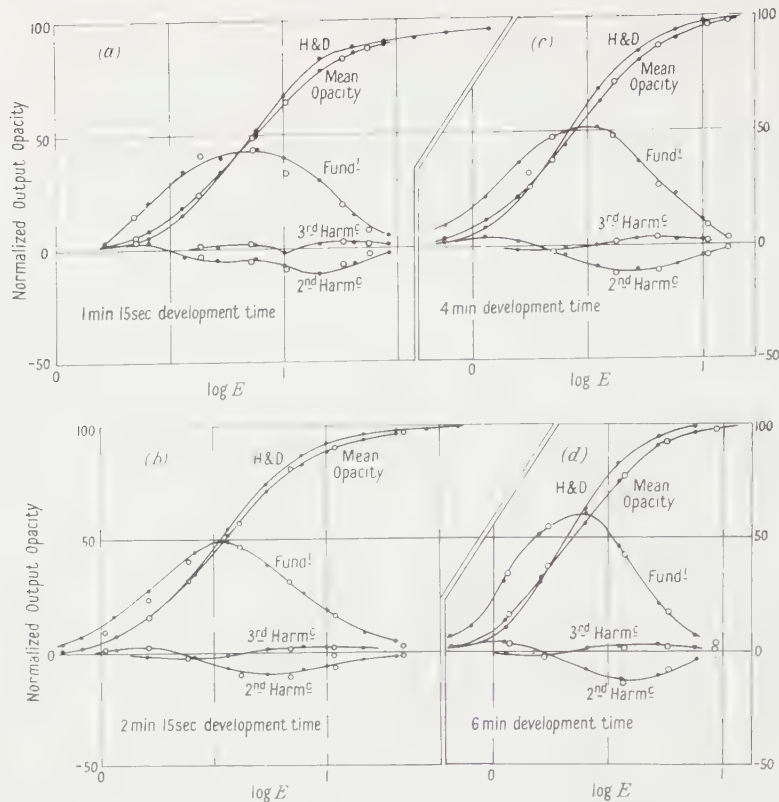


Fig. 6. The output signal for low contrast sine-wave patterns as a function of exposure for different development times.

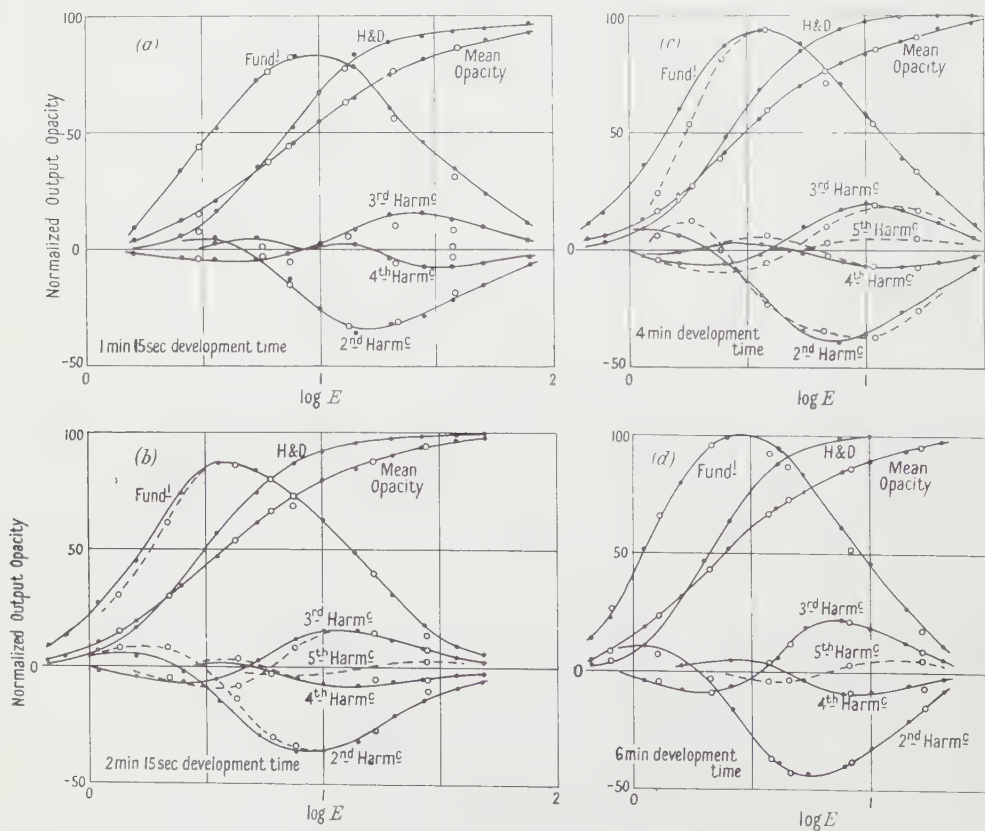


Fig. 7. The output signal for high contrast sine-wave patterns as a function of exposure for different development times.

respectively. The open circles represent the measured values of the fundamental and harmonics distributed along the exposure axis according to the measured mean opacity. The maximum output signal for the longest developing time and highest contrast was normalized to 100 and all the other measurements and calculations of amplitudes were related to this level. The mean opacity is left un-normalized and its scale corresponds to that shown in Fig. 5. For the lower contrast object ($+2\%$) satisfactory agreement is found between the computed and measured values in all cases. Similarly agreement is found for the higher contrast object when the development time is either short or long. For intermediate times the agreement is not so good because of the neighbourhood effect, which, according to Mees (1952) is not very pronounced for short and long development time.

7.2. Influence of the Neighbourhood Effect

The diagrams of Fig. 8, show the agreement on comparing the measured and calculated ratio of harmonic content to the fundamental amplitude as a function of exposure for 8.5% object contrast. The continuous curves represent the computed values and the open circles the measured values. Neglecting

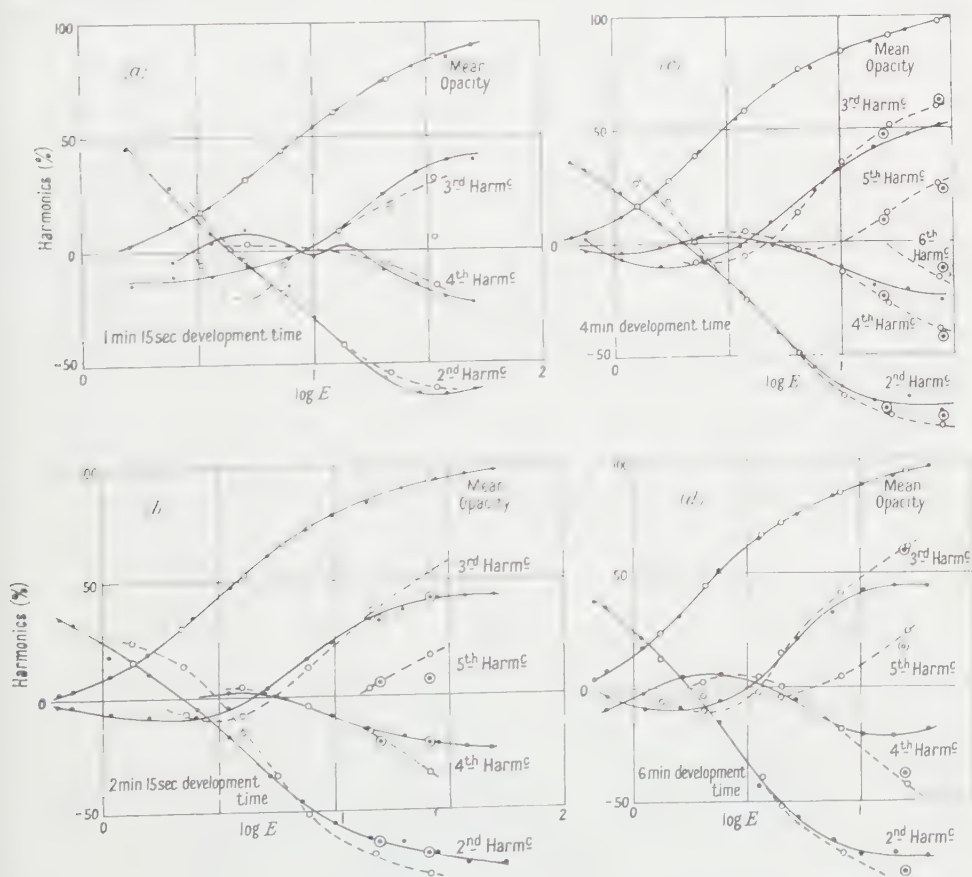


Fig. 8. Percentage of harmonics for a pure sine-wave test object as a function of exposure for different development times.

very low exposure values, where several factors such as fog level or measuring difficulties arising from reduced signal-to-noise ratio may influence the measurements, good agreement is found for the 1 min 15 sec development time. For 2 min 15 sec and higher exposures the agreement is not so good. The ringed points represent the values calculated by the seven-point method while the continuous lines are obtained from the five-point method. Both give the same values and the difference between measured and computed values may be ascribed only to the neighbourhood effect. For four minutes development time the seven-point method gives better agreement than the five-point method which means that the shoulder portion of the H & D curve cannot be satisfactorily represented by the five-term formula (1); it also appears that the neighbourhood effect is now smaller than in the previous case.

As a measure of the neighbourhood effect it is possible to use the difference between the measured and computed percentages of the harmonics present in the developed image of a sine-wave test object. Some results for such a test object of contrast 82.5%, are quoted in the Table.

Dev. time	Log $E=1.2$ harmonics (%)			Log $E=1.4$ harmonics (%)		
	Computed	Measured	Difference	Computed	Measured	Difference
1 min 15 sec	48.3	49.1	1.3	73.5	66.7	-7.2
2 min 15 sec	72.7	83.1	10.4	74.8	102	27.4
4 min	75.5	93.0	18.5	91.6	112	20.4
6 min	101	116	15			

7.3. Determination of the Effective H & D Curve

The form of the effective H & D curve including the micro-non-linearity, may be found using the Eqn (8) or in the case of measurements indicating the presence of higher harmonics a suitably extended version. In Fig. 9 the effective H & D curve and the macroscopic H & D curve are shown for $\log E=1.2$ and for 1 min 15 sec and 4 min development times. The scale of exposure is now arbitrary since the opacity values have been computed for seven equally distributed points along the exposure axis. Using these curves one may immediately find the opacity distribution in a single period of the developed sine-wave image by reading off the opacity values for constant increments of the angle as shown in Fig. 9.

§ 8. THE VARIATION OF THE OUTPUT WITH SPATIAL FREQUENCY

8.1. Experimental Procedure

For higher spatial frequencies the contrast of the effective exposure is significantly lower than that of the printed-on exposure, the frequency response now differing from unity. For this reason a further set of experiments was carried out to investigate the variation with frequency of the output signal resulting from sine-wave test objects. To obtain shorter exposure times and a more pronounced effect of frequency response a fast panchromatic plate was selected (Ilford HP3 plate) and developed in 'Microphen' following recommended procedure. In these experiments the spatial frequency R and exposure were the only parameters varied. A constant fringe contrast of 93% was used. For any selected value of R twelve different exposures were made and nine different spatial frequencies ranging from 2 to 56 lines/mm were used. The resulting sine-wave

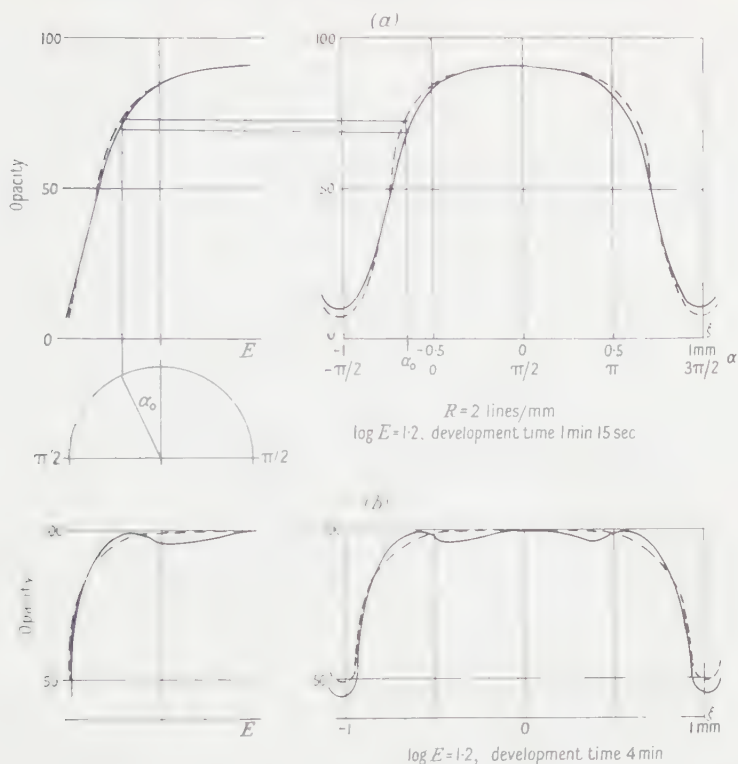


Fig. 9. The H & D micro- and macro-characteristic curves. The reconstruction of opacity distribution in sine-wave image.

patterns, numbering 108, were recorded on three plates across each of which a density wedge was also printed. The exposure conditions were as in previous experiments. After development the macroscopic H & D curves were measured (Fig. 10), and the plates analysed as before. The photographic output signal, its frequency spectrum and mean opacity were measured for each sample, and the highest output signal for the lowest frequency was normalized to 100 as before, so that an opacity of 100 corresponds to density equal to infinity. In this set of experiments the average γ was equal to about unity and in the output signal spectrum no harmonics higher than the fourth could be detected. This made possible the use of the five-point method throughout.

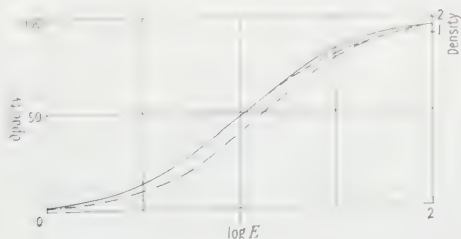


Fig. 10. The measured H & D curves for Ilford HP3 plate.

8.2. Determination of the Frequency Response

To derive the frequency response from the results obtained five opacity values were computed for each specimen using Eqn (8), giving from the H & D

curve five corresponding values of exposure. From these latter the fundamental amplitude in the effective exposure was calculated using Eqn (7). The ratio of the contrast of the effective exposure thus formed to that of the printed-on exposure gives the frequency response for each of the frequencies involved. Spurious harmonics appear in the calculated effective exposure, particularly for larger exposures, because of residual experimental errors and the neighbourhood effect. The root mean square variation of these harmonics was found to be between 2.5% and 7%. In highly exposed images the second harmonic was positive, suggesting the influence of the neighbourhood effect. In other ones the distribution was random suggesting residual experimental errors. Apart from these small effects the effective exposure was found to be distortion free.

The frequency response, Fig. 11, obtained in the manner outlined above was used later to compute the output signal of the photographic emulsion as a function of frequency. The output for each frequency was computed for the contrast in the effective exposure given by the product of the frequency response and the printed-on contrast. The measured amplitudes of fundamental and harmonics, Fig. 12, were distributed along the exposure axis according to the mean opacity curve, which latter is a function of contrast in the effective exposure. Satisfactory agreement between the values computed and measured is seen in the diagrams of Fig. 12. It may be noticed that with increasing frequency first the higher harmonics disappear, followed at higher frequencies by the lower harmonics. Harmonics of frequencies above the ordinary limit of resolution R_{\max} of the emulsion were not detected. It follows that for frequencies higher than $\frac{1}{2}R_{\max}$ the photographic process is linear, and in Eqn (4) all the coefficients but a_1 are zero, irrespective of the shape of the H & D curve.

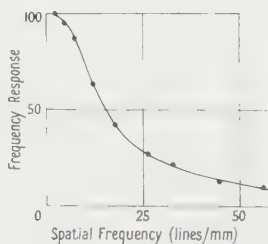


Fig. 11. The indirectly measured frequency response for HP3 plate.

8.3. Representation of Emulsion Characteristics for Given Effective Contrast

The above measurements for test objects of 93% contrast may be usefully represented on a three-dimensional diagram using as coordinates output signal, $\log E$ and R (Fig. 13). The maximum output signal and the best overall response is found on the toe portion of the macro-characteristic H & D curve. (HP3 plate developed in 'Microphen'). It decreases on both sides; greater harmonic distortion is present in the over-exposed than in the under-exposed part of the curve. The presence of detail having a contrast 93% or less cannot be detected outside the base region bounded by the full curve, which represents the limits for the fundamental to be resolved in the image. Similar bounding curves are shown for the harmonics.

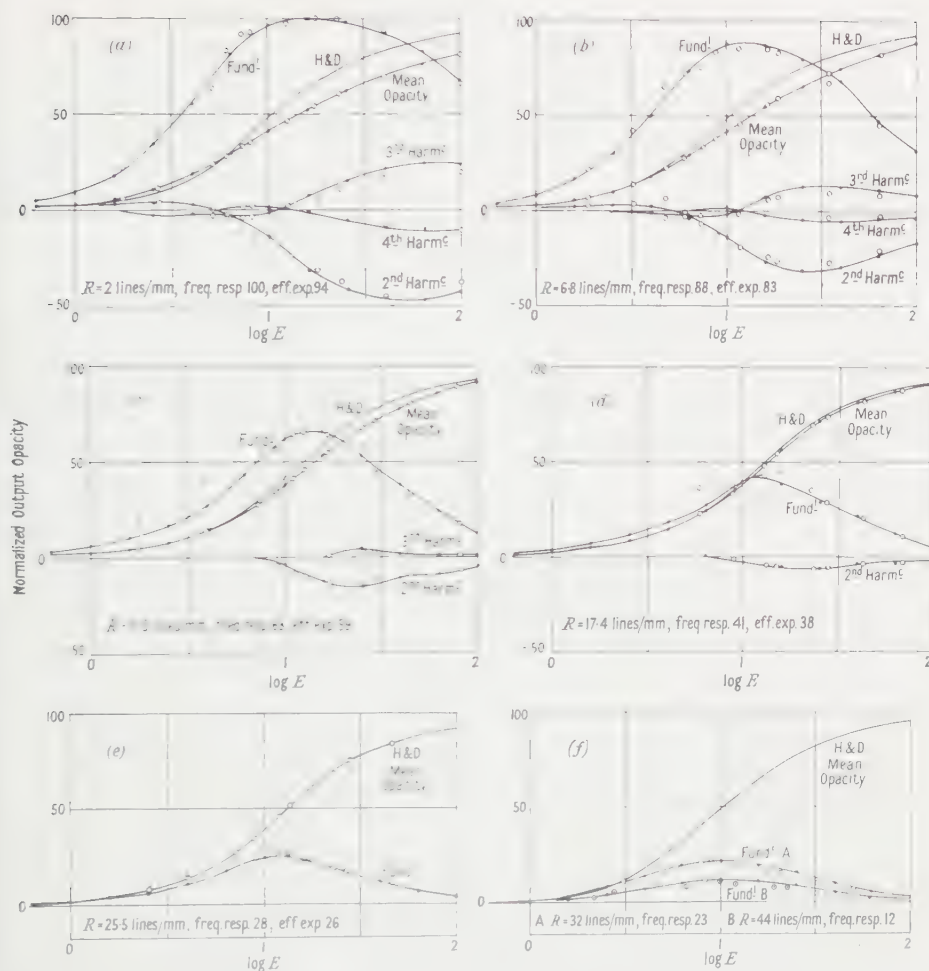


Fig. 12. The output signal as a function of exposure for different spatial frequencies.

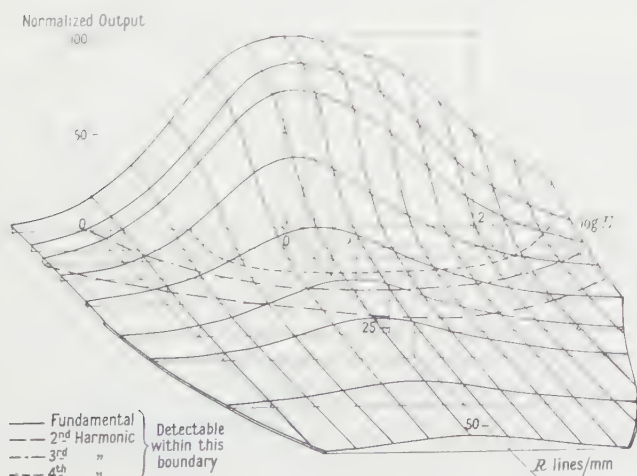


Fig. 13.

§ 9. CONCLUSION AND APPLICATIONS

The apparatus described is particularly suited to the investigation of distortion present in the photographic process, and is in many ways superior to a scanning analyser. For example it deals with larger areas of the specimen, and also gives what is in effect a mean reading of a few hundred measurements within a few seconds. For instance for a measuring time of five seconds the value recorded is an average of $5 \times 67.5 = 337.5$ measuring cycles. This feature makes it possible to record in some cases harmonics as small as 0.5% of the maximum output signal for a sine-wave test object. The same advantage obtains when the instrument is used for measurements of frequency density.

It appears from measurements and calculations described here that the concept of harmonic distortion can be used with great advantage in the study of the non-linear part of the photographic process. Of particular importance is the possibility offered for a fundamental experimental study of the validity of the method of analysis of the photographic process described by Frieser (1935). The results obtained support this theory in considerable detail. Moreover, the same technique has yielded simultaneously a knowledge of both the non-linear response and the frequency response of the emulsion as defined by Frieser.

Some particular results of practical importance have also emerged from these experiments. For example, it is shown theoretically and confirmed by measurement that a signal recorded on the toe portion of the characteristic curve leads to the highest contrast in the image. This was shown qualitatively by MacKenzie (1931) in connection with studies of variable-density sound recording. In this and other cases, a satisfactory account of the final opacity distribution in the photographic image is found using the frequency response to give the effective exposure, and thence the five-point method for the calculation of the fundamental and harmonic amplitudes.

From measurements of the kind described it is possible to select an exposure for which the image of a sine-wave test object will be free from an undesired harmonic. This could be of importance in the photographic production of gratings, for example for use in Moiré fringe metrology. It is also found empirically that harmonics of spatial frequency in excess of the resolution limit for the fundamental frequency of sine-wave test objects are never detectable in the image.

The method clearly lends itself to a direct measurement of the influence of harmonic distortion on the images of any given sets of test objects, and would then provide a more fundamental method for the determination of the photographic characteristics which make for visually acceptable prints. An empirical study not using the concept of harmonic distortion was carried out by Jones and Nelson (1942) to determine tolerances in printing.

A further possibility of the technique is that it gives a measure of the influence of the neighbourhood effect and developer type on image quality.

In delay recording systems, for example, when a developed photographic image is detected photoelectrically and displayed on a television screen, the detector has normally a linear response to light flux. In such cases, therefore, the present technique provides a criterion for photographic speed, image quality and for optimum exposure which can be directly related to the transfer characteristic of the detecting system.

ACKNOWLEDGMENTS

I should like to thank Dr. H. H. Hopkins for suggesting this problem and for helpful discussions. I am also indebted to Messrs. Ilford Ltd., Brentwood, Essex, for supplying information. Thanks are also due to the Ministry of Higher Education in Warsaw and the Cracow Institute of Technology for provision of a research grant.

REFERENCES

- ESPLEY, D. C., 1933, *Proc. Inst. Radio Engrs*, N.Y., **21**, 1439.
FELLGETT, P., 1953, *J. Opt. Soc. Amer.*, **43**, 271.
FLEISHER, H., 1948, *Radiation Laboratory Series*, Vol. 18, *Vacuum Tube Amplifiers* (New York: McGraw Hill).
FREISER, H., 1935, *Kinotechnik*, **17**, 165.
JONES, L. A., and NELSON, C. S., 1942, *J. Opt. Soc. Amer.*, **32**, 588.
KOVASZANAY, L. S. G., and ARMAN, A., 1957, *Rev. Sci. Instrum.*, **28**, 783.
MACKENZIE, D., 1931, *J. Soc. Mot. Pict. Engrs*, **17**, 172.
DU MARACHE, MILLE, 1952, *Thesis*, University of Paris.
MEES, L. E., 1952, *The Theory of Photographic Process* (New York: MacMillan).
MILLER, B. F., 1936, *J. Soc. Mot. Pict. Engrs*, **27**, 302.
VIENOT, J. CH., 1958, *Proc. Phys. Soc.*, **72**, 661.

Angular Dependence of Nuclear Spin-Lattice Relaxation Time for Several Alkali Halide Crystals

By E. R. ANDREW, K. M. SWANSON AND B. R. WILLIAMS

Department of Physics, University College of North Wales, Bangor, Wales

MS. received 12th April 1960

Abstract. The anisotropy of relaxation time for both ^{19}F and ^7Li has been examined in a pure single crystal of lithium fluoride, and is satisfactorily accounted for in terms of Bloembergen's spin-diffusion theory of relaxation. Confirmation is provided by the reduced anisotropy observed in two single crystals of lithium fluoride containing enhanced concentrations (50% and 90%) of ^6Li . The lack of anisotropy of the ^{23}Na relaxation time found in sodium chloride accords with the predictions of the theories of quadrupolar relaxation. A similar observation for the ^{79}Br and ^{81}Br relaxation times in potassium bromide is not inconsistent with van Kranendonk's theory and suggests that covalency does not make a strong contribution to the quadrupolar relaxation process.

§ 1. INTRODUCTION

THE nuclear spin-lattice relaxation time T_1 is not an isotropic characteristic of a crystal, even if cubic, and in general depends upon the orientation of the crystal in the applied magnetic field. In a polycrystalline specimen relaxation proceeds at rates which differ from one crystallite to another. If the relaxation process in a crystallite may be characterized by a single relaxation time, the apparent relaxation time of the whole specimen is an effective average over the assembly of crystallites and if the anisotropy is large the return to equilibrium may differ significantly from exponential form.

Little work has been done on the angular dependence of T_1 . Bloembergen (1949) examined the ^{19}F relaxation time in a single crystal of fluorite, but found no measurable angular dependence. Watkins (1952) found an angular dependence of the ^7Li relaxation time in an x-irradiated single crystal of lithium fluoride; maximum and minimum values of T_1 of 73 and 37 seconds were found with the magnetic field directed along [100] and [111] respectively. Bjorkstam and Uehling (1959) noticed an angular dependence of T_1 for the deuterons in a single crystal of KD_2PO_4 , ranging from 3.5 to 6.5 minutes, while Bloembergen and Sorokin (1958) have reported a 25% variation for the ^{133}Cs relaxation time in caesium bromide.

We have investigated the angular dependence of both the ^7Li and the ^{19}F relaxation times in a pure, unirradiated, single crystal of lithium fluoride containing the lithium isotopes in their natural abundance (92.6% ^7Li), and also of the ^{19}F relaxation time in two single crystals of lithium fluoride enriched in ^6Li , one containing 49.9% ^7Li and the other 9.6% ^7Li . The angular dependence of relaxation of ^{23}Na in sodium chloride and of ^{79}Br and ^{81}Br in potassium bromide have also been examined.

§ 2. EXPERIMENTAL DETAILS

The single crystals of natural lithium fluoride, sodium chloride and potassium bromide were supplied by the Harshaw Chemical Company, Cleveland, U.S.A. All were clear, colourless, cleaved cuboids approximately $1\text{ cm} \times 1\text{ cm} \times 3\text{ cm}$. The single crystals of lithium fluoride containing enriched ^6Li were lent by the United Kingdom Atomic Energy Authority through the kindness of Dr. P. T. Nettle. These crystals were clear, colourless cylinders 6 mm in diameter and 5 cm long. Their crystallographic orientation was determined from cleaved planes at the ends of the cylinders.

Measurements were made at room temperature in the field of 4400 oe of a permanent magnet using a modified Pound-Watkins spectrometer. The relaxation times of the crystal of natural lithium fluoride were long and were measured by a variation of the direct-recovery method. The relaxation times of the other crystals were too short to allow the use of this method, and instead the progressive-saturation method was used.

The direct-recovery method yields the relaxation time T_1 from the exponential return of the nuclear assembly to equilibrium after saturation as registered by the resonance signal measured with very low radio-frequency power. It was generally not possible to record the approach to equilibrium with a sufficiently low level of power to avoid disturbing the system significantly, and a correction had to be made. In the presence of electromagnetic radiation with magnetic amplitude H_1 a magnetically relaxed system approaches equilibrium exponentially with the time constant (Andrew 1955),

$$\tau = T_1 Z = T_1 (1 + a H_1^2 T_1)^{-1}, \quad \dots\dots(1)$$

where Z is the saturation factor. The time constant τ was therefore measured using a sequence of levels of power; a plot of $1/\tau$ against H_1^2 yields a straight line, which when extrapolated to zero power gives T_1 from the intercept. Relative values of H_1 were obtained from a calibrated detector. A typical plot is shown in Fig. 1. The accuracy of the measured values of T_1 is to about 5%. This method of correction avoids the hazardous procedure of calculating Z from the circuit parameters.

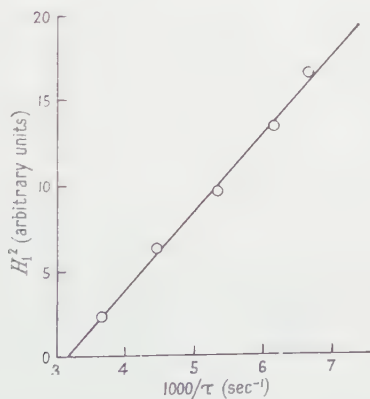


Fig. 1. Typical plot of the reciprocal of the recovery time against H_1^2 .

§ 3. EXPERIMENTAL RESULTS

3.1. *Natural Lithium Fluoride* (7.4% ^6Li)

The ^{19}F relaxation time depended significantly upon orientation. The longest value (340 sec) was obtained with the magnetic field parallel to $[100]$ and the shortest value (180 sec) with the field along $[111]$; along $[110]$ the relaxation time was 210 sec. The angular variation of T_1 as the crystal was rotated about $[100]$ with the field in the (100) plane is shown in Fig. 2(a).

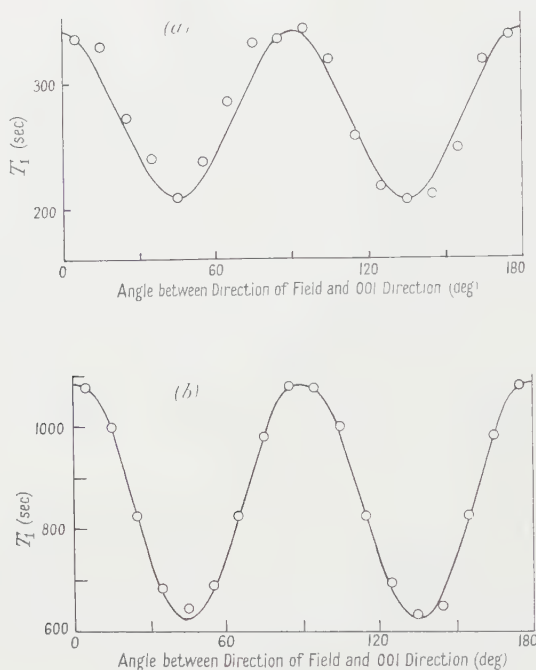


Fig. 2. Angular variation of T_1 in lithium fluoride single crystal containing 92.6% ^7Li . The field is in the (100) plane. (a) ^{19}F relaxation time, (b) ^7Li relaxation time.

The angular variation of the ^7Li resonance, shown in Fig. 2(b), is essentially the same as that found by Watkins for his x-irradiated crystal. For both crystals the maximum value of T_1 was obtained with the magnetic field along $[100]$; for his crystal the maximum value was 73 sec while for our purer crystal it was 1080 sec.

3.2. *Lithium Fluoride containing 50.1% ^6Li*

Since the crystal was in the form of a long cylinder the field could only be applied in a plane normal to the axis of the cylinder. This axis was found to be inclined at an angle $51^\circ 2'$ to the $[100]$ direction and at $60^\circ 45'$ to the $[010]$ direction. As we shall see in § 4 this orientation is not very favourable for a study of angular dependence of T_1 since it does not bring out extreme values. However a variation of 15% in the ^{19}F relaxation time was found and is illustrated in Fig. 3. The absolute values are much shorter than those of the crystal discussed in § 3.1, and indicate a density of paramagnetic relaxation centres some 25 times greater.

3.3. Lithium Fluoride containing 90.4% ^6Li

The cylindrical axis of the specimen was found to be inclined at $25^\circ 0'$ to the $[100]$ direction and $65^\circ 51'$ to the $[010]$ direction. As will be seen in §4 this is a favourable orientation to demonstrate anisotropy of T_1 with the field in the plane normal to the cylindrical axis. The variation of 20% found in the ^{19}F relaxation time is illustrated in Fig. 4.

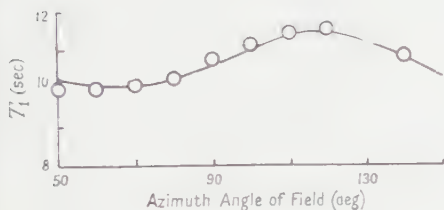


Fig. 3

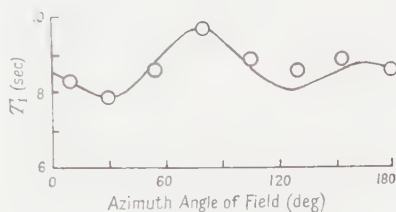


Fig. 4

Fig. 3. Angular variation of T_1 for ^{19}F in lithium fluoride single crystal containing 49.9% ^7Li . The full line follows from Eqn (16). The azimuth angle of the field is measured with respect to the plane containing the specimen axis and the $[100]$ direction.

Fig. 4. Angular variation of T_1 for ^{19}F in lithium fluoride single crystal containing 9.6% ^7Li . The full line follows from Eqn (17). The azimuth angle of the field is measured with respect to the plane containing the specimen axis and the $[100]$ direction.

3.4. Sodium Chloride

The crystal was turned about the c axis so that the magnetic field took a series of orientations in the (001) plane. Within 10% no angular dependence of the ^{23}Na relaxation time was found. The value of T_1 was approximately 10 sec.

3.5. Potassium Bromide

This crystal also was mounted so that the magnetic field took a series of orientations in the (001) plane. Within 10% no angular variation was found for either the ^{79}Br or the ^{81}Br relaxation times. The ratio of relaxation time of ^{81}Br to that of ^{79}Br is found to be 1.2 ± 0.1 . The absolute values of T_1 were estimated to be 0.076 and 0.063 sec for ^{81}Br and ^{79}Br respectively.

§ 4. DISCUSSION

4.1. Lithium Fluoride

The spin-lattice relaxation process for the ^{19}F nuclei must be magnetic in origin, and the diffusion mechanism proposed by Bloembergen (1949) provides the only process capable of accounting for the observed relaxation times in nominally diamagnetic ionic crystals. Excess nuclear spin energy diffuses by spin-exchanges into the vicinity of paramagnetic impurity relaxation centres where the energy is transferred to the lattice. If the relaxation centres are dilute the average distance between a nucleus and its nearest relaxation centre is many atomic distances, and the relaxation time is determined by the time taken by spin-diffusion. Assuming that the relaxation centres are dilute and neglecting

anisotropic effects, Khutsishvili (1956) and de Gennes (1958) find that the relaxation time is given by

$$T_1 = (4\pi DcN)^{-1}, \quad \dots\dots (2)$$

where D is the spin-diffusion coefficient, c is a temperature-dependent relaxation length which is a measure of the range of direct nuclear relaxation around each impurity centre, and N is the number of relaxation centres per unit volume. While neither c nor D can be calculated with accuracy, the value of c is probably not far from 10 Å for lithium fluoride at room temperature, and $D \sim 10^{-11} \text{ cm}^2 \text{ sec}^{-1}$. Thus $N \sim 3 \times 10^{14} \text{ cm}^{-3}$ for the crystal of natural lithium fluoride. The average distance of a fluorine nucleus from an impurity centre is therefore some 300 times the distance between fluorine nearest neighbours. In the enriched specimens, whose relaxation times are shorter, the average distance is still over 100 times the nearest neighbour distance. We are therefore justified in assuming that the relaxation time is determined predominantly by the spin-diffusion process.

As Bloembergen (1949) and Watkins (1952) have shown by a perturbation calculation, the mean transition probability per unit time W_n for mutual spin exchange between a typical nucleus and its n th identical neighbour is proportional to

$$g_{\max}(\nu)(3 \cos^2 \theta_n - 1)^2 r_n^{-6}, \quad \dots\dots (3)$$

where \mathbf{r}_n is the inter-nuclear vector, θ_n is the angle between \mathbf{r}_n and the applied field, and $g(\nu)$ is the normalized resonance line-shape function. As Watkins points out, the factor $g_{\max}(\nu)$ in (3) is only strictly the maximum value of the line-shape function for a Gaussian line shape, though the term is likely to be a good approximation for the near-Gaussian lines considered here.

Expression (3) contains the origins of the angular variation of T_1 which enters in two ways. The factor $g_{\max}(\nu)$ reflects the angular variation of resonance line width, and in physical terms expresses the smaller chance that the neighbour will have the closely similar energy necessary for spin exchange when dipolar broadening is greater. The second factor expresses the angular variation of the dipolar coupling between the two exchanging nuclei. In a crystal containing only one species of magnetic nucleus the angular variations of the two factors tend to offset each other and when summed over all neighbours can often lead to little anisotropy, as we shall see with calcium fluoride presently. However, if two magnetic nuclei are present the unlike nuclei can, through their interaction expressed in the first factor, reduce the spin-exchange probability without any modification of the second factor which is solely concerned with like nuclei. For this reason anisotropy of T_1 is likely to be greater when more than one nuclear magnetic species is present.

The spin-diffusion coefficient D is proportional to $\sum_n W_n r_n^2$, where the sum is taken over all identical nuclear neighbours. Remembering that for lines of similar shape such as those encountered in this work $g_{\max}(\nu)$ is proportional to $S^{-1/2}$, where S is the second moment, we have

$$\frac{1}{T_1} \propto D \propto S^{-1/2} \sum_n (3 \cos^2 \theta_n - 1)^2 r_n^{-4}. \quad \dots\dots (4)$$

For dipolar-broadened resonance lines the second moment is given by the expression of Van Vleck (1948):

$$S = \frac{3}{4} \frac{I+1}{I} \mu^2 \sum_n (3 \cos^2 \theta_n - 1)^2 r_n^{-6} + \frac{1}{3} \sum_f \frac{I_f+1}{I_f} \mu_f^2 (3 \cos^2 \theta_f - 1)^2 r_f^{-6}. \quad \dots\dots (5)$$

The first term in (5) is summed over all identical nuclear neighbours in the cubic lattice and gives their contribution to the second moment, while the second term is summed over all other magnetic nuclei in the lattice; μ and I are the magnetic moment and spin number of the resonant nuclei, while μ_f and I_f refer to other nuclei.

For a crystal containing only one magnetic nuclear species the second term in (5) may be omitted and with (4) we get

$$T_1 \propto \frac{[\sum_n (3 \cos^2 \theta_n - 1)^2 r_n^{-6}]^{1/2}}{\sum_n (3 \cos^2 \theta_n - 1)^2 r_n^{-4}}. \quad \dots\dots (6)$$

In general however both terms in (5) contribute and a more complicated numerator is obtained in (6).

For a crystal with cubic symmetry Van Vleck (1948) shows that the sums in (4), (5) and (6) simplify since

$$\sum_n (3 \cos^2 \theta_n - 1)^2 r_n^{-p} = \frac{1}{2} (a_p + b_p \Lambda), \quad \dots\dots (7)$$

where

$$a_p = \sum_n r_n^{-p} (7 - 9M_n) \quad \text{and} \quad b_p = \sum_n r_n^{-p} (-9 + 15M_n), \quad \dots\dots (8)$$

in which Λ is the sum of the fourth powers of the direction cosines of the applied magnetic field with respect to the cubic crystal axes, and M_n is the corresponding sum for the direction cosines of the internuclear vector \mathbf{r}_n . Substituting (7) and (8) in (6) we find the following expression for the angular variation of relaxation time

$$T_1 \propto \left(\Lambda + \frac{a_6}{b_6} \right)^{1/2} \left(\Lambda + \frac{a_4}{b_4} \right), \quad \dots\dots (9)$$

with a somewhat more complicated expression when more than one magnetic nucleus is present.

Calcium fluoride provides an example of a cubic crystal which, for practical purposes, contains only one magnetic nucleus. The fluorine nuclei form a simple cubic lattice. Summing directly over the nearest 122 neighbours and integrating for the remainder we have found

$$a_6 d^6 = -6.42 \quad \text{and} \quad b_6 d^6 = 33.11, \quad \dots\dots (10)$$

where d is the simple cubic lattice spacing. For the more slowly converging sums a_4 and b_4 a direct sum over the nearest 388 neighbours with integration beyond gave

$$a_4 d^4 = 8.2 \quad \text{and} \quad b_4 d^4 = 30.4. \quad \dots\dots (11)$$

Thus for calcium fluoride (9) becomes

$$T_1 \propto (\Lambda - 0.194)^{1/2} / (\Lambda + 0.27). \quad \dots\dots (12)$$

With the applied field along [100], [110], [111] the right-hand side of (12) takes values 0.71, 0.72, 0.62 respectively, showing, as Bloembergen (1949) found experimentally, that the anisotropy of T_1 is small.

For lithium fluoride the sums in (8) must be carried out over a sodium chloride type lattice. For like neighbours we find

$$\left. \begin{aligned} a_6 d^6 &= 4.01 \\ a_4 d^4 &= 11.95 \end{aligned} \right\} \begin{aligned} b_6 d^6 &= -1.89 \\ a_4 d^4 &= -2.96 \end{aligned} \quad \dots\dots (13)$$

while for unlike neighbours we find

$$a_6' d^6 = -10.44 \qquad b_6' d^6 = 35.0. \qquad \dots\dots (14)$$

Watkins (1952), summing over a smaller number of neighbours, obtained slightly different values. From (4), using (5), (7), (8), (13) and (14) we find for the ^{19}F relaxation time in lithium fluoride

$$T_1 \propto (1 + 33\Lambda)^{1/2} / (1 - 0.25\Lambda). \qquad \dots\dots (15)$$

The range of values of Λ runs from a minimum value of $\frac{1}{3}$ with the field along [111] to a maximum value of 1 with the field along [100]. Using (15) the theoretical values of T_1 along [100], [110] and [111] bear ratios 1:0.62:0.49; the experimental values given in §3.1 have ratios 1:0.62:0.53 in satisfactory agreement. The angular variation of T_1 given by Eqn (15) for orientations of the applied field in the (100) plane is shown in Fig. 2(a); the constant of proportionality in (15) has been adjusted to give the best fit. The agreement with the experimental points provides good support for the concepts of the spin-diffusion relaxation process.

The first factor in (15) is a measure of the resonance line width and experimentally the line width, as measured between derivative turning points, was found to follow this angular behaviour. It would have been more satisfactory to determine the angular variation of the second moment of the line, but unfortunately when the spectrum was recorded with a power level low enough to avoid saturation the signal-to-noise ratio in the skirts was too poor for an accurate evaluation of second moment. It did however seem that the line was broader at all angles than might be expected from dipolar interaction alone. While both factors in (15) contribute significantly to the angular variation of T_1 this first factor is the more important. This angular dependence arises mainly from the interactions of the ^7Li nuclei. A further test of the theory is therefore provided by the behaviour of the two specimens of lithium fluoride in which a proportion of the ^7Li nuclei are replaced by ^6Li nuclei whose magnetic moments are much smaller.

For the specimen containing 49.9% ^7Li the angular variation predicted by (4) is

$$T_1 \propto (1 + 2.8\Lambda)^{1/2} / (1 - 0.25\Lambda). \qquad \dots\dots (16)$$

The orientation of the crystal axes in this specimen was such that as the crystal was rotated about its long cylindrical axis Λ took only the restricted range of values from 0.45 to 0.61. Nevertheless the variation of T_1 given by (16), shown as the full line in Fig. 3, is in satisfactory agreement with the experimental points. For natural lithium fluoride the range of values of T_1 would have been 1.20:1 compared with the range of 1.14:1 in Fig. 3.

For the specimen containing 9.6% ^7Li the angular variation predicted by (4) is

$$T_1 \propto (1 + 0.092\Lambda)^{1/2} / (1 - 0.25\Lambda). \qquad \dots\dots (17)$$

The angular variation caused by the first term is now very small, and in fact the line width was found to be almost independent of orientation. The orientations of the

crystal axes in this specimen were much more favourable, and as the crystal was rotated about its long cylindrical axis Λ took values between 0.40 and 0.99. The angular variation given by (17), which in this case arises almost entirely from the second factor, is shown as the full line in Fig. 4, and agrees reasonably well with the experimental points. For natural lithium fluoride the range of values of T_1 would have been 1.86:1 compared with the range of 1.22:1 in Fig. 4.

The ${}^7\text{Li}$ nuclei may be relaxed by both magnetic and electric quadrupolar mechanisms. From (4), with (5), (7), (8), (13) and (14) the spin-diffusion mechanism gives the following angular dependence of ${}^7\text{Li}$ relaxation time:

$$T_1 \propto (-1 + 9.6\Lambda)^{1/2} / (1 - 0.25\Lambda). \quad \dots\dots (18)$$

This relation gives the full line in Fig. 2 (*b*) which is in good agreement with the experimental points. The angular variation is in fact essentially the same as for ${}^{19}\text{F}$, and confirms Watkins' conclusion that the ${}^7\text{Li}$ relaxation is effected by the spin-diffusion mechanism.

If the spin-lattice relaxation of the ${}^7\text{Li}$ nuclei were predominantly quadrupolar the values of T_1 would not have the observed angular variation. The ${}^7\text{Li}$ nuclei have four equally-spaced energy levels in a strong magnetic field; there is no evidence in these cubic crystals of appreciable perturbation by quadrupole interaction with field gradients created by lattice defects. Mutual spin-exchanges of the type which are the essential feature of the spin-diffusion relaxation process serve here to ensure the maintenance of a Boltzmann distribution of populations of the energy levels (Bloembergen 1954, Abragam and Proctor 1958). Under these conditions a unique spin-lattice relaxation time can be defined for the crystal (Andrew and Swanson 1960), and in the Appendix this is found to be given by

$$\frac{1}{T_1} = \frac{2}{5} (W_1 + 4W_2), \quad \dots\dots (19)$$

where

$$W_1 = W_{3/2 \rightarrow 1/2} = W_{-1/2 \rightarrow -3/2} \quad \text{and} \quad W_2 = W_{3/2 \rightarrow -1/2} = W_{1/2 \rightarrow -3/2}, \quad \dots\dots (20)$$

where $W_{m \rightarrow n}$ is the probability per unit time of a transition between the levels m and n brought about by the interaction between the fluctuating gradient of the crystalline electric field and the nuclear quadrupole moment. Using an ionic model van Krandendonk (1954) has developed the following expressions for W_1 and W_2 for a sodium chloride type lattice:

$$W_1 = AE_1^1(T^*) \quad \text{and} \quad W_2 = 4AE_2^1(T^*) \quad \dots\dots (21)$$

where the constant A has no angular dependence, and where

$$\left. \begin{aligned} E_1^1 &= (1056 + 1440\lambda^2)(D_1 + D_2) + (512 + 2480\lambda^2)D_1 \\ E_2^1 &= (354 - 90\lambda^2)(D_1 + D_2) + (283 - 155\lambda^2)D_4 \end{aligned} \right\} \dots\dots (22)$$

and

$$\left. \begin{aligned} D_1 &= 0.200 - 0.00705/T^{*2} + \dots \\ D_2 &= 0.924 - 0.0547/T^{*2} + \dots \\ D_4 &= 0.276 - 0.0174/T^{*2} + \dots \end{aligned} \right\} \dots\dots (23)$$

In these expressions $T^* = T/\Theta$, where Θ is the Debye temperature, and

$$\lambda^2 = \lambda_1^2 \lambda_2^2 + \lambda_2^2 \lambda_3^2 + \lambda_3^2 \lambda_1^2, \quad \dots\dots (24)$$

where $\lambda_1, \lambda_2, \lambda_3$ are the direction cosines of the applied field with respect to the cubic axes of the crystal. For the range of values of T^* from 0.7 to infinity, the ratio $(D_1 + D_2)/D_4$ has the almost temperature-independent value of 4.1 which we may use without appreciable error in calculating the angular variation of T_1 at room temperature. Over the full range of values of λ^2 from 0 to $\frac{1}{3}$, E_1^1 increases by 58% while E_2^1 decreases by 12%. The angular variations of W_1 and W_2 are thus opposed, and it turns out, using (19), (21) and (22), that there should be no angular variation of T_1 to within 1%. This result contrasts markedly with the predictions of the spin-diffusion theory, and since the latter accord well with experiment it may be concluded that the quadrupolar mechanism contributes relatively little to spin-lattice relaxation in this crystal.

Further evidence for this conclusion is provided by the relative values of T_1 for ^7Li and for ^{19}F in the crystal of natural lithium fluoride. The ratio is approximately 3 at each crystal orientation. The same ratio was found by Bloembergen (1949) for a less pure powdered specimen at 2.1°K, and by Pound (1951) in two crystals of different purity at room temperature, and similar ratios were found by Low and Squire (1958) over a wide range of temperatures. If the quadrupolar mechanism contributed significantly to the ^7Li spin-lattice relaxation the ratio of relaxation times would not be closely similar in samples of different purity and at different temperatures. Using the full expression for D the ratio of the spin-diffusion coefficients for the two nuclei should be about 1.6. The impurity distribution is the same in both cases, though with local differences relative to the two nuclear systems. If we neglect these differences, we conclude from Eqn (2) that the relaxation length c is almost five times greater for ^{19}F than for ^7Li . This is about three times as great as one expects using the relation for c given by Khutsishvili (1956) and de Gennes (1958). However, in view of the simplifying approximations entering into the derivation of (2), and in view of the lack of knowledge of the nature of the relaxation centres, this apparent numerical discrepancy cannot profitably be pursued. Finally the fact that for different specimens of lithium fluoride the values of T_1 for ^7Li differ widely, though always about three times as long as the corresponding values for ^{19}F , provides further evidence that the ^7Li nuclei are magnetically relaxed.

4.2. Sodium Chloride

Although not conclusive, there are several pieces of evidence which suggest that spin-lattice relaxation in sodium chloride is predominantly quadrupolar. First, all reported measurements of T_1 for ^{23}Na at room temperature fall in the relatively restricted range 7–16 seconds; in particular Proctor and Robinson (1956) found the same value for a natural crystal of halite as for a synthetic crystal of high purity. Secondly, the ratio of relaxation times for ^{23}Na and ^{35}Cl is close to that expected if the relaxation mechanism is quadrupolar (Taylor and Bloembergen 1959). Thirdly, the temperature-dependence of T_1 for ^{23}Na is reported to accord with the predictions of van Kranendonk's theory (Kraus 1958, Wikner and Hahn 1958). Examination of the resonance line width and second moment (Proctor and Robinson 1956, Andrew, Bradbury and Eades 1958, 1959, Otsuka, Oshio, Kobayashi and Kawamura 1959) leads to the conclusion that lattice defects do not cause significant deviations from equality of spacing of the four nuclear

magnetic energy levels. Assuming the relaxation mechanism is in fact quadrupolar, the relaxation time is given by (19) and as in the previous section should show no angular variation to within 1% if van Kranendonk's model is adequate. This is consistent with the experimental results (§ 3.4) which revealed no angular variation to within 10%.

The coefficient A in (21) contains, in van Kranendonk's theory, a factor γ^2 , where γ is a dimensionless magnification factor, which is a measure of the increased coupling between the crystalline electric field and the nuclear quadrupole moment caused by polarization of the ionic core. Van Kranendonk took γ to be isotropic, but Taylor and Bloembergen (1959), from ultrasonic experiments, found evidence of some anisotropy of γ , though this is apparently not reflected in a measurable anisotropy of T_1 . The value of γ which it is necessary to assume in van Kranendonk's theory to account for the absolute values of T_1 is in any case some ten times larger than has been calculated for the free sodium ion (Wikner and Das 1958).† Two attempts have been made to account for this type of discrepancy. Yosida and Moriya (1956) have suggested that a small degree of covalent binding would greatly enhance the fluctuating electric field gradient experienced by the nucleus. Their calculations are applied to heavy ions and do not include consideration of sodium chloride; we therefore defer a discussion until the next section where it is relevant. The other approach is that of Kondo and Yamashita (1959), who have considered the modification of the electric field gradient caused by overlap of the ions when bound in a crystal. For sodium chloride this theory gives a relaxation time for ^{23}Na of the right order and gives values of W_1 and W_2 of 0.0063 and 0.0246 sec^{-1} respectively when the field is along $[100]$ and 0.0270 and 0.0196 sec^{-1} when the field is along $[111]$. Substituting in (19) it is found that this model also leads to less than 1% anisotropy of relaxation time.

If the relaxation had been effected by the spin-diffusion process, the angular variation predicted by (4) would have been

$$T_1 \propto (1 + 0.024\Lambda)^{1/2} / (1 - 0.25\Lambda), \quad \dots\dots (25)$$

giving a value of T_1 along $[100]$ which is 17% greater than the value along $[110]$. This variation is rather too small to provide a clear distinction between the two relaxation mechanisms.

4.3. Potassium Bromide

Watkins (1952) has shown that the relaxation mechanism for the ^{79}Br and ^{81}Br nuclei in potassium bromide is predominantly quadrupolar, since the relaxation time of ^{79}Br , which has the larger quadrupole moment, is shorter than that of ^{81}Br , which has the larger magnetic moment. The ratio of relaxation times found here is 1.21, which agrees with the ratio of 1.16 found by Watkins, and both are rather lower than the value of 1.43 found by Wikner and Hahn (1958), and the theoretical ratio, 1.39, given by the square of the ratio of quadrupole moments. It is therefore just possible that there is a small magnetic contribution to the relaxation in the crystal used here.

† Wikner and Das obtain a theoretical value of 25 min for T_1 for ^{23}Na in sodium chloride. The experimental value of 7 min quoted for comparison in their Table IV should be 7 sec. We are grateful to Professor Das for confirmation of this point.

Watkins and Pound (1953) have shown that even in a good crystal of potassium bromide only the central transition between the levels $m = \pm \frac{1}{2}$ is observed. Electric field gradients arising from crystalline defects generate first-order perturbations of the satellite resonance frequencies and prevent their observation. The four nuclear magnetic energy levels are now unequally spaced for almost all bromine nuclei; consequently the spin-exchange process is unable to operate and maintain a Boltzmann distribution of population. A single spin-lattice relaxation time no longer characterizes the spin system. The progressive saturation experiment yields an apparent relaxation time, which, as Yosida and Moriya (1956) have shown, is given by

$$T_1 = \frac{1}{W_1} + \frac{1}{W_2} \quad \dots\dots (26)$$

Taking $\Theta = 177^\circ\text{K}$ for potassium bromide (Seitz 1940) in (23), and using (21), (22), (24) and (26), van Kranendonk's theory is found to predict a relaxation time along [100] which is 17% greater than the value along [110]. Kondo and Yamashita (1959) have not applied their overlap theory to potassium bromide. Yosida and Moriya (1956) have considered the contribution to quadrupolar relaxation through the electric field gradients caused by a small degree of covalent binding. Expressions for W_1 and W_2 of the same form as (21) and (22) are obtained for a sodium chloride type lattice, but with different numerical coefficients which for potassium bromide would considerably enhance the anisotropy of T_1 . Any small magnetic contribution to the relaxation time would somewhat reduce the anisotropy. The lack of observed anisotropy within 10% is therefore not inconsistent with the quadrupolar relaxation theories but suggests that relaxation through covalency plays no marked role in this crystal.

APPENDIX

Consider a system of identical nuclei of spin $\frac{3}{2}$ placed in a magnetic field. If quadrupole perturbations are negligible the four magnetic energy levels are equally spaced. In absence of applied radio-frequency power the transitions which may take place between the levels are shown in Fig. 5, in which W_1 and W_2 refer to transitions effected by the lattice by interaction with the electric quadrupole moments of the nuclei, and α , β and γ are the spin-exchange processes which do not affect the total energy of the system. Δ is given by $4n_0/N$ where n_0

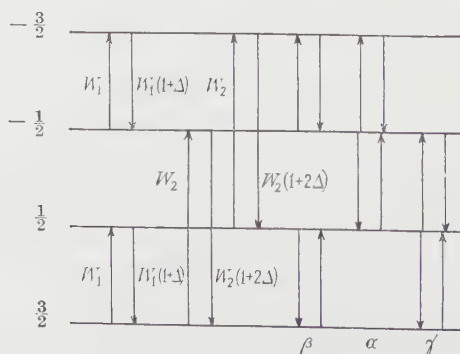


Fig. 5. Diagram illustrating the transitions considered in the Appendix.

is the excess of population in one level over that in the level next above when the system of spins is in thermal equilibrium with the lattice, and where N is the total number of nuclei. Let N_m be the population of level m , and let

$$N_{m+1/2} = N_{m+1} - N_m$$

be the difference in population between adjacent levels. Then we have

$$\begin{aligned}\dot{N}_{-1} &= -N_{-1}(2W_1 + W_2) + N_1W_2 + 2n_0W_1 - 2aW_1(N_{-1} - N_1) \\ &\quad - bW_1(-3N_{-1} + 4N_0 - 3N_1) \\ \dot{N}_0 &= N_{-1}(W_1 - W_2) - 2N_0W_2 + N_1(W_1 - W_2) + 2n_0(2W_2 - W_1) \\ &\quad + 3bW_1(N_{-1} - 2N_0 + N_1) \\ \dot{N}_1 &= N_{-1}W_2 - N_1(2W_1 + W_2) + 2n_0W_1 + 2aW_1(N_{-1} - N_1) \\ &\quad + bW_1(-N_{-1} + 4N_0 - 3N_1), \quad \dots\dots (27)\end{aligned}$$

In these equations the coefficient aW_1 determines the rate of the exchange processes α and γ , bW_1 determines the rate of process β . Both a and b are of the order T_1/T_2 , where T_2 is the spin-spin relaxation time, given in order of magnitude by the reciprocal of the line width. For most solids $T_1 \gg T_2$, and for sodium chloride in particular $T_1/T_2 \sim 10^4$. It is clear therefore that after a time of order T_2 the bracketed quantities in (27) which are prefixed by a or b will be very small; that is to say we shall for practical purposes have N_1 , N_0 and N_{-1} equal. This reflects the fact that the spin-exchange processes bring about and maintain a Boltzmann distribution throughout the longer times during which the much slower spin-lattice processes described by the other terms in (27) are operating.

The total magnetic moment M of the system is proportional to

$$\sum N_m m = \frac{3}{2}N_{-1} + 2N_0 + \frac{3}{2}N_1 = 5N_0, \quad \dots\dots (28)$$

when a Boltzmann distribution prevails. Putting N_{-1} , N_0 , N_1 equal in (27), we find the rate of change of this quantity is

$$\sum \dot{N}_m m = -2(W_1 + 4W_2)(N_0 - n_0). \quad \dots\dots (29)$$

Combining (28) and (29) we find that the nuclear magnetization follows the equation

$$\dot{M} = -\frac{2}{5}(W_1 + 4W_2)(M - M_0),$$

from which we deduce that the spin-lattice relaxation time is given by

$$\frac{1}{T_1} = \frac{2}{5}(W_1 + 4W_2).$$

ACKNOWLEDGMENTS

The authors gratefully acknowledge the helpful advice of Dr. R. G. Eades. One of us (B. R. W.) held a research studentship from the Department of Scientific and Industrial Research.

REFERENCES

- ABRAGAM, A., and PROCTOR, W. G., 1958, *Phys. Rev.*, **109**, 1441.
 ANDREW, E. R., 1955, *Nuclear Magnetic Resonance* (Cambridge: University Press), p. 21.
 ANDREW, E. R., BRADBURY, A., and EADES, R. G., 1958, *Nature, Lond.*, **182**, 1659.
 ——— 1959, *Nature, Lond.*, **183**, 1802.
 ANDREW, E. R., and SWANSON, K. M., 1960, *Proc. Phys. Soc.*, **75**, 582.

- BJORKSTAM, J. L., and UEHILING, E. A., 1959, *Phys. Rev.*, **114**, 961.
- BLOEMBERGEN, N., 1949, *Physica*, **15**, 386.
- 1954, *Proceedings of the Conference on Theoretical Physics, Japan* (Tokyo: Science Council of Japan), p. 757.
- BLOEMBERGEN, N., and SOROKIN, P. P., 1958, *Phys. Rev.*, **110**, 865.
- DE GENNES, P. G., 1958, *J. Phys., Chem. Solids*, **7**, 345.
- KHUTSISHVILI, G. R., 1956, *J. Exp. Theor. Phys. U.S.S.R.*, **31**, 424.
- VAN KRANENDONK, J., 1954, *Physica*, **20**, 781.
- KRAUS, O., 1958, *Bull. Amer. Phys. Soc.*, **3**, 166.
- KONDO, J., and YAMASHITA, J., 1959, *J. Phys. Chem. Solids*, **10**, 245.
- LOW, F. J., and SQUIRE, C. F., 1958, *J. Phys. Chem. Solids*, **5**, 85.
- OTSUKA, E., OSHIO, Y., KOBAYASHI, T., and KAWAMURA, H., 1959, *J. Phys. Soc., Japan*, **14**, 1454.
- POUND, R. V., 1951, *Phys. Rev.*, **81**, 156.
- PROCTOR, W. G., and ROBINSON, W. A., 1956, *Phys. Rev.*, **104**, 1344.
- SEITZ, F., 1940, *The Modern Theory of Solids* (New York: McGraw-Hill), p. 110.
- TAYLOR, E. F., and BLOEMBERGEN, N., 1959, *Phys. Rev.*, **113**, 431.
- VAN VLECK, J. H., 1948, *Phys. Rev.*, **74**, 1168.
- WATKINS, G. D., 1952, *Thesis*, Harvard University.
- WATKINS, G. D., and POUND, R. V., 1953, *Phys. Rev.*, **89**, 658.
- WIKNER, E. G., and DAS, T. P., 1958, *Phys. Rev.*, **109**, 360.
- WIKNER, E. G., and HAHN, E. L., 1958, *Bull. Amer. Phys. Soc.*, **3**, 325.
- YOSIDA, K., and MORIYA, T., 1956, *J. Phys. Soc., Japan*, **11**, 33.

Four Nucleon Reactions with Central Forces

BY P. G. BURKE† AND W. LASKAR‡

† University of London Computer Unit

‡ Department of Physics, University College London

Communicated by E. H. S. Burhop; MS. received 23rd March 1960, in revised form 17th June 1960

Abstract. The four-nucleon reaction has been formulated using the resonating group method and including the three groupings dd , $n^3\text{He}$, and pt . The central potential used is of Gaussian shape with exchange dependence (Serber and symmetrical exchange have been mainly investigated). The wave functions for the nuclear ground states are double Gaussian for deuteron and single Gaussian for t and ^3He , the parameter being determined by variational methods to fit the binding energies.

Coupled integro-differential equations have been derived for each value of the total spin and angular momentum of the corresponding system.

Preliminary results have been obtained by including only one channel for dd and are given here.

§ 1. INTRODUCTION

THE four-nucleon reaction has been formulated using the resonating group method (Wheeler 1937) and including three channels only:

$$\begin{pmatrix} dd \rightarrow dd & dd \rightarrow n^3\text{He} & d \rightarrow pt \\ n^3\text{He} \rightarrow dd & n^3\text{He} \rightarrow n^3\text{He} & n^3\text{He} \rightarrow pt \\ pt \rightarrow dd & pt \rightarrow n^3\text{He} & pt \rightarrow pt \end{pmatrix}$$

Some of the diagonal elements ($n^3\text{He} \rightarrow n^3\text{He}$ and $pt \rightarrow pt$) have been previously investigated by Bransden, Robertson and Swan (1956). The minor of $dd \rightarrow dd$ has also been calculated by Bransden and Robertson (1960). As a first step towards the complete solution we have investigated here the remaining diagonal element $dd \rightarrow dd$ and results concerning the differential cross section will be compared with experimental values given by Blair *et al.* (1948), Rosen and Allred (1952), Brolley *et al.* (1960).

Later on, a comparison with the results obtained with the complete solution now in progress will show the importance of the exchange reaction. Since we are not including any tensor interaction, a choice of central potential of larger range than is normal has been chosen. This interaction has been shown by many workers (see Bransden's (1960) review paper) to give results in close accord with experiment for many light nuclei collisions. As opposed to rather qualitative work done previously (Pruet, Beiduk and Konopinski 1950) we evaluate here numerical solutions of the integro-differential equations in order to calculate the phases and differential cross sections for different values of the energy. Also, three types of exchange forces are considered and the conclusion reached is that a near Serber interaction gives best agreement with experiment both for this work and similar work.

§ 2. THEORY

The notation is that used by Buckingham and Massey (1941).

2.1. *The Interaction and the Wave Function*

The internucleonic interaction is assumed to be purely central and of the form

$$\mathcal{V}(ij) = (wW_{ij} + mM_{ij} + bB_{ij} + hH_{ij}) V(r_{ij}) + \epsilon_{ij} \frac{e^2}{r_{ij}} \quad \dots\dots (2.1)$$

where W, M, B, H are the usual Wigner, Majorana, Bartlett and Heisenberg operators. The constants w, m, b, h give the exchange dependence of the interaction and satisfy

$$\begin{aligned} w + m + b + h &= 1 \\ w + m - b - h &= x. \end{aligned}$$

$x = 0.6$ is the ratio of the singlet to the triplet interaction (Motz and Schwinger 1940).

$$\begin{aligned} r_{ij} &= |\mathbf{r}_i - \mathbf{r}_j| \\ \epsilon_{ij} &= 1 \text{ if } i \text{ and } j \text{ are protons and zero otherwise.} \end{aligned}$$

Denoting protons by even numbers and neutrons by odd numbers, a resonating group wave function of correct symmetry may be written as

$$\begin{aligned} \Psi_s(1234) &= (1 - P_{13}) \phi(12) \phi(34) \sigma_s(12, 34) F_s(12, 34) \\ &\quad + (1 - P_{13}) \phi(234) \sigma_s(1, 234) G_s(1, 234) \\ &\quad + (1 - P_{24}) \eta(134) \sigma_s(2, 134) H_s(2, 134). \quad \dots\dots (2.2) \end{aligned}$$

P_{ij} are exchange operators of Heisenberg type; σ_s is the spin function corresponding to the total spin s of the system ($s = 0, 1, 2$); $\phi(234)$ and $\eta(134)$ are the space part of the wave functions for ${}^3\text{He}$ and t respectively; F, G, H are the scattering functions of the corresponding arguments.

2.2. *Definition of Vectors and Kinetic Energy Terms*

Let the nucleons 1, 2, 3, 4, be denoted by the position vectors $\mathbf{r}_1, \mathbf{r}_2, \mathbf{r}_3, \mathbf{r}_4$ with respect to some arbitrary origin. (To be consistent we take (34) as target deuteron, (342) as ${}^3\text{He}$ and (341) as t .)

There are three linearly independent vectors to describe the system of four particles in the centre-of-mass frame:

$$(34, 12) = \mathbf{R} = \frac{1}{2}(\mathbf{r}_1 + \mathbf{r}_2 - \mathbf{r}_3 - \mathbf{r}_4) \quad (12) = \mathbf{R}_1 = \mathbf{r}_2 - \mathbf{r}_1 \quad (34) = \mathbf{R}_2 = \mathbf{r}_4 - \mathbf{r}_3.$$

Any other vector will be expressed as a linear combination of \mathbf{R}, \mathbf{R}_1 and \mathbf{R}_2 .

$$(13) = \mathbf{r}_3 - \mathbf{r}_1 = -\frac{1}{2}(\mathbf{R}_2 - \mathbf{R}_1) + \mathbf{R} \quad (14) = \mathbf{r}_4 - \mathbf{r}_1 = \frac{1}{2}(\mathbf{R}_2 + \mathbf{R}_1) - \mathbf{R}.$$

$$(23) = \mathbf{r}_3 - \mathbf{r}_2 = -\frac{1}{2}(\mathbf{R}_2 + \mathbf{R}_1) + \mathbf{R} \quad (24) = \mathbf{r}_4 - \mathbf{r}_2 = \frac{1}{2}(\mathbf{R}_2 - \mathbf{R}_1) - \mathbf{R}.$$

The different transformations of variables needed are given in Appendix I.

To deal now with the energy terms, from conservation of energy we have:

$$\mathcal{E} = 2E_d + E(d) = E_{{}^3\text{He}} + E(n) = E_t + E(p) \quad \dots\dots (2.3)$$

where $E_d, E_{{}^3\text{He}}, E_t$ are the binding energies of $d, {}^3\text{He}$ or t respectively and $E(d), E(n), E(p)$ are the energies of the outgoing d, n or p respectively, out of which we deduce from (2.3) the following relations for the k values:

$$\mathcal{E} = 2E_d + \frac{\hbar^2}{2M} k^2(d) = E_{{}^3\text{He}} + \frac{2\hbar^2}{3M} k^2(n) = E_t + \frac{2\hbar^2}{3M} k^2(p)$$

M being the mass of the nucleon (neutron or proton), so that choosing $k(d)$, for instance, we have corresponding values for $k(n)$ and $k(p)$.

Also, the kinetic energy operators can be written and they are given in Appendix I.

2.3. The Coupled Equations for $s=0, 1, 2$

Substituting the form (2.2) for $\Psi_s(1234)$ into the Schrödinger equation of the system, performing the exchange operations included in the interaction, multiplying successively by:

$$\phi(34)\phi(12)\sigma_s^s(34,12), \quad \phi(342)\sigma_s^s(342,1), \quad \eta(341)\sigma_s^s(341,2),$$

summing over spins and integrating over internal variables, taking account of equivalences due to change of variables, of the conservation of energy principle and the consequent symmetry in τ and τ' , and of the binding energy integral equation

$$\int \phi(H - E_{\min})\phi d\tau = 0$$

satisfied by each nuclear wave function respectively to simplify the equations obtained, we get a set of three coupled three-dimensional integro-differential equations for each value of $s=0$ or $s=1$. For $s=2$ we only have one equation:

$$\begin{aligned} 0 = & - \left[\frac{\hbar^2}{2M} \nabla_v^2 + E(d) \right] F_2(\mathbf{v}) \\ & + F_2(\mathbf{v}) \int \phi^2(34)\phi^2(12) [V_{24}^c + (4w - 2m + 4b - 2h)V_{13}] d(34) d(12) \\ & - J_{AA} \int \phi(34)\phi(12) \{ T - \mathcal{E} + V_{24}^c + 2(V_{12} + V_{14}) + [1 + (-1)^l] \\ & \quad \times (w + b - 2m - 2h)V_{13} \} \phi(14)\phi(32) F_2(r') d\mathbf{r}' d\mathbf{s} \end{aligned}$$

(where J_{AA} and V_{24}^c are defined in Appendix II and v, r, r' and s are defined in Appendix I).

This equation only exists when l is even; $1 + (-1)^l = 2$.

Denoting the system dd by A, $n^3\text{He}$ by B and pt by C, the equations can be written symbolically

$$\begin{pmatrix} AA & AB & AC \\ BA & BB & BC \\ CA & CB & CC \end{pmatrix} \begin{pmatrix} F \\ G \\ H \end{pmatrix} = 0$$

For $s=2$ we only have one equation $AAF=0$ given above explicitly. For $s=0$ or 1 we have the three coupled equations with, of course

$$BA = (AB)^\dagger \quad CA = (AC)^\dagger \quad CB = (AC)^\dagger.$$

The systems of equations for $s=0$ and for $s=1$ are given in Appendix II. These equations have been previously published in a matrix form (Burke and Laskar 1958).

§ 3. THE POTENTIAL SHAPE AND THE NUCLEAR WAVE FUNCTIONS

The potential shape is assumed to be the same for all types of exchange and of Gaussian form $V(r) = V_0 \exp(-\mu r^2)$. The value of μ ($\mu = 0.2669 \times 10^{26} \text{ cm}^{-2}$) is that used in previous four and five nucleon calculations (Bransden's review). The value of V_0 ($V_0 = -46.8 \text{ MeV}$) was interpolated from the results obtained by Burke and Robertson (1957).

The wave function for the deuteron is a double Gaussian

$$\phi = \frac{1}{N_d} \{ \exp(-\alpha r^2) + c \exp(-\beta r^2) \}$$

and for any other nuclei, a single Gaussian

$$\phi = \frac{1}{N} \exp \left[-\frac{1}{2} \lambda \sum (r_{ij})^2 \right].$$

The values of the parameters are listed in Table 1, and have been obtained by a variational method. The Table also includes E_{\min} , the variational value of the binding energy.

Table 1				
$\lambda(10^{+26} \text{ cm}^{-2})$	^3He 0.15400	T 0.15715	^4He 0.15780	D $\alpha(10^{+26} \text{ cm}^{-2})=0.0299$ $\beta(10^{+26} \text{ cm}^{-2})=0.186$ $c=2.73$
$E_{\min} \text{ (MeV)}$	-5.975	-6.744	-27.315	-2.133
$E_{\exp} \text{ (MeV)}$	-7.55	-8.3	-28.2	-2.226

§ 4. METHOD OF CALCULATION

In the dd elastic case, after integration over the angular variables, we obtain integro-differential equations of the following form:

$$\left[\frac{d^2}{dr^2} + k^2 - \frac{l(l+1)}{r^2} \right] f_l(r) = U(r) f_l(r) + \int \{k_l^{(1)}(r, r') - \mathcal{E} k_l^{(2)}(r, r')\} f_l(r') dr' \quad (4.1)$$

where $\mathcal{E} = 2E_d(\min) + E(d)$ and $E(d)$ is the energy in the centre-of-mass system of the incident deuteron. $f_l(r)$ and $k_l^{(i)}(r, r')$ are defined as usual:

$$F(\mathbf{r}) = \sum_l \frac{1}{r} f_l(r) P_l(\cos \theta)$$

$$k_l^{(i)}(\mathbf{r}, \mathbf{r}') = \sum_l \frac{2l+1}{4\pi r r'} k_l^{(i)}(r, r') P_l(\cos \Theta) \quad i=1, 2.$$

θ is the angle of scattering in the centre-of-mass frame, Θ is the angle between \mathbf{r} and \mathbf{r}' .

All the kernels are symmetric in r and r' to satisfy the principle of the conservation of energy.

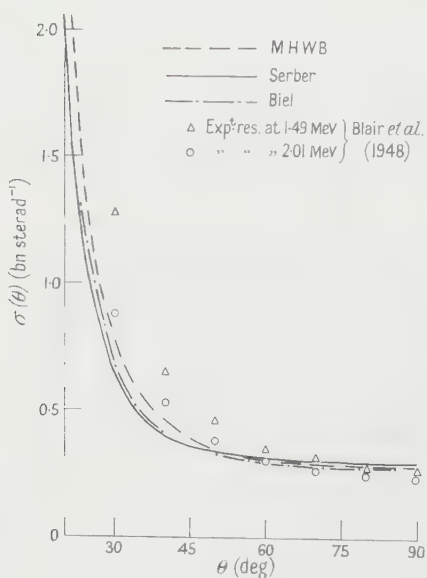


Fig. 1. dd elastic $\sigma(\theta)$ at $E_{\text{lab}} = 1.660$ MeV.

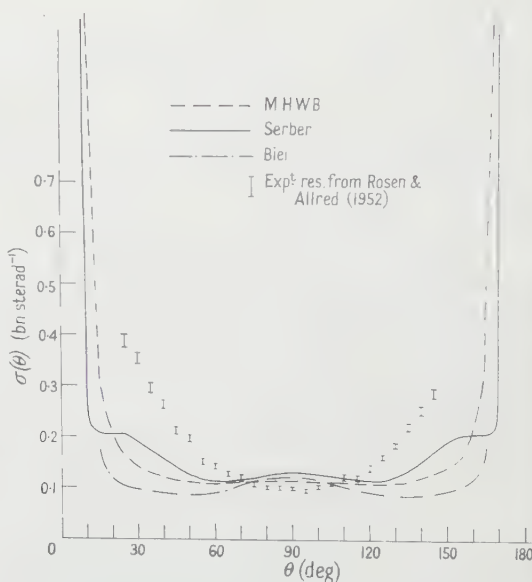


Fig. 2. dd elastic $\sigma(\theta)$ at $E_{\text{lab}} = 10.5$ MeV.

$k_l^{(1)}$ and $k_l^{(2)}$ include, of course, the Coulomb kernels and are the sums of many terms; in the dd case we have about 50 kernels and they cannot be listed here. The authors will be pleased to supply their explicit form to anybody interested. Most of them are of the form

$$k_l^{(k)}(r, r') = \phi_k(r, r') \exp(-\beta_k r^2 - \gamma_k r'^2) \mathcal{J}_{l+\frac{1}{2}}(K_k r r')$$

where $\phi_k(r, r')$ is a polynomial in r and r' , β_k, γ_k, K_k are algebraic expressions in $\alpha, \beta, c, \lambda$ and $\mathcal{J}_{l+\frac{1}{2}}(x) = i^{l-1/2} (\frac{1}{2}\pi x)^{1/2} J_{l-1/2}(ix)$ is the hyperbolic spherical Bessel function, the first two being:

$$\mathcal{J}_{1/2}(x) = \sinh x \quad \mathcal{J}_{3/2}(x) = \frac{\sinh x}{x} - \cosh x.$$

Equation (4.1) is represented as a set of linear simultaneous equations, the unknown being the values of $f_l(r)$ over the range of r required (Robertson 1956). It is necessary to find a solution of (4.1) satisfying the boundary conditions

$$f_l(0) = 0 \quad f_l(r) \sim \sin(kr - \eta \ln 2kr - \frac{1}{2}l\pi + \delta_l + \sigma_l)$$

with

$$\eta = \frac{Mz z' e^2}{\hbar^2 k}, \quad k = \left[\frac{2M}{\hbar^2} E(d) \right]^{1/2}, \quad \sigma_l = \arg \Gamma(l+1+i\eta).$$

The scattering amplitude $f_s(\theta)$ corresponding to the total spin s can be written (Mott and Massey 1933)

$$f_s(\theta) = -\frac{1}{2ik} \sum_l (2l+1) [\exp[2i(\delta_l + \sigma_l)] - 1] P_l(\cos \theta).$$

The differential cross section follows:

$$\sigma(\theta) = \frac{1}{g} [\sigma_0(\theta) + 5\sigma_2(\theta) + 3\sigma_4(\theta)]$$

with

$$\sigma_s(\theta) = |f_s(\theta) + (-1)^s f_s(\pi - \theta)|^2.$$

The differential cross section has been tabulated for $\theta = 5^\circ$ to 175° including S, P, D and F phases.

The calculation was carried out using the Ferranti Mercury digital computer. A programme prepared by B. Haslea was used to calculate the regular and irregular Coulomb functions.

§ 5. TABLES OF RESULTS

The energies for which the calculation has been carried out are given in Table 2.

The values of $k=0.2, 0.4, 0.6$ are regularly spaced to ease interpolation. $k=0.503$ corresponds to $E(d)_{lab} = 10.5$ MeV for which the experimental results of Rosen and Allred (1952) are available for comparison. $k=0.075$ and 0.12 are used for the very low energy.

From these values of k for which effective calculations have been carried out, more results have been obtained by interpolation for $k=0.380, 0.444, 0.540, 0.577$ (in units of 10^{13} cm^{-1}) for which we received, before publication, the experimental results obtained by Dr. J. E. Brolley and others (Brolley *et al.* 1960) from Los Alamos Scientific Laboratory.

The reliability of interpolated values is as good as the direct calculation, as it has been checked for $k=0.503$, for which the results were obtained first by interpolation and then by the complete machine calculations, the results being the same to sufficient accuracy (0.5%).

All this calculation has been carried out for the three following types of exchange forces:

- I M H W B (or symmetrical) i.e. $m=2b$ $h=2w$
 II Serber i.e. $m=w$ $h=b$
 III Biel's mixture (Biel 1957) i.e. $\frac{1}{3}$ M H W B + $\frac{2}{3}$ Serber

(The phases are given in degrees in Tables 3, 4 and 5.)

Table 2. Correspondence between $E(d)$ and k

$k \times 10^{13} \text{ cm}^{-1}$	0.075	0.12	0.200	0.380	0.4	0.444	0.503	0.540	0.577	0.6
$E(d)_{\text{c.m.}} (\text{Mev})$	0.115	0.300	0.830	3	3.200	4.1	5.25	6.05	6.9	7.5
$E(d)_{\text{lab.}} (\text{Mev})$	0.230	0.600	1.660	(6)	6.4	(8.2)	10.5	(12.1)	(13.8)	15

Table 3. Total spin $s=1$

$E(d)_{\text{lab}} (\text{Mev})$	P_3 phases			F_3 phases		
	MHWP	Serber	Biel	MHWP	Serber	Biel
0.230	0.131	0.249	0.193	0	0	0
0.600	0.567	1.457	1.021	0.010	0.010	0.010
0.660	— 0.070	5.340	2.557	0.217	0.221	0.220
(6)	— 9	23	3.8	0.61	0.92	0.84
6.4	— 10.634	23.423	4.709	0.627	1.037	0.891
(8.2)	— 12	27.5	4.8	0.54	1.35	1.08
10.5	— 24.221	30.748	5.235	0.365	1.833	1.299
(12.1)	— 23.5	31.2	5.2	0.17	2.23	1.48
(13.8)	— 20	33.8	5.2	— 0.07	2.77	1.74
15	— 17.759	34.026	5.254	— 0.240	3.214	1.927

Table 4. Total spin $s=0$

$E(d)_{\text{lab}} (\text{Mev})$	S_1 phases			D_1 phases		
	MHWP	Serber	Biel	MHWP	Serber	Biel
0.230	2.386	22.301	9.135	0.010	0.010	0.010
0.600	4.499	48.265	30.637	0.133	0.147	0.141
1.660	0.552	45.853	24.962	1.041	1.267	1.178
(6)	— 23.5	8	— 3	5.1	11.8	9.8
6.4	— 25.483	7.144	— 5.142	6.285	14.388	10.820
(8.2)	— 33.5	— 3	— 13	9	22.5	16.5
10.5	— 41.966	— 12.505	— 23.347	12.940	33.372	24.220
(12.1)	48.2	— 13	— 30	15	38.2	28
(13.8)	— 53	— 25	— 35.1	17.8	44.2	33
15	— 57.389	— 29.419	— 39.641	19.716	49.404	36.897

Table 5. Total spin $s=2$

$E(d)_{\text{lab}} (\text{Mev})$	S_3 phases			D_3 phases		
	MHWP	Serber	Biel	MHWP	Serber	Biel
0.230	— 4.089	— 3.837	— 3.929	0.009	0.009	0.009
0.600	— 13.270	— 12.588	— 12.839	0.112	0.116	0.114
1.660	— 33.377	— 31.944	— 32.468	0.686	0.754	0.729
(6)	— 76	— 72	— 74	— 1.8	0	0
6.4	— 79.274	— 75.515	— 76.926	— 1.851	— 0.308	— 0.878
(8.2)	— 91	— 86	— 89	— 3	— 0.6	— 1.6
10.5	— 98.894	— 93.471	— 95.532	— 4.453	— 0.846	— 2.207
(12.1)	— 104	— 98.7	— 101	— 5	— 0.5	— 2
(13.8)	— 110	— 103.7	— 106.5	— 6	0	— 2
15	— 114.418	— 106.966	— 109.837	— 6.393	0.187	— 2.342

§ 6. CONCLUSION

This paper is related to few-nucleon problems, and deals mainly with the four-nucleon case; the information obtained can be related to the nature of nuclear forces and is of importance for thermonuclear reactions.

With respect to nuclear forces, the comparison at low energy (< 6 Mev) shows no significant difference between the types of exchange force (MHWB, Serber, Biel) and no conclusion can be drawn from the agreement with the experimental results for the cross sections (Blair *et al.* 1948). At higher energy (> 6 Mev), although the three types of force give markedly different results, it is difficult to come to any clear-cut decision concerning the relative merits of each type, because we have included only one grouping in our calculation; in particular no account is taken of the formation of the ^4He grouping. However, between 60° and 120° our results are close enough to the Los Alamos experimental results (Brolley *et al.* 1960) to suggest that the inelastic processes are more important outside this range. Although in the present situation the results favour MHWB type, it is not excluded that the solution of the full system will be in favour of Serber type of exchange, which covers so many cases (Bransden, Hamilton and Robertson 1960); and to make the choice more difficult, between 60° and 120° the results corresponding to the three types of forces are again too close to each other to allow any conclusion except to say that the Wheeler method is able to describe the phenomena. (The other reaction channels become very important for $E(d)_{\text{lab}} > 0.5$ Mev as can be seen from the values of the elastic cross section, even for $\theta \sim 20^\circ$, or from the fact that the classical distance of closest approach must be roughly of the order of the radius of the deuteron.)

The five-nucleon problem is simpler to formulate and should give more conclusive results. Effectively, we only have here two values for the spin ($\frac{3}{2}$ and $\frac{1}{2}$) instead of three (2, 1, 0) in the four-nucleon one.

Only two channels need to be considered

$$\begin{pmatrix} dt \rightarrow dt & dt \rightarrow n^4\text{He} \\ n^4\text{He} \rightarrow dt & n^4\text{He} \rightarrow n^4\text{He} \end{pmatrix}$$

so that the analysis is more relevant to the physical situation.

Furthermore, we expect this problem to be more conclusive, as the results for $dt \rightarrow dt$ appear more sensitive to the exchange type of forces than $dd \rightarrow dd$.

This five-nucleon problem has been studied in conjunction with the four-nucleon one, and results for it should be available soon.

ACKNOWLEDGMENTS

We are greatly indebted to Professor Sir Harrie Massey for the stimulating interest he has shown in this work. It is also a pleasure to thank the staff of the University of London Computer Unit and particularly its Director, Dr. R. A. Buckingham, as well as the staff of the Oxford Computing Laboratory and its Director, Dr. L. Fox, for their assistance in using Ferranti MERCURY Computers.

Finally, one of us (W.L.) wishes to thank the C.N.R.S. (Paris) for his grant during the time this work was performed.

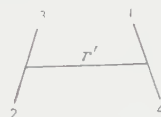
APPENDIX I

I. 1. Table of Kinetic Energy Terms

The following table gives the forms of the kinetic energy operator T in the different possible groupings of the nucleons.

(1) dd (A)

(34, 12)

 $(P_{13})(34, 12) \rightarrow (14, 32)$ 

$$T = -\frac{\hbar^2}{M} \nabla_{34}^2 - \frac{\hbar^2}{M} \nabla_{12}^2 - \frac{\hbar^2}{2M} \nabla_{(34,12)}^2$$

$$T = -\frac{\hbar^2}{M} \nabla_{14}^2 - \frac{\hbar^2}{M} \nabla_{32}^2 - \frac{\hbar^2}{2M} \nabla_{(14,32)}^2$$

(2) n³He (B)

(342, 1)

 $(P_{13})(342, 1) \rightarrow (142, 3)$ 

$$T = -\frac{\hbar^2}{M} \nabla_{34}^2 - \frac{3\hbar^2}{4M} \nabla_{34-2}^2 - \frac{2\hbar^2}{3M} \nabla_{342-1}^2$$

$$T = -\frac{\hbar^2}{M} \nabla_{14}^2 - \frac{3\hbar^2}{4M} \nabla_{(14-2)}^2 - \frac{2\hbar^2}{3M} \nabla_{142-3}^2$$

(3) pt (C)

(341, 2)

 $(P_{24})(341, 2) \rightarrow (321, 4)$ 

$$T = -\frac{\hbar^2}{M} \nabla_{34}^2 - \frac{3\hbar^2}{4M} \nabla_{34-1}^2 - \frac{2\hbar^2}{3M} \nabla_{341-2}^2$$

$$T = -\frac{\hbar^2}{M} \nabla_{32}^2 - \frac{3\hbar^2}{4M} \nabla_{32-1}^2 - \frac{2\hbar^2}{3M} \nabla_{321-4}^2$$

I. 2. Table of Change of Variables

The following Table defines the coordinates \mathbf{r}' and \mathbf{s} corresponding to the different transformation (e.g. AB signifies the transformation $dd \rightarrow n^3\text{He}$).

AA	AB	AC
(34, 12) $\mathbf{v} = \mathbf{R}$	(34, 12) $\mathbf{v} = \mathbf{R}$	(34, 12) $\mathbf{v} = \mathbf{R}$
(14, 32) $\mathbf{r}' = \frac{1}{2}(\mathbf{R}_1 - \mathbf{R}_2)$	(142, 3) $\mathbf{r}' = -\frac{2}{3}(\mathbf{R} + \mathbf{R}_2)$	(321, 4) $\mathbf{r}' = -\frac{2}{3}(\mathbf{R} - \mathbf{R}_2)$
(31, 42) $\mathbf{s} = \frac{1}{2}(\mathbf{R}_1 + \mathbf{R}_2)$	(342, 1) $\mathbf{s} = \frac{2}{3}(\mathbf{R} - \mathbf{R}_1)$	(341, 2) $\mathbf{s} = \frac{2}{3}(\mathbf{R} + \mathbf{R}_1)$
BB	BC	CC
(342, 1) $\mathbf{v} = \frac{2}{3}(\mathbf{R} - \mathbf{R}_1)$	(342, 1) $\mathbf{v} = \frac{2}{3}(\mathbf{R} - \mathbf{R}_1)$	(341, 2) $\mathbf{v} = \frac{2}{3}(\mathbf{R} + \mathbf{R}_1)$
(142, 3) $\mathbf{r}' = -\frac{2}{3}(\mathbf{R} + \mathbf{R}_2)$	(321, 4) $\mathbf{r}' = -\frac{2}{3}(\mathbf{R} - \mathbf{R}_2)$	(321, 4) $\mathbf{r}' = -\frac{2}{3}(\mathbf{R} - \mathbf{R}_2)$
(341, 2) $\mathbf{s} = \frac{2}{3}(\mathbf{R} + \mathbf{R}_1)$	(341, 2) $\mathbf{s} = \frac{2}{3}(\mathbf{R} + \mathbf{R}_1)$	(342, 1) $\mathbf{s} = \frac{2}{3}(\mathbf{R} - \mathbf{R}_1)$

APPENDIX II

The detailed forms of the three coupled equations referred to in §2.3 are given below for the cases $S=0$ and $S=1$. The case $S=2$ is given explicitly in the text. In these equations the quantities $J_{AA}, J_{AB}, J_{AC}, J_{BB}, J_{BC}, J_{CC}$ are the Jacobians of the respective coordinate transformations given in Appendix I. V_{24}^c denotes the coulomb interaction between the protons.

$$S=0$$

$$\begin{aligned}
 0 = & - \left[\frac{\hbar^2}{2M} \nabla_v^2 + E(d) \right] F_0(\mathbf{v}) \\
 & + F_0(\mathbf{v}) \int \phi^2(34) \phi^2(12) [V_{24}^c + (4w + m - 2b - 2h)V_{13}] d(34) d(12) \\
 & + \frac{J_{AA}}{2} \int \phi(34) \phi(12) \{T - \mathcal{E} + V_{24}^c + 2(V_{12} + V_{14}) + [1 + (-1)^i] \\
 & \times (w + 4m - 2b - 2h)V_{13}\} \phi(14) \phi(32) F_0(\mathbf{r}') d\mathbf{r}' d\mathbf{s} \\
 & + J_{AB} \sqrt{3} \int \phi(34) \phi(12) \{T - \mathcal{E} + V_{24}^c + V_{12} + V_{34} + (2w + 2m - b - h) \\
 & \times (V_{13} + V_{24})\} \phi(142) G_0^s(\mathbf{r}') d\mathbf{r}' d\mathbf{s} \\
 & + J_{AC} \sqrt{3} \int \phi(34) \phi(12) \{T - \mathcal{E} + V_{24}^c + V_{12} + V_{34} + (2w + 2m - b - h) \\
 & \times (V_{13} + V_{24})\} \eta(321) H_0^s(\mathbf{r}') d\mathbf{r}' d\mathbf{s} \\
 0 = & BA - \left[\frac{2\hbar^2}{3M} \nabla_v^2 + E(n) \right] G_0(\mathbf{v}) \\
 & + (3w + m - h) G_0(\mathbf{v}) \int \phi^2(342) V_{13} d(34) d(2-34) \\
 & + J_{BB} \int \phi(342) \{T - \mathcal{E} + V_{24}^c + (w + 3m - b)V_{13} + xV_{24} + (2w + 2m + b + h) \\
 & \times (V_{12} + V_{34})\} \phi(142) G_0(\mathbf{r}') d\mathbf{r}' d\mathbf{s} \\
 & + (2m + h) H_0(\mathbf{v}) \int \phi(342) V_{12} \eta(342) d(34) d(2-34) \\
 & + J_{BC} \int \phi(342) \{2(T - \mathcal{E} + V_{24}^c) + (2w + b)V_{14} \\
 & \quad + (2w + 2m + b + h)V_{23} \\
 & \quad + (4w + 4m - b - h)(V_{12} + V_{34})\} \eta(321) H_0(\mathbf{r}') d\mathbf{r}' d\mathbf{s} \\
 0 = & CA + CB - \left[\frac{2\hbar^2}{3M} \nabla_v^2 + E(p) \right] H_0(\mathbf{v}) \\
 & + H_0(\mathbf{v}) \int \eta^2(341) [V_{24}^c + (3w + m - h)V_{24}] d(34) d(1-34) \\
 & + J_{CC} \int \eta(341) \{T - \mathcal{E} + V_{24}^c + (w + 3m - b)V_{24} + xV_{13} + (2w + 2m + b + h) \\
 & \times (V_{12} + V_{34})\} \eta(321) H_0(\mathbf{r}') d\mathbf{r}' d\mathbf{s}
 \end{aligned}$$

N.B. For $s=0$, F_0 is even and the rest of the first equation is even; we write

$$G_0(\mathbf{r}') + G_0(-\mathbf{r}') = 2G_0^s(\mathbf{r}') \quad (\text{similarly for } H).$$

Similarly for $s=1$, F_1 is odd and the rest of the first equation is odd; we write

$$G_1(\mathbf{r}') - G_1(-\mathbf{r}') = 2G_1^a(\mathbf{r}') \quad (\text{similarly for } H).$$

$$S = 1$$

$$\begin{aligned}
 0 = & - \left[\frac{\hbar^2}{2M} \nabla_v^2 + E(d) \right] F_1(\mathbf{v}) \\
 & + F_1(\mathbf{v}) \int \phi^2(34) \phi^2(12) [V_{24}^c + (4w - 2h)V_{13}] d(34) d(12) \\
 & + J_{AA} (2m - b) [1 - (-1)^4] \int \phi(34) \phi(12) V_{13} \phi(14) \phi(32) F_1(\mathbf{r}') d\mathbf{r}' d\mathbf{s} \\
 & - J_{AB} \sqrt{2} \int \phi(34) \phi(12) \{T - \mathcal{E} + V_{24}^c + V_{12} + V_{34} + (2w - 2m + b - h)V_{13} \\
 & \quad + (2w + 2m - b - h)V_{24}\} \phi(142) G_1^a(\mathbf{r}') d\mathbf{r}' d\mathbf{s} \\
 & - J_{AC} \sqrt{2} \int \phi(34) \phi(12) \{T - \mathcal{E} + V_{24}^c + V_{12} + V_{34} + (2w + 2m - b - h)V_{13} \\
 & \quad + (2w - 2m + b - h)V_{24}\} \eta(321) H_1^a(\mathbf{r}') d\mathbf{r}' d\mathbf{s} \\
 0 = & BA - \left[\frac{2\hbar^2}{3M} \nabla_v^2 + E(n) \right] G_1(\mathbf{v}) \\
 & + (3w - m + 2b - h) G_1(v) \int \phi^2(342) V_{13} d(34) d(2 - 34) \\
 & - J_{BB} \int \phi(342) \{T - \mathcal{E} + V_{24}^c + (w - 3m + b - 2h)V_{13} + xV_{24} + (2w + 2m + b + h) \\
 & \quad \times (V_{12} + V_{34})\} \phi(142) G_1(\mathbf{r}') d\mathbf{r}' d\mathbf{s} \\
 & + hH_1(\mathbf{v}) \int \phi(342) V_{12} \eta(342) d(34) d(2 - 34) \\
 & + J_{BC} \int \phi(342) \{bV_{14} - (b + h)(V_{12} + V_{34} - V_{23})\} \eta(321) H_1(\mathbf{r}') d\mathbf{r}' d\mathbf{s} \\
 0 = & CA + CB - \left[\frac{2\hbar^2}{3M} \nabla_v^2 + E(p) \right] H_1(\mathbf{v}) \\
 & + H_1(\mathbf{v}) \int \eta^2(341) [V_{24}^c + (3w - m + 2b - h)V_{24}] d(34) d(1 - 34) \\
 & - J_{CC} \int \eta(341) \{T - \mathcal{E} + V_{24}^c + (w - 3m + b - 2h)V_{24} + xV_{13} + (2w + 2m + b + h) \\
 & \quad \times (V_{12} + V_{34})\} \eta(321) H_1(\mathbf{r}') d\mathbf{r}' d\mathbf{s}.
 \end{aligned}$$

REFERENCES

- BIEL, S. J., 1957, *Proc. Phys. Soc. A*, **70**, 866.
 BLAIR, J. M., FREIER, G., LAMPI, E. E., SLEATOR, W., and WILLIAMS, J. H., 1948, *Phys. Rev.*, **74**, 553.
 BRANDSEN, B. H., 1960, Review paper in *The Proceedings of the London Conference (1959) on Nuclear Forces and the Few-Nucleon Problem* (London: Pergamon Press), 1960.
 BRANDSEN, B. H., HAMILTON, R. A. H., and ROBERTSON, H. H., 1960, *Proc. Phys. Soc.*, **75**, 144.
 BRANDSEN, B. H., and ROBERTSON, H. H., 1958, *Proc. Phys. Soc. A*, **72**, 770.
 BRANDSEN, B. H., ROBERTSON, H. H., and SWAN, P., 1956, *Proc. Phys. Soc. A*, **79**, 877.
 BROLLEY, J. E., PITMAN, T. M., ROSEN, L., and STEWART, L., 1960, *Phys. Rev.*, **117**, 1307.
 BUCKINGHAM, R. A., and MASSEY, H. S. W., 1941, *Proc. Roy. Soc. A*, **179**, 123.
 BURKE, P. G., and LASKAR, W. 1958, *C. R. Acad. Sci, Paris*, **246**, 3044 and 3158f.
 BURKE, P. G., and ROBERTSON, H. H., 1957, *Proc. Phys. Soc. A*, **70**, 777.
 MOTT, N. F., and MASSEY, H. S. W., 1949, *Theory of Atomic Collisions* (Oxford: University Press), 2nd edition.
 MOTZ, L., and SCHWINGER, J., 1940, *Phys. Rev.*, **58**, 26.
 PRUET, J. R., BEIDUK, F. M., and KONOPINSKI, E. J., 1950, *Phys. Rev.*, **77**, 628.
 ROBERTSON, H. H., 1956, *Proc. Camb. Phil. Soc.*, **52**, 538.
 ROSEN, L., and ALLRED, G. C., 1952, *Phys. Rev.*, **88**, 431.
 WHEELER, J. A., 1937, *Phys. Rev.*, **52**, 1107.

Excitation of the 1s-2p Transition of Atomic Hydrogen by Proton and Alpha Particle Impact

BY D. R. BATES

Department of Applied Mathematics, The Queen's University of Belfast

MS. received 6th May 1960

Abstract. Using the distortion approximation the cross sections for the collision processes



are evaluated at H^+ energies between 10 keV and $100\sqrt{10}$ keV (or He^{2+} energies between 40 keV and $400\sqrt{10}$ keV). It is found that the effect of distortion is not as much as in the case of



Optically allowed transitions are in general likely to be less influenced by distortion than are optically forbidden transitions.

§ 1. INTRODUCTION

THE energy of relative motion below which collisions between atomic systems are not described reliably by the first Born approximation is quite high (cf. Bates 1958). Nevertheless few calculations have as yet been carried out using more refined approximations. In the present paper an account is given of the application of the distortion approximation to



and



The only other processes for which this approximation has been employed are



and



(Bates 1959). These two processes involve optically forbidden transitions whereas the two processes now under consideration involve optically allowed transitions. A marked difference in the effect of distortion would be expected.

§ 2. ANALYSES

The distortion approximation (Bates 1959), which is the semi-classical version of the well-known distorted waves approximation (Mott and Massey 1949), takes full account of the secular terms with diagonal matrix elements in the relevant set of coupled differential equations occurring in the collision problem but is otherwise the same as the first Born approximation. According to it the

probability of the target system being excited from state n to state m during the passage of the projectile system at impact parameter ρ is

$$\mathcal{P}_{nm}(\rho) = \left| \frac{1}{v} \int_{-\infty}^{\infty} V_{mn} \exp \left\{ -\frac{i}{v} \gamma_{nm} \right\} dZ \right|^2 \quad \dots\dots (5)^\dagger$$

with

$$V_{mn} = \int \psi_m^*(\mathbf{r}) v(\mathbf{r}, \mathbf{R}) \psi_n(\mathbf{r}) d^3\mathbf{r} \quad \dots\dots (6)$$

and

$$\gamma_{nm} = \int_0^Z \{ \epsilon_n + V_{nn} - \epsilon_m - V_{mm} \} dZ \quad \dots\dots (7)$$

where v is the velocity of relative motion which is taken to be constant and to be directed along the Z axis of a fixed set of Cartesian coordinates with origin on the target system; \mathbf{r} is the position vector of the active electron and $\mathbf{R}(\rho, Z, \Phi)$ is that of the projectile system; $v(\mathbf{r}, \mathbf{R})$ is the interaction potential; $\psi_n(\mathbf{r})$ and $\psi_m(\mathbf{r})$ are the eigenfunctions and ϵ_n and ϵ_m are the eigenenergies of the initial and final states; and all quantities are in atomic units. The excitation cross section is given by

$$Q_{nm} = 2 \int_0^\infty \rho \mathcal{P}_{nm} d\rho \quad (\pi a_0^2). \quad \dots\dots (8)$$

Let \mathcal{Z} be the charge on the projectile system so that for processes (1) and (2) we have

$$v(\mathbf{r}, \mathbf{R}) = \mathcal{Z} \left\{ \frac{1}{R} - \frac{1}{|\mathbf{R} - \mathbf{r}|} \right\}. \quad \dots\dots (9)$$

Analytical expressions for the matrix elements required may readily be derived. Choosing the polar axis to which the eigenfunctions of the target system are referred to coincide with the Z axis we find from (5) that the probabilities of exciting the $2p_0$ and $2p_{\pm 1}$ states are

$$\mathcal{P}_{1s, 2p_0} = \left| \frac{2}{v} \int_0^\infty U(R) Z \sin \gamma_{1s, 2p_0} dZ \right|^2 \quad \dots\dots (10)$$

and

$$\mathcal{P}_{1s, 2p_{\pm 1}} = \left| \frac{2}{v} \int_0^\infty U(R) \rho \cos \gamma_{1s, 2p_{\pm 1}} dZ \right|^2 \quad \dots\dots (11)$$

respectively, with

$$U(R) = \frac{\mathcal{Z} \sqrt{8}}{243 R^3} \left\{ 64 - (64 + 96R + 72R^2 + 27R^3) e^{-3R/2} \right\} \quad \dots\dots (12)$$

$$\gamma_{1s, 2p_0} = \frac{1}{v} \left[\frac{3Z}{8} + \mathcal{Z} \int_0^Z \left\{ \zeta - (2Z^2 - \rho^2) \eta \right\} dZ \right] \quad \dots\dots (13)$$

and

$$\gamma_{1s, 2p_{\pm 1}} = \frac{1}{v} \left[\frac{3Z}{8} + \mathcal{Z} \int_0^Z \left\{ \zeta + (Z^2 - 2\rho^2) \eta \right\} dZ \right] \quad \dots\dots (14)$$

† It may be noted that the formula for \mathcal{P}_{nm} obtained from the distortion approximation differs from the formula obtained from the first Born approximation only in that energies of states of the isolated target system are replaced by the corresponding energies perturbed by the projectile system.

in which

$$\zeta = \frac{1}{24R} \left\{ (24 + 18R + 6R^2 + R^3)e^{-R} - 24(1 + R)e^{-2R} \right\} \dots\dots (15)$$

and

$$\eta = \frac{1}{24R^5} \left\{ 144 - (144 + 144R + 72R^2 + 24R^3 + 6R^4 + R^5)e^{-R} \right\} \dots\dots (16)$$

The probability of exciting any of the $2p(m=0, \pm 1)$ states is

$$\mathcal{P}_{1s, 2p} = \mathcal{P}_{1s, 2p_0} + \mathcal{P}_{1s, 2p_{\pm 1}} \dots\dots (17)$$

§ 3. RESULTS

Numerical methods were used for the integrals occurring in the distortion approximation. The computational work was very lengthy. During the course of it errors of up to several per cent may have accumulated.

For comparison purposes the evaluations were also carried out by the first Born approximation (cf. Bates 1958).

Instead of displaying the probabilities, $\mathcal{P}_{1s, 2p_0}$ and $\mathcal{P}_{1s, 2p_{\pm 1}}$, it is convenient to display the asymptotic coefficients, $a_{2p_0}(\infty)$ and $a_{2p_{\pm 1}}(\infty)$ of ψ_{2p_0} and $\psi_{2p_{\pm 1}}$ in the expansion of the wave function describing the target system after the projectile system has passed. The probabilities and coefficients are of course related through

$$\mathcal{P}_{1s, 2p_0} = |a_{2p_0}(\infty)|^2, \quad \mathcal{P}_{1s, 2p_{\pm 1}} = |a_{2p_{\pm 1}}(\infty)|^2 \dots\dots (18)$$

Fig. 1 (a)-(f) shows $(a_{2p_0}(\infty), \rho)$ and $(a_{2p_{\pm 1}}(\infty), \rho)$ curves for some selected values of \mathcal{E} the energy of the ion; Fig. 2 (a) shows $(a_{2p_0}(\infty), \log \mathcal{E})$ curves for head-on collisions and Fig. 2 (b) $(a_{2p_{\pm 1}}(\infty), \log \mathcal{E})$ curves for collisions in which ρ is $2a_0$. It is apparent that distant encounters are important and that their importance is enhanced as the energy is raised; and it is apparent also that the influence of distortion is most marked in close encounters and at low energies.

The $(Q_{1s, 2p_0}, \log \mathcal{E})$ and $(Q_{1s, 2p_{\pm 1}}, \log \mathcal{E})$ curves are presented in Figs 3 (a) and 3 (b) and the $(Q_{1s, 2p}, \log \mathcal{E})$ curves in Fig. 4. When \mathcal{E} is low allowance for distortion leads to a decrease in $Q_{1s, 2p}$ but when \mathcal{E} is high it leads to a slight increase. Referring to the results of the earlier calculation (Bates 1959) it may be seen that distortion is much less important for processes (1) and (2) than for processes (3) and (4)†. Moreover, its effect is not even the same quantitatively ($Q_{1s, 2s}$ being reduced over the entire \mathcal{E} range). The difference arises from two causes. Firstly distant encounters contribute relatively more to $Q_{1s, 2p}$ than they do to $Q_{1s, 2s}$ and such encounters are less influenced by distortion than are close encounters. Secondly, the trigonometric function occurring in the integrand in equation (10) for $\mathcal{P}_{1s, 2p_0}$ is the *sine* function whereas the corresponding function in the case of $\mathcal{P}_{1s, 2s}$ (like that in Eqn (11) for $\mathcal{P}_{1s, 2p_{\pm 1}}$) is the *cosine* function. From the fact that the interaction makes the initial and final potential energy curves separate as the colliding systems approach so that

$$-\gamma_{1s, 2p_0} - \gamma_{1s, 2p_{\pm 1}}, \quad -\gamma_{1s, 2s} > (\epsilon_{2s, \text{or } 2p} - \epsilon_{1s})Z \dots\dots (19)$$

† For example when \mathcal{E} is 50 kev distortion produces little change in the cross section for process (1) though it reduces that for process (3) by a factor of 1.5; and when \mathcal{E} is 200 kev distortion reduces the cross section for process (2) by a factor of only 1.1 though it reduces that for process (4) by a factor of about 3.

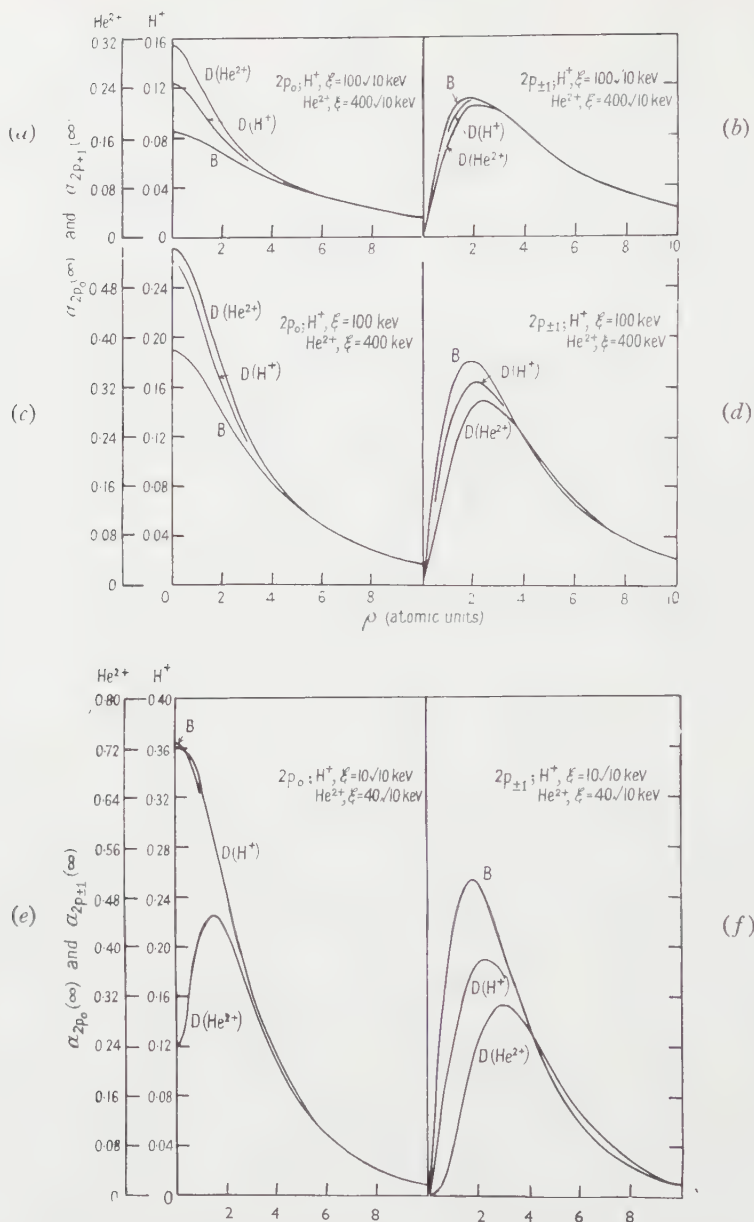


Fig. 1. Asymptotic coefficients $a_{2p_0}(\infty)$ and $a_{2p_{\pm 1}}(\infty)$ plotted against impact parameter ρ . The energy \mathcal{E} of the incident H^+ or He^{2+} ion is as indicated. Curve B of each set of three gives the first Born approximation for H^+ impact and for He^{2+} impact; one of the two curves D gives the distortion approximation for H^+ impact and the other the distortion approximation for He^{2+} impact.

it therefore follows that when \mathcal{E} is high distortion *increases* $Q_{1s, 2p_0}$ though it *decreases* $Q_{1s, 2s}$ (as it does $Q_{1s, 2p_{\pm 1}}$). When the effects of distortion on $Q_{1s, 2p_0}$ and $Q_{1s, 2p_{\pm 1}}$ are opposite in sense the effect on $Q_{1s, 2p}$ is of course reduced by cancellation.

It is clear that distortion is in general to be less important for optically allowed transitions (including ionization) than it is for optically forbidden transitions.

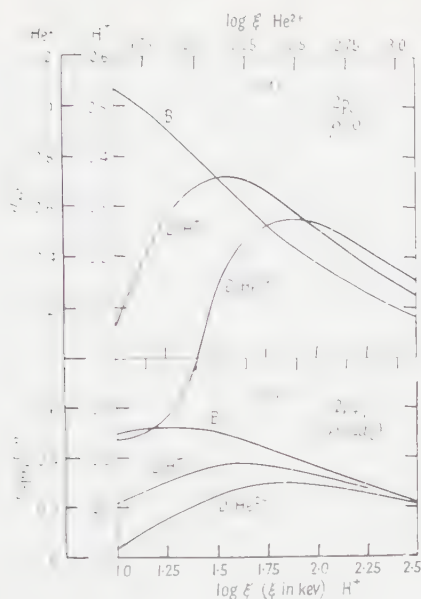


Fig. 2. Asymptotic coefficients $a_{2p_0}(\infty)$ and $a_{2p_{\pm 1}}(\infty)$ plotted against $\log \mathcal{E}$, \mathcal{E} being the energy of the incident ion in keV. In the $2p_0$ case the impact parameter is chosen to be zero (head-on collision) and in the $2p_{\pm 1}$ case it is chosen to be $2a_0$. The designations on the curves are as in the preceding figure.

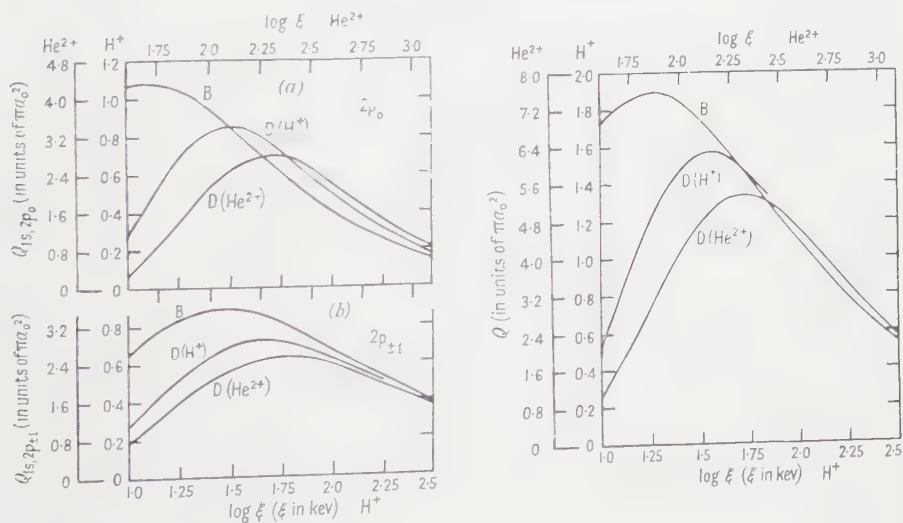


Fig. 3. First Born and distortion approximations to cross sections for H^+ (or He^{2+}) + $H(1s) \rightarrow H^+$ (or He^{2+}) + $H(2p_0)$

and for

$$H^+ \text{ (or } He^{2+}) + H(1s) \rightarrow H^+ \text{ (or } He^{2+}) + H(2p_{\pm 1})$$

plotted against $\log \mathcal{E}$, \mathcal{E} being the energy of the incident ion in keV.

Fig. 4. First Born and distortion approximations to cross sections for H^+ (or He^{2+}) + $H(1s) \rightarrow H^+$ (or He^{2+}) + $H(2p)$

plotted against $\log \mathcal{E}$, \mathcal{E} being the energy of the incident ion in keV. (The curve $D(H^+)$, which is not drawn in full, intersects the curve $D(He^{2+})$ when $\mathcal{E}(H^+)$ is 100 keV and lies almost midway between this curve and the curve B when $\mathcal{E}(H^+)$ is above about 200 keV.)

Kingston, Moiseiwitsch and Skinner (1960) have carried out a study of process (3) with the aid of the second Born approximation (avoiding the common error of including *part* of the term of the fourth order in the interaction). Having verified that the second Born approximation yields results in satisfactory agreement with the exact results of Bates (1959) if the same matrix elements as in the distortion approximation are taken into account, they used it to treat polarization. The intermediate states of most importance in this connection are naturally those in energy resonance† with either the initial or the final states. Kingston *et al.* (1960) found that the virtual transitions through the $2p_{0, \pm 1}$ states, $1s \rightarrow 2p_{0, \pm 1} \rightarrow 2s$ affect the $1s \rightarrow 2s$ excitation cross section greatly. The reason is that the matrix elements for these virtual transitions are strong whereas that for the direct transition is weak.

In the case of processes (1) and (2) the polarizability associated with the $2s$ -state can scarcely influence the cross sections much since the matrix element for the first of the virtual transitions in the $1s \rightarrow 2s \rightarrow 2p_{0, \pm 1}$ sequence is weak and those for the direct transitions, $1s \rightarrow 2p_{0, \pm 1}$, are strong. The position regarding the $1s \rightarrow 2p_0 \rightarrow 2p_{\pm 1}$ and $1s \rightarrow 2p_{\pm 1} \rightarrow 2p_0$ sequences is less certain. These sequences are a manifestation of the tendency of the electronic eigenfunctions to follow the rotation of the internuclear axis. Detailed calculations on them are needed.

ACKNOWLEDGMENTS

Thanks are due to Miss U. Dunwoody for her able assistance with the computing.

The work has been carried out under contract with the United Kingdom Atomic Energy Authority.

REFERENCES

- BATES, D. R., 1958, *Proc. Roy. Soc. A*, **245**, 299.
 ——— 1959, *Proc. Phys. Soc.*, **73**, 227.
 KINGSTON, A. E., MOISEIWITSCH, B. L., and SKINNER, B. G., 1960, *Proc. Roy. Soc. A*, in the press.
 MOTT, N. F., and MASSEY, H. S. W., 1949, *Theory of Atomic Collisions*, 2nd Edn. (Oxford: Clarendon Press) p. 144.

† Such states introduce secular terms (with non-diagonal matrix elements) in the equations arising in the semi-classical treatment.

Pick-up Reactions on a ${}^9\text{Be}$ Target

BY F. H. READ AND J. M. CALVERT

The Physical Laboratories, University of Manchester

MS. received 11th May 1960

Abstract. Absolute differential cross sections have been measured for the ${}^9\text{Be}(p, d){}^8\text{Be}(0)$ and ${}^9\text{Be}(p, p){}^9\text{Be}(0)$ reactions at incident proton energies of 4.85 and 5.49 MeV, and for the ${}^9\text{Be}(d, t){}^8\text{Be}$ reaction at 5.86 MeV; the pick-up reactions have been analysed in terms of the Butler theory. A comparison of the (p, d) results with those at higher proton energies gives the ranges of validity of the Butler theory and the 'transparent-nucleus' Born approximation pick-up theory for the reaction; the neutron reduced width is also deduced from these results. A comparison of the (d, t) results with those at higher deuteron energies shows consistency over a wide energy range; a comparison with the (p, d) reaction gives the triton form-factor $|A_0|^2 N_1^2$. Excitation functions have been measured for the reaction products of ${}^9\text{Be} + p$ for bombarding energies between 3.5 MeV and 6.0 MeV and for the reaction products of ${}^9\text{Be} + d$ for bombarding energies between 3.8 MeV and 6.3 MeV.

§ 1. INTRODUCTION

ABSOLUTE differential cross sections for the reaction ${}^9\text{Be}(p, d){}^8\text{Be}(0)$ have been measured previously at bombarding energies between 5 and 95 MeV (see below), and the results have been analysed either in terms of the Butler pick-up theory (Butler 1951) or the 'transparent-nucleus' Born approximation pick-up theory of Chew and Goldberger (1950). The two methods of analysis differ only in that, whereas in the Butler theory the volume direct interaction is ignored (the integration over the coordinates of the picked-up neutron is cut-off at a finite radius R), in the 'transparent-nucleus' theory there is no cut-off. Use of a cut-off radius seems to be a convenient method of allowing for the interactions which distort the plane proton and deuteron waves at incident proton energies of a few MeV. However, these interactions may be less important at higher energies, thus making the cut-off radius unnecessary. It is of interest therefore to compare these two methods of analysis for a given reaction over a wide range of incident energies. In this paper such a comparison is made for the reaction ${}^9\text{Be}(p, d){}^8\text{Be}$. The results of some of the higher energy measurements have been re-analysed to give the reduced width of the picked-up neutron, and a comparison is made with the results of the present measurements.

Comparison of the (p, d) reaction with the (d, t) reaction on the same nucleus is useful since the same final levels are produced by a pick-up process in each case and the interpretations are analogous. Such a comparison yields the mass-three form-factor, $|A_0|^2 N_1^2$ (Butler and Hittmair 1957), which is a measure of the probability that the mass-three particle (${}^3\text{He}$ or ${}^3\text{H}$) contains a ground state deuteron: due to the similarity of the ${}^3\text{He}$ and ${}^3\text{H}$ wave functions, their form-factors are nearly equal. This information about mass-three particles is important because it allows (${}^3\text{He}, d$) reactions to be used for obtaining proton reduced widths

E

in those cases where the reaction can be analysed in terms of the Butler stripping theory. This then provides a useful method of studying those nuclear levels which are more difficult to study with the (d, n) reaction. Attempts have been made previously (Forsyth *et al.* 1960, Macfarlane and French 1960) to obtain the form factor by comparing (d, t) and (p, d) reactions on the same nuclei, but these comparisons have given values differing by factors of the order of 10. In the present work absolute differential cross sections for the reaction ${}^9\text{Be}(\text{d}, \text{t}){}^8\text{Be}(0)$ have been measured at $E_d = 5.86$ mev, and these, together with previous measurements at $E_d = 3.6$ mev (Fulbright *et al.* 1952), 15.0 mev (Haffner 1956) and 20.0 mev (Vlasov and Ogloblin 1960), have been analysed and compared with the ${}^9\text{Be}(\text{p}, \text{d}){}^8\text{Be}$ measurements mentioned above.

§ 2. APPARATUS AND MEASUREMENTS

The differential cross section measurements were made using a conventional scattering chamber in which two charged particle detectors rotated independently about an axis, containing the target, perpendicular to the beam. The minimum and maximum angles of inclination of the detectors to the beam direction were approximately 16° and 164° respectively. The detectors consisted of thin thallium activated sodium iodide crystals mounted on the end faces of EMI 6097 photomultiplier tubes. Absorbers of varying thickness could be interposed between the target and the detectors without breaking the vacuum; the detectors could also be rotated without breaking the vacuum. The proton and deuteron beams were provided by the 6 MV Van de Graaff generator of Manchester University, and the target was a self-supporting beryllium foil of areal density approximately 0.5 mg cm^{-2} (containing about 2% impurities of carbon and oxygen). The beam was monitored by a Faraday cup and current integrator. The Faraday cup was large and had a small entrance aperture; it also had a biased suppressor plate in front of it. Preliminary experiments showed that there was no loss of secondary electrons from the Faraday cup.

To measure absolute differential cross sections it was necessary to know the calibration of the current integrator, the detector solid angles, the areal density of the self-supporting beryllium target and the amounts of contaminants present in the target. The current integrator was calibrated directly and the detector solid angles were found by direct measurement of the geometry of the scattering chamber. The target thickness was measured by finding proton energy losses in it. One of the detectors was placed at a forward angle (16.3°) and the inclination of the target to a beam of 2.5 mev protons was varied. As the target was rotated, the counting rate of elastically scattered protons changed (giving the effective relative change in target thickness) and the mean pulse height of these detected protons changed (giving the mean energy loss). The detector had previously been calibrated for proton energies. The mean proton energy loss was plotted as a function of the relative target thickness, and a straight line resulted. Using the known proton energy losses in beryllium (Rich and Madey 1954, Whaling 1958), the effective areal density (including the contaminants carbon and oxygen), with the target at any angle to the beam, was calculated to an accuracy within $\pm 4\%$. This method of finding the target density was considerably more accurate than direct measurements with an alpha-particle gauge (Ramavataram and Porat 1958), because the target was non-uniform, and it was not possible to ascertain exactly the part of the target that was hit by the

beam. Finally it was necessary to correct for the amounts of the carbon and oxygen contaminants in the target. To do this, one of the detectors was placed at a laboratory angle of 120° and the yields of the elastic proton groups, per unit charge falling on the target, were measured for the ^9Be , ^{12}C and ^{16}O components of the target (these groups were clearly resolved at this backward angle). Differential cross sections for elastic proton scattering on ^{12}C and ^{16}O have been measured previously (Reich, Phillips and Russell 1956, Sempert, Schneider and Martin 1954). A method of successive approximation then gave the amount of ^9Be in the target and also the differential cross section for the $^9\text{Be}(p, p)^9\text{Be}$ reaction. The ^{12}C and ^{16}O contaminants were found to be 2% and 1% of the ^9Be density respectively. This procedure was carried out several times during the course of the experiments, at three different incident proton energies, and three normalizing points were thereby obtained. In the angular distribution experiments one of the detectors was always placed at the 120° angle to act as a monitor,

The above calibrations gave an absolute normalization to the measured cross sections of $\pm 4.5\%$, but to confirm this the following experiment was performed. Firstly the angular settings of one of the detectors at forward angles were accurately calibrated by using a gold target and a 2 Mev proton beam, and assuming the Rutherford law for the elastic scattering cross section. This detector was then placed at its minimum angle (16.3°), and the differential cross section for elastic proton scattering on ^9Be was measured for low proton energies. The ratio of this measured cross section to the calculated Rutherford cross section was then plotted as a function of the incident proton energy. This ratio was found to be 1.00 (within the accuracy of the assumed calibration) at less than 1.5 Mev, and this was taken to be a weak confirmation of the assumed normalization of the absolute cross sections.

The identities of groups in the charged particle spectra were determined by the known energy calibrations of the detectors, by the changes of energy with changing angle of detection (due to centre-of-mass effects), and by the losses of energy in the various absorbers that could be interposed between the target and the detectors.

§ 3. EXPERIMENTAL RESULTS

In the proton bombardment of the beryllium target the following groups were observed: two proton groups (p_0 , p_1) corresponding to the ground state and first excited state (2.428 Mev) of ^9Be , two deuteron groups (d_0 , d_1) corresponding to the ground state and broad first excited state (2.90 Mev) of ^8Be , an alpha-particle group (z_0) corresponding to the ground state of ^6Li , and two further proton groups corresponding to elastic scattering from the target contaminants ^{12}C and ^{16}O . Excitation functions were measured for the d_0 , p_0 and p_1 groups at different laboratory angles and the results are shown in Fig. 1. Differential cross sections were measured for the d_0 and p_0 groups at $E_{p(\text{lab})} = 4.85$ and 5.49 Mev (corrected for energy losses in the target), and these results are shown in Figs 2 and 3. The full curves in Fig. 2 are the theoretical Butler pick-up angular distributions (see § 4).

The differential cross section for the d_1 group was difficult to measure because of the large width (1.2 ± 0.3 Mev) of the ^8Be first excited state (Ajzenberg-Selove and Lauritsen 1959). The cross section was measured at only one point, $E_p = 5.68$ Mev, $\theta_{\text{lab}} = 39.7^\circ$, and was found to be 17 ± 5 mbn sterad $^{-1}_{\text{lab}}$. The

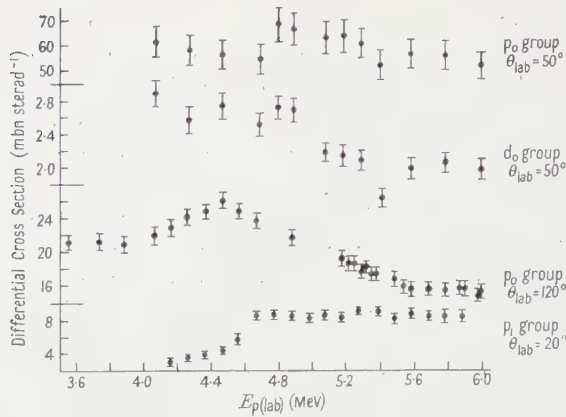


Fig. 1. Excitation functions for the reaction products of ${}^9\text{Be} + \text{p}$.

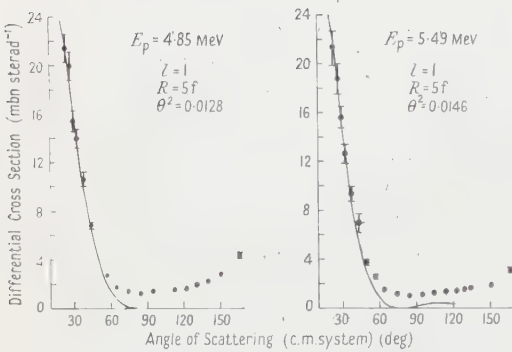


Fig. 2. Differential cross sections for the ground state deuteron group in the ${}^9\text{Be}(\text{p}, \text{d}){}^8\text{Be}$ reaction.

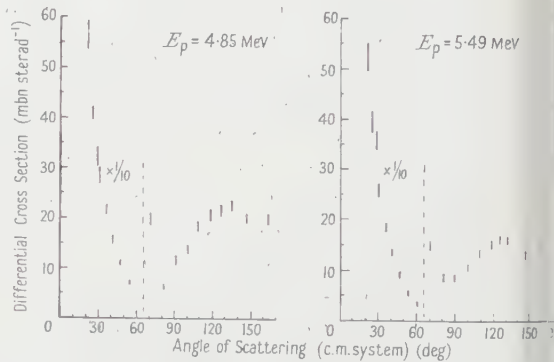


Fig. 3. Differential cross sections for the ground state proton group in the ${}^9\text{Be}(\text{p}, \text{p}){}^8\text{Be}$ reaction.

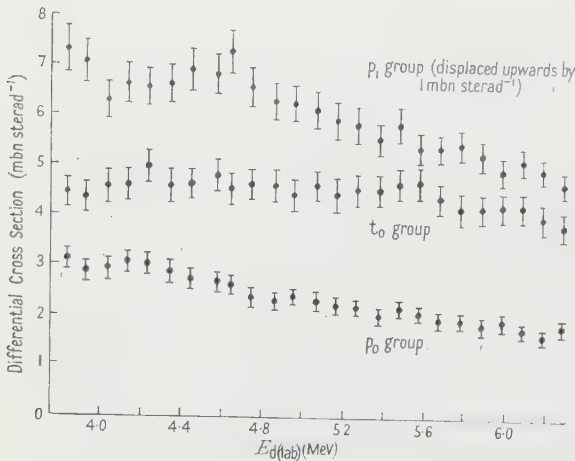


Fig. 4. Excitation functions for the reaction products of ${}^9\text{Be} + \text{d}$, at $\theta_{\text{lab}} = 40^\circ$.

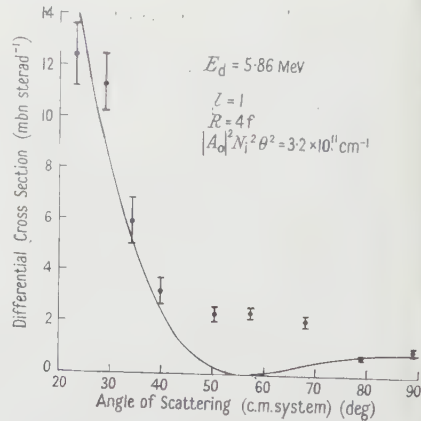


Fig. 5. Angular distributions for the ground state triton group from the ${}^9\text{Be}(\text{d}, \text{t}){}^8\text{Be}$ reaction.

errors shown in the cross sections include the error in the absolute normalization ($\pm 5\%$), the errors due to uncertain background subtractions, and statistical errors due to finite numbers of counts.

In the deuteron bombardment of the beryllium target three main reaction products were observed, as follows: two proton groups (p_0 and p_1) corresponding to the ground state and first excited state (3.37 MeV) of ^{10}Be , and a triton group (t_0) corresponding to the ground state of ^8Be . Weaker proton groups originating from the ^{16}O contaminant were also observed. Excitation functions were measured for the three main groups and the results are shown in Fig. 4. Angular distributions were also measured and the results for the t_0 groups are shown in Fig. 5 (the full curve is calculated from the Butler theory, see § 4). The angular distributions for the two proton groups will appear in a future publication on the $^9\text{Be}(d, p\gamma)^{10}\text{Be}$ (3.37) reaction.

§ 4. DISCUSSION OF THE (p, d) REACTION

Differential cross sections for the $^9\text{Be}(p, d)^8\text{Be}(0)$ reaction have been measured previously at bombarding energies of 12 MeV (Summers-Gill 1958), 16 MeV (Reynolds and Standing 1956), 22 MeV (Cohen *et al.* 1953) and 31.3 MeV (Benveniste, Finke and Martinelli 1956).

Table 1. Neutron Reduced Widths and Cut-off Radii from the $^9\text{Be}(p, d)^8\text{Be}(0)$ Reaction

(1)	(2)	(3)	(4)
4.85	5.0	1.28 ± 0.09	no fit
5.49	5.0	1.46 ± 0.10	no fit
12.0 ^a	3.0	2.4 ± 0.5	1.8
16.5 ^b	3.0 ^b	2.4 ± 0.7	1.2
22.0 ^c	no fit	—	1.2
31.3 ^d	no fit	—	1.2

(1) Incident proton laboratory energies (MeV), (2) cut-off radii using the Butler theory (f), (3) neutron reduced width $\theta^2_{1\frac{1}{2}}$ using the Butler theory (%), (4) neutron reduced width using the 'transparent-nucleus' theory (%).

a, Summers-Gill (1958); b, Reynolds and Standing (1956); c, Cohen *et al.* (1953); d, Benveniste *et al.* (1956).

There have also been some measurements with rather poor accuracy ($\pm 40\%$) at 5 to 8 MeV (Harvey 1951) (these measurements are higher than those of the present work by a factor of about 1.5) and some measurements at 95 MeV (Selove 1956) in which the ground state and first excited state deuterons were unresolved. The results of the first four measurements above, and also the results of the present measurements, have been analysed in terms of the Butler theory (Butler 1951) and also the 'transparent-nucleus' Born approximation theory of Chew and Goldberger (1950). The values of the cut-off radii and neutron reduced widths, θ^2 (see § 4), obtained are summarized in Table 1. Fig. 6 shows some of these angular distributions fitted by the Butler theory. The 16.5 to 95 MeV results have already been analysed in terms of the transparent-nucleus model by several authors (Benveniste, Finke and Martinelli 1956, Glashow and Selove 1956a, b, Dabrowski and Sawicki 1955a, b, 1956a, b, de Pinho Filho 1958). (Benveniste *et al.* use the Butler theory modified by Daitch and French (1952)

to take into account the volume interaction, and it should be noted that this is completely equivalent to the transparent-nucleus model.) The only new thing that we have added to these analyses is the value of θ^2 . The 12 and 16.5 mev results have also been analysed previously (Summers-Gill 1958, Reynolds and Standing 1956) in terms of the Butler theory. The analysis of Summers-Gill contains an error, however, so we have re-analysed these results. The errors in the reduced widths quoted in Table 1 have been estimated from the experimental errors and the errors in fitting the theoretical curves.

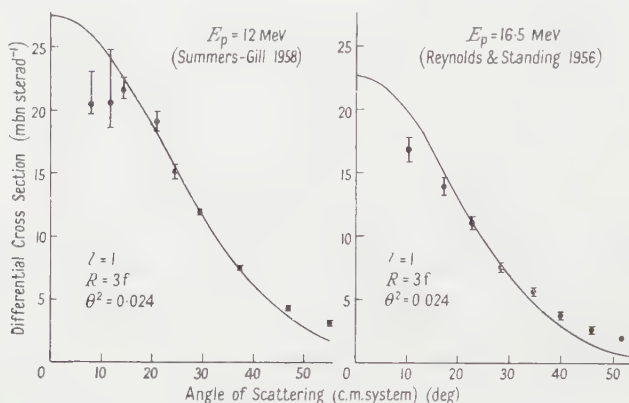


Fig. 6. Angular distributions of the ground state deuteron group, from the ${}^9\text{Be}(p, d){}^8\text{Be}$ reaction.

The 'transparent-nucleus' Born approximation of Chew and Goldberger (1950) assumes that the picked-up neutron is bound to the ${}^8\text{Be}$ core by a central single-particle potential. The differential cross section obtained is (Selove 1956, Glashow and Selove 1956a)

$$\frac{d\sigma}{d\Omega} = \frac{24\pi^2\alpha}{1 + \alpha/\beta - 4\alpha/(\alpha + \beta)} \frac{A(A-1)}{(A+1)^2} \frac{k_d}{k_p} \left(\frac{\beta^2 - \alpha^2}{\beta^2 + q^2} \right)^2 |F|^2 N(n), \quad \dots (1)$$

where $\mathbf{n} = \mathbf{k}_d - (A-1)\mathbf{k}_p/A$ is \hbar^{-1} times the momentum of the picked-up neutron, $\mathbf{q} = \mathbf{k}_p - \frac{1}{2}\mathbf{k}_d$ is \hbar^{-1} times the internal momentum of the neutron in the deuteron, $\hbar\mathbf{k}_p$ and $\hbar\mathbf{k}_d$ are the centre-of-mass momenta of the incident proton and formed deuteron respectively, A is the mass number of the target nucleus, and α and β are the Hulthén wave function parameters. F is the fractional parentage coefficient and takes into account competing processes in which the ${}^8\text{Be}$ core is left in an excited state, $N(n)$ is the momentum density of the neutron,

$$N(n) = (4\pi)^{-1} \int |u(\mathbf{n})|^2 d\Omega_n, \quad \dots (2)$$

where $u(\mathbf{n})$ is the momentum space wave function of the neutron. Analyses of the experimentally measured differential cross sections using Eqns (1) then give $|F|^2 N(n)$ as a function of the neutron momentum $\hbar n$ (n is a function of the angle scattering θ and the incident energy E_p): the results are shown in Fig. 7. It may be seen that the 16.5, 22.0 and 31.3 mev results agree closely, but that the two low energy results do not agree. The 95 mev results also fit in well, if allowance is made for the large errors and the presence of the first excited state deuteron group. (The ratio of $|F|^2 N(n)$ for the ground state group to that for the excited state group is approximately 1 to 2, see Glashow and Selove

1956a, b.) The results at 12 Mev are a special case, lying above the results at other energies. The discrepancy here is a constant multiplying factor of 1.4 in the cross section.

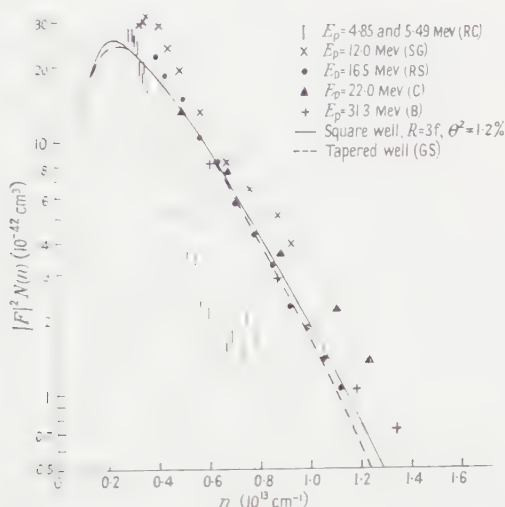


Fig. 7. Values of $|F|^2 N(n)$ obtained from the $^9\text{Be}(p, d)^8\text{Be}$ reaction.

The neutron reduced width has been obtained from the high energy results by calculating the form of $|F|^2 N(n)$ for a square-well potential of radius $3f$ (full curve in Fig. 7). The appropriate formula for the square well is

$$|F|^2 N(n) = \frac{3R\theta^2}{2\pi^2} \left[\frac{n_0^2 + \kappa^2}{(n_0^2 - n^2)(\kappa^2 + n^2)} \right]^2 \left[\frac{\hat{c}j_l(nR)}{\partial R} - \frac{j_l(nR)}{h_l^{(1)}(i\kappa R)} \frac{\partial h_l^{(1)}(i\kappa R)}{\partial R} \right]^2, \quad \dots (3)$$

where we have taken the neutron to be bound in a well of depth V_0 and radius R ; $\hbar^2 \kappa^2 / 2m^*$ is the binding energy of the neutron in the well (1.67 Mev) and m^* is the neutron reduced mass; n_0 is the wave number of the neutron inside the well. n_0 may take one of a series of values, all of which give a zero value of

$$\frac{\hat{c}j_l(n_0 R)}{\partial R} - \frac{j_l(n_0 R)}{h_l^{(1)}(i\kappa R)} \frac{\partial h_l^{(1)}(i\kappa R)}{\partial R}$$

but we have taken the value of n_0 giving the first zero in this quantity, corresponding to the $1p$ state of the neutron. With $R = 3.0f$ this gives $n_0 = 1.083 \times 10^{13} \text{ cm}^{-1}$ and $V_0 = 29.0 \text{ Mev}$, a reasonable value. θ^2 is the dimensionless reduced width ($= \gamma^2 / (3\hbar^2 / 2m^* R^2)$) defined at the radius R (see below). θ^2 would normally carry the subscripts l and j for the orbital and total angular momentum quantum numbers of the picked-up neutron, but in the present reaction these have the unique values 1 and $\frac{3}{2}$ respectively and are therefore omitted. Eqn (3) is particularly easy to use because it contains factors that appear in the Butler stripping cross section, and use may be made of the published numerical tables of Lubitz (1957). Also shown in Fig. 7 (broken curve) is the result of a numerical calculation done by Glashow and Selove (1956a), for a tapered well ($V = -V'$, $r < R - b$; $V = 0$, $r > R + b$; V linear, $R - b < r < R + b$; $R = 3f$, $b = 1f$): they have not calculated the value of θ^2 . The two curves are nearly the same shape however and must therefore give nearly the same value of θ^2 .

Eqn (3) is obtained in the following way. Outside the region of the potential binding the neutron to the ^8Be core (i.e. $r > R$) the neutron wave function must have the form

$$\psi_l^m(\mathbf{r}) = B h_l^{(1)}(i\kappa r) Y_l^m(\Omega_r) \quad \dots\dots (4)$$

(the neglect of the spin wave function will not affect the final result). But the reduced width is defined (Tobocman 1956) at the radius R such that the radial dependence of the part of $\psi(\mathbf{r})$ taking part in the reaction is

$$\left(\frac{3}{R^3}\right)^{1/2} \frac{\theta_l h_l^{(1)}(i\kappa r)}{h_l^{(1)}(i\kappa R)} \text{ for } r > R.$$

However, this must be equated to $FB h_l^{(1)}(i\kappa r)$, since the radial part of Eqn (4) is effectively multiplied by F to allow for the fact that we are dealing only with the ground state of the final ^8Be nucleus. B can therefore be expressed in terms of F and θ . The momentum-space wave function $u(\mathbf{n})$ is the Fourier transform of the complete (unnormalized) wave function for a square well (the exterior part being given by Eqn (4)). We therefore obtain $u(\mathbf{n})$ and hence $N(n)$, in terms of B . Using the relation between B , F and θ , and also using the properties of the spherical Bessel and Hankel functions, we obtain Eqn (3)†.

The results from 16.5 to 31.3 mev (and also at 95 mev, when allowance is made for the presence of the d_1 group) agree quite well, showing the validity of the 'transparent-nucleus' treatment. These results also fit quite well the theoretical curve for a square well of radius $3f$ binding the picked-up neutron to the ^8Be core, with a reduced width θ^2 (defined at the radius $3f$) of 1.2%. There are two interesting points arising from Table 1, apart from the disagreement of the results at 12 mev. Firstly, at 16.5 mev both theories may be used to fit the results, the Butler theory giving a reduced width twice that obtained from the transparent-nucleus theory. This is reasonable, since the Butler theory ignores the volume contribution and predicts too low a cross section; even the magnitude of the discrepancy is reasonable, since the picked-up neutron is loosely bound to the ^8Be core (1.67 mev) and spends about 50% of its time outside the cut-off radius. Secondly, the influence of the Coulomb interaction is apparent at the lowest energies. The use of a larger cut-off radius here would normally give a larger reduced width, but in the present case the larger cut-off radius together with the increasing Coulomb interaction and nuclear interactions gives a reduced width very little different from that obtained at higher energies. It would be interesting, especially at the lower energies, to calculate the differential cross section taking into account the Coulomb interaction (and perhaps also the nuclear interactions) to see if the correct value of θ^2 results.

If the results at 12 mev are multiplied by a factor 0.7, then the reduced widths obtained fit in well with those obtained at other energies.

§ 5. DISCUSSION OF THE (d, t) REACTION

Different cross sections for the $^9\text{Be}(d, t)^8\text{Be}(0)$ reaction have been measured previously at 3.6 mev (Fulbright *et al.* 1952), 15 mev (Haffner 1956) and 20 mev

† This formula may also be obtained from a direct comparison of the differential cross section given by the 'transparent-nucleus' Born approximation theory with the modified form of the Butler cross section given by Daitch and French (1952). The latter includes the volume contribution and is therefore completely equivalent to the 'transparent-nucleus' expression.

(Vlasov and Ogloblin 1960). These results, and those of the present experiments at 5.86 Mev, have been analysed using the Butler stripping theory: in this the cross section for the ${}^9\text{Be}(d, t)$ reaction is (Macfarlane and French 1960)

$$\frac{d\sigma}{d\Omega} = \frac{3m_t^* m_d^*}{2(m_n^*)^2} \frac{k_t}{k_d} \frac{R |A_0|^2 N_i^2 \theta^2}{(\lambda^2 + q^2)^2} \left[\frac{\partial j_1(nR)}{\partial R} - \frac{j_1(nR)}{h_1^{(1)}(ikR)} \frac{\partial h_1^{(1)}(ikR)}{\partial R} \right]^2, \quad \dots\dots (5)$$

where $\mathbf{n} = \mathbf{k}_t - \frac{2}{3}\mathbf{k}_d$, $\mathbf{q} = \frac{2}{3}\mathbf{k}_t - \mathbf{k}_d$, and $\hbar\mathbf{k}_t$, $\hbar\mathbf{k}_d$ are the centre-of-mass momenta of the formed triton and the incident deuteron respectively; $\hbar^2\lambda^2/2m_n^*$ is the binding energy of a neutron in the triton, m_n^* is the neutron reduced mass in the triton; $\hbar^2\kappa^2/2m_n^*$ is the binding energy of the picked-up neutron in ${}^9\text{Be}$ and m_n^* is its reduced mass; m_t^* and m_d^* are the reduced triton and deuteron masses; R is the cut-off radius. θ^2 is defined above, and $|A_0|^2 N_i^2$ is the so called mass-three form-factor, defined by Butler and Hittmair (1957): this form-factor is a measure of the probability that the mass-three particle contains a ground-state deuteron. This form-factor is larger than that defined by Macfarlane and French (1960) by a factor 4π .

The results of these analyses are shown in Table 2, and graphically in Fig. 8. The results of Holt and Marsham (1953) at 8.0 Mev, analysed by Newns (1952) are also included in Table 2, although absolute cross sections were not measured. The full curves in Figs 5 and 8 are the angular distributions according to the Butler theory, Eqn (5). The closeness of fit obtained for the distributions at 5.86 and 15.0 Mev is poor because the measurements do not proceed to small enough angles: one is attempting to fit the curves to a few points near the Butler minimum. The errors in the values of $|A_0|^2 N_i^2$ obtained from these results (column (4) of Table 2) are due to experimental errors and errors in fitting the theoretical curves.

The 'transparent-nucleus' model does not fit these (d, t) results at all well. The nuclear interactions are more important in the (d, t) reaction than in the (p, d) reaction, and it is to be expected that the inclusion of the volume interaction in the former does not improve the fit.

One would expect the value of $|A_0|^2 N_i^2 \theta^2$ found at low energies to be too small because of the Coulomb interaction, and Table 2 does in fact appear to show this. It will be noticed also from Table 2 that the cut-off radius is reasonably constant (apart from the inaccurately obtained value at 15.0 Mev), which supports the validity of the Butler theory as a description of this reaction. Assuming that the neutron reduced width is 1.2%, we obtain a value for the triton form-factor $|A_0|^2 N_i^2 = (40 \pm 10) \times 10^{12} \text{ cm}^{-1}$. This value is considerably larger than that found from other comparisons of (d, t) and (p, d) reactions: Macfarlane and French (1960) and Forsyth *et al.* (1960) both find the value 10^{13} cm^{-1} from such comparisons. The present value is thought to be more accurate than these previous values for two reasons. Firstly the ${}^9\text{Be}(p, d)$ and (d, t) reactions yield consistent values of θ^2 and $|A_0|^2 N_i^2 \theta^2$ respectively over wide ranges of energies, and the neglect of the Coulomb interaction is not important as it is in some of the previous comparisons. Secondly, because the picked-up neutron is only loosely bound to the ${}^8\text{Be}$ core, it has a high probability of being well outside the cut-off radius (e.g. for a square well potential of 3f radius the neutron has a 56% probability of being outside 3f, and 24% of being

† In the notation of Macfarlane and French (1960) this gives $A = 800 \pm 200$.

outside 5f). This means that the neutron may be picked-up at quite large radii and the use of the plane wave approximation will affect the absolute value of the (d, t) cross section less drastically than it might in a more tightly bound case.

Table 2. Triton Form-factors and Cut-off Radii from the ${}^9\text{Be}(\text{d}, \text{t}) {}^8\text{Be}(0)$ Reaction

(1)	(2)	(3)	(4)
3.6 ^a	4.5	20×10^{11}	$(19 \pm 4) \times 10^{12}$
5.86 ^b	4.0	32	27 ± 7
8.0 ^c	4.7 ^d	—	—
15.0 ^e	3.5	70	60 ± 30
20.0 ^f	4.0 ^f	46	38 ± 10

(1) Incident proton laboratory energies (mev), (2) cut-off radii using the Butler theory (f), (3) values of $|A_0|^2 N_i^2 \theta^2$ (cm^{-1}), (4) values of $|A_0|^2 N_i^2$ (cm^{-1}), assuming $\theta_{1\frac{1}{2}}^2 = 1.2\%$.
a, Fulbright *et al.* (1952); b, present work; c, Holt and Marsham (1953); d, Newns (1952); e, Haffner (1956), f, Vlasov and Ogloblin (1960).

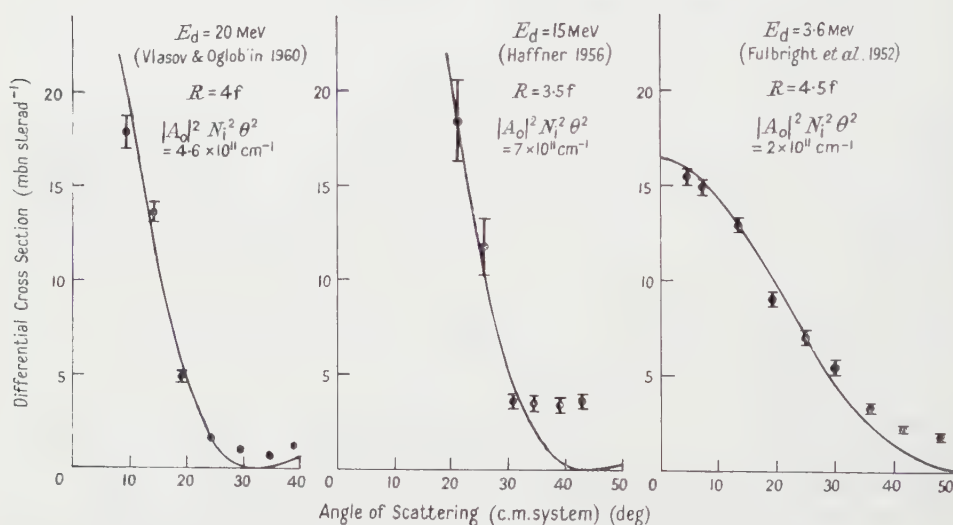


Fig. 8. Angular distributions of the ground state triton group from the ${}^9\text{Be}(\text{d}, \text{t}) {}^8\text{Be}$ reaction.

§ 6. DISCUSSION OF THE EXCITATION FUNCTIONS

Excitation functions for the proton bombardment of ${}^9\text{Be}$ are shown in Fig. 1. Marion, Bonner and Cook (1955), Marion (1956), Marion and Levin (1959) and Hahn *et al.* (1952) have studied ${}^9\text{Be} + \text{p}$ in this energy region, Hahn *et al.* observing the yield of gamma rays and Marion *et al.* of gamma rays and neutrons. Marion and Levin (1959) conclude that there are resonances at 3.5 and 4.6 mev, and have tentatively assigned them to p- and d-wave states having $(J\pi = 2^+, T = 1)$, $(J\pi = 3^-, T = 1)$ respectively. The excitation function for the inelastic proton group (present work) is consistent with there being a resonance at 4.5 mev, but the elastic proton group and the deuteron group do not show this resonance, although the experimental accuracy is rather poor.

The absence of the resonance in the deuteron group supports the $T=1$ assignment of this level of ^{10}B .

The excitation functions for the deuteron bombardment of ^9Be (Fig. 2) do not show any broad resonances; weak narrow resonances might have been missed because of the thickness of the target used (energy loss $\simeq 0.07$ mev). This lack of resonance structure is the result that one might expect since the excitation energy of the compound nucleus, ^{11}B , is high (18.97 to 20.97 mev). Two other investigations have been made in this region of excitation of ^{11}B , and both show a lack of resonance structure. McCrary, Bonner and Ranken (1957) measured the yield of 3.37 mev gamma rays from the deuteron bombardment of ^9Be , and Becker and Barschall (1956) measured the total neutron cross sections for the neutron bombardment of ^{10}B . These results are consistent with those of the present experiment.

§ 7. CONCLUSIONS

The present data and other data on the $^9\text{Be}(p,d)^8\text{Be}$ reaction have been analysed in terms of both the Butler theory and the 'transparent-nucleus' theory: a value of the neutron reduced width θ_{13}^2 of 1.2×10^{-1} results. The present data and other data on the $^9\text{Be}(d,t)^8\text{Be}$ reaction have been analysed in terms of the Butler theory and shown to be consistent over a wide energy range. A comparison of these two reactions gives the triton form-factor

$$|A_0|^2 N_1^2 = (40 \pm 10) \times 10^{12} \text{ cm}^{-1}.$$

ACKNOWLEDGMENTS

The authors wish to thank Professor B. H. Flowers for discussions on the manuscript. One of us (F. H. R.) wishes to thank the Department of Scientific and Industrial Research for a Research Fellowship held during part of this work.

REFERENCES

- AJZENBERG-SELOVE, F., and LAURITSEN, T., 1959, *Nucl. Phys.*, **11**, 1.
 BECKER, R. L., and BARSCHALL, H. H., 1956, *Phys. Rev.*, **102**, 1384.
 BENVENISTE, J., FINKE, R. G., and MARTINELLI, E. A., 1956, *Phys. Rev.*, **101**, 655.
 BUTLER, S. T., 1951, *Proc. Roy. Soc. A*, **208**, 559.
 BUTLER, S. T., and HITTMAIR, O. H., 1957, *Nuclear Stripping Reactions* (London: Pitman).
 CHEW, G. F., and GOLDBERGER, M. L., 1950, *Phys. Rev.*, **77**, 470.
 COHEN, B. L., NEWMAN, E., HANDLEY, T. H., and TIMNICK, A., 1953, *Phys. Rev.*, **90**, 323(L).
 DABROWSKI, J., and SAWICKI, J., 1955 a, *Acta Phys. Polon.*, **14**, 143.
 ——— 1955 b, *Acta Phys. Polon.*, **14**, 407.
 ——— 1956 a, *Acta Phys. Polon.*, **15**, 3.
 ——— 1956 b, *Acta Phys. Polon.*, **15**, 431 (Errata).
 DAITCH, P. B., and FRENCH, J. B., 1952, *Phys. Rev.*, **87**, 900 (L).
 FORSYTH, P. D., DE S. BARROS, F., JAFFE, A. A., and TAYLOR, I. J., 1960, *Proc. Phys. Soc.*, **75**, 291.
 FULBRIGHT, H. W., BRUNER, J. A., BROMLEY, D. A., and GOLDMAN, L. M., 1952, *Phys. Rev.*, **88**, 700.
 GLASHOW, S., and SELOVE, S., 1956 a, *Phys. Rev.*, **102**, 200.
 ——— 1956 b, *Phys. Rev.*, **102**, 1689 (Errata).
 HAFNER, J. W., 1956, *Phys. Rev.*, **103**, 1398.
 HAHN, T. M., SNYDER, C. W., WILLARD, H. B., BAIR, J. K., KLEMA, E. D., and KINGTON, J. D., 1952, *Phys. Rev.*, **85**, 934 (L).

- HARVEY, J. A., 1951, *Phys. Rev.*, **82**, 298 (A).
HOLT, J. R., and MARSHAM, T. N., 1953, *Proc. Phys. Soc. A*, **66**, 1032.
LUBITZ, C. R., 1957, *Numerical Table of Stripping Cross Sections*, Univ. of Michigan Report.
MACFARLANE, M. H., and FRENCH, J. B., 1960, *Rev. Mod. Phys.*, **32**, 567.
MARION, J. B., 1956, *Phys. Rev.*, **103**, 713.
MARION, J. B., BONNER, T. W., and COOK, C. F., 1955, *Phys. Rev.*, **100**, 91.
MARION, J. B., and LEVIN, J. S., 1959, *Phys. Rev.*, **115**, 144.
MCCRARY, J. H., BONNER, T. W., and RANKEN, W. A., 1957, *Phys. Rev.*, **108**, 392.
NEWNS, H. C., 1952, *Proc. Phys. Soc. A*, **65**, 916.
DE PINHO FILHO, A. G., 1958, *Notas de Fisica*, **4**, no. 17.
RAMAVATARAM, K., and PORAT, D., 1958, *Nucl. Instrum.*, **4**, 239.
REICH, C. W., PHILLIPS, G. C., and RUSSELL, J. L., 1956, *Phys. Rev.*, **104**, 143.
REYNOLDS, J. B., and STANDING, K. G., 1956, *Phys. Rev.*, **101**, 158.
RICH, M., and MADEY, R., 1954, *Univ. Cal. Rad. Lab. Report* 2301.
SELOVE, W., 1956, *Phys. Rev.*, **101**, 231.
SEMPERT, M., SCHNEIDER, H., and MARTIN, M., 1954, *Helv. Phys. Acta*, **27**, 313.
SUMMERS-GILL, R. G., 1958, *Phys. Rev.*, **109**, 1591.
TOBOCMAN, W., 1956, *Tech. Report* 29, Case, Inst. of Tech.
VLASOV, N. A., and OGLOBLIN, A. A., 1960, *J. E. T. P.*, **10**, 39.
WHALING, W., 1958, *Handb. d. Phys.*, **34**, 193.

Redetermination of the Panofsky Ratio for Negative Pions Stopped in Hydrogen

By D. P. JONES, P. G. MURPHY†, P. L. O'NEILL‡ AND J. R. WORMALD

Nuclear Physics Research Laboratory, University of Liverpool

MS. received 20th July 1960

Abstract. A lead glass Cerenkov counter has been used as a gamma-ray spectrometer to redetermine the Panofsky ratio for negative pions stopped in hydrogen. The ratio was found to be 1.56 ± 0.05 .

§ 1. INTRODUCTION

THE Panofsky ratio, P , is defined as the ratio of the rates of the two processes which occur when π^- mesons stop in hydrogen,

$$P = \frac{w(\pi^- + p \rightarrow \pi^0 + n)}{w(\pi^- + p \rightarrow \gamma + n)}.$$

As was shown by Anderson and Fermi (1952), and more recently discussed by Hamilton and Woolcock (1960), this ratio is related to low-energy pion nucleon scattering and pion photoproduction data. The published measurements of P , shown in the Table, are not entirely compatible; the experiment described below was carried out to remeasure P with increased accuracy.

P	Reference
0.94 ± 0.30	Panofsky, Aamodt and Hadley 1951.
1.50 ± 0.15	Cassels, Fidecaro, Wetherell and Wormald 1957.
1.87 ± 0.10	Fischer, March and Marshall 1958.
1.60 ± 0.17	Kuehner, Merrison and Tornabene 1959.
1.46 ± 0.10	Koller and Sachs 1959.
1.47 ± 0.10	Derrick, Fetkovich, Fields and Deahl 1959.
1.62 ± 0.06	Samios 1960.
1.56 ± 0.05	This paper.

§ 2. EXPERIMENTAL ARRANGEMENT

The experiment used a lead-glass Cerenkov counter as a gamma-ray spectrometer. The counter consisted of a truncated cone, 8 in. thick, with circular faces 6 in. and 9 in. diameter, of Chance EDF653335 glass, with the 9 in. face in optical contact with an E.M.I. 10 in. photomultiplier. For 129 mev gamma rays it gave a half-width at half-height of 14%.

The experimental arrangement is shown in Fig. 1. 98 mev π^- mesons were slowed down in the polythene absorber A, passed through the monitor counter 1, and stopped in the liquid hydrogen target, B, contained in a copper cylinder 3 in.

† Now at Rutherford High Energy Laboratory, Harwell, Berks.

‡ Now at United Kingdom Atomic Energy Authority, Windscale, Cumberland.

in diameter and 3 in. high with wall thickness $\frac{1}{32}$ in., surrounded by a $\frac{1}{32}$ in. copper radiation shield and an aluminium alloy vacuum tank with $\frac{1}{16}$ in. walls. Gamma rays from the target passed through the veto counter 2 and then a fraction produced electron pairs in the $\frac{1}{16}$ in. lead converter C. The electrons then passed through counter 3 and produced a shower in the Cerenkov counter 4. Counter 3 was of 3 in. diameter to ensure that the showers started near the axis of counter 4. Linear pulses from counter 4 were passed to a pulse height analyser through a gate which was opened by 132 coincidences.

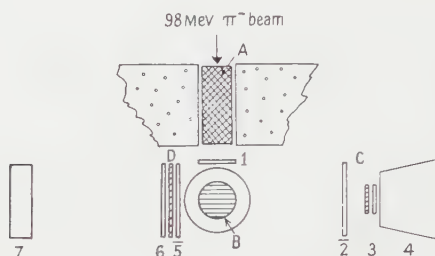


Fig. 1. Experimental arrangement.

The pulse spectrum obtained, corrected for backgrounds obtained on removing either the hydrogen or the lead converter or both, is shown in Fig. 2(a). The 129 mev line from the radiative capture process is not completely resolved from the 55 to 83 mev gamma rays from the π^0 decay. Two further experiments were therefore carried out to determine the individual line shapes separately.

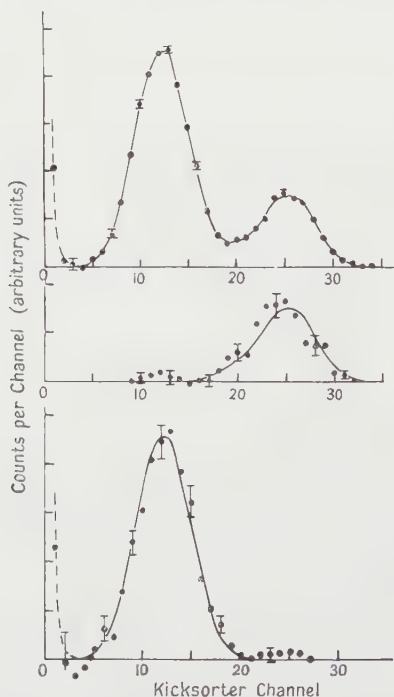


Fig. 2. (a) Total spectrum, (b) spectrum gated by $n\text{-}\gamma$ coincidences, (c) spectrum gated by $\gamma\text{-}\gamma$ coincidences.

To determine the line shape due to the 55 to 83 mev gamma rays use is made of the fact that they are always associated with another gamma ray at a laboratory angle greater than 157° . A fraction of these were detected, after passing through veto counter 5, by conversion into electrons in the second lead converter D, $\frac{1}{8}$ in. thick, the electrons being detected in counter 6. The gate was then opened by $136\overline{25}$ coincidences. The resulting spectrum of pulses from counter 4 contained a background of some of the high energy line due to counter 6 detecting a few of the recoil neutrons. This background was measured by repeating the measurements with the second lead converter, D, removed. The gamma-gated spectrum with this background subtracted is shown in Fig. 2(c).

To determine the line shape for the 129 mev gamma ray the 8.85 mev recoil neutron from the radiative capture process was detected by counter 7, a block of plastic scintillator of 7.5 in. diameter, 2 in. thick; and the gate was opened by $137\overline{25}$ coincidences. Since counter 7 was also sensitive to gamma rays, these were made inoperative by placing the counter 70 cm from the target and using the 15 nsec difference in time of flight. Some random coincidences due to counter 7 detecting background radiation were observed; these were measured by inserting an extra 52 nsec delay between counter 7 and the coincidence circuit. Since counter 7 subtended a smaller solid angle at the target than counter 3, measurements were also made with counter 7 displaced sideways through 3 in., so that the range of angles between the axis of counter 4 and the directions of gamma rays contributing to the neutron-gated spectrum should be the same as for the total spectrum. The final neutron-gated spectrum, combining the results for the two positions of counter 7, and with the random backgrounds subtracted is shown in Fig. 2(b). The statistical accuracy is poor owing to the low counting rate ($\sim 0.5/\text{min}$) in this part of the experiment.

§ 3. RESULTS

The Panofsky ratio is obtained almost directly from the ratio of the number of counts in the low-energy group in Fig. 2(a), to the number in the high-energy group; the counts in the region where the two groups overlap being allocated to them in the ratio of the smooth curves, which are the curves of Figs 2(b) and 2(c) scaled to fit the non-overlapping parts of the total spectrum. A correction is applied to allow for the fact that the cross section for pair-production and Compton scattering in lead is 12% greater for the high-energy gamma rays than for the low-energy group.

A possible source of error has been suggested by Fischer *et al.* (1958) who, in a similar type of experiment, found evidence that a background due to pions interacting in the walls of the target increased by about 20% when the hydrogen was put in. Two tests were made to investigate whether such an effect was important in our experiment. First, the measurement of the total spectrum was repeated using a hydrogen target with inner and outer walls made of 'Mylar' plastic 0.01 in. thick and no radiation shield. No statistically significant change in the total spectrum was observed. Secondly, the target was completely removed; the background counting rate (about 10% of the hydrogen-in rate) then decreased by only $12 \pm 15\%$, indicating that nearly all the background came from interactions in other parts of the apparatus—probably the polythene absorber—and thus would not be affected by the presence of hydrogen in the target.

The principal source of error is the uncertainty in the shape of the pulse spectrum due to the high-energy gamma rays in the region where it overlaps the low-energy spectrum, which gives rise to an estimated standard error of 2.5%. The statistical error due to the number of counts in the total spectrum is 1.5%.

Our result for the Panofsky ratio is

$$P = 1.56 \pm 0.05.$$

ACKNOWLEDGMENTS

We are indebted to Dr. G. Culligan, Dr. S. G. F. Frank, Dr. J. R. Holt and Mr. D. S. E. Rodgers who assembled the Cerenkov counter; and to Mr. J. Barlow, Mr. J. D. Davies, Dr. D. N. Edwards, Dr. T. W. O'Keeffe, and Miss M. Rigby, who assisted in taking the readings.

REFERENCES

- ANDERSON, H. L., and FERMI, E., 1952, *Phys. Rev.*, **86**, 794.
CASSELS, J. M., FIDECARO, G. M., WETHERELL, A. M., and WORMALD, J. R., 1957, *Proc. Phys. Soc. A*, **70**, 405.
DERRICK, M., FETKOVICH, J., FIELDS, T., and DEAHL, J., 1959, *Bull. Amer. Phys. Soc.*, **4**, 401.
FISCHER, J., MARCH, R., and MARSHALL, L., 1958, *Phys. Rev.*, **109**, 533.
HAMILTON, J., and WOOLCOCK, W. S., 1960, *Phys. Rev.*, **118**, 291.
KOLLER, E. L., and SACHS, A. M., 1959, *Phys. Rev.*, **116**, 760.
KUEHNER, J. A., MERRISON, A. W., and TORNABENE, S., 1959, *Proc. Phys. Soc.*, **73**, 545.
SAMIOS, N. P., 1960, *Phys. Rev. Letters*, **4**, 470.
PANOFSKY, W. K. H., AAMODT, R. L., and HADLEY, J., 1951, *Phys. Rev.*, **81**, 565.

Perturbation Theory in Finite Nuclei

By J. DA PROVIDENCIA†

Department of Mathematical Physics, University of Birmingham

Communicated by R. E. Peierls; MS. received 23rd June 1960, in final form 5th September 1960

Abstract. In the surface region of a nucleus the nucleon density is lower than in the interior, and it might be expected that this will reduce the effect of the Pauli principle in suppressing correlations. Since in light nuclei the surface region is more important, one expects perturbation theory to work less well and correlations to be more important, than in uniform nuclear matter.

Calculations with a simple model for ^{16}O show that the second-order correction to the energy is almost exactly the same as for uniform nuclear matter, but that two-body correlations are indeed enhanced considerably.

§ 1. INTRODUCTION

THE application of perturbation theory, starting from independent particles, to uniform nuclear matter has been discussed by several authors. Using non-singular two-body potentials, or potentials with only an r^{-1} singularity, Euler (1937), Huby (1949), and Swiatecki (1956) have shown that ordinary Rayleigh-Schrödinger perturbation theory appears to be well convergent. In this conclusion an important part is played by the Pauli principle, which inhibits virtual transitions to states of low excitation energy. Brueckner and Levinson (1955) (see also Bethe 1956) and others have shown that perturbation theory can be adapted to the case of potentials with strong repulsive cores, using for the repulsive part the smallness of the core radius, rather than the weakness of the forces, to assist the convergence.

These results apply to densities of the order of the normal nuclear densities, which are low enough to make three-body and higher encounters unimportant, yet high enough to make the Pauli principle effective in reducing initial transitions with small energy change. But when the density is low the convergence becomes bad, which may be interpreted as a sign of instability and of a tendency to clustering at low densities. Indeed uniform nuclear matter of low density is unstable and will condense.

Therefore, one might expect the appearance of strong correlations between nucleons in the surface region, where the density is low, but it is not obvious that there is a similarity between a uniform low density and a local region of low density.

There are also some empirical indications that in light nuclei, and in the surface region of heavy nuclei correlations tending to the formation of α -particles may be important (see, for example, Hodgson 1958).

† Now at Faculdade de Ciencias, Universidade de Coimbra, Portugal.

This indicates that perturbation theory might not be adequate for the treatment of finite nuclei, because it does not take properly into account the correlations between nucleons. Even Brueckner theory (Brueckner and Levinson 1955) would not be enough, if four-body clusters were important, because it takes into account two-body correlations only, by considering pairs of nucleons interacting between themselves, in an average field produced by the other nucleons.

The aim of this study is to obtain some indication of the validity of perturbation theory for small nuclei which contain a larger contribution from the surface region. To investigate this point we shall evaluate the binding energy of ^{16}O to second order and the wave function to first order and shall compare the results with the corresponding ones for infinite nuclear matter. If on the surface region the correlations are much larger we should expect the second-order energy per particle and the correlations in the wave function to be larger than in homogeneous nuclear matter.

The results show the existence of stronger correlations on the surface (§6) but this effect does not seem to have influence on the state of convergence of the perturbation series (§3), probably because the effect of the finite excitation energy of a small nucleus offsets the reduced effect of the Pauli principle.

§ 2. PERTURBATION EXPANSION FOR A FINITE NUCLEUS

We wish to study a system of N particles interacting through two-body forces by applying perturbation theory to a system of N independent particles bound by a common potential U . Therefore we write the unperturbed Hamiltonian in the form

$$H = \sum_{i=1}^N h_i \quad \dots\dots (1)$$

with

$$h_i = -\frac{1}{2}\nabla_i^2 + U_i \quad \dots\dots (1a)$$

and the correct Hamiltonian in the form

$$H' = \sum_{i=1}^N -\frac{1}{2}\nabla_i^2 + \sum_{i<j}^N v_{ij}, \quad \dots\dots (2)$$

so that the perturbation is

$$W = \sum_{i<j=1}^N v_{ij} - \sum_{i=1}^N U_i. \quad \dots\dots (3)$$

Let $\Phi_v(x_1 \dots x_N)$ and E_v represent the eigenfunctions and eigenvalues of H and $\Phi'_v(x_1 \dots x_N)$ and E'_v the corresponding quantities for H' . Let also $\phi_i(x)$ and Λ_i be the eigenfunctions and eigenvalues of h . Finally, let the perturbation expansions for the ground state wave function and energy of our system be

$$\Phi_0' = \Phi_0 + \Psi^{(1)} + \dots + \Psi^{(N)} + \dots \quad \dots\dots (4)$$

$$E_0' = E_0 + \epsilon^{(1)} + \epsilon^{(2)} + \dots + \epsilon^{(N)} + \dots \quad \dots\dots (5)$$

The Φ_v 's are determinants of the ϕ_i 's, and Φ_0 is obtained by filling the states corresponding to the lowest N values of the Λ_i 's:

$$\Phi_0(x_1 x_2 \dots x_N) = \mathcal{A}_N \phi_1(x_1) \phi_2(x_2) \dots \phi_N(x_N) \quad \dots\dots (6)$$

where \mathcal{A}_N is the antisymmetrizing operator properly normalized. As is well known

$$E_0 = \sum_{i=1}^N \Lambda_i \quad \dots\dots (7)$$

and

$$\epsilon^{(1)} = \sum_{i < j=1}^N \epsilon_{ij}^{(1)} + \sum_{i=1}^N \epsilon_i^{(1)} \quad \dots\dots (8)$$

where

$$\epsilon_{ij}^{(1)} = \langle \phi_i \phi_j | v | \phi_i \phi_j \rangle \quad \dots\dots (8a)$$

$$\epsilon_i^{(1)} = -\langle \phi_i | U | \phi_i \rangle. \quad \dots\dots (8b)$$

It is convenient, for reasons which will become apparent later, to write $\Psi^{(1)}$ in the form

$$\Psi^{(1)}(x_1 \dots x_N) = \mathcal{A}_N \left\{ \sum_{i < j=1}^N Q_{Nij} \frac{1}{\Lambda_i + \Lambda_j - h_i - h_j} v_{ij} + \sum_{i=1}^N q_{Ni} \frac{1}{\Lambda_i - h_i} (\bar{V}_i - U_i) \right\} \prod_{k=1}^N \phi_k(x_k) \quad \dots\dots (9)$$

where Q_N and q_N are the operators introduced by Gomes, Walecka and Weisskopf (1958), and may be defined by

$$q_N f(x) = \sum_{i=N+1}^{\infty} \phi_i(x) \int_{\xi} \phi_i^*(\xi) f(\xi) \quad \dots\dots (9a)$$

$$Q_N f(x', x'') = \sum_{i=N+1}^{\infty} \sum_{j=N+1}^{\infty} \phi_i(x') \phi_j(x'') \int_{\xi, \xi'} \phi_i^*(\xi') \phi_j^*(\xi'') f(\xi', \xi''). \quad \dots\dots (9b)$$

The operators Q_N and q_N appear obviously as a consequence of the Pauli principle. \bar{V} is the average potential and is defined by

$$\langle \phi_i | \bar{V} | \phi_i \rangle = \sum_{k=1}^N \langle \phi_i \phi_k | v | \phi_i \phi_k \rangle \quad \dots\dots (9c)$$

where we have adopted the convention, which we shall keep, of representing by angular brackets antisymmetric wave functions, so that

$$\langle x' x'' | \psi_{ij} \rangle = \frac{1}{\sqrt{2}} (\psi_{ij}(x', x'') - \psi_{ij}(x'', x')). \quad \dots\dots (10)$$

Eqn (9) suggests the introduction of

$$\psi_{ij}^{(1)}(x', x'') = Q_N \frac{1}{\Lambda_i + \Lambda_j - h' - h''} v(x', x'') \phi_i(x') \phi_j(x'') \quad \dots\dots (11)$$

and of

$$\psi_i^{(1)}(x) = q_N \frac{1}{\Lambda_i - h} (\bar{V} - U) \phi_i(x) \quad \dots\dots (12)$$

with the help of which we may write

$$\epsilon^{(2)} = \sum_{i < j=1}^N \epsilon_{ij}^{(2)} + \sum_{i=1}^N \epsilon_i^{(2)} \quad \dots\dots (13)$$

where

$$\epsilon_{ij}^{(2)} = \langle \phi_i \phi_j | v | \psi_{ij}^{(1)} \rangle \quad \dots\dots (13a)$$

and

$$\epsilon_i^{(2)} = \langle \phi_i | \bar{V} - U | \psi_i^{(1)} \rangle. \quad \dots\dots (13b)$$

Later on we shall need the quantities $\epsilon_{ij}^{(1)}$ and $\epsilon_{ij}^{(2)}$ which we have defined. $\psi_{ij}^{(1)}(x', x'')$ and $\psi_i^{(1)}(x)$ are clearly the important quantities for our problem, but, unfortunately, expressions (11) and (12) are very difficult to evaluate exactly. We have, therefore, employed a variational method (Bethe and Salpeter 1957) already used in atomic physics, which we shall now describe.

Let $X(x_1 x_2 \dots x_N)$ be an arbitrary function. With the help of it, we may write an upper bound for $\epsilon^{(2)}$

$$\epsilon^{(2)} \leq \langle X | H - E_0 | X \rangle + \langle \chi | W - \epsilon^{(1)} | \Phi_0 \rangle + \langle \Phi_0 | W - \epsilon^{(1)} | X \rangle. \quad \dots (14)$$

It is obvious that the right-hand side of the expression is stationary with respect to variations of X , for $X = \Psi^{(1)}$, and then it equals $\epsilon^{(2)}$. Eqn (14) gives an upper bound for $\epsilon^{(2)}$ because $H - E_0$ is positive definite.

Expression (9) suggests that we take

$$X(x_1, \dots, x_N) = \mathcal{A}_N \left\{ \sum_{i < j=1}^N Q_{Nij} G_{ij} + \sum_{i=1}^N q_{Ni} g_i \right\} \prod_{k=1}^N \phi_k(x_k) \quad \dots (15)$$

where G_{ij} and g_i are arbitrary two-body and one-body operators. If we now introduce (15) into (14), and also define

$$\chi_{ij}(x', x'') = Q_{Nij} G_{ij} \phi_i(x') \phi_j(x'') \quad \dots (16)$$

$$\chi_i(x) = q_{Ni} g_i \phi_i(x) \quad \dots (17)$$

we get

$$\epsilon_{ij}^{(2)} \leq \langle \chi_i | h' + h'' - \Lambda_i - \Lambda_j | \chi_{ij} \rangle + \langle \chi_{ij} | v | \phi_i \phi_j \rangle + \langle \phi_i \phi_j | v | \chi_{ij} \rangle \quad \dots (18)$$

$$\epsilon_i^{(2)} \leq \langle \chi_i | h - \Lambda_i | \chi_i \rangle + \langle \chi_i | \bar{V} - U | \phi_i \rangle + \langle \phi_i | \bar{V} - U | \chi_i \rangle. \quad \dots (19)$$

Instead of working with the G_{ij} and g_i we may work with χ_{ij} and χ_i which from (16) and (17) obviously satisfy the restrictions

$$\int_{\xi} \phi_k^*(\xi) \chi_{ij}(x, \xi) = \int_{\xi} \phi_k^*(\xi) \chi_{ij}(\xi, x) = 0, \quad k = 1, 2, \dots, N. \quad \dots (20)$$

$$\int_{\xi} \phi_k^*(\xi) \chi_i(\xi) = 0, \quad k = 1, 2, \dots, N \quad \dots (21)$$

but are otherwise arbitrary.

It is also clear that, when $\chi_{ij}(x', x'') = \psi_{ij}^{(1)}(x', x'')$ and $\chi_i(x) = \psi_i^{(1)}(x)$, the inequalities (18) and (19) become equalities, so that we have a variational method of obtaining approximations for $\epsilon_i^{(2)}$, $\epsilon_{ij}^{(2)}$, $\psi_i^{(1)}$ and $\psi_{ij}^{(1)}$.

§ 3. CALCULATIONS

Euler (1937) and Huby (1949) have calculated the second-order correction to the energy for uniform nuclear matter. Their results were shown by Swiatecki (1956) to be consistent with a rapid convergence for the perturbation series. This convergence was impaired by the fact that Euler and Huby had used forces with a saturating mixture, for which the direct term of the expectation value of the potential energy is zero. Actually this term is the most important for a more realistic mixture, like the Serber mixture, and that is why the convergence is better then.

Nevertheless we are going to use a saturating mixture, because that is the easiest way to obtain saturation, without having to introduce hard cores which invalidate the use of simple perturbation theory.

We have considered the force

$$v(x_1, x_2) = \tau_1 \cdot \tau_2 (g^2 + f^2 \sigma_1 \cdot \sigma_2) u(|\mathbf{r}_1 - \mathbf{r}_2|) \quad \dots\dots (22)$$

with

$$u(|\mathbf{r}_1 - \mathbf{r}_2|) = \exp [- (\mathbf{r}_1 - \mathbf{r}_2)^2], \quad \dots\dots (23)$$

$$g^2 = 0.4447, \quad f^2 = 0.9581, \quad \dots\dots (24)$$

For convenience we have used a unit of length $\rho = 1.791 \times 10^{-13}$ cm, and a unit of energy of $\hbar^2/M\rho^2 = 12.93$ Mev.

The parameters of the force (22) are such that they reproduce the scattering length and effective range for ^3S and ^1S states within 5% (Blatt and Jackson 1949). Moreover they lead to large simplifications in the calculations†.

For the single particle Hamiltonian, the most convenient choice is, from the computational point of view, the harmonic oscillator Hamiltonian (Talmi 1952)

$$h = -\frac{1}{2}\nabla^2 + \frac{1}{2}\nu^2 r^2, \quad \dots\dots (25)$$

We may write

$$\phi_i(x) = (\sigma|\sigma_i)(\tau|\tau_i)(\mathbf{r}|n_i, l_i, m_i) \quad \dots\dots (26)$$

where σ_i , τ_i , n_i , l_i , m_i represent, respectively, the spin, isotopic spin, principal, azimuthal and magnetic quantum numbers of state i . The solutions of the harmonic oscillator are well known and the energy eigenvalues are

$$\Lambda_{n,l} = (2n + l + \frac{3}{2})\nu. \quad \dots\dots (27)$$

To avoid the problem of degeneracy we consider a system of $N = 16$ nucleons, corresponding to the closed configuration $1s^4 1p^{12}$. Therefore the occupied states correspond to $n=0$, $l=0$; $n=0$, $l=1$, $m=-1, 0, +1$.

The parameter ν was chosen so as to minimize the expectation value $\langle \Phi_0 | H' | \Phi_0 \rangle$, because that is the point where the wave functions considered are nearest to Hartree-Fock wave functions. We obtained

$$\nu = 0.954$$

and, at that point

$$\frac{T^{(0)}}{N} = \frac{1}{N} \langle \Phi_0 | -\frac{1}{2} \sum_i \nabla_i^2 | \Phi_0 \rangle = 1.073 = 13.87 \text{ Mev}$$

$$\frac{V^{(0)}}{N} = \frac{1}{N} \langle \Phi_0 | \sum_{i < j} v_{ij} | \Phi_0 \rangle = -1.306 = -16.88 \text{ Mev}$$

$$\frac{T^{(0)} + V^{(0)}}{N} = \frac{1}{N} \langle \Phi_0 | H' | \Phi_0 \rangle = -0.233 = -3.01 \text{ Mev}$$

$$r_0 = N^{-1/3} (\frac{5}{3} \langle \Phi_0 | r^2 | \Phi_0 \rangle)^{1/2} = 0.787 = 1.41 \times 10^{-13} \text{ cm}.$$

We are now going to consider the corrections to these quantities in perturbation theory.

For that we have used the previously described variational method, (14), (18) and (19), where the quantity N plays an important role. Therefore N must be chosen so that it takes into account the different kinds of correlations which may be expected from the perturbation W .

† $\epsilon^{(2)}$ has the following spin coefficients for its direct and exchange parts

$$C_{\text{dir}} = 48 (g^4 + 3f^4)$$

$$C_{\text{ex}} = -12 (g^4 + 6g^2f^2 - 3f^4).$$

Now C_{ex} is zero for our choice of g^2 and f^2 , so we have to evaluate the direct term only.

We have taken

$$\chi_{ij}(x', x'') = Q_N \hat{v}_{ij}(x', x'') \phi_i(x') \phi_j(x'') \quad \dots\dots (28)$$

where

$$\hat{v}_{ij}(x', x'') = \boldsymbol{\tau}' \cdot \boldsymbol{\tau}'' (g^2 + f^2 \boldsymbol{\sigma}' \cdot \boldsymbol{\sigma}'') \beta_{ij} \hat{u}_{ij}(|\mathbf{r}' - \mathbf{r}''|) \quad \dots\dots (28a)$$

with

$$\hat{u}_{ij}(|\mathbf{r}' - \mathbf{r}''|) = \exp \left[- \frac{(\mathbf{r}' - \mathbf{r}'')^2}{\alpha_{ij}} \right] \quad \dots\dots (28b)$$

and

$$\begin{aligned} \chi_i(x) = q_N \left\{ \sum_{n=1}^N \int_{\xi} \phi_n^*(\xi) \hat{v}_i(x, \xi) \phi_n(\xi) \phi_i(x) \right. \\ \left. - \sum_{n=1}^N \int_{\xi} \phi_n^*(\xi) \hat{v}_i(x, \xi) \phi_i(\xi) \phi_n(x) - \gamma_i v r^2 \phi_i(x) \right\} \quad \dots\dots (29) \end{aligned}$$

where

$$\hat{v}_i(x', x'') = \beta_i \frac{\boldsymbol{\tau}' \cdot \boldsymbol{\tau}'' (g^2 + f^2 \boldsymbol{\sigma}' \cdot \boldsymbol{\sigma}'')}{3(g^2 + 3f^2)} \hat{u}_i(|\mathbf{r}' - \mathbf{r}''|) \quad \dots\dots (29a)$$

with

$$\hat{u}_i(|\mathbf{r}' - \mathbf{r}''|) = \exp \left[- \frac{(\mathbf{r}' - \mathbf{r}'')^2}{\alpha_i} \right] \quad \dots\dots (29b)$$

The α_{ij} , β_{ij} , α_i , β_i , γ_i are arbitrary parameters. In principle we might have all the parameters, corresponding to the different values of the indices going from 1 to N , independent. Actually such complication is not necessary. Therefore we have made these parameters vary only with the energy eigenvalues Λ_i . For instance, instead of using 16 different α_{ij} , we have used 2, one α_s and one α_p ; in the same way we have used 3 α_{ij} , namely α_{ss} , $\alpha_{sp} = \alpha_{ps}$, α_{pp} ; etc.

The choice (28) and (29) has the convenience of enabling one to reduce the evaluation of the right-hand sides of (18) and (19) to simple integrations of the form

$$\int_0^\infty \exp(-u^2) u^n du.$$

After minimizing the expressions obtained with respect to the arbitrary parameters, α , β and γ , we get upper bounds for the $\epsilon_{ij}^{(2)}$ and the $\epsilon_i^{(2)}$, and, we hope, reasonable approximations for the $\psi_{ij}^{(1)}$ and $\psi_i^{(1)}$.

Before writing down the upper bounds obtained, let us define

$$\epsilon_{\eta\zeta}^{(2)} = \sum_{i < j \ (l_i, l_j = \eta, \zeta)} \epsilon_{ij}^{(2)}, \quad \epsilon_{\eta}^{(2)} = \sum_{i \ (l_i = \eta)} \epsilon_i^{(2)} \quad \dots\dots (30)$$

where the sums extend over all the values of i and j compatible with the indicated restrictions. η and ζ being either 0 or 1 represent s or p states, so that, for instance, $\epsilon_{sp}^{(2)} = \epsilon_{01}^{(2)}$ gives the total contribution to the second-order energy arising from an interaction between an s and a p state. The evaluation of the perturbation terms on this basis gives the results

$$\begin{aligned} \epsilon_{ss}^{(2)} &\leq -0.215, & \epsilon_{sp}^{(2)} &\leq -0.918, \\ \epsilon_{pp}^{(2)} &\leq -2.496, \\ \epsilon_s^{(2)} &\leq -0.081, & \epsilon_p^{(2)} &\leq -0.076. \end{aligned}$$

Although these results are upper bounds we shall show later that they are close to the correct second-order energies.

It is of interest that the ratio of the two kinds of contributions to $\epsilon^{(2)}$, from single and double excitations, is very small, indicating that the harmonic oscillator potential used is 'nearly' self-consistent. Indeed we have

$$\frac{\epsilon_{ss}^{(2)} + \epsilon_{sp}^{(2)}}{\epsilon_{ss}^{(2)} + \epsilon_{sp}^{(2)} + \epsilon_{pp}^{(2)}} \simeq 4.0.$$

Comparing the value of $\epsilon^{(2)}$ with $T^{(0)} + V^{(0)} = E_0 + \epsilon^{(1)}$, one is tempted to say that perturbation theory works badly, since we had $\frac{1}{16}(T^{(0)} + V^{(0)}) = -0.233$, and now we have $\epsilon^{(2)}/16 \leq -0.236$.

Fortunately Swiatecki (1956) has shown that such a conclusion would be wrong. The ratio $\epsilon^{(2)}/V^{(0)}$ should be more significant and for that we find 18.1%.

In order to compare the quantities already calculated with the corresponding ones for infinite nuclear matter we have simply to introduce the parameters of our forces into Euler's (1937) results.

Table 1

	$N = 16$	$N = \infty$
$\frac{T^{(0)}}{N} = \frac{\langle \Phi_0 -\frac{1}{2} \Sigma \nabla_i^2 \Phi_0 \rangle}{N}$	1.073	1.085
$\frac{V^{(0)}}{N} = \frac{\langle \Phi_0 \Sigma v_{ij} \Phi_0 \rangle}{N}$	-1.306	-1.343
$\frac{T^{(0)} + V^{(0)}}{N} = \frac{\langle \Phi_0 H \Phi_0 \rangle}{N}$	-0.233	-0.258
$\frac{\epsilon^{(2)}}{N} = \frac{\langle \phi_0 \Sigma v \Psi^{(1)} \rangle}{N}$	-0.237	-0.340
$\epsilon^{(2)}$ from single particle excitations		
$= \frac{1}{N} \Sigma_i \langle \phi_i \bar{V} - U \psi_i^{(1)} \rangle$	-0.010	-0.000
$r_0 = N^{-1/3} (\frac{5}{3} \langle \Phi_0 r^2 \Phi_0 \rangle)^{1/2}$	0.787	0.803
$\frac{\epsilon^{(2)}}{V^{(0)}} (\%)$	18.1	25.3

The quantities are given in units of energy of 12.93 mev and units of length of 1.791 fermis.

Looking at Table 1, and considering especially the ratio $\epsilon^{(2)}/V^{(0)}$, we find no indication of a worse convergence for $N = 16$, as the argument about the existence of a large surface region with lower density would imply.

We should not worry about the fact that even $\epsilon^{(2)}/V^{(0)}$ is rather large. This is due in part to the saturating mixture of the forces, as explained before, and in part to the fact that the quantities considered are very large in the region of configuration space corresponding to two particles close together.

To show how the behaviour of an operator for small interparticle distances influences the perturbation correction of first order, we list in Table 2 the potential energy

$$V = \sum_{i < j = 1}^N v(x_i, x_j) \quad \dots\dots (31)$$

and the mean square distance

$$r_{12}^2 = \frac{2}{N(N-1)} \sum_{i < j = 1}^N (\mathbf{r}_i - \mathbf{r}_j)^2 \quad \dots\dots (32)$$

up to first order in W^\dagger . The correction is very important for the potential energy ($\simeq 36\%$), but is not so for the mean square distance ($\simeq 2\%$). Of course this does not mean that $V^{(2)}$ will be necessarily large. $V^{(2)}$ is closely related to $\epsilon^{(3)}$, so that it is small in infinite nuclear matter and, we hope, will be small also in our case.

Table 2. The Importance of the Behaviour of an Operator for Small Interparticle Distances for the Perturbation Correction of First Order

	$N = 16$	$N = \infty$
$\frac{V^{(0)}}{N} = \frac{\langle \Phi_0 \sum v_{ij} \Phi_0 \rangle}{N}$	-1.306	-1.343
$\frac{V^{(1)}}{N} = \frac{2\langle \Phi_0 \sum v_{ij} \Psi^{(1)} \rangle}{N}$	-0.474	-0.680
$V^{(1)}/V^{(0)} (\%)$	36	51
$\frac{1}{2}N(N-1) \nu(r_{12}^2)^{(0)} = \langle \Phi_0 \sum \nu r_{ij}^2 \Phi_0 \rangle$	552	
$\frac{1}{2}N(N-1) \nu(r_{12}^2)^{(1)} = 2\langle \Phi_0 \sum \nu r_{ij}^2 \Psi^{(1)} \rangle$	-12	
$(r_{12}^2)^{(1)}/(r_{12}^2)^{(0)} (\%)$	-2.2	

Up to now, we have found, therefore, no influence on the convergence of the perturbation series, arising from any possible surface clustering.

§ 4. DISCUSSION OF THE MAIN APPROXIMATION

We have made an estimate of the second-order energy, based on a variational method, but we know with certainty only that our number is an upper bound to the energy. We could also find a lower bound, by using the sum rule, since

$$\frac{1}{E_0 - E_1} \sum_{\nu=1}^{\infty} \langle \Phi_0 | W | \Phi_{\nu} \rangle \langle \Phi_{\nu} | W | \Phi_0 \rangle \leq \epsilon^{(2)} \quad \dots\dots (33)$$

but it does not seem interesting, because it leaves a large margin of variation

$$-0.542 \leq \frac{\epsilon^{(2)}}{16} \leq -0.237.$$

Therefore, let us improve our trial wave function in a simple way, by introducing as new arbitrary parameters the components over a finite number of low energy excited states, and let us see how our results are affected by this change.

The trial wave function

$$X'(\lambda_1, \dots, \lambda_{\kappa}; \alpha, \beta, \gamma) = \sum_{\nu=1}^{\kappa} \lambda_{\nu} |\phi_{\nu}\rangle + \left\{ 1 - \sum_{\nu=1}^{\kappa} |\Phi_{\nu}\rangle \langle \Phi_{\nu}| \right\} X(\alpha, \beta, \gamma) \quad \dots\dots (34)$$

is more general than the previous X . Obviously, for the optimum λ 's we have

$$X'(\alpha, \beta, \gamma) = \sum_{\nu=1}^{\kappa} |\Phi_0\rangle \frac{\langle \Phi_{\nu} | W | \Phi_0 \rangle}{E_0 - E_{\nu}} + \left\{ 1 - \sum_{\nu=1}^{\kappa} |\Phi_{\nu}\rangle \langle \Phi_{\nu}| \right\} X(\alpha, \beta, \gamma) \quad \dots\dots (35)$$

so that the first κ excited states are treated exactly.

We have chosen κ so that the fraction of the energy treated exactly is as large as possible, without making the computation too arduous. Of course, that fraction should be appreciable so that we can say that we have indeed improved

† We were able to calculate $(r_{12}^2)^{(1)}$ without making the approximation $\Psi^{(1)} \simeq X$ because r^2 has very few matrix elements between harmonic oscillator wave functions.

the wave function. If the new upper bound to the energy remains very close to the previous one, this indicates that the approximation was probably good.

A new lower bound may also be evaluated:

$$\sum_{\nu=1}^k \frac{|\langle \Phi_0 | W | \Phi_{\nu} \rangle|^2}{E_0 - E_{\nu}} + \frac{1}{E_0 - E_{\kappa+1}} \sum_{\nu=\kappa+1}^{\infty} |\langle \Phi_0 | W | \Phi_{\nu} \rangle|^2 \leq \epsilon^{(2)}. \quad \dots (36)$$

In the calculation with X we have considered only double excitations, because the single excitations give a very small contribution to the energy. And we have chosen κ so that we have treated exactly all the states for which $E_{\nu} - E_0 = \Lambda_{\kappa} + \Lambda_l - \Lambda_i - \Lambda_j \leq 2\nu$. This means that we have treated exactly the excitation from two p states to states $|0; 2; m\rangle$ or $|1; 0; 0\rangle$.

It is interesting to compare the new with the previous sets of lower and upper bounds.

Previously we had

$$-0.542 \leq \frac{\epsilon^{(2)}}{16} \leq -0.237, \quad -5.925 \leq \epsilon_{pp}^{(2)} \leq -2.496$$

but now we have

$$-0.423 \leq \frac{\epsilon^{(2)}}{16} \leq -0.248, \quad -4.023 \leq \epsilon_{pp}^{(2)} \leq -2.679$$

so that the lower bounds have increased ten times faster than the upper bounds have decreased. This indicates that the true value is something like ten times nearer to the upper bound than to the lower bound.

Another interesting fact is that, although the upper bound has changed very little, the part of $\epsilon_{pp}^{(2)}$ treated correctly in the second case was -1.343 , about a half of the total upper bound. In the previous case the corresponding contribution of the first κ levels was -1.269 , which is a number very near to -1.343 .

It seems therefore reasonable to assume that our approximation was good, that the upper bound calculated with X has probably an error of less than 15% and the upper bound calculated with X' an error of less than 10%.

§ 5. THE EFFECT OF THE PAULI PRINCIPLE AT THE NUCLEAR SURFACE

The effect of the Pauli principle is represented in expressions (11) and (12) by the operators Q_N and q_N . Because of them $\psi_{ij}^{(1)}(x', x'')$ and $\psi_i^{(1)}(x)$ have no components inside the 'Fermi sea'. That is very fortunate because those components, if present, would be very large, due to the energy denominators being small.

To estimate the magnitude of this effect we consider the second-order energy calculated without taking the Pauli principle into account. Let us compare

$$\epsilon^{(2), \text{no P.P.}} = \sum_{i < j=1}^N \sum_{k < l=1}^{\infty} \frac{|\langle \phi_i \phi_j | v | \phi_k \phi_l \rangle|^2}{\Lambda_i + \Lambda_j - \Lambda_k - \Lambda_l} + \left\{ \begin{array}{l} \text{single excitations} \\ \text{part of } \epsilon^{(2)} \end{array} \right\} \quad \dots (37)$$

with $\epsilon^{(2)}$. We find $\epsilon^{(2), \text{no P.P.}} \leq -0.761$, so that $\epsilon^{(2), \text{no P.P.}} / \epsilon^{(2)} \simeq 3$, while for infinite nuclear matter this ratio is 4 (de Dominicis 1957). Therefore the Pauli principle seems to be somewhat less effective in reducing the perturbation corrections in finite nuclei than it was in infinite nuclear matter. This is due to the existence of the surface region.

§ 6. TWO-BODY CORRELATIONS AT THE SURFACE

Finally we shall comment on another interesting question related to the finite nucleus problem: how do the two-particle correlations vary with the distance from the centre of the nucleus. A relevant quantity for this point should be the density of potential energy

$$v(x_1) = \int_{x_2, x_3, \dots, x_N} \Phi'^*(x_1, x_2, \dots, x_N) \sum_{i < j} v(x_i, x_j) \Phi'(x_1, x_2, \dots, x_N). \quad \dots (38)$$

Up to first order in perturbation theory we may write

$$v(x) = v^{(0)}(x) + v^{(1)}(x) + \dots \quad \dots (39)$$

We have calculated this with the assumption that $\Psi^{(1)}$ was well approximated by X. This should be all right because the quantity calculated is an average which ought not to be too sensitive to the small details of $\Psi^{(1)}$. The results are plotted in Fig. 1 and show a density of potential energy which goes well above its zero-order part, on the surface region, and has a pronounced maximum. The enhancement of that quantity at the surface may well be due, at least in part, to stronger correlations between the particles.

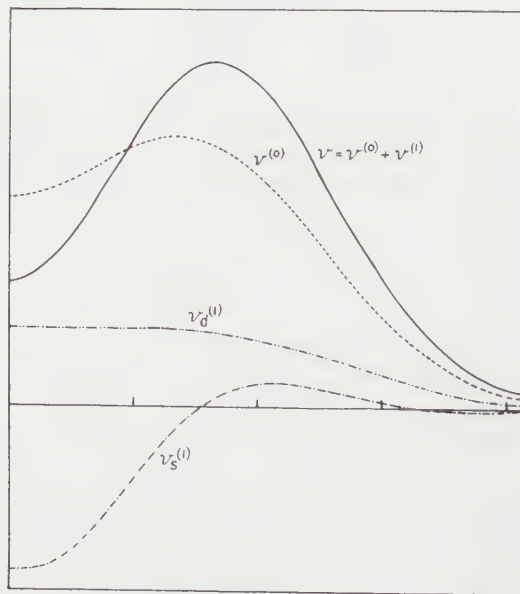


Fig. 1. The density of potential energy up to first order as a function of $\sqrt{\nu}r$. The abscissa scale is as in Fig. 2.

But what is actually happening ought to be better seen by comparing the part of our potential energy density containing no two-body correlations with the part containing all the two-body correlations. We call these quantities, respectively, the uncorrelated density, $v_{\text{uncorr}}(x)$, and the correlated density, $v_{\text{corr}}(x)$; obviously

$$v(x) = v_{\text{uncorr}}(x) + v_{\text{corr}}(x). \quad \dots (40)$$

The first-order correction $v^{(1)}(x)$ is itself formed of two parts. One, $v_d^{(1)}(x)$, arising from double excitations, and containing the $\psi_{ij}^{(1)}(x', x'')$, and the other, $v_s^{(1)}(x)$, arising from single excitations and containing the $\psi_i^{(1)}(x)$:

$$v^{(1)}(x) = v_d^{(1)}(x) + v_s^{(1)}(x). \quad \dots (41)$$

It is clear that

$$v^{(0)}(x) = \sum_{i < j} \int_{x'} \langle \phi_i \phi_j | x x' \rangle v(x, x') \langle x x' | \phi_i \phi_j \rangle \quad \dots\dots (42)$$

$$v_d^{(1)}(x) = 2 \sum_{i < j} \int_{x'} \langle \phi_i \phi_j | x x' \rangle v(x, x') \langle x x' | \psi_{ij}^{(1)} \rangle \quad \dots\dots (43)$$

$$v_s^{(1)}(x) = 2 \sum_{i < j} \int_{x'} \langle \phi_i \phi_j | x x' \rangle v(x, x') \langle x x' | \phi_i \psi_j^{(1)} + \psi_i^{(1)} \phi_j \rangle. \quad \dots\dots (44)$$

From our definitions of v_{corr} and v_{uncorr} we have, up to first-order perturbation theory

$$v_{\text{corr}}(x) = v_d^{(1)}(x), \quad \dots\dots (45)$$

$$v_{\text{uncorr}}(x) = v^{(0)}(x) + v_s^{(1)}(x). \quad \dots\dots (46)$$

We may also regard $v_{\text{uncorr}}(x)$ as an approximation to the zero-order term calculated with Hartree-Fock wave functions, if we assume that $\psi_i^{(1)}$ corrects ϕ_i from lack of self-consistency. In the same way $v_{\text{corr}}(x)$ corresponds to the first-order correction under the same circumstances.

Looking now at Fig. 2, where the quantities v_{corr} and v_{uncorr} are plotted, we see clear evidence of increased correlations at the surface. But we find also evidence for strong correlations in the centre of the nucleus, although over a region with a very small extension. This might be due to lack of self-consistency in our treatment, but, in any case, it does not contradict the idea of stronger correlations where the density of particles is lower, because the density has a very deep minimum precisely at the centre.

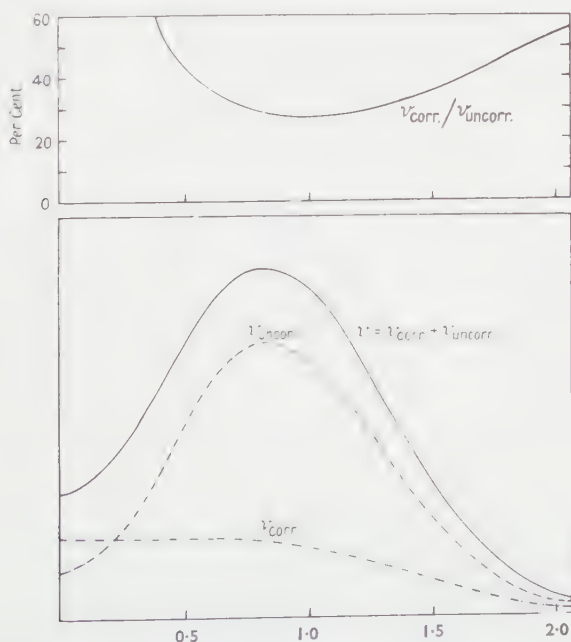


Fig. 2. The correlated and uncorrelated parts of the potential energy density and their ratio, as a function of $\sqrt{r/r}$.

§ 7. INFLUENCE OF A VELOCITY DEPENDENT POTENTIAL

Until now we have been considering a local comparison potential U , namely $U = \frac{1}{2} v^2 r^2$. But the use of harmonic oscillator wave functions does not imply

the use of the harmonic oscillator potential, because such wave functions are eigenfunctions not only of $h = \frac{1}{2}(-\nabla^2 + v^2 r^2)$ but also of

$$h^+ = h + f(h) = -\frac{1}{2}\nabla^2 + U^+, \quad \dots\dots (47)$$

$$U^+ = \frac{1}{2}v^2 r^2 + f(h), \quad \dots\dots (47 a)$$

where f is an arbitrary real function. The eigenvalues of h^+ are

$$\Lambda_i^+ = \Lambda_i + f(\Lambda_i). \quad \dots\dots (48)$$

From the point of view of Hartree-Fock theory, f should be chosen so that

$$\Lambda_i^+ = \langle \phi_i | -\frac{1}{2}\nabla^2 | \phi_i \rangle + \sum_{j=1}^N \langle \phi_i \phi_j | v | \phi_i \phi_j \rangle. \quad \dots\dots (49)$$

As an approximation let us assume

$$f(z) = C + \left(\frac{1}{m^+} - 1 \right) z. \quad \dots\dots (50)$$

and let us calculate the parameters C and m^+ so that (49) is satisfied for the occupied states. We get $1/m^+ = 1.996$, so that the use of this effective mass approximation reduces the perturbation correction by $\frac{1}{2}$. This shows the convenience of using proper velocity dependent potentials for U .

§ 8. CONCLUSIONS

The consideration of the potential energy density has shown that the correlations between particles increase at the surface (§6). Nevertheless this effect does not seem to have influence on the rate of convergence of the perturbation series (§3). This may be due to the larger spacing between the energy levels of finite nuclei, which could compensate the smaller effectiveness of the Pauli principle.

ACKNOWLEDGMENTS

The author wishes to express his deepest gratitude to Professor R. E. Peierls for proposing this problem for investigation, for his constant guidance and for many and very helpful suggestions. He is also very grateful to Professor G. E. Brown and to Professor B. H. Flowers for very useful discussions and suggestions; and to Mr. J. Stuttard for much of the numerical work. Finally he acknowledges a grant from the Comissao de Estudos de Energia Nuclear, Instituto de Alta Cultura.

REFERENCES

- BETHE, H., 1956, *Phys. Rev.*, **103**, 1353.
 BETHE, H., and SALPETER, E. E., 1957, *Hand. d. Phys.*, XXXV, 25 (Berlin: Springer).
 BLATT, J. M., and JACKSON, J. D., 1949, *Phys. Rev.*, **76**, 18.
 BOLSTERLI, M., and FEENBERG, E., 1956, *Phys. Rev.*, **101**, 1349.
 BRUECKNER, K., and LEVINSON, C., 1955, *Phys. Rev.*, **97**, 1344.
 DE DOMINICIS, C., 1957, *Thesis*, University of Birmingham.
 EULER, H., 1937, *Z. Phys.*, **105**, 553.
 GOMES, L., WALECKA, J., and WEISSKOPF, V., 1958, *Annals of Physics*, **3**, 241.
 HODGSON, P. E., 1958, *Nucl. Phys.*, **8**, 1.
 HUBY, R., 1949, *Proc. Phys. Soc. A*, **62**, 62.
 SWIATECKI, W., 1956, *Phys. Rev.*, **101**, 1321; **103**, 264.
 TALMI, I., 1952, *Helv. Phys. Acta.*, **25**, 185.

the transition to the ground state of ^{18}F (Towle and Macefield, private communication, Gow and Alvarez 1954) the calculated branching ratio to a state at 1 Mev excitation is about 5%.

^{18}Ne was produced in the reaction $^{16}\text{O}(^3\text{He}, n)^{18}\text{Ne}$, $Q = -3.210$ Mev (Towle and Macefield, private communication, Dunning and Butler 1959). A beam of about $0.05\ \mu\text{A}$ of 5.2 Mev $^3\text{He}^+$ ions was focused on to a quartz target, $600\text{--}1000\ \mu\text{g cm}^{-2}$ thick. Hollow cylinders cooled to liquid nitrogen temperature and surrounding the beam were placed before and after the target. This system reduced the carbon build-up on the target and eliminated the 2.31 Mev γ -rays from the reactions $^{12}\text{C}(^3\text{He}, p)^{14}\text{N}$ and $^{12}\text{C}(^3\text{He}, n)^{14}\text{O}(\beta^+)^{14}\text{N}$ which had been observed in earlier runs.

The beam could be interrupted by a tantalum shutter situated immediately after the Van de Graaff analysing slits. The shutter was operated electromagnetically, being alternately opened and closed for equal periods. The distance between the target and shutter was 17 feet including a concrete wall 2 feet thick. After passing through the target the beam was collected in a Faraday cup situated 3 feet beyond the target.

Gamma rays emerging from the target at 90° to the beam direction were detected in a $3\text{ in.} \times 3\text{ in.}$ NaI (Tl) crystal mounted on a Du Mont 6363 photomultiplier. The crystal was shielded locally with 2 in. of lead and additional lead shielding was placed between the Faraday cup and counter. The pulse output from the counters was amplified and fed to two 100-channel pulse height analysers. Contacts on the beam shutter were arranged to veto the pulses entering the analysers, so that one analyser counted only during 'beam-off' periods and the other only during 'beam-on' periods. The latter analyser was used as a beam monitor. A pen recorder recording the total pulse counting rate was used to check beam current stability. Variations of photomultiplier gain with counting rate were observed. The difficulty of energy calibration was overcome by placing standard γ -ray sources near the target during some of the runs.

It can be shown that, given equal beam on-off periods T and a nucleus with mean life τ , when equilibrium is established (i.e. after sufficient on-off periods with a constant beam current) the number of counts N recorded in a given time interval obeys the relation

$$N \propto \frac{\tanh x}{x}, \quad \text{where } x = \frac{T}{2\tau}. \quad \dots\dots (1)$$

For ^{18}Ne , τ is about 2.3 seconds and T was chosen as 2 seconds, giving a yield of 94% of the theoretical limit. Any smaller value of T would only increase the background due to other possible shorter lived nuclei.

Pulse height spectra obtained during 'beam-off' periods all show a γ -ray with an energy of about 1 Mev. The measured energy using ^{54}Mn , ^{60}Co and ^{22}Na as energy markers is 1.035 ± 0.010 Mev. Fig. 2 shows a spectrum obtained in twenty minutes running time using ^{54}Mn and ^{60}Co as markers. The possibility of the peak arising from random coincidences between 0.511 Mev annihilation quanta was ruled out by performing the experiment at different beam currents giving different counting rates for the annihilation radiation. Another γ -ray peak at 0.685 Mev was observed in all the spectra. A peak of this energy can arise from the arrival of the two annihilation quanta in the counter, one of which has

been Compton back-scattered in the target assembly. An example of such events is given by Butler and Gosset (1958). The possibility that some of the peak come from a 0.685 MeV γ -ray from the reaction $^{28}\text{Si}(^3\text{He}, n)^{30}\text{S}(\beta^+)^{30}\text{P}^*$ cannot however be excluded.

In order to check that the 1.035 MeV γ -ray came from a nucleus with a mean life near 2.3 seconds, the periods T were varied. Periods of 2, 10 and 50 seconds were used, 2 seconds being the shortest period that was consistent with accurate timing of the switching. From these results and using relation (1) the mean life of the nucleus was calculated as 2.5 ± 0.6 seconds in good agreement with the known mean life of ^{18}Ne .

To conclude then, a γ -ray has been observed which can be identified with a transition from the 1.04 MeV level in ^{18}F which is fed by the positron decay of

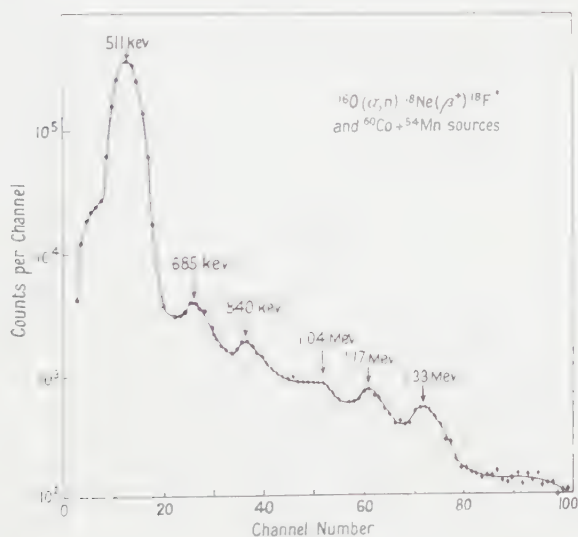


Fig. 2. Gamma-ray spectrum following irradiation of target, with ^{54}Mn and ^{60}Co as energy markers.

^{18}Ne . It is probable that the level excited in ^{18}F is the analogue of the ground state of ^{18}Ne and has the assignment $0^+, T = 1$. This confirms the assignment made by Hinds and Middleton. Also Butler and Dunning (private communication) have repeated their earlier work on the decay of ^{18}Ne (Butler and Dunning 1960) and obtain results in agreement with ours.

ACKNOWLEDGMENTS

We would like to express our thanks to Dr. K. W. Allen for many helpful suggestions. Also we would like to thank Mr. A. R. D. Norman, Mr. V. Shepherd and the operating crew of the Van de Graaff for their assistance during the experiments. We are grateful to Dr. J. W. Butler for his comments on this work and for communicating his results prior to publication.

REFERENCES

- AJZENBERG-SELOVE, F., and LAURITSEN, T., 1959, *Nucl. Phys.*, **11**, 1.
ALLEN, K. W., ECCLESHALL, D., and YATES, M. J. L., 1959, *Proc. Phys. Soc.*, **74**, 660.
ALMQVIST, E., BROMLEY, D. A., and KUEHNER, J. A., 1958, *Bull. Amer. Phys. Soc.*, [II], **3**, 27.
BROMLEY, D. A., ALMQVIST, E., GOVE, H. E., LITHERLAND, A. E., PAUL, E. B., and FERGUSON, A. J., 1957, *Phys. Rev.*, **105**, 957.
BUTLER, J. W., and DUNNING, K. L., 1960, *Bull. Amer. Phys. Soc.*, [II], **5**, 101.
BUTLER, J. W., and GOSSET, C. R., 1958, *Phys. Rev.*, **112**, 1257.
DUNNING, K. L., and BUTLER, J. W., 1959, *Bull. Amer. Phys. Soc.*, [II], **4**, 444.
ELLIOT, J. P., and FLOWERS, B. H., 1955, *Proc. Roy. Soc. A*, **229**, 536.
GOW, J. P., and ALVAREZ, L. W., 1954, *Phys. Rev.*, **94**, 365.
HINDS, S., and MIDDLETON, R., 1959 a, *Proc. Phys. Soc.*, **73**, 721.
—— 1959 b, *Proc. Phys. Soc.*, **74**, 762.

Rate of Energy Loss and Ranges of Carbon and Oxygen Ions in Solids

BY D. I. PORAT† AND K. RAMAVATARAM‡

The Physical Laboratories, The University, Manchester

Communicated by B. H. Flowers; MS. received 17th May 1960

Abstract. The rate of energy loss of carbon and oxygen ions passing through carbon, aluminium, nickel, silver, and gold absorbers has been measured in the energy interval of 0.36 to 3.2 mev. Ranges of the carbon and oxygen ions in these stopping materials were obtained by numerical integration of the rate of energy loss against energy curve. The relative accuracy of the results is to about 2% and the absolute accuracy is to better than 5%.

§ 1. INTRODUCTION

SUFFICIENT data are available on the rate of energy loss of protons passing through matter (Allison and Warshaw 1953, Bethe and Ashkin 1952, Whaling 1958). Bethe's theory of electronic stopping, based on the Born approximation, is used to calculate the stopping power for protons at higher energies where experimental data are not available (Aron, Hoffman and Williams 1949, Rich and Madey 1954). The accuracy of the theory was substantiated in numerous experiments with protons especially at higher energies (Bakker and Segrè 1951, Sachs and Richardson 1953). In the case of heavy ions such as C, N, O... moving at velocities v comparable with the classical Bohr orbit velocity v_0 , one cannot calculate the rate of energy loss suffered by the ion from present theories. The ions undergo a process of continual capture and loss of electrons in their passage through matter. A charge se^* , smaller than ze , is effective in the interaction with the stopping atoms, thus reducing the rate of energy loss in electronic collisions. This effective charge se^* would have to take into account also the excited states of the particle's bound electrons. The process of charge exchange constitutes in itself one mode of energy loss which has not been estimated theoretically as yet. In addition one has to consider energy losses from nuclear collisions in a screened field, which gain in importance with the increase of the atomic number of the ion and with the decrease of its velocity.

The limitations of the present theories, in their application to the stopping of slow, heavy ions have been summarized in an earlier paper (Porat and Ramavataram 1959) which will be referred to as I henceforth. The velocities of carbon ions of 0.36 and 3.2 mev kinetic energy are $1.10v_0$ and $3.27v_0$ respectively; the velocities of oxygen ions of the above energies are $0.95v_0$ and $2.83v_0$. The criterion for the application of Bohr's theory of electronic stopping ($v_0 \ll v \ll se^*v_0$) is thus not fulfilled. The energy loss in carbon, aluminium, nickel, silver and gold was determined experimentally. The stopping elements were chosen because they represent a wide range on the scale of atomic numbers and also possess the necessary chemical stability and mechanical strength.

† Now at Cambridge Electron Accelerator, Harvard University, Cambridge, Mass., U.S.A.

‡ On leave from the Physics Department, Osmania University, Hyderabad, India.

§ 2. EXPERIMENTAL

The experiments were performed with the Manchester University Van de Graaff generator. The energy E_1 of the beam was measured by an electrostatic analyser whose field settings were earlier calibrated in terms of energy using known nuclear resonance reactions (Hunt and Firth 1955). A self-supporting foil of the stopping material of accurately determined surface density was then interposed in the path of the beam and the reduced energy E_2 was measured as before. In the limit of very thin foils, the ratio of energy loss to foil thickness can be taken as the rate of energy loss. The experimental set-up was described in detail in I and is shown in the block diagram of figure 1. The electrostatic analyser is capable of focusing ions up to an energy $z' \times 1$ mev, where z' is the charge state of the moving ion. The measurements of the rate of energy loss dE/dx could be extended to 3.2 mev due to the availability of C^{4+} and O^{4+} ions. The various charge states were identified by the modulation method described in I. Table 1 shows the number of foils used and their surface densities which were measured by alpha particle absorption (Ramavataram and Porat 1959). The uniformity

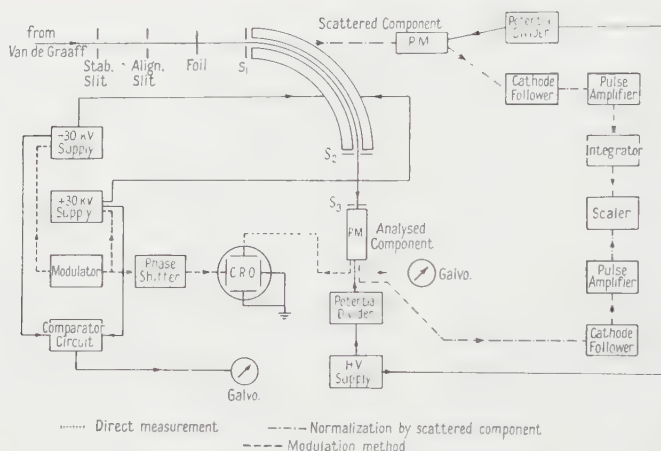


Figure 1. General diagram of apparatus: Alternative methods of measurement (described in paper I). Arrows indicate the direction of flow of information.

Table 1. Foils used for the Measurement of dE/dx

Stopping element	C	Al	Ni	Ag	Au
Number of foils	3	8	5	8	12
Surface density ($\mu\text{g cm}^{-2}$)	38.9-39.9	45.2-111	117-168	93.6-222	169-239

of foil thickness was also checked by the same method and was found to be better than 1%. Those foils which were not destroyed by exposure to the particle beam were also measured after the experiment. The surface density of the foils tended, generally, to increase slightly after the stopping power experiment, the maximum increase recorded being 5%. Average values of the surface density were used in calculating dE/dx . The comparatively large number of foils used enabled one to obtain independent dE/dx values, resulting in a better statistical accuracy of the final curves. The measurements were performed in two

stages at an interval of six months. Although the electrostatic analyser was dismantled in the intervening period, re-assembled and calibrated against nuclear resonance reactions, the results obtained from the two independent sets of measurements lie on one curve well within the experimental errors.

§ 3. RESULTS

3.1. Rate of Energy Loss for C and O Ions

The experimental points for carbon and oxygen ions are plotted in figures 2 and 3 respectively and are based on 106 independent measurements for carbon ions and 89 for oxygen ions. $(dE/dx)_{\text{NPTL}}$ is composed of the electronic stopping power $(dE/dx)_e$ and only part of the nuclear stopping power $(dE^*/dx)_n$ since instrument geometry excluded detection of those particles which were deflected to large angles in close, energetic collisions. The contribution of these large angle collisions to the stopping power were calculated using Bohr's (1948) approximate theory of nuclear collisions in a screened field and following the

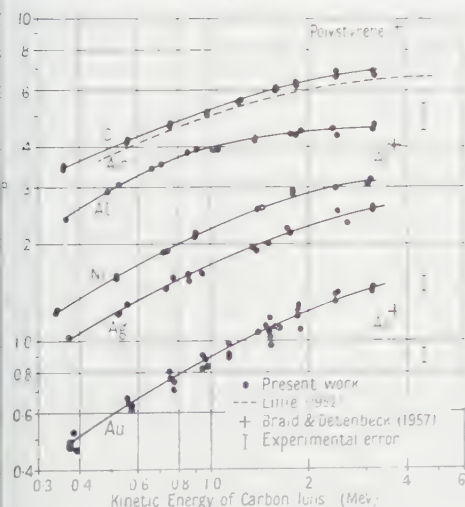


Figure 2. Stopping power for carbon ions.

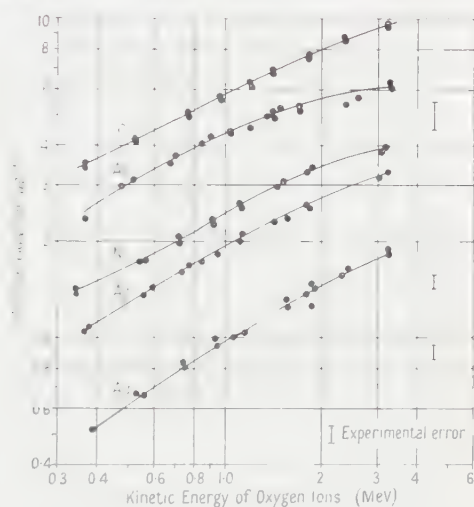


Figure 3. Stopping power for oxygen ions.

procedure described in 1. The experimental values were then corrected to give $(dE/dx)_e$. The correction is small and amounts to 3.9% for 360 keV oxygen ions passing through nickel and is smaller in all other cases. Any inaccuracies in this correction should therefore have a negligible effect on the final values of $(dE/dx)_e$. Tables 2 and 3 summarize the results for carbon and oxygen ions, respectively. Electronic stopping power $(dE/dx)_e$ is listed under column (a) while the calculated nuclear stopping power $(dE/dx)_n$ is under column (b). The rate of energy loss is seen to increase with energy and is higher for oxygen ions than for carbon ions of the same velocity. Few data from previous work are available for comparison with the present measurements. Braid and Detenbeck (1957) used a time-of-flight method to measure the velocity loss of 3.67 MeV carbon ions passing through thin foils of polystyrene, aluminium and gold. The rate of energy loss for the above absorbers expressed in units of $\text{keV} \times \text{cm}^2 \mu\text{g}^{-1}$ is 9.55, 3.97 and 1.24 respectively. These data are indicated by crosses in figure 2 and appear to be about 13 and 17% lower (for Al and Au, respectively) than our results. Lillie (1952) measured the range of ^{13}C and ^{11}B ions in a cloud chamber filled with a mixture of O_2 and N_2

and converted his data to range in air. Whaling (1958) differentiated the range curves to obtain dE/dx for both ions in air. Using Whaling's data we calculate the rate of energy loss for ^{12}C ions on the assumption that the electronic energy loss is equal for the two carbon isotopes moving at the same velocities. The nuclear energy losses will be somewhat different because the mass of the ion enters into the expression of these losses. However, the contribution of this mode of energy loss was shown to be only a few per cent of the total stopping power (see tables 2 and 3) at energies of 0.5 MeV and above. Lillie's results are shown in figure 2 (broken line). The slope as well as the position of the curve is in good agreement with the

Table 2. Stopping Power for Carbon Ions Passing through Solids
 dE/dx (keV cm² μg^{-1})

Energy (keV)	Velocity (units of v_0)	Carbon		Aluminium		Nickel		Silver		Gold	
		(a)	(b)	(a)	(b)	(a)	(b)	(a)	(b)	(a)	(b)
360	1.10	3.42	0.118	2.36	0.097	1.24	0.078	1.01	0.055	0.475	0.037
400	1.16	3.56	0.108	2.56	0.088	1.34	0.071	1.06	0.051	0.496	0.035
600	1.42	4.17	0.078	3.27	0.064	1.69	0.053	1.32	0.038	0.650	0.027
800	1.64	4.67	0.061	3.68	0.051	1.98	0.042	1.54	0.031	0.773	0.022
1000	1.83	5.08	0.051	3.93	0.043	2.21	0.036	1.71	0.026	0.882	0.019
1200	2.00	5.43	0.043	4.11	0.036	2.40	0.030	1.85	0.022	0.970	0.016
1400	2.16	5.76	0.038	4.24	0.032	2.57	0.027	1.98	0.020	1.06	0.014
1600	2.32	6.04	0.034	4.36	0.029	2.70	0.024	2.08	0.018	1.13	0.013
1800	2.46	6.30	0.031	4.42	0.026	2.83	0.022	2.17	0.016	1.20	0.012
2000	2.58	6.50	0.028	4.48	0.024	2.93	0.020	2.25	0.015	1.26	0.011
2200	2.71	6.64	0.026	4.51	0.022	2.97	0.018	2.33	0.014	1.32	0.010
2400	2.83	6.76	0.024	4.58	0.020	3.01	0.017	2.40	0.013	1.36	0.010
2600	2.94	6.81	0.023	4.60	0.019	3.05	0.016	2.46	0.012	1.40	0.009
2800	3.06	6.87	0.022	4.62	0.018	3.09	0.015	2.50	0.012	1.42	0.009
3000	3.16	6.87	0.020	4.65	0.017	3.11	0.015	2.54	0.011	1.44	0.008
3200	3.27	6.88	0.019	4.68	0.016	3.14	0.014	2.57	0.010	1.45	0.008

Table 3. Stopping Power for Oxygen Ions Passing through Solids
 dE/dx (keV cm² μg^{-1})

Energy (keV)	Velocity (units of v_0)	Carbon		Aluminium		Nickel		Silver		Gold	
		(a)	(b)	(a)	(b)	(a)	(b)	(a)	(b)	(a)	(b)
360	0.949	3.43	0.257	2.30	0.205	1.35	0.164	1.02	0.116	—	—
400	1.00	3.63	0.230	2.52	0.189	1.42	0.152	1.10	0.107	0.517	0.072
600	1.23	4.43	0.167	3.32	0.139	1.79	0.113	1.40	0.082	0.707	0.056
800	1.42	5.11	0.133	3.91	0.111	2.13	0.092	1.68	0.067	0.833	0.047
1000	1.58	5.72	0.111	4.35	0.093	2.41	0.077	1.89	0.057	0.935	0.041
1200	1.73	6.22	0.094	4.72	0.078	2.64	0.066	2.09	0.049	1.05	0.035
1400	1.87	6.78	0.082	4.96	0.070	2.87	0.059	2.24	0.044	1.16	0.031
1600	2.00	7.13	0.074	5.18	0.062	3.09	0.053	2.39	0.039	1.28	0.028
1800	2.12	7.62	0.067	5.37	0.056	3.27	0.048	2.53	0.036	1.38	0.026
2000	2.24	8.02	0.062	5.54	0.053	3.39	0.045	2.67	0.034	1.46	0.025
2200	2.35	8.45	0.057	5.66	0.048	3.51	0.041	2.79	0.031	1.53	0.023
2400	2.45	8.79	0.053	5.73	0.045	3.61	0.039	2.89	0.029	1.61	0.021
2600	2.55	9.02	0.050	5.80	0.042	3.69	0.036	2.98	0.027	1.67	0.020
2800	2.65	9.27	0.046	5.87	0.040	3.78	0.034	3.08	0.026	1.73	0.019
3000	2.74	9.50	0.044	5.92	0.038	3.85	0.037	3.17	0.025	1.79	0.018
3200	2.83	9.70	0.042	5.98	0.036	3.86	0.031	3.22	0.023	1.84	0.017

present measurements. Finally, there are data available on the rate of energy loss of C and O ions of low velocity in silver from the work by Telkovskii and Pistunovitch (1957) who find dE/dx for 21.5 keV C ions and 28 keV O ions to be 0.73 and 0.96 keV \times cm² μ g⁻¹, respectively. This energy loss appears to be rather high and cannot be explained by an increase of the energy loss at low energies due to nuclear collisions.

3.2. Ranges

The ranges R of 3.2 MeV carbon and oxygen ions in the five stopping materials were obtained by numerical integration of the expression

$$R = \int_{E_{\text{final}}}^{E_{\text{initial}}} \frac{dE}{(dE/dx)_e + (dE/dx)_n}.$$

The integration was performed on the Manchester University electronic computer MERCURY using the trapezium rule at energy intervals of 100 keV down to 100 keV kinetic energy of the ions and at energy intervals of 10 keV below that. The computed ranges below about 400 keV cannot claim the same degree of accuracy as the other data in the present measurements for the following reasons: (a) The values of $(dE/dx)_e$ used in the integration were obtained by extrapolating the measured $(dE/dx)_e$ curve as they could not be evaluated from the Fermi-Teller (1947) theory for reasons stated in the introduction. (b) $(dE/dx)_n$ was calculated on the basis of Bohr's theory of nuclear collisions in a screened field which is of the inverse-square type at the higher particle velocities and approximates to the inverse-cube field as the velocity of the ion is reduced. The large angle scattering which reduces the average range of the particle beam has been neglected in the integration.

The lower limit of the integration was determined in each case at an ion energy E_{final} at which the screening parameters ζ (Bohr 1948, § 2.1) is equal to unity and where the scattering approaches a spherically symmetrical distribution.

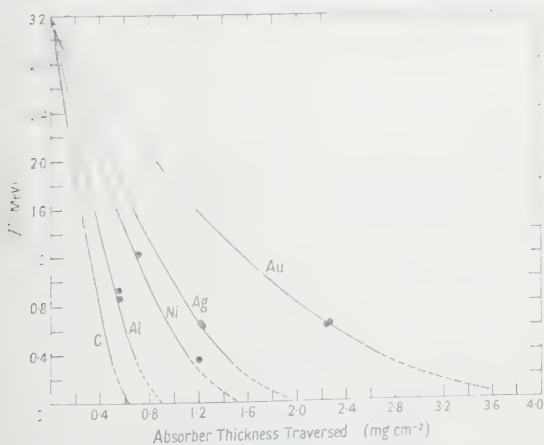


Figure 4. Range-energy relations for carbon ions.

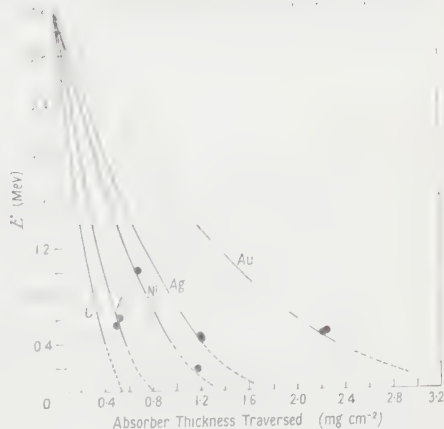


Figure 5. Range-energy relations for oxygen ions.

The range below 400 keV is shown in figures 4 and 5 by broken lines to indicate the approximate nature of the values. The circles in these figures relate to range intervals as determined experimentally with 'thick' absorbers. It is seen that

the circles lie slightly above the calculated curves, a fact which confirms qualitatively our procedure in separating the nuclear energy losses into small angle multiple, and large angle single collisions. The geometry of our experiment excluded the latter and hence showed an apparently increased range. A quantitative treatment of the influence of instrument geometry in relation to large angle scattering is given in I.

ACKNOWLEDGMENTS

The authors wish to express their thanks to Professor S. Devons, for his constant interest, to Professor B. H. Flowers for his suggestions in the preparation of this paper and to the Atomic Energy Research Establishment, Harwell, and the University of Manchester for their support.

REFERENCES

- ALLISON, S. K., and WARSHAW, S. D., 1953, *Rev. Mod. Phys.*, **25**, 779.
ARON, W. A., HOFFMAN, B. G., and WILLIAMS, F. C., 1949, UCRL-121 (University of California Radiation Laboratory).
BAKKER, C. J., and SEGRÈ, E., 1951, *Phys. Rev.*, **81**, 489.
BETHE, H. A., and ASHKIN, J., 1952, *Experimental Nuclear Physics*, **1**, 166 (New York: John Wiley).
BOHR, N., 1948, *Mat.-fys. Medd.*, **18**, No. 8.
BRAID, T. H., and DETENBECK, R. W., 1957, *Bull. Amer. Phys. Soc.*, [II], **2**, 225.
FERMI, E., and TELLER, E., 1947, *Phys. Rev.*, **72**, 399.
HUNT, S. E., and FIRTH, K., 1955, *Phys. Rev.*, **99**, 786.
LILLIE, A. B., 1952, *Phys. Rev.*, **87**, 716.
PORAT, D. I., and RAMAVATARAM, K., 1959, *Proc. Roy. Soc. A*, **252**, 394.
RAMAVATARAM, K., and PORAT, D. I., 1959, *Nucl. Instrum.*, **4**, 239.
RICH, M., and MADEY, R., 1954, UCRL-2301 (University of California Radiation Laboratory).
SACHS, D. C., and RICHARDSON, J. R., 1953, *Phys. Rev.*, **89**, 1165.
TELKOVSKII, V. G., and PISTUNOVITCH, V. I., 1957, *Sov. Phys. (Doklady)*, **2**, 184.
WHALING, W., 1958, *Handb. d. Phys.*, **34** (Berlin: Springer).

Explanation of some 'Forbidden' Transitions in Paramagnetic Resonance

BY B. BLEANEY AND R. S. RUBINS

Clarendon Laboratory, Oxford

MS. received 10th June 1960

Abstract. The abnormal intensity of some 'forbidden' hyperfine transitions in the paramagnetic resonance spectra of ions with $S=1$ or more is shown to be due to cross terms in the spin Hamiltonian. These arise from off-diagonal terms in the electronic and nuclear interactions, and the computed transition intensities agree closely with measurements on vanadium fluosilicate. In a powder an apparent doubling of the hyperfine transitions is shown to be due to the combined effect of these terms and others due solely to the electronic splitting.

§ 1. INTRODUCTION

IN the paramagnetic resonance spectra of ions which have a more than doubly degenerate ground state, split by the crystalline electric field by amounts of the order 10^{-2} to 10^{-1} cm^{-1} , and which also have a hyperfine structure, a number of extra hyperfine lines have often been observed which appear to correspond to transitions in which the nuclear magnetic quantum m changes by ± 1 . These were first reported by Bleaney and Ingram (1951) in manganese ammonium sulphate and manganese fluosilicate (both diluted); they appeared when the external magnetic field was at an angle between parallel and perpendicular to the crystal axis, and were inexplicably large in intensity. The purpose of this paper is to show that they arise from second-order effects due to cross terms in the spin Hamiltonian between the 'fine structure' splitting and the hyperfine structure splitting.

§ 2. THEORY

We consider an ion with spin $S(>\frac{1}{2})$ and a fine structure term of the second degree with axial symmetry; for simplicity we shall assume that the spectroscopic splitting factor and the hyperfine structure are both isotropic, as is closely the case for ions such as d^5 and f^7 , or d^3 in an octahedral field, where such effects are usually observed. The spin Hamiltonian is then

$$\mathcal{H} = g\beta\mathbf{H} \cdot \mathbf{S} + D\{S_z^2 - \frac{1}{3}S(S+1)\} + \mathbf{AS} \cdot \mathbf{I} - g_I\beta\mathbf{H} \cdot \mathbf{I} \quad \dots\dots (1)$$

If H is at an angle θ to the crystal axis, and the Zeeman energy is the largest term, the latter can be diagonalized by choosing the direction of H as the new z axis. With axial symmetry this change can be treated as a rotation through an angle θ about the y axis, and the Hamiltonian then becomes

$$\begin{aligned} \mathcal{H} = & g\beta HS_z + \frac{1}{2}D\{S_z^2 - \frac{1}{3}S(S+1)\}\{3\cos^2\theta - 1\} \\ & + D(S_zS_x + S_xS_z)\cos\theta\sin\theta + \frac{1}{4}D(S_+^2 + S_-^2)\sin^2\theta \\ & + \mathbf{AS} \cdot \mathbf{I} - g_I\beta\mathbf{H} \cdot \mathbf{I} \quad \dots\dots (2) \end{aligned}$$

Zero-order wave functions $|M, m\rangle$ (where M, m are the electronic and nuclear magnetic quantum numbers), which would be appropriate to an ion in a very large magnetic field, are admixed by the off-diagonal terms in this Hamiltonian. The effect on the energy of first-order admixtures due to terms in A and D has been evaluated by Bleaney (1951). For our purpose there are important second-order admixtures arising from cross products of the terms in D and A . These consist of products $(S_z S_+)(S_- I_+)$, $(S_z S_-)(S_+ I_-)$ and other products formed by permutation of the components of S , whose energy coefficients are of order $(DA/\text{Zeeman energy})$. Such terms can be reduced to an equivalent operator

$$\frac{1}{8} DA \sin 2\theta (I_+ + I_-) \left\{ \frac{(2S_z - 1)[S(S+1) - S_z^2 + S_z]}{W_{M-} - W_{M-1}} + \frac{(2S_z + 1)[S(S+1) - S_z^2 - S_z]}{W_{M-} - W_{M+1}} \right\} \dots\dots (3)$$

and if $D \ll g\beta H$, we can take the energy denominators as

$$W_{M+1} - W_M = W_{M-} - W_{M-1} = g\beta H,$$

when (3) reduces to

$$\frac{3DA \sin 2\theta}{4g\beta H} (I_+ + I_-) \{S_z^2 - \frac{1}{3}S(S+1)\}. \dots\dots (4)$$

The importance of the terms in (3) and (4) derives from the fact that they contain operators connecting the hyperfine states with the same M , which differ in energy only by AM . Hence a nuclear state $|m\rangle$ becomes admixed with states $|m \pm 1\rangle$ by amounts of order $3D \sin 2\theta / 4g\beta H$ and transitions of the type $\Delta M = \pm 1, \Delta m = \pm 1$ become allowed with intensities of the order of the square of this admixture coefficient, relative to the intensities of the ordinary transitions in which m does not change. Detailed evaluation of these gives for the relative intensity the expression

$$\left\{ \frac{3D \sin 2\theta}{4g\beta H} \right\}^2 \left\{ 1 + \frac{S(S+1)}{3M(M-1)} \right\}^2 \{I(I+1) - m^2 + m\} \dots\dots (5)$$

for the transitions $|M, m\rangle \longleftrightarrow |M-1, m-1\rangle$ and $|M, m-1\rangle \longleftrightarrow |M-1, m\rangle$.

These lines are strongest in the electronic $|+\frac{1}{2}\rangle \longleftrightarrow |-\frac{1}{2}\rangle$ transition, and their angular dependence is such that they vanish parallel or perpendicular to the symmetry axis, being strongest at $\theta = 45^\circ$. Their intensity is surprisingly large, for at this angle they would rival the $\Delta m = 0$ transitions in intensity for a value of $D/g\beta H$ as small as $1/12$.

Under such conditions transitions with $\Delta m = \pm 2$ will also have appreciable intensity. It is readily seen that these arise from admixtures due to the repeated application of the cross-product terms already considered, together with cross products of the form $(DS_+^2)(AS_-I_+)^2$ and $(DS_-^2)(AS_+I_-)^2$. By means of perturbation theory it can be shown that the relative intensity of the transitions $|M, m \pm 1\rangle \longleftrightarrow |M-1, m \mp 1\rangle$ is, assuming $D, A \ll g\beta H$,

$$\left[\frac{1}{2} \left\{ \frac{3D \sin 2\theta}{4g\beta H} \right\}^2 \left\{ 1 + \frac{S(S+1)}{3M(M-1)} \right\}^2 \pm \frac{3DA \sin^2 \theta}{16(g\beta H)^2} \left\{ 1 + \frac{S(S+1)}{3M(M-1)} \right\} \right]^2 \times \{I^2 - m^2\} \{I(I+1)^2 - m^2\} \dots\dots (6)$$

Positions of Lines

The energy of the state $|M, m\rangle$ due to the hyperfine terms is

$$AMm + m(A^2/2g\beta H)\{M^2 - S(S+1)\} + M(A^2/2g\beta H)\{I(I+1) - m^2\} - g_I\beta Hm \\ + \left\{ \frac{3D \sin 2\theta}{4g\beta H} \right\}^2 \left\{ \frac{2Am}{M} \right\} \{M^2 - \frac{1}{3}S(S+1)\}^2 \dots\dots (7)$$

where all second-order terms have been included, together with the one important third-order term arising from the cross products considered above. An idea of the appearance of the spectrum is obtained by omitting at first the energy terms which vanish at high frequencies; then for an ion with $S=3/2$, $I=3/2$ and D large enough to separate out the three electronic transitions, the spectrum will be roughly as in Fig. 1. For the central transition, the $\Delta m = \pm 1$

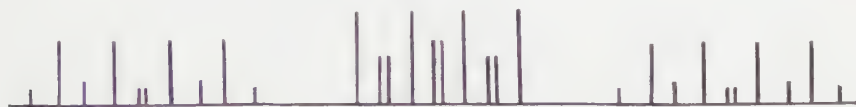


Fig. 1. Schematic plot of spectrum for $S=3/2$, $I=3/2$ showing the $\Delta m = \pm 1$ lines.

lines occur as doublets, with splitting $2g_I\beta H$, centred on the points midway between the main lines, and with greatest intensity at the centre. For the outer transitions, half of the $\Delta m = \pm 1$ lines are displaced by an amount A towards the higher frequencies, while the other half are equally displaced in the opposite sense; hence one line at each end of a hyperfine set falls outside the main hyperfine structure lines. For an ion with a higher value of S , the displacement is $\pm 2A$ for the $|\pm 5/2\rangle \leftrightarrow |\pm 3/2\rangle$ transitions, and $\pm 3A$ for the $|\pm 7/2\rangle \leftrightarrow |\pm 5/2\rangle$ transitions.

To this must be added the second-order displacements. As would be expected, the term in $A(D/g\beta H)^2$ is the most important if D is large. However, for the electronic $|\pm \frac{1}{2}\rangle \leftrightarrow |\mp \frac{1}{2}\rangle$ transition this term shifts the two components of the $\Delta m = \pm 1$ doublets equally, and so does not affect the splitting of each doublet, which is

$$[(A^2/g\beta H)\{S(S+1) - \frac{1}{4}\} + 2g_I\beta H]. \dots\dots (8)$$

Measurement of the splitting at different field strengths makes it possible to determine both quantities in (8). This is not usually a very precise method of determining g_I , but it may be of use in fixing its sign (strictly only its sign relative to g can be found, but the latter is usually known in the cases we are considering). If there were a nuclear electric quadrupole interaction (with a corresponding term $P\{I^2 - \frac{1}{3}I(I+1)\}$ in the Hamiltonian), a term $2P(2m-1)$ would have to be included between the modulus signs in Eqn (8). This would increase the splitting of the doublets at one end and decrease it at the other. Thus equal spacing in the doublets serves as rather a delicate test of such an interaction, though caution must be observed in using this test, since terms in I_z^2 which would give similar effects may arise from higher order effects neglected in our treatment.

The positions of the $\Delta m \pm 2$ lines can be easily seen. For the central electronic transition they form doublets spaced by twice the amount given by Eqn (8), centred on all the main hyperfine lines except the outside ones. For the

outer electronic transitions they will be displaced sideways, but by twice the amount (in first order) for the $\Delta m = \pm 1$ transitions.

It may be noted that these sideways displacements give the sign of A relative to g_I , by observing whether the sideways displacement is added to or subtracted from that due to $g_I\beta H$ in the outer transition with positive M . The sign of M is, however, only identified if that of D is known; otherwise only the sign of the product Dg_I is determined.

§ 3. SPECTRUM OF VANADIUM FLUOSILICATE

Measurements were made on crystals of zinc fluosilicate, $\text{ZnSiF}_6 \cdot 6\text{H}_2\text{O}$, containing about 1% of divalent vanadium. The V^{2+} ion, $3d^3$, has a singlet orbital ground state in this salt, with spin $S=3/2$; it is situated in a crystal field of axial symmetry. The only stable isotope of appreciable abundance is ^{51}V , with a nuclear spin of $7/2$. The spin Hamiltonian (1) is thus applicable to this ion with the following values of the parameters: $S=3/2$, $I=7/2$, $g = +1.971 \pm 0.002$, $g_I = +0.80 \times 10^{-3}$, $D = +876 \pm 1 \text{ gauss} = +808 \pm 1 \times 10^{-4} \text{ cm}^{-1}$, $A = -91.25 \pm 0.10 \text{ gauss} = -84.2 \pm 0.1 \times 10^{-4} \text{ cm}^{-1}$.

These parameters were determined from measurements at wavelengths of approximately 1.3 and 3.2 cm respectively, for which the magnetic fields at the centre of the spectra were 8200 and 3400 gauss respectively. The value of D is so large that perturbation theory can be used only for angles where $\sin 2\theta$ is rather small. This is illustrated by the spectra shown in Fig. 2 which show the central electronic transition $|+1/2\rangle \longleftrightarrow |-1/2\rangle$ with the magnetic field at an angle of 78° to the crystal axis. At the shorter wavelength the $\Delta m = \pm 1$ lines can be seen clearly as unresolved doublets, whose intensity in the centre is nearly equal to that of the $\Delta m = 0$ lines. Eqn (5) predicts a relative intensity of 0.5 for the central unresolved pair; this is in fair agreement with the observed intensity when allowance is made for the fact that the intensity of the $\Delta m = 0$ lines must be diminished by an amount corresponding to the intensity of the 'forbidden lines' since the total intensity of all the hyperfine lines is a constant. The increase of intensity of the $\Delta m = \pm 1$ lines towards the centre, with a corresponding decrease in the $\Delta m = 0$ lines, is clearly seen. The $\Delta m = \pm 2$ lines are not resolved from the $\Delta m = 0$ lines.

At the longer wavelength the intensity of the forbidden transitions is considerably greater. The $\Delta m = \pm 1$ lines now appear as resolved doublets, and the $\Delta m = \pm 2$ lines are also clearly visible with a splitting about twice as great. The $\Delta m = 0$ lines have sunk to negligible intensity, except for the two outside lines.

Under such conditions perturbation theory is quite inadequate, and to avoid its limitations the Oxford University MERCURY computer was used. The method was based on a library programme written by Dr. J. S. Rollett of the Oxford University Computing Laboratory which uses Givens' method to find the eigenvalues and eigenfunctions of the real symmetric $(2S+1)(2I+1)$ matrix. The problem was solved for the two field strengths mentioned earlier in this section, and intensities of various types of transition were plotted against the angle θ between the magnetic field and the crystal axis. Fig. 3 shows the relative intensities of the middle lines for several types of 'forbidden' transition in the central electronic transition $M = |+1/2\rangle \longleftrightarrow |-1/2\rangle$. From the calculations for $H = 3400$ gauss one finds that (a) $\Delta m = 0$ and ± 1 transitions are of comparable

intensity at 5° from the parallel or perpendicular directions; (b) $\Delta m = \pm 1$ and ± 2 transitions are of comparable intensity near 10° from parallel or perpendicular while $\Delta m = 0$ transitions have dropped to zero; (c) near 45° $\Delta m = \pm 3$ and ± 4 transitions should be the most intense; (d) the curves are approximately symmetrical about $\theta = 45^\circ$ (the symmetry is not exact because of the DS_z^2 term, which gives rise to terms varying as $3\cos^2\theta - 1$ and $\sin^2\theta$ in the spin Hamiltonian (2); the former of these is the more important because of its effect on the energy denominators in (3)).

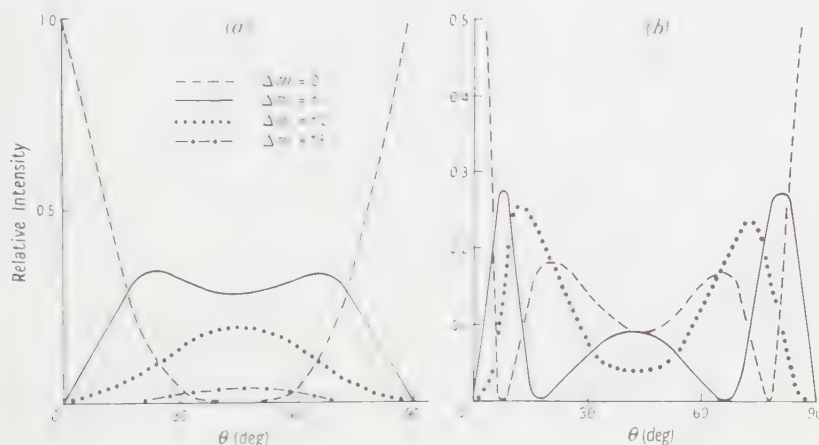


Fig. 3. Computed intensities of the 'forbidden' transitions as a function of the angle θ between H and the symmetry axis, for vanadium fluosilicate: (a) $H = 8200$ gauss; (b) $H = 3400$ gauss.

In the absence of off-diagonal terms the $\Delta m = 0$ transitions would have unit intensity. For clarity, the $\Delta m = \pm 3$ and higher transitions have been omitted from (b); the ± 3 transitions have intensity ~ 0.20 for $\theta = 20^\circ$ to 65° , while the ± 4 and ± 5 transitions have broad maxima at $\theta = 45^\circ$ of 0.14 and 0.04 respectively.

Predictions (a), (b) and (d) have been verified experimentally, but the complexity of the spectrum near 45° , where the various electronic transitions overlap, makes it impossible to be sure that the most intense transitions are those corresponding to $\Delta m = \pm 3$ and ± 4 . The graphs for $H = 8200$ gauss agree generally with experiment but the prediction that the $\Delta m = 0$ and ± 2 transitions should be equally intense near $\theta = 25^\circ$ and 65° could not be verified owing to the overlapping of the $\Delta m = 0$ transitions. The main difficulties in attempting an accurate quantitative comparison between theory and experiment are (i) the observed lines are rather wide (~ 20 gauss), particularly on the outer electronic transitions $|\pm 3, 2\rangle \leftrightarrow |\pm 1, 2\rangle$; (ii) in the experiments the microwave frequency was maintained constant and the field varied, while in the calculation the field was assumed constant; (iii) experimentally the microwave magnetic field was not always perpendicular to the steady field, though this was assumed in the calculation.

The splitting of the $\Delta m = \pm 1$ doublets as given by Eqn (8) is 10 gauss at the shorter wavelength, which (together with a somewhat larger line width due to field inhomogeneity) accounts for their not being resolved. At the longer wavelength this formula gives a splitting of 11 gauss, but the computer calculation shows that perturbation theory is not sufficiently accurate in this

case and gives splittings of 16 and 19 gauss near $\theta = 78^\circ$. This accounts for the resolution of the doublets shown in Fig. 2(b).

§ 4. THE SPECTRUM OF A POWDER

The spectrum of an ion for which $S \geq 1$, and whose Hamiltonian contains a term DS_z^2 as in Eqn (1), is a function of the angle between H and the crystal axis. The electronic transitions have a first-order displacement proportional to $D(3\cos^2\theta - 1)$, except for the central transition $|+1/2\rangle \leftrightarrow |-1/2\rangle$ which has only second-order displacement of order $D^2/g\beta H$. In a powder consisting of a number of crystallites randomly oriented, the outer transitions are therefore smeared out, while the central transition may still give a fairly well resolved hyperfine structure, provided that $D^2/g\beta H$ is not too large. A similar position holds for the 'forbidden' hyperfine lines, and for a powder they may therefore be observed in the central electronic transition. Thus their intensity may be used to estimate a value of D , when it cannot be measured directly, by using Eqn (5), averaged over all values of θ from 0 to $\frac{1}{2}\pi$, with a weighting proportional to $\sin\theta$ to allow for the number of crystallites at various angles. This averaging results in $\sin^2 2\theta$ in Eqn (5) being replaced by $8/15$.

An independent estimate of D in a powder can be obtained from a doubling of the hyperfine lines, which results from second and higher order effects. These are of two kinds: shifts of order $D^2/g\beta H$, which are the same for all hyperfine lines, and shifts of order $D^2 A/(g\beta H)^2$ which are proportional to the distance of the hyperfine line from the centre of the spectrum. The former are given by Bleaney (1951), while the latter arise from the last term in Eqn (7). The terms which depend on the angle θ produce a shift in the position of the line $|+1/2, m\rangle \leftrightarrow |-1/2, m\rangle$ by an amount

$$\Delta H = x(y \cos^2 \theta - \sin^2 \theta) \sin^2 \theta \quad \dots\dots (9)$$

where

$$x = (D^2/16g\beta H)\{4S(S+1) - 3\}$$

and

$$y = 8(1 - \delta) \text{ where } \delta = (Am/4g\beta H)\{4S(S+1) - 3\}.$$

The number of ions whose spectrum lies in the range of field H to $H + \Delta H$ is proportional to $\Delta n = \sin\theta(d\theta/dH)\Delta H$, and evaluation of this quantity would give details of the line shape which results from the angular variation in (8). We shall confine our attention to the intensity peaks in the line shape which occur where $(\Delta n/\Delta H)$ is infinite. From Eqn (9) the quantity $\sin\theta(d\theta/dH)$ is inversely proportional to $\cos\theta\{(y+2)\sin^2\theta - y\cos^2\theta\}$, and is therefore infinite at $\theta_1 = \frac{1}{2}\pi$ and at θ_2 , where $\tan^2\theta_2 = \{y/(y+2)\}$. Peaks in the spectrum corresponding to these two values of θ will therefore occur at fields which differ by

$$\delta H = x \left\{ 1 + \frac{y^2}{4(y+1)} \right\}. \quad \dots\dots (10)$$

Since y is a function of m , the splitting of the hyperfine components will vary within the central electronic transition. In making a similar calculation for the forbidden lines, allowance must be made for the fact that the transition probability is proportional to $\sin^2 2\theta$ (see Eqn 5) so that there is no intensity peak at $\theta_1 = \pi/2$. Hence the forbidden lines are not split, though they will be broadened.

When δ is small, (10) reduces to $\delta H = (25x/9)(1 - 32\delta/45)$, and since δ is proportional to m , the splitting varies linearly from one end of the hyperfine structure to the other. In fact the splitting is always greatest at the high field end, since this corresponds to negative values of m if A is positive, and vice versa.

The spectrum of a sample of modelling clay is shown in Fig. 4, for wavelengths of 1.3 and 3.2 cm. The effects described above are clearly seen at the longer wavelength, where both x and the term in y which depends on m are more important; the six main lines are double peaked and the forbidden doublets broadened, the effects being greater at the high field end. At the shorter wavelength the line doubling has disappeared while the $\Delta m = \pm 1$ lines can only just be seen. From the latter spectrum one obtains the values:

$$I = \frac{5}{2}, \quad A = 94.9 \pm 0.3 \text{ gauss} = (88.7 \pm 0.3)10^{-4} \text{ cm}^{-1}, \quad g = 2.0013 \pm 0.0006.$$

Since these are very close to those commonly observed for ^{55}Mn in ionic compounds, we assume that the spectrum is due to a trace of this isotope. Then, taking $S = 5/2$, the value of D can be estimated both from the size of the splitting of the $\Delta m = 0$ lines, which gives $|D| = 70$ to 80 gauss, and from the intensities of the $\Delta m = \pm 1$ lines, which gives about 125 gauss. An independent estimate of D can be obtained from two extra lines which can be seen outside the main spectrum when more sensitive apparatus is used. These are asymmetrical in shape, the symmetry being reversed for the two lines; this is consistent with their belonging to the electronic transitions $|\pm 3/2\rangle \longleftrightarrow |\pm 1/2\rangle$. These move as $\pm D(3 \cos^2 \theta - 1)$, with intensity peaks at $\theta = \frac{1}{2}\pi$. Identification of the two observed lines with the outer hyperfine lines in these transitions at the points of maximum intensity yields a value for $|D|$ of 113 ± 5 gauss, neglecting any additional splitting due to a cubic field term which might be about 10 gauss. This value is in reasonable agreement with those obtained above, and the fact that D is roughly equal to A would place the remaining weak hyperfine lines of the outer transitions so close to the strong central transitions that they would not be detected.

At the shorter wavelength the average separation of the $\Delta m = \pm 1$ lines is found to be 16 ± 1 gauss. This is in good agreement with the calculated value of 15.5 gauss given by Eqn 8, with $g_I = 0.754 \times 10^{-3}$, the nuclear resonance value for ^{55}Mn . The difference in the splittings at either end is less than 2 gauss. This may be due to third-order contributions, which are estimated to amount to about 1 gauss, but suggests that any nuclear electric quadrupole interaction term P would be less than about 10^{-5} cm^{-1} .

A more accurate check of the theory for a powder is obtained by applying it to a substance which has been measured both as a powder and as a single crystal, so that the value of D is known. The work of Hurd, Sachs and Hershberger (1954) on the spectrum of Mn^{2+} in CaCO_3 (calcite) provides just such a check, with the advantage that the lines in the single crystal were very narrow so that accurate measurements could be made, while any broadening in the powder must be due to the effects of the random orientations. The powder spectrum is shown in Fig. 5 of their paper, and is very similar to the modelling clay spectrum at 3 cm wavelength in our Fig. 4(b). Since the value of D found by Hurd *et al.* (1954) is 81 gauss (the parameter D used by them is equal to $\frac{1}{2}D$ in our nomenclature), the agreement with the theory of

this section is very satisfactory, both as regards the doubling of the lines in the powder and the intensities and positions of the $\Delta m = \pm 1$ lines. In the single crystal spectrum the latter are not visible owing to the overlapping of the five electronic transitions, but in their Fig. 4 Hurd *et al.* show the variation with angle of the positions of the hyperfine lines in the central $|+1/2\rangle \leftrightarrow |-1/2\rangle$ transition; this agrees closely with that predicted by our Eqn (7). The doubling of the outer electronic transitions at intermediate angles observed by them in the crystal is due to the presence of two ions whose cubic axes are not identical, as pointed out by McConnell (1956).

§ 5. DISCUSSION

The theory given above applies only to an ion with a splitting of the form DS_z^2 (the spin operator O_2^0 in the nomenclature of Baker, Bleaney and Hayes (1958)), but similar effects would arise from splitting operators of any degree provided that the magnetic field (assumed to give the strongest term in the Hamiltonian) is not directed along an axis of two-fold or higher symmetry. If the direction of H is taken as the z axis, the operators O_n^m referred to this axis will include those with $m = \pm 1$, which are of the form $f(S_z)S_{\pm}$. These will have cross terms with $AS_{\mp}I_{\pm}$ similar to those treated in this paper, and give rise to transitions of the type $\Delta m = \pm 1$. Such lines have been observed for Eu^{2+} in CaF_2 , where the ionic state is $S_{7/2}$ with a cubic field splitting.

Since the intensity of the forbidden lines increases as D approaches $g\beta H$ in magnitude, it is pertinent to enquire what happens in the other extreme case of $D \gg g\beta H$. This may again be answered by perturbation theory, but since DS_z^2 is now the most important term, and it is already diagonal, no rotation of axes is required. If H is in the plane $y=0$ at an angle θ to the z axis, the Zeeman energy is $g\beta H\{S_z \cos \theta + \frac{1}{2}(S_+ + S_-) \sin \theta\}$. There will then be cross terms similar to those considered in § 2, but arising from products such as $(HS_+)(AS_-I_+)$. The terms of this kind amount to

$$(\frac{1}{4}Ag\beta H \sin \theta)(S_+S_- + S_-S_+)(I_+ + I_-),$$

which is equivalent to

$$(\frac{1}{4}Ag\beta H \sin \theta)(I_+ + I_-) \left\{ \frac{S(S+1) - S_z^2 - S_z}{W_M - W_{M+1}} + \frac{S(S+1) - S_z^2 + S_z}{W_M - W_{M-1}} \right\} \dots (11)$$

for the state $S_z = M$. This is essentially similar to Eqn (3), and calculation of the intensities of the forbidden lines proceeds as in § 2. To a first approximation the energy denominators are $-D(2M+1)$ and $+D(2M-1)$ respectively, except that the term involving both states $|\pm 1/2\rangle$ must be excluded since perturbation theory is then invalid. The energy difference between the states $|+1/2\rangle$ and $|-1/2\rangle$ is of order $g\beta H$, but it would still not be correct to use (11) with this as a denominator. The reason can be seen from the fact that this pair of states behaves for small values of $g\beta H/D$ like an isolated doublet with anisotropic g tensor and A tensor

$$g_{\parallel} = g, \quad A_{\parallel} = A; \quad g_{\perp}/g_{\parallel} = A_{\perp}/A_{\parallel} = \{S(S+1) + \frac{1}{4}\}^{1/2}$$

for which the spin Hamiltonian can be transformed into one where the only off-diagonal terms are of the form $S_{\pm}I_{\pm}$, with energy of order A . Thus terms of the form (11) would appear only through incorrect use of perturbation theory, and must be excluded whenever the two states whose energy difference appears in one denominator are $|\pm 1/2\rangle$.

The theory given in the preceding paragraph is essentially similar to that used by Baker and Bleaney (1958) for another special case, the ground doublet of a rare earth ion. There it was shown that for resonance within the doublet the effect is to produce an interaction of the form $\mathbf{H} \cdot \mathbf{g}_n' \cdot \mathbf{I}$, where \mathbf{g}_n' is anisotropic and is of order (hyperfine energy/energy of excited electronic states); another special case has been given by Elliott (1957). We have here considered the case of transitions between states with different values of $|M|$, which require quanta of order D , rather than $g\beta H$.

The method of dynamical polarization of nuclei used by Abragam and Proctor (1958) and others depends on terms in the spin Hamiltonian of the form $S_z I_{\pm}$, which are essentially similar to those in Eqn (3). In view of the large intensities of the 'forbidden' transitions produced by the latter, the question arises whether the substances considered by us would be advantageous in producing high degrees of nuclear polarization. The main difficulty would arise from the multitude of such transitions since it would be impracticable to apply 'pumping' power to a number of them unless a corresponding number of different microwave frequencies was used. The theory developed in this paper would also apply to hyperfine interactions with ligand nuclei, and a more favourable case might be one where the interaction energy is too small to give a resolved hyperfine structure. This would reduce the complexity of the spectrum, the forbidden lines forming satellites similar to those described by Baker, Hayes and O'Brien (1960). Paradoxically, the theory of §2 suggests that the intensity of such satellites would be of the order $(D/g\beta H)^2$ even in the limit of vanishing A . In this limit, however, the perturbation denominators (of order AS_z) vanish and should be replaced by $g_I\beta H$, so that the satellite intensity would be of order $(D/g\beta H)^2 (A/g_I\beta H)^2$. This is worse by a factor $(D/g\beta H)^2$ than for the system considered by Baker, Hayes and O'Brien (1960) apart from the difficulty of saturating more than one electronic transition at a time with a single pumping frequency.

ACKNOWLEDGMENTS

We are indebted to the Board of Admiralty and the United States Air Force Cambridge Research Center (through the European Office of the Air Research Development Command) for financial assistance in building apparatus; the work has been carried out during the tenure by one of us (R. S. R.) of a Research Studentship of the Department of Scientific and Industrial Research. We wish to express our thanks to Dr. J. M. Baker for helpful discussion, and Dr J. S. Rollett for advice in writing the computer programme.

REFERENCES

- ABRAGAM, A., and PROCTOR, W. G., 1958, *C.R. Acad. Sci., Paris*, **246**, 2253.
 BAKER, J. M., and BLEANEY, B., 1958, *Proc. Roy. Soc. A*, **245**, 156.
 BAKER, J. M., BLEANEY, B., and HAYES, W., 1958, *Proc. Roy. Soc. A*, **247**, 141.
 BAKER, J. M., HAYES, W., and O'BRIEN, M. C. M., 1960, *Proc. Roy. Soc. A*, **254**, 373.
 BLEANEY, B., 1951, *Phil. Mag.*, **42**, 441.
 BLEANEY, B., and INGRAM, D. J. E., 1951, *Proc. Roy. Soc. A*, **205**, 336.
 ELLIOTT, R. J., 1957, *Proc. Phys. Soc. B*, **70**, 119.
 HURD, F. H., SACHS, M., and HERSHBERGER, W. D., 1954, *Phys. Rev.*, **93**, 373.
 MCCONNELL, H. M., 1956, *J. Chem. Phys.*, **24**, 904.

Note added in proof. Sierro, Lacroix and Muller (1959) and Ludwig and Woodbury (1960) have suggested independently that forbidden hyperfine transitions will occur if the electronic fine structure term competes with the Zeeman energy term, though they give no detailed calculations. From investigations of forbidden $\Delta m = \pm 1$ transitions in the spectrum of Mn^{2+} in $\text{ZnSiF}_6 \cdot 6\text{H}_2\text{O}$, Friedman and Low (1960) suggest that the relative intensities of such transitions vary as $(D/A)^2 \cos^2 \theta \sin^2 \theta$; but this expression fails to predict the correct variation of intensity with microwave frequency. These authors use a 3×3 matrix to justify their result; if in their ensuing calculation $2\alpha^2/(U - W)$ had been neglected in comparison with ϵ , agreement with the theory of § 2 of this paper would have been obtained.

Forbidden $\Delta m = \pm 1$ lines in the spectrum Mn^{2+} in single crystals of calcite (see § 4) have recently been observed by Kikuchi and Matarrese (1960).

FRIEDMAN, E., and LOW, W., 1960, *Phys. Rev.*, **120**, 408.

KIKUCHI, C., and MATARRESE, L. M., 1960, *J. Chem. Phys.*, **33**, 601.

LUDWIG, G. W., and WOODBURY, H. H., 1960, *Bull. Amer. Phys. Soc.*, [II], **5**, 158.

SIERRO, J., LACROIX, R., and, MULLER, K. A., 1959, *Helv. Phys. Acta.*, **32**, 286.

Quadrupole-quadrupole Interaction in the Rare Earths

By B. BLEANEY

The Clarendon Laboratory, Oxford

MS. received 30th August 1960

THE thermal and magnetic properties of cerium ethylsulphate have been extensively studied at low temperatures. The $^2F_{5/2}$ state of the Ce^{3+} ion is split by the crystal field (Elliott and Stevens 1952) into three doublets, which may be conveniently labelled X, Y, Z. These lie at 0, $\delta_1 = 4.7 \pm 0.1 \text{ cm}^{-1}$ (Meyer and Smith 1959, Cooke, Whitley and Wolf 1955) and $\delta_2 = 100$ to 150 cm^{-1} respectively, the corresponding states being characterized to a fairly good approximation by $J = \pm \frac{5}{2}$, $\pm \frac{1}{2}$ and $\pm \frac{3}{2}$. The interaction specific heat of the spin system when only the lowest doublet is populated was found by Cooke, Whitley and Wolf to be about six times greater than that expected for magnetic dipole interaction alone, and this has been confirmed by Johnson and Meyer (1959). The extra interaction has been attributed to electric quadrupole-quadrupole (EQ) interaction, and a detailed comparison has been made by the latter authors with the theory of Finkelstein and Mencher (1953). On this theory the interaction between two ions each in the ground doublet is a second order effect of the EQ interaction, which results in a pair of ions, one in the X^+ state and the other in the X^- state, having a slightly different energy from a pair with both in the same state (X^+ or X^-). This splitting lies between 10^{-1} and 10^{-2} cm^{-1} for nearest and next nearest neighbours but, as will be shown below, there are first order effects of the EQ interaction which are much larger. These could be detected spectroscopically by observation at millimetre wavelengths of the transition between the X and Y doublets. With suitable polarization of the oscillatory magnetic field, transitions are allowed between any pair of the four states, X^\pm , Y^\pm , provided that they consist of admixtures of the $J_Z = \pm \frac{5}{2}$ and $\mp \frac{1}{2}$ states as assumed by Elliott and Stevens in the interpretation of magnetic resonance measurements on the dilute salt (Bogle, Cooke and Whitley 1951).

For simplicity, we consider a pair of ions in nearest neighbour positions, where the line joining them lies along the trigonal axis of the crystal. The EQ interaction can then be written in the form

$$\mathcal{H}_Q = A \{ 4 O_{a2}^0 O_{b2}^0 - 4 (O_{a2}^{+1} O_{b2}^{-1} + O_{a2}^{-1} O_{b2}^{+1}) + (O_{a2}^{+2} O_{b2}^{-2} + O_{a2}^{-2} O_{b2}^{+2}) \}, \quad \dots (1)$$

where the subscripts a, b refer to the two ions, and the O_n^m are spin operators defined as

$$O_2^0 = 3J_z^2 - J(J+1), \quad O_2^{\pm 1} = \frac{1}{2}(J_+ J_z + J_- J_z), \quad O_2^{\pm 2} = J_+^2, \quad \dots (2)$$

The coefficient A (in cm^{-1}) is

$$A = \frac{3e^2 \langle r_a^2 \rangle \langle r_b^2 \rangle \langle J_{a,z} J_b \rangle \langle J_{b,z} J_a \rangle}{8\epsilon R^5 \hbar c}, \quad \dots (3)$$

where R is the distance between the ions, $\langle r^2 \rangle$ the mean square radius of the $4f$ electrons on each ion, and $\langle J || z || J \rangle$ is a coefficient defined by Elliott and Stevens

(1953) (for Ce^{3+} it has the value $-2/35$). Our Hamiltonian is written in terms of operator equivalents, but is otherwise identical with that of Finkelstein and Mencher, except for the constant ϵ in the denominator of (3). This is an effective dielectric constant which has been introduced to allow for screening of the electric potential by the intervening molecules. In cerium ethylsulphate these are mostly water molecules with a considerable polarizability so that ϵ might well be large.

The most important first order elements of the interaction arise from the first term in (1). If both ions are in the ground doublet X, they give an interaction energy of $+346A$, if both are in doublet Y they give $+213A$, but if one is in X and the other in Y the interaction energy is $-272A$. This can easily be understood classically, since for the doublet X the charge density lies close to the equatorial plane, while for Y it is close to the axis; for two ions whose centres lie on this axis the electrostatic energy is high if both quadrupoles are rotating in the equatorial plane or both along the axis, and low if one is equatorial and the other axial. In first order the energy is the same for both states of a doublet. Thus at a low temperature where both the nearest neighbours are in X, the energy required to raise an ion to Y would be $\delta_1 + 2(-272 - 346)A = \delta_1 - 1236A$ (EQ interaction with the six next nearest neighbours would only change the coefficient of A by about 13%). At temperatures where one or both nearest neighbours are already in Y, the energy required would be $\delta_1 - 133A$ and $\delta_1 + 970A$ respectively. Observation of the transition $X \longleftrightarrow Y$ at various temperatures would provide a direct determination of these quantities, and perhaps also of the interaction with next nearest neighbours (a full interpretation of the spectrum would obviously require the inclusion of some smaller terms here neglected for simplicity).

If we follow Johnson and Meyer in attributing all the excess interaction energy below 1°K to EQ interaction, a value of A can be obtained from their results. As there appear to be some numerical errors in Finkelstein and Mencher (e.g. the constant c_1 in their equation 27a should be -4), the second order interaction for nearest neighbours has been recalculated, and yields

$$Q_1 = A^2(800\delta_1^{-1} + 2750\delta_2^{-1}) \quad \dots\dots(4)$$

where Q_1 is as defined by Johnson and Meyer except that it, δ_1 and δ_2 are here expressed in cm^{-1} . Their experimental result $Q_1 = 0.06 \text{ cm}^{-1}$ and the values of δ_1 , δ_2 given below lead to $A = 0.018 \text{ cm}^{-1}$. Then the first order interaction energies given above for pairs are of order 4 to 6 cm^{-1} , and the energy required at low temperatures to raise an ion to the Y doublet would be negative. This would lead to a ground state with a mixture of ions in X and Y states, in contradiction to susceptibility measurements, but this difficulty is probably unreal, since in these circumstances the experiments giving $\delta_1 = 4.7 \text{ cm}^{-1}$ would require re-interpretation. However, Elliott and Heap (private communication) have pointed out that an EQ interaction of the calculated sign would lead to a specific heat anomaly which is flatter than an ordinary Schottky curve, since less energy would be required to raise an ion to the Y doublet at low temperatures than at higher temperatures where some of the neighbours are already in the Y states. This disagrees with the results of Meyer and Smith, who find an anomaly which is sharpened rather than flattened. A change of sign of the quadrupole interaction energy could explain the observed shape without reversing the sign of the second order interaction, but it seems difficult to think of any mechanism (such as polarization of the intervening molecules) which would produce such a change.

These results suggest that not all of the excess interaction observed below 1°K can be attributed to EQ interaction; in addition, the value of A derived above implies a value of $\langle r^2 \rangle$ of a few square angström units, while crystal field calculations which involve $\langle r^2 \rangle$ lead to much smaller values. The excess interaction might partly or wholly be due to exchange interaction, but in an experiment involving transitions between the X and Y doublets effects due to exchange interaction would be of the same order as observed in resonance experiments on the transition $X^+ \leftrightarrow X^-$, in contrast with the EQ interaction which enters in first order in the former experiment and second order in the latter.

A better knowledge of the size of the EQ interaction is of interest, since the first order interaction would be important in cases where it is comparable with or greater than the splitting between levels involving orbital states which are not simply time reversed. As the EQ interaction varies as R^{-5} , it would be very much more important in the lanthanon metals, for instance, than in the rather dilute ethylsulphates. When the local symmetry is cubic, as in the lanthanon nitrides (LnN), the ground state may be a Γ_3 triplet or Γ_8 quartet, with degenerate states which would have a first order interaction. A case of particular interest is UO_2 , where the ground state is a Γ_3 triplet (Hutchinson and Candela 1957), and possibly also NpO_2 , where the ground state is probably a Γ_8 quartet, since reduction of $\langle r^2 \rangle$ by internal screening effects may be less important for 5f than for 4f ions.

Finally we mention that although interaction with a nuclear electric quadrupole is generally taken to be zero in a solid when the local symmetry is cubic, this would not be true for the Γ_3 triplet or Γ_8 quartet discussed in the preceding paragraph. In such cases an appropriate spin Hamiltonian for the nuclear electric quadrupole interaction would be similar to that for a free atom with $J=1$ and $J=3/2$ respectively.

ACKNOWLEDGMENT

The author wishes to thank Dr. R. J. Elliott for many interesting discussions.

REFERENCES

- BOGLE, G. S., COOKE, A. H., and WHITLEY, S., 1951, *Proc. Phys. Soc. A*, **64**, 931.
 COOKE, A. H., WHITLEY, S., and WOLF, W. P., 1955, *Proc. Phys. Soc. B*, **68**, 415.
 ELLIOTT, R. J., and STEVENS, K. W. H., 1952, *Proc. Roy. Soc. A*, **215**, 437.
 ——— 1953, *Proc. Roy. Soc. A*, **218**, 553.
 FINKELSTEIN, R., and MENCHER, A., 1953, *J. Chem. Phys.*, **21**, 472.
 HUTCHINSON, C. A., and CANDELA, G. A., 1957, *J. Chem. Phys.*, **27**, 707.
 JOHNSON, C. E., and MEYER, H., 1959, *Proc. Roy. Soc. A*, **253**, 199.
 MEYER, H., and SMITH, P. L., 1959, *J. Chem. Phys. Solids*, **9**, 285.

The Estimation of Antiferromagnetic Exchange Interactions

BY A. DANIELIAN† AND K. W. H. STEVENS

University of Nottingham

MS. received 22nd April 1960

Abstract. The estimation of the interaction energies between the magnetic ions in antiferromagnetic crystals is investigated and it is shown that they may be obtained from measurements of the magnetic susceptibility in the paramagnetic phase.

High temperature power series expansions of the zero-field susceptibility—well known in connection with ferromagnetic systems—are analytically continued by means of the transformation $1/w = 1/z - \theta$ so that the series no longer diverge at the ferromagnetic Curie point and the domain of convergence is extended towards lower temperatures.

§ 1. INTRODUCTION

THE problem of understanding the interactions between magnetic ions in crystals has been studied for some time, but it cannot be said that they are well understood. For comparatively weak interactions magnetic resonance experiments on pairs of ions seem to be the most promising line of attack (Griffiths, Cooke *et al.* 1959, Judd 1959). Where the interactions are stronger, or where paramagnetic resonance is unsuitable, it seems that we shall have to rely on the older methods, such as the measurement of magnetic susceptibilities. It is a striking observation that although the Néel points of a good many antiferromagnetics are known, it is comparatively difficult to find, in the literature, any estimates of the magnitudes of the interactions. One reason for this is that it is not easy to pass from a measurement of the Néel temperature, even when this is supplemented by a knowledge of the antiferromagnetic superlattice, to values of the exchange interactions, for this requires the solution of a co-operative problem.

Some time ago Dr. W. S. Carter, of this laboratory, undertook magnetic susceptibility and specific heat measurements on two polymorphic phases of manganous sulphide, the so-called β modifications. Their crystal structures are very similar and have the important feature that the dominant exchange interactions are almost certainly between nearest neighbours, and the next nearest neighbour interactions are most probably negligible in comparison. Further the manganous ions, $\text{Mn}^{2+} 3d^5$, are almost certainly in the 6S state and can be expected to have g -values very close to 2. They thus seem to be ideal substances in which to study exchange interactions. One unforeseen drawback was that the manganous lattice is close-packed, face-centred cubic in one modification and hexagonal in the other, and there is no satisfactory theory of the Néel temperature for these cases. (If only nearest neighbour interactions are used no Néel temperature is predicted (Ziman 1953).) We were thus led

† Now at the Wheatstone Physics Laboratory, King's College, London.

to consider the possibility of obtaining the interactions from the susceptibilities at temperatures in the paramagnetic phase. There is nothing immediately new in this, for the asymptotic Curie temperature α in $\chi = C/(T + \alpha)$ is known to provide a measure of the interactions. However, in our problem the susceptibility could not be said to follow a Curie-Weiss law in the temperature range in which results were obtained, so the above method was ruled out. In any case it is essentially a very high temperature method and usually requires some extrapolation. We have therefore examined the problem of determining the interactions from measurements of susceptibility made above the Néel temperature but still below the Curie-Weiss region (Danielian and Stevens 1957). In this paper we shall present a general account of the method. In a following paper we shall consider specifically the sulphides of manganese sulphide and, in less detail, the case of α manganous sulphide.

§ 2. GENERAL METHOD

We assume that each ion interacts only with its nearest neighbours. The Hamiltonian, with isotropic interaction and an external magnetic field H , is thus

$$\mathcal{H} = -g\beta\mathbf{H} \cdot \sum \mathbf{S}_i - 2J \sum_{\substack{\text{nearest} \\ \text{neighbours}}} \mathbf{S}_i \cdot \mathbf{S}_j \quad \dots\dots (1)$$

where, $\mathbf{S}_i, \mathbf{S}_j \dots$ represent spin variables located at the i th, j th \dots sites, J is the exchange integral, g the splitting factor and β the Bohr magneton.

Our object is to find ways of estimating J , assuming that it is negative (antiferromagnetic coupling), and that the spin values and g 's are known. The partition function Z is given by

$$Z = \text{trace} [\exp \{-\mathcal{H}/kT\}] \quad \dots\dots (2)$$

and the zero field susceptibility by

$$\chi = \left[\frac{\partial^2}{\partial H^2} (kT \ln Z) \right]_{H=0} \quad \dots\dots (3)$$

Following Van Vleck (1937) the high temperature susceptibility can be expanded in a power series in J/kT , so that

$$\chi = \frac{C}{T} \sum_{n=0}^{\infty} \frac{a_n}{t^n} \quad \dots\dots (4)$$

where

$$t = \frac{kT}{J} \quad \text{and} \quad C = \frac{Ng^2\beta^2 S(S+1)}{4J}.$$

The a_n 's depend on the spin values and on the structure of the lattice of magnetic ions. In principle they can all be calculated, but in practice the labour involved in calculating more than the first few is so great that only a limited number are known (Brown and Luttinger 1955, Brown 1956, Domb and Sykes 1957a, b, Rushbrooke and Wood 1955, 1958). It will be noted that with J negative the values of t of physical interest are also negative.

In the formal theory of power series it is usual to work with complex variables, and we therefore introduce the function

$$S(z) = \sum_{n=0}^{\infty} a_n z^n \quad \dots\dots (5)$$

where $z = 1/t + iv$ is complex. If J is known, to each temperature T there corresponds a (negative) value of t , which is represented by a point on the

negative real axis in the z plane. Thus the behaviour of $S(z)$ on the negative real axis determines the antiferromagnetic susceptibility. Similarly the behaviour on the positive real axis determines the susceptibility of the same magnetic system only with the sign of J reversed, that is, ferromagnetically coupled. A power series has a circle of convergence, the radius of which is determined by the singularity nearest the origin. All known a_n 's are positive and it is generally supposed that all the a_n 's are positive, in which case the first singularity of $S(z)$ lies on the positive real axis and the radius R of the circle of convergence is given by

$$R = \lim_{n \rightarrow \infty} (a_n)^{-1/n}.$$

Consider the variation of $S(z)$ on moving from the origin along the positive real axis. It will vary smoothly within its circle of convergence and diverge at $z = +R$. Physically this corresponds to the variation of the susceptibility from infinitely high temperatures downwards and since in ferromagnetically coupled systems the susceptibility becomes infinite at the Curie temperature T_c , it is assumed that this corresponds to the first singularity on the positive axis,

$$\text{i.e. } \frac{1}{t_c} \equiv R \text{ or } \frac{kT_c}{|J|} = \frac{1}{R}. \quad \dots\dots (6)$$

Thus estimates of R may be used to relate T_c to J (Rushbrooke and Wood 1955, 1958, Domb and Sykes 1957a).

Suppose though that z is varied from 0 along the negative real axis. $S(z)$ now determines the susceptibility of the antiferromagnetically coupled spin system. Again a smooth variation will be found within the circle of convergence, but on crossing this circle $S(z)$ will not converge, and a meaningless result will be obtained. This does not mean that anything drastic happens to the susceptibility on crossing the circle, but only that the expansion of

$$\chi = \left[\frac{\partial^2}{\partial H^2} (kT \ln Z) \right]_{H=0}$$

in powers of J/kT is no longer valid. In using such a power series for an antiferromagnetic it seems unfortunate that a peculiarity in the corresponding ferromagnetically coupled system should limit the value of the expansion.

The expression

$$J\chi = J \left[\frac{\partial^2}{\partial H^2} (kT \ln Z) \right]_{H=0} \quad \dots\dots (7)$$

can be written in terms of $1/t = J/kT$, and $1/t$ can then be replaced by z , giving a function $G(z)$. Within the circle of convergence

$$G(z) = kCzS(z) \quad \dots\dots (8)$$

but outside, $G(z)$ exists but is not given by the above equation. Our problem is to determine $G(z)$ outside the circle, knowing it inside. Where this is too ambitious we would particularly like to know it along the negative real axis. Questions which then arise, but which we only mention here, are whether $G(z)$ will have a singularity on the negative real axis, what sort of singularity it is and whether it corresponds physically to the Néel temperature. If it does, as seems likely, it can hardly be a simple pole, for the susceptibility of an antiferromagnetic remains finite at its Néel temperature.

The formal determination of $G(z)$, by analytical continuation, is well established (Titchmarsh 1939). Bearing in mind that only the first few a_n 's are actually known we cannot use completely general methods, but must choose a transformation which makes as few assumptions as possible about the unknown a_n 's. Such a transformation, due to Euler, is to set $1/w = 1/z - \theta$ where θ is an arbitrary constant. Substitution for z in $zS(z)$ gives

$$zS(z) = F(w) = w \sum_{n=0}^{\infty} b_n w^n \quad \dots\dots (9)$$

where

$$b_n = \sum_{r=0}^n (-1)^r a_{n-r} C_r \theta^r$$

showing that b_n depends on a_0, a_1, \dots, a_n only. $F(w)$ is convergent within its circle of convergence in the w plane. The transformation takes circles into circles (or straight lines) so that the function

$$G(z) \equiv \frac{kCz}{1-\theta z} \sum_{n=0}^{\infty} \left\{ \frac{b_n z^n}{(1-\theta z)^n} \right\} \quad \dots\dots (10)$$

is well behaved and equals $G(z)$ in a circle in the z plane which is the transform of the circle of convergence of $F(w)$ in the w plane. Our purpose is to ensure that this new expression for $G(z)$ is valid along more of the negative real axis than is the direct expansion in z .

Suppose first that $G(z)$ has only two singularities, one at F on the positive real axis at distance R from the origin (the Curie point), and the other, A, on the negative real axis at distance a . Then $a \geq R$, since F is the singularity nearest to the origin. We must choose θ so that, in the w plane, the transform F' of F is further from the origin than the transform A' of A. For then the circle of convergence of $F(w)$ is determined by A' and $G(z)$ converges in a region which extends right up to A. In particular it contains the whole of the negative real axis between 0 and A. The required condition is that $|R/(1-\theta R)| > |a/(1+\theta a)|$ that is, $\theta > 1/2R$. If $\theta > 1/R$, A' and F' lie on the negative real axis. If $1/R > \theta > 1/2R$, A' and F' lie on opposite sides of the origin. The point at infinity X' and the origin O' in the w plane, are inverse points with respect to all circles having O' as centre. The transformation is bilinear, so the domain of convergence of $G(z)$ is the circle which passes through A and has $z=0$ and $z=1/\theta$ as inverse points. It now easily follows that this circle has radius $a(1+\theta)/(1+2a\theta)$ and centre at $z = -a^2\theta/(1+2a\theta)$. It intersects the positive real axis at $z = a(1+2a\theta)$ so the condition $\theta > 1/2R$ ensures that F does not lie inside the circle for any value of a greater than R .

The condition that $G(z)$ has only two singularities can now be relaxed, for the above reasoning holds provided that it has no singularities within the above circle. Hence we can assume that there are other singularities. Then for any chosen value of $\theta (> 1/2R)$ we construct the circles which pass through the singularities and have $z=0$ and $z=1/\theta$ as inverse points. They belong to a coaxial family having the line $\Re(z) = 1/2\theta$ as radical axis. The circles to the left of this line do not enclose F and form a set, one of which encloses no singularities of $G(z)$. This particular circle is the domain of validity of the expansion $G(z)$. It cannot lie entirely within $|z|=R$, for this circle contains no singularities. The nearest approach to this situation occurs if it is enclosed

in $|z|=R$ except at $z=-R$, where it touches $|z|=R$. However if this happens $z=-R$ must be a singularity of $G(z)$, such that A exists and A and F are equidistant from the origin. Apart from this special case, the domain of validity of $G(z)$ contains more of the negative real axis than does the direct expansion in powers of z and it is therefore reasonable to suppose that it gives a better description of the antiferromagnetic susceptibility.

It has been suggested (Rushbrooke and Wood 1958) that series such as (10) may be obtained by considering χ^{-1} instead of χ in the first place, since the former does not tend to infinity and hence is not limited by the singularity at F. Although in practice this procedure leads to the same result it involves an assumption which we feel is not justifiable, namely, the singularity at F is a simple pole which is eliminated by considering the reciprocal of χ . (It is of interest to note that in the case of the Ising plane square net exact calculations have shown that in the vicinity of the Curie point $\chi \propto T^{-1}(1 - T_c/T)^{-7/4}$ (Fisher 1959).)

§ 3. APPLICATION OF THE TRANSFORMED SERIES

The formal theory, given above, is modified in practice because the a_n 's will only be known up to a certain value of n , say N . For any chosen value of θ the b_n 's are then determined up to b_N . Setting $kT/|J|=t$, the approximate susceptibility is then

$$\chi_N(t) = \frac{kC}{|J|(t+\theta)} \sum_0^N \frac{(-1)^n b_n}{(t+\theta)^n}. \quad \dots\dots(11)$$

The first term in the expansion, $kCb_0/|J|(t+\theta)$ equals $kC/(kT+\theta|J|)$, since $b_0=1$ in all cases, and is very similar to the Curie-Weiss law so frequently used to describe susceptibilities. It is not, however, the Curie-Weiss law, because θ is not unique. It can be made unique if we add the requirement that b_1 shall vanish. Then $0=b_1=a_1-a_0\theta$ so that $\theta=a_1/a_0$. This particular value of θ is that used in the theoretical Curie-Weiss law and we may therefore say that the use of the Curie-Weiss law is equivalent to performing an Euler transformation to reduce the coefficient of $(T+\alpha)^{-2}$ (α being the Curie-Weiss constant) to zero. In general the terms in $(T+\alpha)^{-3}$, $(T+\alpha)^{-4}$, etc... will not vanish, but this does not matter provided that T is sufficiently high for their contribution to the susceptibility to be negligible. It is perhaps worth remarking that if the Néel temperature corresponds to a singularity in $G(z)$ it will be determined by the b_n 's for large values of n and it is therefore unlikely that there will be a simple relation between the Curie-Weiss constant and the Néel temperature.

The expression for b_n is such that $\partial b_n/\partial\theta = -nb_{n-1}$ so that

$$\frac{\partial \chi_N}{\partial \theta} = \frac{kC}{|J|} (-1)^{N+1} \frac{(N+1)b_N}{(t+\theta)^{N+2}}. \quad \dots\dots(12)$$

It follows then that the Curie-Weiss law, obtained with $N=1$ and $b_1=0$ implies that $\partial\chi_1/\partial\theta$ is an extremum. Also for any given value of t the variation of $\chi_N(t)$ with θ can be obtained from the particular values of θ for which b_N vanishes. That is, from the roots of

$$\sum_{r=0}^N (-1)^r a_{N-r} C_r \theta^r = 0. \quad \dots\dots(13)$$

It seems reasonable to assume that the spread in values of $\chi_N(t)$, (θ always

being greater than $1/2R$), gives an indication of the error caused by truncation of the full series for the susceptibility.

In Figs 1 and 2, $a\chi_N^{-1}(t)$, ($a=kC_I|J|$) is plotted against t for various θ with $N=6$. Curve A is $\chi_N^{-1}(t)$ maximum and curve X is with $\theta=0$, i.e. without analytical continuation. As θ increases, $\chi_N^{-1}(t)$ tends to a straight line—the extrapolation of the high temperature region. Curve A and this straight line provide an estimate of the variation of $\chi_N(t)$ with θ , which in turn is an indication of the error involved through the truncation of the series, since if all the terms were available $\chi_N(t)$ would be independent of θ .

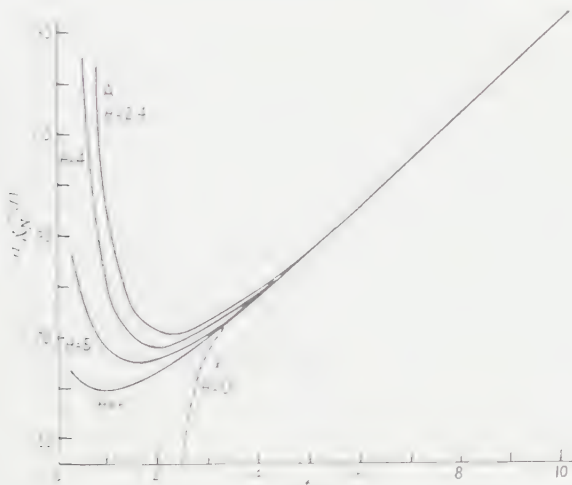


Fig. 1. The reciprocal susceptibility plotted against reduced temperature for a simple cubic lattice of magnetic spin moments with $S = \frac{1}{2}$ ($t_c = 1.7$ (Rushbrooke and Wood 1958)).

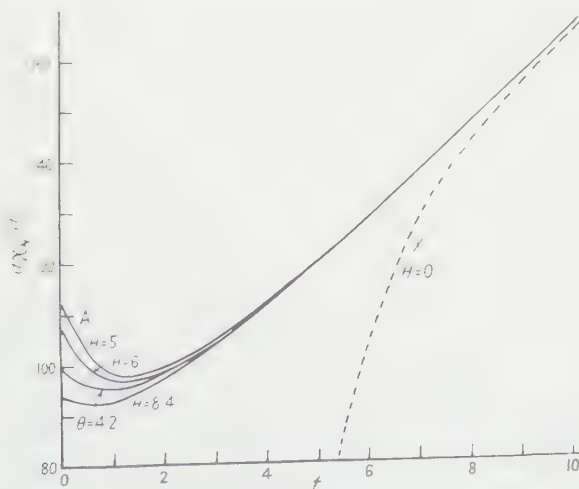


Fig. 2. The reciprocal susceptibility plotted against reduced temperature for a face-centred cubic lattice of magnetic moments with $S = \frac{1}{2}$ ($t_c = 4.2$ (Rushbrooke and Wood 1958)).

§ 4. CORRESPONDING POINTS

In reduced units ($t = kT/|J|$) the truncated susceptibility is

$$\chi_N(t) = \frac{kC}{|J|(t+\theta)} \sum_0^N \frac{(-1)^n b_n}{(t+\theta)^n}$$

so that for any specified spin system and chosen value of θ a curve of $|J|\chi_N(t)$ against t can be drawn. The theoretical expression for the observed susceptibility is

$$\chi_N(T) = \frac{kC}{[kT+\theta|J|]} \sum_0^N \frac{(-1)^n b_n |J|^n}{[kT+\theta|J|]^n} \quad \dots\dots (14)$$

so that

$$t[|J|\chi_N(t)] = kT\chi_N(T). \quad \dots\dots (15)$$

Assuming, then, that the theoretical expression for the susceptibility is a good approximation to the observed susceptibility at temperature T , one multiplies the observed susceptibility by kT . The curve of $|J|\chi_N(t)$ against t is then examined to find the value t for which the product $t(|J|\chi_N(t))$ equals the product $kT\chi_N(T)$. The points T and t may then be called 'corresponding points'. They are related by $kT = |J|t$, so that J is determined. The interest in this result is that the value of J is found from the susceptibility at a single temperature, so that an estimate of the error can be found by using a range of temperatures. In this, though, it is worth remembering that the theoretical susceptibility $\chi_N(T)$ is likely to be most accurate at the highest temperatures.

A further method is provided by the observation that

$$\frac{\partial}{\partial t} \left\{ \frac{|J|}{k} \chi_N(t) \right\} = \left(\frac{|J|}{k} \right)^2 \frac{\partial}{\partial T} \left\{ \chi_N(T) \right\} \quad \dots\dots (16)$$

so that the slope of the $[(|J|\chi_N(t)/k), t]$ curve is equal to $(|J|/k)^2$ times the slope of the experimental $[\chi_N(T), T]$ curve at 'corresponding points'. Should one have a situation in which the g -value of the ion is not known, so that C is not known, the two methods can be combined to give C and J . If, as is customary, the experimental results are displayed by plotting $\chi^{-1}(T)$ against T the first method is still easy to apply. For the second method it is more convenient to use the result

$$\frac{\partial}{\partial t} \left[\frac{|J|}{k} \chi_N(t) \right]^{-1} = \frac{\partial}{\partial T} \left[\chi_N(T) \right]^{-1}. \quad \dots\dots (17)$$

§ 5. CONCLUSION

In the following paper (Danielian and Stevens 1961) we shall give specific examples of the use of this method. Here it seems appropriate to make some general comments.

There is a striking difference between the results of the transformation when applied to a magnetic face-centred cubic lattice from those for body-centred cubic and simple cubic lattices (Figs 1 and 2). In the latter it seems that A is approximately at the same distance from the origin as F, whereas in the former A may not even exist. Thus the value of the transformation is greatest when applied to a face-centred cubic lattice (or hexagonal close-packed). It is interesting to note that if an Ising type of interaction is used it can be proved

rigorously that A and F are equidistant from the origin for simple cubic and body-centred cubic lattices, and it appears that the use of the Heisenberg interaction may change this only slightly.

Power series expansions can also be obtained for the specific heats of spin systems and it is possible that extensions following the same argument as that used for susceptibilities may prove of value in some cases.

REFERENCES

- BROWN, H. A., 1956, *Phys. Rev.*, **104**, 624.
BROWN, H. A., and LUTTINGER, J. M., 1955, *Phys. Rev.*, **100**, 685.
COOKE, A. H., LAZENBY, R., MCKIM, F. R., OWEN, J., and WOLF, W. P., 1959, *Proc. Roy. Soc. A*, **250**, 97.
DANIELIAN, A., and STEVENS, K. W. H., 1957, *Proc. Phys. Soc. B*, **70**, 326.
——— 1961, *Proc. Phys. Soc.*, **77**, 124.
DOMB, C., and SYKES, M. F., 1957 a, *Proc. Roy. Soc. A*, **240**, 214.
——— 1957 b, *Proc. Phys. Soc. B*, **70**, 896.
FISHER, M. E., 1959, *Physica*, **25**, 521.
GRIFFITHS, J. H. E., OWEN, J., PARK, J. G., and PARTRIDGE, M. F., 1959, *Proc. Roy. Soc. A*, **250**, 84.
JUDD, B. R., 1959, *Proc. Roy. Soc. A*, **250**, 110.
RUSHBROOKE, G. S., and WOOD, P. J., 1955, *Proc. Phys. Soc. A*, **68**, 1161.
——— 1958, *Mol. Phys.*, **1**, 257.
TITCHMARSH, E. C., 1939, *The Theory of Functions* (Oxford: University Press).
VAN VLECK, J. H., 1937, *J. Chem. Phys.*, **5**, 320.
ZIMAN, J. M., 1953, *Proc. Phys. Soc. A*, **66**, 89.

Exchange Interactions in the Polymorphic Forms of MnS

BY A. DANIELIAN† AND K. W. H. STEVENS

University of Nottingham

MS. received 22nd April 1960

Abstract. Analytically continued high temperature power series expansions developed in the preceding paper are applied to the susceptibilities of the polymorphic forms of MnS, all three of which are known to be antiferromagnetic. An isotropic Heisenberg interaction is assumed between nearest neighbours only.

Estimates of the exchange interaction are obtained using experimental data from the region above the Néel temperature but below the Curie-Weiss region. It is found that $|J|/k$ is $(12.4 \pm 0.5)^\circ\text{K}$ for β -MnS (zinc blende) and $(10.7 \pm 0.5)^\circ\text{K}$ for β -MnS (wurtzite). In the case of α -MnS difficulty occurs, using $g=2$, because general arguments show that it is not possible to fit the experimental susceptibility. A fit can be obtained with $g=1.8$, but as this is an arbitrary assumption it seems that a full understanding of the properties of α -MnS must await further experiments.

§ 1. INTRODUCTION

MANGANOUS sulphide exists in three polymorphic forms: α -MnS with a NaCl structure and β -MnS, which can either have the zinc blende or the wurtzite structure. All three forms have been examined from the magnetic point of view by neutron diffraction and by susceptibility measurements (Carter and Stevens 1956, Corliss, Elliott and Hastings 1956, Banewicz and Lindsay 1956, 1958). We have been primarily concerned with the β -forms but have also considered certain problems arising with α -MnS. All three are antiferromagnetic with Néel temperatures of approximately 100°K (zinc blende), 80°K (wurtzite), 154°K (α -MnS).

The interest in the β forms arises because their crystal structures, which are very similar, indicate that the exchange interactions between the nearest neighbours are much greater than those between the next nearest neighbours. The lattices can be regarded as made up of interlocking tetrahedra, each sulphur ion being at the centre of a tetrahedron of manganese ions and vice versa. In the zinc blende structure the manganese ions lie on a face-centred cubic lattice, in the wurtzite on a hexagonal close-packed lattice. The exchanges between nearest neighbour manganese ions can be either direct or super-exchanges via the sulphur ions at the centres of the tetrahedra of manganese ions. On the other hand it is comparatively difficult to find a path via sulphur ions along which a manganese ion can interact with its next nearest neighbours—which strongly suggests that such interactions will be small. This is confirmed by the neutron scattering result, for the observed antiferromagnetic super-lattices (ordering of the 'third kind') are consistent with dominant nearest neighbour interactions.

† Now at the Wheatstone Physics Laboratory, King's College, London.

In α -MnS the observed ordering is of the 'second kind', in which half the nearest neighbours of a given magnetic ion are aligned parallel to it and the other half anti-parallel; on the other hand all the next nearest neighbours are aligned anti-parallel to it. Hence it seems likely that the dominant exchange interactions are between next nearest neighbours, but there seems less reason to suppose that the next largest interaction, that between nearest neighbours, is quite so negligible.

§ 2. METHOD OF POWER SERIES

Considering the β forms we suppose that each manganous ion is in the $3d^5\ ^6S$ state and has a g -value of approximately 2. There is no independent evidence for this, but whenever Mn^{2+} ions have been examined by paramagnetic resonance the g -value has been close to 2, in accordance with theoretical expectations (e.g. Low 1956, Maxwell and McGuire 1953). We also suppose that the interactions between nearest neighbours are described by $-J\mathbf{S}_i\cdot\mathbf{S}_j$, where J is negative. This is the usual assumption to make, but it seems to be based more on analogy with the interactions between free spins ($S = \frac{1}{2}$) than on theory. It is by no means the most general interaction which could be used, even assuming isotropic coupling, but it is the simplest. Our problem is to determine J from the high temperature susceptibility results. For this, we use the power series method described in the preceding paper (Danielian and Stevens 1961). The same formulae (i.e. those appropriate to a face-centred cubic lattice) may be used for the susceptibilities of both forms since, as has been shown by Domb and Sykes (1957), the a_n 's are identical up to a_5 , and the a_6 's differ only slightly.

In Fig. 1 we show the theoretical curves for $a\chi_6^{-1}(t)$, [$a=kC/|J|$], $\chi_6(t)$ being given by

$$\chi_6(t) = \frac{kC}{|J|(t+\theta)} \sum_0^{\infty} \frac{(-1)^n b_n}{(t+\theta)^n}$$

and where

$$t = \frac{kT}{J}, \quad C = \frac{Ng^2\beta^2S(S+1)}{3k}, \quad g = 2, \quad S = \frac{5}{2}.$$

The curves A ($\theta=60$) and D ($\theta=120$) are plotted to show the variation with θ , while curve X ($\theta=0$) is without analytical continuation. As indicated in the preceding paper this variation is a measure of the error incurred through the truncation of the series, and as our estimates of J are made in the region $t > 35$, where the variation is less than 2%, it becomes evident that the errors so incurred are small.

In Table 1 the experimental results of Carter and Stevens (1956) are used to obtain estimates of $|J|/k$ at various temperatures, by the method of determining 'corresponding points' described in the preceding paper. Only curves A and D are used—to show the effect of varying θ .

Having obtained estimates of J , we now plot the theoretical curves of the susceptibilities as a function of T . In Fig. 2 the experimental results are shown by 'points'. Curves A represent the theoretical susceptibility of the zinc blende form, A₁ being that corresponding to $\theta=120$, $|J|/k=12.5\text{ K}$ and A₂ to $\theta=60$, $|J|/k=12.4\text{ K}$. Curve B represents the theoretical susceptibility of the wurtzite form with $\theta=120$, $|J|/k=10.8\text{ K}$.

From these results a clear picture emerges. The interpretations based on the assumptions made above are consistent with experimental results which are

in themselves subject to an error of the order of 2%. We conclude that for the zinc blende form $|J|/k = (12.45 \pm 0.05)^\circ\text{K}$ and for the wurtzite form $|J|/k = (10.75 \pm 0.05)^\circ\text{K}$. (The \pm in these results is only the variation with θ .) These values may be compared with their respective Néel temperatures of 100°K

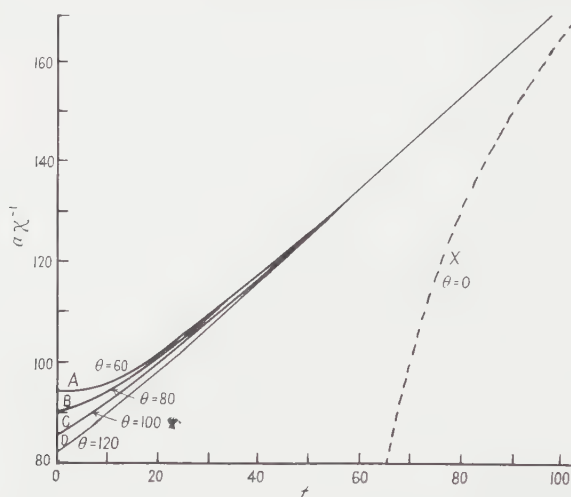


Fig. 1. The reciprocal magnetic susceptibility plotted against reduced temperature for a face-centred cubic lattice of magnetic spin moments with $S=5/2$.

and 80°K . It should be noted that in our quantitative deductions no weight is attached to so-called 'good fit' of the theoretical curves to the experimental results, e.g. to curve A_1 compared with A_2 , as we are unable to determine θ more precisely. Had this been possible, the value of J would have been determined more precisely.

Table 1

Zinc blende form								
$T (^\circ\text{K})$	450	400	350	300	250	200	150	100
$\chi^{-1}_M (T)$	324	312	301	289	279	270	263	255
$t \begin{cases} \theta=60 \\ \theta=120 \end{cases}$	$\begin{cases} 36.3 \\ 36.0 \end{cases}$	$\begin{cases} 32.5 \\ 32.0 \end{cases}$	$\begin{cases} 28.5 \\ 28.0 \end{cases}$	$\begin{cases} 25.0 \\ 24.2 \end{cases}$	$\begin{cases} 21.0 \\ 20.2 \end{cases}$	$\begin{cases} 16.8 \\ 16.1 \end{cases}$	$\begin{cases} 12.7 \\ 11.9 \end{cases}$	$\begin{cases} 8.5 \\ 7.9 \end{cases}$
$ J /k \begin{cases} \theta=60 \\ \theta=120 \end{cases}$	$\begin{cases} 12.4 \\ 12.5 \end{cases}$	$\begin{cases} 12.3 \\ 12.5 \end{cases}$	$\begin{cases} 12.3 \\ 12.5 \end{cases}$	$\begin{cases} 12.0 \\ 12.4 \end{cases}$	$\begin{cases} 11.9 \\ 12.4 \end{cases}$	$\begin{cases} 11.9 \\ 12.4 \end{cases}$	$\begin{cases} 11.8 \\ 12.6 \end{cases}$	$\begin{cases} 11.8 \\ 12.7 \end{cases}$
Wurtzite form								
$\chi^{-1}_M (T)$	292	281	271	260	250	239	229	218
$t \begin{cases} \theta=60 \\ \theta=120 \end{cases}$	$\begin{cases} 42.0 \\ 41.5 \end{cases}$	$\begin{cases} 37.7 \\ 37.0 \end{cases}$	$\begin{cases} 32.9 \\ 32.2 \end{cases}$	$\begin{cases} 28.5 \\ 27.8 \end{cases}$	$\begin{cases} 23.8 \\ 23.1 \end{cases}$	$\begin{cases} 19.3 \\ 18.6 \end{cases}$	$\begin{cases} 14.7 \\ 14.0 \end{cases}$	$\begin{cases} 10.0 \\ 9.4 \end{cases}$
$ J /k \begin{cases} \theta=60 \\ \theta=120 \end{cases}$	$\begin{cases} 10.7 \\ 10.8 \end{cases}$	$\begin{cases} 10.6 \\ 10.8 \end{cases}$	$\begin{cases} 10.6 \\ 10.9 \end{cases}$	$\begin{cases} 10.5 \\ 10.8 \end{cases}$	$\begin{cases} 10.5 \\ 10.8 \end{cases}$	$\begin{cases} 10.4 \\ 10.8 \end{cases}$	$\begin{cases} 10.2 \\ 10.7 \end{cases}$	$\begin{cases} 10.0 \\ 10.6 \end{cases}$

$|J|/k$ in deg K, χ_M : 'molar susceptibility'.

§ 3. α -MANGANOUS SULPHIDE

We have applied the same analysis to α -MnS, neglecting the interactions between nearest neighbours, so that the magnetic lattice is equivalent to a simple cubic lattice with antiferromagnetic interactions between nearest neighbours. Without going into as great detail we note that in this case a discrepancy arises (also noted by Wojtowicz 1957). This is shown by curve C_2 of Fig. 2 (the

equivalent of curves A and B, with $g=2$) the slope of which could never fit the experimental points. On the other hand curve C_1 with $g=1.8$ and $|J|/k=8.5^\circ\text{K}$ (Table 2) seems to be quite consistent with them. We therefore have to consider one of the following possibilities: (a) $g=1.8$; (b) $g=2$, but there are other interactions, e.g. near neighbour or a more generalized next nearest neighbour interaction; (c) $g=2$, but there are a sufficient number of vacant manganese lattice sites, manganese ions in states other than $3d^5\ ^6S$ etc. to cause a reduction of the susceptibility by about 20%, which is what an effective g -value of 1.8 would imply.

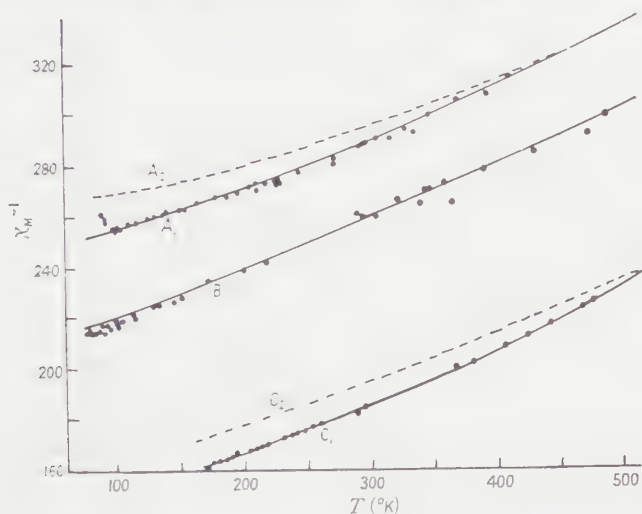


Fig. 2. The reciprocal magnetic susceptibility of the polymorphic forms of MnS.

This third possibility seems to be the least likely, as it requires 20% vacancies, or more than 20% of the sites having reduced moments. It may be possible to arrive at a more definite conclusion if experimental results at higher temperatures become available (in the Curie region, where $\chi_M = C/T$, the effect of the interactions, whatever their form may be, can be disregarded). If we assume that the experimental curve at higher temperatures would continue to be consistent with C_1 , then g must be 1.8. On the other hand it can be argued that this is a rather drastic change in the g -value. It then seems that the answer lies in the direction of the suggestions made under (b).

In Table 2, estimates of J at various temperatures are shown, assuming $g=1.8$.

Table 2

α -MnS	500	450	400	350	300	250	200	175
$T(^{\circ}\text{K})$	500	450	400	350	300	250	200	175
χ_M^{-1}	234	221	208	197	185	176	166	162†
t	59.2	53.4	47.7	41.4	35.6	29.4	23.7	20.9
$ J /k$	8.5	8.4	8.4	8.4	8.5	8.4	8.4	8.4

† Experimental results from Banewicz and Lindsay (1958).

In the case of a simple cubic lattice there is an alternative method for obtaining an estimate of J , using an expression based on the constant coupling approximation obtained by Kasteleijn and Van Kranendonk (1956), namely

$$\frac{kT_N}{4JS(S+1)} = 0.806$$

where T_M is the Néel temperature. On substituting the experimental value, $T_N = 154^\circ\text{K}$, $|J|/k = 5.46^\circ\text{K}$.

§ 4. CONCLUSION

Where there is a straightforward problem such as Mn^{2+} ions interacting with nearest neighbours only, it is possible, using susceptibility results taken above the Néel temperature, to obtain consistent values of the exchange interaction by means of analytically continued power series expansions. It is suggested that estimates so obtained are more reliable than those based on other approximations. Power series expansions provide a greater number of exact coefficients than such approximations as the 'molecular field', 'Bethe' or 'constant coupling' methods. Also those theories which relate J directly to the Néel temperature are based on theories of cooperative processes, which introduce approximations the effects of which are not easily assessed.

Another problem comparable with that of the β forms of MnS seems to be the understanding of the interactions in the chloro-iridates (Griffiths *et al.* 1959, Cooke *et al.* 1959, Judd 1959). A good deal of progress has been made with this, using various experimental techniques. Difficulties still remain with α - MnS , but there is the possibility that future developments in the method of power series may help to resolve them.

Finally, we feel we should comment on the interpretation of the MnS susceptibility by Wojtowicz (1957). He suggests the application of the Bethe approximation with an Ising type interaction, and obtains a simple closed expression for the susceptibility. Unfortunately his analysis is in error for the presence of the states $S_z \doteq \pm \frac{1}{2}$, $\pm \frac{3}{2}$ was overlooked. This omission accounts for his widely different values for J . When the correct analysis is made the formulae are far from simple or easy to apply, and we are unable to see that this method has any advantages over power series.

ACKNOWLEDGMENTS

We would like to thank Dr. W. S. Carter for stimulating our interest in his work on β -manganous sulphides.

REFERENCES

- BANEWICZ, J. J., and LINDSAY, R., 1956, *Phys. Rev.*, **104**, 318.
 — 1958, *Phys. Rev.*, **110**, 634.
 CARTER, W. S., and STEVENS, K. W. H., 1956, *Proc. Phys. Soc. B*, **69**, 1006.
 COOKE, A. H., LAZENBY, R., MCKIM, F. R., OWEN, J., and WOLF, W. P., 1959, *Proc. Roy. Soc. A*, **250**, 97.
 CORLISS, L., ELLIOTT, N., and HASTINGS, J., 1956, *Phys. Rev.*, **104**, 924.
 DANIELIAN, A., and STEVENS, K. W. H., 1961, *Proc. Phys. Soc.*, **77**, 116.
 DOMB, C., and SYKES, M. F., 1957, *Proc. Phys. Soc. B*, **70**, 896.
 GRIFFITHS, J. H. E., OWEN, J., PARK, J. G., and PARTRIDGE, M. F., 1959, *Proc. Roy. Soc. A*, **250**, 84.
 JUDD, B. R., 1959, *Proc. Roy. Soc. A*, **250**, 110.
 KASTELEIJN, P. W., and VAN KRANENDONK, J., 1956, *Physica*, **22**, 317, 367.
 LOW, W., 1956, *Phys. Rev.*, **101**, 1827.
 MAXWELL, L. R., and MCGUIRE, T. R., 1953, *Rev. Mod. Phys.*, **25**, 279.
 WOJTOWICZ, P. J., *Phys. Rev.*, **107**, 429.

The Mössbauer Effect in Tin from 120°K to the Melting Point

By A. J. F. BOYLE, D. ST. P. BUNBURY, C. EDWARDS AND
H. E. HALL

The Physical Laboratories, University of Manchester

Communicated by B. H. Flowers; MS. received 18th June 1960

Abstract. Measurements have been made of the intensity of the recoilless resonance absorption of the 24 keV γ -ray from the decay of $^{119}\text{Sn}^m$ in metallic tin from 120°K to the melting point. Values of the Debye-Waller factor deduced from these results tend towards the values calculated for a Debye Θ of 142°K at low temperatures; the behaviour of the Debye-Waller factor at higher temperatures indicates considerable anharmonicity of the lattice vibrations. Comparison with evidence from the thermal expansion and specific heat suggests that the quartic term in the interatomic potential is positive, and that the ratio of quartic to cubic terms is of the same order as the ratio of cubic to quadratic terms.

In the last few degrees below the melting point the resonance absorption shows a rapid drop accompanied by an increase in line width. It is suggested that this effect is due to enhanced self-diffusion in the solid, and it is estimated that the diffusion coefficient reaches a value of $10^{-8}\text{ cm}^2\text{ sec}^{-1}$ about 0.6°K below the melting point.

§ 1. INTRODUCTION

THE primary purpose of the experiments to be described in this paper was to investigate the way in which the recoilless γ emission discovered by Mössbauer (1958) is affected by the transition from solid to liquid; for this purpose the 24 keV γ -ray of $^{119}\text{Sn}^m$ in metallic tin was used. The experiments show that the effect disappears continuously in the last few degrees below the melting point, and this result is attributed to self-diffusion in the solid. In addition, measurements of the intensity of the effect down to liquid air temperatures have yielded some information about the nature of the atomic vibrations in tin.

For the purpose of this paper it is convenient to express the emission of γ -rays from a solid in a way analogous to the elegant result derived by Van Hove (1954) for the scattering of x-rays or neutrons by an assembly of atoms. Van Hove shows that the differential cross section for scattering with momentum change $\hbar\mathbf{x}$ and energy change $\hbar\omega$ is proportional to a quantity $S(\mathbf{x}, \omega)$ which is the Fourier transform in space and time of a time dependent pair correlation function. $S(\mathbf{x}, \omega)$ is given by

$$S(\mathbf{x}, \omega) = \frac{1}{2\pi} \int_{-\infty}^{\infty} e^{i\omega t} dt \sum_{ij} \langle \exp[-i\mathbf{x} \cdot \mathbf{r}_i(0)] \exp[i\mathbf{x} \cdot \mathbf{r}_j(t)] \rangle, \quad \dots\dots (1)$$

where $\mathbf{r}_i(t)$ is the Heisenberg position operator of the i th atom and the symbol $\langle \rangle$

denotes an average value in thermal equilibrium. For emission of a γ -ray from a given atom the equivalent result (Marshall and Schiffer, private communication) is that the probability of the emitted γ -ray having wave number k is

$$p(k) = \frac{1}{2\pi} \int_{-\infty}^{\infty} \exp [ic(k - k_0)t] \exp (-\frac{1}{2} \Gamma_{\gamma} |t|) \langle \exp [-i\mathbf{k} \cdot \mathbf{r}(t)] \exp [i\mathbf{k} \cdot \mathbf{r}(0)] \rangle dt, \quad \dots\dots (2)$$

where $\hbar ck_0$ is the energy of the γ transition and Γ_{γ} its width. The correlations in $\langle e^{-i\mathbf{k} \cdot \mathbf{r}(t)} e^{i\mathbf{k} \cdot \mathbf{r}(0)} \rangle$ at small times give the emission of γ -rays with recoil; at large times this factor tends asymptotically to

$$\exp (-2W) = \exp (-k^2 \bar{x}^2), \quad \dots\dots (3)$$

where \bar{x}^2 is the mean square displacement of the atom (assumed Gaussian) in the direction of emission of the γ -ray. The factor (3) is the Debye-Waller factor, familiar in x-ray crystallography, and from Eqn (2) we see that this fraction of the γ -rays is emitted as a sharp line with the energy and width of the nuclear transition. The cross section for resonance absorption is likewise multiplied by this factor. For a Debye solid

$$2W = \frac{3E_{\gamma}^2}{Mc^2 \bar{k}^2} \left[\frac{1}{4} + \left(\frac{T}{\Theta} \right)^2 \int_0^{\Theta} \frac{x dx}{e^x - 1} \right], \quad \dots\dots (4)$$

where E_{γ} is the energy of the γ -ray and M the mass of the emitting atom.

§ 2. EXPERIMENTAL METHOD

The resonance absorption was measured by moving the source so as to destroy the resonance by the Doppler effect. The source was driven by a flat-topped saw-tooth waveform, so that it was stationary and moving for equal periods of time; a feedback amplifier was used to ensure that the motion of the source followed the driving waveform. Pulses from a scintillation counter were passed through a single-channel pulse height analyser and then gated into separate counting channels for the stationary and moving periods; the counting rate was obtained by simultaneously gating pulses from a standard oscillator. The velocity in the moving part of the waveform was such as to shift the emission line off resonance by about ten half-widths. This velocity was calculated from the frequency of the driving waveform and the amplitude of motion (about 0.2 mm, measured with a micrometer-eyepiece microscope).

To obtain maximum recoilless emission the source was maintained within a few degrees of liquid air temperature throughout the experiments, by enclosing it in a chamber surrounded by liquid air. The absorber was situated in the vacuum space below this liquid air vessel. It was held between graphite disks clamped in an aluminium ring; the graphite disks were machined so as to preserve the shape of the absorber when it was melted. Palladium foils placed on either side of the absorber served both to absorb unwanted x-rays and as thermal radiation shields. Absorber temperatures above room temperature were obtained by electrical heating; for temperatures below room temperature the absorber was connected thermally to the liquid air vessel, and electrical heating was again used to obtain temperatures up to room temperature. The temperatures of source and absorber were measured by copper-constantan thermocouples in contact with them; the thermocouples were calibrated in liquid nitrogen and at the melting point of tin.

Since the temperatures of source and absorber were normally different, a small correction had to be made to the results to allow for the thermal shift reported previously (Boyle *et al.* 1960); this never amounted to more than 7%. The apparent absorption actually measured was less than the true absorption because of the finite source velocity used; this factor was allowed for in the subsequent reduction of the results.

§ 3. THE DEBYE-WALLER FACTOR

To convert the measured absorptions into values of the Debye-Waller factor it was necessary to know the fraction of recoilless γ -rays emitted by the source. To this end measurements were made with three absorber thicknesses of approximately 0.001 in., 0.003 in. and 0.008 in. After correcting for background to the 24-keV photopeak passed by the single-channel analyser and for the thermal shift, the values of absorption as a function of absorber thickness were plotted on double logarithmic graph paper for six selected temperatures. These six sets of three points could then be compared with a calculated curve of apparent fraction of recoilless γ -rays absorbed as a function of $n\sigma_0 e^{-2W}$, where n is the number of atoms per cm^2 , and σ_0 is the absorption cross section at resonance. In this way six values of the fraction of recoilless γ -rays emitted by the source were obtained; they agreed within the experimental error and had a mean value of 19.4%. All the results could then be expressed as fractions of recoilless γ -rays absorbed, and using the known value of σ_0 and the measured values of n , e^{-2W} could be found from the theoretical absorption curve. The results are shown as a function of temperature in Fig. 1. A slight extrapolation of these results yields an expected Debye-Waller factor for the source of 40%; after correction for self-absorption due to finite source thickness we expect a recoilless emission of 23%. The presence of ^{113}In K x-rays in the source could account for the difference between this value and the directly measured value of 19.4%; this latter estimate is probably about 10% too low, however, because of broadening

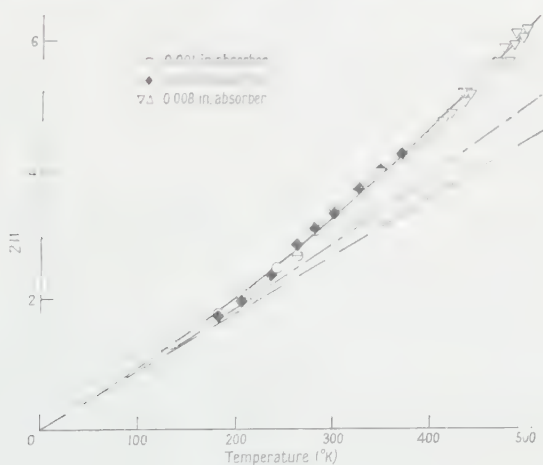


Fig. 1. Temperature dependence of the Debye-Waller factor. Broken line, Eqn (5) for $\Theta=142^\circ\text{K}$; chain curve, corrected for change in Θ due to thermal expansion; full curve, corrected for change in Θ due to thermal expansion, and for the effect of anharmonicity at constant volume.

of the emission line by self-absorption. Fortunately, the corresponding error in our values of the Debye–Waller factor for the absorber is of second order in the source and absorber broadenings, and is probably less than 1%.

For $T > \frac{1}{2}\Theta$ the high temperature approximation to Eqn (4) is not in error by more than 7%, and we may put

$$2W = k^2 \bar{x}^2 = \frac{3E_v^2 T}{Mc^2 k \Theta^2}. \quad \dots (5)$$

The broken line in Fig. 1 represents Eqn (5) with $\Theta = 142^\circ\text{K}$. Measurements of the specific heat of tin indicate a Debye Θ of 195°K below 2°K , but the effective value of Θ falls rapidly to a minimum of 125°K at about 12°K . In view of these large deviations from the Debye law, an effective Θ of 142°K for the Debye–Waller factor does not seem unreasonable. But the experimental results deviate more and more from the linear law of Eqn (5) as the temperature rises. The result $\bar{x}^2 \propto T$ at high temperatures depends only on the assumption of harmonic forces; an explanation of the non-linear relation between W and T shown in Fig. 1 must therefore be sought in terms of anharmonicity of the lattice vibrations.

Anharmonicity can affect \bar{x}^2 in two ways. First, the effective Debye Θ will be altered by thermal expansion; this is the effect considered by Zener and Bilinsky (1936). If we assume that all lattice frequencies are changed in the same proportion by expansion

$$\frac{\partial \ln \Theta}{\partial \ln V} = \frac{V\beta}{C_v K}, \quad \dots (6)$$

where β is the coefficient of cubic expansion and K is the isothermal compressibility. From Eqn (6) we have

$$\frac{d \ln \Theta}{dT} = \frac{V\beta^2}{C_v K}, \quad \dots (7)$$

and if we further assume Gruneisen's law that $\beta \propto C_v$

$$\begin{aligned} \ln \left(\frac{\Theta}{\Theta_0} \right) &= \frac{V}{K} \left(\frac{\beta}{C_v} \right)^2 \int_0^T C_v dT \\ &\simeq \frac{V\beta^2}{3RK} \left(T - \frac{3}{8}\Theta \right), \end{aligned} \quad \dots (8)$$

since the specific heat is almost classical in the temperature range with which we are concerned. If we insert numbers into Eqn (8) we find that the value of \bar{x}^2 given by Eqn (5) has to be increased by a fraction $(2.63 \times 10^{-4})(T - \frac{3}{8}\Theta)$; values thus corrected are shown by the chain line in Fig. 1. It can be seen that this correction is too small by a factor of more than 3 to account for the experimental results. The correction is not very certain because we have, for example, ignored the very large anisotropy in the thermal expansion of tin; but it seems most unlikely that our estimate could be in error by so large a factor, and there is indeed a second mechanism by which anharmonicity can increase \bar{x}^2 . Even at constant volume \bar{x}^2 is not proportional to T at high temperatures if the forces are anharmonic. To estimate the magnitude of this effect consider a particle bound in the one-dimensional potential

$$V(x) = \frac{1}{2}ax^2 + bx^3 + cx^4; \quad \dots (9)$$

it is then easily shown that in classical conditions (cf. Peierls 1956) the specific heat is, including only the lowest order corrections,

$$C_v = kT \left\{ 1 + \frac{kT}{a} \left[15 \left(\frac{b}{a} \right)^2 - 6 \left(\frac{c}{a} \right) \right] \right\}, \quad \dots\dots(10)$$

and the mean square displacement is

$$\overline{x^2} = \frac{kT}{a} \left\{ 1 + \frac{kT}{a} \left[45 \left(\frac{b}{a} \right)^2 - 12 \left(\frac{c}{a} \right) \right] \right\}. \quad \dots\dots(11)$$

This model therefore leads us to expect a fractional deviation in $\overline{x^2}$ about three times that in the specific heat; more or less according to the sign and magnitude of the quartic term in the potential. The measured expansion coefficient and specific heat of tin show that the fractional excess in C_v at high temperatures, excluding the electronic specific heat, is moderately well represented by

$$\frac{\Delta C_v}{C_v} = 1.38 \times 10^{-4} (T - 50). \quad \dots\dots(12)$$

If a correction of 4.5 times this amount is added to the previous correction to the value of W calculated from Eqn (5) we obtain the full curve of Fig. 1, which is in excellent agreement with the experimental results. This factor of 4.5 implies that in Eqn (9)

$$\frac{c}{a} = 1.5 \left(\frac{b}{a} \right)^2. \quad \dots\dots(13)$$

In view of the grossly over-simplified model used to derive this result too much significance should not be attached to it; but it is perhaps worth pointing out that for a 12-6 interatomic potential $ac/b^2 = 1.26$.

§ 4. DIFFUSION NEAR THE MELTING POINT

Experimental values of absorption in the 0.008 in. absorber near the melting point are shown in Fig. 2. The full line corresponds to the full curve of Fig. 1. It is clear that there is a significant decrease in resonance absorption below the value expected from the Debye-Waller factor in the last few degrees below the melting point. Measurements of line width were also made at temperatures approximately 0.8 and 8°K below the melting point, by taking additional readings with a source velocity corresponding approximately to the half-width; it was found that 0.8°K below the melting point the width of the absorption line had increased by a factor of $1.97^{+0.75}_{-0.54}$.

To see how such an effect might arise, consider the effect of diffusion on the factor $\langle e^{-i\mathbf{k} \cdot \mathbf{r}(t)} e^{i\mathbf{k} \cdot \mathbf{r}(0)} \rangle$ in Eqn (2). In an ideal lattice this tends asymptotically to e^{-2W} at infinite time, but if any diffusion occurs this is no longer true. In fact, the wavelength of 24 keV γ -rays is sufficiently short that if the atom has jumped to another lattice site at time t , $\langle e^{-i\mathbf{k} \cdot \mathbf{r}(t)} \rangle$ is effectively zero. The value of $\langle e^{-i\mathbf{k} \cdot \mathbf{r}(t)} e^{i\mathbf{k} \cdot \mathbf{r}(0)} \rangle$ is thus the value in the absence of diffusion multiplied by the chance that the atom concerned has not diffused from its original lattice site, i.e.

$$\langle e^{-i\mathbf{k} \cdot \mathbf{r}(t)} e^{i\mathbf{k} \cdot \mathbf{r}(0)} \rangle \simeq e^{-2W} \exp[-\Gamma_D |t|], \quad \dots\dots(14)$$

where Γ_D is the mean jump frequency of the atoms in the diffusion process. Eqn (2) thus becomes

$$p(k) = \frac{1}{2\pi} \int_{-\infty}^{\infty} \exp[ic(k - k_0)t] \exp[(\frac{1}{2}\Gamma_\gamma + \Gamma_D)|t|] e^{-2W} dt. \quad \dots\dots(15)$$

The effect of diffusion is thus to increase the width of the absorption line by a factor $(\Gamma_\gamma + 2\Gamma_D)/\Gamma_\gamma$ and thus to reduce its maximum height by the same factor. When this absorption line is folded with the emission line of width $\frac{1}{2}\Gamma_\gamma$, we find that the actual reduction in resonant absorption is by a factor $(\Gamma_\gamma + \Gamma_D)/\Gamma_\gamma$.

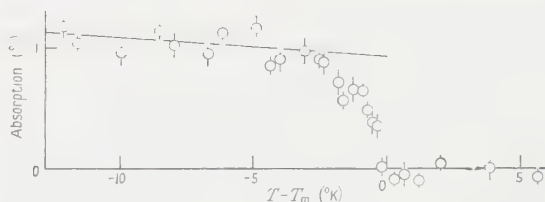


Fig. 2. Resonance absorption in the 0.008 in. absorber near the melting point. The full line corresponds to the full curve in Fig. 1.

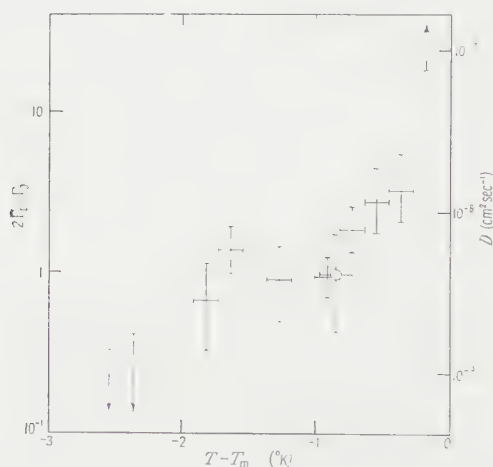


Fig. 3. Diffusion near the melting point. The point marked by a circle was deduced from the width of the resonance absorption, and the other points from its amplitude (Fig. 2).

Values of $2\Gamma_D/\Gamma_\gamma$, calculated from the measured reduction in absorption are shown in Fig. 3; a point calculated from the change in line width is also shown; the agreement with the other points provides some confirmation of Eqn (15). The diffusion coefficient D may be estimated from the relation for a random walk in three dimensions

$$\Gamma_D = 6D/\delta^2, \quad \dots\dots (16)$$

where δ is the step length. A tin atom has four nearest neighbours at 3.02 Å, and two others at 3.16 Å. We therefore have taken a mean value of 3.1 Å to obtain the approximate values of diffusion coefficient indicated on the right-hand ordinate of Fig. 3. Measurements of self-diffusion in tin (Fensham 1950) only extend up to 223.1°K (8.8°K below the melting point), where $D = 2.65 \times 10^{-10} \text{ cm}^2 \text{ sec}^{-1}$ along the tetrad axis and $D = 0.93 \times 10^{-10} \text{ cm}^2 \text{ sec}^{-1}$ perpendicular to it. Our results could reasonably be extrapolated to join these smoothly, but they indicate a greatly accelerated rise in diffusion near the melting point. Such an effect has been found by conventional methods in indium close to the melting point by Eckert and Drickamer (1951). This encourages us to believe that our proposed explanation of

the behaviour of the Mössbauer effect near the melting point is indeed correct. We may also mention that very rapid recrystallization of an unmelted absorber foil was observed at temperatures where the Mössbauer effect was reduced.

§ 5. CONCLUSION

Our experiments show that the intensity of the Mössbauer effect is essentially determined by the mean square displacement of the emitting atom during the lifetime of the excited state, in accordance with Eqn (2). The effect of diffusion may be thought of crudely as defining rather precisely the time at which the γ -ray was emitted, and thereby broadening its energy. It is essentially because of diffusion that the effect is not observed in the liquid; but there seems to be no reason in principle why it should not be observed in a liquid if the diffusion coefficient were sufficiently low and the lifetime sufficiently short.

Our analysis in §3 shows that measurements of the Debye-Waller factor may give useful information about lattice anharmonicity, if a more thorough theoretical analysis can be given. For this purpose the Mössbauer effect has the advantage over x-ray diffraction that it readily yields absolute values of the Debye-Waller factor.

ACKNOWLEDGMENTS

We should like to thank Dr. S. F. Edwards, Dr. A. Herzenberg and Dr. J. O. Newton for a number of helpful discussions, and Mr. J. R. Rook for computing the theoretical absorption integrals. One of us (C.E.) is indebted to the Department of Scientific and Industrial Research for financial support.

REFERENCES

- BOYLE, A. J. F., BUNBURY, D. ST. P., EDWARDS, C., and HALL, H. E., 1960, *Proc. Phys. Soc.*, **76**, 165.
ECKERT, R. E., and DRICKAMER, H. G., 1951, *J. Chem. Phys.*, **20**, 13.
FENSHAM, P. J., 1950, *Aust. J. Sci. Res. A*, **3**, 91; **4**, 229.
MÖSSBAUER, R. J., 1958, *Z. Phys.*, **151**, 124.
PEIERLS, R. E., 1956, *Quantum Theory of Solids*, § 2.3 (Oxford: University Press).
VAN HOVE, L., 1954, *Phys. Rev.*, **95**, 249.
ZENER, C., and BILINSKY, S., 1936, *Phys. Rev.*, **50**, 101.

Diamagnetism of Many-Fermion Systems

By G. L. SEWELL

Mathematical Institute, The University, Liverpool

*Communicated by H. Fröhlich; MS. received 26th February 1960, in
revised form 1st June 1960*

Abstract. A set of simple theoretical criteria are established for the occurrence of the Meissner effect in a many-electron system. The criteria are of a qualitative nature and involve only the single- and two-particle excitations of the system.

§ 1. INTRODUCTION AND DISCUSSION

THE Bardeen-Cooper-Schrieffer (1957, to be referred to as BCS) theory of superconductivity has given rise to a number of gauge-invariant theoretical derivations of the Meissner effect (e.g. Bogoliubov 1959, Rickayzen 1959 and Nambu 1960). However, although these derivations may be basically correct, they are all very complicated mathematically and are based on approximations (e.g. the random phase approximation) whose physical significance is not clear. Is it therefore difficult to see from these theories which properties of superconductors are the ones responsible for the Meissner effect. For example, though the energy gap in the one-electron spectrum of a superconductor is important in the above theories, it is clear that the existence of the gap is not of itself a sufficient criterion for the Meissner effect, as may be seen by considering the case of an insulator.

The object of the present paper is to propose a set of simple theoretical criteria for the occurrence of the Meissner effect in a many-electron system. The criteria are of a qualitative nature and involve only the properties of the single- and two-particle excitation spectra of the model.

Since we do not deduce the relevant properties of these spectra from first principles, but merely postulate them, it is of interest to note that, according to the BCS theory, our criteria are all satisfied by Fröhlich's electron-phonon model (Fröhlich 1952) in its condensed phase. However, the present theory makes no use of the BCS theory as such, and would also be valid if our criteria could be satisfied by a model in which there was no formation of 'Cooper pairs'.

Our theory is based on a model representing a homogeneous, isotropic 'medium' of interacting fermions, and is applicable whether the interactions occur via static two-body forces or via some field (e.g. a phonon field). It is thus sufficiently general to apply to the rotational properties of 'nuclear matter' (cf. Migdal 1959), since the Coriolis forces acting on a rotating system are equivalent to the Lorentz forces due to a magnetic field. The relevance of our theory to the properties of real solids will be discussed at the end of this section.

We have been able to show that the model will exhibit the Meissner effect, provided that the following criteria are satisfied.

(a) The set of electron-hole pair states (i.e. states generated by operating on the ground state with $\psi(x_1)\psi^+(x_2)$, ψ being the electron wave operator) of

total momentum \mathbf{p} contains a single bound state which lies below and is separated by an energy gap 2ϵ from the continuum of scattering states of the same total momentum. This automatically means that the single-particle spectrum contains an energy gap ϵ , for the energy of a scattering pair is equal to the sum of the energies of a pair of independently-moving particles, since energy is conserved in scattering processes. The states in the BCS theory that correspond to our electron-hole bound pair excitations are longitudinal collective oscillations (Anderson 1958).

(b) The single-particle excitations are equivalent to the creations of quasi-particles which move through some self-consistent field. It is immaterial to our theory whether these quasi-particles are 'clothed' electrons and holes, as in Landau's theory of Fermi liquids (Landau 1956), or whether they are based on 'complexes' of electrons and holes, as in Bogoliubov's treatment of the BCS theory (Bogoliubov 1958). In either case, we are able to formulate the theory in a way that satisfies the principle of electron number conservation.

(c) The interactions are sufficiently weak for all scattering processes to be neglected, except in the bound states. Thus, we neglect the scatterings between pairs in the so-called scattering states, and also the virtual scatterings which lead to the 'clothing' of the quasi-particles. On the other hand, we do not neglect the self-consistent field through which the particles move, since it is this which leads to the energy gap.

We shall henceforth refer to these criteria as hypotheses (a), (b) and (c).

In describing the magnetic properties of the model we write the Fourier transform, $\mathbf{J}(\mathbf{q})$, of the density of the equilibrium current induced by the magnetic field, vector potential \mathbf{A} , as

$$\left. \begin{aligned} \mathbf{J}(\mathbf{q}) &= \mathbf{J}_d(\mathbf{q}) + \mathbf{J}_p(\mathbf{q}), \\ \mathbf{J}_d(\mathbf{q}) &= \frac{n_0 e^2}{mc} \mathbf{A}(\mathbf{q}) \end{aligned} \right\} \dots\dots (1.1)$$

where

is the diamagnetic part of \mathbf{J} , n_0 being the number of electrons per unit volume, and \mathbf{J}_p is the paramagnetic part. This latter part arises from the electron-hole pairs of total momentum $\hbar\mathbf{q}$ that are excited by the applied field. As is well known, the Meissner effect will occur if \mathbf{J}_d is not cancelled by \mathbf{J}_p in the London limit ($\mathbf{q} \rightarrow 0$). In general, we may write

$$\mathbf{J}_p = \mathbf{J}_A + \mathbf{J}_B, \quad \dots\dots (1.2)$$

the two parts arising from the excitations of scattering and bound pairs, respectively. The latter excitations are found by a simple invariance argument to contribute only to the longitudinal part of \mathbf{J}_p , and are therefore not directly relevant to the magnetic properties of the model. Their significance will be discussed below. The current \mathbf{J}_A is formed from the excitations of pairs of independently-moving quasi-particles (by our criteria (b) and (c)) and is therefore given by the single-particle excitation energies and wave functions (i.e. matrix elements of ψ, ψ^\dagger). It is found that the energy gap in the single-particle spectrum, together with the restrictions imposed on the wave functions by the Fermi anti-commutation rules, ensures that $\mathbf{J}_A \neq 0$ in the London limit, and therefore the model exhibits the Meissner effect.

Since the bound pair excitations do not contribute to the transverse part of the current, it might be imagined that their existence is inessential to our theory. This is not so, however, since if we were to assume that there were no bound

states and that the scattering states possessed the properties we have postulated, then Eqns (1.1) and (1.2) would lead to a gauge-dependent equilibrium current

$$\mathbf{J}(\mathbf{q}) = -\frac{n_0 e^2}{mc} \mathbf{A}(\mathbf{q}).$$

However, our formalism is gauge-invariant, and therefore the derivation of the above equation constitutes a *reductio ad absurdum* proof that the set of pair states of momentum \mathbf{p} must possess at least one bound state if our other requirements are to be satisfied. The number of bound states within this set will clearly depend on the nature of the interactions. For simplicity, we consider only models for which this number is unity.

In setting up our theory, we shall proceed as follows. In § 2, we shall formulate the general properties of the model, and in particular we shall express the current due to a given applied field in terms of single-particle propagators. In § 3, we shall formulate the required properties of these propagators. In § 4, we shall derive the Meissner effect on the basis of §§ 2 and 3.

We can extend our theory to a real metal by assuming that, on condensation to the superconducting phase, the properties of the *conduction band* may be described essentially by our model. However, in considering the diamagnetic properties of a real solid, we must take interband transitions into account, and, in general, we may express the contribution \mathbf{J}_A to the paramagnetic current as

$$\mathbf{J}_A = \mathbf{J}_C + \mathbf{J}_I \quad \dots\dots (1.3)$$

the two parts being due to transitions within the conduction band and interband transitions, respectively. In the normal phase, these two contributions combine to cancel \mathbf{J}_d in the London limit. It is important to realise that, whereas only the electrons near the Fermi surface contribute to \mathbf{J}_C , all the particles in the system contribute more or less equally to \mathbf{J}_I . This latter part of the current is therefore practically unchanged by the superconducting transition, since this involves only a minute proportion of the electrons. On the other hand, the alterations, due to the condensation, of the properties of the electrons near the Fermi surface leads to a 'freezing-out' of the current \mathbf{J}_C , as in our model, and thus to a change in the paramagnetic current. Consequently, \mathbf{J}_d is not cancelled by \mathbf{J}_p in the condensed state, so that the system exhibits a Meissner effect.

In an insulator, there is no current \mathbf{J}_C , but the interband transitions lead to a cancellation of \mathbf{J}_d by \mathbf{J}_I and thus to a normal diamagnetism.

§ 2. THE MODEL

Our model will consist of an assembly of interacting electrons in a volume Ω , within which conditions are homogeneous and isotropic. We shall describe our system in Heisenberg representation, denoting a typical field operator at the space-time point $(\mathbf{x}, t) \equiv x$ by $Q(\mathbf{x}, t)$ or $Q(x)$. The electron wave of spin $(\alpha = \pm \frac{1}{2})$ will be denoted by $\psi_\alpha(x)$ (complex conjugate $\psi_\alpha^+(x)$) and will be quantized according to the exclusion principle. Thus, we may write

$$\left. \begin{aligned} \psi_\alpha(x) &= \Omega^{-1/2} \sum_{\mathbf{p}} \psi_\alpha(\mathbf{p}, t) \exp i\mathbf{p} \cdot \mathbf{x}, \\ \{\psi_\alpha^+(\mathbf{p}, t), \psi_\beta(\mathbf{p}', t)\}_+ &= \delta_{\alpha\beta} \delta_{\mathbf{p}\mathbf{p}'}, \text{ etc.} \end{aligned} \right\} \quad \dots\dots (2.1)$$

where

The Lagrangian for the system will be of the form

$$L = L_0 + L_1, \quad \dots\dots (2.2)$$

where, in units for which $\hbar = 2m = c = 1$,

$$L_0 = \sum_{\alpha} \int [\frac{1}{2}i(\psi_{\alpha}^+ \dot{\psi}_{\alpha} - \dot{\psi}_{\alpha}^+ \psi_{\alpha}) - \nabla \psi_{\alpha}^+ \cdot \nabla \psi_{\alpha} + \zeta \psi_{\alpha}^+ \psi_{\alpha}] d^3\mathbf{x} \quad \dots\dots (2.3)$$

represents the free electronic part of the system, with single-particle excitation energies measured from the chemical potential ζ , and L_1 represents a spin-conserving interaction. The form of this interaction will not be specified. Thus, it might be a static two-body interaction

$$L_1 = \sum_{\alpha, \beta} \int \psi_{\alpha}^+(x) \psi_{\beta}^+(x') V(\mathbf{x} - \mathbf{x}') \delta(t - t') \psi_{\beta}(x') \psi_{\alpha}(x) d^4x' d^3\mathbf{x}, \quad \dots\dots (2.4a)$$

or it might be an interaction between the electrons and a field f (e.g. a phonon field), so that

$$L_1 = g \sum_{\alpha} \int \psi_{\alpha}^+(x) \psi_{\alpha}(x) f(x) d^3\mathbf{x} + L_f, \quad \dots\dots (2.4b)$$

where g is an interaction constant and L_f is the Lagrangian for the free field f .

The operators representing the total energy and momentum of the system (including the field f in case (2.4b)) will be denoted by H and \mathbf{P} respectively. As is well known (cf. Schweber *et al.* 1955, p. 372), these are temporal and spatial displacement operators, so that any Heisenberg operator $Q(x)$ may be written

$$Q(x) = \exp i(\mathbf{P} \cdot \mathbf{x} + Ht) Q(0) \exp -i(\mathbf{P} \cdot \mathbf{x} + Ht). \quad \dots\dots (2.5)$$

In addition to H and \mathbf{P} , other important constants of the motion are the total number of electrons N and the total electronic spin σ given by

$$N = \sum_{\alpha} \int \psi_{\alpha}^+ \psi_{\alpha} d^3\mathbf{x}, \quad \sigma = \sum_{\alpha} \alpha \int \psi_{\alpha}^+ \psi_{\alpha} d^3\mathbf{x}.$$

The electron current density operator is

$$\mathbf{j}(x) = ie \sum_{\alpha} (\psi_{\alpha} \nabla \psi_{\alpha}^+ - \nabla \psi_{\alpha} \psi_{\alpha}^+). \quad \dots\dots (2.6)$$

We shall denote the N -particle physical vacuum (i.e. ground state) by ϕ_N . Since we are measuring single-particle energies from the chemical potential, it follows that the energies for the vacuum states $\phi_N, \phi_{N+1}, \phi_{N+2}$ etc., are all equal, and we shall measure the energies of all excited states of the system from this vacuum energy.

2.1. Propagators

The single-particle propagators for the system are

$$G^{(1)}(x, x') = \sum_{\alpha} G_{\alpha}^{(1)}(x, x'),$$

where

$$G_{\alpha}^{(1)}(x, x') = \langle \phi_N | T \psi_{\alpha}(x) \bar{\psi}_{\alpha}(x') | \phi_N \rangle = \langle \phi_{N+1} | T \psi_{\alpha}(x) \bar{\psi}_{\alpha}(x') | \phi_{N+2} \rangle, \quad \dots\dots (2.7)$$

$$F_{\alpha}(x, x') = \langle \phi_{N+2} | T \psi_{\alpha}^+(x) \bar{\psi}_{-\alpha}^+(x') | \phi_N \rangle \quad \dots\dots (2.8)$$

and

$$\bar{F}_{\alpha}(x, x') = \langle \phi_N | T \bar{\psi}_{-\alpha}(x) \psi_{\alpha}(x') | \phi_{N+2} \rangle, \quad \dots\dots (2.9)$$

where T is the chronological operator. As will be shown in the Appendix, the

invariance of the model under space-reflections and spin-reversals leads to the relation

$$\left. \begin{aligned} \bar{F}_{-\alpha}(x, x') &= -\bar{F}_{\alpha}(Rx, Rx'), \\ \text{where} \quad Rx &\equiv (-\mathbf{x}, t). \end{aligned} \right\} \dots\dots (2.9a)$$

There are no other single-particle propagators, since matrices between vacuum states such as $\langle \phi_N | T\psi_{\alpha}(x)\psi_{-\alpha}^{+}(x') | \phi_N \rangle$ and $\langle \phi_N | T\psi_{\alpha}^{+}(x)\psi_{-\alpha}(x') | \phi_N \rangle$, etc. are seen to be zero because of the requirements of spin and number conservation.

The propagators F, \bar{F} were first introduced by Gorkhov (1958). F represents the process in which an electron created at x' emerges as a hole at x in the $(N+2)$ -vacuum, and \bar{F} represents the one in which a hole created at x' emerges as an electron at x . Both of these processes are charge-conserving.

It is worth pointing out that, by contrast with BCS, the occurrence of these processes is not essential to our theory. We simply take into account the possibility of their occurrence for the sake of generality.

It is convenient to express the single-particle propagators in terms of their Fourier components. Thus, by (2.1) and (2.7)–(2.9a), we obtain that, for $t > t'$,

$$\left. \begin{aligned} G_{\alpha}^{(1)}(x, x') &= \Omega^{-1} \sum_{\mathbf{p}} G_{\alpha}(\mathbf{p}, t-t') \exp i\mathbf{p} \cdot (\mathbf{x} - \mathbf{x}') \\ G_{\alpha}^{(1)}(x', x) &= -\Omega^{-1} \sum_{\mathbf{p}} \bar{G}_{\alpha}(\mathbf{p}, t-t') \exp -i\mathbf{p} \cdot (\mathbf{x} - \mathbf{x}') \\ F_{\alpha}(x, x') &= \Omega^{-1} \sum_{\mathbf{p}} F_{\alpha}(\mathbf{p}, t-t') \exp -i\mathbf{p} \cdot (\mathbf{x} - \mathbf{x}') \\ \text{and} \quad \bar{F}_{\alpha}(Rx, Rx') &= \Omega^{-1} \sum_{\mathbf{p}} \bar{F}_{\alpha}(\mathbf{p}, t-t') \exp i\mathbf{p} \cdot (\mathbf{x} - \mathbf{x}'), \end{aligned} \right\} \dots\dots (2.10)$$

where

$$\left. \begin{aligned} G_{\alpha}(\mathbf{p}, t-t') &= \langle \phi_N | \psi_{\alpha}(\mathbf{p}, t) \psi_{\alpha}^{+}(\mathbf{p}, t') | \phi_N \rangle \\ \bar{G}_{\alpha}(\mathbf{p}, t-t') &= \langle \phi_{N+2} | \psi_{\alpha}^{+}(\mathbf{p}, t) \psi_{\alpha}(\mathbf{p}, t') | \phi_{N+2} \rangle \\ F_{\alpha}(\mathbf{p}, t-t') &= \langle \phi_{N+2} | \psi_{\alpha}^{+}(\mathbf{p}, t) \psi_{-\alpha}^{+}(-\mathbf{p}, t') | \phi_N \rangle \\ \text{and} \quad \bar{F}_{\alpha}(\mathbf{p}, t-t') &= \langle \phi_N | \psi_{-\alpha}(-\mathbf{p}, t) \psi_{\alpha}(\mathbf{p}, t') | \phi_{N+2} \rangle. \end{aligned} \right\} \dots\dots (2.11)$$

The two-particle propagator relevant to the diamagnetic properties of the model is

$$\left. \begin{aligned} G^{(2)} &= G^{(2)}(x_1, x_2; x_1', x_2') = \sum_{\alpha\beta} \langle \phi_N | T\psi_{\alpha}(x_1)\psi_{\alpha}^{+}(x_2)\psi_{\beta}(x_1')\psi_{\beta}^{+}(x_2') | \phi_N \rangle \\ \text{with} \quad t_1, t_2 &> t_1', t_2'. \end{aligned} \right\} \dots\dots (2.12)$$

This propagator may be expressed by field-theoretical methods in terms of single-particle propagators, and propagators describing scattering processes. Thus, using (2.7)–(2.9a), we may rewrite (2.12) as

$$G^{(2)} = G^{(1)}(x_1, x_1')G^{(1)}(x_2, x_2') + G_0^{(2)} + G_{\text{int}}^{(2)}, \quad \dots\dots (2.13)$$

where

$$G_0^{(2)} = \sum_{\alpha} [\bar{F}_{\alpha}(Rx_1, Rx_1')F_{\alpha}(x_2, x_2') - G_{\alpha}^{(1)}(x_1, x_2')G_{\alpha}^{(1)}(x_1', x_2)] \quad \dots\dots (2.14)$$

is the part of $G^{(2)}$ due to processes in which an electron and hole are propagated independently of one another from x_1', x_2' to x_1, x_2 ; and $G_{\text{int}}^{(2)}$ is the part due to the interactions between the pair, including interactions in bound states (cf. Schweber *et al.* 1955, p. 395).

On the other hand, we can also express $G^{(2)}$ in terms of the wave functions for the spinless electron-hole pair states. These states are generated by operating on the vacuum state with $T\psi_a(x_1)\psi_a^+(x_2)$, and we shall denote them by

$$\left. \begin{array}{l} \phi_N, \mathbf{p}, \theta, \text{ momentum } \mathbf{p}, \text{ energy } E_\theta(\mathbf{p}), \\ \text{with } \theta = a \text{ for scattering states} \\ \text{and } \theta = b \text{ for bound states.} \end{array} \right\} \dots\dots (2.15)$$

The wave functions for these states are

$$\left. \begin{array}{l} \chi_\theta(x_1, x_2) = \langle \phi_{N\mathbf{p}\theta} | \sum_a T\psi_a(x_1)\psi_a^+(x_2) | \phi_N \rangle \\ \text{and} \\ \bar{\chi}_\theta(x_1, x_2) = \langle \phi_N | \sum_a T\psi_a(x_1)\psi_a^+(x_2) | \phi_{N\mathbf{p}\theta} \rangle. \end{array} \right\} \dots\dots (2.16)$$

It now follows from (2.8), (2.12), (2.15) and (2.16) that we may rewrite $G^{(2)}$ as,

$$\left. \begin{array}{l} G^{(2)} = G^{(1)}(x_1, x_2)G^{(1)}(x_1', x_2') + G_A^{(2)} + G_B^{(2)}, \\ \text{where} \\ G_A^{(2)} = \sum \bar{\chi}_a(x_1, x_2)\chi_a(x_1', x_2') \\ \text{and} \\ G_B^{(2)} = \sum \bar{\chi}_b(x_1, x_2)\chi_b(x_1', x_2'). \end{array} \right\} \dots\dots (2.17)$$

$G_B^{(2)}$ may thus be regarded as the part of $G^{(2)}$ that arises from bound electron-hole pair excitations. On comparing (2.13) and (2.17) we obtain

$$G_A^{(2)} + G_B^{(2)} = G_0^{(2)} + G_{\text{int}}^{(2)}. \dots\dots (2.18)$$

It is now convenient to express the coordinates x_1, x_2 of a pair in terms of their centre-of-mass coordinate x , and their relative displacement, 2ξ . Thus,

$$\left. \begin{array}{l} x_1, x_2 = x \pm \xi, \quad \xi = (\xi, \tau) \\ \text{and} \\ x_1', x_2' = x' \pm \xi'. \end{array} \right\} \dots\dots (2.19)$$

As is well known (cf. Schweber *et al.*, p. 398), the frequencies in $t-t'$ that occur in $G_B^{(2)}$ correspond to the energies of bound states, and do not occur in $G_0^{(2)}$, whose frequencies are the energies of scattering states. Consequently, by (2.18), all the terms comprising $G_B^{(2)}$ are contained in $G_{\text{int}}^{(2)}$, so that we may write

$$G_{\text{int}}^{(2)} = G_B^{(2)} + G_{\text{scat}}^{(2)}$$

the last term arising due to scattering processes in which an electron and a hole set out and finish independently of one another. In accordance with our hypothesis (c), we shall neglect this contribution. Hence, we may rewrite (2.13) as

$$G^{(2)} = G_0^{(2)} + G^{(1)}(x_1, x_2)G^{(1)}(x_1', x_2') + G_B^{(2)}. \dots\dots (2.20)$$

2.2. The Correlation Function

As is well known (cf. Nakajima 1956), the diamagnetic properties of the system are given by the form of the correlation function

$$\left. \begin{array}{l} C_{\mu\nu}(\mathbf{x} - \mathbf{x}', t - t') = \langle \phi_N | j_\mu(x) j_\nu(x') | \phi_N \rangle, \\ \text{Fourier transform} \\ C_{\mu\nu}(\mathbf{q}, t - t') = \int C_{\mu\nu}(\mathbf{x} - \mathbf{x}', t - t') \exp i\mathbf{q} \cdot (\mathbf{x} - \mathbf{x}') d^3\mathbf{x} \end{array} \right\} \dots\dots (2.21)$$

where μ, ν denote vectorial components. It may easily be seen from (2.6), (2.12) and (2.19) that

$$C_{\mu\nu}(\mathbf{x} - \mathbf{x}', t - t') = LG^{(2)}, \dots\dots (2.22)$$

where

$$L\phi(x_1, x_2; x_1', x_2') \equiv -e^2 \left(\frac{\partial^2 \phi}{\partial \xi_\mu \partial \xi_\nu'} \right)_{\xi, \xi' \rightarrow 0; \tau, \tau' \rightarrow +0} \quad \dots\dots (2.23)$$

Hence by (2.20), (2.22), (2.23),

$$C_{\mu\nu} = C_{A\mu\nu} + C_{B\mu\nu}, \quad \dots\dots (2.24)$$

where

$$\left. \begin{aligned} C_{A\mu\nu} &= LG_0^{(2)}, \\ C_{B\mu\nu} &= LG_B^{(2)}. \end{aligned} \right\} \quad \dots\dots (2.25)$$

In deriving (2.23), we have equated to zero the term

$$LG^{(1)}(x_1, x_2)G^{(1)}(x_1', x_2') = \langle \phi_N | j_\mu(x) | \phi_N \rangle \langle \phi_N | j_\nu(x') | \phi_N \rangle,$$

since the vacuum state ϕ_N is not current-carrying.

The Fourier transform $C_{A\mu\nu}(\mathbf{q}, t-t')$ can now be expressed in terms of single-particle Green's functions. In fact, it follows from (2.10), (2.14), (2.19), (2.21), (2.23) and (2.25) and the relation $\sum_{\mathbf{p}} = \{\Omega/(2\pi)^3\} \int d^3\mathbf{p}$ that

$$C_{A\mu\nu}(\mathbf{q}, t) = \frac{e^2}{(2\pi)^3} \sum_{\alpha} \int d^3\mathbf{p} (2p_\mu + q_\mu)(2p_\nu + q_\nu) [G_\alpha(\mathbf{p}, t)\bar{G}_\alpha(\mathbf{p} + \mathbf{q}, t) - F_\alpha(\mathbf{p} + \mathbf{q}, t)\bar{F}_\alpha(\mathbf{p}, t)]. \quad \dots\dots (2.26)$$

We shall now show that C_B is of the form

$$C_{B\mu\nu}(\mathbf{q}, t) = \phi(\mathbf{q}^2) q_\mu q_\nu \exp iE_b(\mathbf{q})t, \quad \dots\dots (2.27)$$

where ϕ is some scalar function; and we shall presently deduce from this formula that the bound pair excitations are irrelevant to the diamagnetic properties. To prove (2.27), we note that, by (2.6), (2.16), (2.17), (2.19) and (2.25),

$$C_{B\mu\nu}(\mathbf{x} - \mathbf{x}', t - t') = \sum_{i,j} \langle \phi_N | j_\mu(x) | \phi_{N\mathbf{p}i} \rangle \langle \phi_{N\mathbf{p}j} | j_\nu(x') | \phi_N \rangle. \quad \dots\dots (2.28)$$

Moreover, by (2.5) and (2.15), we may write

$$\langle \phi_{N\mathbf{p}b} | j(x') | \phi_N \rangle = \mathbf{B} \exp i(\mathbf{p} \cdot \mathbf{x}' + E_b(\mathbf{p})t'), \quad \dots\dots (2.29)$$

where \mathbf{B} is independent of x' . By our hypothesis (a), there exists only one bound state $\phi_{N\mathbf{p}b}$ for given \mathbf{p} . Therefore, since the system is isotropic, it follows that the direction of \mathbf{B} is given by that of \mathbf{p} alone, there being no other vectors available. Hence \mathbf{B} is of the form

$$\mathbf{B} = b(\mathbf{p}^2)\mathbf{p}.$$

Using this formula, Eqn (2.27) immediately follows from (2.21), (2.28) and (2.29).

2.3. The Paramagnetic Current

The Fourier transform of the paramagnetic part of the equilibrium current (Eqn (1.1)) due to an applied magnetic field, vector potential \mathbf{A} , is given (Nakajima 1956) by

$$J_{\mathbf{p}, \mu}(\mathbf{q}) = K_{\mu\nu}(\mathbf{q}) A_\nu(\mathbf{q}), \quad \dots\dots (2.30)$$

where the response function K is related to the correlation function by the formula

$$K_{\mu\nu}(\mathbf{q}) = \int_0^\infty C_{\mu\nu}(\mathbf{q}, -i\lambda) d\lambda.$$

Thus, by (2.24), we may write

$$K_{\mu\nu}(\mathbf{q}) = K_{\Delta\mu\nu}(\mathbf{q}) + K_{B\mu\nu}(\mathbf{q}), \quad \dots\dots (2.31)$$

where

$$K_{\Delta\mu\nu}(\mathbf{q}) = \int_0^\infty C_{\Delta\mu\nu}(\mathbf{q}, -i\lambda) d\lambda; \quad K_{B\mu\nu}(\mathbf{q}) = \int_0^\infty C_{B\mu\nu}(\mathbf{q}, -i\lambda) d\lambda. \quad \dots\dots (2.32)$$

We shall gauge the vector potential transversely, so that

$$q_\nu A_\nu(\mathbf{q}) = 0. \quad \dots\dots (2.33)$$

It now follows immediately from (2.27) and (2.32) that, in this gauge

$$K_{B\mu\nu}(\mathbf{q}) A_\nu(\mathbf{q}) = 0,$$

and therefore, by (2.30) and (2.31),

$$J_{D,\mu}(\mathbf{q}) = K_{\Delta\mu\nu}(\mathbf{q}) A_\nu(\mathbf{q}). \quad \dots\dots (2.34)$$

Thus, by (2.26), (2.32) and (2.34), we are able to express the paramagnetic current in terms of single-particle propagators.

§ 3. SINGLE-PARTICLE EXCITATIONS

Since ψ^+ , ψ are creation and destruction operators, respectively, it follows that states of spin α , momentum \mathbf{p} and electron number $(N+1)$ can be generated either by operating on the N -vacuum with $\psi_\alpha^+(\mathbf{p}, t)$ or on the $(N+2)$ -vacuum with $\psi_{-\alpha}(-\mathbf{p}, t)$. For this reason, it is convenient to combine $\psi_{-\alpha}$ and ψ_α^+ into a single operator Ψ_α (cf. Nambu 1960), given by

$$\Psi_\alpha(x) = \Omega^{-1/2} \sum \Psi_\alpha(\mathbf{p}, t) \exp -i\mathbf{p}\mathbf{x}, \quad \left. \begin{array}{l} \end{array} \right\}$$

$$\text{with } \Psi_\alpha(x) = \begin{pmatrix} \psi_\alpha^+(x) & 0 \\ 0 & \psi_{-\alpha}(x) \end{pmatrix}, \quad \Psi_\alpha(\mathbf{p}, t) = \begin{pmatrix} \psi_\alpha^+(\mathbf{p}, t) & 0 \\ 0 & \psi_{-\alpha}(-\mathbf{p}, t) \end{pmatrix} \quad \dots\dots (3.1)$$

Introducing

$$\tau_1 = \begin{pmatrix} 0 & 1 \\ 1 & 0 \end{pmatrix}, \quad \tau_2 = \begin{pmatrix} 1 & 0 \\ 0 & -1 \end{pmatrix}, \quad \dots\dots (3.2)$$

it is seen that

$$\Psi_\alpha^+(x) = \tau_1 \Psi_{-\alpha}(x) \tau_1; \quad \Psi_\alpha^+(\mathbf{p}, t) = \tau_1 \Psi_{-\alpha}(-\mathbf{p}, t) \tau_1. \quad \dots\dots (3.3)$$

Similarly, we shall combine each eigenstate ϕ_{Nr} of the N -particle system with the corresponding state of the $(N+2)$ -particle system to form single-column matrices

$$\Phi_r = \begin{pmatrix} \phi_{Nr} \\ \phi_{N+2,r} \end{pmatrix}, \quad \Phi_r' = \begin{pmatrix} \phi_{N+2,r} \\ \phi_{Nr} \end{pmatrix}, \quad \left. \begin{array}{l} \text{with } \Phi = \begin{pmatrix} \phi_N \\ \phi_{N+2} \end{pmatrix}, \quad \Phi' = \begin{pmatrix} \phi_{N+2} \\ \phi_N \end{pmatrix} \text{ for the vacuum.} \end{array} \right\} \quad \dots\dots (3.4)$$

The matrices Φ_r , Φ_r' are eigenvectors of H , and will be the operands of Ψ , Ψ^\dagger in our subsequent theory. It may be seen from (3.1) and (3.4) that all the single-particle excitations of spin α may be generated by operating on Φ with $\Psi_\alpha(x)$.

The equations of motion for the system may be deduced from the Lagrangian L (Eqns (2.2)–(2.4)). The Heisenberg equations for ψ_α^+ and ψ_α may be combined by means of (3.1) and (3.2) into a single equation for Ψ_α , of the form

$$i\Psi_\alpha(x) - (\nabla^2 + \zeta)\tau_2\Psi_\alpha(x) = \int U(\mathbf{x}, \mathbf{x}')\Psi_\alpha(\mathbf{x}', t) d^3\mathbf{x}' \quad \dots\dots (3.5)$$

The left-hand side of this equation arises from the free-electronic part of the Lagrangian and the right-hand side from the interactions. The operator U is a 2×2 matrix

$$U = \begin{pmatrix} U_1 & 0 \\ 0 & U_2 \end{pmatrix},$$

where U_1 and U_2 are spin-independent operators formed from the field variables describing the system.

According to our hypothesis (b), the single-particle excitations of the system are given by creations of quasi-particles. The equation of motion for the 'bare' quasi-particles can be obtained by replacing the operator U , in (3.5), by a 2×2 Hermitian matrix $U_0(\mathbf{x}, \mathbf{x}')$, whose elements are c -numbers, and which is not necessarily diagonal. This matrix represents a spin-independent self-consistent field, which we shall define below (after Eqns (3.6)).

Since our model is translationally invariant, it follows that U_0 depends on the coordinates \mathbf{x}, \mathbf{x}' only through their difference. Hence we may write

$$U_0(\mathbf{x}, \mathbf{x}') = U_0(\mathbf{x} - \mathbf{x}'),$$

and the equation of motion for the 'bare' quasi-particles is

$$\left. \begin{aligned} i\dot{\Psi}_\alpha(\mathbf{x}) - (\nabla^2 + \zeta)\tau_2\Psi_\alpha(\mathbf{x}) &= \int U_0(\mathbf{x} - \mathbf{x}')\Psi_\alpha(\mathbf{x}', t) d^3\mathbf{x}', \\ \text{or} \quad i\dot{\Psi}_\alpha(\mathbf{p}, t) + (\mathbf{p}^2 - \zeta)\tau_2\Psi_\alpha(\mathbf{p}, t) &= U_0(\mathbf{p})\Psi_\alpha(\mathbf{p}, t), \end{aligned} \right\} \dots\dots (3.6)$$

where $U_0(\mathbf{p})$ is the Fourier transform of $U_0(\mathbf{x})$. The first Eqn (3.6) represents a zero-order approximation to (3.5), so that the properties of the 'clothed' quasi-particles can be obtained by first solving (3.6) and then treating $U - U_0$ as a perturbation.

As may be seen from (3.6), the matrix $U_0(\mathbf{p})$ represents the self-energy for a quasi-particle of momentum \mathbf{p} . This matrix is defined by the self-consistency requirement that the perturbation $U - U_0$ does not change this self-energy (cf. Nambu 1960). Thus, by taking the perturbations to a sufficiently high order, U_0 may be calculated to any desired accuracy.

Having defined U_0 , we may now proceed to derive the properties of the single-particle excitations from (3.6), instead of (3.5), since, according to our hypothesis (c), the 'clothing' of the quasi-particles may be neglected. With the single-column matrix Φ_r , defined in (3.4), as operand, either of the Eqns (3.6) will yield a pair of linear simultaneous equations for $\psi_{\alpha}^+\phi_{N,r}$ and $\psi_{-\alpha}\phi_{N+2,r}$. Since both of these states contain $N+1$ particles, it follows that our formulation satisfies the principle of electron number conservation.

The second Eqn (3.6) may be easily solved. For, if $\omega_1(\mathbf{p})$ and $\omega_2(\mathbf{p})$ are the latent roots of the matrix

$$(\mathbf{p}^2 - \zeta)\tau_2 - U_0(\mathbf{p}),$$

then it follows that Ψ_α is the form

$$\Psi_\alpha(\mathbf{p}, t) = \Psi_{\alpha 1}(\mathbf{p}) \exp i\omega_1(\mathbf{p})t + \Psi_{\alpha 2}(\mathbf{p}) \exp i\omega_2(\mathbf{p})t, \quad \dots\dots (3.7)$$

where $\Psi_{\alpha 1}$ and $\Psi_{\alpha 2}$ are time-independent operators. Similarly, on applying (3.6) to the operand Φ_r , it is seen that the resultant simultaneous equations for $\psi_{\alpha}^+(\mathbf{p}, t)\phi_{N,r}$ and $\psi_{-\alpha}(-\mathbf{p}, t)\phi_{N+2,r}$ yield

$$\Psi_\alpha(\mathbf{p}, t)\Phi_r = \begin{pmatrix} u_1 \\ v_1 \end{pmatrix} \phi_{N+1, r_1} \exp i\omega_1(\mathbf{p})t + \begin{pmatrix} u_2 \\ v_2 \end{pmatrix} \phi_{N+1, r_2} \exp i\omega_2(\mathbf{p})t, \quad \dots\dots (3.8)$$

where the states ϕ and the coefficients u, v are time-independent. The frequencies ω_1, ω_2 are real, since U_0 is Hermitian.

Since the model is invariant under spin-reversals and space-reflections, it follows that $\omega_1(\mathbf{p}), \omega_2(\mathbf{p})$ are the frequencies not only of $\Psi_\alpha(\mathbf{p}, t)$ but also of $\Psi_{-\alpha}(-\mathbf{p}, t)$, and therefore, by (3.3), they are the frequencies of $\Psi_\alpha^+(\mathbf{p}, t)$. On the other hand, the frequencies of this latter operator may be seen to be $-\omega_1(\mathbf{p}), -\omega_2(\mathbf{p})$ by taking the complex conjugate of Eqn (3.7). Hence, $\omega_1(\mathbf{p})$ and $\omega_2(\mathbf{p})$ are equal and opposite. Defining ω_1 as the positive frequency, we may write

$$\omega_1(\mathbf{p}) = -\omega_2(\mathbf{p}) = \omega(\mathbf{p}) > 0. \quad \dots\dots (3.9)$$

It follows from (3.7) that $\omega(\mathbf{p}), \Psi_{-1}(\mathbf{p}), \Psi_{-2}(\mathbf{p})$ represent the energy, the creation operator and the destruction operator, respectively, for a quasi-particle of momentum \mathbf{p} and spin α .

Moreover, if Φ_r is replaced by the vacuum state Φ in (3.8), the term corresponding to a negative energy state (i.e. negative frequency) must be omitted, since the vacuum is defined as the state of least energy. Thus, by (3.1), (3.4), (3.8) and (3.9),

$$\left. \begin{aligned} \psi_\alpha^+(\mathbf{p}, t)\phi_N = u_\alpha(\mathbf{p})\phi_{N+1, \alpha, \mathbf{p}} \exp i\omega(\mathbf{p})t \\ \text{and} \quad \psi_{-\alpha}(-\mathbf{p}, t)\phi_{N+2} = v_{-\alpha}(-\mathbf{p})\phi_{N+1, \alpha, \mathbf{p}} \exp i\omega(\mathbf{p})t, \end{aligned} \right\} \quad \dots\dots (3.10)$$

where $\phi_{N+1, \alpha, \mathbf{p}}$ is a normalized eigenstate of momentum \mathbf{p} and spin α . The coefficients u, v are related by the equation

$$|u_\alpha(\mathbf{p})|^2 + |v_\alpha(\mathbf{p})|^2 = 1, \quad \dots\dots (3.11)$$

which follows from (3.10) on taking the expectation value, for the vacuum state ϕ_N , of the anticommutation relation of (2.1). Also, since the system is invariant under spin-reversal and space-reflections, it follows that

$$|u_\alpha(\mathbf{p})|^2 = |u_{\pm\alpha}(\pm\mathbf{p})|^2; |v_\alpha(\mathbf{p})|^2 = |v_{\pm\alpha}(\pm\mathbf{p})|^2. \quad \dots\dots (3.12)$$

We may express the single-particle propagators, given in Eqns (2.11), in terms of the single-particle wave functions. Thus, by (3.10),

$$\left. \begin{aligned} G_\alpha(\mathbf{p}, t) &= |u_\alpha(\mathbf{p})|^2 \exp -i\omega(\mathbf{p})t \\ \bar{G}_\alpha(\mathbf{p}, t) &= |v_\alpha(\mathbf{p})|^2 \exp -i\omega(\mathbf{p})t \\ F_\alpha(\mathbf{p}, t) &= u_{-\alpha}(-\mathbf{p})v_\alpha^+(\mathbf{p}) \exp -i\omega(\mathbf{p})t \\ \text{and} \quad \bar{F}_\alpha(\mathbf{p}, t) &= u_{-\alpha}^+(-\mathbf{p})v_\alpha(\mathbf{p}) \exp -i\omega(\mathbf{p})t. \end{aligned} \right\} \quad \dots\dots (3.13)$$

§ 4. MEISSNER EFFECT

We can now formulate the response function K_A in terms of the single-particle wave functions. For it follows from (2.26), (2.32) and (3.13) that

$$\begin{aligned} K_{A\mu\nu}(\mathbf{q}) &= \frac{e^2}{(2\pi)^3} \sum_\alpha \int d^3\mathbf{p} (2p_\mu + q_\mu)(2p_\nu + q_\nu) \\ &\times \frac{[|u_\alpha(\mathbf{p})|^2 \bar{v}_\alpha(\mathbf{p} + \mathbf{q}) - u_{-\alpha}(-\mathbf{p})v_{-\alpha}(-\mathbf{p} - \mathbf{q}) \bar{v}_\alpha(\mathbf{p}) \bar{v}_\alpha(\mathbf{p} + \mathbf{q})]}{\omega(\mathbf{p}) + \omega(\mathbf{p} + \mathbf{q})}. \quad \dots\dots (4.1) \end{aligned}$$

Because of the energy gap in the one-particle spectrum, the denominator in the above integrand is never zero; and, moreover, it follows from (3.11) that the numerator is always finite. Therefore, if the integrand possesses any discontinuities, these will be finite. Consequently, we may obtain the London limit for K_A simply by putting $\mathbf{q} = 0$ in the integral in (4.1), since in this limit any finite discontinuities integrate out to zero. On putting $\mathbf{q} = 0$ in this integral, it

may be seen from (3.12) that the integrand vanishes. Therefore, by (2.34), the paramagnetic current is zero in the London limit, which means that the model exhibits the Meissner effect.

APPENDIX

In order to prove the relation (2.9a), we note that the matrix element

$$f_{\alpha}(x-x') \equiv \langle \phi_N | \psi_{-\alpha}(x) \psi_{-\alpha}(x') | \phi_{N+2} \rangle \quad \dots\dots (A1)$$

is invariant under any contact transformation

$$\begin{aligned} Q &\rightarrow S^+ Q S \quad (S \text{ unitary}), \\ | > &\rightarrow S^+ | > . \end{aligned}$$

Since the model is invariant under spin-reversals and space-reflections, it follows that H is left unchanged by the transformation

$$\left. \begin{aligned} \psi_{1/2}(x) &\rightarrow \psi_{-1/2}(Rx), \\ \psi_{-1/2}(x) &\rightarrow -\psi_{1/2}(Rx), \end{aligned} \right\} \quad \dots\dots (A2)$$

the reflection operator R being defined in (2.9a). The vacuum states ϕ_N , ϕ_{N+2} are therefore unchanged by the transformation, except possibly for a constant phase factor, so that we may write

$$\left. \begin{aligned} \phi_N &\rightarrow \lambda_N \phi_N \\ \phi_{N+2} &\rightarrow \lambda_{N+2} \phi_{N+2}, \end{aligned} \right\} \quad \dots\dots (A3)$$

and

where the λ 's are numerical constants of unit modulus. Hence, it follows from (A1-3) that

$$\left. \begin{aligned} f_{\alpha}(x-x') &= -\lambda f_{-\alpha}(Rx-Rx'), \\ \lambda &= \lambda_N^+ \lambda_{N+2}. \end{aligned} \right\} \quad \dots\dots (A4)$$

where

On the other hand, it follows from (A1), that, at $t=t'$,

$$\begin{aligned} f_{\alpha}(x-x') &= -\langle \phi_N | \psi_{-\alpha}(x') \psi_{\alpha}(x) | \phi_{N+2} \rangle \quad (\text{Fermi anticommutation rules}) \\ &= -f_{-\alpha}(x'-x) = -f_{-\alpha}(Rx-Rx'); \end{aligned}$$

and hence, by (A4), $\lambda=1$.

Therefore, by (A1) and (A4),

$$\langle \phi_N | \psi_{\alpha}(x) \psi_{-\alpha}(x') | \phi_{N+2} \rangle = -\langle \phi_N | \psi_{-\alpha}(Rx) \psi_{\alpha}(Rx') | \phi_{N+2} \rangle.$$

The relation (2.9a) follows immediately from this equation.

ACKNOWLEDGMENT

The author would like to express his thanks to Professor H. Fröhlich for numerous helpful discussions on the subject of this paper.

REFERENCES

- ANDERSON, P. W., 1958, *Phys. Rev.*, **112**, 1900.
 BARDEEN, J., COOPER, L. N., and SCHRIEFFER, J. R., 1957, *Phys. Rev.*, **108**, 1175.
 BOGOLIUBOV, N. N., 1958, *Nuov. Cim.*, **7**, 794.
 ——— 1959, *On the Principle of Compensation* (Lab. Theor. Phys., Dubna: Joint Inst. Nucl. Res.), p. 267.
 FRÖHLICH, H., 1952, *Proc. Roy. Soc. A*, **215**, 291.
 GORKHOV, L. P., 1958, *Soviet Physics, J.E.T.P.*, **7**, 505.
 LANDAU, L. D., 1956, *Soviet Physics*, **3**, 920.
 MIGDAL, A. B., 1959, *Nuclear Physics*, **13**, 655.
 NAKAJIMA, S., 1956, *Proc. Phys. Soc. A*, **69**, 441.
 NAMBU, Y., 1960, *Phys. Rev.*, **117**, 648.
 RICKAYZEN, G., 1959, *Phys. Rev.*, **115**, 795.
 SCHWEBER, S. S., BETHE, H. A., DE HOFFMANN, F., 1955, *Mesons and Fields*, Vol. 1 (Evanston, Illinois: Row Peterson and Co.).

Absorption Spectrum of Tellurium Monosulphide in the Ultra-violet Region

BY H. MOHAN AND K. MAJUMDAR

Department of Physics, University of Allahabad,
Allahabad, India

MS. received 26th January 1960

Abstract. Two new band systems in absorption have been observed in the quartz ultra-violet region ($\lambda 2190-2450$) by vaporizing tellurium in a vacuum along with the sulphide of a group IIb element. The bands, which are degraded to the violet, have been classified and attributed to a new molecule TeS .

§ 1. INTRODUCTION

THE diatomic molecules formed with an atom of group VIb or of group VIIb as one of the constituents are the molecules which have been comparatively well studied as regards their band spectra. However, our knowledge regarding the spectra of diatomic sulphides in general is not very satisfactory except for those of group IVb elements.

Sen Gupta (1932) and Mathur (1937) investigated the electronic spectra of the sulphides of group IIb elements. They observed only certain regions of continuous absorption for all the six molecules tried, viz. ZnS , CdS , HgS (Sen Gupta) and CaS , SrS , BaS (Mathur) and inferred that while the normal electronic states for these molecules have deep minima, the upper states are repulsive in character. It was further asserted that these molecules were ionic in nature, being of the type $\text{M}^{2+}\text{S}^{2-}$ and by the absorption of light, both the electrons from S^{2-} are simultaneously transferred to M^{2+} giving rise to two normal atoms.

Band spectra of the diatomic sulphides of the group Vb elements have also been studied but satisfactory results could not be obtained except for the molecule NS (Fowler and Bakkar 1932, Herman and Herman 1950).

No experimental data have so far been reported regarding spectra of diatomic sulphides of group VI atoms except in the case of OS and SS . During the course of the present investigations, it was observed that when a mixture of tellurium metal powder and a sulphide of any one of the atoms of group IIb is heated to about 1000°C in a vacuum, tellurium monosulphide is formed in the vapour state and it was possible to study its absorption spectrum.

The present communication is concerned with the study of the absorption spectrum of this new molecule.

§ 2. EXPERIMENTAL DETAILS

The investigation was carried out with a vacuum graphite tube furnace which is illustrated in Fig. 1. This furnace has been in use in this laboratory for a considerable length of time and was originally designed to carry out investigations in thermal ionization (Saha, Sur and Majumdar 1926). The graphite tube G, which is held in a horizontal position by means of graphite blocks

F, attached to the electrodes E, is heated by a heavy electric current from a 10kw variable step-down transformer. The four walls W, the top L and the bottom B of the furnace chamber are hollow. These, as well as the electrodes carrying the current, are kept cool by a continuous flow of water. M is a concentric cylindrical covering which, when put in position, reduces loss of heat by radiation, thereby increasing the temperature of the furnace tube.

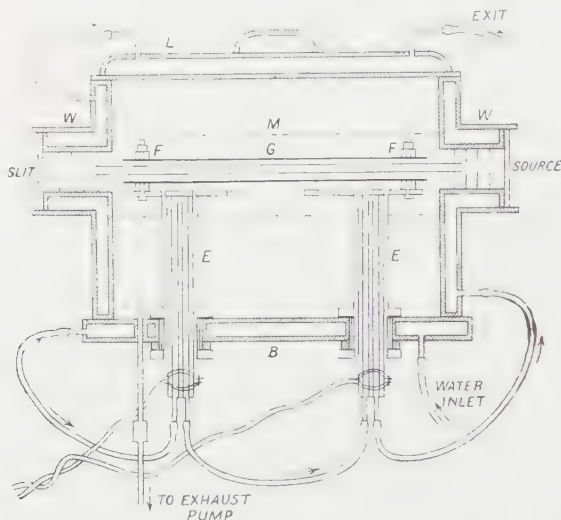


Fig. 1. Vacuum graphite tube furnace.

A small quantity of a mixture of tellurium metal (specpure, Johnson Matthey & Co., England) powder and a sulphide of Zn, Cd or Hg (Analar, British Drug Houses Ltd., England) was introduced into the absorption tube and after evacuation of the chamber, the graphite tube was electrically heated to the desired temperature. To minimize rapid effusion of vapours from the open ends of the absorption tube, it was found necessary to introduce some nitrogen.

A quartz hydrogen discharge lamp was used as a source of ultra-violet continuum while a copper arc provided the comparison spectrum. The spectra were photographed on Ilford N40 process plates using a Leitz medium size quartz spectrograph, which had a reciprocal dispersion of about 5 \AA mm^{-1} in the extreme quartz ultra-violet region. Exposures of the order of 15 to 20 minutes were sufficient to obtain a satisfactory impression of the absorption spectrum. The most favourable temperature for appearance of the bands was found to be between 1000°C and 1100°C .

Violet-degraded bands appeared in the region $\lambda\lambda 2190\text{--}2450$ in all the three cases tried, i.e. when any one of the sulphides, ZnS, CdS or HgS, was used as one of the components of the experimental mixture. However, in the case of the mixture with CdS, the resonance line of cadmium ($\lambda 2288$) appeared with great strength and broadening with the result that a number of absorption bands were masked by its presence. It may be mentioned here that attempts to obtain these new bands by putting a mixture of tellurium and sulphur instead of tellurium and a sulphide in the absorption tube did not prove successful.

This method of studying the absorption spectrum of TeS suggested that the spectrum of the molecule SeS may also be studied in a similar manner, i.e. by

heating a mixture of selenium and zinc sulphide. Attempts made in this direction, however, did not yield any positive result. It is surmised that since SeS is a lighter molecule the corresponding bands would lie in the Schumann region, which was beyond the region of our investigation.

§ 3. RESULTS

Reproduction of the recorded spectrum is given in Fig. 2 (Plate). The spectrum consists of a number of violet-degraded bands in the region $\lambda\lambda 2190-2450$ and these have been classified into two systems:

System I $\lambda\lambda 2190-2360$

System II $\lambda\lambda 2310-2450$.

System I

The wavelengths of the band heads, the corresponding wave numbers and a visual estimate of their intensities are entered in columns 1, 2 and 3 respectively of Table 1. Entries in the last column denote the probable vibrational assignments.

Table 1

Wavelength (Å)	Intensity	Wave number (cm ⁻¹)	Classification
2197.03†	0	45502	(5, 1)
2226.01	1	44909	(4, 1)
2228.31	1	44863	(3, 0)
2250.65	2	44418	(3, 1)
2254.02	3	44351	(2, 0)
2277.40	5	43896	(2, 1)
2280.75	6	43832	(1, 0)
2304.95	2	43371	(1, 1)
2308.19	9	43310	(0, 0)
2330.22	4	42901	(1, 2)
2333.35	5	42844	(0, 1)
2359.19	3	42374	(0, 2)

† Measurement uncertain.

Table 2. Deslandres Arrangement for System I

$\nu' \backslash \nu''$	0	1	2
5		45502 (0)	
4		44909 (1)	
3	44863 (1)	44418 (2)	
2	44351 (3)	43896 (5)	
1	43832 (6)	43371 (2)	42901 (4)
0	43310 (9)	42844 (5)	42374 (3)

Table 2 shows the Deslandres arrangement for the various bands. The Condon curve that can be drawn through the strong bands is nearly of the type

expected with such relative values of w_e as occur here. The following vibrational constants are suggested for the system:

$$\begin{aligned} \nu_e &= 43282.7 \text{ cm}^{-1} \\ w_e'' &= 470.0 \text{ cm}^{-1} & w_e''x_e'' &= 1.4 \text{ cm}^{-1} \\ w_e' &= 524.2 \text{ cm}^{-1} & w_e'x_e' &= 0.8 \text{ cm}^{-1}. \end{aligned}$$

System II

Table 3 gives the wavelengths of the band heads, their wave numbers and a visual estimate of their intensities. Since the available data for this system are fragmentary, only a provisional analysis could be possible and the assignments made therefrom are entered in the last column of this table.

The Deslandres arrangement and the intensity distribution of the various bands have been shown in Table 4.

Table 3

Wavelength (Å)	Intensity	Wave number (cm ⁻¹)	Classification
2310.50	1	43267	(2, 0)
2338.61	7	42747	(1, 0)
2364.45	2	42280	(1, 1)
2367.51	10	42226	(0, 0)
2386.70	2	41886	(2, 3)
2391.16	3	41808	(1, 2)
2394.35	5	41752	(0, 1)
2421.76	2	41279	(0, 2)
2449.63†	1	40810	(0, 3)

† Measurement uncertain.

Table 4. Deslandres Arrangement for System II

$\nu' \backslash \nu''$	0	1	2	3
2	43267 (1)			41886 (2)
1	42747 (7)	42280 (2)	41808 (3)	
0	42226 (10)	41752 (5)	41279 (2)	40810 (1)

§ 4. DISCUSSION

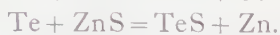
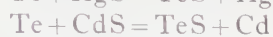
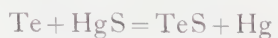
4.1. Identification of the Absorbing Molecule

The following facts support the assignment of the present spectrum to the diatomic molecule TeS.

(i) The new bands appear only when the experimental mixture, e.g. (ZnS + tellurium), was put into the absorption tube and no bands appeared when the clean and empty tube was heated to the same degree and the spectrum of the emergent light was photographed. This fact indicates that the spectrum is not due to any impurity in the graphite tube.

(ii) The same violet-degraded bands appeared in all the three cases, i.e. when any one of the three mixtures, viz. (ZnS + tellurium), (CdS + tellurium) or (HgS + tellurium) was used in the experiment. A single constituent, i.e. either a sulphide or the tellurium metal, when put in the absorption tube and

subjected to similar experimental conditions, did not give rise to these bands. It can, therefore, be safely concluded that the present spectrum is due to the TeS molecule which is common in the following reactions:



The appearance of the absorption lines of the respective atoms further supports the simple mechanism of the process.

(iii) In view of the high temperature (1000°C – 1100°C) maintained in the absorption tube and the simple analysis of the observed bands, the spectrum under reference cannot be attributed to a polyatomic molecule like S_4 or S_8 or S_8 identified by Wieland *et al.* (1934).

(iv) The vibrational analysis of the experimental data gives a value for the ground state frequency which one could expect from empirical considerations. The fact that the w_e'' values for TeO and TeSe are 496 cm^{-1} and 318 cm^{-1} respectively suggests that the w_e'' value for TeS should lie between these two values. Clark (1935, 1937) and Majumdar and Varshni (1954) predicted the value of w_e'' for TeS as 476 cm^{-1} and 467 cm^{-1} respectively. The present value 470 cm^{-1} for w_e'' obtained from experimental results confirms these empirical predictions.

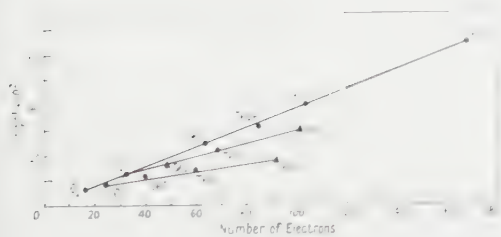


Fig. 3. Variation of w_e'' with number of electrons.

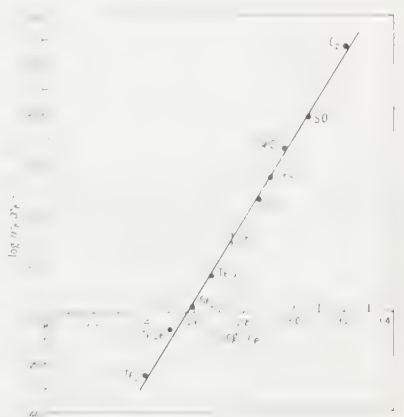


Fig. 4. Graph showing variation of $\log w_e'' x_e''$ with $\log w_e''$ for different molecules of the group.

(v) There exist various regularities among the different spectral constants of the molecules formed out of elements group VIb. A plot of the value of w_e'' against the number of electrons has been found to give straight line curves. Similarly when $\log w_e'' x_e''$ values are plotted against $\log w_e''$ values for the various members of this molecular group, a straight line can be drawn approximately passing through the points. Our values for w_e'' and $w_e'' x_e''$ fit nearly at the right places in these curves. These points have been illustrated in Figs 3 and 4. Studies of this type are sometimes very useful in anticipating hitherto unknown constants of molecules (Barrow and Jevons 1939, Varshni 1955).

4.2. Probable Electronic Transition and other Features of the Spectrum

Studies of the band systems of S_2 molecule in the Schumann region by Maeder (1948), Maeder and Miescher (1948) seem to bear a close analogy with the present findings. These authors have reported violet-degraded bands due to S_2 molecule in the region $\lambda\lambda 1600$ – 1900 . As TeS is a heavier molecule in the same group, the corresponding spectrum is expected to lie towards the longer wavelength side and this is what has been observed in the present case. It thus appears that the present spectrum is an analogue of the Schumann spectrum of S_2 , arising from the transition $d^3II-x^3\Sigma$. However, a study of the band spectrum of SeS is expected to throw more light on this point.

A close examination of the various bands in system I shows that the bands at 44418 cm^{-1} and 44863 cm^{-1} are diffuse while the band at 44909 cm^{-1} on the shorter wavelength is again sharp. It is just possible, as is quite common with the spectra of the diatomic molecules belonging to this molecular group, that this phenomenon is due to predissociation. However, a study of this system of bands in emission is desirable to support this argument. Similar features of predissociation have been detected in the case of TeSe molecule by Dr. D. Sharma in this laboratory.

ACKNOWLEDGMENTS

The authors are grateful to the Council of Scientific and Industrial Research, New Delhi, for financial assistance and for the award of a research fellowship to one of them (H. M.). They are also thankful to Professor K. Banerjee, Head of the Department of Physics, for providing facilities to carry out this investigation and to Dr. D. Sharma for useful discussions.

REFERENCES

- BARROW, R. F., and JEVONS, W., 1939, *Proc. Roy. Soc. A*, **169**, 45.
CLARK, C. H. D., 1935, *Trans. Faraday Soc.*, **31**, 585.
—— 1937, *Nature, Lond.*, **139**, 508.
FOWLER, A., and BAKKAR, C. J., 1932, *Proc. Roy. Soc. A*, **136**, 28.
HERMAN, R., and HERMAN, L., 1950, *C.R. Acad. Sci., Paris*, **230**, 1516.
MAEDER, R., 1948, *Helv. Phys. Acta*, **21**, 411.
MAEDER, R., and MIESCHER, E., 1948, *Nature, Lond.*, **161**, 393.
MAJUMDAR, K., and VARSHNI, Y. P., 1954, *Ind. J. Phys.*, **28**, 209.
MATHUR, L. S., 1937, *Proc. Roy. Soc. A*, **162**, 83.
SAHA, M. N., SUR, N. K., and MAJUMDAR, K., 1926, *Z. Phys.*, **40**, 648.
SEN GUPTA, P. K., 1932, *Proc. Roy. Soc. A*, **138**, 84.
VARSHNI, Y. P., 1955, *D.Phil. Thesis*, University of Allahabad.
WIELAND, K., WEHRLI, M., and MIESCHER, E., 1934, *Helv. Phys. Acta*, **7**, 843.

Z-centres in Sodium Chloride containing Calcium

By J. E. CAFFYN† AND B. K. RIDLEY‡

† Northampton College of Advanced Technology, London

‡ Mullard Research Laboratories, Salfords, Redhill, Surrey

MS. received 29th March 1960§, in revised form 29th July 1960

Abstract. The optical absorption of single crystals of sodium chloride containing calcium as impurity has been measured. Results are given which show a new band at $345\text{ m}\mu$ and from measurements of the bandwidth of the F-band it is deduced that the Z_1 -band is present in specimens, x-ray coloured, at room temperature.

The growth of the Z-bands on bleaching in samples containing differing amounts of calcium impurity and the effect of quenching was also studied. Rate equations are used to discuss the coloration of NaCl and are also applied to the complex $(\text{Ca}^{2+}, \text{F}, 2\text{F}^-)$ to explain the coloration of the crystals containing Ca^{2+} .

§ 1. INTRODUCTION

IT is well known that the presence of certain divalent metals in alkali halides give rise to Z-bands on the long wavelength side of the F-band (Pick 1939, Heiland and Kelting 1949, Camagni *et al.* 1954). So far, only the alkaline earths have been found to produce these bands, and unpublished work by the authors on alkali halides containing variously copper, nickel and manganese does not change this picture. Seitz (1951) pictures the centre giving rise to the Z_1 -band as being an electron trapped by the extra positive charge on an alkaline earth ion occupying substitutionally an alkali ion site, and therefore the Z_1 -centre should be similar, in optical behaviour, to the F-centre. The close proximity of the F- and Z-bands in NaCl and KCl support this view. We might expect that the electron capture cross sections of the two centres would not differ very much, so that under conditions where the F-band is produced the Z_1 -band should appear also, if both types of centre are present in about the same proportions. In fact, it is found that the Z_1 -band only appears when the F-band is bleached with F-light. In particular, Pick (1939b) has found that NaCl containing alkaline earth ions gives only the F-band on x-irradiation but not any of the Z-bands, the Z_1 -band appearing only when the specimen is irradiated with light absorbed by the F-band. Evidence is given here that in fact, the Z_1 -band is produced by x-irradiation and manifests itself by an apparent broadening of the F-band.

The width of the F-band is due to the random thermal motion of ions surrounding the F-centre and as such should depend predominantly on temperature. It is found, however, that quite large variations occur among crystals of the same material (Mador *et al.* 1953, for bandwidth measurements with KBr). This is also found here for NaCl and is attributed to the presence of Z-centres.

It is of interest to ask whether all the alkaline earth ions present as impurity form Z-centres or whether some or most are not simply substitutional but are present as

§ Work originally submitted on 28th October 1959, but lost in post until 29th March 1960.

more complex centres and/or aggregates at dislocations (Caffyn and Schneider 1955). Also, it is known that the alkaline earths enhance the colourability of crystals (Etzel 1952, Hummel 1950, Etzel and Maurer 1950). The mechanism of this effect is not well understood and it is therefore of interest to find out the quantitative dependence of the enhancement upon the concentration of impurity. The results presented are of work on NaCl containing calcium.

§ 2. EXPERIMENTAL DETAILS

Single crystals were grown from Analar material using the Kyropoulos technique, calcium being incorporated by direct addition of the chloride to the NaCl melt. The calcium was quantitatively detected by the ethylenediamine-tetra-acetate (E.D.T.A.) method (Chalmers 1954). Optical absorption measurements at liquid nitrogen temperatures were made with a grating spectrophotometer having a spectral bandwidth of 10 Å throughout the range, and measurements were made at room temperature with a Unicam S.P. 500. The specimens were cleaved from the parent crystal, and were about 0.05 cm thick. For optical bleaching a cadmium vapour lamp was used in conjunction with an appropriate Ilford filter. An x-ray tube with a copper target, operating at 40 kV and 20 mA, was used for x-irradiation.

The mole fractions of calcium in the specimens measured ranged from about 1×10^{-6} to over 6×10^{-3} .

§ 3. ABSORPTION BANDS OF NaCl. Ca^{2+} : EXPERIMENTAL RESULTS

The results of absorption measurements on specimens containing a large amount of calcium (mole fraction greater than 10^{-3}) which have undergone various thermal and optical treatments are presented in Figs 1 to 5. The following observations can be made.

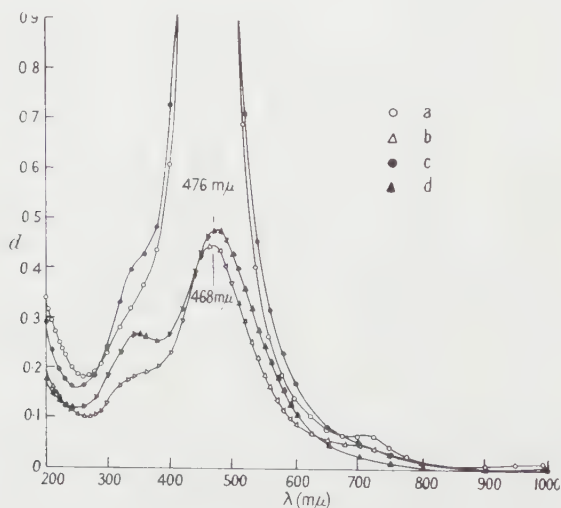


Fig. 1. Absorption spectra of NaCl . Ca^{2+} (mole fraction of $\text{Ca}^{2+} = 5.7 \times 10^{-3}$) at room temperature. a, x-rayed 5 hours; b, x-rayed 5 hours, bleached 2 hours with F-light; c, quenched from 600°C , x-rayed 5 hours; d, quenched from 600°C , x-rayed 5 hours and bleached 2.5 hours with F-light.

(i) A band at $345\text{ m}\mu$ is present which has not been reported before. This band only appears in high calcium content crystals, and is enhanced by quenching the specimen from elevated temperatures. Since the quenching process tends to freeze in calcium liberated from internal boundaries or associates it would point to an association between the band and substitutional calcium, e.g. a centre comprised of two calcium ions, or, since the presence of calcium enhances the density of vacancies of both types, a centre comprised of a calcium ion and a negative ion vacancy, i.e. a helium-like centre. The band was also found to occur in additively coloured specimens, which supports the view that it is associated

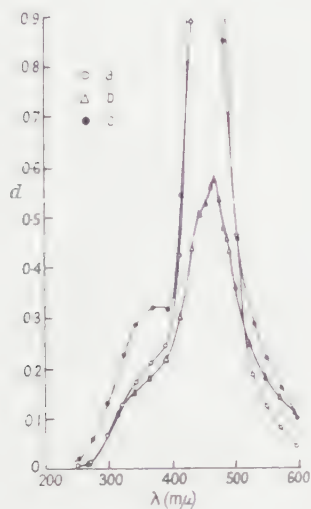


Fig. 2. Absorption spectra of $\text{NaCl} : \text{Ca}^{2+}$ (mole fraction of $\text{Ca}^{2+} = 6.1 \times 10^{-3}$) measured at about 150°K . a, x-rayed 2 hours; b, x-rayed 2 hours, bleached 1 hour, with F-light; c, quenched from 600°C , x-rayed 2 hours.

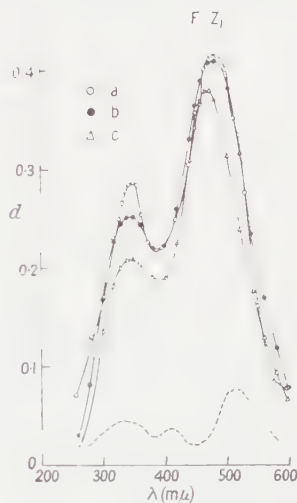


Fig. 3. Absorption spectra of $\text{NaCl} : \text{Ca}^{2+}$ (mole fraction of $\text{Ca}^{2+} = 5.4 \times 10^{-3}$) after quenching from 600°C . a, x-rayed 7 hours, bleached 16 hours with F-light, measured at about 150°K ; b, x-rayed 7 hours, bleached 16 hours with F-light, measured at room temperature; c, x-rayed 7 hours, bleached 16 hours with F-light, measured at room temperature after 70 hours in dark. Broken line, subtraction curve showing thermally bleached bands.

with trapped electrons and not trapped holes. Optically bleaching the F-band only makes the $345\text{ m}\mu$ band more apparent but does not markedly reduce it, indicating again that it arises from trapped electrons and not trapped holes. Figs 3 to 5 show that the band is thermally bleached more rapidly than the F-band. Since the band lies on the short wavelength side of the F-band it is improbable that the faster bleaching is due to more rapid thermal ionization of the trapped electrons; more likely, it is due to the low binding energy of the components of the centre. This view is supported by the fact that the band is not regenerated after thermal bleaching by subsequent F-band bleaching (Fig. 5).

(ii) The low temperature absorption measurements of specimens which have been coloured and partially bleached with light absorbed in the F-band show the presence of the Z_1 -band, and probably the Z_2 -band as well (Figs 2 and 3).

The Z-bands manifest themselves in the absorption spectra obtained at room temperature by the shift in wavelength of the peak of the F-band towards the red. The Z-bands thermally bleach more rapidly than the F-band but can be regenerated by irradiating in the F-band, showing that the thermal bleaching is due to

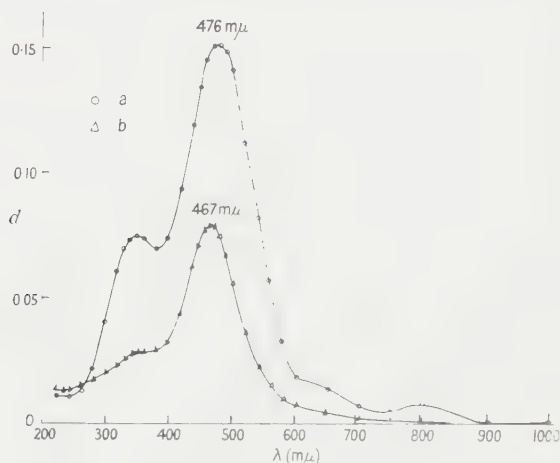


Fig. 4. Absorption spectra of NaCl. Ca^{2+} at room temperature after quenching from 600°C (mole fraction $\text{Ca}^{2+} = 5.4 \times 10^{-3}$). a, x-rayed 4.5 hours, bleached with F-light 15 hours; b, after 15 minutes at 110°C .

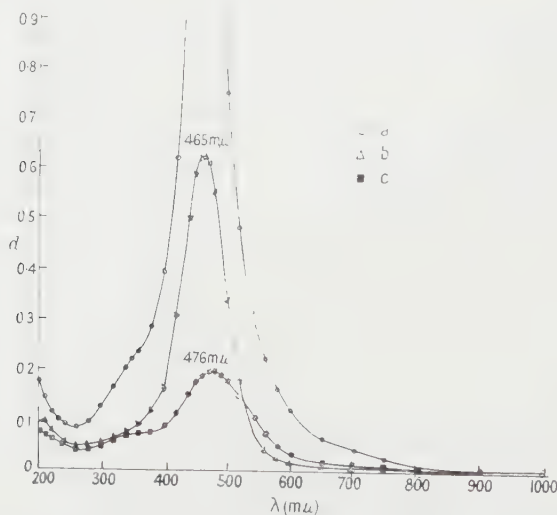


Fig. 5. Absorption spectra of NaCl. Ca^{2+} at room temperature after quenching at 600°C (mole fraction $\text{Ca}^{2+} = 5.4 \times 10^{-3}$). a, x-rayed 3 hours; b, after 15 minutes at 100°C ; c, after bleaching with F-light for 1 hour.

thermal ionization of the trapped electrons. The Z-bands are enhanced by quenching, indicating that calcium, like manganese (Caffyn and Schneider 1955) resides in the crystal, probably at dislocations, as aggregates or associates which disperse at elevated temperatures; quenching then freezes in a more uniform distribution of Ca^{2+} ions giving rise to incipient Z-centres and other complexes.

§ 4. MEASUREMENTS OF THE WIDTH OF THE F-BAND

The width of the F-band was measured by plotting $(\log_{10} d_0/d)^{1/2}$ against the photon energy E , where d_0 was the optical density at the peak, and d was the optical density at E . Since the shape of the F-band is Gaussian, two straight lines were obtained which intersected at $E = E_0$, the photon energy at the peak, one line being for E greater than E_0 , the other for E less than E_0 (Fig. 6). The slope was given by $(\log_{10} 2)^{1/2}/\sigma$, where 2σ was the bandwidth.

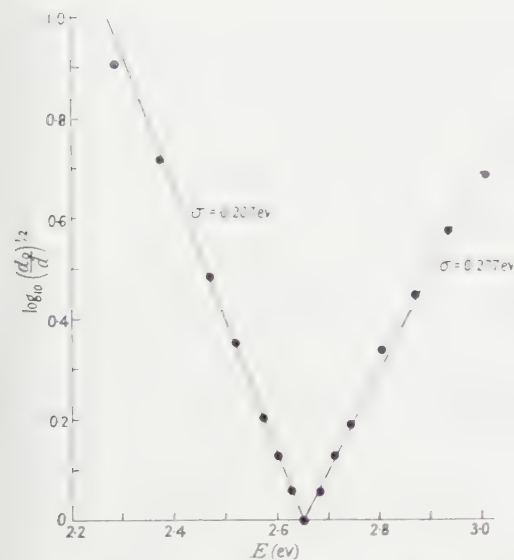


Fig. 6. Measurement of the width of the F-band in NaCl.

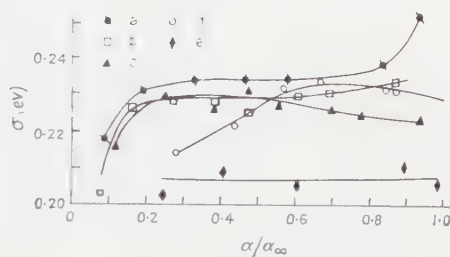


Fig. 7. Dependence of the half-width of the F-band in NaCl. Ca^{2+} on the degree of coloration. The five curves correspond to five different mole fractions of calcium: a, 6.3×10^{-3} , b, 220×10^{-6} , c, 16×10^{-6} , d, 3×10^{-6} (Korth), e, 1×10^{-6} (Harshaw).

It was found that the NaCl F-band was an asymmetrical Gaussian curve (Fig. 6) being broader on the short wavelength side. In this, NaCl is similar to KBr (Mador *et al.* 1953). The Table shows the results of measurements of bandwidth taken from the long-wavelength side of the F-band in x-rayed specimens from various sources, along with their calcium content. The values are accurate to within 0.005 ev.

Specimen	m.f. of Calcium $\times 10^6$	Bandwidth (ev)
Harshaw	1	0.414
Korth (a)	5	0.440
(b)	5	0.464
Manchester (Analar)	19	0.436
Durham (Analar) (a)	15	0.428
(b)	15	0.434
(c)	20	0.482
(d)	20	0.470

The variation from specimen to specimen suggests that, as in the case of the short wavelength side of the F-band, other bands in the range $465\text{ m}\mu$ to $540\text{ m}\mu$, are intruding, and these are likely to be Z-bands due to the presence of alkaline earth impurity.

Measurements of bandwidth were also carried out on crystals containing a high proportion of calcium, when the crystals were (a) well-annealed, (b) quenched, and (c) during the growth of the F-band. It was found that (1) the bandwidth increased with quenching; (2) the bandwidth varied during the growth of the F-band. With pure crystals there was no variation during growth (Fig. 7); (3) the bandwidth increased slightly with calcium content above a mole-fraction of 10^{-5} , but rapidly for mole fractions from 10^{-6} to 10^{-5} ; (4) the bandwidth in crystals which had been thermally bleached for a while was much smaller than in crystals which had been freshly coloured, and, in fact, approached the value 0.414 eV found in the purest specimens.

From these results it is concluded that the broadening was due to Z-bands formed during x-irradiation.

§ 5. THE GROWTH OF ABSORPTION BANDS

By assuming that the true width of the F-band was that found in the purest specimens, i.e. 0.414 eV , it was possible to obtain the Z-band intensity in any case by subtracting a Gaussian curve of this width from the experimental absorption band. In well annealed specimens containing mole fractions of calcium between $\sim 10^{-4}$ to 6.3×10^{-3} which had been x-rayed the ratio between the Z-band intensities remained remarkably constant at about 0.1. It appears, therefore, that the increase of Z-centre concentration in well-annealed crystals due to the addition

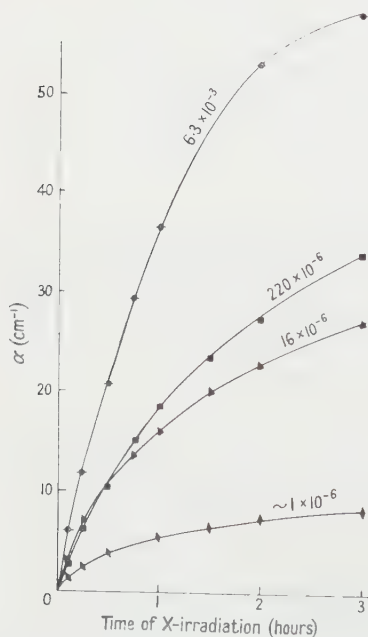


Fig. 8. Growth of the F-band. The figures on the curves indicate mole fractions of calcium.

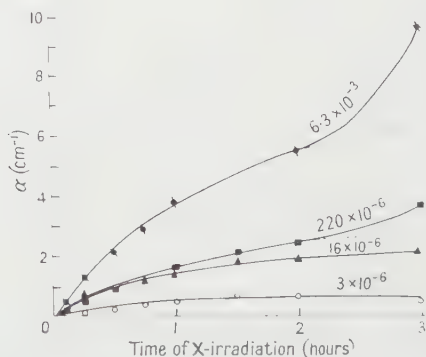


Fig. 9. Growth of the Z-band. The figures on the curves indicate mole fractions of calcium.

of calcium is always accompanied by a proportional increase in F-centre concentration. Quenching, however, increased this ratio.

To find more quantitatively the relations between calcium concentration, Z-centre concentration and F-centre concentration, the intensities of the F-band and of the Z-band were plotted against time (Figs 8 and 9). The intensity of the Z-bands was found by the method of subtracting a Gaussian curve. The growth curves had the expected exponential form over the first three hours of irradiation;

$$\text{i.e. } \alpha = \alpha_{\infty} \{1 - \exp(-\nu t)\}$$

where α = absorption coefficient of the band peak at time t , ν = growth constant and α_{∞} = saturation absorption coefficient, but deviations from this curve occurred for the Z-band in the higher calcium content specimens with long irradiation times.

To obtain colour centre concentrations from the experimental values of α it was necessary to make the following assumptions:

(1) the Z-band measured was the Z_1 -band, (2) the rate of thermal ionization of either centre was negligible, (3) the Z_1 -band was the same width as the F-band and had the same oscillator strength associated with it and (4) the crystals were coloured uniformly.

The assumption that the oscillator strengths are the same, or nearly so, is reasonable in the light of the results obtained by Camagni *et al.* (1954). The similarity of the Z_1 -centre and the F-centre models makes the other assumptions a reasonable first approximation. (However, assumption (2) will not be as valid for Z_1 -centres as for F-centres.) To justify assumption (4) the specimens used were as thin as possible.

The following formula was then used to calculate colour centre densities:

$$n = 7.24 \times 10^{15} \frac{\alpha_{\nu} W}{f}$$

where W is the bandwidth and f the oscillator strength ($=0.55$ for the F-band in NaCl) (see Herring 1956 for a discussion of this formula and its relation to the usual Smakula formula). The results are presented as plots of $\log N_c$ against $\log n_i$ in Fig. 10, where N_c is the total concentration of calcium ions in the crystal and n_i is the colour centre concentration.

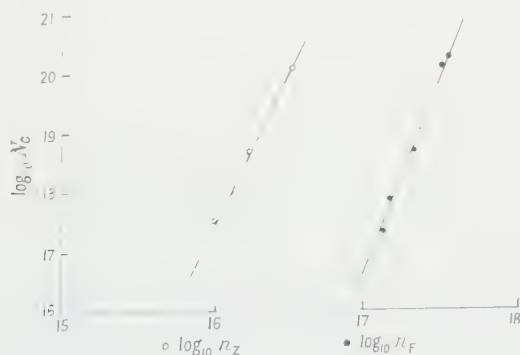


Fig. 10. Dependence of Z-centre and F-centre concentrations on the concentration of calcium.

It is seen that the points lie on a straight line in each case. The slopes are both near to 6 so that the various concentrations are related by the empirical formulae

$$n_z \simeq K_z N_c^{1/6} \qquad n_F \simeq K_F N_c^{1/6}$$

where K_z and K_F are constants. The first of these results indicates that only a small proportion of the calcium produces Z-centres, and the second result points to an apparent increase of the Schottky product for vacancies due to calcium.

§ 6. COLORATION BY X-RAYS

To approach an explanation of these results let us consider what happens when a pure crystal is irradiated with x-rays. A review of the theories of growth of colour intensity has been given by Przibram (1956) but these are rather vague in content. Here we would like to consider the coloration process in a specific way though several simplifications will be made to clarify the relation to the above experimental results.

6.1. Pure NaCl

At room temperature most of the oppositely charged vacancies will be associated into pairs which will only feebly attract electrons or holes. We assume, therefore, that x-rays not only produce free electrons and holes but also break up vacancy pairs. We could now write down the rate equations for the various elements involved, and these would contain terms referring to the dissociation of pairs and the association of vacancies, the capture and emission of electrons and holes by and from the two types of vacancy, and the generation and direct recombination of electrons and holes. In order to reduce the complexity of these equations and make the germane points clear let us assume that

- (1) the thermal emission of electrons and holes is negligible;
- (2) the two types of imperfection have exactly similar properties in that the one's relation to electrons is exactly reflected by the other's relation to holes. This means that at all times $n=p$ and $x=y$, where n and p refer to electron and hole densities, and x and y refer to the densities of negative ion vacancies and positive ion vacancies.
- (3) The rate equations for electrons and holes are governed mainly by generation and direct recombination.

The various rate equations can then be reduced to the following three:

$$\begin{aligned} \frac{dn}{dt} &= gI - rnp \\ \frac{dn_F}{dt} &= Ynx - \sigma pn_F - \epsilon_F In_F + \epsilon_x Ix \\ \frac{dn_p}{dt} &= -(\alpha I + \theta)np + (\beta_0 + \beta_1)xy \end{aligned}$$

where I = flux density of x-rays, n_F = density of F-centres, n_p = density of pairs, g = generation rate, r = direct recombination rate, Y = electron capture rate of a negative ion vacancy, σ = hole capture rate of an F-centre, ϵ_F = rate of x-ray ejection of an F-centre electron, ϵ_x = rate of ejection of a valence band electron into a negative ion vacancy directly, α = dissociation rate due to x-rays of a pair,

θ = thermal dissociation rate of a pair, β_0 = thermal association rate of vacancies, and β_1 = x-ray association rate of vacancies.

If the density of new vacancies produced by x-rays is negligible then

$$x = N_p - n_F - n_p$$

where N_p is the total density of vacancies of one sign.

At the steady state we can solve for n , n_F and n_p . From now on in this subsection, n , n_F and n_p will refer to steady state values. We obtain

$$\begin{aligned} n &= [gI/r]^{1/2} \\ n_F &= 2RN_p [\{G(G+1)\}^{1/2} - G] \\ n_p &= N_p [1 + 2(G - \{G(G+1)\}^{1/2})] \end{aligned}$$

where

$$R = \frac{Yn + \epsilon_x I}{(\sigma + Y)n + I(\epsilon_F + \epsilon_x)}, \quad G = \frac{(\alpha I + \theta)}{4N_p(\beta_0 + \beta_1)(1 - R)^2}.$$

Two simple results are possible depending upon the value of the factor G . When $G \gg 1$

$$n_F = \left[\frac{Y(gI/r)^{1/2} + \epsilon_x I}{(\sigma + Y)(gI/r)^{1/2} + I(\epsilon_F + \epsilon_x)} \right] N_p \quad \dots\dots (1)$$

i.e. n_F depends linearly upon N_p and will not be influenced greatly by the x-ray intensity. When $G \ll 1$

$$n_F = \left[\frac{Y(gI/r)^{1/2} + \epsilon_x I}{\sigma(gI/r)^{1/2} + \epsilon_F I} \right] \left[\frac{\alpha I + \theta}{\beta_0 + \beta_1} N_p \right]^{1/2} \quad \dots\dots (2)$$

i.e. n_F depends upon the square root of N_p (quasi-bimolecular reaction) and is more dependent upon the x-ray intensity. If capture of electrons and holes is more important than the direct action of x-rays on negative ion vacancies and F-centres, or vice versa, n_F is just dependent upon the square root of the x-ray intensity. The experimental results of Belar (1926) agree with this. It should be pointed out that the presence of the capture and ejection rates in the equations indicates the role of the electrons, holes and x-rays in influencing the equilibrium between associated and unassociated vacancies: the formation of F-centres is effectively a withdrawal of free vacancies and this leads to a greater dissociation of pairs.

6.2. $\text{NaCl} \cdot \text{Ca}^{2+}$

Before we look at the similar problem in $\text{NaCl} \cdot \text{Ca}^{2+}$ we must find an explanation for the apparent increase in negative ion vacancies due to the presence of calcium. Etzel (1952) suggests that the enhancement of the F-band by alkaline earth impurities is due to the production of positive ion vacancies by the divalent impurity which, by increasing the chances of hole capture, reduces the rate of direct recombination and allows more electrons to be captured by negative ion vacancies already present in the crystal. In support of this he has shown that the V-band is enhanced by the presence of calcium in NaCl, and this has been observed by the author. However comparison of the magnitude of this enhancement with results obtained with $\text{NaCl} \cdot \text{Mn}^{2+}$ (Fig. 11 is a typical example) shows that it is relatively small in $\text{NaCl} \cdot \text{Ca}^{2+}$, whereas the enhancement of the F-band in both cases can be comparable. Further, consideration of the kinetics of electron and hole capture and recombination shows that although an increase in hole capture

rate could certainly increase the rate of formation of F-centres it is unlikely to increase the saturation F-centre density, provided this is attained in a time short enough for thermal regeneration of the trapped electrons to be negligible. This

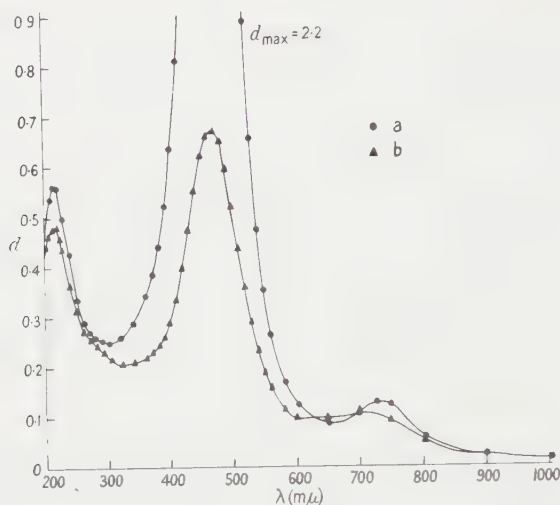


Fig. 11. Absorption spectra of NaCl . Mn²⁺ (mole fraction of Mn²⁺ = 480×10^{-6}) at room temperature: a, x-rayed 7 hours; b, bleached with F-light for 0.5 hour.

condition is easily attained using normal x-ray intensities, therefore it would appear that the enhancement of the F-band is due to the production of negative ion vacancies by the divalent ion. It is quite feasible that this can occur through the accentuation of mis-match in the lattice by the presence of the impurity (Shulman 1953). A model showing how this can produce negative ion vacancies will now be described.

At the temperature of growth of the crystal there is a large number of vacancies present and as the crystal cools these vacancies tend to diffuse to the surface and disappear. It is reasonable to suppose that calcium ions, being misfits in the lattice, act as traps for vacancies of either type so that instead of diffusing out of the crystal some vacancies remain trapped in associates involving calcium. The experimental results suggest that the main associate formed consists of six imperfections. Since the F-band is more dominant than the Z-band we suggest that the associate consists of a calcium ion plus positive ion vacancy and two vacancy pairs, the whole being electrically neutral relative to the NaCl matrix. Its dissociation can be represented thus:



Such an associate is unlikely to capture an electron or a hole to form a colour centre at room temperature.

We can now look at the kinetics of x-ray coloration in the same way as we did for pure NaCl with the additional simplifications that:

(1) the density of vacancies generated from the associates swamp the intrinsic vacancy density so that if w is the concentration of free calcium ions then $x = 2w$ and $y = 3w$, where x and y have the same meaning as before;

(2) the condition of detailed balance of charges is not destroyed so that $n=p$, $y=w+x$, and $n_V=n_F+n_Z$, at all times, where n_Z is the density of calcium ions with a trapped electron.

The rate equations concerning the F-centres, Z-centres and associates (density n_c) are

$$\begin{aligned}\frac{dn_F}{dt} &= Y_x n x - \sigma_F p n_F - \epsilon_F I n_F + \epsilon_x I x, \\ \frac{dn_Z}{dt} &= Y_w n w - \sigma_Z p n_Z - \epsilon_Z I n_Z + \epsilon_w I w, \\ \frac{dn_c}{dt} &= -(\alpha_c I + \theta_c) n_c + (\beta_0 + \beta_1)_c w x^2 y^3,\end{aligned}$$

where the suffix c refers to the associate. If N_{ca} is the total concentration of calcium free and in associates then

$$w = N_{ca} - n_p - n_Z \quad x = 2(N_{ca} - n_p) - n_F.$$

If we use the simplifying assumptions and put $n=p$, $Y_x=Y_w=Y$, $\sigma_F=\sigma_Z=\sigma$, $\epsilon_F=\epsilon_Z$, and $\epsilon_x=\epsilon_w$ etc., the steady state solutions can be obtained. These are governed by a factor G_c defined thus

$$G_c = \frac{(\alpha_c I + \theta_c)}{6 N_{ca}^5 2^2 3^3 (\beta_0 + \beta_1)_c (1-R)^6}$$

where R is the quantity defined in § 6.1. When $G \gg 1$

$$n_Z = \left[\frac{Y(gI/r)^{1.2} + \epsilon_x I}{(\sigma + Y)(gI/r)^{1.2} + I(\epsilon_F + \epsilon_x)} \right] N_{ca} \quad \dots\dots (3)$$

$$n_F = 2n_Z$$

i.e. this is very much the same as Eqn (1). When $G \ll 1$

$$n_Z = \left[\frac{Y(gI/r)^{1.2} + \epsilon_x I}{(\sigma + Y)(gI/r)^{1.2} + \epsilon_F I} \right] \left[\frac{(\alpha_c I + \theta_c)}{2^2 3^3 (\beta_0 + \beta_1)_c} N_{ca} \right]^{1.6} \quad \dots\dots (4)$$

$$n_F = 2n_Z.$$

The dependence upon x-ray intensity in this case should be much smaller than that predicted for the parallel condition in pure NaCl (Eqn (2)). This experiment, however, has not been done. Eqn (4) is of the form found by experiment provided N_{ca} is, if not equal to, at least proportional to the total density of calcium in the crystal. (It should be mentioned that I was kept constant in the experiments.)

As far as NaCl. Ca²⁺ is concerned the real state of affairs seems more complicated. Thus another associate exists which gives rise to the 345 mμ band, the latter and the Z-band are enhanced by quenching without this operation markedly affecting the F-band, and deviations from the simple Z-band growth curves occur at long irradiation times. If the calcium exists as associates of the type suggested quenching should not alter the F-band to Z-band ratio. However, the quenching operation was performed with small specimens. There was therefore a larger surface to volume ratio here than in the as-grown crystals and the excess vacancies may have diffused out faster than the calcium leaving a greater concentration of calcium ion plus positive ion vacancy complexes behind. Without further experimental work on quenching it seems useless to speculate further.

§ 7. CONCLUSION

The results of the present investigation of colour centres in NaCl. Ca^{2+} suggest that calcium can exist in the crystal:

(1) In associates of the form $(\text{Ca}^{2+}, \oplus, 2\oplus\ominus)$

(2) In associates of unknown form (but possibly $(\text{Ca}^{2+}, \oplus, \text{Ca}^{2+})$) giving rise to the 345 μ band.

(3) As single ions giving rise to the Z_1 -band.

It is also suggested that the calcium ion can trap during cooling vacancy pairs, which relieve the mis-match in the lattice around the ion, and so calcium can enhance the F-band in the coloured crystal.

The study of the width of the F-band indicates that Z-centres are formed along with F-centres when the crystal is irradiated with x-rays. In this the effect of x-ray coloration is different from that of additive coloration.

The results of the investigation on the growth of colour bands on x-irradiation have been explained by a simple analysis of x-ray coloration in which it is assumed that the action of the x-rays at room temperature is, not only to provide free electrons and holes, but also to break up associates.

ACKNOWLEDGMENTS

The authors would like to express their debt to Dr. F. A. Kroger whose contribution to discussion was invaluable. They would also like to acknowledge the facilities provided by Professors J. E. P. Wagstaff and G. D. Rochester in the Physics Department of the Durham Colleges, and they would like to thank the members of staff of the Faculty who put apparatus at their disposal. Thanks are also due to the Royal Society for a grant, and to Dr. J. Markham of Zenith Radio Corporation Ltd., Illinois, Dr. Korth of Kiel, and Mr. W. Smith of the University of Manchester for providing some of the specimens. One of us (B. K. R.) would like to acknowledge the maintenance grants received from St. Cuthbert's Society, University of Durham, the Gateshead Borough Council, and the Department of Scientific and Industrial Research.

REFERENCES

- BELAR, M., 1926, *Akad. Wiss., Wien, Ber.*, IIa, **135**, 187.
 CAFFYN, J. E., and SCHNEIDER, E. E., 1955, *Report of the Conference on Defects in Crystalline Solids* (London: Physical Society), p. 74.
 CAMAGNI, P., *et al.*, 1954, *Phil. Mag.*, **45**, 225.
 CHALMERS, R., 1954, *Analyst*, **79**, 519.
 ETZEL, H. W., 1952, *Phys. Rev.*, **87**, 906.
 ETZEL, H. W., and MAURER, R. J., 1950, *J. Chem. Phys.*, **18**, 1003.
 HEILAND, G., and KELTING, H., 1949, *Z. Phys.*, **126**, 689.
 HERRING, C., 1956, *Photoconductivity Conference (Atlantic City)* (New York: Wiley), p. 81.
 HUMMEL, H., 1950, *Thesis*, Göttingen.
 MADOR, I. L., MARKHAM, J. J., and PLATT, R. T. JR., 1953, *Phys. Rev.*, **91**, 1277.
 PICK, H., 1939 a, *Ann. Phys. Lpz.*, **35**, 73.
 ——— 1939 b, *Z. Phys.*, **114**, 129.
 PRZIBRAM, K., 1956, *Irradiation Colours and Luminescence* (London: Pergamon).
 SEITZ, F., 1951, *Phys. Rev.*, **83**, 134.
 SHULMAN, J. H., 1953, *J. Phys. Chem.*, **51**, 749.

The Hartree Energies of the Helium Sequence

BY M. COHEN AND A. DALGARNO

Department of Applied Mathematics, The Queen's University of Belfast

MS. received 30th August 1960

IN an earlier note (Dalgarno 1960) a theory was presented which made possible the exact calculation of all terms of the series expansions of the Hartree-Fock energies of atomic systems in inverse powers of the nuclear charge Z . A variational method was applied to obtain an approximate value for the first non-trivial term of the expansion corresponding to the helium sequence. We have now solved the appropriate equation exactly and have thereby obtained an exact value for this term.

We merely reproduce the necessary equations from the earlier note. The Hartree energy of the helium sequence is given in atomic units by

$$E = -Z^2 + \frac{5Z}{8} + \epsilon_2 + O(Z^{-1}) \quad \dots\dots (1)$$

where

$$\epsilon_2 = 2(u_0, v_1 u_1) \quad \dots\dots (2)$$

$$u_0 = (Z^3/\pi)^{1/2} \exp(-Zr) \quad \dots\dots (3)$$

$$v_1 = \frac{1}{r} - \left(\frac{1}{r} + Z\right) \exp(-2Zr) - \frac{5Z}{8} \quad \dots\dots (4)$$

and u_1 is the well-behaved solution of

$$\left(-\frac{1}{2}\nabla^2 - \frac{Z}{r} + \frac{Z^2}{2}\right)u_1 + v_1 u_0 = 0. \quad \dots\dots (5)$$

Then it may be shown that

$$u_1 = \left\{ \left(\frac{5r}{8} + \frac{3}{16Z^2r}\right) - \left(\frac{1}{4Z} + \frac{3}{16Z^2r}\right) \exp(-2Zr) + \frac{3}{8Z} \left(\int_r^\infty \frac{\exp(-2Zr')}{r'} dr' - \ln r \right) \right\} u_0 \quad \dots\dots (6)$$

and

$$\begin{aligned} \epsilon_2 &= \frac{-13}{432} - \frac{9}{32} \ln \frac{4}{3} \quad \dots\dots (7) \\ &= -0.1110031755\dots, \end{aligned}$$

which may be compared with the result -0.111003 obtained by Dalgarno (1960).

The form of (6) is of interest and suggests that in variational determinations of Hartree-Fock orbitals (cf. Roothan, Sachs and Weiss 1960), terms involving $\ln r$ and r^{-1} should be included in the trial wave functions.

REFERENCES

- DALGARNO, A., 1960, *Proc. Phys. Soc.*, **75**, 439.
 ROTHAN, C. C. J., SACHS, L. M., and WEISS, A. W., 1960, *Rev. Mod. Phys.*, **32**, 186.

Fine Structure in the $^{12}\text{C}(\gamma, n)^{11}\text{C}$ Activation Curve

By I. M. THORSON AND L. KATZ

Department of Physics, University of Saskatchewan, Canada

MS. received 9th June 1960

Abstract. Fine structure in the $^{12}\text{C}(\gamma, n)^{11}\text{C}$ activation curve has been examined in great detail. Eighteen breaks were found between threshold and 23 MeV. The positions of these breaks and the integrated cross sections of the corresponding levels for the (γ, n) reaction are listed. Independent measurements in other laboratories have indicated that resonance photon absorption into discrete levels may also be present for the (γ, p) reaction. The failure to observe structure in the (p, γ) inverse reaction thus remains unexplained.

§ 1. INTRODUCTION

A NUMBER of attempts have recently been made to confirm the existence of discrete energy levels for strong photon absorption, implied by the fine structure observed in the (γ, n) yield curves of some light elements (Katz *et al.* 1954, Goldenberg and Katz 1954, Penfold and Spicer 1955, Sadeh 1959, King and Katz 1959).

Gove, Litherland and Batchelor (1959) studied the $^{11}\text{B}(p, \gamma_0)^{12}\text{C}$ cross section (where γ_0 represents gamma transitions to the ground state) with a proton energy resolution of a few keV but failed to find any fine structure in it. Detailed balancing would imply that such structure should have been observed (Brown and Levinger 1958) if we also assume that the (γ, p) reactions exhibit the same structure as (γ, n) . Gemmell, Morton and Titterton (1959) using cyclotron accelerated protons with energy resolutions of 60 to 100 keV observed two small maxima in the $^{11}\text{B}(p, \gamma)^{12}\text{C}$ cross section.

Carroll and Stephens (1960) used the monochromatic capture gamma rays from the $\text{T}(p, \gamma)^4\text{He}$ reaction, in the energy region from 20.3 to 20.8 MeV, to study photon attenuation in carbon absorbers; they found structure in the total photon capture cross section so measured. Earlier measurements from the same laboratory (Wolf and Stephens 1958, Cohen and Stephens 1959) failed to reveal any structure in similar experiments, though those experiments were presumably of lower sensitivity. Day (1959, private communication) also using the $\text{T}(p, \gamma)^4\text{He}$ gamma rays was able to cover an energy range from 21 to 24.5 MeV with good sensitivity, but failed to find any fine structure in the $^{12}\text{C}(\gamma, n)^{11}\text{C}$ cross section curve. He would have detected bumps in the cross section 0.6 mbn high and integrated cross sections of 0.3 MeV mbn.

In this paper we report on new measurements of the fine structure in the $^{12}\text{C}(\gamma, n)^{11}\text{C}$ activations curve using bremsstrahlung whose peak energy could be varied in fine steps†, and compare these results with other measurements on the photon absorption cross section of carbon.

† A preliminary report on these measurements was given at the 1958 Washington Photonuclear Conference.

§ 2. EXPERIMENTAL TECHNIQUE

To obtain increased sensitivity in the present experiment, the scintillation technique reported by Cohen and McElhinney (1956) was used. In this method, plastic scintillators (type NE101†) are used as samples. After irradiation in the betatron beam, positrons from the ^{11}C activity within the body of the scintillator produced by the $^{12}\text{C}(\gamma, n)^{11}\text{C}$ reactions are stopped in the scintillator itself, and the resulting scintillations detected with a photomultiplier. A similar technique was recently adopted by Sadeh (1959) using samples of anthracene.

Twenty plastic samples were used, each 5 cm in diameter and 3 cm high. They were tested for uniformity by irradiating each with a given x-ray dose at a specific energy. After allowing for counting statistics, a statistical scatter of less than 0.5% remained‡. Stability of the counting system was monitored with a small ^{60}Co source imbedded in one of the plastic scintillators. The system showed slow long-time drift, negligible for the present experiment.

During the course of this experiment the energy stability of the betatron was checked frequently. Long term drifts seldom exceeded 10 keV, and appropriate corrections were always applied. Calibration of the energy scale was carried out according to the method outlined by Katz (1959). Previous measurements suffer mainly from a deficiency in the following respect. The betatron energy scale is almost without exception established from (γ, n) threshold measurements, and since the $^{12}\text{C}(\gamma, n)$ threshold is the highest available, fine structure in this reaction lies in an extrapolated part of the energy scale. In previous measurements this difficulty, coupled with the large errors resulting from other less sensitive techniques for detecting the calibrating thresholds, resulted in large variations in the location of the fine structure breaks. A conservative estimate would indicate that the energy scale in the present experiment is known to within ± 40 keV near threshold (see Fig. 1) and ± 70 keV at 24 MeV.

§ 3. RESULTS

The breaks in the $^{12}\text{C}(\gamma, n)^{11}\text{C}$ activation curve as a function of maximum bremsstrahlung energy are shown in Figs 1 to 11. The positions of these breaks and the integrated cross section represented by the magnitude of the discontinuities at each break are given in Table 1.

Older measurements of yield are liable to error due to previous uncertainties in the energy scale. These errors are aggravated by the steepness of the $^{12}\text{C}(\gamma, n)$ curve in the region of normalization, since at 22 MeV the yield changes by about a factor of two per MeV. For this reason we have adopted for absolute normalization the average of the two most recent yield determinations at 22 MeV.

Cook (1957) gave a value of $1.35 \pm 0.2 \times 10^6$ reactions/100 r mole at 22 MeV, while Haslam and Roalsvig (1958, private communication) found 1.15×10^6 at the same energy. We have taken a value of $1.25 \pm 0.2 \times 10^6$ and calculated

† Made by Nuclear Enterprises, Winnipeg, Canada.

‡ In the beginning of these experiments difficulty was experienced with a variable counting rate. This was finally traced to the 19.7 min activity of ^{211}Bi deposited on the surface of the scintillators from the decay chain of the naturally occurring ^{222}Rn in the air. Keeping the scintillators in airtight containers eliminated this trouble.

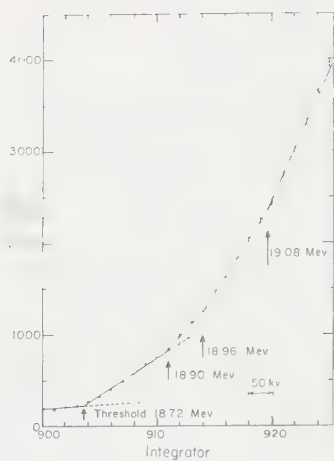


Fig. 1.

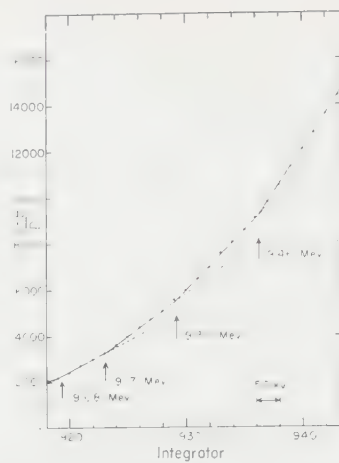


Fig. 2.

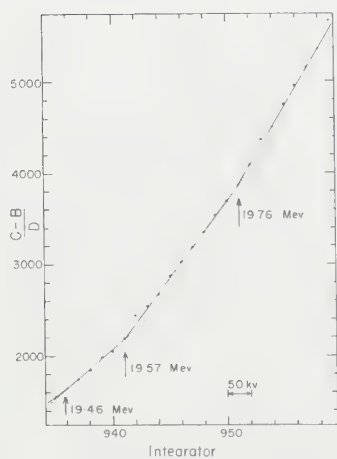


Fig. 3.

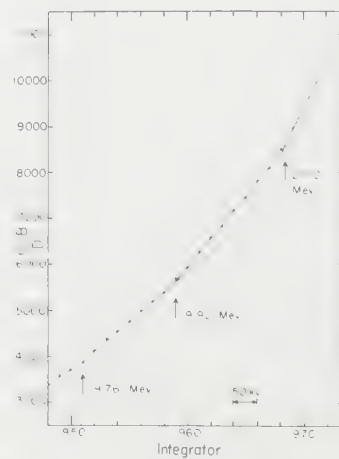


Fig. 4.

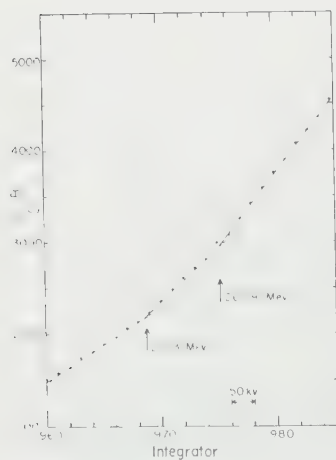


Fig. 5.

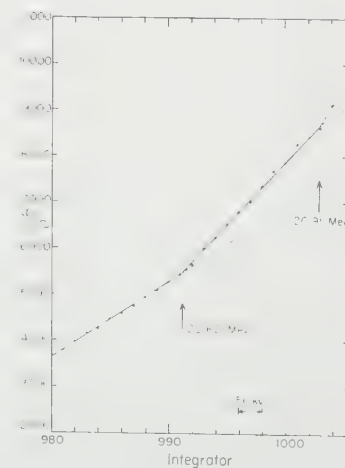


Fig. 6.

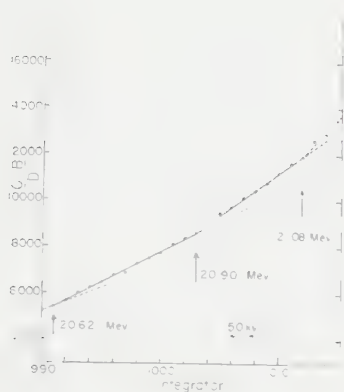


Fig. 7.

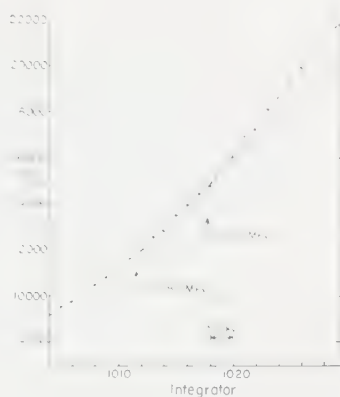


Fig. 8.

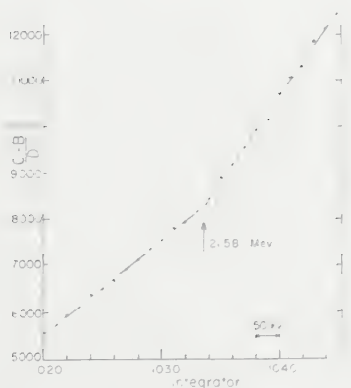


Fig. 9.

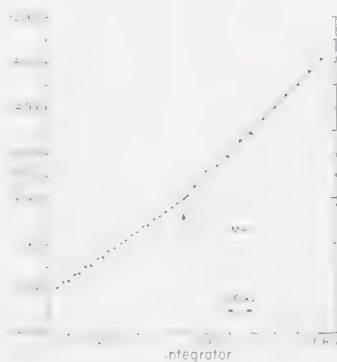


Fig. 10.

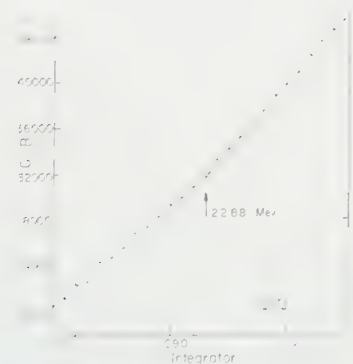


Fig. 11.

Figs 1-11. Activation yield from the $^{12}\text{C}(\gamma, n)^{11}\text{C}$ reaction, per unit dose after correction for background, plotted as a function of the peak bremsstrahlung energy.

integrated cross sections from the equation (Katz *et al.* 1954)

$$\int_0^{E_0} (\sigma_{\gamma,n})_i dE_\gamma = \int_0^{E_0} G_i \sigma_i(E_\gamma) dE_\gamma = \frac{\Delta\alpha(E_0)}{0.6023P(E_i, E_0)} \text{ (mev bn)}$$

where $(\sigma_{\gamma,n})_i$ is the cross section for (γ, n) reactions in the i th level, $\sigma_i(E_\gamma)$ is the photon capture cross section in the i th level, $\Delta\alpha(E_0)$ is the change in activity at bremsstrahlung peak energy E_0 due to the level at E_i (in neutrons/100 r mole), $P(E_i, E_0)$ the number of photons in the bremsstrahlung spectrum measured in photons 100 r in the interval from E_i to E_0 and G_i the neutron branching ratio from the level involved.

Table 1. Positions of Breaks and the Integrated (γ, n) Cross Section of the Photon Absorption Levels corresponding to these Breaks in the $^{12}\text{C}(\gamma, n)^{11}\text{C}$ Reactions

(1)	(2)	(3)	(4)
18.73 Threshold			
18.90	0.0125		18.86
18.96	0.0155		18.96
19.08	0.0194	19.10	19.10
19.17	0.0236		
19.30	0.0378		
19.46	0.0583		
19.57	0.0708	19.55 ± 0.05	19.56
19.76	0.0626		
19.92	0.127	19.95 ± 0.05	19.95
20.13	0.206		
20.29	0.282	20.35 ± 0.05	20.37
20.62	0.616	20.75 ± 0.05	20.75
20.90	0.657		
21.08	0.761		
21.22	0.956		
21.58	3.13		
22.02	2.80		
22.88	4.12		

(1) Energy of break E_i (mev) (energies are to within ± 0.04 mev near threshold and ± 0.07 mev near 23 mev); (2) $\int (\sigma_{\gamma,n})_i dE_\gamma$ (mev mbn) (relative values are given to 3 significant figures, absolute values are probably known to within 20%); (3) Spicer and Penfold (1955) E_i (mev); (4) Sadeh (1959) E_i (mev) (Sadeh quotes his energies to within ± 0.02 mev; this seems rather optimistic).

§ 4. DISCUSSION

Agreement between the positions of the breaks in the present experiment and measurements by Spicer and Penfold (1955) and by Sadeh (1959) is satisfactory, as can be seen from Table 1.

The integrated cross sections of the various levels (level strengths) are plotted against the break positions in Fig. 12. Also shown on the same figure are the spacings between the breaks as a function of the corresponding mean ^{12}C excitation energy. Since these breaks were observed in the reaction yield curve obtained by varying the peak bremsstrahlung energy E_0 , each break is seen on top of a 'background' of yield from all previous breaks. Now if we tentatively assume that the level spacings and level strengths are statistically distributed in the narrow energy region from 18.73 to 23 mev, then the build-up of yield

'back-ground' would tend to mask the weaker levels at the higher energies and we should expect to find level spacing and level strength to increase with energy.

We find in fact that while the level spacing increases only slightly with energy the strength increases by a factor of the order of 400 (Fig. 12). This almost exponential increase of level strength with energy towards the peak of the giant resonance (22.5 Mev) while the spacing remains almost constant, shows an intimate and direct relation between it and the giant resonance phenomena. The integrated cross section represented by all the breaks is 14 ± 3 Mev mbn.



Fig. 12. Spacing between breaks, D in Mev, plotted as circles at the mid-point energy and the integrated cross section in Mev mbn of each level represented by the break discontinuities, plotted as lines at the break position energy.

The experiment of Carroll and Stephens (1960), in which the absorption of monochromatic gammas from $\text{T}(\text{p}, \gamma)^4\text{He}$ through carbon absorbers were studied, showed three resonances. Their properties are summarized in Table 2.

Table 2. Levels found in the Photon Absorption Cross Section of Carbon by Carroll and Stephens

Level Position (Mev)	20.15	20.46	20.92
Width (Mev)	165 ± 30	145 ± 30	~ 300
Height (mbn)	6.5 ± 2	7 ± 3	
Integrated cross section (Mev mbn)	1.1 ± 0.6	1 ± 0.75	6.6 ± 1.2

Total integrated cross section 20.00 to 21.20 Mev; 8.7 ± 2.6 Mev mbn.

Penfold and Spicer (1955) have shown that if a level has a width Γ we may expect the corresponding break to be of the order of Γ below it. With this to guide us, we identify the breaks at 19.92 ± 0.05 , 20.29 ± 0.05 and 20.62 ± 0.06 Mev with the three levels observed by Carroll and Stephens. The separations between the breaks and the levels are 230 ± 60 (165 ± 30), 170 ± 60 (145 ± 30) and 300 ± 70

(~ 300) respectively, with the Carroll and Stephens level width shown in the brackets. A level corresponding to our break at 20.13 mev was not seen by them.

Levels listed by Ajzenberg-Selove and Lauritsen (1959) can be similarly identified with the breaks, taking into consideration their tabulated widths. However, in view of the relatively large energy errors, such identification is not very significant.

The level at 21.58 ± 0.06 mev was investigated in a careful set of independent experiments in our laboratory by Lindemberger (private communication). Least square lines were fitted to the experimental points above and below the break. His results are shown in Fig. 13(a). To indicate more clearly the nature of this break an arbitrary straight line designated by α_0 was drawn, and the deviations of the measured points from this line are shown in Fig. 13(b); the break in this case was found at 21.72 ± 0.06 mev. These measurements again emphasize that even with great care, present-day betatron energy calibration techniques are limited to approximately ± 70 kev at 23 mev.

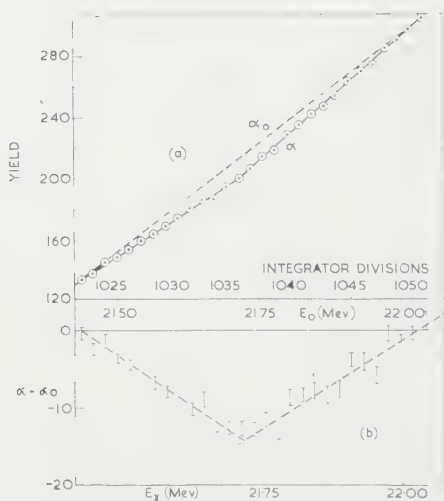


Fig. 13. (a) The activation yield from the $^{12}\text{C}(\gamma, n)^{11}\text{C}$ reaction in the region of 21.50 to 22.00 mev. α is the experimental curve, while α_0 is an arbitrary straight line. (b) The difference between the measured points α and the straight line α_0 . The bars on the experimental points represent the standard deviation calculated from counting statistics.

Ajzenberg-Selove and Lauritsen (1959) tabulate a level at 21.80 mev from values reported in the literature for the $^{11}\text{B}(\text{p}, n)$, ^{11}C , $^{12}\text{C}(\gamma, \text{p})$, ^{11}B and $^{12}\text{C}(\gamma, 3\alpha)$ reactions. This is some 150 kev above the mean value of the break position. Our results would thus imply that the level width is 150 ± 70 kev. The experimental points shown in Fig. 13(b) are not inconsistent with a level about 150 kev wide centred around a point 150 kev above the break.

In the energy range from 20.00 to 21.20 mev, Carroll and Stephens report an integrated cross section of 8.7 ± 2.6 mev mbn. In the same energy range, allowing for the difference between break position and level position, we find an integrated cross section of 2.3 ± 0.5 mev mbn. Experimentally it is found that the (γ, p) cross section in carbon is approximately 2 times that of (γ, n) (see for example Barber *et al.* (1955) and Penner and Leiss (1959)); thus for comparison,

our integrated cross section should be multiplied by approximately 3, giving a value in good agreement with that of Carroll and Stephens. This implies that the levels seen by them contain a large contribution from absorbed photons leading to (γ, p) reactions and we conclude that fine structure exists in this reaction also.

A more direct proof for fine structure in the $^{12}\text{C}(\gamma, p)^{11}\text{B}$ reaction comes from the work of Cohen and McElhinney (1956). Using nuclear plates and an energy resolution of 0.2 MeV they found a number of peaks in the proton energy distribution.

According to detailed balancing (Brown and Levinger 1958) the (γ, p) cross section is found by summing over all members j of the configuration of the final nucleus $A-1$. That is the (γ, p) cross section is obtained by summing from the ground state in A to all final states χ_i in $A-1$. Similarly the (p, γ) cross section sums all reactions which start from the ground state χ_0 in $A-1$ and includes all final states in A to which the emitted photon can go.

Penner and Leiss (1959) have shown that in the energy region of interest the (γ, p) reactions leave the residual ^{11}B nucleus in its ground state. Conversely in their work on the (p, γ) reactions Gove *et al.* (1959) measured the cross section for γ transitions to the ^{12}C ground state. Assuming that an undetected low energy cascade photon was not present, then detailed balancing should hold.

The fact that Gove *et al.* (1959) found the (p, γ_0) cross section smooth, with no fine structure, is thus an anomaly which is difficult to understand.

REFERENCES

- AJZENBERG-SELOVE, F., and LAURITSEN, T., 1959, *Nucl. Phys.*, **11**, 1.
 BARBER, W. C., GEORGE, W. D., and REAGAN, D. D., 1955, *Phys. Rev.*, **98**, 73.
 BROWN, G. E., and LEVINGER, J. S., 1958, *Proc. Phys. Soc.*, **71**, 733.
 CARROLL, E. E., JR., and STEPHENS, W. E., 1960, *Phys. Rev.*, **118**, 1256.
 COHEN, L., and McELHINNEY, J., 1956, *Rev. Sci. Instrum.*, **27**, 773.
 COHEN, L. D., and STEPHENS, W. E., 1959, *Phys. Rev. Letters*, **2**, 263.
 COOK, B. C., 1957, *Phys. Rev.*, **106**, 300.
 GEMMEL, D. S., MORTON, A. H., and TITTERTON, E. W., 1959, *Nucl. Phys.*, **10**, 33.
 GOLDENBERG, J., and KATZ, L., 1954, *Phys. Rev.*, **95**, 471.
 GOVE, H. E., LITTLERLAND, A. E., and BATCHELOR, R., 1959, *Phys. Rev. Letters*, **3**, 177.
 KATZ, L., 1959, *Canad. J. Phys.*, **37**, 1455.
 KATZ, L., HASLAM, R. N. H., CAMERON, A. G. W., and MONTALBETH, R., 1954, *Phys. Rev.*, **95**, 464.
 KING, H., and KATZ, L., 1959, *Canad. J. Phys.*, **37**, 1357.
 PENFOLD, A. S., and SPICER, B. M., 1955, *Phys. Rev.*, **100**, 1377.
 PENNER, S., and LEISS, J. E., 1959, *Phys. Rev.*, **114**, 1101.
 SADEH, D., 1959, *C. R. Acad. Sci., Paris*, **249**, 531.
 SPICER, B. M., and PENFOLD, A. S., 1955, *Phys. Rev.*, **100**, 1375.
 WOLF, M. M., and STEPHENS, W. E., 1958, *Phys. Rev.*, **112**, 890.

Strong Coupling in Optically Allowed Atomic Transitions produced by Electron Impact

By M. J. SEATON

Department of Physics, University College London

MS. received 2nd June 1960

Abstract. Optically allowed transitions have long-range interaction potentials, behaving asymptotically as s_1/r^2 where s_1 is proportional to the dipole matrix element. In calculating cross sections many angular momentum states l must therefore be considered. When the coupling is strong the usual Born approximation leads to violations of conservation conditions which are serious for the smaller values of l . Three variants of the first Born approximation are considered: I is the Born approximation for the total scattering amplitude, II the Born approximation for the reactance matrix and III (suggested by Percival) the Born approximation for the proper phase of the scattering matrix. Approximations II and III satisfy conservation conditions and make some allowance for processes such as $a \rightarrow a' \rightarrow a$, $a \rightarrow a' \rightarrow a''$ and of $a \rightarrow a''$ competing with $a \rightarrow a'$.

Considering the case of exact resonance, and replacing the potentials by their asymptotic forms, one obtains equations for which exact analytic solutions may be obtained. The exact solutions are compared with those obtained using approximations I, II and III.

§ 1. INTRODUCTION

STRONG coupling in electron-atom collisions may occur both for optically allowed and for optically forbidden transitions. Allowance for strong coupling presents different types of problems in these two cases. On making an analysis in terms of states of definite angular momentum, $\hbar[l(l+1)]^{1/2}$, of the colliding electron, it is usually found that comparatively few values of l give significant contributions to the cross sections for optically forbidden transitions. When strong coupling occurs in such cases it is necessary to make detailed calculations for the most important values of l . In many cases only one value of l need be considered.

The characteristic feature of optically allowed transitions is that the interaction potential has a very long range and in consequence many values of l are important. For strong optically allowed transitions one may find a value l_0 of l such that the coupling is weak for $l > l_0$ but becomes strong for $l < l_0$. Our problem is to find approximate methods which will be accurate for $l > l_0$, and which will give reasonable results for $l < l_0$. Purcell (1952) has considered this problem in a semi-classical treatment and a rather crude quantum mechanical treatment has previously been given by Seaton (1955). In calculating the $a \rightarrow a'$ cross section this earlier work makes some allowance for back-coupling, $a \rightarrow a' \rightarrow a$, but does not consider processes such as $a \rightarrow a' \rightarrow a''$ or $a \rightarrow a''$ competing with $a \rightarrow a'$.

In the present paper we consider three different ways of using the first Born approximation. Consideration of some exactly soluble equations gives some indication of the accuracy which may be obtained. One of our methods has been used by Van Regemorter (1960) in calculating cross sections for strong allowed transitions in Ca^+ produced by electron impact. Further applications of our methods will be given in later papers.

§ 2. FORMULATION FOR ELECTRON-HYDROGEN COLLISIONS

The nature of the problem to be considered is best appreciated by considering the partial wave formulation for electron-hydrogen collisions (Percival and Seaton 1957). We neglect electron exchange, which will be important only for small values of l .

2.1. The Radial Equations

Let the atom states be nl_1 , the velocity of the colliding electron be v_n and its angular momentum be $\hbar[l_2(l_2+1)]^{1/2}$. The radial equations are

$$\left[\frac{d^2}{dr^2} - \frac{l_2(l_2+1)}{r^2} + k_n^2 \right] F(nl_1 l_2 L | r) = \sum_{n'l_1' l_2' L} U(nl_1 l_2 L, n'l_1' l_2' L | r) \times F(n'l_1' l_2' L | r) \quad \dots\dots (2.1)$$

where $k_n = mv_n/\hbar$ and $\hbar[L(L+1)]^{1/2}$ is the total angular momentum. On making multipole expansions of the potentials we have $U = \sum_\lambda U_\lambda$ with

$$U_0(nl_1 l_2 L, n'l_1' l_2' L | r) = \frac{2me^2}{\hbar^2} \delta(l_1 l_2, l_1' l_2') \left\{ -\frac{\delta(n, n')}{r} + y_0(nl_1 n'l_1' | r) \right\} \quad \dots\dots (2.2)$$

and

$$U_\lambda(nl_1 l_2 L, n'l_1' l_2' L | r) = \frac{2me^2}{\hbar^2} f_\lambda(l_1 l_2 l_1' l_2'; L) y_\lambda(nl_1 n'l_1' | r) \quad \dots\dots (2.3)$$

for $\lambda > 0$, where

$$y_\lambda(nl_1 n'l_1' | r) = \frac{1}{r^{\lambda+1}} \int_0^r P_{nl_1}(r_0) r_0^\lambda P_{n'l_1'}(r_0) dr_0 + r^\lambda \int_r^\infty P_{nl_1}(r_0) \frac{1}{r_0^{\lambda+1}} P_{n'l_1'}(r_0) dr_0 \quad \dots\dots (2.4)$$

where $P_{nl_1}(r)$ is an atomic radial function. The coefficients f_λ are zero unless: (i) $l_1 l_2 L$ and $l_1' l_2' L$ satisfy the usual relations for vector-coupling, (ii) l_1, l_2 and l_1', l_2' satisfy the parity conservation condition, $(-1)^{l_1+l_2} = (-1)^{l_1'+l_2'}$, and (iii) λ is such that

$$|l_1 - l_1'| \leq \lambda \leq (l_1 + l_1'), \quad l_1 + l_1' + \lambda = \text{even integer} \quad \dots\dots (2.5)$$

and

$$|l_2 - l_2'| \leq \lambda \leq (l_2 + l_2'), \quad l_2 + l_2' + \lambda = \text{even integer}. \quad \dots\dots (2.6)$$

Considering large values of r ,

$$y_\lambda(nl_1 n'l_1' | r) = \frac{1}{r^{\lambda+1}} s_\lambda(nl_1 n'l_1') + O(r^{-\lambda-2}) \quad \dots\dots (2.7)$$

where

$$s_\lambda(nl_1 n'l_1') = \int_0^\infty P_{nl_1}(r) r^\lambda P_{n'l_1'}(r) dr. \quad \dots\dots (2.8)$$

Due to the orthonormality of atom functions, $s_0(nl_1 n'l_1) = \delta(n, n')$ and rU_0 goes to zero for large values of r . Further analysis shows that† $U_0 \rightarrow 0$ exponentially for $r \rightarrow \infty$. For r large the dominant interactions are those for the dipole term, $\lambda = 1$. From (2.5) it is seen that these occur only for $l_1' = l_1 \pm 1$, which is the condition for the transitions to be optically allowed.

† We consider only transitions between bound states; see Castillejo, Percival and Seaton (1960).

2.2. Boundary Conditions

We now use a, a' for the states $nl_1l_2L, n'l_1'l_2'L$ and use k for k_n, l for l_2 . We consider only those functions $F(a|r)$ satisfying $F(a|0)=0$. With N states a we can then obtain N linearly independent sets of solutions of the Eqns (2.1). Let the functions of the i th set be $F(a, i|r)$ and for their asymptotic forms use the notation

$$F(a, i|r) \sim k^{-1/2} \{ \sin(kr - \frac{1}{2}l\pi) p_{ai} + \cos(kr - \frac{1}{2}l\pi) q_{ai} \}. \quad \dots\dots (2.9)$$

We consider two special cases: the functions $F_{\mathbf{R}}(a, a'|r)$ having asymptotic forms specified by the reactance matrix \mathbf{R} and the functions $F_{\mathbf{S}}(a, a'|r)$ specified by the scattering matrix \mathbf{S} . The asymptotic forms are

$$F_{\mathbf{R}}(a, a'|r) \sim k^{-1/2} \{ \sin(kr - \frac{1}{2}l\pi) \delta_{aa'} + \cos(kr - \frac{1}{2}l\pi) R_{aa'} \} \quad \dots\dots (2.10)$$

and

$$F_{\mathbf{S}}(a, a'|r) \sim k^{-1/2} \{ \exp[-i(kr - \frac{1}{2}l\pi)] \delta_{aa'} - \exp[+i(kr - \frac{1}{2}l\pi)] S_{aa'} \}. \quad \dots\dots (2.11)$$

One obtains the matrix relations $\mathbf{R} = \mathbf{q} \cdot \mathbf{p}$ and $\mathbf{S} = (\mathbf{1} + i\mathbf{R})(\mathbf{1} - i\mathbf{R})$. The cross sections are expressed in terms of the transmission matrix \mathbf{T} :

$$\mathbf{T} \equiv \mathbf{1} - \mathbf{S} = \frac{-2i\mathbf{R}}{1 - i\mathbf{R}} = - \frac{2i\mathbf{q}}{\mathbf{p} - i\mathbf{q}}. \quad \dots\dots (2.12)$$

The cross section for $n'l_1' \rightarrow nl_1$ is

$$Q(n'l_1' \rightarrow nl_1) = \frac{\pi \Omega(nl_1, n'l_1')}{k^2(2l_1 + 1)} \quad \dots\dots (2.13)$$

where

$$\Omega(nl_1, n'l_1') = \sum_{l_2l_2'} (2L + 1) |T(nl_1l_2L, n'l_1'l_2'L)|^2. \quad \dots\dots (2.14)$$

Since $U(a, a'|r)$ is real and symmetric, \mathbf{R} must be real and symmetric ($\mathbf{R} = \mathbf{R}^*, \mathbf{R} = \tilde{\mathbf{R}}$) and from $\mathbf{S} = (\mathbf{1} + i\mathbf{R})(\mathbf{1} - i\mathbf{R})$ it follows that \mathbf{S} must be symmetric and unitary; hence $\mathbf{S} = \tilde{\mathbf{S}}, |\mathbf{S}|^2 = \mathbf{1}$. From the conservation condition, $|\mathbf{S}|^2 = \mathbf{1}$, we have $|\mathbf{T}|^2 = 2\Re\mathbf{T}$, $\Re\mathbf{T}$ being the real part of \mathbf{T} . We seek approximate solutions satisfying these conditions.

§ 3. THE BORN APPROXIMATION

The Born approximation is obtained assuming U to be small. The usual form of the approximation, which will be referred to as approximation I, has the advantage that the total scattering amplitude may be calculated without making a partial wave analysis. Approximation I has the disadvantage, not only that there may be considerable error if the assumption of U small is not justified, but also that, from the expression for the total amplitude, it is difficult to estimate to what extent such errors may be introduced.

Our discussion considers the partial wave analysis. The assumption that U should be small will then be justified if it leads to a matrix \mathbf{T} satisfying $\mathbf{T} \ll \mathbf{1}$. Approximation I always violates the conservation conditions but this is not serious for $\mathbf{T} \ll \mathbf{1}$.

Having calculated the Born partial wave integrals we may calculate \mathbf{T} in a number of different ways which are all equivalent for $\mathbf{T} \ll \mathbf{1}$ but which differ for larger values of \mathbf{T} . We may expect to obtain some improvement if we calculate \mathbf{T} in such a way that the conservation conditions are satisfied.

3.1. Elastic Scattering

Three different ways of using the first Born approximations are first considered for elastic scattering.

Let the solutions of

$$\left[\frac{d^2}{dr^2} - \frac{l(l+1)}{r^2} - U(r) + k^2 \right] F(r) = 0 \quad \dots\dots (3.1)$$

satisfy $F(0) = 0$, $F(r) \sim k^{-1/2} \sin(kr - \frac{1}{2}l\pi + \eta_l)$. The exact scattering amplitude is

$$f(\theta) = \frac{-1}{2iR} \sum_l (2l+1) P_l(\cos \theta) T(l) \quad \dots\dots (3.2)$$

where $T(l) = 1 - S(l)$, $S(l) = \exp 2i\eta_l$ and η_l is real. First consider $U(r)$ to be small, giving $\eta_l \ll 1$. We then have that

$$\eta_l \simeq \tan \eta_l \simeq -\frac{1}{2i} (1 - \exp 2i\eta_l) \quad \dots\dots (3.3)$$

and that these are all approximately equal to the Born integral

$$B(l) = -\frac{1}{2} \pi \int_0^\infty U(r) J_{l+\frac{1}{2}}^2(kr) r dr. \quad \dots\dots (3.4)$$

The following three approximations are equivalent for small η_l but differ for large η_l .

Approximation I. We have $T = 1 - e^{2i\eta} \simeq -2i\eta$, giving

$$T_I = -2iB. \quad \dots\dots (3.5)$$

Substituting (3.5) in (3.2), the sum may be evaluated to obtain

$$f_I = - \int_0^\infty \frac{\sin(Kr)}{Kr} U(r) r^2 dr \quad \dots\dots (3.6)$$

where $K = 2k \sin \theta/2$. This is the usual first Born approximation for the scattering amplitude (Mott and Massey 1949, p. 119).

Approximation II. We use the Born approximation for $\tan \eta$. Putting $R = \tan \eta$ we have $T = 1 - e^{2i\eta} = -2iR/(1-iR)$. Approximation II is $R = B$,

$$T_{II} = -2iB/(1-iB). \quad \dots\dots (3.7)$$

Approximation III. We use the Born approximation for η (Percival 1960). Putting $\eta = B$ we have

$$T_{III} = 1 - e^{2iB}. \quad \dots\dots (3.8)$$

To consider the behaviour of these expressions when U becomes large let us put $U = \alpha u$ and let α vary. The exact expression gives $|T|^2 = 4 \sin^2 \eta$ and the conservation condition is $|T|^2 \leq 4$. Since η increases with α , $|T|^2$ will be an oscillatory function of α for α large. In approximation I, $|T_I|^2 = 4B^2$ which increases as α^2 and becomes greater than 4 for α large. In approximation II $|T_{II}|^2 = 4B^2/(1+B^2)$, which is always less than 4 but approaches 4 for $\alpha \rightarrow \infty$, corresponding to a phase η_{II} of $\pi/2$. Approximation III gives $|T_{III}|^2 = 4 \sin^2 B$ which has the correct general behaviour of an oscillatory function for α large. Percival (1960) has published graphs illustrating these trends in particular cases.

Let us next consider how, for a given function U , $|T(l)|^2$ will depend on l . Our main interest is in potentials which are large and of long range and we wish to evaluate sums of the type

$$\sum_{l=0}^{\infty} (2l+1) |T(l)|^2. \quad \dots\dots (3.9)$$

The trend of $|T(l)|^2$ for a fixed potential, as l decreases, will be similar to the trend of $|T(l)|^2$ for fixed l as the potential increases. Suppose that there is a value l_0

of l such that $|T(l)| \ll 1$ for $l > l_0$ but that $T_l(l)$ becomes large for $l < l_0$. For large l our three approximations give similar results which differ little from the exact results. For small l approximation I will overestimate the contribution to the sum by an amount which may lead to large errors. Approximation II will be much better but may still overestimate the sum if the potential is strong enough to make $|T(l)|^2$ an oscillatory function of l for l small. In such cases $|T_{\text{III}}(l)|^2$ will also be an oscillatory function and should give better results. When l is small, approximation III may not give $|T(l)|^2$ accurately for any given small value of l but, assuming l_0 to be large, it should give a good estimate for the sum. Approximations II and III should give good results for the sum whenever there is a large contribution from the weak interaction region of $l > l_0$.

3.2. The Many-Channel Case

We define a matrix \mathbf{B} with elements

$$B(nl_1l_2L, n'l_1'l_2'L) = -\frac{\pi}{2} \int_0^\infty J_{l_1+\frac{1}{2}}(kr) U(nl_1l_2L, n'l_1'l_2'L | r) J_{l_1'+\frac{1}{2}}(k'r) r dr. \quad \dots\dots (3.10)$$

Our variants of the first Born approximation are

$$\mathbf{T}_I = -2i\mathbf{B} \quad \dots\dots (3.11)$$

$$\mathbf{T}_{\text{II}} = -2i\mathbf{B}/(1-i\mathbf{B}) \quad \dots\dots (3.12)$$

$$\mathbf{T}_{\text{III}} = 1 - e^{2i\mathbf{B}}, \quad \dots\dots (3.13)$$

approximation III being due to Percival (1960). The matrix $e^{2i\mathbf{B}}$ may be defined as a power series but is best calculated on diagonalizing \mathbf{B} . Let $\mathbf{BY} = \mathbf{Yb}$ where \mathbf{Y} is a unitary matrix, \mathbf{b} a diagonal matrix with diagonal elements b_j . Then $\mathbf{B} = \mathbf{YbY}^\dagger$ and $e^{2i\mathbf{B}} = \mathbf{Y}e^{2i\mathbf{b}}\mathbf{Y}^\dagger$ where $e^{2i\mathbf{b}}$ is a diagonal matrix with diagonal elements $\exp 2ib_j$.

The matrices \mathbf{T}_{II} and \mathbf{T}_{III} satisfy the conservation conditions. Approximation II involves a matrix inversion and approximation III involves a matrix diagonalization.

In using these methods the first step is to calculate the matrix \mathbf{B} . Practical methods for doing this will be described in a later paper. For the moment we try to get some idea of the usefulness of these methods by considering the situation obtained when the potentials are replaced by their asymptotic forms.

§ 4. THE BETHE APPROXIMATION

The Bethe approximation is usually obtained on replacing $e^{i\mathbf{K}\cdot\mathbf{r}}$ by $1 + i\mathbf{K}\cdot\mathbf{r}$ in the expression for Born total amplitude, \mathbf{K} being $\mathbf{k}' - \mathbf{k}$. This gives non-zero results only for optically allowed transitions. An alternative derivation (Seaton 1955) is to use the Born approximation after replacing $1/|\mathbf{r}_1 - \mathbf{r}_2|$ by

$$\frac{1}{r_2} + \frac{\mathbf{r}_1 \cdot \mathbf{r}_2}{r_2^3}, \quad \dots\dots (4.1)$$

\mathbf{r}_1 being the coordinate of the atomic electron and \mathbf{r}_2 that of the colliding electron. In terms of the partial-wave multipole analysis, this means that we put all $y_\lambda = 0$ for $\lambda \neq 1$ and replace all $y_1(nl_1n'l_1' | r)$ by $s_1(nl_1n'l_1')/r^2$.

Having made these approximations in the potentials we consider each of the three variants of the Born approximation.

On replacing y_1 by s_1/r^2 we obtain, in place of **B**, a matrix **B'** where

$$B'(nl_1l_2L, n'l_1'l_2'L) = -\frac{2me^2}{\hbar^2}f_1(l_1l_2l_1'l_2'; L)s_1(nl_1n'l_1')\frac{\pi}{2}\int_0^\infty J_{l_2+\frac{1}{2}}(kr)\frac{1}{r}J_{l_2'+\frac{1}{2}}(k'r)dr. \quad \dots\dots (4.2)$$

Evaluation of the integral gives, for $(k'/k) \leq 1$,

$$B'(nl_1l_2L, n'l_1'l_2'L) = -\frac{2me^2}{\hbar^2}f_1(l_1l_2l_1'l_2'; L)s_1(nl_1n'l_1')\left(\frac{k'}{k}\right)^{l_2+l_2'+1} \frac{E_1(\frac{1}{2}(l_2+l_2'+1), \frac{1}{2}(l_2'-l_2); (k'/k)^2)}{(l_2+l_2'+1)} \quad \dots\dots (4.3)$$

where $l_2' = l_2 \pm 1$ and where the functions E_1 are tabulated by Seaton (1955).

For the exact resonance case, $k = k'$ implying $n = n'$, we have $E_1 = 1$ and

$$B'(nl_1l_2L, nl_1'l_2'L) = -\frac{2me^2}{\hbar^2}f_1(l_1l_2l_1'l_2'; L)s_1(nl_1nl_1') \frac{1}{(1+l_2+l_2')}. \quad \dots\dots (4.4)$$

The long-range parts of the potentials dominate for large l_2, l_2' and therefore the Born integral B equals the Bethe integral B' in the limit of large l_2, l_2' . In the special case of exact resonance the long range parts dominate for small k and $B = B'$ in the limit of $k = 0$.

§ 5. EXACT RESONANCE

We shall consider transitions between the states $nl_1, nl_1', l_1' = l_1 \pm 1$, of a hydrogen energy level n . We have $l_2' = l_2 \pm 1$, so that the coupled equations contain at least three functions $F(nl_1l_2L)$. In the approximation of retaining only long-range parts of the potentials explicit solutions of these equations may be obtained. We first consider the case of similar equations containing only two functions.

5.1. The Two-Channel Case

In place of $l' = l \pm 1$ we first consider $l' = l$,

$$\begin{aligned} \left(\frac{d^2}{dr^2} - \frac{l(l+1)}{r^2} + k^2\right)F_1 &= \frac{A}{r^2}F_2 \\ \left(\frac{d^2}{dr^2} - \frac{l(l+1)}{r^2} + k^2\right)F_2 &= \frac{A}{r^2}F_1. \end{aligned} \quad \dots\dots (5.1)$$

Putting $F_\pm = (F_1 \pm F_2)/\sqrt{2}$,

$$\left(\frac{d^2}{dr^2} - \frac{l(l+1)}{r^2} + k^2\right)F_\pm = \pm \frac{A}{r^2}F_\pm \quad \dots\dots (5.2)$$

and

$$F_\pm \sim (1/\pi l)^{1/2} F_{\pm l}(kr) \sim \sin(kr - \frac{1}{2}l\pi) \quad \dots\dots (5.3)$$

where

$$\mu^\pm(\mu^\pm + 1) = l(l+1) \pm A. \quad \dots\dots (5.4)$$

There are two roots for μ^+ and two for μ^- ; we choose those giving $F_\pm(0) = 0$.

Defining η^\pm by $F_\pm \sim \sin(kr - \frac{1}{2}l\pi + \eta^\pm)$ we obtain

$$\eta^\pm \sim \frac{1}{2}\pi \left\{ (2l+1) - [(2l+1)^2 + 4A]^{1/2} \right\}. \quad \dots\dots (5.5)$$

With $T_\pm = 1 - \exp 2i\eta^\pm$ we obtain $T_{11} = T_{22} = \frac{1}{2}(T_+ + T_-)$ and

$$T_{12} = T_{21} = \frac{1}{2}(T_+ - T_-).$$

It should be noted that acceptable solutions exist only for $|A| < (l + \frac{1}{2})^2$ (Mott and Massey 1949, p. 40).

The Born integral is $B_{12} = -\gamma$ where

$$\gamma = -\frac{\pi}{2}\int_0^\infty \frac{1}{r}J_{l+\frac{1}{2}}^2(kr)dr = \frac{\pi A}{2(2l+1)} \quad \dots\dots (5.6)$$

(Watson 1948). Table 1 gives the solutions for **T**.

Table 1. The \mathbf{T} matrix for the Exact Resonance Two-Channel Case

	Approximation			Exact
	I	II	III	
$T_{11} = T_{22}$	0	$2\gamma^2/(1+\gamma^2)$	$2 \sin^2 \gamma$	$1 - \frac{1}{2}(\exp 2i\eta^- + \exp 2i\eta^+)$
$T_{12} = T_{21}$	$2i\gamma$	$2i\gamma/(1+\gamma^2)$	$i \sin 2\gamma$	$\frac{1}{2}(\exp 2i\eta^- - \exp 2i\eta^+)$

Fig. 1 shows some results for $l=2$ and A variable. Exact solutions do not exist for $|A| > 6.25$. Approximation I gives $|T_{12}| > 1$, violating the conservation condition for large A , and gives $T_{11}=0$ for all A . Approximation II gives good results up to the maximum of $|T_{12}|$ but beyond this it overestimates $|T_{12}|$ and underestimates $|T_{11}|$. Approximation III continues to give good results up to larger values of A .

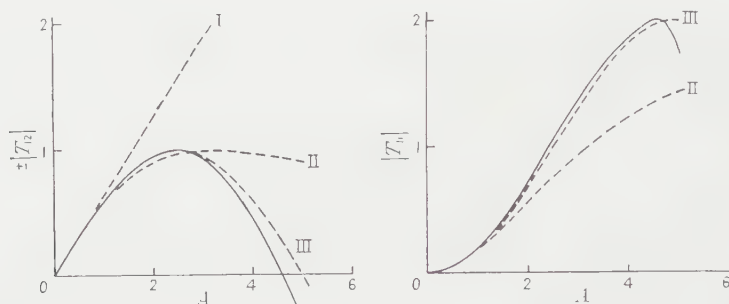


Fig. 1. $|T|$ plotted against A (for $l=2$) for the exact resonance two-channel problem. Full line curves are used for the exact solutions, broken curves for approximations I, II and III.

5.2. A Three-Channel Case

We consider coupling between the states ns , np . We label the states by subscripts $\nu=1, 2, 3$ according to the scheme

ν	nl_1	l_2	L
1	ns	l	l
2	np	$l-1$	l
3	np	$l+1$	l

Retaining only asymptotic forms of dipole potentials we have

$$U_{11} = U_{22} = U_{33} = U_{23} = 0$$

and

$$U_{12} = \frac{l^{1/2}\beta}{r^2}, \quad U_{13} = -\frac{(l+1)^{1/2}\beta}{r^2} \quad \dots\dots (5.7)$$

where

$$\beta = \frac{2me^2}{\hbar^2} \frac{s_1(ns, np)}{[3(2l+1)]^{1/2}} \quad \dots\dots (5.8)$$

We have here used $f_1(0l1l-1; l) = [l/3(2l+1)]^{1/2}$

and

$$f_1(0l1l+1; l) = -[(l+1)/3(2l+1)]^{1/2}$$

(Percival and Seaton 1957). The radial equations may be written

$$r^2 \left(\frac{d^2}{dr^2} + k^2 \right) \mathbf{F} = \mathbf{A}\mathbf{F} \quad \dots\dots (5.9)$$

where \mathbf{F} is the vector† with components F_1, F_2, F_3 and \mathbf{A} is the matrix

$$\mathbf{A} = \begin{pmatrix} l(l+1) & l^{1/2}\beta & -(l+1)^{1/2}\beta \\ l^{1/2}\beta & (l-1)l & 0 \\ -(l+1)^{1/2}\beta & 0 & (l+1)(l+2) \end{pmatrix} \dots (5.10)$$

To solve (5.9) we diagonalize \mathbf{A} . Put $\mathbf{AX} = \mathbf{Xa}$ where \mathbf{X} is unitary and \mathbf{a} diagonal. The eigenvalues are

$$\left. \begin{aligned} a_1 &= l(l+1) \\ a_2 &= l^2 + l + 1 - (2l+1)x \\ a_3 &= l^2 + l + 1 + (2l+1)x \end{aligned} \right\} x = \left[1 + \frac{\beta^2}{(2l+1)} \right]^{1/2} \dots (5.11)$$

$$\text{With } \mathbf{G} = \mathbf{X}^+ \mathbf{F}, \quad r^2 \left(\frac{d^2}{dr^2} + k^2 \right) \mathbf{G} = \mathbf{aG} \dots (5.12)$$

and we may take the solutions to be

$$G_i = -2i \exp \left[-\frac{1}{2} i \pi \mu_i \right] \left(\frac{1}{2} \pi k r \right)^{1/2} J_{\mu_i + \frac{1}{2}}(kr) \dots (5.13)$$

where $\mathbf{a} = \boldsymbol{\mu}(\boldsymbol{\mu} + 1)$. To obtain $G(0) = 0$,

$$\left. \begin{aligned} \mu_1 &= l \\ \mu_2 &= -\frac{1}{2} + \left[\left(l - \frac{1}{2} \right)^2 - C \right]^{1/2} \\ \mu_3 &= \frac{1}{2} + \left[\left(l + \frac{1}{2} \right)^2 - C \right]^{1/2} \end{aligned} \right\} C = (2l+1)(x-1) \dots (5.14)$$

$$\text{Acceptable solutions exist only for } C \geq \left(l - \frac{1}{2} \right)^2 \text{ giving} \quad \frac{1}{4}(2l-1)(2l+3) \geq (2l+1)^{1/2}\beta \dots (5.15)$$

The asymptotic forms are

$$\mathbf{G} \sim e^{-ikr} \mathbf{1} - e^{+ikr} \boldsymbol{\sigma} \dots (5.16)$$

where $\boldsymbol{\sigma} = e^{-i\pi\boldsymbol{\mu}}$ and, using $\mathbf{F} = \mathbf{XG}$,

$$\mathbf{F} \sim e^{-ikr} \mathbf{1} - e^{+ikr} \mathbf{S}' \dots (5.17)$$

where $\mathbf{S}' = \mathbf{X}\boldsymbol{\sigma}\mathbf{X}^+$. The elements of \mathbf{S} , defined in terms of $\exp \{ \pm i(kr - \frac{1}{2}l\pi) \}$, are obtained from those of \mathbf{S}' on multiplying by suitable phase factors. The final expressions for \mathbf{T} are

$$\left. \begin{aligned} DT_{11} &= \beta^2 \{ (2l+1)(1+q) + r \} \\ DT_{12} &= i\beta l^{1/2} \{ 2(l+1)(1+q+r) + \beta^2 r \} \\ DT_{13} &= -i\beta (l+1)^{1/2} \{ 2l(1+q-r) - \beta^2 r \} \\ DT_{22} &= D(1-q) + (l+1)\beta^2(1+q) - l[(4l+3)x^2 + 1]r \\ DT_{23} &= -\beta^2 \frac{[l(l+1)]^{1/2}}{(2l+1)} \{ (2l+1)(1+q) + r \} \\ DT_{33} &= D(1-q) + l\beta^2(1+q) + (l+1)[(4l+1)x^2 - 1]r \end{aligned} \right\} \dots (5.18)$$

$$\text{where } \left. \begin{aligned} D &= 4l(l+1) + (2l+1)\beta^2 \\ q &= \frac{1}{2} \{ \exp i\pi\eta_2 + \exp(-i\pi\eta_3) \} \\ r &= \frac{1}{2x} \{ \exp i\pi\eta_2 - \exp(-i\pi\eta_3) \} \end{aligned} \right\} \dots (5.19)$$

$$\text{and } \left. \begin{aligned} \eta_2 &= \left(l - \frac{1}{2} \right) - \left[\left(l - \frac{1}{2} \right)^2 - C \right]^{1/2} \\ \eta_3 &= \left[\left(l + \frac{3}{2} \right)^2 + C \right]^{1/2} - \left(l + \frac{3}{2} \right) \end{aligned} \right\} \dots (5.20)$$

$$\text{Considering the Born approximation for (5.9), the only non-zero elements of } \mathbf{B} \text{ are } B_{12} = B_{21} = -\frac{1}{2} l^{-1/2} \beta, \quad B_{13} = B_{31} = \frac{1}{2} (l+1)^{-1/2} \beta \dots (5.21)$$

where β is defined by (5.8) and where we have used (4.4). Introducing

$$\theta = -\frac{1}{2} l^{-1/2} \beta, \quad \phi = \frac{1}{2} (l+1)^{-1/2} \beta, \dots (5.22)$$

$$\gamma = (\theta^2 + \phi^2)^{1/2} = \frac{1}{2} \left\{ \frac{(2l+1)}{l(l+1)} \right\}^{1/2} \beta \dots (5.23)$$

we obtain the expressions of Table 2 for approximations I, II and III.

† The symbol \mathbf{F} is also used for the 3×3 matrix obtained from three linearly independent sets of solutions.

Table 2. Approximations I, II and III for the Exact Resonance Three-Channel Case

	I	II	III
T_{11}	0	$2\gamma^2/(1+\gamma^2)$	$2\sin^2\gamma$
T_{12}	$-2i\theta$	$-2i\theta/(1+\gamma^2)$	$-i(\theta/\gamma)\sin 2\gamma$
T_{13}	$-2i\phi$	$-2i\phi/(1+\gamma^2)$	$-i(\phi/\gamma)\sin 2\gamma$
T_{22}	0	$2\theta^2/(1+\gamma^2)$	$2(\theta/\gamma)^2\sin^2\gamma$
T_{23}	0	$2\theta\phi/(1+\gamma^2)$	$2(\theta\phi/\gamma^2)\sin^2\gamma$
T_{33}	0	$2\phi^2/(1+\gamma^2)$	$2(\phi/\gamma)^2\sin^2\gamma$

Calculations have been made for H 2s, 2p. In atomic units $s_1(2s, 2p) = 3\sqrt{3}$ and $\beta = 6/(2l+1)^{1/2}$. According to (5.15) acceptable exact solutions of (5.9) exist only for $l \geq 3$. Fig. 2 shows results for

$$\Omega_{\nu\nu'}(l) = (2l+1) |T_{\nu\nu'}(l)|^2. \quad \dots\dots (5.24)$$

The coupling is strong for the smaller values of l but not so strong that the $|T_{\nu\nu'}|^2$ are oscillatory functions of l . In all cases approximations II and III are better than I. For the direct coupling cases, Ω_{12} and Ω_{13} , approximations II and III give good results for the whole range of l considered. For the other cases there is

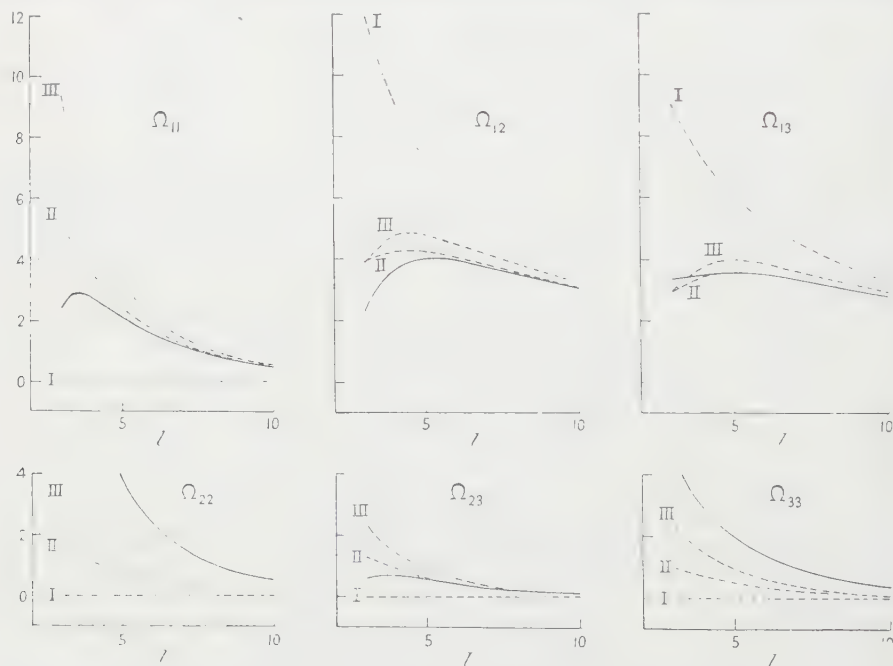


Fig. 2. $\Omega_{\nu\nu'}(l)$ plotted against l for the exact resonance three-channel problem. Full line curves are used for exact results, broken curves for approximation I, II and III.

no direct coupling and transitions take place only through processes of the type $\nu \rightarrow \nu' \rightarrow \nu''$. For large l approximations II and III give good results for Ω_{11} and Ω_{23} but are not so good for Ω_{22} and Ω_{33} . This may be understood as follows. The conservation condition gives relations of the type

$$\Omega_{12} + \Omega_{22} + \Omega_{32} = 2(2l+1)\Re T_{22}. \quad \dots\dots (5.25)$$

For large l the left-hand side is dominated by the direct-coupling contribution, Ω_{12} . Approximations II and III for large l therefore give good results for $\Re T_{22}$

but the exact solutions show that the imaginary part of T_{22} is somewhat larger than the real part. In II and III this imaginary part is zero and $|T_{22}|^2$ is underestimated. In such cases the conservation condition alone does not ensure that good results are obtained.

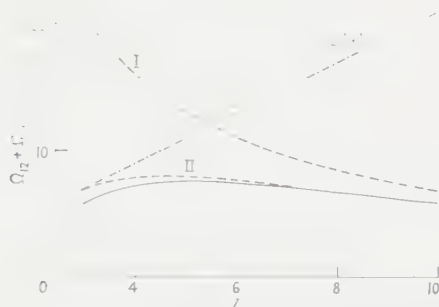


Fig. 3. $\Omega_{12}(l) + \Omega_{13}(l)$ plotted against l . Curves show exact results (full line), approximations I and II, and the upper limit of $2l+1$.

From the conservation condition it follows that

$$\Omega_{12}(l) + \Omega_{13}(l) \dots\dots\dots (5.26)$$

should not exceed $2l+1$. Fig. 3 shows (5.26) plotted against l . Approximation I is seen to give values greater than $2l+1$ for $l < 6$.

ACKNOWLEDGMENTS

I would like to thank Dr. I. C. Percival for discussions, particularly those relating to his work on approximation III.

REFERENCES

- CASTILLEJO, L., PERCIVAL, I. C., and SEATON, M. J., 1960, *Proc. Roy. Soc. A*, **254**, 259.
 MOTT, N. F., and MASSEY, H. S. W., 1949, *Theory of Atomic Collisions*, 2nd edn (Oxford: Clarendon Press), pp. 40, 119.
 PERCIVAL, I. C., 1960, *Proc. Phys. Soc.*, **76**, 206.
 PERCIVAL, I. C., and SEATON, M. J., 1957, *Proc. Camb. Phil. Soc.*, **53**, 654.
 PURCELL, E. M., 1952, *Astrophys. J.*, **116**, 457.
 VAN REGEMORTER, H., 1960, *Mon. Not. R. Astr. Soc.*, **121**, 213.
 SEATON, M. J., 1955, *Proc. Phys. Soc. A*, **68**, 457.
 WATSON, G. N., 1948, *Bessel Functions*, 2nd edn (Cambridge: University Press), p. 403.

The Evaluation of Partial Wave Integrals in the Born Approximation

BY M. J. SEATON

Department of Physics, University College London

MS. received 2nd June 1960

Abstract. The Born partial wave integrals may be evaluated on making a harmonic analysis of the integrals occurring in the Born total scattering amplitude. This provides a convenient method for numerical evaluation of the partial wave integrals.

The paper includes the proofs of an addition theorem for solid harmonics and a multiplication theorem for spherical Bessel functions.

§ 1. INTRODUCTION

USE of the Born approximation in a collision problem involves evaluation of integrals of the type

$$(\mathbf{k}_j|V_{ji}|\mathbf{k}_i) = \int \exp(-i\mathbf{k}_j \cdot \mathbf{r}) V_{ji}(\mathbf{r}) \exp(+i\mathbf{k}_i \cdot \mathbf{r}) d^3\mathbf{r}. \quad \dots\dots (1.1)$$

On making a partial wave analysis we obtain integrals

$$(k_j l_j m_j|V_{ji}|k_i l_i m_i) = \int \phi^*(k_j l_j m_j|\mathbf{r}) V_{ji}(\mathbf{r}) \phi(k_i l_i m_i|\mathbf{r}) d^3\mathbf{r} \quad \dots\dots (1.2)$$

where

$$\phi(klm|\mathbf{r}) = Y_{lm}(\mathbf{r}) f_l(kr),$$

Y_{lm} being a normalized spherical harmonic, \mathbf{r} the unit vector specifying the direction of \mathbf{r} and

$$f_l(x) = \left(\frac{\pi}{2x}\right)^{1/2} J_{l+1/2}(x)$$

being a spherical Bessel function.

It is usually possible to evaluate (1.1) without making a partial wave analysis but such an analysis is of interest for several reasons. Using (1.1) alone it is often difficult to estimate the accuracy of a Born cross section but, since the assumptions made in deriving the Born approximation are valid for large relative angular momenta, an estimate of accuracy is easier to make when the integrals (1.2) have been evaluated. A defect of the usual Born approximation is that the scattering amplitude obtained from (1.1) is not consistent with conservation theorems. Once the Born partial wave integrals have been evaluated they may be used in alternative expressions for the scattering amplitude which satisfy the conservation theorems. A further reason for making a Born partial wave analysis is that, in a more elaborate treatment of the collision problem, only small values of the angular momenta are usually considered. To obtain the total cross section it is necessary to add the contributions from large angular momenta as calculated in the Born approximation.

1.1. Elastic Scattering by a Central Potential

In order to illustrate the ideas underlying the method used in the more general case, we first consider elastic scattering by a central potential. Let the potential be $V(r)$, the velocity of the incident particle be \mathbf{v}' and the velocity after scattering be \mathbf{v} . We define

$$u(r) = \frac{2m}{\hbar^2} V(r), \quad \mathbf{k}' = m\mathbf{v}'/\hbar \quad \text{and} \quad \mathbf{k} = m\mathbf{v}/\hbar.$$

Since the scattering is elastic, $k = k'$. The Born total amplitude is (Mott and Massey 1949)

$$f(K) = -\frac{1}{4\pi} \int e^{i\mathbf{K} \cdot \mathbf{r}} u(r) d^3\mathbf{r} \quad \dots\dots(1.3)$$

where $\mathbf{K} = \mathbf{k}' - \mathbf{k}$ and $K = [2k^2(1 - \cos \omega)]^{1/2}$ where ω is the angle between \mathbf{k} and \mathbf{k}' . Carrying out the angular integrations in (1.3) we obtain

$$f(K) = -\int_0^\infty u(r) f_0(Kr) r^2 dr \quad \dots\dots(1.4)$$

where

$$f_0(x) = \frac{\sin x}{x}.$$

The required partial wave integrals are

$$L(kl) = -k \int_0^\infty u(r) f_l^2(kr) r^2 dr. \quad \dots\dots(1.5)$$

Thus the Born approximation for the tangent of the phase is

$$(\tan \eta_l)_{\text{Born}} = L(kl). \quad \dots\dots(1.6)$$

We show that the integrals (1.5) may be evaluated on making a harmonic analysis of the simpler integrals (1.4). We use the Bessel function relation (Watson 1948)

$$f_0(Kr) = \sum_l (2l+1) P_l(\cos \omega) f_l^2(kr), \quad \dots\dots(1.7)$$

where $K = [2k^2(1 - \cos \omega)]^{1/2}$, to obtain

$$f(K) = \frac{1}{k} \sum_l (2l+1) P_l(\cos \omega) L(kl) \quad \dots\dots(1.8)$$

and hence,

$$L(kl) = \frac{k}{2} \int_{-1}^{+1} f(K) P_l(\cos \omega) d \cos \omega. \quad \dots\dots(1.9)$$

For numerical calculations, the use of (1.4) and (1.9) is much simpler than direct calculation using (1.5).

The aim of the present paper is to obtain expressions similar to (1.9) for inelastic collisions. We require a generalization of the Bessel function relation (1.7). This is obtained in §3. The proof requires an addition theorem for solid harmonics which is obtained in §2

§ 2. AN ADDITION THEOREM FOR SOLID HARMONICS

The normalized spherical harmonic $Y_{lm}(\mathbf{r})$ is defined by

$$Y_{lm}(\mathbf{r}) = \frac{(-1)^m}{2^l l!} \left[\frac{(2l+1)(l-m)!}{4\pi(l+m)!} \right]^{1/2} e^{im\phi} (\sin\theta)^m \left[\frac{\partial}{\partial \cos\theta} \right]^{l-m} (\sin\theta)^2 \dots\dots (2.1)$$

(Condon and Shortley 1935, Edmonds 1957) where \mathbf{r} is the unit vector with direction specified by the polar angles θ, ϕ . It may be shown that

$$\int Y_{lm}^*(\mathbf{r}) Y_{l'm'}(\mathbf{r}) d\mathbf{r} = \delta_{ll'} \delta_{mm'}, \dots\dots (2.2)$$

where the integration is over the unit sphere, and that

$$Y_{l-m}(\mathbf{r}) = (-1)^m Y_{lm}^*(\mathbf{r}). \dots\dots (2.3)$$

The solid harmonic $\mathcal{Y}_{lm}(\mathbf{r})$ is defined by

$$\mathcal{Y}_{lm}(\mathbf{r}) = r^l Y_{lm}(\mathbf{r}). \dots\dots (2.4)$$

We wish to express $\mathcal{Y}_{lm}(\mathbf{r}_1 + \mathbf{r}_2)$ in terms of

$$\mathcal{Y}_{l_1 m_1}(\mathbf{r}_1) \mathcal{Y}_{l_2 m_2}(\mathbf{r}_2).$$

We use the fact that the \mathcal{Y}_{lm} are angular momentum eigenfunctions.

Let us define $\mathbf{L} = -i\mathbf{r} \times \nabla$. We then have

$$\left. \begin{aligned} \mathbf{L}^2 \mathcal{Y}_{lm}(\mathbf{r}) &= l(l+1) \mathcal{Y}_{lm}(\mathbf{r}) \\ L_z \mathcal{Y}_{lm}(\mathbf{r}) &= m \mathcal{Y}_{lm}(\mathbf{r}) \end{aligned} \right\} \dots\dots (2.5)$$

Consider two vectors \mathbf{r}_1 and \mathbf{r}_2 and define

$$\mathbf{r} = \mathbf{r}_1 + \mathbf{r}_2 \quad \text{and} \quad \mathbf{r}' = \mathbf{r}_1 - \mathbf{r}_2. \dots\dots (2.6)$$

We then have

$$\nabla = \frac{1}{2}(\nabla_1 + \nabla_2) \quad \text{and} \quad \nabla' = \frac{1}{2}(\nabla_1 - \nabla_2) \dots\dots (2.7)$$

and defining the angular momentum operators

$$\mathbf{L}_1 = -i\mathbf{r}_1 \times \nabla_1, \quad \mathbf{L}_2 = -i\mathbf{r}_2 \times \nabla_2, \quad \mathbf{L} = -i\mathbf{r} \times \nabla, \quad \mathbf{L}' = -i\mathbf{r}' \times \nabla' \dots\dots (2.8)$$

we obtain

$$\mathbf{L} + \mathbf{L}' = \mathbf{L}_1 + \mathbf{L}_2. \dots\dots (2.9)$$

By (2.5), $\mathcal{Y}_{lm}(\mathbf{r})$ is an eigenfunction of \mathbf{L}^2 and L_z . Further, \mathbf{L}' operating on $\mathcal{Y}_{lm}(\mathbf{r})$ gives zero. Therefore, by (2.9), $\mathcal{Y}_{lm}(\mathbf{r})$ is also an eigenfunction of

$$(\mathbf{L}_1 + \mathbf{L}_2)^2 \quad \text{and} \quad L_{1z} + L_{2z}. \dots\dots (2.10)$$

Let us now introduce the solid harmonic, $\mathcal{Y}_{l_1 l_2 l m}(\mathbf{r}_1, \mathbf{r}_2)$, which is a simultaneous eigenfunction of \mathbf{L}_1^2 , \mathbf{L}_2^2 , $(\mathbf{L}_1 + \mathbf{L}_2)^2$ and $L_{1z} + L_{2z}$. This is given by

$$\mathcal{Y}_{l_1 l_2 l m}(\mathbf{r}_1, \mathbf{r}_2) = \sum_{m_1 m_2} C_{m_1 m_2 m}^{l_1 l_2 l} \mathcal{Y}_{l_1 m_1}(\mathbf{r}_1) \mathcal{Y}_{l_2 m_2}(\mathbf{r}_2) \dots\dots (2.11)$$

where $C_{\alpha\beta\gamma}^{abc}$ is a vector-coupling coefficient. We adopt the usual phase conventions (Condon and Shortley 1935, Edmonds 1957) and in particular the convention which gives

$$\mathcal{Y}_{l_1 l_2, l_1+l_2, l_1+l_2} = \mathcal{Y}_{l_1 l_1} \mathcal{Y}_{l_2 l_2}. \dots\dots (2.12)$$

Since $\mathcal{Y}_{lm}(\mathbf{r}_1 + \mathbf{r}_2)$ and $\mathcal{Y}_{l_1 l_2 l m}(\mathbf{r}_1, \mathbf{r}_2)$ are both eigenfunctions of $(\mathbf{L}_1 + \mathbf{L}_2)^2$ and $L_{1z} + L_{2z}$ an expansion of the type

$$\mathcal{Y}_{lm}(\mathbf{r}_1 + \mathbf{r}_2) = \sum_{l_1 l_2} a(l_1 l_2 l) \mathcal{Y}_{l_1 l_2 l m}(\mathbf{r}_1, \mathbf{r}_2) \dots\dots (2.13)$$

must exist. Operation with $(L_{1x} + iL_{1y}) + (L_{2x} + iL_{2y})$ shows that $a(l_1 l_2 l)$ is independent of m (see Condon and Shortley 1935, p. 49) and consideration of powers of r_1 , r_2 and r shows that $a(l_1 l_2 l)$ will be zero unless $l = l_1 + l_2$. To determine $a(l_1 l_2 l)$ we consider the case of $m = l$. From (2.12) and (2.13),

$$\mathcal{Y}_l(\mathbf{r}_1 + \mathbf{r}_2) = \sum a(l_1 l_2 l) \mathcal{Y}_{l_1}(\mathbf{r}_1) \mathcal{Y}_{l_2}(\mathbf{r}_2). \quad \dots (2.14)$$

Using (2.1) we obtain

$$\mathcal{Y}_{l-l}(\mathbf{r}) = \frac{1}{l!l!} \left[\frac{(2l+1)!}{4\pi} \right]^{1/2} (x - iy)^l \quad \dots (2.15)$$

and therefore, by (2.3),

$$\mathcal{Y}_l(\mathbf{r}) = \frac{(-1)^l}{2!l!} \left[\frac{(2l+1)!}{4\pi} \right]^{1/2} (x + iy)^l. \quad \dots (2.16)$$

Using the binomial theorem we obtain

$$\mathcal{Y}_l(\mathbf{r}_1 + \mathbf{r}_2) = \sum_{l_1 l_2} \left[\frac{4\pi(2l+1)!}{(2l_1+1)!(2l_2+1)!} \right]^{1/2} \mathcal{Y}_{l_1}(\mathbf{r}_1) \mathcal{Y}_{l_2}(\mathbf{r}_2) \quad \dots (2.17)$$

and therefore

$$a(l_1 l_2 l) = \delta(l_1 + l_2, l) \left[\frac{4\pi(2l+1)!}{(2l_1+1)!(2l_2+1)!} \right]^{1/2}. \quad \dots (2.18)$$

§ 3. A MULTIPLICATION THEOREM FOR SPHERICAL BESSEL FUNCTIONS

The plane wave $e^{i\mathbf{p} \cdot \mathbf{r}}$ may be expanded in the form

$$e^{i\mathbf{p} \cdot \mathbf{r}} = \sum_L (2L+1) P_L(\cos \alpha) i^L f_L(pr) \quad \dots (3.1)$$

where α is the angle between \mathbf{p} and \mathbf{r} , $P_L(\cos \alpha)$ is a Legendre polynomial and f_L is the spherical Bessel function,

$$f_L(x) = \left(\frac{\pi}{2x} \right)^{1/2} J_{L+1/2}(x). \quad \dots (3.2)$$

The multiplication theorem is obtained from

$$e^{i\mathbf{K} \cdot \mathbf{r}} = e^{i\mathbf{K}' \cdot \mathbf{r}} \times e^{-i\mathbf{K}'' \cdot \mathbf{r}} \quad \dots (3.3)$$

where $\mathbf{K} = \mathbf{K}' - \mathbf{K}''$.

The spherical harmonic addition theorem is

$$\left. \begin{aligned} P_L(\cos \alpha) &= \sum_M \frac{4\pi}{(2L+1)} Y_{LM}^*(\hat{\mathbf{p}}) Y_{LM}(\hat{\mathbf{p}}) \\ &= \sum_M \frac{4\pi}{(2L+1)} Y_{LM}(\hat{\mathbf{p}}) Y_{LM}^*(\hat{\mathbf{p}}). \end{aligned} \right\} \quad \dots (3.4)$$

Using (3.1) and (3.3) we have

$$\begin{aligned} & \sum i^\lambda Y_{\lambda\mu}(\hat{\mathbf{K}}) Y_{\lambda\mu}^*(\hat{\mathbf{p}}) f_\lambda(Kr) \\ &= 4\pi \sum_{lm'l'm'} i^{l'-l} Y_{lm}(\hat{\mathbf{K}}) Y_{l'm'}(\hat{\mathbf{K}}') Y_{lm}^*(\hat{\mathbf{p}}) Y_{l'm'}^*(\hat{\mathbf{p}}) f_l(kr) f_{l'}(k'r) \end{aligned} \quad \dots (3.5)$$

and from the orthonormality of the $Y_{\lambda\mu}(\hat{\mathbf{p}})$ (Eqn (2.2)),

$$\begin{aligned} i^\lambda Y_{\lambda\mu}(\hat{\mathbf{K}}) f_\lambda(Kr) &= 4\pi \sum_{lm'l'm'} i^{l'-l} Y_{lm}(\hat{\mathbf{K}}) Y_{l'm'}(\hat{\mathbf{K}}') f_l(kr) f_{l'}(k'r) \\ &\quad \times \int Y_{\lambda\mu}(\hat{\mathbf{p}}) Y_{lm}^*(\hat{\mathbf{p}}) Y_{l'm'}^*(\hat{\mathbf{p}}) d\hat{\mathbf{p}}. \end{aligned} \quad \dots (3.6)$$

For the special case of $\lambda = 0$ it is readily shown that (3.6) gives the Bessel function relation (1.8). For the general case we use a result of Racah (1942), that the integral on the right-hand side of (3.6) is equal to

$$(-1)^{\lambda_l \lambda + l + l'} \left[\frac{(2l+1)(2l'+1)C_{l\lambda l'}}{8\pi} \right]^{1/2} C_{m'lm}^{l'l\lambda} \dots\dots (3.7)$$

where

$$C_{l\lambda l'} = \int_{-1}^{+1} P_l(t) P_\lambda(t) P_{l'}(t) dt. \dots\dots (3.8)$$

It should be noted that $C_{l\lambda l'}$ is zero unless $l + \lambda + l'$ is even and $l + l' \geq \lambda \geq |l - l'|$. An explicit expression for $C_{l\lambda l'}$ is given by Condon and Shortley (1935, p. 182). On substituting (3.7) in (3.6) the sum over m, m' may be carried out to give the coupled angular momentum functions

$$Y_{l'l\lambda\mu}(\mathbf{k}', \mathbf{k}) = \sum_{mm'} C_{m'm\mu}^{l'l\lambda} Y_{l'm'}(\mathbf{k}') Y_{lm}(\mathbf{k}). \dots\dots (3.9)$$

Using the orthonormality relations for these functions we obtain

$$\begin{aligned} \int \int Y_{l'l\lambda\mu}^*(\mathbf{k}', \mathbf{k}) f_\lambda(Kr) Y_{\lambda\mu}(\mathbf{K}) d\mathbf{k} d\mathbf{k}' \\ = (-1)^l [2\pi(2l+1)(2l'+1)C_{l\lambda l'}]^{1/2} f_l(kr) f_{l'}(k'r). \dots\dots (3.10) \end{aligned}$$

Since $\mathbf{K} = \mathbf{k}' - \mathbf{k}$, the solid harmonic addition theorem gives us $Y_{\lambda\mu}(\mathbf{K})$ in terms of $Y_{\lambda_1\lambda_2\lambda\mu}(\mathbf{k}', -\mathbf{k})$ where

$$\lambda = \lambda_1 + \lambda_2. \dots\dots (3.11)$$

Using the relation

$$\mathcal{Y}_{\lambda_1\lambda_2\lambda\mu}(\mathbf{k}', -\mathbf{k}) = (-1)^{\lambda_2} Y_{\lambda_1\lambda_2\lambda\mu}(\mathbf{k}', \mathbf{k})$$

(Condon and Shortley 1935, Edmonds 1957) we obtain

$$Y_{\lambda\mu}(\mathbf{K}) = \sum_{\lambda_1\lambda_2} \left[\frac{4\pi(2\lambda+1)!}{(2\lambda_1+1)!(2\lambda_2+1)!} \right]^{1/2} \frac{k'^{\lambda_1} k^{\lambda_2}}{K^\lambda} (-1)^{\lambda_2} Y_{\lambda_1\lambda_2\lambda\mu}(\mathbf{k}', \mathbf{k}). \dots\dots (3.12)$$

We make a spherical harmonic analysis of $f_\lambda(Kr)/K^\lambda$:

$$\frac{f_\lambda(Kr)}{K^\lambda} = \sum_{\mathcal{L}} \left(\frac{2\mathcal{L}+1}{2} \right) P_{\mathcal{L}}(\cos \omega) F_{\lambda\mathcal{L}}(k'r, kr) \dots\dots (3.13)$$

where ω is the angle between \mathbf{k} and \mathbf{k}' . We then have

$$F_{\lambda\mathcal{L}} = \int_{-1}^{+1} \frac{f_\lambda(Kr)}{K^\lambda} P_{\mathcal{L}}(\cos \omega) d\cos \omega \dots\dots (3.14)$$

and

$$K = [k^2 + k'^2 - 2kk' \cos \omega]^{1/2}. \dots\dots (3.15)$$

Substitution of (3.12) and (3.15) in (3.10) gives

$$\begin{aligned} (-1)^l [2\pi(2l+1)(2l'+1)C_{l\lambda l'}]^{1/2} f_l f_{l'} \\ = \sum_{\lambda_1\lambda_2\mathcal{L}} \left[\frac{4\pi(2\lambda+1)!}{(2\lambda_1+1)!(2\lambda_2+1)!} \right]^{1/2} k'^{\lambda_1} k^{\lambda_2} (-1)^{\lambda_2} \left(\frac{2\mathcal{L}+1}{2} \right) (l'l\lambda | P_{\mathcal{L}} | \lambda_1\lambda_2\lambda) F_{\lambda\mathcal{L}} \end{aligned} \dots\dots (3.16)$$

where

$$(l'l\lambda | P_{\mathcal{L}} | \lambda_1\lambda_2\lambda) = \int \int Y_{l'l\lambda\mu}^*(\mathbf{k}', \mathbf{k}) P_{\mathcal{L}}(\cos \omega) Y_{\lambda_1\lambda_2\lambda\mu}(\mathbf{k}', \mathbf{k}) d\mathbf{k}' d\mathbf{k} \dots\dots (3.17)$$

is independent of μ and is zero unless $l' + \lambda_1 + \mathcal{L}$ and $l + \lambda_2 + \mathcal{L}$ are both even.

Eqn (3.16) is the required multiplication theorem. It may be written

$$f_l(kr)f_{l'}(k'r) = \sum_{\mathcal{L}} \mathcal{Q}_{\lambda\mathcal{L}}(kl, k'l') \int_{-1}^{+1} \frac{f_{\lambda}(Kr)}{K^{\lambda}} P_{\mathcal{L}}(\cos \omega) d \cos \omega \quad \dots\dots (3.18)$$

where

$$\mathcal{Q}_{\lambda\mathcal{L}}(kl, k'l') = \frac{(-1)^{\mathcal{L}}(2\mathcal{L}+1)}{[2(2l+1)(2l'+1)C_{l\lambda l'}]^{\frac{1}{2}}} \sum_{\lambda_1, \lambda_2} \delta(\lambda_1 + \lambda_2, \lambda) \left[\frac{(2\lambda+1)!}{(2\lambda_1+1)!(2\lambda_2+1)!} \right]^{\frac{1}{2}} k'^{\lambda_1} k^{\lambda_2} (l'l\lambda | P_{\mathcal{L}} | \lambda_1\lambda_2\lambda) \quad \dots\dots (3.19)$$

It may be shown (Racah 1942) that

$$\begin{aligned} (l'l\lambda | P_{\mathcal{L}} | \lambda_1\lambda_2\lambda) &= (-1)^{\mathcal{L}-\lambda_1} l' - l + \lambda, -\lambda_2 \\ &\times \frac{1}{2} [(2l+1)(2l'+1)(2\lambda_1+1)(2\lambda_2+1)C_{l'\mathcal{L}\lambda_1}C_{l\mathcal{L}\lambda_2}]^{\frac{1}{2}} \\ &\times W(\lambda_1\lambda_2l'l; \lambda\mathcal{L}) \quad \dots\dots (3.20) \end{aligned}$$

where W is a Racah coefficient. The Table gives $\mathcal{Q}_{\lambda\mathcal{L}}$ for $\lambda=0, 1$ and 2 .

λ	\mathcal{L}	l	l'	$\mathcal{Q}_{\lambda\mathcal{L}}(kl, k'l')$
0	l	l	l	$+\frac{1}{2}$
1	l	l	$l+1$	$+\frac{1}{2}k'$
1	$l+1$	l	$l+1$	$-\frac{1}{2}k$
2	$l-1$	l	l	$+\frac{1}{2}kk'(2l+3)/(2l+1)$
2	l	l	l	$-\frac{1}{2}(k^2+k'^2)$
2	$l+1$	l	l	$+\frac{1}{2}kk'(2l-1)/(2l+1)$
2	l	l	$l+2$	$+\frac{1}{2}k'^2$
2	$l+1$	l	$l+2$	$-kk'$
2	$l+2$	l	$l+2$	$+\frac{1}{2}k^2$

Note: $\mathcal{Q}_{\lambda\mathcal{L}}(kl, k'l') = \mathcal{Q}_{\lambda\mathcal{L}}(k'l', kl)$

§ 4. BORN INTEGRALS

The multiplication theorem allows us to obtain Born partial wave integrals on making a harmonic analysis of the integrals occurring in the Born total collision amplitude. The theory could be given in a very general form but we prefer to illustrate its essentials by considering the case of collisions of charged particles with hydrogen atoms.

4.1. Coulomb Interactions

The particular simplicity of the Born approximation for Coulomb potentials is a consequence of the relation (Bethe 1930),

$$\int \frac{e^{i\mathbf{K} \cdot \mathbf{r}}}{r} d^3\mathbf{r} = \frac{4\pi}{K^2} \quad \dots\dots (4.1)$$

This may be proved on introducing a factor e^{-cr} ($c > 0$) into the integrand and letting $c \rightarrow 0$ after the integration has been carried out. By a simple change of origin we obtain

$$\int \frac{e^{i\mathbf{K} \cdot \mathbf{r}_2}}{r_{12}} d^3\mathbf{r}_2 = \frac{4\pi}{K^2} e^{i\mathbf{K} \cdot \mathbf{r}_1} \quad \dots\dots (4.2)$$

For collisions of charged particles with hydrogen atoms we require

$$\int \left[\frac{1}{r_{12}} - \frac{1}{r_2} \right] e^{i\mathbf{K} \cdot \mathbf{r}_2} d^3\mathbf{r}_2 = \frac{4\pi}{K^2} [e^{i\mathbf{K} \cdot \mathbf{r}_1} - 1] \quad \dots\dots (4.3)$$

In the partial wave theory we use the expansion

$$\left[\frac{1}{r_{12}} - \frac{1}{r_2} \right] = \sum_{\lambda} P_{\lambda}(\cos \beta) \Gamma_{\lambda}(r_1, r_2) \quad \dots\dots (4.4)$$

where β is the angle between \mathbf{r}_1 and \mathbf{r}_2 and

$$\Gamma_{\lambda}(\mathbf{r}_1, \mathbf{r}_2) = \begin{cases} \frac{r_1^{\lambda}}{r_2^{\lambda+1}} - \frac{\delta_{\lambda,0}}{r_2} & r_1 < r_2 \\ \frac{r_2^{\lambda}}{r_1^{\lambda+1}} - \frac{\delta_{\lambda,0}}{r_2} & r_1 > r_2 \end{cases} \quad \dots\dots (4.5)$$

On substituting (4.4) in (4.3) and using (3.1) and (3.4) we obtain

$$\int_0^{\infty} \Gamma_{\lambda}(r_1, r_2) f_{\lambda}(Kr_2) r_2^2 dr_2 = \frac{(2\lambda+1)}{K^2} \{f_{\lambda}(Kr_1) - \delta_{\lambda,0}\}. \quad \dots\dots (4.6)$$

4.2. The Born Total Amplitude

For collisions of charged particles with hydrogen atoms the Born amplitudes are proportional to

$$\begin{aligned} & \left(nl_1 m_1 \mathbf{k} \left| \frac{1}{r_{12}} - \frac{1}{r_2} \right| n' l_1' m_1' \mathbf{k}' \right) \\ &= \int \int \psi_{nl_1 m_1}^*(\mathbf{r}_1) \left[\frac{1}{r_{12}} - \frac{1}{r_2} \right] e^{i\mathbf{K} \cdot \mathbf{r}_2} \psi_{n' l_1' m_1'}(\mathbf{r}_1) d^3 \mathbf{r}_1 d^3 \mathbf{r}_2 \quad \dots\dots (4.7) \end{aligned}$$

where $\mathbf{K} = \mathbf{k}' - \mathbf{k}$. Using (4.3),

$$\begin{aligned} & \left(nl_1 m_1 \mathbf{k} \left| \frac{1}{r_{12}} - \frac{1}{r_2} \right| n' l_1' m_1' \mathbf{k}' \right) \\ &= \frac{4\pi}{K^2} (nl_1 m_1 | e^{i\mathbf{K} \cdot \mathbf{r}} - 1 | n' l_1' m_1') \quad \dots\dots (4.8) \end{aligned}$$

and, using the plane wave expansion for $e^{i\mathbf{K} \cdot \mathbf{r}}$,

$$\begin{aligned} & (nl_1 m_1 | e^{i\mathbf{K} \cdot \mathbf{r}} - 1 | n' l_1' m_1') \\ &= 4\pi \sum_{\lambda \mu} i^{\lambda} Y_{\lambda \mu}^*(\hat{\mathbf{K}}) (l_1 m_1 | Y_{\lambda \mu}(\hat{\mathbf{r}}) | l_1' m_1') (nl_1 | f_{\lambda}(Kr) - \delta_{\lambda,0} | n' l_1'). \quad \dots\dots (4.9) \end{aligned}$$

The angular integral is given by

$$(lm | Y_{\lambda \mu} | l' m') = (-1)^{l-l'+\lambda+\mu} \left[\frac{(2l'+1)(2\lambda+1)}{8\pi} C_{l\lambda l'} \right]^{1/2} C_{m' \lambda m}^{l' \lambda l}. \quad \dots\dots (4.10)$$

Evaluation of the Born integral (4.7) is thus reduced to evaluation of the radial integral

$$(nl_1 | f_{\lambda}(Kr) - \delta_{\lambda,0} | n' l_1') = \int_0^{\infty} P_{nl}(r) [f_{\lambda}(Kr) - \delta_{\lambda,0}] P_{n' l_1'}(r) dr \quad \dots\dots (4.11)$$

where the hydrogen atom functions are

$$\psi_{nlm}(\mathbf{r}) = Y_{lm}(\hat{\mathbf{r}}) \frac{1}{r} P_{nl}(r). \quad \dots\dots (4.12)$$

4.3. Partial Wave Integrals

We use the coupled angular momentum functions

$$\psi_{n l_1 k l_2 L M}(\mathbf{r}_1, \mathbf{r}_2) = \sum_{m_1 m_2} C_{m_1 m_2 L}^{l_1 l_2 L} \psi_{n l_1 m_1}(\mathbf{r}_1) Y_{l_2 m_2}(\hat{\mathbf{r}}_2) f_{l_2}(kr_2) \quad \dots\dots (4.13)$$

where it may be noted that $f_l(kr)$ has asymptotic form

$$f_l(kr) \sim (kr)^{-1} \sin(kr - \frac{1}{2}l\pi). \quad \dots\dots (4.14)$$

The matrix elements

$$\left(nl_1 k l_2 LM \left| \frac{1}{r_{12}} - \frac{1}{r_2} \right| n' l_1' k' l_2' L' M' \right) \quad \dots\dots (4.15)$$

are diagonal with respect to LM and are independent of M . Using the expansion (4.5) we obtain

$$\begin{aligned} & \left(nl_1 k l_2 LM \left| \frac{1}{r_{12}} - \frac{1}{r_2} \right| n' l_1' k' l_2' LM \right) \\ &= \sum_{\lambda} f_{\lambda}(l_1 l_2 l_1' l_2'; L) (nl_1 k l_2 | \Gamma_{\lambda}(r_1, r_2) | n' l_1' k' l_2') \end{aligned} \quad \dots\dots (4.16)$$

where the coefficients

$$f_{\lambda}(l_1 l_2 l_1' l_2'; L) = (l_1 l_2 L | P_{\lambda} | l_1' l_2' L) \quad \dots\dots (4.17)$$

are tabulated by Percival and Seaton (1957) and where

$$\begin{aligned} & (nl_1 k l_2 | \Gamma_{\lambda} | n' l_1' k' l_2') \\ &= \int_0^{\infty} \int_0^{\infty} P_{nl_1}(r_1) f_{l_2}(kr_2) \Gamma_{\lambda}(r_1, r_2) P_{n'l_1'}(r_1) f_{l_2'}(k'r_2) r_2^2 dr_1 dr_2. \end{aligned} \quad \dots\dots (4.18)$$

Using the multiplication theorem (3.18) we have

$$\begin{aligned} & (nl_1 k l_2 | \Gamma_{\lambda} | n' l_1' k' l_2') = \sum_{\mathcal{L}} \mathcal{Q}_{\lambda \mathcal{L}}(kl, k'l') \\ &= \int_{-1}^{+1} P_{\mathcal{L}}(\cos \omega) \left\{ \int \int P_{nl_1}(r_1) \Gamma_{\lambda}(r_1, r_2) \frac{f_{\lambda}(Kr_2)}{K^{\lambda}} P_{n'l_1'}(r_1) r_2^2 dr_1 dr_2 \right\} d \cos \omega. \end{aligned} \quad \dots\dots (4.19)$$

By (4.6) the double integral in braces is equal to

$$(2\lambda + 1) \frac{(nl_1 | f_{\lambda}(Kr) - \delta_{\lambda,0} | n' l_1')}{K^{\lambda+2}} \quad \dots\dots (4.20)$$

and therefore

$$\begin{aligned} & (nl_1 k l_2 | \Gamma_{\lambda} | n' l_1' k' l_2') \\ &= (2\lambda + 1) \sum_{\mathcal{L}} \mathcal{Q}_{\lambda \mathcal{L}}(kl, k'l') \int_{-1}^{+1} P_{\mathcal{L}}(\cos \omega) \frac{(nl_1 | f_{\lambda}(Kr) - \delta_{\lambda,0} | n' l_1')}{K^{\lambda+2}} d \cos \omega. \end{aligned} \quad \dots\dots (4.21)$$

REFERENCES

- BETHE, H., 1930, *Ann. Phys.*, **Lfz.**, **5**, 325.
 CONDON, E. U., and SHORTLEY, G. H., 1935, *The Theory of Atomic Spectra* (Cambridge: University Press).
 EDMONDS, A. R., 1957, *Angular Momentum in Quantum Mechanics* (Princeton: University Press).
 MOTT, N. F., and MASSEY, H. S. W., 1949, *The Theory of Atomic Collisions*, 2nd edn, Chapter VII (Oxford: Clarendon Press).
 PERCIVAL, I. C., and SEATON, M. J., 1957, *Proc. Camb. Phil. Soc.*, **53**, 654.
 RACAH, G., 1942, *Phys. Rev.*, **62**, 438.
 WATSON, G. N., 1948, *The Theory of Bessel Functions*, 2nd edn, (Cambridge: University Press), p. 363.

The Calculation of Born Partial Wave Integrals for some Transitions in H Produced by Electron Impact

By J. LAWSON, W. LAWSON AND M. J. SEATON

Department of Physics, University College London

MS. received 2nd June 1960

Abstract. Using methods described in a companion paper by Seaton, the partial wave integrals are calculated for transitions involving the states 1s, 2s and 2p.

§ 1. INTRODUCTION

IN the preceding paper (Seaton 1961, to be referred to as I), methods have been given for the calculation of Born partial wave integrals. In the present paper we give numerical results for electron impact transitions involving H 1s, 2s and 2p. These will be used in the following paper (Burke and Seaton 1961) to obtain improved cross section estimates.

§ 2. BORN CROSS SECTIONS

2.1. Total Scattering Amplitudes

Let \mathbf{v}' be the velocity of an electron incident on state $n'l_1'$ of a hydrogen atom and put $\mathbf{k}' = m\mathbf{v}'/\hbar$. The cross section for the transition $n'l_1' \rightarrow nl_1$ is

$$Q(n'l_1' \rightarrow nl_1) = \frac{\pi\Omega(nl_1, n'l_1')}{k'^2(2l_1' + 1)} \quad \dots\dots (2.1)$$

where the *collision strength* $\Omega(a, a')$ is a dimensionless number and $\Omega(a, a') = \Omega(a', a)$.

Let Ω_I be the value of Ω obtained in the Born approximation for the total scattering amplitude. Using atomic units,

$$\Omega_I(nl_1, n'l_1') = \frac{kk'}{2\pi^2} \sum_{m_1 m_1'} \int \left| \left(nl_1 m_1 \mathbf{k} \left| \frac{1}{r_{12}} - \frac{1}{r_2} \right| n'l_1' m_1' \mathbf{k}' \right) \right|^2 d\cos\omega \quad \dots\dots (2.2)$$

where ω is the angle between \mathbf{k} and \mathbf{k}' . Using Eqn (4.8) of paper I, referred to as (I, 4.8), we obtain

$$\Omega_I = 8kk' \sum_{m_1 m_1'} \int \frac{|(nl_1 m_1 | e^{i\mathbf{K} \cdot \mathbf{r}} - 1 | n'l_1' m_1')|^2}{K^4} d\cos\omega \quad \dots\dots (2.3)$$

where $\mathbf{K} = \mathbf{k}' - \mathbf{k}$, $K^2 = k^2 + k'^2 - 2kk' \cos\omega$.

The H atom wave functions are written as

$$\psi_{nl_1 m_1}(\mathbf{r}) = Y_{l_1 m_1}(\hat{\mathbf{r}}) \frac{1}{r} P_{nl}(r)$$

where Y_{lm} is a normalized spherical harmonic. We express the matrix element in (2.3) in terms of the radial matrix elements

$$(nl_1 | f_\lambda(Kr) - \delta_{\lambda,0} | n'l_1') = \int_0^\infty P_{nl_1}(r) \{f_\lambda(Kr) - \delta_{\lambda,0}\} P_{n'l_1'}(r) dr \quad \dots\dots (2.4)$$

where $f_\lambda(x) = (\pi/2x)^{1/2} J_{\lambda+1/2}(x)$. Using (1, 4.9) and carrying out the summation over m_1, m_1' we obtain

$$\Omega_1 = 4kk'(2l_1+1)(2l_1'+1) \sum_{\lambda} (2\lambda+1) C_{l_1 l_1'} \int \frac{|(nl_1|f_\lambda(Kr) - \delta_{\lambda,0}|n'l_1')|^2}{K^4} d\cos\omega. \quad \dots\dots (2.5)$$

The coefficient $C_{l_1 l_1'}$ is defined by (1, 3.8); the following numerical values are required:

$$C_{000} = 2, \quad C_{011} = C_{110} = C_{101} = 2/3, \quad C_{121} = 4/15.$$

The values of λ occurring in (2.5) are such that $|l_1 - l_1'| \leq \lambda \leq (l_1 + l_1')$ and that $(\lambda + l_1 + l_1')$ is even.

2.2. The Reactance Matrix

We use the coupled angular momentum representation

$$\psi_{nl_1 k l_2 L M}(\mathbf{r}_1, \mathbf{r}_2) = \sum_{m_1 m_2} C_{m_1 m_2 L}^{nl_1 l_2} \psi_{n l_1 m_1}(\mathbf{r}_1) Y_{l_2 m_2}(\mathbf{r}_2) f_{l_2}(kr_2). \quad \dots\dots (2.6)$$

The Born approximation to the reactance matrix is

$$R(nl_1 k l_2 L, n'l_1' k' l_2' L) = -2(kk')^{1/2} (nl_1 k l_2 L \left| \frac{1}{r_{12}} - \frac{1}{r_2} \right| n'l_1' k' l_2' L). \quad \dots\dots (2.7)$$

Using (I, 4.21) we obtain

$$R(nl_1 k l_2 L, n'l_1' k' l_2' L) = -2(kk')^{1/2} \sum (2\lambda+1) f_\lambda(l_1 l_2 l_1' l_2'; L) \sum_{\mathcal{L}} \mathcal{Q}_{\lambda \mathcal{L}}(kl_2, k'l_2') \int_{-1}^1 \frac{(nl_1|f_\lambda(Kr) - \delta_{\lambda,0}|n'l_1')}{K^4} P_{\mathcal{L}}(\cos\omega) d\cos\omega. \quad \dots\dots (2.8)$$

The coefficients f_λ are tabulated by Percival and Seaton (1957) and the coefficients $\mathcal{Q}_{\lambda \mathcal{L}}$ are given in I.

The collision strength is

$$\Omega(nl_1, n'l_1') = \sum_{l_2 l_2' L} (2L+1) |T(nl_1 k l_2 L, n'l_1' k' l_2' L)|^2 \quad \dots\dots (2.9)$$

where \mathbf{T} is the transmission matrix. This is given in terms of the reactance matrix \mathbf{R} by $\mathbf{T} = -2i\mathbf{R}(1-i\mathbf{R})$. For $\mathbf{R} = \mathbf{1}$ we have $\mathbf{T} \simeq -2i\mathbf{R}$ and, using the Born approximation (2.7) for \mathbf{R} ,

$$\Omega_1 = \sum_{l_2 l_2' L} (2L+1) |-2iR(nl_1 k l_2 L, n'l_1' k' l_2' L)|^2. \quad \dots\dots (2.10)$$

From the usual expansion of a plane wave in terms of spherical Bessel functions it is readily shown that (2.2) is equivalent to (2.10) with \mathbf{R} defined by (2.7).

§ 3. RESULTS FOR H 1s, 2s AND 2p

3.1. Formulae

We take k_1 to be the value of k going with 1s, k_2 that going with 2s and 2p. In atomic units,

$$k_1^2 = k_2^2 + 0.75. \quad \dots\dots (3.1)$$

Let us define

$$\left. \begin{aligned} x &= K_{11}^2 = 2k_1^2(1 - \cos\omega) \\ y &= K_{12}^2 = k_1^2 + k_2^2 - 2k_1 k_2 \cos\omega \\ z &= K_{22}^2 = 2k_2^2(1 - \cos\omega). \end{aligned} \right\} \quad \dots\dots (3.2)$$

We then obtain

$$\left. \begin{aligned} A &= \frac{(1s|f_0(K_{11}r) - 1|1s)}{K_{11}^2} = \frac{1}{x} \left\{ \frac{1}{(1+x/4)^2} - 1 \right\} \\ B &= \frac{(1s|f_0(K_{12}r)|2s)}{K_{12}^2} = \left(\frac{2^8\sqrt{2}}{3^6} \right) \left\{ \frac{1}{(1+4y/9)^3} \right\} \\ C &= \frac{(2s|f_0(K_{22}r) - 1|2s)}{K_{22}^2} = \frac{1}{z} \left\{ \frac{(1-z)(1-2z)}{(1+z)^4} - 1 \right\} \\ D &= \frac{(2p|f_0(K_{22}r) - 1|2p)}{K_{22}^2} = \frac{1}{z} \left\{ \frac{(1-z)}{(1+z)^4} - 1 \right\} \\ E &= \frac{(1s|f_1(K_{12}r)|2p)}{K_{12}^3} = \frac{2^8}{3^5\sqrt{6}y} \left\{ \frac{1}{(1+4y/9)^3} \right\} \\ F &= \frac{(2s|f_1(K_{22}r)|2p)}{K_{22}^3} = \sqrt{3} \frac{1}{z} \left\{ \frac{(z-1)}{(1+z)^4} \right\} \\ G &= \frac{(2p|f_2(K_{22}r)|2p)}{K_{22}^4} = 2 \frac{1}{z} \left\{ \frac{1}{(1+z)^4} \right\} \end{aligned} \right\} \dots\dots (3.3)$$

Using the notation

$$\overline{X^2} = \int_{-1}^{+1} X^2 d\cos\omega \quad \dots\dots (3.4)$$

we obtain from (2.5)

$$\left. \begin{aligned} \Omega_I(1s, 1s) &= 8k_1^2 \overline{A^2} \\ \Omega_I(1s, 2s) &= 8k_1 k_2 \overline{B^2} \\ \Omega_I(1s, 2p) &= 24k_1 k_2 (\overline{yE^2}) \\ \Omega_I(2s, 2s) &= 8k_2^2 \overline{C^2} \\ \Omega_I(2s, 2p) &= 24k_2^2 (\overline{zF^2}) \\ \Omega_I(2p, 2p) &= 24k_2^2 [\overline{D^2} + 2(\overline{zG^2})] \end{aligned} \right\} \dots\dots (3.5)$$

With the neglect of energy differences between 2s and 2p, $\Omega_I(2s, 2p)$ is infinite but a finite result is obtained on redefining z as $k_2^2 + k_2'^2 - 2k_2 k_2' \cos\omega$ with $k_2 \neq k_2'$. This will be discussed in the following paper by Burke and Seaton (1961).

For given total angular momentum L we have five states denoted by $\nu = 1, 2, 3, 4$ and 5. They are

ν	nl_1	k	l_2	L
1	1s	k_1	l	l
2	2s	k_2	l	l
3	2p	k_2	$l-1$	l
4	2p	k_2	$l+1$	l
5	2p	k_2	l	l

For given $L (=l)$ the states $\nu = 1$ to 4 all have the same parity (even or odd for $(l_1 + l_2)$ even or odd) but $\nu = 5$ has the opposite parity. Therefore the states $\nu = 1$ to 4 are coupled together but $\nu = 5$ is not coupled to the others.

Using the notation

$$X_l = \int_{-1}^{+1} X P_l(\cos\omega) d\cos\omega \quad \dots\dots (3.6)$$

we obtain from (2.8)

$$\left. \begin{aligned} R_{11} &= -k_1 A_l \\ R_{12} &= -(k_1 k_2)^{1/2} B_l \\ R_{13} &= + (k_1 k_2)^{1/2} \left(\frac{3l}{2l+1} \right)^{1/2} \{k_2 E_l - k_1 E_{l-1}\} \\ R_{14} &= + (k_1 k_2)^{1/2} \left(\frac{3(l+1)}{2l+1} \right)^{1/2} \{k_2 E_l - k_1 E_{l+1}\} \\ R_{22} &= -k_2 C_l \\ R_{23} &= + k_2^2 \left(\frac{3l}{2l+1} \right)^{1/2} \{F_l - F_{l-1}\} \\ R_{24} &= + k_2^2 \left(\frac{3(l+1)}{2l+1} \right)^{1/2} \{F_l - F_{l+1}\} \\ R_{33} &= -k_2 D_{l-1} - \frac{k_2^3(l-1)}{(4l^2-1)} H_{l-1} \\ R_{34} &= + 3k_2^3 \frac{[l(l+1)]^{1/2}}{(2l-1)} I_l \\ R_{44} &= -k_2 D_{l+1} - \frac{k_2^3(l+2)}{(2l+1)(2l+3)} H_{l+1} \\ R_{55} &= -k_2 D_l + \frac{k_2^3}{(2l+1)} H_l \end{aligned} \right\} \dots\dots (3.7)$$

where

$$H_l = (2l+3)G_{l-1} - 2(2l+1)G_l + (2l-1)G_{l+1} \quad \dots\dots (3.8)$$

and

$$I_l = G_{l-1} - 2G_l + G_{l+1}. \quad \dots\dots (3.9)$$

Due to the fact that $z=0$ for $\omega=0$, the integrals F_l and G_l are divergent. These integrals occur in (3.7) only in the linear combinations $F_l - F_{l-1}$, H_l and I_l and these linear combinations may be expressed in terms of convergent integrals.

3.2. Numerical Methods

After some preliminary hand computing all final results were obtained using the electronic computer of the Department of Physics, University College London.

In principle it is possible to evaluate the harmonic integrals using systematic generating procedures obtained from the recurrence relations

$$(2l+1)tP_l(t) = (l+1)P_{l+1}(t) + lP_{l-1}(t). \quad \dots\dots (3.10)$$

In practice it was found that these generating procedures gave excessive cancellation and that, working in floating point to 25 binary digits, some of the results were of low accuracy. All final results were therefore obtained by numerical integration but some use was made of recurrence relations. As an illustrative example we consider the evaluation of B_l and E_l . From (3.3), $B = (2/\sqrt{3})yE$ and therefore, using (3.2) and (3.6),

$$\frac{1}{2}\sqrt{3}(2l+1)B_l = (2l+1)(k_1^2 + k_2^2)E_l - 2k_1k_2\{(l+1)E_{l+1} + lE_{l-1}\}. \quad \dots\dots (3.11)$$

This gives B_l once E_l has been calculated.

Table 1. The Born Approximation for the Reactance Matrix

k_1	l	R_{11}	R_{12}	R_{13}	R_{14}	R_{22}	R_{23}	R_{24}	R_{33}	R_{34}	R_{44}	R_{55}
0.9	0	0.5782	-0.1821	0.0000	-0.0147	2.4186	0.0000	-1.7774	0.0000	0.0000	-0.7503	0.0000
	1	0.0810	-0.0257	-0.1775	+0.0006	0.2820	1.0262	-1.1295	1.8381	0.1311	-0.2103	0.6366
	2	0.0124	-0.0029	-0.0624	0.0005	0.0288	0.8749	-0.7664	+0.0819	0.1010	-0.0955	0.2416
	3	0.0019	-0.0003	-0.0172	0.0001	0.0026	0.6478	-0.5663	-0.0489	0.0590	-0.0532	0.1223
	4	0.0003	-0.0000	-0.0044	0.0000	0.0002	0.4994	-0.4472	-0.0390	0.0364	-0.0406	0.0735
1.0	0	0.5966	-0.2212	0.0000	-0.0353	2.5681	0.0000	-0.6250	0.0000	0.0000	-0.1819	0.0000
	1	0.0966	-0.0632	-0.2018	+0.0015	0.8181	0.3608	-0.7144	2.1515	-0.0589	-0.1402	0.9431
	2	0.0171	-0.0146	-0.1335	0.0035	0.2504	0.5534	-0.6434	0.4931	+0.0612	-0.1244	0.4431
	3	0.0031	-0.0030	-0.0693	0.0019	0.0703	0.5437	-0.5339	+0.0681	0.0769	-0.0902	0.2422
	4	0.0006	-0.0006	-0.0332	0.0009	0.0183	0.4708	-0.4392	-0.0294	0.0630	-0.0629	0.1488
	5	0.0001	-0.0001	-0.0155	0.0004	0.0045	0.3973	-0.3674	-0.0413	0.0470	-0.0446	0.0998
	6	0.0000	-0.0000	-0.0072	0.0002	0.0011	0.3380	-0.3141	-0.0354	0.0350	-0.0328	0.0714
	7	0.0000	-0.0000	-0.0033	0.0001	0.0002	0.2924	-0.2738	-0.0279	+0.0266	-0.0250	0.0536
1.2	0	0.6176	-0.2139	0.0000	-0.0519	2.1406	0.0000	-0.2060	0.0000	0.0000	0.3375	0.0000
	1	0.1258	-0.0974	-0.1751	-0.0001	1.0144	0.1189	-0.3308	1.9125	-0.1511	+0.1275	1.0181
	2	0.0283	-0.0366	-0.1655	+0.0087	0.5107	0.2562	-0.3943	0.7459	-0.0456	-0.0049	0.5763
	3	0.0065	-0.0124	-0.1238	0.0077	0.2486	0.3333	-0.4005	0.2878	+0.0175	-0.0522	0.3546
	4	0.0015	-0.0039	-0.0844	0.0052	0.1156	0.3532	-0.3754	0.0883	0.0435	-0.0611	0.2328
	5	0.0003	-0.0012	-0.0555	0.0032	0.0516	0.3395	-0.3390	+0.0061	0.0487	-0.0559	0.1614
	6	0.0001	-0.0004	-0.0360	0.0019	0.0222	0.3118	-0.3020	-0.0235	0.0451	-0.0471	0.1173
	7	0.0000	-0.0001	-0.0234	0.0011	0.0093	0.2811	-0.2688	-0.0309	0.0387	-0.0386	0.0886
	8	0.0000	-0.0000	-0.0152	0.0007	0.0038	0.2525	-0.2405	-0.0300	0.0323	-0.0314	0.0691
	9	0.0000	-0.0000	-0.0099	0.0004	0.0015	0.2275	-0.2169	-0.0265	0.0268	-0.0258	0.0553
	10	0.0000	-0.0000	-0.0065	0.0002	0.0006	0.2063	-0.1971	-0.0227	0.0223	-0.0214	0.0453
	11	0.0000	-0.0000	-0.0043	0.0001	0.0002	0.1883	-0.1805	-0.0193	0.0187	-0.0180	0.0377
	12	0.0000	-0.0000	-0.0028	0.0001	0.0001	0.1731	-0.1664	-0.0165	0.0159	-0.0153	0.0319
	13	0.0000	-0.0000	-0.0019	0.0001	0.0000	0.1601	-0.1543	-0.0141	0.0137	-0.0132	0.0274

Table 1 (*continued*)

k_1	l	R_{11}	R_{12}	R_{13}	R_{14}	R_{22}	R_{23}	R_{24}	R_{33}	R_{34}	R_{11}	R_{55}
1.5	0	0.6237	-0.1817	0.0000	-0.0556	1.7585	0.0000	-0.0874	0.0000	0.0000	0.5302	0.0000
	1	0.1621	-0.1113	-0.1311	-0.0046	0.9801	0.0505	-0.1535	1.6157	-0.1464	0.3124	0.9694
	2	0.0469	-0.0579	0.1496	+0.0108	0.6105	0.1189	0.2114	0.7937	-0.0927	0.1459	0.6195
	3	0.0139	-0.0275	0.1375	0.0137	0.3837	0.1787	-0.2484	0.4220	-0.0417	+0.0503	0.4208
	4	0.0041	-0.0123	-0.1149	0.0121	0.2370	0.2191	-0.2647	0.2171	-0.0049	-0.0006	0.2976
	5	0.0012	-0.0053	-0.0916	0.0095	0.1430	0.2394	-0.2652	0.1009	+0.0175	-0.0251	0.2176
	6	0.0004	-0.0022	-0.0715	0.0070	0.0843	0.2440	-0.2559	0.0364	0.0289	0.0348	0.1638
	7	0.0001	-0.0009	-0.0553	0.0051	0.0486	0.2382	-0.2413	+0.0022	0.0331	-0.0369	0.1265
	8	0.0000	-0.0004	-0.0427	0.0037	0.0275	0.2266	-0.2246	-0.0145	0.0332	0.0352	0.1000
	9	0.0000	-0.0001	-0.0330	0.0026	0.0151	0.2125	0.2079	-0.0216	0.0311	-0.0319	0.0808
	10	0.0000	-0.0001	0.0256	0.0019	0.0084	0.1978	-0.1922	0.0235	0.0282	-0.0283	0.0664
	11	0.0000	-0.0000	-0.0199	0.0014	0.0045	0.1836	-0.1778	-0.0229	0.0250	-0.0248	0.0555
	12	0.0000	-0.0000	0.0155	0.0010	0.0024	0.1706	-0.1650	-0.0213	0.0221	-0.0217	0.0470
	13	0.0000	-0.0000	-0.0122	0.0007	0.0013	0.1587	-0.1535	-0.0193	0.0194	-0.0190	0.0403
2.0	0	0.6024	-0.1395	0.0000	-0.0484	1.4060	0.0000	-0.0390	0.0000	0.0000	0.5230	0.0000
	1	0.2024	-0.1059	-0.0856	-0.0092	0.8673	0.0225	-0.0681	1.3123	-0.1158	0.4026	0.8607
	2	0.0765	-0.0710	-0.1087	+0.0079	0.6082	0.0528	-0.0997	0.7456	-0.0959	0.2590	0.6032
	3	0.0298	-0.0442	-0.1148	0.0152	0.4416	0.0842	-0.1279	0.4742	-0.0694	0.1598	0.4453
	4	0.0117	-0.0261	0.1107	0.0172	0.3227	0.1128	-0.1502	0.3073	-0.0439	0.0923	0.3387
	5	0.0046	-0.0149	-0.1011	0.0165	0.2346	0.1359	-0.1656	0.1964	-0.0223	0.0470	0.2633
	6	0.0018	-0.0083	-0.0900	0.0146	0.1688	0.1524	0.1746	0.1212	-0.0056	+0.0173	0.2083
	7	0.0007	-0.0045	-0.0786	0.0124	0.1201	0.1625	-0.1781	0.0703	+0.0065	-0.0015	0.1674
	8	0.0003	-0.0024	-0.0680	0.0103	0.0845	0.1673	-0.1773	0.0362	0.0146	-0.0129	0.1365
	9	0.0001	-0.0013	-0.0586	0.0085	0.0587	0.1677	0.1735	+0.0139	0.0194	-0.0192	0.1127
	10	0.0000	-0.0007	-0.0505	0.0070	0.0404	0.1650	-0.1677	-0.0003	0.0220	-0.0223	0.0942
	11	0.0000	-0.0003	-0.0435	0.0057	0.0275	0.1603	-0.1608	-0.0089	0.0229	-0.0232	0.0796
	12	0.0000	-0.0002	-0.0375	0.0047	0.0186	0.1542	-0.1533	-0.0137	0.0227	-0.0230	0.0680
	13	0.0000	-0.0001	-0.0324	0.0038	0.0125	0.1475	-0.1456	-0.0162	0.0218	-0.0220	0.0587

In the numerical integrations it was found that the integrands tend to vary rapidly for small ω and it was therefore convenient to work with

$$X_l = \int_0^\pi X P_l(\cos \omega) \sin \omega d\omega \quad \dots\dots (3.12)$$

in which ω , rather than $\cos \omega$, is taken as integration variable.

The procedure finally adopted was to calculate the following integrals by numerical methods:

$$\left. \begin{aligned} a_l &= \int_0^\pi (8+x)(4+x)^{-2} P_l(\cos \omega) \sin \omega d\omega \\ b_l &= \int_0^\pi y^{-1}(1+4y/9)^{-3} P_l(\cos \omega) \sin \omega d\omega \\ c_l &= \int_0^\pi (1+z)^{-4} P_l(\cos \omega) \sin \omega d\omega. \end{aligned} \right\} \quad \dots\dots (3.13)$$

The functions $\sin \omega P_l(\cos \omega)$ for $l=0(1)14$ were generated, using (3.10), at the intervals (in degrees)

$$\omega = 0(1)30, 30(2)90, 90(5)180.$$

The integrals in (3.7) were then obtained from a_l , b_l and c_l using systematic generating procedures.

3.3. Numerical Results

Table 1 gives the Born reactance matrix for $k_1=0.9, 1.0, 1.2, 1.5$ and 2.0 and Table 2 gives the collision strengths. For $\Omega_1(2p, 2p)$ we consider separately the contributions from $\lambda=0$ and $\lambda=2$.

Table 2. Collision Strengths

k_1	$\Omega_I(1s, 1s)$	$\Omega_I(1s, 2s)$	$\Omega_I(1s, 2p)$	$\Omega_I(2s, 2s)$	$\Omega_I(2p, 2p)$		
					$\lambda=0$	$\lambda=2$	Total
0.9	1.4194	0.1408	0.4660	24.370	41.653	10.672	52.324
1.0	1.5417	0.2483	1.0385	35.819	68.678	13.607	82.286
1.2	1.7326	0.3283	1.8827	38.253	76.481	13.713	90.194
1.5	1.9213	0.3759	2.8823	38.984	78.855	13.714	92.569
2.0	2.0907	0.4075	4.1622	39.332	79.934	13.714	93.648

It was checked that the values of Ω_I in Table 2, obtained from (2.5), are in satisfactory agreement with values obtained from (2.10) and values of \mathbf{R} given in Table 1. In most cases this check involves making extrapolations of the results of Table 1 to larger values of l .

For $l=0$ to 4, spot checks show our results for the $1s-2s$ transition to be in satisfactory agreement with those of Bates and Miskelly (1957).

REFERENCES

- BATES, D. R., and MISKELLY, D., 1957, *Proc. Phys. Soc. A*, **70**, 539.
 BURKE, V. M., and SEATON, M. J., 1961, *Proc. Phys. Soc.*, **77**, 199.
 PERCIVAL, I. C., and SEATON, M. J., 1957, *Proc. Camb. Phil. Soc.*, **53**, 654.
 SEATON, M. J., 1961, *Proc. Phys. Soc.*, **77**, 184.

The Calculation of Electron-Hydrogen Collision Cross Sections Using the Born Approximation for the Reactance Matrix

By V. M. BURKE† AND M. J. SEATON

Department of Physics, University College, London

MS. received 2nd June 1960

Abstract. In a companion paper Lawson, Lawson and Seaton have calculated the Born \mathbf{R} matrix for H 1s, 2s and 2p. Using these results the transmission matrix is calculated from $\mathbf{T} = -2i\mathbf{R}(\mathbf{I} - i\mathbf{R})$. In another companion paper Seaton has shown that this should give results which are better than those obtained from the Born approximation for the total scattering amplitude.

The following cross sections are calculated: elastic (1s-1s, 2s-2s, 2p-2p); momentum loss (1s-1s, 2s-2s, 2p-2p, 2s-2p); inelastic (1s-2s, 1s-2p m_l); transitions between fine structure levels (2s $_{1/2}$ -2p $_{1/2}$, 2s $_{1/2}$ -2p $_{3/2}$, 2p $_{1/2}$ -2p $_{3/2}$). Comparison with experiment shows our results for 1s-2p to be much better than those obtained from the usual Born total amplitude.

§ 1. INTRODUCTION

WE consider all interactions involving H 1s, 2s and 2p. Calculations of the reactance matrix \mathbf{R} in the Born approximation (Lawson, Lawson and Seaton 1961) give an indication of the strengths of the potential interactions. For 1s-1s there is strong interaction only for the $l=0$ partial wave. For 1s-2s and 1s-2p the coupling is not strong; for the optically allowed 1s-2p transition many partial waves must be considered but for 1s-2s the convergence of the partial wave analysis is much more rapid. For the diagonal terms in the interactions with excited states, 2s-2s and 2p-2p, there is fairly strong interaction for a number of partial waves and the quadrupole term in the 2p-2p interaction is important for the higher partial waves. Finally, there is strong coupling between 2s-2p, particularly at the lower energies.

We wish to calculate cross sections making some allowance for strong interactions. In the usual form of the Born approximation for the total scattering amplitude, valid when all interactions are weak, the transmission matrix \mathbf{T} is calculated from

$$\mathbf{T}_I = -2i\mathbf{R} \text{ (Born)}. \quad \dots\dots (1.1)$$

This is referred to as approximation I. The exact relation between \mathbf{T} and \mathbf{R} is $\mathbf{T} = -2i\mathbf{R}/(\mathbf{I} - i\mathbf{R})$. For \mathbf{R} real and symmetric this gives the conservation condition $|\mathbf{T}|^2 = 2\Re\mathbf{T}$, $\Re\mathbf{T}$ being the real part of \mathbf{T} . Approximation II is

$$\mathbf{T}_{II} = -2i\mathbf{R} \text{ (Born)} / \{\mathbf{I} - i\mathbf{R} \text{ (Born)}\}. \quad \dots\dots (1.2)$$

Approximation I does not satisfy the conservation condition and this may lead to serious errors when the interactions are not weak. In such cases approximation II, which satisfies the conservation condition, should give better results (Seaton 1961).

†Now at Physics Department, University of California, Berkeley.

Since both I and II are based on the Born approximation, no account is taken of electron exchange. The error so introduced will be most serious when the first few partial waves give the dominant contributions to the cross sections. Exact solutions of the coupled integro-differential equations, obtained on allowing for exchange, are being calculated for the first few partial waves (John 1960, Burke, Burke, McCarroll and Percival, to be published). Eventually the exchange results for small l will be used together with the present results for larger values of l .

§ 2. CROSS SECTION EXPRESSIONS

2.1. Neglect of Spin Variables

Using nl_1 for the atom quantum numbers, the cross sections are given by

$$Q(n'l_1' \rightarrow nl_1) = \frac{\pi \Omega(nl_1, n'l_1')}{k'^2(2l_1' + 1)} \quad \dots\dots (2.1)$$

where $k' = mv'/\hbar$ and where the total energy is

$$E_{n'l_1'} + \frac{1}{2}mv'^2 = E_{nl_1} + \frac{1}{2}mv^2. \quad \dots\dots (2.2)$$

The collision strength Ω is given by

$$\Omega(nl_1, n'l_1') = \sum_{l_2 l_2'} (2L + 1) |T(nl_1 l_2 L, n'l_1' l_2' L)|^2 \quad \dots\dots (2.3)$$

where l_2, l_2' specify the angular momenta of the colliding electron and L specifies the total angular momentum.

2.2. Transitions Involving Specification of Spin Variables

For transitions between fine-structure levels,

$$Q(n'l_1' j_1' \rightarrow nl_1 j_1) = \frac{\pi \Omega(nl_1 j_1, n'l_1' j_1')}{k'^2(2j_1' + 1)}. \quad \dots\dots (2.4)$$

Using a jj coupling representation,

$$\Omega(nl_1 j_1, n'l_1' j_1') = \frac{1}{2} \sum_{l_2 l_2' j_2 J} (2J + 1) |T(nl_1 j_1 l_2 j_2 J, n'l_1' j_1' l_2' j_2' J)|^2 \quad \dots\dots (2.5)$$

where the factor $\frac{1}{2}$ enters the right-hand side when we average over spin directions of the incident electron. We have

$$T(nl_1 j_1 l_2 j_2 J, n'l_1' j_1' l_2' j_2' J) = \sum_{SL} A \begin{pmatrix} \frac{1}{2} & l_1 & j_1 \\ \frac{1}{2} & l_2 & j_2 \\ S & L & J \end{pmatrix} T(nl_1 l_2 L, n'l_1' l_2' L) A \begin{pmatrix} \frac{1}{2} & l_1' & j_1' \\ \frac{1}{2} & l_2' & j_2' \\ S & L & J \end{pmatrix} \quad \dots\dots (2.6)$$

where A is the transformation coefficient between jj and LS coupling and where, since we neglect exchange, we take T to be independent of S . From the unitary character of the transformation coefficient we obtain

$$\sum_{j_1 j_1'} \Omega(nl_1 j_1, n'l_1' j_1') = 2\Omega(nl_1, n'l_1').$$

§ 3. CALCULATION OF THE \mathbf{T} MATRIX

We denote the states by subscripts ν :

ν	nl_1	l_2	L
1	1s	l	l
2	2s	l	l
3	2p	$l-1$	l
4	2p	$l+1$	l
5	2p	l	l

The states $\nu=1$ to 4 have the same parity and are coupled together but $\nu=5$ has a different parity and is not coupled to the others.

The \mathbf{R} matrix was taken from the work of Lawson, Lawson and Seaton (1961). Putting

$$\mathbf{T} = \mathbf{X} + i\mathbf{Y} \quad \text{..... (3.1)}$$

with \mathbf{X} and \mathbf{Y} real, the relation $\mathbf{T} = -2i\mathbf{R}/(1-i\mathbf{R})$ gives

$$\mathbf{X} = \frac{2\mathbf{R}}{\mathbf{R} + \mathbf{R}^{-1}}, \quad \mathbf{Y} = \frac{-2}{\mathbf{R} + \mathbf{R}^{-1}}. \quad \text{..... (3.2)}$$

The matrix inversions were carried out on a DEUCE computer. Fixed point arithmetic was used throughout, all numbers being to 19 binary places. The method used for inverting \mathbf{R} and \mathbf{R}^{-1} was the usual elimination method for solving linear coupled equations. This was then improved by an iteration procedure. If \mathbf{r}_0^{-1} was the first approximation to \mathbf{r}^{-1} the error $\delta\mathbf{r}_0^{-1}$ is defined by

$$\mathbf{r}\mathbf{r}_0^{-1} = \mathbf{1} + \delta\mathbf{r}_0^{-1} \quad \text{..... (3.3)}$$

$$\text{so that} \quad \mathbf{r}\mathbf{r}_0^{-1}(\mathbf{1} - \delta\mathbf{r}_0^{-1}) = \mathbf{1} - (\delta\mathbf{r}_0^{-1})^2. \quad \text{..... (3.4)}$$

An improved estimate is then

$$\mathbf{r}_1^{-1} = \mathbf{r}_0^{-1}(\mathbf{1} - \delta\mathbf{r}_0^{-1}) = \mathbf{r}_0^{-1}(2 - \mathbf{r}\mathbf{r}_0^{-1}). \quad \text{..... (3.5)}$$

The iterations were continued until succeeding iterations had converged to within the error in multiplication.

Calculations were made for all the values of l considered by Lawson, Lawson and Seaton. Table 1 gives results for $l=0$ to 4.

§ 4. CALCULATION OF TOTAL COLLISION STRENGTHS

The collision strength Ω is calculated from sums of the type

$$\Omega = \sum_{l=0}^{\infty} \Omega^l. \quad \text{..... (4.1)}$$

In many cases the sums are rather slowly convergent. In approximation I, Ω_I may be calculated directly (Lawson, Lawson and Seaton 1961) and, making extrapolations where necessary, it was thus possible to check most of the sums $\Sigma \Omega_I^l$. In a few cases the sums $\Sigma \Omega_{II}^l$ could be evaluated using the calculated values of Ω_{II}^l and making extrapolations. In others it was convenient to use

$$\Omega_{II} = \Omega_I + \sum_l \{\Omega_{II}^l - \Omega_I^l\} \quad \text{..... (4.2)}$$

but this did not always give a sufficiently rapid convergence. Use was therefore made of the fact that the expressions of approximation II become simple in the limit of $k_2=0$ (Seaton 1961), k_2 being the value of k going with 2s and 2p, and could therefore be evaluated up to very large values of l . Some use was made of

$$\sum_{l=l_0}^{\infty} \Omega^l \simeq \frac{1}{2} \Omega^{l_0} + \int_{l_0}^{\infty} \Omega^l dl \quad (l_0 \text{ large}). \quad \text{..... (4.3)}$$

Finally, values of Ω_{II} were obtained using

$$\Omega_{II}(k_2) = \Omega_{II}(k_2=0) + \Omega_I(k_2) + \sum_{l=0}^{\infty} \{\Omega_{II}^l(k_2) - \Omega_{II}^l(k_2=0) - \Omega_I^l(k_2)\}. \quad \text{.... (4.4)}$$

This form was particularly useful for 2s-2s and 2p-2p. The reason for fairly rapid convergence of the sum in (4.4) may be understood as follows. For large l , $\Omega_{II}^l(k_2)$ for 2s-2s or 2p-2p may be considered to have two contributions. The first comes from the 2s-2s or 2p-2p interaction and for large l is given reliably by $\Omega_I^l(k_2)$. This part vanishes in the limit of $k_2 \rightarrow 0$. The second part comes from 2s-2p coupling, 2s \rightarrow 2s being due to 2s \rightarrow 2p \rightarrow 2s. For large l this part of $\Omega_{II}^l(k_2)$ tends to be equal to that calculated for $k_2=0$.

Divergence of the sums for Ω (2s, 2p) will be discussed in § 7.2.

Table 1. $\mathbf{T} = \mathbf{X} + i\mathbf{Y}$ Calculated in Approximation II

k_1	l	X_{11}	X_{12}	X_{13}	X_{14}	X_{22}	X_{23}	X_{24}	X_{33}	X_{34}	X_{44}	X_{55}
0.9	0	0.4997	-0.0577	0.0000	+0.0674	1.7534	0.0000	-0.1507	0.0000	0.0000	1.4772	0.0000
	1	0.0234	-0.0348	-0.1274	-0.0459	1.2243	0.3100	+0.1433	1.4736	-0.2198	1.0522	0.5768
	2	0.0054	-0.0462	-0.0110	-0.0057	1.1433	+0.0441	0.0927	0.6690	-0.5605	0.5128	0.1103
	3	0.0005	-0.0129	+0.0001	-0.0006	0.8475	-0.0390	0.0467	0.4847	-0.4238	0.3713	0.0295
	4	0.0000	-0.0031	0.0001	-0.0001	0.6186	-0.0337	0.0312	0.3461	-0.3099	0.2775	0.0107
1.0	0	0.5173	-0.1255	0.0000	-0.0020	1.6812	0.0000	-0.3210	0.0000	0.0000	0.2624	0.0000
	1	0.0275	-0.0318	-0.1542	+0.0250	0.9849	0.1756	-0.2904	1.6065	-0.0330	0.5910	0.9415
	2	0.0242	-0.0718	-0.0828	-0.0205	0.8162	0.2841	+0.0273	0.5873	-0.3197	0.5309	0.3283
	3	0.0076	-0.0485	-0.0099	-0.0062	0.7344	+0.0467	0.0615	0.3922	-0.3635	0.3762	0.1108
	4	0.0018	-0.0225	+0.0002	-0.0022	0.5837	-0.0287	0.0529	0.3187	-0.2965	0.2798	0.0433
1.2	0	0.5378	-0.1559	0.0000	-0.0741	1.6168	0.0000	-0.1658	0.0000	0.0000	0.2026	0.0000
	1	0.0438	-0.0869	-0.1429	+0.0267	0.9995	0.0574	-0.3229	1.5526	-0.1084	0.1133	1.0180
	2	0.0336	-0.0497	-0.1528	+0.0106	0.5512	0.2804	-0.2307	0.7094	-0.0978	0.2185	0.4986
	3	0.0254	-0.0632	-0.0576	-0.0063	0.4666	0.2097	-0.0725	0.2954	-0.1776	0.2566	0.2234
	4	0.0125	-0.0495	-0.0135	-0.0061	0.4317	0.0768	+0.0017	0.2206	-0.2043	0.2322	0.1028
1.5	0	0.5477	-0.1540	0.0000	-0.0769	1.4965	0.0000	-0.0798	0.0000	0.0000	0.4372	0.0000
	1	0.0637	-0.1181	-0.1203	+0.0061	0.9716	0.0258	-0.1747	1.4325	-0.1356	0.1836	0.9689
	2	0.0313	-0.0563	-0.1486	0.0269	0.5582	0.1491	-0.2129	0.7698	-0.1026	0.0934	0.5546
	3	0.0313	-0.0451	-0.0984	0.0143	0.3427	0.1820	-0.1675	0.3361	-0.0745	0.1016	0.3008
	4	0.0239	-0.0487	-0.0457	0.0017	0.2773	0.1525	-0.0939	0.1752	-0.0938	0.1203	0.1628
2.0	0	0.5254	-0.1384	0.0000	-0.0642	1.3190	0.0000	-0.0413	0.0000	0.0000	0.4940	0.0000
	1	0.0885	-0.1208	-0.0887	-0.0053	0.8566	0.0158	-0.0816	1.2574	-0.1234	0.2785	0.8511
	2	0.0301	-0.0698	-0.1118	+0.0201	0.5438	0.0702	-0.1155	0.7160	-0.1131	0.1380	0.5335
	3	0.0244	-0.0439	-0.0948	0.0225	0.3431	0.1129	-0.1253	0.3835	-0.0768	0.0752	0.3309
	4	0.0228	-0.0357	-0.0657	0.0156	0.2298	0.1223	-0.1114	0.2035	-0.0546	0.0551	0.2059

Table 1 (continued)

k_1	l	Y_{11}	Y_{12}	Y_{13}	Y_{14}	Y_{22}	Y_{23}	Y_{24}	Y_{33}	Y_{34}	Y_{41}	Y_{55}
0.9	0	-0.8580	+0.0138	0.0000	0.0741	-0.3181	0.0000	0.5523	0.0000	0.0000	0.6591	0.0000
	1	-0.1366	-0.0378	0.0750	0.0311	-0.0616	-0.2012	0.8867	0.6556	0.3730	0.0086	-0.9060
	2	-0.0239	-0.0008	0.0825	0.0340	0.0870	0.7336	0.6521	-0.1264	0.1147	0.0144	-0.4565
	3	-0.0038	+0.0010	0.0261	0.0071	-0.0547	-0.7447	0.6479	+0.0238	-0.0451	0.0338	-0.2411
	4	-0.0006	0.0002	0.0073	0.0013	0.0311	0.6875	0.6155	0.0365	0.0350	0.0310	-0.1462
1.0	0	0.8567	0.0070	0.0000	0.1312	-0.5903	0.0000	0.2621	0.0000	0.0000	0.5167	0.0000
	1	0.1573	+0.0252	0.0534	0.0253	-0.5576	+0.0350	0.7585	-0.7502	-0.0979	0.4070	-0.9983
	2	-0.0218	-0.0218	0.1819	0.0369	-0.1556	-0.5037	0.7754	0.5480	-0.2298	0.1456	-0.7408
	3	-0.0053	+0.0006	0.1106	0.0219	-0.0962	-0.6769	0.6736	-0.1115	-0.1158	0.0858	-0.4576
	4	0.0011	0.0018	0.0555	0.0083	-0.0627	-0.6619	0.6169	+0.0172	-0.0746	0.0663	-0.2912
1.2	0	-0.8658	-0.0057	0.0000	0.0830	0.7529	0.0000	0.0311	0.0000	0.0000	-0.5686	0.0000
	1	-0.2126	+0.0765	0.0548	0.0540	0.8928	+0.0547	0.2812	-0.8075	+0.0349	-0.1175	-0.9998
	2	-0.0284	+0.0032	0.1982	0.0094	-0.5753	-0.1434	0.5892	-0.8611	-0.0526	+0.1042	-0.8652
	3	-0.0049	-0.0079	0.2067	0.0095	-0.2815	-0.4441	0.6211	-0.4167	-0.1051	0.1168	-0.6300
	4	-0.0017	-0.0004	0.1489	0.0081	0.1547	0.5429	0.5917	-0.1378	-0.0938	0.0985	0.4416
1.5	0	-0.8735	-0.0001	0.0000	0.0535	-0.8505	0.0000	0.0103	0.0000	0.0000	-0.8173	0.0000
	1	-0.2850	+0.0927	0.0527	0.0466	-0.9667	+0.0309	0.1001	-0.8799	0.0374	-0.5205	-0.9995
	2	0.0666	0.0562	0.1673	+0.0084	-0.8143	-0.0250	0.2594	-0.9269	0.0660	0.2233	-0.8953
	3	-0.0124	0.0176	0.2215	-0.0109	0.5640	0.1738	0.3951	0.6567	+0.0190	-0.0506	0.7149
	4	-0.0023	0.0023	0.2065	-0.0108	0.3494	0.3383	0.4547	0.3571	-0.0319	+0.0264	-0.5468
2.0	0	-0.8658	0.0136	0.0000	0.0399	-0.9365	0.0000	0.0096	0.0000	0.0000	-0.8582	0.0000
	1	-0.3664	0.0960	0.0451	0.0339	-0.9729	0.0148	0.0444	-0.9523	+0.0361	-0.6731	-0.9889
	2	-0.1334	0.0895	0.1251	+0.0073	-0.8655	-0.0059	0.1079	-0.9306	0.0860	-0.4596	-0.8845
	3	-0.0457	0.0570	0.1766	-0.0143	-0.7043	-0.0723	0.1834	-0.7408	0.0841	-0.2860	-0.7432
	4	-0.0147	0.0304	0.1939	-0.0243	-0.5398	-0.1533	0.2496	-0.5285	0.0544	-0.1601	-0.6077

§ 5. ELASTIC SCATTERING

5.1. Total Cross Sections

Table 2 gives results for $k_1^2 = 0.75, 0.81, 1.00, 1.44, 2.25$ and 4.00 , $k_1^2 = 0.75$ being the threshold for excitation of $n=2$. The partial collision strengths are defined by

$$\left. \begin{aligned} \Omega^l(1s, 1s) &= (2l+1)|T_{11}(l)|^2, \\ \Omega^l(2s, 2s) &= (2l+1)|T_{22}(l)|^2, \\ \Omega^l(2p, 2p) &= (2l+1)\{|T_{33}(l)|^2 + 2|T_{34}(l)|^2 + |T_{44}(l)|^2 + |T_{55}(l)|^2\} \end{aligned} \right\} \dots\dots (5.1)$$

For $\Omega(1s, 1s)$ the differences between approximations I and II are largely due to the strong interaction for $l=0$. The coupling with $2s$ and $2p$ is of minor importance.

The effect of $2s-2p$ coupling on $\Omega(2s, 2s)$ and $\Omega(2p, 2p)$ is most marked for k_2 small. In particular, for $k_2=0$, approximation I, which neglects this coupling, gives $\Omega(2s, 2s) = \Omega(2p, 2p) = 0$, while approximation II gives non-zero values.

5.2. Diffusion Cross Sections

Table 2 shows that the cross sections are large for elastic scattering by H atoms in the $n=2$ level but since large contributions come from large values of l the elastic scattering will be mainly through small angles. The diffusion (momentum loss) cross section is defined by

$$Q_d = 2\pi \int_0^\pi I(\theta)(1 - \cos \theta) \sin \theta d\theta \quad \dots\dots (5.2)$$

where $I(\theta)$ is the cross section for scattering per unit solid angle. Small angle scattering contributes less to Q_d than to the total cross section,

$$Q = 2\pi \int_0^\pi I(\theta) \sin \theta d\theta. \quad \dots\dots (5.3)$$

Putting

$$I(\theta) = \sum_\lambda A_\lambda P_\lambda(\cos \theta) \quad \dots\dots (5.4)$$

one has (Percival and Seaton 1957),

$$\begin{aligned} A_\lambda(n_1' l_1' \rightarrow n_1 l_1) &= \frac{(-1)^{l_1+l_1'}}{4k'^2(2l_1'+1)} \\ &\times \sum_{LL''l_2l_2''l_2'l_2'''} \{Z(l_2 L l_2'' L''; l_1 \lambda) Z(l_2' L l_2''' L'''; l_1' \lambda) \\ &\times T(n l_1 l_2 L, n' l_1' l_2' L) T^*(n l_1 l_2'' L'', n' l_1' l_2''' L''')\}. \end{aligned} \quad \dots\dots (5.5)$$

With

$$Q_d(n' l_1' \rightarrow n l_1) = \frac{\pi \Omega_d(n l_1, n' l_1')}{k'^2(2l_1'+1)} \quad \dots\dots (5.6)$$

one obtains

$$\Omega_d(n l_1, n' l_1') = 4(2l_1'+1)k'^2 \{A_0(n' l_1' \rightarrow n l_1) - \frac{1}{3} A_1(n' l_1' \rightarrow n l_1)\}. \quad \dots\dots (5.7)$$

For $\lambda=0$ and 1 one may use explicit expressions for the Z coefficients. The expression for Ω_d contains cross-terms between $T(l)$ and $T(l \pm 1)$. We use expansions of the type

$$\Omega_d = \sum_l \Omega_d^{(l)} \quad \dots\dots (5.8)$$

and group the terms in such a way that the convergence is not too slow. While the quantities Ω^l depend only on $|T_{vv'}(l)|^2$ and are necessarily positive, the $\Omega_d^{(l)}$ may be positive or negative. The sum Ω_d is, of course, always positive.

Table 2. Collision Strengths for Elastic Scattering

l	$k_1^2 = 0.75$		$k_1^2 = 0.81$		$k_1^2 = 1.00$		$k_1^2 = 1.44$		$k_1^2 = 2.25$		$k_1^2 = 4.00$	
	I	II	I	II	I	II	I	II	I	II	I	II
0	1.3020	0.9823	1.3375	0.9859	1.4236	1.0015	1.5256	1.0389	1.5558	1.0629	1.4513	1.0257
1	0.0687	0.0683	0.0787	0.0576	0.1119	0.0765	0.1898	0.1413	0.3154	0.2558	0.4914	0.4262
2	0.0024	0.0024	0.0031	0.0030	0.0059	0.0053	0.0160	0.0097	0.0440	0.0271	0.1170	0.0935
3	0.0001	0.0001	0.0001	0.0001	0.0003	0.0006	0.0012	0.0047	0.0054	0.0079	0.0248	0.0187
4	0.0000	0.0000	0.0000	0.0000	0.0000	0.0000	0.0001	0.0014	0.0006	0.0051	0.0049	0.0066
$\Sigma_{l=5}$	0.0000	0.0000	0.0000	0.0000	0.0000	0.0000	0.0000	0.0004	0.0001	0.0048	0.0013	0.0129
$\Omega(1s, 1s) =$	1.3732	1.0530	1.4194	1.0466	1.5417	1.0839	1.7326	1.1964	1.9213	1.3636	2.0907	1.5836
0	0.000	3.240	23.399	3.176	26.331	3.175	18.328	3.181	12.369	2.963	7.907	2.617
1	0.000	8.033	0.955	4.508	8.032	3.843	12.348	5.388	11.527	5.635	9.026	5.041
2	0.000	7.200	0.017	6.552	1.254	3.452	5.216	3.174	7.455	4.873	7.398	5.224
3	0.000	5.143	0.000	5.048	0.138	3.840	1.730	2.079	4.121	3.049	5.461	4.296
4	0.000	3.467	0.000	3.452	0.012	3.102	0.481	1.893	2.022	1.791	3.749	3.098
$\Sigma_{l=5}$	0.000	9.551	0.000	9.548	0.002	9.430	0.156	8.412	1.490	6.977	5.791	8.142
$\Omega(2s, 2s) =$	0.000	36.634	24.370	32.284	35.819	26.842	38.253	24.127	38.984	25.288	39.332	28.418
0	0.000	3.240	2.252	2.617	0.132	0.336	0.456	0.364	1.124	0.859	1.313	0.980
1	0.000	8.033	46.350	15.711	66.540	16.689	57.072	15.453	44.287	15.325	31.822	14.261
2	0.000	7.200	1.892	8.009	9.251	9.574	17.853	11.625	21.043	13.247	20.104	13.583
3	0.000	5.143	0.757	5.577	2.332	5.795	5.934	6.107	10.112	8.193	12.833	10.298
4	0.000	3.467	0.383	3.735	1.256	4.123	2.502	3.941	4.888	4.667	7.975	6.957
$\Sigma_{l=5}$	0.000	9.551	0.691	10.20	2.774	11.87	6.377	14.24	11.115	16.56	19.601	22.03
$\Omega(2p, 2p) =$	0.000	36.634	52.325	45.85	82.286	48.39	90.194	51.73	92.569	58.85	93.648	68.12

The following are the expressions finally used:

$$\Omega_d^{(l)}(2s, 2s) = (l+1)|T_{22}(l) - T_{22}(l+1)|^2, \quad \dots\dots (5.9)$$

$$\Omega_d^{(l)}(2s, 2p) = (c_l - d_l - d_{l-1}), \quad \dots\dots (5.10)$$

$$\Omega_d^{(l)}(2p, 2p) = (e_l - g_l - g_{l-1}) + (f_l - i_l - i_{l-1}) - h_l \quad \dots\dots (5.11)$$

where

$$\begin{aligned} c_l &= (2l+1)\{|T_{23}(l)|^2 + |T_{24}(l)|^2\}, \\ d_l &= \mathcal{R} \left\{ \left[\frac{(l+1)(l+2)(2l+1)}{(2l+3)} \right]^{1/2} T_{24}(l) T_{24}^*(l+1) \right. \\ &\quad + [(2l+1)(2l+3)]^{-1/2} T_{24}(l) T_{23}^*(l+1) \\ &\quad \left. + \left[\frac{l(l+1)(2l+3)}{(2l+1)} \right]^{1/2} T_{23}(l) T_{23}^*(l+1) \right\}, \\ e_l &= (2l+1)\{|T_{33}(l)|^2 + |T_{44}(l)|^2 + 2|T_{34}(l)|^2\}, \\ f_l &= (2l+1)|T_{55}(l)|^2, \\ g_l &= \mathcal{R} \left\{ \frac{l(2l+3)}{(2l+1)} T_{33}(l) T_{33}^*(l+1) + \frac{(l+2)(2l+1)}{(2l+3)} T_{44}(l) T_{44}^*(l+1) \right. \\ &\quad + 2[l(l+2)]^{1/2} T_{34}(l) T_{34}^*(l+1) \\ &\quad + [(l+1)(2l+1)(2l+3)]^{-1} T_{44}(l) T_{33}^*(l+1) \\ &\quad + \frac{2}{(2l+3)} \left[\frac{(l+2)}{(l+1)} \right]^{1/2} T_{44}(l) T_{34}^*(l+1) \\ &\quad \left. + \frac{2}{(2l+1)} \left[\frac{l}{(l+1)} \right]^{1/2} T_{34}(l) T_{33}^*(l+1) \right\}, \\ h_l &= 2\mathcal{R} T_{55}(l) \left\{ \frac{1}{l} T_{33}(l) + \frac{1}{(l+1)} T_{44}(l) - \frac{2}{[l(l+1)]^{1/2}} T_{34}(l) \right\}^*, \\ i_l &= \frac{l(l+2)}{(l+1)} \mathcal{R} T_{55}(l) T_{55}^*(l+1). \quad \dots\dots (5.12) \end{aligned}$$

Numerical results are given in Table 3.

§ 6. INELASTIC COLLISIONS

Results for 1s-2s and 1s-2p transitions are given in Table 4.

6.1. 1s-2s Transitions

At the lower energies there is rapid convergence in the expansion for $\Omega_I(1s, 2s)$, the dominant contribution being from $l=0$. In approximation II the contribution from small l is very much reduced but there is a larger contribution from large l (due to $1s \rightarrow 2p \rightarrow 2s$). Our results show that it is important to allow for strong interactions but our method may not do this accurately at the lower energies.

The work of Marriott (1958) shows that exchange is important for the $l=0$ contribution to $\Omega(1s, 2s)$ but his results will be unreliable due to neglect of 2s-2p coupling. To make a reliable calculation of $\Omega(1s, 2s)$ at low energies it will be necessary to allow both for exchange and for 2s-2p coupling.

Table 3. Collision Strengths for Diffusion Cross Sections

l	$k_2^2=0.00$		$k_2^2=0.06$		$k_2^2=0.25$		$k_2^2=0.69$		$k_2^2=1.50$		$k_2^2=3.25$	
	I	II	I	II	I	II	I	II	I	II	I	II
$\Omega_d^{(l)}$ (2s, 2s)	0.000	0.027	18.259	0.346	12.250	0.486	5.073	0.401	2.424	0.289	1.161	0.215
	0.000	0.381	0.513	0.013	2.579	0.380	2.030	0.604	1.093	0.388	0.537	0.219
	0.000	0.353	0.008	0.263	0.389	0.031	0.825	0.280	0.618	0.327	0.333	0.199
	0.000	0.224	0.000	0.212	0.043	0.095	0.283	0.069	0.344	0.201	0.226	0.160
	0.000	0.305	0.000	0.300	0.004	0.260	0.109	0.148	0.318	0.195	0.419	0.312
$\Omega_d(2s, 2s) =$	0.000	1.289	18.781	1.133	15.265	1.252	8.319	1.502	4.796	1.401	2.676	1.104
$\Omega_d^{(l)}$ (2s, 2p)	0.000	0.360	10.292	0.037	0.625	-0.039	0.004	-0.018	-0.003	-0.005	-0.001	-0.001
	0.000	0.476	13.495	1.288	2.212	+0.815	0.192	+0.102	+0.008	-0.003	-0.001	-0.003
	0.000	0.748	3.635	0.881	2.591	1.174	0.547	0.534	0.070	0.078	+0.003	+0.001
	0.000	0.568	0.475	0.546	1.390	0.603	0.701	0.639	0.161	0.160	0.017	0.022
	0.000	0.815	0.052	0.817	0.704	0.855	1.287	1.028	1.021	1.017	0.563	0.588
$\Omega_d(2s, 2p) =$	72.000	2.967	27.949	3.568	7.521	3.408	2.731	2.285	1.257	1.248	0.580	0.608
$\Omega_d^{(l)}$ (2p, 2p)	0.000	3.240	4.041	1.533	0.546	0.137	-0.327	0.086	-0.167	0.158	-0.054	0.111
	0.000	5.088	+38.027	8.008	+41.044	7.507	+25.542	4.696	+15.224	3.342	+8.560	2.485
	0.000	1.512	-0.646	1.138	-2.623	1.408	-1.493	1.801	-0.611	1.398	-0.203	0.881
	0.000	0.405	-0.118	0.455	-0.071	0.346	-0.527	0.064	-0.420	0.209	-0.192	+0.252
	0.000	0.094	0.012	0.10	+0.144	0.28	+0.060	0.30	-0.189	0.05	-0.30	-0.06
$\Omega_d(2p, 2p) =$	0.000	10.339	41.552	11.23	39.039	9.68	23.255	6.95	13.837	5.16	7.81	3.67

6.2. 1s-2p Transitions

Due to the long range of the 1s-2p interaction there is a larger contribution from large values of l . Our results for $\Omega(1s, 2p)$ should therefore be more accurate than those for $\Omega(1s, 2s)$.

When 1s-2p transitions are produced by a unidirectional electron beam, the Ly α radiation emitted is polarized and its intensity depends on the angle between the direction of the electron beam and the direction of observation. The theory is discussed by Percival and Seaton (1958), who allow for the fact that the Ly α natural line width is of a magnitude comparable with the hyperfine structure separations.

The theoretical expressions involve the cross sections

$$Q(1s \rightarrow 2p m_l) = \frac{\pi}{k_1^2} \Omega(1s, 2p m_l). \quad \dots\dots (6.1)$$

$$\text{Evidently} \quad \Omega(1s, 2p) = \sum_{m_l} \Omega(1s, 2p m_l) \quad \dots\dots (6.2)$$

and $\Omega(1s, 2p m_l = +1) = \Omega(1s, 2p m_l = -1)$. For $m_l = 0$ we have

$$\Omega(1s, 2p 0) = \sum_{l=0}^{\infty} \left[\frac{l(2l-1)}{(2l+1)} \right]^{1/2} T_{14}(l-1) + \left[\frac{(l+1)(2l+3)}{(2l+1)} \right]^{1/2} T_{13}(l+1) \right]^2 \quad (6.3)$$

(Percival and Seaton 1957) and, in approximation I,

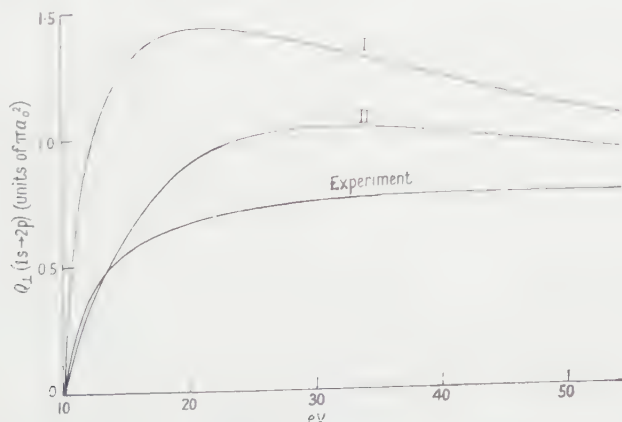
$$\Omega_I(1s, 2p 0) = \frac{6}{k_1^2} \int_{|k_1-k_2|}^{k_1+k_2} \frac{(K^2 + k_1^2 - k_2^2) |1s|f_1|2p\rangle|^2}{K^5} dK \quad \dots\dots (6.4)$$

(Percival and Seaton 1958, Eqn (6.13)). Values of $\Omega(1s, 2p 0)$ are included in Table 4.

A cross section $Q_{\perp}(1s \rightarrow 2p)$ has been measured by Fite, Stebbings and Brackmann (1959). This is obtained on counting the photons emitted perpendicular to the electron beam and calculating the cross section assuming an isotropic photon distribution. From the theory of Percival and Seaton (1958) we obtain

$$Q_{\perp}(1s \rightarrow 2p) = 0.918Q(1s \rightarrow 2p) + 0.246Q(1s \rightarrow 2p 0). \quad \dots\dots (6.5)$$

In the Figure the experimental results are compared with those calculated in approximations I and II. Approximation II is seen to be much superior to approximation I.



The cross section $Q_{\perp}(1s \rightarrow 2p)$ is defined in the text. The Figure shows experimental results of Fite, Stebbings and Brackmann (1959) and results calculated using approximations I and II.

§ 7. TRANSITIONS BETWEEN FINE STRUCTURE LEVELS

7.1. *Transitions between the 2p_j Levels*

Using (2.5), (2.6) it may be shown that

$$\left. \begin{aligned} \Omega(2p_{1/2}, 2p_{1/2}) + \Omega(2p_{1/2}, 2p_{3/2}) &= \frac{2}{3}\Omega(2p, 2p) \\ \Omega(2p_{1/2}, 2p_{3/2}) + \Omega(2p_{3/2}, 2p_{3/2}) &= \frac{4}{3}\Omega(2p, 2p) \end{aligned} \right\} \dots\dots (7.1)$$

Having calculated $\Omega(2p, 2p)$ it remains to calculate any one of the $\Omega(2p_j, 2p_{j'})$. We choose $\Omega(2p_{1/2}, 2p_{3/2})$. Using the explicit expressions for the transformation coefficients we obtain

$$\Omega(2p_{1/2}, 2p_{3/2}) = \sum_l \Omega^{(l)}(2p_{1/2}, 2p_{3/2}) \dots\dots (7.2)$$

with

$$\begin{aligned} \Omega^{(l)}(2p_{1/2}, 2p_{3/2}) &= \frac{2}{3} \{ (2l-1) |T_{44}(l-1)|^2 + (2l+1) |T_{55}(l)|^2 + (2l+3) |T_{33}(l+1)|^2 \\ &\quad + (2l-1) |T_{34}(l-1)|^2 + (2l+3) |T_{34}(l+1)|^2 \} \\ &\quad - \frac{1}{18} \left\{ \frac{(2l-1)}{l^2} \left| (2l-1)T_{44}(l-1) + (l+1)T_{55}(l) \right|^2 \right. \\ &\quad + \frac{1}{l^2(2l+1)^3} \left| (2l+1)(2l^2-l+1)T_{55}(l) + 4l^2(2l+3)T_{33}(l+1) \right. \\ &\quad + (2l-1)T_{44}(l-1) \left. \right|^2 + \frac{8}{l(l+1)(2l+1)^3} \left| -(2l+1)T_{55}(l) \right. \\ &\quad + l(2l+3)T_{33}(l+1) - (2l-1)(l+1)T_{44}(l-1) \left. \right|^2 \\ &\quad + \frac{1}{(l+1)^2(2l+1)^3} \left| (2l+1)(2l^2+5l+4)T_{55}(l) + (2l+3)T_{33}(l+1) \right. \\ &\quad + 4(l+1)^2(2l-1)T_{44}(l-1) \left. \right|^2 + \frac{(2l+3)}{(l+1)^2} \left| (2l+3)T_{33}(l+1) + lT_{55}(l) \right|^2 \}. \end{aligned} \dots\dots (7.3)$$

Numerical results are given in Table 5.

In approximation I, $\Omega(2p_{1/2}, 2p_{3/2})$ is determined by the quadrupole part of the 2p-2p interaction. One has

$$\Omega_I(2p_{1/2}, 2p_{3/2}) = \frac{2}{3}\Omega_2(2p, 2p) \dots\dots (7.4)$$

where $\Omega_2(2p, 2p)$ is the quadrupole part of $\Omega(2p, 2p)$ calculated in approximation I. In approximation II there is also a contribution from the two dipole interactions involved in $2p_{1/2} \rightarrow 2s_{1/2} \rightarrow 2p_{3/2}$ and this gives the major contribution at the lower energies.

7.2. *2s-2p Transitions*

These have been discussed by Seaton (1955, 1961). With exact resonance, $\Omega^I(2s, 2p)$ behaves as l^{-1} for l large and the sum for $\Omega(2s, 2p)$ is divergent. We consider the case of a small energy difference,

$$\Delta\epsilon = |k_{2s}^2 - k_{2p}^2|. \dots\dots (7.5)$$

We then obtain expressions of the form

$$\Omega(2s, 2p) = 72 \{ \ln(4k_2^2/\Delta\epsilon) - \mu \}. \dots\dots (7.6)$$

Table 5. Results for Ω ($2p_{1/2}, 2p_{3/2}$)

l	$k_2^2 = 0.00$		$k_2^2 = 0.06$		$k_2^2 = 0.25$		$k_2^2 = 0.69$		$k_2^2 = 1.50$		$k_2^2 = 3.25$	
	I	II	I	II	I	II	I	II	I	II	I	II
$\Omega^{(b)}$ ($2p_{1/2}, 2p_{3/2}$)	0	0.000	1.190	0.375	0.028	0.021	0.183	0.026	0.172	0.040	0.107	0.033
	1	0.000	2.880	2.883	2.750	1.924	1.016	0.483	0.526	0.215	0.299	0.144
	2	0.000	2.576	2.711	2.083	2.502	1.339	1.184	0.743	0.454	0.427	0.248
	3	0.000	2.242	2.383	1.384	2.381	1.265	1.506	0.812	0.746	0.489	0.371
	8.21	0.000	6.082	6.5	2.827	7.78	5.340	8.80	6.891	9.02	7.820	8.84
$\Omega(2p_{1/2}, 2p_{3/2}) =$	0.000	14.971	7.115	14.9	9.071	14.51	9.142	12.00	9.143	10.48	9.143	9.63

Table 6. Results for Ω ($2p, 2s$)

l	$k_2^2 = 0.00$		$k_2^2 = 0.06$		$k_2^2 = 0.25$		$k_2^2 = 0.69$		$k_2^2 = 1.50$		$k_2^2 = 3.25$	
	I	II	I	II	I	II	I	II	I	II	I	II
$\Omega(2s, 2p)$	0	36.000	0.360	0.328	1.563	0.172	0.170	0.029	0.031	0.007	0.006	0.002
	1	54.000	1.785	2.830	7.688	2.062	1.483	0.569	0.314	0.127	0.062	0.027
	2	30.000	4.800	4.870	14.403	4.682	4.423	2.326	1.177	0.677	0.254	0.150
	3	21.000	6.857	6.815	16.259	6.425	7.601	4.426	2.622	1.732	0.657	0.471
	4	16.200	7.705	7.682	14.924	7.400	9.564	5.856	4.250	3.179	1.270	1.018
$72 \mu =$	0.000	156.33	52.66	155.33	102.78	157.34	139.32	167.14	167.27	182.30	195.11	202.66

In approximation I

$$72\mu_I = \frac{2}{7}(1 - \eta^{-7}) + \frac{1}{2} \sum_{p=1}^5 p^{-1}(1 - \eta^{-p}) + \frac{1}{2} \ln \eta, \quad \eta = 1 + 4k_2^2. \quad \dots\dots (7.7)$$

For $l\Delta\epsilon/k_2^2 \ll 1$, $\Omega^l(2s, 2p)$ is effectively independent of $\Delta\epsilon$ and may be calculated with $\Delta\epsilon = 0$. This condition is satisfied for the values of l for which Ω_{II}^l differs significantly from Ω_I^l and therefore

$$72(\mu_{II} - \mu_I) = \sum_l \{ \Omega_I^l(2s, 2p) - \Omega_{II}^l(2s, 2p) \} \quad \dots\dots (7.8)$$

where the right-hand side is calculated with $\Delta\epsilon = 0$. Table 6 gives values of $72\mu_I$, $72\mu_{II}$ and $\Omega^l(2s, 2p)$.

7.3. $2s_{1/2}$ - $2p_j$ Transitions

We have

$$\begin{aligned} \Omega(2s_{1/2}, 2p_{1/2}) &= 48 \{ \ln(4k_2^2/\Delta\epsilon') - \mu \} \\ \Omega(2s_{1/2}, 2p_{3/2}) &= 96 \{ \ln(4k_2^2/\Delta\epsilon'') - \mu \} \end{aligned} \quad \dots\dots (7.9)$$

where $\Delta\epsilon' = 3.23 \times 10^{-7}$, $\Delta\epsilon'' = 2.98 \times 10^{-6}$. Numerical results are given in Table 7. The differences between approximations I and II are small because the expressions (7.9) are dominated by the logarithmic terms. This means the main contribution comes from distant encounters for which the interactions are weak. The work of Seaton (1961) suggests that the approximation II results may be correct to within about 1%.

Table 7. Results for $\Omega(2s_{1/2}, 2p_j)$

k_2^2	$\Omega(2s_{1/2}, 2p_{1/2})$		$\Omega(2s_{1/2}, 2p_{3/2})$	
	I	II	I	II
0.06	614	545	1014	877
0.25	649	613	1084	1012
0.69	673	655	1133	1096
1.50	692	682	1170	1150
3.25	711	706	1208	1197

ACKNOWLEDGMENTS

We wish to thank Mr. W. Lawson and Mrs. J. Lawson for assistance with the computations. The work was supported by the Atomic Energy Research Establishment, to whom we are indebted for permission to publish.

REFERENCES

- FITE, W. L., STEBBINGS, R. F., and BRACKMANN, R. T., 1959, *Phys. Rev.*, **116**, 356.
 JOHN, T. L., 1960, *Proc. Phys. Soc.*, **76**, 532.
 LAWSON, J., LAWSON, W., and SEATON, M. J., 1961, *Proc. Phys. Soc.*, **77**, 192.
 MARRIOTT, R., 1958, *Proc. Phys. Soc.*, **72**, 121.
 PERCIVAL, I. C., and SEATON, M. J., 1957, *Proc. Camb. Phil. Soc.*, **53**, 654.
 ——— 1958, *Phil. Trans. Roy. Soc. A*, **251**, 113.
 SEATON, M. J., 1955, *Proc. Phys. Soc. A*, **68**, 457.
 ——— 1961, *Proc. Phys. Soc.*, **77**, 174.

LETTERS TO THE EDITOR

Antiferromagnetic Behaviour of GdB_6

A number of metals form hexaborides in which individual metal atoms and boron octahedra are arranged in the CsCl structure; and it has been suggested, on the basis of a theoretical analysis (Longuet-Higgins and Roberts 1954), that in CaB_6 satisfactory covalent bonding orbitals linking the boron atoms can be built up if the two valency electrons of the calcium are also used in them, so that the crystal is effectively built up of Ca^{2+} and B_6^{2-} ions. In LaB_6 an extra valence electron is present, and the high metallic conductivity and the magnitude of the Hall coefficient (Lafferty 1951) show that this electron must have a wave function rather like that of a conduction electron in a simple metal. (CaB_6 has a conductivity markedly inferior to that of LaB_6 (Samsonov and Grodshstein 1956), but it is not yet clear whether it is the semiconductor indicated by the models of Longuet-Higgins and Roberts and of Yamazaki (1957) or a poor metallic conductor as the more recent theoretical work of Flodmark (1959) suggests.)

GdB_6 must be similar to LaB_6 in many respects, but here there is a half-filled 4f electron shell on each gadolinium atom. The possibility therefore exists of significant magnetic interactions through indirect exchange involving the conduction electrons, since such an interaction through the three conduction electrons per atom in pure gadolinium gives rise to its ferromagnetism. Above room temperature GdB_6 is a well-behaved Curie-Weiss paramagnetic, with a negative θ value and an effective moment close to that for Gd^{3+} (Benoit and Blum 1952†).

We have measured the susceptibility of GdB_6 between 2°K and 300°K, using a sample prepared by Johnson, Matthey and Co. from highly pure materials and a force-measuring method incorporating a new type of balance shortly to be described in detail elsewhere. The susceptibility is shown as a function of temperature in Fig. 1, and a sharp maximum strongly suggestive of antiferromagnetic

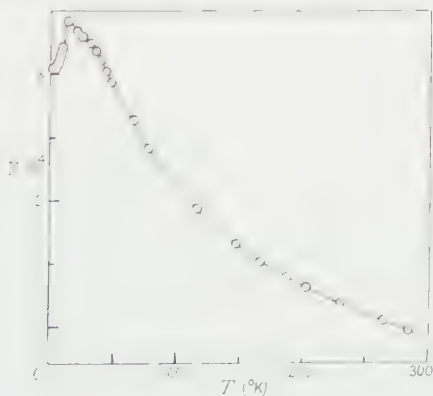


Fig. 1. Susceptibility χ in e.m.u. per gramme plotted against temperature T .

† These authors and Klemm, Schüth and v. Stackelberg (1932) have also examined other rare earth hexaborides.

ordering can be seen at about 13°K . The reciprocal susceptibility is accurately linear in temperature above 100°K , below which a gradual departure from linearity sets in. From the linear portion we derive the values $p_{\text{eff}} = 7.78 \pm 0.05$ Bohr magnetons per gadolinium atom and $\theta = -60^\circ\text{K}$, as compared with those of $7.63 \mu_B$ and -49°K given by Benoit and Blum; the theoretical value for Gd^{3+} is $7.94 \mu_B$.

Field-dependence of the susceptibility was looked for carefully but the magnetization-field curves of Fig. 2 show that none was found even at 2°K .

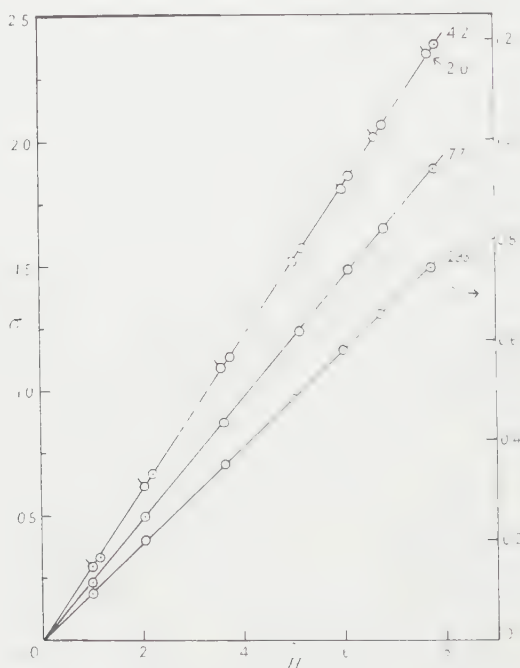


Fig. 2. Magnetization σ in e.m.u. per gramme plotted against magnetic field H in kilooersteds for four temperatures. The scale on the right refers only to the 293°K values.

In GdB_6 the gadolinium atoms are about 4.1 \AA apart (Andrieux quoted by Bertaut and Blum 1952), and direct interactions must therefore be very weak. Super-exchange through boron atoms may play a part, but the most likely source of antiferromagnetism is an indirect exchange through the conduction electrons. It has been pointed out to the authors (Elliott, private communication) that EuB_6 is likely to contain Eu^{2+} in a $4f^7$ configuration†, and examination of this material should therefore throw light on the part played by conduction electrons.

The electrical resistivity of GdB_6 is to be examined for spin disorder contributions, and it is hoped that the spin arrangement will be studied by low temperature neutron diffraction.

† A similar conclusion was reached on the basis of work function studies by Samsonov and Neshpor (1958).

The authors' thanks are due to the Royal Society and the Atomic Energy Research Establishment, Harwell, for financial support of the programme of which this work forms a part.

Department of Physics,
Imperial College,
London.
1st July 1960.

B. R. COLES.
D. GRIFFITHS.

Note added in proof.

Dr. T. Cole of the Ford Scientific Laboratory (U.S.A.) has observed paramagnetic resonance absorption in a sample of this material at room temperature, finding a g -value very close to 2.0 in agreement with an $^8\text{S}_{7/2}$ configuration for the gadolinium atoms.

- BENOIT, R., and BLUM, P., 1952, *C.R. Acad. Sci., Paris*, **234**, 2428.
BERTAUT, F., and BLUM, P., 1952, *C.R. Acad. Sci., Paris*, **234**, 2621.
FLODMARK, S., 1959, *Ark. Fys.*, **14**, 513.
KLEMM, W., SCHÜTH, W., and v. STACKELBERG, M., 1932, *Z. Phys. Chem. B*, **19**, 321.
LAFFERTY, J. M., 1951, *J. Appl. Phys.*, **22**, 299.
LONGUET-HIGGINS, H. C., and ROBERTS, M. DE V., 1954, *Proc. Roy. Soc. A*, **224**, 336.
SAMSONOV, G. V., and GRODSHTEIN, A. E., 1956, *Z. Fiz. Khim.*, **30**, 379.
SAMSONOV, G. V., and NESHPOR, V. S., 1958, *Dokl. Akad. Nauk, S.S.S.R.*, **122**, 1021.
YAMAZAKI, M., 1957, *J. Phys. Soc., Japan*, **12**, 1.

The Optical Absorption of Gallium Arsenide in the Reststrahlen Band

Measurements of the absolute absorption coefficients of gallium arsenide have been made through the reststrahlen band. The results are shown in the Figure.

Simultaneous measurements of the transmission t and reflection r coefficients were made on plane parallel-sided specimens at normal incidence, and the absorption coefficients α determined from the equation

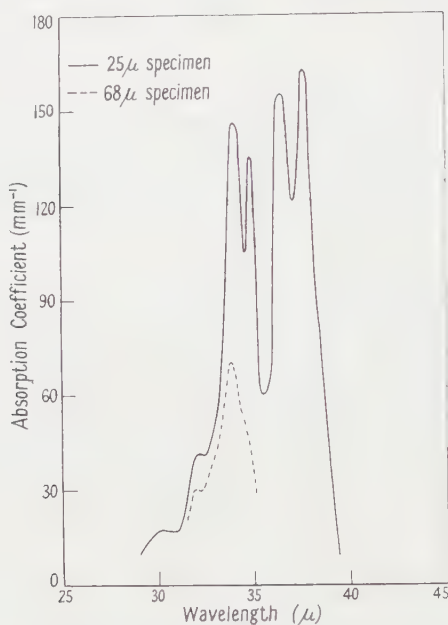
$$[(1-r)^2/t] - t = 2 \sinh \alpha l$$

where l is the thickness of the specimen. The only assumption made in the derivation of this equation is that the intensities are additive (Smith 1946).

The two small bands at 30.2 and 32μ are probably due to summation bands of transverse acoustic with transverse and longitudinal optic phonons respectively. The strong peak at 34μ is, presumably, due to the absorption of a photon and the emission of a single long wavelength longitudinal optic phonon. This would require the energy of the LO phonon to be 0.0364 eV which is in very good agreement with the value of 0.036 eV found from electrical measurements of tunnel diodes made by Hall, Racette and Ehrenreich (1960). The peak at 34.9μ is only found in the 25μ specimen and is, we believe, associated with the discrete structure of k space as explained below. The two peaks at 36.5 and 37.7μ are, presumably, due to the emission of single long wavelength transverse optic phonons. The value of 36.5μ is very close to the value we deduce for the TO phonons at $k=0$

from the cut-off frequencies of two phonon summation bands, and the ratio of the LO frequency to the TO frequency which is thus 1.074 is close to the value of 1.079 deduced by Ehrenreich (1960) in a recent re-analysis of the reflectivity.

All of these strong peaks must be associated with sharp transitions since the spectral slit width of the spectrometer was approximately $1.0\text{--}1.5\mu$ which is close to the half-width of most of the strong peaks.



Optical absorption of GaAs at 25°C.

A possible explanation for the appearance of the bands at 34 and 34.9μ can be given. It can be shown by group theoretical arguments that the three optical branches of the phonon spectrum become degenerate at $k=0$, but for small finite values of k the effect of the Coulomb forces is to cause the frequency of the longitudinal branch to increase fairly rapidly to a value ω_l given by the equation:

$$(\omega_l/\omega_t)^2 = \epsilon_0/\epsilon_\alpha$$

where ω_t is the frequency of the transverse optic branch near $k=0$, and ϵ_0 and ϵ_α are the static and infra-red dielectric constants—for a fuller discussion of the behaviour of the Coulomb forces near $k=0$ see Kellermann (1940). In the intermediate range, however, the vibrational modes will contain mixtures of longitudinal and transverse components, and the photon will couple with the latter. Now the wavelength of the phonon is nearly the same as the wavelength of the photon in the crystal, since wave-vector is conserved in the interaction with an accuracy of the order of $2\pi/l$ set by the uncertainty principle (the phonon states have wave-vectors that are integral multiples of $2\pi/l$, and the uncertainty principle will always allow transitions to a few of these states in the immediate neighbourhood of the photon wave-vector). The wavelength of the photon in the crystal is approximately $10\mu (\lambda/\epsilon_\alpha^{1/2})$ and thus the wavelength of the phonons emitted in the

crystal is comparable with the thickness of our specimens. It seems reasonable to assume that these phonons contain a mixture of longitudinal and transverse polarizations.

The appearance of the 34.9μ peak in the thinner specimen can now be understood. The wave-vector of the photon is approximately 625 mm^{-1} and in the 25μ specimen the phonon states are spaced at intervals of 250 mm^{-1} ($2\pi/l$), thus the transitions are mainly to states 2 and 3 (i.e. states for which $k=4\pi/l$ and $k=6\pi/l$) but there will be a definite though smaller probability of transitions to state 1. However, in state 1 the admixture of transverse polarization is, presumably, much greater and its energy correspondingly less so that it is reasonable to expect that this transition will be quite strong and that it will have a lower energy. This is confirmed by the results. In the case of the 68μ specimen the phonon states are spaced at intervals of 92 mm^{-1} (thus transitions will be mainly to states 6 and 7) and the chances of resolving discrete structure on the long wavelength side would be very much less.

The only explanation we can offer for the appearance of two peaks associated with transverse optic phonons near $k=0$ is that the coupling between these modes and electromagnetic radiation is so strong that the resonance is split. There are of course two transverse optical branches, but on any simple theory these should be degenerate near $k=0$.

We have no satisfactory explanation for the observed increase in absorption coefficient with decreasing specimen thickness.

These measurements form part of a study of the lattice bands of gallium arsenide, of which the experimental details and complete results are to be published later.

We would like to thank Mr. S. J. Brooks and Miss C. A. Nash for preparing the specimens and assisting with the development of the experimental techniques. We would also like to thank Drs. W. Cochran, R. J. Elliott and T. P. McLean for some very valuable discussions, and Dr. D. H. Parkinson for generous support and encouragement. The gallium arsenide crystals used in this investigation were very kindly supplied by Dr. C. Hilsum of the Services Electronics Research Laboratories. This letter is published by the permission of the Controller, Her Majesty's Stationery Office.

Royal Radar Establishment,
Great Malvern,
Worcs.
17th August 1960

S. J. FRAY.
F. A. JOHNSON.
J. E. QUARRINGTON.
N. WILLIAMS.

EHRENREICH, H., 1960, *Phys. Rev.*, to be published.
HALL, R. N., RACETTE, J. H., and EHRENREICH, H., 1960, *Phys. Rev. Letters*, **4**, 456.
KELLERMANN, E. W., 1940, *Phil. Trans. Roy. Soc.*, **238**, 513.
SMITH, T., 1946, *Proc. Phys. Soc.*, **58**, 472.

Note added in proof.—More recent work with much higher resolution has led us to change our ideas. We now believe that the vibration spectrum near $k=0$ is strongly influenced by the actual boundary conditions which in turn will depend on the size, shape and orientation of the specimen. The increase in the absorption coefficient with decreasing thickness seems to be consistent with this idea.

The Calculation of Debye Characteristic Temperatures

In a recent research note Joshi and Mitra (1960) give the elastic constants for a number of solids and the Debye characteristic temperature at 0°K , θ_0 , obtained from these by numerical integration. It may be pointed out that θ_0 for the cubic and hexagonal crystals (with the exception of AgBr, AgCl and FeS₂) listed by Joshi and Mitra may be readily calculated from the tables of DeLaunay (1956, 1959) and Wolcott (1959), the numerical integrations so to speak having been performed in advance. The three exceptions above involve substances for which the elastic constants happen to fall outside the range currently covered by the tables. Crystals of lower symmetry still require numerical techniques as preparation of tables for these is not practicable.

There is also a serious question as to whether the θ_0 calculated from low temperature adiabatic elastic constants should agree with the low temperature value of θ found calorimetrically. Evidence for magnesium (Slutsky and Garland 1957), zinc (Garland and Dalven 1958) and cadmium (Garland and Silverman 1960) shows considerable discrepancies well outside experimental error, between the values of θ_0 determined from low temperature heat capacities and those calculated from elastic constants. These discrepancies, which occur in the hexagonal crystals and not in cubic ones, may be of some fundamental significance.

European Research Office,
United States Department of the Army,
Frankfurt am Main,
Germany.

N. M. WOLCOTT.

6th October 1960.

DELAUNAY, J., 1956, *Solid State Physics*, Vol. II (New York: Academic Press).

— 1959, *J. Chem. Phys.*, **30**, 91.

GARLAND, C. W., and DALVEN, R., 1958, *Phys. Rev.*, **111**, 1232.

GARLAND, C. W., and SILVERMAN, J., 1960, *Phys. Rev.*, **119**, 1218.

JOSHI, S. K., and MITRA, S. S., 1960, *Proc. Phys. Soc.*, **76**, 295.

SLUTSKY, L. J., and GARLAND, C. W., 1957, *Phys. Rev.*, **107**, 972.

WOLCOTT, N. M., 1959, *J. Chem. Phys.*, **31**, 536.

REVIEWS OF BOOKS

Electrons and Phonons, by J. M. ZIMAN. Pp. xiv + 554. (London: Clarendon Press: Oxford University Press, 1960.) 84s.

This is undoubtedly a book of substance. It says in its 500 pages exactly what is known about electrons and phonons in metal and semiconductors, how they interact and why the transport properties of these solids are what they are. To the present reviewer it represents something near the ideal in a book.

It is aimed at those who want to know how quantum mechanics is to be applied to problems of electron transport in solids, and assumes that they know their standard techniques up to about mathematical physics honours degree or first year postgraduate level. It also assumes that the reader will work and does not need to be pandered to. The book is about the title, and contains mercifully little standard 'methods of quantum theory' and other introductory matter which so often devours a lot of space in works at this level.

It uses the minimum of mathematical verbiage consistent with completeness. The reader is hardly ever left in doubt as to where the argument is intended to go, for the concise mathematics is backed up by lucid plain English. When an argument is incomplete, it is pointed out, and the words 'guess' and 'approximation' are used with their real meanings at the appropriate places.

The usefulness of a book after the first reading rests on two main factors, its reliability and its indexing. On both counts this book seems exemplary. It is already indispensable to me.

So in style and presentation the book is good. In content it is new. It is new because it deals with substances as they really are, with complex energy surfaces, anisotropic elastic behaviour, screened electron interactions, plasma waves, and shows that a determined physicist can get somewhere without replacing everything by spheres and uniformity.

To sum up, I can only echo ruefully the quotation which so aptly introduces the chapter on imperfection scattering: "All things are literally better, lovelier and more beloved for the imperfections that have been divinely appointed, that the law of human life may be Effort, and the law of human judgement Mercy"—the book is too damned perfect for a reviewer's enjoyment. W. M. LOMER.

Mechanik Deformierbarer Körper, by M. PÄSLER. Pp. 199. (Berlin: Walter de Gruyter, 1960.) DM. 5.80.

The series of concise textbooks issued under the name of the *Göschen Sammlung* have long been a feature of the German scientific literature. The present volume fully maintains the tradition. Two main topics are considered: elasticity and hydrodynamics. In the former both static deformations and waves propagation are treated, in the latter viscous as well as non-viscous fluids.

The mathematical apparatus required is reviewed in an opening chapter—in the main vector algebra, the properties of tensors and a discussion of the wave equation. The treatment is neat and elegant throughout and the book constitutes a welcome addition to the series. M. BLACKMAN.

Introduction to Practical Infra-Red Spectroscopy, by A. D. CROSS. Pp. viii + 80. (London: Butterworth's Scientific Publications, 1960.) 17s. 6d.

This book is primarily intended for the many organic and analytical chemists who have come to use the methods of infra-red spectroscopy without any

background in the field of spectroscopy as a whole. In the first half of the book the author describes in a simple, straightforward manner both the experimental techniques and the elementary theory of infra-red spectroscopy as an analytical tool. A valuable comparative table of commercial double-beam spectrometers is included. The second half of the book consists of correlation charts and tables of characteristic group frequencies, with brief notes on their use for the interpretation of spectra. Spectroscopists will be pleased to observe that wave numbers are used in preference to wavelength throughout.

This is a practical book written in a clear and concise style, and it will be useful to all analytical spectroscopists. Even at 80 pages, and with paper covers, it is good value for 17s. 6d.

I. M. M.

Die Entstehung von Sternen durch Kondensation diffuser Materie, by G. R. BURBIDGE, F. D. KAHN, R. EBERT, S. v. HOERNER and ST. TEMESVÁRY. Pp. vi + 330. (Berlin, Göttingen, Heidelberg: Springer, 1960.) DM. 38.

Contemporary astrophysics is much concerned with attempts to ascertain the ages of the stars and to account for their formation from dust and gas in the galaxy. These topics turn very largely for their observational material to the celebrated Hertzsprung–Russell diagram, which displays the relation between absolute magnitude and colour as it occurs in different classes of objects, as, for example, in open and in globular clusters. The volume under review, *Die Entstehung von Sternen durch Kondensation diffuser Materie*, publishes three essays which each gained a prize in a special competition. A great deal of material has been collected very industriously by the prize winners, and the volume is most useful in that it presents a convenient summary of contemporary views on the subject. This was perhaps the natural result of a competition of this sort: one might wonder whether the nine essays submitted which did not gain a prize indulged in adventure, or criticism, or whether they were merely unsuccessful attempts at reporting contemporary fashion. One may wish to consult a book because it epitomizes contemporary views—as *Die Entstehung von Sternen* does very successfully—or because it contains a lucid account of standard development. An example of the latter is Smart's *Stellar Dynamics*, which was actually criticized when it appeared for not concerning itself with accounts of the latest views on the galaxy, or with a critique of the observational facts as they were then understood. Had the book done so, it would now be unreadable, but in fact its standard mathematical development makes it still most useful, although twenty years have elapsed since its publication. The present volume is of a very different character and will be read only as long as people care what astrophysicists thought in 1958. For all this, the reviewer is very glad to possess the book and expects to consult it frequently. There is no doubt about the enormous contemporary importance of the topics which the essayists report.

R. V. D. R. WOOLLEY.

General Crystallography. A Brief Compendium, by W. F. DE JONG. Pp. ix + 281. (San Francisco, London: W. H. Freeman and Co., 1960.) 38s.

This is a translation from Dutch of a book which first appeared in 1951. A number of sections have been revised and new material has been added. The translation has been well done, although the use of the word 'particle' for an atom seems inappropriate nowadays, for example. The subject is treated under

four separate headings entitled Geometric, Structural, Chemical and Physical Crystallography respectively. It is clearly in the first of these that the author's greatest interest lies. In a book which sets out to "serve undergraduate students as a summary of the modern view of crystallography" it is inappropriate to devote so large a proportion of the space to classical crystallography, with many references to works of the last century in the German language. Very few of these are available to the English-speaking reader, nor is it likely that the modern student would find them useful. The remaining sections provide good introductions to the topics with which they deal, although the treatment is necessarily superficial in places. For example, only one page is devoted to "The crystal as a dielectric", and this includes half a page concerned with ferroelectricity.

This is an excellent book of its kind, but the balance of the treatment lessens its value as an introductory text, at least for physicists. W. COCHRAN.

The Special Theory of Relativity, by J. AHARONI. Pp. viii+285. (Oxford: Clarendon Press: Oxford University Press, 1959.) 45s.

The author builds most of the usual formal apparatus of special relativity theory, often supplying much elementary detail in derivations. He sets out the Lorentz transformation and Maxwell's theory at length, includes a rather difficult chapter on general field theory, reminiscent of Corson or Rzewuski, and deals briefly with the elementary relativistic dynamics of particles and fluids. The number of concrete applications described by way of illustration is rather limited, and there are no exercises to test the student's understanding of what purports to be an introductory book.

The book's most unusual feature, embodying the author's intention to expound applications to quantum theory, is a final chapter of 87 pages, occupying almost one-third of the text, on spinors. Again there is a great deal of elementary detail (for example, two pages are devoted to writing out the γ -matrices explicitly) perhaps at the expense of more fundamental considerations. The author announces in a Preface the admirable intention to introduce tensors and spinors as representations of the rotation and Lorentz groups, but makes precise statements of very few theorems in representation theory and proves even fewer. Consequently, the student may acquire some manipulative technique, but is unlikely to gain a deep understanding of the subject, and for this reason the book cannot be recommended to the theoretical physicist or applied mathematician as a serious introduction to tensor and spinor analysis and their relativistic applications. F. A. E. PIRANI.

Exploding Wires, edited by W. G. CHACE and H. K. MOORE. Pp. 373. (London: Chapman and Hall; New York: Plenum Press, 1959.) 76s.

The rapid and violent fusion of a thin wire by a high voltage capacitive discharge presents an interesting field of study in itself and the phenomenon has a wide variety of applications. Interest in this subject has only recently been aroused and this monograph, the first in its field, is a record of an American conference on Exploding Wire Phenomena held in April 1959.

In the experimental field much effort has been taken in electrical circuit design to transfer the optimum electrical energy into the wire before rupture and so ensure a vigorous explosion. Several theories of the various phases of the explosion are put forward together with experimental results in support of

the theories. A complete understanding of the processes of explosion is, however, still lacking and, in particular, considerable theoretical and experimental attention has been focused on the 'current dwell' phase of the explosion. This effect, the presence of which depends on prevailing experimental conditions, is characterized by a period of constant and low amplitude current conduction through the wire terminating in complete rupture. The relevant characteristics of this phase are studied as a function of the electrical discharge circuit parameters, dimensions and material of the wire and the ambient gas pressure.

In view of the rapidity of the processes under investigation many optical and electrical diagnostic techniques are described, capable of resolution in the sub-microsecond time region. These techniques give information on wire diameters, temperature, resistance and physical state as a function of time during the electrical discharge. The performance of the photographic and cinematographic equipment is of a high standard as is illustrated by many prints.

Such a rapid explosion is necessarily a potent source of shock waves and visible radiation. Many applications of exploding wires stem from these two aspects, particularly to those problems requiring a highly reproducible source of sound or radiation whose time origin and duration as well as intensity are accurately controllable. The various phases of the explosion process also serve as a useful model for the study of hydrodynamic flow at elevated pressures and temperatures. Other applications cited include the production of rapidly moving sources of plasma, metallic bonding of various materials and the design of specialized electrical fuses.

This collection of original papers will prove very useful to workers dealing with any aspect of exploding wires or of high-speed photography.

C. B. WHEELER.

The Scientific Papers of Sir Geoffrey Ingram Taylor, Vol. 2, *Meteorology, Oceanography and Turbulent Flow*, edited by G. K. BATCHELOR. Pp. x+515. (Cambridge: University Press, 1960.) 75s.

The phenomenon of G. I. Taylor is known to physicists and applied mathematicians all over the world. He is the latest and by no means the least of the great line of British mathematical physicists in the tradition of Stokes, Kelvin and Rayleigh. His work is characterized by two closely correlated features—the depth of the physical insight and the relative simplicity of the mathematical treatment which follows, and nowhere are these admirable traits better illustrated than in the present collection.

The volume opens with the great memoir of 1915 on atmospheric turbulence. This contribution, written when Sir Geoffrey was still in his twenties, arose primarily from studies of the formation of the fogs of the Grand Banks, near Newfoundland, during the voyage of the *Scotia*, but it became much more than a report on a meteorological phenomenon. It is remarkable in many ways: for its anticipation of many of the fundamental developments of later years, including the vorticity-transport and mixing-length theories of turbulence; for the adroit use of somewhat meagre data from observations and for the maturity and clarity of the style. Sir Geoffrey's handwriting has long been famous among his friends (it is to be hoped that somewhere in this series a page of a Taylor MS. will be reproduced, just as Hardy's meticulous script formed the wrapper of *A Mathematician's Apology*), but when the words have been deciphered

the English is always a delight to read. The 1915 paper is one of the foundation stones of what is now called 'micrometeorology', and it was followed by others almost as famous, including investigations on the propagation of the diurnal wave of temperature in the lower layers of the atmosphere, the skin-friction of the earth's surface and the formation of fog and mist.

In 1921 there was published in the *Proceedings of the London Mathematical Society* a short paper on diffusion by continuous movements. In this Taylor generalized the problem of the random or drunkard's walk by the introduction of Lagrangian correlation, and he gave a simple equation which related the scatter of particles in a turbulent fluid to the double integral of the correlation coefficient. From this grain of mustard seed has grown a veritable forest. In 1935-36 came the truly remarkable series of five papers which created the statistical theory of turbulence. These were written at a time when the somewhat loose concept of the *Mischungssteg* had been used with considerable success by Prandtl and his followers at Göttingen to predict phenomena in boundary-layer turbulence, but in Taylor's treatment concepts such as the 'scale of turbulence' were defined precisely and an explicit relation, which could be tested in wind-tunnel experiments, was derived between the rate of dissipation of energy, the mean square variation of the downstream component of velocity and the average 'size' of the smallest eddies.

Although the papers in this collection cover an enormous field, from the physics of the atmosphere and the oceans to flow in wind tunnels and chimneys, they show a remarkable likeness in their approach to a subject. A paper by G. I. Taylor nearly always begins with some facts of observation, after which there is a lucid and penetrating physical explanation which leads naturally to an elegant but usually simple mathematical analysis. The end-point is almost invariably a comparison of the 'theoretical' and 'observed' values, and the agreement is nearly always so close that the reader cannot escape the conclusion that the problem really has been solved. No one can read through these papers without being conscious that he is in the presence of a great applied mathematician, a natural philosopher in the true sense of the word, whose physical intuition rather than his mathematical skill is the dominant characteristic of his mind.

This volume should be accessible to every physicist, and the scientific world as a whole is grateful to Dr. Batchelor, the Ministry of Supply, Trinity College, the Cambridge University Press and indeed to all who have made possible the publication of the series. It goes without saying that the printing and format are of the high standard that one has learned to expect of the Cambridge University Press.

O. G. SUTTON.

The Science of Mechanics in the Middle Ages, by MARSHALL CLAGETT. Pp. xxix + 711. (Wisconsin, London: Oxford University Press, 1959.) 50s.

The Science of Mechanics in the Middle Ages is a guide and a source book in the development of mechanics in the period before Galileo. Numerous original texts are studied with great care and detail and presented critically. Forty-five original documents are included in the English translation, some of which are accompanied by their original Latin texts. Among the articles are *The Book on the Balance* attributed to Euclid, Archimedes on *Heaviness and Lightness*, a selection from the manuscripts of Leonardo da Vinci, and a selection from Copernicus on the *Revolutions of the Celestial Orbs*.

Principles of Electricity and Magnetism, by E. M. PUGH and E. W. PUGH. Pp. xi + 430. (Reading, Mass.: Addison-Wesley, 1960.) 49s.

This is an elementary textbook which starts in the usual manner with a presentation and discussion of the basic experimental laws and which leads ultimately to Maxwell's equations. Very little is assumed of the reader's mathematical knowledge, so that there appears, wherever necessary, a brief utilitarian account of matters such as vector algebra, theory of complex variables, line integration, etc.

The style of writing is clear and fluent, and the emphasis is mainly on fundamental notions. The presentation is based on many years of experience by the authors and undoubtedly this has led to the many original and excellent examples to be found at the end of each chapter. The authors seem to have relied a great deal on these examples: it might have been better at this level of presentation to have included some of the illustrative exercises in the text. This is particularly pertinent to the chapters dealing with electrostatic problems and the magnetic fields of electric currents.

Some discussion is given of the propagation of electromagnetic waves through different media, with application given to the problem of power transmission as a function of frequency. This treatment is very brief, and in many instances, the relevant formulae are given without derivation, but with particular reference to standard text-books.

A careful description of the rival systems of units is given at the beginning of the text and the m.k.s. system is chosen for later use.

It is curious that two new textbooks on electromagnetism, covering essentially the same material in a similar manner should have been issued by the same publishing company within the last year.

L. GOLDFARB.

Progress in Automation, Vol. 1, edited by A. D. BOOTH. Pp. viii + 231. (London: Butterworths Scientific Publications, 1960.) 42s.

The aim of this volume is to record some recent contributions made in England to the growth of automation. It opens with a breezy and readable survey of the history and basic concepts of the subject by the Editor, who traces it perhaps farther back than most of its practitioners would recognize. Notions such as binary coding (including error-detecting codes), feedback and Fourier analysis are touched on briefly but lucidly, and a short but adequate bibliography is given. A charming touch is added by the news that men can now apparently be replaced by pigeons in such tasks as the inspection of transistors, unacceptable specimens being rejected with a flick of the beak.

Despite the gentleness of this introduction, however, the bulk of the book is not for the general reader. The first half deals mainly with specialized devices for transducing and processing data, and the second with examples of industrial applications and the problems of automatic inspection. The physicist will find familiar nucleonic and other monitoring techniques discussed, and experimentalists in general might well pick up some labour-saving ideas. But the volume as a whole is designed (by contrast with others on this much dramatized subject), to excite only those actively engaged in the field.

D. M. MACKAY.

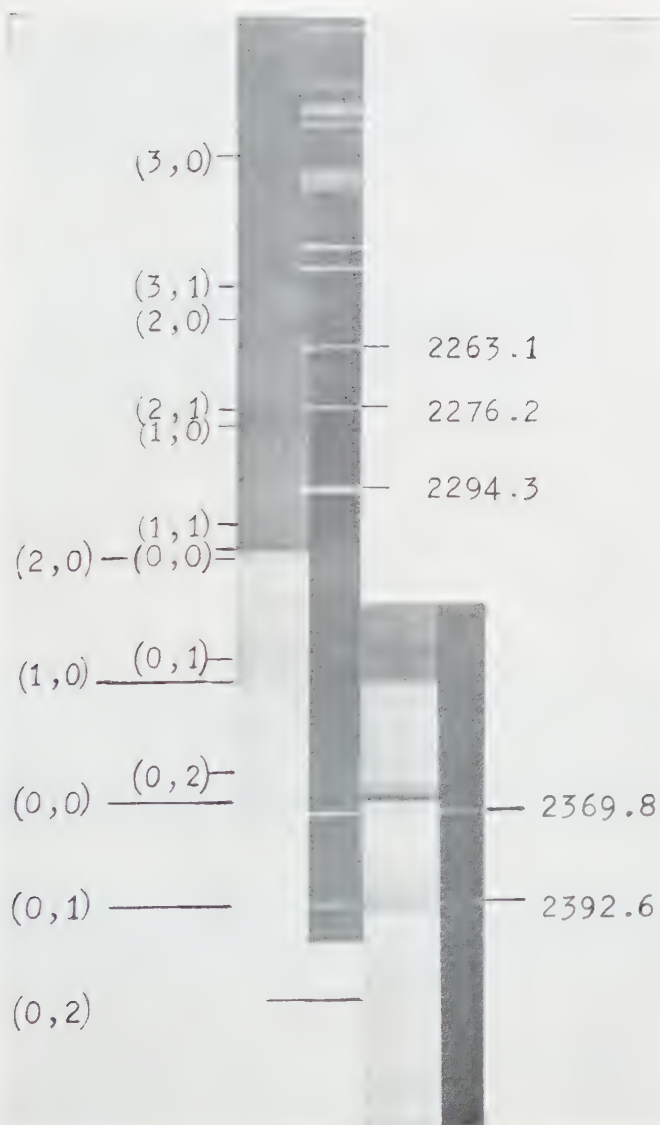


Fig. 2. Absorption spectrum of tellurium monosulphide.

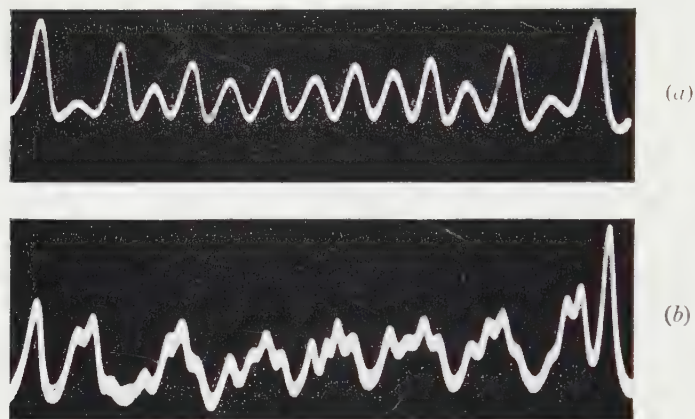


Fig. 2. Central $|+1/2\rangle \leftrightarrow |-1/2\rangle$ transition for dilute vanadium fluosilicate, with H at 78° from the crystal axis: (a) wavelength 1.3 cm ($H \sim 8200$ gauss), (b) wavelength 3.2 cm ($H \sim 3400$ gauss); the line at the extreme right is abnormally intense through an accidental coincidence with a line belonging to an outer electronic transition.

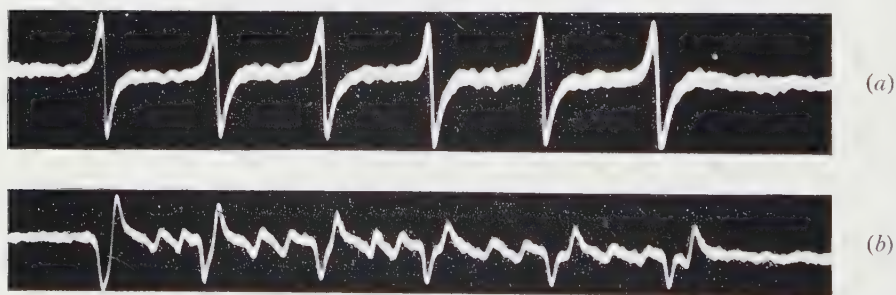


Fig. 4. Spectrum of modelling clay at (a) 1.3 cm, (b) 3.2 cm wavelength. The spectrum is attributed to the $|+1/2\rangle \leftrightarrow |-1/2\rangle$ transition of a trace of $^{55}\text{Mn}^{2+}$. High field is towards the right.

A Further Explanation of the Shape of the Hysteresis Loop of 'Square Loop' Ferrites

By J. E. KNOWLES

Mullard Research Laboratories, Salfords, Surrey

MS. received 16th June 1960

Abstract. In an earlier paper it was assumed that the individual grains of a 'square loop' ferrite have rectangular hysteresis loops. This hypothesis has now been given a theoretical justification, based on a model due to Néel. It was also possible to estimate the number of times (14) that the energy of a typical domain wall passed through a minimum in the course of a magnetization reversal.

§ 1. INTRODUCTION

A MODEL has recently been proposed for the domain configuration in a polycrystalline 'square loop' ferrite. (Knowles 1960, hereafter referred to as I). It was observed that a particular grain of the material possessed two 180° domain walls, the motion of which was impeded by 'obstacles' which were presumably due to stresses, chemical inhomogeneities and voids in the material. The hysteresis loop of the grain did not show a well-defined 'knee' but was otherwise essentially rectangular in character. On the basis of this observation it was assumed that all grains in the material had one or two 180° walls, that they all possessed perfectly rectangular hysteresis loops, and that the coercive force of these loops varied slightly from grain to grain.

The validity of this hypothesis will now be investigated on the basis of theories due to Néel (1942, 1943).

§ 2. THE 'AVERAGE' HYSTERESIS LOOP OF A SINGLE GRAIN

The effect of any kind of inhomogeneity (which for convenience will subsequently be referred to as stresses), will be to cause the wall energy E to fluctuate as the wall moves across the grain in a manner illustrated by Fig. 1. In the

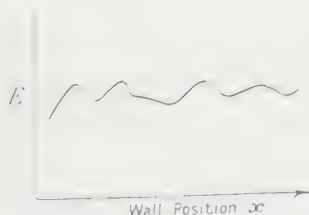


Fig. 1. Schematic representation of the wall energy as a function of position.

absence of an external field the wall will lie in a minimum. If now a small field H_1 is applied, the wall will move reversibly until the driving pressure balances the opposing force or

$$2MH_1 = \left(\frac{dE}{dx} \right)_1.$$

If the field is increased to H_2 so that $2MH_2 > (dE/dx)_{\max}$ then the wall will move irreversibly to a position where $(dE/dx)_2$ again has a value equal or greater than $2MH_2$. On increasing the field still further the wall will move until it again reaches a position where $(dE/dx)_3$ has a value greater than $2MH_3$ and so on. At first sight it would seem that the magnetization would change with field rather in the manner indicated in Fig. 2(a), but as Tebble (1955) has pointed out, this pre-supposes that as the wall moves across a grain it constantly encounters regions of increasing stress. This is rather improbable, for the wall is more likely to encounter a very high stress gradient quite early on in its travel so that the magnetization would change with field rather as indicated in Fig. 2(b). Thus it is desirable to determine the shape of the hysteresis loop produced by domain walls moving across many similar grains, the motion of the walls being impeded by stresses of variable magnitude.

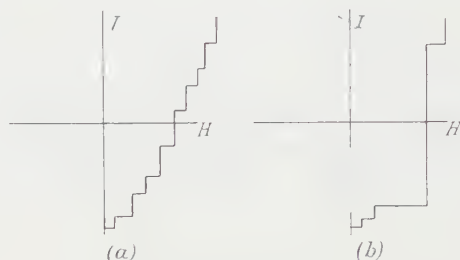


Fig. 2. Possible (I, H) curves for a single grain.

A solution is possible upon the basis of a model due to Néel. In order to analyse the movement of a domain wall impeded by stress gradients it is necessary to assume that the wall energy varies with position in a manner which is both physically plausible and susceptible to mathematical treatment. Néel, as a first approximation, assumed that the different sections of a plane wall had the same energy, and that the variation of wall energy with wall position could be represented diagrammatically (Fig. 3) by a 'contour polygonal' consisting of a

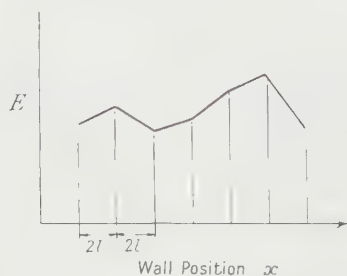


Fig. 3. A Néel 'contour polygonal'.

series of straight lines of equal projection $2l$ upon the abscissa. There is no correlation between the gradients of consecutive sides, and the magnitudes of the gradients are scattered in a Gaussian manner about some mean value. This mean gradient, which is of course an intrinsic property of the material, will here be designated by H_s where H_s is the limiting field required to force a wall up a side of that gradient. In a second approximation, which is not required here, the

contour polygonal was given a more realistic shape by rounding off the peaks and valleys with parabolic arcs.

Consider now a large number of very similar cubic grains of side L , each grain supporting one 180° wall. All the grains are orientated so that the magnetization is along the field direction. At moderately large field strengths it is supposed that the wall is adjacent to one face of the grain, so that during the course of a magnetization reversal each wall travels a distance L . It is further assumed that the wall energy as a function of position in each grain is given by a contour polygonal of the type shown in Fig. 3. The shape of the contour polygonal varies from grain to grain, but the parameters H_c , $2l$ and N , the number of sides of the polygonal, are everywhere the same.

Then, as Néel has pointed out, if a field H , where H is not very small, is applied all slopes having a gradient greater than $-H$ will be impassable barriers to the motion of the walls. In general each grain will contain a different number of such barriers, the average number n per grain being given by a conventional Gaussian expression of the type

$$n = \frac{N}{2} \int_H^\infty \frac{2}{\sqrt{\pi}} \exp(-p^2) dp.$$

The mean distance t travelled by the walls before encountering the first barrier in their path may then be shown to be given by

$$t = L(1 - e^{-n})/n.$$

Thus t is proportional to the change in magnetization, from remanence, produced by a field H .

Using these two results of Néel hysteresis loops were calculated for $N = 20$, 50 and 500 and for two distributions of the slopes of the contour polygonal about the mean value H_c . Fig. 4 shows on one diagram the frequency size distribution

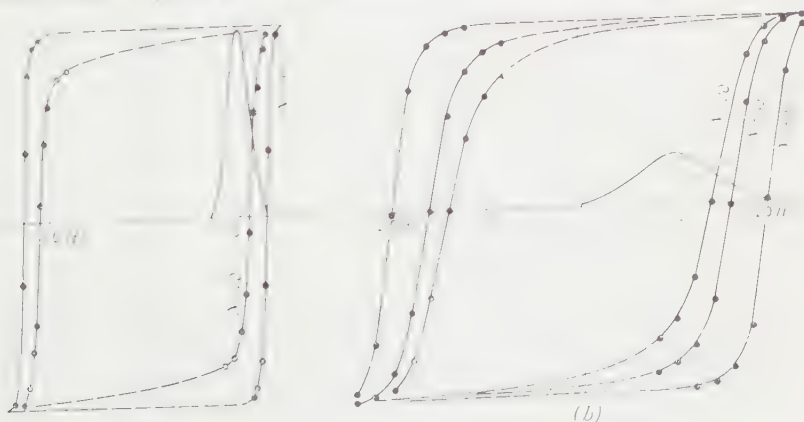


Fig. 4. Theoretical hysteresis loops of an assembly of single grains.

of the gradients of the sides, and the corresponding hysteresis loops. The low field portions of the loops to which the theory does not apply, have been sketched in with broken lines. For a very narrow distribution of the gradients the hysteresis loops are very rectangular, and the coercive force varies very slowly with N . For a much wider distribution of the gradients (Fig. 4(b)) the loops are still substantially rectangular and there is a rather more pronounced variation of coercive force with N .

Thus the assumption made in I, that all grains have perfectly rectangular loops the coercive force of which varies slightly from grain to grain, may be substantially justified provided there is a narrow distribution of stress gradient in the material. It would seem desirable that the material be very homogeneous and show a small magnetostrictive effect, and in order that the spread of the grain coercive force be small the grains should be of the same size and of a compact shape.

It is also possible on the basis of Néel's paper to calculate N , and hence the average number of minima of the characteristic function encountered in the path of a domain wall during the course of a magnetization reversal, i.e. in the distance L . This ratio, designated by $1/\alpha$, is obtained by determining the value of the constants in the Rayleigh low field region where

$$I = aH + bH^2 \quad \dots\dots (1)$$

$$\text{or} \quad \mu = \mu_0 + 4\pi bH \quad \text{where} \quad \mu_0 = 4\pi a \quad \dots\dots (2)$$

$$\text{and} \quad \alpha = a/0.45bM. \quad \dots\dots (3)$$

§ 3. THE EXPERIMENTAL DETERMINATION OF α

A FX1394 core 1 in. outer diameter, of manganese magnesium ferrite was demagnetized by heating to 320°C. Its permeability as a function of the magnetizing field was then measured on a bridge of the inductive ratio arm type: when in balance the potential difference across the specimen was a linear function of the magnetizing field. The (μ, H) curve at 15 kc/s has been plotted in Fig. 5; it may be seen that the curve is linear for inductions up to about 1% of B_{\max} showing that Eqn (2) is valid in this region.

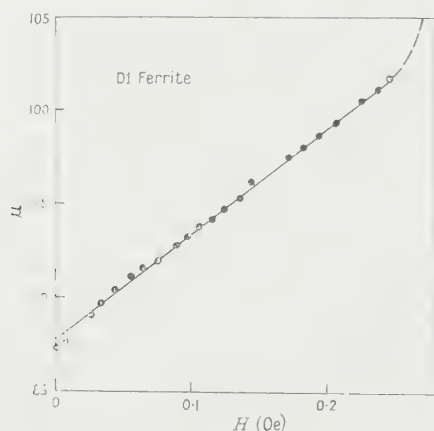


Fig. 5. The variation of the initial permeability of D1 ferroxcube with the magnetizing field.

In calculating α from the foregoing equations, it is necessary to deduct the permeability due to rotations, μ_0^{rot} , from the experimental value. For a polycrystalline sample it may be shown that for $K < 0$ (Smit and Wijn 1959)

$$\mu_0^{\text{rot}} = 1 + 2\pi M^2/K$$

$M \simeq 220$ e.m.u. cm^{-3} and $K \simeq 2 \times 10^4$ erg cm^{-3} . Hence $\mu_0^{\text{rot}} \simeq 16.2$ compared with the total initial permeability of 87.8; thus a permeability of 71.6 may be attributed to wall movements.

From Fig. 5 and Eqns (1)–(3) we find $a = 5.70$, $b = 4.46$ and hence $\alpha = 0.0735$ or $1/\alpha = 13.6$. Néel shows that $N = 4/\alpha$, so N in this case is about 55, and each domain wall traverses an average of about fourteen stress minima during the course of a complete magnetization reversal.

Néel gives for the coercive force an expression

$$H_c = 3ra \cdot 2\pi\lambda b$$

where λ is a constant equal to 0.81 and r , a reduced coercive force, may be shown to be equal to 1.32 for $1/\alpha = 13.6$. Substituting for a and b , $H_c \simeq 1.0$ Oe compared with the nominal value of 1.25 Oe. This agreement is closer by about a factor of two than any of the examples quoted by Néel.

ACKNOWLEDGMENTS

The author is indebted to the management of the Mullard Research Laboratories for permission to publish this paper, and also to Mr. J. Roche of Southampton University for some stimulating discussions. The permeability measurements were made by Mr. S. Longley.

REFERENCES

- KNOWLES, J. E., 1960, *Proc. Phys. Soc.*, **75**, 885.
NÉEL, L., 1942, *Cah. de Phys.*, No. 12.
——— 1943, *Cah. de Phys.*, No. 13.
SMIT, J., and WIJN, H. P. J., 1959, *Ferrites* (Philips' Technical Library), p. 244.
TEBBLE, R. S., 1955, *Proc. Phys. Soc. B*, **68**, 1017.

The Elastic Scattering of ^3He by C, Mg, Al and Cu

By G. PARRY, H. D. SCOTT AND S. SWIERSZCZEWSKI

Physics Department, University of Liverpool

MS. received 18th August 1960

Abstract. Angular distributions of 5.5 MeV ^3He particles elastically scattered by C, Mg, Al and Cu have been measured by magnetic analysis at angles of observation between 20° and 132.5° . The curves of the ratio of observed cross section to calculated Coulomb cross section show a decrease with angle for C, Mg and Al and an increase at large angles for Cu. The curves also show maxima and minima.

§ 1. INTRODUCTION

SINCE Farwell and Wegner (1954) first observed the variation with energy of the alpha particle scattering cross section many authors have observed pronounced maxima and minima in the angular distributions of scattered alpha particles (Bleuler and Tendam 1955, Eisberg, Igo and Wegner 1955, Seidlitz, Bleuler and Tendam 1958, Shook 1959, Aguilar *et al.* 1960). The optical model of the nucleus has been applied to analysis of the results of scattering of alpha particles and of heavy ions (Halbert, Hunting and Zucker 1960). The Fraunhofer diffraction formula for an absorbing disk (Bethe and Placzek 1940) and the sharp cut-off model of Blair (1954, 1957) have also been applied to analyse alpha particle scattering (Yavin and Farwell 1959, Aguilar *et al.* 1960) and ^3He scattering (Greenlees and Rowe 1960), and from these analyses values for interaction radii are obtained. The radii obtained from experiments with energy of incident particles around 40 MeV are in agreement with values predicted otherwise. Seidlitz, Bleuler and Tendam (1958) using 18 MeV alpha particles obtained somewhat larger values for R and suggested a possible dependence on energy of R derived this way. Zucker (1959) and Halbert, Hunting and Zucker (1960) were not able to get a reasonable fit to their heavy ion scattering data, nor to derive reasonable R values with incident nitrogen ions of energy 18 MeV.

In the present work an attempt is made to investigate the angular distributions of elastically scattered ^3He particles with energy close to the Coulomb barrier. The results have been analysed using the Fraunhofer diffraction formula, and the sharp cut-off model to obtain values for the interaction radii.

§ 2. EXPERIMENTAL METHOD

The 5.5 MeV ^3He beam from the 37 in. cyclotron of the University of Liverpool was used to bombard C, Mg, Al and Cu targets. As the divergence from the pure Coulomb scattering was expected to be small and the scattering cross sections are very large at small angles of observation the exposures at different angles varied over a wide range. The difficulty of timing and integrating the beam current introduces the possibility of error at small exposures. The targets used were as thin as possible and the beam was reduced by means of slits in front of the target chamber. The Coulomb cross section is proportional to Z^2 and small impurities of heavier elements in the target can give rise to particle groups obscuring the groups being studied. By analysing the scattered ^3He magnetically it was possible to separate the groups arising from different elements and inelastic events.

The extracted beam of singly charged ^3He was collimated by means of three separate slit systems, focused by magnetic lenses and passed into the target chamber 14 ft from the cyclotron. The scattered particles were magnetically analysed using the apparatus described by Green and Middleton (1956) and Dalton, Hinds and Parry (1957). The particles were recorded on nuclear plates which were exposed for angles of observation in the range 20° to 132.5° at 2.5° intervals, except for carbon whose spectrum became out of range of the magnetic analyser at angles over 90° (laboratory system).

All the targets used were self-supporting. Al and Mg targets were prepared by evaporation on to glass. The separated isotope ^{65}Cu target was obtained from the Atomic Energy Research Establishment, Harwell. By means of maintaining an arc between two graphite electrodes in vacuum it was possible to deposit a carbon film on glass, and from this film a robust carbon target was prepared. The thicknesses of the targets were found by weighing and are shown in the Table.

Target	Thickness (mg cm^{-2})
C natural mixture	0.12 ± 0.03
Mg natural mixture	1.00 ± 0.05
^{27}Al	0.06 ± 0.01
^{65}Cu isotopic	0.70 ± 0.05

No observable amounts of impurities were detected in the spectra for the Mg, Al and Cu targets. In the carbon spectrum a strong impurity group was present. The impurity group at larger angles splits into several components where Cu and Zn can be identified from their positions. The presence of the impurities in the carbon target is very likely due to insufficient cooling of the brass and copper parts in the graphite arc arrangement.

The exposures were adjusted to give adequate statistics and they were varied from about 1 to 600 microcoulombs. Because of the difficulty mentioned previously for small angles of observation it was not possible to make exposures at angles smaller than 20° . As the Mg and Cu targets are relatively thick the exposures at small angles had to be particularly small and hence the errors are large for angles less than 30° .

§ 3. RESULTS

The ratios of the experimental cross sections to the calculated Coulomb cross sections are shown in Figs 1 to 4. The Coulomb cross section for the natural Mg target was calculated as for the ^{24}Mg isotope (78.6% abundance). The errors shown on the points include the statistical errors and those due to the uncertainty in monitoring the exposure (the latter important only at small angles), but not those introduced by the uncertainty in target thickness.

A general feature of the results is that for C, Mg and Al there is a decrease with angle of the experimental cross section relative to calculated Coulomb cross section. For copper there is a decrease up to about 80° and then a large increase with angle. The curves also show maxima and minima. The periodicity of the variations is comparable with that of the patterns observed at higher energies. When the results are analysed in terms of Fraunhofer's diffraction formula for an absorbing disk, to obtain a fit high values between 10 and 20 fermis have to be used for the interaction radii.

On the basis of the sharp cut-off theory of Blair (1957) the ratio of experimental to Coulomb cross section should show a gross negative slope and a value for the interaction radius can be obtained.

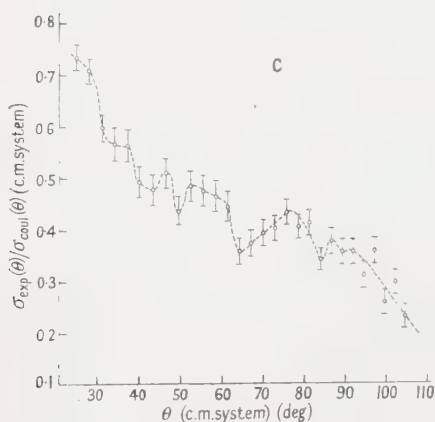


Fig. 1. Elastic scattering of ^3He by carbon. The observed cross section for the centre-of-mass system relative to calculated Coulomb cross section as a function of centre-of-mass angle.

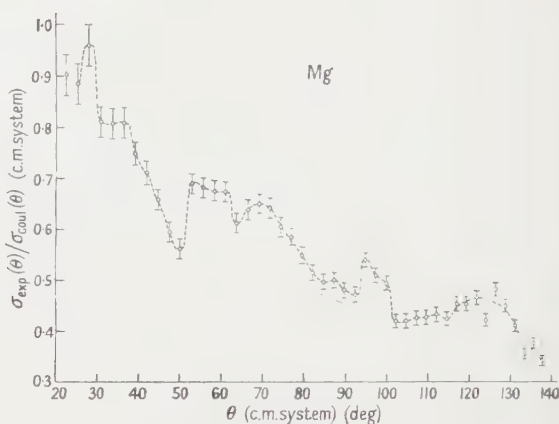


Fig. 2. Elastic scattering of ^3He by magnesium. The observed cross section for the centre-of-mass system relative to calculated Coulomb cross section as a function of centre-of-mass angle.

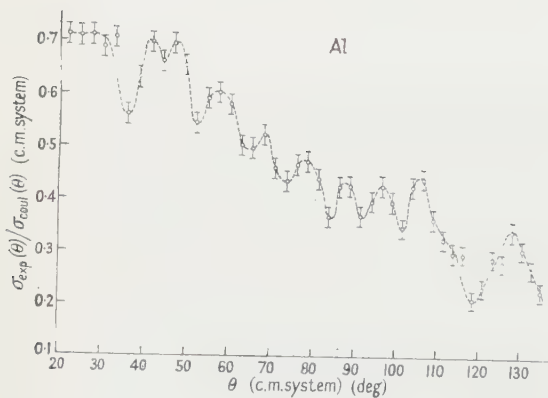


Fig. 3. Elastic scattering of ^3He by aluminium. The observed cross section for the centre-of-mass system relative to calculated Coulomb cross section as a function of centre-of-mass angle.

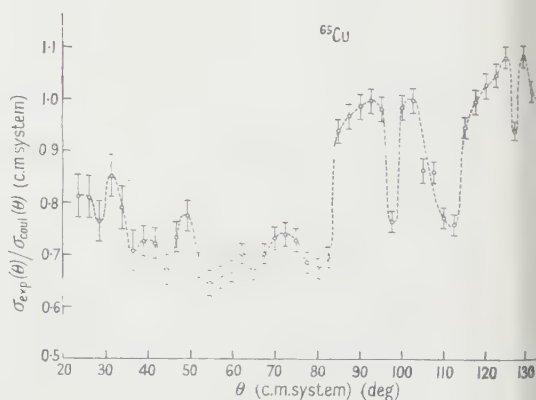


Fig. 4. Elastic scattering of ^3He by copper 65. The observed cross section for the centre-of-mass system relative to calculated Coulomb cross section as a function of centre-of-mass angle.

We make use of the formula given by Greenlees and Rowe (1960)

$$R = \frac{Z_1 Z_2 e^2}{2E} (1 + \operatorname{cosec} \frac{1}{2}\phi)$$

where ϕ is the angle at which the ratio of observed to Coulomb cross section reaches

the value 0.25, Z_1 and Z_2 are the atomic numbers of the target and incident nucleus and E is the energy of incident particles.

The following values for R were obtained :

carbon	$R = (4.18 \pm 1.1) \times 10^{-13} \text{ cm}$
magnesium	$R = (7.30 \pm 0.35) \times 10^{-13} \text{ cm}$
aluminium	$R = (8.27 \pm 0.99) \times 10^{-13} \text{ cm}.$

Because of the nature of the curve for copper a value for R could not be obtained.

An analysis of the results in terms of the optical model is being carried out by Hodgson (1960, private communication).

ACKNOWLEDGMENT

One of us (S. S.) thanks the Polish Academy for a grant which enabled him to undertake the work.

REFERENCES

- AGUILAR, J., BURCHAM, W. E., CATALA, J., ENGLAND, J. B. A., MCKEE, J. S. C., and ROTBLAT, J., 1960, *Proc. Roy. Soc. A*, **254**, 395.
 BETHE, H., and PLACZEK, G., 1940, *Phys. Rev.*, **57**, 1075.
 BLAIR, J. S., 1954, *Phys. Rev.*, **95**, 1218.
 — 1957, *Phys. Rev.*, **108**, 827.
 BLEULER, E., TENDAM, D. J., 1955, *Phys. Rev.*, **99**, 1605.
 DALTON, A. W., HINDS, S., and PARRY, G., 1957, *Proc. Phys. Soc. A*, **70**, 586.
 EISBERG, R. M., IGO, G., and WEGNER, H. E., 1955, *Phys. Rev.*, **99**, 1606.
 FARWELL, G. W., and WEGNER, H. E., 1954, *Phys. Rev.*, **95**, 1212.
 GREEN, T. S., and MIDDLETON, R., 1956, *Proc. Phys. Soc. A*, **69**, 16.
 GREENLESS, G. W., and ROWE, P. C., 1960, *Nucl. Phys.*, **15**, 687.
 HALBERT, M. L., HUNTING, C. E., and ZUCKER, A., 1960, *Phys. Rev.*, **117**, 1545.
 SEIDLITZ, L., BLEULER, E., and TENDAM, D. J., 1958, *Phys. Rev.*, **110**, 682.
 SHOOK, G. N., 1959, *Phys. Rev.*, **114**, 310.
 YAVIN, A. J., and FARWELL, G. W., 1959, *Nucl. Phys.*, **12**, 1.
 ZUCKER, A. J., 1959, *Proc. of the International Conference on the Nuclear Optical Model*, Florida, p. 247.

Spin Correlation Measurements in p-p Scattering at 382 and 320 MeV

BY J. V. ALLABY, A. ASHMORE†, A. N. DIDDENS‡, J. EADES,
G. B. HUXTABLE§ AND K. SKARSVÅG||

Nuclear Physics Research Laboratory, University of Liverpool

MS. received 8th April 1960

Abstract. An account is given of the measurement of the spin correlation coefficients C_{nn} and C_{KP} in p-p scattering at 90° centre-of-mass scattering angle. C_{nn} was measured at 382 and 320 MeV, C_{KP} at 382 MeV. The method of calibrating the polarization analysers is described and details given of the corrections for random coincidences and for the geometrical contribution to asymmetry. The experimental results were:

$$\begin{aligned} C_{nn} \quad 382 \text{ MeV}, & \quad +0.41 \pm 0.09, \\ C_{nn} \quad 320 \text{ MeV}, & \quad +0.77 \pm 0.11, \\ C_{KP} \quad 382 \text{ MeV}, & \quad +0.63 \pm 0.10. \end{aligned}$$

The results are discussed in relation to the 310 MeV phase shift analyses and the potential models of Gammel and Thaler, and Bryan.

§ 1. INTRODUCTION

THE use of spin correlation measurements to obtain information about the p-p elastic scattering matrix has been discussed by Wolfenstein (1954, 1956), Oehme (1955), Smorodinsky (1955), Kanellopoulos and Brown (1957 a, b), Puzikov, Ryndin and Smorodinsky (1957), and Skarsvåg (1958 a). A relativistic version of the formalism has been given by Stapp (1956). It is shown that measurements of five suitably chosen quantities over the whole angular range would determine the scattering matrix at any angle, and that spin correlation measurements are particularly useful for this purpose.

There are two spin correlation coefficients that can be measured using an unpolarized proton beam, and without the aid of a magnet for rotating polarization directions. The notation of Wolfenstein (1956) will be used in defining the coefficients. Fig. 1 shows the directions involved. \mathbf{p} and \mathbf{p}' are the momenta of the incident and scattered protons in the centre-of-mass system, θ being the angle of scattering in that system. Unit vectors \mathbf{K} and \mathbf{P} are defined in the scattering plane in the directions $\mathbf{p}' - \mathbf{p}$ and $\mathbf{p}' + \mathbf{p}$ respectively. For non-relativistic kinematics these vectors are respectively perpendicular to the directions of motion of the scattered and recoil protons in the laboratory system. A unit vector \mathbf{n} is defined perpendicular to the scattering plane and

† Now at Queen Mary College, University of London.

‡ Now at CERN, Geneva.

§ Now at Atomic Energy Research Establishment, Harwell.

|| Now at Joint Establishment for Nuclear Energy Research, Kjeller, Norway.

is chosen in the upward direction. The two spin correlation coefficients are then defined by the expectation values,

$$C_{nn} = \langle \sigma_1 \cdot \mathbf{n} \quad \sigma_2 \cdot \mathbf{n} \rangle \quad \dots\dots (1a)$$

$$C_{KP} = \langle \sigma_1 \cdot \mathbf{K} \quad \sigma_2 \cdot \mathbf{P} \rangle \quad \dots\dots (1b)$$

where σ_1 and σ_2 are the spins of the incident and target protons. In the particular case of scattering at 90° in the centre-of-mass system C_{nn} is simply related to the proportion t of the triplet contribution to the differential cross section,

$$C_{nn} = 2t - 1. \quad \dots\dots (2)$$

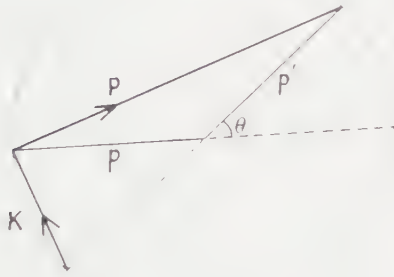


Fig. 1. Definition of vectors.

Spin correlation is measured by the polarization analysis in coincidence of the scattered and recoil protons. At the energies of the experiment described here the best polarization analyser is a second elastic scattering through a small angle from a light nucleus, in this case carbon. For the measurement of C_{nn} the second scatterings are to the left or right in the same plane as the first scattering, whereas for the measurement of C_{KP} they are through an angle in the upward and downward direction in the perpendicular plane. These directions are shown



Fig. 2. Directions of second scattering.

in Fig. 2 using L, R, U, D, to indicate left, right, upward and downward. The hydrogen first target is marked 1 and the carbon second targets 2l and 2r. Genuine events were defined by six-fold coincidences between the counters arranged as shown in Fig. 3.

The number of genuine six-fold coincidence counts for a fixed number of monitor counts will be denoted by using two of the letters L, R, U, D, the first indicating the direction of scattering from target 2l and the second from target 2r. The numbers of genuine counts in the various positions can be written:

$$\begin{aligned} LL &= N_0 a \epsilon_1 \epsilon_{2l} \epsilon_{2r} [1 + P_1 P_{2l} + P_1 P_{2r} + C_{nn} P_{2l} P_{2r}] \\ RR &= N_0 a \epsilon_1 \epsilon_{2l} \epsilon_{2r} [1 - P_1 P_{2l} - P_1 P_{2r} + C_{nn} P_{2l} P_{2r}] \\ RL &= N_0 a \epsilon_1 \epsilon_{2l} \epsilon_{2r} [1 - P_1 P_{2l} + P_1 P_{2r} - C_{nn} P_{2l} P_{2r}] \\ LR &= N_0 a \epsilon_1 \epsilon_{2l} \epsilon_{2r} [1 + P_1 P_{2l} - P_1 P_{2r} - C_{nn} P_{2l} P_{2r}] \quad \dots\dots (3a) \\ UU &= DD = N_0 a \epsilon_1 \epsilon_{2l} \epsilon_{2r} [1 + C_{KP} P_{2l} P_{2r}] \\ DU &= UD = N_0 a \epsilon_1 \epsilon_{2l} \epsilon_{2r} [1 - C_{KP} P_{2l} P_{2r}] \quad \dots\dots (3b) \end{aligned}$$

N_0 is the number of protons incident on the hydrogen target, ϵ_1 is the efficiency of the first scattering, ϵ_{2l} and ϵ_{2r} are the efficiencies of the two second scatterings, P_1 is the polarization in the first scattering, P_{2l} and P_{2r} are the polarization analysing powers of the two second scatterings; efficiency in a scattering is the product of differential cross section, solid angle, and number of atoms per cm^2 of the target. Owing to the finite size of the hydrogen target the first scattering efficiency has to be multiplied by the factor a (< 1) to give the number of coincidences between the two sides. In the particular case of 90° centre-of-mass scattering angle $P_1 = 0$, so that $LL = RR$ and $RL = LR$. The measured asymmetries are given by

$$\begin{aligned} e_{nn} &= C_{nn} P_{2l} P_{2r} = \frac{RR + LL - RL - LR}{RR + LL + RL + LR}, \quad \dots\dots (4a) \\ e_{KP} &= C_{KP} P_{2l} P_{2r} = \frac{UU + DD - UD - DU}{UU + DD + UD + DU}. \quad \dots\dots (4b) \end{aligned}$$

Owing to the relativistic transformation from the centre-of-mass to the laboratory system the directions \mathbf{K} and \mathbf{P} will not be quite perpendicular to the directions of motion of the scattered and recoil protons in the laboratory system. Thus the measured coefficient defined by Eqn (4b) will not be quite equal to the expectation value defined in Eqn (1b). It is convenient to define C_{KP} as the measured coefficient and make a correction to the theoretical value using Eqn (57) of Stapp (1956). No such correction arises for C_{nn} .

Measurements have been made at 90° centre-of-mass scattering angle of C_{nn} at 382 MeV (Ashmore *et al.* 1958), C_{KP} at 382 MeV (Ashmore, Diddens and Huxtable 1959), C_{nn} at 320 MeV (Allaby *et al.* 1959) and C_{nn} at 315 MeV (Vasilevsky *et al.* 1959). The present paper gives a detailed account of the first three measurements using the Liverpool synchrocyclotron. They will be referred to hereafter as C_{nn} 382, C_{KP} 382 and C_{nn} 320.

At 310 MeV sufficient information has been obtained from single, double and triple scattering experiments (Chamberlain *et al.* 1957) to make possible a phase shift analysis. This was done by Stapp, Ypsilantis and Metropolis (1957) who used partial waves up to H waves and found eight sets of phase shifts that gave satisfactory fits to the experimental data. Sets 5, 7 and 8 were eliminated on the basis of Tripp's (1956) analysis of his experiment on the reaction $p + p \rightarrow d + \pi^+$. Ciffra *et al.* (1959) and MacGregor, Moravcsik and Stapp (1959) have extended the analysis by calculating the one-pion exchange contribution for high orbital angular momentum values and using the phase shift analysis for the lower values.

Sets 3 and 4 were thus shown not to be separate solutions but to merge respectively with sets 1 and 2, and set 6 was shown to be rather improbable. The $C_{nn}382$ and $C_{KP}382$ measurements were undertaken at the full energy of the proton beam from the Liverpool synchrocyclotron. At this energy inelastic scattering is about 4% of the total p - p cross section, and still has negligible effect on the elastic scattering (R. J. N. Phillips, private communication). The measurement $C_{nn}320$ was undertaken to eliminate the variation with energy in making comparisons with the 310 MeV phase shift analysis (§5).

It is interesting also to compare the results with the predictions of the static potential models such as those of Gammel and Thaler (1957) and Signell and Marshak (1958). Considerable success has been achieved by these authors in fitting nucleon-nucleon scattering data up to 300 MeV. The former potential was adjusted with the aim of fitting the 310 MeV p - p data and is correspondingly more successful at this energy. It will give phase shifts similar to set 1 of Stapp, Ypsilantis and Metropolis (1957). In a review of the phenomenology of the nucleon-nucleon interaction Gammel and Thaler (1959) argue that only set 1 can reasonably be derived from a static local potential.

§ 2. EXPERIMENTAL DETAILS

2.1. The Scattering Table

The scattering table consisted of a triangular angle iron framework which could be wheeled into position and then raised from the floor on three jacks. Two main arms carrying the counters and shielding blocks were arranged at approximately the correct laboratory angle of 85° between the scattered protons. These arms pivoted about the same vertical axis and could be adjusted over a small range of angles. The liquid hydrogen first target, in the form of a vertical cylinder, was mounted so that its axis could be made to coincide with the axis of rotation of the arms. A section through the horizontal first scattering plane is shown in Fig. 3(a) and a vertical section through the right arm in Fig. 3(b).

The liquid hydrogen target was similar to the one described by Whalin and Reitz (1955), and consisted of a vertical cylindrical tube of 0.001 in. thick Mylar cemented between brass collars of which the upper one was fastened to the base of the cylindrical liquid-hydrogen reservoir. The lower one was connected to a filling tube from the reservoir. A tube from the top of the target up to the atmosphere was used as an outlet for gas from the target, and could be closed to empty the contents of the target into the reservoir. The liquid-hydrogen reservoir had a capacity of about 5 l. and was surrounded by an annular liquid-nitrogen jacket. Both were attached to the top plate of an aluminium alloy vacuum vessel. This vessel was connected on to the vacuum pipe conveying the incident proton beam. On the opposite side of the vessel an extension pipe 4 ft long was connected with an 0.005 in. thick Mylar window at the far end. The whole system was maintained at a pressure of the order of 10^{-5} mm by means of a pump on the proton beam pipe. The argon filled ionization chamber used as a monitor was attached to the far end of the extension pipe. Protons would have to be scattered backwards from this chamber to get into one of the counters. Exit ports with windows of 0.005 in. thick Mylar were provided in the target vacuum vessel in the directions of the scattered protons.

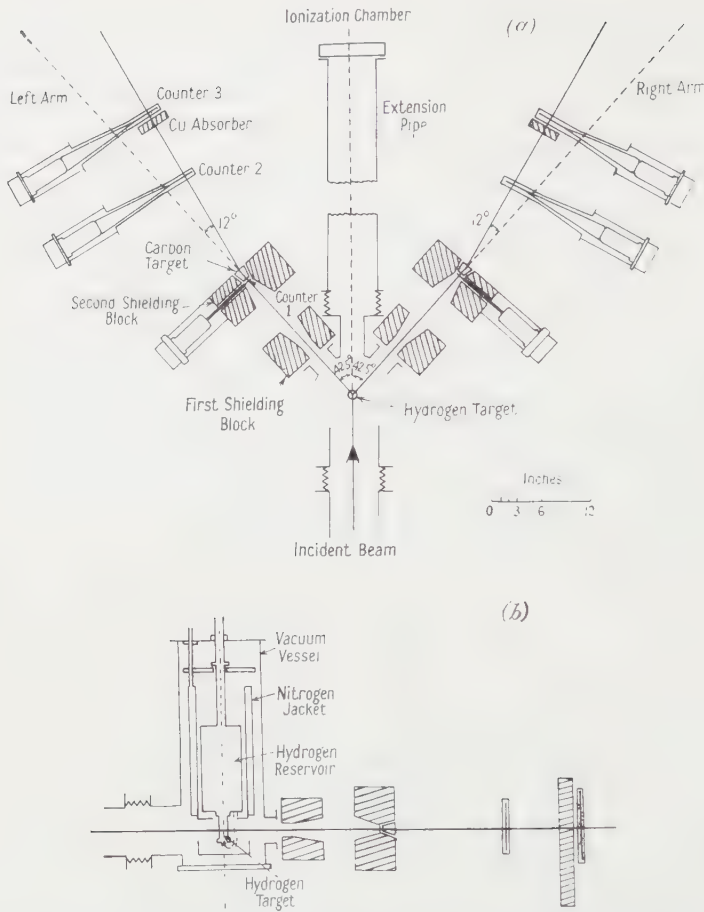


Fig. 3. Experimental arrangement, (a) section in first scattering plane, (b) section through one arm perpendicular to first scattering plane. Arrangement shown as for measurement of C_{nn} .

Two copper shielding blocks were provided on each arm, the first to shield the counters from background protons scattered from the region of the proton pipe exit and the second to shield the counters from protons scattered from the hydrogen target and not passing through the carbon second target. The thickness of these blocks was made about equal to the range of protons with the full beam energy. In C_{nn} 382 the holes through the shielding blocks had a rectangular section but in the subsequent measurements they were specially shaped to get the best possible shielding, and at the same time tapered to avoid the possibility of protons being scattered first from the hydrogen target and then from one of the inside faces of a shielding block into the counters. The lateral extent of the first shielding blocks was also increased and some heavy concrete shielding introduced around them.

The carbon second target on each arm was mounted in the hole through the second shielding block. The scintillator of each counter 1 was placed immediately before the target on the end of a light guide through a slot in the block. Thin aluminium windows over the ends of the hole through the block provided a light seal. Events were selected by six-fold coincidences between counters 1, 2

and 3 of each arm. The inclusion of counters 1 was important in selecting events involving scattering in the carbon targets. The thickness of the copper absorber between the counters 2 and 3 was chosen to confine the second scattering as far as was reasonably possible to elastic events. Counters 2 and 3 on each arm were mounted in a cradle supported on bearings on the second shielding block and the back support. The counters were fixed on an arm which could be offset from the cradle so as to define the second scattering angle ψ_0 indicated in Fig. 3(a). Rotation of the cradle about its axis enabled these counters to be brought into the R, U, L and D positions defined in §1. On the basis of experimental data from Harwell, Rochester and Uppsala, referred to in §§ 2.5 and 5.1, a second scattering angle of 12° was chosen. A stop was arranged so that the counter arm could repeatedly be set to precisely the same angle.

2.2. The Electronic Equipment

Plastic scintillators 0.25 in. thick and RCA 6342 photomultipliers were used in all the counters. Pulses from the photomultipliers of counters 1, 2 and 3 on each arm were fed through 130 Ω cables to a fast triple coincidence circuit with a resolving time $2\tau = 10$ nsec (Skarsvag 1958b). The output pulses from these two circuits were fed to a somewhat slower double coincidence circuit (Collinge, Eccleshall and Merrison 1956). This circuit was arranged to resolve counts in successive radio frequency pulses so that its effective resolving time $2\tau' = 55$ nsec, the period of the radio frequency of the synchrocyclotron as the beam is extracted. Provision was made for counting both the input channels at the same time as the output channel of the double coincidence circuit. These input counts, i.e. triple coincidences from each of the arms, were a useful check on drifts in the apparatus. An identical double coincidence circuit was also provided for simultaneously counting coincidences with the input from one arm delayed by a radio frequency period. Since the six-fold rates were less than 1 per minute they were counted by two scalers in parallel to guard against spurious counts.

The proton beam was monitored by passing it through an argon filled ionization chamber whose position is indicated in Fig. 3(a). This chamber was connected to a current integrator. A check was provided on variations due to bubbling in the hydrogen target and to lateral movements of the incident proton beam. In $C_{im}382$ this was done by means of a double coincidence counter telescope arranged below beam level to count protons scattered from the target. Subsequently the double coincidence rate from the counters 1 on the two arms was used for this purpose. This involved the use of a scale of 4 with a resolving time of 40 nsec (Collinge and Huxtable 1958).

2.3. Reduction of Proton Beam Energy

The extracted proton beam from the synchrocyclotron has an energy of 382 MeV and is focused by the bending magnet into a spot about 0.4 in. square just beyond the end of the proton exit pipe. $C_{im}382$ and $C_{kp}382$ were measured with this beam. For $C_{im}320$ the beam was reduced in energy by means of a polyethylene absorber placed just outside the synchrocyclotron tank. Scattering in this absorber reduced by a factor of about 10 the amount of the beam collected by the bending magnet and focused in the experimental area. Also the focused

spot was considerably larger than for the full energy beam and the background was increased. Improvements were made by modifications to the collimators in the proton beam pipe and by the introduction of extra shielding round the scattering table. It was thus possible to establish reasonable conditions with a proton energy of 320 mev and a beam spot about 1.0 in square.

2.4. First Scattering Geometry

The limitations on the solid angle that may be used in the first scattering arise mainly from the resultant energy spread of the scattered protons and in the geometrical correction to the observed asymmetry arising from finite geometry. It is the energy spread which gives rise to the correction for inelastic scattering in the second target (§ 5.3), and it must be kept sufficiently small for the correction to be estimated from available experimental data on inelastic scattering to the excited states of carbon. For C_{nn} measurements where both scatterings are in the same plane, it is possible to take advantage of the fact that for both effects the vertical dimensions contribute much less than the horizontal ones. The details of the first scattering geometry used in the three measurements are given in Table 1.

Table 1. First Scattering Geometry

Horizontal dimensions are given before vertical ones.

	$C_{nn}382$	$C_{KP}382$	$C_{nn}320$
Beam spot at hydrogen target (in.)	0.4×0.4	0.4×0.4	1.0×1.0
Diameter of hydrogen target (in.)	0.5	1.0	1.0
Scintillator size in counters 1 (in.)	0.375×2.0	1.0×1.0	0.75×2.0
Angle subtended at hydrogen target (deg)	1.07×5.73	2.85×2.85	2.14×5.73
Solid angle subtended at hydrogen target (sterad)	1.88×10^{-3}	2.50×10^{-3}	3.75×10^{-3}
Energy spread (std. dev., mev)	5	9	7

The corrections for inelastic scattering and finite geometry showed that the choice of geometry for $C_{nn}382$ was rather severe but that for $C_{KP}382$ it was just a little too relaxed. For $C_{nn}320$ the geometry was near the best compromise between correction difficulty and counting rate.

2.5. Second Scattering Geometry

As is shown in § 2.6 the factor in each of the second scatterings which determines the statistical error in the observed asymmetry is $P^2(\psi) d\sigma/d\omega(\psi)$, where $P(\psi)$ is the polarization and $d\sigma/d\omega(\psi)$ the differential cross section for elastic scattering through the angle ψ . It is adequate to consider protons with the energy corresponding to scattering half-way through the carbon second target. The second scattering geometry was chosen for $C_{nn}382$ and not subsequently altered, giving a mean scattering energy near 175 mev. At that time use was made of experimental data available at 155 mev (Alphonse, Johansson and Tibell 1957 a, b, Hillman, Johansson and Tyren 1957) and at 220 mev (Chesnut, Hafner and Roberts 1956). In optimizing the statistical error care must be taken not to reduce the analysing power so that the measured asymmetry becomes of the order of the geometrical correction. Negligible energy spread was introduced in the second scattering since the carbon target was tapered so that all protons detected in the counters 2 and 3 had to traverse its full length.

A mean second scattering angle of 12° was chosen and details of the geometry are given in Table 2. The limit to the thickness of the carbon target is set by multiple scattering. It was chosen to be 6.2 g cm^{-2} giving an r.m.s. projected scattering angle of 1.13° . Differential cross section and polarization data have become available at other energies and are shown at 180 mev in Fig. 4. Values of $P^2(\psi) d\sigma/d\omega(\psi)$ are also plotted to emphasize the considerations affecting the choice of scattering angle and angular width parallel to the scattering plane. The angular size in the perpendicular plane has a negligible effect on the polarization and was decided by the rapid fall of differential cross section with increasing angle.

Table 2. Second Scattering Geometry

The first dimension of each counter is parallel to the second scattering plane, i.e. horizontal for C_{nn} and vertical for C_{KP} .

Scintillator size in counter 2 (in.)	2.25×6
Angle subtended at carbon target (deg)	9.2×24.5
Scintillator size in counter 3 (in.)	3×8
Angle subtended at carbon target (deg)	7.3×19.7
Solid angle subtended at carbon target (sterad)	0.044

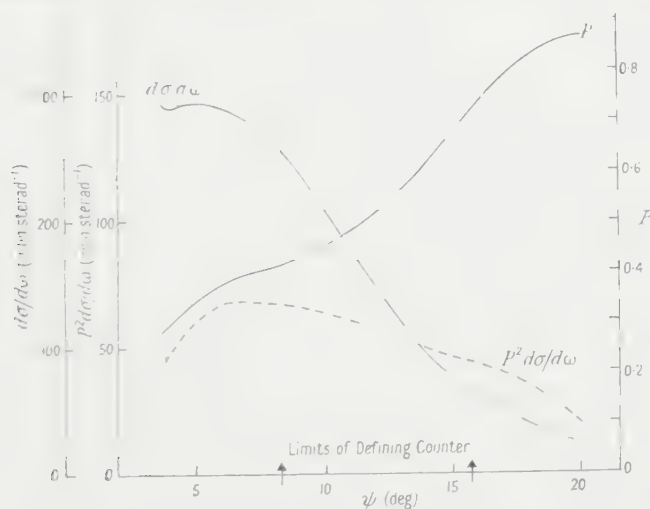


Fig. 4. Experimental data on the elastic scattering of 180 mev protons from carbon (Maris and Tyren 1957 b).

2.6. The Statistical Error in the Correlation Coefficient

The asymmetry measured in a spin correlation experiment can be written

$$e = (G_+ - G_-)/(G_+ + G_-) = P_{2l}P_{2r}C \quad \dots\dots (5)$$

where from Eqns (3)

$$G_+ = LL + RR \text{ for } C = C_{nn}, \quad UU + DD \text{ for } C = C_{KP},$$

$$G_- = LR + RL \text{ for } C = C_{nn}, \quad DU + UD \text{ for } C = C_{KP}.$$

The standard deviation δe in e is given by

$$\delta e^2 = \frac{1}{4}(1 - e^2)^2(G_+^{-1} + G_-^{-1}).$$

Then from Eqns (3) the standard deviation δC in C is given by

$$\delta C^2 = \frac{1 - (CP_{2l}P_{2r})^2}{4N_0 a \epsilon_1 \epsilon_{2l} P_{2l}^2 \epsilon_{2r} P_{2r}^2} + C^2 \left[\frac{\delta(P_{2l}P_{2r})}{P_{2l}P_{2r}} \right]^2. \quad \dots\dots (6)$$

In these experiments the first term in Eqn (6) was predominant and $(CP_{2l}P_{2r})^2 \ll 1$, so that,

$$\delta C^2 \simeq (4N_0 a \epsilon_1 \epsilon_{2l} P_{2l}^2 \epsilon_{2r} P_{2r}^2)^{-1}.$$

Thus the factors to be optimized are $a\epsilon_1$ in the first scattering and $\epsilon_2 P_2^2$ in the second scatterings. The factor a approaches unity as the dimensions of the effective target become small compared with those of the two first counters.

§ 3. EXPERIMENTAL PROCEDURE

3.1. Alignment

Alignment of the components on the scattering table was carried out with the table level but not in position near the exit of the proton beam vacuum pipe. The components on each arm have to be aligned along the perpendicular to the vertical axis of rotation of the two arms through the centre of the hole in the second shielding block (Fig. 3(a)). The point of intersection of the two perpendiculars defines the position for the centre of the hydrogen target. For alignment of the counters and shielding blocks this point was defined by the tip of a vertical rod fixed on the axis of rotation of the two arms. The centre of the hole in the second shielding block was defined by cross wires. Adjustments were made on each arm in the following order using a theodolite (sometimes a long steel ruler and plumb line were used instead). (i) The axis of rotation of the cradle carrying counters 2 and 3 was aligned using adjustments on the backbearing. (ii) The first shielding block was aligned. (iii) Counter 1 was set centrally in the hole in the second shielding block. (iv) The second scattering angle was set to 0° and counters 2 and 3 then aligned.

Adjustments (i) and (iv) were checked by observing the movement of the central spots on the scintillators in counters 2 and 3 as the cradle was rotated, and could thus be adjusted to an accuracy of about $3'$ in angle. The hydrogen target in its vacuum vessel was then mounted on the scattering table and adjusted to its correct position.

The scattering table was then wheeled as near as possible to its correct position near the exit of the proton pipe. It was jacked up and levelled with the defining lines of the two arms at the known height of the centre of the beam spot. The vacuum connections were then made through bellows from the hydrogen target vacuum vessel and to the extension pipe carrying the ionization chamber.

3.2. Setting up in the Proton Beam

Initial measurements were made with both second scattering angles at 0° . The lateral position of the beam spot was adjusted by means of the proton bending magnet current to give the maximum triple coincidence counting rates in the two arms. Photomultiplier e.h.t. voltages were set on their plateaux and cable lengths adjusted for the centres of delay curves. A beam photograph was taken at the ionization chamber and the two arms set as close as possible to the correct first scattering angle (42.5°) by measuring distances from the centre of the beam spot to the centres of the back bearings. The ionization chamber was adjusted

so that the proton beam traversed it centrally. Final adjustment of the angle between the two arms was made by measuring six-fold coincidences as the angle was varied over a small range. Range curves were taken and the thickness of the copper absorber between counters 2 and 3 set to 2 ($C_{nn}320$) or 3 ($C_{nn}382$ and $C_{KP}382$) standard deviations below the mean range, allowing for a second scattering angle of 12° . The choice of 2 standard deviations made the correction for inelastic scattering more reliable in $C_{nn}320$ than in $C_{KP}382$ but brought the operating point rather near the knee of the range curve.

A critical test of the alignment was the profile curve of the first scattered beam. This was taken by setting the second scattering angle to various small values and rotating the cradle carrying counters 2 and 3 to the L and R positions for C_{nn} measurements or to the U and D positions for C_{KP} measurements. In $C_{nn}382$ only the triple coincidence rates in the two arms were used but in $C_{KP}382$ and $C_{nn}320$ the six-fold coincidence rates were also used. The profile curves have flat tops and steep sides and their symmetry is sensitive to the alignment. Fine adjustments can thus be made to the height and levelling of the scattering table for C_{KP} measurements and to the position of the hydrogen target in the first scattering plane for C_{nn} measurements.

3.3. Counting Procedure

Numerical information about the measurement of the correlation asymmetry is given in Table 3. For $C_{nn}382$ and $C_{KP}382$ the beam intensity was chosen so that the percentage of random coincidences was small enough to make the error in their estimation negligible. For $C_{nn}320$ the maximum available internal beam of the synchrocyclotron was used, the intensity at the target being reduced by multiple scattering in the polyethylene degrader (§2.3). Runs of about three-quarters of an hour duration in each position were made in the sequence RL, RR, LR, LL for C_{nn} measurements or UU, DU, DD, UD for C_{KP} measurements, thus reducing the effect of drifts in the experimental conditions. The evidence from the triple coincidence counts in the two arms indicated that the magnitude of any drifts was small. Daily checks were made of the bending magnet current, counter e.h.t. voltage settings, range and profile curves and adjustments made if required. In $C_{KP}382$ the beam height was found to drift so that the profile curve had to be checked several times a day.

The number of random coincidences was estimated as described in §4.1. Measurements of the single, double, triple and quadruple coincidence rates required for this purpose were made at intervals throughout the experiment. Adequate statistical accuracy was quickly achieved in these measurements but they were susceptible to changes in beam conditions. In particular the duty cycle is rather critically dependent on the field of the cyclotron magnet. A scintillation counter in the proton beam enabled the beam pulse profile to be displayed on an oscilloscope in the counting room. The field could thus be chosen to give the best possible duty cycle and adjusted when necessary.

The numbers of total, random and genuine coincidence counts in the four positions are given in Table 4. A χ^2 test was applied to the numbers from individual runs in each position and no deviations were found that could not reasonably be statistical ones. It should be found that $RR=LL$, $RL=LR$, $UU=DD$, $UD=DU$. The data in Table 4 confirm these equalities within the statistical error.

Table 3. Counting Information

	C_{nn382}	C_{KP382}	C_{nn320}
Beam intensity (protons per sec)	1.4×10^9	1.4×10^9	0.8×10^9
Counting rate per hour	10	27	27
Random coincidences (% of total)	16	10	7
Hours used for measurement of asymmetry	138	70	186

Table 4. Numbers of Counts in the Four Positions

		RR or UU	LL or DD	RL or UD	LR or DU
C_{nn382}	Total	381	377	301	246
	Random	52	52	65	39
	Genuine	329	325	236	207
C_{KP382}	Total	515	541	394	371
	Random	46	46	46	46
	Genuine	469	495	348	325
C_{nn320}	Total	1419	1419	1083	1008
	Random	88	89	94	84
	Genuine	1331	1330	989	924

§ 4. TREATMENT OF RESULTS

4.1. Random Coincidences

An analysis was made to determine the contributions to the six-fold random coincidences. A rough estimate of their magnitude was made from observations on the single counting rates in the six counters, the double and triple coincidence counting rates in the two arms, and the duty cycle. It was found that for C_{KP382} and C_{nn320} 90% of the random coincidence counting rate was due to the contributions,

$$2\tau S[(_{321}G_1)(G_{23}) + (_{32}G)(_1G_{123})] \dots\dots (7a)$$

$$2\tau S[(_{321}G) + (_{321}G_1)][(_1G_{123}) + (G_{123})]. \dots\dots (7b)$$

For C_{nn382} the following contribution was also important

$$3\tau^2 S^2[(_{321}G_1)(G_2)(G_3) + (_3G)(_2G)(_1G_{123})]. \dots\dots (7c)$$

τ is the effective resolving time of the fast coincidence circuit, S is the inverse of the duty cycle. The G 's are genuine counting rates with the numbers indicating which counters are in coincidence. Counters on the left or right arm are distinguished by whether the numbers precede or follow the G . Thus $_{321}G_1$ is the genuine four-fold coincidence counting rate between all three counters on the left arm and counter 1 on the right arm. The numbers associated with each G indicate all the counters involved so that, for example, $(_1G_{123})$ is not included in (G_{23}) and (G_2) does not include any of the coincidences in which counter 2 on the right arm is involved.

Apart from a small correction term ($\sim 10\%$) the random six-fold coincidence counting rate could be expressed in terms of measurable quantities not requiring a knowledge of the resolving time and duty cycle.

$$\frac{(_{321}G_1)(G_{23})(R_{1'23})}{(N_1)[(G_{23}) + (G_{123}) + (_1G_{123})]} + \frac{(_1G_{123})(_{32}G)(_{321}R)}{(_1N)[(_{32}G) + (_{321}G) + (_{321}G_1)]} + (_{321}R_{1'2'3'}) \dots\dots (8)$$

The N 's are total counting rates as directly measured. The R 's are random coincidence counting rates, in this case measured ones with the primed numbers indicating counters delayed by one radio-frequency period. Apart from contributions in the correction term, the first two terms of formula (8) are equivalent to the contributions (7a) and (7c) and the third term to the contribution (7b).

The genuine counting rates in formula (8) can be expressed in terms of measured rates. Thus for the first term,

$$(G_{23}) + (G_{123}) + ({}_1G_{123}) \simeq (N_{23}) - (R_{23}) \quad \dots\dots (9a)$$

$$(G_{23}) \simeq (N_{23}) - (N_{123}) - (R_{23}) + (R_{123}) \quad \dots\dots (9b)$$

$$({}_{321}G_1) = a[({}_{321}N) - ({}_{321}R)]. \quad \dots\dots (9c)$$

In this formula the random triple coincidence rates were given with sufficient accuracy by,

$$(R_{123}) = (R_{123'}) + (R_{1'23}) - (R_{1'23'}) \quad \dots\dots (10)$$

where the double prime indicates delay by two radio-frequency periods. The factor a was defined in § 1 and can be estimated either from the geometry of the first scattering or from the ratio of the genuine coincidence rate between the two first counters to the singles rate in one of them, arising from scattering in the hydrogen. These two estimates agreed reasonably well. Corresponding formulae were used for the second term in formula (8) in which case it is the singles rate in the right-hand first counter which is involved in the factor a .

The term $({}_{321}R_{1'23'})$ in formula (8) was continuously measured as described in § 2.2. Only the correction term required a knowledge of τS and was estimated from the single, double and triple counting rates involved. As mentioned in § 3.3 the counting rates involved in the first two terms of formula (8) were measured at intervals throughout the experiment. For $C_{\text{in}} 382$ a slightly modified formula was used to take account of the larger contribution (7c).

The estimated numbers of random coincidences are given in Table 4. From cross checks the error on these numbers was estimated to be $\pm 15\%$.

4.2. Geometrical Correction

A contribution to the asymmetry arises from the finite dimensions of the second target (defined by the first counter), and the variation with second scattering angle of the differential cross section and polarization. In the horizontal plane there is a constant angle of 85° between the scattered and recoil protons. For example, in Fig. 6(a) both protons are scattered to the left side of the second targets so that in this case LL is favoured and RR disfavoured in C_{in} measurements, since the differential cross section decreases with increasing angle. In the vertical plane the projected directions of the scattered and recoil protons are in line. In the case shown in Fig. 6(b) one proton is scattered upwards and the other downwards so that DU is favoured and UD disfavoured in C_{KP} measurements. Some cancellation occurs since it is $LL + RR$ and $DU + UD$ that are involved in the asymmetry. Also the favoured and disfavoured positions change with the scattering points on the first and second targets. There is a net contribution to the asymmetry which is evaluated in the Appendix.

It is shown there that in the Liverpool experiments the contribution is approximately $\pm (d_1/D_1)^2 K^2$ (Eqn (16)). d_1 is the half-width of the first

counter in the second scattering plane (horizontal for C_{nn} , vertical for C_{KP}), D_1 is the distance from the hydrogen target to the first counters, and K is the linear coefficient of variation of differential cross section with second scattering angle around 12° . The plus sign is for C_{KP} and the minus sign for C_{nn} . Values of d_1/D_1 can be deduced from Table 1 and values of K are given in the Appendix (Table 8). The resulting corrections to the asymmetry along with the measured and corrected values are given in Table 5. The error in the correction arises firstly from the error in K and then from the approximations made. It was estimated to be $\pm 20\%$.

Table 5. Geometrical Corrections to the Measured Asymmetries

	C_{nn}^{382}	C_{KP}^{382}	C_{nn}^{320}
Measured asymmetry (e_1)	$+0.192 \pm 0.035$	$+0.178 \pm 0.027$	$+0.163 \pm 0.016$
Correction	-0.005 ± 0.001	$+0.057 \pm 0.012$	-0.021 ± 0.005
Corrected asymmetry (e')	$+0.187 \pm 0.035$	$+0.235 \pm 0.030$	$+0.142 \pm 0.017$

§ 5. THE CALIBRATION OF THE POLARIZATION ANALYSIS

5.1. Experimental Arrangements

For the measurement of the polarization P_2 in the second scattering the energy of the unpolarized external proton beam was reduced to the required value by means of a polyethylene absorber placed just outside the cyclotron tank. Elastic scattering from a first carbon target through an angle of approximately 20° was used to produce a primary polarization P_0 of approximately 0.95. Using each arm in turn for a second scattering the polarization P_2 was determined by measuring the asymmetry,

$$E = (L - R)/(L + R) = P_0 P_2 \quad \dots\dots (11)$$

where L and R are numbers of genuine triple coincidence counts for a fixed number of monitor counts with the second scattering to the left and right. The first scattering angle was chosen to give the maximum polarization and the value of P_0 was obtained using the experimental data from Harwell at 135 meV (Dickson and Salter 1957), from Uppsala at 155 meV and 175 meV (Alphonse, Johansson and Tibell 1957b, Hillman, Johannsson and Tyren 1957, Maris and Tyren 1957b) and from Rochester at 220 meV (Chesnut, Hafner and Roberts 1956).

The conditions of the correlation experiment were reproduced as far as possible. From the first shielding block onwards (Fig. 3) there was no change. The hydrogen target in its vacuum casing and the extension pipe were removed, and the carbon first target mounted at the end of the proton beam vacuum pipe. By moving back the scattering table and swinging it round, the first counter on the arm being calibrated was set to the chosen first scattering angle. The thickness of the polyethylene absorber was chosen to make the mean range measured by the counter telescope the same as in the correlation measurement. Extra collimators were introduced after the proton bending magnet to define a beam spot about 1.0 in. square at the first target. This target was considerably larger in area than the beam spot and 4.1 g cm^{-2} thick. Its distance from the second target was about 45 in. and its effective width was defined by a collimator in the

form of a narrow vertical slit placed about 10 in. from the first target. The width of the slit was 0.25 in. for $C_{nn}382$ and $C_{kp}382$, and 0.4 in. for $C_{nn}320$. It was convenient to have both scatterings in the horizontal plane so that for the $C_{kp}382$ calibration the whole telescope (counters and shielding blocks) was rotated through 90° about its axis compared with its position for the correlation measurement. To cancel any effect of energy and intensity distribution across the first target the left and right arms were calibrated with first scatterings to the left and right respectively.

5.2. Experimental Procedure

The method of alignment and setting up in the proton beam has been described in §3.2. Beam photographs were used as reference points in setting the first scattering angle to the chosen value. An air-filled ionization chamber was used as a monitor in the calibration experiments.

Because of the intensity distribution across the second target, arising from the variation of differential cross section with first scattering angle, the profile curve should not be quite symmetrical about 0. In the calibration for $C_{nn}382$ small adjustments of the back pivot and defining collimator were used to compensate for the larger variation for carbon than for hydrogen, whereas in $C_{kp}382$ and $C_{nn}320$ no adjustments were made and a correction to the asymmetry E was calculated. An unexplained discrepancy occurred in $C_{kp}382$, the angular asymmetry being twice the predicted value of 0.25. In $C_{nn}320$ the angular asymmetries were 0.15 and 0.05 for the left and right arms, compared with the predicted value of 0.10.

Due to the loss of protons by scattering in the polyethylene absorber the available beam (1 in. square) at the first target was of the order of $5 \cdot 10^7$ protons per second. This gave a triple coincidence counting rate averaging about 10 per minute so that approximately 10 hours running time on each arm was required to measure the asymmetry with reasonable accuracy. The time was divided between the left and right positions in the ratio to give the smallest statistical error.

The number of random coincidences was shown to be given sufficiently well by Eqn (10). Measurements of the three terms were made at intervals throughout the calibration experiment. The number of random coincidences averaged a few per cent of the genuine ones and the time devoted to their measurement was such that the statistical error was appreciably less than that in the number of genuine coincidences.

5.3. Corrections

In deducing the value of P_2 from the observed numbers of genuine coincidences the following corrections were made:

(i) The polarization P_0 produced in the first scattering was corrected for (a) finite angular resolution in the first scattering and (b) for inelastic scattering in the first target. Some experimental data are available on the differential cross section and polarization for inelastic scattering to the various energy levels of carbon. The data used were those of Alphonse, Johansson and Tibell (1957 a, b), Hillman (private communication), Hillman, Johansson and Tyren (1957), Maris and Tyren (1957 a, b).

(ii) The observed asymmetry E_1 was corrected (a) in C_{nn} 382 for a slight misalignment deduced from the profile curve, (b) in C_{KP} 382 and C_{nn} 320 for the intensity distribution across the second target. The method of calculating the correction is indicated in the Appendix. In C_{KP} 382 no allowance was made for the unexplained discrepancy, which could possibly mean that the correction (ii)(b) should be doubled. This would reduce the value of C_{KP} from 0.63 to 0.57 (Table 7).

(iii) Using the corrected values P_0 and E' the polarization P'_2 , defined in the Appendix, was calculated. This was then corrected for differences between the calibration and correlation measurements, in (a) mean range and (b) inelastic scattering. The correction (iii)(a) should be zero but was not so in C_{nn} 382 and C_{KP} 382 where the calibrations were done before the correlation measurements. From the experimental data referred to in § 5.1 and from the present calibration measurements the mean value for the variation of polarization with mean range was found to be $+(12 \pm 2) \times 10^{-3} (\text{g cm}^{-2})^{-1} \text{Cu}$. The correction (iii)(b) arises from the greater variation of energy with scattering angle for scattering from hydrogen than for carbon. It was estimated using the same experimental data as for correction (i)(b). In C_{KP} 382 this estimate was a little difficult since the energy resolution was such that there was some contribution from states about which data were not available. Although the correction is small it was considered advisable to reduce the width of the first counters in C_{nn} 320.

The results of the calibrations are given in Table 6 together with the size of the corrections and other relevant information. For C_{nn} 382 and C_{KP} 382 the measured analysing powers correspond well with the polarizations at 12° for the mean energy of scattering in the second target as measured by Hillman, Johansson and Tyren (1957) and Maris and Tyren (1957b). For C_{nn} 320 the analysing powers are lower than would be expected from the data of Dickson and Salter (1957) by $15 \pm 7\%$. The use of their values would give C_{nn} 320 = $+0.55 \pm 0.08$ which is in better agreement with the theoretical values (§ 6).

§ 6. RESULTS AND DISCUSSION

The results of the measurements of C_{nn} and C_{KP} for 90° centre-of-mass scattering angle are given in Table 7 together with the values calculated from the sets of phase shifts at 310 MeV. These sets include the ones from the original conventional phase shift analysis and the ones from the modified analysis with the one-pion exchange contribution replacing the higher partial waves. Values of t , the amount of triplet scattering expressed as a proportion of the total scattering, calculated from C_{nn} by means of formula (2) are also given in Table 7. The predominance of triplet scattering is a clear indication of the importance of spin dependent forces, since for central forces only singlet states contribute to the scattering at 90° in the centre of mass.

The main conclusion from the phase shift analysis is that set 6 is definitely eliminated by the C_{KP} 382 measurement. Set 2 of the conventional analysis is favoured by the C_{nn} 320 measurement, but this preference disappears in the modified analysis of the MacGregor, Moravcsik and Stapp (1959). If set 1 is chosen smooth variation of phase shifts with energy can be obtained (J. K. Perring, private communication), and a static local potential can be used.

Table 6. Results and Corrections in the Calibrations

Calibration	$C_{nn,38.2}$		$C_{kp,38.2}$		$C_{nn,320}$	
	L	R	L	R	L	R
Mean range (g cm^{-2} Cu)	22.0	22.3	24.65	24.75	14.2	14.5
Standard deviation (g cm^{-2} Cu)	1.05	1.1	1.0	1.0	0.85	0.85
Absorber setting (g cm^{-2} Cu)	19.49	19.84	21.28	21.28	12.23	12.51
First scattering angle (deg)						
P_0 elastic	17.2		17.2		20.2	
Correction (i)(a)	0.96 ± 0.03		0.96 ± 0.03		0.96 ± 0.03	
Correction (i)(b)	0.015		0.020		-0.007	
P_0 corrected	-0.024		0.033		0.021	
	0.921 ± 0.03		0.907 ± 0.03		0.932 ± 0.03	
Measured asymmetry E_1						
Correction (ii)(a)	0.601 ± 0.012	0.604 ± 0.012	0.564 ± 0.013	0.551 ± 0.011	0.384 ± 0.010	0.399 ± 0.011
Correction (ii)(b)	$+0.003 \pm 0.004$	$+0.006 \pm 0.004$	0 ± 0.015	0 ± 0.010	0 ± 0.010	0 ± 0.010
Corrected asymmetry E'	0.604 ± 0.013	0.610 ± 0.013	$+0.027 \pm 0.006$	$\pm 0.021 \pm 0.006$	$\pm 0.021 \pm 0.004$	$\pm 0.021 \pm 0.004$
	0.656 ± 0.026	0.662 ± 0.026	0.591 ± 0.021	0.578 ± 0.020	0.405 ± 0.015	0.420 ± 0.015
E'/P_0			0.652 ± 0.032	0.637 ± 0.031	0.435 ± 0.021	0.451 ± 0.022
Correlation Measurement						
Mean range (g cm^{-2} Cu)	24.2	24.0	23.8	23.9	14.6	14.2
Standard deviation (g cm^{-2} Cu)	1.5	1.5	2.55	2.8	1.65	1.8
Absorber setting (g cm^{-2} Cu)	19.43	19.18	15.61	15.45	10.45	10.36
Correction (iii)(a)	$+0.024 \pm 0.008$		-0.010 \pm 0.003			
Correction (iii)(b)	-0.005 \pm 0.003		-0.024 \pm 0.011			
$P_2'(\Psi_0)$	0.675 ± 0.029	0.681 ± 0.029	0.618 ± 0.034	0.603 ± 0.033	0.422 ± 0.022	0.438 ± 0.023
$[P_2'(\Psi_0)P_{2f}'(\Psi_0)]^{-1}$	2.18 ± 0.17		2.68 ± 0.24		5.42 ± 0.45	

Table 7. Measured and Calculated Values of C_{nn} and C_{kp} for 90° Centre-of-mass Scattering Angle

Calculated values of C_{kp} include the relativistic correction (§ 1).		Energy (mev)	Measured value	Proportion of triplet	Set No.	Values calculated from phase shifts at 310 mev		
Coefficient						SYM	CMMS	MMS
C_{nn}	VVYT	315	$+0.52 \pm 0.20$	0.76 ± 0.10	1	$+0.35 \pm 0.08$	$+0.38$	$+0.41$
	AADE	320	$+0.77 \pm 0.11$	0.89 ± 0.06	2	$+0.71 \pm 0.05$	$+0.61$	$+0.40$
	ADHS	382	$+0.41 \pm 0.09$	0.70 ± 0.04	3	$+0.30 \pm 0.08$	merges with set 1	
C_{kp}	ADH	382	$+0.63 \pm 0.10$		4	$+0.49 \pm 0.06$	merges with set 2	
					6	$+0.43 \pm 0.08$	$< 15\%$ Prob. $< 0.1\%$ Prob.	
					1	$+0.39 \pm 0.05$	$+0.44$	$+0.50$
					2	$+0.53 \pm 0.10$	$+0.49$	$+0.45$
					3	$+0.28 \pm 0.05$		
					4	$+0.53 \pm 0.09$		
					6	-0.31 ± 0.04		

VVYT, Vasilevsky *et al.* (1959). AADE, Allaby *et al.* (1959). ADHS, Ashmore *et al.* (1958). ADH, Ashmore, Diddens and Huxtable (1959). SYM, Stapp, Ypsilantis and Metropolis (1957) conventional. Cut-off above H waves. CMMS, Cziffra *et al.* (1959) modified. Cut-off above H waves. MMS, MacGregor, Moravcsik and Stapp (1959) modified. Cut-off above F waves.

Lee, Gammel and Thaler (1960) have shown that phase shifts similar to those of set 2 can be obtained by using a non-local singlet potential, but with a rather large non-local distance of approximately 0.8 fermi. Comparisons with all the experimental results can be made with the predictions of static local potentials. The variation of the correlation coefficients with energy is given in Fig. 5 for the potential of Gammel and Thaler (1957). Agreement with the experimental points is poor. Better agreement has been obtained by Bryan (1960) using a potential based on meson theory with a stronger shorter range spin orbit potential. His values of the correlation coefficients are indicated in Fig. 5.

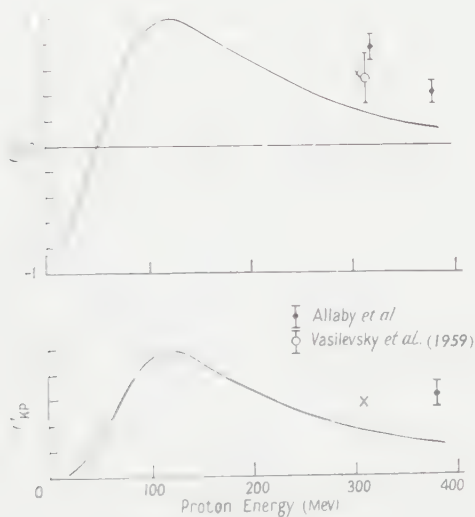


Fig. 5. Variation with energy of C_{nn} and C_{KP} as given by the potential of Gammel and Thaler (1957). Points are the experimental values from Table 7. Crosses are the values given by the potential of Bryan (1960).

Further measurements of the correlation coefficients and other parameters are needed to fix the phase shifts in the region of 300 mev. Correlation measurements at angles other than 90° may help. For example, sets 1 and 2 give widely separated values of C_{KP} for angles between 20° and 40° . Angular distributions have been given by Cziffra *et al.* (1959) and by MacGregor, Moravcsik and Stapp (1959). An experiment is being prepared at Liverpool to measure C_{KP} at 380 mev and 40° .

APPENDIX

Evaluation of the Geometrical Correction

The first scattering geometry is shown in Fig. 6 (a) and (b) for the horizontal and vertical planes. It is convenient to use the same quantities χ and d_1 in the second scattering plane, i.e. the horizontal plane for C_{nn} and the vertical plane for C_{KP} . ξ and b_1 are used for the corresponding quantities in the perpendicular plane. The origin of the axes O is at the centre of the hydrogen target and $P(x, y, z)$ is the point of scattering. It is assumed that the angle between the scattered and recoil protons is 90° .

The second scattering geometry is shown in Fig. 7. This can be applied to all four positions of both arms by the choice of symbols given below. Since $x, y, z \ll D_1$ and all angles are small ($< 17^\circ$) the relation between the actual scattering angle ψ and its central value ψ_0 can be written

$$D_2\psi \simeq D_2(\psi_0 + \eta) + s[(D_1 + D_2)\chi + \rho]$$

or

$$\psi - \psi_0 \simeq \eta + sF/D_2 \quad \dots\dots (12)$$

where $F = (D_1 + D_2)\chi + \rho$ and the choice of symbols is for C_{nn} : $\rho_l = (-x + y)/\sqrt{2}$, $\rho_r = (x + y)/\sqrt{2}$, $s_l = s_r = +1$ for R and -1 for L; for C_{KP} : $\rho_l = -z$, $\rho_r = +z$, $s_l = +1$ for U and -1 for D, $s_r = -1$ for U and $+1$ for D. The subscripts l and r refer to the left and right arms.

The variation of differential cross section and polarization with second scattering angle are represented by,

$$d\sigma/d\omega_2(\psi) = d\sigma/d\omega_2(\psi_0)[1 - K(\psi - \psi_0) - L(\psi - \psi_0)^2] \quad \dots\dots (13a)$$

$$P_2(\psi) = P_2(\psi_0)[1 - k(\psi - \psi_0) - l(\psi - \psi_0)^2]. \quad \dots\dots (13b)$$

Using the experimental data of Alphonse, Johansson and Tibell (1957b), Dickson and Salter (1957), Hillman, Johansson and Tyren (1957) and Maris and Tyren (1957a), values of K, L, k, l were deduced and are given in Table 8.

The genuine six-fold coincidence counting rate from a volume element $\delta x, \delta y, \delta z$ of the hydrogen target at P into intervals $\delta\chi$ at χ and $\delta\xi$ at ξ is

$$\delta G = Q(S_l S_r \pm C S_l' S_r') \delta\xi \delta\chi \delta x \delta y \delta z. \quad \dots\dots (14)$$

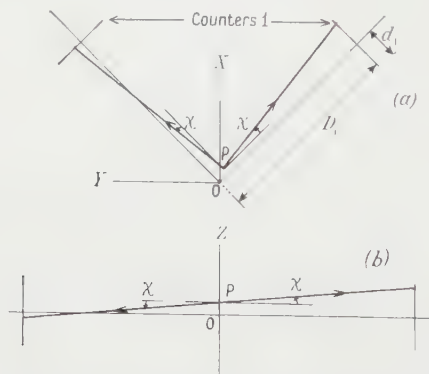


Fig. 6. Geometry of the first scattering, (a) horizontal plane (b) vertical plane. The vertical scattering planes are shown folded back into the plane perpendicular to the incident beam direction.

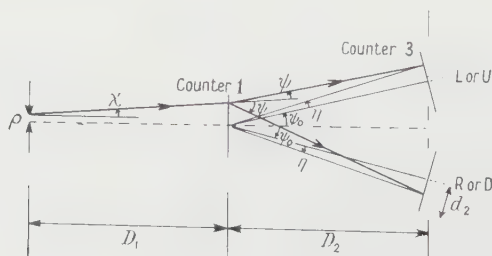


Fig. 7. Geometry of the second scattering.

Q is a constant, it being assumed that the variation with χ of the differential cross section in the first scattering is negligible. C is C_{nn} or C_{KP} ,

$$S = (2b_2 D_2) \int_{-d_2/D_2}^{d_2/D_2} d\sigma d\omega_2(\psi) d\eta, \quad S' = (2b_2 D_2) \int_{-d_2/D_2}^{d_2/D_2} d\sigma d\omega_2(\psi) P_2(\psi) d\eta.$$

The plus sign is for LL, RR, UU, DD and the minus sign for LR, RL, UD, DU; b_2 is the dimension in the perpendicular plane corresponding to d_2 . Variations of $d\sigma/d\omega_2$ and P_2 with scattering angle in this plane are small and can be neglected.

The integrals S and S' can be evaluated using Eqns (12) and (13) with the appropriate allocation of symbols for the different positions. In multiplying the integrals for the two arms it is convenient to take account of the fact that the quantities of interest are,

$$G_+ = LL + RR \text{ for } C_{nn}, \quad UU + DD \text{ for } C_{KP};$$

$$G_- = LR + RL \text{ for } C_{nn}, \quad UD + DU \text{ for } C_{KP}.$$

Several terms disappear in these sums and the term in D_2^{-4} can be neglected. χ enters dG through the factor F defined in Eqn (12). ξ only appears in $\delta\xi$.

Limits for integration over ξ and χ are determined respectively by the dimensions b_1 and d_1 , and by the need to consider only genuine coincidences between the two arms. Then from Fig. 6 the limits for χ are

$$[-y \pm (\chi/2d_1 - |x|)]/\chi/2D_1 \text{ for } C_{nn}, \quad \pm (d_1 - |z|)/D_1 \text{ for } C_{KP}.$$

For ξ the terms for C_{nn} and C_{KP} are interchanged and d_1 is replaced by b_1 . In many cases a rectangular block is a good approximation to the effective target. If $2X, 2Y, 2Z$ are the dimensions of the block then the limits for integration are $\pm (X, Y, Z)$, provided that $X \leq \chi/2d_1$ and $Z \leq d_1$ which was the case in the present measurements. Outside these values of X and Z coincidences between the two arms are impossible. The corresponding value for Y is larger and is unlikely to be reached in any reasonable geometry.

After integrating it is found that

$$G_{\pm} = R[T \pm e'T'] \quad \dots\dots (15)$$

where

$$\begin{aligned} R &= 2QSXYZ(4b_1d_1/D_1^2)(1 - \frac{1}{2}X/\chi/2d_1)(1 - \frac{1}{2}Z/d_1) \\ &\quad \times \{d\sigma/d\omega_{2l}(\psi_0)\}\{d\sigma/d\omega_{2r}(\psi_0)\}h^2(4b_2d_2/D_2^2)^2, \\ e' &= (j/h)^2e = (j/h)^2CP_{2l}(\psi_0)P_{2r}(\psi_0), \\ h &= 1 - \frac{1}{3}L(d_2/D_2)^2, \quad j = 1 - \frac{1}{3}(L + l - Kk)(d_2/D_2)^2. \end{aligned}$$

The product $(1 - \frac{1}{2}X/\chi/2d_1)(1 - \frac{1}{2}Z/d_1)$ is the factor a occurring in Eqn (3). It is convenient to use the asymmetry e' since the analysing powers measured in the calibration experiments include the effect of finite geometry and are

$$P_2'(\psi_0) = j/hP_2(\psi_0)$$

so that

$$e' = CP_{2l}'(\psi_0)P_{2r}'(\psi_0).$$

T and T' can be written

$$\begin{aligned} T &= 1 \pm p(K/h)^2(d_1/D_1)^2f(U, V, -1) - 2(L/h)(d_1/D_1)^2f(U, V, +1), \\ T' &= 1 \pm p[(K+k)/j]^2(d_1/D_1)^2f(U, V, -1) - 2[(L+l-Kk)/j](d_1/D_1)^2f(U, V, +1) \end{aligned}$$

where

$$f(U, V, m) = \frac{1}{3}(1 + D_1/D_2)^2[1 - V/d_1 + \frac{1}{2}(V/d_1)^2] + \frac{1}{3}(U/d_1)^2 \\ + m\frac{1}{2}(D_1/D_2)^2(V/d_1)^2[1 - \frac{1}{3}(1 - \frac{1}{2}V/d_1)^{-1}] \\ U = Y/\sqrt{2} \text{ for } C_{nn}, \quad 0 \text{ for } C_{KP}; \\ V = X/\sqrt{2} \text{ for } C_{nn}, \quad Z \text{ for } C_{KP}; \\ p = +1 \text{ for } C_{nn}, \quad -1 \text{ for } C_{KP}.$$

The measured asymmetry e_1 is

$$e_1 = (G_+ - G_-) / (G_+ + G_-).$$

Inserting the values of T and T' in this equation, expanding by the binomial theorem and neglecting second-order terms

$$e' = e_1 - pf(U, V, -1)(d_1/D_1)^2\{(K/h)^2 - e_1^2[(K+k)/j]^2\} \\ - 2e_1f(U, V+1)(d_1/D_1)^2[(L/h) - (L+l-Kk)/j]. \quad \dots\dots (16)$$

In the present measurements the second correction term is of the order of 10% of the first. Also $e_1^2 \ll 1$ (Table 5), h and $j \simeq 1$, and $D_2 \simeq D_1$ so that the first correction term is approximately $\pm K^2(d_1/D_1)^2\gamma$ where the minus sign is for C_{nn} and the plus sign for C_{KP} and

$$\gamma = \frac{4}{3}\left[1 - \frac{V}{d_1} + \frac{1}{2}\left(\frac{V}{d_1}\right)^2\right] + \frac{1}{3}\left(\frac{U}{d_1}\right)^2 - \frac{1}{2}\left(\frac{V}{d_1}\right)^2\left[1 - \frac{1}{3}\left(1 - \frac{1}{2}\frac{V}{d_1}\right)^{-1}\right].$$

γ is of the order of unity having the value 4/3 for a point target and falling to 5/6 for C_{nn} when $U/d_1 = V/d_1 = 1$ and $\frac{1}{2}$ for C_{KP} when $V/d_1 = 1$.

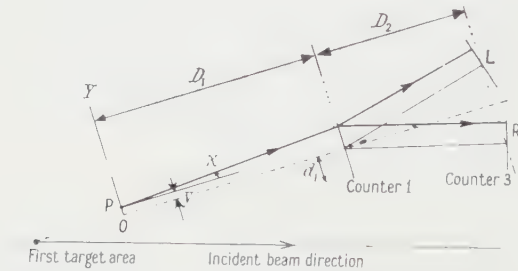


Fig. 8. Geometry of the calibration experiments.

Table 8. Coefficients for the Second Scattering (angles in radians)						
Proton beam energy	K	L	k	l	A	B
382 MeV	$+10.6 \pm 0.6$	-21	-3.8 ± 0.25	0	$+13.8 \pm 1.0$	-66
320 MeV	$+8.9 \pm 0.6$	+7	-3.3 ± 0.2	-13	$+18.9 \pm 1.2$	-164

In the calibration experiment a similar correction arises from the intensity distribution across the second target, due to the variation of differential cross section with first scattering angle. The geometry is shown in Fig. 8. It is convenient to choose the position of the defining collimator O as the origin of the axes, since this may be regarded as the effective source of the protons. The procedure is exactly the same as in the correlation experiment except that only one arm is involved and integration over the source has only to be performed for the Y direction.

The genuine triple coincidence counting rate from an element δy at P into an element of angle $\delta\chi$ at χ is,

$$\delta G_{\pm} = \text{const.} \delta y (1 - A\chi - B\chi^2) \delta\chi (S \pm P_0 S') \quad \dots\dots (17)$$

where the plus sign is for L and the minus sign for R since the first scattering is to the left. $1 - A\chi - B\chi^2$ represents the variation of differential cross section with first scattering angle. P_0 is the polarization of the first scattered beam which may be assumed constant over the range of χ involved. Values of A and B were deduced from the data of Maris and Tyren (1957 b) and are given in Table 8. S and S' are the same as in Eqn (14) with $p = -y$, $s = -1$ for L and $+1$ for R in Eqn (12) for $\psi = \psi_0$. The limits of integration are $(\pm d_1 - y)/D_1$ for χ and $\pm Y$ for y , Y being half the width of the defining collimator.

The integration gives

$$G_{\pm} = \text{const.} \cdot \left[1 - \frac{1}{3} \left(\frac{d_1}{D_1} \right)^2 (z \pm \beta) + E' \left[1 - \frac{1}{3} \left(\frac{d_1}{D_1} \right)^2 (z' \pm \beta') \right] \right],$$

where

$$\begin{aligned} z &= B \left[1 - \left(\frac{Y}{d_1} \right)^2 \right] + \left(\frac{L}{h} \right) \left[\left(1 - \frac{D_1}{D_2} \right)^2 + \left(\frac{Y}{d_1} \right)^2 \right] \\ z' &= B \left[1 - \left(\frac{Y}{d_1} \right)^2 \right] + \left[\frac{(L - l - Kk)}{l} \right] \left[\left(1 + \frac{D_1}{D_2} \right)^2 + \left(\frac{Y}{d_1} \right)^2 \right] \\ \beta &= A \left(\frac{K}{h} \right) \left[1 + \frac{D_1}{D_2} + \left(\frac{Y}{d_1} \right)^2 \right] \\ \beta' &= A \left[\frac{(K - k)}{l} \right] \left[1 + \frac{D_1}{D_2} + \left(\frac{Y}{d_1} \right)^2 \right] \\ E' &= P_0 P_2(\psi_0) \left(\frac{j}{h} \right) = P_0 P_2'(\psi_0). \end{aligned}$$

The observed asymmetry $E_1 = (G_+ - G_-)/(G_+ + G_-)$. Expanding by the binomial theorem and neglecting second-order terms

$$E' = E_1 + \frac{1}{3} (d_1/D_1)^2 [\beta - E_1(\alpha - \alpha') - E_1^2 \beta']. \quad \dots\dots (18)$$

In the present measurements the correction terms in E_1 and E_1^2 are approximately 10^{-1} of the leading correction term.

By use of Eqn (18), E' was calculated from E_1 and since P_0 is known the value of $P_2'(\psi_1)$ was deduced.

ACKNOWLEDGMENTS

We acknowledge a valuable discussion with Professor O. Chamberlain, particularly on the geometrical correction to the asymmetry. The detailed design of the scattering table was done by Mr. C. A. Amery. Throughout the series of experiments we have had the whole-hearted co-operation of the cyclotron crew under Mr. B. S. Halliday. A. N. D. is indebted to C.E.R.N. and K. S. to the Royal Norwegian Council for Scientific and Industrial Research for the provision of fellowships. K. S. was here on leave of absence from the Joint Establishment for Nuclear Energy Research, Kjeller. J. V. A., J. E. and G. B. H. are indebted to the Department of Scientific and Industrial Research for the provision of maintenance grants.

REFERENCES

- ALLABY, J. V., ASHMORE, A., DIDDENS, A. N., and EADES, J., 1959, *Proc. Phys. Soc.*, **74**, 482.
- ALPHONCE, R., JOHANSSON, A., and TIBELL, G., 1957 a, *Nucl. Phys.*, **3**, 185.
- 1957 b, *Nucl. Phys.*, **4**, 672.
- ASHMORE, A., DIDDENS, A. N., and HUXTABLE, G. B., 1959, *Proc. Phys. Soc.*, **73**, 957.
- ASHMORE, A., DIDDENS, A. N., HUXTABLE, G. B., and SKARSVÅG, K., 1958, *Proc. Phys. Soc.*, **72**, 289.
- BRYAN, R. A., 1960, *Nuovo Cim.*, **16**, 895.
- CHAMBERLAIN, O., SEGRÈ, E., TRIPP, R. D., WIEGAND, C., and YPSILANTIS, T. J., 1957, *Phys. Rev.*, **105**, 288.
- CHESNUT, W. G., HAFNER, E. M., and ROBERTS, A., 1956, *Phys. Rev.*, **104**, 449.
- COLLINGS, B., ECCLESHALL, D., and MERRISON, A. W., 1956, *J. Sci. Instrum.*, **33**, 72.
- COLLINGS, B., and HUXTABLE, G. B., 1958, *Nucl. Instrum.*, **3**, 116.
- CZIFFRA, P., MACGREGOR, M. H., MORAVCSIK, M. J., and STAPP, H. P., 1959, *Phys. Rev.*, **114**, 880.
- DICKSON, J. M., and SALTER, D. C., 1957, *Nuovo Cim.*, **6**, 235.
- GAMMEL, J. L., and THALER, R. M., 1957, *Phys. Rev.*, **107**, 291.
- 1959, *Prog. Elem. Part. and Cosmic Ray Phys.*, **5**, 99.
- HILLMAN, P., JOHANSSON, A., and TYREN, H., 1957, *Nucl. Phys.*, **4**, 648.
- KANELLOPOULOS, T. V., and BROWN, G. E., 1957 a, *Proc. Phys. Soc.*, **70**, 690.
- 1957 b, *Proc. Phys. Soc.*, **70**, 703.
- LEE, C., GAMMEL, J. L., and THALER, R., 1960, *Nuclear Forces and the Few Nucleon Problem* (Pergamon Press), Vol. **1**, p. 43.
- MACGREGOR, M. H., MORAVCSIK, M. J., and STAPP, H. P., 1959, *Phys. Rev.*, **116**, 1248.
- MARIS, TH. A. J., and TYREN, H., 1957 a, *Nucl. Phys.*, **4**, 637.
- 1957 b, *Nucl. Phys.*, **4**, 662.
- OEHME, R., 1955, *Phys. Rev.*, **98**, 216.
- PUZIKOV, L., RYNDIN, R., and SMORODINSKY, YA., 1957, *Nucl. Phys.*, **3**, 436.
- SIGNELL, P. S., and MARSHAK, R. E., 1958, *Phys. Rev.*, **109**, 1229.
- SKARSVÅG, K., 1958 a, *Nucl. Phys.*, **8**, 55.
- 1958 b, *Nucl. Instrum.*, **3**, 336.
- SMORODINSKY, YA., 1955, *Dok. Akad. Nauk. S.S.S.R.*, **104**, 713.
- STAPP, H. P., 1956, *Phys. Rev.*, **103**, 425.
- STAPP, H. P., YPSILANTIS, T. J., and METROPOLIS, N., 1957, *Phys. Rev.*, **105**, 302.
- TRIPP, R. D., 1956, *Phys. Rev.*, **102**, 862.
- VASILEVSKY, T. M., VISHNIAKOV, V. V., YLIESCUA, E., and TIAPKIN, A. A., 1959, Kiev International Conference on *The Physics of High Energy Particles*.
- WHALIN, E. A., and REITZ, R. A., 1955, *Rev. Sci. Instrum.*, **26**, 59.
- WOLFENSTEIN, L., 1954, *Phys. Rev.*, **96**, 1654.
- 1956, *Ann. Rev. Nucl. Sci.*, **6**, 43.

Spin-Lattice Relaxation Times in Sapphire and Chromium-doped Rutile at 34.6 Gc/s

By J. H. PACE, D. F. SAMPSON AND J. S. THORP

Physics Department, Royal Radar Establishment, Malvern

MS. received 15th August 1960

Abstract. The paper describes measurements made at 34.6 Gc/s on synthetic sapphire (Fe^{3+} in Al_2O_3) and chromium-doped rutile (Cr^{3+} in TiO_2) in the temperature range 1.4°K to 56°K. Spin-lattice relaxation times of up to 5 milliseconds at helium temperatures are reported. The main features of the temperature dependence of the relaxation times show a broad similarity with the results previously reported by the authors for ruby, but there are insufficient data to show whether the relaxation times are substantially independent of frequency as was found for ruby.

MEASUREMENTS of spin-lattice relaxation times in ruby, made by a pulse saturation method at 34.6 Gc/s, have recently been reported by the authors (Pace, Sampson and Thorp 1960a). These were undertaken to assess the suitability of ruby for maser operation at millimetre wavelengths and it was shown that because of the long relaxation times available it appeared to be a promising material. This note describes corresponding measurements made on synthetic sapphire (Fe^{3+} in Al_2O_3) and chromium-doped rutile (Cr^{3+} in TiO_2) both of which possess some advantages as alternative materials. In ruby the chromium ion has a spin of $s = 3/2$ and the zero field splitting is 11.59 Gc/s. In sapphire, however, iron has a spin of $s = 5/2$ and the zero field splitting of 31.2 Gc/s is considerably larger; the resulting spectrum of six levels affords both a wider choice of transition and the possibility of low field maser operation (Bogle and Symmons 1959a). Chromium in rutile has a spin of $s = 3/2$ as in ruby, giving a spectrum only four levels, but the zero field splitting of 43.3 Gc/s (Gerritsen *et al.* 1959) is of the same order as that of sapphire and the exceptionally high value of the dielectric constant enables unplated samples to resonate as multimode cavities of reasonable Q (Foner and Momo 1960).

To obtain estimates of the maximum available relaxation times orientations were chosen so that cross-relaxation effects (Bloembergen *et al.* 1959) were minimized. Convenient orientations fulfilling this condition were ($\theta = 90^\circ$, $\phi = 0^\circ$) for sapphire, at which the spectra for the two non-equivalent ions in the unit cell coincide, and ($\theta = 90^\circ$, $\phi = 0^\circ$) for the chromium-doped rutile; the energy level diagrams for these orientations are shown in Figs 1 and 2 respectively. A limited number of samples of known concentration were available and measurements were made on a sapphire crystal containing 0.03% Fe and a rutile crystal containing 0.07% Cr, both of which gave line widths of about 20 gauss. Analysis for impurities has not yet been completed. In the sapphire, however, no lines

R

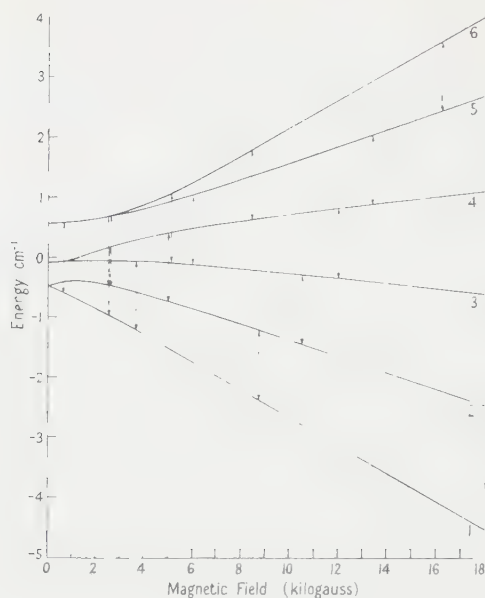


Fig. 1. Energy level diagram for sapphire at $\theta = 90^\circ$, showing 34.6 Gc/s transitions.

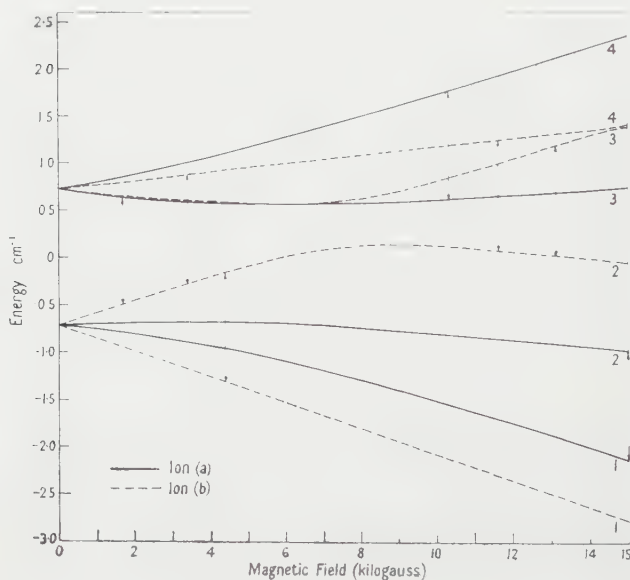


Fig. 2. Energy level diagram for chromium-doped rutile at $\theta = 90^\circ$, $\phi = 0^\circ$, showing 34.6 Gc/s transitions.

other than those due to iron were found; in the rutile some very weak lines were detected which were well removed from those due to chromium. As in the previous measurements the overall accuracy was estimated to be to within $\pm 10\%$ and the minimum measurable relaxation time, set by the receiver recovery, was about 10 microseconds. The observed relaxation times for the sapphire sample are given in Table 1.

Table 1. Relaxation times in sapphire, Fe^{3+} in Al_2O_3 ; $\theta = 90^\circ$; 34.6 Gc/s.

Transition	Field (Oe)	Relaxation time (milliseconds)			
		1.4°K	4.2°K	10.1°K	20.2°K
4-5	13500	4.0	1.8	0.77	0.45
3-4	11900	4.1	1.6	0.80	0.55
2-3	10500	4.1	1.5	0.80	0.55
1-2	8800	4.0	2.0	0.80	0.50
3-6	4850	11.2	—	—	0.9
2-3	4750	13.5	—	—	0.9
1-3	3550	12.5	—	—	1.1
2-5	2800	11.7	—	—	—
2-6	2350	13.2	—	—	—

At and above 56 K the relaxation time for all transitions was less than 10 microseconds. Measurements on the high order lines occurring below 4850 oersted were restricted because their intensities were some 20 dB less than those of the first-order transitions.

The corresponding results for the chromium-doped rutile crystal are given in Table 2.

Table 2. Spin-lattice relaxation times of Cr^{3+} in TiO_2 at 34.6 Gc/s, $\theta = 90^\circ$.

Transition	Field O(e)	Relaxation time (milliseconds)			
		1.4 K	4.2°K	10.1°K	20.3°K
1-2	15000	6.0	4.5	2.2	0.6
3-4	10300	4.7	2.5	2.0	0.6
2-3	13100	5.6	2.5	1.6	0.6
1-2	4400	about 4 at 4.2°K			
2-3	1700	about 3 at 4.2°K			
2-4	11600	3.9	2.1	1.4	0.6
2-4	3400	about 3 at 4.2°K			

Again the relaxation times for all transitions at and above 56 K were less than 10 microseconds and the low field transitions were weak.

The main features of the temperature dependence of the relaxation times show a broad similarity with the results previously reported for ruby (Pace, Sampson and Thorp 1960 b). In sapphire the relaxation time varies approximately as (temperature) $^{-1}$ up to about 10 K, in agreement with theory (Van Vleck 1940); this effect has also been found in potassium chromicyanide (Shapiro and Bleombergen 1959) and in nickel fluosilicate (Bowers and Mims 1959) when cross-relaxation effects are negligible. In the chromium-doped rutile the relaxation time varies approximately as (temperature) $^{-1.2}$ up to 10 K; the departure from a (temperature) $^{-1}$ law is probably due to the rather high chromium content and is similar to the temperature variation found in the higher concentration ruby samples previously studied. In both materials the transition to a region where

the relaxation time varies at least as rapidly as (temperature)⁻⁵ occurs at about 20°K; this is considerably lower than the corresponding temperature for ruby and suggests that high temperature maser operation (Ditchfield and Forrester 1958) would be unlikely. Some relaxation time measurements at lower frequencies have been reported. In sapphire Bogle and Symmons (1959b) using a pulse saturation method found that $T_1 = 7 \pm 2$ milliseconds at 4.2°K and 9 Gc/s in a sample containing 0.005% Fe; in rutile Gerritsen *et al.* (1959) using a c.w. saturation method obtained a value of 40 milliseconds at 4.2°K and 23.7 Gc/s for a sample containing 0.12% Cr. At present there are insufficient data on the variation of the spin-lattice relaxation times with concentration to deduce from the above results and the 34.6 Gc/s measurements whether the relaxation times are substantially independent of frequency as was previously found for ruby. However, the fact that relaxation times of up to 5 milliseconds at 34.6 Gc/s can be obtained at helium temperatures in material giving useful line widths suggests that both sapphire and chromium-doped rutile would be promising materials for millimetre wavelength masers.

ACKNOWLEDGMENT

This paper is published by permission of the Controller, Her Majesty's Stationery Office.

REFERENCES

- BLOEMBERGEN, N., SHAPIRO, S., PERSHAN, P. S., and ARTMAN, J. D., 1959, *Phys. Rev.*, **114**, 445.
BOGLE, G. S., and SYMMONS, H. F., 1959 a, *Aust. J. Phys.*, **12**, 1.
— 1959 b, *Proc. Phys. Soc.*, **73**, 531.
BOWERS, K. D., and MIMS, W. B., 1959, *Phys. Rev.*, **115**, 285.
DITCHFIELD, C. R., and FORRESTER, P. A., 1958, *Phys. Rev. Letters*, **1**, 448.
FONER, S., and MOMO, L. R., 1960, *J. Appl. Phys.*, **31**, 742.
GERRITSEN, H. J., HARRISON, S. E., LEWIS, H. R., and WITTKKE, J. P., 1959, *Phys. Rev. Letters*, **2**, 153.
PACE, J. H., SAMPSON, D. F., and THORP, J. S., 1960 a, *Phys. Rev. Letters*, **4**, 18.
— 1960 b, *Proc. Phys. Soc.*, **76**, 697.
SHAPIRO, S., and BLOEMBERGEN, N., 1959, *Phys. Rev.*, **116**, 1453.
VAN VLECK, J. H., 1940, *Phys. Rev.*, **57**, 426.

Spin-Lattice Relaxation in Cerium Magnesium Nitrate at Liquid Helium Temperature: A New Process

By C. B. P. FINN, R. ORBACH AND W. P. WOLF

Clarendon Laboratory, Oxford

Communicated by B. Bleaney; MS. received 22nd June 1960

Abstract. The spin-lattice relaxation time of Ce^{3+} in cerium magnesium nitrate has been measured as a function of temperature and of magnetic fields up to 1000 gauss. In the temperature range between 3° and 1.9°K , the relaxation time is found to vary exponentially with inverse temperature, changing by a factor of 350. A theoretical treatment of spin-lattice relaxation appropriate to rare earth salts leads to predictions which agree both with the experimentally observed temperature dependence and with the magnitude of the relaxation time. The dominant relaxation process is one in which a phonon of high energy ($\gg kT$) is absorbed by the spin system resulting in a transition from one of the ground state doublet levels to the nearest excited level. Then, in a separate step, another high energy phonon is emitted and a transition is effected to the other level of the ground state doublet. The net result of this 'two-step direct process' can be interpreted as spin-lattice relaxation: i.e. there results a net change in population between the ground state doublet levels which brings the spin system towards thermal equilibrium with the lattice. Such a mechanism, which is quite different from those which have been envisaged up to now for spin-lattice relaxation, should be appropriate for many of the rare earth salts.

§ 1. INTRODUCTION

SPIN-LATTICE relaxation in magnetic rare earth salts presents quite a different problem from that which has been considered in the past in connection with iron group salts (e.g. see Van Vleck 1940). In the rare earths, spin-orbit coupling is in general strong compared with crystal field effects, and the states of an ion are thus primarily functions of $\mathbf{J} = \mathbf{L} + \mathbf{S}$, and therefore contain non-zero components of orbital angular momentum. Through the orbital angular momentum, direct interaction between the magnetic states and the lattice vibrations is possible by means of orbit-lattice interactions, and the magnetic spin temperature is thus relatively strongly coupled to that of the lattice. For this reason spin-lattice relaxation times are generally very short ($T_1 \sim 10^{-12}$ sec at normal temperatures), and low temperatures ($\sim 20^\circ\text{K}$) are often necessary to eliminate spin-lattice relaxation broadening of paramagnetic resonance absorption ($T_1 \gtrsim 10^{-8}$ sec). At even lower temperatures ($T_1 \sim 10^{-3}$ sec), the increase, however, relaxation times may become quite long ($T_1 \sim 10^{-3}$ sec), the increase occurring very rapidly as the temperature decreases. Thus, some early measurements of T_1 in cerium magnesium nitrate (Cooke, Duffus and Wolf 1953) showed that T_1 increases roughly as T^{-10} near 2°K , and so far there has been no explanation of this striking result.

We have now made further measurements of T_1 in this substance and examined possible mechanisms to account for the observed relaxation times. We find that the results can be satisfactorily explained in terms of a new kind of phonon process. This process depends on the fact that the crystal field splittings of the ground multiplet are smaller than available single phonon energies, so that direct phonon-induced transitions can take place between the different magnetic states. This is a condition which may be expected to hold also in other rare earth salts. The particular substance, cerium magnesium nitrate, was chosen for several practical reasons. The spectroscopic ground state of Ce^{3+} is relatively simple, $^2F_{5/2}$, and under the action of the crystal field splits into three Kramers' doublets, the eigenfunctions of which can be specified fairly precisely from magnetic measurements. At temperatures below 4°K only one of these is appreciably populated, and as there is no nuclear hyperfine structure and all the ions are magnetically equivalent, the substance behaves very much like an assembly of ideal $S = \frac{1}{2}$ spins, save for an anisotropic g factor ($g_{\parallel} \ll g_{\perp}$). Hence we do not have to consider special effects which can occur when there are more than two states at energies comparable with kT , or when there is more than one magnetic ion per unit cell. Further, spin-spin interactions are known to be very small (Cooke, Duffus and Wolfe 1953) and it is therefore possible to measure T_1 in steady fields, large compared with internal fields (~ 50 Oe), which are readily attainable in practice. This simplifies the theoretical picture considerably. Though these special conditions help to clarify the situation in this particular salt, the mechanism which we propose may be expected to operate also in other cases.

§ 2. THE EXPERIMENTS

Measurements were made on a large single crystal ($4\text{ cm} \times 1\text{ cm} \times 1\text{ cm}$) using the method of Casimir and du Pré (1938) at frequencies of 175, 500 and

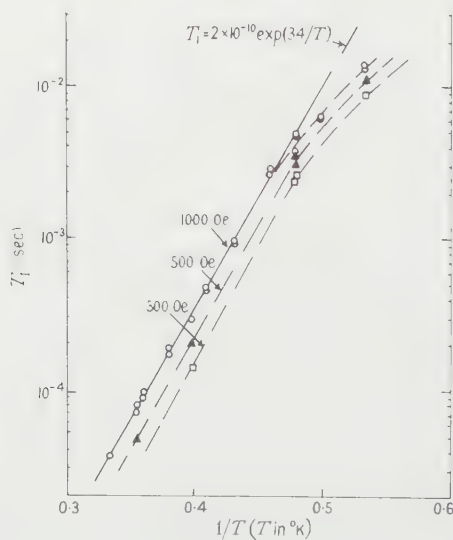


Fig. 1. A plot of the measured relaxation time for Ce^{3+} in cerium magnesium nitrate against $1/T$ for three field strengths—300, 500 and 1000 Oe. The solid line is a plot of $T_1 = 2 \times 10^{-10} \exp(34/T)$ against $1/T$.

900 c/s and d.c. fields of 300, 500 and 1000 Oe. The fields were applied along the direction of maximum g perpendicular to the crystal axis. The experimental procedure and apparatus employed were the same as those described by Benzie and Cooke (1950). At most temperatures good agreement was found between the values of T_1 deduced from measurements at the three frequencies, indicating that the system has one dominant relaxation time. The results are given in Fig. 1. In all fields an extremely rapid variation of T_1 with temperature was observed, T_1 increasing by a factor of about 350 between 3° and 1.9°K . Outside this temperature range the limited range of frequencies available to us at the time prevented quantitative measurements, but the trend indicated that T_1 varies much less rapidly between 1.9° and 1.1°K . Above 3°K it would seem that T_1 continues its rapid variation, since no paramagnetic resonance absorption has been observed above 10°K , even at 10^{10} c/s (Cooke, Duffus and Wolf 1953).

§ 3. THEORY

In most rare earth salts with an odd number of electrons, and in cerium magnesium nitrate in particular, only one Kramers' doublet is appreciably populated at temperatures in the liquid helium range. In a magnetic field H_0 which is large compared with internal fields this is split into two discrete states which we denote by $|a\rangle$ and $|b\rangle$, separated in energy by $g\beta H_0 \equiv \hbar\omega_s$.

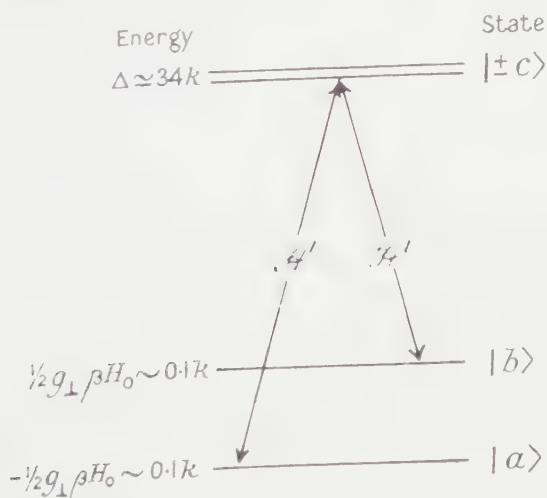


Fig. 2. An illustration of a two-step phonon relaxation process. The perturbation Hamiltonian \mathcal{H}' connects state $|b\rangle$ with state $|±c\rangle$, and, in a separate step, state $|±c\rangle$ with $|a\rangle$. This results in a net relaxation from state $|b\rangle$ to state $|a\rangle$.

We denote the first excited states of the ion in the crystalline field by $|±c\rangle$, and their energy relative to the mean ground state energy by Δ . In general the doublet $|±c\rangle$ may be split by H_0 , but in the particular case which we shall consider here, the splitting is zero to second order (see below) and for simplicity we shall therefore consider only a single value of Δ . If Δ is less than the maximum phonon energy $k\theta_1$, an ion which is in the upper state of the ground doublet $|b\rangle$ may absorb a phonon of energy $\Delta - \frac{1}{2}\hbar\omega_s$ and make a transition to the $|±c\rangle$ state. Then, in a separate step, a second phonon is emitted with energy $\Delta + \frac{1}{2}\hbar\omega_s$ and relaxation takes place from the $|±c\rangle$ level to the other lower state of the ground doublet (see Fig. 2). These conditions apply to the case of cerium magnesium

nitrate, for which Bailey (1959) has shown that $\theta_D \simeq 60^\circ\text{K}$ at low temperatures, and (unpublished) that $\Delta = 34 \pm 1$ K. Leask and Wolf (to be published) found $\Delta = 37^\circ \pm 3^\circ\text{K}$ from susceptibility measurements. We thus envisage a two-step process†, the net effect of which is a transition between the ground state doublet levels, the absorption of one phonon of energy $\Delta - \frac{1}{2}\hbar\omega_s$ and the emission of another phonon with energy $\Delta + \frac{1}{2}\hbar\omega_s$, the difference in phonon energies being equal to the change of Zeeman energy $\hbar\omega_s \equiv g\beta H_0$.

This two-step direct relaxation process differs markedly from previous one- and two-phonon relaxation mechanisms. In the usual theory, considering the iron group salts for a concrete example (Van Vleck 1940), the *one*-phonon (or direct) relaxation processes arise from terms in the so-called 'effective Hamiltonian' which are linear in the strain. Only phonons of energy $\hbar\omega_s$ are utilized as it is only these phonons which have the proper energy (equal to the Zeeman energy) and are thus on 'speaking terms' with the spin system. As crystal fields in the iron group salts are usually so large that $\Delta \gg k\theta_D$, and spin-orbit coupling is so small that the spin and the orbit are to first order uncoupled, the Hamiltonian must be constructed by considering virtual transitions to and from the excited states. These virtual transitions mix in spin-orbit and orbit-lattice terms which then couple the spin magnetic moment to the lattice vibrational modes. For the *two*-phonon Raman processes the effective Hamiltonian is built up in much the same way, only now one must go to a higher order perturbation, the orbit-lattice terms being taken twice. Then the strain will appear in second order allowing all phonons to take part in the relaxation process, the energy of a given phonon being changed by the Zeeman energy upon being scattered. The direct one-phonon process matrix element of the effective Hamiltonian may be larger than in the Raman case, but more phonons can take part in the latter and it is generally more effective in spin-lattice relaxation at intermediate temperatures. At very low temperatures, of the order of a few degrees, there are so many fewer phonons thermally excited that the direct one-phonon process will then be dominant.

In the rare earth salts, however, all this is changed for two reasons. First, $\Delta \ll k\theta_D$ and we can make a real phonon induced transition to the excited state. Secondly, the spin-orbit interaction is much stronger in the rare earth salts and the magnetic states contain orbital angular momentum in zero order, and not as a result of a relatively weak perturbation. Under such conditions the effective Hamiltonian is just the orbit-lattice interaction and is linear in the strain. It can induce real transitions directly between the ground state and the excited state, the phonons taking part having the energy $\Delta \pm \frac{1}{2}\hbar\omega_s$. Because we do not have to go to a high order of perturbation theory, the matrix element of the rare earth effective Hamiltonian is several orders of magnitude larger than in the iron group salts. Relatively few phonons with energies much greater than kT can then give rise to the relatively short relaxation times observed in rare earth salts.

As Van Vleck (1940) has pointed out, the primary perturbations which give rise to direct spin-lattice relaxation processes are orbit-lattice interactions linear in the strain, which come about from Jahn-Teller distortions of the complex

† It has been pointed out by Dr. B. Bölger (private communication) that a somewhat similar process has been thought of by Lloyd and Pake (1954) in quite a different context. We are indebted to Dr. Bölger for this communication.

surrounding each magnetic ion. There are always additional perturbations present which are second order in the strain, but these are in general much smaller than the first-order Jahn-Teller terms and at low temperatures may be neglected. Unfortunately, however, the detailed crystal structure of the double nitrates has not been determined, so that the form and strength of the Jahn-Teller distortions are unknown. We therefore consider an orbit-lattice perturbation Hamiltonian \mathcal{H}' which we believe from general considerations may have the form

$$\mathcal{H}' = (\cos \phi V_2^{+1} + \sin \phi V_2^{-1} + \cos \phi' V_4^{+1} + \sin \phi' V_4^{-1})\epsilon, \dots (1)$$

where ϵ is the strain, V_l^m are terms in the crystal field potential (e.g. see Stevens 1952) and ϕ and ϕ' are phase factors specifying the direction of the strain. Within a manifold of constant J , the V_l^m may be replaced by their operator equivalents,

$$V_2^{\pm 1} = \frac{1}{2}\alpha A_2^1 \bar{r}^2 [J_z J_{\pm} + J_{\pm} J_z], \dots (2)$$

$$V_4^{\pm 1} = \frac{1}{2}\beta A_4^1 \bar{r}^4 \{ [7J_z^3 - 3J(J+1)J_z - J_{\pm} J_{\pm} + J_{\pm} [7J_z^3 - 3J(J+1)J_z - J_z] \}. \quad (3)$$

Here, α and β are proportionality constants defined and tabulated by Stevens (1952), and $A_2^1 \bar{r}^2$ and $A_4^1 \bar{r}^4$ are appropriate crystal field parameters.

The transition probability per unit time W for the absorption of a phonon by one ion initially in state $|b\rangle$ and finally in one of the states $|\pm c\rangle$ under the action of \mathcal{H}' is, according to first-order time dependent perturbation theory (e.g. Landau and Lifshitz 1958)

$$W = \frac{2\pi}{h^2} \frac{12\pi}{(2\pi)^3} \int k^2 dk |\langle \pm c | \mathcal{H}' | b \rangle|^2 \delta(\omega_i - \omega_f), \dots (4)$$

where ω_i and ω_f are the initial and final energies of the system. V is the crystal volume, $k = \omega/v$, where ω is the phonon frequency and v its velocity. We have neglected dispersion in the phonon spectrum and assumed that all three phonon modes interact in the same way and have the same velocity, which justifies our use of $12\pi V k^2 / (2\pi)^3$ for the density of final states. We have also assumed that the amplitude of displacement of the rare earth ion is the same as that of a neighbouring ion. These are all crude approximations, but in view of our lack of information regarding the Jahn-Teller distortions they are adequate.

The magnitude of the matrix element of \mathcal{H}' may be computed from known magnetic properties of the Ce^{3+} ion in the double nitrate. Neglecting for simplicity admixtures through the crystalline field between the ground multiplet $^2F_{5/2}$ and the states $^2F_{7/2}$ which are at 2250 cm^{-1} , the three Kramers' conjugate states have the form (Elliott and Stevens 1952, Judd 1955 a)

$$\cos \theta |J_z = \pm 1/2\rangle \mp \sin \theta |J_z = \mp 5/2\rangle, \dots (5a)$$

$$|J_z = \pm 3/2\rangle, \dots (5b)$$

where θ has two values differing by $\frac{1}{2}\pi$. Using the values of the crystal field parameters as estimated by Judd (1955 b), we find the ground state doublet to be,

$$|\pm\rangle \simeq 0.9 |J_z = \pm 1/2\rangle \mp 0.4 |J_z = \mp 5/2\rangle. \dots (6)$$

In the presence of a d.c. magnetic field perpendicular to the Z axis these combine into the eigenstates,

$$\begin{aligned} |b\rangle &= 1/\sqrt{2}(|+\rangle + |-\rangle), \\ |a\rangle &= 1/\sqrt{2}(|+\rangle - |-\rangle), \end{aligned} \dots (7a)$$

with relative energies $E_b - E_a = g_{\perp} \beta H_0 \equiv \hbar \omega_s$.

Specific heat (Bailey 1959) and magnetic susceptibility (Leask and Wolf, to be published) measurements have shown that the first excited state $|\pm c\rangle$ is the doublet $|J_z = \pm 3/2\rangle$, and that its energy is $\Delta \simeq 34^\circ\text{K}$. This doublet is unaffected in first order by a magnetic field perpendicular to the Z axis, i.e. $g_\perp = 0$. This is true even if we allow for possible admixtures of the $J = 7/2$ multiplet, justifying our earlier assumption that both components of the doublet $|\pm c\rangle$ are at the same energy Δ . The third doublet belonging to ${}^2F_{5/2}$ is considerably higher in energy ($\sim 150^\circ\text{K}$) and we shall neglect its effect.

The matrix elements of \mathcal{H}' between the components $|a\rangle$ and $|b\rangle$ of the ground state doublet and $|J_z = \pm 3/2\rangle$ are readily found from Eqns (2), (3), (6) and (7). We find

$$\langle J_z = \pm 3/2 | V_2^{+1} | b \rangle = (0.91)(-2/35)A_2^1 \bar{r}^2 \quad \dots\dots (8a)$$

$$\langle J_z = \pm 3/2 | V_2^{-1} | b \rangle = (-6.3)(-2/35)A_2^1 \bar{r}^2 \quad \dots\dots (8b)$$

$$\langle J_z = \pm 3/2 | V_4^{+1} | b \rangle = (-69)(2/315)A_4^1 \bar{r}^4 \quad \dots\dots (8c)$$

$$\langle J_z = \pm 3/2 | V_4^{-1} | b \rangle = (25)(2/315)A_4^1 \bar{r}^4 \quad \dots\dots (8d)$$

with a similar set for state $|a\rangle$. Collecting terms and averaging over the different strain directions (ϕ and ϕ'), we find finally for the square of the matrix element of our interaction Hamiltonian,

$$|\langle J_z = \pm 3/2 | \mathcal{H}' | b \rangle|^2 = (2/35)^2 [14A_2^1 \bar{r}^2 + 22A_4^1 \bar{r}^4] \epsilon^2 \equiv G^2 \epsilon^2 \quad \dots\dots (9)$$

which defines G^2 . Inserting Eqn (9) into our expression for W , Eqn (4), multiplying by the number of spins in the state $|b\rangle$ and integrating we find for the total probability per unit time for transitions between states $|b\rangle$ and $|\pm c\rangle$, W_{up} ,

$$W_{\text{up}} = \frac{3G^2}{2\pi\hbar\rho v^5} \left(\frac{\Delta - \frac{1}{2}\hbar\omega_s}{\hbar} \right)^3 N_b \bar{N}(\Delta - \frac{1}{2}\hbar\omega_s); \quad \dots\dots (10)$$

where ρ is the crystal density, $\hbar\omega_s$ is the splitting of the Kramers' doublet $= g_\perp \beta H_0$, v the phonon velocity, and we designate by N_a , N_b , $N_{\pm 3/2}$ the number of spins in the $|a\rangle$, $|b\rangle$, $|J_z = \pm 3/2\rangle$ levels respectively. The term $\bar{N}(\Delta - \frac{1}{2}\hbar\omega_s)$ represents the phonon equilibrium occupation number evaluated at energy $\Delta - \frac{1}{2}\hbar\omega_s$ and enters through the square of the matrix element of the strain ϵ :

$$\bar{N}(\Delta - \frac{1}{2}\hbar\omega_s) = \frac{1}{\exp\{(\Delta - \frac{1}{2}\hbar\omega_s)/kT\} - 1}. \quad \dots\dots (11)$$

We must now consider the process going in the reverse direction. That is, we must find the total transition probability per unit time W_{down} for the emission of a phonon of energy $\Delta - \frac{1}{2}\hbar\omega_s$ and the accompanying transition from the state $|J_z = \pm 3/2\rangle$ to the state $|b\rangle$. We can then find the *net* transition probability per unit time W_1 by subtraction. From Eqn (10) and an analogous expression for W_{down} we find

$$W_1 = W_{\text{up}} - W_{\text{down}} = \frac{3G^2}{2\pi\hbar\rho v^5} \left(\frac{\Delta - \frac{1}{2}\hbar\omega_s}{\hbar} \right)^3 \{N_b \bar{N}(\Delta - \frac{1}{2}\hbar\omega_s) - N_{\pm 3/2} [\bar{N}(\Delta - \frac{1}{2}\hbar\omega_s) + 1]\}. \quad \dots\dots (12)$$

The next step in our calculation is to consider the relaxation from the $|J_z = \pm 3/2\rangle$ states to the state $|a\rangle$. Exactly as before we find the net transition probability per unit time for such transitions to be

$$W_2 = \frac{3G^2}{2\pi\hbar\rho v^5} \left(\frac{\Delta + \frac{1}{2}\hbar\omega_s}{\hbar} \right)^3 \{N_{\pm 3/2} [\bar{N}(\Delta + \frac{1}{2}\hbar\omega_s) + 1] - N_a \bar{N}(\Delta + \frac{1}{2}\hbar\omega_s)\}. \quad \dots\dots (13)$$

We are now finally in a position to calculate the spin-lattice relaxation time between our Kramers' doublet states, $|b\rangle$ and $|a\rangle$. The relevant rate equations are

$$\frac{dN_b}{dt} = -W_1; \quad \frac{dN_a}{dt} = W_2. \quad \dots\dots (14)$$

Subtracting the latter from the former Eqn and neglecting $\frac{1}{2}\hbar\omega_s$ compared with Δ in the first bracketed term in Eqns (12) and (13) we have

$$\frac{d}{dt}(N_b - N_a) = -W_1 - W_2 \simeq -\frac{3G^2}{2\pi\hbar\rho v^5} \left(\frac{\Delta}{\hbar}\right)^3 \{N_b \bar{N}(\Delta - \frac{1}{2}\hbar\omega_s) - N_a \bar{N}(\Delta + \frac{1}{2}\hbar\omega_s) + N_{\pm 3/2} [\bar{N}(\Delta + \frac{1}{2}\hbar\omega_s) - \bar{N}(\Delta - \frac{1}{2}\hbar\omega_s)]\}. \quad (15)$$

We consider the term in curly brackets. Assuming $\Delta \gg kT \gg \hbar\omega_s$, it reduces to

$$\exp(-\Delta/kT) \{N_b \exp(\hbar\omega_s/kT) - N_a - N_{\pm 3/2}(\hbar\omega_s/kT)\}. \quad \dots\dots (16)$$

At low temperatures ($T \ll \Delta/k$) we can neglect the last term. In this approximation, Eqn (15) becomes,

$$\frac{d}{dt}(N_b - N_a) = -\frac{3G^2}{2\pi\hbar\rho v^5} \left(\frac{\Delta}{\hbar}\right)^3 \exp(-\Delta/kT) \{N_b \exp(\hbar\omega_s/kT) - N_a\}. \quad \dots\dots (17)$$

This form for the rate equation leads in the usual sense (Orbach 1960) to the spin-lattice relaxation time T_1 ,

$$\frac{1}{T_1} = \frac{3G^2}{2\pi\hbar\rho v^5} \left(\frac{\Delta}{\hbar}\right)^3 \exp(-\Delta/kT). \quad \dots\dots (18)$$

This form for the relaxation time is actually quite general and should apply to many of the rare earth salts. It is to be noted that because of the way Δ appears in (18), all else being equal, T_1 at a given temperature T , will not be a monotonic function of the crystal field splitting Δ from one salt to another, but in fact will be shortest for the salt in which $\Delta/kT \sim 3$ and will increase for other values of Δ .

Experimentally, as can be seen from Fig. 1, the relaxation time is found to vary exponentially with T^{-1} and a slope $\Delta/k \sim 34$ K. The value of Δ thus obtained is in very good agreement with that calculated from specific heat and susceptibility data. It thus appears that our basic process and the resulting form for the relaxation time are consistent with experiment.

We can make an approximate estimate of the absolute magnitude of T_1 for our mechanism by extrapolating some highly tentative values for the appropriate crystal field parameters. Previous work (Orbach 1960) has indicated that as a first approximation we may take the phenomenological crystal field perturbation coefficients $A_2^0\bar{r}^2$, $A_4^0\bar{r}^4$ to be of the same order of magnitude as the values of the zero-order terms. They can be treated as a perturbation because they are multiplied by the strain ϵ which is small.

Judd (1955 b) gives the values for the zero-order crystal field parameters

$$A_2^0\bar{r}^2 \sim -70 \text{ cm}^{-1}; \quad A_4^0\bar{r}^4 \sim -30 \text{ cm}^{-1}; \quad A_4^3\bar{r}^4 \sim \pm 900 \text{ cm}^{-1}. \quad \dots\dots (19)$$

Hence, it is not unreasonable to assume

$$A_2^1\bar{r}^2 \sim 50 \text{ cm}^{-1}, \quad A_4^1\bar{r}^4 \sim 500 \text{ cm}^{-1}. \quad \dots\dots (20)$$

We let $\Delta/k = 34^\circ\text{K}$ and find $G^2 = 1.4 \times 10^{-28}$. Using $v = 2.3 \times 10^5 \text{ cm sec}^{-1}$, $\rho = 2 \text{ g cm}^{-3}$, we find from Eqn (18) that

$$T_1 \sim 10^{-10} \exp(34/T) \text{ sec}, \quad \dots\dots (21)$$

in very reasonable agreement with our experimental results.

§ 4. CONCLUSIONS

The experimental results presented in this paper have shown that the spin-lattice relaxation time for Ce^{3+} in the double nitrate varies exponentially with the inverse temperature in the temperature region between 1.9° and 3°K . By using a theory for paramagnetic relaxation appropriate to the rare earth salts we are able to explain both the temperature dependence and the magnitude of the relaxation time. It must be emphasized that although the temperature range in which we have been able to measure is small, the magnitude of T_1 changes by two orders within it. Thus, the theory appears to be significant over a wide range of values of the relaxation time, though tested in only a narrow temperature range.

ACKNOWLEDGMENTS

We wish particularly to thank Dr. R. J. Elliott for many very helpful discussions, and Professor B. Bleaney for suggesting this investigation and his continued interest. We should also like to thank Professor J. H. Van Vleck and Dr. A. H. Cooke for their useful comments and criticisms. We are indebted to Dr. C. A. Bailey for supplying us with his experimental specific heat results on cerium magnesium nitrate prior to publication.

This work was carried out during the tenure by R. O. of a National Science Foundation Postdoctoral Fellowship, and by C. B. P. F. of a grant from the Department of Scientific and Industrial Research. It was also supported in part by the United States Air Force Cambridge Research Center, through the European Office of Air Research and Development Command.

REFERENCES

- BAILEY, C. A., 1959, *Phil. Mag.*, **4**, 833.
 BENZIE, R. J., and COOKE, A. H., 1950, *Proc. Phys. Soc. A*, **63**, 201.
 CASIMIR, H. G. B., and DU PRÉ, F. K., 1938, *Physica*, **5**, 507.
 COOKE, A. H., DUFFUS, H. J., and WOLF, W. P., 1953, *Phil. Mag.*, **44**, 623.
 ELLIOTT, R. J., and STEVENS, K. W. H., 1952, *Proc. Roy. Soc. A*, **215**, 437.
 JUDD, B. R., 1955 a, *Proc. Roy. Soc. A*, **227**, 552.
 ——— 1955 b, *Proc. Roy. Soc. A*, **232**, 458.
 LANDAU, L. D., and LIFSHITZ, E. M., 1958, *Quantum Mechanics* (London: Pergamon Press), p. 133.
 LLOYD, J. P., and PAKE, G. E., 1954, *Phys. Rev.*, **94**, 579.
 ORBACH, R., 1960, *Ph.D. Thesis*, University of California.
 STEVENS, K. W. H., 1952, *Proc. Phys. Soc. A*, **65**, 209.
 VAN VLECK, J. H., 1940, *Phys. Rev.*, **57**, 426.

Note added in proof. An alternative approach outlined in a forthcoming paper by one of us (R.O.; *Proc. Phys. Soc.*, in the press), which treats this problem using higher order perturbation techniques, shows that in addition to the exponential temperature dependence of T_1 on $1/T$, a term is also present for which T_1 varies inversely as the seventh power of temperature, *viz.*

$$\frac{1}{T_1} = \frac{9G^2(6!)}{8\pi^3\rho^2v^{10}k^2\Delta^2} \left(\frac{kT}{\hbar}\right)^7.$$

A comparison with Eqns (18) and (21) shows that this term will only be important at the very lowest and highest of temperatures. It may account for the curvature of our experimental results at the low temperature end of Fig. 2.

The Energy Transferred in Inelastic Ion-Atom Collisions

By J. B. HASTED

University College, London

MS. received 21st July 1960

Abstract. Multiply charged target ion abundances for Ne⁺ A 75 keV collisions are calculated from the theory of Russek and Thomas and compared with experimental data of Afrosimov and Fedorenko. The electron energy distribution for 'hard scattering' is also calculated, and shows a maximum at about 200 eV.

FROM the statistical theory developed by Russek and Thomas (1958) to account for the multiple ionization produced in an energetic collision between two atomic systems it is possible to calculate the relative differential multiple ionization cross sections provided that assumptions are made concerning the amount of energy E_1 transferred from one system to the other in such collisions. This quantity may only be calculated on the basis of further assumptions concerning the mechanism of transfer (see also Firsov 1959). However the energy transferred E_1 has recently been measured for certain ion-atom collisions by Afrosimov and Fedorenko (1957), using retardation techniques in which the slow ion kinetic energies are measured after their mass analysis. It is possible to use this information, together with data obtained by Everhart *et al.* (1960) in assessing the validity of Russek and Thomas's conclusions.

Afrosimov and Fedorenko have measured ion abundances for target ions $I_{A^{n+}}$, $n = 1$ to 6, formed at laboratory coordinate scattering angles $77^\circ < \phi < 90^\circ$ by the impact of 75 keV Ne⁺ projectile ions on argon gas, as a function of retarding potential V_2 . At any scattering angle ϕ , the inelastic energy loss E_1 is given by

$$E_T(\phi) = 2 \cos \phi \left(\frac{m_2 E_2 E_1}{m_1} \right)^{1/2} - \left(\frac{m_1 + m_2}{m_1} \right) E_2 \quad \dots (1)$$

where m_2 and E_2 are the target ion mass and kinetic energy after collision; m_1 is the projectile ion mass, E_1 is the projectile kinetic energy, approximately unchanged by collision.

Everhart has measured the relative probabilities P_n ($n = 0$ to 5) of scattering, by argon, of 75 keV Ne⁺ projectile ions into a laboratory coordinate angle $\theta = 5^\circ$, accompanied by the removal of $n + 1$ electrons from the Ne⁺ projectile. He finds at this energy $P_0 \approx P_1$, $P_1 \approx P_2$, $P_2 \approx P_3$, $P_3 \approx P_4$. This condition can only be satisfied by Russek and Thomas's calculations provided $E_1/\epsilon = 14$, where ϵ is the cell size into which their energy scale is divided. It is defined as one quarter of the mean energy per electron for removal of a shell of eight electrons; arguments are adduced for the assumption that any electron acquiring more than this 'uniform ionization energy' can escape regardless of how many others also escape.

To remove eight electrons from neon requires an energy of 953 eV, the sum of the ionization potentials iE . Since spectroscopic values of the seventh and eighth are not available, they must be found by extrapolation through the iso-electronic series, following the method of Glockler (1934):

$$\begin{aligned} iE_{\text{Ne VIII}} &= 3iE_{\text{F VII}} - 3iE_{\text{O VI}} + iE_{\text{N V}} = 238.9 \text{ eV} \\ iE_{\text{Ne VII}} &= 3iE_{\text{F VI}} - 3iE_{\text{O V}} + iE_{\text{N IV}} = 207.1 \text{ eV.} \end{aligned} \quad \dots (2)$$

Thus the Russek-Everhart value of E_T for this collision is $14 \times 953.4/32 \approx 470$ eV.

We now require to know which value of ϕ studied by Fedorenko corresponds to $\theta = 5^\circ$. Using the formula

$$\tan \theta = \frac{m_2 \left[\cos \phi \pm \left(\cos^2 \phi - \frac{m_1 + m_2}{m_2} \cdot \frac{E_T}{E_1} \right)^{1/2} \right] \sin \phi}{m_1 + m_2 - m_2 \left[\cos \phi \pm \left(\cos^2 \phi - \frac{m_1 + m_2}{m_2} \cdot \frac{E_T}{E_1} \right)^{1/2} \right] \cos \phi} \dots\dots (3)$$

we find that the nearest corresponding value is $\phi = 84^\circ$. (The experiment is carried out at $\Delta\phi = 2^\circ$ intervals.) For this value $\theta = 3^\circ$ or $5^\circ 3'$, the second ('hard scattering') value, with two plus signs in the equation, corresponding to the faster target ions to which Fedorenko's retardation curves refer. For $\phi = 84^\circ$, Fedorenko gives $E_T = 490$ ev, which is in such (fortuitously?) good agreement with the Russek-Everhart value that further comparisons seem worthwhile.

Russek and Thomas calculate the probabilities of ionization $P_n(E_T)$ for $n=1$ to 8. It should be possible from Afrosimov and Fedorenko's retarding potential data and angular distribution data to compute hard scattering ion abundance as a function of E_T , that is $I_{An+}(E_T)$, $n=2$ to 4. This function may or may not be of the form predicted by Russek and Thomas.

We first obtain $I_{An+}(E_T)$ at each value of ϕ for which hard scattering experimental data are available, using the relation $dI_{An+}/dV_2 = I_{An+}(E_2)$, and Eqn (1). This function is multiplied by the angular distribution function $I_{An+}(\phi)$ at the identical projectile energy $E_1 = 75$ kev, using data obtained with a high enough retardation level (200 ev) to eliminate soft scattering. The resulting $I_{An+}(\phi, E_T)$, $n=2$ to 4, is now normalized so that its maximum value corresponds with that of $P_n(E_T)$, and the two functions are compared in Fig. 1, with units of E_T/ϵ as energy scale.

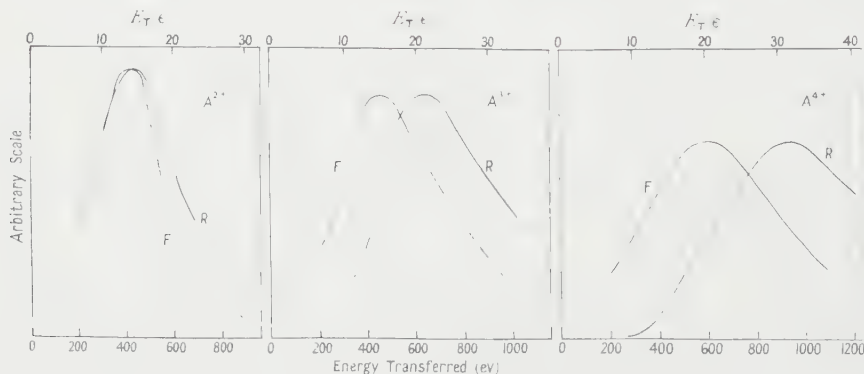


Fig. 1. Comparison of Fedorenko's experimental ion abundances, F, ($\text{Ne}^+ \text{A}$, 75 keV) with Russek's calculated ionization probabilities, R, as a function of energy transferred.

The correspondence is encouraging although as the ion charge increases a systematic discrepancy becomes more and more apparent. The experimental maximum abundances occur at lower transferred energies than those predicted by Russek and Thomas.

It is assumed in the above derivation of $I_{An+}(\phi, E_T)$ that the angular resolution is small compared with the $\Delta\phi = 2^\circ$ intervals chosen. If this is not so the retardation curves $I_{An+}(V_2)$ will not yield true values of $I_{An+}(E_2)$, at a single value of ϕ . Since the angle of emission is only defined to $\pm 1.25^\circ$, this represents a source of inaccuracy in the derivation. For $n=4$ the limits of energy are set by the contributions from angles $\phi < 78^\circ$, for which extrapolated data must be used.

It would seem that the energy transferred in an inelastic collision of this type is fundamental to any theory formulated to account for the data. In the 'soft scattering' dominant in single ionization there are arguments for supposing that the energy is not much greater than the minimum necessary for ionization. On this assumption Firsov (1959) is able to calculate ionization cross sections which are in fair agreement with the experimental data. But for multiple ionization there is a greater admixture of 'hard scattering', with a much larger transfer of energy dissipated during the short time of collision in Auger transitions rather than in radiation. Thus we would expect the ejected electrons to possess considerable kinetic energy distribution, as has been shown experimentally in the work of Blauth (1957). The overall energy distribution of the electrons ejected in the hard scattering only, may be estimated in the following way.

The proportions of hard and soft collisions are obtained from the ratio of areas under the angular distribution curves $I(\phi)$ taken with $V_2=200$ v and $V_2=0$.

$$\frac{{}_nI_h}{{}_nI_{s+h}} = \frac{\int {}_nI_{200}(\phi)d\phi}{\int {}_nI_0(\phi)d\phi}. \quad \dots\dots (4)$$

The total collision cross sections for the production of A^n have been published earlier by Fedorenko and Afrosimov (1956), so that we can obtain the total hard and soft collision cross sections for $n=1$ to 5†. These allow us to weight the transferred energy distribution curves correctly:

$$\frac{h\sigma_{n1}}{h\sigma_{n2}} = \frac{\int {}_nI(E_T)dE_T}{\int {}_nI(E_T)dE_T}. \quad \dots\dots (5)$$

Performing all the integrals graphically, and assuming that the kinetic energy is uniformly divided among the ejected electrons,

$$E_e = \frac{1}{n}(E_T - iE_n) \quad \dots\dots (6)$$

we sum the weighted $I(E_1)$ curves to give, very approximately, the total hard scattering electron energy distribution curve shown in Fig. 2.

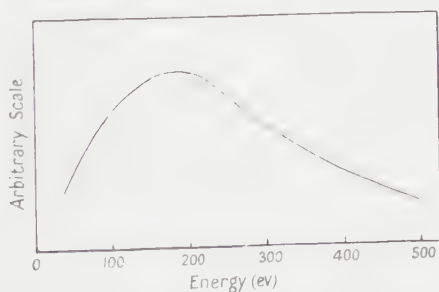


Fig. 2. Hard scattering electron energy distribution calculated for $\text{Ne}^+ \text{A}$, 75 kev collisions.

Comparison of this distribution curve, having a characteristic maximum at 200 eV, with experiment may enable us to decide whether a significant proportion of transferred energy is lost in any other way—for instance, to a radiation continuum. It must however be remembered that: (i) A proportion of the collisions in which electrons are removed from the argon will also involve their removal from

† The data for $n=1$ and 5 have been included in this calculation but are not shown in Fig. 1 because they are too approximate. The retardation curve for $n=1$ is taken as identical with the others given by Fedorenko.

the neon. Thus in Eqn (6) some unknown but possibly small proportion of neon ionization potentials should be inserted. (ii) The assumption of equipartition of kinetic energy among the electrons is open to question. (iii) The low energy soft scattering electrons may not be separated from the hard so easily as expected, since they form such a large proportion of the total.

REFERENCES

- AFROSIMOV, V. V., and FEDORENKO, N. V., 1957, *J. Tech. Phys. (U.S.S.R.)*, **27**, 2557, 2573.
English translation, 1958, *Soviet Phys., Tech Phys.*, **2**, 2378, 2391.
BLAUTH, E., 1957, *Z. Phys.*, **147**, 228.
EVERHART, E. E., ZIEMBA, F. P., LOCKWOOD G. J., and MORGAN, G. H., 1960, *Phys. Rev.* **118**, 1552.
FEDORENKO, N. V., and AFROSIMOV, V. V., 1956, *J. Tech. Phys. (U.S.S.R.)*, **26**, 1941.
English translation, 1956, *Soviet Phys., Tech. Phys.*, **1**, 1872.
FIRSOV, O. B., 1959, *J. Exp. Theor. Phys. (U.S.S.R.)*, **36**, 1517. English Translation, 1959, *Soviet Phys., J.E.T.P.*, **9**, 1076.
GLOCKLER, G., 1934, *Phys. Rev.*, **46**, 111.
RUSSEK, A., and THOMAS, M. T., 1958, *Phys. Rev.*, **109**, 2015.

The Measurement of Indirect (J) Coupling between Nuclei in Liquids in Magnetic Resonance by the Transient Method

By J. G. POWLES AND A. HARTLAND

Physics Department, Queen Mary College, London

MS. received 2nd June 1960

Abstract. An improved method of determining the indirect nuclear spin coupling J in magnetic resonance by the transient method is described. The reduction of self-diffusion method is described. The reduction of self-diffusion attenuation by complex pulse trains permits the observation of J modulation for times up to about one second and measurement of J to $\pm 1\frac{1}{2}\%$ or better. Chemical shifts δ can also be determined. Expressions are given for the echo modulation in some special cases and also a general method for obtaining them when $J \ll \delta$. The modulation patterns in methyl alcohol, ethyl alcohol and 2-bromo-5-chloro-thiophene are given.

THE chemical shift δ and the indirect coupling J between magnetic nuclei in liquids in the nuclear magnetic resonance experiment can be determined either by a transient or by a steady-state experiment. The original investigations of J coupling were made by the transient 'echo' method (Hahn and Maxwell 1951, 1952, McNeil, Slichter and Gutowsky 1951) but J values are at present determined more accurately by the steady-state high resolution method or in special cases by the modulated wiggles method (Reilly 1956). A disadvantage of the latter methods is that an expensive magnet is required and the accuracy attained is not likely to improve for some time. We have therefore reconsidered the transient method.

We suggest here a simple modification of Hahn and Maxwell's experiment which we feel makes the accuracy of the transient method in determining J and in many cases δ , comparable with, if not better than, that which can be achieved by present high resolution equipment.

In Hahn and Maxwell's experiment a $90^\circ, \pi, 90^\circ$ radio-frequency pulse sequence is applied to the nuclear system and an 'echo' (Hahn 1950) appears at time 2τ . If there are at least two sets of nuclei at resonance which are chemically shifted and have indirect coupling the *amplitude* of the echo is modulated. For the simplest case of two protons with chemical shift δ c/s and indirect coupling J c/s the modulation is given by (Hahn and Maxwell 1951)

$$\frac{1}{4} \left| \frac{2\delta^2 + J^2}{\delta^2 + J^2} - \frac{4\delta^2}{\delta^2 + J^2} \sin^2 \frac{1}{2} \pi J t \sin^2 \left\{ \frac{1}{2} \pi (\delta^2 + J^2)^{1/2} t \right\} \right| \quad \dots\dots (1)$$

which for $J \ll \delta$ reduces to

$$\frac{1}{2} \left| 1 - \frac{1}{2} (1 - \cos \pi J t) (1 - \cos \pi \delta t) \right| \quad \dots\dots (1')$$

where t is the time at which the echo occurs. δ and J may be determined by varying t and obtaining a multiple exposure photograph. However the amplitude of the echo is attenuated both by incoherent dephasing causing decay of transverse magnetization T_2 and, more importantly in these experiments, by attenuation due

to self-diffusion of the nuclei in the inhomogeneity of the main field required to produce the echo. Hence Eqn (1) must be multiplied by $\exp(-t/T_2 - t^3/T_D^3)$ where $T_D^3 = 12/\Delta\gamma^2 G^2$ for a linear field gradient G gauss cm^{-1} at the sample and Δ is the self-diffusion constant of the liquid (Carr and Purcell 1952, 1954). In a typical liquid and experimental situation we might have $T_2 = 5$ seconds and $T_D = 0.1$ second. Since J values may be of order 5 c/s for protons this T_D value means that little more than half a period of the J variation can be observed and so the accuracy of the determination of J is necessarily poor. We are surprised at the accuracy quoted for instance by Crawford and Foster (1956).

It has been shown by Carr and Purcell (1952, 1954) that the effects of self-diffusion can be reduced by use of a $90^\circ, \tau, 180^\circ, 2\tau, 180^\circ, \dots$ pulse sequence. If the echo at time $t(=2n\tau)$ is the n th echo of a sequence T_D^3 is increased by the factor n^2 . Moreover the magnetization available for signal is doubled, which is helpful. The use of a $90^\circ, \tau, 180^\circ$ pulse sequence gives quite a different modulation from Eqn (1) as shown elsewhere (Powles 1959). It is

$$\left| \frac{\delta^2}{\delta^2 + J^2} \cos \pi J t + \frac{J}{(\delta^2 + J^2)^{1/2}} \sin \pi J t \sin \{ \pi (\delta^2 + J^2)^{1/2} t \} + \frac{J^2}{\delta^2 + J^2} \cos \pi J t \cos \{ \pi (\delta^2 + J^2)^{1/2} t \} \right| \quad \dots\dots (2)$$

and for $J \ll \delta$ this becomes

$$|\cos \pi J t|. \quad \dots\dots (2')$$

Eqn (2') can be given a simple physical interpretation (Powles 1959) and is formally the Fourier transform of the steady-state signal after the chemical shift has been removed.

The upper diagram in Fig. 1 (a) shows the steady-state absorption spectrum for a pair of spins $\frac{1}{2}$ with a chemical shift of δ c/s and an indirect interaction of J c/s for $J \ll \delta$. Below is shown what we call a collapsed spectrum in which the chemical shift has been removed. It is the Fourier transform of this spectrum which gives the echo amplitude modulation of Eqn (2'). The Bloch decay after a 90° pulse would be the Fourier transform of the upper spectrum. Other parts of the figure show complete and collapsed spectra for other cases discussed below. The collapsed spectrum approximation is only valid when $J \ll \delta$.

The expressions for the second and third echoes are more and increasingly complex. We find

$$\left| \frac{\delta^2}{\delta^2 + J^2} \cos \pi J t + \frac{\delta^2 J}{(\delta^2 + J^2)^{3/2}} 2 \sin \pi J t \sin \{ \frac{1}{2} \pi (\delta^2 + J^2)^{1/2} t \} + \frac{J^2}{\delta^2 + J^2} \times \cos \pi J t \cos \{ \pi (\delta^2 + J^2)^{1/2} t \} + \frac{J^3}{(\delta^2 + J^2)^{3/2}} \sin \pi J t \sin \{ \pi (\delta^2 + J^2)^{1/2} t \} \right| \dots\dots (3)$$

for the second echo at time $t(=4\tau)$ in a $90^\circ, \tau, 180^\circ, 2\tau, 180^\circ$ pulse sequence and

$$\left| \frac{\delta^4}{(\delta^2 + J^2)^2} \cos \pi J t + \frac{\delta^2 J}{(\delta^2 + J^2)^{3/2}} 3 \sin \pi J t \sin \{ \frac{1}{3} \pi (\delta^2 + J^2)^{1/2} t \} + \frac{\delta^2 J^2}{(\delta^2 + J^2)^2} \cos \pi J t [2 \cos \frac{2}{3} \pi (\delta^2 + J^2)^{1/2} t + \cos \{ \frac{1}{3} \pi (\delta^2 + J^2)^{1/2} t \} - 1] + \frac{J^3}{(\delta^2 + J^2)^{3/2}} \sin \pi J t \sin \{ \pi (\delta^2 + J^2)^{1/2} t \} + \frac{J^4}{(\delta^2 + J^2)^2} \cos \pi J t \cos \{ \pi (\delta^2 + J^2)^{1/2} t \} \right| \dots\dots (4)$$

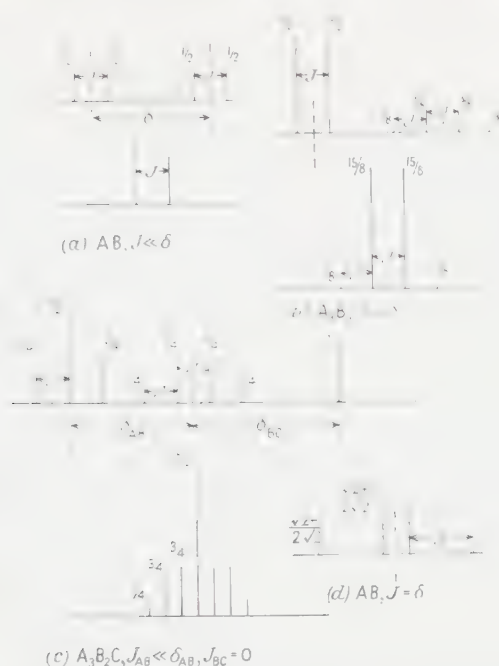


Fig. 1. The steady-state spectrum (above) and the 'collapsed' spectrum (below) for various nuclear groups which are discussed in the text.

for the third echo at time t . We see no simple way of obtaining the n th echo. The echo modulation disappears if $\delta = 0$ and/or $J = 0$ as expected (Gutowsky, McCall and Slichter 1953). For $J \ll \delta$ both (3) and (4) give $|\cos \pi J t|$ and so together with (2') we assume that when $J \ll \delta$ the n th echo at t is given by $|\cos \pi J t|$ independent of n .

We have not yet calculated the echo amplitude modulation in the general case for more complicated groups of nuclei but it is not difficult to show that for $J \ll \delta$ and $n \leq 10$ any echo at t in a $90^\circ, 180^\circ, 180^\circ, \dots$ pulse sequence is given by the Fourier transform of the 'collapsed' steady-state spectrum. For example, for methyl alcohol at temperatures sufficiently low that the hydroxyl proton exchange rate is slow (i.e. $\ll J$) the high resolution spectrum is as shown in the upper part of Fig. 1(b). The lower part of Fig. 1(b) shows the collapsed spectrum and the Fourier transform of this is

$$\frac{1}{16} |15 \cos \pi J t + \cos 3\pi J t|. \quad \dots (5)$$

This is expected to be a good approximation for methyl alcohol at 21.5 Mc/s where $J/\delta \simeq 0.1$.

Fig. 2 (Plate) shows a single exposure photograph of echoes in methyl alcohol at -71°C at 21.5 Mc/s. The pulses are not visible and the spacing between echoes is exactly 20 msec. The envelope was independent of pulse spacing, i.e. n , and is given by Eqn (5) (which is little different from $|\cos \pi J t|$) multiplied approximately by $\exp(-t/T_2')$ with $J = 4.95 \pm 0.05$ c/s and $T_2' = 0.5$ second. We emphasize that previous results in methyl alcohol (Hahn and Maxwell 1952) using the $90^\circ, \tau, 90^\circ$ sequence and multiple exposure suffered an attenuation constant T_2' of about 0.1 second. Hence modulation barely beyond the first minimum in Fig. 2 was observed and so the determination of J was rather poor. The advantage in getting the result in a single shot is also appreciable.

Ethyl alcohol is more complex. In this case we allow rapid exchange of the hydroxyl proton to annul modulation due to $J_{\text{CH}_2-\text{OH}}$. Since

$$J_{\text{CH}_3-\text{CH}_2}/\delta_{\text{CH}_3-\text{CH}_2}=0.12$$

we again have the simplified situation and it may be shown that the modulation to be expected (see Fig. 1 (c)) is

$$\frac{1}{12} |5 + 3 \cos \pi Jt + 3 \cos 2\pi Jt + \cos 3\pi Jt|. \quad \dots (6)$$

The experimental result at 25°C shown in Fig. 3 (Plate) fits this very well with $J=6.93 \pm 0.10$ c/s and $T_2' \approx 0.6$ second. The results for the 90°, τ , 90° and the 90°, τ , 180° single shot multiple exposure method only extend to about the first minimum in Fig. 3.

If J is comparable with δ the signals are much more difficult to interpret since the pattern is very sensitive to pulse spacing or n . Even so the study of the second and third echoes rather than the first already gives appreciable relief from the self-diffusion attenuation and also the modulation is more detailed than for the single echo (see Fig. 4). This may be ascribed physically to the greater 'mixing up' of the magnetization by the pulses.

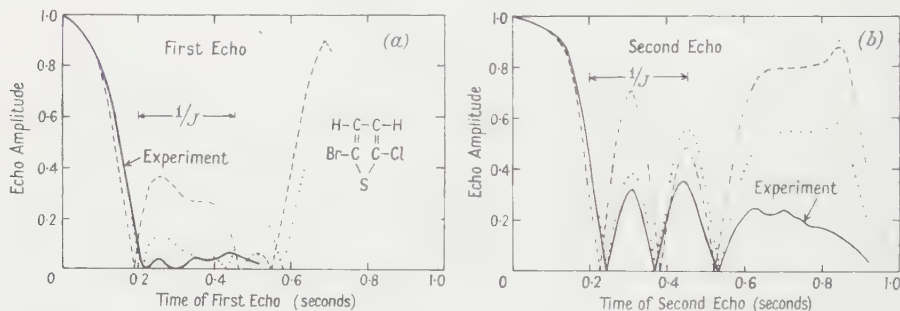


Fig. 4. Echo envelope modulation from multiple shot experiments in 2-bromo-5-chlorothiophene at 25°C; (a) for the first echo and (b) for the second echo in a 90°, τ , 180°, τ , echo₁, τ , 180°, τ , echo₂ sequence. The theoretical curves for $\delta=3.97$ c/s and $J=3.87$ c/s are shown broken. The dotted curve is for the same parameters but with 20% impurity protons. No attenuation has been applied to the theoretical curves.

Fig. 4 shows the echo amplitude modulation for the first and second echoes determined by single shot multiple exposure for 2-bromo-5-chlorothiophene at 25°C. The increase in detail and the decrease in attenuation with even the second echo is evident. This molecule has only two inequivalent protons and $J/\delta=0.98$ at 21.5 Mc/s. The theoretical curves for the pure material (Eqns (2) and (3)) apart from T_2 and T_D attenuation factors, for $\delta=3.97$ c/s and $J=3.87$ c/s are the broken curves in Fig. 4. The agreement between theory and experiment is greatly improved if we assume that the sample was impure and that 20% of the protons were not subject to J interaction. Eqns (2) and (3) are readily modified to allow for this and the revised theoretical curves are given in Fig. (4) by the dotted curves. We estimate the parameters of 2-bromo-5-chlorothiophene at 25°C to be $\delta=3.97 \pm 0.15$ c/s at 21.5 Mc/s and $J=3.87 \pm 0.10$ c/s. An excellent fit is obtained for the second echo upon adding an attenuation corresponding to $T_D=0.6$ second. The impurities are probably dibromo and dichloro compounds in which the protons are not chemically shifted and which are difficult to separate from the bromo chloro compound.

We also find agreement for the third echo. We have experimental results for up to 60 echoes but there seems to be no simple way of interpreting them in terms of J and δ .

We are at present investigating a variety of materials at various temperatures having various complexities of nuclear groupings and relative J and δ values in order to evaluate the method for the determination of J and δ . In principle it should be more accurate than the present steady-state experiment since the accuracy is determined mainly by the natural T_2 (e.g. 5 seconds or more) whereas the steady-state experiment is limited by an arbitrary magnetic field stability and/or homogeneity corresponding at present to an effective T_2 of about 0.3 second.

ACKNOWLEDGMENTS

The apparatus used has been described elsewhere (Luszczynski and Powles 1959). The sample of 2-bromo-5-chloro-thiophene was kindly prepared for us by Dr. M. A. Whitehead of our Chemistry Department according to a recipe generously provided by Professor H. S. Mosher of Stanford University. One of us (A. H.) was supported by a grant from the Department of Scientific and Industrial Research.

REFERENCES

- CARR, H. Y., and PURCELL, E. M., 1952, *Phys. Rev.*, **88**, 415.
— 1954, *Phys. Rev.* **94**, 630.
CRAWFORD, G. J. B., and FOSTER, J. S., 1956, *Canad. J. Phys.*, **34**, 653.
GUTOWSKY, H. S., MCCALL, D. W., and SLICHTER, C. P., 1953, *J. Chem. Phys.*, **21**, 279.
HAHN, E. L., 1950, *Phys. Rev.*, **80**, 580.
HAHN, E. L., and MAXWELL, D. E., 1951, *Phys. Rev.*, **84**, 1246.
— 1952, *Phys. Rev.* **88**, 1070.
LUSZCZYNSKI, K., and POWLES, J. G., 1959, *J. Sci. Instrum.*, **36**, 57.
MCNEIL, E. R., SLICHTER, C. P., and GUTOWSKY, H. S., 1951, *Phys. Rev.*, **84**, 1245.
POWLES, J. G., 1959, *Rep. Progr. Phys.*, **22**, 433 (London: Physical Society).
REILLY, C. A., 1956, *J. Chem. Phys.*, **25**, 604.

The S Wave Pion-Pion Interaction

BY G. R. ALLCOCK AND A. N. KAMAL

Department of Theoretical Physics, University of Liverpool

MS. received 8th April 1960, in revised form 18th May 1960

Abstract. The pion-pion interaction has been studied with an explicit appeal to the standard quantum field theory. Lowest order perturbation theory calculations indicate that the usual renormalization procedure may imply an indefinite quantization metric. An alternative procedure, using a regulator cut-off near the nucleon mass, is therefore adopted, and on this basis the following conclusions are drawn. The short range pion-pion interaction is found to be highly repulsive in states of isobaric spin $I=0$ and 2, giving a hard-core scattering. The short range repulsion vanishes in the states with $I=1$. The long range interaction is attractive in the even isobaric spin states but is very small.

An 'effective' pion-pion coupling constant is obtained in terms of a_0 and a_2 , the hard-core radii in states of isobaric spin $I=0$ and 2, and μ , the meson rest mass:

$$\lambda_{\text{eff}} \simeq \frac{16\pi}{5} a_0 \mu \simeq \frac{16\pi}{2} a_2 \mu.$$

§ 1. INTRODUCTION

IT is commonly believed nowadays that the pion-pion interaction plays an important role in pion-nucleon scattering processes. The experiments on the scattering of negative pions by protons show a pronounced peak in the π^- -p total cross section around 900 mev pion laboratory kinetic energy (Shapiro, Leavitt and Chen 1953, Cool, Madansky and Piccioni 1954, Cool, Piccioni and Clark 1956, Erwin and Kopp 1958, Burrowes *et al.* 1959, Crittendon *et al.* 1959). Dyson (1955) and Takeda (1955) have attempted to explain this peak on the basis of a resonant pion-pion interaction. Dyson (1955) suggests that the incident pion forms a resonant state, with a 'cloud-pion', with total isobaric spin $I=0$. Takeda (1955) assumes a resonant state between the two pions with total isobaric spin $I=1$, and shows that this too may lead to an understanding of the π^- -p scattering peak. Wong and Ross (1959) have shown recently, however, that a possible explanation of the 900 mev peak through a nucleon isobar cannot be ruled out.

Recent experiments on pion production at energies well below the 900 mev resonance also appear to indicate the presence of a strong pion-pion interaction. Perkins *et al.* (1959) have measured the $\pi^- + p \rightarrow \pi^+ + \pi^- + n$ cross section between 260 mev and 430 mev pion laboratory kinetic energy. The theoretical estimate for this cross section made by Rodberg (1957) on the basis of a pion-nucleon interaction alone compares very poorly with the experimental results. Perkins *et al.* (1959) and Rodberg (1959) have shown, however, that the experimental results can be fitted with the inclusion of a strong pion-pion interaction. The size of the cross section at low energies suggests an S-wave pion-pion interaction

and the rise in cross section with energy requires the inclusion also of P-wave interaction.

Chew† and Mandelstam (1959) have attacked the problem of the pion-pion interaction through the double dispersion relation. Chew expects the singularity due to the exchange of a pion pair to give the longest range interaction and expects the higher singularities to give a constant contribution. The short range interaction (the residual contributions from branch lines corresponding to the exchange of four pions, six pions, etc., and those due to other short range processes) is thus expected to be represented by one parameter only.

The treatment of the present paper also embodies these basic physical considerations but makes a more explicit appeal to standard quantum field theory for the determination of the magnitudes and the signs of the long and short range contributions. The approximation made in this work should remain valid up to about 2 GeV pion laboratory kinetic energy, though pion-pair production may necessitate some modifications above the threshold at approximately 1 GeV. The results obtained are quoted below.

(i) The short range interaction in states $I = 0$ and 2 is highly repulsive, giving hard-core scattering. This feature is not in disagreement with Rodberg's (1959) results on the low energy behaviour of S-waves. However, in order to obtain a quantitative fit it is necessary to assume a very large effective core radius (half a pion Compton wavelength) in the $I = 0$ state. This cannot be understood on the basis of the present approach.

(ii) The long range effects are primarily due to the exchange of pairs of virtual S-wave pions. Although the resultant long range interaction is attractive its contribution to the total scattering is negligibly small.

(iii) In view of these results, an S-wave resonance appears incompatible with standard meson theory.

(iv) The strong repulsion vanishes in states with total isobaric spin 1. The dynamics of such states are therefore likely to be much more complicated.

(v) An 'effective' 4-meson coupling constant λ_{40} has been obtained in terms of a_0 and a_2 , the hard-core radii in states of isobaric spin $I = 0$ and 2, and μ the meson rest mass:

$$\lambda_{40} \sim \frac{16\pi}{5} a_{00} \mu \sim \frac{16\pi}{2} a_{20} \mu.$$

§ 2. METHOD AND DISCUSSION

Before we set out to discuss the results obtained in this work it is necessary that we examine the pion nucleon Hamiltonian density. In the pseudoscalar neutral theory one writes

$$H_{\text{int}}(x) = ig\bar{\psi}\gamma_5\psi\phi - \delta m\bar{\psi}\psi - \frac{1}{2}\delta\mu^2\phi^2 + \frac{1}{4}\lambda\phi^4. \quad \dots\dots (1)$$

It is well known that in the pseudoscalar theory the square diagrams (Fig. 4) of the perturbation expansion give an infinite contribution. The usual mass and coupling constant renormalizations remove all other divergences. To remove the square diagram divergences Matthews (1950) introduced the term $\frac{1}{4}\lambda\phi^4$. The coefficient λ could in principle have an infinite part $\delta\lambda$ and a finite part λ_1 , i.e. $\lambda = \lambda_1 - \delta\lambda$. The part $\delta\lambda$ was to play the role of a counter term. The renormalization was to be effected by combining the contributions of the square diagrams with that of a 4-meson vertex at which λ operates. The divergent

† 1959 Kiev Conference Report, unpublished

contributions were then to be cancelled against the counter term $\delta\lambda$, leaving a finite remainder, and a finite coupling constant λ_1 to be determined by experiments. Salam (1951) and Ward (1952) showed that this cancellation could be effected in all orders of perturbation theory, $\delta\lambda$ being formally defined as a power series in g_1 and λ_1 . The term by term renormalizability of the field theory derived from the interaction Hamiltonian (1) was thus demonstrated, for any values of the renormalized constants g_1 and λ_1 .

During recent years, however, it has become apparent that the considerations outlined above are not sufficient to guarantee a perturbation expansion whose individual terms conform to the requirement of unitarity. There is at least one further condition to be imposed; namely that the Hamiltonian should be so constructed that the imposition of a positive quantization metric results in an energy spectrum bounded from below. The renormalized relativistic perturbation expansion for the fields does lead automatically to an energy spectrum of this type, but implies at the same time a quantization metric which is positive definite if, and only if, the Hamiltonian conforms to the condition just set out.

We shall now examine the Hamiltonian of the present theory, and shall find that it has the desirable property enunciated above, provided λ is non-negative. We begin by remarking that all nucleon factors in the Hamiltonian are limited in magnitude by the anti-canonical quantization rules.[†] Accordingly, the presence or absence of a lower bound to the Hamiltonian hinges upon the form of the meson factors therein. Now one can always find states in which the meson field ϕ at a given time exhibits a spectrum of arbitrarily large eigenvalues, while that shown by its conjugate momentum density $\partial\phi/\partial t$ remains within prescribed limits. (A specific example of such a state is given in the Appendix, where the present arguments are set out with greater rigour.) Since the Hamiltonian is a functional of ϕ , $\partial\phi/\partial t$ and various nucleon factors, its behaviour with respect to these states is dominated by the term containing the highest power of ϕ , i.e. by the term $\frac{1}{4}\lambda\phi^4$ in the neutral theory, $\frac{1}{4}\lambda(\phi_1\phi_1)^2$ in the charge independent theory. As the fourth power of a self-adjoint operator is positive when the quantization metric is positive, this evidently implies that the energy spectrum will extend to infinity in the direction given by the sign of λ . Thus we must choose

$$\lambda \equiv (\lambda_1 - \delta\lambda) \geq 0. \quad \dots\dots (2)$$

The most immediate consequence of Eqn (2) is that it forbids one to choose arbitrarily the magnitude of the renormalized coupling constant λ_1 . Rather, λ_1 has to be chosen greater than $\delta\lambda$, where $\delta\lambda$ is by definition adjusted to cancel out the divergent contributions coming from the various square diagrams, etc. We have evaluated $\delta\lambda$ to the fourth order in g (§ 3), and have found, in this order,

$$\delta\lambda = 24\pi^2 g^4 \ln\left(\frac{m^2 + \Lambda_0^2}{m^2}\right) + O(\mu^2/m^2), \quad \dots\dots (3)$$

where Λ_0 is a regulator mass and m the nucleon mass. Thus in fourth order $\delta\lambda$ is positive, and, in the usual renormalization theory, infinite. Hence, in view of inequality (2), the cancellation of divergences by the usual renormalization method

[†] Strictly speaking, these limits are infinite. However, we believe that it is sensible to argue as though they were finite, because they do become finite if the theory is modified by enclosing the fields in a large box, and cutting out the short wavelength components (cf. Caianiello 1956).

can only be accomplished at the expense of introducing indefinite metric terms in fourth order. Accordingly, we now argue that these square diagram divergences ought not to be cancelled by the formal renormalization method. It seems that we should regard them as representing an essential physical feature of the theory. The following developments are based entirely on this attitude.

We are now in a position to discuss the meson-meson interaction itself. The square diagrams represent a meson meson interaction whose divergent part corresponds to a local interaction characterized by a coupling constant $\delta\lambda$. We put forward the apparently reasonable conjecture that this local interaction, like the original local interaction $\frac{1}{4}\lambda\phi^4$, will be repulsive, i.e.

$$\delta\lambda \geq 0. \quad \dots\dots(4)$$

This conjecture is certainly supported by Eqn (3), but no adequate proof is available at present.[†] Accepting Eqn (4), we see that the square diagrams produce a short range interaction with a repulsive divergent part, which must not be renormalized away. It is shown in §4 that the repulsion is likely to be exceedingly strong, even for the regulator mass usually contemplated. In the charge-independent theory the divergent part operates in states of total isobaric spin 0 and 2 and in these states the resultant repulsion is expected to outweigh the more complicated velocity-dependent effects which are contributed by the convergent terms from the square diagrams.[‡] This rules out the possibility of an $I=0$ resonant state. The $I=1$ state contribution is convergent but is essentially velocity dependent. It is not studied in the present paper.

It seems reasonable to assume that the short range repulsion will produce relativistic hard-sphere scattering, so that the energy dependence of the S-phase shift in states of (even) isobaric spin I will be given by

$$\delta_I = -ka_I\mu/a_0. \quad \dots\dots(5)$$

Here μ is the meson mass, k and ω the barycentric momentum and energy, and a_I the hard-sphere radius. A closer examination of the meson-meson vertex function indicates that $a_0 \sim 5a_2/2$. In fact the S-wave scattering appears primarily as the Born term of a single 4-meson vertex at which an effective coupling constant λ_{eff} operates, giving λ_{eff} in terms of the meson rest mass and the ranges of interaction as

$$\lambda_{\text{eff}} \simeq \frac{16\pi}{5} a_0 \mu \simeq \frac{16\pi}{2} a_2 \mu. \quad \dots\dots(6)$$

In order to get a better understanding of the problem a solvable case has been obtained by treating the neutral theory in the fixed source approximation (§§6 and 7). In this approximation Fig. 1(a) is replaced by Fig. 1(b), representing the emission of two neutral mesons by a fixed, highly repulsive source. In the spirit of the same approximation Fig. 2(a), representing the scattering of two neutral mesons through exchange of a neutral pion pair, can be approximated by Fig. 2(b) in which the neutral pion pair is exchanged between two fixed, highly repulsive sources. The long range effects from Figs 1(b) and 2(b) can be solved to a high degree of accuracy provided the repulsion is sufficiently strong, and the core radius not too large. They do indeed reduce to the Born terms of an effective coupling. The effective coupling constant, which includes all radiative

[†] The methods used by Moffat (1959, 1960) might perhaps be applied to resolve this matter.

[‡] The reader is referred to an earlier work on meson-meson interaction by Mitra and Saxena (1957).

corrections at the vertices, appears moreover as a function of the range r_0 of the repulsion, and the meson mass μ . These findings tend to confirm the assumptions which we make in treating the relativistic problem.

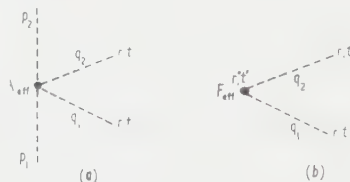


Fig. 1. Virtual emission of S wave pions, (a) by a pion, (b) by a fixed source.

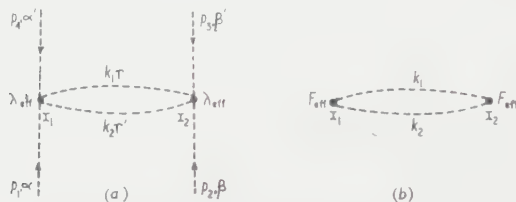


Fig. 2. Virtual exchange of two S-wave pions, (a) between two pions, (b) between two fixed sources.

Returning to the relativistic charge independent theory, it is found that the long range interaction in states of isobaric spin 0 and 2 is attractive, the attraction being somewhat larger in the $I=0$ state. For large separations and slow mesons the interaction potential, apart from an isobaric factor of magnitude 5/3 or 1 respectively, is

$$V^{(2)}(r) \sim - \frac{36\mu}{25\pi^{1/2}} \frac{a_0^2 \exp(-2\mu r)}{r^2(\mu r)^{1/2}},$$

where the radius a_0 is defined by Eqn (6).

A phase shift analysis, § 8, shows that the major contribution to the phase shift is made by the 'hard core'. The phase shift due to the long range attractive part of the interaction is very small indeed, and becomes even less significant at higher energies. This conclusion is not modified by consideration of the relativistic long range term, Fig. 2(a).

Diagrams of the type shown in Fig. 3, representing two successive hard-sphere scatterings, have also been considered. It was found that the contribution from the second-order graph, Fig. 3, with the usually contemplated cut-offs, was negligibly small compared with that of the first-order graph, representing a single hard-sphere scattering.



Fig. 3. Re-scattering correction.

§ 3. THE LOWEST ORDER SQUARE DIAGRAM

The fourth-order effect we are interested in is shown in Fig. 4. Three more graphs are obtained by reversing the internal nucleon lines. For reasons of symmetry all the external meson lines have been directed inwards.

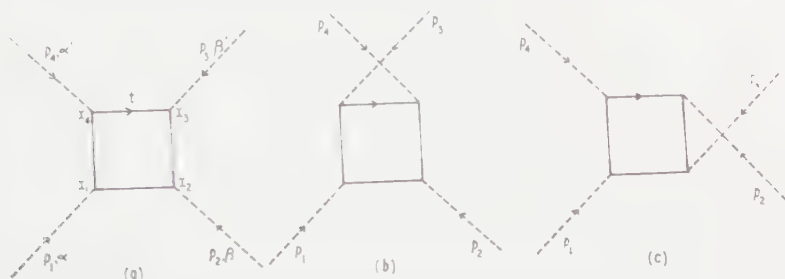


Fig. 4. Three basic square diagrams. Three more diagrams may be obtained by reversing the nucleon lines.

In the pseudoscalar neutral meson theory, the 'square box' contribution, in the momentum space, is written as (Fig. 4(a))

$$F(p_1, p_4, p_3, p_2) = -g^4 \int d^4t \frac{\text{Tr}_t(t \cdot m)(t - p_4 \cdot m)(t + p_2 + p_3 \cdot m)(-t - p_1 - p_2 - p_3 + m)}{(t^2 - m^2)\{(t + p_3)^2 - m^2\}\{(t + p_2 + p_3)^2 - m^2\}\{(t + p_1 + p_2 + p_3)^2 - m^2\}} \quad \dots\dots (7)$$

where $\mathbf{p} = \gamma_{\mu} p_{\mu}$ and $A B = A^{\mu} B_{\mu} = \mathbf{A} \cdot \mathbf{B}$. The integral over t is logarithmically divergent. Following Dyson (1950) the divergent part of the integral is defined by setting all the external 4-momenta equal to zero. Thus

$$F(p_1, p_2, p_3, p_4) = F(0, 0, 0, 0) + F_c(p_1, p_2, p_3, p_4).$$

The last term on the right is a convergent integral over t . It will be seen later that for very slow mesons F_c is small enough to be neglected. From Eqn (7), setting all the momenta equal to zero, and working out the trace, one obtains

$$F(0, 0, 0, 0) = -4g^4 \int d^4t \frac{1}{(t^2 - m^2)^2}. \quad \dots\dots (8)$$

The divergent integral in Eqn (8) has been evaluated with various cut-off techniques. The results are given below.

(i) Feynman cut-off (Feynman 1950).

$$F(0, 0, 0, 0) = -4\pi^2 g^4 \left[\frac{m^2}{\Lambda^2} \ln \frac{m^2 + \Lambda^2}{m^2} + \ln \frac{m^2 + \Lambda^2}{m^2} - 1 \right], \quad \dots\dots (9)$$

where Λ is a cut-off mass.

(ii) Regulator technique (Gupta 1953).

$$F(0, 0, 0, 0) = -4\pi^2 g^4 \ln \frac{m^2 + \Lambda_0^2}{m^2}, \quad \dots\dots (10)$$

where Λ_0 is a regulator mass.

(iii) Direct non-covariant integration.

$$F(0, 0, 0, 0) = -8\pi^2 g^4 \left[\ln \frac{T + T_0}{m} - \frac{T}{T_0} \right], \quad \dots\dots (11)$$

where T is the cut-off 3-momentum and

$$T_0 = (T^2 + m^2)^{1/2}.$$

Alternatively, the divergent part of the integral in Eqn (7) may be defined by setting the external momenta each equal to their free particle values p_i^0 (Salam 1951). Thus

$$F(p_1, p_2, p_3, p_4) = F(p_1^0, p_2^0, p_3^0, p_4^0) + F_c'(p_1, p_2, p_3, p_4).$$

One obtains, from Eqn (7), on using the following set of 4-momenta,

$$\begin{aligned} p_1^0 &= (\mu, 0, 0, 0) = p_2^0, \\ p_3^0 &= (-\mu, 0, 0, 0) = p_4^0, \end{aligned} \quad \dots\dots (12)$$

$$F(p_1^0, p_2^0, p_3^0, p_4^0) = -\pi^2 i g^4 \left[4 \ln \left(\frac{m^2 + \Lambda_0^2}{m^2} \right) + \frac{236}{15} \frac{\mu^2}{m^2} - \frac{61}{5} \frac{\mu^2}{m^2 + \Lambda_0^2} + O \left(\frac{\mu^4}{m^4} \right) \right] \quad \dots\dots (13)$$

where Λ_0 is a regulator mass.

A comparison with Eqn (10) shows that $F(0, 0, 0, 0)$ differs from $F(p_1^0, p_2^0, p_3^0, p_4^0)$ only in terms of the order μ^2/m^2 and higher. This feature is common to all square diagrams.

Eqns (9), (10) and (11) agree in indicating a positive $\delta\lambda$. The implications of this result for the renormalization programme have already been discussed.

§ 4. THE PION-PION INTERACTION AT SHORT DISTANCES

The square diagrams represent a very short range interaction, the nature of which is examined in this section.

4.1. The Pseudoscalar Neutral Theory

The term in the meson-meson scattering matrix arising from the processes shown in Fig. 4, and the three similar processes obtained by reversing the nucleon lines in Fig. 4, is

$$\langle f | S^{(4)} | i \rangle \sim - \frac{6\pi^2 i g^4}{(\omega_1 \omega_2 \omega_3 \omega_4)^{1/2}} \delta^{(4)}(p_1 + p_2 + p_3 + p_4) \ln \left(\frac{m^2 + \Lambda_0^2}{m^2} \right). \quad \dots\dots (14)$$

On the other hand, a pure potential scattering, by a potential

$$\begin{aligned} V(\mathbf{r}_1 - \mathbf{r}_2) &= 0, \quad |\mathbf{r}_1 - \mathbf{r}_2| > R, \\ &= V_0, \quad |\mathbf{r}_1 - \mathbf{r}_2| < R, \end{aligned}$$

would produce for the same matrix element, in Born approximation,

$$-i(2\pi)^4 \delta^{(4)}(p_1 + p_2 + p_3 + p_4) \frac{8\pi R^3}{3} V_0. \quad \dots\dots (15)$$

Comparing (14) and (15) we see that if we choose $R = m^{-1}$, and $\Lambda_0 = m$, we get (with $g^2/4\pi \sim 14$),

$$V_0 \simeq 5 \times 10^3 m.$$

This indicates a large repulsion.

4.2. Charge Independent Theory

In the charge independent theory the fourth-order term in the meson-meson scattering matrix arising from Fig. 4(a) differs from the expression given in Eqn (7) by the inclusion of an extra factor depending on the isobaric spin indices $\alpha, \beta, \beta', \alpha'$ of the mesons 1, 2, 3 and 4 respectively. This factor is

$$\begin{aligned} D_{\alpha\alpha', \beta\beta'} &= \text{Tr}(\tau_\alpha \tau_{\alpha'} \tau_{\beta'} \tau_\beta) \\ &= 2(\delta_{\alpha\alpha'} \delta_{\beta\beta'} - \delta_{\alpha\beta'} \delta_{\alpha'\beta} + \delta_{\alpha\beta} \delta_{\alpha'\beta'}). \end{aligned} \quad \dots\dots (16)$$

Accordingly, the scattering amplitude obtained from the six square diagrams is now

$$\langle f | S^{(4)} | i \rangle = \frac{1}{2^{(\omega_1 + \omega_2 + \omega_3 + \omega_4)/2}} \delta^{(4)}(p_1 + p_2 + p_3 + p_4) R_{\alpha, \alpha', \beta, \beta'}^{p_1, p_2, p_3, p_4}, \quad \dots (17)$$

with

$$\begin{aligned} R_{\alpha, \alpha', \beta, \beta'}^{p_1, p_2, p_3, p_4} = & D_{\alpha\alpha', \beta'\beta} F(p_1, p_4, p_3, p_2) \\ & + D_{\alpha\beta', \alpha'\beta} F(p_1, p_3, p_4, p_2) \\ & + D_{\alpha\alpha', \beta\beta'} F(p_1, p_4, p_2, p_3). \quad \dots (18) \end{aligned}$$

The isobaric spin dependence of the scattering matrix can conveniently be expressed in terms of the following operators (Mitra and Saxena 1957),

$$\left. \begin{aligned} M_{\alpha\alpha', \beta\beta'} &= \delta_{\alpha\alpha'} \delta_{\beta\beta'}, \\ N_{\alpha\beta, \alpha'\beta'} &= \delta_{\alpha\alpha'} \delta_{\beta\beta'} - \delta_{\alpha\beta'} \delta_{\alpha'\beta}, \\ Q_{\alpha\alpha', \beta\beta'} &= \delta_{\alpha\alpha'} \delta_{\beta\beta'} - \delta_{\alpha\beta'} \delta_{\alpha'\beta}. \end{aligned} \right\}, \quad \dots (19)$$

M and Q are symmetric in exchange of α and β and α' and β' while N is skew-symmetric. Mesons being Bose particles, M and Q are non-zero in states with total isobaric spin 0 or 2 and even angular momentum, while N is non-zero in states with total isobaric spin 1 and odd angular momentum.

The eigenvalues of these operators are given below; the subscripts indicate the total isobaric spin.

$$\left. \begin{aligned} M_0 &= 3; & M_1 &= M_2 = 0, \\ N_1 &= 2; & N_0 &= N_2 = 0, \\ Q_0 &= Q_2 = 2; & Q_1 &= 0. \end{aligned} \right\} \quad \dots (20)$$

Using the relations

$$\begin{aligned} D_{\alpha\alpha', \beta'\beta} &= 2(M_{\alpha\beta, \alpha'\beta'} + N_{\alpha\beta, \alpha'\beta'}), \\ D_{\alpha\beta', \alpha'\beta} &= 2(M_{\alpha\beta, \alpha'\beta'} - N_{\alpha\beta, \alpha'\beta'}), \\ D_{\alpha\alpha', \beta\beta'} &= 2(Q_{\alpha\beta, \alpha'\beta'} - M_{\alpha\beta, \alpha'\beta'}), \end{aligned}$$

and the notations

$$\begin{aligned} F_1 &= F(p_1, p_4, p_3, p_2), \\ F_2 &= F(p_1, p_3, p_4, p_2), \\ F_3 &= F(p_1, p_4, p_2, p_3), \end{aligned}$$

one obtains for (18) (dropping the isobaric spin indices),

$$\begin{aligned} R &= 2(M + N)F_1 + 2(M - N)F_2 + 2(Q - M)F_3 \\ &= 2M(F_1 + F_2 - F_3) + 2N(F_1 - F_2) + 2QF_3. \quad \dots (21) \end{aligned}$$

F_2 and F_3 differ from F_1 only in terms of the order p^2/m^2 . F_1 is given by Eqn (13).

We have

$$\left. \begin{aligned} R_{I=0} &= -40\pi^2 i g^4 \left\{ \ln \left(\frac{m^2 + \Lambda_0^2}{m^2} \right) + O(p^2/m^2) \right\} \\ R_{I=1} &= g^4 O(p^2/m^2), \\ R_{I=2} &= -16\pi^2 i g^4 \left\{ \ln \left(\frac{m^2 + \Lambda_0^2}{m^2} \right) + O(p^2/m^2) \right\}. \end{aligned} \right\} \quad \dots (22)$$

Eqns (22) indicate a strong repulsion both in the states $I=0$ and 2.

It will be seen that the divergent part of (21) is energy independent, and that it contains the isobaric factor

$$\delta_{\alpha\alpha'} \delta_{\beta'\beta} + \delta_{\alpha\beta} \delta_{\alpha'\beta'} + \delta_{\alpha\beta'} \delta_{\alpha'\beta}.$$

Both these features are exhibited by the Born term of an effective coupling $\frac{1}{4}\lambda_{\text{eff}}(\phi_i\phi_i)^2$, moreover, it can be shown in a general manner that the same isobaric and energy dependences appear with the leading contribution from all the higher order square diagrams. Accordingly the main contribution of all these diagrams, in states of even isobaric spin, may be summed up through a single parameter λ_{eff} , which may be related to the radius of the repulsive region by Eqn (6). On the other hand, the interaction in states of odd isobaric spin is non-divergent (since the above isobaric spin factor vanishes in these states) but it is essentially energy dependent. This feature is also common to all the higher order square diagrams.

§ 5. THE LONG RANGE PION-PION INTERACTION

The exchange of a single pion being forbidden, the longest range pion-pion interaction takes place through exchange of a pion pair. In the following we shall use an effective 4-meson coupling constant λ_{eff} , which is assumed to include all short range radiative corrections, as explained in §§ 2 and 4.

5.1. Neutral Theory

The process shown in Fig. 2(a), and a similar process in which lines p_3 and p_4 are interchanged, give the following contribution to the scattering matrix, $\langle f|S^{(2)}|i\rangle =$

$$\frac{-18\lambda_{\text{eff}}^2}{(16\omega_1\omega_2\omega_3\omega_4)^{1/2}} \int d^4x_1 d^4x_2 \Delta_F^2(x_1 - x_2) [\exp\{-i(p_1 + p_4)x_1 - i(p_2 + p_3)x_2\} \\ + \exp\{-i(p_1 + p_3)x_1 - i(p_2 + p_4)x_2\}], \quad \dots\dots (23)$$

with

$$\Delta_F(x) = \frac{i}{(2\pi)^4} \int \frac{\exp(-ipx)}{p^2 - \mu^2} d^4p. \quad \dots\dots (24)$$

At low energies, the above matrix element can be produced by a potential $V^{(2)}(r)$, which is obtained in terms of the Hankel function of the first kind K_1 .

$$V^{(2)}(r) = -\frac{9\lambda_{\text{eff}}^2\mu}{32\pi^3} \frac{K_1(2\mu r)}{\mu^2 r^2}. \quad \dots\dots (25)$$

This potential is attractive and behaves asymptotically as

$$V^{(2)}(r) \sim -\frac{9\lambda_{\text{eff}}^2\mu}{64\pi^{5/2}} \frac{\exp(-2\mu r)}{(\mu r)^{5/2}} \left(1 + \frac{3}{16\mu r} + \dots\right).$$

At short distances the repulsion takes over, and the interaction in the neutral theory is therefore represented by a short range repulsion with an attractive long range tail.

5.2. Charge Independent Theory

In the charge independent theory the strongest long range interaction should arise from the exchange of S-wave pions. According to the preceding arguments, § 2, the emission of these pions may be properly described through the Born term of the interaction $\frac{1}{4}\lambda_{\text{eff}}(\phi_i\phi_i)^2$. Thus the vertex factors of the neutral theory must now be augmented by the following isobaric spin operators, Fig. 2(a),

$$\frac{1}{3}(\delta_{\alpha\alpha'}\delta_{\gamma'\gamma} + \delta_{\alpha\gamma'}\delta_{\alpha'\gamma} + \delta_{\alpha\gamma}\delta_{\alpha'\gamma'}) \text{ at } x_1, \\ \frac{1}{3}(\delta_{\gamma'\gamma}\delta_{\beta\beta'} + \delta_{\gamma'\beta}\delta_{\gamma\beta'} + \delta_{\gamma\beta}\delta_{\gamma'\beta'}) \text{ at } x_2.$$

The neutral theory contribution from Fig. 2(a) will thus appear multiplied by a factor,

$$C_{\alpha\beta, \alpha'\beta'} = \frac{1}{9}(\delta_{\alpha\alpha'}\delta_{\gamma'\gamma} + \delta_{\alpha\gamma'}\delta_{\alpha'\gamma} + \delta_{\alpha\gamma}\delta_{\alpha'\gamma'}) (\delta_{\gamma'\gamma'}\delta_{\beta\beta'} + \delta_{\gamma'\beta}\delta_{\gamma\beta'} + \delta_{\gamma'\beta'}\delta_{\gamma\beta}) \\ = \frac{1}{9}(2M + \frac{9}{2}Q + \frac{5}{2}N)_{\alpha\beta, \alpha'\beta'}.$$

The diagram with p_3 and p_4 interchanged gives the factor $C_{\alpha\beta, \beta'\alpha'}$. Using (20) for the eigenvalues of the isobaric spin operators, the contribution to the scattering matrix from the two second-order graphs (Fig. 2(a)) is summarized as follows:

$$\begin{aligned} \langle f|S^{(2)}|i\rangle &= J_1 + J_2 \text{ in the neutral theory,} \\ &= \frac{5}{3}(J_1 + J_2) \text{ in the } I=0 \text{ state,} \\ &= \frac{5}{9}(J_1 - J_2) \text{ in the } I=1 \text{ state,} \\ &= J_1 + J_2 \text{ in the } I=2 \text{ state,} \end{aligned}$$

where J_1 and J_2 are the parts of the matrix element (23) arising from the first and second exponential factors respectively. We see that the potentials in the states with isobaric spin 0 and 2 are given by multiplying the expression (25) by 5/3 and 1 respectively. The effect on the scattering is discussed in § 8 and found to be very small. It must be stressed, however, that the long range force produced by the virtual P-wave mesons is not included in the above analysis. While it is difficult to estimate this effect, it seems rather probable that it will not be important in states of total isobaric spin 0 and 2.

§ 6. AN 'EFFECTIVE' COUPLING CONSTANT FOR PION-PION INTERACTION

In the following the one parameter approximation to the short range pion-pion interaction is investigated in more detail, within the context of a solvable problem with a fixed source, which produces pion pairs. The Hamiltonian density for the system is given by Eqn (26). Assuming a large positive interaction constant F at the source one can obtain the propagator for the two mesons at r and r' , Fig. 1(b). The same problem is also treated through the perturbation theory and a comparison of the two results indicates that the perturbation theory yields essentially the same result as the exact theory, provided a suitable effective coupling constant is used.

We take the Hamiltonian density

$$H(x) = \frac{1}{2}[\pi^2 + \nabla(\phi)^2 + \mu^2\phi^2 + F(\mathbf{r})\phi^2], \quad \dots\dots(26)$$

with $F(\mathbf{r})$ zero for $r > r_0$, and very large and positive for $r < r_0$. The fields π and ϕ satisfy the usual commutation relations

$$[\phi(t, \mathbf{r}), \pi(t, \mathbf{r}')] = i\delta^{(3)}(\mathbf{r} - \mathbf{r}').$$

The field equation is

$$\ddot{\phi} - \nabla^2\phi + \mu^2\phi + F(\mathbf{r})\phi = 0. \quad \dots\dots(27)$$

The solution of this equation can be written down in terms of spherical harmonics as follows

$$\left. \begin{aligned} \phi(t, \mathbf{r}) &= \sum_{l,m} \frac{1}{r} \phi_{l,m}(t, r) Y_{l,m}(\theta, \varphi), \\ \pi(t, \mathbf{r}) &= \sum_{l,m} \frac{1}{r} \pi_{l,m}(t, r) Y_{l,m}^*(\theta, \varphi) \end{aligned} \right\} \quad \dots\dots(28)$$

where the $Y_{l,m}(\theta, \varphi)$ satisfy the usual orthogonality condition

$$\int d(\cos \theta) d\varphi Y_{l'm'}^*(\theta, \varphi) Y_{l,m}(\theta, \varphi) = \delta_{ll'} \delta_{mm'}.$$

In spherical polar coordinates Eqn (27) becomes

$$\ddot{\phi}_{l,m} - \frac{\partial^2}{\partial r^2} \phi_{l,m} + \frac{l(l+1)}{r^2} \phi_{l,m} + \mu^2 \phi_{l,m} + F(r) \phi_{l,m} = 0. \quad \dots\dots (29)$$

We will solve Eqn (29) for S-waves only.

Put

$$\phi_{00}(t, r) = \psi(t, r),$$

then Eqn (29) assumes the form

$$\ddot{\psi} - \frac{\partial^2}{\partial r^2} \psi + \mu^2 \psi + F(r) \psi = 0. \quad \dots\dots (30)$$

The solutions of Eqn (30) are conveniently chosen in the form

$$\exp(i\omega t) \psi_\omega(r),$$

where the radial factor $\psi_\omega(r)$ obeys the equation

$$\frac{\partial^2}{\partial r^2} \psi_\omega(r) + (q^2 - F(r)) \psi_\omega(r) = 0, \quad \dots\dots (31)$$

with

$$q^2 = (\omega^2 - \mu^2).$$

Provided $\omega^2 \ll F$ the solution for Eqn (31) is

$$\left. \begin{aligned} \psi_\omega(r) &= \sin q(r - r_0), & r > r_0, \\ &= 0, & r < r_0. \end{aligned} \right\} \quad \dots\dots (32)$$

The propagator for two mesons at space-time points (t, \mathbf{r}) and (t', \mathbf{r}') satisfies the equation

$$\begin{aligned} \left(\frac{\partial^2}{\partial t^2} - \frac{\partial^2}{\partial r^2} + \mu^2 + F \right) \langle 0 | T \psi(t, r) \psi(t', r') | 0 \rangle \\ = -i \delta(t - t') \delta(r - r'), \quad r, r' > 0. \quad \dots\dots (33) \end{aligned}$$

It obeys Feynman boundary conditions in the time variables, and vanishes when either r or r' , or both, are zero. Evidently the propagator can be constructed from the solutions (32).

In the absence of interaction Eqn (33) is easily solved by using a representation of the delta function satisfying the same boundary conditions as the propagator. One such representation is

$$\delta(r - r') = \frac{2}{\pi} \int_0^\infty \sin qr \sin qr' dq, \quad \dots\dots (34)$$

and the corresponding solution is (the S-wave propagator of Eqn (33) being denoted by \mathbb{K})

$$\mathbb{K}_{\text{free}}(t, r; t', r') = \frac{i}{\pi^2} \int_0^\infty dq \int_{-\infty}^\infty d\omega \exp\{i\omega(t - t')\} \frac{\sin qr \sin qr'}{\omega^2 - q^2 - \mu^2}.$$

To obtain the solution in the presence of interaction we merely replace the free waves $\sin qr$ by the perturbed waves $\sin q(r - r_0)$ and obtain

$$\mathbb{K}_{\text{perturbed}}(t, r; t', r') = \frac{i}{\pi^2} \int_0^\infty dq \int_{-\infty}^\infty d\omega \exp\{i\omega(t - t')\} \frac{\sin q(r - r_0) \sin q(r' - r_0)}{\omega^2 - q^2 - \mu^2}.$$

The difference, having done the ω integration and setting $t = t'$, is

$$\begin{aligned}\Delta \mathbf{K} &\equiv \mathbf{K}_{\text{perturbed}} - \mathbf{K}_{\text{free}} \\ &= -\frac{1}{\pi} \int_0^\infty \frac{dq}{\omega_q} \left[\frac{1}{2} \sin 2qr_0 \sin q(r+r') - \sin^2 qr_0 \cos q(r+r') \right], \dots\dots (35)\end{aligned}$$

with $\omega_q^2 = (q^2 + \mu^2)$.

The asymptotic behaviour for large r may be obtained most simply by performing the q integration with the approximation $\sin qr_0 \simeq qr_0 + O(r_0^3)$ giving

$$\Delta \mathbf{K} = -\frac{\mu r_0}{\pi} K_1(2\mu r) + O(r_0^2) \dots\dots (36)$$

where r has been put equal to r' , i.e. the two mesons are created at the same space-time point. Eqn (36) expresses the change in the propagator at large distances in the strong coupling limit.

The same problem can be treated in the perturbation theory, using an effective coupling F_{eff} different from F . Referring to Fig. 2(b) the lowest perturbation term in the difference in the propagators \mathbf{K} is,

$$\Delta \mathbf{K} = -i4\pi r r' \int F_{\text{eff}}(\mathbf{r}'') \Delta_F(t-t'', \mathbf{r}-\mathbf{r}'') \Delta_F(t'-t'', \mathbf{r}'-\mathbf{r}'') dt'' d^3\mathbf{r}''.$$

Going over to the momentum space and performing the elementary integrations, we obtain, setting $\mathbf{r} = \mathbf{r}'$, $t = t'$,

$$\begin{aligned}\Delta \mathbf{K} &= \frac{2}{\pi^2} F_0 \frac{r_0^3}{3} \int_0^\infty \frac{\sin q_1 r \sin q_2 r}{q_1^2 - q_2^2} \left(\frac{1}{\omega_1} - \frac{1}{\omega_2} \right) q_1 q_2 dq_1 dq_2 \\ &= -\frac{F_0}{3\pi} r_0^3 \mu K_1(2\mu r) + \text{higher order terms in } r_0, \dots\dots (37)\end{aligned}$$

where F_0 is defined by

$$\begin{aligned}F_{\text{eff}}(r) &= F_0, & r < r_0, \\ &= 0, & r > r_0.\end{aligned}$$

Comparing (37) and (36) we see that the lowest perturbation term gives essentially the same spatial structure as the exact theory (they differ in higher orders of r_0). Equating the first terms in (37) and (36) we obtain

$$F_0 = 3\mu r_0^2. \dots\dots (38)$$

Eqn (38) expresses the effective coupling constant in terms of the radius r_0 . In the fixed source approximation, therefore, the sum of all the 4-meson vertex parts may be replaced by a single 2-meson vertex at which the coupling constant F_{eff} operates. We will use this coupling constant in perturbation theory to get the long range pion-pion interaction in the fixed source approximation.

§ 7. THE LONG RANGE PION-PION INTERACTION IN THE FIXED SOURCE APPROXIMATION

We will evaluate the long range potential due to a pion pair exchange in the fixed source approximation. On comparing this potential with the one obtained in § 5, for very slow mesons, one obtains a relation between λ_{eff} , μ and r_0 .

Fig. 2(b) contributes a term in the scattering matrix

$$S^{(2)} = \frac{1}{2(2\pi)^8} \int_{-\infty}^{\infty} \frac{F_{\text{eff}}(\mathbf{r}_1) F_{\text{eff}}(\mathbf{r}_2) \exp \{i(k_1 - k_2)(x_2 - x_1)\}}{(k_1^2 - \mu^2)(k_2^2 - \mu^2)} d^4 k_1 d^4 k_2 d^4 x_1 d^4 x_2.$$

The corresponding potential is

$$V^{(2)}(r) = -\frac{r_0^2}{r^2} \frac{1}{(2\pi)^2} \int_{-\infty}^{\infty} \frac{\sin k_1 r \sin k_2 r}{k_2^2 - k_1^2} \left(\frac{1}{\omega_{k_1}} - \frac{1}{\omega_{k_2}} \right) k_1 k_2 dk_1 dk_2$$

with $r = |\mathbf{r}_2 - \mathbf{r}_1|$ and $\omega_k^2 = k^2 + \mu^2$.

Integrating over k_1 and k_2 we obtain

$$V^{(2)}(r) = -\frac{r_0^2}{2\pi r^2} \mu K_1(2\mu r). \quad \dots\dots (39)$$

$V^{(2)}$ behaves asymptotically as

$$V^{(2)}(r) \sim -\frac{r_0^2}{4r^2} \left(\frac{\mu}{\pi r} \right)^{1/2} \exp(-2\mu r) \left(1 + \frac{3}{16\mu r} + \dots \right).$$

It will be seen that the potential (25) obtained from the relativistic neutral theory depends on the separation r in the same way as the potential (39) above. To compare them in absolute magnitude we eliminate λ_{eff} from (25), in favour of r_0 . The formula appropriate to this step, in the relativistic neutral theory, is

$$\lambda_{\text{eff}} = 16\pi r_0 \mu / 3. \quad \dots\dots (40)$$

When (40) is substituted in (25), there results a potential sixteen times larger than the fixed source potential (39), the radii r_0 in the two cases being understood to be equal. This discrepancy seems at first sight rather alarming; nevertheless it does not indicate a wrong numerical factor in the preceding calculations! It arises because the fixed source model fails to take into account two essential features of the full problem. Firstly, the two virtual mesons concerned in the full problem are Bose particles of the same type as the two real mesons. The corresponding exchange effects are felt in the formula (40) relating the coupling constant and the core radius. They can be eliminated by supposing the two virtual mesons to be quanta of a field different from that describing the real mesons. When this is done, the long range attractive force, expressed in terms of r_0 , falls to one quarter of its former value. The remaining factor of one quarter stems from the fact that recoil is not taken into account in the fixed source model. To investigate this effect, one must take the virtual and real mesons as quanta of different fields. Then, as in other force problems in field theory, the long range potential appears as the same function of the coupling constant whether the sources are held fixed or allowed to recoil. But the interaction Hamiltonians which describe these two cases can readily be shown to produce S-wave phase shifts appropriate to core radii in the ratio 2:1. Thus, if the core radius is held fixed, the coupling constant is halved when the sources are fixed, and the long range force is consequently diminished by a further factor of one quarter. We conclude that the fixed source model should not be taken very literally, though it does serve to demonstrate that an infinite short range repulsion can be accurately represented for many purposes by a weak positive local coupling.

§ 8. PHASE SHIFT ANALYSIS

The S-wave phase shifts for the attractive two-meson exchange potential (Eqn 25) have been evaluated in the Born approximation, allowing of course for the influence of the repulsive core. The Table gives the S-wave phase shifts for different values of r_0 and the barycentric momentum of one pion.

Core radius	Barycentric momentum (μ)	δ_0^{core} (deg)	$\delta_0^{\text{attractive}}$ (deg)
m^{-1}	0.5	- 4.24	+ 0.77
m^{-1}	1.0	- 8.48	+ 1.37
$2m^{-1}$	0.5	- 8.48	+ 1.97
$2m^{-1}$	1.0	- 16.96	+ 3.61

It will be seen from the Table that the attractive two-meson exchange potential contributes only a very small fraction of the total phase shift. At larger energies the contribution becomes even less significant.

ACKNOWLEDGMENTS

One of us (A. N. K.) is grateful to the Pakistan Atomic Energy Commission and the Colombo Plan Authorities for financial support.

APPENDIX

In this Appendix the inequality (2), namely $\lambda \geq 0$, is derived with full mathematical argument. The method used is an adaptation of one employed by Baym (1960) to demonstrate the non-unitary nature of the well-known cubic self-coupled scalar meson theory.†

Assuming throughout a positive quantization metric, we take a real space function $a(\mathbf{x})$, and define a unitary operator U by the equation

$$U = \exp -i \int d^3\mathbf{x} a(\mathbf{x}) \partial\phi(\mathbf{x})/\partial t. \quad \dots\dots (A1)$$

(It is understood that the operators in this equation, and in the following ones, refer to some fixed, but otherwise arbitrary, time.) The operator U excites $\phi(\mathbf{x})$ by an amount $a(\mathbf{x})$, leaving unaltered all the other variables which appear in the full Hamiltonian \mathcal{H} . We have

$$\begin{aligned} U^{-1}\phi(\mathbf{x})U &= \phi(\mathbf{x}) + a(\mathbf{x}), \\ U^{-1}\partial\phi(\mathbf{x})/\partial t U &= \partial\phi(\mathbf{x})/\partial t, \text{ etc.} \end{aligned} \quad \dots\dots (A2)$$

Let expectation values in the lowest eigenstate of \mathcal{H} be denoted by angular brackets. The positive metric implies that

$$\langle U^{-1}\mathcal{H}U \rangle - \langle \mathcal{H} \rangle \geq 0. \quad \dots\dots (A3)$$

We evaluate (A3) with the help of (A2). The terms linear in $a(\mathbf{x})$ cancel out in view of the stationary character of the energy expectation in the vicinity of an eigenstate. The remaining terms give,

$$\begin{aligned} \lambda \int d^3\mathbf{x} \{ \frac{1}{4}a^4(\mathbf{x}) + \langle \phi(\mathbf{x}) \rangle a^3(\mathbf{x}) + \frac{3}{2} \langle \phi^2(\mathbf{x}) \rangle a^2(\mathbf{x}) \} \\ \geq -\frac{1}{2} \int d^3\mathbf{x} \{ (\nabla a(\mathbf{x}))^2 + (\mu^2 - \delta\mu^2)a^2(\mathbf{x}) \}. \end{aligned} \quad \dots\dots (A4)$$

This inequality is valid for any function $a(\mathbf{x})$ such that the various integrals exist. If we take any such function, $f(\mathbf{x})$ say, and now set $a(\mathbf{x}) = cf(\mathbf{x})$, with c some constant, then (A4) obviously gives $\lambda \geq 0$ in the limit $c \rightarrow \infty$. The above proof can evidently be extended without difficulty to the charge independent theory.

† We wish to thank one of the referees of this paper for drawing our attention to Baym's work.

REFERENCES

- BAYM, G., 1960, *Phys. Rev.*, **117**, 886.
BURROWES, H. C., CALDWELL, D. O., FRISCH, D. H., HILL, D. A., RITSON, D. M., and SCHLUTER, R. A., 1959, *Phys. Rev. Letters*, **2**, 119.
CAIANIELLO, E. R., 1956, *Nuovo Cim.*, **3**, 223.
COOL, R., MADANSKY, L., and PICCIONI, O., 1954, *Phys. Rev.*, **93**, 637.
COOL, R., PICCIONI, O., and CLARK, D., 1956, *Phys. Rev.*, **103**, 1082.
CRITTENDON, R. R., SCANDRETT, J. H., SHEPHARD, W. D., WALTER, W. D., and BALLAM, J., 1959, *Phys. Rev. Letters*, **2**, 120.
DYSON, F. J., 1950, *Phys. Rev.*, **75**, 1636.
— 1955, *Phys. Rev.*, **99**, 1037.
ERWIN, A. R., (Jr), and KOPP, J. K., 1958, *Phys. Rev.*, **109**, 1364.
FEYNMAN, R. P., 1950, *Phys. Rev.*, **76**, 769.
GUPTA, S. N., 1953, *Proc. Phys. Soc. A*, **66**, 129.
MANDELSTAM, S., 1959, *Phys. Rev.*, **115**, 1741.
MATTHEWS, P. T., 1950, *Phil. Mag.*, **41**, 185.
MITRA, A. N., and SAXENA, R. P., 1957, *Phys. Rev.*, **108**, 1083.
MOFFAT, J. W., 1959, *Nucl. Phys.*, **13**, 150.
— 1960, *Nucl. Phys.*, **14**, 682.
PERKINS, W. A., CARIS, J. C., KENNY, R. W., KNAPP, E. A., and PEREZ-MENDEZ, V., 1959, *Phys. Rev. Letters*, **3**, 56.
RODBERG, L. S., 1957, *Phys. Rev.*, **106**, 1090.
— 1959, *Phys. Rev. Letters*, **3**, 58.
SALAM, A., 1951, *Phys. Rev.*, **82**, 217.
SHAPIRO, A. M., LEAVITT, S. P., and CHEN, F. F., 1953, *Phys. Rev.*, **92**, 1073.
TAKEDA, G., 1955, *Phys. Rev.*, **100**, 440.
WARD, J. C., 1952, *Phys. Rev.*, **84**, 897.
WONG, W. N., and ROSS, M., 1959, *Phys. Rev. Letters*, **3**, 398.

The Photoproduction Reaction $^{60}\text{Ni}(\gamma, \pi^-)^{60}\text{Cu}$

By P. V. MARCH AND T. G. WALKER

Natural Philosophy Department, University of Glasgow

MS. received 15th June 1960

Abstract. The cross section for the reaction $^{60}\text{Ni}(\gamma, \pi^-)^{60}\text{Cu}$ has been measured using bremsstrahlung having maximum energies from 120 meV to 320 meV. Radio-chemical separation techniques were used to separate the ^{60}Cu from the other activities produced by the irradiation. A comparison with previous results for the reaction $^{11}\text{B}(\gamma, \pi^-)^{11}\text{C}$ indicates that the reaction is due predominantly to surface production.

§ 1. INTRODUCTION

IN a previous communication (Hughes and March 1958) measurements were reported of the cross section for the reaction $^{11}\text{B}(\gamma, \pi^-)^{11}\text{C}$. This reaction is of interest since it represents the photoproduction of a π -meson from a complex nucleus resulting in the nucleus remaining in a bound state; it is thus more amenable to theoretical treatment (Laing and Moorhouse 1957) than meson production accompanied by the emission of nucleons. The present measurements were made to study this reaction in other elements and to look for evidence of any activity below the threshold energy for meson production similar to that noted in the previous work.

Photomeson production in complex nuclei resulting in the nucleus remaining in a bound state can be either $^Z_Z\text{X}(\gamma, \pi^-)^{Z-1}_{Z-1}\text{Y}$, $^Z_Z\text{X}(\gamma, \pi^+)^{Z-1}_{Z-1}\text{Y}$ or $^Z_Z\text{X}(\gamma, \pi^0)^Z_Z\text{Y}$. If the residual nuclei are β -emitters the cross sections of the reactions can be found by measuring the β -activity. The (γ, π^-) type of reaction can be studied much more readily than the (γ, π^+) reaction because the residual nucleus in the former is a positron emitter and advantage can be taken of the annihilation quanta to use coincidence counting and so eliminate much of the background counting rate. Another advantage of studying the (γ, π^-) reaction is that the residual nucleus can only be produced by the reaction $^Z_Z\text{X}(p, n)^{Z-1}_{Z-1}\text{Y}$ and it is possible to detect and remove the proton contamination of a bremsstrahlung beam, whereas, the residual nucleus of the (γ, π^+) reaction can be produced by the reaction $^Z_Z\text{X}(n, p)^{Z-1}_{Z-1}\text{Y}$ and neutron contamination of bremsstrahlung beams is much more difficult to detect and reduce. The π^0 production reaction cannot be studied by activation techniques. Thus the present work was confined to the investigation of the reaction $^Z_Z\text{X}(\gamma, \pi^-)^{Z-1}_{Z-1}\text{Y}$.

An inspection of the periodic table and consideration of the cross sections involved ($5 \cdot 10^{-6}$ of the total cross section for π^- production) show that for a (γ, π^-) reaction in elements heavier than boron it is necessary to use radio-chemical separation techniques in order to eliminate the photospallation products which would have positron activities of similar half-life to the (γ, π^-) activity. Practical considerations restrict the activities suitable for investigation to those with half-lives in the range 10 minutes to 10 hours.

The most promising elements are ^{45}Sc , ^{60}Ni and ^{63}Cu . The high cost of ^{45}Sc in the quantities required reduced the choice to ^{60}Ni and ^{63}Cu . In this paper the results are reported for the reaction $^{60}\text{Ni}(\gamma, \pi^-)^{60}\text{Cu}$.

Other reactions of interest that may be studied using the same technique are those of the type $^Z_A\text{X}(\gamma, \pi^-)^{Z+1}_{A-1}\text{X}$ where cross sections of a similar magnitude to those for (γ, π^-) may be expected. Thus it may be possible to study the reactions $^{48}\text{Ti}(\gamma, \pi^-)^{47}\text{V}$ and $^{52}\text{Cr}(\gamma, \pi^-)^{51}\text{Mn}$ which result in positron emitters with half-lives of 34 minutes and 44 minutes respectively.

§ 2. EXPERIMENTAL PROCEDURE

The nickel samples were irradiated in the uncollimated beam of the Glasgow 330 MeV synchrotron. Each sample consisted of 12 g of nickel powder packed uniformly into a Perspex box of dimensions 1 in. \times 1 in. \times $\frac{1}{4}$ in. and was irradiated between two pieces of polythene (CH_2) each 1 in. \times 1 in. \times $\frac{1}{16}$ in. The reaction $^{12}\text{C}(\gamma, n)^{11}\text{C}$ occurring in the polythene was used to monitor the beam and to measure the absorption occurring in the nickel sample. This was done by counting the 20.5 min positron activity of the ^{11}C (Barber, George and Reagan 1955). During the irradiations a continuous record was made of the beam intensity. The samples were irradiated for 60 minutes in a flux of approximately 10^{10} equivalent quanta per minute.

Measurement of the positron activities induced in a nickel sample showed that a mixture of half-lives was present and that the counting rate was about 200 times greater than that expected for the reaction $^{60}\text{Ni}(\gamma, \pi^-)^{60}\text{Cu}$. This demonstrated the necessity for chemical separation if the ^{60}Cu activity was to be detected.

The nickel powder used was Mond Nickel Powder, grade A, the impurities being: oxygen 0.1%, carbon 0.05–0.1%, iron <0.01% and sulphur <0.001%. A comparison with the previous work on boron yields an estimate of 10^{-3} for the ratio of the ^{60}Cu activity induced per gramme of nickel powder to the ^{11}C activity induced per gramme of carbon for samples exposed simultaneously to bremsstrahlung having a maximum energy of 320 MeV. Thus the carbon impurity of the nickel powder must be eliminated in the chemical separation of the copper. The effect of the other impurities is negligible.

After exposure the nickel powder was dissolved in aqua regia and a known amount of copper carrier was added together with hold-back carriers for cobalt, iron, manganese, chromium, vanadium, titanium, scandium, potassium and carbon. The solution was filtered to remove traces of undissolved nickel and the copper was then precipitated as the sulphide using hydrogen sulphide. After filtering the precipitate was washed, folded up in the filter paper and placed in a copper box of dimensions 1 in. \times 1 in. \times $\frac{1}{4}$ in. with walls thick enough to absorb 3 MeV positrons. This box was placed between two 1.5 in. \times 2 in. sodium iodide scintillators mounted on E.M.I. photomultipliers and the 0.51 MeV photons resulting from the annihilation of the positrons were counted in coincidence. The pulses from one photomultiplier were used to gate those from the other and the coincident pulses were fed to a single-channel pulse analyser so that only pulses corresponding to the photoelectric peak of the annihilation quanta were counted.

In general counting began on the separated copper activity about 28 minutes after the end of the irradiation and continued for an hour.

The stability of the counting system was checked periodically during the runs by counting a standard ^{22}Na source and throughout the runs the clipping levels were monitored by displaying the coincidence output on a 100-channel kicksorter.

After the counting, the filter paper containing the copper sulphide was burnt and the precipitate weighed to determine the efficiency of the chemical separation. The weight of the precipitate was usually about 150 mg and the efficiency about 95%. Dummy runs in which the copper carrier was omitted showed that no other carrier was precipitated by the chemical processing.

For each irradiation the positron activities of the separated copper and of the polythene irradiated simultaneously were measured. After making allowance for the efficiency of the chemical separation of the copper, the ratio of the positron activity of copper produced per gramme of the nickel sample to the positron activity per gramme of carbon in the polythene monitor was determined. The measurements were made with bremsstrahlung having maximum energies between 120 mev and 320 mev.

§ 3. RESULTS

The most abundant isotope of nickel is ^{58}Ni (67.9%) but a (γ, π^-) reaction in this isotope results predominantly in the formation of the 3-sec isomer of ^{58}Cu . The (γ, π^-) reaction which was observed occurred in ^{60}Ni (26.2%), the positron emission detected being the decay of ^{60}Cu which has a half-life of 24 minutes (Ajzenberg Selove and Lauritsen 1959). A small contribution to the activity observed will have been made by the other isotopes ^{62}Ni (3.7%), ^{61}Ni (1.2%) and ^{64}Ni (1%), the product nuclei ^{62}Cu , ^{61}Cu and ^{64}Cu having half-lives of 10.1 minutes, 3.5 hours and 12.8 hours respectively (Ajzenberg-Selove and Lauritsen 1959). The contribution of these isotopes to the activity observed was estimated by assuming that the cross section per atom was the same as that for the reaction $^{60}\text{Ni}(\gamma, \pi^-)^{60}\text{Cu}$; the contribution was estimated to be 10% in a typical irradiation and is mainly due to the 10.1-minute and 3.3-hour activities. Contributions from reactions of the type $(\gamma, \pi^- n)$ and $(\gamma, \pi^- 2n)$ are expected to be small.

The difference in the half-lives of ^{60}Cu and ^{11}C was taken into account in calculating the ratio of the production rates of the ^{60}Cu and the ^{11}C activities, allowance also being made for any beam fluctuations occurring during the irradiations.

The only major modification of the value observed for the ratio of the ^{60}Cu activity to the ^{11}C activity is due to the different efficiencies for counting the two activities. This difference arises because the positron decay of ^{11}C goes directly to the ground state of ^{11}B whereas the positron decay of ^{60}Cu goes to excited states of ^{60}Ni which subsequently decay by γ -ray emission to the ground state. These γ -rays are in coincidence with the quanta resulting from the annihilation of the positrons and increase the efficiency for detecting the ^{60}Cu activity. This increase of efficiency was determined experimentally to be 40%.

The ratio of the production rate of ^{60}Cu per atom of ^{60}Ni to that of ^{11}C per atom of ^{12}C is shown in Fig. 1 as a function of the maximum energy of the bremsstrahlung. It is very small at energies below the threshold for meson production and rises at higher energies to a value five times greater at 320 mev.

In view of the very low cross section for the (γ, π^-) reaction compared with spallation processes it is necessary to confirm that the activity observed is in fact due to ^{60}Cu . The first check is that of the half-life of the activity observed.

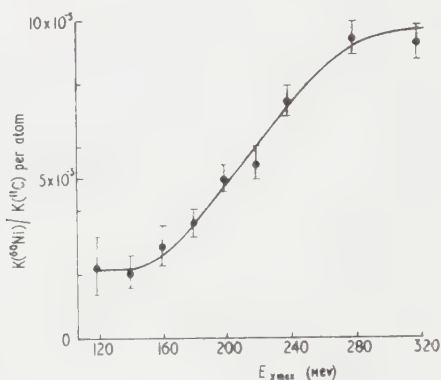


Fig. 1. The ratio of the production rate of ^{60}Cu per atom of ^{60}Ni to that of ^{11}C per atom of ^{12}C as a function of $E_{\gamma \text{ max}}$, the maximum energy of the bremsstrahlung.

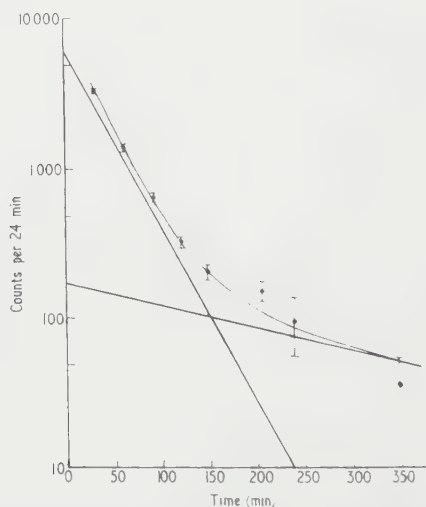


Fig. 2. The decay curve of the copper activity produced by bremsstrahlung having a maximum energy of 320 MeV. The curve superimposed on the experimental points is the sum of the 24-min and 3.3-h components shown.

The decay curve of the copper activity produced by bremsstrahlung having a maximum energy of 320 MeV is shown in Fig. 2. The contribution of the 10.1 min activity produced by the reaction $^{62}\text{Ni}(\gamma, \pi^-)^{62}\text{Cu}$ is estimated to be about 7.5% of the counting rate at 34 min, 2% at 62 min and negligible for subsequent observations.

The remaining activity is consistent with a 95% component of half-life 24 min and a 5% component of half-life 3.3 hours. The 3.3-h activity is presumably due to the reaction $^{61}\text{Ni}(\gamma, \pi^-)^{61}\text{Cu}$ and possibly also to $^{62}\text{Ni}(\gamma, \pi^-)^{61}\text{Cu}$.

A conclusive identification of the ^{60}Cu activity can be made by measuring the γ -ray spectrum following the positron emission. Its two major components both involve positron emission followed by two γ -rays in coincidence, the energy of both γ -rays being greater than that of the annihilation quanta (0.51 mev). In none of the spallation products of similar half-life does this occur. Thus a comparison of the number of pulses in the photoelectric peak due to annihilation quanta with the number of pulses having a greater pulse height will yield different results for positron emission, (a) without subsequent γ -ray emission, (b) with a single coincident high energy γ -ray and (c) with two coincident high energy γ -rays. The latter possibility can only occur in the present experiment if the activity is due to ^{60}Cu . The experimental values obtained for the number of pulses in the photoelectric peak of the annihilation quanta and the number of pulses of greater pulse height for ^{11}C , ^{22}Na and the separated copper activity are given in Table 1 for irradiations with bremsstrahlung having a maximum energy of 320 mev.

Table 1

Isotope	Number of pulses		Ratio of numbers
	Photoel. peak	> Peak	> Peak/Peak
^{11}C	2178 ± 47	17 ± 9	0.0078 ± 0.0042
^{22}Na	2277 ± 48	481 ± 23	0.211 ± 0.012
^{60}Cu	1276 ± 40	506 ± 30	0.396 ± 0.026

The ^{22}Na positron emission is followed by a single γ -ray of energy 1.28 mev. A direct comparison can be made between the ^{22}Na and ^{60}Cu results because the efficiencies of detection of the high energy γ -rays are similar and therefore, assuming that the γ -rays are emitted in random directions, the ratio found for ^{60}Cu should be approximately twice that for ^{22}Na . The results show conclusively that the positron activity of the separated copper is followed by two high energy γ -rays in coincidence, thus confirming the activity as due to ^{60}Cu . These results on the spectra of pulses observed for the different activities also gave a direct measurement of the relative efficiencies for the detection of the ^{11}C and ^{60}Cu activities.

The counting rates obtained with bremsstrahlung of maximum energy 140 mev and 120 mev were too low to obtain significant determinations of the half-life or pulse height spectrum of the activity produced at these energies. The activity observed below the threshold energy for meson production must have a half-life very similar to that of ^{60}Cu , otherwise its presence would have been observed in the decay curve at 320 mev. It may be due to the 20.5-min activity of ^{11}C produced by the reaction $^{12}\text{C}(\gamma, n)^{11}\text{C}$ in the carbon impurity of the nickel sample, the chemical processing having perhaps failed to eliminate all the carbon present originally. On the other hand, this activity may represent an effect similar to that noted in the previous work with ^{11}B where an unexplained activity of half-life identical with that produced in the (γ, π^-) reaction was detected at energies below 140 mev. The ^{11}B work showed that second-order reactions such as (γ, p) followed by (p, n) were not responsible for this activity.

The cross section for the reaction $^{60}\text{Ni}(\gamma, \pi^-)^{60}\text{Cu}$ was obtained from the ratio of production rates by using the results of Barber, George and Reagan (1955) for the cross section of the reaction $^{12}\text{C}(\gamma, n)^{11}\text{C}$ and assuming a bremsstrahlung spectrum for a tungsten target of 0.020 in. effective thickness. The value of the cross section averaged over the photon energy range 140 to 320 MeV was found to be $3.6 \pm 0.1 \times 10^{-29} \text{ cm}^2$. Table 2 shows the cross section as a function of photon energy together with the results obtained previously for $^{11}\text{B}(\gamma, \pi^-)^{11}\text{C}$ multiplied by a factor $A^{2/3}$.

Table 2

Photon energy	140-170	170-200	200-230	230-260	260-290	290-320
Cross section for $^{60}\text{Ni}(\gamma, \pi^-)^{60}\text{Cu}$	2.2 ± 0.5	4.2 ± 0.6	6.1 ± 0.6	5.9 ± 0.7	2.6 ± 0.9	0.2 ± 1.2
$A^{2/3}$ extrapolation of ^{11}B results	8.6	9.3	9.6	9.6	8.6	5.9
Units: 10^{-29} cm^2						

The ^{11}B results were in good agreement with the theoretical predictions of Laing and Moorhouse (1957) for meson production at the nuclear surface only. An $A^{2/3}$ variation would be expected for surface production and a variation proportional to A would be expected for volume production for which the predicted value for ^{11}B is approximately six times larger than that observed. The experimental values for ^{60}Ni are smaller than the $A^{2/3}$ extrapolation of those for ^{11}B , strongly suggesting that surface production rather than volume production is responsible for this type of reaction. The $A^{2/3}$ variation is only expected to hold for the average effect of many elements, any particular element may depart from the general trend because of details of its own particular structure. Thus the lack of precise agreement with the $A^{2/3}$ extrapolation is not unexpected, indeed it should be pointed out that in ^{11}B the odd unpaired neutron might be expected to cause enhancement of the surface photoproduction of π^- -mesons. Such an enhancement has been reported previously by Littauer and Walker (1952) and Luckey (1953).

ACKNOWLEDGMENTS

The authors wish to thank Professor P. I. Dee for his encouragement and Dr. W. McFarlane and the synchrotron crew for their valuable cooperation during the irradiations. One of us (T.G.W.) wishes to thank the Department of Scientific and Industrial Research for the award of a maintenance grant.

REFERENCES

- AJZENBERG-SELOVE, F., and LAURITSEN, T., 1959, *Nucl. Phys.*, **11**, 1.
 BARBER, W. C., GEORGE, W. D., and REAGAN, D. D., 1955, *Phys. Rev.*, **98**, 73.
 HUGHES, I. S., and MARCH, P. V., 1958, *Proc. Phys. Soc.*, **72**, 259.
 LAING, E. W., and MOORHOUSE, R. G., 1957, *Proc. Phys. Soc. A*, **70**, 629.
 LITTAUER, R. M., and WALKER, D., 1952, *Phys. Rev.*, **86**, 838.
 LUCKEY, P. D., 1953, *Phys. Rev.*, **90**, 711.

The Quasi-particle Approximation in Superconductivity

By P. G. HARPER

Division of Electrotechnology, National Standards Laboratory, Commonwealth Scientific and Industrial Research Organization, Sydney, Australia

Communicated by H. Fröhlich; MS. received 8th June 1960

Abstract. A derivation of the Bardeen, Cooper and Schrieffer and the Bogoliubov secular equations by a common method shows that it is necessary to neglect a large number (proportional to V^n) of small matrix elements (proportional to V^{-n}) where V is the volume of the system and n an arbitrary positive integer. A generalization of the Bogoliubov fermion transformation which diagonalizes these terms takes the form of an infinite series whose convergence may depend on the form of the interaction.

§ 1. INTRODUCTION

IN the Bardeen, Cooper and Schrieffer (1957) theory of superconductivity a total Hamiltonian is considered in which the lattice coordinates are eliminated and a resulting interaction between electrons introduced, additional to the Coulomb interaction. This interaction, denoted by H_1 , written in terms of electron annihilation and creation operators, has the general two-body interaction form

$$H_1 = \sum_{\mathbf{k} \mathbf{k}' \mathbf{l} \mathbf{l}' s s'} V_{\mathbf{k}' \mathbf{k} \mathbf{l} \mathbf{l}'} a_{\mathbf{k}' s}^\dagger a_{\mathbf{k} s}^\dagger a_{\mathbf{l}' s'} a_{\mathbf{l} s'} \quad \dots\dots (1)$$

where momentum is conserved, $\mathbf{k}' + \mathbf{k}'' = \mathbf{l}' + \mathbf{l}''$ and s denotes the spin state. $V_{\mathbf{k}' \mathbf{k} \mathbf{l} \mathbf{l}'}$ is given by

$$V_{\mathbf{k}' \mathbf{k} \mathbf{l} \mathbf{l}'} = \frac{\hbar \omega_{\mathbf{w}} |M_{\mathbf{w}}|^2}{(\epsilon_{\mathbf{k}} - \epsilon_{\mathbf{k}'})^2 - (\hbar \omega_{\mathbf{w}})^2}, \quad \mathbf{w} = \mathbf{k} - \mathbf{k}'$$

which is attractive in the region $(\epsilon_{\mathbf{k}'} - \epsilon_{\mathbf{k}})^2 < (\hbar \omega_{\mathbf{w}})^2$. Here $\epsilon_{\mathbf{k}} = \hbar^2 k^2 / 2m$, $\omega_{\mathbf{w}}$ is the frequency of a phonon momentum \mathbf{w} and $M_{\mathbf{w}} / V^{1/2}$ denotes the matrix element for the electron-lattice interaction.

Bardeen, Cooper and Schrieffer (to be referred to as BCS) now remark that the greatest number of matrix elements of H_1 having the same sign will be obtained from states having pairs of electrons $\mathbf{k}'', \mathbf{l}''$ both occupied (or unoccupied); for the ground state it is natural to choose $\mathbf{k}'' + \mathbf{l}'' = 0$. For further coherence the total spin of a pair is taken to be zero. The Hamiltonian is effectively reduced to

$$H_{\text{red}} = H_0 - \sum_{\mathbf{k} \mathbf{k}'} V_{\mathbf{k}' \mathbf{k}} a_{\mathbf{k}'}^\dagger a_{\mathbf{k}}^\dagger a_{-\mathbf{k}'} a_{-\mathbf{k}} \quad \dots\dots (2)$$

where the interaction has been further limited to the attractive region so that $V_{\mathbf{k}' \mathbf{k}} > 0$. The operators $a_{\mathbf{k}}$ and $a_{\mathbf{k}}^\dagger$ refer to states of opposite spin. H_0 denotes the Hamiltonian for the free electrons. In this case though the reduced interaction is proportional to V , the perturbing matrix elements to all orders are independent of V and therefore, in the limit $V \rightarrow \infty$, become vanishingly small. One may not, however, conclude that in this limit the eigenstates of H_0 become exact, and indeed, it is the spirit of the BCS method to obtain by means of suitably

coherent wave functions a non-vanishing energy from a large number (proportional to V) of small (independent of V) matrix elements. This cannot be accomplished by any finite order perturbation.

§ 2. BCS AND BOGOLIUBOV SECULAR EQUATIONS

In order to discuss the matrix elements and re-derive the secular equations, it proves convenient to define adjacent eigenstates of H_{red} by the requirement that they are connected solely by $a_{\mathbf{k}+}$, $a_{-\mathbf{k}-}^\dagger$, i.e. that $\langle 0|a_{\mathbf{k}+}|1\rangle$, $\langle 0|a_{-\mathbf{k}-}^\dagger|1\rangle$ are both finite. This follows from the work of Valatin (1958) and the fermion transformation of Bogoliubov (1958). Adopting the notation of the latter, the above matrix elements are denoted by u_k , $-v_k$ respectively.

From (2)

$$[a_{\mathbf{k}+}, H] = \epsilon_k a_{\mathbf{k}+} - \sum_{\mathbf{k}'} V_{\mathbf{k}\mathbf{k}'} a_{-\mathbf{k}'} a_{\mathbf{k}'+}^\dagger \dots \dots \dots (3)$$

where, following Bogoliubov, ϵ_k may now be taken to be measured relative to the chemical potential introduced into H_{red} . In the H_{red} eigenstate representation, (3) taken between states $|0\rangle$ and $|1\rangle$ gives,

$$(W - \epsilon_k)u_k = \left(\sum_{\mathbf{k}'} V_{\mathbf{k}\mathbf{k}'} u_{\mathbf{k}'} v_{\mathbf{k}'} \right) v_k \dots \dots \dots (4)$$

where W denotes the excitation energy, i.e. $W = \langle 1|H_{\text{red}}|1\rangle - \langle 0|H_{\text{red}}|0\rangle$. Similarly

$$[a_{-\mathbf{k}-}^\dagger, H] = -\epsilon_k a_{-\mathbf{k}-}^\dagger - \sum_{\mathbf{k}'} V_{\mathbf{k}\mathbf{k}'} a_{\mathbf{k}'+}^\dagger a_{-\mathbf{k}'-}^\dagger a_{\mathbf{k}+} \dots \dots \dots (5)$$

which gives

$$(W + \epsilon_k)v_k = \left(\sum_{\mathbf{k}'} V_{\mathbf{k}\mathbf{k}'} u_{\mathbf{k}'} v_{\mathbf{k}'} \right) u_k \dots \dots \dots (6)$$

It follows immediately from (4) and (6) that

$$W = W_k = \pm (\epsilon_k^2 + C_k^2)^{1/2}, \quad \frac{1}{2} \sum_{\mathbf{k}'} V_{\mathbf{k}\mathbf{k}'} \frac{C_{\mathbf{k}'}}{(\epsilon_{\mathbf{k}'}^2 + C_{\mathbf{k}'}^2)^{1/2}} = C_k$$

which gives the quasi-particle energy W_k in terms of the BCS integral equation. Since W_k may take both signs it follows that there are two types of excited state which may be labelled by \mathbf{k} . Using the notation of Kuper (1959), the complete Bogoliubov transformation may be presented as

$$\begin{aligned} \langle 0|a_{\mathbf{k}+}|\mathbf{k}+\rangle &= u_k; & \langle 0|a_{\mathbf{k}+}^\dagger|-\mathbf{k}-\rangle &= v_k \\ \langle 0|a_{-\mathbf{k}-}^\dagger|\mathbf{k}+\rangle &= -v_k; & \langle 0|a_{-\mathbf{k}-}^\dagger|-\mathbf{k}-\rangle &= u_k \end{aligned} \dots \dots \dots (7)$$

where $|\mathbf{k}+\rangle$, $|\mathbf{k}-\rangle$ denote the two possible excited states.

Though BCS suppose $V_{\mathbf{k}\mathbf{k}'}$ to describe an attractive two-body force acting only near the Fermi surface, the derivation leaves it arbitrary and might, for example, be applied to a space-dependent force $V_{\mathbf{k}\mathbf{k}'} = V_{\mathbf{k}-\mathbf{k}'}$.

The Fröhlich electron-lattice Hamiltonian may be treated in similar fashion. Thus in Fröhlich's notation (1952)

$$[a_{\mathbf{k}+}, H_F] = \epsilon_k a_{\mathbf{k}+} + \sum_{\mathbf{w}} D_w (b_{\mathbf{w}}^\dagger + b_{-\mathbf{w}}) a_{\mathbf{k}'+}, \quad \mathbf{w} = \mathbf{k}' - \mathbf{k}.$$

Upon taking matrix elements between the ground state $\langle 0|$ and the excited state $|\mathbf{k}+\rangle$, one gets

$$(W_k - \epsilon_k)u_k = \sum_{\mathbf{k}'} D_w \langle 0|b_{\mathbf{w}}^\dagger|-\mathbf{k}'-, \mathbf{k}+\rangle v_{\mathbf{k}'}. \dots \dots \dots (8)$$

From the phonon equation of motion

$$[b_{\mathbf{w}}^\dagger, H_F] = -\hbar\omega b_{\mathbf{w}}^\dagger - D_w \sum_{1,s} a_{1s}^\dagger a_{1's}, \quad 1' - 1 = \mathbf{w},$$

the matrix element on the right-hand side of (8) is given, using the relations (7), as

$$(W_k + W_{k'} + \hbar\omega) \langle 0 | b_{\mathbf{w}}^\dagger | -\mathbf{k}', -, \mathbf{k} + \rangle = D_w (u_{k'} v_k + u_k v_{k'}). \quad \dots\dots (9)$$

Substituting into (8), one obtains

$$\left(W_k + \epsilon_k - \sum_{k'} \frac{D_w^2}{W_k + W_{k'} + \hbar\omega} v_{k'}^2 \right) u_k = \left(\sum_{k'} \frac{D_w^2}{W_k + W_{k'} + \hbar\omega} u_{k'} v_{k'} \right) v_k. \quad \dots\dots (10)$$

Similarly, from the equation of motion for $a_{-\mathbf{k}-}^\dagger$,

$$\left(W_k + \epsilon_k - \sum_{k'} \frac{D_w^2}{W_k + W_{k'} + \hbar\omega} u_{k'}^2 \right) v_k = \left(\sum_{k'} \frac{D_w^2}{W_k + W_{k'} + \hbar\omega} u_{k'} v_{k'} \right) u_k. \quad \dots\dots (11)$$

From (10) and (11) it follows immediately that

$$W_k = \epsilon_k \pm (\xi_k^2 + C_k^2)^{1/2},$$

$$\frac{1}{2} \sum_{k'} \frac{D_w^2}{W_k + W_{k'} + \hbar\omega} \frac{C_{k'}}{(C_{k'}^2 + \xi_{k'}^2)^{1/2}} = C_k$$

where

$$\gamma_k = \frac{1}{2} \sum_{k'} \frac{D_w^2}{W_k + W_{k'} + \hbar\omega}$$

and

$$\xi_k = \epsilon_k - \frac{1}{2} \sum_{k'} \frac{D_w^2}{W_k + W_{k'} + \hbar\omega} (u_{k'}^2 + v_{k'}^2). \quad \dots\dots (12)$$

The Eqns (12) represent the Bogoliubov solution (1958) and will not be further discussed.

§ 3. THE NEGLECTED MATRIX ELEMENTS

Returning to the BCS reduced Hamiltonian equation of motion (3), it is noticed that the assumed matrix elements (7) allow the operator $a_{-\mathbf{k}'} a_{\mathbf{k}'}^\dagger a_{-\mathbf{k}}^\dagger$ to have matrix elements between the states $|0\rangle$ and $|-\mathbf{k}', -, \mathbf{k} + \rangle$ thus,

$$\langle 0 | a_{-\mathbf{k}'} | -\mathbf{k}' - \rangle \langle -\mathbf{k}' - | a_{\mathbf{k}'}^\dagger | -\mathbf{k}', -, \mathbf{k} + \rangle \langle -\mathbf{k}', -, \mathbf{k} + | a_{-\mathbf{k}}^\dagger | -\mathbf{k}', -, \mathbf{k} + \rangle$$

$$= \langle 0 | a_{-\mathbf{k}'} a_{\mathbf{k}'}^\dagger a_{-\mathbf{k}}^\dagger | -\mathbf{k}', -, \mathbf{k} + \rangle, \quad \mathbf{k}' \neq \mathbf{k}.$$

Consequently, it follows from (3) that the matrix element $\langle 0 | a_{\mathbf{k}} | \mathbf{l}, \mathbf{k} + \rangle$ is also finite, where \mathbf{l} denotes any excited pair of quasi-particles, $-\mathbf{l} = \mathbf{l} +$. The above matrix element is proportional to $V_{kl} \propto V^{-1}$ where V is the volume of the system. \mathbf{l} may take roughly all occupied \mathbf{l} state values and therefore the number of such elements is proportional to V . The operator $a_{-\mathbf{k}}$ is seen to have similar matrix elements.

In Eqns (3), (5), intermediate states containing an extra quasi-particle pair must now be added and this leads to further V^2 elements of $a_{\mathbf{k}}$, containing two arbitrary pairs, i.e.

$$\langle 0 | a_{\mathbf{k}} | \mathbf{l}_1, \mathbf{l}_2, \mathbf{k} + \rangle \propto V^{-2}.$$

Inserting these as intermediate states in the right-hand side of (3) leads to matrix elements

$$\langle 0 | a_{\mathbf{k}} | \mathbf{l}_1, \mathbf{l}_2, \mathbf{l}_3, \mathbf{k} + \rangle \propto V^{-3}$$

and so on to indefinite order. Quite generally,

$$\langle 0 | a_{\mathbf{k}} | \mathbf{l}_1, \mathbf{l}_2, \mathbf{l}_3 \dots \mathbf{l}_n, \mathbf{k} + \rangle \propto V^{-n}$$

the number of such elements being proportional to V^n . Consequently a perturbation treatment of these extra terms in (3) to any finite order leads to an

energy correction proportional to V^{-1} . In the BCS theory, such second-order terms were dismissed on the grounds that they became vanishingly small in the limit $V \rightarrow \infty$. Conjecturing this to be true for all orders (as is now shown to be the case), it was concluded that their solution in this limit was exact. The same argument applied to the original reduced interaction regarded as a perturbation to the eigenstates of H_0 would lead to the contrary conclusion that eigenstates of H_0 in the limit $V \rightarrow \infty$ become exact.

The Bogoliubov fermion transformation, namely,

$$\begin{aligned} a_{\mathbf{k}+} &= u_{\mathbf{k}} \alpha_{\mathbf{k}+} + v_{\mathbf{k}} \alpha_{-\mathbf{k}-}^{\dagger} \\ a_{-\mathbf{k}} &= u_{\mathbf{k}} \alpha_{-\mathbf{k}-} - v_{\mathbf{k}} \alpha_{\mathbf{k}+}^{\dagger} \end{aligned}$$

defines operators $\alpha_{\mathbf{k}+}, \alpha_{-\mathbf{k}-}$ which, from the above matrix elements of $a_{\mathbf{k}+}$ etc., connect eigenstates of the interaction Hamiltonian differing by one excited quasi-particle \mathbf{k} plus an arbitrary number of quasi-pairs, $\mathbf{l}_1, \mathbf{l}_2$, etc. Alternatively, if $\alpha_{\pm \mathbf{k} \pm}$ is defined to connect only adjacent eigenstates, then the exact diagonalizing transformation becomes

$$\begin{aligned} a_{\mathbf{k}+} &= \alpha_{\mathbf{k}+} \left\{ u_{\mathbf{k}} + \sum_{\mathbf{l}_1} \langle 0 | a_{\mathbf{k}+} | \mathbf{l}_1, \mathbf{k} + \rangle b_{\mathbf{l}_1} + \sum_{\mathbf{l}_1, \mathbf{l}_2} \langle 0 | a_{\mathbf{k}+} | \mathbf{l}_1, \mathbf{l}_2, \mathbf{k} + \rangle b_{\mathbf{l}_1} b_{\mathbf{l}_2} + \dots \right\} \\ &+ \alpha_{-\mathbf{k}-} \left\{ v_{\mathbf{k}} + \sum_{\mathbf{l}_1} \langle -\mathbf{k}-, \mathbf{l}_1 | \alpha_{\mathbf{k}+} | 0 \rangle b_{\mathbf{l}_1}^{\dagger} + \sum_{\mathbf{l}_1, \mathbf{l}_2} \langle -\mathbf{k}-, \mathbf{l}_1, \mathbf{l}_2 | a_{\mathbf{k}+} | 0 \rangle b_{\mathbf{l}_1}^{\dagger} b_{\mathbf{l}_2}^{\dagger} + \dots \right\} \end{aligned}$$

$a_{-\mathbf{k}-}$ = similar expression where $b_{\mathbf{l}} = \alpha_{\mathbf{l}+} \alpha_{-\mathbf{l}-}$. This is a volume independent transformation satisfying the fermion commutation rules and which may be interpreted as follows. The leading (Bogoliubov) terms do not exactly diagonalize the reduced Hamiltonian but lead to non-diagonal elements involving quasi-pairs \mathbf{l}_1 . These are removed by the second terms $\langle 0 | a_{\mathbf{k}+} | \mathbf{l}_1, \mathbf{k} + \rangle \alpha_{\mathbf{k}+} b_{\mathbf{l}_1}$ etc. which however introduce non-diagonal terms in two quasi-pairs $\mathbf{l}_1, \mathbf{l}_2$. These in turn are removed by third-order terms of the transformation which again lead to triple pair non-diagonals $\mathbf{l}_1, \mathbf{l}_2, \mathbf{l}_3$, and so on. For an arbitrary interaction there is no reason why the process should converge, though for a sufficiently velocity-dependent interaction it may do so, since this might tend to limit the matrix elements

$$\langle 0 | a_{\mathbf{k}+} | \mathbf{l}_1 \mathbf{l}_2 \dots, \mathbf{k} + \rangle$$

etc.

§ 4. CONCLUSION

In the derivation of the BCS secular equation for quasi-particle excitation energies, the form of the attractive two-body interaction is quite arbitrary, the method applying, for example, to purely spatial forces. The consideration given here of the neglected matrix elements suggests that the success of the approximation may depend upon some as yet unstated restriction on the interaction.

ACKNOWLEDGMENT

The author wishes to thank Professor H. Fröhlich for stimulating discussions.

REFERENCES

- BARDEEN, J., COOPER, L. N., and SCHRIEFFER, J. R., 1957, *Phys. Rev.*, **106**, 162.
- BOGOLIUBOV, N. N., 1958, *J. Expt. Theoret. Phys. (U.S.S.R.)*, **34**, 58.
- FRÖHLICH, H., 1952, *Proc. Roy. Soc. A*, **215**, 291.
- KUPER, C. G., 1959, *Advanc. Phys.*, **8**, 1.
- VALATIN, J. G., 1958, *Nuovo Cim.*, **7**, 843.

A Revision of Kellermann's Calculations of the Specific Heats of Sodium Chloride

BY B. DAYAL AND B. B. TRIPATHI

Department of Physics, Banaras Hindu University, India

MS. received 21st September 1960

Abstract. In the well-known work on the lattice vibrations and the specific heats of sodium chloride, Kellermann has not assigned a correct statistical weight to several frequencies and has, further, omitted one point of the Brillouin zone. His results have, therefore, been revised to take these factors into account.

DAYAL AND SINGH (1960) have pointed out that some of the earlier workers have not used the correct number of frequencies for the purpose of evaluation of specific heats of solids. If the basic vectors of the reciprocal lattice are subdivided into n points each, it is obvious that the total number of points of the Brillouin zone should be exactly n^3 , whereas the numbers considered by them differ considerably from this value. This has resulted in a non-uniform distribution of points in the Brillouin zone.

The well-known work of Kellermann (1940, 1941) on the vibration frequencies and the specific heats of sodium chloride also falls in the same category. His value of n is 10 and the number of frequencies, including the origin, should, therefore, be exactly $6 \times 1000 = 6000$. The number considered by him is, however, 6700. He has not stated how he arrived at this figure but it is probable that he did not assign the correct statistical weight to the frequencies on the boundary of the zone. This work is well known and has been extensively quoted in almost all textbooks and reviews on the subject. We have, therefore, thought it advisable to recalculate his results by a proper assignment of the statistical weight.

While going through his work we found that he has inadvertently omitted the point (7, 7, 1) which falls on the boundary of the zone and should not have been left out. On the other hand a new point (10, 5, 0) has been included, which is not a point of any of the thousand basic cells into which the Brillouin zone has been sub-divided. This is not permissible because it will lead to more than one thousand points and to a non-uniform distribution. According to Kellermann, this point has been included because it happens to be a corner of the zone. This purpose could have been achieved only if a different value of n , say 8 or 12 had been selected. In the present revision we have omitted the point (10, 5, 0) and included (7, 7, 1). Each point has been weighted according to the number of similar points in the whole of the zone. The weight of the points on the surface of the boundary has, however, been divided by two, because each point is shared by two polyhedra. This gives exactly 10^3 or 1000 points.

The coupling coefficients and the frequencies of the point (7, 7, 1) have not been given by Kellermann. We have calculated them and obtained the following values.

Attractive coupling coefficients:

$$\begin{aligned} {}^c\left[\begin{smallmatrix} 1 & 1 \\ x & x \end{smallmatrix}\right] \frac{v_a}{e^2} &= {}^c\left[\begin{smallmatrix} 1 & 1 \\ y & y \end{smallmatrix}\right] \frac{v_a}{e^2} = +0.790, & {}^c\left[\begin{smallmatrix} 1 & 1 \\ z & z \end{smallmatrix}\right] \frac{v_a}{e^2} &= -1.583. \\ {}^c\left[\begin{smallmatrix} 1 & 2 \\ x & x \end{smallmatrix}\right] \frac{v_a}{e^2} &= {}^c\left[\begin{smallmatrix} 1 & 2 \\ y & y \end{smallmatrix}\right] \frac{v_a}{e^2} = +5.756, & {}^c\left[\begin{smallmatrix} 1 & 2 \\ z & z \end{smallmatrix}\right] \frac{v_a}{e^2} &= -11.516. \\ {}^c\left[\begin{smallmatrix} 1 & 1 \\ x & z \end{smallmatrix}\right] \frac{v_a}{e^2} &= {}^c\left[\begin{smallmatrix} 1 & 1 \\ y & z \end{smallmatrix}\right] \frac{v_a}{e^2} = -0.851, & {}^c\left[\begin{smallmatrix} 1 & 1 \\ x & y \end{smallmatrix}\right] \frac{v_a}{e^2} &= -2.103. \\ {}^c\left[\begin{smallmatrix} 1 & 2 \\ x & z \end{smallmatrix}\right] \frac{v_a}{e^2} &= {}^c\left[\begin{smallmatrix} 1 & 2 \\ y & z \end{smallmatrix}\right] \frac{v_a}{e^2} = -0.258, & {}^c\left[\begin{smallmatrix} 1 & 2 \\ x & y \end{smallmatrix}\right] \frac{v_a}{e^2} &= +0.862. \end{aligned}$$

Repulsive coupling coefficients:

$$\begin{aligned} {}^R\left[\begin{smallmatrix} 1 & 1 \\ x & x \end{smallmatrix}\right] \frac{v_a}{e^2} &= {}^R\left[\begin{smallmatrix} 1 & 1 \\ y & y \end{smallmatrix}\right] \frac{v_a}{e^2} = {}^R\left[\begin{smallmatrix} 1 & 1 \\ z & z \end{smallmatrix}\right] \frac{v_a}{e^2} = -7.850. \\ {}^R\left[\begin{smallmatrix} 1 & 2 \\ x & x \end{smallmatrix}\right] \frac{v_a}{e^2} &= {}^R\left[\begin{smallmatrix} 1 & 2 \\ y & y \end{smallmatrix}\right] \frac{v_a}{e^2} = -6.407, & {}^R\left[\begin{smallmatrix} 1 & 2 \\ z & z \end{smallmatrix}\right] \frac{v_a}{e^2} &= +11.052. \end{aligned}$$

The other repulsive coefficients are all zero.

Frequencies (in units of 10^{13} sec^{-1}):

$$\begin{array}{lll} \omega_1 = 3.61 & \omega_2 = 3.59 & \omega_3 = 2.80 \\ \omega_4 = 2.76 & \omega_5 = 2.75 & \omega_6 = 1.86. \end{array}$$

The specific heats have been calculated by numerical computation. For this purpose the frequencies have been divided into steps of $\Delta\omega = 2\pi\Delta\nu = 0.3 \times 10^{13} \text{ sec}^{-1}$. An Einstein function corresponding to the mid-point of each step multiplied by its statistical weight gives the contribution of each step to the specific heat. The statistical weight has been obtained from the number of points lying in each step. The results of calculation are given in the Table.

Specific Heats of Sodium Chloride						
$T (^{\circ}\text{K})$	20	30	40	50	60	100
C_V (revised) ($\text{cal deg}^{-1} \text{ g}^{-1} \text{ mol}^{-1}$)	0.184	0.618	1.24	1.90	2.52	4.12
C_V (Kellermann) ($\text{cal deg}^{-1} \text{ g}^{-1} \text{ mol}^{-1}$)	0.157	0.577	1.19	1.84	2.45	4.12

It is found that the revised specific heat at the lowest temperature is about 17% higher than the original value calculated by Kellermann. The difference gradually decreases at higher temperatures. This was anticipated in general terms by Dayal and Singh. Since the experimental values are almost the same as those of Kellermann's original calculations, the difference between the revised theoretical and the experimental values can be obtained from the Table.

REFERENCES

- DAYAL, B., and SINGH, S. P., 1960, *Proc. Phys. Soc.*, **76**, 777.
 KELLERMANN, E. W., 1940, *Phil. Trans. Roy. Soc. A*, **238**, 513.
 ——— 1941, *Proc. Roy. Soc. A*, **178**, 17.

Diffraction by an Irregular Screen of Limited Extent

By B. H. BRIGGS

Cavendish Laboratory, Cambridge

Communicated by J. A. Ratcliffe; MS. received 21st March 1960

Abstract. The problem considered is the nature of the diffraction pattern produced by an irregular diffracting screen of limited extent. In particular, the deductions which may be made about the screen from measurements of the correlation of the wave disturbances at separated points in the diffraction pattern are discussed. It is shown that such measurements can give information about either the size of the irregularities in the screen or about its overall extent depending on the distance from the screen at which the measurements are made. Close to the screen, the measured auto-correlation function of the diffraction pattern is shown to be the same as that of the small scale irregular structure in the screen. Observations of this function can, therefore, be used to determine the size of the irregularities in the screen. Far from the screen this is no longer true, and the auto-correlation function is determined by the angular distribution of power over the screen as seen from the observing point; it is in fact equal to the Fourier transform of this angular power distribution. Measurements made at a large distance, therefore, give no information about the small scale structure of the screen, but can be used to determine the distribution of power over it. The distance from the screen at which the transition takes place may be calculated by multiplying the size of the small irregularities by the overall length of the screen, and dividing by the wavelength of the radiation. If nothing is known about the nature of the screen or its distance, it is impossible to decide upon the correct interpretation of the measurements. However, in most experiments enough is known to enable the correct interpretation to be made. Several examples are discussed including measurements of the angular diameter of stars, measurements of the small scale structure of the ionospheric layers, and the problem of reflection from irregular ionized trails produced by meteors.

§ 1. INTRODUCTION AND STATEMENT OF THE PROBLEM

THE problem discussed in this paper concerns the diffraction pattern produced by an irregular screen of limited extent, as shown in Fig. 1. Only a two-dimensional problem will be treated, in which the screen does not vary in a direction at right angles to the plane of the figure. An irregular wave disturbance exists over a limited region of length $2x_0$. The irregular wave front which leaves the screen will be described by a complex function $f(x)$. The fluctuations of this function in amplitude and phase will be closely related to the irregular structure of the screen itself. The screen may be self-luminous, or it may transmit a wave incident from above.

The fluctuations of the wave front may be described by the correlation function $\rho_f(\xi)$ of the function $f(x)$. This correlation function is given by†

$$\rho_f(\xi) = \int_{-\infty}^{+\infty} f(x)f^*(x+\xi) dx \bigg/ \int_{-\infty}^{+\infty} |f(x)|^2 dx. \quad \dots\dots (1)$$

† We suppose throughout either that the random functions have zero mean value, or that the mean is removed before evaluating the correlation functions.

If the function $\rho_f(\xi)$ falls to a small value when $\xi = l$ the value of l may be used to describe the 'size' of the irregularities. If $l \ll x_0$, so that the screen contains a large number of irregularities, then $\rho_f(\xi)$ will depend almost entirely on the small scale structure, and hardly at all on x_0 . *It is convenient to measure all lengths in terms of the wavelength λ as a unit. This will be done throughout the paper, unless otherwise stated*†.

The above description of the wave front leaving the screen applies at any one instant. We shall also suppose, however, that the small irregularities change with time in a random manner, while preserving the same statistical properties.

Now consider the diffraction pattern produced in another plane $A'B'$ parallel to the diffracting screen AB and distant z from it (Fig. 1). At any instant this diffraction pattern can be represented by another complex function $g(y)$. In the experiments with which we shall be concerned, measurements are made of the correlation between the wave disturbances at spaced points in the pattern. The object of the measurements is to obtain information about the nature of the diffracting screen which produced the pattern.

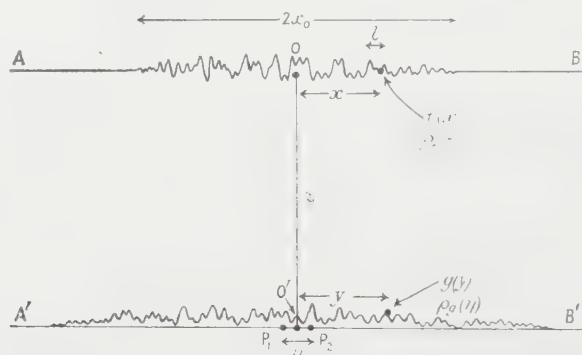


Fig. 1. Diagram to illustrate the measurement of the correlation of the wave disturbances at two points P_1 and P_2 , separated by a distance η .

The methods used for the measurement of correlation, and the interpretation of the results, are different in different experiments. In some radio experiments the wave field $g(y)$ is measured directly at two or more points, and the correlation afterwards evaluated from the records. This has been done, for example, in experiments on waves reflected from the ionosphere, and from meteor trails.‡ In other experiments the correlation has been measured by observing the 'visibility' of the fringes produced when waves from two points are combined with a variable phase difference. It can be shown (Zernike 1938) that the visibility of these fringes, defined by the usual optical method, is equal to the correlation between the wave disturbances at the two points. Thus the Michelson stellar interferometer can be regarded as an instrument for the determination of the correlation of the wave disturbances at the two mirrors. In radio astronomy the same principle is used; the two aerials of the radio interferometer correspond to the two mirrors of Michelson's method.

† It should be noted that this convention is *not* used in the companion paper by Mercier (1961).

‡ The correlation which has been determined has usually been of the wave amplitude $|g(y)|$ only, because it is more difficult to measure the phase. The relation of the correlation of amplitude to the complex correlation has been discussed by Ratcliffe (1956). The correlation interferometer of Brown and Twiss (1954) is based on the same principle.

If the correlation of the wave disturbances at two points is measured for different separations of the points, a correlation function is determined for the diffraction pattern $g(y)$. Two different interpretations of this correlation function have been made. It has sometimes been supposed that the function gives information about the small scale structure of the diffracting screen. This interpretation is based upon a theorem due to Booker, Ratcliffe and Shinn (1950) which states that the correlation function of $g(y)$ is the same as that of the wave front $f(x)$ very close to the screen. In this way information has been obtained about the sizes of the irregularities present in ionospheric layers from observations of reflected waves. A similar method has been used to investigate the irregular structure of the solar corona by observing the waves from a radio star which have passed through it. The second interpretation is based upon a result due to Zernike (1938), which was originally proved for a self-luminous optical source of finite size. This method leads to the conclusion that the correlation function is the Fourier transform of the function which represents the angular distribution of power from the source. This depends only on the brightness distribution over the source (i.e. in our terminology, over the diffracting screen) and has nothing to do with the small scale structure. This interpretation is the basis of the various methods for the determination of the angular diameters and brightness distributions of sources, both optical and radio (e.g. Bracewell 1958).

The two different interpretations which have been made are at first sight conflicting, and it is the object of this paper to reconcile them. The problem appears in an acute form in connection with experiments on waves reflected from meteor trails. Since a trail contains irregularities, and is also of limited length, it is not clear whether correlation measurements will give information about the small scale structure, or about the overall length of the trail.

In order to resolve these difficulties, it will be necessary to distinguish between two types of correlation function. Consider first the diffracting screen itself. The correlation function defined by (1) will be called the 'space average' correlation function. It should be noted that from its definition, it cannot be a function of x . If, now, instead of one screen we have a statistical assembly, a different type of correlation function can be defined in terms of an 'assembly average' as follows

$${}_{as}\rho_f(\xi) = \overline{f(x)f^*(x+\xi)} / \overline{|f(x)|^2}. \quad \dots\dots(2)$$

We have here used an obvious notation to indicate an assembly average, and the symbol ${}_{as}\rho_f(\xi)$ for the resulting 'assembly average' correlation function. Now this function could in principle be a function of x as well as ξ , but this would imply that the size of the small irregularities was different at different points. We shall postulate that this is not the case, and therefore the function ${}_{as}\rho_f(\xi)$ will be independent of x for the type of screen we wish to consider. If also the screen contains many irregularities (i.e. $x_0 \gg l$) the assembly average correlation function will be equal to an assembly average of the space correlation function. That is

$${}_{as}\rho_f(\xi) = \overline{\rho_f(\xi)}. \quad \dots\dots(3)$$

Now consider the diffraction pattern $g(y)$. There is no reason to suppose that the fluctuations of $g(y)$ will be similar for all values of y . Thus a relation like (3) will *not* hold for the correlation functions of $g(y)$, and we must carefully

distinguish between the space average correlation function $\rho_g(\eta)$ defined in a similar way to (1), and the assembly average correlation function ${}_{(a)}\rho_g(\eta)$, defined as in (2). The function ${}_{(a)}\rho_g(\eta)$ will be a function of y as well as η , as will be shown in §2.

In the experimental measurements, the correlation is measured for fixed points in the diffraction pattern by means of an average in time. We suppose that the screen changes irregularly in detail, but preserves its statistical properties. In other words, the different members of a statistical assembly are presented in time sequence, and an average in time is equivalent to an average over the assembly. Thus the experiments measure the *assembly average* correlation function. But the theorem of Booker, Ratcliffe and Shinn applies to the space average correlation functions. It is incorrect in principle to apply this theorem to the measured correlation functions. We shall show in §2, however, that for some conditions the theorem of Booker, Ratcliffe and Shinn holds for the assembly average correlation functions. The conditions for which this result holds will provide the criterion which determines the correct interpretation of the measurements.

Since the experiments measure ${}_{(a)}\rho_g(\eta)$ we shall now determine how this quantity is related to the diffracting screen, and how it varies with distance from the screen and across the diffraction pattern.

§ 2. THE EVALUATION OF THE ASSEMBLY AVERAGE CORRELATION FUNCTION OF THE DIFFRACTION PATTERN DUE TO A LIMITED IRREGULAR SCREEN

We shall make use of several results developed by Ratcliffe (1956) and shall use a similar notation. We first introduce the angular spectrum $F(S)$ produced by the screen (Fig. 2). The quantity $F(S) dS$ gives the amplitude of the plane

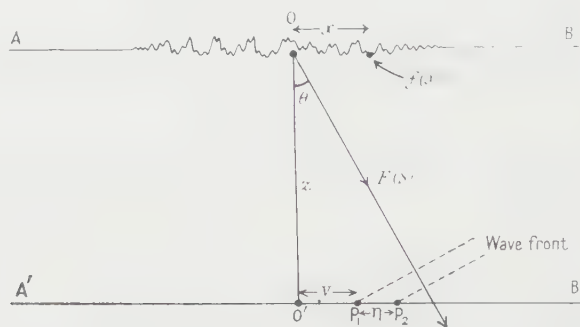


Fig. 2. Diagram to illustrate the calculation of the assembly average correlation function for points P_1 and P_2 , separated by η and distant y from O' .

waves diffracted into directions between S and $S + dS$, where $S = \sin \theta$. $F(S)$ is the Fourier transform of $f(x)$ and this symmetrical relationship between the two functions will be written

$$f(x) \longleftrightarrow F(S). \quad \dots\dots (4)$$

We may note here that if the screen contains irregularities of size l , then $F(S)$ will extend over a range of values of S of the order of $1/l$, and will be small for larger values of S . The phases of the plane waves in the angular spectrum are referred to the point $x=0$. We shall assume that the aperture is symmetrical or approximately symmetrical, and take $x=0$ near the centre.

The auto-correlation function of the diffraction pattern $g(y)$, defined as in (1) by a space average, is the Fourier transform of $|F(S)|^2$. Thus

$$\rho_g(\eta) \longleftrightarrow |F(S)|^2. \quad \dots\dots (5)$$

Provided the screen does not contain structure smaller than the wavelength (which would produce evanescent waves in the angular spectrum), both the functions in (5) are independent of the distance z from the screen. From this fact there follows the theorem of Booker, Ratcliffe and Shinn

$$\rho_g(\xi) = \rho_f(\xi). \quad \dots\dots (6)$$

The correlation $\rho_F(\sigma)$ between the values of F for angles S and $S + \sigma$ is defined by

$$\rho_F(\sigma) = \int_{-1}^{+1} F(S)F^*(S + \sigma) dS / \int_{-1}^{+1} |F(S)|^2 dS. \quad \dots\dots (7)$$

By analogy with (5), this is the Fourier transform of $|f(x)|^2$. Thus

$$\rho_F(\sigma) \longleftrightarrow |f(x)|^2. \quad \dots\dots (8)$$

We can alternatively define the correlation within the spectrum $F(S)$ by means of an assembly average correlation function as follows

$${}_{(a)}\rho_F(\sigma) = \overline{F(S)F^*(S + \sigma)} / \overline{|F(S)|^2}. \quad \dots\dots (9)$$

This function could in principle be a function of S , but it is not difficult to show that it is not, provided we are not concerned with large values of S . This can be seen from the description given by Ratcliffe (1956, p. 222) of the way the correlation inside the spectrum arises. If the screen were of infinite extent, there would be no correlation between $F(S)$ and $F(S + \sigma)$, however small the value of σ . If, now, another screen is placed below the first, so as to limit the area of the first which is effective, each plane wave of the spectrum $F(S)$ is diffracted coherently in passing through the lower screen. Correlation is therefore introduced into the spectrum, and provided S is not large, the correlation is independent of S . Thus for the function $F(S)$ the assembly average correlation function will be the same as the assembly average of the space average correlation function. That is, ${}_{(a)}\rho_F(\sigma) = \rho_F(\sigma)$. Hence from (8)

$${}_{(a)}\rho_F(\sigma) \longleftrightarrow \overline{|f(x)|^2}. \quad \dots\dots (10)$$

The quantity $\overline{|f(x)|^2}$ is the mean distribution of power over the screen. It will be constant or slowly varying over a range $x = x_0$ to $x = +x_0$, and zero outside this range. This variation of power over the screen may arise because it is illuminated unevenly, because it is of limited extent, or because some limiting aperture is placed beneath it as discussed above. Mathematically, these situations can all be described by a suitable variation of $\overline{|f(x)|^2}$ over the screen.

It follows from (10) by a well-known property of Fourier transforms that ${}_{(a)}\rho_F(\sigma)$ will fall to a small value when $\sigma > \sigma_0$, where

$$\sigma_0 = 1/x_0. \quad \dots\dots (11)$$

We shall now evaluate the assembly average correlation of the wave disturbances at two points in the diffraction pattern separated by a distance η . Let the two points P_1 and P_2 have coordinates y and $y + \eta$ (Fig. 2). The distances travelled by a wave front of a plane wave of the angular spectrum in reaching

P_1 and P_2 from the phase reference point O are $[Sy + Cz]$ and $[S(y + \eta) + Cz]$, where $C = \cos \theta$. The total wave disturbance at P_1 is therefore

$$g(y) = \int_{-1}^{+1} F(S) \exp \{2\pi i(Sy + Cz)\} dS.$$

The total wave disturbance at P_2 is

$$g(y + \eta) = \int_{-1}^{+1} F(S) \exp \{2\pi i[S(y + \eta) + Cz]\} dS.$$

From (2), the assembly average correlation function is given by

$$\begin{aligned} \overline{|g(y)|^2}_{(a)\rho_g(\eta)} &= \int_{-1}^{+1} \int_{-1}^{+1} \overline{F(S')F^*(S)} \exp \{2\pi i[S'y - S(y + \eta) + C'z - Cz]\} dS dS'. \end{aligned}$$

Now put $S' = S + \sigma$; then $S'y - S(y + \eta) = \sigma y - S\eta$ and $C'z - Cz = -S\sigma z$ (to the first order in S and σ). The range of the integration over σ will be much less than over S , because $F(S)$ and $F(S')$ will be uncorrelated when $\sigma > 1/x_0$, while $F(S)$ extends over a range of the order of $1/l$. Thus

$$\begin{aligned} \overline{|g(y)|^2}_{(a)\rho_g(\eta)} &= \int_{-1}^{+1} \int_{\sigma} \overline{F^*(S)F(S + \sigma)} \exp \{2\pi i[\sigma(y - Sz) - \eta S]\} dS d\sigma \\ &= \int_{-1}^{+1} \int_{\sigma} {}_{(a)}\rho_F^*(\sigma) \overline{|F(S)|^2} \exp \{2\pi i[\sigma(y - Sz) - \eta S]\} dS d\sigma \\ &= \int_{-1}^{+1} \left[\int_{\sigma} {}_{(a)}\rho_F(\sigma) \exp \{-2\pi i(y - Sz)\sigma\} d\sigma \right]^* \overline{|F(S)|^2} \exp(-2\pi i\eta S) dS \\ &= \int_{\sigma=-1}^{+1} \overline{|f(y - Sz)|^2} \overline{|F(S)|^2} \exp(-2\pi i\eta S) dS. \end{aligned} \quad \dots\dots (12)$$

In this derivation Eqns (9) and (10) have been used. Apart from the normalizing factor $\overline{|g(y)|^2}$, which does not affect the shape of the correlation function, ${}_{(a)}\rho_g(\eta)$ is the Fourier transform of a function $|H(S)|^2$, where

$$|H(S)|^2 = \overline{|f(y - Sz)|^2} \overline{|F(S)|^2}. \quad \dots\dots (13)$$

Thus

$${}_{(a)}\rho_g(\eta) \longleftrightarrow |H(S)|^2. \quad \dots\dots (14)$$

A comparison of Eqns (5) and (14) shows that the space average correlation function is the Fourier transform of the ordinary angular power spectrum $|F(S)|^2$ while the assembly average correlation function is the Fourier transform of $|H(S)|^2$. We shall call $|H(S)|^2$ the 'effective angular power spectrum'. It should be noted that it is not a true angular power spectrum in the usual sense, since it varies with y and z . The true angular power spectrum $|F(S)|^2$ is, of course, independent of y and z . Similarly the assembly average correlation function ${}_{(a)}\rho_g(\eta)$ varies with y and z , but the space average correlation function $\rho_g(\eta)$ does not.

We shall now consider how ${}_{(a)}\rho_g(\eta)$ varies with distance z from the screen. Consider first the case $y = 0$ so that the observing points P_1 and P_2 are near the origin O' , as in Fig. 1. Then

$$\overline{|g(y)|^2}_{(a)\rho_g(\eta)} = \int_{-1}^{+1} \overline{|f(-Sz)|^2} \overline{|F(S)|^2} \exp(-2\pi i\eta S) dS. \quad \dots\dots (15)$$

If we were to observe the screen from O' , we see from Fig. 3 that the intensity of the part of the screen which lies in a direction θ from the normal would

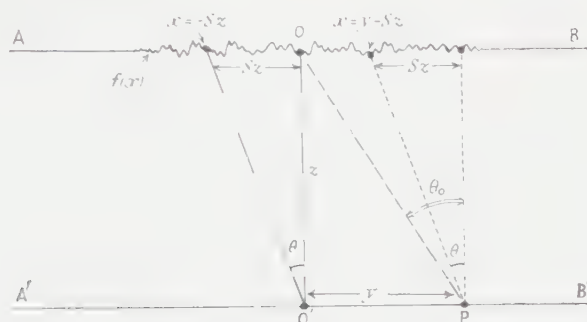


Fig. 3. Diagram to illustrate the variation of mean power over the screen, as seen from the points O' and P .

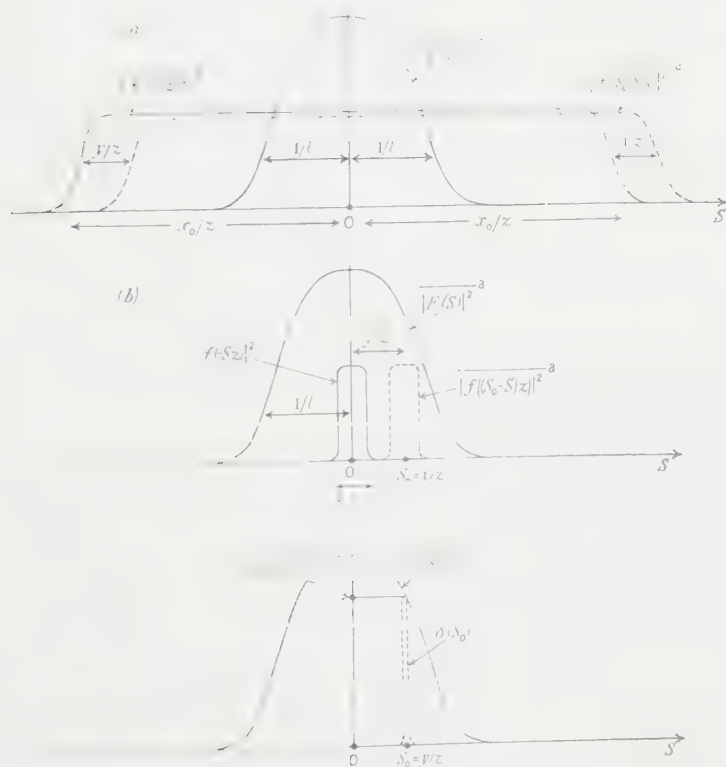


Fig. 4. The effective angular spectrum is obtained by multiplying the curve $\overline{|F(S)|^2}$ by the curve $\overline{|f\{(S_0 - S)z\}|^2}$. The diagrams illustrate three cases: (a) close to the screen, (b) far from the screen, (c) very far from the screen.

be obtained from the function $\overline{|f(x)|^2}$ by writing $x = -z \tan \theta$. Thus for small angles, the term $\overline{|f(-S_0 z)|^2}$ in (15) represents the variation of mean power over the screen as seen from the observing point O' . It will be constant, or only slowly varying, for $|S| < x_0/z$, and zero for $|S| > x_0/z$. The other term in

the integral $\overline{|F(S)|^2}^a$ is independent of z . It will be appreciable for $|S| < 1/l$ and small when $|S| > 1/l$.

In order to illustrate the variation of the effective angular power spectrum $|H(S)|^2$ with increasing distance from the screen, consider the special case where $\overline{|f(x)|^2}^a$ is constant over the illuminated portion of the screen, and falls rapidly to zero at the edges. Very close to such a screen we have the situation illustrated in Fig. 4(a). The function $\overline{|f(-Sz)|^2}^a$ is constant over the range of angles for which $\overline{|F(S)|^2}^a$ is appreciable. The effective angular spectrum is therefore $\overline{|F(S)|^2}^a$ itself. The condition for this to hold is $x_0/z \gg 1/l$. If x'_0, z', l' are the actual values of x_0, z and l (not expressed in terms of the wavelength λ as a unit), this condition becomes

$$x'_0 l' \gg \lambda z'. \quad \dots (16)$$

Also, from (5) and (15) (if $\overline{|f(-Sz)|^2}^a$ can be taken as constant) we have

$$({}_a)\rho_g(\eta) = \rho_f(\eta) = ({}_a)\rho_f(\eta). \quad \dots (17)$$

Thus, if condition (16) holds, the theorem of Booker, Ratcliffe and Shinn can be applied to the *assembly average* correlation functions. Measurements of $({}_a)\rho_g(\eta)$ give information about the small scale structure of the diffracting screen.

At a greater distance from the same screen, the situation shown in Fig. 4(b) will arise. The function $\overline{|f(-Sz)|^2}^a$ now extends over a smaller range of angles. If this range is much less than $1/l$, the function $\overline{|F(S)|^2}^a$ may be assumed to be constant over this range. The effective angular spectrum is then $\overline{|f(-Sz)|^2}^a$. The condition for this is

$$x'_0 l' \ll \lambda z'. \quad \dots (18)$$

Measurements of $({}_a)\rho_g(\eta)$ now give information, not about the small irregularities, but about the overall size $2x_0$ of the illuminated region. Since $({}_a)\rho_g(\eta)$ is the Fourier transform of $\overline{|F(-Sz)|^2}^a$ it is the same in form as $({}_a)\rho_F(\sigma)$. It is in fact the Fraunhofer diffraction pattern which would be produced by an aperture with no irregularities, and in which the illumination varied like $\overline{|f(x)|^2}^a$. Conversely, the mean distribution of power over the screen can be determined from the Fourier transform of the measured auto-correlation function.

There will be an intermediate range of distances where $x'_0 l' \simeq \lambda z'$, and here the two functions $\overline{|F(S)|^2}^a$ and $\overline{|f(-Sz)|^2}^a$ extend over roughly the same ranges of values of S , and are equally important in determining the effective angular power spectrum. If the variation of mean power over the screen is known, the function $\overline{|f(-Sz)|^2}^a$ can be calculated for any value of z . Then $|H(S)|^2$ can be determined as the Fourier transform of $({}_a)\rho_g(\eta)$, and $\overline{|F(S)|^2}^a$ can then be found from (13). In this way information about the small scale structure of the screen can be obtained even in this transition region. For example, in many radio applications, the distribution of power over the screen is determined by the polar diagram of a transmitting aerial, and can be assumed to be known. This point will be discussed further in § 3.2.

It is possible to give a very simple interpretation of these results. Suppose, as in Fig. 5, that the diffracting screen, of length $2x_0$, contains small irregularities of size l which are randomly distributed over the screen, and that it is illuminated from above by a plane wave. Each irregularity scatters a cone of radiation which extends over a range of angles ϕ_1 , where $\phi_1 \sim 2/l$. Now suppose that observations are made at a point P, and that the effective portion of the screen subtends an angle ϕ_2 at P, where $\phi_2 \sim 2x_0/z$. Then if $\phi_1 < \phi_2$ all the irregularities scatter radiation to P. The width of the angular spectrum at P is determined by the length of the screen, and is equal to ϕ_2 . On the other hand, if $\phi_1 > \phi_2$ radiation can reach P only from irregularities near the centre of the screen. The width of the angular spectrum is now ϕ_1 . Thus in the first case, measurements at P give information about ϕ_2 and hence about the size $2x_0$ of the screen. In the second case, the measurements give ϕ_1 , and hence the value of l . The conditions (16) and (18) can be obtained immediately from this simple argument.

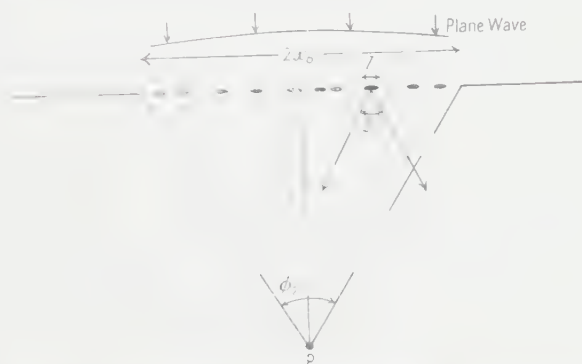


Fig. 5. The small irregularities scatter over an angle ϕ_1 . The screen subtends an angle ϕ_2 at P. If $\phi_1 > \phi_2$ the effective angular spectrum is determined by ϕ_2 and therefore by $2x_0$. If $\phi_1 < \phi_2$, the effective angular spectrum is determined by ϕ_1 , and therefore by l .

Also, it should be pointed out that an expression similar to (15) has been used in the literature, and has probably been regarded as almost self-evident. Our object has been not to derive a new result, but to point out the mistakes which can arise through failure to distinguish between the space average and the assembly average correlation functions and through an incorrect application of the theorem of Booker, Ratcliffe and Shinn.

We have so far discussed only the case in which correlation measurements are made near the origin O as in Fig. 1. Let us now return to the more general case, in which the correlation is measured at a distance y from O', as in

Fig. 2. Eqns (12) and (13) hold, and the function which multiplies $|\overline{F(S)}|^2$ is now $|\overline{f(y - Sz)}|^2$ or $|\overline{f'(S_0 - S)z}|^2$ where $S_0 = y/z$. This is again just the variation of mean power over the screen as seen from the observing point, as can be seen from Fig. 3. The curves which represent $|\overline{f(y - Sz)}|^2$ in Figs. 4(a) and (b) must therefore be moved a distance S_0 along the S axis, as shown dotted.

Consider first Fig. 4(a), which applies close to the screen. The effective angular power spectrum will not be altered appreciably until $|S_0| > x_0/z$. Therefore the assembly average correlation function $\omega\rho_g(\eta)$ has the same form

for all values of $|y|$ less than x_0 . For values of $|y|$ greater than this the effective angular spectrum begins to get narrower, and so the linear scale of the irregularities in the diffraction pattern begins to increase.

It is of interest to consider also how the mean power in the diffraction pattern varies with y . From (12), if $\eta = 0$

$$\overline{|g(y)|^2}^a = \int_{-1}^{+1} \overline{|f(y - Sz)|^2}^a \overline{|F(S)|^2}^a dS. \quad \dots\dots (19)$$

Thus the mean power in the diffraction pattern, $\overline{|g(y)|^2}^a$ depends upon the area under the function obtained by multiplying the two curves in Figs 4 (a) and (b). For Fig. 4 (a) we see that this area is constant for $|y| < x_0$ but begins to decrease when $|y| > x_0$. Thus the mean power in the diffraction pattern begins to decrease just where its linear scale begins to increase. There is a range of values of y from $-x_0$ to $+x_0$ for which the linear scale of the pattern and the mean power are constant. This is just what would be expected close to the screen.

Further away from the screen, the curves of Fig. 4 (b) apply. Consideration of the shapes of these curves shows that the power will decrease quite rapidly as y increases, and will have fallen appreciably when $y = z/l$, i.e. when $S_0 = 1/l$. For the shapes of the curves which were assumed, the pattern scale will not vary much because the width of the effective angular spectrum is always determined mainly by the function $\overline{|f(y - Sz)|^2}^a$.

At intermediate distances, where the functions $\overline{|f(-Sz)|^2}^a$ and $\overline{|F(S)|^2}^a$ have roughly the same widths, the power and the linear scale of the pattern will change quite rapidly as soon as y departs from zero.

If we go to a very large distance from the screen, the function $\overline{|f(y - Sz)|^2}^a$ becomes a δ -function centred on $S_0 = y/z$ as shown in Fig. 4 (c). The mean power then becomes from (19)

$$\overline{|g(y)|^2}^a = \int_{-1}^{+1} \delta(S_0) \overline{|F(S)|^2}^a dS = \overline{|F(S_0)|^2}^a. \quad \dots\dots (20)$$

Thus at large distances the mean power in the diffraction pattern varies like the angular spectrum or 'scattering polar diagram' of the small irregularities, as would be expected.

§ 3. APPLICATIONS

We shall briefly consider some experimental measurements to which these results may be applicable.

3.1. Measurements of Angular Diameters of Stars

The star may be assumed to consist of an aggregate of independent radiators, and the angular spectrum of the small irregularities will extend over 90° . The condition (18) will always be satisfied, and the measurements give information about the size of the source. If ${}_{(a)}\rho_g(\eta)$ is measured, the angular distribution of brightness of the source can be determined as its Fourier transform.

3.2. Measurements of Ionospheric Irregularities

In experiments on waves reflected from the ionosphere, which often has an irregular structure, the reflecting layer is 'illuminated' by a transmitter on the ground. The variation of mean power over the layer $\overline{|f(x)|^2}^a$ depends on the

polar diagram of the transmitting aerial, and can be calculated if this polar diagram is known. Observations of the diffraction pattern produced over the ground by the reflected wave are made with spaced receiving aerials. Let the receiving aerials have identical polar diagrams $R(S)$. The effective angular spectrum at $y=0$ (close to the transmitter) will then be

$$|H(S)|^2 = \overline{|f(-Sz)|^2} \overline{|R(S)|^2} \overline{|F(S)|^2}. \quad \dots\dots (21)$$

The assembly average correlation function of the diffraction pattern is the Fourier transform of (21). Conversely, the expression (21) can be determined as the Fourier transform of the measured correlation function, and $\overline{|F(S)|^2}$ can then be found if the aerial polar diagrams are known. In this way, information is obtained about the small scale structure of the reflecting layer, since $\overline{|F(S)|^2}$ is the Fourier transform of $\overline{\rho_r(\xi)}$ (from Eqns (5) and (6)). A further correction is necessary to allow for the phase variation which exists over the screen due to the fact that a point source is used. It can be shown that the diffraction pattern on the ground has a linear scale which is twice that which would have been observed with plane wave illumination (Ratcliffe 1956, p. 262).

In practice the aerial polar diagrams are broad, while the function $\overline{|F(S)|^2}$ usually extends over less than 10° . Thus the corrections for the aerial polar diagrams are small, and can easily be carried out with sufficient accuracy. This method has been used by Briggs and Phillips (1950) and others.

Similar considerations apply to observations of the scintillations of radio stars produced by transmission through the ionospheric irregularities. In this case, however, the 'illumination' over the layer is uniform, and $\overline{|f(-Sz)|^2}$ can be taken as constant. Also in practice no correction is necessary for the receiving aerials, since the function $\overline{|F(S)|^2}$ spreads over only a few minutes of arc, and no correction is needed for the use of a point source, owing to the large distance of the radio star. The measurements therefore give direct information about the sizes of the irregularities which cause the scintillations (Spencer 1955, Jones 1960).

3.3. Measurements on Waves Propagated by Ionospheric Forward Scattering

In these experiments the wavelengths used are shorter than those which can be reflected by the ionosphere in the normal way. A transmitting aerial 'illuminates' a small region of the ionosphere, and the waves scattered by irregularities in the electron density are observed at a point several thousands of kilometres away. The transmitting and receiving aerials are highly directional, and are pointed at the same region of the ionosphere, close to the midpoint of the path.

In principle, measurements of the correlation between the voltages induced in separated receiving aerials can be used to give information about the sizes of the irregularities which cause the scattering. The corrections for the aerial polar diagrams and for the use of a point source are necessary, as described in §3.2. In practice the polar diagrams are usually so narrow, that the expression (21) is dominated by the terms which represent the aerials, and depends very little on $\overline{|F(S)|^2}$.

Special experiments have been made by Hagfors (1959) in which the aerial polar diagrams were broader than usual, in an attempt to obtain information about the small irregularities. Even then, an important correction for the aerial polar diagrams was necessary.

Similar considerations will apply in experiments on scattering by tropospheric irregularities.

3.4. *Measurements on Waves Scattered by the Solar Corona*

Observations have been made of the scattering of the waves from a radio star when it passes behind the solar corona. The experiments have been used to obtain information about the scale of the irregular structure of the solar corona (Hewish 1955).

The effective angular spectrum depends partly on the size of the irregularities and partly on the mean gradient of scattering power, which varies with radial distance from the Sun. Hewish (1958) has, in effect, used an expression like (15) to compute the resultant angular spectrum. The effect of the gradient of scattering power is particularly important low down in the corona, and has the effect of making the angular spectrum unsymmetrical, even if the irregularities scatter isotropically.

3.5. *Measurements on Waves Reflected by Meteor Trails*

The ionized trail produced by a meteor can be thought of as an irregular linear reflector of limited length. The reflection coefficient will decrease gradually to zero at each end, but for the purposes of this discussion it will be assumed to fall to zero rather suddenly. Let the overall length of the trail be $2x_0$ and suppose that it contains irregularities of size l . Then the results of §2 will apply.

The diffraction pattern produced by the reflected wave has been observed at spaced receiving points (Kent 1960). When the experiments were started it was not clear whether they would give information about x_0 or l . We now see that this depends upon the distance z from the trail. For example, if the length of the trail is 10 km, if the small irregularities are 100 m in size, and if the wavelength is 10 m, Eqns (16) and (18) show that at distances less than 100 km the correlation measurements give the value of l , but at distances greater than 100 km they lead to a determination of the value of x_0 . To put it another way, if observations are made at a distance of 100 km, they give information about the small irregularities provided these are larger than 100 m in size. An irregularity size smaller than this could not be measured at the given distance, and the trail would behave exactly as it would do if it were completely irregular, i.e. as if the irregularities were small compared with the wavelength.

For the conditions of Kent's experiments in which the waves were reflected obliquely by the meteor trails, it appeared that the width of the angular spectrum was determined by the length of the trail rather than by the size of the irregularities (Kent 1960).

§ 4. CONCLUSIONS

It has been shown that measurements of the assembly average correlation between the wave disturbances at spaced points in a diffraction pattern must be interpreted with care. They can give information about either the size of the irregularities in the diffracting screen, or upon its overall extent, depending on

the distance from the screen at which the observations are made. If nothing is known about the nature of the screen or its distance, it is impossible to decide upon the correct interpretation. Fortunately, in most experiments enough is known to enable the correct interpretation to be used, and several examples have been discussed in §3. Measurements on waves reflected from meteor trails, which first prompted this investigation, present a border-line case, and experiments of this type must be interpreted with special care.

ACKNOWLEDGMENTS

The author is greatly indebted to his colleagues at the Cavendish Laboratory for valuable discussions of this problem, and particularly to Mr. J. A. Ratcliffe and Mr. R. P. Mercier. The problem was first raised by Dr. G. S. Kent in connection with experiments on waves reflected by meteor trails. It was first solved, by a method different from that given here, by Mr. Mercier, whose work will be published separately (Mercier 1960). The work forms part of an investigation of tropospheric and ionospheric irregularities, supported by a grant from the Department of Scientific and Industrial Research.

APPENDIX

The results obtained in §2 can be deduced in a slightly different way as follows. From (15), by the use of the convolution theorem (Ratcliffe 1956, p. 257), it follows that $\gamma_{\text{avg}}(\eta)$ is proportional to the convolution of the Fourier transform of $|F(S)|^2$ with the Fourier transform of $|f(-Sz)|^2$. Now the Fourier transform of $|F(S)|^2$ is ${}_{(a)}\rho_f(\eta)$ and the Fourier transform of $|f(-Sz)|^2$ is ${}_{(a)}\rho_F(\eta/z)$. Thus

$${}_{(a)}\rho_g(\eta) \propto \text{convolution of } {}_{(a)}\rho_f(\eta) \text{ with } {}_{(a)}\rho_F(\eta/z). \quad \dots\dots (22)$$

Close to the screen, ${}_{(a)}\rho_f(\eta/z)$ falls to zero very rapidly as soon as η departs from zero. Hence the convolution gives very nearly ${}_{(a)}\rho_f(\eta)$. Far from the screen ${}_{(a)}\rho_F(\eta/z)$ decreases only slowly as η departs from zero, and the convolution gives ${}_{(a)}\rho_F(\eta/z)$. The expression (22) is an extension of the theorem of Booker, Ratcliffe and Shinn, and it applies to the assembly average correlation functions. The conditions (16) and (18) can easily be obtained from (22).

REFERENCES

- BOOKER, H. G., RATCLIFFE, J. A., and SHINN, D. H., 1950, *Phil. Trans. Roy. Soc. A*, **242**, 579.
 BRACEWELL, R. N., 1958, *Proc. Inst. Radio Engrs, N.Y.*, **46**, 97.
 BRIGGS, B. H., and PHILLIPS, G. J., 1950, *Proc. Phys. Soc. B*, **63**, 907.
 BROWN, R. H., and TWISS, R. Q., 1954, *Phil. Mag.*, **45**, 663.
 HAGFORS, T., 1959, *Geofys. Publ.*, **21**, Nr. 2.
 HEWISH, A., 1955, *Proc. Roy. Soc. A*, **228**, 238.
 ——— 1958, *Mon. Not. R. Astr. Soc.*, **118**, 534.
 JONES, I. L., 1960, *J. Atmos. Terr. Phys.*, **19**, 26.
 KENT, G. S., 1960, *J. Atmos. Terr. Phys.*, **19**, 272.
 MERCIER, R. P., 1961, *Proc. Phys. Soc.*, **77**, 318.
 RATCLIFFE, J. A., 1956, *Rep. Progr. Phys.*, **19**, 188 (London: Physical Society).
 SPENCER, M., 1955, *Proc. Phys. Soc. B*, **68**, 493.
 ZERNIKE, F., 1938, *Physica*, **5**, 785.

Diffraction by Finite Irregular Objects

BY R. P. MERCIER

Cavendish Laboratory, Cambridge†

Communicated by J. A. Ratcliffe; MS. received 21st March 1960

Abstract. In this paper a theory is given of statistical correlation in the complex amplitude of a scalar wave diffracted by an irregular object of limited extent. The theory is one-dimensional, and uses the Fresnel integral to calculate the amplitude at the receiver. Two well-known results appear as special cases. In the first the correlation function of the complex amplitude in the wave is shown to be the same as the correlation function of the complex amplitude at the object if the object is an infinite plane; this is the basis of irregularity measurement in the ionosphere. In the second the correlation function of the complex amplitude is shown to depend upon the angular distribution of mean power over the source. This is the basis of the Michelson method for measuring the angular diameter of a star. The criterion which distinguishes between the two cases is expressed in terms of the overall size of the object, the irregularity size, the wavelength and the distance from the object.

The similar case of diffraction by a cylindrical object is considered. Here, the criterion distinguishing the two cases involves only the irregularity size and the wavelength. An application to lunar radio echoes is discussed, and it is concluded that the irregularities in the lunar surface cause phase fluctuations much greater than one radian, and these phase fluctuations are correlated over a distance of some 15 metres.

§ 1. INTRODUCTION

WE are concerned in this paper with the propagation of a wave from an irregular source, either a self-luminous object, or a scattering object. The problem is to find information about the irregular structure of the wave at the object, and therefore about the irregular structure of the object itself. It has been shown (Booker, Ratcliffe and Shinn 1950) that the correlation of the complex amplitude, with a spatial average over an infinite plane, is independent of the distance of the plane from the source. When the source is an infinite plane, and the fluctuations in complex amplitude are statistically stationary, it is sufficient to consider an average over an assembly of sources instead of a spatial average. In practice this is achieved by a time average; no other average can in fact be experimentally determined. An interpretation of the correlation function is sometimes supposed to give the size of the irregularities in the source.

It is clear then that if only time averages can be obtained, we cannot apply the theorem of Booker, Ratcliffe and Shinn when the source is limited in extent. The purpose of the present paper is to show that when the source becomes small enough, the correlation function actually measures the overall angular diameter of the source, and to calculate where the transition takes place.

† Now at the Department of Physics, University College, London.

§ 2. CORRELATION IN THE WAVE DIFFRACTED BY A PLANE TWO-DIMENSIONAL IRREGULAR OBJECT

The model is a simple screen, varying only in the x -direction, extending from $-x_0$ to x_0 . Let the complex amplitude at the screen be $f(x)$. Then, according to the formula used in Fresnel diffraction theory (Mercier 1959), the complex amplitude $g(y)$ at the receiver is

$$g(y) = \sqrt{\left(-\frac{i}{\lambda z}\right)} \int_{-x_0}^{x_0} f(x) \exp \left\{ -\frac{\pi i (x-y)^2}{\lambda z} \right\} dx \quad \dots\dots (1)$$

where z, y are indicated in Fig. 1 and λ = wavelength.



Fig. 1. Coordinate system for diffraction by a plane source or screen.

The amplitude $f(x)$ is irregular in some way over the screen, and the irregularities in $f(x)$ are assumed to be much smaller than $2x_0$. Let a correlation function of $f(x)$ be defined:

$$\rho_f(\xi) = \frac{\overline{f(x)f^*(x-\xi)}}{\overline{f(x)f^*(x)}} \quad \dots\dots (2)$$

The average, indicated by a bar, is over assemblies (time average).† Suppose $\rho_f(\xi)$ to become small for $\xi \sim l$, so that l is a measure of the irregularity size. We assume that if x is not too near $\pm x_0$, $\rho_f(\xi)$ is a function of only ξ .

The correlation function of g between a point on the axis and a point at a distance η , is defined in the same way,

$$\rho_g(\eta) = \frac{\overline{g(0)g^*(\eta)}}{\overline{g(0)g^*(0)}}$$

Now,

$$\overline{g(0)g^*(\eta)} = \frac{1}{\lambda z} \int_{-x_0}^{x_0} dx \int_{-x_0}^{x_0} dx' \overline{f(x)f^*(x')} \exp \left\{ -\frac{\pi i}{\lambda z} [x^2 - (x' - \eta)^2] \right\} \quad \dots\dots (3)$$

We shall in this paper consider only the correlation of g on the axis of the object. The off-axis correlation is considered by Briggs (1961).

† In the accompanying paper by Briggs the assembly average correlation function is denoted by ${}_{(a)}\rho_f(\xi)$.

Make a change of variable in the integral (3) to x, ξ , where $\xi = x' - x$. Except near the points $x = \pm x_0$, $\overline{f(x)f^*(x')}$ will be a function of ξ only, so that we have, approximately,

$$\overline{g(0)g^*(\eta)} = \frac{\overline{ff^*}}{\lambda z} \int_{-x_0}^{x_0} dx \int d\xi \rho_f(\xi) \exp \left\{ -\frac{2\pi i x(\eta - \xi)}{\lambda z} \right\} \exp \left\{ -\frac{\pi i(\eta - \xi)^2}{\lambda z} \right\}. \quad (4)$$

The effective range of integration of ξ is determined by $\rho_f(\xi)$ and is much less than $2x_0$, because the irregularity size l is much less than $2x_0$. Performing the x -integration in (4) we have

$$\overline{g(0)g^*(\eta)} = \frac{\overline{ff^*}}{\lambda z} \int d\xi \rho_f(\xi) \exp \left\{ -\frac{\pi i(\eta - \xi)^2}{\lambda z} \right\} \frac{\sin(2\pi x_0(\xi - \eta)/\lambda z)}{\pi(\xi - \eta)/\lambda z}. \quad \dots\dots (5)$$

Now, if the screen were infinite, so that $x_0 \rightarrow \infty$, the last factor in the integrand of (5) would be $\lambda z \delta(\xi - \eta)$, where $\delta(x)$ is the Dirac delta function. Thus

$$\overline{g(0)g^*(\eta)} \rightarrow \overline{ff^*} \rho_f(\eta) \quad \rho_g(\eta) \rightarrow \rho_f(\eta). \quad \dots\dots (6)$$

Therefore, for an infinite screen, the correlation at a distance z from the source is the same as the correlation at the source. This is a special case of the theorem proved by Booker, Ratcliffe and Shinn (1950). Their result was obtained using spatial averages and then, as they showed, the source need not be infinite.

Next, consider the other extreme, where

$$2x_0 l / \lambda z \ll 1. \quad \dots\dots (7)$$

If $\eta \sim l$, the last factor in the integrand of (5) may be written as $2x_0$, and also condition (7) implies that $(\eta - \xi)^2 / \lambda z \ll 1$, so that the exponential factor in (5) is one. Therefore

$$\overline{g(0)g^*(\eta)} = \frac{2x_0}{\lambda z} \overline{ff^*} \int \rho_f(\xi) d\xi. \quad \dots\dots (8)$$

Clearly $\rho_g(\eta)$ does not fall to zero when $\eta \sim l$, and the scale of correlation in $g(y)$ is now larger than in $f(x)$. The size is determined by the zero of the last factor in the integrand of (5), this is given by

$$\left| \frac{2x_0(\xi - \eta)}{\lambda z} \right| = 1$$

which, together with condition (7), implies

$$\frac{2x_0 \eta}{\lambda z} = 1.$$

The distance over which $g(y)$ is correlated is therefore

$$\eta = \frac{\lambda z}{2x_0} = \frac{\lambda}{\theta} \quad \dots\dots (9)$$

where θ is the angle subtended by the source at the receiver.

§ 3. THE MICHELSON STELLAR INTERFEROMETER

Let us now recall the usual theory of Michelson's method of measuring star diameters. The image of a point on the star is seen by means of the two paths SA_1 and SA_2 . A system of fringes is seen by the eye, with a fringe separation determined by the separation of the inner mirrors. A system of fringes due to some other point on the star is shown dotted in Fig. 2.

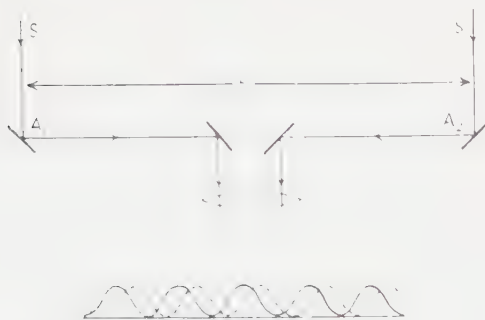


Fig. 2. Diagram to illustrate Michelson's method for the measurement of stellar diameters.

Let B be the distance between the outer mirrors. The separation between the two fringe systems is determined by B . If we have only two sources on the limbs of the star, the fringe system will be least distinct when B is adjusted so that the maximum of one system coincides with the minimum of the other. Then $B = \lambda / (2\theta)$, where θ is the angular diameter of the star. To take account of all the points on the star one assumes that they radiate incoherently, and performs an integration giving the fringe intensity. It is found that the fringes become indistinguishable when $B = \lambda / \theta$ approximately.

In terms of correlation theory the wave from the star is correlated over a distance B , if B is adjusted so that the fringes of the Fraunhofer pattern disappear (see Zernike 1938). This correlation distance has been denoted by η in the diffraction theory. The diffraction theory finds for the correlation distance the same value λ / θ (Eqn (9)) as is found in the usual theory. The usual theory presupposes that the light sources at different points of the star are uncorrelated, viz. condition (7). In terms of θ this condition states that unless $l \ll \lambda / \theta$ the correlation distance will not equal λ / θ .

We may summarize the theory as follows:

- (i) if $l \ll \lambda / \theta$ the correlation distance at the receiver is λ / θ ,
- (ii) if $l \gg \lambda / \theta$ the correlation distance at the receiver is l .

Fig. 3 shows in a rough way how the correlation distance at the receiver depends on l , for a fixed wavelength.

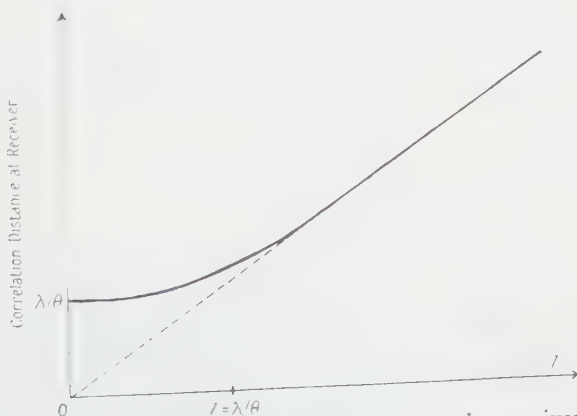


Fig. 3. The variation of correlation distance at the receiver with l .

§ 4. INTERPRETATION OF EXPERIMENTAL RESULTS

The experimental problem is to decide whether a measured correlation distance is really l or λ/θ or something in between l and λ/θ . If one were allowed to suppose that the correlation distance l in the complex amplitude at the source were independent of λ , then it would be easy to interpret an observed correlation. For, by altering the wavelength at which the measurement is made, the correlation distance at the receiver would vary as λ (equal to λ/θ) if $l \ll \lambda/\theta$, or would remain fixed (equal to l) if $l \gg \lambda/\theta$.

However, it is certainly not always true that l is independent of wavelength. We may take as an example a deep phase screen, i.e. a diffracting screen which produces phase fluctuations greater than one radian. In this case

$$l = L/\phi_0 \quad \dots\dots (10)$$

where L = distance over which phase fluctuations in the screen are correlated, and ϕ_0 = r.m.s. phase fluctuation (see Hewish 1951, Ratcliffe 1956). Now, if L is independent of λ , as it is in the known cases, then l will depend on λ through ϕ_0 . Here various possibilities arise. In the case of a rough or 'wavy' reflecting surface, with r.m.s. depth h

$$\phi_0 = 2\pi h/\lambda \quad \dots\dots (11)$$

so that

$$l = L\lambda/2\pi h \propto \lambda. \quad \dots\dots (12)$$

A deep phase screen may also be formed by transmission through an irregular ionized medium, and l will depend on λ in a way determined by the dispersion of the medium.

Thus the variation of the correlation distance with wavelength does not provide a reliable guide to the interpretation of the measurements unless something is known about the nature of the screen.

§ 5. THE THEORY FROM A QUALITATIVE POINT OF VIEW

We here describe a simple qualitative picture of the statistical study of an irregular diffracting screen. Each irregularity of the object scatters a wave over an angular spectrum whose width is of the order λ/l . Since we are only interested in the average irregularity, we may consider the same one to be repeated over and over again from one end of the object to the other. If in this way we gain a view of the whole angular spectrum of width λ/l (see Fig. 4) then the correlation distance at the receiver is l . The whole angular spectrum will be viewed if the angle subtended by the source is much greater than the width of the irregularity spectrum:

$$\theta \gg \lambda/l \quad \text{or} \quad \frac{2x_0 l}{\lambda z} \gg 1. \quad \dots\dots (13)$$

This is the criterion obtained in § 2 (7).

This is the converse of the Abbe theory of resolution of a microscope. In order that a detail be resolved when seen through a microscope the angle subtended by the object lens at the detail must be greater than the width of the angular spectrum of the detail.

We have not introduced angular spectra explicitly into the mathematical theory; however, this is done by Briggs (1960).



Fig. 4. Irregularities repeated at random over the source.

§ 6. CORRELATION IN THE WAVE DIFFRACTED BY A CYLINDRICAL IRREGULAR OBJECT

Suppose the object, instead of being plane, is bent into a circular arc of the order of a radian, and that the radiation is, on the average, directed radially outward from each point (see Fig. 5). When the irregularities are thus tilted more towards the edge of the source, one always sees the whole angular spectrum of width l/λ , provided only that $l > \lambda$. It is not possible to see the edge of the source unless $l \sim \lambda$. The following diffraction theory will illustrate this.



Fig. 5. Coordinate system for diffraction by a cylindrical object.

The coordinate system is shown in Fig. 5. Angles are measured from a reference line OR and the object is assumed to extend over an arc $\pm \psi_0$. The receiver is at P, and $\angle POR = \nu$. The distance to a point Q on the object from P is r , and $\angle QOR = \psi$. The radius is a , and the distance $OP = z$.

The complex amplitude $f(\psi)$ is assumed to be statistically stationary over the range $|\psi| < \psi_0$ and we define a correlation function

$$\rho_f(\mu) = \frac{f(\psi)f^*(\psi+\mu)}{f(\psi)f^*(\psi)} \quad \dots\dots (14)$$

$\rho_f(\mu)$ falls to zero at $\mu = \mu_0$, say; the irregularity size is $l = a\mu_0$. The complex amplitude at P is

$$g(\nu) = \sqrt{\left(-\frac{i}{\lambda z}\right)} \int_{-\psi_0}^{\psi_0} a d\psi f(\psi) \exp\left\{-\frac{2\pi i r(\psi-\nu)}{\lambda}\right\} \quad \dots\dots (15)$$

($r(\psi-\nu)$ is read, r is a function of $\psi-\nu$.) Assuming $a \ll z$,

$$\begin{aligned} r &= [a^2 + z^2 - 2az \cos(\psi-\nu)]^{1/2} \\ &= z[1 - 2(a/z) \cos(\psi-\nu)]^{1/2} \\ &= z - a \cos(\psi-\nu). \end{aligned} \quad \dots\dots (16)$$

The correlation function of the complex amplitude at P is†

$$\rho_g(\nu) = \frac{\overline{g(0)g^*(\nu)}}{\overline{g(0)g^*(0)}}. \quad \dots\dots(17)$$

From (15):

$$\begin{aligned} \overline{g(0)g^*(\nu)} &= \frac{a^2}{\lambda z} \int_{-\psi_0}^{\psi_0} d\psi \int_{-\psi_0}^{\psi_0} d\psi' \overline{f(\psi)f^*(\psi')} \exp \left\{ -\frac{\pi ia}{\lambda} [\cos(\psi' - \nu) - \cos \psi'] \right\} \\ &= \frac{a^2}{\lambda z} \int_{-\psi_0}^{\psi_0} d\psi \int d\psi_1 \left[\overline{f(\psi)f^*(\psi + \psi_1)} \exp \left\{ -\frac{\pi ia}{\lambda} [\cos(\psi + \psi_1 - \nu) - \cos \psi] \right\} \right] \\ &= \frac{a^2}{\lambda z} \overline{ff^*} \int_{-\psi_0}^{\psi_0} d\psi \int d\psi_1 \left[\rho_f(\psi_1) \right. \\ &\quad \times \exp \left\{ -\frac{2\pi ia}{\lambda} \sin \psi \sin(\psi_1 - \nu) - \frac{4\pi ia}{\lambda} \cos \psi \sin^2 \frac{\psi_1 - \nu}{2} \right\} \left. \right]. \quad \dots\dots(18) \end{aligned}$$

The substitution $\psi' = \psi + \psi_1$ has been made. The integral with respect to ψ cannot be performed as it stands; however we may discuss its behaviour well enough if we make the approximations $\sin \psi = \psi$, $\cos \psi = 1$; consistently, one may put $\sin(\psi_1 - \nu) = \psi_1 - \nu$. Eqn (18) becomes, accordingly,

$$\begin{aligned} \overline{g(0)g^*(\nu)} &= \frac{a^2}{\lambda z} \overline{ff^*} \int_{-\psi_0}^{\psi_0} d\psi \int d\psi_1 \rho_f(\psi_1) \exp \left\{ -\frac{2\pi ia\psi(\psi_1 - \nu)}{\lambda} \right\} \exp \left\{ -\frac{\pi ia(\psi_1 - \nu)^2}{\lambda} \right\} \\ &= \frac{a^2}{\lambda z} \overline{ff^*} \int d\psi_1 \rho_f(\psi_1) \frac{\sin [2\pi a\psi_0(\psi_1 - \nu)/\lambda]}{\pi a(\psi_1 - \nu)/\lambda} \exp \left\{ -\frac{\pi ia(\psi_1 - \nu)^2}{\lambda} \right\}. \quad \dots\dots(19) \end{aligned}$$

We may expect this integral to behave like (5), §2. The behaviour of the integral may be discussed now in terms of the quantity $2a\psi_0\mu_0/\lambda = 2\psi_0 l/\lambda$ instead of $2x_0 l/\lambda z$. First, suppose

$$2\psi_0 l/\lambda \gg 1. \quad \dots\dots(20)$$

Since $\psi_0 \lesssim 1$ this means $l \gg \lambda$. The second factor in (19) cannot really be a delta function because ψ_0 cannot tend to infinity; none the less its oscillations are such that only the part of $\rho_f(\psi_1)$ near $\psi_1 = \nu$ is important, the oscillations cancel each other out elsewhere.

$$\text{Hence} \quad \overline{g(0)g^*(\nu)} \propto \rho_f(\nu), \quad \rho_g(\nu) = \rho_f(\nu). \quad \dots\dots(21)$$

Therefore the angle over which the wave front is correlated is independent of the distance z .

On the other hand, if $l/\lambda \sim 1$, then $\overline{g(0)g^*(\nu)}$ will fall to zero when

$$0 \sim \sin \left\{ \frac{2\pi a\psi_0(\psi_1 - \nu)}{\lambda} \right\} \sim \sin \left\{ 2\pi - \frac{2\pi a\psi_0\nu}{\lambda} \right\}$$

or

$$\nu \simeq \frac{\lambda}{2a\psi_0}.$$

The linear extent of correlation in the wave front at a distance z is

$$z\nu = \frac{z\lambda}{2a\psi_0} = \frac{\lambda}{\psi_0\theta} \quad \dots\dots(22)$$

where θ is the angle subtended by the source at P. (22) is essentially the formula used in the theory of the Michelson interferometer. Thus the interferometer measures the overall diameter of the source only if $l \sim \lambda$.

† As before, we only consider correlation on the axis of the source.

§ 7. THE REFLECTION OF RADIO WAVES FROM THE MOON

Radio echoes have been successfully received from the moon, in a number of experiments, since 1947. Results using different wavelengths have been accumulated over a wavelength range of about 150:1. Some attempt will be made here to interpret the data in terms of a diffraction process for the moon.

A radio echo received from the moon fades in an irregular way, with a period dependent on the wavelength, but of the order of one second. This fading is due to the libration of the moon; i.e., an oscillation of the moon about its axis, at the rate of about 3 degrees per day. One may regard the fading as due to a Doppler shift in the echo from the limbs of the moon, or as due to a rotation of the reflected wave about the moon's axis in step with the libration. Since no wave theory has been used in previous discussions of the problem, the Doppler shift explanation was always used, (see Pawsey and Bracewell 1955). With the wave theory it is simpler to use the second approach.

We must modify the preceding theory slightly, because of the fact that the radiated wave is produced by reflection from the moon. Hence the angular spectrum of the irregularities is no longer centred on the normal to the surface, but is inclined to it. The complex amplitude at the lunar surface is no longer statistically stationary. To make it so one must take account of the extra phase $2\pi a(1 - \cos\psi)/\lambda$ involved in reflection. If we write the complex amplitude at the surface in the form

$$f(\psi) \exp \left\{ -\frac{2\pi ai}{\lambda} (1 - \cos\psi) \right\} \simeq f(\psi) \exp \left(-\frac{\pi i a \psi^2}{\lambda} \right)$$

then $f(\psi)$ will be statistically stationary. It may then be shown that (21) becomes

$$\rho_g(\nu) = \rho_f \left(\frac{\nu}{2} \right). \quad \dots\dots (23)$$

If the width of $\rho_g(\nu)$ is ν_0 , the width of $\rho_f(\nu)$ is $\nu_0/2$.

Now, let the libration rate of the moon be ω radians/sec, then the wave reflected from the moon is turned at twice that rate past the receiver. If the fading is correlated over a time τ_0 , then $g(\nu)$ is correlated over an angle $\nu_0 = 2\omega\tau_0$.

If $2l \gg \lambda$, then $\rho_g(\nu) = \rho_f(\frac{1}{2}\nu)$ and the irregularity size l at the moon is given by

$$l = a \frac{\nu_0}{2} = a\omega\tau_0. \quad \dots\dots (24)$$

If $l \sim \lambda$, then the angular width of correlation at the receiver is (Eqn (22)) $\lambda/(2a\psi_0)$.

Therefore
$$\tau_0 = \frac{\lambda}{4a\omega\psi_0} = \frac{\lambda}{\psi_0^4 (\text{limb velocity})}^\dagger. \quad \dots\dots (25)$$

Measurements made on three frequencies are collected in the Table below.

f	λ	τ_0	f_0	l	a'	Observer
(Mc/s)	(m)	(sec)	(c/s)	(m)		
20	15	—	0.15	6.7	a	Kerr and Shain 1951
120	2.5	1	—	1	$a/3$	Evans 1957
400	0.75	—	2	0.5	$2a/3$	Fricker <i>et al.</i> 1958

λ , f = wavelength and frequency of observation; τ_0 = typical period of correlation in fading, if reported; f_0 = typical frequency of fading, if reported. (— indicates that no measurement was reported; roughly, $\tau_0 = f_0^{-1}$); l = irregularity size, calculated from (24); a' = effective radius of the moon, given by the observer, on Doppler shift argument.

[†] According to the Doppler shift argument, which applies in this case, the frequency shift is $\tau_0^{-1} = 4v/\lambda$, where v is the limb velocity (Pawsey and Bracewell, p. 301), which agrees approximately with this (Eqn (25)).

The measurements indicate approximately that

$$\tau_0 \propto \lambda. \quad \dots\dots (26)$$

This conclusion is consistent with the postulate of a perfectly rough moon. For in this case $\tau_0 \propto \lambda$ (25). None the less all the observers, except perhaps Kerr and Shain agree that the moon is nearly a specular reflector. Direct measurements of the depth of the reflecting region using pulses have shown that most of the received power comes from the central part of the moon.

If we then rule out the possibility of a completely rough moon, and assume on the contrary $l \gg \lambda$, l follows from (24), and is given in the above Table. Since $l \propto \lambda$, the average angular spectrum of each irregularity is independent of frequency. It must be noted that the values of l obtained from (24) are comparable with λ , and so (23) and (24) are only roughly applicable.

The moon now appears to behave like a deep phase screen, as described in § 2. It produces phase fluctuations ϕ , with a scale L such that $l = L/\phi_0$, where $\phi_0 = \text{r.m.s. } \phi, \gg 1$. The actual value of ϕ_0 may be estimated from the observed depth of fading, but this has not yet been done by the author. Since at the longest wavelength used (15m) the moon did appear to be completely rough, it may be that the irregularities in the lunar surface are some 15m across.

Each irregularity in the lunar surface acts like a nearly specular reflector, and the tilts of these reflectors to the horizontal are given by the observed widths of the angular spectra ; viz., up to about 20° , for an effective radius of $a/3$.

It must be stressed that since neither extreme case $l \ll \lambda$ or $l \gg \lambda$ is strictly applicable, any further work should be directed toward a more precise calculation of correlation in the wave front when $l \sim \lambda$.

A recent note by Hargreaves (1959) has discussed these questions. He concluded from the experimental data that the width of the angular spectrum is constant, and postulated two models to explain this. He tried to distinguish between a deep phase screen and a faceted surface, maintaining that the facets of the surface will each give specular reflection provided they be larger than a Fresnel zone. Now the condition for specular reflection is not this, but that the irregularity be large compared to a wavelength. The comparison with a Fresnel zone is relevant only in calculating the amplitude of the reflected wave. There is in fact no difference between a faceted surface and a deep phase screen ; the former is a special case of the latter, and the same mathematical model serves for both.

§ 8. CONCLUSION

A simple theory of diffraction by irregular objects is given, which shows how the correlation size in the diffracted wave depends not only on the small scale irregularities in the object but also on the size of the object and the distance from it. The theory includes both the cases of irregularity size measurement in the ionosphere, and the Michelson method of measuring the angular diameter of a star.

The diffraction by a curved object is examined and illustrated by recent experiments on radio echoes from the moon. It is concluded that the irregularities in the lunar surface cause phase fluctuations much greater than one radian, and that these phase fluctuations are correlated over a distance of some 15m.

ACKNOWLEDGMENTS

The author is much indebted to Dr. G. S. Kent, Dr. B. H. Briggs and Mr. J. A. Ratcliffe for their help and criticism. The problem was brought to his attention by Dr. Kent in connection with reflections from meteor trails. Discussion with Dr. Briggs was helpful especially in the interpretation of moon echoes.

The author was in receipt of a Special Scholarship from the National Research Council of Canada when the work was carried out.

REFERENCES

- BOOKER, H. G., RATCLIFFE, J. A., and SHINN, D. H., 1950, *Phil. Trans. Roy. Soc. A*, **242**, 856.
BRIGGS, B. H., 1961, *Proc. Phys. Soc.*, **77**, 305.
EVANS, J. V., 1957, *Proc. Phys. Soc. B*, **70**, 1105.
FRICKER, S. J., INGALLS, R. P., MASON, W. C., STONE, M. L., and SWIFT, D. W., 1958, *Mass. Inst. Tech., Technical Report No. 187*.
HARGREAVES, J. K., 1959, *Proc. Phys. Soc.*, **73**, 536.
HEWISH, A., 1951, *Proc. Roy. Soc. A*, **209**, 81.
KERR, F. J., and SHAIN, C. A., 1951, *Proc. Inst. Radio Engrs*, **39**, 230.
MERCIER, R. P., 1959, *Phil. Mag.*, **4**, 763.
PAWSEY, L. J., and BRACEWELL, R. N., 1955, *Radio Astronomy* (Oxford: University Press).
RATCLIFFE, J. A., 1956, *Rep. Progr. Phys.*, **19**, 188.
ZERNIKE, F., 1938, *Physica*, **5**, 785.

The Separation of Symmetrical and Asymmetrical Wave-front Aberrations in the Twyman Interferometer

BY P. HARIHARAN AND D. SEN

National Physical Laboratory of India, New Delhi, India

MS. received 6th July 1960

Abstract. By reflecting the two wave fronts emerging from a Twyman interferometer back through the interferometer once again, it is possible to obtain two separate interferograms showing, respectively, the symmetrical and asymmetrical parts of the wave aberration of an optical system. These can then be analysed to obtain the various aberration coefficients of the system in a very simple manner.

§ 1. INTRODUCTION

THE interference pattern obtained with a lens in a Twyman interferometer is essentially a contour map of the wave front leaving the lens aperture, in which each fringe passes through all the points having the same optical path difference. The patterns produced by wave fronts having certain particular aberrations are easily recognized and can also be synthesized from theoretical considerations, as was first shown by Kingslake (1926) and more recently by Coleman, Clark and Coleman (1947). In theory, therefore, it should be possible to identify the various aberrations of a lens from a study of the interferogram obtained with it. However, when many aberrations are present simultaneously, the quantitative analysis of such an interferogram to obtain the individual aberrations is notoriously difficult.

The problem can be considerably simplified, if, as pointed out by Bates (1947), the number of aberration coefficients to be evaluated at one time is reduced by isolating either the symmetrical or the asymmetrical part of the wave aberration. Thus, the asymmetrical aberrations can be measured separately with an inverting interferometer such as that described by Gates (1955), or by Saunders (1955), in which the wave front which is being studied is made to interfere with its own mirror image. However, a better solution which would facilitate immediate visual interpretation would be if the symmetrical and asymmetrical parts of the aberration could be directly displayed in separate interferograms taken on the same instrument at the same setting. The present paper shows how this can be done by modifying the Twyman interferometer in a very simple fashion.

§ 2. CLASSIFICATION OF ABERRATIONS

The most convenient method of classifying wave-front aberrations is that outlined by Hopkins (1950), which utilizes the coordinate system shown in Fig. 1. In this, AO_0 is the optical axis of the lens, A being the axial point of the exit pupil and O_0 the paraxial image, O is the Gaussian image of an extra-axial object point, O_0O is the Gaussian image plane, perpendicular to AO_0 , and AO_0O is the tangential plane. The obliquity of the principal ray AO is measured by O_0O , the Gaussian image height, which is expressed for convenience as a

fraction σ of the maximum value of O_0O . Any point R in the pupil is defined in polar coordinates by its perpendicular distance from AO (expressed as a fraction r of the maximum semi-aperture) and the angle ϕ which the plane RAO makes with the meridian plane AO_0O .



Fig. 1. Coordinate system used in the analysis of wave-front aberrations.

From formal considerations, it can be shown that $W(\sigma, r, \phi)$, the aberration of the element of wave front associated with the ray passing through R , can be represented by the sum of a series of terms, each of which is the product of a coefficient and powers of r^2 , σ^2 and $\sigma \cos \phi$. If the reference sphere considered has its centre at the Gaussian image point, this series takes the form

$$W(\sigma, r, \phi) = {}_0c_{40}r^4 + {}_0c_{31}\sigma r^3 \cos \phi + {}_2c_{22}\sigma^2 r^2 \cos^2 \phi + {}_2c_{20}\sigma^2 r^2 + {}_3c_{11}\sigma^3 r \cos \phi + \dots \quad (1)$$

The first five terms of this series are the so-called Seidel aberrations, and, by an obvious extension of the nomenclature applied to these, the general aberration terms can be classified into three categories. Thus, spherical aberration terms are those which are independent of ϕ , comatic aberration terms involve odd powers of $\cos \phi$, and astigmatic aberration terms involve even powers of $\cos \phi$. With this terminology, it is seen that the 'symmetrical' part of the aberration involves spherical aberration and astigmatic terms, while the 'asymmetrical' part comprises the comatic terms, so that we can express the total wave-front aberration $W(\sigma, r, \phi)$ in the form

$$W(\sigma, r, \phi) = W_{\text{even}}(\sigma, r, \phi) + W_{\text{odd}}(\sigma, r, \phi) \quad (2)$$

where W_{even} represents the sum of the terms involving even powers of $\cos \phi$, and W_{odd} represents the sum of the terms involving odd powers of $\cos \phi$.

In theory, an investigation of the wave-front aberration over the pupil for a number of values of σ should make possible the identification of the aberration terms present, and the assignment of a value to each coefficient. However, when all the aberrations are present, the task is rather difficult, since there are five coefficients to be determined simultaneously for the primary aberrations alone. A considerable simplification can obviously be effected if W_{even} and W_{odd} , i.e. the sums of the terms depending on even powers of $\cos \phi$ and the terms depending

on odd powers of $\cos \phi$, can be evaluated separately. In this case the number of coefficients to be determined at one time is reduced to three and two, respectively, if we consider only the primary aberrations.

§ 3. THEORY OF THE METHOD

The separation of the 'odd' and 'even' parts of the total wave-front aberration is effected in the Twyman interferometer basically by inverting the two wave fronts emerging from the interferometer and reflecting them back through the interferometer once again. This can be done either by means of a corner-cube, or a combination of a lens and a plane mirror placed at its focus. In practice, the latter is preferable. The paths of the rays in a Twyman interferometer modified in this fashion are shown schematically in Fig. 2. As can be seen from

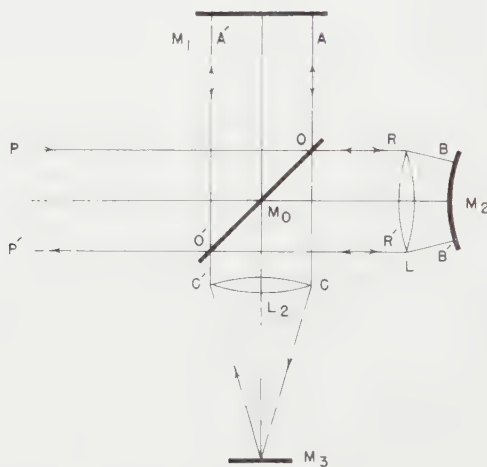


Fig. 2. Paths of the rays in the modified Twyman interferometer.

this, any ray entering the interferometer from the left and incident on the semi-reflecting mirror M_0 at O is divided into two rays, one of which traverses the reference path $POAOC$ (which we shall term the A path) and the other the path $POBOC$ (which we shall term the B path) in which the lens system under test is located. When these rays are reflected back through the interferometer by means of the plane mirror M_3 placed at the focus of the lens L_2 , each of them is further divided into two rays, one of which returns along the path $C'O'A'O'P'$ (the A' path) while the other returns along the path $C'O'B'O'P'$ (the B' path) giving us four rays in all. We can term any ray which has made the to-and-fro journey through the interferometer a double-passed ray (Hariharan and Sen 1960), and identify it by two letters, the first corresponding to the path followed by the ray on the outward journey and the second to that followed by it on the return journey. Accordingly, the four double-passed rays emerging from the interferometer may be termed the AA' ray ($POAOCC'O'A'O'P'$), the AB' ray ($POAOCC'O'B'O'P'$), the BA' ray ($POBOCC'O'A'O'P'$), and the BB' ray ($POBOCC'O'B'O'P'$). Of these, the BB' ray traverses the lens system four times, while the AB' and BA' rays traverse it twice, and the AA' ray does not traverse it at all.

Since the combination of the lens L_2 and mirror M_3 inverts the wave fronts emerging from the interferometer before sending them back through the interferometer, it is easily seen that if on the outward journey the BB' ray corresponding to a given point P in the field traverses the pupil at a point R with the coordinates (r, ϕ) , the point R' at which it traverses it when it is reflected back through the interferometer will be diametrically opposite to R in the pupil and will therefore have the coordinates $(r, \pi + \phi)$. In the same manner, while the corresponding BA' ray traverses the pupil at the point R , the AB' ray traverses it at R' . At these two points, all the terms in the expressions for the total wave-front aberration in which the exponent of $\cos \phi$ is even (i.e. the spherical aberration and astigmatic terms) will have the same value, while the terms for which this index is odd (i.e. the comatic terms) will be of equal magnitude but will have opposite signs.

If, then, we assume for the sake of simplicity that the end mirrors M_1 , M_2 of the interferometer are set normal to the principal rays in the two paths, so that the only variations in the optical paths of the beams are those due to the lens system under test, we can express the total optical paths of the four double-passed rays at any point in the field in the form

$$D_{AA'} = D \text{ (say)} \quad \dots\dots (3)$$

$$D_{BA'} = D + 2W_{\text{even}} + 2W_{\text{odd}} + \Delta D \quad \dots\dots (4)$$

$$D_{AB'} = D + 2W_{\text{even}} - 2W_{\text{odd}} + \Delta D \quad \dots\dots (5)$$

$$\text{and } D_{BB'} = D + 2W_{\text{even}} + 2W_{\text{odd}} + \Delta D + 2W_{\text{even}} - 2W_{\text{odd}} + \Delta D \\ = D + 4W_{\text{even}} + 2\Delta D \quad \dots\dots (6)$$

where W_{even} is the sum of the spherical aberration and astigmatic terms at the point R in the pupil, W_{odd} is the sum of the comatic aberration terms at the same point, and ΔD is the difference in the lengths of the A and B paths for the principal ray.

It follows, therefore, that if the AB' and BA' rays are made to interfere (the AA' and BB' rays being eliminated by a suitable arrangement), the path difference between them is given by the relation

$$D_{BA'} - D_{AB'} = 4W_{\text{odd}}. \quad \dots\dots (7)$$

Features of the wave front which depend on even powers of $\cos \phi$ will therefore disappear, while features which depend on odd powers of $\cos \phi$ will be doubled. Hence, asymmetric errors such as distortion and coma will be shown in this interferogram, independent of the effects of change of focus, spherical aberration and astigmatism.

Similarly, if the AA' and BB' rays are made to interfere (the AB' and BA' rays being eliminated by a suitable arrangement) the path difference between them is given by the relation

$$D_{BB'} - D_{AA'} = 4W_{\text{even}} + 2\Delta D. \quad \dots\dots (8)$$

so that features of the wave-front which depend on odd powers of $\cos \phi$ disappear, while features which depend on even powers of $\cos \phi$ are doubled. Accordingly, only symmetric errors such as change of focus, spherical aberration and astigmatism will be recorded in this interferogram.

Any tilt of the reference mirror M_1 with respect to the mean plane of the wave front under investigation normally results in an increase in the number of fringes in the single-passed interferogram. Such a tilt can be considered

equivalent to the introduction of an additional 'odd' aberration term in the expression for the total optical path difference. This term is automatically eliminated in the interferogram formed by the AA' and BB' rays, which is therefore unaffected by a tilt of the reference mirror. However, it is doubled in the interferogram formed by the BA' and AB' beams and consequently results in twice the number of additional fringes across the field in this case.

§ 4. OPTICAL SYSTEM

The optical system of the modified Twyman interferometer is shown in Fig. 3. The interferometer is illuminated with a parallel beam of monochromatic light from the collimator L_1 and the beams emerging from the interferometer through the lens L_2 are reflected back again through it by the plane mirror M_2 placed at its focus. The double-passed beams emerging from the interferometer through L_1 are brought to a focus at E by means of the semi-reflecting mirror M_4 .

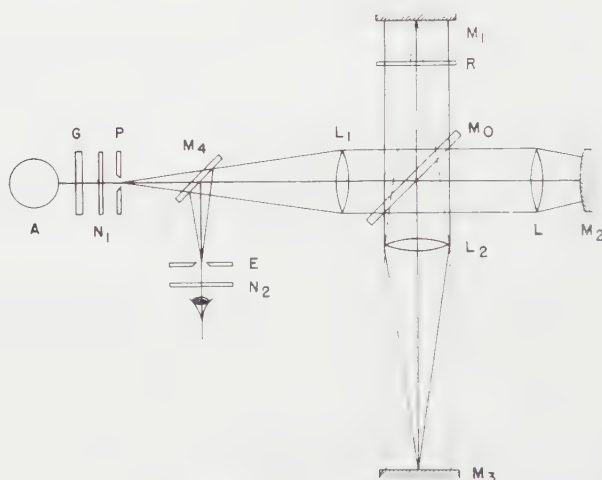


Fig. 3. Optical system of the modified Twyman interferometer. A, mercury arc; G, green filter; P, pinhole; L_1 , L_2 , objective lenses; M_0 , beam divider; M_1 , M_2 , M_3 , plane mirrors; M_4 , auxiliary semi-reflecting mirror; E, exit stop; L, lens system under test; N_1 , N_2 , polarizers; R, quarter-wave plate.

The double-passed beams are separated from the single-passed beams reflected back directly from the mirrors M_1 , M_2 by shifting the pinhole P very slightly off-axis, so that the beam from the lens L_1 makes a small angle with the normals to M_1 and M_2 . The images formed at E by the two sets of beams then move off the axis in opposite directions by equal amounts. By shifting the eye stop E, it is possible to view either the normal interference pattern, or the pattern produced by the double-passed beams at will.[†]

[†] Note added in Proof.—Images due to multiple-passed beams of higher orders are also formed in this instrument. Among these, the images due to multiple-passed beams of odd orders, such as the third and the fifth, coincide with the single-passed image and are therefore eliminated along with it. Only the images due to multiple-passed beams of even orders, such as the fourth and the sixth, coincide with the double-passed image. However, the intensity of these higher order images falls off quite rapidly, so that the image formed by the quadruple-passed beams is normally weak enough not to affect the double-passed fringes.

The two combinations of double-passed rays required are selected by means of a system consisting of two polarizers and a quarter-wave plate. The beam from the collimator is initially polarized in the vertical plane by means of the polarizer N_1 , and the quarter-wave plate R is introduced in the A path, as shown in Fig. 3, with its optic axis in azimuth $+45^\circ$. It is then easily seen that the AB' and BA' beams, both of which traverse the quarter-wave plate twice, have their planes of polarization rotated through 90° so that they emerge polarized in the horizontal plane, while the AA' beam which traverses the quarter-wave plate four times and the BB' beam which does not traverse it at all emerge polarized in the vertical plane. Hence, when the polarizer N_2 is set with its axis parallel to that of N_1 , the AB' and BA' beams are extinguished and the interference pattern due to the AA' and BB' beams alone is visible, while when N_2 is rotated through 90° from this position, the AA' and BB' beams are extinguished so that the interference pattern due to the AB' and BA' beams alone is visible.

No particular difficulty was experienced in securing the double-passed fringes with this arrangement, once the Twyman interferometer had been initially adjusted, according to the usual procedure, to give the normal, single-passed fringes. Only two precautions were found necessary. One was to adjust the distance of the combination of the lens L_2 and mirror M_3 from M_1 approximately so that the latter was imaged on itself. The other was to verify that the axis of L_2 coincided with the principal ray, and that the mirror M_3 was normal to it, since any appreciable deviation from these conditions introduces shear between the AB' and BA' wave fronts. For this, M_3 was first set so that the image of the pinhole P formed by the double-passed rays when the lens L_2 was removed coincided with the image formed by the single-passed beams reflected back from M_1 and M_3 . After this, L_2 was replaced and adjusted so that M_3 was at its focus, and the two images of the pupil formed by the AB' and BA' beams exhibited no shear relative to one another.

§ 5. MEASUREMENTS

Two typical sets of interferograms obtained with this arrangement, with an uncorrected lens, are shown in Figs 4 and 5 (Plate). Both sets were made under the same conditions, except that for the second set the reference mirror was slightly tilted. In each of these sets, the first picture is the normal, single-passed interferogram, while the second and third are the double-passed interferograms showing the 'even' and 'odd' components, respectively, of the wave-front aberrations. As has been pointed out in the theoretical discussion, the wave-front aberrations are doubled in the latter two interferograms, so that the contour interval in them is only half of that in the single-passed interferogram. It is apparent from these photographs that the tilt of the reference mirror has no effect at all on the interference pattern formed by the AA' and BB' rays, which shows only the 'even' part of the wave-front aberration.

Each of the double-passed interferograms in Fig. 4 was analysed following a procedure similar to that outlined by Gates (1955). This analysis is further simplified in the present case by the fact that the spherical aberration terms and the astigmatic terms can be easily separated. Thus, in the interferogram showing the 'even' part of the aberration, the astigmatic terms vanish when $\phi = \pi/2$. This makes it possible to evaluate the defocusing and spherical aberration terms

directly from measurements in the sagittal plane. The astigmatic terms are then readily obtained by subtracting the wave aberrations in the sagittal plane from those in the tangential plane.

The analytical expressions for the 'odd' and 'even' parts of the wave-front aberration, taken to as many terms as necessary to secure a good fit, are given below each interferogram. The theoretical fringe patterns given by these expressions are also presented. The analytical expression for the total wave-front aberration is merely the sum of these expressions, and the theoretical interferogram obtained by combining them is plotted below the single-passed interferogram. A comparison of the two shows excellent agreement, confirming the validity of this technique.

§ 6. CONCLUSIONS

The present paper shows how the problem of analysing the aberrations of a lens system can be considerably simplified by modifying the Twyman interferometer so that the symmetrical and asymmetrical parts of the wave-front aberration are presented in separate interferograms. Each of these can be resolved into its component terms with relative ease. The accuracy of the method is verified experimentally by comparing the contour map obtained by plotting the sum of these terms with the interferogram of the original wave front.

ACKNOWLEDGMENT

The authors wish to thank the Director, National Physical Laboratory of India, for permission to publish this paper.

REFERENCES

- BATES, W. J., 1947, *Proc. Phys. Soc.*, **59**, 940.
- COLEMAN, H. S., CLARK, D. G., and COLEMAN, M. F., 1947, *J. Opt. Soc. Amer.*, **37**, 671.
- GATES, J. W., 1955, *Proc. Phys. Soc. B*, **68**, 1065.
- HARIHARAN, P., and SEN, D., 1960, *J. Opt. Soc. Amer.*, **50**, 357.
- HOPKINS, H. H., 1950, *Wave Theory of Aberrations* (Oxford: Clarendon Press), p. 48.
- KINGSLAKE, R., 1926, *Trans. Opt. Soc. Lond.*, **27**, 94, **28**, 1.
- SAUNDERS, J. B., 1955, *J. Opt. Soc. Amer.*, **45**, 133.

Features of the Elastic Wave Surface for a Zinc Crystal

By M. J. P. MUSGRAVE AND M. F. MARKHAM

National Physical Laboratory

MS. received 11th July 1960

Abstract. In recent years the elastic wave surfaces for certain crystals have been calculated from observed values of physical constants. The surfaces show geometrical features which have interesting physical interpretation.

Experiments designed to verify the existence of one of the cuspidal edges on the wave surface for zinc are described.

As an example of the use of a general method of computation for the elastic wave surfaces of anisotropic media (Musgrave 1954a), the zonal section of the wave surface in the hexagonal crystal zinc was given (Musgrave 1954b). The form of the T_2 -wave sheet with its cuspidal edges has been considered startling particularly since it implies that there are five waves whose associated energy fluxes travel along any ray inclined at less than 26° to the zonal axis. Accordingly, some experimental evidence further to that reported by Markham (1957) and Musgrave (1959) has been sought which might help to authenticate for remaining sceptics the form of the wave surface presented.

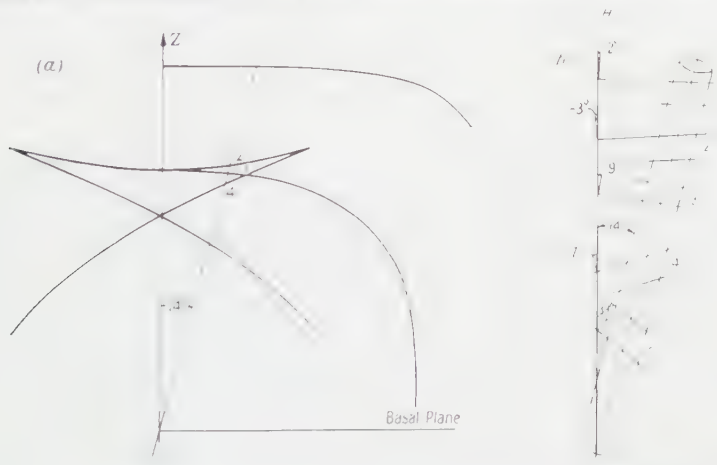


Fig. 1 (a). Part of a zonal section of elastic wave surface of zinc showing how five waves have associated energy fluxes along a ray at 14° to the zonal axis.

Fig. 1 (b). The circularly cylindrical seeded crystal with the detail of the cuts made to provide the five specimens.

Fig. 1 (a) shows the relevant section of the wave surface and a ray making an angle of 14° with the zonal axis. The quasi-longitudinal (1), truly transverse (3) and quasi-transverse (2, 4, 5) waves should have associated energy fluxes along this ray. To verify this, a single crystal of zinc was grown in the shape of a circular cylinder whose axis was at 14° to the zonal axis. This particular orientation was chosen in order to achieve a maximum distinction of the wave normals 2, 3 and 4. Specimens with pairs of parallel faces were prepared from the large crystal as indicated in Fig. 1 (b). The normals to these faces were those of the tangent

planes at the points on the wave surface defined by the radius vector at 14° to the zonal axis. In each of the five specimens, the energy flux of the wave with appropriate displacement vector should therefore be parallel to the generators of the original cylinder.

In so far as was possible by mounting transmitting and receiving transducers at different sites on the plane faces of the specimens, it was verified that the maximum amplitude was received when the line joining the centres of the transducers was parallel to the generators of the original cylinder. In each case, however, accurate measurement of the time of transit was made using apparatus described by Markham (1957) and recently refined. In conjunction with the perpendicular distances between the parallel faces, accurate determinations of the relevant phase velocities were made. The details of the specimens and the observed velocities are given in the Table where values of the phase velocities calculated from the constants used by Musgrave (1954 b) (set A) and those given by Huntington (1958) (set B) are also included.

(1)	(2)	(3)	(4)	(5)	(6)	
					A	B
1	L	2°	1.0460	2987 ± 3	2700	2990
2	T_2	-3°	1.2830	2324 ± 3	2313	2277
3	T_1	9°	1.1983	2357 ± 3	2392	2343
4	T_2	-17°	1.1470	2044 ± 3	2014	1990
5	T_2	39°	0.9596	1817 ± 3	1835	1797

(1) Specimen number, (2) wave, (3) angle of wave normal to zonal axis θ , (4) distance between parallel faces (cm), (5) observed velocity (m sec $^{-1}$), (6) calculated velocity (m sec $^{-1}$).

Set A, used to calculate the wave surface from which the specifications for the test pieces were made, was derived from the values of Bridgeman (1924) and Hanson (1934). The two sets A and B are significantly different but both satisfy the inequalities for the existence of the cuspidal edges (Musgrave 1957) so that the qualitative features of the propagation remain unaltered. However, a comparison of the observed and calculated phase velocities shown in the Table appears to offer confirmatory evidence for the value of the individual constant c_{33} from the later set B while the other observations are consistent with the general pattern of anisotropy given by B but with a slightly higher value of c_{44} .

We wish to acknowledge the care exercised by Dr. L. M. T. Hopkin, Metallurgy Division, in the growth of the seeded crystal and in the preparation of the specimens. The work described has formed part of the research programme of the National Physical Laboratory and is published with the permission of the Director.

REFERENCES

- BRIDGEMAN, P. W., 1924, *Proc. Nat. Acad. Sci. Wash.*, **10**, 411.
HANSON, A. W., 1934, *Phys. Rev.*, **45**, 324.
HUNTINGTON, H. B., 1958, *Solid State Physics*, **7**, 213 (New York : Academic Press).
MARKHAM, M. F., 1957, *Brit. J. Appl. Phys.*, Suppl. No. 6.
MUSGRAVE, M. J. P., 1954 a, *Proc. Roy. Soc. A*, **226**, 339,
— 1954 b, *Proc. Roy. Soc. A*, **226**, 356.
— 1957, *Proc. Camb. Phil. Soc.*, **53**, 897.
— 1959, *Rep. Progr. Phys.*, **22**, 74 (London : Physical Society).

The Application of Ray Tracing Methods to Radio Signals from Satellites

By I. N. CAPON

University Mathematical Laboratory, Cambridge

Communicated by K. G. Budden; MS. received 3rd June 1960

Abstract. A method of calculating the effect that an ionosphere of given form will have on a radio signal emitted by an earth satellite is described. The method is based on ray tracing techniques, involving the integration of a system of differential equations.

Results of very high accuracy may be obtained. Some results obtained with an ionospheric model in which the electron density increases linearly up to the F2 peak, and then decays according to the Chapman law, are presented and discussed. These results relate to the received characteristics of the signal, including the Doppler shift, the Faraday effect and the refraction.

One of the models considered varies slowly with latitude, and this has a marked effect on the results. The effect of a 10% change in scale height is also shown, and is much smaller than that due to an ionospheric slope.

§ 1. INTRODUCTION

RADIO signals received from artificial earth satellites are affected by the ionosphere. Suitable measurements of the characteristics of these signals contain information about the structure of the ionosphere, but the problem of interpreting these measurements in terms of electron density distributions is complicated. At present, one of the most promising methods is to assume some model for the ionosphere and to calculate the signal that would then be received from a satellite whose position and velocity are known. This process is repeated until reasonable agreement with experimental results is obtained.

The purpose of this paper is firstly to describe a method of calculating the signal received at a given point on the earth, knowing the ionospheric structure, and secondly to present some preliminary results obtained with some simple models, including those in which the electron density varies with geographical position as well as with altitude.

The signal characteristics which are computed include the Doppler frequency shift, and also the changes in bearing and elevation of the signal. As these calculations have all been made for a frequency of 20 Mc/s, it is justifiable to neglect collisions among the electrons, and to use ray tracing techniques. One such technique has been described by Haselgrove (1957 a, b), and its application to signals from satellites is outlined in § 3 of this paper. This method has previously been used mainly for two-dimensional problems, but in this paper the three-dimensional problem is considered. The three-dimensional case has also been studied by Haselgrove (1960), using Cartesian coordinates. In addition, the ionosphere is doubly-refracting in the presence of the earth's magnetic field, and

Y

therefore there will be two rays, known as the Ordinary and Extraordinary rays, which will reach the receiver along different three-dimensional paths. These paths bear no simple relation to each other, and must be computed separately. The fluctuations in phase of the two rays causes Faraday fading of the signal.

Section 4 of this paper describes the models of the ionosphere in use, and in § 5 some of the results obtained are presented and discussed.

§ 2. NOTATION

The notation in this paper is as follows: r, θ, ϕ spherical polar coordinates of points on the ray path, with the origin at the centre of the earth and the axis through the observer; e, m charge and mass of the electron; N electron density; $X = Ne^2/\epsilon_0 m$, using rationalized units; $Y = f_H^2/f^2$, where f_H is gyro-frequency and f the signal frequency; μ is the refractive index; $\cos \alpha_r, \cos \alpha_\theta, \cos \alpha_\phi$ direction cosines of the wave-normal at (r, θ, ϕ) ; p_r (etc.) $= \mu \cos \alpha_r$ (etc.); P the phase path length; ψ the angle between the wave-normal and the earth's magnetic field and $\cos \beta_r, \cos \beta_\theta, \cos \beta_\phi$ are the direction cosines of the earth's magnetic field.

The refractive index μ is given by the Appleton-Hartree formula, viz.

$$\mu^2 = 1 + Xq$$

where q is a root of $aq^2 + 2bq + c = 0$ and

$$a = (1 - X) - Y^2 + XY^2 \cos^2 \psi$$

$$b = (1 - X) - \frac{1}{2} Y^2 \sin^2 \psi$$

$$c = 1 - X.$$

It should be noted that as a consequence of these definitions, we have the relation

$$p_r^2 + p_\theta^2 + p_\phi^2 = \mu^2$$

and hence the four variables are not independent. One of the variables could be eliminated from the equations, but it is more convenient to retain them all and to use the above relation to control the accuracy of the numerical solution of the problem; see § 3.

§ 3. THE CALCULATION OF THE RAY PATH

The ray tracing procedure of Haselgrove consists essentially of integrating a system of differential equations, three of which describe the rate of change of the wave-normal direction at points on the ray path, while three further equations describe the path itself. It should be noted that in general the wave-normal is not tangent to the ray path. The equations in use are

$$\frac{dr}{dP} = \frac{1}{\mu^2} \left\{ p_r + \frac{\mu \cos \beta_r - p_r \cos \psi}{2\mu^2 \sin \psi} \frac{\partial \mu^2}{\partial \psi} \right\}$$

$$\frac{dp_r}{dP} = \frac{1}{2\mu^2} \frac{\partial \mu^2}{\partial r} + p_\theta \frac{d\theta}{dP} + p_\phi \sin \theta \frac{d\phi}{dP}$$

$$\begin{aligned}\frac{d\theta}{dP} &= \frac{1}{r\mu^2} \left\{ p_\theta + \frac{\mu \cos \beta_\theta - p_\theta \cos \psi}{2\mu^2 \sin \psi} \frac{\partial \mu^2}{\partial \psi} \right\} \\ \frac{dp_\theta}{dP} &= \frac{1}{2r\mu^2} \frac{\partial \mu^2}{\partial \theta} - \frac{p_\theta}{r} \frac{dr}{dP} + p_\phi \cos \theta \frac{d\phi}{dP} \\ \frac{d\phi}{dP} &= \frac{1}{r\mu^2 \sin \theta} \left\{ p_\phi + \frac{\mu \cos \beta_\phi - p_\phi \cos \psi}{2\mu^2 \sin \psi} \frac{\partial \mu^2}{\partial \psi} \right\} \\ \frac{dp_\phi}{dP} &= \frac{1}{2r\mu^2 \sin \theta} \frac{\partial \mu^2}{\partial \phi} - \frac{p_\phi}{r} \frac{dr}{dP} - p_\phi \cot \theta \frac{d\theta}{dP}.\end{aligned}$$

The right-hand sides of these equations can be computed, and hence the equations can be integrated numerically. The integration process in use is a 'step-by-step' process, and is in fact the variant of the Runge-Kutta process due to Gill (1951), which allows the step-length to be changed at the end of every sub-interval. Advantage is taken of this feature in the present computer programme: the step-length is adjusted to ensure that at every stage

$$|p_r^2 + p_\theta^2 + p_\phi^2 - \mu^2| < \epsilon$$

where ϵ is the maximum error tolerated. This quantity varies during the operation of the programme, but is generally of the order of 10^{-6} or less. In addition, the step-length is reduced at any point at which the refractive index or any of its derivatives is discontinuous. Such points are made to be at the end of a sub-interval by a process due to Wheeler (1959).

The Haselgrove method enables us to find the destination of any ray, given only the initial conditions. It now remains to compute the ray joining a given transmitter position to a given receiver position. A suitable initial direction is first determined by a simple calculation, described below. The path of this ray is then traced through the model ionosphere under test. In general, this trial ray will not reach the receiving site, indeed it may not reach the ground at all. Other trial rays are computed, and their terminal positions and directions used to correct the initial direction until the ray passing through the receiver is found.

The first trial ray may of course be taken as the straight line joining the receiver and transmitter, but it has been found worthwhile to do a preliminary, two-dimensional ray tracing, neglecting the earth's magnetic field, and using a simple 'uniform slab' model of the ionosphere. The electron density of the slab must of course be given an appropriate value, but this may be found by computing the total electron content below the satellite, or below some other representative point. These preliminaries increase the accuracy of the starting vector very considerably, and occupy a trivial amount of computing time.

The correction of the initial direction in order to find the required ray is essentially a process of interpolation. Initially we have to correct two direction cosines simultaneously, but the azimuthal direction, $\cos z_\phi$, rapidly attains its final value, and thereafter we need only correct $\cos z_r$. The third direction cosine then follows from $\cos^2 z_r + \cos^2 z_\theta + \cos^2 z_\phi = 1$. No real difficulty has been encountered in these processes, although considerable effort has been put, and is being put, into decreasing the number of iterations required while maintaining a guarantee that even the most difficult rays can be computed automatically. The computing time required is heavily dependent upon the number of iterations

required, as the tracing of a single ray requires far more computing time than any of the subsidiary calculations involved.

The total time required depends heavily upon the accuracy and type of results required. For example, for either magneto-ionic component the Doppler frequency shift can be computed in less than five minutes to an accuracy far greater than could ever be observed. But finding the Faraday fading rate requires a knowledge of the difference between the Doppler frequency shifts for the two components. If each of these shifts is found to an accuracy of somewhat better than 1 part in 10^5 , this will give the Faraday fading rate to within about 3%, and to do this requires a time of the order of 10–15 minutes of the computer EDSAC II. Further accuracy is obtainable at the cost of increased computer time.

§ 4. IONOSPHERIC MODELS AND TRANSITS CONSIDERED

Some of the preliminary results obtained by the method given above are presented in § 5. In all of these results the earth's magnetic field is taken to be that of a simple dipole oriented along the earth's axis.

The ionospheric models used all have the following features:

(a) The base level is constant at 90 km. (b) They have one maximum of electron density, chosen to simulate the maximum of the F2 layer. The altitude of this maximum is given by $A = K_1\lambda + K_2$ where λ is the geographical latitude. The electron density at the maximum is given by $N_0 = K_3\lambda + K_4$. (c) Below the maximum, the electron density varies linearly with altitude. Above the peak, the Chapman law

$$N = N_0 \exp \frac{1}{2} \left[1 - \left\{ \frac{h}{H} + \exp \left(- \frac{h}{H} \right) \right\} \right]$$

is used, where h = height of satellite above maximum and H = scale height.

This family of models has been chosen for mathematical simplicity, rather than maximum physical reality.

Three of the above family of models are shown in the results given below. They are as follows:

- | | | |
|----------|---|--------------------------|
| Model 1. | $K_1 = -1.25 \text{ km deg}^{-1}$ | $K_2 = 367.5 \text{ km}$ |
| | $K_3 = -0.035 \times 10^6 \text{ electrons cm}^{-3} \text{ deg}^{-1}$ | |
| | $K_4 = 3.25 \times 10^6 \text{ electrons cm}^{-3}$ | $H = 100 \text{ km.}$ |
| Model 4. | $K_1 = K_3 = 0$ | $K_2 = 305 \text{ km}$ |
| | $K_4 = 1.5 \times 10^6 \text{ electrons cm}^{-3}$ | $H = 100 \text{ km.}$ |
| Model 6. | As model 4, but with $H = 110 \text{ km.}$ | |

Models 2, 3 and 5 are intermediate cases, not shown here. In models 4 and 6, the ionosphere is radially stratified, while model 1 has the height and the intensity of the maximum dependent upon latitude.

The orbit in use is that of revolution 3471 of Sputnik III, and the observer is taken to be at 50.87° N , 1.12° W . The transit is from the south-west towards the

orth for such an observer, at a high and rising altitude. An abbreviated table of positions is given in Table 1.

Table 1. Satellite Positions

Height is measured from the centre of the earth, latitude and longitude are of sub-satellite point

Ray ref. no.	Height (km)	Latitude (deg N)	Longitude (deg W)	Time from apex (min)
20	7132.5	44.53	19.83	-11.90
24	7158.5	46.45	17.94	-11.23
28	7184.5	48.31	15.92	-10.57
32	7210.4	50.12	13.75	-9.90
36	7236.3	51.86	11.43	-9.23
40	7262.0	53.53	8.93	-8.57
44	7287.6	55.13	6.23	-7.90
48	7313.0	56.65	3.32	-7.23
52	7338.1	58.08	0.18	-6.57
56	7362.9	59.40	-3.20	-5.90
60	7387.4	60.61	-6.82	-5.23
64	7411.5	61.70	-10.70	-4.57
68	7435.3	62.66	-14.83	-3.90
72	7458.6	63.47	-19.20	-3.23
76	7481.4	64.12	-23.77	-2.57

§ 5. RESULTS

The potential output of a ray tracing programme such as that described above is extremely large. The entire ray path is available if required, together with the wave-normal direction and geomagnetic field strength and direction at points on it. This amount of information is, however, comparatively useless because of its sheer bulk. In the results given here, only conditions at the receiver are considered, but other information is available— notably conditions at the transmitter.

The received, Doppler-shifted frequency differs from the emitted frequency by an amount

$$\frac{\mu f_0}{c} (\dot{r} p_r + r \dot{\theta} p_\theta + r \sin \theta \dot{\phi} p_\phi)$$

where the dot indicates time differentiation, f is nominal transmitter frequency, and the variables take values appropriate to the transmitter position. The difference between the frequency shifts for Ordinary and Extraordinary rays is the Faraday fading rate.

An abbreviated table of Doppler shifts is given as Table 2, while the derived fading rates are plotted in Fig. 1. Table 2 also gives the angle M between the geomagnetic field and the Ordinary ray at the transmitter, to the nearest degree. Fig. 2 is a plot of the difference in phase path length, in wavelengths, for the two components: this is essentially a plot of the number of Faraday fades experienced by the signal. The abscissa in both figures is time, measured from the apex of the orbit.

From the Appleton-Hartree formula, it appears that the number of Faraday fades should be a minimum when the propagation is most nearly transverse, as then the two refractive indices, and hence the two rays, are most nearly coincident. It is, however, noticeable that the minimum in Fig. 2 does not appear at the time when the ray leaves the satellite transverse to the field. However, this shift of

Table 2. Frequency Shifts for Various Models (c/s)

The column M gives the angle between the geomagnetic field and the wave-normal at the satellite in the case of Model 1, Ordinary ray.

Ref. no.	No. ions.	M (deg)	Model 1		Model 4		Model 6	
			Ord.	Extra.	Ord.	Extra.	Ord.	Extra.
20	356.63	41	307.31	304.36	317.77	315.61	317.45	315.20
24	326.26	42	286.23	283.99	293.23	291.54	292.69	290.99
28	283.09	42	251.50	249.78	256.05	254.72	255.44	254.08
32	222.37	42	198.85	197.49	201.83	200.74	201.26	200.14
36	140.76	42	125.27	124.15	127.43	126.50	127.04	126.09
40	41.18	46	33.58	32.61	35.59	34.77	35.49	34.65
44	63.78	46	64.22	65.09	61.84	62.60	61.61	62.38
48	157.69	50	152.33	153.12	149.30	150.00	148.76	149.48
52	230.96	53	221.39	222.10	217.55	218.20	216.81	217.47
56	283.39	56	270.94	271.59	266.20	266.82	265.33	265.96
60	319.39	58	304.94	305.55	299.22	299.82	298.31	298.90
64	343.74	59	327.82	328.39	321.02	321.59	320.13	320.69
68	360.16	59	343.05	343.54	335.11	335.44	334.26	334.62
72	371.19	59	353.08	353.28	344.01	343.61	343.61	343.61
76	378.52	59	359.53	359.25	349.03	347.97	347.97	347.97

the minimum may be ascribed to the fact that the ray is initially refracted upwards, and thus becomes more nearly transverse in a region of high electron density, which is of greater importance in determining the ray path.

The number of Faraday fades may also be determined by approximate methods, which neglect the refraction of the signal. The results of one such calculation, using Model Ionosphere 4, are also shown in Fig. 2. In this case, the neglect of refraction has increased the calculated number of fades over most of the



Fig. 1. Faraday fading rate (c/s) as a function of time for the various models considered.

A, Model 1; B, Model 4; C, Model 6; N, approximate calculation.

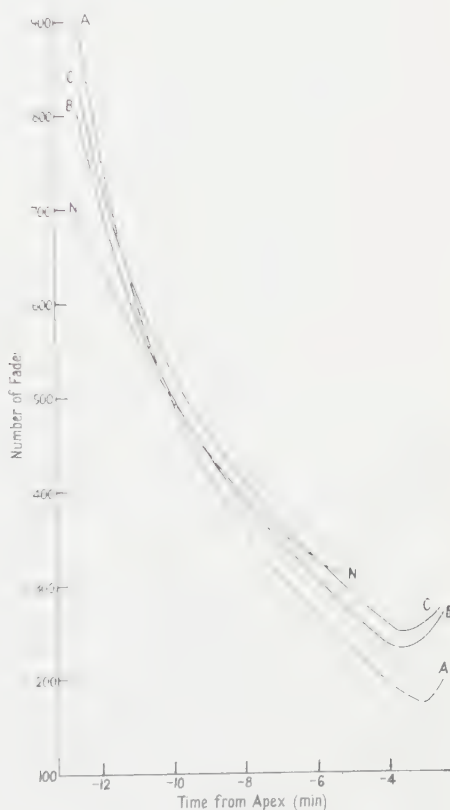


Fig. 2. Number of Faraday fades as a function of time.

transit, while decreasing the Faraday fading rate. The author is indebted to Mr. A. W. Nichol for these results, and to Mr. D. McL. A. Wilson who developed the method used: see Wilson (1959).

Fig. 3 gives the co-elevation of the received signal at the observer for the case of no ionosphere, and for the Ordinary rays for Models 1 and 4. The Extraordinary ray directions are very close to the Ordinary ray directions in each case, and are not shown. The difference between the no-ionosphere case and either of the other curves shown is the refraction in the vertical plane, or change in

elevation, produced by the relevant model ionosphere. The chief feature of these curves is the rapid increase in refraction near the horizon.

In Fig. 4, the shifts in apparent azimuth from the no-ionosphere case are plotted against time for models 1 and 4. The curves for model 6 are very similar to those for model 4. As all of the ionospheric models considered here are not dependent upon longitude, there is no change in bearing when the transmitter

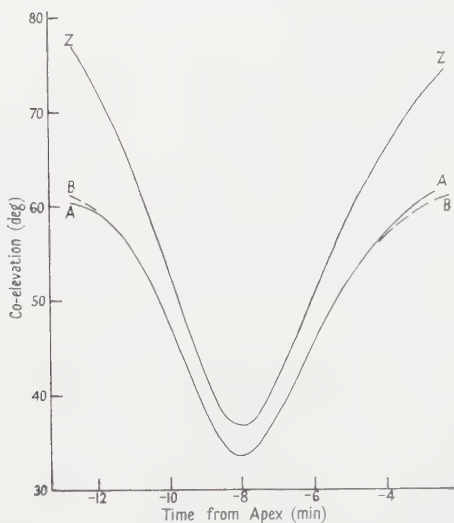


Fig. 3. Co-elevation of the received signal (degrees) as a function of time.

A, Model 1; B, Model 4; Z, no ionosphere; O, Ordinary ray; E, Extraordinary ray.

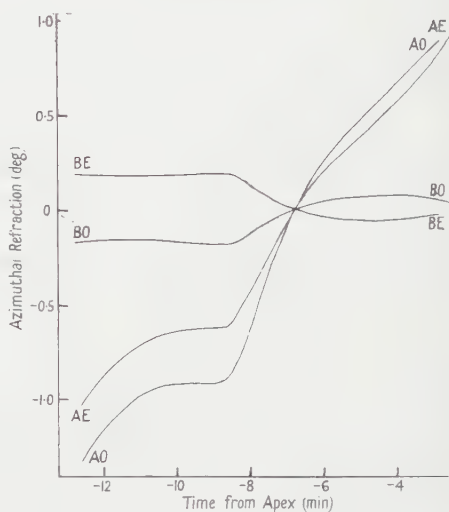


Fig. 4. Apparent shift in azimuth (degrees) as a function of time.

and receiver lie in the same magnetic meridian. Thus the four curves shown in Fig. 4 have a common zero, and it is this fact which largely accounts for the abrupt changes in gradient shown by the curves.

The azimuthal refraction for Model 4 is entirely due to the earth's magnetic field, as the model is radially stratified. The two components are refracted in opposite directions, either side of the geometrical path from transmitter to receiver. This refraction is quite small, and probably not detectable at present. The refraction for model 1 is about five times larger, in general, and is in the same sense for each of the components, although the difference between them is little altered from the case of model 4, except in the neighbourhood of the magnetic meridian, which is crossed at -6.42 minutes.

§ 6. CONCLUSIONS

The results given here by no means exhaust the information available, even for the case of a single transit. It is hoped, however, that the accuracy and universality of the method have been adequately demonstrated.

It is intended that calculations of the kind described here should be used to compare experimental results with what would be expected from various models of the ionosphere.

ACKNOWLEDGMENTS

I wish to thank Dr. K. G. Budden, Dr. K. Weekes and Mr. A. W. Nichol for much helpful advice and criticism, and Dr. M. V. Wilkes for permission to use the computer EDSAC II at the University Mathematical Laboratory, Cambridge. For a description of this machine, see Barron and Swinnerton-Dyer (1960).

REFERENCES

- BARRON, D. W., and SWINNERTON-DYER, H. P. F., 1960, *The Computer Journal*, **3**, 28.
GILL, S., 1951, *Proc. Camb. Phil. Soc.*, **47**, 96.
HASELGROVE, J., 1957 a, *Radio Ray Tracing in the Ionosphere and Solar Corona* (University of Cambridge Doctoral Thesis).
—— 1957 b, *Proc. Phys. Soc. B*, **70**, 653.
—— 1960, *Proc. Phys. Soc. B*, **75**, 357.
WHEELER, D. J., 1959, *The Computer Journal*, **2**, 23.
WILSON, D. McL. A., 1959, *Two Investigations of the Ionosphere* (University of Cambridge Doctoral Thesis).

Internal Conversion of ^{141}Ce

By J. R. COOK

Department of Physics Applied to Medicine, The Middlesex Hospital Medical School,
London

Communicated by J. E. Roberts; MS. received 16th February 1960

Abstract. The K conversion coefficient of the 141 keV gamma ray of ^{141}Ce has been measured by a scintillation spectrometer as 0.405 ± 0.01 . This indicates that the radiation is probably electric quadrupole.

§ 1. INTRODUCTION

THE gamma-ray spectrum of ^{141}Ce is known to consist of a single line of energy 141 keV. A fraction is internally converted with the production of a 36 keV x-ray. The conversion coefficient has been given by Heath (1952) using a scintillation spectrometer as $\alpha_K = 0.46 \pm 0.02$. According to Heath this value lies between extrapolated values of the magnetic dipole and electric quadrupole coefficients, and he concluded that the radiation was mixed but mainly magnetic dipole.

In the present experiment an attempt has been made to measure α_K with higher accuracy.

§ 2. EXPERIMENTAL METHOD

The source (of weight 0.1 g) was mounted in foil of negligible absorbing power 0.5 cm from the crystal cap of a scintillation spectrometer. The magnesium oxide reflector had a thickness of 2 mm and the aluminium outer cover was 1 mm thick. A lead collimator of thickness 0.4 cm was used so that the gamma and x-rays entered the central area of the crystal face approximately at right angles. This was done in order to avoid uncertainties in the geometrical efficiency. In order to avoid any slight change of spectrometer window width as a function of discriminator bias voltage the maxima of the x- and γ -ray photoelectric peaks were counted over approximately the same bias voltages. It is evident from Fig. 1 that the area under these peaks could be determined accurately. The background was estimated by replacing the collimator with a solid lead block of the same external dimensions and repeating the experiment. The background count did not vary appreciably over the peak regions. Contributions to the peaks from lead fluorescent radiation and bremsstrahlung were also negligible. The 1 mm cap thickness was sufficient to absorb the β -rays completely.

The experiment was repeated until three consistent measurements were obtained under conditions of high stability. Let A_x be the observed area under the γ -ray photoelectric peak and A_y that under the x-ray photoelectric peak; R_x the observed ratio of area under photoelectric peak to total area of the 141 keV

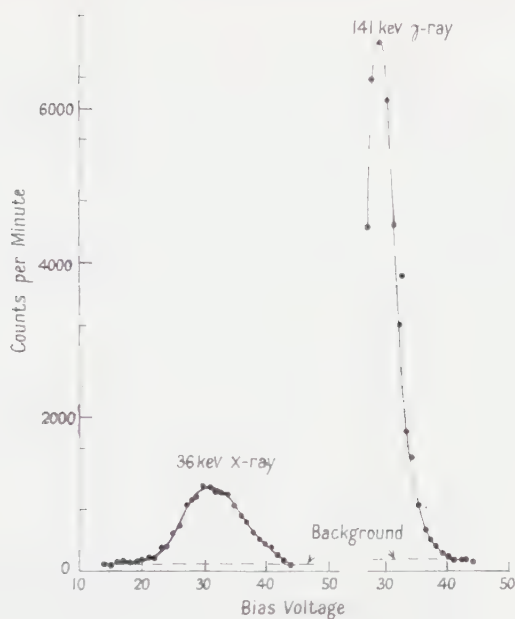


Fig. 1. Comparison of areas.

scintillation spectrum; R_y the ratio of area under the photoelectric peak to the total area of the 36 keV scintillation spectrum; K_y the theoretical fraction of the K x-rays of iodine excited by the 36 keV x-ray which escape from the crystal surface, expressed in terms of the number which does not escape (photoelectric peak); E_r the theoretical efficiency of the crystal to 141 keV rays; E_y the theoretical efficiency of the crystal to 36 keV x-rays; Δx the calculated fractional reduction of the 141 keV ray in the 1 mm Al cap + 2 mm MgO; Δy the calculated fractional reduction of the 36 keV x-ray in the Al cap + 2 mm MgO; and w_K the fluorescent yield of an atom with $Z=59$. Then the conversion coefficient

$$\alpha_K = \frac{A_y(1 + K_y)}{A_x} \frac{R_x E_x \Delta x}{R_y E_y \Delta y w_K} \cdot \frac{1}{w_K}.$$

§ 3. DETERMINATION OF NUMERICAL FACTORS

3.1. Ratios R_x , R_y

Below 100 keV the ratio of peak to total area is unity (i.e. $R_y=1$) since the Compton process is negligible, but at 141 keV it is necessary to determine the ratio experimentally. Fig. 2 shows the spectrum with the lead collimator and the source in the same position. A background correction was made as described above. The Compton pulses are distributed roughly from 0 to 100 keV as a result of fluctuation processes. A peak occurs at an energy about 90 keV due to lead fluorescent radiation from the collimator. This peak and the x-ray peak were subtracted from the total pulse spectrum leaving an area due to the Compton process plus the 141 keV photoelectric peak. The sharp rise below 5 bias volts was neglected since it was due probably to bremsstrahlung and not to a true Compton process (the area measured is shown between the dotted lines and background). The value of R_x was found to be 0.89.

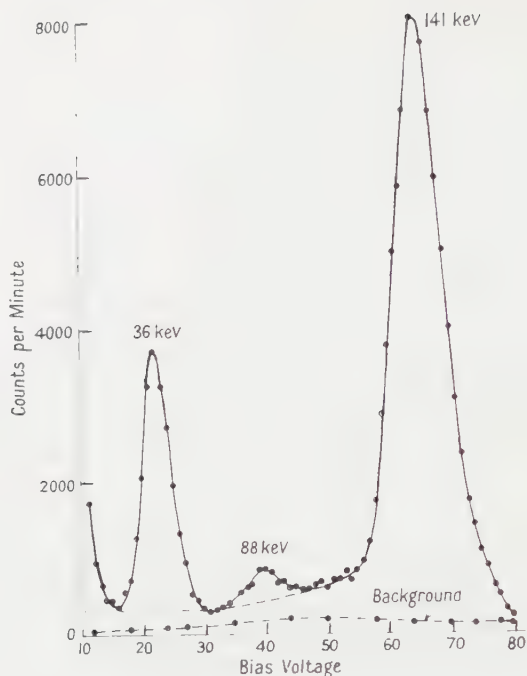


Fig. 2. Complete ^{141}Ce spectrum with collimation.

3.2. Value of K_y

The 36 keV x-rays of ^{141}Ce can excite the 33 keV x-rays of iodine which, being emitted isotropically, can escape from the front face of the crystal. Novey (1953) has calculated the fraction of the full incident energy peak which is lost (the difference peak being approximately 3 keV in the present case) for a beam of x-rays incident normally on the crystal. A more recent calculation by Sterk and Wapstra (1953) has been used in the present work since it includes the Auger effect. The accuracy of this correction should be reasonably high since the gamma rays were collimated. For 36 keV x-rays, $K_y = 0.29$ compared with the value 0.27 given by Novey.

3.3. Values of E_x , E_y

With the particular collimator used in the experiment some 141 keV gamma rays may traverse as little as 1.1 cm of NaI, but the efficiency (calculated from the absorption coefficients) is high (about 98%). Most of the 141 keV gamma rays are absorbed in 2.54 cm of crystal in which case $E_x = 1.0$ and $E_x/E_y = 1.0$.

3.4. Values of Δx , Δy

From the data on the absorption coefficients of Al and Mg (White 1952), Δx was calculated as 0.95 and Δy as 0.805.

3.5. Fluorescent Yield w_K

The experimental data has been discussed by Burhop (1952) who suggests a value for $w_K = 0.91$ for $Z = 59$. This value should however be regarded as an extrapolation from data of lower Z .

3.6. Value of α_K

The ratio A_y/A_x was 0.272 ± 0.003 . Errors in some of the other factors are difficult to determine accurately. Probably the most serious errors lie in the values of R_x estimated as 0.89 ± 0.01 , and $w_K = 0.91 \pm 0.01$. Application of the usual error formula gives $\alpha_K = 0.405 \pm 0.01$ which may be compared with Heath's value of 0.46 ± 0.02 . Theoretical values of the K shell internal conversion coefficients have been given by Sliv and Band (1956). Graphical interpolation gives a value for $\alpha_2 = 0.42$ and $\beta_1 = 0.435$. The experimental value 0.405 therefore suggests an α_2 conversion.

ACKNOWLEDGMENT

The author is grateful to Professor J. E. Roberts for encouragement in this work.

REFERENCES

- BURHOP, E. H. S., 1952, *The Auger Effect* (Cambridge: University Press).
HEATH, R. L., 1952, *Phys. Rev.*, **87**, 1132.
NOVEY, T. B., 1953, *Phys. Rev.*, **89**, 672.
SLIV, L. A., and BAND, I. M., 1956, *Acad. Sci. U.S.S.R.*, Report 57, University of Illinois.
STERK, M. J., and WAPSTRA, A. H., 1953, *Physica*, **19**, 669.
WHITE, G. R., 1952, *Nat. Bur. Stds*, Report No. 1003.

Absence of Doppler Shift for Gamma Ray Source and Detector on Same Circular Orbit

BY D. C. CHAMPENEY AND P. B. MOON

Department of Physics, University of Birmingham

MS. received 29th August 1960

Abstract. An experiment is described showing that for a source and absorber of ^{57}Fe placed at opposite ends of a rotor the Mössbauer absorption is unaffected by rotation. This is contrary to the situation with the source at the centre when relativistic effects cause a frequency shift between source and absorber.

REPORTING a test of the effect of circular motion on the resonant frequency of the gamma-ray transition in ^{57}Fe , Hay, Schiffer, Cranshaw and Egelstaff (1960) point out that one can treat the acceleration as an effective gravitational field and calculate the frequency shift from the difference of potential between source and absorber, or one can obtain the same answer by using the time dilatation of special relativity.

For their arrangement, with the source at the centre and the absorber at the periphery of the rotating system, the same result also follows from the argument that since source and absorber have relative velocity v ($\ll c$) in a direction perpendicular to the line joining them, there exists a transverse Doppler effect giving a fractional frequency shift $v^2/2c^2$.

It is perhaps surprising that the naïve use of this formula, without any account being taken of acceleration, should give the correct answer; an indication of the subtleties that may be involved is obtained by considering source and absorber to move on the same circle, e.g. at opposite points on the periphery. Their pseudo-gravitational potentials are equal, so are their time-dilatations, yet their relative velocity is $2v$.

We are indebted to several of our colleagues for interesting comments on this problem, involving such matters as Coriolis forces on photons and the difference between the lines-of-flight of photons and the line joining instantaneous positions of source and absorber.

Since in this laboratory we were undertaking a 'source at centre' experiment similar to that of Hay *et al.*, we decided also to make an experimental test of the 'peripherally opposite' arrangement. A null result, besides confirming the consensus of theoretical opinion, would give an important check on the absence of Doppler effect due to mechanical vibration of the rotor.

The source of ^{57}Co in a matrix of ^{56}Fe , was in the form of a slightly convex foil F, 0.001 in. thick, hard-soldered to a short thin steel cylinder C which fitted inside the tubular steel rotor (Fig. 1) against the rim R; the absorber was a similar foil of natural iron (2% ^{57}Fe) in the other tip of the rotor. This assembly was spun within an evacuated glass vessel provided with a thin window, behind which was a proportional counter for the 14 keV gamma radiation (Fig. 2). Two standard speeds were chosen: 100 rev/sec and 600 rev/sec and in separate experiments two different methods were used to restrict the counting of gamma rays to those few degrees of the rotor's azimuthal position within which the counter could 'see' the source through the absorber.

In the first method, the counts were displayed on the screen of a 100-channel kicksorter by a device that caused each gamma ray to deliver to the kicksorter an impulse proportional to the azimuth of the rotor at the instant in question; the counts in the four channels corresponding most nearly to the 'seeing' position were totalled. A typical record is shown in Fig. 3.

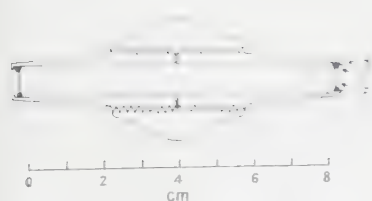


Fig. 1. Diagram of the rotor.

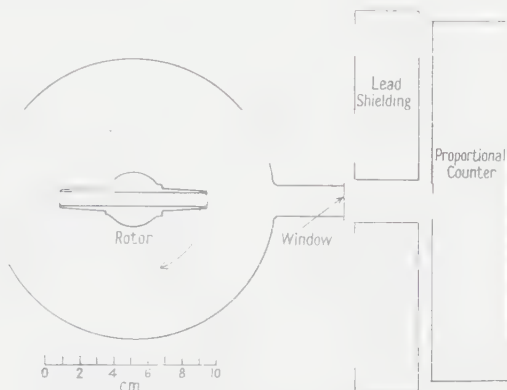


Fig. 2. Plan of the rotor, vacuum vessel, shielding and counter.

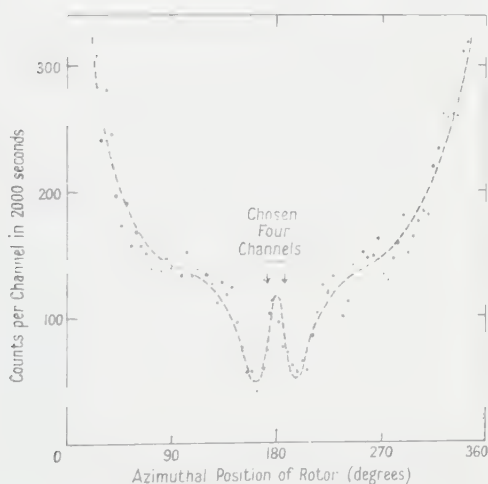


Fig. 3. Plot of typical kicksorter record. The channel number is expressed in terms of the angular position of the rotor.

In the second method, the successive interception of two light beams by one arm of the rotor opened and closed an electronic gate; a scale-of-two device prevented the gate from responding to the other arm of the rotor.

After subtraction of background (measured by placing $\frac{1}{8}$ in. aluminium over the window) the events recorded at 600 rev/sec were found by the first method to be $(0.4 \pm 3)\%$ less and by the second method to be $(2.0 \pm 2.5)\%$ more than those at 100 rev/sec; combining these two results we obtain $(+0.8 \pm 2.0)\%$.

The width of the resonance was measured for the actual source and absorber by the method described by Cordey-Hayes, Dyson and Moon (1960); it was thence calculated that a fractional shift $\frac{1}{2}(2v)^2/c^2$ would have given a 9.4% higher counting rate at the higher speed. In comparison with this figure, our result with its associated probable error may be taken as satisfactory evidence in favour of a null result.

As an incidental check that the null result was not due to instrumental deficiencies, an experiment with the source at the centre gave an increase in counting rate of $(7.1 \pm 1.7)\%$ at 900 rev/sec in agreement with an expected increase of 5.4%.

REFERENCES

- CORDEY-HAYES, M., DYSON, N. A., and MOON, P. B., 1960, *Proc. Phys. Soc.*, **75**, 810.
HAY, H. J., SCHIFFER, J. P., CRANSHAW, T. E., and EGELSTAFF, P. A., 1960, *Phys. Rev. Letters*, **4**, 165.
RUDERFER, M., 1960, *Phys. Rev. Letters*, **5**, 191.

Note added in proof.—It may be pointed out that the experiment is equivalent to that proposed by Ruderfer (1960) to test for the effects of other drift. No special care was taken to obtain readings in more than one direction, but when our results are interpreted according to Ruderfer's ideas they indicate an average value for $v \sin \theta$, over the six days of experimentation, of $17 \pm 43 \text{ m sec}^{-1}$, where v is the magnitude of the component of the ether drift velocity in the plane of rotation of the rotor and θ is the angle between this component and the counting axis.

Neutron Scattering from a Liquid on a Jump Diffusion Model

By C. T. CHUDLEY† AND R. J. ELLIOTT

Clarendon Laboratory, Oxford

MS. received 20th July 1960

Abstract. The incoherent inelastic scattering cross section of slow neutrons from liquids is calculated using a simple model in which the liquid is assumed to have appreciable short range order in a quasi-crystalline form. Diffusive motion takes place in large discrete jumps, between which the atoms oscillate as in a solid. The model predicts a definite, easily calculable cross section which is not dominated by diffusion effects as when continuous diffusion is assumed, but shows a characteristic variation with angle which could be looked for experimentally. The related pair correlation functions are dominated at small \mathbf{r} and t by vibrational effects. Although simple and extreme the model explains several aspects of the observations of Brockhouse and Pope in 1959 and others. A brief discussion of the coherent scattering cross sections for the model is given although explicit formulae are not obtained.

§ 1

OBSERVATION of the inelastic scattering cross section of slow neutrons from liquids promises to be an important method in determining their basic properties, since these cross sections contain more information than any other type of measurement. Several preliminary results have been reported mainly on two liquids of rather different kinds, water (Brockhouse 1959, Hughes *et al.* 1959), and lead (Pelah, Whittemore and McReynolds 1959, Turberfield, to be published). More recently Brockhouse and Pope (1959) have reported much more detailed results on lead. These results have been transformed using the formalism of van Hove (1954) who showed that the inelastic cross sections were related to the Fourier transform of the correlation function $G(\mathbf{r}, t)$ between pairs of atoms. In the classical form $G(\mathbf{r}, t)$ is the probability of finding an atom at \mathbf{r} at time t if there was an atom at the origin at $t = 0$. It is well known that in the scattering of energetic particles (e.g. x-rays) where the energy transfer is unimportant the differential scattering cross section is the Fourier transform of the instantaneous pair correlation function $G(\mathbf{r}, 0)$.

In fact

$$\frac{\partial^2 \sigma}{\partial \Omega \partial \epsilon} = \frac{a^2 k'}{hk} \Gamma(\mathbf{x}, \omega) \quad \dots\dots (1)$$

$$\Gamma(\mathbf{x}, \omega) = \iint \exp i(\mathbf{x} \cdot \mathbf{r} - \omega t) G(\mathbf{r}, t) d\mathbf{r} dt \quad \dots\dots (2)$$

where a is the appropriate scattering length, \mathbf{k} and \mathbf{k}' the wave vectors of the incident and outgoing neutrons. The momentum transfer is

$$\hbar \mathbf{x} = \hbar(\mathbf{k} - \mathbf{k}')$$

† Now at Atomic Energy Establishment, Winfrith, Dorset.

and ϵ is the energy lost by the neutron on collision

$$\epsilon = h\omega = \hbar^2(k^2 - k'^2)/2m_0.$$

For interpretation the experimental results are most conveniently displayed as $G(\mathbf{r}, t)$ and Brockhouse's measurement are the first sufficiently detailed to allow its evaluation. However, several Fourier transformations are required on data taken in a limited range of \mathbf{x} and ω , and the extrapolation of this data to cover the whole range may give rise to errors.

The present status of the theory of liquids is totally inadequate for the interpretation of such results, and at the present time the best method of approach appears to be to compare the results with simple models representing various extreme cases. Pioneer work of this kind was done by Vineyard (1958) who discussed, free, oscillatory and diffuse motion and evaluated $G(\mathbf{r}, t)$ in a classical approximation. Schofield (1960) has pointed out that one must proceed to the classical limit with care; crudely speaking because the energy transfers $\hbar\omega$ may all be lost if $\hbar \rightarrow 0$ is taken in $G(\mathbf{r}, t)$. He notes that it is safer to consider not $G(\mathbf{r}, t)$ but

$$\gamma'(\mathbf{x}, t) = \gamma\left(\mathbf{x}, t + \frac{i\hbar}{2kT}\right) \quad \dots\dots (3)$$

where γ is defined as

$$\gamma(\mathbf{x}, t) = \int \exp[i(\mathbf{x} \cdot \mathbf{r})] G(\mathbf{r}, t) d\mathbf{r}. \quad \dots\dots (4)$$

Thus for evaluation of the data it is convenient to have predictions of G , γ' and Γ for particular simple models. It has become clear from both the water and lead results (Brockhouse and Pope 1959) that a part of the diffusive motion in liquids takes place in comparatively large diffusive jumps. It therefore seemed of some interest to evaluate the predictions of a specific model of diffusion by large jumps. Brockhouse (1958) was the first to suggest that such a model might be applicable and to investigate some of its properties.

§ 2. MODEL

The model used is basically that proposed by Frenkel for liquids close to the melting point in which he assumes that the liquid has locally a lattice-like structure. It is known from x-ray scattering that $G(\mathbf{r}, 0)$ is peaked at about the expected atomic spacing. In the model the atomic motion is largely oscillatory as in the solid but because of the randomness left in the structure and the high density of vacancies compared with a solid an atom can occasionally jump into a neighbouring lattice site. If the observed coefficient of self-diffusion in lead $D = 2.5 \times 10^{-5} \text{ cm}^2 \text{ sec}^{-1}$ (Hall and Rothman 1956) is due to large jumps of an interatomic spacing $l = 3.5 \times 10^{-8} \text{ cm}$ the time between jumps

$$\tau = l^2/6D \sim 7 \times 10^{-12} \text{ sec}.$$

Assuming a Debye model of a solid the average time of oscillation is the inverse of the mean frequency $\bar{\nu}$

$$\frac{1}{\bar{\nu}} = \frac{4\hbar}{3k\theta} = 7 \times 10^{-13} \text{ sec}$$

assuming a Debye temperature of 80°K . Thus the atom performs many oscillations between jumps and it seems that this quasi-crystalline model would be a good first approximation.

If we assume that during the jumping process the atom moves as a free particle the time in transit

$$\tau' = l \left(\frac{M}{2kT} \right)^{1/2} \sim 1.5 \times 10^{-12} \text{ sec}$$

where M is the mass of the lead atom. This is much shorter than the time between jumps, and will be neglected in considering the diffusion process.

It is convenient to divide a discussion of $G(\mathbf{r}, t)$ into the self-correlation function $G_s(\mathbf{r}, t)$ which defines the probability of finding the atom which began at the origin at \mathbf{r} at t , and $G_d(\mathbf{r}, t)$, the correlation function of different atoms. G_d is further conveniently subdivided into its mean value—the density ρ —and fluctuations about this mean which die away in a few atomic radii (G_d'). ρ remains constant and since its contribution to scattering occurs only at $\mathbf{x}=0$, $\omega=0$, which cannot be observed, it may be neglected.

In substances where the nuclear scattering is incoherent because of isotope and spin effects only G_s is observable. Since protons have a very large incoherent cross section this is always the dominant effect in hydrogenous materials. In coherent scatterers like lead it is possible to effect an approximate separation of the effects of G_s and G_d (Brockhouse and Pope 1959, Egelstaff, unpublished). It is also very much more difficult to make a calculation of G_d than one of G_s . Accordingly we devote most of the rest of the paper to an evaluation of G_s on our model, giving only a brief discussion of G_d in a later section.

Taking the view that the atomic motion is oscillatory about well-defined points between which the atom moves by diffusion we write

$$G_s(\mathbf{r}, t) = \int G_s^D(\mathbf{R}, t) G_s^V(\mathbf{r} - \mathbf{R}, t) d\mathbf{R} \quad \dots\dots (5)$$

where G^D describes the diffusive and G^V the vibrational motion. The Fourier transform of (5) is a simple product

$$\gamma_s(\mathbf{x}, t) = \gamma_s^D(\mathbf{x}, t) \gamma_s^V(\mathbf{x}, t) \quad \dots\dots (6)$$

while

$$\Gamma_s(\mathbf{x}, \omega) = 2\pi \int \Gamma_s^D(\mathbf{x}, \omega') \Gamma_s^V(\mathbf{x}, \omega - \omega') d\omega'. \quad \dots\dots (7)$$

In writing (5) it has been assumed that the oscillatory and diffusive motions are completely uncorrelated, and that the diffusion takes place very rapidly so that the oscillatory motion has gone on for the whole time interval t .

§ 3. THE DIFFUSIVE MOTION

The diffusion equation for discrete jumps in space is a difference equation. If $P(\mathbf{r})$ is the probability of finding a particle at \mathbf{r} , and it can jump to a distribution of sites \mathbf{l} from \mathbf{r} , of which there are n

$$\frac{\partial P(\mathbf{r})}{\partial t} = \frac{1}{n\tau} \sum_{\mathbf{l}} [P(\mathbf{r} + \mathbf{l}) - P(\mathbf{r})]. \quad \dots\dots (8)$$

Thus $G_s^D(\mathbf{r}, t)$ is a solution of this equation with the boundary condition

$$G_s^D(\mathbf{r}, 0) = \delta(\mathbf{r}). \quad \dots\dots (9)$$

The equation is conveniently solved by considering the Fourier transform of G_s

$$G_s^D(\mathbf{r}, t) = (2\pi)^{-3} \int \exp(-i\mathbf{x} \cdot \mathbf{r}) \exp(-f(\mathbf{x})t) d\mathbf{x} \quad \dots\dots (10)$$

where

$$f(\mathbf{x}) = - \sum_{\mathbf{l}} (\exp(i\mathbf{x} \cdot \mathbf{l}) - 1) / n\tau. \quad \dots\dots (11)$$

This may now be evaluated for various arrangements of sites. For example, if the diffusion is on a simple cubic lattice of spacing a

$$f(\mathbf{x}) = (3 - \cos \kappa_x a - \cos \kappa_y a - \cos \kappa_z a) / 3. \quad \dots\dots (12)$$

The actual form of $G(\mathbf{r}, t)$ is more difficult to find although in this case it is possible to give the result in closed form. At lattice point $(\alpha a, \beta a, \gamma a)$

$$G(\mathbf{r}, t) = \exp(-t/\tau) I_\alpha(t/3\tau) I_\beta(t/3\tau) I_\gamma(t/3\tau) \quad \dots\dots (13)$$

where I_n is the Bessel function of imaginary argument. It will be noticed that at the origin the decay is not given simply by $\exp(-t/\tau)$ but is modified by a probability that it will return.

For a close-packed lattice with atomic distance a

$$f(\mathbf{x}) = [1 - \cos(\kappa_x a / \sqrt{3}) \cos(\kappa_y a / \sqrt{3}) \cos(\kappa_z a / \sqrt{3})] / \tau. \quad \dots\dots (14)$$

Since it is not certain that the long range order implied by these lattices does not exist in a liquid an alternative model is to assume jumps of a fixed distance l but in random directions, although this probably overestimates the randomness of the motion. The sum in (11) is now replaced by an integral and

$$f(\mathbf{x}) = \frac{1}{\tau} \left(1 - \frac{\sin \kappa l}{\kappa l} \right). \quad \dots\dots (15)$$

If the jumps have a distribution $q(l)$

$$f(\mathbf{x}) = \frac{1}{\tau} \int \left(1 - \frac{\sin \kappa l}{\kappa l} \right) q(l) dl / \int q(l) dl. \quad \dots\dots (16)$$

The case of jumps of fixed length is a well-known problem in the theory of random walks and is treated in detail by Chandrasekhar (1943). After one jump the distribution function has a contribution $\delta(\mathbf{r} - \mathbf{l})$. After two jumps $G_s^{(2)}$ has two steps:

$$\begin{aligned} G_s^{(2)} &= 2Z & 0 < \mathbf{r} < \mathbf{l}, \\ &= Z & \mathbf{l} < \mathbf{r} < 2\mathbf{l}, \\ &= 0 & \mathbf{r} > 2\mathbf{l}, \end{aligned}$$

where Z is a constant. Expressions after three and four jumps are given in the reference cited, and after many jumps G_s takes on a Gaussian distribution

$$G_s(\mathbf{r}, t) = \left(\frac{1}{4\pi Dt} \right)^{3/2} \exp\left(-\frac{r^2}{4Dt}\right). \quad \dots\dots (17)$$

This formula is of course obtained at all times in the limit of small jumps when the difference equation (8) becomes a differential equation.

In the foregoing work the discrete nature of the jumping in space has been emphasized but it has been assumed that this takes place at a uniform rate. A better approximation was proposed by Vineyard (1958) and extended by Schofield (1960) using the Langevin equation as for Brownian motion. They demonstrate that these effects can be included by replacing t in the exponent of (10) by

$$\zeta = t + \frac{1}{\eta} (e^{-\eta t} - 1) \quad \dots\dots (18)$$

where $\eta = kT / MD$.

The form of these results means that the usual methods of discussing the width of the distribution G_s as a function of time must be interpreted with care. At small times the jumping process produces peaks in G_s at the average value of l but does not broaden the central peak. After one or two jumps have taken place, however, all such bumps and discontinuities have been smoothed out, particularly if there is a distribution of jump lengths, and after those times the form of G_s is given by (17). Thus, if measurements are made on the central peak of G_s (as is usual in substances with coherent scattering since the outer tails are obscured by G_d , and is certainly the case with Brockhouse and Pope (1959)), the diffusive broadening is not observed until times of two or three times τ .

§ 4. THE VIBRATIONAL MOTION

The form of $G_s(\mathbf{r}, t)$ in crystals has been extensively discussed by van Hove (1954), Vineyard (1958) and others, so that we give only the relevant results. For a cubic crystal

$$G_s^V(\mathbf{r}, t) = \left(\frac{L}{2\pi}\right)^{3/2} \exp(-Lr^2) \quad \dots\dots(19)$$

where

$$L^{-1} = 2(M(0) - M(t)),$$

and the quantum mechanical expression for $M(t)$ is

$$\frac{\hbar}{2M} \int \frac{g(\nu)}{\nu} \left[1 - \exp\left(-\frac{\hbar\nu}{kT}\right) \right]^{-1} \left[\exp(i\nu t) + \exp\left\{-\nu\left(it + \frac{\hbar}{kT}\right)\right\} \right] d\nu, \quad \dots\dots(20)$$

$g(\nu)$ is the density of modes per unit frequency range. (20) contains all the complications due to the phonon spectrum, and the cross sections computed from it are conveniently divided into processes where a fixed number of phonons are created or destroyed. The most important contributions to the cross section come from elastic no-phonon processes where $\Gamma_s \sim \delta(\omega)$, one-phonon creation processes where

$$\Gamma_s^{(1)} = e^{-2W} \kappa^2 g(\omega) / \omega (1 - \exp(-\hbar\omega/kT)) \quad \dots\dots(21)$$

and a similar term with an appropriate temperature factor for destruction processes. The first term in (21) is the Debye-Waller factor and

$$W = \frac{1}{2} \kappa^2 M(0). \quad \dots\dots(22)$$

In the limits of high temperatures or high incident neutron energies many-phonon processes are important and this detail is not observed. Under these conditions it is possible to approximate to the width function (20) of G_s . The classical result (Vineyard 1958) is

$$L^{-1} = \int \frac{g(\nu) 2kT}{M\nu^2} (1 - \cos \nu t) d\nu \quad \dots\dots(23)$$

and Schofield (1960) gives an improved form for the appropriate γ' . The oscillatory nature of this width is rapidly damped out and as demonstrated by Vineyard the width increases with time quadratically at first and saturates with minor oscillations after $t \sim 1/\bar{\nu}$, at a value corresponding to the Debye-Waller factor. For a Debye spectrum this value is $L^{-1} = 12\hbar^2 T / Mk\theta^2$ where θ is the Debye temperature.

§ 5. RESULTS

The predictions of the diffusive model can be displayed in various ways using formulae (5)–(7). The integration in (5) to form G_s is tedious but the general behaviour is clear. At short times G_s takes the form of a Gaussian whose width increases with time as described by (20) or (23) and saturates at a value L beyond $t \sim 1/\bar{\nu}$. The diffusion at first causes peaks to appear in the wings of G_s at times of about τ and only when $t \sim 2\tau$ does the central peak of G_s become broadened by the diffusion.

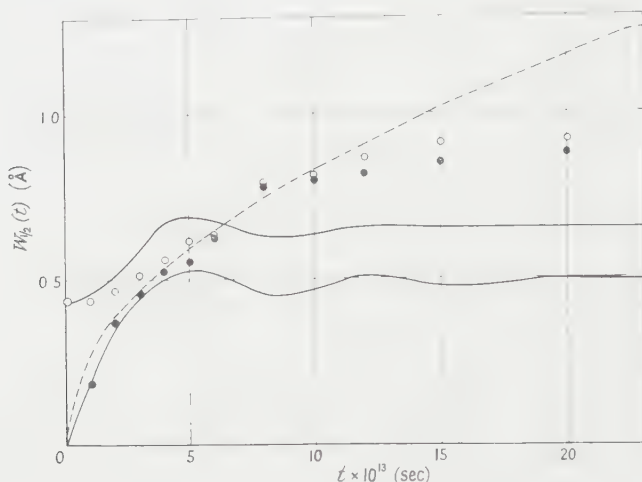


Fig. 1. The width at half height of G_s (full circles) and the first peak of G_d (open circles) in liquid Pb after Brockhouse and Pope (1959). The lower full curve is the width of G_s predicted using a Debye crystal model from Eqn (23). The upper full curve is obtained by adding the vibrational width to the original width of G_d at $t=0$ using (28). The broken curve is that given by continuous diffusion.

A comparison with experiment is made most conveniently by comparing the widths of the central peak of G_s , which is essentially the same as the central peak of G in a coherent scatterer. This explicitly excludes the peaks which appear in the wings at short times. Thus the width is predicted to have a plateau between about $1/\bar{\nu}$ and 2τ . In Fig. 1 the results of Brockhouse and Pope are compared, the widths being predicted for Debye oscillations and continuous diffusion appropriate to his experimental conditions. This jump model predicts a width like the Debye model with some slight increase at large t and a very considerable increase at $t \sim 10^{-11}$ sec to raise the curve up to the diffusion value. The experimental results do show a rapid rise at short times followed by near saturation with a small slope. The magnitude of the saturation value is, however, almost twice as large as that predicted by the Debye theory. Thus, while the jump diffusion model is satisfactory in predicting a saturation of the width below the diffusion value in this time region, there appears to be a further source of broadening not treated in the model. One possibility arises from the fact that the nearest neighbours of one atom are found with a considerable spread about their mean distance. From the width of the first peak of $G_d(\mathbf{r}, 0)$ this is about $\delta_0 \sim 0.4$ Å in lead. An atom whose nearest neighbours are more distant than the average might be expected to move out more freely and so $G_s(\mathbf{r}, t)$ takes up a

width similar to that of the first peak of $G_d(\mathbf{r}, 0)$ at a rate appropriate to free motion. Such a width added to the vibrational width would certainly give reasonable agreement with experiment.

The cross section results transformed only once from their energy dependence to give $\gamma'(\mathbf{x}, t)$ are probably a more reliable source of comparison with theory. $\gamma_s'(\mathbf{x}, t)$ is given in a very convenient form for the above model

$$\gamma_s'(\mathbf{x}, t) = \exp \left[-\frac{1}{2} \kappa^2 L(t) - f(\mathbf{x}) \zeta \right] \quad \dots\dots (24)$$

using (11), (18) and (23) or its improvement given by Schofield. At small κ , $f(\mathbf{x})$ has in all cases the form $D\kappa^2$ which is appropriate to continuous diffusion. This is because small κ reflects the behaviour of G_s at large \mathbf{r} where the discreteness of the jumping process is not noticeable. Conversely at large κ , $f(\mathbf{x})$ oscillates in the true lattices but allowing for disorder as in (15) or (16) it saturates, and leads to a term in Γ independent of κ . This reflects the fact that at small \mathbf{r} , G_s is given by the vibrational motions.

If the quasi-lattice model with phonons is applicable, the best mode of comparison is with $\Gamma(\mathbf{x}, \omega)$. The zero-phonon contribution is broadened in energy (sometimes called the quasi-elastic contribution) and has Lorentzian form

$$\Gamma_s^0(\mathbf{x}, \omega) = e^{-2W} \frac{2f(\mathbf{x})}{\omega^2 + f(\mathbf{x})^2} \quad \dots\dots (25)$$

One-phonon creation processes give

$$\Gamma_s^{+1}(\mathbf{x}, \omega) = \frac{h\kappa^2}{4\pi^2 M} e^{-2W} \int \frac{g(\nu) d\nu}{\nu [1 - \exp(-\hbar\nu/kT)]} \cdot \frac{f(\mathbf{x})}{(\omega + \nu)^2 + f(\mathbf{x})^2} \quad \dots\dots (26)$$

and one-phonon destruction processes

$$\Gamma_s^{(-1)}(\mathbf{x}, \omega) = \frac{h\kappa^2}{4\pi^2 M} e^{-2W} \int \frac{g(\nu) d\nu}{\nu [\exp(\hbar\nu/kT) - 1]} \cdot \frac{f(\mathbf{x})}{(\omega - \nu)^2 + f(\mathbf{x})^2} \quad \dots\dots (27)$$

In the improved formulation of Schofield (1960), using (18) for the diffusive term in this product, the result is an infinite series of which the term in (25)–(27) is only the first. The effect of this series is to give a somewhat narrower function than the Lorentzian but having basically the same form.

The energy width of the quasi-elastic scattering is thus seen to depend on \mathbf{x} like $f(\mathbf{x})$, i.e. it rises like $D\kappa^2$ at small κ and then saturates. The single-phonon contributions also have an extra broadening in energy because of the diffusion terms and the amount depends on the angle through $f(\mathbf{x})$. In a crystal the spread of these contributions is independent of angle, and because of the jump nature of the diffusion the extra broadening is a comparatively small effect, although it does lead to an increase in width with increasing angle. Fig. 2 shows a typical result actually evaluated for lead, although experimentally this would be difficult to separate from the G_d . In a hydrogenous substance the comparison with experiment is simpler. In his experiments with water Brockhouse (1959) notes that the energy width does increase with scattering angle but less rapidly than is expected for free or diffusional motion, which is the form of result predicted here. It would appear to be instructive to compare the inelastic cross sections with the crystal phonon form. Unfortunately the best results in this form by Hughes *et al.* (1959) on water show a considerable structure due to rotations. It would be interesting to have experiments on a more symmetrical hydrogenous (and hence incoherent) molecular scatterer like methane.

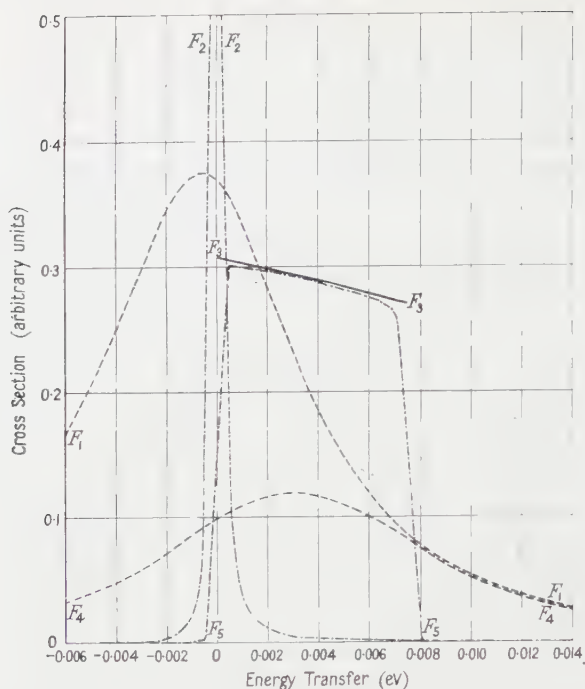


Fig. 2. Neutron scattering cross sections as a function of energy transfer predicted by the model for the scattering of thermal energy neutrons at a scattering angle of 90° from liquid lead at a temperature of 600°K (the melting point) with a Debye temperature of 88°K . The cross sections shown are:

- F_1 , no-phonon cross section on a continuous diffusion model;
- F_2 , no-phonon cross section on a jump diffusion model;
- F_3 , one-phonon gain cross section of lead as a Debye solid;
- F_4 , one-phonon gain cross section on the continuous diffusion model;
- F_5 , one-phonon gain cross section on the jump diffusion model.

The model of jump diffusion is therefore seen to lead to quite definite predictions about the nature of the neutron scattering in a liquid, which can be compared with the experimental results in various ways. The data at present available seem to indicate that it does agree with many salient features, and it will be of some interest to see how far this crude model can explain the more detailed results which it is hoped will shortly be available.

§ 6. DISCUSSION OF G_d

In conclusion it seems appropriate to add a brief discussion of the behaviour of G_d on the jump diffusion model. It is much more difficult to do this on a quantitative basis than it is for G_s unless one makes even more sweeping approximations—like the convolution approximation of Vineyard which is certainly bad at small distances where the crystalline structure is important. It is possible to give some discussion of G_d on an *ad hoc* basis—and in particular of the first peak which is its most prominent feature. At $t=0$ the width of this peak is finite (δ_0) because of the randomness in the positions of the shell of first neighbours. At short times the vibrations cause an increase in width

$$w = (\delta_0^2 + L^{-1})^{1/2}$$

where L is given by (25). Results for a Debye model are shown in Fig. 1. ω increases slightly with time and then saturates in a manner similar to the experiment but at a low value. The jump diffusion again does not influence the width much until $t \sim 2$ or 3τ . At $t < \tau$ (the mean jump time) atoms in the first neighbour shell cannot jump to the origin because it is occupied, and rearrangements within the first shell will not affect the width of the first peak. At $t > 2\tau$ all the peaks of G_d will be rapidly ironed out.

An alternative method of approach is through the inelastic cross sections on the basis of a lattice-like theory involving phonons. The one-phonon processes in solids lead to $d^2\sigma/d\Omega d\epsilon$ which are a few δ -functions of energy which vary in their position with angle. These lines will in a liquid be broadened in angle (i.e. in κ) because of the smooth variation of $G_d(\mathbf{r})$. They will be broadened in energy because of the diffusive motions. If diffusion is by jumps the first form of broadening will be dominant except possibly in the case of very slow neutrons. A quasi-phonon picture of this type has been partly worked out by Butterworth and Marshall (1957).

ACKNOWLEDGMENTS

We are particularly indebted to Mr. P. Egelstaff for many illuminating discussions on this subject. The work forms part of a thesis to be submitted to the University of Reading by one of us (C. T. C.), who is indebted to Professor W. E. Lamb, Jr., and Professor B. Bleaney for permission to work in the Clarendon Laboratory. The work was performed under contract with the United Kingdom Atomic Energy Authority.

REFERENCES

- BROCKHOUSE, B. N., 1958, *Nuovo Cim. Suppl.*, **9**, 45.
 ——— 1959, *Phys. Rev. Letters*, **2**, 287.
 BROCKHOUSE, B. N., and POPE, N. K., 1959, *Phys. Rev. Letters*, **3**, 259.
 BUTTERWORTH, I., and MARSHALL, W., 1957, *Proceedings of Meeting on the Use of Slow Neutrons to Investigate the Solid State* (Stockholm: Swedish A.E.C.), p. 31.
 CHANDRASEKHAR, S., 1943, *Rev. Mod. Phys.*, **15**, 1.
 HALL, L. D., and ROTHMAN, S., 1956, *Trans. Amer. Inst. Mining Met. Engrs*, **206**, 199.
 VAN HOVE, L., 1954, *Phys. Rev.*, **95**, 249.
 HUGHES, D. J., PALEVSKY, H., KLEY, W., and TUNELLO, E., 1959, *Phys. Rev. Letters*, **3**, 91.
 PELAH, I., WHITTEMORE, W. L., and McREYNOLDS, A. W., 1959, *Phys. Rev.*, **113**, 767.
 SCHOFIELD, P., 1960, *Phys. Rev. Letters*, **4**, 239.
 VINEYARD, G. H., 1958, *Phys. Rev.*, **110**, 999.

Gamma Rays Corresponding to a Dipole or a High Quadrupole Excitation of Carbon 12 by 150 MeV Protons

BY N. GILBERT†

Department of Mathematical Physics, University of Birmingham

Communicated by R. E. Peierls; MS. received 9th June 1960

Abstract. The process $^{12}\text{C}(p, p'\gamma)^{12}\text{C}$ is formulated in direct interaction theory using the sum rule for the group of dipole states at about 20 MeV and for a group of quadrupole states that we assume to be at about 30 MeV. The angular correlation (p', γ) is discussed and it is shown that for some (p', γ) and (p, p') angles the emission of an E2 γ -ray in this range of energy has an appreciable probability.

§ 1. INTRODUCTION

IN this paper we are interested in the γ -ray following the inelastic scattering of high energy protons on carbon. We shall consider the cross section for $^{12}\text{C}(p, p'\gamma)^{12}\text{C}$ taking into account the possible emission of either E1 or E2 γ -rays and shall discuss the $(p, p'\gamma)$ angular function for these two cases.

In §2 we shall discuss the process using the theory of direct interaction and give a general formula for a γ -ray of any multipole order.

In §3 we shall consider the simple case of a nucleon described by a plane-wave function and show how we can use the sum rule for the intermediate excited states; knowing that the 1^- states are grouped in a narrow range of energies at about 20 MeV and supposing that the 2^+ states have the same property at a high excitation energy. In this way, we avoid giving a description of the excited states of the nucleus. Calculations are made for ^{12}C .

In §4 we use the formalism of distorted waves given by McCauley and Brown (1958) and show how we can use the sum rule with the same approximations. The calculations are performed for the ^{12}C nucleus and we give the results as functions of p scattering angle and γ emission angle.

In a final section we shall compare the results obtained without and with distortion of the nucleon wave functions.

§ 2. DESCRIPTION OF THE PROCESS CONSIDERED AND AMPLITUDE FOR THE $(p, p'\gamma)$ SCATTERING

Within the framework of the theory of direct interaction, we shall consider a process in two steps as follows.

(a) The incident proton (space coordinate \mathbf{r}_0) interacts with one nucleon i (space coordinate \mathbf{r}_i) of the nucleus which changes its state and goes to a higher level while the proton is scattered with an energy E_t . Then we can write the

† Now at Laboratoire de Physique Nucleaire, Orsay (Seine et Oise), France.

nucleon-nucleus interaction as a sum of nucleon-nucleon interactions:

$$V_N(\mathbf{r}_0, \mathbf{r}_1 \dots \mathbf{r}_A) = \sum_{i=1}^A V_N(\mathbf{r}_0 - \mathbf{r}_i).$$

(b) The nucleus goes back to its initial state by emission of a γ -ray. This electromagnetic interaction involves only charged particles in the nucleus. Let the corresponding Hamiltonian be $\sum_{i=1}^Z H_E(\mathbf{r}_i)$.

We neglect the possible process of a γ -ray emission at first, involving the scattering of the proton by the nucleus in the intermediate state (because of the non-conservation of energy in the intermediate state). This process has a fairly small probability. With this description of the process we write the scattering amplitude A as

$$A = \sum_{\text{int states}} \left[\frac{\langle \psi_0(\mathbf{r}_1 \dots \mathbf{r}_A) | \sum_{i=1}^Z H_E(\mathbf{r}_i) | \psi_{\text{int}}(\mathbf{r}_1 \dots \mathbf{r}_A) \rangle \times \langle \psi_{\text{int}}(\mathbf{r}_1 \dots \mathbf{r}_A) \phi_f(\mathbf{r}_0) | \sum_{i=1}^A V_N(\mathbf{r}_0 - \mathbf{r}_i) | \psi_0(\mathbf{r}_1 \dots \mathbf{r}_A) \phi_0(\mathbf{r}_0) \rangle}{E_0 - E_{\text{int}}} \right]$$

where we carry out the sum over all the possible intermediate excited states of the nucleus described by $\psi_{\text{int}}(\mathbf{r}_1 \dots \mathbf{r}_A)$ reached in the step (a), $\psi_0(\mathbf{r}_1 \dots \mathbf{r}_A)$ is the wave function of the nucleus in its ground state, $\phi_f(\mathbf{r}_0)$ and $\phi_0(\mathbf{r}_0)$ are the final and initial proton wave functions, E_0 is the initial total energy of the system in the centre of mass $p^{12}\text{C}$, E_{int} is the intermediate total energy, and is a complex number, the imaginary part of which is the half-width of the single-particle excitation.

We can write $H_E(\mathbf{r}_i)$ as do Austern and Sachs (1952)

$$H_E(\mathbf{r}_i) = ie \left(\frac{2\pi\hbar\omega_\gamma}{V} \right)^{1/2} (\mathbf{u} \cdot \mathbf{r}_i) \exp(i\mathbf{k}_\gamma \cdot \mathbf{r}_i)$$

where \mathbf{u} is the polarization vector for the γ , \mathbf{k} is its wave number and V the normalization volume.

We write the exponential as a sum of partial waves. The ground state of ^{12}C being $J=0^+$, the l th term of the electromagnetic Hamiltonian will always lead to a unique state $J=l(-)^l$. Writing

$$\exp(i\mathbf{k}_\gamma \cdot \mathbf{r}_i) = 1 + \sum_{l=1}^{\infty} \sum_{m=-l}^{+l} k_\gamma^l r_i^l F_{lm}(\hat{k}_\gamma, \hat{r}_i),$$

A becomes

$$A = ie \left(\frac{2\pi\hbar\omega_\gamma}{V} \right)^{1/2} \left[\sum_{1-\text{int states}} \frac{\langle \psi_0 | \sum_{i=1}^Z \mathbf{u} \cdot \mathbf{r}_i | \psi_{\text{int}} \rangle \langle \psi_{\text{int}} \phi_f | \sum_{i=1}^A V_N(\mathbf{r}_0 - \mathbf{r}_i) | \psi_0 \phi_0 \rangle}{E_0 - E_{\text{int}}} + \sum_{l=1}^{\infty} \sum_{m=-l}^{+l} \sum_{\text{int states}} \frac{\langle \psi_0 | \sum_{i=1}^Z (\mathbf{u} \cdot \mathbf{r}_i) (k_\gamma r_i)^l F_{lm}(\hat{k}_\gamma, \hat{r}_i) | \psi_{\text{int}} \rangle \langle \psi_{\text{int}} \phi_f | \sum_{i=1}^A V_N(\mathbf{r}_0 - \mathbf{r}_i) | \psi_0 \phi_0 \rangle}{E_0 - E_{\text{int}}} \right].$$

In the following calculations we shall keep only the two first terms corresponding to dipole and quadrupole excitation in the intermediate state.

§ 3. SCATTERING AMPLITUDE WITH PLANE-WAVE FUNCTIONS FOR THE NUCLEONS

In this section we consider the particular and not very realistic case where

$$\phi_0(\mathbf{r}_0) = V^{-1/2} \exp(i\mathbf{k}_0 \cdot \mathbf{r}_0), \quad \phi_f(\mathbf{r}_0) = V^{-1/2} \exp(i\mathbf{k}_f \cdot \mathbf{r}_0),$$

\mathbf{k}_0 and \mathbf{k}_f being the initial and final wave numbers.

We know from experiments on excitation of nuclei by γ -rays that excited levels obtained in a dipole transition are grouped in a very narrow range of energy at about 20 MeV for carbon, and we expect this grouping also on theoretical grounds (Brown and Bolsterli 1959). Then in this case, to perform the sum over intermediate states $J=1^-$, we may replace E_{int} by an average value

$$\bar{E}_{\text{int}} = E_i + \bar{E}_1 + iW_1,$$

\bar{E}_1 being the average excitation energy and $2W_1$ the corresponding width, and then use the sum rule. In order to estimate effects of interference from quadrupole transitions we assume that the corresponding levels are also localized in a narrow range of energy (higher and wider than for the dipole states). Strong quadrupole transitions in this region have not yet been observed experimentally but would be expected theoretically. These would correspond to $T=1$ intermediate states. Then it is possible to perform sum rule over intermediate states taking an average value of excitation energy \bar{E}_2 . We neglect the first level $J=2^+$ at 4.4 MeV which has $T=0$ since we will take only that part of V_N which excites $T=1$ resonances, and it is far enough away in energy to be expected not to affect the results greatly in the energy region above the dipole resonance, although one should include it for completeness.

In this problem we have to look only at small angles of scattering for the proton (smaller than 25°) since A becomes very small for larger angles. We can say now that, to a good approximation, \mathbf{K} is perpendicular to \mathbf{k}_f and use a reference system with \mathbf{K} as polar axis and \mathbf{k}_f as the Oz axis. If we denote the direction of the emitted γ -ray in this system by $\theta_\gamma, \phi_\gamma$ (Fig. 1) we can write

$$\begin{aligned} \mathbf{u} \cdot \mathbf{r}_i &= a_\gamma r_i \sin \theta_{i\frac{1}{2}} (\exp(i\phi_i) + \exp(-i\phi_i)) \\ &\quad - ib_\gamma r_i \sin \theta_{i\frac{1}{2}} (\exp(i\phi_i) - \exp(-i\phi_i)) + ic_\gamma r_i \cos \theta_i \\ F_{1m}(\hat{\mathbf{k}}_\gamma \cdot \hat{\mathbf{r}}_i) &= 4\pi i Y_1^{m*}(\theta_\gamma, \phi_\gamma) Y_1^m(\theta_i, \phi_i) \end{aligned}$$

with

$$\begin{aligned} a_\gamma &= -\sin \phi_\gamma - i \cos \phi_\gamma \cos \theta_\gamma \\ b_\gamma &= \cos \phi_\gamma - i \sin \phi_\gamma \cos \theta_\gamma \\ c_\gamma &= \sin \theta_\gamma. \end{aligned}$$

To calculate A , we describe the nucleus of carbon 12 in an independent-particle model. In (jj) coupling the ^{12}C ground state has the configuration $(1s)^4(1p_{3/2})^8$ with two closed shells. We write its wave function as a Slater determinant, using as radial functions the harmonic oscillator solutions, the parameter of which is $\nu = 0.234 f^{-2}$

$$\text{for an s nucleon} \quad u_s(r) = \frac{2\nu^{3/4}}{\pi^{1/4}} \exp(-\tfrac{1}{2}\nu r^2)$$

$$\text{for a p nucleon} \quad u_p(r) = \frac{2\sqrt{2}\nu^{5/4}}{\sqrt{3}\pi^{1/4}} r \exp(-\tfrac{1}{2}\nu r^2).$$

For the nucleon-nucleon potential we shall use the Kerman, Thaler and McManus results. Replacing the V_N matrix element by the M scattering matrix

and using their notation we can write with their approximations:

$$\langle \phi_f(\mathbf{r}_0) \psi_{\text{int}}(\mathbf{r}_1 \dots \mathbf{r}_A) | L_N(\mathbf{r}_0 - \mathbf{r}_i) | \phi_0(\mathbf{r}_0) \psi_0(\mathbf{r}_1 \dots \mathbf{r}_A) \rangle = \frac{2\hbar^2}{(2\pi)^2 M} \cdot \langle \psi_{\text{int}}(\mathbf{r}_1 \dots \mathbf{r}_A) | \\ \times [A + B\sigma_{0n}\sigma_{1n} + C(\sigma_{0n} + \sigma_{1n}) + E\sigma_{0p}\sigma_{1p} + F\sigma_{0q}\sigma_{1q}] \exp(i\mathbf{K} \cdot \mathbf{r}_i) | \psi_0(\mathbf{r}_1 \dots \mathbf{r}_A) \rangle$$

where $\mathbf{K} = \mathbf{k}_0 - \mathbf{k}_f$.

A , B , C , E and F are of the form:

$$A = A_S + A_T \tau_0 \cdot \tau_1 \dots \dots$$

A_S , $A_T \dots \dots$ being functions of the only K momentum transfer.

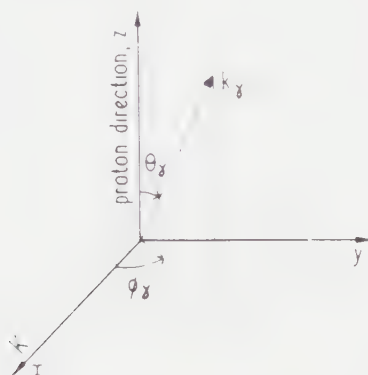


Fig. 1. Reference system used.

In this problem we are interested in $T=1$ transitions so the only A_T , $B_T \dots \dots$ parts give a contribution to the transition amplitude. Carrying out the matrix elements corresponding to the target nucleon spin part, M is reduced to $A_T + C_T \sigma_{0n}$. We calculate A_T and C_T from the Kerman, McManus and Thaler results (they give them for a 156 MeV energy, nearly ours) for a same transfer momentum (this will correspond to a scattering angle in the two nucleon centre-of-mass system equal to 2θ).

Let us call $u_1; u_2 \dots u_A$ the A individual wave functions of the nucleons in the nucleus, we apply then the sum rule over the intermediate states and obtain A as a sum of five different terms:

$$A = ie \left(\frac{2\pi\hbar\omega_\gamma}{V^3} \right)^{1,2} \frac{2\hbar^2}{(2\pi)^2 M} [A_T + C_T \sigma_{0n}] \left\{ \frac{1}{E_0 - E_f - E_1 + iW_1} \left[\sum_{i=1}^Z \langle u_i(\mathbf{r}_i) | \right. \right. \\ \times \exp(i\mathbf{K} \cdot \mathbf{r}_i) (u \cdot \mathbf{r}_i) | u_i(\mathbf{r}_i) \rangle - \sum_{i \neq j} \langle u_i(\mathbf{r}_i) | \exp(i\mathbf{K} \cdot \mathbf{r}_i) | u_j(\mathbf{r}_i) \rangle \langle u_j(\mathbf{r}_j) | \mathbf{u} \cdot \mathbf{r}_j | u_j(\mathbf{r}_j) \rangle \Big] \\ + \frac{k_\gamma}{E_0 - E_f - E_2 + iW_2} \cdot \left[\sum_{i=1}^Z \langle u_i(\mathbf{r}_i) | \exp(i\mathbf{K} \cdot \mathbf{r}_i) \cdot (\mathbf{u} \cdot \mathbf{r}_i) r_i \sum_m F_{1m} | u_i(\mathbf{r}_i) \rangle \right. \\ + \sum_{i \neq j} \langle u_i(\mathbf{r}_i) | \exp(i\mathbf{K} \cdot \mathbf{r}_i) | u_i(\mathbf{r}_i) \rangle \cdot \langle u_j(\mathbf{r}_j) | (\mathbf{u} \cdot \mathbf{r}_j) r_j \sum_m F_{1m} | u_j(\mathbf{r}_j) \rangle \\ \left. \left. - \sum_{i \neq j} \langle u_i(\mathbf{r}_i) | \exp(i\mathbf{K} \cdot \mathbf{r}_i) | u_j(\mathbf{r}_i) \rangle \cdot \langle u_j(\mathbf{r}_j) | (\mathbf{u} \cdot \mathbf{r}_j) r_j \sum_m F_{1m} | u_i(\mathbf{r}_j) \rangle \right] \right\} \dots \dots (1)$$

we expand $\exp(i\mathbf{K} \cdot \mathbf{r}_i)$ in partial waves and keep only the $l=1$ and $l=2$ terms respectively for the dipole and quadrupole matrix elements. Performing then the

calculations we find:

$$A = ie \left(\frac{2\pi\hbar\omega_\gamma}{V^3} \right)^{1/2} \frac{2\hbar^2}{(2\pi)^2 M} (A_T + C_T \sigma_{0n}) \left\{ \frac{\cos\phi_\gamma \cos\theta_\gamma - i \sin\phi_\gamma M_1}{\Delta E_1 + iW_1} + \frac{\sin\theta_\gamma (\cos 2\phi_\gamma \cos\theta_\gamma - i \sin 2\phi_\gamma)}{\Delta E_2 + iW_2} M_2 \right\}$$

where

$$\begin{cases} \Delta E_1 = E_0 - E_f - \bar{E}_1 \\ \Delta E_2 = E_0 - E_f - \bar{E}_2 \end{cases} \quad \begin{cases} M_1 = \frac{K}{3\nu} \left(9 - \frac{K^2}{\nu} \right) \exp \left(-\frac{K^2}{4\nu} \right) \\ M_2 = k_f \frac{K^2}{4\nu^2} \left(15 - \frac{K^2}{\nu} \right) \exp \left(-\frac{K^2}{4\nu} \right). \end{cases}$$

The cross section of this process is related to A by

$$\frac{d^4\sigma}{d\Omega_p d\Omega_\gamma dE_p dE_\gamma} = \frac{2\pi}{\hbar} \rho(E_\gamma) \rho(E_p) \delta(E_0 - E_f - E_\gamma) \frac{1}{\text{flux of incident protons}} \frac{1}{2} \text{Tr} AA^+$$

the trace is taken on the 0- proton spin.

We perform the integration over E_p and inserting the expression for A we obtain

$$\frac{d^3\sigma}{d\Omega_p d\Omega_\gamma dE_\gamma} = 4(2\pi)^{-5} \frac{e^2 k_f E_\gamma^3}{\hbar c k_0 \hbar^2 c^2} [|A_T|^2 + |C_T|^2] |M|^2$$

where

$$\begin{aligned} |M|^2 = & \frac{\cos^2\phi_\gamma \cos^2\theta_\gamma + \sin^2\phi_\gamma}{(\Delta E_1)^2 + W_1^2} M_1^2 + \sin^2\theta_\gamma \frac{\cos^2\theta_\gamma (1 + \cos 2\phi_\gamma)^2 + \sin^2 2\phi_\gamma}{(\Delta E_2)^2 + W_2^2} M_2^2 \\ & + 2 \sin\theta_\gamma \left[\cos\theta_\gamma (1 + \cos 2\phi_\gamma) \right. \\ & \times \frac{(\Delta E_1 \cdot \Delta E_2 + W_1 W_2) \cos\phi_\gamma \cos\theta_\gamma + (\Delta E_1 \cdot W_2 - \Delta E_2 \cdot W_1) \sin\phi_\gamma}{\{(\Delta E_1^2 + W_1^2)\} \{(\Delta E_2^2 + W_2^2)\}} \\ & \left. + \sin 2\phi_\gamma \frac{(\Delta E_2 \cdot W_1 - \Delta E_1 \cdot W_2) \cos\phi_\gamma \cos\theta_\gamma + (\Delta E_1 \cdot \Delta E_2 + W_1 W_2) \sin\phi_\gamma}{\{(\Delta E_1^2 + W_1^2)\} \{(\Delta E_2^2 + W_2^2)\}} \right] \\ & \times M_1 M_2. \end{aligned}$$

Numerical Calculations

We choose the average excitation energies and widths to be $\bar{E}_1 = 20$ mev, $W_1 = 2$ mev (given experimentally) and $\bar{E}_2 = 30$ mev, $W_2 = 3$ mev (arbitrary values).

Let us confine ourselves to the case where the γ -ray is measured in the plane of the incident and scattered proton directions ($\phi_\gamma = 0$ or π). The angular correlation which we get is $\cos^2\theta_\gamma$ for the dipole and $\sin^2 2\theta_\gamma$ for the quadrupole and

$$\frac{d^3\sigma}{d\Omega_\gamma d\Omega_p dE_\gamma} = \cos^2\theta_\gamma T_1 + \sin^2 2\theta_\gamma T_2 + 2\epsilon \sin 2\theta_\gamma \cos\theta_\gamma T_I$$

where

$$T_1 = 4(2\pi)^{-5} \frac{e^2 k_f E_\gamma^3}{\hbar c k_0 \hbar^2 c^2} [|A_T|^2 + |C_T|^2] \frac{M_1^2}{(\Delta E_1)^2 + W_1^2}$$

$$T_2 = 4(2\pi)^{-5} \frac{e^2 k_f E_\gamma^3}{\hbar c k_0 \hbar^2 c^2} [|A_T|^2 + |C_T|^2] \frac{M_2^2}{(\Delta E_2)^2 + W_2^2}$$

$$T_I = 4(2\pi)^{-5} \frac{e^2 k_f E_\gamma^3}{\hbar c k_0 \hbar^2 c^2} [|A_T|^2 + |C_T|^2] \frac{[\Delta E_1 \Delta E_2 + W_1 W_2] M_1 M_2}{[(\Delta E_1)^2 + W_1^2][(\Delta E_2)^2 + W_2^2]}$$

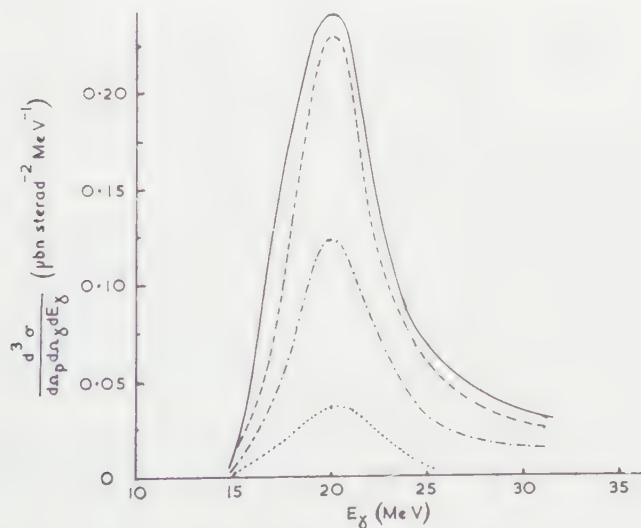
and

$$\begin{aligned} \epsilon &= +1, & \text{if } \phi &= 0 \\ &= -1, & \text{if } \phi &= \pi. \end{aligned}$$

Table 1

 $\phi_\gamma=0$; T_1 , T_2 , T_I are given in $\mu\text{bn sterad}^{-2}\text{MeV}^{-1}$

$E_\gamma(\text{MeV})$	40	30	24	20	15
$\theta=5^\circ$ $\left\{ \begin{array}{l} T_1 \\ T_2 \\ T_I \end{array} \right.$	0.009	0.034 0.05 0.007	0.081 0.002 -0.008	0.242 $0.3 \cdot 10^{-3}$ $\sim 10^{-3}$	0.012
$\theta=10^\circ$ $\left\{ \begin{array}{l} T_1 \\ T_2 \\ T_I \end{array} \right.$	0.016 0.03 0.022	0.028 0.08 0.009	0.076 0.005 -0.01	0.23 $0.8 \cdot 10^{-3}$ 0.004	0.013
$\theta=15^\circ$ $\left\{ \begin{array}{l} T_1 \\ T_2 \\ T_I \end{array} \right.$	0.008 0.03 0.014	0.015 0.08 0.003	0.043 0.006 -0.009	0.124 $0.9 \cdot 10^{-3}$ $\sim 10^{-3}$	0.006
$\theta=20^\circ$ $\left\{ \begin{array}{l} T_1 \\ T_2 \\ T_I \end{array} \right.$	0.002 0.015 0.002	0.004 0.05 0.003	0.01 0.003 -0.004	0.036 $0.6 \cdot 10^{-3}$ $\sim 10^{-3}$	0.002

Fig. 2. Differential cross section as a function of γ -energy for $\theta_\gamma=0$, $\phi_\gamma=0$.

We give in Table 1 the values of T_1 , T_2 , T_I for different angles θ between the incident and scattered proton directions and different values of E_γ . We plot the cross section as a function of E_γ for these same angles θ for: (a) $\theta_\gamma=0$ which gives the maximum of the dipole term and zero for the quadrupole (Fig. 2) and (b) $\theta_\gamma=\frac{1}{4}\pi$ which gives the maximum for the quadrupole term (Fig. 3).

The interference term gives a contribution to the cross section only between the two peaks corresponding to the two excitations in the intermediate state.

For θ smaller than 5 or 10° , we get one peak only due to the dipole excitation and an E1 γ -ray emission. For $\theta \gtrsim 10^\circ$, two peaks appear. If we look at their variation with θ for the same (p', γ) angle, we see that the dipole decreases with increasing θ while the quadrupole has a maximum at about 15° . The quadrupole excitation of the nucleus in the intermediate state can have an appreciable contribution to the process, but always smaller than the dipole one.

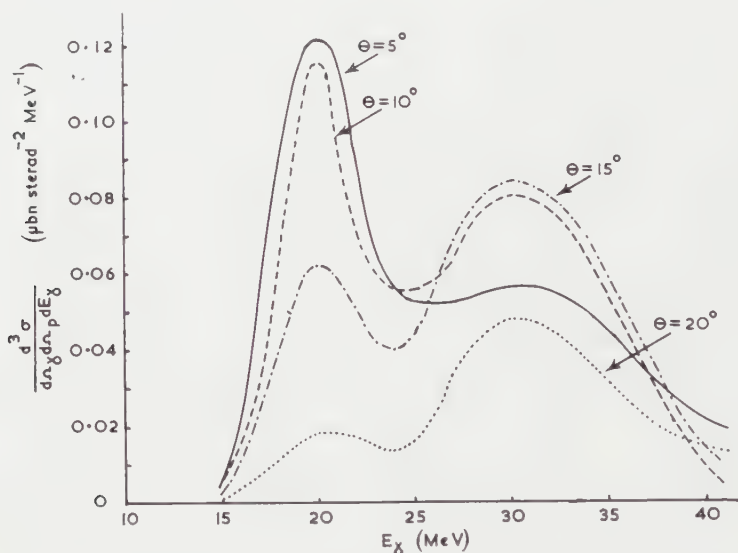


Fig. 3. Differential cross section as a function of γ -energy for $\theta_\gamma = \frac{1}{4}\pi$, $\phi_\gamma = 0$.

§ 4. CROSS SECTION WITH DISTORTED WAVE FUNCTIONS FOR NUCLEONS

We assume the distortion of the nucleon wave function by the nucleus to be well represented by an imaginary Gaussian potential $V(\mathbf{r}) = -iV_0 \exp(-r^2/r_0^2)$. We use the approximate wave function given by McCauley and Brown (1958)

$$\phi(\mathbf{r}) = V^{-1/2} \exp\{i\mathbf{k} \cdot \mathbf{r} + iS(\mathbf{r})\}.$$

We take the z axis along the incident direction of the nucleon (total energy E). If the incident nucleon strikes the i th nucleon of the nucleus at z , we must write the wave functions as

$$S_0(\mathbf{r}) = -\frac{E_0}{k_0} \int_{-\infty}^z V(\mathbf{r}) dz \quad (\text{O}z \text{ axis along } \mathbf{k}_0) \text{ for the incident nucleon}$$

$$S_f(\mathbf{r}) = -\frac{E_f}{k_f} \int_z^{+\infty} V(\mathbf{r}) dz' \quad (\text{O}z' \text{ axis along } \mathbf{k}_f) \text{ for the scattered nucleon.}$$

We consider cases where the angle between the incident and the scattered proton directions are smaller than 20 – 25° , so we may neglect this deflection and write

$$\phi_f^*(\mathbf{r}_0) \cdot \phi_0(\mathbf{r}_0) = \frac{1}{V} \exp(i\mathbf{K} \cdot \mathbf{r}_0) \exp\left(-\frac{E_0}{k_0} \int_{-\infty}^{+\infty} V(\mathbf{r}) dz\right) \left(\frac{E_0}{k_0} \simeq \frac{E_f}{k_f}\right)$$

$V(r)$ being a central potential, the integration over z will give a function of $b^2 = r^2 - z^2$ that can be written as

$$\Gamma(b_0) = \exp \left(-\frac{E_0}{k_0} \int_{-\infty}^{\infty} V(\mathbf{r}) dz \right) = \exp(-\alpha e^{-b_0^2/r_0^2}) \quad \text{where} \quad \alpha = \sqrt{\pi}(E_0/k_0) V_0 r_0.$$

In the following calculations we take an approximate form for $\Gamma(b)$ (Squires 1958) so that we can carry the integrations out analytically:

$$\Gamma(b_0) = 1 - a \exp(-\mu b_0^2); \quad \text{for } {}^{12}\text{C}: a = 0.734, \mu = 0.125 \text{ f}^{-2}.$$

If the nucleon-nucleon potential is of short range compared with the i th particle in the nucleus we can set approximately $\Gamma(b_0) = \Gamma(b_i)$. We keep only the two first terms in the expansion of the electromagnetic part in partial waves and get two matrix elements corresponding to a dipole and a quadrupole excitation. As in §3, we sum for each of them, on the intermediate states, using the same nucleon-nucleon potential. We obtain the same expression (1) for A but here the $\exp(i\mathbf{K} \cdot \mathbf{r}_i)$ of (1) is multiplied by $\Gamma(b_i)$. We keep it on its general form because we cannot expand it in a simple way in partial waves. The selection of intermediate states is given by the electromagnetic part of each term. The calculations were then carried out with the same nuclear model as before. The integrations were performed analytically in cylindrical coordinates (b, z, ϕ) if

$$\frac{K^2}{\nu} = x, \quad \frac{K^2}{\nu + \mu} = y, \quad \frac{\nu}{\nu + \mu} = \beta$$

we get

$$A = ie \left(\frac{2\pi \hbar \omega_\gamma}{V^3} \right)^{1/2} \frac{2\hbar^2}{(2\pi)^2 M} (A_T + C_T \sigma_{0n}) \left[\frac{\cos \phi_\gamma \cos \theta_\gamma - i \sin \phi_\gamma}{\Delta E_1 + i W_1} M_1 \right. \\ \left. + \frac{\sin \theta_\gamma \cos \theta_\gamma M_{20} + \sin 2\theta_\gamma (\cos \theta_\gamma \cos 2\phi_\gamma - i \sin 2\phi_\gamma) M_{21}}{\Delta E_2 + i W_2} \right]$$

with

$$M_1 = \frac{1}{3} \left[\frac{x^{1/2}}{\nu^{1/2}} (9-x) \exp \left(-\frac{x}{4} \right) - x\beta \frac{y^{1/2}}{(\nu + \mu)^{1/2}} (9-y) \exp \left(-\frac{y}{4} \right) \right] \\ M_{20} = \frac{k_\gamma}{2} \left[\frac{x}{2\nu} (15-x) \exp \left(-\frac{x}{4} \right) \right. \\ \left. - \frac{2a}{\nu + \mu} \left[7 + \beta - 8\beta^2 + y \left(-\frac{\beta}{4} + 4\beta^2 \right) - \frac{1}{4}\beta^2 y^2 \right] \exp \left(-\frac{y}{4} \right) \right] \\ M_{21} = \frac{k_\gamma}{2} \left[\frac{x}{2\nu} (15-x) \exp \left(-\frac{x}{4} \right) - a\beta \frac{y}{\nu + \mu} \left(\frac{3}{2} + 6\beta - \frac{1}{2}y \right) \exp \left(-\frac{y}{4} \right) \right]$$

M_1 corresponds to the dipole excitation with emission of an E1 γ -ray, M_{20} and M_{21} correspond to the quadrupole excitation with emission of an E2 γ -ray.

Now the cross section can be written as

$$\frac{d^3\sigma}{d\Omega_\gamma dE_\gamma} = 4(2\pi)^{-5} \frac{e^2 k_t E_\gamma^3}{\hbar c k_0 \hbar^2 c^2} [|A_T|^2 + |C_T|^2] |M|^2$$

where

$$\begin{aligned}
 |M|^2 = & (\cos^2 \phi_\gamma \cos^2 \theta_\gamma + \sin^2 \theta_\gamma) \frac{M_1^2}{(\Delta E_1)^2 + W_1^2} \\
 & + \sin^2 \theta_\gamma \frac{\cos^2 \theta_\gamma (M_{20} + \cos 2\phi_\gamma M_{21})^2 + \sin^2 2\phi_\gamma M_{21}^2}{(\Delta E_2)^2 + W_2^2} \\
 & + \frac{2 \sin \theta_\gamma}{[(\Delta E_1)^2 + W_1^2][(\Delta E_2)^2 + W_2^2]} \left\{ \cos \theta_\gamma \{(\Delta E_1 \Delta E_2 + W_1 W_2) \cos \phi_\gamma \cos \theta_\gamma \right. \\
 & + (\Delta E_1 W_2 - \Delta E_2 W_1) \sin \phi_\gamma \} (M_{20} + \cos 2\phi_\gamma M_{21}) \left. \right\} M_1 + \sin 2\phi_\gamma \\
 & \left\{ (\Delta E_2 W_1 - \Delta E_1 W_2) \cos \phi_\gamma \cos \theta_\gamma + (\Delta E_1 \Delta E_2 + W_1 W_2) \sin \phi_\gamma \right\} M_{21} M_1 \left. \right\}.
 \end{aligned}$$

We notice that the $(p, p'\gamma)$ correlation calculated in §§ 3 and 4 is the same for the dipole term but it is different for the quadrupole.

Numerical Results

We use the same average excitation energies, and the same widths as in § 3.

We start to consider the simple case where the proton is measured in the plan determined by the incident and scattered proton directions ($\phi_\gamma = 0$ or π)

$$\frac{d^3\sigma}{d\Omega_p d\Omega_\gamma dE_\gamma} = \cos^2 \theta_\gamma T_1 + \sin^2 2\theta_\gamma T_2 + \epsilon \sin 2\theta_\gamma \cos \theta_\gamma T_I$$

where

$$\begin{aligned}
 \epsilon &= +1 & \text{if } \phi_\gamma &= 0 \\
 &= -1 & \text{if } \phi_\gamma &= \pi
 \end{aligned}$$

$$T_1 = 4(2\pi)^{-5} \frac{e^2 k_f}{\hbar c k_0} \frac{E_\gamma^3}{\hbar^2 c^2} [|A_T|^2 + |C_T|^2] \frac{M_1^2}{(\Delta E_1)^2 + W_1^2}$$

$$T_2 = (2\pi)^{-5} \frac{e^2 k_f}{\hbar c k_0} \frac{E_\gamma^3}{\hbar^2 c^2} [|A_T|^2 + |C_T|^2] \frac{(M_{20} + M_{21})^2}{(\Delta E_2)^2 + W_2^2}$$

$$T_I = 4(2\pi)^{-5} \frac{e^2 k_f}{\hbar c k_0} \frac{E_\gamma^3}{\hbar^2 c^2} [|A_T|^2 + |C_T|^2]$$

$$\times \frac{\Delta E_1 \Delta E_2 + W_1 W_2}{[(\Delta E_1)^2 + W_1^2][(\Delta E_2)^2 + W_2^2]} (M_{20} + M_{21}) M_1.$$

The (p', γ) correlations are the same as in § 3 for dipole and quadrupole terms. Our approximations of taking a potential with a zero range and of neglecting the proton scattering angle in the nucleon wave functions lead still to a $\sin^2 2\theta_\gamma$ correlation function for the quadrupole but without these simplifying assumptions we should probably have found a correlation, the symmetry axis of which would not be exactly the recoil direction; as we might expect if we look at the experimental results for the lower quadrupole excitation at 4.4 meV (Levinson and Barnerjee 1958). We give in Table 2, the values of T_1 , T_2 and T_I as functions of E_γ and for different proton scattering angles, and we have plotted the cross section as function of E_γ for:

(a) $\theta_\gamma = 0$, which corresponds at a maximum dipole and no quadrupole contribution (Fig. 4), (b) $\theta_\gamma = \frac{1}{2}\pi$, which corresponds to a maximum quadrupole contribution (Fig. 5). When θ is smaller than about $5-10^\circ$ we obtain only one peak at $E_\gamma \simeq 20$ meV which is given by the dipole term. But when θ is greater, we get two peaks of the same order of magnitude. If the interference is then

destructive it can be made constructive between these two peaks by changing ϕ into $\pi - \phi$. Now we consider the general case where $\phi_\gamma \neq 0$. At first we shall look at the variation of dipole and quadrupole peaks as function of θ_γ and ϕ_γ angles.

Let us fix ϕ_γ . The variations of these two peaks are given in Fig. 6 and Fig. 7 (a) and (b).

Table 2

T_1, T_2, T_I are given in $\mu\text{bn sterad}^{-2} \text{mev}^{-1}$						
$E_\gamma(\text{Mev})$	40	30	24	20	15	
$\theta = 5^\circ$	T_1	0.01	0.016	0.038	0.12	0.006
	T_2		0.01	$0.25.10^{-3}$	$0.2.10^{-4}$	$\sim 10^{-6}$
	T_I		0.003	-0.004	$\sim 10^{-3}$	$\sim 10^{-4}$
$\theta = 10^\circ$	T_1	0.0068	0.012	0.033	0.10	0.006
	T_2	0.01	0.028	0.0015	$\sim 0.2.10^{-3}$	$0.2.10^{-4}$
	T_I	0.01	0.007	-0.003	$\sim 3.10^{-3}$	$\sim 10^{-4}$
$\theta = 15^\circ$	T_1	0.003	0.005	0.016	0.045	0.002
	T_2	0.0125	0.035	0.0025	0.0005	$\sim 0.2.10^{-4}$
	T_I	0.01	0.005	-0.007	$\sim 10^{-3}$	10^{-4}
$\theta = 20^\circ$	T_1	0.0005	0.001	0.003	0.009	0.0005
	T_2	0.008	0.0187	0.0012	$\sim 0.2.10^{-3}$	$\sim 10^{-5}$
	T_I	0.004	0.003	-0.002	$\sim 10^{-3}$	$\sim 10^{-4}$

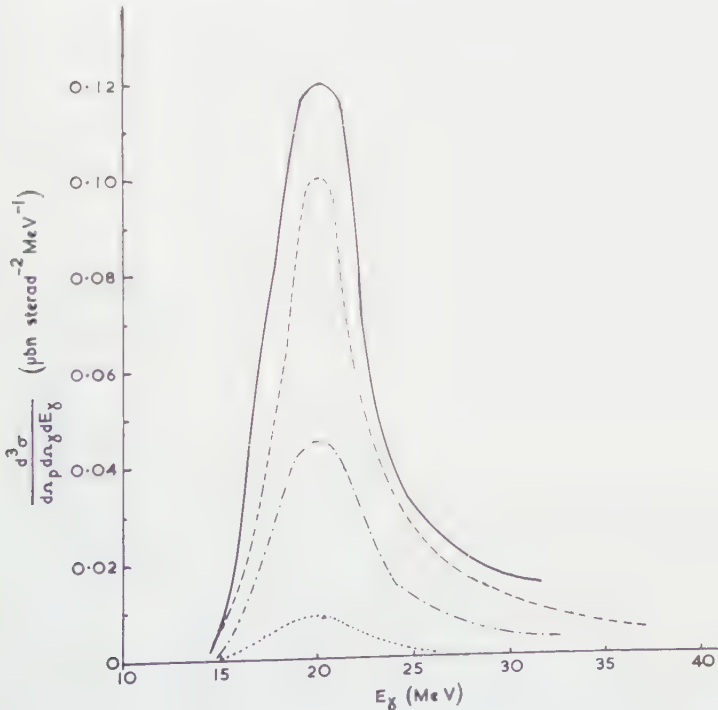


Fig. 4. Differential cross section as a function of γ -energy for $\theta_\gamma = 0, \phi_\gamma = 0$.

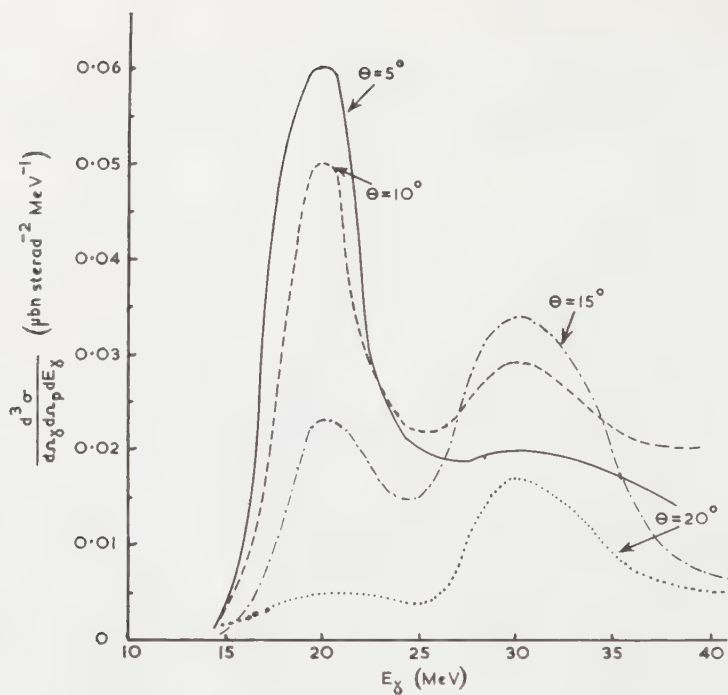


Fig. 5. Differential cross section as a function of γ -energy for $\theta_\gamma = \frac{1}{4}\pi$, $\phi_\gamma = 0$.

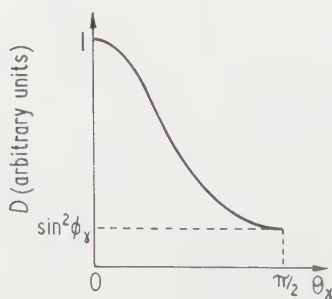


Fig. 6. Variation of the dipole peak D with θ_γ when ϕ_γ is fixed.

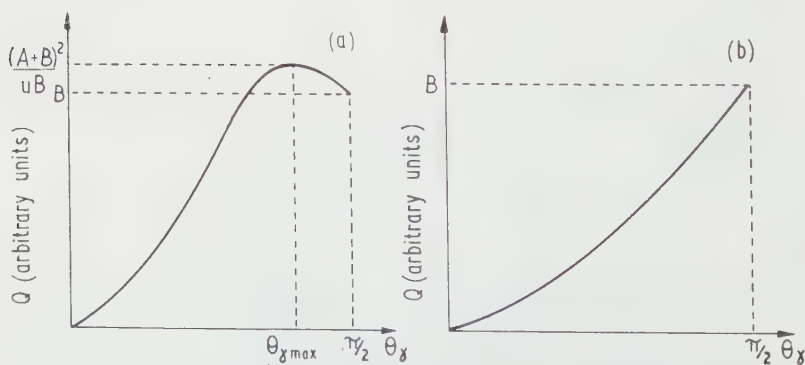


Fig. 7. Variation of the quadrupole peak Q with θ_γ when ϕ_γ is fixed. (a) $(A+B)/2B < 1$ (for ϕ_γ outside the $\beta_2 - \beta_1$ range); (b) $(A+B)/2B \geq 1$ (for $\beta_2 \leq \phi_\gamma \leq \beta_1$).

We have defined $A = (M_{20} + \cos 2\phi_\gamma M_{21})^2$, $B = \sin^2 2\phi_\gamma M_{21}^2$ and β_1 and β_2 in the range $0 - \frac{1}{2}\pi$ are defined by

$$\cos 2\beta_1 = \frac{-M_{20} - (2M_{21}^2 - M_{20}^2)^{1/2}}{2M_{21}^2}$$

$$\cos 2\beta_2 = \frac{-M_{20} + (2M_{21}^2 - M_{20}^2)^{1/2}}{2M_{21}^2}.$$

For the quadrupole peak the $\theta_{\gamma(\max)}$ is the value of θ_γ which gives the maximum in the case (a) and is

$$\sin^2 \theta_{\gamma(\max)} = (A + B)/2B.$$

Taking now this maximum of Q , Q_{\max} , we can look at its variation with ϕ_γ (Fig. 8). We see that the most favourable angle for observing the γ -ray corresponding to a quadrupole excitation of the nucleus in the intermediate state will be $\phi_\gamma = \beta_2$, $\theta_\gamma = \frac{1}{2}\pi$. We give in Table 3 the values of β_2 and β_1 for different proton scattering angles.

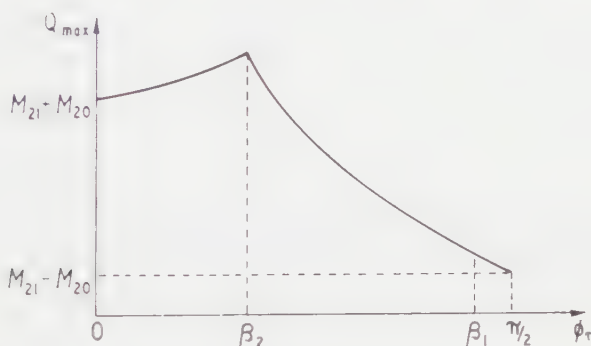


Fig. 8. Variation of Q_{\max} with ϕ_γ .

Table 3

θ (deg)	5	10	15	20
β_1	$63^\circ 36'$	$59^\circ 50'$	$57^\circ 51'$	$58^\circ 54'$
β_2	$26^\circ 42'$	$37^\circ 36'$	$40^\circ 42'$	$41^\circ 9'$

Table 4

M_1 , M_{20} and M_{21} are given in 10^{-13} cm

E_γ (mev)	40	30	24	20	15
$\theta = 5^\circ$	M_1	2.78	2.66	2.6	2.44
	M_{20}	0.07	-0.11	-0.15	-0.20
	M_{21}	1.19	0.82	0.62	0.40
$\theta = 10^\circ$	M_1	2.77	2.84	2.88	2.88
	M_{20}	1.28	0.77	0.54	0.34
	M_{21}	2.56	1.79	1.36	0.81
$\theta = 15^\circ$	M_1	2.17	2.29	2.35	2.39
	M_{20}	1.85	1.35	1.06	0.65
	M_{21}	2.92	2.18	1.74	1.07
$\theta = 20^\circ$	M_1	1.20	1.29	1.32	1.34
	M_{20}	2.12	1.41	1.12	0.71
	M_{21}	2.72	2.06	1.66	1.04

Table 5

T_1 , T_2 and T_I are given in $\mu\text{bn sterad}^{-2}\text{MeV}^{-1}$

E_γ (MeV)	40	30	24	20	15
$\theta = 5^\circ$ $\begin{cases} T_1 \\ T_{20} \\ T_{21} \end{cases}$		0.016 0.012.10 ⁻³ 0.033	0.038 0.03.10 ⁻³ 0.002	0.12 0.01.10 ⁻³ 0.024.10 ⁻²	0.006 0.005.10 ⁻³ 0.002.10 ⁻²
$\theta = 10^\circ$ $\begin{cases} T_1 \\ T_{20} \\ T_{21} \end{cases}$	0.0068 0.0053 0.02	0.012 0.01 0.06	0.033 0.52.10 ⁻² 0.003	0.10 0.08.10 ⁻³ 0.05.10 ⁻²	0.006 0.001.10 ⁻² 0.006.10 ⁻²
$\theta = 15^\circ$ $\begin{cases} T_1 \\ T_{20} \\ T_{21} \end{cases}$	0.003 0.008 0.02	0.005 0.02 0.055	0.016 0.001 0.004	0.045 0.023.10 ⁻² 0.06.10 ⁻²	0.0024 0.002.10 ⁻² 0.006.10 ⁻²
$\theta = 20^\circ$ $\begin{cases} T_1 \\ T_{20} \\ T_{21} \end{cases}$	0.0005 0.006 0.009	0.001 0.014 0.03	0.003 0.0009 0.002	0.009 0.0002 0.0004	0.005 0.2.10 ⁻⁴ 0.4.10 ⁻⁴

To look at the cross sections, we give in Table 4, the values of the three quantities M_1 , M_{20} , M_{21} , functions of E_γ , and for four proton scattering angles and in Table 5 the values of T_1 , T_{20} , T_{21} defined by:

$$T_1 = 4(2\pi)^{-5} \frac{e^2 k_f}{\hbar c} \frac{E_\gamma^3}{k_0 \hbar^2 c^2} [|A_T|^2 + |C_T|^2] \frac{M_1^2}{(\Delta E_1)^2 + W_1^2}$$

$$T_{20} = 4(2\pi)^{-5} \frac{e^2 k_f}{\hbar c} \frac{E_\gamma^3}{k_0 \hbar^2 c^2} [|A_T|^2 + |C_T|^2] \frac{M_{20}^2}{(\Delta E_2)^2 + W_2^2}$$

$$T_{21} = 4(2\pi)^{-5} \frac{e^2 k_f}{\hbar c} \frac{E_\gamma^3}{k_0 \hbar^2 c^2} [|A_T|^2 + |C_T|^2] \frac{M_{21}^2}{(\Delta E_2)^2 + W_2^2}.$$

There the cross section is given directly by

$$\begin{aligned} \frac{d^3\sigma}{d\Omega_p d\Omega_\gamma dE_\gamma} &= (\cos^2 \phi_\gamma \cos^2 \theta_\gamma + \sin^2 \phi_\gamma) T_1 + \sin^2 \theta_\gamma \\ &\times [\cos^2 \theta_\gamma (T_{20}^{1/2} + \cos 2\phi_\gamma T_{21}^{1/2})^2 + \sin^2 2\phi_\gamma T_{21}] + 2 \sin \theta_\gamma \\ &\times \left\{ \cos \theta_\gamma \frac{(\Delta E_1 \Delta E_2 + W_1 W_2) \cos \phi_\gamma \cos \theta_\gamma + (\Delta E_1 W_2 - \Delta E_2 W_1) \sin \phi_\gamma}{[(\Delta E_1)^2 + W_1^2]^{1/2} [(\Delta E_2)^2 + W_2^2]^{1/2}} \right. \\ &\times (T_{20}^{1/2} + \cos 2\phi_\gamma T_{21}^{1/2}) T_1^{1/2} + \sin 2\phi_\gamma \\ &\times \frac{(\Delta E_2 W_1 - \Delta E_1 W_2) \cos \phi_\gamma \cos \theta_\gamma + (\Delta E_1 \Delta E_2 + W_1 W_2) \sin \phi_\gamma}{[(\Delta E_1)^2 + W_1^2]^{1/2} [(\Delta E_2)^2 + W_2^2]^{1/2}} \\ &\left. \times T_{21}^{1/2} T_1^{1/2} \right\}. \end{aligned}$$

The numerical calculations have been performed for several particular cases and the cross sections plotted. Some of them are shown here on Fig. 9.

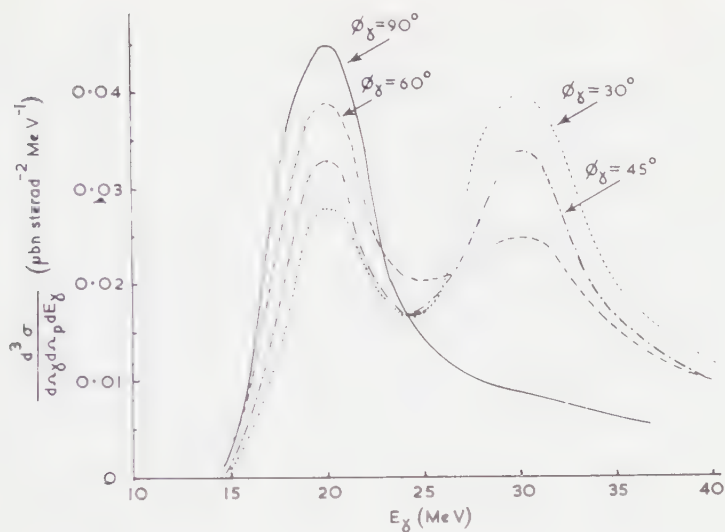


Fig. 9. Differential cross section as a function of γ -energy for $\theta = 15^\circ$ and $\theta_\gamma = \frac{1}{4}\pi$.

We find that for θ greater than $5-10^\circ$ and for some $(\theta_\gamma, \phi_\gamma)$ the emission of an E2 γ -ray coming from the scattering of protons by carbon is not negligible. The energy of this γ -ray can be approximately 30 MeV but the results are not very sensitive when we vary this energy in a not too large range and it can be greater or smaller.

On the other hand; the experimental results (Tyrén and Maris 1957) on the proton scattering by ^{12}C give two peaks in the cross section for excitation energies in the neighbourhood of 20 MeV corresponding to a dipole excitation of the nucleus. But we could not find these two peaks in the dipole with the sum rule approximation employed here.

§ 5. CONCLUSIONS

We have calculated cross sections for the $(p, p'\gamma)$ reaction in carbon and have found the probability of emission of a dipole γ -ray to be quite appreciable. We also considered the possible quadrupole emission to $T=1, J=2^+$ states at an energy above the dipole resonance. Such states have not been observed, but on fairly general theoretical grounds one would expect the $T=1$ quadrupole strength to be distributed in this region. We may have assumed the strength to be too bunched or at a too low energy but our calculations illustrate possible effects both in dipole-quadrupole interference and in quadrupole absorption.

The calculations presented here indicate optimum values of angles and energies for observing these processes, this is of importance since experiments are now being carried out on the 155 MeV synchrocyclotron at Orsay (France).

Comparing results of §§ 3 and 4 we see that the distortion does not change the dipole-quadrupole angular correlation but does decrease the absolute values of the cross section by about a factor two for the dipole and about three for the quadrupole.

ACKNOWLEDGMENTS

I should like to thank Professor G. E. Brown for suggesting the problem and giving me much help and encouragement, and Mme P. Benoist for helpful criticism. I am also very grateful to Professor R. E. Peierls in whose Department this work was carried out.

REFERENCES

- AUSTERN, N., BUTLER, S. T., and McMANUS, H., 1953, *Phys. Rev.*, **92**, 350.
AUSTERN, N., and SACHS, R. G., 1952, *Phys. Rev.*, **81**, 701.
BROWN, G. E., and BOLSTERLI, M., 1959, *Phys. Rev. Lett.*, **3**, 472.
KERMAN, A. K., McMANUS, H., and THALER, R. M., 1959, *Ann. Phys., Lpz.*, **8**, 551.
LEVINSON, C. A., and BARNERJEE, M. K., 1958, *Ann. Phys., Lpz.*, **3**, 67.
McCAULEY, G. P., and BROWN, G. E., 1958, *Proc. Phys. Soc.*, **71**, 893.
SQUIRES, E. J., 1958, *Nucl. Phys.*, **6**, 504.
TYRÉN, H., and MARIS, TH. A. J., 1957, *Nucl. Phys.*, **3**, 52.

Multiple Geiger Counter Coincidences due to Gamma Radiation

BY J. C. BARTON† AND E. G. MICHAELIS‡§

† Northern Polytechnic, London

‡ Birkbeck College, London

MS. received 11th May 1960, in revised form 12th July 1960

Abstract. Triple coincidences produced in Geiger counters by single gamma rays have been found to contribute to the rate of genuine coincidences in unscreened cosmic ray telescopes at great depths below ground.

The effect has been examined by a separate anti-coincidence experiment and has been shown to be compatible with the hypothesis of successive Compton scatters of a single gamma ray quantum in the three counters.

§ 1. INTRODUCTION

AN anomaly in the depth-intensity relation of cosmic rays below ground was postulated by Barnóthy and Forró (1948) who measured two-fold coincidences with a Geiger-counter telescope at water-equivalent depths of about 1000 metres. Subsequent experiments by Miesowicz, Jurkiewicz and Massalski (1950) and Miesowicz and Massalski (1950) indicated that local radioactivity could influence the rate of genuine, as distinct from accidental, two-fold coincidences, and the authors suggested that Barnóthy and Forró's results could be explained in this way. A laboratory investigation by Gierula (1951) confirmed the hypothesis that a single gamma quantum could discharge two Geiger counters, having undergone Compton scattering in the first. On this assumption Gierula was able to account quantitatively for the observed coincidence rate. The process was also investigated by Barnóthy and Forró (1951), who evaluated the contribution of single ^{60}Co gamma rays to the coincidence rate between two Geiger counters. Even earlier Dunworth (1940) had pointed out that the effect could be of importance in gamma-gamma coincidence experiments unless precautions were taken to avoid it. Rather surprisingly the effect does not seem to have been considered as a possible source of error in determining the resolving time of a coincidence system by placing radioactive sources near the counters.

The first part of this paper describes experiments carried out at great depths in the Lake Shore gold mine in Northern Ontario using the three-fold Geiger counter telescope which was described previously (Barton 1956). The results suggested that there might be a contribution to the genuine triple coincidence rate by single γ -rays from the surrounding rock, discharging three counters in succession. To see whether such an effect was possible, a subsequent experiment, described in § 4, was performed in a coal mine in this country. This experiment confirmed that the presence of a γ -ray source could enhance the triple coincidence rate of the telescope. Finally, to study the effect in greater detail, an experiment was devised to measure it under laboratory conditions, and this work is reported in § 5.

§ Now at C.E.R.N., Geneva.

A preliminary account of these investigations was presented to the Physical Society Conference at Durham in September 1958.

§ 2. OBSERVATIONS AT LAKE SHORE MINE

The apparatus (Barton 1956) consisted of twelve Geiger counters each 60 cm long and 3.8 cm in diameter, arranged in three rows of four, placed one above the other. An event required the discharge of at least one counter in each row and hodoscope records showed which of the counters in the top and bottom rows had been discharged in each event.

The sea-level counting rate was 9.0 ± 0.2 per second; the results obtained at Lake Shore are summarized in Table 1.

Table 1

Depth (ft)	Time (days)	Number of events	Rate (day ⁻¹)
2000	3	158	53 ± 4
4000	13	445	34 ± 2
6000	27	846	31 ± 1
8000	54	1483	27 ± 1

These events cannot all be attributed to a known component of the cosmic radiation, for despite the scarcity of our knowledge of its intensities deep underground there is no indication that its flux is independent of depth (Barrett *et al.* 1952). It can therefore be concluded that the majority of the events recorded at the three deeper levels were due to some other effect.

This conclusion is reinforced by information from the hodoscope records. These enable the projected angles between the incident radiation and the vertical to be divided into four groups, centred respectively on 0° , $26\frac{1}{2}^\circ$, 45° and 56° . The records show no evidence of any asymmetry between either side of the vertical; in this case the number of channels contributing to each angular group are 4, 6, 4 and 2 respectively. In addition to the events showing the discharge of one counter in each row there are some multiple events, to which a unique direction cannot be assigned. Results from the hodoscope records are shown in Table 2.

Table 2

Depth (ft)	Inclination to vertical (deg)				Multiple events
	0	$26\frac{1}{2}$	45	56	
2000	49	60	30	8	11
4000	147	179	85	33	1
6000	249	348	183	60	6
8000	437	612	306	117	11

The figures for the three greater depths are again inconsistent with the known behaviour of the cosmic radiation underground, which, if the zenith angle distribution is represented by $\cos^n \theta$, has a value for the exponent $n \ll 3$ (Barrett *et al.* 1952). It is also seen that the events are not due to accidental coincidences, which would be distributed in proportion to the number of

channels. Moreover, the calculated frequency of accidentals is only about 1% of the observed rates.

A simple consideration shows that the angular distribution at the greater depths is compatible with that which would be produced by an isotropic radiation.

§ 3. NATURE OF THE ISOTROPIC RADIATION

The radioactive contamination of the apparatus was extremely small and quite inadequate to account for the events. The counter walls were of 2 mm glass; thus it was very improbable that any naturally occurring beta ray should discharge two counters simultaneously. The source of the radiation was therefore sought in the gamma radiation from the surrounding rock.

Slack (1952) has given results on the background radiation due to rocks of the Canadian Shield in which the Lake Shore mine is situated. Except for the thin ore-bearing fissures, the rock is almost entirely syenite-porphry, a type of granite which has a relatively small uranium and thorium content. Dr. Turner of the Royal Marsden Hospital has measured the alpha activity of rock samples from the Lake Shore Mine and obtained values consistent with the measurements of Slack.

The expected counting rate of a single counter due to the γ -rays was calculated using the theory of Karr and Lamkin (1949) and found to agree with the observed value of 10sec^{-1} . This shows that there was no other important source of radioactivity present in the mine.

§ 4. THE COAL MINE EXPERIMENT

The sensitivity of the three-fold Geiger counter telescope to gamma rays was confirmed by measurements carried out at Harworth Colliery, Bircotes, Doncaster. There the apparatus was placed at a water-equivalent depth of 2110 m and the effect of 2.62 MeV gamma rays from a radio-thorium source on the three-fold coincidence rate was studied. The low cosmic ray intensity at such a depth made it possible to employ a very weak source giving about 10^4 disintegrations per second, which increased the single counter rates on average by about 2.5 counts per second and had a negligible effect on the accidental rate.

The source was attached to the outside of the pressure-vessel in which the apparatus was contained. A thickness of 1.8 cm of lead was interposed to screen off the lower energy gamma rays. The observed three-fold coincidence rates were:

without source: 26 ± 1 per day; with source: 49 ± 5 per day.

This clearly establishes the effect suggested by the anomaly in the results of the earlier experiment. Moreover, when the source was placed so that the gamma ray flux passed through the apparatus at about 45° to the vertical the angular distribution showed some asymmetry. This and the distribution of events in the different channels again showed that the observed effect was not due to accidental coincidences.

§ 5. THE ANTI-COINCIDENCE EXPERIMENT

In order to study the coincidences produced by gamma rays under laboratory conditions the following experiment was devised. Four pairs of

Geiger counters were used to form a telescope for measuring two-, three- and four-fold coincidences. The number of coincidences due to cosmic rays was kept to a minimum by (i) enclosing the counters in a screen of anti-coincidence counters, (ii) requiring in the coincidence that the rays travelled close to the horizontal and (iii) operating at a depth of 60 m water-equivalent in Holborn tube station.

In this way it was possible to use a gamma-ray source which was weak enough for accidental coincidences to be negligible.

The apparatus used is shown in Fig. 1. The coincidence counters (B, C, D, E) were 36 cm long and the anti-coincidence ones (A) 60 cm; all diameters were 3.8 cm. Additional anti-coincidence counters were placed at each end of the apparatus. All counters were operated with electronic quenching units. The resolving time of the coincidence circuits was 3 microseconds but check experiments were made at other values. The anti-coincidence circuit was a transistor version of a circuit due to Hodson (1948)[†].

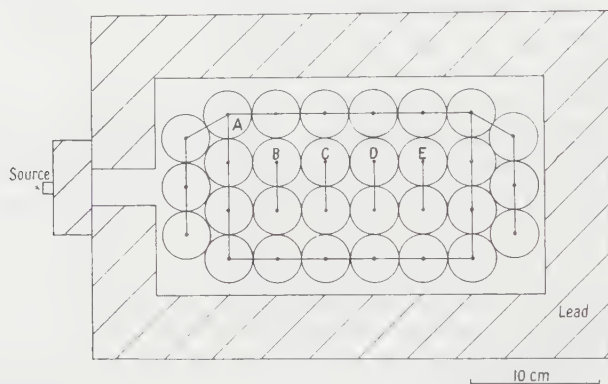


Fig. 1. The anti-coincidence apparatus.

A radio-thorium source with an activity of several microcuries was used and a 3 cm lead filter ensured that the gamma rays were mostly of 2.62 MeV. No correction was made for the decay of the source during the course of the experiment, but readings were taken in such a way that the results would hardly be affected. The coincidence rates were monitored throughout the experiment but the results are not given since they were consistent with those to be expected from single μ -mesons traversing the apparatus. The results for the anti-coincidence rates are given in Table 3.

In the absence of the thorium source the anti-coincidence rates were still appreciable. This can be explained partly by a small leakage of cosmic ray particles through the anti-coincidence screen and partly by the background radioactivity of the laboratory and, possibly, of the apparatus itself. It is therefore necessary to use the figures for the differences between the rates measured with and without the source. No correction has been applied for accidental coincidences since their rate was always less than the statistical error on the same reading. In the case of the three-fold rates this also applies to the

[†] It was essential in the present experiment to be certain that the efficiency of the anti-coincidence screen was not affected by the single counting rate of the anti-coincidence counters. This independence was established by subsidiary experiments.

accidental coincidence of a genuine two-fold event with a count in the third channel.

It is seen from the Table that the rate of two-fold coincidences due to high energy gamma rays could be very easily distinguished from other effects and that the existence of triple coincidences was clearly established. Any four-fold effect was certainly an order of magnitude less frequent.

Table 3

Single counter rates: (sec ⁻¹)						
	B	C	D	E		
Without source	3.62 ± 0.11	3.47 ± 0.11	3.62 ± 0.11	3.40 ± 0.11		
With source	13.16 ± 0.15	11.13 ± 0.14	9.86 ± 0.13	8.87 ± 0.12		
Difference	9.54 ± 0.19	7.66 ± 0.18	6.24 ± 0.17	5.47 ± 0.16		
Anti-coincidence counting rates						
Two-fold rates: (hour ⁻¹)						
	-A+B+C	-A+C+D	-A+D+E	-A+B+D	-A+C+E	-A+B+E
Without source	28 ± 6	23 ± 5	10 ± 4	7 ± 2	1 ± 1	2 ± 1
With source	237 ± 12	218 ± 11	136 ± 9	49 ± 2	46 ± 4	32 ± 2
Difference	209 ± 13	195 ± 12	126 ± 10	42 ± 3	45 ± 4	30 ± 2
Three-fold rates: (hour ⁻¹)						
	-A-B-C-D	A+C-D-E	-A+B+C+E	-A+B+D+E		
Without source	0.180 ± 0.032	0.234 ± 0.037	0.036 ± 0.016	0.027 ± 0.014		
With source	0.490 ± 0.046	0.456 ± 0.044	0.121 ± 0.018	0.131 ± 0.019		
Difference	0.310 ± 0.056	0.222 ± 0.057	0.085 ± 0.024	0.104 ± 0.024		
Four-fold rates: (hour ⁻¹)						
	-A+B+C+D+E					
Without source	0.028 ± 0.009					
With source	0.018 ± 0.007					
Difference	-0.010 ± 0.011					

The results can be summarized by calculating the ratios of different rates. Thus the probability that a gamma ray, having caused a discharge in counters B, is also registered by C, is given by

$$\frac{-A+B+C}{B} = \frac{209}{9.54 \times 3600} = 0.0061 \pm 0.0004.$$

Similarly the probability that a gamma ray is able to discharge a third counter, having already caused a double coincidence, is given by

$$\frac{-A+B+C+D}{-A+B+C} = \frac{0.310}{209} = 0.0015 \pm 0.0003.$$

Similar ratios can be calculated for other pairs of results and are found to be in general agreement with those quoted.

The average ratio for two-fold coincidences between adjacent counters to singles is 0.0063 ± 0.0003 ; for three-fold to two-fold coincidences it is 0.0013 ± 0.0002 . The smaller rates observed for coincidences between non-adjacent counters suggest that the gamma rays are often scattered at large angles.

§ 6. COMPARISON OF EXPERIMENTAL RESULTS

We have referred earlier to previous work on two-fold coincidences in Geiger counters caused by gamma rays. Of the experiments mentioned that of Gierula deserves special attention. In a careful laboratory investigation he studied the effect as a function of gamma-ray energy and of scattering angle.

No anti-coincidence screen was used, but a strong gamma source and a short resolving time enabled accurate results to be obtained. Gierula showed in particular that for 2.62 Mev gamma rays the second counter was most frequently discharged when the gamma ray was scattered at about 30° in the first counter. He discusses the difficulty of defining the efficiency of a two-fold telescope for gamma rays, but his results are consistent with the ratio of double coincidences to single counting rates obtained by us if allowance is made for the different geometries of the two experiments.

Regarding the three-fold effect we can compare the results obtained in the two mine experiments with those of the anti-coincidence experiment. The results are summarized in Table 4.

Table 4

	Rate of one row of counters (sec^{-1})	Triple coincidence rate due to gamma rays (h^{-1})
Lake Shore Mine	40	1.2 ± 0.1
Harworth Colliery	10	1.0 ± 0.2
Holborn experiment	8	0.31 ± 0.06

The similar order of magnitude of the three results suggests that the same effect was indeed being measured in each case. The relatively smaller three-fold rate in the first experiment was due to the lower energy of the γ -rays emerging from the rock compared with the 2.62 Mev of the γ -rays used in the other experiments. The rate in the Holborn experiment would be expected to be smaller because of the less favourable geometry. Allowing for these differences the agreement between the three experiments is as good as could be expected.

§ 7. INTERPRETATION AND CONCLUSIONS

In the case of the two-fold coincidences Gierula showed that the observed angular distribution and absolute intensity were consistent with the hypothesis that the gamma ray was Compton-scattered in the wall of the first counter. It is an obvious extension of this idea to postulate that the gamma ray can again be Compton-scattered in the second counter and then interact also in the third. This process is indicated schematically in Fig. 2(a).

Gierula was able to make an exact calculation for the probability of double coincidences, but the complicated geometry of the problem makes it difficult to extend his method. Very general considerations are, however, sufficient to estimate the order of magnitude of the effects.

It has been shown by Bradt *et al.* (1946) that the detection efficiency of Geiger counters is roughly proportional to the energy of the gamma ray, except at very low energies. For the counters used in these experiments the efficiency is about 1.6% for 2.62 Mev gamma rays. We may also assume that in the Compton-scattering process the differential cross section for all energies of the forward scattered gamma ray is roughly constant and that the total cross section falls off inversely with energy. In this way one can estimate from a fairly simple analysis that the ratio of two-fold coincidences to singles should be about one third of the single counter efficiency; similarly the ratio of triple to double coincidences should be one sixth of that efficiency. In comparing these

theoretical estimates of 0.54% and 0.27% with the experimental values of $0.63 \pm 0.03\%$ and $0.13 \pm 0.02\%$ it must be remembered that they make no allowance for the gamma rays being so scattered that they do not reach the subsequent counters. While this assumption should be satisfied for the first scatter where the energy is high and the collimation good, it is not surprising that there is a considerable loss after the second scatter. The results for coincidences between non-adjacent counters can be explained in a similar fashion.



Fig. 2. Possible mechanisms whereby a gamma ray could discharge three counters.

There are various other processes which might contribute to the triple coincidences. The possibility of a secondary electron penetrating from one counter into another has been considered, but the thickness of the counter walls is sufficient to prevent this process from becoming important. A few of the secondary electrons may produce bremsstrahlung which is detected in one of the other counters (Fig. 2(b)), but at the energies involved here this process is very improbable. Again it is possible for the incident gamma ray to be scattered by the 'double Compton' process and to cause a triple coincidence in the manner shown in Fig. 2(c). It was predicted by Heitler and Nordheim (1934) that this process would be less common than normal Compton scattering by a factor of order $e^2 hc$ and this estimate has been confirmed by recent experimental work (e.g. Bracci *et al.* 1956). Hence it is of relatively little importance in the experiments discussed here.

We conclude that, due to its sensitivity to single gamma rays, an unscreened three-fold Geiger counter telescope is not a suitable instrument for investigating the cosmic radiation at depths of more than about 1000 ft below ground. Quite large thicknesses of lead would be necessary to ensure that there is no significant contribution from effects due to local gamma radiation. If our interpretation of the three-fold coincidences due to gamma rays is correct then the frequency of four-fold coincidences should be very small, hence the multiple events included in Table 2 can probably be attributed to cosmic rays and thus provide a lower bound to the cosmic ray intensity at these depths. It is also possible to estimate the flux at the higher levels by assuming that the events

recorded at 8000 ft are entirely due to γ -rays and that the γ -ray intensity and spectrum are independent of depth. Unfortunately we regard these assumptions as being too questionable for it to be possible to place much reliance on the values thus found.

ACKNOWLEDGMENTS

We are indebted to Mr. W. T. Robson, The Mine Superintendent, for the excellent facilities he provided at the Lake Shore Mine, to Mr. D. A. Tanfield and Mr. W. Briggs of the National Coal Board, for their assistance in arranging the experiment at Harworth Colliery, and to Dr. P. T. Trent and the London Transport Executive for permission to use the Holborn Laboratory. We also thank Dr. Turner for making the analysis of the rock samples, Dr. D. K. Butt for his advice on the radio-thorium source and Dr. Gierula for a valuable discussion. The work carried out in mines was financed by a grant from the University of London Central Research Fund.

REFERENCES

- BARNÓTHY, J., and FORRÓ, M., 1948, *Phys. Rev.*, **74**, 1300.
— 1951, *Rev. Sci. Instrum.*, **22**, 415.
BARRETT, P. H., BOLLINGER, L. M., COCCONI, G., EISENBERG, Y., and GREISEN, K., 1952, *Rev. Mod. Phys.*, **24**, 133.
BARTON, J. C., 1956, *J. Sci. Instrum.*, **33**, 308.
BRACCI, A., COCEVA, C., COLLI, L., and LOVATI, R. D., 1956, *Nuovo Cim.*, **3**, 203.
BRADT, H., GUGELOT, P. C., HUBER, O., MEDICUS, H., PREISWERK, P., and SCHERRER, P., 1946, *Helv. Phys. Acta*, **19**, 77.
DUNWORTH, J. V., 1940, *Rev. Sci. Instrum.*, **11**, 167.
GIERULA, J., 1951, *Acta Physica Polonica*, **11**, 36.
HEITLER, W., and NORDHEIM, L., 1934, *Physica*, **1**, 1059.
HODSON, A. L., 1948, *J. Sci. Instrum.*, **25**, 11.
KARR, P. M., and LAMKIN, J. C., 1949, *Phys. Rev.*, **76**, 1843.
MIESOWICZ, M., JURKIEWICZ, L., and MASSALSKI, J. M., 1950, *Acta Physica Polonica*, **10**, 69.
MIESOWICZ, M., and MASSALSKI, J. M., 1950, *Acta Physica Polonica*, **10**, 274.
SLACK, H. A., 1952, *Trans. Amer. Geophys. Union*, **33**, 897.

Measurement of Townsend's Ionization Coefficients and Attachment Coefficients in Oxygen

BY A. N. PRASAD AND J. D. CRAGGS

Department of Electrical Engineering, The University of Liverpool

MS. received 19th May 1960

Abstract. Pre-breakdown currents and breakdown potentials have been measured in oxygen over a pressure range of 60–600 mm Hg and an E/p range of 35 to 50 $\text{v cm}^{-1}(\text{mm Hg})^{-1}$. From the semi-logarithmic plots of current against electrode separation, the Townsend ionization coefficient α/p , and attachment coefficient η/p and a generalized secondary coefficient γ (where present) have been evaluated employing the modified Townsend current growth equation. From the values of α/p and η/p so obtained and from the earlier measurements, the mean cross section for ionization and attachment have been evaluated and by comparison with those obtained from low pressure (single collision) experiments, the electron attachment in O_2 under high pressure swarm conditions has been interpreted in terms of the dissociative attachment process. Lastly, from the measured values of α/p , η/p and γ , values of the breakdown gap d_s have been evaluated for the E/p range 40–50, employing the modified Townsend breakdown criterion and by comparison with the measured values, the uniform field breakdown in O_2 at threshold has been interpreted in terms of the Townsend build-up processes up to a pd of approximately 250 mm Hg cm.

§ 1. INTRODUCTION

WHILE considerable data are available on electron attachment in oxygen at low pressures (\sim a few mm Hg) and low values of E/p ($\text{v cm}^{-1}(\text{mm Hg})^{-1}$) ($E/p < 30$) (Loeb 1955) and the mechanism of negative ion formation has been interpreted in terms of the dissociative attachment process (Massey 1950, Craggs, Thorburn and Tozer 1957), there appears to be very little information on electron attachment in O_2 and its influence on uniform field breakdown at high pressures and/or high values of E/p . Thus while the recent evaluations of Townsend's primary ionization coefficient α/p and attachment coefficient η/p in O_2 by Harrison and Geballe (1953) are over an extensive range of E/p ($25 < E/p < 60$), the measurements were conducted at pressures below 60 mm Hg and no investigations of uniform field breakdown in O_2 were undertaken. Similarly in a subsequent study of ionization and attachment in O_2 by DeBitetto and Fisher (1958), while values of α/p , η/p and Townsend's secondary coefficient γ were obtained at a pressure of approximately 300 mm Hg, the measurements were confined to one particular value of E/p (≈ 35) and no measurements of breakdown potential were undertaken. Further the values of α/p and η/p obtained differed appreciably from those by Harrison and Geballe. In some earlier studies in this laboratory on ionization and attachment in dry air (Prasad 1959, Prasad and Craggs 1960) at high pressures (up to one atmosphere), it was shown that electron attachment in air at these pressures could be interpreted

in terms of dissociative attachment in the constituent O_2 (Craggs, Thorburn and Tozer 1957, Buchel'Nikova 1958). However, since the maximum partial pressure of O_2 in these studies was only 140 mm Hg approximately, the present study of ionization and attachment in oxygen over an extensive range of pressure was undertaken.

From studies referred to above (Craggs, Thorburn and Tozer 1957) and from the mass spectrometric observations (Thorburn 1954), the negative ion formation in O_2 at electron energies greater than 1 eV appears to consist of:



with an appearance potential of 4.7 eV, and



occurring at energies greater than 17.1 eV, with a further possible O_2^- ion resulting from either collision stabilization of the O_2^{-*} (Eqn (1a)) in a three-body collision at high pressures or from charge exchange processes such as $O^- + O_2 \rightarrow O_2^- + O$.† However since continuous processes (Eqn (1b) above) have cross sections which in general appear to be much smaller than those for the resonant capture process (Craggs, Thorburn and Tozer 1957) and occur at relatively high energies, any contributions to the negative ion formation in O_2 from these processes in high pressure swarm conditions where mean energies are less than 10 eV can in general be neglected as an approximation (Harrison and Geballe 1953).

Thus, assuming that the negative ion formation in O_2 at high pressures results solely from the resonant capture process together with possible further charge exchange and/or collision stabilization processes, following the theories developed by Harrison and Geballe (1953) and Prasad (1959), the growth of pre-breakdown ionization currents and the condition for breakdown in uniform field conditions at high pressures can be expressed by

$$\frac{I}{I_0} = \left[\frac{\alpha}{\alpha - \eta} e^{(\alpha - \eta)d} - \frac{\eta}{\alpha - \eta} \right] / \left[1 - \frac{\gamma\alpha}{\alpha - \eta} (e^{(\alpha - \eta)d} - 1) \right] \quad \dots\dots (2)$$

and

$$\frac{\gamma\alpha}{\alpha - \eta} [e^{(\alpha - \eta)d} - 1] = 1 \quad \dots\dots (3)$$

respectively.

In these equations α and γ are Townsend's primary and secondary ionization coefficients respectively, d the electrode separation and η an attachment coefficient, defined analogous to α as the mean number of attachments per electron per cm of drift in the field direction, describing the rate of negative ion formation due to the processes indicated above.

The authors find that the measurements of pre-breakdown currents in O_2 over extensive ranges of pressure and E/p conform to the above theory and justify the assumptions made regarding the mode of negative ion formation.

§ 2. EXPERIMENTAL PROCEDURE AND RESULTS

A detailed description of the apparatus and the technique and accuracies of the measurements has been published earlier (Hopwood, Peacock and Wilkes 1956, Prasad 1959) and will not be dealt with here. Two cathodes, one of

† We are indebted to the referee for pointing out that this reaction is believed to be endothermic and therefore will have a low probability in a cold gas.

dural (a widely used aluminium alloy) and one of platinum, have been employed in this study. Pre-dried compressed O_2 of 99.5% purity supplied in a cylinder by Messrs. British Oxygen Gases Ltd. has been employed throughout the present work. The gas was, however, dried by passing it through a cold trap containing a mixture of solid CO_2 and acetone as a further precaution. Pre-breakdown currents were measured at $p=60$ and 150 mm Hg (at $20^\circ C$) employing the dural cathode and at $p=100, 150, 200, 300$ and 600 mm Hg employing the platinum cathode, while breakdown potentials were measured employing both the cathodes at $p=150, 300$ and 700 mm Hg. However one further set of pre-breakdown current measurements were obtained employing spectroscopically pure O_2 at $p=60$ mm Hg employing the dural cathode for purposes of comparison.

§ 3. STABILITY OF I_0

Since in all the pre-breakdown current measurements, the stability of the photo-emission I_0 is of great importance, current measurements were repeatedly checked for reproducibility. It was found with both the cathodes that after an initial warming up time of approximately 60 minutes, the intensity of the ultra-violet light from the lamp attained stability and all current measurements could be reproduced to within 5%, provided that the occurrence of sparks or the passage of high currents ($I > 10^{-7}$ amp), which tended to alter the cathode surface, were avoided. It was however found with both the cathodes that the value of I_0 obtained decreased approximately exponentially with increase in pressure of O_2 .

Though this effect could not be confirmed in the case of the dural cathode, owing to the limited number of runs conducted, it was found to be quite pronounced in the case of the Pt cathode where an increase of pressure from 10 mm Hg to 500 mm Hg produced a decrease in I_0 of approximately a factor of four. These figures were obtained by measuring the saturation currents at a gap of $\frac{1}{2}$ cm and voltages of a few tens of volts to a few hundred volts. Since a true 'saturation' could not be obtained in all cases, current values corresponding to $E/p=5$ where ionization is very small were considered in all cases to give a measure of I_0 . It was further found on decreasing the pressure progressively, by pumping, that the value of I_0 increased to within a few per cent of its original value at each pressure, thus confirming that I_0 was truly dependent on pressure. While the approximately exponential fall in I_0 with increase in p would suggest absorption of ultra-violet light by O_2 (Weissler 1956) possible pressure dependent cathode effects cannot be ruled out. If however this effect is due to absorption, since the ultra-violet light is admitted to the chamber via the h.v. bushing (Hopwood, Peacock and Wilkes 1956) and hence traverses approximately 50 cm before reaching the cathode, variation in the gap of even 2.5 cm, the maximum employed in this study, would not cause any appreciable change in I_0 . In either case since it was observed that the value of I_0 at any particular value of p was very stable, it was felt that no particular corrections were necessary in the current measurements due to these effects.

For the sake of brevity the $(\log I, d)$ plots obtained at 60, 200 and 300 mm Hg only are indicated in Figs 1(a), (b), 2 and 3 respectively where the values of I_0 were obtained by extrapolation bearing in mind the pressure dependence of I_0 as mentioned above. The value of I_0 obtained thus, was further confirmed for the 300 mm Hg run by the measurement of the saturation current

(cf. Fig. 3). In the case of the measurements obtained at a pressure of 60 mm Hg, no upcurving was observed in the $(\log I, d)$ plots for $E/p < 42.5$ even at electrode separations of 3 cm corresponding to a pd of 180 mm Hg cm (Fig. 1(a)). On the other hand, for $E/p \geq 45$, the upcurving in these plots was very small while the values of currents were approximately 10^{-7} amp and hence to obtain a greater accuracy in the evaluation of γ , the value of I_0 was reduced by four orders of magnitude approximately, by reducing the intensity of the ultra-violet light by the introduction of filters, and the curves were thus extended to greater values of d . The plots so obtained are indicated in Fig. 1(b). In the case of the runs conducted at higher pressures no upcurving was observed in the $(\log I, d)$ plots for the E/p range of 34 to 38, while current growth investigations at higher values of E/p were not undertaken owing to the very rapid growth of I over a small range of d ($0.4 < d < 1.5$ cm). Thus except at the low pressure of 60 mm Hg and at high values of E/p (≥ 45), no measurements of γ were possible in this study.

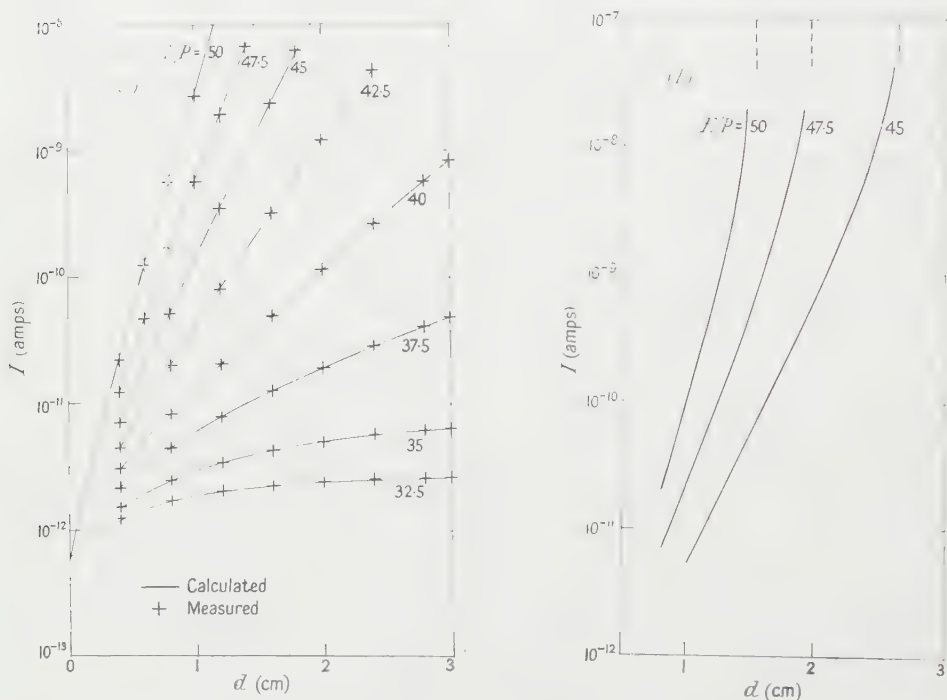


Fig. 1. Ionization currents in dry oxygen at 60 mm Hg pressure for various constant values of the parameter E/p ($\text{v cm}^{-1} (\text{mm Hg})^{-1}$) obtained with a dural cathode.

It is seen from Figs 1 to 3 that the $(\log I, d)$ plots exhibit curvatures characteristic of Eqn (2). The values of the coefficients α , η and γ in the case of the runs at 60 mm Hg were obtained from these current growth plots by a process of curve fitting employing Eqn (2) such that the measured and calculated values of I at any particular value of d agreed within 5%, the figure of reproducibility of current measurements in this study. While it was possible to achieve this agreement for current measurements at pressures less than 150 mm Hg for all values of d , at higher pressures this was possible only for

current measurements at $d > 0.8$ cm. In the range $d = 0.4$ to 0.8 cm, it was found that the calculated values of I were consistently lower than the measured values (see Figs 2 and 3). It was further found that at any particular value of d in this range this difference increased with pressure and decreased with E/p . Thus at $d = 0.4$ cm and $E/p = 35$, while this difference was only approximately 7% at $p = 200$ mm Hg, it increased to 15% (approximately) at $p = 300$ mm Hg and to 33% (approximately) at 600 mm Hg. Finally at these high pressures ($p \geq 200$ mm Hg) an abnormally low value of I_0 had to be assumed compared with analogous conditions in dry air (Prasad 1959). Since this effect was rather puzzling consecutive sets of runs were undertaken starting



Fig. 2. As in Fig. 1 but at a pressure of 200 mm Hg obtained with a platinum cathode.

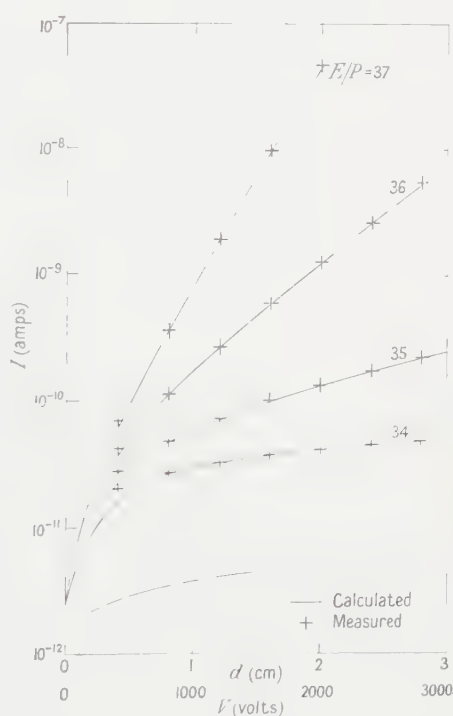


Fig. 3. As in Fig. 1 but at a pressure of 300 mm Hg obtained with a platinum cathode. Lower curve represents current voltage characteristic at $p = 300$ mm Hg and $d = 0.5$ cm.

at a pressure of 100 mm Hg and increasing it to 200 and finally to 300 mm Hg, great care being taken to avoid the passage of large currents ($I > 10^{-8}$ A) and the occurrence of sparks so as to prevent any change in cathode surface due to these. As mentioned earlier, these measurements confirmed that I_0 was progressively reduced with increase in pressure. The shape of $(\log I, d)$ curves at $p = 300$ mm Hg was further confirmed by undertaking several sets of runs. Lastly, apparent values of α/p were obtained from those of the $(\log I, d)$ plots which exhibited no pronounced curvatures (Prasad 1959) and these were in good agreement with the values of $(\alpha - \eta)/p$ from the low pressure measurements,

thus confirming that no particular pressure dependent effects were occurring in the growth of ionization and attachment over the entire pressure range studied.

It was hence decided to ignore the discrepancies between the measured and calculated values of I at small values of d (see later discussion) and to evaluate those values of α/p and η/p which gave the maximum measure of agreement between the measured and calculated values of I (i.e. agreement to within 5%) over the widest possible range of d ($d=0.8$ to 3 cm). The values of α/p and η/p so obtained are indicated in Figs 4 and 5 together with the data from the recent studies of Harrison and Geballe (1953). The values of η/p obtained from the various low pressure swarm experiments at low values of E/p ($E/p < 25$) are also included in Fig. 5 for comparison. The vertical lines in the curves

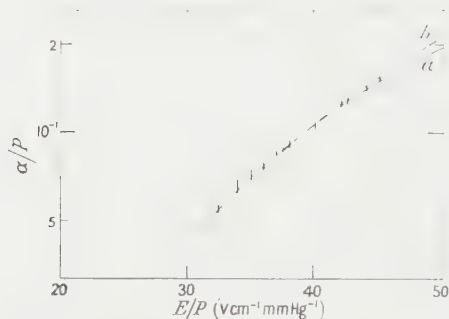


Fig. 4. Values of α/p as a function of E/p in dry oxygen (20°C): *a*, present work; *b*, Harrison and Geballe (1953).

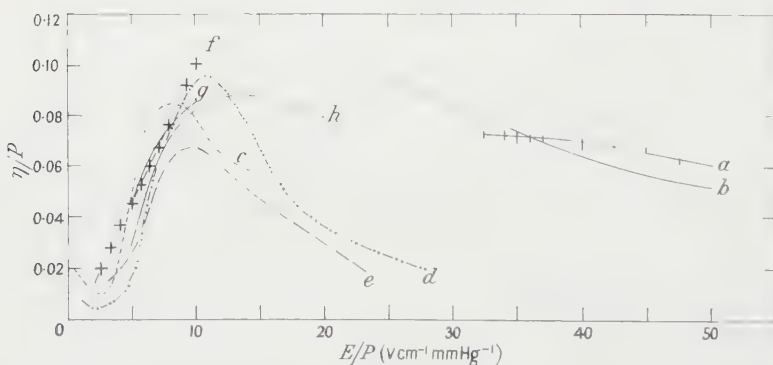


Fig. 5. Values of η/p as a function of E/p in dry oxygen: *a*, present work; *b*, Harrison and Geballe (1953); *c*, Bradbury (1933); *d*, Kuffel (1959); *e*, Herreng (1952); *f*, Doehring (1952); *g*, Chanin *et al.* (1959); *h*, Huxley *et al.* (1959).

relating to this study in these figures represent the scatter between the results obtained at various pressures including those obtained at 60 mm Hg employing spectroscopically pure O_2 . These results thus further confirm that no particular pressure effects were occurring in the growth of ionization in O_2 .

From the pre-breakdown current measurements conducted at 60 mm Hg with the dural cathode (Figs 1(a) and 1(b)) values of γ were obtained for $E/p > 45$. These, together with the calculated and measured values of sparking distance d_s , are indicated in Table 1. Since no measurements of γ were

available with the platinum cathode, these together with values of γ for the dural electrode have been calculated employing the measured values of breakdown potential and these data are presented in Table 2. The mean values of the breakdown potentials V_s obtained at various pressures for both the electrode materials are indicated in Fig. 6 where these are in addition plotted as $V_s/pd(=E/p)_s$ as functions of pd (mm Hg cm) to illustrate the dependence of the breakdown potential on the cathode material.

Table 1

E/p (v cm ⁻¹ (mm Hg ⁻¹))	45.0	47.5	50.0
γ measured	1.8×10^{-6}	2.4×10^{-6}	3.2×10^{-6}
pd_s (mm Hg cm) calculated	158	117	91
pd_s (mm Hg cm) measured	160	117	92.5

Table 2

E/p (v cm ⁻¹ (mm Hg ⁻¹))	40	42.5	45.0	47.5	50.0
γ (calc.) dural	1.1×10^{-7}	3.0×10^{-7}	1.1×10^{-6}	2.4×10^{-6}	3.1×10^{-6}
γ (calc.) platinum	3.8×10^{-7}	5.4×10^{-7}	1.7×10^{-6}	3.8×10^{-6}	5.6×10^{-6}

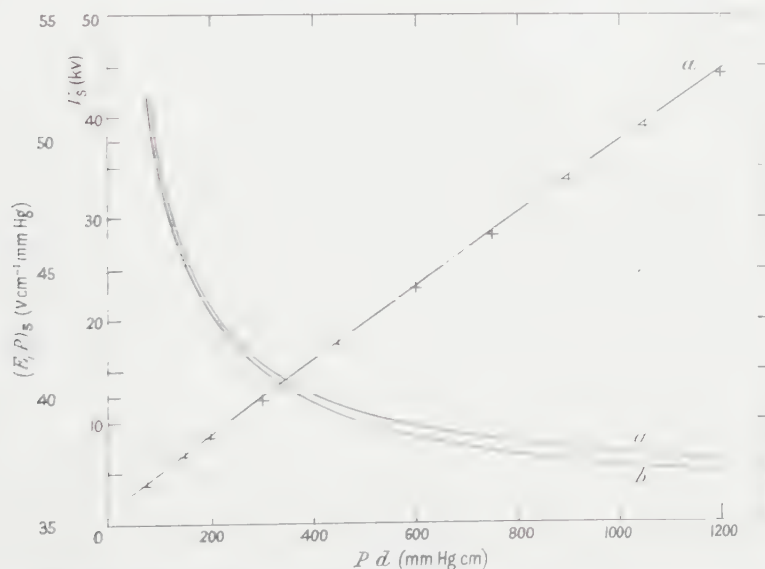


Fig. 6. Observed breakdown potentials and values of E/p at breakdown in oxygen as functions of pd . Curve *a*, dural cathode; experimental points and curve *b*, platinum cathode.

§ 4. DISCUSSION

In view of the good reproducibility of the current measurements (reproducible to within 5%) at $d=0.4$, 0.8 and 1.2 cm in the runs at all pressures and the saturation current measurements it is difficult at present to explain either the abnormally low and pressure dependent values of I_0 or the discrepancy between the measured and calculated values of I for $d \leq 0.8$ cm at high pressures. It

is felt however that diffusion to the cathode of some of the neutral atomic oxygen arising from the electron attaching collisions (cf. Eqn (1a)) coupled with the normal adsorption of O_2 on the cathode surface and the consequent increase in the average cathode work function might be responsible for these effects, though the detailed mechanisms are somewhat obscure. In addition, calculations of the current employing Eqn (2) and mean values of α/p and η/p for $0 < d < 1$ mm, indicate that a marked current growth occurs over a very small distance from the cathode ($d < 1$ mm) and thus any small disturbances of the field (due for instance to the holes in the anode) or the cathode surface condition would have an appreciable influence on the values of I at these gaps. Thus in the absence of careful measurements of both the effective average work function of the cathode and current growth at very small gaps, no special allowances can be made at present for these effects. It is worth while to note that since these effects become appreciable at $p > 200$ mm Hg only, they would not in general be noticeable in pre-breakdown current measurements in air even at a pressure of one atmosphere (Prasad 1959). However, as mentioned earlier, the apparent values of α/p obtained from the linear ($\log I, d$) plots at the high pressures ($p > 200$ mm Hg) agree well with those of $(\alpha - \eta)/p$ from the low pressure runs, thus confirming that no particular pressure dependent processes were occurring in the growth of either ionization or attachment. Finally the good agreement between the values of breakdown potentials obtained at various pressures further confirms this view, thus justifying the procedure adopted for the evaluation of α/p and η/p in this study.

§ 5. IONIZATION AND ATTACHMENT IN O_2

Considering now the values of α/p and η/p obtained in this study (see Figs 4 and 5), it is seen that there is very little scatter between the values obtained at various pressures. Further, the values of α/p obtained in this study (Fig. 4) are in good agreement with those obtained by Harrison and Geballe (1953). On the other hand, while the values of η/p from this study (Fig. 5) are in general agreement with the earlier measurements (Harrison and Geballe 1953), it is seen that the mean curve of $(\eta/p, E/p)$ indicates marked departures at both low and high values of E/p ($E/p \simeq 30$ and 45 respectively) from the latter measurements.

Considering now the values of η/p obtained from the low pressure swarm experiments (Fig. 5), it is seen that though there is general agreement in the measurements by various workers for $E/p < 8$ (approximately), there are marked differences in the maximum values of η/p observed (η/p maximum ranges from 6.7×10^{-2} to 10.2×10^{-2}) and the general shape of the $(\eta/p, E/p)$ curve. In this connection it is worth while to point out that the reduction in the values of η/p beyond the maximum of the $(\eta/p, E/p)$ curve (i.e. for $E/p > 10$ to 12) which has been attributed earlier to onset of ionization (Craggs, Thorburn and Tozer 1957, Tozer *et al.* 1958) appears to be in fact due to experimental errors, since the values of α/p at these values of E/p , i.e. $12 < E/p < 25$ (see Fig. 4) are far too low to account for the observed reductions. Some recent measurements by Chatterton (unpublished) in this laboratory on an apparatus employing the electron filter techniques developed by Bradbury (Loeb 1955) indicate that at these values of E/p , where low pressures are employed, appreciable errors occur due either to the collection of negative ions at the grids or the loss of electron

population by diffusion unless corrected for. It would thus appear that beyond a value for E/p of approximately 10, the results from experiments employing electron filter techniques are apt to be seriously in error. On the other hand, the observations from diffusion experiments of the type developed by Townsend and subsequent workers (Loeb 1955) do not suffer from these errors. In these experiments however the exact corrections to be applied for the presence of both the negative ions in appreciable quantities and the onset of appreciable ionization are somewhat obscure. However, as mentioned earlier, errors due to ionization cannot be appreciable at these values of E/p ($10 < E/p < 20$). Thus it is suggested that the observations of Huxley, Crompton and Bagot (1959) who employ the diffusion techniques and those of Doehring (1952) and Chanin, Phelps and Biondi (1959) who, while employing the time-of-flight methods, correct for any possible diffusion losses, represent the true picture of electron attachment at these values of E/p . From these latter measurements (Fig. 5) it can be seen that the $(\eta/p, E/p)$ curve does not have a pronounced peak at E/p of approximately 10 (as would appear from the recent studies of Kuffel (1959) for example) but has in fact a broad maximum over the E/p range of 10 to 16 and η/p decreases very slowly with further increase of E/p . The results from this study further confirm the above suggestion, since they appear to extrapolate into such a broad maximum, contrary to the observations of Harrison and Geballe which suggest on extrapolation a relatively sharp peak in the $(\eta/p, E/p)$ curve at low E/p .

Finally, considering the values of the cross section for electron attachment and total ionization in O_2 obtained from low pressure (single collision) experiments, recent measurements of Buchel-Nikova (1958), who employs a pulsed electron beam method, yield a peak cross section for the dissociative attachment process,



of $1.3 \pm 0.2 \times 10^{-18} \text{ cm}^2$ at an energy of 6.2 eV with an appearance potential of 4.63 ± 0.04 eV, contrary to the earlier measured value of $2.25 \pm 0.3 \times 10^{-18}$ at 6.7 eV obtained by Craggs, Thorburn and Tozer (1957). The latter authors employed an apparatus based on the design of Lozier (Marriott and Craggs 1954) and utilize the cross section data of Tate and Smith (1932) for positive ion formation in O_2 as standards. However Craggs *et al.* suggest that an error of some 28% occurs in the experiments of Tate and Smith at low energies (20 and 40 eV) arising from the increase in the maximum path length of the electrons in the beam due to the collimating magnetic field used and hence adopt a positive ion cross section of only 0.75 of the Tate and Smith value at 20 eV as a final standard for the evaluation of the cross section for the formation of O^- from O_2 .

Similarly, in their measurements of total ionization in O_2 by electron impact, Craggs *et al.* (1957) employ the value of ionization cross section for 40 eV electrons given by Tate and Smith as a standard and obtain ionization cross sections over the energy range 14–40 eV. While these are in good agreement with those of Tate and Smith for energies greater than 30 eV, below this energy, these values differ appreciably. Thus at 20 eV Craggs *et al.* obtain an ionization cross section which is some 25% lower than that given by Tate and Smith. This difference is attributed by the authors to errors in the electron path length in the experiments of Tate and Smith, as stated above. In a more recent study of ionization of atomic oxygen, Fite and Brackmann (1959) obtain relative cross section measurements which appear to confirm the general shape of the total ionization cross

section curve as obtained by Tate and Smith; however to obtain absolute values of cross section, these authors also had to employ the data of Tate and Smith as standards. Thus it would appear that in the absence of an investigation of the ionization cross section data in O_2 by a direct method, the existing results appear to be somewhat unsatisfactory.

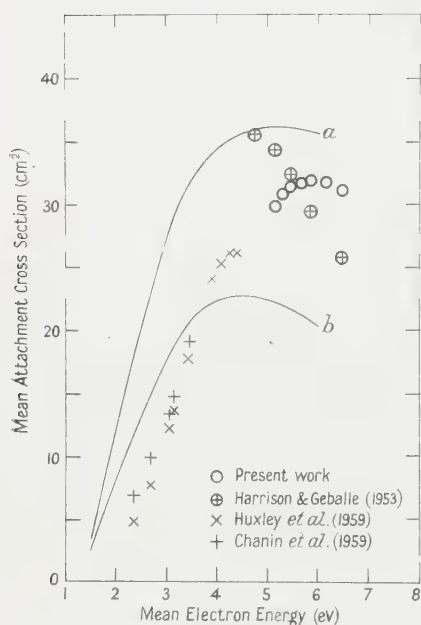


Fig. 7. Mean values of attachment cross sections in oxygen for a Maxwellian form of electron energy distribution. Values calculated (a) from the data of Craggs *et al.* (1957), (b) from the data of Buchel'Nikova (1958).

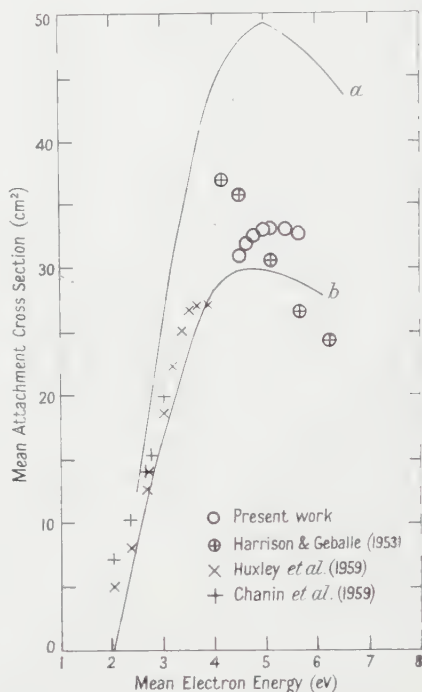


Fig. 8. As in Fig. 7 but with a Druyvesteyn form of electron energy distribution.

In view of these considerations it was decided to calculate the cross sections for ionization and dissociative attachment in O_2 from the present study and to compare them with the corresponding data obtained from the various single collision experiments, employing the methods developed originally by Emeleus, Lunt and Meek (1936). In the absence of the comprehensive data necessary to calculate the energy distribution of the electrons, a knowledge of which is required in the above methods, it was decided to employ as approximations both the Maxwellian distribution and Druyvesteyn's distribution for conditions of constant mean free path and elastic collisions. Full details of the method have been outlined in an earlier publication by the authors (Prasad and Craggs 1960) and will not be dealt with here. The recent measurements of electron drift and agitational velocities in O_2 (Huxley, Crompton and Bagot 1959) have been employed in these calculations. Mean cross sections for electron attachment and ionization in O_2 thus obtained for both the Maxwellian and Druyvesteyn distributions are indicated in Figs 7 to 9 as functions of mean energy. For the

sake of clarity and for reasons mentioned before, the attachment data obtained from the measurements of Chanin, Phelps and Biondi (1959) and Huxley, Crompton and Bagot (1959) only are included in Figs 7 and 8 together with the results from this study and those from the measurements of Harrison and Geballe (1953).

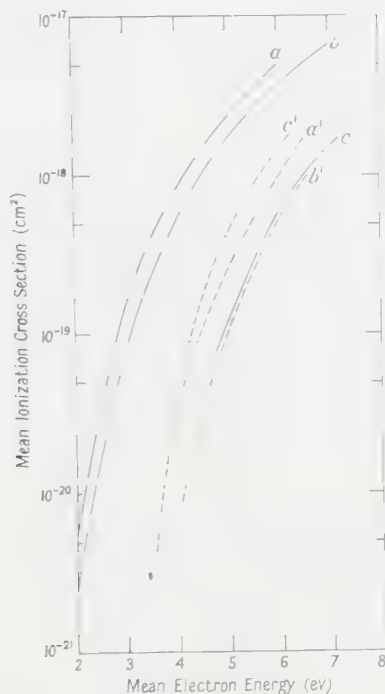


Fig. 9. Mean values of ionization cross sections in oxygen for a Maxwellian form of electron energy distribution: a , calculated from the data of Tate and Smith (1932); b , calculated from the data of Craggs *et al.* (1957); c , observed values from this study and Harrison and Geballe (1953). For a Druyvesteyn form of electron energy distribution: a' , calculated from the data of Tate and Smith; b' , calculated from the data of Craggs *et al.*; c' , observed values from this study and Harrison and Geballe (1953).

Considering the electron attachment data (Figs 7 and 8), it can be seen that the results from this study are in good agreement with those of Chanin *et al.* and Huxley *et al.* and yield a consistent picture of the electron attachment in O_2 as stated earlier although they differ appreciably from those of Harrison and Geballe. Further, while in the case of the Maxwellian distribution (Fig. 7) the results from this and the earlier studies are reconcilable with the data of Craggs *et al.* and of Buchel'Nikova and no satisfactory conclusions can be drawn, but in the case of the Druyvesteyn distribution the results from all the swarm experiments seem to be in good agreement with the data from the measurements of Buchel'Nikova. Similarly in the case of ionization data also (Fig. 9) the data of both Craggs *et al.* and Tate and Smith appear to yield cross sections far in excess of those observed in the swarm experiments for the Maxwellian distribution; in the case of the Druyvesteyn distribution on the other hand, the data of Tate and Smith appear to yield cross sections in agreement with the

observed cross sections, although the data of Craggs *et al.* are not entirely irreconcilable with the observed values. It would thus appear that the observed cross sections for attachment and ionization in the swarm experiments are consistent with the data from the measurements of Buchel'Nikova and Tate and Smith respectively, if the electron energy distribution is assumed to be of the Druyvesteyn form. It should however be emphasized (Heylen and Lewis 1960) that in the absence of a precise knowledge of the electron energy distribution from either measurements or detailed calculations, conclusions such as those above based on the assumption of the distribution function should be interpreted with caution, although in this study in view of the simultaneous evaluation of both a low energy process (attachment) and a high energy process (ionization) this assumption is critically tested.

Lastly, from the measurements of the cross sections for electron attachment resulting from the continuous processes (Eqn (1*b*)) obtained by Craggs *et al.*, the contribution to the attachment from these processes under swarm conditions have been evaluated by the above methods for mean energies less than 6 eV. From these calculations it was found that such contributions are negligible compared with the attachment resulting from the low energy dissociative process, thus confirming the assumption made earlier regarding the mechanism of attachment for low energy swarm conditions.

§ 6. UNIFORM FIELD BREAKDOWN IN O₂

The values of γ obtained in this study for $E/p = 40$ to 50 range both for the dural and platinum cathodes, both measured and calculated (Tables 1 and 2) are over an order of magnitude lower than those in dry air (Prasad 1959) for analogous conditions and correspond more to the values obtained in humid air with a partial pressure of H₂O of 5 mm Hg in a total pressure of 150 mm Hg (Prasad and Craggs 1959). These values thus appear to be contrary to the recent measurements of DeBitetto and Fisher (1958) who obtain $\gamma = 0.045$ at $E/p \approx 35$ ($p = 300$ mm Hg) with a nickel cathode. Further, while values of γ do not vary appreciably with E/p for $E/p > 42.5$, below this γ falls sharply with decrease in E/p ; for example calculations employing the observed values of V_s and assuming the breakdown criterion (Eqn (3)), yield a γ value of 4×10^{-9} at $E/p = 38$ for the dural cathode. On the other hand, by plotting $\log \gamma$ as a $f(pd_s)$ for both the cathodes (assuming γ to be independent of E/p) it was found that γ varies exponentially with pd_s according to a relationship of the form $\gamma = \gamma_0 \exp(-\mu pd_s)$, indicating some form of photo-absorption mechanism (Meek 1959), though in the absence of detailed investigations this conclusion cannot at present be confirmed.

The good agreement between the measured and calculated values of d_s (Table 1) over the E/p range of 42.5 to 50 suggests that at these high values of E/p (up to $pd \approx 250$) the uniform field breakdown in O₂ at threshold is conditioned by a Townsend build-up mechanism. The small but definite dependence of the breakdown potential on the cathode material (Fig. 6) further confirms this view. However at lower values of E/p (i.e. at higher values of pd , where the E/p at breakdown tends to an asymptotic value and α/p tends to η/p (Fig. 6)), no direct measurements of γ were possible in this study (since the value of γ approaches 10^{-9}) and hence the validity of the Townsend criterion for breakdown cannot at present be established, although the continued dependence of

V_s on the cathode material at these values of pd_s suggests such a criterion. It is possible that under these conditions the Townsend build-up processes are operative initially, though the actual advent of breakdown is conditioned by some form of space charge distortion, since rough calculations (Meek and Craggs 1953) indicate the presence of appreciable space charge fields at the head of a single electron avalanche, particularly at high pressures (\sim one atmosphere). Thus in the absence of investigations of a temporal nature, the detailed mechanisms of breakdown at these values of pd_s ($pd > 300$) cannot at present be specified.

§ 7. CONCLUSIONS

From a comparison of the values of the mean cross sections for attachment obtained in this study over an extensive range of pressures, and those from the earlier experiments with the calculated cross sections from the low pressure electron beam studies, it is concluded that the electron attachment in O_2 under high pressure swarm conditions can be interpreted satisfactorily in terms of the dissociative attachment process (Harrison and Geballe 1953, Craggs, Thorburn and Tozer 1957). Further, from a simultaneous comparison of the data relating to both ionization and attachment in O_2 obtained from the various swarm experiments with those from the low pressure (single collision) electron beam experiments, it would appear that the electron energy distribution in the former experiments is of the Druyvesteyn form, although in the absence of direct experimental evidence, or detailed calculations, this conclusion cannot at present be confirmed. Finally, from the measured values of γ and the static breakdown potentials, it is seen that the uniform field breakdown at threshold in O_2 can be interpreted in terms of the Townsend build-up mechanisms up to $pd \simeq 250$ mm Hg cm.

ACKNOWLEDGMENTS

The authors wish to thank Dr. B. A. Tozer for many valuable discussions. One of us (A.N.P.) is grateful to the University of Liverpool for the award of a Fellowship.

REFERENCES

- BRADBURY, N. E., 1933, *Phys. Rev.*, **44**, 883.
 BUCHEL'NIKOVA, N. A., 1958, *Zh. Eksper. Teor. Fiz.*, **35**, 1119.
 CHANIN, L. M., PHELPS, A. V., and BIONDI, M. A., 1959, *Phys. Rev. Letters*, **2**, 344.
 CRAGGS, J. D., THORBURN, R., and TOZER, B. A., 1957, *Proc. Roy. Soc. A*, **240**, 473.
 DEBITETTO, D. J., and FISHER, L. H., 1958, *Phys. Rev.*, **111**, 390.
 DOEHRING, A., 1952, *Z. Naturf.*, **79**, 253.
 EMELEUS, K. G., LUNT, R. W., and MEEK, C. A., 1936, *Proc. Roy. Soc. A*, **156**, 394.
 FITE, W. L., and BRACKMAN, R. T., 1959, *Phys. Rev.*, **113**, 815.
 HARRISON, M. A., and GEBALLE, R., 1953, *Phys. Rev.*, **91**, 1.
 HERRENG, P., 1952, *Cah. d. Phys.*, **38**, 7.
 HEYLEN, A. E. D., and LEWIS, T. J., 1960, *Proceedings of the 4th International Conference on Ionization Phenomena in Gases (Uppsala)*. (Amsterdam: North Holland Publishing Co.)
 HOPWOOD, W., PEACOCK, N. J., and WILKES, A., 1956, *Proc. Roy. Soc. A*, **235**, 334.
 HUXLEY, L. G., CROMPTON, R. W., and BAGOT, C. H., 1959, *Austr. J. Phys.*, **12**, 303.
 KUFFEL, E., 1959, *Proc. Phys. Soc.*, **74**, 297.
 LOEB, L. B., 1955, *Basic Processes of Gaseous Electronics* (University of California Press).

- MARRIOTT, J., and CRAGGS, J. D., 1954, *E.R.A. Report L/T308*.
- MASSEY, H. S. W., 1950, *Negative Ions* (Cambridge: University Press).
- MEEK, J. M., 1959, *Nature, Lond.*, **183**, 1805.
- MEEK, J. M., and CRAGGS, J. D., 1953, *Electrical Breakdown of Gases* (Oxford : University Press).
- PRASAD, A. N., 1959, *Proc. Phys. Soc.*, **74**, 33.
- PRASAD, A. N., and CRAGGS, J. D., 1959, *E.R.A. Report L/T390*.
- 1960 *Proceedings of the 4th International Conference on Ionization Phenomena in Gases (Uppsala)* (Amsterdam: North Holland Publishing Co.)
- TATE, J. T., and SMITH, P. T., 1932, *Phys. Rev.*, **39**, 270.
- THORBURN, R., 1954, *Applied Mass Spectrometry* (London : Institute of Petroleum), p. 185.
- TOZER, B. A., THORBURN, R., and CRAGGS, J. D., 1958, *Proc. Phys. Soc.*, **72**, 1081.
- WEISSLER, G. L., 1956, *Handb. d. Phys.*, **21**, 304 (Berlin: Springer).

A Study of the Reactions $^{12}\text{C}(^3\text{He}, \text{n})^{14}\text{O}$ and $^{16}\text{O}(^3\text{He}, \text{n})^{18}\text{Ne}$

By J. H. TOWLE AND B. E. F. MACEFIELD

Atomic Weapons Research Establishment, Aldermaston, Berks.

MS. received 13th June 1960

Abstract. The time-of-flight and slow-neutron threshold techniques in conjunction with ^3He particles of energies of up to 11 mev, have been used to measure the Q value of the $^{16}\text{O}(^3\text{He}, \text{n})$ reaction and to locate levels in ^{14}O and ^{18}Ne . The Q value, -3.199 ± 0.006 mev, requires a mass defect of 10.649 ± 0.008 mev for ^{18}Ne . Levels were found in ^{14}O at 5.905 ± 0.012 , 6.30 ± 0.03 , and 6.586 ± 0.012 mev; and in ^{18}Ne at 1.880 ± 0.010 , 3.362 ± 0.011 and 3.608 ± 0.012 mev.

Excitation functions were measured between 2.0 and 5.7 mev for both reactions. Angular distributions of the $^{12}\text{C}(^3\text{He}, \text{n})$ reaction measured at 4.65, 4.98 and 5.26 mev, have been compared with theory for a double stripping process. The data suggest that a direct process is competing strongly with compound nucleus formation in this energy region.

§ 1. INTRODUCTION

THE $(^3\text{He}, \text{n})$ reactions are of interest from two viewpoints. The reaction mechanism is of interest, since direct interaction and compound nucleus formation may both be expected to play a substantial role. Also, since two protons are added to the target nuclei, they enable the levels of proton-rich nuclei to be studied, and these are usually difficult to produce by alternative reactions. Thus, whereas the energy levels of many pairs of mirror nuclei ($T_z = \pm \frac{1}{2}$) have been compared, as yet very little has been done towards the correlation of levels in isobars having $T_z = \pm 1$.

The $^{12}\text{C}(^3\text{He}, \text{n})^{14}\text{O}$ reaction has been studied in the energy range 1.0 to 2.8 mev by Bromley *et al.* (1957). The threshold was found to be 1449.6 ± 2.8 kev. The 0° and 90° excitation functions were obtained, and angular distributions of the neutrons were measured at bombarding energies of 1.89, 2.16, 2.40 and 2.51 mev. The results, together with those of similar measurements on the $^{12}\text{C}(^3\text{He}, \text{p})^{14}\text{N}$ reaction, could not easily be explained as resulting from either compound nuclear or direct processes, but rather from a mixture of the two.

Since the angular distributions of direct reactions become, in general, increasingly asymmetric with increasing bombarding energy, whereas the compound nuclear process becomes more isotropic owing to interference cancellations, it was thought that a contribution from a direct process would be better revealed in experiments at higher bombarding energies than those used by Bromley *et al.* Measurements of the 0° and 90° excitation functions in the range 2.0 to 5.7 mev, and of differential cross sections at 4.65, 4.98 and 5.26 mev, are reported in this paper.

Ajzenberg and Franzen (1954) in a study of the $^{14}\text{N}(\text{p}, \text{n})^{14}\text{O}$ reaction, using nuclear emulsions, found broad or unresolved levels in ^{14}O at about 6.2, 7.5 and 9.3 mev. In the $^{12}\text{C}(^3\text{He}, \text{n})^{14}\text{O}$ reaction at energies between threshold and

2.8 MeV (Bromley *et al.* 1957), there was no evidence for a second threshold corresponding to a level in ^{14}O with an excitation energy of up to 1.0 MeV. In the present work on this reaction we have observed three excited state thresholds, using ^3He particles of energies between 2.5 and 11 MeV. All the measurements were made using the 6 MV Van de Graaff accelerator. Energies greater than 6 MeV were obtained using the doubly charged ^3He beam which had previously been much enhanced by the insertion of a gas stripper tube a short way along the accelerating tube. This facility is to be described elsewhere. In addition, the neutron spectrum from this reaction was observed using a time-of-flight spectrometer at bombarding energies up to 5.5 MeV in a search for low lying excited states of ^{14}O . The time-of-flight measurements were restricted to bombarding energies below 6 MeV, since the beam current of doubly charged ions attainable ($\sim 0.5 \mu\text{A}$), was insufficient for the application of this technique.

When the present work was begun, no previous work on the $^{16}\text{O}(^3\text{He}, n)^{18}\text{Ne}$ reaction had been reported. This paper reports measurements of the neutron spectrum made at bombarding energies up to 6 MeV, and observations of slow neutron thresholds corresponding to the ground and three excited states of ^{18}Ne using ^3He particles of energies up to 10 MeV. The 0° and 90° excitation functions measured between threshold and 5.7 MeV are also given.

Two preliminary reports concerning the ground state Q value of this reaction have recently appeared. Dunning and Butler (1959), report the threshold as 3.811 ± 0.015 MeV, corresponding to a Q value of -3.206 ± 0.013 MeV, also a possible threshold which would correspond to a level in ^{18}Ne at 0.114 ± 0.015 MeV. Using nuclear emulsion detectors and 5.52 MeV ^3He particles, Ajzenberg-Selove and Dunning (1960) find the Q value to be -3.20 ± 0.05 MeV.

§ 2. EXPERIMENTAL PROCEDURE

2.1. Targets

The carbon targets were made by placing metal foil backings near an arc discharge maintained *in vacuo* between pure graphite electrodes. Oxygen targets were made by vacuum evaporation of SiO_2 , Nb_2O_5 or Cr_2O_3 to thicknesses between 50 and $300 \mu\text{g cm}^{-2}$, the material and thickness used depending on the yield and energy resolution required. For all except the threshold experiments, the target materials were deposited over a circular area 1 in. in diameter, on a gold backing 0.005 in. thick. In the threshold experiments where good uniformity over a large area was required, the target areas were 1.5 in. in diameter, located centrally on tantalum disks 2.5 in. in diameter and 0.005 in. thick. The thicknesses of the targets were determined by weighing.

2.2. Excitation Functions and Angular Distributions

The excitation functions were measured with two long counters placed at angles of 0° and 90° to the incident beam. The distance between the target and the face of each counter was 60 cm corresponding to an angular acceptance of $\pm 10^\circ$. Small corrections have been made to allow for neutrons arising elsewhere than at the target, and for neutrons scattered into the counters from surrounding materials. The former correction was determined from measurements made with a clean gold backing in place of the target, and the latter by inserting a cone of paraffin wax between target and counter. The corrections applied to the results

obtained with the carbon target were both between 1% and 2% over the whole energy range. The yield from the oxygen target was much smaller than with carbon, and the counts observed when bombarding a clean backing formed a larger fraction of the total. The corrections applied were 10% and 20% at 4.2 MeV for the 0° and 90° counters respectively, decreasing with increasing yield to 3% and 7% at 5.5 MeV.

The target box formed an effective Faraday-cup and a ring maintained at -100 v with respect to the target was used to suppress secondary electrons. A current integrator measured the total charge collected at the target. The detection efficiency of the long counters had previously been determined at several energies between 0 and 5 MeV using neutron sources of known strength (McTaggart 1960, unpublished). It was thus possible to plot the excitation functions on an absolute scale.

The angular distributions were measured using a long counter which could be rotated about the target at a distance of 100 cm, the angular acceptance being $\pm 6^\circ$. The counts in this counter were normalized to a fixed number of counts recorded by a second long counter fixed at an angle of 90°, 60 cm away from the target. As with the excitation functions, experimentally determined corrections have been applied to allow for counts due to neutrons other than those leaving the target within the acceptance angle of the counter. The total corrections applied were not greater than 10% and 20% at 0° and 140° respectively. The correction to the shape of the angular distribution due to the finite acceptance angle of the detector is small compared with these and has not been applied.

2.3. Time of Flight Spectrometer

This facility has been described previously (Batchelor and Towle 1959). A comparison with a long counter showed that the neutron counting efficiency of the detector was constant within 10% over the energy range 0.6 to 4.0 MeV. In some of the measurements the random background counts were reduced by means of pulse shape discrimination against γ -rays. This development will be described elsewhere (Batchelor *et al.* 1960).

The time to pulse height converter was adjusted so that each channel of the 100 channel analyser corresponded to approximately 2 nsec. The time scale was calibrated in terms of the known delay in a coaxial cable by means of a double pulse generator.

2.4. Threshold Experiments

The arrangement of the target and counters used in the measurement of neutron thresholds is shown in Fig. 1. Counter A which is more sensitive to

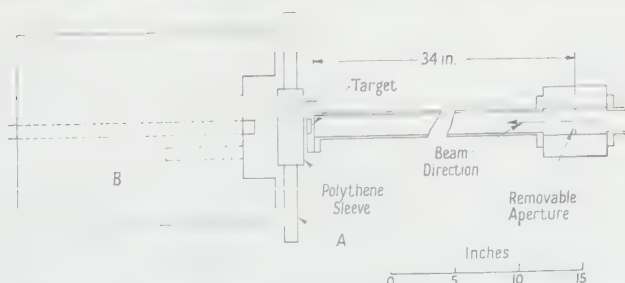


Fig. 1. Target and counter arrangement for the threshold experiments. A and B are the 'slow'- and 'fast'-neutron counters respectively.

neutrons emitted at threshold (≈ 50 kev) than to fast neutrons, consists of a BF_3 counter of 1 in. diameter and 12 in. long with a sleeve of polythene 6 in. long and 0.5 in. thick as moderator. The parts of the BF_3 tube not covered by polythene were enclosed in a layer of cadmium foil 0.02 in. thick to attenuate the thermal neutron background. The fast neutron counter B, is a long counter having a similar BF_3 tube to the above. The efficiency of the long counter, which is fairly constant in the range 0.01 to 5.0 Mev was effectively reduced for threshold neutrons since these were considerably attenuated on traversing the polythene moderator of the 'slow' counter. Thus the ratio of the efficiencies of the 'slow' and 'fast' counters for threshold neutrons was further enhanced.

The simultaneous use of slow- and fast-neutron counters facilitates the differentiation between thresholds and compound nuclear resonances, as shown by Bonner and Cook (1954). This is of particular importance for thresholds corresponding to excited states, where a large background of fast neutrons usually exists. Further, the ratio of the counts in the detectors is independent of target uniformity. Fig. 2 shows the variation of the counter ratio (slow/fast)

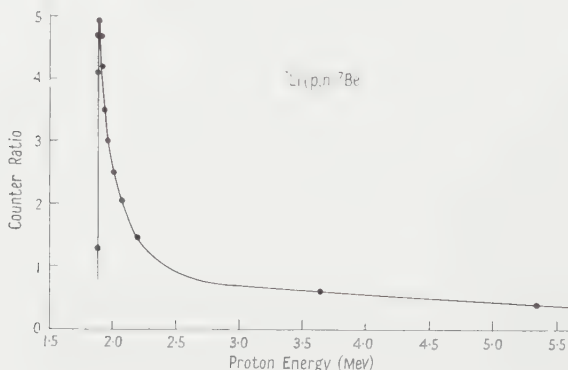


Fig. 2. Counter ratio plot for the ${}^7\text{Li}(p, n){}^7\text{Be}$ reaction.

through the ${}^7\text{Li}(p, n){}^7\text{Be}$ threshold, obtained using a Li_2O target 5 kev thick. This curve applies essentially to a single group of neutrons, since the yield of slow neutrons above the excited state threshold at 2.37 Mev is very small (Marion, Bonner and Cook 1955). The ratio rises sharply to a value of 4.9 at threshold where the neutron energy is 30 kev, and falls to one half of this value for 0.23 Mev neutrons.

Preliminary measurements on the ${}^{16}\text{O}({}^3\text{He}, n){}^{18}\text{Ne}$ reaction showed that in order to obtain meaningful and reproducible results, it was essential to reduce to an absolute minimum the background counts due to beam striking diaphragms and slits, and at the same time to confine the beam to a small area of a target of uniform thickness. The target was therefore set up at a distance of 32 ft from the beam stabilizing slits. Midway between these slits and the target, the beam passed through an electrostatic strong focus lens. A diaphragm with a 0.25 in. diameter aperture was placed 3 ft from the target. This diaphragm could be moved into or out of the path of the beam by means of an actuator mechanism operated electrically from a switch in the control room. By observing the beam impinging on a quartz plate placed in the target position, it was seen that the aperture restricted the beam to a circular spot 0.3 in. in diameter at the target centre. By careful

adjustment of the focusing lenses, all of the analysed beam current could be brought through the aperture onto the target without incurring any measurable loss.

The preliminary experiments also showed that in order to obtain consistent day to day measurements of the threshold energies in terms of the magnetic field of the 90° analysing magnet, it was essential to define the path of the beam in the magnet within narrow limits. This was achieved by placing a slit 0.1 cm wide at a distance 70 cm from the entrance face of the magnet which has a 60 cm radius. The stabilizing slits which were 80 cm from the exit face were also adjusted to 0.1 cm gap. The beam emerging from the accelerator was focused onto the first slit by means of an electrostatic strong focus lens.

The procedure of the experiment was as follows. After each change was made in the beam energy, the diaphragm was inserted and both strong focus lenses, together with the machine focus control, were adjusted for maximum current on target. The diaphragm was then removed, but if in consequence the current on target increased, it was replaced and the beam was refocused. When there was no measurable loss of current due to the diaphragm, this was removed, the target current was switched to the integrator, and the neutron counts were recorded.

This attention to uniformity of the target, beam impact location, and attenuation of background has enabled useful information to be obtained from the yield curves as well as the ratio plots. The excited state thresholds are well defined in the slow-neutron yield curves. The threshold energies obtained from runs made in some cases weeks apart agree within the uncertainty (10 to 15 keV) of each measurement.

2.5. Energy Calibration

The energy of the ^3He beam was determined by measuring the proton resonance frequency in the field of the analysing magnet. This magnetometer was calibrated against the threshold of the reaction $^6\text{Li}(^3\text{He}, n)^8\text{B}$ which has been

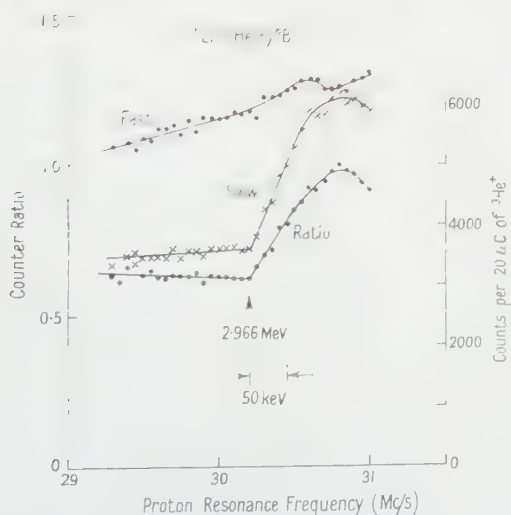


Fig. 3. Plots of the 'slow' and 'fast' counts, and 'slow'/'fast' ratio through the threshold of the $^6\text{Li}(^3\text{He}, n)^8\text{B}$ reaction.

measured absolutely to be 2.9661 ± 0.0017 MeV (Dunning, Butler and Bondelid 1958). In Fig. 3 are shown the yield curves and ratio plot obtained for this threshold with the present apparatus. The target was a 50 keV thickness of ${}^6\text{Li}_2\text{O}$ on a thick tantalum backing. The proton resonance frequencies at threshold measured in three runs at weekly intervals are 30.19 ± 0.025 , 30.19 ± 0.025 and 30.22 ± 0.025 Mc/s giving a mean of 30.20 ± 0.015 Mc/s. Thus in the relation between proton resonance frequency ν (Mc/s) and particle energy T (MeV)

$$\nu^2 q^2 = K m_0 T (1 + T/2m_0 c^2)$$

where m_0 is the rest mass of the bombarding particle expressed in a.m.u. and q is its charge in units of the electronic charge, we find that $K = 101.86 \pm 0.12$. This threshold conveniently calibrates both ends of the energy scale used, since the magnetic field required for 3 MeV ${}^3\text{He}^+$ ions would correspond also to 12 MeV ${}^3\text{He}^{2+}$ ions.

§ 3. RESULTS

3.1. ${}^{12}\text{C}({}^3\text{He}, n){}^{14}\text{O}$

With bombarding energies of 5.2 and 5.5 MeV, the neutron spectrum was observed at several angles between 0° and 140° . The target thickness was $240 \mu\text{g cm}^{-2}$. Only the ground state group was observed. The upper limit of the range of excitation in ${}^{14}\text{O}$ covered was 3.0 MeV, corresponding to the lowest neutron energy observable in the run at 0° with 5.5 MeV ${}^3\text{He}$ particles. In this spectrum (Fig. 8(a)) the maximum possible intensity of any unobserved group was 0.08 of the ground state group.

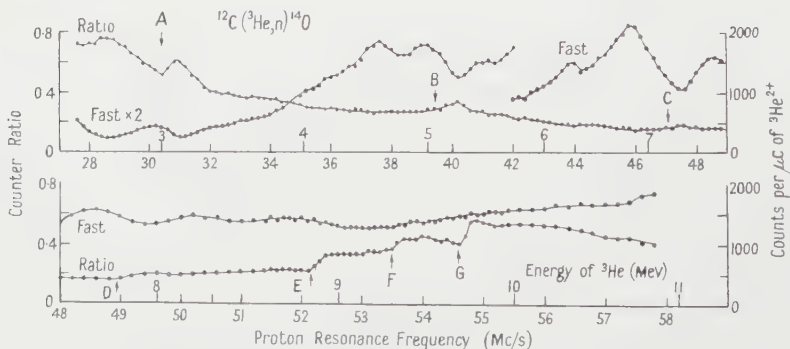


Fig. 4. Plots of the counter ratio and 'fast' counts for the ${}^{12}\text{C}({}^3\text{He}, n){}^{14}\text{O}$ reaction. The statistical error in the ratio varies between 1% and 2%.

Fig. 4 shows plots of the counts per μC measured by the 'fast' counter, and the 'slow' to 'fast' ratio for bombarding energies between 2.5 and 11.0 MeV. Targets of thickness 70 and $150 \mu\text{g cm}^{-2}$ were used below and above 4.5 MeV respectively. Providing the 'fast' and 'slow' counters subtend the same solid angle at the target, the counter-ratio decreases monotonically until a new threshold is reached. In Fig. 4, the ratio begins to increase at seven places marked A to G. However, only at E, F and G are there corresponding increases in the yield of slow neutrons. At A, B, C and D, the individual yield curves are both falling, and the 'fast' yield is falling more rapidly than the 'slow', resulting in an increase in the 'slow' to 'fast' ratio. This effect is explained by the marked variation with

bombarding energy of the angular distribution of neutrons (Figs 6 and 7), together with the fact that owing to its proximity to the target, the 'slow' counter subtends a larger angle than the 'fast' counter. To prove the validity of this interpretation, the regions immediately including the anomalies A to G were re-examined with the counters arranged differently. The counters were in the same relative position as in Fig. 1, but further from the target, the long counter face being 1 ft away. With this arrangement, which gave approximately equal acceptance angles for the two counters, increases in the counter ratio did not appear at A, B, C and D, but the shapes of the yield and ratio curves at E, F and G were similar to those obtained previously. Thus there was no evidence for an excited state threshold below that at E which is at 8.84 MeV. In order to obtain good statistics, it was necessary to use the counters in the close-up position for most of this work.

Measurements made with a clean tantalum backing in place of the target, revealed background counts which formed not more than 5% of the counts due to the $150\ \mu\text{g cm}^{-2}$ carbon target, over the whole range of bombarding energy covered. This small background could not significantly affect the result of these experiments, and it has not been subtracted.

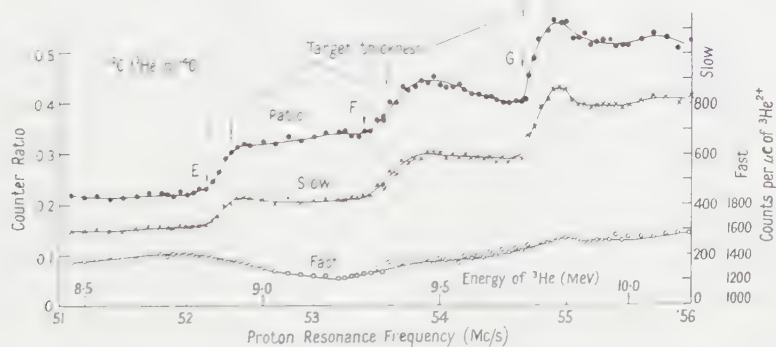


Fig. 5. Excited state thresholds (E, F and G), in the $^{12}\text{C}(^3\text{He}, n)^{14}\text{O}$ reaction. At each energy, 6000 counts were recorded in the 'slow' counter.

Fig. 5 shows in detail the results of a run taken with better statistics in the energy region including the thresholds at E, F, and G. At E and G, the slow neutron yield and counter ratio rise in an energy interval corresponding to the target thickness of 60 keV, and this has been taken for the upper limit on the width of the corresponding levels in ^{14}O . The rise at F occupies an interval some two to three times greater than this. In general there are three effects which may lead to these functions taking an interval in excess of the target thickness to reach their maxima. These are: (a) a geometrical effect due to the slow opening out of the forward projected cone of neutrons as the bombarding energy is increased, (b) emission of neutrons with angular momentum greater than zero, and (c) excitation of a broad level or two or more closely spaced levels. The possibility of (a) is ruled out since 'normal' thresholds were observed at E and G and also since the profiles of the yield and ratio curves obtained through E, F, and G with the alternative counter geometry are essentially the same as in Fig. 5. Possibility (b) is unlikely since the yield of slow neutrons is no less than at the (presumably s-wave) thresholds E and G, and also since the yield after the initial rise falls

at the same rate as at the latter. Explanation (c) is the most likely, in which case the most plausible interpretation of this feature is that it is due to the excitation of a single level of width about 0.12 meV, the level 'shape' being integrated in the slow neutron yield and ratio plots. The possibility that this threshold is due to two (or more) unresolved levels cannot be ruled out however, in which case the above conclusion on the level width, and the remarks concerning the resulting reduced width (§4) would be invalidated.

Table 1. Threshold Energies in $^{12}\text{C}(^3\text{He}, n)^{14}\text{O}$, and Energy Levels in ^{14}O

(1)	(2)	(3)	(4)	(5)
52.16 ± 0.03	52.167 ± 0.025	8.841 ± 0.014	5.905 ± 0.012	$\lesssim 0.06$
52.18 ± 0.04	—	—	—	—
53.60 ± 0.10	53.60 ± 0.10	9.333 ± 0.036	6.30 ± 0.03	0.12 ± 0.03
54.63 ± 0.03	54.63 ± 0.025	9.694 ± 0.015	6.586 ± 0.012	$\lesssim 0.06$
54.63 ± 0.04	—	—	—	—

(1), Proton resonance frequencies at threshold (Mc/s); (2), mean values of these;
(3), threshold energy (meV); (4) ^{14}O level (meV); (5), level width (meV).

The results of the measurements are shown in Table 1. The reaction Q values were obtained from the threshold energies using an approximate relativistic expression due to Langsdorf, Monahan and Reardon (1954).

$$E_{\text{th}}(0^\circ) = |Q| \left(1 + \frac{m_1}{m_2} + \frac{|Q|}{2m_2c^2} \right)$$

where m_1 and m_2 are the atomic masses of the incident and target atoms respectively. In calculating the excitation energies of the levels in ^{14}O , the ground state Q value was taken to be -1.159 ± 0.003 meV (Bromley *et al.* 1957).

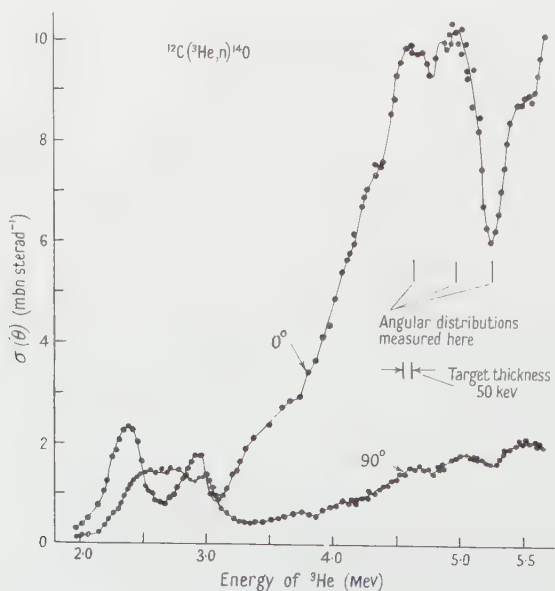


Fig. 6. Excitation curves for the $^{12}\text{C}(^3\text{He}, n)^{14}\text{O}$ reaction measured at 0° and 90° .

The 0° and 90° yield curves measured between 2.0 and 5.7 MeV are shown in Fig. 6. Since there is no evidence for a level in ^{14}O below 5.9 MeV, both the excitation curves and the angular distributions apply to the ground state group only. The energy scale has been corrected for energy loss in the target. The target thickness also determines the energy resolution, and is indicated in the figure. The error on the absolute cross section is about $\pm 15\%$, due mainly to the uncertainty in the target thickness. The shapes of the curves are in good agreement with those of Bromley *et al.* where they overlap (2.0 to 2.7 MeV), but our absolute values are 30% lower. Deposition of carbon on the target from pump oil would have made the cross sections obtained in the present work too large however. Partial stripping of the singly charged ^3He beam between the analysing magnet and the target could lead to an overestimate of the beam intensity and hence to an underestimate of the cross sections. However, comparisons of yields obtained with singly and doubly charged beams of the same energy have shown that this effect is too small to explain the discrepancy. The more prominent resonances in the 90° excitation curve are at 2.5, 3.0, 3.75, 4.7, 5.05 and 5.55 MeV.

Angular distributions measured at 4.65, 4.98 and 5.26 MeV (these energies are marked in Fig. 6) were converted to the centre-of-mass system, and are shown in Fig. 7. The curves drawn in this figure were calculated from a

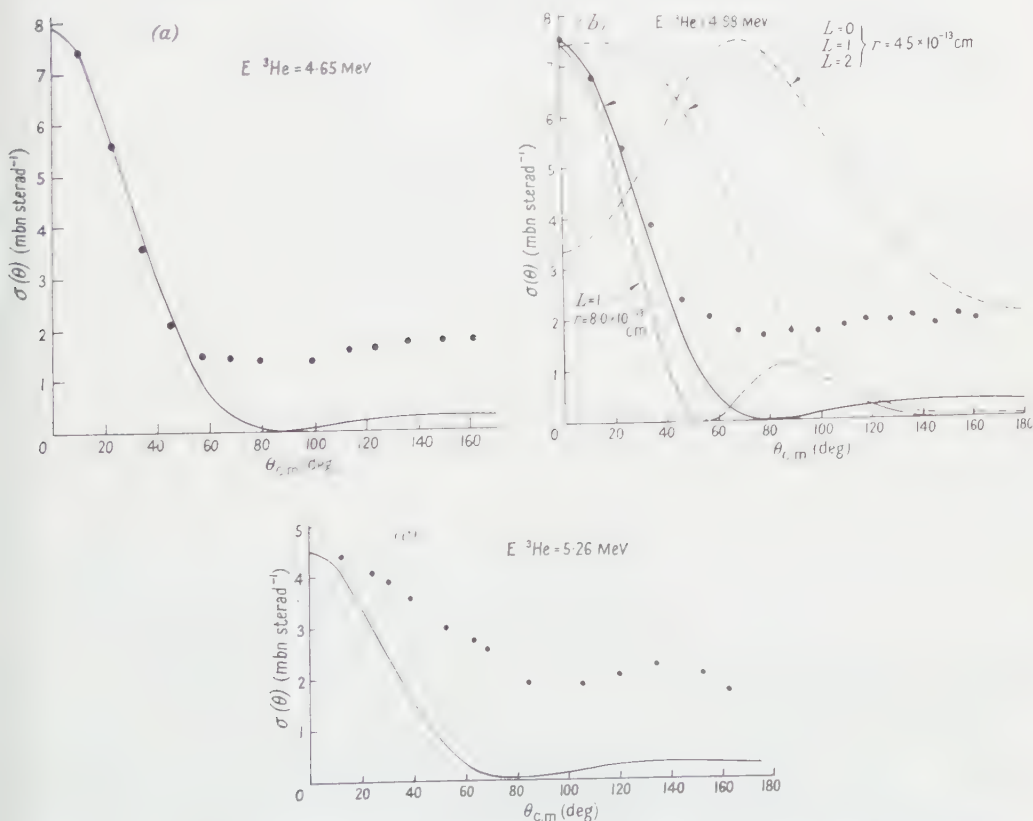


Fig. 7. Angular distributions of the $^{12}\text{C}(^3\text{He}, n)^{14}\text{O}$ reaction at (a) 4.65 MeV, (b) 4.98 MeV and (c) 5.26 MeV. The statistical errors on the points after subtraction of background are not greater than $\pm 4\%$.

theoretical formula for the double stripping process due to H. C. Newns (private communication). If only one value $L\hbar$, of the total orbital angular momentum of the captured particles is considered, this is the form

$$\sigma(\theta) = A [\exp(-K^2/4\gamma^2)] |J_L(kr)|^2$$

where k is the wave number of the captured 'particle' and r is the stripping radius. The exponential term which is independent of L , takes account of the internal motion of the ${}^3\text{He}$ particle, and is analogous to the $G^2(K)$ factor in deuteron stripping. Since the ground states of ${}^{12}\text{C}$ and ${}^{14}\text{O}$ both have spin and parity 0^+ , then the stripping process, if it occurs, must be characterized by $L=0$. With $L=0$, a good fit was obtained to the forward maxima of the angular distributions at 4.65 and 4.98 MeV, by taking $r=4.5$ fermi, which is the Gamow radius given by $r=1.70+1.22A^{1/3}$ fermi, for $A=12$. The fit to the experimental points at 5.26 MeV using the same value of r is very poor (Fig. 7). Also shown in 7(b) for comparison, are theoretical curves for $L=1$ and $L=2$ using the same value of r , and a curve for $L=1$ with $r=8$ fermi. The latter shows that an unrealistically large stripping radius would be required to fit an $L=1$ distribution. The curves have been normalized to have the same maximum intensity as observed at $\theta=0^\circ$.

3.2. ${}^{16}\text{O}({}^3\text{He}, n){}^{18}\text{Ne}$

The neutron spectrum has been observed in order to measure the Q value of this reaction, and to locate any levels at low excitation in ${}^{18}\text{Ne}$. Fig. 8(b) shows a time spectrum obtained at 20° with 4.36 MeV ${}^3\text{He}$ particles. The target

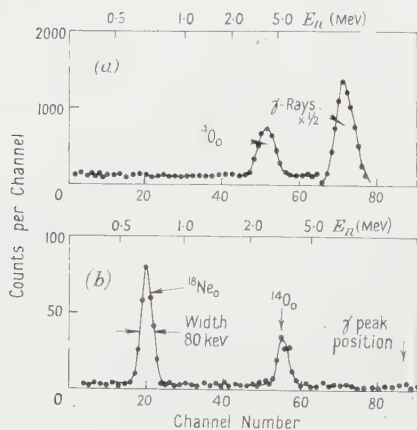


Fig. 8. Time-of-flight spectra from $({}^3\text{He}, n)$ reactions on ${}^{12}\text{C}$ and ${}^{16}\text{O}$. (a) Carbon target, thickness $240 \mu\text{g cm}^{-2}$, (b) SiO_2 target, $90 \mu\text{g cm}^{-2}$ thick + $9 \mu\text{g cm}^{-2}$ carbon. The data for curve (b) were obtained using pulse shape discrimination against γ -rays.

was a deposit of SiO_2 of thickness $90 \mu\text{g cm}^{-2}$, and the flight path was 171 cm. The ground state group ${}^{18}\text{Ne}_0$ was observed together with that from the ${}^{12}\text{C}({}^3\text{He}, n){}^{14}\text{O}$ reaction, the latter arising from carbon contamination of the target. From the observed yields, and the cross sections of these reactions (Figs 6 and 13), the thickness of the carbon deposit was estimated to be about $9 \mu\text{g cm}^{-2}$. This contaminant group from ${}^{12}\text{C}({}^3\text{He}, n){}^{14}\text{O}$ has been used as an energy calibration, the Q value being taken as -1.159 ± 0.003 MeV (Bromley *et al.* 1957). This method of calibration was convenient since use of the pulse

shape discrimination technique to reduce γ -ray background had eliminated the γ -ray peak, normally used to infer the zero of the time scale. Calibration on a nearby peak also makes the energy measurement less sensitive to any possible systematic error in the time to pulse height conversion factor. Allowance was made for the mean energy loss of the ^3He particles in the C and SiO_2 deposits. Two other similar measurements were made at 25° and 35° , both with 4.55 MeV ^3He particles. The mean Q value obtained from these three measurements is $-3.200 \pm 0.020\text{ MeV}$. Taking a more recent result for the $^{12}\text{C}(^3\text{He}, n)^{14}\text{O}$ Q value of $-1.1477 \pm 0.0007\text{ MeV}$ (J. W. Butler, private communication), we find a $^{16}\text{O}(^3\text{He}, n)^{18}\text{Ne}$ Q value of $-3.199 \pm 0.020\text{ MeV}$. The measured Q value is thus very insensitive to that of the calibration reaction in this experiment.

There is no evidence from any of these runs for a level in ^{18}Ne at 114 keV as suggested by Dunning and Butler (1959). In Fig. 8(b) the neutron group corresponding to such a level would appear on the low energy side of the group $^{18}\text{Ne}_0$ with a spacing of 1.5 times the group width at half height. A further measurement of the spectrum at 0° with 6 MeV ^3He particles produced no evidence for a level below 1.5 MeV excitation in ^{18}Ne . In this run the target was of SiO_2 160 keV thick, and the flight path was 72 cm . The maximum intensity of any unobserved group was 0.06 of that of the ground state group.

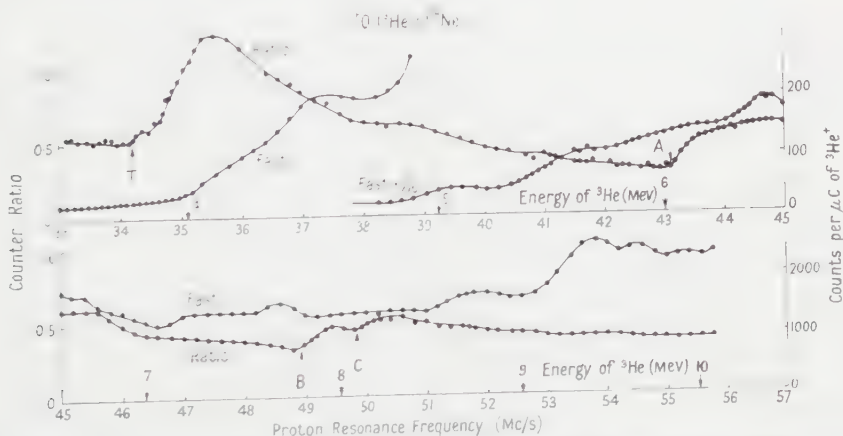


Fig. 9. Plots of the counter ratio and 'fast' counts for $^{16}\text{O}(^3\text{He}, n)^{18}\text{Ne}$. The statistical error in the ratio is 3.5% near the ground state threshold T, decreasing to 2.5% at higher bombarding energies.

Fig. 9 shows plots of the 'fast'-neutron counts and the counter ratio obtained when bombarding a Nb_2O_5 target of thickness $300\mu\text{g cm}^{-2}$ with ^3He particles in the energy range 3.5 to 10 MeV . The abrupt increases in the counter ratio beginning at T, A, B and C, indicate the location of thresholds corresponding to the ground state and three excited states of ^{18}Ne . The ratio curve has an unusual feature, namely the point of inflection closely following the threshold at T.

All four thresholds were studied further using thinner targets. Fig. 10 shows the variation of the 'slow'- and 'fast'-neutron yields and the counter ratio, in the region of the ground state threshold, using a target of Nb_2O_5 , $100\mu\text{g cm}^{-2}$ thick. At threshold T the slow-neutron yield rises in an interval corresponding approximately to the target thickness. At R, about 70 keV above

threshold, this yield rises again, but it is noted that the curve following R can be extrapolated smoothly back to T such that the background level forms a line tangential to the extrapolated curve at this point. The yield immediately above threshold is due to a small number of s-wave neutrons. Only s-wave neutrons can give rise to a yield curve of non-zero slope at the threshold. The further rise in the yield after point R is due to neutrons of higher angular momenta (for intensity reasons probably $l=1$). This explains why the counter ratio continues to rise over an energy interval some five times the target thickness.

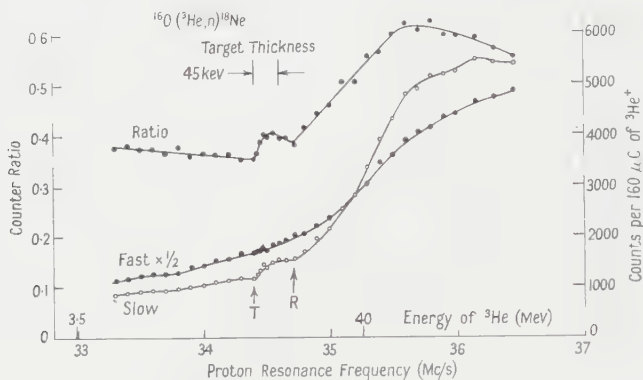


Fig. 10. Plots of the 'slow' and 'fast' counts, and counter ratio in the region of the ground state threshold (marked T), of $^{16}\text{O}(^3\text{He}, n)^{18}\text{Ne}$. The relation between proton resonance frequency and ^3He energy is different to that in the other figures (see text).

As seen in Figs 9 and 10 the yield of slow neutrons defining the threshold is very small. In view of this it was necessary to verify this result with targets of different composition since there was a slight possibility that these neutrons were due to Nb, the Ta backing, or a contaminant. Similar measurements were made with targets of Cr_2O_3 on a Ta backing and SiO_2 on a backing of Au. Both targets were of thickness $95 \mu\text{g cm}^{-2}$. The results obtained are very similar to those shown in Fig. 10, and the yield of slow neutrons was in each case proportional to the number of ^{16}O atoms in the target. These measurements (as in Fig. 10) concerning the ground state threshold, were made using a different beam analysing magnet from that used in the other measurements. The proton resonance magnetometer was calibrated before and after these runs against the threshold of the $^6\text{Li}(^3\text{He}, n)^8\text{B}$ reaction. The values of the proton resonance frequency for this latter threshold were 30.373 ± 0.025 and 30.370 ± 0.025 Mc/s, giving a calibration constant of 103.03 ± 0.13 for this magnet (see §2.5). The Q value of the $^{16}\text{O}(^3\text{He}, n)^{18}\text{Ne}$ reaction obtained from the threshold measurements (Table 2), is -3.199 ± 0.006 MeV, in excellent agreement with the time-of-flight result.

Fig. 11 shows the results obtained of a more detailed study in the region of the excited state threshold at A (Fig. 9) using a different 'slow' counter. Some 200 keV above threshold resonances occur in both 'slow' and 'fast' neutron yields, and it was found necessary to improve the differentiation between threshold neutrons, and neutrons of a few hundred keV energy. An improvement was achieved by replacing the 'slow' counter used previously with one composed of two BF_3 tubes each with a sleeve of polythene only 0.25 in. thick.

The target was a $96\ \mu\text{g cm}^{-2}$ deposit of Cr_2O_3 . The ratio plot indicates only one threshold in this region. The excited state thresholds at B and C are revealed more clearly in Fig. 12. These results were obtained using a Nb_2O_5 target of thickness $100\ \mu\text{g cm}^{-2}$ and the usual counter arrangement shown in Fig. 1. The slow neutron yields and ratio plots at all three excited state thresholds rise in an interval equal to the calculated target thicknesses, indicating the emission of predominantly s-wave neutrons.

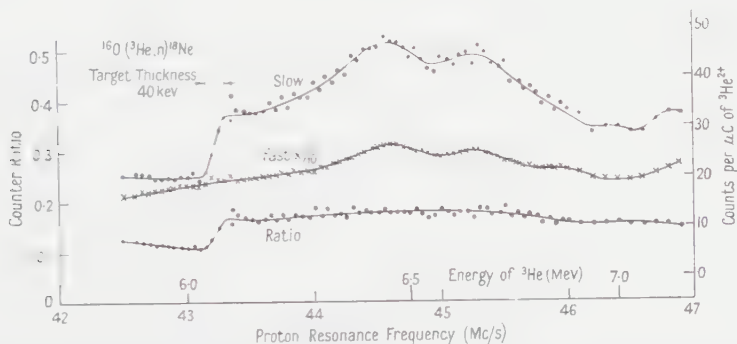


Fig. 11. The first excited threshold in the $^{16}\text{O}(^3\text{He}, n)^{18}\text{Ne}$ reaction, using a modified 'slow' counter. At each energy 2000 'slow'-neutron counts were recorded.

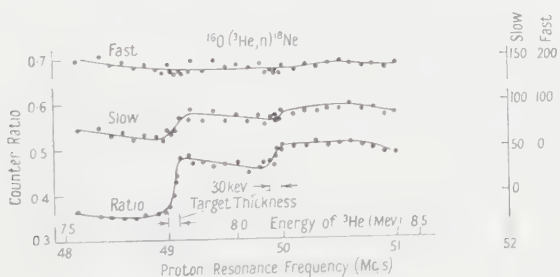


Fig. 12. The second and third excited state thresholds in the $^{16}\text{O}(^3\text{He}, n)^{18}\text{Ne}$ reaction. At each energy, 6000 'slow'-neutron counts were recorded.

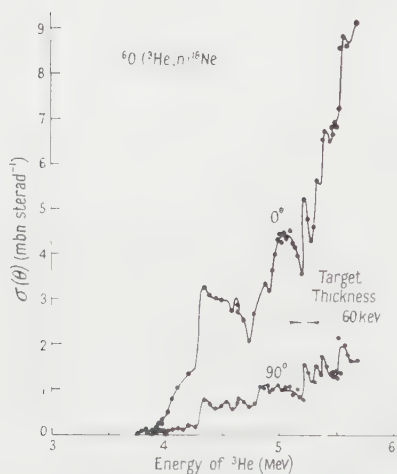
The results of several measurements of these threshold energies are given in Table 2. The Q values and corresponding level energies are also given. In these measurements, a point by point subtraction of background has not been made. At several bombarding energies near each excited state threshold however, measurements were made with clean tantalum backings in place of the target. The yield from the backing was about 25% of that from a $100\ \mu\text{g cm}^{-2}$ target, and proportionately less for the thicker targets used. This background was not sufficient to affect significantly the results obtained even with the thinnest target.

The 0° and 90° excitation functions measured from threshold to 5.7 MeV are shown in Fig. 13. Only the ground state group is produced in this energy region. The energy scale has been corrected for the thickness of the target ($90\ \mu\text{g cm}^{-2}$ SiO_2). The target thickness, which determines the energy resolution, is indicated in the figure.

Table 2. Threshold Energies in $^{16}\text{O}(^3\text{He}, n)^{18}\text{Ne}$ and Energy Levels in ^{18}Ne

(1)	(2)	(3)	(4)	(5)
34.38 ± 0.04	34.390 ± 0.022	3.802 ± 0.007	-3.199 ± 0.006	0
34.40 ± 0.03				
34.37 ± 0.06				
43.10 ± 0.04	43.100 ± 0.016	6.038 ± 0.009	-5.079 ± 0.008	1.880 ± 0.010
43.08 ± 0.03				
43.07 ± 0.03				
43.14 ± 0.03				
49.02 ± 0.02	48.995 ± 0.012	7.800 ± 0.010	-6.561 ± 0.009	3.362 ± 0.011
48.90 ± 0.04				
48.98 ± 0.04				
49.01 ± 0.03				
48.99 ± 0.02				
49.92 ± 0.02	49.905 ± 0.016	8.092 ± 0.011	-6.807 ± 0.010	3.608 ± 0.012
49.89 ± 0.04				
49.88 ± 0.03				

(1) Proton resonance frequencies at threshold (Mc/s); (2) mean values of these;
 (3) threshold energy (mev); (4) Q value (mev); (5) ^{18}Ne level (mev).

Fig. 13. Excitation curves for the $^{16}\text{O}(^3\text{He}, n)^{18}\text{Ne}$ reaction measured at 0° and 90° .

§ 4. DISCUSSION

The resonances in the excitation function suggest that the $^{12}\text{C}(^3\text{He}, n)^{14}\text{O}$ reaction proceeds to some extent via a compound nucleus. Since the angular distributions change rapidly with energy, a measurement of the variation with energy of the total cross section would be required to locate the resonances accurately. The approximate resonance energies, taken from the positions of the peaks in the 90° curve, are at 2.5, 3.0, 3.75, 4.7, 5.05 and 5.55 mev. The resonances at 2.5 and 3.0 mev are particularly prominent, and at higher energies the forward peaking of the yield becomes very pronounced. These results may be compared with data obtained for the $^{12}\text{C}(^3\text{He}, p)^{14}\text{N}$ reaction in the same

range of bombarding energy by Johnston *et al.* (1958). The excitation curves measured at several angles for three proton groups, indicated resonances at 2.5, 2.7, 3.0, 3.6, 4.4 and 4.8 mev, which may be compared with the above values. If these reactions proceed by compound nucleus formation, the excitation functions for the ground state neutron group (well above threshold), and of the proton group leading to the 2.3 mev, $T=1$ state in ^{14}N , should be similar in shape. The curves measured for this proton group at 7° and 90° are in fact very similar to those in Fig. 6. Further, the $(^3\text{He}, n)$ cross section is roughly twice the $(^3\text{He}, p)$ cross section for excitation of the analogue state as expected from considerations of isotopic spin (Bromley *et al.* 1957). The angular distributions of the proton group measured at 4.5 and 4.75 mev differ from that of the neutron group at 4.65 mev (Fig. 7), since they peak at both 0° and 180° and have a minimum at about 90° . Hinds and Middleton (1960) have measured angular distributions in the $^{12}\text{C}(^3\text{He}, p)^{14}\text{N}$ reaction at bombarding energies of 5.98, 8.83, 9.37 and 10.14 mev. The group corresponding to the 2.3 mev level of ^{14}N consistently gave fairly good s-wave stripping curves, but the peak intensity varied rapidly with energy. The angular distributions of the neutrons measured at 4.65 and 4.98 mev are consistent with the theory for double stripping, but without more extensive data cannot be taken as good evidence for this process. However, the consistent forward peaking of both the neutron and the proton groups over a wide range of bombarding energy is very suggestive of a contribution from a direct reaction.

The excitation function of the $^{16}\text{O}(^3\text{He}, n)^{18}\text{Ne}$ reaction (Fig. 13), shows about 15 resonances between 3.9 and 5.7 mev, corresponding to levels in the compound nucleus ^{19}Ne between 11.7 and 13.2 mev with an average spacing of 0.1 mev. A feature of this reaction is the very small yield at threshold. This suggests the absence of levels in the compound nucleus at this excitation having $J = \frac{1}{2}^+$, resulting in the almost complete inhibition of s-wave neutron emission. In the centre-of-mass system, $\sigma(0^\circ) / \sigma(90^\circ)$ lies between 2 and 4 for bombarding energies between 4.2 and 5.7 mev. This suggests some contribution from a direct process. Double stripping, if it occurs, must be characterized by $L=0$ as in the $^{12}\text{C}(^3\text{He}, n)$ reaction.

Thus it is concluded that both compound nuclear and direct processes are contributing to the $(^3\text{He}, n)$ reactions on ^{12}C and ^{16}O , and that neither predominates in the region of bombarding energy studied which, it may be noted, hardly exceeds the height of the Coulomb barrier which is about 5 mev for ^{12}C . Comparable contributions from both processes are expected in (d, n) reactions at energies below the Coulomb barrier (Peaslea 1948), but it is questionable whether $(^3\text{He}, n)$ and (d, n) reactions are analogous in this respect. A feature of this work which is difficult to explain is the fact that good stripping angular distributions were obtained on resonances in the yield curve, and a more symmetric distribution off resonance. This is the opposite to what one might naïvely expect, if the resonances are to be associated with compound nucleus formation. Similar effects were observed in the $^{12}\text{C}(^3\text{He}, p)$ reaction where, as the bombarding energy was increased, the angular distributions became more strongly peaked at forward and backward angles, the peaking being enhanced on resonances (Johnston *et al.* 1958). In the $^{12}\text{C}(d, p)^{13}\text{C}$ reaction, Bonner *et al.* (1956) observed a similar apparent enhancement of the stripping contribution on resonances which correspond to known compound nuclear levels. The results were explained in

terms of a small compound nuclear amplitude interfering with a large stripping amplitude. It is not possible however on the present evidence to draw any definite conclusion on this point for the ($^3\text{He}, n$) reactions.

The Q value of -3.199 ± 0.006 mev obtained for the $^{16}\text{O}(^3\text{He}, n)$ reaction is in good agreement with the value of -3.206 ± 0.013 mev reported by Dunning and Butler. The present measurement requires a mass-defect of 10.649 ± 0.008 mev for ^{18}Ne , and hence an end point of 3.439 ± 0.012 mev for the β^+ decay of ^{18}Ne . This is to be compared with a previous measurement of 3.2 ± 0.2 mev for this end point by Gow and Alvarez (1954).

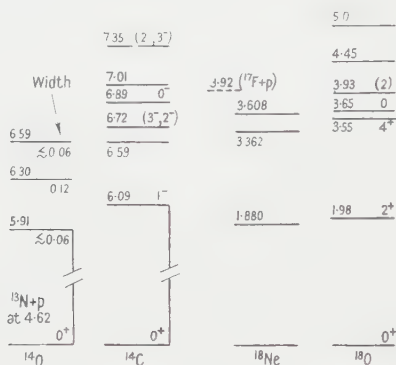


Fig. 14. Energy levels (in mev) in $T_z = \pm 1$ pairs.

In Fig. 14, the energy level diagrams obtained for ^{14}O and ^{18}Ne are shown alongside those of their analogous isobars ^{14}C and ^{18}O . Recent data on ^{18}O were obtained by Silbert and Jarmie (private communication to A. E. Litherland; A. E. Litherland, R. Batchelor, A. J. Ferguson and H. E. Gove 1960, private communication). There is no evidence in the present work for an excited state in ^{14}O below 5.9 mev, in agreement with the measurements on the $^{14}\text{N}(p, n)^{14}\text{O}$ reaction. Since the binding energy of the last proton in ^{14}O is 4.62 mev, the levels reported here are unbound, and some information on their properties may be inferred from the observed widths. The reduced widths θ^2 in units

Table 3. Reduced Widths of Levels in ^{14}O for Emission of s, p and d wave Protons

Energy level (mev)	Width (mev)	Reduced width θ^2		
		s	p	d
5.905	$\lesssim 0.06$	$\lesssim 0.025$	$\lesssim 0.11$	$\lesssim 1.4$
6.30	0.12	0.03	0.09	0.9
6.586	$\lesssim 0.06$	$\lesssim 0.013$	$\lesssim 0.04$	$\lesssim 0.3$

of $3\hbar^2/2\mu R^2$, were calculated with $R=1.5A^{1/3}$ fermi, for s, p and d wave protons using the barrier penetrabilities given by Sharp, Gove and Paul (1955), and are given in Table 3. Higher angular momenta gave reduced widths much greater than the Wigner limit ($\theta^2 \gg 1$) and were not considered further. This table is of use in correlating these $T=1$ levels with those of ^{14}C . Data

taken from Ajzenberg-Selove and Lauritsen (1959) and Warburton and Pinkston (1960) on the first six levels of ^{14}C , including the angular momentum transfer l_n and reduced width θ_n^2 obtained from the $^{13}\text{C}(\text{d}, \text{p})^{14}\text{C}$ reaction, are given in Table 4. The 7.01 meV level is expected to have a small neutron reduced width since it was not observed in the $^{13}\text{C}(\text{d}, \text{p})^{14}\text{C}$ reaction. It is thought that the 6.09 and 6.89 meV levels have the predominant configuration $\text{p}_{1/2}, 2\text{s}_{1/2}$

Table 4. Properties of Levels in ^{14}C from Ajzenberg-Selove and Lauritsen (1959) and Warburton and Pinkston (1960)

Energy level (meV)	$J\pi$	l_n	θ_n^2
6.09	1-	0	0.40 ($J=1^-$)
6.59			$\lesssim 0.01$
6.72	3-, (2-)	2	0.11 ($J=3^-$)
6.89	0(-)	0, 1	0.39 ($J=0^-$)
7.01			small
7.35	2-, 3-	2	0.11 ($J=2^-$)

for the two extra-core neutrons, also that the 6.72 and 7.35 meV levels have the configuration $\text{p}_{1/2}\text{d}_{5/2}$ (Warburton, Rose and Hatch 1959). It is unlikely that any one of the levels observed in ^{14}O is the analogue of the 6.09 meV level of ^{14}C , since the ^{14}O level would be expected to decay by s-wave proton emission with $\theta^2 \sim 0.4$, which value is some ten times greater than those in Table 3. The same argument applies to the 6.89 meV level of ^{14}C if it has odd parity. The levels at 5.91 and 6.59 meV in ^{14}O however, may be analogous to those at 6.72 and 7.35 meV in ^{14}C . If this is so, these ^{14}O levels would be expected to decay by emission of d-wave protons with $\theta^2 \sim 0.1$, and this requirement is consistent with the values in Table 3. Considering now the level in ^{14}O at 6.3 meV, the s-wave value of θ^2 is ten times smaller than that of the ^{14}C levels at 6.09 and 6.89 meV, and the value for d-waves is eight times larger than that of the levels at 6.72 and 7.35 meV. Thus the only levels in Table 4 which seem at all likely to correspond to the 6.3 meV level are those at 6.59 and 7.01 meV. The small reduced widths of these levels are perhaps not inconsistent with the s-wave value of approximately 0.03 in Table 3.

The levels located in ^{18}Ne are bound states, since the binding energy of the last proton is 3.92 meV. There is no evidence for a low lying level as suggested by Dunning and Butler. The 1.88 and 1.98 meV levels are probably members of the same isobaric triplet. The second and third levels also occur at similar energies in the two nuclei, but spins and parities need to be measured before further comparisons can safely be made. A depression of the levels of ^{14}O and ^{18}Ne with respect to their possible analogue states is evident in Fig. 14, and the effect is probably quite large in ^{14}O . This phenomenon occurs also in the $T = -\frac{1}{2}$ members of mirror pairs, and is particularly large for the virtual first excited state of ^{13}N and for the weakly bound first level of ^{17}F . Calculations have shown (Ehrman 1951, Thomas 1952) that the level depressions in ^{13}N and ^{17}F do not refute the principle of charge symmetry of nuclear forces, since they can be explained in terms of the Coulomb dependence of the level shifts (Wigner and Eisenbud 1947).

Information on the spins and parities of the levels in ^{14}O and ^{18}Ne may probably be obtained from measurements of angular distributions in the

$^{12}\text{C}(^3\text{He}, n)^{14}\text{O}$ and $^{16}\text{O}(^3\text{He}, n)^{18}\text{Ne}$ reactions if these are consistent with a stripping interpretation as pursued in §3.1. Good stripping patterns were obtained for the similar reaction $^{16}\text{O}(^3\text{He}, p)^{18}\text{F}$ at bombarding energies of 5.0 and 9.16 MeV by Hinds and Middleton (1959), and the interpretations were in harmony with previous spin assignments to levels in ^{18}F .

ACKNOWLEDGMENTS

We are indebted to Dr. K. W. Allen and Mr. R. Batchelor for their interest and helpful comments, also to Dr. H. C. Newns for communicating his work prior to publication.

REFERENCES

- AJZENBERG, F., and FRANZEN, W., 1954, *Phys. Rev.*, **94**, 409.
 AJZENBERG-SELOVE, F., and DUNNING, K. L., 1960, *Bull. Amer. Phys. Soc.*, [II], **5**, 36.
 AJZENBERG-SELOVE, F., and LAURITSEN, T., 1959, *Nucl. Phys.*, **11**, 1.
 BATCHELOR, R., GILBOY, W. B., PURNELL, A. D., and TOWLE, J. H., 1960, *Nucl. Instrum.*, **8**, 146.
 BATCHELOR, R., and TOWLE, J. H., 1959, *Proc. Phys. Soc.*, **73**, 193 and *A.W.R.E. Report* NR/P-12/58 (Unclassified).
 BONNER, T. W., and COOK, C. F., 1954, *Phys. Rev.*, **96**, 122.
 BONNER, T. W., EISINGER, J. T., KRAUS, A. A., and MARION, J. B., 1956, *Phys. Rev.*, **101**, 209.
 BROMLEY, D. A., ALMQVIST, E., GOVE, H. E., LITHERLAND, A. E., PAUL, E. B., and FERGUSON, A. J., 1957, *Phys. Rev.*, **105**, 957.
 DUNNING, K. L., and BUTLER, J. W., 1959, *Bull. Amer. Phys. Soc.*, [II], **4**, 444.
 DUNNING, K. L., BUTLER, J. W., and BONDELID, R. O., 1958, *Phys. Rev.*, **110**, 1076.
 EHRLMAN, J. B., 1951, *Phys. Rev.*, **81**, 412.
 GOW, J. D., and ALVAREZ, L. W., 1954, *Phys. Rev.*, **94**, 365.
 HINDS, S., and MIDDLETON, R., 1959, *Proc. Phys. Soc.*, **74**, 762.
 ———, 1960, *Proc. Phys. Soc.*, **75**, 745.
 JOHNSTON, R. L., HOLMGREN, H. D., WOLICKI, E. A., and GEER-ILLSLEY, E., 1958, *Phys. Rev.*, **109**, 884.
 LANGSDORF, A. S., MONAHAN, J. E., and REARDON, W. A., 1954, *Argonne National Laboratory Report* ANL-5219.
 MARION, J. B., BONNER, T. W., and COOK, C. F., 1955, *Phys. Rev.*, **100**, 91.
 PEASLEA, D. C., 1948, *Phys. Rev.*, **74**, 1001.
 SHARP, W. T., GROVE, H. E., and PAUL, E. B., 1955, *Graphs of Coulomb Functions*, Atomic Energy of Canada Ltd., TPI-70.
 THOMAS, R. G., 1952, *Phys. Rev.*, **88**, 1109.
 WARBURTON, E. K., and PINKSTON, W. T., 1960, *Phys. Rev.*, **118**, 733.
 WARBURTON, E. K., ROSE, H. J., and HATCH, E. N., 1959, *Phys. Rev.*, **114**, 214.
 WIGNER, E. P., and EISENBUD, L., 1947, *Phys. Rev.*, **72**, 29.

The Reaction $^{51}\text{V}(\gamma, \alpha)^{47}\text{Sc}$ and some Remarks on (γ, α) Reactions

By J. H. CARVER

Research School of Physical Sciences, Australian National University, Canberra

MS. received 31st May 1960

Abstract. The $^{51}\text{V}(\gamma, \alpha)^{47}\text{Sc}$ reaction has been studied using induced radioactivity techniques up to gamma-ray energies of 32 mev. The cross section has a maximum value of 0.95 mbn at an energy of 22 mev and an integrated cross section to 32 mev of 12 ± 2 mev mbn. The statistical model gives a satisfactory interpretation of the ratio of the $^{51}\text{V}(\gamma, \alpha)$ cross section to the $^{51}\text{V}(\gamma, n)$ cross section measured by Goldemberg and Katz in 1954. It is probable that this interpretation can be applied to the (γ, α) yields from other middle-weight nuclei but it is not appropriate for the heavy nuclei ($Z > 50$). It is suggested that the roughly constant (γ, α) yields observed in the heavy nuclei may arise from direct electric dipole interactions with preformed 'alpha particles' in the nuclear surface.

§ 1. INTRODUCTION

EXCEPT for some of the very light nuclei the (γ, α) cross section of an element amounts to but a small fraction, at most a few per cent, of the total integrated gamma-ray absorption cross section (Erdos, Scherrer and Stoll 1957, Toms and McElhinney 1958). The (γ, α) yields are at their maximum for middle-weight nuclei ($Z \sim 25$) and in this region the integrated cross section is about 10 mev mbn. With increasing atomic number the yield at first decreases rapidly and then levels off at a roughly constant value for $Z > 50$. According to Erdos, Scherrer and Stoll (1957) the integrated cross sections for these heavy nuclei are about 0.3 mev mbn.

It is to be expected that for the medium and heavy nuclei studies of the (γ, α) process would have some bearing on the problem of the preformation of alpha particles within, or at any rate on the surface of the nucleus. From a study of (p, α) reactions Hodgson (1958) has suggested that a surface nucleon spends about 0.4 of its time in an alpha-like cluster. Wilkinson (1959) has reached a similar conclusion from an analysis of reactions induced in complex nuclei by slow k^- mesons, while analysis of alpha-decay rates in the heavy elements also indicates considerable preformation (Perlman and Rasmussen 1957). It will be suggested here (§5) that direct electric dipole interactions with preformed surface 'alpha particles' are responsible for the (γ, α) yields in the heavy nuclei.

In the present experiments the reaction $^{51}\text{V}(\gamma, \alpha)^{47}\text{Sc}$ has been studied by the method of induced radioactivity for gamma-ray energies up to 32 mev. The method yields unambiguous results since there are no other radioactive end products to obscure the yield of 3.4-day ^{47}Sc and no radiochemical separation is needed. The $^{51}\text{V}(\gamma, \alpha)$ reaction lies in the region of maximum (γ, α) yields. As an example of the (γ, α) yields in heavy nuclei a similar method has been used to measure the yield (at one energy) of the $^{207}\text{Pb}(\gamma, \alpha)^{203}\text{Hg}$ reaction.

§ 2. MEASUREMENT OF THE $^{51}\text{V}(\gamma, \alpha)^{47}\text{Sc}$ CROSS SECTION

One-gramme samples of vanadium oxide (V_2O_5) were irradiated with bremsstrahlung from the Canberra electron synchrotron. Each irradiation was for a period of three hours and the beam was monitored by measuring the 8.15-hr $\text{Ta}(\gamma, n)$ activity induced in tantalum disks placed on either side of the vanadium sample.

^{47}Sc decays by β^- emission with a half-life of 3.4 days and a gamma ray with energy of 160 keV is emitted in 74% of the transitions (Lidosky and Fisher 1956). A $1\frac{1}{2}$ in. diameter \times 2 in. long NaI(Tl) crystal was used to observe the gamma-ray spectrum from the irradiated vanadium samples. There was an intense short-lived activity which was mainly the annihilation radiation of ^{15}O produced in the $^{16}\text{O}(\gamma, n)^{15}\text{O}$ reaction. After this short-lived activity had decayed a pure 160 keV gamma-ray spectrum was found. A typical gamma-ray spectrum, observed five hours after the end of the irradiation, is shown in Fig. 1. This 160 keV gamma-ray line was found to decay with the 3.4-day half-life of ^{47}Sc and one of the measured decay curves is shown in Fig. 2.

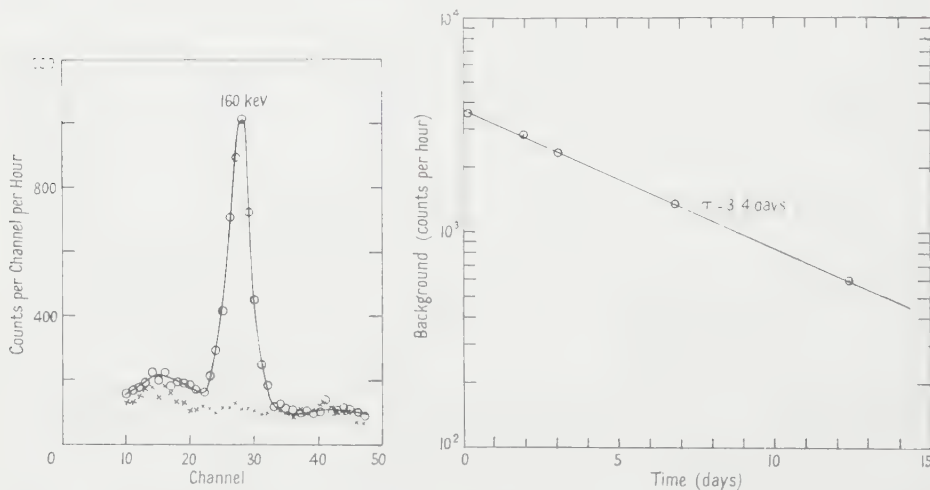


Fig. 1. Gamma-ray spectrum of ^{47}Sc produced in the $^{51}\text{V}(\gamma, \alpha)$ reaction. (The crosses represent the background spectrum.)

Fig. 2. Decay curve for the 160 keV gamma-ray line of ^{47}Sc .

According to the mass table of Wapstra (1958) the threshold for the $^{51}\text{V}(\gamma, \alpha)^{47}\text{Sc}$ reaction is 10.2 MeV but owing to the inhibiting effect of the Coulomb barrier (height 9.4 MeV) the yield was very small below a bremsstrahlung energy of 16 MeV. The measured yield curve and the derived cross section for the reaction are shown in Fig. 3. The absolute cross section scale is based on the value of Berman and Brown (1954) for the $^{63}\text{Cu}(\gamma, n)^{62}\text{Cu}$ cross section and was obtained by comparing the yield of the 160 keV gamma rays of 3.4-day ^{47}Sc with the yield of the annihilation radiation of 10-min ^{62}Cu . This determination was made by means of a number of 5-min irradiations of copper and tantalum disks and the relative copper to tantalum activities were compared with the relative scandium to tantalum activities obtained from the three-hour irradiations. The relative photo-peak efficiency of the NaI(Tl) crystal for 160 keV and 511 keV gamma rays was obtained from measured photo-fractions and calculated total crystal efficiencies (Mott and Sutton 1958).

The integrated cross section for the $^{51}\text{V}(\gamma, \alpha)$ reaction is

$$\int_0^{32} \sigma dE = 12 \pm 2 \text{ mev mbn.}$$

The cross section has a maximum value of 0.95 mbn at a gamma-ray energy of 22 Mev. Erdos, Sherrer and Stoll (1957) have measured the yield of this reaction for 32 Mev bremsstrahlung. They have not determined the shape of the cross section curve but estimate the integrated cross section as $5.5 \cdot 2 \text{ mev mbn}$ which is rather less than the present value. Dyal and Hummel (1959) have studied this reaction to 25 Mev and find a peak cross section of 0.81 mbn at a gamma-ray energy of 23 Mev in fair agreement with the present experiments.

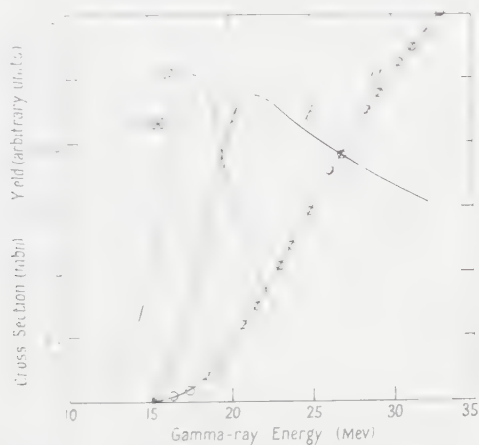


Fig. 3. *a*, activation curve for the $^{51}\text{V}(\gamma, \alpha)^{47}\text{Sc}$ reaction; *b*, the derived $^{51}\text{V}(\gamma, \alpha)$ cross section; *c*, the $^{51}\text{V}(\gamma, \alpha)$ cross section calculated by means of the statistical theory; *d*, the $^{51}\text{V}(\gamma, n)$ cross section of Goldemberg and Katz (1954) used in the calculation of curve *c*. (Note difference in cross section scale for curve *d*.)

§ 3. COMPARISON WITH THE STATISTICAL MODEL

Any calculation of the emission of complex particles, such as alpha particles, involves the question of the preformation of these particles within the nucleus. Should additional (small) factors be included in the equations to represent the assembly of these complex particles from the individual nucleons? Le Conteur (1959) argues that for the statistical model this question should be answered in the negative and states that, assuming thermodynamic equilibrium, the assembling of particles is completely taken into account through the dependence of the emission probabilities upon the binding energies of these complex particles. This is the assumption that is usually made when considering the emission of complex particles and it will be adopted here.

Accordingly at a gamma-ray energy E the ratio of the (γ, α) cross section $\sigma_{\gamma\alpha}$ to the total gamma-ray absorption cross section $\sigma_{\gamma\text{total}}$ is given by

$$\sigma_{\gamma\alpha}/\sigma_{\gamma\text{total}} = \Gamma_{\alpha}/\Gamma \quad \dots\dots (1)$$

where Γ is the total width ($\Gamma = \Gamma_n + \Gamma_p + \Gamma_{\alpha} + \text{etc.}$) and Γ_{α} is the particle width for alpha-particle emission given by

$$\Gamma_{\alpha} D(E) = \frac{2M}{\hbar^2 \pi^2} \int_0^{\epsilon_{\alpha}} \frac{\epsilon \sigma_{\alpha}(\epsilon)}{D(E_{\alpha} - \epsilon)} d\epsilon \quad \dots\dots (2)$$

where $D(E)$ is the level spacing of the compound nucleus, $D(E_{\alpha} - \epsilon)$ that of the

residual nucleus, ϵ is the energy of the emitted alpha particle, ϵ_α its maximum possible energy and $\sigma_\alpha(\epsilon)$ is the cross section for the inverse process of compound nucleus formation by alpha-particle capture. Similar expressions can be written down for $\sigma_{\gamma n}/\sigma_{\gamma \text{ total}}$ and $\sigma_{\gamma p}/\sigma_{\gamma \text{ total}}$. The relative probabilities for emitting protons, neutrons and alpha particles were calculated from these expressions as a function of gamma-ray energy. The semi-empirical formula of Cameron (1958) was used to calculate the level densities. The cross sections for the inverse reactions of particle capture were taken from the data of Blatt and Weisskopf (1953) using a nuclear radius of $1.5A^{1/3} \times 10^{-13}$ cm for protons and neutrons and $(1.5A^{1/3} + 1.0) \times 10^{-13}$ cm for alpha particles. Q -values were obtained from the table of Wapstra (1958).

The relative (γ, α) cross section calculated from Eqns (1) and (2) is not exactly comparable with that measured by induced radioactivity since it includes those events in which the emission of an alpha particle is followed by further particle emission. This is easily allowed for by altering the limits of integration in Eqn (2). Of these multiple processes the $(\gamma, \alpha n)$ reaction leading to 85-day ^{46}Sc is likely to be the most important. The $(\gamma, \alpha p)$ reaction is energetically favoured by about 2.5 MeV but for the gamma-ray energies of the present experiment the Coulomb barrier makes this reaction less important than the $(\gamma, \alpha n)$. The integrated $(\gamma, \alpha n)$ cross section to 32 MeV is calculated to be only 0.15 of the measured integrated (γ, α) cross section. A search was made for ^{46}Sc activity but, as would be expected from these calculations, none was detected.

Goldemberg and Katz (1954) and Nathans and Halpern (1954) have measured the photo-neutron yield from ^{51}V up to gamma-ray energies of 22 MeV with similar results. The $^{51}\text{V}(\gamma, 2n)$ threshold is at 20.2 MeV and for the present comparison the effect of this and any other multiple neutron reactions will be neglected. At a gamma-ray energy of 22 MeV the $^{51}\text{V}(\gamma, \alpha)$ cross section as measured in this experiment is 2.5% of the $^{51}\text{V}(\gamma, n)$ cross section reported by Goldemberg and Katz (1954). The statistical calculations suggest a value of 2.7% for this ratio. A more detailed comparison with the statistical theory is shown in Fig. 3, curve *c*. This curve has been derived from the calculated ratio of the (γ, α) to (γ, n) cross sections and Goldemberg and Katz's measured values for the $^{51}\text{V}(\gamma, n)$ cross section to 22 MeV (Fig. 3, curve *d*). It is seen that there is excellent agreement between these values calculated from the statistical theory and the measured $^{51}\text{V}(\gamma, \alpha)$ cross section (Fig. 3, curve *b*). These results suggest therefore, that the statistical theory gives an adequate account of the data at least up to gamma-ray energies of 22 MeV. It should be noted however, that, if this interpretation is also true at higher energies, the large high energy tail to the $^{51}\text{V}(\gamma, \alpha)$ cross section implies a similarly large tail to the total cross section which, on this basis, would be expected to amount to 15 mbn at 32 MeV. Such a large tail to the total cross section is not expected from the general systematics of these photonuclear reactions so that the statistical model may not account for the (γ, α) cross section at high energies.

§ 4. (γ, α) YIELDS IN HEAVY NUCLEI

The results of Erdos, Scherrer and Stoll (1957) show that for heavy nuclei ($Z > 50$) the (γ, α) yields are about $(1-2) \times 10^3$ α 's per mole R, i.e. about $(5-10) \times 10^{-5}$ of the total photonuclear yield.

The magnitude of the (γ, α) yield has been confirmed by measuring the yield of the $^{207}\text{Pb}(\gamma, \alpha)^{203}\text{Hg}$ reaction. ^{203}Hg has a half-life of 47 days and emits 279 keV gamma rays (Strominger, Hollander and Seaborg 1958). It is convenient to measure the yield for this reaction in terms of that for the $^{204}\text{Pb}(\gamma, n)$ reaction since ^{203}Pb decays with a 2.2-day half-life and emits the same gamma rays. Samples of natural lead (21.7% ^{207}Pb , 1.4% ^{204}Pb) were irradiated for 30 hr at a bremsstrahlung energy of 32 MeV and the induced radioactivity was measured with a $1\frac{1}{2}$ in. diameter \times 2 in. long NaI(Tl) crystal. The relative yields of the two reactions were found to be $^{207}\text{Pb}(\gamma, \alpha)/^{204}\text{Pb}(\gamma, n) = (8 \pm 2) \times 10^{-5}$. Assuming that the neutron multiplicity for lead is the same as for tantalum (Carver and Turchinets 1958) and that the (γ, n) cross sections for ^{207}Pb and ^{204}Pb are the same, it follows that, at 32 MeV, the $^{207}\text{Pb}(\gamma, \alpha)$ yield is $(6 \pm 2) \times 10^{-5}$ of the total photonuclear yield.

It is convenient to relate these (γ, α) yields to the corresponding (γ, p) yields. For the very heavy nuclei ($Z > 70$) the (γ, p) yield for 23 MeV bremsstrahlung is about 2×10^{-3} of the total photonuclear yield (Wilkinson 1956). Experiments in this laboratory (Carver, Taylor and Turchinets 1960, Taylor 1960) show that the (γ, p) yields increase by a factor of about 5 between 23 and 32 MeV. Thus at 32 MeV it is estimated that the relative yields for lead are $Y(\gamma, \alpha)/Y(\gamma, p) \approx 0.6\%$.

§ 5. POSSIBLE DIRECT EFFECTS ON THE (γ, α) YIELDS IN HEAVY NUCLEI

While the statistical model may give a fair account of the (γ, α) cross section for vanadium and for other middle-weight nuclei, it fails by several orders of magnitude to explain the yields observed for the heavy nuclei (§4). The integrated (γ, α) cross sections equal about 0.3 MeV mbn for the heavy nuclei ($Z > 50$) and they do not decrease appreciably with increasing atomic number. The behaviour of the yield as a function of atomic weight is similar to that observed for (γ, p) cross sections (Weinstock and Halpern 1954) and it is tempting to seek an explanation of these (γ, α) yields in terms of direct interactions similar to those invoked to explain the (γ, p) yields (Courant 1951, Wilkinson 1956). Hodgson (1958) and Wilkinson (1959) have suggested that the surface regions of the heavy nuclei may contain preformed alpha particles and it is possible that direct interactions with these preformed, surface alpha particles are responsible for the (γ, α) yields in heavy nuclei.†

Direct emission of alpha particles following the absorption of electric dipole radiation by a nucleus with $N = Z$ cannot occur if electric polarization of the nucleus or the alpha particle is neglected. This follows from the fact that electric dipole absorption requires a separation of the charge and mass centres of the absorbing system. In the more general case in which $N \neq Z$ the effective charge e_α for the alpha particle can be obtained in the usual way by subtracting the motion of the centre of mass. The result is, in units of the electronic charge, $e_\alpha = 2(N - Z)/A$. This may be compared with the effective charge of a proton of $e_p = N/A$. Since the cross sections are proportional to the squares of the

† The importance of direct effects is also evident from studies of fast neutron reactions. In particular the comparatively large (n, α) cross sections ($\sim 0.3\text{--}3.0$ mbn) observed by Coleman *et al.* (1959) with 14.5 MeV neutrons probably result from direct interactions with 'alpha particles' in the nuclear surface.

effective charges this factor introduces a term $4(N-Z)^2/N^2$ into the ratio of the (γ, α) to (γ, p) direct cross sections.

The neutron excess of the heavy nuclei is such that the effective charge factor does not of itself lead to very small ratios of (γ, α) to (γ, p) cross sections. In the case of ^{207}Pb for example $N=125$, $Z=82$ and $4(N-Z)^2/N^2=0.47$. Two further factors must be estimated before it is possible to compare the (γ, α) and (γ, p) cross sections. Firstly, the number of alpha particles which may be considered to exist preformed within the nucleus; secondly, the probability, relative to that for protons, that after a direct interaction such an alpha particle escapes from the nucleus before losing its energy to the general nuclear motion.

The mean free path of an alpha particle in nuclear matter is very short, of the order of 1–2 fermis. It is therefore necessary to consider the emission of alpha particles from the surface of the nucleus only. The results of Hodgson (1958) and of Wilkinson (1959) indicate that in the surface layer of a heavy nucleus the nucleons spend about 0.4 of their time in alpha-like clusters. We follow this suggestion and assume that the surface layer has a thickness of 2.4 fermis (Hill 1957). For lead these assumptions suggest that there are about eight preformed alpha particles in the nuclear surface so that the relative number of alpha particles and protons is about 0.1.

The relative probability of escape for protons and alpha particles can be estimated very roughly as follows. First, owing to the short mean free path of alpha particles in nuclear matter, an alpha particle will only be emitted if in the initial interaction it moves away from the centre of the nucleus. Since initial motions towards and away from the nuclear centre are equally likely, this effect reduces by a factor of two the escape probability of alpha particles relative to protons. The relative escape probabilities are also influenced by the barrier penetrabilities and to evaluate this factor requires some knowledge of the momentum distribution of alpha particles and protons in the nucleus. In the absence of any detailed information two extreme assumptions will be made: (a) that there is a uniform energy distribution, up to the maximum energy, of particles reaching the nuclear surface, (b) that all particles are emitted with the maximum energy. It is further assumed (Erdos, Scherrer and Stoll 1957) that for a heavy nucleus like lead, gamma rays of about 25 mev give the most important contributions to the yields of charged particles. The penetrabilities for alpha particles relative to protons calculated in this way are 0.2 for assumption (a) and 0.5 for assumption (b). Recalling the additional factor of two introduced to account for the absorption of alpha particles within the nucleus, the estimated ratio of the escape probabilities of alpha particles and protons is 0.1 and 0.25.

Collecting the three factors, the calculated ratios of the cross sections for lead is

$$\begin{aligned}\frac{\sigma(\gamma, \alpha)}{\sigma(\gamma, p)} &= 0.47 \times 0.1 \times (0.1-0.25) \\ &= 0.5-1\%.\end{aligned}$$

The agreement between this calculated value and the measured value of approximately 0.6% (§4) is better than expected considering the extreme crudeness of the calculations. It is concluded therefore that the (γ, α) yields in the heavy nuclei may arise from direct interactions with preformed alpha-like clusters

of nucleons in the nuclear surface. For middle-weight nuclei, such as vanadium, the usual statistical, evaporation theory seems to give a satisfactory account of the yields.

REFERENCES

- BERMAN, A. I., and BROWN, K. L., 1954, *Phys. Rev.*, **96**, 83.
BLATT, J. M., and WEISSKOPF, V., 1953, *Theoretical Nuclear Physics* (New York : John Wiley).
CAMERON, A. G. W., 1958, *Canad. J. Phys.*, **36**, 1040.
CARVER, J. H., TAYLOR, R., and TURCHINETZ, W., 1960, *Aust. J. Phys.*, **13**, 617.
CARVER, J. H., and TURCHINETZ, W., 1958, *Proc. Phys. Soc.*, **71**, 613.
COLEMAN, R. F., HAWKER, B. E., O'CONNOR, L. P., and PERKIN, J. L., 1959, *Proc. Phys. Soc.*, **73**, 215.
COURANT, E. D., 1951, *Phys. Rev.*, **82**, 703.
DYAL, P., and HUMMEL, J. P., 1959, *Phys. Rev.*, **115**, 1264.
ERDOS, P., SCHERRER, P., and STOLL, P., 1957, *Helv. Phys. Acta*, **30**, 639.
GOLDEMBERG, J., and KATZ, L., 1954, *Canad. J. Phys.*, **32**, 49.
HILL, D. L., 1957, *Encyclopaedia of Physics* (Ed. S. Flugge) (Berlin : Springer), **39**, 178.
HODGSON, P. E., 1958, *Nucl. Phys.*, **8**, 1.
LE COUTEUR, K. J., 1959, *Nuclear Reactions* (Eds P. M. Endt and M. Demeur), **1**, 318.
LIDOSKY, L. S., and FISHER, V. K., 1956, *Phys. Rev.*, **104**, 759.
MOTT, W. E., and SUTTON, R. B., 1958, *Encyclopaedia of Physics* (Ed. S. Flugge) (Berlin : Springer), **45**, 86.
NATHANS, R., and HALPERN, J., 1954, *Phys. Rev.*, **93**, 437.
PERKIN, J. L., and RASMUSSEN, J. O., 1957, *Encyclopaedia of Physics* (Ed. S. Flugge) (Berlin : Springer), **42**, 171.
STROMINGER, D., HOLLANDER, J. M., and SEABORG, G. T., 1958, *Rev. Mod. Phys.*, **30**, 585.
TAYLOR, R. B., 1960, *Nucl. Phys.*, **19**, 453.
TOMS, M. E., and McELHINNEY, J., 1958, *Phys. Rev.*, **111**, 561.
WADSWORTH, A. H., 1958, *Encyclopaedia of Physics* (Ed. S. Flugge) (Berlin : Springer), **38**, 1, 1.
WEINSTOCK, E. V., and HALPERN, J., 1954, *Phys. Rev.*, **94**, 165.
WILKINSON, D. H., 1956, *Physica*, **22**, 1039.
—, 1959, *Phil. Mag.*, **4**, 215.

Scale Times and Scale Lengths of Variables : with Geomagnetic and Ionospheric Illustrations

By SYDNEY CHAPMAN

Geophysical Institute, College, Alaska

and

High Altitude Observatory, Boulder, Colorado†

MS. received 17th June 1960

Abstract. The conception of the atmospheric scale height (relating to the proportionate variation of barometric pressure) is generalized to apply to any scalar and vector functions of time and/or position. Examples are given relative to magnetic fields and the ionosphere. The scale length and scale time here defined enable precision to be given to often used terms such as 'slow variation', distance (or time) 'small in relation to the scale of variation' of another quantity.

§ 1. INTRODUCTION

IN 1936 I introduced the conception and term *scale height* in connection with general atmospheres subject to gravity. The definition of the scale height H was

$$H = -1/[d(\ln p)/dh], \quad \dots\dots(1)$$

where p denotes pressure, h height, and \ln the Napierian logarithm. In an atmosphere of uniform composition at absolute temperature T , subject to a uniform gravity field g ,

$$H = kT/mg = RT/Wg, \quad \dots\dots(2)$$

which is positive. Here k denotes Boltzmann's constant, R the gas constant (8.314×10^7); m and W denote respectively the mean molecular mass and (chemical) mean molecular 'weight'.

If T is uniform, H is constant, and

$$p = p_0 e^{-h/H}. \quad \dots\dots(3)$$

Previously the rather cumbersome name 'height of the homogeneous atmosphere' had been used for H in this specially simple case. The Eqn (1) generalized the conception, making it applicable to atmospheres in which T , W and g (and hence also H) may vary with height.

§ 2. SCALE LENGTH

Consider a scalar function f of one space variable s ; s may, for example, be a Cartesian coordinate, or a distance along a line (perhaps the path of a particle), not necessarily straight. Let Δf denote the change in f in going from s to $s + \Delta s$. The *proportionate* change of f is $\Delta f/f$. The mean *rate* of proportionate change over this interval of length is $(\Delta f/\Delta s)/f$. The rate of proportionate change at s is $(df/ds)/f$ or $d(\ln f)/ds$.

† There engaged in a programme of research supported by the National Bureau of Standards and the Sacramento Peak Observatory of the Air Force Cambridge Research Center.

By analogy with the conception and name *scale height* for the rate of proportionate variation of atmospheric pressure, we write

$$L = 1/[d(\ln f)/ds], \quad \dots\dots (4)$$

and name L the scale length of f (for its rate of proportional space variation).

In general L will be a function of s , positive or negative. In the special case when L is independent of s , integration of (4) gives

$$f = f_0 e^{s/L}. \quad \dots\dots (5)$$

If L is large (by any chosen standard), the rate of proportionate (space) variation of f is small (by that standard), and vice versa.

In an interval Δs that is small compared with L , the proportionate change of f , namely $\Delta f/f$, is approximately $\Delta s/L$, and consequently small.

The Eqns (1) and (4) are completely analogous except as regards the minus sign in (1). Thus the *scale height* is the negative *scale length* of p . In an atmosphere the pressure always decreases upwards, so that its scale length is negative. The scale height is consequently positive.

2.1. Other Aeronomic Scale Heights

This section was added later (5th July 1960), after reading a preprint of a paper, "Solar Extreme Ultra-violet Attenuation Profiles of the Upper Terrestrial Atmosphere", by H. E. Hinteregger, of the Geophysics Research Directorate, Bedford, Massachusetts, U.S.A. In this paper he introduced the notation H_p , discussed what is here denoted by H , and derived the special case (5 g) based on the general formula (5 d).

The scale height H refers to the atmospheric pressure p . This can be indicated by adding the suffix p . Similar scale heights can be defined for the associated variables n, g, m, T and the mass density ρ . These scale heights can likewise be denoted by H with the corresponding suffix.

For an atmosphere on a spherical earth of radius a , the gravitational scale height H_g at height h is given by

$$H_g = \frac{1}{2}(a+h), \quad \dots\dots (5 a)$$

if we neglect the contribution to g made by the atmosphere itself.

Clearly

$$H_m = H_w. \quad \dots\dots (5 b)$$

It is easily shown that

$$\frac{1}{H_p} = \frac{1}{H_g} - \frac{1}{H_T}, \quad \frac{1}{H_p} = \frac{1}{H_n} + \frac{1}{H_m}. \quad \dots\dots (5 c)$$

The height variation of H_p , depending on non-uniformity of one or more of the variables g, m and T , is given by

$$\frac{1}{H_p} \frac{dH_p}{dh} = -\frac{1}{H_T} + \frac{1}{H_m} + \frac{1}{H_g}. \quad \dots\dots (5 d)$$

Hence

$$\frac{1}{H_T} = -\frac{1}{H_p} \frac{dH_p}{dh} + \frac{1}{H_m} + \frac{1}{H_g}. \quad \dots\dots (5 e)$$

In an isothermal atmosphere of uniform composition,

$$H_T = H_m = H_w = \infty, \quad H_p = H_n = H_\rho. \quad \dots\dots (5 f)$$

For an atmosphere in which T varies but m is constant, (5 *d*) takes the form (given by Hinteregger)

$$\frac{1}{H_n} = \frac{1}{H_p} \left(1 + \frac{dH_p}{dh} \right) \quad \dots\dots (5g)$$

if the variation of gravity is ignored.

§ 3. SCALE TIME

If f is a scalar function of time t , we may similarly define a time T by

$$T = 1/[d(\ln f)/dt], \quad \dots\dots (6)$$

and name it the *scale time* of f (for its rate of proportionate time change). The scale time may be positive or negative. In general T will be a function of t . In the special case when it is constant, integration of (6) gives

$$f = f_0 e^{t/T}. \quad \dots\dots (7)$$

The proportionate time change of f is rapid if T is small, slow if T is large.

The proportionate change $\Delta f/f$ in a time interval Δt that is small compared with T is approximately $\Delta t/T$.

§ 4. SCALAR FUNCTIONS OF POSITION AND TIME

If f is a scalar function of both position and time, we can similarly define its scale time and one or more scale lengths. There will be only one scale length if f , as in § 2, depends on only one space variable. But if f is a function of position in three-dimensional space, and consequently a function of three orthogonal Cartesian coordinates x, y, z , we can define three scale lengths, each as in

$$L_x = 1/[\partial(\ln f)/\partial x]. \quad \dots\dots (8)$$

This gives the scale length of the rate of proportionate variation of f along the x direction. We may call L_x, L_y, L_z *partial* scale lengths.

An invariant positive scale length L can be defined, which is independent of the choice of axes, by

$$\frac{1}{L^2} = (\text{grad } \ln f)^2. \quad \dots\dots (9)$$

This is equivalent to

$$\frac{1}{L^2} = \frac{1}{L_x^2} + \frac{1}{L_y^2} + \frac{1}{L_z^2}. \quad \dots\dots (10)$$

Hence L is less than or equal to the least of the partial scale lengths.

In any displacement $d\mathbf{r}$, of magnitude dr , small compared with L , the proportionate change of f will be small if dr/L is small.

§ 5. CHANGING VECTOR FUNCTIONS : SCALE TIMES

For the magnitude F of a vector function of time \mathbf{F} a scale time T may be defined by

$$T = 1/[d(\ln F)/dt]. \quad \dots\dots (11)$$

'Partial' scale times T_x, T_y, T_z may be defined also for each orthogonal Cartesian component of \mathbf{F} , namely F_x, F_y, F_z . In their case, however, it is most appropriate to modify the definition of scale time as follows:

$$\frac{1}{T_x} = \frac{1}{F} \frac{dF_x}{dt}. \quad \dots\dots (12)$$

Here the time derivative dF_x/dt is divided by F rather than by F_x . Division by F_x would give an infinite partial scale time if \mathbf{F} were perpendicular to the Ox axis at the point considered, so that $F_x = 0$. With the definition (12) it is easy to show that

$$\frac{1}{T} = \frac{l}{T_x} + \frac{m}{T_y} + \frac{n}{T_z}, \quad \dots\dots (13)$$

where l, m, n denote the direction cosines of \mathbf{F} (so that $F_x = lF$, etc.). The right-hand side of (13) is an invariant for change of the orthogonal axes.

§ 6. NON-UNIFORM VECTOR FUNCTIONS : THE SCALE LENGTH

Nine partial scale lengths L_{uv} may be defined for \mathbf{F} , a vector function of position defined by orthogonal Cartesian coordinates x, y, z . Here L_{uv} , where u and v may each represent any of the variables x, y, z , is defined by

$$\frac{1}{L_{uv}} = \frac{1}{F} \frac{\partial F_u}{\partial v}. \quad \dots\dots (14)$$

As in § 5, the division of the derivative is by F and not by the component F_u .

Clearly F/L_{uv} is an element of $\nabla\mathbf{F}$, the gradient tensor of \mathbf{F} . The sum of the squares of the nine elements is invariant for change of orthogonal Cartesian axes. In the notation used by Chapman and Cowling (1939), in association with the late E. A. Milne, this sum is $w : \bar{w}$ (Chapter 1, note especially p. 17), where \bar{w} denotes $\nabla\mathbf{F}$, and $\bar{\bar{w}}$ the conjugate dyadic. It is convenient to define the scale length L of \mathbf{F} as the positive magnitude

$$L = F(w : \bar{w})^{1/2}. \quad \dots\dots (15)$$

With this definition,

$$\frac{1}{L^2} = \sum \sum \frac{1}{L_{uv}^2}. \quad \dots\dots (16)$$

Clearly L is less than any of the partial scale lengths (unless all vanish except one, which L will then equal).

The variation of the magnitude F in any displacement $d\mathbf{r}$ will be small if dr/L is small.

6.1. The Scale Length of a Vector Field derived from a Potential, near a Neutral Point

If a vector field \mathbf{F} has a potential V , such that $\mathbf{F} = \text{grad } V$, we can express V , for the region near a point P_0 , in terms of coordinates x, y, z relative to P_0 , by

$$V = V_0 + X_0x + Y_0y + Z_0z + \frac{1}{2}(ax^2 + by^2 + cz^2 + 2fyz + 2gzx + 2hxy) + \dots$$

where X_0, Y_0, Z_0 denote the components F_x, F_y, F_z of \mathbf{F} at P_0 , and a, b, c, f, g, h are constants characteristic of this point. At a neutral point, X_0, Y_0, Z_0 are all zero, that is, $\mathbf{F} = 0$. To calculate the scale length $L(\mathbf{F})$ for such a point, it is convenient to use the expression for V relative to the principal axes at O of the quadratic $V = 0$, neglecting all higher powers of x, y, z . This is legitimate because L is invariant for change of orthogonal axes. Relative to such axes, f, g, h are all zero.

Thus at a point P with such coordinates x, y, z , relative to the neutral point,

$$w : \bar{w} = a^2 + b^2 + c^2, \quad F = (a^2x^2 + b^2y^2 + c^2z^2)^{1/2}.$$

Hence $L(\mathbf{F})$ is given by

$$L(\mathbf{F})^2 = (a^2x^2 + b^2y^2 + c^2z^2)/(a^2 + b^2 + c^2).$$

Thus L will depend on the direction of the point P relative to O .

The scale length $L(F)$ of the magnitude F of the vector field can be calculated from (10) for a point P near a neutral point in a similar way. The result is

$$\frac{1}{L(F)^2} = \frac{a^4x^2 + b^4y^2 + c^4z^2}{(a^2x^2 + b^2y^2 + c^2z^2)^2}.$$

These formulae take a slightly simpler form in the case when the potential of the field satisfies Laplace's equation, because then

$$a + b + c = 0.$$

This signifies that one of the three quantities a, b, c has a sign opposite to that of the other two. Let this one be c (the choice can always be made thus by naming the axes appropriately). Then

$$c = -(a + b),$$

and the above expressions for $L(\mathbf{F})$ and $L(F)$ can be re-written with this simplification.

The result is specially simple for points near a neutral line. In this case one of the three coefficients a, b, c is zero. Suppose $c = 0$, then $a = -b$. In this case

$$L(\mathbf{F}) = r/\sqrt{2}, \quad L(F) = r,$$

where

$$r^2 = x^2 + y^2.$$

§ 7. THE SCALE LENGTH FOR THE MAGNETIC FIELD OF AN INFINITELY LONG RECTILINEAR ELECTRIC CURRENT

In this case $H = 2i/r$, where r denotes the distance from the line. Taking the line as z axis, the components X, Y, Z of H are given in terms of x, y, z by

$$X = -2iy/r^2, \quad Y = 2ix/r^2, \quad Z = 0. \quad \dots\dots (17)$$

Hence

$$\partial X/\partial x = 4ixy/r^4 = -\partial Y/\partial y, \quad \dots\dots (18)$$

$$\partial X/\partial y = 2i(y^2 - x^2)/r^4 = \partial Y/\partial x. \quad \dots\dots (19)$$

Hence in this case it follows that

$$w : \bar{w} = 8i^2/r^4 \quad \dots\dots (20)$$

and

$$L = r/\sqrt{2}. \quad \dots\dots (21)$$

§ 8. THE SCALE LENGTH FOR THE FIELD OF A POINT DIPOLE

For the field of a point dipole the value of $w : \bar{w}$ can with some labour be inferred using orthogonal Cartesian coordinates and the expression for V :

$$V = mz/r^3. \quad \dots\dots (22)$$

The result obtained for $w : \bar{w}$ is most simply expressed in terms of r and θ as

$$w : \bar{w} = 18m^2(1 + 2\cos^2\theta)/r^8. \quad \dots\dots (23)$$

Another method of obtaining this result is by using the expression for w in spherical polar coordinates r, θ, ϕ . Denoting the corresponding components of \mathbf{H} by R, Θ, Φ , we have for the terms in w :

$$\begin{aligned} & \frac{\partial R}{\partial r} & \frac{\partial \Theta}{\partial r} & \frac{\partial \Phi}{\partial r} \\ & \frac{1}{r} \frac{\partial R}{\partial \theta} - \frac{\Theta}{r} & \frac{1}{r} \frac{\partial \Theta}{\partial \theta} + \frac{R}{r} & \frac{1}{r} \frac{\partial \Phi}{\partial \theta} & \dots\dots (24) \\ & \frac{1}{r \sin \theta} \frac{\partial R}{\partial \phi} - \frac{\Phi}{r} & \frac{1}{r \sin \theta} \frac{\partial \Theta}{\partial \phi} - \frac{\Phi}{r} \cot \theta & \frac{1}{r \sin \theta} \frac{\partial \Phi}{\partial \phi} + \frac{R}{r} + \frac{\Theta}{r} \cot \theta \end{aligned}$$

(Morse and Feshbach 1953, p. 64). For the dipole field

$$R = 2m \cos \theta / r^3, \quad \Theta = m \sin \theta / r^3, \quad \Phi = 0. \quad \dots\dots (25)$$

Using (24) and (25) the result (23) is readily obtained.

The value of H is $(m/r^3)(1 - 3 \cos^2 \theta)^{1/2}$. Hence the scale length L is given by

$$L = \frac{r}{3\sqrt{2}} \left(\frac{1 + 3 \cos^2 \theta}{1 + 2 \cos^2 \theta} \right)^{1/2}. \quad \dots\dots (26)$$

Along the dipole axis ($\theta = 0$) the second factor is $(4/3)^{1/2}$ or 1.154. As θ increases from its polar value (zero) to its equatorial value (90°), this factor decreases to 1. Thus L is nearly constant over any sphere concentric with the dipole. It is less than r by a factor that varies between 3.57 (for $\theta = 0$) and 4.24 (for $\theta = 90^\circ$).

§ 9. THE SCALE LENGTH OF A CIRCULAR LINE CURRENT

At a great distance compared with a , the radius of a circular line current, the magnetic field tends to equality with that of a dipole of moment m given by

$$m = \pi a^2 i.$$

Hence its scale length tends towards the value given by (26).

Close to the line current, at a distance s small compared with a , the field approximates to that of an infinitely long rectilinear current i . Hence its scale length (see (21)) approximates to $s/\sqrt{2}$.

Near the centre of the circle, and within a sphere of any radius less than a , the magnetic potential of the field is given by

$$V = 2\pi i \sum_{n=0}^{\infty} (-1)^{n+1} \frac{1.3 \dots (2n-1)}{2.4 \dots 2n} \left(\frac{r}{a} \right)^{2n+1} P_{2n+1}(\cos \theta) \quad \dots\dots (27)$$

in terms of polar coordinates r, θ, ϕ ; see, for example, Chapman and Bartels (1940, p. 895).

Here V will be considered only as far as the second term, of degree 3 in r . It is convenient to express it in terms of Cartesian coordinates, thus:

$$V = -\frac{2\pi i z}{a} \left\{ 1 + 3 \frac{x^2 + y^2}{4a^2} - \frac{z^2}{2a^2} \right\}. \quad \dots\dots (28)$$

At the origin (indicated by the subscript zero),

$$X_0 = Y_0 = 0, \quad Z_0 = 2\pi i/a = H_0. \quad \dots\dots (29)$$

Near the origin,

$$\begin{aligned} X &= (3xz/2a^2)H_0, & Y &= (3yz/2a^2)H_0 \\ Z &= H_0 \{1 - (3/4a^2)(2z^2 - x^2 - y^2)\}. \end{aligned} \quad \dots\dots (30)$$

Hence, to this degree of accuracy,

$$\left. \begin{aligned} \frac{\partial X}{\partial x} = \frac{\partial Y}{\partial y} = \frac{3z}{2a^2} H_0, \quad \frac{\partial X}{\partial y} = \frac{\partial Y}{\partial x} = 0 \\ \frac{\partial X}{\partial z} = \frac{\partial Z}{\partial x} = \frac{3x}{2a^2} H_0, \quad \frac{\partial Y}{\partial z} = \frac{\partial Z}{\partial y} = \frac{3y}{2a^2} H_0, \quad \frac{\partial Z}{\partial z} = -\frac{3z}{a^2} H_0. \end{aligned} \right\} \dots\dots (31)$$

Hence

$$w : \bar{w} = (3H_0 r / 2a^2)^2 2(1 + 2 \cos^2 \theta). \dots\dots (32)$$

Near the origin, neglecting higher terms

$$H = H_0 \left\{ 1 - \frac{3r^2}{4a^2} (3 \cos^2 \theta - 1) \right\}. \dots\dots (33)$$

Hence, to the present degree of accuracy, the scale length L is given by

$$L = \frac{a^2/r}{3 (\cos^2 \theta + 1/2)^{1/2}}. \dots\dots (34)$$

To obtain the next approximation to L it is necessary to include in the calculations the next higher terms in X , Y , Z and their derivatives. The correction factor to be applied to (34) is here given only for the equatorial plane, $\theta = 90^\circ$: it is

$$1 + \frac{1}{8a^2/r^2 + 5}.$$

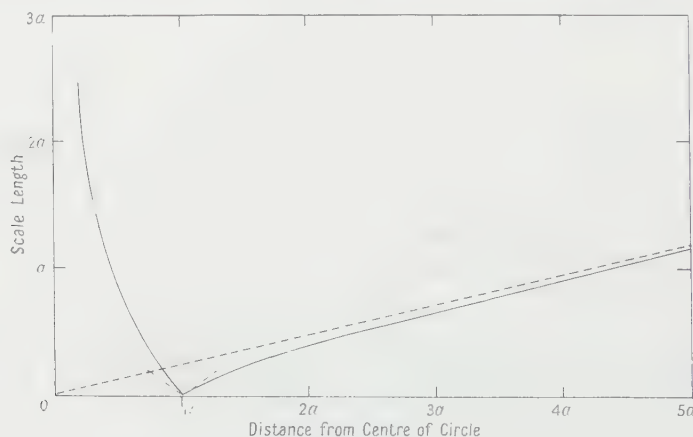
Even for r as large as $\frac{1}{2}a$, this factor, 1.027, differs little from 1.

Similarly for $r > a$ the following is the correction factor applicable to (26) for points in the equatorial plane ($\theta = 90^\circ$); the factor is given to order $(a/r)^4$

$$1 - \frac{3}{4}(a/r)^2 \frac{1 + (10/9)(a/r)^2}{1 + (15/8)(a/r)^2 + (35/24)(a/r)^4}.$$

The second term in this factor has the values 0.028, 0.045, 0.076, 0.153 when r/a has the values 5, 4, 3, 2.

From these results it is easy to draw a graph of L for points in the plane $\theta = 90^\circ$, as shown in the Figure; L is zero at $r = a$, implying an infinite field gradient there;



The scale length of the magnetic field of a line current, flowing in a circle of radius a , at different distances from the centre, in the plane of the circle. At the circle L is zero; the tangents there are shown by chain lines, and the asymptote of the graph at infinite distance by a broken line.

at the origin L is infinite, and L also tends to infinity with r , implying zero field gradients at the origin and at infinity.

§ 10. THE IONOSPHERE : SCALE LENGTHS AND TIMES FOR ABSORPTION AND IONIZATION

Other simple examples of scale lengths and times relate to the ionosphere—particularly for a plane stratified atmosphere of constant scale height H , ionized by monochromatic radiation (Chapman 1931 a).

In this case the rate of absorption of photons is given, for incidence of sunlight at zenith angle χ , by

$$q = q_0 \exp(1 - z - e^{-z} \sec \chi) \text{ cm}^{-3} \text{ sec}^{-1}. \quad \dots\dots (35)$$

Here q_0 denotes the maximum rate of absorption for *vertical* incidence of sunlight ($\chi=0$), and z denotes height measured in scale-height units from the absorption peak level at vertical incidence. The peak level corresponding to (35) is at

$$z = \ln \sec \chi. \quad \dots\dots (36)$$

If we write

$$z' = z - \ln \sec \chi \quad \dots\dots (37)$$

(35) can be expressed as

$$q = q_x \exp(1 - z' - e^{-z'}) \quad \dots\dots (38)$$

where q_x is the maximum rate of absorption at zenith angle χ . It is given by

$$q_x = q_0 \cos \chi. \quad \dots\dots (39)$$

Note that (38) is the form assumed by (35) when $\chi=0$, q_x being replaced by q_0 .

Hence it readily follows that the scale length for the proportionate variation of absorption is given by

$$L_{\text{absorption}} = 1/(e^{-z'} - 1) \quad \dots\dots (40)$$

in terms of H as the unit of length.

At the absorption peak ($z'=0$) the height variation of q is zero, by definition, and correspondingly L is infinite. Below the peak level ($z' < 0$), where q is increasing upward, L is positive and decreases downwards, tending towards the value $e^{-z'}$ (and zero, as z' tends to $-\infty$). Above the peak level, where q decreases upwards, L is negative, and decreases upwards, tending to the value -1 , that is, to equality with the scale height.

Consider an ionospheric layer where the rate of recombination is expressible by zn^2 , where n denotes the number density of electrons. When near-equilibrium conditions prevail, n is given approximately by

$$n = (\alpha q)^{1/2}. \quad \dots\dots (41)$$

The corresponding scale length for the proportionate variation of electric density with height is then given approximately by

$$L_{\text{ionization}} = \frac{1}{2} L_{\text{absorption}}. \quad \dots\dots (42)$$

As regards the scale *time* for q , it is convenient to use (35) rather than (38), because q_x and z in (38) are both functions of time, through χ . This is given as follows, for a station in colatitude θ , at a season when the sun's declination is δ , and at a time of day when the sun's hour angle is ϕ :

$$\cos \chi = \sin \delta \cos \theta + \cos \delta \sin \theta \cos \phi. \quad \dots\dots (43)$$

Hence

$$d\chi/dt = -(d\phi/dt) \cos \delta \sin \theta \sin \phi \quad \dots\dots (44)$$

and $d\phi/dt$ is constant (2π per day or $2\pi/86400$ per second). The minus sign

appears here because $\sin \chi$, unlike $\sin \phi$, is always positive; and in the forenoon, when ϕ is negative, χ is decreasing.

It may easily be shown that the scale time for proportionate change of q at the level z , time ϕ , season δ , and colatitude θ is given by

$$T_{\text{absorption}} = \frac{(86400/2\pi)e^z \cos^2 \chi}{\cos \delta \sin \theta \sin \phi} \text{ seconds.} \quad \dots\dots (45)$$

At noon ($\phi = 0$) the rate of change of q is zero and T is infinite—at all heights, latitudes, seasons, and times of sunlight.

At sunrise and sunset $\chi = 90^\circ$ and $T = 0$, implying infinitely rapid proportionate variation of q ; but this applies only to an atmosphere that is plane stratified. For an atmosphere on a spherical earth $\sec \chi$ in (35) must be replaced by another function $\text{Ch}(x, \chi)$ (Chapman 1931 b, Wilkes 1954), and $\cos \chi$ in (45) must be replaced by $1/\text{Ch}(x, \chi)$. The function $\text{Ch}(x, \chi)$ is not infinite at $\chi = 90^\circ$.

At the equinoxes $\delta = 0$ and (45) takes the form (reckoning T in days instead of seconds)

$$T_{\text{absorption}} = a \cos^2 \phi / \sin \phi \quad \dots\dots (46)$$

where

$$a = (e^z \sin \theta) / 2\pi. \quad \dots\dots (47)$$

From sunrise to noon the variation of T is indicated by the following table of T/a or $\cos^2 \phi / \sin \phi$:

ϕ (deg)	90	80	70	60	50	40	30	20	10	0
$T/a = \cos^2 \phi / \sin \phi$	0	0.03	0.12	0.29	0.54	0.91	1.5	2.6	5.6	∞

The higher the level, and the greater the value of $e^z \sin \theta$, the longer the interval around noon during which T will be large, and q slowly varying. This is illustrated by graphs of q as a function of a by Chapman (1931 b, Fig. 1), also reproduced by Chapman and Bartels (1940, p. 509). The higher the level, the more 'square-shouldered' is the graph.

Contrariwise for low levels, where z is negative and $e^z \sin \theta$ is small, the briefer is the interval around noon during which L is large and the proportionate variation of q small; there the graph of q near its noon maximum is narrow; this also is shown in the diagram referred to.

For an ionized layer of the kind described above, for which (41) is valid, we have a formula analogous to (42), namely

$$T_{\text{ionization}} = \left(\frac{1}{2}\right) T_{\text{absorption}}. \quad \dots\dots (48)$$

Also during the night, when the ionizing radiation is absent,

$$T_{\text{ionization}} (\text{night}) = -1/\alpha n. \quad \dots\dots (49)$$

This increases from sunset to dawn, corresponding to the decrease in n and its rate of change.

REFERENCES

- CHAPMAN, S., 1931 a, *Proc. Phys. Soc.*, **43**, 26.
 — 1931 b, *Proc. Phys. Soc.*, **43**, 483.
 — 1936, *Rep. Progr. Phys.*, **3**, 42 (London: Physical Society).
 CHAPMAN, S., and BARTELS, J., 1940, *Geomagnetism* (Oxford: Clarendon Press), p. 895.
 CHAPMAN, S., and COWLING, T. G., 1939, *The Mathematical Theory of Non-uniform Gases* (Cambridge: University Press).
 MORSE, P. M., and FESHBACH, H., 1953, *Methods of Theoretical Physics* (New York: McGraw-Hill).
 WILKES, M. V., 1954, *Proc. Phys. Soc. B*, **67**, 304.

Integrable Many Body Wave Functions for a System of Bose Particles

By S. F. EDWARDS AND M. A. NAQVI

Department of Theoretical Physics, the University, Manchester

Communicated by B. H. Flowers; MS. received 21st June 1960

Abstract. It is shown that, by means of a parametric representation, a variational calculation for a system of Bose particles can be carried through using explicit trial wave functions which describe a state with a fixed number of particles and include pair correlations. For the ground state the results of previous work are obtained as the first term in a steepest descent calculation. An effective Schrödinger equation is obtained for the relative motion of two particles. The application of the method to excited states is discussed; in particular for the case of a vortex line in the system it is shown that the method leads to an analysis which is similar to that for the ground state and could be carried through in the same way.

§ 1. INTRODUCTION

IN the theory of many boson systems it has proved possible to go beyond the independent particle or 'gas' model approximation and to calculate the contributions to the energy of the system arising from the terms corresponding to excitation of pairs of particles into states of opposite momenta. As is well known, this possibility was first demonstrated by Bogoliubov (1947) with the aid of his canonical transformation method. Recently several authors (Girardeaux and Arnowitt 1959, Valatin and Butler 1958) have provided a variational basis for the method by using an explicit form of the pair type wave function within the second quantization framework. In this paper a variational calculation will be performed on an explicit pair correlation wave function for a fixed number N of particles by means of parametric representation of the wave function which allows the integrations to be performed exactly, the results of previous work being obtained for large N as the first term in a steepest descent calculation. An effective Schrödinger equation is deduced for the interaction of two particles in the form

$$\{E - \nabla_{12}^2 - v(r_{12}) + F(\mathbf{r}_{12}, \phi)\} \phi(\mathbf{r}_{12}) = 0,$$

where F represents the effect of all the remaining particles and is a complicated functional of ϕ . The total energy deduced from this effective Schrödinger equation is then a lower bound. It is also shown that extensions of the ground state wave functions can be made in order to discuss the case of vortex lines (or rings) in the many body system, and which lead by a variational calculation to an effective Schrödinger equation for two particles in the presence of the vortex line.

§ 2. THE PARAMETRIC INTEGRAL REPRESENTATION

We shall use in this work real functions $\phi(\mathbf{r})$ as integration variables. We start with the definition of the functional integration given by Bogoliubov and Shirkov (1959). Consider a real function $\phi(\mathbf{r})$ satisfying periodic boundary conditions

over a box of volume V . The Fourier expansion of $\phi(\mathbf{r})$, i.e.

$$\phi(\mathbf{r}) = \sum_{\mathbf{K}} \phi_{\mathbf{F}}(\mathbf{K}) \frac{e^{i\mathbf{K} \cdot \mathbf{r}}}{V^{1/2}} \quad \dots\dots (2.1)$$

with $\mathbf{K} = (2\pi/V^{1/3})(n_x, n_y, n_z)$, and the n 's integers, gives a function $\phi_{\mathbf{F}}$ defined at a set of discrete points in \mathbf{K} space. These points are symmetrical with respect to the transformation $\mathbf{K} \rightarrow -\mathbf{K}$. Since $\phi(\mathbf{r})$ is real we have

$$\phi_{\mathbf{F}}^*(\mathbf{K}) = \phi_{\mathbf{F}}(-\mathbf{K}). \quad \dots\dots (2.2)$$

Thus

$$\phi_{\mathbf{F}}(\mathbf{K}) = u(\mathbf{K}) + iv(\mathbf{K}),$$

where $u(\mathbf{K})$ is a real even function of \mathbf{K} and $v(\mathbf{K})$ is a real odd function. For the purpose of functional integration we will regard $u(\mathbf{K}) = u(-\mathbf{K})$, and $v(\mathbf{K}) = -v(-\mathbf{K})$ as integration variables. The volume element of function space is thus given by

$$\delta\phi = \delta u_0 \prod_{\mathbf{K} > 0} \delta u_{\mathbf{K}} \delta v_{\mathbf{K}}. \quad \dots\dots (2.3)$$

The restriction $\mathbf{K} > 0$ means that we cover only half of \mathbf{K} space; for example by introducing a new index symbol j such that as j goes through $1, 2, \dots$; \mathbf{K}_j takes on all values lying in one-half of the space, and as j goes through the negative integers we cover the field points corresponding to $-\mathbf{K}$. Further $v(0)$ is not regarded as an integration variable since this is always zero.

With these definitions a functional integral written as

$$I = \int F\{\phi(\mathbf{r})\} \delta\phi,$$

means that through a Fourier expansion we are to go over to an expression in terms of the $u_{\mathbf{K}}, u_{-\mathbf{K}}, v_{\mathbf{K}}, v_{-\mathbf{K}}$; put $u_{\mathbf{K}} = u_{-\mathbf{K}}, v_{\mathbf{K}} = -v_{-\mathbf{K}}$; and then integrate, independently from $-\infty$ to $+\infty$ over all the $u_{\mathbf{K}}$'s and $v_{\mathbf{K}}$'s lying in half of \mathbf{K} space.

§ 3. THE WAVE FUNCTION

We shall consider a spatially uniform, many body system, i.e. one for which the number of particles N and their volume V are infinite while N/V remains finite. For the variational many body wave function of a Bose system we shall take the form

$$\Psi(\mathbf{r}_1 \dots \mathbf{r}_N) = \int \prod_{i=1}^N \{1 + \beta\phi(\mathbf{r}_i)\} Z(\phi) \delta\phi, \quad \dots\dots (3.1)$$

where

$$Z(\phi) = A \exp \left[-2 \sum_{\mathbf{K} > 0} \epsilon_{\mathbf{K}} (u_{\mathbf{K}}^2 + v_{\mathbf{K}}^2) - \epsilon_0 u_0^2 \right]. \quad \dots\dots (3.2)$$

In these expressions A, β are constants, while $\epsilon(\mathbf{K})$ is a positive even function of \mathbf{K} to be specified later

We shall, in this section, obtain Ψ explicitly in order to illustrate the operations implied in (3.1). Expanding the product in (3.1) we have

$$\prod_{i=1}^N \{1 + \beta\phi(\mathbf{r}_i)\} = 1 + \beta \sum_i \phi(\mathbf{r}_i) + \frac{1}{2} \beta^2 \sum_{i \neq j} \phi(\mathbf{r}_i) \phi(\mathbf{r}_j) + \dots \dots\dots (3.3)$$

Substituting (3.3) in (3.1) we integrate term by term. We have for the first term

$$\int Z(\phi) \delta\phi = A \int \delta u_0 \exp[-\epsilon_0 u_0^2] \prod_{\mathbf{K} > 0} \int r_{\mathbf{K}} \delta r_{\mathbf{K}} \delta \theta_{\mathbf{K}} \exp[-2\epsilon_{\mathbf{K}} r_{\mathbf{K}}^2], \quad \dots\dots (3.4)$$

where in (3.4) we have changed from 'Cartesian' coordinates $u_{\mathbf{k}}, v_{\mathbf{k}}$ to 'polar' coordinates $r_{\mathbf{k}}, \theta_{\mathbf{k}}$. We require the first term to be unity, hence from (3.4)

$$A = \frac{\epsilon_0^{1/2}}{\pi^{1/2}} \prod_{\mathbf{k} > 0} \frac{2\epsilon_{\mathbf{k}}}{\pi}. \quad \dots\dots (3.5)$$

The second, fourth, sixth terms, etc., give no contribution as they reduce to odd powers of the u 's and the v 's. For the third term we have, using (2.1),

$$I_3 = \frac{A\beta^2}{2V} \sum_{i \neq j} \int \delta\phi Z(\phi) \left[u_0 + \sum_{\mathbf{k} > 0} \{ (u_{\mathbf{k}} + iv_{\mathbf{k}}) \exp(i\mathbf{K} \cdot \mathbf{r}_i) + (u_{\mathbf{k}} - iv_{\mathbf{k}}) \exp(-i\mathbf{K} \cdot \mathbf{r}_i) \} \right] \\ \times [\text{similar expression with } \mathbf{r}_j \text{ replacing } \mathbf{r}_i]. \quad \dots\dots (3.6)$$

Using polar variables this becomes

$$I_3 = \frac{A\beta^2}{V} \sum_{i \neq j} \int \delta\phi Z(\phi) \left\{ u_0 + \sum_{\mathbf{k} > 0} 2r_{\mathbf{k}} \cos(\theta_{\mathbf{k}} + \mathbf{K} \cdot \mathbf{r}_i) \right\} + \left\{ u_0 + \sum_{\mathbf{l} > 0} 2r_{\mathbf{l}} \cos(\theta_{\mathbf{l}} + \mathbf{l} \cdot \mathbf{r}_j) \right\}. \\ \dots\dots (3.7)$$

Multiplying out the product in (3.7) those terms for which $\mathbf{K} \neq \mathbf{l}$ will vanish on integration over $\theta_{\mathbf{k}}$ or $\theta_{\mathbf{l}}$. Such terms would correspond to excitation of two particles into unrelated momentum states. Eqn (3.7) thus reduces to

$$I_3 = \frac{A\beta^2}{2V} \sum_{i \neq j} \int \delta\phi Z(\phi) \left\{ u_0^2 + 2 \sum_{\mathbf{k} > 0} r_{\mathbf{k}}^2 [\cos \mathbf{K} \cdot (\mathbf{r}_i - \mathbf{r}_j) + \cos(2\theta_{\mathbf{k}} + \mathbf{K} \cdot \mathbf{r}_i + \mathbf{K} \cdot \mathbf{r}_j)] \right\}, \\ \dots\dots (3.8)$$

where the function in the square bracket is obtained by writing a product of cosines as a sum of cosines. Again the second term in the square bracket, which would correspond to excitation of a pair of particles into the same state (thus violating momentum conservation), vanishes on integrating over $\theta_{\mathbf{k}}$. Carrying out the Gaussian integration we get

$$I_3 = \frac{\beta^2}{2V} \sum_{i \neq j} \left\{ \frac{1}{2\epsilon_0} + \sum_{\mathbf{k} > 0} \frac{1}{\epsilon_{\mathbf{k}}} \cos \mathbf{K} \cdot (\mathbf{r}_i - \mathbf{r}_j) \right\}. \quad \dots\dots (3.9)$$

Writing $g_{\mathbf{F}}(\mathbf{K})$ for the reciprocal of $\epsilon(\mathbf{K})$ and noting that ϵ is even, we have

$$I_3 = \frac{\beta^2}{4} \sum_{i \neq j} g(\mathbf{r}_i - \mathbf{r}_j), \quad \dots\dots (3.10)$$

where g is the Fourier transform of $g_{\mathbf{F}}$. A fairly lengthy calculation gives for the fifth term

$$I_5 = \frac{\beta^4}{32} \sum_{\substack{i, j, k, l, \\ \text{all different}}} g(\mathbf{r}_i - \mathbf{r}_j) g(\mathbf{r}_k - \mathbf{r}_l). \quad \dots\dots (3.11)$$

Specifying $\beta = i\sqrt{2}$ we see from (3.5), (3.10) and (3.11) that (3.1) leads to

$$\Psi(\mathbf{r}_1 \dots \mathbf{r}_N) = 1 - \frac{1}{2} \sum_{i \neq j} g(\mathbf{r}_i - \mathbf{r}_j) + \frac{1}{8} \sum_{\substack{i, j, k, l, \\ \text{all different}}} g(\mathbf{r}_i - \mathbf{r}_j) g(\mathbf{r}_k - \mathbf{r}_l) - \dots\dots \\ \dots\dots (3.12)$$

Thus our wave function differs from the product type wave function

$$\Psi_{\text{P}} = \prod_{i < j} \{1 - g(\mathbf{r}_i - \mathbf{r}_j)\} \quad \dots\dots (3.13)$$

in so far as it does not contain 'linked' terms of the type $g(12)g(23)$ for example. It has been shown by Lee, Huang and Yang (Huang 1958) that (3.12) is also the coordinate representation of the pair type wave function underlying Bogoliubov's transformation.

Finally we may note some points about (3.12):

(a) The sequence of signs in (3.12) is appropriate when the forces are of a purely repulsive type. For the ground state of such a system $g(\mathbf{r})$ would be positive everywhere (nodes in g not being energetically favourable), and would vanish as $\mathbf{r} \rightarrow \infty$. (b) The use of the Gaussian form (3.2) for $Z(\phi)$ requires that $\epsilon(\mathbf{K})$, and hence the Fourier transform $g_F(\mathbf{K})$ of $g(\mathbf{r})$, should be positive everywhere. This restriction would in general not be satisfied for the function appearing in (3.13) even for purely repulsive forces. However, a modification of the functional representation (3.1) can be made which allows $g_F(\mathbf{K})$ to be positive, negative or zero. As a result of this modification the calculations become much longer but one is led to exactly the same formulae as one gets when $g_F(\mathbf{K})$ is always positive. We shall not, therefore, discuss this modification but obtain the formulae assuming $g_F(\mathbf{K})$ to be positive. (c) The absence of the linked terms in (3.12) has the consequence that the method cannot be applied to a system with strong inter-particle forces (for example, repulsive cores). It is possible, by using a product of exponentials instead of powers in (3.1), to obtain a wave function which contains the linked terms; that is, we take the wave function to be

$$\Psi(\mathbf{r}_1 \dots \mathbf{r}_N) = \int \exp \left\{ \sum_i \beta \phi(\mathbf{r}_i) \right\} Z(\phi) \delta \phi. \quad \dots (3.14)$$

Expanding the exponential as a power series we obtain, instead of (3.3), a series in which any two or more of the indices i, j, k etc. can be equal to each other. Term by term integration then leads to an expression which is similar to (3.12) but contains also the linked terms. However, the disadvantage of this wave function is that the many body integrals which are needed for calculating the energy (see (4.2)) cannot be evaluated in a closed form. The difficulty that one meets here is of the same type as that which occurs in the calculation of the partition function of an imperfect gas.

It is of interest to note that the product function (3.13) can be represented by an expression only slightly different from (3.14). If one attempts to calculate the normalization and other integrals (see §§ 4 and 5) on the basis of (3.14) one is led to functional integrals of the type

$$\int \exp \left\{ b \int e^{\theta(\mathbf{r})} d\mathbf{r} - \sum_{\mathbf{K}} \theta_{\mathbf{F}}^2(\mathbf{K}) \epsilon_{\mathbf{K}} \right\} \delta \theta, \quad \dots (3.15)$$

where b is a constant and the subscript F denotes the Fourier transform. These integrals, unlike those arising from (3.1), cannot be evaluated in a closed form. This is of course the reflection in the functional method of the difficulties occasioned by the linked terms in a straightforward procedure.

§ 4. NORMALIZATION

We shall take as the Hamiltonian of the system the expression

$$H = \sum_i -\frac{\hbar^2}{2m} \nabla_{\mathbf{r}_i}^2 + \sum_{i < j} v(r_{ij}). \quad \dots (4.1)$$

The two body interaction v will not be specified except to the extent that it has no singularities, since, as found by other authors, the amount of correlation included in the pair type wave function is not sufficient to give a finite value of the potential energy for such a case. The energy of the system is given by

$$E = \frac{\int \Psi^* H \Psi}{\int \Psi^* \Psi}, \quad \dots (4.2)$$

and in this section we shall exhibit, in some detail, the calculation of the normalization integral appearing in (4.2) in order to illustrate the procedure. It is convenient for this calculation to work in momentum representation.

The wave function (3.1) written in momentum representation becomes

$$\Psi_F(\mathbf{K}_1 \dots \mathbf{K}_N) = \int \delta\phi \prod_{i=1}^N \{V^{1/2} \delta_{\mathbf{K}_i 0} + \sqrt{2i} \phi_F(\mathbf{K}_i)\} Z(\phi), \quad \dots (4.3)$$

where the subscript F is used, as in the previous section, to denote the Fourier transforms. If A is the value of the normalization we have

$$A = \sum_{\mathbf{K}_1, \mathbf{K}_N} \int \delta\phi \delta\psi \prod_{i=1}^N \{V \delta_{\mathbf{K}_i 0} - \sqrt{2i} \psi_F(-\mathbf{K}_i) V^{1/2} \delta_{\mathbf{K}_i 0} + \sqrt{2i} V^{1/2} \delta_{\mathbf{K}_i 0} \phi_F(\mathbf{K}_i) + 2\psi_F(-\mathbf{K}_i) \phi_F(\mathbf{K}_i)\}, \quad \dots (4.4)$$

In (4.4) we have used the integration variable ψ_i for the functional representation of Ψ_F^* as it is necessary to distinguish the two integration variables in the product $\Psi_F^* \Psi_F$. We note that with respect to summation over the \mathbf{K} 's the expression (4.4) behaves as a separable product of functions of the \mathbf{K} 's and that on summing over each \mathbf{K} from $-\infty$ to $+\infty$ we get the same contribution from each term of the product. Hence

$$A = \int \delta\phi \delta\psi \left[\sum_{\mathbf{K}} \{V \delta_{\mathbf{K} 0} + i \sqrt{2} V^{1/2} \delta_{\mathbf{K} 0} \phi_F(\mathbf{K}) - i \sqrt{2} V^{1/2} \delta_{\mathbf{K} 0} \psi_F(-\mathbf{K}) + 2\psi_F(-\mathbf{K}) \phi_F(\mathbf{K})\} \right]^N Z(\phi) Z(\psi). \quad \dots (4.5)$$

As we are interested in the limiting case of $N \rightarrow \infty$, the evaluation of the integral may be carried through by the method of steepest descents. We use the relation

$$a^N = \frac{N!}{2\pi i} \oint dz \exp \{-(N+1) \log z + az\} \quad \dots (4.6)$$

to write (4.5) in the form

$$A = \frac{N!}{2\pi i} \oint dz \exp \{-(N+1) \log z + Vz\} \int \delta\phi \delta\psi \exp [i \sqrt{2} V^{1/2} z \times \{\phi_F(0) - \psi_F(0)\} + 2z \sum_{\mathbf{K}} \psi_F(-\mathbf{K}) \phi_F(\mathbf{K})] Z(\phi) Z(\psi). \quad \dots (4.7)$$

Writing

$$\begin{aligned} \phi_F(\mathbf{K}) &= u(\mathbf{K}) + iv(\mathbf{K}) \\ \psi_F(\mathbf{K}) &= x(\mathbf{K}) + iy(\mathbf{K}), \end{aligned} \quad \dots (4.8)$$

we have by definition of functional integration

$$\begin{aligned} A &= \frac{N!}{2\pi i} \oint dz e^{-(N+1) \log z + Vz} \frac{\epsilon_0}{\pi} \prod_{\mathbf{K} > 0} \frac{4\epsilon_{\mathbf{K}}^2}{\pi^2} \int \delta u_0 \delta x_0 \prod_{\mathbf{K} > 0} \delta u_{\mathbf{K}} \delta v_{\mathbf{K}} \delta x_{\mathbf{K}} \delta y_{\mathbf{K}} \\ &\times \exp \left[\sqrt{2i} V^{1/2} z (u_0 - x_0) + 2z x_0 u_0 - \epsilon_0 (u_0^2 + x_0^2) \right. \\ &\left. + \sum_{\mathbf{K} > 0} \{4z x_{\mathbf{K}} u_{\mathbf{K}} - 2\epsilon_{\mathbf{K}} (x_{\mathbf{K}}^2 + u_{\mathbf{K}}^2) + 4z y_{\mathbf{K}} v_{\mathbf{K}} - 2\epsilon_{\mathbf{K}} (y_{\mathbf{K}}^2 + v_{\mathbf{K}}^2)\} \right], \quad \dots (4.9) \end{aligned}$$

where we have substituted the expressions (3.4) and (3.5) for $Z(\phi)$ and $Z(\psi)$.

We now make an orthogonal transformation in function space to new variables:

$$\begin{aligned} \theta_{\mathbf{K}} &= \frac{u_{\mathbf{K}} + x_{\mathbf{K}}}{\sqrt{2}}, & \mu_{\mathbf{K}} &= \frac{v_{\mathbf{K}} + y_{\mathbf{K}}}{\sqrt{2}}, \\ \eta_{\mathbf{K}} &= \frac{u_{\mathbf{K}} - x_{\mathbf{K}}}{\sqrt{2}}, & \nu_{\mathbf{K}} &= \frac{v_{\mathbf{K}} - y_{\mathbf{K}}}{\sqrt{2}}. \end{aligned} \quad \dots (4.10)$$

The functional part \mathcal{J} of the integral (4.9) then becomes

$$\mathcal{J} = \int \delta\theta_0 \delta\eta_0 \prod_{\mathbf{K} > 0} \delta\theta_{\mathbf{K}} \delta\eta_{\mathbf{K}} \delta\mu_{\mathbf{K}} \delta\nu_{\mathbf{K}} \exp \left[2iV^{1/2}z\eta_0 - (\epsilon_0 + z)\eta_0^2 - (\epsilon_0 - z)\theta_0^2 - \sum_{\mathbf{K} > 0} \{2(\epsilon_{\mathbf{K}} + z)(\eta_{\mathbf{K}}^2 + \nu_{\mathbf{K}}^2) + 2(\epsilon_{\mathbf{K}} - z)(\theta_{\mathbf{K}}^2 + \mu_{\mathbf{K}}^2)\} \right]. \quad \dots (4.11)$$

Thus, in the new variables, \mathcal{J} is a product of separate Gaussian integrals. On carrying these out we obtain

$$\mathcal{J} = \frac{\pi}{(\epsilon_0 - z^2)^{1/2}} \prod_{\mathbf{K} > 0} \frac{\pi^2}{4(\epsilon_{\mathbf{K}}^2 - z^2)} \exp [-z^2 V / (\epsilon_0 + z)]. \quad \dots (4.12)$$

Hence (4.9) becomes

$$A = \frac{N!}{2\pi i} \epsilon_0 \prod_{\mathbf{K} > 0} \epsilon_{\mathbf{K}}^2 \oint dz \exp \left[Vz - (N+1)\log z - z^2 V / (\epsilon_0 + z) + \sum_{\mathbf{K} = -\infty}^{+\infty} \log (\epsilon_{\mathbf{K}}^2 - z^2)^{-1/2} \right], \quad \dots (4.13)$$

where the property that $\epsilon_{\mathbf{K}} = \epsilon_{-\mathbf{K}}$ has been used.

The point of stationary phase ξ is therefore given by the equation

$$V - \frac{(N+1)}{\xi} + \sum_{\mathbf{K} = -\infty}^{+\infty} \frac{\xi}{(\epsilon_{\mathbf{K}}^2 - \xi^2)} - 2 \frac{\xi V}{(\epsilon_0 + \xi)} + \frac{\xi^2 V}{(\epsilon_0 + \xi)^2} = 0. \quad \dots (4.14)$$

As in the previous section we define

$$g_{\mathbf{F}}(\mathbf{K}) = 1/\epsilon(\mathbf{K}). \quad \dots (4.15)$$

Using the fact that when N, V both tend to infinity while $N/V (= \rho, \text{ the number density})$ remains finite, summation may be replaced by integration, that is

$$\sum_{\mathbf{K}} \rightarrow \frac{V}{8\pi^3} \int d\mathbf{K},$$

and Eqn (4.14) becomes

$$\rho = \xi + \frac{\xi^2}{8\pi^3} \int \frac{g_{\mathbf{F}}^2(\mathbf{K})}{\{1 - \xi^2 g_{\mathbf{F}}^2(\mathbf{K})\}} d\mathbf{K} - \frac{2\xi^2 g_{\mathbf{F}}(0)}{1 + \xi g_{\mathbf{F}}(0)} + \frac{\xi^3 g_{\mathbf{F}}^2(0)}{\{1 + \xi g_{\mathbf{F}}(0)\}^2}. \quad \dots (4.16)$$

The stationary phase being found from (4.16), the integral (4.13) is then given by

$$A = N! \{2\pi f''(\xi)\}^{-1/2} \xi^{-N-1} \exp \left[V \left\{ \xi - \frac{\xi^2 g_{\mathbf{F}}(0)}{1 + \xi g_{\mathbf{F}}(0)} \right\} \right] \prod_{\mathbf{K} = -\infty}^{+\infty} \{1 - \xi^2 g_{\mathbf{F}}^2(\mathbf{K})\}^{-1/2}, \quad \dots (4.17)$$

where $f(\xi)$ is the function in the square bracket of the expression in (4.13).

As will already be clear, the aim of the present method is to obtain the ratio (4.2) as a functional of g , the latter then being found by the normal variational procedure. It is argued in the Appendix that with our choice (3.12) of the many-body wave function there is probably no loss of generality in taking $g_{\mathbf{F}}(\mathbf{K}=0)$ to be zero. We shall assume this to be the case for the further calculations, a considerable simplification of the formulae thereby resulting; for example the last two terms in (4.16) now drop out of the equation for the stationary phase.

§ 5. CALCULATION OF THE ENERGY

The calculation of energy is made simpler by calculating first the momentum and the pair position distribution functions. Denoting these by $\mathcal{N}(\mathbf{K})$ and $M(\mathbf{r}_1, \mathbf{r}_2)$ we have

$$\frac{1}{N} \mathcal{N}(\mathbf{K}_1) = \frac{\sum_{\mathbf{K}_2 \dots \mathbf{K}_N} \Psi_{\mathbf{F}}^*(\mathbf{K}_1 \dots \mathbf{K}_N) \Psi_{\mathbf{F}}(\mathbf{K}_1 \dots \mathbf{K}_N)}{\sum_{\mathbf{K}_1 \dots \mathbf{K}_N} \Psi_{\mathbf{F}}^* \Psi_{\mathbf{F}}}, \quad \dots (5.1)$$

$$\frac{2}{N(N-1)} M(\mathbf{r}_1, \mathbf{r}_2) = \frac{\int \Psi^*(\mathbf{r}_1 \dots \mathbf{r}_N) \Psi(\mathbf{r}_1 \dots \mathbf{r}_N) d\mathbf{r}_3 \dots d\mathbf{r}_N}{\int \Psi^* \Psi d\mathbf{r}_1 \dots d\mathbf{r}_N}, \quad \dots (5.2)$$

Because of the symmetry of the Hamiltonian and the wave functions with respect to interchange of particles, the energy is given by the expression

$$E = \frac{\hbar^2 V}{16m\pi^3} \int K^2 \mathcal{N}(\mathbf{K}) d\mathbf{K} + \int v(\mathbf{r}_1 - \mathbf{r}_2) M(\mathbf{r}_1 \mathbf{r}_2) d\mathbf{r}_1 d\mathbf{r}_2, \quad \dots (5.3)$$

where in the first (kinetic energy) term the usual replacement of summation by integration has been made.

Consider the numerator on the right of (5.1), denoting this by \mathcal{N}_1 ; using the manipulations given in the last section this becomes

$$\begin{aligned} \mathcal{N}_1(\mathbf{K}_1) &= \frac{(N-1)!}{2\pi i} \oint dz \exp(-N \log z + Vz) \frac{\epsilon_0}{\pi} \prod_{\mathbf{K} > 0} \frac{4\epsilon_{\mathbf{K}}^2}{\pi^2} \int \delta\theta_0 \delta\eta_0 \\ &\times \prod_{\mathbf{K} > 0} \delta\theta_{\mathbf{K}} \delta\eta_{\mathbf{K}} \delta\mu_{\mathbf{K}} \delta\nu_{\mathbf{K}} \{ V\delta_{\mathbf{K},0} - 2V^{1/2} \delta_{\mathbf{K},0} \eta_{\mathbf{K}_1} + \theta_{\mathbf{K}_1}^2 - \eta_{\mathbf{K}_1}^2 + \mu_{\mathbf{K}_1}^2 \\ &- \nu_{\mathbf{K}_1}^2 + 2i(\theta_{\mathbf{K}_1} \mu_{\mathbf{K}_1} - \eta_{\mathbf{K}_1} \nu_{\mathbf{K}_1} + \theta_{\mathbf{K}_1} \nu_{\mathbf{K}_1} - \eta_{\mathbf{K}_1} \mu_{\mathbf{K}_1}) \} \\ &\times \exp[F(\theta_{\mathbf{K}}, \eta_{\mathbf{K}}, \mu_{\mathbf{K}}, \nu_{\mathbf{K}}; (\epsilon_{\mathbf{K}}, z)], \quad \dots (5.4) \end{aligned}$$

where F is the same function as appears in the exponent in (4.11). As before the functional integral separates into a product of integrals, and consequently the four terms in the curly brackets vanish on integration since for these there is a factor in the product of integrals in which the integrand is odd. The second term in the curly bracket gives a contribution which vanishes if we take $g_F(0)$ to be zero. The contributions of the remaining terms may be evaluated as before, the only difference being that in this case there is a factor in the product of integrals in which the integrand is a Gaussian multiplied by the second power of the argument.

Disregarding the difference between N and $N-1$, the equation for the stationary phase is the same as before and one is led to the formula

$$\mathcal{N}_1(\mathbf{K}_1) = \left\{ V\delta_{\mathbf{K},0} + \frac{\xi g_F^2(\mathbf{K}_1)}{1 - \xi^2 g_F^2(\mathbf{K}_1)} \right\} \frac{(N-1)!}{(2\pi)^{N/2}} \frac{e^{V\xi}}{(\xi)^{1/2}} \prod_{\mathbf{K} > 0} \frac{1}{\{1 - \xi^2 g_F^2(\mathbf{K})\}^{1/2}}. \quad \dots (5.5)$$

Dividing (5.5) by (4.17) and multiplying by N we get for the momentum distribution the expression

$$\mathcal{N}(\mathbf{K}) = \left\{ V\xi\delta_{\mathbf{K},0} + \frac{\xi^2 g_F^2(\mathbf{K})}{1 - \xi^2 g_F^2(\mathbf{K})} \right\}. \quad \dots (5.6)$$

The calculation of the numerator in (5.2) is fairly lengthy but nothing new is involved: we quote here the result, the work being given in the Appendix. We obtain for the pair distribution the expression

$$M(\mathbf{r}_1 \mathbf{r}_2) = \frac{\xi^2}{2} \left\{ \frac{\rho^2}{\xi^2} - 2g_2(\mathbf{r}_1 - \mathbf{r}_2) + \frac{1}{2}g_1^2(\mathbf{r}_1 - \mathbf{r}_2) + \frac{1}{2}g_2^2(\mathbf{r}_1 - \mathbf{r}_2) \right\}, \quad \dots (5.7)$$

where

$$\begin{aligned} g_1(\mathbf{r}) &= \frac{1}{8\pi^3} \int \frac{g_F(\mathbf{K})}{1 - \xi g_F(\mathbf{K})} e^{i\mathbf{K} \cdot \mathbf{r}} d\mathbf{K} \\ g_2(\mathbf{r}) &= \frac{1}{8\pi^3} \int \frac{g_F(\mathbf{K})}{1 + \xi g_F(\mathbf{K})} e^{i\mathbf{K} \cdot \mathbf{r}} d\mathbf{K}. \end{aligned} \quad \dots (5.8)$$

The Eqns (5.3), (5.6), (5.7), (5.8) and (4.16) allow us to calculate the total energy of the system. However, to carry out the variation of the energy with respect to $g_F(\mathbf{K})$ it is necessary to express both terms in (5.3) in one representation. If we use momentum representation and define

$$v(\mathbf{K}) = \int v(\mathbf{r}) e^{i\mathbf{K} \cdot \mathbf{r}} d\mathbf{r}, \quad \dots\dots (5.9)$$

then after some manipulations we obtain an expression for the energy per particle which we give below in the form given by Girardeaux and Arnowitt (1959) in their pair theory of bosons:

$$\begin{aligned} \frac{E}{N} = & \frac{1}{2} \rho \bar{v}(0) + \frac{1}{8\pi^3 \rho} \int \left[\left\{ \frac{\hbar^2}{2m} K^2 + \xi \bar{v}(\mathbf{K}) + \frac{1}{2} I_2(\mathbf{K}) \right\} \frac{\xi^2 g_F^2(\mathbf{K})}{1 - \xi^2 g_F^2(\mathbf{K})} \right. \\ & \left. + \left\{ \frac{1}{2} I_1(\mathbf{K}) - \xi \bar{v}(\mathbf{K}) \right\} \frac{\xi g_F(\mathbf{K})}{1 - \xi^2 g_F^2(\mathbf{K})} \right] d\mathbf{K}, \quad \dots\dots (5.10) \end{aligned}$$

where

$$\left. \begin{aligned} I_1(\mathbf{K}) &= \frac{1}{8\pi^3} \int v(\mathbf{K} - \mathbf{K}') \frac{\xi g_F^2(\mathbf{K}')}{1 - \xi^2 g_F^2(\mathbf{K}')} d\mathbf{K}' \\ I_2(\mathbf{K}) &= \frac{1}{8\pi^3} \int v(\mathbf{K} - \mathbf{K}') \frac{\xi^2 g_F^2(\mathbf{K}')}{1 - \xi^2 g_F^2(\mathbf{K}')} d\mathbf{K}' \end{aligned} \right\} \quad \dots\dots (5.11)$$

These formulae together with (4.16), which for $g(0)=0$ is

$$\rho = \xi + \frac{1}{8\pi^3} \int \frac{\xi^2 g_F^2(\mathbf{K})}{1 - \xi^2 g_F^2(\mathbf{K})} d\mathbf{K}, \quad \dots\dots (5.12)$$

form a complete set of equations of the variational problem. They are identical in form with those given by Girardeaux and Arnowitt (1959) if one uses $\xi g_F(\mathbf{K})$ instead of $g_F(\mathbf{K})$ as the variational function. We may note, however, that our derivation of these formulae requires $g_F(\mathbf{K}=0)$ to be zero; otherwise one would obtain additional terms in the formulae depending on this number (see for example (4.16)).

§ 6. THE VARIATIONAL EQUATION

The variational problem for the expression (5.10) has been discussed previously (Girardeaux and Arnowitt 1959) from the point of view of the function $g_F(\mathbf{K})$. In this section we will describe an alternative approach to this problem, based on varying (5.10) with respect to the pair distribution function (5.7). This results in a Schrödinger type equation for the pair function.

Let

$$\left. \begin{aligned} \psi(\mathbf{K}) &= \xi g_F(\mathbf{K}) \\ \psi_1(\mathbf{r}) &= \xi g_1(\mathbf{r}) \\ \psi_2(\mathbf{r}) &= \xi g_2(\mathbf{r}). \end{aligned} \right\} \quad \dots\dots (6.1)$$

In coordinate representation Eqns (5.10) and (5.12) become

$$\begin{aligned} \frac{E}{N} = \mathcal{E} = & \frac{\hbar^2}{2m\rho} \int (\nabla \psi_1 \cdot \nabla \psi_2) d\mathbf{r} + \frac{\rho}{2} \int v \left\{ 1 - 2 \frac{\xi}{\rho^2} \psi_2 \right. \\ & \left. + \frac{1}{2\rho^2} \psi_1^2 + \frac{1}{2\rho^2} \psi_2^2 \right\} d\mathbf{r}, \quad \dots\dots (6.2) \end{aligned}$$

$$\rho = \xi + \frac{1}{8\pi^3} \int \frac{\psi^2(\mathbf{K})}{1 - \psi^2(\mathbf{K})} d\mathbf{K}. \quad \dots\dots (6.3)$$

Further, if $\psi_F(\mathbf{r})$ denotes the Fourier transform of $\psi(\mathbf{K})$, then the restriction $g_F(\mathbf{K}=0)=0$ becomes

$$\int \psi_F(\mathbf{r}) d\mathbf{r} = 0. \quad \dots\dots (6.4)$$

We shall consider a situation where the inter-particle forces are repulsive and the particles are constrained to occupy a finite but large volume V by an external field ('box'). The presence of the box does not directly affect the internal energy of the system but it makes the particle density an arbitrary parameter depending on the external conditions. Hence in finding the minimum value of \mathcal{E} we do not need to vary with respect to ρ .

Let

$$\Phi^2(\mathbf{r}) = 1 - \frac{2\xi}{\rho^2} \psi_2 + \frac{1}{2\rho^2} \psi_1^2 + \frac{1}{2\rho^2} \psi_2^2. \quad \dots\dots (6.5)$$

We can determine this quantity, which from (5.7) is proportional to the pair distribution, by minimizing \mathcal{E} with respect to variations of ϕ , that is from the equation

$$\frac{\delta \mathcal{E}}{\delta \Phi(\mathbf{r})} = 0. \quad \dots\dots (6.6)$$

Carrying out the functional differentiation we write (6.6) as

$$\left[-\frac{\hbar^2}{m} \nabla_{\mathbf{r}}^2 + v(\mathbf{r}) + \mathcal{E} + F(\mathbf{r}, \Phi) \right] \Phi(\mathbf{r}) = 0, \quad \dots\dots (6.7)$$

where

$$F(\mathbf{r}, \Phi) = G(\mathbf{r}, \Phi) - \frac{\hbar^2 \nabla_{\mathbf{r}}^2 \Phi}{m \Phi} - \mathcal{E},$$

with \mathcal{E} given by (6.2) and $G(\mathbf{r}, \Phi)$ by

$$\begin{aligned} G(\mathbf{r}, \Phi) = & \frac{\hbar^2}{2m\rho^2} \int \{ \nabla \psi_2(\mathbf{s}) \cdot \nabla_{\mathbf{s}} F_1(\mathbf{s} - \mathbf{x}) + \nabla \psi_1(\mathbf{s}) \cdot \nabla_{\mathbf{s}} F_2(\mathbf{s} - \mathbf{x}) \} \\ & \times R(\mathbf{x}, \mathbf{r}) d\mathbf{x} d\mathbf{s} + \frac{\lambda}{\rho} \int R(\mathbf{x}, \mathbf{r}) d\mathbf{x}. \quad \dots\dots (6.8) \end{aligned}$$

The parameter λ is brought in by the restriction (6.4), the matrix R satisfying the equation

$$\begin{aligned} 2\delta(\mathbf{r} - \mathbf{x}) = & \int \left[\frac{1}{\rho^2} \psi_1(\mathbf{r}) F_1(\mathbf{r} - \mathbf{s}) + \frac{1}{\rho^2} \psi_2(\mathbf{r}) F_2(\mathbf{r} - \mathbf{s}) \right. \\ & \left. - 2 \frac{\xi}{\rho^2} F_2(\mathbf{r} - \mathbf{s}) - \frac{2}{\rho^2} \psi_2(\mathbf{r}) \theta(\mathbf{s}) \right] R(\mathbf{s}, \mathbf{x}) d\mathbf{s}, \quad \dots\dots (6.9) \end{aligned}$$

while F_1 , F_2 and θ are given by

$$F_1(\mathbf{r} - \mathbf{s}) = \frac{1}{8\pi^3} \int \frac{1}{\{1 - \psi(\mathbf{K})\}^2} e^{i\mathbf{K} \cdot (\mathbf{r} - \mathbf{s})} d\mathbf{K}, \quad \dots\dots (6.10)$$

$$F_2(\mathbf{r} - \mathbf{s}) = \frac{1}{8\pi^3} \int \frac{1}{\{1 + \psi(\mathbf{K})\}^2} e^{i\mathbf{K} \cdot (\mathbf{r} - \mathbf{s})} d\mathbf{K}, \quad \dots\dots (6.11)$$

$$\theta(\mathbf{s}) = \frac{1}{8\pi^3} \int \frac{2\psi(\mathbf{K})}{\{1 - \psi^2(\mathbf{K})\}^2} e^{-i\mathbf{K} \cdot \mathbf{s}} d\mathbf{K}. \quad \dots\dots (6.12)$$

Eqn (6.7), combined with (6.5) and (6.8) to (6.12), determines the probability 'amplitude' for a pair of particles to be at a certain distance from each other. The term $F(\mathbf{r}, \Phi)$ in this equation thus reflects the effect of all the other particles on the motion of the pair, and (6.7) is the extension of the Schrödinger equation for two particles in the presence of the rest.

§ 7. THE EXTENSION OF THE METHOD TO OTHER STATES

'Phonon' excitations are obtained by multiplying the parametric wave function by $\phi_F(\mathbf{K})$. This gives a wave function which is symmetric and orthogonal to the ground state and is roughly equivalent to multiplying the ground state wave function by $\sum_i \exp(i\mathbf{K} \cdot \mathbf{r}_i)$. Another class of excitations with integrable wave functions are obtained by using products of single body wave functions with the ground state wave functions. For example if one wished to describe a vortex line in liquid helium, the wave function of a single particle could be expected in cylindrical coordinates to be of the form $\exp(im\chi_i)f(\rho_1)$ where $f(\rho_1)$ vanishes at the origin and tends to unity at infinity, χ_1 is the azimuthal angle and m the angular quantum number. A trial many-body parametric wave function could then be

$$\int \prod_{\alpha} \exp(im\chi_{\alpha})f(\rho_{\alpha})\{1 + \phi(\mathbf{r}_{\alpha})\}Z(\phi)\delta\phi.$$

It will be seen that this is again integrable and an analysis parallel to §§ 4, 5, 6 can be performed leading to a pair of effective Schrödinger equations, a single body equation for f being the effective Schrödinger equation for a single particle in the presence of the vortex line, and a two body equation for ϕ being the Schrödinger equation for a pair of particles in the presence of all the others and the vortex line. For example if one considers the two particle correlation to be as in the ground state, then the analysis will lead to a one particle equation, which in cylindrical coordinates is of the form

$$\left\{ E + \frac{\partial^2}{\partial \rho^2} + \frac{1}{\rho} \frac{\partial}{\partial \rho} - \frac{m^2}{\rho^2} + H(\rho, \Phi) \right\} f(\rho) = 0,$$

where m is the quantum number associated with the vortex line and H is due to the effects of the rest of the particles on the one considered.

§ 8. CONCLUSION

We have shown that the method of parametric representation provides a fairly direct procedure for calculating the contribution of pair correlations to the energy of a system of Bose particles. The formulae (5.10) to (5.12) obtained for the ground state energy per particle are, naturally, the same as given by other authors (Girardeaux and Arnowitt 1959). There is a slight difference, relating to the normalization of the correlation function (see the remark at the end of § 5), between our results and those given previously, but this is probably of little importance so far as the applications of the formulae are concerned.

In § 6 we have considered the variational problem for the ground state energy from the point of view of the pair distribution function (6.5), and have shown that this leads to a Schrödinger type Eqn (6.7) for the square root of this quantity.

In the last section we have discussed the extensions of the method to excited states. A new feature here is that an explicit trial wave function corresponding to the presence of vortex lines in the many body system can be written down which would allow the integrations to be performed by the analysis developed in the previous sections. A variational calculation along the lines considered in § 6 would then lead to a pair of effective Schrödinger equations: a single body equation for the state of one particle, and a two body equation describing the state of a pair of particles in the presence of the vortex line and all the other particles.

APPENDIX

1. THE PAIR DISTRIBUTION FUNCTION

The wave function is

$$\Psi(\mathbf{r}_1 \dots \mathbf{r}_N) = \int \left[\prod_j \left\{ 1 + i\sqrt{2} \sum_{\mathbf{K}} (u_{\mathbf{K}} + iv_{\mathbf{K}}) \exp(i\mathbf{K} \cdot \mathbf{r}_j) \right\} \right. \\ \left. \times A \exp \left[-2 \sum_{\mathbf{K} > 0} \epsilon_{\mathbf{K}} (u_{\mathbf{K}}^2 + v_{\mathbf{K}}^2) \right] \delta(u_0) \right] \delta\phi, \quad (\text{A.1.1})$$

where $A = \prod_{\mathbf{K} < 0} 2\epsilon_{\mathbf{K}}/\pi$, and we have used the relation

$$\frac{\epsilon_0^{1,2}}{\pi^{1,2}} \exp(-\epsilon_0 u_0^2) \rightarrow \delta(u_0) \quad \text{as} \quad \epsilon_0 \rightarrow \infty. \quad \dots (\text{A.1.2})$$

Hence

$$\Psi^*(\mathbf{r}_1 \dots \mathbf{r}_N) = \int \left[\prod_j \left\{ 1 - i\sqrt{2} \sum_{\mathbf{K}} (x_{\mathbf{K}} - iy_{\mathbf{K}}) \exp(-i\mathbf{K} \cdot \mathbf{r}_j) / V^{1/2} \right\} \right. \\ \left. \times A \exp \left[-2 \sum_{\mathbf{K} > 0} \epsilon_{\mathbf{K}} (x_{\mathbf{K}}^2 + y_{\mathbf{K}}^2) \right] \delta(x_0) \right] \delta\psi, \quad \dots (\text{A.1.3})$$

where after taking the complex conjugate, different symbols $(x_{\mathbf{K}}, y_{\mathbf{K}})$ have been used for the integration variables.

Let

$$p(\mathbf{r}_1 \mathbf{r}_2) = \int \Psi^*(\mathbf{r}_1 \dots \mathbf{r}_N) \Psi(\mathbf{r}_1 \dots \mathbf{r}_N) d\mathbf{r}_3 \dots d\mathbf{r}_N. \quad (\text{A.1.4})$$

Substituting the expressions (A.1.1) and (A.1.3), carrying out the integrations over $\mathbf{r}_3 \dots \mathbf{r}_N$, and using the relation (4.6) and the even odd properties of $u_{\mathbf{K}}, x_{\mathbf{K}}, v_{\mathbf{K}}, y_{\mathbf{K}}$ we obtain

$$p(\mathbf{r}_1 \mathbf{r}_2) = \frac{(N-2)!}{2\pi i} \oint dz \exp[-(N-1) \log z + Vz] \int \left[\prod_{j=1}^2 \left\{ 1 + \frac{i\sqrt{2}}{V^{1/2}} u_0 \right. \right. \\ \left. \left. + i \frac{\sqrt{2}}{V^{1/2}} \sum_{\mathbf{K} \neq 0} (u_{\mathbf{K}} \cos \mathbf{K} \cdot \mathbf{r}_j - v_{\mathbf{K}} \sin \mathbf{K} \cdot \mathbf{r}_j) \right\} \right. \\ \left. \times \left\{ 1 - i\sqrt{2} \frac{x_0}{V^{1/2}} - i \frac{\sqrt{2}}{V^{1/2}} \sum_{\mathbf{K} \neq 0} (x_{\mathbf{K}} \cos \mathbf{K} \cdot \mathbf{r}_j - y_{\mathbf{K}} \sin \mathbf{K} \cdot \mathbf{r}_j) \right\} \right. \\ \left. \times \exp \left\{ i\sqrt{2} z V^{1/2} (u_0 - x_0) + 4z \sum_{\mathbf{K} > 0} (u_{\mathbf{K}} x_{\mathbf{K}} + v_{\mathbf{K}} y_{\mathbf{K}}) + 2u_0 x_0 z \right. \right. \\ \left. \left. - 2 \sum_{\mathbf{K} > 0} \epsilon_{\mathbf{K}} (u_{\mathbf{K}}^2 + x_{\mathbf{K}}^2 + v_{\mathbf{K}}^2 + y_{\mathbf{K}}^2) \right\} \delta(u_0) \delta(x_0) \right] A^2 \delta\phi \delta\psi. \quad \dots (\text{A.1.5})$$

Because of the δ functions in u_0 and x_0 the integration over these variables can be carried out, with the result that those terms which have these numbers as

powers drop out of the expression and those which have them in the exponent are put equal to one. As in the previous calculations we make the transformation

$$\begin{aligned}\theta_{\mathbf{K}} &= \frac{u_{\mathbf{K}} + x_{\mathbf{K}}}{\sqrt{2}}, & \mu_{\mathbf{K}} &= \frac{v_{\mathbf{K}} + y_{\mathbf{K}}}{\sqrt{2}}, \\ \eta_{\mathbf{K}} &= \frac{u_{\mathbf{K}} - x_{\mathbf{K}}}{\sqrt{2}}, & \nu_{\mathbf{K}} &= \frac{v_{\mathbf{K}} - y_{\mathbf{K}}}{\sqrt{2}},\end{aligned}$$

and obtain p in terms of these variables as

$$\begin{aligned}p(\mathbf{r}_1, \mathbf{r}_2) &= \frac{(N-2)!}{2\pi i} \oint dz \exp[-(N-1)\log z + Vz] \int \prod_{j=1}^2 \left[1 + \frac{4i}{V^{1/2}}\right. \\ &\quad \times \sum_{\mathbf{K}>0} (\eta_{\mathbf{K}} \cos \mathbf{K} \cdot \mathbf{r}_j - \nu_{\mathbf{K}} \sin \mathbf{K} \cdot \mathbf{r}_j) + \frac{4}{V} \left\{ \sum_{\mathbf{K}>0} (\theta_{\mathbf{K}} \cos \mathbf{K} \cdot \mathbf{r}_j - \mu_{\mathbf{K}} \sin \mathbf{K} \cdot \mathbf{r}_j) \right\}^2 \\ &\quad \left. - \frac{4}{V} \left\{ \sum_{\mathbf{K}>0} (\eta_{\mathbf{K}} \cos \mathbf{K} \cdot \mathbf{r}_j - \nu_{\mathbf{K}} \sin \mathbf{K} \cdot \mathbf{r}_j) \right\}^2 \right] \exp \left\{ -2 \sum_{\mathbf{K}>0} (\epsilon_{\mathbf{K}} + z) \right. \\ &\quad \times (\eta_{\mathbf{K}}^2 + \nu_{\mathbf{K}}^2) - 2 \sum_{\mathbf{K}>0} (\epsilon_{\mathbf{K}} - z)(\mu_{\mathbf{K}}^2 + \theta_{\mathbf{K}}^2) \Big\} A^2 \prod_{\mathbf{K}>0} \delta \eta_{\mathbf{K}} \delta \theta_{\mathbf{K}} \delta \mu_{\mathbf{K}} \delta \nu_{\mathbf{K}}. \\ &\dots\dots (A.1.6)\end{aligned}$$

The evaluation of the functional integral is simplified by the further transformation to 'polar' variables:

$$\begin{aligned}\theta_{\mathbf{K}} &= r_{\mathbf{K}} \cos \phi_{\mathbf{K}}, & \eta_{\mathbf{K}} &= s_{\mathbf{K}} \cos \lambda_{\mathbf{K}}, \\ \mu_{\mathbf{K}} &= r_{\mathbf{K}} \sin \phi_{\mathbf{K}}, & \nu_{\mathbf{K}} &= s_{\mathbf{K}} \sin \lambda_{\mathbf{K}}.\end{aligned}$$

Expanding the product in (A.1.6) and dropping some of the terms which vanish on integrating over the angles $\phi_{\mathbf{K}}, \lambda_{\mathbf{K}}$ we obtain

$$\begin{aligned}p(\mathbf{r}_1, \mathbf{r}_2) &= \frac{(N-2)!}{2\pi i} \oint dz \exp[-(N-1)\log z + Vz] \\ &\quad \times \int \left[1 + \frac{4}{V} \left\{ \sum_{\mathbf{K}>0} r_{\mathbf{K}} \cos(\phi_{\mathbf{K}} + \mathbf{K} \cdot \mathbf{r}) \right\}^2 - \frac{4}{V} \left\{ \sum_{\mathbf{K}>0} s_{\mathbf{K}} \cos(\lambda_{\mathbf{K}} + \mathbf{K} \cdot \mathbf{r}) \right\}^2 \right. \\ &\quad + \frac{4}{V} \left\{ \sum_{\mathbf{K}>0} r_{\mathbf{K}} \cos(\phi_{\mathbf{K}} + \mathbf{K} \cdot \mathbf{r}_2) \right\}^2 - \frac{4}{V} \left\{ \sum_{\mathbf{K}>0} s_{\mathbf{K}} \cos(\lambda_{\mathbf{K}} + \mathbf{K} \cdot \mathbf{r}_2) \right\}^2 \\ &\quad - \frac{16}{V} \left\{ \sum_{\mathbf{K}>0} s_{\mathbf{K}} \cos(\lambda_{\mathbf{K}} + \mathbf{K} \cdot \mathbf{r}_1) \right\} \left\{ \sum_{\mathbf{K}>0} s_{\mathbf{K}} \cos(\lambda_{\mathbf{K}} + \mathbf{K} \cdot \mathbf{r}_2) \right\} \\ &\quad + \frac{16}{V^2} \left\{ \sum_{\mathbf{K}>0} r_{\mathbf{K}} \cos(\phi_{\mathbf{K}} + \mathbf{K} \cdot \mathbf{r}_1) \right\}^2 \left\{ \sum_{\mathbf{K}>0} r_{\mathbf{K}} \cos(\phi_{\mathbf{K}} + \mathbf{K} \cdot \mathbf{r}_2) \right\}^2 \\ &\quad + \frac{16}{V^2} \left\{ \sum_{\mathbf{K}>0} s_{\mathbf{K}} \cos(\lambda_{\mathbf{K}} + \mathbf{K} \cdot \mathbf{r}) \right\}^2 \left\{ \sum_{\mathbf{K}>0} s_{\mathbf{K}} \cos(\lambda_{\mathbf{K}} + \mathbf{K} \cdot \mathbf{r}_2) \right\}^2 \\ &\quad - \frac{16}{V^2} \left\{ \sum_{\mathbf{K}>0} r_{\mathbf{K}} \cos(\phi_{\mathbf{K}} + \mathbf{K} \cdot \mathbf{r}_1) \right\}^2 \left\{ \sum_{\mathbf{K}>0} s_{\mathbf{K}} \cos(\lambda_{\mathbf{K}} + \mathbf{K} \cdot \mathbf{r}_2) \right\}^2 \\ &\quad \left. - \frac{16}{V^2} \left\{ \sum_{\mathbf{K}>0} s_{\mathbf{K}} \cos(\lambda_{\mathbf{K}} + \mathbf{K} \cdot \mathbf{r}_1) \right\}^2 \left\{ \sum_{\mathbf{K}>0} r_{\mathbf{K}} \cos(\phi_{\mathbf{K}} + \mathbf{K} \cdot \mathbf{r}_1) \right\}^2 \right] \\ &\quad \times \exp \left\{ -2 \sum_{\mathbf{K}>0} (\epsilon_{\mathbf{K}} - z) r_{\mathbf{K}}^2 - 2 \sum_{\mathbf{K}>0} (\epsilon_{\mathbf{K}} + z) s_{\mathbf{K}}^2 \right\} \\ &\quad \times A^2 \prod_{\mathbf{K}>0} r_{\mathbf{K}} \delta \phi_{\mathbf{K}} \delta r_{\mathbf{K}} s_{\mathbf{K}} \delta \lambda_{\mathbf{K}} \delta s_{\mathbf{K}}. \\ &\dots\dots (A.1.7)\end{aligned}$$

The remaining calculation is straightforward, the work consists in picking out those terms which do not vanish on angular integrations. Ignoring the difference between N and $N-2$ the equation for the stationary phase is the same as in the previous calculations, and one obtains

$$\begin{aligned} p(\mathbf{r}_1, \mathbf{r}_2) = & \left[\left\{ 1 - \frac{1}{V} \sum_{\mathbf{K} > 0} \frac{1}{(\epsilon_{\mathbf{K}} - \xi)} - \frac{1}{(\epsilon_{\mathbf{K}} + \xi)} \right\}^2 - \frac{4}{V} \sum_{\mathbf{K} > 0} \frac{1}{(\epsilon_{\mathbf{K}} + \xi)} \cos \mathbf{K} \cdot (\mathbf{r}_1 - \mathbf{r}_2) \right. \\ & + \frac{2}{V^2} \left\{ \sum_{\mathbf{K} > 0} \frac{1}{(\epsilon_{\mathbf{K}} - \xi)} \cos \mathbf{K} \cdot (\mathbf{r}_1 - \mathbf{r}_2) \right\}^2 + \frac{2}{V^2} \left\{ \sum_{\mathbf{K} > 0} \frac{1}{(\epsilon_{\mathbf{K}} + \xi)} \cos \mathbf{K} \cdot (\mathbf{r}_1 - \mathbf{r}_2) \right\}^2 \Big] \\ & \times \frac{(N-2)!}{\{2\pi f''(\xi)\}^{1/2}} e^{V\xi} \frac{1}{\xi^{N-1}} \prod_{\mathbf{K}} \frac{\epsilon_{\mathbf{K}}^2}{(\epsilon_{\mathbf{K}}^2 - \xi^2)}. \end{aligned} \quad \text{..... (A.1.8)}$$

Taking $g(\mathbf{K})$ as the inverse of $\epsilon(\mathbf{K})$, using the even property of these functions, and changing from summations to integrations we have

$$\begin{aligned} p(\mathbf{r}_1, \mathbf{r}_2) = & \left[\left\{ 1 + \frac{\xi}{8\pi^3} \int \frac{g_{\mathbf{F}}^2}{1 - \xi^2 g_{\mathbf{F}}^2} d\mathbf{K} \right\}^2 - \frac{2}{8\pi^3} \int \frac{g_{\mathbf{F}}}{1 + \xi g_{\mathbf{F}}} \exp [i\mathbf{K} \cdot (\mathbf{r}_1 - \mathbf{r}_2)] d\mathbf{K} \right. \\ & + \frac{1}{2} \left\{ \frac{1}{8\pi^3} \int \frac{g_{\mathbf{F}}}{1 - \xi g_{\mathbf{F}}} \exp [i\mathbf{K} \cdot (\mathbf{r}_1 - \mathbf{r}_2)] d\mathbf{K} \right\}^2 + \frac{1}{2} \left\{ \frac{1}{8\pi^3} \int \frac{g_{\mathbf{F}}}{1 + \xi g_{\mathbf{F}}} \right. \\ & \times \exp [i\mathbf{K} \cdot (\mathbf{r}_1 - \mathbf{r}_2)] d\mathbf{K} \Big\}^2 \frac{(N-2)!}{\{2\pi f''(\xi)\}^{1/2}} e^{V\xi} \prod_{\mathbf{K}=-\infty}^{\infty} \frac{1}{\{1 - \xi^2 g_{\mathbf{F}}^2(\mathbf{K})\}^{1/2}}. \end{aligned} \quad \text{..... (A.1.9)}$$

Thus from (5.2), (4.17), (5.8) and (5.12) we obtain the pair distribution function as

$$M(\mathbf{r}_1, \mathbf{r}_2) = \frac{\xi^2}{2} \left\{ \frac{\rho^2}{\xi^2} - 2g_2(\mathbf{r}_1 - \mathbf{r}_2) + \frac{1}{2}g_1^2(\mathbf{r}_1 - \mathbf{r}_2) + \frac{1}{2}g_2^2(\mathbf{r}_1 - \mathbf{r}_2) \right\}. \quad \text{..... (A.1.10)}$$

2. THE RESTRICTION (6.4)

If we use the product type function (3.13) as a trial wave function, then there is no loss of generality in requiring $g(\mathbf{r})$ to satisfy a restriction of type (6.4). This can be seen as follows:

Let

$$\int g(\mathbf{r}) d\mathbf{r} = \lambda, \quad \text{..... (A.2.1)}$$

and write (3.13) as

$$\Psi_{\mathbf{P}} = \left(1 + \frac{\lambda}{V} \right)^{N(N-1)/2} \prod_{i < j} \{ 1 - u(\mathbf{r}_{ij}) \}, \quad \text{..... (A.2.2)}$$

where

$$u(\mathbf{r}) = \frac{g(\mathbf{r}) - \lambda/V}{1 + \lambda/V}. \quad \text{..... (A.2.3)}$$

Evidently u satisfies a restriction of type (6.4), that is

$$\int u(\mathbf{r}) d\mathbf{r} = 0. \quad \text{..... (A.2.4)}$$

Now in calculating the energy, the constant factor $(1 - \lambda/V)^{N(N-1)/2}$ cancels from the numerator and denominator of (4.2), hence the equations have the same form with respect to u as they have with respect to g .

In view of the relation between our wave function (3.1) and the product type, the above considerations suggest that the use of the restriction (6.4) in the calculation of the formulae is not a serious shortcoming. As we have already shown (see the calculations of §4) this restriction could be relaxed but the formulae would then become more cumbersome.

ACKNOWLEDGMENTS

We wish to thank Professor B. H. Flowers for several discussions. One of us (M. A. N.) would like to acknowledge a Turner and Newall Fellowship during the tenure of which this work was carried out.

REFERENCES

- BOGOLIUBOV, N. N., 1947, *J. Phys. (U.S.S.R.)*, **11**, 23.
BOGOLIUBOV, N. N., and SHIRKOV, D., 1959, *Introduction to the Theory of Quantized Fields* (New York : Interscience).
GIRARDEAUX, M., and ARNOWITT, R., 1959, *Phys. Rev.*, **113**, 755.
HUANG, K., 1958, *The Many Body Problem* (London: Methuen).
VALATIN, J. G., and BUTLER, D., 1958, *Nuovo Cim.*, **10**, 37.

An Approximate Method for the Calculation of Multipole Polarizabilities of Atoms

By A. L. STEWART

Department of Physics, The Queen's University of Belfast†

MS. received 3rd August 1960

Abstract. The method devised by Vinti in 1932 is modified to calculate values of the multipole polarizabilities and nuclear quadrupole shielding factors of the two electron systems. The results are used to compute the long range interaction energy curve for a proton and a helium atom.

VALUES of the dipole, field gradient quadrupole and higher order multipole polarizabilities of atoms and ions are required in many connections but their estimation by conventional quantum mechanical methods is a formidable task even for simple two-electron atomic systems (Baber and Hassé 1937, Dalgarno, Davison and Stewart 1960). Thus there has been a persistent search for methods which permit rapid calculation of these quantities (Dalgarno and Lewis 1957, Allen 1960).

The problem is essentially the evaluation of the matrix element sum

$$S = \sum_{\substack{n, \\ n \neq 0}} (E_0 - E_n)^{-1} (\phi_0, h_1 \phi_n) (\phi_n, h_2 \phi_0) \quad \dots\dots (1)$$

for a many electron atom with energy eigenvalues E_n , in rydbergs, and associated eigenfunctions ϕ_n , the perturbations h_1 and h_2 being functions of the electron coordinates expressed in atomic units. This expression may be related, using the Unsöld (1927) approximation, to the matrix element sum

$$T = \sum_{\substack{n, \\ n \neq 0}} (\phi_0, h_1 \phi_n) (\phi_n, h_2 \phi_0) = (\phi_0, h_1 h_2 \phi_0) - (\phi_0, h_1 \phi_0) (\phi_0, h_2 \phi_0) \quad \dots\dots (2)$$

giving

$$S \simeq \epsilon^{-1} T, \quad \dots\dots (3)$$

where ϵ is an average value of $E_0 - E_n$. In the same way the sum

$$U = \sum_{\substack{n, \\ n \neq 0}} (E_0 - E_n) (\phi_0, h_1 \phi_n) (\phi_n, h_2 \phi_0) \quad \dots\dots (4)$$

may be evaluated by the Unsöld method, which yields

$$U \simeq \epsilon_1 T \quad \dots\dots (5)$$

where ϵ_1 is a second average value of $E_0 - E_n$, or expressed exactly as (Dalgarno and Lewis 1955)

$$U = \left(\phi_0, h_1 \sum_i \left\{ \nabla_i^2 h_2 + 2 \nabla_i h_2 \cdot \nabla_i \right\} \phi_0 \right) - \left(\phi_0, h_1 \phi_0 \right) \left(\phi_0, \sum_i \left\{ \nabla_i^2 h_2 + 2 \nabla_i h_2 \cdot \nabla_i \right\} \phi_0 \right), \quad \dots\dots (6)$$

† Now at Department of Applied Mathematics, The Queen's University of Belfast.

where the suffix i specifies the coordinates of the i th electron. Some manipulation then of (3), (5) and (6) gives

$$S \simeq \epsilon_1 \epsilon^{-1} U^{-1} T^2, \quad \dots\dots (7)$$

which is a generalization of the expression derived by Vinti (1932) for the special case of the optical dipole oscillator strength sum.

If we follow Vinti and set the disposable parameter $\epsilon_1 \epsilon^{-1}$ equal to the constant unity then Eqn (7) simply states that T is the geometric mean of S and U . Although $\epsilon_1 \epsilon^{-1}$ will in general not be unity it will almost certainly be adequately represented by a constant, the zero-order term in its expression as a power series in ζ^{-1} , where ζ is the charge on the atomic nucleus, by virtue of its form as a ratio of two similar quantities. Thus we assume

$$\epsilon_1 \epsilon^{-1} \simeq (\epsilon_1 \epsilon^{-1})_0 = S_0 U_0 T_0^{-2}, \quad \dots\dots (8)$$

where the suffix zero indicates the zero-order term in the expansion of each of the quantities as a power series in ζ^{-1} , and (7) becomes

$$S \simeq (S_0 U_0 T_0^{-2}) U^{-1} T^2, \quad \dots\dots (9)$$

each term of which is easily calculated.

To assess the accuracy of Eqn (9) it is used to estimate the multipole polarizabilities α_l and nuclear quadrupole shielding factors γ_∞ of the ground states of the two-electron systems by inserting in (1), (2) and (4)

$$h_1 = h_2 = r_1^l P_l(\cos \theta_1) + r_2^l P_l(\cos \theta_2), \quad S = -\frac{1}{4} \alpha_l$$

and

$$h_1 = r_1^{-3} P_2(\cos \theta_1) + r_2^{-3} P_2(\cos \theta_2), \quad h_2 = r_1^2 P_2(\cos \theta_1) + r_2^2 P_2(\cos \theta_2), \quad S = -\frac{1}{4} \gamma_\infty,$$

respectively, (r_i, θ_i, ϕ_i) being the electron coordinates in polar form. For this purpose it would be misleading to adopt for ϕ_0 a more complex representation than that usually employed in calculations using conventional methods and so we take

$$\phi_0 = \frac{N^2}{4\pi} \{ \exp(-Zr_1) + c \exp(-kZr_1) \} \{ \exp(-Zr_2) + c \exp(-kZr_2) \} \quad \dots\dots (10)$$

in which the variational parameters Z , c and k have been determined by Green *et al.* (1954). The relevant values of S_0 are taken from the papers of Dalgarno and Stewart (1956) and Dalgarno, Davison and Stewart (1960).

The results for the dipole polarizability α_1 , field gradient quadrupole polarizability α_2 and nuclear quadrupole shielding factor γ_∞ are presented in the first columns of Tables 1, 2 and 4 respectively where they are compared with the estimates based on Eqn (10) using conventional methods (Das and Bersohn 1956, Wikner and Das 1957) in the second columns and with the very precise values of Dalgarno and Stewart (1960) displayed in the third columns. These last are computed from the perturbation series, based on zero-order screened hydrogen-like orbitals, with an additional term added so that the very accurate values measured by Essen (1953) and computed by Dalgarno, Davison and Stewart (1960) for helium are reproduced. The higher order multipole polarizabilities are given in Table 3.

The comparison shows that Eqn (9) predicts values for the dipole and quadrupole polarizabilities which are at least as accurate as those given by the conventional method based on the same field free wave functions (10). The

values predicted for the screening factor are not so good, almost certainly because Eqn (8) gives a poor estimate of $\epsilon_1\epsilon^{-1}$. This is apparent since for this case $(\epsilon_1\epsilon^{-1})_0 = 10.3$ which, being very different from unity, shows that ϵ_1 and ϵ are quite dissimilar.

Table 1. The Dipole Polarizabilities α_1 of the Helium Iso-electronic Sequence (in units of a_0^3)

Atom	Eqn (9)	Wikner and Das	Dalgarno and Stewart†
H ⁻	83.54	100.4	95.09
He	1.387	1.47	1.390
Li ⁺	0.1981	0.206	0.1936
Be ²⁺	0.05374	0.0549	0.05247
B ³⁺	0.02016	0.0211	0.01969
C ⁴⁺	0.009162	—	0.008980

$$\dagger \alpha_1 = 9(\zeta - 0.359375)^{-4} + 2.879(\zeta - 0.359375)^{-6}.$$

Table 2. The Field Gradient Quadrupole Polarizabilities α_2 of the Helium Iso-electronic Sequence (in units of a_0^5)

Atom	Eqn (9)	Das and Bersohn	Dalgarno and Stewart†
H ⁻	1493	1614	1499
He	2.208	2.29	2.270
Li ⁻	0.1099	0.113	0.1112
Be ²⁺	0.01503	0.0152	0.01514
B ³⁺	0.003382	0.00342	0.003402
C ⁴⁺	0.001027	—	0.001031

$$\dagger \alpha_2 = 30(\zeta - 0.450564)^{-6} + 3.39(\zeta - 0.450564)^{-8}.$$

Table 3. Octupole and Higher Order Polarizabilities of the Helium Iso-electronic Sequence (Eqn (9))

Atom	$\alpha_3(a_0^7)$	$\alpha_4(a_0^9)$	$\alpha_5(a_0^{11})$
H ⁻	6.500×10^4	5.036×10^6	6.101×10^8
He	9.186	70.51	855.6
Li ⁺	0.1605	0.4341	1.859
Be ²⁺	0.01107	0.01511	0.03268
B ³⁺	0.001498	0.001228	0.001596
C ⁴⁺	0.0003031	0.0001658	0.0001437

Table 4. The Nuclear Quadrupole Shielding Factors γ_∞ of the Helium Iso-electronic Sequence

Atom	Eqn (9)	Das and Bersohn	Dalgarno and Stewart†
H ⁻	0.6597	1.141	1.005
He	0.3354	0.416	0.3970
Li ⁺	0.2240	0.256	0.2484
Be ²⁺	0.1678	0.185	0.1809
B ³⁺	0.1341	0.145	0.1422
C ⁴⁺	0.1117	—	0.1172

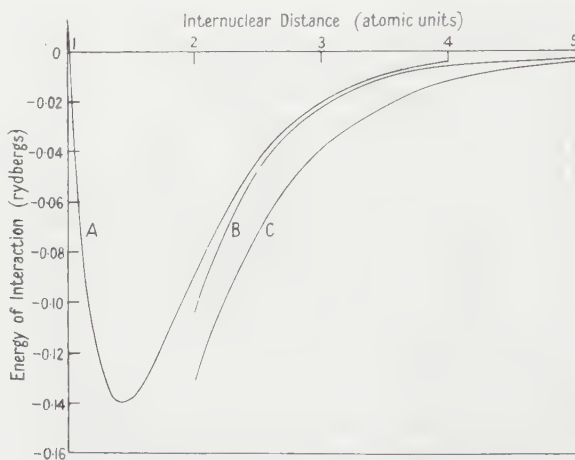
$$\dagger \gamma_\infty = 0.6667(\zeta - 0.309221)^{-1} + 0.01305(\zeta - 0.309221)^{-3}.$$

Kyle and Merzbacher (1960) have recently presented a method for summing (1) when h_1 and h_2 are the interaction energy between a proton and an atom. Their method yielded useful results for hydrogen but they concluded that their method failed for helium. If in (1) we let h_1 and h_2 be the interaction energy between a

proton and a helium atom and expand the interaction in inverse powers of the nuclear separation R we get

$$S = E_2 = - \sum_{l=1}^{\infty} \frac{\alpha_l}{R^{2l+2}}, \quad \dots\dots (11)$$

where E_2 is the interaction energy to second order. Using the values for the polarizabilities presented in Tables 1, 2 and 3 this semi-divergent series can be summed for any value of R and so the method presented in this note is applicable to the problem considered by Kyle and Merzbacher. The computed interaction energy curve is displayed in curve B of the Figure together with the total interaction energy curves, A and C, favoured by Fallon, Mason and Vanderslice (1960) for small and large nuclear separations respectively and which are based in part on experimental scattering data. It is considered unlikely that the



Energy of interaction between a proton and a helium atom.

difference between curves B and C, the latter being considered more reliable than curve A at large internuclear distances, at separations greater than four atomic units, is due to the use of the harmonic expansion of h_1 and h_2 to obtain (11) or to the neglect of higher order interactions.

REFERENCES

- ALLEN, L. C., 1960, *Phys. Rev.*, **118**, 167.
 BABER, T. D., and HASSÉ, H. R., 1937, *Proc. Camb. Phil. Soc.*, **33**, 253.
 DALGARNO, A., DAVISON, W. D., and STEWART, A. L., 1960, *Proc. Roy. Soc. A*, **257**, 115.
 ———, 1957, *Proc. Roy. Soc. A*, **240**, 284.
 DALGARNO, A., and STEWART, A. L., 1956, *Proc. Roy. Soc. A*, **238**, 276.
 ———, 1960, *Proc. Roy. Soc. A*, **257**, 534.
 DAS, T. P., and BERSOHN, R., 1956, *Phys. Rev.*, **102**, 733.
 ESSEN, L., 1953, *Proc. Phys. Soc. B*, **66**, 189.
 FALLON, R. J., MASON, E. A., and VANDERSLICE, J. T., 1960, *Astrophys. J.*, **131**, 12.
 GREEN, L. C., MULDER, M. M., LEWIS, M. N., and WOLL, J. W., 1954, *Phys. Rev.*, **93**, 757.
 KYLE, H. L., and MERZBACHER, E., 1960, *Proc. Phys. Soc.*, **75**, 164.
 UNSÖLD, A., 1927, *Z. Phys.*, **43**, 563.
 VINTI, J. P., 1932, *Phys. Rev.*, **41**, 813.
 WIKNER, E. G., and DAS, T. P., 1957, *Phys. Rev.*, **107**, 497.

A Lattice Model of a Classical Hard Sphere Gas: II

By D. M. BURLEY†

Mathematics Department, University of Glasgow

Communicated by C. Domb; MS. received 27th June 1960.

Abstract. It was shown in a previous publication that the antiferromagnetic Ising model could be transformed into a model of a hard sphere lattice gas. It was seen that, for the model on the loose packed lattices, a transition from an ordered to a disordered phase was suggested. No firm results could be obtained, however, since the approximation used for the ordered phase was inadequate. It is now shown that the pressure and free energy curves of both phases can be calculated on the Bethe and 'ring' approximations. In each case a transition is shown to occur and to be of the second order.

§ 1. ORDERED PHASE ON THE BETHE APPROXIMATION

1.1. Introduction

IN a previous publication (Burley 1960, referred to as I hereafter), the transformation of the antiferromagnetic Ising model to a simple lattice model of a hard sphere gas was considered. It was found that for loose packed lattices, two regions, one ordered and the other disordered, were necessary to describe the whole range of densities. The treatment of the disordered phase was found to be satisfactory and it was shown that this phase could be studied on various approximate methods and also from exact series expansions. For the ordered phase, a simple approximation was used and was found to be unsatisfactory since although a phase transition appeared to be necessary no firm results could be obtained.

In this paper, it is shown that the ordered phase can be treated on both the Bethe and ring approximations. Comparisons are then made to the same degree of approximation and in each case a second-order transition is noted.

1.2. Derivation of Basic Equations

The simplest approximation used in I was the Bethe approximation. The problem of calculating the partition function and thermodynamic properties of the Ising model of an antiferromagnetic on this approximation was studied originally by Easthope (1937) and in more detail by Ziman (1951) and Kasteleijn (1956). Although their results could be used, they are not in a convenient form for the lattice gas problem, so the method and notation of Kikuchi (1951) will be used to derive the required equations. The method used here is a simple extension of Kikuchi's method and hence various steps in the analysis will be omitted.

The extension of the method is to divide the lattice, with coordination number q , into two inter-penetrating sub-lattices, which will be called lattice 1 and lattice 2. The different configurations to be considered must now be treated in relation to the sub-lattice on which the systems, making up the configuration, occur. The probabilities of occurrence of the configurations, required for the Bethe approximation, are set out in Tables 1 and 2.

† Now at Department of Applied Mathematics, The University, Sheffield 10.

Table 1

Config.	Lattice	Prob.
+	1	x_1
-	1	x_2
+	2	x_3
-	2	x_4

Table 2

Config.		Lattice 2	Prob.
Lattice 1			
+	—————	+	y_1
+	—————	-	y_2
-	—————	+	y_3
-	—————	-	y_4

By definition these probabilities are not independent and the following connecting relations can be written down immediately

$$\left. \begin{aligned} x_1 + x_2 &= 1 & x_1 &= y_1 + y_2 & x_3 &= y_1 + y_3 \\ x_2 &= y_3 + y_4 & x_4 &= y_2 + y_4 \end{aligned} \right\} \dots\dots (1)$$

These five equations are independent and can be seen to imply $x_3 + x_4 = 1$. Thus among the eight variables x_i and y_i there are three independent variables which may be taken most conveniently as $x_1 - x_2$, $x_3 - x_4$ and $y_2 + y_3$.

For a lattice, with coordination number q , consisting of N points, the entropy S , and the energy E , of the assembly can be written

$$S/kN = \frac{1}{2}(q-1) \sum_{i=1}^4 x_i \ln x_i - \frac{1}{2}q \sum_{i=1}^4 y_i \ln y_i$$

and

$$E/N = \frac{1}{2}q\epsilon(2y_2 + 2y_3 - 1) + \frac{1}{2}mH(x_1 - x_2 + x_3 - x_4)$$

where ϵ is the interaction energy between neighbouring spins, m is the magnetic moment of a single spin and H is the external magnetic field. The entropy here is calculated on the assumption that the probabilities of occurrence of larger configurations depend exactly on the probabilities shown in Tables 1 and 2. The free energy can now be calculated from the equation

$$F = E - ST$$

and minimizing it with respect to the three independent variables gives the following basic equations

$$\left. \begin{aligned} \mu &= \left(\frac{x_2}{x_1} \right)^{q-1} \left(\frac{y_1 y_2}{y_3 y_4} \right)^{q/2} = \left(\frac{x_4}{x_3} \right)^{q-1} \left(\frac{y_1 y_3}{y_2 y_4} \right)^{q/2} \\ z^4 &= y_2 y_3 / y_1 y_4 \end{aligned} \right\} \dots\dots (2)$$

where $z = \exp(-\epsilon/kT)$ and $\mu = \exp(-2mH/kT)$. The free energy can then be calculated as

$$-F/NkT = -\frac{1}{2}q \ln z + \frac{1}{4}(q-1) \ln(x_1 x_2 x_3 x_4) - \frac{1}{4}q \ln(y_1 y_4) \dots\dots (3)$$

and the magnetization as

$$I/I_0 = y_4 - y_1 \dots\dots (4)$$

where I_0 is the magnetization at absolute zero.

1.3. Lattice Gas Problem

It is now necessary to convert the antiferromagnetic Ising model to the lattice gas model used in I. This was achieved by noticing that as $T \rightarrow 0$, $\mu \rightarrow 0$ and $z \rightarrow \infty$ (since $\epsilon < 0$) while $\omega = \mu z^{2q}$ (as defined here) remains finite. It was then shown that neglect of all terms of order μ or z^{-1} and retaining only terms in ω , implied that no two positive spins could be neighbours on the

lattice, which in the notation of Table 2 implies that $y_1=0$. From Eqn (2) it can be seen that putting $y_1=0$ satisfies the conditions $\mu \rightarrow 0$ and $z \rightarrow \infty$, and calculating $\omega = z^{2q}$ gives the two equations

$$\omega = \left(\frac{x_2}{x_1}\right)^{q-1} \left(\frac{y_2}{y_4}\right)^q = \left(\frac{x_4}{x_3}\right)^{q-1} \left(\frac{y_3}{y_4}\right)^q. \quad \dots\dots (5)$$

If we put $y_1=0$ in (1) and let $\alpha = y_2/y_4$, $\beta = y_3/y_4$ and $x_1' = x_1/y_4$ etc., then

$$\left. \begin{aligned} x_1' &= \alpha, & x_2' &= 1 + \beta, & x_3' &= \beta, & x_4' &= 1 + \alpha \\ y_4 &= (1 + \alpha + \beta)^{-1}. \end{aligned} \right\} \quad \dots\dots (6)$$

Substitution of these values into the right-hand side of (5) gives

$$x(1-\beta)^{q-1} = \beta(1-x)^{q-1} \quad \dots\dots (7)$$

and the proportion of molecules present in the gas is given by x where

$$2x = 1 - I/I_0 = (\alpha + \beta)/(1 + \alpha + \beta). \quad \dots\dots (8)$$

The pressure of the lattice gas can be calculated from the free energy of the antiferromagnetic (3) as

$$P/kT = \frac{1}{2}(q-1) \ln(x_2 x_4) - \frac{1}{2}q \ln y_4. \quad \dots\dots (9)$$

To study the case where $y_1=0$, it is now required to calculate α and β (in terms of x) from (7) and (8) and then to substitute into (9). It is not easy to solve (7) in general but considering first the simple quadratic lattice, $q=4$, the equation gives

$$(\alpha - \beta)[\alpha\beta(3 + \alpha + \beta) - 1] = 0. \quad \dots\dots (10)$$

The first factor in this equation gives $x = \beta$ and leads to the disordered phase discussed in I, while the second factor leads to the ordered phase. For this phase (8) and (10) give

$$\alpha + \beta = \frac{2x}{1-2x}, \quad \alpha\beta = \frac{1-2x}{3-4x} \quad \dots\dots (11)$$

which gives on substitution

$$P/kT = -\frac{1}{2} \ln(1-2x) + 3 \ln 2(1-x) - \frac{3}{2} \ln(3-4x). \quad \dots\dots (12)$$

This function has been calculated independently by Dr. H. N. V. Temperley (private communication).

For values of q larger than four, Eqn (7) is more difficult to solve but in the simple cubic case, $q=6$, a similar analysis gives

$$\begin{aligned} P/kT = & -3 \ln(1-2x) + 5 \ln 2(1-x) - (5/2) \ln 2(5-6x) \\ & + (5/2) \ln \{(5-8x) - (5-16x+16x^2)^{1/2}\}. \end{aligned} \quad \dots\dots (13)$$

1.4. The Transition Points

It was pointed out in I that the transition point, if one occurs, must be obtained from the intersection of the free energy curves of the two phases. The free energy can be calculated from the pressure by

$$F/MkT = \int \frac{P}{kT} \frac{dx}{x^2} \quad \dots\dots (14)$$

where M is the number of molecules of the gas present. (It should be noted here that in I in Eqns (15) and (18) and in Fig. 6, m should be replaced by M . Also in the expansion given in Eqn (10) the first term should be $-x \ln x$.)

For $q=4$, the integrations can be performed easily and give for the disordered phase

$$F/MkT = \frac{1}{x} \{x \ln x - 3(1-x) \ln(1-x) + 2(1-2x) \ln(1-2x)\} \quad \dots\dots (15)$$

and for the ordered phase

$$F/MkT = \frac{1}{2x} \{(1-2x) \ln(1-2x) - 6(1-x) \ln 2(1-x) + (3-4x) \ln(3-4x)\} \quad \dots\dots (16)$$

The integration for $q=6$ can also be performed but since the results are essentially the same as the case $q=4$, they will not be reproduced.

The graph of the free energies determined by (15) and (16) is shown in Fig. 1, and the graph for the pressure, from (12) and the corresponding equation in I, in Fig. 2.

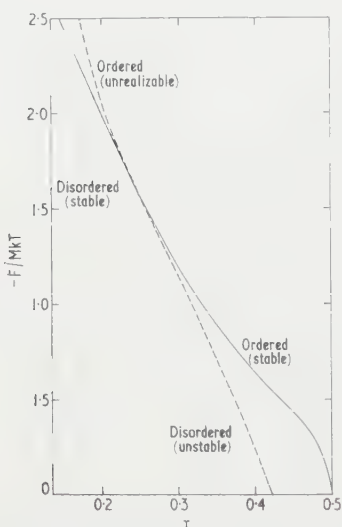


Fig. 1. Simple quadratic lattice, free energy plotted against number density for the Bethe approximation.

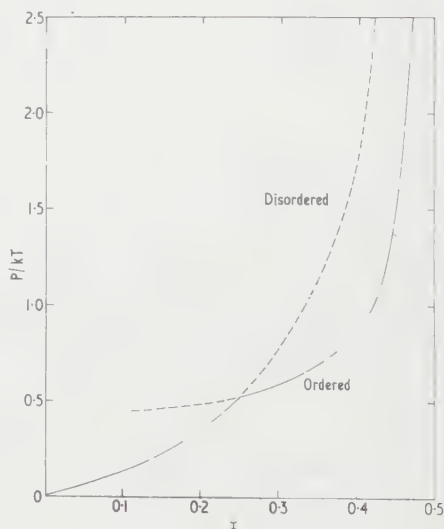


Fig. 2. Simple quadratic lattice, pressure plotted against number density for the Bethe approximation.

Two significant facts may be noted from Fig. 1. The first is that the two curves touch at $x=0.25$. This is easily proved to be the case since the free energies and the pressures are equal at this point, and since the pressure is effectively the gradient of the free energy curve, the two curves must touch. The second fact that can be deduced from Fig. 1 is that the free energy of the ordered phase is always less than or equal to that of the disordered phase and hence the ordered phase is always more stable. It will now be shown, however, that for $x < 0.25$ the ordered phase is physically unrealizable. Remembering the definitions $\alpha = y_2/y_4$ and $\beta = y_3/y_4$, it may be observed that these parameters represent measurable quantities and hence must be real. From (11) since α and β are the roots of

$$\theta^2 - \frac{2x}{1-2x} \theta + \frac{1-2x}{3-4x} = 0$$

the condition that the roots remain real reduces to

$$\frac{4(1-x)^2(4x-1)}{(1-2x)^2(3-4x)} \geq 0.$$

Thus the ordered phase only exists if $x \geq 0.25$. Physically this means that, although the pressure and free energy curves exist for $x < 0.25$, since Eqns (8), (9) and (10) involve only functions of $\alpha + \beta$ and $\alpha\beta$, which always remain real, in this region the measurable quantities α and β become complex and hence the ordered solution becomes spurious. Thus at the value $x = 0.25$ the ordered solution ceases to be meaningful and a transition occurs from the ordered to the disordered phase.

For $q = 6$, a similar analysis can be carried out and the results are the same except that the transition occurs at $x = 1/6$. For a general Bethe lattice with coordination number q , the transition point occurs at $x = 1/q$, as pointed out by Easthope (1937).

§ 2. ORDERED PHASE ON THE RING APPROXIMATION

In I it was pointed out that, when only terms of the type $\omega = \mu z^{2q}$ were considered, the ring approximation, derived from the work of Rushbrooke and Scoins (1955), was equivalent to the approximation of Kikuchi (1951). This approximation, for the loose packed lattices, assumes that the probabilities of occurrence of all larger configurations of lattice sites depend exactly on the probabilities of Tables 1 and 2 and the probabilities of the nine different types of squares of four lattice sites which can be drawn on the lattice. It has been found possible to make a complete study of the antiferromagnetic on the approximation, and for the loose packed lattices some calculations have been made. Since they are quite complicated, the derivation and numerical results will be reserved for a further publication and the formulae relevant to this paper will be quoted.

For the simple quadratic lattice the pressure is given in terms of two physical quantities α and β (slightly different from the quantities for the Bethe approximation) by

$$P/kT = 2 \ln(1 + \alpha + \beta) - \frac{1}{2} \ln(1 + \alpha + 2\beta + \beta^2) - \frac{1}{2} \ln(1 + \beta + 2\alpha + \alpha^2) \dots\dots (17)$$

where

$$\omega = \frac{\alpha(1 + \alpha + \beta)^4}{(1 - \alpha)^3(1 - \alpha + 2\beta + \beta^2)} = \frac{\beta(1 + \alpha + \beta)^4}{(1 - \beta)^3(1 - \beta + 2\alpha + \alpha^2)} \dots\dots (18)$$

and the number density x is given by

$$2x = \frac{\alpha + \beta + \alpha^2 + \beta^2}{1 + 2\alpha + 2\beta + \alpha^2 + \beta^2} \dots\dots (19)$$

A reduction of the right-hand side of (18) leads to two factors, the first of which gives $\alpha = \beta$ which again produces the disordered phase, with the pressure given in I (13). The other factor which determines the ordered phase reduces to

$$1 + 2(\alpha + \beta) + \alpha^2 + \beta^2 + \alpha\beta - \alpha\beta(\alpha + \beta) - \alpha\beta(\alpha^2 + \beta^2) = 0. \dots\dots (20)$$

The calculation of α and β between Eqns (19) and (20) can be performed and substitution into (17) gives

$$P/kT = -\frac{1}{2} \ln 2(1 - 2x) + \frac{1}{2} \ln \{5 - 16x + 12x^2 + 16x^3 - 16x^4 + (3 - 6x + 4x^2)(1 + 4x - 20x^2 + 16x^3 + 16x^4)^{1/2}\} \dots\dots (21)$$

The evaluation of the free energy from (14) can be performed for the disordered phase, since the necessary integrals have been obtained by Chessin (1959) and gives

$$F/MkT = (1/x)\{(1-x)\ln(1-x) + x\ln x - (1-2x)\ln[2x + (1-4x+8x^2)^{1/2}]\} - 2\ln\frac{1}{2}[(1-2x) + (1-4x+8x^2)^{1/2}]. \quad \dots\dots (22)$$

For the ordered phase the integral of the second term of (21) is very complicated and it was performed numerically using Simpson's rule, which was found to be accurate enough. The results for the free energy are plotted in Fig. 3 and for the pressure in Fig. 4.

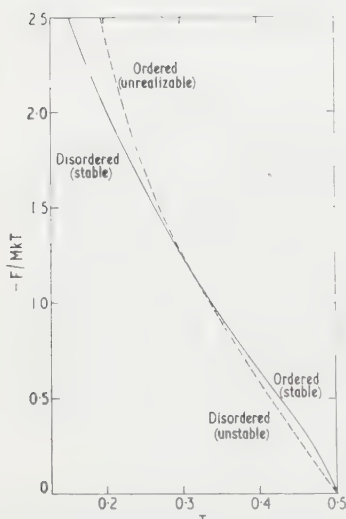


Fig. 3. Simple quadratic lattice, free energy plotted against number density for the ring approximation.

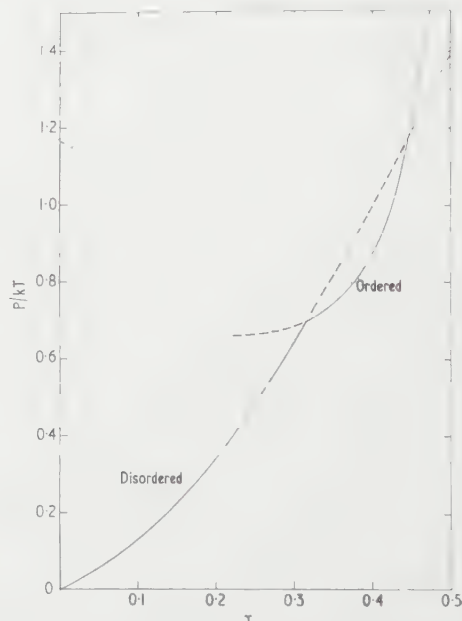


Fig. 4. Simple quadratic lattice, pressure plotted against number density for the ring approximation.

It is noted from Fig. 3 that the situation is similar to that for the Bethe approximation, that is, the curves touch at a certain point and the ordered phase always has the lower free energy. As in §1.4, it is noted that Eqns (17), (19) and (20) are functions of $\alpha + \beta$ and $\alpha\beta$ only, where α and β are parameters measuring some physical quantity. Thus it is required that α and β remain real and putting in the condition for reality gives, after some complicated manipulations, that the ordered phase can only exist for

$$x \geq \frac{1}{4}(3 - \sqrt{3}) = 0.3170.$$

It is easily shown that the pressures of the two phases are equal to this point and hence that the free energy curves have the same gradient. The values of the free energies can also be shown to be equal to within the error of the Simpson's rule integration.

For the simple cubic lattice, $q=6$, the equation corresponding to (18) leads to

$$\alpha(1+\beta)^{11}(1+\beta+2\alpha+\alpha^2)^7 = \beta(1+\alpha)^{11}(1+\alpha+2\beta+\beta^2)^7. \quad \dots\dots (23)$$

This equation has one factor which gives $\alpha = \beta$, which produces the results for the disordered phase I (13). The other factor could be derived and the ordered phase calculated completely, but the manipulation is very heavy. Since there appears to be no essential difference between the calculations for the simple cubic and simple quadratic lattices, and since the critical point can be evaluated easily, detailed results from (23) were not obtained. The critical point occurs at the value of α calculated by first differentiating Eqn (23) partially with respect to α and then putting $\alpha = \beta$. This leads to the equation

$$4\alpha^3 - 8\alpha^2 + 1 = 0$$

which has one negative root, which is of no importance, and two positive roots at $\alpha = 0.3946$ and 1.9331 . The corresponding values of x are 0.1904 and 0.3499 , the smaller value giving the transition point, while the larger value gives the second point of intersection of the ordered and disordered pressure curves (see Fig. 4 of I) and presumably has no physical significance.

§ 3. CONCLUSION

The characteristics of the transition which has been shown to occur on the Bethe approximation and on the ring approximation for the loose packed lattices are as follows. The two free energy curves, one obtained from the ordered phase and the other from the disordered phase, were shown to touch at a certain point and the ordered phase always had a lower free energy. It was shown, however, that below this point the ordered phase becomes physically unrealizable because it leads to measurable quantities being complex. These characteristics are just those required for a phase transition of the second order. This transition is a transition from an ordered to a disordered phase and the value of x at which it occurs will be called the transition point. The transition points for the Bethe approximation were shown to be $x = 1/q$ in agreement with those given by Easthope (1937). For the ring approximation, the transition values were $x = 0.3170$ for the simple quadratic and $x = 0.1904$ for the simple cubic. These values are larger than those obtained for the Bethe approximation and in disagreement with the results of Table 3 in I.

It is interesting to speculate on the behaviour of the lattice gas if it could be studied exactly. It has been shown by Fisher (1960) that when treated exactly, transitions of the Ising model are usually associated with points of inflection, while approximate methods show discontinuities in slope. This would seem to imply that the discontinuity in slope of the pressure curves in Figs 2 and 4 may be replaced by a point of inflection. Thus the free energy curves would have three or four point contact at the transition point and show a high order transition. On the other hand the two curves could be identical, have no discontinuity in slope or point of inflection, and show no transition.

The general problem when the repulsion between molecules is not infinite, that is $\varepsilon \neq \infty$, has been considered by Temperley (1959). It is now possible, using the results of §§ 1.2 and 1.3, to study the problem completely on the Bethe approximation and with more difficulty on the Kikuchi approximation. The closely related problem of calculating the transition curve for an antiferromagnetic has been solved by Kasteleijn (1956) for the Bethe approximation and the author has obtained results for the loose packed lattices on the Kikuchi approximation which will be presented for publication in due course. The more interesting problem of the use of the Kikuchi approximation for an antiferromagnetic on a close packed lattice seems possible, but it has not yet been studied in detail.

REFERENCES

- BURLEY, D. M., 1960, *Proc. Phys. Soc.*, **75**, 262.
CHESSIN, P. L., 1959, *J. Chem. Phys.*, **31**, 159.
EASTHOPE, C. E., 1937, *Proc. Camb. Phil. Soc.*, **33**, 502.
FISHER, M. F., 1960, *Proc. Roy. Soc. A*, **256**, 66.
KASTELEIJN, P. W., 1956, *Physica*, **22**, 387.
KIKUCHI, R., 1951, *Phys. Rev.*, **81**, 988.
RUSHBROOKE, G. S., and SCOINS, H. I., 1955, *Proc. Roy. Soc. A*, **230**, 74.
TEMPERLEY, H. N. V., 1959, *Proc. Phys. Soc.*, **74**, 183, 432.
ZIMAN, J. M., 1951, *Proc. Phys. Soc. A*, **64**, 1108.

Variation of Photovoltaic Response with Magnetic Field for a Germanium p-n Junction

By W. DUNSTAN

Department of Physics, Northern Polytechnic, London, N.7

MS. received 12th August 1960

Abstract. Measurements are described of the variation with magnetic field of the open-circuit voltage of a germanium p-n junction photocell, the illumination being parallel to the junction plane, and the field perpendicular to the illumination. The effect depends on the orientation of the field, vanishes when the latter is less than about 0.1 Wb m^{-2} , and is proportional to illumination. A fairly complete discussion of the operation of the cell is attempted, both with and without field; a partial explanation of the results is obtained.

§ 1. INTRODUCTION

THE photovoltaic properties of p-n junctions have been noted by Pietonpol (1951); a one-dimensional treatment of the theory for illumination parallel to the junction plane has been given by Rittner (1954). Under illumination, some of the additional minority carriers generated pass across the junction (in the 'reverse' direction in the language of rectifier theory), giving rise to a current in the external circuit.

The carriers will have a component of velocity away from the illuminated surface, although the total current in this direction must vanish. Under the action of a magnetic field perpendicular to the planes of current flow, one might expect the minority carrier velocity vectors to be rotated through an angle, producing a variation in flow across the junction, the sign of the change depending on the sense of the field. No effect is to be anticipated if the field is perpendicular to the junction plane. The actual results, however, are somewhat more complicated than the above simple considerations might suggest.

§ 2. DESCRIPTION OF APPARATUS

The specimen was a germanium p-n junction, produced by Standard Telephones and Cables Ltd., type PG 40A. The manufacturers state that the junction is made by diffusing gold into n-type germanium (antimony doped, resistivity 5–15 ohm cm); the dimensions are $0.75 \text{ mm} \times 0.75 \text{ mm} \times 0.5 \text{ mm}$, the last being perpendicular to the junction plane.

The cell was mounted as shown in Fig. 1; it was capable of rotation about a direction parallel to the incident light, but was otherwise rigidly supported: the wooden block was clamped to the base of the electromagnet. The source was a 60 watt tungsten filament lamp. This was replaced, for measurements of variation of the effect with intensity, by a 'Pointolite' a.c. tungsten arc. Some care is necessary in aligning the apparatus to ensure that the response is unaltered

on rotation in the absence of a field. A jet of cold air was directed at the specimen to minimize heating by the incident light.

Since a small change in response is to be measured, measurements of open-circuit voltage are capable of greater accuracy than those of short-circuit current. The potential difference was determined with a potentiometer; with the galvanometer used the accuracy of measurement was $3\text{--}4\text{ }\mu\text{V}$.

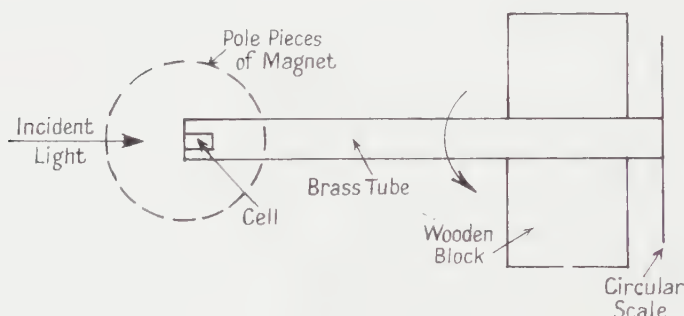


Fig. 1. Sketch of apparatus.

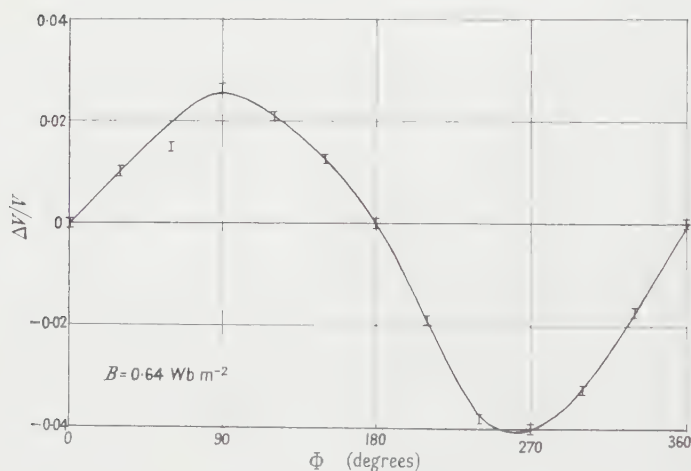


Fig. 2. Variation with orientation.

§ 3. RESULTS

Fig. 2 shows the fractional change in open-circuit voltage as the cell is rotated in a field of 0.64 Wb m^{-2} ; the zero values correspond to a field perpendicular to the plane of the junction. Fig. 3 represents the variation with field of change of potential for the two positions (90° and 270° in Fig. 2) of the maximum effect; the intensity is about twice that used in obtaining Fig. 2; for $\Phi = 270^\circ$, ΔV is negative. It will be seen that at about 0.1 Wb m^{-2} the alteration is comparable to the sensitivity of the apparatus.

A few readings of short-circuit current (external resistance 1 ohm) were also taken, in a field of 0.64 Wb m^{-2} . In this case the asymmetry is rather more

marked, the values being 2.98, 3.00, 2.90 mA for orientations of 0, 90°, 270° respectively.

Both the total and the change in e.m.f. for the same two positions were found to vary linearly with light intensity over a range of about 6 to 1. The relative intensities were calculated from the inverse square law, using a point source; no absolute measurements were made.

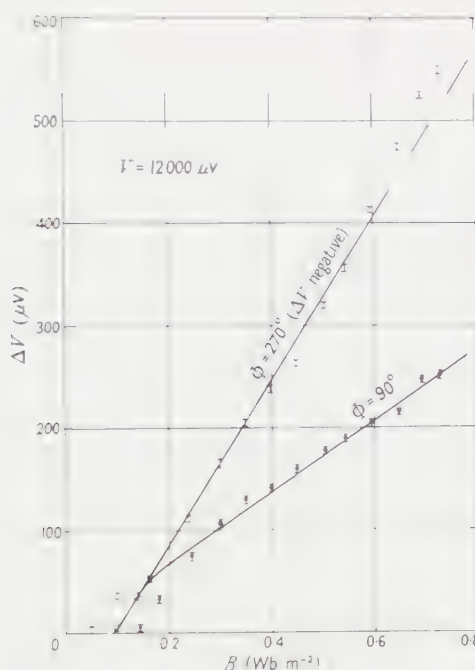


Fig. 3. Variation with field.

§ 4. THEORY

The junction is supposed to be very sharp, and confined to the immediate neighbourhood of the plane xy (Fig. 4); outside this region, electrical neutrality is assumed. The magnetic field is directed parallel to the positive oz axis. Considering the n -region, which is taken to be homogeneous, we have for the current densities:

$$\left. \begin{aligned} J_x^+ &= pe\mu_p E_x - eD_p \frac{\partial \Delta p}{\partial x} + \theta_p J_y^+ \\ J_x^- &= neb\mu_p E_x + ebD_p \frac{\partial \Delta p}{\partial x} - b\theta_p J_y^- \\ J_y^+ &= pe\mu_p E_y - eD_p \frac{\partial \Delta p}{\partial y} - \theta_p J_x^+ \\ J_y^- &= neb\mu_p E_y + ebD_p \frac{\partial \Delta p}{\partial y} + b\theta_p J_x^- \end{aligned} \right\} \dots\dots (1)$$

where b is the ratio of electron to hole mobility, $\theta_p = \mu_p B$, μ_p and D_p are the hole

mobility and diffusivity, p and n the hole and electron densities and Δp is the increase in p due to illumination.

Now

$$\text{div } \mathbf{J} = \text{div } (\mathbf{J}^+ + \mathbf{J}^-) = 0 \quad \dots\dots (2)$$

$$-\frac{1}{e} \text{div } \mathbf{J}^+ = \frac{\Delta p}{\tau} \quad \dots\dots (3)$$

where τ is the hole lifetime.

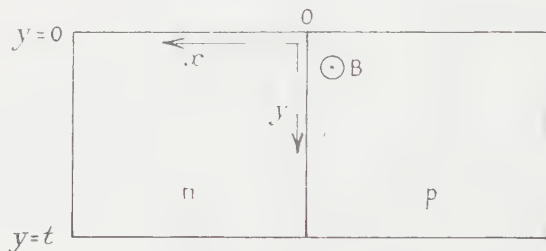


Fig. 4. Choice of axes.

Solving Eqns (1) for the current densities, neglecting terms in θp^2 , substituting in (2) and (3), and simplifying, we obtain

$$\begin{aligned} (1+b)\mu_p \left(E_y \frac{\partial \Delta p}{\partial y} + E_x \frac{\partial \Delta p}{\partial x} \right) + (b-1)D_p \left(\frac{\partial^2 \Delta p}{\partial x^2} + \frac{\partial^2 \Delta p}{\partial y^2} \right) \\ + \theta_p(b^2-1)\mu_p \left(E_x \frac{\partial \Delta p}{\partial y} - E_y \frac{\partial \Delta p}{\partial x} \right) = 0 \end{aligned} \quad \dots\dots (4)$$

and

$$\begin{aligned} \mu_p \left(E_y \frac{\partial \Delta p}{\partial y} + E_x \frac{\partial \Delta p}{\partial x} \right) - D_p \left(\frac{\partial^2 \Delta p}{\partial x^2} + \frac{\partial^2 \Delta p}{\partial y^2} \right) \\ - \theta_p \mu_p \left(E_x \frac{\partial \Delta p}{\partial y} - E_y \frac{\partial \Delta p}{\partial x} \right) = -\frac{\Delta p}{\tau}. \end{aligned} \quad \dots\dots (5)$$

Here we have used the results $\text{div } \mathbf{E} = 0$, and $\text{curl } \mathbf{E} = 0$ (since $\partial H / \partial t = 0$).

Eliminating the first term of (5) by means of (4), writing P for Δp , and dropping the subscript p everywhere, we find

$$\frac{\partial^2 P}{\partial x^2} + \frac{\partial^2 P}{\partial y^2} = \frac{b+1}{2b} \cdot \frac{1}{D\tau} P - \frac{(b+1)\mu\theta}{2D} \left(E_x \frac{\partial P}{\partial y} - E_y \frac{\partial P}{\partial x} \right). \quad \dots\dots (6)$$

Case a. $\theta = 0$. (It is convenient to treat this first, and to suppose that the application of a field produces only small changes.) (6) now becomes

$$\frac{\partial^2 P}{\partial x^2} + \frac{\partial^2 P}{\partial y^2} = \gamma^2 P \quad \dots\dots (7)$$

where

$$\gamma^2 = \frac{b+1}{2b} \frac{1}{D\tau}.$$

Solutions will be of the form $P = \text{const. exp } (\alpha x + \beta y)$ with $\alpha^2 + \beta^2 = \gamma^2$.

A convenient representation is in the form of definite integrals:

$$\begin{aligned} P = \int_0^\infty C^{++}(q) \exp(\alpha_q x + \beta_q y) dq + \int_0^\infty C^{+-}(q) \exp(\alpha_q x - \beta_q y) dq \\ + \text{two similar terms with } \exp(-\alpha_q x \pm \beta_q y), \end{aligned}$$

where q is a variable such that $\alpha_q = 0$ when $q = 0$, $\beta_q = 0$ when $q = \infty$ and α_q and β_q are positive.

The boundary conditions, assuming surface absorption with the liberation of Q pairs of carriers per cm^2 per sec are

$$\left. \begin{aligned} y=0: \quad & \frac{1}{e} J_y^+ = Q - sP \\ y=t: \quad & \frac{1}{e} J_y^+ = sP \end{aligned} \right\} \dots\dots (8)$$

where s is the surface recombination velocity. J_y^+ is given by (1), with $\theta = 0$. At both faces $J_y = J_y^+ + J_y^- = 0$. Now if b does not differ from unity in order of magnitude, the conduction current, which equals the difference of the two diffusion currents, is at most of the order of either of the latter. (For germanium, with $b \simeq 2$, the conduction current equals the hole diffusion current.) Hence the hole conduction current, forming a fraction $p/(p + nb)$ of the total, will be negligible compared with the hole diffusion current in n-type material. Similar considerations, if $1/b$ is not greatly different from unity, will apply to electrons in p-type semiconductors.

Thus we may write approximately

$$\begin{aligned} y=0: \quad & -D \frac{\partial P}{\partial y} = Q - sP \\ y=t: \quad & -D \frac{\partial P}{\partial y} = sP. \end{aligned}$$

Substituting, and dropping the subscript q :

$$\begin{aligned} & \int_0^\infty [C^{++}(q)(-\beta D + s) + C^{+-}(q)(\beta D + s)] \exp \alpha x dq \\ & \quad + \text{similar term with } \exp(-\alpha x) = Q \\ & \int_0^\infty [C^{++}(q)(-\beta D - s) \exp \beta t + C^{+-}(q)(\beta D - s) \exp(-\beta t)] \exp \alpha x dq \\ & \quad + \text{similar term} = 0. \end{aligned}$$

These equations can be satisfied for all x only if $\alpha = 0$, i.e. $q = 0$, $\beta = \gamma$ or if, for a particular value of q , the terms in square brackets vanish identically. This second form of solution can exist only in conjunction with the first, which relates Q to the coefficients $C(0)$.

The second choice gives rise to a compatibility equation, the solution of which reduces to

$$\exp \beta t = \frac{\beta D - s}{\beta D + s}.$$

(More precisely, there are two compatibility equations for the pairs of constants C^{--} , C^{+-} , and C^{+-} , C^{--} . The two equations are, however, identical.)

This is a transcendental equation for β (which is positive by hypothesis); it is easily seen to have no real roots. Complex roots appear unsuited to the nature of the problem, and are certainly impossible in the case of a specimen extending to infinity in the positive y direction, when the above conditions reduce simply to $\beta D + s = 0$.

It may be noted that in addition to the solutions discussed above, we may also have

$$P = \exp(\pm \gamma x)(A + By)$$

$$P = \exp(\pm \gamma y)(L + Mx).$$

To satisfy the boundary conditions, however, we find that we must have $A = B = M = 0$. In consequence, there is no concentration gradient in the x direction under uniform illumination.

To calculate the short-circuit current, we consider the junction region, supposed sufficiently narrow for recombination to be negligible. The hole current density will depend on the difference of electrochemical potential $\tilde{\mu}$ for holes between the two sides of the junction, and for sufficiently small currents we may write

$$J^- = \lambda \Delta \tilde{\mu}$$

where λ is a constant. Now

$$\Delta \tilde{\mu} = kT \ln p/p' + e\Delta\phi$$

p' being the hole density in the p-region, and ϕ the electrostatic potential. If $Q = 0$, $\Delta \tilde{\mu}$ of course vanishes.

Under illumination, $\Delta \tilde{\mu}$ changes by $d\Delta \tilde{\mu}$ given by

$$d\Delta \tilde{\mu} = kT \ln (P + p_0)/p_0$$

if ϕ is unaltered, and disregarding the change in p' ; p_0 is here the value in the dark for the n-region. To find λ , consider the junction as a rectifier with very small applied voltage V . Shockley's equation then gives for the holes

$$J^+ = \frac{ep_0 D}{L} \frac{eV}{kT}$$

where $L = (D\tau)^{1/2}$. In this case $d\Delta \tilde{\mu}$ is simply eV . Hence

$$\lambda = \frac{ep_0 D}{LkT}$$

so that under illumination

$$J^+ = \frac{ep_0 D}{LkT} kT \ln \frac{p_0 + P}{p_0}$$

$$\simeq \frac{eDP}{L} \quad \dots\dots (9)$$

for $P \ll p_0$.

For a specimen extending to $y = \infty$ the solution of (7) subject to (8) reduces simply to

$$P = \frac{Q}{D\gamma + s} \exp(-\gamma y). \quad \dots\dots (10)$$

Substituting, and integrating with respect to y from 0 to ∞ , the total hole current is found to be

$$\frac{QeD}{D\gamma + s} \left(\frac{2b}{b+1} \right)^{1/2},$$

with a similar term for the electrons. For $D\gamma \gg s$, this becomes

$$QeL \frac{2b}{b+1},$$

which differs only by the introduction of the last factor from the result of Rittner (1954).

Case b. $\theta \neq 0$. Eqn (6) is clearly not soluble as it stands. We may show, however, that if E_x and E_y do not differ in order of magnitude from their values in zero magnetic field, then the coefficient of θ is much smaller than the other terms in (6). Under short-circuit conditions, we may take $J_y = 0$, everywhere, and hence, using (2), J_x is independent of x .

From (1), with $\theta = 0$

$$\frac{1}{e} J_y = (p + nb)\mu E_x + (b - 1)D \frac{\partial P}{\partial y} = 0$$

and so, introducing (10) (semi-infinite specimen),

$$E_y \simeq \frac{b-1}{nb} \frac{D\gamma P}{\mu}$$

$\partial P / \partial x$ is zero for $\theta = 0$, and presumably never exceeds γP in magnitude. Thus

$$\frac{\mu E_y}{D} \frac{\partial P}{\partial x} \sim \frac{\gamma^2 P^2}{n},$$

which is smaller than $\gamma^2 P$ in the ratio P/n . Again

$$\frac{1}{e} J_x = (p + nb)\mu E_x = \frac{DP}{L} + \frac{D'N}{L'}$$

using (9); the second term on the right represents the electron flow, and is taken to be of the same order as the first. If this is correct,

$$\frac{\mu E_x}{D} \frac{\partial P}{\partial y} \sim \frac{P^2 \gamma}{nL},$$

where (10) has again been used. Since $L \sim 1/\gamma$, this term is also negligible.

We therefore attempt to solve (7) with the new boundary conditions

$$y=0: \quad -D \frac{\partial P}{\partial y} - \theta \left[(p_0 + P)\mu E_x - D \frac{\partial P}{\partial x} \right] = Q - sP$$

$$y=t: \quad -D \frac{\partial P}{\partial y} - \theta \left[(p_0 + P)\mu E_x - D \frac{\partial P}{\partial x} \right] = sP.$$

Once more the terms involving E_x are found to be smaller than

$$D \frac{\partial P}{\partial y}$$

in the ratio $(p_0 + P)/n$; accordingly they are neglected.

Proceeding in straightforward style as in case *a*, we find that the compatibility equation for the second form of solution reduces to

$$\exp 2\beta t = \frac{(\beta D - s)^2 - \theta^2(\gamma^2 - \beta^2)D^2}{(\beta D + s)^2 - \theta^2(\gamma^2 - \beta^2)D^2},$$

an equation which will possess a real root for sufficiently large values of θ . In the case $t = \infty$, we have simply

$$\beta D + s \pm \theta \alpha D = 0, \quad \dots\dots\dots(11)$$

the choice of sign arising from the two exponentials in α . Using $\alpha^2 + \beta^2 = \gamma^2$, we obtain for β the values

$$-\frac{2Ds \pm [4D^2s^2 + 4D^2(1 + \theta^2)(\theta^2D^2\gamma^2 - s^2)]^{1/2}}{2D^2(1 + \theta^2)} \quad \dots\dots\dots(12)$$

giving a positive root if

$$|\theta| > s/\gamma D. \quad \dots\dots (13)$$

If the positive sign is taken in front of α in (11), θ must be negative, and vice versa.

Thus at $x=0$ we now have

$$P = \frac{Q}{D\gamma + s} \exp(-\gamma y) + C' \exp(-\beta y)$$

with β given by (12).

The value of the constant C' presumably can be obtained only from considerations of continuity as we enter the junction region, where a space charge exists. This will not be attempted here.

§ 5. DISCUSSION AND CONCLUSIONS

It will be noted that while the theory relates to short-circuit current, the results are for open-circuit voltage. In the latter case, there is presumably a circulating current in the specimen, and J_y is no longer zero everywhere. It will be small, however, except at the ends of the specimen, where of course the condition $J_x=0$ may be used; it seems probable that E_x and E_y never become large enough to make (7) an unreasonable approximation.

It is natural to associate the appearance of the second solution of (7) with the existence of the 'critical' field illustrated in Fig. 3. There should of course be two such fields, one for each half of the junction; since the variation of C' with θ is unknown, no conclusion can be drawn as to the effect of exceeding the second of these values on the shape of the $(\Delta V, B)$ curve.

As far as numerical agreement is concerned, if we take a minority carrier lifetime of $100 \mu\text{sec}$, and adopt the usual values of μ and D , Eqn (13) gives for s values of the order of 10 and 30 cm sec^{-1} for n- and p-type respectively. These are lower than one would expect. It may be pointed out, however, that Woodbury and Tyler (1957) find that for gold-doped germanium $\tau < 3 \mu\text{sec}$: s of course varies inversely as $\tau^{1/2}$ in (13). The theory may therefore be satisfactory.

ACKNOWLEDGMENTS

The author's thanks are due to Dr. M. E. Pillow, Head of this Department, for facilities to carry out the experimental work, and to Messrs. G. W. Dickson and R. Benham for the construction of apparatus. He is also indebted to Messrs. Standard Telephones and Cables Ltd., for the information quoted above on the specimen used.

REFERENCES

- PIETONPOL, W. J., 1951, *Phys. Rev.*, **82**, 120.
 RITTNER, E. S., 1954, *Photoconductivity Conference, Atlantic City* (New York: Wiley), p. 246.
 WOODBURY, H. H., and TYLER, W. W., 1957, *Phys. Rev.*, **105**, 84.

A Perturbation-Variation Calculation of Eigenvalues

By A. DALGARNO AND A. L. STEWART

Department of Applied Mathematics, The Queen's University of Belfast

MS. received 12th September 1960

Abstract. A variational method, based upon perturbation theory, is used to calculate the eigenvalues of the helium sequence. With a trial wave function containing essentially only one variable parameter, the resulting errors range from 0.3 ev for H^- to 0.01 ev for Ne^{8+} .

§ 1. INTRODUCTION

CALCULATIONS of eigenvalues by the Rayleigh-Schrödinger perturbation theory are capable of high accuracy and have the advantage that by suitable choice of the zero-order eigenfunctions a single calculation suffices to yield eigenvalues of all the members of a given iso-electronic sequence. The results suffer by comparison with those of the variational method in that they do not (in general) provide bounds to the correct eigenvalues. The merits of the two procedures can be combined by evaluating the expectation value of the Hamiltonian over the perturbed eigenfunction.

§ 2. THEORY

In Rayleigh-Schrodinger perturbation theory, the Hamiltonian of an atomic system is decomposed into $H + V$ and the eigenvalue E and the eigenfunction Ψ are expanded according to

$$E = \sum_{n=0}^{\infty} E_n, \quad \Psi = \sum_{n=0}^{\infty} \psi_n \quad \dots\dots (1)$$

such that

$$(H - E_0) \psi_0 = 0 \quad \dots\dots (2)$$

$$(H - E_0) \psi_1 + (V - E_1) \psi_0 = 0 \quad \dots\dots (3)$$

$$(H - E_0) \psi_2 + (V - E_1) \psi_1 - E_2 \psi_0 = 0 \quad \dots\dots (4)$$

from which it may be shown that

$$E_1 = (\psi_0, V \psi_0) \quad \dots\dots (5)$$

$$E_2 = (\psi_1, V \psi_0) \quad \dots\dots (6)$$

$$E_3 = (\psi_1, V \psi_1) - E_1(\psi_1, \psi_1) \quad \dots\dots (7)$$

where for convenience we require that

$$(\psi_0, \psi_1) = 0. \quad \dots\dots (8)$$

If now we substitute

$$\Psi_t = \psi_0 + \psi_1 \quad \dots\dots (9)$$

into the energy integral, it follows that

$$E = E_0 + E_1 + \frac{E_2 + E_3}{1 + (\psi_1, \psi_1)} \quad \dots\dots (10)$$

is an upper bound to the eigenvalue. The perturbation expansion

$$E = E_0 + E_1 + E_2 + E_3 \quad \dots\dots (11)$$

follows from (10) on retaining terms up to third order only.

We may improve the bound (10) by selecting ψ_1 as the trial function in the conventional variational method

$$\Psi_t = \psi_0 + \lambda \psi_1. \quad \dots\dots (12)$$

Variation of λ then leads to the quadratic equation

$$(\psi_1, \psi_1)(E - E_0 - E_1)^2 - (E_3 - E_2)(E - E_0 - E_1) - E_2^2 = 0. \quad \dots\dots (13)$$

Expressions (10), (11) and (13) involve only wave functions needed for the evaluation of the second-order energy E_2 .

2.1. The Hydrogenic Approximation

For the helium sequence, we select as the zero-order unperturbed wave function

$$\psi_0 = \frac{Z^3}{\pi} \exp \{-Z(r_1 + r_2)\} \quad \dots\dots (14)$$

where Z is the nuclear charge and \mathbf{r}_1 and \mathbf{r}_2 are the position vectors of the two electrons referred to the nucleus as origin. Then, measuring energy in rydbergs,

$$E_0 = -2Z^2, \quad h = \frac{2}{|\mathbf{r}_1 - \mathbf{r}_2|}, \quad E_1 = \frac{5Z}{4}. \quad \dots\dots (15)$$

Hylleraas (1930) has determined the first-order perturbed function ψ_1 by minimizing the functional

$$E_2 = (\psi_1, [H - E_0]\psi_1) + 2(\psi_1, [h - E_1]\psi_0) \quad \dots\dots (16)$$

with respect to an eight-parameter representation of ψ_1 , obtaining $E_2 = -0.314\,63$ and $E_3 = 0.015\,53/Z$. His work has been extended by Hylleraas and Midtdal (1956) and by Stewart (1957) using more flexible representations of ψ_1 , and the most accurate estimate of E_2 presently available is $-0.315\,311$ (Hylleraas and Midtdal 1956). The third-order energy E_3 has not been evaluated with the more flexible forms of ψ_1 and the original result for E_3 (Hylleraas 1930) remains the best theoretical value.

We have used the first-order function obtained by Hylleraas to evaluate (10) and (12) and to solve (13). Expression (10) becomes

$$E = -2Z^2 + \frac{5Z}{4} - \frac{(0.314\,63 - 0.015\,53/Z)}{1 + 0.244\,44/Z^2} \quad \dots\dots (17)$$

and (12) becomes

$$E = -2Z^2 + \frac{5Z}{4} - 0.31463 + \frac{0.015\,53}{Z}. \quad \dots\dots (18)$$

In the Table, the results are compared with the very accurate eigenvalues obtained by Pekeris (1958) by individual variational calculations. Expressions (10) and (13) yield upper bounds to the eigenvalues but are less accurate than the perturbation expansion (12). Very little improvement is obtained by the

introduction of the variable parameter in (12), the best choice of λ being nearly unity.

Eigenvalues of the Helium Sequence (ryd)

Z	$\zeta = Z$			ζ variable		
	Pekeris	Eqn (18)	Eqn (10)	Eqn (13)	Eqn (10)	Eqn (13)
1	-1.055019	-1.04910	-0.99035	-1.00259	-1.03354	-1.03957
2	-5.807449	-5.80687	-5.78919	-5.79100	-5.80332	-5.80428
3	-14.559827	-14.55945	-14.55127	-14.55180	-14.55785	-14.55821
4	-27.311132	-27.31075	-27.30607	-27.30629	-27.30980	-27.30999
5	-44.061943	-44.06152	-44.05851	-44.05862	-44.06089	-44.06100
6	-64.812493	-64.81204	-64.80994	-64.81001	-64.81158	-64.81165
7	-89.562890	-89.56241	-89.56086	-89.56091	-89.56205	-89.56211
8	-118.313190	-118.31269	-118.31150	-118.31153	-118.31240	-118.31244
9	-151.063425	-151.06290	-151.06196	-151.06199	-151.06266	-151.06270
10	-187.813613	-187.81308	-187.81231	-187.81233	-187.81287	-187.81289

2.2. The Screening Approximation

Dalgarno and Stewart (1960) have pointed out that the perturbation expansion corresponding to the screening approximation may be readily obtained from the perturbation expansion for the hydrogenic approximation. The screening approximation follows from choosing as unperturbed eigenfunction

$$\psi_0(\mathbf{r}_1, \mathbf{r}_2) = \frac{\zeta^3}{\pi} \exp\{-\zeta(r_1 + r_2)\} \quad \dots\dots (19)$$

where ζ is an arbitrary parameter. Then

$$E_0(\zeta) = -2\zeta^2, \quad h(\zeta) = \frac{2}{|\mathbf{r}_1 - \mathbf{r}_2|} - 2(Z - \zeta) \left(\frac{1}{r_1} + \frac{1}{r_2} \right), \quad E_1(\zeta) = \frac{5\zeta}{4} - 4\zeta(Z - \zeta) \quad \dots\dots (20)$$

and the (unnormalized) first-order perturbed wave function is given by

$$\psi_1' = \psi_1(\zeta) - (Z - \zeta)(r_1 + r_2)\psi_0(\zeta). \quad \dots\dots (21)$$

The third-order perturbation expansion becomes

$$E_2(\zeta) = E_0(Z) + E_1(Z) + E_2(Z) + \frac{ZE_3(Z)}{\zeta}, \quad \dots\dots (22)$$

but this is not useful since it provides no means of selecting the parameter ζ . It is necessary to use (10) or (13) which provide upper bounds to the eigenvalues.

We have evaluated (10) and solved (13), adopting for ψ_1 the eight-parameter representation of Hylleraas (1930). Minimization of E with respect to ζ then leads to the values given in the last two columns of the Table. Again very little improvement is obtained by the introduction of the parameter λ in (12). The results of (10), which are based on a trial function containing essentially the single variable parameter ζ , are in error by less than 0.02 ev for $Z \geq 3$, by 0.06 ev for $Z = 2$ and by 0.3 ev for $Z = 1$.

The error in the region of large Z is nearly equal to the difference between the value of E_2 used in the present calculations and the best available value of E_2 , which suggests that it may be largely eliminated by the use of a more flexible representation of ψ_1 .

REFERENCES

- DALGARNO, A., and STEWART, A. L., 1960, *Proc. Roy. Soc. A*, **257**, 534.
HYLLERAAS, E., 1930, *Z. Phys.*, **65**, 209.
HYLLERAAS, E., and MIDTDAL, J., 1956, *Phys. Rev.*, **103**, 829.
PEKERIS, C. L., 1958, *Phys. Rev.*, **112**, 1649.
STEWART, A. L., 1957, *Proc. Phys. Soc. A*, **70**, 756.

The Polymorphism of Thallium and Other Halides at Low Temperatures

BY M. BLACKMAN AND I. H. KHAN

Physics Department, Imperial College, London

MS. received 27th June 1960

Abstract. Thin layers of caesium, rubidium and thallium halides have been evaporated on to amorphous bases at low temperatures, and examined by electron diffraction. All the caesium halides examined, as well as thallium chloride and thallium bromide, showed both the rocksalt structure as well as the normal caesium chloride structure. In general the abnormal structure gave the weaker pattern which decreased in intensity as the layer was heated and disappeared before room temperature was reached. Thallium iodide showed a caesium chloride structure at low temperatures changing to the normal orthorhombic form only in the neighbourhood of room temperature. The rubidium salts showed a rather persistent broad ring pattern at low temperatures in addition to the normal rocksalt rings. The diffuse ring pattern is consistent with a caesium chloride structure for the rubidium halides.

§ 1. INTRODUCTION

IT has been known for some time that the caesium and thallium halides (CsCl, CsBr, CsI, TlCl, TlBr, TlI) possess the rocksalt structure when formed, by deposition *in vacuo*, as thin oriented layers on the cleavage face of crystals of the rocksalt types (Schulz 1951a, Pashley 1952, Lüdemann 1957). Deposits on amorphous bases at room temperature were examined by Meyerhof and Ungelenk (1959). The electron diffraction transmission patterns showed rings characteristic of the normal structure for CsI, TlCl, TlBr, and TlI, whereas CsCl gave rings of both the rocksalt and the normal structure when the deposits were formed slowly. It was suggested that the alkali halide bases were not essential to the formation of the rocksalt structure, that nuclei with this structure are in fact formed but change into the normal state too rapidly to be observed.

The present experiments are also concerned with thin layers of caesium and thallium halides on amorphous bases, the main difference being that these layers are deposited on to bases maintained at low temperatures. It will be shown that in all the cases examined (TlCl, TlBr, TlI, CsCl, CsBr, CsI) abnormal structures do occur at low temperatures. When heated these disappear before room temperature is reached, with the one exception of CsCl. The results confirm the view that the abnormal forms can exist independently of the base.

The investigations were extended to cover the rubidium halides (RbCl, RbBr, RbI), using the same technique. In all these cases an extra diffraction pattern was found at low temperatures. This consisted of rings which were always broad, but the position and the spacing of the rings did coincide with what would be expected for the CsCl structure. This rather unusual change from a rocksalt structure to a caesium chloride structure appears to have been

reported only once previously. Schulz (1951b) found that rubidium bromide has the caesium chloride structure when formed from solution on a silver substrate. The conditions must have been rather unusual in this case, as attempts to reproduce this by Khan (1959) were unsuccessful.

§ 2. EXPERIMENTAL PROCEDURE AND RESULTS

2.1. *Experimental Procedure*

The apparatus used consisted of an electron diffraction camera in conjunction with a low temperature unit (Blackman and Lisgarten 1957) which allowed the temperature of the base to be set at values varying between that of liquid oxygen and 120°C. The specimens were prepared by evaporation *in situ*, with the base at a low temperature; the base was carried on an electron microscope grid set at an angle of about 45° both to the electron beam and to the stream of halide vapour.

Great care had to be taken to prevent the formation of an ice layer on the specimen during the experiment—particularly as photographic film was used. The evaporation was carried out slowly, the maximum rate being determined in preliminary experiments—the criterion being that the breadth of the diffraction rings should not be altered as compared with those obtained with the slowest rates of evaporation. After a layer of suitable thickness had been formed, the specimen was heated slowly, the diffraction pattern being photographed at intervals.

2.2. *Experimental Results*

2.2.1. *Caesium bromide.*

Caesium bromide was evaporated on to formvar initially at -160°C at a rate of about 12 \AA min^{-1} . As the deposit was built up an extra diffraction pattern was observed consisting of broad rings (Fig. 1(a)†). The specimen was then heated at a rate of about four degrees per minute. At -135°C sharp rings began to appear, the transition to a sharp ring pattern taking place in a temperature interval of about six degrees. The rings were due to both the rocksalt structure and the normal structure, the rocksalt rings being weaker (Fig. 1(b)). On further heating the rocksalt rings weakened still further and could not be observed above -110°C .

Another set of evaporation experiments was carried out with the base at different fixed temperatures. The three types of ring pattern were observed, depending on the temperature of the base. The results, which are shown in Table 1, refer to a low rate of deposition and a thickness of about 150 Å.

Table 1. Structure of CsBr Deposits

Temperature of base (deg c)	Type of pattern
-180 to -140	Diffuse rings
-140 to -115	Sharp rings—CsCl and NaCl structure
-115	Sharp rings—CsCl structure

The temperature at which the NaCl type pattern is observed to disappear is to some extent a function of the rate of heating. This rate was kept reasonably low, and was the same in all experiments of this type. The thickness of the deposit

† All figures are printed as Plates.

was also arranged to be the same as far as possible. The rocksalt type rings were not observed in relatively thick deposits, nor when the rate of deposition was high.

Similar experiments were also carried out on carbon and on silicon monoxide bases. The results were materially the same as with formvar.

2.2.2. *CsCl*, *CsI*, *TlCl*, and *TlBr*.

In all these cases, broad diffuse rings were obtained from deposits on bases at the lowest temperatures. On heating, the sharp rings corresponding to both types of structures appeared. Except in the case of *CsCl* the rocksalt type rings were much weaker than those due to the normal structure and disappeared well before room temperature was reached. In the case of *CsCl*, the rocksalt type gave initially the more intense rings; these became weaker as the temperature was raised and were not observed above 120°C.

2.2.3. *TlI*.

The results for thallium iodide differed in many respects from those previously discussed. At the lowest temperature a diffuse ring pattern was found, consisting of four rings (Fig. 2(a)). An unusually sharp ring pattern was obtained either by warming the diffuse ring pattern or by direct deposition at a suitable low temperature. The pattern is that to be expected of the *CsCl* structure, and persists unchanged even when kept for hours at -30°C (Fig. 2(b)). As the layer is heated extra rings appear and the pattern slowly becomes that of the normal orthorhombic structure at room temperature. As the *CsCl* form is the stable form above 175°C, experiments were also carried out in which a thick layer of *TlI* was heated up to above 175°C, or deposited at a fast rate on an amorphous base above the transformation temperature. These special measures were necessary as the vapour pressure above 175°C is rather high. In both types of experiment the initial pattern of the orthorhombic form changed to that of the *CsCl* form.

2.2.4. *RbI*, *RbBr*, *RbCl*.

Rubidium iodide was deposited on to a formvar base at -100°C at a rate of about 5 Å min⁻¹. A broad ring pattern appeared consisting of two fairly intense inner rings and a weak outer ring. The initial effect of heating a layer of about 100 Å in thickness (at a rate of 5°C min⁻¹) was to cause a slight lessening in the diffuseness of the rings; at about -85°C, however, sharp rings appeared which were of the rocksalt type. The broad rings still persisted and it was evident that the centre of gravity of these broad rings did not coincide with the position of strong rocksalt type rings. The broad rings were however consistent with those to be expected for a *CsCl* structure and for this, and other reasons (see §4), have been indexed as such (Fig. 3). With increasing temperature the broad ring pattern became less distinct and disappeared at about -40°C.

Similar results were found with rubidium bromide and chloride, i.e. the broad ring pattern appeared first at the low temperatures; on heating, rocksalt rings were obtained with the broad ring pattern still present and at higher temperatures this pattern disappeared. In no case were sharp rings of the *CsCl* type obtained.

§ 3. MEASUREMENTS OF LATTICE CONSTANTS

The lattice constants of the abnormal structures of all the halides were measured by comparison with the normal structures (except in the case of TII) both ring patterns appearing on the same plate. As the patterns were taken at low temperatures, and the lattice constants of the CsCl form are known at room temperature, it was necessary to allow for thermal contraction. In some cases it was necessary to change the data from x.u. to ångströms.

The lattice constant of thallium iodide with the CsCl form was measured by comparison with TlCl. A thin specimen of TlCl was formed by vacuum deposition on to a thin layer of formvar carried on an electron microscope grid. This was placed close to and as nearly as possible at the same level as the TII specimen. By a slight movement of the beam one could obtain one or other of the patterns. The lattice constants obtained are given in Table 2.

Table 2. Lattice Constants of the Abnormal Forms

Deposit	Structure	Spacing a_0 (Å)	Temperature (°C)
CsCl	NaCl	6.923 ± 0.010	- 46
CsBr	NaCl	7.253 ± 0.010	- 118
CsI	NaCl	7.631 ± 0.010	- 125
TlCl	NaCl	6.320 ± 0.010	- 65
TlBr	NaCl	6.594 ± 0.010	- 60
TII	CsCl	4.205 ± 0.007	+ 15
RbCl	CsCl	3.97 ± 0.12	- 80
RbBr	CsCl	4.24 ± 0.13	- 43
RbI	CsCl	4.59 ± 0.16	- 80

§ 4. COMMENTS AND DISCUSSION

All the experiments show that a slow deposition of the thallium, caesium and rubidium halides on to a base at sufficiently low temperature, leads to a layer giving a very diffuse diffraction pattern. This is presumably due to very small crystallite size, as increasing the rate of deposition does lead to less diffuse rings. As the layer is heated reasonably sharp ring patterns are obtained.

The substances examined are found to fall into several categories. The caesium salts, thallium chloride and bromide all show rings due to both the rocksalt structure as well as the normal structure. The strong rings of the normal structure are associated with the broad ring structure in the sense that the centres of gravity of the broad rings coincide with either intense rings or a group of intense rings. The exception is caesium chloride where the rocksalt type rings are the more intense. It is reasonable to assume that in all these cases nuclei of both structures are present initially, even when the corresponding diffuse rings are too weak to be observed.

When the temperature of the deposit is increased, the rocksalt type rings weaken in intensity and are not visible at room temperature (except in the case of CsCl). It follows that crystals with the abnormal structure can exist as such, without any obvious influence due to the base.

Thallium iodide is rather exceptional in that the CsCl form appears at low temperatures, without any admixture of the normal orthorhombic form. It is also noteworthy that the ring pattern from this layer is unusually sharp indicating

relatively large crystals. Since the orthorhombic form is considered to be the stable structure below 175°C , one is left with the problem as to whether one is dealing with a metastable or a stable thermodynamic form. This question could be answered satisfactorily only by calorimetric measurements in the neighbourhood of room temperature where a change to the orthorhombic form is observed. A further point of note is that in none of the experiments (including those at high temperatures) was the rocksalt form observed; though this form does appear as an oriented layer on alkali halide bases (Schulz 1951 a, Khan 1959).

The rubidium salts gave results of a rather unexpected nature. The broad ring pattern found at low temperature does not seem to be related to the sharp ring pattern of the normal form—in contrast to the results for CsBr and CsI. Except for a lessening in the diffuseness with temperature, the pattern merely fades out as the temperature increases though it does not disappear until a relatively high temperature is reached (-40°C for RbI). While it is not surprising that a CsCl structure could be formed at low temperatures, it is unexpected that there should be no signs of broad rings corresponding to the NaCl structure. The position of the diffuse rings force one to the conclusion, however, that one is dealing with the CsCl structure. Though the measurements of the lattice spacings are rather inaccurate these show that the anion-cation distance increased by from 5% to 8% in going over to the CsCl form. As the error here is about 50%, these results are consistent with the 4% increase one would expect theoretically.

Another pointer in this direction is to be found in the behaviour of the potassium salts (as shown by recent, unpublished, experiments by Cooper-Smith). These give a broad ring pattern at the lowest temperatures, but this pattern transforms readily on heating into an NaCl type ring pattern which is directly related to the broad ring pattern.

It appears therefore that the rubidium salts differ in their behaviour from both the caesium and the potassium salts, and show a preference for the abnormal form when deposited at low temperatures in the form of very small crystals.

ACKNOWLEDGMENTS

One of the authors (I.H.K.) would like to express his thanks to the Commonwealth Relations Office (London) and to the British Council for a research fellowship and a maintenance grant.

REFERENCES

- BLACKMAN, M., and LISGARTEN, N. D., 1957, *Proc. Roy. Soc. A*, **239**, 93.
KHAN, I. H., 1959, *Ph.D. Thesis*, University of London.
LÜDEMANN, H., 1957, *Z. Naturf.*, **12a**, 226.
MEYERHOF, K., and UNGELENK, J., 1959, *Acta Cryst.*, **12**, 32.
PASHLEY, D. W., 1952, *Proc. Phys. Soc. A*, **65**, 33.
SCHULZ, L. G., 1951 a, *Acta Cryst.*, **4**, 487.
— 1951 b, *J. Chem. Phys.*, **19**, 504.

Moving Striations and Anode Spots in Neon

By J. R. M. COULTER†, N. H. K. ARMSTRONG
AND K. G. EMELEUS

Physics Department, Queen's University, Belfast

MS. received 9th June 1960

Abstract. An experimental study has been made of boundary conditions at the positive end of positive columns in neon which were traversed by waves of ionization (moving striations) proceeding towards the Faraday dark space. The striations were generated from small anode spots, which usually oscillated with increasing amplitude until they became detached from the anode. Closely similar processes took place at the negative end of a capillary tube when the discharge was passed through the capillary into a wide tube. A few typical time-resolved photographs of the oscillations have been reproduced to illustrate the nature of the phenomena and their dependence on pressure and current, and possible causes of the oscillations are discussed briefly.

§ 1. INTRODUCTION

THE positive column of a glow discharge often consists of luminous balls, called 'moving striations', which move with speeds of the order of 100 m sec^{-1} from near the anode to the Faraday dark space. The changes in electron and ion concentrations and in space-potential through the striations are too large for them to be linear plasma-ion waves (Armstrong, Emeleus and Neill 1951). They have in fact more nearly the properties of mobile low-voltage arcs, or 'balls of fire', although it is generally assumed that they mark the passage of a wave of ionization rather than bodily motion of portions of ionized gas.

Comparatively little is known about their theory (Emeleus and Oleson 1959, Pekarek 1960). Since knowledge of boundary conditions is often basic for understanding oscillations, we have now made a study of the ends of some oscillating columns. This paper contains an account of the results for the positive end; results for the negative (Faraday dark space) end will be described elsewhere (Coulter 1960). Our results support Pupp's suggestion (1935) that the formation of moving striations depends on the existence of a positive anode fall in potential, and confirm the observation of Takamine, Suga and Yanagihara (1933) that moving striations may be generated by the catastrophic growth of the oscillations of small anode spots.

§ 2. APPARATUS

The positive end of the discharge tube used for most of the experiments is shown in Fig. 1. The anode A was a pointed zirconium rod, 2 mm in diameter, movable by an iron slug C enclosed in glass, so that its tip could be positioned either to the right of the inset glass capillary B of 2.5 mm internal diameter, inside B, or projecting on its left-hand side. The tube was 2.5 cm in diameter and 108 cm

† Now at Stevens Institute of Technology, Hoboken, New Jersey.

long. The cathode was a blunt zirconium rod, 4.5 mm in diameter, mounted axially at the far (negative) end of the tube with a similar arrangement for moving it; it was usually kept well to the left of B. In some other experiments a tube like that of Fig. 1 was used, but without the capillary B, and with a blunt zirconium rod 4.5 mm in diameter as anode.

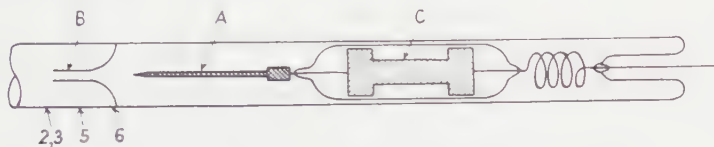


Fig. 1. Anode end of discharge tube. The approximate position of the tip of the anode in Figs 2, 3, 5 and 6 is shown by the arrows.

The tubes were attached to a vacuum and gas-filling manifold at the cathode end, and were baked, and the electrodes glowed inductively before use. The discharges were passed through British Oxygen Gases Ltd's 'spectrally pure' neon, kept clean by a liquid nitrogen trap beyond the cathode, and by the sputtering of the zirconium during operation. No spectroscopic impurity was noticed whilst the discharges were passing. Current was drawn from a 1300 v battery of accumulators.

The moving striations and anode glow were examined by (a) a photomultiplier, with output fed to a cathode-ray oscilloscope, (b) direct photography of an image of the tube reflected from a flat rectangular stainless steel mirror (10 cm \times 5 cm) rotating about an axis parallel to its long side and the axis of the tube (Coulter 1959). Both methods serve to detect intermittence and give the frequency of the oscillations. The first method gives more accurate measurements of frequency and fluctuations in luminosity than the second, but the second reveals more detail of what is taking place. Essentially, the second method gives a series of successive pictures of the tube (see Appendix).

§ 3. RESULTS

In all the discharges studied, moving striations were present in the main positive column. With the tube of Fig. 1, they also occurred in the capillary and to the right of it, if the anode were in a suitable position. The striations did not penetrate appreciably into the Faraday dark space, but formed a complex pattern near the latter (Cooper, Coulter and Emeleus 1958). In most cases, the striations developed from a small oscillating spot on the anode or at the negative end of the capillary. The spot underwent a kind of growing relaxation oscillation, and ultimately appeared to peel off as a moving striation. Only results obtained with the pointed anode will be described in detail. Those found with the blunt anode were similar, but more complicated because of the frequent presence of several unsymmetrically placed spots to which the discharge passed alternately, and because there was considerable rotation of even a single spot. The tube of Fig. 1 was designed to minimize this type of motion, and to pin down the anode spot on or near the point of the anode, particularly when the pointed end only just emerged from the capillary. With the blunt anode, the anode spots were diffuse and yellow in colour; with the pointed anode they were smaller and bright red. The difference in their spectra is probably due to the difference in current density in the two cases.

3.1. Anode Projecting from Capillary

Figs 2 and 3 (Plate I) are typical rotating mirror photographs (§ 2(b)) showing the growth of moving striations from anode spots. The discharge parameters were, for Fig. 2, $p = 8.5$ mm Hg, $i = 20$ mA, exposed length of anode $l = 1.0$ mm, distance from tip of cathode to capillary $d = 16.3$ cm; and for Fig. 3, $p = 8.5$ mm Hg, $i = 40$ mA, $l = 1.0$ mm, $d = 32.8$ cm. The row of bright dots at the right of each figure is the oscillating anode spot. The bright bars inclined down to the left are striations moving away towards the Faraday dark space. In Fig. 2 the speed of the striations varies considerably, in Fig. 3 it is more nearly constant. In each case, as found by Takamine, Suga and Yanagihara (1933), the striations are formed as a result of the oscillations of the anode spot increasing in amplitude until it appears to move off and develop into a striation occupying the wider cross section of the main tube. The frequency of oscillation of the spot was $2.04 \times 10^4 \text{ sec}^{-1}$, about 16 times that of the striations in Fig. 2, and $2.02 \times 10^4 \text{ sec}^{-1}$, or about 15 times that of the striations in Fig. 3.

In both instances, the moving striations ultimately develop from a sort of residual accumulation in front of the anode of two or three of the last stages of growth of the spots. Also, in both, in spite of the small dimensions of the anode, there is a retrograde motion of the spots to behind their initial positions. Inspection of the original pictures shows that, at least for the first discharge, the spot is most intense at the beginning and end of each of the oscillations. In Fig. 3, the spot has apparently stopped oscillating near the middle of the growth sequences for about $100 \mu\text{sec}$.

The mobility of the spots over the anode surface and the tendency to form multiple spots were increased by increasing the projecting length of anode l . For example, with $l = 1.0$ cm, $p = 34.7$ mm Hg and $i = 30$ mA, four spots were obtained. Of these, the smallest was at the pointed tip of the anode; the other three were more diffuse, and arranged asymmetrically on the anode surface where it left the capillary. The striation frequency was 1730 sec^{-1} . The striations were produced by growth of the spot on the tip, which had a frequency of $3 \times 1730 \text{ sec}^{-1}$. The other spots oscillated with apparently constant amplitude and period, and a frequency of $2 \times 1730 \text{ sec}^{-1}$, and did not give rise to moving striations.

It would be expected that increase of pressure alone would have much the same effect as increasing l , since from similarity considerations the nature of the discharge is likely to depend on the ratio of l to the free path, or to the product lp . This was found to be the case. For example, with $i = 30$ mA and $l = 4$ mm, a single oscillating spot was present for $p = 8.5$ mm Hg, and two spots for $p = 21.9$ and 34.7 mm Hg. In this instance, however, both spots grew, and ultimately combined to form a moving striation. The ratio of spot frequency to striation frequency decreased with increase in pressure, for example, with a current of 30 mA, from 18:1 for $p = 8.5$ mm, to 4:1 for $p = 34.7$ mm. The change in ratio may be connected with increase in current density through decrease in size of the spots, since a change in the same sense was found when the current was increased at constant pressure.

The effects of moving the cathode closer to the pointed anode were the same as for a blunt anode (Coulter 1960). The ratio of spot frequency to striation frequency remained constant until the tip of the anode entered the region where striations branched. If the anode were moved into the Faraday dark space an anode spot persisted, but it was now yellow, and although it oscillated with high

frequency (sometimes $> 30\,000\text{ sec}^{-1}$) it did not produce detectable propagating waves.

The photomultiplier records (§2(a)) give further information about the oscillations of the spots. A typical cathode-ray oscilloscope trace is shown in Fig. 4. This shows the growth of the luminosity in the stepped process leading up to the launching of a striation, which took place when maximum light intensity was reached, and just after. These traces show that the period of oscillation of a spot increases during the growth cycle; this can also be seen from the mirror photographs. In this instance (Fig. 4), the oscillations had a second large peak between the maximum at the end of one growth cycle and the beginning of the next, for every other cycle. When this second maximum was present, a striation which had almost formed at the principal maximum did not move away until it received sufficient additional impetus in the following spot excursion (cf. Figs 2 and 3). Sometimes the double maximum and delayed launching occurred in each cycle. In many instances the amplitude of the light oscillations increased nearly exponentially in each cycle to near the maximum. The spot oscillations were accompanied by voltage fluctuations of the same frequency between anode and cathode, with maximum amplitude of order of 1 volt.

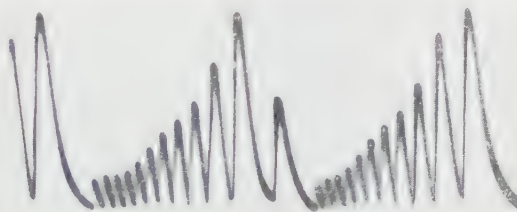


Fig. 4. Oscilloscopic record of the a.c. component of light from an anode spot. The discharge parameters were: $p=7.3\text{ mm Hg}$, $i=13.2\text{ mA}$, $V=320\text{ volts}$, $l=1.0\text{ mm}$. Time increases from left to right, the total time interval being 9.6 msec .

The photomultiplier experiments also showed that when the pressure and electrode separation were constant and the current was varied, regular oscillations of the spot only occurred for certain values of the current. For intermediate values of current the oscillations of the spot were very irregular. Similar effects are known for the striations.

3.2. Anode Inside Capillary

The current density in the capillary was about 70 times that in the main tube, and the discharge in the capillary very much brighter. It was examined with the rotating mirror. A typical picture is shown in Fig. 5 (Plate II), for $p=21.9\text{ mm Hg}$, $i=27.5\text{ mA}$, and the anode 1.0 cm from the negative end of the capillary. Striations, with frequency $1.13 \times 10^4\text{ sec}^{-1}$ and mean velocity 150 msec^{-1} , are generated by a minute oscillating spot at the tip of the anode. They produce an oscillating spot at the end of the capillary, which in turn produces striations in the main tube, like an oscillating anode spot on a projecting anode. At lower pressure the moving striations in the capillary are less regular, particularly just prior to launching of the striation in the wide tube (Coulter 1959). The effects of this irregularity die down in a short distance in the wide tube, and the striations in the latter appear quite regular.

3.3. *Anode behind Capillary*

This position yielded little new. Striations occurred in and on each side of the capillary. Oscillating spots were present on the anode and at the negative end of the capillary. The conical section between the capillary and the anode section was dark; striations approaching it from the anode produced a standing wave pattern like that near the true Faraday dark space (Cooper, Coulter and Emeleus 1958). At no time did we succeed in stabilizing all three sets of striations simultaneously; this is in accord with the observation that, in a tube with constant cross section, the stability conditions involve both current density and electrode separation (Pigg, Burton and Oleson 1957). The frequency in the capillary was several times that in the wide tubes, and the frequencies in the two wider sections nearly the same.

3.4. *Nearly Stable Anode Spots*

When the current was reduced to such small values that moving striations became difficult to observe (e.g. 5 mA at a pressure of 5 mm Hg), the anode spots persisted, although with reduced intensity. It was then found that if the anode projected from the capillary, oscillations could not always be detected in the anode glow with higher frequency than that of the striations. The striations were apparently launched by the spot increasing steadily in size until some critical unstable extension was reached. Both the mirror photographs and the photomultiplier failed to show any spot frequency higher than that of the striations. When the anode was inside the capillary an oscillation pattern like that shown in Fig. 6 (Plate II) was obtained; the discharge parameters were $p = 4.35$ mm Hg, $i = 5$ mA. The thin vertical line is the negative end of the capillary. There are moving striations of normal type at all times near the anode. At the other end of the capillary these are transformed periodically into very slow striations. A spot also forms at the negative end of the capillary and grows to form the main moving striations in the wide tube. The latter were of feeble intensity and do not show in the Plate. The slow striations at the end of the capillary and the terminal spot have nearly the same speed, about 12 m sec^{-1} , and merge into one another.†

§ 4. SUMMARY AND DISCUSSION

The experiments have shown that moving striations may be formed from small anode spots. The latter can grow, usually periodically, less often monotonically, until a striation moves off. Moving striations can also start at a sharp constriction in a tube in much the same way that they start at a small metal anode. The coupling of the oscillations of the spot and of the main column is reminiscent of the interaction of the local oscillations at the point of entry of the air stream into an organ pipe with the main oscillations of the pipe (Armstrong, Emeleus and Neill 1951). The experiments do not show that conditions cannot exist under which moving striations can occur without anode spots, or an equivalent gas anode (Coulter, Armstrong and Emeleus 1958), although we have not encountered such.

Synchronization of the anode spot and positive column oscillations requires some feed-back from the latter to the former. This may be provided by Donahue and Dieke's fast 'negative' waves, which move towards the anode in the main column (Armstrong, Emeleus and Neill 1951), or by voltage pulses from the external circuit (Steele 1950). Our experiments do not discriminate between these possibilities. Existence of some direct reaction of the striations on the

† Here and elsewhere, the possibility of radial motion in the tube is ignored.

spots may be indicated by the way in which the former linger before moving off, and by the apparent effect of developing striations in the wide tube on those in the capillary (§3). It must however be remembered that, as with an organ pipe, there may be a number of widely differing ways for maintaining the main oscillations, here the moving striations.

Conversely the experiments show that the instability of small anode spots may be partly governed by the same factors that determine the movement of striations. An oscillating anode spot is somewhat like a moving striation in a tube of variable, roughly conical, cross section based on the anode. The current density in the spot, although not constant, is higher than in the main tube and comparable with the current density in the capillary; it might therefore be anticipated that the frequency of the spot would usually be higher than the frequency of the corresponding moving striations in the wide tube and comparable with the capillary frequency, as has been found to be the case. The spot is different from the moving striations in that it is not confined laterally by a glass wall. How far this may alter its properties fundamentally, by giving different transverse boundary conditions for the plasma and space charges in it, is not known. It may not be of much importance as we have noticed moving striations, in other gases, in 'constricted' positive columns which were detached from the tube wall. It is possible that the lack of stability of small anode spots is related to the large curvature of the space-charge sheets in them, but, as with other discharge forms, it is also conceivable that electrophoresis has a more important role than has been realized; in this connection, it has been claimed that anode spots cannot form without some gas emission from the anode (Thomas and Duffendack 1930). Further useful information would probably be gained if time-resolved spectra, which have been obtained for moving striations (Sloane and Minnis 1935, Rutscher 1960), could also be obtained for oscillating anode spots.

ACKNOWLEDGMENTS

We would like to thank A. W. Cooper, L. W. Kerr, N. L. Oleson and H. L. Steele for discussion of parts of this work.

APPENDIX

Summarized Data for Plates

Figures	p	i	V	f_a	f_s	s	v_a	v_c	L	T
2	8.5	20	242	1275	2.04	16.2	—	—	3.3	1.3
3	8.5	40	301	1345	2.02	32.7	90	—	3.1	1.6
5	21.9	27.5	232	2305	1.13	11.1	156	65	3.1	1.1
6	4.35	5	380	2200	2.45	21.6	12	180–220	2.9	0.9

p =pressure (mm Hg), i =current (mA), V =tube voltage (v), f_a =frequency of striations at anode (sec^{-1}), f_s =frequency of anode spot ($\text{sec}^{-1} \times 10^{-4}$), s =anode-cathode distance (cm), v_a =velocity of striations at anode (m sec^{-1}), v_c =velocity of striations in capillary (m sec^{-1}), L =length of tube included (cm), T =time included from top to bottom (msec).

In Figs 2 and 3 the tip of the anode was 1.0 mm to the left of the capillary; in Figs 5 and 6 the tip of the anode was 1.0 cm and 0.7 cm respectively inside the capillary.

In Fig. 2 the faint spots to the left of the main anode spots are reflections in the tube, and the same is true of the faint short inclined streaks in a similar position in Fig. 5.

In Figs 2, 3, 5 and 6 time increases from top to bottom and the anode is at the right.

REFERENCES

- ARMSTRONG, E. B., EMELEUS, K. G., and NEILL, T. R., 1951, *Proc. R. Irish Acad. A*, **54**, 291.
- COOPER, A. W., COULTER, J. R. M., and EMELEUS, K. G., 1958, *Nature, Lond.*, **181**, 1326.
- COULTER, J. R. M., 1959, *Ph.D. Thesis*, Belfast.
- 1960, *J. Electron. and Control*, **9**, 41.
- COULTER, J. R. M., ARMSTRONG, N. H. K., and EMELEUS, K. G., 1958, *Physica*, **24**, 828.
- EMELEUS, K. G., and OLESON, N. L., 1959, *Proc. Phys. Soc.*, **73**, 526.
- PEKAREK, L., 1960, *Proc. 4th Int. Conf. on Ionization Phenomena in Gases, Uppsala* (Amsterdam: North-Holland), I, 306.
- PIGG, M. K., BURTON, J. B., and OLESON, N. L., 1957, *Proc. 3rd Int. Conf. on Ionization Phenomena in Gases, Venice* (Milan: Italian Physical Society), p. 833.
- PUPP, W., 1935, *Physik. Z.*, **36**, 61, and an earlier series of papers.
- RUTSCHER, A., 1960, *Proc. 4th Int. Conf. on Ionization Phenomena in Gases, Uppsala* (Amsterdam: North-Holland), I, 286.
- SLOANE, R. H., and MINNIS, C. M., 1935, *Proc. Phys. Soc.*, **47**, 1019.
- STEELE, H. L., 1950, *3rd Ann. Conf. on Gaseous Electronics* (New York: American Physical Society).
- TAKAMINE, T., SUGA, T., and YANAGIHARA, A., 1933, *Sci. Pap. Inst. Phys. Chem. Res. Tokyo*, No. 403.
- THOMAS, C. H., and DUFFENDACK, O. S., 1930, *Phys. Rev.*, **35**, No. 72.

Stresses at a Crack in an Elastomer

By E. H. ANDREWS

The Natural Rubber Producers' Research Association, Welwyn Garden City, Herts.

MS. received 5th July 1960

Abstract. A microscopical, photoelastic technique has been used to investigate the distributions of stress and strain around a crack in a highly elastic material, natural rubber. The finite strains encountered in such a material give rise to a distortion of the principal-stress map, an effect which has no parallel in classical elasticity and which leads to a complex dependence of the stresses upon the external constraint. The strain energy at a point is however simply related to the external constraint when the latter is expressed in terms of a stored energy parameter T , which is defined. The same parameter is shown to govern the distortion of the stress field. The decay of strain energy in a direction perpendicular to the crack axis is much more gradual when the strains are finite, but the rate of decay along the axis in the elastomer is similar, both in form and magnitude, to that predicted by infinitesimal-strain theory.

§ 1. INTRODUCTION

THE stress distribution around a crack of known geometry in a strained lamina may be calculated by means of classical elasticity theory. Thus Inglis (1913) treated the problem of an elliptical hole and extrapolated his results to the case of a crack. The calculation fails however if the material displays such properties as plasticity or high elasticity which violate the assumptions of Hookean behaviour and infinitesimal strain. Theoretical treatments exist for the plastic-elastic problem (see e.g. Hill 1950) but are mathematically intractable in the case of finite strain. In consequence of this, methods have been developed for the empirical determination of stresses at a crack in a highly elastic medium and these are described, together with the results obtained, in the present paper. A separate publication will discuss the application of this work to the theory of rupture in elastomers.

§ 2. EXPERIMENTAL METHOD

2.1. Apparatus

The investigation involved the photoelastic measurement of stresses in a microscopic region surrounding the tip of a crack in a thin sheet of transparent rubber. It was carried out using a Cooke, Troughton and Simms universal polarizing microscope fitted with a strip-film camera. Magnifications from $100\times$ to $600\times$ were employed. The specimen, illustrated in Fig. 1 and containing the crack to be studied, was mounted in a specially designed extensometer attached to the stage of the microscope. The extensometer, which has been previously described (Andrews 1957), also carries a compensator cut from the same sheet of rubber as the specimen and which intercepts the

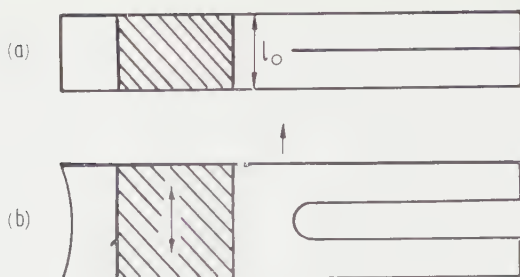


Fig. 1. 'Pure shear' test piece (a) unstrained (b) strained.

plane-polarized beam illuminating the region of the crack tip. The direction of extension of the compensator is perpendicular to that of the specimen. The extensions of both specimen and compensator are given directly by micrometers which record the movement of the securing clamps. These extensions were calibrated against the strains actually existing in the central regions of the test piece (shaded in Fig. 1) and compensator respectively in a preliminary experiment, and in all results quoted the small corrections necessary have been applied.

2.2. Material and its Properties

The rubber sheet employed was cast from pre-vulcanized latex, and combined the properties of toughness, transparency and uniform thickness (of the order of 0.2 mm). Although the stress-strain and stress-optical behaviour of an elastomer is describable up to moderate strains in terms of the theory of large elastic deformations (Treloar 1958), the high strains encountered near the crack tip made preliminary calibration of these properties essential. This consisted in measuring the principal stresses and optical retardation in the material under conditions of general two-dimensional strain (plane stress) by

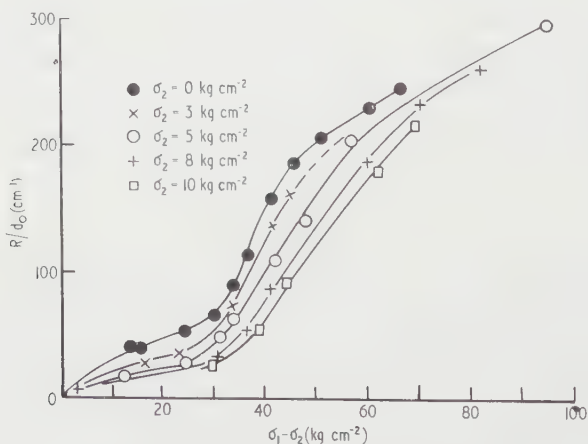


Fig. 2. The optical retardation per unit thickness of the undeformed sheet R/d_0 as a function of the principal-stress difference $\sigma_1 - \sigma_2$ for various σ_2 . R is measured in wavelengths of 5461 ångström units.

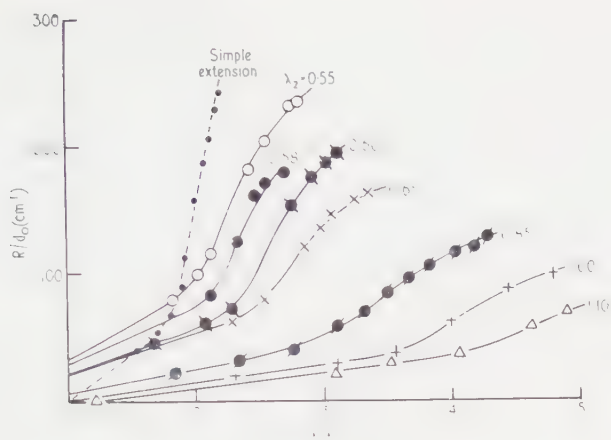


Fig. 3. R/d_0 as a function of the product of the principal extension ratios $\lambda_1 \lambda_2$ for various λ_2 .

the methods of Rivlin and Saunders (1951) and Treloar (1948). From these measurements the graphical data of Figs 2 and 3 were obtained in forms suitable for applications to the stress analysis problem.

2.3. Procedure I

This method was used to determine the stresses along the axis of symmetry of the crack at various extensions of the test piece. The specimen containing the crack was extended under the microscope until the curvature of the opened tip just fitted one of the circles on an inscribed eyepiece graticule. This is a simple way of measuring the deformed tip radius ρ_0 . Using crossed 'nicols' and white light, the compensator was extended beneath the crack causing a black fringe to appear and move inwards towards the tip. By means of an eyepiece scale the position and width of the black fringe were measured as functions of the strain in the compensator. At the black fringe the retardation R in the specimen is equal, though opposite, to that introduced by the compensator.

With the compensator again relaxed the isoclinic fringe system at the crack tip was observed by rotation of the crossed polarizer and analyser. Photographs were taken of the fringes at different rotations and from these records a map of

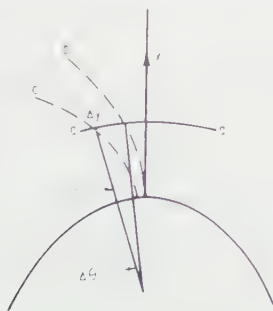


Fig. 4. Method of calculating the curvature ρ of the lines of major principal stress. a , line of principal stress; b , c , isoclinic fringes; $\rho = \Delta y / \Delta \theta$.

principal-stress directions can be derived in the conventional way (see e.g. Jessop and Harris 1949). The whole principal-stress map is not required, however, for the determination of stresses along the crack axis. All that is needed is a knowledge of the curvature radius ρ of the lines of major principal stress σ_1 at their intersection with the axis of symmetry (the x axis). The method by which these data were obtained is indicated in Fig. 4. The lateral shift Δy of the isoclinic fringe caused by a small rotation $\Delta\theta$ of the plane of polarization about the symmetrical position, gave immediately a value for the curvature ρ . Since Δy varied with the distance (x) from the tip, ρ was obtained as a function of x .

The whole procedure was repeated for different extensions of the test piece and for test pieces of different width l_0 (see Fig. 1).

2.4. Procedure II

This method, which is analogous to that of Post (1953) for brittle materials, is more suitable for points off the axis of symmetry than is procedure I. The position of the black fringe was measured as a function of the compensator extension exactly as before, except that now a squared graticule was used to 'map' the fringe over the whole (x, y) plane. No observations of isoclinic fringes were made, but instead the actual deformed thickness d of the sheet was measured from point to point over the (x, y) plane. At the extreme tip ($x=0$) both upper and lower surfaces of the sheet could be brought into focus successively and the thickness read off on the fine focus micrometer of the microscope. Thereafter micrometer readings at focus were taken only on the upper surface, the deformation being assumed symmetrical about the median plane of the sheet. Departure of this median plane from the horizontal was negligible. With a 4 mm objective lens these measurements could be made to within 2μ giving an accuracy to some 5%. From these data the extension ratio $\lambda_3 (= d/d_0)$ perpendicular to the plane of the sheet could be determined at any point in that plane.

§ 3. ANALYTICAL METHODS

3.1. Derivation of the Axial Stresses from Procedure I

The compensator stress σ_c for each known extension was first obtained from the stress-strain curve of the material in simple extension. The optical retardation caused by the compensator was then read off in Fig. 2 on the curve $\sigma_2=0$. This same retardation could be brought about by a whole series of different states of plane stress (σ_1, σ_2) and the locus of these stress states was immediately obtainable from Fig. 2 as a plot of $\sigma_1 - \sigma_2$ against σ_2 for constant R . This locus must include the actual state of stress in the specimen at all points along the black fringe. A series of such loci, one for each extension of the compensator, and thus for each position of the black fringe, is given in Fig. 5.

The Lamé-Maxwell equation of equilibrium (see e.g. Jessop and Harris 1949) gives the following expression for the minor principal stress σ_2 along the axis of the crack,†

$$\sigma_2(x) = \int_0^x \frac{\sigma_1 - \sigma_2}{\rho} dx \quad \dots (1)$$

† This assumes plane stress. Departures from this condition can be shown to be negligible.

where x is a point on the axis of symmetry, the extreme tip of the crack being at $x=0$. As defined earlier ρ is the curvature radius of the lines of major principal stress at their intersection with the x axis. At $x=0$, $\rho=\rho_0$ the deformed tip radius.

Values for $\sigma_2(x)$ were obtained from Eqn (1) using the compensator stress σ_c as a first approximation to $\sigma_1 - \sigma_2$ and integrating graphically with respect to x . This approximate value for σ_2 was next used in Fig. 5 to read off an improved value for $\sigma_1 - \sigma_2$ for the fringe position concerned, and the process

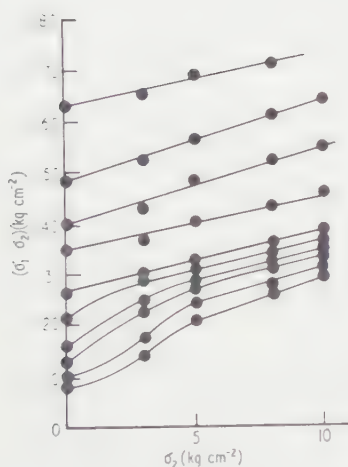


Fig. 5. Loci of stress states producing constant optical retardations.

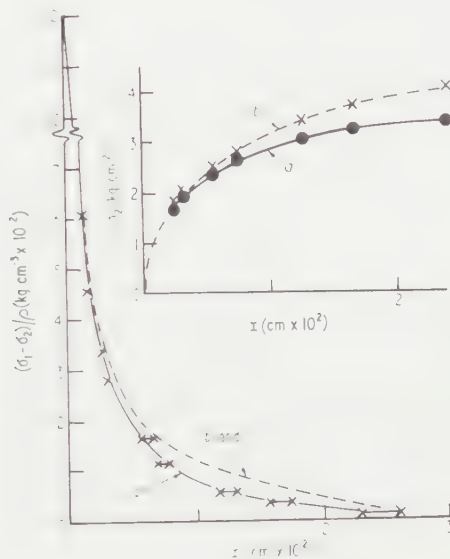


Fig. 6. Determination of the stresses by procedure I; *a*, first, *b*, second and *c*, third approximations.

was repeated until convergent results were obtained. In practice the second approximation of σ_2 gave stresses within 2% of the exact solution. The successive approximation procedure is shown for an actual case in Table 1, and Figs 5 and 6.

3.2. Derivation of the Strain from Procedure II

It has been shown how measurements of the deformed sheet thickness give the value of λ_3 at any point. Since rubber is effectively incompressible

$$\lambda_3 = 1/\lambda_1\lambda_2 \quad \dots\dots(2)$$

λ_1 , λ_2 being the principal extension ratios at a point in the (x, y) plane. The retardation at a point on the black fringe was read off on the simple-extension curve in Fig. 3 using the known extension of the compensator, and a locus of possible strain states ($\lambda_1\lambda_2$ against λ_2) giving rise to the same retardation was plotted. At the same point (x, y) however the value of $\lambda_1\lambda_2$ was known from measurements of λ_3 and the state of strain ($\lambda_1\lambda_2$), λ_2 was therefore uniquely determined.

Table 1. Derivation of Stresses along the Axis by Procedure I
 $T = 1.04 \text{ kg cm}^{-1}$; $l_0 = 3.315 \text{ cm}$

λ_c	Compensator $\sigma_c (\text{kg cm}^{-2})$	Fringe position $x (\text{cm} \times 10^2)$	$\rho^{-1} (\text{cm}^{-1})$	Successive approximations			Results	
				$(\sigma_1 - \sigma_2)/\rho$	σ_2	$(\sigma_1 - \sigma_2)$	$\sigma_1 (\text{kg cm}^{-2})$	
1.694	8.0	3.2-3.7	0.11	0.9	1.5	3.4	4.1	18.1
1.853	10.0	2.3-2.6	1.12	11.2	24.1	3.4	4.1	25.6
2.085	12.7	1.58-1.75	2.69	34.2	66.0	3.2	3.7	28.2
2.320	16.0	1.19-1.32	3.47	55.5	90.0	3.1	3.4	29.3
2.725	21.5	0.70-0.79	5.38	116	153	2.6	2.8	31.2
3.076	26.5	0.58-0.67	6.27	166	185	2.3	2.5	32.0
3.641	35.0	0.32	8.06	282	290	1.9	2.0	39.5
3.960	40.0	0.27	8.50	340	366	1.7	1.8	44.9
4.465	48.5	0.16	9.40	456	498	1.4	1.5	54.5
4.850	63.0	0.13	9.64	607	636	1.2	1.2	67.5
	107	0	11.20	1200	1200	0	0	107

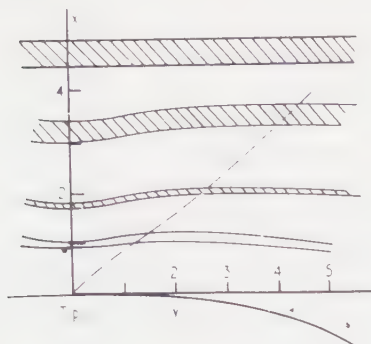


Fig. 7. Successive positions of the black fringe with the maximum-stress trajectory (broken line). The units of x, y are 14.6μ .

Table 2. Derivation of Strains along the Maximum-stress Trajectory, Procedure II

$T = 0.845 \text{ kg cm}^{-1}$; $l_0 = 2.066 \text{ cm}$; $d_0 = 0.229 \text{ mm}$

Compensator	Fringe position ($\text{cm} \times 10^2$)		Specimen thickness		Results	
	x	y	$d(\mu)$	λ_3	λ_2	λ_1
λ_c	0	0	79	0.35	0.35	8.30
—	0.14	0.18	83	0.36	0.52	5.30
5.02	0.15	0.19	83	0.36	0.54	5.10
4.81	0.18	0.23	83	0.36	0.57	4.83
4.38	0.28–0.30	0.40	85	0.37	0.62	4.32
3.74	0.48–0.54	0.66	91	0.40	0.68	3.72
3.36	0.68–0.72	—	95	0.42	0.79	3.04
2.41						

This method was used to measure the strains at points along the axis (for comparison with the results of procedure I) and also at points along the trajectory of maximum stress. This trajectory is defined as the locus

$$\frac{\partial \sigma_1}{\partial y} = 0 \quad \dots\dots (3)$$

σ_1 being a maximum. Since σ_2 is at most points considerably smaller than σ_1 , and since λ_3 changes only slowly with y , it can be assumed with sufficient accuracy that the trajectory crosses the black fringe at the point where its x coordinate is a maximum. This is illustrated in Fig. 7 which shows successive positions of the black fringe together with the maximum-stress trajectory as a broken line.

The calculation of the principal extension ratios along the maximum-stress trajectory from the experimental data for an actual case is given in Table 2.

3.3. Form of the External Constraint

The deformation of the test piece as a whole was characterized by a stored energy parameter T . This is defined (Rivlin and Thomas 1953) as the elastic energy that would be lost from the test piece per unit area of freshly cleaved surface if the crack were to propagate without external work being supplied. For a sheet, thickness d_0

$$T = \frac{1}{d_0} \frac{\partial E}{\partial c} \bigg|_l \quad \dots\dots (4)$$

where E is the total elastic stored energy in the test piece, c the crack length and the suffix l indicates that the constrained boundaries of the test piece do not move. It is important to realise that this definition involves only a *virtual* propagation of the crack and that there exists a T value for every state of strain of the test piece. *Actual* propagation of the crack will occur at some *particular* value of T .

The usefulness of the stored energy parameter lies in the fact that it is readily calculated in some cases where the boundary conditions for the test piece in terms of stress are very complicated. For a test piece of the kind used in this investigation, for instance, Rivlin and Thomas (1953) have shown that

$$T = W_0 l_0 = l_0 (C_1 + C_2) (\lambda^2 + \lambda^{-2} - 2) \quad \dots\dots (5)$$

where l_0 is the width of the specimen, W_0 the stored energy density in the pure shear region of the specimen (shaded in Fig. 1), C_1 and C_2 are elastic constants of the rubber and λ is the extension ratio in the pure shear region. For the rubber used in these experiments $C_1 = 1.00 \text{ kg cm}^{-2}$ and $C_2 = 1.36 \text{ kg cm}^{-2}$.

§ 4. RESULTS

4.1. *The Form of the Principal Stress Map and the Curvature of the Lines of Principal Stress*

Examples of complete principal-stress maps, given in Figs 8 and 9, show the effect of increasing the external constraint on the test piece. Lines of principal stress are represented by solid, and isoclinic fringes by broken lines respectively. As T increases the whole stress map opens out as if all linear dimensions were being magnified in the same proportion. A striking illustration of this is provided by the behaviour of ρ the curvature of the lines of major principal stress at their intersection with the x axis. In Fig. 10, ρ^{-1} is plotted against the distance x with the strained tip radius ρ_0 as a scaling factor for both quantities. Data from all experiments define a single curve

$$\rho_0/\rho = f(x/\rho_0). \quad \dots\dots (6)$$

It is also found that ρ_0 is proportional to T (Fig. 11) so that T can also be used as a scaling factor for distances.

This change in the principal-stress map is important because it has no parallel in classical elasticity theory. Reference to the Lamé–Maxwell equation shows that this strain distortion of the stress field, by making ρ a function of the external constraint, leads to a considerably more complex relation between the latter and the local stresses than in the classical case. For instance the ratio σ_2/σ_1 at a point, which is constant in classical theory, must, in the elastomer, decrease as T increases. A second consequence stems from the enlargement of the curvature radii ρ' of the lines of *minor* principal stress, since these govern the decay of major principal stress in the direction of y

$$\frac{\partial \sigma_1}{\partial y} = - \frac{\sigma_1 - \sigma_2}{\rho'}. \quad \dots\dots (7)$$

As T and therefore ρ' increase, the rate of stress decay along the boundary of the crack is diminished. The situation in a brittle material is analogous to that in the elastomer at vanishing T , when little strain distortion has occurred, so that under all finite stresses the value of $\partial \sigma_1 / \partial y$ must be smaller in an elastomer than in a brittle substance. (A factor of the order of the strained radius divided by

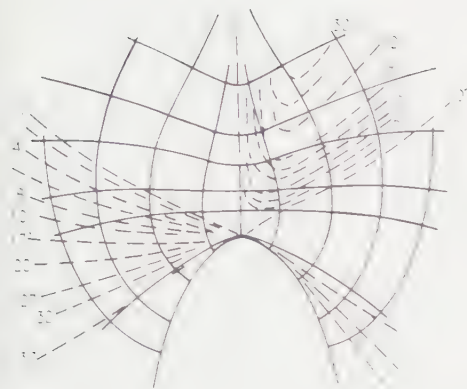


Fig. 8. Principal-stress map (isoclinics shown as broken lines) at $T=0.16 \text{ kg cm}^{-1}$.

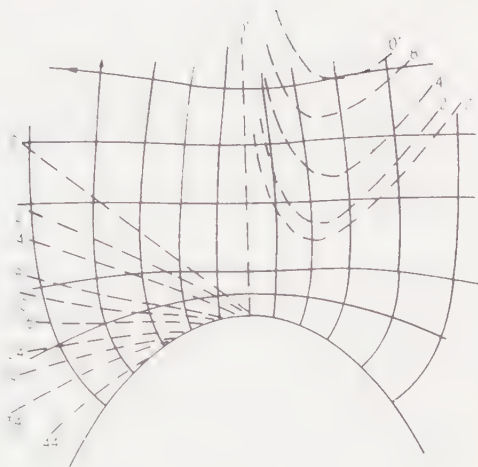


Fig. 9. Principal-stress map at $T=0.65 \text{ kg cm}^{-1}$.

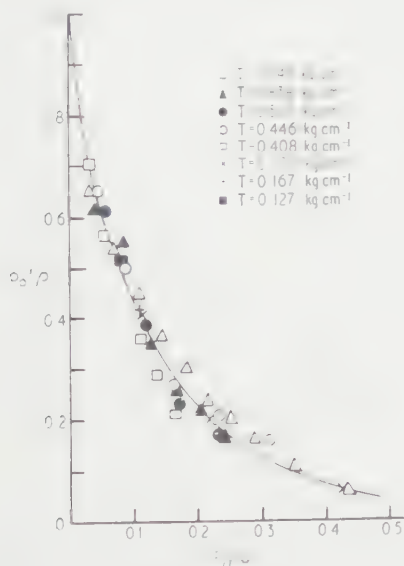


Fig. 10.

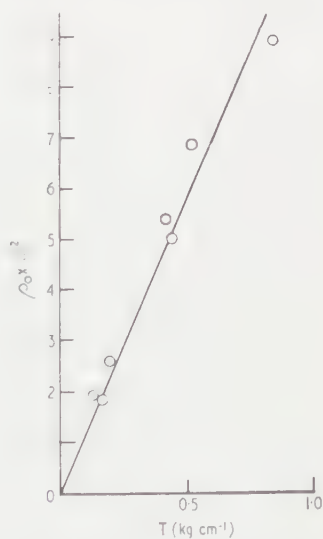


Fig. 11. Dependence of the deformed tip radius upon T .

the unstrained radius is involved.) Since, as will be shown, the stress decay along the crack axis is almost identical in brittle and elastomeric media it follows that a much larger volume of material is under high stress at the tip of a crack in an elastomer.

4.2. The Stresses and Stored Energy Along the Axis from Procedure I

The stresses σ_1 , σ_2 are given in Table 3 as functions of x (distance measured along the axis from the tip in the deformed state) for test pieces of different widths l_0 and for several values of T . As discussed above the minor principal

Table 3. Stress Distribution along Crack Axis

	T (kg cm ⁻¹)	x (cm × 10 ²)	σ_1 (kg cm ⁻²)	σ_2 (kg cm ⁻²)	W ((kg cm)cm ⁻³)
Test piece A $l_0 = 2.710$ cm	0.191	0.07	42.7	1.2	21.8
		0.14	33.4	1.9	15.5
		0.20	29.7	2.5	13.3
		0.27	25.8	2.8	11.2
		0.34	24.3	3.1	10.5
		0.41	23.5	3.3	9.9
		0.68	21.5	3.8	9.0
	0.408	0.07	57.0	1.0	27.0
		0.14	35.9	1.4	17.2
		0.20	30.2	1.7	14.7
		0.27	27.4	1.9	12.0
		0.41	23.1	2.1	9.6
		0.54	20.8	2.3	8.4
		0.68	19.0	2.5	7.6
Test piece B $l_0 = 1.620$ cm	0.505	0.09	59.0	1.0	27.8
		0.18	34.9	1.4	16.6
		0.26	29.7	1.7	13.4
		0.35	27.6	1.9	12.2
		0.53	25.5	2.3	10.9
		0.70	22.5	2.5	9.4
		0.88	21.7	2.7	8.7
		1.76	16.2	3.2	6.6
	0.838	0.09	65.0	2.0	29.7
		0.18	47.8	2.5	24.4
		0.26	38.6	2.8	19.6
		0.35	34.3	3.0	16.5
		0.53	32.4	3.4	14.9
		0.70	30.4	3.7	14.0
		0.88	28.4	3.9	12.8
		1.76	26.8	4.6	11.8
Test piece C $l_0 = 3.315$ cm	0.446	2.63	23.5	4.8	10.0
		0.11	57.6	1.6	27.3
		0.18	39.5	2.3	19.7
		0.26	32.2	2.7	15.0
		0.35	31.5	3.0	14.6
		0.53	29.4	3.4	13.2
		0.70	27.1	3.6	11.9
		0.88	25.4	3.9	11.0
	1.040	0.13	67.5	1.2	30.3
		0.16	54.5	1.5	26.4
		0.27	44.9	1.8	23.0
		0.32	39.5	2.0	19.7
		0.63	32.0	2.5	14.6
		0.75	31.2	2.8	14.3
		1.26	29.3	3.4	13.1
		1.66	28.2	3.7	12.6
		2.45	25.6	4.1	11.1
		3.45	18.1	4.1	7.5

Table 4. Strains Derived by Procedure II

$T(\text{kg cm}^{-1})$ $(l_0 = 2.066 \text{ cm})$	Maximum-stress trajectory				Axis		$W'(\text{kg cm})\text{cm}^{-3}$
	$x(\text{cm} \times 10^2)$	λ_1	λ_2	$W'(\text{kg cm})\text{cm}^{-3}$	$x(\text{cm} \times 10^2)$	λ_1	
0.434 $(l_0 = 2.066 \text{ cm})$	0	6.7	0.39	65	0	6.7	65
	0.16	4.50	0.54	25.6	0.14	4.52	25.6
	0.19	4.30	0.57	23.7	0.15	4.38	24.2
	0.24	4.05	0.60	21.0	0.19	3.89	19.4
	0.31	3.81	0.63	18.6	0.25	3.62	16.5
	0.44	3.13	0.76	12.4	0.43	3.17	12.5
	0.75	2.67	0.82	8.8	0.75	2.71	8.8
	0	8.3	0.35	90	0	8.3	90
	0.14	5.30	0.52	36.5	0.13	5.25	35.8
	0.15	5.10	0.54	33.2	0.14	5.20	34.5
0.845 $(l_0 = 2.066 \text{ cm})$	0.18	4.83	0.57	30.0	0.16	4.97	31.8
	0.29	4.32	0.62	24.0	0.28	4.07	21.3
	0.51	3.72	0.68	17.9	0.48	3.50	16.1
	0.70	3.04	0.79	11.8	0.69	3.15	12.8
	0	7.1	0.37	70	0	7.1	70
	0.16	4.43	0.58	25.0	0.14	4.90	30.8
	0.23	4.16	0.58	22.0	0.20	4.31	23.6
	0.37	3.85	0.59	18.9	0.35	3.56	16.0
	0.73	3.00	0.73	11.4	0.73	3.14	12.5
	0	7.1	0.37	70	0	7.1	70
0.628 $(l_0 = 1.900 \text{ cm})$	0.16	4.43	0.58	25.0	0.14	4.90	30.8
	0.23	4.16	0.58	22.0	0.20	4.31	23.6
	0.37	3.85	0.59	18.9	0.35	3.56	16.0
	0.73	3.00	0.73	11.4	0.73	3.14	12.5
	0	7.1	0.37	70	0	7.1	70
	0.16	4.43	0.58	25.0	0.14	4.90	30.8
	0.23	4.16	0.58	22.0	0.20	4.31	23.6
	0.37	3.85	0.59	18.9	0.35	3.56	16.0
	0.73	3.00	0.73	11.4	0.73	3.14	12.5
	0	7.1	0.37	70	0	7.1	70

stress σ_2 at a point does not, like σ_1 , increase steadily with T , but tends rather to decrease.

A more analytical treatment of the results is possible if they are expressed in terms of the strain energy density W . The known stress-strain data for the material have therefore been used to convert the stresses to the stored energy at a point in the (x, y) plane. Although W contains less explicit information than the separate stresses, it is a quantity which can be directly compared with the parameter T . In Fig. 12, the reciprocal of the energy is plotted as a function of $(x + \alpha)/T$, T being used as a scaling factor for distance as discussed earlier. A small shift α along the x axis has been introduced to bring the data for all values of T into coincidence and is shown inset as a function of T for the four test pieces used. (Results for test piece D were obtained by procedure II.) The early, linear portion of the curve is thus described by the equation,

$$\frac{1}{W} = \frac{K_1(x + \alpha)}{T} \quad \dots\dots (8)$$

where K_1 is a dimensionless constant of value 9.0. It is clear from this result, as well as the findings of §4.1, that the stress field at the tip of a given crack is entirely governed by the parameter T . This general conclusion was anticipated by Thomas (1955) who measured strains in a rubber sheet around a notch of measurable radius. It will be shown later that the constant α is in the nature of an unstrained tip radius. Its observed variation with T is probably the result of a small amount of crack propagation during the course of the experiments.

4.3. Results from Procedure II

The results obtained by this method are given in Table 4 which shows the principal extension ratios and stored energy as functions of the x coordinate

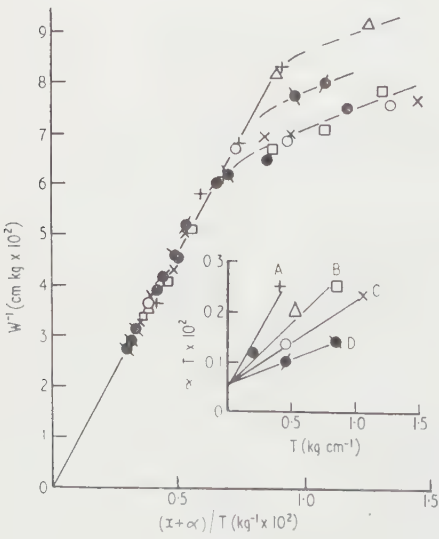


Fig. 12. Reduced curve for axial stored energy. Shift factor inset as a function of T for various test pieces A to D.

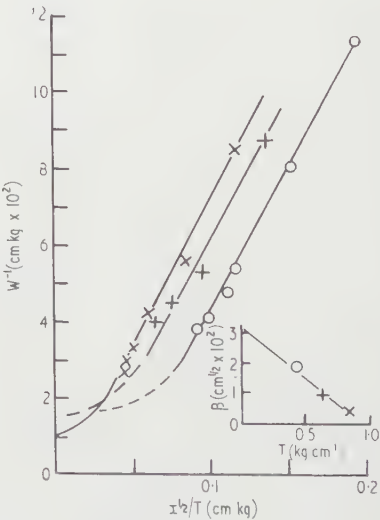


Fig. 13. Stored energy along the maximum-stress trajectory. Shift factor required to bring the results into coincidence is shown inset.

along both the axis and the maximum-stress trajectory for three values of T . Two of the axial solutions have already been displayed in Fig. 12 alongside the results from procedure I and are seen to agree very closely with the latter.

The stored energies along the maximum-stress trajectory are plotted in Fig. 13 in reciprocal form against $x^{1/2}/T$. The replacement of x by its square root produces linearity over most of the experimental range, though near the tip the plots must curve to intercept the W^{-1} axis at a positive value. As in the case of the axial energies the results may be superimposed by shifting the curves along the distance axis to give a 'master' curve

$$\frac{1}{W} = \frac{K_2(x^{1/2} - \beta)}{T} \quad \dots\dots(9)$$

where K_2 is a constant of value $0.72 \text{ cm}^{1/2}$ and β is the shift factor whose dependence upon T is shown inset in Fig. 13.

The parameter β is the apparent intercept of the linear portion of the curve with the distance axis and is a measure of the non-linearity at small x . Its physical significance may be inferred from the results for classical materials. Fig. 14 shows the empirical data obtained by Post (1953) on a brittle plastic containing a notch of measurable radius. His results for the maximum-stress trajectory have been plotted in the form used for the elastomer and a very similar

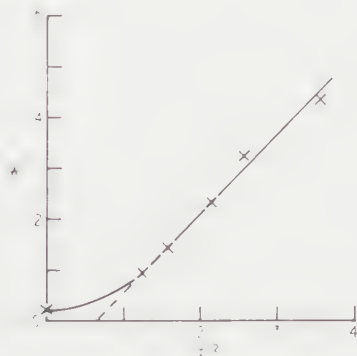


Fig. 14. Stored energy along the maximum-stress trajectory in a brittle material (empirical data of Post (1953). Arbitrary units).

curve results. The initial curvature, which reflects the fact that at low x the maximum-stress trajectory coincides with the x axis, persists until x is roughly twice the tip radius. The quantity β^2 is then approximately equal to the tip radius, and Post's results suggest that this equivalence is maintained as the (unstrained) tip radius is reduced to crack dimensions. It therefore seems reasonable in the case of the elastomer to identify β^2 with an unstrained tip radius. The fact that β decreases with increasing T is, like the variation in z , attributable to a small growth of the crack during the experiments and the true value of β is obtained by extrapolating to zero T . If this reasoning is correct it indicates an unstrained tip radius of some 10μ for the elastomer.

4.4. Comparison of the Axial Stored Energy with the Results of Infinitesimal Strain Theory

The classical solution for stresses along the axis is sufficiently simple to be expressed in terms of stored energy and thus compared with the results for the elastomer.

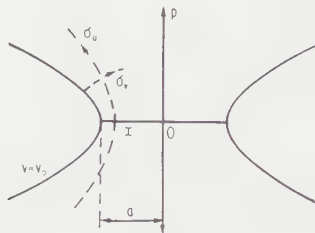


Fig. 15.

Use may be made of Neuber's solution (1945) for the stresses at a deep external notch in a tensile-loaded plate, sketched in Fig. 15. The nominal stress is p and the perimeter of the notch is the hyperbola $v = v_0$ (constant). The curvilinear coordinates are related to the Cartesian in the following manner:

$$\left. \begin{aligned} y/a &= \sin u \cos v \\ x'/a &= \cos u \sin v. \end{aligned} \right\} \dots\dots (10)$$

Since x' is measured from the origin O and the tip of the crack lies at $x' = a$,

$$\frac{x'}{a} \equiv 1 - \frac{x}{a} \dots\dots (11)$$

where x is the distance measured from the tip in accordance with previous usage.

Neuber's solution for stresses along the axis reduces to

$$\left. \begin{aligned} \sigma_u &= \frac{p}{\cos v} \left(\frac{\sin v_0}{v_0 + \sin v_0 \cos v_0} \right) \left(1 + \frac{\cos^2 v_0}{\cos^2 v} \right) \\ \sigma_v &= \frac{p}{\cos^2 v} \left(\frac{\sin v_0}{v_0 + \sin v_0 \cos v_0} \right) (\cos^2 v - \cos^2 v_0) \\ \tau_{uv} &= 0. \end{aligned} \right\} \dots\dots (12)$$

The case of a crack of zero tip radius is obtained by letting $\cos v_0 \rightarrow 0$, whence

$$\sigma_v = \sigma_u = 2p/\pi \cos v$$

i.e. a state of biaxial tension rising to infinity at the tip $\cos v = \cos v_0 = 0$. Now along the x axis, $\sin u = 0$ and, from (10)

$$\cos v = (1 - x'^2/a^2)^{1/2}$$

so that,

$$\sigma_u^2 + \sigma_v^2 = \frac{8p^2}{\pi^2} \frac{1}{(1 - x'^2/a^2)}.$$

The left-hand side is proportional to W and the right-hand side to W_0 , the stored energy density a large distance from the tip, so that

$$W = \frac{8W_0}{\pi^2} \frac{1}{(1 - x'/a)(1 + x'/a)}.$$

At small x , where $x' \simeq a$,

$$W \simeq \frac{4W_0a}{\pi^2 x}. \quad \dots (13)$$

This is of the same form as the equation obtained empirically for the elastomer, which is, from (5) and (8),

$$W = \frac{W_0 l_0}{9(x + \alpha)}. \quad \dots (14)$$

Allowing a formal equivalence between the dimensions l_0 and $4a$, the rates of decay of W along the x axis are almost identical.

The classical derivation for a tip of zero radius contains the singularity $\sigma_y = \infty$ at $x=0$ so that a preferable treatment is to allow $\cos \epsilon_0 \rightarrow \epsilon$ where $\epsilon \ll 1$. An exactly similar calculation leads to the equation

$$W \simeq \frac{4W_0a}{\pi^2} \left\{ \frac{1 + (1 + x/\gamma)^{-2}}{x + \gamma} \right\}$$

where $2\gamma = \epsilon^2 a$. Neuber gives $\cos^2 \epsilon_0 = (1 + a/r)^{-1}$, where r is the unstrained tip radius, so that if $a \gg r$, then $2\gamma = r$. For $x > r$ this reduces rapidly to

$$W \simeq \frac{4W_0a}{\pi^2(x + r)} \quad \dots (15)$$

which is precisely the form of the empirical equation (14) with $\alpha \equiv \gamma$. Using measured values of α for test piece D (on which the tip radius was earlier calculated from the behaviour of β)

$$x \simeq 5 \mu$$

and an independent estimate of $r \simeq 10 \mu$ is obtained in agreement with the previous value.

§ 5. DISCUSSION

Since the stress distribution at a crack in an elastomer must be given by classical elasticity theory when the strains tend to zero, the classical solution may be regarded as the limiting case of a more general, finite-strain solution. The most important characteristic of the system under finite strain is that the *distribution* of stress (as typified for example by the principal-stress map) depends upon the external constraint. This dependence has been shown experimentally to be a simple one provided the external constraint is expressed in suitable terms, and the stored energy parameter T appears well suited to this purpose.

The fact that the stress *distribution* as well as the stress *level* is a function of the applied constraint when the strains are finite has a number of consequences. In the first place it leads to variations in the ratio σ_2/σ_1 at a point and secondly to large changes in the volume of material subjected to high strain. Although the first of these is only of academic interest, the volume effect has important repercussions in rupture theory where energy losses in the highly strained region of the propagating crack contribute largely to the energy of rupture (Mullins 1959).

Although the differences between the results for finite and infinitesimal strain are important, the similarities are also striking. In particular the decay of stored energy along the crack axis is, for small x , identical in form and quantitatively similar to that predicted by classical theory. This is in spite of the facts that (i) classical theory is totally inapplicable to strains of the magnitude

encountered and (ii) the stress-strain curve of the elastomer is strongly non-linear. It appears then that the spatial distribution of elastic stored energy close to the tip of a crack may be expressed in simple mathematical terms even when the elastic behaviour of the medium is complex. It is not possible to say at this stage whether this result is fortuitous or whether it reflects some more general principle of energy distribution in a strained body.

ACKNOWLEDGMENT

This work forms part of a programme of research undertaken by 'The Board of the Natural Rubber Producers' Research Association.

REFERENCES

- ANDREWS, E. H., 1957, *J. Sci. Instrum.*, **34**, 115.
HILL, R., 1950, *The Mathematical Theory of Plasticity* (Oxford: Clarendon Press).
INGLIS, C. E., 1913, *Trans. Instn Nav. Archit., Lond.*, **60**, 219.
JESSOP, H. T., and HARRIS, F. C., 1949, *Photoelasticity* (London: Cleaver-Hume Press).
MULLINS, L., 1959, *I.R.I. Trans.*, **35**, 213.
NEUBER, H., 1945, *Theory of Notch Stresses*, David Taylor Model Basin, U.S. Navy.
POST, D., 1953, *Memorandum Report 175*, Naval Research Laboratory, Washington D.C.
RIVLIN, R. S., and SAUNDERS, D. W., 1951, *Phil. Trans. Roy. Soc. A*, **243**, 251.
RIVLIN, R. S., and THOMAS, A. G., 1953, *J. Polym. Sci.*, **10**, 291.
THOMAS, A. G., 1955, *J. Polym. Sci.*, **18**, 177.
TRELOAR, L. R. G., 1948, *Proc. Phys. Soc.*, **60**, 135.
—— 1958, *Physics of Rubber Elasticity*, 2nd Edn (Oxford: Clarendon Press).

Polarization of Protons from Low Resonances in $^{12}\text{C}(\text{d}, \text{p})^{13}\text{C}$

BY A. G. GREGORY AND P. B. TREACY

Research School of Physical Sciences, Australian National University, Canberra

Communicated by E. W. Titterton; MS. received 16th May 1960

Abstract. The polarization of protons from the $^{12}\text{C}(\text{d}, \text{p})^{13}\text{C}$ reaction has been measured at deuteron energies from 790 to 1100 kv at angles of 45° , 60° , 90° , 120° and 135° , using a carbon polarimeter. Published angular distributions have been analysed in conjunction with the present results in terms of compound nucleus theory. Previous assignments of 1^+ and 2^- for the first two resonance levels are confirmed. Analysis of the present results seems to imply a ratio of reduced width amplitudes for d to s wave deuterons larger than that suggested by previous measurements of the angular distribution. However, in fitting these results, it was found necessary to assume phase angles other than those required in the usual theory of resonance reactions.

§ 1. INTRODUCTION

POLARIZATION, being essentially an interference effect, is more sensitive to the nature of reaction mechanisms and parameters than is the reaction cross section. It is to be expected therefore that an analysis of the energy and angle dependence of polarizations in the vicinity of suitable nuclear resonances will yield information additional to that obtained from normal angular distributions. In the case of $^{12}\text{C}(\text{d}, \text{p})^{13}\text{C}$ angular distributions have been reported (Phillips 1950, Sarma *et al.* 1957) of protons leading to the ground state of ^{13}C at bombarding energies from 0.8 Mev to 1.7 Mev, which range covers the first five resonances. The analysis of these distributions in terms of Legendre polynomials shows a large A_1 term which is attributed to interference between two levels of the compound nucleus ^{14}N corresponding to bombarding energies of 0.96 and 1.16 Mev. Suggested nuclear spins and parities for these levels are 1^- and 2^- . Such conditions seem very favourable to the existence of large polarizations, and indeed, quite large values have been reported (Jurić and Čirilov 1958) at a deuteron energy of 1060 kev. The existence of a negative ' Q ' value for the (d, n) reaction was a deciding factor in the present choice of ^{12}C for a (d, p) reaction relatively free from knock-on proton background.

The polarization of a beam of protons produced in a nuclear reaction may be deduced from measurements of right left asymmetries resulting when suitable materials are interposed in the beam. As shown by Simon (1953) for spin $\frac{1}{2}$ outgoing particles the asymmetries are of the form

$$P_1(\theta_1)P_2(\theta_2)\cos\phi_2 = \frac{L-R}{L+R} \quad \dots\dots(1.1)$$

where L and R are scattered intensities at angles θ_2 to left and right of the scatterer, $P_1(\theta_1)$ is the polarization produced in the initial reaction, $P_2(\theta_2)$ the polarization

which would be produced by the elastic scattering of an unpolarized beam of protons, and ϕ_2 is the azimuthal angle between the normals to the planes of the two reactions. In the convention used here P_1 is positive when the greater of L and R is on the same side of the scatterer as the scatterer is of the target. Carbon was chosen as the best scattering material for these experiments as it provides better energy resolution and a smaller range of scattering angles than does helium and it is more convenient to use. A carbon scatterer was also employed by Juric and Cirilov (1958). They used foils to reduce the proton energy to 1.75 MeV, where their calculations indicated that the value of $P_2(\theta_2)$ should be very high over a small range of θ_2 , although critically dependent on energy. More extensive calculations since published (Phillips and Miller 1959) confirm this and also predict that for protons of about 3 MeV energy scattered through 45° , $P_2(\theta_2)$ should be about 20% and not sensitive to small variations of energy or angle. The present experiments were carried out in this region.

§ 2. APPARATUS

The apparatus consisted of two distinct units, the target and analysing chambers. These are shown diagrammatically in Fig. 1. The target chamber consisted of a dural cylinder of $4\frac{1}{2}$ in. internal diameter and 5 in. depth. An axial tube passing through an 'O' ring seal in the lid provided a rotatable water cooled support on which targets in the form of 1.16 in. thick carbon plates could be screwed, the lower part of the support being cut back so that the target face passed through the cylinder axis. For lining-up purposes a quartz plate was attached to the support below the target, which could be raised to bring the quartz into the target position. The analysing chamber consisted of a similar

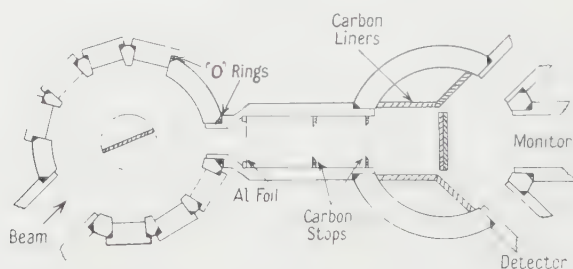


Fig. 1. Schematic cross section of apparatus with the analyser in the 45° position.

dural cylinder which could be connected to the target chamber at various angles to the beam direction by means of a short tube which fitted into any one of eight ports at 15° intervals round the target chamber. The connecting tube contained an aluminium foil in which scattered deuterons were stopped, and two carbon stops were placed so as to minimize the number of scattered protons reaching the analyser. The scatterer was in the form of a 20 micron polystyrene sheet held in a carbon frame and could be raised so as to expose an identical, but empty, frame to the proton flux when making background runs. Carbon liners in the analysing chamber were employed to reduce the neutron background. Electrostatic quadrupole lenses were used to focus the beam on the target at a distance of 10 ft from the analysing magnet of the 1.2 MeV h.t. set. Stable beam spots of less than $\frac{1}{4}$ in. cross section could be obtained.

In order to investigate the azimuthal variation of asymmetry it was possible to rotate the whole scattering chamber about the axis of the connecting tube. To check any intrinsic asymmetries in the detection system an azimuth of 90° was used. The detectors were two caesium iodide crystals each 0.01 in. thick and 1 in. diameter cemented to 2 in. Dumont type 6292 photomultipliers which subtended a solid angle of $1/20$ sterad at the scatterer, the illuminated area of which was also about 1 in. in diameter. A photomultiplier in the 'straight through' position could be used as a monitor. Pulses from the two 45° counters were amplified and passed through a spectrum sorter which allowed both spectra to be displayed simultaneously on the screen of a 100 channel kicksorter.

§ 3. EXPERIMENTAL PROCEDURE AND RESULTS

At the beginning of each set of runs at any angle θ the beam was lined up on the quartz disk, then the target set at an angle of $\theta/2$ to the beam direction. At each energy three runs were made with the scatterer alternatively in, out and in again. Null runs, with $\phi = 90^\circ$ were made at five energies at each of three angles. It was found sufficiently accurate to use a beam-current integrator as monitor rather than the straight-through detector. At energies from 790 to 945 keV each run was given 1000 microcoulombs, higher energies being given half this. About 1000 scattered protons would be recorded in each detector under these conditions at 850 keV.

Thick targets were used in preference to thin ones so that beam currents of up to $150\mu\text{A}$ could be used for long periods without causing noticeable damage, and build-up of carbon deposits could be ignored. The use of such targets entailed a more complicated treatment of results since protons observed at any given deuteron energy E arose from reactions at all energies up to E . Thus any polarization derived from a single observation would be a composite value, with little significance. The results were therefore treated as follows.

At each angle separate yield curves were obtained for protons scattered to left- and right-hand detectors. Then, with a correction of about 1% for variations of dE/dx with energy, the 'thin target' yields appropriate to any given energy were given by the slopes of the yield curves at this energy. Eqn (1.1) then gave the required polarization with L and R as the slopes of the yield curves.

Some factors which could introduce errors into this type of experiment are the finite sizes of target, scatterer and detectors combined with the variation with angle of the cross sections for the (d, p) and (p, p) reactions. An algebraic expression was derived containing the contributions of each of these factors. The largest contribution was found to arise from the variation of the (d, p) reaction and Phillips' (1950) results were used to estimate the maximum error from this source which amounted to 0.5%.

Fig. 2 shows a typical pair of spectra of protons scattered from the polystyrene target. The excellent resolution from background in these spectra permitted good accuracy in estimating the areas under the peaks even at the lowest energies used and from such areas the left and right yield curves were obtained. Errors quoted for the final polarizations are those involved in estimating the slopes of these curves, and are due to the spread of values obtained at each point. Graphs 1-5, Fig. 3 show P_1P_2 as functions of energy. It was necessary to leave the results in this form owing to a discrepancy between the efficiency predicted by Phillips and Miller (1959) and the maximum values of

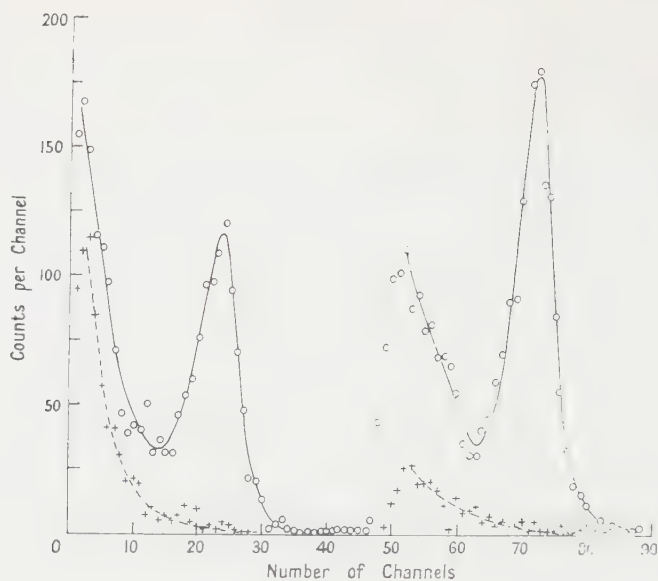


Fig. 2. A typical pair of spectra at 850 kv with $\theta=45^\circ$. The two peaks represent protons scattered at 45° on opposite sides of the polystyrene foil.

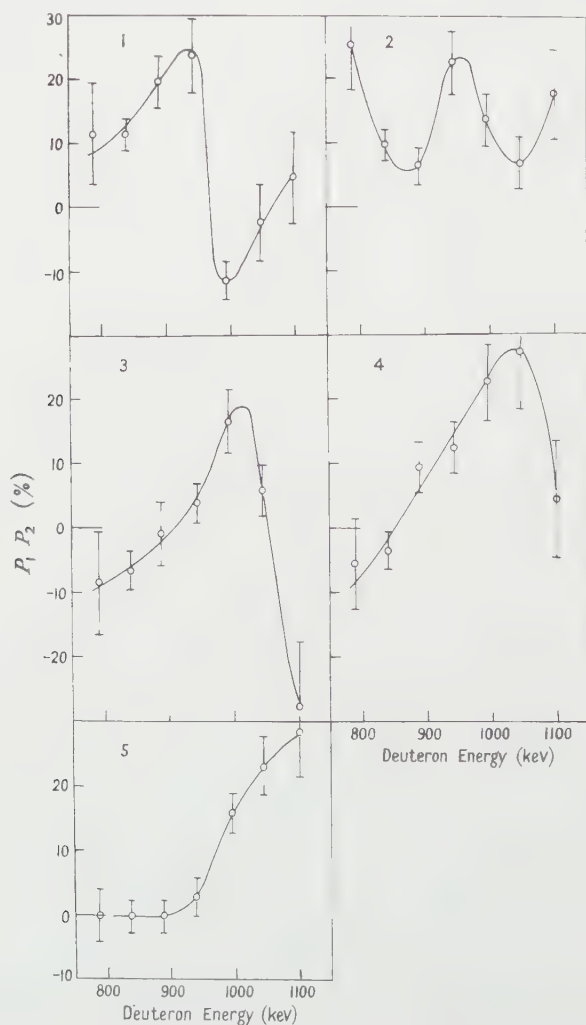


Fig. 3. P_1P_2 as a function of deuteron energy.
1, $\theta=45^\circ$; 2, $\theta=135^\circ$; 3, $\theta=60^\circ$; 4, $\theta=120^\circ$; 5, $\theta=90^\circ$.

P_1P_2 found in these experiments. The latter require P_2 to be at least 25% as compared with the predicted value of less than 20%.

The null runs gave a resultant value of 0.6% with a r.m.s. deviation of 4.4%.

§ 4. ANALYSIS OF RESULTS

4.1. Angular Distributions

Defining the differential cross section as

$$\frac{d\sigma}{d\Omega} = \sum_n A_n P_n(\cos\theta) \quad \dots\dots (4.1)$$

one may plot the energy dependence of the A_i . Fig. 4 shows values of A_0 to A_4 inferred from the data of Sarma *et al.* (1957) (Table and Fig. 2, for $\theta_{\text{cm}} = 161^\circ$). The fact that higher A_i are negligible, i.e. less than 1% of A_0 , is clear evidence that the compound-nucleus mechanism operates.

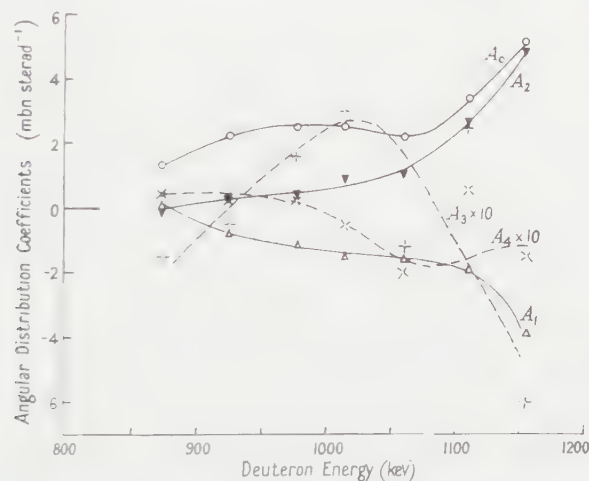


Fig. 4. Angular distribution coefficients, defined by the relation $d\sigma/d\Omega = \sum_n A_n P_n$.

The total cross section is $4\pi A_0$, and, disregarding the possibility of complex behaviour due to adjacent levels having equal spins and parities (Teichmann 1950), there seem to be resonances at 0.96 and 1.16 Mev. A_1 is resonant at both of these energies and A_2 strongly so at only 1.16 Mev. It has been postulated (Phillips 1950, Sarma *et al.* 1957) that the levels are of opposite parities and the nearly isotropic distribution at 0.96 Mev is due to predominant s-wave deuteron capture to form a ($J^\pi = 1^-$) level. At 1.16 Mev $J^\pi = 2^-$ has previously been assumed on the basis of limited anisotropy and (Sarma *et al.* 1957) in order to guarantee approximate equality of the reduced widths for neutron and proton emission to the first excited state of ^{13}C . It is better here to argue on the basis of the relative magnitudes of A_0 , A_2 and A_4 as follows.

Using Phillips' data on (d, p) and (d, n) cross sections and assuming his value of 0.200 Mev for the total width of the 1.16 level, one can deduce that the partial deuteron width is 10 keV or 7 keV for $J = 1$ or $J = 2$, respectively. Taking 7 keV as a minimum one finds that the sum rule limit restricts the deuteron angular momentum to 2 or less. This limits J^π to 0^+ , 1^- , 2^+ or 3^- . Anisotropy coefficients for the significant J^π assignments are listed in the Table. These were

calculated using formulae as given by Sharp *et al.* (1954) and Coulomb wave functions with the Wigner-Eisenbud theory.

Anisotropies for Compound Levels of $^{12}\text{C}(\text{d}, \text{p})$				
J^π	A_2/A_0	A_4/A_0	Min A_4/A_0	Max A_2/A_0 at Min A_4/A_0
1^-	$\frac{\pm 0.17\sqrt{(\Gamma_0\Gamma_2) - \frac{1}{2}\Gamma_2}}{\Gamma_0 + \Gamma_2}$	0	0	0.015
2^+	$\frac{\frac{1}{2}\Gamma_1 + \frac{4}{7}\Gamma_3 \pm 0.27\sqrt{(\Gamma_1\Gamma_3) - \frac{4}{7}\Gamma_3}}{\Gamma_1 + \Gamma_3}$	$\mp 2.16\sqrt{(\Gamma_1\Gamma_3) - \frac{4}{7}\Gamma_3}$	0	0.50
2^-	$\frac{\frac{1}{2} + \chi}{1 + \chi}$	0	0	1
3^+	$\frac{\frac{6}{7} + \frac{8}{7}\chi}{1 + \chi}$	$\frac{\frac{1}{7}(1 + 6\chi)}{1 + \chi}$	$\frac{1}{7}$	$\frac{6}{7}$

Γ_i =partial width for protons of angular momentum i ; χ =the ratio of probabilities of outgoing channel spin 0 to 1.

In the Table the alternative signs in cross terms arise from uncertainties of signs (but not phases) of proton reduced-width amplitudes. An interaction radius of 3.96×10^{-13} cm was used in calculating phase factors.

Experimental angular distributions at the higher resonance (Fig. 4) require $A_2/A_0 \simeq 1$, $A_4/A_0 \simeq 0$ which lead to the assignments $J^\pi = 2^-$, $\chi \rightarrow \infty$ or $J^\pi = 3^+$, $\chi \rightarrow 0$. On the available data it appears that the minimum value of $A_4/A_0 = \frac{1}{7}$ is too large to permit the latter assignment. Furthermore in this case the 0.96 mev level would be required to be of odd parity to account for the observed interference terms, giving the possible J^π values of 0^- , 1^- , or 2^- . The first two of these cannot give the required A_1 term, whilst 2^- requires $A_2/A_0 \geq \frac{1}{2}$ which is not the case. A 2^- assignment for the 1.16 mev level leads to either 0^+ or 1^+ at 0.96 mev. The former is ruled out on the basis that A_1 , A_3 and B_3 are non-zero (see below). We are thus left with the assignments: 2^- at 1.16 mev and 1^+ at 0.96 mev.

Also of interest from the Table is the fact that the previous assignment 3^+ for levels at 1.30 and 1.44 mev are not compatible with measured values of A_2/A_0 and A_4/A_0 .

4.2. Polarization Results

The evidence from measured angular distributions (Phillips 1950, Sarma *et al.* 1957) is that the $^{12}\text{C}(\text{d}, \text{p})$ process for deuteron energies to 1.4 mev can be described in terms of interfering levels of the compound nucleus ^{14}N . In analysing resonance reactions the natural description is in terms of the differential polarization (Simon and Welton 1953, Eqn (3.2)), which may be written

$$\frac{dP(\theta)}{d\Omega} = i'f(\theta) \quad \frac{d\sigma(\theta)}{d\Omega} = \sum_n B_n P_n^1(\cos\theta), \quad \dots\dots (4.2)$$

where i' is the spin of the outgoing particle, $f(\theta)$ the polarization P_1 defined in § 1 and $d\sigma/d\Omega$ the differential cross section at the energy and angle considered; P_n^1 is an associated Legendre polynomial of order $(n, 1)$. In the present experiments no attempt was made to measure the absolute cross sections and in order to obtain

the B_n we have used the results of Sarma *et al.* (1957), normalized to their experimental results at 161° . Values of n up to 4 have been shown to be important, and only odd n -values occur in the interference of levels of opposite parities such as to be described here. Since $P_n^1(\theta)$ and $P_n^1(\pi - \theta)$ are equal or opposite as n is odd or even one may write

$$\frac{1}{2} \left\{ f(\theta) \frac{d\sigma(\theta)}{d\Omega} + f(\pi - \theta) \frac{d\sigma(\pi - \theta)}{d\Omega} \right\} = B_1 P_1^1(\cos \theta) + B_3 P_3^1(\cos \theta).$$

The five experimental values of $f(\theta)$ at each deuteron energy were analysed by the method of least squares and the results plotted with probable errors are shown in Fig. 5. They are fitted to theoretical curves calculated by the method described later.

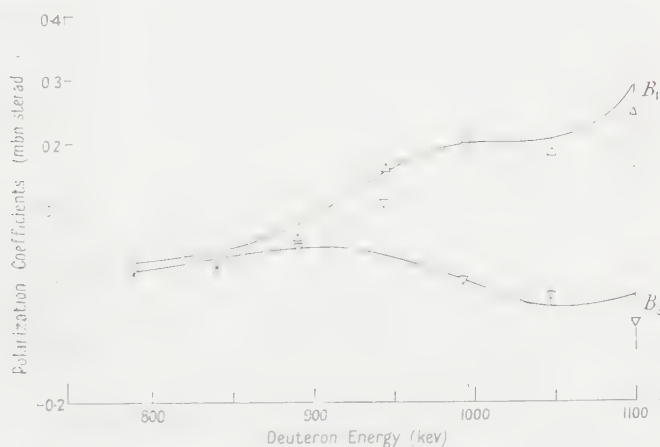


Fig. 5. Polarization distribution coefficients, defined by the relation $dP/d\Omega = \sum_n B_n P_n^1$.

As already discussed in § 2 the polarization $f(\theta)$ cannot be calculated absolutely unless P_2 is known, preferably from data on double scattering (cf. Phillips and Miller 1959). From the present experiments only relative values of B_1 and B_3 will be discussed. Values of B_1 and B_3 for the case of interfering $(1^+, 2^-)$ levels were computed using Simon and Welton's method, with phases as corrected by Huby (1954). Since B_3 is small compared to B_1 , contributions of d-wave deuterons to B_1 were neglected. Fig. 6 shows phase angles, including Coulomb and nuclear effects, calculated assuming total widths $\Gamma(0.96) - \Gamma(1.16) - 0.20$ mev and interaction radius $R = 3.96 \times 10^{-13}$ cm. Since the B 's are proportional to sine functions of these it is evident that, as B_1 does not change sign although B_3 does, these phase angles cannot be used for fitting the results of Fig. 5. The curves drawn in Fig. 5 were computed using additive phases $\alpha_1 = 1.87$, $\alpha_3 = -1.65$ radians, and ratios of reduced width amplitudes

$$\frac{\gamma(\text{d-wave deuterons})}{\gamma(\text{s-wave deuterons})} = \frac{\gamma_2}{\gamma_0} = 2.4. \quad \dots (4.3)$$

These curves fit reasonably well except for one point in B_3 . The reason for this discrepancy is not clear.

It is of interest to compare the ratio (4.3) with the ratio for channel spin 1 which comes from the angular distributions. Unfortunately data on A_3 are meagre, and seem to imply a phase angle changing far too rapidly to be explained

on the basis of interference between levels at 0.96 and 1.16 mev. However, from an examination of Figs 4 and 6, it seems that we can fit the A_3 curve at 1030 kv

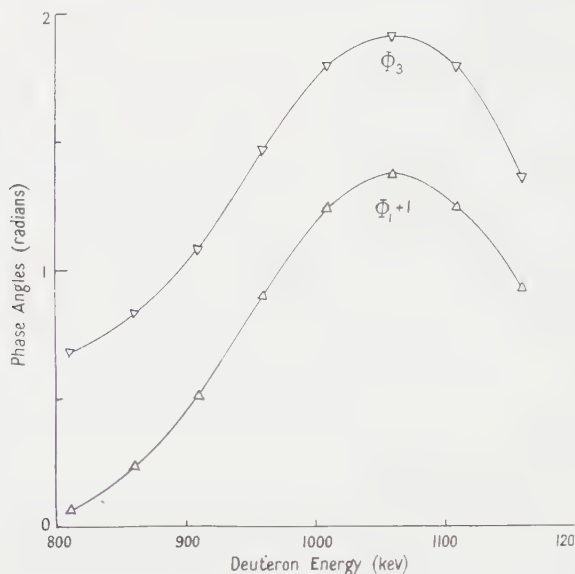


Fig. 6. Phase angles, including Coulomb and nuclear effects, calculated assuming total widths $\Gamma(0.96) = \Gamma(1.16) = 0.20$ mev and interaction radius $R = 3.96 \times 10^{-13}$ cm.

with an additive phase of -1.9 radians whilst the similarity of the A_1 and B_1 curves (Figs 4 and 5) leads to the assignment of 2.74 radians as the A_1 additive phase. This implies

$$\gamma_2/\gamma_0 = 0.2. \quad \dots\dots (4.4)$$

The uncertainty of curve-fitting to A_3 is stressed, and contribution from higher levels cannot be ruled out. Both (4.3) and (4.4) can, of course, change sign if a phase difference of 180° is inserted between α_1 and α_3 .

§ 5. CONCLUSIONS

Angular distributions and polarizations taken together confirm the assignments

$$0.96 \text{ mev}, \quad J^\pi = 1, \quad \Gamma = 0.20 \text{ mev}$$

$$1.16 \text{ mev}, \quad J^\pi = 2, \quad \chi \rightarrow \infty, \quad \Gamma = 0.20 \text{ mev}.$$

No reliable assignments exist for higher levels. The result (4.3) seems to be implied by the polarization measurements, while (4.4) which is suggested by the angular distribution measurements is subject to the objections mentioned in § 4.

Our main conclusion is that the apparent discrepancy between theoretical predictions of phase angles and experimental results previously noted elsewhere (Thomson *et al.* 1952) seems to be confirmed in the present experiments.

ACKNOWLEDGMENTS

The authors wish to thank Professor E. W. Titterton for his encouragement and interest in this work and also Dr. F. C. Barker for much helpful advice.

REFERENCES

- HUBY, R., 1954, *Proc. Phys. Soc. A*, **67**, 1103.
JURIĆ, M. K., and CIRILOV, S. D., 1958, *Phys. Rev.*, **112**, 1224.
PHILLIPS, G. C., 1950, *Phys. Rev.*, **80**, 164.
PHILLIPS, G. C., and MILLER, P. D., 1959, *Phys. Rev.*, **115**, 1268.
SARMA, N., GOVINDJEE, M., and ALLAN, H. R., 1957, *Proc. Phys. Soc. A*, **70**, 68.
SHARP, W. T., KENNEDY, J. M., SEARS, B. J., and HOYLE, M. G., 1954, *Atomic Energy of Canada Ltd., Report 97* (Chalk River, Ontario).
SIMON, A., 1953, *Phys. Rev.*, **92**, 1050.
SIMON, A., and WELTON, T. A., 1953, *Phys. Rev.*, **90**, 1036.
TEICHMANN, T., 1950, *Phys. Rev.*, **77**, 506.
THOMSON, D. M., COHEN, A. V., FRENCH, A. P., and HUTCHINSON, G. W., 1952, *Proc. Phys. Soc. A*, **65**, 745.

Activation Cross Sections with 14 Mev Neutrons

By S. K. MUKHERJEE, A. K. GANGULY AND N. K. MAJUMDER

Saha Institute of Nuclear Physics, Calcutta

MS. received 12th July 1960, in revised form 30th August 1960

Abstract. Some activation cross sections have been measured for the elements Na, Al, Sc, Cr, Cu, Ag and Bi using 14.8 mev neutrons from the (DT) reaction. The cross section values with their experimental errors are as follows:

$^{23}\text{Na}(n, p)^{23}\text{Ne}$ 29 mbn \pm 10%, $^{23}\text{Na}(n, \alpha)^{20}\text{F}$ 222 mbn \pm 10%, $^{27}\text{Al}(n, p)^{27}\text{Mg}$ 77 mbn \pm 10%, $^{45}\text{Sc}(n, 2n)^{44\text{m}}\text{Sc}$ 149 mbn \pm 15%, $^{45}\text{Sc}(n, 2n)^{44}\text{Sc}$ 179 mbn \pm 15%, $^{45}\text{Sc}(n, \alpha)^{42}\text{K}$ 63 mbn \pm 15%, $^{50}\text{Cr}(n, 2n)^{49}\text{Cr}$ 32 mbn \pm 10%, $^{52}\text{Cr}(n, p)^{52}\text{V}$ 105 mbn \pm 10%, $^{65}\text{Cu}(n, p)^{65}\text{Ni}$ 29 mbn \pm 10%, $^{107}\text{Ag}(n, 2n)^{106}\text{Ag}$ (8.2 days) \sim 6500 mbn, $^{107}\text{Ag}(n, 2n)^{106}\text{Ag}$ (24 min) 662 mbn \pm 10%, $^{109}\text{Ag}(n, 2n)^{108}\text{Ag}$ 833 mbn \pm 10%, $^{109}\text{Ag}(n, p)^{109}\text{Pd}$ 2.7 mbn \pm 20%, $^{109}\text{Ag}(n, \alpha)^{106}\text{Rh}$ 12 mbn \pm 25%, $^{209}\text{Bi}(n, p)^{209}\text{Pb}$ 0.7 mbn \pm 15%, $^{209}\text{Bi}(n, \alpha)^{206}\text{Tl}$ 0.6 mbn \pm 15%. The cross sections were measured in relation to 556 mbn for the cross section of $^{63}\text{Cu}(n, 2n)^{62}\text{Cu}$ and 117 mbn for the cross section of $^{27}\text{Al}(n, \alpha)^{24}\text{Na}$ reactions. It has been found that the (n, α) cross section values follow more or less the empirical curve given by Blosser, Goodman and Handley in 1958.

§ 1. INTRODUCTION

ACTIVATION cross section measurements with 14 mev neutrons started with the pioneer work of Paul and Clarke (1953). In a classical paper, they presented the cross sections of (n, 2n), (n, p) and (n, α) reactions for some 38, 25 and 34 nuclides respectively. They found that the experimental cross sections for the (n, 2n) process were in qualitative agreement with the predictions from the statistical theory of Weisskopf. They, however, found that the discrepancies between the theoretical predictions and the experimental results were very wide in the case of (n, p) and (n, α) reactions for heavy nuclei and suggested the existence of direct processes which contribute to the reaction mechanism even at these low energies. But as the method of absolute beta measurement adopted by Paul and Clarke (1953) was somewhat approximate, a more accurate measurement on the activation cross section was necessary in order to correlate the experimental data with the theoretical predictions. With this in view accurate measurements of cross sections were undertaken by several workers (Yasumi 1957, Rayburn 1958, 1959, Blosser *et al.* 1955, Blosser, Goodman and Handley 1958, Dvantiev, Levkoskii and Malievskii 1957, Coleman *et al.* 1959, Scalan and Fink 1958, Poularikas and Fink 1959, Preiss and Fink 1960, Mukherjee, Ganguly and Majumder 1960).

A systematic and detailed study of the neutron reaction cross sections at 14 mev to test the agreement or otherwise of these experimental data with the theoretical predictions from the current theories was also undertaken in the present investigation. The present paper is one of such reports on cross section measurements. The results presented contain some new measurements on reaction cross sections together with measurements of some cross sections which had previously been reported by other workers.

§ 2. EXPERIMENTAL DETAILS

2.1. Measurement of Cross Section

The measured cross sections of $^{63}\text{Cu}(n, 2n)^{62}\text{Cu}$ giving rise to the 9.73 minute activity of ^{62}Cu and $^{27}\text{Al}(n, \alpha)^{24}\text{Na}$ giving rise to the 14.97 hour activity of ^{24}Na have been adopted as our standards and all cross sections reported in this paper have been determined in relation to these cross sections. Yasumi's (1957) value of 556 mbn for the cross section of $^{63}\text{Cu}(n, 2n)^{62}\text{Cu}$ and Schmitt and Halperin's (1959) value of 117 mbn for the cross section of $^{27}\text{Al}(n, \alpha)^{24}\text{Na}$ have been taken as the best available values. Some of the cross section values have been cross checked with reference to both Cu and Al activity.

2.2. Neutron Irradiation

The samples irradiated, either in foil or in powder form, were of spectroscopically pure quality except in the case of Na and Al. The compound of Na used was of E. Merck guaranteed reagent quality. For Al samples chemically pure aluminium foils were used. Foil samples in the form of disks of 1 inch diameter and powder samples pressed in a Perspex sample pan of 1 inch diameter were sandwiched between two reference foils (in our case they were Cu or Al disks of 1 inch diameter of 1 mil thick) and irradiated by 14.8 mev neutrons at 0 degree to the incident deuteron beam, the bombarding time being dependent on the half-life of the respective product nuclei.

The samples were activated with monoenergetic neutrons of 14.8 mev energy, resulting from the (D, T) reaction by accelerated deuteron ions of 200 kev energy from a radio-frequency Cockcroft Walton type accelerator, falling on a direct refrigerant cooled tritiated zirconium target. The target cooling was designed to handle a continuous high beam current of the order of milliamperes without appreciable rise of target temperature and described by Mukherjee, Majumder and Ganguly (1969). The neutron yield was maintained constant in the region 10^{10} to 10^{11} neutrons per second from the target during the course of irradiation, the yield being monitored by a long calibrated counter and also by standard foil activity.

2.3. Counting Techniques and Analysis of Irradiated Samples

The resulting activities were followed up to background in every case in an end window beta counter. The radioactive samples were counted on saturation back scattering with aluminium backing. The compound decay curves thus obtained were analysed and the component activities separated. A typical reduction from the decay curves in the case of Ag for the analysis of ^{109}Ag reactions are shown (see Figure). The assignment of nuclear reactions to the component activities was made by means of the established half-lives and energies of the radiations of the product nuclei. Usual corrections such as geometry, back scattering, source absorption, window and air absorption were applied to determine the absolute beta disintegration rate including the probability of K-capture for β^+ -activity.

The geometrical efficiency of the end window counters employed was determined with the help of standard sources of different energies, manufactured by the Tracer Laboratory, U.S.A. Our samples had diameters equal to those of the standard sources.

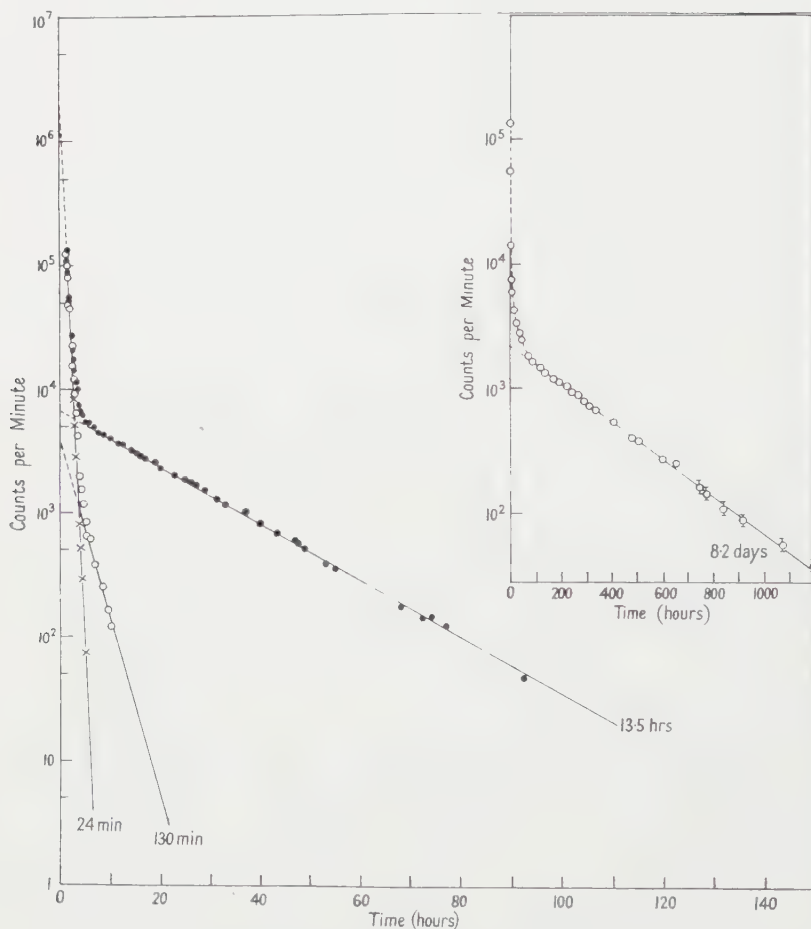
(1)	(2)	(3)	(4)	Results		(7)
				(5)	(6)	
^{23}Na	(n, p)	^{23}Na	40.2 sec	$29 \pm 10\%$	265	(i) 80 mbn for (Li + D) neutrons Jelley & Paul (1950).
	(n, α)	^{20}F	10.7 sec	$222 \pm 10\%$	—	(ii) $33.9 \pm 45\%$, Paul & Clarke (1953)
^{27}Al	(n, p)	^{27}Mg	9.45 min	$77 \pm 10\%$	146	(i) 118.7 mbn for (Li + D) neutrons Jelley & Paul (1950)
						(i) $79 \pm 7\%$ Forbes (1952)
						(ii) $52.4 \pm 18\%$ Paul & Clarke (1953)
						(iii) $87.2 \pm 8\%$ Yasumi (1957)
						(iv) $79 \pm 15\%$ Haling <i>et al.</i> (1957)
						(v) 53 ± 5 Poularikas & Fink (1959)
						(vi) 79 Hudson & Morgan (1959)
^{45}Sc	(n, 2n)	^{44}mSc	2.44 days	$149 \pm 15\%$	201	—
	(n, 2n)	^{44}Sc	3.92 hr	$179 \pm 15\%$	—	—
	(n, α)	^{42}K	12.52 hr	$63 \pm 15\%$	—	—
^{50}Cr	(n, 2n)	^{49}Cr	42 min	$32 \pm 10\%$	—	(i) $25.4 \pm 8\%$ Rayburn (1958)
^{52}Cr	(n, p)	^{52}V	3.8 min	$105 \pm 10\%$	50	(i) $77.7 \pm 14\%$ Paul & Clarke (1953)
						(ii) 87 ± 13 Thompson <i>et al.</i> (1958)
						(iii) 110 mbn at 15 mev Kern <i>et al.</i> (1959)
^{65}Cu	(n, p)	^{65}Ni	2.56 hr	$29 \pm 10\%$	7.9	(i) 28.6 for (Li + D) neutrons Wäffler (1950)
						(ii) $19 \pm 20\%$ Forbes (1952)
						(iii) 27 ± 11 Poularikas & Fink (1959)

(1)	(2)	(3)	(4)	(5)	(6)	(7)
^{107}Ag	(n, 2n) (n, 2n)	^{106}Ag ^{106}Ag	8.2 days 24.3 min	~ 6500 $662 \pm 10\%$	14.00	(i) $519 \pm 50\%$ Paul & Clarke (1953) (ii) $458 \pm 11\%$ Yasumi (1957)
^{109}Ag	(n, 2n)	^{108}Ag	2.3 min	$833 \pm 10\%$	15.00	(i) $311 \pm 50\%$ Paul & Clarke (1953) (ii) $604 \pm 11\%$ Yasumi (1957)
^{109}Ag	(n, p)	^{109}Pd	13.5 hr	$3.7 \pm 20\%$	2.03	(i) 7.8 for (1,1 + 1) neutrons Wäfler (1950) (ii) 10.5 ± 2 Dvantičev <i>et al.</i> (1957) (iii) $12.5 \pm 15\%$ Coleman <i>et al.</i> (1959)
^{209}Bi	(n, α)	^{206}Rh	130 min	$1.2 \pm 25\%$	—	—
	(n, p)	^{209}Pb	3.3 hr	$0.7 \pm 15\%$	0.043	(i) $1.33 \pm 20\%$ Coleman <i>et al.</i> (1959) (ii) 0.83 ± 0.40 Poularikas & Fink (1959)
	(n, α)	^{206}Tl	4.4 min	$0.6 \pm 15\%$	0.00005	(i) $1.2 \pm 85\%$ Paul & Clarke (1953) (ii) $0.52 \pm 15\%$ Coleman <i>et al.</i> (1959) (iii) 1.1 ± 0.3 Poularikas & Fink (1959)

(1) Element; (2) reaction; (3) product nucleus; (4) half-life; (5) observed cross section σ_{obs} (mbn); (6) theoretical cross sections calculated from statistical theory σ_{cal} (mbn); (7) previous measurements.

Note. The theoretical cross sections (presented in the table of results above) have been calculated according to the statistical theory of Weisskopf and are taken from the tables of Paul and Clarke (1953) and Yasumi (1957).

The radioactive samples were counted with a thick aluminium backing ($\sim 0.85 \text{ g cm}^{-2}$) which ensured saturation back scattering throughout the energy range of the β -particles involved in our measurements. The value for saturation back-scattering factor in aluminium was taken from Burt (1949).



Analysis of complex decay curve of Ag.

The factor for the source absorption correction was derived assuming a uniform sample thickness and an exponential absorption of the beta particles in the sample. Correction due to source absorption was calculated according to the following formula

$$f_s = \frac{1}{\mu t} [1 - \exp(-\mu t)]$$

where f_s is the source absorption correction factor, μ the mass absorption coefficient in $\text{cm}^2 \text{ mg}^{-1}$ and t the sample thickness in mg cm^{-2} .

In view of the high energies of the beta particles (0.6 MeV to 5 MeV) involved in our measurements, the errors involved in using a comparatively thicker window 2.8 mg cm^{-2} (as against 1.4 mg cm^{-2} by Paul and Clarke (1953) and 0.7 mg cm^{-2}

by Poularikas and Fink (1959)) after the extrapolation for the window thickness, have been estimated and are negligible for β -energies greater than 1 MeV. For beta energies less than 1 MeV, the corrections due to absorption in the window were taken into account. At β -ray energies of the order of 1 MeV, the window correction becomes negligible as it is less than 1% and need not be taken into account.

In the cases of β -decay the necessary corrections due to K-capture have been incorporated. In the cases where branching ratios are not known experimentally the theoretical values from the work of Feenberg and Trigg (1950) have been employed.

Finally, the cross sections reported in the Table are the average of at least three separate runs and the errors mentioned are the deviations from the average value.

§ 3. CONCLUSIONS

It is interesting to note that the (n, α) cross section values determined in the present work as well as in the cases of ^{79}Br , ^{81}Br reported earlier (Mukherjee, Ganguly and Majumder 1960) fall more or less on the empirical curve given by Blosser, Goodman and Handley (1958), except in the case of $^{109}\text{Ag}(n, \alpha)^{106}\text{Rh}$.

It is found that our results are in general agreement with the reports of other workers to the effect that $\sigma_{\text{obs}}/\sigma_{\text{cal}}$ (statistical theory) > 1 for (n, p) and (n, α) reactions (the calculated values of cross sections for different elements presented in this paper are taken from the tables of Paul and Clarke (1953) and Yasumi (1957)) suggesting the existence of processes other than the compound nucleus formation, namely, direct interaction.

When silver is irradiated with 14-MeV neutrons, the 8.2-day isomer of ^{106}Ag is produced along with the usual 24.3-minute activity of ^{106}Ag . The 8.2-day isomer decays with orbital electron capture, giving rise to a complex gamma spectrum. The cross section for this 8.2-day activity is calculated assuming that the end window counter has an efficiency of 1% for these gamma rays. It is found that the ratio of the cross sections for the formation of the two isomers by the $(n, 2n)$ process is $\sigma(8.2\text{-day})/\sigma(24\text{-min}) \sim 10$ for an incident neutron energy of 14 MeV. This is in qualitative agreement with the value $\sigma(8.2\text{-day})/\sigma(24\text{-min}) \sim 20$ as reported by Pool (1938) using 20-MeV neutrons.

ACKNOWLEDGMENTS

The authors are grateful to Dr. B. D. Nag Chaudhuri for providing them with all necessary facilities and for his continued association with and encouragement for this work and also to Dr. D. N. Kundu for his timely advice and helpful guidance in course of the work. Thanks are due to Shri Barin Chatterjee and Shri Naresh Sen for their wholehearted co-operation in the preparation of the materials of this paper and also in the operation of the C.W. Generator and computation of the data.

REFERENCES

- BLOSSER, H. G., GOODMAN, C. D., and HANDLEY, T. H., 1958, *Phys. Rev.*, **110**, 531.
 BLOSSER, H. G., GOODMAN, C. D., HANDLEY, T. H., and RANDOLPH, M. L., 1955, *Phys. Rev.*, **100**, 429.
 BUTT, B. P., 1949, *Nucleonics*, **5**, 28.
 COLEMAN, R. F., HAWKER, B. E., O'CONNOR, L. P., and PERKIN, J. L., 1959, *Proc. Phys. Soc.*, **73**, 215.

- DVANTIEV, B. G., LEVKOSSKII, V. N., and MALIEVSKII, A. D., 1957, *Proc. Acad. Sci. U.S.S.R.*, **113**, 537.
- FEENBERG, E., and TRIGG, G. L., 1950, *Rev. Mod. Phys.*, **22**, 399.
- FORBES, S. G., 1952, *Phys. Rev.*, **88**, 1309.
- HALING, R. K., PECK, R. A., Jr., and EUBANK, H. P., 1957, *Phys. Rev.*, **106**, 971.
- HUDSON, O. M., Jr., and MORGAN, IRA L., 1959, *Bull. Amer. Phys. Soc.*, [II], **4**, 97.
- JELLEY, J. V., and PAUL, E. B., 1950, *Proc. Phys. Soc.*, **63**, 112.
- KERN, B. D., THOMPSON, W. E., and FERGUSON, J. M., 1959, *Nucl. Phys.*, **10**, 226.
- MUKHERJEE, S. K., GANGULY, A. K., and MAJUMDER, N. K., 1960, *Proceedings of the Symposium on Low Energy Nuclear Physics, Waltair (India)*, p. 289.
- MUKHERJEE, S. K., MAJUMDER, N. K., and GANGULY, A. K., 1960, *Ind. J. Phys.*, **34**, 307.
- PAUL, E. B., and CLARKE, R. L., 1953, *Canad. J. Phys.*, **31**, 267.
- POOL, M. L., 1938, *Phys. Rev.*, **53**, 116.
- POULARIKAS, A., and FINK, R. W., 1959, *Phys. Rev.*, **115**, 989.
- PREISS, I. L., and FINK, R. W., 1960, *Nucl. Phys.*, **15**, 326.
- RAYBURN, L. A., 1958, *Bull. Amer. Phys. Soc.*, [II], **3**, 337, 365.
- 1959, *Bull. Amer. Phys. Soc.*, [II], **4**, 288.
- SCALAN, R., and FINK, R. W., 1958, *Nucl. Phys.*, **9**, 334.
- SCHMITT, H. W., and HALPERIN, J., 1959, *Bull. Amer. Phys. Soc.*, [II], **4**, 385.
- THOMPSON, W. E., FERGUSON, J. M., and KERN, B. D., 1958, *Bull. Amer. Phys. Soc.*, [II] **3**, 210.
- WÄFFLER, H., 1950, *Helv. Phys. Acta*, **23**, 239.
- YASUMI, S., 1957, *J. Phys. Soc., Japan*, **12**, 443.

The Hamiltonian Formalism of Damping in a Tuned Circuit

By K. W. H. STEVENS

Department of Physics, University of Nottingham

MS. received 30th May 1960

Abstract. The idea behind this work is the supposition that it should be possible to introduce damping into the quantum mechanical discussion of a harmonic oscillator without a detailed description of the damping mechanism. A study is therefore made of an L, C circuit coupled to an artificial (or transmission) line, using a Hamiltonian formalism. The whole system is conservative but, for the transmission line case, the L, C circuit behaves as if it is damped. The most probable form for the Hamiltonian does not exhibit the damping in an obvious way. It is shown that by a suitable change of variables the Hamiltonian can be split into two time-dependent commuting parts, one of which has the form

$$e^{-2\alpha t} \frac{\tilde{P}^2}{2C} + e^{2\alpha t} \frac{\tilde{Q}^2}{2L}$$

which has been previously used in a study of 2-level masers, and which does display the damping. The new operators \tilde{Q} and \tilde{P} are studied and it is shown that they are related to the charges and currents in the L, C circuit, but with the noise components due to the resistive loss (the transmission line) omitted. They are thus perhaps more natural variables to use than the actual charges and currents which do contain noise components. The problem of coupling a spin system to the current in the inductance is studied and the transition is made to the analogous problem of a spin system interacting with a damped mode of a cavity resonator. The analysis is compared with one given previously by Stevens and Josephson in 1959 and it is shown that the results previously obtained in a heuristic way are valid provided that noise fluctuations are negligible.

§ 1. INTRODUCTION

A PROBLEM of some importance in quantum electronics is that of describing the coupling between a spin system and a damped oscillator, which may be a cavity mode, a lattice mode or perhaps a spin wave. The difficulty lies in the description of the damping, in a reasonably tractable way. If one considers a mode of a resonant cavity important sources of damping are the resistive losses in the walls, and it is clearly not going to be a simple matter to describe these on a microscopic scale. Nor is it likely to be a profitable thing to do, for there are strong reasons to suppose that, having gone through an involved analysis, the results will condense into a macroscopic form depending primarily on the shape of the cavity, the frequency of the mode being studied and its Q -factor. Details such as whether or not the cavity is made of copper or of brass may be expected to disappear, unless there is interest in thermal noise at frequencies comparable with the collision frequencies of the electrons in the walls of the cavity. Where there is no

such interest it is a challenging problem to try and formulate the description of the damping in a way which avoids those details which may ultimately be expected to disappear.

A step in this direction was taken (Stevens 1958, to be referred to as I) when it was shown that the damped equation

$$L \frac{d^2 Q}{dt^2} + R \frac{dQ}{dt} + \frac{Q}{C} = 0$$

can be obtained from a Hamiltonian

$$\mathcal{H} \equiv e^{-Rt/L} \frac{P^2}{2AL} + e^{Rt/L} \frac{AQ^2}{2C}$$

using Hamilton's equations:

$$\dot{Q} = \frac{\partial \mathcal{H}}{\partial P}, \quad \dot{P} = -\frac{\partial \mathcal{H}}{\partial Q}.$$

Further, if the Hamiltonian is formally quantized the Schrödinger equation can be solved without approximations. This result alone does not, of course, imply that the formalism has any physical significance. To examine its physical content the problem of the interaction of such a damped oscillator (a specific cavity mode) and a spin system was studied (Stevens and Josephson 1959, to be referred to as II) using the Hamiltonian

$$\mathcal{H} \equiv \hbar\omega_0 S_z + \left(e^{-Rt/L} \frac{P^2}{2AL} + e^{Rt/L} \frac{AQ^2}{2C} \right) + \mu ag\beta QS_x.$$

While it was not possible to obtain general solutions of the resulting Schrödinger equation a number of interesting results were obtained. For example it was found that the motion of a single spin is oscillatory, with the period of oscillation lengthening continuously, a result which seems plausible on physical grounds when it is remembered that the energy available to the whole system is continuously being dissipated. Again, a threshold for spontaneous oscillation was found when there were many spins in the cavity. It was however appreciated that thermal noise fluctuations had been omitted and that the Hamiltonian used was open to question. The difficulty was that although

$$e^{-Rt/L} \frac{P^2}{2AL} + e^{Rt/L} \frac{AQ^2}{2C}$$

might describe the cavity alone (ignoring noise), and $\hbar\omega_0 S_z$ should be correct for the spin system alone, there was no certainty that the two Hamiltonians added together, with the interaction term $\mu ag\beta QS_x$ would correctly describe the interacting systems. While it is legitimate to add the Hamiltonians of conservative systems (with interaction terms) it is not clear what one should do when one of the terms represents a non-conservative system.

Our purpose in this paper is to show how these difficulties can largely be resolved, by considering a rather more familiar example of damping—a series L, C circuit across which is coupled an infinitely long transmission line of characteristic resistance R . This study was first suggested to me by Professor M. H. L. Pryce. The L, C circuit behaves as if it is damped, except that it is driven by any voltage waves which come towards it along the line. While in most of the analysis it does not matter whether one proceeds by classical or by quantum

methods one important difference is that classically it can be supposed, if necessary, that there are no voltage waves travelling towards the circuit. The equation

$$L \frac{d^2 Q}{dt^2} + R \frac{dQ}{dt} + \frac{Q}{C} = 0$$

is then rigorously valid for the charge. In quantum mechanics there is always a voltage wave going towards the circuit, and the above equation is never valid, except as an approximation. However, as we shall show, if the variables which described the circuit and the transmission line are changed appropriately, the Hamiltonian can be written as the sum of two commuting parts, the first (and simplest) having the damped form

$$e^{-Rt/L} \frac{\tilde{P}^2}{2C} + e^{Rt/L} \frac{\tilde{Q}^2}{2L}.$$

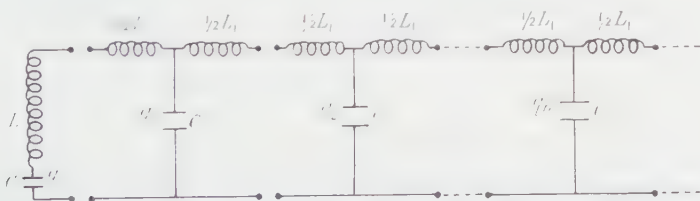
Further, the interaction with a spin system adds terms of the form

$$k S_x (\tilde{Q} + R e^{-Rt/L} \tilde{P})$$

together with more complicated terms which describe the interaction of the spin with the noise terms due to the resistance. The Hamiltonian used in II is therefore in error in omitting these noise terms, as was known, but it is otherwise valid, provided that the interpretations of P and Q are slightly modified. As no significant use was made of the meanings of P and Q this is a trivial correction.

§ 2. THE HAMILTONIAN

While we shall ultimately wish to consider the resonant circuit connected to a transmission line it is convenient to begin by supposing that it is connected to an artificial line, as in the Figure. The details of the termination have been deliberately omitted because we wish to emphasize that these are unimportant. We shall only consider time intervals which are sufficiently short that no signals launched by the tuned circuit have time to travel down to the far end of the line and back again. Thus an observer at the tuned circuit would, in the time interval allowed, have no means of knowing how the line is terminated, or even whether it is terminated. By increasing the number of sections in the line the time interval can be made as large as necessary. The change to a transmission line is made by letting L_1 and C_1 tend to zero so that $(L_1/C_1)^{1/2}$ tends to R .



An L, C circuit coupled across an artificial line of identical sections. The n th condenser has charge q_n .

Provided that the termination is not resistive the circuit and artificial line form a conservative system and it is reasonable to expect that the circuit equations can be obtained from an appropriate Hamiltonian. The standard way to obtain a Hamiltonian is via the Lagrangian, which is chosen so that the equations

$$\frac{d}{dt} \left(\frac{\partial \mathcal{L}}{\partial \dot{q}_n} \right) - \frac{\partial \mathcal{L}}{\partial q_n} = 0, \quad n = 1, 2, \dots$$

where q_n represent convenient variables, reproduce the circuit equations. It might be expected that the charges on the condensers should be taken as variables, but this is, in fact, not a suitable choice because the sum of the charges is constant, thus providing a dynamical constraint. This point is made by Jeans (1943, p. 499), with the implication that no Lagrangian exists. (There is, of course, no difficulty with a single tuned circuit, but only with coupled circuits.) Leech (1958, p. 40) gives a Lagrangian—a rather peculiar function which does not, for example, have the dimensions of energy. Nevertheless, Hamiltonians exist, and furthermore they are equal to the energy. Taking the charges as dynamical variables and identifying the conjugate momenta from Hamilton's equations, a Hamiltonian is

$$\mathcal{H} \equiv \frac{q^2}{2C} + \frac{(p-p_1)^2}{2L} + \frac{1}{2C_1} \sum q_n^2 + \frac{1}{2L_1} \sum (p_n - p_{n+1})^2 \dots\dots (1)$$

where the variables with subscripts refer to the artificial line and those without to the tuned circuit. This Hamiltonian is constructed by adding the squares of the charges divided by twice the capacities in which they are found and the squares of differences of successive p 's divided by twice the inductances which link the corresponding charges. It was obtained by inspection and not through a Lagrangian. Conservation of charge is then achieved because

$$\dot{q} + \sum \dot{q}_n = \frac{\partial \mathcal{H}}{\partial p} + \sum \frac{\partial \mathcal{H}}{\partial p_n} = 0.$$

Also $\dot{q} = (p-p_1)/L$ and, as the current in L is \dot{q} , $(p-p_1)^2/2L$ represents the energy stored in L . The other inductive terms can be similarly identified, showing that the Hamiltonian is, in fact, equal to the total energy. All the circuit equations are obtained correctly from

$$\begin{aligned} \dot{q} &= \frac{\partial \mathcal{H}}{\partial p}, & \dot{p} &= -\frac{\partial \mathcal{H}}{\partial q} \\ \dot{q}_n &= \frac{\partial \mathcal{H}}{\partial p_n}, & \dot{p}_n &= -\frac{\partial \mathcal{H}}{\partial q_n}. \end{aligned}$$

In Hamiltonian mechanics the coordinates and conjugate momenta are treated on an equal footing and we were therefore led to study the Hamiltonian

$$\mathcal{H} \equiv \frac{P^2}{2C} + \frac{(Q-Q_1)^2}{2L} + \frac{1}{2L_1} \sum (Q_n - Q_{n+1})^2 + \frac{1}{2C_1} \sum P_n^2$$

which is similar to (1), except that the p 's and q 's have been interchanged and capitals introduced to emphasize that the Q_n 's are not now charges. In the theory which follows we shall use this second form for the Hamiltonian, mainly because it can be deduced from a Lagrangian formulation of the circuit equations (as was pointed out to me by Dr. C. A. Bates), and is therefore less intuitive, and also because the final expressions obtained are then similar to those used in I and II. From Hamiltonian's equations it is seen that

$$\dot{Q} = \frac{P}{C} = \frac{q}{C} \quad \text{and} \quad \dot{Q}_n = \frac{P_n}{C_1} = \frac{q_n}{C_1}$$

so the Q 's are integrals with respect to time of the charges and the P 's are charges.

§ 3. THE EQUATIONS FOR P AND Q

The Hamiltonian

$$\mathcal{H} \equiv \frac{P^2}{2C} + \frac{(Q - Q_1)^2}{2L} + \frac{1}{2L_1} \sum (Q_n - Q_{n+1})^2 + \frac{1}{2C_1} \sum P_n^2$$

together with Hamilton's equations

$$\begin{aligned} \dot{Q} &= \frac{\partial \mathcal{H}}{\partial P}, & \dot{Q}_n &= \frac{\partial \mathcal{H}}{\partial P_n} \\ \dot{P} &= -\frac{\partial \mathcal{H}}{\partial Q}, & \dot{P}_n &= -\frac{\partial \mathcal{H}}{\partial Q_n} \end{aligned}$$

contains the information that the tuned circuit is coupled across an artificial line, which effectively damps it, and is driven by any incident voltage waves. It does however seem reasonable to observe that this is by no means obvious. We shall therefore examine Hamilton's equations in some detail and obtain the differential equations which P and Q , the coordinates associated with the tuned circuit, satisfy. The theory will be given as if the P 's and Q 's are classical variables. In quantum mechanics, using a Heisenberg representation, instead of $\dot{Q}_n = \partial \mathcal{H} / \partial P_n$ etc. one has $\dot{Q}_n = [Q_n, \mathcal{H}]$ etc. The equations are identical in form with those of the classical theory.

For a general value of n Hamilton's equations give

$$\dot{Q}_n = \frac{\partial \mathcal{H}}{\partial P_n} = \frac{P_n}{C_1}, \quad \dot{P}_n = -\frac{\partial \mathcal{H}}{\partial Q_n} = -(2Q_n - Q_{n+1} - Q_{n-1})/L_1$$

so that $\ddot{Q}_n = \omega_0^2 (Q_{n+1} + Q_{n-1} - 2Q_n)$ where $\omega_0^2 = 1/L_1 C_1$. The solution of this difference equation, valid for $n \geq 2$ is

$$Q_n = \sum \{ A_\epsilon e^{i(\omega t - n\epsilon)} + \bar{A}_\epsilon e^{-i(\omega t - n\epsilon)} + A_{-\epsilon} e^{i(\omega t + n\epsilon)} + \bar{A}_{-\epsilon} e^{-i(\omega t + n\epsilon)} \}$$

where $\omega^2 = 4\omega_0^2 \sin^2 \epsilon / 2$ and ω and ϵ can be taken as positive without loss of generality. Then, since $P_n = C_1 \dot{Q}_n$,

$$P_n = C_1 \sum \{ i\omega A_\epsilon e^{i(\omega t - n\epsilon)} + \dots \}, \quad n \geq 2$$

where the \dots is intended to indicate that similar terms with ϵ reversed and conjugate complexes have been omitted. The use of this device simplifies the appearance of the formulae and leads to no confusion. The A_ϵ are constants, and from the quadratic form of the Hamiltonian it can be inferred that they are related to the amplitudes of the normal modes. Hamilton's equations for the tuned circuit and first section of the line give

$$\begin{aligned} \dot{Q} &= \frac{P}{C}, & \dot{P} &= -\frac{Q - Q_1}{L} \\ \dot{Q}_1 &= \frac{P_1}{C_1}, & \dot{P}_1 &= \frac{Q - Q_1}{L} + \frac{Q_2 - Q_1}{L_1} \end{aligned}$$

and it then follows that

$$\begin{aligned} Q_1 &= 2Q_2 - Q_3 + \ddot{Q}_2 / \omega_0^2 \\ &= \sum \left[A_\epsilon e^{i(\omega t - 2\epsilon)} \left\{ 2 - e^{-i\epsilon} - \frac{\omega^2}{\omega_0^2} \right\} + \dots \right] \end{aligned}$$

and

$$P_1 = C_1 \sum \left[i\omega A_\epsilon e^{i(\omega t - 2\epsilon)} \left\{ 2 - e^{-i\epsilon} - \frac{\omega^2}{\omega_0^2} \right\} + \dots \right]$$

Also, $\dot{P} + \dot{P}_1 = (Q_2 - Q_1)/L_1$, so that

$$\dot{P} = \sum \left[A_\epsilon e^{i(\omega t - 2\epsilon)} \left\{ \frac{1 - e^{i\epsilon}}{L_1} + \omega^2 C_1 \left(2 - e^{-i\epsilon} - \frac{\omega^2}{\omega_0^2} \right) \right\} + \dots \right].$$

Next

$$L\ddot{P} = -(\dot{Q} - \dot{Q}_1) = -\frac{P}{C} + \dot{Q}_1$$

so that

$$\begin{aligned} L\ddot{P} + \left(\frac{L_1}{C_1} \right)^{1/2} \dot{P} + \frac{P}{C} &= \sum \left[A_\epsilon e^{i(\omega t - 2\epsilon)} \left\{ i\omega \left(2 - e^{-i\epsilon} - \frac{\omega^2}{\omega_0^2} \right) \right. \right. \\ &\quad \left. \left. + \left(\frac{L_1}{C_1} \right)^{1/2} \left[\frac{1 - e^{i\epsilon}}{L_1} + \omega^2 C_1 \left(2 - e^{-i\epsilon} - \frac{\omega^2}{\omega_0^2} \right) \right] \right\} + \dots \right] \\ &= \sum \left[A_\epsilon e^{i(\omega t - 2\epsilon)} \left\{ \omega_0(1 - e^{i\epsilon}) + \left(2 - e^{-i\epsilon} - \frac{\omega^2}{\omega_0^2} \right) \left(i\omega + \frac{\omega^2}{\omega_0} \right) \right\} + \dots \right]. \end{aligned}$$

.....(2)

On passing to the limit $L_1 \rightarrow 0$, $C_1 \rightarrow 0$ so that $(L_1/C_1)^{1/2} \rightarrow R$, which converts the artificial line into a transmission line, $\omega_0 = (1/L_1 C_1)^{1/2} \rightarrow \infty$, $\omega^2 = 4\omega_0^2 \sin^2 \epsilon/2$ becomes $\omega = \epsilon\omega_0$ for finite values of ω and the terms in A_ϵ and \bar{A}_ϵ on the right-hand side of (2) disappear, leaving only the terms in $A_{-\epsilon}$ and $\bar{A}_{-\epsilon}$. As these are the terms which describe the waves on the line which are travelling towards the circuit we see that the equation for P , the charge operator, is that of a damped oscillator driven by the incident waves. In the classical problem there need be no such incident waves, but in quantum mechanics the $A_{-\epsilon}$ and $\bar{A}_{-\epsilon}$ are operators related to the amplitudes of the normal modes. Their expectation values may be zero, but they cannot be dropped except as an approximation. As we shall show elsewhere (see Senitsky (1959) for a similar problem) when the $A_{-\epsilon}$ and $\bar{A}_{-\epsilon}$ correspond to zero point oscillations they nevertheless drive the circuit so as to maintain its zero point energy, which would otherwise decay because of the damping term, $R\dot{P}$.

It is not necessary, in the following considerations, to go to the limit $L_1, C_1 \rightarrow 0$ with $(L_1/C_1)^{1/2} \rightarrow R$, but it is convenient to set $(L_1/C_1)^{1/2} = R$.

Equation (2) can be written in the alternative form

$$\left(L \frac{d^2}{dt^2} + R \frac{d}{dt} + \frac{1}{C} \right) (P + X) = 0$$

where

$$\begin{aligned} X = - \sum \left[e^{-2i\epsilon} A_\epsilon \left\{ \omega_0(1 - e^{i\epsilon}) + \left(2 - e^{-i\epsilon} - \frac{\omega^2}{\omega_0^2} \right) \left(i\omega + \frac{\omega^2}{\omega_0} \right) \right\} \right. \\ \left. \times \left\{ \frac{e^{i\omega t} - \lambda e^{-\alpha t + i\Omega t} - (1 - \lambda)e^{-\alpha t - i\Omega t}}{-L\omega^2 + iR\omega + 1/C} \right\} + \dots \right] \end{aligned} \quad \text{.....(3)}$$

λ is a constant to be chosen later, $\alpha = R/2L$ and $\Omega = (1/LC - R^2/4L^2)^{1/2}$. The main point to be noted about X is that it contains linear combinations of the solutions $e^{-\alpha t} e^{\pm i\Omega t}$ of

$$\left(L \frac{d^2}{dt^2} + R \frac{d}{dt} + \frac{1}{C} \right) z = 0$$

so that it vanishes at $t=0$. The general solution is

$$P + X = e^{-\alpha t} [U \sin \Omega t + V \cos \Omega t]$$

where U and V are independent of time. For reasons shortly to become clear U and V are chosen so that

$$P + X = e^{-\alpha t} \left[P_0 \cos \Omega t - \frac{\sin \Omega t}{\Omega} \left(\frac{R}{2L} P_0 + \frac{1}{L} Q_0 \right) \right]$$

where P_0 and Q_0 are the respective values of P and Q at $t=0$ ($X=0$ when $t=0$). The requirement $\dot{Q}=P/C$ is met by integrating (3) and choosing λ so that

$$\frac{1}{i\omega} - \frac{\lambda}{i\Omega - \alpha} + \frac{1-\lambda}{\alpha + i\Omega} = 0.$$

Then

$$Q + Y = e^{-\alpha t} \left[Q_0 \cos \Omega t + \frac{\sin \Omega t}{\Omega} \left(\frac{P_0}{C} + \frac{R}{2L} Q_0 \right) \right]$$

where

$$Y = -\frac{1}{C} \sum \left[e^{-2i\epsilon} A_\epsilon \left\{ \omega_0 (1 - e^{i\epsilon}) + \left(2 - e^{-i\epsilon} - \frac{\omega^2}{\omega_0^2} \right) \left(i\omega + \frac{\omega^2}{\omega_0} \right) \right\} \right. \\ \left. \times \left\{ \frac{e^{i\omega t}}{i\omega} - \frac{\lambda e^{-\alpha t + i\Omega t}}{i\Omega - \alpha} + \frac{(1-\lambda)e^{-\alpha t - i\Omega t}}{\alpha + i\Omega} \right\} / \left(-L\omega^2 + i\omega R + \frac{1}{C} \right) + \dots \right].$$

§ 4. CHANGE OF VARIABLES

It is now of interest to consider the Poisson bracket of $Q + Y$ with $P + X$, thus:

$$[Q + Y, P + X] = e^{-2\alpha t} \left[Q_0 \cos \Omega t - \frac{\sin \Omega t}{\Omega} \left(\frac{P_0}{C} + \frac{R}{2L} Q_0 \right), P_0 \cos \Omega t - \frac{\sin \Omega t}{\Omega} \right. \\ \left. \times \left(\frac{R}{2L} P_0 + \frac{Q_0}{L} \right) \right] \\ = e^{-2\alpha t} [Q_0, P_0] = e^{-2\alpha t}.$$

This result suggests that new conjugate variables \tilde{Q}, \tilde{P} given by

$$\tilde{Q} = (Q + Y) = e^{-\alpha t} \left[Q_0 \cos \Omega t + \frac{\sin \Omega t}{\Omega} \left(\frac{P_0}{C} + \frac{R}{2L} Q_0 \right) \right] \\ \tilde{P} = e^{2\alpha t} (P + X) = e^{\alpha t} \left[P_0 \cos \Omega t - \frac{\sin \Omega t}{\Omega} \left(\frac{R}{2L} P_0 + \frac{1}{L} Q_0 \right) \right]$$

can be defined, for $[\tilde{Q}, \tilde{P}] = 1$.

A more formal approach is to determine a transformation matrix T (it is now convenient to use quantum mechanical formalism) such that $\tilde{Q} = T^* Q T = Q + Y$ with $T^* T = 1$. The matrix T certainly exists, as is readily proved by expressing it as a power series in t . Also, since $Y=0$ when $t=0$, $T=1$ when $t=0$. Then $\tilde{P} = T^* P T$ and similarly the sets of variables \tilde{P}_n, \tilde{Q}_n can be defined by $\tilde{P}_n = T^* P_n T$, $\tilde{Q}_n = T^* Q_n T$. The result $\tilde{P} = e^{2\alpha t} (P + X)$ will, for the moment, be assumed, for it is easier to prove it when the analysis has been taken slightly further. By differentiation it next follows that

$$\dot{\tilde{Q}} = e^{-2\alpha t} \frac{\tilde{P}}{C} \quad \text{and} \quad \dot{\tilde{P}} = -e^{2\alpha t} \frac{\tilde{Q}}{L}.$$

Suppose now that a Hamiltonian \mathcal{H}' is obtained in terms of the new conjugate variables \tilde{P}, \tilde{Q} and \tilde{P}_n, \tilde{Q}_n . It follows from Hamilton's equations that $\dot{\tilde{Q}} = \partial \mathcal{H}' / \partial \tilde{P}$, $\dot{\tilde{P}} = -\partial \mathcal{H}' / \partial \tilde{Q}$ and on comparison with the above results the conclusion is reached that the new Hamiltonian must consist of two time-dependent commuting terms, thus:

$$\mathcal{H}' \equiv e^{-2\alpha t} \frac{\tilde{P}^2}{2C} + e^{2\alpha t} \frac{\tilde{Q}^2}{2L} + \mathcal{H}_2(\tilde{P}_n, \tilde{Q}_n, t).$$

This is the main result which we wished to demonstrate, that by changing from P, Q and P_n, Q_n to $\tilde{P}, \tilde{Q}, \tilde{P}_n, \tilde{Q}_n$, using a time-dependent transformation, the Hamiltonian splits into two commuting parts, the first of which has the damped harmonic oscillator form which was investigated in I.

§ 5. THE TRANSFORMATION MATRIX T

The transformation matrix T relates Q and \tilde{Q} thus:

$$\tilde{Q} = T^* Q T = e^{-\alpha t} \left[Q_0 \cos \Omega t + \frac{\sin \Omega t}{\Omega} \left(\frac{P_0}{C} + \frac{R}{2L} Q_0 \right) \right].$$

Now in a Schrödinger representation a ket vector varies with time according to $|t\rangle = \exp(-i\mathcal{H}t/\hbar)|0\rangle$ where $|0\rangle$ is the ket at $t=0$. Thus the constant operators P_0 and Q_0 can be written as

$$\begin{aligned} P_0 &= \exp(-i\mathcal{H}t/\hbar) P \exp(i\mathcal{H}t/\hbar) \\ Q_0 &= \exp(-i\mathcal{H}t/\hbar) Q \exp(i\mathcal{H}t/\hbar). \end{aligned}$$

We therefore set $T = T_1 \exp(i\mathcal{H}t/\hbar)$ with the requirement that

$$T_1^* Q T_1 = e^{-\alpha t} \left[Q \cos \Omega t + \frac{\sin \Omega t}{\Omega} \left(\frac{P}{C} + \frac{R}{2L} Q \right) \right].$$

The factor $e^{-\alpha t}$ is removed (see I) by setting $T_1 = \exp\{(i\alpha t/2\hbar)(PQ + QP)\} T_2$. Then T_2 must be chosen so that

$$T_2^* Q T_2 = Q \left\{ \cos \Omega t + \frac{R}{2L\Omega} \sin \Omega t \right\} + P \frac{\sin \Omega t}{C\Omega}. \quad \dots (4)$$

Using the results $\exp(i\lambda P^2/\hbar) Q \exp(-i\lambda P^2/\hbar) = Q + 2\lambda P$

$$\exp(-i\mu Q^2/\hbar) P \exp(i\mu Q^2/\hbar) = P + 2\mu Q$$

it is seen that the relation (4) is obeyed with

$$T_2 = \exp(i\mu_1 Q^2/\hbar) \exp(-i\lambda P^2/\hbar) \exp(i\mu_2 Q^2/\hbar),$$

so that $T_2^* Q T_2 = Q + 2\lambda(P + 2\mu_2 Q)$

provided that $2\lambda = (\sin \Omega t)/C\Omega$ and

$$4\lambda\mu_2 = \left(\cos \Omega t + \frac{R}{2L\Omega} \sin \Omega t - 1 \right).$$

That is, $\lambda = \frac{\sin \Omega t}{2\Omega C}$, $\mu_2 = C \left\{ \frac{R}{4L} - \frac{\Omega}{2} \tan \frac{1}{2} \Omega t \right\}$.

Thus a transformation matrix T equal to

$$\exp \left\{ \frac{i\alpha t}{2\hbar} (PQ + QP) \right\} \exp \left\{ \frac{i\mu_1 Q^2}{\hbar} \right\} \exp \left\{ \frac{-i\lambda P^2}{\hbar} \right\} \exp \left\{ \frac{i\mu_2 Q^2}{\hbar} \right\} \exp \left\{ \frac{i\mathcal{H}t}{\hbar} \right\}$$

is determined. It is not unique because, for example, μ_1 is undetermined.

Applying the transformation to P gives

$$T^*PT = e^{\alpha t} [(1 + 4\lambda\mu_1)P_0 + \{2\mu_2(1 + 4\lambda\mu_1) + 2\mu_1\}Q_0]$$

and
$$T^*PT = e^{\alpha t} \left[P_0 \cos \Omega t - \frac{\sin \Omega t}{\Omega} \left(\frac{R}{2L} P_0 + \frac{1}{L} Q_0 \right) \right]$$

is obtained with
$$\mu_1 = -\frac{1}{2}\Omega C \left[\frac{R}{2L\Omega} + \tan \frac{1}{2}\Omega t \right].$$

The transformation matrix T is still not unique, for T_2 can be multiplied by any unitary operator which does not involve P and Q .

§ 6. THE MEANINGS OF \tilde{Q} AND \tilde{P}

It is now of interest to examine the physical interpretation of the new variables, \tilde{Q} and \tilde{P} . In this we shall assume that the initial charge distribution on the line is such that an observer at the tuned circuit would see an incoming signal which is random, and which corresponds to that expected from a resistance R at temperature T . \tilde{Q} is defined in two ways, either as $Q + Y$ or as

$$e^{-\alpha t} \left[Q_0 \cos \Omega t + \frac{\sin \Omega t}{\Omega} \left(\frac{P_0}{C} + \frac{R}{2L} Q_0 \right) \right].$$

The first definition suggests that it is a complicated variable, for Y is by no means simple. On the other hand, the second definition suggests that it is really not very complicated. This paradox is resolved as follows. It seems probable that most physicists, when they think of the charge on the condenser of a damped, tuned circuit, automatically smooth it, in the sense that they ignore the noise fluctuations which it has. When they need to introduce noise they will do so, but normally the presence of noise is forgotten. Thus what is usually thought of as the charge is not really the charge, but is a 'smoothed' charge. Our variable Q is defined as $(1/C) \int q dt$, where q is the true charge, including its noise fluctuations. The new variable \tilde{Q} , which varies in a smooth manner with time, is to be interpreted as $(1/C) \int \tilde{q} dt$, where \tilde{q} is the 'smoothed' charge. Thus we recognize that the variable which has a complicated behaviour with time is Q , and that adding Y to it to give \tilde{Q} is the process of subtracting the noise terms. Since

$$\tilde{P} = C e^{2\alpha t} \tilde{Q}$$

we recognize that it is related to the smoothed charge on the condenser. In a sense then, \tilde{Q} and \tilde{P} are the variables which one might expect a physicist to use, as describing most closely his smoothed picture of the time integral of charge and charge respectively.

In cases where the excitations are well above noise level it would seem reasonable to forget the difference between Q and \tilde{Q} , which is what happened in I. We therefore conclude that the interpretation of the analysis given in I is only valid for excitations large compared with noise. The mathematical treatment, given in terms of P and Q in I, is immediately applicable to \tilde{P} and \tilde{Q} in

$$e^{-2\alpha t} \frac{\tilde{P}^2}{2C} + e^{2\alpha t} \frac{\tilde{Q}^2}{2L}.$$

§ 7. COUPLING TO A SPIN SYSTEM

It is now of interest to consider our model of an L, C circuit coupled to a line, when there is a spin system in the coil of the inductance. We assume that there is also an external magnetic field H present. The current in the circuit is \tilde{P} ,

which equals $-(Q-Q_1)/L$ and we may assume that the field set up at the spin is transverse to H , in which case we expect additional terms in the Hamiltonian,

$$\mathcal{H}_s + g\beta HS_z + k(Q-Q_1)S_x$$

where k is a coupling constant between spin system and coil and \mathcal{H}_s is the Hamiltonian of the spin system. This Hamiltonian may not, however, be complete, for there are magnetic fields set up by the currents on the line and the spin may also be coupled to these. It might therefore be better to use, as coupling term, an expression such as

$$\sum Q_i \mathbf{a}_i \cdot \mathbf{S} + \sum P_i \mathbf{b}_i \cdot \mathbf{S}$$

where the \mathbf{a}_i and \mathbf{b}_i are vectors and, for the sake of generality, we have also included terms linear in the P 's. The difficulty now arises that although it might be possible to evaluate all the various interactions for a specified geometry we are primarily interested in a mathematical analogue between our circuit coupled to a line and a damped mode of a cavity resonator. Thus a detailed knowledge of all the couplings in the circuit case is probably not going to be of much value for the cavity analogue. If the damping in the cavity is supposed to be due to resistive losses in the wall we expect that the electronic motions in the walls, which give rise to the absorption, also give rise to emission—black-body radiation if the wall is at a uniform temperature T . This emission will drive all the cavity modes, and a spin system in the cavity will be exposed to the magnetic fields set up in the modes. If, however, we are primarily interested in the coupling to one of the modes and if, at $t=0$, we assume that the energy in this mode is well above the equilibrium noise energy kT , ($kT \gg \hbar\omega$), it would seem a reasonable approximation to assume that the spin system is coupled only to the smoothed 'current', that is, to $C\ddot{Q}$. From $L\ddot{Q} + R\dot{Q} + \tilde{Q}/C = 0$ we have

$$C\ddot{Q} = -(\tilde{Q} + R e^{-2\alpha t} \tilde{P})/L$$

so that a Hamiltonian

$$\begin{aligned} \mathcal{H} \equiv \mathcal{H}_s + g\beta HS_z + \left(e^{-2\alpha t} \frac{\tilde{P}^2}{2C} + e^{2\alpha t} \frac{\tilde{Q}^2}{2L} \right) + \mathcal{H}_2(\tilde{P}_n, \tilde{Q}_n, t) \\ + kS_x(\tilde{Q} + R e^{-2\alpha t} \tilde{P}) \end{aligned}$$

seems indicated. This is very similar to the Hamiltonian used in II, apart from some differences in notation, for the additional term $R e^{-2\alpha t} \tilde{P} S_x$ and for the commuting term $\mathcal{H}_2(\tilde{P}_n, \tilde{Q}_n, t)$, which can be dropped (or transformed away).

In order that the formalism of II can be directly applied it is convenient to make another change of variables, by setting $\tilde{P} = (C/AL)^{1/2} P$ and $\tilde{Q} = (AL/C)^{1/2} Q$, where it is to be understood that P and Q are new variables, which are not the same as P and Q used earlier in this paper. They are introduced solely to agree with the formalism in II. Then, dropping \mathcal{H}_s , \mathcal{H}_2 , setting $g\beta H = \hbar\omega_0$ and $k(AL/C)^{1/2} = \mu ag\beta$, \mathcal{H} becomes

$$\mathcal{H} \equiv \hbar\omega_0 S_z + \left(e^{-Rt/L} \frac{P^2}{2AL} + e^{Rt/L} \frac{AQ^2}{2C} \right) + \mu ag\beta S_x \left(Q + R \frac{C}{AL} e^{-Rt/L} P \right)$$

which, apart from the extra term in PS_x , is identical with the Hamiltonian used in II. This extra term causes no complications, and is absorbed by modifying the definition (in II) of p_+ , by choosing ϕ so that $p_+ = \exp(\pm i\phi)q_+$, where

$$\exp(-i\phi)[(\cosh\theta + i\sinh\theta) + R(C/L)^{1/2}(\sinh\theta + i\cosh\theta)] = (\cosh 2\theta)^{1/2}.$$

K is unaltered, and because the behaviour of $\langle S_z \rangle$ is independent of the changes in the transformation the results in II are unaltered.

Thus as a result of this further study it is possible to see what the underlying assumptions made in II were, the main conclusion being that the analysis given there is valid provided that the thermal energy ($\sim kT$) of the cavity mode can be neglected in comparison with the stored energy.

ACKNOWLEDGMENT

I would like to thank Professor M. H. L. Pryce for a very stimulating discussion on damping.

REFERENCES

- JEANS, SIR JAMES, 1943, *The Mathematical Theory of Electricity and Magnetism*, 5th Edn (Cambridge: University Press).
- LEECH, J. W., 1958, *Classical Mechanics* (London: Methuen).
- SENITSKY, I. R., 1959, *Phys. Rev.*, **115**, 227.
- STEVENS, K. W. H., 1958, *Proc. Phys. Soc.*, **72**, 1027.
- STEVENS, K. W. H., and JOSEPHSON, B., Jr., 1959, *Proc. Phys. Soc.*, **74**, 561.

Upper Limits for the Radiative Capture Cross Sections of ^{27}Al and ^{31}P for ^{16}O Ions

By R. F. COLEMAN, D. N. HERBERT AND J. L. PERKIN

Atomic Weapons Research Establishment, Aldermaston, Berks.

MS. received 7th September 1960

Abstract. The radiative capture cross sections of ^{27}Al and ^{31}P for ^{16}O ions with energies a few meV above the expected thresholds for these reactions (~ 30 meV) have been found to be not greater than 0.2 and $18\mu\text{bn}$ respectively. Activation methods were used and care was taken to avoid errors due to impurities in the targets and the recoil into the targets of reaction products from elsewhere in the irradiation assembly.

A calculation based on the statistical theory of the compound nucleus predicts a cross section of $2\mu\text{bn}$ for the capture in aluminium of ^{16}O ions at the energy used in these experiments. Various possible reasons for this over-estimation of the cross section are discussed.

§ 1. INTRODUCTION

RADIATIVE capture cross sections involving excitation energies of the compound nucleus of greater than 15 meV have been measured for some nuclides with neutrons (Perkin, O'Connor and Coleman 1958), protons (Kelly 1950, Cohen 1955), deuterons (Blair, Hintz and Van Patter 1954, Carver and Jones 1959) and α -particles (Ball, Fairhall and Halpern 1959). The magnitude of these cross sections is of the order of 10^{-3} to 10^{-4} of the corresponding total reaction cross section for excitation energies of 15 to 25 meV.

At these excitation energies Lane (1959) and Lane and Lynn (1959) have shown that the capture of neutrons and protons is predominantly a direct process. On the other hand, Carver and Jones (1959) have shown that the cross section of the $^{64}\text{Zn}(\text{d}, \gamma)^{66}\text{Ga}$ reaction is in agreement with that calculated from the statistical theory of the compound nucleus. The purpose of the present experiments was to find the validity of the statistical theory as applied to the capture of heavy ions. The only previous work reported of this nature is that of Reasbeck and Fremlin (1958). In these experiments a search was made for the products of the reactions $^{19}\text{F}(^{13}\text{C}, \gamma)^{32}\text{P}$ and $^{51}\text{V}(^{13}\text{C}, \gamma)^{64}\text{Cu}$ using ^{13}C ions of mean energy 50 to 60 meV. Thick target yields of the order of 10^{-9} to 10^{-8} were found but the possibility that the ^{32}P and ^{64}Cu activities observed originated from reactions with impurities in the targets could not be eliminated.

A similar activation technique was used in the present work using ^{16}O ions. The choice of targets was restricted by the maximum energy of the ^{16}O ions available and the small number of nuclides which form on capture a radioactive nucleus with a convenient half-life. The availability of the target in a form of high and known purity was also essential. These conditions were best met by the reactions $^{27}\text{Al}(^{16}\text{O}, \gamma)^{43}\text{Sc}$ (3.9 h) and $^{31}\text{P}(^{16}\text{O}, \gamma)^{47}\text{V}$ (31 min.) The Q -values for these reactions are 14.4 and 12.4 meV respectively and their effective thresholds are expected to be about 30 to 32 meV.

§ 2. EXPERIMENTAL DETAILS

Currents of about $0.08\ \mu\text{A}$ of magnetically analysed ^{16}O , 6^+ ion beams with energies up to 38 mev were obtained with the A.W.R.E. Tandem Van de Graaff (Allen *et al.* 1959). Thick targets for irradiation were placed across the end of a Faraday cup. This cup and all the collimators defining the oxygen beam were made of high purity gold to reduce the bombardment of the target by nuclei recoiling from reactions between the oxygen beam and any light elements. The deposition on the surface of the targets of any volatile matter during the irradiations was suppressed by means of a liquid nitrogen trap positioned around the entrance to the Faraday cup.

The aluminium targets consisted of disks turned from a $\frac{1}{4}$ in. diameter bar of spectroscopically pure metal. Before irradiation the surface layers were removed with sodium hydroxide. After an irradiation of some 4 hours about $300\ \mu\text{g}$ of scandium carrier was added and the target was dissolved. The solution was adjusted to pH 1.5 and scandium was extracted into 0.5 M thenoyltrifluoroacetone (T.T.A.) in benzene. After thoroughly washing the organic extract, the scandium was back extracted into 1 M nitric acid. This solution was then divided into two portions. The majority was evaporated on a $30\ \mu\text{g cm}^{-2}$ plastic film for counting and the remainder was used for determining the chemical yield by means of a spectrophotometric method developed by Herrington and Monk (1957) based on the colour of the 8-hydroxyquinoline scandium complex.

The phosphorus targets were in the form of lithium phosphate, prepared from spectroscopically pure lithium hydroxide and sodium di-hydrogen phosphate and compacted under pressure. After irradiation the targets were dissolved in dilute hydrochloric acid with $300\ \mu\text{g}$ of vanadium and 1 mg of titanium carriers. The vanadium was reduced with sulphur dioxide and separated from the solution on a titanium hydroxide precipitate. This was then dissolved in 1 M hydrofluoric acid and passed through an anion column in the fluoride form. After evaporating the effluent to dryness the residue was re-dissolved in 0.1 M hydrochloric acid. The bulk of this solution was evaporated on a plastic film for counting and the remainder was used to determine the chemical yield using a spectrophotometric method utilizing the colour of the tungsto-vanado-phosphoric acid complex.

The separated scandium and vanadium sources were counted in a 4π gas flow proportional counter. An anticoincidence ring of Geiger counters was used to reduce the background of this counter to 0.3 c/s.

§ 3. CONTAMINATION OF THE TARGETS BY RECOIL NUCLEI

The residual nuclides from the two capture reactions examined could also be produced from other reactions between ^{16}O and any nuclide of higher atomic number and at least as great a mass as that of either ^{27}Al or ^{31}P respectively. These nuclides could be present in the targets and in material exposed to the oxygen beam and in a position such that reaction products could recoil into the targets. In order to detect these recoils, thick gold foils (10 parts per million total impurity) were irradiated and processed for scandium or vanadium. No reactions were possible between the oxygen ions of the energy used and gold because of the high Coulomb barrier. The yields from these gold foils together with those from the aluminium and lithium phosphate targets are given in Table 1.

Table 1

Thick target yields of 3.9-hour scandium isotopes for 38 MeV ^{16}O ions		
Target	Al	Au
Yield (10^{-12} atoms per ^{16}O ion)	52 ± 4	46 ± 5
Thick target yields of ^{47}V for 36 MeV ^{16}O ions		
Target	Li_3PO_4	Au
Yield (10^{-12} atoms per ^{16}O ion)	≤ 80	≤ 15

The yields of scandium are quoted as for 3.9-hour scandium isotopes. This is because ^{44}Sc and ^{43}Sc have practically the same half-life and could not be distinguished from one another at the low level of activity observed. The yield from aluminium at 38 MeV is only slightly greater than that from gold, setting a limit of not more than 10^{-11} atoms per ^{16}O ion for the yield from the capture reaction. The origin of the scandium activity on the gold and most of that on the aluminium targets was found to be the reaction between ^{16}O and traces of silicon (presumably from silicone grease used on O-rings) on the edges of the collimators. No vanadium activity was found from the oxygen ion irradiation of either lithium phosphate or gold. The upper limits for the yields were higher than those for scandium because the chemical yields were smaller and the period required for chemical separation before counting could begin was relatively longer.

§ 4. IMPURITIES IN THE ALUMINIUM TARGETS

The small difference between the yields of scandium activity from aluminium and gold targets could be due to impurities in the aluminium. An analysis of the aluminium was therefore carried out using mainly neutron activation methods because of the low concentrations of the impurities. The yields of 3.9-hour scandium isotopes from the impurities found were measured by irradiating suitable compounds of these impurities with oxygen ions.

The results obtained are given in Table 2. Relatively high yields were obtained from impurities a few mass units heavier than aluminium and scandium. This is presumably because of the higher probability of forming 3.9-hour scandium by compound nucleus processes and stripping reactions respectively in these two regions.

Table 2

Thick target yields of 3.9-hour scandium isotopes from the irradiation of impurity elements with 35.4 MeV oxygen ions and the concentrations of these elements in the aluminium targets used.

(1)	(2)	(3)	(4)
Si	SiO_2	0.51	3 ± 1 (a)
P	KH_2PO_4	0.81	0.8 (a)
S	ZnS	2.1	≤ 0.3 (b)
Cl	NaCl	0.041	2 ± 1 (a)
K	K_2CO_3	0.024	10 ± 5 (a)
Ca	CaCO_3	0.0036	1 (d)
Sc	Sc_2O_3	≤ 0.0004	0.22 (a)
Ti	Ti	0.066	1 (c)
V	V_2O_5	0.0026	< 10 (c)
Cr	Cr_2O_3	≤ 0.00007	< 1 (c)
Mn	Mn_3O_4	≤ 0.00006	< 10 (c)

Analytical methods: (a) slow neutron activation, (b) fast neutron activation, (c) colorimetric, (d) spectrographic (data from Johnson Matthey).

(1) Element; (2) compound irradiated; (3) yield $\times 10^{12}$ per part per million of element if present in an aluminium target; (4) concentration in the aluminium targets (parts per million).

The yields in the Table are for 1 part per million of an impurity element in an aluminium target. These were obtained by multiplying the observed yield from the irradiated compound of each impurity by the ratio of the stopping cross sections of aluminium and the particular compound irradiated. In the absence of any comprehensive stopping cross section data for ^{16}O ions these ratios were calculated using proton stopping cross section data (Whaling 1958). It was assumed that these ratios for oxygen ions were the same as those for protons of the same velocity and that the stopping cross section of a compound was the sum of the atomic stopping cross sections of its constituents.

From the figures for the yield and concentration for each element in Table 2, the total 3.9-hour scandium isotope yield from the impurities in the aluminium targets is of the order of 3×10^{-12} atoms per ^{16}O ion.

§ 5. RESULTS AND DISCUSSIONS

From the results in the Tables it is evident that the thick target yield of ^{43}Sc from the $^{27}\text{Al}(^{16}\text{O}, \gamma)^{43}\text{Sc}$ reaction at 38 MeV is not more than 10^{-11} atoms per ^{16}O ion, and that at least 30% of this upper limit is from the yield of 3.9-hour scandium isotopes from impurities in the targets.

An upper limit for the average value of the cross section in the energy range 30 to 38 MeV can be obtained from the expression $(dY/dE) \times \epsilon$ where Y is the yield for an incident ^{16}O ion of energy E and ϵ is the average atomic stopping power for ^{16}O ions in this energy range in aluminium. The latter was calculated from the work of Papineau (1956) and Heckmann *et al.* (1960) and from the differentiation of an extrapolated range-energy curve obtained by Oganessian (1959). Both these methods gave the same result, namely approximately 2.2×10^{-13} eV cm². The capture cross section is therefore not greater than $0.2 \mu\text{bn}$. This limit is some two or three orders of magnitude less than that found in the experiments of Reasbeck and Fremlin (1958).

Similar calculations for the $^{31}\text{P}(^{16}\text{O}, \gamma)^{47}\text{V}$ reaction result in an upper limit of 8×10^{-11} for the thick target yield of ^{47}V from lithium phosphate at 36 MeV and a mean cross section in the energy range 31 to 36 MeV not greater than $18 \mu\text{bn}$.

The magnitude of the capture cross section expected on the basis of the statistical theory of the compound nucleus was calculated using the relationship $\sigma(\text{capture}) = \sigma(\text{compound nucleus}) \times \Gamma_\gamma / \Gamma_{\text{total}}$. The expressions used to calculate the radiation width Γ_γ and the total width Γ_{total} (taken to be of the order of the neutron width) were those of Lane (1959) and Lane and Lynn (1959). Only the reaction with aluminium was considered as this had the lowest upper limit for the cross section. The cross section for the formation of the compound nucleus was taken from the theoretical work of Thomas (1959). It was assumed that the cross section for direct reactions was relatively small and could be neglected. The value of the capture cross section calculated in this manner is approximately $2 \mu\text{bn}$, i.e. at least one order of magnitude greater than that found.

This discrepancy is not unexpected considering the assumptions made and the uncertainties associated with the application of the statistical theory at high excitation energies (some 40 MeV in the present experiments). In particular the constants in the level density formula used may not be correct at high energies. Also at these energies the photon absorption form factor used in the calculation of the γ -ray width is not known accurately and could lead to a large error in the cross section.

Another possible source of error in the calculations which would, in this case, result in an over-estimation of the capture cross section is the assumption that the density of states ρ_I of spin I for the final states of the residual nucleus is given by $(2I+1)\rho_0$. The density is better represented by the expression $(2I+1)\rho_0 \exp(-I^2/2S^2)$ (Newton 1956), where S , a 'cut-off' parameter, is of the order of 4 and probably increases with the excitation energy. As the compound states formed will in general have a high spin, this high spin cut-off of the final bound states reduces the probability of E1 γ -ray transitions. The probability of neutron emission is relatively unaffected because of the greater range of angular momentum of the emitted neutrons. Also the states reached by neutron emission are generally at a higher excitation energy than those reached by capture which are mainly lower than the binding energy. The corresponding value of S for neutron emission is, therefore, probably larger.

Finally, in the particular case considered the odd-odd nature of the final nucleus after neutron emission gives rise to a larger value of S (Lang and Le Couteur 1959).

§ 6. CONCLUSIONS

The radiative capture cross sections of ^{27}Al and ^{31}P for ^{16}O ions with energies a few MeV above the expected thresholds for these reactions have been found to be not greater than 0.2 and $18\mu\text{bn}$ respectively. A calculation based on the statistical theory of the compound nucleus predicts a cross section of $2\mu\text{bn}$ for the first of these reactions. Various possible reasons for this over-estimation of the cross section have been discussed, but as the full extent of the discrepancy between theory and experiment is not known no definite conclusions can be drawn.

ACKNOWLEDGMENTS

We would like to thank Dr. N. MacDonald for examining many of the theoretical implications of this work and Dr. A. M. Lane and Mr. J. E. Lynn for useful discussions.

REFERENCES

- ALLEN, K. W., JULIAN, F. A., ALLEN, W. D., PYRAH, A. E., and BLEARS, J., 1959, *Nature, Lond.*, **184**, 303.
 BALL, J. B., FAIRHALL, A. W., and HALPERN, I., 1959, *Phys. Rev.*, **114**, 305.
 BLAIR, J. M., HINTZ, N. M., and VAN PATTEN, D. M., 1954, *Phys. Rev.*, **96**, 1023.
 CARVER, J. H., and JONES, G. A., 1959, *Nucl. Phys.*, **11**, 400.
 COHEN, B. L., 1955, *Phys. Rev.*, **100**, 206.
 HECKMANN, H. H., PERKINS, B. L., SIMON, W. G., SMITH, F. M., and BARKAS, W. H., 1960, *Phys. Rev.*, **117**, 544.
 HERRINGTON, J., and MONK, R. G., 1957, *Atomic Weapons Research Establishment, Report No. 0-39/56*.
 KELLY, E. L., 1950, *University of California Radiation Laboratory, Report UCRL 1044*.
 LANE, A. M., 1959, *Nucl. Phys.*, **11**, 625.
 LANE, A. M., and LYNN, J. E., 1959, *Nucl. Phys.*, **11**, 646.
 LANG, D. W., and LE COUTEUR, K. J., 1959, *Nucl. Phys.*, **14**, 21.
 NEWTON, T. D., 1956, *Canad. J. Phys.*, **34**, 804.
 OGANESEYAN, YU. TS., 1959, *J. Exp. Theor. Phys.*, **36**, 936.
 PAPINEAU, A., 1956, *C.R. Acad. Sci., Paris*, **242**, 2933.
 PERKIN, J. L., O'CONNOR, L. P., and COLEMAN, R. F., 1958, *Proc. Phys. Soc.*, **72**, 505.
 REASBECK, P., and FREMLIN, J. H., 1958, *Proc. Conf. on Reactions in Complex Nuclei, Gatlinburg, Oak Ridge National Laboratory, Report ORNL 2606*.
 THOMAS, T. D., 1959, *Phys. Rev.*, **116**, 703.
 WHALING, W., 1958, *Encyclopaedia of Physics*, Vol. 34, (Berlin: Springer).

Some Notes on Theories of Helium

By F. J. PEARSON

Department of Applied Physics, Lanchester College of Technology, Coventry

MS. received 16th June 1960

Abstract. Attention is directed to that approximation to the quantum mechanical partition function for an imperfect fluid which is afforded by assuming the commutation of the kinetic and potential energy operators. The corresponding grand partition function is developed in the form of a cluster integral series, and discussion of its behaviour at low temperature is facilitated by a further approximation. This leads to equations for the pressure and density which are similar to the classical expressions of Mayer, and which afford a qualitative description of the condensation of helium into liquids I and II. Numerical calculation shows not unreasonable agreement with experiment. Finally the theories of Chester and Feynman are discussed in more detail in relation to these cluster integral expansions.

§ 1. INTRODUCTION

THEORIES of helium based on quantum statistical mechanics usually start from the density matrix $\rho^N(\mathbf{r}^N, \mathbf{r}^N)$ for an assembly of N systems occupying volume V at temperature T , which has been given by von Neumann (1927), Husimi (1940) and others, in the form:

$$\rho^N(\mathbf{r}^N, \mathbf{r}^N) = \sum_i \Psi_i^*(\mathbf{r}^N) \left\{ \exp \left(-\frac{\mathcal{H}(\mathbf{r}^N)}{kT} \right) \right\} \Psi_i(\mathbf{r}^N), \quad \dots\dots(1.1)$$

where $\mathcal{H}(\mathbf{r}^N)$ is the Hamiltonian operator, and the $\Psi_i(\mathbf{r}^N)$ are any complete orthonormal set of wave functions for the assembly. The \mathbf{r}^N denote the set of N position vectors $\mathbf{r}_1, \mathbf{r}_2 \dots \mathbf{r}_N$. The reduced density matrix $\rho_h^N(\mathbf{r}^h)$ for a group of h systems out of N can then be defined thus:

$$\rho_h^N(\mathbf{r}^h) = \int \dots \int_{(N-h)} \rho^N(\mathbf{r}^N, \mathbf{r}^N) d\mathbf{r}^{N-h}. \quad \dots\dots(1.2)$$

Both $\rho^N(\mathbf{r}^N, \mathbf{r}^N)$ and $\rho_h^N(\mathbf{r}^h)$ are normalized to the partition function Z_N according to:

$$Z_N = \int \dots \int_{(N)} \rho^N(\mathbf{r}^N, \mathbf{r}^N) d\mathbf{r}^N = \int \dots \int_{(h)} \rho_h^N(\mathbf{r}^h) d\mathbf{r}^h. \quad \dots\dots(1.3)$$

There are four previous attempts at the evaluation of Z_N which are of importance in the present context. The first is the expansion in powers of Planck's constant \hbar , developed by Wigner (1932) and Kirkwood (1933), which Chester (1954c) has summarized in a form which can be rewritten:

$$Z_N = \int \dots \int_{(N)} \exp[-\beta V(\mathbf{r}^N)] \left\{ \sum_i \Psi_i^*(\mathbf{r}^N) \exp[-\beta \mathcal{H}_0(\mathbf{r}^N)] \Psi_i(\mathbf{r}^N) + O(\hbar^2) + O(\hbar^4) + \dots \right\} d\mathbf{r}^N. \quad \dots\dots(1.4)$$

Here, the Hamiltonian has been separated into kinetic and potential energy contributions $\mathcal{H}_0(\mathbf{r}^N)$ and $V(\mathbf{r}^N)$ respectively, and $\beta = 1/kT$. The first term of (1.4) can be derived from (1.1) and (1.3) by ignoring the fact that $\mathcal{H}_0(\mathbf{r}^N)$ and $V(\mathbf{r}^N)$ do not commute. It will form what we shall call the exchange approximation, because this assumption of commutation implies that more weight is being given to the exchange effect of the statistics, entailed by the proper symmetry of the $\Psi_i(\mathbf{r}^N)$, than to the diffraction effect of the quantum mechanics.

The second approach, that of an expansion in terms of the interaction potential, was originally developed by Green (1951) and by Goldberger and Adams (1952). Calculations were limited to classical statistics, however, until Chester (1954a) showed that

$$Z_N = f_N(\beta) - \beta \sum_{n=1}^{\infty} \sum_{(q_j)} \frac{1}{n!} V_{q_1 q_2} V_{q_2 q_3} \dots V_{q_n q_1} \sum_j \left[\exp(-\beta E_{q_j}) / \prod_{i \neq j} (E_{q_j} - E_{q_i}) \right], \quad \dots (1.5)$$

where $f_N(\beta)$ is the perfect fluid partition function. The E_{q_j} are unperturbed (kinetic) energy levels, and the $V_{q_i q_j}$ are the matrix elements of the potential energy with respect to the complete orthonormal set, $\Psi_i(\mathbf{r}^N)$ of (1.1), which are now taken to be unperturbed energy eigenfunctions. In his application of (1.5) to liquid helium, however, Chester (1954b) confined attention to only the first two terms thus:

$$Z_N \simeq f_N(\beta) - \beta \sum_j V_{jj} \exp(-\beta E_j). \quad \dots (1.6)$$

These two terms are, in fact, included in the above exchange approximation, which can, in point of fact, be derived from (1.5) as follows. The $V_{q_i q_j}$ in (1.5) vanish if the states q_i and q_j differ in that more than two systems occupy different unperturbed energy levels. Since a typical assembly contains about 10^{23} systems, excitation of only two of them can result in there being little difference between E_{q_i} and E_{q_j} for non-zero $V_{q_i q_j}$. On making the approximation $E_{q_i} = E_{q_j}$, therefore, the exchange approximation itself follows from (1.5). However, the number of terms in each sum in (1.5) in which E_{q_i} is very slightly different from E_{q_j} is, of course, very large. Consequently, it does not necessarily follow that the *major* contribution to the partition function comes from terms for which $E_{q_i} = E_{q_j}$.

Thirdly, Feynman (1953) used the space-time approach to quantum mechanics in order to write the partition function as an integral over trajectories. On assuming that helium atoms ... "move freely among each other" ... he showed that

$$Z_N \simeq \left(\frac{h^2}{2\pi m' kT} \right)^{3N/2} \frac{K_\beta}{N!} \int \dots \int_{(N)} R_N(\mathbf{r}^N) \sum_P \left[\exp \left(-\frac{2\pi m' kT}{h^2} \sum_{i=1}^N \sum |\mathbf{r}_i - P\mathbf{r}_i|^2 \right) \right] d\mathbf{r}^N \quad \dots (1.7)$$

where m' is the effective mass of the helium atom, K_β is a normalization constant, P is the permutation operator, and the function $R_N(\mathbf{r}^N)$ is expected to be qualitatively very similar to the distribution function for a classical gas. Chester (1954c) therefore suggested writing it in the form $\exp[-\beta V'(\beta)]$, where $V'(\beta)$ is a quasi-interaction potential slightly dependent upon temperature. With this modification, therefore, (1.7) differs from the exchange approximation only

in that the true mass is replaced by the effective mass, $I(\mathbf{r}^N)$ is replaced by $I'(\beta)$, and a constant K_3 corrects the normalization. In his subsequent work, Feynman ignored these last two points, so that, in effect, he confined his attention to the exchange approximation, with the mass of the systems as an adjustable parameter.

Finally, Kikuchi (1954) applied Bethe's method for the Ising model to (1.7) by assuming that $R_N(\mathbf{r}^N)$ was non-vanishing only when the \mathbf{r}^N were located on a simple cubic lattice, and that $|\mathbf{r}_i - P\mathbf{r}_i|$ was negligible except when it equalled the lattice constant. This application of the quasi-crystalline approach to essentially the exchange approximation is asserted to lead to a second-order change at a temperature of $2.9m/m' ^\circ\text{K}$.

It seems therefore that the exchange approximation is worthy of further study. We hope to be able to demonstrate the relation between some of these previous attempts at evaluating Z_N and the classical work of Mayer (1948) relating to the condensation of an imperfect classical gas into a liquid. Since theories of helium usually consider a phase change between liquid I and liquid II, we must first show that the Bose-Einstein condensation of the perfect fluid can be regarded as a first-order change, and also establish some necessary formulae relating to the perfect fluid.

§ 2. THE PERFECT BOSE-EINSTEIN FLUID

The density matrices for the perfect fluid have been investigated by Husimi (1940). He showed that, if in (1.1) we substitute for the $\Psi_i(\mathbf{r}^N)$ a determinant or permanent of one-particle energy eigenfunctions, $\psi_l(\mathbf{r}_j)$ say, with the appropriate normalization factor, we obtain, for Fermi-Dirac or Bose-Einstein assemblies respectively,

$$\rho^N(\mathbf{r}^N, \mathbf{r}^N) = \frac{1}{N!} \pm |\rho(\mathbf{r}_i, \mathbf{r}_j|\beta)|_N, \quad \dots\dots (2.1)$$

where

$$\rho(\mathbf{r}_i, \mathbf{r}_j|\beta) = \sum_l \exp(-\beta\epsilon_l) \psi_l(\mathbf{r}_i) \psi_l^*(\mathbf{r}_j). \quad \dots\dots (2.2)$$

The notation $\pm| \cdot |_N$ denotes a permanent (+) or determinant (−) of order N . In general, out of a pair of alternate signs, the upper one refers to Bose-Einstein, the lower to Fermi-Dirac, statistics. Furthermore, in (2.2), the ϵ_l are the (kinetic) energy levels of the independent systems. Husimi then deduced another algebraic identity

$$\sum_{N=h}^{\infty} \lambda^N \rho_h^N(\mathbf{r}^h) N! / (N-h)! = \pm |\sigma(\mathbf{r}_i, \mathbf{r}_j|\lambda)|_h \sum_{N=0}^{\infty} \lambda^N f_N(\beta), \quad \dots\dots (2.3)$$

where

$$\sigma(\mathbf{r}_i, \mathbf{r}_j|\lambda) = \sum_l \frac{\lambda \exp(-\beta\epsilon_l)}{1 \mp \lambda \exp(-\beta\epsilon_l)} \psi_l(\mathbf{r}_i) \psi_l^*(\mathbf{r}_j). \quad \dots\dots (2.4)$$

Now, in (2.3) and (2.4), it is well known that, for $\lambda \leq 1$,

$$\sigma(\mathbf{r}_i, \mathbf{r}_j|\lambda) = \left(\frac{2\pi mkT}{h^2} \right)^{3/2} \sum_{l \geq 1} \frac{(\pm)^{l+1} \lambda^l}{l^{3/2}} \exp \left[- \frac{2\pi mkT}{h^2} \frac{\pi r_{ij}^2}{l} \right], \quad \dots\dots (2.5)$$

and

$$\sum_{N=0}^{\infty} \lambda^N f_N(\beta) = \exp \left\{ V \left(\frac{2\pi mkT}{h^2} \right)^{3/2} \sum_{l \geq 1} \frac{(\pm)^{l+1} \lambda^l}{l^{5/2}} \right\} = G(\lambda), \text{ say.} \quad \dots\dots (2.6)$$

Then, from (2.1)–(2.4), and from (1.2), we can set up a third algebraic identity:

$$\sum_{N=h}^{\infty} \frac{\lambda^N}{(N-h)!} \int \dots \int_{(N-h)} \pm \left| \sum_i \exp(-\beta \epsilon_i) \psi_i(\mathbf{r}_i) \psi_i^*(\mathbf{r}_j) \right|_N d\mathbf{r}^{N-h} \\ = G(\lambda) \pm \sum_i \frac{\lambda \exp(-\beta \epsilon_i)}{1 \mp \lambda \exp(-\beta \epsilon_i)} \psi_i(\mathbf{r}_i) \psi_i^*(\mathbf{r}_j) \Big|_h \dots \dots (2.7)$$

where $G(\lambda)$ is given, for $\lambda \leq 1$, by (2.6). Eqn (2.7) is a purely algebraic relation involving one-particle energy eigenfunctions $\psi_i(\mathbf{r}_i)$, the associated unperturbed (kinetic) energy levels ϵ_i , and the parameter λ , ≤ 1 . Furthermore, when λ corresponds to the absolute activity λ_0 of the *perfect* assembly, $G(\lambda_0)$ or $\Sigma \lambda_0^N f_N(\beta)$ becomes the corresponding grand partition function.

Now, it is usually thought that the thermodynamic functions for the perfect assembly deduced from (2.6) (with $\lambda = \lambda_0$) exhibit a third-order transition. Kahn (1938) and Goldstein (1946), however, consider it to be a first-order change. We suggest that this latter view affords an approximation to the condensation of *gaseous* helium into liquid II.

A first-order change is one in which a heterogeneous region of mixed liquid and vapour appears on a pV , TV or TS diagram. Across this region there are discontinuities in certain thermodynamic functions. For example, in an obvious notation, the discontinuities in entropy S and volume V are related to the latent heat L of the transition, and to the derivative dp/dT along the phase boundary, by the well-known equation:

$$S_2 - S_1 = (V_2 - V_1) dp/dT = L/T \quad (S_2 > S_1). \quad \dots \dots (2.8)$$

Furthermore, *within* this heterogeneous region, the specific heat C_p and the derivatives $(\partial V/\partial T)_p$, $(\partial S/\partial T)_p$ and $(\partial V/\partial p)_T$ are all infinite. Also, if $(\partial p/\partial V)_T$ vanishes throughout a finite range of volumes so that $p = p(T)$ within this range, we have a first-order change with C_p infinite, implying a latent heat.

Now consider the following equations, for a perfect Bose–Einstein fluid, which follow from (2.6) (with $\lambda = \lambda_0$):

$$p = kT \left(\frac{2\pi mkT}{h^2} \right)^{3/2} \sum_{l \geq 1} \lambda_0^l / l^{5/2}, \quad \dots \dots (2.9)$$

$$E = \frac{3}{2} V kT \left(\frac{2\pi mkT}{h^2} \right)^{3/2} \sum_{l \geq 1} \lambda_0^l / l^{5/2} = \frac{3}{2} pV, \quad \dots \dots (2.10)$$

and

$$\rho = \frac{N}{V} = \left(\frac{2\pi mkT}{h^2} \right)^{3/2} \sum_{l \geq 1} \lambda_0^l / l^{3/2}. \quad \dots \dots (2.11)$$

London (1938) gave appropriate pV , VT and pT diagrams when he drew attention to the failure of (2.11) to take account, at low temperatures, of the systems flooding into the lowest energy level. His pV and TV diagrams display a region throughout which $(\partial p/\partial V)_T$ and $(\partial T/\partial V)_p$ vanish, extending from that value of the volume at which this flooding first becomes important, down to zero volume. This can be looked upon as a heterogeneous region within which C_p is given by

$$C_p = \left[\frac{\partial}{\partial T} (E + pV) \right]_p = \frac{5p}{2} \left(\frac{\partial V}{\partial T} \right)_p. \quad \dots \dots (2.12)$$

It is therefore infinite because of $(\partial V/\partial T)_p$. This is characteristic of a first-order change. The latent heat is given by (2.8) and (2.9) with $\lambda_0 = 1$, and $V_1 = 0$,

and V_2 is given by (2.11) with $\lambda_0 = 1$, whence

$$L = \frac{5}{2} NkT \sum l^{-5/2} / \sum l^{-3/2}. \quad \dots\dots (2.13)$$

In (2.13) it is well known that $\sum l^{-5/2} = 1.341$ and $\sum l^{-3/2} = 2.612$. Consequently, the latent heat of vaporization of the perfect fluid is given by $L = 2.54T$ cal mole⁻¹, a result which bears comparison, to the present crude level of approximation, with the experimental results collected by Squire (1953) for the latent heat of vaporization of liquid helium II.

Further support for our new point of view comes also from the well-known equation of the vaporization curve of the perfect fluid. Its gradient, of about 2.3 atm deg⁻¹, is nearly five times that of the experimental vaporization curve of liquid helium II, to which, however, it is a better approximation than to the slope of -81 atm deg⁻¹ of the lambda line on the more usual interpretation.

London (1938), on the other hand, took this perfect fluid to be a model of liquid helium. Consequently, the thermodynamic discontinuities which he investigated were across the upper boundary of our heterogeneous region, which comprises his model of liquid helium II. It therefore has $(\partial p, \partial V)_T$ zero and C_p infinite, which can hardly be regarded as satisfactory. Furthermore, the rest of this paper is concerned with the addition of gaseous imperfections to the perfect fluid theory, and we believe that this is necessarily more profitably regarded as a step towards achieving a better description of the condensation of helium *vapour* into liquids I and II.

§ 3. THE CLUSTER INTEGRAL EXPANSIONS

The summation in the integrand of the first term of (1.4) is an unperturbed or perfect fluid density matrix normalized to the corresponding partition function. Consequently, if we make the usual determinantal or permanent substitution for the $\Psi_i(\mathbf{r}^N)$, we can use (2.1) in the form:

$$\sum_i \Psi_i^*(\mathbf{r}^N) \exp[-\beta \mathcal{H}_0(\mathbf{r}^N)] \Psi_i(\mathbf{r}^N) = \frac{1}{N!} \left| \sum_k \exp(-\beta \epsilon_k) \psi_k(\mathbf{r}_i) \psi_k^*(\mathbf{r}_j) \right|_N. \quad \dots\dots (3.1)$$

We can also follow classical theory and write:

$$\exp[-\beta V(\mathbf{r}^N)] = \prod_{i>j}^N \exp[-\beta \phi(\mathbf{r}_{ij})] = \prod_{i>j}^N (1 + f_{ij}), \quad \dots\dots (3.2)$$

where $\phi(\mathbf{r}_{ij})$ is the intermolecular pair potential energy. With the aid of (3.1) and (3.2), therefore, the first term of (1.4) can be rewritten

$$Z_N = \frac{1}{N!} \int \dots \int \prod_{i>j}^N (1 + f_{ij}) \left| \sum_k \exp(-\beta \epsilon_k) \psi_k(\mathbf{r}_i) \psi_k^*(\mathbf{r}_j) \right|_N d\mathbf{r}^N. \quad \dots\dots (3.3)$$

Now we select from $\prod_{i>j}^N (1 + f_{ij})$ a sum of a number of products of f_{ij} factors relating to a group of l suffices, each term of which contains each suffix 1 to l mentioned at least once, the sum exhausting all the possibilities of these suffices, and we denote it by $C_l(\mathbf{r}^l)$. Furthermore, there are $N!/l!(N-l)!$ ways of

selecting these l points out of the total number N . Hence (3.3) becomes

$$Z_N = \sum_{l=0}^N \frac{1}{l!} \int \dots \int_{(l)} C_l(\mathbf{r}^l) \left[\frac{1}{(N-l)!} \times \int \dots \int_{(N-l)} \pm \sum_k \exp(-\beta \epsilon_k) \psi_k(\mathbf{r}_i) \psi_k^*(\mathbf{r}_j) |_{N-l} d\mathbf{r}^{N-l} \right] d\mathbf{r}^l. \quad \dots (3.4)$$

Here, we have taken $C_0(\mathbf{r}^1)$ as unity by definition. It then follows that

$$\sum_{N=0}^{\infty} \lambda^N Z_N = \sum_{N=0}^{\infty} \sum_{l=0}^{\infty} \frac{\lambda^N}{l!} \int \dots \int_{(l)} C_l(\mathbf{r}^l) \times \left[\frac{1}{(N-l)!} \int \dots \int_{(N-l)} \pm \sum_k \exp(-\beta \epsilon_k) \psi_k(\mathbf{r}_i) \psi_k^*(\mathbf{r}_j) |_{N-l} d\mathbf{r}^{N-l} \right] d\mathbf{r}^l. \quad \dots (3.5)$$

If we interchange the orders of summation, this becomes

$$\sum_{N=0}^{\infty} \lambda^N Z_N = \sum_{l=0}^{\infty} \frac{1}{l!} \int \dots \int_{(l)} C_l(\mathbf{r}^l) \times \left[\sum_{N=l}^{\infty} \frac{\lambda^N}{(N-l)!} \int \dots \int_{(N-l)} \pm \sum_k \exp(-\beta \epsilon_k) \psi_k(\mathbf{r}_i) \psi_k^*(\mathbf{r}_j) |_{N-l} d\mathbf{r}^{N-l} \right] d\mathbf{r}^l. \quad \dots (3.6)$$

The summation in the square bracket in (3.6) can then be expressed in terms of the $\sigma(\mathbf{r}_i, \mathbf{r}_j | \lambda)$ of (2.4) by means of the algebraic identity (2.7), which holds, *inter alia*, for that value of λ corresponding to the true absolute activity, Λ say, of the imperfect assembly. We finally obtain, then, for the logarithm of the grand partition function:

$$\ln(\text{GPF}) = \ln G(\Lambda) + \ln \left[1 + \sum_{l \geq 2} \frac{1}{l!} \int \dots \int_{(l)} C_l(\mathbf{r}^l) \pm \sigma(\mathbf{r}_i, \mathbf{r}_j | \Lambda) |_l d\mathbf{r}^l \right], \quad \dots (3.7)$$

where $G(\Lambda)$ and $\sigma(\mathbf{r}_i, \mathbf{r}_j | \Lambda)$ are given by (2.6) and (2.5) respectively (with $\lambda = \Lambda$, ≤ 1). While this is an *exact* reduction of the exchange approximation, it is not yet in a suitable form for comparison with other work (although it is clearly some sort of cluster integral expansion). However, a further approximation will facilitate our discussion, while our qualitative conclusions will still apply to (3.7).

§ 4. THE DIAGONAL APPROXIMATION

Now consider the expansion, to begin with, of the permanent of order l in the argument of the second logarithm of (3.7). The elements $\sigma(\mathbf{r}_i, \mathbf{r}_j | \Lambda)$ of this permanent are characterized by the suffices i and j . We regard these suffices, of which there are l in all, as l numbered points. Then the whole expansion can be thought of as a sum of products of factors $\sigma(\mathbf{r}_i, \mathbf{r}_j | \Lambda)$, each factor having two suffices. The suffices of a typical product represent the selection, from these l points, of n_s 'closed rings' of s points numbered consecutively from 1 to s .

A typical product must then be multiplied by the complicated sum of products of f_{ij} factors represented by $C_l(\mathbf{r}^l)$. The resulting integral remains, as yet, intractable, and we are compelled to introduce an approximation which can best

be illustrated by reference to $l-6$ rings of one and two rings of three in the expansion of the permanent. This particular term will be given by

$$\sigma^{l-6}(\mathbf{r}, \mathbf{r}|\Lambda)\sigma(\mathbf{r}_1\mathbf{r}_2|\Lambda)\sigma(\mathbf{r}_2\mathbf{r}_3|\Lambda)\sigma(\mathbf{r}_3\mathbf{r}_1|\Lambda)\sigma(\mathbf{r}_4\mathbf{r}_5|\Lambda)\sigma(\mathbf{r}_5\mathbf{r}_6|\Lambda)\sigma(\mathbf{r}_6\mathbf{r}_4|\Lambda).$$

The approximation, in this case, consists in writing

$$C_l(\mathbf{r}^l) \simeq C_{l-6}(\mathbf{r}^{l-6})(f_{12}f_{23}f_{31})(f_{45}f_{56}f_{64}). \quad \dots\dots (4.1)$$

It implies that we are treating *exactly* the diagonal product term in the expansion of the permanent. The only approximation is in our consideration of the effect of the off-diagonal elements of the permanent.

The resulting l -fold space integral of the term involving (4.1) therefore becomes the product of two 'chain integrals' of three factors $\sigma(\mathbf{r}_i\mathbf{r}_j|\Lambda)f_{ij}$ and the configurational integral

$$\int \dots \int C_{l-6}(\mathbf{r}^{l-6}) d\mathbf{r}^{l-6}.$$

And, out of all these integrals we can integrate a factor V . Consequently, if we define

$$g_s = \int \dots \int_{(s-1)} [\sigma(\mathbf{r}_1\mathbf{r}_2|\Lambda)f_{12}][\sigma(\mathbf{r}_2\mathbf{r}_3|\Lambda)f_{23}] \dots [\sigma(\mathbf{r}_s\mathbf{r}_1|\Lambda)f_{s1}] d\mathbf{r}^{s-1}, \quad \dots\dots (4.2)$$

it then follows that the term of order l in the summation in (3.7) can be written as a sum of products, each product corresponding to the selection of n_s closed rings of s points out of l , with the appropriate combinatorial factor, $g(n_s)$ say. We therefore obtain

$$\begin{aligned} & \frac{1}{l!} \int \dots \int C_l(\mathbf{r}^l) [\sigma(\mathbf{r}_i\mathbf{r}_j|\Lambda)]_l d\mathbf{r}^l \\ &= \frac{1}{l!} \sum_{(n_s)}^{(l)} g(n_s) \left(\int \dots \int \sigma^{n_s}(\mathbf{r}\mathbf{r}|\Lambda) C_{n_s}(\mathbf{r}^{n_s}) d\mathbf{r}^{n_s} \right) \dots \dots (V_{s2}^{g_s})^{n_2} (V_{s3}^{g_s})^{n_3} \dots (V_{ss}^{g_s})^{n_s} \dots \end{aligned} \quad \dots\dots (4.3)$$

where

$$g(n_s) = l! / \prod_s n_s! s^{n_s}, \quad \text{with} \quad \sum_s s n_s = l. \quad \dots\dots (4.4)$$

Strictly speaking, the term with $s=2$ in (4.3) gives incorrect weight to f_{12} . This could easily be corrected at the cost of increased mathematical complexity, but we shall ignore it as a further approximation unlikely to affect the *singularities* of the theory.

On substituting (4.3) and (4.4) into (3.7) we can carry out the summation with respect to l in the following manner:

$$\begin{aligned} \ln(\text{GPF}) \simeq \ln G(\Lambda) + \ln \left\{ \left[\prod_{s \geq 2} \sum_{(n_s)} \frac{1}{n_s!} \left(\frac{V_{ss}^{g_s}}{s} \right)^{n_s} \right] \sum_{(n_1)} \frac{\sigma^{n_1}(\mathbf{r}\mathbf{r}|\Lambda)}{n_1!} \right. \\ \left. \times \int \dots \int C_{n_1}(\mathbf{r}^{n_1}) d\mathbf{r}^{n_1} \right\}. \quad \dots\dots (4.5) \end{aligned}$$

Then, clearly,

$$\ln(\text{GPF}) \simeq \ln G(\Lambda) + V \sum_{s \geq 2} \frac{g_s}{s} + \ln \sum_{(n_1)} \frac{\sigma^{n_1}(\mathbf{r}\mathbf{r}|\Lambda)}{n_1!} \int \dots \int C_{n_1}(\mathbf{r}^{n_1}) d\mathbf{r}^{n_1}. \quad \dots\dots (4.6)$$

Now the logarithm of the grand partition function must be proportional to the volume V because:

$$\frac{pV}{kT} = \ln(\text{GPF}) = V \frac{\partial}{\partial V} \ln(\text{GPF}). \quad \dots\dots(4.7)$$

The first two terms on the right-hand side of (4.6) are already proportional to V (see Eqn (2.6) with $\lambda = \Lambda, \leq 1$). In the summation in the argument of the third term, we will be able to integrate out various powers of V because of the difference between the f_{ij} -linkages comprising the $C_{n_1}(\mathbf{r}^{n_1})$ and the corresponding classical reducible cluster integral. The third term of (4.6) will therefore be of the form

$$\ln[1 + aV + bV^2 + cV^3 + \dots]. \quad \dots\dots(4.8)$$

This must be proportional to V . The series in the square bracket must therefore be the exponential series. Its logarithm will consequently reduce to the sum of all the terms proportional to V from the summation with respect to n_1 in (4.6). We will therefore have to reject all those linkages in $C_{n_1}(\mathbf{r}^{n_1})$ which make the integral differ from the classical reducible cluster integral b_{n_1} (whose definition includes a factor $1/n_1!$). Consequently (4.6) becomes:

$$\ln(\text{GPF}) = \ln G(\Lambda) + V \sum_{s \geq 2} \frac{g_s}{s} + V \sum_{l \geq 2} b_l \sigma^l(\mathbf{r}\mathbf{r}|\Lambda). \quad \dots\dots(4.9)$$

Now, in (4.9) the chain integrals g_s defined by (4.2) can be reduced by means of lemma II of Rushbrooke and Scoins (1951) as follows:

$$g_s = \frac{(2\pi)^{3s/2}}{2\pi^2} \int_0^\infty u^2 \mathcal{G}^s(u, \Lambda) du, \quad \dots\dots(4.10)$$

where

$$u \mathcal{G}(u, \Lambda) = \frac{1}{(2\pi)^{1/2}} \int_{-\infty}^{+\infty} r_{12} f_{12} \sigma(\mathbf{r}_1 \mathbf{r}_2 | \Lambda) \sin ur_{12} dr_{12}. \quad \dots\dots(4.11)$$

Eqn (4.10) enables us to effect the second summation in (4.9) in the following closed form:

$$\begin{aligned} \ln(\text{GPF}) = \ln G(\Lambda) - \frac{V}{2\pi^2} \int_0^\infty u^2 \ln[1 - (2\pi)^{3/2} \mathcal{G}(u, \Lambda)] du \\ + V \sum_{l \geq 2} b_l \sigma^l(\mathbf{r}\mathbf{r}|\Lambda) - \frac{V}{2\pi^2} \int_0^\infty u^2 (2\pi)^{3/2} \mathcal{G}(u, \Lambda) du. \quad \dots\dots(4.12) \end{aligned}$$

The last term in (4.12) can be rewritten thus:

$$\frac{V}{(2\pi)^{1/2}} \int_{-\infty}^{+\infty} u^2 \mathcal{G}(u, \Lambda) du = V \lim_{r \rightarrow 0} \frac{1}{(2\pi)^{1/2}} \int_{-\infty}^{+\infty} u^2 \mathcal{G}(u, \Lambda) \frac{\sin ur}{ur} dr = -V \sigma(\mathbf{r}\mathbf{r}|\Lambda), \quad \dots\dots(4.13)$$

so defining

$$b_1 = 1, \quad \dots\dots(4.14)$$

we obtain from (4.12), (4.13), (4.14), (2.5) and (2.6) the following approximation for an imperfect Bose-Einstein fluid:

$$\ln(\text{GPF}) = VP(\Lambda, \frac{5}{2}) + V \sum_{l \geq 1} b_l P^l(\Lambda, \frac{3}{2}) - \frac{V}{2\pi^2} \int_0^\infty u^2 \ln[1 - (2\pi)^{3/2} \mathcal{G}(u, \Lambda)] du, \quad \dots\dots(4.15)$$

whence

$$p = kTP(\Lambda, \frac{5}{2}) + kT \sum_{l \geq 1} b_l P^l(\Lambda, \frac{3}{2}) - \frac{kT}{2\pi^2} \int_0^\infty u^2 \ln[1 - (2\pi)^{3/2} \mathcal{G}(u, \Lambda)] du, \quad \dots\dots(4.16)$$

and

$$\rho = \frac{N}{V} = P(\Lambda, \frac{3}{2}) + \frac{P(\Lambda, \frac{1}{2})}{P(\Lambda, \frac{3}{2})} \sum_{l=1}^{\infty} l b_l P^l(\Lambda, \frac{3}{2}) + \frac{(2\pi)^{3/2}}{2\pi^2} \int_0^{\infty} \frac{u^2 \Lambda \partial \mathcal{G}(u, \Lambda) / \partial \Lambda}{1 - (2\pi)^{3/2} \mathcal{G}(u, \Lambda)} du, \quad \dots (4.17)$$

where

$$P(\Lambda, n/2) = \left(\frac{2\pi m k T}{h^2} \right)^{3/2} \sum_{s=1}^{\infty} \Lambda^s / s^{n/2}, \quad \dots (4.18)$$

and, explicitly,

$$u \mathcal{G}(u, \Lambda) = \left(\frac{2\pi m k T}{h^2} \right)^{3/2} \sum_{l=1}^{\infty} \frac{\Lambda^l}{l^{3/2}} \frac{1}{(2\pi)^{1/2}} \int_{-\infty}^{\infty} r f(r) \exp \left[- \frac{2\pi m k T}{h^2} \frac{\pi r^2}{l} \right] \sin ur \, dr, \quad \dots (4.19)$$

and

$$u \Lambda \frac{\partial \mathcal{G}(u, \Lambda)}{\partial \Lambda} = \left(\frac{2\pi m k T}{h^2} \right)^{3/2} \sum_{l=1}^{\infty} \frac{\Lambda^l}{l^{1/2}} \frac{1}{(2\pi)^{1/2}} \int_{-\infty}^{\infty} r f(r) \exp \left[- \frac{2\pi m k T}{h^2} \frac{\pi r^2}{l} \right] \sin ur \, dr. \quad \dots (4.20)$$

These Eqns (4.15)–(4.20) constitute what we shall call the diagonal approximation (to the exchange approximation) because the effect of the diagonal terms in the permanents of order l in (3.7) is embodied *exactly* in the second terms of Eqns (4.15)–(4.17) (which we shall call the ‘diagonal series’). On the other hand, only *approximate* account is taken of the *off-diagonal* terms by means of the third, integrated terms (which we shall call the ‘off-diagonal integrals’). And, it appears that these off-diagonal integrals well might play an important part in the condensation of helium gas into liquids I and II.

The first terms of (4.16) and (4.17) are the corresponding expressions for the perfect fluid, while their classical limit is obtained by ignoring the third term in either equation, and by retaining only the first power of Λ in the various series. It is easily verified that we then regain the well-known equations of Mayer (1948), i.e.

$$p = kT \sum b_l z^l \quad \dots (4.21)$$

$$\rho = \sum l b_l z^l \quad \dots (4.22)$$

where

$$z = \left(\frac{2\pi m k T}{h^2} \right)^{3/2} \Lambda. \quad \dots (4.23)$$

Also, of course, Mayer succeeded in eliminating z between (4.21) and (4.22) to obtain the well-known virial expansion. And all these classical equations refer to the condensation of a gas into a liquid. Because of the relation between (4.21)–(4.23) and (4.16)–(4.18) (which were derived from (3.7)) this suggests that theories based on (3.7) (and hence, ultimately, on the first term of (1.4)) should similarly refer to the condensation of helium vapour into liquids I and II, and not to the lambda transition in the liquid phase, which has hitherto been the conventional approach.

We can therefore now take over the work of Mayer in discussing the dependence of (4.16) and (4.17) on the classical cluster integral series. The best we can hope for at the present stage is to show that the phenomena of condensation of the gas into liquids I and II can at least be covered by these equations if we make certain assumptions about their asymptotic behaviour which are certainly not obviously false. We shall assume that condensation of the gas into liquid I is a predominantly ‘classical’ process described by the divergence of the diagonal

series, and we shall investigate the possibility that condensation into liquid II is a 'quantal' process described by the divergence of the off-diagonal integral (which is an approximation, in closed form, to the sum of terms arising from the off-diagonal elements of the permanents appearing in (3.7)). We shall therefore first consider the diagonal series in more detail.

§ 5. THE SINGULARITIES OF THE EQUATIONS

Following Mayer's well-known arguments, we are mainly interested here in the divergence of the diagonal series constituting essentially the second terms of the right-hand sides of (4.16) and (4.17). Consider therefore, in an obvious notation, the series

$$\sum_{l \geq 1} l b_l P^{l-1}(\Lambda, \frac{3}{2}) = 1 + \sum_{l \geq 2} \frac{l P^{l-1}(\Lambda, \frac{3}{2})}{l!} \int \dots \int \left[\begin{array}{c} \text{reducible cluster} \\ \text{of } l \text{ points} \end{array} \right] d\mathbf{r}^{l-1} \quad \dots\dots (5.1)$$

and the integrals u_n introduced by Rushbrooke and Scoins (1953) defined by

$$u_1 = \int_0^\infty f(r) d\mathbf{r}, \quad \dots\dots (5.2)$$

$$u_{n+1} = \int_0^\infty [1 + f(r)] g_n(r) d\mathbf{r} \quad (n \geq 1). \quad \dots\dots (5.3)$$

Here, $g_n(r)$ is an *open* cluster integral of $n+2$ points with two major points a distance r apart, while all the integrands in (5.1), (5.2) and (5.3) are appropriate sums of products of factors f_{ij} . If $g_n(r)$ is 'closed' by multiplying by $f(r)$ and integrating, the corresponding irreducible cluster integral is obtained. Specifically, therefore,

$$g_n(r) = \frac{1}{n!} \int \dots \int_{(n)} [\text{open cluster of } n \text{ points} + 2 \text{ major points}] d\mathbf{r}^n. \quad \dots\dots (5.4)$$

So from (5.3) and (5.4), we obtain:

$$u_{n+1} = \frac{1}{n!} \int \dots \int_{(n+1)} [\text{partially closed cluster of } n \text{ points} + 2 \text{ major points}] d\mathbf{r}^n \quad \dots\dots (5.5)$$

which can be rewritten in the form:

$$u_{l-1} = \frac{2}{(l-1)!} \int \dots \int_{(l-1)} [\text{partially closed cluster of } l \text{ points}] d\mathbf{r}^{l-1}. \quad \dots\dots (5.6)$$

The combinatorial factor occurring in the transition from (5.5) to (5.6) arises from the number of ways of selecting the two major points from the total number of points comprising the cluster.

We now introduce the approximation of replacing the reducible cluster integrals b_l in (5.1) by the integrals u_{l-1} of (5.6), which comprise the sum of an open and an irreducible cluster of l points. It then follows that

$$\sum_{l \geq 1} l b_l P^{l-1}(\Lambda, \frac{3}{2}) \simeq 1 + \sum_{l \geq 2} \frac{u_{l-1}}{2} P^{l-1}(\Lambda, \frac{3}{2}) = 1 + \frac{1}{2} \sum_{l \geq 1} u_l P^l(\Lambda, \frac{3}{2}). \quad \dots\dots (5.7)$$

But Rushbrooke and Scoins (1953) showed that

$$1 + \sum_{n \geq 1} u_n \rho^n = 1 / (1 - \sum k \beta_k \rho^k) \quad \dots\dots (5.8)$$

where the β_k are the irreducible cluster integrals and ρ can be regarded here as a parameter. Consequently, from (5.7) and (5.8) we obtain the important approximate result that

$$\sum_{l \geq 1} l b_l P^{l-1}(\Lambda, \frac{3}{2}) \simeq 1 + \frac{\sum_{K \geq 1} k \beta_k P^k(\Lambda, \frac{3}{2})}{2(1 - \sum_{K \geq 0} k \beta_k P^k(\Lambda, \frac{3}{2}))}. \quad \dots\dots (5.9)$$

There are therefore two possible conditions for the singularity of the diagonal series (5.9). Either

$$1 - \sum k \beta_k P^k(\Lambda, \frac{3}{2}) = 0 \quad \dots\dots (5.10)$$

or $\sum k \beta_k P^k(\Lambda, \frac{3}{2})$ is itself singular. These conclusions ought to be compared with those of Born and Fuchs (1938), who showed exactly that the singularity of the classical series $\sum b_l z^l$ (where z is the classical fugacity) occurs when either

$$1 - \sum k \beta_k \rho^k = 0 \quad \dots\dots (5.11)$$

(where ρ is the number density), or when $\sum k \beta_k \rho^k$ is singular. Although our results are similar, as indeed we expect, they are, of course, based on the approximations which led to (5.9).

If, however, the 'classical' condensation into liquid helium I occurs when (5.10) is satisfied, then the diagonal series does *not* diverge suddenly. Hence $(\partial p / \partial V)_T$ will tend monotonically to zero without any discontinuity, indicative of the critical point. If, on the other hand, $\sum k \beta_k P^k(\Lambda, \frac{3}{2})$ is singular, for a smaller value of $P(\Lambda, \frac{3}{2})$ than the smallest real root of (5.10), then the diagonal series will diverge suddenly, corresponding to condensation with a discontinuity in $(\partial p / \partial V)_T$. Furthermore, this singularity must occur when $\sum k \beta_k P^k(\Lambda, \frac{3}{2}) < 1$ (the β_k being positive at these low temperatures), so that the diagonal series (5.9) will be positive when condensation is imminent. At the same time, it can be shown that the off-diagonal integrals will make negative contributions to the right-hand sides of (4.16) and (4.17). However, it is rather difficult to predict the total effect of both these terms in (4.16) and (4.17), although the experimental values of the pressure and density of helium vapour, when condensation is imminent, are less than the theoretical values predicted by the first (perfect fluid) terms on the right-hand sides of (4.16) and (4.17).

But it is also worth noting that the off-diagonal integrals themselves will diverge when

$$1 - (2\pi)^{3/2} \mathcal{G}(u, \Lambda) = 0. \quad \dots\dots (5.12)$$

This condition is peculiar to Bose-Einstein fluids, being absent from both classical and Fermi-Dirac statistics, and shows that the condensation of helium vapour may ultimately be modified by a purely quantal effect suggestive of the formation of liquid helium II. Furthermore (5.12) arises, in effect, from the property of statistical attraction which, in the perfect fluid, gives rise to the need for taking specific account of the systems flooding into the lowest energy level when $\Lambda = 1$. However, in the case of the imperfect fluid, the series $P(\Lambda, \frac{1}{2})$ in (4.17) tends monotonically to infinity as Λ tends to unity. Consequently, it is clearly of interest to estimate for what values of Λ and T (5.12) is satisfied at the place $u = 0$.

Now, physically, the classical condensation into liquid I is characterized by the divergence of the diagonal series (when $\sum k\beta_k P^k(\Lambda, \frac{3}{2})$ is singular). This occurs for increasing Λ as T decreases. Ultimately, there will occur a sufficiently low temperature at which (5.12) is first satisfied in addition. This temperature will be that of the triple line separating liquids I and II on the conventional pV diagram; and it will be given by the simultaneous solution of (5.12) with the condition that $\sum k\beta_k P^k(\Lambda, \frac{3}{2})$ is singular. However, this implies that the phase boundaries (on the conventional phase diagram) between the vapour and liquid I, and between the vapour and liquid II, are given by quite different equations; whereas, in actual fact, the boundary is continuous through the lambda point, and almost certainly has a continuous gradient there. Thus, it is difficult to believe that two different mathematical conditions are involved. Consequently, Chester (1959, private communication) and Rushbrooke (1959, private communication) have suggested that it might be possible to regard the singularity of $\sum k\beta_k P^k(\Lambda, \frac{3}{2})$ as prescribing the phase boundary between the vapour and *both* liquids I and II, while the additional condition (5.12) might constitute an approximate equation for the phase boundary *between* liquids I and II, i.e. for the lambda line. The simultaneous satisfaction of these two conditions will again lead to a theoretical prediction of the lambda temperature; and it will also determine the corresponding Λ , subject to the severe approximations inherent in (5.12). It is therefore now convenient to write down some obvious approximations to the singularity of $\sum k\beta_k P^k(\Lambda, \frac{3}{2})$ suitable for numerical computation.

Firstly, using the 'netted chain' technique of Rushbrooke and Scoins (1953) it can be shown that one suitable approximation to this singularity is given by

$$1 - P(\Lambda, \frac{3}{2})\beta_1 - 2P^2(\Lambda, \frac{3}{2})\beta_2 = 0. \quad \dots\dots (5.13)$$

Secondly, it is possible to estimate the radius of convergence of $\sum k\beta_k P^k(\Lambda, \frac{3}{2})$ by means of the Cauchy-Hadamard theorem. This value of $P(\Lambda, \frac{3}{2})$ corresponding to the singularity is then given by

$$P(\Lambda, \frac{3}{2}) = \left\{ \lim_{n \rightarrow \infty} (\beta_n)^{1/n} \right\}^{-1}. \quad \dots\dots (5.14)$$

An approximation to (5.14) of the same order as (5.13) is clearly

$$P(\Lambda, \frac{3}{2}) \simeq \beta_2^{-1/2}. \quad \dots\dots (5.15)$$

At the same time, from (4.19) and (5.12) we have explicitly for the quantal condensation

$$1 - \left(\frac{2\pi mkT}{h^2} \right)^{3/2} \sum_{l \geq 1} \frac{\Lambda^l}{l^{3/2}} \int f(r) \exp \left[- \frac{2\pi mkT}{h^2} \frac{\pi r^2}{l} \right] d\mathbf{r} = 0. \quad \dots\dots (5.16)$$

We now require to discuss the numerical solutions of these equations, using appropriate potential functions for helium, bearing in mind that (5.16) is less exact than (5.13) or (5.15).

§ 6. NUMERICAL CALCULATIONS

Firstly, $\phi(r)$ has been given in the form of a Lennard-Jones type potential by de Boer (1950, 1951) thus

$$\phi(r) = 4\epsilon \left\{ \left(\frac{\sigma}{r} \right)^{12} - \left(\frac{\sigma}{r} \right)^6 \right\} \quad \dots\dots (6.1)$$

where $\epsilon = 1.41 \times 10^{-15}$ erg and $\sigma = 2.561 \times 10^{-8}$ cm.

Secondly, Guggenheim (1950) has given a general method of arriving at a square-well approximation to (6.1) from which it follows that

$$\begin{aligned} e^{-\phi(r)/kT} &= 0 \text{ for } r < 2.166 \times 10^{-8} \text{ cm} \\ &= e^{12.26/T} \text{ for } 2.166 \times 10^{-8} \text{ cm} < r < 3.251 \times 10^{-8} \text{ cm} \\ &= 1 \text{ for } r > 3.251 \times 10^{-8} \text{ cm.} \end{aligned} \quad \dots\dots (6.2)$$

Because of the difficulty of eliminating Λ between (5.13) or (5.15) and (5.16), we shall first solve (5.13) and (5.15) for T assuming $\Lambda = 1$, using both (6.1) and (6.2), and then discuss the corresponding value of Λ obtained from (5.16) on substituting representative values of T . In the case of (6.1), the work is simplified by using tables of classical virial coefficients (equivalent to β_1 and β_2) provided by Hirschfelder, Curtiss and Bird (1954). The square-well potential (6.2) enables β_1 and β_2 to be calculated by direct integration; the only result worth quoting here being that for β_2 for a square well of depth d and radii r_1 and r_2 with $r_1 < r_2 < 2r_1$, i.e.,

$$\begin{aligned} \beta_2 = \frac{\pi^2}{12} \{ &-5r_2^6 - e^{d/kT} [r_1^6 - 18r_1^4r_2^2 + 32r_1^3r_2^3 - 15r_2^6] \\ &+ e^{2d/kT} [2r_1^6 - 36r_1^4r_2^2 + 32r_1^3r_2^3 + 18r_1^2r_2^4 - 16r_2^6] \\ &- 6e^{3d/kT} (r_1^2 - r_2^2)^3 \}. \end{aligned} \quad \dots\dots (6.3)$$

The results may be tabulated thus:

	(6.1)	(6.2)	
(5.13)	10°K	12°K(6.4)
(5.15)	9.6°K	11°K	

i.e. they are all of the order of 10 K (compared with the actual 2.19°K), while parabolic extrapolation to the solution of (5.14) with $\Lambda = 1$, based on tabulated values of β_1 and β_2 using (6.1), reduces this temperature to 6.7 K. However, it is notoriously difficult to derive, from even the classical theory of condensation, numerical results which agree closely with experiment. Numerical work on helium is overshadowed by the astonishingly good results of the London perfect fluid model, which well might be purely fortuitous. Indeed, if we follow Temperley (1954) and assume that β_{11} is of order $(\frac{1}{3}\pi\sigma^3)''$, where σ is defined in (6.1), then (5.14) gives:

$$P(1, \frac{3}{2}) = 1/\frac{4}{3}\pi\sigma^3, \quad \dots\dots (6.5)$$

whence the resulting lambda temperature is 2.36 K. This implies that further work on condensation theory might well lead to much improvement, although the mathematical difficulties are obviously considerable.

However, to return to (5.16), this is most easily integrated in terms of the square-well potential. The resulting integration involves the error functions $\text{erf}(r_1)$ and $\text{erf}(r_2)$ which can be replaced by their arguments in the present context. We therefore obtain simply

$$1 - \frac{2}{\pi^{1/2}} \left\{ e^{d/kT} (r_2 - r_1) - r_2 \right\} \sum_{l \geq 1} \Lambda^l = 0. \quad \dots\dots (6.6)$$

If Λ is less than unity, the series $\sum \Lambda^l$ can be summed in closed form to give

$$\sum \Lambda^l = \frac{\Lambda}{1 - \Lambda} = \frac{\pi^{1/2}}{2\{e^{d/kT}(r_2 - r_1) - r_2\}} = b \text{ say.} \quad \dots\dots (6.7)$$

Now for temperatures in the range under discussion, and for the potential (6.2), then b is very large, i.e. of the order, say, of 10^6 – 10^8 . Under these conditions Λ is given by

$$\Lambda = \frac{b}{1+b} \simeq 1 - \frac{1}{b}, \quad \dots\dots(6.8)$$

indicating that it is very nearly unity (so near unity, in fact, that we are justified in taking it to be actually equal to unity in our above numerical work). However, it is well known that specific account has to be taken, in perfect fluid theory, of the systems flooding into the lowest energy level when Λ is given by

$$\Lambda \sim 1 - x/N \quad \dots\dots(6.9)$$

where x is a numerical factor of the order of unity, and N is of the order of 10^{23} . On comparing (6.8) and (6.9) we see that, in the present problem, Λ is not yet sufficiently close to unity for it to be necessary to introduce this correction. At the same time, (6.7) shows that $\Sigma \Lambda^l$ has a finite (though very large) sum. Consequently, the series $P(\Lambda, \frac{1}{2})$ in (4.17) also has a finite sum (the sum of the series $\Sigma \Lambda^l/l^{1/2}$ lying between b and $\ln b$).

So we can summarize our results at this stage in the following manner:

(1) Eqns (4.16)–(4.18) represent an approximation to the exact reduction (3.7) of the exchange approximation constituting the first term of (1.4).

(2) Also, they exhibit two singularities, one given by the singularity of $\Sigma k \beta_k P^k(\Lambda, \frac{3}{2})$ and corresponding to the classical condensation of helium vapour into liquid I: the other given by (5.16), and either corresponding to the quantal condensation into liquid II, or giving the equation for the lambda line.

(3) Numerical calculation yields a result for the lambda temperature of the right order of magnitude, and illustrates the probable difficulties in refining the present approach (i.e. based upon a consideration of the condensation of helium vapour).

(4) The quantal condensation occurs for a value of Λ very nearly unity, but not so near unity that the series $P(\Lambda, \frac{1}{2})$ in (4.17) diverges.

However, this draws attention to a further limitation to approaches based on the exchange approximation, that as Λ increases, then $P(\Lambda, n/2)$ ultimately diverges, while $P(\Lambda, \frac{1}{2})$ tends monotonically to infinity. In other words, it seems that the present method is reaching its limit, and that different techniques will be required if a more satisfactory description of the lambda transition in the liquid phase is desired. Consequently, it may not be out of place to demonstrate in more detail the relation, to the exchange approximation, of certain other theories of helium.

§ 7. THE WORK OF CHESTER AND FEYNMAN

The theory of helium developed by Chester (1954b) is based essentially on the pair approximation to the partition function of Eqn (1.7), which is included in the exchange approximation to the grand partition function of (3.7). A pair approximation to this latter function is clearly

$$\ln(\text{GPF}) \simeq \ln G(\Lambda) + \frac{V}{2} \int f(r_{12}) + |\sigma(\mathbf{r}_1 \mathbf{r}_2 | \Lambda)|_2 d\mathbf{r}_{12}. \quad \dots\dots(7.1)$$

It is easily seen that (7.1) does not describe any vapour-liquid condensation, because of the neglect of higher order terms. In order to discuss Chester's use of it in greater detail, however, we return to Eqn (3.4) for Z_N . A pair approximation can be written

$$\ln Z_N \simeq \ln f_N(\beta) + \frac{V}{2} \int f(r_{12})^+ \left| \sum_k \exp(-\beta \epsilon_k) \psi_k(\mathbf{r}_1) \psi_k^*(\mathbf{r}_2) \right|_2 d\mathbf{r}_{12}. \quad \dots\dots (7.2)$$

In this case, however, we do not have satisfactory expressions for $f_N(\beta)$ or the second-order permanent. It might, nevertheless, be plausible to form a sort of 'average' (rather than 'grand') partition function by replacing the permanent in the integrand by $|\sigma(\mathbf{r}_1 \mathbf{r}_2 | \lambda)|_2$ but it must be remembered, on so doing, that λ will no longer be the true absolute activity, but rather that activity, λ_i say, which the assembly would have if it were perfect. Furthermore, $\sigma(\mathbf{r} \mathbf{r} | \lambda_i)$ is now, by definition, the number density. Whence from (2.4) and (7.2) we obtain the correction F_1 to the free energy of the perfect fluid in the form:

$$F_1 = -\frac{V k T}{2} \left(\frac{2 \pi m k T}{h^2} \right)^{3/2} \left\{ \int f(r) \left[\left(\frac{N}{V} \right)^2 + \left(\sum_i \frac{\lambda_i^2}{V^2} \exp \left[-\frac{2 \pi m k T}{h^2} \frac{\pi r^2}{V} \right] \right)^2 \right] d\mathbf{r} \right\}. \quad \dots\dots (7.3)$$

This is what Chester's treatment implies. In order to arrive at his precise equations, however, the following additional modifications to (7.3) are necessary:

(1) Replace $f(r) = e^{-\phi(r)/kT} - 1$ by $-\phi(r)/kT$, which leads to difficulties of convergence.

(2) Take specific account, in the usual way, of the systems flooding into the lowest energy level.

(3) Drop $(N/V)^2$ as an irrelevant constant, when discussing the behaviour of the specific heat derived from (7.3), although this term is important for the stability of the assembly (see, for example, Chester 1955).

This shows how his work represents an approximation to (3.7) which is so severe that it will not describe a first-order phase change. Whether or not one is justified in using it as a theory of a liquid is, of course, another question.

The theory of helium put forward by Feynman (1953) is based essentially on the expansion of the partition function by a similar technique to that used in developing the off-diagonal integral. In Feynman's original derivation, this point is obscured by the complication of the treatment. Consequently, certain subsequent remarks by Temperley (1954) and ter Haar (1954) on the validity of Feynman's expansion may not be relevant.

For these reasons, it is worth while deriving his equations again by a direct method which also draws attention to the inherent approximations. We begin by writing

$$b_{ij} x_0^{-3} = \sum_k \exp(-\beta \epsilon_k) \psi_k(\mathbf{r}_i) \psi_k^*(\mathbf{r}_j) = x_0^{-3} \exp[-\pi x_0^{-2} \mathbf{r}_{ij}^2], \quad \dots\dots (7.4)$$

where

$$x_0^2 = h^2 / 2 \pi m k T. \quad \dots\dots (7.5)$$

The exchange approximation of Eqn (3.3) then becomes

$$Z_N = (N!x_0^{3N})^{-1} \int \dots \int \exp(-\beta V(\mathbf{r}^N)) \pm |b_{ij}|_N d\mathbf{r}^N. \quad \dots (7.6)$$

We now expand the permanent of order N in the integrand of (5.3) as a sum of products of n_l closed rings of l points as outlined above in the derivation of (4.5). The first approximation necessary to obtain Feynman's result can be illustrated with reference to $N=6$ rings of one and two closed rings of three, given by $b_{12} b_{23} b_{31} b_{45} b_{56} b_{64}$, say. The approximation, in this case, consists in writing

$$V(\mathbf{r}^N) \simeq (\phi_{12} + \phi_{23} + \phi_{31}) + (\phi_{45} + \phi_{56} + \phi_{64}) + V(\mathbf{r}^{N-6}). \quad \dots (7.7)$$

The resulting space integral becomes the product of two 'chain integrals' of three factors $b_{ij} \exp[-\beta \phi_{ij}]$ and the classical configurational integral

$$\int \dots \int \exp[-\beta V(\mathbf{r}^{N-6})] d\mathbf{r}^{N-6}.$$

If we now consider a general term in the expansion of the permanent corresponding to the selection of n_l closed rings of l points, the second approximation implicit in Feynman's treatment can be written

$$\int \dots \int \exp[-\beta V(\mathbf{r}^{n_l})] d\mathbf{r}^{n_l} \simeq V^{n_l}. \quad \dots (7.8)$$

If, therefore, we define

$$f_1 = 1 \quad \dots (7.9)$$

and

$$f_l = \int \dots \int [\exp(-\beta \phi_{12}) b_{12}] [\exp(-\beta \phi_{23}) b_{23}] \dots [\exp(-\beta \phi_{l1}) b_{l1}] d\mathbf{r}^{l-1} \quad \dots (7.10)$$

it follows from (7.6) and (7.10) that

$$Z_N \simeq (N!x_0^{3N})^{-1} \sum_l g(n_l) (Vf_1)^{n_1} (Vf_2)^{n_2} \dots (Vf_l)^{n_l} \quad \dots (7.11)$$

where

$$g(n_l) = N! / \prod_l n_l! l^{n_l} \quad \text{with} \quad \sum_l l n_l = N. \quad \dots (7.12)$$

Hence from (7.11) and (7.12) we find that

$$Z_N = x_0^{-3N} \sum \prod_{(l, n_l)} (Vf_l)^{n_l} / n_l! l^{n_l}. \quad \dots (7.13)$$

Consequently

$$(\text{GPF}) = \sum_{N=0}^{\infty} \Lambda^N Z_N = \exp \left[V \sum_l \frac{f_l}{l} \left(\frac{\Lambda}{x_0^3} \right)^l \right]. \quad \dots (7.14)$$

This is substantially what Feynman obtains. We shall call it the 'simple Feynman approximation' because this derivation draws attention to an obvious improvement upon the approximation constituting Eqn (7.8). As it stands, this implies that in the classical limit (7.14) will reduce to the grand partition function

for a perfect, rather than an imperfect, gas. The 'improved Feynman approximation' arises when we use classical imperfect gas theory to replace (7.8) by the exact relation

$$\frac{1}{n_1!} \int \dots \int_{(n_1)} \exp[-\beta V(\mathbf{r}^{n_1})] d\mathbf{r}^{n_1} = \sum_{(\sum s m_s = n_1)} \prod (V b_s)^{m_s} / m_s! \dots (7.15)$$

This leads to

$$\ln(\text{GPF}) \simeq \sum V b_s z^s + \sum_{s \geq 2} V f_l z^l / l, \dots (7.16)$$

where b_s and z are respectively the classical reducible cluster integral and the fugacity Λx_0^3 . We now replace b_s by a simple chain of the f_{ij} factors of Eqn (3.1), which can be done in $s! / 2s$ ways, whence

$$b_s \simeq \frac{1}{2s} \int \dots \int_{s-1} f_{12} f_{23} \dots f_{s1} d\mathbf{r}^{s-1} = \gamma_s / s \text{ say}, \dots (7.17)$$

except when $s=2$, as discussed below. Then we can express the f_l and γ_s of (7.16) and (7.17) in terms of their Fourier transforms $\Phi(u)$ and $F(u)$ by means of lemma II of Rushbrooke and Scoins (1951). We find that

$$\ln(\text{GPF}) = Vz + \frac{V}{2\pi^2} \int_0^\infty u^2 \sum_{s \geq 2} \frac{[(2\pi)^{3/2} z F(u)]^s}{s} du \\ + \frac{V}{2\pi^2} \int_0^\infty u^2 \sum_{s \geq 2} \frac{[(2\pi)^{3/2} z \Phi(u)]^s}{s} du. \dots (7.18)$$

The terms with $l, s=2$ are, of course, not strictly correct, as remarked above. We ignore this, however, by way of further approximation, capable of correction at the cost of increased mathematical complexity unlikely to affect the singularities of the theory. Furthermore, in (7.18) we have

$$u\Phi(u) = (2\pi)^{-1/2} \int_{-\infty}^{+\infty} r \sin ur \{ \exp[-(\beta\phi(r) + \pi r^2/x_0^2)] \} dr, \dots (7.19)$$

and

$$uF(u) = (2\pi)^{-1/2} \int_{-\infty}^{+\infty} r \sin ur \{ \exp[-\beta\phi(r)] - 1 \} dr. \dots (7.20)$$

It is, perhaps, worth noting here that Matsubara (1951) looked upon the exponent in the integrand of (7.19) as indicating that the pair potential energy function $\phi(r)$ was modified by $\pi r^2/x_0^2$ in a manner peculiar to Bose-Einstein statistics. It is easily shown, however, that the analogous Fermi-Dirac equations only differ from (7.21) below in that the negative signs preceding the last integral, and appearing in the argument of the integrand, are replaced by positive signs. Consequently, Matsubara's point of view does not appear to be correct.

Now if the helium atom has an incompressible core, we can sum (7.18) in the following closed form:

$$\ln(\text{GPF}) = V \left[z - (2\pi)^{-2} \int_{-\infty}^{+\infty} u^2 \ln \{ 1 - (2\pi)^{3/2} z F(u) \} du \right] \\ + V \left[z - (2\pi)^{-2} \int_{-\infty}^{+\infty} u^2 \ln \{ 1 - (2\pi)^{3/2} z \Phi(u) \} du \right]. \dots (7.21)$$

The first term of (7.21) refers to classical behaviour on roughly the same lines as the simplest form of the theory of Born and Green (1946-8), while the second term is, in fact, what Feynman obtains. Eqs for p, ρ and $(\partial p / \partial \rho)_T$ deduced

from (7.21) represent the summation in closed form of the series:

$$p = kT \sum B_l z^l, \quad \dots\dots (7.22)$$

$$\rho = \sum l B_l z^l, \quad \dots\dots (7.23)$$

and

$$\left(\frac{\partial p}{\partial \rho} \right)_T = \frac{\rho kT}{\sum l^2 B_l z^l}, \quad \dots\dots (7.24)$$

where

$$lB_l = \gamma_l + f_l \quad \text{and} \quad B_1 = 1. \quad \dots\dots (7.25)$$

There are two values of the fugacity z at which these series diverge, given by the following equations:

$$1 - (2\pi)^{3/2} z F(u) = 0 \quad \dots\dots (7.26)$$

and

$$1 - (2\pi)^{3/2} z \Phi(u) = 0. \quad \dots\dots (7.27)$$

These equations are essentially approximations to (5.13) and (5.16). However, this extension of Feynman's treatment has led to series expansions for p and ρ in powers of the classical fugacity rather than $P(\Lambda, \frac{2}{3})$. Nevertheless, (7.26) and (7.27) correspond to two first-order transitions from helium vapour to liquids I and II rather than to the third-order transition in the liquid phase suggested by Feynman.

Finally, Penrose and Onsager (1956) have discussed various mathematical criteria for the onset of Bose-Einstein condensation in the London approach to the liquid helium problem. They have applied these criteria to the simple Feynman approximation, and they have concluded that this condensation can occur in liquid helium II, but not in liquid helium I. These conclusions are based essentially on the application of some of the equations of this section to the lambda transition in the *liquid* phase. In the present context, therefore, where the equations describe the first-order gas-liquid phase changes, they appear to be irrelevant.

§ 8. CONCLUSIONS

We have seen that the exchange approximation is capable of describing, to a limited extent, the condensation of helium vapour into liquids I and II. Also, the theories of Chester and Feynman turn out to be special cases of this approximation. It finally appears that an adequate description of the lambda transition in the liquid phase well might have to await the development of a satisfactory theory of the ordinary classical liquid to which helium I approximates.

ACKNOWLEDGMENTS

The earlier portion of this paper formed part of the author's thesis for the degree of Doctor of Philosophy of the University of Durham in June 1955; and some of the subsequent work was carried out in the Department of Physics of the City of Birmingham College of Advanced Technology under the guidance of Professor G. S. Rushbrooke of King's College, Newcastle upon Tyne.

It is a pleasure to pay tribute to Professor Rushbrooke for having suggested the problem in the first place, and for his patient and stimulating supervision

of much of this work, and to Dr. G. V. Chester, for having discussed it at the Physical Society Conference on Co-operative Phenomena and Phase Transitions, July 1959.

REFERENCES

- DE BOER, J., 1950, *Physica*, **16**, 545.
 — 1951, *Physica*, **17**, 993.
 BORN, M., and FUCHS, K., 1938, *Proc. Roy. Soc. A*, **166**, 391.
 BORN, M., and GREEN, H. S., 1946–48, see, for example, GREEN, H. S., 1952, *The Molecular Theory of Fluids* (Amsterdam: North-Holland).
 CHESTER, G. V., 1954 a, *Phys. Rev.*, **93**, 606.
 — 1954 b, *Phys. Rev.*, **94**, 246.
 — 1954 c, *Phys. Rev.*, **93**, 1412.
 — 1955, *Phys. Rev.*, **99**, 1062.
 FEYNMAN, R. P., 1953, *Phys. Rev.*, **91**, 1291.
 GOLDBERGER, H., and ADAMS, E. N., 1952, *J. Chem. Phys.*, **20**, 240.
 GOLDSTEIN, L., 1946, *J. Chem. Phys.*, **14**, 276.
 GREEN, H. S., 1951, *J. Chem. Phys.*, **19**, 995.
 GUGGENHEIM, E. A., 1950, *Thermodynamics* (Amsterdam: North-Holland).
 TER HAAR, D., 1954, *Phys. Rev.*, **95**, 896.
 HIRSCHFELDER, J. O., CURTISS, C. F., and BIRD, R. B., 1954, *Molecular Theory of Gases and Liquids* (New York: Wiley).
 HUSIMI, K., 1940, *Proc. Phys. Math. Soc. Japan*, **22**, 264.
 KAHN, B., 1938, *Thesis*, University of Amsterdam: *Theory of the Equation of State*.
 KIKUCHI, T., 1954, *Phys. Rev.*, **96**, 563.
 KIRKWOOD, J. G., 1933, *Phys. Rev.*, **44**, 31.
 LONDON, F., 1938, *Phys. Rev.*, **54**, 947.
 MATSUBARA, T., 1951, *Progr. Theor. Phys., Japan*, **6**, 714.
 MAYER, J. E., 1948, see, for example, MAYER, J. E., and MAYER, M. G., 1948, *Statistical Thermodynamics* (New York: Wiley).
 VON NEUMANN, J., 1927, *Gott. Nachr. 245 and Math. Grundle. der Quantenmechanik* (Berlin: Springer).
 PENROSE, K., and ONSAGER, L., 1956, *Phys. Rev.*, **104**, 576.
 RUSHBROOKE, G. S., and SCOINS, H. I., 1951, *Phil. Mag.*, **42**, 582.
 — 1953, *Proc. Roy. Soc. A*, **216**, 203.
 SQUIRE, C. F., 1953, *Low Temperature Physics* (New York: McGraw-Hill).
 TEMPERLEY, H. N. V., 1954, *Proc. Phys. Soc. A*, **67**, 233, 901.
 WIGNER, E., 1932, *Phys. Rev.*, **40**, 749.

LETTERS TO THE EDITOR

Cubic Crystal Field Splitting of the Gd^{3+} Ion

The question of whether the cubic field splitting for an S state is proportional, to a first approximation, to the cubic crystal field or to its square was recently the subject of several papers, both theoretical and experimental (Watanabe 1960, Low and Rosenburger 1959). However certain points, which we think important, seem to be left in the background.

It is not perfectly correct that the matrix elements of the crystalline potential appear only in even powers in an approximation involving the fundamental configuration l^{2l+1} alone (Watanabe 1957). What can be proved is that a perturbation Hamiltonian including only the crystalline potential and the spin-orbit interaction contributes to even order approximation only (Lacroix 1957). Hence, if such an approximation contains n matrix elements of crystalline potential and m matrix elements of spin-orbit interaction, $n+m$ is necessarily even, but n and m may be odd†.

In the case of Gd^{3+} , the approximation involving only the $4f^7$ configuration is not adequate to account for the experimental splitting. It appears that the numerical estimate according to this approximation (Lacroix 1958) gives a result ten times smaller than the paramagnetic resonance measurements (Ryter 1957) on Gd^{3+} in CaF_2 which leads to a splitting of 0.149 cm^{-1} . Hence it follows that the crystalline field acts on the Gd^{3+} ion through an excited configuration.

The previously proposed mechanisms of this type (Lacroix 1958) proved to be inadequate and we think that the splitting is due to a mechanism in which the crystalline potential plays a role only through matrix elements connecting states of the excited configuration. In this case, the relevant excited configurations are $4f^65f$ and $4f^55d^2$.

In this mechanism the first non-zero approximation is the seventh, which is linear in the cubic crystalline potential, quartic in the spin-orbit interaction and quadratic in the configuration interaction. As terms quadratic in the cubic potential appear only from the eighth approximation onwards, one can presume that the splitting is mostly linear in the crystalline field.

A way of evaluating the relative importance of the approximations of successive orders is to consider the ratio R of the splittings $\Gamma_6 - \Gamma_8$ and $\Gamma_7 - \Gamma_8$, since its value deviates from $R=3/5$ under perturbations of ninth order. The measurements made by Ryter (1957) on Gd^{3+} in CaF_2 give $R=0.596$, while Low and Rosenburger (1959) obtain $R=0.613$ and 0.580 for Gd^{3+} in $SrCl_2$ and ThO_2 respectively. This shows that the ninth approximation contributes only a few per cent to the splitting. Hence one can estimate roughly that the effect of the approximation of eighth order, i.e. of the terms quadratic in the cubic field, is not larger than 20 or 30% of the splitting.

We intend to perform more precise numerical work on this problem.

Institut de Physique,
University of Geneva,
Switzerland.

R. LACROIX.

6th October 1960.

† After having written this letter, we have noticed a paper by Powell, Gabriel and Johnston (*Phys. Rev. Letters*, 1960, 5, 145), where the same criticism is raised against the theory of Watanabe.

- LACROIX, R., 1957, *Helv. Phys. Acta*, **30**, 479.
 — 1958, *Arch. Sci. (Geneva) Fasc. Spec. AMPERE*, **11**, 141.
 LOW, W., and ROSENBERGER, U., 1959, *Phys. Rev.*, **116**, 621.
 RYTER, C., 1957, *Helv. Phys. Acta*, **30**, 353.
 WATANABE, H., 1957, *Progr. Theor. Phys. (Kyoto)*, **18**, 405.
 — 1960, *Phys. Rev. Letters*, **4**, 410.

On the Validity of Two Conjectures Relating to Resonance Collisions

The first-order coupled differential equations

$$\left. \begin{aligned} \dot{c}_1 &= if(t)e^{-i\alpha t}c_2 \\ \dot{c}_2 &= if(t)e^{i\alpha t}c_1 \end{aligned} \right\} \dots\dots (1)$$

with initial conditions

$$|c_1(-\infty)| = 1, \quad c_2(-\infty) = 0 \dots\dots (2)$$

arise in the theory of resonance and near resonance collisions. Only $|c_2(\infty)|^2$ is required.

In the special case

$$f(t) = A \operatorname{sech} Bt \dots\dots (3)$$

the equations can be treated analytically. Rosen and Zener (1932) have shown that here

$$|c_2(\infty)|^2 = \sin^2 \frac{\pi}{B} \operatorname{sech}^2 \frac{\pi z}{2B}, \dots\dots (4)$$

This may be rewritten in the form

$$|c_2(\infty)|^2 = \frac{\sin^2 \left(\frac{\pi}{2} \frac{\int_{-\infty}^{\infty} f(t) dt}{\int_{-\infty}^{\infty} f(t) dt} \right)}{\left(\int_{-\infty}^{\infty} f(t) e^{i\alpha t} dt \right)^2} \dots\dots (5)$$

Rosen and Zener have conjectured that (5) is valid for any function $f(t)$ which is non-singular. Supporting evidence is given by the fact that this conjecture is certainly correct if α is zero and also if $f(t)$ is very small.

Interest in resonance collisions and therefore in Eqn (1) has recently revived. Takayanagi (1952) has made use of (5) in some calculations. Its correctness has been questioned by Bates and Lynn (1959).

Gurnee and Magee have postulated the alternative formula

$$|c_2(\infty)|^2 = \left| \sin \left(\frac{\pi}{2} \int_{-\infty}^{\infty} f(t) e^{i\alpha t} dt \right) \right|^2 \dots\dots (6)$$

which like (5) is correct in the cases of small $f(t)$ and α equal to zero. This has been adopted by Karmohapatro and Das (1958), Karmohapatro (1959, 1960), and Rapp and Ortenburger (1960) in their work on charge transfer. Bates and Lynn have pointed out that it fails to reproduce the correct result in the case of Eqn (3) and therefore cannot be correct.

It can be seen that the two suggested solutions are not compatible for large values of α . Thus

$$\text{Rosen-Zener: } |c_2(\infty)|^2 \sim \left\{ \frac{\sin I(0)}{I(0)} \right\}^2 |I(\alpha)|^2,$$

$$\text{Gurnee-Magee: } |c_2(\infty)|^2 \sim |I(\alpha)|^2,$$

where

$$I(\alpha) = \int_{-\infty}^{\infty} f(t) e^{i\alpha t} dt.$$

In order to examine the validity of the Rosen-Zener and Gurnee-Magee conjectures, the Eqns (1) were integrated numerically on a DEUCE computer using a 4-stage Runge-Kutta method. It was found that the numerical solutions were accurate to at least 5 decimal places.

The functions used were

$$(i) f_1(t) = A \operatorname{sech} Bt,$$

$$(ii) f_2(t) = A \exp(-Bt^2),$$

$$(iii) f_3(t) = 2A \exp[-\{(Bt)^2 + (\log 2)^2\}^{1/2}],$$

chosen so that

$$f_3(0) = f_1(0),$$

$$f_3(\pm\infty) \sim f_1(\pm\infty).$$

Sample results are given in the accompanying Table. From there it may be seen that apart from case (i), the formula (5) of Rosen and Zener is exact only when α is zero and is a good approximation when $\alpha \lesssim \frac{1}{2}$. It is also seen that the formula (6) of Gurnee and Magee gives good results over a much smaller range.

Values of $ c_2(\infty) ^2$									
α	$f_1(t) = \frac{1}{2} \operatorname{sech} t$			$f_2(t) = \exp(-t^2)$			$f_3(t) = 2 \exp[-\{t^2 + (\log 2)^2\}^{1/2}]$		
	(i)	(ii)	(iii)	(i)	(ii)	(iii)	(i)	(ii)	(iii)
0	—	1.000000	1.000000	0.959889	0.959883	0.959883	0.034977	0.034973	0.034973
0.25	—	0.860360	0.987106	0.925912	0.930350	0.969969	0.031524	0.030158	0.150902
0.5	—	0.569934	0.858997	0.830830	0.847093	0.991140	0.024072	0.020162	0.612699
1.0	0.158832	0.158832	0.343307	0.536576	0.582198	0.964181	0.011772	0.005972	0.882237
2.0	0.007442	0.007442	0.018250	0.086118	0.129906	0.368226	0.003009	0.000411	0.099106
4.0	0.000014	0.000014	0.000034	0.000100	0.000322	0.001054	0.000153	0.000004	0.001026

(i) Exact numerical solution; (ii) Rosen-Zener formula; (iii) Gurnee-Magee formula.

Since in many applications

$$\alpha = \sqrt{\frac{M}{2E}} \Delta$$

where M and E are the mass and energy of the incident particle and Δ is the energy difference between the initial and final states, all quantities being in atomic units, it follows that the Rosen-Zener formula is valid for

$$E \gtrsim 2M\Delta^2;$$

or if E and Δ are expressed in ev and M on the chemical (^{16}O) scale, that

$$E \gtrsim 135M\Delta^2.$$

As an example, the case quoted by Karmohapatro

$$A^+(2P_{1/2}) + A \rightarrow A + A^+(2P_{3/2}) + 0.18 \text{ ev}$$

gives the criterion

$$E \gtrsim 180 \text{ ev.}$$

Karmohapatro actually used the Gurnee-Magee formula which has a more restricted range than the Rosen-Zener formula.

It is a pleasure to thank Professor D. R. Bates for his interest and advice.

This investigation has been supported by the Air Force Cambridge Research Center, Geophysics Research Directorate, of the Air Research and Development Command, U.S. Air Force, through its European Office, under Contract No. AF 61(052)-131.

Department of Applied Mathematics,
The Queen's University of Belfast.

B. G. SKINNER.

19th October 1960.

- BATES, D. R., and LYNN, N., 1959, *Proc. Roy. Soc. A*, **253**, 141.
 GURNEE, E. F., and MAGEE, J. L., 1957, *J. Chem. Phys.*, **26**, 1237.
 KARMOHAPATRO, S. B., 1959, *J. Chem. Phys.*, **30**, 538.
 — 1960, *Proc. Phys. Soc. A*, **76**, 416.
 KARMOHAPATRO, S. B., and DAS, T. P., 1958, *J. Chem. Phys.*, **29**, 240.
 RAPP, D., and ORTENBURGER, I. B., 1960, *J. Chem. Phys.*, **33**, 1230.
 ROSEN, N., and ZENER, C., 1932, *Phys. Rev.*, **40**, 502.
 TAKAYANAGI, K., 1952, *Sci. Rep. Saitama Univ. A*, **1**, 9.

REVIEWS OF BOOKS

Modern Geometrical Optics, by MAX HERZBERGER. Pp. xii + 504. (New York, London: Interscience Publishers, 1959.) \$15.00.

A book by so well-known a researcher as Dr. Herzberger will be eagerly read by all interested in Geometrical Optics. It gives the results of fourteen years' work and embodies the methods and ideas put forward in numerous papers.

It has been a subject of reproach for many years that optical workers do not publish their work in book form, so that often there has been no fundamental explanation of principles, nor even a consistent development of the writer's notation. Thus the task of following the writings of different workers has been laborious and often abandoned by the very people that could benefit most, namely those engaged in industry and dealing with and designing optical systems. Such people have little time for serious theoretical investigation and are often poorly equipped mathematically.

Dr. Herzberger says "those who most need a thorough knowledge of the theory of optics are the designers of optical lenses. . . and, unfortunately the acquaintance of the average designer with higher mathematics is limited." This statement will not seriously be contested. However no amount of knowledge of optical theory will make a good lens designer. Some guiding principles must be imparted to the learner, such as were given in the lectures of the late S. D. Chalmers and A. E. Conrady. This book does not aim at supplying this need but, with a view to equipping the lens designer with optical knowledge, Dr. Herzberger has made use of any mathematical tools that he finds convenient. Thus ray tracing is done by vectorial methods (introduced to opticians by Dr. Silberstein), in dealing with Gaussian optics the author uses matrices and a new tool (Gaussian brackets), and for image formation utilizes Hamilton's characteristic function.

H. D. Taylor and A. E. Conrady endeavoured to teach lens design by elementary methods. At present there is a great dearth of optical designers (at least in England) and the elementary character of the textbooks may have been a deterrent to the entry of mathematicians to the profession. It will be interesting to see if the treatment in the present book will attract them. The electronic computer and modern methods of estimating optical performance by considering the imagery of a grating with the aid of Fourier functions seem to be attractive to mathematicians but the strictly practical value of the techniques has yet to be proved in the design of optical systems.

The more advanced parts of Dr. Herzberger's mathematics are explained in Appendices. Strictly speaking this should bring them within the reach of any one of pass degree standard, but it is doubtful if in fact the reasoning in this book could be followed by anyone less well equipped than with an honours degree in mathematics, and used to a fairly high standard of mathematical demonstration.

It is to be hoped that 'practical opticians' will not be deterred by the formidable treatment of optics in this book and that others will be encouraged to take up the study of optical design.

The book is beautifully printed without apparent errors and is provided with a Bibliography and an Index as well as the mathematical Appendix. H. W. L.

Numerische Mathematik, edited by R. SAUER, E. STIEFEL, J. TODD and A. WALTHER. Pp. 180. (Berlin, Göttingen, Heidelberg: Springer.) Vol. 1, Part 1, January 1959. Part 3, July 1959. DM. 16.80 per part.

This is a new international journal concerned with general problems of computation, including the development of new numerical methods and the exploitation of digital computers by numerical analyst and programmer alike. The interval of publication may vary but at present appears to be roughly quarterly. The editorial board is distinguished, and covers nine countries, Germany and the U.S.A. being most prominent.

The issues under review include contributions on evaluating roots of polynomials, error propagation, Tschebyscheff approximation, orthogonal polynomials, quadratic integers, and the computer language ALGOL, and these set a high standard. Altogether the new journal is very welcome; the price is also very high.

R. A. BUCKINGHAM.

Proceedings of the First National Biophysics Conference, Columbus, Ohio, March 1957, edited by H. QUASTLER and H. J. MOROWITZ. Pp. xxviii+208. (Yale: University Press; London: Oxford University Press, 1960.) 120s.

This book contains 214 communications of which about half are summaries and the remainder papers of length between five and ten pages. The communications may be listed as follows: an introduction on (a) careers and training in biophysics and (b) a historical review; part I, physical biology (182 communications); part II, effects of physical agents on living material. The papers and abstracts are sufficient to inform a physicist of the kind of work that is being done in biophysics. From it he may select items which he considers worth further study. As might be expected, there is a wide variation in quality between the different papers. No one person would be interested in more than a small fraction.

R. W. DITCHBURN.

Beam and Wave Electronics in Microwave Tubes, by R. G. E. HUTTER. Pp. xii+378. (Toronto, London, New York: Van Nostrand, 1960.) 73s. 6d.

Microwave devices range over a very extensive field. Any writer on the subject must of necessity be consciously selective in his choice of material. In this book it is the author's intention to present the basic physics of microwave tubes rather than produce design data for the engineer. This is a wise distinction. It is not always clear that design in this field is approached through a full and clear understanding of basic principles. In microwave tubes there occurs an extremely complicated interaction of electromagnetic fields and electron beams, in which many simplifications are forced on the theoretician. Even then the mathematical complexity is considerable. The approach of the designer on the other hand is often semi-empirical backed by theory, previous experience and experiment.

In the early chapters of the book the author deals with the properties of waveguide and cavity structures in the absence of the electron beam. Some of this material is conventional and can be found in any elementary textbook on waveguides. The chapter on 'slow-wave' structures is however of particular application to microwave tubes. These waveguides are either of the 'slotted' type,

which are employed in the magnetron and linear accelerator, or of the wire-loaded variety (e.g. the helix), commonly employed in the travelling-wave amplifier.

Rather more than half of the book is devoted to the complicated problem of beam interaction. An extensive literature has emerged during the past decade on this subject. Most of the analysis is based on 'small amplitude' theory and so does not apply to power amplifiers. The author's approach is systematic, dealing in turn with beams across gaps (e.g. klystrons and diodes), then with beams in drift spaces, in interaction with 'slow waves' and lastly in crossed electric and magnetic fields. The mathematical detail is adequately supported by many graphical illustrations.

Following this discussion, a simplified picture of coupling between waves and beams is developed from an equivalent circuit analysis as favoured by Pierce in his early work in this field.

To sum up, this is a book for the specialist providing a comprehensive account of the mathematical foundations of this complicated subject. Physicists in allied fields of magnetohydrodynamics and gas discharge physics may however find some parts of the subject of value in their researches. W. WALKINSHAW.

Basic Data of Plasma Physics, by SANBORN C. BROWN. Pp. viii + 336. (London: Chapman and Hall; New York: John Wiley, 1960.) 52s.

To those who have listened to Dr. Brown lecturing on the phenomena of electrical discharges, it will come as no surprise that he has had many requests for the notes on the course he gives in association with Professor W. P. Allis at Massachusetts Institute of Technology. Dr. Brown is not only an unusually able expositor but is also well known for his own very important contributions to the subject, especially as a pioneer of the microwave method.

This book contains the class notes for a graduate course given at the Massachusetts Institute of Technology during 1959, augmented by a large collection of published data. They are very good notes and only occasionally can one find a place where the accompanying remarks of a lecturer would be necessary for a student not already familiar with the subject.

There are sixteen chapters, the first twelve are concerned with the basic collision phenomena of discharges, their combined action in electrical breakdown and the effects of space charge. The last four chapters deal with corona glow, microwave and arc discharges. Quite properly there is no discussion of plasma dynamics or thermonuclear discharges.

As a source for reference and as an inspiration and guide to those who would see the high standards maintained at M.I.T. spread to other universities, this is a valuable book. It should pass through further editions which deserve a type face more pleasing than the typewriter form used for the sake of speed in this edition.

R. L. F. BOYD.

Selected Lectures in Modern Physics for School Science Teachers, edited by H. MESSEL. Pp. 328. (London: Macmillan and Co., 1960.) 30s.

This excellent volume looks as if it may provide me with a lasting interest for my leisure hours, for I have gladly written several appreciative reviews of it already and am prepared to go on doing so. I ought to hark back to the first, however, written in 1958. In January of that year, the Nuclear Research Foundation

sponsored a Summer School for Science Teachers at the University of Sydney, and published at the time the lectures delivered, in a form which was very much like the present book, though rather less polished. The twenty-three lectures include nuclear energy (H. Messel); low-energy nuclear physics (E. W. Titterton); high-energy nuclear physics (Sir Marcus Oliphant); ultra-high-energy nuclear physics (D. D. Millar); radio-astronomy (J. P. Wild); Newton's laws of motion and space travel (J. M. Blatt); transistor electronics (R. E. Aitchison); superfluids (S. T. Butler); isotopes in medicine (E. P. George); and physics and geology (J. C. Jaeger). It is a wide range of current interests, and the contributions are very well written at a standard that the ordinary school teacher can follow easily, and that the physicist also will welcome for its clarity. In this edition, the only obvious difference is that the previously good illustrations are rather better. It is strongly to be recommended for the school science library, and is very good value for a private purchase.

G. R. NOAKES.

Heat and Thermodynamics, 5th edn, by J. K. ROBERTS and A. R. MILLER. Pp. xx+619. (London, Glasgow: Blackie and Son, 1960.) 45s.

This is a new edition of an old favourite and as such should require little comment. However, the time must come when not only a textbook itself but also the habit of publishing new editions of it will have to be revised. The present volume is dangerously near to this stage. When the first edition came out in 1928 it had 545 pages, which is fairly long as textbooks for the students' course go. Its second edition kept to 570 pages, but by now it has increased to 619. New material certainly requires additional space, but space might be saved by omission or streamlining of apparatus description and illustration, now often more than half a century old. Should there be a sixth edition of this book, it can certainly do with some firmer handling which should, for example, reduce to one the two almost identical illustrations on pages 149 and 151. At 45s. this book is a bargain for those who know how to find things in it, but this will not be easy for the average student.

K. MENDELSSOHN.

Progress in Elementary Particle and Cosmic Ray Physics, Vol. V, edited by J. G. WILSON and S. A. WOUTHUYSEN. Pp. xii+461. (Amsterdam: North-Holland Publishing Co., 1960.) 85s.

The present volume retains the title and form of Volume IV and contains the following five review articles: Weak interactions (A. Lundby), The nucleon-nucleon interaction (J. L. Gammel and R. M. Thaler), Antinucleon theory (J. McConnell), Cosmic ray jets (D. H. Perkins), and The absorption and decay of negative muons (R. M. Tennent). Each article is excellent in its own way, but perhaps the most fascinating and satisfying is the first which is a clear account of recent experimental and theoretical work on the weak interactions. The discovery of the violation of parity conservation in weak interactions has had momentous consequences in lepton physics and has led to the solution of the classical problem of β -decay. In this connection it is interesting to note the parallelism between the use of high-energy γ -particles by Rutherford to elucidate the extra-nuclear structure of the atom—a low-energy system—and of the θ - and τ -particles by Lee and Yang to give the clue to the solution of the problem of β -decay.

The second and third articles are authoritative surveys in their respective fields, but the article on the nucleon-nucleon interaction is rather too detailed and technical to make it interesting to the non-specialist.

The fourth article is concerned with the study of ultra-high energy interactions, (10^{12} – 10^{15} eV), induced by cosmic rays in nuclear emulsions. These interactions are undoubtedly similar to low-energy extensive showers and their study by the emulsion technique can give valuable information, for example, about the nature of the primary and secondary particles, unobtainable at present by any other method. This long article is an important contribution to the literature of the subject.

The final article is a careful and competent analysis of the extensive experimental data on the absorption and decay of negative muons in complex nuclei, a subject in which experiment has now outrun theory.

G. D. R.

Integraltafeln zur Quantenchemie, Vol. IV, by H. PREUSS. Pp. viii + 145. (Berlin, Göttingen, Heidelberg: Springer, 1960). DM. 45.

This volume is the fourth in a series of sets of tables of values of some of the simpler integrals which occur in the calculation of molecular wave functions, when these are expressed in the form of linear combinations of Slater determinants defined in terms of radial exponential functions multiplied by polynomials. It is well known that there is no possibility of tabulating all the required integrals for moderately spaced intervals of all the parameters occurring in the case of a general molecule. If each parameter (after eliminating seven of these by symmetry and change of scale) were given 10 values there would be over 10^{10} integral values. Only a negligible proportion of these would be appropriate for calculations on actual molecules. Hence any volume of integrals can only apply to a restricted range. The present volume is particularly restricted. It provides the values for part of the requirements for diatomic molecules when the expansion functions are restricted to functions of 1s type. The molecules for which the values could be used could not be much more complicated than HeH or LiH systems. It would take about 100 times the space of this volume if the same ranges of parameters were treated for all the integrals which would be required for such still modest systems as CO or NO. It is the difficult mathematical nature of the problem which causes this situation, but this must be considered if an investigator plans to use or construct tables with moderately close equal intervals. The easy alternative is to use an electronic machine to get the full set for CO etc. in ten minutes. If this is not feasible, the construction of tables with parameter values clustered round zones associated with particular molecules might be worth consideration.

The volume commences with an interesting fifty-page review of selected topics from the whole range of problems in molecular integral evaluation. The particular tables which are reported consist of a minor set of values of an auxiliary function, then of the overlap, the nuclear potential, the kinetic energy, the hybrid and exchange integrals for 1s functions in a diatomic molecule. The exchange integral is only quoted for all parameters equal, but the others are given for all combinations of fourteen values of each independent parameter.

S. F. BOYS.

Foundations of Electromagnetic Theory, by J. R. REITZ and F. J. MILFORD. Pp. xi+387. (Reading, Massachusetts: Addison-Wesley, 1960.) 49s.

One often wonders: what is the reason that textbooks on electromagnetism are published in such an abundance, although there is already a very good selection of standard works on the market? The answer is provided, perhaps, by the authors of the present book when they say: "The advanced undergraduate student in Science approaches the subject of electricity with a qualitative understanding of atomic phenomena. At the same time, he has acquired a good background in mathematics, and for the first time in his career he is in the position of being able to solve some of the important mathematical problems of classical physics." The great educational power inherent in the study of electromagnetism is indeed well known to anyone who has had the opportunity to observe the mental development of his students during a course in this subject. Hence the successful lecturer's desire to write up his cherished lecture-notes in the form of a book. Under these circumstances it is only natural that any new textbook in this field will reflect to a great extent the special interests of the author. In the present case this has the effect that the best, and somewhat unproportionally long, chapters of this book are devoted to the microscopic theory of dielectrics and the magnetic properties of matter. A special chapter on the elementary theory of plasmas is also included. The rest is the rather customary stuff. We only regret that the general discussion of Maxwell's equations appears at a rather late stage and that the chapters on electromagnetic radiation and boundary value problems on the general electromagnetic field occupy a rather small proportion of the text.

The style is clear and vivid, many useful illustrations help the understanding, and there is a good selection of problems. In some cases, however, in particular when new concepts are introduced, the presentation could have been made more logical and the style less *ex cathedra*.
P. ROMAN.

Correspondence of Isaac Newton, edited by H. W. TURNBULL, with an introduction by E. N. DA C. ANDRADE. Volume 1 (1661-1675). Pp. xxxvii+467. (Cambridge: University Press, 1959.) £7 7s. Volume 2 (1676-1687). Pp. xii+551. (Cambridge: University Press, 1960.) £7 7s.

The Correspondence of Isaac Newton, which is published for the Royal Society by the Cambridge University Press in seven volumes, presents a fascinating account of the development of science during the latter half of the seventeenth century and beginning of the eighteenth.

The publication of Newton's scientific work is very incomplete, and it has been considered impossible to collect and present a series of his work sufficiently complete and sufficiently worthy of him. The present collection of correspondence, which includes not only letters to and from Newton but also correspondence between contemporaries which throws light on Newton's work, gives perhaps a much more valuable account of the scientific work of this period and of Newton himself than a full collection of his works could do.

From the correspondence there emerges a picture of Newton's character, which explains why his published work was so incomplete. He was a man who shrank from any sort of publicity and from controversy to such an extent that he refused to publish the result of some of his work. On the other hand, he responded readily to courtesy and frank enquiry.

The range of Newton's interests was very wide, for, beside the work in exact science for which he is so well known, he was almost equally interested in theology and in alchemy and chemistry, and for many years was a most able administrator in the employ of the Royal Mint.

The first two volumes of the correspondence are already published, one in 1959 and the other in 1960. The third volume in the series is expected to be ready early in 1961.

The introduction by Professor E. N. da C. Andrade and the preface by the Editor of the volumes provide an excellent and most interesting guide to the contents of the books.

A.C.S.

The Technique of Photomicrography, by D. F. LAWSON. Pp. xvi+256. (London: George Newnes, 1960.) 55s.

In writing this book the author has drawn upon years of practical experience in the fields of photomacrography and photomicrography. This has resulted in a comprehensive treatment of the subject which leads from a description of the optical microscope components to the final mounting of the prints. Instruments which, so far, have had limited use as tools in physics are described, such as ultra-violet, infra-red, reflecting and interference microscopes. The various aspects are considered in a practical manner to help the experimenter record the information available in the best possible way. A noteworthy feature of the book is the 150 excellent plates, although most of them will be unfamiliar to the physicist as they have primarily been chosen from natural history. Also some of the specimen preparation techniques will be of limited interest to readers of the *Proceedings of the Physical Society* (e.g. technique for photographing pickled cauliflower). These however are small points and the book is recommended to those who are already using the technique as well as those requiring an introduction to the subject.

T. EVANS.

Dynamical Analogies, 2nd edn, by Harry F. OLSON. Pp. xi+278. (Princeton, New Jersey, Toronto, New York, London: D. Van Nostrand Company, 1958.)

This is a second edition of a book whose first edition appeared in 1943. It is now thoroughly revised and enlarged and includes important new chapters on magnetic and mobility and analogies, noise, distortion and feedback.

Instrument Construction, No. 1, Jan. 1959 (translated from the Russian). Pp. 37. (London: Taylor & Francis Ltd., 1959.) £6 yearly.

This is the English translation of the Russian monthly journal *Priborostroenie*, and appears from January 1959 onwards. In general it is expected to appear two to three months after the corresponding Russian issue. The contents of the first issue include a report on a Congress held at the Manometer Factory in Moscow: short, concise articles of fifteen hundred to two thousand words on a wide range of subjects including automation, the theory and construction of electrical circuits, and experimental developments in their various fields.

The translated journal is produced for the Department of Scientific and Industrial Research by the British Scientific Instrument Research Association.



Fig. 2. Single shot echo sequence in methyl alcohol at -71°C . The modulation corresponds to Eqn (5) with $J = 4.95 \pm 0.05$ c/s. Echo separation is 20 msec.

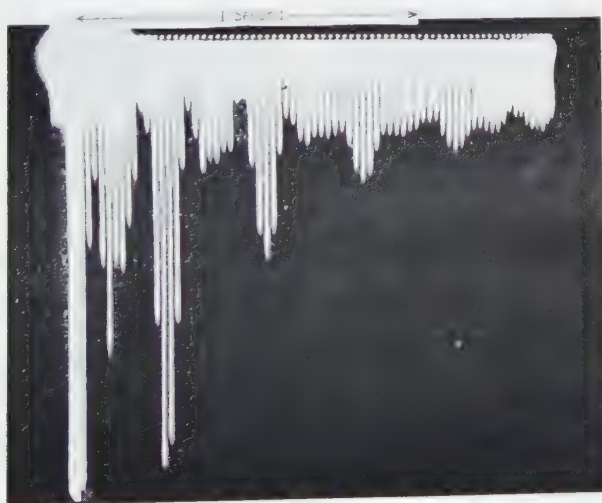


Fig. 3. Single shot echo sequence for ethyl alcohol at 25°C . The modulation fits Eqn (6) with $J = 6.93 \pm 0.10$ c/s.

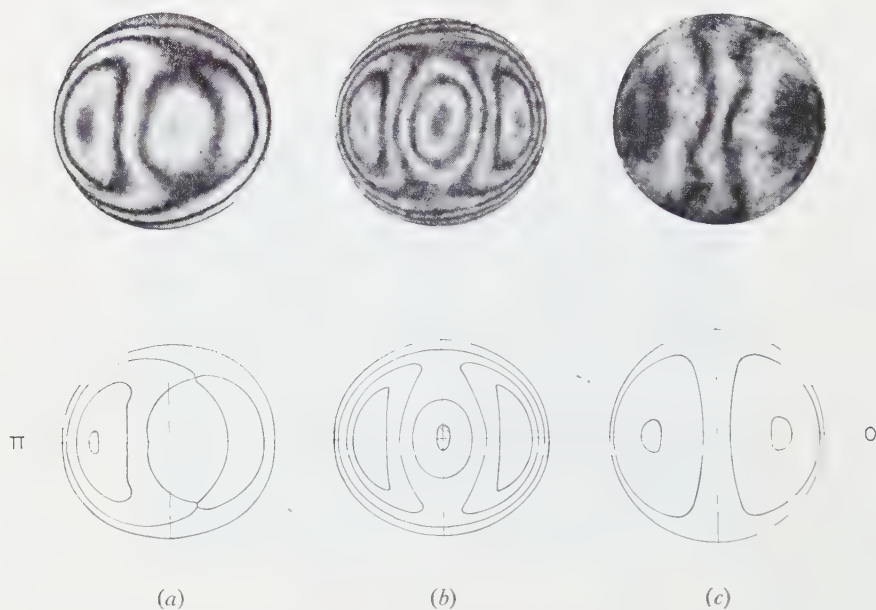


Fig. 4. Interferograms obtained with the modified Twyman interferometer, compared with the patterns obtained by plotting the expressions for the most important aberration terms: (a) normal interferogram; (b) double-passed interferogram showing only the 'even' terms; (c) double-passed interferogram showing only the 'odd' terms.

$$\begin{aligned}
 (a) \quad 2W &= 0.25 - 3.99r^2 + 4.33r^4 - 2.75r^2 \cos^2 \phi + 1.72r^4 \cos^2 \phi \\
 &\quad + 1.85r \cos \phi - 1.57r^3 \cos \phi \\
 (b) \quad 4W_{\text{even}} &= 0.50 - 7.98r^2 + 8.66r^4 - 5.50r^2 \cos^2 \phi + 3.44r^4 \cos^2 \phi \\
 (c) \quad 4W_{\text{odd}} &= 3.70r \cos \phi - 3.14r^3 \cos \phi.
 \end{aligned}$$

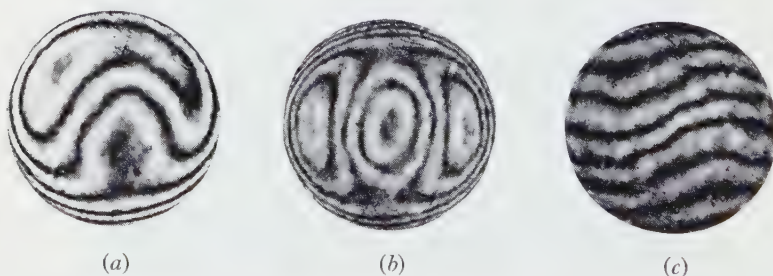
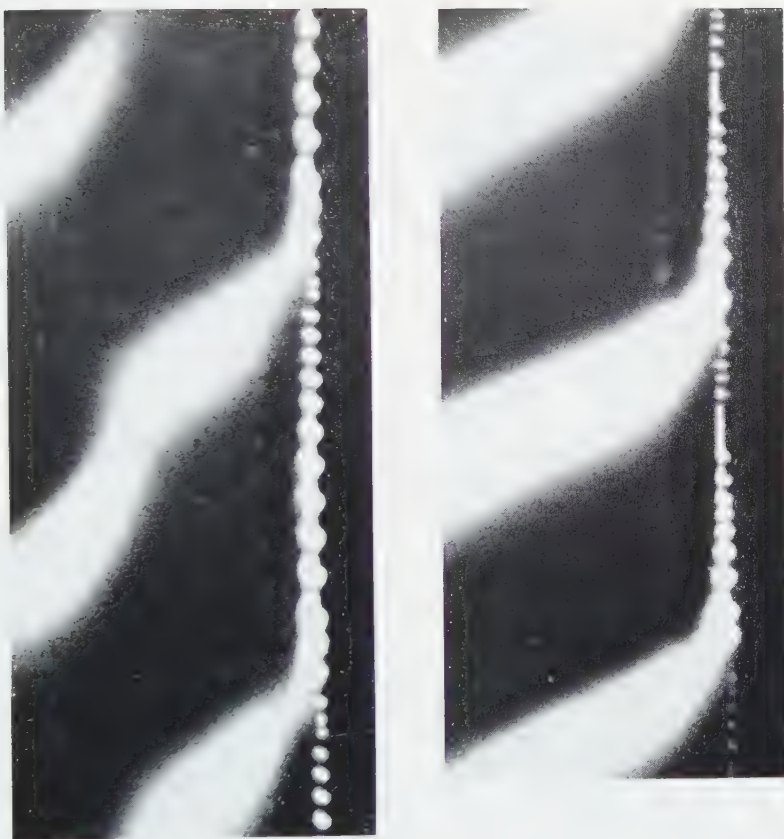
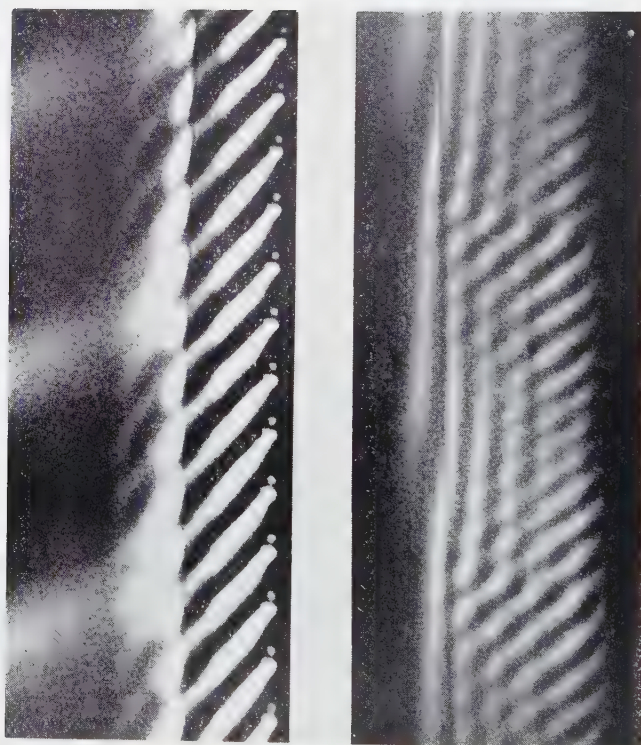


Fig. 5. Interferograms obtained with the same lens as in Fig. 4, but with the end mirror M_1 tilted slightly: (a) normal interferogram; (b) double-passed interferogram showing only the 'even' terms; (c) double-passed interferogram showing only the 'odd' terms.



Figs 2 and 3. For details see Appendix.



Figs 5 and 6. For details see Appendix.

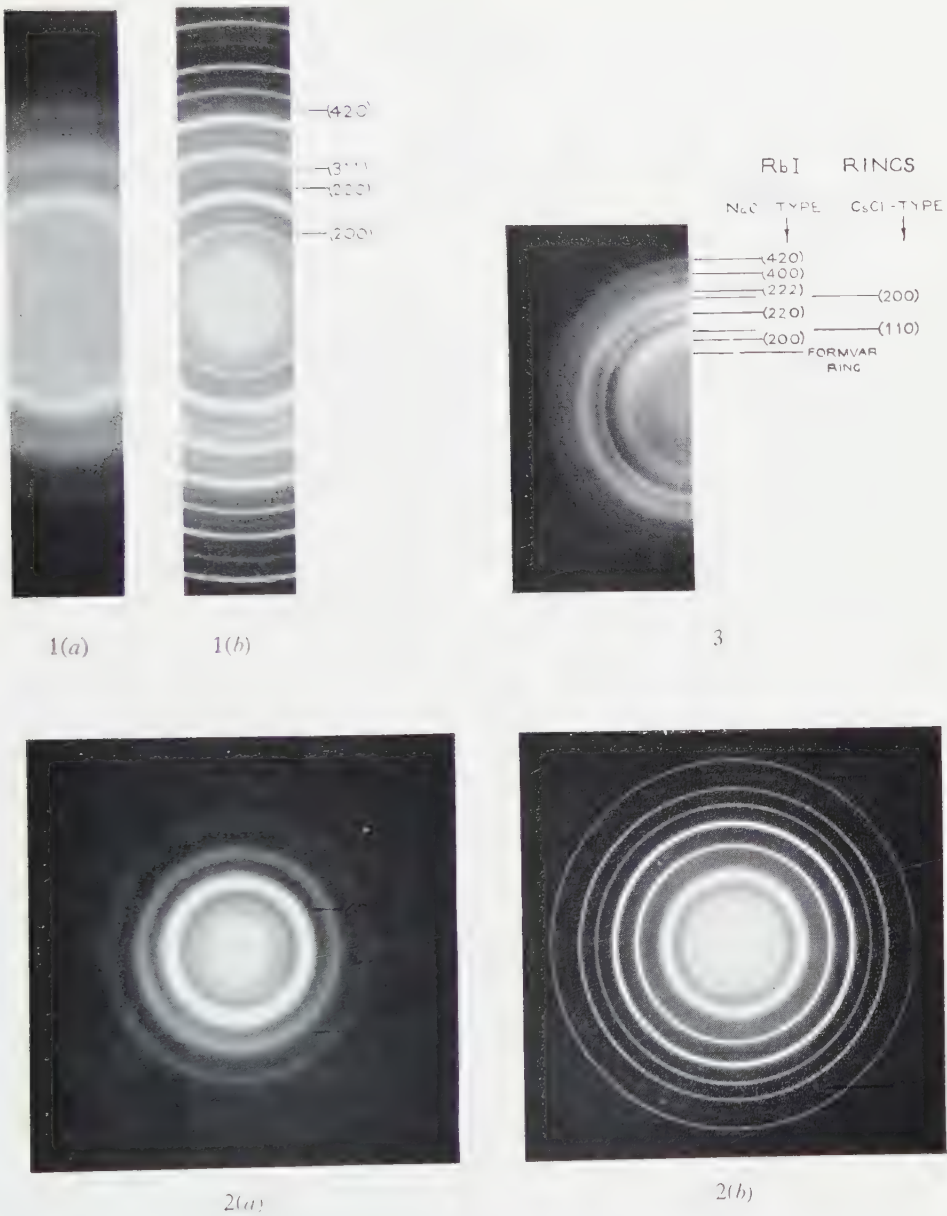


Fig. 1. Transmission patterns obtained from a deposit of caesium bromide on formvar; (a) broad ring pattern at -160°C and (b) ring patterns due to the normal and to abnormal structure at -118°C . The rocksalt type rings are indexed.

Fig. 2. Transmission patterns from a deposit of thallium iodide on formvar; (a) broad ring pattern at -100°C and (b) caesium chloride structure obtained by heating the deposit to -60°C .

Fig. 3. Diffraction pattern from a deposit of rubidium iodide formed at a low temperature and heated to -80°C . The rings are indexed.

Paramagnetic Resonance Spectrometry at Zero Magnetic Field

By G. S. BOGLE, H. F. SYMMONS, V. R. BURGESS
AND J. V. SIERINS

Division of Physics, Commonwealth Scientific and Industrial Research Organization,
Sydney

MS. received 22nd August 1960, in revised form 26th September 1960

Abstract. The need for direct measurements of paramagnetic resonance absorption spectra in zero magnetic field is discussed. Two spectrometers have been built which together cover the range of 8 to 18 Gc/s; with one of these a spectrum is recorded over a range of nearly 6 Gc/s in a time of two minutes with a sensitivity sufficient to detect about 10^{17} Fe^{3+} ions at 80 K. Polycrystalline samples may be used, and examples are shown of the spectra of a dilute ferric chelate compound. A technique is described for obtaining the absorption line shape free from the effects of the associated anomalous dispersion.

§ 1. INTRODUCTION

THE ultimate aim of paramagnetic resonance absorption studies is to determine completely the behaviour of the energy levels of paramagnetic ions or molecules as a function of magnetic field. In conventional paramagnetic resonance experiments the sample under investigation is subjected to fixed frequency microwave radiation and, in effect, the absorption coefficient is plotted as a spectrum against applied magnetic field up to some 10 000 gauss. Absorption lines occur at the fields where two energy levels of the paramagnetic ions are separated by one microwave quantum, and if the ground energy level in zero field is multiple, with splittings within a few cm^{-1} , the spectrum is multiple with a structure dependent on the inclination of the field to the crystal axes. Because of this anisotropy the maximum information is obtainable only with monocrystalline samples, polycrystals giving a spectrum which is in general diffuse and structureless. The choice of this approach—varying field at fixed frequency—instead of the reverse, was dictated partly by the early concentration of microwave development in a few narrow frequency bands, and partly by the necessity to use high Q cavity resonator techniques to increase sensitivity and so offset the small size of most single crystal samples.

To interpret the results of such experiments a theoretical model is needed: this has been provided by the spin-Hamiltonian of Pryce (1950) and Abragam and Pryce (1951). This model has been highly successful in interpreting many different spectra, but it should be noted that these have mostly been measured under conditions such that the energy equivalent of the steady magnetic field is much greater than the zero-field energy splittings. In other words, the spin-Hamiltonian has largely been tested only at relatively high magnetic fields, and hardly any measurements are available for the opposite case of zero field.

As far as we know, the only substance which has been carefully studied both at relatively high fields and also near zero field is gadolinium ethylsulphate. For this material Bleaney, Scovil and Trenam (1954) found a discrepancy of 90 Mc/s

or 7%—many times the experimental error—between one of the measured zero-field splitting frequencies and that predicted from the high field measurements. This discrepancy has not been explained. Evidently the theory of paramagnetism in crystals is in need of refinement. A first step has been taken recently by Koster and Statz (1959), who have produced, by completely general group-theoretical arguments, a secular matrix which contains more elements than that of the spin-Hamiltonian.

Measurements at and near zero field are not only necessary for the further development of theory, but are important, too, for the design of zero-field masers (Bogle and Symmons 1959). The development of wide-band microwave generators and ancillary equipment has now made such measurements possible, and we have therefore begun the construction of a series of wide-band spectrometers for use at zero field, of which two, covering the range 7.8 to 18.0 Gc/s, are described below.

§ 2. PRINCIPLES OF THE METHOD

In the absence of an applied magnetic field the absorption frequency of a paramagnetic crystal is, of course, independent of its orientation, which can only affect the intensity of absorption. Samples may therefore be studied in polycrystalline form, and their absorption intensity may be shown to be substantially the same as for favourably oriented material. Thus a broad-band spectrometer may be constructed simply by connecting a microwave generator to a detector through a piece of waveguide containing a polycrystalline sample, the relatively large size of which partly compensates for the sensitivity lost by giving up the conventional cavity technique.

The fractional absorption of power in a conveniently sized sample of dilute paramagnetic material is only of the order of 0.1% at liquid air temperature. This is much smaller than the changes of transmitted power, over a paramagnetic line width, caused by imperfections of the waveguide system and the frequency dependence of the microwave generator power, so that some method of modulating the intensity, or frequency, of the absorption must be used. We have used magnetic modulation in almost the same way as the well-known Stark modulation is used in the microwave spectroscopy of gases. The modulation consists of a field of 80 gauss which is effectively switched on and off 3000 times a second. For the sake of brevity we shall limit our discussion to the case of ions which have doublet levels in zero field (e.g. Fe^{3+} , Gd^{3+}). When a magnetic field is applied the levels split and each absorption line of a single ion splits into four separate components with frequency separations (of the order of $g\beta B/h$) which depend on the orientation of the crystal axes relative to the modulating field. For a randomly oriented sample the absorption profile is a smooth curve typified by the dotted line of Fig. 1(a), spread over a range of about $g\beta B/h$ above and below the zero-field frequency ν_0 . The actual shape of the curve depends on the type of transition considered and need not be symmetrical about ν_0 , but these details will be ignored for the present; the essential feature is that the absorption line is broadened and weakened. In Fig. 1(b) we show the algebraic difference between the two curves of Fig. 1(a). It is clear that it may be obtained experimentally by scanning the microwave frequency, applying modulation to the sample and recording phase-sensitively the resulting modulation of transmitted power. Fig. 2 shows an actual chart record so obtained.

In principle, it would be desirable to apply a modulation field such that $g\beta B/h$ was much greater than the zero-field line width, for then the dotted curve of Fig. 1(a) would be nearly flattened out and the output chart of Fig. 1(b) would be a close approximation to the line shape in zero field. In practice, the switching of such a large field presents difficulties. However, the same net effect can be achieved by proceeding in stages with the aid of an external steady field, switching from 0 to 80 gauss in the first stage, then from 80 to 160, and so on. Fig. 3 shows the results of the first two stages.

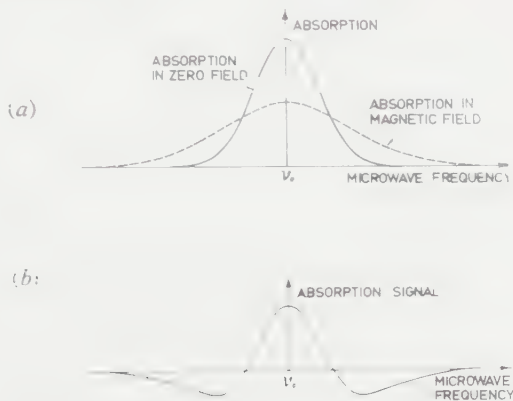


Fig. 1. (a) Absorption curves for a perfectly randomly oriented sample.
(b) Phase-sensitive detector output.

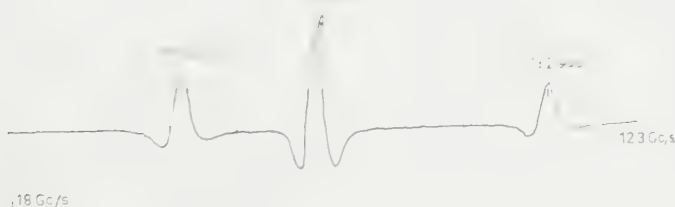


Fig. 2. The absorption spectrum of (Al, Fe) acetylacetonate at 80°K, between 18 and 12 Gc/s.
The amplitude of magnetic field modulation was 80 gauss.

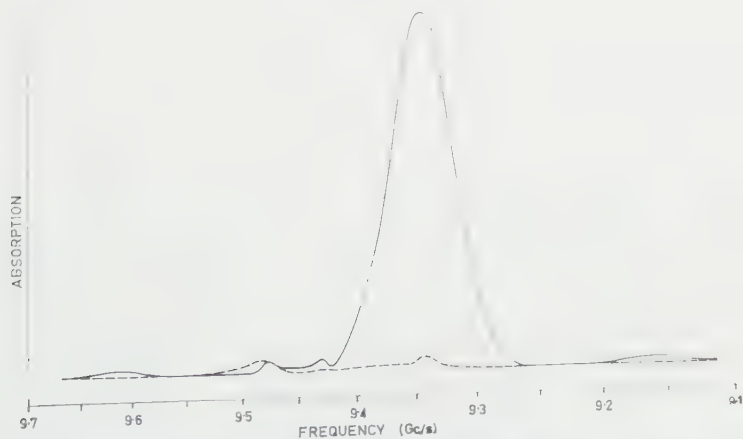


Fig. 3. The 9.35 Gc/s absorption line of (Al, Fe) acetylacetonate at 80°K. The full line results from modulating from zero to 100 gauss, and the dotted line from modulating from 100 to 200 gauss.

§ 3. DESCRIPTION OF THE SPECTROMETERS

Two spectrometers have been built, one covering the frequency range known as J-band (12.4–18.0 Gc/s) and the other 7.8–12.4 Gc/s, which is slightly more than X-band. Both can be operated at liquid air or liquid helium temperatures.

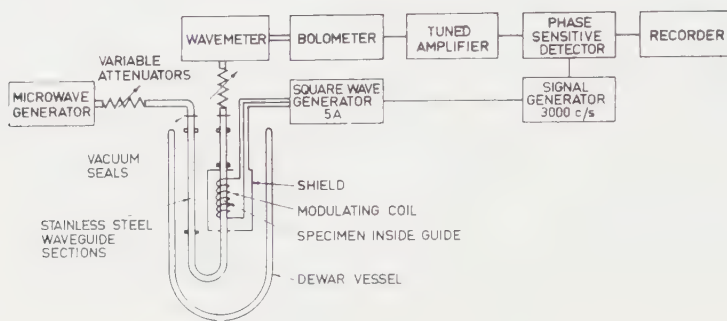


Fig. 4. The J(K_u) band transmission system.

The J-band spectrometer is shown schematically in Fig. 4. The microwave generator is a Hewlett-Packard sweep oscillator, model 687A, which contains a Huggins HO-4B backward-wave oscillator. The frequency may be swept electronically at various rates over the entire J-band, the frequency varying linearly (within 6%) with time. The slowest rate, at which the band is swept in 130 seconds, is well suited to our purpose. The transmitted power is detected by a broad-band bolometer and mounting (Narda type 604 and 529 respectively). The modulating coil is wound around the waveguide with spacers which allow the liquid coolant to circulate between the two and so prevent heat from the coil affecting the temperature of the waveguide and sample. The coil produces 16 gauss per ampere, and is supplied with a 5A square-wave current from a transistor circuit. The waveguide is slotted to prevent eddy currents. Unwanted pick-up from the coil is reduced by a shield pierced to allow free convection of the coolant within it. The bolometer amplifier is a Sanders transistorized voltage standing wave ratio amplifier, which can be operated selectively at 1000 or 3000 c/s with a bandwidth of about 200 c/s. The various charts of J-band absorption spectra which are shown in this paper were each taken in a time of 130 seconds. We believe that their frequency range—nearly 6 Gc/s—exceeds that of any microwave spectrum previously recorded in a single run.

The generator for the X-band spectrometer (Fig. 5) is a klystron (Varian X-13) which must be tuned mechanically. At present, spectra are measured point by point. The reflection system used here has the advantage of compactness, but the disadvantage of uncertainty whether all the power reaching the detector has traversed the paramagnetic sample. We now consider a transmission system to be preferable. In Fig. 6 we show a plot of the absorption spectrum of Fe³⁺ in Al[(CH₃CO)₂CH]₃ in the X-band at 90 K, and in Fig. 5 a detailed plot of the 9.3 Gc/s line at 80°K for modulation both from 0 to 100 and from 100 to 200 gauss. These results were taken without a phase-sensitive detector. Since the 100 to 200 gauss modulation curve in Fig. 3 is so flat, the 0 to 100 gauss modulation curve gives nearly the true line shape. The whole width at half intensity is 80 ± 5 Mc/s. We believe that this is the first determination of a paramagnetic resonance line shape at zero field.

A paper dealing in detail with these results is in preparation, and will appear later.

The major experimental problem which we have encountered is the avoidance of what we term 'interferometer fringes'. By this we mean the sharp wiggles on the chart of Fig. 7. These fringes only occur near absorption lines. We

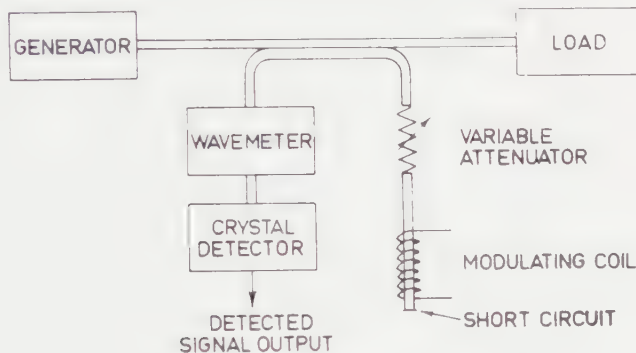


Fig. 5. The X-band reflection system.

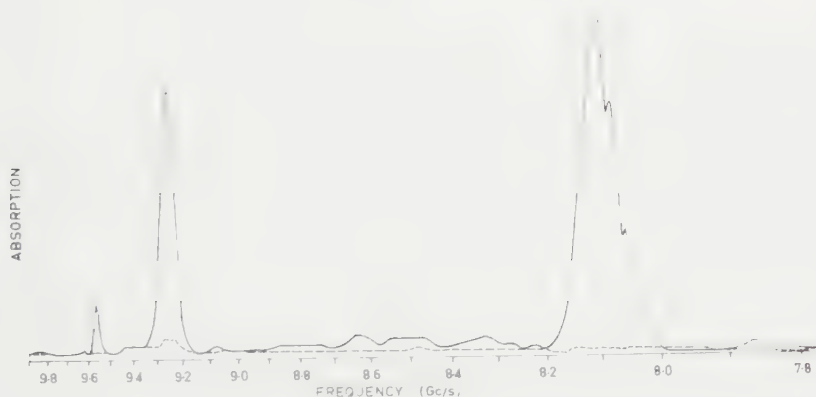


Fig. 6. The absorption spectrum of (Al, Fe) acetylacetonate at 90°K, between 8 and 10 Gc/s. The peak at 9.56 Gc/s is an 'interferometer fringe' (see text); other fringes are also discernible.

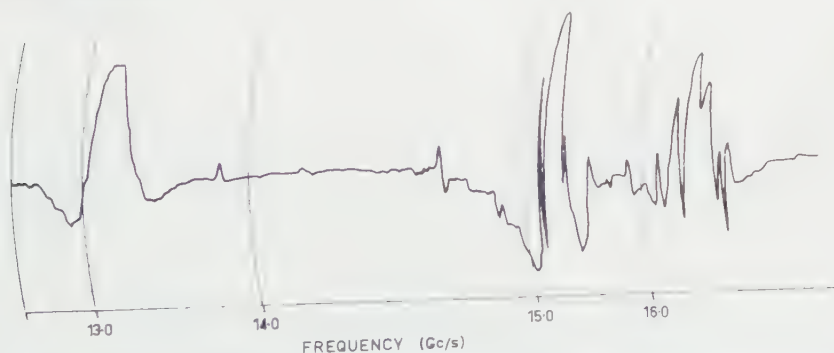


Fig. 7. The absorption spectrum of (Al, Fe) acetylacetonate at 80 K showing undamped 'interferometer fringes'. The reversed scale results from a different method of sweeping frequency.

have not worked out a quantitative theory of the fringes, but think they may be understood qualitatively in the following way: owing to waveguide reflections produced at the external attenuators, the vacuum seals, the waveguide bends and the sample itself, some length or lengths of the waveguide must act like an interferometer in that the transmission shows peaks at a succession of frequencies which correspond to orders of interference. If the 'interferometer' includes the sample, its effective length is perturbed when the frequency approaches a paramagnetic absorption line because of the associated anomalous dispersion. However, when the modulation field is switched on the anomalous dispersion is much reduced, and so the transmission peaks of the interferometer are shifted in frequency. Proceeding in this way one can understand the presence of fringes on the chart, and their shapes, and the fact that they are reversed after crossing the absorption line.

The remedy for fringes is to introduce some microwave attenuation at the sample, which can be done by painting parts of the sample-holder with a suspension of colloidal graphite in water ('aquadag'). This damps any waveguide resonances enclosing the sample, and the associated transmission peaks or dips are broadened and weakened so that they are much less sensitive to modulation. An attenuation of 3 to 6 dB is generally sufficient. The improvement may be seen by comparing Figs 2 and 7.

It is perhaps hardly necessary to mention that ferromagnetic materials must be scrupulously kept out of the sample space. A sliver of steel wool almost too small to be seen with the naked eye produced effects which were much larger than the absorptions shown in Figs 2 and 7. We have found that 'non-magnetic' stainless steel (type 18/8 F.S.L.) is weakly ferromagnetic at low temperatures, and that if this is used for the waveguide inside the modulating coil similar spurious signals occur.

§ 4. SENSITIVITY

In the case of the electronically swept J-band spectrometer the choice of the modulation frequency of 3000 c/s, which is unusually high for bolometer detection, is made desirable by the noise characteristics of the backward wave oscillator. The noise power per cycle per second of bandwidth is 55 and 61 dB below the carrier level at 1000 and 3000 c/s respectively.

The minimum number of Fe^{3+} ions which can be detected at 80°K is of the order of 10^{17} . The sensitivity of the present equipment is limited almost equally by the backward wave oscillator noise and the transistor amplifier noise.

ACKNOWLEDGMENTS

We are grateful to Mr. G. J. Troup and Mr. J. M. Hammond of the Weapons Research Establishment, South Australia, for preparing for us the acetylacetonate specimens used in the above experiments, and to Dr. I. D. Campbell, of the Defence Standards Laboratory, Melbourne, for the loan of a J-band wavemeter.

REFERENCES

- ABRAGAM, A., and PRYCE, M. H. L., 1951, *Proc. Roy. Soc. A*, **205**, 135.
- BLEANEY, B., SCOVIL, H. E. D., and TRENAM, R. S., 1954, *Proc. Roy. Soc. A*, **223**, 15.
- BOGLE, G. S., and SYMMONS, H. F., 1959, *Aust. J. Phys.*, **12**, 1.
- KOSTER, G. F., and STATZ, H., 1959, *Phys. Rev.*, **113**, 445.
- PRYCE, M. H. L., 1950, *Proc. Phys. Soc. A*, **63**, 25.

The Thermomagnetic Behaviour of Cobalt Ferrite

BY L. F. BATES AND A. J. PACEY

University of Nottingham

MS. received 18th August 1960

Abstract. The small heat changes accompanying the magnetization of cobalt ferrite were measured with two rod specimens. One had been heat-treated to destroy uniaxial anisotropy, the other was untreated. A new method of analysis of the results is described, and while its application to these specimens may not have led to conclusive results, it appears to give useful information when applied to materials of less complex magnetic behaviour.

§ 1. INTRODUCTION

MUCH work has been done on cobalt ferrite specimens of low density, e.g. of about 2.9 to 3.2 g cm^{-3} (Guillaud 1953, Vautier 1954). Such specimens tend to show single domain behaviour, and any domain walls are anchored by the pores in the material, so that reversal of magnetization takes place mainly by the rotation of magnetization vectors. This gives rise to high coercivities of the order of 1000 Oe .

Two samples of cobalt ferrite (CoFe_2O_4) were available. They were in the form of rods, some 0.4 cm in diameter and 27 cm long, and were of relatively high density (4.51 g cm^{-3} , representing 85% packing). Their coercivities were correspondingly low (250 Oe), but they were not technically saturated until fields of some thousands of oersteds were applied. Magnetization loops, measured for a 950 Oe cycle (Fig. 1) showed the characteristic constriction discussed by Wijn, van der Heide and East (1957) for a variety of cobalt ferrous ferrites. It seems that the constriction is caused by a minimum in the domain wall energy associated with a uniaxial component of anisotropy.

Conner and Artman (1958) attributed this anisotropy to a precipitation effect. However, Wijn *et al.* found no second phase, and they explained it by a directional ordering process. They envisaged that at a sufficiently high temperature an ordering occurs by which an easy direction of magnetization is induced close to the direction of the magnetization vectors. Hence, to produce uniaxial anisotropy, a specimen must be annealed at an appropriate temperature. Alternatively, to destroy the uniaxial anisotropy, the specimen should be annealed at a temperature above the Curie point, where there is no intrinsic magnetization to encourage ordering, and then quenched to room temperature while exposed to an alternating magnetic field. These treatments were determined largely by Eckert (1957), who found that the best annealing temperature for the production of a constricted magnetization loop was about 10°C below the Curie point.

In the present work measurements were made on a specimen which showed a constriction, and on one whose constriction had been removed by heating the specimen up to 600°C and then cooling it at a rate of $15^\circ \text{C min}^{-1}$ down to 500°C ,

and at a slower rate thereafter. (The Curie temperature was $540^{\circ}\text{C}.$) The cooling was carried out in an alternating field of about 100 Oe amplitude, and with the specimen in an atmosphere of carbon dioxide.

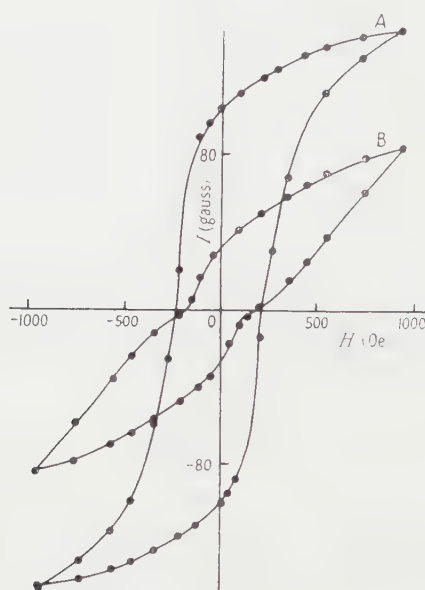


Fig. 1. Magnetization loops for cobalt ferrite; A, after heat treatment; B, untreated.

§ 2. MAGNETOTHERMAL MEASUREMENTS

It has been suggested (Sherry 1954) that in magnetothermal measurements reversible and irreversible changes can be separated by the direct method of measuring thermal changes (Bates and Sherry 1955) only if the coercivity of the specimen is greater than the magnitude of the field steps which are made. Several sets of measurements of the reversible component of magnetization were made using a series of different field steps, and it was confirmed that the coercivities of the specimens were large enough for the direct method to be used with confidence. The relevant thermal curves of the heat changes during a half cycle of magnetization are given in Fig. 2. By convention, we always start with the specimen in a negative field.

The reversible heating was much smaller than the irreversible heating in both specimens, so that calibration could be based on Warburg's law. Half the area of the hysteresis loop ($H_{\text{max}} = 950$ Oe) for the untreated specimen was $33\,800 \text{ erg cm}^{-3}$. The irreversible heating for a half cycle, calibrated by loading, was found to be $32\,300 \text{ erg cm}^{-3}$, after allowing for porosity, i.e. for the actual density of the specimen in comparison with the density obtained from x-ray data (Christoffel 1957). The corresponding figures for the heat-treated specimen were $66\,100$ and $67\,700 \text{ erg cm}^{-3}$, respectively. The results for both specimens were unusual in that some reversible heating, instead of cooling, was observed in negative fields (cf. Fig. 2) an indication of a large contribution due to magneto-crystalline anisotropy.

In the analysis of the observations it was decided to use the differential form of the Stoner and Rhodes (1949) equation, namely

$$\left(\frac{\partial Q_R'}{\partial H}\right)_S = a \left[I + H \left(\frac{\partial I_R}{\partial H}\right)_T \right] + bH \left(\frac{\partial I_R}{\partial H}\right)_T \quad \dots\dots (1)$$

where $a = -(T/I_0)(dI_0/dT)$ and $b = (T/K)(dK/dT)$. When several processes

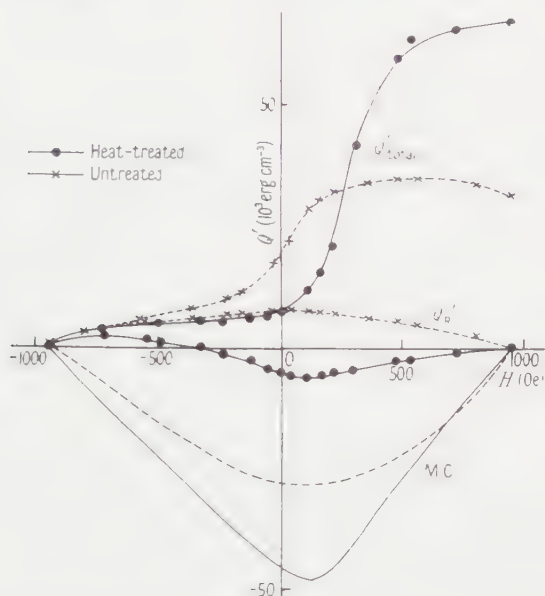


Fig. 2. Magnetothermal curves (Q', H) for cobalt ferrite. (Note that curve M.C. (Weiss magnetocaloric effect) is calculated using the expression $a(HI - H_1I_1)$ for the M.C. effect.)

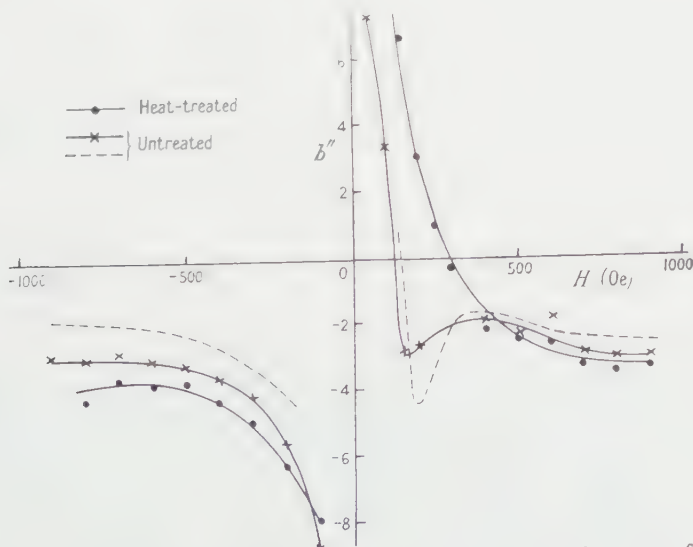


Fig. 3. Variation of b'' with H for cobalt ferrite. Of the untreated curves: full line, using the differential form of the Stoner and Rhodes equation in both cases; broken line, using $a(HI - H_1I_1)$ for the M.C. effect.

are operative, $\partial Q_R'/\partial H$ cannot be represented thus simply. We then introduce a variable coefficient b'' , and write

$$\left(\frac{\partial Q_R'}{\partial H}\right)_S = a \left[I + H \left(\frac{\partial I_R}{\partial H} \right)_T \right] + b'' H \left(\frac{\partial I_R}{\partial H} \right)_T. \quad \dots\dots (2)$$

The differential form of the equation has two advantages over the usual form

$$\Delta Q_R' = a(HI - H_1 I_1) + b \int_{H_1}^H H dI_R. \quad \dots\dots (3)$$

Firstly, $\Delta Q_R'$ and $\int H dI_R$ both refer to reversible changes, whereas it seems that $HI - H_1 I_1$ refers to both reversible and irreversible effects. Lack of definiteness is avoided by using the differential form of the equation, as it is clear that $I + H \partial I_R / \partial H$ refers to reversible effects only. The importance of this procedure may be seen on comparing the different values of b'' (Fig. 3) given by the two equations. Secondly, cumulative errors due to the summation of readings of $\Delta Q_R'$ are avoided.

It was found impossible to measure $(T/I_0)(dI_0/dT)$ since the specimens were not technically saturated even in fields of 7000 Oe. The value $a = +0.33$ from the results of Pauthenet (1952) was assumed.

§ 3. HIGH FIELD VALUES OF b''

Values of b'' were calculated and plotted against H (Fig. 3). The curves for the two specimens were very similar, except in the region 0 to 400 Oe. For very small fields b'' moved towards infinity in both cases, but in the case of untreated cobalt ferrite it passed through a minimum value at about 180 Oe. In high fields b'' approached a constant value of 3.0, compared with 3.25 for the heat-treated specimen. In comparing these values with $(T/K)(dK/dT)$ it is to be remembered that cobalt ferrite exhibits two kinds of anisotropy. There is a cubic component, which is fundamental to the material, as well as a uniaxial component, which is dependent on the thermal history of the specimen. Since the high field value of b'' is little changed by the heat treatment, it might be expected that b'' would be determined by the cubic anisotropy. However, although the first anisotropy constants at 20 °C are $3.0 \times 10^6 \text{ erg cm}^{-3}$ for the cubic component, and $0.52 \times 10^6 \text{ erg cm}^{-3}$ for the uniaxial component, respectively, the measurements of Foner and Artman (1958) give $(T/K)(dK/dT)$ equal to 3.0 in both cases (Shenker 1957, gives 3.25 for the cubic component). If these results are applicable to the present specimens, it may be that the uniaxial anisotropy contributes to b'' in the case of the untreated specimen.

§ 4. LOW FIELD VALUES OF b''

Recently, attempts have been made to analyse the measurements of b'' in low fields. Several magnetization processes are active in this region, and the Stoner and Rhodes equation is modified to the form given by Teale and Rowlands (1957) which, using the notation of Saunders and Tebble (1960) with one minor difference noted below, may be expressed as

$$\left(\frac{\partial Q_R'}{\partial H}\right)_S = a \left\{ I + H \left(\frac{\partial I_R}{\partial H} \right)_T \right\} + \left(\sum_{n=1}^N b_n V_n \right) \left(\frac{\partial I_R}{\partial H} \right)_T. \quad \dots\dots (4)$$

Here, $V_n = (\partial F_n / \partial I)_T$ for the n th magnetization process. F_n is defined by

$\sum_{n=1}^N dF_n = HdI$; b_n is a constant of the form $(T/A_n)(dA_n/dT)$, where A_n is given by $F_n = A_n f(I/I_0)$. Comparing Eqns (2) and (4),

$$b''H = \sum_{n=1}^N b_n V_n.$$

But, since $\sum dF_n = HdI$, it follows that $\sum V_n = H$. Therefore

$$(b'' - b_1)H = \sum_{n=2}^N (b_n - b_1) V_n \quad \text{..... (5)}$$

where b_1 replaces b of the original Stoner and Rhodes equation.

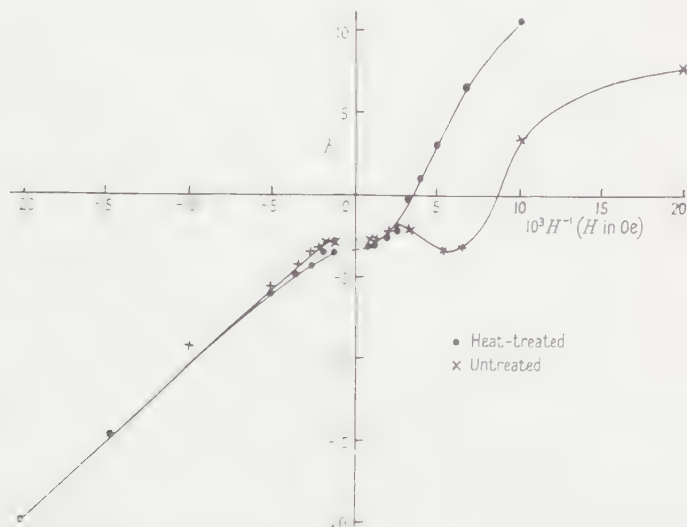


Fig. 4. Variation of b'' with $1/H$ for cobalt ferrite.

Now Saunders and Tebble (1960) noticed that many (b'', H) curves approximate to rectangular hyperbolae. This means that the graph of b'' plotted against $1/H$ is a straight line of the form

$$b'' = p + q/H, \text{ or } (b'' - p)H = q. \quad \text{..... (6)}$$

By comparing Eqns (5) and (6), Saunders and Tebble showed that if the $(b'', 1/H)$ curve is a straight line,

$$\sum_{n=2}^N (b_n - b_1) V_n$$

must be constant (b_n replaces S_n in their notation). Such a straight line is obtained for cobalt ferrite in negative fields (Fig. 4). In the simplest case, for which n is 2, the last expression becomes $(b_2 - b_1)I_2$. If this is constant, then I_2 is constant. However, the analysis is not unambiguous. It is easily seen that if $I_2 = A + BH$, once again, the $(b'', 1/H)$ curve is a straight line. To avoid this ambiguity in the Saunders and Tebble treatment, it was decided to plot $(b'' - b_1)H$ against H , so that by using Eqn (5), the form of V_n could be seen. The plot, using smoothed values of b'' gave almost a straight line for negative fields (Fig. 5), which shows that cobalt ferrite obeys $I_2 = A + BH$ rather than $V_2 = \text{const.}$

The validity of plotting $(b'' - b_1)H$ may be questioned on the grounds that b'' cannot be measured very accurately, and therefore values of $b'' - b_1$ may be

subject to very large error. However, in the low field region, $b'' - b_1$ becomes large and significant. A more serious objection is that the Stoner and Rhodes equation is itself of doubtful validity in the region of the coercive point where irreversible effects predominate. We therefore think that the form of $(b'' - b_1)H$ cannot be regarded as more than qualitatively significant.

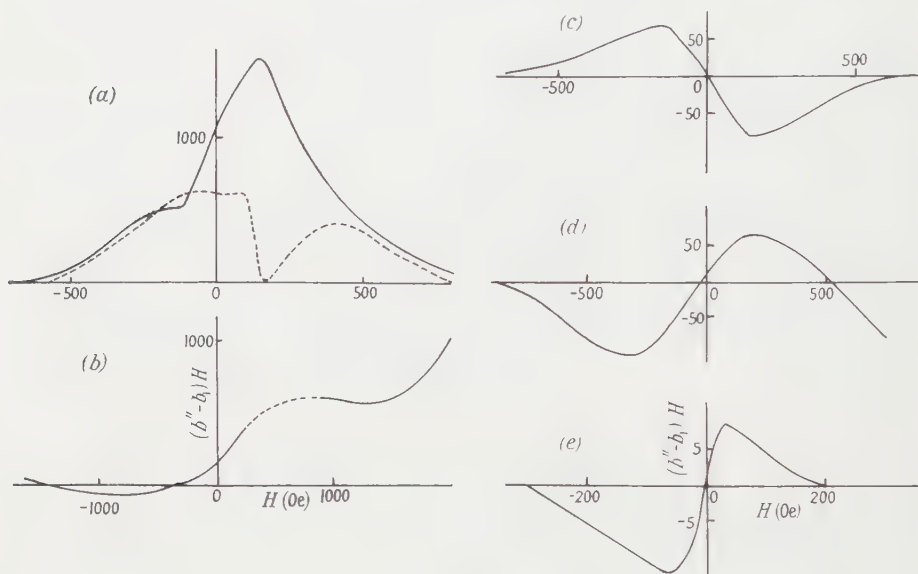


Fig. 5. Variation of $(b'' - b_1)H$ with H . (a) Cobalt ferrite: full line, heat-treated specimen; broken line, untreated specimen; (b) alcomax II (Bates and Simpson; the broken section of the curve was calculated using extrapolated values of Q_R); (c) nickel ferrite (Bates and Clow); (d) cobalt (Teale); (e) nickel (Teale).

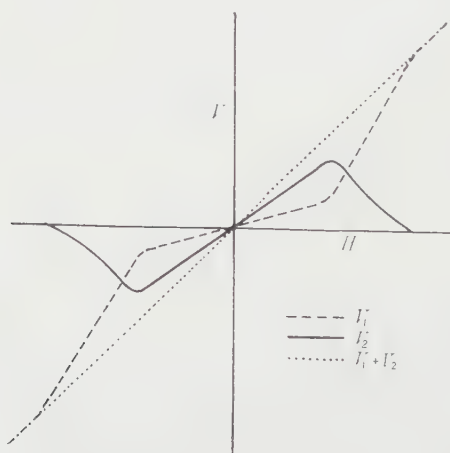


Fig. 6. Explanation of the shape of the $((b'' - b_1)H, H)$ curve.

For the sake of comparison, $((b'' - b_1)H, H)$ curves for cobalt, nickel, nickel ferrite and alcomax II are plotted in Fig. 5. The values of b'' are taken from Teale (1955), Bates and Clow (1960) and Bates and Simpson (1955), and where necessary have been recalculated using the differential form of the Stoner and

Rhodes equation. By convention, values of b_1 are chosen such that $(b'' - b_1)H$ is zero in the maximum negative field. This is necessary because in some cases $(T/K)(dK/dT)$ is not known. Where it is known, however, it is in every case very close to the value of b_1 which has been adopted. Cobalt and nickel show curves of very similar shape, each with a trough in negative fields and a peak in positive fields. The curve for nickel ferrite is also similar, but inverted. This characteristic shape can be explained fairly simply, as follows.

Consider a specimen in which a single domain wall effect is the principal magnetization process in low fields, while rotation of magnetization vectors is the principal process in high fields. If the free energy due to rotations is F_1 and that due to the domain wall effect is F_2 , then $V_1 = (\partial F_1 / \partial I)_T$ and $V_2 = (\partial F_2 / \partial I)_T$. Now, consider the variation of V_1 and V_2 with H (Fig. 6). Since $V_1 + V_2 = H$, a graph of $V_1 + V_2$ against H will be a straight line of unit gradient. In large negative fields, where rotations alone are operative, V_1 follows this line, V_2 being zero. But, as the field increases (i.e. becomes less negative) rotations become less and less important, and V_1 approaches the axis of abscissae. When this happens, V_2 decreases from zero to take up a negative value such that $V_1 + V_2$ remains equal to H . Hence, as the field passes through zero, the graph of V_2 is a straight line with a gradient which approaches unity. Then, in positive fields, the domain wall effect disappears, V_2 falls again to zero, and V_1 increases in its place. But, $(b'' - b_1)H = (b_2 - b_1)V_2$, (from Eqn (5), with $n=2$); hence the $((b'' - b_1)H, H)$ graph will give a curve of the same shape as that for V_2 ; this is in agreement with the experimental results for cobalt, nickel and nickel ferrite (inverted). Further, if the (V_2, H) curve has a gradient which approaches unity, the gradient of $((b'' - b_1)H, H)$ can be used to estimate roughly a limiting value for $b_2 - b_1$ so that an approximate value for b_2 can be obtained. Data for cobalt, nickel and nickel ferrite are given in Table 1.

Table 1. Estimated Values of b_2

Material	b_1	$b_2 - b_1$	b_2
Cobalt	-1.14	0.1	-1
Nickel	-4.8	1.5	-3
Nickel Ferrite	-0.26	-0.6	-1

Since we do not claim more than qualitative significance for the graphs from which these figures are obtained, not much weight is to be put upon them. However, the orders of magnitude of b_2 which are given by this method are well within the range of various predicted values for the several materials. This seems to confirm that the simple two-process model which has been used in this explanation is applicable to these three cases.

It remains now to consider the more complex curves for $(b'' - b_1)H$ given by cobalt ferrite and alcomax II, whose graphs have a peak in positive field regions. Here, other effects must occur. It is suggested that where rotational processes play an important part in the reversal of magnetization, the function V_1 does not approach zero in the simple manner so far envisaged. Yet, it seems that the peaks in these graphs are comparable with those given by cobalt and nickel, and that their explanation is of a similar nature.

If the region where domain wall or other effects occur is centred on the coercive point, then for high coercivity materials, such as alcomax, rotations may continue to be the dominant process almost up to zero fields. The effect of this is to remove the trough in the (V_2, H) graph, leaving only the peak in positive fields. When heat-treated and untreated cobalt ferrite are compared, it is seen that, apart from the region of the coercive point, values of $(b'' - b_1)H$ are similar. In the region of the coercive point the heat-treated specimen shows a peak, which indicates a positive value of $b_2 - b_1$. On the other hand, the untreated specimen shows a trough, corresponding to the minimum in the values of b'' , and a negative value of $b_2 - b_1$ is indicated. In trying to explain these results, the effect of the uniaxial anisotropy comes first to mind. But the values available for $(T/K)(dK/dT)$ are the same for both kinds of anisotropy.

If the values of $(T/K)(dK/dT)$ hold for the present specimens, $b_2 - b_1$ will be zero, and the uniaxial anisotropy will have no effect on $(b'' - b_1)H$.

Wijn, van der Heide and Fast (1957) explain the constriction in the hysteresis loop in terms of a directional ordering process similar to that which causes the uniaxial anisotropy. According to them, directional ordering "takes place in the Bloch wall itself. This must be understood in such a way that the gradual change of the direction of the magnetic moments in the Bloch wall enhances a discontinuous change of that of the 'directional ordering' through the wall. As a consequence, the 180° walls are much more strongly bound to their equilibrium positions than would be the case without ordering." This means that there is a minimum in the free energy F_2 of the Bloch wall, which produces a curve for V_2 of the shape required in Fig. 6, although only the peak will appear. This is shown on the $((b'' - b_1)H, H)$ graph as a trough, which indicates the negative value of $b_2 - b_1$ already mentioned. It is difficult to calculate what b_2 should be for the process envisaged by Wijn *et al.*, so the negative sign cannot be confirmed.

With the heat-treated specimen, the prominent peak indicates a fairly large positive value of $b_2 - b_1$. Since b_1 , i.e. $(T/K)(dK/dT)$, is about -3 , it is evident that b_2 is considerably greater (less negative) than -3 . The predicted values of b_2 are given in Table 2. It will be seen that the highest values are those for rotations against shape anisotropy, domain wall movement governed by magneto-static energy, or by the Lilley disperse field theory. We think it is one of these three processes which occurs, though it is impossible to decide which from the analysis of these experiments.

Table 2. Predicted Values for b_1 and b_2

Rotations against crystal anisotropy energy	$(T/K_1)(dK_1/dT)$	-3.2
Rotations against strain anisotropy energy	$(T/\lambda_s)(d\lambda_s/dT)$	$-1.9\dagger$
Rotations against shape anisotropy energy	$\left. \begin{array}{l} \\ \end{array} \right\} (2T/I_0)(dI_0/dT)$	-0.66
Wall movement against magnetostatic energy		
Wall movement: Kersten (1943)	$(T/\gamma)(d\gamma/dT)$	-1.95
Wall movement: strain theory	$(T/I_0)(dI_0/dT) + (T/2\lambda_s)(d\lambda_s/dT)$	-1.2
Wall movement: Lilley (1952)	$(2T/\lambda_s)(d\lambda_s/dT) - (T/K)(dK/dT)$	-0.6

\dagger Estimated from the results of Guillaud (1953).

§ 5. CONCLUSION

The magnetothermal behaviour of these specimens of cobalt ferrite is generally similar to that of other materials, b'' in high fields being in reasonable agreement with $(T/K)(dK/dT)$. In the present work, however, $(b'' - b_1)H$ has been examined for the first time. This analysis does not seem to be very significant quantitatively, but the method is useful in that it indicates whether the magnetic behaviour of the material can be represented by a simple two-process model, or whether the magnetization processes are more complex. Some indication of the sign of b_2 is also given.

ACKNOWLEDGMENTS

We are indebted to Dr. E. W. Gorter of Philips' Research Laboratories, Eindhoven for the provision of the cobalt ferrite rods. One of us (A.J.P.) thanks the Department of Scientific and Industrial Research for a maintenance allowance which has enabled the work to be undertaken.

REFERENCES

- BATES, L. F., and CLOW, H., 1960, *Proc. Phys. Soc.*, **75**, 17.
 BATES, L. F., and SHERRY, N. P. R., 1955, *Proc. Phys. Soc. B*, **68**, 642.
 BATES, L. F., and SIMPSON, A. W., 1955, *Proc. Phys. Soc. B*, **68**, 849.
 CHRISTOFFEL, D. A., 1957, *Thesis*, University of Nottingham.
 ECKERT, O., 1957, *Proc. Instn Elect. Engrs*, **104 B**, 428.
 FONER, S., and ARTMAN, J. O., 1958, *J. Appl. Phys.*, **29**, 443.
 GUILLAUD, C., 1953, *Rev. Mod. Phys.*, **25**, 64.
 KERSTEN, M., 1943, *Grundlagen einer Theorie der Ferromagnetischen Hysterese und Koerzitivkraft* (Leipzig: Hirzel).
 LILLEY, B. A., 1952, *Thesis*, University of Leeds.
 PAUTHENET, R., 1952, *Ann. Phys.*, **7**, 710.
 SAUNDERS, N. H., and TEBBLE, R. S., 1960, *Proc. Phys. Soc.*, **76**, 282.
 SHENKER, H., 1957, *Phys. Rev.*, **107**, 1246.
 SHERRY, N. P. R., 1954, *Thesis*, University of Nottingham.
 STONER, E. C., and RHODES, P., 1949, *Phil. Mag.*, **40**, 481.
 TEALE, R. W., 1955, *Thesis*, University of Leeds.
 TEALE, R. W., and ROWLANDS, G. R., 1957, *Proc. Phys. Soc. B*, **70**, 1123.
 VAUTIER, R., 1954, *Ann. Phys.*, **9**, 322.
 WIJN, H. P. J., VAN DER HEIDE, H., and EAST, J. F., 1957, *Proc. Instn Elect. Engrs*, **104 B**, 412.

The Irreversible Change of Magnetization produced in 'Square Loop' Ferrite by Pulsed Magnetic Fields

By J. E. KNOWLES

Mullard Research Laboratories, Salfords, Surrey

MS. received 27th June 1960, in revised form 22nd August 1960

Abstract. A core of square loop ferrite was examined under pulse magnetization conditions. Starting from remanence the irreversible change of magnetization produced by a series of very short pulses was measured by a ballistic galvanometer method. The results were interpreted on the basis of a domain wall model, which enabled an estimate to be made of the ratio of the time spent by the walls in reversible motion to the time spent in irreversible motion. From this ratio was deduced the average number of times that the domain wall energy passed through a maximum during the course of a magnetization reversal. The result so obtained, twenty-five, agreed well with that obtained by an independent method, due to Néel.

§ 1. INTRODUCTION

EXPERIMENTS by Newhouse (1957) and by Verkruijsen (unpublished) had shown that if a series of very short demagnetizing pulses of large amplitude was applied to a magnetic core initially at remanence, the irreversible change of magnetization could be very small. Newhouse, working with molybdenum permalloy found that pulses of 0.63 Oe and of 100 nsec duration caused no change in the permanent state of magnetization, although the coercive force was only 0.07 Oe. Verkruijsen, working with Ferroxcube rings, obtained similar results. Both workers deduced the magnetic state of their samples by observing pulse shapes displayed on an oscilloscope, which made the determination of accurate data rather difficult.

In the method to be described a ballistic galvanometer was used to overcome this limitation, although this too had certain disadvantages: in particular no data could be obtained concerning the output of a core due to reversible processes. As a preliminary the behaviour of domain walls under pulse conditions was observed.

§ 2. DOMAIN OBSERVATIONS

Using a technique described earlier (Knowles 1960, to be referred to as I) a grain with a domain structure similar to that of I was located on a toroidal specimen of manganese-magnesium ferrite. A continuous train of pulses of a known duration in the range 10–100 nsec was applied and their amplitude slowly increased. The domain walls were seen to move across the grain in just the same way as I when they were driven by a slowly increasing uninterrupted field, that is, as the amplitude of the pulses was increased the magnetization changed by what appeared to be Barkhausen jumps. Of course, the domain walls could only be observed at successive remanence positions since the walls were in motion only for about 10^{-5} of any given period.

In view of these observations, it appeared reasonable to try and explain the behaviour of a square loop ferrite when driven with short pulses upon the basis of an existing domain wall model (Knowles 1960, 1961, to be referred to as II).

§ 3. EXPERIMENTAL WORK

3.1. Method

A small core of manganese-magnesium ferrite was, in principle, provided with three windings: (a) a primary coil connected to a battery circuit, (b) a coil connected to a generator of pulses of variable amplitude and duration, and of negative sign, (c) a secondary coil connected to a ballistic galvanometer.

Coil (a) was used to put the core into a cyclic state, the core being left at positive remanence (A in Fig. 1). (a) and (c) were then open circuited and a very long train of pulses of a known duration and amplitude were passed through (b), the repetition rate being 100 c/s. These drove the material down to some point B_1 on the left-hand limb of a hysteresis loop and no further change in magnetization was produced by subsequent pulses. When the pulse train terminated, the material returned to a remanence position C_1 , which from the normal hysteresis loop of the material may be supposed to be about level with B_1 . (b) was then open circuited and a large positive pulse of about 0.1 sec duration was passed through (a). This returned the material to the normal positive remanence position along the path C_1DA , and the swing of the ballistic galvanometer was an indication of the irreversible change in magnetization produced by the pulse train.

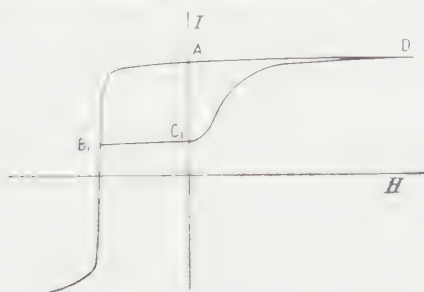


Fig. 1. Diagram showing the derivation of the remanence curves.

This procedure was repeated a number of times for a fixed pulse duration and various pulse amplitudes and so a form of hysteresis loop, or remanence curve, could be drawn. The whole process was then repeated for a different value of pulse duration.

Measurements were made upon an 8-mm diameter toroid of 'square loop' manganese-magnesium ferrite. To reduce spurious effects due to the windings the toroid was wound with two coils of $4\frac{1}{2}$ turns of (90 \times 46 s.w.g.) wire, connected in parallel to reduce their self-capacitance (Smit and Wijn 1959). This composite winding served both as primary (a) and pulse winding (b). The secondary (c) consisted of $4\frac{1}{2}$ turns of 44 s.w.g. wire which was laded with the other. Both coils were terminated in copper leaves adjacent to the core, connection between the components of the circuit being made by copper links (Fig. 2).

The three stages in making an observation then became:

(1) Connect 1-2 (and incidentally, 3-4, the galvanometer circuit being broken elsewhere) and cycle the core with a field of 5 Oe.

(2) Connect 1-4 and pass pulse train. The single strand of 44 s.w.g. wire has now become part of the pulse circuit and there is no possibility of any 'ringing' due to this winding.

(3) Connect 1-2 and 3-4; pass positive pulse and observe galvanometer deflection.

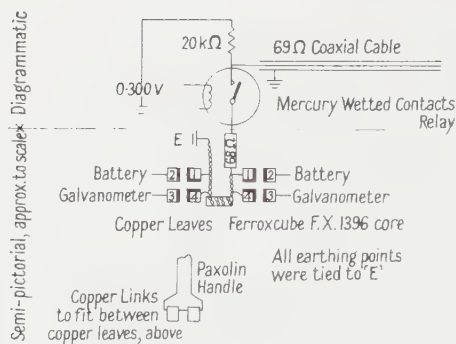


Fig. 2. The layout of the pulse generator and associated equipment.

3.2. Experimental Results

A series of remanence curves obtained at room temperature ($22 \pm 1^\circ\text{C}$) are shown in Fig. 3. For clarity only the left-hand side of the loops has been drawn and the field scale has not been placed in the conventional position. The normal loop may be considered to be very nearly coincident with that for 800 nsec. It may be seen that the pulse duration was changed logarithmically from $12\frac{1}{2} \sqrt{2}$ nsec to 800 nsec. The number of pulses applied ranged from 6000 for the longest pulses to 360 000 for the shortest pulses. The shapes of pulses of $12\frac{1}{2} \sqrt{2}$ and 800 nsec duration are shown in Fig. 4: their rise time appeared to be comparable with the 3 nsec rise time of the oscilloscope used to observe them.

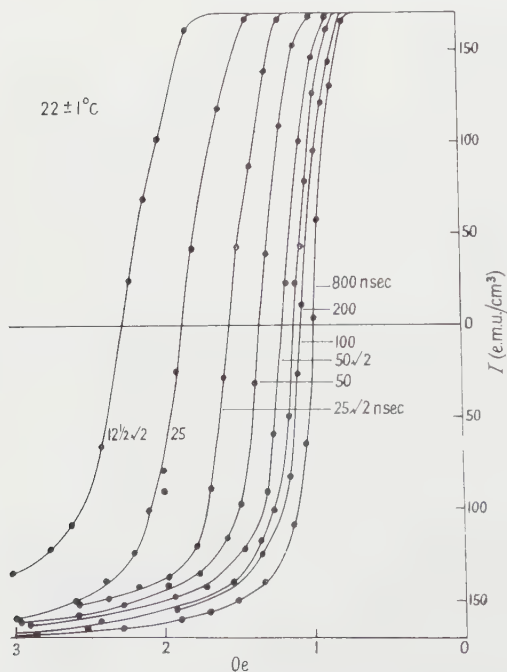


Fig. 3. Remanence curves obtained with various values of pulse duration.

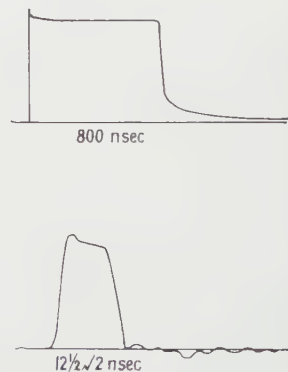


Fig. 4. Typical pulse shapes.

To interpret these results, suppose that the field was kept constant at say 1.4 Oe, and that the pulse duration was increased continuously from $12\frac{1}{2}\sqrt{2}$ to 25 nsec. The magnetization of the specimen would change by an amount ΔI_1 , i.e. this part of the magnetization had what may be called a 'break free' time of between $12\frac{1}{2}\sqrt{2}$ and 25 nsec. Increasing the pulse duration to $25\sqrt{2}$ nsec we find a further part ΔI_2 of the magnetization had a break free time of between 25 and $25\sqrt{2}$ nsec, and so on. Thus a form of histogram may be plotted of ΔI against the (geometrical) mean of the pulse durations. For convenience ΔI was plotted against $\log t$ (Fig. 5). For each value of the applied field $\log t$ appeared to be scattered in a roughly Gaussian mode about a mean value. The half-width of the peak remained fairly constant at $t_1/t_2 \simeq 1.9$ for fields in the range 1.4–1.8 Oe.

The time corresponding to the peak of a curve might be called the mean break free time, and Fig. 5 shows that as the field was increased this time diminished. Accurate values cannot be obtained from these curves, however, so the mean break free time t_b for a given field H will be defined in the following way: 'If a train of pulses of duration t produces a loop with a coercivity H , then t is the mean break free time t_b corresponding to a field H '. As the loops have steep sides the value of t_b so obtained is not sensitive to the exact mode of definition.

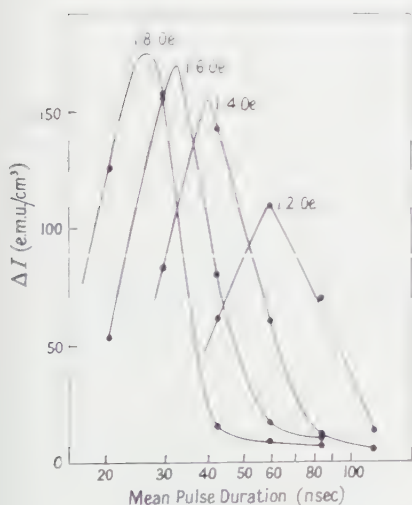


Fig. 5. Experimental plot of ΔI against pulse duration.

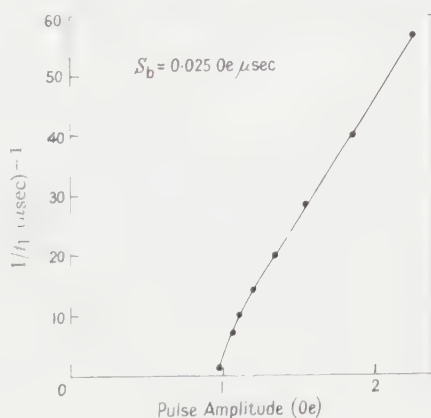


Fig. 6. Experimental plot of the reciprocal of the 'break free' time against field.

From Fig. 3 a curve of $1/t_b$ as a function of H was derived and has been plotted on Fig. 6. It may be seen that for moderate values of field the curve is linear. By analogy with the conventional expression

$$(H - H_0)\tau = S_w$$

a parameter S_b may be defined. S_b was found to be $0.025 \mu\text{sec Oe}$ which may be compared with a value of S_w of $1.25 \mu\text{sec Oe}$.

It would be of interest to investigate the change in magnetization produced by 1, 2, 3... n pulses, but as the subsequent argument will demonstrate quantitative results cannot be obtained because of the time constant of the circuit.

The self-inductance of the wound toroid is about $2.6\mu \times 10^{-9}\text{H}$ where μ is the permeability of the ferrite. The resistance of the associated circuit is 68Ω and so the time constant is $0.038\mu\text{nsec}$. The total permeability when the material is at a point on the steep side of the loop is of the order 10^4 , giving rise to a time constant of 380nsec which is generally longer than the duration of the applied pulses. On the other hand, when the material has attained equilibrium each pulse will drive it along the line B_1C_1 (Fig. 1) where the permeability is about 30, corresponding to a time constant of 1.2nsec . Thus only results obtained with a long series of pulses are meaningful since the time constant of the circuit under these conditions is known to be much less than the duration of the applied pulses.

An attempt will now be made to explain these experimental results on the basis of domain wall theory.

§ 4. THEORY

4.1. Elementary Considerations

Consider a 180° wall in a grain of the material, and suppose that inhomogeneities cause the domain wall energy E to be a function of the wall position z , the wavelength of the fluctuations being large compared with the wall thickness (Kersten 1938). E is assumed to be uniform throughout the wall, and the magnitudes of the maxima of dE/dz may be supposed to be distributed in a Gaussian manner about some mean value (Néel 1942, 1943). If there is no external field then the wall will rest in a position where E is a minimum. Let a slowly increasing field be applied; then the wall will move in a reversible manner until it reaches the point where dE/dz is a maximum, the field strength now being H_0 . As the field is further increased the wall will become unstable and move irreversibly until it encounters a region where dE/dz is sufficiently large to bring it to rest.

Suppose now, the wall again being in the zero field position, that a pulse field of magnitude H is applied. If the pulse is of very short duration then, although $H > H_0$, the wall may not have time to reach the place where dE/dz is a maximum before the pulse ends, when it will fall back to its equilibrium position. Again, if the drive field terminates when the wall is moving irreversibly in the region between the maximum of dE/dz and the maximum of E , then the wall will again fall back to its initial position. It is therefore important in this context to distinguish between two meanings of the word 'reversible'. It might be used to describe the state of the wall when it is possible to move it through a continuum of equilibrium positions, or alternatively it might merely imply that when the drive field ceases the wall reverts to its initial position. To avoid ambiguity the word will be used only in the first sense.

The mean time taken for a domain wall to travel between an initial position where E is a minimum to the nearest maximum of E may be correlated with the mean 'break free' time t_b defined earlier.

4.2. A Theoretical Derivation of the Break Free Time

Let us consider the dynamic behaviour of a single 180° wall traversing a cubic grain of the material, the applied field H being parallel to the wall. Following Kersten (1938) let the domain wall energy E vary sinusoidally with its displacement z so that

$$E = E_0 (1 - \cos 2\pi z/\lambda), \quad \dots\dots (1)$$

If the wall is moving with velocity $v = \dot{z}$ the forces acting upon it are: (a) that due to viscous damping, $\beta \dot{z}$, (b) that due to stiffness, $dE/dz = (2\pi E_0/\lambda) \sin 2\pi z/\lambda$, (c) that due to the applied field, $2HI_s$.

The equation of motion of the wall, which is assumed to have a negligible inertia, is then

$$\beta \dot{z} + (2\pi E_0/\lambda) \sin 2\pi z/\lambda = 2HI_s. \quad \text{..... (2)}$$

The critical field H_0 required to move the wall up to the maximum of dE/dz is given by

$$\begin{aligned} \{(2\pi E_0/\lambda) \sin 2\pi z/\lambda\}_{\max} &= 2H_0 I_s \\ 2H_0 I_s &= 2\pi E_0/\lambda. \end{aligned}$$

or

Eqn (2) may therefore be written

$$\beta \dot{z} + 2H_0 I_s \sin 2\pi z/\lambda = 2HI_s. \quad \text{..... (3)}$$

The break free time $t_{b,g}$, say, of this wall in a single grain may be obtained by integrating (3) from $t=0$ to $t=t_{b,g}$ and from $z=0$ to $z=\lambda/2$.

Writing $h = H_0/H$, for $h < 1$ we obtain

$$Ht_{b,g} = \frac{\beta\lambda}{2\pi I_s} \frac{1}{(1-h^2)^{1/2}} \left[\frac{\pi}{2} + \tan^{-1} \frac{h}{(1-h^2)^{1/2}} \right]$$

or

$$Ht_{b,g} = \frac{\beta\lambda}{2I_s} \Psi'(h), \text{ say.} \quad \text{..... (4)}$$

It will be noted that when $h \rightarrow 1$, $\Psi'(h) \rightarrow \infty$ and when the applied field is very large $h \rightarrow 0$ and $\Psi'(h) \rightarrow 0.50$, or

$$Ht_{b,g} = \frac{\beta\lambda}{2I_s} \cdot \frac{1}{2}. \quad \text{..... (5)}$$

(4) may be written as

$$\frac{1}{h} = \frac{\beta\lambda}{2I_s H_0} \Psi'(h) \frac{1}{t_{b,g}}. \quad \text{..... (6)}$$

($1/t_{b,g}$) in multiples of $2I_s H_0/\beta\lambda$ has been plotted against H/H_0 , i.e. $1/h$, in Fig. 7. For moderate field strengths the curve is very nearly linear, the reciprocal slope $S_{b,g}$ of the corresponding curve of $1/t_{b,g}$ against H being given by (5) above, i.e.

$$S_{b,g} = \frac{\beta\lambda}{2I_s} \cdot \frac{1}{2}. \quad \text{..... (7)}$$

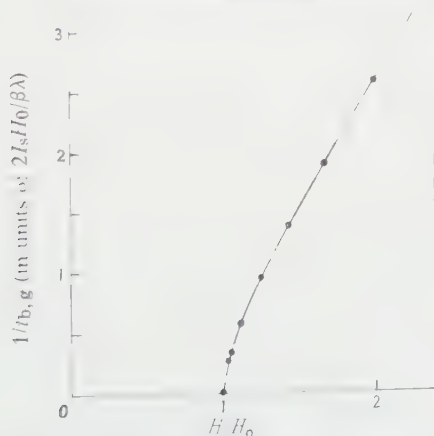


Fig. 7. A normalized theoretical curve of the reciprocal of the 'break free' time against field.

It may be seen that there is a close resemblance between the experimental and theoretical curves of Figs 6 and 7. It must be remembered though that Fig. 7 was obtained on the assumption that the magnetization was everywhere parallel to the field and that the wall energy varied sinusoidally with its position, but neither of these assumptions held for the actual sample.

It may be remarked here that the sinusoidal model of the variation of wall energy against displacement might be extended by considering it to be comprised of a number of half wavelengths of sine curves of different amplitudes and wavelengths, see for example Fig. 8. The magnitudes of the maxima of the wall energy gradients might be postulated to be distributed in a Gaussian mode about some mean value.

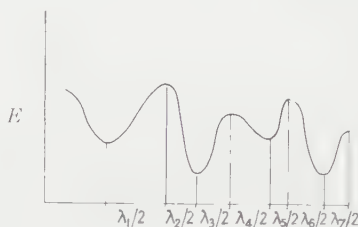


Fig. 8. Schematic variation of wall energy with wall position.

4.3. *A Theoretical Derivation of the Relationship $(H - H_0')\tau_g = S_{w, g}$*

The relationship will now be derived between the applied field and the time taken for a grain of material to reverse its magnetization. The theoretical relationship between this time and the reversal time of the polycrystalline assembly was given in I.

Suppose that in the course of a magnetization reversal the domain walls move a distance $n\lambda$ where n is an integer. The time τ_g taken for the wall to move through this distance is obtained by integrating (3) from $z = 0$ to $z = \lambda$ and multiplying by n .

Then

$$H\tau_g = \frac{\beta n\lambda}{2I_s} \frac{1}{(1 - h^2)^{1/2}}$$

or

$$\tau_g = \frac{\beta n\lambda}{2I_s H_0} \frac{h}{(1 - h^2)^{1/2}}. \quad \dots\dots (8)$$

From Eqn (8) a curve may be plotted of $1/\tau_g$ in multiples of $2I_s H_0/\beta n\lambda$ against H/H_0 (Fig. 9).

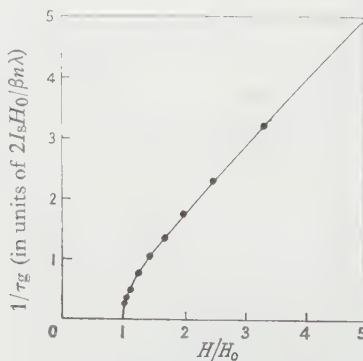


Fig. 9. A normalized theoretical curve of the reciprocal of the reversal time of a grain against field.

This curve closely resembles Fig. 7, and for moderate fields the corresponding curve of $1/\tau_g$ against H is of the conventional form:

$$\text{where} \quad (H - H_0')\tau_g = S_{w,g} \quad H_0' \simeq 0.4H_0 \quad \text{and} \quad S_{w,g} = \beta n\lambda/2I_s. \quad \dots\dots (9)$$

From Eqn (8) it is apparent that for a given value of h , e.g. under coincident current conditions here $h \simeq 0.5$, a material with a large coercive force, corresponding to a large value of H_0 , will switch faster than an otherwise identical material with a small coercive force. From Eqns (7) and (9) $S_{w,g}/S_{b,g} = 2n$.

To obtain theoretical values of S_w and S_b for a polycrystalline sample both $S_{w,g}$ and $S_{g,b}$ must be multiplied by the same averaging factors and hence S_w/S_b is also equal to $2n$.

Substituting the experimental values $S_w = 1.25 \mu\text{sec Oe}$ and $S_b = 0.025 \mu\text{sec Oe}$, n is found to be equal to 25, that is the domain wall traverses about 25 wall energy maxima in the course of a magnetization reversal. The application of an independent method, due to Neel (1942, 1943) for determining this ratio was described in II. It was stated that for a specimen of the same composition to that examined here, but of greater dimensions, a value for n (or $1/\alpha$) of 14 was found. This method has since been applied to a specimen nominally identical to that used in the pulse experiments and a value for n of 21 was obtained.

Thus there is quite good agreement between values yielded by two independent methods for the average number of wall energy maxima traversed by a domain wall during the course of magnetization reversal.

4.4. A Fuller Theoretical Description of the Behaviour of the Domain Walls

It is assumed that the wall energy fluctuates with wall position as described earlier and illustrated in Fig. 8.

In equilibrium the walls will rest at positions where E is a minimum. Suppose that pulses of magnitude H and duration t are applied. The behaviour of the individual walls will be governed by the magnitude H_0 of the field required to drive a wall over the first maximum of dE/dz , and by the duration of the applied pulse; there are three possibilities:

(i) Those walls for which $H < H_0$. A field of magnitude H can never move these walls irreversibly however long the pulses.

(ii) For other walls $H > H_0$ but the pulse duration is too short for the walls to reach the position where E is a maximum, i.e. $t < t_b$, and these walls will remain 'trapped'.

(iii) $H > H_0$ and $t > t_b$. These walls will break free and travel until either: (a) they reach a gradient for which $H < H_0$, i.e. become class (i) walls, (b) at the end of the pulse they will move, either forwards or backwards, to the nearest position where E is a minimum when all the possibilities (i), (ii) and (iii) will recur with the next pulse.

A great simplification is introduced if only those fields are considered which are sufficiently powerful to reverse the bulk of the magnetization if applied for a long period. In this case H is nearly always greater than H_0 , i.e. there will be a negligible number of class (i) walls.

The analysis is complicated by virtue of the fact that the distances λ between adjacent maxima of E (these regions will be referred to as valleys) are distributed about a mean value, and that the magnetization of the grains does not in general lie along the field direction. These possibilities will be considered separately.

Case I. It is assumed that the material consists of N grains, the magnetization in each lying along the field direction. Each grain contains M valleys, the widths of which are distributed about a mean value $\bar{\lambda}$. There is one domain wall per grain.

If a wall ceases its motion over a valley of width λ then when a pulse of duration t is applied from (5), for large values of H , the wall will be trapped if

$$Ht \leq \frac{\beta}{4I_s} \lambda. \quad \dots\dots (10)$$

The probability P that a wall ceases its motion in a valley of width less than or equal to λ depends on two factors: (a) the relative number of valleys of a given width, (b) the width λ of the valley.

If an appropriate distribution function is assumed P may, in principle, be calculated.

Thus for a given value of the product Ht the fraction of walls remaining untrapped at the end of each pulse is P , and the number of walls set in motion by the first pulse is NP , by the second pulse NP^2 and so on. The mean distance travelled by the walls is during the duration of each pulse approximately

$$\bar{d} = \frac{2I_s}{\beta} Ht.$$

After a number m of pulses have been applied, the walls remaining untrapped will have been driven across the grains and subsequent pulses will not produce any further change in the irreversible component of magnetization. The change in magnetization produced by m pulses is therefore $I_m \propto NdP(1 - P^m)/(1 - P)$ or $I_m \propto HtP(1 - P^m)/(1 - P)$. It will be noted that for a given value of Ht , P is a constant and so I_m is also a constant, in agreement with experiment.

Case II. The case where λ has everywhere the same value $\bar{\lambda}$ and where, as was assumed in I, the magnetization vectors all lie within a cone of semi-vertical angle $54^\circ 44'$ (or 55° say) will now be considered.

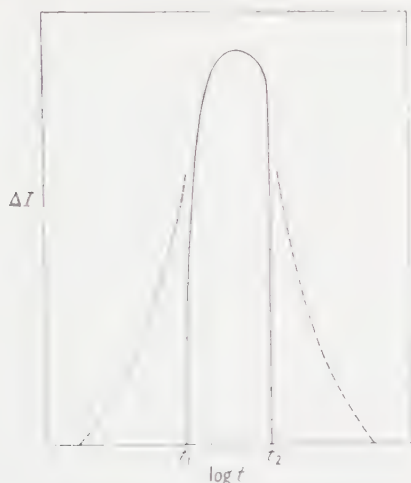
For those grains where the magnetization makes an angle θ with the field from (5)

$$t_{b,g}(\theta) = \frac{\beta\bar{\lambda}}{4I_s H \cos \theta} \quad 0 < \theta < 55^\circ. \quad \dots\dots (11)$$

The resolved component of the magnetization making an angle $\theta \rightarrow (\theta + \Delta\theta)$ with the field is given by $\Delta I/2$ where

$$\Delta I = \frac{2I_s \sin \theta \cos \theta}{1 - \cos 55^\circ} \Delta\theta. \quad \dots\dots (12)$$

Thus as the duration of the applied pulses is increased from zero, no change in magnetization is produced until the pulse duration is $t_1 = \beta\bar{\lambda}/4I_s H$ when those grains where the magnetization lies along the field direction will have their magnetization reversed. As the pulse duration is increased, grains where the magnetization makes successively larger angles with the field will switch until finally all grains will be switched when the pulse duration is $t_2 = \beta\bar{\lambda}/4I_s H \cos 55^\circ$. It will be noted that $t_2/t_1 \simeq 1.73$; thus explaining the invariance with field of the half-widths of the curves of Fig. 5. In fact the half-width was 1.9, which may be accounted for by the size distribution of the widths of the valleys and by the geometry of the toroidal sample. A curve of ΔI against $\log t$, plotted from Eqns (11) and (12), is shown in Fig. 10. The broken lines have been sketched in on the basis that the widths of the valleys all lie between 0 and $2\bar{\lambda}$. The scale of the ordinate is, of course, a function of the spacing of the curves comprising a set like those of Fig. 3; this fixes the value of $\Delta\theta$ to be used in (12)

Fig. 10. Theoretical curve of ΔI against pulse duration.

The curves of Fig. 3 were mostly obtained with pulse durations increasing in the ratio $\sqrt{2}:1$, and the corresponding maximum value of ΔI in Fig. 10 will now be estimated. From (12) the maximum value of ΔI occurs when $\theta = 45^\circ$. Let the pulse durations bracketing ΔI_{\max} be t_a and t_b .

$$\text{From (11),} \quad \frac{t_a}{t_b} = \frac{\cos \theta_b}{\cos \theta_a} = \sqrt{2}$$

or

$$\sqrt{2} = \frac{\cos(\pi/4 - \Delta\theta/2)}{\cos(\pi/4 + \Delta\theta/2)}, \quad \text{say.}$$

Hence $\Delta\theta/2 \approx 0.1715$.

From (12) the change in magnetization on increasing the pulse duration from t_b to t_a is $\Delta I_{\max} \approx 0.811 I_s$. For the sample $I_R \approx 0.75 I_s$, and so $\Delta I_{\max} \approx 1.1 I_R$. From Figs 3 and 5 it may be seen that this value is in good accord with experiment.

§ 6. DISCUSSION

Newhouse states that pulses of large amplitude can be applied without causing a permanent change in magnetization provided each pulse is followed by a pulse of opposite polarity at some arbitrary time afterwards; this was verified on the present equipment. This behaviour may be explained on the basis of the domain wall model. In general the valleys will not be symmetrical and whilst a domain wall may be 'trapped' if driven, say, to the right, it may be free if driven to the left with a similar pulse of opposite polarity. Obviously on average the converse will be equally true, and the observed behaviour will follow.

It is unfortunate that the time constant of the core and associated circuit is too long for satisfactory single pulse data to be obtained. It would be possible by changing the proportions of the core to decrease the time constant by a factor of three without decreasing the sensitivity of the apparatus, but this improvement would not be significant. A single 2-mm diameter core would have a maximum time constant under optimum conditions of 8 nsec, but the galvanometer sensitivity would have to be impracticably large.

ACKNOWLEDGMENTS

The author wishes to thank the management of Mullard Research Laboratories for permission to publish this paper, and Dr. K. Hoselitz, Dr. E. W. Gorter and Dr. F. W. Harrison for some valuable discussions. He is also indebted to Mr. P. Moore for advice concerning the pulse generator.

REFERENCES

- KERSTEN, M., 1938, *Probleme der technischen Magnetisierungs Kurve* (Berlin : Springer), summarized by STEWARD, K. H., 1954, *Ferromagnetic Domains* (Cambridge : University Press).
- KNOWLES, J. E., 1960, *Proc. Phys. Soc.*, **75**, 885.
- 1961, *Proc. Phys. Soc.*, **77**, 225.
- NÉEL, L., 1942, *Cah. Phys.*, **12**, 1.
- 1943, *Cah. Phys.*, **13**, 18.
- NEWHOUSE, V. L., 1957, *Proc. Inst. Radio Engrs, N.Y.*, **45**, 1484.
- SMIT, J., and WIJN, H. P. J., 1959, *Ferrites* (Eindhoven : Philips Technical Library), § 28.

Note added in proof.—A curve corresponding to Fig. 9 has been published by Rodbell and Bean in 1956.

RODBELL, D. S., and BEAN, C. P., 1956, *Phys. Rev.*, **103**, 886.

The Range-Energy Relation for High Energy μ -mesons

By F. ASHTON

Department of Physics, The University of Leeds

Communicated by J. G. Wilson; MS. received 8th September 1960

Abstract. The range-energy relation for μ -mesons with energies up to 1000 GeV has been studied by comparing the sea-level energy spectrum of cosmic rays with the underground depth-intensity curve. No significant divergence from accepted theory has been found.

§ 1. INTRODUCTION

THE difficulty of producing beams of high energy μ -mesons from accelerating machines means that experiments on the interactions of these particles are still in the province of cosmic rays. Fast μ -mesons interact with matter in a variety of ways and the individual types of interaction have been studied to some extent in various experiments. The comparatively low flux of the particles, particularly at high energies, has limited the accuracy of many of these experiments and further investigation is very desirable. The overall effect of the interactions can be examined by studying the relation between the range and energy of the particles. Such measurements can be made at low energies by stopping the μ -mesons in an absorber in the laboratory but above a few GeV the thickness of absorber becomes very large and an indirect method must be used.

One approach to this problem has been made recently by Dayon and Potapov (1959) and Ashton, Nash and Wolfendale (1959) who compared the momentum spectrum of μ -mesons underground with that at sea level. In this way energies up to the order of 15 GeV were studied. Higher energies can be studied by comparing the sea-level spectrum with the underground depth intensity curve and it is with these measurements that the present work is concerned.

§ 2. THE INTEGRAL SPECTRUM AND THE DEPTH-INTENSITY CURVE

A cosmic-ray spectrograph with a maximum detectable momentum of 1000 GeV/c has been constructed at Durham (near sea-level) and a preliminary measurement of the differential momentum spectrum of μ -mesons has been made (Ashton *et al.* 1960). This spectrum has been converted to an integral spectrum by numerical integration with the result shown in Fig. 1. At the energies under consideration there is no significant difference between energy and momentum so that a direct transformation from momentum to energy can be made.

Many workers have measured the rate of μ -mesons underground and George (1925) has collected the data for a wide range of depths. Barrett *et al.* (1952)

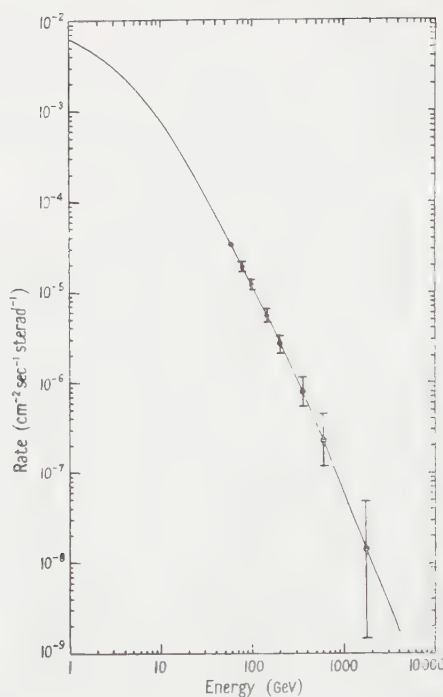


Fig. 1. The integral spectrum of μ -mesons at sea level.

have also made a similar survey for depths greater than 100 metres water equivalent (m.w.e.) below sea level. George and Barrett *et al.* have derived values for the vertical intensity by correcting the published rates for the angular distribution of particles and the effect of showers. The best estimate of the variation of vertical intensity with depth is shown in Fig. 2; the curve of George has been taken for depths between sea level and 100 m.w.e. and for greater depths that of Barrett *et al.* has been used. At great depths Barrett *et al.* had at their disposal some results of Bollinger (1951) and it is considered that the depth-intensity curve is well established down to 1900 m.w.e. Below this depth there is only the rather uncertain measurement of Miyazaki (1949) at 3000 m.w.e.

§ 3. THE THEORETICAL RANGE-ENERGY RELATION

The known energy loss processes for high energy μ -mesons are ionization and excitation, bremsstrahlung, electron pair production and nuclear interaction. George (1952) and Barrett *et al.* (1952) have evaluated the contributions from the various processes as a function of energy.

The processes will be considered in turn. Following Rossi and Greisen (1941), Barrett *et al.* (1952) and Greisen (private communication) the ionization energy loss process may be considered in two parts, large energy transfers (> 10 kev), in which the electron can essentially be considered as free, and small energy transfers (< 10 kev) in which the transition probability for the system formed by the primary particle and the atom as a whole must be considered. For a μ -meson of energy E and spin $\frac{1}{2}$, Bhabha (1938) and Massey and Corben

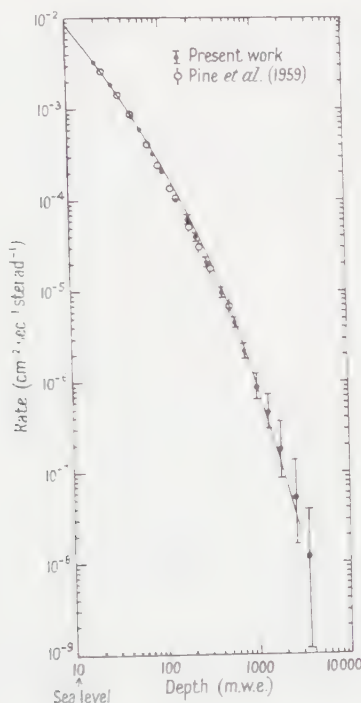


Fig. 2. Comparison of the predicted rates of μ -mesons underground (experimental points) with the best smooth curve through the measured rates.

(1939) give the probability per g cm^{-2} of producing an electron with energy E' to $E' + dE'$ as

$$\chi(E, E') dE' = \frac{2\mu_e}{\beta^2} \frac{\pi N(Z/A) r_0^2}{(E')^2} \left\{ 1 - \frac{\beta^2}{E_m'} + \frac{1}{2} \left(\frac{E'}{E + \mu} \right)^2 \right\} dE',$$

where μ_e , r_0 are the mass and classical radius of the electron and

$$E_m' = \frac{E^2}{(E + \mu^2 c^2 / 2\mu_e)}$$

is the maximum transferable energy. Using this equation the mean energy loss for energy transfers $E' > \eta$ is given by

$$K(>\eta) = \int_{\eta}^{E_m'} \chi(E, E') E' dE' \\ = 0.0766 \left\{ \ln \left(\frac{E_m'}{\eta} \right) - 1 + \frac{1}{4} \left(\frac{E_m'}{E + \mu} \right)^2 \right\} \text{MeV} (\text{g cm}^{-2})^{-1}$$

for $E \gg \eta$ and $\beta \simeq 1$.

The energy loss for energy transfers less than η has been calculated by Bethe (1930, 1932, 1937)

$$K(<\eta) = 0.0766 \left\{ \ln \left[\frac{2\mu_e \beta^2 \eta}{(1 - \beta^2) I^2(Z)} \right] - \beta^2 \right\} \text{MeV} (\text{g cm}^{-2})^{-1}$$

where $I(Z) = Z \times 13.5 \text{ eV}$. In the above equation the increase in energy transfer with energy is due to the relativistic increase of the electric field perpendicular to the direction of motion of the particle. For condensed materials the equation has to be modified since the increase of the electric field at large impact parameters

is opposed by the polarization of the medium. According to Fermi (1939, 1940) and Halpern and Hall (1940, 1948) the density correction Δ which must be subtracted from $K(<\eta)$ is given by

$$\Delta = \frac{2\mu_e \pi N Z r_0^2}{\beta^2 A} \left\{ \ln \left(\frac{\epsilon - 1}{1 - \beta^2} \right) - 1 \right\},$$

for $\beta > 1/\epsilon^{1/2}$, i.e. $E > 323$ Mev for μ -mesons, where ϵ is the equivalent dielectric constant of the medium.

$$\begin{aligned} \epsilon &= 1 + \frac{ZN\rho e^2}{A\pi\mu_e v_0^2} \quad \text{where } h\nu_0 = I(Z) \\ &= 1.06 \text{ for rock with } Z=10, \quad A=20, \quad \rho=1.9 \text{ g cm}^{-3}. \end{aligned}$$

Thus

$$\Delta = 0.0766 \left\{ \ln \left(\frac{0.06}{1 - \beta^2} \right) - 1 \right\} \text{ Mev (g cm}^{-2}\text{)}^{-1}$$

and

$$K(<\eta) - \Delta = 0.0766 \ln \left(\frac{2\mu_e \eta}{0.06 I^2(Z)} \right) \text{ Mev (g cm}^{-2}\text{)}^{-1}$$

for μ -mesons with $\beta \simeq 1$ i.e. $E > 1$ Gev. The total energy loss due to ionization and excitation is $K(<\eta) - \Delta + K(>\eta)$.

$$\left(\frac{dE}{dx} \right)_{\text{ionization}} = 1.51 + 0.0766 \left[\ln E_m' + \frac{1}{4} \left(\frac{E_m'}{E + \mu} \right)^2 \right] \text{ Mev (g cm}^{-2}\text{)}^{-1}.$$

The contribution to the energy loss due to bremsstrahlung, pair production and nuclear interaction have been taken from George (1952):

$$\left(\frac{dE}{dx} \right)_{\text{bremsstrahlung}} = 1.5 \times 10^{-7} E \left\{ \ln \left(\frac{E}{\mu c^2} \right) - 0.23 \right\} \text{ Mev (g cm}^{-2}\text{)}^{-1},$$

$$\left(\frac{dE}{dx} \right)_{\text{pair production}} = 1.6 \times 10^{-6} E \text{ Mev (g cm}^{-2}\text{)}^{-1},$$

$$\left(\frac{dE}{dx} \right)_{\text{nuclear}} = 5.0 \times 10^{-7} E \text{ Mev (g cm}^{-2}\text{)}^{-1},$$

where E is in Mev. The total energy loss for μ -mesons with $E > 1$ Gev is the sum of the four independent losses.

$$\begin{aligned} \frac{dE}{dx} &= 1.51 + 0.0766 \left\{ \ln E_m' + \frac{1}{4} \left(\frac{E_m'}{E + \mu} \right)^2 \right\} + 0.15 \times 10^{-6} E \left\{ \ln \left(\frac{E}{\mu c^2} \right) - 0.23 \right\} \\ &\quad + 2.1 \times 10^{-6} E \text{ Mev (g cm}^{-2}\text{)}^{-1}. \end{aligned}$$

The range-energy relation is best derived by splitting the region of integration of energy loss into two parts, above and below 1 Gev. Above 1 Gev the equation can be integrated directly. Below 1 Gev the most accurate result is derived from the calculations of Sternheimer (1959) who gives the range of a 1 Gev μ -meson in rock as 545 g cm^{-2} .

The result is

$$R = 545 + \int_1^E \left(1 / \frac{dE}{dx} \right) dE.$$

The integration has been performed numerically and the range-energy relation is shown in Fig. 3.

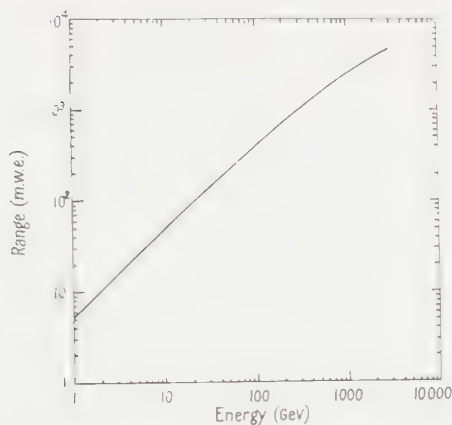


Fig. 3. The theoretical range-energy relation for μ -mesons.

§ 4. COMPARISON OF THE INTEGRAL SPECTRUM, THE RANGE-ENERGY RELATION AND THE DEPTH-INTENSITY CURVE

From the integral spectrum and the range energy relation the expected rates at various depths underground have been calculated and these are shown in Fig. 2 (closed circles). Bollinger (1951), by a Monte Carlo calculation, has shown that fluctuations in the range of high energy μ -mesons are not serious. The rates underground have been normalized so that the predicted rate at 40 m.w.e. below sea level is the same as the rate given by George at this depth. The justification for this normalization is that Ashton, Nash and Wolfendale (1959) measured the energy loss of μ -mesons reaching this depth and found that it was not inconsistent with that expected theoretically. The agreement between the measured rates and the expected rates is quite good although the measured rates at intermediate depths (~ 200 m.w.e.) are distributed a little above the predicted rates. More accurate measurements are required of both the sea-level spectrum and the depth-intensity curve to determine whether this effect is real. It is thus concluded that the energy loss of μ -mesons with energy up to 1000 GeV is close to that expected from theory. It is interesting to note that at 200 GeV the ionization and excitation loss contributes 80% of the total energy loss and at 1000 GeV 43%.

Recently Pine, Davisson and Greisen (1959) have performed a similar experiment at sea level with a spectrograph of maximum detectable momentum 175 GeV c and have reached a similar conclusion. The closeness of the results of the two experiments in the common energy region below 175 GeV is apparent from Fig. 2 where the experimental points of Pine *et al.* are also shown (open circles).

ACKNOWLEDGMENTS

The experimental work included in this paper was carried out in the Physics Department of the Durham Colleges in the University of Durham. The author would like to thank Professor G. D. Rochester for the facilities of his laboratory and Dr. A. W. Wolfendale of Durham for constant advice and encouragement. He would also like to thank Professor K. Greisen of Cornell University for helpful correspondence.

REFERENCES

- ASHTON, F., BROOKE, G., GARDENER, M., HAYMAN, P. J., JONES, D. G., KISDNASAMY, S., LLOYD, J. L., TAYLOR, F. E., WEST, R. H., and WOLFENDALE, A. W., 1960, *Nature, Lond.*, **185**, 364.
- ASHTON, F., NASH, W. F., and WOLFENDALE, A. W., 1959, *Proc. Roy. Soc. A*, **253**, 163.
- BARRETT, P. H., BOLLINGER, L. M., COCCONI, G., EISENBERG, Y., and GREISEN, K., 1952, *Rev. Mod. Phys.*, **24**, 133.
- BETHE, H., 1930, *Ann. Phys.*, **5**, 325.
- 1932, *Z. Phys.*, **76**, 293.
- 1937, *Rev. Mod. Phys.*, **9**, 245.
- BHABHA, H. J., 1935, *Proc. Roy. Soc. A*, **152**, 559.
- 1938, *Proc. Roy. Soc. A*, **164**, 257.
- BOLLINGER, L. M., 1951, *Ph.D. Thesis*, Cornell University.
- DAYON, M. I., and POTAPOV, L. I., 1959, *J. Exp. Theor. Phys.*, **36**, 697.
- FERMI, E., 1939, *Phys. Rev.*, **56**, 1242.
- 1940, *Phys. Rev.*, **57**, 485.
- GEORGE, E. P., 1952, *Progress in Cosmic Ray Physics*, Vol. I (ed. J. G. Wilson), (Amsterdam: North-Holland), p. 395.
- HALPERN, O., and HALL, H., 1940, *Phys. Rev.*, **57**, 460.
- 1948, *Phys. Rev.*, **73**, 477.
- MASSEY, H. S. W., and CORBEN, H. C., 1939, *Proc. Camb. Phil. Soc.*, **35**, 463.
- MIYAZAKI, Y., 1949, *Phys. Rev.*, **76**, 1733.
- PINE, J., DAVISSON, R. J., and GREISEN, K., 1959, *Nuovo Cim.*, **14**, 1181.
- ROSSI, B., and GREISEN, K., 1941, *Rev. Mod. Phys.*, **13**, 240.
- STERNHEIMER, R. M., 1959, *Phys. Rev.*, **115**, 137.

Scattering Cross Sections of Gamma Radiation

By V. LAKSHMINARAYANA AND S. JNANANANDA

Laboratories for Nuclear Research, Andhra University, Waltair, India

MS. received 7th June 1960, in revised form 20th September 1960

Abstract. Total cross sections of gamma rays from sources cobalt 60, scandium 46, caesium 137, chromium 51 and cerium 141 in the elements graphite, aluminium and copper are determined, using a scintillation spectrometer of good figures of merit and modified narrow beam geometry. The values of total scattering cross section are obtained by subtracting the theoretical values of photoelectric and pair cross sections from the total experimental values. For energies greater than 320 kev good agreement is observed between theoretical and experimental values of total scattering cross section, while at the energy 145 kev definite deviations are observed. The deviations are ascribed to the over-estimation of total scattering cross section by the use of atomic charge distribution predicted by the Thomas-Fermi model.

§ 1. INTRODUCTION

THE passage of gamma radiation through matter is characterized by an exponential decrease in its intensity. A large number of processes (Fano 1953) are operative in the interaction of gamma radiation with matter, resulting in intensity attenuation. Of these, 'scattering' is of special interest inasmuch as it is one of the main processes of interaction in the low energy region. Electronic scattering with (incoherent) or without (coherent) energy change forms a large part of this interaction, the nuclear scattering probability (cross section) being of much smaller magnitude.

The cross section for incoherent scattering (Compton scattering) is represented by the well-known Klein-Nishina (1929) formula, applicable to the case of a free electron. An electron in the atom can be considered free if the momentum transfer q to the electron greatly exceeds the momentum of the electron motion within the atom. If this condition be not fulfilled, Compton scattering will be complicated by the binding effects and become less frequent than that predicted by the Klein-Nishina formula. In such cases this expression is to be multiplied by the incoherent scattering function $S(q, z)$ which takes up a value of unity at high energies and decreases to zero at low energies. Thus the differential cross section for incoherent scattering $(d\sigma/d\Omega)_{\text{incoh}}$ in a direction θ , by the z electrons of an atom is given by

$$\left(\frac{d\sigma}{d\Omega}\right)_{\text{incoh}} = \frac{zr_0^2}{2} \left[1 + \frac{h\nu}{mc^2}(1 - \cos\theta)\right]^{-2} \left\{1 + \cos^2\theta + \frac{(h\nu/mc^2)^2(1 - \cos\theta)^2}{1 + (h\nu/mc^2)(1 - \cos\theta)}\right\} S(q, z) \quad \dots\dots(1)$$

where $r_0 = e^2/mc^2$ is the classical electron radius and $h\nu/mc^2$ the incident photon energy in units of electron rest energy.

Differential cross section for coherent (Rayleigh) scattering can similarly be written as

$$\left(\frac{d\sigma}{d\Omega}\right)_{\text{coh}} = \frac{r_0^2}{2} (1 + \cos^2 \theta) [F(q, z)]^2 \quad \dots\dots (2)$$

where $F(q, z)$, the atomic form factor, is somewhat complementary to $S(q, z)$ in that it represents the probability that the z electrons of an atom take up the recoil momentum without absorbing any energy. The total scattering cross section can be obtained by adding Eqns (1) and (2) for various angles θ , and then making a numerical integration.

Values of $F(q, z)$ and $S(q, z)$ depend on the assumed type of charge distribution within an atom. Several types of charge distributions have been proposed, but the one proposed by Thomas (1926) and Fermi (1928) is most frequently used. Grodstein (1957) used the values computed with this distribution in his evaluation of the total scattering cross sections for various elements over a wide range of energies. However, this type of charge distribution is found to be very approximate. Evaluation of coherent scattering cross sections by more exact methods has received great attention (Brown, Peierls and Woodward 1954, Brenner, Brown and Woodward 1954, Brown and Mayers 1956, 1957) in recent years in efforts to study Delbruck scattering. These exact calculations as well as recent experimental studies (Bernstein and Mann 1958) have shown that the values of coherent scattering cross sections are over-estimated in the computations using form factor formalism. It is therefore considered useful to obtain some experimental data on scattering cross sections for comparison with the values obtained by methods outlined above.

§ 2. METHOD

(a) *Experimental.* The simplest method for obtaining the scattering cross section is to determine the total cross section and subtract from it all other contributions determined theoretically. To obtain good accuracy in this procedure the subtracted contribution should be amenable to accurate computation. Thus a low energy region (0.145 to 1.33 Mev) is selected in the present investigation on light elements.

(b) *Theoretical.* To evaluate the total cross section it is assumed that only three interaction processes, photoelectric absorption, scattering and pair production, are operative in the chosen energy region.

For energies of 320 and 145 keV the photoelectric cross sections are obtained by the evaluation of K shell cross sections using the Heitler (1936) non-relativistic formula combined with the Stobbe (1930) correction factor and correcting for the contribution of L and M shells, using the ratios of $\Gamma_{(K+L+M)}/\Gamma_K$ given by White (1952). For all other energies the photoelectric cross sections are obtained by interpolation from a smooth curve drawn on a large graph sheet using the values of total cross sections from Grodstein's tables.

For energies greater than 662 keV the scattering in light elements is completely incoherent. Consequently the values of cross sections at these energies are computed, using the Klein-Nishina formula for free electrons. For energies of 320 and 145 keV the total scattering cross sections are obtained by interpolation from a smooth curve of the data given in Grodstein's tables.

Pair cross sections are calculated for 1.119 and 1.332 MeV using Hough's approximate formula (1948) for energies less than $4.2 mc^2$. These Born approximation values K_B are corrected using the z dependence formula $K_{NB} = K_B (1 + az^2)$ to obtain the non-Born values. The value of the constant a for

1.332 mev is taken from West's (1956) data. For 1.119 mev the Born value is retained since the value of a is not available. Since the absolute magnitude of cross section is quite small at this energy, retention of the Born value will not affect the total cross section.

Partial cross sections obtained as outlined above, are added to give the total cross section and are included in Table 1. Errors in total cross section, thus computed, may not exceed 3 to 5%. For energies of 320 and 145 kev the photoelectric cross sections computed from the non-relativistic formula should yield good accuracy, since the approximations made in obtaining the formula are valid for low z materials. At higher energies, since the values are obtained by interpolation, the accuracy is rather small and may give an error of about 2%. For energies greater than 662 kev the scattering cross section should be accurate to within 1%, the accuracy increasing with increase in energy. For energies of 320 and 145 kev the accuracy of total scattering cross section may be to within about 2%. Errors in pair cross section may be of the order of 2%. But the errors in pair cross section are not likely to interfere with the overall accuracy since the absolute magnitudes are small at the present energies.

Table 1. Total Cross Sections of Gamma Rays (barns per atom)

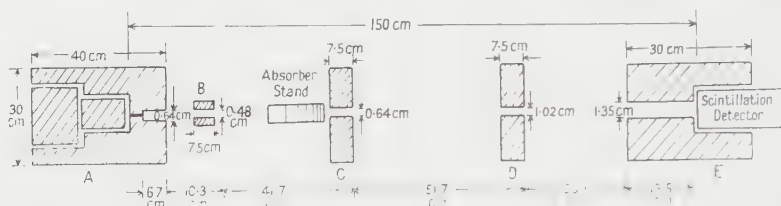
Energy (mev)	Elements	Graphite	Aluminium	Copper
1.332	Exptl	1.10 ± 0.01	2.37 ± 0.01	5.34 ± 0.02
	Theor.	1.10	2.37	5.35
1.119	Exptl	1.19 ± 0.01	2.58 ± 0.02	5.82 ± 0.02
	Theor.	1.20	2.60	5.83
0.662	Exptl	1.54 ± 0.01	3.35 ± 0.02	7.56 ± 0.04
	Theor.	1.54	3.33	7.61
0.320	Exptl	2.02 ± 0.01	4.47 ± 0.03	11.06 ± 0.03
	Theor.	2.05	4.56	11.24
0.145	Exptl	2.62 ± 0.02	5.87 ± 0.02	22.52 ± 0.10
	Theor.	2.74	6.29	25.26

§ 3. EXPERIMENTAL DETAILS

Total cross sections for gamma rays are usually determined by simple transmission experiments with a narrow beam geometry. Most of the earlier workers used Geiger-Muller counters for the detection of gamma rays. But they have several disadvantages for the detection of gamma radiation inasmuch as they have very small efficiency and are not energy selective. Colgate (1952) was the first to employ an energy selective scintillation detector but his instrument does not seem to have adequate resolution (as can be noted from the necessity for making a correction for the low energy gamma rays included in the high energy peak of cobalt 60 source). Colgate reported a deviation of the total experimental cross section from the theoretical values and ascribed it to the insufficiency in the theoretical photoelectric cross section. Howland and Kreger (1954), however,

obtained experimental values of the cross section which are in agreement with the theoretical values by proper positioning of the absorber to make the cross section a maximum.

In the present investigation a scintillation spectrometer of good figures of merit was employed as a detector in a modified geometrical set up. The geometrical arrangement of the collimator system employed is shown in the Figure. The changes in this arrangement from that adopted by Davisson and Evans (1952) were made primarily to make the solid angle so small that the cross section is more or less insensitive to absorber positioning. Various contrivances were provided to effect accurate collimation by an optical method. A scintillation spectrometer of high stability and high efficiency was assembled for use as detector. The stability was tested and found adequate for the purpose. The linearity was tested by plotting a number of spectra and was found to be quite satisfactory.



Graphite, aluminium and copper were used as absorbers. They were obtained in highly pure form (purity greater than 99.9%) and machined to diameters of $\frac{3}{4}$ in. and cut into pieces of required lengths with a high degree of precision. The thickness of each one of these absorbers was measured to an accuracy better than 0.1%. Sources of ^{60}Co , ^{46}Sc , ^{137}Cs , ^{51}Cr and ^{141}Ce used in the present investigation were obtained either from Harwell or Amersham. All the sources (except ^{137}Cs) were obtained in the standard radiographic capsules with groove dimensions of 4 mm \times 4 mm. ^{137}Cs was obtained in the standard form (CDCC5), the active pellet dimensions being of the order of 3 mm \times 3 mm and the activity 5 mc. The activity of each one of the other sources was about 10 mc.

Simple transmission experiments were conducted to obtain total cross sections. Photopeak of the spectrum of the required energy was accepted symmetrically in the channel. Count rates were taken with progressive increase of absorber thicknesses. The best estimate of the linear attenuation coefficient μ , was obtained by the method of least squares employing the formula

$$\mu = \ln 10 \sum_{r=1}^K x_r \log \left(\frac{N_0}{N_r} \right) / \sum_{r=1}^K x_r^2 \quad \dots\dots (3)$$

where N_0 is the direct count rate and N_r is the count rate with an absorber of thickness x_r . The experimental uncertainties involved were mainly due to statistical errors. Sufficiently large counting periods were adopted to ensure that these errors did not exceed 0.5%. Each experimental run was repeated eight times and the mean values $\bar{\mu}$ and standard deviations were computed. The atomic cross sections were determined from these values and included in Table 1 together with the theoretical values.

Corrections were made for the counting losses in the system due to finite resolution and for the radiation scattered at small angles in the absorber and included in the detector, the maximum angle of scattering contributing to this effect being 55' 40".

§ 4. RESULTS

It can be observed from the data given in Table 1 that the agreement is good for energies greater than 662 kev and deviations become noticeable at lower energies. At 320 kev the agreement can be taken as within the limits of combined error of theory and experiment. The sum of photoelectric and pair cross sections (theoretically computed) is subtracted from the total experimental value and the results are compared with the theoretically expected values of total scattering cross sections. This information is furnished by Table 2.

Table 2. Scattering Cross Sections (barns per atom)

Graphite

(1)	(2)	(3)	(4)	(5)	(6)
1.332	1.10 ± 0.01	0.001	1.009 ± 0.01	1.10 ± 0.005	-0.1 ± 1.4
1.119	1.19 ± 0.01	—	1.19 ± 0.01	1.20 ± 0.006	-0.8 ± 1.3
0.662	1.54 ± 0.01	—	1.54 ± 0.01	1.54 ± 0.015	0.0 ± 1.7
0.320	2.02 ± 0.01	—	2.02 ± 0.01	2.05 ± 0.040	-1.5 ± 2.4
0.145	2.62 ± 0.02	—	2.62 ± 0.02	2.74 ± 0.056	-4.4 ± 2.6

Aluminium

(1)	(2)	(3)	(4)	(5)	(6)
1.332	2.37 ± 0.01	0.003	2.367 ± 0.01	2.37 ± 0.01	-0.1 ± 0.9
1.119	2.58 ± 0.02	—	2.58 ± 0.02	2.60 ± 0.01	-0.8 ± 1.2
0.662	3.35 ± 0.02	—	3.35 ± 0.02	3.33 ± 0.03	$+0.1 \pm 1.5$
0.320	4.47 ± 0.03	0.02 ± 0.0002	4.45 ± 0.03	4.54 ± 0.09	-2.0 ± 2.7
0.145	5.87 ± 0.02	0.24 ± 0.004	5.63 ± 0.02	6.06 ± 0.12	-7.1 ± 2.5

(1) Energy (mev); (2) present experimental value; (3) theoretical sum (pair + photoelectric); (4) column (2) - column (3); (5) theoretical value of scattering cross section; (6) percentage deviation.

It can be seen from this table that the agreement is good for energies greater than 662 kev. At these energies for both aluminium and graphite the scattering is completely incoherent. Thus it can be concluded that the Klein-Nishina formula accurately predicts the values of scattering cross sections for free electrons. The agreement is not quite so good at 320 kev, while definite deviations do exist at 145 kev. At such low energies the contribution due to coherent scattering and binding effects in incoherent scattering become appreciable. This fact evidently shows that the values of $S(q, z)$ and $F(q, z)$ are over-estimated in their computation using Thomas-Fermi atomic charge distribution.

The magnitudes of deviation observed at 145 kev are high and at least a part of it must be ascribed to the dilution effect of high energy gamma rays emitted by impurities present in the source. The effect of such dilution can only account for a small part of the observed deviation since the intensities of these high energy gamma rays are not significantly high. Thus a large part of the deviation has to be ascribed to the over-estimation of the total scattering cross section as mentioned above.

ACKNOWLEDGMENTS

The authors wish to express their thanks to the Department of Atomic Energy, Government of India, for sponsoring this scheme of work and the award of a Senior Research Assistantship to one of them (V. L. N.)

REFERENCES

- BERNSTEIN, A. M., and MANN, A. K., 1958, *Phys. Rev.*, **110**, 805.
BRENNER, S., BROWN, G. E., and WOODWARD, J. B., 1954, *Proc. Roy. Soc. A*, **227**, 59.
BROWN, G. E., and MAYERS, D. F., 1956, *Proc. Roy. Soc. A*, **234**, 387.
—— 1957, *Proc. Roy. Soc. A*, **242**, 89.
BROWN, G. E., PEIERLS, R. E., and WOODWARD, J. B., 1954, *Proc. Roy. Soc. A*, **227**, 51.
COLGATE, S. A., 1952, *Phys. Rev.*, **87**, 592.
DAVISSON, C. M., and EVANS, R. D., 1952, *Rev. Mod. Phys.*, **24**, 79.
FANO, U., 1953, *Nucleonics*, **11**, 8, 55.
FERMI, E., 1928, *Z. Phys.* **48**, 73.
GRODSTEIN, G. W., 1957, *National Bureau of Standards Circular* 583.
HEITLER, W., 1936, *The Quantum Theory of Radiation* (London: Oxford University Press).
HOUGH, P. V. C., 1948, *Phys. Rev.*, **73**, 266.
HOWLAND, P. R., and KREGER, W. E., 1954, *Phys. Rev.*, **95**, 407.
KLEIN, O., and NISHINA, Y., 1929, *Z. Phys.*, **52**, 853.
STOBBE, M., 1930, *Ann. Phys., Lpz.*, **7**, 661.
THOMAS, L. H., 1926, *Proc. Camb. Phil. Soc.*, **23**, 542.
WEST, H. I., JR, 1956, *Phys. Rev.*, **101**, 915.
WHITE, G. R., 1952, *National Bureau of Standards Report* No. 1003.

The Isobaric Triplets in the Nuclear 2p-shell and the Charge Independence of Nuclear Forces

By W. M. FAIRBAIRN

Department of Mathematics, The College of Science and Technology, Manchester

MS. received 11th July 1960

Abstract. The positions of the lowest lying $T=1$ levels in the 2p-shell nuclei with $T_3=0$ are calculated from the experimental positions of the ground states of the nuclei with $T_3=-1$ and the energy differences between the ground states of the nuclei with $T=\frac{1}{2}$. Coulomb forces are considered as a perturbation in the shell model and it is shown that, apart from small terms which depend on symmetry, the method is equivalent to that used by Wilkinson (1956). The corrections due to symmetry are of the same order of magnitude as the significant differences which Wilkinson found between the experimental and the calculated positions of the $T=1$, $T_3=0$ levels, and when these corrections are included the differences are no longer significant. The energy shift due to the charge dependence of nuclear forces caused by the pion mass difference is calculated and is shown to be appreciable. There is good agreement between theory and experiment for the isobars with $A=14$.

§ 1. INTRODUCTION

THE evidence in favour of charge independence of the specifically nuclear force is slight in comparison with the amount of evidence which supports the less restrictive conditions of charge symmetry. The evidence obtained from low and medium energy nuclear reactions is difficult to analyse since most of the intermediate states which are involved are in regions where there can be much mixing of isotopic spin states by the Coulomb forces. Other evidence comes from the energy levels of isobaric multiplets, in particular, the low-lying levels in isobaric triplets with atomic number $A \approx 40$. The qualitative agreement between the positions of these levels and their expected positions assuming charge independence is well established (Burcham 1955). A quantitative comparison has been made by Wilkinson (1956, all references in the present paper to Wilkinson's results are to this paper). Wilkinson concluded that the quantity Δ , which denotes the difference between the calculated and the experimental values of the position of the lowest $T=1$ level in nuclei with $T_3=0$, was significantly positive, at least in the nuclear 2p-shell. He showed that the calculated positions were on the average 35 keV higher than those determined experimentally and he explained this discrepancy by a 1% departure from charge independence.

In this paper we investigate the effect on the values of Δ when account is taken of the symmetry of the nuclear wave function. The next section is devoted to obtaining formulae for the theoretical Coulomb energies and energy differences of the nuclei in the 2p-shell. In §3 we use these formulae to discuss the effect of including symmetry in Wilkinson's methods, and in §4 we estimate the corrections to the values of Δ which he obtained. These corrected values are discussed in §5 where it is shown that they are no longer significantly positive.

Another charge dependent force between nucleons is that due to the difference between the masses of the neutral and the charged pions (Blin-Stoyle and Kearsley 1960). The effect on the calculated positions of the energy levels of this departure from charge independence is discussed in §6 where it is found that there are still discrepancies between the calculated and the experimental positions of the levels with $T=1$ and $T_3=0$. This may be due to our assumption of states with maximum symmetry in L - S coupling for the 2p-shell nuclei.

§ 2. THEORETICAL COULOMB ENERGIES

If nuclear forces are charge independent and if Coulomb forces are neglected a particular state of the nucleus with atomic number A and spin J can be characterized also by its isobaric spin T and third component T_3 . The isobaric spin vector \mathbf{T} for the nucleus is related to the isobaric spin vectors $\boldsymbol{\tau}_i = (\tau_{1i}, \tau_{2i}, \tau_{3i})$, $i=1, 2, \dots, A$, of its constituent nucleons by

$$\mathbf{T} = \frac{1}{2} \sum_{i=1}^A \boldsymbol{\tau}_i.$$

Similarly
$$T_3 = \frac{1}{2} \sum_{i=1}^A \tau_{3i} = \frac{1}{2}(A - 2Z),$$

where $-Ze$ is the nuclear charge. To this approximation the various energy levels of the nucleus can be labelled by A, J, T and T_3 , all of these being good quantum numbers.

When Coulomb and other charge dependent interactions are included in the nuclear Hamiltonian the isobaric spin T of a nuclear level is no longer a good quantum number. These interactions mix in states with values of T different from that given by a charge independent Hamiltonian and they also cause a shift in the energy of the levels: the energy shifts will be calculated by first-order perturbation theory since the charge dependent interactions are a very small part of the total nuclear Hamiltonian. Thus the energy shifts are given by the matrix elements $\langle AJTT_3 | H_{\text{pert}} | AJTT_3 \rangle$.

The nuclear states $|AJTT_3\rangle$ will be chosen as shell model states for which L, S and the symmetry $[\alpha]$ are also good quantum numbers: that is, we shall assume L - S coupling since only the lighter nuclei will be considered. The energy shifts are obtained for states characterized by A, T, T_3, L, S and $[\alpha]$. In this section H_{pert} is chosen to be the Coulomb interaction H_c but in §6 a different charge dependent interaction will be considered.

Using the isobaric spin formalism $H_c = \sum_{i < j} H_c(ij),$

where
$$H_c(ij) = \sum_{t=0}^2 a_t T_t(ij) e^2 / r_{ij} \\ = \{T_0(ij) - T_1(ij) + \sqrt{\frac{2}{3}} T_2(ij)\} e^2 / r_{ij}$$

is the Coulomb interaction between two nucleons: r_{ij} is the distance between the two nucleons,

$$T_0(ij) = 1 + \frac{1}{3}(\boldsymbol{\tau}_i \cdot \boldsymbol{\tau}_j), \quad T_1(ij) = \tau_{3i} + \tau_{3j}, \quad \text{and} \quad T_2(ij) = \{3\tau_{3i}\tau_{3j} - \boldsymbol{\tau}_i \cdot \boldsymbol{\tau}_j\} / \sqrt{6}.$$

The first-order energy shift due to the Coulomb interaction is

$$\langle AJTT_3 | H_c | AJTT_3 \rangle \quad \dots\dots (2.1)$$

and will be denoted by $E_c(AJTT_3)$.

Since the transformation properties of the $T_i(ij)$ are known the method of Elliott (1953) can be used to express (2.1) in terms of two-particle matrix elements. This reduction gives

$$E_c(A|TT_3) = e^2 \frac{1}{2} (A-1) \sum \langle (A-1) | T T T | (A-2) T'' : (2) L_2 [\gamma_2] T_2 \rangle^2 \\ \times \sum_{t, t_2} a_t C_{TT_3 0}^{TT_3} U(T'' T T_2 t; T_2 T) \langle T_2 - T_i(12) \| T_2 \rangle \langle L_2 [\gamma_2], r_{ij}^{-1} \| L_2 [\gamma_2] \rangle, \quad \dots (2.2)$$

where $\langle (A) | (A-2) : (2) \rangle$ is the fractional parentage coefficient for removing two particles from the state with A particles, the symbols $\langle . \| . \rangle$ denote reduced matrix elements, C and U are Clebsch-Gordan vector coupling coefficients and U -functions (Jahn 1951) respectively. The first summation is over all the states of the two particles and of the $A-2$ particles which are allowed by the fractional parentage coefficients. When $T_2=0$ $\langle T_2 \| T_i(12) \| T_2 \rangle = 0$ for all t , and thus the contributions to the Coulomb energy of the nucleus come only from two-particle states with $T_2=1$. The corresponding reduced matrix elements are $\langle T_2=1 \| T_0(12) \| T_2=1 \rangle = \frac{4}{3}$; $\langle T_2=1 \| T_1(12) \| T_2=1 \rangle = 2\sqrt{2}$; $\langle T_2=1 \| T_2(12) \| T_2=1 \rangle = 2(5/3)^{1/2}$.

If a shell model configuration is assumed for the nuclear state the expression (2.2) can be simplified further. Let the state be described by the configuration $(1s)^4(2p)^{[x]} L S T J$, where $A = m + 4$. Using the symbol m to include the quantum numbers $[x] L S (J)$ the Coulomb energy is

$$E(m|TT_3) = e^2 F_0(1s, 1s) + m e^2 \{ F_0(1s, 2p) - \frac{1}{6} G_1(1s, 2p) \} \\ - m e^2 \{ F_0(1s, 2p) - \frac{1}{6} G_1(1s, 2p) \} \sqrt{3} C_{TT_3 0}^{TT_3} \sum_{(m-1)} U(T' T_2' 1; \frac{1}{2} T) \\ \times \langle (m) T | (m-1) T' : (1) \rangle^2 \\ + \frac{1}{8} m(m-1) e^2 \sum_{(m-2), (2)} \{ F_0(2p, 2p) + \frac{6}{5} (-1)^{L_2} W(1111; L_2 2) F_2(2p, 2p) \} \\ - \frac{1}{4} m(m-2) \sqrt{2} C_{TT_3 0}^{TT_3} U(T'' T 11; 1 T) + \frac{2\sqrt{10}}{3} C_{TT_3 0}^{TT_3} U(T'' T 12; 1 T) \\ \times \langle (m) T | (m-2) T'' : (2) L_2 T_2 = 1 \rangle^2, \quad \dots (2.3)$$

where F_k and G_k are the Slater integrals for the Coulomb potential r_{ij}^{-1} and the Racah W -functions are related to the U -functions by

$$U(abcd; ef) = (2e+1)^{1/2} (2f+1)^{1/2} W(abcd; ef).$$

The symbols $\langle (m) | (m-1) : (1) \rangle$ are the fractional parentage coefficients for removing one 2p-particle from the state with m 2p-particles and are tabulated by Jahn and van Wieringen (1951); the symbols $\langle (m) | (m-2) : (2) \rangle$ are the fractional parentage coefficients for removing two 2p-particles (in the state defined by L_2 and T_2) from the state with m 2p-particles and are tabulated by Elliott, Hope and Jahn (1953). These coefficients satisfy the following relationships:

$$m \sum_{(m-1)} (-1)^{T'-T+1/2} (2T'+1)^{-1} \langle (m) T | (m-1) T' : (1) \rangle^2 = 1, \\ m(m-1) \sum_{(m-2), (2)} \langle (m) T | (m-2) T'' : (2) T_2 = 1 \rangle^2 = \frac{1}{4} \{ 3m(m-2) + 4T(T+1) \}, \\ m \sum_{(m-2), (2)} U(T'' T 11; 1 T) \langle (m) T | (m-2) T'' : (2) T_2 = 1 \rangle^2 = \{ 2T(T+1) \}^{1/2}, \\ m(m-1) \sum_{(m-2), (2)} U(T'' T 12; 1 T) \langle (m) T | (m-2) T'' : (2) T_2 = 1 \rangle^2 \\ = \{ (2T-1) 2T(T+1)(2T+3) \}^{1/2} / 5^{1/2}.$$

When these results and the normalization properties of the fractional parentage coefficients are used formula (2.3) gives the following expressions for the Coulomb energy $E_c(mTT_3)$:

$$\begin{aligned}
 (a) \quad E_c(m, \tfrac{1}{2}, \pm \tfrac{1}{2}) &= e^2 F_0(1s, 1s) + (m \mp 1) e^2 \{F_0(1s, 2p) - \tfrac{1}{6} G_1(1s, 2p)\} \\
 &\quad + \tfrac{1}{8} (m-1)(m-1 \mp 2) e^2 F_0(2p, 2p) \\
 &\quad + \tfrac{1}{5} m(m-1) e^2 F_2(2p, 2p) \sum_{(m-2), (2)} \{1 \mp 3W(T'' \tfrac{1}{2} 11; 1 \tfrac{1}{2})\} (-1)^{L_2} W(1111; L_2 2) \\
 &\quad \times \langle (m) | (m-2) T'' : (2) L_2 T_2 = 1 \rangle^2, \\
 (b) \quad E_c(m, 1, 0) &= e^2 F_0(1s, 1s) + m e^2 \{F_0(1s, 2p) - \tfrac{1}{6} G_1(1s, 2p)\} \\
 &\quad + \tfrac{1}{8} m(m-2) e^2 F_0(2p, 2p) \\
 &\quad + \tfrac{1}{5} m(m-1) e^2 F_2(2p, 2p) \sum_{(m-2), (2)} \{1 - 3W(T'' 112; 11)\} (-1)^{L_2} W(1111; L_2 2) \\
 &\quad \times \langle (m) | (m-2) T'' : (2) L_2 T_2 = 1 \rangle^2, \\
 (c) \quad E_c(m, 1, \pm 1) &= e^2 F_0(1s, 1s) + (m \mp 2) e^2 \{F_0(1s, 2p) - \tfrac{1}{6} G_1(1s, 2p)\} \\
 &\quad + \tfrac{1}{8} (m \mp 2)(m-2 \mp 2) e^2 F_0(2p, 2p) \\
 &\quad + \tfrac{1}{10} m(m-1) e^2 F_2(2p, 2p) \sum_{(m-2), (2)} \{2 \mp 9W(T'' 111; 11) + 3W(T'' 112; 11)\} \\
 &\quad \times (-1)^{L_2} W(1111; L_2 2) \langle (m) | (m-2) T'' : (2) L_2 T_2 = 1 \rangle^2. \\
 &\quad \dots\dots (2.4)
 \end{aligned}$$

These five expressions show that the Coulomb energy of the state $(1s)^4(2p)^m$ depends on the quantum numbers $[\alpha] LS$ only through the terms involving the Slater integral $F_2(2p, 2p)$, because these terms are the only ones which contain the fractional parentage coefficients $\langle (m) | (m-2) : (2) \rangle$. Thus the symmetry of the nuclear state contributes to the Coulomb energy through the terms in (2.4) which contain $F_2(2p, 2p)$: we shall call these the symmetry terms.

The Coulomb energy differences in an isobaric multiplet can be found from (2.4). The members of an isobaric multiplet have the same value of A but different values of Z , and hence of T_3 . Assuming that the Slater integrals depend on A but not on Z and defining

$$\Delta E_c(m, T, T_3, T_3') = E_c(m, T, T_3') - E_c(m, T, T_3)$$

we obtain

$$\begin{aligned}
 (a) \quad \Delta E_c(m, \tfrac{1}{2}, \tfrac{1}{2}, -\tfrac{1}{2}) &= 2e^2 \{F_0(1s, 2p) - \tfrac{1}{6} G_1(1s, 2p)\} + \tfrac{1}{2} (m-1) e^2 F_0(2p, 2p) \\
 &\quad + \tfrac{6}{5} m(m-1) e^2 F_2(2p, 2p) \sum_{(T_2=1)} W(T'' \tfrac{1}{2} 11; 1 \tfrac{1}{2}) (-1)^{L_2} W(1111; L_2 2) \\
 &\quad \times \langle (m) | (m-2) : (2) \rangle^2, \\
 (b) \quad \Delta E_c(m, 1, 1, 0) &= 2e^2 \{F_0(1s, 2p) - \tfrac{1}{6} G_1(1s, 2p)\} + \tfrac{1}{2} (m-2) e^2 F_0(2p, 2p) \\
 &\quad + \tfrac{9}{10} m(m-1) e^2 F_2(2p, 2p) \sum_{(T_2=1)} \{W(T'' 111; 11) - W(T'' 112; 11)\} \\
 &\quad \times (-1)^{L_2} W(1111; L_2 2) \langle (m) | (m-2) : (2) \rangle^2, \\
 (c) \quad \Delta E_c(m, 1, 0, -1) &= 2e^2 \{F_0(1s, 2p) - \tfrac{1}{6} G_1(1s, 2p)\} + \tfrac{1}{2} m e^2 F_0(2p, 2p) \\
 &\quad + \tfrac{9}{10} m(m-1) e^2 F_2(2p, 2p) \\
 &\quad \times \sum_{(T_2=1)} \{W(T'' 111; 11) + W(T'' 112; 11)\} (-1)^{L_2} W(1111; L_2 2) \\
 &\quad \times \langle (m) | (m-2) : (2) \rangle^2. \\
 &\quad \dots\dots (2.5)
 \end{aligned}$$

In each of these expressions the first two terms depend only on m but the last term depends on the symmetry and contains $F_2(2p, 2p)$.

§ 3. THE EFFECT OF NUCLEAR SYMMETRY

We can use formulae (2.4: a, b, c) to compare Wilkinson's method of calculating the positions of $T=1$, $T_3=0$ levels in isobaric triplets with the theoretical predictions of the L - S coupling shell model. The Slater integrals for the Coulomb potential are inversely proportional to the scale parameter in the radial part of the single-particle wave functions and this scale parameter is related to the size of the nucleus. In general the radius of the nucleus is taken to be proportional to $A^{1/3}$ and the Slater integrals will then be inversely proportional to $A^{1/3}$. Over small ranges of A (such as the 2p-shell nuclei, which we shall be considering) the variation of the radius with $A^{1/3}$ may not be strictly accurate but, since we wish to compare our results with those of Wilkinson who used the $A^{1/3}$ variation, we shall take the Slater integral to be proportional to $A^{-1/3}$.

When the symmetry terms in formulae (2.4) are omitted

$$(A-1)^{1/3}E_c(A-5, \frac{1}{2}, -\frac{1}{2}) = A^{1/3}E_c(A-4, 1, 0)$$

$$\text{and } (A-1)^{1/3}E_c(A-5, \frac{1}{2}, \frac{1}{2}) = A^{1/3}E_c(A-4, 1, 1).$$

These give $\{E_c(A-4, 1, 0) - E_c(A-4, 1, 1)\}$

$$= \left(1 - \frac{1}{A}\right)^{1/3} \{E_c(A-5, \frac{1}{2}, -\frac{1}{2}) - E_c(A-5, \frac{1}{2}, \frac{1}{2})\} \quad \dots\dots (3.1)$$

which is the formula used by Wilkinson. Eqn (3.1) connects the Coulomb energy difference $\Delta E_c(A-4, 1, 1, 0)$ and $\Delta E_c(A-5, \frac{1}{2}, \frac{1}{2}, -\frac{1}{2})$ which are given by formulae (2.5: a, b). Since (3.1) gives the correct Coulomb energy differences apart from the symmetry terms, corrections to Wilkinson's results come from the symmetry terms in formulae (2.5).

The contributions of the symmetry terms to the Coulomb energy differences are given in Table 1 for the states $(1s)^4(2p)^m$ of greater symmetry. The states for which ΔE_c is tabulated are those which give the correct spin J for the nuclear energy level and they have been arranged with the most probable state first for each isobar. The experimental Coulomb differences for the nuclei with odd A are also listed in Table 1.

An examination of the last column of Table 1 shows that in general the symmetry terms contribute less to $A^{1/3}\Delta E_c(A-4, 1, 1, 0)$ than they do to $(A-1)^{1/3}\Delta E_c(A-5, \frac{1}{2}, \frac{1}{2}, -\frac{1}{2})$. Thus if (3.1) is used to estimate $\Delta E_c(A-4, 1, 1, 0)$ from the experimental value of $\Delta E_c(A-5, \frac{1}{2}, \frac{1}{2}, -\frac{1}{2})$ there could be a tendency to over-estimate and this would result in calculated positions of the first $T=1$, $T_3=0$ levels in even nuclei which are too high. Thus the effect of nuclear symmetry could explain the significantly positive value of Δ which Wilkinson found in the 2p-shell nuclei.

§ 4. ESTIMATION OF SYMMETRY EFFECTS

Since the inclusion of the symmetry terms in the calculation of Coulomb energies could account for Wilkinson's positive value of Δ in the 2p-shell we try in this section to estimate the quantitative effect of including these terms which involve $F_2(2p, 2p)$. To obtain such an estimate we must choose a state in L - S coupling to represent the actual nucleus: in all cases we shall take the state of maximum symmetry which gives the correct value for J and T . We estimate the position of the $T=1$, $T_3=0$ level in an isobaric triplet by the following method.

Table 1

$A-4$	J, T	$[\alpha]LS$	T_3', T_3	(5)	(6)
1	$\frac{3}{2}, \frac{1}{2}$	[1] $1\frac{1}{2}$	$\frac{1}{2}, -\frac{1}{2}$	—	0.84
2	0, 1	[2] 00	1, 0	—	
		[11] 11		—	
		[2] 00	0, -1	+0.1	
		[11] 11		-0.2	
3	$\frac{3}{2}, \frac{1}{2}$	[3] $1\frac{1}{2}$	$\frac{1}{2}, -\frac{1}{2}$	+0.24	1.645
		[21] $1\frac{3}{2}$		-0.2	
		[21] $1\frac{1}{2}$		—	
		[21] $2\frac{3}{2}$		-0.2	
		[21] $2\frac{1}{2}$		-0.08	
4	2, 1	[31] 11	1, 0	+0.07	
		[31] 21		0.08	
		[31] 20		+0.22	
		[31] 31		-0.08	
		[31] 11	0, -1	-0.16	
		[31] 21		+0.03	
		[31] 20		-0.28	
		[31] 31		-0.16	
5	$\frac{3}{2}, \frac{1}{2}$	[41] $1\frac{1}{2}$	$\frac{1}{2}, -\frac{1}{2}$	-0.32	1.853
		[41] $2\frac{1}{2}$		-0.256	
6	0, 1	[42] 00	1, 0	-0.43	
		[33] 11		+0.12	
		[411] 11		-0.02	
		[42] 00	0, -1	+0.03	
		[33] 11		-0.08	
		[411] 11		-0.42	
7	$\frac{3}{2}, \frac{1}{2}$	[43] $1\frac{1}{2}$	$\frac{1}{2}, -\frac{1}{2}$	+0.128	2.763
		[43] $2\frac{1}{2}$		+0.1408	
8	1, 1	[431] 11	1, 0	-0.29	
		[431] 10		-0.27	
		[431] 21		-0.42	
		[431] 11	0, -1	-0.47	
		[431] 10		-0.44	
		[431] 21		-0.32	
9	$\frac{1}{2}, \frac{1}{2}$	[441] $1\frac{1}{2}$	$\frac{1}{2}, -\frac{1}{2}$	-0.64	3.004
		[432] $1\frac{1}{2}$		-0.4	
		[432] $2\frac{3}{2}$		-0.2	
		[333] $0\frac{1}{2}$		-0.2	
10	0, 1	[442] 00	1, 0	-0.8	
		[433] 11		-0.2	
		[442] 00	0, -1	-0.4	
		[433] 11		-0.4	
11	$\frac{1}{2}, \frac{1}{2}$	[443] $1\frac{1}{2}$	$\frac{1}{2}, -\frac{1}{2}$	-0.4	3.542

Column (5) gives the symmetry terms in ΔE_c (m, T, T_3', T_3) in units of $e^2 F_2(2p, 2p)$.
 Column (6) gives the experimental values of ΔE_c for A odd in meV (Ajzenberg-Selove and Lauritsen 1959).

(i) The experimental values of $A^{1/3}\Delta E_c(A-4, \frac{1}{2}, \frac{1}{2}, -\frac{1}{2})$ for $A=5, 7, 11, 13, 15$ are used to estimate the value of $A^{1/3}F_2(2p, 2p)$. The experimental data are reasonably accurate for these mirror pairs (apart from $A=5$): the $A=9$ data are not used because of the large Thomas shift in ${}^9\text{B}$ which is unstable against proton emission. With our hypothesis of states of maximum symmetry this analysis gives 0.75 Mev as the approximate value of $A^{1/3}e^2F_2(2p, 2p)$.

(ii) This value of $F_2(2p, 2p)$ is used to estimate $\Delta E_c(m, 1, 1, 0)$ for m even and from this the position of the $T=1, T_3=0$ level is obtained. The positions so calculated and the experimental values are given in Table 2.

Table 2

Atomic number $A=m+4$	Level position (mev)		Δ (mev)
	Exptl	Calc.	
6	3.56	3.55	-0.01
8	16.67	16.73	+0.06
10	1.739	1.697 (1.729)	-0.042
12	15.11	15.15	+0.04
14	2.312	2.251(L-S) 2.299(j-j) (2.272, L-S) (2.342, j-j)	-0.061 -0.013

Values in brackets are calculated from $T_3 = \pm 1$ states.

For $A=14$ the symmetry correction has been estimated also in $j-j$ coupling which is probably more reliable and that result is tabulated as well. For $A=10$ the approximate values obtained in (1) for $F_0(2p, 2p)$ and $\frac{1}{6}F_0(1s, 2p) - G_1(1s, 2p)$ were used to estimate the Coulomb energy difference for $A=9$; this gives a Thomas shift in ${}^9\text{B}$ of 0.17 Mev. The position of the first $T=1$ level in ${}^{10}\text{B}$ was estimated from this calculated value of $\Delta E_c(5, \frac{1}{2}, \frac{1}{2}, -\frac{1}{2})$. In these two cases ($A=10, 14$) the experimental data for $\Delta E_c(m, 1, 0, -1)$ is fairly reliable and the positions of the $T_3=+1$ and $T_3=-1$ states can be used to estimate the position of the $T_3=0$ state. These results are also given in Table 2.

The method can be used to estimate the Coulomb energy difference between the states with $T=1$ and $T_3=0$ or -1 . Using the experimental data for $A^{1/3}\Delta E_c(A-4, \frac{1}{2}, \frac{1}{2}, -\frac{1}{2})$ estimates can be found for $\Delta E_c(A-5, 1, 0, -1)$: these are given in Table 3. For $A=8$ the calculated value of $A^{1/3}\Delta E_c(5, \frac{1}{2}, \frac{1}{2}, -\frac{1}{2})$ has been used.

Table 3

Atomic number $A=m+4$	$\Delta E_c(m, 1, 0, -1)$ (mev)	
	Exptl	Calc.
6	1.66	1.67
8	2.09	2.07
10	2.823	2.781
12	3.13	3.14
14	3.618	3.624

Experimental values are from Ajzenberg-Selove and Lauritsen (1959).

§ 5. DISCUSSION OF RESULTS

An examination of Table 2 shows that the significantly positive average value of 35 kev for Δ which Wilkinson found has disappeared when the symmetry effects have been included. The numerical results given depend on our hypothesis of using only states of maximum symmetry but the calculations show that the symmetry effects are of the same order of magnitude as Wilkinson's values for Δ . Using harmonic oscillator wave functions

$$F_2(2p, 2p) = \left(\frac{2}{\pi}\right)^{1/2} \left(\frac{5}{12a_0}\right),$$

where by the definition of Swiatecki (1951) the nuclear radius $R = 1.924a_0$. Our estimate of 0.75 mev for $A^{1/3}e^2F_2(2p, 2p)$ gives $R = 1.23A^{1/3} \times 10^{-13}$ cm which is in reasonable agreement with other estimates of the nuclear radius. Thus the neglect of symmetry effects can lead to errors which are of the same order as Wilkinson's average of 35 kev for Δ .

There remains the problem of whether or not Δ has still a significantly positive value when symmetry effects are included. Table 2 shows that the assumption of states of maximum symmetry removes completely the tendency for Δ to be positive in the 2p-shell. In fact, the present positive values of Δ for $A=8$ and $A=12$ could be caused by the Thomas shift since the lowest $T=1$ states in ^8Be and ^{12}C are only just stable against proton emission. For the same reason the calculated value of $\Delta E_c(A-4, 1, 0, -1)$ for $A=8$ and 12 should be low: this is true for $A=8$ but not for $A=12$.

It might seem that the adjusted values of Δ are significantly negative when the symmetry effects are considered. However, the numerical values listed in Table 2 are based on L - S coupling wave functions of maximum symmetry, and for the 2p-shell nuclei intermediate coupling gives a much better account of most of the properties of these nuclei. The coupling changes from nearly pure L - S to nearly pure j - j as A goes from 5 to 15. The admixture of other states of the $(1s)^4(2p)^m$ configuration will alter the symmetry corrections which have been calculated. The amount of mixing caused by the deviation from pure L - S coupling is not known with precision, although there is some knowledge for many of the nuclei. However, we shall discuss the effect of mixing in a qualitative way only.

The calculated position of the $T=1$, $T_3=0$ level in ^6Li is unchanged. In ^8Be and ^{12}C the levels may be changed slightly: the former level being raised, the latter lowered. The level in ^{10}B should be raised. The j - j coupling result for ^{14}N is expected to be more accurate than that obtained using L - S coupling. Thus the change to intermediate coupling is likely to make Δ smaller (in absolute magnitude) for $A=8$ and $A=10$ but to have little effect on the other values.

Similarly the values of $\Delta E_c(m, 1, 0, -1)$ would be altered. The only appreciable change would be in $\Delta E_c(4, 1, 0, -1)$: this would be decreased.

§ 6. THE PION MASS DIFFERENCE

The Coulomb forces which have been considered as a perturbation to the forces of specifically nuclear origin is the obvious example of a charge dependent force between two nucleons and is also the most important cause of the differences in the energy levels of isobaric multiplets. However, since the mass of the neutral pion differs from that of the charged pions the nuclear forces themselves will have a dependence on charge which will be reflected in the positions of the energy levels. Blin-Stoyle and Kearsley (1960) have investigated this effect for $A=6$.

Using the form of potential given by Blin-Stoyle and Kearsley the position of the $T_3=0$ level (relative to the $T_3=\pm 1$ levels) in an isobaric triplet of the nuclear 2p-shell must be altered by an amount

$$\begin{aligned} & \frac{1}{3} \left(\frac{g\mu}{2M} \right)^2 \left(\frac{\delta\mu}{\mu} \right) m(m-1) \sum_{T''=1}^{T=1} U(T''112; 11) \langle (m)T=1|(m-2)T'':(2)L_2T_2=1 \rangle^2 \\ & \{ [1+2(-1)^{L_2}] F_0(2p, 2p) + \frac{6}{5} [2+(-1)^{L_2}] W(1111; L_22) F_2(2p, 2p) \} \\ & + \frac{10}{3} \left(\frac{g\mu}{2M} \right)^2 \left(\frac{\delta\mu}{\mu} \right) m(m-1) U(21LJ; 1L) \\ & \times \sum_{(m-2)} \langle (m)LT=1S=1|(m-2)L''T''S'':(2)L_2=1T_2=1S_2=1 \rangle^2 \\ & \times U(L''L12; 1L) U(T''112; 11) U(S''112; 11) B(2p, 2p), \quad \dots\dots (6.1) \end{aligned}$$

for the configuration $(1s)^4(2p)^m$. F_0 and F_2 are the Slater integrals for the central potential $(\mu-2/r)\exp(-\mu r)$, and B is the integral defined by Elliott (1953, p. 354) for a tensor potential which in this case is $(\mu+1/r)\exp(-\mu r)$. The levels with $T=\frac{1}{2}$ are unaffected, as also are those with $T=0$. Formula (6.1) gives the amount by which the value of $\Delta E_c(m, 1, 1, 0)$ given in (2.5 (b)) should be increased and also by which the value of $\Delta E_c(m, 1, 0, -1)$ given in (2.5 (c)) should be decreased to allow for the pion mass difference. The value of (6.1) for the states of greater symmetry of the even nuclei in the 2p-shell are listed in Table 4. The numerical values given there have been calculated using harmonic oscillator wave functions with the same definition of the radial parameter as before.

Table 4

$m=A-4$	$[\alpha]LS$	(3)	(4)
2	[2] 00	$+6F_0+2.4F_2$	-0.384
	[11] 11	$-6F_0+0.4F_2+20B$	+0.244
4	[31] 11	$-0.58F_2-1.7B$	+0.034
	[31] 21	$+1.4F_2-7B$	-0.119
	[31] 20	$-12F_0-0.6F_2$	+0.356
	[31] 31	$+0.32F_2-3.6B$	-0.034
6	[42] 00	$+6F_0+2.76F_2$	-0.298
	[33] 11	$-6F_0+0.4F_2+12B$	+0.135
8	[431] 11	$-0.58F_2+8.5B$	+0.053
	[431] 10	$-12F_0+1.38F_2$	+0.139
	[431] 21	$+1.4F_2+7B$	-0.058
10	[442] 00	$+6F_0+2.4F_2$	-0.207
	[433] 11	$-6F_0+0.4F_2+20B$	+0.115
	$j-j$	$-2F_0+\frac{16}{15}F_2+\frac{80}{3}B$	+0.008

Column (3) gives the correction to the positions of the $T_3=0$ levels in units of

$$\frac{1}{3} \left(\frac{g\mu}{2M} \right)^2 \left(\frac{\delta\mu}{\mu} \right) = 0.096 \times 10^{13} \text{ meV cm}^{-1}.$$

Column (4) gives the calculated corrections in meV.

The numerical values obtained for this correction are appreciable and, except in the case of $A=14$ with j - j coupling, they are all of the wrong sign to explain the values and signs of Δ listed in Table 2. The magnitude of the corrections are similar in magnitude to the symmetry corrections obtained previously.

When admixtures of other states are allowed the comparison between theory and experiment is improved, especially for $A=6$ and $A=10$. However, the experimental data used for $A=6$ is not reliable and the theoretical results listed in Tables 2 and 3 for $A=10$ depend on the estimated value of the Thomas shift in 9B . Also it can be seen from the magnitudes and signs of the corrections which are listed in Table 4 that the numerical values as well as depending on the choice of nuclear radius are critically dependent on the admixtures allowed. A 'suitable' choice of the states mixed could ensure that the effect of the pion mass difference compensated for the previous discrepancy Δ between the calculated and the experimental positions of the $T=1$, $T_3=0$ levels.

§ 7. CONCLUSIONS

We have investigated the problem of including symmetry effects in Wilkinson's method for calculating the position of the first $T=1$ level of nuclei with $T_3=0$ in the nuclear $2p$ -shell. The results show that the inclusion of these effects tends to nullify Wilkinson's conclusion that Δ is significantly positive for these nuclei and the specific nuclear forces are not charge independent. The values of Δ which have been obtained are very much smaller than those found by Wilkinson and some are positive, some negative.

The remaining discrepancies between the calculated and the experimental energy levels can be due to effects neglected in our calculation of the Coulomb energies, or to errors in the experimental data, or to the specific nuclear forces being charge dependent. As an example of the last possibility we have calculated the effect of the pion mass difference. These calculations show that the resultant correction to the position of the $T=1$, $T_3=0$ levels are probably not of the correct sign to explain the values previously found for Δ . Also they are larger than required but this could be due to using only the second-order potential without a repulsive core or to the choice of the radial parameter in the harmonic oscillator wave functions.

It is perhaps significant that in one of the two nuclei for which the calculations are most accurate—that for $A=14$ with j - j coupling—there is very good agreement between the calculated and the experimental results: the discrepancy is 0.005 mev for $\Delta E_c(10, 1, 1, 0)$ and 0.002 mev for $\Delta E_c(10, 1, 0, -1)$. In the other nucleus— $A=6$ with L - S coupling—it is unfortunate that the experimental data are not reliable. It has been seen that for the remaining nuclei ($A=8, 10, 12$) a judicious mixing of states could give reasonable agreement between theory and experiment.

We conclude that the Coulomb forces provide the major part of the energy differences between the levels of an isobaric multiplet and that there is little evidence of any other deviation from charge independence. The effect of the pion mass difference is of the correct sign and magnitude in the only case ($A=14$) for which the calculations are reliable to the accuracy required in looking for small departures from charge independence. For the other nuclei it is difficult to

judge how accurately the present calculations estimate probable deviations from charge independence, but the deviation between theory and experiment is not significantly of one sign.

REFERENCES

- AJZENBERG-SELOVE, F., and LAURITSEN, T., 1959, *Nucl. Phys.*, **11**, 1.
BLIN-STOYLE, R. J., and KEARSLEY, M. J., 1960, *Proc. Phys. Soc.*, **75**, 147.
BURCHAM, W. E., 1955, *Reports on the Progress of Nuclear Physics*, **4**, 171 (London: Pergamon Press).
ELLIOTT, J. P., 1953, *Proc. Roy. Soc. A*, **218**, 345.
ELLIOTT, J. P., HOPE, J., and JAHN, H. A., 1953, *Phil. Trans. Roy. Soc. A*, **246**, 241.
JAHN, H. A., 1951, *Proc. Roy. Soc. A*, **205**, 192.
JAHN, H. A., and VAN WIERINGEN, H., 1951, *Proc. Roy. Soc. A*, **209**, 502.
SWIATECKI, W. J., 1951, *Proc. Roy. Soc. A*, **205**, 238.
WILKINSON, D. H., 1956, *Phil. Mag.*, **1**, 1031.

The Lifetime of the 364 keV Level in ^{131}Xe

By W. D. HAMILTON†

Department of Physics, University of Birmingham

Communicated by P. B. Moon; MS. received 14th March 1960

Abstract. The nuclear resonant scattering technique for γ -rays was used to measure the lifetime of the 364 keV level in ^{131}Xe , and to determine the mixing ratio of the E2+M1 ground state transition. Doppler broadening of the emission level, which compensates the recoil losses of the 364 keV gamma ray, is provided by the preceding 608 keV β^- -transition from ^{131}I when the source, methyl iodide, is in the gaseous phase, the scatterer being solid xenon.

The measured lifetime of $(1.4 \pm 0.4) \times 10^{-11}$ sec is in agreement with Sunyar's estimated value of 2×10^{-11} sec. A 0.34% M1 admixture was found for the 364 keV transition, and is of the order expected from internal conversion coefficient measurements.

§ 1. INTRODUCTION

IN the extensive studies of the β -decay of ^{131}I to the excited states of xenon, the lifetime of the 364 keV level was shown by Bell, Graham and Petch (1952) to be less than 10^{-10} sec. More recently Sunyar (1957), using a coincidence method to detect the 364 keV γ -ray and the preceding 608 keV β^- -transition, found the mean life to be of the order of 3×10^{-11} sec. It should be possible to determine such a lifetime more accurately from a measurement of the resonant scattering cross section (see Metzger 1959), where the resonance condition for the scattering of the 364 keV γ -ray is provided by the persistence of nuclear recoil following the β -emission.

The total energy in β -decay, except for the small amount taken by nuclear recoil, is distributed between the β -particle and the neutrino, the recoiling nucleus receiving its momentum principally from the β -particle. The most probable β -momentum occurs at approximately half the maximum momentum, and must equal that of the γ -ray if it is to compensate adequately for the energy losses of the latter in conserving linear momentum with the nucleus when emitted and resonantly absorbed. In the present case the β -particle and γ -ray have momenta 1.93 mc and 0.71 mc respectively, permitting the 364 keV γ -ray to be sufficiently broadened to allow it to overlap the absorption level.

For lifetimes longer than 10^{-13} sec a gaseous source is necessary to prevent the recoiling nucleus losing its momentum in a collision before emitting the gamma ray. While ease in preparation and handling the source during the experiment are obligatory conditions, it is also necessary to consider if the molecule will break up during the β - γ cascade, or whether the nuclear recoil energy will be taken by the whole molecule. The recoil energy in the centre-of-mass system is available for bond rupture, and for iodine in a molecule of low mass this is only a small fraction of the total recoil energy, while an additional complication is the change

† Now at the Physics Institute, Uppsala University, Sweden.

in chemical form of the recoiling atom. It was thus decided to use methyl iodide (^{131}I) for which the change in the amount of line overlap would be little affected whether the molecule or the free xenon atom recoiled.

In constructing the broadening of the 364 keV level (Fig. 1) by a geometrical method, the β - ν correlation was ignored as the recoil distribution remains symmetrical with little change in shape in the region of interest. The 608 keV β -transition is allowed by Gamow-Teller selection rules ($\Delta I = 1$; no), and consequently there is no β - γ angular correlation. The 364 keV γ -ray of momentum 0.71 mc is displaced in energy by 1.08 eV on emission and subsequent absorption by the xenon atom, while the maximum recoil energy imparted to the nucleus by the β -particle of momentum 1.93 mc is 2.97 eV. The area under the curve has been normalized to unity, and the ordinate represents the fraction of incident γ -rays on the scatterer which satisfy the resonance condition.

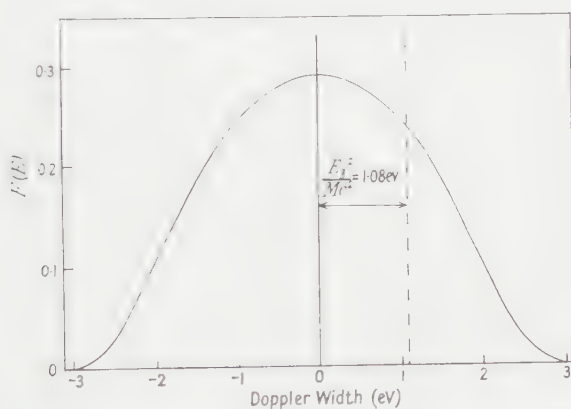


Fig. 1. The Doppler broadening of the 364 keV transition due to β -recoil for a gaseous source. The broken line represents the displacement of the absorption level when the xenon atom accepts the nuclear recoil.

§ 2. EXPERIMENTAL METHOD

A gas scatterer would be unsuitable because of its low density and it was necessary to develop a method which allowed the xenon to be solidified. A thin-walled copper cylinder was embedded in styrofoam, and a narrow well of liquid nitrogen at the back of the cylinder permitted it to be cooled rapidly. The outlet tube from the cylinder was connected to the copper-glass seal of the vacuum line and xenon reservoir, by a section of thin-walled stainless steel tubing which completed the thermal insulation. The container dimensions were height 3.2 cm and diameter 3.5 cm, and were sufficient to hold 15 litres of xenon gas when solidified, although in the present case only 10.5 litres were used. The well measured 1 cm wide by 0.2 cm thick, and extended the height of the cylinder into a styrofoam container of liquid nitrogen; this size of well permitted a rapid solidification of the gas. The fraction of gas present in the container was known from a manometer which indicated the total gas pressure, while radiographs showed the solid xenon to have a cylindrical form. It was possible to thaw the xenon by using a small heating coil which was wound directly on the copper outlet tube of the cylinder.

As it would have been inconvenient to replace the solid xenon by a comparison scatterer and maintain the geometrical arrangement, the resonance effect was observed by comparing the counting rates when the source was alternatively gaseous and solid. From the order of the lifetime it would be expected that when the source was solid, the only significant contribution to the elastic peak would be from Rayleigh scattering, while for a gaseous source, both Rayleigh and resonant scattering would contribute to the peak.

The 20 mc source of 0.075 mm methyl iodide was contained in a conical glass ampoule having a volume 1.5 ml and enclosed in a copper container of which the temperature could be controlled. The finite volume of the source gave a small change in geometry on condensation, but this was reproducible by arranging for selective solidification on the base of the cone which faced the scatterer. The solid angle of the conical ampoule was greater than the angle subtended by the scatterer at the source position, and γ -rays incident on the scatterer from any region of the source penetrated the base of the cone normally. Thus for small changes in the effective source position, the absorption remained constant.

The scattered radiation was detected in a scintillation counter using a $1\frac{1}{2}$ in. diameter by 1 in. thick NaI(Tl) crystal mounted on a 6295 Dumont photomultiplier. The geometrical arrangement of the apparatus was such that source-scatterer and detector-scatterer distances were both of the order 10 cm, with a mean scattering angle of 105° ; this was a compromise to give minimum background counting rate due to the scattered radiation and to direct penetration through the heavy alloy shielding.

§ 3. RECORDING OF RESULTS

The scattered spectra were recorded on a Marshall pulse height analyser set at 100 channels. The number of the counts resonantly scattered was determined from the difference in the counting rates in a ten-channel section of the spectra when the source was solid and gaseous; the ten-channel interval was selected by direct calibration. The correction for the small change in source geometry on condensation was made from a comparison of the scattered spectra when the scatterer was absent, and for which the source was alternatively solid and gaseous. From this comparison the spectrum obtained for a gaseous source when the scatterer was present could be normalized relative to the spectrum for a solid source.

Despite efforts to reduce the construction material to a minimum there was appreciable scattering from the empty container so that the actual resonance effect was only 10% above background. Since the comparison of several counting rates increased the probable error it was necessary to count for 30 min periods for a particular source condition to obtain adequate statistics.

Direct calibration of the source was made at 1 metre giving 2.97×10^5 counts per minute in the selected ten-channel section, the counting rate being corrected to a standard time when the first measurements were made. This counting rate was adjusted by a factor relating the detection efficiency for this measurement and when the crystal was detecting the resonantly scattered radiation.

§ 4. EXPERIMENTAL RESULTS

In Fig. 2 the number of resonantly scattered counts recorded on different days is shown, the solid line being the mean value and having a slope corresponding to the 8-day half-life of ^{131}I .

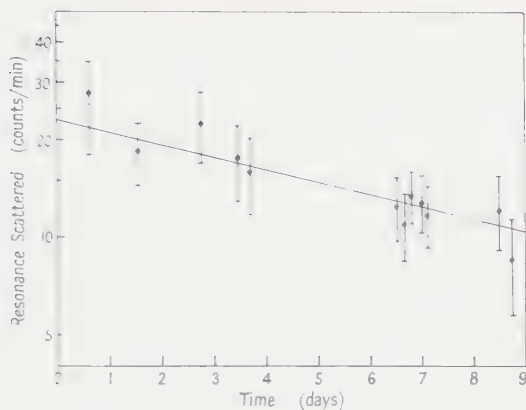


Fig. 2. The change in resonance scattering intensity with decay of the source. The line is the mean value of the results with a gradient corresponding to an 8-day half-life.

The percentage of resonantly scattered radiation as a function of source temperature (Fig. 3) was found to follow the vapour pressure curve of methyl iodide, as was the fraction of source in the vapour phase (circles on Fig. 3). The latter was determined by recording the counting rate from a slitted section of the source ampoule at various temperatures. A regular temperature change, with selective condensation of the source at the opposite end of the ampoule to that being observed, was achieved by immersing the ampoule in a hot oil bath and cooling through a small temperature gradient. These measurements gave the boiling point of methyl iodide as 45°C indicating that the pressure in the ampoule was greater than atmospheric, and was consistent within the accuracy of the source specifications.

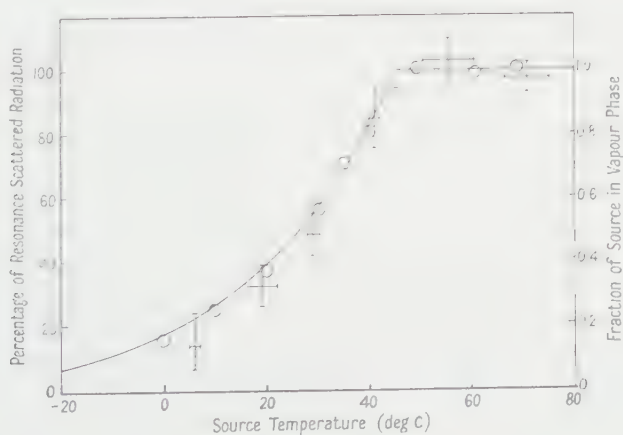


Fig. 3. The variation in resonance scattered intensity with source temperature is compared with the fraction of source in the vapour phase. This fraction is represented by the theoretical curve based on vapour pressure data; the circles being a direct measurement for a slitted section of the source with a counting rate of 1000 counts per minute at 50°C .

An important factor which was included in the evaluation of the resonant scattering cross section was the correction for the attenuation of the radiation

resonantly scattered by the solid xenon. The attenuation of the resonantly absorbed and re-emitted radiation will be similar to that from a distributed cylindrical source. Evans and Evans (1948) showed that such a cylindrical source is equivalent to a line source on the axis of an absorbing cylinder for which the transmission probability could be determined.

The resonant scattered counting rate was compared with the number of photons incident on the scatterer and found to be smaller by the factor 1.06×10^{-6} . Corrections were applied for the geometrical arrangement of source, scatterer and detector, and for the attenuation of the radiation by the scatterer of which 2.65×10^{21} atoms cm^{-2} are ^{131}Xe . The differential resonant scattering cross section at a scattering angle of 105° was evaluated as

$$\sigma(105^\circ) = 2.96 \times 10^{-26} \text{ cm}^2 \text{ sterad}^{-1}.$$

When line broadening is due to a preceding recoil then, from Metzger,

$$\sigma(\theta) = \sigma_{\max} \frac{\pi}{2} \frac{\Gamma_\gamma^2}{\Gamma} F(E) \frac{f(\theta)}{4\pi} \text{ cm}^2 \text{ sterad}^{-1}.$$

We may substitute in the above equation for the peak cross section

$$\sigma_{\max} = 2.78 \times 10^{-20} \text{ cm}^2 \text{ per } ^{131}\text{Xe nucleus}, F(E) = 0.26 \text{ ev}^{-1},$$

the angular distribution function $f(105^\circ) = 1.05$, and Γ_γ/Γ the branching ratio for the 364 keV γ -decay mode, whence we obtain $\Gamma_\gamma = 3.3 \times 10^{-5} \text{ ev}$ for the level width associated with the 364 keV γ -ray. The corresponding half-life is $t_{1/2} = 1.4 \times 10^{-11} \text{ sec}$. Uncertainty in geometrical factors contributes mainly to the probable error which was put at 20%. It has been assumed that the xenon atom was free to recoil but should the molecule have accepted the recoil energy the value of the lifetime would have been decreased by 9%.

§ 5. THE MIXING RATIO OF THE 364 keV TRANSITION

The K electron conversion coefficients and the relative conversion coefficients for different shells have been determined by Bell and Graham (1952), and by Verster, Nijgh, van Leishout and Bakker (1951). These results, when compared with the theoretical values of Rose (1958), suggest the possibility of a small admixture of M1 with E2 radiation. The ratio of E2 to M1 radiation in the transition is denoted by δ^2 , where δ is the ratio of the reduced matrix elements for E2 and M1 radiation. Internal conversion coefficients depend upon δ^2 and are thus not particularly sensitive to a small admixture; angular correlations between successive γ -transitions, and the equivalent case of the angular distribution of resonantly scattered radiation, give δ which enters as an interference term.

The angular correlation expression for a γ - γ cascade of which both stages are mixed has been derived by Rose (1954). This is simplified considerably for resonantly scattered radiation in which the initial and final states are the same, so that both stages of the equivalent cascade have the same multiplicities and mixing ratio.

The angular distribution of resonantly scattered radiation is expressed as

$$W(\theta) = \sum_\nu A_\nu P_\nu(\cos \theta),$$

in which the coefficients A_ν have the form

$$A_\nu = \{F_\nu(LLJ_iJ) + \delta^2 F_\nu(L'L'J_iJ) + 2\delta F_\nu(L'LJ_iJ)\}^2$$

where $L' = L + 1$ and $\nu = 0, 2, 4, \dots$

The quadrupole component of the radiation requires the expression to be expanded to include the coefficient A_4 . After substitution for the coefficients $F_\nu(LLJ_iJ)$ in the spin sequence $\frac{3}{2}^+(E2+M1)\frac{5}{2}^+(E2+M1)\frac{3}{2}^+$ (see Wapstra, Nijgh, and van Lieshout, 1959), and normalization to give $A_0=1$, the angular distribution function becomes

$$f(\theta) = 1 + \frac{P_2(\cos \theta)}{(1+\delta^2)^2} \{0.374 - 0.191\delta^2 - 1.898\delta\}^2 + \frac{P_4(\cos \theta)}{(1+\delta^2)^2} \{0.705\delta^2\}^2.$$

From the best fit of this expression to the resonant scattering cross section measured at three angles, it should be possible to determine the magnitude and sign of δ .

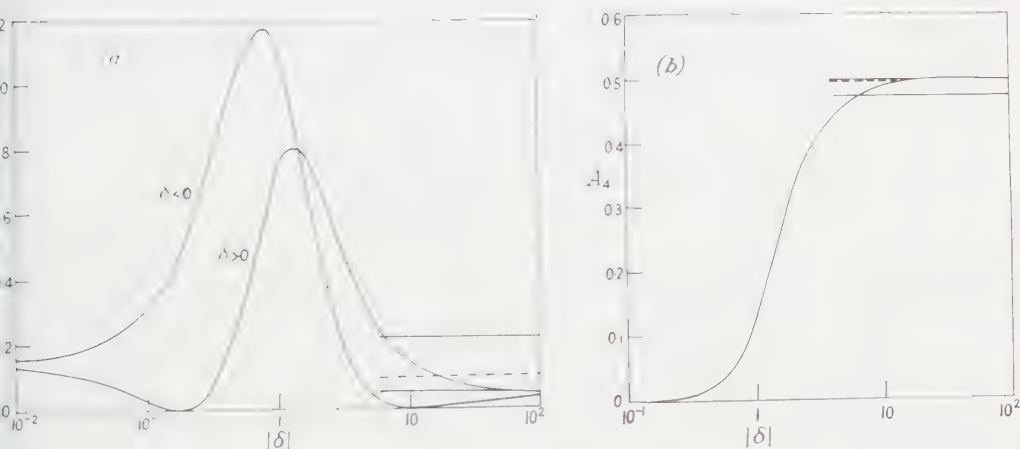


Fig. 4 (a and b). The coefficients A_2 and A_4 are shown as a function of δ for the $\frac{5}{2}(E2+M1)\frac{3}{2}(E2+M1)\frac{5}{2}$ resonant scattered transition. The best fit of the experimental data for a positive value of δ is shown by the broken line, with the limits of the error indicated by the solid lines.

§ 6. EXPERIMENTAL METHOD AND RESULTS

The source-scatterer and scatterer-detector distances were increased to 15 cm and 22 cm respectively, to improve the angular resolution of the detector; this required the source strength to be raised to 100 mc of ^{131}I . The activity was contained in 0.004 mm of elementary iodine, and together with 0.045 mm of hydrogen was enclosed in a glass ampoule, similar to that used previously. When the ampoule was heated to above the boiling point of iodine it was expected that a large fraction of the source would exist as hydrogen iodide for which the resonance condition exists. Further, it was assumed that the fraction of the source as hydrogen iodide was constant at the upper temperature since the temperature cycle was similar in every case. The improved geometry gave a well-defined elastic peak at 364 keV in the scattered spectra, and this was compared when the source was solid and gaseous. The ratio of resonant to Rayleigh scattered counts was determined and, from the calculated differential cross section for Rayleigh scattering, the relative magnitudes of the differential cross section at the three angles were found. The results are presented in the Table.

Scattering angle (deg)	$\frac{C_{\text{resonant}}}{C_{\text{Rayleigh}}}$	$\sigma(\theta)_{\text{Rayleigh}}$ ($\times 10^{-27} \text{ cm}^2 \text{ sterad}^{-1}$)	$\sigma(\theta)_{\text{resonant}}$ ($\times 10^{-27} \text{ cm}^2 \text{ sterad}^{-1}$)
103	0.358	4.11	6.93
119	0.330	3.64	5.66
135	0.320	3.59	5.42

Fitting these results to the angular distribution function the values $A_2 = 0.090$ and $A_4 = 0.494$ were found, corresponding to $\delta = +17$. The fraction of M1 radiation $1/(1 + \delta^2)$ is then 0.34%. A fit is also possible for $\delta = -4.7$ corresponding to a 4.5% M1 admixture, but this would not appear an acceptable alternative since the quite accurate measurements of Verster *et al.* should have indicated such an admixture.

Although the measurements for the resonant scattering distribution are free from the corrections associated with the coincidence technique for a γ - γ cascade, there is a relatively large error introduced in the present experiment, since the resonant counting rate is obtained from the difference in counting rates of Rayleigh plus resonant, and Rayleigh alone. The experimental error would permit an M1 admixture from zero to 2.7% for a positive value of δ , while a small admixture for a negative value of δ cannot be excluded.

§ 7. DISCUSSION OF RESULTS

Since the multipole character of the radiation enters into the calculation only through the angular distribution of the resonant scattering, the small admixture of M1 radiation will not significantly alter the lifetime of $(1.5 \pm 0.4) \times 10^{-11}$ sec, which is in good agreement with Sunyar's value of 2×10^{-11} sec. The experimental lifetime is some 200 times faster than would be expected for a pure E2 transition on the single-particle model. This disagreement is not unexpected as there is a large discrepancy between the quadrupole moment of an odd-N nucleus on the single-particle model and the experimental value of -0.12 barns for ^{131}Xe . Narumi and Nagai (1960) have accounted for this value of the quadrupole moment by assuming configuration mixing.

ACKNOWLEDGMENTS

The author gratefully acknowledges the encouragement given by Professor P. B. Moon and the interest he has taken in the work, and thanks Drs J. C. Charlton and D. J. Jenkins of the Radiochemical Centre, Amersham, for advice given concerning the sources, which were prepared under their direction at the centre.

The experimental work was carried out while the author was in receipt of a Research Studentship from the Ministry of Education for Northern Ireland.

REFERENCES

- BELL, R. E., and GRAHAM, R. L., 1952, *Phys. Rev.*, **86**, 212.
 BELL, R. E., GRAHAM, R. L., and PETCH, H. E., 1952, *Canad. J. Phys.*, **30**, 35.
 EVANS, R. D., and EVANS, R. O., 1948, *Rev. Mod. Phys.*, **20**, 305.
 METZGER, F. R., 1959, *Progr. Nucl. Phys.*, **7**, 54.
 NARUMI, H., and NAGAI, H., 1960, *Nucl. Phys.*, **16**, 193.
 ROSE, M. E., 1954, *Phys. Rev.*, **93**, 477.
 ———, 1958, *Internal Conversion Coefficients* (Amsterdam: North Holland).
 SUNYAR, A. W., 1957, *Bull. Amer. Phys. Soc.*, [II], **2**, 37.
 VERSTER, N. F., NIJGH, G. J., VAN LIESHOUT, R., and BAKKER, C. J., 1951, *Physica*, **17**, 637.
 WAPSTRA, A. H., NIJGH, G. J., and VAN LIESHOUT, R., 1959, *Nuclear Spectroscopy Tables* (Amsterdam: North Holland).

Electron Collisions with Na Atoms

By A. SALMONA† AND M. J. SEATON‡

†Institute Henri Poincaré, Paris

‡Department of Physics, University College, London

MS. received 12th July 1960

Abstract. Measurements have been made of total collision cross sections (Brode 1929), of cross sections for 3s–3p excitation (Haft 1933, Christoph 1935) and, at thermal energies, of cross sections for elastic scattering with electron exchange (Dehmelt 1958). In all cases the measured cross sections are very large.

The distinguishing feature of electron–Na collisions is the very strong coupling between the 3s and 3p states. It has been shown previously (Seaton 1955) that the Bethe approximation gives good results for the 3s–3p cross section when allowance is made for effects of strong coupling. The present paper gives results of calculations for energies above the 3p excitation threshold and also for the limit of zero kinetic energy. Further work is being done for energies in the immediate vicinity of the 3p threshold.

For the higher energies the Bethe approximation is used to calculate partial wave integrals and the transmission matrix is then obtained by two different methods, both of which ensure that conservation conditions are satisfied exactly (Percival 1960, Seaton 1961). The only potential considered is $V(3s, 3p)$. For energies not too close to the 3p threshold these calculations give good results for the 3s–3p cross section and fairly good results for the total cross section. This shows that a substantial part of the elastic scattering is due to the process $3s \rightarrow 3p \rightarrow 3s$.

At very low energies exchange effects and polarization effects are both large and a much more elaborate theory is required. The coupled integro-differential equations, of Hartree–Fock type, are discussed in detail. It is shown that the coupling between 3s and 3p accounts for 99.4% of the atom polarizability. Solutions of the coupled equations for 3s and 3p are obtained for the case of zero kinetic energy. The calculated zero-energy elastic cross section is $380\pi a_0^2$ and the exchange cross section is $440\pi a_0^2$. These calculated values are consistent with those obtained experimentally.

§ 1. INTRODUCTION

THE alkali atoms have very large total cross sections for electron impact (see Massey and Burhop 1952). Thus the Na total cross section, which has values of several hundred πa_0^2 at low energies, may be compared with the Ne total cross section which has a maximum value of a little under $4\pi a_0^2$. It is obvious that the alkali cross sections are largely determined by interactions with the valence electron. Previous calculations (Salmona and Frenkiel 1959) have shown that a static central field model is quite inadequate to explain the experimental results; for Na such a model gives a zero-energy cross section of $22\pi a_0^2$, which is too small by at least an order of magnitude. To obtain improved results it is necessary to allow for exchange and polarization.

1.1. Discussion of Experimental Results

Fig. 1 shows the Na total cross section, as measured by Brode (1929) using the Ramsauer method, and the 3s-3p cross section as measured by Haft (1933) and Christoph (1935) and corrected by Bates, Fundamirsky, Leech and Massey (1950). Since the 3s-3p cross section is much larger than any other Na inelastic cross section it may be subtracted from the total cross section to obtain the cross section for elastic scattering. This is shown in Fig. 1. The sharp peak which occurs in the elastic cross section at the 3p excitation threshold is undoubtedly a cusp of the type discussed by Wigner (1948). At the higher energies the elastic and inelastic cross sections are still large and are of comparable magnitude. It is evident that strong coupling between 3s and 3p must be taken into account in calculating both the elastic and the inelastic cross sections.

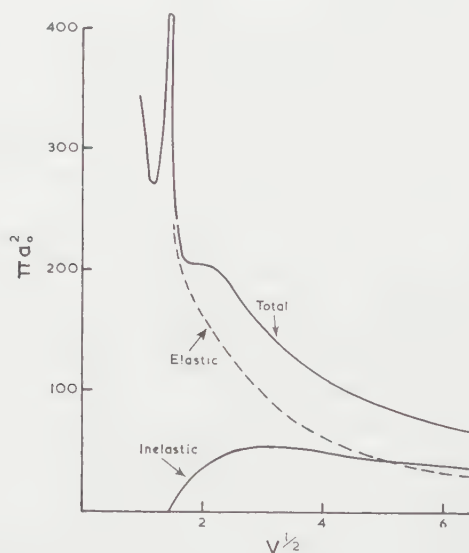


Fig. 1. Na cross sections in units of πa_0^2 as functions of $V^{1/2}$, V being the energy of the incident electrons in eV. The total cross section is from Brode (1929) and the inelastic cross section (3s→3p) from the results of Haft (1933) and Christop (1935). The broken curve for the elastic cross section is obtained on subtracting the inelastic from the total cross section.

Such coupling will remain important below the first excitation threshold, representing virtual excitation. Coupling between the 3s state and the np states introduces a long-range polarization potential V_p (Castillejo, Percival and Seaton 1960) behaving asymptotically as

$$V_p \sim -\frac{\alpha e^2}{2r^4} \quad \dots\dots (1.1)$$

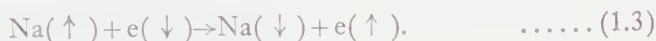
where

$$\alpha = \frac{e^2 \hbar^2}{m} \sum_{n=3}^{\infty} \frac{f(np, 3s)}{(E_{np} - E_{3s})^2} \quad \dots\dots (1.2)$$

is the atom polarizability. The oscillator strength $f(3p, 3s)$ is much greater than all other $f(np, 3s)$. Using experimental f -values of Filippov and Prokofjew (1929) we find that 99.4% of the polarizability comes from 3s-3p coupling.

For collision calculations this is a very fortunate situation; by including only one virtual state we can calculate polarization effects very accurately.

While the older experimental work shows that polarization effects must be large, more recent work shows that, at low energies, exchange effects must also be large. Using optical pumping and micro-wave techniques, Dehmelt (1958) has measured the cross section, Q_{exch} , for the process in which the spin of the electron is reversed due to electron exchange at thermal energies:



He obtains $Q_{\text{exch}} \geq 260\pi a_0^2$ at a temperature of 400°K . This cross section depends on $[\Lambda(0) - \Lambda(1)]$ where $\Lambda(0)$, $\Lambda(1)$ are scattering lengths for singlet and triplet interactions. Dehmelt suggests that the experimental results may be explained by the fact that Na has a bound singlet state of small binding energy and that $\Lambda(0)$ will therefore be large compared with $\Lambda(1)$.

1.2. Theory

We consider two special problems, the scattering at fairly high energies and in the limit of zero kinetic energy. We are continuing the study of electron collisions with Na and plan, in particular, to study the region of the peak in the elastic cross section.

On making an analysis in terms of states of definite total angular momentum, at the higher energies one finds that many such states have to be considered. Exchange effects are then unimportant. We make the rather drastic approximations of considering the only potential to be the $3s-3p$ interaction potential, $V(3s, 3p)$, and of replacing this potential by its asymptotic form. These approximations are valid for large angular momenta. The fact that we get fairly good results for summations over all angular momenta depends on the fact that we employ methods which ensure that conservation conditions are satisfied quite rigorously.

In the limit of zero kinetic energy it is necessary to consider only the state of zero angular momentum, but for this state an elaborate treatment is required, including the solution of coupled integro-differential equations.

§ 2. ENERGIES BEYOND THE FIRST EXCITATION THRESHOLD

We consider a central field model, neglecting exchange. Define a Hamiltonian

$$H_{\text{cf}}(\mathbf{r}) = -\frac{1}{2}\nabla^2 + V_{\text{cf}}(r) \quad \dots\dots (2.1)$$

where atomic units are used and where V_{cf} is the static potential for the Na⁺ core. The wave functions for the valence electron are

$$\psi(n_1 l_1 m_1 | \mathbf{r}) = Y_{l_1 m_1}(\hat{\mathbf{r}}) \frac{1}{r} P_{n_1 l_1}(r), \quad \dots\dots (2.2)$$

the radial functions satisfying

$$\mathcal{H}_{\text{cf}}^{(l_1)} P_{n_1 l_1}(r) = E_{n_1 l_1} P_{n_1 l_1}(r) \quad \dots\dots (2.3)$$

where

$$\mathcal{H}_{\text{cf}}^{(l)} = -\frac{1}{2} \left[\frac{d^2}{dr^2} - \frac{l(l+1)}{r^2} \right] + V_{\text{cf}}(r). \quad \dots\dots (2.4)$$

Using a notation similar to that of Percival and Seaton (1957), we introduce the vector-coupled functions

$$\Psi(n_1 l_1 l_2 LM) = \sum_{m_1 m_2} C_{m_1 m_2 M}^{l_1 l_2 L} \psi(n_1 l_1 m_1 | \mathbf{r}_1) Y_{l_2 m_2}(\mathbf{r}_2) \frac{1}{r_2} F_{n_1 l_1 l_2 L}(r_2), \quad \dots (2.5)$$

the $F_{n_1 l_1 l_2 L}$ being radial functions for the colliding electron. Taking the complete wave functions,

$$\Psi = \sum_{n_1 l_1} \Psi(n_1 l_1 l_2 LM), \quad \dots (2.6)$$

to be solutions of

$$(H - E)\Psi = 0 \quad \dots (2.7)$$

where

$$H = H_{\text{cf}}(\mathbf{r}_1) + H_{\text{cf}}(\mathbf{r}_2) + \frac{1}{r_{12}}, \quad \dots (2.8)$$

we obtain the radial equations

$$\left\{ \mathcal{H}_{\text{cf}}^{(l_2)} - \frac{1}{2} k^2 \right\} F_{n_1 l_1 l_2 L}(r) + \sum_{\lambda n' l'_1 l'_2} f_{\lambda}(l_1 l_2 l'_1 l'_2; L) y_{\lambda}(n_1 l_1 n'_1 l'_1 | r) F_{n' l'_1 l'_2 L}(r) = 0 \quad \dots (2.9)$$

where k^2 is numerically equal to the kinetic energy of the colliding electron in units of 13.60 eV, the atomic electron being in the level $n_1 l_1$. Expressions for the coefficients f_{λ} are given by Percival and Seaton (1957) and

$$y_{\lambda}(ab|r) = \frac{1}{r^{\lambda+1}} \int_0^r P_a(r_0) P_b(r_0) r_0^{\lambda} dr_0 + r^{\lambda} \int_r^{\infty} P_a(r_0) P_b(r_0) \frac{1}{r_0^{\lambda+1}} dr_0. \quad \dots (2.10)$$

The dipole interactions y_1 behave as r^{-2} for large r :

$$y_1(ab|r) \sim \frac{1}{r^2} s_1(ab), \quad \dots (2.11)$$

$$s_1(ab) = \int_0^{\infty} P_a(r) P_b(r) r dr. \quad \dots (2.12)$$

All other interactions are of shorter range.

From experimental f -value measurements one obtains $s_1(3s, 3p) = 19.0$ (Seaton 1955). This large value of $s_1(3s, 3p)$ shows that $y_1(3s, 3p)$ will tend to be the dominant interaction in (2.9) and since this interaction is of long range it will remain important for large values of the angular momentum quantum number l_2 . These large values of l_2 give important contributions to the high energy cross sections and we must therefore consider approximations which are valid for large l_2 and which continue to give reasonable results for small l_2 . In particular, for small l_2 , it is necessary to ensure that the conservation conditions are satisfied.

Our basic approximation is to consider only the long range interactions; we replace $y_1(3s, 3p|r)$ by $s_1(3s, 3p)/r^2$ and put all other y_{λ} equal to zero. We then use two different forms of the Born approximation, referred to as approximations II and III. These are discussed in detail by Percival (1960) and by Seaton (1961). Approximation II is the Born approximation for the reactance matrix and III the Born approximation for the proper phases of the scattering matrix. In both approximations conservation conditions are satisfied exactly.

The use of these methods is described by Seaton (1961) and we therefore give only the final results. Fig. 2 shows the inelastic cross section and

Fig. 3 the elastic cross section. Approximation III is seen to be rather better than II. As is to be expected from the results obtained in an exactly soluble problem (Seaton 1961), the theoretical results for the inelastic process are better than those for the elastic process.

Fig. 4 shows that the theory, which tends to over-estimate the inelastic cross section and under-estimate the elastic cross section, gives good results for the total cross section. As a further check we have calculated the total cross section for Cs. The trend in going from Na to Cs is seen, in Fig. 4, to be reproduced correctly by the theory.

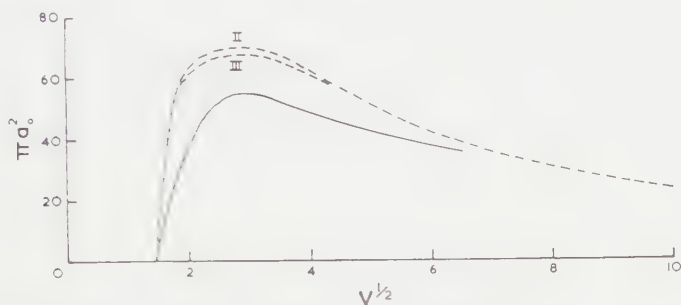


Fig. 2. The Na inelastic cross section ($3s \rightarrow 3p$). The full line curve is the experimental cross section, the broken curves the results calculated in approximations II and III.

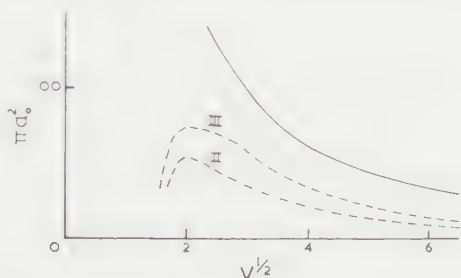


Fig. 3. The Na elastic cross section for energies above the $3p$ excitation threshold. Full line curve experimental, broken curves from approximations II and III.

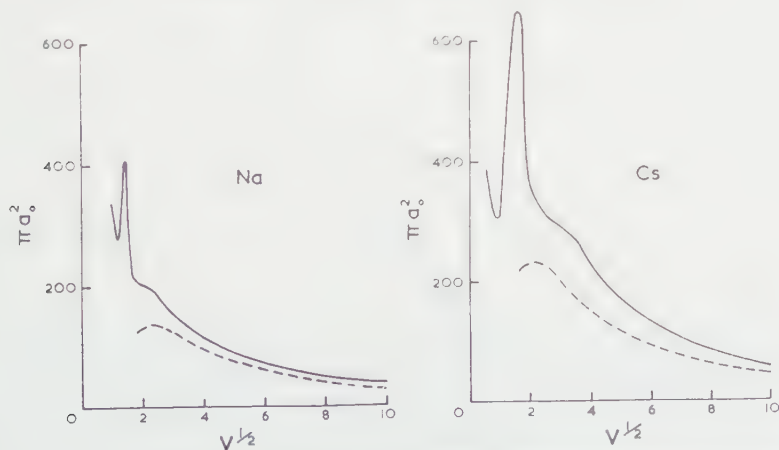


Fig. 4. Total cross sections for Na and Cs. Full line curves are experimental results of Brode (1929), broken curves are from calculations in approximation III.

We have considered a theory which is fairly crude, and which fails completely as the excitation threshold is approached, but it is good enough to show that the great strength of the 3s-3p interaction explains the main trend of the experimental results at the higher energies.

§ 3. EXCHANGE EQUATIONS

For calculations at lower energies a more refined theory is required. The present section is of the nature of a digression concerning some properties of exchange equations, a subject previously discussed by Seaton (1953).

3.1. The Na^+ Core

For the ten electrons of the Na^+ core we consider orbital functions $a_i(\mathbf{x}_j)$, $\mathbf{x}_j = (\mathbf{r}_j, \sigma_j)$ representing the space and spin coordinates. The complete wave function has the determinant form

$$D(a_1 a_2 \dots a_{10}) = \frac{1}{\sqrt{10!}} \begin{vmatrix} a_1(\mathbf{x}_1) a_2(\mathbf{x}_2) \dots a_{10}(\mathbf{x}_{10}) \\ a_1(\mathbf{x}_2) \\ \vdots \\ a_1(\mathbf{x}_{10}) \dots a_{10}(\mathbf{x}_{10}) \end{vmatrix} \dots \dots \dots (3.1)$$

Without altering D one may replace $a_i(\mathbf{x})$ by

$$a_i(\mathbf{x}) + \sum_{j \neq i} C_j a_j(\mathbf{x}) \dots \dots \dots (3.2)$$

and hence no essential restriction results from imposing the orthonormality condition

$$(a_i | a_j) = \delta_{ij}. \dots \dots \dots (3.3)$$

The orbitals are determined by the variational condition

$$\delta(a_1 a_2 \dots a_{10} | H_{10} | a_1 a_2 \dots a_{10}) = 0 \dots \dots \dots (3.4)$$

where H_{10} is the ten-electron Hamiltonian. From (3.3) and (3.4) one obtains

$$H_{\text{HF}} a_i = E_i a_i \dots \dots \dots (3.5)$$

where H_{HF} is the Hartree-Fock Hamiltonian,

$$H_{\text{HF}} = -\frac{1}{2} \nabla^2 - \frac{11}{r} + V - W, \dots \dots \dots (3.6)$$

$$V a_i = \sum_{j=1}^{10} v(a_j a_j) a_i, \dots \dots \dots (3.7)$$

$$W a_i = \sum_{j=1}^{10} v(a_j a_i) a_j, \dots \dots \dots (3.8)$$

$$v(a_j a_k | \mathbf{x}) = \int \frac{a_j^*(\mathbf{x}_0) a_k(\mathbf{x}_0)}{|\mathbf{r} - \mathbf{r}_0|} d\mathbf{x}_0. \dots \dots \dots (3.9)$$

The term $j=i$ is included in the definition of $V a_i$, $W a_i$ but cancels in $(V - W) a_i$. The parameter E_i in (3.5) is adjusted so as to obtain solutions which may be made to satisfy $(a_i | a_i) = 1$. For $i \neq j$ there is no need to introduce Lagrange multipliers in order to obtain solutions which satisfy $(a_i | a_j) = 0$; for $E_i \neq E_j$, from the fact that H_{HF} is Hermitian, it follows that $(a_i | a_j) = 0$ and for $E = E_j$ one can choose the functions spin and angular coordinates to be such that $(a_i | a_j) = 0$.

3.2. Addition of a Valence Electron

On adding a valence electron with orbital b , we have a determinant function $D(a_1 a_2 \dots a_{10} b)$. Retaining the a_i calculated for Na^+ , b is determined from

$$\delta(a_1 a_2 \dots a_{10} b | H_{11} | a_1 a_2 \dots a_{10} b) = 0, \quad \dots (3.10)$$

$$(b|b) = 1, \quad (a_i|b) = 0. \quad \dots (3.11)$$

This gives

$$H_{\text{HF}} b = E_b b \quad \dots (3.12)$$

where the operator, H_{HF} , is identical with that occurring in (3.5) but in $(I - W)b$ there is no longer the type of cancellation which occurs between the $j=i$ terms of (3.7), (3.8). The parameter E_b is adjusted to obtain solutions which satisfy $(b|b)=1$; for $E_b \neq E_i$ these satisfy $(a_i|b)=0$.

3.3. Radial Equations for the Atom

Let the configuration be $1s^2 2s^2 2p^6 n_1 l_1$ and let the radial functions be $P_{nl}(r)$ where nl is $1s, 2s, 2p$ or $n_1 l_1$. The radial equations are obtained on carrying out the integrations over spin and angular coordinates and then varying the radial functions. Using standard techniques (Condon and Shortley 1935, Hartree 1957) one obtains

$$\mathcal{H}_{\text{HF}}^{(0)} P_{nl}(r) = E_{nl} P_{nl}(r) \quad \dots (3.13)$$

where

$$\mathcal{H}_{\text{HF}}^{(0)} = -\frac{1}{2} \left[\frac{d^2}{dr^2} - \frac{l(l+1)}{r^2} \right] - \frac{11}{r} + V - W^{(0)}, \quad \dots (3.14)$$

$$V = 2y_0(1s1s) + 2y_0(2s2s) + 6y_0(2p2p), \quad \dots (3.15)$$

$$W^{(0)} P_{nl} = \frac{1}{(2l+1)} \left\{ y_l(1s nl) P_{1s} + y_l(2s nl) P_{2s} \right. \\ \left. + \left(\frac{3l}{2l-1} \right) y_{l-1}(2p nl) P_{2p} + \left(\frac{3l+3}{2l+3} \right) y_{l+1}(2p nl) P_{2p} \right\} \quad \dots (3.16)$$

and where y_λ is defined by (2.10). Introducing

$$(nl|n'l) = \int_0^\infty P_{nl} P_{n'l} dr, \quad \dots (3.17)$$

one has $(nl|n'l) = 0$ for $E_{nl} \neq E_{n'l}$.

Solutions of (3.13) have been obtained by Fock and Petrashen (1934) and, rather more accurately, by Hartree (1948).

3.4. Radial Equations for the Collision Problem

With orbitals ϕ for the colliding electron one could construct determinant functions

$$D(a_1 a_2 \dots a_{10} b \phi). \quad \dots (3.18)$$

The complete wave function could be taken to be a linear combination of such determinants. The quantum numbers would be $n_1 l_1 m_{l_1} m_{s_1}$ for the valence-electron orbital b and $kl_2 m_{l_2} m_{s_2}$ for the orbital ϕ .

It is convenient to use an LS coupling representation. Let γ stand for the quantum numbers

$$\gamma = 1s^2 2s^2 2p^6 n_1 l_1 k l_2 S L M_S M_L. \quad \dots (3.19)$$

The functions Ψ_γ are obtained from the functions (3.18) using vector-coupling formulae. The complete wave function is

$$\Psi(\gamma') = \sum_\gamma \Psi_\gamma(\gamma') \quad \dots\dots (3.20)$$

where γ' is introduced in specifying boundary conditions. If one uses the reactance matrix the radial functions for the colliding electron have asymptotic form

$$F_\gamma(\gamma'|r) \sim k^{-1/2} \{ \sin(kr - \frac{1}{2}l_2\pi) \delta(\gamma, \gamma') + \cos(kr - \frac{1}{2}l_2\pi) R(\gamma, \gamma') \}. \quad \dots\dots (3.21)$$

The radial functions may be determined from a Hulthén-Kohn type of variational principle:

$$\delta \left\{ (\gamma'' | H - E | \gamma) + \frac{\hbar^2}{2m} R(\gamma'', \gamma') \right\} = 0. \quad \dots\dots (3.22)$$

When (3.22) is satisfied for all variations in the functions F_γ , the errors in the calculated cross sections will be proportional to expressions of quadratic order in the errors in the wave functions.

In obtaining the radial equations from (3.22) we impose the orthogonality conditions

$$(1s|kl_2) = 0 \quad \text{and} \quad (2s|kl_2) = 0 \quad \text{for} \quad l_2 = 0, \quad \dots\dots (3.23)$$

$$(2p|kl_2) = 0 \quad \text{for} \quad l_2 = 1 \quad \dots\dots (3.24)$$

but we do not impose the condition $(n_1 l_1 | k l_2) = 0$ for $l_1 = l_2$. The question of orthogonality relations will be discussed in §3.5.

The radial equations are

$$\begin{aligned} \{ \mathcal{H}_{\text{HF}}^{(l_2)} - \frac{1}{2}k^2 \} F_{n_1 l_1 k l_2 S L} + \sum_{\lambda n_1' l_1' l_2'} \{ f_\lambda(l_1 l_2 l_1' l_2'; L) y_\lambda(n_1 l_1 n_1' l_1') F_{n_1' l_1' k l_2' S L} \\ + (-1)^{l_1 + l_2 - S - L} [\delta_{\lambda, 0} \delta_{l_1, l_2'} \delta_{l_2, l_1'} (E_{n_1 l_1} - \frac{1}{2}k'^2) (n_1 l_1 | k' l_2') \\ + f_\lambda(l_1 l_2 l_2' l_1'; L) y_\lambda(n_1 l_1 k' l_2') \} P_{n_1' l_1'} \} = 0 \quad \dots\dots (3.25) \end{aligned}$$

where

$$E_{n_1 l_1} - \frac{1}{2}k^2 = E_{n_1' l_1'} - \frac{1}{2}k'^2. \quad \dots\dots (3.26)$$

In deriving these equations we have used the Eqns (3.13) satisfied by the atomic radial functions.

In (3.25), all interactions with the Na^+ core are contained in the operator $\mathcal{H}_{\text{HF}}^{(l_2)}$; all other terms represent interactions with the valence electron. If the operator $H_{\text{HF}}^{(l_2)}$ were replaced by

$$\mathcal{H}^{(l_2)} = -\frac{1}{2} \left[\frac{d^2}{dr^2} - \frac{l_2(l_2+1)}{r^2} \right] - \frac{1}{r} \quad \dots\dots (3.27)$$

the Eqns (3.25) would be identical with the equations, discussed by Percival and Seaton (1957), for electron collisions with H atoms.

3.5. Orthogonality Conditions

It is readily shown that the solutions of (3.25) will satisfy the orthogonality conditions (3.23), (3.24) and also that imposition of these conditions does not involve any essential restriction on the radial functions.

In general we have not the same freedom to impose an orthogonality condition $(n l_1 | k' l_2') = 0$ for $l_1 = l_2'$. Consider the case of $3sksS$ where S is the total-spin quantum number. Let us put

$$F_{3sksS} = F_{3sksS}^0 + c P_{3s} \quad \dots\dots (3.28)$$

where F_{3skS}^0 is orthogonal to P_{3s} . The complete wave function is then seen to contain a linear combination of the wave function for

$$1s^2 2s^2 2p^6 3s^2 S.$$

For the triplet interaction, $S=1$, this part vanishes and, without introducing any essential restriction, one could replace F_{3skS} by the orthogonal function F_{3skS}^0 . For the singlet interaction, $S=0$, the situation is different since the $3s^2$ function no longer vanishes.

The importance of retaining the term $\delta_{l,l'}(nl_1|k'l'_2)$ in (3.25) is that we allow, in effect, for the possibility of the complete wave function containing admixtures of functions for states such as $3s^2$ and the coefficients of these admixtures are determined from a variational principle.

§ 4. CROSS SECTION EXPRESSIONS

We consider elastic scattering below the first excitation threshold. The radial functions F_{3sklS} then have phases $\eta_l(S)$, and the transmission matrix \mathbf{T} has diagonal elements

$$T_l(S) = 1 - \exp 2i\eta_l(S). \quad \dots\dots (4.1)$$

The elastic cross section is

$$Q = \frac{1}{4} \frac{\pi}{k_{3s}^2} \sum_l (2l+1)(2S+1) |T_l(S)|^2 \quad \dots\dots (4.2)$$

$$= \frac{\pi}{k_{3s}^2} \sum_l (2l+1) \{ \sin^2 \eta_l(0) + 3 \sin^2 \eta_l(1) \} \quad \dots\dots (4.3)$$

where the factor $\frac{1}{4}$ in (4.2) comes from averaging over spin orientations. For the exchange process (1.3) we use the representation of uncoupled spins,

$$T_l(m_{s_1} m_{s_2}, m'_{s_1} m'_{s_2}) = \sum_{SM_S} C_{m_{s_1} m_{s_2} M_S}^{\frac{1}{2} \frac{1}{2} S} T_l(S) C_{m'_{s_1} m'_{s_2} M_S}^{\frac{1}{2} \frac{1}{2} S}. \quad \dots\dots (4.4)$$

The exchange cross section is

$$Q(\text{exch}) = \frac{\pi}{k_{3s}^2} \sum_l (2l+1) |T_l(+\frac{1}{2} - \frac{1}{2}, -\frac{1}{2} + \frac{1}{2})|^2 \quad \dots\dots (4.5)$$

$$= \frac{\pi}{k_{3s}^2} \sum_l (2l+1) \sin^2 (\eta_l(0) - \eta_l(1)). \quad \dots\dots (4.6)$$

For $k_{3s} \rightarrow 0$,

$$\eta_0(S) = N\pi + \Lambda(S)k_{3s} + O(k_{3s}^2) \quad \dots\dots (4.7)$$

where Λ is the scattering length and N is an integer. When polarization is taken into account, the higher order phases ($l > 0$) behave as k_{3s}^2 . The zero-energy elastic cross section is

$$Q = \{ \Lambda^2(0) + 3\Lambda^2(1) \} \pi a_0^2 \quad \dots\dots (4.8)$$

and the zero-energy exchange cross section is

$$Q(\text{exch}) = \{ \Lambda(0) - \Lambda(1) \}^2 \pi a_0^2, \quad \dots\dots (4.9)$$

Λ being in atomic units.

§ 5. THE ZERO ENERGY CROSS SECTIONS

We consider scattering by $3s$ allowing for virtual excitation of $3p$. In general, for each value of l , we have three states $3sk_{3s}l$, $3pk_{3p}l-1$ and $3pk_{3p}l+1$ but for $l=0$ we have only $3sk_{3s}s$ and $3pk_{3p}p$.

5.1. The Radial Equation

Introducing the notation

$$P_1 = P_{3s}, \quad E_1 = E_{3s}, \quad k_1 = k_{3s}, \quad F_1 = F_{3s} k_1 s \quad \dots (5.1)$$

and

$$P_2 = P_{3p}, \quad E_2 = E_{3p}, \quad k_2 = k_{3p}, \quad F_2 = F_{3p} k_2 p \quad \dots (5.2)$$

the radial equations are

$$\begin{aligned} (\mathcal{H}_{\text{HF}}^{(0)} - \frac{1}{2} k_1^2) F_1 + y_0 (P_1 P_1) F_1 - 3^{-1/2} y_1 (P_1 P_2) F_2 \\ + (-1)^s [(E_1 - \frac{1}{2} k_1^2) (P_1 | F_1) P_1 + y_0 (P_1 F_1) P_1 - 3^{-1/2} y_1 (P_1 F_2) P_2] = 0, \end{aligned} \quad \dots (5.3)$$

$$\begin{aligned} (\mathcal{H}_{\text{HF}}^{(2)} - \frac{1}{2} k_2^2) F_2 - 3^{-1/2} y_1 (P_1 P_2) F_1 + y_0 (P_2 P_2) F_2 + (2/5) y_2 (P_2 P_2) F_2 \\ + (-1)^s [-3^{-1/2} y_1 (P_2 F_1) P_1 + (E_2 - \frac{1}{2} k_2^2) (P_2 | F_2) P_2 \\ + y_0 (P_2 F_2) P_2 + (2/5) y_2 (P_2 F_2) P_2] = 0. \end{aligned} \quad \dots (5.4)$$

With $E_1 = -0.180$, $E_2 = -0.111_5$ and $k_1 = 0$ we have $k_2^2 = -0.137$. We put $\kappa^2 = -k_2^2 = +0.137$. We seek solutions $F_1(r)$, $F_2(r)$ of (5.3), (5.4) satisfying $F_1(0) = F_2(0) = 0$ and

$$F_1(r) \sim r + \Lambda(S), \quad F_2(r) \sim 0. \quad \dots (5.5)$$

It may be shown (Castillejo, Percival and Seaton 1960) that

$$F_2 \sim \frac{2}{\kappa^2 \sqrt{3}} \frac{s_1}{r^2} F_1 \quad \dots (5.6)$$

where $y_1(P_1 P_2 | r) \sim s_1 / r^2$.

We first studied separately the effects of polarization and of exchange.

5.2. Polarization without Exchange

We neglected all exchange terms and also the quadrupole term $y_2(P_2 P_2)$. The following equations were solved:

$$\{\mathcal{H}_{\text{cf}}^{(0)} + y_0(P_1 P_1)\} F_1^{(\text{cf})} = 0, \quad \dots (5.7)$$

$$\{\mathcal{H}_{\text{cf}}^{(1)} + y_0(P_2 P_2) + \frac{1}{2} \kappa^2\} F_2^{(1)} = 3^{-1/2} y_1(P_1 P_2) F_1^{(\text{cf})}, \quad \dots (5.8)$$

$$\{\mathcal{H}_{\text{cf}}^{(0)} + y_0(P_1 P_1)\} F_1^{(1)} = 3^{-1/2} y_1(P_1 P_2) F_2^{(1)} \quad \dots (5.9)$$

where

$$\mathcal{H}_{\text{cf}}^{(l)} = -\frac{1}{2} \left\{ \frac{d^2}{dr^2} - \frac{l(l+1)}{r^2} \right\} + V. \quad \dots (5.10)$$

The central field function is $F_1^{(\text{cf})}$ and the first approximation to the radial function allowing for polarization is $F_1^{(1)}$. The asymptotic forms were taken to be

$$F_1^{(\text{cf})} \sim r + \Lambda(\text{cf}), \quad \dots (5.11)$$

$$F_2^{(1)} \sim \frac{2}{\kappa^2 \sqrt{3}} \frac{s_1}{r} F_1^{(\text{cf})} + C e^{-\kappa r}, \quad \dots (5.12)$$

$$F_1^{(1)} \sim r + \Lambda(p). \quad \dots (5.13)$$

To obtain the required solution of (5.8) we obtained two solutions by outward integration satisfying $F_2^{(1)}(0) = 0$ and two solutions by inward integration having different values of the constant C in (5.12). The solution satisfying both boundary conditions was then obtained by matching at intermediate values of r . It may be noted that, due to the long range of the coupling potential, the asymptotic forms (5.12), (5.13) are good approximations only for very large

values of r . In order to obtain Λ from functions calculated out to $r=24$ it was necessary to use asymptotic forms correct to terms of order r^{-3} . Neglecting the term in $\exp(-\kappa r)$ we have

$$F_1 \sim r + \Lambda - \frac{2s_1^2}{3\kappa^2} \left[r^{-1} + \frac{\Lambda}{3} r^{-2} - \frac{s_1^2}{9\kappa^2} r^{-3} \dots \right],$$

$$F_2 \sim \frac{2s_1}{\kappa^2\sqrt{3}} \left[r^{-1} + \Lambda r^{-2} - \frac{2s_1^2}{3\kappa^2} r^{-3} \dots \right].$$

These calculations gave $\Lambda(\text{cf})=2.4$, $\Lambda(\text{p})=-36$, a result which shows the effect of polarization to be very large.

5.3. Exchange without Polarization

Before attempting to improve the polarization calculations, by further iteration with equations of the type (5.7) to (5.9), we tried to estimate the effect of exchange using a Kohn type of variational calculation. As trial functions we took

$$F_1 = F_1^{(\text{cf})} + cP_1, \quad \dots\dots (5.14)$$

the parameter c being varied, and $F_2=0$. These calculations gave $\Lambda(0)=+60$, $\Lambda(1)=-29$.

5.4. Exchange and Polarization

Having shown that the effects of polarization and of exchange are both large, we continued with an iterative treatment in which both effects were included simultaneously. In Eqns (5.3), (5.4) we made the approximations of replacing $\mathcal{H}_{\text{HF}}^{(l)}$ by $\mathcal{H}_{\text{cf}}^{(l)}$, thereby neglecting exchange with the Na^+ core, and of omitting the quadrupole terms, $y_2(P_2P_2)F_2$ and $y_2(P_2F_2)P_2$.

Starting with

$$F_1^{(0)} = F_1^{(\text{cf})}, \quad F_2^{(0)} = F_2^{(\text{p})} \quad \dots\dots (5.15)$$

we solved the equations

$$\{\mathcal{H}_{\text{cf}}^{(0)} + y_0(P_1P_1)\}F_1^{(n)} = 3^{-1/2}y_1(P_1P_2)F_2^{(n-1)} \\ + (-1)^n[E_1(P_1|F_1^{(n-1)})P_1 + y_0(P_1F_1^{(n-1)})P_1 - 3^{-1/2}y_1(P_1F_2^{(n-1)})P_2],$$

\dots\dots (5.16)

$$\{\mathcal{H}_{\text{cf}}^{(1)} + y_0(P_2P_2) + \frac{1}{2}\kappa^2\}F_2^{(n)} = 3^{-1/2}y_1(P_1P_2)F_1^{(n-1)} \\ - (-1)^n[-3^{-1/2}y_1(P_2F_1^{(n-1)})P_1 + E_1(P_2|F_2^{(n-1)})P_2 + y_0(P_2F_2^{(n-1)})P_2]$$

\dots\dots (5.17)

to obtain

$n=$	0	1	2	3	4
$\Lambda(0)=$	2.4	-10.0	-14.0	-13.9	—
$\Lambda(1)=$	2.4	9.6	5.3	9.5	6.6.

To consider the convergence, write Eqns (5.16), (5.17) as

$$\mathcal{L}[F^{(n)}] = \phi[F^{(n-1)}], \quad \dots\dots (5.18)$$

We say that the solutions converge to a single function if, for large n , $F^{(n)} \rightarrow G$, independent of n . This was found to be the case for $S=0$. For $S=1$ we obtained convergence to two functions, $F^{(2n)} \rightarrow G_1$, $F^{(2n+1)} \rightarrow G_2$ where

$$\mathcal{L}[G_1] = \phi[G_2], \quad \mathcal{L}[G_2] = \phi[G_1]. \quad \dots\dots (5.19)$$

A similar effect was found by John (1960) for elastic scattering by H. The

required solution of $\mathcal{L}[G] = \phi[G]$ is clearly $G = \frac{1}{2}(G_1 + G_2)$. This gives $\Lambda(1) = 8$.

Fig. 5 shows the radial functions obtained in the final iterations.

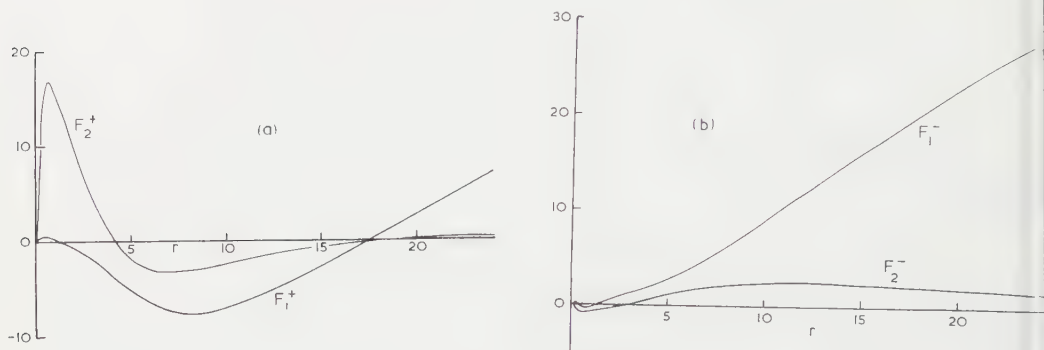


Fig. 5. Radial functions for zero-energy scattering. (a) Singlet interaction. The function F_1^+ is from the 3rd iteration, F_2^+ from the 2nd iteration. (b) Triplet interaction. The function F_1^- is the mean of the functions obtained in the 3rd and 4th iterations, F_2^- the mean from the 2nd and 3rd iterations.

5.5. Corrections for Exchange with the Na^+ Core

We obtained an estimate of the effect of the exchange terms $y_0(1sks)$ and $y_0(2sks)$. To illustrate the method, consider that we were to iterate on the term $y_0(1sks)$. We would solve equations of the form

$$\mathcal{L}F_1^{(n)} = [\lambda^{(n)} + y_0(P_{1s}F_1^{(n-1)})]P_{1s}. \quad \dots\dots (5.20)$$

At each stage of the iteration, $\lambda^{(n)}$ would be adjusted to give solutions satisfying

$$(P_{1s}|F_1^{(n)}) = 0; \quad \dots\dots (5.21)$$

the convergence would then be rapid (Seaton 1951). For large n , the parameter $\lambda^{(n)}$ would tend to zero and one would have

$$\mathcal{L}F_1 = y_0(P_{1s}F_1)P_{1s}. \quad \dots\dots (5.22)$$

The first function to be obtained is

$$\mathcal{L}F_1^{(0)} = \lambda^{(0)}P_{1s}. \quad \dots\dots (5.23)$$

It is seen that the constant $\lambda^{(0)}$ represents an effective mean value of the function y_0 . It has been found previously that this first correction already gives a good estimate of the exchange interaction (Seaton 1951).

The method outlined (Eqn (5.23)) was used to obtain corrections to the results of the final iterations of §5.4. The corrections were not large, the final corrected results being

$$\Lambda(0) = -12, \quad \Lambda(1) = +9.$$

§ 6. DISCUSSION OF THE ZERO ENERGY CROSS SECTIONS

The results of Fig. 1 suggest that the zero-energy elastic cross section is at least as great as the calculated value, $Q = 380\pi a_0^2$.

The calculated exchange cross section, $Q(\text{exch}) = 440\pi a_0^2$, is consistent with the measurement of Dehmelt, $Q(\text{exch}) \geq 260\pi a_0^2$. However, our calculations do not confirm the suggestion of Dehmelt that in calculating $Q(\text{exch})$

only the singlet interaction need be considered. With $\Lambda(0) = -12$, $\Lambda(1) = +9$, the triplet interaction is nearly as strong as the singlet interaction. In this connection it should be noted (§3.5) that our wave functions contain an admixture of $3s^2\ ^1S$ functions and therefore make allowance for the effect discussed by Dehmelt.

REFERENCES

- BATES, D. R., FUNDAMINSKY, A., LEECH, J. W., and MASSEY, H. S. W., 1950, *Phil. Trans. Roy. Soc. A*, **243**, 93.
 BRODE, R. E., 1929, *Phys. Rev.*, **34**, 673.
 CASTILLEJO, L., PERCIVAL, I. C., and SEATON, M. J., 1960, *Proc. Roy. Soc. A*, **254**, 259.
 CHRISTOPH, W., 1935, *Ann. Phys., Lpz.*, **23**, 51.
 CONDON, E. U., and SHORTLEY, G. H., 1935, *The Theory of Atomic Spectra* (Cambridge: University Press), ch. VI.
 DEHMELT, H. G., 1958, *Phys. Rev.*, **109**, 381.
 FILIPPOV, A., and PROKOFJEV, W., 1929, *Z. Phys.*, **56**, 458.
 FOCK, V., and PETRASHEN, M. J., 1934, *Phys. Z. Sowjet.*, **6**, 368.
 HAFT, G., 1933, *Z. Phys.*, **82**, 73.
 HARTREE, D. R., 1948, *Proc. Roy. Soc. A*, **193**, 299.
 ——— 1957, *The Calculation of Atomic Structures* (London: Chapman and Hall).
 JOHN, T. L., 1960, *Proc. Phys. Soc.*, **76**, 532.
 MASSEY, H. S. W., and BURHOP, E. H. S., 1952, *Electronic and Ionic Impact Phenomena* (Oxford: Clarendon Press), ch. I.
 PERCIVAL, I. C., 1960, *Proc. Phys. Soc.*, **76**, 206.
 PERCIVAL, I. C., and SEATON, M. J., 1957, *Proc. Camb. Phil. Soc.*, **53**, 654.
 SALMONA, A., and FRENKIEL, P., 1959, *J. Phys. Radium*, **20**, 492.
 SEATON, M. J., 1951, *Proc. Roy. Soc. A*, **208**, 408.
 ——— 1953, *Phil. Trans. Roy. Soc. A*, **245**, 469.
 ——— 1955, *Proc. Phys. Soc. A*, **68**, 457.
 ——— 1961, *Proc. Phys. Soc.*, **77**, 174.
 WIGNER, E. P., 1948, *Phys. Rev.*, **73**, 1002.

Improvements in the Lattice Model of a Liquid

BY H. N. V. TEMPERLEY

Atomic Weapons Research Establishment, Aldermaston, Berks.

MS. received 5th August 1960

Abstract. A new type of approximation is introduced, with the objects of examining further the transition of a fluid of non-attracting rigid molecules, and of improving the lattice model of a liquid by reducing the ratio of mesh size to molecular volume. The approximation is first checked by applying it to some simple two-dimensional lattices, reproducing many known results and predicting some new ones. The probable qualitative behaviour of the isotherm of a two-dimensional fluid of rigid non-attracting molecules is determined, available evidence suggesting the existence of a finite region in which the fluid phase is metastable. Some preliminary results on the effect of reducing the lattice mesh size suggest that simple lattice models of a liquid do give physically sensible results in spite of their crudity.

§ 1. INTRODUCTION

THE question whether a gas of non-attracting rigid spheres would show a transition to an ordered configuration as the free volume was gradually diminished was finally settled by the machine calculations of Alder and Wainwright (1957) and Wood and Jacobson (1957). The sharpness of the transition is quite apparent even in quite small assemblies, and its onset probably lies at between 1.8 and 1.5 times the close-packed volume. The corresponding two-dimensional assembly has been studied experimentally by Turnbull and Cormia (1960) and a similar transition was found at about 1.2 times the close-packed area, this figure being almost independent of the 'temperature', or random kinetic energy imparted to the spheres. This is to be expected theoretically.

In attempts to find possible analytic reasons for these transitions, various 'lattice' models have been studied by Temperley (1959 a, b) and Burley (1960). According to such models, the 'hard core' of a molecule is described by assuming that it 'occupies' two or more contiguous sites, e.g. one lattice point and its nearest neighbours. The latter model is equivalent to an extreme case of the order-disorder model, in which for example neighbouring A-A pairs are forbidden altogether. The fact that, in such a situation, no transition is possible unless the number of A molecules attains a certain minimum value was pointed out by Easthope (1937). The model can also be treated as an extreme case of the Onsager-Ising problem when the interactions between neighbours are in the antiferromagnetic direction and large (Temperley 1959 a). The following conclusions can be drawn from Temperley's papers (1959 a, b).

(a) One can use these simple models as reasonable representations of the solid-gas transition at high pressures.

(b) The Mayer z -series cannot describe the disordered state right up to the transition curve, because it diverges before this as the result of singularities (*not* on the positive real axis) of little real significance.

(c) Unlike the gas-liquid transition, the solid-gas transition involves some sort of ordering parameter, so the Mayer theory has to be modified, to take account of the unequal occupation of sub-lattices in the ordered state.

(d) The virial series probably holds right up to the transition curve and does not necessarily have a singularity even there. It may well be possible to extrapolate it to even higher densities, corresponding physically to a supercooled liquid.

(e) Although the analytical details of the liquid-vapour transition (the result of attractive forces) are still uncertain, it is clear that they are quite different from those of the solid-gas transition, the result of repulsive forces.

The lattice model of a liquid or compressed gas is a reasonable first approximation, but it is open to the criticism that the coordinates of the centre of a molecule are, in an actual liquid, continuously variable, whereas the model only allows it to be in a discrete set of positions, in other words we are using a mesh that is comparable with the size of the molecule. A reduction in the size of the mesh is equivalent to the assumption that a molecule 'occupies' a larger number of sites, and we shall examine the effect of making this change. In the language of Burley's (1960) paper, we are increasing the effective number of neighbours of a particular site so that our modified models correspond to 'close-packed' lattices. Burley (1960) suggests that such lattices show different analytic behaviour from 'loose-packed' lattices, in that their virial coefficients all seem to be positive. In later work Burley (private communication) has found a transition for the plane triangular lattice which is first order, in contrast with the second-order transitions found for the loose-packed lattices. Its location agrees with that found from Eqn (21) below.

§ 2. A NEW APPROXIMATION METHOD

Until some analytic results are discovered for 'completely rigid' molecules, one must rely on approximations or series expansions. We now describe an approximation method that, besides reproducing many of the results quoted by Burley (1960), leads in a natural way to transitions to the ordered state and to descriptions of the latter, and also enables us to follow the effect of a reduction of mesh size.

Various workers, see, for example, Newell and Montroll (1953) have made use of a matrix technique. The assembly is supposed to be built up by adding lattice sites a row at a time. Each row of the matrix corresponds to one possible mode of occupation of the last row of lattice sites and each column of the matrix to one possible mode of occupation of the last-but-one row. We determine the element pq in the matrix as the modification in the Boltzmann factor for the whole assembly caused by adding a row with mode of occupation p to an assembly whose outer row had mode of occupation q , the various possible modes of occupation being enumerated, for example, by binary numbers. The most natural application of this process is evidently to two-dimensional lattices with interactions between neighbouring sites only, but it is obviously of much greater generality. If, for example, interactions extended between three successive rows of the lattice instead of between neighbouring rows, we could make one row of the matrix correspond to each configuration of the assembly consisting of the *two* rows s and

$s+1$ of the lattice, while the columns would correspond to the configuration of the assembly formed by combining rows $s-1$ and s . It is possible to set up the matrices corresponding to a wide range of problems in statistical mechanics, the essential difficulty is to solve the resulting problem by determining the eigenvalues.

The connection between this work and stochastic theory is obvious. If T is the matrix defined as above, T_{pq} is proportional to the probability that its outer row will have configuration p , given that the next to outer row has configuration q . $T_{pq}T_{qr}$ represents the probability that a row with configuration r will be followed by a row with configuration q and then by a row with configuration p and so on, so that the various terms of the matrix product T^{n-1} describe an assembly with n rows. If we insist that the first and last rows are identical, all the possibilities are included in the trace of T^n , which is known asymptotically if we can determine the top eigenvalue of T . For the rigid molecule type of problem that we are considering in this paper, the elements of T are zero or unity, corresponding to the fact that rigid molecules interact with an energy of infinity or zero, according as they do or do not overlap.

The approximation that we use is equivalent to a less severe version of the stochastic problem. We try to set up a matrix, the element (mn) of which is the probability that the $(s+1)$ th row contains m molecules, given that the s th row contains n molecules, nothing yet being said about the $(s+2)$ th row. This probability is evidently the ratio $P(m, n)/Q(n)$ where $Q(n)$ is the number of ways in which n molecules can be disposed in row s , nothing being said about row $s+1$, while $P(m, n)$ is the number of ways in which m molecules can be disposed in row $s+1$ and n molecules at the same time in row s . Clearly we must have

$$\sum_n P(m, n) = Q(n)$$

so that our quantities defined above are genuine probabilities and we have a stochastic matrix. In practice, it is more convenient to work with the more symmetrical quantity $P(m, n)/[Q(m)Q(n)]^{1/2}$. The rules of matrix multiplication ensure that the trace of any power of this matrix is identical with that of the former one, though in general it is not stochastic. For quite a number of models generating functions for the P 's and Q 's are very readily obtainable.

§ 3. PARTICULAR EXAMPLES OF THE 'MATRIX' APPROXIMATION

3.1. Plane Square Lattice

We consider first the plane square lattice (simple quadratic) with interactions between nearest neighbours only. We can divide the lattice into two interlacing sub-lattices A and B (Fig. 1) and, in the completely ordered state, one



Fig. 1.

of these will be empty, the other completely filled, while, in the disordered state they will be equally occupied. In our first treatment, we build up the lattice

by adding diagonal rows one at a time, thus rows of A sites and B sites will alternate (Fig. 1). If the total number of sites in each row is L , then the quantity $Q(n)$ is given simply by $\binom{L}{n}$, since, if we are considering one diagonal row only, we can fill up any or all of the L sites without causing any overlap. To determine the quantity $P_{2L}(m, n)$, the number of ways in which m A sites and n B sites, in two contiguous rows each of L sites, can be occupied without any overlaps, we can set up a recurrence relation. We use the condition that, if an A site is occupied both neighbouring B sites must be empty, and vice-versa. Let

$$p_l(w, z) = \sum_m \sum_n P_l(m, n) w^m z^n$$

be the generating function for a double row of l sites in all, the left-hand site being an A site. Let $q_l(w, z)$ be the same generating function for a double row totalling l sites, the left-hand one being a B site. Then, enumerating the two possible modes of occupation of the left-hand site in each case, we must have

$$p_l = w p_{l-2} + q_{l-1} \quad \dots\dots (1)$$

because, if the left-hand A site is occupied, the neighbouring B site must be empty, but the next A site can be empty or occupied. If we leave the left-hand A site empty, the neighbouring B site can be empty or occupied. Similarly

$$q_l = z q_{l-2} + p_{l-1} \quad \dots\dots (2)$$

These recurrence relations can be solved by means of generating functions. If $p(x, z, w)$ stands for $\sum_l p_l x^l$, we find

$$p \sim [1 - x^2 - x^2 w - x^2 z + x^4 w z]^{-1} \quad \dots\dots (3)$$

This gives results that are sufficiently good for long rows. (Strictly speaking, the expression p has a numerator, a polynomial of low degree in x , whose terms depend on the 'boundary conditions' i.e. on the occupations of the end sites.) From (3) we find without difficulty that the asymptotic form of $P_{2L}(m, n)$ must be

$$P_{2L}(m, n) \sim 0(1) \binom{L-m}{n} \binom{L-n}{m} \quad \dots\dots (4)$$

To expand expressions such as (3), the following identity has been found very valuable:

$$\begin{aligned} [S - Tw - Uz + Vz w]^{-1} &\equiv \sum_{r=0}^{\infty} \sum_m \sum_n \binom{m+r}{r} \binom{n+r}{r} w^m z^n \\ &\times \frac{V^{m+n+1}}{T^{n+r+1} U^{m+r+1}} (TU - SV)^r \quad \dots\dots (5) \end{aligned}$$

which can be arrived at, first by expansion in ascending powers of w , then in ascending powers of z .

Our estimate for the (m, n) element in our stochastic-type matrix is therefore given by

$$P_{2L}(m, n) / [Q(m)Q(n)]^{1/2} = \binom{L-m}{n} \binom{L-n}{m} / \left[\binom{L}{m} \binom{L}{n} \right]^{1/2} \quad \dots\dots (6)$$

Strictly speaking, we ought now to solve the eigenvalue problem posed by expression (6), but consideration shows that we can infer the final consequences of the approximation directly.

In the disordered state, there is no distinction between different rows, so we expect the dominant contribution to the number of arrangements of NM molecules on NL sites to come from micro-states in which the occupations of each row are nearly equal. In the ordered state, we have asymmetry between the occupations of the two sub-lattices, but there still is no distinction between different pairs of rows. If we constrained the occupation numbers of different pairs of rows to be alike, the contribution to the partition function would be just the N th power of expression (6), and we assume this to be dominant. If (6) can be increased by allowing m and n to become unequal, subject to the constraint that $m+n=2M$, then we take the maximum value. Our process is thus a simple generalization of that of 'selecting the maximum term' but rigorous generalizations of the principle of steepest descents to assemblies described by stochastic type matrices, rather than simple generating functions, are almost certainly possible.

A further check on the validity of this assumption is that, as will be seen below, the results agree with those of Burley (1960). These, in turn, rest on the theorem of Rushbrooke and Scoins (1955), according to which the only contributions to the irreducible cluster series come from molecules grouped on single sites, neighbouring pairs or multiply-connected groups of sites. Since certain groups of sites, e.g. $:::$, can be shown to give a zero contribution if the molecules are rigid, Burley's type of approximation turns out to be particularly good for the 'rigid' case. It can be improved further, but we reserve this for another paper.

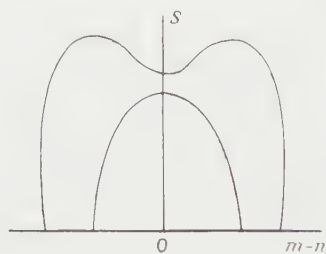


Fig. 2.

We can also think of (6) as analogous to Bethe's approximation, in which we first work out the exact partition function for a 'sample' assembly and then apply a correction to allow for the effect of the remaining molecules. Looked at in this way, the 'sample' assembly is now a whole double row, the partition function of which is given by the numerator of (6), while the denominator of (6) corrects for the fact that arrangements in successive pairs of rows are *not* independent. The thermodynamic consequences of (6) can now be worked out. The relation between m and n must be such as to make (6) a maximum, subject to $m+n=2M$. Taking logarithms and differentiating (or letting m and n each change by 1) leads us to the condition

$$(L-m)^3n = (L-n)^3m \quad \dots\dots (7)$$

the solutions of which are

$$m=n=M \text{ or } \frac{m}{n} = M \pm (L-M) \left(\frac{4M-L}{3L-4M} \right)^{1/2} \quad \dots\dots (8)$$

so that the symmetric (disordered) solution is the only one for $M < \frac{1}{4}L$, while for $M > \frac{1}{4}L$ it is easily seen to make the entropy a minimum and therefore to be unstable, while the unsymmetric (ordered) solution is stable (Fig. 2). The

virial is easily determined from the equation $\partial P / \partial T = \partial S / \partial V$, for altering the volume is equivalent to altering the length of each row, that is L , keeping M constant. We find, with $x = M/L$,

$$\begin{aligned} \frac{vPv}{kT} &= 3 \log(1-x) - 2 \log(1-2x) \quad (\text{disordered}) \quad \dots\dots (9) \\ &= 3 \log(1-x) - 2 \log(1-2x) + \frac{3}{2} \log\left(\frac{4-8x}{3-4x}\right) \quad (\text{ordered}) \\ &\dots\dots (10) \end{aligned}$$

(9) is identical with the Bethe type approximation, quoted by Burley (1960) (his section 3.2), while (10) agrees closely with the virial for the ordered state plotted in his Fig. 3 but derived from a quite different model. Our approximation predicts a 'second-order' type of change. The 'order' $(m-n)/(m+n)$ is zero at the actual transition point but rises according to a square root law as we go to higher densities. This is not inconsistent with the machine calculations, which gave a region in which the two isotherms overlap. It must be remembered that, if the transition were strictly second order the ordering entropy is very small until we take M sufficiently above the transition value. Put in another way, the 'thermodynamic driving force' is small, so we would expect the transition to be sluggish.

3.2. Plane Square Lattice (*Aliter*)

It is interesting to examine the result of building up the lattice by adding rows straight across the lattice rather than building it up along the diagonals. The typical pair of rows is shown in Fig. 3. The partition function for the

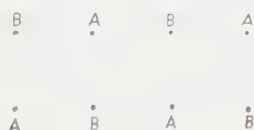


Fig. 3.

pair of rows can be formed by a recurrence relation in a way quite analogous to that already used, the three possible modes of occupation of the left-hand pair of sites being considered separately, and recurrence relations being set up as before. The generating function is found to be

$$(1 - x^2 - x^2w - x^2z + x^2wz + x^3wz)^{-1} \quad \dots\dots (11)$$

which also lends itself to expansion by means of (5). The correcting factor is obtained by enumerating the modes of occupation of a single sample row which, this time, consists of A and B sites alternately, the expected numbers on them being $\frac{1}{2}m$, $\frac{1}{2}n$ respectively, since m is the expected number on L A sites, so that we have the same problem as that solved by generating function (3). Our estimate for the factor contributed to the partition function by one row of sites is then found to be

$$\frac{\sum_r \binom{m+r}{r} \binom{n+r}{r} \binom{2m+2n-L+2r}{L-m-n-2r}}{\binom{\frac{1}{2}L-\frac{1}{2}m}{\frac{1}{2}n} \binom{\frac{1}{2}L-\frac{1}{2}n}{\frac{1}{2}m}} \quad \dots\dots (12)$$

In evaluating the logarithm of the numerator of (12) it is, as usual, sufficiently accurate to replace the series by its maximum term, which leads to a quadratic for r . Maximizing with respect to m and n , subject to $m+n=2M$ we obtain the following pair of equations for mn and r

$$Lr^2 + 2rmn - mn(L - 2M) = 0 \quad \dots\dots (13)$$

$$m = n \text{ or } r^2(4LM - 4M^2 - 4mn) - r(L - 2M) \\ \times (2LM - 4M^2 - 4mn) - mn(L - 2M)^2 = 0, \quad \dots\dots (14)$$

For the disordered state, we find the virial (differentiating with respect to L as before)

$$\frac{xP\epsilon}{kT} = -\log(1-x) + \log[2x + (1-4x+8x^2)^{1/2}] \quad \dots\dots (15)$$

identical with that quoted by Burley (1960, Eqn (13)) as the consequence of the 'ring approximation' of Rushbrooke and Scoins (1955). Examination of Eqns (14) and (15) shows that the behaviour of the partition function is qualitatively just the same as before, i.e. for small x , the only maximum is given by $m=n$ but, above the critical value, the disordered solution corresponds to a minimum of the partition function, the value of $(m-n)$ corresponding to the two maxima increasing from zero as before, the critical value of x being determined by the equation

$$8x^2 - 12x + 3 = 0 \quad \text{with the relevant root } x = 0.317 \quad \dots\dots (16)$$

corresponding to a critical volume of 1.60 times close packing.

3.3. Plane Triangular Lattice (Molecules Rigid Hexagons)

There are now three sub-lattices (Fig. 4) and our sample assembly is chosen in the manner shown. We can derive a recurrence relation as before by considering the four permissible modes of occupation of the left-hand set of points

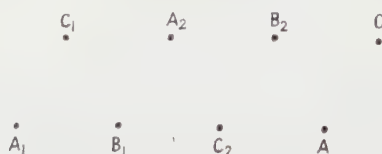


Fig. 4.

A_1, B_1, C_1 in conjunction with the modes of occupation of A_2, B_2, C_2 that are compatible with them. The generating function is found to be

$$[1 - x^2 - x^2(w + v + z) + x^4(wv + wz + vz) - x^6wvz]^{-1}. \quad \dots\dots (17)$$

This can be expanded, as before, by applying (5) to one pair of variables, e.g. w and z . The single row is made up of groups of three sites taken in the order ABCA and, since only this row is involved (it is to be filled up as if the other rows were not there) we have only to prevent occupation of pairs of neighbouring sites in the row. The generating function for this problem is found to be

$$[1 - x^3 - x^3(w + v + z) - x^6(wvz)]^{-1} \quad \dots\dots (18)$$

which, since all the terms involving x are of the same sign, can be expanded by the multinomial theorem. We arrive at the following as our estimate of the factor in the partition function per row added.

$$\frac{\left(\frac{2}{3}L - \frac{m}{p} - n\right)! \left(\frac{2}{3}L - \frac{m}{n} - p\right)! \left(\frac{2}{3}L - \frac{n}{m} - p\right)!}{\sum_{r=0}^{\frac{2}{3}L} \left(\frac{1}{3}L - r\right)! [r!(m-r)!(n-r)!(p-r)!(\frac{1}{3}L + r - m - n - p)!]} \dots\dots\dots (19)$$

where, as usual, it is understood that no terms with negative factorials occur and $0!$ is interpreted as 1. This time we must maximize the denominator with respect to r . Proceeding as before, we obtain for the virial in the disordered state

$$\frac{pPv}{kT} = -\log(1-x) + 3\log(1-2x) - 2\log(1-3x) \dots\dots\dots (20)$$

which again is identical with the result of the ring approximation given by Burley (1960, Eqn (12)).

Searching for the value of x , equal to $3M/2L$ for this lattice, at which the symmetric solution ceases to give a maximum in the partition function, we find

$$3x^2 - 5x + 1 = 0: \text{relevant root } x = 0.232 \dots\dots\dots (21)$$

corresponding to a critical volume of $1.43 \times$ close packing.

Burley (private communication) has arrived at an equivalent result by another method. A closer study of the model showed him that there are now *three* branches of the virial consistent with the entropy being stationary, and two of them correspond to ordered states. Their qualitative behaviour is shown in Fig. 9. The relation

$$TS = \int p dv = - \int \frac{p dx}{x^2}$$

clearly shows that, where relevant, the lowest of the three curves must correspond to the largest entropy. Furthermore, we can, in exactly the same manner as in the discussion of the van der Waals, Bragg-Williams and similar models, use the rule of equal areas to identify the points L and M in Fig. 9, between which an overall gain of entropy results from breaking an assembly with uniform density x into two assemblies with densities x_L and x_M .

Thus, the 'solidification density', x_L , is slightly less than the density, x_C , at which the disordered state becomes unstable relative to an ordered one of equal density. Whether a further extrapolation of the disordered virial beyond C would lead to its passing through a maximum, as that for the square lattice does, is at present uncertain, but the portion of the disordered virial beyond C would only be of physical significance if transfers between the two sub-lattices were prevented.

3.4. Plane Square Lattice Interactions Extending as far as Second Neighbours

There are now four sub-lattices and our sample assembly is as shown in Fig. 5, but the interactions still only occur between sites in the same or neighbouring rows. The enumeration of modes of occupation can at once be made to depend on the simple generating function (3), the actual generating function for the problem being simply

$$[1 - x^2 - x^2(z_A + z_D) - x^2(z_B + z_C) + x^4(z_A + z_D)(z_B + z_C)]^{-1} \dots\dots\dots (22)$$

This is equivalent to (3) except for the fact that, at each station, there are always *two* mutually exclusive ways of placing a molecule, i.e. we can occupy the A or D site, but not both, and either alternative prevents the occupation of the nearest

B and C sites. The problem of filling a single row is precisely that solved by (3). Our estimate of the contribution to the partition function per added row is a factor

$$\frac{(\frac{1}{2}L - m_A - m_D)!}{m_B!m_C!(\frac{1}{2}L - m_A - m_B - m_C - m_D)!} \frac{(\frac{1}{2}L - m_B - m_C)!}{m_A!m_D!(\frac{1}{2}L - m_A - m_B - m_C - m_D)!} \\ \left[\binom{\frac{1}{2}L - m_A}{m_C} \binom{\frac{1}{2}L - m_C}{m_A} \binom{\frac{1}{2}L - m_B}{m_D} \binom{\frac{1}{2}L - m_D}{m_B} \right]^{1/2} \dots\dots (23)$$

which leads to the following expression for the virial in the disordered state:

$$\frac{xP_v}{kT} = -\log(1-x) + 2\log(1-2x) - \log(1-4x). \dots\dots (24)$$

In the light of Burley's work on the triangular lattice, a study was made of expression (23), and it was indeed found that, for certain values of x , there are

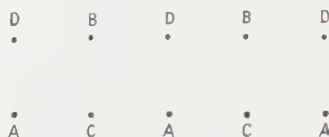


Fig. 5.

three real solutions of the equations obtained by maximizing (23) with respect to the m 's. There is always the disordered solution, all four m 's equal, and the two ordered virials behave qualitatively as in Fig. 9. They correspond to two different modes of ordering, y being a parameter measuring the degree of order.

Branch CD: $m_A = m_C = M(1+y)$; $m_B = m_D = M(1-y)$.

Branch CME: $m_A = m_B = M(1 + \frac{1}{2}y^2 + \dots)$; $m_C = M(1 + y - \frac{1}{2}y^2 + \dots)$;
 $m_D = M(1 - y - \frac{1}{2}y^2 + \dots)$.

It was also verified that these are the only physically significant solutions (apart from those arising from permutations among the four sub-lattices). It will be seen that the more relevant branch, CME, corresponds to the more unsymmetrical occupation of sub-lattices, and it is reasonable that this gives the larger entropy. It, in fact, involves the solution of a seventh-degree equation, whereas an explicit form for the equation of branch CD can be given.

For the value of x corresponding to the point C we find

$$4x^2 - 6x + 1 = 0 : \text{relevant root } x = 0.191 \dots\dots (25)$$

corresponding to 1.31 times the close-packed volume.

3.5. Squares Covering q^2 Sites

We can proceed in an analogous way as the mesh becomes finer. For $q=3$ Fig. 6 shows that, of any three successive stations A, B, and C, no more than one may be occupied, and also that station A may be occupied in three mutually exclusive ways A_1, A_2, A_3 . The necessary generating function for $P(m, n)$ is obtained from (17) in just the same way that we obtained (22) from (3), that is we write $w_1 + w_2 + w_3$ for w , $v_1 + v_2 + v_3$ for v etc. As we have mentioned above, since

the interactions now extend beyond pairs of neighbouring rows, each row or column of the stochastic matrix now describes the configuration of $q-1$ successive rows in the lattice. For $q=3$, the generating function for $Q(m)$ is obtained from (17) by replacing w by $w_1 + w_2$ etc., while that for $Q(n)$ is similarly obtained by replacing w by $w_2 + w_3$ etc. The expression $(Q(m)Q(n))^{1/2}$ does not maintain



Fig. 6.

symmetry between the nine sub-lattices, those with suffix 2 being treated in a special way, but this is easily remedied by introducing another factor involving A_1 and A_3 etc. and taking the cube root. With the labelling given in Fig. 6 and putting for short $m_A = m_{A1} + m_{A2} + m_{A3}$ etc., we obtain for $P(m, n)$ the product of

$$\frac{(\frac{1}{3}L - m_B - m_C)!}{m_{A1}!m_{A2}!m_{A3}!(\frac{1}{3}L - m_A - m_B - m_C)!} \dots\dots (26)$$

with two similar expressions.

Instead of $(Q(m)Q(n))^{1/2}$ we write

$$\left[\frac{(\frac{1}{3}L - m_{B1} - m_{B2} - m_{C1} - m_{C2})!}{m_{A1}!m_{A2}!(\frac{1}{3}L - m_{A1} - m_{A2} - m_{B1} - m_{B2} - m_{C1} - m_{C2})!} \times \text{six similar expressions} \right. \\ \cdot \frac{(\frac{1}{3}L - m_{A2} - m_{B3} - m_{C2} - m_{C3})!}{m_{A2}!m_{A3}!(\frac{1}{3}L - m_{A2} - m_{A3} - m_{B2} - m_{B3} - m_{C2} - m_{C3})!} \\ \left. \times \frac{(\frac{1}{3}L - m_{B1} - m_{B3} - m_{C1} - m_{C3})!}{m_{A1}!m_{A3}!(\frac{1}{3}L - m_{A1} - m_{A3} - m_{B1} - m_{B3} - m_{C2} - m_{C3})!} \right]^{1/3} \dots\dots (27)$$

and symmetry between the sub-lattices is restored while preserving the spirit of the 'matrix approximation'. For a general value of q we have, according to this further assumption, the following disordered virial series obtained from the appropriate generalization of (26) and (27):

$$\frac{Pv}{kT} = 2 \log(1 - q(q-1)x) - \log(1 - q^2x) - \log(1 - (q-1)^2x). \dots\dots (28)$$

We have found closed expressions for the ordered virial series only in the special cases described by Eqns (10) and (15). It is of interest to see what becomes of (28) in the limiting case when q becomes very large. Each molecule then occupies a large number of lattice sites, and we are back to Zwanzig's (1956) model of oriented rigid squares in a two-dimensional continuum. Introducing b the side of the square, we have $x = b^2/vq^2$, where v is the 'volume' (actually area) available per molecule, we find without difficulty that

$$\frac{Pv}{kT} = 1 + \frac{2b^2}{v} + \frac{3b^4}{v^2} + \frac{4b^6}{v^3} + \frac{5b^8}{v^4} + \dots \dots\dots (29)$$

whereas the correct coefficients (Zwanzig 1956) are 1, 2, 3, 3.67, 3.77 respectively. In spite of the simplicity of expression (28) and of the approximations that led to it, these results are closer to the truth than those of the best other approximations

so far available. The results of the latter are listed by Temperley (1957). The 'ring' and 'netted ring' approximations there mentioned refer to rings of molecules in cluster-integrals, and have nothing to do with the 'ring' approximation mentioned by Burley (1960), which refers to rings of sites on the lattice.

In Table 1 we list the ratio of the close-packing density to the density at point A, Fig. 7 or C, Fig. 9, at which order can set in without any change of density. This represents the actual transition density for the 'loose-packed' lattices, but for the 'close-packed' lattices the transition sets in at a slightly lower density,

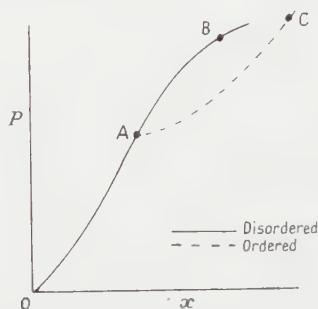


Fig. 7.

which would correspond to a slightly higher figure than in the Table. The ratio is listed against the effective number of lattice points covered by the molecule. For example, for the nearest neighbour model on the square lattice, this number is two because close-packing corresponds to occupation of just one half of the lattice-points. The tendency of the ratio to diminish with smaller mesh size

No. of points	2 (square)	3 (hexagon)	4 (square)	9 (square)	∞ (square)
Effective no. of neighbours	4	6	8	24	∞
Ratio of densities	1.60	1.43	1.31	1.11	(1.00)

is clearly marked. Bearing in mind that the transition may actually set in at a lower density, the general run of the figures agrees well with the observation of Turnbull and Cormia (1960) that a transition occurs for a two-dimensional assembly of spheres at an area of about 1.2 times that of close packing.

§ 4. DISCUSSION

The possibilities of this type of approximation are by no means exhausted. It seems to be particularly suitable for the 'rigid molecule' case but could be applied to other models also. There are possibilities of improving it further. For example, we can specify the configurations of our 'sample' rows more closely than stating merely the total number of molecules in each. If we improve the treatment in § 3.1 by specifying, besides the number of molecules in row A, the numbers occupying contiguous sites in that row, with a similar specification for row B (Fig. 1), we improve the approximation (9) to the better one (15).

The results suggest that we do make mistakes about the position and nature of the transition if we use a lattice mesh that corresponds to only one point per liquid 'cell', but that little further improvement is likely once we introduce a reasonable

number of mesh points into each cell. Actually, the machine calculations are hardly able to distinguish between the situations shown in Figs 7 and 9. A transition occurring near the point A in Fig. 7 would only involve a small change of density and might escape notice, though the calculations certainly do seem to suggest an isotherm with two definitely separated, but overlapping, portions.

A point of some interest concerns the signs of the higher virial coefficients and the related question whether the metastable disordered virial goes through a maximum, as suggested in Fig. 7, or rises monotonically. Burley (1960) has suggested that this virial goes through a maximum for the 'loose-packed' lattices but is monotonic for the 'close-packed' ones. There is insufficient evidence at the moment to check this conjecture for the plane triangular lattice. If we refer to the corresponding antiferromagnetic problem, cf. Brooks and Domb (1951), there is certainly a region where the ordered state is stable, the probable shape being sketched in Fig. 8. The peculiarity of this lattice is that the transition is

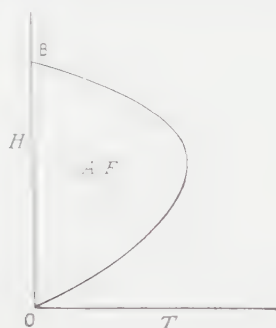


Fig. 8.

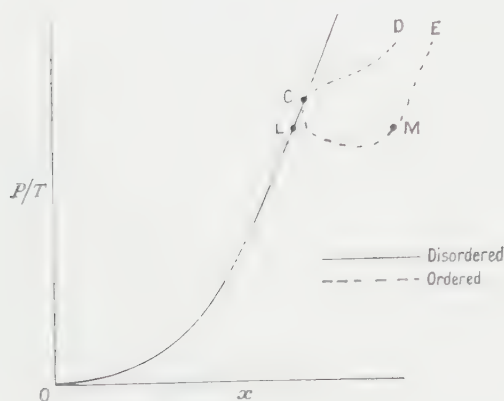


Fig. 9.

absent for $H=0$, but our rigid case corresponds to point B in Fig. 8. The best analytic approximation so far available involves a ring of only three lattice sites and is insufficiently accurate to settle this point. It is hoped to present and discuss some further numerical and analytic results on the triangular lattice in another paper. Only a few coefficients are known for other 'close-packed' lattices so we must rely on indirect evidence at present. Zwanzig's (1956) continuous models

may be regarded as equivalent to extreme cases of the 'close-packed' lattices (interactions occurring between a site and a great many 'neighbours'). Even here Temperley (1957) found some definite instances of negative virial coefficients, and gave reasons for expecting others.

§ 5. CONCLUSIONS

The evidence at present available suggests that, in spite of its obvious crudity, the 'lattice' model of a gas or liquid does not do any great violence to the physics of the problem. As in other numerical calculations it is advisable to examine the effect of altering the size of the coordinate mesh, and we find that it is permissible to use a relatively coarse mesh. The likely behaviour of the isotherm of a 'rigid molecule liquid' is as sketched in Fig. 9.

ACKNOWLEDGMENTS

Some of the results of this paper have been derived, independently and by other means, by Dr. D. M. Burley. I wish to thank him for helpful discussions and correspondence, also for letting me see his unpublished results. I should also like to thank the Director of the Atomic Weapons Research Establishment for permission to publish this paper.

REFERENCES

- ALDER, B. J., and WAINWRIGHT, T. E., 1957, *J. Chem. Phys.*, **27**, 1208.
BROOKS, J. E., and DOMB, C., 1951, *Proc. Roy. Soc. A*, **207**, 343.
BURLEY, D. M., 1960, *Proc. Phys. Soc.*, **75**, 262.
EASTHOPE, C. E., 1937, *Proc. Camb. Phil. Soc.*, **33**, 502.
RUSHBROOKE, G. S., and SCOINS, H. I., 1955, *Proc. Roy. Soc. A*, **230**, 74.
NEWELL, G. F., and MONTROLL, E. W., 1953, *Rev. Mod. Phys.*, **25**, 353.
TEMPERLEY, H. N. V., 1957, *Proc. Phys. Soc. B*, **70**, 537.
— 1959 a, b, *Proc. Phys. Soc.*, **74**, 183, 432.
TURNBULL, D., and CORMIA, R. L., 1960, *J. Appl. Phys.*, **31**, 674.
WOOD, W. W., and JACOBSON, T. D., 1957, *J. Chem. Phys.*, **27**, 1207.
ZWANZIG, R. W., 1956, *J. Chem. Phys.*, **24**, 855.

The Effect of Electrodes in a Linear Pinched Discharge

By M. G. HAINES

Physics Department, Imperial College of Science and Technology,
London, S.W.7

*Communicated by R. Latham; MS. received 29th January 1960, in revised form
5th April 1960*

Abstract. A linear pinched discharge in fully ionized hydrogen or deuterium is examined theoretically under an idealized steady-state condition, when there is a pressure and an energy balance and no instabilities. Under this condition, the Joule heating caused by the axial current is balanced by bremsstrahlung radiation losses and by axial heat conduction and diffusion to the electrodes. A partial analytical solution is found assuming that the transport coefficients have the usual power dependencies on temperature throughout the plasma. It is shown that all the energy not radiated is carried to the anode, the cathode even having a negative total heat flux at its surface due to thermal effects of diffusion by the current-carrying electrons. The maximum temperature in the discharge is shown to vary directly with the voltage across the tube and only insensitively to other parameters. Further relations are derived involving the dimensions of the discharge, the current and the maximum temperature. The temperature, the line density and the electric field are plotted showing their variation along the axis. The relative importance of heat conduction and radiation losses is seen to depend only on the total axial current which is flowing. A typical example of a discharge shows that temperatures of 10^6 to 10^7 °K are quite feasible in the presence of heat losses to the electrodes.

§ 1. INTRODUCTION

THE linear pinched discharge is probably the most useful geometrical configuration for the examination of properties of hot ionized gases provided the electrodes have only a small effect on the gas or plasma. The effect and magnitude of the heat losses from the plasma to the electrodes is examined in this paper to see whether fairly high temperatures can be attained despite the presence of electrodes. The aim of this paper is also to produce algebraic relations involving the voltage and current applied to the discharge and the temperature, the particle line density and dimensions of the plasma. These will help the experimentalist to design a linear pinched discharge to give required temperatures.

The column of ionized gas is assumed to be stable. Since the conditions imposed on the plasma in this problem are such as to maintain a pressure balance and no acceleration of the plasma, Rayleigh–Taylor instabilities will be absent. The importance of the ‘static’ magnetohydrodynamic instabilities for a plasma in this configuration have not yet been assessed experimentally. Nevertheless, in spite of the possible presence of instabilities, the solution of this problem of heat losses to electrodes is believed to be of interest.

In order to be able to solve the problem without too many complications, the steady-state situation only is considered. This situation will hold in a pinched discharge after a certain relaxation time, but it is not envisaged, of course, that it

will then hold indefinitely. It will be shown later that the anode receives a large amount of heat, but it is assumed that, during the time when this steady state exists, the temperature of the anode is very little altered because of its own high thermal capacity and conductivity.

A qualitative examination shows that the coefficients of both thermal and electrical conductivity of a fully ionized gas depend on its temperature in such a way that near the electrodes where the gas is cool, the thermal conduction is low and the Joule heating is high compared with the centre of the discharge. Thus the gas near the centre of the discharge might effectively be isolated from the electrodes thermally and be at quite a high temperature. Superimposed on this, the electrons which carry the current also carry heat by diffusion in the direction of the anode, thus shifting the maximum temperature towards the anode and destroying the symmetry about the centre of the discharge. Throughout the plasma heat is also lost by Bremsstrahlung radiation. This ought to be included in the treatment so that the relative magnitudes of the two forms of heat loss can be assessed.

A quantitative analysis of the problem will now be given which will confirm this qualitative picture to a large extent. The m.k.s. system of units is used.

§ 2. BASIC EQUATIONS

2.1. *The Steady-state Model*

The fully ionized hydrogen or deuterium in the linear pinched discharge is assumed to possess azimuthal symmetry when viewed in cylindrical coordinates. It is also assumed to be stable and isolated in the radial direction from the side walls of the containing vessel. The plasma is bounded axially at $z=0$ by the anode and at $z=z_0$ by the cathode. In order that suitable boundary conditions should be imposed on the energy equation, it is assumed that the electrodes are kept by external means at a fixed temperature T_0 . In the radial direction the plasma is bounded at $r=a$, this outside radius of the plasma being less than the internal radius of the vessel. An axial current \mathcal{I} is the only current flowing, and it is this which interacts with the associated azimuthal magnetic field to produce the radial pinch force.

Because of this isolation of the plasma from the side walls it is reasonable to assume (due to the large thermal conductivity) that its temperature is fairly uniform across the radius, and that it is a function of z only. This simplifies the problem without affecting the main effect of the axial heat conduction.

In the steady state envisaged, there is a pressure balance everywhere in the plasma. If the electrical current has an axial component only, the pressure balance conditions can be written as

$$\frac{\partial p}{\partial r} = -i_z B_\phi \quad \dots\dots (1)$$

$$\frac{\partial p}{\partial z} = 0. \quad \dots\dots (2)$$

The energy balance in the steady state can be written in the form

$$\frac{\partial q_z}{\partial z} + \frac{1}{r} \frac{\partial(rq_r)}{\partial r} + \beta n^2 T^{1/2} = i_z E_z. \quad \dots\dots (3)$$

This equation means that, for an element of plasma, the axial and radial heat conduction and the bremsstrahlung radiation losses are balanced by the Joule

heating. β ($=1.42 \times 10^{-40}$ m.k.s.) is the bremsstrahlung radiation coefficient and n is the number density of electrons.

Ohm's law contains a thermoelectric term for this problem, and this is written as

$$i_z = \sigma E_z + \phi \frac{\partial T}{\partial z} \quad \dots\dots (4)$$

where σ is the electrical conductivity and ϕ is the thermoelectric coefficient.

The heat flux vectors for this problem contain a thermal diffusion term as well as the thermal conduction term

$$q_z = -\lambda \frac{\partial T}{\partial z} + \psi i_z \quad \dots\dots (5)$$

$$q_r = -\lambda \frac{\partial T}{\partial r} \quad \dots\dots (6)$$

All these transport coefficients are dependent on temperature in the following way:

$$\left. \begin{aligned} \lambda &= \kappa T^{5.2} & \text{where } \kappa &= 8.7 \times 10^{-12} \text{ m.k.s.} \\ \sigma &= \alpha T^{3.2} & \text{where } \alpha &= 1.1 \times 10^{-3} \text{ m.k.s.} \\ \phi &= \gamma T^{3.2} & \text{where } \gamma &= 0.69 \times 10^{-4} \text{ m.k.s.} \\ \psi &= -\zeta T & \text{where } \zeta &= 2.85 \times 10^{-4} \text{ m.k.s.} \end{aligned} \right\} \quad \dots\dots (7)$$

These values have been taken from Marshall (1958) where the logarithmic terms have been fixed at a value of 27. The coefficients are related by $\kappa/\alpha\gamma^2 = 1.63$ and $\zeta/\gamma = 4.11$, these being purely numerical.

In Eqns (4), (5), (6) and (7) the effect of the magnetic field on the transport coefficients has been ignored until § 5.3 for the sake of simplicity. Thus, since in general this would reduce the conduction coefficients, the worst possible case is being studied. Similarly in the energy equation (3) no account has been taken of magnetic bremsstrahlung radiation. This heat loss is unimportant below temperatures of 5×10^7 °K. Also the magnitude of this loss is considerably reduced due to the large absorption of the radiation by the plasma (see Trubnikov and Kudryavtsev 1958).

The application of Faraday's law of induction shows that in the steady state the axial electric field E_z is uniform across the radius. From Eqn (4) it thus follows that i_z is also uniform because of the assumptions made about the transport coefficients and the temperature.

The relevant component of Maxwell's equation which is applicable to an axial current is

$$\frac{1}{r} \frac{\partial}{\partial r} (r B_\phi) = \mu i_z \quad \dots\dots (8)$$

From Eqns (1) and (8), the radial distribution of number density of ions or electrons and the Bennett (1934) relation are derived:

$$n(r, z) = \frac{2N(z)}{\pi a^2} \left[1 - \frac{r^2}{a^2} \right] \quad \dots\dots (9)$$

$$16\pi N(z) k T(z) = \mu \mathcal{I}^2 \quad \dots\dots (10)$$

where the pressure p is given by

$$p(r, z) = 2n(r, z) k T(z),$$

the line density of ions or electrons by

$$N(z) = \int_0^a 2\pi n(r, z) r dr$$

and the total axial current by

$$\mathcal{J} = \int_0^a 2\pi i_z r dr$$

with the condition that $n=p=0$ at $r=a$.

Also, Eqn (2) yields

$$\frac{\partial}{\partial z} [n(r, z) T(z)] = 0. \quad \dots\dots (11)$$

From Eqns (10) and (11) it can be seen that both $n(r, z)T(z)$ and $N(z)T(z)$ are independent of z . Therefore, this simple model, where axial current only flows, is consistent with the bounding radius of the plasma a being independent of z .

In Eqn (3), though the temperature T is assumed fairly uniform over the radius, q_r , the radial heat flux, is not zero in the plasma due to the large value of λ , the thermal conductivity. However, at $r=a$, q_r is zero due to the radial isolation of the plasma. Thus q_r is eliminated from Eqn (3) by integrating over the radius. For this Eqn (9) is used for the radial dependence of n , giving

$$\pi a^2 \frac{\partial q_z}{\partial z} + \frac{4}{3} \beta \frac{N^2}{\pi a^2} T^{1/2} = \mathcal{J} E_z. \quad \dots\dots (12)$$

$N(z)$ can be eliminated from this using Eqn (10), to give

$$\pi a^2 \frac{\partial q_z}{\partial z} + \frac{\mathcal{J}^4}{\pi a^2 \alpha T^{3/2} \mathcal{J}_m^2} = \mathcal{J} E_z \quad \dots\dots (13)$$

where

$$\mathcal{J}_m = \left(\frac{192}{\alpha \beta} \right)^{1/2} \frac{\pi k}{\mu} = 1.21 \times 10^6 \text{ A} \quad \dots\dots (14)$$

and is the current which flows when Joule heating balances bremsstrahlung losses only; in this problem, in which there are heat conduction losses also, the axial current \mathcal{J} is always less than this in the steady state. Perhaps an advantage of electrodes is that a steady state can exist in a plasma using lower currents!

2.2. The Differential Equation for Temperature

Equations (4), (5) and (7) can be used in the energy equation (13) to obtain q_z , E_z and the transport coefficients entirely in terms of the temperature which is then the only function of z in the equation

$$\pi a^2 \kappa \frac{d}{dz} \left(T^{5/2} \frac{dT}{dz} \right) + \mathcal{J} (\zeta - \gamma) \frac{dT}{dz} + \frac{\mathcal{J}^2}{\pi a^2 \alpha T^{3/2}} \left(1 - \frac{\mathcal{J}^2}{\mathcal{J}_m^2} \right) = 0. \quad \dots\dots (15)$$

By suitable changes of variables, namely $\xi = \pi a^2 T^{5/2} / z_0 \mathcal{J}$ and $x = z/z_0$, this becomes

$$\frac{2}{5} \alpha \kappa \xi \frac{d^2 \xi}{dx^2} + \frac{4}{25} \alpha \kappa \left(\frac{d\xi}{dx} \right)^2 + \frac{2}{5} \alpha (\zeta - \gamma) \frac{d\xi}{dx} + 1 - \frac{\mathcal{J}^2}{\mathcal{J}_m^2} = 0. \quad \dots\dots (16)$$

This is now in a suitable form for analysis.

§ 3. FIRST INTEGRATION

3.1. Properties of the Differential Equation

The properties of Eqn (16) can be seen by plotting $\frac{2}{5}\alpha\kappa\xi(d^2\xi/dx^2)$ against $d\xi/dx$ as shown in Fig. 1.



Fig. 1. A plot of $\frac{2}{5}\alpha\kappa\xi(d^2\xi/dx^2)$ against $d\xi/dx$.

The plotted curve is a parabola with zeros of $\frac{2}{5}\alpha\kappa\xi(d^2\xi/dx^2)$ occurring at

$$\left[\frac{d\xi}{dx}\right]_1 = -\frac{5}{4\kappa}(\zeta - \gamma)(1 - s) \quad \dots\dots(17)$$

and at

$$\left[\frac{d\xi}{dx}\right]_2 = -\frac{5}{4\kappa}(\zeta - \gamma)(1 + s)$$

and a maximum positive value at

$$\left[\frac{d\xi}{dx}\right]_2 = -\frac{5}{4\kappa}(\zeta - \gamma).$$

For this s is defined by

$$\begin{aligned} s &= \left[1 - \frac{4\kappa}{\alpha(\zeta - \gamma)^2} \left(1 - \frac{\mathcal{J}^2}{\mathcal{J}_m^2}\right)\right]^{1/2} \quad \dots\dots(18) \\ &= \left[1 - \frac{1}{1.47} \left(1 - \frac{\mathcal{J}^2}{\mathcal{J}_m^2}\right)\right]^{1/2} \end{aligned}$$

and has a value depending on the current \mathcal{J} in the range 0.5654 ($\mathcal{J}=0$) to 1 ($\mathcal{J}=\mathcal{J}_m$).

It can be seen from Fig. 1 that, for the special problem under consideration where the plasma is held between electrodes both at a low temperature T_m , only part of this curve can be used, namely $d\xi/dx > [d\xi/dx]_1$.

Since $d^2\xi/dx^2 \rightarrow 0$ as $d\xi/dx \rightarrow [d\xi/dx]_1$, $d\xi/dx$ can in no circumstances pass through the value $[d\xi/dx]_1$. This can be seen more clearly in Fig. 2 which presents qualitatively a plot of $d\xi/dx (=v)$ against x (using the work of following sections). This shows that there are three branches to the curve, none of which are accessible

from any other in any one physical case where the differential equation holds throughout the plasma. In this problem, where there are two boundary conditions fixing the temperature at the electrodes, and a peak value of ξ (where $d\xi/dx=0$) is required at some point in between, the part of the curve to be used is that where $d\xi/dx > [d\xi/dx]_1$. There is thus a limiting gradient approaching $[d\xi/dx]_1$ at the cathode. It will be shown in § 3.3 that this does not prevent the attainment of very low temperatures there, necessary to satisfy the boundary condition. In fact, as $[d\xi/dx]_1$ is approached, with increasing x , ξ tends to a low value.

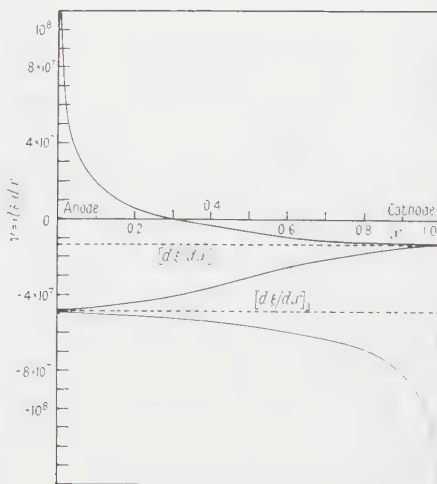


Fig. 2. A qualitative sketch of $d\xi/dx$ against x .

3.2. First Integration and Boundary Conditions

If $d\xi/dx$ is replaced by a parameter v in Eqn (16) it can be written in the form

$$-\int \frac{d\xi}{\xi} = \int \left[\frac{2\alpha\kappa}{5} v dv / \left(\frac{4\alpha\kappa}{25} v^2 + \frac{2\alpha}{5} (\xi - \gamma) v + 1 - \frac{\mathcal{J}^2}{\mathcal{J}_m^2} \right) \right]. \dots (19)$$

This can now be integrated using the boundary condition that, when $v=0$, ξ has a maximum value of ξ_m . Then the solution is

$$\begin{aligned} \left(\frac{\xi_m}{\xi} \right)^{4/5} &= \frac{4\alpha\kappa v^2/25 + 2\alpha(\xi - \gamma)v/5 + 1 - \mathcal{J}^2/\mathcal{J}_m^2}{1 - \mathcal{J}^2/\mathcal{J}_m^2} \\ &\times \left[\frac{4\kappa v/5(\xi - \gamma)(1+s) + 1}{4\kappa v/5(\xi - \gamma)(1-s) + 1} \right]^{1/s}. \dots (20) \end{aligned}$$

3.3. The Heat Flux to the Electrodes

The original energy equation (13) can be integrated from the anode ($z=0$) to the cathode ($z=z_0$) to give

$$\pi a^2 \left[q_z \right]_0^{z_0} + \frac{\mathcal{J}^4}{\pi a^2 \alpha \mathcal{J}_m^2} \int_0^{z_0} \frac{dz}{T^{3/2}} = \mathcal{J} V \dots (21)$$

where V is the potential in volts of the anode with respect to the cathode, that is

$$V = \int_0^{z_0} E_z dz. \dots (22)$$

Now Eqn (4) can be written in the form

$$\frac{\mathcal{J}}{\pi a^2 \alpha T^{3/2}} = \frac{i_z}{\alpha T^{3/2}} = E_z + \gamma \frac{dT}{dz}. \quad \dots\dots (23)$$

Therefore, if the temperatures of the anode and cathode are the same ($= T_0$), Eqn (23) can be integrated to give

$$\frac{\mathcal{J}}{\pi a^2 \alpha} \int_0^z \frac{dz}{T^{3/2}} = V. \quad \dots\dots (24)$$

Using Eqn (24), Eqn (21) becomes

$$[\pi a^2 q_z]_{\text{cathode}} - [\pi a^2 q_z]_{\text{anode}} + \mathcal{J} V \mathcal{J}^2 / \mathcal{J}_m^2 = \mathcal{J} V. \quad \dots\dots (25)$$

In this equation $[\pi a^2 q_z]_{\text{cathode}}$ = heat transferred to the cathode per second, $-\pi a^2 q_z]_{\text{anode}}$ = heat transferred to the anode per second, $\mathcal{J} V \mathcal{J}^2 / \mathcal{J}_m^2$ = total bremsstrahlung radiation loss per second, $\mathcal{J} V$ = total Joule heating per second.

Firstly, the heat flux to the cathode will be examined. It was noted in §2.1 that there is a limiting value of $[d\xi/dx]_1$ that can be obtained at the cathode. It can easily be shown that as v approaches $[d\xi/dx]_1$ in Eqn (20), large values of ξ_m can be obtained, that is, the temperature at the cathode can be very small in comparison with the maximum temperature in the plasma despite the small gradient of ξ .

Now the heat flux vector q_z can be written, using Eqns (5) and (7) as

$$q_z = -\kappa T^{5/2} \frac{dT}{dz} - \zeta T \frac{\mathcal{J}}{\pi a^2}. \quad \dots\dots (26)$$

Since $d\xi/dx$ is very close to $[d\xi/dx]_1$ at the cathode, the heat flux to the cathode can be written as

$$[\pi a^2 q_z]_{\text{cathode}} = -\frac{T_0 \mathcal{J}}{2} [\zeta(1+s) + \gamma(1-s)] \quad \dots\dots (27)$$

where

$$\frac{d\xi}{dx} = \frac{5}{2} \frac{\pi a^2}{\mathcal{J}} T^{3/2} \frac{dT}{dx} \quad \dots\dots (28)$$

and where $[d\xi/dx]_1$ is given by Eqn (17).

Thus, the heat flux to the cathode is a negative quantity. This is due to the dominant influence of the thermal effect of diffusion of the electrons which form the current. These electrons are emitted from the cathode and essentially carry their thermal energy with them. This effect is greater than the effect of thermal conduction to the cathode. As a typical example of the value of this heat flux, if $T_0 = 5 \times 10^2$ deg K, $\mathcal{J} = 10^6$ A, then from Eqn (27) the heat flux from the cathode is about 10^4 w. This is a small quantity in comparison with the Joule heating in the plasma, for, if $V = 10^3$ v, the Joule heating is 10^8 w.

All the heat generated in the plasma is thus either radiated or transferred to the anode. The heat flux at the anode will now be considered. The order of magnitude of $[d\xi/dx]_{\text{anode}}$ can be assessed from Eqn (25) using Eqns (26), (27) and (28).

$$\mathcal{J} V \left(1 - \frac{\mathcal{J}^2}{\mathcal{J}_m^2}\right) = \frac{2}{5} \kappa T_0 \mathcal{J} \left[\frac{d\xi}{dx}\right]_{\text{anode}} + \zeta T_0 \mathcal{J} - \frac{1}{2} T_0 \mathcal{J} [\zeta(1+s) + \gamma(1-s)]. \quad \dots\dots (29)$$

On inserting values in this for the typical case (as above) of $T_0 = 5 \times 10^2$ °K, $\mathcal{J} = 10^5$ A and $V = 10^3$ V, $[d\xi/dx]_{\text{anode}}$ is seen to be about 6×10^{11} . Then, when Eqn (20) is applied at the anode, $2v\kappa/5(\zeta - \gamma) \sim 10^4 \gg 1$ and $4\alpha\kappa v^2/25 \sim 10^8 \gg 1$, and thus the smaller powers of v in each factor can be ignored, thus giving

$$\frac{T_m^2}{T_0^2} = \left(\frac{\xi_m}{\xi_0}\right)^{4/5} = \frac{4\alpha\kappa}{25(1 - \mathcal{J}^2/\mathcal{J}_m^2)} \left[\frac{d\xi}{dx}\right]_{\text{anode}}^2 \left[\frac{1-s}{1+s}\right]^{1/s} \dots\dots (30)$$

Also in Eqn (29), the heat flux at the cathode and the thermal effect of diffusion at the anode can be ignored in comparison with the thermal conduction to the anode. Using this approximation, Eqns (29) and (30) can be combined to give the following important result:

$$V \left[1 - \frac{\mathcal{J}^2}{\mathcal{J}_m^2}\right]^{1/2} = \left(\frac{\kappa}{\alpha}\right)^{1/2} \left(\frac{1+s}{1-s}\right)^{1/2s} T_m \dots\dots (31)$$

In this equation it is to be noted that the maximum temperature is proportional to the applied voltage, and only weakly dependent on the current due to the inclusion of bremsstrahlung radiation losses. For no radiation losses, i.e. $\mathcal{J}_m = \infty$, Eqn (31) becomes

$$T_m = 3.62 \times 10^3 V \dots\dots (32)$$

It is interesting that in this first-order approximation the temperature of the electrodes, being much less than T_m , is not included in the result.

If there were no thermal effects of diffusion or thermoelectric effects, the discharge would be symmetrical about $\approx = \frac{1}{2}\xi_0$ and the anode and cathode would have equal effects. Then in Eqn (31) the factor $[(1+s)/(1-s)]^{1/2s}$ (which has a value of 3.109 when $\mathcal{J}_m = \infty$) would be replaced by a factor of 2. Therefore with thermal effects of diffusion and thermoelectric effects the maximum temperature is reduced to two-thirds approximately of what it would be without these effects. The case of heat losses to electrodes without thermal diffusion effects has been reported by Haines (1959 b) at the Uppsala Conference.

3.4. Comparison of Conduction and Radiation Losses

On examining Eqn (25) it can be seen that the ratio of heat lost by conduction and diffusion to the heat lost by bremsstrahlung radiation depends only on the current which flows in the discharge. In fact, it can be written as

$$\frac{\text{heat lost by conduction and diffusion}}{\text{heat lost by bremsstrahlung radiation}} = \frac{\mathcal{J}_m^2}{\mathcal{J}^2} - 1 \dots\dots (33)$$

where \mathcal{J}_m is given by Eqn (14). When $\mathcal{J} = \mathcal{J}_m/\sqrt{2}$ the two heat losses are the same. This corresponds to a current of 8.55×10^5 A. For currents less than this, the conduction and diffusion effects are greater, and for currents greater than this, bremsstrahlung radiation is dominant.

§ 4. SECOND INTEGRATION

4.1. Graphical Integration

There is no analytic integration of Eqn (20), and thus a second integration can only be found numerically. Because the values of the transport coefficients are only known to 10%, the best method of integration for this problem is graphical.

If $1/v (= dx/d\xi)$ is plotted against ξ/ξ_m , the area under the curves, as shown in Fig. 3, gives a value of $1/\xi_m$. This can be done for a specific value of $\mathcal{J}/\mathcal{J}_m$.

The value taken is $\mathcal{J}_m = \infty$, which is the case when radiation losses are absent. As ξ/ξ_m approaches unity, asymptotic solutions to Eqn (20) are used to calculate the area.

From the calculated area, a value of ξ_m for $\mathcal{J}_m = \infty$ is obtained as shown below:

$$\xi_m = \frac{\pi a^2 T_m^{5/2}}{z_0 \mathcal{J}} = 5.89 \times 10^6. \quad \dots\dots (34)$$

To include the effect of radiation losses in Eqn (34), an approximate algebraic result can be obtained using the fact that the area measured in Fig. 3 depends to a large extent on the value of $[dv/d\xi]_1$ at the cathode. This quantity varies with $\mathcal{J}/\mathcal{J}_m$ as $(1-s)^{-1}$ as given in Eqn (17). Therefore an approximate algebraic correction to Eqn (34) to include radiation losses can be written as

$$T_m^{5/2} = 1.36 \times 10^7 \frac{z_0}{\pi a^2} (1-s) \mathcal{J}. \quad \dots\dots (35)$$

This equation is consistent with Eqn (31) which shows that as \mathcal{J} approaches \mathcal{J}_m the temperature T_m is reduced to zero.

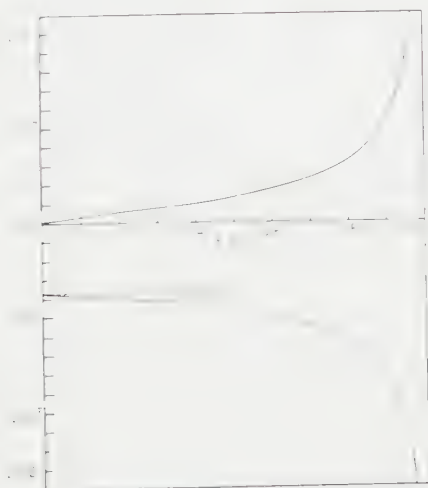


Fig. 3. A plot of $1/v$ against ξ/ξ_m for $\mathcal{J}_m = \infty$.

4.2. The Variation of Temperature between the Electrodes

By measuring the areas swept out by the curves in Fig. 3 as a function of ξ/ξ_m , a plot of T/T_m against v can be made using the value of ξ_m given in Eqn (34). This is shown in Fig. 4, again for the case when radiation is absent.

It can be seen from this (and from the ratio of the areas on either side of the ξ/ξ_m axis in Fig. 3) that the maximum temperature is displaced towards the anode. In fact, the value of x at T_m is 0.308.

The ratio of the mean temperature \bar{T} in plasma to the maximum temperature T_m can be better estimated from a plot of $(\xi/\xi_m)^{2/3} v$ against ξ/ξ_m . The ratio of the total area under this curve to the area under the curves of Fig. 3 gives the value of \bar{T}/T_m . This is

$$\bar{T}/T_m = 0.827. \quad \dots\dots (36)$$

4.3. Variation of Line Density between the Electrodes

From Eqn (10) it can be seen that the line density N varies inversely with temperature. Thus a plot of N would be the inverse of the curve shown in Fig. 4.

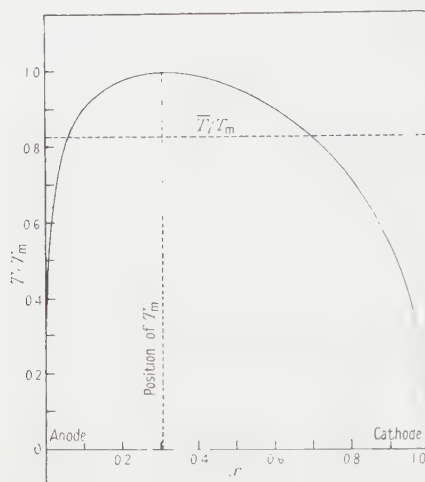


Fig. 4. Distribution of temperature between the electrodes for $\mathcal{J}_m = \infty$.

The mean line density \bar{N} , which is the line density of particles at the start of the discharge, can be found from a plot of $(\xi_m, \xi)^{2/5}/v$ against ξ/ξ_m . The ratio of the total area under this curve to the area under the curves of Fig. 3 gives the ratio \bar{N}/N_m where N_m is the line density (a minimum) at the point where the temperature is T_m (the maximum). From this,

$$\bar{N}/N_m = 1.435. \quad \dots\dots (37)$$

Since N_m is related to T_m by the Bennett relation, Eqn (10), \bar{N} is related from Eqn (37) to the current \mathcal{J} and temperature T_m by

$$\bar{N}T_m = 2.60 \times 10^{15} \mathcal{J}^2. \quad \dots\dots (38)$$

4.4. Variation of Electric Field between the Electrodes

The variation of electric field with temperature is given by Eqn (23). In terms of v and ξ , it can be written as

$$E_z = \frac{T_m}{\alpha z_0 \xi_m} \left(\frac{\xi_m}{\xi} \right)^{3/5} \left(1 - \frac{2\alpha\gamma}{5} v \right). \quad \dots\dots (39)$$

Using $dx = d\xi/v$, the mean electric field \bar{E}_z can be found from

$$\bar{E}_z = \frac{T_m}{\alpha z_0} \int \left(\frac{\xi_m}{\xi} \right)^{3/5} \left(\frac{1}{v} \right) d \left(\frac{\xi}{\xi_m} \right). \quad \dots\dots (40)$$

Now, Eqn (31) gives

$$\bar{E}_z = \frac{V}{z_0} = 3.039 \times 10^{-7} \frac{T_m}{\alpha z_0} \quad \dots\dots (41)$$

for the case when $\mathcal{J}_m = \infty$. Therefore a plot of $(\xi_m/\xi)^{3/5}/v$ against ξ/ξ_m should give an area equal to 3.039×10^{-7} . In fact, it does agree.

A plot of E_z/\bar{E}_z against x can now be made making use of Eqns (39), (41) and § 4.2. This is shown in Fig. 5.

The electric field is strongly negative at the anode and strongly positive at the cathode to compensate for the strong thermoelectric effects in these regions. Throughout the central part of the plasma, E_z is of the same order as \bar{E}_z .

From Gauss's theorem, the charge density q_v is given by

$$\nabla \cdot \mathbf{D} = q_v.$$

The relevant component of this is

$$\frac{dE_z}{dz} = \epsilon q_v. \quad \dots\dots (42)$$

Thus, from Fig. 5, it can be seen that everywhere in the plasma there is an excess of positive charge, and at the electrodes especially there are sheaths of positive charge.

The conditions for a limitation to the applied electric field to prevent run-away electrons is discussed in the following section.

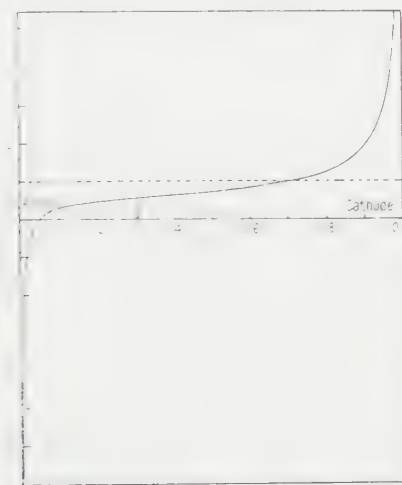


Fig. 5. Distribution of electric field between the electrodes for $\mathcal{J}_m = \infty$.

§ 5. VALIDITY OF RESULTS

5.1. Mean Free Path Considerations

The assumptions made with regard to the form of transport coefficients and to the concept of temperature at a point are probably only valid (i) if the temperature and particle density do not change considerably over a mean free path for collision, and (ii) if the electric field does not accelerate electrons in a mean free path to an energy more than kT .

The first condition can be written for this problem as

$$\left| \frac{dT}{dz} \right| \frac{l}{T} < 1 \quad \dots\dots (43)$$

where l is the mean free path.

From Marshall (1958) an estimate of the mean free path can be found, giving, in m.k.s. units,

$$\frac{l}{T} = 4.5 \times 10^{-9} \frac{n}{T}, \quad \dots\dots (44)$$

$|dT/dz|l/T$ has its largest value at the anode. From Eqns (28) and (29), the gradient of the temperature at the anode can be written approximately as

$$\left| \frac{dT}{dz} \right| \simeq \frac{i_z V}{\kappa T_0^{5/2}}.$$

Therefore, using Eqn (10) and the approximation $N \simeq \pi a^2 n$, (43) becomes

$$6.3 \times 10^4 \frac{V}{\mathcal{J} T_0^{1/2}} < 1. \quad \dots\dots (45)$$

In applying (45) to an experimental case it must be remembered that it is possible to have a slip temperature at the electrodes, so that T_0 could be much larger than the electrode temperature. Also it is possible that the ion and electron temperature are different. This case has not been studied here.

The condition $|\partial n/\partial z|l/n < 1$, results in the same inequality (45) due to Eqn (11).

The second condition is the condition to prevent runaway electrons. The critical electric field E_c , which must not be exceeded is given by Dreicer (1958) in m.k.s. units as

$$E_c = 1.69 \times 10^{-12} n/T \text{ volts m}^{-1}. \quad \dots\dots (46)$$

Therefore the condition to prevent runaway electrons is

$$\left| \frac{E_z}{E_c} \right| < 1. \quad \dots\dots (47)$$

$|E_z/E_c|$ has a large value at the anode due to the large thermoelectric effect. From Eqn (23) the electric field at the anode becomes, approximately,

$$|E_z| = \gamma \left| \frac{dT}{dz} \right|. \quad \dots\dots (48)$$

It is gratifying to note that E_c and T/l have the same functional dependence. Since, from Eqns (7), (44) and (46), $E_c < \gamma T/l$ it follows using Eqn (48) that, if the condition (45) holds, condition (47) must also hold at the anode.

At the point in the plasma where the temperature is a maximum, Eqn (23) gives

$$E_z = \frac{\mathcal{J}}{\pi a^2 \alpha T_m^{3/2}}.$$

From Eqn (10) and using the approximation $N \simeq \pi a^2 n$, the result as obtained by Haines (1959 a) is arrived at

$$\frac{E_z}{E_c} \simeq \frac{10^7}{N^{1/2}}. \quad \dots\dots (49)$$

Since electrons grow into the runaway region it is preferable if N , the line density, is at least 10^{18} . Because n has a small value near the surface of the plasma, it is difficult to avoid runaway electrons here. Thus these are two conditions for the prevention of runaway electrons.

5.2. Detailed Atomic Effects

In the preceding analysis no account has been taken of atomic processes such as recombination, ionization and charge exchange. These might have important effects near the electrodes.

5.3. Magnetic Effects on Transport Coefficients

So far in this paper, no account has been taken of the effects of the azimuthal magnetic field on the transport coefficients. Intuitively, the magnetic field would tend to reduce the transport of heat and give rise to higher plasma temperatures. On the axis of the column of the plasma ($r=0$), there will be no effect, but elsewhere the effect could be important. For this case, bearing in mind that the radial Hall current i_r cannot flow, Eqns (4), (5) and (6) become

$$i_z = \left(\sigma^{\text{II}} + \frac{\sigma^{\text{III}}}{\sigma^{\text{II}}} \right) E_z + \left(\frac{\sigma^{\text{III}}}{\sigma^{\text{II}}} \phi^{\text{II}} - \phi^{\text{III}} \right) \frac{\partial T}{\partial r} + \left(\frac{\sigma^{\text{III}}}{\sigma^{\text{II}}} \phi^{\text{III}} + \phi^{\text{II}} \right) \frac{\partial T}{\partial z} \quad \text{..... (50)}$$

$$q_z = -\lambda^{\text{II}} \frac{\partial T}{\partial z} + \lambda^{\text{III}} \frac{\partial T}{\partial r} + \psi^{\text{II}} i_z \quad \text{..... (51)}$$

$$q_r = -\lambda^{\text{II}} \frac{\partial T}{\partial r} - \lambda^{\text{III}} \frac{\partial T}{\partial z} + \psi^{\text{III}} i_z. \quad \text{..... (52)}$$

Here the nomenclature is the same as Marshall (1958). These coefficients are related to the corresponding coefficients defined in Eqn (7), but they also contain as factors functions of $\omega\tau$ where $\omega = eB/m$ and τ is the electron collision time. To obtain the greatest divergence from the previous analysis, $\omega\tau$ should be made very large. Then, $i_z \rightarrow (\sigma/1.931)E_z$, $q_r \rightarrow 0$, and $q_z \rightarrow -(2.5/3.305)\zeta T i_z$. The heat is thus seen to be transported entirely in the z direction and only by the thermal effects of diffusion of the electrons which carry the current. The energy equation (3) reduces to a first-order equation, namely,

$$\frac{2.5}{3.305} \zeta i_z \frac{\partial T}{\partial z} + \beta n^2 T^{1/2} = \frac{i_z^2 1.931}{\alpha T^{3/2}} \quad \text{..... (53)}$$

which now replaces Eqn (15). Thus there is only one boundary condition which is that the temperature of the cathode is T_0 . The temperature is then a maximum near the anode. The difficulty of having the anode itself at a low temperature is overcome by having a very large temperature gradient near the anode which causes the term $\lambda^{\text{II}} \partial T / \partial z$ in Eqn (51) to be non-zero in this small region and invalidates Eqn (53) as $z \rightarrow 0$.

However, the interesting point is that on integration of Eqn (53) one obtains relations of substantially the same algebraic dependence and with numerical factors which differ only slightly from those in Eqns (31) and (35).

$$V \left(1.931 - \frac{\mathcal{J}^2}{\mathcal{J}_m^2} \right) = 1.46 \zeta T_m \quad \text{..... (54)}$$

$$T_m^{5/2} = \frac{3.305}{\alpha \zeta} \frac{z_0}{\pi a^2} \left(1.931 - \frac{\mathcal{J}^2}{\mathcal{J}_m^2} \right) \mathcal{J} = 2.04 \times 10^7 \frac{z_0}{\pi a^2} \left(1 - \frac{\mathcal{J}}{1.931 \mathcal{J}_m} \right) \mathcal{J}. \quad \text{..... (55)}$$

With radiation losses absent, Eqn (54) reduces to

$$T_m = 4.64 \times 10^3 V \quad \text{..... (56)}$$

(cf. Eqn (32)).

Therefore, whilst the magnetic field affects the mode of transport of energy and causes the temperature to maximize nearer the anode, the algebraic results derived in this analysis are very little affected.

It is of interest to note that the radiation and conduction losses tend to cause a peak temperature near the centre of the discharge, while the thermal effects of diffusion, prominent in a strong magnetic field, shift the peak towards the anode.

§ 6. SUMMARY AND CONCLUSIONS

It can be concluded that, within the limits of validity as set out in the preceding section, the steady-state model of a linear pinched discharge in fully ionized hydrogen or deuterium predicts temperatures of 10^6 to 10^7 K with an apparatus of modest size.

The anode receives all the heat in excess of that radiated, while the cathode is not heated at all by the plasma. Also the maximum temperature is displaced towards the anode so that it is at an approximate distance of one-third of the length of the tube from the anode. These two effects of asymmetry are due to thermal effects of diffusion by the electrons which carry the current.

A most interesting result obtained is that the voltage V is proportional to the maximum temperature T_m , as given in Eqn (31), repeated below.

$$V \left[1 - \frac{\mathcal{I}^2}{\mathcal{I}_m^2} \right]^{1/2} = \left(\frac{\kappa}{\alpha} \right)^{1/2} \left(\frac{1+s}{1-s} \right)^{1/2s} T_m. \quad \dots\dots (31)$$

Evidence in support of this is given by Artsimovich (1958). The functional dependence on current is due to the inclusion of bremsstrahlung radiation losses. The relative magnitude of bremsstrahlung radiation losses and heat conduction losses is shown to depend only on the total current flowing. In terms of the length of the discharge z_0 , the pinch radius a , and the maximum temperature T_m , the total axial current \mathcal{I} has the following functional dependence.

$$T_m^{5/2} = 1.36 \times 10^7 (1-s) \frac{z_0 \mathcal{I}}{\pi a^2}. \quad \dots\dots (35)$$

Finally, the mean line density of ions or electrons \bar{N} is related to T_m and \mathcal{I} by

$$\bar{N} T_m = 2.60 \times 10^{15} \mathcal{I}^2. \quad \dots\dots (38)$$

ACKNOWLEDGMENTS

The author wishes to thank members of the High Temperature Physics Group of Imperial College, especially Dr. R. Latham, Dr. D. W. Allan and Mr. N. J. Phillips for valuable discussions, and the Department of Scientific and Industrial Research for the provision of a maintenance grant.

REFERENCES

- ARTSIMOVICH, L. A., 1958, *Proceedings of the Second International Conference on the Peaceful Uses of Atomic Energy*, **31**, 6 (Geneva: United Nations).
 BENNETT, W. H., 1934, *Phys. Rev.*, **45**, 890.
 DREICER, H., 1958, *Proceedings of the Second International Conference on the Peaceful Uses of Atomic Energy*, **31**, 57 (Geneva: United Nations).
 HAINES, M. G., 1959 a, *Proc. Phys. Soc.*, **76**, 250.
 — 1959 b, *Proceedings of the Fourth International Conference on Ionization Phenomena in Gases*, Uppsala (Amsterdam: North-Holland).
 MARSHALL, W., 1958, *Kinetic Theory of an Ionized Gas*, A.E.R.E. T/R 2419 (Harwell).
 TRUBNIKOV, B. A., and KUDRYAVTSEV, V. S., 1958, *Proceedings of the Second International Conference on the Peaceful Uses of Atomic Energy*, **31**, 93 (Geneva: United Nations).

Fluorescence and Other Yields of the L_{II} Shell in Pu

By L. SALGUEIRO†, J. G. FERREIRA†, J. J. H. PARK
AND M. A. S. ROSS

Department of Natural Philosophy, University of Edinburgh

MS. received 22nd March 1960

Abstract. A study has been made of the L x-radiations emitted after the disintegration of ^{242}Cm to determine, as accurately as possible, the fluorescence and other yields of the L_{II} sub-shell in Pu. Observations have been made (i) on the total intensity per disintegration of the L x-rays by observing the L x-ray photons in coincidence with α -particles from ^{242}Cm , (ii) on the relative intensity of the L x-rays from the L_{II} and L_{III} sub-shells. The sensitivity of the curved crystal spectrograph used for the latter observations had previously been determined.

The experimental results are: fluorescence yield $\omega_2 = 0.413 \pm 0.02$, Coster-Krönig yield $f_{23} = 0.22 \pm 0.08$, and Auger yield $a_2 = 0.37 \pm 0.08$. The total fluorescence yield of the L shells is $\bar{\omega} = 0.486 \pm 0.01$. The values of ω_2 and $\bar{\omega}$ are independent of previous work on fluorescence yields, but for the distribution of yields between f_{23} and a_2 it was necessary to use an extrapolated value of ω_3 .

§ 1. INTRODUCTION

THE fluorescence and other yields of the L sub-shells in the heavy elements are not yet known with sufficient accuracy, and it appears that information concerning the L_{II} shell yields is particularly uncertain. For example, in the case of bismuth (the element which has been most widely studied for the evaluation of fluorescence yields), recent estimates of the fluorescence yield of the L_{II} shell vary from 0.32 to 0.66 (Kinsey 1948, Ross *et al.* 1955, Burde and Cohen 1956, Tousset and Moussa 1958, Risch 1958). The present work has been undertaken with the object of obtaining, for one of the heavy elements, values as accurate as possible for the fluorescence and Coster-Krönig yields of the L_{II} shell.

The identities connecting the L sub-shell yields for fluorescence ω , Auger electrons a and Coster-Krönig transfers f , in the notation of Ross *et al.* (1955) are:

$$(L_I \text{ shell}) \quad \omega_1 + a_1 + f_{12} + f_{13} = 1 \quad \dots\dots (1)$$

$$(L_{II} \text{ shell}) \quad \omega_2 + a_2 + f_{23} = 1 \quad \dots\dots (2)$$

$$(L_{III} \text{ shell}) \quad \omega_3 + a_3 = 1. \quad \dots\dots (3)$$

A complete analysis of the yields thus involves the determination of six quantities, three of which relate to the L_I shell, two to the L_{II} shell and one to the L_{III} shell. If, however, the primary ionization is effectively confined to the L_{II} and L_{III} shells, the yields then involve only three independent quantities. To estimate these, much less information is required than in the general case,

† On leave from the University of Lisbon.

and the cumulative effect of experimental error is correspondingly reduced. We have therefore made a study of the L-shell fluorescence in an example of this restricted case, choosing for this purpose the α -disintegration $^{242}\text{Cm} \rightarrow ^{238}\text{Pu}$, a disintegration in which all γ -transitions are of E2 polarity.

The equations giving ω_2 and f_{23} in terms of experimentally determined quantities are derived assuming that no ionization occurs in the L_I shell, and at a later stage account is taken of the error involved in this assumption. The total number per disintegration of L-shell vacancies and of L x-ray quanta are represented respectively by I and F . The ratio of the number of ionization vacancies in the L_{III} shell to the number in the L_{II} shell is represented by C_3' , and the ratio of the number of photons from the L_{III} shell to the number from the L_{II} shell by F_3' . This notation replaces the quotients $C_3/C_2 (=C_3')$, and $F_3/F_2 (=F_3')$ of the equations of Ross *et al.* (1955). Taking n_2 and n_3 as the number of vacancies per disintegration in the L_{II} and L_{III} shells, we write

$$\left. \begin{aligned} n_2 + n_3 &= I \\ \omega_2 n_2 + \omega_3 (n_3 + f_{23} n_2) &= F \\ n_2 C_3' &= n_3 \\ \omega_2 n_2 F_3' &= \omega_3 (n_3 + f_{23} n_2) \end{aligned} \right\} \dots\dots (4)$$

Hence

$$\omega_2 = F(1 + C_3')/I(1 + F_3') \dots\dots (5)$$

and

$$f_{23} = \omega_2 F_3' / \omega_3 - C_3' \dots\dots (6)$$

To evaluate ω_2 and f_{23} by this method it is necessary to know five experimental quantities, I , F , C_3' , F_3' and ω_3 . Two of these, F and F_3' , have been measured by us. A value for ω_3 , 0.455 ± 0.01 , has been obtained by extrapolating to higher Z the experimental values of Kustner and Arends (1935) and Stephenson (1937). Estimates of I and C_3' have been based on published data relating to the disintegrations of ^{242}Cm and ^{238}Np . Where it has been necessary to refer to calculated internal conversion coefficients, those of Sliv and Band (1956) have been used.

§ 2. THE α -DISINTEGRATION OF ^{242}Cm : VALUES OF I AND C_3'

The α -particle and γ -ray spectra of ^{242}Cm have been studied by Asaro (1953), Asaro, Reynolds and Perlman (1952), Stephens, Asaro and Perlman (1955), Newton, Rose and Milsted (1956) and Perlman *et al.* (1957). Further information is included in the *Table of Isotopes* (Strominger, Hollander and Seaborg 1958). The α -particle emission leads to the ground state of ^{238}Pu and to the rotational levels of this state. The excitation energies and intensities, and the spins of these levels, also the observed intensity of γ -radiation, are shown in Table 1.

The conversion electron spectrum of the 44 keV transition in ^{238}Pu has been studied repeatedly in the α -decay of ^{242}Cm and the β -decay of ^{238}Np . We have selected the data listed in Table 2 as the most reliable for the estimation of the relative intensities of conversion and emission in this transition.

The relative intensities of conversion of the 102 keV transition have been similarly treated, using the results of Slatis *et al.* and Passell, and the calculations of Sliv. For the much weaker 157 keV transition, the relative intensities have

been based purely on Sliv's values. The final relative intensities are shown in Table 3.

Table 1. States of ^{238}Pu produced from ^{242}Cm

Level energy (kev)	Relative intensity	Spin	γ -ray energy (kev)	γ -ray intensity (%)
0	73.7	0^+		
44	26.3	2^+	44	$(3.9 \pm 0.7) \times 10^{-2}$
146	0.035	4^+	102	$\dagger(3.5 \pm 0.8) \times 10^{-3}$
303	0.007†	6^+	157	$(2.3 \pm 0.4) \times 10^{-3}$
others	very weak			

† Chosen to fit the γ -ray intensity of Newton, Rose and Milford (1956) using Sliv's conversion coefficients.

‡ Including K x-rays with an intensity of about $0.4 \times 10^{-3} \%$.

Table 2. Relative Intensities in Conversion and Emission of the 44 kev Transition

Author	L_I	L_{II}	L_{III}	$\Sigma(M+N+O)$	γ -ray
Slatis, Rasmussen and Atterling (1954)†	—	1	0.732	0.530	—
Passell (1954)†	<0.032	1	0.795 ± 0.03	0.538	—
Smith and Hollander (1956)	—	1	0.820 ± 0.03	—	—
Sliv (calc.)	0.035	1	0.857	—	0.003
Experimental mean values	—	1	0.782 (± 0.03)	0.534 (± 0.02)	—
Selected values	0.03	1	—	—	0.003

† Results for ^{238}Np .

Table 3. Relative Intensities of Conversion and Emission

Transition energy (kev)	Shell of Conversion				$\Sigma(M+N+O)$	γ -ray	Total
	K	L_I	L_{II}	L_{III}			
44		0.03	1	0.782	0.534	0.003	2.349
102		0.05	1	0.630	0.5	0.152	2.332
157	0.188	0.09	1.05	0.57	(0.5?)	1.0	3.4
+K shell transfers†		+	+	+			
		0.00	0.05	0.09			

† The transfer of ionization from the K shell to the L shell by K x-ray and K Auger emission has been estimated from the data of Nijgh *et al.* (1959).

Taking the absolute intensities of the 44, 102 and 157 kev transitions to be 0.26331, 0.00042 and 0.00007 per disintegration respectively, the values of n_1 , n_2 and n_3 are 0.00337, 0.11230 and 0.08778. Accuracy is not claimed for the fourth and fifth significant figures—but these are given here since the calculations have to be carried out to five-figure accuracy if the result is to be quoted to three figures.

We may now consider the consequences of the non-zero value of n_1 . Since Coster-Krönig yields of approximately $f_{12}=0.1$ and $f_{13}=0.6$ are applicable,

the greater part of n_1 is likely to be transferred to n_2 and n_3 , thus modifying C_3' and I . We therefore write

$$C_3' \simeq (n_3/n_2)(1 + f_{13}n_1/n_3 - f_{12}n_1/n_2) = 0.80 \pm 0.03$$

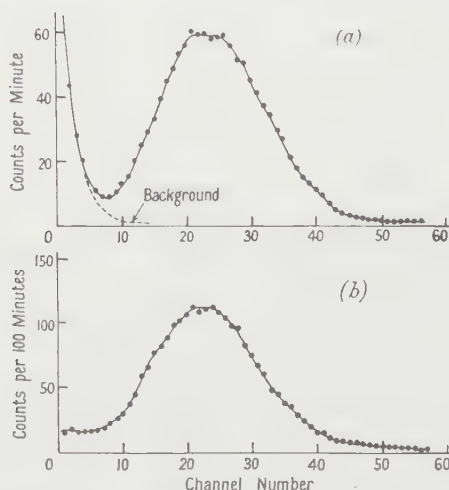
$$I = n_2 + n_3 + n_1(f_{12} + f_{13}) = 0.2025 \pm 0.005.$$

A deduction may also be required for the fluorescence $\omega_1 n_1 = 0.0004$, which is present in the observed value F_{obs} .

§ 3. THE DETERMINATION OF F

The number of L x-ray photons emitted per disintegration of ^{242}Cm has been determined by observing the number of such photons emitted in coincidence with the α -particles of ^{242}Cm . Since it has been shown by Falk-Vairant *et al.* (1954) that the L x-rays following de-excitation by internal conversion of the first rotational level of an even-even nucleus are radiated isotropically with respect to the direction of the α -particles, the required absolute intensity can be found from a knowledge of the photon angular aperture. The α -particles were detected in a parallel-plate gridded ionization chamber, and the photons in a sodium iodide crystal. The window of the crystal was specially thin and consisted of 5 mg cm^{-2} Al, 7 mg cm^{-2} araldite and 6 mg cm^{-2} MgO. The source support was 0.68 mg cm^{-2} Al and the window of the ionization chamber was 3.1 mg cm^{-2} polythene. The chamber was filled with a continuously purified mixture of argon and 10% methane at atmospheric pressure. Special arrangements were made to maintain equal pressures outside and inside the window when the gas was changed.

A carrier-free ^{242}Cm source of $1.5 \mu\text{C}$ strength was prepared for us by Dr. Milsted of Harwell. This source contained a detectable but not important contamination of $^{243}\text{Cm} + ^{244}\text{Cm}$. The spectra of α -particles and photons were obtained using a Hutchinson-Scarrott pulse spectrograph of Sunvic construction having a measured dead-time of $740 \mu\text{sec}$. A single-channel pulse-height analyser (Park 1956) with $5 \mu\text{sec}$ resolving time was used to select and count



Pulse height analyses of L x-ray spectra. (a) Total L x-ray spectrum of ^{242}Cm source with spectrum of background pulses shown as a broken line. (b) L x-ray spectrum in coincidence with α -particles of ^{242}Cm . Random coincidences with background pulses raise the low energy end of this spectrum.

the α -particle gating pulses. Using this analyser the measured coincidence resolving interval was $2\tau = 7.5 \mu\text{sec}$. The coincident photon pulses were recorded on the pulse spectrograph. Typical pulse-height analyses of (a) the total L x-ray spectrum and (b) the coincident L x-ray spectrum are shown in the Figure. Preliminary experiments were performed to determine the angular apertures Ω_α and Ω_γ for α -particles and photons, and to determine the correction for ^{243}Cm contamination of the source.

The α -particle aperture was required only for the contamination measurements. It was determined to sufficient accuracy by observing the count of all L x-ray photons and the count of coincidences of these photons with α -particles. $\Omega_\alpha/4\pi$ was 0.020 ± 0.001 .

The photon aperture enters as a factor into the determination of F , and Ω_γ must therefore be known with high accuracy. The collimator for photons was made adjustable by using different accurately measured spacers of brass tubing (internal diameter 6.4 cm) interposed between the wall of the ionization chamber and the aperture plate (aperture diameter 1.2635 ± 0.001 cm). The angle Ω_γ could thus be measured geometrically with accuracy to 0.2% . The proportionality between Ω_γ and the photon counting rate was checked and the maximum allowable value of $\Omega_\gamma/4\pi$ was found to be 0.011.

An estimate was required of the error introduced into the observed value of F by the ^{243}Cm contamination of the source, the highest energy α -particles from this isotope having energies similar to those from ^{242}Cm . If the numbers of gating pulses from ^{242}Cm and ^{243}Cm are respectively $N_{\alpha 1}$ and $N_{\alpha 2}$, and the numbers of coincident L x-ray photons in a solid angle of 4π are N_{X1} and N_{X2} then $F_{(242)} = N_{X1}/N_{\alpha 1}$ and $F_{\text{obs}} = (N_{X1} + N_{X2})/(N_{\alpha 1} + N_{\alpha 2})$.

From a knowledge of the decay scheme of ^{243}Cm and of the observed line shape in the α -particle spectrum, the fraction of all ^{243}Cm α -particles which lie within the gating group was estimated to be 11.8%. L-shell vacancies would be produced in about 0.37 of these cases, the corresponding fraction for ^{242}Cm being 0.20. The total intensity of ^{243}Cm α -particles was deduced from the observed intensity of the 226 and 278 keV γ -ray lines which have been shown by Asaro (1953) to arise from ^{243}Cm and to have a total intensity of 0.30 per disintegration of the parent nucleus. Taking account of the efficiency of the crystal detector and of the angular apertures for photons and α -particles in our experiment, it was found that, in the gating group, 85 out of a total of about 21 000 α -particles per minute were attributable to ^{243}Cm . Assuming that in the disintegrations of ^{242}Cm and ^{243}Cm there is isotropic emission of the L x-rays and equal total fluorescence yields, we deduce that $F_{\text{obs}} = 1.0031 F_{(242)}$. This correction is clearly so small that further refinement in relation to sub-shells is unnecessary.

In the coincidence experiments to determine F_{obs} no upper limit was set to the size of pulse entering the gating circuit. The discriminator voltage determining the minimum pulse size was adjusted to admit all α -particle pulses from ^{242}Cm and reject as many as possible from ^{243}Cm . The adjustment was made by matching the rate of counting of the gating pulses to the integrated rate of counting in the ^{242}Cm peak of the α -particle spectrum, due allowance being made for dead-time losses. The results of four determinations of F_{obs} are shown in Table 4. Counts were taken of the gating pulses N_α , of all photons N_γ , and of the L x-ray photons detected in coincidence with α -particles

$\Omega_\gamma N_X/4\pi$. After each observed count entered in the table (the duration of the count in minutes is shown in brackets) and beneath the observed count, the corrected counting rate per minute is shown. Dead-time corrections were applied to all counts and correction for random coincidences to $\Omega_\gamma N_X/4\pi$. The counting rate for N_γ is required only for dead-time and random coincidence corrections and it is therefore uncorrected for background counts (which were about 282 per minute).

Table 4. Data for the Evaluation of F_{obs}

Date	N_α	N_γ	$\Omega_\gamma N_X/4\pi$	$\Omega_\gamma/4\pi$	$F_{\text{obs}}(\%)$
17.8.59	211145(10)	90395(100)	996(80)	0.00516	9.226
	21152	914.2	10.070		± 0.3
18.8.59	530881(25)	as	2467(200)	0.00516	9.057
	21273	above	9.942		± 0.2
19.8.59	355943(17)	as	13100(1060)	0.00516	9.237
	20974	above	9.998		± 0.1
21.8.59	415878(20)	74004(50)	25109(1000)	0.01088	9.385
	20830	1507.6	21.267		± 0.07

Uncorrected weighted mean $F_{\text{obs}} = (9.31 \pm 0.1)\%$.

Fully corrected $F = 0.0986 \pm 0.001$.

The mean correction for absorption of the L x-rays in the path between source and crystal was evaluated knowing the absorption coefficients and superficial density of each material traversed, and the relative intensities of the various lines in the x-ray spectrum as reported in § 4 below. The efficiency of the crystal detector was taken as unity for this radiation. The resulting mean correction factor was 1.067.

The weighted mean of the four observations of F_{obs} is $(9.31 \pm 0.1)\%$. After applying the corrections for absorption, for ^{243}Cm contamination of the source, and for ionization of the L_I shell, we obtain $F = 0.0986 \pm 0.001$.

§ 4. MEASUREMENT OF F_3' BY CRYSTAL SPECTROGRAPH

We have determined the relative intensities of all recorded lines in the L x-ray spectrum of plutonium following the α -disintegration of ^{242}Cm . The observations were made with a curved crystal spectrograph having a mica crystal, 0.25 mm in thickness, bent to a cylinder of 20 cm radius. The spectrum was recorded on Ilford G5 plates, the electron-sensitive emulsion being 200μ in thickness and covered with a layer of black paper. The intensity calibration of the spectrograph used in this manner had been experimentally determined by Cochran (1955) for thirteen energies of radiation in the range from about 9 to 36 keV.

For the experiment to determine F_3' , a 3 mc carrier-free source of ^{242}Cm was used, deposited on a circular area 7 mm in diameter, and covered with 14.5 mg cm^{-2} Al foil. The spectrograph exposure time was 112 days. After photographic development of the plate in the Elon developer as used by Cochran, densitometry measurements were made on the spectrum using a Hilger and Watts non-recording microphotometer. The integrated density of each line was converted to intensity using Cochran's calibration, corrected for absorption in the aluminium cover of the source, and divided by the quantum energy to give the relative number of quanta. Our results may be compared with those

of Barton, Robinson and Perlman (1951) obtained with a quartz crystal spectrograph and proportional counter filled with xenon and methane. These authors applied corrections to the observed counts for absorption between source and counter, for counter efficiency, and for the coefficient of reflection of the quartz crystal. Our results and those of Barton *et al.* are shown in Table 5 together with the relative numbers of photons in the uranium spectrum derived from the relative intensity data of Allison (1928)†. The total photon yield for each sub-shell in the uranium spectrum (including weak lines) has also been found from Allison's spectrum. The total photon yields of the plutonium sub-shells have been obtained by two methods, using Allison's data for scaling up to include weak lines. Method (i) uses the total intensity in all observed lines of a sub-shell and method (ii) the intensities in the lines β_1 and β_2 . The second method should minimize errors introduced by the energy-dependent correction factors. Values of F_3' deduced by both methods are shown in Table 5. The inconsistency in the values of F_3 obtained from the data of Barton *et al.* suggests to us that their estimates of β_1 and β_2 may be respectively too small and too large, and that in consequence, the Barton values of F_3' tend to be high. We therefore adopt the value 1.12 ± 0.06 for F_3' .

Table 5. Relative Numbers of Photons in the Pu L x-ray Lines emitted after ^{242}Cm decay

Line	Transition	Barton <i>et al.</i> (1951)	Present work	Allison (uranium)
α_2	$L_{III}-M_{IV}$	13	11.1 ± 1.7	11.1
α_1	$L_{III}-M_V$	100	100 ± 4.5	100
β_2	$L_{III}-N_V$	28	25.0 ± 1.4	23.2
β_3	$L_{III}-O_V$	6	7.2 ± 0.7	5.1
L_{III} shell total	(i)	153.1	149.3	145.2
	(ii)	175.2	156.4	
β_1	$L_{II}-M_{IV}$	91	107.6 ± 4.5	39.1
γ_1	$L_{II}-N_{IV}$	23	21.6 ± 0.7	8.1
γ_2	$L_{II}-O_{IV}$	4	3.9 ± 0.4	1.4
L_{II} shell total	(i)	120.2	135.6	49.5
	(ii)	115.2	136.2	
F_3' :	Method (i)	1.27	1.10 ± 0.055	
	Method (ii)	1.52	1.15 ± 0.08	

†The observed value for this line was 29.0, but this includes the β_1 line in the L x-ray spectrum of uranium produced in the disintegration of ^{238}Pu , the daughter product of ^{242}Cm . The mean age of the source in our experiment was 305 days. From this information we calculate the $U\beta_1$ contribution to be 4.8, but deduct only 4.0.

§ 5. EVALUATION OF ω_2 AND f_{23}

The data for the evaluation of ω_2 and f_{23} are collected below:

$$\begin{aligned}
 C_3' &= 0.80 \pm 0.03 & I &= 0.2025 \pm 0.005 \\
 F_3' &= 1.12 \pm 0.06 & F &= 0.0986 \pm 0.001 \\
 \omega_3 &= 0.455 \pm 0.01
 \end{aligned}$$

† Since Allison's spectrum was excited by electron bombardment of uranium, the relative intensity of ionization in the L_{II} and L_{III} shells differs from that in our spectrum.

On substitution in Eqns (5), (6) and (2) we obtain

$$\omega_2 = 0.413 \pm 0.02$$

$$f_{23} = 0.22 \pm 0.08$$

$$a_2 = 0.37 \pm 0.08.$$

A measurement of some interest is the total L-shell fluorescence yield following conversion of a low energy E2 nuclear transition. Using our data without the corrections which removed the effects of the L_I sub-shell, we have $I = 0.2035 \pm 0.005$, $F = 0.0990 \pm 0.001$, so that $\bar{\omega} = F/I = 0.486 \pm 0.01$.

ACKNOWLEDGMENTS

This work has been assisted in many ways by Professor Norman Feather. Our thanks are also due to Dr. Milsted who prepared the ^{242}Cm sources at Harwell.

Two of the authors (L.S. and J.G.F.) were given leave of absence from the University of Lisbon and awarded a grant from the Instituto para a cultura (Portugal), a third (J.P.) was maintained by a Scholarship Award from the Office of Atomic Energy of the Republic of Korea and by a grant from the W.D. Brodie Memorial Fund of the University of Edinburgh.

REFERENCES

- ALLISON, S. K., 1928, *Phys. Rev.*, **32**, 1.
 ASARO, F., 1953, *Thesis*, University of California Radiation Laboratory Report No. 2180.
 ASARO, F., REYNOLDS, F. L., and PERLMAN, I., 1952, *Phys. Rev.*, **87**, 277.
 BARTON, G. W., ROBINSON, H. P., and PERLMAN, I., 1951, *Phys. Rev.*, **81**, 208.
 BURDE, J., and COHEN, S. G., 1956, *Phys. Rev.*, **104**, 1085.
 COCHRAN, A. J., 1955, *Thesis*, University of Edinburgh.
 FALK-VAIRANT, P., TEILLAC, J., VALLADAS, G., and BENOIST, P., 1954, *C.R. Acad. Sci., Paris*, **238**, 1409.
 KINSEY, B. B., 1948, *Canad. J. Res.*, **26**, 404.
 KUSTNER, H., and ARENDS, E., 1935, *Ann. Phys., Lpz.*, **22**, 443.
 NEWTON, J. O., ROSE, B., and MILSTED, J., 1956, *Phil. Mag.*, **1**, 981.
 NIJGH, G. J., WAPSTRA, A. H., and VAN LIESHOUT, R., 1959, *Nuclear Spectroscopy Tables* (Amsterdam: North-Holland).
 PARK, E. C., 1956, *J. Sci. Instrum.*, **33**, 257.
 PASSELL, T. O., 1954, *Thesis*, University of California Radiation Laboratory Report No. 2528.
 PERLMAN, I., ASARO, F., HARVEY, B. G., and STEPHENS, F. S., 1957, *Bull. Amer. Phys. Soc.*, **2**, 394.
 RISCH, K., 1958, *Z. Phys.*, **150**, 87.
 ROSS, M. A. S., COCHRAN, A. J., HUGHES, J., and FEATHER, N., 1955, *Proc. Phys. Soc. A*, **68**, 612.
 SLATIS, H., RASMUSSEN, J. O., and ATTERLING, H., 1954, *Phys. Rev.*, **93**, 646.
 SLIV, L. A., and BAND, I. M., 1956, *Leningrad Physico-Technical Institute Report* (translation: 1958, Reports 57 ICC K1, 58 ICC L1, Physics Department, University of Illinois).
 SMITH, W. G., and HOLLANDER, J. M., 1956, *Phys. Rev.*, **101**, 746.
 STEPHENS, F. S., ASARO, F., and PERLMAN, I., 1955, *Phys. Rev.*, **100**, 1543.
 STEPHENSON, R. J., 1937, *Phys. Rev.*, **51**, 637.
 STROMINGER, D., HOLLANDER, J. M., and SEABORG, E. T., 1958, *Rev. Mod. Phys.*, **30**, 585.
 TOUSSET, J., and MOUSSA, A., 1958, *J. Phys. Radium*, **19**, 39.

Selective Pressure Broadening of Si and F Spectral Lines†

By M. B. K. SARMA‡

Department of Physics, Osmania University, Hyderabad, India

MS. received 18th March 1960, in revised form 22nd September 1960

Abstract. The behaviour of the Si I, II, III and IV and F II and III spectral lines in highly condensed discharges, in the range 2900–6000 Å, at pressures varying from 3 mm to 35 cm, is given. The lines originating from the higher energy levels are found to be more sensitive to pressure.

§ 1. INTRODUCTION

THE discharges produced by passing high voltage condensed sparks through capillary tubes result in large current densities and a large number of electrons and ions are produced. A radiating atom in such a discharge will naturally be surrounded by these particles, and, therefore will be subjected to enormous electric fields. Hence, the characteristics of the lines produced in this way may safely be attributed to the Stark effect produced by inter-electronic and ionic electric fields. This is confirmed to be true to a large extent by a comparative study of the pressure broadening and Stark displacements of neon and argon by Maissel (1959).

The study of either the pressure broadening or the Stark effect of silicon and fluorine spectral lines has not been carried on till now even though they are astrophysically important. It is very difficult to obtain the Stark displacements for ionized atomic lines. Hence it is thought worth while to investigate the pressure broadening of these lines in condensed discharges. The similarity of the conditions (high percentage of ions and great temperatures) in the condensed discharges and high temperature stars makes this investigation important from an astrophysical point of view.

§ 2. EXPERIMENTAL

SiF_4 gas was used to obtain the spectrum of silicon as was suggested by Fowler (1926). It was possible to get the fluorine spectrum also incidentally. The gas was prepared by heating barium fluosilicate up to 400°C.

The pressure of the SiF_4 gas was varied systematically in the capillary tube (inner diameter 1.5 mm and length 1 cm) from 3 mm to 35 cm. Condensers of total capacity of 0.05 μF were used and these were charged to 26 kv. Both the silicon and the fluorine lines were recorded on the same plates.

§ 3. RESULTS

3.1. Silicon

Si I, II, III and IV lines are observable on the plates. The majority of these lines are found to be sensitive to pressure and merge with the continuum at high pressures as can be seen from the Tables.

† A part of the Thesis presented for Ph.D. degree to the Osmania University in 1958.

‡ Now at Berkeley Astronomical Department, University of California, Berkeley 4, California.

The Si I lines are not as sensitive as those of Si II, III or IV. None of the Si I lines disappeared at high pressures but many of the Si II, III and IV lines merged with the continuum at high pressures.

Si I. One Si I line, 2881.6 ($3p^2\ ^1D_2-4s\ ^1P_1$) showed asymmetrical reversal at 7 mm pressure. The reversal is very prominent at high pressures.

Si II. There are some unclassified lines at 3188 and 5180 which are very sensitive to pressure. They are diffuse at 3 mm pressure and disappear at high pressures. The lines arising from the energy levels F are found to be affected only after 3 mm pressure. From this behaviour of the above two groups of lines, it appears that the lines at 3188 and 5180 might have originated from levels higher than F.

Si III. All the Si III lines recorded on the plates are sensitive to pressure and all except a few have merged with the continuum at high pressures.

Si IV. The Si IV lines are not as strong as Si II or Si III lines. All these lines grow diffuse as the pressure is raised and merge with the continuum at high pressures.

3.2. Fluorine

No neutral fluorine lines are recorded on the plates.

F II. The most sensitive lines in F II are those at 4275–4278. They are diffuse at 3 mm pressure and become more diffuse as the pressure is raised and merge with the continuum at high pressures.

F III. Only three classified F III lines are recorded and these lines are all sensitive to pressure.

Multiplet No.	Wavelength	Broadening		Classification	Remarks	
		Class	Direction		Broadened at	Merged at
Si I						
1	2881.6	B	R > V	$3p^2\ ^1D-4s\ ^1P$	7 mm	—
2	5684.5	B	D	$4s\ ^3P-5p\ ^3P$	7 cm	—
3	5780.4	B	D	$4s\ ^3P-5p\ ^3D$	7 cm	—
4	2987.6	E	—	$3p^2\ ^1D-4s\ ^3P$		
Si II						
1	2904.0	A	D	$3d\ ^2D-5f\ ^2F$	7 mm	35 cm
2	4128.1	B	S	$3d\ ^2D-4f\ ^2F$	10 mm	—
3	5041.0	B	R	$4p\ ^2P-4d\ ^2D$	3 cm	—
4	3853.0	C	—	$3p^2\ ^2D-4p\ ^2P$		
5	5540.7	E	—	$4s\ ^4P-4p\ ^4S$		
Si III						
1	3086.2	A	D	$3d\ ^3D-4p\ ^3P$	10 cm	35 cm
2	3185.2	A	R	$4p\ ^1P-5s\ ^1S$	7 mm	35 cm
3	3230.4	A	R	$4p\ ^3P-5s\ ^3S$	7 mm	35 cm
4	3590.7	A	R	$4p\ ^1P-4d\ ^1D$	7 cm	35 cm
5	3796.0	A	D	$4p\ ^3P-4d\ ^3D$	10 cm	35 cm
6	4552.5	B	S	$4s\ ^3S-4p\ ^3P$	10 cm	35 cm
7	4665.8	B	D	$4s\ ^3P-4p\ ^3P$	10 cm	—
8	4813.2	A	D	$4f\ ^3F-5g\ ^3G$	3 mm	35 cm

Multiplet No.	Wavelength	Broadening		Classification	Remarks	
		Class	Direction		Broadened at	Merged at
Si iv						
1	3149.7	A	D	4p ² P-4d ² D	10 cm	35 cm
2	3762.4	A	D	4d ² D-5p ² P	7 cm	35 cm
3	4088.8	A	D	4s ² S-4p ² P	3 cm	35 cm
4	4631.3	A	D	5f ² F-6g ² G	10 mm	35 cm
F II						
1	3057.0	A	R	3p ³ P-4s ³ S	7 cm	35 cm
2	3296.2	A	D	3p ¹ D-3d' ¹ P	10 mm	35 cm
3	3406.5	A	D	3p' ¹ D-3d' ³ D	10 mm	35 cm
4	3416.4	A	D	3p ³ P-4s ³ S	15 cm	35 cm
5	3473.5	A	D	3p' ³ D-3d' ³ F	10 mm	35 cm
6	3541.9	B	D	3p' ¹ P-3d' ¹ P	15 cm	—
7	3544.3	B	D	3s' ³ D-3d' ³ P	15 cm	—
8	3640.9	B	D	3p' ³ F-3d' ³ F	10 cm	—
9	3679.6	A	D	X-3p ¹ P	15 cm	35 cm
10	3792.4	A	D	3p' ³ P-3d' ³ P	10 mm	35 cm
11	3944.3	A	D	3p' ³ P-3d' ³ D	10 mm	35 cm
12	4083.9	A	D	3p ¹ P-3d ¹ D	7 cm	35 cm
13	4109.2	B	D	3s' ³ D-3p' ³ D	10 cm	—
14	4192.6	A	D	X-3p ¹ S	7 cm	20 cm
15	4207.1	B	D	3s'' ³ P-3p'' ³ S	7 cm	20 cm
19	4246.1	A	S	3d ⁵ D-4f ⁵ F	10 mm	35 cm
20	4275.2	A	S	3p'' ³ D-3d'' ³ F	3 mm	25 cm
21	4446.2	A	D	3d ³ D-4f ³ F	3 mm	35 cm
22	4933.2	A	D	3p' ¹ D-3d' ¹ P	10 mm	35 cm
23	5001.9	A	D	3p' ¹ D-3d' ¹ D	10 mm	35 cm
24	5173.2	A	D	3p'' ¹ D-3d'' ¹ D	3 mm	25 cm
25	3202.7	C	—	3s' ¹ D-3p' ¹ D		
26	3377.4	C	—	3p'' ³ S-3d'' ³ P		
27	3606.8	C	—	3s ³ P-3p ³ P		
28	3847.0	C	—	3s ⁵ S-3p ⁵ P		
29	3902.8	C	—	3s' ³ D-3p' ³ F		
30	3501.4	E	—	3p ⁵ P-3d ⁵ D		
31	3535.1	E	—	3s' ³ D-3p' ³ P		
32	3704.5	E	—	3p' ³ F-3d' ³ G		
33	3971.6	E	—	3s'' ³ P-3p'' ³ D		
34	4024.7	E	—	4s ³ S-3p ³ P		
35	4103.1	E	—	3p ³ P-3d ³ D		
36	4118.7	E	—	3s' ³ D-3'p ³ D		
37	4299.2	E	—	3s' ¹ D-3'p ¹ P		
F III						
1	3154.4	A	D	3p ² P-3d ² D	25 cm	35 cm
2	3174.1	A	D	3s ² P-3p ² D	20 cm	35 cm

Explanation of Tables

At 3 mm pressure almost all the lines are sharp. As the pressure is raised, different groups of lines start broadening at different pressures and merge with the continuum at different pressures. All these lines are classed as A in the tables and the pressures at which they show broadening and merge with the continuum are given in the remarks column. There are some groups of lines which broaden at different pressures but still survive at 35 cm pressure. These

lines are classed as B. Those lines which do not show any broadening characteristics but which become faint as the pressure is raised are classed as C and those lines which are not at all affected by pressure—these lines are as sharp and strong at 35 cm pressure as they are at 3 mm pressure—are classed as E.

In the broadening characteristics S denotes symmetrical and D denotes diffuse, i.e. the broadening is symmetrical but not as prominent as the S type.

As it is noticed that all the lines of a single multiplet behaved similarly in all respects, only the shortest wavelength of the multiplet is given in the Tables. The unclassified lines are not given. The classification of the spectral lines is taken from Moore (1945) and the original papers.

§ 4. CONCLUSIONS

From the classification of the spectral lines and their susceptibility to pressure, it is noticed that those lines which originate from higher energy levels are the most sensitive ones. It is also noticed that the lines of a single multiplet behave similarly.

When a source emitting light is subjected to electric fields, the perturbation theory of Stark effect predicts that large Stark displacements are to be expected in the spectra when two terms which may combine according to optical selection rules lie close together. For the higher energy levels, the probability of their nearness to other levels is very great and the greater sensitivity of the lines arising from them may be attributed to the perturbations of these levels. Hence the behaviour of the silicon and fluorine spectral lines in the highly condensed discharges may be attributed to a large extent to the Stark effect produced by the inter-electronic and ionic electric fields. But to confirm this conclusively, a knowledge of the Stark displacements for these lines in electric fields is necessary.

ACKNOWLEDGMENTS

The author wishes to thank Dr. R. S. Narayan, Head of the Department of Physics, Osmania University for his guidance throughout this work. He also wishes to express his gratitude to the Osmania University and the Government of India, for awarding a scholarship during the period of this work.

REFERENCES

- FOWLER, A., 1926, *Phil. Trans. Roy. Soc.*, **225**, 1.
MAISSEL, L. I., 1959, *Proc. Phys. Soc.*, **74**, 97.
MOORE, C. E., 1945, *Revised Multiplet Table, Contributions from the Princeton University Observatory*, No. 20.

A 'Level Crossing' Experiment in Mercury

By J. N. DODD

Department of Physics, University of Otago, Dunedin, New Zealand

MS. received 18th July 1960

Abstract. A change of the intensity of resonance fluorescence may take place when Zeeman states of the excited level have the same energy. The fields at which these 'level crossings' occur in ^{199}Hg and ^{201}Hg have been measured. Combined with recent determinations of the hyperfine coupling constants, the results yield values for g_J of the 3P_1 states: $g_J(199) = 1.48634 \pm 0.00005$, $g_J(201) = 1.48606 \pm 0.00015$.

§ 1. THE LEVEL CROSSING TECHNIQUE

THE level crossing technique of Colgrove, Franken, Lewis and Sands (1959) provides a simple method for studying hyperfine structures. The measurement of the field at which a 'cross-over' occurs in ^{199}Hg has recently been reported by Hirsch (1960); in the experiments described here the 'cross-over' fields in both ^{199}Hg and ^{201}Hg have been observed and measured.

In the presence of a magnetic field, two Zeeman states, originating from different hyperfine levels of an excited level may have the same energy. The field at which this occurs depends primarily on the hyperfine coupling constants and the g -values of the levels. Consider two such states, differing in m by two, which are connected to a common ground level Zeeman state by emission of σ^- and σ^+ radiation respectively. The spatial distribution of resonance fluorescence due to these transitions changes sharply at the 'cross-over'; the theory of the effect is based on that given by Breit and Lowen (1934) and is closely related to the depolarization of resonance fluorescence in near zero fields, where many states satisfying the above conditions, intersect. From a classical point of view, one can think of the transitions between excited and ground states as circularly polarized oscillators which radiate independently. But at 'cross-over', the oscillators have the same frequency and radiate coherently. In particular, if atoms are excited by linearly polarized σ light, the intensity of light from these two states, observed in the direction of the electric vector of the incident beam, falls sharply as one passes through the 'cross-over' field. The variation of intensity is expressed by a term of the form $Q/[1^2 + (k_1 - k_2)^2]$, where k_1 and k_2 are the frequencies of the crossing levels, 1 is the radiation damping constant and Q is a product of matrix elements between the excited levels and the ground level. Other terms in the expression for the intensity represent radiation from incoherent sources and sum to a constant value.

§ 2. APPLICATION TO EXPERIMENTS IN MERCURY

2.1. The 6^3P_1 Level of ^{199}Hg

In zero field, the $F = \frac{3}{2}$ and the $F = \frac{1}{2}$ hyperfine levels are separated by $3a/2$, where a is the magnetic dipole coupling constant. In the presence of a

magnetic field, the Zeeman states $|\frac{3}{2}, -\frac{3}{2}\rangle$ and $|\frac{1}{2}', \frac{1}{2}\rangle^\dagger$ have the same energy at a field given approximately by $B = ah/g_J \beta$. These states make optical transitions to the ground level state $|\frac{1}{2}, -\frac{1}{2}\rangle$ by the emission of σ^- and σ^+ radiation respectively. The measurement of B , by observation of the proton precessional frequency, $f_p = g_p \beta B/h$, leads to the determination of a/g_J for the level. On solving for a/g_J and including various correction terms, one obtains

$$\frac{a}{g_J} = \frac{f_p}{g_p} \left(1 - \frac{\alpha}{2} + \frac{3k}{4} \right).$$

The term $\alpha = g_I/g_J$ arises from the effect of B on the nuclear magnetic moment; using $g_I = 0.5423 \times 10^{-3}$ (Cagnac and Brossel 1959) and $g_J = 1.4838$ (Brossel and Bitter 1952) one obtains $\alpha = 365 \times 10^{-6}$. The term k is due to the perturbation by the 3P_0 and 3P_2 levels; calculation of the first order perturbation gives

$$k = \frac{a}{g_J^2} \frac{4}{9} \left(\frac{1}{\delta} - \frac{1}{8\delta'} \right)$$

at the cross-over field, where δ is the $^3P_1 - ^3P_0$ spacing, and δ' is the $^3P_2 - ^3P_1$ spacing. From spectroscopic information and known values of a and g_J , one obtains $k = 54 \times 10^{-6}$. In the experiment performed, second order correction terms are negligible. The maximum of the 'level crossing' signal occurs at a field slightly different from that given by $k_1 = k_2$, since Q is also a slowly varying function of the magnetic field due to the decoupling of J and I in the level denoted $|\frac{1}{2}', \frac{1}{2}\rangle$. The effect shifts the resonance by a factor of the order $(\Gamma/a)^2$ which is less than one part per million, and hence is neglected.

Use of the value $g_p = (328.731)^{-1}$ obtained from recent measurements by Liebes and Franken (1959), leads to the result $a/g_J = 328.684 f_p$, where the constant should be accurate to within about six parts per million.

Theory predicts that the width of the signal at half-height should be $3\Gamma/2 = 3/2\tau' \text{ sec}^{-1}$ where τ' is the coherence time, which Boutron, Barrat and Brossel (1957) have shown to be slightly greater than the natural life of the excited states, $\tau = 1.18 \times 10^{-7} \text{ sec}$. A resonance width of about 1.3 gauss is expected.

2.2. The 6^3P_1 Level of ^{201}Hg

In this case there are three hyperfine levels $F = \frac{1}{2}$, $F = \frac{3}{2}$, $F = \frac{5}{2}$ separated by $-3a/2 + 9b/4$ and $-5a/2 - 5b/4$ respectively, where b is the electric quadrupole coupling constant. Of these levels $F = \frac{1}{2}$ is the highest and $F = \frac{5}{2}$ is the lowest, a being negative. In the presence of a magnetic field the Zeeman states $|\frac{5}{2}, \frac{5}{2}\rangle$ and $|\frac{3}{2}', \frac{1}{2}\rangle$ have the same energy at a field given approximately by $B = -2ah/g_J \beta$. On solving for a/g_J and including correction terms one obtains

$$\frac{a}{g_J} = \frac{1}{2} \frac{f_p}{g_p} \left(1 - \frac{\alpha}{2} + \frac{3k}{4} + \frac{b}{4a} \right) / \left(1 + \frac{b}{4a} - \frac{b^2}{8a^2} \right).$$

The terms in b/a are due to the effect of the quadrupole moment; the equation is exact in these terms. The coupling constants may be calculated from the zero-field spacing of the hyperfine levels measured by Stager and Kohler (1960); one obtains $b/a = 0.0513527$. Using $g_I = -0.200 \times 10^{-3}$ (Cagnac and Brossel 1959) one obtains $\alpha = -135 \times 10^{-6}$. The perturbation k has the same form as for ^{199}Hg ; $k = -20 \times 10^{-6}$. These values lead to the result $a/g_J = -164.427 f_p$.

† The notation is $|F, m_F\rangle$; the quotation marks indicate that F is not a good quantum number in the presence of a magnetic field.

§ 3. EXPERIMENT

A fused quartz cell containing natural mercury vapour at room temperature was situated in a homogeneous magnetic field of about 7000 gauss; on this was imposed a sinusoidal modulating field, amplitude about 3 gauss and frequency 9 c/s. The vapour was irradiated by σ -polarized light from a mercury lamp, and the intensity of resonance fluorescence, in a direction at right angles to the incident beam, was measured by a photomultiplier tube. The 'level crossing' signal was displayed on a cathode-ray screen; the signal-to-noise ratio achieved was better than ten in the case of ^{199}Hg and rather poorer in the case of ^{201}Hg .

The uncertainty in the position of the maximum of the signal on the screen was less than 0.2 gauss. A proton magnetometer was then placed in the exact position previously occupied by the cell and the frequency f_p adjusted to give a proton resonance signal in the same position on the screen. The mercury cell and the proton magnetometer were firmly mounted on a movable structure on which they could be accurately positioned; movement of the structure between two accurately determined positions ensured that rapid substitution into the correct location could be made.

The frequency f_p was measured by a Bendix wavemeter, whose 1 Mc/s crystal was checked against standard transmissions from radio station WWV of the National Bureau of Standards.

In attempts to discover systematic errors, the mechanical arrangement was re-aligned several times, the mercury cell was operated at ice and room temperatures, the 9 c/s modulating field was replaced by one at 50 c/s, the source lamp was excited by power from 3000 Mc/s, 166 Mc/s and d.c. sources. It was confirmed that the magnetic field was unaffected by the movements made during the substitution procedure. None of these alterations changed the measured value of f_p by as much as 1 kc/s.

The width of the signal, as estimated from the trace on the oscilloscope screen, was 1.5 ± 0.2 gauss, in agreement with the predicted value.

§ 4. RESULTS

The measured value of f_p for the ^{199}Hg 'cross-over' was 30.197 ± 0.001 Mc/s (7092.2 gauss). This gives $a/g_J = 9925.27 \pm 0.35$ Mc/s.

The measured value of f_p for the ^{201}Hg 'cross-over' was 22.323 ± 0.002 Mc/s (5242.9 gauss). This gives $a/g_J = -3670.50 \pm 0.36$ Mc/s.

From these and the previously measured value of g_J for the 6^3P_1 level one could determine the a -values for the levels. However, in view of the recent accurate determinations of a from the zero-field splitting measurements by Stager and Kohler (1960), it is more appropriate to use these to calculate a new value for g_J .

For ^{199}Hg , $a = 14752.37 \pm 0.02$ Mc/s leading to $g_J = 1.48634 \pm 0.00005$.

For ^{201}Hg , $a = 5454.569 \pm 0.005$ Mc/s leading to $g_J = 1.48606 \pm 0.00015$.

These are rather higher than the value obtained by Brossel and Bitter (1952) for the even isotopes ($g_J = 1.4838 \pm 0.0005$); the author would like to point out that a value of 1.4866 ± 0.0010 has been obtained by W. L. McLean (1955) of this laboratory.

ACKNOWLEDGMENTS

The author wishes to thank Professor R. R. Nimmo and Mr. R. W. N. Kinnear for their help, and to record his indebtedness to Mr. A. E. Adam for

his technical assistance. The work has been supported by a grant from the N.Z. Research Committee.

Note added in Proof. Since performing the above experiments the author has redetermined the value of g_J for the even isotopes by using the 'double resonance' method with an oscillating field of frequency 4344 Mc/s. The value 1.48635 ± 0.00030 has been obtained. Results will be published (Dodd, *Proc. Phys. Soc.*, in the press).

REFERENCES

- BOUTRON, F., BARRAT, J.-P., and BROSSEL, J., 1957, *C.R. Acad. Sci., Paris*, **245**, 2250.
BREIT, G. and LOWEN, L. S., 1934, *Phys. Rev.*, **46**, 590.
BROSSEL, J., and BITTER, F., 1952, *Phys. Rev.*, **86**, 308.
CAGNAC, B., and BROSSEL, J., 1959, *C. R. Acad. Sci., Paris*, **249**, 77.
COLGROVE, F. D., FRANKEN, P. A., LEWIS, R. R., and SANDS, R. H., 1959, *Phys. Rev. Letters*, **3**, 420.
HIRSCH, H. R., 1960, *Bull. Amer. Phys. Soc.*, [II], **5**, 274.
LIEBES, S., and FRANKEN, P. A., 1959, *Phys. Rev.*, **116**, 633.
MCLEAN, W. L., 1955, *Thesis*, University of Otago.
STAGER, C., and KOHLER, R., 1960, *Bull. Amer. Phys. Soc.*, [II], **5**, 274.

The Hartree Perturbation Method for Helium

BY A. DALGARNO AND J. M. MCNAMEE

Department of Applied Mathematics, The Queen's University of Belfast

MS. received 1st September 1960

Abstract. The Hartree perturbation method is used to calculate the dipole polarizability, the electric field at the nucleus, the quadrupole polarizability and the nuclear shielding factor of helium using a twelve-term representation of the unperturbed Hartree wave functions. It is pointed out that the method yields lower bounds for the dipole and quadrupole polarizabilities. The absolute error in the predicted values of any of the quantities is less than 4.3%.

§ 1. INTRODUCTION

THE extension of the Hartree-Fock procedure to the calculation of the effects of perturbations on atomic systems has been carried out recently by Dalgarno (1959), Kaneko (1959) and Allen (1960). Dalgarno applied the method to the calculation of the dipole and quadrupole polarizabilities of helium and concluded that the intrinsic accuracy of the method was such that the determination of the unperturbed orbital might provide the major source of error. A twelve-parameter representation of the unperturbed orbital has since become available (Roothan, Sachs and Weiss 1960) and it is desirable to repeat and extend the calculations.

§ 2. THEORY

Let \mathbf{r} be the position vector of an electron referred to the nucleus and let $u^{(0)}(\mathbf{r})$ be the unperturbed Hartree orbital for helium which is the solution of the equation

$$\left(-\frac{1}{2}\nabla^2 - \frac{2}{r} + \int \frac{|u^{(0)}(\mathbf{r}')|^2}{|\mathbf{r}-\mathbf{r}'|} d\mathbf{r}' - \epsilon_0\right) u^{(0)}(\mathbf{r}) = 0. \quad \dots\dots (1)$$

Then according to Dalgarno (1959) and Kaneko (1959), the first-order perturbed function $u^{(1)}(\mathbf{r})$ corresponding to a perturbation $h(\mathbf{r}_1) + h(\mathbf{r}_2)$ is the solution of

$$\begin{aligned} \left(-\frac{1}{2}\nabla^2 - \frac{2}{r} + \int \frac{|u^{(0)}(\mathbf{r}')|^2}{|\mathbf{r}-\mathbf{r}'|} d\mathbf{r}' - \epsilon_0\right) u^{(1)}(\mathbf{r}) + h(\mathbf{r})u^{(0)}(\mathbf{r}) \\ = -2 \int \frac{u^{(1)}(\mathbf{r}')u^{(0)}(\mathbf{r}')}{|\mathbf{r}-\mathbf{r}'|} d\mathbf{r}' u^{(0)}(\mathbf{r}) + \epsilon_1 u^{(0)}(\mathbf{r}) \quad \dots\dots (2) \end{aligned}$$

and the second-order energy is given by

$$\epsilon_2 = 2(u^{(1)}, hu^{(0)}). \quad \dots\dots (3)$$

Dalgarno (1959) showed that expression (3) was correct to first order in the error of the unperturbed Hamiltonian appearing in (1). It is clear from general considerations that (3) is actually an upper bound to the second-order energy.

Most recent calculations of second-order energies (cf. Sternheimer 1954) employ a method which for helium is equivalent to ignoring the right-hand side of (2). The resulting value is correct only to zero order. We shall call the more accurate procedure method I and the less accurate method II.

Equation (2) may usually be solved by direct numerical integration (Kaneko 1959) and can always be solved by variational methods (Dalgarno 1959). Thus the functional

$$J = \left(u_t^{(1)}, \left[-\frac{1}{2} \nabla^2 - \frac{2}{r} + \int \frac{|u^{(0)}(\mathbf{r}')|^2}{|\mathbf{r} - \mathbf{r}'|} d\mathbf{r}' - \epsilon_0 \right] u_t^{(1)} \right) + 2(u_t^{(1)}, hu^{(0)}) \\ + 2 \left(u_t^{(1)}, \left[\int \frac{u_t^{(1)}(\mathbf{r}') u^{(0)}(\mathbf{r}')}{|\mathbf{r} - \mathbf{r}'|} d\mathbf{r}' \right] u^{(0)} \right) \dots\dots (4)$$

may be minimized with respect to some selected trial function $u_t^{(1)}$.

§ 3. CALCULATIONS

3.1. The Dipole Polarizability

For the dipole polarizability α_d , the perturbation is given in spherical polar coordinates by

$$h = r \cos \theta \dots\dots (5)$$

and

$$\alpha_d = -4(u^{(0)}, r \cos \theta u^{(1)}). \dots\dots (6)$$

Writing

$$u^{(1)}(\mathbf{r}) = f(r) \cos \theta \dots\dots (7)$$

reduces (2) to a second-order differential equation in the single variable r which has been solved by Kaneko (1959). We use the variational method and write

$$u_t^{(1)}(\mathbf{r}) = \sum_{n=1} a_n r^n \cos \theta u^{(0)}(\mathbf{r}), \dots\dots (8)$$

adopting for $u^{(0)}$ the twelve-parameter representation obtained by Roothan, Sachs and Weiss (1960).

Minimization of J with respect to a_n yields the results shown in Table 1. A check on the correctness of the minimization procedure is provided by the fact that after minimization, $J = \alpha_d$. The final value $0.1959 \times 10^{-24} \text{ cm}^3$ agrees with the value $0.196 \times 10^{-24} \text{ cm}^3$ obtained by Dalgarno† (1959) and Kaneko (1959). Table 1 also includes the values of α_d obtained by a similar procedure except that the right-hand side of (2) was ignored (method II). The most accurate theoretical value of α_d is $0.2045 \times 10^{-24} \text{ cm}^3$ (C. Schwartz 1960, private communication) and the most accurate experimental value is $0.205 \times 10^{-24} \text{ cm}^3$. The

Table 1. Dipole Polarizability of Helium

				$\alpha_d(\text{\AA}^3)$	
$-a_1$	$-a_2$	$-a_3$	$-a_4$	(I)	(II)
0.673473	—	—	—	0.15767	—
0.203864	0.386412	—	—	0.195906	—
0.218176	0.363629	0.007035	—	0.195925	—
0.236081	0.321773	0.032511	-0.004225	0.195940	0.2204

† Due to an error of transcription, Dalgarno reported a value of $0.207 \times 10^{-24} \text{ cm}^3$. This actually refers to his iterated functional $J^{(i)}$. The value of the quadrupole polarizability was given correctly.

effect of the self-consistency condition is therefore to reduce the error from $+6.8\%$ to -4.3% , the lower value being a lower bound to the polarizability.

3.2. The Electric Field at the Nucleus

It has been pointed out by Sternheimer (1954) that the electric field induced at the helium nucleus by an external electric field may be written in the form

$$E = 2 \left(u^{(0)}, \frac{\cos \theta}{r^2} u^{(1)} \right) \quad \dots\dots (9)$$

which must be equal to unity for a neutral atom. Expression (9) therefore provides a test of the accuracy of $u^{(1)}$.

Using the solution $u^{(1)}$ obtained in method II yields a value for E of 1.23 whereas using the solution for the complete form of (2) yields a value for E of 1.00, showing that the accuracy of $u^{(1)}$ at small values of r is much improved.

3.3. The Quadrupole Polarizability

For the quadrupole polarizability α_q , the perturbation h is given by

$$h = \frac{1}{2} r^2 (3 \cos^2 \theta - 1). \quad \dots\dots (10)$$

Writing

$$u^{(1)}(\mathbf{r}) = f(r)(3 \cos^2 \theta - 1) \quad \dots\dots (11)$$

reduces (2) to a second-order differential equation in r , which may be integrated numerically. We use instead the variational method, adopting as trial function

$$u_t^{(1)}(\mathbf{r}) = \sum_{n=2} b_n r^n (3 \cos^2 \theta - 1) u^{(0)}(\mathbf{r}). \quad \dots\dots (12)$$

The results are given in Table 2. The final value 0.0965 \AA^5 is somewhat larger than the value 0.0942 \AA^5 obtained by Dalgarno (1959) using the two-term representation of $u^{(0)}$ given by Green, Mulder, Lewis and Woll (1954) and somewhat smaller than the value 0.0983 \AA^5 obtained by Dalgarno (1959) using the two-term representation of $u^{(0)}$ given by Löwdin (1953). The most accurate value previously available is 0.0942 \AA^5 , computed by Dalgarno, Davison and Stewart (1960) using a six-term representation of the wave function of helium (Hylleraas 1929) which takes account of correlation. Since the value 0.0965 \AA^5 obtained here is a lower bound (provided the representation employed for $u^{(0)}$ is accurate), it seems that the Hylleraas wave function does not provide a very accurate description of the electron density at large values of r .

Table 2. Quadrupole Polarizability of Helium

			$\alpha_q(\text{\AA}^5)$	
$-b_1$	$-b_2$	$-b_3$	(I)	(II)
0.640298	—	—	0.08265	0.084712
0.138850	0.256785	—	0.096533	0.097910
0.132088	0.263650	-0.001463	0.096534	0.0979097

Table 2 includes also the values of α_q obtained by method II. The effect of self-consistency is a reduction of α_q by only 1.5%. The results of §3.2 suggest, however, that the improvement will be much greater for quantities which are strongly weighted at small values of r such as the nuclear shielding factor.

3.4. *The Nuclear Shielding Factor*

The nuclear shielding factor for helium is given by

$$\gamma_{\infty} = \left(u^{(1)}, \left[\frac{3 \cos^2 \theta - 1}{r^3} \right] u^{(0)} \right) \dots\dots (12)$$

(Sternheimer 1954), where $u^{(1)}$ is the solution of (2) for the perturbation (10). We obtain $\gamma_{\infty} = 0.388$ using method I and $\gamma_{\infty} = 0.417$ using method II. The most accurate estimate available is 0.397 (Dalgarno, Davison and Stewart 1960) so that marked improvement results from the inclusion of the self-consistency condition.

3.5. *Results for Li^+ and H^-*

We have also obtained results for Li^+ based upon the twelve-term representation of Roothaan, Sachs and Weiss (1960) and for H^- , based upon the two-term representations of Green *et al.* (1954). For Li^+ , we obtain $\alpha_d = 0.0281 \text{ \AA}^3$ and $\alpha_q = 0.00464 \text{ \AA}^3$ using method I and $\alpha_d = 0.0304 \text{ \AA}^3$ and $\alpha_q = 0.00472 \text{ \AA}^3$ using method II. For the electric field induced at the nucleus we obtain with method I $E = 0.667$, which is the correct value, whereas with method II we obtain $E = 0.763$. For γ_{∞} , method I gives 0.248, and method II 0.257.

For heavier ions of the helium sequence the improvement resulting from the use of method I will be insignificant.

Hartree wave functions are not available for H^- but, if we adopt the orbital given by Green *et al.* (1954), α_q is 11.8 \AA^3 according to method I and 14.9 \AA^3 according to method II. These values are much smaller than the correct value of 26.8 \AA^3 (C. Schwartz 1960, private communication). For the electric field induced at the nucleus, method I yields a value of 1.8 and method II a value of 3.2, the correct value being 2.0. The error is therefore reduced from 60% to 10%.

REFERENCES

- ALLEN, L. C., 1960, *Phys. Rev.*, **118**, 167.
 DALGARNO, A., 1959, *Proc. Roy. Soc. A*, **251**, 282.
 DALGARNO, A., DAVISON, W. D., and STEWART, A. L., 1960, *Proc. Roy. Soc. A*, **257**, 115.
 GREEN, L. C., MULDER, M. M., LEWIS, M. N., and WOLL, J. W., 1954, *Phys. Rev.*, **93**, 757.
 HYLLERAAS, E., 1929, *Z. Phys.*, **54**, 347.
 KANEKO, S., 1959, *J. Phys. Soc. Japan*, **14**, 1600.
 LÖWDIN, P. O., 1953, *Phys. Rev.*, **90**, 120.
 ROTHAAAN, C. C. J., SACHS, L. M., and WEISS, A. W., 1960, *Rev. Mod. Phys.*, **32**, 186.
 STERNHEIMER, R. M., 1954, *Phys. Rev.*, **96**, 951.

Rotational Translational Relaxation Time in H_2 Calculated from Thermal Conductivity

By B. N. SRIVASTAVA AND A. K. BARUA

Indian Association for the Cultivation of Science, Calcutta-32, India

MS. received 17th May 1960, in revised form 27th June 1960

Abstract. An approximate method has been developed for obtaining the value of Z , the number of collisions required to make a rotational translational energy transfer in a diatomic gas from the thermal conductivity data, and the geometry of the apparatus employed in the conductivity measurements. The values of Z for H_2 calculated at different temperatures are in fair agreement with the values obtained by other methods. They also show that Z increases with rise of temperature.

§ 1. INTRODUCTION

THE fact that the relaxation of the rotational and the vibrational energies will have some effect on the transport processes, and particularly on the thermal conductivity of polyatomic molecules, is well recognized but the exact calculation of this effect from theory is extremely complicated. This has led several investigators to start with the simplifying assumption of local chemical equilibrium. In this way Hirschfelder (1957) has developed a formal treatment of the thermal conductivity of a pure polyatomic gas which is expected to hold when all reactions including rotational-translational transfer are fast. The experiments of Srivastava and his co-workers (Srivastava and Srivastava 1959, Srivastava and Barua 1960 a) have shown that at least at the temperatures of their experiments the condition of local chemical equilibrium is not satisfied owing to the comparatively slow rate of rotational-translational transfer of energy (vibrational excitation being negligible at these temperatures). On account of this relaxation of the rotational energy the value of the thermal conductivity of a pure polyatomic gas is smaller than that given by Hirschfelder's theory. It is therefore natural to expect that accurate measurement of the thermal conductivity of a polyatomic gas will throw some light on the transfer of internal energy among the molecules.

Unfortunately, due to the difficulty in treating transport processes, very little advance has till now been made in providing a rigorous treatment of the transport phenomena of polyatomic molecules. The first formal treatment of the transport processes taking into account relaxation effects has been given by Uhlenbeck and Wang Chang (1951). They considered translational motion classically and internal motions quantum mechanically. The generalized Boltzmann equation was, however, solved by perturbation methods only for the two limiting cases, viz. (i) energy exchange between translational and internal motion is not difficult and (ii) energy exchange between translational and internal motion is difficult. In our present investigation we shall be concerned only with the relaxation of rotational energy which may be considered to fall under category (i). For this case, as shown by Uhlenbeck and Wang Chang (1951), the coefficient of thermal

conductivity may be written as the sum of terms representing the effects of translational and internal degrees of freedom so that the heat flux vector \mathbf{q} may be written in the form

$$\mathbf{q} = -(K^{\text{tr}} + K^{\text{int}}) \frac{\partial T}{\partial \mathbf{r}}, \quad \dots\dots (1)$$

where K^{tr} and K^{int} are the values of K corresponding to the translational and the internal degrees of freedom respectively. The expressions for K^{tr} , K^{int} and τ , the relaxation time, are complicated and involve differential collision cross sections which have not yet been evaluated for any realistic molecular model. Hence the expressions obtained by Uhlenbeck and Wang Chang cannot be utilized to calculate the thermal conductivity and the relaxation time theoretically even for this limiting case.

In a recent paper Srivastava and Barua (1960 b) have shown that it is possible to calculate approximately the value of Z for a diatomic molecule by knowing the thermal conductivity and the geometry of the apparatus. They, however, assumed accommodation effects to be negligible. This is open to question and needs further examination. We have, therefore, in this paper examined in detail the recent data of Waelbroeck and Zuckerbrodt (1958) on the thermal conductivity of H_2 down to very low pressures with a view to disentangling the effects of relaxation and accommodation on the thermal conductivity of H_2 . An attempt has also been made to utilize the extensive data of Johnston and Grilly (1946) to determine Z at different temperatures for H_2 and thereby throw some light on the conflicting theories regarding the temperature dependence of Z .

§ 2. CALCULATION OF RELAXATION TIME

Hirschfelder's expression for the thermal conductivity K of a pure polyatomic gas based on the assumption of local chemical equilibrium is

$$K = K_{\text{mon}}[1 - \delta_{\text{f}} + \delta_{\text{f}}C_{\text{p}}/C_{\text{pf}}], \quad \dots\dots (2)$$

where K_{mon} is the thermal conductivity of a gas when it is treated as monatomic, $\delta_{\text{f}} = \rho DC_{\text{pf}}/K_{\text{mon}}$ (ρ being the density and D the self-diffusion coefficient) and $C_{\text{pf}} = 5R/2$. Eqn (2) may also be written in the form

$$K = K_{\text{mon}} + \rho DC_{\text{p}}^{\text{int}}. \quad \dots\dots (3)$$

Due to the comparatively slow rate of rotational-translational transfer of energy it is expected that $C_{\text{p}}^{\text{int}}$ in Eqn (3) will have a smaller effective value $C_{\text{p}}^{\text{'int}}$ which may be obtained from Eqn (3) by knowing the experimental value of K and the value of ρD or δ_{f} from values calculated by Hirschfelder (1957), since for this particular case Eqn (1) still holds. We assume the system to be initially in translational equilibrium and the rotational energy $E_{\text{R}}(t)$ to be unexcited. Then, as usual, we represent the growth of the rotational energy with the characteristic relaxation time τ by the equation

$$E_{\text{R}}(t) = E_{\text{R}}^{\infty} [1 - e^{-t/\tau}], \quad \dots\dots (4)$$

where E_{R}^{∞} is the equilibrium value of $E_{\text{R}}(t)$. Due to the collision process, the system acquires the requisite amount of rotational energy (corresponding to $C_{\text{p}}^{\text{'int}}$) in a certain time $n\tau$ where n is a positive number (integral or fractional). By taking the average of $E_{\text{R}}(t)$ over $n\tau$ we have

$$\overline{E_{\text{R}}(t)} = \frac{1}{n\tau} \int_0^{n\tau} E_{\text{R}}(t) dt = E_{\text{R}}^{\infty} \left[1 + \frac{1}{n} (e^{-n} - 1) \right]. \quad \dots\dots (5)$$

Let $C_R' \simeq C_p'^{\text{int}}$ denote the effective value of the rotational molar specific heat as determined from the thermal conductivity measurements in the manner explained above. Then from Eqn (5), assuming $E_R^\infty = C_R T$, and $\overline{E_R(t)} = C_R' T$ if the temperature is not too low, we get

$$C_R' = C_R \left[1 + \frac{1}{n} (e^{-n} - 1) \right] \quad \text{..... (6)}$$

where the equilibrium value of the molar rotational specific heat $C_R = C_p - 5R/2$. Hence Eqn (6) may be utilized to obtain n from the experimental value of K . We assume that the diatomic molecule as it leaves the hot surface starts building up the rotational energy during collisions at the expense of translational energy and this process continues till the molecule reaches the cold surface after which there is no further building up. Thus the amount of rotational energy acquired by the molecule, which is a measure of $n\tau$, will depend on the time of transit t' of the molecule from the hot to the cold surface in the conductivity cell employed. Evidently therefore we can put

$$t' = r/\bar{c} \simeq n\tau \quad \text{..... (7)}$$

where r is the distance between the hot and the cold surface of the conductivity cell and \bar{c} is the mean speed of the molecules given by the relation $\bar{c} = \sqrt{(8kT/\pi m)}$. Hence

$$\tau \simeq \frac{1}{n} \frac{r}{\bar{c}} \quad \text{..... (8)}$$

The time between two collisions is given on the rigid sphere model by the relation

$$\tau_c = \frac{\eta}{1.271p}, \quad \text{..... (9)}$$

where η is the viscosity and p the pressure in dynes cm^{-2} . The number of collisions, Z , required to produce the rotational-translational transfer is calculated from the relation

$$\tau = Z\tau_c. \quad \text{..... (10)}$$

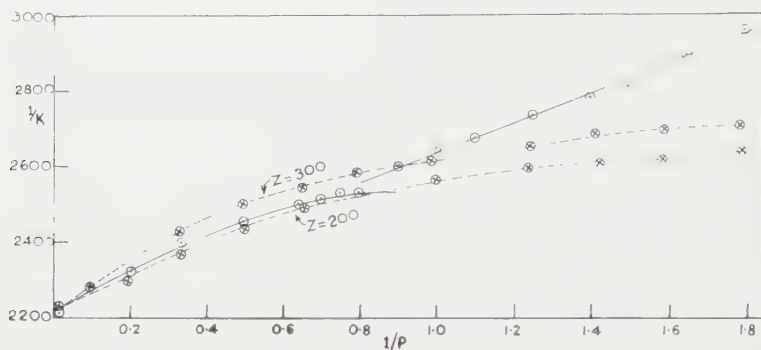
§ 3. COMPARISON WITH EXPERIMENT

Recently, Srivastava and Barua (1960b) have estimated the Z values of O_2 , N_2 , H_2 from Eqn (10) by utilizing their thermal conductivity data at 45°C and at a pressure of 10 cm of Hg. They, however, neglected the accommodation effect as they could not calculate its magnitude on account of their experimental data being taken at a single pressure. To investigate this point further we have examined in detail the recent thermal conductivity data of H_2 at 45°C obtained by Waelbroeck and Zuckerbrodt (1958) down to very low pressures. The full line in the Figure represents the $(1/K, 1/p)$ plot (p in cm of Hg) obtained from the graph given by Waelbroeck and Zuckerbrodt (1958). It may be seen that a straight line may be drawn in the low pressure region but the graph takes a definite bend when the high pressure region is approached. If we assume the rotational accommodation coefficient to be negligibly small compared with the translational accommodation coefficient, then the bend in the Figure should be attributed to the presence of relaxation effect. It is impossible to disentangle the accommodation and relaxation effects analytically as the dependence of relaxation upon pressure cannot be explicitly calculated theoretically. It is however possible to calculate the value of K with the help of Eqns (10), (8), (6) and (3) by using assumed

values of Z . These values which take into consideration the relaxation of rotational energy will be designated as K_r . The two broken lines in the Figure show the $(1/K_r, 1/p)$ plots for K_r obtained by assuming $Z=300$ and $Z=200$. For this calculation the geometry of the apparatus III described by Waelbroeck and Zuckerbrodt (1958) was utilized. It is seen that the broken lines reproduce the bend in the $(1/K, 1/p)$ plot quite well and the agreement is better for $Z=200$. In the lower pressure region the $(1/K_r, 1/p)$ plots are nearly parallel to the $1/p$ axis and the full line in this region may be reproduced by the equation

$$1/K_r + A/p = 1/K, \quad \dots\dots (11)$$

where A is a constant depending on the translational accommodation coefficient. From the graphs for $Z=200$, $A=0.0017$ so that the contribution of A/p to $1/K$ at 10 cm of Hg is quite small, which shows that the error caused by neglecting the accommodation effects at 10 cm pressure by Srivastava and Barua (1960b) must be very small indeed.



$1/K$ plotted against $1/p$ (p in cm Hg).

The earlier attempts to deal theoretically with the relaxation of rotational and vibrational energies were not very successful (e.g. Rice 1931, Zener 1933, Landau and Teller 1937). However, more recent investigations of Brout (1954), Parker (1959) and others enable us to evaluate Z , the number of collisions required to bring about a rotational and vibrational energy transfer, and these values of Z are in fair agreement with the experimental values obtained by other methods. Brout's quantum mechanical treatment shows that Z for rotational-translational energy transfer is independent of temperature whereas Parker finds it to be temperature dependent. It would be interesting to find what temperature dependence is shown by the values of Z thus determined experimentally from the thermal conductivity measurements. For this purpose we have examined the extensive thermal conductivity data of Johnston and Grilly (1946) for H_2 extending over a wide range of temperatures. However, a close examination of their data for H_2 shows that their values are consistently lower than those obtained by other workers (e.g. Archer 1935, Gregory 1935, Keyes 1951, etc.). This discrepancy may be attributed to some systematic error in the values obtained by Johnston and Grilly. In order to correct for this we took the values of the thermal conductivity of H_2 at 30°C and 45°C obtained recently by Srivastava and Barua (1960a) as standard and the (thermal conductivity, temperature) curves of Johnston and Grilly at a pressure of 10 cm of Hg were laterally shifted to coincide with the values reported by Srivastava and Barua.

The values of the thermal conductivity K of H_2 at 10 cm of Hg were obtained graphically from the tables given by Grilly, Taylor and Johnston (1946) and are recorded in the Table. In order to obtain Z from these data, the force constants (Lennard-Jones 12:6 model) utilized were those determined from viscosity data (Hirschfelder, Curtiss and Bird 1954). The results of this calculation are shown in the Table, the effect of the two isomeric forms of H_2 being ignored.

$T(^{\circ}K)$	$K \times 10^5$ at 10 cm of Hg	$\tau \times 10^{-8}$ (sec)	$\tau_c \times 10^{-10}$ (sec)	Z
254.4	38.48	16.21	4.655	348
277.7	40.85	18.44	4.950	373
293.3	42.30	23.12	5.124	451
324.3	45.15	27.22	5.480	497
341.3	46.50	29.10	5.665	514

The values of Z thus obtained are in fair agreement with those obtained by other methods (Stewart and Stewart 1948, Griffith 1950). For H_2 the variation of Z with temperature is in the same direction as obtained theoretically by Parker, i.e. Z increases with increasing temperature.

REFERENCES

- ARCHER, C. T., 1935, *Phil. Mag.*, **19**, 901.
 BROUT, R., 1954, *J. Chem. Phys.*, **22**, 1189.
 GREGORY, H. S., 1935, *Proc. Roy. Soc. A*, **149**, 35.
 GRIFFITH, W., 1950, *J. Appl. Phys.*, **21**, 1319.
 GRILLY, E. R., TAYLOR, W. J., and JOHNSTON, H. L., 1946, *J. Chem. Phys.*, **14**, 436.
 HIRSCHFELDER, J. O., 1957, *J. Chem. Phys.*, **26**, 274, 282.
 HIRSCHFELDER, J. O., CURTISS, C. F., and BIRD, R. B., 1954, *Molecular Theory of Gases and Liquids* (New York : Wiley).
 JOHNSTON, W., and GRILLY, E. R., 1946, *J. Chem. Phys.*, **14**, 223.
 KEYES, F. G., 1951, *Trans. Amer. Soc. Mech. Engrs.*, **71**, 966.
 LANDAU, L., and TELLER, E., 1937, *Physik Z. Sowjetunion*, **11**, 18.
 PARKER, J. G., 1959, *Phys. Fluids*, **2**, 449.
 RICE, O. K., 1931, *Phys. Rev.*, **38**, 1943.
 SRIVASTAVA, B. N., and BARUA, A. K., 1960 a, *J. Chem. Phys.*, **32**, 427.
 ——— 1960 b, *Symposium on Rate-processes in Physico-Chemical Reactions* (Indian Chemical Society).
 SRIVASTAVA, B. N., and SRIVASTAVA, R. C., 1959, *J. Chem. Phys.*, **30**, 1200.
 STEWART, J. L., and STEWART, E. S., 1948, *J. Acoust. Soc. Amer.*, **20**, 585.
 UHLENBECK, G. E., and WANG CHANG, C., 1951, *Univ. of Michigan*, CM-681.
 WAELEBROECK, F. G., and ZUCKERBRODT, P., 1958, *J. Chem. Phys.*, **28**, 524.
 ZENER, C., 1933, *Proc. Camb. Phil. Soc.*, **29**, 136.

The $^{58}\text{Ni}(\text{d}, \text{p})^{59}\text{Ni}$ and $^{60}\text{Ni}(\text{d}, \text{p})^{61}\text{Ni}$ Reactions

By A. W. DALTON†, G. PARRY, H. D. SCOTT
AND S. SWIERSZCZEWSKI

Physics Department, University of Liverpool

MS. received 16th September 1960

Abstract. In the present investigation targets of natural nickel and isotopically pure ^{60}Ni were bombarded by deuterons with energies of 8.9 mev and 8.6 mev respectively. From the resulting proton energy spectra a number of angular distribution measurements have been made for the $^{58}\text{Ni}(\text{d}, \text{p})^{59}\text{Ni}$ and $^{60}\text{Ni}(\text{d}, \text{p})^{61}\text{Ni}$ reactions and spin and parity assignments made to states of ^{59}Ni and ^{61}Ni . The results have also been compared with the gross structure peaks in the proton spectra recently reported by Schiffer, Lee and Zeidman.

§ 1. INTRODUCTION

THE energies of proton groups resulting from the deuteron bombardment of nickel have been studied by Harvey (1951), McFarland, Bretscher and Shull (1953) and Pratt (1954a, b). The latter investigated the angular distribution of four proton groups resulting from a bombardment with 3 mev deuterons, and made spin and parity assignments for the final states on the basis of compound nucleus formation. More recently, while the present work was in progress, Paris and Buechner (1958a, b) reported the results of a high resolution study of the reactions $^{58}\text{Ni}(\text{d}, \text{p})^{59}\text{Ni}$ and $^{60}\text{Ni}(\text{d}, \text{p})^{61}\text{Ni}$ using 7.0 mev deuterons. Since then more comprehensive tables of excited states of ^{59}Ni up to an excitation of 7.533 mev and excited states of ^{61}Ni up to an excitation of 6.857 mev have been completed by Paris (1959). Angular distribution measurements from the $^{60}\text{Ni}(\text{d}, \text{p})^{61}\text{Ni}$ reaction have also been made by Enge and Fisher (1959) at a deuteron bombarding energy of 7.5 mev.

In the present investigation targets of natural nickel and isotopically pure ^{60}Ni were bombarded by deuterons with energies of 8.9 mev and 8.6 mev respectively. From the resulting proton energy spectra a number of angular distribution measurements have been made for the $^{58}\text{Ni}(\text{d}, \text{p})^{59}\text{Ni}$ and $^{60}\text{Ni}(\text{d}, \text{p})^{61}\text{Ni}$ reactions and spin and parity assignments made to states of ^{59}Ni and ^{61}Ni . The results have also been compared with the gross structure peaks in the proton spectra reported by Schiffer, Lee and Zeidman (1959).

§ 2. PROCEDURE AND RESULTS

The protons from the targets were magnetically analysed using the apparatus described in a previous paper (Dalton *et al.* 1960).

The natural nickel target was prepared from a thin metallic foil of thickness 1.8 mg cm^{-2} and the isotopically pure ^{60}Ni target of thickness 0.85 mg cm^{-2} was obtained from the Atomic Energy Research Establishment, Harwell. Thickness determinations were made by direct weighing. Natural nickel contains 67.76% ^{58}Ni , 26.16% ^{60}Ni , 1.25% ^{61}Ni , 3.66% ^{62}Ni and 1.16% ^{64}Ni .

† Now at the United Kingdom Atomic Energy Authority, Seascale, Cumberland.

so that by comparing the proton spectra obtained from the two targets the proton groups arising from the ^{58}Ni component in the natural nickel target could be distinguished from those due to the ^{60}Ni component. This is illustrated in Fig. 1 in which the proton spectra obtained at 15° to the incident deuteron beam are shown. Exposures were about 260 microcoulombs for the

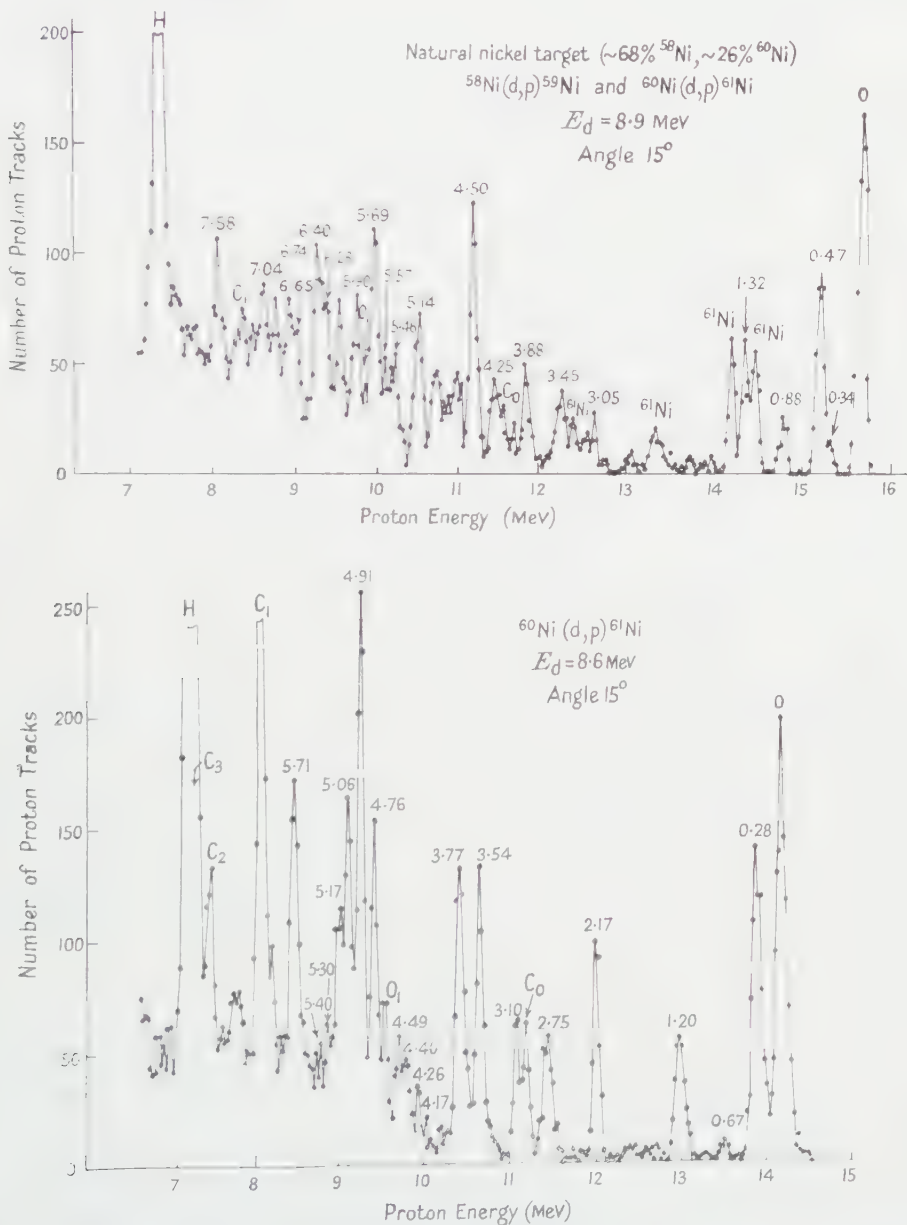


Fig. 1. Energy spectra of protons emitted at 15° from targets of natural nickel and ^{60}Ni bombarded by 8.9 MeV and 8.6 MeV deuterons respectively.

natural target and about 700 microcoulombs for the ^{60}Ni target. The protons resulting from carbon and oxygen impurities in the natural nickel target were

much less than that normally experienced in an exposure of this kind. Identification of the proton groups from the two isotopes was made using the known energy calibration of the spectrograph and these groups are labelled with the excitation energy of the final state in mev. The groups labelled C_0 , C_1 , C_2 , C_3 , O_1 and H are due to carbon, oxygen and hydrogen impurities in the target. From the spectra at different angles it was possible to obtain angular distributions of many of the proton groups observed corresponding to levels in ^{56}Ni and ^{61}Ni . These have been fitted with Butler type stripping curves for which the nuclear radius parameter R has been allowed to vary about the Gamow-Critchfield (1949) value. The results of these calculations have been tabulated and the two reactions will be dealt with separately.

2.1. $^{60}\text{Ni}(d, p)^{61}\text{Ni}$

The proton groups observed in our investigation were correlated with the levels in ^{61}Ni using the table published by Paris of the relative number of protons associated with each level at angles of 30° , 50° and 70° to the direction of the incident deuteron beam. Table 1 contains the results of the investigation of this reaction. The corresponding results of Enge and Fisher are listed for comparison although their cross sections are uncertain because of difficulties in measuring the true target thickness. It will be seen that the l -value assignments in both sets of data agree well. It has been possible in our analysis to assign an l -value of 1 to the weak distribution corresponding to the 0.660 mev level, and also an l -value of 0 for the quite strong distribution corresponding to the level at 3.749 mev. However, a transition to the low-lying level at 0.915 mev was not observed.

There is some ambiguity in the assignment of l -values to angular distributions of some groups. It is found that the experimental distribution often lies between two curves calculated for successive l -values using the Gamow-Critchfield radius. In such cases the experimental distribution is fitted better by reducing the radius parameter for the lower l -value rather than by increasing the radius parameter for the higher l -value. However, at high excitation when both $l=0$ and $l=1$ curves peak at 0° , it is possible to obtain acceptable fits to forward peaking distributions by using both these l -values and corresponding small or large values for the radius parameter. In such cases we have again tended to favour the assignment of the lower l -value.

It will be seen by comparing columns (5) and (10) in the table that the cross sections at the peak of the proton groups have increased on average by a factor four for an increase in beam energy of 1.1 mev, and the values of the reduced width are correspondingly much higher than those tentatively put forward by Enge and Fisher in their report. This could be due to the effect of the Coulomb barrier and possibly to the uncertainty of the target thickness in the experiment of Enge and Fisher. Column (7) is given in order to present the dimensionless form of the reduced width designated $(2J_f+1)\theta^2$ by Macfarlane and French (1959) which is less dependent upon the magnitude of the radius parameter R than the value quoted in kev units.

The ground state spin and parity of the even-even nucleus ^{60}Ni is 0^+ so that the selection rules for the stripping reaction limit the spins and parities of the final state to two possible values, except in the case of an $l=0$ transition for

Table 1. $^{60}\text{Ni}(d, p)^{61}\text{Ni}$

(1)	(2)	(3)	(4)	(5)	(6)	(7)	(8)	(9)	(10)
0	1 +3	$\frac{1}{2}^-, \frac{3}{2}^-$ $\frac{5}{2}^-, \frac{7}{2}^-$	5.68 5.68	6000 1980	48 119	0.024 0.060	$\begin{cases} 0 \\ 0.068 \end{cases}$	1 3	1528 246
0.28	1	$\frac{1}{2}^-, \frac{3}{2}^-$	5.12	4340	46	0.019	0.284	1	1154
0.67	1	$\frac{1}{2}^-, \frac{3}{2}^-$	5.43	204	1.8	0.0008	0.660	—	—
1.20	1	$\frac{1}{2}^-, \frac{3}{2}^-$	4.80	1860	20	0.0073	$\begin{cases} 1.104 \\ 1.137 \\ 1.190 \end{cases}$	1 — 1	131 — 311
2.17	—	—	—	1820	—	—	2.127	1	615
2.75	2	$\frac{3}{2}^-, \frac{5}{2}^+$	5.90	2200	36	0.020	$\begin{cases} 2.645 \\ 2.704 \\ 2.770 \end{cases}$	— 2 1	— 387 90
3.10	0	$\frac{1}{2}^+$	5.10	3150	5.5	0.0022	3.069	0	980
3.54	2	$\frac{3}{2}^-, \frac{5}{2}^-$	5.15	3910	86	0.036	3.503	2	998
3.77	0	$\frac{1}{2}^+$	4.0	6590	19	0.0047	3.749	—	—
4.17	—	—	—	—	—	—	4.158	—	—
4.26	—	—	—	—	—	—	4.247	1 or 2	96
4.40	—	—	—	—	—	—	$\begin{cases} 4.369 \\ 4.381 \end{cases}$	— —	— —
4.49	—	—	—	—	—	—	4.471	—	—
4.76	2	$\frac{3}{2}^+, \frac{5}{2}^+$	4.51	4200	120	0.038	4.756	(2)	1140
4.91	0	$\frac{1}{2}^+$	3.75	12100	39	0.0086	4.911	0	2930
5.06	0 or 1	$\frac{1}{2}^+$ $\frac{1}{2}^-, \frac{3}{2}^-$	3.0 6.48	6160	27 13	0.0037 0.0089	$\begin{cases} 5.059 \\ 5.092 \end{cases}$	0 —	1630 —
5.17	0 or 1	$\frac{1}{2}^+$ $\frac{1}{2}^-, \frac{3}{2}^-$	3.0 6.48	3900	17 8.8	0.0025 0.0058	5.181	0	880
5.30	—	—	—	—	—	—	$\begin{cases} 5.289 \\ 5.303 \end{cases}$	— —	— —
5.40	—	—	—	—	—	—	$\begin{cases} 5.389 \\ 5.434 \end{cases}$	— —	— —
5.71	2	$\frac{3}{2}^+, \frac{5}{2}^+$	3.9	5110	205	0.049	$\begin{cases} 5.697 \\ 5.736 \end{cases}$	1 or 2 2	693 483

(1) Excitation energy (MeV) of level or group of levels; (2) l -value of in-going neutron; (3) spin and parity assignments from the selection rules; (4) radius R (f) chosen for Butler stripping curves; (5) value of the cross section ($\mu\text{bn sterad}^{-1}$) at the peak of the angular distribution; (6) reduced width $(2J_f + 1)\gamma$ (keV); (7) reduced width expressed in dimensionless form $(2J_f + 1)\theta^2$; (8) levels in ^{61}Ni determined by Paris (1959) corresponding to the proton groups observed in the present investigation; (9) l -value assignments made by Enge and Fisher (1959); (10) value of the cross section ($\mu\text{bn sterad}^{-1}$) at the peak of the angular distribution from the investigation of Enge and Fisher.

which the final state must have spin and parity $\frac{1}{2}^+$. We are therefore in a position to assign the spin and parity value of $\frac{1}{2}^+$ to five excited states in ^{61}Ni . These are at excitations 3.069, 3.749, 4.911, 5.059 and 5.181 mev. The assignment for the level at 5.059 mev is made because the table published by Paris shows that approximately 80% of the proton group with excitation energy 5.06 mev in our investigation is associated with the level at 5.059 mev. Possible spins and parities for other levels are shown in column (3). The ground state of ^{61}Ni has been shown to be $\frac{3}{2}^-$, as predicted by the shell model theory, by Nussbaum *et al.* (1956) from measurements on the decay rates of ^{61}Co and ^{61}Cu . This investigation also shows the spin and parity of the first excited state at 0.068 mev to be $\frac{5}{2}^-$, and the states at 0.284 mev and 0.660 mev to be either $\frac{1}{2}^-$ or $\frac{3}{2}^-$. Our results are therefore compatible with all these assignments.

2.2. $^{58}\text{Ni}(d, p)^{59}\text{Ni}$

In Table 2 are listed the results of the investigation into this reaction. There are no previous measurements of angular distributions of this reaction at a deuteron bombarding energy sufficient to produce the well-established stripping mechanism. The proton groups observed in our investigation have again been correlated with the levels in ^{59}Ni using the table published by Paris. From this data it is thought that approximately 80% of the proton group with excitation 5.14 mev is associated with the level at 5.144 mev. Similarly we consider that the 5.46 mev group is predominantly due to a level at 5.453 mev and the 5.57 mev group due to a level at 5.563 mev. The groups at excitations 7.04 mev and 7.58 mev have not been correlated since they are probably due to the combined effect of five or more states in ^{59}Ni . The proton groups with excitation energies of 6.65 mev and 6.74 mev together correspond to at least five levels in ^{59}Ni but appear to show an overall $l=2$ distribution. It will be seen that other definite proton groups have been observed, but angular distribution measurements have not been possible for these mainly because of the difficulty of allowing for the contribution from the $^{60}\text{Ni}(d, p)^{61}\text{Ni}$ reaction. The distribution to the 4.501 mev level is exceptionally strong and corresponds to an $l=2$ transition. It would therefore appear that this is the $d_{5/2}$ level for this nucleus. The ground state spin of the even-even nucleus ^{58}Ni is 0^+ , so that the selection rules give the same limitations on spin and parity assignments as for the case of the $^{60}\text{Ni}(d, p)^{61}\text{Ni}$ reaction. In the ^{59}Ni nucleus we can assign spin and parity uniquely to three levels. These are the levels at 5.144, 5.563 and 5.676 mev, which must all be $\frac{1}{2}^+$, although the first two depend upon the correlating assumptions mentioned previously. Possible spins and parities of other levels are shown in column (4). The ground state spin has previously been determined as $\frac{3}{2}^-$ by Pratt (1954b) and Trumphy (1957). Pratt also fixes the spin and parity of the level at 0.341 mev as $\frac{7}{2}^-$, so that our results are compatible with both these assignments. The other assignments made by Pratt of a possible level at 1.1 mev with spin and parity $\frac{7}{2}^-$ and one at 1.62 mev with spin and parity $\frac{1}{2}^-$ could not be checked because of the contribution from the $^{60}\text{Ni}(d, p)^{61}\text{Ni}$ reaction.

2.3. Gross Structure of the Proton Spectra

A comparison has also been made with the gross structure peaks in the proton spectra reported by Schiffer, Lee and Zeidman (1959). In Fig. 2 is

Table 2. $^{58}\text{Ni}(d, p)^{59}\text{Ni}$

(1)	(2)	(3)	(4)	(5)	(6)	(7)
0	0	1	$\frac{1}{2}^-, \frac{3}{2}^-$	6.36	55	0.035
0.341	0.34	3	$\frac{5}{2}^-, \frac{7}{2}^-$	6.45	36	0.023
0.466	0.47	1	$\frac{1}{2}^-, \frac{3}{2}^-$	6.45	29	0.019
0.880	0.88	1	$\frac{1}{2}^-, \frac{3}{2}^-$	5.88	7.1	0.0039
1.309	1.32	1	$\frac{1}{2}^-, \frac{3}{2}^-$	5.48	21	0.0098
3.058	3.05	—	—	—	—	—
3.420 } 3.457 } 3.541 }	3.45	1 — 3	$\frac{1}{2}^-, \frac{3}{2}^-$ $\frac{1}{2}^-, \frac{3}{2}^-$ $\frac{1}{2}^-, \frac{3}{2}^-$	6.45 6.45	8.3 29	0.0054 0.19
3.862	3.88	—	—	—	—	—
4.261	4.25	—	—	—	—	—
4.501	4.50	2	$\frac{3}{2}^+, \frac{5}{2}^-$	5.90	87	0.047
5.144 } 5.209 } 5.390 }	5.14	0	$\frac{1}{2}^+$	4.0	23	0.0059
5.424 } 5.453 } 5.503 }	5.46	2	$\frac{3}{2}^+, \frac{5}{2}^+$	5.3	41	0.0182
5.523 } 5.563 } 5.603 }	5.57	0	$\frac{1}{2}^+$	3.5	14	0.0026
5.686	5.69	0	$\frac{1}{2}^+$	4.0	31	0.0077
5.889	5.90	—	—	—	—	—
6.278 } 6.298 }	6.28	—	—	—	—	—
6.373	6.40	—	—	—	—	—
6.599 } 6.642 } 6.702 } 6.720 } 6.743 }	6.65 } 6.74 }	2	$\frac{3}{2}^+, \frac{5}{2}^+$	5.3	83	0.036
	7.04	—	—	—	—	—
	7.58	—	—	—	—	—

(1) Levels in ^{59}Ni (MeV) determined by Paris (1959) corresponding to the proton groups observed in the present investigation; (2) excitation energy (MeV) of the observed proton groups; (3) l -value of in-going neutron; (4) spin and parity assignments from the selection rules; (5) radius R (f) chosen for Butler stripping curves; (6) reduced width $(2J_f + 1)\gamma$ (keV); (7) reduced width expressed in dimensionless form $(2J_f + 1)\theta^2$.

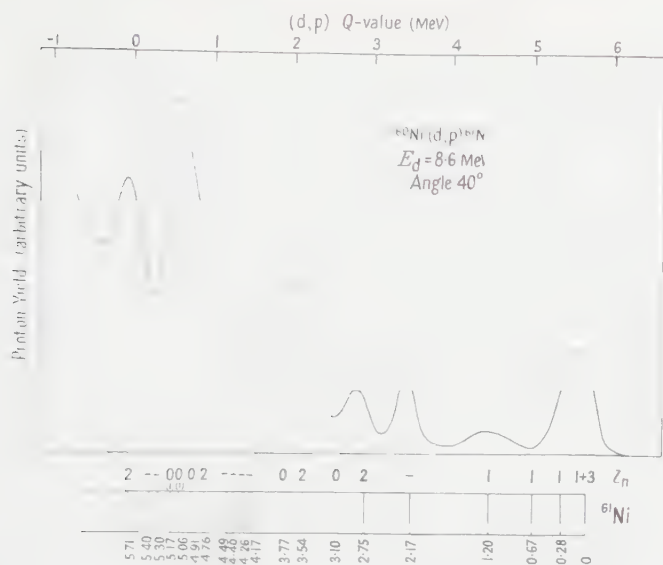


Fig. 3. Gross structure proton spectrum for the $^{60}\text{Ni}(d, p)^{61}\text{Ni}$ reaction at an angle of 40° to the incident beam direction.

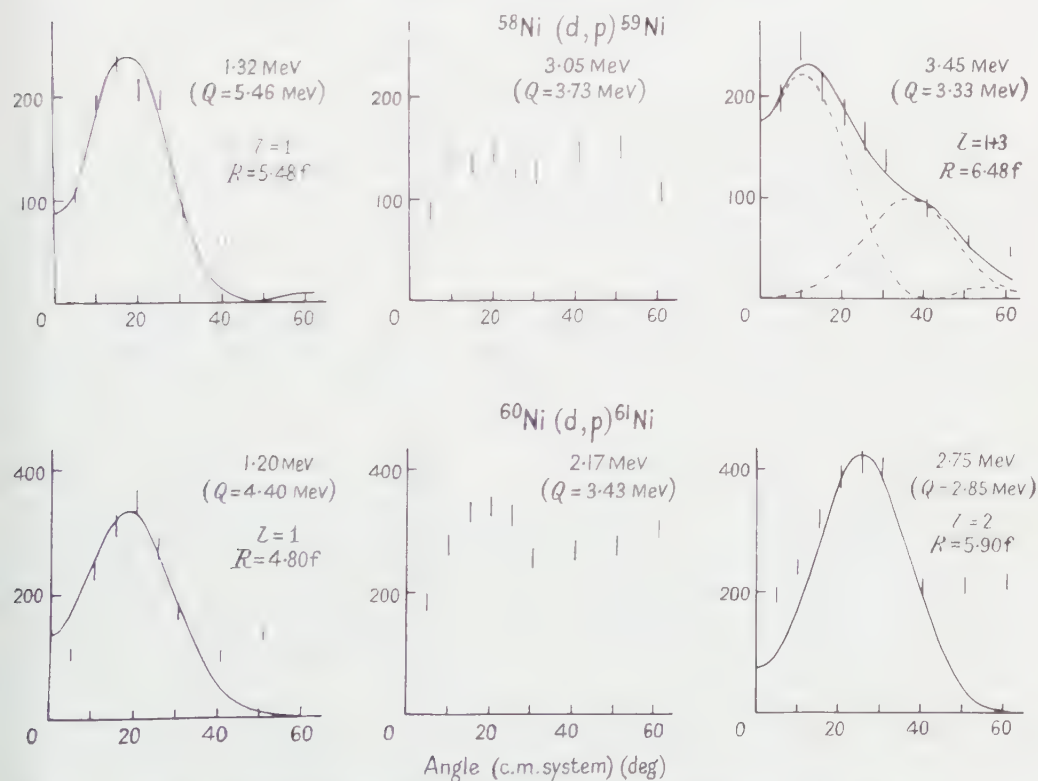


Fig. 4. Angular distributions of groups observed in the vicinity of $Q = 4.2$ MeV for the $^{58}\text{Ni}(d, p)^{59}\text{Ni}$ reaction, and $Q = 3.8$ MeV for the $^{60}\text{Ni}(d, p)^{61}\text{Ni}$ reaction. The distributions are labelled by the excitation energy of the corresponding final state and also by the Q -value of the final state.

2.3 mev. In addition there appears to be an $l=2$ group midway between these two groups with a Q -value of about 1.3 mev. This would not be apparent in a gross structure spectrum due to the proximity of strong $l=0$ groups.

In Fig. 3 is shown the gross structure proton spectrum for the $^{60}\text{Ni}(d, p)^{61}\text{Ni}$ reaction, again at an angle of 40° to the incident deuteron beam. A similarity is again seen between this and the spectrum published by Schiffer, Lee and Zeidman for an angle of observation of 30° to a 10 mev deuteron beam, although their Q -values differ from ours sometimes by as much as 1 mev. The angular distribution assignments for the gross peaks again correspond fairly well with our results except for the $l=4$ assignment for a peak with Q -value about 3.8 mev. The proton group with Q -value 3.43 mev has a large contribution up to and probably beyond 60° . This is also shown in Fig. 4 together with the angular distributions of the groups observed on either side. In the analysis of Enge and Fisher a value of $l=1$ has been assigned to the distribution corresponding to the level at 2.127 mev. In our analysis the points up to 30° could possibly be fitted by an $l=1$ distribution but this has not been done because of the uncertainty involved. Once again there appears to be an $l=2$ transition in a region where strong $l=0$ contributions would make its recognition difficult in gross structure spectra.

ACKNOWLEDGMENT

We wish to thank Dr. H. C. Newns for helpful discussions on the interpretation of the results.

REFERENCES

- DALTON, A. W., KIRK, A., PARRY, G., and SCOTT, H. D., 1960, *Proc. Phys. Soc. A*, **75**, 95.
 ENGE, H. A., and FISHER, R. A., 1959, *Massachusetts Institute of Technology, Progress Report of Laboratory for Nuclear Science*, May 1959.
 GAMOW, G., and CRITCHFIELD, C. L., 1949, *Theory of the Atomic Nucleus* (Oxford: University Press), p. 11.
 HARVEY, J. A., 1951, *Phys. Rev.*, **81**, 353.
 MCFARLAND, C. E., BRETSCHER, M. M., and SHULL, F. B., 1953, *Phys. Rev.*, **89**, 892A.
 MACFARLANE, M. H., and FRENCH, J. B., 1959, *Stripping Reactions and the Structure of Light and Intermediate Nuclei* (New York: University of Rochester), pp. 152, 370.
 NUSSBAUM, R. H., WAPSTRA, A. H., BRUIL, W. A., STERK, M. J., NIJGH, G. J., and GROBBEN, N., 1956, *Phys. Rev.*, **101**, 905.
 PARIS, C. H., 1959, *Massachusetts Institute of Technology, Progress Report of Laboratory for Nuclear Science*, May 1959.
 PARIS, C. H., and BUECHNER, W. W., 1958 a, *Bull. Amer. Phys. Soc.*, **3**, 38.
 — 1958 b, *Massachusetts Institute of Technology, Progress Report of Laboratory for Nuclear Science*, February 1958.
 PRATT, W. W., 1954 a, *Phys. Rev.*, **94**, 1086.
 — 1954 b, *Phys. Rev.*, **95**, 1517.
 SCHIFFER, J. P., LEE, L. L., and ZEIDMAN, B., 1959, *Phys. Rev.*, **115**, 427.
 TRUMPY, G., 1957, *Nucl. Phys.*, **2**, 664.

The Electrical Resistivities and Magnetic Susceptibilities of some Stable and Metastable Uranium-Molybdenum Alloys

By L. F. BATES AND R. D. BARNARD†

Department of Physics, University of Nottingham

MS. received 8th July 1960, in revised form 30th September 1960

Abstract. The magnetic susceptibilities and electrical resistivities of a series of quenched γ body-centred cubic uranium-molybdenum alloys were measured over the temperature ranges 293°–1200°K and 90°–1200°K, respectively. U-15, 20, 25 at. % Mo each possessed a small negative temperature coefficient of resistivity below about 200°C in the metastable γ -state, and a positive coefficient in the stable γ -region.

All samples exhibited a Pauli weak spin paramagnetism which increased with temperature, and in addition possessed an exchange contribution shown to be independent of composition over the range 15–30 at. % Mo. The bearing of the results on our understanding of the electronic structure of the γ -alloys is discussed.

§ 1. INTRODUCTION

FOR pure uranium the general forms of the resistivity-temperature (Dahl and Van Dusen 1947) and susceptibility-temperature (Bates and Hughes 1954) relations have been determined. These have shown that sharp discontinuities occur at 663°C and 770°C in both the electric and the magnetic properties, and are associated with the structural phase changes α - β and β - γ . The crystallography of these phases is now well understood; the structures of α and β are orthorhombic and tetragonal, respectively (Jacob and Warren 1937, Tucker 1951), while the γ -phase is body-centred cubic (Wilson and Rundle 1949). Consequently, much interest attaches to the low temperature behaviour of body-centred cubic uranium, as this is the simplest structure which the element exhibits.

In the present investigation we have examined the resistivity and susceptibility behaviours of a series of uranium-molybdenum alloys in the high temperature γ -phase and in the temperature range 290 K to about 600 K. In addition, the resistivities were measured in the range 90 to 290 K. For measurements below 600 K the γ -phase was retained in metastable equilibrium by initial quenching of the alloys to room temperature from the stable γ -region. It was therefore hoped that low temperature susceptibility and resistivity data could be obtained for pure γ -uranium by extrapolating the results for the alloys to zero molybdenum content. This procedure was adopted by Ames and McQuillan (1954) to determine the resistivity-temperature relation for pure β body-centred cubic titanium from observations on quenched β Ti-Nb alloys, but these authors did not obtain precise numerical values. In the present work, too, no reliable values were so obtained for pure uranium for two reasons. Firstly, the

† Now at E.R.A. Research Laboratory, Cleve Road, Leatherhead, Surrey.

extrapolation indicated an extremely high resistivity value at 0°K , which is unacceptable for a pure metal; the alloys were nevertheless of considerable interest because they showed a small negative temperature coefficient of resistivity below 200°C .

Secondly, for a number of years it was believed that the addition of between 10 and 30 at. % molybdenum to uranium was sufficient to retain the body-centred cubic structure at room temperature on quenching. This is now believed to be a simplification of what occurs; the low molybdenum content alloys tend to form a strained, partly transformed structure, which was not detectable by x-ray techniques, and was observed only after detailed metallographic investigation; further details are given below.

Previous investigations (Chandrasekhar and Hulm 1958, Berlincourt 1959) also showed that uranium-molybdenum quenched γ -alloys are characterized by a small negative temperature coefficient of resistivity below room temperature. This abnormal alloy behaviour persists down to a few degrees absolute, where the alloys become superconducting. It was considered desirable to extend the observations above room temperature and to include the region where the γ -phase is in stable equilibrium. A remarkable minimum in the resistance-temperature curve was observed in three of the four alloys investigated here, the relevant coefficient being positive in the stable γ -region in each case.

It was believed that measurement of the magnetic susceptibility as a function of temperature would give information concerning electronic changes which might account for anomalous resistivity behaviour, and possibly indicate the presence of randomly orientated localized moments. If any such moments were present, then an appropriate spin disorder contribution would be included in the resistivity. No randomly oriented local moments were found, and a Pauli weak spin type susceptibility was considered sufficient to explain the results.

The results are discussed below in terms of the hypothesis proposed by Chandrasekhar and Hulm (1958), which has been extended by Blatt (1961) in the light of some recent Hall effect measurements by Berlincourt (1959). It now seems possible, with the electronic specific heat measurements by Goodman *et al.* (1960) and the magnetic susceptibility results on metastable U-Mo alloys, to begin to understand the electronic structure of the γ -phase alloys.

§ 2. EXPERIMENTAL PROCEDURE

2.1. Alloy Preparation

The alloy ingots were prepared at Harwell in an argon arc furnace from molybdenum (Johnson Matthey) and uranium of purity given in Table 1.

Table 1. Impurity Content (parts per million) of Uranium

B	C	Fe	Al	Si	N ₂	Cr	Mn	H ₂	O ₂
0.05	800	100	65	25	20	5	10	10	50

The ingots were then wrapped in molybdenum foil, sealed in quartz under a pressure of less than 10^{-4} mm Hg and homogenized for 2 weeks at 1000°C . After water-quenching with fracture of the quartz capsule, each ingot was machined to give a cylinder 4 cm long and 4 mm diameter. Surface strain introduced by machining was removed by a further anneal of 2 hours at 950°C .

followed by requeenching. Prior to investigation the specimens were subjected to both metallographic and x-ray examination to verify the existence of the γ -phase.

2.2. X-ray and Metallographic Observations

X-ray powder photographs of the filings taken from the specimens showed the typical body-centred cubic pattern. The calculated lattice parameters obeyed Vegard's law and extrapolated, when account had been taken of thermal expansion, to the high temperature value of pure γ -uranium. However, metallographic observations performed at the Fulmer Research Institute showed that in the 10–20 at. % molybdenum range the alloys were weakly anisotropic, the structure being considered to be a distorted γ or body-centred tetragonal phase, the axial ratio at 10 at. % Mo being 0.98. To avoid, as far as possible, complications due to this tetragonality in the quenched alloys, only specimens in the range 15–30 at. % Mo were considered. The bearing of this anisotropy on the physical properties will be discussed later.

2.3. Electrical Resistivity Measurements

Separate sets of apparatus were used for resistivity measurements above room temperature and below room temperature; both were of the conventional current–potential type. Special precautions were taken with the high temperature apparatus to avoid oxidation of the specimens, and also to prevent their contamination by diffusion from the supports. Oxidation was almost completely prevented by continuously evacuating the furnace tube, the ultimate pressure being less than 3×10^{-5} mm Hg. The ends of the specimen were wrapped in molybdenum foil so that the specimens did not touch the stainless steel supports. Also, the potential probes which were spot welded to the specimen were no. 40 s.w.g. molybdenum wires. These precautions were sufficient to prevent contamination of the samples. No special precautions were necessary with the low temperature apparatus, details of which have been published elsewhere (Bates and Loasby 1958).

2.4. Magnetic Susceptibility Measurements

The room temperature mass susceptibilities were measured with a standard apparatus employing a modification of the Gouy method (Bates and Loasby 1958). A tantalum rod of the same dimensions as the specimens was used as a standard; it had been separately calibrated against an aqueous solution of nickel chloride (Nettleton and Sugden 1939). Susceptibility readings were taken for various magnetic fields between 7 and 16 kilo-oersteds, so that corrections to the apparent molar susceptibility $\chi_M(\text{app})$ could, if necessary, be applied for ferromagnetic impurity, using the formula due to Honda and Owen (cf. Bates 1951)

$$\chi_M(\text{true}) = \chi_M(\text{app}) - 2\sigma/H \quad \dots\dots(1)$$

where σ is the saturation magnetic moment of the impurities per mole and H the applied Gouy field. However, in the present instance the susceptibility was independent of field strength. High temperature susceptibility measurements, relative to the room temperature values, were made with an apparatus described by Bates and Hughes (1954).

§ 3. EXPERIMENTAL RESULTS

3.1. Electrical Resistivity

The resistivities of the γ -phase U-Mo alloys are shown as a function of temperature in Fig. 1. The results below room temperature are in reasonable agreement with those previously reported (Chandrasekhar and Hulm 1958,

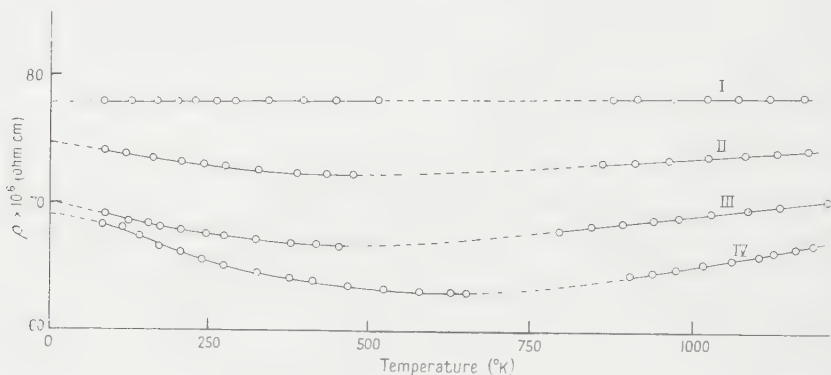


Fig. 1. Electrical resistivity plotted against temperature of γ U-Mo alloys. I, U-30 at. % Mo; II, U-25 at. % Mo; III, U-20 at. % Mo; IV, U-15 at. % Mo.

Berlincourt 1959). Observations above room temperature were taken until breakdown of the metastable γ -phase occurred and the equilibrium α -phase set in. It was possible to take readings up to about 350°C before precipitation of the α -phase, whose onset was recognized by a pronounced discontinuity in the slope of the resistivity-temperature curve which does not appear in Fig. 1, because it lies in the region indicated by the broken line. Further observations were not taken until the temperature had been raised to that of the stable γ -region, above 575–650°C, depending on the composition of the particular alloy. Readings were then taken up to 900°C. In the curves for the uranium-rich alloys, there were therefore temperature regions in which no experimental values

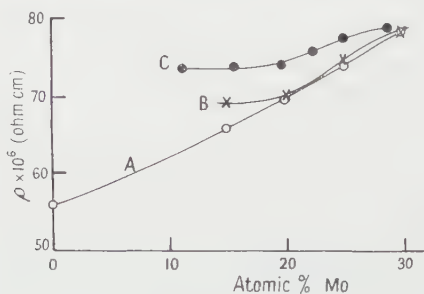


Fig. 2. Electrical resistivity plotted against composition at 0°K and 1100°K of γ U-Mo alloys. A, resistivities at 1100°K (present investigation); B, extrapolated resistivities at 0°K (present investigation); C, resistivities at 0°K (Chandrasekhar and Hulm 1958).

could be obtained. It was possible, however, to interpolate between the two portions of the graph, and estimate with a reasonable degree of accuracy the form of the curves where the γ -phase was decomposing. These regions are shown by broken lines in Fig. 1.

Fig. 2 shows the concentration dependence of the resistivity at 1100°K and 0°K. Although observations were only taken down to liquid oxygen temperatures, reasonably accurate extrapolations for ρ_0 , the resistivity at 0°K, could be made on the basis of the results of Chandrasekhar and Hulm (1958), which are plotted for comparison in Fig. 2. The present investigation gave rather lower values than those of Chandrasekhar and Hulm; it may be that purer metals were used in the present alloys. Apart from the difference in absolute magnitude, the resistivity-concentration curves vary in the same manner. Significant features of the curves are the negative temperature coefficients of resistivity both above and below room temperature, the resistivity minimum exhibited by three of the four samples, and the weak concentration dependence of the resistivity.

3.2. Magnetic Susceptibility

The molar magnetic susceptibilities of the same specimens in the metastable and stable γ -states are shown as a function of temperature in Fig. 3. The isothermal susceptibility-composition graphs, shown in Fig. 4, include the

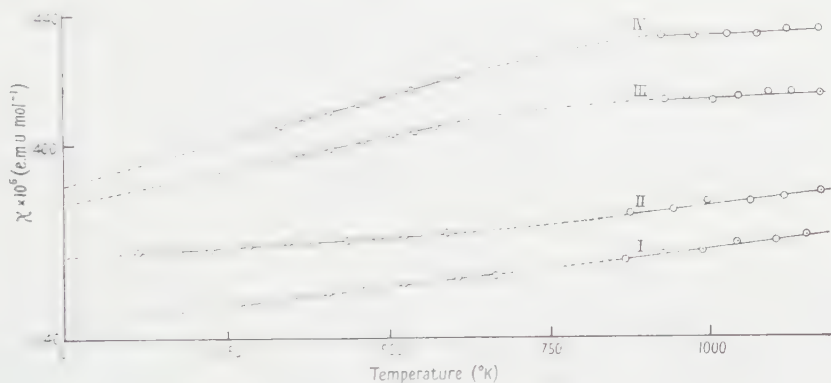


Fig. 3. Molar susceptibility plotted against temperature of γ U-Mo alloys. I, U-30 at. % Mo; II, U-25 at. % Mo; III, U-20 at. % Mo; IV, U-15 at. % Mo.

value at 1100°K for the pure uranium used in the preparation of the alloys. The temperature dependence of the susceptibility for U-15 at. % Mo is high and positive in low temperature regions, and this effect lessens with rise of temperature. In contrast to this behaviour, U-25 at. % Mo has a susceptibility which increases slowly at low temperatures and more rapidly at high temperatures. Although the apparatus was not suitable for measurements below room temperature, tentative linear extrapolations were made for the susceptibilities at 0°K. Such linear extrapolation was shown by Loasby (1958) to be valid for γ U-25 at. % Mo down to liquid oxygen temperatures.

The susceptibilities of both uranium and molybdenum are markedly sensitive to impurities, but, in spite of differences in absolute magnitude for different samples it is now well established that both elements have a susceptibility which increases with temperature. The recorded values at room temperature for different samples of pure α -uranium have in recent years steadily decreased, presumably because of better methods of purification. The uranium used here had a susceptibility of $1.60 \pm 0.02 \times 10^{-6}$ e.m.u. g⁻¹ at room temperature, compared with $1.72 \pm 0.02 \times 10^{-6}$ given by Bates and Hughes (1954).

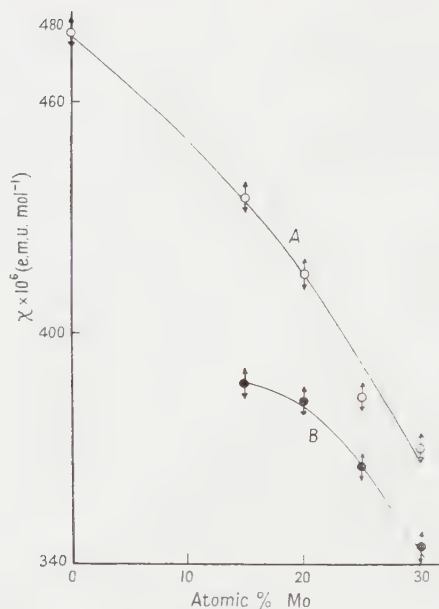


Fig. 4. Susceptibility plotted against composition at 0°K and 1100°K of γ U-Mo alloys A, susceptibilities at 1100°K; B, extrapolated susceptibilities to 0°K.

§ 4. DISCUSSION

The weak linear dependence of ρ_0 , shown in Fig. 2, instead of the expected relation $\rho_0 \propto c(1-c)$, where c is the concentration of the solute, is thought to be a consequence of a decreasing density of states at the Fermi surface with increasing molybdenum composition, and also to an increase in the effective number of free electrons. The decrease of the density of states alone, found by Goodman *et al.* (1960) from electron specific heat measurements, is not sufficient to account for the weak concentration dependence of ρ_0 .

The possibility that the negative temperature coefficient is a characteristic of the distorted γ -tetragonal phase, and not of the body-centred cubic γ -phase, should not be overlooked, especially as the degree of tetragonality increases with decreasing concentration of molybdenum. For, the negative slope of the resistivity-temperature graph also increases with decreasing molybdenum content. However, the existence of this anomalous behaviour in alloys with between 20 and 30 at. % Mo, where tetragonality is not observed, and the continuity of the resistivity curves of the stable and metastable alloys, leaves little doubt that it is typical of the γ body-centred cubic U-Mo alloys. Incidentally, similar behaviour was observed by the authors with U-Zr and U-Nb quenched γ -alloys; in the latter system a similar anomalous behaviour was shown by a U-50 at. % Nb sample in which there was no indication of a tetragonal structure. Similar behaviour has also been reported in quenched body-centred cubic Ti-Nb (Ames and McQuillan 1954), Ti-Mo (Yoshida and Tsuya 1956) and Ti-V (Brotzen *et al.*, 1955) alloys, and also in the γ -phase of neptunium metal (Lee *et al.* 1959).

The increase in susceptibility with temperature of the alloys is in accord with explanations of the behaviours of uranium and molybdenum which have been

discussed by Kriessman and Callen (1954) in connection with other transition elements, in which special forms for the density of states energy curves are postulated. These are based on a Pauli weak spin type paramagnetism, which is proportional to $N(E_0)$, the density of states at the Fermi surface. Exchange interaction effects which, if positive, tend to increase the difference between the number of positive and negative electron spins, result in a larger measured susceptibility than that given by the Pauli expression:

$$\chi_M' = 2\mu^2\Omega N(E_0) \quad \text{at } 0^\circ\text{K} \quad \dots\dots (2)$$

where χ_M' is the molar susceptibility, μ is the Bohr magneton, Ω is the molar volume and $N(E_0)$ the number of states per unit volume and energy. Stoner (1936) concluded that the exchange interaction is temperature independent and that the measured molar susceptibility χ_M may be separated into two terms; χ_M' , the calculated value without exchange, and a constant term in K , involving the exchange interaction. The relation between these quantities is:

$$1/\chi_M = 1/\chi_M' - K.$$

The electronic specific heat measurements of Goodman *et al.* enable $N(E_0)$, and thus χ_M' , to be calculated directly. From the values of the observed susceptibility extrapolated to 0°K , χ_M and K may be obtained as functions of molybdenum concentration. The values so found are given in Table 2; those of χ_M are corrected for the diamagnetism of the radon and krypton cores, $2\cdot5$ and $29\cdot0 \times 10^{-6}$ e.m.u. mol $^{-1}$, respectively.

Table 2

Alloy (at. % Mo)	$\chi_M' \times 10^6$ (e.m.u. mol $^{-1}$)	$\chi_M \times 10^6$ (e.m.u. mol $^{-1}$)	$(1/\chi_M') \times 10^{-1}$ (mol e.m.u. $^{-1}$)	$(1/\chi_M) \times 10^{-1}$ (mol e.m.u. $^{-1}$)	$K \times 10^{-1}$ (mol e.m.u. $^{-1}$)
15	210 ± 2	412 ± 4	476 ± 4	243 ± 2	233 ± 6
20	206 ± 2	407 ± 4	484 ± 4	246 ± 2	238 ± 6
25	201 ± 2	390 ± 4	497 ± 4	256 ± 2	241 ± 6
30	195 ± 2	369 ± 4	514 ± 5	271 ± 2	243 ± 7

The constancy of K within the limits of experimental error shows that the exchange interaction is independent of molybdenum concentration over the γ -phase range, and since $\chi_M > \chi_M'$ the exchange interaction must be positive, as indeed is the case for nearly all the transition elements.

In a recent paper, Chandrasekhar and Hulm (1958) discussed the resistivity of the γ U-Mo alloys, using a collective electron model. The electrons are assumed to lie in two overlapping bands, one of high density of states, the other a low broad s band, whose electrons carry most of the current. This model is identical with that with overlapping s and d bands proposed by Mott (1936) for the transition elements; but in the case of uranium the high narrow band is probably constructed of 5f and 6d hybridized orbitals. However, the proposed explanation does not involve the nature of the bands, apart from the fact that the s electrons are more mobile than those which we shall label the d electrons.

The resistivity of the transition metals is determined mainly by scattering processes in which the s electrons are transferred to the d band; the probability of such processes at 0°K is proportional to $N(E_0)$. Taking account of the variation of Fermi energy with temperature, Jones (1956) found that the thermal

resistivity ρ_{th} is given by

$$\rho_{\text{th}}(ET) = \rho_{\text{th}}(E_0T) \left[1 - \frac{\pi^2 k^2 T^2}{6} \left\{ 3 \left(\frac{1}{N} \frac{dN}{dE} \right)^2 - \frac{1}{N} \frac{d^2 N}{dE^2} \right\}_{E=E_0} \right]. \quad \dots\dots (4)$$

The appropriate expression for alloys of transition elements, assuming that thermal and residual resistivities (ρ_{th} and ρ_0 , respectively) are additive, is

$$\rho = \rho_{\text{th}} + \rho_0 = (\rho_{\text{th}}(E_0T) + \rho_0(E_0)) \left[1 - \frac{\pi^2 k^2 T^2}{6} \left\{ 3 \left(\frac{1}{N} \frac{dN}{dE} \right)^2 - \frac{1}{N} \frac{d^2 N}{dE^2} \right\}_{E=E_0} \right]. \quad \dots\dots (5)$$

Chandrasekhar and Hulm assumed that dN/dE was large and $\rho_{\text{th}}(E_0T)$ increased slowly with temperature, the net result being a decrease of ρ with temperature. This hypothesis is well in accordance with the high temperature resistivity measurements, for here $\rho_{\text{th}}(E_0T)$ (which is proportional to T at high temperatures) is the dominant term. Clearly, according to this formula a resistivity minimum can occur, provided the expansion of $N(E)$ is valid only at fairly low temperatures. The variation of the Pauli susceptibility with temperature is given by

$$\chi_M' = 2\mu^2 \Omega N(E_0) \left[1 - \frac{\pi^2 k^2 T^2}{6} \left\{ \left(\frac{1}{N} \frac{dN}{dE} \right)^2 - \frac{1}{N} \frac{d^2 N}{dE^2} \right\}_{E=E_0} \right]. \quad \dots\dots (6)$$

Blatt (1961) has given an analysis of the Hall effect and resistivity data obtained by Berlincourt (1959) below 100°K and has shown that, for all the alloys which the latter investigated,

$$\left(\frac{1}{N} \frac{d^2 N}{dE^2} \right)_{E=E_0} > \left(\frac{1}{N} \frac{dN}{dE} \right)_{E=E_0}^2.$$

Hence the susceptibility should increase according to a T^2 expression. Although qualitative agreement exists with the susceptibility results presented in Fig. 3, a T^2 dependence of the susceptibility is not found, especially in the case of U-15 at. % Mo, and the increases observed are very much smaller than those indicated by Blatt's numerical results.

The linear variation of the susceptibility with temperature is difficult to explain; in fact this has for a number of years been a serious weakness for the application of the theory to other transition elements. It is unlikely to be due to failure of the degeneracy condition $E_0 > kT$, since even at 1000°K , kT is only 0.086 eV. Lattice expansion with temperature would tend to increase $N(E)$, but might decrease the exchange interaction, thus resulting in a lower susceptibility. It may be that the result of a Pauli susceptibility which increases as T^2 , and an exchange interaction which decreases as some function of T , would result in a small linear increase with temperature.

The application of a rigid band model for γ -uranium in which the energy states are progressively filled up or depleted according to the conventional valency of the solute, cannot be applied to the U-Mo alloy system, as the elements are not close neighbours in the periodic table. Further, no change in $N(E_0)$ with composition is to be expected from such a model if uranium and molybdenum both contribute six electrons to the bands. Although uranium and molybdenum may be exercising their valencies of six, the observed decrease of $N(E_0)$ might be due to a modified band shape, partly as a result of a decreasing lattice parameter with Mo content, and also because of changes in the potential field.

No explanation can be given at present for the independence of the exchange interaction K with composition. This result is very surprising in view of the large value of K , $22.5 \times 10^3 \text{ mol e.m.u.}^{-1}$, for pure molybdenum, which, like

the alloys, has a body-centred cubic structure. The calculated value of K was taken from the susceptibility results of Kriessman (1953) and the electron specific heat measurements of Horowitz and Daunt (1953).

ACKNOWLEDGMENTS

The authors are indebted to Dr. G. K. Williamson, formerly of the Metallurgy Division, Atomic Energy Research Establishment, Harwell, and Dr. W. E. Gardner, for the provision of the alloys and also for much valuable discussion. Their thanks are also due to Dr. F. J. Blatt (Michigan State University) for allowing reference to work prior to publication, and to the Director of the Atomic Energy Research Establishment for permission to publish our results.

REFERENCES

- AMES, S. L., and MCQUILLAN, A. D., 1954, *Acta Metallurgica*, **2**, 831.
BATES, L. F., 1951, *Modern Magnetism* (Cambridge: University Press), p. 135.
BATES, L. F., and HUGHES, D., 1954, *Proc. Phys. Soc. B*, **67**, 28.
BATES, L. F., and LOASBY, R. G., 1958, *Proc. Phys. Soc.*, **72**, 757.
BERLINICOURT, T. G., 1959, *J. Phys. Chem. Solids*, **11**, 12.
BLATT, F. J., 1961, *J. Phys. Chem. Solids*, **17**, 177.
BROTZEN, F. R., HARMON, E. L., and TROIANO, A. R., 1955, *Trans. Amer. Inst. Min. (Metall.) Engrs*, **203**, 413.
CHANDRASEKHAR, B. S., and HULM, J. K., 1958, *J. Phys. Chem. Solids*, **7**, 259.
DAHL, A. I., and VAN DUSEN, 1947, *J. Res. Nat. Bur. Stand.*, **39**, 53.
GOODMAN, B. B., HILLAIRET, J., VEYSSIE, J., and WEIL, L., 1960, *C.R. Acad. Sci., Paris*, No. 3, 542.
HOROWITZ, M., and DAUNT, J. G., 1953, *Phys. Rev.*, **91**, 1099.
JACOB, C., and WARREN, B., 1937, *J. Amer. Chem. Soc.*, **59**, 2588.
JONES, H., 1956, *Handb. d. Phys.*, **19**, 227 (Berlin: Springer).
KRIESSMAN, C. J., 1953, *Rev. Mod. Phys.*, **25**, 122.
KRIESSMAN, C. J., and CALLEN, H. B., 1954, *Phys. Rev.*, **94**, 837.
LEE, J. A., EVAN, J. P., HALL, R. O. A., and KING, E., 1959, *J. Phys. Chem. Solids*, **11**, 278.
LOASBY, R. G., 1958, *Proc. Phys. Soc.*, **72**, 425.
MOTT, N. F., 1936, *Proc. Roy. Soc. A*, **153**, 699.
NETTLETON, H. R., and SUGDEN, S., 1939, *Proc. Roy. Soc. A*, **173**, 313.
STONER, E. C., 1936, *Proc. Roy. Soc. A*, **154**, 656.
TUCKER, C. W., Jr., 1951, *Acta Cryst.*, **4**, 425.
WILSON, A. S., and RUNDLE, R. E., 1949, *Acta Cryst.*, **2**, 126.
YOSHIDA, S., and TSUYA, Y., 1956, *J. Phys. Soc. Japan*, **11**, 1206.

Electrical and Optical Properties of GaAs-InAs Alloys

By J. C. WOOLLEY, C. M. GILLETT AND J. A. EVANS

Department of Physics, University of Nottingham

MS. received 23rd August 1960, in revised form 24th October 1960

Abstract. Solid specimens of GaAs-InAs alloys, showing a composition spread of less than 3 mol %, have been prepared by a slow directional freeze technique. These specimens have been used for measurements of Hall effect and conductivity as a function of temperature and for infra-red transmission measurements to determine the optical energy gap E_G . The electrical measurements show that there is mixed conduction in the alloys and hence the values of Hall mobility have no significance. The optical measurements to determine the variation of E_G with composition are in good agreement with values obtained by diffuse reflection methods on single phase powder samples. The values of E_G show a linear variation over most of the composition range.

§ 1. INTRODUCTION

RECENT work has shown that in many alloy systems involving III-V compounds, solid solution occurs throughout the whole range of composition (Folberth 1955, Woolley and Smith 1958 a, 1958 b). Woolley and Smith (1958 a) showed this to be the case for the GaAs-InAs alloy system. Although in many cases the data are limited, electrical and optical measurements have been reported on many alloy systems including the following: InAs-InP (Folberth 1955), GaSb-InSb (Woolley, Evans and Gillett 1959, Woolley and Gillett 1960), InSb-In₂Te₃ (Woolley, Gillett and Evans 1960), GaAs-InAs (Abrahams, Braunstein and Rosi 1959). Abrahams *et al.* (1959) investigated the variation of optical energy gap, Hall electron mobility and lattice thermal conductivity as a function of composition for alloys of the GaAs-InAs system. Some of their alloys, however, were very inhomogeneous, showing a considerable spread in composition. The present paper reports an investigation of the electrical and optical properties for the GaAs-InAs alloy system, using specimens more homogeneous than those of Abrahams *et al.*

§ 2. EXPERIMENTAL PROCEDURE

2.1. Preparation of Alloys

Each of the two compounds concerned was first prepared separately by the standard method. The problem in the preparation of the alloys is to obtain solid ingot specimens in a good equilibrium condition. Thus although with powdered specimens homogeneous samples can be obtained by annealing for one or two weeks some 10 or 20°C below the solidus (Woolley and Smith 1958 a), the approach to equilibrium with solid ingots is very much slower and even months of annealing give specimens which still show a range of composition. A suitable method for preparation of solid ingots is the directional freezing

technique described previously (Woolley, Evans and Gillett 1959) provided a sufficiently slow movement of the freezing surface is maintained. Most of the alloys used here were prepared in this way, an ingot of initial composition 30 mol % GaAs, 70 mol % InAs being frozen at the rate of approximately 0.5 cm per day. X-ray measurements on sections of the ingot showed these to be of a similar homogeneity to that of the GaSb-InSb alloys prepared in this way, i.e. with a composition spread of 5 mol % in the least homogeneous samples but with a considerably smaller spread in the majority of specimens used.

The variation of composition with position along the directionally frozen ingot was determined and the results are shown in Fig. 1. The resulting range of composition for this ingot extended from 82 mol % GaAs, 18 mol % InAs to 11 mol % GaAs, 89 mol % InAs. To cover the range of composition from 80–100 mol % GaAs, ingots of the appropriate composition were made up and annealed at 930°C for six weeks. As indicated above, these alloys were less homogeneous than the specimens produced by directional freezing.

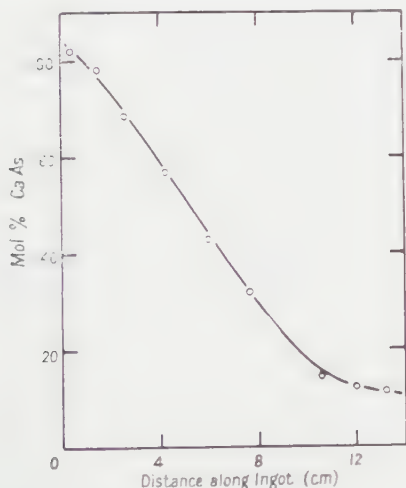


Fig. 1. Variation of composition with position along a directionally frozen ingot.

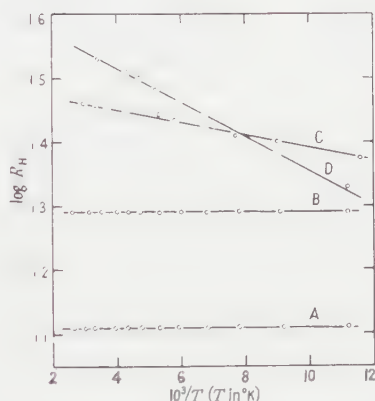


Fig. 2. Log R_H plotted against $10^3/T$ for various typical specimens: A, 29 mol % GaAs, 71 mol % InAs; B, 43 mol % GaAs, 57 mol % InAs; C, 57 mol % GaAs, 43 mol % InAs; D, 68 mol % GaAs, 32 mol % InAs.

2.2. Physical Measurements

Both the electrical and optical measurements were performed as described previously (Woolley, Gillett and Evans 1960), the values of Hall coefficient R_H and conductivity σ being determined in the temperature range 90 K to 400 K. The variation of R_H as a function of temperature is shown for typical specimens in Fig. 2.

The optical energy gaps of three alloys, 65 mol % GaAs, 35 mol % InAs, 50 mol % GaAs, 50 mol % InAs and 35 mol % GaAs, 65 mol % InAs, were determined using the diffuse reflection technique described by Fochs (1956) in which good single-phase powdered alloys were used. These optical measurements were kindly performed by Dr. P. D. Fochs and typical results are shown in Fig. 3.

For the remaining alloys, sections cut from the ingots were ground to parallel-sided plates and polished with diamond paste so giving specimens of thickness in the range 100–150 μ . Measurements were made of the percentage transmission through the various specimens as a function of wavelength and a graph of $\log I_0/I$ against λ plotted for each specimen. Two such graphs are shown in Fig. 4, A for a homogeneous specimen and B for a less homogeneous sample from the directionally frozen ingot. An increase in absorption coefficient of 150 cm^{-1} above the extrapolated background value was chosen as the criterion for the absorption edge wavelength so that the resultant values of optical energy gap E_G agreed with those obtained from powders by the diffuse reflection technique.

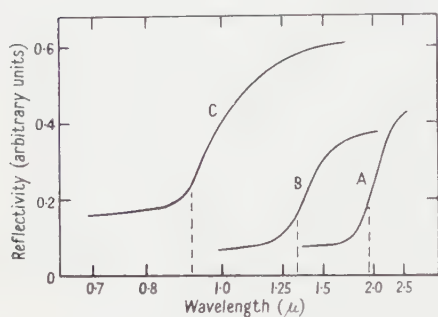


Fig. 3. Variation of reflectivity with wavelength for diffuse reflection measurements on typical alloys: A, 35 mol % GaAs, 65 mol % InAs; B, 65 mol % GaAs, 35 mol % InAs; C, GaAs.

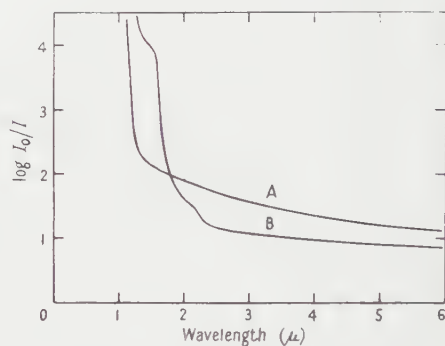


Fig. 4. Variation of $\log I_0/I$ with wavelength for transmission measurements on typical alloys: (A) good homogeneous specimen; (B) less homogeneous specimen.

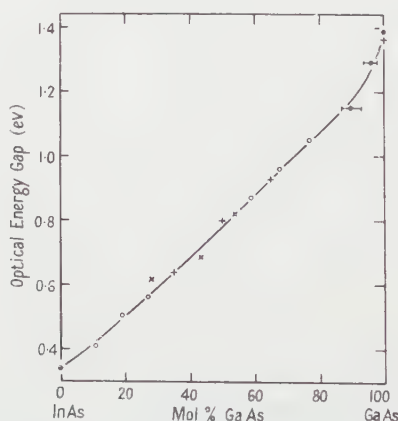


Fig. 5. Variation of optical energy gap E_G with composition. Key: ○ single phase, directionally frozen solid specimen; × partially multiphase, directionally frozen solid specimen; + single phase powder; ● annealed solid ingot specimen.

The variation of E_G with composition is shown in Fig. 5 where results from four types of specimen are distinguished, viz., (i) good homogeneous directionally frozen specimens giving $(\log I_0/I, \lambda)$ curves as in Fig. 4, curve A; (ii) somewhat multiphase directionally frozen specimens giving $(\log I_0/I, \lambda)$ curves as in Fig. 4,

curve B; (iii) good homogeneous powder specimens and (iv) annealed solid ingot specimens. Results with alloys of types (ii) and (iv) are obviously less reliable than the others because of their spread in composition.

§ 3. RESULTS AND DISCUSSION

3.1. Hall Measurements

Hall effect measurements on alloys containing less than 70 mol % GaAs indicated an n-type behaviour whereas no Hall voltage was detectable for the 78 mol % GaAs and 82 mol % GaAs alloys. On investigating the thermoelectric power of these two specimens, they were found to give a p-type effect at room temperature while the alloys of lower GaAs content showed n-type thermoelectric behaviour.

These results and the form of the (R_H , temperature) curves (Fig. 2) would indicate that all the specimens show mixed conduction. Hence the application of the simple single carrier equations for interpretation of Hall data is invalid and so the electrical measurements cannot give mobility values of any significance. It is perhaps worthy of note however that if the simple σR_H values are plotted as a function of composition they give values which, while being lower than those quoted by Abrahams, Braunstein and Rosi (1959), have a similar variation with composition up to approximately 70 mol % GaAs. The question of mixed conduction is not discussed by Abrahams *et al.*

3.2. Energy Gap

In Fig. 5 the energy gap of the GaAs-InAs system is plotted as a function of composition. An essentially linear variation of energy gap with composition is obtained up to about 80 mol % GaAs, beyond which a more rapid increase is observed up to a value of 1.37 ± 0.01 eV characteristic of GaAs. Alloys in the range 80-100 mol % GaAs were annealed solid ingots and consequently were not in as good an equilibrium condition as many specimens prepared by the directional freezing technique. This is reflected in the larger scatter of experimental points in this range.

The results may be compared with similar results for other alloy systems. The GaSb-InSb system (Woolley, Evans and Gillett 1959) shows a similar variation with a corresponding rapid variation of E_g at the GaSb end of the composition range, while the GaAs-GaP system (Folberth 1955) shows a linear variation of E_g with composition throughout the whole composition range. In the Ge-Si system, a definite discontinuity is observed in the variation of E_g with composition and this can be attributed to a change from Ge type to Si type band structure. Such a simple change cannot explain the form of the graphs for the GaSb-InSb or the GaAs-InAs systems and more complex effects must be postulated in these cases (Woolley and Gillett 1960). Before this can be done further data on the properties of the alloys must be obtained, and this will require the preparation of samples which are both purer and more homogeneous than those used here.

ACKNOWLEDGMENTS

The authors are indebted to Professor L. F. Bates for the facilities of his laboratory and to Dr. P. D. Fochs, Associated Electrical Industries (Woolwich)

for performing some of the optical measurements. The work described forms part of an investigation carried out for the Admiralty.

REFERENCES

- ABRAHAM, M. S., BRAUNSTEIN, R., and ROSI, F. D., 1959, *J. Phys. Chem. Solids*, **10**, 204.
FOCHS, P. D., 1956, *Proc. Phys. Soc.*, **69**, 70.
FOLBERTH, O. G., 1955, *Z. Naturf.*, **10a**, 502.
JOHNSON, E. R., and CHRISTIAN, S. M., 1954, *Phys. Rev.*, **95**, 560.
WOOLLEY, J. C., EVANS, J. A., and GILLETT, C. M., 1959, *Proc. Phys. Soc.*, **74**, 244.
WOOLLEY, J. C., and GILLETT, C. M., 1960, *J. Phys. Chem. Solids*, **17**, 34.
WOOLLEY, J. C., GILLETT, C. M., and EVANS, J. A., 1960, *J. Phys. Chem. Solids*, **16**, 138.
WOOLLEY, J. C., and SMITH, B. A., 1958 a, *Proc. Phys. Soc.*, **72**, 214.
—— 1958 b, *Proc. Phys. Soc.*, **72**, 867.

One-dimensional Chains with Random Spacing between Atoms

By R. E. BORLAND†

Mathematics Department, Imperial College of Science and Technology, London

Communicated by P. Dean; MS. received 3rd October 1960

Abstract. The calculation of the integrated density of states for positive electron energies of a one-dimensional chain of atoms whose spacing is given by a probability distribution function is reduced to the form of an integral equation. This equation is simplified considerably when the atoms are distributed at random. In this case, an explicit solution for the integrated density of states is found, which is rigorously valid for δ -function atomic potentials, and may be valid generally. It is shown that the solution gives good agreement with the machine results of Lax and Phillips (1958) for the δ -function case.

§ 1. INTRODUCTION

OWING to the considerable difficulty involved in exact calculations for three-dimensional disordered crystals, there is still much interest in exact calculations on one-dimensional crystals exhibiting various kinds of disorder, not only to provide qualitative insight, but also to provide standards against which to check the validity of certain three-dimensional approximate models.

A type of disorder which is of importance, both in the theory of impurity bands in semiconductors and in the theory of liquids, is that possessed by a chain of identical atoms whose spacing is given by a probability distribution function. In this paper we consider the calculation of the integrated density of states at positive electron energies for this disordered chain.



We use the one-electron approximation and assume that the shape of an atomic potential is not modified by the presence of adjacent atoms. Thus our representation of the problem consists of a chain of identical potential shapes, which we term atomic potentials, connected by regions of zero potential, each of which we term a 'spacing region'. In the Figure PQ and P'Q' represent atomic potentials and Q'P a 'spacing region'.

† Now at the Mathematics Division, National Physical Laboratory, Teddington.

§ 2. DERIVATION OF THE INTEGRAL EQUATION

James and Ginzburg (1953) defined the phase ϕ of a real solution $\psi(E, x)$ of the wave equation by

$$\tan \phi(E, x) = -b\psi'(E, x)/\psi(E, x) \quad \dots\dots (1)$$

and the conditions that $-\pi/2 \leq \phi(E, 0) < \pi/2$ and that ϕ changes continuously with x , E being the energy of the electron, and b an arbitrary positive constant. They showed that if the phase increase along a length of chain is $\Delta\phi$, then the number of zeros of ψ in the chain is $\Delta\phi/\pi$, to within unity, and consequently the number of states with energy less than E is equal to $\Delta\phi/\pi$, to within two.

We define the integrated density of states $N(k)$ as the average number of states per atom with energy less than E (equal to k^2 in atomic units), so that $N(k)$ is the average phase increase per atom divided by π . If we choose b equal to $1/k$, then it can be shown that the phase increase in a length x of the 'spacing region' is kx . It follows that if $\langle S \rangle$ is the average length of the 'spacing region', the contribution to $N(k)$ due to the spacing alone is

$$N_s(k) = k\langle S \rangle/\pi = 1/\pi\mu \quad \dots\dots (2)$$

where μ is defined as $1/k\langle S \rangle$.

The problem is to find the average phase increase $\langle \Phi \rangle$ per atomic potential. Then the contribution to $N(k)$ due to the atomic potentials is

$$N_A(k) = \langle \Phi \rangle/\pi \text{ so that finally } N(k) = N_s(k) + N_A(k).$$

If the phase at point P (see Figure) is ϕ , then the phase at point Q is defined as $D\phi$, where $D\phi$ is uniquely specified by the electron energy and the form of the atomic potential, the arbitrary constant b having been fixed. We introduce a reduced phase, denoted by primed symbols, which is restricted to the range $-\pi/2 \leq \phi' < \pi/2$ by subtracting integral multiples of π from ϕ . If $\Phi(\phi)$ is the phase increase due to the atomic potential, and $n\pi \leq \phi' + \Phi(\phi') < (n+1)\pi$ then

$$D\phi' = \phi' + \Phi(\phi') - n\pi. \quad \dots\dots (3)$$

Note that $\Phi(\phi') = \Phi(\phi)$ and is an unreduced phase increase, whereas $D\phi'$ is a reduced phase.

We now define a probability distribution function $\rho(\phi')$ such that the probability that the phase at point P at the extreme left of a typical atomic potential (see Figure) lies in the interval $d\phi'$ is given by $\rho(\phi')d\phi'$. We then have

$$\int_{-\pi/2}^{+\pi/2} \rho(\phi')d\phi' = 1 \quad \dots\dots (4)$$

$$\int_{-\pi/2}^{+\pi/2} \rho(\phi')\Phi(\phi')d\phi' = \langle \Phi \rangle. \quad \dots\dots (5)$$

This definition of $\rho(\phi')$ is justified only for disordered chains. For perfectly periodic chains $\rho(\phi')$ may have singularities.

The probability that the phase θ' at point P', immediately to the left of the adjacent atom specified by P'Q' (see Figure), transforms into the interval $d\phi'$ at P is equal to the probability that the phase $D\theta'$ at Q' is transformed into the interval $d\phi'$ at P by the spacing Q'P = S . Since the phase increase from Q' to P is kS equal to Ψ say, it follows that if the probability that the spacing lies in the interval

dS is $p(S)dS$, then the probability that the phase increase lies in the interval $d\Psi$ is

$$\frac{1}{k} p\left(\frac{\Psi'}{k}\right) d\Psi'.$$

Therefore, the probability that the phase $D\theta'$ at Q' will transform into the phase interval $d\phi'$ at P is

$$\frac{1}{k} \sum_{n=0}^{\infty} p\left(\frac{\phi' - D\theta' + n\pi}{k}\right) d\phi' \quad \text{if } D\theta' \leq \phi'$$

or

$$\frac{1}{k} \sum_{n=1}^{\infty} p\left(\frac{\phi' - D\theta' + n\pi}{k}\right) d\phi' \quad \text{if } D\theta' > \phi'.$$

To find $\rho(\phi')d\phi'$ we must integrate these contributions for all values of θ' appropriately weighted. Therefore,

$$\begin{aligned} \rho(\phi') &= \frac{1}{k} \int_{D\theta' = -\pi/2}^{D\theta' = \pi/2} \rho(\theta') \sum_{n=0}^{\infty} p\left(\frac{\phi' - D\theta' + n\pi}{k}\right) d\theta' \\ &\quad - \frac{1}{k} \int_{D\theta' = \pi/2}^{D\theta' = \pi/2} \rho(\theta') \sum_{n=1}^{\infty} p\left(\frac{\phi' - D\theta' + n\pi}{k}\right) d\theta' \end{aligned}$$

i.e., simplifying,

$$\begin{aligned} \rho(\phi') &= \frac{1}{k} \int_{\theta' = -\pi/2}^{\pi/2} \rho(\theta') \sum_{n=1}^{\infty} p\left(\frac{\phi' - D\theta' + n\pi}{k}\right) d\theta' \\ &\quad + \frac{1}{k} \int_{D\theta' = -\pi/2}^{D\theta' = \phi'} \rho(\theta') p\left(\frac{\phi' - D\theta'}{k}\right) d\theta'. \end{aligned} \quad \text{..... (6)}$$

Equation (6) is a general integral equation for the spacing disorder problem. The approach to this problem is similar to the method of Schmidt (1957), the difference being that Schmidt expresses his equations in terms of a finite number of possible transformations (i.e. those due to the presence of atoms of different kinds) whereas here we consider a continuous range of possible transformations.

§ 3. SOLUTION OF THE INTEGRAL EQUATION WHEN THE ATOMS ARE DISTRIBUTED AT RANDOM

In this case the atoms have an equal probability of lying anywhere along the chain, except that they must not overlap, this condition being implied by our initial assumption that the atomic potential is not modified by the presence of other atoms. It can be shown that the required probability distribution function for the spacing is given by

$$p(S)dS = \frac{1}{\langle S \rangle} \exp(-S/\langle S \rangle) dS. \quad \text{..... (7)}$$

Inserting Eqn (7) into the general integral equation (6) and using $\mu = 1/k\langle S \rangle$, we obtain

$$\rho(\phi') = \text{constant} \times \exp(-\mu\phi') + \mu \exp(-\mu\phi') \int_{D\theta' = -\pi/2}^{D\theta' = \phi'} \rho(\theta') \exp(\mu D\theta') d\theta'.$$

Multiplying by $\exp(\mu\phi')$ and differentiating with respect to ϕ' , we get

$$\mu\rho(\phi') + \frac{d\rho(\phi')}{d\phi'} = \mu\rho(D^{-1}\phi') \frac{d(D^{-1}\phi')}{d\phi'} \quad \text{..... (8)}$$

where $D\theta' = \phi'$ implies $\phi' = D^{-1}\theta'$. Eqn (8) is equally valid for unreduced phase, provided we assume that $\rho(\phi)$ is a periodic function with period π and is normalized to unity in a phase interval of length π . Multiplying Eqn (8) expressed in terms of unreduced phase by $d\phi$ and integrating from $\phi = 0$ to $\phi = \psi$ we obtain,

$$\begin{aligned}\rho(\psi) &= \rho(0) + \mu \int_{\phi=0}^{\phi=\psi} \rho(D^{-1}\phi) d(D^{-1}\phi) - \mu \int_{\phi=0}^{\psi} \rho(\phi) d\phi \\ &= \rho(0) + \mu \int_{\phi=D^{-1}0}^{D^{-1}\psi} \rho(\phi) d\phi - \mu \int_{\phi=0}^{\psi} \rho(\phi) d\phi \\ &= \rho(0) + \mu \int_{\phi=D^{-1}0}^0 \rho(\phi) d\phi - \mu \int_{\phi=D^{-1}\psi}^{\psi} \rho(\phi) d\phi\end{aligned}$$

$$\text{i.e.} \quad \rho(\psi) = A - \mu \int_{D^{-1}\psi}^{\psi} \rho(\phi) d\phi \quad \dots\dots\dots (9)$$

where A is a constant.

We can relate A to the average phase change per atomic potential $\langle \Phi \rangle$ by integrating (9) over an interval of length π . We obtain

$$1 = \pi A - \mu \int_{\psi=0}^{\pi} \int_{\phi=D^{-1}\psi}^{\psi} \rho(\phi) d\phi d\psi.$$

Changing the order of integration, and using $D\psi = \psi + \Phi(\psi)$ we obtain

$$1 = \pi A - \mu \int_{\phi=0}^{\pi} \rho(\phi) \Phi(\phi) d\phi = \pi A - \mu \langle \Phi \rangle$$

$$\text{i.e.} \quad \langle \Phi \rangle = \pi A / \mu - 1 / \mu. \quad \dots\dots\dots (10)$$

Hence

$$N_A(k) = \langle \Phi \rangle / \pi = A / \mu - 1 / \pi \mu.$$

But we have already shown that $N_S(k) = 1 / \pi \mu$, so

$$N(k) = N_A(k) + N_S(k) = A / \mu. \quad \dots\dots\dots (11)$$

The constant A is determined by normalizing the solution $\rho(\psi)$ of Eqn (9).

Now it can be shown that for a fixed electron energy $U \leq \Phi(\phi) < U + \pi$ for all ϕ . If $n\pi \leq U < (n+1)\pi$, we shall denote the corresponding Φ by Φ_n . We define

$$f(\psi) = \psi - \Phi_n(D^{-1}\psi) + n\pi = D^{-1}\psi + n\pi. \quad \dots\dots\dots (12)$$

Eqn (9) then becomes

$$\rho(\psi) = A - n\mu - \mu \int_{f(\psi)}^{\psi} \rho(\phi) d\phi. \quad \dots\dots\dots (13)$$

We can certainly write down a solution valid when $0 \leq \mu < 1/\text{max value of } \psi - f(\psi)$, by iteration in Eqn (13). We obtain

$$\rho(\psi) = (A - n\mu) \left[1 + \sum_{n=1}^{\infty} (-\mu)^n K^n \right] = (A - n\mu) \rho'(\psi) \text{ say} \quad \dots\dots\dots (14)$$

where

$$K^n = \int_{t_n=f(\psi)}^{\psi} \int_{t_{n-1}=f(t_n)}^{t_n} \dots \int_{t_1=f(t_2)}^{t_2} dt_1 dt_2 \dots dt_n. \quad \dots\dots\dots (15)$$

Normalizing $\rho(\psi)$ we obtain,

$$A - n\mu = 1 / \int_0^{\pi} \rho'(\psi).$$

Finally therefore,

$$N(k) = 1/\mu \int_0^\pi \rho'(\psi) d\psi + n, \quad \dots\dots (16)$$

provided the iterated solution is valid.

§ 4. REPRESENTATION OF ATOMIC POTENTIALS BY δ -FUNCTIONS

We now consider the case when the atomic potential is represented by $-2k_0$ multiplied by a δ -function. Lax and Phillips (1958), using this model as a representation of the one-dimensional impurity band problem, have obtained machine results accurate to about 1%.

It can be shown in a straightforward manner that the transformation of phase across a δ -function is given by

$$\tan D^{-1}\psi = \tan \psi - 2\alpha \quad \dots\dots (17)$$

where $\alpha = k_0/k$. Furthermore $\Phi(\psi) < \pi$, so that in Eqn (13) $n = 0$ and $f(\psi) = D^{-1}\psi$. Hence $-\pi/2 \leq f(\psi) < \psi$. If the phase origin is moved back to $-\pi/2$, then clearly

$$\mu \int_{f(\psi)}^\psi \rho(\phi) d\phi \leq \mu \int_0^\psi \rho(\phi) d\phi.$$

Therefore the error in the iterated solution converges to zero for all values of μ , by the standard theory of the Volterra integral equation.

Expressing Eqn (17) in explicit form, we obtain

$$D^{-1}\psi = \psi - \Delta + \frac{i}{2} \log \left(\frac{1 + z_0 e^{2i\psi}}{1 + z_0^* e^{-2i\psi}} \right) \quad \dots\dots (18)$$

where $\Delta = \tan^{-1} \alpha$ and $z_0 = i\alpha/(1 + i\alpha)$.

The first three terms of

$$\int_0^\pi \rho'(\psi) d\psi$$

can be readily evaluated. The result is

$$\int_0^\pi \rho'(\psi) d\psi = \pi \{ 1 - \mu\Delta + \mu^2 [\Delta^2 - \frac{1}{2} Li_2(\cos^2 \delta, 2\delta)] \dots \}$$

where $\delta = \pi/2 - \Delta$, and $Li_2(r, \theta)$ is the real part of the dilogarithmic function of $r \exp(i\theta)$. For high energies and consequently small μ , this is obviously a very good approximation. Now $D^{-1}\psi$ is equal to $\psi - \Phi(D^{-1}\psi)$, and the average value of $\Phi(D^{-1}\psi)$ is equal to Δ . Thus we can get a crude approximation to the remaining integrals by replacing the lower limit of integration, $D^{-1}\psi$, by $\psi - \Delta$. Furthermore, we replace K^2 by its average value $\Delta^2 - \frac{1}{2} Li_2(\cos^2 \delta, 2\delta)$. We finally obtain the 'high energy' approximation,

$$\begin{aligned} \int_0^\pi \rho'(\psi) d\psi &\simeq \pi \left\{ 1 - \mu\Delta + \frac{[\mu^2 \Delta^2 - \frac{1}{2} \mu^2 Li_2(\cos^2 \delta, 2\delta)]}{1 + \mu\Delta} \right\} \\ &= \pi \left[\frac{1 - \frac{1}{2} \mu^2 Li_2(\cos^2 \delta, 2\delta)}{1 + \mu\Delta} \right] \\ \text{i.e. } N(k) &\simeq \frac{1 + \mu\Delta}{\pi\mu [1 - \frac{1}{2} \mu^2 Li_2(\cos^2 \delta, 2\delta)]}. \quad \dots\dots (19) \end{aligned}$$

On comparing the results given by this approximate formula with those of Lax and Phillips (1958), we find good agreement at 'high energies' as

expected (see Table). Our μ is equal to $\epsilon k_0/k$ in the notation of Lax and Phillips.

Integrated Density of States at Positive Energies			
ϵ	k/k_0	$N(k)$ given by Eqn (19)	Machine results of Lax and Phillips
10	π	0.144	0.174
10	2π	0.2431	0.249
10	4π	0.4244	0.431
10	6π	0.6166	0.628
10	8π	0.8126	0.826
10	10π	1.0101	1.018
10	20π	2.0051	2.039
0.5	0.71	0.7772	0.752
0.5	1.00	0.8801	0.884
0.25	0.35	1.005	0.894
0.25	0.50	1.037	1.006
0.25	0.71	1.2160	1.200
0.25	1.00	1.5204	1.528
0.1	0.05π	1.24	1.044
0.1	0.10π	1.457	1.442
0.1	0.15π	1.8774	1.888
0.1	0.20π	2.3271	2.342

As a further check on the explicit solution, it can easily be shown that it correctly predicts one negative bound state per atom when the mean spacing is infinitely large. The simplicity of evaluation in this case, derives from the fact that $D^{-1}\psi$ tends to zero for all ψ as k tends to zero. Simultaneously, the mean spacing must be allowed to tend to infinity, in order to keep μ constant whilst the limit is derived.

Furthermore it is reassuring that for the δ -function atomic potential we can obtain the optical model result as an approximate solution at high energies of the integral equation. If we express Eqn (13) in terms of a new variable $z = \tan \psi$ we obtain,

$$\rho(z) = A - \mu \int_{z' = z - 2\alpha}^{z' = z} \rho(z') \frac{dz'}{1 + z'^2}. \quad \dots (20)$$

For high energies α is small and we can therefore assume that $\rho(z)/(1 + z^2)$ is constant over an interval of length 2α ,

$$\begin{aligned} \text{i.e.} \quad \rho(z) &\simeq A - \frac{2\mu\alpha\rho(z)}{1 + z^2} \\ \rho(z) &\simeq \frac{A(1 + z^2)}{1 + 2\mu\alpha + z^2}. \end{aligned}$$

But

$$1 = \int_0^\pi \rho(\psi) d\psi = \int_{-\infty}^{+\infty} \frac{\rho(z) dz}{1 + z^2} \simeq A \int_{-\infty}^{+\infty} \frac{dz}{1 + 2\mu\alpha + z^2}$$

$$\text{i.e.} \quad A \simeq (1 + 2\mu\alpha)^{1/2}/\pi.$$

Hence $N(k) = A/\mu \simeq (1 + 2\mu\alpha)^{1/2}/\pi\mu$ which is the optical model result.

§ 5. IMPURE CRYSTALS

The model considered in § 3 has a very close connection with a one-dimensional crystal containing a small concentration of impurity atoms. James and Ginzburg (1953) have shown that provided the atomic potentials of the host cells are symmetric and the energy lies within one of the allowed bands of the pure crystal, then the arbitrary constant b in the definition of phase can always be chosen to give a linear relationship between the initial and final phase of a host cell. This choice of b at a particular energy value enables us to regard the host lattice potential as zero provided that the other parameters are suitably changed. Thus the only assumption that has to be made is that the impurity atoms are distributed at random on a continuous domain rather than at lattice sites. This is certainly justified for low impurity concentrations.

§ 6. SUMMARY

We have shown that the problem of calculating the integrated density of states for positive electron energies of a one-dimensional chain of atoms whose spacing is given by a probability distribution function can be reduced to the problem of finding the solution to an integral equation. Furthermore, this integral equation has been considerably simplified for the case where the atoms are distributed at random. We have shown that in this case the integrated density of states can be written down explicitly for energies which are sufficiently high, and it may be that the solution is valid for all energies. Certainly this is true when the atoms are represented by δ -functions. We have obtained numerical results for this latter case which agree with the machine results of Lax and Phillips (1958).

Note added in proof.—Frisch and Lloyd (1960) have independently solved the particular case of the δ -function potential.

ACKNOWLEDGMENT

I wish to thank Dr. E. P. Wohlfarth for his interest and encouragement in this work.

REFERENCES

- FRISCH, H. L., and LLOYD, S. P., 1960, *Phys. Rev.*, **120**, 1175.
 JAMES, H. M., and GINZBURG, A. S., 1953, *J. Phys. Chem.*, **57**, 840.
 LAX, M., and PHILLIPS, J. C., 1958, *Phys. Rev.*, **110**, 41.
 SCHMIDT, H., 1957, *Phys. Rev.*, **105**, 425.

On the Inversion Temperature Function of the First Order (One Phonon) Scattering and the Determination of Debye Characteristic Temperatures†

BY M. L. CANUT AND J. L. AMORÓS

Sección de Termodinámica Cristalina, Departamento de Cristalografía Física, C.S.I.C. Madrid

Communicated by K. Lonsdale; MS. received 20th September 1960

Abstract. Starting from Laval's expression for the first-order thermal diffuse scattering (TDS_1), a new expression for the inversion temperature of TDS_1 , $T_{\max} = m\Theta_D^2 d_{hkl}^2 k/3h^2$, has been obtained, valid for a crystal of any symmetry. T_{\max} is attained when $(\bar{u}^2)^{1/2}/d_{hkl} = 16\%$. Every crystalline substance has a definite range where the above formula holds: the upper limit is T_{mp} and the lower limit is Θ_D . The melting temperature defines a d_{\max} for which the inversion phenomenon can be observable. The inversion curves of TDS_1 have been calculated for some metallic, ionic and molecular crystals. It is shown that KCl, Pb and Al, for which the inversion phenomenon has been reported, are not special cases. In molecular crystals this effect will be observable mainly at low temperatures. A method is given for determining Debye characteristic temperatures of crystals of any symmetry. This method is tested using Cartz's experimental T_{\max} for lead.

§ 1. INTRODUCTION

X-RAY and electron scattering by a crystal are obviously dependent on temperature. However, the different contributions to the total scattering of a crystal undergoing thermal agitation are differently dependent on temperature. In this way, the temperature factor modifying the Bragg intensity is given (for $T > \Theta$) by the well-known Debye-Waller (James 1954) expression

$$\exp(-2B(\sin^2 \theta)/\lambda^2) = \exp\left(-\frac{12h^2}{km\Theta^2} \frac{\sin^2 \theta}{\lambda^2} T\right). \quad \dots\dots (1)$$

According to Laval (1942) the temperature factors for first-, second- and third-order (one, two, three phonon) scattering are given by

$$kT \exp[-2B_j |\mathbf{X}|^2 T] \quad \dots\dots (2)$$

$$k^2 T^2 \exp[-2B_j |\mathbf{X}|^2 T] \quad \dots\dots (3)$$

$$k^3 T^3 \exp[-2B_j |\mathbf{X}|^2 T] \quad \dots\dots (4)$$

if the equipartition law holds. \mathbf{X} is the reciprocal lattice vector.

† Partially supported by the Directorate of Solid State Sciences, Air Force Office of Scientific Research, through the European Office of Air Research and Development Command, Contract No. AF 61 (514)-1146.

The temperature factor for independent molecular motion is (Amorós, Canut and de Acha 1960)

$$1 - \exp [-2B(\sin^2 \theta)/\lambda^2] \quad \dots\dots (5)$$

(cf. the well-known Debye temperature factor for independent atomic motion, Debye 1954).

A full knowledge of the temperature dependence of each contribution to the total scattering will thus be of great value in the full interpretation of the experimental x-ray diffuse scattering of crystals.

In this paper, attention will be paid to the first-order (one-phonon) scattering (hereafter called TDS_1), and second-order (two-phonon) scattering (hereafter called TDS_2).

§ 2. THE TEMPERATURE DEPENDENCE OF THE THERMAL DIFFUSE SCATTERING

First-, second- and third-order diffuse scattering each increases from absolute zero up to a given temperature where a maximum is attained, then decreases with increasing temperature. This fact was predicted by Laval (1941), who expressed the temperatures of the maximum intensity of TDS_1 , TDS_2 and TDS_3 as

$$T_1 = 1/2 B_j |\mathbf{X}|^2 \quad \dots\dots (6)$$

$$T_2 = 2T_1 \quad \dots\dots (7)$$

$$T_3 = 3T_1 \quad \dots\dots (8)$$

if the equipartition law is assumed.

Born (1943) defined an 'inversion temperature' T_h , that makes the function (valid when $T > \Theta$)

$$\sigma_2 \propto T \exp [-T/T_h] \quad \dots\dots (9)$$

a maximum when $T = T_h$. However, as Born pointed out, the approximation involved, $\exp (-2M) = 1 - 2M$, makes (9) only valid for $2M < 1$. Born expressed the inversion temperature for the particular case of cubic crystals as

$$T_h = T_0 / \Sigma h^2 \quad \dots\dots (10)$$

where

$$T_0 = \frac{mka^2\Theta^2}{12\pi^2\hbar^2} = \frac{\Theta}{12\pi^2} \left(\frac{a}{l}\right)^2 \quad \dots\dots (11)$$

and

$$l = \hbar / (mk\Theta)^{1/2} = 6.96 \times 10^{-8} / (\mu\Theta)^{1/2} \text{ cm} \quad \dots\dots (12)$$

μ is the atomic weight relative to O = 16; l is Born's 'dynamical lattice constant'. Born's theory predicts also a difference in the temperature dependence of low- and high-order spots. Born and Lonsdale (1942) gave a table of T_0 for some cubic elements.

The experimental data reported by Laval (1941) for KCl showed very clearly that the diffuse scattering associated with the 006 reflection decreases with increasing temperature.

Lonsdale (1948) suggested that lead should show a decrease of diffuse intensity for high-order planes. Cartz (1955) was able to detect this inversion phenomenon

in lead by using the diffractometer technique. Later, Burgers, Kooy and Tiedema (1956) showed this phenomenon photographically.

Recently, Laberrigue (1959) reported a decrease of the diffuse intensity of the 444 Al reflection with increasing temperature, by using the electron-diffraction technique.

Cartz (1955) gave also a list of substances where the effect of temperature on diffuse scattering had been studied. In all cases an increase of diffuse scattering with temperature was reported except for phloroglucinol dihydrate where no change was observed in the range studied.

From the literature it would appear that the inversion of diffuse scattering is only observable in special cases. In this paper we are going to show from the theoretical standpoint that, on the contrary, it must be a general case and it is only necessary to select appropriate experimental conditions for observation; and also (following Cartz 1954) that the inversion temperature phenomenon gives a new method for determining the Debye characteristic temperatures for many substances.

§ 3. RESTATEMENT OF THE PROBLEM

Born's formulae (10, 11) are only valid for cubic crystals and their extension to the other crystallographic systems would give a complicated expression in terms of $h, k, l, a, b, c, \alpha, \beta, \gamma$.

We shall start with Laval's formula for TDS_1 .

From (1) and (2) we obtain as temperature factor for TDS_1

$$kT \exp\left(-\frac{12h^2 \sin^2 \theta}{km\Theta^2} T\right). \quad \dots\dots (13)$$

The maximum of this function satisfies

$$(T_{\max})_1 = \frac{k}{12h^2} m \Theta^2 \frac{\lambda^2}{\sin^2 \theta} \quad \dots\dots (14)$$

$$= \frac{k}{3h^2} m \Theta^2 d_{hkl}^2. \quad \dots\dots (15)$$

Every crystalline substance has a definite temperature range where (15) holds. The upper limit of T_{\max} is obviously the melting temperature and the lower limit is the characteristic temperature of the substance, as the equipartition law has been applied. These two extreme temperatures define the upper and lower spacings for which (15) applies. The consequence is that only certain sets of crystal planes will be potentially able to show the phenomenon.

Experimental conditions impose further limits on observation of T_{\max} : (a) through λ , defining the limit of the sphere of reflection, and (b) through F_{geom}^2 , as TDS_1 is proportional to this factor. Accordingly, the inversion phenomenon will be observable only for those (hkl) planes having a spacing within the limiting range, which also have F_{geom}^2 big enough to give observable TDS_1 and $2d_{hkl} > \lambda$.

From (7) and (15) we obtain for the T_{\max} of TDS_2

$$(T_{\max})_2 = \frac{2k}{3h^2} m \Theta^2 d_{hkl}^2 \quad \dots\dots (16)$$

and in a similar way, from (8) and (15) we obtain for the T_{\max} of TDS_3

$$(T_{\max})_3 = \frac{3k}{3h^2} m\Theta^2 d_{hkl}^2. \quad \dots\dots (17)$$

The upper limit is fixed by the melting temperature of the substance, but as the maxima of TDS_2 and TDS_3 are, respectively, twice and three times the T_{\max} of TDS_1 , the lower limit (being the formula valid for $T > \Theta$) will be extended in the region of the lower spacings.

§ 4. RELATION BETWEEN $\overline{u^2}$ AND T_{\max}

Substituting Θ from the Debye-Waller (James 1954) formula

$$\overline{u^2} = 3h^2 T / 4\pi^2 m k \Theta^2 \quad \dots\dots (18)$$

in (15), making $T = (T_{\max})_1$

$$(T_{\max})_1 / T = 1 = (1/4\pi^2)(d_{hkl}^2 / \overline{u^2}) \quad \dots\dots (19)$$

or

$$(\overline{u^2})^{1/2} / d_{hkl} = 0.16. \quad \dots\dots (20)$$

Therefore TDS_1 reaches its maximum value for a given crystallographic plane when $(\overline{u^2})^{1/2}$ is a definite fraction 0.16 of its spacing.

Similarly

$$(\overline{u^2})^{1/2} / d_{hkl} = 0.22 \quad \dots\dots (21)$$

when the maximum for TDS_2 is reached and

$$(\overline{u^2})^{1/2} / d_{hkl} = 0.28 \quad \dots\dots (22)$$

for TDS_3 .

Grüneisen (1926) stated that melting takes place when $(\overline{u^2})^{1/2}$ is of the order of 0.10 of the shortest interatomic distance.

Our results have a clear physical meaning: the Bragg intensity (corresponding to diffraction from ideal planes) decreases with T because thermal vibrations make the plane less and less perfect. TDS increases when thermal disorder is introduced, but it will increase only up to the point where the plane retains its physical meaning relative to the effect we are considering (one, two or three phonons). TDS begins to decrease when, as the result of thermal agitation, the plane begins to lose its reality, that is, to 'melt'. Later the whole structure melts.

§ 5. PREDICTED RANGE OF THE INVERSION PHENOMENON IN METALLIC, IONIC AND MOLECULAR CRYSTALS

Our expression (15) allows us to compute T_{\max} in real cases, when Θ and m are known, and to plot the inversion curves of TDS_1 as $(T_{\max})_1$ against d_{hkl} . Fig. 1 shows a set of inversion curves corresponding to different crystal types: metals (Na, Pb, Al, Ag, Au), ionic crystals (KCl, NaCl), and molecular crystals (acridine III, benzene, naphthalene, anthracene, hexamine). Since T_{\max} is proportional to d_{hkl}^2 , the inversion curves are hyperbolae. If no constancy of Θ is assumed, the curves will be only slightly different, not affecting the validity of our study.

Figure 1 and Table 1 show that Pb, KCl and Al are by no means exceptional cases and that the inversion phenomenon of TDS_1 is universal. In general, the inversion phenomenon will be observable mainly at high temperatures in metals, at low temperatures in molecular crystals, and at moderate temperatures in ionic crystals.

Table 1. Values of $m\Theta^2$, T_{mp} and d_{max} , Θ and d_{min} for Different Crystalline Substances

	Substance	$m\Theta^2 \cdot 10^{-18}$ g (°K) ^a	$T_{mp}(^{\circ}\text{K})$	$d_{max}(\text{\AA})$		$\Theta (^{\circ}\text{K})$	$d_{min}(\text{\AA})$
				TDS ₁	TDS ₂		
Molecular	Acridine III	0.5171	381	2.60	1.81	41	0.39
	Benzene	1.1307	278	1.54	1.09	93	0.65
	Naphthalene	1.7699	353	1.38	0.97	90	0.73
	Anthracene	2.2619	490	1.45	1.01	87	0.70
	Hexamine	3.1353	536	1.28	0.91	116	0.78
Ionic	KCl	3.3028	1049	1.74	1.24	231	0.57
	NaCl	3.8313	1074	1.64	1.16	281	0.61
	Na	0.8589	370	2.00	1.44	150	0.49
Metals	Pb	2.6642	600	1.45	1.02	88	0.69
	Al	6.8135	933	1.15	0.80	390	0.88
	Ag	8.2794	1234	1.18	0.82	215	0.86
	Au	9.4529	1336	1.20	0.86	170	0.82

Of course the curves of Fig. 1 will be extended beyond the limit Θ if zero-point energy is taken into account.

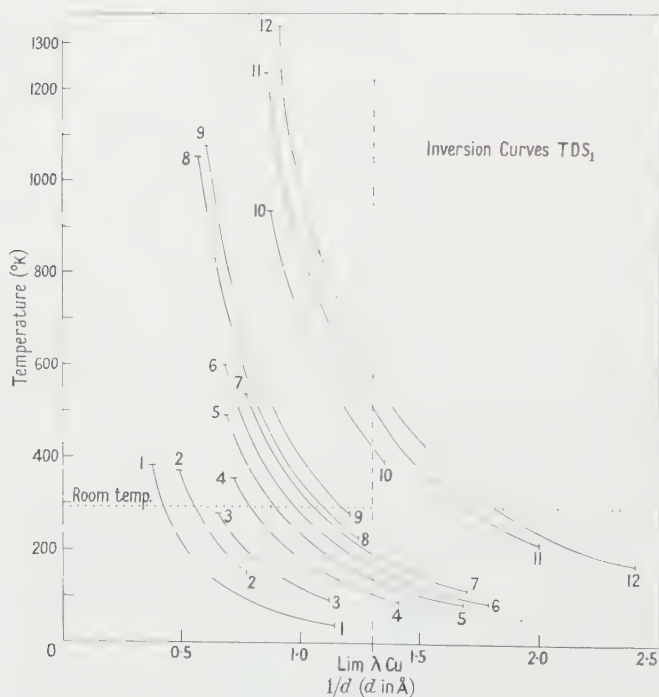


Fig. 1. Theoretical inversion curves of TDS₁ for some metallic, ionic and molecular crystals as a function of $1/d$. Temperature range between T_{mp} and Θ .
 1, acridine III; 2, Na; 3, benzene; 4, naphthalene;
 5, anthracene; 6, Pb; 7, hexamine; 8, KCl;
 9, NaCl; 10, Al; 11, Ag; 12, Au.

The values of d_{\max} for TDS_1 and TDS_2 define a region in reciprocal space where the inversion phenomenon for a given substance depends only on first-order diffuse scattering.

The fact that organic crystals show high intensity and complex diffuse patterns was to be expected as observation at room temperature is in general near to their melting points. This can be also an explanation for the intense and complicated diffuse pattern for Na. Comparison between the diffuse scattering of different crystals should be made at temperatures lying at corresponding points of the hyperbola (T_{mp}/Θ).

In our opinion, molecular crystals are the substances for which the inversion effect can best be shown experimentally. Experiment has shown that strong diffuse maxima appear for high $\sin \theta$ in Laue and oscillation photographs at room temperature, and superimposed on these there are also continuous diffuse areas. Two good examples are hexamine and acridine III. Hexamine has a medium translational-vibration amplitude at room temperature and acridine III a very high one. Figs 2 and 3 represent the variation of the temperature factor of TDS_1 plotted against absolute temperature for constant values of $|\mathbf{X}|$, the reciprocal lattice vector. These curves have been computed applying the equipartition law for $T > \theta$, and taking into account zero point energy for $T < \theta$.

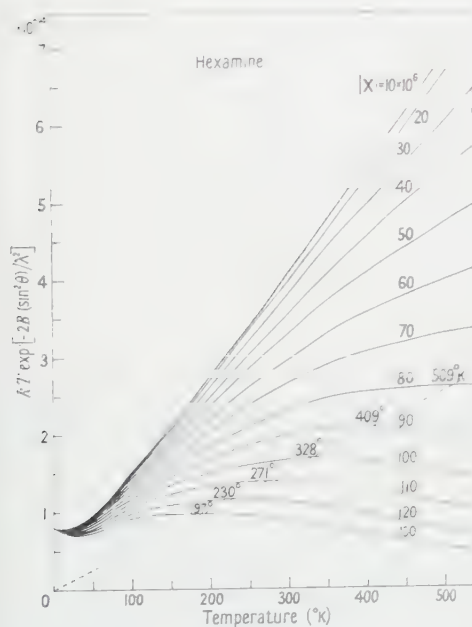


Fig. 2. Hexamine: Temperature factor of TDS_1 plotted against absolute temperature for constant values of $|\mathbf{X}|$. Broken straight line: the locus of the maxima of TDS_1 . The temperature of the maximum for each curve $|\mathbf{X}| = \text{const.}$ is indicated.

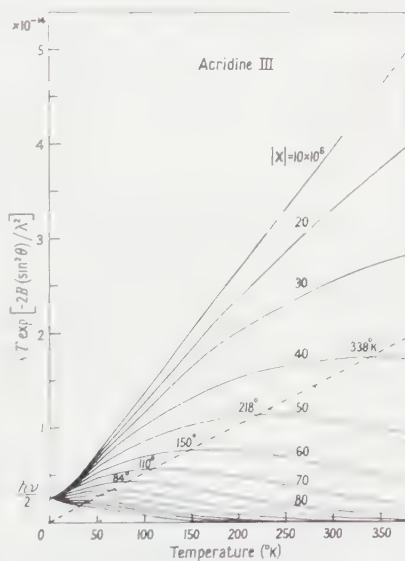


Fig. 3. Acridine III: Temperature factor of TDS_1 plotted against absolute temperature for constant values of $|\mathbf{X}|$. Broken straight line: the locus of the maxima of TDS_1 . The temperature of the maximum for each $|\mathbf{X}| = \text{const.}$ curve is indicated.

In order to compute these curves, Θ_1 for hexamine and acridine III had to be calculated. That for hexamine has been calculated from the data for the elastic constants given by Haussühl (1958), and by using de Launay's method (1959).

The value obtained, $\Theta_D = 116^\circ\text{K}$, coincides with the value obtained, using Cruickshank's method (1956), from $(\bar{u}^2)^{1/2} = 0.15 \text{ \AA}$ obtained by Andresen (1957) by neutron-diffraction techniques.

In the case of acridine III we have used Cruickshank's method and $(\bar{u}^2)^{1/2} = 0.37 \text{ \AA}$ obtained by x-ray diffraction technique by Phillips (1956). The value obtained is $\Theta = 41^\circ\text{K}$, a very low value indeed as was expected from the very unusual thermal parameter. This fact is in agreement with our own experimental work which showed very strong diffuse scattering at room temperature for acridine III (Amorós, de Acha and Canut 1961).

The broken line of Figs 2 and 3 are the loci of T_{\max} for each $|\mathbf{X}|$. It can easily be seen that for small $|\mathbf{X}|$ (points near the origin of reciprocal space) the temperature factor is a linear function of temperature except near to 0°K and that a maximum only occurs for a given range of $|\mathbf{X}|$.

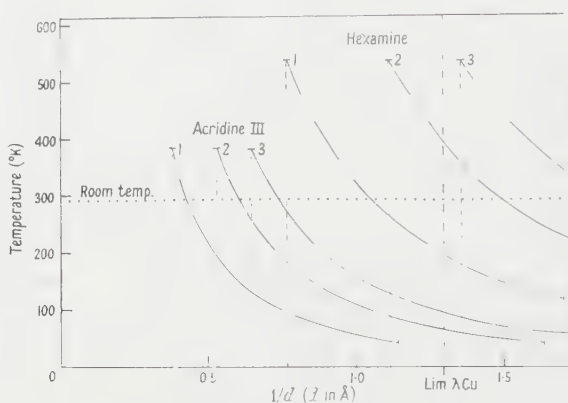


Fig. 4. Hexamine and acridine III: Theoretical inversion curves of TDS_1 , TDS_2 and TDS_3 as a function of $1/d$.

According to this, photographs of these crystals taken at low temperatures and compared with others in identical positions at room temperature will show at the lower temperature a decrease of diffuse scattering in the central part of the photograph and an increase (or at least a constancy) of the diffuse-intensity maxima in the back-reflection regions.

Figure 4 represents the TDS_1 , TDS_2 and TDS_3 inversion curves for hexamine and acridine III. The figure clearly shows the regions where the decrease of the thermal diffuse scattering is only due to the one-phonon contribution.

In the case of acridine, we have disregarded polymorphism. At and above room temperature the II form is the more stable one, but the region of stability of acridine III has not yet been determined (Phillips 1956).

§ 6. DETERMINATION OF DEBYE CHARACTERISTIC TEMPERATURES FROM THE INVERSION TEMPERATURES

The phenomenon of inversion allows us to determine the Debye characteristic temperatures of a given crystal of any symmetry, because from (15) we obtain

$$\Theta_D = \left(\frac{(T_{\max})_1}{d_{hkl}^2} \frac{3h^2}{km} \right)^{1/2} \dots\dots (23)$$

Careful measurements with a diffractometer at different temperatures and very near to a given reciprocal lattice point (in order to have the maximum contribution of TDS_1) will enable us to plot the temperature dependence of TDS_1 and to determine T_{\max} . The precision of the method will evidently depend on the precision of the temperature measurements and the location of the $(2\theta, \phi)$ coordinates in reciprocal space.

Moreover, the variation of T_{\max} along different directions in reciprocal space provides the possibility of determining Θ_{\max} and Θ_{\min} which are required when dealing with those crystal structures which are highly anisotropic (Tarassov 1954).

In another paper we shall fully describe this experimental way of determining Θ . However, a proof of the validity of the method can be given by using the values of T_{\max} for lead determined by Cartz.

Figure 5 shows the calculated TDS_1 , TDS_2 and TDS_3 inversion curves of lead. From Cartz's graphs we have measured the approximate experimental T_{\max} for the $\bar{4}40$, $\bar{2}4\bar{2}$, $\bar{2}40$ and $\bar{3}3\bar{1}$; these values are plotted in the figure. The

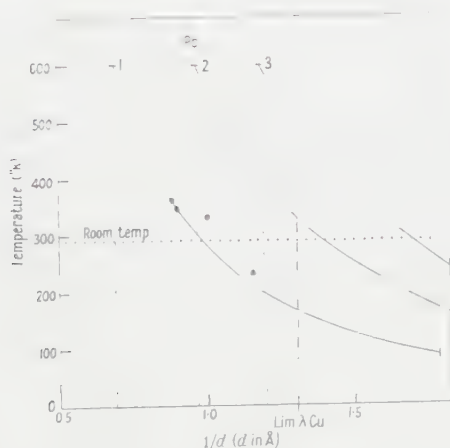


Fig. 5. Lead: Theoretical inversion curves of TDS_1 , TDS_2 and TDS_3 in terms of $\Theta = 88^\circ\text{K}$. The experimental T_{\max} from Cartz are marked.

corresponding Θ_D values calculated with (23) are given in Table 2. Two points, namely $\bar{2}40$ and $\bar{3}3\bar{1}$ lie on the theoretical curve and the corresponding Θ_D 's calculated with (23) are in good agreement with the Θ values determined by other methods. The values corresponding to $\bar{4}40$ and $\bar{2}4\bar{2}$ give higher Θ_D values; the reason for this might be that the measurements are made at points where the TDS_2 contribution was high.

Table 2. Values of Θ_D for Lead Calculated by (23) in Terms of Cartz's Experimental Values of T_{\max}

hkl	d_{hkl}	$T_{\max}(^\circ\text{K})$	$\Theta_D(^\circ\text{K})$
$\bar{4}40$	0.87	235	92
$\bar{2}4\bar{2}$	1.01	330	94
$\bar{2}40$	1.11	345	88
$\bar{3}3\bar{1}$	1.14	360	87

This method can be applied to a crystal of any symmetry. It is not necessary to determine the absolute value of the diffuse scattering. It is only necessary to detect the inversion point.

ACKNOWLEDGMENT

We wish to thank Miss M. C. Moreno for her valuable help in the computation.

REFERENCES

- AMORÓS, J. L., DE ACHA, A., and CANUT, M. L., 1961, *Bull. Soc. Franç. Minér. Crist.*, in the press.
- AMORÓS, J. L., CANUT, M. L., and DE ACHA, A., 1960, *Z. Krist.*, **114**, 39.
- ANDRESEN, A. F., 1957, *Acta Cryst.*, **10**, 107.
- BORN, M., 1943, *Rep. Progr. Phys.*, **9**, 294 (London: Physical Society).
- BORN, M., and LONSDALE, K., 1942, *Nature, Lond.*, **150**, 490.
- BURGERS, W. G., KOOY, C. L. D., and TIEDEMA, T. J., 1956, *Proc. K. Ned. Akad. Wetensch. B*, **59**, 195.
- CARTZ, L., 1954, *Thesis*, University of London.
- 1955, *Proc. Phys. Soc. B*, **68**, 951.
- CRUICKSHANK, D. W. J., 1956, *Acta Cryst.*, **9**, 1005.
- DEBYE, P., 1954, *The Collected Papers of Peter J. W. Debye* (New York: Interscience).
- GRÜNEISEN, E., 1926, *Handb. d. Phys.*, **10**, 1.
- HAUSSÜHL, S., 1958, *Acta Cryst.*, **11**, 58.
- JAMES, R. W., 1954, *The Crystalline State*. Vol. 2. *The Optical Principles of the Diffraction of X-rays* (London: Bell), p. 642.
- LABERRIGUE, A., 1959, *Ann. Phys., Paris.*, **4**, 385.
- DE LAUNAY, J., 1959, *J. Chem. Phys.*, **30**, 91.
- LAVAL, J., 1941, *Bull. Soc., Franç. Minér. Crist.*, **64**, 138.
- LONSDALE, K., 1948, *Crystals and X-rays* (London: Bell), p. 199.
- PHILLIPS, D. C., 1956, *Acta Cryst.*, **9**, 237.
- TARASSOV, V. V., 1954, *Travaux Inst. Crist. Acad. Sci., U.R.S.S.*, **10**, 322.

Elastic Scattering of Slow Electrons by Helium Atoms

By B. L. MOISEWITSCH†

Upper Air Laboratory, Department of Physics, University of Colorado

MS. received 26th August 1960, in revised form 7th September 1960

Abstract. The scattering length for elastic collisions between electrons and helium atoms is calculated with full allowance for distortion and exchange by the exact numerical integration of the appropriate integro-differential equation for the zero-order partial wave. The resulting cross section $26a_0^2$ for electrons of zero impact energy is in good agreement with the available experimental data, so that the effect of polarization which is neglected in the present calculation is probably small.

RECENTLY a considerable amount of experimental information concerning the momentum transfer cross section Q_m for slow electrons in helium has been derived by the investigation of the behaviour of electron swarms. These data are summarized in the Table. The values of Q_m found by Phelps, Fundingsland and Brown (1951), by Gould and Brown (1954) and by Anderson and Goldstein (1956) were obtained from measurements of electron conductivity using microwave techniques while the values of Q_m found by Bowe (1960) and by Phelps, Pack and Frost (1960) were obtained from measurements of drift velocity. Phelps, Pack and Frost found good agreement with the drift velocity data of Townsend and Bailey (1923), Nielson (1936) and Hornbeck (1951) for values of the ratio E/p of the electric field strength to the gas pressure greater than $0.05 \text{ v cm}^{-1} (\text{mm Hg})^{-1}$. For E/p between 0.01 and $0.05 \text{ v cm}^{-1} (\text{mm Hg})^{-1}$ they obtained somewhat smaller values for the drift velocity than were found by Townsend and Bailey so that, whereas the momentum transfer cross section derived by Phelps, Pack and Frost is approximately constant for electron energies less than about 2 ev , the momentum transfer cross section derived from the drift velocity data of Townsend and Bailey decreases quite rapidly as the electron energy falls below about 1 ev †. However, apart from this early work of Townsend and Bailey at low values of E/p , the experimental data quoted above are consistent with a constant value of Q_m for electrons with energies less than about 2 ev . The arithmetic mean of the experimental values for Q_m is $22a_0^2$ which in fact coincides with the constant value that Phelps, Pack and Frost found best fitted their drift velocity data.

The first theoretical investigation of the elastic scattering of electrons by helium atoms in which both distortion and exchange were taken into account was carried out by Morse and Allis (1933) who solved numerically the appropriate integro-differential equations for the zero-order and first-order partial waves for a range of electron energies up to about 120 ev . For the ground state of the

† On leave of absence from the Department of Applied Mathematics, The Queen's University of Belfast.

‡ It has been suggested by Kivel (1959) that this decrease in Q_m is due to polarization.

helium atom they chose a Hartree wave function and obtained satisfactory agreement with the experimental data for the total elastic cross section found by Ramsauer and Kollath (1932) for electron energies greater than about 2 ev. The gradient of their (phase shift, wave number) curve at zero wave number gives 1.5_5a_0 for the scattering length a which results in an elastic cross section $Q(0) = 30a_0^2$ for zero energy incident electrons since (cf. Massey 1956)

$$Q(0) = 4\pi a^2. \quad \dots\dots (1)$$

At very low electron energies the cross section for momentum transfer is practically the same as the elastic cross section. Hence we see that the elastic cross section at zero energy estimated from the calculations of Morse and Allis (1933) is about 35% greater than the elastic cross section $22a_0^2$ derived from the mean of the experimental values for Q_m .

Experimentally Determined Values of the Momentum Transfer Cross Section Q_m
for Slow Electrons in Helium†

$Q_m(a_0^2)$	Mean Electron Energy (ev)	Reference
19	0.04	Phelps, Fundingsland and Brown (1951)
18 to 19 ± 2	0 to 2.2	Gould and Brown (1954)
23 to 26	0.04 to 0.4	Anderson and Goldstein (1956)
28 ± 1	0.13 to 4	Bowe (1960)
22	0 to 2	Phelps, Pack and Frost (1960)

A more recent calculation has been carried out by Moiseiwitsch (1953) employing variational methods. He obtained a scattering length having the value $1.46a_0$ corresponding to an elastic cross section of $27a_0^2$ at zero electron impact energy. However Moiseiwitsch adopted the very simple helium ground state wave function

$$\psi(r_1, r_2) = \frac{\lambda^3}{\pi a_0^3} \exp \left[-\frac{\lambda(r_1 + r_2)}{a_0} \right], \quad \dots\dots (2)$$

where r_1 and r_2 are the radial coordinates of the two atomic electrons and $\lambda = 27/16$, so that the reliability of his calculation is difficult to estimate.

In view of the considerable amount of experimental data at very low electron energies which have recently become available it was considered worth while to recalculate the scattering length by exact numerical integration making allowance for both distortion and exchange and using for the ground state wave function of helium

$$\psi(r_1, r_2) = \frac{N^2}{\pi a_0^3} u(r_1)u(r_2), \quad \dots\dots (3)$$

where

$$u(r) = \exp(-Zr/a_0) + C \exp(-2Zr/a_0), \quad \dots\dots (4)$$

with $Z = 1.4558$, $C = 0.6$ and $N = 1.484233$. This function was determined by Green *et al.* (1954) using the variational method for bound states and provides an accurate representation of the Hartree wave function for helium.

† Since this paper was submitted for publication, Pack and Phelps (1960) have reported the value $19a_0^2$ for Q_m at mean electron energies in the range 0.003 to 0.05 ev which they derived from measurements of drift velocity.

For electrons of zero energy and zero angular momentum the radial equation describing the scattering is given by

$$\left[\frac{d^2}{dr_3^2} - \frac{2m}{\hbar^2} V(r_3) \right] f(r_3) = \int_0^\infty \int_0^\infty f(r_1) K(r_1, r_2, r_3) dr_1 dr_2, \quad \dots\dots (5)$$

where the asymptotic behaviour of $f(r)$ for large r is

$$f(r) \sim a - r. \quad \dots\dots (6)$$

The static potential V of the helium atom is given by

$$V(r_3) = \iint \left(\frac{e^2}{r_{13}} + \frac{e^2}{r_{23}} - \frac{2e^2}{r_3} \right) |\psi(r_1, r_2)|^2 d\mathbf{r}_1 d\mathbf{r}_2 \quad \dots\dots (7)$$

while the form of the kernel $K(r_1, r_2, r_3)$ is too complicated to present here. The value of the scattering length a obtained by numerical integration of Eqn (5) is found to be $1.442a_0$, which gives $26.1a_0^2$ for the total elastic cross section in the limit of zero energy. This is about 18% greater than the value $22a_0^2$ derived from the mean of the experimental values for Q_m and so is in rather better agreement with experiment than previous calculations. The remaining discrepancy between theory and experiment is probably due, at least in part, to the neglect of the polarization of the helium atom by the incoming electron.

ACKNOWLEDGMENT

It is a pleasure to acknowledge the assistance given by Mrs. N. Scott in the calculation of the scattering length.

The work reported in this article was partially supported by the United Kingdom Atomic Energy Authority and partially by the National Science Foundation of the U.S.A. under contract NSF-Y/22.8/329 IGY.

REFERENCES

- ANDERSON, J. M., and GOLDSTEIN, L., 1956, *Phys. Rev.*, **102**, 933.
 BOWE, J. C., 1960, *Phys. Rev.*, **117**, 1416.
 GOULD, L., and BROWN, S. C., 1954, *Phys. Rev.*, **95**, 897.
 GREEN, L. C., MULDER, M. M., LEWIS, M. N., and WOLL, J. W., 1954, *Phys. Rev.*, **93**, 757.
 HORNBECK, J. A., 1951, *Phys. Rev.*, **83**, 374.
 KIVEL, B., 1959, *Phys. Rev.*, **116**, 1484.
 MASSEY, H. S. W., 1956, *Handb. d. Phys.*, **36/II** (Berlin: Springer).
 MOISEWITSCH, B. L., 1953, *Proc. Roy. Soc. A*, **219**, 102.
 MORSE, P. M., and ALLIS, W. P., 1933, *Phys. Rev.*, **44**, 269.
 NIELSON, R. A., 1936, *Phys. Rev.*, **50**, 950.
 PACK, J. L., and PHELPS, A. V., 1960, *Phys. Rev. Letters*, **5**, 532.
 PHELPS, A. V., FUNDINGSLAND, O. T., and BROWN, S. C., 1951, *Phys. Rev.*, **84**, 559.
 PHELPS, A. V., PACK, J. L., and FROST, L. S., 1960, *Phys. Rev.*, **117**, 470.
 RAMSAUER, C., and KOLLATH, R., 1932, *Ann. Phys., Lpz.*, **12**, 529.
 TOWNSEND, J. S., and BAILEY, V. A., 1923, *Phil. Mag.*, **46**, 657.

The Elastic Scattering of Electrons and Positrons by Hydrogen Atoms

BY A. E. KINGSTON AND B. G. SKINNER

Department of Applied Mathematics, The Queen's University of Belfast

Communicated by D. R. Bates; MS. received 7th September 1960

Abstract. The expression for the differential cross section obtained from the second Born approximation by including only terms to the third order in the interaction energy is employed to calculate the differential and total cross sections for the elastic scattering of electrons and positrons by hydrogen atoms. Allowance is made for both distortion and polarization by evaluating the terms which correspond to transitions through the 1s, 2s and 2p intermediate states. It is found that for electrons with impact energies below 100 eV the effect of distortion and polarization is to increase the total cross section appreciably above the first Born cross section. For positrons, distortion and polarization decrease the total cross section.

CONSIDER an encounter between a hydrogen atom and a particle having the same mass as an electron and Z times the charge. The second Born approximation to the elastic scattering amplitude is

$$f = f_{B1} + f_{B2}, \quad \dots\dots(1)$$

f_{B1} being the first Born approximation to the scattering amplitude and f_{B2} being the second Born correction term to the scattering amplitude, so that, in atomic units

$$f_{B1} = -\frac{1}{2\pi} \int \exp\{i(\mathbf{k}_0 - \mathbf{k}_0') \cdot \mathbf{r}_1\} V_{00}(\mathbf{r}_1) d\mathbf{r}_1 \quad \dots\dots(2)$$

$$f_{B2} = \frac{1}{4\pi^2} \sum_m \iint \exp\{i(\mathbf{k}_0 \cdot \mathbf{r}_1' - \mathbf{k}_0' \cdot \mathbf{r}_1)\} \frac{\exp i k_m |\mathbf{r}_1 - \mathbf{r}_1'|}{|\mathbf{r}_1 - \mathbf{r}_1'|} \\ \times V_{0m}(\mathbf{r}_1) V_{m0}(\mathbf{r}_1') d\mathbf{r}_1 d\mathbf{r}_1' \quad \dots\dots(3)$$

in which \mathbf{k}_0 and \mathbf{k}_0' represent the initial and final momenta, and

$$V_{nm}(\mathbf{r}_1) = Z \int \phi_n^*(\mathbf{r}_2) \left(\frac{1}{r_1} - \frac{1}{|\mathbf{r}_1 - \mathbf{r}_2|} \right) \phi_m(\mathbf{r}_2) d\mathbf{r}_2, \quad \dots\dots(4)$$

the ϕ 's being the eigenfunctions of the hydrogen atom in the state indicated by the subscript (cf. Massey 1956).

It has been customary to take the second Born approximation to the differential cross section to be

$$I(\theta) = |f_{B1} + f_{B2}|^2. \quad \dots\dots(5)$$

The corresponding formula based on the Schwinger variational method with plane wave trial function is

$$I(\theta) = \left| \frac{f_{B1}^2}{f_{B1} - f_{B2}} \right|^2 \quad \dots\dots(6)$$

(Massey and Mohr 1934, Mower 1953, Newstein 1955, Moiseiwitsch and

Williams 1959). These formulae are in error. If we introduce the quantities

$$\alpha = \frac{\mathcal{R}f_{B2}}{f_{B1}}, \quad \dots\dots(7)$$

$$\beta = \frac{\mathcal{I}f_{B2}}{f_{B1}}, \quad \dots\dots(8)$$

which are both of the order Z , we can write (5) as

$$I(\theta) = |f_{B1}|^2 \{1 + 2\alpha + (\alpha^2 + \beta^2)\} \quad \dots\dots(9)$$

and (6) as

$$I(\theta) = |f_{B1}|^2 \{1 + 2\alpha + (3\alpha^2 - \beta^2) + \dots\dots\}. \quad \dots\dots(10)$$

Neither expression is correct to the fourth order in Z ; thus if we define

$$\gamma = \frac{\mathcal{R}f_{B3}}{f_{B1}}, \quad \dots\dots(11)$$

where f_{B3} is the third Born correction to the scattering amplitude, we find that to the fourth order in Z

$$I(\theta) = |f_{B1}|^2 \{1 - 2\alpha + (\alpha^2 + \beta^2 + 2\gamma)\} \quad \dots\dots(12)$$

so that the fourth-order term is actually $\alpha^2 + \beta^2 + 2\gamma$, not $\alpha^2 + \beta^2$ as in (9) nor $3\alpha^2 - \beta^2$ as in (10). Instead of arbitrarily including some fourth-order terms as in (9) and (10) and neglecting others which may be about the same magnitude but of opposite sign, it is better to retain only third-order terms (Kingston, Moiseiwitsch and Skinner 1960).

To the third order in the interaction energy the differential cross section is

$$I(\theta) = f_{B1}(f_{B1} + 2\mathcal{R}f_{B2}) \quad \dots\dots(13)$$

and the total cross section is

$$Q = 2\pi \int_0^\pi f_{B1}(f_{B1} + 2\mathcal{R}f_{B2}) \sin \theta d\theta, \quad \dots\dots(14)$$

where θ is the angle of scattering.

The second Born correction term f_{B2} involves a summation over an infinite number of intermediate states. Its evaluation is greatly simplified by making the approximation introduced by Massey and Mohr (1934) in which the free electron wave number k_m associated with the hydrogen atom in the intermediate state m is replaced by the wave number k_0 of the incident electron. Although this approximation is satisfactory for $\mathcal{R}f_{B2}$ provided the angle of scattering is not small, it is invalid for $\mathcal{I}f_{B2}$ and so cannot be used to evaluate the expressions (13) and (14) for the total elastic cross section. Each term of the summation must be treated separately. Using a method described in a previous paper (Kingston, Moiseiwitsch and Skinner 1960), we have computed the following terms in this infinite sum: the term corresponding to the 1s intermediate state (which allows for distortion of the wave function of the atom) and the terms corresponding to the 2s and 2p intermediate states (which allow partially for polarization of the atom)†.

If we denote the contribution to f_{B2} from a transition through the intermediate state m by f_{B2}^m , then we refer to the results obtained from putting $f_{B2} = f_{B2}^{1s}$,

† We have not calculated the terms corresponding to higher intermediate states. Approximate allowance for these terms may be made, if desired, noting that the total polarizability of atomic hydrogen is 1.35 times the contribution to the polarizability from the first excited state. The correction is very small.

Table 1. Elastic Scattering of Electrons by Hydrogen Atoms: Differential Cross Sections (in units of πa_0^2)

$\cos \theta$	$k_0 = 2$			$k_0 = 3$			$k_0 = 4$		
	(1)	(2)	(3)	(1)	(2)	(3)	(1)	(2)	(3)
1.0	1.000(0)†	1.187(0)	2.702(0)	1.000(0)	1.087(0)	2.152(0)	1.000(0)	1.050(0)	1.879(0)
0.984375	9.120(-1)	1.088(0)	1.388(0)	8.165(-1)	8.928(-1)	9.108(-1)	7.048(-1)	7.442(-1)	7.451(-1)
0.96875	8.345(-1)	1.001(0)	1.114(0)	6.768(-1)	7.441(-1)	7.379(-1)	5.184(-1)	5.504(-1)	5.505(-1)
0.9375	7.048(-1)	8.536(-1)	8.655(-1)	4.828(-1)	5.362(-1)	5.322(-1)	3.086(-1)	3.308(-1)	3.326(-1)
0.875	5.184(-1)	6.396(-1)	6.289(-1)	2.754(-1)	3.113(-1)	3.125(-1)	1.406(-1)	1.529(-1)	1.538(-1)
0.75	3.086(-1)	3.933(-1)	3.908(-1)	1.197(-1)	1.389(-1)	1.400(-1)	4.938(-1)	5.466(-2)	5.462(-2)
0.5	1.406(-1)	1.883(-1)	1.895(-1)	4.048(-2)	4.839(-2)	4.839(-2)	1.440(-2)	1.617(-2)	1.615(-2)
0.0	4.938(-2)	7.025(-2)	7.004(-2)	1.154(-2)	1.412(-2)	1.412(-2)	3.810(-3)	4.306(-3)	4.306(-3)
-0.5	2.441(-2)	3.587(-2)	3.570(-2)	5.306(-3)	6.537(-3)	6.537(-3)	1.716(-3)	1.942(-3)	1.942(-3)
-1.0	1.440(-2)	2.155(-2)	2.145(-2)	3.025(-3)	3.737(-3)	3.737(-3)	1.073(-3)	1.098(-3)	1.098(-3)

(1) First Born approximation; (2) distortion approximation; (3) distortion-polarization approximation.

† The number in brackets denotes the power of 10 by which the other number should be multiplied.

$f_{B2} = f_{B2}^{2s} + f_{B2}^{2p}$ and $f_{B2} = f_{B2}^{1s} + f_{B2}^{2s} + f_{B2}^{2p}$ as the distortion, polarization and distortion-polarization approximations respectively.

In Table 1 we compare the values for the differential cross section obtained using the first Born approximation with those obtained from the third-order expression for the differential cross section (13), using the distortion and the distortion-polarization approximations. At small angles of scattering the third-order approximation results rise much more sharply than the first Born results. This trend is as required to give agreement with experimental data in the case of helium (cf. Moiseiwitsch and Williams 1959).

Table 2 gives the total elastic cross sections according to the first Born approximation and according to the third-order expression (14) with the distortion and distortion-polarization approximations.

Table 2. Elastic Scattering of Electrons by Hydrogen Atoms:
Total Cross Section (in units of πa_0^2)

Wave number k_0 (in a_0^{-1})	First Born approximation	Third-order approximation Eqn (14)		Massey-Mohr approximation	
		(1)	(2)	Eqn (5)	Eqn (6)
0.5	2.90	6.55	8.09	97.7	0.219
1.0	1.54	2.74	3.32	12.08	1.116
2.0	0.523	0.674	0.705	1.378	0.502
3.0	0.247	0.281	0.287	0.431	0.234
4.0	0.142	0.153	0.156	0.203	0.135

(1) Distortion approximation ; (2) distortion-polarization approximation.

Table 3. Elastic Scattering of Positrons by Hydrogen Atoms:
Total Cross Section (in units of πa_0^2)

Wave number k_0 (in a_0^{-1})	First Born approximation	Third-order approximation Eqn (14)	
		(1)	(2)
2	0.523	0.372	0.341
3	0.247	0.213	0.207
4	0.142	0.131	0.128

(1) Distortion approximation; (2) distortion-polarization approximation.

We have also calculated the total cross sections using the expressions (5) and (6) with f_{B2} obtained from the Massey-Mohr approximation (Moiseiwitsch and Williams 1959). They are given in the last two columns of Table 2. It is evident that these are less accurate than the first Born cross sections.

The cross sections for the elastic scattering of positrons by hydrogen atoms have also been calculated and are displayed in Table 3. It is seen that the effect of distortion and polarization is to increase the total cross section for electrons but to decrease the cross section for positrons.

The total elastic cross section obtained by using the third-order distortion-polarization approximation should be quite accurate for impact energies greater

than about 50 eV ($k_0 \gtrsim 2a_0^{-1}$). At lower energies fourth-order terms must become significant as must electron exchange (or the formation of positronium).

ACKNOWLEDGMENTS

We are indebted to Professor D. R. Bates and Dr. B. L. Moiseiwitsch for their interest and encouragement. This work was supported partially by the Atomic Energy Authority.

REFERENCES

- KINGSTON, A. E., MOISEWITSCH, B. L., and SKINNER, B. G., 1960, *Proc. Roy. Soc. A*, **258**, 237.
MASSEY, H. S. W., 1956, *Handb. d. Phys.*, **36/II**, 264.
MASSEY, H. S. W., and MOHR, C. B. O., 1934, *Proc. Roy. Soc. A*, **146**, 880.
MOISEWITSCH, B. L., and WILLIAMS, A., 1959, *Proc. Roy. Soc. A*, **250**, 337.
MOWER, L., 1953, *Phys. Rev.*, **89**, 947.
NEWSTEIN, M. C., 1955, *Tech. Rep. Mass. Inst. Tech.*, No. 4.

A Thermal Motion Effect in the Electron Spin Resonance of a Free Radical in Solution

BY J. G. POWLES AND M. H. MOSLEY

Physics Department, Queen Mary College, University of London

MS. received 25th July 1960

Abstract. The electron resonance hyperfine triplet at 9.5 mm wavelength of the peroxyamine disulphonate ion has been measured in a series of solutions of water and glycerol from 20% to 72% glycerol by weight and over a temperature range from -46° to 65°C . There is a temperature and solution dependent broadening which affects the individuals of the triplet differently. The high field line is broadened first with falling temperature. The effect is thought to be due to the motionally attenuated anisotropic electron-nuclear interaction. The anisotropic interaction is estimated to be comparable with the isotropic one. The anisotropy of the g factor, $\Delta g/g$, is 2×10^{-3} . These parameters allow the prediction of a static spectrum of the ion in agreement with experiment (Weissmann and Banfill 1953). The effect of thermal motion of the ion is shown by the close relation between the value and temperature dependence of the thermal reorientation correlation frequency and the variation of the electron resonance signal with temperature and nature of the solvent.

§ 1. INTRODUCTION AND EXPERIMENTAL RESULTS

WE have measured the electron spin resonance absorption signal of the peroxyamine disulphonate ion ($\text{ON}(\text{SO}_3)_2^{2-}$) at 9.5 mm wavelength in solution in a series of mixtures of glycerol and water over the temperature range -46° to $+65^{\circ}\text{C}$.

The ion was prepared as its potassium salt as described by Palmer (1954). The salt was dissolved in water and the glycerol added to give the required mixture. An added trace of ammonium hydroxide gave a sample stable for several hours.

The spectrometer was of the reflection cavity type using a directional coupler with field modulation at 15kc/s produced by coils mounted on the cavity. Synchronous detection and chart display gives a plot of the derivative of the absorption ξ as a function of magnetic field $d\xi/dH$ as in Fig. 1. The lower than usual modulation frequency was used with a view to high resolution work. The higher than usual microwave frequency was used in anticipation of frequency dependent effects since spectrometers at 3 cm are more readily available.

The signal from the peroxyamine disulphonate ion in solution is a well-known (Pake, Townsend and Weissmann 1952, Townsend, Weissmann and Pake 1953) hyperfine triplet with a spacing, ΔH_{hfs} 13 gauss and a width, δH_{iso} of each line of about one gauss depending on the concentration of the solution, as in Fig. 1(a). The triplet is due to the hyperfine interaction of the unpaired electron with the ^{14}N nucleus which has spin $I=1$.

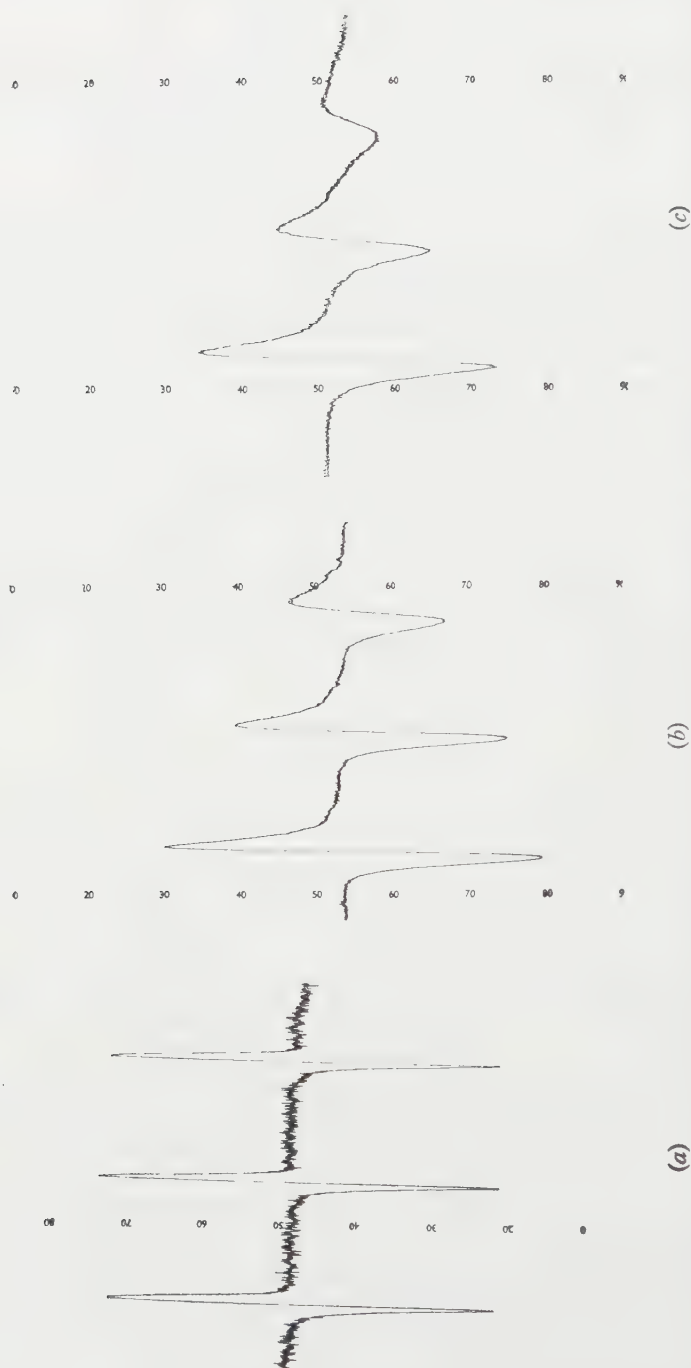


Fig. 1. The hyperfine triplet for the peroxylamine disulphonate ion concentration 0.01M in 1 : 1 water/glycerol by volume (at 25 °C) solution: (a) at 25 °C, the usual triplet, (b) at -22 °C, showing asymmetric broadening, (c) at -28 °C, showing considerable asymmetry but still a recognisable triplet.

We have found that lowering the temperature of the solution affects the hyperfine triplet *asymmetrically*. All three lines are broadened and $(d\xi/dH)_{\max}$ is reduced but the high field line is the most affected and the central line is affected to an intermediate extent, as shown in Figs 1(b) and 1(c). In the absence of saturation and when the hyperfine lines are distinct the total intensity for each hyperfine line should be constant. If the line preserves its shape, it is easy to show that for any symmetrical line shape $(d\xi/dH)_{\max} \propto (\text{width})^{-2}$; we have confirmed this relation for our measurements. The actual line shapes are as near as we can tell Lorentzian. Since it is rather easier to measure the peak intensities ($\propto (d\xi/dH)_{\max}$) we shall use these in the analysis below. It was not possible to compare intensities at different temperatures and so we shall discuss only ratios of the three hyperfine line intensities at given temperatures. Some of these ratios are given in Fig. 3.

The asymmetry is independent of concentration in the range below 0.1 Molar and is therefore not due to exchange narrowing. The effect is independent of the direction of field sweep and the signals are not saturated. The normal hyperfine line width depends on concentration presumably due to exchange narrowing (Pake and Tuttle 1959).

As the temperature is lowered the spectrum changes and the triplet pattern is lost. For all solutions we found an abrupt disappearance of the signal at -46°C , which is the eutectic temperature of glycerol/water. This prevented the attainment of a sufficiently high viscosity with lowered temperature to observe a continuous change-over from hyperfine triplet to anisotropic broad line as observed by Hausser (1959) in other systems. Peroxylamine disulphonate only appears to dissolve to a sufficient extent in water or water containing mixtures suggesting that the solution of the ion may be accompanied by solvation.

The temperature at which the asymmetry appears depends on the solution as shown in Fig. 2(a).

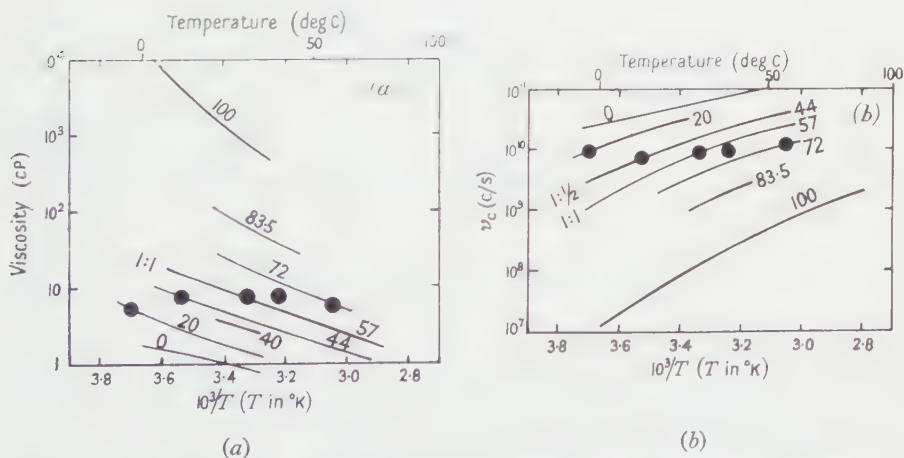


Fig. 2. (a) The viscosity of a series of solutions of glycerol water (indicated by % glycerol by weight) as a function of temperature. The points indicate that the temperature at which 5% asymmetry appears is at constant viscosity although the actual temperature varies between -3°C and 54°C . (b) A plot similar to (a) but for the solvent molecular correlation frequency, as described in the text.

§ 2. PRELIMINARY INTERPRETATION OF THE RESULTS

In view of the possibility that the effect is associated with motional averaging of the anisotropic hyperfine interaction we plot in Fig. 2(a) the macroscopic viscosity of the solutions as a function of temperature (Sheely 1932). We have confirmed and extended the measurements of viscosity on some of the solutions using an Ostwald viscometer and the results are included in Fig. 2(a).

We also plot in Fig. 2(a) the temperature at which the high to low field line intensity ratio is 0.95 for the different solutions. This shows that a given asymmetry appears at constant viscosity.

With a motional effect still in mind we estimated the motional correlation frequencies ν_c of the solvent molecules using values for glycerol deduced from proton magnetic resonance (Luszczynski, Kail and Powles 1960) and for water from dielectric loss ν_D (Smyth 1955) assuming $\nu_c = 3\nu_D$ (Bloembergen, Purcell and Pound 1948). No results are available for solutions of water and glycerol but we have made plausible interpolations between the values for the pure liquids with the aid of viscosity data. The asymmetry appears at a constant correlation frequency, which is approximately 10^{10} c/s for an asymmetry of 5%.

Asymmetry has also been reported for free radicals in solution by Ebsworth and Weil (1959), McGarvey (1956, 1957), McConnell and Thurston (quoted by McConnell 1956) and Deguchi (1960). McConnell (1956) has given a general explanation of this effect which we consider in § 3. We feel it likely that an explanation may be more soundly based for our rather simple radical and spectrum.

We think the origin of the line broadening is that as the temperature is lowered the motional averaging of the anisotropic interaction of the electron with the nucleus and of effects due to anisotropy of the g factor are reduced. The anisotropic interactions are not well known. Weissmann and Banfill (1953) from a study of the same ion in dilute mixed crystals with potassium hydroxylamine disulphonate find intervals between triplet hyperfine lines between 6 and 27 gauss depending on orientation. We have prepared similar mixed crystals but were unable to find the signal. In the frozen liquid we would have a 'powder average' and the absorption line would be broad and weak and our equipment proved too insensitive to observe it.

A preliminary interpretation may be based on an obvious generalization of the Bloembergen, Purcell and Pound (1948) theory to anisotropic broadening in electron resonance. We assume that besides the isotropic line width δH_{iso} there is another motionally dependent contribution which can be written

$$\delta H_{\text{aniso}}^2 = \Delta H^2 \frac{2}{\pi} \tan^{-1} \left[\frac{\sqrt{3} g \beta \delta H_{\text{aniso}}}{h \nu_c} \right] \quad \dots\dots (1)$$

where ΔH is the 'rigid lattice' line width and ν_c is the motional correlation frequency. We are concerned with the motionally narrowed line. The argument of \tan^{-1} is then small and

$$\delta H_{\text{aniso}} \simeq \Delta H^2 \frac{2\sqrt{3}}{\pi} \frac{g\beta}{h\nu_c} \quad \dots\dots (1')$$

If both lines have the same (Lorentzian) shape we get for the resultant line width

$$\delta H = \delta H_{\text{iso}} + \delta H_{\text{aniso}} \quad \dots\dots (2)$$

Since $(d\xi/dH)_{\max} \propto (\delta H)^{-2}$ we have for the ratio of the intensities of the high to the low field hyperfine lines m_h/m_l ,

$$m_h/m_l = [1 + \delta H_{\text{aniso}}/\delta H_{\text{iso}}]^{-2} \quad \dots\dots (3)$$

assuming that the high field line is affected first as explained in §3. If we assume that the motional correlation frequency for the radical is the same as that of the solvent molecules we obtain from Fig. 2(b) $\nu_c \simeq 10^{10}$ c/s when $m_h/m_l = 0.95$. This value of ν_c may be a little high since the ion is rather larger than the solvent molecules. Also $\delta H_{\text{iso}} = 0.94$ gauss. Hence from Eqns (3) and (1') we find $\Delta H \simeq 9$ gauss. The anisotropic splittings should be in the range approximately $\Delta H_{\text{hfs}} \pm \Delta H$, i.e. 4 to 22 gauss. This is similar to the range 6 to 27 gauss observed by Weissmann and Banfill (1953). This reasonable order of magnitude for the anisotropic contribution suggests that our interpretation is substantially correct.

Further, ΔH having been found, the temperature variation of m_h/m_l , given in Fig. 3(b), should give the temperature dependence of the motional correlation frequency, $\nu_c(T)$ using Eqns (1') and (3). We assume, as is suggested by the plot in Fig. 2(b), that

$$\nu_c(T) = \nu_0 \exp(-\Delta E/kT) \quad \dots\dots (4)$$

over a small temperature range and calculate ΔE . We find for the 1:1 by volume (at 25°C) solution $\Delta E \simeq 7$ kcal mole⁻¹ (0.3 eV). From Fig. 2(b) the temperature dependence of $\nu_c(T)$ itself corresponds to $\Delta E \simeq 8$ kcal mole⁻¹.

The excellence of the correlation with ν_c both in magnitude and in variation with temperature strongly supports our interpretation that the effect is due to the motionally attenuated anisotropic interaction. We have still however to explain the asymmetry and this is attempted in the next section.

§ 3. INTERPRETATION OF THE ASYMMETRY

We base our interpretation on McConnell's theory (1956) although a more detailed theory of relaxation in these systems has been given recently (Stephen and Fraenkel 1960). This is essentially an extension of Bloembergen, Purcell and Pound's (1948) theory of motional narrowing of nuclear dipole interaction.

The axially symmetric Hamiltonian of Bleaney and Stevens (1953) is used, namely,

$$\mathcal{H} = \beta[g_{\parallel}H_rS_r + g_{\perp}(H_pS_p + H_qS_q)] + AI_rS_r + B(I_pS_p + I_qS_q) \quad \dots\dots (5)$$

where p, q, r refer to the radical and r is the axis of symmetry. For complete motional averaging one gets the isotropic Hamiltonian

$$\mathcal{H}_0 = g\beta H_0 S_z + a\mathbf{S} \cdot \mathbf{I} \quad \dots\dots (6)$$

where $g = \frac{1}{3}(g_{\parallel} + 2g_{\perp})$ and $a = \frac{1}{3}(A + 2B)$ and H_0 is the applied field.

When $I=1$ as for ¹⁴N Eqn (6) gives the three equally spaced ($a/g\beta$ gauss) lines of equal intensity of Fig. 1(a). The sign of a is not determined. The other part of the Hamiltonian $\mathcal{H} - \mathcal{H}_0$, contains angular functions and so is motion dependent and contributes to relaxation T_1' and line width δH_{aniso} . McConnell shows that if

$$|\Delta g\beta H_0| \gg |b| \quad \dots\dots (7)$$

where $\Delta g = g_{\parallel} - g_{\perp}$ and $b = A - B$ the contributions to T_1 and δH from this source are

$$\frac{1}{T_1'} = \frac{4\pi}{15} \frac{(\Delta g \beta H_0 + b I_z)^2 h^{-2} \nu_c}{1 + (\nu_c/\nu_r)^2} \quad \dots\dots (8)$$

and

$$\delta H_{\text{aniso}}^2 = \frac{32}{135\pi} (\Delta g \beta H_0 + b I_z)^2 (g\beta)^{-2} \tan^{-1} \frac{\sqrt{3} g \beta \delta H_{\text{aniso}}}{h \nu_c} \quad \dots\dots (9)$$

where ν_c is the motional correlation frequency as before and the electron resonance frequency is ν_r in the field H_0 . The required dependence of δH_{aniso} on the particular hyperfine line ($I_z = 1, 0, -1$) appears explicitly in Eqn (9). For the motionally reduced case,

$$\delta H_{\text{aniso}} \simeq \frac{32\sqrt{3}}{135\pi} (\Delta g \beta H_0 + b I_z)^2 (g\beta h)^{-1} \nu_c^{-1} \quad \dots\dots (9')$$

and for not too severe broadening we again use Eqn (2).

If a is positive (or negative) the high field line, which is broadened most, corresponds to $I_z = -1$ (or $+1$) and we have from Eqn (9)

$$(\Delta g \beta H_0 \mp b)^2 > (\Delta g \beta H_0 \pm b)^2 \text{ if } a \gtrless 0$$

i.e. $\Delta g \beta H_0 b \leq 0$ according as $a \gtrless 0$.

Consider the line intensities m at high, intermediate and low field, which are proportional to $(\delta H_{\text{iso}} + \delta H_{\text{aniso}})^{-2}$ for $I_z = \mp 1, 0, \pm 1$. Then for a given temperature and solution

$$m_1 : m_i : m_h = [\delta H_{\text{iso}} + \delta H_{\text{aniso}}(I_z = \pm 1)]^{-2} : [\delta H_{\text{iso}} + \delta H_{\text{aniso}}(I_z = 0)]^{-2} : [\delta H_{\text{iso}} + \delta H_{\text{aniso}}(I_z = \mp 1)]^{-2} \quad \dots\dots (10)$$

Thus the relative line intensities depend only on the magnetic parameters of the radical and on ν_c . In Eqn (10) the upper or lower sign is to be taken for $a \gtrless 0$ and then $\Delta g \beta H_0 b \leq 0$ and since also $|\Delta g \beta H_0| > |b|$ by Eqn (7), Eqn (10) shows the observed behaviour.

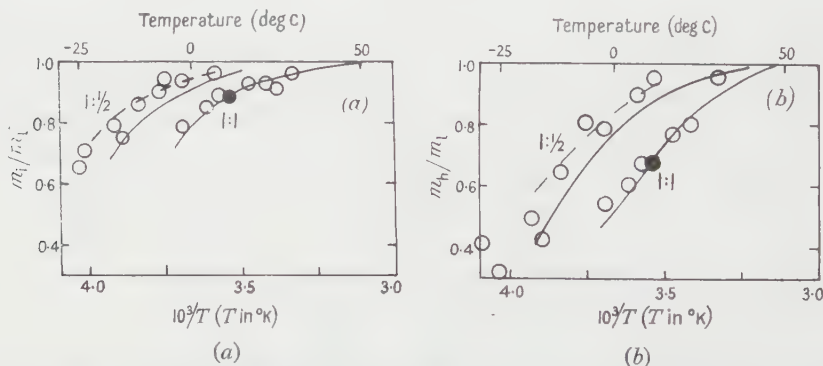


Fig. 3. Plots of relative intensities of the hyperfine lines as a function of temperature and solution. (a) intermediate field/low field lines, (b) high field/low field lines. The full lines are the theoretical values for anisotropy parameters chosen to produce a fit for the 1 : 1 solution at 10°C (solid points) as discussed in § 3. The broken lines are theoretical curves for the 1 : $\frac{1}{2}$ solution but for the parameters 20% smaller.

We measure, for example, for a 1 : 1 solution of glycerol/water, at +10°C $m_1 : m_i : m_h = 1 : 0.89 : 0.68$ (Fig. 3) and from Fig. 2(b) $\nu_c \simeq 3.3 \times 10^9$ c/s.

$\delta H_{\text{iso}} = 0.94$ gauss. Hence from Eqn (10) we find

$$|\Delta g \beta H_0| = 4.4 \times 10^{-19} \text{ erg} \quad \text{and} \quad |b| = 2.7 \times 10^{-19} \text{ erg} = 0.0014 \text{ cm}^{-1}, \quad \dots\dots (11)$$

Thus $|\Delta g \beta H_0|/b = 1.6$, i.e. greater than 1 as assumed in the theory Eqn (7) although the approximation is a poor one. Even at 3 cm wavelength the approximation would be quite invalid and a more profound analysis than McConnell's would be required.

With the parameters of Eqn (11) and values of $\nu_c(T)$ from Fig. 2(b) we have calculated the curves for m_i/m_l and m_b/m_l given in Fig. 3 for the 1:1 and 1:½ solutions. The fit is satisfactory for the 1:1 solution. A better fit to the 1:½ results could be obtained by taking values of $|\Delta g \beta H_0|$ and $|b|$ about 20% smaller. In view of the uncertainty in the values of $\nu_c(T)$ and in the accuracy of the theory the agreement is satisfactory. However the deduced values of the parameters must be regarded as very approximate.

The anisotropic part of the interaction may be compared with the isotropic part. Since $\Delta H_{\text{hfs}} = 13$ gauss $= |a/g\beta|$ we find

$$|b/a| = 1.1 \quad \text{and} \quad |\Delta g \beta H_0/a| = 1.8 \quad \text{for} \quad H_0 = 11380 \text{ gauss (9.5 mm wavelength)}$$

i.e. $|\Delta g/g| = 2 \times 10^{-3}$. Also $g = 2.0052$ (assuming DPPH has $g = 2.0036$).

Apart from uncertainties in signs we have all the parameters to determine the spectrum of the stationary radical. It would be of interest to determine these parameters also from the spectrum of the radical in dilute solid solution in a non-magnetic host. This might allow an estimate of the contribution, if any, of solvated water to the anisotropic part of the electron spin Hamiltonian in solution.

For the Hamiltonian of Eqn (5) the deviation of any line from the centre $H_0 (= h\nu/g\beta)$ is

$$H_0 \frac{\Delta g}{g} \left(\cos^2 \theta - \frac{1}{3} \right) + \frac{a}{g\beta} \left[\left(1 + \frac{2}{3} \frac{b}{a} \right)^2 \cos^2 \theta + \left(1 - \frac{1}{3} \frac{b}{a} \right)^2 \sin^2 \theta \right]^{1/2} I_z \text{ gauss}$$

since $|\Delta g/g| \ll 1$. Hence since $|b/a| = 1.1$ and $\Delta H_{\text{hfs}} = |a/g\beta| = 13$ gauss the extrema of the spacing between triplets (i.e. ignoring the displacement of the centre of gravity) are 8 and 22 gauss for $\theta = 90^\circ$ or 0° if $b/a > 0$ and $3\frac{1}{2}$ and 18 gauss if $b/a < 0$. The values reported by Weissmann and Banfill (1953) are 6 and 17 gauss which seems to correspond with our values and suggest that possibly $b/a > 0$.

A consideration of Eqn (8) for T_1' shows that this would not lead to asymmetric saturation of the hyperfine lines to give signals of the observed form. More recent theories also indicate symmetric saturation (Kivelson 1957, Stephen and Fraenkel 1960). This together with the observed relation $(d\xi/dH)_{\text{max}} \propto \delta H^2$, which does not hold for saturation, further confirms our direct observation that selective saturation does not explain our asymmetry.

ACKNOWLEDGMENTS

The electromagnet was provided by a grant from the Department of Scientific and Industrial Research. We acknowledge considerable help in the preparation of samples from the Chemistry Department of Queen Mary College.

REFERENCES

- BLEANEY, B., and STEVENS, K. W. H., 1953, *Rep. Progr. Phys.*, **16**, 108 (London: Physical Society).
- BLOEMBERGEN, N., PURCELL, E. M., and POUND, R. V., 1948, *Phys. Rev.*, **73**, 679.
- DEGUCHI, Y., 1960, *J. Chem. Phys.*, **32**, 1584.
- EBSWORTH, E. A. V., and WEIL, J. A., 1959, *J. Phys. Chem.*, **63**, 1890.
- HAUSSER, K. H., 1959, *Z. Naturf.*, **14a**, 425.
- KIVELSON, D., 1957, *J. Chem. Phys.*, **27**, 1087.
- LUSZCZYNSKI, K., KAIL, J. A. E., and POWLES, J. G., 1960, *Proc. Phys. Soc.*, **75**, 243.
- MCCONNELL, H. M., 1956, *J. Chem. Phys.*, **25**, 709.
- MCGARVEY, B. R., 1956, *J. Phys. Chem.*, **60**, 71.
- 1957, *J. Phys. Chem.*, **61**, 1232.
- PAKE, G. E., TOWNSEND, J., and WEISSMANN, S. I., 1952, *Phys. Rev.*, **85**, 682.
- PAKE, G. E., and TUTTLE, T. R., 1959, *Phys. Rev. Letters*, **3**, 423.
- PALMER, W. G., 1954, *Experimental Inorganic Chemistry* (Cambridge: University Press).
- SHEELY, M. L., 1932, *Industr. Engng Chem.*, **24**, 1060.
- SMYTH, C. P., 1955, *Dielectric Behaviour and Structure* (New York: McGraw-Hill), p. 128.
- STEPHEN, M. J., and FRAENKEL, G. K., 1960, *J. Chem. Phys.*, **32**, 1435.
- TOWNSEND, J., WEISSMANN, S. I., and PAKE, G. E., 1953, *Phys. Rev.*, **89**, 606.
- WEISSMANN, S. I., and BANFILL, D., 1953, *J. Amer. Chem. Soc.*, **75**, 2534.

Molecular Motion in Liquid Toluene by Proton Magnetic Resonance Relaxation

By J. G. POWLES AND D. J. NEALE

Physics Department, Queen Mary College, University of London

MS. received 22nd August 1960

Abstract. Measurements are reported of the proton spin-lattice relaxation time T_1 at 47.5 Mc/s for both the methyl and ring protons in liquid toluene over a wide temperature range by recovery from saturation of the high resolution signal. The two sets of protons relax independently and show a very different dependence on temperature. The ring proton T_1 has a minimum of 1.4 sec at -108°C while the methyl proton T_1 is still falling at the lowest temperature -131°C to which the liquid could be supercooled. The results are interpreted in terms of a complex thermal motion of the toluene molecules about more than one axis together with internal motions of the methyl group relative to the molecule. Plausible generalizations of current theories of magnetic resonance relaxation are made to facilitate the analysis. It is suggested that very considerably increased information about molecular liquids is obtainable from magnetic resonance measurements by such a study of each chemical type of proton within a molecule, when present.

§ 1. INTRODUCTION

IN the whole liquid range, -131° to $+110.6^\circ\text{C}$ (including supercooling below the melting point at -95.0°C) the proton magnetic resonance spectrum of toluene ($\text{CH}_3\text{C}_6\text{H}_5$) consists of two single, well separated lines with intensities in the ratio three to five corresponding to the methyl and ring protons. We have measured the proton magnetic resonance spin-lattice relaxation times T_1 at 47.5 Mc/s, of each type of proton over the above temperature range by a method which has considerable advantages over the usual transient methods. The T_1 values are interpreted in terms of the thermal motions of the toluene molecules in the liquid. A general interpretation is given in § 3 and a more detailed one together with a discussion of the parameters is given in §§ 4 and 5.

§ 2. EXPERIMENTAL ARRANGEMENT AND RESULTS

We have constructed a moderately high resolution nuclear magnetic resonance equipment using the bridged T single coil system (see e.g. Leane, Richards and Schaefer 1959) together with a Varian 12 in. magnet without super-stabilizer. The resolution and stability is about 15 c/s at the operating frequency for protons of 47.5 Mc/s. This is sufficient to allow the study of the relaxation of individual groups of chemically shifted protons in many molecules. Thus the two sets of protons in toluene give signals separated by 230 c/s, as in Fig. 1 (a).

The experiment consists in setting on one or other, or sometimes both, of the signals at high radio-frequency level sufficient to saturate and then reducing the radio-frequency level suddenly to well below saturation and applying a

triangular calibrated field sweep of low amplitude. The low radio-frequency field then acts as a probe and inspects the magnitude of the longitudinal magnetization $M_z(t)$ at suitable intervals. Its recovery was always exponential, i.e. $M_z(t) = M_0[1 - \exp(-t/T_1)]$ and so T_1 may be deduced. The rate of sweep and radio-frequency level were adjusted to avoid both saturation and ringing. $M_z(t)$ is proportional to the oscilloscope deflection which was recorded by a camera with a moving film (Fig. 1(a)).

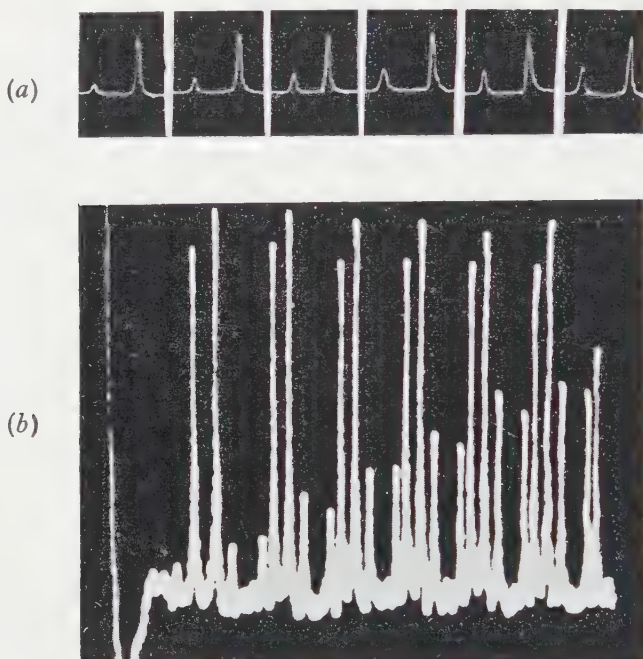


Fig. 1. (a) Showing the recovery of the methyl proton signal in toluene after saturation. The ring proton signal remains constant. The flyback signal has been removed. (b) Double sweep display showing the recovery of the methyl proton signal from saturation.

It was sometimes convenient to use a fixed film, a slow (i.e. $> T_1$) oscilloscope time-base sweep, and sweep the magnetic field rapidly (i.e. $< T_1$) over a small range thus obtaining a result as in Fig. 1(b).

The lower temperature limit of measurement was determined by the spontaneous crystallization of the supercooled liquid. The material was of Analar grade and was not further purified ($n_{D20} = 1.4963 \pm 0.0005$, boiling point 110.6°C). Oxygen was removed by a freeze-pump-thaw technique. Any contamination by oxygen was clearly indicated by the approach of T_1 to a constant value above a certain temperature. Saturation by the probing signal was indicated by a signal not linearly proportional to the radio-frequency level and by an apparent fall in T_1 with increasing temperature.

The signal-to-noise ratio is smaller than in the usual high resolution experiment because of the inhomogeneity broadening and because the signal has to be displayed several times within a time T_1 . Thus the integrating time constant must be less than say $T_1/10$ which may be $1/10$ sec as compared with

the usual 1 sec or more. At the higher temperatures loss of signal occurs because of the Boltzmann factor and a fall in sensitivity. Nevertheless the signal-to-noise ratio was never below 5 for toluene.

The accuracy of measurement of T_1 was to about $\pm 7\%$ for the longest T_1 's depreciating to about $\pm 15\%$ for the shortest ones. Even with this rather poor accuracy the method is superior to the transient method of determining T_1 , at least for multiple T_1 's longer than about 1 second. This is because of the well-known difficulty of resolving two or more exponential decays when the decay times are not very different. For instance, Fig. 2 shows the plot of a function of signal amplitude $A(t)$ after the 90° pulse of a 180° , t , 90° pulse sequence (Carr and Purcell 1954) for toluene at 21°C . This should be

$$A(t)/A(\infty) = \frac{3}{8}[1 - 2 \exp(-t/T_{1\text{methyl}})] + \frac{5}{8}[1 - 2 \exp(-t/T_{1\text{ring}})].$$

In fact the experimental curve would be taken to be a straight line for the accuracy achieved here (Luszczynski and Powles 1959a), i.e. a single relaxation time of 11.4 sec at 21.5 Mc/s. This evidently explains a value $T_1 = 12.5$ sec at 7 Mc/s reported by Giulotto (1956) for toluene at 25°C . (T_1 should be frequency independent for toluene at room temperature, see Eqn (3).) As

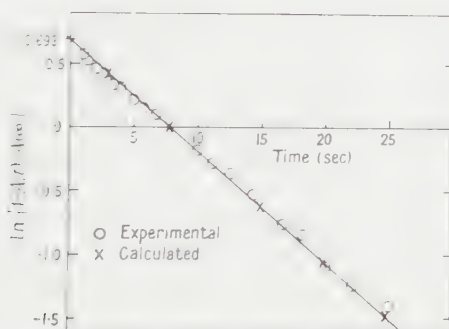


Fig. 2. The longitudinal relaxation in toluene at 21°C by the transient 90° , t , 180° pulse method. The straight line corresponds to $T_1 = 11.4$ sec. Calculated points (crosses) assume $T_{1\text{methyl}} = 9$ sec and $T_{1\text{ring}} = 13$ sec giving a curve not distinguishable from the straight line within experimental error.

shown in Fig. 2 the results can equally well be fitted to the above formula with $T_{1\text{methyl}} = 9$ sec and $T_{1\text{ring}} = 13$ sec. This compares favourably with 9.8 and 15.3 sec by the present method (Fig. 3). Nederbragt and Reilly (1956) using an adiabatic fast passage method report 9 and 16 sec at 40 Mc/s at 25°C which may be compared with our values of 10.5 and 16 seconds. Bonera *et al.* (1960) have recently reported a slight curvature on a plot similar to Fig. 2 thus confirming the inequality of the two relaxation times. However their accuracy of determination of the T_1 values is still poor for the reasons given above.

We have found the values 5 and 12.5 sec at 25°C from a transient experiment at 1 Mc/s by another method (Powles and Cutler 1957). These low values may indicate a field dependent effect at low fields.

Saturation and subsequent recovery of one proton signal had no discernable effect on the other (Fig. 1) and so the two relaxations appear to this extent to be independent.

§ 3. DISCUSSION OF THE RESULTS AND PRELIMINARY INTERPRETATION

The striking and unexpected features of the results given in Fig. 3 are that although the magnitudes of $T_{1\text{methyl}}$ and $T_{1\text{ring}}$ are similar at room temperature their variation with temperature is quite different and $T_{1\text{ring}}$ exhibits a minimum while $T_{1\text{methyl}}$ does not.

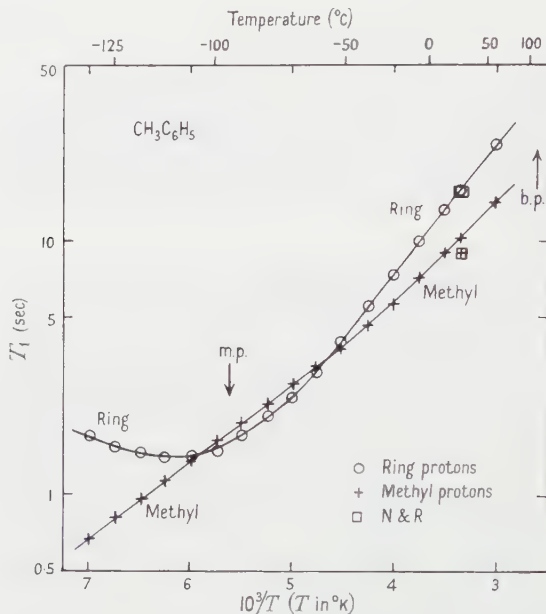


Fig. 3. Values of T_1 for the ring and methyl protons in liquid toluene as a function of temperature. m.p. indicates the melting point; N & R, values due to Nederbragt and Reilly (1956).

Present theories of magnetic relaxation in liquids are inadequate to deal with such a complex situation with both inter- and intramolecular nuclear dipolar interactions as well as the possibility of complex molecular motions and even internal motions. We shall use what seem to be reasonable generalizations.

For a motional correlation frequency ν_c greater than the interaction in terms of frequency, i.e. in this case $\nu_c \gtrsim 10^4$ c/s, the spin-lattice relaxation time of an isolated pair of nuclei of spin $\frac{1}{2}$ at separation d resonant at ν_r c/s is given by (Kubo and Tomita 1954, Solomon 1955)

$$\frac{1}{T_1} = \frac{3}{10} \frac{1}{2\pi\nu_r} \frac{\gamma^4 \hbar^2}{d^6} \left[\frac{(\nu_r, \nu_c)}{1 + (\nu_r/\nu_c)^2} + \frac{4(\nu_r, \nu_c)}{1 + (2\nu_r/\nu_c)^2} \right] = \frac{I}{1.42\nu_r} f(\nu_r/\nu_c) \quad \dots\dots(1)^\dagger$$

where

$$I = 1.42 \times \frac{3}{10} \times \frac{1}{2\pi} \times \frac{\gamma^4 \hbar^2}{d^6}.$$

T_1 has a minimum value when $\nu_c = 1.62\nu_r$ given by

$$1/T_{1\text{min}} = I/\nu_r. \quad \dots\dots(2)$$

[†] The introduction of the new symbol I is justified when more complex situations are studied below.

When $\nu_c \gg \nu_r$,

$$\frac{1}{T_1} = \frac{3}{2} \frac{\gamma^4 \hbar^2}{2\pi d^6} \frac{1}{\nu_c} = 3.52 \frac{I}{\nu_c}. \quad \dots\dots (3)$$

In the case of a trio of spins $\frac{1}{2}$ disposed on an equilateral triangle of side d , Hubbard (1958) has shown, implicitly, that in Eqn (3) I is multiplied by the factor 2 to a good approximation, just as is the second moment of the static magnetic interaction (Van Vleck 1948).

We shall make the plausible assumption that for other than an isolated pair, Eqn (1) may be used but with the factor appropriate to the powder average of the second moment of the static magnetic interaction.

The effect of interactions external to the group is even less firmly established but it seems reasonable to generalize Eqn (3) for a pair of nuclei to

$$\frac{1}{T_1} = \frac{3}{2} \frac{\gamma^4 \hbar^2}{2\pi} \frac{d^{-6} + \frac{1}{2} B\pi(N/V)a^{-3}}{\nu_c} \quad \dots\dots (4)$$

where $B=6/5$ (Skrotskii and Kokin 1959) although Bloembergen, Purcell and Pound (1948) find $B=3/2$; N/V is the number of protons per cm^3 and a is an effective radius of the diffusing molecule. For toluene the second term in Eqn (4) is $2 \times 10^{-3} \text{ \AA}^{-6}$ which may be compared with $d^{-6} = 31.5 \times 10^{-3} \text{ \AA}^{-6}$ for the proton separation in the methyl group and $4.4 \times 10^{-3} \text{ \AA}^{-6}$ for the separation between ring protons. For other than pairs of nuclei the first term tends to be even bigger than the second.

The correlation frequencies for re-orientational and translational motions are not equal but are often approximately so. The relaxation due to 'external' interactions for any ν_c has been considered by Skrotskii and Kokin (1959) but for the simple case of pairs only. They find that the dependence on ν_c is similar to that for the internal interaction except when $\nu_c < \nu_r$ and so

$$\frac{1}{T_1} = \frac{I}{1.42\nu_r} f\left(\frac{\nu_r}{\nu_{cR}}\right) + \frac{E}{1.42\nu_r} f\left(\frac{\nu_r}{\nu_{cT}}\right) \quad \dots\dots (5)$$

for $\nu_{cT} > \nu_r$ where ν_{cR} and ν_{cT} are the correlation frequencies for re-orientational and translational thermal motion. We shall take I appropriate to the nuclear grouping under discussion and $E = 1.42(9.50)\gamma^4 \hbar^2 (N/V)a^{-3}$ as indicated by Eqn (4).

It must be recognized in calculating I and E that there are two sets of nuclei with similar but not identical resonant frequencies. In powder second-moment calculations non-resonant nuclei are less effective in causing transverse relaxation by the factor 2.9. But for the motional case the matter is less clear since the relaxing effect of the static and precessing magnetizations (which roughly speaking lead to the two terms in Eqn (1)) are not, one would think, much affected by the slight differences in effective γ (i.e. ν_r). Following Solomon (1955) we find for two almost identical nuclei at fixed separation d with one spin system initially saturated and the other at equilibrium that the equations of motion of the two longitudinal magnetizations I_{1Z} and I_{2Z} are

$$I_{1Z} = I_0 \{1 - \frac{1}{2} [\exp(-\frac{3}{2}\delta t) + \exp(-\frac{1}{2}\delta t)]\}$$

and

$$I_{2Z} = I_0 \{1 - \frac{1}{2} [\exp(-\frac{3}{2}\delta t) - \exp(-\frac{1}{2}\delta t)]\} \quad \dots\dots (6)$$

when $\nu_c \gg \nu_r$ and where $\delta = \hbar^2 \gamma^4 / 2\pi \nu_c d^6$. (The relaxation rate is $\frac{3}{2}\delta$ for identical nuclei, Eqn 3.) Thus the recovery of the saturated system I_{1Z} is not

exponential and is accompanied by a temporary *increase* in the signal from the other system \bar{I}_{22} . We have observed neither of these effects when saturating one system only and feel therefore that relaxation due to non-resonant nuclei must be small. Therefore, the second term in Eqn (4) and E in Eqn (5) may well be reduced in toluene by 3/8 for the ring and 5/8 for the methyl protons. Since these contributions are in any case rather small we expect to make little error in doing this, or indeed in neglecting them in our case of multiple groups of nuclei. This conclusion has received general support (Bovey 1960). When both systems are initially saturated Solomon's analysis leads to Eqn (6) without the terms in $\exp(-\frac{1}{2}\delta t)$, i.e. recovery of both systems at the same rate as for identical nuclei. This result is confirmed implicitly by Miyake and Chujo (1957). We therefore first analyse the results ignoring the second term in Eqn (5) and reconsider it later.

Since $T_{1\text{ring}}$ has a minimum we can deduce $\nu_{c\text{ring}}$ as a function of temperature from Eqn (1) assuming that I/ν_r is independent of temperature and equal to $T_{1\text{min}}^{-1}$; $\nu_{c\text{ring}}$ is given in Fig. 4 and $I/\nu_r = 0.70 \text{ sec}^{-1}$. The I/ν_r value for a pair of protons only, with the same separation (2.47 \AA) as the ring ones, is already 3.3 sec^{-1} and so the actual interaction is very weak. (It may appear later that our conclusions rely heavily on the observation of a minimum for $T_{1\text{ring}}$. This is not so since if we accept only the values of $T_{1\text{ring}}$ above, say, -50°C we would calculate $\nu_{c\text{ring}}$ as for $\nu_{c\text{methyl}}$ below. The plausible value of I/ν_r is about 6 sec^{-1} and using Eqn (3) we find $\nu_{c'\text{ring}}$ as given in Fig. (4). The difference between $\nu_{c'\text{ring}}$ and $\nu_{c\text{methyl}}$ is still very marked and our subsequent interpretation is not greatly affected. To make $\nu_{c'\text{ring}} = \nu_{c\text{methyl}}$ would require $I/\nu_r \simeq 50 \text{ sec}^{-1}$, an unacceptable value.)

To obtain $\nu_{c\text{methyl}}$ from $T_{1\text{methyl}}$ we use Eqn (1) with $I/\nu_r = 52 \text{ sec}^{-1}$ appropriate to the isolated methyl group at 47.5 Mc/s . The result is shown in Fig. 4.

Within the uncertainties of this analysis, the correlation frequency for the two types of protons differ both in their variation with temperature and by a factor of about 45 in magnitude. The latter contrasts with the T_1 values themselves which do not differ by more than the factor 2, except at low temperatures.

We now consider some independent evidence for the motion of the toluene molecule. The molecule is slightly polar ($\mu = 0.37$ Debye) and Fig. 4 shows the correlation frequency ν_D for the dielectric relaxation (Whiffen and Thompson 1946, Petro and Smyth 1957). We ought to compare ν_c with $\alpha\nu_D$ for the same re-orientational motion (Bloembergen, Purcell and Pound 1948). The factor α depends on the model and is 3 for the Brownian motion of a sphere. $\nu_{c\text{methyl}}$ and $3\nu_D$ are strikingly similar in magnitude and behaviour with temperature in the range in which ν_D is available (Fig. 4). This is very satisfactory since the electric dipole moment is in the direction of the C-CH₃ bond. However at lower temperatures $\nu_{c\text{methyl}}$ and $3\nu_D$ diverge considerably. It is likely, from a general consideration of the behaviour of re-orientational correlation frequencies in liquids (Powles 1961, to be published), that the dielectric relaxation at low temperatures will behave as indicated by the broken line in Fig. 4. In particular it would be most unusual for the slope of the $(\ln \nu_D, -1/T)$ curve to decrease with decreasing temperature as suggested by $\nu_{c\text{methyl}}$. The divergence between $\nu_{c\text{methyl}}$ and $3\nu_D$ at low temperatures is explained in §4.

It is related to the rather abrupt change in slope of the $(\ln T_1, -1/T)$ curve near -60°C . A similar effect has been observed in the methyl proton relaxation in polydimethyl siloxanes (Powles and Hartland 1960).

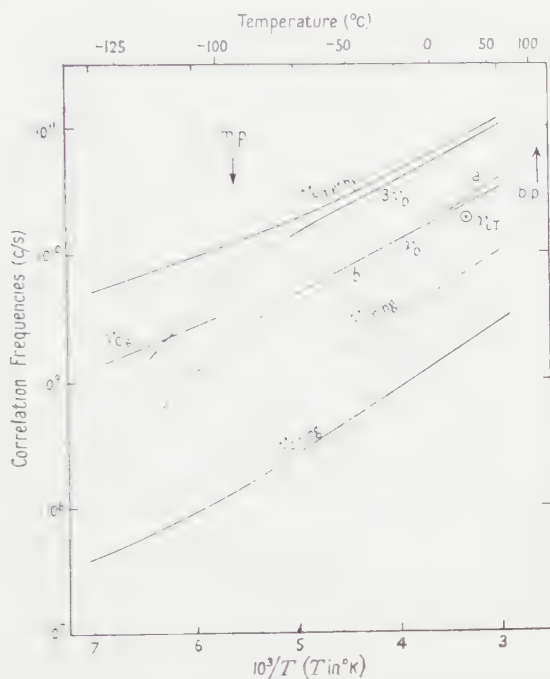


Fig. 4. Correlation frequencies as a function of temperature for toluene. $\nu_{c \text{ ring}}$ deduced from $T_1 \text{ ring}$ using Eqn (1); $\nu_{c \text{ methyl}}$ deduced from $T_1 \text{ methyl}$ using Eqn (1); ν_D is the correlation frequency for dielectric loss, *a*, Petro and Smyth (1957); *b*, Whiffen and Thompson (1946), and a plausible extrapolation at low temperatures; ν_{cT} is discussed in § 4; ν_{cT} is a translational correlation frequency discussed in § 5; $\nu_{c' \text{ ring}}$ is an alternative value of $\nu_{c \text{ ring}}$ discussed in § 2

§ 4. INTERPRETATION USING A MODEL FOR THE MOTION OF THE MOLECULE

The proton relaxation results in liquid toluene can be plausibly explained by the following simplified picture of the motions of the toluene molecules. From a consideration of the shape and constitution of the molecule we propose that for the molecule as a whole there are two distinguishable motions. A C_6 motion of re-orientation about an axis perpendicular to the plane of the ring and a C_2 motion about the C-CH₃ axis (Fig. 5). In addition to this the methyl group can have a C_3 motion of re-orientation about its own C_3 axis relative to the ring. Evidently the relaxation of the methyl protons is affected by the C_3 and C_6 motions but not by C_2 except in so far as they are carried round with the ring. The ring protons are affected by C_6 and C_2 but very little by C_3 . The dielectric relaxation is affected only by the motion C_6 . The translational motion of the molecules is considered later since it is of importance for the intermolecular interaction contribution to relaxation.

In view of the double motion of the methyl protons we now use a generalization of Eqn (1)

$$\frac{1}{T_{1 \text{ methyl}}} = \frac{I_{C_3}}{1.42\nu_r} f\left(\frac{\nu_r}{\nu_{C_3}}\right) + \frac{I_{C_6}}{1.42\nu_r} f\left(\frac{\nu_r}{\nu_{C_6}}\right) + \text{intra- and intermolecular terms} \quad \dots\dots(7)$$

where I_{C_3} and I_{C_4} depend on assumptions about the various ν_c 's.[†] It seems likely from the study of other molecular liquids and solids with molecules containing methyl groups (e.g. Luszczynski and Powles 1959b) that at low temperatures the methyl group C_3 re-orientation is often much faster than the

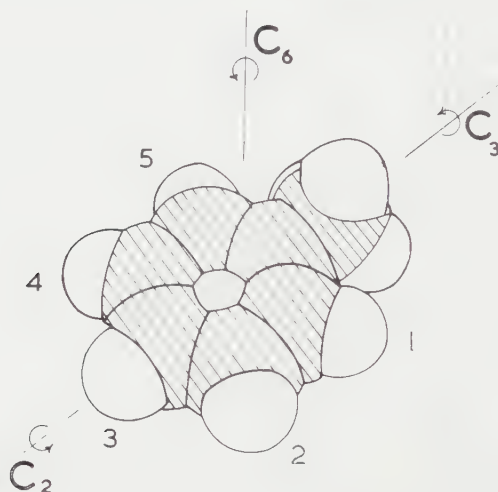


Fig. 5. Illustrating the various axes of re-orientation of the toluene molecule discussed in the text.

molecular re-orientation, i.e. in this case $\nu_{C_3} \gg \nu_{C_4}$ for $T \lesssim T_{m.p.}$. But at higher temperatures the two frequencies become comparable, i.e. $\nu_{C_3} \simeq \nu_{C_4}$ for $T \gtrsim T_{m.p.}$. This seems plausible physically. At low temperatures the methyl group undergoes re-orientation in a more or less fixed environment. As the temperature rises the increasingly rapid re-orientation of the whole molecule increasingly disturbs the CH_3-C_3 re-orientation until the two motions become inextricably mixed.

Since both ν_{C_3} and $\nu_{C_4} \gg \nu_r$ we have, using Eqn (3)

$$\frac{1}{T_{1 \text{ methyl}}} \simeq 3 \cdot 52 I_{C_3} / \nu_{C_3} \quad \text{for } T \lesssim T_{m.p.} \quad \dots \dots (8a)$$

and

$$\simeq 3 \cdot 52 (I_{C_3} + I_{C_4}) / \nu_c = 3 \cdot 52 I_{CH_3} / \nu_c \quad \text{for } T \gtrsim T_{m.p.} \quad \dots \dots (8b)$$

apart from intra- and intermolecular terms. We suppose $I_{C_3} = \frac{1}{4} I_{CH_3} = 13 \nu_r \text{ sec}^{-2}$ in the present context and if we use Eqn (8a) to calculate ν_{C_3} we get the result shown on Fig. 4 for temperatures below the melting temperature. ν_{C_3} is in better agreement with the extrapolated values of $3\nu_D$ than $\nu_{C_{\text{methyl}}}$ as would be expected. Above the melting temperature the original analysis is still valid preserving the agreement of ν_c with $3\nu_D$. A more detailed analysis to effect the change-over from Eqn (8a) to (8b) would give quite satisfactory agreement over a wide temperature range. It would leave the difficulty that the slope of ν_{C_3} would be too small at the lowest temperatures. This could be due to a

[†] A rather similar generalization has been made by Stejskal and Gutowsky (1958). However the magnitude of the interaction constants given there appear to be suspect. They do not, for instance, find Hubbard's (1958) result for the isotropic re-orientation of the methyl group.

distribution of correlation frequencies setting in at low temperatures (e.g. Powles and Luszczynski 1959) as is common for dielectric relaxation. Measurements of the dielectric relaxation at low temperatures would give valuable independent information.

We suggest therefore that the unexpectedly small fall of $\nu_{\text{e methyl}}$ at low temperatures is an apparent effect associated with the double motion of the methyl group.

Turning now to the ring protons we consider the possibility that $\nu_{\text{e ring}}$ is in fact ν_{C_1} . Since both ν_{C_1} and $\nu_{\text{C}_2} \gg \nu_{\text{C}_3}$, the interaction to be associated with the ring proton T_1 is motionally reduced considerably below the rigid lattice value. The external interaction of the ring protons with the methyl protons in the same molecule is also motionally attenuated and possibly reduced by the non-resonant effect discussed in §3. The C_2 motion does not modulate the interaction of protons 1 with 2 and 4 with 5 (Fig. 5) which therefore cannot contribute much to T_1 . Allowing for complete motional attenuation by ν_{C_1} and remembering that I/ν_{r} for the static ring protons is 6.0 sec^{-1} we estimate $I/\nu_{\text{r}} \approx 6.0(1/4)(3/5) = 0.9 \text{ sec}^{-1}$. This value must be increased somewhat for the interaction with methyl protons and protons in other molecules. The former, however, are modulated at $\nu_{\text{e methyl}}$ and the latter at ν_{C_1} and again by the translational motion, expected to be also at the rate ν_{C_1} approximately. All are much larger than ν_{C_1} and ν_{r} . These contributions should therefore be small. Hence the theoretical interaction constant is about 0.8 sec^{-1} and compares favourably with the experimental value of 0.7 sec^{-1} .

One objection to the curve of $\nu_{\text{e ring}}$ in Fig. 4 is that, like $\nu_{\text{e methyl}}$, it does not fall at low temperatures as rapidly as might be expected. This is because the minimum of $T_{1 \text{ ring}}$ in Fig. 3 is not symmetric. The behaviour has been observed in other molecular liquids (Luszczynski and Powles 1959b, Luszczynski, Kail and Powles 1960). Skrotskii and Kokin (1959) suggest that for pairs of nuclei the T_1 curve near the minimum should in fact be asymmetric rather in the manner observed here for the ring protons. Results at different resonant frequencies would be valuable.

The special motions postulated raise an apparent difficulty in that the dielectric absorption measurements giving ν_{D} in Fig. 4 also give the correct molecular electric dipole moment based essentially on the Langevin-Debye formula $\mu^2/3kT$ (μ can be obtained with some confidence from measurements on the pure liquid since it is low). This formula assumes isotropic re-orientation of the dipole. It can be shown however that the restricted dipolar motion C_6 together with the isotropic distribution of that axis, ensured by the slower motions C_2 etc., give the same formula. The agreement is therefore unaffected.

§ 5. DISCUSSION OF THE CORRELATION FREQUENCIES

We must also explain the factor of about 45 between the correlation frequencies for the C_2 and C_6 motions and the difference in their behaviour with temperature. There are at least four ways of looking at this problem.

One is to regard the molecule as being spheroidal in shape and undergoing re-orientational diffusion in a viscous medium. If we assume the toluene molecule is an oblate spheroid of axial ratio about 3 a calculation by Perrin (1934)

shows that $\nu_{C_6}/\nu_{C_2} \simeq 1.1$. This is quite inadequate to explain our factor of 45 (significant differences are in fact only to be expected for very long prolate spheroids). Further, the activation energies for the two motions should be equal, and equal to that for the viscosity. They are in fact 1.8 for ν_{C_6} , 2.3 for ν_{C_2} and 2.08 kcal mol⁻¹ for the viscosity. This adverse result is in accord with dielectric relaxation studies which suggest that the internal friction model for motion of a molecule is usually a poor approximation for a pure liquid.

On the other hand we may regard the two re-orientations as thermally activated processes (Glasstone, Laidler and Eyring 1941, Kauzmann 1942). The difference of 0.5 kcal mol⁻¹ in the activation energies corresponds to a factor 2.3 between ν_{C_6} and ν_{C_2} leaving a factor 20 to be explained. This might be interpreted as a difference in activation entropy of amount 6 cal mol⁻¹ deg C⁻¹, the higher activation entropy being associated with the methyl C₆ motion. Using the 'absolute' reaction rate theory for which

$$\nu_c = kT/h \exp(-\Delta E^\ddagger/kT + \Delta S^\ddagger/k)$$

we find at 25°C for ν_{C_2} , $\Delta S^\ddagger = -8$ cal mol⁻¹ deg⁻¹ to which it is difficult to attach a meaning (but see Kauzmann 1942). However caution is required in the use of activation theory at all since $\Delta E^\ddagger/kT \sim 3$ at the higher temperatures whereas Montroll and Shuler (1958) suggest that $\Delta E^\ddagger/kT \gtrsim 5$ is necessary.

Again we have the simple picture of vibrations in potential wells separated by energy barriers. The barriers would then be as discussed above, i.e. rather similar in magnitude but the frequencies of vibration would differ by the factor 20. A factor 3 of this would be provided if we assume there are six wells for the C₆ motion and two for C₂. However, the moments of inertia differ and in fact $(I_{C_6}/I_{C_2})^{1/2} \simeq 1.8$. This leaves an unexplained factor of $20 \times 1.8/3 = 12$.

Finally we have to consider the possibility of a cage release mechanism of re-orientation as suggested by Bauer (1944) for water. In this case our correlation frequencies reflect the lifetimes of cybotactic groupings. This last explanation may well be the most likely one.

As regards the translational motion of the molecules we have used reaction rate theory as applied to viscosity (Glasstone, Laidler and Eyring 1941) and assumed the jump step is a molecular diameter to calculate for toluene at 25°C, $\nu_{cT} \simeq 2 \times 10^{10}$ c/s. Although this calculation is crude it supports our assumption that the intermolecular nuclear dipole interaction is modulated at a frequency greater than ν_{C_2} . The molecule may therefore re-orient and translate at the same time. In this connection it would be interesting to study toluene in solution in perdeuterotoluene.

We present only a simplified picture of the motions of the toluene molecule in liquid toluene. Our proposals are a first approximation on which a more refined theory may be based when more data become available. The data required from nuclear magnetic resonance are relaxation of the transverse magnetization and the relaxation of the longitudinal magnetization for various resonant frequencies.

We are at present applying this technique to other molecular liquids in which more than one proton type is present since it seems to extend considerably the information obtainable in the study of thermal motions in liquids by magnetic resonance.

§ 6. CONCLUSION

The strikingly different magnetic resonance relaxation of the two types of protons in the toluene molecule in liquid toluene have been interpreted in terms of a complex thermal motion of the molecule. It is suggested that the molecule re-orientates about an axis perpendicular to the plane of the ring much faster than about an axis in the ring and containing the methyl group. There is a close relation between the methyl proton relaxation and dielectric relaxation. It seems likely that translation occurs at the faster rate and so tends to be in a direction parallel to the plane of the ring. This analysis illustrates the complexity of the thermal motions to be expected in molecular liquids and the power of magnetic resonance methods in elucidating them.

ACKNOWLEDGMENTS

The electromagnet was provided by a grant from the Department of Scientific and Industrial Research who also provided a maintenance grant for one of us (D. J. N.). The T_1 measurements at 21.5 Mc s were made by Mr. A. Hartland and at 1 Mc s by Dr. D. Cutler in this laboratory. We also acknowledge the loan of a pen recorder from the Central Research Fund of the University of London.

REFERENCES

- BAUER, E., 1944, *Cah. Phys.*, **21**, 43.
BLOEMBERGEN, N., PURCELL, E. M., and POUND, R. V., 1948, *Phys. Rev.*, **73**, 679.
BONERA, G., CHIOLDI, L., LANZI, G., and RIGAMONTI, A., 1960, *Nuovo Cim.*, **17**, 198.
BOVEY, F. A., 1960, *J. Chem. Phys.*, **32**, 1877.
CARR, H. Y., and PURCELL, E. M., 1954, *Phys. Rev.*, **94**, 630.
GIULOTTO, L., 1956, *Arch. Sci.*, **9**, 218 (5th Coll. Ampere).
GLASSTONE, S., LAIDLER, K. J., and EYRING, H., 1941, *The Theory of the Rate Process* (New York: McGraw-Hill).
HUBBARD, P. S., 1958, *Phys. Rev.*, **109**, 1153.
KAUZMANN, W., 1942, *Rev. Mod. Phys.*, **14**, 12.
KUBO, R., and TOMITA, D., 1954, *J. Phys. Soc., Japan*, **9**, 888.
LEANE, J. B., RICHARDS, R. E., and SCHAEFER, T. P., 1959, *J. Sci. Instrum.*, **36**, 220.
LUSZCZYNSKI, K., KAIL, J. A. E., and POWLES, J. G., 1960, *Proc. Phys. Soc.*, **75**, 243.
LUSZCZYNSKI, K., and POWLES, J. G., 1959 a, *J. Sci. Instrum.*, **36**, 57.
—— 1959 b, *Proc. Phys. Soc.*, **74**, 408.
MIYAKE, A., and CHUJO, R., 1957, *Busseiron Kenkyu*, **11**, 2, 769 (English summary 1958, *Reports Progress in Polymer Physics in Japan*, **1**, 171).
MONTROLL, E. W., and SHULER, K. E., 1958, *Advanc. Chem. Phys.*, **1**, 361.
NEDERBRAGT, E. W., and REILLY, C. A., 1956, *J. Chem. Phys.*, **24**, 1110.
PERRIN, F., 1934, *J. Phys. Radium*, (7) **5**, 497.
PETRO, A. J., and SMYTH, C. P., 1957, *J. Amer. Chem. Soc.*, **79**, 6142.
POWLES, J. G., and CUTLER, D., 1957, *Nature, Lond.*, **180**, 1344.
POWLES, J. G., and HARTLAND, A., 1960, *Nature, Lond.*, **186**, 26.
POWLES, J. G., and LUSZCZYNSKI, K., 1959, *Physica*, **25**, 455.
SKROTSKII, G. V., and KOKIN, A. A., 1959, *J. Exp. Theor. Phys.* (English translation), **36** (9), 335.
SOLOMON, I., 1955, *Phys. Rev.*, **99**, 559.
STEJSKAL, E. O., and GUTOWSKY, H. S., 1958, *J. Chem. Phys.*, **28**, 388.
VAN VLECK, H. J., 1948, *Phys. Rev.*, **74**, 1168.
WHIFFEN, D. H., and THOMPSON, H. W., 1946, *Disc. Faraday Soc.*, **42A**, 142

Stationary Properties of the Hartree-Fock Approximation

BY M. COHEN AND A. DALGARNO

Department of Applied Mathematics, The Queen's University of Belfast

MS. received 21st September 1960

Abstract. The theorem is proved that the first order correction to the expectation value of any operator which can be expressed as a sum of one-electron operators vanishes if Hartree-Fock wave functions are used in its evaluation.

IT has been shown that the first-order correction to the charge density of an atomic system vanishes if Hartree-Fock wave functions are used in its evaluation (Møller and Plesset 1934). The theorem may be replaced by the more powerful assertion that *the first-order correction to the expectation value of any operator which can be expressed as a sum of one-electron operators vanishes if Hartree-Fock wave functions are used in its evaluation.*

We restrict ourselves to a consideration of closed shell systems for which the Hartree-Fock wave function $\psi^{(0)}$ may be put in the form of a single determinant. Then

$$\psi^{(0)} = \mathcal{A} \prod_{i=1}^N u_i^{(0)} \quad \dots\dots (1)$$

where \mathcal{A} is the normalized antisymmetrizing operator (cf. Condon and Shortley 1935) and the orbitals $u_i^{(0)}$ satisfy the eigenvalue equations

$$H_i u_i^{(0)}(\mathbf{r}_i) = \epsilon_i^{(0)} u_i^{(0)}(\mathbf{r}_i) \quad \dots\dots (2)$$

with

$$H_i = -\frac{1}{2} \nabla_i^2 - \frac{Z}{r_i} + \sum_k (\beta_{ik} - \alpha_{ik}), \quad \dots\dots (3)$$

β_{ik} and α_{ik} being defined according to

$$\beta_{ik} = \int \frac{|u_k^{(0)}(\mathbf{r}_k)|^2}{|\mathbf{r}_i - \mathbf{r}_k|} d\mathbf{r}_k \quad \dots\dots (4)$$

$$\alpha_{ik} u_i(\mathbf{r}_i) = \int \frac{u_k^{(0)*}(\mathbf{r}_k) u_i(\mathbf{r}_k)}{|\mathbf{r}_i - \mathbf{r}_k|} d\mathbf{r}_k u_k^{(0)}(\mathbf{r}_i); \quad \dots\dots (5)$$

α_{ik} vanishes unless $u_k^{(0)}$ and u_i are associated with parallel spins. The total wave function (1) satisfies the equation

$$H' \psi^{(0)} = E^{(0)} \psi^{(0)} \quad \dots\dots (6)$$

where

$$H' = \sum_{i=1}^N H_i - \sum_{i < k} \sum \int (\beta_{ik} - \alpha_{ik}) |u_i^{(0)}(\mathbf{r}_i)|^2 d\mathbf{r}_i \quad \dots\dots (7)$$

and

$$E^{(0)} = \sum_{i=1}^N \epsilon_i^{(0)} - \sum_{i < k} \sum \int (\beta_{ik} - \alpha_{ik}) |u_i^{(0)}(\mathbf{r}_i)|^2 d\mathbf{r}_i, \quad \dots\dots (8)$$

it being understood that H_i operates only on functions of \mathbf{r}_i .

The exact Hamiltonian is given by

$$H = -\frac{1}{2} \sum_i \nabla_i^2 - \sum_i \frac{Z}{r_i} + \sum_{i,k} \sum \frac{1}{|\mathbf{r}_i - \mathbf{r}_k|} \quad \text{..... (9)}$$

and the exact wave function Ψ satisfies the equation

$$(H - E)\Psi = 0. \quad \text{..... (10)}$$

We expand Ψ and E according to

$$\Psi = \sum_{s=0}^{\infty} \psi^{(s)}, \quad E = \sum_{s=0}^{\infty} E^{(s)},$$

the superscript indicating the order in the perturbation $v = H - H'$. Then the zero-order contribution to the expectation value $(\Psi, L\Psi)$ of an operator L is given by

$$L^{(0)} = (\psi^{(0)}, L\psi^{(0)}), \quad \text{..... (11)}$$

and the first-order contribution is given by

$$L^{(1)} = 2\{(\psi^{(0)}, L\psi^{(1)}) - L^{(0)}(\psi^{(0)}, \psi^{(1)})\} \quad \text{..... (12)}$$

where $\psi^{(1)}$ is the well-behaved solution of

$$(H' - E^{(0)})\psi^{(1)} + \{v - (\psi^{(0)}, v\psi^{(0)})\}\psi^{(0)} = 0. \quad \text{..... (13)}$$

The first-order contribution can be written alternatively (Dalgarno and Stewart 1957) as

$$L^{(1)} = 2\{(\psi^{(0)}, \tau\chi^{(1)}) - (\psi^{(0)}, v\psi^{(0)})(\psi^{(0)}, \chi^{(1)})\} \quad \text{..... (14)}$$

where

$$(H' - E^{(0)})\chi^{(1)} + \{L - L^{(0)}\}\psi^{(0)} = 0. \quad \text{..... (15)}$$

If now L is a sum of one-electron operators

$$L = \sum_i L_i(\mathbf{r}_i) \quad \text{..... (16)}$$

and we write

$$\chi^{(1)} = \sum_{j=1}^N \mathcal{A} \prod_{i \neq j} u_i^{(0)} w_j^{(1)}, \quad \text{..... (17)}$$

(15) is reduced to a set of one-electron equations for $w_j^{(1)}$. The perturbation v can be written as

$$v = \sum_i \sum_j v_{ij} \quad \text{..... (18)}$$

where

$$v_{ij} = \frac{1}{|\mathbf{r}_i - \mathbf{r}_j|} - (\beta_{ij} - \alpha_{ij}) - (\beta_{ji} - \alpha_{ji}) + \int (\beta_{ij} - \alpha_{ij}) |u_i^{(0)}(\mathbf{r}_i)|^2 d\mathbf{r}_i. \quad \text{..... (19)}$$

Substituting (17) into (14) and using (19), it may be shown by employing the techniques described by Hartree (1957) that the individual contributions

$$(\psi^{(1)}, v_{ij}\chi^{(1)}) - (\psi^{(0)}, v_{ij}\psi^{(0)})(\psi^{(0)}, \chi^{(1)})$$

to $L^{(1)}$ all vanish identically.

A comparison is given in the Table of the expectation values for helium of some one-electron operators computed using analytic Hartree wave functions (Green, Mulder, Lewis and Woll 1954) and computed using the very accurate variational wave functions of Pekeris (1959). The error is less than 1% for all but one of the operators. By contrast, the error in the expectation value of the two-electron operator $1/r_1 r_2$ is 5% and for $\delta(\mathbf{r}_1 - \mathbf{r}_2)$ is 79%, whereas the energy (which is stationary with respect to first-order variations) is in error by 1.5%.

Expectation Values for Helium

L	Hartree	Exact	% Error
∇_1^4	52.7	54.1	2.6
$\delta(\mathbf{r}_1)$	1.79 ₅	1.81	0.8 ₅
$1/r_1^2$	5.99	6.02	0.4 ₂
$1/r_1$	1.69	1.69	0.0 ₆
r_1	0.927	0.929	0.3 ₁
r_1^2	1.18	1.19	0.9 ₈
$\delta(\mathbf{r}_1 - \mathbf{r}_2)$	0.19	0.11	79
$1/r_1 r_2$	2.85	2.71	5.1
H	2.86	2.90	1.4 ₅

REFERENCES

- CONDON, E. U., and SHORTLEY, E. H., 1935, *The Theory of Atomic Spectra* (Cambridge: University Press).
- DALGARNO, A., and STEWART, A. L., 1957, *Proc. Roy. Soc. A*, **240**, 347.
- GREEN, L. C., MULDER, M. M., LEWIS, M. N., and WOLL, J. W., 1954, *Phys. Rev.*, **93**, 757.
- HARTREE, D. R., 1957, *The Calculation of Atomic Structures* (New York: Wiley).
- MØLLER, C., and PLESSET, M. S., 1934, *Phys. Rev.*, **46**, 618.
- PEKERIS, C. L., 1959, *Phys. Rev.*, **115**, 1216.

The Luminescent Decay of Various Crystals for Particles of Different Ionization Density

By J. C. ROBERTSON AND J. G. LYNCH

Department of Natural Philosophy, The University, Glasgow

MS. received 8th June 1960, in revised form 9th November 1960

Abstract. New measurements of the decay of the luminescence produced in LiI(Eu), NaI(Tl), KI(Tl), CsBr(Tl) and three CsI crystals of varying thallium concentration have been made for particles with different ionization densities. The decay time of the luminescence is found to depend on the average ionization density ρ . In all cases except LiI(Eu) two components are found in the decay. The dependence of the decay times and efficiency, the relative voltage pulse height per unit energy, on thallium concentration for different particles has been studied in CsI. The ratio τ_e'/τ_α' has been found to increase with the average Z of the crystal where τ_e' and τ_α' are the average decay times for electrons and alpha particles respectively.

§ 1. INTRODUCTION

IN the scintillation counter the light produced by an ionizing particle in a luminescent material is converted into an electrical current pulse with the same time variation. Measurements by Storey, Jack and Ward (1958) indicated that in CsI(Tl) the decay time of the luminescence was dependent on the average ionization density ρ due to the ionizing particle. Robertson and Ward (1959) described a technique which employs this difference to distinguish between alpha particles and electrons, electrons and protons, and protons and alpha particles. It is of practical as well as theoretical interest to see whether this difference in decay time is found in any other crystals and, if so, whether any other crystal would be more suitable for practical use.

§ 2. EXPERIMENTAL METHOD

Measurements of the decay times of the luminescence produced by alpha particles, protons of varying energies and electrons have been made in LiI(Eu), NaI(Tl), KI(Tl) and CsBr(Tl). Measurements have also been made on a standard Harshaw CsI(Tl) crystal, a CsI crystal with very low thallium concentration and a CsI crystal with high thallium concentration. The CsBr(Tl), NaI(Tl), KI(Tl) and LiI(Eu) crystals were obtained from the Harshaw Chemical Company. All the crystals supplied by this Company had a molar concentration of 0.1% of thallium. The CsI crystals of high and low thallium concentrations (3% and 0.009% respectively) were obtained from Aberdeen University.

The crystals were mounted directly on to the face of a Du Mont 6292 photo-multiplier with silicone grease. A highly reflecting aluminium cylinder with an end window of thickness 1 mg cm^{-2} was used as a light reflector.

The current pulses from the photomultiplier were integrated (the leakage time constant being $86.5 \mu\text{sec}$) and were then fed through a cathode follower and matched delay to a Tektronix Type 541 cathode ray oscilloscope. Measurements were made on a short and long time scale in each case, the length of the delay line being chosen according to the length of the decay time to be measured. Photographs were taken of the individual pulses produced by each type of particle.

The time base speeds on the Tektronix oscilloscope were calibrated using a crystal controlled standard frequency oscillator Furzehill Type G.415. The probable error in the calibration was $\pm 1\%$; our measurements were corrected according to this calibration.

^{137}Cs gamma rays ($E = 661 \text{ keV}$) were used to produce photoelectrons in the crystal; a ^{210}Po source (5.3 MeV) was used to give the alpha particles. High energy protons were obtained from the reaction ${}^3_2\text{He}(\text{d}, \text{p}){}^4_2\text{He}$. Lower energy protons were obtained using aluminium absorbers. Very low energy protons were obtained from the ${}^2_1\text{H}(\text{d}, \text{p}){}^3_1\text{H}$ reaction. In order to keep the pulse height on the oscilloscope constant, various values of the photomultiplier voltage were used. The change in photomultiplier gain at these different voltages was later measured using a Hutchinson-Scarrott 100-channel pulse height analyser. Knowing the difference in gain at the voltages used, all the graphs of the voltage pulses could be normalized to the same gain.

§ 3. ANALYSIS

Two methods of analysis were used. The first was identical with that described by Storey, Jack and Ward (1958). In the second method of analysis the values of the decay time τ' , over four lifetimes of the short component of the decay for electrons, were measured assuming that the decay was purely exponential.

§ 4. RESULTS

Values of the long and short components, t and τ respectively, of the decay time of the luminescence produced by α -particles, protons and electrons in the crystals studied are shown in Tables 1 to 4. The subscripts α , p and e are used to denote the type of particle producing the luminescence.

Table 1. LiI(Lu)

Particle	Electron	Proton	Proton	Proton	Proton	Alpha
Energy (mev)	0.66	15	10	6	3	3.5
Short component (μ sec)		All gave value	$\tau=0.94 \pm 0.06 \mu$ sec			
Long component		No long component detected				
$^{\infty}\epsilon$	$1+0.05$	0.87 ± 0.03	—	—	—	—

Table 2. NaI(Tl)

Particle	Electron	Proton	Proton
Energy (MeV)	0.66	2.5	14.9
Short component τ (μsec)	0.23 ± 0.01	0.21 ± 0.01	0.23 ± 0.01
Long component t (μsec)	1.5 ± 0.08	1.5 ± 0.08	1.5 ± 0.08
${}^5 \epsilon$	1 ± 0.05	—	1.15 ± 0.06
I_{max}/E	1 ± 0.1	—	1 ± 0.1
R	0.43	0.4	0.38

Since all our results could be normalized to the same electronic gain, we have been able to estimate the relative voltage pulse height per unit energy (or efficiency) for the different particles. Two efficiencies are given in the tables: $^{\infty}\epsilon$ is the efficiency for infinite time based on the assumption that there is no contribution to the light output from components longer than t in each case and $^x\epsilon$ is defined as the efficiency for light emitted in the time range up to $x\mu\text{sec}$. The same subscripts are used to distinguish the different particles.

Table 3. KI(Tl)

Particle	Electron	Proton	Proton	Proton	Proton	Alpha
Energy (mev)	0.66	14.02	9.7	6.8	3.14	3.4
Short compt						
τ (μsec)	0.24 ± 0.01	0.2 ± 0.02	0.22 ± 0.02	0.2 ± 0.01	0.2 ± 0.008	0.21 ± 0.01
Long compt						
t (μsec)	2.5 ± 0.1	1.8 ± 0.09	1.6 ± 0.1	1.56 ± 0.08	1.6 ± 0.08	1.76 ± 0.09
$^{0.5}\epsilon$	1 ± 0.05	1.31 ± 0.06	1.27 ± 0.06	1.28 ± 0.06	1.27 ± 0.06	1.07 ± 0.05
$^{\infty}\epsilon$	1 ± 0.05	1.29 ± 0.08	1.28 ± 0.07	1.22 ± 0.06	1.53 ± 0.08	1.06 ± 0.08
I_{max}/E	1 ± 0.1	1.54 ± 0.15	1.93 ± 0.19	1.3 ± 0.13	1.53 ± 0.15	1.53 ± 0.15
R	0.44	0.39	0.35	0.38	0.39	0.3

Table 4. CsBr(Tl)

Particle	Electron	Proton	Proton	Proton	Proton	Alpha
Energy (mev)	0.66	3.14	6.8	9.7	14.9	3.4
Short compt						
τ (μsec)	2.57 ± 0.13	1.92 ± 0.07	2 ± 0.12	2.32 ± 0.06	2.5 ± 0.08	2.3 ± 0.15
Long compt						
t (μsec)	24.23 ± 1.5	13.3 ± 0.8	14.6 ± 0.9	14.5 ± 0.9	16.5 ± 1.1	14.5 ± 1.34
$^6\epsilon$	1 ± 0.05	0.92 ± 0.05	0.94 ± 0.05	0.95 ± 0.05	0.90 ± 0.05	0.78 ± 0.04
$^{\infty}\epsilon$	1 ± 0.05	0.96 ± 0.05	1.01 ± 0.05	1.08 ± 0.05	0.96 ± 0.05	0.7 ± 0.04
I_{max}/E	1.0 ± 0.1	1.19 ± 0.1	1.2 ± 0.1	1.15 ± 0.1	0.89 ± 0.09	0.88 ± 0.09
R	0.53	0.61	0.61	0.58	0.61	0.34

Table 5. Values of τ_{α}' , the Average Lifetime after 4 Lifetimes of Electron Short Component

Crystal	τ_{α}'	τ_e'	τ_e'/τ_{α}'
LiI(Eu)	0.9	0.9	1
NaI(Tl)	0.335^{\dagger}	0.35	1.04^{\dagger}
KI(Tl)	0.43	0.48	1.13
CsBr(Tl)	2.86	3.52	1.23
CsI(Tl)	1.17	1.6	1.37

† The value quoted here as τ_{α}' is in fact the value for a low energy proton. Hence τ_e'/τ_{α}' will be slightly greater than 1.04.

Derived values of I_{max}/E , the relative peak current per unit energy and of R , the ratio of the light output in the long components found in the pulses to the total light output observed are also given.

Table 5 gives the values of τ_{α}' and τ_e' as defined earlier. The values of τ_e'/τ_{α}' are also shown.

Table 6 gives the values of $\tau'_{\alpha, p, e}$ and $\infty\epsilon_{\alpha, p, e}$ for three CsI crystals of different thallium concentrations. $\tau'_{\alpha, p, e}$ was measured over the first $4\mu\text{sec}$ of the voltage pulse from these crystals assuming the decay to be purely exponential. $\infty\epsilon_{\alpha, p, e}$ in the Harshaw crystal (Tl concentration 0.1%) was not measured since the geometry of this crystal differed from that of the other two.

Table 6. Variation of $\tau'_{\alpha, p, e}$ and $\infty\epsilon_{\alpha, p, e}$ in CsI(Tl) with Varying Thallium Concentration

Thallium concentration	τ'_α (μsec)	τ'_p (μsec)		τ'_e (μsec)	$\infty\epsilon_\alpha$	$\infty\epsilon_p$		$\infty\epsilon_e$
		3.14 Mev	15 Mev			3.14 Mev	15 Mev	
0.009%	1.55 ± 0.05	1.77 ± 0.06	1.5 ± 0.05	1.58 ± 0.02	0.036	0.08	0.6	0.746
0.1%	1.17 ± 0.05	—	—	1.6 ± 0.02	—	—	—	—
3%	1.07 ± 0.05	1.23 ± 0.06	1.5 ± 0.05	1.58 ± 0.02	0.746	0.9	1.07	1

In the results given for NaI(Tl), Table 2, no measurements were made with alpha particles since they were stopped in the window in the air-tight aluminium container in which the crystal was mounted. Since the exact thickness of the aluminium window was not known $\infty\epsilon$ has not been measured for low energy protons. Our value of τ_e is in good agreement with the result of Eby and Jentschke (1954) who quote $\tau_e = 0.25\mu\text{sec}$. Nicholson and Snelling (1955) find a value of $0.34\mu\text{sec}$ for the decay time for electrons. This fits our average value τ'_e given in Table 5.

For KI(Tl) our value of $\infty\epsilon_p/\infty\epsilon_e = 1.29 \pm 5\%$, where $\infty\epsilon_p$ is in this case the value of efficiency for 14.02 Mev protons. This value is in agreement with the result ($1.42 \pm 5\%$) obtained by Kienle and Segel (1959). Our value of $\infty\epsilon_\alpha/\infty\epsilon_e = 1.07$ is in good agreement with the value found by Kienle and Segel and with the value (1.08) found by Franzen, Peele and Scherr (1950).

$\infty\epsilon$ was not measured for lower energy protons or for alpha particles in LiI(Eu) since to prevent the crystal being exposed to air it was completely enclosed in silicone grease. The layer of silicone grease was thin enough to have a negligible effect on the energy of 15 Mev protons. Shenk and Neiler (1954) find that in LiI(Eu), $\infty\epsilon$ first increases and then decreases with increasing ionization density ρ due to the exciting particle. Our results do not agree with this. The difference may be due to different europium concentrations. Nicholson and Snelling find $\tau = 1.4\mu\text{sec}$ for their crystal LiI(0.03% Eu).

As a test of the method used, measurements were made on a standard CsI(Tl 0.1%) Harshaw crystal. The results obtained agreed with those of Storey, Jack and Ward (1958), $t = 7\mu\text{sec}$ for all particles, $\tau_\alpha = 0.425 \pm 0.01\mu\text{sec}$ and $\tau_e = 0.7 \pm 0.025\mu\text{sec}$.

For CsBr(pure), the pulse heights produced by electrons and alpha particles were only slightly greater than the luminescence of the glass of the photomultiplier. τ'_p is estimated as $10.5 \pm 1\mu\text{sec}$ for protons of energy 14.9 Mev.

No luminescence was produced in a pure NaCl crystal.

§ 5. DISCUSSION

Our results are consistent with the picture that the detailed shape of the decay of the luminescence depends on the average ionization density ρ due to the particle producing the luminescence.

In addition we find:

- (i) $\tau_{\alpha} \leq \tau_e$.
- (ii) τ increases for all particles as Z of the cation increases.
- (iii) t_e for CsBr(Tl) and KI(Tl) $> t_{\alpha, p}$.
- (iv) Our measurements for CsI, in accord with those of Jones and Ward (1960), indicate that τ_{α} decreases with increasing thallium concentration and reaches a minimum at approximately the concentration present in the standard Harshaw crystals. τ_e for electrons, on the other hand, remains constant with varying thallium concentration. The behaviour of τ_p' , τ_e' and τ_{α}' indicates that this mechanism again depends on the ionization density ρ due to the particle.
- (v) $\tau_e' \sim \tau_{\alpha}'$.
- (vi) τ_{α} in CsI decreases as thallium concentration increases while τ_e decreases much less markedly.
- (vii) In CsI (0.1% Tl) and KI(Tl) τ_e first increases and then decreases with the ionization density ρ of the ionizing particle. In CsBr(Tl) τ_e decreases steadily as the ionization density increases.

Any model which is proposed to explain the luminescent properties of the alkali halides must account for these facts.

The conventional picture for the process producing the luminescence is one in which the electrons produced by the ionizing particle are released thermally from traps emitting radiation or in radiationless transitions. The measured decay times show that these radiationless transitions must increase with increasing ionization density due to the exciting particle. This would explain the behaviour of τ_{α} , but we should expect that the efficiency of light emission would decrease as the ionization density produced by the particle increases. Our results in CsI(Tl) and KI(Tl) indicate that this is not the case.

The variation in decay times with ionization density ρ may be explained by assuming that two different sets of electron traps exist at different energy levels. It is necessary in this case to postulate that the relative population of such sets of traps is related to the ionization density ρ due to the particle. Since τ_e' remains constant with decreasing thallium concentration it seems that one of the sets of traps must be independent of thallium. In addition to explain the behaviour of efficiency it is necessary to introduce some form of quenching.

In Table 5 the ratio τ_e'/τ_{α}' can be seen to increase as Z of the crystal increases. From the practical point of view it would be of interest therefore to study crystals of very large Z ; of the crystals studied it is seen that none has properties more suitable than CsI(Tl) for use in a technique similar to that of Robertson and Ward (1959).

ACKNOWLEDGMENTS

The authors are indebted to Professor P. I. Dee and Dr. W. Jack for helpful discussions during the course of this work. They also wish to acknowledge the receipt of Research Studentships of the Department of Scientific and Industrial Research. Thanks are due to Dr. D. A. Jones, Department of Natural Philosophy of Aberdeen University, who kindly supplied the CsI crystals of high and low thallium concentrations.

REFERENCES

- EBY, F. S., and JENTSCHKE, W. K., 1954, *Phys. Rev.*, **96**, 911.
FRANZEN, W., PEELE, R. W., and SCHERR, R., 1950, *Phys. Rev.*, **79**, 742.
JONES, D. A., and WARD, A., 1960, *Proc. Phys. Soc.*, **75**, 931.
KIENLE, P., and SEGEL, R. E., 1959, *Phys. Rev.*, **113**, 909.
NICHOLSON, K. P., and SNELLING, G. F., 1955, *Brit. J. Appl. Phys.*, **6**, 104.
ROBERTSON, J. C., and WARD, A., 1959, *Proc. Phys. Soc.*, **73**, 523.
SHENK, J., and NEILER, J. H., 1954, *Nucleonics*, **12**, 28.
STOREY, R. S., JACK, W., and WARD, A., 1958, *Proc. Phys. Soc.*, **72**, 1.

Air Bubbles in Ice

By A. E. CARTE

National Physical Research Laboratory, South African Council for Scientific and Industrial Research, Pretoria

MS. received 8th July 1960

Abstract. The opacity of ice formed from water containing dissolved air is due to the presence of bubbles of air in the ice. Both bubble concentration and sizes were found to depend on the rate of freezing. Bulk water saturated with air at 0°C was found to freeze into ice containing about six bubbles per mm^3 when freezing proceeded at 0.5 mm min^{-1} and 300 per mm^3 at a rate of 5 mm min^{-1} . Bubbles were formed at the ice-water boundary when the concentration of dissolved air reached a critical value which, for rates of freezing greater than 2 mm min^{-1} , corresponded to a supersaturation ratio of 30. Agitation of the water could prevent the critical concentration from being attained and clear ice then formed.

Other factors which influenced bubble concentrations and sizes were the amount of dissolved air, pressure, thickness of the layer of water ahead of the growing ice and escape of bubbles by buoyancy.

The magnitude and extent of the air concentration gradient ahead of the ice were estimated from theory.

Bubbles in ice were found to change shape with time particularly when under the influence of a temperature gradient.

§ 1. INTRODUCTION

AIR bubbles in ice can form from air originally dissolved in water before freezing. Bubbles in rime and in hailstones may originate in this way (Coste 1940, Puzanov and Akkuratov 1952, Blanchard 1957). They may also be air entrapped during growth by accretion of ice crystals or of super-cooled water droplets which froze on impact. Examination of the internal structure of hailstones, including the concentration and orientation of air bubbles, has already added to the understanding of the growth of hailstones (Weickmann 1953, List 1958). At the same time the need has been emphasized for further basic knowledge of the various processes involved, in particular regarding the formation of air bubbles. The present investigation was confined to bubbles in ice which were formed by freezing bulk water containing dissolved air.

§ 2. THE GROWTH OF DISKS OF ICE

Circular disks of ice $\frac{1}{2} \text{ mm}$ in thickness were formed by freezing a film of water held between two glass disks separated by a Perspex ring. A cold copper needle made contact at or near to the centre of the disk causing radial freezing to start from that point. Clear or opaque rings of ice could be formed by changing the rate of cooling during freezing (see Plate I (a)). Opacity was due

to numbers of tiny bubbles and threads of air. Sections cut through hailstones often display analogous ring structures.

Similar results were obtained by cooling from the periphery, making the ice grow radially inwards. There was one noticeable difference, however. The water was subjected to greater pressure as freezing progressed. Very often the glass cracked or shattered and at this instant a ring of air bubbles, larger than those already within the ice, formed at the ice-water boundary. The ice often cracked as well under the strains produced by the pressure thus adding to its opacity. Meteorological implications of the cracking of the ice shell when a water drop freezes, and how this is influenced by the release of dissolved air, have been discussed by Mason and Maybank (1960).

These simple experiments demonstrated how variations in the opacity of ice can be brought about by alterations in the rate of freezing or by pressure effects. The next experiments were designed to investigate further the effect of the growth rate of ice on the formation of air bubbles.

§ 3. APPARATUS FOR GROWING SHEETS OF ICE

A film of water was introduced between two glass plates which were separated by brass strips $\frac{1}{2}$ mm in thickness as shown in Fig. 1. Cooling was effected by placing a small block of solid carbon dioxide on one brass strip.

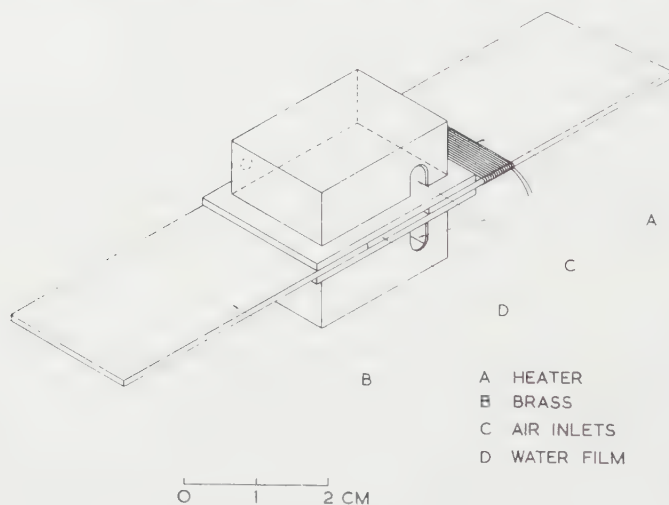


Fig. 1. Apparatus for growing thin sheets of ice.

The rate of cooling could be controlled by means of a small electrical heater wound on this strip. A very slow stream of cool, dry air was passed through transparent boxes covering both glass surfaces to prevent condensation of moisture.

The whole cell was cooled to a temperature of 0°C and filled with distilled water, also at 0°C , which had been shaken to saturate it with air. The cell was placed on a thermally-insulated microscope stage with the water film in a horizontal plane. The solid carbon dioxide was placed on one end and ice on the other to maintain the water temperature at 0°C . A stereo-microscope was used to observe freezing and to measure the growth rate of the ice. Magnifications up to $\times 160$ were used.

A larger cell holding a film of water 1 mm in thickness was used for growth rates below 1 mm min^{-1} . The temperature of the starting edge, as measured by a thermocouple, was adjusted continuously throughout a run in order to keep the growth rate steady.

§ 4. OBSERVATIONS

Supercooling of the water usually made freezing rapid and uncontrollable for about the first millimetre of growth. The leading edge of the ice was invariably serrated. The serrations were very thin dendrites in contact with the glass surfaces. Faster growth produced bigger serrations. Air bubbles formed at the straight part of the leading edge from which the serrations protruded. The bubbles were not carried ahead as the ice advanced but grew until covered over by ice. Slower growth of ice produced fewer but larger bubbles than faster growth. Threads of air, rather than bubbles, began to form at rates less than about 1 mm min^{-1} . These cylindrical threads were always arranged parallel to the direction of growth of the ice and could be several millimetres in length. The birth of a bubble close by either temporarily reduced the thread diameter or even terminated its growth.

In addition to the easily visible bubbles and threads of diameters or widths of the order of tens of microns there were always micron-size bubbles and threads of air in the ice. These will be referred to as minor bubbles and threads. Their numbers also increased with the rate of freezing. They contribute greatly to the opacity of the ice. Most, if not all, of the large bubbles do not originate by nucleation at the leading edge but start off as minor threads of air which appear to be squeezed out of the ice. The strip of ice from the leading edge to about 0.1 mm behind is a scene of constant activity for this is where the minor bubbles and threads originate and move in spurts along what must be fissures in the ice, towards the leading edge. At this stage these fissures must contain water. The minute volumes of air which succeed in escaping from the ice grow rapidly until they are completely enveloped by the advancing ice. These bubbles are oval with their long axes parallel to the ice growth direction. Most of them are egg-shaped with the pointed end pointing in the same direction as the direction of growth (Plate I (c)). A bubble appears to grow as a sphere until it has reached a diameter equal to its final maximum width. Half the sphere is then protruding ahead of the ice into the water. Thereafter only this part grows producing the final oval or cylindrical shape.

Minor threads and bubble chains were usually arranged along or parallel to crystal boundaries (as revealed by polarized light) which are not necessarily parallel to the direction of growth (see top half of Plate I (d)). Another observation which linked bubble formation with crystal structure rather than a random nucleation process in the water was the occasional persistence of a fixed avenue of escape for minor volumes of air, leading to the formation of a string of bubbles in a line parallel to the growth direction (Plate I (b)). Sometimes a cluster of bubbles formed when several spurts of air arrived at the same point in the water in rapid succession. The first bubbles were pushed away from the leading edge and rose to the upper glass surface.

There is a tendency for bubbles to form in waves even when the ice growth rate is constant. A particularly well-defined series of waves can be seen in Plate I (e). Evidently bubbles may reduce the local supply of dissolved air to

such an extent that further bubble formation is inhibited until the concentration has built up again. The rapid growth of bubbles at the interface indicates that considerable air supersaturation is reached there. Clear ice follows immediately after a wave of bubbles. Thereafter the density of minor bubbles increases and the next wave follows.

The average distance between waves of bubbles formed at various rates of freezing was measured. Results are given in Table 1.

Table 1. Rates of Freezing R and Corresponding Wavelengths λ and Supersaturations immediately after Bubble Formation† $(C/C_0)_{\text{red}}$

R (mm min ⁻¹)	λ (mm)	$(C/C_0)_{\text{red}}$
1.7	0.7	—
2.5	0.5	14
3.5	0.4	14
3.8	0.3	17

† See § 9.

In some experiments supercooling of the water was prevented (by seeding the starting point with ice) in order to obtain a uniform growth rate from near the start. A region of clear ice formed before the bubble formation commenced. At rates greater than about 2 mm min⁻¹ the first bubbles to form were the same size as those which formed later. At lower rates the size and concentration of bubbles increased at first, then became constant. Results relevant to water saturated with air at 0°C are shown in Table 2.

Table 2. Observed Width y of Clear Ice Zone and Calculated Air Supersaturation† $(C/C_0)_{\text{max}}$ for Various Rates of Freezing R

R (mm min ⁻¹)	y (mm)	$(C/C_0)_{\text{max}}$
1.6	0.5	12
2.0	0.8	22
2.5	0.8	27
3.2	0.75	31
3.8	0.5	26
5.1	0.4	27

† See § 9.

An estimate of the extent of the concentration gradient ahead of the interface can be obtained by growing ice simultaneously from two opposite directions. The air bubble concentration is greater in the region where the two ice surfaces meet. Plate I(d) shows a typical example and indicates that the region of increased bubble (and dissolved air) concentration extends for no more than 0.1 mm when the growth rate is 2.5 mm min⁻¹.

§ 5. MEASUREMENTS OF BUBBLE SIZE AND CONCENTRATION

Measurements were made of the sizes and average concentration of air bubbles formed at various constant growth rates from water saturated with air at 0°C ; the results are shown in Figs 2, 3 and 4. Several hundred bubbles were

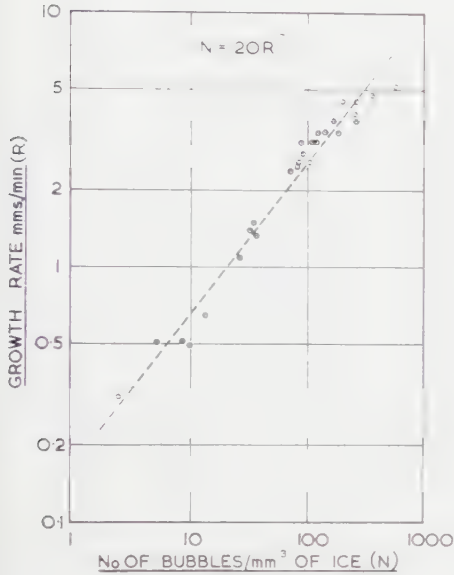


Fig. 2. Bubble concentration against ice growth rate.

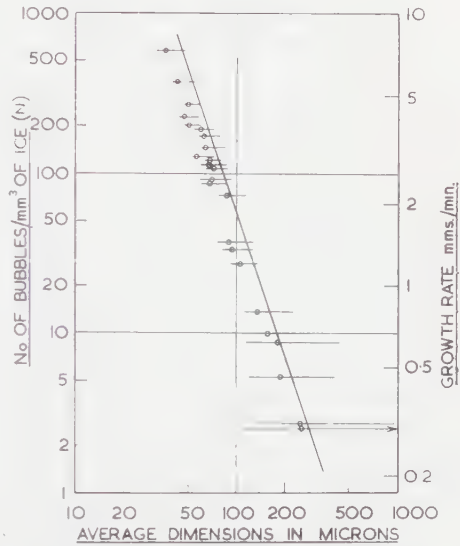


Fig. 3. Size of bubbles against concentration and ice growth rate.

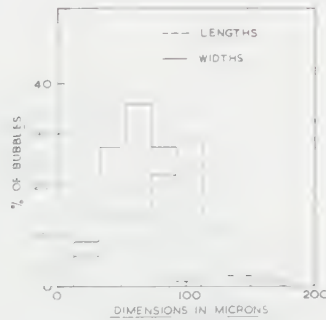


Fig. 4. Size distribution of bubbles for $R = 2.5 \text{ mm min}^{-1}$.

observed in each cubic millimetre of ice which had been grown at a rate of 5 mm min^{-1} whereas there were only 5 to 10 at a rate of 0.5 mm min^{-1} . At the latter rate most of the expelled air was in the form of cylindrical threads of lengths large compared to their diameters. The scatter of points about the straight line which has been drawn in Fig. 2 is considered to be greater than the errors of observation. This means that the number of air bubbles per unit volume of ice is mainly but not wholly dependent upon the rate of growth of the ice. Occasionally, adjacent regions of a given specimen of ice which had been grown at the same rate proved to have bubble concentrations which differed by as

much as 50%. Measurements were made in a volume large enough to eliminate local variations such as those caused by waves of bubbles. Despite these differences, the growth rate of ice formed from water saturated with air at 0°C may be determined to within useful limits from measurements of bubble concentration using the relationship given by the broken line in Fig. 2:

$$N = 20R^{1.7} \quad \dots\dots (1)$$

where N is the average number of air bubbles per mm³ of ice and R is the rate of growth of the ice in mm min⁻¹.

Figure 3 illustrates how the bubbles diminish in size as their numbers increase when the ice growth rate is increased. The rate of growth scale was derived from Eqn (1) and the bubble concentration N . The horizontal lines were drawn from points representing average bubble widths to points representing lengths. The ringed points show the diameter of spheres equal in volume to the average volume per observed bubble. Bubbles were assumed to be prolate spheroids, or, in the appropriate cases, cylinders. A typical distribution of bubble sizes formed at a constant freezing rate is shown in Fig. 4. The bubbles were more uniform in width than in length.

Some experiments were made with water containing less than the saturation value of air at 0°C. The object was to establish whether diminished air content would reduce either the number of bubbles or their size, or whether both would be affected, for a given freezing rate.

Water was saturated with air at 40°C. Its dissolved air content was then half that of water saturated at 0°C. Fewer and smaller bubbles appeared and their total volume was about half those in water saturated at 0°C. Further experiments with even less dissolved air showed conclusively that at a given freezing rate both fewer and smaller bubbles form as the air content is reduced. Clear ice formed from water which had been boiled long enough to expel all air.

The straight line in Fig. 3 indicates the number of spherical bubbles of a given diameter there would be if all the dissolved air appeared as bubbles of equal sizes. The solubility of air in water at 0°C was taken as 29.3 cm³ l⁻¹. The position of the ringed points relative to the straight line shows that only $\frac{1}{2}$ to $\frac{2}{3}$ of the air originally dissolved in the water appears as bubbles in the ice. This neglects air contained in minor bubbles and threads whose volume is estimated to be exceedingly small relative to that of the big bubbles. It would account for only a small fraction of the air not yet accounted for unless the air in these minor bubbles and threads is under pressure. In fact this must be so otherwise they would not tend to make their way towards the leading edge during growth. Unfortunately the pressure cannot be estimated.

Work by Komabayasi (1959) leads to another possibility for accounting for air not visible as bubbles. He determined the free oxygen content of blocks of clear ice. It proved to be 45% (4.6 cm³ l⁻¹ of ice) of the oxygen in water saturated with air at 0°C. The oxygen might have been present in the ice in the gaseous state as bubbles too small to be observed. Also, he argued, it might have been present as individual molecules because 4.6 cm³ oxygen per litre ice corresponds to only one O₂ molecule per 3×10^5 H₂O molecules. The small solubility of air in ice as measured by Scholander *et al.* (1953) would appear to exclude the latter possibility.

Some of the dissolved air that is expelled from the ice may escape by diffusion through the water. There is, as has been shown, an air concentration gradient ahead of growing ice but it extends for a very short distance. Air will have a greater chance of diffusing away if the ice advances slowly. There is, however, no evidence from present work of the total bubble volume being less at small growth rates than at greater rates.

Thus dissolved air which does not appear as bubbles when the water has been frozen may be present as bubbles too small to be seen; part of it may possibly be present as individual molecules within the ice structure or it may have escaped by diffusion through the water ahead of the growing ice. The latter possibility is discussed at greater length in §§ 9 and 10.

§ 6. VERTICAL GROWTH OF ICE

The results obtained thus far apply to thin sheets of ice formed from a horizontal film of water confined between glass plates. At small rates of growth some of the bubbles were seen to escape from their point of formation and to rise to the upper glass surface. These bubbles were readily distinguished from the others: firstly, they were in contact with the upper surface and secondly, they were more nearly spherical than interior bubbles. There was some tendency for them to form in clusters. This happened when a stream of tiny bubbles emerged in rapid succession from the same point. They constituted from 5 to 60% of the total bubble volume and up to half the total number.

Some ice sections were accordingly grown vertically upwards to find out how many bubbles would escape. There proved to be no precise relationship between the number of escaping bubbles and ice growth rate. Streams of tiny bubbles might escape from one point on the leading edge while none escaped from other parts growing at the same rate.

Sections were cut from bulk ice grown vertically upwards and vertically downwards under otherwise identical conditions. There was no difference between ice grown upwards and that grown downwards when the rate was greater than 2 mm min^{-1} . Differences were observed at smaller rates. There were more bubbles and threads, although the average length of threads was less in ice grown downwards than in that grown upwards. For example, at 0.4 mm min^{-1} upwards only threads formed (2 per mm^3) while at the same rate downwards, in addition to 2 shorter threads per mm^3 , there were 5 bubbles per mm^3 . The important observation, however, was that the total bubble volume was almost the same for both. These results can be explained readily. A number of air bubbles do escape when growth is vertically upwards but they have so little time for growth in the supersaturated region that the volume of air carried away is not appreciable. When growth is vertically downwards buoyant escape is impossible, giving more bubbles per unit volume of ice. Threads of air will therefore have less chance of reaching great length.

§ 7. EFFECT OF AGITATION OF WATER

The picture is changed completely if the water ahead of the ice is kept moving. This prevents a localised build-up of dissolved air. Completely clear ice may be formed if the water is agitated sufficiently and the freezing is not too rapid.

§ 8. STABILITY OF BUBBLES

The conditions under which air bubbles in ice retain their characteristic appearance were next considered. Many hailstones are at a temperature very close to 0°C by the time they reach the ground and are collected for structural examination. Therefore, as a starting point, the effects of raising the temperature of an ice specimen were investigated. It has long been known that melting of ice proceeds preferentially from boundaries. The boundary may be that between ice and impurity, including air, or simply between adjacent ice crystals. Thus one might expect air bubbles to change in shape as soon as the ice begins to melt.

A section of ice was warmed slowly from one end until melting commenced. Bubbles near this end became spherical, and those within microns of one another often merged to produce a bubble of irregular shape (compare Plates I(e) and I(f)). At the same time movements of the minor bubbles and threads were noted, the latter often becoming a row of tiny bubbles. The region close to the melting edge also became slightly more opaque. Further melting produced visible pools of water round the bubbles. Small bubbles vanished altogether as their surrounding pools increased in size and the air dissolved.

In order to exaggerate these early melting phenomena associated with air bubbles the experiment was repeated with water partially saturated with CO_2 , thereby attaining a far higher concentration of dissolved gas than possible with air. Bubble-free regions of ice were seen to contain many more striations than when the water had been saturated with air. The striations were parallel to crystal boundaries, as revealed by polarized light. When melting commenced there was a spectacular increase in opacity in ice near the melting edge hitherto clear except for the faint striations. An interesting feature of this experiment was that the increased opacity persisted if this region was again cooled below 0°C .

Changes in bubble shape and coalescence of nearly touching bubbles occurred even if the ice was kept continuously at -5° to -10°C . The difference was that changes at -5°C took hours or days as compared to seconds at 0°C .

Other changes occurred if there was a temperature gradient in the ice. Ice sublimed from the warmer ends of air bubbles and was deposited at the colder ends, thereby distorting the original shape. A temperature difference of about 0.1°C across a bubble produced marked distortion within minutes. The cold end became rough in appearance with ill-defined outlines.

§ 9. AIR SUPERSATURATION AHEAD OF A MOVING ICE-WATER INTERFACE

The experimental results have shown qualitatively how the dissolved air concentration in water immediately ahead of an advancing ice front must increase with time. A limit to the increase is imposed by bubble formation and subsequent growth. The concentration build-up and the extent of the concentration gradient may be derived theoretically for certain conditions. This provides further insight into the processes leading to bubble formation and indicates conditions under which dissolved air will not form bubbles but will be transported by diffusion through the water.

Pohl (1954) has obtained an expression which gives the solute concentration C at a plane, distance x ahead of a plane solid-liquid interface at time t after the start of freezing, provided the interface advances at a constant rate R . If

the initial concentration of solute throughout the liquid is everywhere C_0 then an approximation of Pohl's equation which is valid for small values of D and k is

$$\frac{C}{C_0} = 1 + \frac{(1-k)}{k} \left[\exp\left(-\frac{Rx}{D}\right) - \exp\left\{-\frac{R}{D}(1-k)(x+kRt)\right\} \right], \quad \dots\dots (2)$$

where D is the diffusivity of solute in liquid and is equal to $1.1 \times 10^{-5} \text{ cm}^2 \text{ sec}^{-1}$ for air in water at 0°C . k is the distribution coefficient, which is defined as the ratio of the concentrations of solute at the interface in the solid and in the liquid respectively.

The distribution coefficient k may reasonably be taken as a constant for the range of velocities considered (Pfann 1957). The solubility and diffusivity of air in ice are both exceedingly small (Scholander *et al.* 1953). Therefore air is rejected from ice when water freezes, so that for this system k must be less than unity and probably k is very much less than 1. The value which has been used in Eqn (2) is $k=0.01$. A smaller value does not markedly affect the results and would not alter significantly the ensuing conclusions. Values greater than 0.01 substantially reduce the calculated values of C/C_0 and would lead to results inconsistent with experimental observations as shown later.

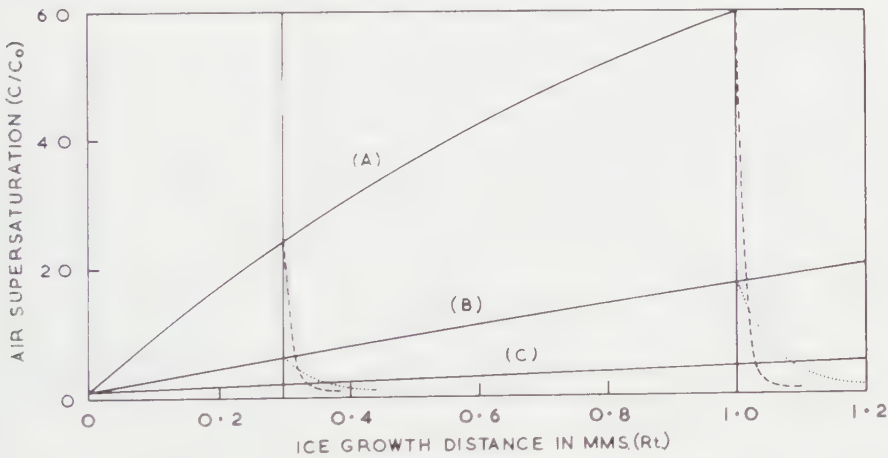


Fig. 5. Calculated air supersaturation in water ahead of growing ice. Values assumed for R in mm min^{-1} : curve A, 6; B, 1.2; C, 0.24.

The curves shown in Fig. (5) were obtained from Eqn (2) using $k=0.01$. The solid lines indicate how the dissolved air concentration increases in the water in contact with an ice front advancing at 6, 1.2 and 0.24 mm min^{-1} respectively. The concentration gradients which develop ahead of the ice after growth has proceeded for 0.3 mm and for 1 mm are shown by the dashed curves for 6 mm min^{-1} and by the dotted curves for 1.2 mm min^{-1} .

The calculated maximum air supersaturation (assuming that the water is initially saturated) reached at an ice-water interface before the onset of bubble formation is given in Table 2. The indication is that at all rates greater than 2 mm min^{-1} , bubble formation commences when C/C_0 is about 30. Smaller supersaturations are sufficient at smaller rates. After bubbles have formed,

the air supersaturation in water at the interface rises from its reduced value $(C/C_0)_{\text{red}}$ until it again reaches the critical value for bubble formation. This increase takes place in the time that it takes for the ice to advance a distance of one wavelength as given in Table 1. Values of $(C/C_0)_{\text{red}}$ may therefore be calculated using the corresponding values of rates and wavelengths given in Table 1. As shown in Table 1 $(C/C_0)_{\text{red}}$ is about 15 when $R > 2 \text{ mm min}^{-1}$.

Supersaturations may also be deduced from observations of the rate of growth of bubbles. As already mentioned, bubbles grow as spheres up to radius b (where $2b$ = final maximum width of bubble) in time $t = b/R$ (where R = rate of freezing). From diffusion theory, the rate of volume increase of an air bubble, radius b , in air-supersaturated water is

$$\frac{dV}{dt} = -AD \left(\frac{\partial C}{\partial r} \right)_b,$$

where A is the area of the water-air boundary, D is the diffusion constant of air in water and $(\partial C/\partial r)_b$ is the dissolved air concentration gradient at the water-air boundary of the bubble. Epstein and Plesset (1950) have shown that the concentration gradient at the bubble boundary rapidly attains a steady state and then

$$\left(\frac{\partial C}{\partial r} \right)_b \simeq \frac{C_\infty - C_0}{b}$$

where C_∞ is the initial dissolved air concentration, which is assumed to remain unchanged with time at a great distance from the bubble. C_0 is the dissolved air concentration at saturation and is equal to 0.0293 (for growth $C_\infty > C_0$).

The above relationships lead readily to the following expressions for the growth of bubbles in air-supersaturated water of concentration C_∞ , provided that the initial radius is very much less than final radius in the case of spherical bubbles.

For a spherical bubble growing by diffusion through its whole surface area or a cylindrical bubble with a hemispherical cap protruding into the water:

$$C_\infty - C_0 = bR/2D. \quad \dots\dots (3a)$$

For a spherical bubble half protruding into the water:

$$C_\infty - C_0 = bR/D. \quad \dots\dots (3b)$$

The supersaturations required to produce bubbles under the various conditions may be found by substituting experimentally-determined values for b and R in Eqns (3a) and (3b).

The conditions for which the results in Table 3 are valid do not apply strictly to bubbles growing at a moving ice interface. The dissolved air concentration will not be radially symmetrical with respect to a bubble because the concentration falls off rapidly with distance from the interface. Secondly, there is continuous generation of air at the interface. Unless this latter effect exerts a dominating influence, it is reasonable to conclude that the supersaturations at the ice-water interface when bubble growth commences must be at least equal to, and will probably be greater than, the values in column (4) of Table 3 because part of the bubble is screened from diffusing material by the ice.

Table 3. Calculated Air Supersaturation Ratios C_{∞}/C_0 which are required to produce Bubbles of Maximum Widths $2b$ at Various Rates of Freezing R

(1)	(2)	(3)	(4)
0.2	120	5	—
0.5	120	9	—
1	94	25	13
2	70	37	19
3	58	45	23
5	32	41	21

(1) R (mm min⁻¹); (2) $2b$ (microns); (3), (4) C_{∞}/C_0 ; (3) diffusion through a hemisphere; (4) diffusion through a spherical surface.

Calculated values of C_{∞}/C_0 for cylindrical threads are likely to be more reliable because there is no uncertainty as to the area through which diffusion takes place (a hemisphere) and dI/dt is constant and accurately known. Also, threads form at small rates of freezing when the air concentration ahead of the ice tails off slowly so that the concentration surrounding the hemisphere in the water will be reasonably uniform.

The curves of Fig. 5 thus fit in with experimental results as well as can be expected in view of the uncertainties and assumptions. The maximum supersaturations, as calculated from the width of the clear ice zone (Table 2), lie between the limits of supersaturation required to cause the observed rate of growth of bubbles, assuming firstly diffusion through a hemisphere and secondly diffusion through a spherical surface (Table 3). The width of the region of increased concentration of bubbles where two ice surfaces meet is consistent with the rapid decrease of air concentration shown in Fig. 5.

If in Eqn (2) values of k much greater than 0.01 had been used, unrealistically low values would have been obtained for the calculated supersaturation. For example $k=0.1$ gives $C/C_0=10$ (instead of 60 for $k=0.01$) after growth has proceeded for 1 mm at 6 mm min⁻¹. Table 3 shows that $C/C_0=10$ would not allow sufficiently rapid growth of the bubbles even if no part of them was screened by the ice from diffusion.

§ 10. CONCLUSION

To review briefly the mechanism of bubble formation from dissolved air: when a plane ice front advances air is driven to crystal boundaries, as are solid impurities. At rates greater than 2 mm min⁻¹ the concentration of air in water at the moving boundary increases until a supersaturation ratio of thirty is reached. Minute volumes of air appear in the ice close to the water and some are forced into the water where they grow until enveloped by ice. The supersaturation in the vicinity of a bubble is by then reduced to about 15. It builds up again and the process is repeated, leading to bubbles of approximately the same size as long as the freezing rate is constant.

Bubble formation proved to be partly dependent upon time at rates smaller than 2 mm min⁻¹. Bubbles form at supersaturations less than thirty, but as freezing proceeds the average supersaturation increases as do the number and size of bubbles until a quasi-steady state is reached.

Average bubble sizes and concentrations depend not only upon the rate of freezing but also upon the amount of dissolved air, changes of pressure during the process of freezing, movement of the water and, to a lesser extent, upon escape of bubbles by buoyancy.

The thickness of the layer of water ahead of the ice may also have an effect. Dissolved air would escape in the event of the water being open to the atmosphere if the supersaturated region extended right through the water. The results given in Table 2 and Fig. 5 show that this would happen at rapid rates of freezing only if the water film was less than 0.1 mm thick. A thickness of 0.2 mm would be necessary to prevent loss to the atmosphere for a freezing rate of 1 mm min^{-1} . Greater thicknesses would be needed at smaller rates.

Bubbles in ice at temperatures above -10°C lose their characteristic shapes in time, particularly when in a region of a temperature gradient or if they are close together.

Application of these results to air bubbles in hailstones will be described elsewhere.

ACKNOWLEDGMENTS

I should like to thank Mr. W. C. Hattingh for his assistance with the experimental observations and Mr. G. Gafner for advice on the diffusion theory.

REFERENCES

- BLANCHARD, D. C., 1957, *Artificial Stimulation of Rain* (London: Pergamon Press), p. 233.
 COSTE, J. H., 1940, *Quart. J. R. Met. Soc.*, **66**, 365.
 EPSTEIN, P. S., and PLESSET, M. S., 1950, *J. Chem. Phys.*, **18**, 1505.
 KOMABAYASHI, M., 1959, *J. Met. Soc. Japan*, [II], **37** 22.
 LIST, R., 1958, *Z. Angew. Math. Phys.*, **9a**, 180.
 MASON, B. J., and MAYBANK, J., 1960, *Quart. J. R. Met. Soc.*, **86**, 176.
 PFANN, W. G., 1957, *Solid State Physics*, **4**, 423.
 POHL, R. G., 1954, *J. Appl. Phys.*, **25**, 1170.
 PUZANOV, V. P., and AKKURATOV, V. I., 1952, *Meteorologiya i Gidrologiya*, **6**, 29.
 SCHOLANDER, P. F., FLAGG, W., HOCK, R. J., and IRVING, L., 1953, *J. Cell. Comp. Physiol.*, **42**, suppl. 1, p. 1.
 WEICKMANN, H., 1953, *Thunderstorm Electricity* (ed. Byers, H. R.) (Chicago: University Press), p. 66.

The Design and Construction of a 29 Mev Microtron

By D. K. AITKEN, F. F. HEYMANN, R. E. JENNINGS
AND P. I. P. KALMUS

Department of Physics, University College, London

MS. received 10th May 1960

Abstract. An account is given of the design and construction of a microtron having a 20-ton magnet with a pole diameter of 80 inches. Details are given of the major components, phase stability is considered, and the particle dynamics relevant to vertical focusing and to beam extraction are developed.

This accelerator was brought into operation in the summer of 1958, and provides an extracted electron beam of about 10^{-8} A mean at an energy of 29 Mev. The microtron is pulsed at a repetition rate of 100 pulses/sec, and has an electron pulse duration of about $2\mu\text{sec}$. By use of a quadrupole lens system the extracted beam can be focused to a spot about 2 mm in diameter, the corresponding angular spread being certainly less than 1° .

§ 1. INTRODUCTION

SINCE 1950 several microtrons have been constructed which accelerate electrons to energies of a few Mev (Redhead *et al.* 1950, Henderson *et al.* 1953a, Kaiser 1956, Carrelli and Porreca 1957). In this type of accelerator electrons are accelerated by passing successively through a single resonant cavity situated towards the edge of a magnetic field, and the final energy obtained can be increased, in principle, simply by using a magnet with larger poles so that the electrons can cross the cavity a larger number of times. Thus for a final energy of 29 Mev a magnet having a diameter of about 2 metres is required assuming that operation is in the fundamental mode (energy gain of one rest mass per orbit) at a frequency of 3000 Mc/s. In practice, however, it is found that a number of further requirements have to be met, of which the more important are given below.

(i) The tolerances on the uniformity of the magnetic field are far closer for a 29 Mev microtron than for one of a few Mev. During acceleration the orbit diameter increases to about 2 metres and precession can cause serious attenuation of the beam since all the orbits have to pass through holes of 1 cm diameter as they enter and leave the cavity.

(ii) Some deviation from a completely uniform field is necessary for vertical focusing; such deviation, however, must not cause serious precession.

(iii) Phase stability conditions also impose restrictions on the magnetic field as lack of uniformity can cause quite serious changes in path length and hence phase at the resonator, particularly for the larger orbits.

(iv) It is a considerable advantage to use a longer pulse, as a more than proportional increase in the final beam current can be achieved by lengthening the microwave pulse from $2\mu\text{sec}$ (as used in the smaller $4\frac{1}{2}$ Mev microtron at University College) to $3\mu\text{sec}$.

(v) Extraction of the beam requires more careful design as the introduction of iron tubes will have a comparatively larger perturbing effect on the previous orbits than in smaller microtrons.

Some of these requirements will now be discussed together with the more important design features of the 29 MeV microtron which was brought into operation at University College London in the summer of 1958 (Aitken and Jennings 1958).

§ 2. DESIGN OF THE MACHINE

As the later orbits in a machine of this size are large, small irregularities in the field will cause comparatively large movements of these orbits. If this movement is across the hole in the resonator (i.e. along the common diameter AB in Fig. 1) serious attenuation of the beam will result. It can be shown that such a precession is dependent on the first Fourier sine component of the field around the orbit, corresponding to a uniform tilt of one pole relative to the other about AB. A field symmetrical about AB would eliminate the sine components and was aimed at in design and manufacture. However as the maximum permissible uniform variation of field was calculated to be only 1 part in 10^4 per metre normal to AB, final adjustments are made by means of graded D shaped pole-face windings. To compensate for the precession along AB, D coils would only be required on one side of this diameter but to satisfy phase stability conditions two sets are used, one on each side of the diameter.

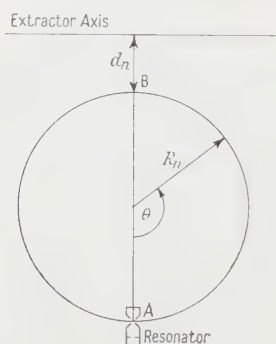


Fig. 1. Diagram showing one of the later orbits in the microtron.

Precession normal to AB, although not so serious to the operation of the machine, must still be reduced to a minimum, and a series of concentric pole-face windings are mounted on each pole to compensate for the small drop in field obtained towards the centre in a magnet of this type which has its return path at the periphery of the castings. The windings are spaced at radial intervals of 2 inches and can be separately energized.

2.1. Magnet and Vacuum Chamber

The design of the magnet and vacuum chamber is shown in Fig. 2; the pole diameter is 80 inches and the gap is 5 inches. The upper pole rests on the return path R which consists of a series of blocks freely resting on the lower pole. These blocks were carefully ground and the variation in h is less than one-thousandth of an inch from the mean. Although small gaps in the ring of return blocks are necessary, these were reduced to the absolute minimum

and were arranged symmetrically about AB. For a magnetic flux density in the gap of 1070 gauss as required for the fundamental mode, the design was such that the flux density in the iron nowhere exceeded 5500 gauss so that the magnet could be run at higher fields if required at a later date. The coils consist of a set of separate pancakes wound *in situ* with copper strip $\frac{5}{8}$ in. \times 0.030 in. insulated with 'Lewmex' and a current of 7 A is required for operation in the fundamental mode. To gain access to the inside of the vacuum chamber the upper pole can be lifted by means of three jacks which are built in and are driven through a common gear box from an electric motor mounted on the top pole.

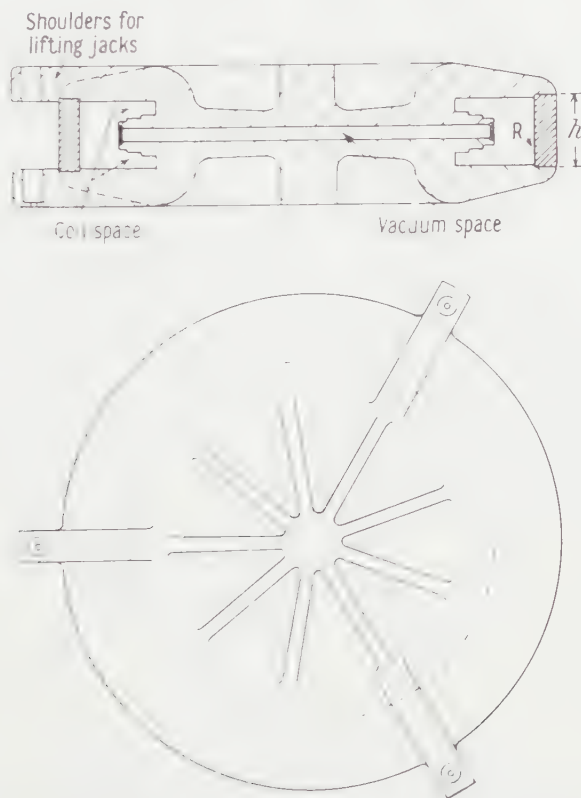


Fig. 2. Design of the magnet and vacuum chamber. The material used is high permeability dynamo steel.

The vacuum chamber is formed by mounting a ring of aluminium strip ($\frac{3}{4}$ in. thick) between the poles, grooves for rubber vacuum rings being machined in the top and bottom edges of the strip after bending and welding. The height of this strip is such that while there is still sufficient force to compress the O rings, most of the weight of the upper casting is taken by the return blocks. The vacuum chamber is evacuated using a 6 in. diffusion pump backed by a Kinney pump and after opening the chamber for a quick adjustment it is possible to reach the operating pressure of about 10^{-4} mm of mercury in one hour.

The pole faces and the seating rings for the blocks were machined to an accuracy far better than normally expected with castings of such large dimensions. After an initial assembly of the whole magnet it was possible to re-arrange

the return blocks in such a way as to reduce what 'tilt' there was across AB (Fig. 1) to a minimum, making use of the very small variation in height of the return blocks. The resulting magnetic field was such that the machine would just operate without the D correcting coils, but a considerable increase in beam was obtained when the current in these coils was adjusted to the optimum value.

A great advantage of the microtron is that the magnetic field is constant. Nevertheless a definite procedure must be adopted when switching on to bring the large mass of steel (~ 20 tons) to a repeatable field configuration. It was found that this could best be achieved by cycling the magnet through seven sub-cycles (current $\pm 30\%$ about the required value) and approaching the required value in a given sense.

The magnetic field is stabilized by stabilizing the current using a six-phase grid-controlled rectifier set (Davies *et al.* 1961†). In this way the current is stabilized to better than 1 in 10^3 over a period of several hours after an initial warming-up time.

2.2. Radio-frequency Supply

The source of microwave power is a 2 MW magnetron ($\lambda = 10$ cm) which is pulsed at 100 p/s from a modulator which utilizes a Blumlein delay line. The attenuator used was made to a slightly modified Harwell design (Kingdon 1955) in which water flows through a glass tube which crosses slant-wise across the guide, the attenuation being adjusted by insertion of a glass rod into the tube. The design of the cavity (Fig. 3) is rather similar to that used on the smaller $4\frac{1}{2}$ MeV machine, apart from small changes in shape to improve the shunt impedance. The cones are electroformed, and the cavity is tuned by electrically heated rods attached to one of the cones.

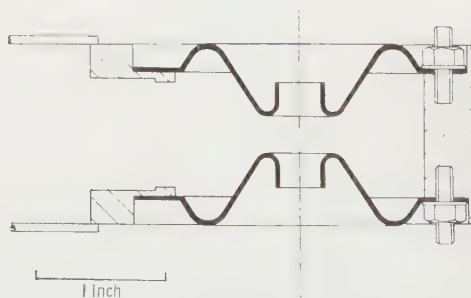


Fig. 3. Design of the cavity.

In small microtrons, the acceleration time is comparatively negligible but at 29 MeV it corresponds to about $0.5 \mu\text{sec}$. In addition part of the radio-frequency pulse is 'wasted' due to the build-up time of the cavity, so that less than $1 \mu\text{sec}$ remains for particle acceleration to full energy if a $2 \mu\text{sec}$ pulse is used. As the magnetron is being run at a repetition rate of only 100 p/s, it has been possible to increase the pulse length to $3 \mu\text{sec}$ and thus obtain a large increase in output beam.

By mounting the waveguide system and magnetron on a movable platform and by using a sliding seal where the waveguide enters the vacuum chamber

† This paper gives further details of the magnetic field, etc.

it is possible to make quick adjustments to the radial position of the cavity. This is very useful as the cavity position can thus be easily adjusted relative to the vertical focusing field.

§ 3. PHASE STABILITY

The problem regarding loss of beam due to phase fluctuation is basically the following. In the machine the electrons are travelling at $v \approx c$ and each orbit increases in length by effectively the wavelength λ of the radio-frequency supply. The length of the final orbit is about 60λ corresponding to $60 \times 360^\circ \approx 20\,000^\circ$ of radio-frequency phase. The width of the phase stable region at a given voltage (Henderson *et al.* 1953b) is of the order of 20° so that a fractional variation in length of any of the later orbits by anything of the order of $20/20\,000$, i.e. 10^{-3} , is serious. This corresponds to a change in the average magnetic flux density around an orbit by 1 gauss.



Fig. 4. Diagrammatic representation of a phase stable region. $\bar{\alpha}$ is the mean phase angle for the transit of an electron across the accelerating gap.

The problem can be developed a little as follows. Let the magnetic flux density be B , the peak voltage on the cavity be V and the average energy gain per transit of the electron be eV_R . The corresponding phase stable region is shown diagrammatically in Fig. 4 (upper curve), ΔE being the error in energy relative to the resonant electron. Now consider what happens, if, as the electron completes orbit X and starts orbit Y it moves from an average magnetic flux around the orbit of B to $B + \Delta B$. The corresponding energy of the resonant electron will increase by the factor $1 + \Delta B/B$, so the electrons being accelerated will be deficient in energy by an amount $neV_R \Delta B/B$ where n is the orbit number (differences between n and $n+1$ etc. are ignored). In the phase stable diagram the conditions on leaving the cavity are plotted so that as the electrons leave to start orbit Y they have the correct phase but are deficient in energy. The appearance of the phase stable region will alter very

little provided $\Delta B \ll B$; strictly it will be the same as for a voltage $V(1 - \Delta B/B)$ with a magnetic field B , except that the errors ΔE will be increased by $1 + \Delta B/B$. Relative to this new region values of ΔE and $\bar{\gamma}$ for the electrons fall in the shaded area, which is approximately the first region displaced downwards by an amount $neV_R \Delta B/B$.

Thus only those electrons in the area common to the two curves are phase stable, and these will move around the new stable region. Those electrons outside the stable region will eventually be lost, but it may well happen that the perturbation only lasts for one or two orbits and that, on returning to the original field, many of these fall inside the original stable region; the electrons which have moved into the unshaded area will, however, now be lost. If the average field slowly changes as the orbits increase in size, there will in general be a steady loss of particles. Provided all the electrons are not lost at a large change in the average field between one orbit and the next, the overall change in field can be quite large and some electrons will in general survive. The larger the rate of change of the average field, the greater will be the attenuation of the beam.

Due to such perturbations the energy spread of the beam will tend to be decreased, as also will the beam current. Much depends on the density of electrons in the phase stable region, particularly near the edges, as to how serious this effect will be.

The two treatments, in phase and energy, are complementary, the error in energy causing a corresponding change in phase at the next transit. Some idea of the permissible variation in magnetic field can be obtained as follows; values of $neV_R \Delta B/B \simeq 0.01 eV_R$ although serious would not be impossibly large. For $n=56$, $\Delta B/B=1/5600$ and $\Delta B \simeq \frac{1}{5}$ gauss (this is the extreme case; for earlier orbits ΔB can be proportionately larger); this accuracy is not too difficult to achieve when it is remembered that this is a variation on the average field and is, generally speaking, less severe than the requirements of the magnetic field regarding precession. However, some loss from this cause is inevitable unless an extremely complex system of correcting coils is employed.

§ 4. VERTICAL FOCUSING

4.1. Cavity Forces

The vertical motion of the electrons in a microtron due to the electromagnetic forces in the resonator has been investigated by Bell (1953 a, b) and, for energies greater than a few MeV, the motion is represented by the matrix transformation (to first order in n^{-1})

$$\begin{bmatrix} z_{n+1} \\ p_{n+1} \end{bmatrix} = \begin{bmatrix} 1 - \frac{1}{2(n+1)} & \frac{\lambda}{m_0 c} \left(1 - \frac{1}{2(n+1)} \right) \\ -\frac{Km_0 c}{4l(n+1)} & 1 + \frac{1}{2(n+1)} - \frac{K\lambda}{4l(n+1)} \end{bmatrix} \begin{bmatrix} z_n \\ p_n \end{bmatrix} \dots\dots(1)$$

where K is a constant approximately equal to unity depending on the detailed resonator field configuration, l is the length of the resonator gap and λ is the free space wavelength of the radio frequency, z_n and p_n are the vertical displacement and vertical momentum on leaving the resonator at the beginning of the n th

orbit. The steady magnetic field is assumed to be uniform and at right angles to the resonator axis.

The general solution of such an iterative equation, in which the matrix elements vary only slowly with n , has been shown to be (Le Couteur 1951)

$$z \simeq A_n \sin (\phi + \sum \mu_n) \quad \dots\dots (2)$$

where

$$\cos \mu_n = \frac{1}{2}(\beta_{11} + \beta_{22}) \text{ and } A_n^2 = \frac{D\beta_{12}}{\sin \mu_n}$$

the matrix elements being denoted by β , and where D and ϕ are determined by the initial conditions. Here $\cos \mu_n = 1 - K\lambda/8l(n+1)$, and making the approximations appropriate to large n the solution

$$z \simeq An^{1/4} \sin [(K\lambda n/l)^{1/2} + \phi] \quad \dots\dots (3)$$

is obtained. The motion is oscillatory with amplitude increasing as $n^{1/4}$, which thus doubles in going from the 4th to the 56th orbit.

The situation is much worse than this if allowance is made for a slight angular deviation θ of the resonator axis from a plane normal to the steady magnetic field, such as must occur in practice. A suitable modification to Bell's treatment leads to the inhomogeneous transformation (to first order)

$$\begin{bmatrix} z_{n+1} \\ p_{n+1} \end{bmatrix} = \begin{bmatrix} 1 - \frac{1}{2(n+1)} & \frac{\lambda}{m_0 c} \left(1 - \frac{1}{2(n+1)}\right) \\ -\frac{Km_0 c}{4l(n+1)} & 1 + \frac{1}{2(n+1)} - \frac{K\lambda}{4l(n+1)} \end{bmatrix} \begin{bmatrix} z_n \\ p_n \end{bmatrix} + \frac{1}{2} \begin{bmatrix} 0 \\ \theta m_0 c \end{bmatrix} \quad \dots\dots (4)$$

Writing the solutions to this equation in the form

$$z_n' = z_n + a_n, \quad p_n' = p_n + b_n$$

in which z_n, p_n are solutions of the homogeneous Eqn (1), we can find approximate expressions for a_n and b_n by putting $a_{n+1} = a_n, b_{n+1} = b_n$.

Then

$$\begin{bmatrix} \beta_{11} - 1 & \beta_{12} \\ \beta_{21} & \beta_{22} - 1 \end{bmatrix} \begin{bmatrix} a_n \\ b_n \end{bmatrix} + \frac{1}{2} \begin{bmatrix} 0 \\ \theta m_0 c \end{bmatrix} \simeq 0$$

from which a_n is given by

$$2a_n \simeq \frac{\beta_{12} \theta m_0 c}{(\beta_{11} - 1)(\beta_{22} - 1) - \beta_{12} \beta_{21}} \quad \dots\dots (5)$$

and the complete solution is

$$z_n' \simeq \frac{2l\theta n}{K} + An^{1/4} \sin [(K\lambda n/l)^{1/2} + \phi]. \quad \dots\dots (6)$$

It is seen that the mean line of the vertical oscillation is displaced by an amount $2\theta l n/K$; nearly all the beam will be lost when this quantity equals the radius ρ of the resonator hole. Inserting typical values at $n=60$ gives a maximum permissible tilt $\theta_m < K\rho/2ln \simeq \frac{1}{4}^\circ$. The electrical axis of the resonator is not known to this accuracy, which requires location of the electroformed end faces to approximately 0.001 in. It would therefore be very difficult to operate a microtron without additional focusing forces.

In passing it is of interest to note that it is necessary to include the resonator focusing forces. If these forces could be neglected, (4) would be

$$\begin{bmatrix} z_{n+1} \\ p_{n+1} \end{bmatrix} = \begin{bmatrix} 1 & \lambda/m_0c \\ 0 & 1 \end{bmatrix} \begin{bmatrix} z_n \\ p_n \end{bmatrix} + \begin{bmatrix} 0 \\ \theta m_0c \end{bmatrix}.$$

Here the motion is no longer oscillatory since $\frac{1}{2}(\beta_{11} + \beta_{22}) = 1$ and Eqns (2) are not valid. The matrix can however be approximated for large n by the pair of differential equations

$$\frac{dz}{dn} = \frac{\lambda}{m_0c} p_n, \quad \frac{dp}{dn} = \theta m_0c.$$

These have the solution $z \simeq \frac{1}{2}\theta\lambda n^2$, putting $z_1 = 0$, $p_1 = \theta m_0c$ instead of the previous linear dependence on n . The maximum permissible tilt indicated by this expression is about one hundredth of that when resonator focusing is included.

4.2. Magnet Forces

A magnetic field gradient can provide vertical focusing forces much greater than those due to the resonator (Bell 1953 b) and for some configurations give rise to damped oscillations, while effects due to resonator misalignment can be greatly reduced. Such a gradient should be symmetrical about the common orbit diameter as indicated in a previous section, and such that the average field for each orbit is nearly constant, to satisfy phase stability requirements.

The natural fall-off field from a circular pole magnet fulfils these conditions and smaller microtrons have successfully operated with the resonator situated in this region.

For small displacements from the median plane the restoring force is

$$\left| z \frac{ev}{c} \frac{dB_r}{dz} \right| = \left| z \frac{ev}{c} \frac{dB_z}{dr} \right|,$$

since the magnetic flux B does not vary with time (Gaussian units used). Then the change in vertical momentum of an electron in passing from the resonator to the edge of the fall-off region (a distance L) is given by

$$(p_1 - p_0) = - \int_0^L \left| ez \frac{dB_z}{dr} \right| \frac{dx}{c} \quad (v \simeq c).$$

Understanding by $|dB_z/dr|$ its average value in the range $0 \leq x \leq L$ and neglecting the variation of z in this distance,

$$(p_1 - p_0) = - \frac{L}{c} \left| ez_0 \frac{dB_z}{dr} \right|, \quad z_1 = z_0$$

or in matrix notation:

$$\begin{bmatrix} z_1 \\ p_1 \end{bmatrix} = \begin{bmatrix} 1 & 0 \\ - \left| \frac{eL}{c} \frac{dB_z}{dr} \right| & 1 \end{bmatrix} \begin{bmatrix} z_0 \\ p_0 \end{bmatrix}.$$

Until re-entry to the fall-off field the motion is drifting only, and

$$\begin{bmatrix} z_2 \\ p_2 \end{bmatrix} = \begin{bmatrix} 1 & \frac{2\pi R}{\gamma m_0c} \\ 0 & 1 \end{bmatrix} \begin{bmatrix} z_1 \\ p_1 \end{bmatrix}$$

where R is the radius of the orbit, $\gamma = 1/(1 - \beta^2)^{1/2}$ and assuming that $L \ll 2\pi R$. The motion in the fall-off region $-L \leq x \leq 0$ to re-entry to the resonator is given by the first transformation, so that

$$\begin{bmatrix} z_3 \\ p_3 \end{bmatrix} = \begin{bmatrix} g_{11} & g_{12} \\ g_{21} & g_{22} \end{bmatrix} \begin{bmatrix} z_0 \\ p_0 \end{bmatrix}$$

where(7)

$$g_{11} = g_{22} = 1 - \frac{2\pi L}{B_0} \left| \frac{dB_z}{dr} \right|,$$

$$g_{12} = \frac{\lambda}{m_0 c}, \quad g_{21} = -\frac{4\pi L m_0 c}{B_0 \lambda} \left| \frac{dB_z}{dr} \right| \left(1 - \frac{\pi L}{B_0} \left| \frac{dB_z}{dr} \right| \right).$$

Here B_0 , the value of the steady magnetic field, has been substituted for $\gamma m_0 c^2 e R$ and, corresponding to the fundamental mode of operation, $\gamma \lambda / 2\pi = (n+1)\lambda / 2\pi$ for R .

In crossing the resonator the change in the vertical displacement is negligible and, if we neglect resonator focusing forces and for the moment any effects due to tilt of the resonator, there will be no change in the vertical momentum so that the transformation (7) applies for one complete orbit. It is easily verified that the determinant of the matrix is unity.

The effective length of the focusing region $2L$ will be some function of orbit radius R . For the fall-off field due to a circular magnet it is a reasonable approximation to put $L = \alpha R$ where α is a constant, for all but the first and last few orbits, so that

$$\begin{bmatrix} z_{n+1} \\ p_{n+1} \end{bmatrix} = \begin{bmatrix} h_{11} & h_{12} \\ h_{21} & h_{22} \end{bmatrix} \begin{bmatrix} z_n \\ p_n \end{bmatrix}$$

where(8)

$$h_{11} = h_{22} = 1 - \frac{(n+1)\alpha\lambda}{B_0} \left| \frac{dB_z}{dr} \right|_M,$$

$$h_{12} = \frac{\lambda}{m_0 c}, \quad h_{21} = -\frac{2(n+1)m_0 c \alpha}{B_0} \left| \frac{dB_z}{dr} \right|_M \left(1 - \frac{(n+1)\alpha\lambda}{2B_0} \left| \frac{dB_z}{dr} \right|_M \right)$$

and $|dB_z/dr|_M$ denotes the average fall-off field of the magnet. The elements of the matrix vary only slowly provided that

$$\frac{\alpha\lambda}{B_0} \left| \frac{dB_z}{dr} \right|_M \ll 1$$

in which case Eqns (2) are valid. For z to be oscillatory we must have

$$-2 < h_{11} + h_{22} < 2$$

or

$$n < \frac{2B_0}{\alpha\lambda \left| \frac{dB_z}{dr} \right|_M}.$$

Here

$$\cos \mu_n = 1 - \frac{(n+1)\alpha\lambda}{B_0} \left| \frac{dB_z}{dr} \right|_M$$

and for small μ_n ,

$$\mu_n \simeq \left[\frac{2(n+1)\alpha\lambda}{B_0} \left| \frac{dB_z}{dr} \right|_M \right]^{1/2}, \quad A_n \simeq \frac{A}{(n+1)^{1/4}}.$$

It is seen that the oscillations become more rapid with slowly damped

amplitude as n increases. In order to keep stable vertical oscillations throughout the machine it is necessary to choose $(\alpha\lambda/B_0)|dB_z/dr|_M < 1/30$, and this in turn makes the phase change of the motion initially only $20\text{--}25^\circ$ per orbit, corresponding to weak initial focusing. As the cavity emits a diverging beam into the first orbit there will be a loss in beam intensity until the vertical motion has gone through its first maximum, that is, during the first 4.5 orbits. A typical oscillation for $(\alpha\lambda/B_0)|dB_z/dr|_M = 1/25$ is shown in Fig. 5(b), the points being obtained from the difference equation equivalent to the transformation (8); it is seen that the motion becomes unstable between the 50th and 60th orbit. (The displacement is in arbitrary units, the frequency being independent of the amplitude†.)

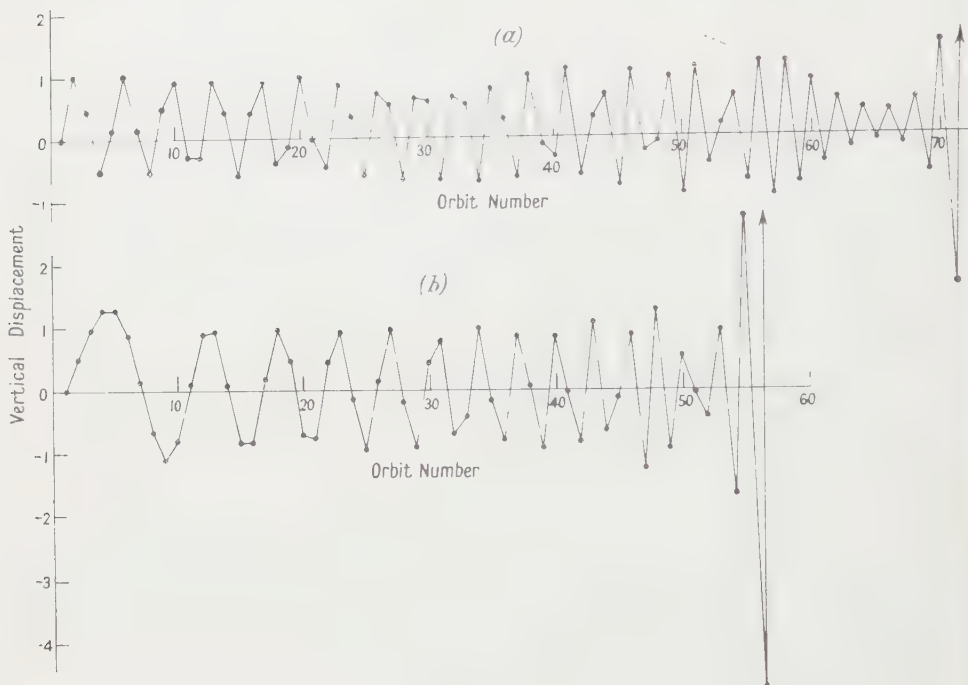


Fig. 5.

The initial loss of intensity can be reduced by introducing a more localized and steeper gradient at the resonator, for instance by placing small steel shims on the pole faces. Considering this type of configuration alone, the matrix elements of (7) are now independent of n , and the approximate solution, including the effects due to resonator tilt is,

$$z_n \simeq \frac{B_0}{8\pi L \left| \frac{dB_z}{dr} \right|_L} \theta \lambda + A \sin \left[\left(\frac{4\pi L}{B_0} \left| \frac{dB_z}{dr} \right|_L \right)^{1/2} n + \phi \right], \quad \dots\dots (9)$$

where $|dB_z/dr|_L$ denotes the average slope of the field over a fixed length of $2L$. Eqn (9) represents an oscillation of fixed amplitude and frequency displaced by an amount $B_0\theta\lambda/8\pi L|dB_z/dr|_L$ from the median plane. Beam losses due to

† Although this analysis is not so appropriate for the first and last orbits as for the others, the general behaviour is correctly given.

resonator tilt will be small provided this displacement is much less than the resonator radius ρ . Putting $L = 5$ cm, $|dB_z/dr|_L = 20$ gauss cm^{-1} the phase change per orbit is equal to 65° and losses due to tilt will be small if $\theta < 1^\circ$ (corresponding to a displacement of about 1 mm from the median plane), a much easier requirement than with resonator forces only.

Inclusion of the magnet fall-off field results in eventual vertical instability as before, but it is now possible to remove the instability to higher orbits than the 60th, while still retaining adequate focusing in the early orbits. A typical oscillation is shown in Fig. 5(a) in which

$$\frac{\alpha\lambda}{B_0} \left| \frac{dB_z}{dr} \right|_M = \frac{1}{60}, \quad \frac{\pi L}{B_0} \left| \frac{dB_z}{dr} \right|_L = \frac{1}{2}.$$

Here the effects of a resonator tilt, $\theta\lambda = 1.0$, are included where λ is to be taken in the same units as the vertical displacement. It is seen that a much larger tilt of the resonator is now permissible. The decrease in amplitude between the 60th and 70th orbits is not typical.

§ 5. INITIAL MAGNETIC FIELD ADJUSTMENTS

A lead target of sufficient thickness to stop a 29 MeV electron beam is mounted on a carriage movable to any desired position along the common diameter. It is thus possible to measure the beam current in any orbit along this diameter, and with a coating of fluorescent material on the target the beam profile can also be observed. A mirror system allows this to be done from outside the 2-foot thick concrete screening wall which surrounds the microtron.

With the resonator situated in the magnet fall-off field alone orbits were observed only up to the 25th and these with only low current of the order of 10^{-10} A mean. The field gradient at the resonator was approximately 8 Oe cm^{-1} and the field itself 17 Oe below the main field. When the resonator was moved radially outwards into a steeper field gradient the current in the earlier orbits increased while the number of orbits obtainable decreased. For a gradient of 21 Oe cm^{-1} and field drop of 50 Oe the final orbit was the 16th, with earlier orbit currents of approximately 10^{-9} A. This change in the number of orbits with the resonator position was attributed to precession normal to the common diameter due to the field error, and it was found that depression of the central field, whilst keeping that at the resonator fixed, increased the number of orbits obtainable to about 35, with currents of the order of $2-3 \times 10^{-10}$ A. The central field was depressed by passing a suitable current through the 32 in. radius shim coil.

It seemed probable that this limitation was due to vertical overfocusing by the fall-off field at around the 35th orbit, as discussed previously. An approximation to a localized gradient at the resonator was achieved by placing steel washers on the pole faces on the common diameter, the optimum radial position being determined experimentally. With this arrangement a current of approximately 10^{-8} A was observed in the 56th orbit. To obtain these last few orbits it was found necessary to energize the D shaped shim coil, mentioned in § 2.

The field near the resonator, due to the combined effect of the steel shims and the magnet fall-off is shown in Fig. 6. Apart from providing a nearly

constant length of vertical focusing field, the contribution due to the steel shims has some additional features, listed below.

(i) A large fall-off rate whilst keeping the field at the resonator equal to the central field. This keeps precession perpendicular to the common diameter small and satisfies the requirements of phase stability.

(ii) The initial orbits are focused over their whole path, giving better vertical acceptance to higher orbits.

(iii) The 1st orbit is in a relatively high field, which can improve the phase acceptance. This is so since electrons spend rather longer in the first transit of the resonator than in subsequent transits, and therefore take longer than 2 cycles to complete the first orbit. Although the shortening of the duration of this orbit due to the higher field is only approximately 1%, this corresponds to 7° of phase correction at re-entry to the resonator and is significant.

(iv) The higher field over part of the first orbit tends to correct for its slight skewness with respect to the resonator diameter, which is due to the large change of velocity during the first transit (Henderson *et al.* 1953 a).

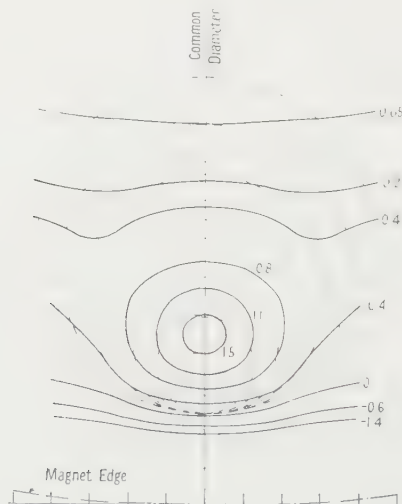


Fig. 6. Field recontours near the sonator. The numbers represent the excess field expressed as a percentage of the central field. Orbits 1-6 are shown by the broken lines. The axes are marked in 1 in. intervals.

§ 6. BEAM EXTRACTION

An attractive feature of microtrons is the comparatively large spacing between orbits which greatly simplifies the problem of extraction. For a microtron operating in the fundamental mode the spacing between orbits at the position diametrically opposite the cavity is λ/π , i.e. about 3 cm in our case. This is more than sufficient to allow the insertion of an iron tube tangential to an orbit, thereby providing a field-free region for extraction of electrons. Extraction at this position also has the advantage that owing to 180° focusing the beam cannot be larger than the resonator aperture at this point.

Extraction by means of single iron tubes has been achieved on smaller microtrons (Henderson *et al.* 1953 a, Kaiser 1956, Brannen and Ferguson 1956)

but perturbation of previous orbits caused by the presence of the iron can impose severe limitations in applying this method to a larger machine. Hence various calculations were made and the chief points of interest arising from these are listed below.

The magnetic flux density inside a long tube of permeability μ , when it is placed in an external uniform field (see Fig. 7) having an unperturbed value B_0 perpendicular to the tube axis is given by

$$B_z = \frac{4B_0}{\mu(1 - a^2/b^2)}, \quad B_y = 0$$

provided $\mu \gg 1$, the flux density being uniform. A simple calculation shows that in our case an iron tube having $a/b \simeq \frac{3}{4}$ can provide adequate magnetic shielding. The flux density outside the tube has the values

$$B_z = B_0 \left(1 - \frac{b^2}{y^2}\right), \quad B_y = \frac{2B_0 b^2 z}{y^3}$$

in the region where $y \gg z$ and provided $\mu \gg 1$. This departure from uniformity causes horizontal and vertical perturbations of the orbits.

For the conditions under consideration, the orbit precession along the common diameter caused by an iron tube having a diameter larger than about $\frac{1}{2}$ cm is sufficiently large to cause complete loss of the beam. This precession can however be almost eliminated by providing a 'dummy' extractor tube similar to the real one but extending in the opposite direction.

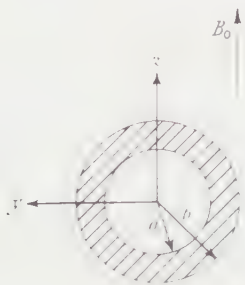


Fig. 7.

Approximate calculations of the vertical motion of the electrons due to the presence of the extractor and dummy tubes were carried out. An electron travelling above the median plane will experience a downward force in the perturbed field near the extractor. This force will be greatest when the electron is closest to the extractor and will decrease rapidly at greater distances. The effect of the vertical force in each orbit can therefore be considered to a good approximation as an impulse occurring at the point of closest approach, this impulse resulting in a sharp change in vertical momentum at this point. The impulse experienced by an electron moving at a height z_n above the median plane is found by integrating over the orbit and is given by $I_n z_n$ where

$$I_n = - \frac{6B_0 b^2 e \pi}{c R_n^2} \frac{\xi}{(\xi^2 - 1)^{5/2}}$$

and

$$\xi = \frac{R_n + d_n}{R_n} \dots \dots (\text{see Fig. 1}).$$

The relations between the vertical displacements (z_n) and momenta (p_n) at the point of closest approach of successive orbits are

$$z_{n+1} = z_n + \frac{2\pi R_n}{\gamma m_0 c} p_n$$

$$= z_n + \frac{\lambda}{m_0 c} p_n$$

$$p_{n+1} = I_{n+1} z_{n+1} + p_n.$$

By also writing down the expression for z_{n+2} the momenta can be eliminated giving the following relation between the heights in three successive orbits

$$z_{n+2} = z_{n+1} \left(2 + \frac{\lambda}{m_0 c} I_{n+1} \right) - z_n.$$

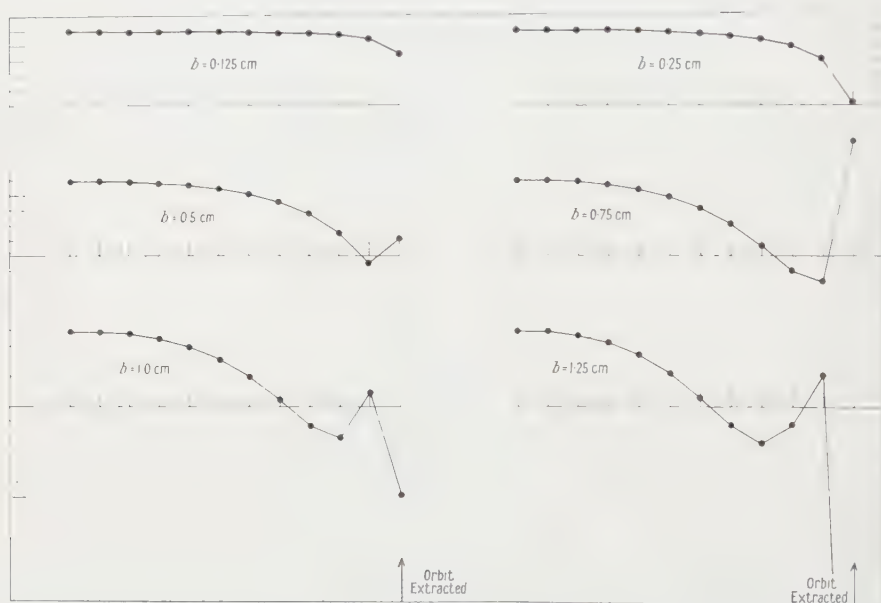


Fig. 8. Perturbation caused by extractor tubes of different radii b . The vertical scale gives the height of the orbits with respect to the median plane (arbitrary units). The position of the orbits is indicated on the horizontal scale.

The vertical motion of the beam due to the presence of the extractor can thus be followed through successive orbits (other focusing forces are ignored). This is shown in Fig. 8 for various extractor tube diameters. It can be seen that the effect of a uniform tube of small diameter is to focus the beam in the vertical plane, but larger tubes cause overfocusing leading to loss of beam. The maximum permissible radius given by this approximate treatment (in general valid until overfocusing occurs) appears to be about $\frac{1}{2}$ cm.

As it is the portion of the extractor and dummy tubes which is nearest to the common diameter (and hence to previous orbits) which has the greatest effect, a tapered tube is used, smaller at its entrance than at its exit. Such a

tube also has room for the extracted beam to diverge, and also allows for some bending of the beam due to the imperfect screening of the field.

The above mentioned considerations led to the actual design which is shown in Fig. 9. For convenience the iron tubes were constructed from short sections ranging from $\frac{1}{4}$ in. outside diameter at the entrance to $\frac{3}{4}$ in. outside diameter at the exit, the sections being welded together. The extractor and dummy tubes were placed in a slotted brass tube which can be displaced and tilted in horizontal and vertical planes by remotely controlled motors situated outside the magnetic field. These adjustments can be made while the machine is operating to find the position for maximum extraction.

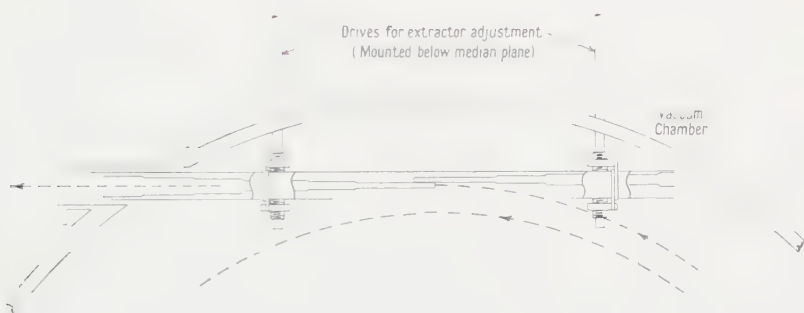


Fig. 9. Beam extraction system.

§ 7. SUMMARY OF OPERATING CHARACTERISTICS

The operation of the machine is found to be relatively insensitive to small radial variations of the magnet field, and correction of the natural depression towards the centre of the magnet by means of the concentric shim coils is not found to be critical. However, the value of the field at the resonator relative to the central field is critical, especially for the higher orbits. Two of the shim coils, of 30 in. and 32 in. radius, are used for this adjustment, as coarse and fine controls.

Slow variations of the main magnet current of $\pm 2\%$ produce a drop of roughly 50% in the extracted beam intensity (N.B. the beam position remains constant). In fact since the current supply is stabilized to 0.1% over a period of 10 hours, no trouble is experienced from this cause. In passing it may be mentioned that sudden variations in magnet voltage of more than a few tenths per cent completely stop the beam until eddy currents decay and the field distribution has resumed its former shape.

The extraction efficiency from the 56th orbit is 25–30%, this being the ratio of extracted current measured outside the machine to current in the 55th orbit measured internally. The latter orbit shows marked radial spread on the lead probe, due to the presence of the extractor tubes. It is hoped that magnetic shimming in this region will reduce this effect and correspondingly improve the extraction efficiency.

The extracted beam profile just outside the machine (35 in. from the common diameter) is a horizontal strip 7 mm \times 1 mm. The corresponding vertical and horizontal angular divergences are less than $\frac{1}{10}^\circ$ and less than 1° respectively.

The extracted beam current is usually of the order of 3×10^{-9} A mean, the electrons being obtained by field emission from the resonator lips. On favourable occasions extracted currents of $1-2 \times 10^{-8}$ A, with internal current approximately 4 times this figure, have been obtained. The variation of beam current with orbit number is shown in Fig. 10 where it is seen that, apart from losses

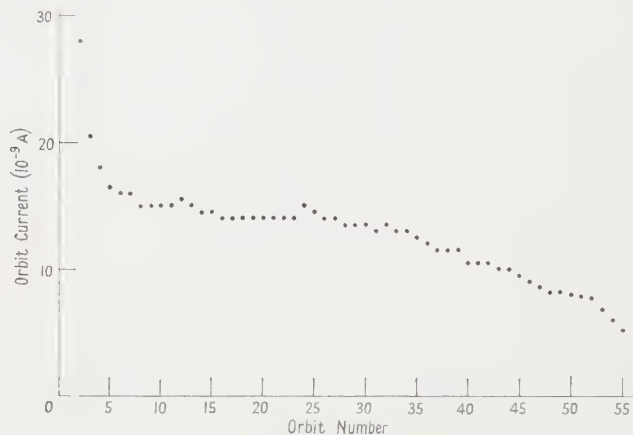


Fig. 10. Variation of beam current with orbit number (not corrected for variations in beam loading, acceleration time, etc.).



Fig. 11. Possible arrangement for operation at a higher energy.

in the early orbits, the current remains roughly constant up to the 30th, subsequently dropping to about one-third of this value in the penultimate orbit. It is considered that this current fall is due to small irregularities still remaining in the magnetic field, such irregularities having a predominant effect on the later orbits. It is hoped to reduce this attenuation by the use of additional shim coils. Some loss of beam in the later orbits is to be expected as a result of the

long acceleration time ($\sim 0.5 \mu\text{sec}$ for 56 orbits), but with the present pulse length to the magnetron this will not exceed 25%.

Operation of the machine is found to be very insensitive to pressure. This is usually about 10^{-4} mm Hg, although there is little change in beam current up to 10^{-3} mm Hg, when flashover in the waveguide system occurs.

An electron resonance probe is used to monitor the magnet field with an accuracy to a few parts in 10^4 . The uncertainty in the final orbit radius, given by the size of the extractor tubes, resonator orifice and variations of the magnetic field in these two regions, is approximately 2%, so that the beam energy is known absolutely to this accuracy. Higher accuracy than this, probably a few tenths of one per cent, could be achieved at some sacrifice to beam intensity, using three defining slits in the last orbit, situated in the nearly uniform field away from the resonator and extractor.

It is hoped at a later date to increase the final energy of the machine to 50–60 MeV using a modified resonator excited to a higher peak voltage with an appropriate increase of the magnetic field (Aitken 1957). Here the chief problem is the small size of the first orbit which can no longer clear the resonator. Numerical calculations on the first orbit trajectory have shown that it is not feasible to allow the beam to re-enter the resonator through a radial slot half way through the first orbit, as previously suggested. However a possible solution is to guide this orbit round the resonator by means of steel tubes, increasing its period from one to two cycles of the radio frequency (see Fig. 11). A preliminary set-up along these lines has had fairly encouraging results.

ACKNOWLEDGMENTS

The authors would like to thank Professor Sir Harrie Massey for his support of, and continued interest in this project. They are grateful to Dr. P. W. Higgs for checking some of the calculations, and would like to acknowledge the radiation shielding calculations and design carried out by Mr. L. R. Day. Finally the authors wish to thank members of the technical staff of the department for work connected with the construction of the microtron.

This work was supported by the Department of Scientific and Industrial Research.

REFERENCES

- AITKEN, D. K., 1957, *Proc. Phys. Soc. A*, **70**, 550.
 AITKEN, D. K., and JENNINGS, R. E., 1958, *Nature, Lond.*, **181**, 1726.
 BELL, J. S., 1953 a, *Proc. Phys. Soc. B*, **66**, 802.
 — 1953 b, *Atomic Energy Research Establishment*, Report T/M 75.
 BRANNEN, E., and FERGUSON, H. I. S., 1956, *Rev. Sci. Instrum.*, **27**, 833.
 CARRELLI, A., and PORRECA, F., 1957, *Nuovo Cim.*, **6**, 729.
 DAVIES, G. R., JENNINGS, R. E., PORRECA, F., and RAND, R. E., 1961, *Nuovo Cim.*, in the press.
 HENDERSON, C., HEYMANN, F. F., and JENNINGS, R. E., 1953 a, *Proc. Phys. Soc. B*, **66**, 654.
 — 1953 b, *Proc. Phys. Soc. B*, **66**, 41.
 KAISER, H. F., 1956, *Instn Radio Engrs: Transactions on Nuclear Science*, N.S.3. 17.
 KINGDON, B. E., 1955, *J. Brit. Instn Radio Engrs*, **15**, 471.
 LE COUTEUR, K. J., 1951, *Proc. Phys. Soc. B*, **64**, 1073.
 REDHEAD, P. A., LECAINE, H., and HENDERSON, W. J., 1950, *Canad. J. Res. A*, **28**, 73.

Nuclear and Relativistic Effects in Atomic Spectra

By A. P. STONE

Clarendon Laboratory, Oxford†

MS. received 1st June 1960, in revised form 13th October 1960

Abstract. The electronic Hamiltonian for a general atom is obtained as far as terms in $1/c^2$ and m/M_A by reducing a relativistic wave equation with four components for each electron and nucleon to an approximately relativistic form with two components per particle. The presence of non-Hermitian terms in the reduced Hamiltonian is explained. Relativistic corrections to the Coulomb and nuclear interactions and the effect of the intrinsic magnetic moments are treated by first-order perturbation theory. The electronic Hamiltonian is obtained in the centre-of-mass system of the atom. The hyperfine structure interaction is obtained by expressing all electron-nucleon terms as multipole expansions, giving the previously known hyperfine structure expansion with recoil corrections. The exact operator for the nuclear field effect in isotope shift is obtained from the Coulomb interaction. The presence of other corrections depending on nuclear structure is indicated. Terms referring only to s electrons are not considered as the reduction procedure used does not cover the contact approach of particles (cf. Ma 1956). The usual calculation of the normal mass effect in isotope shift is investigated for non-s-electron configurations and is shown to be justified if 0.1% of the spin-orbit interaction and the whole of the other relativistic perturbations are negligible in comparison with the term value.

§ 1. INTRODUCTION

Up to now there has been no comprehensive general treatment of the nucleus in atomic spectra. The nucleus was first considered as a fixed point charge interacting electrostatically with the atomic electrons. Hughes and Eckart (1930) showed that the motion of the nucleus introduces a correction to the electronic energy in the centre-of-mass system of the atom (the mass effect in isotope shift). Another correction (the nuclear field effect in isotope shift) arises from the distributed nature of the nuclear charge (Bodmer 1958 and references therein). Relativistic corrections in the hydrogen atom, including the effect of the intrinsic magnetic moments of the proton and electron, have been treated by Barker and Glover (1955; for a summary of earlier work see Ishidzu 1951). Relativistic effects for the electrons of two-electron atoms have been treated by Sucher and Foley (1954), and of n-electron atoms by Perl (1953); these authors treat the nucleus as a fixed point charge.

The effect of nuclear structure on the hyperfine structure of hydrogen and helium isotopes has been treated in some detail (Low 1950, Adams 1951, Sessler and Foley 1955). Schwartz (1955) has obtained the general (unretarded) hyperfine structure interaction due to the spin and orbital currents of a stationary

† Now at the Department of Mathematics, University of Hull.

nucleus and recoil effects have also been discussed (Gartenhaus and Schwartz 1957). Bohr and Weisskopf (1950) have investigated the effect of nuclear structure on the magnetic dipole hyperfine structure due to a stationary nucleus.

In the present paper a unified approach is made to the problem of the effect of the nucleus in atomic spectra. The nucleons are treated as individual particles in order to start from a relativistic wave equation of the Dirac type for a general atom. In §2 this wave equation is reduced to an approximately relativistic Pauli form as far as terms in $1/c^2$. The Breit operators correcting all Coulomb interactions and phenomenological terms giving the effect of the intrinsic magnetic moments of the particles are treated as perturbations and reduced as far as terms in $1/c^2$ in §2.1, where this procedure is justified. Nuclear interactions are introduced phenomenologically and relativistic corrections to the nuclear interactions are obtained in §2.2. Apart from the intrinsic moment terms, radiative corrections to the fine structure (Salpeter 1952) and to the hyperfine structure (Newcomb and Salpeter 1955) of relative order $\alpha(m/M)$ are not considered.

The electronic Hamiltonian is obtained in the centre-of-mass system of the whole atom. Operators in the centre-of-mass system are defined in §3. In §4 the interactions between electrons and nucleons are separated into hyperfine structure and non-hyperfine structure terms by means of multipole expansions. The hyperfine structure terms are not considered in detail but the relation of the present approach to previous work is discussed in §4.3. The approximate non-hyperfine structure electronic Hamiltonian is given in §5.

Ma (1956) has shown that the contact interaction between a stationary point nucleus and an electron, obtained by reducing the Dirac equation to an approximately relativistic form, changes into a core interaction when the reduction is carried out rigorously. The reduction procedure has to be modified for distances of the electron from the nucleus of less than about $e^2/2mc^2$. This modification is not extended to the general atom in the present work and all contact interactions are omitted. In view of Ma's work the conclusions of previous writers on the s-electron energies are in need of revision.

In their treatment of the normal mass effect in isotope shift, Hughes and Eckart (1930) neglected all interactions except the Coulomb interactions. In heavy elements the spin-orbit interaction can amount to an appreciable fraction of the term value and should be taken into account. In §6 it is shown that the Hughes-Eckart formula for the normal mass shift is correct to a good approximation when the spin-orbit and other smaller interactions are included in the electronic Hamiltonian (Eqn (17)). Configurations involving s electrons require a knowledge of the contact interactions but it is possible that the Hughes-Eckart formula applies also to them.

All terms whose expectation values vanish when the nuclear and electronic wave functions separately have definite parity, and terms of relative order $(m/M)^2$, are omitted.

§ 2. REDUCTION OF THE RELATIVISTIC WAVE EQUATION

The unperturbed wave equation for the nucleons and electrons will be taken to be

$$\left[\sum (\alpha_a \cdot \mathbf{P}_a + \beta_a m_a c^2) + V + \sum_{a>b} \beta_a \beta_b J_{ab} - E \right] \Psi = 0, \quad \dots\dots (1)$$

where α_a, β_a are the Dirac matrices acting on the four components of Ψ corresponding to particle a . The sign of these matrices is not important; replacing them by $-\alpha_a, -\beta_a$ merely exchanges the roles of the upper and lower pairs of components for particle a .

The interactions $V, J_{ab}(=J_{ba})$ are to depend only on the inter-particle vectors $\mathbf{R}_{cd} = \mathbf{R}_c - \mathbf{R}_d$, where \mathbf{R}_a is the position vector of particle a in an external frame of reference and \mathbf{P}_a is the conjugate momentum. V consists of the static Coulomb interactions and, possibly, nuclear interactions. The terms in J_{ab} are a form of nuclear interaction considered by Breit (1937) in the two-body case; here there is nothing to prevent the occurrence of many-body forces. Spin-dependent nuclear forces are considered in §2.2. Write

$$E = W + \sum m_a c^2, \quad J \equiv \sum_{a>b} J_{ab},$$

$$K_a \equiv V + J - 2 \sum_b J_{ab},$$

and let Ψ'_0 denote the components of Ψ which are largest when all the particles are in positive-energy states. The correct set of components Ψ'_0 is recognized by the fact that it contains two components per particle and obeys an equation reducing to the Schrödinger equation in the non-relativistic limit (Eqn (2)). By eliminating the smaller components of the wave function, Eqn (1) may be reduced to an equation for Ψ'_0 , correct as far as terms in $1/c^2$ provided that R_{ab} is large enough to make

$$|W - K_a| < 2m_a c^2.$$

The reduced wave equation may be written in the form

$$H_R \Psi'_0 = W \Psi'_0, \quad \dots\dots (2)$$

$$H_R = H_0 + H_I + H_{II} + H_{III},$$

$$H_0 = \sum \mathbf{P}_a^2 / 2m_a + V + J,$$

$$H_I = - \sum \mathbf{P}_a^4 / 8m_a^3 c^2 - \sum_{a \neq b} (\mathbf{P}_a^2 / 2m_a^2 c^2) J_{ab},$$

$$H_{II} = \sum (1/2m_a^2 c^2) \nabla_a K_a \times \mathbf{P}_a \cdot \mathbf{S}_a,$$

$$H_{III} = \sum (\hbar^2 / 4m_a^2 c^2) [\nabla_a^2 K_a + \nabla_a K_a \cdot \nabla_a],$$

where $\mathbf{S}_a = \frac{1}{2} \hbar \boldsymbol{\sigma}_a$. The reduced Hamiltonian H_R is not Hermitian because the equation

$$[W - V - J] \Psi'_0 = [\sum (\mathbf{P}_a^2 / 2m_a) + t(1/c^2)] \Psi'_0, \quad \dots\dots (3)$$

where $t(1/c^2)$ denotes terms in $1/c^2$, has been used in obtaining H_I . In other words, the usual procedure for evaluating the relativistic terms by taking their expectation values with a wave function satisfying (3) has already begun. The expectation value of H_I with such a wave function will thus be real and correct to the present order of approximation.

2.1. Breit Operators and Intrinsic Moments

For their work on hydrogen, Barker and Glover (1955) used a Bethe-Salpeter equation in which the Coulomb interaction is corrected by the Breit operator (Breit 1930) and the intrinsic magnetic moments of the proton and electron were introduced phenomenologically, following Pauli (1933), by adding to the interactions an operator U_{IM} . In the present theory the Coulomb interactions are made relativistically invariant up to terms in $1/c^2$ (Breit 1937) by the addition of

Breit operators for each pair of charged particles. The Breit operator is known to give correct results when its expectation value is taken (Breit 1932, Brown and Ravenhall 1951). The effect of the intrinsic magnetic moments $\mu_a \epsilon_a \hbar / 2m_a c$ ($\epsilon_a = e_a$ for charged particles, $\epsilon_a = e$ for neutrons) is taken into account by Pauli terms which may be taken in the form of a sum of two-particle operators, each identical with an operator U_{IM} of Barker and Glover apart from notation and the omission of contact interactions in the present work.

The expectation value of these Breit and intrinsic moment terms is the expectation value with Ψ_0 of

$$M_R = M_1 + M_2 + M_3 + M_4, \quad \dots (4)$$

$$M_1 = - \sum_{a>b} (e_a e_b / 2m_a m_b c^2) (R_{ab}^{-1} \mathbf{P}_a \cdot \mathbf{P}_b + R_{ab}^{-3} \mathbf{R}_{ab} \mathbf{R}_{ab} : \mathbf{P}_a \mathbf{P}_b),$$

$$M_2 = - \sum_{a=b} (g_{sa} e e_b / 2m_a m_b c^2) \nabla_a R_{ab}^{-1} \times \mathbf{P}_b \cdot \mathbf{S}_a,$$

$$M_3 = \sum_{a=b} (\mu_a \epsilon_a e_b / m_a^2 c^2) \nabla_a R_{ab}^{-1} \times \mathbf{P}_a \cdot \mathbf{S}_a,$$

$$M_4 = \sum_{a>b} (g_{sa} g_{sb} e^2 / 4m_a m_b c^2) \nabla_b \nabla_a R_{ab}^{-1} : \mathbf{S}_a \mathbf{S}_b,$$

where $g_{sa} = 2(\epsilon_a - \epsilon_a / \epsilon_a) e$. For the hydrogen atom M_R is precisely the operator obtained by Barker and Glover by applying a Foldy-Wouthuysen (1950) transformation to their Bethe-Salpeter equation, but without the contact terms. Thus the operator (4) may be considered to be the correct one for terms in $1/c^2$.

It is noteworthy that each term of M_R has a simple physical meaning. M_1 is the electromagnetic correction to the static Coulomb interaction for the motion of the particles (Darwin 1920). M_2 is the sum of the interactions between the magnetic moment of particle a and the magnetic field produced by the motion of particle b . M_3 is the sum of the spin-orbit interactions between the intrinsic moment of particle a and the effective magnetic field produced by its motion in the electric field of the other particles. The corresponding spin-orbit interaction for the Dirac part of the magnetic moments, $e_a \hbar / 2m_a c$ is contained in the term H_{II} (Eqn (2)). The Thomas precession, included automatically in the reduced Hamiltonian obtained from a relativistic wave equation, gives rise to a subtractive term (Case 1954) of the same form as the spin-orbit interaction in H_{II} . This explains the difference of a factor 2 in the coefficients of H_{II} , M_3 . M_4 is the interaction between the magnetic moments of the particles after omitting the contact interaction of Sessler and Foley (1953; quantum-mechanical derivation in Sucher and Foley 1954).

2.2. Relativistic Corrections to Nuclear Interactions

In §2 the relativistic wave equation for the atom was reduced as far as terms in $1/c^2$ assuming the types of nuclear forces appearing in Eqn (1). The relativistic corrections in $1/c^2$ to the nuclear forces have to be determined and this can be done for more general forces than those considered in §2. The approximate relativistic corrections to any nuclear interactions which are independent of velocity and depend on position through the inter-nucleon vectors $\mathbf{R}_{\nu\sigma}$ only will be found by requiring the reduced form of the nuclear wave equation to be Lorentz invariant, as was done by Breit (1937) for one particle. It is assumed that the corrections may be evaluated by taking expectation values. This method yields those correction terms which are bilinear in the nucleon momenta (Eqn (7)),

and these are the only terms giving electron-nucleon terms when the nucleon momentum \mathbf{P}_ν is given by its expression in the centre-of-mass system of the atom (Eqn (10)).

In order to apply a Lorentz transformation to the nuclear wave equation it is convenient to introduce a multiple-time formalism. Let the wave equation for the nucleons, interacting through a field ϕ , be

$$H\Psi = \sum_\nu (H_\nu + H'[\phi(\mathbf{R}_\nu, t)])\Psi = i\hbar(\partial\Psi/\partial t), \quad \dots\dots (5)$$

where H_ν is the Dirac Hamiltonian for nucleon ν . Let the function

$$\Phi(\mathbf{R}_1, t_1; \dots; \mathbf{R}_A, t_A),$$

with a separate time for each nucleon, satisfy

$$i\hbar(\partial\Phi/\partial t_\nu) = (H_\nu + H'[\phi(\mathbf{R}_\nu, t_\nu)])\Phi, \\ \partial\Phi/\partial t = 0.$$

If we define the wave function by $\Psi = \Phi(\mathbf{R}_1, t; \dots; \mathbf{R}_A, t)$ we obtain the wave equation (5):

$$i\hbar(\partial\Psi/\partial t) = i\hbar \sum_\nu (\partial\Phi/\partial t_\nu)_{t_\nu=t} - H\Psi.$$

If Φ_0 has two components per nucleon the reduced wave equation is obtained by putting $t_\nu = t$ in an equation of the form

$$(H_R + Q)\Phi_0 = \sum[i\hbar(\partial/\partial t_\nu) - Mc^2]\Phi_0, \quad \dots\dots (6)$$

where H_R is the Hamiltonian (2) for nucleons only and Q is the relativistic correction in $1/c^2$ to the nuclear interaction $U \equiv V + J$. The exact form of the nuclear spin-orbit interaction of type H_{II} is not required.

Applying a Lorentz transformation to the wave equation (6) one finds that the expectation value of $H_R + Q$ is invariant in form if, for instance,

$$Q = \text{Herm} (1/2M^2c^2) \sum_{\nu > \sigma} \left[K_{\nu\sigma} \mathbf{P}_\nu \cdot \mathbf{P}_\sigma + \mathbf{R}_{\nu\sigma} \nabla_\nu U : \mathbf{P}_\nu \mathbf{P}_\sigma \right], \quad \dots\dots (7)$$

provided only that $\sum_{\nu > \sigma} K_{\nu\sigma} = 2J - U$. Herm indicates that the Hermitian part is to be taken.

The full correction to the proton Coulomb interaction is contained in M_R (Eqn (4)). For the Coulomb interaction, $K_{\nu\sigma}$ may be chosen so that Q reduces to M_1 . M_1 and the expressions found by Breit (1937, 1938) are all equivalent to (7) as far as the resulting electron-nucleon terms of §3 are concerned.

§ 3. THE CENTRE OF MASS SYSTEM

The internal energy of the atom is the energy in the centre-of-mass system of the electrons and nucleons. In §§3-4.3 the various terms found in §§2-2.2 are divided into electron, nucleon, and electron-nucleon terms in the centre-of-mass system. Only terms involving electronic operators are required in the present work.

Let the N electrons of mass m be distinguished by Latin suffixes and the A nucleons of mass M by Greek suffixes. Internal coordinates will be measured from the classical centre of mass of the nucleus, \mathbf{R} :

$$\mathbf{r}_k = \mathbf{R}_k - \mathbf{R}, \quad k = 1, 2, \dots, N \\ \mathbf{s}_\nu = \mathbf{R}_\nu - \mathbf{R}, \quad \nu = 2, 3, \dots, A \\ \mathbf{R} \equiv (1/A) \sum \mathbf{R}_\nu. \quad \dots\dots (8)$$

Define \mathbf{X} by

$$(Nm + AM)\mathbf{X} = m\sum \mathbf{R}_k + M\sum \mathbf{R}_\nu$$

and let the momenta conjugate to $\mathbf{r}_k, \mathbf{s}_\nu, \mathbf{X}$ be $\mathbf{p}_k, \mathbf{q}_\nu, \mathbf{P}$, respectively. Then

$$\mathbf{P} = \sum \mathbf{P}_\alpha.$$

In the centre-of-mass system, $\sum \mathbf{P}_\alpha = 0$ and

$$\mathbf{P}_k = \mathbf{p}_k, \quad \dots\dots (9)$$

$$\mathbf{P}_\nu = \mathbf{q}_\nu' - (1/A)\sum \mathbf{p}_k, \quad \dots\dots (10)$$

$$\mathbf{q}_\nu' \equiv \mathbf{q}_\nu - (1/A)\sum \mathbf{q}_\sigma.$$

Eqns (8), (10) hold also for $\nu = 1$ with the definitions

$$\mathbf{s}_1 \equiv -\sum_{\nu=2}^A \mathbf{s}_\nu, \quad \mathbf{q}_1 \equiv 0.$$

The total orbital angular momentum of the atom is the generator of an infinitesimal rotation for the coordinate part of the wave function, $\sum \mathbf{L}_\nu + \sum \mathbf{L}_k$, where

$$\mathbf{L}_\nu \equiv \mathbf{s}_\nu \times \mathbf{q}_\nu, \quad \mathbf{L}_k \equiv \mathbf{r}_k \times \mathbf{p}_k.$$

Although \mathbf{s}_1 is not an independent coordinate the sum over ν may include $\nu = 1$ since \mathbf{q}_1 vanishes. The nuclear angular momenta which occur naturally in the electron-nucleon interactions are

$$\mathbf{L}_\nu' \equiv \mathbf{s}_\nu \times \mathbf{q}_\nu', \quad \nu = 1, 2, \dots, A. \quad \dots\dots (11)$$

These angular momenta include the nucleon recoil correction (Gartenhaus and Schwartz 1957).

The electronic Hamiltonian in the centre-of-mass system is found from (2), (4), (7) using Eqns (9), (10) for the momenta. The term H_0 (Eqn (2)) becomes

$$\sum \mathbf{p}_k^2/2m + T_A + (\sum \mathbf{p}_k)^2/2AM + V_e + V_{ep} + V_p + U, \quad \dots\dots (12)$$

where $T_A \equiv \sum \mathbf{q}_\nu'^2/2M$; V_e, V_{ep}, V_p are the electron, electron-proton and proton Coulomb interactions, respectively, and U is the specifically nuclear interaction of §2.2.

The electron and electron-nucleon terms from H_I (Eqn (2)), Q (Eqn (7)), and the proton-proton part of M_R (Eqn (4)) are

$$-\sum \mathbf{p}_k^4/8m^3c^2 - (\sum \mathbf{p}_k)^4/8A^3M^3c^2 \quad \dots\dots (13a)$$

$$-(1/2A^2M^2c^2)(\sum \mathbf{p}_k)^2(T_A + V_p + U) \quad \dots\dots (13b)$$

$$+ (1/2A^2M^2c^2) \left[\sum_{\nu < \sigma} \mathbf{R}_{\nu\sigma} \nabla_\nu (V_p + U) - (1/M) \sum \mathbf{q}_\nu' \mathbf{q}_\nu' \right] : \sum \mathbf{p}_k \sum \mathbf{p}_l. \quad \dots\dots (13c)$$

The second term of (13a) can be neglected. Since the mass of the nucleus is

$$M_A \approx AM + (T_A + V_p + U)/c^2,$$

(13b) combines with the isotope shift term of (12) to give the usual term

$$(\sum \mathbf{p}_k)^2/2M_A$$

(Hughes and Eckart 1930).

By a simple extension of the virial theorem the expectation value of (13c) is zero, provided that the nuclear forces are of the types considered in §2.2.

There is no direct coupling between electrons and nucleons from nuclear forces depending on velocity through $\mathbf{P}_\nu - \mathbf{P}_\sigma$.

Of the remaining terms, H_{II} , H_{III} (Eqn (2)) and M_3 (Eqn (4)) are dealt with in §4.2. The electron-nucleon parts of M_1 , M_2 , M_4 are considered in §4.3 and their purely electronic parts are included in the final electronic Hamiltonian in §5.

§ 4. INTERACTIONS WITH THE NUCLEUS

The electron-nucleon interactions may be expressed as multipole expansions by the use of tensor operators (Racah 1942, Edmonds 1957). The preliminary multipole expansion of $R_{k\nu}^{-3}$ is derived in the Appendix (Eqn (A4)), together with the expansions used in §4.2.

4.1. The Coulomb Interaction

The Coulomb interaction V_{ep} is

$$\begin{aligned} V_{ep} &= - \sum_{k,\nu} ee_\nu / |\mathbf{r}_k - \mathbf{s}_\nu| \\ &= - \sum_{k,\nu,n} ee_\nu [\max(r_k, s_\nu)]^{-2n-1} \mathcal{Y}(\mathbf{r}_k \cdot \mathbf{s}_\nu; n), \dots\dots (14) \end{aligned}$$

where the solid harmonics \mathcal{Y} are given in terms of Legendre polynomials by

$$\mathcal{Y}(\mathbf{r} \cdot \mathbf{s}; n) = (rs)^n P_n(\mathbf{r} \cdot \mathbf{s} / rs). \dots\dots (15)$$

For $r_k > s_\nu$, with a nucleus containing Z protons, the non-hyperfine structure part of (14) is $-\sum Ze^2/r_k$. The correction for taking this to be valid over the whole of space is

$$\sum_{k,\nu} ee_\nu (r_k^{-1} - s_\nu^{-1}), \quad r_k < s_\nu. \dots\dots (16)$$

This is therefore the exact operator for the nuclear field effect in isotope shift. Smaller nuclear structure corrections arising from the non-hyperfine structure operators of §4.3 are of relative order $\alpha(m/M)$ and are neglected.

4.2. The Spin-Orbit Interaction

In the centre-of-mass system the relevant spin-orbit terms from H_{II} , M_3 (Eqns (2, 4)) are

$$\frac{e(1+2\mu_e)}{2m^2c^2} \left[\sum_{k \neq l} e \nabla_k \mathbf{r}_{kl}^{-1} - \sum_{k,\nu} e_\nu \nabla_k R_{k\nu}^{-1} \right] \times \mathbf{p}_k \cdot \mathbf{s}_k,$$

where $\mathbf{r}_{kl} \equiv \mathbf{r}_k - \mathbf{r}_l$. By (A5) the second sum for $r_k > s_\nu$ gives multipole terms of all even orders, the non-hyperfine structure terms being

$$\frac{Ze^2(1+2\mu_e)}{2m^2c^2} \sum r_k^{-3} \mathbf{L}_k \cdot \mathbf{s}_k.$$

For $r_k < s_\nu$, (A6) shows that the multipole terms are of even order ≥ 2 .

H_{III} (Eqn (2)) contains contact interactions and s electron terms which are not dealt with in this paper.

4.3. The Hyperfine Structure Interaction

The main magnetic hyperfine structure interaction is contained in M_1 , M_2 , M_4 (Eqn (4)), other hyperfine structure terms having been found in §§4.1, 4.2. In the centre-of-mass system the electron-nucleon part of these operators contains purely electronic terms since the nucleon momenta (10) contain \mathbf{p}_k . The principal

non-hyperfine structure terms (i.e. neglecting nuclear structure corrections) are, for $r_k > s_\nu$,

$$\frac{-Ze^2}{2mAMc^2} \sum_{k,l} (r_k^{-1} \mathbf{p}_k \cdot \mathbf{p}_l + r_k^{-3} \mathbf{r}_k \mathbf{r}_k : \mathbf{p}_k \mathbf{p}_l + g_{se} r_k^{-3} \mathbf{r}_k \times \mathbf{p}_l \cdot \mathbf{S}_k),$$

$$g_{se} = -2(1 + \mu_e).$$

The principal hyperfine structure terms, neglecting nuclear structure and the recoil of the nucleus as a whole, may be transformed into the usual form of the magnetic hyperfine structure interaction (Schwartz 1955, Eqn (A8)), but with nucleon recoil effects included by the occurrence of \mathbf{L}_ν' (Eqn (11)) instead of \mathbf{L}_ν . The exchange magnetic moment of the nucleus is not included in this derivation. The s-electron hyperfine structure terms have not been obtained; the nucleon spin part comes from the electron-nucleon spin-spin interaction at small distances and the proton orbital part comes from the hyperfine structure interaction for $r_k < s_\nu$. There are nuclear structure correction terms of all multipole orders. The retardation part of M_R (Eqn (4)) affects only these corrections.

Bohr and Weisskopf (1950) calculated the effect of smoothed-out distributions of nuclear spin and orbital magnetic moments on the magnetic dipole hyperfine structure, using relativistic wave functions for an orbital electron. As far as terms in $1/c^2$ their method is similar to the present approach, without the recoil effects and small corrections and without treating the nucleons individually.

§ 5. THE ELECTRONIC HAMILTONIAN

Terms of the electronic Hamiltonian have been given in §§ 3, 4.1, 4.2, 4.3. There are also some purely electronic terms in M_1 , M_2 , M_4 (Eqn (4)). The resulting non-hyperfine structure electronic Hamiltonian for $r_k > s_\nu$, as far as terms in $1/c^2$, omitting nuclear structure terms such as (16), contact and 'divergence' terms, terms of relative order $(m/M)^2$ and terms neglected on parity considerations, is

$$H_e = \sum_{i=1}^7 H_i, \quad \dots\dots (17)$$

$$H_1 = \sum \mathbf{p}_k^2 / 2m - \sum Ze^2 / r_k - \sum_{k>l} e^2 / r_{kl},$$

$$H_2 = (\sum \mathbf{p}_k)^2 / 2M_A,$$

$$H_3 = - \sum \mathbf{p}_k^4 / 8m^3 c^2,$$

$$H_4 = \sum (Ze^2(1 + 2\mu_e) / 2m^2 c^2) r_k^{-3} \mathbf{L}_k \cdot \mathbf{S}_k$$

$$+ \sum_{k,l} (Ze^2(1 + \mu_e) / m M_A c^2) r_k^{-3} \mathbf{r}_k \times \mathbf{p}_l \cdot \mathbf{S}_k,$$

$$H_5 = \sum_{k \neq l} (e^2 / 2m^2 c^2) r_{kl}^{-3} \mathbf{r}_{kl} \times [2(1 + \mu_e) \mathbf{p}_l - (1 + 2\mu_e) \mathbf{p}_k] \cdot \mathbf{S}_k,$$

$$H_6 = - \sum_{k>l} (e^2 / 2m^2 c^2) (r_{kl}^{-1} \mathbf{p}_k \cdot \mathbf{p}_l + r_{kl}^{-3} \mathbf{r}_{kl} \mathbf{r}_{kl} : \mathbf{p}_k \mathbf{p}_l)$$

$$- \sum_{k,l} (Ze^2 / 2m M_A c^2) (r_k^{-1} \mathbf{p}_k \cdot \mathbf{p}_l + r_k^{-3} \mathbf{r}_k \mathbf{r}_k : \mathbf{p}_k \mathbf{p}_l),$$

$$H_7 = \sum_{k>l} (eg_{se} / 2mc^2) (r_{kl}^{-3} \mathbf{S}_k \cdot \mathbf{S}_l - 3r_{kl}^{-5} \mathbf{r}_{kl} \mathbf{r}_{kl} : \mathbf{S}_k \mathbf{S}_l).$$

In H_4 , H_6 , AM has been replaced by M_A .

§ 6. THE NORMAL MASS EFFECT IN ISOTOPE SHIFT

The Hamiltonian H_e (Eqn (17)) contains the term H_2 for the mass effect in isotope shift (Hughes and Eckart 1930). The division of the mass effect into the normal and specific effects is represented by

$$H_2 = \sum \mathbf{p}_k^2 / 2M_A + \sum_{k>l} \mathbf{p}_k \cdot \mathbf{p}_l / M_A. \quad \dots\dots (18)$$

The normal effect arises from the first term of (18) and is the effect of the reduced mass of the electron. The resulting energy shift for a single isotope will now be evaluated by applying the method of Hughes and Eckart (1930) to the Hamiltonian H_e .

Write

$$H_e = H_0(M_A) + H_p,$$

$$H_0(M_A) \equiv \sum \mathbf{p}_k^2 (M_A + m) / 2mM_A - \sum Ze^2/r_k + \sum e^2/r_{kl} \\ + [(1 + 2\mu_e)(1 + 2m/M_A) - 2\mu_e(m/M_A)] \times \sum (Ze^2/2m^2c^2)r_k^{-3} \mathbf{L}_k \cdot \mathbf{S}_k.$$

Then $H_0(M_A)$ contains the main part of H_e , using the reduced mass of the electron and including all spin-orbit terms in $\mathbf{L}_k \cdot \mathbf{S}_k$. Making the transformation

$$r_k = \beta^{-1}r'_k, \quad p_k = \beta p'_k,$$

with

$$\beta \equiv M_A / (M_A + m),$$

yields

$$H_0(M_A) = \beta H'_0(\infty)$$

if terms of order $\mu_e(m/M_A) \times (\text{spin-orbit interaction})$ are neglected. These terms are of the same order of magnitude as the radiative corrections to the fine structure found by Salpeter (1952).

If $(m/M_A)H_p$ can also be neglected one can write $H_p = \beta H'_p$ and the transformed wave equation becomes

$$\beta[H'_0(\infty) + H'_p]\Psi' = W\Psi'.$$

If W_0 is the energy for infinite nuclear mass it follows that $W = \beta W_0$ and the normal shift is, as usual,

$$W - W_0 = -(m/M_A)W.$$

Compared with the normal shift the undetermined shifts due to the fine structure and its radiative corrections are of relative magnitudes $(0.1\% \text{ spin-orbit interaction/term value})$ and $(\langle H_p \rangle_{av}/\text{term value})$. Shifts of these orders are usually negligible.

Since contact interactions have not been considered, s-electron configurations are not covered by this section.

§ 7. DISCUSSION

The method of expanding the Hamiltonian in powers of $1/c^2$ has proved satisfactory for the electronic operators up to terms in $1/c^2$ even when the nuclear Hamiltonian, with certain types of nuclear forces, is taken into account. The nuclear forces whose relativistic corrections were obtained in §2.2 were restricted to local, velocity-independent interactions. Non-local interactions (Frahn and Lemmer 1957) may require different relativistic corrections, yet the terms of (13b) arising from the relativistic correction Q (Eqn (7)) are essential for the

derivation of the isotope shift term H_2 (Eqn (17)) which Hughes and Eckart (1930) derived by treating the nucleus as a single particle. Again, (13c) has zero expectation value, by the virial theorem, because of the presence of terms from Q , thus avoiding an awkward correction to H_2 .

The terms referring to the contact approach of particles remain to be determined by rigorous reduction of the relativistic Hamiltonian and its perturbations.

ACKNOWLEDGMENTS

The author is indebted to Dr. M. J. Kearsley, Professor H. Primakoff and Dr. G. R. Satchler for helpful discussions. Much of this work was done while in receipt of a Maintenance Grant from the Department of Scientific and Industrial Research.

REFERENCES

- ADAMS, E. N., 1951, *Phys. Rev.*, **81**, 1.
 BARKER, W. A., and GLOVER, F. N., 1955, *Phys. Rev.*, **99**, 317.
 BODMER, A. R., 1958, *Nucl. Phys.*, **9**, 371.
 BOHR, A., and WEISSKOPF, V. F., 1950, *Phys. Rev.*, **77**, 94.
 BREIT, G., 1930, *Phys. Rev.*, **36**, 383.
 ——— 1932, *Phys. Rev.*, **39**, 616.
 ——— 1937, *Phys. Rev.*, **51**, 248.
 ——— 1938, *Phys. Rev.*, **53**, 153.
 BROWN, G. E., and RAVENHALL, D. G., 1951, *Proc. Roy. Soc. A*, **208**, 552.
 CASE, K. M., 1954, *Phys. Rev.*, **95**, 1323.
 COURANT, R., and HILBERT, D., 1953, *Methods of Mathematical Physics*, I (New York: Interscience Publishers), pp. 368, 369.
 DARWIN, C. G., 1920, *Phil. Mag.*, **39**, 537.
 EDMONDS, A. R., 1957, *Angular Momentum in Quantum Mechanics* (Princeton: University Press).
 FOLDY, L. L., and WOUTHUYSEN, S. A., 1950, *Phys. Rev.*, **78**, 29.
 FRAHN, W. E., and LEMMER, R. H., 1957, *Nuovo Cim.*, **6**, 664.
 GARTENHAUS, S., and SCHWARTZ, C., 1957, *Phys. Rev.*, **108**, 482.
 HUGHES, D. S., and ECKART, C., 1930, *Phys. Rev.*, **36**, 694.
 ISHIDZU, T., 1951, *Progr. Theor. Phys.*, Japan, **6**, 48, 154.
 LOW, F., 1950, *Phys. Rev.*, **77**, 361.
 MA, S. T., 1956, *Nucl. Phys.*, **2**, 347.
 NEWCOMB, W. A., and SALPETER, E. E., 1955, *Phys. Rev.*, **97**, 1146.
 PAULI, W., *Handb. d. Phys.*, **24**, 1 (Berlin: Springer).
 PERL, W., 1953, *Phys. Rev.*, **91**, 852.
 RACAH, G., 1942, *Phys. Rev.*, **62**, 438.
 SALPETER, E. E., 1952, *Phys. Rev.*, **87**, 328.
 SCHWARTZ, C., 1955, *Phys. Rev.*, **97**, 380.
 SESSLER, A. M., and FOLEY, H. M., 1953, *Phys. Rev.*, **92**, 1321.
 ——— 1955, *Phys. Rev.*, **98**, 6.
 SUCHER, J., and FOLEY, H. M., 1954, *Phys. Rev.*, **95**, 966.
 SZEGÖ, G., 1939, *Orthogonal Polynomials*, American Mathematical Society Colloquium Publications, Vol. 23, p. 80.

APPENDIX

MULTIPOLE EXPANSIONS

The multipole expansion of $R_{k\nu}^{-3}$ or, dropping suffixes, $|\mathbf{r}-\mathbf{s}|^{-3}$ may be effected by means of the polynomials $P(x; \lambda, n)$ defined by

$$(1-2hx+h^2)^{-\lambda} \equiv \sum_{n=0}^{\infty} h^n P(x; \lambda, n). \quad \dots (A1)$$

These polynomials have the property

$$(n+\lambda)P(x; \lambda, n) = \lambda[P(x; \lambda+1, n) - P(x; \lambda+1, n-2)] \dots\dots (A2)$$

(Szegő 1939), which holds for all integers n if $P(x; \lambda, n)$ is put equal to zero for negative values of n . Write

$$\mathcal{Y}(\mathbf{r} \cdot \mathbf{s}; \lambda, n) \equiv (rs)^n P(\mathbf{r} \cdot \mathbf{s}/rs; \lambda, n).$$

Then \mathcal{Y} reduces to the solid harmonic (15) for $\lambda = \frac{1}{2}$. The expansion (A1) may now be written

$$|\mathbf{r} - \mathbf{s}|^{-\lambda} = \sum_{n=0}^{\infty} [\max(r, s)]^{-2n-\lambda} \mathcal{Y}(\mathbf{r} \cdot \mathbf{s}; \lambda/2, n). \dots\dots (A3)$$

This series is absolutely convergent for $r \neq s$ (Courant and Hilbert 1953) so that rearrangement of terms is permissible. By (A2) one obtains

$$\mathcal{Y}(\mathbf{r} \cdot \mathbf{s}; 3/2, n) = \sum (2l+1)(rs)^{n-l} \mathcal{Y}(\mathbf{r} \cdot \mathbf{s}; l),$$

where the summation is over even values of l from 0 to n if n is even and over odd values of l from 1 to n if n is odd. Using this result in (A3) with $\lambda = 3$ gives, for $r > s$,

$$|\mathbf{r} - \mathbf{s}|^{-3} = \sum_{n=0}^r (2n+1)r^{-2n-3}(1-s^2/r^2)^{-1} \mathcal{Y}(\mathbf{r} \cdot \mathbf{s}; n). \dots\dots (A4)$$

The expansion for $r < s$ is obtained by interchanging r, s . This is the desired multipole expansion since $\mathcal{Y}(\mathbf{r} \cdot \mathbf{s}; n)$ is the scalar product of two tensor operators depending on \mathbf{r}, \mathbf{s} respectively (Racah 1942).

If \mathbf{a} is a vector of odd parity belonging to the same system as \mathbf{r} , (A3) with $\lambda = 1$ gives, omitting terms on parity considerations,

$$\begin{aligned} \nabla_r |\mathbf{r} - \mathbf{s}|^{-1} \cdot \mathbf{a} &\rightarrow \sum_{n \text{ even}} [r^{-2n-1} \nabla_r \mathcal{Y}(\mathbf{r} \cdot \mathbf{s}; n) \cdot \mathbf{a} \\ &\quad - (2n+1)r^{-2n-3} \mathcal{Y}(\mathbf{r} \cdot \mathbf{s}; n) \mathbf{r} \cdot \mathbf{a}], \quad r > s, \dots\dots (A5) \end{aligned}$$

$$\rightarrow \sum_{n \text{ even}} s^{-2n-1} \nabla_r \mathcal{Y}(\mathbf{r} \cdot \mathbf{s}; n) \cdot \mathbf{a}, \quad r < s. \dots\dots (A6)$$

The sum over n even includes $n=0$.

Ultra-violet Extensions of the Arc Spectra of the Alkaline Earths: The Absorption Spectrum of Magnesium Vapour

By K. CODLING

Physics Department, Imperial College, London

Communicated by W. R. S. Garton; MS. received 17th October 1960

Abstract. The principal series of magnesium has been photographed, in absorption, in the ultra-violet region between 2400 Å and 1600 Å by means of a 3-metre vacuum spectrograph and a large King furnace. Measurement of twenty-four new members of the series against accurate copper standards leads to a revised value of 61670.6 cm^{-1} for the ionization potential of Mg I, an increase of 1.5 cm^{-1} on the value previously accepted.

§ 1. INTRODUCTION

THE following work on magnesium was undertaken as a continuation of investigations of the spectra of the alkaline earth metals, results for one of these, Ba, having already been published (Garton and Codling 1960); work on Ca is almost complete whilst work on Sr is in progress. Unlike the spectra of Ba, Sr and Ca, that of Mg exhibits no auto-ionization phenomena in the region 2400 Å–1400 Å. This is to be expected, since the first ionization potential of magnesium corresponds to a wavelength of 1620 Å; also there is no empty d shell in magnesium corresponding to the 3d, 4d and 5d shells of Ca, Sr and Ba.

The magnesium principal series has received comparatively little attention to date. Moore (1949) lists only the 3p, 4p and 5p members of the $3snp \ ^1P_1$ series and the 3P_1 series is given to the 7th member. The ionization potential of magnesium given by Moore (1949) is based on the Paschen (1931) limit.

§ 2. EXPERIMENTAL

The absorption spectra have been photographed with a 3-metre normal incidence vacuum spectrograph provided with a Bausch and Lomb aluminized replica grating of 30 000 lines to the inch, blazed at 1500 Å in the first order. A 12 in. \times 3 in. plate covers a wavelength range of 800 Å.

As explained previously (Garton and Codling 1960), the absorption vessel used in these experiments is a large King furnace, the basic part of which is a graphite tube 13 in. in length and of $\frac{3}{4}$ in. bore. A nickel liner 8 in. long is used to contain the metal, since the alkaline earths quickly react with the graphite to form their respective carbides. This nickel liner is insulated from the graphite tube by mica foil and has washers of nickel, at intervals along the tube, to retain the alkaline earth metal and to ensure an even distribution along the tube length. The furnace is run in an atmosphere of helium at a pressure of approximately 2 mm Hg. The furnace is heated to a temperature of 750°C. There is no lithium fluoride window between furnace and slit. This necessitates a differential pumping system, and, whilst there is a pressure of 2 mm Hg on the furnace side

of the slit, a pressure of less than 1 micron is maintained in the body of the spectrograph.

In the work on Ba, internal wavelength standards were used, these being mainly Ca and Sr impurities in the absorption spectrum itself. Since then, however, improvement has been made in the comparison wavelengths used. Between flash-tube and furnace is placed a molybdenum hollow cathode, of $\frac{1}{32}$ in. wall, $1\frac{1}{4}$ in. long with $\frac{1}{2}$ in. internal diameter. In this are excited the emission spectra of Cu I and Cu II. The hollow cathode runs in pure helium at a pressure of 1 or 2 mm of mercury, and is placed on the optical axis of the system about three feet away from the spectrograph slit. The exposure time required is only of the order of twenty seconds in the region 2400 Å–1600 Å, although there is no condensing lens between cathode and slit.

To provide a background continuum a 'Lyman' flash-tube is used (Garton 1953). The absorption spectrum of the alkaline earth metal vapour is first photographed, the light from the flash-tube passing centrally through the hollow cathode. The copper emission spectrum is subsequently superimposed.

§ 3. SPECTROGRAMS

The spectra were photographed on Ilford Q2 plates and measured with a Zeiss comparator capable of accuracy to a tenth of a micron. On the 12 in. plates used, the reciprocal dispersion was 0.003 Å per micron. Due to the

Table 1. Principal Series Mg I $3s^2\ ^1S_0 - 3snp\ ^1P_1^0$

n	$\lambda_{\text{vac}} (\text{\AA})$	$T_n (\text{cm}^{-1})$	n^* (Limit $T_\infty = 61669.14 \text{ cm}^{-1}$)	n^* (Limit $T_\infty = 61670.64 \text{ cm}^{-1}$)
3	2852.956	35051.36	2.0304	2.0304
4	2026.479	49346.67	2.9842	2.9840
5	1827.965	54705.64	3.9697	3.9693
6	1747.806	57214.59	4.9634	4.9625
7	1707.078	58579.63	5.9598	5.9584
8	1683.428	59402.60	6.9583	6.9560
9	1668.446	59936.01	7.9572	7.9538
10	1658.322	60301.92	8.9590	8.9540
11	1651.177	60562.86	9.9595	9.9530
12	1645.936	60755.70	10.9608	10.9518
13	1641.973	60902.34	11.963	11.951
14	1638.895	61016.72	12.969	12.954
15	1636.480	61106.76	13.969	13.950
16	1634.517	61180.15	14.980	14.957
17	1632.934	61239.46	15.981	15.953
18	1631.616	61288.93	16.989	16.956
19	1630.520	61330.13	17.992	17.952
20	1629.586	61365.28	19.004	18.957
21	1628.795	61395.08	20.010	19.956
22	1628.116	61420.69	21.016	20.954
23	1627.528	61442.87	22.022	21.950
24	1627.016	61462.21	23.028	22.945
25	1626.561	61479.40	24.049	23.954
26	1626.164	61494.41	25.060	24.953
27	1625.814	61507.65	26.068	25.947
28	1625.501	61519.49	27.079	26.945
29	1625.220	61530.13	28.096	27.946

N.B. $n=3$ member is taken from Moore (1949) tables.

breadth of the Mg lines, the series members were not measurable to a greater accuracy than ± 1 micron. The copper emission spectrum has recently been given with an accuracy to 0.001 Å and better (Reader *et al.* 1960) but a greater accuracy than 0.004 Å for the Mg lines is not claimed.

§ 4. RESULTS

Table 1 shows the vacuum wavelengths and wave numbers of principal series lines from 3s3p to 3s29p $^1P_1^0$. Columns 4 and 5 give the effective quantum numbers n^* of each line for two different limits, the limit in column 4 being the one given by Moore (1949), 61669.14 cm⁻¹; the limit referred to in column 5 is 1.5 cm⁻¹ greater than this, viz. 61670.64 cm⁻¹.

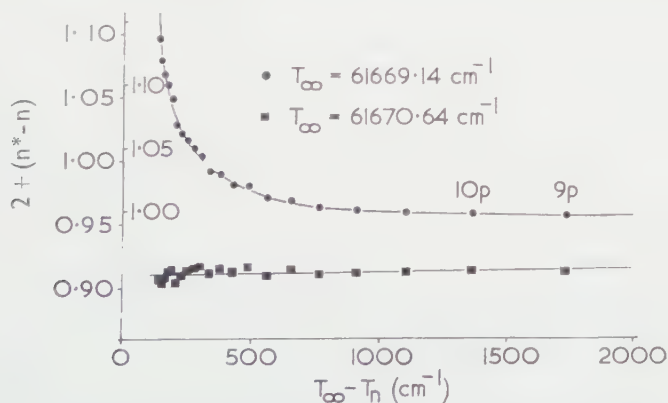
In addition, Table 2 shows six high series members of the triplet series, measured with an accuracy to 0.01 Å; their effective quantum number n^* given in column 4 was determined using the second of the two limits mentioned previously.

Table 2. 3s²1S₀-3snp 3P_1 . Limit = 61670.64 cm⁻¹

n	λ_{vac} (Å)	T_n (cm ⁻¹)	n^*
21	1629.21	61379.4	19.41
22	1628.46	61407.7	20.43
23	1627.82	61431.9	21.44
24	1627.27	61452.6	22.44
25	1626.79	61470.7	23.43
26	1626.36	61487.0	24.45

§ 5. INTERPRETATION

If a plot is made of quantum defect $n^* - n$ against $T_\infty - T_n$ (where T_∞ is the ionization limit in cm⁻¹) using the Moore (1949) limit of 61669.14 cm⁻¹, there is a steady rise in quantum defect as one goes to higher series members—as shown in the Figure. However, if the limit 61670.64 cm⁻¹ is used, the curve becomes a straight line. Following Shenstone and Russell (1932), the best value of the ionization limit is that which gives the closest approach to a straight line. The figure, therefore, indicates that the second limit is the better one. It is conceivable that the gradual increase in quantum defect at higher series members when the Moore limit is used may be caused not by an error in this limit, but by a real



Magnesium principal series; variation in quantum defect.

shift of the upper terms, due perhaps to resonance collisions. To try to exclude this possibility only those plates taken at low vapour pressure of Mg were measured and, as previously stated, the Mg was in a helium atmosphere of only 2 mm Hg pressure. The limit $T_\infty = 61670.6 \text{ cm}^{-1}$ is believed to be correct to $\pm 0.1 \text{ cm}^{-1}$, a second decimal place in either limit being meaningless, since the limit has been changed by such a relatively large amount.

As the quantum defect curve is so close to a straight line for the second limit, term values T_n have been fitted to a Ritz formula:

$$T_n = T_\infty - \frac{R}{(n + \mu + \alpha \bar{\nu}_n)^2}$$

$$\bar{\nu}_n = T_\infty - T_n.$$

Values of μ and α from the plot are $\mu = -1.0500$ and $\alpha = 2.75 \times 10^{-6}$. Using these values the agreement between T_n (observed) and T_n (calculated) is on average 0.1 cm^{-1} , for terms $3s6p^1P_1$ and above. One cannot however expect the lowest members of the series to fit closely to a Ritz formula, as is shown in the $3s3p$ member in particular.

With the advent of rocket spectroscopy on a large scale, it is hoped that these results will be of some use in the analysis of the absorption features from the hot stars.

ACKNOWLEDGMENTS

The author is glad to express great appreciation of the help and encouragement of Dr. W. R. S. Garton, Reader in Physics. The work has been in part performed under a supporting contract of the Atomic Energy Research Establishment, in the form of a Research Studentship awarded to the author.

REFERENCES

- GARTON, W. R. S., 1953, *J. Sci. Instrum.*, **30**, 119.
 GARTON, W. R. S., and CODLING, K., 1960, *Proc. Phys. Soc.*, **75**, 87.
 MOORE, C. E., 1949, *Circ. Nat. Bur. Stand.*, No. 467, Vol. I.
 PASCHEN, F., 1931, *S.B. Preuss. Akad. Wiss.*, **32**, 709.
 READER, J., MEISSNER, K. W., and ANDREW, K. L., 1960, *J. Opt. Soc. Amer.*, **50**, 221.
 SHENSTONE, A. G., and RUSSELL, H. N., 1932, *Phys. Rev.*, **39**, 415.

The Ohmic Heating of Positive Ions in an Impure Plasma

By A. A. WARE AND J. A. WESSON

Research Laboratory, Associated Electrical Industries, Aldermaston Court, Berks.

Communicated by D. R. Click; MS received 31st August 1960

Abstract. It is shown that in a plasma which is heated by an electric current the direct heating of the positive ions can be increased markedly by the presence of a small concentration of impurity ions. With favourable impurity concentrations, this heating is sufficient to explain the observed ion temperature in ZETA and SCEPTRE.

§ 1. INTRODUCTION

WHEN a current is passed through an ionized pure gas most of the heat generated is given to the electrons, and only a small fraction of the order m/M , goes directly to the positive ions, m and M being the electron and ion masses respectively. If the only energy loss from the electrons is that to the positive ions, the electron temperature will rise faster than the ion temperature until the temperature difference is sufficient for this loss to be comparable with the rate of heating of the electrons.† The positive ion and electron temperatures will then rise together, but the electron temperature will always be greater than the ion temperature. If, however, the electron temperature is prevented from rising owing to a heat loss mechanism peculiar to the electrons, then the ion temperature will rise until the rate of ion heating is equal to the rate of energy loss to the electrons. Because of the low rate of ion heating this temperature will be only slightly in excess of the electron temperature.

It will be shown in this paper that the presence of a small percentage of impurity ions with a charge different from that of the initial positive ions can lead to a marked change in the proportion of heat passing directly to the positive ions. In the case where energy losses hold the electron temperature constant, a suitable proportion of impurity ions can lead to the positive ion temperature rising well above the electron temperature. This result is of considerable interest in connection with the high current pinched discharge, where the observed positive ion temperatures (Thonemann *et al.* 1958, Allen *et al.* 1958) are about ten times higher than the electron temperature (Kaufman and Williams 1958).

The positive ion heating mechanism considered here has been referred to in an earlier publication by Ware (1959). Following the discovery by Hughes and Kaufman (1959) of a Doppler shift of impurity spectral lines in SCEPTRE III, it was shown in this earlier paper that the deuterons must have larger drift velocities than the impurity ions, indicating that there was mass motion of the gas as a whole. Secondly, it was pointed out that there would be considerable direct ohmic heating of the deuterons. However, it was not realized at the time that the heating mechanism was independent of the mass motion. In the following theory the ionized gas will be assumed to have no mass motion for the sake of

† It is assumed that the electric field is not large enough to cause runaway conditions.

convenience, but, since the heating rates involve only the relative drift velocities between different types of ions, the results are independent of any net mass motion.

§ 2. MOMENTUM TRANSFER

Consider a uniform fully ionized plasma composed of x types of particle having charges $Z_a e, Z_b e \dots Z_x e$ (where e is the charge on a proton) and masses $m_a, m_b \dots m_x$. If an electric field is applied to the plasma and a quasi-steady state is reached in which the mean acceleration of each type of particle is negligible, the equation of momentum transfer for particles of type r is,

$$n_r Z_r e \mathbf{E} + \sum_s \mathbf{F}_{rs} = 0 \quad \dots\dots(1)$$

where n_r is the concentration of particles of type r and \mathbf{F}_{rs} is the force per unit volume acting on these particles due to collisions with particles of type s .

An approximate expression can be obtained for the forces \mathbf{F}_{rs} by assuming that the velocity distributions of the particles of types r and s are Maxwellian about their respective mean velocities. The true distributions will deviate from this form and neglect of this fact may involve considerable error. In the absence of solutions for the distribution functions for such gas mixtures this approximation must be made.

Let \mathbf{v}_r be the mean velocity of particles of type r . If the relative speed $|\mathbf{v}_r - \mathbf{v}_s|$ is much less than the mean thermal speed of either particles of type r or of type s , the frictional force density is given by an equation of the form

$$\mathbf{F}_{rs} = a_{rs}(\mathbf{v}_s - \mathbf{v}_r), \quad \dots\dots(2)$$

where (Wesson, to be published, Herdan and Liley 1960)

$$a_{rs} = \left(\frac{\pi}{2}\right)^{1/2} \frac{8e^4 \ln \Lambda_{rs}}{3k^3 z} n_r n_s Z_r^2 Z_s^2 \left(\frac{1}{m_r} + \frac{1}{m_s}\right) \left(\frac{T_r}{m_r} + \frac{T_s}{m_s}\right)^{-3/2} \quad \dots\dots(3)$$

where T_r is the temperature of the component r . Λ_{rs} is the well-known ratio of the Debye length to an average distance of closest approach for particles of types r and s . Under the conditions of interest Λ_{rs} is much greater than unity, and the variation of $\ln \Lambda_{rs}$ with the temperatures, particle densities, charges and masses of the components is slow. We shall therefore put all such terms equal to $\ln \Lambda$, where (Rosenbluth, Macdonald and Judd 1957)

$$\Lambda = \frac{3}{2e^3} \left(\frac{k^3 T^3}{\pi n}\right)^{1/2},$$

$\frac{3}{2}kT$ being the mean energy of all the particles present and n the total particle concentration.

§ 3. OHMIC HEATING

If the equations of type (1) are multiplied by \mathbf{v}_r (scalar product) and the x equations added together, the resulting equation reduces to

$$\mathbf{j} \cdot \mathbf{E} = \sum_r \sum_{s \neq r} \mathbf{F}_{rs} \cdot (\mathbf{v}_s - \mathbf{v}_r) \quad \dots\dots(4)$$

where \mathbf{j} is the current density in the plasma. The left-hand side is the total rate at which heat is generated per unit volume. On the right-hand side, a particular term $\mathbf{F}_{rs} \cdot (\mathbf{v}_s - \mathbf{v}_r)$ represents the rate of conversion of energy of drift motion to heat due to the frictional force \mathbf{F}_{rs} .

The heat generated by \mathbf{F}_{rs} will increase the thermal energy of the r and s type particles. The relative proportions in which this energy is shared between

the two types of particles will depend on their relative masses and temperatures. In the special case where there is a large inequality of mass and the temperature difference is not too great, it can be shown that most of the heat is received by the lighter type of particle (Wesson, to be published).

§ 4. THE HEATING OF A DEUTERIUM PLASMA CONTAINING IMPURITY IONS

A deuterium plasma containing a single type of impurity ion with charge Ze will now be considered. The subscripts e, d and i will be used to identify the variables associated with the electrons, deuterons and impurity ions respectively, and the problem will be treated in one dimension, allowing vector quantities to be replaced by scalars. The inequalities $m_i \gg m_d$ and $m_i/T_i \gg m_d/T_d$ will be assumed.

There are three momentum balance equations of the type

$$n_e Z e e E + a_{ed}(v_d - v_e) + a_{ei}(v_i - v_e) = 0, \quad \dots\dots (5)$$

and these can be solved for the three relative drift velocities which take the form

$$v_e - v_d = \frac{a_{di} n_e Z e - a_{ei} n_d Z_d}{a_{ed} a_{di} + a_{ie} a_{ed} + a_{di} a_{ie}} e E. \quad \dots\dots (6)$$

Before considering the heating of the plasma it is of interest to consider the ratio $(v_d - v_i)/(v_d - v_e)$. Using Eqns (3) and (6) and the assumptions already made

$$\begin{aligned} \frac{v_d - v_i}{v_d - v_e} &= \frac{1 - Z^{-1}}{1 - (m_d/m_e)^{1/2} (T_e/T_d)^{3/2}}, \\ &\simeq \frac{1 - Z^{-1}}{1 + 60 (T_e/T_d)^{3/2}}. \end{aligned}$$

The value of this ratio is independent of the concentrations of the three components. If $Z \gg 1$ then, for $T_d = T_e$, $(v_d - v_i)/(v_d - v_e) \simeq 1/60$, and for $T_d = 10T_e$, $(v_d - v_i)/(v_d - v_e) \simeq \frac{1}{3}$. If velocities are measured relative to the mass velocity, v_d approaches $-m_e v_e/m_d = -v_e/3672$ as the impurity concentration approaches zero. Thus with a sufficiently low impurity concentration v_i has the same sign as v_e . Considering now the case where the deuteron concentration approaches zero, v_i approaches $-Z m_e v_e/m_i$ and so v_d becomes much greater than it would be in a pure deuterium plasma provided Z and T_e/T_d are not too large.

Since $m_i \gg m_d$ most of the heat generated by the frictional force F_{di} will go to the deuterons. In the case of the other two friction forces F_{ie} and F_{de} the electrons will receive most of the heat. Since, in addition, energy will be exchanged between the three types of particles due to their difference in temperature, the equation of energy balance for the deuterons takes the form (Spitzer 1958)

$$\frac{3}{2} n_d k \frac{dT_d}{dt} = F_{di}(v_i - v_d) + b_{de}(T_e - T_d) + b_{di}(T_i - T_d), \quad \dots\dots (7)$$

where

$$b_{rs} = \left(\frac{\pi}{2k} \right)^{1/2} 8e^4 \ln \Lambda \frac{n_r n_s Z_r^2 Z_s^2}{m_r m_s} \left(\frac{T_r}{m_r} + \frac{T_s}{m_s} \right)^{-3/2}.$$

To illustrate the importance of direct ion heating we shall take the case of a deuterium plasma with a small concentration of Ov ions in which the electron temperature is kept constant by some energy loss mechanism. For small impurity ion concentrations, the loss to the oxygen ions can be neglected.

Fig. 1 shows the rate of heating of the deuterons due to F_{di} and the rate of energy loss to the electrons for $T_d = 10T_e = 2 \times 10^6$ °K, $n_d = 10^{14}$ cm $^{-3}$ and $E = 3$ v cm $^{-1}$. $\ln \Lambda$ has been put equal to 12. The neglect of the energy loss to the oxygen ions becomes unjustifiable for concentrations greater than about 10%, but if it were taken into account the only result would be a more rapid increase of the energy loss for concentrations above this value. It is seen that over a range of impurity concentrations the direct heating is greater than the energy loss to the electrons, resulting in an increasing deuteron temperature. The heating is a maximum at about 8% oxygen concentration.

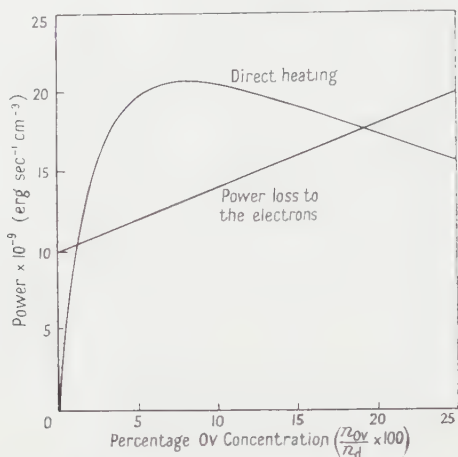


Fig. 1. Variation of the rates of heating and cooling of the deuterons with percentage Ov concentration.

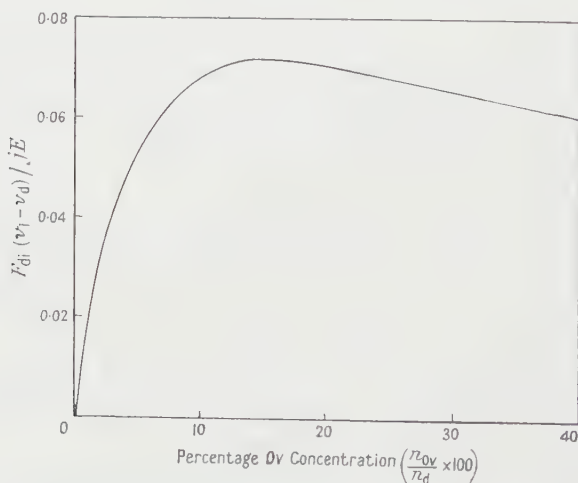


Fig. 2. Variation of the fraction of the total energy input going into direct heating of the deuterons with percentage Ov concentration.

The value of dT_d/dt is positive for all values of T_d less than 2×10^6 °K for the conditions chosen, so that it will be possible for the deuterons to reach this temperature.

In Fig. 2 the ratio $F_{\text{di}}(v_i - v_d)/jE$ is shown. This ratio is the fraction of the total energy input which goes into direct heating of the deuterons. The maximum value is about $7 \cdot 0$ compared with $0 \cdot 027 \cdot 0$ in a pure deuterium plasma.

The rate of heating of the deuterons due to the presence of the impurity ions, $F_{\text{di}}(v_i - v_d)$, can be compared with the rate at which they would be heated in a pure deuterium plasma. It was shown by Spitzer (1956) that this latter rate was too slow to account for the ion temperatures observed in ZETA even if the most favourable condition for ion heating, $T_e = 3T_d$, existed. If this condition does exist then, for $n_d = 10^{14} \text{ cm}^{-3}$, the rate of heating is given by

$$\left(\frac{d\epsilon_d}{dt}\right)_0 = 1 \cdot 89 \times 10^{10} T_d^{-1 \cdot 2}.$$

(This differs slightly from Spitzer's value because he took $\ln \Lambda$ to be 15.) With the same value of n_d and with $n_i = 10^{13} \text{ cm}^{-3}$, $E = 3 \text{ v cm}^{-1}$ and T_e constant at $2 \times 10^5 \text{ }^\circ\text{K}$, the rate of heating is

$$\frac{d\epsilon_d}{dt} = \frac{1 \cdot 14 T_d^{3 \cdot 2}}{(1 + 0 \cdot 88 \times 10^{-10} T_d^{3 \cdot 2})^2} - 770(T_d - 2 \times 10^5).$$

The ratio $(d\epsilon_d/dt)/(d\epsilon_d/dt)_0$ is greater than unity when T_d is within the range $2 \times 10^4 \text{ }^\circ\text{K}$ to $4 \times 10^6 \text{ }^\circ\text{K}$. At $T_d = 2 \times 10^5 \text{ }^\circ\text{K}$ this ratio is 2.4 and at $2 \times 10^6 \text{ }^\circ\text{K}$ it is 50. This shows that the rate of heating due to the presence of impurity ions can be much greater than that by electron-ion collisions in a pure plasma.

§ 5. POSITIVE ION HEATING IN THE TOROIDAL PINCH DISCHARGE

The results of the above calculations are of importance in the study of the high current toroidal pinch discharge, where not only is the electron temperature observed to be held at a low value (Kaufman and Williams 1958) (about $2 \times 10^5 \text{ }^\circ\text{K}$), but the measured temperatures of various impurity ions are about ten times as high (Butt *et al.* 1958, Allibone *et al.* 1958). In such discharges highly ionized impurity ions are certainly present, but unfortunately with unknown concentrations. The above calculations show that if the only heat loss from the positive ions is to the electrons, favourable impurity concentrations will lead to sufficient heating to produce the observed temperatures.

In order to test this hypothesis a series of experiments was carried out in this Laboratory on SCEPTRE IV by Hughes and Williams (private communication) who added small concentrations of Ne to the deuterium flowing through the tube. In all these experiments the addition of further impurity led to a reduction in the Ov Doppler broadening. These results are consistent with the above heating mechanism provided the amount of impurity which enters the discharge from the tube walls is itself beyond the optimum for positive ion heating (see Fig. 2). It is quite possible that the impurity concentration is high enough for this to be the case.

The suggested theory of ion heating implies that the impurity ions will have a velocity with respect to the centre-of-mass velocity in the opposite direction to the electric field. Measurements on SCEPTRE III (Hughes and Kaufman 1959) have shown a velocity of Ov ions of the order 10^6 cm sec^{-1} in the direction of

the electric field. This may be due to the plasma having a mass velocity in this direction as suggested by Ware.

It is possible that the observed magnetic field fluctuations in devices such as SCEPTRE III give rise to electric fields which cause direct heating of the positive ions by the mechanism described in this paper.

§ 6. CONCLUSIONS

It has been shown that the addition of small concentrations of impurity ions to a deuterium plasma causes a large change in the drift velocity of the deuterons with respect to the mass velocity of the plasma. The effect is most marked when the deuteron temperature is large compared with the electron temperature. Because of the relative motion between the deuterons and impurity ions there is appreciable direct ohmic heating of the deuterons. With favourable impurity concentrations the order of magnitude of this heating is sufficient to explain the observed ion temperature in ZETA and SCEPTRE. Attempts to verify this heating mechanism experimentally have been inconclusive.

ACKNOWLEDGMENTS

The authors acknowledge the benefit of many helpful discussions with Mr. B. S. Liley, and they wish to thank Messrs Hughes and Williams for carrying out the experiments referred to above. Part of this work was supported by a contract from the Atomic Energy Research Establishment, Harwell, and the authors wish to thank Dr. T. E. Allibone, F.R.S., Director of the Research Laboratory, Associated Electrical Industries Ltd., for permission to publish this paper.

REFERENCES

- ALLEN, N. L., *et al.*, 1958, *Nature, Lond.*, **181**, 222.
ALLIBONE, T. E., CHICK, D. R., THOMSON, G. P., and WARE, A. A., 1958, *Proc. 2nd U.N. Int. Conf. on the Peaceful Uses of Atomic Energy*, **32**, 169.
BUTT, E. P., *et al.*, 1958, *Proc. 2nd U.N. Int. Conf. on the Peaceful Uses of Atomic Energy*, **32**, 42.
HERDAN, R., and LILEY, B. S., 1960, Associated Electrical Industries, Research Laboratory, *Research Reports* Nos. A.1004 and A.1005.
HUGHES, T. P., and KAUFMAN, S., 1959, *Nature, Lond.*, **183**, 7.
KAUFMAN, S., and WILLIAMS, R. V., 1958, *Nature, Lond.*, **182**, 557.
ROSENBLUTH, M. N., MACDONALD, W. M., and JUDD, D. L., 1957, *Phys. Rev.*, **107**, 1.
SPITZER, L., Jr., 1958, *Nature, Lond.*, **181**, 221.
— 1956, *Physics of Fully Ionized Gases* (New York: Interscience Publishers), section 5.3.
THONEMANN, P. C., *et al.*, 1958, *Nature, Lond.*, **181**, 217.
WARE, A. A., 1959, *Nature, Lond.*, **183**, 8.

The Heat Capacities of Some Copper-Manganese Alloys

By J. M. TITMAN

Physics Department, The University, Sheffield

MS. received 21st September 1960

Abstract. The anomalous behaviour of the heat capacities at the Néel points of copper-manganese alloys containing 80 and 85 at. % Mn is more marked than that observed in other metallic antiferromagnetics. The entropies associated with the anomalies are 0.20 and 0.35 cal mol⁻¹ deg⁻¹, respectively, and are significantly less than the value $R \ln(2S+1)$ predicted by localized theories of antiferromagnetism. It is concluded that these results indicate that the appropriate model of antiferromagnetism in metals is not one based on completely localized moments.

§ 1. INTRODUCTION

CONSIDERABLE attention has been given in the literature to the anomalous behaviour of the specific heat at the Néel points of non-metallic antiferromagnetics (Lidiard 1954a, Nagamiya, Yosida and Kubo 1955). Less information of this kind is available for antiferromagnetic metals and alloys, although small anomalies, probably associated with antiferromagnetism, have been reported to occur in the heat capacities of α -Mn (Shomate 1945) and Cr (Beaumont, Chihara and Morrison 1960).

The purpose of this note, therefore, is to report measurements of the specific heat between 77°K and 380°K of manganese-rich copper-manganese alloys. Meneghetti and Sidhu (1957) and Bacon *et al.* (1957) have shown by neutron diffraction techniques that such alloys, containing more than 69% manganese, are strongly antiferromagnetic when quenched from the γ -phase (Dean *et al.* 1945). The temperatures at which the antiferromagnetic order is destroyed in these alloys coincides with those at which the lattice undergoes a martensitic transformation from face-centred tetragonal to face-centred cubic.

§ 2. EXPERIMENTAL METHOD

The specimens used in these experiments contained 65, 69, 80 and 85 at. % of manganese respectively, and were similar to those used by Bacon *et al.* They were prepared by melting Analar grade manganese and copper together in an argon arc furnace. Each specimen was annealed in the γ field for about 100 hours, and quenched in water. This procedure was used by Bacon *et al.* to obtain the γ -phase at room temperature.

The calorimetric measurements were made in an adiabatic calorimeter of standard form. The combined heater and thermometer, a coil of 47 s.w.g. copper wire, was attached to the specimen by a thin layer of 'Araldite'. Suitable corrections, amounting to about 5% of the total, were made to the heat capacity, to allow for the presence of these extra materials. The corrections were estimated by conducting the experiments with a specimen of high purity copper.

§ 3. EXPERIMENTAL RESULTS

The specific heats at constant pressure of the 65% and 80% Mn specimens are shown in Fig. 1 and that of the 85% specimens in Fig. 2. The curve for the 69% specimen lies about 1% higher at all temperatures than that of the 65% specimen. No anomalous behaviour was detected, but the specific heat at high temperatures is considerably in excess of the Dulong and Petit value. The curve for the 65% specimen does not deviate by more than 1% from the curve

$$C_p = D(338) + 3.72 \times 10^{-3} T \text{ cal mol}^{-1} \text{ deg}^{-1} \quad \dots\dots (1)$$

where $D(338)$ is the Debye function corresponding to a Debye temperature of 338°K .

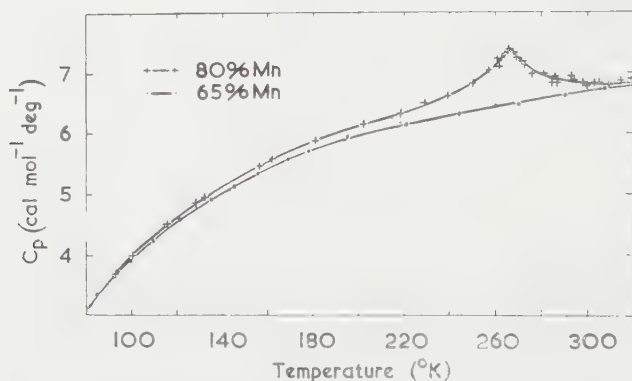


Fig. 1. The heat capacities of the 65 and 80% Mn alloys.

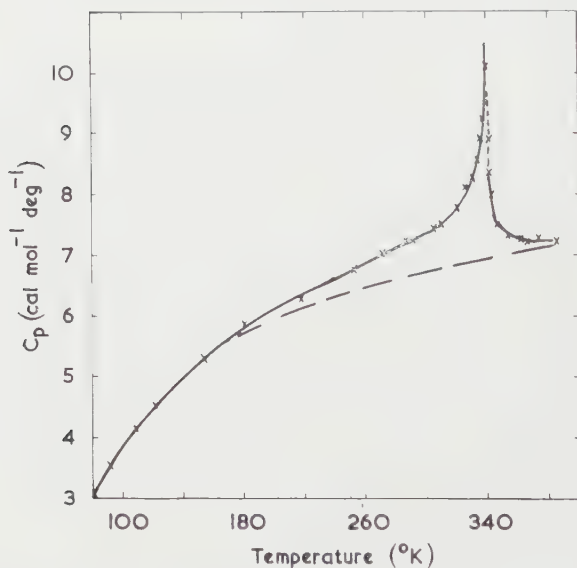


Fig. 2. The heat capacity of the 85% Mn alloy.

The maxima in the curves for the 80 and 85% specimens occur at temperatures which are within a few degrees of the Néel points given by Bacon *et al.* for these alloys. The difference in shape of the two anomalies is presumably due to a stronger tendency to short range order in the 80% specimen.

Since a martensitic transformation accompanies the disappearance of the magnetic order, it is possible that a latent heat may be observed. However, Burkhart and Read (1953) have obtained a latent heat of only 2×10^{-3} cal g⁻¹ for the In-Tl martensitic transformation, in which similar crystallographic changes take place. A cooling curve of the 85% specimen was made and no latent heat could be detected. It is concluded that the latent heat is small in the present case also.

An attempt has also been made to determine the entropy associated with the magnetic ordering. Unfortunately, it is not possible to make an independent estimate of the various non-magnetic contributions to the total heat capacity, but it seems reasonable to assume that they can be represented by Eqn 1. This curve almost coincides with those for the 80 and 85% specimens above and below the anomalies, as indicated by the broken line in Fig. 2. The excess heat capacity above this curve was assumed to be due entirely to the decrease in magnetic order. Thus the entropies associated with the anomalies were found to be 0.20 and 0.35 cal mol⁻¹ deg⁻¹ for the 80 and 85% specimens respectively.

A summary of the experimental results is given in the Table.

at. % Mn	Sp. Ht. Max (°K)	Entropy (cal mol ⁻¹ deg ⁻¹)			ΔC (cal mol ⁻¹ deg ⁻¹)	
		Exptl	A	B	Exptl	B
80	267	0.20	1.10	0.005	0.61	0.014
85	340	0.35	1.17	0.03	3.26	0.09

A, localized model; B, collective electron theory.

§ 4. DISCUSSION

The molecular field theory of antiferromagnetism and its modifications regard the magnetic moments as localized on lattice sites and hence the entropy is merely a configurational one and equal to $R \ln (2S+1)$ cal mol⁻¹ deg⁻¹, where R is the gas constant, and S is the spin quantum number. This result is always obtained, whatever the details of the theory, providing one assumes complete disorder above the Néel point. The smallest value for S obtained in the present case is $S = \frac{1}{2}$ (Bacon *et al.* 1957), and thus one obtains the values 1.10 and 1.17 cal mol⁻¹ deg⁻¹ for the 80 and 85% specimens, respectively.

When reasonable estimates could be made, experiments on non-metallic antiferromagnetics have yielded values of the entropy in the neighbourhood of $R \ln (2S+1)$ (Friedberg 1952, 1953, Nagamiya, Yosida and Kubo 1955). The present results show that copper-manganese alloys, in common with other metallic antiferromagnetics, have relatively small specific heat anomalies at their Néel points. However, the entropy in the copper-manganese case is only about five times smaller than $R \ln (2S+1)$, in contrast to a reduction of about 300 times in the Cr case.

As has already been pointed out (Lidiard 1954b, Nagamiya, Yosida and Kubo 1955), the collective electron theory of antiferromagnetism does not necessarily predict an entropy of $R \ln (2S+1)$, owing to the non-localized character of the d-electrons in this case. However, this theory, based on Stoner's (1939) model for ferromagnetics, is unlikely, at least in its simplest form, to be of more than qualitative usefulness. For completeness, values of the entropy and change in specific heat at the Néel point, ΔC , based on this

model are given in the Table. They were calculated from the appropriate equations given by Lidiard (1954b) and Stoner (1939) using values of the effective moment given by Bacon *et al.* (1957) and assuming 6 electrons in the d-shell. The validity of the calculations is open to question, since the values of the effective moments used were obtained from a completely localized model.

Although they differ considerably from the experimental values, they serve to emphasize that the small specific heat anomalies observed in metallic anti-ferromagnetics may be more easily explained on a non-localized model.

§ 5. CONCLUSION

The maxima of the anomalies in the specific heats of the two copper-manganese alloys are within a few degrees of the Néel points given by Bacon *et al.* and therefore are certainly of antiferromagnetic origin. The departures of the entropy from the value $R \ln (2S+1)$ is significant, and the experimental results do not lend support to a description of the antiferromagnetism of copper-manganese alloys in terms of a completely localized model.

ACKNOWLEDGMENTS

The author wishes to thank Drs. R. Street, N. H. March and P. Gaunt for many useful discussions.

REFERENCES

- BACON, G. E., DUNMUR, I. W., SMITH, J. H., and STREET, R., 1957, *Proc. Roy. Soc. A*, **241**, 223.
BEAUMONT, R. H., CHIHARA, H., and MORRISON, J. A., 1960, *Phil. Mag.*, **5**, 188.
BURKHART, M. W., and READ, T. A., 1953, *Trans. Amer. Inst. Mech. Engrs*, **197**, 1516.
DEAN, R. S., LONG, J. R., GRAHAM, T. R., POTTER, E. V., and HAYES, E. T., 1945, *Trans. Amer. Soc. Metals*, **34**, 443.
FRIEDBERG, S. A., 1952, *Physica*, **18**, 714.
— 1953, *Physica*, **19**, 1072.
LIDIARD, A. B., 1954 a, *Rep. Progr. Phys.*, **22**, 201 (London: Physical Society).
— 1954 b, *Proc. Roy. Soc. A*, **224**, 161.
MENEGHETTI, D., and SIDHU, S. S., 1957, *Phys. Rev.*, **101**, 537.
NAGAMIYA, T., YOSIDA, K., and KUBO, R., 1955, *Advanc. Phys.*, **4**, 1.
SHOMATE, C. H., 1945, *J. Chem. Phys.*, **13**, 326.
STONER, E. C., 1939, *Proc. Roy. Soc. A*, **169**, 339.

Positronium Formation in Helium

By H. S. W. MASSEY AND A. H. MOUSSA

University College, London

MS. received 21st March 1960

Abstract. The cross section for formation of positronium on impact of a positron with a normal helium atom is calculated by Born's approximation for positron energies up to 125 ev. As judged by the size of the maximum cross sections obtained at positron energy of 27 ev, the coupling between elastic scattering and positronium formation is far from weak. This suggests that virtual formation of positronium may play an important part in the elastic scattering of slow positrons by helium atoms. The coupled equations for dealing with this effect are derived.

§ 1. INTRODUCTION

ONE of the outstanding problems in the theory of the scattering of slow electrons by atoms is the evaluation of the importance of polarization, the distortion of the atom by the presence of the colliding electron. For electrons the effective potential due to polarization, being attractive, will be of the same sign as that due to the mean field of the undistorted atom. On the other hand, for positrons the two act in opposite sense. One might therefore be able to obtain information useful for sorting out the contributions from different effects if comparison could be made between corresponding cross sections for electron and for positron impact.

Some evidence of a semi-empirical character has been obtained (Massey and Moussa 1958) which suggests that, for the scattering of positrons with energies between 15 and 20 ev by helium, neon and argon atoms, polarization is indeed important and reduces the cross sections substantially below the value expected on the basis of scattering by the undistorted atomic field alone. The variational method used by Massey and Moiseiwitsch (1951) to examine the importance of polarization in the scattering of electrons in hydrogen was therefore applied to the positron case. No appreciable effect was obtained when trial functions of the same form as for the electron case were used. There is, however, an important difference between the two cases. At energies below the threshold for any inelastic collision, polarization arises from virtual transitions to intermediate states. These states will, for electrons, be excited, including ionized, atomic states, but for positrons there is the additional possibility of positronium formation. In a sense this makes up for the fact that there is no positron analogue of electron exchange which is always allowed for in the calculations for electrons—both positronium formation and electron exchange are rearrangement collisions. Some idea of the importance of positronium formation for hydrogen can be gleaned from the size of the maximum cross section for the process as calculated by the Born approximation. This was found by Massey and Mohr (1954) to be very high, πa_0^2 , which is close to the allowable maximum, and suggests that the coupling concerned is not weak. In

view of this, Moussa (1959) carried out a further variational calculation for positron scattering in hydrogen using a trial function which allowed for the possibility of virtual positronium formation. Only a small change was thereby introduced in the resulting cross sections but a similar calculation by Spruch and Rosenberg (1959) has been reported in which a large effect was obtained, so large in fact that even the sign of the scattering length was changed, indicating a dominance of the polarization potential. To clear the matter thoroughly it would be possible to treat the problem as one of close coupling and solve the coupled integro-differential equations numerically on a high speed electronic computer.

Meanwhile, we must remember that the experimental results for positrons refer to helium not hydrogen and it by no means follows that virtual positronium formation would be so important in this case. We may indeed reach a position in which we can understand the importance of polarization in positron-hydrogen collisions but not in positron-helium collisions which are the only ones for which we have any observational evidence. As a first step, however, it is worthwhile evaluating the cross sections for real positronium formation in helium by Born's approximation to see whether they come out large enough to offer hope of a strong back-coupling on elastic scattering. We report in this paper the result of such a calculation which seems to indicate that at any rate the coupling, while not so strong as for hydrogen, is still not very weak.

§ 2. GENERAL FORMULATION

If we denote the coordinates of the positron and of the two electrons relative to the helium nucleus as centre as \mathbf{r}_1 , \mathbf{r}_2 and \mathbf{r}_3 respectively, then, in atomic units, the wave equation is

$$\left\{ -\frac{1}{2}(\nabla_1^2 + \nabla_2^2 + \nabla_3^2) + \frac{2}{r_1} - \frac{2}{r_2} - \frac{2}{r_3} + \frac{1}{r_{23}} - \frac{1}{r_{12}} - \frac{1}{r_{13}} - E \right\} \Psi = 0, \quad \dots\dots (1)$$

where

$$E = E_0 + \frac{1}{2}k_0^2,$$

k_0 being the wave number of the incident positron and E_0 the energy of the ground state of helium.

We now make the usual approximation of ignoring any states except the initial state and the final states in which the positron and an electron are bound in the ground states of ortho- and para-positronium leaving a helium ion in its ground state. We ignore the small energy difference between the ortho- and para-states. A wave function of the correct symmetry, consistent with the Pauli principle, is then

$$\begin{aligned} \Psi = & \psi_0(r_2, r_3) F_0(\mathbf{r}_1) \chi_1(1, 23) \\ & + \phi_0(r_3) \omega(r_{12}) [G^p(\mathbf{s}_{12}) \chi_1(3, 12) + G^o(\mathbf{s}_{12}) \chi_2(3, 12)] \\ & + \phi_0(r_2) \omega(r_{13}) [G^p(\mathbf{s}_{13}) \chi_1(2, 31) - G^o(\mathbf{s}_{13}) \chi_2(2, 31)] \quad \dots\dots (2) \end{aligned}$$

where

$$\mathbf{s}_{12} = \frac{1}{2}(\mathbf{r}_1 + \mathbf{r}_2), \quad \mathbf{r}_{12} = \mathbf{r}_1 - \mathbf{r}_2. \quad \dots\dots (3)$$

The spin functions χ_1, χ_2 are given by

$$\chi_1(1, 23) = \frac{1}{\sqrt{2}} (\alpha_2 \beta_3 - \alpha_3 \beta_2) \alpha_1, \quad \dots\dots (4)$$

$$\chi_2(3, 12) = \frac{1}{\sqrt{6}} [(\alpha_1 \beta_2 + \alpha_2 \beta_1) \alpha_3 - 2\alpha_1 \alpha_2 \beta_3]. \quad \dots\dots (5)$$

ψ_0, ϕ_0 are the wave functions for the ground states of neutral and ionized helium respectively, ω that for the ground state of positronium.

For ψ_0 we use the simple variational form

$$\psi_0 = (Z^3/\pi) \exp[-Z(r_2 + r_3)], \quad \dots\dots (6)$$

and take for E_0 the corresponding value $-Z^2$. If now we substitute (2) in the wave equation (1), using the relations

$$\begin{aligned} \nabla_1^2 + \nabla_2^2 &= 2\nabla_{r_{12}}^2 + \frac{1}{2}\nabla_{s_{12}}^2, \quad \left(-\frac{1}{2}\nabla^2 - \frac{2}{r} + 2\right) \exp(-2r) = 0, \\ \left(-\nabla_{12}^2 - \frac{1}{r_{12}} + \frac{1}{4}\right) \exp(-\frac{1}{2}r_{12}) &= 0, \quad \dots\dots (7) \end{aligned}$$

multiply by $\phi_0(r_3)\omega(r_{12})\chi_2(3, 12)$, integrate over the space of r_3, r_{12} and sum over spins we obtain

$$\begin{aligned} (\nabla_{s_{12}}^2 - \kappa^2)G^0(s_{12}) + \frac{1}{2} \iint \phi_0(r_3)\omega(r_{12}) \left\{ \nabla_{s_{12}}^2 + \kappa^2 - \frac{8}{r_1} + \frac{8}{r_3} - \frac{4}{r_{23}} - \frac{4}{r_{12}} \right\} \\ \times \omega(r_{13})\phi_0(r_2) \{ \sqrt{3}G^p(s_{13}) + G^0(s_{13}) \} d\mathbf{r}_{12} d\mathbf{r}_3 \\ = \sqrt{3} \iint \phi_0(r_3)\omega(r_{12}) \left\{ \nabla_1^2 + k_0^2 - \frac{4}{r_1} - 2(Z-2) \left(\frac{1}{r_2} + \frac{1}{r_3} \right) - \frac{2}{r_{23}} \right. \\ \left. + \frac{2}{r_{12}} + \frac{2}{r_{13}} \right\} \psi_0(r_2, r_3) F_0(r_1) d\mathbf{r}_{12} d\mathbf{r}_3. \quad \dots\dots (8) \end{aligned}$$

It is to be noted that we have not assumed that $\psi_0(r_2, r_3)$ is the exact solution for the helium ground state wave function but have used the approximate form (6) explicitly. This is in accordance with the procedure adopted in other cases where an approximate bound state wave function is used (Hochberg, Massey and Underhill 1954, Massey and Moiseiwitsch 1954).

In a similar way we obtain an equation for $G^p(s_{12})$ which differs in that $\sqrt{3}G^p(s_{13}) + G^0(s_{13})$ in the integrand on the left-hand side is replaced by $-G^p(s_{13}) - \sqrt{3}G^0(s_{13})$ and the numerical factor on the right-hand side becomes 1 instead of $\sqrt{3}$. The equation for F_0 results if we substitute (2) in (1), multiply on the left by $\psi(r_2, r_3)\chi(12, 3)$, integrate over the space of r_2, r_3 and sum over spins. It is

$$\begin{aligned} \left(\nabla_1^2 + k_0^2 - \frac{2}{r_1} \right) F_0 - 2 \iint \psi_0^2(r_2, r_3) \left\{ \frac{Z-2}{r_2} + \frac{Z-2}{r_3} + \frac{1}{r_{23}} - \frac{1}{r_{12}} - \frac{1}{r_{13}} \right\} d\mathbf{r}_2 d\mathbf{r}_3 \\ = \frac{1}{2} \iint \psi_0(r_2, r_3) \left\{ \nabla_{s_{12}}^2 + \kappa^2 + \frac{8}{r_1} - \frac{8}{r_2} + \frac{4}{r_{23}} - \frac{4}{r_{13}} \right\} \\ \times \{ G^p(s_{12}) + \sqrt{3}G^0(s_{12}) \} \omega(r_{12})\phi_0(r_3) d\mathbf{r}_2 d\mathbf{r}_3. \quad \dots\dots (9) \end{aligned}$$

Solutions of these coupled integro-differential equations are required which have the asymptotic form

$$\begin{aligned} F_0(r) &\sim e^{ik_0 z} + f_0(\theta, \phi)r^{-1}e^{ik_0 r}, \\ G^0(s) &\sim g^0(\vartheta)s^{-1}e^{i\kappa s}, \\ G^p(s) &\sim g^p(\vartheta)s^{-1}e^{i\kappa s}, \quad \dots\dots (10) \end{aligned}$$

where $\kappa^2 = 4E + 9$. The cross section for capture of an electron into the ground state of ortho-positronium is then given by

$$Q^0 = \pi \frac{\kappa}{k_0} \int_0^\pi |g^0(\vartheta)|^2 \sin \vartheta d\vartheta. \quad \dots\dots (11)$$

In this paper we only calculate Q^0 to the accuracy of Born's first approximation. This means that on the right-hand side of Eqn (8) is represented a plane wave and the terms under the integral sign on the left-hand side

of (8) are also neglected. In doing so we not only suppose that the coupling between the Eqns (8) and (9) is weak but also that the terms on the left-hand sides of these equations, which arise from the mean interaction between the colliding systems in their initial and final states, are unimportant.

With this approximation we have

$$g^0(\vartheta) = \frac{\sqrt{3}}{2} \frac{Z^3}{\pi^3} \int \int \int \left\{ \frac{2}{r_1} + (Z-2) \left(\frac{1}{r_2} + \frac{1}{r_3} \right) + \frac{1}{r_{23}} - \frac{1}{r_{12}} - \frac{1}{r_{13}} \right\} \\ \times \exp \{ -Zr_2 - (Z+2)r_3 - \frac{1}{2}r_{12} + i(\mathbf{k}_0 \cdot \mathbf{r}_1 - \boldsymbol{\kappa} \cdot \mathbf{s}_{12}) \} d\mathbf{r}_3 d\mathbf{r}_{12} d\mathbf{s}_{12}. \dots\dots (12)$$

Here $\boldsymbol{\kappa}$ is the wave vector of the relative motion of the positronium and the helium ion after the impact and ϑ is the angle between $\boldsymbol{\kappa}$ and \mathbf{k}_0 . A similar expression is obtained for the case in which the electron is captured into the ground state of para-positronium except that the numerical factor in $g^p(\vartheta)$ is $1/2$ instead of $\sqrt{3}/2$.

Integration over $d\mathbf{r}_3$ is readily carried out to give

$$g^0(\vartheta) = \frac{2\sqrt{3}Z^3}{\pi^2(Z+2)^3} \int \int \exp \{ -Zr_2 - \frac{1}{2}r_{12} + i(\mathbf{k}_0 \cdot \mathbf{r}_1 - \boldsymbol{\kappa} \cdot \mathbf{s}_{12}) \} \\ \times \left\{ \frac{2}{r_1} - \frac{1}{r_{12}} + \left(\frac{2}{r_1} + Z+2 \right) e^{-(Z+2)r_1} + \frac{2Z-2}{r_2} + Z^2-4 \right. \\ \left. - \left(\frac{2}{r_2} + Z+2 \right) e^{-(Z+2)r_2} \right\} d\mathbf{r}_{12} d\mathbf{s}_{12}. \dots\dots (13)$$

It is now convenient to change the variables to $\boldsymbol{\rho}_1$ and $\boldsymbol{\rho}_2$ where

$$\boldsymbol{\rho}_1 = -\mathbf{r}_{12}, \quad \boldsymbol{\rho}_2 = \mathbf{r}_2.$$

Writing then

$$\mathbf{k}_0 - \frac{1}{2}\boldsymbol{\kappa} = \mathbf{k}_1, \quad \boldsymbol{\kappa} - \mathbf{k}_0 = \mathbf{k}_2, \dots\dots (14)$$

we have

$$g^0(\vartheta) = \frac{2\sqrt{3}Z^3}{\pi^2(Z+2)^3} \{ (4-Z^2)I_1 + 2I_2 - 2(Z-1)I_3 + (Z+2)I_4 + 2I_5 - 2I_6 \\ - 2I_7 - (Z+2)I_8 \}, \dots\dots (15)$$

where

$$I_l = \int \int \alpha_l \exp \{ -\frac{1}{2}\rho_1 - Z\rho_2 + i(\mathbf{k}_1 \cdot \boldsymbol{\rho}_1 - \mathbf{k}_2 \cdot \boldsymbol{\rho}_2) \} d\boldsymbol{\rho}_1 d\boldsymbol{\rho}_2, \\ \alpha_1 = 1, \quad \alpha_2 = \rho_1^{-1}, \quad \alpha_3 = \rho_2^{-1}, \quad \alpha_4 = \exp \{ -(Z+2)\rho_2 \}, \quad \alpha_5 = \rho_2^{-1} \exp \{ -(Z+2)\rho_2 \} \\ \alpha_6 = (|\boldsymbol{\rho}_1 + \boldsymbol{\rho}_2|)^{-1}, \quad \alpha_7 = \exp \{ -(Z+2)|\boldsymbol{\rho}_1 + \boldsymbol{\rho}_2| \} / |\boldsymbol{\rho}_1 + \boldsymbol{\rho}_2|, \\ \alpha_8 = \exp \{ -(Z+2)|\boldsymbol{\rho}_1 + \boldsymbol{\rho}_2| \}. \dots\dots (16)$$

§ 3. EVALUATION OF THE INTEGRALS

Of the integrals I_1 to I_8 the first five are easily calculated by simple analytical methods. The remaining three present more difficulty. By using the formula

$$(|\boldsymbol{\rho}_1 + \boldsymbol{\rho}_2|)^{-1} \exp \{ -\gamma|\boldsymbol{\rho}_1 + \boldsymbol{\rho}_2| \} = \frac{1}{2\pi^2} \int \frac{\exp \{ i\mathbf{p} \cdot (\boldsymbol{\rho}_1 + \boldsymbol{\rho}_2) \}}{p^2 + \gamma^2} d\mathbf{p} \dots\dots (17)$$

and the parametrization technique of Feynman (1949) we find

$$I_6 = 30\pi^2 Z \int_0^1 \int_0^1 \frac{y(1-y)x^3}{(r^2 - q^2)^{7/2}} dy dx, \dots\dots (18)$$

where

$$r^2 = \frac{1}{4}xy + Z^2x(1-y) + k_1^2xy + k_2^2x(1-y), \dots\dots (19)$$

$$q^2 = k_1^2x^2y^2 + k_2^2x^2(1-y)^2 - 2\mathbf{k}_1 \cdot \mathbf{k}_2 x^2y(1-y). \dots\dots (20)$$

If we write

$$r^2 - q^2 = Bx + Cx^2$$

then we find, after carrying out the integration over x , that

$$I_6 = 4\pi^2 Z \int_0^1 y(1-y) \frac{15B^2 + 20BC + 8C^2}{B^3(B+C)^{5/2}} dy. \quad \dots\dots (21)$$

It is still possible to carry out the final integration analytically but it yields a very lengthy algebraical expression. To reduce the tedium and minimize errors, it was thought best to complete the integration numerically.

A similar procedure was followed for I_7 and I_8 which are given by

$$I_7 = 16\pi^2 Z \int_0^1 \frac{y(1-y)}{(D^2 - 4AC)^3} \left\{ \frac{N}{(B+C)^{5/2}} - 8A^{1/2}(3D^2 + 4AC) \right\} dy, \quad \dots\dots (22)$$

$$I_8 = 32\pi^2 Z(Z+2) \int_0^1 \frac{y(1-y)}{(D^2 - 4AC)^4} \left[6A^{-1/2}(D^4 - 16A^2C^2) \right. \\ \left. + 48A^{1/2}(D^3 + 3D^2C + 4ACD + 4AC^2) \right. \\ \left. - (A+C+D)^{-7/2}(17D^2 + 24C^2 + 12AD + 12DC + 4AC) \right. \\ \left. + (A+C+D)^{-5/2}(D^2 - 4AC) \left(\frac{5}{2}N - \frac{\partial N}{\partial A} - \frac{\partial N}{\partial B} \right) \right] dy, \quad \dots\dots (23)$$

where

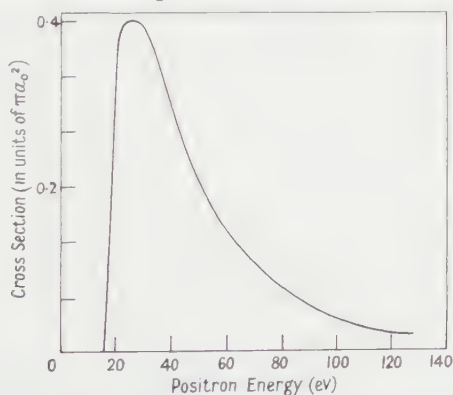
$$D = B - A, \quad A = (Z+2)^2,$$

$$N = \frac{15}{4}D^5 + 5D^4\left(\frac{9}{2}A + C\right) + 2D^3(A^2 + 25AC + C^2) + 12D^2A(A^2 + 5AC + 5C^2) \\ + 4DAC(10A^2 + 15AC + 6C^2) + 8A^3C(2A + C). \quad \dots\dots (24)$$

Having evaluated the integrals numerically for a suitable range of values of ϑ for each chosen k_0 , the total cross section Q was calculated by a further numerical integration from the formula (11).

§ 4. RESULTS AND DISCUSSION

To the approximation we are using $Q^0 = 3Q^p$. The Figure illustrates the total cross section $Q^0 + Q^p$ for production of positronium as a function of positron energy. The maximum value is $0.4\pi a_0^2$ for a positron energy of 27 eV. This is to be compared with the maximum possible cross section for inelastic collisions with s state positrons, $0.5\pi a_0^2$ and for p state, $1.5\pi a_0^2$.



Calculated cross sections for formation of positronium on impact of positrons with normal helium atoms.

As a large part of the contribution comes from positrons with these angular momenta, it is clear that Born's approximation gives values approaching the allowable limits. This certainly suggests that the coupling is not weak. On

the other hand, it must be remembered that, apart from assuming the coupling between initial and final states to be weak, we have neglected distortion of the waves representing the initial motion of the positrons in the field of the helium atom, and the final motion of the positronium in the field of the helium ion. Strictly we can only judge whether the coupling is strong or weak from cross sections calculated when this distortion is allowed for. Here we are in a peculiar position. If polarization is unimportant in positron-helium atom collisions, then the distortion will arise from a repulsive atomic field, reducing the cross sections and hence the effective strength of the coupling. This would be consistent but so also is the other possibility. The coupling could be strong so giving rise to a large polarization. This in turn would reduce the distortion of the positron wave so that the relatively large magnitude of the cross section we have calculated, neglecting distortion, would really be consistent with strong coupling.

It seems then that we cannot be sure from our calculation that the contribution from virtual positronium formation in helium to the dynamical polarization of the atom by an incident positron will be large. On the other hand, it does not exclude this possibility. A more accurate solution of the problem in terms of coupled integro-differential equations of the form (8) and (9) would therefore be well worth while and is now being undertaken.

ACKNOWLEDGMENTS

We are especially indebted to Mrs. W. Lawson for carrying out much of the lengthy numerical work involved and also to her husband, Mr. W. Lawson for invaluable assistance in the operation of the departmental electronic computer.

REFERENCES

- FEYNMAN, R. P., 1949, *Phys. Rev.*, **76**, 769.
HOCHBERG, S., MASSEY, H. S. W., and UNDERHILL, L. H., 1954, *Proc. Phys. Soc. A*, **67**, 957.
MASSEY, H. S. W., and MOHR, C. B. O., 1954, *Proc. Phys. Soc. A*, **67**, 695.
MASSEY, H. S. W., and MOISEWITSCH, B. L., 1951, *Proc. Roy. Soc. A*, **205**, 483.
— 1954, *Proc. Roy. Soc. A*, **227**, 38.
MASSEY, H. S. W., and MOUSSA, A. H., 1958, *Proc. Phys. Soc.*, **71**, 38.
MOUSSA, A. H., 1959, *Proc. Phys. Soc.*, **74**, 101.
SPRUCH, L., and ROSENBERG, L., 1959, *Res. Report*, CX-40, New York University.

LETTERS TO THE EDITOR

Relative Intensities in the Triplet System of CO Bands

Pillow and Rowlatt (1960) have calculated the relative intensities of CO triplet bands by the 'distortion method' (Pillow 1951). Pillow's distortion method is supposed to yield the vibrational wave functions for a 'Morse oscillator'. Ta-You Wu (1952) has pointed out that the wave functions obtained by the 'distortion process' do not exactly correspond to the Morse wave functions, especially for higher vibrational quantum numbers. Firstly, there is a lack of orthogonality in the wave functions thus obtained; secondly, they have the

(1)	(2)	(3)	(4)	(5)	(1)	(2)	(3)	(4)	(5)
7500	0, 0	0.007	1	1	5325	5, 0	0.142	75.3	90
8620	0, 1	0.044	3.4	3	5660	5, 1	0.008	3.4	6
10080	0, 2	0.124	5.1	5	6500	5, 2	0.062	14.9	11
12090	0, 3	0.202	4.0	4	7280	5, 3	0.031	4.7	6
6900	1, 0	0.031	5.8	5	5040	6, 0	0.133	87.7	99
7550	1, 1	0.114	14.9	13	5520	6, 1	0.002	0.8	—
9050	1, 2	0.161	10.2	11	6090	6, 2	0.073	22.7	23
10640	1, 3	0.090	3.0	3	6760	6, 3	—	—	—
6430	2, 0	0.068	17.0	16	4800	7, 0	0.112	90.2	120
7210	2, 1	0.144	22.8	24	5220	7, 1	0.023	13.0	6
8230	2, 2	0.074	6.9	7	5730	7, 2	0.047	18.4	14
9524	2, 3	—	—	—	6320	7, 3	0.020	5.2	3
6010	3, 0	0.107	35.1	35	4580	8, 0	0.086	83.2	105
6700	3, 1	0.112	23.7	23	4960	8, 1	0.055	38.4	49
7545	3, 2	0.004	0.5	—	5420	8, 2	0.017	8.4	11
8620	3, 3	0.057	4.4	3	5940	8, 3	0.043	14.6	15
5644	4, 0	0.134	56.3	60					
6250	4, 1	0.051	14.3	20					
6990	4, 2	0.018	3.3	2					
7900	4, 3	0.080	8.7	10					

(1) $\lambda(\text{\AA})$; (2) v', v'' ; (3) square of overlap integrals; (4) I_1 (our calculation by numerical integration); (5) I_2 (Pillow and Rowlatt).

same amplitude near both the turning points; and lastly, in the distortion process, the centre of the wave function for the v th vibrational level is shifted from the equilibrium internuclear distance by an amount $(v+1)x_0/a$, which is not exactly true. The error introduced in the vibrational wave functions, and consequently in the overlap integrals on account of these factors, increases with the vibrational quantum numbers. Hence it was considered worth while to calculate the

overlap integrals for the various bands of this system by the method of numerical integration (Jarman and Nicholls 1952, Tawde and Sreedhara Murthy 1959) using Morse wave functions. The molecular constants have been adopted from Herzberg (1950) and the approximate mean wavelengths and their vibrational assignments are the same as quoted by Pillow and Rowlatt (1960). The relative intensities given in the Table have been calculated on the assumption of equal population of all vibrational levels in the upper state, i.e. for $T \rightarrow \infty$. For comparison, relative intensities obtained by Pillow and Rowlatt have also been inserted in the Table.

Further experimental work is in progress to determine the variation of electronic transition moment for this band system.

Department of Spectroscopy,
Banaras Hindu University,
Varanasi-5,
India.

N. L. SINGH.
D. C. JAIN.

3rd January 1961.

- HERZBERG, G., 1950, *Molecular Spectra and Molecular Structure I*, 2nd Edn (New York: Van Nostrand).
JARMAN, W. R., and NICHOLLS, R. W., 1952, *Scientific Report No. 4*, contract No. AF 19(122)-470 (London, Canada: Dept. of Physics, University of Western Ontario).
PILLOW, M. E., 1951, *Proc. Phys. Soc. A*, **64**, 772.
PILLOW, M. E., and ROWLATT, A. L., 1960, *Proc. Phys. Soc. A*, **75**, 162.
TAWDE, N. R., and SREEDHARA MURTHY, N., 1959, *Physica*, **25**, 610.
WU, TA-YOU, 1952, *Proc. Phys. Soc. A*, **65**, 967.

REVIEWS OF BOOKS

Accélérateurs de Particules et Progrès Scientifique, by N. FELICI. Pp. 161. (Paris: Dunod, 1960.) 12.50 n fr.

This little book is written for the reader who wishes to know something of the achievements of the modern science of accelerators, and of its possible contribution to systems of philosophy. The treatment is lucid and non-mathematical, although it demands some general acquaintance with, and interest in, the principles of modern physics. The early chapters review some of the main results of atomic and nuclear physics and lead up to the Cockcroft-Walton experiment and the invention of the cyclotron. More detailed chapters follow, in which the several types of accelerator are dealt with individually. The reasons for the growth of the accelerator family are particularly well discussed; the principles of operation of those employing time-varying fields are introduced by interesting analogies with electric motors. In the final chapter the author ranges widely, in a way unusual in a physics text, into general philosophy. He has much to say on the doctrines of Epicurus and Lucretius, and concludes that nuclear physics has something to add not only to the body, but also to the spirit, of knowledge. The book may be recommended both for its technical approach (although it lacks references for further reading) and for its attempt to set its subject within a wide general framework.

W. E. B.

Kommunikation und Kybernetik in Einzeldarstellungen, Vol. 1, *Grundlagen und Anwendungen der Informationstheorie*, edited by W. MEYER-EPPLER. Pp. xviii + 446. (Berlin, Göttingen, Heidelberg: Springer, 1959.) DM 98.

In this book Professor W. Meyer-Eppler of Bonn, whose premature death has been recently reported, has left behind him a lasting monument of his astounding erudition and industry. It is almost unbelievable that an able physicist could immerse himself with equal fervour into every ramification of this new science, from mathematics to neurophysiology, from communication engineering to linguistics, and that he could create not just a compilation but a well-organized, systematic work, closely reasoned on every page. It is the result of seven years of indefatigable work, and it might well remain the last encyclopaedia of information theory written by a single author.

The introductory chapter with its rich jargon of 'semantics', 'ecto-semantics' and so on, which the beginner would be well advised to skip, is followed by a remarkably clear and well-illustrated synopsis of signal analysis and by a somewhat brief section on channel capacity. The chapter on 'statistic of symbols', which is really an introduction to statistical communication theory is rather hard reading, but richly larded with illuminating examples. The chapter on 'disturbed systems' (communication in the presence of noise) is somewhat formal and rather insufficient for beginners. Chapter VI on coding on the other hand is a remarkable didactic effort for making this rather dry subject palatable. The real strength of the book starts revealing itself in Chapter VII which in 80 pages gives as good an introduction to sensory organs as receivers of information as the restricted space permits. The next chapter on 'signs and symbols' is overloaded with terminology ('taxes, taxemes, taxoids', etc.) but well-chosen examples and fine illustrations reassure the reader from time to time that he is not by mistake reading a German book on philosophy. This is followed by a chapter on acoustical and optical signs, with an amazing wealth of optical, phonetical and linguistic information, perhaps a little mixed in the effort of keeping the discussion on a general level. This is continued in the closing chapters X and XI on communication by languages, spoken and written, in which the author has condensed hundreds of articles and books on phonetics, linguistics, experimental psychology and communication engineering. These are the chapters which make the book unique as an encyclopaedia, and an invaluable introduction to remote branches for the mathematician, physicist or engineer who wants to take an interest in the human terminal of communication channels. The Index is exemplary, but a Glossary would have been desirable. It may be hoped that it will be supplied in later editions, but in view of the hundreds of most unfamiliar terms it could not run over less than some 20 pages.

This book connects so many fields that few libraries will be able to dispense with it, and there cannot be many experts who will not be surprised how much they can learn from it.

D. GABOR.

Applications of Thermo-electricity, by H. J. GOLDSMID. Pp. xv + 118. (London: Methuen Monographs, 1960.) 10s. 6d.

The interest in thermoelectricity has had its ups and downs; this applies both to its theory and its application. The present phase commenced when it

became apparent that semiconducting materials have thermoelectric coefficients an order of magnitude higher than have metals. Many new devices become thus practical possibilities. Of this, Goldsmid's book gives a competent, reliable and eminently readable account.

Naturally, Goldsmid's monograph leans heavily on Ioffe's *Semiconductor Thermoelements and Thermoelectric Cooling*, but it does also contain some additional material. Being about half its size and being priced about a quarter, it does not supersede Ioffe's book, but it makes the field accessible to a much wider public.

W. EHRENBURG.

Figures of Equilibrium of Celestial Bodies, by ZDENEK KOPAL. Pp. vi+135. (Madison: University of Wisconsin Press, 1960.)

The book presents an account of the hydrostatic theory of self-gravitating celestial bodies such as the earth, other planets and the stars. This theory takes account of all the effects produced by rotational or tidal distortion and should be applicable to the prediction of the orbits of artificial satellites.

Qualitätsbewertung Optischer Bilder, by E. H. LINFOOT. Pp. 58. (Braunschweig: Vieweg and Sohn, 1960.) DM 9.8.

This short monograph stems from a course of lectures delivered by the author during a visit at the Technische Hochschule in Brunswick. After a short note on the diffraction image, a second chapter gives the elements of the Fourier treatment of optical image formation. This really serves the author to introduce the reader to the concepts and notation used in chapter 3, where the relation between an object and its image is specified in three possible ways, and where the interrelations of these quantities and the so-called frequency response (Übertragungsfaktor) are discussed. It is this which, to the reviewer's mind, constitutes the real attractions of this useful little book.

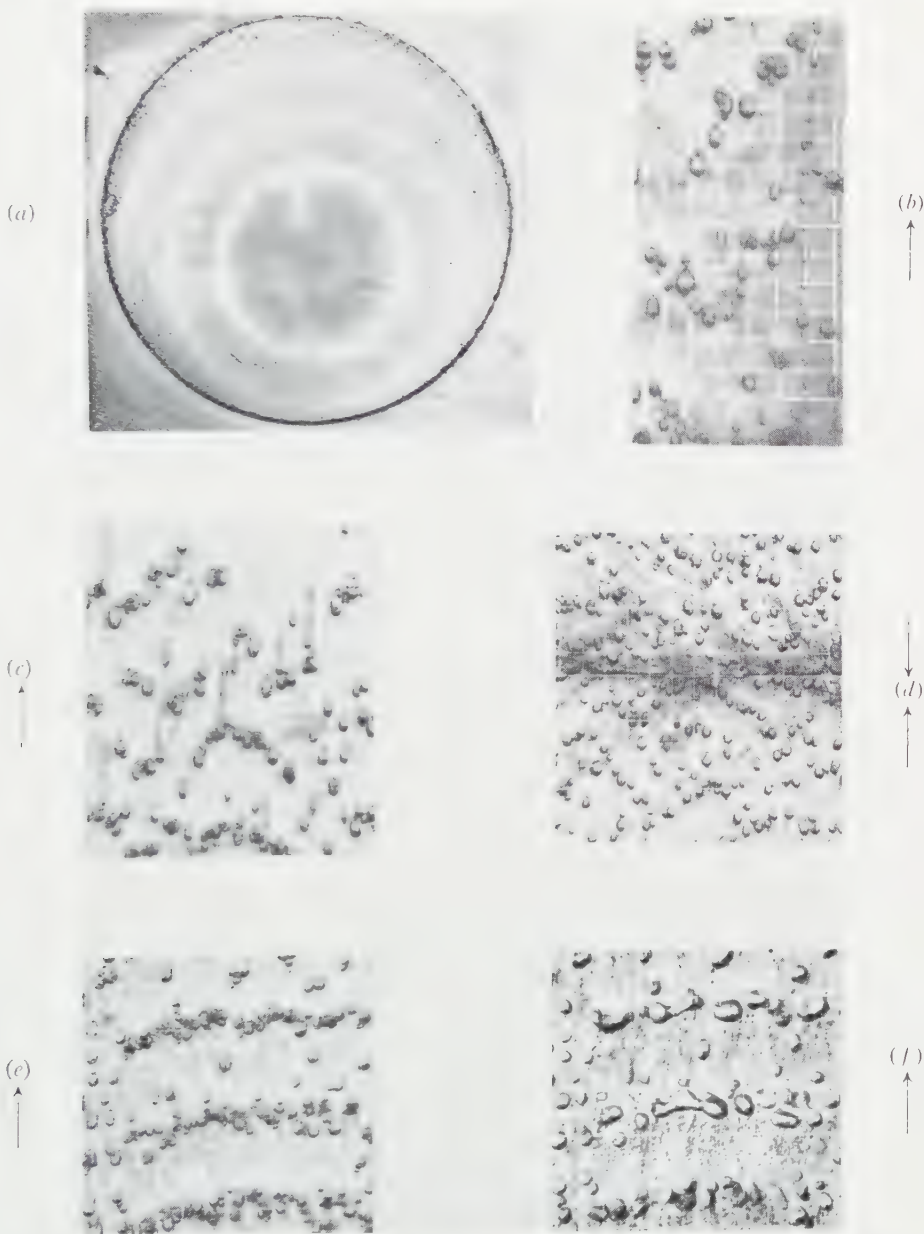
The lack of fidelity of the image is measured by the mean squared difference of the two functions describing the distributions of intensity in the image and object respectively. It is a matter for surprise that Dr. Linfoot's well-known concern for consistency and rigour should have allowed him to overlook mentioning that the photometric units used for the object and image planes have to be suitably chosen for this quantity to be unique and meaningfully defined. Fortunately, this kind of blemish is absent from the book as a whole.

The two other object-image relations are defined as the relative structural content and the correlation quality respectively. The former rests essentially on the Schwarz inequality to measure the amount of variation of a function, and the latter uses a cross-product formula between object and image. These are important concepts in a field which is rapidly developing, and it is useful to have a treatment of them in a separate monograph.

Chapters 4 and 5 would appear to be less satisfactory in that the photographic process is in effect linearized by restricting the discussion to low contrast detail. This is reasonable near to the limit of resolution, but one would not expect this to enlarge our knowledge of the role of the mid-frequencies in relation to image quality. Nevertheless both the earlier chapters and these later ones will be read with interest by the increasing numbers of workers in this field.

H. H. HOPKINS.

Plate I



(a) Thin disk of ice, 9 mm in diameter.

(b) Chain of bubbles parallel to growth direction.

(c) Oval bubbles and cylindrical threads of air.

(d) Junction of two thin sheets of ice grown from opposite directions.

(e) Waves of bubbles.

(f) Same ice as in (e) after one week at temperature of about -5°C .

Length in microns of side of one small square of graticule scale: (b) 140; (c) 170; (d) 140; (e) and (f) 110. Direction of growth of ice: as indicated by the arrows.

On the Theory of Spin-Lattice Relaxation in Paramagnetic Salts

By R. ORBACH

Clarendon Laboratory, Oxford

MS. received 4th November 1960

Abstract. A spin-Hamiltonian approach to the theory of spin-lattice relaxation in paramagnetic salts is developed in which the orbit-lattice interaction is treated as a perturbation connecting states of the overall spin-Hamiltonian. The approach is much simpler than previous treatments where the spin-orbit and Zeeman effects were treated as perturbations, and is applicable to a wide range of salts including both the iron group and the rare earth group.

It is found that, for Kramers salts (ions with an odd number of electrons), many previous results apply quite generally, regardless of the relative size of the spin-orbit and crystalline field terms, but there are important exceptions. For the case of large crystalline field splittings, the relaxation rate (inverse of the relaxation time T_1) varies as H^4T and T^9 for direct and Raman processes respectively, as Van Vleck has previously shown. The so-called Van Vleck cancellation leading to these dependences is derived in a very simple and quite general manner. For small crystal field splittings Δ , less than, or of the order of, the lattice Debye temperature, the relaxation rate varies as H^4T and $a \exp(-\Delta/kT) + bT^9$ for direct and Raman processes respectively. The two coefficients a and b are such that the T^9 term is important only at low temperatures where the exponential term is quite small. These results are in marked contrast with earlier theories.

THIS note will outline an alternative approach to that of Van Vleck (1940) and more recently Mattuck and Strandberg (1960) for the computation of the 'effective Hamiltonian', \mathcal{H}_{eff} , found in spin-lattice relaxation expressions. The method is applicable over a wide range of paramagnetic salts and does not suffer from the limitations of these two approaches.

In these treatments the static Stark interaction of the paramagnetic ion with the surrounding medium \mathcal{H}_0 (in the notation of Van Vleck) is treated as being diagonal. The Zeeman interaction \mathcal{H}_Z ; the spin-orbit interaction \mathcal{H}_{so} ; and the interaction between the orbital moment of the paramagnetic ion and the fluctuations in the crystalline electric fields set up by the lattice waves, the orbit-lattice interaction, \mathcal{H}_{ol} ; are all treated as perturbations on \mathcal{H}_0 . This approach applies only when $\mathcal{H}_0 \gg \mathcal{H}_{\text{so}}$. Because there are many cases when the reverse is true (e.g. the rare earth salts, iron group salts where the deviation from crystalline cubic symmetry is small) such treatments must often fail. We shall, however, similarly assume that \mathcal{H}_Z and \mathcal{H}_{ol} are always less than \mathcal{H}_0 and \mathcal{H}_{so} , though our treatment can easily be extended to the case of large Zeeman splittings.

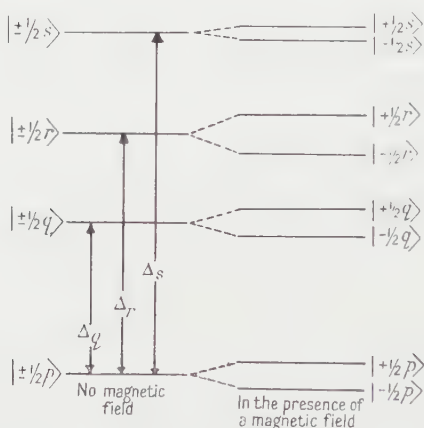
We propose that $\mathcal{H}_0 + \mathcal{H}_{\text{so}}$ be treated as diagonal and let the orbit-lattice interaction \mathcal{H}_{ol} alone be considered as the dynamic perturbing term connecting states of the overall Hamiltonian. Because \mathcal{H}_0 and \mathcal{H}_{so} can in principle always be diagonalized, the method is then appropriate for a very wide range of situations.

When it is found inconvenient to treat the effects of \mathcal{H}_{so} exactly we can instead take \mathcal{H}_{ol} as connecting states of the spin-Hamiltonian (Bleaney and Stevens 1953) wherein \mathcal{H}_{so} and \mathcal{H}_Z have been treated as accurately as need be. The point of our approach in such salts (where $\mathcal{H}_{so} \ll \mathcal{H}_0$) is that most of the work has already been done for us by the spin-Hamiltonian formalism. All we need do is compute the matrix elements of \mathcal{H}_{ol} between the already adequately described states. Our treatment then gives in a simple manner all the results found by Van Vleck (1940) for iron group salts and also by Finn, Orbach and Wolf (1961) for rare earth salts.

We find it useful to expand \mathcal{H}_{ol} into a series of terms,

$$\mathcal{H}_{ol} = \sum_{l,m} a_{lm} Y_l^m \equiv \sum_{l,m} V_l^m \quad \dots\dots (1)$$

where V_l^m is that part of the dynamic crystalline potential which transforms as the respective spherical harmonic Y_l^m . The V_l^m 's contain the lattice displacements expanded in powers of the lattice strain, and for simplicity we shall keep only the linear terms. Using such an expansion (1) we can make use of all the formal simplifications first elaborated by Stevens (1952) in calculating the matrix elements of the crystalline electric field between spin-Hamiltonian states.



A hypothetical level diagram for a Kramers salt in a uniaxial crystalline field in the presence of spin-orbit coupling. In the absence of a magnetic field each level is doubly degenerate (left side of the figure), p, q, r, \dots being odd integers. The splittings on the right side of the figure represent the level structure in the presence of a magnetic field.

To give a concrete example of the formalism we propose, consider a system of Kramers' conjugate states as shown in the Figure. Each level is supposed to be doubly degenerate so that $p, q, r, \dots = 2\lambda + 1$ where λ is an integer. This would be the case, for example, for any paramagnetic ion with an odd number of electrons in an axially distorted cubic field. We assume also that the splittings between any of the excited states and the ground doublet are much greater than kT .

To calculate the spin-lattice relaxation time between the ground states $|+\frac{1}{2}p\rangle$ and $|-\frac{1}{2}p\rangle$ we make use of standard time dependent perturbation theory (Landau and Lifshitz 1958). In this approximation, the transition probability

per unit time W to go between $|\pm \frac{1}{2}p\rangle$ and $|\mp \frac{1}{2}p\rangle$ by interaction of the spin system with the lattice is

$$W(+\frac{1}{2}p; -\frac{1}{2}p) = \frac{2\pi}{\hbar} |\langle -\frac{1}{2}p | \mathcal{H}_{\text{eff}} | +\frac{1}{2}p \rangle|^2 \rho(E), \quad \dots\dots (2)$$

where \mathcal{H}_{eff} is the appropriate coupling Hamiltonian (the same as Van Vleck's effective Hamiltonian) and $\rho(E)$ is the density of final states. We consider first the so-called direct relaxation process; that is, when only one phonon is emitted in the transitions from $|\pm \frac{1}{2}p\rangle$ to $|\mp \frac{1}{2}p\rangle$. We take, therefore, $\mathcal{H}_{\text{eff}} = \mathcal{H}_{\text{ol}}$ in (2). Using the expansion (1) for convenience and examining a representative general term, Eqn (2) becomes

$$W(+\frac{1}{2}p, n_{lm}; -\frac{1}{2}p, n_{lm} + 1) = \frac{2\pi}{\hbar} |\langle -\frac{1}{2}p | V_l^m | \frac{1}{2}p \rangle|^2 \rho(E) \quad \dots\dots (3)$$

where we have shown explicitly the emission of a phonon of occupation number n_{lm} of the type associated with the term V_l^m in our expansion of \mathcal{H}_{ol} . In the case of zero magnetic field, Kramers' theorem tells us that $\langle -\frac{1}{2}p | V_l^m | \frac{1}{2}p \rangle = 0$. This can be seen as follows: for such a matrix element to be non-vanishing, we must have $m = -p$. By hypothesis, p is odd. Time reversal (Elliott and Stevens 1952) dictates

$$\langle -\frac{1}{2}p | V_l^m | \frac{1}{2}p \rangle = (-1)^m \langle \frac{1}{2}p | V_l^{m*} | -\frac{1}{2}p \rangle = -\langle \frac{1}{2}p | V_l^{m*} | -\frac{1}{2}p \rangle,$$

because m is odd. The Hermitian conjugate of the matrix element is

$$\langle \frac{1}{2}p | V_l^{m*} | -\frac{1}{2}p \rangle$$

and thus we must have $\langle \frac{1}{2}p | V_l^{m*} | -\frac{1}{2}p \rangle = -\langle \frac{1}{2}p | V_l^{m*} | -\frac{1}{2}p \rangle$. This can only be true if the matrix element is identically zero. As this is true for any term in the sum (1) (i.e. for arbitrary l), it is true for the sum as a whole. Thus, in (3), the matrix elements all vanish and no spin-lattice relaxation may take place. This is not true in the presence of a magnetic field. The states $|\pm \frac{1}{2}p\rangle$ are then subject to admixture from the other excited states and finite matrix elements of V_l^m are then allowed between the modified ground state doublet. For a first-order Zeeman splitting, this mixing is proportional to field, and thus the matrix element of V_l^m between the ground state levels is proportional to the field. As shown by Van Vleck (1940) this leads to a relaxation time inversely proportional to the fourth power of the magnetic field and inversely proportional to the first power of the temperature. For a full account of the details of the relationship between W and the spin-lattice relaxation time see Orbach (1960).

The process described above is referred to as the 'direct' process because \mathcal{H}_{ol} appears only once, and thus only one phonon is involved. Our conclusions are in complete agreement with Van Vleck, but we have not had to regard \mathcal{H}_{so} as a perturbation to obtain the result. Hence, it is valid for the appropriater are earth salts as well as for the iron group salts.

For the next higher order effect, we consider the case when \mathcal{H}_{ol} acts twice. This is just the so-called Raman process wherein a phonon is scattered inelastically from one energy state to another. Again the matrix element of \mathcal{H}_{ol} is zero between $|\pm \frac{1}{2}p\rangle$ states, but it is not zero *a priori* between $|\pm \frac{1}{2}p\rangle$ and the excited states. We shall examine this case in some detail. The transition probability per unit time to go from state $|\pm \frac{1}{2}p\rangle$ to $|\mp \frac{1}{2}p\rangle$ is given by (2); only now,

$$\langle -\frac{1}{2}p | \mathcal{H}_{\text{eff}} | \frac{1}{2}p \rangle = \sum_{\pm t} \frac{\langle -\frac{1}{2}p | \mathcal{H}_{\text{ol}} | \frac{1}{2}t \rangle \langle \frac{1}{2}t | \mathcal{H}_{\text{ol}} | +\frac{1}{2}p \rangle}{\hbar\omega_{tp}}. \quad \dots\dots (4)$$

We sum over the excited states $|\pm \frac{1}{2}t\rangle$ and $\hbar\omega_{lm}$ is the energy difference between the initial state and the intermediate state. We again use the expansion (1) of \mathcal{H}_{0l} and consider a typical term in the sum. The transition probability per unit time to go from the state $|\pm \frac{1}{2}p\rangle$ to $|\mp \frac{1}{2}p\rangle$ with the accompanying absorption and emission of phonons associated with V_l^m and $V_{l'm'}$, having occupation numbers n_{lm} and $n_{l'm'}$ respectively, is then,

$$W(+\frac{1}{2}p, n_{lm}, n_{l'm'}; -\frac{1}{2}p, n_{lm}-1, n_{l'm'}+1) \\ = \frac{2\pi}{\hbar} \left| \sum_t \left[\frac{\langle -\frac{1}{2}p | V_{l'm'} | \frac{1}{2}t \rangle \langle \frac{1}{2}t | V_l^m | \frac{1}{2}p \rangle}{-\Delta_l + \hbar\omega_{lm}} \right. \right. \\ \left. \left. + \frac{\langle -\frac{1}{2}p | V_l^m | -\frac{1}{2}t \rangle \langle -\frac{1}{2}t | V_{l'm'} | \frac{1}{2}p \rangle}{-\Delta_l - \hbar\omega_{l'm'}} \right] \right|^2 \rho(E). \quad \dots\dots (5)$$

The second term in (5) follows by considering transitions to the Kramers conjugate of the intermediate state in the first term. By hypothesis, p and t are odd. It is easily seen then that if m is odd, then m' is even and vice versa in order that we have non-vanishing matrix elements. Hence, $m+m'$ will be odd. Then, because

$$\begin{aligned} \langle -\frac{1}{2}p | V_l^m | -\frac{1}{2}t \rangle \langle -\frac{1}{2}t | V_{l'm'} | +\frac{1}{2}p \rangle &= (-1)^{m+m'} \langle +\frac{1}{2}p | V_l^{m*} | +\frac{1}{2}t \rangle \\ &\times \langle +\frac{1}{2}t | V_{l'm'}^* | -\frac{1}{2}p \rangle \\ &= -\langle -\frac{1}{2}p | V_{l'm'} | \frac{1}{2}t \rangle \langle \frac{1}{2}t | V_l^m | \frac{1}{2}p \rangle, \end{aligned}$$

by time inversion and Hermitian conjugation, the numerator of the second term in (5) has the opposite sign from the first. Combining, (5) reduces to

$$W = \frac{2\pi}{\hbar} \left| \sum_t \left[\langle -\frac{1}{2}p | V_{l'm'} | \frac{1}{2}t \rangle \langle \frac{1}{2}t | V_l^m | \frac{1}{2}p \rangle \right] \left[\frac{1}{-\Delta_l + \hbar\omega_{lm}} - \frac{1}{-\Delta_l - \hbar\omega_{l'm'}} \right] \right|^2 \rho(E). \quad \dots\dots (6)$$

If we assume that $\Delta_l \gg \hbar\omega_{lm}$ and that the predominant phonon energies are much greater than \mathcal{H}_Z so that the difference in energy between $\hbar\omega_{lm}$ and $\hbar\omega_{l'm'}$, equal to the Zeeman splitting, is negligible compared with $\hbar\omega_{lm}$ or $\hbar\omega_{l'm'}$, then the terms in the square bracket almost cancel and (6) reduces to

$$W = \frac{2\pi}{\hbar} \left| \sum_t \left[\frac{(\hbar\omega_{lm} + \hbar\omega_{l'm'})}{\Delta_l^2} \langle -\frac{1}{2}p | V_{l'm'} | \frac{1}{2}t \rangle \langle \frac{1}{2}t | V_l^m | \frac{1}{2}p \rangle \right] \right|^2 \rho(E), \quad \dots\dots (7)$$

which is the expression Van Vleck (1940) finds for Ti^{3+} in the alum, an equivalent case. This is, of course, just the so-called 'Van Vleck cancellation' and we see that it is merely a statement of time reversal symmetry and applies regardless of the relative size of \mathcal{H}_0 and \mathcal{H}_{so} . As was shown by Van Vleck, Eqn (7) leads to a relaxation time inversely proportional to the ninth power of the temperature and independent of the field.

In the presence of a magnetic field, two effects occur. First, the Kramers pairs are split by the field as shown in the Figure. This means that the energy denominators Δ_l in (5) are altered by $+\frac{1}{2}\mathcal{H}_Z$ in the first term and $-\frac{1}{2}\mathcal{H}_Z$ in the second, where \mathcal{H}_Z is to be evaluated in the t th excited state. This will tend to lessen the cancellation between the two terms, but only if $\mathcal{H}_Z > \hbar\omega_{lm} \sim kT$ will this effect be dominant over the one described above in the absence of the field. In the usual paramagnetic resonance experiments, this inequality is never satisfied. There is another effect of the magnetic field, however, which is much

more important and arises in much the same manner as in the direct process. In the presence of the field, the Kramers states will be mixed, and the time invariance destroyed. There will appear in the split Kramers eigenvectors other states whose amplitudes will be proportional to $\mathcal{H}_z/(\mathcal{H}_0 + \mathcal{H}_{so})$ and no cancellation will occur in (5) using these admixed states. The significant point is that now it is the *excited* states which can be mixed rather than the *ground* state. The denominator $\mathcal{H}_0 + \mathcal{H}_{so}$ then refers to, say, $\Delta_q - \Delta_r$ rather than to the splitting Δ_q as it would for admixtures into the ground state. As $\Delta_q - \Delta_r$ may be very much less than Δ_q , *excited* state admixtures may be much more important than *ground* state admixtures. This effect is to be compared with (7) in which it was shown that, in the absence of a field, cancellation was avoided at best to order $\hbar\omega, \Delta_q \sim kT, \Delta_q$. Thus, for the field effect to be dominant,

$$\left| \frac{\mathcal{H}_z \Delta_q}{(\Delta_q - \Delta_r) kT} \right| \gtrsim 1. \quad \dots\dots (8)$$

If this inequality is satisfied, then, as shown by Kronig and Bouwkamp (1938), the relaxation time will be inversely proportional to the square of the magnetic field and inversely proportional to the seventh power of the temperature. If not, then our previous result holds, of a relaxation time inversely proportional to the ninth power of the temperature and independent of field.

If Δ_l is not greater than the phonon energy $\hbar\omega_{lm}$ then yet another result occurs which has been described by Finn, Orbach and Wolf (1961). The first term in (5) has a resonance at $\Delta_l = \hbar\omega_{lm}$ and they show that direct excitations between the ground state and the excited state may occur with the absorption or emission of a phonon of energy $\hbar\omega_{lm} = \Delta_l$. This leads to a spin-lattice relaxation time proportional to $\exp(\Delta_l/kT)$ for $\Delta_l \gg kT$. Such a term will arise whenever $\Delta_l \ll k\theta_D$, θ_D being the Debye temperature of the lattice. The non-resonant contribution from the first term and the contribution of the second term in (5) lead to the previously found term in the relaxation time which is inversely proportional to the ninth power of the temperature and is field independent. However, its contribution is generally much less than that due to the first term and it can be neglected except, perhaps, at very low temperatures where $\exp(\Delta_l/kT)$ may be quite large.

The above treatments have all been applied to Kramers systems in uniaxial fields. Should we, however, not have this situation but, say, a paramagnetic ion with an even number of electrons, then $\langle -\frac{1}{2}p | \mathcal{H}_{ol} | \frac{1}{2}p \rangle$ does not vanish and, as shown by Kronig and Bouwkamp (1938), the relaxation time due to direct processes goes inversely as the square of the magnetic field and inversely as the first power of the temperature. Further, for Raman processes, the cancellation in (5) does not occur because m and m' may both be even or odd, so that under time reversal no net change of sign occurs in any term. In such a case, again as described by Kronig and Bouwkamp (1938), the relaxation time due to Raman processes will go inversely as the seventh power of the temperature, and be field independent.

There will, of course, be some cases which we have not covered here, but the basic approach which we have outlined should be applicable to them. As there are no restrictions on the relative size of \mathcal{H}_0 and \mathcal{H}_{so} , and as the method makes use of the convenient spin-Hamiltonian formalism, in principle the essential character of paramagnetic spin-lattice relaxation can be determined in a very wide range of systems.

ACKNOWLEDGMENTS

In acknowledgment, I should like to thank Professor B. Bleaney for a critical appraisal of the manuscript and Dr. R. J. Elliott for many helpful discussions. This work was carried out during the tenure of a National Science Foundation Postdoctoral Fellowship.

REFERENCES

- BLEANEY, B., and STEVENS, K. W. H., 1953, *Rep. Progr. Phys.*, **16**, 108 (London: Physical Society).
ELLIOTT, R. J., and STEVENS, K. W. H., 1952, *Proc. Roy. Soc. A*, **215**, 437.
FINN, C. B. P., ORBACH, R., and WOLF, W. P., 1961, *Proc. Phys. Soc.*, **77**, 261.
KRONIG, R. DE L., and BOUWKAMP, C. J., 1938, *Physica*, **5**, 521.
LANDAU, L. D., and LIFSHITZ, E. M., 1958, *Quantum Mechanics* (London: Pergamon Press), p. 140.
MATTUCK, R. D., and STRANDBERG, M. W. P., 1960, *Phys. Rev.*, **119**, 1204.
ORBACH, R., 1960, *Thesis*, University of California, Berkeley, California.
STEVENS, K. W. H., 1952, *Proc. Phys. Soc. A*, **65**, 209.
VAN VLECK, J. H., 1940, *Phys. Rev.*, **57**, 426.

Application of the Schwinger Variational Method to Zero-Energy Electron-Hydrogen Scattering

By H. E. SARAPH

Department of Physics, University College, London

MS. received 6th October 1960

Abstract. The problem is formulated in terms of the radial exchange equations. The Schwinger method, with polynomial trial functions, is used to calculate the scattering length. With 3-term polynomials one obtains $\Lambda^+ = -9.72$, $\Lambda^- = -2.35$ compared with $\Lambda^+ = -8.095$, $\Lambda^- = -2.350$ from exact numerical integrations.

§ 1. INTRODUCTION

THE Schwinger variational method has previously been applied in two different ways to the problem of elastic scattering of electrons by hydrogen atoms.

Newstein (1955) has considered the integral equation satisfied by the complete wave function $\Psi(\mathbf{r}_1, \mathbf{r}_2)$ and obtains stationary expressions for the direct amplitude f and the exchange amplitude g . In principle this method gives an exact formulation of the problem but in practice one is restricted to the use of very simple trial functions Ψ^t . It is unlikely that these simple functions will make adequate allowance for the strong interactions which are important at low energies.

Altshuler (1953) considers the central field model, thus neglecting exchange and other effects of distortion of the atom. The problem is reduced to that of solving radial equations of the form

$$\left\{ \frac{d^2}{dr^2} - \frac{l(l+1)}{r^2} + k^2 \right\} \phi_l(r) = U(r)\phi_l(r),$$

atomic units being used. Here one may use much more elaborate trial functions ϕ_l^t . Altshuler shows that good results may be obtained using polynomials. However, at low energies the neglected exchange effects are known to be very large and the central field model will not give physically significant results.

We consider the application of the Schwinger method to the exchange radial equations, discussed by Bransden, Dalgarno, John and Seaton (1958):

$$\left\{ \frac{d^2}{dr^2} - \frac{l(l+1)}{r^2} + k^2 \right\} \phi_l^\pm = (U \pm W_l)\phi_l^\pm \quad \dots\dots (1)$$

where W_l is an exchange operator.

§ 2. A STATIONARY EXPRESSION FOR THE SCATTERING LENGTH

In the zero energy limit Eqn (1) is

$$\frac{d^2}{dr^2} \phi = (U \pm W)\phi \quad \dots\dots (2)$$

where

$$U = -2 \left(1 + \frac{1}{r} \right) e^{-2r}$$

$$W\phi = 4re^{-r} \left\{ \frac{1}{r} \int_0^r 2r' e^{-r'} \phi(r') dr' + \int_r^\infty 2e^{-r'} \phi(r') dr' - \frac{1}{2} \int_0^\infty 2r' e^{-r'} \phi(r') dr' \right\}$$

and where $2r \exp(-r)$ is the normalized ground state wave function of the hydrogen atom.

Equation (2) will be satisfied by solutions of the integral equation

$$\phi^\pm(r) = r + \int_0^\infty G(r, r_0) \{ U(r_0) \pm W(r_0) \} \phi^\pm(r_0) dr_0$$

where

$$G(r, r_0) = \begin{cases} -r, & r \leq r_0 \\ -r_0, & r \geq r_0 \end{cases}$$

and such solutions will satisfy the boundary conditions

$$\phi(0) = 0, \quad \phi(r) \sim r + \Lambda^\pm$$

where Λ^\pm is the scattering length. The zero-energy elastic cross section is

$$Q = \{ (\Lambda^-)^2 + 3(\Lambda^+)^2 \} \pi a_0^2.$$

Using polynomial trial functions

$$\phi^b = \sum_{i=1}^N c_i r^i \quad \dots\dots (3)$$

the Schwinger stationary expression for the scattering length is (Altshuler 1953)

$$\Lambda^\pm = \frac{c_\alpha c_\beta A_\alpha^\pm B_\beta^\pm}{c_\alpha c_\beta (D_{\alpha\beta}^\pm - E_{\alpha\beta}^\pm)}, \quad \alpha, \beta = 1 \dots N$$

where the summation convention is used and where

$$A_\alpha^\pm = B_\alpha^\pm = \int_0^\infty r(U \pm W) r^\alpha dr$$

$$D_{\alpha\beta} = D_{\beta\alpha} = \int_0^\infty r^\alpha r^\beta (U \pm W) dr$$

$$E_{\alpha\beta} = E_{\beta\alpha} = \int_0^\infty \int_0^\infty r^\alpha \{ U(r) \pm W(r) \} G(r, r_0) \{ U(r_0) \pm W(r_0) \} r_0^\beta dr_0 dr.$$

We find the extremum of Λ from

$$\frac{\partial \Lambda}{\partial c_i} = 0, \quad i = 1 \dots N.$$

The N equations can be written in the form

$$\{ \Lambda_{\text{ext}} (D_{i\alpha} - E_{i\alpha}) - A_i B_\alpha \} c_\alpha = 0.$$

The c_α 's can only be determined if the compatibility condition holds:

$$[\Lambda_{\text{ext}} (D_{ij} - E_{ij}) - A_i B_j] = 0.$$

Since the matrix $(A_i B_j)$ is of rank one, there is only one non-zero root for Λ_{ext} . As Altshuler (1953) has shown, this is given by

$$\Lambda_{\text{ext}} = \frac{\begin{vmatrix} \mathcal{N}_{11} & \mathcal{N}_{12} & \dots & \mathcal{N}_{1N} \\ \mathcal{M}_{21} & \mathcal{M}_{22} & \dots & \mathcal{M}_{2N} \\ \vdots & \vdots & \ddots & \vdots \\ \mathcal{M}_{N1} & \mathcal{M}_{N2} & \dots & \mathcal{M}_{NN} \end{vmatrix} + \dots + \begin{vmatrix} \mathcal{M}_{11} & \mathcal{M}_{12} & \dots & \mathcal{M}_{1N} \\ \vdots & \vdots & \ddots & \vdots \\ \mathcal{M}_{N-1,1} & \mathcal{M}_{N-1,2} & \dots & \mathcal{M}_{N-1,N} \\ \mathcal{N}_{N1} & \mathcal{N}_{N2} & \dots & \mathcal{N}_{NN} \end{vmatrix}}{|\mathcal{M}_{ij}|}$$

where

$$\mathcal{M}_{ij} = A_i B_j, \quad \mathcal{M}_{ij} = D_{ij} - E_{ij}.$$

§ 3. RESULTS AND DISCUSSION

Using functions (3) with $N=3$ we obtain:

$$\Lambda = -9.72, \quad \Lambda = 2.35.$$

These results may be compared with those obtained by exact numerical integration (John 1960) of Eqn (2):

$$\Lambda = -8.095, \quad \Lambda = -2.350.$$

ACKNOWLEDGMENT

The author is indebted to Dr. M. J. Seaton for suggesting the problem and for his supervision and continued encouragement in this work. The work was supported by the Atomic Energy Research Establishment, to whom thanks are due for permission to publish.

REFERENCES

- ALTSHULER, S., 1953, *Phys. Rev.*, **89**, 1278.
 BRANDEN, B. H., DALGARNO, A., JOHN, T. L., and SEATON, M. J., 1958, *Proc. Phys. Soc.*, **71**, 877.
 JOHN, T. L., 1960, *Proc. Phys. Soc.*, **76**, 532.
 NEWSTEIN, M. C., 1955, *Massachusetts Institute of Technology, Technical Report No. 4*.

Polarization of 9 Mev Protons Elastically Scattered from C and Al†

BY D. HOARE, A. B. ROBBINS‡ AND G. W. GREENLEES

Department of Physics, Birmingham University

MS. received 4th November 1960

Abstract. The polarization of 9 mev protons, elastically scattered from C and Al, has been measured using a double scattering technique. The polarization was obtained from the left-right scattering asymmetry from helium as recorded in photographic emulsions. Angular distributions from the polarization and elastic scattering cross section are compared with predictions of optical model calculations. The general features of the scattering from aluminium are described by the optical model calculation, while the scattering from carbon appears to have strong contributions from sources other than the shape-elastic scattering.

A RECENT paper (Robbins and Greenlees 1960) presented results on the polarization of 9.1 mev protons elastically scattered from Mg. These results were obtained using a double scattering technique with He as an analyser. The present paper gives results obtained with C and Al as the first target using the same apparatus. The target thickness was 0.8 mev in the case of C and 1.0 mev for Al, making the energies at the target centres 9.2 and 9.1 mev respectively. Differential cross sections for elastic scattering were also obtained with the same targets and the results have been compared with the predictions of an optical model analysis.

The optical model programme was made available by Mr. B. Easlea and used on the University of London MERCURY Computer. This programme, which is discussed fully elsewhere (B. Easlea, to be published), uses a real potential $Vf(r)$ where $f(r)$ is the Saxon-Woods form factor, an imaginary potential with both volume and surface form factors, $f(r)$ and $df(r)/dr$, and a real spin-orbit potential

$$v_s \frac{1}{r} \frac{df(r)}{dr} (\sigma \cdot \mathbf{l}).$$

The parameters for the imaginary potential are quoted as W_c and W_s , where W_c is the magnitude of the potential at $r=0$ and W_s is the magnitude at $r=R$ ($R=r_0A^{1/3}$). Initially, a set of parameters was chosen and a visual comparison made of the model predictions and the experimental results. Adjustments were then made to the parameters in an attempt to improve the agreement between the curves. For each target (C and Al) about twenty sets of parameters were tried but no systematic study of the parameter space was undertaken.

Carbon.

The results for carbon, together with an optical model curve, are given in Fig. 1. The curve giving the polarization of protons of about 8 mev as a

† This work was supported in part by the National Science Foundation, U.S.A.

‡ On leave of absence from Rutgers University, New Jersey, U.S.A.

function of the angle of scattering from helium has two peaks, at 70° (negative polarization) and 120° (positive polarization). At three of the angles of scattering from the carbon target polarizations were measured using the two possible analyser angles, and pairs of results are given in the figure. The sign convention used is that $(\mathbf{K}_{\text{in}} \times \mathbf{K}_{\text{out}})$ is positive.

The optical model predictions shown in Fig. 1 are typical of the results obtained. In all cases the model gave a negative peak in the polarization around 60° , which was not present experimentally, and the cross sections predicted were too low to fit the experimental data.

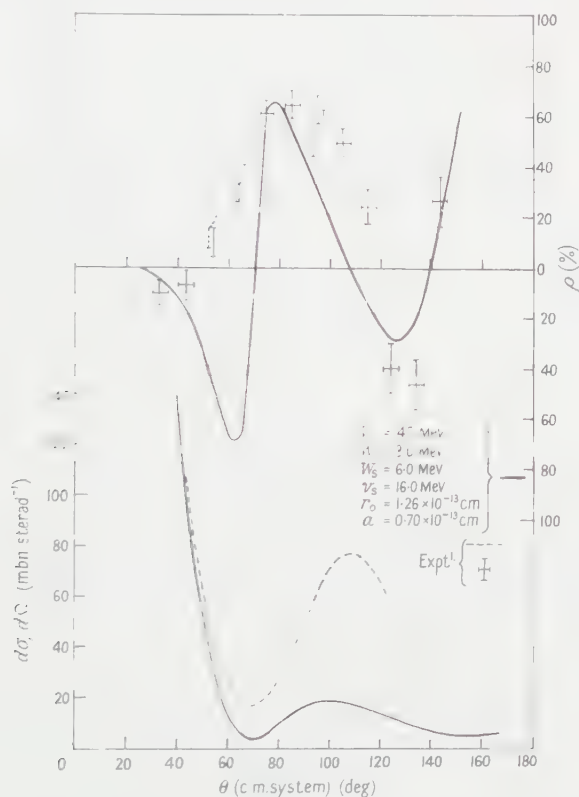


Fig. 1. Differential cross sections and polarizations for the elastic scattering of 9.2 ± 0.4 MeV protons from carbon. The full lines show the prediction of an optical model analysis using the parameters quoted in the figure.

Strzalkowski *et al.* (1960) have reported variations of the polarization with energy around 9 MeV in the elastic scattering for carbon at 40° . Nevertheless, the shapes of the polarization angular distributions at 8.2 MeV given by these authors and by Rosen and Brolley (1958) at 10 MeV, are both very similar to the present results; this indicates that the main features of the curve are relatively insensitive to the energy. Variations with energy have been observed in the elastic scattering cross sections from carbon at backward angles (Gibson, Prowse and Rotblat 1957) which have been attributed to compound nucleus effects, but the magnitude of the effects is insufficient to explain the present discrepancy between calculation and experiment. One can only conclude that the model, as used here, is unsatisfactory for carbon in the 10 MeV region.

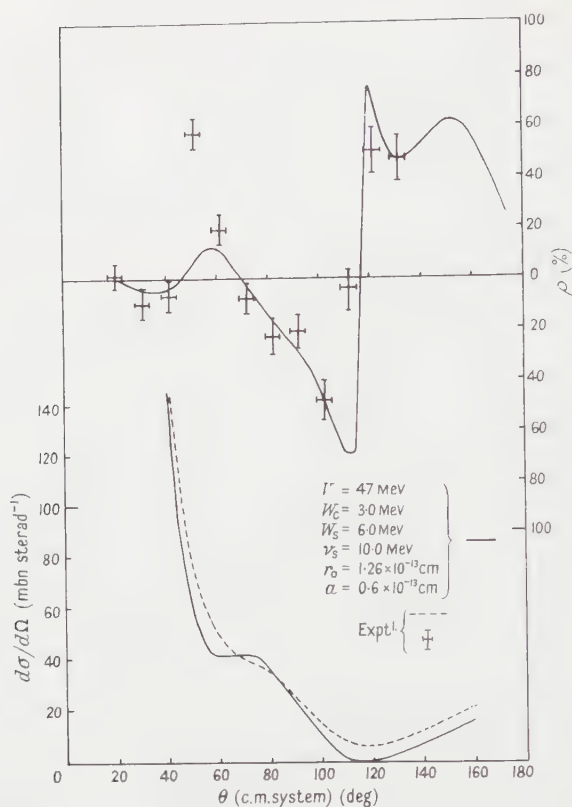


Fig. 2. Differential cross sections and polarizations for the elastic scattering of 9.1 ± 0.5 MeV protons from aluminium. The full lines show the prediction of an optical model analysis using the parameters quoted in the figure.

Aluminium.

The cross section and polarization data obtained using an Al target are shown in Fig. 2 together with an optical model curve. Apart from one point (51°), the polarization results are well represented by the model and reasonable representation is made of the cross section data. The departure at backward angles in the latter may be attributed to a compound elastic contribution since such effects are known to occur in this energy region (Greenlees and Rolph 1960).

REFERENCES

- GIBSON, W. M., PROWSE, D. J., and ROTBLAT, J., 1957, *Proc. Roy. Soc. A*, **243**, 237.
 GREENLEES, G. W., and ROLPH, P. M., 1960, *Proc. Phys. Soc.*, **75**, 201.
 ROBBINS, A. B., and GREENLEES, G. W., 1960, *Phys. Rev.*, **118**, 803.
 ROSEN, L., and BROLLEY, J. E., 1958, *Proceedings of the Second International Conference on the Peaceful Uses of Atomic Energy* (Geneva: United Nations), **14**, 116.
 STRZALKOWSKI, A., BOKHARI, M. S., AL-JEBOORI, A., and HIRD, B., 1960, *Proc. Phys. Soc.*, **75**, 502.

The Emission of Charged Particles from the Bombardment of Silver with Nitrogen Ions

By J. S. LILLEY

Physics Department, University of Birmingham

Communicated by W. E. Burcham; MS. received 18th July 1960

Abstract. A silver foil of 4.4 mg cm^{-2} was bombarded with the internal $^{14}\text{N}^{6+}$ beam from the 150 cm Birmingham cyclotron, and the reaction products were recorded in C2 emulsion. The energy and angular distributions of the emitted protons and α -particles were measured and the results at large angles have been compared with the predictions of evaporation theory. Good agreement was obtained by assuming that the Coulomb barrier is reduced at high nuclear excitations.

The presence of competing direct processes is discussed briefly.

§ 1. INTRODUCTION

ONE of the important uses of a heavy ion as a bombarding particle in nuclear physics is its ability to produce a highly excited compound nucleus with a good probability of uniform energy distribution. By introducing many low-energy nucleons simultaneously into the target nucleus it is possible to produce this excitation without having to resort to the high velocity necessary if the bombarding particle is a proton or an α -particle.

For example the velocity of a 70 Mev nitrogen ion corresponds to 5 Mev per nucleon. Such a complex particle will interact very strongly with nuclear matter, and the mean free path of its constituent nucleons is so small that their kinetic energy will probably be distributed throughout the nucleus before any of them has time to escape. Consequently direct processes will be unimportant and the subsequent emission of charged and neutral particles will obey a statistical evaporation process.

Recent experiments at Oak Ridge (Zucker 1958, Halbert and Zucker 1959) using 28 Mev ^{14}N ions and light target elements have shown that charged particle emission may be satisfactorily interpreted in terms of the simple theory of particle evaporation (Blatt and Weisskopf 1952). The presence of direct processes was, however, indicated by asymmetries in the α -particle distributions.

Until quite recently high-energy heavy ion beams of sufficient intensity have not been available to allow a detailed study to be made of their interaction with medium to heavy elements. Some work has been done, however (Fremlin 1959), and the results suggest that nearly all these reactions go by way of a compound nucleus. The yields of stripping products are reduced and, for all but the heaviest elements, fission should not be an important mechanism for de-excitation. Evaporation is expected to be the dominant mode of decay, and experiments should provide considerable insight as to the nature of this process.

In 1956 Parfanovich, Rabin and Semchinova investigated the interaction of 115 MeV ^{14}N ions with nuclear emulsion. Detailed examination of the energy and angular distribution of the prongs radiating from the interaction stars showed several interesting and unexpected features. An analysis of the silver and bromine stars showed that α -particles appeared twice as frequently as protons. Moreover the angular distribution of the former was strongly peaked in the forward direction, whereas the protons were emitted approximately isotropically. These observations are not in accord with the predicted results of an evaporation process.

A similar star analysis has been carried out at this laboratory (Lilley 1959, M.Sc. Thesis, Birmingham, unpublished). The reactions were produced in a 400 micron C2 emulsion with the extracted 120 MeV ^{14}N beam from the 150 cm Birmingham cyclotron. The ratio of protons to α -particles was found to be 1.7 ± 0.5 and an increase in the number of protons was observed at forward angles. The α -particle distribution was approximately isotropic, although the number observed was too small to be significant.

Although the study of individual stars provides useful information regarding the emission of charged particles, a most extensive analysis of many hundreds of events would be required to give good statistical accuracy. However, the technique suffers from a more serious drawback since the composition of nuclear emulsion is complex. It was difficult to determine whether a particular interaction involved a light nucleus or a heavy nucleus, and it was impossible to distinguish between silver and bromine stars. Furthermore, it was important to avoid preferential selection of the most visible stars and it is possible that part of the discrepancy between the analyses done by the author and by Parfanovich, Rabin and Semchinova was due to a bias of this nature. The E1 emulsion used by the Russian workers was considerably less sensitive than C2 emulsion and a number of $(^{14}\text{N}, p)$ and $(^{14}\text{N}, 2p)$ stars may have been overlooked, especially if the protons were of high energy.

Clearly it was important to devise a different experiment to provide an independent check of the above observations and a description of this work is given in the remainder of the paper. Nuclear emulsion was again used to record the charged particles, but the reactions were generated in a silver foil which was placed in the path of a beam of $^{14}\text{N}^{6+}$ ions. The energy of the incident ions covered a wide range from zero to 120 MeV. The high potential barrier between the nitrogen and silver nuclei, however, allowed only the faster particles to interact and it was possible to account satisfactorily for the forward motion of the centre of mass.

§ 2. EXPERIMENTAL DETAILS

2.1. Apparatus

The target chamber used for the bombardments is illustrated in Fig. 1. During the experiment it was supported inside the cyclotron vacuum tank on the end of a standard $1\frac{1}{2}$ in. probe of which only the beginning is indicated. The heavy ion beam current to the inner coaxial rod was observed with a vibrating reed electrometer. The size of the chamber was limited to allow it to be inserted through a 10 cm diameter air lock.

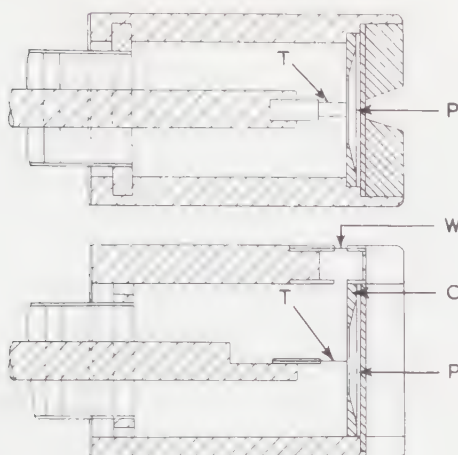


Fig. 1. The target chamber used for the internal heavy ion bombardments.

A $5\text{ cm} \times 5\text{ cm}$ nuclear plate P was backed against a $1\frac{1}{2}\text{ mm}$ heavy alloy plate which formed the side of the chamber facing the ion source. The beam was collimated with a series of 4 mm. lead stops and a tungsten heavy-alloy mask C. The latter was designed to screen the emulsion from the bulk of the reaction products and scattered heavy ions produced in the collimator. At the same time it accepted particles emitted from the target foil T over a continuous angular range from 10° to 170° . A 5-micron gold window W stopped the overwhelming flux of 11.5 mev doubly charged nitrogen ions which are also accelerated by the cyclotron in the manner described by Walker *et al.* (1954).

2.2. Thin Foil Experiments

2.2.1. Exposures.

Thin foils of silver and gold, each having a stopping power approximately equivalent to 10 microns of emulsion, were bombarded with the internal nitrogen beam and the emitted reaction products were detected with 200 micron C2 nuclear emulsion. A typical exposure of 15 minutes was given for the silver target with a beam current reading of 10^{-10} amp . Longer bombardments would have been desirable but it was found that after about 30 minutes general fogging of the emulsion was too severe. Background plates were exposed with the foil withdrawn from the path of the beam.

During each run the target foil was positioned at an angle of 45° to the beam direction. This arrangement allowed the whole angular distribution to be obtained from one plate, and so eliminated the problem of accurate beam integration.

During the examination of the processed plates the position of each track was noted relative to the centre of the plate which during the exposure was nearest to the target foil. The tracks of the emitted particles appeared to radiate from this point and it was important to locate its position accurately since an uncertainty here would have lead to a false asymmetry in the observed angular distribution.

2.2.2. Background.

The presence of extraneous γ and x radiation has already been mentioned above. Its effect on the nuclear emulsion was controlled by limiting the exposure to less than 30 minutes. More serious sources of background were those that produced unwanted tracks. They fall naturally into three separate categories.

(i) Nitrogen ions were scattered both elastically and inelastically by the target nuclei. Generally the reaction products could be distinguished in a high flux of these scattered heavy ions. However this background increased rapidly for angles less than 70° and accurate scanning was impossible below 45° .

(ii) Stray protons and α -particles were produced from interactions in the collimator and at the edges of the heavy-alloy screen. These tracks were also more numerous in the forward direction and over the range of angles concerned were always recognized by their direction in the plate.

(iii) Collisions between high-energy neutrons and hydrogen nuclei in the gelatin produced a large number of unwanted proton tracks. Most of these lay entirely below the surface of the emulsion and could easily be recognized. The general direction of the tracks indicated that a large fraction of the neutrons were generated from reactions in the collimator and the leading face of the target chamber. Consequently, when scanning backward angles, care had to be exercised in order that a knock-on proton was not mistaken for a true reaction proton.

2.2.3. The effect of the cyclotron field.

The experiment was performed within the cyclotron magnetic field of 15 600 oersteds. It can easily be shown that, as a result of this, the number of particles striking the emulsion is reduced at backward angles and increased at

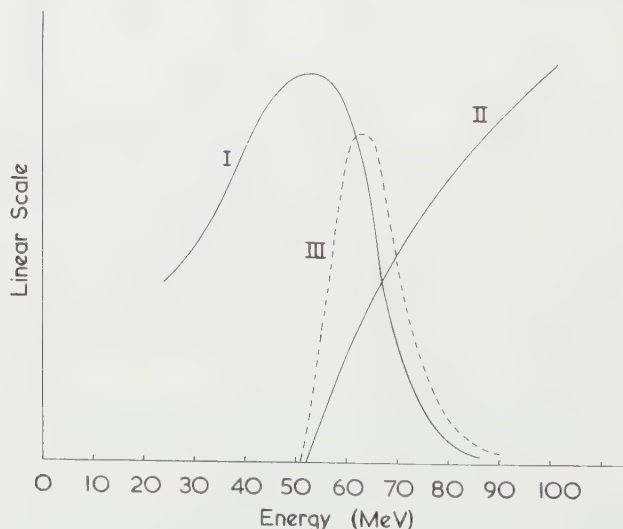


Fig. 2. Curve I represents the energy distribution of the internal ^{14}N beam incident on the target foil. Curve II is a graphical plot of Eqn (1) showing how the cross section for the formation of a compound nucleus varies with the laboratory energy of the incident ^{14}N ion. Curve III is the product of I and II and illustrates how the Coulomb barrier between the interacting nuclei limited the effective energy distribution to a comparatively narrow energy interval.

forward angles. The effect was calculated and generally found to be unimportant, amounting to a few per cent at most angles.

2.2.4. Conversion to centre-of-mass system.

A typical energy spectrum of the internal ^{14}N beam incident on the target at a radius of 63 cm is shown in Fig. 2. This curve was derived from the observed range distribution of ^{13}N ions produced in a stripping reaction (Chackett and Fremlin 1954). Although the detailed shape of the energy spectrum was not reproducible, the high-energy fall off was found to be similar over a wide range of machine operating conditions. This was utilized in the present work to estimate the mean excitation energy of the compound nuclei produced during the bombardments.

The variation with energy of the cross section for the formation of a compound nucleus is given classically by the formula

$$\sigma_c(E) = \pi R^2 \left(1 - \frac{(A_1 + A_2)}{A_2} \frac{V(R)}{E} \right), \quad \dots\dots (1)$$

where A_1 and A_2 are the mass numbers of the incident particle and the target nucleus respectively, E is the kinetic energy of the incident particle in the laboratory system and $V(R)$ is the Coulomb barrier between the interacting nuclei. The interaction radius $R = 1.4(A_1^{1/3} + A_2^{1/3})$ fermis and it was assumed that there was no distortion of either the target nucleus or the projectile.

A more accurate expression is obtained by including the wave nature of particles. However, over the energy range considered, the de Broglie wavelength of a nitrogen ion is much less than the nuclear radius and the classical approach is valid.

The above excitation function was combined with the beam energy distribution and it was found that the experiment was effectively carried out with a beam of mean energy 62 Mev and width at half height of 15 Mev (see Fig. 2). The mean energy of the bombarding ions being known, the corrections for the forward motion of the centre of mass were applied to the observed energy and angular distributions of the emitted protons and α -particles.

2.3. Thick Foil Experiments

The results of the experiments described in the previous section were cut off at forward angles. Below 45° the dense background of scattered nitrogen ions completely masked the more lightly ionizing reaction products. Now one of the important features observed by Parfanovich, Rabin and Semchinova was the strong forward concentration of α -particles and in order to verify this it was necessary to extend the range of observation to small angles. This was done by using a target foil thick enough to stop completely the incident particles. Since the energies of the majority of the heavy ions lay close to that of the potential barrier for silver, most of the nuclear reactions occurred at the top of the foil and the degree of activation fell rapidly inside the foil as the energy of the beam was reduced. A calculation based on the available heavy ion range-energy data and Eqn (1) showed that the interactions occurred at a mean depth of 5 microns. It was thus possible to apply a reasonably precise correction to the observed particle ranges.

Unfortunately, the α -particles and protons transmitted through the target were seriously degraded in energy and many of the low-energy particles were not recorded at all. At 45° in the laboratory system the mean target thickness was equivalent to 112 microns of emulsion which corresponded to proton and α -particle cut-off energies of 3.9 MeV and 15.2 MeV respectively.

The bombardments using thick silver and gold targets were carried out in an exactly similar manner to those with thin foils. The only serious source of background was from protons and α -particles originating in the collimator and heavy-alloy screen edges. At 45° it was possible to recognize these particles by their direction relative to those from the target, but at smaller angles this method of discrimination became more and more uncertain. A more accurate determination of the background was obtained from measurements made on the plate exposed in the gold foil bombardment.

§ 3. RESULTS

The corrected angular distributions for both the thin and thick foil experiments are summarized in Fig. 3. It can be seen that these results confirm those of Parfanovich, Rabin and Semchinova in showing that there is a predominance of α -particles in the forward direction. A similar though less pronounced increase is also found for protons.

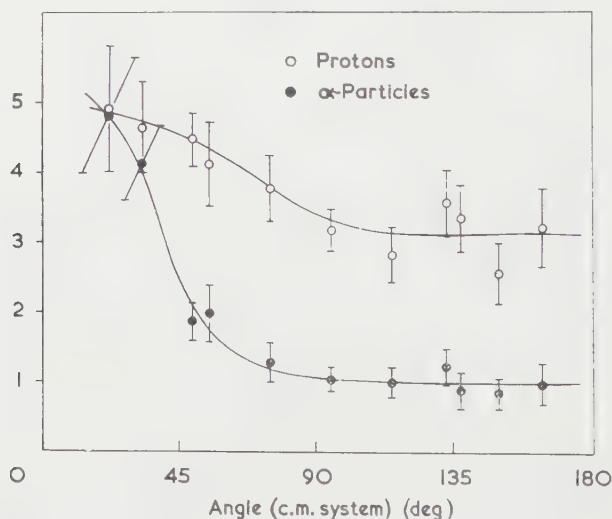


Fig. 3. The centre-of-mass angular distributions of protons and α -particles from the interaction of nitrogen with silver.

The excess of singly-charged particles observed previously by the author is strikingly confirmed at all angles. Indeed the ratio of protons to α -particles is even greater than before, being 3 to 1 in favour of protons over the interval 90° to 180°.

The centre-of-mass energy distributions of each particle emitted in different angular ranges are shown in Figs 4 and 5. A small variation in the mean laboratory energy was observed. This was completely accounted for by the forward motion of the centre of mass. The majority of the particles have

energies well below that of the classical Coulomb barrier of the compound nucleus ^{121}Xe or ^{123}Xe which is approximately 10 MeV for protons and 20 MeV for α -particles. This is in agreement with the emulsion star work done by Parfanovich and by the author and the present method has the advantage that there was no uncertainty as to the nature of the target nuclei. In the emulsion star work silver and bromine reactions could not be distinguished.

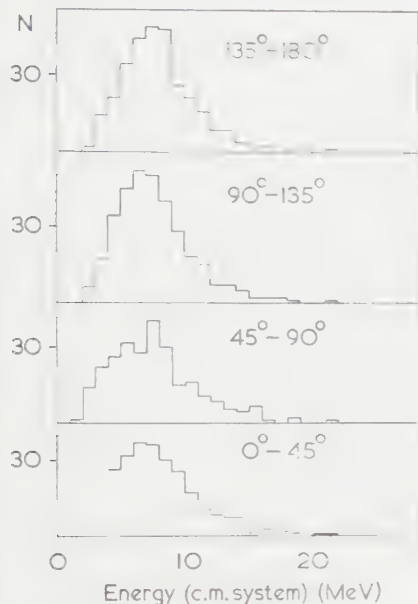


Fig. 4. Centre-of-mass energy spectra of protons emitted in different angular ranges.

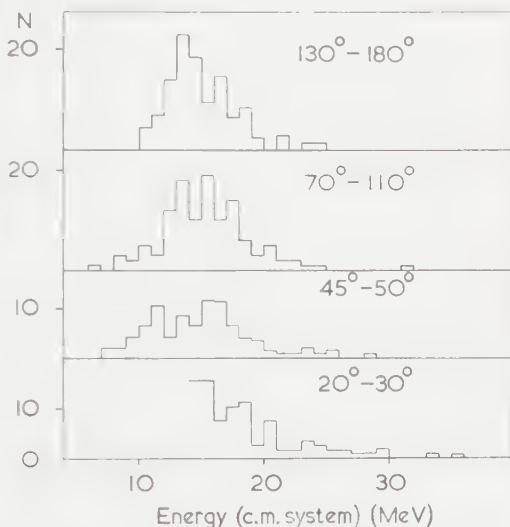


Fig. 5. Centre-of-mass energy spectra of α -particles emitted in different angular ranges.

It will be noticed that the energy spectra do not alter significantly over the entire angular range, and also that the angular distributions are approximately isotropic in the backward hemisphere. These observations suggest that evaporation plays the main part in this type of interaction and that at backward angles nearly all the particles were emitted in this way. Indeed the products of direct interactions are usually rare at large angles because of the difficulty of conserving the momentum of the incident particle, and it is expected that the results from this region will be most characteristic of compound nucleus processes. The following section outlines the method by which the experimental data were compared with predictions based on the Weisskopf theory of evaporation.

§ 4. DISCUSSION

4.1. Theory of Evaporation

If a nucleus is excited to an energy E_0 , the energy distribution of an evaporated particle i is given by (Weisskopf 1937)

$$P(\epsilon)d\epsilon = \frac{\gamma_i \sigma_c}{\omega_0(E_0)} \epsilon \omega(E_0 - Q_i - \epsilon) d\epsilon, \quad \dots\dots (2)$$

where $\gamma_i = g_i m_i / \pi^2 \hbar^3$. Q_i is the binding energy of the emitted particle, m_i is

its mass and g_i is the number of spin states it can assume. σ_c is the cross section for the formation of a compound nucleus by the inverse process, that is by the absorption of the emitted particle. For neutrons σ_c is equal to σ_0 , the geometric cross section of the residual nucleus, but for positively charged particles the process is opposed by Coulomb interaction. If V_i is the height of the Coulomb barrier, classical theory gives

$$\sigma_c = \sigma_0(1 - V_i/\epsilon), \quad \dots\dots(3)$$

which is similar in form to Eqn (1).

Thermodynamics relates the level density $\omega(E)$ to the entropy $S(E)$ of the nucleus as follows:

$$\ln \omega(E) = S(E).$$

Also $1/T = dS/dE$, which defines the nuclear temperature.

Using the Fermi gas model of the nucleus, the important relationship between the temperature and the excitation energy is given by

$$E = aT^2, \quad \dots\dots(4)$$

whence

$$\omega(E) = C \exp 2(aE)^{1/2}. \quad \dots\dots(5)$$

a is a parameter which depends on the atomic weight and the neutron excess of the nucleus (Le Couteur 1950). C depends on the odd-even nature of the nucleus.

Substitution of these formulae into Eqn (2) yields the result

$$P(\epsilon)d\epsilon = \frac{C_i \gamma_i \sigma_c}{\omega_0(E_0)} \exp 2(a_i R_i)^{1/2} \epsilon \exp \left\{ -\frac{(\epsilon - V_i)}{T(R_i)} \right\} d\epsilon, \quad \dots\dots(6)$$

where

$$R_i = (E_0 - Q_i - V_i) \gg (\epsilon - V_i).$$

The total emission probability is obtained by integrating (6) after substituting for σ_c from Eqn (3):

$$P_i = \frac{C_i \gamma_i \sigma_0}{\omega_0(E_0)} \exp 2(a_i R_i)^{1/2} T^2(R_i), \quad \dots\dots(7)$$

whence

$$\frac{P_i}{P_j} = \frac{C_i g_i m_i}{C_j g_j m_j} \frac{T^2(R_i)}{T^2(R_j)} \exp 2[(a_i R_i)^{1/2} - (a_j R_j)^{1/2}]. \quad \dots\dots(8)$$

The use of Eqn (3) represents an approximation in the treatment which is more serious for small excitation energies. This objection was overcome by introducing a penetration coefficient K such that

$$V_i = KV_0, \quad \dots\dots(9)$$

where $V_0 = Z_1 Z_2 e^2 / R$ is the Coulomb barrier height. The effective nuclear radius was taken to be $R = r_0 A^{1/3} + \rho$ with $\rho = 0$ fermis for protons and 1.2 fermis for α -particles.

The values of K were determined from the relation

$$\int_0^\infty \sigma_c \epsilon \exp \left(-\frac{\epsilon}{T(R_i)} \right) d\epsilon = \sigma_0 T^2(R_i) \exp \left(-\frac{KV_0}{T(R_i)} \right). \quad \dots\dots(10)$$

The left-hand side of the equation was integrated numerically with values of σ_c for protons and α -particles given by Blatt and Weisskopf (1952), p. 352. A graph was plotted of K as a function of T/V_0 from which it was possible to determine the effective potential barrier for any nucleus at any temperature.

Using the above relations it is possible to evaluate the energy spectra and emission probabilities of various types of particle from a given nucleus of known excitation. In the bombardments of emulsion and silver foils described in this paper the excitation energy was sufficient for several charged particles to be emitted. The experimentally observed energy spectra cannot be related to a unique temperature, but must be considered to be a superposition of distributions from nuclei with temperatures ranging from a maximum to a minimum below which the nucleus decays by γ -emission. It was therefore necessary to sum the emission probabilities over the whole of the de-excitation process.

This has been done as an integration by Le Couteur (1950) and more recently Dostrovsky, Rabinowitz and Bivins (1958) published a detailed set of results obtained by using a Monte-Carlo method. For very high excitation energies the treatment of Le Couteur is valid, but at the comparatively low temperatures produced in the present experiments fluctuations in the binding energies of the different particles are important and each nucleus had to be considered individually as it was formed. The problem was simplified by assuming that each emitted particle always carried away a quantity of energy corresponding to the mean value of its particular energy spectrum. The emission ratios were evaluated for each possible nucleus as it was formed and hence the total relative numbers of emitted α -particles, protons and neutrons were determined for the different values of nuclear temperature T . The overall energy spectra were obtained as a combination of spectra calculated for different T from Eqn (6). The proton and neutron binding energies were taken from the data of Zeldes (1958) and the α -particle binding energies were calculated from the *Tables of Isotopic Masses* compiled by Wapstra (1955).

From Eqn (6) it is clear that a graph of $\ln [P(\epsilon)/\sigma_c\epsilon]$ against ϵ should be linear, and a value for the nuclear temperature and hence the constant a may be calculated from a measurement of the slope. The experimental proton and α -particle data were analysed in this way and the values for the nuclear temperature obtained were $T_p = 1.8 \text{ Mev}$ and $T_\alpha = 2.2 \text{ Mev}$. Since the energy distributions do not refer to a unique excitation, these values correspond to mean temperatures of the evaporating nuclei. Knowing R_i , the mean excitation energy of the residual nuclei, to be about 50 Mev, the parameter a was given by Eqn (4) to be approximately $a = A/10$, where A is the atomic weight. This is within the range of values quoted for this coefficient by other investigators.

The emission ratio $N_p/N_\alpha = 3.2 \pm 0.3$ experimentally. This ratio is very sensitive to the height of the Coulomb barrier V_i especially for the relatively low excitation energies used in the experiment. In order to obtain agreement between theory and experiment it was necessary to assume, in agreement with other work, that there is a considerable lowering of V_i at high excitations by thermal expansion and surface vibrations (Le Couteur 1950, Bagge 1938). The relationship between the effective barrier and the excitation energy E modifies Eqn (9) to the form

$$V_i = \frac{KV_0}{1 + E/\text{const.}}$$

The constant is usually taken to be 200 Mev for nuclei in the region $A = 100$, and this value was used in the calculations.

A value of 2.6 for the proton to α -particle ratio was calculated using values for V_0 of 9.2 Mev for protons and 18.4 Mev for α -particles. These numbers

correspond to a nuclear radius coefficient r_0 of 1.55 fermis for protons and 1.25 fermis for α -particles. It must be stressed, however, that V_0 was treated as a parameter in these calculations to give a good fit to the data. No attempt was made to determine the sensitivity of the theoretical predictions to the various parameters and no doubt adequate fits could be obtained with different values for these quantities.

The theoretical energy spectra are compared with the experimental points in Fig. 6. The excess of low-energy particles evident in the proton distribution has been observed in the evaporative emission from cosmic ray stars (Harding, Lattimore and Perkins 1949, Page 1950). Le Couteur suggested that these

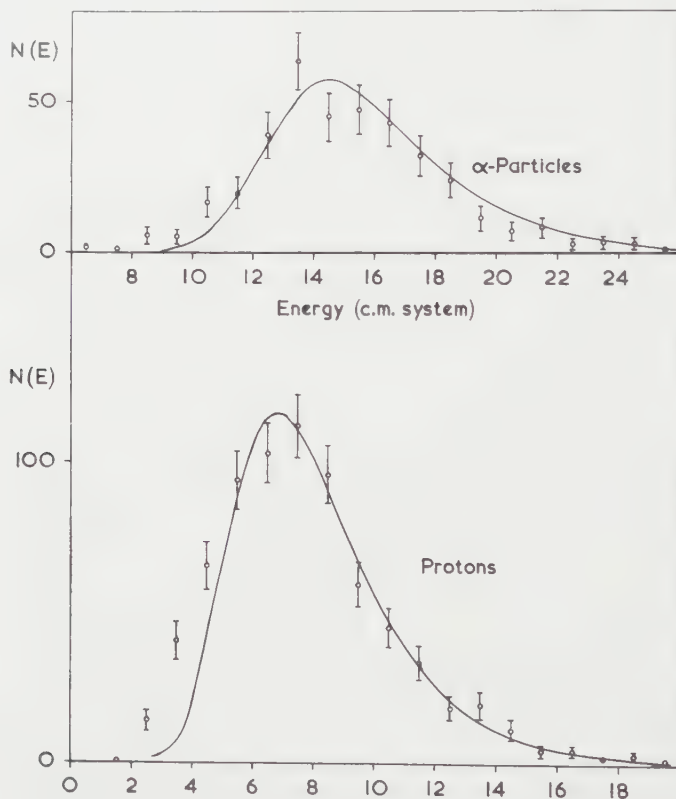


Fig. 6. Experimental centre-of-mass energy spectra of α -particles (upper graph) and protons (lower graph), emitted at backward angles. The solid curves are calculated evaporation spectra with $a = A/10$, and V_0 equal to 9.2 Mev for protons and 18.4 Mev for α -particles.

might be 'decay' protons which are produced when the excitation energy lies below that required for the release of a neutron and above the region in which de-excitation by γ -emission is likely. A rough estimate suggests that between 0.1 and 0.3 proton per interaction may be emitted in this way. This would satisfactorily account for the observed low-energy tail in the proton distribution. Low energy α -particles could, in principle, be emitted in a similar way. However, owing to their low penetrating power and high Coulomb barrier they compete very unfavourably with the protons and so are not to be expected.

On the whole it seems that, within the limits of the available experimental data, the backward emission of particles may be satisfactorily interpreted in terms of an evaporative mechanism based on well-established ideas. A more accurate computation will need to include the distribution in energy of the evaporated particles. Moreover, the cross section σ_c need not necessarily agree with that calculated for the ground state with a Coulomb barrier modified according to a rough energy dependence. The emission probabilities are also very dependent on the level density factor a . The present work suggests approximate values for the parameters, but more accurate absolute measurements, with monoenergetic heavy ions, over a range of excitation energies, and target nuclei, are needed to supply a more critical test of the theory.

4.2. Remarks on the Forward Distribution

The asymmetries in the proton and α -particle distributions indicate clearly that competing direct interactions are important. Unfortunately, heavy ion reactions are so complex that several different mechanisms may have contributed to the observed distributions. However, many of these processes are inhibited by the rather special conditions used in the experiments.

For example the complex stripping processes which have been observed by several workers (Chackett, Fremlin and Walker 1954, Miller 1952) are important for light target nuclei with high bombarding energies where glancing collisions can occur which involve the nuclear forces. A totally different process, which is favoured by similar conditions, is brought about by the great deal of angular momentum which may be imparted to a nucleus by a heavy bombarding ion (Ericson and Strutinski 1958). The characteristic distribution of the emitted particles has been recently demonstrated at Yale in the reaction between 160 Mev oxygen ions and nickel (Knox, Quinton and Anderson 1959).

All these reactions are expected to have been unimportant in the present experiments, however, because the effective incident energy lay close to the Coulomb barrier between the interacting nuclei. Glancing collisions were restricted to the few ions with energies well above the average and, in general, nuclear interaction could occur only when the collision was almost head-on.

A direct mechanism which may have been important in this case is closely related to the high linear momentum of the heavy ion. The impulse generated on impact is transmitted through the target nucleus in a manner similar to the passage of a shock wave through a liquid drop. The far side of the nucleus becomes violently distorted with a highly modified Coulomb field in its vicinity. Enhanced evaporation will certainly occur in such circumstances favouring low-energy α -particles and with a definite forward bias.

It is impossible to test this theory with the present data and further work will clearly be hampered by the masking effect of the isotropically evaporated particles. However, at very forward angles the α -particle distribution is enhanced five-fold and a careful study of the energy spectrum over a range of bombarding energies should lead to a better understanding of this part of the interaction.

ACKNOWLEDGMENTS

The author is indebted to Dr. J. H. Fremlin for his advice and assistance throughout the course of this work, and to Professor W. E. Burcham for many

helpful discussions. It is also a pleasure to thank Mr. W. Hardy and the cyclotron staff for the excellent heavy ion bombardments.

The work was carried out whilst the author was in receipt of a Department of Scientific and Industrial Research maintenance grant.

REFERENCES

- BAGGE, E., 1938, *Ann. Phys. Lpz.*, **33**, 389.
BLATT, J. M., and WEISSKOPF, V. F., 1952, *Theoretical Nuclear Physics* (New York: John Wiley).
CHACKETT, K. F., and FREMLIN, J. H., 1954, *Phil. Mag.*, **45**, 735.
CHACKETT, K. F., FREMLIN, J. H., and WALKER, D., 1954, *Phil. Mag.*, **45**, 173.
DOSTROVSKY, I., RABINOWITZ, P., and BIVINS, R., 1958, *Phys. Rev.*, **111**, 1659.
ERICSON, T., and STRUTINSKI, V., 1958, *Nucl. Phys.*, **8**, 284.
FREMLIN, J. H., 1959, *Nuclear Reactions*, Vol. 1 (Amsterdam: North Holland).
HALBERT, M. L., and ZUCKER, A., 1959, *Phys. Rev.*, **114**, 132.
HARDING, J. B., LATTIMORE, S., and PERKINS, D. D., 1949, *Proc. Roy. Soc. A*, **196**, 325.
KNOX, W. J., QUINTON, A. R., and ANDERSON, C. E., 1959, *Phys. Rev. Letters*, **2**, 402.
LE COUTEUR, K. J., 1950, *Proc. Phys. Soc. A*, **63**, 259.
MILLER, J. F., 1952, *Thesis*, U.C.R.L. Report 1902.
PAGE, N., 1950, *Proc. Phys. Soc. A*, **63**, 250.
PARFANOVICH, D. M., RABIN, N. V., and SEMCHINOVA, A. M., 1956, *J. Exp. Theor. Phys.*, **31**, 188.
WALKER, D., FREMLIN, J. H., LINK, W. T., and STEPHENS, K. G., 1954, *Brit. J. Appl. Phys.*, **5**, 157.
WAPSTRA, A. H., 1955, *Physica*, **21**, 367, 385.
WEISSKOPF, V. F., 1937, *Phys. Rev.*, **52**, 295.
ZELDES, N., 1958, *Nucl. Phys.*, **7**, 27.
ZUCKER, A., 1958, *Nucl. Phys.*, **6**, 420.

Negative Oxygen Ions from a Glow Discharge Source

By W. S. WHITLOCK AND J. E. BOUNDEN

Services Electronics Research Laboratory, Baldock, Herts.

MS. received 3rd October 1960

Abstract. A simple source of O^- ions suitable for accelerator applications is described. Negative atomic ion currents of over $2\mu A$ can be directly extracted at 10 keV energy for a low-pressure cold-cathode oxygen discharge source which incorporates an electrostatic constrictor electrode. The input power is only 25 watts and the gas consumption $14\text{ cm}^3\text{ h}^{-1}$ of oxygen at atmospheric pressure.

Mass analysis of the beam has shown the primary components to be O^- and O_2^- ions whilst the main impurity ions are OH^- , Cl^- and NO_2^- .

A study has been made of the relationship between the negative ion yield and various source operating conditions. The O^- and O_2^- ion yields are shown to be related to the striated structure of the positive column. With a singly striated column the beam is composed mainly of atomic ions. Only when a doubly striated column is formed does the O_2^- yield become large. Ion production processes are discussed in terms of this relationship.

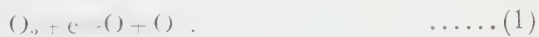
§ 1. INTRODUCTION

WITH the increasing tempo of negative ion studies and the construction of tandem Van de Graaff accelerators the demand for negative ion sources has grown. Accelerator requirements may call for negative ion currents of tens of microamperes but there are requirements for which a few microamperes are sufficient. When large negative ion currents are required, sources which utilize medium-energy charge-transfer reactions appear most promising (for example Weinman and Cameron 1956). Such sources, however, are relatively complex and may have large power consumptions.

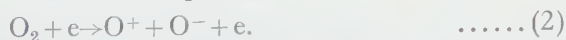
The source described here utilizes low-energy reactions in a direct extraction system. It generates a useful current of O^- ions, yet is simple, reliable and has a low power consumption.

§ 2. FUNDAMENTAL PROCESSES

Negative atomic oxygen ions may be formed by dissociative attachment of low-energy electrons to oxygen molecules, i.e.



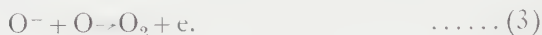
This process has a mean effective cross section of about $3 \times 10^{-19}\text{ cm}^2$ when the mean electron energy lies between 4–8 eV (Tozer, Thorburn and Craggs 1958, Thompson 1959b, Biondi 1960). At higher electron energies, i.e. greater than 17 eV, O^- ions may be formed from the process



The cross section for this process is of the same order of magnitude as that for (1).

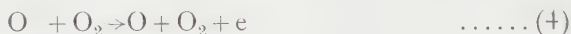
In the positive column of an oxygen glow discharge the electron temperature is about 3 eV (Thompson 1959a) which is favourable to the production of a large number of negative oxygen ions. Using the above data it can be shown that for a discharge current density of 1 ma cm^{-2} and an oxygen pressure of 10^{-2} mm Hg , the rate of production of O^- ions is of the order of $10^{12} \text{ ions cm}^{-3} \text{ sec}^{-1}$. The equilibrium concentration of negative ions will be determined by loss processes.

It has been reported (Thompson 1959a) that the main loss of negative ions can occur in the gas phase because loss to the walls may be restricted by radial electric fields. Where the walls are insulators a flow of energetic electrons maintains these at a negative potential with respect to the plasma. An important O^- gas destruction process is that due to associative detachment collisions with atoms, i.e.

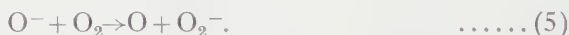


As the cross section value for (3) is relatively large (Thompson 1959, private communication) it is desirable to keep the concentration of atoms in the discharge small. At low gas pressures the atom concentration in the discharge depends on the efficiency of the source walls in recombining the atoms to form molecules.

Detachment collisions of the form



may also contribute as a loss process and atomic negative ions may also be lost in charge transfer collisions with neutral molecules, i.e.



However reactions (4) and (5) are endothermic with an O^- energy threshold of a few electron volts so that the importance of detachment and charge transfer will depend critically on the energy of the ions involved and on the particular discharge conditions.

Volume recombination and destruction due to electron collisions are not normally important as negative ion loss processes in low-pressure glow discharges.

§ 3. SOURCE DESIGN

In principle the source is similar to those of Emeleus and Sayers (1938) and Fite (1953) who extended some early work of Bennett and Darby (1936). Negative ions are extracted through a small hole in the anode of a low-pressure glow-discharge system. Of the sources referred to, that of Fite gave the largest negative ion yield; $1.4 \times 10^{-7} \text{ A}$ of O^- through a hole 0.05 cm in diameter with a gas pressure of about 0.1 mm Hg. This O^- current is insufficient for many applications so that a new source design was investigated.

In the Fite source the optimum extracted O^- current density was $8 \times 10^{-5} \text{ A cm}^{-2}$ and if this current density is reproduced then microamperes of negative ion current can be drawn through an aperture 0.1–0.2 cm in diameter. Increasing the aperture area, however, also increases the efflux of gas from the source. Hence, in order to keep the gas consumption down to a reasonable level the present source is operated with an oxygen gas pressure of about 10^{-2} mm Hg . Despite this low operating pressure the negative ion current density exceeds $10^{-4} \text{ A cm}^{-2}$ due principally to the influence of the 'constrictor' electrode described below.

Figure 1 shows the constructional details of the present source. The source body consists of a Kodial glass cylinder terminated by Nilo K spinnings. To each spinning a stainless steel flange is argon-arc welded. One flange carries the cathode, gas inlet and Pirani gauge. The other flange is made the anode of the discharge and possesses a central aperture 0.15 cm in diameter through which the ions are extracted. The overall dimensions are such that at a pressure of about 10^{-2} mm Hg a short positive column just forms. At lower pressures the source impedance rapidly increases and the positive column disappears so that the discharge characteristics are unsuited to negative ion production.

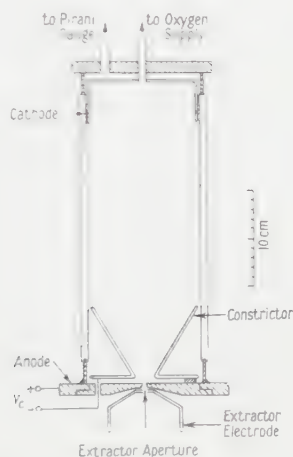


Fig. 1. Details of ion source.

In Fite's source an aperture electrode was positioned on the cathode side of the anode. In order to increase the extracted ion current this electrode was operated at a negative potential so that the discharge was concentrated on the centre of the anode. This idea has been extended in the present source in that a metal cone has been mounted above the anode. When the potential of this 'constrictor' is made negative with respect to the anode, the discharge is concentrated on to the extraction hole. With this arrangement ions may be extracted from a relatively high density plasma whilst the cathode current loading and associated cathode sputtering rates are maintained at a low value.

As previously mentioned, O^- ions may be lost due to associative detachment collisions with oxygen atoms. In order to encourage atom recombination on electrode surfaces both the constrictor and cathode electrodes are of copper for it has been shown (Greaves and Linnett 1959) that copper oxide has a high recombination coefficient with respect to oxygen atoms. Copper films which are sputtered onto the glass walls during the operation of the source should also contribute to atom recombination.

§ 4. EXPERIMENTAL METHOD

The ion source and associated supplies were normally operated at about 10 kV below earth potential. Both electrons and ions were extracted through the anode aperture and across a 0.05 cm gap by an electrode at earth potential.

The composite beam was then focused by means of an einzel lens into a conventional 60° magnetic mass analyser. Beam currents were measured by means of collector cups subjected to a transverse magnetic field in order to suppress secondary electrons. The beam was focused over the 100 cm path length into a spot about 5 mm in diameter. When a detailed mass spectrogram was required the beam size was decreased by means of beam defining slits.

A working pressure of about 1×10^{-5} mm Hg was maintained in the main vacuum chamber by two mercury diffusion pumps. Commercial oxygen was fed into the ion source via a needle valve and liquid nitrogen trap.

§ 5. EXPERIMENTAL RESULTS

5.1. Initial Beam Composition

The negative ion mass spectrum was found to be very dependent on the impurity gases in the source. During the first hour of source operation the beam consisted mainly of H^- , O^- , OH^- , O_2^- , Cl^- and a heavy ion which appeared to be NO_2^- . This heavy ion was generally dominant and NO_2^- is well known (e.g. Branscomb 1957) as an impurity in oxygen discharges. Most of the chlorine appeared to originate from the glass walls. After a few hours' operation, during which time the source was cleaned by the discharge, the yield of most of the impurity negative ions fell to a negligible amount. Ultimately the beam consisted of O^- , O_2^- and NO_2^- . A detailed investigation was then carried out to study the variation of beam composition and intensity with source operating conditions.

5.2. Beam Composition and Intensity

Figure 2(a) shows the variation of the total collected O^- ion current with discharge current, I_d . Also plotted (broken curve) is the O^-/O_2^- current ratio. This latter curve was not very reproducible in terms of absolute ratios but was repeatable in form. At about 18 mA the O^- current reaches its maximum value and a further increase in I_d only results in a lower negative ion yield.

Figure 2(b) shows the approximate total extracted current, i.e. electrons plus negative ions, plotted against I_d . As most of the negative ion beam consists of O^- ions it is seen that over 99% of the total beam consists of electrons. However, this electron component is easily rejected by a magnetic field and represents a power loss of less than 50 watts.

The next two figures are plotted with source oxygen gas pressure as a parameter. Fig. 2(c) shows an increasing O^- current with pressure whilst the O^-/O_2^- current ratio falls. As before, the O^-/O_2^- curve was not very reproducible and the general form only is shown in Fig. 2(c).

The negative constrictor potential V_c with respect to the anode, had a very marked influence on the negative ion beam composition and intensity. As seen from Fig. 3(a) the O^- current is large at low values of V_c whilst the O_2^- current is small. At high values of V_c the O^- and O_2^- currents are roughly equal in intensity. The large changes in negative ion beam composition appeared to be connected with changes in the structure of the positive column. With V_c set to about 50 volts the visible glow in front of the anode consists of two parts, a faint hemispherical region extending some 2 cm in front of the anode and within this a brighter hemispherical 'striation' about 0.5 cm in

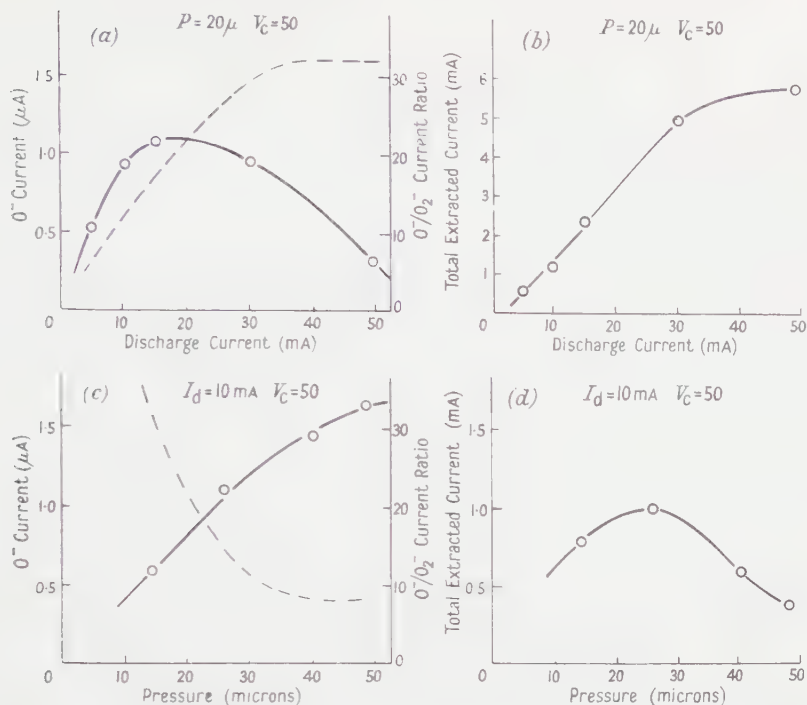


Fig. 2. Variation of beam characteristics with source current and pressure.

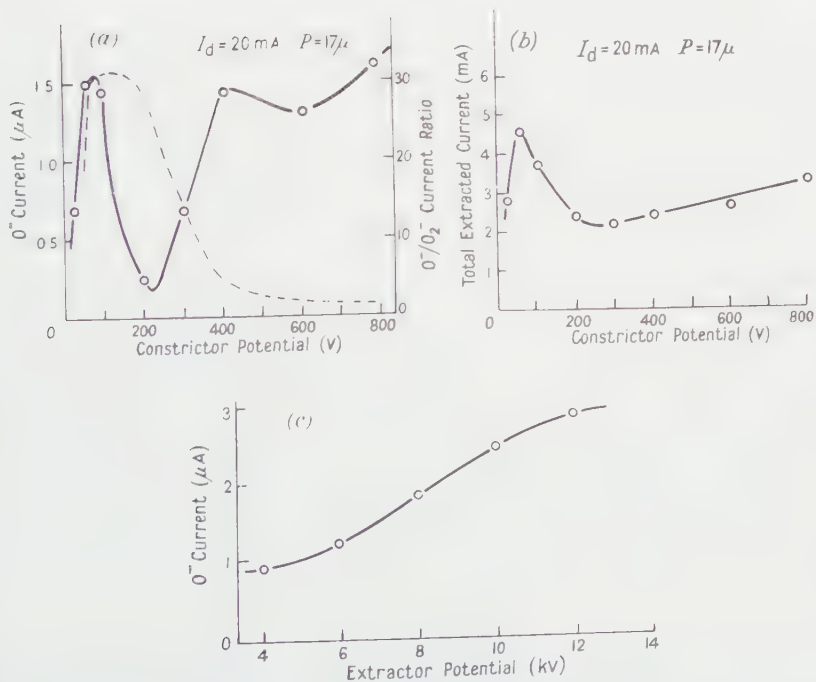


Fig. 3. Variation of beam characteristics with constrictor and extractor potential.

diameter located over the extraction hole. As V_c is increased to about 150 v this striation breaks away from the anode and moves axially down the discharge tube. When V_c equals about 300 v a second striation forms at the anode. As V_c is further increased this second striation grows in size whilst the first striation moves axially along the source to a position about 3 cm from the anode. The peak values of the O^- current therefore occur when either the first or the second striation is located at the extraction aperture. The O_2^- current, however, is large only when the first striation has moved away from the anode. The electron current also shows a maximum when a striation is located at the extraction aperture.

Figure 3(c) shows the value of O^- current as a function of the potential difference across the extractor gap.

Optimum conditions for source operation were found to be as follows. With $I_d = 18$ mA, an oxygen pressure of 2×10^{-2} mm of mercury, $V_c = 80$ v and an extraction voltage of 10 kv, the collected O^- , O_2^- and NO_2^- currents are $2.5 \mu A$, $0.3 \mu A$ and $0.1 \mu A$ respectively. If V_c is increased to 800 v then these currents become $2.6 \mu A$, $2.4 \mu A$ and $0.3 \mu A$ respectively. When operated under the conditions described above the power consumption of the source is small, the anode-cathode potential difference being 1.1 kv for $I_d = 18$ mA. At low values of V_c the constrictor current is about 3 mA but at $V_c = 800$ v this current rises to 15 mA. Thus an O^- current of over $2 \mu A$ can easily be obtained for a source input power of 25 watts. The gas consumption at a source pressure 2×10^{-2} mm of mercury is $14 \text{ cm}^3 \text{ h}^{-1}$ of oxygen at atmospheric pressure. The source has been operated for over 30 hours without apparent deterioration in performance.

§ 6. DISCUSSION OF RESULTS

In considering the implications of the results of these measurements it must be borne in mind that they have been influenced by particular experimental conditions. For example, about 20% of the extracted O^- and O_2^- ions were lost due to detachment collisions with residual gas molecules in the analyser system. The beam also suffered some attenuation in the ion optical system due to aberrations and aperture losses. The attenuation was not large and should not have influenced the relative proportions of the various ions produced by the source as indicated by mass analysis.

It is important to stress the effect of small impurity concentrations on this type of source. In the present case, the most troublesome impurities were water vapour and nitrogen. The former leads to the formation of OH^- which could be mistaken for O^- if the spectrometer resolution was inadequate. Nitrogen contamination leads to the formation of NO_2^- and although these ions are easily rejected from the main beam their presence in the source appears to reduce the concentration of O^- and O_2^- . The mechanisms of formation of NO_2^- , discussed by Branscomb (1957), have yet to be positively identified. In this investigation the relative proportion of NO_2^- was greatest at low pressures and low values of V_c , i.e. conditions under which the extracted O_2^- current was least.

There is evidence (Lunt and Gregg 1940) to suggest that few negative ions are to be found in the Faraday dark space. Therefore it is assumed that most of the negative ions are generated in the short positive column. The rate

of production of O^- ions is given by

$$R = N \int_0^{\infty} n_v \sigma_v v dv$$

where N is the neutral molecule density, $n_v dv$ the number of electrons per unit volume with velocities between v and $v + dv$, and σ_v the appropriate cross section of the ion forming reaction. For the present source an approximate value for R is 10^{13} ions $\text{cm}^{-3}\text{sec}^{-1}$. So far as O^- loss processes are concerned it is interesting to note that the O^- drain to the anode represents a loss of at least 10^{13} ion sec^{-1} . This suggests that a large proportion of the O^- ions formed in the short positive column is drawn rapidly into the anode and that destructive collisions in the gas are not significant. This interpretation is supported by Fig. 2(c) which shows an almost linear increase of O^- current with pressure, i.e. $R \propto N$.

An unexpected source characteristic was the marked influence of the constrictor potential on the negative ion beam composition. Merely by changing the potential of this electrode the yield of O_2^- ions may be increased thirty-fold. At low values of V_c the beam consists mainly of O^- ions. Under this condition a single hemispherical striation rests on the extraction aperture and it is probable that most of the extracted O^- ions are generated by dissociative attachment collisions, reaction (1) within this striation.

The origin of the O_2^- current presents a more difficult problem, particularly as the mechanisms of O_2^- production in gas discharges generally are not fully resolved. Negative molecular oxygen ions may be formed directly by radiative attachment but the cross section for this reaction is small, i.e. less than 10^{-20}cm^2 . Molecular negative ions may also be formed by direct attachment followed by a stabilizing collision or by attachment during a three-bodied collision. Such processes are unlikely to account for the O_2^- yield of 10^{13} ions sec^{-1} observed in the present source, particularly as the lifetime of the excited O_2^- ion is very short, i.e. of the order of 10^{-10}sec (Bloch and Bradbury 1935) and the gas pressure too low for multi-collision processes to be significant. Under suitable conditions a high rate of O_2^- production can result from charge transfer or ion exchange collisions involving O^- ions and it is suggested that such collisions are effective in the present source in the following way.

When V_c is small, the extracted O^- ions originate in the single striation which rests on the anode. On increasing V_c this first striation moves away from the anode and the extracted O^- current falls. A similar effect was observed by Fite (1953). A further increase in V_c initiates a second striation and the O^- current regains its previous value whilst the O_2^- current rapidly increases until it equals the O^- current. It is now suggested that the second striation supplies the O^- current whilst the O_2^- ions are produced in the inter-striation region by charge transfer from the O^- ions which come from the first striation. It is assumed that these atomic ions are accelerated by the electric field between the striations to an energy above the threshold value for the charge transfer reaction (5).

ACKNOWLEDGMENTS

The authors are grateful to the members of the Physics Department, University College, London, for valuable discussions and to Miss P. M. Dunmow for experimental help. Acknowledgment is made to the Admiralty for permission to publish this paper.

REFERENCES

- BENNETT, W. H., and DARBY, P. F., 1936, *Phys. Rev.*, **49**, 97.
BIONDI, M. A., 1960, *Proc. Int. Conf. Uppsala*, Vol. **1**, 72.
BLOCH, F., and BRADBURY, N. E., 1935, *Phys. Rev.*, **48**, 689.
BRANSCOMB, L. M., 1957, *Advanc. Elect. and Electron Phys.*, **9**, 43.
EMELEUS, K. G., and SAYERS, J., 1938, *Proc. R. Irish Acad.*, **44**, 87.
FITE, W. L., 1953, *Phys. Rev.*, **89**, 411.
GREAVES, J. C., and LINNETT, J. W., 1959, *Trans. Faraday Soc.*, **55**, 1346.
LUNT, R. W., and GREGG, A. H., 1940, *Trans. Faraday Soc.*, **36**, 1062.
THOMPSON, J. B., 1959 a, *Proc. Phys. Soc.*, **73**, 818.
—— 1959 b, *Proc. Phys. Soc.*, **73**, 821.
TOZER, B. A., THORBURN, R., and CRAGGS, J. D., 1958, *Proc. Phys. Soc.*, **72**, 1081.
WEINMAN, J. A., and CAMERON, J. R., 1956, *Rev. Sci. Instrum.*, **27**, 288.

An Investigation of Some (t, d) Reactions in Light Nuclei at 5.5 Mev

By F. DE S. BARROS†, P. D. FORSYTH‡, A. A. JAFFE
AND I. J. TAYLOR

The Physical Laboratories, University of Manchester

MS. received 5th October 1960

Abstract. A broad range magnetic spectrograph has been used to analyse the deuterons emitted from targets of natural boron, carbon, silicon dioxide and aluminium bombarded with 5.5 Mev tritons. The angular distributions of the majority of the deuteron groups from the reactions observed in ^{10}B , ^{12}C , ^{13}C , ^{16}O , ^{27}Al and ^{28}Si have been measured and information has also been obtained on (t, d) reactions in ^{24}Mg , ^{28}Si , and ^{40}Ca because of the presence of these nuclei as impurities in the targets. In all cases the measured excitation energies of the final nuclei are in good agreement with the accepted values. The angular distributions have been compared with the stripping theory and also with published data on (d, p) transitions between the same initial and final nuclear states. Where possible the ratios of the yields of corresponding (t, d) and (d, p) reactions have been compared with the predictions of stripping theory to extract values of the proportionality constant of the momentum transform of the deuteron within the triton, $|A_0|^2 N_i^2$. The values obtained vary between $18.0 \times 10^{12} \text{ cm}^{-1}$ for the transition from ^{10}B to the ground state of ^{11}B and $1.3 \times 10^{12} \text{ cm}^{-1}$ for the transitions from ^{16}O to the ground state of ^{17}O and from ^{28}Si to the 3.630 Mev excited state of ^{29}Si .

At 5.5 Mev triton bombarding energy, therefore, a constant value of $|A_0|^2 N_i^2$ cannot be used to extract values of nucleon reduced widths from studies of (t, d) reactions.

§ 1. INTRODUCTION

IN this work, (t, d) reactions in several light target nuclei have been investigated using a triton beam of 5.53 Mev incident energy. Deuteron groups leading to discrete levels in the final nuclei have been observed and angular distributions and absolute cross sections have been measured. Little previously published information is available at present on (t, d) reactions induced at similar, or higher, bombarding energies.

The primary aim of these experiments was to verify the predictions of the theory of single particle stripping from mass-3 particles (Newns 1952, Butler and Salpeter 1952, Butler and Hittmair 1957) as in the case of a previous investigation of some (^3He , d) reactions (Forsyth *et al.* 1960). At the maximum

† On leave of absence from the Brazilian Centre for Physical Research.

‡ Now at the Rice Institute, Houston, U.S.A.

bombarding energies available by acceleration in the Manchester University Van de Graaff generator, the (t, d) reaction is more suitable for this purpose than the (^3He , d) reaction since Coulomb effects will be less important. Also, as discussed by Forsyth *et al.*, it is of particular interest to compare the behaviour of the mass-3 stripping reactions with the corresponding deuteron stripping reaction between the same initial and final states. For the (t, d) reactions comparison may be made with the (d, p) reactions which have, in general, been studied more widely and thoroughly than the (d, n) reactions which were used for comparison with the results of the (^3He , d) reaction.

In the present work deuterons were observed, using a broad range magnetic spectrograph, in a series of exposures with targets of natural boron, carbon, silicon dioxide and aluminium. Most of the experimental details have already been given in an account of the (t, p) reactions which were recorded simultaneously on the same photographic plates (Jaffe *et al.* 1960).

Table 1

(1)	(2)	(3)	(4)	(5)	(6)
$^{10}\text{B}(\text{t}, \text{d}_0)^{11}\text{B}$	0	1	5.5	5.0(a)	5.2 (18°)
$^{10}\text{B}(\text{t}, \text{d}_1)^{11}\text{B}$	2.126	1	6.5	6.0(a)	0.6 (24°)
$^{10}\text{B}(\text{t}, \text{d}_2)^{11}\text{B}$	4.449	1	5.5	5.5(a)	4.0 (25°)
$^{10}\text{B}(\text{t}, \text{d}_3)^{11}\text{B}$	5.027	1	5.5	5.5(a)	1.6 (25°)
$^{10}\text{B}(\text{t}, \text{d}_4)^{11}\text{B}$	6.769	1	5.5	5.0(a)	20.0 (14°)
$^{10}\text{B}(\text{t}, \text{d}_5)^{11}\text{B}$	6.806	1	5.5	—	0.6 (14°)
$^{10}\text{B}(\text{t}, \text{d}_6)^{11}\text{B}$	7.301	1	5.5	—	1.9 (14°)
$^{12}\text{C}(\text{t}, \text{d}_0)^{13}\text{C}$	0	1	6.0	4.5(b)	34.0 (13°)
$^{13}\text{C}(\text{t}, \text{d}_0)^{14}\text{C}$	0	1	5.9	5.4(c)	22.3 (18°)
$^{16}\text{O}(\text{t}, \text{d}_0)^{17}\text{O}$	0	2	5.3	5.1(d)	9.8 (19°)
$^{24}\text{Mg}(\text{t}, \text{d}_0)^{25}\text{Mg}$	0	2	5.7	5.3(e)	—
$^{24}\text{Mg}(\text{t}, \text{d}_1)^{25}\text{Mg}$	0.569	0	5.7	5.3(e)	—
$^{27}\text{Al}(\text{t}, \text{d}_0)^{28}\text{Al}$	0	0	7.0	6.6(f)	13.6 (12°)
$^{27}\text{Al}(\text{t}, \text{d}_1)^{28}\text{Al}$	0.030	0	7.5	6.6(f)	8.7 (12°)
$^{27}\text{Al}(\text{t}, \text{d}_2)^{28}\text{Al}$	1.020	2	5.5	5.4(f)	1.7 (33°)
$^{27}\text{Al}(\text{t}, \text{d}_3)^{28}\text{Al}$	1.370	2	5.5	—	2.7 (33°)
$^{27}\text{Al}(\text{t}, \text{d}_4)^{28}\text{Al}$	2.138	0	6.5	6.6(f)	2.0 (12°)
$^{27}\text{Al}(\text{t}, \text{d}_5)^{28}\text{Al}$	2.203	2	5.5	5.4(f)	0.7 (23°)
$^{27}\text{Al}(\text{t}, \text{d}_6)^{28}\text{Al}$	2.279	2	5.5	5.4(f)	1.1 (16°)
$^{27}\text{Al}(\text{t}, \text{d}_7)^{28}\text{Al}$	2.489	0	6.5	6.6(f)	0.3 (16°)
$^{27}\text{Al}(\text{t}, \text{d}_8)^{28}\text{Al}$	2.664	2	5.5	5.4(f)	1.1 (17°)
$^{28}\text{Si}(\text{t}, \text{d}_0)^{29}\text{Si}$	0	0	5.7	5.4(g)	—
$^{28}\text{Si}(\text{t}, \text{d}_1)^{29}\text{Si}$	1.271	2	5.7	5.4(g)	—
$^{28}\text{Si}(\text{t}, \text{d}_2)^{29}\text{Si}$	3.071	2	4.5	5.4(g)	0.3 (44°)
$^{28}\text{Si}(\text{t}, \text{d}_3)^{29}\text{Si}$	3.630	3	6.7	5.4(g)	1.8 (33°)
$^{28}\text{Si}(\text{t}, \text{d}_4)^{29}\text{Si}$	4.936	1	6.7	5.4(g)	1.4 (23°)
$^{40}\text{Ca}(\text{t}, \text{d}_0)^{41}\text{Ca}$	0	3	4.6	6.0(h)	—
$^{40}\text{Ca}(\text{t}, \text{d}_3)^{41}\text{Ca}$	2.456	1	5.1	6.0(h)	—

(1) Reaction; (2) measured excitation (mev); (3) *L*-values; (4) radius (10^{-13} cm); (5) radius used by Macfarlane and French (1960) in (d, p) analyses (10^{-13} cm); (6) differential cross section at the centre-of-mass angle shown (mbn sterad $^{-1}$). (a) Evans and Parkinson (1954), (b) Green and Middleton (1956), (c) McGruer *et al.* (1955), (d) Burge *et al.* (1951), (e) Holt and Marsham (1953 a), (f) Enge *et al.* (1956), (g) Holt and Marsham (1953 b), (h) Bockelman and Buechner (1957).

§ 2. RESULTS

2.1. Spectra

In the course of this investigation deuteron groups leading to levels of ^{11}B , ^{13}C , ^{14}C , ^{17}O , ^{25}Mg , ^{28}Si , ^{40}K and ^{41}Ca were observed. The measured excitation energies of these nuclei, which are shown in Table 1, were in excellent agreement with the values given by Ajzenberg-Selove and Lauritsen (1959) and Endt and Braams (1957). The results for the individual targets are discussed below.

2.1.1. Natural boron target.

This target consisted of a $30\ \mu\text{g cm}^{-2}$ layer of natural boron evaporated on to a $14\ \mu\text{g cm}^{-2}$ carbon foil. Spectra of the deuterons observed at 60° to the incident beam for two different field settings are shown in Fig. 1. Deuteron groups leading to the ground state and the first six excited states of ^{11}B at (1) 2.126, (2) 4.449,

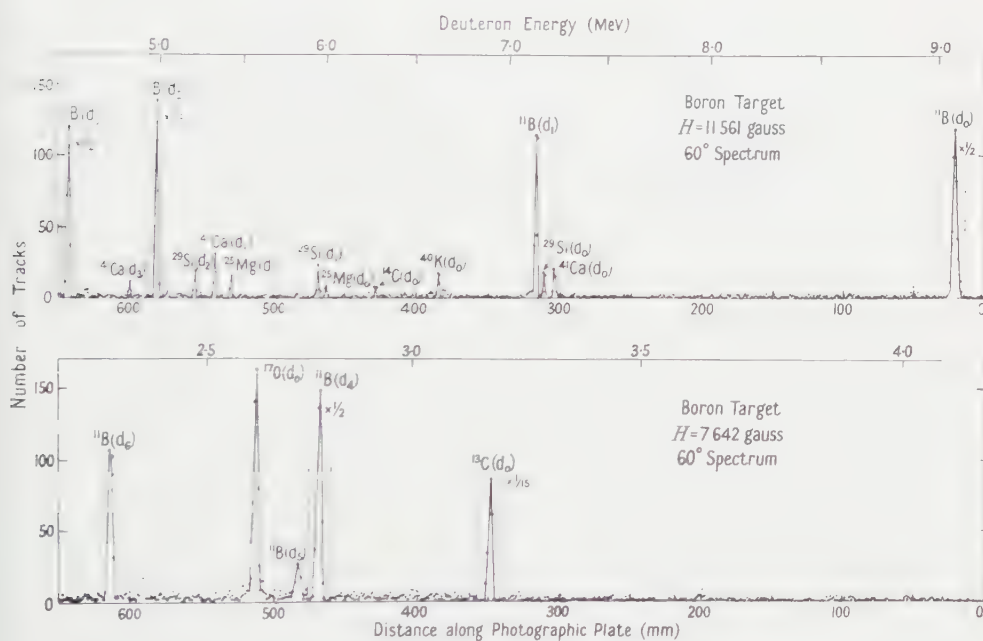


Fig. 1. The 60° deuteron spectrum from the boron target bombarded with 5.53 MeV tritons.

(3) 5.027, (4) 6.769, (5) 6.806 and (6) 7.301 MeV were identified. These excitation energies were determined with an accuracy to ± 10 keV. Deuterons from the $^{11}\text{B}(t, d)^{12}\text{B}$ reaction were absent because it has a relatively low Q value (-2.894 MeV).

The reaction $^{13}\text{C}(t, d)^{14}\text{C}$ was observed due to the presence of ^{13}C in the natural carbon backing for the boron target.

As shown in Fig. 1, deuteron groups from the reactions in ^{16}O , ^{24}Mg , ^{28}Si , ^{39}K and ^{40}Ca , which were present as contaminants, were also observed. The

contamination amounted to about 12% of the total target thickness (Muto *et al.* 1960). The following reactions were observed in these nuclei: $^{16}\text{O}(\text{t}, \text{d})^{17}\text{O}$ (ground state); $^{24}\text{Mg}(\text{t}, \text{d})^{25}\text{Mg}$ (ground state, 0.569, 0.973 MeV); $^{28}\text{Si}(\text{t}, \text{d})^{29}\text{Si}$ (ground state, 1.271, 2.025 MeV); $^{39}\text{K}(\text{t}, \text{d})^{40}\text{K}$ (ground state); $^{40}\text{Ca}(\text{t}, \text{d})^{41}\text{Ca}$ (ground state, 1.937, 2.456 MeV). The excitations were determined with an accuracy to ± 6 keV. The deuteron groups to the third excited state of ^{29}Si at 2.426 MeV and the second excited state of ^{41}Ca at 2.014 MeV (Endt and Braams 1957) were not detected above the background.

2.1.2. Carbon target.

The ground state deuteron group from the $^{12}\text{C}(\text{t}, \text{d})^{13}\text{C}$ reaction was observed from the triton bombardment of a $35 \mu\text{g cm}^{-2}$ thick natural carbon target and this group was also present on spectra obtained with each of the other targets, since carbon films were used as backing in each case.

The relative intensities of this group from the different targets were used to verify the consistency of the measurements of the thickness of the targets.

2.1.3. Silicon dioxide target.

As can be seen from the spectrum shown in Fig. 2, the reactions leading to the ground state of ^{17}O and the excited state at 0.865 ± 0.005 MeV were observed and also those leading to the fourth, fifth and ninth excited states of ^{29}Si at measured excitations of 3.071, 3.630 and 4.936 MeV (± 0.010 MeV) respectively. The deuteron groups leading to the sixth, seventh and eighth excited states of

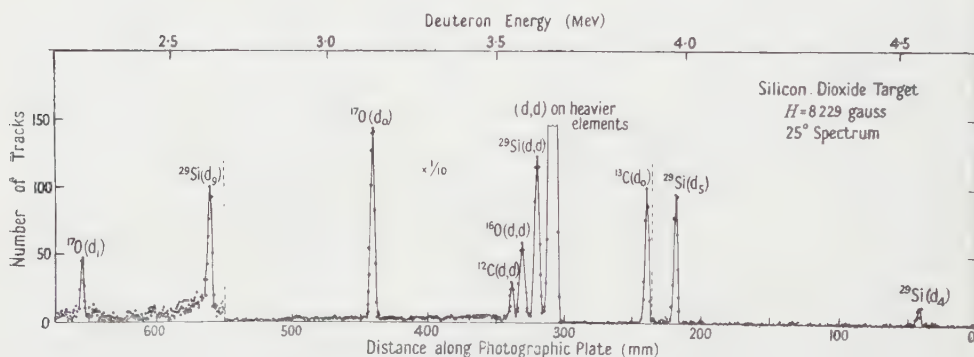


Fig. 2. The 25° deuteron spectrum from the silicon dioxide target bombarded with 5.53 MeV tritons.

^{29}Si at 4.078, 4.840 and 4.897 MeV (Endt and Braams 1957) could not be studied from these spectra because the sixth excited state group was always obscured by electrically scattered deuterons, which arose from the presence of HD molecules in the incident beam, and the seventh and eighth excited state groups are evidently very weak (maximum differential cross section less than $0.01 \text{ mbn sterad}^{-1}$).

2.1.4. Aluminium target.

Deuteron groups leading to the ground state of ^{28}Al and to excited states at (1) 0.030, (2) 0.973, (3) 1.020, (4) 1.370, (5) 1.630, (6) 2.138, (7) 2.203, (8) 2.279, (9) 2.489, (10) 2.582, and (11) 2.664 MeV, (± 5 keV) are shown in Fig. 3.

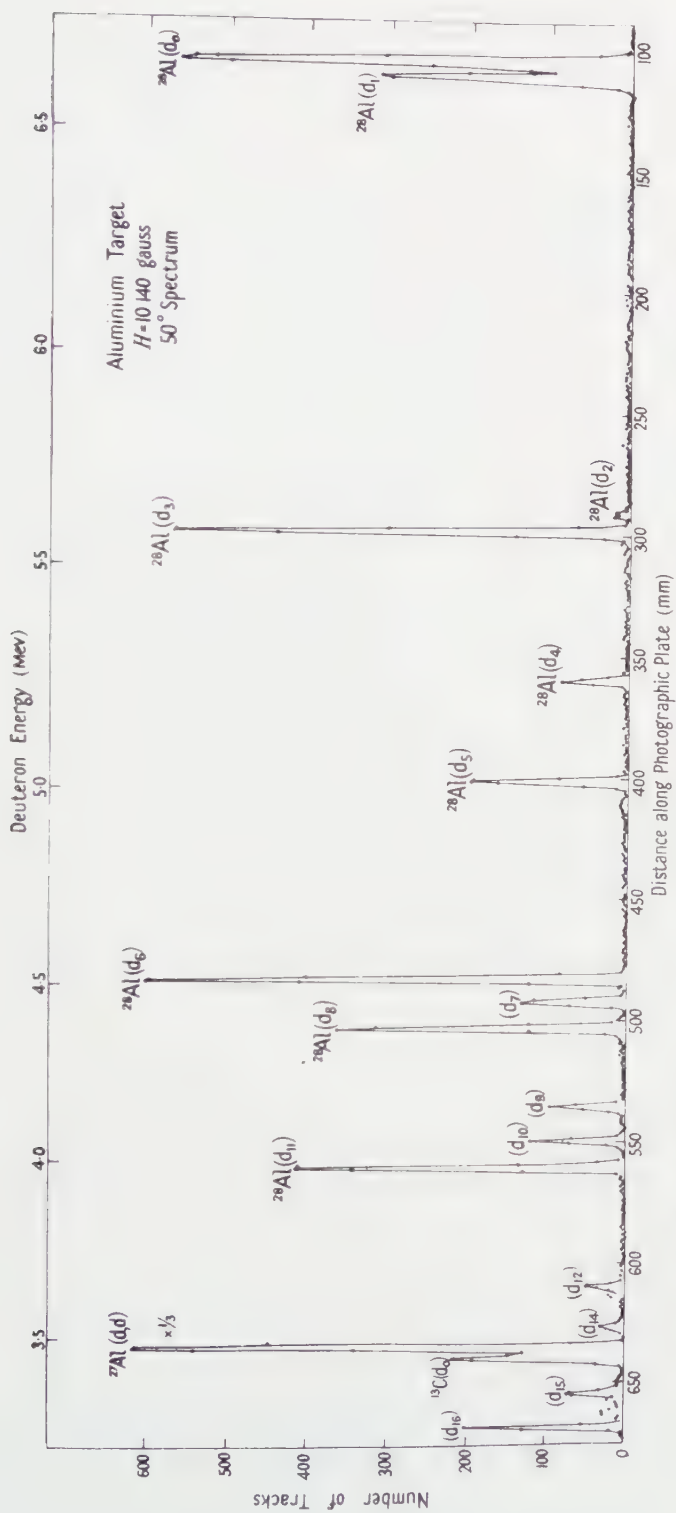


Fig. 3. The 50' deuteron spectrum from the aluminium target bombarded with 5.53 mev tritons.

The excitation energies corresponding to groups leading to higher excited states of ^{28}Al could not be measured accurately since at most of the angles these groups were either obscured by elastically scattered deuteron groups or were not recorded on the plates.

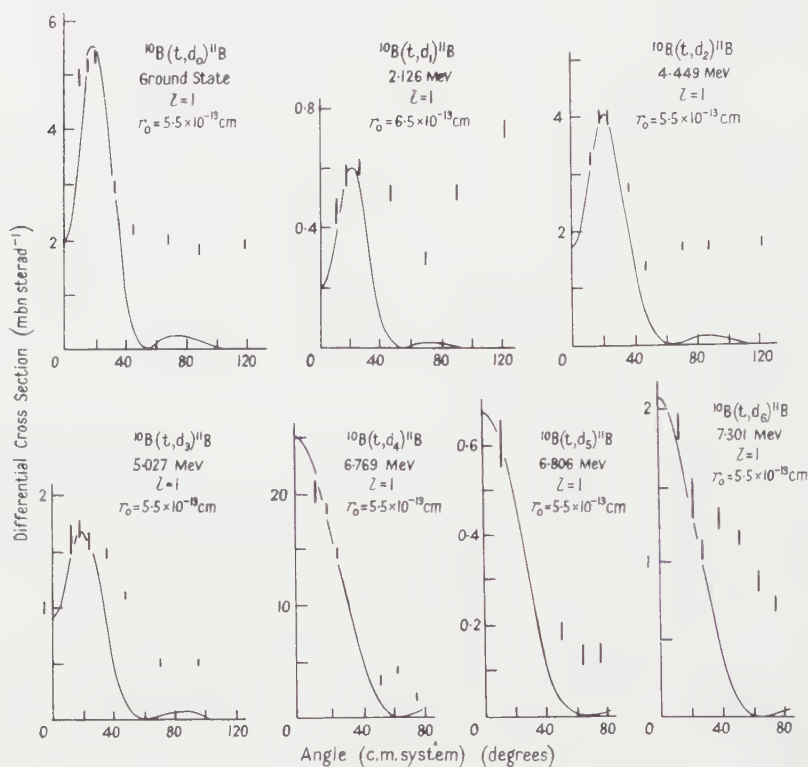


Fig. 4. Angular distributions of deuteron groups from the reaction $^{10}\text{B}(t, d)^{11}\text{B}$.

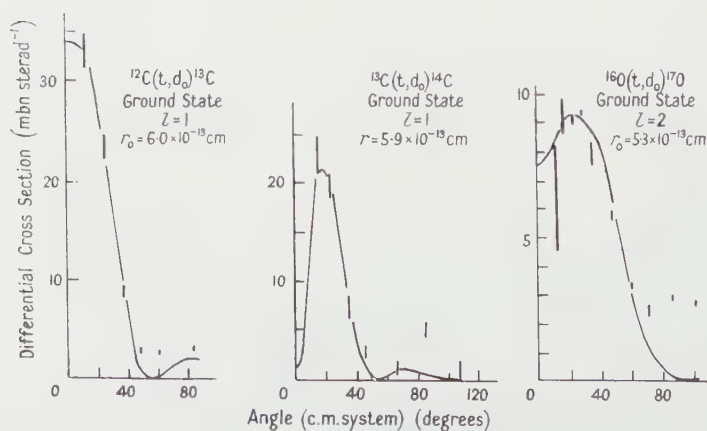


Fig. 5. Angular distributions of the ground state deuteron groups from the reactions $^{12}\text{C}(t, d)^{13}\text{C}$, $^{13}\text{C}(t, d)^{14}\text{C}$ and $^{16}\text{O}(t, d)^{17}\text{O}$.

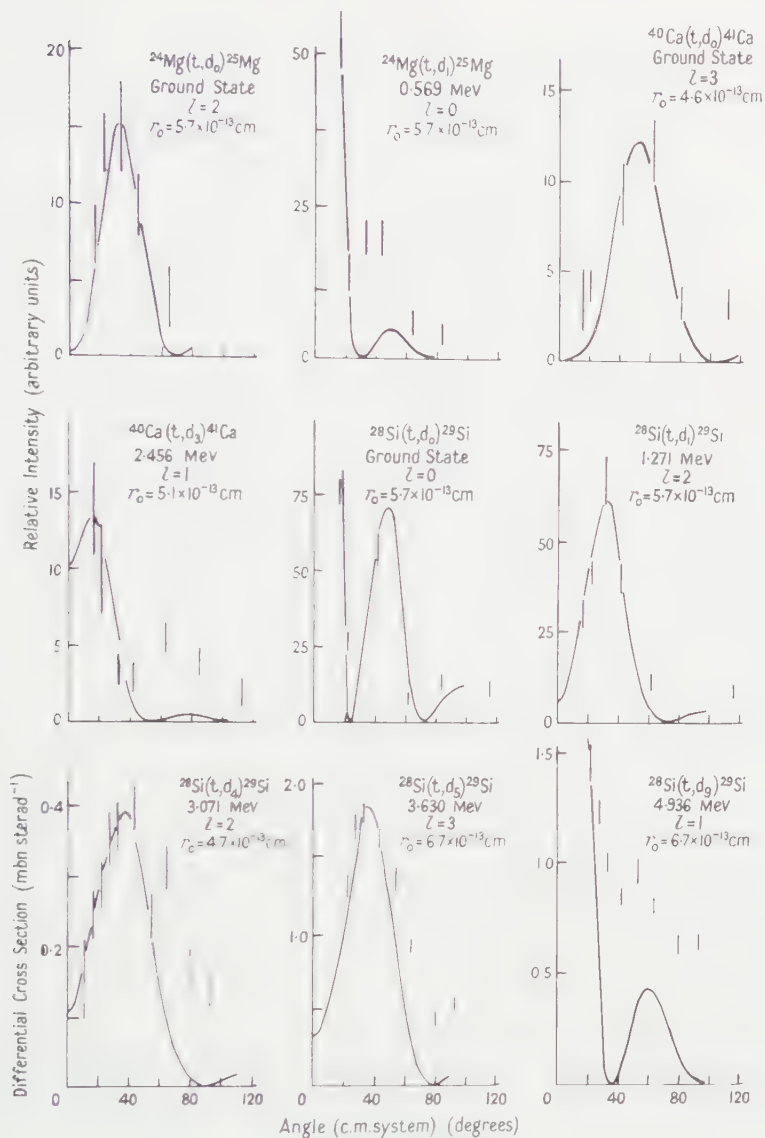


Fig. 6. Angular distributions of deuteron groups from the reactions $^{24}\text{Mg}(t, d)^{25}\text{Mg}$, $^{28}\text{Si}(t, d)^{29}\text{Si}$ and $^{40}\text{Ca}(t, d)^{41}\text{Ca}$. Absolute cross sections were not measured for several of the transitions. In these cases the scales show the relative intensities of groups arising from the same target nucleus.

2.2. Angular Distributions and Differential Cross Sections

The angular distributions and differential cross sections for the deuteron groups observed from the above targets are shown in Figs 4 to 7. The maximum absolute cross sections are given in Table 1 and the accuracy was estimated to be to $\pm 15\%$.

Little information on the reaction $^{16}\text{O}(t, d_1)^{17}\text{O}$ could be obtained since the deuteron group was observed only at a limited number of angles. The angular

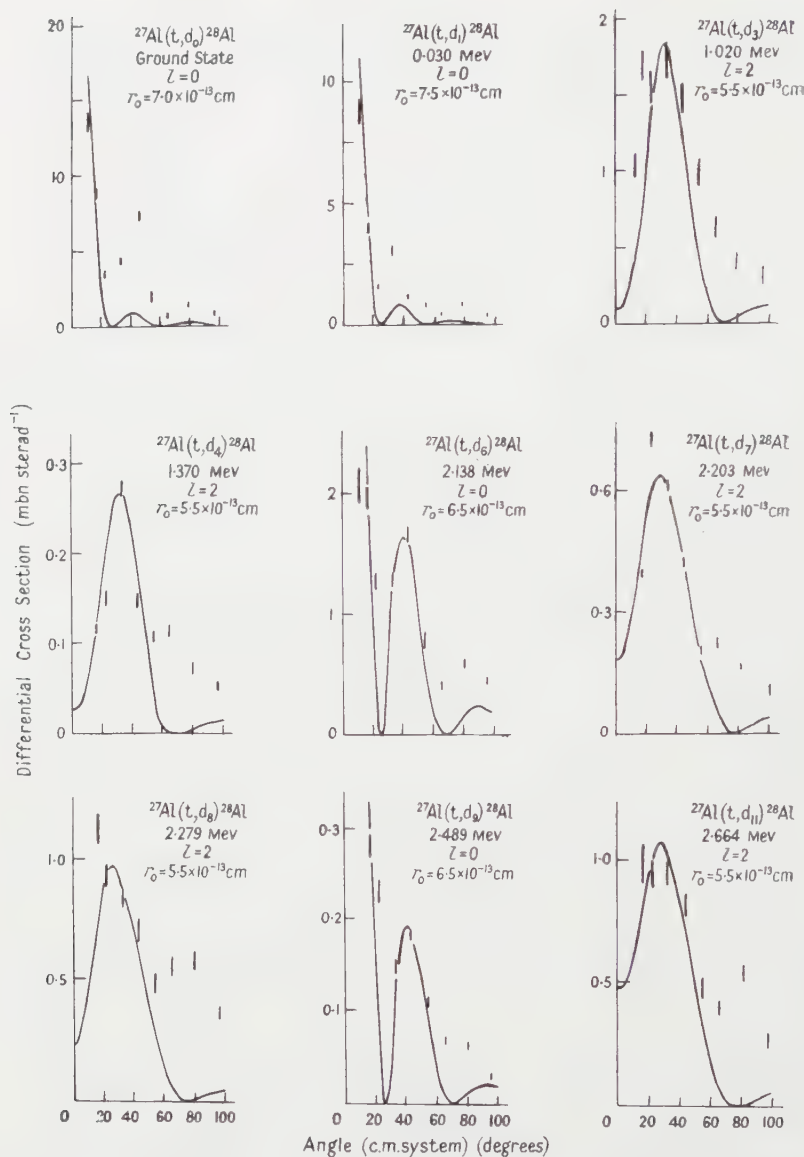


Fig. 7. Angular distributions of the deuteron groups from the $^{27}\text{Al}(t, d)^{28}\text{Al}$ reaction.

distribution appeared to peak close to the 0° direction but observations could not be made below 20° (c.m.) where the measured differential cross section was $1 \text{ mbn sterad}^{-1}$.

The d_2 group from the $^{27}\text{Al}(t, d)^{28}\text{Al}$ was too weak ($0.06 \text{ mbn sterad}^{-1}$) to yield a reliable angular distribution. The d_5 and d_{10} groups from this reaction had angular distributions which were isotropic to within 30% and average differential cross sections of 0.40 and $0.15 \text{ mbn sterad}^{-1}$, respectively.

Apparently reliable angular distributions of the deuteron groups arising from the (t, d) reactions in the ^{24}Mg , ^{28}Si , and ^{40}Ca impurities in the boron target were obtained, and these are shown in Fig. 6. Further (t, d) transitions arising from these and other impurities were observed but the angular distributions could not be constructed because the deuteron groups overlapped with each other or were obscured by larger groups arising from $^{10}\text{B}(\text{t}, \text{d})^{11}\text{B}$ reactions.

§ 3. DISCUSSION OF RESULTS

3.1. Angular Distributions

The results described above have been compared with the predictions of the Butler theory of stripping as applied to (^3He , d) and (t, d) reactions (Butler and Salpeter 1952, Butler and Hittmair 1957, Forsyth *et al.* 1960). Most of the transitions observed in the present investigation have been previously studied via (d, p) reactions and these data have been reviewed by Macfarlane and French (1960) who have re-analysed the results in a uniform manner using the Butler theory of (d, p) stripping. The numerical table of Butler-Born approximation stripping cross sections computed by Lubitz (1957, "Numerical Table of Butler-Born Approximation Stripping Cross Sections", Univ. of Michigan Report, unpublished) and used by Macfarlane and French to analyse the (d, p) results has also been used here to fit the angular distributions and to compare the magnitude of the absolute differential cross sections with the predictions of the Butler theory.

The l -values which gave the best fit with the (t, d) angular distributions were invariably found to be the same as had been required to fit those of the corresponding (d, p) reactions. Also, similar values of the interaction radius were used, as can be seen in Table 1. This reflects the close similarity between the corresponding (d, p) and (t, d) angular distributions which even extends to the deviations from the theoretical curves observed for many of the studied transitions, as is mentioned below.

$^{10}\text{B}(\text{t}, \text{d})^{11}\text{B}$. The angular distributions of the d_0 , d_2 , d_3 and d_4 groups (Fig. 4) exhibit similar deviations from the theoretical curves as those of the corresponding proton groups from the $^{10}\text{B}(\text{d}, \text{p})^{11}\text{B}$ reaction studied at 7.7 mev by Evans and Parkinson (1954).† The relatively high yield of the d_0 , d_2 and d_3 groups at large angles, which cannot be explained by simple stripping theory, has also been observed in the angular distributions of the corresponding proton groups in the (d, p) investigation mentioned above. The relative yields to different excited states of the (t, d) and (d, p) reactions are closely similar. The high cross section for the (t, d) reaction leading to the fourth excited state confirms the single-particle character of this state indicated by the (d, p) results of Evans and Parkinson. The d_1 group is weak and has an angular distribution which cannot be explained by the simple stripping theory, although there is some evidence of an

† Although Evans and Parkinson (1954) could not resolve the fourth and fifth excited state proton groups from the (d, p) reaction, the transition leading to the fifth excited state has been observed to be relatively weak by Van Patter *et al.* (1951). As can be seen in Table 1, the intensity of the d_3 group is considerably smaller than that of the d_4 group. Hence it is reasonable to compare the angular distribution of the unresolved p_4 and p_5 groups with that of the d_4 group.

$l=1$ component. A similar result was obtained in a previous observation of the mirror reaction $^{10}\text{B}(^3\text{He}, d_1)^{11}\text{C}$ (Forsyth *et al.* 1960) and it was suggested that other direct interaction mechanisms might be responsible for the anomalous behaviour. The angular distributions of the p_5 and p_6 groups from the (d, p) reaction in ^{10}B , leading to excited states of ^{11}B at 6.81 and 7.30 mev, respectively, have not been reported (Ajzenberg-Selove and Lauritsen 1959). The d_5 and d_6 angular distributions can be fitted assuming $l=1$ which is consistent with the tentative assignments of spins and parities of $3/2^-$ and $5/2^-$ for the fifth and sixth excited states of ^{11}B (Ajzenberg-Selove and Lauritsen 1959). The low cross section for the transition leading to the fifth excited state is consistent with this state having a mixed configuration as would be required by the shell-model calculations of Kurath (1956).

$^{12}\text{C}(t, d)^{13}\text{C}$, $^{16}\text{O}(t, d)^{17}\text{O}$, $^{13}\text{C}(t, d)^{14}\text{C}$. The angular distributions of the deuteron groups from these reactions (Fig. 5) were fitted with the stripping theory using the l -values obtained from the corresponding (d, p) results (Macfarlane and French 1960).

$^{24}\text{Mg}(t, d)^{25}\text{Mg}$. Although the theoretical fits of the d_0 and d_1 angular distributions (Fig. 6) must be regarded as tentative since the deuteron groups arose from the small ^{24}Mg contamination of the boron target, the l -values and radii employed agree well with the parameters used in previous investigations of the corresponding (d, p) reactions (Holt and Marsham 1953 a, Hinds *et al.* 1958).

$^{27}\text{Al}(t, d)^{28}\text{Al}$. The theoretical fits to the angular distributions shown in Fig. 7 have been made using the l -values obtained from investigation of the corresponding (d, p) reaction (Enge *et al.* 1956). The radii which yield the best fits are in good agreement with those used by Enge *et al.* except for those cases ($l=0$) where the peaks of the angular distributions were not observed, thus making the fits uncertain. Although some of the angular distributions show complex structures, the deviations from the theoretical curves are generally closely similar to those observed in the corresponding (d, p) angular distributions. For example, the large cross sections of the d_3 and d_8 groups at small angles were observed for the p_3 and p_8 groups by the above authors who employed small $l=0$ components to improve the fits of the angular distributions of these groups. Both the (t, d) and (d, p) transitions to the fifth and tenth excited states of ^{28}Al are approximately isotropic. The relative yields of the (t, d) and (d, p) reactions leading to different excited states of ^{28}Al are also in excellent agreement.

$^{28}\text{Si}(t, d)^{29}\text{Si}$. The angular distributions shown in Fig. 6 have been fitted with Butler theory using the l -values indicated by the investigation of the corresponding (d, p) reactions by Holt and Marsham (1953 b). However, the proton angular distributions leading to the fourth and fifth excited states of ^{29}Si required an $l=0$ component which does not appear to be present in the (t, d) angular distributions.

$^{40}\text{Ca}(t, d)^{41}\text{Ca}$. Once again the theoretical fits (see Fig. 6) are tentative since the ^{40}Ca was present as a contaminant in the boron target, but the l -values used agree with those employed to fit the corresponding (d, p) angular distributions (Bockelman and Buechner 1957) though the radii are slightly smaller.

3.2. The Absolute Cross Sections

For those angular distributions in which the experimental points showed a maximum within the angular range studied, a comparison of the measured peak differential cross sections with predictions of the theory yielded values of

$(2J_f + 1)|A_0|^2 N_i^2 \theta^2$. The quantity $(2J_f + 1)\theta^2$, where J_f is the spin of the final nucleus and θ^2 is the nucleon reduced width, has in many cases been calculated by Macfarlane and French (1960) from the results of previous investigations of the (d, p) reaction. Hence the proportionality factor of the momentum transform of the deuteron within the triton, $|A_0|^2 N_i^2$, which is defined by Butler and Hittmair (1957), could be extracted for the transitions and the values obtained are listed in Table 2. A constant value of $|A_0|^2 N_i^2$ would be expected if the simple theory of stripping was valid and the assumed momentum transform was a good approximation. The errors associated with measurements of the cross sections of the (t, d) and (d, p) reactions are such that an experimental error of $\pm 50\%$ should be assigned to the values of $|A_0|^2 N_i^2$. A comparison of the yields of the corresponding (t, d) and (d, p) transitions characterized by an $l=0$ angular momentum transfer could not be made reliably since the first maxima of the (t, d) angular distributions occurred at too small an angle to be observed. The values of $|A_0|^2 N_i^2$ obtained for these cases should therefore be treated with reserve and are shown in parenthesis in Table 2.

The derived values of $|A_0|^2 N_i^2$ vary over a range of from 1.3 to $18 \times 10^{12} \text{ cm}^{-1}$, the larger values corresponding to the results obtained for the lighter target nuclei, ^{10}B , ^{12}C and ^{13}C . A possible explanation of the variation between the lighter and heavier target nuclei is that Coulomb interactions are important, as has been suggested in the case of the investigations of $(^3\text{He}, \text{d})$ reactions (Forsyth *et al.* 1960). The low value obtained from the $^{16}\text{O}(\text{t}, \text{d})^{17}\text{O}$ reaction ($Q = -2.113 \text{ MeV}$) might thus be a result of the relatively low energy of the outgoing deuteron.

Table 2

(1)	(2)	(3)	(4)	(5)
$^{10}\text{B}(\text{t}, \text{d}_0)^{11}\text{B}$	1	0.80	0.044 ^(a)	18.2
$^{10}\text{B}(\text{t}, \text{d}_2)^{11}\text{B}$	1	0.46	—	—
$^{10}\text{B}(\text{t}, \text{d}_3)^{11}\text{B}$	1	0.20	—	—
$^{10}\text{B}(\text{t}, \text{d}_4)^{11}\text{B}$	1	2.28	—	—
$^{10}\text{B}(\text{t}, \text{d}_5)^{11}\text{B}$	1	0.06	—	—
$^{10}\text{B}(\text{t}, \text{d}_6)^{11}\text{B}$	1	0.26	—	—
$^{12}\text{C}(\text{t}, \text{d}_0)^{13}\text{C}$	1	0.48	0.066 ^(b)	7.3
$^{13}\text{C}(\text{t}, \text{d}_0)^{14}\text{C}$	1	0.71	0.063	11.2
$^{16}\text{O}(\text{t}, \text{d}_0)^{17}\text{O}$	2	0.48	0.35	1.3
$^{27}\text{Al}(\text{t}, \text{d}_0)^{28}\text{Al}$	0	0.71	0.15	(4.8)
$^{27}\text{Al}(\text{t}, \text{d}_1)^{28}\text{Al}$	0	0.33	0.08	(4.4)
$^{27}\text{Al}(\text{t}, \text{d}_3)^{28}\text{Al}$	2	0.47	0.13	3.5
$^{27}\text{Al}(\text{t}, \text{d}_4)^{28}\text{Al}$	2	0.06	—	—
$^{27}\text{Al}(\text{t}, \text{d}_6)^{28}\text{Al}$	0	0.62	0.05	(21.3)
$^{27}\text{Al}(\text{t}, \text{d}_7)^{28}\text{Al}$	2	0.17	0.04	4.3
$^{27}\text{Al}(\text{t}, \text{d}_8)^{28}\text{Al}$	2	0.30	0.11	2.7
$^{27}\text{Al}(\text{t}, \text{d}_9)^{28}\text{Al}$	0	0.09	0.01	(9.0)
$^{27}\text{Al}(\text{t}, \text{d}_{11})^{28}\text{Al}$	2	0.29	0.11	2.7
$^{28}\text{Si}(\text{t}, \text{d}_1)^{29}\text{Si}$	2	0.03	0.01	3.0
$^{28}\text{Si}(\text{t}, \text{d}_5)^{29}\text{Si}$	3	0.13	0.10	1.3
$^{28}\text{Si}(\text{t}, \text{d}_9)^{29}\text{Si}$	1	0.11	0.05	2.2

(1) Reaction; (2) l -value; (3) $(2J_f + 1)|A_0|^2 N_i^2 \theta^2$ (10^{12} cm^{-1}); (4) $(2J_f + 1)\theta^2$, calculated by Macfarlane and French (1960) from the results of the (d, p) investigations listed in the footnote of Table 1; (5) $|A_0|^2 N_i^2$ (10^{12} cm^{-1}).

(a) The value obtained by Jaffe and Husain (1960, private communication) at 6 MeV, (b) the value reported by Mayo and Hamburger (1960).

Recently Macfarlane and French (1960) have reviewed the available data on (d, t) reactions in target nuclei with masses between ${}^6\text{Li}$ and ${}^{23}\text{Na}$. For each reaction they evaluated a factor Λ which is directly proportional to the quantity $|A_0|^2 N_i^2$ as defined by Butler and Hittmair and adopted in this paper. In the majority of the reactions, which were analysed, the incident deuteron energy was about 15 meV and they found that Λ is approximately constant with an average value of 195 ± 35 , which is equivalent to a value of $14.4 \times 10^{12} \text{ cm}^{-1}$ for $|A_0|^2 N_i^2$. More recently, a similar analysis has been made by Hamburger (1960).

The ${}^{12}\text{C}(\text{t}, \text{d}){}^{13}\text{C}$ and ${}^{13}\text{C}(\text{t}, \text{d}){}^{14}\text{C}$ reactions are the only ones studied by us which involve the same initial and final nuclear states as in the (d, t) reactions analysed by Macfarlane and French (1960). The incident triton energy of 5.5 meV used in the present work is such that the results for the ${}^{12}\text{C}(\text{t}, \text{d}){}^{13}\text{C}$ reaction should correspond closely to those of the inverse reaction ${}^{13}\text{C}(\text{d}, \text{t}){}^{12}\text{C}$ studied at a deuteron energy of 3.29 meV. However, our value of $|A_0|^2 N_i^2$ is only about one third as large as that from the value $\Lambda = 290$ obtained by Macfarlane and French for the latter reaction. The discrepancy appears to be incapable of explanation other than by experimental errors in the absolute cross sections unless a large sharp resonance occurs in the ${}^{12}\text{C}(\text{t}, \text{d}){}^{13}\text{C}$ reaction at a triton bombarding energy of about 5.2 meV, which seems unlikely. The above value of Λ is, however, abnormally large compared with the value $\Lambda = 190$ derived by Macfarlane and French from other measurements of the ${}^{13}\text{C}(\text{d}, \text{t}){}^{12}\text{C}$ reaction at an incident energy of 14.8 meV. Our value of $|A_0|^2 N_i^2$ for the ${}^{13}\text{C}(\text{t}, \text{d}){}^{14}\text{C}$ reaction agrees well with that derived from the results of the ${}^{14}\text{C}(\text{d}, \text{t}){}^{13}\text{C}$ reaction, although the latter results were obtained at the high deuteron energy of 14.9 meV so that the reactions are not energetically the inverse of one another.

§ 4. CONCLUSION

The angular distributions of the observed (t, d) reactions at 5.5 meV can be fitted with the Butler theory of deuteron stripping modified to the case of mass-3 particles. The degree of agreement is then about as good as that obtained with the corresponding (d, p) reactions. The results indicate that at bombarding energies of below 6 meV a constant value of $|A_0|^2 N_i^2$ cannot be used to extract reduced widths from (t, d) reactions except, perhaps, for a very light target nuclei. The analysis of (d, t) reactions by Macfarlane and French, however, indicates that this should be possible at higher triton bombarding energies.

ACKNOWLEDGMENTS

The authors wish to thank Professor S. Devons for helpful criticisms of the manuscript of this paper. They also wish to thank Mrs. S. Ramavataram and Professor Jiro Muto for their help in the analysis of the results and Miss Claire Aston for her assistance in scanning the photographic plates. One of us (F. de S. B.) acknowledges the receipt of a research grant from the Brazilian Government (C.A.P.E.S.) and another (P.D.F.) a research fellowship from the Department of Scientific and Industrial Research.

REFERENCES

- AJZENBERG-SELOVE, F., and LAURITSEN, T., 1959, *Nucl. Phys.*, **11**, 1.
 BOCKELMAN, C. K., and BUECHNER, W. W., 1957, *Phys. Rev.*, **107**, 1366.
 BURGE, E. J., BURROWS, H. B., GIBSON, W. M., and ROTBLAT, J., 1951, *Proc. Roy. Soc. A*, **210**, 534.

- BUTLER, S. T., and HITTMAIR, O. H., 1957, *Nuclear Stripping Reactions* (London: Pitman).
- BUTLER, S. T., and SALPETER, E. E., 1952, *Phys. Rev.*, **88**, 133.
- ENDT, P. M., and BRAAMS, C. M., 1957, *Rev. Mod. Phys.*, **29**, 683.
- ENGE, H. A., ANGLEMAN, C. C., and JARREL, D. L., 1956, *Progr. Report, Lab. Nucl. Sci.*, M.I.T.
- EVANS, N. T. S., and PARKINSON, W. C., 1954, *Proc. Phys. Soc. A*, **67**, 684.
- FORSYTH, P. D., BARROS, F. DE S., JAFFE, A. A., TAYLOR, I. J., and RAMAVATARAM, S., 1960, *Proc. Phys. Soc.*, **75**, 291.
- GREEN, T. S., and MIDDLETON, R., 1956, *Proc. Phys. Soc. A*, **69**, 28.
- HAMBURGER, A. I., 1960, *Phys. Rev.*, **118**, 1271.
- HINDS, S., MIDDLETON, R., and PARRY, G., 1958, *Proc. Phys. Soc.*, A, **71**, 49.
- HOLT, J. R., and MARSHAM, T. N., 1953 a, *Proc. Phys. Soc. A*, **66**, 258.
- 1953 b, *Proc. Phys. Soc. A*, **66**, 467.
- JAFFE, A. A., BARROS, F. DE S., FORSYTH, P. D., MUTO, J., TAYLOR, I. J., and RAMAVATARAM, S., 1960, *Proc. Phys. Soc.*, **76**, 914.
- KURATH, D., 1956, *Phys. Rev.*, **101**, 216.
- MACFARLANE, M. H., and FRENCH, J. B., 1960, *Rev. Mod. Phys.*, **32**, 567.
- MAYO, S., and HAMBURGER, A. I., 1960, *Phys. Rev.*, **117**, 832.
- MCGRUE, J. N., WARBURTON, E. K., and BENDER, R. S., 1955, *Phys. Rev.*, **100**, 235.
- MUTO, J., BARROS, F. DE S., and JAFFE, A. A., 1960, *Proc. Phys. Soc.*, **75**, 929.
- NEWNS, H. C., 1952, *Proc. Phys. Soc. A*, **65**, 916.
- VAN PATTTER, D. M., BUECHNER, W. W., and SPERDUTO, A., 1951, *Phys. Rev.*, **81**, 233.

The 2^3S Excitation in Helium

By G. S. HIGGINSON AND L. W. KERR

Physics Department, Queen's University, Belfast

MS. received 12th September 1960

Abstract. A simple diffusion method has been employed to measure the shape of the excitation probability curve above the threshold of the 2^3S excitation in helium. The results are in substantial agreement with those of Schulz and Fox.

INELASTIC collisions between electrons and helium near the threshold of excitation are of special interest because of the relative simplicity of the electronic structure of helium. The classical experimental study of the inelastic collision of electrons with helium atoms is that of Maier-Leibnitz (1935). The special importance of his work is that simple electrical measurements only are involved and that by making use of classical diffusion theory an absolute measurement of the total inelastic collision cross section as a function of incident electron energy may be obtained.

Other methods are open to criticism in that the absolute value of the cross section obtained may have a large inherent error arising from difficulties in experimental techniques, or uncertainties in the theories required in the calculations.

The Maier-Leibnitz experiment would appear to be potentially the most reliable method of determining absolute inelastic cross sections, but it suffers from the defect (Kerr 1950) that diffusion of metastable atoms from the collision region on to the electron collector surface will produce secondary emission there, the direction of the current being such as to result in over-estimation of the collision cross section, possibly by a factor of two. Comparison of Maier-Leibnitz' value of $5 \times 10^{-18} \text{ cm}^2$ for the X type maximum of the 2^3S excitation with that of Schulz and Fox (1957), $4 \times 10^{-18} \pm 30\% \text{ cm}^2$, indicates that the error may be of this order. It is possible however to measure the secondary current alone and thus to correct for its effect. The measurements are still quite direct, and the final experimental error in the absolute cross section should not be more than a few per cent.

It is the purpose of this note to report some preliminary measurements of the secondary emission occurring in an experiment of the Maier-Leibnitz type. One of us (G. S. H.) hopes to obtain later the corrected absolute cross section values.

In the apparatus employed (Fig. 1) near planar geometry is used instead of the cylindrical geometry of Maier-Leibnitz. A beam of electrons (approximately 10^{-8} A) from an indirectly heated cathode A passes axially through a cylindrical collision chamber B of length 2.0 cm and diameter 9 cm, which is held at a positive potential of V volts with respect to the cathode. The collector electrode C, spaced 0.1 mm from B, is maintained at 10 volts below cathode potential. The retarding potential thus established between B and C is

sufficient to prevent any electrons from reaching C in measurable quantities ($< 10^{-13}$ A) over the range of gas pressure used (0.27–0.33 mm Hg). If V is increased from zero, no current is recorded by an electrometer connected to C until potentials in excess of the first excitation potential in helium (allowing for contact potential difference) are reached.



Fig. 1. Diagram of apparatus.

A current in the sense of an electron loss from the collector plate is then recorded due to secondary emission produced by metastable atoms which have diffused from B colliding with the collector C. For potentials only slightly in excess of the excitation value, the secondary emission current is likely to be closely related to the number of metastable atoms formed in the collision chamber, and consequently, the form of the collector current voltage characteristic, after correction for changes in cathode emission as the potential V is increased, will be closely associated with the shape of the excitation probability curve.

A secondary emission curve obtained in this way with a tantalum collector is shown in Fig. 2 as curve 1, a curve for an oxidized copper collector obtained by Kerr (1950) is shown as curve 2, while the cross section measurements of Schulz and Fox (1957) are shown as curve 3. All three curves are normalized

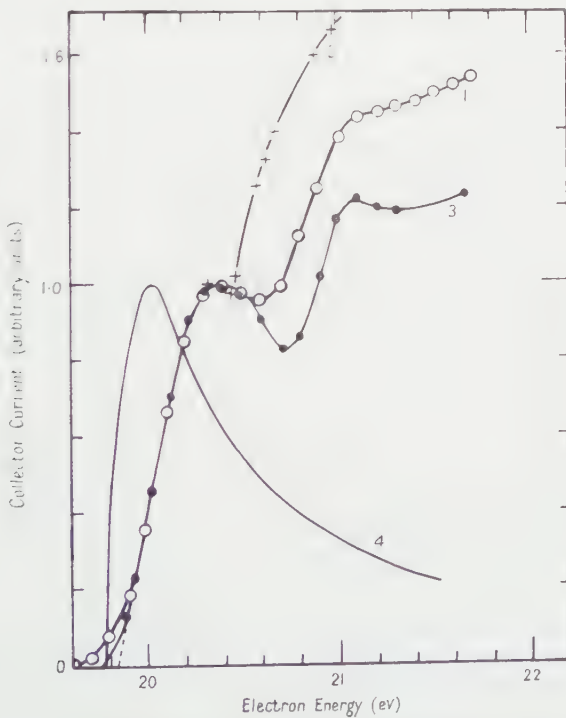


Fig. 2. Excitation probability curves in helium; 1, experimental curve; 2, Kerr (1950); 3, Schulz and Fox (1957); 4, Maier-Leibnitz (1935).

and corrected for contact potentials so that the 2^3S peaks coincide. The slope of the curves above threshold are in substantial agreement, the threshold being at 19.82 eV and the peak 0.6 eV above threshold. They do not agree with the steeper inclination of Maier-Leibnitz' curve 4 nor with the theoretical curve of Massey and Moiseiwitsch (1953). Above the 2^3S peak the curves do not agree. The greater spread of the electron energy distribution in our experiments compared with that used by Schulz and Fox could account for a loss of resolution and for the long tail below threshold, but the relative displacement of the curves can hardly be accounted for in this way. It may be due to different relative efficiencies of 2^3S and 2^1S secondary emission in the three experiments or to differences in the diffusion parameters for the two types of metastables. Some support is lent to the second explanation by the variation with gas pressure, curve 1 being obtained at 0.30 mm Hg and curve 2 at 0.68 mm Hg.

ACKNOWLEDGMENT

The authors are indebted to Professor K. G. Emeleus for helpful discussions and encouragement.

REFERENCES

- KERR, L. W., 1950, *Thesis*, Queen's University, Belfast.
MAIER-LEIBNITZ, H., 1935, *Z. Phys.*, **95**, 499.
MASSEY, H. S. W., and MOISEWITSCH, B. L., 1953, *Proc. Phys. Soc. A*, **66**, 406.
SCHULZ, G. J., and FOX, R. E., 1957, *Phys. Rev.*, **106**, 1179; also private communication.

Luminescence Excitation Spectrum of Diamond near the Fundamental Absorption Edge†

By J. C. MALE

Department of Physics, King's College, London

MS. received 4th October 1960

Abstract. Luminescence excitation spectra have been obtained, at room temperature, for 13 natural diamonds comprising six of type I, three of type IIa, three of 'intermediate' type and a single, semiconducting diamond. Excitation peaks, corresponding in detail to the well-known absorption bands at 5.250 eV, 5.363 eV and 5.391 eV were detected in all except the semiconducting crystal, and indications of further structure in this energy region were seen. In the region of fundamental optical absorption, broad excitation bands with maxima at 5.51 eV, 5.56 eV and 5.73 eV occur in all but the semiconducting crystal. The semiconducting diamond showed unique features consistent with the presence of an acceptor level within 0.35 eV of the valence band. The luminescence emission spectrum appears to be independent of the quantum energy of the exciting radiation.

Luminescence decay times of 10 milliseconds have generally been found but for the semiconducting diamond, the decay time was six seconds.

§ 1. INTRODUCTION

PREVIOUS published work on diamond, concerned with the energy band structure in the region of fundamental optical absorption, has established that the forbidden energy-gap is approximately 5.6 eV for direct transitions. Robertson, Fox and Martin (1934) first distinguished between diamonds which transmit light appreciably up to a quantum energy of 5.5 eV (2250 Å), which they classed as type II, and those which show a heavy absorption continuum for wavelengths below 3000 Å (type I). This absorption continuum has recently been positively correlated with the presence of up to 0.25% of nitrogen impurity (Kaiser and Bond 1959). Robertson *et al.* also observed absorption bands at 2300 Å and 2355 Å, which were later confirmed by Bai (1944) and Ramanathan (1946). These bands are sometimes associated with the well-known 4150 Å absorption system in type I diamond (Clark, Ditchburn and Dyer 1956). These workers suggest that the bands do not occur in pure, type II diamond, but only in 'intermediate' types, being masked in type I by the absorption continuum. Custers (1954) showed that type I diamonds will transmit light to wavelengths near 2250 Å if sufficiently thin samples are used and, subsequently Raal (1959), working with parallel-sided slabs of thickness 0.04 to 0.5 mm, showed that weak transmission down to the primary absorption limit occurred in type I diamonds and he observed absorption bands in the regions 2290–2310 Å

† Paper read during the Conference on Diamond Physics at Reading University on 23rd September 1960.

and 2350–2370 Å, whose integrated intensity was proportional to the integrated intensity of the 4150 Å system.

Halperin and Arbell (1959), working with single crystals of zinc sulphide, have observed that excitation spectra reveal fine structure much more sensitively than do absorption measurements and that structure appears well within the region of lattice absorption, where the absorption coefficient is too great to permit transmission measurements. The present paper shows that such is also the case with diamond and the study of excitation spectra appears to have great potentialities for the elucidation of the energy band structure.

§ 2. EXPERIMENTAL

The measurements were made with a modified, single-beam, Hilger quartz spectrograph (Type E498). A specially selected, low-noise photomultiplier tube (E.M.I. 6256B) was mounted so that it could track slowly along behind the focal plane of the spectrograph. The diamonds, small industrial stones of linear dimensions approximately 1.5 mm, were mounted in black wax over holes of diameter 0.3 mm or 0.45 mm drilled in brass slips. These slips were then clipped over a drilled aperture of diameter 1 mm in a steel slide, which could be inserted in an exactly reproducible position immediately in front of the photo-cathode, so that the smallest aperture moved exactly in the focal plane. The apertures in the steel slide and brass slip were aligned by eye and the arrangement allowed the widest possible cone of light from the crystal to reach the photo-cathode. When the luminescence intensity was large enough to permit it, a slit of width 50μ was incorporated in the focal plane between the brass slip and the crystal, giving a mean effective slit-width of approximately 0.0015 ev over the range studied.

With this arrangement, spectra were reproducible to within 1.5 Å (0.005 ev) at 5.5 ev. Greater precision was achieved by including an intense mercury line in each spectrum after it had been run and before the steel slide had been removed, comparing its position with that of the same line in the calibration charts and correcting the spectrum accordingly. This gave reproducibility within ± 0.15 Å (0.0005 ev) for the peak at 5.391 ev in six specimens where it was sharply resolved. Other factors, such as the finite slit-widths, inaccuracy of the calibration charts, finite time constant of the recording circuit, etc., lead to ± 0.002 ev as an estimate of the reliability of the absolute energies of the sharp peaks.

The light source was a hydrogen discharge lamp operated from a highly stabilized power unit. The signal from the photomultiplier was fed, via a cathode-follower unit to a Brown, strip-chart recorder. For those diamonds which transmitted some ultra-violet light, a slip of gelatine filter (Wratten series 2B), transmitting only above 4000 Å, was introduced between the diamond and the photo-cathode. A check showed that this did not contribute appreciably to the luminescence radiation. The spectra were corrected for the variation with wavelength of the hydrogen source intensity and so represent relative luminescence intensity per unit incident exciting energy. In practice, this correction was small below 5.5 ev and increased to a factor of about 10 at 5.9 ev.

For the measurement of fast luminescence decay times, a rotating chopper in front of the spectrometer entrance-slit provided pulses of exciting radiation.

The photomultiplier output was taken directly to the Y plates of a Tektronix type 545 oscilloscope and the display was photographed. Sufficient intensity was obtained here by using, as light source, a low-pressure mercury discharge lamp, operated on direct current.

Fluorescence spectra were obtained photographically, exciting radiation in the appropriate wavelength intervals being collected from the spectrum of a mercury discharge lamp formed in the Hilger spectrometer and focused on to the diamond with a quartz lens.

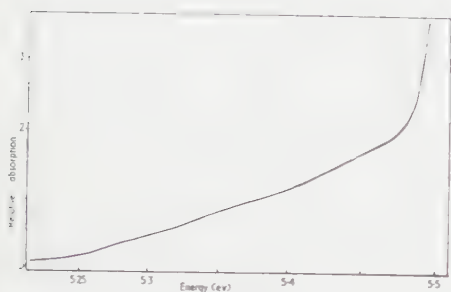


Fig. 1. Ultra-violet absorption for X.120 (type IIa). The 'relative absorption' plotted is proportional to the logarithm of the ratio of incident to transmitted intensities.

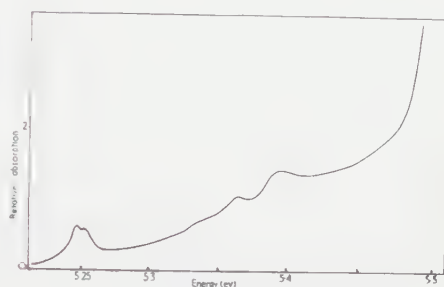


Fig. 2. Ultra-violet absorption for K.82 ('intermediate' type). The 'relative absorption' plotted is proportional to the logarithm of the ratio of incident to transmitted intensities.

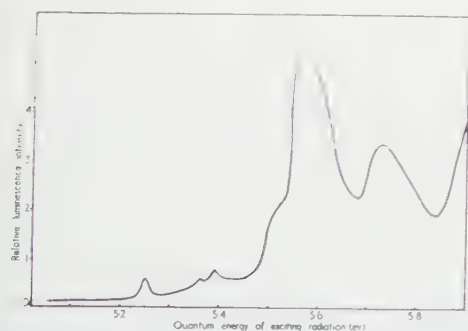


Fig. 3. Excitation spectrum for X.120 (type IIa).

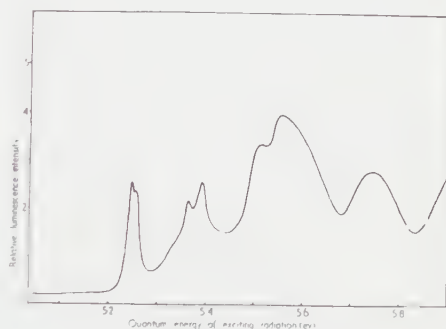


Fig. 4. Excitation spectrum for K.82 ('intermediate' type).

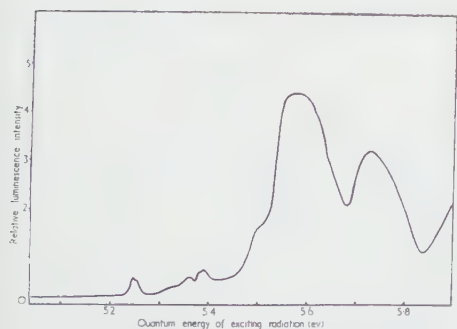


Fig. 5. Excitation spectrum for Co.21 (type I).

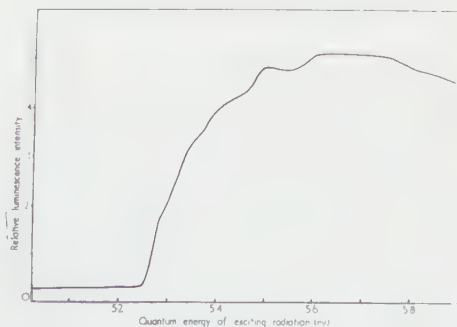


Fig. 6. Excitation spectrum for A.100 (type IIb).

§ 3. RESULTS

Excitation spectra have been obtained for 13 natural diamonds, including six of type I, three of type IIa, having ultra-violet absorption spectra similar to Fig. 1, and three which can be classed as 'intermediate' types, following Clark, Ditchburn and Dyer (1956), having ultra-violet absorption spectra similar to Fig. 2. Also a single, semiconducting diamond (type IIb) (Custers 1952) was examined. Typical excitation spectra for each type are shown in Figs 3 to 6. In all, except the IIb crystal, excitation peaks were seen at 2300 Å (5.391 eV), 2312 Å (5.363 eV) and 2360 Å (5.25 eV), corresponding in energy to the absorption bands of the 'intermediate' type diamonds. In the three 'intermediate' crystals and in one of the type I crystals, the luminescence intensity was sufficient to show that the 5.25 eV peak had components at 5.255 eV (2359 Å) and 5.247 eV (2363 Å), corresponding exactly in energy to absorption bands, first reported by Martin (1957).

Further fine structure appears in K.82 (Fig. 4) and is more clearly resolved in Co 21 (Fig. 5) in an excitation maximum at 5.382 eV and a less sharp maximum near 5.33 eV. A suggestion of absorption near 5.33 eV can be seen in Fig. 2, although no definite signs of absorption at 5.382 eV have been seen so far.

The excitation bands near 5.25 eV, 5.36 eV and 5.39 eV always appear with approximately the same relative intensity.

The features of the spectra at energies above 5.45 eV, i.e. in the region of fundamental absorption, do not appear to bear any fixed intensity relation to the sharp peaks below 5.45 eV. The main features consist of broad excitation bands with maxima near 5.51 eV and 5.56 eV and a further maximum near 5.73 eV. The positions of the 5.51 eV and 5.56 eV peaks vary from specimen to specimen within a range of 0.03 eV and this is probably partly due to variations in their relative intensity. That this is not the whole explanation is indicated by differences in shape as well and, in Co 21, further structure can be seen (Fig. 5). The band at 5.73 eV is very constant in position and always bears approximately the same intensity relation to the 5.56 eV band.

It is possible that further bands exist at energies above 5.9 eV, but it was, unfortunately, not possible to explore this region with the apparatus available.

The type IIb, semiconducting diamond, A.100, has an excitation spectrum quite distinct from all the others (Fig. 6), the only possibly common feature being a peak near 5.50 eV. Its ultra-violet absorption spectrum was similar to Fig. 1.

The decay time of the luminescence was found to be 10 milliseconds for all parts of the excitation spectrum, again with the exception of the IIb crystal which showed phosphorescence with a decay time of 6 seconds. Phosphorescence of IIb diamonds has also been noted by Custers (1952) and Dyer and Matthews (1958), but these authors do not quote decay times.

Spectra of the visible luminescence emission have been obtained for three of the 'intermediate' diamonds and for the IIb diamond. These specimens were chosen because they luminesced particularly strongly.

Even so, exposure times of the order of a day were required, using Ilford H.P.S. plates. Densitometer records of the plates were made, and compared for luminescence excited by wavelengths below 2275 Å (5.45 eV) and by wavelengths between 2275 Å and 2500 Å (5.45 eV and 4.95 eV). No significant differences were noticed, all the spectra showing the usual main features of diamond luminescence for both regions of excitation. A further check to see

whether the various regions of the luminescence spectrum could be differentially excited was made by inserting filters between the diamond and the photo-cathode during the measurement of excitation spectra. Excitation spectra for emission in the wavelength ranges 3200–4700 Å, 4800–6000 Å and 5500 Å upwards were obtained by using Wratten series 35, 61 and 22 filters respectively. No change in the relative intensities of the excitation bands was observed.

§ 4. DISCUSSION

It is convenient to consider the regions either side of 5.45 eV separately.

On the low-energy side of this dividing line, the excitation peaks have been shown to occur at energies identical with the energies of absorption bands observed in 'intermediate' type crystals. The excitation peaks have been detected in both type I and type IIa crystals, including an extremely 'perfect' type IIa diamond (K.80) which has been used by Dean (1960) for detailed studies on the temperature-dependence of ultra-violet absorption, and in which he did not detect the presence of absorption bands.

Martin (1957) has measured the temperature-dependence of the absorption bands at 2359 Å and 2363 Å and found that they shifted some 4 Å towards lower wavelengths on cooling from room temperature to -180°C . This corresponds to a mean rate of shift of $4 \times 10^{-5} \text{ eV deg}^{-1}$, whereas the mean rate of shift of the intrinsic energy gap is as much as $2 \times 10^{-4} \text{ eV deg}^{-1}$ (Dean 1960).

It is concluded, therefore, that the centres responsible for these absorption and excitation bands are present in varying concentrations in both type I and type IIa diamonds, but their appearance in absorption is much more difficult to detect. No trace of the 5.25 eV band is discernible, either in absorption or excitation, in the single type IIb diamond examined. It should have been easily detected if of comparable intensity with its occurrence in type I and IIa.

It has been suggested by Seitz (1954), in connection with the α and β bands in alkali halide crystals, that weak absorption bands close to the fundamental absorption edge may be due to electronic transitions in host crystal atoms adjacent to defects and that the great variability of these bands indicates that they cannot be due to intrinsic absorption. If this interpretation is correct for the 5.25 eV, 5.36 eV and 5.39 eV bands in diamond, the relevant defect is unlikely to be nitrogen, since there is no correlation between the strength of the bands and the nitrogen concentration as indicated by the strength of the type I absorption continuum.

The 4150 Å absorption system has also been observed in emission by Dyer and Matthews (1958), the emission lines appearing as the approximate mirror image of the absorption lines. If this system is connected with 5.25 eV and 5.37 eV bands, it is possible that corresponding emission of these bands may exist; but it would be expected to be very weak indeed, in view of the fact that much lower-energy decay processes are available. Weak, ultra-violet emission has recently been detected in diamond X.120 (see Figs 1 and 5) (Male and Prior 1960). Emission peaks occur near 5.278 eV and 5.125 eV which are thought to be due to an intrinsic process, involving phonon participation. Taking Clark's value of 5.33 eV for the indirect energy gap less an exciton binding energy, which he calculates from ultra-violet absorption measurements (Clark 1958), the low-energy edges of the emission peaks at 5.09 eV and 5.25 eV are consistent, with phonon energies of 0.16 eV and 0.08 eV.

The excitation bands at energies greater than 5.45 eV should correspond to fundamental lattice absorption. The shape and relative intensity of the 5.51 and 5.56 eV bands vary between different specimens, while the 5.73 eV band appears to be specimen-independent. It is of interest that the general form of these bands is very similar to corresponding bands observed in cadmium sulphide (Halperin and Arbell 1959) and zinc sulphide (Klick 1953) at low temperature. Investigation of the temperature-dependence of the diamond effects is obviously desirable and is projected in the near future.

The excitation spectrum of the IIb diamond is dominated by a region of continuous excitation, whose low-energy threshold is at 5.25 eV. Many workers, for example Austin and Wolfe (1956), Brophy (1955), have established the existence of an acceptor level at 0.35 eV above the valence band in IIb diamond and a threshold at 5.25 eV for the excitation of photoconductivity has been observed by Bell and Leivo (1958). The luminescence-excitation threshold at 5.25 eV can, therefore, be interpreted as corresponding to the excitation of electrons from this acceptor level to the conduction band.

The quantum efficiency of luminescence excitation in diamond has not been measured absolutely but it is generally much weaker than the efficiency of cadmium sulphide, which may be as much as 30%, and only rarely is it detectable in normal ultra-violet transmission measurements.

A large body of experimental data shows that the luminescence spectrum of crystals, excited in the fundamental absorption region, is independent of the exciting wavelength (Broude, Prikhot'ko and Rashba 1959) and the present observations do not conflict with this generalization. Broude *et al.* also conclude that energy transfer in crystals with a large forbidden energy gap is almost entirely due to excitons. Luminescence due to direct or indirect exciton decay is strongly inhibited, even in nearly perfect crystals, the exciton acting only to transfer energy from the host-lattice to structural defects and impurities, which become excited and emit characteristic radiation.

The scintillations produced in diamond by bombardment with alpha particles consist of a rapid main pulse, followed by a train of small after-pulses lasting 50 milliseconds at room temperature. Dean (1960) has shown that this after-pulse emission is predominantly blue, while the main pulse (rise-time less than 10^{-9} sec) is partly green. These results led to the expectation that the blue and green components of normal diamond luminescence might have different decay times. Since no rapidly decaying component has been detected for the luminescence considered in these experiments, the mechanisms involved in ultra-violet and alpha particle stimulated luminescence must differ in some important respect, although the spectra of the actual emission are very similar.

ACKNOWLEDGMENTS

I am indebted to the Department of Scientific and Industrial Research for a maintenance grant and I should like to thank Professor F. C. Champion for useful discussion.

REFERENCES

- AUSTIN, I. G., and WOLFE, R., 1956, *Proc. Phys. Soc. B*, **69**, 329.
- BAI, K. S., 1944, *Proc. Ind. Acad. Sci. A*, **19**, 253.
- BELL, D. W., and LEIVO, W. J., 1958, *Phys. Rev.*, **111**, 1227.

- BROPHY, J. J., 1955, *Phys. Rev.*, **99**, 1336.
- BROUDE, V. L., PRIKHOT'KO, A. F., and RASHBA, E. I., 1959, *Sov. Phys. Uspekhi*, **2**, 38.
- CLARK, C. D., 1958, *J. Phys. Chem. Solids*, **8**, 481.
- CLARK, C. D., DITCHBURN, R. W., and DYER, H. B., 1956, *Proc. Roy. Soc. A*, **234**, 363.
- CUSTERS, J. F. H., 1952, *Physica*, **18**, 489.
- 1954, *Physica*, **20**, 183.
- DEAN, P. J., 1960, *Ph.D. Thesis*, University of London.
- DYER, H. B., and MATTHEWS, I. G., 1958, *Proc. Roy. Soc. A*, **243**, 320.
- HALPERIN, A., and ARBELL, H., 1959, *Phys. Rev.*, **113**, 1216.
- KAISER, W., and BOND, W. L., 1959, *Phys. Rev.*, **115**, 857.
- KLICK, C. C., 1953, *Phys. Rev.*, **89**, 274.
- MALE, J. C., and PRIOR, J. R., 1960, *Nature, Lond.*, **186**, 1037.
- MARTIN, R. W., 1957, *M.Sc. Thesis*, University of London.
- RAAL, F. A., 1959, *Proc. Phys. Soc. B*, **74**, 647.
- RAMANATHAN, K. G., 1946, *Proc. Ind. Acad. Sci. A*, **24**, 137.
- ROBERTSON, R., FOX, J. J., and MARTIN, A. E., 1934, *Trans. Roy. Soc. A*, **232**, 463.
- SEITZ, F., 1954, *Rev. Mod. Phys.*, **26**, 7.

The Variation of the Fracture Energy of Brittle Plastics with Temperature

BY N. L. SVENSSON

Department of Mechanical Engineering, University of Melbourne

MS. received 16th September 1960

Abstract. A method for the determination of the fracture energy of brittle plastics is described. A crack is propagated down the length of a rectangular specimen under controlled conditions and the variation of crack opening with length determined. From these results the fracture energy may be calculated. The method has been applied to determine the variation of fracture energy for polymethyl-methacrylate and polystyrene with temperature in the temperature range 20 to 80°C. The results of tests carried out at room temperature show good agreement with similar results obtained by other investigators.

§ 1. INTRODUCTION

WHEN a crack propagates through a solid material, work is done in overcoming the atomic binding forces, this work appearing in the form of surface energy. Some energy may also be irreversibly dissipated in permanent deformation of the material immediately ahead of the propagating crack. The sum of these energies per unit area of crack surface produced is known as the fracture energy.

Griffith (1920) suggested that the condition to be satisfied for a crack to propagate through a solid material is that the strain energy released by the spread of the crack should be in excess of the fracture energy absorbed in the formation of the fresh surfaces. If this excess energy release is small the crack will grow very slowly but if the excess is large, energy is available for acceleration of the material and a rapid crack propagation results.

If this hypothesis is valid it should be possible to determine the fracture energy by measuring the strain energy associated with a crack growing slowly under controlled conditions. Several experimental techniques have been devised for such measurements. Obreimoff (1930) relied on anisotropy in the structure of the material (mica) whilst Roesler (1956) required that the material should be extremely brittle (glass). Kies (1953) developed a method suitable for the determination of the fracture energy in polymethyl-methacrylate. In this test, specimens were subjected to a tensile loading and a crack caused to propagate across the specimen. By measuring the length of the crack at the transition from slow to fast propagation the fracture energy could be calculated.

Subsequently Benbow and Roesler (1957) devised a form of test in which the strain energy stored in the specimen could be continually determined. In this test, a crack was caused to propagate down the length of a rectangular specimen by opening the crack with a wedge. Special grips and the provision of some axial compressive load caused the crack to spread down the centre of the specimen.

The tests reported in this paper were carried out on a modified form of Benbow and Roesler specimen. These modifications consisted of doubling the length of the specimen with the crack growing from the centre, and the provision of a measurable end load. These changes enabled a more accurate theoretical analysis to be made and a closer compliance of experimental conditions and theoretical assumptions. The theoretical analysis was carried out to determine the method for calculating the fracture energy. This predicted a linear relationship between two independent parameters which was verified by the experimental results. Consequently values of the fracture energy were determined for specimens of polymethyl-methacrylate (Perspex) and polystyrene (Styron and Lustrex).

§ 2. EXPERIMENTAL METHOD

2.1. Principle

The form of specimen used for the determination of the fracture energy is shown in Fig. 1. In Appendix I it is shown that the fracture energy can be determined from measurements of the crack opening δ , crack length L , and axial force Q . In order to obtain simultaneous readings of δ and L it was decided that the crack should grow sufficiently slowly for visual observations to be made.

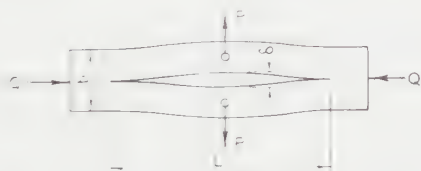


Fig. 1. Test piece used in experiments.

A rigid straining frame as shown in Fig. 2 (Plate) was therefore devised in order to achieve this control. The splitting force was transmitted to the specimen through two pins passing through two specimen-holding blocks. These blocks were forced apart by the rotation of a calibrated nut on a screw fixed to one of them. The movement of the nut was taken to be a measure of the opening of the crack. The necessary axial load was applied through two calibrated compression springs. The initial crack was a longitudinal saw cut in the centre of the specimen with a swallow tail shape cut with a jeweller's saw.

2.2. Experimental Technique

Some preliminary experiments were carried out to determine the magnitude of the axial force required to maintain a straight crack. The effect of axial load on the crack shape for Perspex specimens at room temperature is shown in Fig. 3. As a result of these tests the axial load was adjusted to be 250 lb for each test. Due to the low velocity of propagation the crack would continue growing for some time. It was found that most of this growth occurred in the first five minutes after increasing the crack opening. Consequently all crack length readings were taken five minutes after the crack opening had been increased a further amount.

The complete straining frame was placed in an insulated cabinet which was provided with heating elements and a circulating fan. The power supplied to the heaters could be controlled to maintain the temperature in the cabinet to $\pm \frac{1}{2}^{\circ}\text{C}$. The cabinet was provided with a glass door which enabled the various readings to be made without disturbing the test conditions.

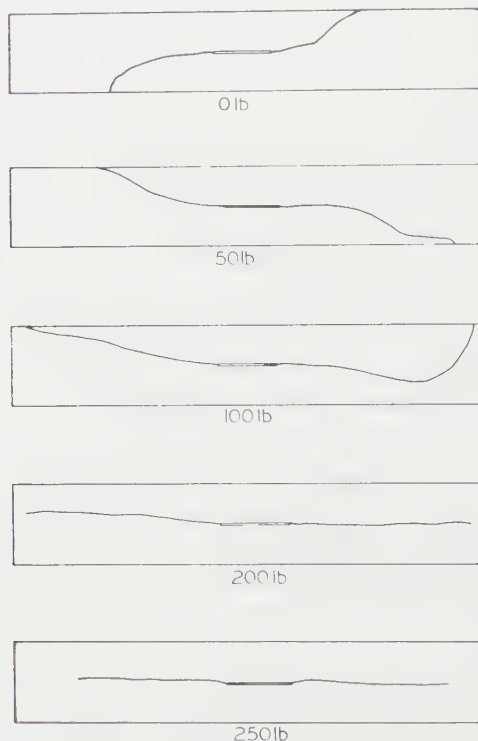


Fig. 3. Effect of axial load on shape of crack.

A centrally loaded, simply supported beam specimen was also placed in the cabinet during the tests for the determination of the modulus of elasticity at the test temperature.

The expression derived in Appendix I for the calculation of fracture energy is

$$T = \frac{1}{4} \frac{Eb^3\delta^2S}{L^4} \quad \dots\dots (1)$$

where S is a factor which depends on the crack length L , and b the width of the specimen. As a result of the method adopted for measuring crack opening, the origin from which δ is measured is difficult to assess. Eqn (1) may be rewritten as

$$\delta = \left(\frac{4T}{Eb^3} \right)^{1/2} \frac{L^2}{\sqrt{S}} \quad \dots\dots (2)$$

If δ is plotted as a function of L^2/\sqrt{S} the experimental points should fall on a straight line, the slope of which is a measure of the fracture energy. For

ease in computation L^2/\sqrt{S} has been calculated for the materials used in these tests and plotted in Fig. 4 as a function of L .

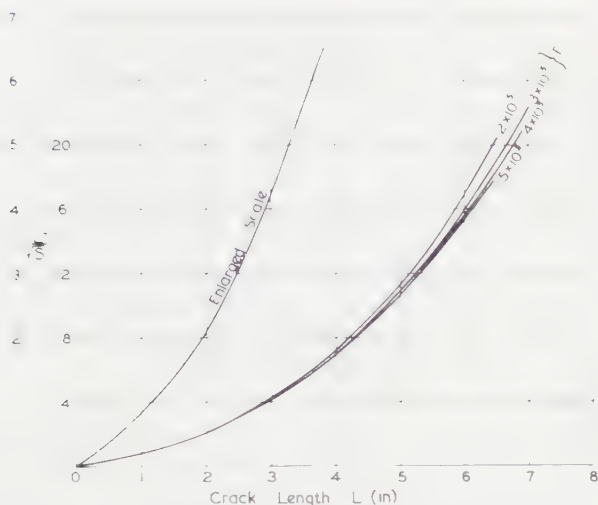


Fig. 4. Variation of L^2/\sqrt{S} with crack length L .

§ 3. EXPERIMENTAL RESULTS

A series of tests was carried out on a number of Perspex and Styron specimens at various temperatures. When the tests were carefully executed the crack growth was generally found to be continuous with crack opening. In some cases, however, the crack propagated in a series of jumps with large changes in crack opening between jumps. The data obtained from such tests were not considered in the analysis of the results. Some typical experimental

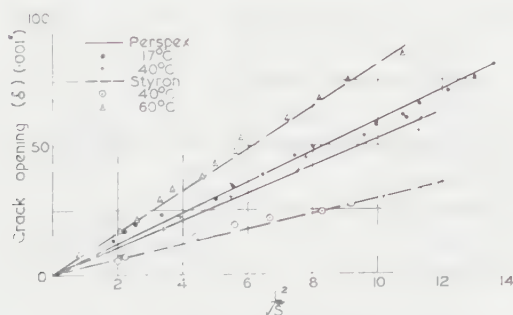


Fig. 5. Typical experimental results.

results are shown plotted as δ against L^2/\sqrt{S} in Fig. 5. The slope of the line of best fit was determined for each set of experimental data and the fracture energy calculated.

At the conclusion of the tests at higher temperatures it was observed that there was some residual deformation present. This indicated that some of the strain energy which had been supplied to the specimen had been dissipated in creep relaxation during the test. Thus the apparent fracture energy T_a as

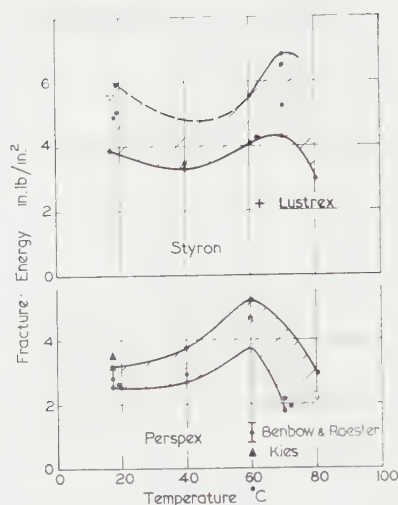


Fig. 6. Variation of fracture energy with temperature.

Results of Fracture Tests

Temperature (°c)	Crack opening (in.)		Fracture energy (in. lb in ⁻²)		Crack length (in.)
	δ	δ_r	T_a	T_r	
Polystyrene					
17	0.078	0.003	4.18	3.86	5.26
18	0.082	0.002	5.16	4.90	5.30
19	0.038	0	5.04	5.04	4.21
19	0.078	0	5.93	5.93	5.53
40	0.105	0.005	3.64	3.30	5.85
40	0.043	0.004	4.19	3.44	5.37
60	0.113	0.035	10.5	5.55	5.26
60	0.110	0.025	6.8	4.06	5.02
62	0.103	0.033	9.14	4.22	4.79
70	0.188	0.110	25.0	4.30	5.43
70	0.190	0.117	35.3	5.21	4.91
70	0.120	0.063	30.1	6.82	4.06
70	0.170	0.106	45.6	6.49	4.43
80	0.123	0.102	100.5	2.93	3.08
Polymethyl-methacrylate					
17	0.086	0	3.19	3.19	5.68
19	0.063	0.001	2.69	2.60	5.22
20	0.077	0.003	2.74	2.53	5.61
40	0.089	0.002	3.91	3.74	5.37
40	0.073	0	2.62	2.62	5.12
40	0.085	0.005	3.28	2.90	5.65
60	0.125	0.019	5.21	3.76	5.48
60	0.122	0.021	6.83	4.69	5.16
60	0.113	0.021	7.86	5.20	4.47
70	0.115	0.023	3.38	2.16	5.53
70	0.098	0.035	4.32	1.79	5.08
72	0.142	0.060	6.05	1.92	5.70
80	0.118	0.048	6.08	2.14	4.89
80	0.125	0.035	5.72	2.97	5.53

calculated from the experimental results is in fact the sum of the true fracture energy T_r and the corresponding energy of permanent deformation T_d . By taking measurements of the residual crack opening at the conclusion of a test it was possible to estimate the true fracture energy as shown in Appendix II. The results of the tests carried out were so analysed and are summarized in the Table and shown in Fig. 6.

Some additional tests were carried out on Lustrex polystyrene specimens at 17°C. In some of these, the crack grew slowly and continuously whilst in others the growth was discontinuous. In the case of the slow crack propagation some stress crazing was observed in the vicinity of the tip of the crack and the fracture energy was calculated to be 19.4 in. lb in⁻². The results for discontinuous crack growth were analysed by calculating the strain energy in the system before and after the crack jump. This calculation gave a value for the fracture energy of 5.6 in. lb in⁻².

§ 4. DISCUSSION

Only a few results are available to compare this determination of fracture energy with those of other investigators. Benbow and Roesler quote fracture energies as 2.8 in. lb in⁻² for polymethyl-methacrylate and 14.6 in. lb in⁻² for polystyrene. Kies obtained a value of 3.5 in. lb in⁻² for polymethyl-methacrylate.

The results for polymethyl-methacrylate show reasonable agreement amongst the three sets of results. In the case of polystyrene, however, the results of Benbow and Roesler show a considerable difference, but since their result falls between the values obtained on Lustrex polystyrene it is possible that there had been some stress crazing present. During the tests of Styron polystyrene no stress crazing was observed at any time although the cracks propagated slowly. Thus it may be concluded that the fracture energy for polystyrene at room temperature is of the order of 5 in. lb in⁻². Higher apparent values would be obtained if some additional area of crack surface is formed through stress crazing.

The scatter bands representing the results which are shown in Fig. 6 indicate that there is probably some significant change in the fracture energy with temperature. In Perspex the fracture energy appears to increase with temperature reaching a maximum at about 60°C. The fracture energy then falling sharply as the material approaches its softening temperature. In the case of Styron there appears to be a minimum in the fracture energy at about 40°C and a maximum at 70°C.

It is suggested that an explanation of this variation of fracture energy with temperature is as follows. The energy associated with a cleavage failure will decrease with temperature due to the greater thermal energy of the molecules. On the other hand the strain energy absorbed in shear deformation preceding the growth of the crack will increase to a maximum and then fall. The increase is due to an increase in ductility at a substantially constant shear stress at moderate temperatures. As the temperature is increased the ductility still increases but the shear stress drops considerably until it is very low when the material softens.

Thus the fracture energy should first fall with temperature, rise to a maximum and then fall to a low value at the softening temperature. This characteristic is

shown by the results obtained from Styron but apparently the minimum for Perspex occurs at a temperature less than those investigated.

The results plotted on Fig. 5 indicate that the fracture energy can be readily calculated from the gradient of the curve of δ against L^2/\sqrt{S} . An important feature of the test is that measurements are made on a continually moving crack so that problems of crack initiation and the corresponding energy requirements are of no concern. At the higher temperatures, considerable creeping was observed and consequently the corrections required were very large in the case of Styron. Thus the absolute magnitudes of the results at these temperatures may be somewhat suspect but it is likely that the trend observed is a valid one.

ACKNOWLEDGMENTS

The author wishes to acknowledge the assistance of Messrs D. G. Havard, B. R. Little and R. Sawczak in carrying out most of the experimental work.

APPENDIX I

DERIVATION OF FRACTURE ENERGY EXPRESSION

The expression to be used for calculating the fracture energy may be derived by considering the changes in strain energy in the system consequent on the growth of the crack. Since the straining frame is rigid compared with the specimen any energy stored within it will be negligible. Consequently it is only necessary to consider strain energy changes in the specimen.

In carrying out the test the crack opening δ is increased by a small amount and then the crack slowly grows an additional increment. When the crack has ceased growing its length L is measured and a curve relating crack width and length may be drawn.



Fig. 7. Loading of test piece.

The energy required to form the new surfaces can then be obtained from the energy balance:

$$\begin{matrix} \text{initial strain} \\ \text{energy} \end{matrix} + \begin{matrix} \text{work done to} \\ \text{increase } \delta \end{matrix} = \begin{matrix} \text{final strain} \\ \text{energy} \end{matrix} + \begin{matrix} \text{work done in} \\ \text{fracture.} \end{matrix} \quad (\text{A1})$$

If U is the strain energy corresponding to δ and L , Eqn (A1) becomes

$$U + P\Delta\delta = U + \Delta U + 2Tt\Delta L \quad \dots\dots (\text{A2})$$

where T is the fracture energy per unit surface area. Then in the limit

$$T = \frac{P}{2t} \frac{d\delta}{dL} - \frac{1}{2t} \frac{\partial U}{\partial L}. \quad \dots\dots (\text{A3})$$

It may be assumed that the total strain energy consists of the sum of that due to bending and shear stresses. It is also assumed that the simple theories of bending and shear stress distribution apply.

Consider first the strain energy due to bending moments. The forces and moments acting on one half of a specimen are as shown in Fig. 7. The strain energy due to bending may be determined from

$$U_B = 4 \int_0^{L/2} \frac{M_x^2 dx}{2EI}$$

where

$$M_x = \frac{1}{2}Qy + \frac{1}{2}Px - M_0 = -EI \frac{d^2y}{dx^2}.$$

The deflected shape of the beam can be determined from this differential equation and hence the bending moment distribution. The bending strain energy is then given by

$$U_B = \frac{P^2 L^3}{16EI} \frac{(1 - \cos u)(u - \sin u)}{u^3 \sin^2 u} \quad \dots\dots (A4)$$

where

$$u^2 = \frac{QL^2}{8EI}.$$

In the limit as $u \rightarrow 0$ then $U_B \rightarrow P^2 L^3 / 192EI$. Thus Eqn (A4) may be rewritten as

$$U_B = \frac{P^2 L^3}{192EI} \psi(u) \quad \dots\dots (A5)$$

where

$$\psi(u) = 12 \frac{(1 - \cos u)(u - \sin u)}{u^3 \sin^2 u}.$$

Assuming a parabolic distribution of shearing stress, the associated strain energy is given by

$$U_s = 4 \int_0^{L/2} \frac{6}{5} \frac{(P/2)^2}{Gtb} dx = \frac{P^2 L b^2}{160GI}. \quad \dots\dots (A6)$$

Thus the total strain energy is

$$U = U_B + U_s = \frac{P^2 L^3}{192EI} \left[\psi(u) + \frac{6}{5} \frac{b^2 E}{L^2 G} \right]. \quad \dots\dots (A7)$$

For a given specimen with a specified end load the quantity in brackets is a function of the crack length only.

Thus

$$U = \frac{P^2 L^3}{192EI} \lambda(L). \quad \dots\dots (A8)$$

Since the force P is not directly measured, the expression for strain energy should be obtained in terms of δ .

Thus

$$\phi = \frac{\partial U}{\partial P} = \frac{PL^3 \lambda}{96EI}$$

and

$$U = \frac{48EI\delta^2}{L^3 \lambda}. \quad \dots\dots (A9)$$

Substituting for U and P in Eqn (A3) leads to the expression for the fracture energy

$$T = \frac{1}{4} \frac{Eb^3 \delta^2}{L^4} S \quad \dots\dots (A10)$$

where

$$S = \frac{1}{\lambda} \left[\frac{2L}{\delta} \frac{d\delta}{dL} + \frac{L}{\lambda} \frac{d\lambda}{dL} + 3 \right].$$

Generally the quantity $(L/\delta)(d\delta/dL)$ is sensibly equal to 2, thus

$$S = \frac{1}{\lambda} \left[7 + \frac{L}{\lambda} \frac{d\lambda}{dL} \right]. \quad \dots\dots (A11)$$

For any given end load S is a function of L and E . Thus it is possible to draw a family of curves of L^2/\sqrt{S} plotted against L for a series of values of E . Such a family of curves has been plotted in Fig. 4.

APPENDIX II

DETERMINATION OF THE 'TRUE' FRACTURE ENERGY

During testing at elevated temperatures the specimens acquired a permanent deformation which therefore absorbed some of the strain energy supplied. Hence it is necessary to estimate the amount of energy so absorbed in order to calculate the true fracture energy consumed by the fracture process alone.

The tests were carried out by straining the specimen to a fixed crack opening and then waiting for some time for the crack to grow. During this time the specimen would suffer creep relaxation with consequent dissipation of energy. The effect of this creep is that a residual crack opening becomes apparent when the splitting force is removed. The theory on which this method for fracture energy determination is based assumes that only elastic deformation occurs so that all displacements are recoverable. Thus, to allow for the effects of creep only, the recoverable part of the crack opening should be considered. At the conclusion of the test the net or recoverable crack opening is

$$\delta_u = \delta - \delta_r$$

where δ is the imposed crack opening at the end of the test and δ_r is the residual crack opening at the end of the test.

Since Benbow and Roesler showed that the nominal stress at the tip of the crack remains constant for all crack lengths it may be assumed that the residual crack opening is proportional to the imposed crack opening. Thus the fracture energy should be calculated from the gradient of the net crack opening curve plotted against L^2/\sqrt{S} . Hence the true fracture energy may be determined from the apparent value as

$$T_r = T_a \left(\frac{\delta - \delta_r}{\delta} \right)^2.$$

REFERENCES

- BENBOW, J. J., and ROESLER, F. C., 1957, *Proc. Phys. Soc. B*, **70**, 201.
 GRIFFITH, A. A., 1920, *Phil. Trans. Roy. Soc.*, **221**, 163.
 KIES, J. A., 1953, *U.S. Naval Research Laboratory Report*, 237.
 OBREIMOFF, J. W., 1930, *Proc. Roy. Soc. A*, **127**, 290.
 ROESLER, F. C., 1956, *Proc. Phys. Soc. B*, **69**, 981.

A Note on Non-equilibrium Elastic Constants

BY M. A. JASWON† AND B. J. SHAW‡

† Department of Mathematics, Imperial College, London, S.W.7

‡ Department of Metallurgy, Imperial College, London, S.W.7

MS. received 14th November 1960

Abstract. A new tensor invariant is introduced into elasticity, viz. the work done by a system of fixed initial stresses in generating second-order dilatations. The effect of the latter can therefore be systematically accounted for, in a crystal of any symmetry class, when making lattice theory calculations of non-equilibrium elastic constants. Two examples of such calculations are included.

THE total energy of a crystal, as a function of the six Cartesian strain parameters $e_i (i=1, 2, \dots, 6)$, must usually be calculated as the sum of a number of distinct contributions none of which by itself could maintain equilibrium. If W stands for such a contribution, per atom, e.g. W is a volume potential or a potential arising from central interatomic forces, then $(\partial W / \partial e_i)_0 \neq 0$ at the equilibrium configuration. Hence, the conventional elastic constant identification, which follows from the expansion

$$W = W_0 + \sum_i \left(\frac{\partial W}{\partial e_i} \right)_0 e_i + \frac{1}{2} \sum_{ij} \left(\frac{\partial^2 W}{\partial e_i \partial e_j} \right)_0 e_i e_j \quad \dots\dots (1)$$

does not necessarily retain its validity. For instance, the shear constant c_{66}^W associated with W is not given by $c_{66}^W / V_0 = \frac{1}{4} (\partial^2 W / \partial e_6^2)_0$ unless we arrange for the deformation to be dilatationless. This complication stems from the fact that a second-order dilatation inevitably accompanies e_1, \dots , and it now makes a contribution to W that must be accounted for when defining c_{ij}^W . The problem has previously been recognized (Huntington 1958), and people have devised *ad hoc* methods for eliminating the unwanted dilatation in particular cases, but no explicit general formula ever seems to have been put forward. How a dilatationless procedure would work for non-cubic crystals, and to what extent it could cope with cross-constants such as c_{14}^W or c_{45}^W , remain open to question. It is the purpose of the present paper to point out that a simple solution of the problem exists, applicable to all the constants c_{ij}^W characteristic of any symmetry class.

Our argument is as follows. The first summation in (1) represents the work done by a system of fixed stresses $P_i = (\partial W / \partial e_i)_0$, which are required to maintain the equilibrium configuration at $e_i = 0$. They may, however, also do second-order work, which would be included within the second summation. Thus, the pair of strains e_1, e_2 involve a second-order dilatation

$$(1 + e_1)(1 + e_2) - (1 + e_1 + e_2) = e_1 e_2$$

which, to the same order, is equivalent to equal strains $\frac{1}{2}e_1e_2$ along the coordinate axes 1, 2. This yields a strain energy contribution

$$\frac{1}{2} \left(\frac{\partial W}{\partial e_1} + \frac{\partial W}{\partial e_2} \right)_0 e_1 e_2$$

with similar contributions from e_2e_3 and e_3e_1 . We therefore arrive at a principal-axes energy

$$\frac{1}{2} \sum_{1,2,3} \left(\frac{\partial^2 W}{\partial e_i \partial e_j} \right)_0 e_i e_j - \frac{1}{2} \sum_{1,2,3} \left(\frac{\partial W}{\partial e_1} + \frac{\partial W}{\partial e_2} \right)_0 e_1 e_2 \quad \dots\dots (2)$$

corrected for the presence of $e_1e_2 + e_2e_3 + e_3e_1$. Equivalently, expression (2) provides the energy associated with a set of principal strains

$$e_1 - \frac{1}{2}e_1e_2 - \frac{1}{2}e_1e_3, \quad e_2 - \frac{1}{2}e_2e_3 - \frac{1}{2}e_2e_1, \quad e_3 - \frac{1}{2}e_3e_1 - \frac{1}{2}e_3e_2 \quad \dots\dots (3)$$

that involve no second-order dilatation, and it thus enables us to dispense with specialized procedures for eliminating the latter. If so,

$$c_{12}^W V_0 = \left(\frac{\partial^2 W}{\partial e_1 \partial e_2} \right)_0 - \frac{1}{2} \left(\frac{\partial W}{\partial e_1} + \frac{\partial W}{\partial e_2} \right)_0, \quad \dots\dots (4)$$

with analogous formulae for c_{23}^W , c_{31}^W ; no corrections are required for c_{11}^W , c_{22}^W , c_{33}^W . The introduction of (3) in place of e_1 , e_2 , e_3 becomes unnecessary when $(\partial W / \partial e_i)_0 = 0$ since the extra summation in (2) then vanishes.

To calculate c_{66}^W , we in effect rotate the coordinate axes 1, 2 through 45° about their common normal, introduce strains $e_1' = e_6$, $e_2' = -e_6$ and compute $(\partial^2 W / \partial e_6^2)_0$, making an allowance for the dilatation $-e_6^2$. This procedure yields the equation

$$\frac{1}{2} 4c_{66}^W e_6^2 V_0 = \frac{1}{2} \left(\frac{\partial^2 W}{\partial e_6^2} \right)_0 e_6^2 + \frac{1}{2} \left(\frac{\partial W}{\partial e_1'} + \frac{\partial W}{\partial e_2'} \right)_0 e_6^2,$$

whence

$$4c_{66}^W V_0 = \left(\frac{\partial^2 W}{\partial e_6^2} \right)_0 + \left(\frac{\partial W}{\partial e_1} + \frac{\partial W}{\partial e_2} \right)_0 \quad \dots\dots (5)$$

on bearing in mind the invariance properties of

$$\left(\frac{\partial W}{\partial e_1} + \frac{\partial W}{\partial e_2} \right).$$

Analogous formulae hold for c_{44}^W , c_{55}^W . A superior approach is to examine how (2) transforms under an arbitrary rotation of axes. First,

$$\sum_{1,2,3} \left(\frac{\partial^2 W}{\partial e_i \partial e_j} \right)_0 e_i e_j \rightarrow \sum_{ij} \left(\frac{\partial^2 W}{\partial e_i \partial e_j} \right)_0 e_i e_j,$$

where the second summation now extends over all six strain parameters instead of only e_1 , e_2 , e_3 . Also

$$\sum_{1,2,3} \left(\frac{\partial W}{\partial e_1} + \frac{\partial W}{\partial e_2} \right)_0 e_1 e_2 \rightarrow \sum_{1,2,3} \left(\frac{\partial W}{\partial e_1} + \frac{\partial W}{\partial e_2} \right)_0 (e_1 e_2 - e_6^2) + 2 \sum_{4,5,6} \left(\frac{\partial W}{\partial e_4} \right)_0 (e_4 e_1 - e_5 e_6)$$

as follows from the properties of the strain determinant $||e_1e_2e_3||$. Accordingly, the tensor invariant energy of the system, corrected for the second-order dilatation

$$e_1e_2 + e_2e_3 + e_3e_1 - e_4^2 - e_5^2 - e_6^2,$$

takes the form

$$\frac{1}{2} \sum_{ij} \left(\frac{\partial^2 W}{\partial e_i \partial e_j} \right)_0 e_i e_j - \frac{1}{2} \sum_{1,2,3} \left(\frac{\partial W}{\partial e_1} + \frac{\partial W}{\partial e_2} \right)_0 (e_1 e_2 - e_6^2) - \sum_{4,5,6} \left(\frac{\partial W}{\partial e_4} \right)_0 (e_4 e_1 - e_5 e_6). \dots\dots (6)$$

This useful expression does not seem to have previously appeared in the literature (Leibfried 1955). It verifies (5), and also indicates the corrections to be associated with c_{14}^W , c_{56}^W , etc.,

$$\left. \begin{aligned} 4c_{56}^W V_0 &= \left(\frac{\partial^2 W}{\partial e_5 \partial e_6} \right)_0 + \left(\frac{\partial W}{\partial e_4} \right)_0 \\ 2c_{14}^W V_0 &= \left(\frac{\partial^2 W}{\partial e_1 \partial e_4} \right)_0 - \left(\frac{\partial W}{\partial e_4} \right)_0 \end{aligned} \right\} \dots\dots (7)$$

As a first application of the theory, we calculate c_{ij}^W for a volume potential

$$W = W(V), \quad V = V_0(1 + e_1 + e_2 + e_3 + e_1e_2 + e_2e_3 + e_3e_1 - e_4^2 - e_5^2 - e_6^2).$$

Writing

$$\begin{aligned} \frac{\partial W}{\partial e_1} &= \frac{dW}{dV} \frac{\partial V}{\partial e_1} = \frac{dW}{dV} V_0(1 + e_2 + e_3), \quad \text{etc.}, \\ \frac{\partial^2 W}{\partial e_1 \partial e_2} &= \frac{d^2 W}{dV^2} V_0^2(1 + e_2 + e_3)^2 + \frac{dW}{dV} V_0, \quad \text{etc.}, \end{aligned}$$

it may be readily shown that

$$c_{11}^W = c_{12}^W = \left(\frac{d^2 W}{dV^2} \right)_0 V_0, \quad c_{66}^W = c_{14}^W = c_{56}^W = 0, \quad \text{etc.}, \quad \dots\dots (8)$$

as expected. As a second example, we calculate c_{ij}^W for a W arising from central forces between nearest neighbouring atoms in rhombohedral crystal structures. It is convenient to think of the rhombohedral cell, of angle α , as generated from a unit cube†, whose edges define a Cartesian reference frame, by the homogeneous deformation

$$0, 0, 0 \rightarrow 0, 0, 0; \quad 1, 0, 0 \rightarrow 1 + \lambda, \lambda, \lambda; \quad 0, 1, 0 \rightarrow \lambda, 1 + \lambda, \lambda; \quad 0, 0, 1 \rightarrow \lambda, \lambda, 1 + \lambda$$

where $\cos \alpha = (2\lambda + 3\lambda^2)/(1 + 2\lambda + 3\lambda^2)$. With this orientation of coordinate system, the six independent elastic constants of a face-centred crystal (e.g. crystalline mercury, for which $\cos \alpha = -1/7$) are seen to be $c_{11} = c_{22} = c_{33}$, $c_{12} = c_{23} = c_{31}$, $c_{44} = c_{55} = c_{66}$, $c_{45} = c_{56} = c_{64}$, $c_{14} = c_{25} = c_{36}$, $c_{15} = c_{16} = c_{24} = c_{26} = c_{34} = c_{35}$.

Writing

$$W = \frac{1}{2} \sum_{i=1}^6 \phi(a_i) + \frac{1}{2} \sum_{i=1}^6 \psi(b_i)$$

where a_1 denotes the current distance from $[0, 0, 0]$ of the atom at

$$\frac{1}{2}[1 + 2\lambda, 1 + 2\lambda, 2\lambda],$$

† For a cube of edge l , replace ϕ_0' , ϕ_0'' by $l\phi_0'$, $l^2\phi_0''$, etc., in the subsequent formulae, the derivatives being evaluated at la_0 , lb_0 . Choice of $l = (1 + 2\lambda + 3\lambda^2)^{-1/2} \equiv (1 - \cos \alpha)^{1/2}$ ensures a rhombohedron of unit edge.

and where b_1 has a similar significance for the atom at $\frac{1}{2}[1, \bar{1}, 0]$, there being six atoms of each type, we obtain

$$\begin{aligned} \left(\frac{\partial W}{\partial e_1} + \frac{\partial W}{\partial e_2} \right)_0 &= \frac{\phi_0'}{a_0} + \frac{\psi_0'}{b_0} (1 + 4\lambda + 6\lambda^2), \\ \left(\frac{\partial^2 W}{\partial e_1 \partial e_2} \right)_0 &= \frac{a_0^2 \phi_0'' - a_0 \phi_0'}{16a_0^4} + \frac{b_0^2 \psi_0'' - b_0 \psi_0'}{16b_0^4} (1 + 4\lambda + 12\lambda^2)(1 + 2\lambda)^2, \\ \left(\frac{\partial^2 W}{\partial e_6^2} \right)_0 &= \frac{a_0^2 \phi_0'' - a_0 \phi_0'}{4a_0^4} + \frac{\phi_0'}{a_0} + \frac{b_0^2 \psi_0'' - b_0 \psi_0'}{4b_0^4} (1 + 4\lambda + 12\lambda^2)(1 + 2\lambda)^2 \\ &\quad + \frac{\psi_0'}{b_0} (1 + 4\lambda + 6\lambda^2), \\ \left(\frac{\partial W}{\partial e_6} \right)_0 &= -\frac{\phi_0'}{2a_0} + \frac{\psi_0'}{2b_0} (1 + 8\lambda + 12\lambda^2), \\ \left(\frac{\partial^2 W}{\partial e_3 \partial e_6} \right)_0 &= \frac{b_0^2 \psi_0'' - b_0 \psi_0'}{4b_0^4} \lambda (1 + 3\lambda)(1 + 2\lambda)^2, \\ \left(\frac{\partial^2 W}{\partial e_5 \partial e_6} \right)_0 &= -\frac{\phi_0'}{4a_0} + \frac{b_0^2 \psi_0'' - b_0 \psi_0'}{b_0^4} \lambda (1 + 3\lambda)(1 + 2\lambda)^2 \\ &\quad + \frac{\psi_0'}{4b_0} (1 + 8\lambda + 12\lambda^2). \end{aligned}$$

In these formulae, a_0 and b_0 denote the initial lengths of a_i , b_i respectively; ϕ_0' denotes $d\phi/da_i$ evaluated at a_0 , etc. Substituting into (4), (5), (7) yields c_{12}^W , c_{66}^W , c_{36}^W , c_{56}^W for this structure, no corrections being required for the remaining constants. The calculation has also been effected for a body-centred cell. Well-known results for face-centred cubic and body-centred cubic crystals may be deduced on setting $\lambda = 0$, $\phi_0 = \psi_0$, $a_0 = b_0$.

The deformation $e_1 = e_2 = e_3 = \Delta/3$, equivalent to a dilatation Δ plus a second-order dilatation $\Delta^2/3$, is associated with a strain energy $\frac{1}{2}K\Delta^2V_0$ where

$$K = \frac{1}{9}(c_{11}^W + \dots 2c_{12}^W + \dots). \quad \dots (9)$$

If so,

$$KV_0 = \frac{1}{9} \sum_{1,2,3} \left(\frac{\partial^2 W}{\partial e_i \partial e_j} \right)_0 - \frac{2}{9} \sum_{1,2,3} \left(\frac{\partial W}{\partial e_i} \right)_0 = \left(\frac{d^2 W}{d\Delta^2} \right)_0 - \frac{2}{3} \left(\frac{dW}{d\Delta} \right)_0$$

on bearing in mind

$$\frac{dW}{d\Delta} = \frac{1}{3} \sum_{1,2,3} \frac{\partial W}{\partial e_i}, \quad \frac{d^2 W}{d\Delta^2} = \frac{1}{9} \sum_{1,2,3} \frac{\partial^2 W}{\partial e_i \partial e_j}.$$

It follows, since $V = V_0(1 + \Delta + \Delta^2/3)$, that

$$K = \left(\frac{d^2 W}{dV^2} \right)_0 V_0,$$

in agreement with the thermodynamic definitions

$$K = -V \frac{dp}{dV}, \quad p = -\frac{dW}{dV}.$$

ACKNOWLEDGMENT

One of us (B.J.S.) acknowledges a maintenance grant provided by the United Kingdom Atomic Energy Authority.

REFERENCES

- HUNTINGTON, H. B., 1958, *Solid State Physics*, Vol I (edited by F. Seitz and D. Turnbull) (New York: Academic Press), p. 213.
LEIBFRIED, G., 1955, *Handb. d. Phys.*, Vol. 7, (Berlin: Springer), p. 104.

The Reduced Equation of State of the Inert Gas Solids at the Absolute Zero

By I. J. ZUCKER

Northampton College of Advanced Technology, St. John Street, London, E.C.1

MS. received 5th May 1960, in revised form 4th October 1960

Abstract. It is shown that a law of corresponding states exists amongst the inert gases in the solid phase even when quantum effects are large. The theoretical treatment is based on the Einstein model of a crystal modified to account for large vibrations of the crystal atoms. Using a Lennard-Jones 12-6 potential for the interaction energy between a pair of atoms, reasonable agreement is obtained between theoretical and experimental values for the equilibrium volumes and energies of the rare gas crystals at the absolute zero.

§ 1. INTRODUCTION

IF a law of corresponding states exists amongst a group of substances, then it is possible to express the equations of state of this group in a single reduced equation provided that the thermodynamic variables are expressed in a suitable way. De Boer (1948) showed that if classical statistics were obeyed then such a law will exist amongst a group of substances, if the forces between the atoms of the substances were central, and that the interaction between atoms could be expressed in the form $\epsilon f(\sigma/r)$. ϵ and σ are respectively a characteristic energy and length, r is the interatomic distance and f is a universal function. The free energy could then be written as

$$F^* = F(V^*, T^*) \quad \dots\dots (1.1)$$

where $F^* = F/N\epsilon$, $V^* = V/N\sigma^3$, and $T^* = kT/\epsilon$; V and T are the molar volume and absolute temperature respectively, whilst N is Avogadro's number and k is Boltzmann's constant.

If on the other hand quantum statistics are obeyed, then if all other conditions are the same as before, De Boer showed that F^* now depended on a third quantity, Λ^* , defined by

$$\Lambda^* = h/\sigma(m\epsilon)^{1/2} \quad \dots\dots (1.2)$$

h being Planck's constant and m the mass of the atom of the substance considered. Λ^* may be considered as a measure of quantum effects. Physically these quantum effects appear as zero-point energy E_0 and it would be expected that the larger Λ^* is, the larger will be the proportion of E_0 to the total energy. In the Table some relevant data for the inert gas solids are tabulated, and from this it will be observed that the proportion of E_0 does indeed increase with Λ^* .

The Λ^* given in the Table were determined from parameters obtained for the following intermolecular potential:

$$\epsilon f\left(\frac{\sigma}{r}\right) = 4\epsilon \left[\left(\frac{\sigma}{r}\right)^{12} - \left(\frac{\sigma}{r}\right)^6 \right] = \phi(r). \quad \dots\dots (1.3)$$

Element	M	σ (Å)	ϵ (10^{-16} erg)	V_0 (exptl) ($\text{cm}^3 \text{ g mol}^{-1}$)	V_0^*	F_0 (exptl) (cal g mol^{-1})	F_0^*	Δ^*	E_0 (cal g mol^{-1})	$\frac{E_0}{F_0 + E_0}$ (%)	Ref.
Xe	131.3	3.920	318	33.6	0.926	3830	8.36	0.062	123	3.1	1
Kr	83.7	3.604	228	26.3	0.940	2678	8.14	0.102	141	5.0	2
A	39.9	3.400	169	22.6	0.951	1850	7.60	0.184	179	8.8	2
Ne	20.3	2.831	49.6	14.0	1.024	448	6.26	0.574	143	24.2	2
D ₂	4.0	2.920	50.8	20.3	1.343	276	3.77	1.22	217	44.2	1
H ₂	2.0	2.920	50.8	22.9	1.515	183	2.50	1.73	235	56.2	1
⁴ He	4.0	2.556	14.1	21.2†	2.107	12	0.59	2.68	47	79.7	1
³ He	3.0	2.556	14.1	32.0†	3.181	4.5	0.22	3.09	—	—	1

(1) De Boer (1948)

(2) Zucker (1956)

† Under 25 atmospheres pressure.

‡ Under 30 atmospheres pressure.

Given that such a law holds for the inert gas solids, De Boer and Blaisse (1948) and Salter (1954) attempted to calculate V_0^* and F_0^* , the equilibrium values of V^* and F^* at $T=0$, as a function of Λ^* . Both achieved some success for the heavier elements with Λ^* small, but both attempts failed when applied to the hydrogen and helium isotopes. (The hydrogen isotopes are not members of the inert gas group, but in the solid state they behave so much like the latter that they are often treated as such.) The reason for this breakdown in both cases is that the theories employed were in each instance based on the harmonic approximation of lattice dynamics. Quantum effects in the shape of zero-point energy correspond to a negative pressure, however, and this tends to increase the equilibrium volume of the crystal. The forces between the constituent atoms tend to become weaker, the vibrations of the latter about their equilibrium positions become large, and the harmonic approximation is no longer valid. Recently Bernardes (1958), trying a different approach, used a variation technique in attempting to find a wave function to describe a crystal in terms of a suitable combination of ground state and first excited states of the individual atoms considered as confined in spherical boxes. Bernardes obtained a series for the energy of the crystal in terms of two variation parameters, but this also failed to converge rapidly enough in the cases of the lighter elements with large Λ^* . Dugdale and MacDonald (1954), basing their approach on an equation proposed by Domb (1952) to account for the large zero-point energy of helium, succeeded in some measure in calculating V_0^* and F_0^* for all the elements considered. These results will be discussed later.

The approach described below is similar to that of Salter's but is based on the Einstein model of a crystal. But not only are the normal harmonic terms in the expansion of the potential energy considered, but also the first two anharmonic terms. With the harmonic terms alone results similar to Salter are obtained. The additional terms clearly show the range of validity of the harmonic approximation.

§ 2. THEORY

The potential energy of a single atom displaced from its equilibrium position in an Einstein crystal due to the mean field of all the other atoms may be shown to be (see Appendix I)

$$W = W_0 + W_2(x^2 + y^2 + z^2) + W_4(x^4 + y^4 + z^4) + W_6(x^6 + y^6 + z^6) + \dots \quad (2.1)$$

where

$$\begin{aligned} W_0 &= \frac{1}{2} \sum_{\mathbf{A}} \phi(\mathbf{A}), & W_2 &= \frac{1}{6} \sum_{\mathbf{A}} \left[\phi^{ii}(\mathbf{A}) + \frac{2}{\mathbf{A}} \phi^i(\mathbf{A}) \right] \\ W_4 &= \frac{1}{72} \sum_{\mathbf{A}} \left[\phi^{iiii}(\mathbf{A}) + \frac{4}{\mathbf{A}} \phi^{iii}(\mathbf{A}) \right] \\ W_6 &= \frac{1}{2160} \sum_{\mathbf{A}} \left[\phi^{vi}(\mathbf{A}) + \frac{6}{\mathbf{A}} \phi^v(\mathbf{A}) \right] \quad \dots \quad (2.2) \end{aligned}$$

x, y, z , are the displacement components of the atom, and $\sum_{\mathbf{A}}$ implies summation over all lattice points of the crystal. These summations for various lattices and for intermolecular potentials of the form (1.3) are well known, and were first carried out by Lennard-Jones and Ingham (1925). The first term of (2.1) is the classical static lattice energy of the undisplaced atom. The second term

gives the contribution to the potential energy due to the harmonic motion of the atom. The third and fourth terms are higher order contributions. (2.1) was given by Henkel (1955) up to the W_4 term for a particular $\phi(r)$ and for a face-centred cubic lattice. In the above form the expansion may be applied to any central potential $\phi(r)$ and to any cubic lattice. The elements considered here are all assumed to condense into face-centred cubic structures. In fact the isotopes of hydrogen and helium appear to form hexagonal close-packed structures. However, the difference between a hexagonal close-packed and face-centred cubic structure is so small that in the present approximations this difference is not important.

Consider first a classical crystal at the absolute zero, i.e. $T=0=T^*$. There is no zero-point energy and hence the total energy is just the static lattice energy. For an Einstein crystal this is just NW_0 , and for the $\phi(r)$ used here the reduced energy as a function of volume becomes

$$F^* = \frac{6.066}{V^{*4}} - \frac{14.454}{V^{*2}}. \quad \dots\dots(2.3)$$

Differentiation of F^* with respect to V^* and equation to zero gives V_0^* and thus F_0^* . Consider now a crystal in which the vibration of the atoms is so small that only the harmonic term in (2.1) is significant in the potential energy. The Schrödinger equation for such a potential is easily solved giving the zero-point energy for a harmonic Einstein crystal as

$$E_{0(\text{harm})} = \frac{3hN}{4\pi} \left(\frac{2W_2}{m} \right)^{1/2} \quad \dots\dots(2.4)$$

whence

$$E_0^*(\text{harm}) = 0.4255\Lambda^* R^{1/2} / V^{*7/3} \quad \dots\dots(2.5)$$

$$R = 132.66 - 64.01V^{*2}.$$

This is the same result as obtained by Salter (1954) apart from two minor modifications as Salter used a Debye model and considered only nearest and next nearest neighbour interactions. E_0^* thus appears as a function of V^* and Λ^* , and hence V_0^* and F_0^* may be calculated as a function of Λ^* in the same way as before. But it will immediately be observed that if V^* is greater than 1.4, R , which is essentially the reduced form of W_2 , becomes negative and thus E_0^* becomes negative. The elements after neon in the Table are therefore beyond the scope of this treatment. The same sort of difficulty occurs in the work of De Boer and Blaisse (1948) when V^* becomes greater than 1.3. Both failures are due to the breakdown of the harmonic approximation.

Consider now the first anharmonic term in (2.1). The inclusion of this term as a perturbation by Henkel (1955), Johns (1958) and Zucker (1956, 1958) has shown that in the treatment of the heavier inert gases improvements are obtained. The additional contribution to the zero-point energy is found to be

$$E_{0(\text{anharm})} = \frac{9h^2N}{32\pi^2m} \frac{W_4}{W_2} \quad \dots\dots(2.6)$$

which in reduced form becomes

$$E_0^*(\text{anharm}) = 0.2639\Lambda^{*2} \frac{S}{RV^{*2/3}} \quad \dots\dots(2.7)$$

$$S = 172 - 24.622V^{*2}.$$

S is essentially the reduced form of W_4 . The free energy of a crystal in reduced form including the first anharmonic term as a perturbation may thus be written

$$F^* = \frac{6.066}{V^{*4}} - \frac{14.454}{V^{*2}} + \frac{0.4255\Lambda^* R^{1/2}}{V^{*7/3}} + \frac{0.2639\Lambda^{*2} S}{RV^{*2/3}} \dots (2.8)$$

This is an improvement on the results of Salter but the range in which (2.8) is valid is not altered since $R^{1/2}$ still becomes imaginary for V^* greater than 1.4. The extra term does, however, help to define clearly when (2.8) is valid. Since the anharmonic term has been treated as a perturbation it is required that $E_{0,\text{anhar}}^*/E_{0,\text{harm}}^*$ should be some fraction—say about a fifth. Then no matter how small Λ^* is (2.8) breaks down for V^* greater than 1.4. But the larger Λ^* is the smaller V^* must be for the condition to hold that the anharmonic term is a perturbation. Thus for $\Lambda^*=0.5$, V^* should be less than 1.2, and for $\Lambda^*=1.0$, V^* should be less than 1.0. This range will just cover the elements up to deuterium.

For the lighter gases it is apparent that the term with W_4 is no longer a perturbation. But it was observed that when V^* is greater than 2.6 that S becomes negative indicating that for larger volumes an additional term is necessary. The next order term was thus included in the calculations. The governing factor of the reduced form of W_6 is given by $T=343.2-18.0V^{*2}$. This does not become negative until V^* is greater than 4.4. Although large Λ^* will reduce the range over which this approximation holds it was hoped that this would be sufficient to cover all the elements considered. The necessary calculation was to find the lowest eigenvalue of the Schrödinger equation with a potential given by (2.1). This is separable into three equations of the form

$$\left[-\frac{\partial^2}{\partial x^2} + \frac{8\pi^2 m}{h^2} (W_2 x^2 + W_4 x^4 + W_6 x^6) \right] \Psi = \frac{8\pi^2 m E}{h^2} \Psi \dots (2.9)$$

The eigenvalues of such an equation may be found numerically to any degree of accuracy by a method due to Coulson and McWeeny (1948) and described in

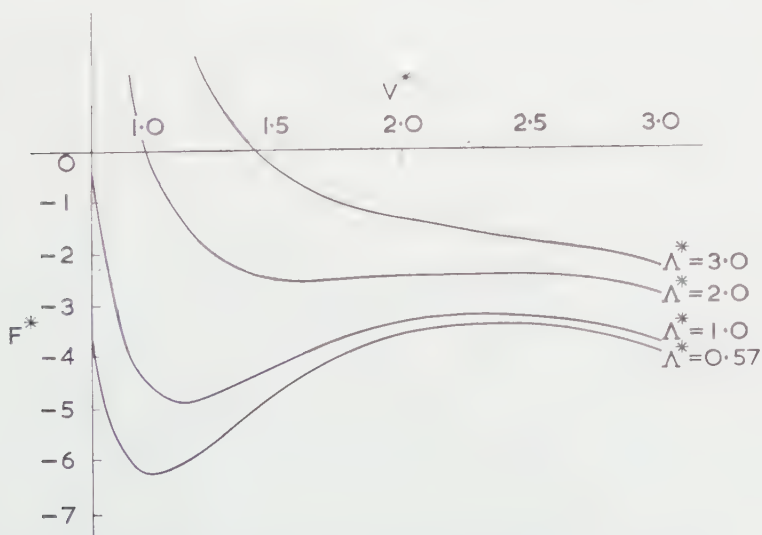


Fig. 1. Variation of energy with volume for selected values of Λ^* .

Appendix II. The energy of a crystal at the absolute zero is found to be

$$F^* = \frac{6.066}{V^{*4}} - \frac{14.454}{V^{*2}} + \frac{3}{8\pi^2} \Lambda^{*2} \lambda_0^* \quad \dots\dots (2.10)$$

where λ_0^* is the lowest eigenvalue of (2.9) in reduced form. F^* was evaluated for values of V^* ranging from 0.8 to 3.5 and for Λ^* ranging from zero to 3.5. V_0^* and F_0^* were obtained directly from these results. Curves of F^* against V^* for selected values of Λ^* , and of F_0^* and V_0^* against Λ^* are shown in Figs 1 to 3 together with other relevant information.

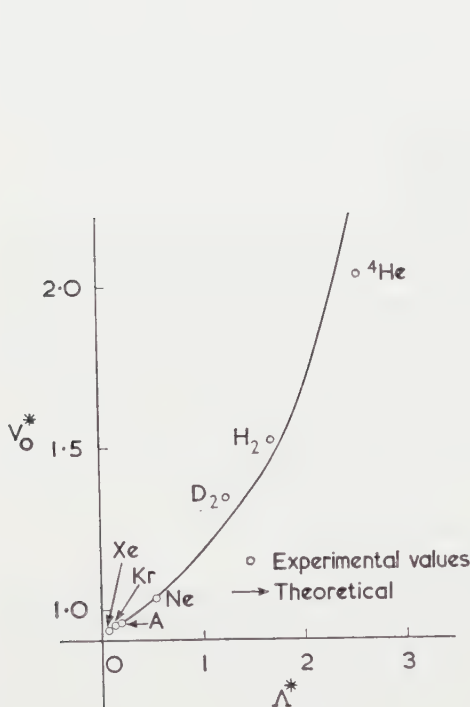


Fig. 2. Variation of equilibrium volume with Λ^* at $T=0$.

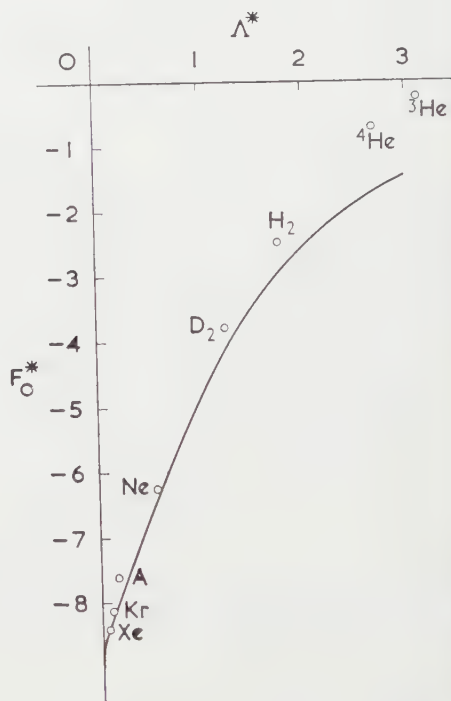


Fig. 3. Variation of equilibrium energy with Λ^* at $T=0$.

§ 3. DISCUSSION

The most interesting aspects of these calculations are to be seen in the graphs of F^* against V^* shown in Fig. 1. Physically it would be expected that as V^* increased indefinitely, F^* , the free energy, should pass through a minimum—the equilibrium value for the crystal—and then tend to zero. This certainly occurs for a classical crystal with $\Lambda^*=0$. On the introduction of quantum effects this trend is first observed, but at some value of V^* depending on the size of Λ^* , F^* begins to diverge from zero, becoming more negative. This divergence only appears at large values of V^* . In order to explain this a closer examination of the Einstein model on which these calculations are based is necessary.

The Einstein model assumes that each atom of the crystal is independent of all the others. Each atom is confined to a cell from which all others are

excluded. Each atom is assumed to be governed by the mean potential field due to all the other atoms at rest in their mean positions. These rest positions are assumed to be situated at the centres of the atomic cells, which are identified as the lattice sites of the atoms. The model just described is remarkably similar to the cell model of a liquid used by Lennard-Jones and Devonshire (1939), and the results given by the latter may be used to illustrate certain facets of the Einstein model. Lennard-Jones and Devonshire calculated the mean field in which an atom vibrates in its cell as a function of V^* employing the same form of $\phi(r)$ as used here. Their results are illustrated in Fig. 4. For V^* of the

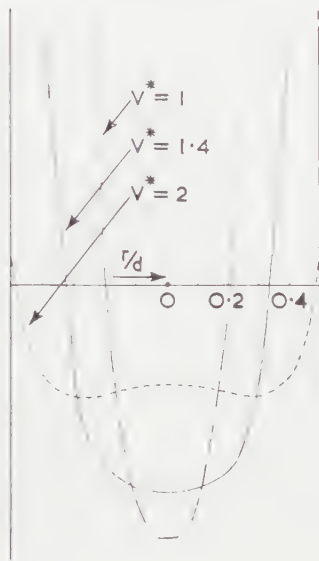


Fig. 4. Potential energy of an atom in a cell as a function of volume.

order of 1.0 the shape of the potential field is parabolic, i.e. it may be represented with terms involving only squares of the distances of the atoms from their static equilibrium positions. The vibrations of the atom in such a field are those of a harmonic oscillator. The harmonic approximation is valid in this region and indeed is applicable to the heavier elements with small Λ^* and $V_0^* \simeq 1$. As V^* increases the potential field is no longer parabolic. The harmonic approximation is no longer valid, and the Henkel approximation attempts to account for the change by introducing fourth and higher order terms in the displacement of the atom from equilibrium.

The examination of this model suggests two possible explanations for the eventual divergence of F^* from zero at large V^* . From Fig. 4 it is seen that at large V^* the potential field is not even approximately that of a parabola. The appearance of the potential is more like a square-well. Thus it may be necessary to include many more higher order terms than already considered in the expansion (2.1). The other possible explanation concerns the walls of the potential field. In solving the Schrödinger equation for the given potential it is tacitly assumed that the potential field tends to infinity at large distances from the equilibrium position of the atom. This assumption is plausible for

small V^* when the crystal is tightly bound and the atoms are confined rigorously to their cells. At large V^* , however, the atoms are less tightly bound and the mean field they produce is much weaker. The height of the potential barrier can no longer be considered infinite. At large enough V^* the atoms may leak through or over the confining potential field. The crystal would break down into a liquid which may exhibit lattice-like properties—as appears to be the case with helium.

In spite of the failure at large V^* the F^* against V^* curves behave as expected at small V^* , and the minima can be determined for Λ^* up to about 2.5. This includes the elements in the Table up to ^4He and this is a definite improvement on Salter, De Boer and Bernardes. Graphs of F_0^* and V_0^* against Λ^* are shown together with experimental results in Figs 2 and 3. The agreement is quite good and indicates the validity of a law of corresponding states applying to the rare gas solids.

It should be pointed out here that ^4He and ^3He exist only in the solid phase under minimum pressures of 25 and 30 atmospheres respectively. In reduced terms these pressures correspond to 0.30 and 0.36 respectively. For a true comparison with experiment the values of V^* and F^* should be found not at the minimum, where $P^*=0$, but when the negative slope ($P^*=-\partial F^*/\partial V^*$) of the F^* curves for the appropriate Λ^* are the above values. But for the large V^* and Λ^* applicable to these elements while the minima of the F^* curves are in some doubt, the slopes are even less trustworthy. Hence the theoretical curves in Figs 1 and 2 refer solely to the minima. Estimates for ^4He indicate that the differences in F^* and V^* for $P^*=0.3$ and for $P^*=0$ are less than 5%. Also the effect on the theoretical curves in Figs 2 and 3 would be to shift both in the correct direction as far as agreement with experiment is concerned. Nevertheless should reliable F^* curves be obtained then the values of F^* and V^* should be found at the appropriate equilibrium pressures.

It is interesting to note that Dugdale and Domb (1957) obtain from the results of Dugdale and MacDonald (1954) similar curves to those shown in Fig. 1. As Λ^* increases the energy minimum becomes shallower, and Dugdale and Domb show one curve appropriate to ^3He for which F^* is always positive and has no minimum at all.

Domb comments that this might correspond to an interesting distinction between solid ^3He and solid ^4He . The Simon melting equation may be written

$$\frac{P}{a} = \left(\frac{T_f}{T_0} \right)^c = 1 \quad \text{..... (3.1)}$$

T_0 is the melting temperature at zero pressure, T_f is the melting temperature at a pressure P , c is a constant, and a is another constant representing the internal pressure of the solid. a is found to be positive for all substances except ^3He . Thus solid ^3He cannot exist under zero pressure in any circumstances, indicating no energy minimum. ^4He does not exist in the solid phase under zero pressure since the free energy of the liquid phase is less than that of the solid. This, however, does not preclude the existence of solid ^4He under zero pressure in some metastable condition, whereas this would be impossible for ^3He .

Dugdale and MacDonald's results are obtained using a 10-6 Lennard-Jones potential, but on using other plausible potentials this disappearance of the energy minimum is not obtained. Further Fisher and Zucker (1961) have

shown that the non-linear differential equation which Dugdale and MacDonald employed to derive their results cannot possibly account for the properties of the inert gas solids when a full solution is attempted. Dugdale and MacDonald's results depend on stopping an iterative procedure at a particular stage. The results of the present approximation agree qualitatively with those of Dugdale and MacDonald but seem to have a sounder theoretical basis and offer possibilities of further inquiry, for example, any central additive potential may be examined.

§ 4. CONCLUSION

The model employed above supports the idea that a modified law of corresponding states exists amongst the inert gas crystals even when quantum effects are large. Further refinements, however, are necessary to investigate more fully the properties of ^3He .

ACKNOWLEDGMENTS

The writer is indebted to Professor C. Domb and Dr. M. E. Fisher for many stimulating discussions and comments. Thanks are also due to the University of London Computer Unit for use of the MERCURY and to Dr. M. J. Bernal for help in preparing the necessary computing programmes.

APPENDIX I

Consider a typical atom in a lattice and make it the origin O , of a coordinate system. Let \mathbf{h} be the displacement vector of the atom from equilibrium with components (x, y, z) . Let \mathbf{A} be the position vector of any other typical atom which is considered at rest in its equilibrium position. The components of \mathbf{A} will be (n_1d, n_2d, n_3d) where d is the lattice constant, and (n_1, n_2, n_3) are numbers depending on the type of lattice. The potential energy of the displaced atom is thus

$$W(\mathbf{h}) = \sum_{\mathbf{A}} [\phi(|\mathbf{A} - \mathbf{h}|) - \frac{1}{2}\phi(|\mathbf{A}|)]. \quad \text{.....(I.1)}$$

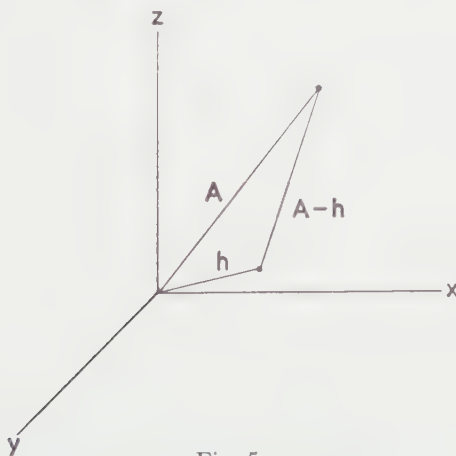


Fig. 5.

The $\frac{1}{2}\phi(|\mathbf{A}|)$ is subtracted so that when $\mathbf{h} = 0$ one obtains the static lattice energy. Expanding $W(\mathbf{h})$ as a Taylor series about the origin up to the sixth-order term one has

$$W(\mathbf{h}) = \sum_{\mathbf{A}} \left[\frac{1}{2}\phi(|\mathbf{A}|) + \sum_{n=1}^6 (-1)^n (\mathbf{h} \cdot \nabla)^n \phi|_{\mathbf{h}=0} \right]. \quad \text{.....(I.2)}$$

The quantities $(\mathbf{h} \cdot \nabla)^n \phi|_{h=0}$ may be evaluated simply thus

$$\begin{aligned} (\mathbf{h} \cdot \nabla) \phi|_{h=0} &= (\mathbf{h} \cdot \mathbf{A}) \frac{\phi^i}{|\mathbf{A}|} \\ (\mathbf{h} \cdot \nabla)^2 \phi|_{h=0} &= (\mathbf{h} \cdot \mathbf{h}) \frac{\phi^i}{|\mathbf{A}|} + (\mathbf{h} \cdot \mathbf{A})^2 \left[\frac{\phi^{ii}}{|\mathbf{A}|^2} - \frac{\phi^i}{|\mathbf{A}|^3} \right], \text{ etc., with finally} \\ &\vdots \\ (\mathbf{h} \cdot \nabla)^6 \phi|_{h=0} &= 15(\mathbf{h} \cdot \mathbf{h})^3 \left[\frac{\phi^{iii}}{|\mathbf{A}|^3} - \frac{3\phi^{ii}}{|\mathbf{A}|^4} + \frac{3\phi^i}{|\mathbf{A}|^5} \right] \\ &+ 45(\mathbf{h} \cdot \mathbf{h})^2 (\mathbf{h} \cdot \mathbf{A})^2 \left[\frac{\phi^{iv}}{|\mathbf{A}|^4} - \frac{6\phi^{iii}}{|\mathbf{A}|^5} + \frac{15\phi^{ii}}{|\mathbf{A}|^6} - \frac{15\phi^i}{|\mathbf{A}|^7} \right] \\ &+ 15(\mathbf{h} \cdot \mathbf{h}) (\mathbf{h} \cdot \mathbf{A})^4 \left[\frac{\phi^v}{|\mathbf{A}|^5} - \frac{10\phi^{iv}}{|\mathbf{A}|^6} + \frac{45\phi^{iii}}{|\mathbf{A}|^7} - \frac{105\phi^{ii}}{|\mathbf{A}|^8} + \frac{105\phi^i}{|\mathbf{A}|^9} \right] \\ &+ (\mathbf{h} \cdot \mathbf{A})^6 \left[\frac{\phi^{vi}}{|\mathbf{A}|^6} - \frac{15\phi^v}{|\mathbf{A}|^7} + \frac{105\phi^{iv}}{|\mathbf{A}|^8} - \frac{420\phi^{iii}}{|\mathbf{A}|^9} + \frac{945\phi^{ii}}{|\mathbf{A}|^{10}} - \frac{945\phi^i}{|\mathbf{A}|^{11}} \right]. \end{aligned}$$

It remains to evaluate such quantities as $(\mathbf{h} \cdot \mathbf{h})^n (\mathbf{h} \cdot \mathbf{A})^m$. As typical examples showing how this was achieved, consider $(\mathbf{h} \cdot \mathbf{A})^2$ and $(\mathbf{h} \cdot \mathbf{h})(\mathbf{h} \cdot \mathbf{A})^2$.

$$(\mathbf{h} \cdot \mathbf{A})^2 = d^2(n_1^2 x^2 + n_2^2 y^2 + n_3^2 z^2) + 2d^2(n_1 n_2 xy + n_2 n_3 yz + n_3 n_1 zx).$$

Since the summations involved are made over all lattice points which run over all integral values from $-\infty$ to $+\infty$ all terms involving odd powers of (n_1, n_2, n_3) vanish. (Consequently all odd-order terms of W in (I.2) also vanish.) Further since the (n_1, n_2, n_3) are interchangeable, in highly symmetric lattices terms such as $d^2(n_1^2 x^2 + n_2^2 y^2 + n_3^2 z^2)$ may be written as

$$\frac{1}{3} d^2 (n_1^2 + n_2^2 + n_3^2) (x^2 + y^2 + z^2),$$

which equals $\frac{1}{3} |\mathbf{A}|^2 (x^2 + y^2 + z^2)$. Now consider $(\mathbf{h} \cdot \mathbf{h})(\mathbf{h} \cdot \mathbf{A})^2$. This is equal to

$$(x^2 + y^2 + z^2) \frac{1}{3} |\mathbf{A}|^2 (x^2 + y^2 + z^2) = \frac{1}{3} |\mathbf{A}|^2 (x^4 + y^4 + z^4 + 2x^2 y^2 + 2y^2 z^2 + 2z^2 x^2).$$

The cross product terms are difficult to treat satisfactorily and $x^2 y^2 + y^2 z^2 + z^2 x^2$ is replaced by $\frac{1}{3} (x^4 + y^4 + z^4)$. That this is a reasonable approximation may be seen from the following considerations. First the two quantities have the same symmetry properties. Secondly both have the same value when integrated over a sphere. Thirdly only the lowest eigenvalue is required, and a first-order perturbation treatment using the cross-product terms yields the same value for the lowest eigenvalue as using the approximation to the cross-product terms.

Other quantities such as $(\mathbf{h} \cdot \mathbf{A})^6$ may be treated similarly. Thus

$$x^4 y^2 + y^4 z^2 + z^4 x^2 \text{ becomes } \frac{1}{5} (x^6 + y^6 + z^6),$$

and $x^2 y^2 z^2$ reduces to $(x^6 + y^6 + z^6)/45$. On making all these substitutions (I.2) finally becomes the result (2.1) given in the text.

APPENDIX II

The Schrödinger equation with a potential W given by (2.1) is immediately separable into three equations of the same form. In reduced notation this form of the equation reads

$$\left(-\frac{\partial^2}{\partial x^2} + \alpha^2 x^2 + \beta^2 x^4 + \gamma^2 x^6 \right) \Psi = \lambda \Psi \quad \dots\dots (II.1)$$

where

$$\begin{aligned}\alpha^2 &= \frac{8\pi^2 W_2^*}{\Lambda^{*2}}, & W_2^* &= \frac{2^{2/3} R}{V^{*14/3}} \\ \beta^2 &= \frac{8\pi^2 W_4^*}{\Lambda^{*2}}, & W_4^* &= \frac{2^{1/3} 35 S}{3 V^{*16/3}} \\ \gamma^2 &= \frac{8\pi^2 W_6^*}{\Lambda^{*2}}, & W_6^* &= \frac{140 T}{3 V^{*6}} \\ \lambda &= \frac{8\pi^2 E^*}{\Lambda^{*2}}.\end{aligned}$$

Coulson and McWeeny (1948) have indicated how the eigenvalues of (II.1) may be found. Ψ is expanded in terms of an infinite set of harmonic oscillator functions of arbitrary argument.

Let

$$\Psi = \sum_i a_i X_i \quad \dots\dots (II.2)$$

where

$$X_i = N_i H_i \exp(-\frac{1}{2}\alpha_0 x^2),$$

H_i are the hermite polynomials, N_i being normalizing constants. α_0 is quite arbitrary. Substituting (II.2) into (II.1) recurrence relations between x^n and the H_i are applied. On multiplying through by a conjugate set of functions $\Sigma_r a_r X_r$ and integrating over all space, a recurrence relation between the coefficients a_r is found. This relation is

$$\begin{aligned}a_{r+6} D \left[\frac{(r+6)!}{r!} \right]^{1/2} + a_{r+4} [C + 3D(2r+5)] \left[\frac{(r+4)!}{r!} \right]^{1/2} \\ + a_{r+2} [B + 2C(2r+3) + 15D(r^2 + 3r + 3)] \left[\frac{(r+2)!}{r!} \right]^{1/2} \\ + a_r [(A+B)(2r+1) + 3C(2r^2 + 2r + 1) + 5D(4r^3 + 6r^2 + 8r + 3) - \lambda] \\ + a_{r-2} [B + 2C(2r-1) + 15D(r^2 - r + 1)] \left[\frac{r!}{(r-2)!} \right]^{1/2} \\ - a_{r-4} [C + 3D(2r-3)] \left[\frac{r!}{(r-4)!} \right]^{1/2} + a_{r-6} D \left[\frac{r!}{(r-6)!} \right]^{1/2} = 0 \\ \dots\dots (II.3)\end{aligned}$$

where

$$A = \alpha_0, \quad B = \frac{\alpha^2 - \alpha_0^2}{2\alpha_0}, \quad C = \frac{\beta^2}{4\alpha_0^2}, \quad D = \frac{\gamma^2}{8\alpha_0^3}.$$

For consistency the infinite determinant formed by the above recurrence relations must vanish. The eigenvalues of this determinant are the energy eigenvalues. It will be observed that two infinite determinants may be formed, one for even and one for odd eigenvalues. This is always the case for a symmetric potential function. Further, if β^2 and γ^2 vanish the determinants become diagonal giving the eigenvalues of a harmonic oscillator. As it is, most of the off-diagonal terms are zero. Since only the lowest eigenvalue was required, only the even order determinant was considered. To evaluate λ_0^* a value must be given to the arbitrary parameter α_0 ; α_0 was chosen to minimize the diagonal term of the determinant which contains α_0 . This ensures the rapid

convergence of the approximations to λ_0^* resulting from the solutions of the determinants of 1, 2, n , rows and columns. In this case α_0 is the smallest positive root of the quartic

$$\alpha_0^4 - \alpha^2 \alpha_0^2 - 3\beta^2 \alpha_0 - \frac{45\gamma^2}{4} = 0. \quad \dots\dots (II.4)$$

In practice the required degree of accuracy for λ_0^* was obtained by solving the determinant of order seven. The necessary computations were carried out on the University of London digital computer.

REFERENCES

- BERNARDES, N., 1958, *Phys. Rev.*, **112**, 1534.
 COULSON, C. A., and McWEENY, R., 1948, *Proc. Camb. Phil. Soc.*, **44**, 413.
 DE BOER, J., 1948, *Physica*, **14**, 139.
 DE BOER, J., and BLAISSE, B. S., 1948, *Physica*, **14**, 149.
 DOMB, C., 1952, *Changement de Phases* (Paris: Société de Chimie Physique), p. 338.
 DUGDALE, J. S., and DOMB, C., 1957, *Progress in Low Temperature Physics*, **2**, 338.
 DUGDALE, J. S., and MACDONALD, D. K. C., 1954, *Phil. Mag.*, **45**, 811.
 FISHER, M. E., and ZUCKER, I. J., 1961, *Proc. Camb. Phil. Soc.*, **57**, 107.
 HENKEL, J. H., 1955, *J. Chem. Phys.*, **23**, 681.
 JOHNS, T. F., 1958, *Phil. Mag.* (8), **3**, 229.
 LENNARD-JONES, J. E., and DEVONSHIRE, A. F., 1939, *Proc. Roy. Soc. A*, **169**, 317, **170**, 464.
 LENNARD-JONES, J. E., and INGHAM, A. E., 1925, *Proc. Roy. Soc. A*, **107**, 636.
 SALTER, L., 1954, *Phil. Mag.*, **45**, 360.
 ZUCKER, I. J., 1956, *J. Chem. Phys.*, **25**, 915.
 ———, 1958, *Phil. Mag.* (8), **3**, 987.

A Scanning Instrument for the Measurement of Optical Frequency Response†

By K. G. BIRCH

Department of Physics, Imperial College, London

MS. received 9th September 1960

Abstract. The instrument described measures alternatively the distribution of intensity in the image of a narrow slit (the spread function), or the frequency response function, which latter is the Fourier transform of the spread function. For the former use a slow scan with an exploring slit is used while for the direct determination of the frequency response curve a continuous scanning with a grating of slits arranged around the periphery of a variable speed drum is employed with a single frequency electrical detector.

The in-focus aberration-free image of a line source has been measured together with the axial variation of central intensity and good agreement with the theoretical curves has been obtained. The frequency response curves obtained by taking the Fourier transforms of four out-of-focus spread functions numerically agree well with the direct determinations of the frequency response with the scanning drum. Further the frequency response curves for a well corrected lens in different focal planes have been compared with results obtained by Hopkins theoretically.

§ 1. INTRODUCTION

THE frequency response function of an optical system is the inverse Fourier transform of the image of an incoherently illuminated line source, the latter being the so-called line spread function. The instrument to be described here is designed to measure independently both the frequency response and the spread function, and eliminate any need to evaluate one from the other by numerical harmonic analysis. An independent knowledge of both functions is desirable both as a means of confirming theoretical results and for the accumulation of practical information on image quality. A comparison of the frequency response function obtained as the numerical Fourier transform of the measured line spread function with that measured directly affords a useful initial test of the complete apparatus. Comparison of the measured frequency response function of a lens having a known wave front aberration with that predicted theoretically affords both a test of the theory of these calculations and also a further check on the operation of the apparatus.

§ 2. DESCRIPTION OF THE APPARATUS

In the apparatus to be described a lens under test is arranged in conjunction with a collimator to produce an enlarged image of the entrance slit, that is the line spread function. A slow scan of the spread function with a slit aperture serves to measure the line spread function itself, whilst a variable velocity scanning drum

† The contents of this paper form part of the subject matter of a thesis which has been approved by the University of London for the award of the Ph.D. degree.

carrying a series of equally spaced narrow scanning slits is used to determine the frequency response. The apparatus consists therefore of a basic unit to form the spread function image and two separate scanning units.

2.1. Illuminating System and Object Slit

To form the line spread function the object presented to the test lens must be a narrow incoherently illuminated slit source, which behaves like a self-luminous line source. The width of this slit must not exceed about one quarter of the resolution limit of the test lens. For an F/5 aperture system this would require a slit source of width equal to half a micron. To avoid the need for an adjustable slit reducing to this width it is convenient to form a reduced image of a normal spectrometer slit with a microscope objective as illustrated in Fig. 1. The slit is illuminated with either a mercury arc or a tungsten Pointolite lamp as source, the mercury source to provide the monochromatic light necessary in the confirmation of theoretical studies and the white light source for the testing of lenses in conditions similar to those obtaining in practice. The light sources are operated from a Westat constant potential power unit which supplies an operating output of 1.6 A at a voltage of $200 \pm 0.4\text{ v}$. To ensure uniform illumination despite movements of the mercury arc the sources are imaged on to the object slit using Köhler illumination.

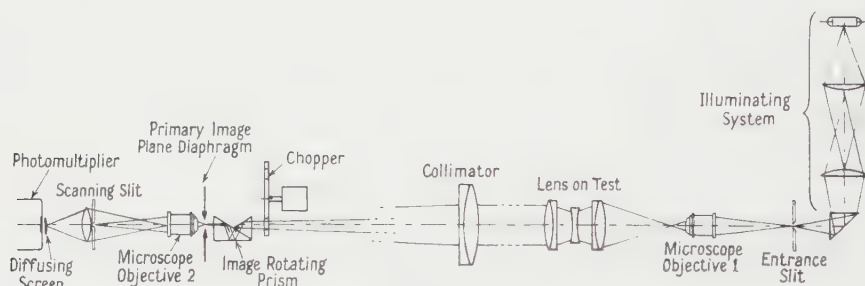


Fig. 1. Basic optical system.

When the test lens is in an off axis position and it is to be tested in any given azimuth it is necessary to bring the line source parallel to this azimuth. To achieve this the entrance slit is rotatable in its mount besides having conventional linear adjustments in three perpendicular directions. The housing of the light source is also rotatable to bring the length of the mercury arc parallel to the length of the slit.

2.2. Test Lens Mounting and Collimator

The microscope objective imaging the entrance slit is focused on a register plate mounted on a nodal slide and the test lens is positioned to have its principal focus in this plane. The nodal slide, which is of the conventional T-bar construction, may accommodate lenses of 25 cm to 150 cm focal length and examine their performance up to a maximum angular field of $\pm 30^\circ$. Axial movement of the test lens on the nodal slide is indicated by means of a pointer and a millimetre scale attached to the slide base. A dial gauge attached to the lens mount and impinging on an adjustable stop attached to a stationary portion of the nodal slide allows sub-division of this scale to 0.01 mm, which is the accuracy with which the lens, and hence change of focal plane, can be positioned.

The collimated beam leaving the test lens (Fig. 1) is brought to a focus by a highly corrected collimator objective which is of 8-inch diameter and 115 inches in focal length. The collimator is mounted on the end of the nodal slide base to avoid the large shifts of the image of the entrance slit which would arise from relative movement between it and the test lens.

2.3. *The Primary Image Plane, Chopper and the Image Rotating Prism*

The focal plane of the collimator is the primary image plane containing the spread function required. The position of this plane is indicated by a diaphragm which is set in position axially by auto-collimation and is centred on the optical axis during the initial lining up of the apparatus when the diaphragm acts as one of a number of pin-holes defining the optical axis.

The image rotating prism placed before the diaphragm (Fig. 1) is used to bring the direction of variation of intensity in the spread function perpendicular to the slit of the scanning system. This is needed when the entrance slit is rotated for testing a lens in differing azimuths. The type of image rotating prism used has perpendicular incidence of the light at the two air-glass surfaces. This is to reduce the amount of aberration introduced by the prism. Under these conditions the principal aberration introduced is astigmatism and is less than one eighth of a wavelength.

The light beam may be chopped at a frequency of 1000 cycles per second by means of a disk with 40 apertures around its circumference, and which is driven by a $1500 \text{ rev min}^{-1}$ synchronous motor. This is used in the determination of the line spread function, an alternating current amplifier then being used to amplify the photomultiplier output. The position of the chopper in the optical system was chosen for ease of mounting in a position independent of the mounting of the basic optical system and also to obtain a beam diameter allowing a chopper of small size.

2.4. *Detector and Electronic Measuring Circuits*

The light passing through the scanning systems is collected directly on to the diffusing screen before the photomultiplier by a lens which images the exit pupil of the second microscope objective on to the diffusing screen. The scanning system acts as an aperture before this lens causing the patch of light on the diffusing screen to be stationary but varying in intensity. The diffusing screen ensures a uniform spread of light over the photocathode, so reducing the risk of fatigue of the photosensitive surface and other disturbing effects.

The photomultiplier, an E.M.I. type 6094B with an antimony-caesium photocathode and eleven dynodes is energized by a constant voltage high potential unit able to supply 2000 volts with less than 0.1% change for 10% input voltage variation. A potentiometer unit is used to adjust the total voltage applied to the photomultiplier resistance chain.

The current output of the photomultiplier is converted into a voltage signal and amplified in the first portion of a frequency selective amplifier (Figs 2 and 3). This amplifier also selects the frequency of interest and further amplifies it before splitting the output to feed an oscilloscope and a measuring circuit (Fig. 2). The measuring circuit is a standard Mullard 510 amplifier used to feed an Elliott a.c. measuring pen recorder.

The frequency selective amplifier, Fig. 3, has a cathode follower input to match its input impedance approximately with the output impedance of the

photomultiplier. This stage is followed by a voltage amplifier with negative feedback to ensure linearity of amplification. The output of this stage may be fed to auxiliary apparatus but is usually used to feed the tuned amplifier stages. The first of these is constructed on valves 3 and 4 in conjunction with network 1, shown in Fig. 3. The input signal to the stage as applied to the grid of valve 3 is amplified and the output applied to the cathode follower stage, valve 5. The feedback from the cathode of this stage is via the network which may be tuned to have maximum impedance at a particular frequency, in practice 1000 cycles per second. Signals at other frequencies pass through the network and cause incoming signals at these frequencies to have reduced gain through the stage. A further stage of tuned amplification is added on valves 6 and 7.

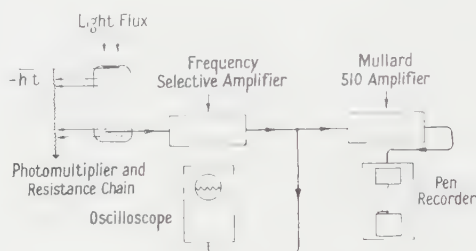


Fig. 2. Schematic circuit diagram.

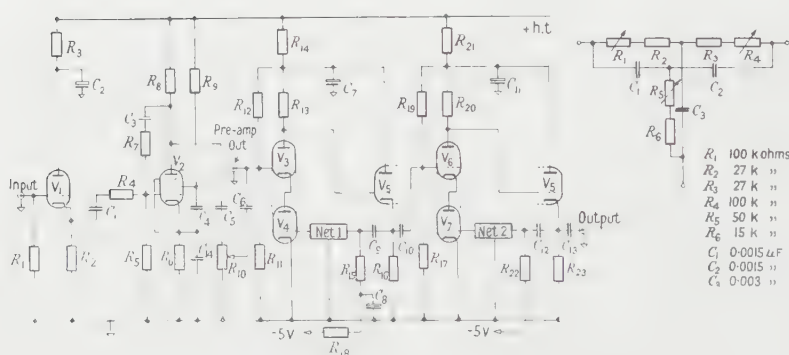


Fig. 3. Frequency selective amplifier and tuning network.

The h.t. supply to both frequency selective stages is decoupled by the pairs (R_{14} , C_7), (R_{21} , C_{11}), to prevent oscillations passing into these circuits from either the h.t. supply or other stages and for the same reason the negative biasing of network 1 is also decoupled. All the power supplies including the h.t., grid biasing and heater current are supplied from batteries or accumulators to ensure constancy of supply and freedom from mains hum and other oscillations.

A single-stage tuned amplifier passing negligible signal at 100 cycles per second to either side of 1000 cycles per second is difficult to design but two stages as described suitably tuned are sufficient to give the required characteristics to the amplifier. Further the two stages may be stagger-tuned to give a flatter topped frequency-gain characteristic with a quick cut-off, a condition that is better suited to the measurements to be made.

2.5. Measurement of the Line Spread Function

The line spread function from the test lens is formed in the focal plane of the collimator and a magnified image of this is formed on the scanning slit, which is suspended beneath a supporting table. This table, of cast aluminium alloy and machined flat to take the many attachments, is supported above the optical system which produces the spread function image. It rests on three steel legs of adjustable length which are themselves supported independently of the main apparatus. On the table a synchronous motor, operating through a reduction gear box, rotates a cam designed to give the cam follower slide a linear motion. This motion is transferred by a lever arm to the slit carrying slide which moves with a linear velocity of 0.204 mm per second. The mounting of the moving mechanical components on the supporting table prevents the passing of vibrations into the optical system forming the line spread function.

The light passing through the scanning slit is collected on to the photomultiplier whose output is recorded to indicate the variation of flux passing through the slit. If the length of the spread function is brought parallel to the length of the scanning slit and perpendicular to its motion the variation of the photomultiplier output with time will indicate the variation of intensity in the spread function with respect to an axis perpendicular to the length of the spread function.

2.6. Measurement of the Frequency Response

The enlarged image of the spread function is projected on to a scanning drum as illustrated in Fig. 4. This drum is also suspended from the supporting table, which is mounted above the main apparatus. Twenty-four narrow slits of equal width are evenly spaced around the drum, and the flux passing through the slits is collected on the photomultiplier in the same manner as before. The output of the photomultiplier when the scanning drum is rotated consists of a regular series of current pulses in which each pulse has a time varying amplitude corresponding to the distribution of intensity in the line spread function. The frequency response is given by the inverse Fourier transform of any one of the pulses, and the Fourier transform of the sequence of pulses will be zero except at frequencies corresponding to the fundamental and harmonics of the frequency of repetition, at which frequencies the Fourier transform of the sequence will have values directly proportional to that of a single pulse. Hence the frequency response may be measured at these discretely spaced frequencies. This is easily understood if the spread function scanned is considered in terms of its Fourier spectrum and the scanning drum is considered as an infinite screen having a series of slits

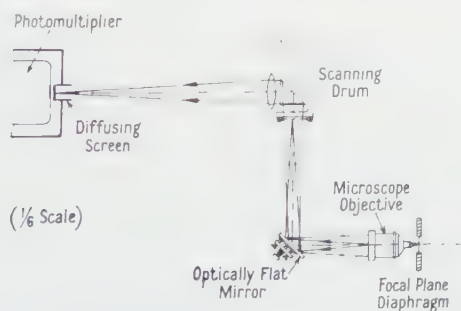


Fig. 4. Scanning system for the determination of optical frequency response.

spaced at a period p and moving at uniform velocity over the spread function. As these slits scan across the infinite series of sine waves constituting the spectrum of the spread function, a detector placed to accept light from all of them will only produce a constant signal as the scanning screen moves across, unless there are present sine-wave components of period $p, p/2, p/3, \dots, p/n$. For other frequencies the photomultiplier signals associated with light passing through the individual slits will vary in phase and the total amplitude from the detector will thus be constant with no alternating current component.

In practice the amplitudes of the accepted fundamental and harmonic components are measured separately by varying the velocity of the scanning drum, thereby causing each of the spatial frequencies to correspond in turn with a fixed electrical frequency which is that to which the amplifier is tuned. The speed of rotation of the drum is varied from a high speed at which the spatial frequency $1/p$ gives rise to an electrical frequency of 1000 cycles per second; reducing the speed then brings the spatial frequencies $2/p, 3/p, \dots, n/p$ to the same condition. As each spatial frequency component is in this manner brought into resonance the a.c. signal shown on the cathode-ray oscilloscope (see Fig. 2) will in each case rise to a maximum. This is used merely as a coarse adjustment of the speed of rotation of the scanning drum; for fine control the trace on the pen recorder chart is maximized by making further small changes in the speed of rotation. When the signal has been maximized it is recorded for a few seconds to form a level trace on the pen recorder chart and the mean value of the trace measured. The amplitudes of the traces corresponding to $p, p/2, p/3, \dots$, are normalized and replotted at equally spaced values on the abscissa to give the frequency response. The scale of spatial frequency at which the normalized amplitudes are recorded may be evaluated from the dimensions of the scanning drum and the magnification through the optical system from the object plane of the test lens to the scanning drum. If the slits of the scanning drum are spaced at 15 mm intervals and the magnification through the system is 30 times the spatial frequency $1/p$ is equivalent to 2 lines/mm in the object plane of the test lens. The harmonics $2/p, 3/p, 4/p, \dots$ are equivalent to 4, 6, 8 \dots lines/mm and the spatial frequency scale may be extended to the 50th harmonic, 100 lines/mm. Alternatively the power of the second microscope objective may be increased to change the magnification through the system and the first ten harmonics used to cover the spatial frequency range 4–40 lines/mm.

2.7. *Anti-vibration Mounting*

The complete optical system, including the Ross nodal slide, the collimating lens and the auxiliary systems performing the scanning operations, has a total length exceeding seventeen feet. This system requires to be mounted on a suitably rigid base which must be isolated from vibrations present in the building in which it is housed. To this end a basic frame of six-inch I-section rolled steel joists was constructed from two eighteen-foot long girders strapped together in five positions by separating pieces of length two feet six inches. This frame was supported at its two ends by double sandwiches of foam rubber and half-inch block board. This mounting has proved successful in eliminating unwanted vibrations from the optical system.

§ 3. THEORY OF RESPONSE MEASUREMENTS

The properties of a moving scanning screen may be specified by means of its transparency at time $t=0$ given as a function of u' , a length coordinate fixed in

space along the length of the screen. If this transparency function is denoted by $Z(u')$ and the screen moves with a constant velocity γ , the transparency will be given by $Z(u' - \gamma t)$ at any other time t . If a spread function, with intensity distribution $G(u')$, is scanned by the moving screen the total flux through the screen at time t will be given by

$$F(t) = \int_{-\infty}^{+\infty} G(u') Z(u' - \gamma t) du'.$$

For an infinite periodic scanning screen the transparency may be represented by a Fourier series of the form

$$Z(u') = \sum_{n=-\infty}^{+\infty} z_n \exp[-i(2\pi n/p)u']$$

in terms of which the total flux passing through the screen is

$$\begin{aligned} F(t) &= \sum_{n=-\infty}^{+\infty} z_n \int_{-\infty}^{+\infty} G(u') \exp[-i(2\pi n/p)(u' - \gamma t)] du' \\ &= \sum_{n=-\infty}^{+\infty} z_n \exp[i(2\pi n/p)\gamma t] \int_{-\infty}^{+\infty} G(u') \exp[-i(2\pi n/p)u'] du'. \end{aligned}$$

The integral here defines the inverse Fourier transform $g(n/p)$ of the spread function so that

$$F(t) = \sum_{n=-\infty}^{+\infty} z_n g(n/p) \exp[i2\pi(n\gamma/p)t].$$

This expression indicates that the time-varying flux passing through the slits of the scanning drum may be represented by a Fourier series in time, having complex coefficients $z_n g(n/p)$ where n takes on the value zero and all integral values. If the scanning screen has a transparency that is repeated with period p , $s_1 = 1/p$ is the spatial frequency corresponding to the fundamental period of the scanning screen transparency and $s_n = n/p$ is the spatial frequency corresponding to the $(n-1)$ th harmonic. The above time-varying light flux is converted to a time-varying electrical signal by the photomultiplier, which is used in conjunction with the frequency selective amplifier to select the electrical frequency $\nu = n\gamma/p = \gamma s_n$, when the speed of rotation γ is given a suitable value. The output of the system is then proportional to $g(n/p)z_n = g(s_n)z_n$ and so measures the product of the value of the Fourier transform of the spread function and z_n , the appropriate coefficient of the transfer admittance of the scanning screen.

If the scanning screen consists of a series of slits, separated by a period p and each width kp , where $k < 1$, the coefficients of the transfer admittance are given by

$$z_n = (1/p) \int_{-kp/2}^{+kp/2} \exp[i(2\pi n/p)u'] du' = (1/p) [(p/n\pi) \sin n\pi k]$$

or omitting the constant factor k

$$z_n = (\sin n\pi k)/n\pi k.$$

With scanning slits of width 0.1 mm, and a spacing of 15 mm, the value of k is $1/150$. The coefficient of the ninth harmonic, for example, is then equal to $(\sin \pi/15)/(\pi/15) = 0.993$. The coefficients z_n may thus be assumed to be equal to unity since the correction factor to be applied to the measured value of $g(s_n)$, for all spatial frequencies less than or equal to $10/p$, would be less than 1%. The correction factor is however sensitive to variation in k which depends on the slit

widths. These may be effectively increased by misalignment of the spread function relative to the scanning slits; a misalignment of the spread function by only 2° will reduce the amplitude of the ninth harmonic to 87% of the correct value. It is therefore clear that the spread function and the scanning slits must be aligned to within $30'$.

The influence on the measured frequency response of the finite width of the entrance slit must be considered. The above treatment has assumed this width to be infinitely small in which case all spatial frequencies would be present in its transform with equal amplitude. Because of the finite slit width the higher spatial frequencies have smaller amplitudes. The spatial frequency spectrum of a slit of width u has the form $(\sin \pi su)/\pi su$ where s is the reduced spatial frequency defined by $s = (\lambda/n \sin \alpha) R$ where R is measured in lines/mm, λ is the wavelength and $n \sin \alpha$ the numerical aperture. The width u is then measured in a reduced unit of length defined by $(\lambda/n \sin \alpha)$. This latter choice makes the conventional resolution limit of the lens equal to 0.61 units. A quarter of the resolution limit is thus equal to 0.15 and for a spatial frequency of $s = 1$ the amplitude of this spatial frequency in the spectrum of the object slit is $(\sin 0.15\pi)/0.15\pi = 0.97$ of that for an infinitely narrow slit. Even for a perfect lens the frequency response will have reduced to less than 0.40 when $s = 1$ so that the finite width of this slit leads to a maximum error of 0.015, the response for zero spatial frequency being normalized to unity.

Writing $z(n)$ and $g(n/p)$ in terms of their respective moduli and arguments, namely

$$z_n = \frac{1}{2}\alpha_n \exp i\phi_n; \quad g(n/p) = T(n/p) \exp i\theta(n/p)$$

and noting that both z_n and $g(n/p)$ are amplitudes of the Fourier spectra of two essentially non-negative real functions the flux passing through the scanning screen at the frequency $\nu = n\gamma/p$ may be expressed in the form

$$F(t) = \sum_{n=0}^{\infty} |z_n| T(n/p) \cos \{2\pi(n\gamma/p)t + \phi_n + \theta(n/p)\}.$$

Again because $Z(u')$ and $G(u')$ are both non-negative and real $\phi_0 = \theta(0) = 0$, so that this may be normalized to make $F(t) = 1$ when $s_n = n\gamma/p$ is zero giving

$$F(t) = \sum_{n=0}^{\infty} \frac{|z_n|}{|z_0|} T(s_n) \cos \{2\pi\gamma s_n t + \phi_n + \theta(s_n)\}.$$

The output of the photomultiplier at the frequency s_n is thus a pure cosine term of amplitude $T(s_n)$ modulated by the transfer admittance of the scanning screen at that spatial frequency, $T(s_n)$ is the modulus of the frequency response and the factor $\theta(s_n)$, which causes a lateral shift of the cosine signal from the zero of the scanning screen transparency, is the argument of the frequency response. The effect of the transfer admittance of the scanning screen has been shown above to be negligible for this apparatus.

§ 4. MEASUREMENTS AND RESULTS

To confirm the correct operation of the apparatus it is sufficient to show that it is accurately measuring the spread function and the frequency response function in a known case, and to show that the latter is correctly the Fourier transform of the former. The spread function scanning mechanism was therefore used to confirm the only known theoretical results, namely the variation of intensity in the true focal plane and along the optical axis for an aberration free system. The variation of

intensity across the focused image of an incoherent line source formed by a perfect lens having a circular aperture has been calculated, among others, by Rayleigh (1888). Later Selwyn (1943) provided additional numerical values, and an alternative derivation using Fourier analysis has been given by Steel (1952) together with the calculation of the variation of intensity along the optical axis, that is, with defocusing.

The test lens used throughout in obtaining the results given below was an achromatic doublet of 50 cm focal length. This was mounted such that plates containing measured circular apertures could be used in order to change the numerical aperture. The spread functions shown in Fig. 5 were obtained by defocusing the test lens in equal steps, working with a numerical aperture of 0.01, corresponding to $F/50$ relative aperture, and the entrance slit being illuminated by mercury green light ($\lambda = 5461 \text{ \AA}$). Then a defocusing of 1.098 cm corresponds to one wavelength of optical path difference between marginal and axial rays.

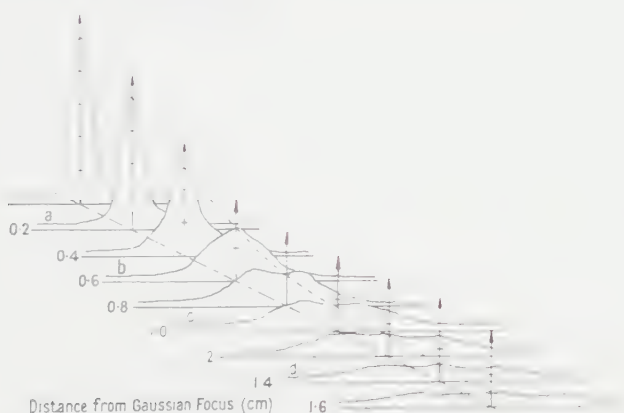


Fig. 5. Variation of the line spread function with defocusing.

The gain of the electronic system was first kept constant for all these readings and also for measuring the intensity variation along the optical axis. This latter, shown in Fig. 5 as a dotted line, was plotted separately (Fig. 6, curve *a*) to confirm the theoretical result. The spread function with the maximum value of central intensity corresponds closely to the theoretical curve for the Gaussian focal plane, and the variation of intensity in this spread function was accurately measured. The curve shown (Fig. 6, curve *b*) is the mean of four recorded

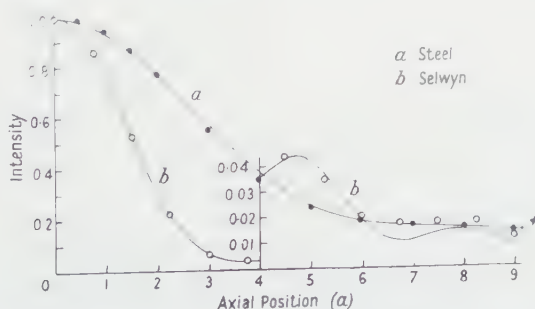


Fig. 6. Comparison with theoretical curves of the variations of intensity in the image of a line source in the two principle axes.

traces, in measuring which further gain of the detector was obtained by increasing the voltage applied to the photomultiplier resistance chain for the region where the intensity falls below 4% of the maximum value. The change of gain may be calibrated against photomultiplier voltage and the recorded traces corrected accordingly. The comparison of the measured intensity variation in the focused spread function with the theoretical curve shown in Fig. 6 (curve *b*) shows errors of less than 0.01 up to the second subsidiary maximum. This is good evidence of satisfactory linearity and accuracy of the electronic recording system and shows the test lens to be satisfactorily corrected. The agreement for the axial variation of intensity with defocusing with errors nowhere in excess of 0.03 confirms this.

To test the operation of the scanning drum in measuring the frequency response directly the spread functions for four different planes of focus, curves *a*, *b*, *c* and *d* of Fig. 5, were accurately measured and the Fourier transforms of these calculated using a simple procedure based on Whittaker's interpolation theorem. The test lens was then reset in each of the focal planes and the frequency response function determined directly using the scanning drum. Comparison of these two sets of results, shown in Fig. 7, confirms that the apparatus is working correctly and with good accuracy. In particular the scanning drum measures reliably the Fourier transform of the spread function.

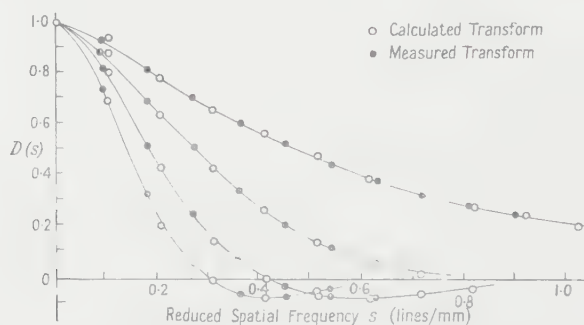


Fig. 7. Comparison of measured and calculated response curves.

It will be seen in Fig. 7 that on each curve the first calculated value of the Fourier transform of the spread function is always slightly greater than the measured Fourier transform even when the remaining values fit satisfactorily. This is also seen in Fig. 8, where the calculated Fourier transform of the aberration free spread function, curve *b* of Fig. 6, is compared with the known theoretical frequency response of a perfectly corrected system. It is theoretically impossible

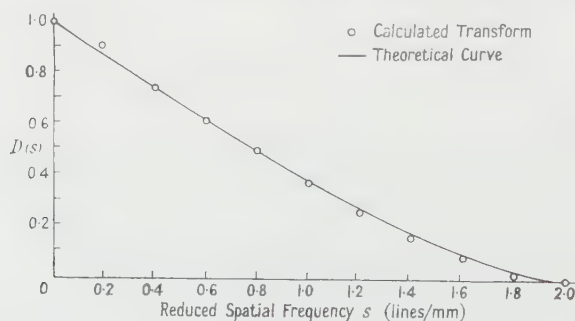


Fig. 8. Response curve of an aberration free lens.

for an optical system to have a response greater than that of a perfectly corrected system and this suggests that the calculated point lying above the theoretical curve must include a systematic error inherent in the method of calculation. This is easily understood in general terms, since the spread function is assumed to be zero beyond a given point. This implies in fact an approximation in the spread function for larger values of the variable, which would lead to errors in the transform for small values of the variable.

A further, and important, test of the correct operation of the scanning drum is available from a comparison of the measured frequency response for a lens having specified amounts of wave front aberration with that derived theoretically (Hopkins 1953). Such results are available for defect of focus with an unaberrated system. To study the frequency response for this case the test lens is first accurately focused and then defocused by specific amounts. The frequency response is measured for each of these focal settings and the results compared with the theoretical curve. The defocusing coefficient W_{20} measures the path difference introduced between the marginal and axial rays. Results obtained are shown in Fig. 9, where W_{20} is increased in steps of $1/\pi$ wavelengths. The curve $n=3$ thus corresponds approximately to the introduction of one wavelength of wave front aberration and shows the characteristically quick decrease in the response from that of a perfectly focused lens, $n=0$. The slight lack of agreement between the practical and theoretical curves for $n=0, 1$ and 2 corresponds to a difference in focal setting of less than $\lambda/10$, the effect of which would be observable in its effects on the response of a nearly perfectly focused lens but which would have negligible effect for large focusing errors. The small discrepancies shown in Fig. 9 may be interpreted to mean that the true focal plane can be set with a higher accuracy using measurement of frequency response than by other means. Having regard to this fact the agreement between the measured and calculated frequency response is satisfactory confirmation of the accuracy of the apparatus.

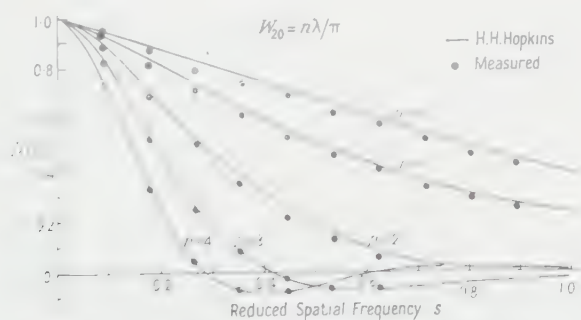


Fig. 9. Response curves for a defocused lens.

To check the reproducibility of results two sets of measurements for identical settings of the same test lens were taken over a period of two weeks, the second set being measured after the apparatus had been dismantled for cleaning and then re-assembled. The agreement of the two sets of results, shown in Fig. 10, is within the experimental error for the greater majority of the readings and is always within ± 0.03 .

To facilitate comparison with theory all of the above results were measured for monochromatic light, but the apparatus is equally suitable for use with white light sources. In appropriate cases filters may be necessary to match the spectral

composition of the illuminant and the spectral response of the detector to that of the detector intended to be used with the lens under test.

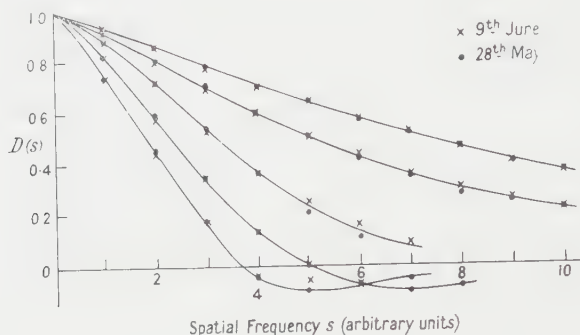


Fig. 10. Consistency of results.

§ 5. CONCLUSIONS

The instrument has proved capable of measuring both the spread function and the frequency response to an accuracy to better than ± 0.02 . The numerical apertures of the test lens, lying between F 70 and F 25, and the intensity of the light sources used in the above confirmation of theoretical results were much smaller than those which would normally be used in the routine testing of photographic lenses, and even so the detector was not used at maximum sensitivity or gain. The instrument may thus be expected to measure to at least this accuracy under more favourable conditions; for example, when examining test lenses with apertures of the order of F/16 and greater in white light. Increasing the aperture of the test lens by a factor k increases the light flux by a factor k^2 . There is however a need to decrease the entrance slit width by $1/k$ but there still remains an increase in light flux by the factor k . Of equal importance is the fact that the instrument is simple to operate and remains stable in its alignment over long periods of time.

The apparatus in its present form has some inherent limitations. The most serious of these is that the value of the response at zero frequency, $s=0$, which is required for normalization is not directly measured. This is of no great consequence when a comparison is to be made with theoretical relations as the measured response may be normalized at a finite value of s , but in the practical testing of lenses, when the expected response is not known, the absence of a simple and reliable normalization could prove to be a more serious shortcoming. Again the frequency response is measured only at a discretely spaced set of spatial frequencies and for this reason automatic recording of the response with decreasing scanning speed, that is, with detection of a changing spatial frequency, may suffer from overshooting of the pen recorder on passing through the successive resonances.

ACKNOWLEDGMENTS

I wish to thank Dr. H. H. Hopkins for suggesting this problem and for the many discussions and helpful criticisms relating thereto.

REFERENCES

- HOPKINS, H. H., 1953, *Proc. Roy. Soc. A*, **217**, 408.
- RAYLEIGH, LORD, 1888, *Encyclopedia Britannica*, 9th Edition, Wave theory, Section 12.
- SELWYN, E. W. H., 1943, *Proc. Phys. Soc.*, **55**, 286.
- STEEL, W. H., 1952, *Rev. Opt. (théor. instrum.)*, **31**, 334.

Ferromagnetic Resonance in Nickel-Copper Alloys

By D. M. S. BAGGULEY AND M. HEATH

The Clarendon Laboratory, Oxford

MS. received 25th October 1960

Abstract. Ferromagnetic resonance absorption has been measured in a series of nickel-copper alloys having compositions Ni 50% Cu 50%, Ni 45% Cu 55%, Ni 42% Cu 58% by weight. The temperature range over which measurements were made included the individual Curie points of the alloys. The experiments were carried out at 3.19 cm and 8.8 mm wavelength. Absorption lines were observed in both the ferromagnetic and paramagnetic phases, and the line-width was found to be a maximum at the Curie point. It was also frequency dependent, being roughly twice as great at 8.8 mm as compared with 3.19 cm. The g -factor had the value 2.22 ± 0.02 for the ferromagnetic phase of each alloy.

FERROMAGNETIC resonance absorption has been investigated in a series of nickel-copper alloys throughout a temperature range sufficient to include their individual Curie points. The alloy compositions were: Ni 50% Cu 50%, Ni 45% Cu 55%, Ni 42% Cu 58% by weight. The corresponding Curie temperatures were 100°K, 40°K and 25°K. Quantitative data on the line-widths and the spectroscopic splitting factor g have been obtained both in the ferromagnetic and the paramagnetic phases. These experiments provide the first extensive set of measurements of resonance absorption above the Curie point of a ferromagnetic metal.

The experiments described in this paper have been carried out at 3.19 cm and 8.8 mm wavelength using conventional microwave spectrometers with magnetic field modulation. Plane disk-shaped samples having approximate dimensions 5 mm diameter by 0.1 mm thickness were etched, and annealed in helium gas at 850°C for three hours. Each sample was then mounted freely in a small envelope of 'Melinex' plastic thus avoiding any strain. The envelope was fixed lightly to the wall of the cavity resonator using vacuum grease. Typical records of the differential absorption line obtained for the Cu 55% alloy are given in Fig. 1. Here Fig. 1(a) refers to a temperature well below the Curie temperature T_c , and the curve in Fig. 1(b) was obtained well above the Curie point at about $2T_c$. The steady magnetic field could be applied either parallel or perpendicular to the plane of the sample, and so provided two values for the line-width and two resonance conditions from which the g -factor could in principle be calculated without any additional measurement of the magnetization of the sample.

The temperature dependence of the line-width for the Cu 50% and Cu 58% alloys is given in Fig. 2. A similar temperature dependence is obtained for the Cu 55% alloy. The line-width passes through a maximum at the Curie



Fig. 1. Differential absorption lines for the Ni 45% Cu 55% alloy taken at 8.8 mm wavelength; (a) refers to a temperature well below the Curie point (about $\frac{1}{4}T_c$), (b) refers to a temperature well above the Curie point (about $2T_c$).

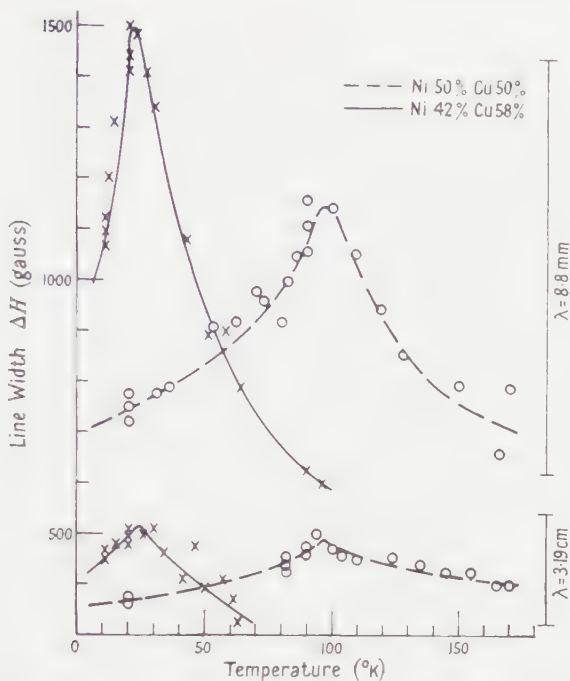


Fig. 2. The temperature dependence of the line-width for two nickel-copper alloys.

point. It has the same magnitude for both the parallel and perpendicular geometries (with an accuracy to 15%) but is frequency dependent, the width at 8.8 mm wavelength being roughly two to three times that observed at 3.19 cm wavelength.

The zero point on the differential absorption curve locates the magnetic field at resonance H_0 . From this field value the spectroscopic splitting factor g may be derived using the electromagnetic theory of Young and Uehling (1954), with the approximation that the imaginary part of the high frequency permeability for these dilute alloys is small at resonance ($\mu_{hf} = \mu_1 - j\mu_2$ and $\mu_2 \ll \mu_1 \sim 1$). The resonance conditions for the parallel and perpendicular geometries are then

$$\frac{h\nu}{g\beta} = [H_0(H_0 + 4\pi M)]^{1/2} - \frac{1}{2}(\Delta H) \quad \dots\dots (1)$$

$$\frac{h\nu}{g\beta} = H_0 - 4\pi M - \frac{1}{2}(\Delta H). \quad \dots\dots (2)$$

Here M is the magnetization of the sample, ΔH is one half the width in gauss between the maximum and minimum values of the differential absorption curve, and anisotropy terms are assumed to be negligible. The term ΔH which gives rise to a shift in the position of the resonance line occurs because the power loss in the sample is a function of both the real and the imaginary parts of the high frequency permeability. It does not imply the use of any specific mechanism for producing the line-width and should not arise in the case of spherical particles, the dimensions of which are small compared with the skin depth (Bagguley and Harrick 1954). This type of shift has been recognized previously for the cases of spin resonance from conduction electrons (Feher and Kip 1955, Dyson 1955) and for manganese in copper (Owen, Browne, Arp and Kip 1957).

The absorption line shape should be asymmetric when these conditions apply and this is well established for our results at temperatures below the Curie point. Above the Curie point, where the absorption line is much weaker in intensity, the asymmetry is present at 3.19 cm wavelength but is not well established at 8.8 mm wavelength.

The g -factor calculated from Eqns (1) and (2) has the value 2.22 ± 0.02 for the ferromagnetic phase of each alloy. As the temperature increases through the Curie point the g -factor slowly decreases to reach a value of 2.12 ± 0.04 when the temperature is about $2T_C$. If, on the other hand, the g -factor is obtained by solving Eqns (1) and (2) without including the line shift term in the paramagnetic phase where the line shape asymmetry is not so well established, the g value falls sharply to 2.0 ± 0.05 at the Curie point. A sharp change of this kind was also observed by Bagguley and Harrick (1954) when using pure nickel colloids, but in their samples no correction should be necessary for the line shift.

ACKNOWLEDGMENTS

This work was supported by a research grant from the British Board of Admiralty. One of us (M. H.) wishes to thank the Department of Scientific and Industrial Research for a maintenance allowance.

REFERENCES

- BAGGULEY, D. M. S., and HARRICK, N. J., 1954, *Proc. Phys. Soc. A*, **67**, 648.
DYSON, F. J., 1955, *Phys. Rev.*, **98**, 349.
FEHER, G., and KIP, A. F., 1955, *Phys. Rev.*, **98**, 337.
OWEN, J., BROWNE, M. E., ARP, V., and KIP, A. F., 1957, *J. Phys. Chem. Solids*, **2**, 85.
YOUNG, J. A., and UEHLING, E. A., 1954, *Phys. Rev.*, **94**, 544.

P-wave Pion-Pion Resonance

By A. N. KAMAL

Department of Theoretical Physics, University of Liverpool

MS. received 1st September 1960

Abstract. A new phenomenological coupling constant in the pion-pion interaction is introduced through an interaction Lagrangian of the form

$$\mathcal{L}_{\text{int}} = \lambda_1 (\phi \times \phi_{,\mu}) \cdot (\phi \times \phi^{,\mu}).$$

It is found that this type of interaction leads to a P-wave pion-pion resonance when summation is made over the 'chain-diagrams'. The width of the resonance is adjusted by a cut-off and λ_1 is determined by the position of the resonance and the cut-off.

THE P-wave pion-pion resonance has been the subject of much discussion recently (Dyson 1955, Takeda 1955, Frazer and Fulco 1959, 1960, Ball 1960, Drell and Zachariasen 1960, and Chew and Mandelstam 1960). Dyson (1955) and Takeda (1955) were among the first to employ the notion of a pion-pion resonant interaction to explain the enhancement in the total $\pi^- - p$ cross section around 900 MeV pion laboratory kinetic energy. More recently, Frazer and Fulco (1959, 1960) have been able to explain the isobaric vector part of the nucleon electromagnetic structure through the introduction of a P-wave pion-pion resonance. The fit with the experiment is secured by suitably adjusting the position and the width of the resonance.

The difficulty in producing the P-wave resonance on the basis of field theory may be summarized as follows. Summing over the chain-diagrams, Okubo (1960) has shown that the $\lambda_0 \phi^4$ theory leads only to S-wave interaction at short distances. The P-wave contribution is attractive and comes from the long range cross-diagrams. The attraction in the P-state turns out to be much smaller than that required by Rodberg (1959) to fit the double pion production data. In order that one can produce resonance in this state one needs to increase the strength of attraction and hence demand a much larger coupling constant. That a large coupling constant is indeed required to fit the electromagnetic structure of nucleons has been borne out by the calculations of Baker and Zachariasen (1960). If one adopts the point of view recently expressed by Allcock and Kamal (1961) one finds it difficult to explain such a large coupling constant. According to Allcock and Kamal (1961), the coupling constant λ_0 is related to the size of the repulsive core in the states of isobaric spin 0 and 2, and the value of λ_0 required by Baker and Zachariasen (1960) demands an extremely large core radius.

The difficulty in producing a resonance with only one parameter λ_0 , has also been encountered in the treatment which Chew and Mandelstam (1960) have developed using the double dispersion representation. They have shown that two classes of solution to their integral equations exist—the 'S-dominant'

and the 'P-dominant' solutions. The first type of solution gives a smooth behaviour of the S-wave amplitude and no resonances appear. This seems to contain essentially the same physics as the field theory above. The second type of solution produces a resonance with the help of a new parameter descriptive of a short-range attractive P-wave interaction. Yet a third parameter, namely a cut-off, is required to obtain the correct resonance width.

Thus, both from the point of view of field theory and dispersion theory, new parameters seem necessary. The question then arises as to how the new parameters can be introduced. Lee and Vaughn (1960) have realised the necessity of short range interactions to produce the P-wave resonance and have suggested the introduction of a vector boson which interacts with the isovector part of the pion current in the Lagrangian. They have shown that the vector boson propagator exhibits a resonant structure.

The purpose of the present work is to show that one can also produce a resonance in the state with $T=1, J=1$ just by introducing a new term in the interaction Lagrangian of the form

$$\mathcal{L}_{\text{int}} = \lambda_1 (\phi \times \phi_{,\mu}) \cdot (\phi \times \phi^{,\mu}) \quad \dots\dots (1)$$

with a new coupling constant λ_1 .

Each bracket in the above Lagrangian is a vector in the isobaric spin space and Eqn (1) is one of the two possible isoscalars quadratic in the field derivatives. At low energies this type of interaction simulates the effect of the square diagrams (Igi and Kawarabayashi 1958, Mitra and Saxena 1957) in the $T=1, J=1$ state, just as $\lambda_0(\phi_\alpha\phi_\alpha)^2$ simulates them in the $J=0$ states. The two terms, $\lambda_0(\phi_\alpha\phi_\alpha)^2$ and $\lambda_1(\phi \times \phi_{,\mu}) \cdot (\phi \times \phi^{,\mu})$, contain therefore the first two terms in the expansion of the square diagram in powers of the external momenta. The interaction will also contribute in the states with $T=0$ and $T=2$ but in the present work only the $T=1$ contribution will be studied.

The resonance in the $T=1, J=1$ state is produced by summing over the graphs shown in Fig. 1, using a positive λ_1 to give attraction. Consistent with the philosophy of Allcock and Kamal (1961), we will regularize the divergent integrals to give them finite values, so introducing a second new parameter.

We define the T -matrix as follows:

$$S_{\alpha\beta,\alpha'\beta'} = 1 - i(2\pi)^4 \delta^4(p_1 + p_2 - q_1 - q_2) T_{\alpha\beta,\alpha'\beta'},$$

with the ingoing mesons having momenta p_1 and p_2 and charge indices α, β respectively, the outgoing ones having momenta q_1 and q_2 and charge indices α', β' respectively. In writing down the iterated T -matrix below, the $T=1$ state contribution has been picked out by the use of the appropriate projection operator. Denoting the iterated T -matrix by T' , we obtain for the $T=1, J=1$ state (the eigenvalues of the isobaric spin factors have been fed in),

$$T' = T_0 + \lambda_1 F T'$$

or

$$T' = \frac{T_0}{1 - \lambda_1 F} \quad \dots\dots (2)$$

T_0 is the Born contribution to T' ,

$$T_0 = -\frac{6\lambda_1}{\omega^2} (\mathbf{p} \cdot \mathbf{q}) \quad \dots\dots (3)$$

where \mathbf{p} and \mathbf{q} are the barycentric momenta and ω is the pion energy in the

barycentric frame of reference. The integral F is obtained from

$$\frac{3i}{(2\pi)^4} \int \frac{(k_1 - k_2)_\mu (k_1 - k_2)_\nu dk_1 dk_2 \delta^4(p_1 + p_2 - k_1 - k_2)}{(k_1^2 - \mu^2)(k_2^2 - \mu^2)}$$

(with k_1 and k_2 the intermediate momenta), by (a) combining the denominators (variable u), (b) regularizing the integral once (variable L and regulator

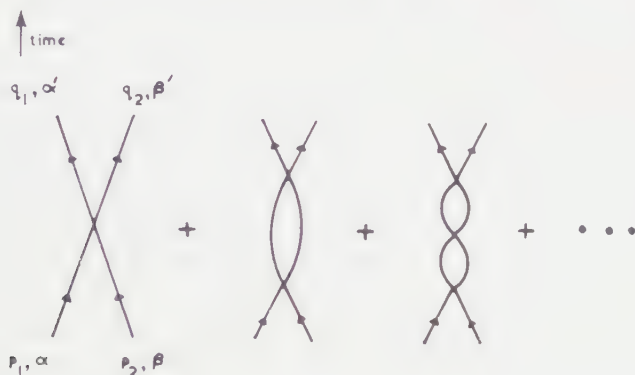


Fig. 1. Chain diagrams.

mass M , (c) shifting the origin and remembering that the terms of the form $(q_1 + q_2)_\nu (q_1 - q_2)_\nu$ and $(p_1 + p_2)_\mu (p_1 - p_2)_\mu$ vanish. F is finally given by

$$F = - \frac{6i}{(2\pi)^4} \int_0^1 du \int_0^{M^2} dL \int \frac{k_1^2 dk_1}{[k_1^2 + k^2 u(1-u) - \mu^2 - L]^3}; \dots\dots (4)$$

k is the total barycentric energy of the two pions. Writing s for k^2 , the imaginary part of F is given by

$$\mathcal{I}F(s) = \frac{1}{16\pi} \left[\frac{(s - 4\mu^2)^{3/2}}{s^{1/2}} \theta(s - 4\mu^2) - \frac{\{s - 4(M^2 + \mu^2)\}^{3/2}}{s^{1/2}} \theta\{s - 4(M^2 + \mu^2)\} \right]. \dots\dots (5)$$

For large enough regulator mass M the second term does not contribute in the energy range of interest.

The real part of F , regularizing F once again and expanding in inverse powers of M^2 , is

$$\begin{aligned} \mathcal{R}F(s) = \frac{3}{8\pi^2} \left[2M^2(\ln 2 - \tfrac{1}{2}) + \frac{s}{6}(2 \ln r - \ln 2 - \tfrac{2}{3}) - \frac{8}{3}\mu^2 - 2\mu^2 \ln r \right. \\ \left. + 4\mu^2 \frac{(s - 4\mu^2)^{1/2}}{s^{1/2}} \ln \frac{s^{1/2} + (s - 4\mu^2)^{1/2}}{2\mu} \right. \\ \left. + \frac{(s - 4\mu^2)^{3/2}}{3s^{1/2}} \ln \frac{s^{1/2} + (s - 4\mu^2)^{1/2}}{2\mu} + O\left(\frac{s^2}{M^2}\right) \right] \dots\dots (6) \end{aligned}$$

where r is the ratio M/μ .

Expression (2) can be rewritten as

$$T'(s) = \frac{T_0}{\lambda_1} \left[\frac{1}{\lambda_1} - \mathcal{R}F(s) - \frac{i}{16\pi} \frac{(s-4\mu^2)^{3/2}}{s^{1/2}} \theta(s-4\mu^2) \right]^{-1}. \quad \dots\dots (7)$$

The position of resonance is defined by the condition

$$1/\lambda_1 - \mathcal{R}F(s_r) = 0. \quad \dots\dots (8)$$

Near resonance we can expand $\mathcal{R}F(s)$ as

$$\mathcal{R}F(s) \simeq \mathcal{R}F(s_r) + (s-s_r)\mathcal{R}F'(s_r) + \text{higher derivatives.}$$

Hence we can write, near resonance,

$$\begin{aligned} T'(s) &= T_0 \left[-(s-s_r)\mathcal{R}F'(s_r) - \frac{i}{16\pi} \frac{(s-4\mu^2)^{3/2}}{s^{1/2}} \theta(s-4\mu^2) \right]^{-1} \\ &= \frac{T_0}{4\lambda_1 \mathcal{R}F'(s_r)} \left[\nu_r - \nu - i\Gamma \left(\frac{\nu^3}{\nu + \mu^2} \right)^{1/2} \theta(\nu) \right]^{-1} \quad \dots\dots (9) \end{aligned}$$

where the width Γ is defined by

$$\Gamma = \frac{1}{16\pi} \frac{1}{\mathcal{R}F'(s_r)} \quad \dots\dots (10)$$

and ν is related to s by $4\nu = s - 4\mu^2$.

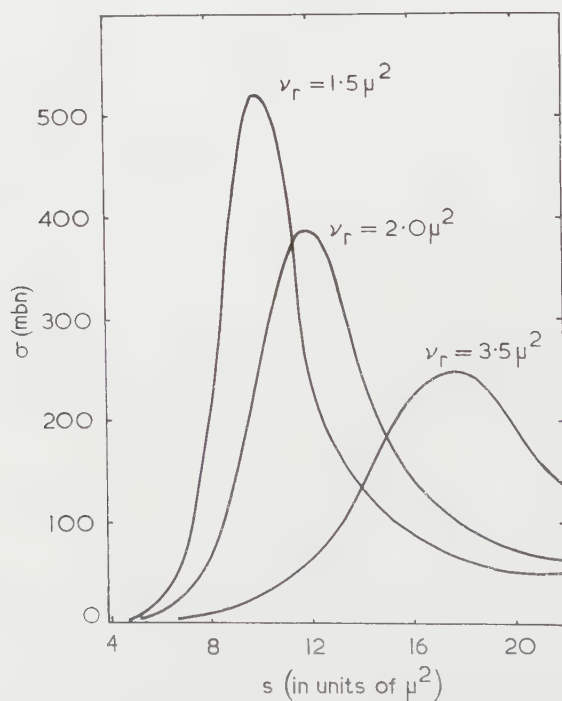


Fig. 2. The total cross section for $\pi^+-\pi^-$ scattering in $T=1, J=1$ state.

Equation (9) has a striking resemblance to the propagator of an intermediate unstable particle whose mass must be greater than 2μ in order that the real part of the denominator may vanish in the physical region. The approximate expression (9) represents the exact expression (7) remarkably well over the energy range of interest ($4\mu^2 \leq s \leq 20\mu^2$). The width of the resonance Γ is adjusted by the magnitude of the regulator mass M , through Eqn (10). It is found that a width of 0.42 at $\nu_r = 1.5\mu^2$ requires $M = 9\mu$, which is a reasonable cut-off. A narrower resonance would necessitate a larger regulator mass. Once the regulator mass is fixed the magnitude of λ_1 is determined by Eqn (8). For $M = 9\mu$ we find

$$\lambda_1 = +0.77\mu^{-2}.$$

Assuming that no scattering takes place in states other than the $T=1$, $J=1$ state, one can calculate the total cross section for $\pi^+\pi^-$ scattering implied by Eqn (9). In Fig. (2) we have plotted the total $\pi^+\pi^-$ scattering cross section, under the above assumption, with $\Gamma=0.42$ and $\nu_r=1.5\mu^2$, $2.0\mu^2$ and $3.5\mu^2$. Our curves have similar shapes to those given by Frazer and Fulco (1960).

ACKNOWLEDGMENTS

The author finds great pleasure in thanking Dr. G. R. Allcock for suggesting the investigation, encouragement and numerous valuable discussions. A financial grant from the Pakistan Atomic Energy Commission and the Colombo Plan Authorities is gratefully acknowledged.

REFERENCES

- ALLCOCK, G. R., and KAMAL, A. N., 1961, *Proc. Phys. Soc.*, **77**, 278.
 BAKER, M., and ZACHARIASEN, F., 1960, *Phys. Rev.*, **118**, 1659.
 BALL, J. S., 1960, *Phys. Rev. Letters*, **5**, 73.
 CHEW, G. F., and MANDELSTAM, S., 1960, Pre-print, U.C.R.L. 9126.
 DRELL, S. D., and ZACHARIASEN, F., 1960, *Phys. Rev. Letters*, **5**, 66.
 DYSON, F. J., 1955, *Phys. Rev.*, **99**, 1037.
 FRAZER, W. R., and FULCO, J. R., 1959, *Phys. Rev. Letters*, **2**, 365.
 ——— 1960, *Phys. Rev.*, **117**, 1609.
 IGI, K., and KAWARABAYASHI, K., 1958, *Progr. Theor. Phys., Japan*, **20**, 576.
 LEE, B. W., and VAUGHN, M. T., 1960, *Phys. Rev. Letters*, **4**, 578.
 MITRA, A. N., and SAXENA, R. P., 1957, *Phys. Rev.*, **108**, 1083.
 MIYAMOTO, Y., 1960, *Progr. Theor. Phys., Japan*, **24**, 840.
 OKUBO, S., 1960, *Phys. Rev.*, **118**, 357.
 RODBERG, L. S., 1959, *Phys. Rev. Letters*, **3**, 58.
 TAKEDA, G., 1955, *Phys. Rev.*, **100**, 440.

Note added in proof.—Ideas similar to those expressed in this paper have been arrived at by Miyamoto (1960).

Diffusion Narrowing of Nuclear Magnetic Resonance in Aluminium and Copper

BY C. P. FLYNN AND E. F. W. SEYMOUR

Physics Department, University of Leeds

MS. received 23rd August 1960

Abstract. An apparatus has been developed by means of which nuclear resonance signals have been observed at temperatures up to 1300°K. The variation of the line shape and width of the ^{63}Cu resonance at high temperatures is found to follow quantitatively the predictions of Kubo and Tomita for motional narrowing. In conjunction with the theoretical value of the frequency factor D_0 ($0.28 \text{ cm}^2 \text{ sec}^{-1}$) in the expression $D = D_0 \exp(-E/RT)$ for the coefficient of self-diffusion, the results yield a value $48.1 \pm 0.9 \text{ kcal mol}^{-1}$ for the activation energy for self-diffusion in copper, in agreement with the results of the most recent radio-tracer measurements. A similar change in shape and width of the ^{27}Al resonance cannot be used to determine the activation energy in aluminium because of the presence of a line-broadening mechanism of uncertain origin. The data are not inconsistent, however, with the theory and the known activation energy of about 31 kcal mol^{-1} .

§ 1. INTRODUCTION

IN a rigid lattice the width of a nuclear magnetic resonance line depends on the strength of the interactions between neighbouring nuclei, and between the nuclei and the lattice. Motion of the nuclei may reduce this width by effectively time-averaging the interaction between nuclei. An alternative description of this process may be given in terms of the spin spin relaxation time T_2 , the reciprocal of which is related to the line width, and which is lengthened when the interaction between a pair of nuclei is interrupted by a movement of either. Diffusional motion has been investigated in several metals by observation over an appropriate temperature range either of line width using a steady state technique, or of T_2 using a pulse technique (Gutowsky 1951, Holcomb and Norberg 1955, Li and Na; Seymour 1953, Spokas and Slichter 1959, Al; Masuda 1958, Cd).

In this paper an apparatus is described with which resonance signals have been observed at temperatures up to 1300°K. Measurements of the steady state resonance line widths of copper and aluminium nuclei in the pure metals are reported, and are interpreted as far as possible in terms of the theory of Kubo and Tomita (1954), with the objects both of confirming the theory and of deriving activation energies for self-diffusion.

§ 2. THEORETICAL CONSIDERATIONS

The interaction of usual interest which is affected by the motion is the magnetic dipolar coupling between nuclei. On the assumption of stochastic

nuclear motion with correlation time τ , Bloembergen, Purcell and Pound (1948) found that if only components of the frequency spectrum of this interaction for which the frequency is less than $1/2\pi T_2$ were considered to contribute to the line width,

$$\frac{1}{T_2^2} = \frac{2}{\pi T_2^{*2}} \tan^{-1}(2\tau/T_2), \quad \dots\dots(1)$$

where T_2^* is characteristic of the rigid lattice. Together with the conventional equation for the coefficient of self-diffusion, $D = D_0 \exp(-E/RT)$ and $D = d^2/6\tau_d$ where E is the activation energy, d the distance between neighbouring lattice sites, and τ_d the mean jump-time of the ions, which may be identified with the correlation time τ ; Eqn (1) provides a description of the line width as a function of temperature in terms of the constants of the diffusion process. However, the description is not accurate since it does not specify the line shape which in practice often changes during the transition. The line shape may be approximately Gaussian in the rigid lattice becoming Lorentzian in the strongly narrowed region. It follows that the theory is only quantitatively valuable when the line shape is not changing, i.e. for $\tau \ll T_2^*$; values of T_2 obtained in this region by pulse techniques have been successfully interpreted using Eqn (1). However this region is inaccessible for line width measurements since the observed width is here usually determined by other factors, including spin-lattice relaxation and magnet inhomogeneity.

A more sophisticated treatment of the narrowing process has been given by Kubo and Tomita (1954). They have developed, by means of the quantum statistics of irreversible processes, a description of the motional narrowing of a line which is Gaussian in the rigid lattice. They find that the line shape throughout the transition is given by

$$g(\omega) = \frac{\exp(\sigma^2\tau^2)}{\pi\sigma} \sum_{n=0}^{\infty} \frac{(-1)^n}{n!} (\sigma\tau)^{2n} \frac{\sigma\tau + n/\sigma\tau}{(\sigma\tau + n/\sigma\tau)^2 + (\omega/\sigma)^2} \quad \dots\dots(2)$$

where σ is the dispersion of the rigid lattice Gaussian line shape, given by $(2\pi\sigma^2)^{-1/2} \exp(-\omega^2/2\sigma^2)$, and $\omega = 2\pi\nu$ is the angular frequency deviation from the resonance centre. This series reduces to a simple Lorentzian shape in the limit $\sigma\tau \ll 1$. Although the series converges rapidly for $\sigma\tau \lesssim 1$, it is not useful for $\sigma\tau \gtrsim 1.5$ and we have found it necessary, for larger values of $\sigma\tau$, to redevelop their general result (Eqn (6.17) of Kubo and Tomita's paper) in a series in inverse powers of $\sigma\tau$:

$$g(\omega) = \sigma^{-1} \left\{ \frac{\exp(-\omega^2/2\sigma^2)}{(2\pi)^{1/2}} + \frac{\sum_{n=0}^{\infty} [(-2)^n(n+1)!/(2n)!](\omega/\sigma)^{2n}}{2\pi\sigma\tau} \right. \\ \left. - \frac{(3-6\omega^2/\sigma^2+\omega^4/\sigma^4)\exp(-\omega^2/2\sigma^2)}{24(2\pi)^{1/2}(\sigma\tau)^2} \right. \\ \left. + O(\sigma\tau)^{-3} - \dots \right\}. \quad \dots\dots(3)$$

The first three coefficients of the series (3) are given as functions of ω/σ in Table 1. To our knowledge the quantitative validity of Kubo and Tomita's result has not hitherto been tested experimentally. It is clear, however, that

if Eqns (2) and (3) give an adequate description of the line shapes throughout a transition region, then an activation energy for the motion may be obtainable from the values of τ found by fitting the theoretical curves to the experimental results.

It has been suggested by Nowick (1951) that the use of a theoretical value of D_0 in conjunction with a single value of D determined experimentally may

Table 1

The Coefficients $A_n(\omega/\sigma)$ in the Expansion $g(\omega) = \sigma^{-1} \sum_n (\sigma\tau)^{-n} A_n(\omega/\sigma)$

ω/σ	0	0.2	0.4	0.6	0.8	1.0	1.2	1.4
A_0	+0.3989	+0.3910	+0.3683	+0.3332	+0.2897	+0.2420	+0.1942	+0.1497
A_1	+0.1061	+0.0978	+0.0748	+0.0422	+0.0071	-0.0238	-0.0458	-0.0567
A_2	-0.0497	-0.0452	-0.0317	-0.0136	+0.0051	+0.0204	+0.0288	+0.0305
ω/σ	1.6	1.8	2.0	2.2	2.4	2.6	2.8	
A_0	+0.1109	+0.0790	+0.0540	+0.0355	+0.0224	+0.0136	+0.0079	
A_1	-0.0572	-0.0499	-0.0382	-0.0254	-0.0139	-0.0051	+0.0008	
A_2	+0.0266	+0.0204	+0.0113	+0.0040	-0.0017	-0.0045	-0.0057	

lead to a more accurate value of E than can be obtained by deducing values of both D_0 and E from measurements of D over a limited temperature range. Spokas and Slichter (1959) have used this idea in developing a convenient semi-empirical method of determining E from pulse-technique measurements of T_2 . They choose to determine τ and hence D at the 'narrowing temperature' T_N , defined as the temperature at which the extrapolation of the high temperature linear logarithmic plot of $1/T_2$ against T reaches the rigid lattice value $1/T_2^*$. They assert that at the temperature T_N the correlation time τ is related to the rigid lattice 'line width' $\delta\omega_0$ by the equation $\delta\omega_0\tau = b$, where b has approximately the same value for all metals. This value is found to be 5.9 from the results of Holcomb and Norberg (1955). Thus E may be found from

$$\frac{d^2\delta\omega_0}{6D_0} \exp\left(\frac{E}{RT_N}\right) = b \simeq 5.9, \quad \dots\dots (4)$$

where D_0 takes its theoretical value. In view of the success of this method we have thought it advisable to establish it on the basis of the results of Kubo and Tomita. At the highest temperatures Eqn (2) reduces to

$$g(\omega) = (\pi\sigma)^{-1} \frac{\sigma\tau}{(\sigma\tau)^2 + (\omega/\sigma)^2}$$

which defines a Lorentzian line for which $T_2 = \frac{1}{2}g(\nu)_{\max} = (\sigma^2\tau)^{-1}$. For the low temperature rigid lattice Gaussian line of dispersion σ , $T_2^* = (\pi/2\sigma^2)^{1/2}$. Hence the condition that $1/T_2$ extrapolates to $1/T_2^*$ is $\sigma\tau_N = (2/\pi)^{1/2}$. To make the definition of the rigid lattice line width $\delta\omega_0$ precise, we take $\delta\omega_0 = 2\sigma$, which is simply the peak to peak derivative width of the Gaussian line, and we obtain

$$\frac{d^2\delta\omega_0}{6D_0} \exp\left(\frac{E}{RT_N}\right) = \left(\frac{8}{\pi}\right)^{1/2} = 1.59. \quad \dots\dots (5)$$

The difference between the value 1.59 and the experimental one is not important

in view of the logarithmic sensitivity of the activation energy to the value of b . In the case of aluminium the difference affects E to the extent of $1.6 \text{ kcal mol}^{-1}$ which is within the experimental uncertainty of Spokas and Slichter's results.

Nowick's suggested use of the theoretical value of D_0 is particularly relevant to the treatment of results of steady state line width measurements, which are inevitably restricted to a small range of temperature. If the line shapes conform to the theory of Kubo and Tomita a reliable estimate of the activation energy should be obtainable by choosing a value of τ for best fit near the centre of the transition region, where the line width is most sensitive to the value of this parameter.

§ 3. APPARATUS

It was found that a radio-frequency bridge circuit was preferable to the Watkins-Pound type of spectrometer for the measurements in metals at high temperatures. The spin-lattice relaxation time decreases with increasing temperature and the available signal power is therefore increased. It is necessary to take advantage of this increase by using a large radio-frequency field, owing to the adverse effects on signal-to-noise ratio inherent in the use of high temperatures. These effects include a decreased nuclear polarization, and the increased noise temperature and decreased quality factor of the specimen coil. Since the Watkins-Pound circuit operates at poor noise figures at high radio-frequency levels its use would squander the increase of signal power due to the accelerated relaxation. A bridge circuit similar to that described by Anderson (1949), the output of which was matched to the input of a cascode pre-amplifier, was therefore used. The remainder of the radio-frequency and audio-frequency apparatus, and the recording potentiometer, were conventional. All the measurements were made at a frequency of 6.7 Mc/s .

The sample was surrounded by a furnace consisting of a fused silica tube of inside diameter 15 mm on which was wound a non-inductive heating coil of 28 s.w.g. platinum wire which was cemented in place. The annular space between the tube and a surrounding copper water jacket was packed with a refractory powder. The furnace fitted a magnet gap of 30 mm and remained cold on the outside while temperatures up to 1500°K were maintained on the inside.

Insulating materials for use with the radio-frequency coil at these temperatures must be chosen with care, since for many materials the losses become prohibitively high. Fused silica, mica and porcelain were found to be satisfactory. In addition fused silica fibre in the form of tape, yarn and sleeving proved of immense use†.

Both foil and powder samples have been used successfully. The first observations of the narrowing of the copper resonance were made using a mixture of powdered copper and barium chloride, which sintered to a hard mass in which the copper particles were isolated. This type of specimen was contained in a thin-walled fused silica tube carrying a platinum radio-frequency coil which was covered by fibrous silica sleeving. The measurements reported below were made using samples consisting of metallic foils separated by mica sheets. A platinum radio-frequency coil was wound directly round the sheets and anchored by passing the wire through holes in the protruding ends of the

† Obtainable from British Refrasil Co. Ltd., Stillington, Co. Durham.

mica. A platinum, 13% platinum-rhodium thermojunction was introduced between the mica sheets and the whole coil and sample covered with a paste of good quality powdered porcelain. The life of such a specimen before deterioration of the insulation was adequate to study in detail the line shape throughout the region of a line width transition.

§ 4. THE ^{27}Al LINE SHAPE TRANSITION

The activation energy for self-diffusion in aluminium cannot be measured by radio-tracer methods since a suitable isotope is not available. Two nuclear resonance investigations have been made; the first by Seymour (1953) using the steady state technique, and the second by Spokas and Slichter (1959) using pulse techniques. References to estimates of the activation energy from other types of measurement are given in the paper by Spokas and Slichter. Seymour analysed the data obtained in the region of the line width transition by means of Eqn (1) using the peak to peak derivative width of the resonance as a measure of $1/T_2$. The activation energy of $21 \pm 2 \text{ kcal mol}^{-1}$ obtained in this way is in very poor agreement with the expected value of 33 kcal mol^{-1} (Nowick 1951). In the region of severe narrowing, Spokas and Slichter find that the decay of phase coherence is exponential (corresponding to a Lorentzian steady state line shape), and that T_2 varies with temperature in a manner consistent with an activation energy for self-diffusion of about 31 kcal mol^{-1} . They also point out that the steady state line shape must change during the

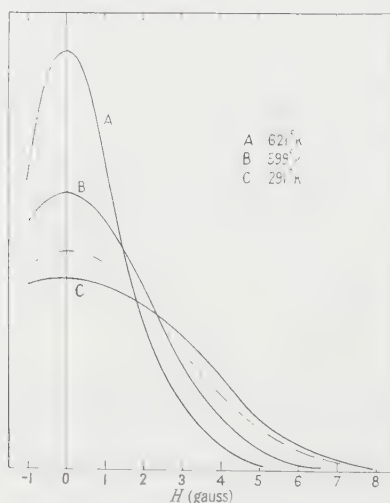


Fig. 1. The observed shapes of the ^{27}Al resonance line in the transition region. The broken line represents the theoretical dipolar line shape.

line width transition. This of course implies that Seymour's analysis is inappropriate and that a more sophisticated treatment of the line width data is necessary. We have therefore attempted to apply the equations of Kubo and Tomita to this case.

The ^{27}Al line width transition has been re-investigated with the apparatus described above, using a sample consisting of foils 0.001 in. thick. The sensitivity of the apparatus was such that the narrowed resonance at about 400°C

could be observed at noise figures of about 10 on an oscilloscope display. The transition was found to occur in precisely the temperature range reported in the earlier work, and the line shape was found to change in the same temperature interval: the central peak sharpens and the wings become more pronounced as the temperature increases, as shown in Fig. 1. The change is very roughly from Gaussian to Lorentzian but the rigid lattice curve has a more rounded central region and even less marked wings than a Gaussian curve. Further, the measured second moment of the rigid lattice line is about 10 G^2 , and is considerably greater than that (7.6 G^2) expected from dipolar interactions alone. This discrepancy has been reported by other workers (for instance, Gutowsky 1951), but a satisfactory explanation has not been given. The theoretical dipolar line shape is shown as a broken line in the figure.

It is unfortunate that the presence of this considerable additional line width, of uncertain origin, inhibits a precise analysis of the transition by means of the Kubo and Tomita equation. We have, however, computed the line shapes corresponding to the theoretical dipolar interaction and the activation energy deduced by Spokas and Slichter from their higher temperature results, and compared them with our experimental curves. The latter would be expected to be the wider throughout the transition owing to the extra interaction present. The experimental curves are indeed consistently rather wider than the computed ones, although the difference is too small to allow any deduction about the shape characteristic of the excess width alone, or about its temperature dependence. We therefore conclude that the steady state results are not inconsistent with the activation energy assumed (31 kcal mol^{-1}).

We may also attempt to obtain an estimate of the activation energy from the theoretical value of D_0 ($0.45\text{ cm}^2\text{ sec}^{-1}$, Nowick 1951) and Eqn (4) or (5). In this case we do not have an exact interpretation of the narrowing temperature T_N , so we arbitrarily use the temperature (600°K) at which the line width is halved. Using $\delta\omega_0 = 6 \times 10^4\text{ sec}^{-1}$ and $d = 2.85\text{ \AA}$, we obtain 30 or 32 kcal mol^{-1} depending on which value of b is used. This is of course only a rough estimate, but the agreement with the result of Spokas and Slichter from higher temperature measurements is none the less gratifying.

§ 5. THE ^{63}Cu AND ^{65}Cu LINE SHAPE TRANSITIONS

Unlike the aluminium resonance, the copper resonances are closely Gaussian in shape at room temperature. Moreover the activation energy for self-diffusion in copper is known from radio-tracer experiments to be $47.12 \pm 0.33\text{ kcal mol}^{-1}$. The corresponding value of D_0 is $0.20 \pm 0.03\text{ cm}^2\text{ sec}^{-1}$ (Kuper *et al.* 1954, 1955), and the theoretical value $0.28\text{ cm}^2\text{ sec}^{-1}$ (Zener 1951). Thus, while the predictions of Kubo and Tomita could not be subjected to experimental verification in the case of aluminium, it was anticipated that the investigation of copper would be more fruitful in this respect.

The character of the resonances of both copper isotopes was found to change at temperatures in the region of 950 K . The peak to peak widths ΔH of the derivatives of the resonances decreased as shown in Fig. 2. The line shapes also changed during the narrowing. Several shapes recorded for the ^{63}Cu resonance (the stronger of the two resonances) in the transition region are shown by the points in Fig. 3. The curves are shown as a function of ω/σ where σ is the dispersion of a Gaussian curve of second moment 5.6 G^2 , which

is the theoretical value for dipolar broadening. The measurements were taken using approximately the optimum modulation amplitude and have been corrected for modulation broadening (Flynn and Seymour 1960, and to be published). For the ^{63}Cu resonance the signal-to-noise ratio on the potentiometer recorder deteriorated from about 100 at room temperature to about 15 just before the onset of narrowing. The ratio improved on narrowing and then decreased at still higher temperatures, being about 4 at 1300°K .

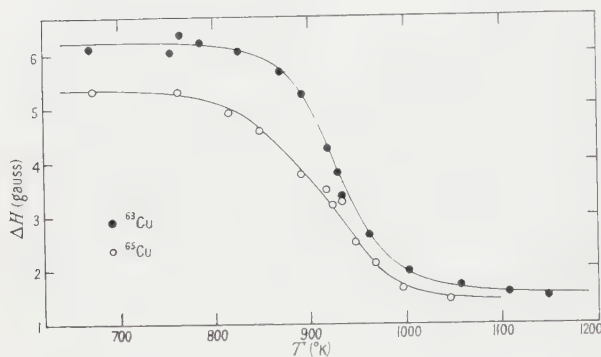


Fig. 2.

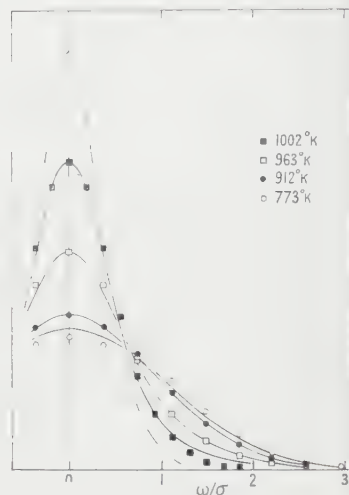


Fig. 3.

Fig. 2. The peak to peak widths ΔH of the derivatives of the ^{63}Cu and ^{65}Cu resonances as a function of temperature.

Fig. 3. The shapes of the ^{63}Cu resonance line in the transition region. The points represent the experimental results and the smooth curves the theoretical shapes. The broken line is the observed residual line shape.

The known contributions to the residual width ΔH of the lines after narrowing are spin-lattice relaxation and magnetic field inhomogeneity. The former may be estimated to be about 0.2 G from an extrapolation of the room temperature relaxation time measurements of Redfield (1956). The field inhomogeneity amounted to about 0.6 G . This leaves about half of the residual width unaccounted for. It is possible that the remainder has an origin similar to that of an extra temperature-independent contribution to T_2 observed by Spokas and Slichter for aluminium above the narrowing temperature. They suggest that the contribution may arise from quadrupolar effects. For the present purpose it will be assumed that all mechanisms contributing to the residual width are independent of temperature in the range in which the dipolar contribution is changing. Certainly, to the accuracy of the measurements, the variation of the spin-lattice relaxation time in this range is negligible. The observed line shape $f(\omega)$ in the transition region may then be written

$$f(\omega) = \int_{-\infty}^{\infty} g(\omega - \omega') h(\omega') d\omega'$$

where $g(\omega)$ represents the dipolar broadening alone and $h(\omega)$ the residual shape.

To correct the narrower experimental line shapes accurately for so large a broadening as the residual curve would be impossible: instead we have computed a series of dipolar curves $g_0(\omega)$ from the theory of Kubo and Tomita (Eqns (2) and (3) above) corresponding to a selection of values of $\sigma\tau$, with σ put equal to the theoretical value $16\,800\text{ sec}^{-1}$ for dipolar broadening. We have then folded the computed curves with the observed residual curve $h(\omega)$ to produce curves

$$f_0(\omega) = \int_{-\infty}^{\infty} g_0(\omega - \omega') h(\omega') d\omega'.$$

By a process of trial the values of $\sigma\tau$ required to fit the observed curves at three temperatures through the transition were found. These values are given in column 2 of Table 2. Fig. 3 shows the predicted line shapes $f_0(\omega)$ as smooth curves together with the corresponding experimental points $f(\omega)$. The broken line shows the observed residual line shape $h(\omega)$. The computed curve for $\sigma\tau = \infty$ is also shown and compared with the experimental points obtained at 773°K , a temperature just below that at which narrowing becomes appreciable. The worst agreement is for this last curve; as mentioned earlier, however, this is the region of minimum visibility of the resonance. The second moment of this experimental rigid lattice line when corrected for the residual width was found to be $5.5 \pm 0.5\text{ G}^2$ in good agreement with the theoretical value for dipolar broadening of 5.6 G^2 .

Table 2

Temperature ($^\circ\text{K}$)	Values of $\sigma\tau$		
	(1)	(2)	(3)
1002	$0.21 \begin{smallmatrix} -0.04 \\ +0.05 \end{smallmatrix}$	0.17	0.20
963	$0.54 \begin{smallmatrix} -0.03 \\ +0.08 \end{smallmatrix}$	0.46	0.54
912	$2 \begin{smallmatrix} -1 \\ -3 \end{smallmatrix}$	1.8	2.2
773	∞		

(1) From observed line shapes; (2) from results of Kuper *et al.* (1954, 1955); (3) from $D = 0.28 \exp(-48.1/RT)\text{ cm}^2\text{ sec}^{-1}$.

The values of $\sigma\tau$ deduced here are in good agreement with those (shown in column 2 of the table) calculated from the diffusion coefficients measured by Kuper *et al.* However, useful values of both D_0 and E cannot be deduced from the present measurements because of the restricted temperature range; our values of $\sigma\tau$ could be obtained with any value of E between 30 and 60 kcal mol^{-1} with appropriate values of D_0 . It is necessary therefore to make use of the theoretical value of D_0 . Taking $D_0 = 0.28\text{ cm}^2\text{ sec}^{-1}$, the best-known value of $\sigma\tau$, i.e. that at 963°K which is roughly the centre of the transition range, yields a value of $E = 48.1 \pm 0.9\text{ kcal mol}^{-1}$. The values of $\sigma\tau$ that this activation energy gives for the other temperatures are quite satisfactory, as shown in the last column of Table 2. This value of E is in good agreement with the radio-tracer results of Kuper *et al.*

§ 6. CONCLUSION

It was the intention in these investigations of the high temperature line width changes in aluminium and copper to try to obtain quantitative confirmation of

the theory of Kubo and Tomita relating to motional narrowing of nuclear magnetic resonances, and also to obtain estimates of the activation energies for self-diffusion in these metals. In the case of copper the Kubo and Tomita theory was fully tested and good agreement was found for the line shapes during the narrowing. It was therefore possible to deduce a value for the activation energy with some confidence. In order to do so, however, it was necessary to assume a value for the frequency factor D_0 . On taking the theoretical value, E was found to be 48.1 ± 0.9 kcal mol⁻¹ in satisfactory agreement with the most recent results of conventional measurements.

In the case of aluminium the line shape could not be adequately described by the theory, owing to the presence of an interaction other than the magnetic dipolar one between nuclei. The theory could not be used directly, therefore, to obtain a value for the activation energy. However it was checked, using the theory for the dipolar interaction alone, and taking the value of Spokas and Slichter for the activation energy, that the computed lines were always narrower than the observed ones throughout the transition. It follows that the experimental results are not inconsistent with an activation energy of 31 kcal mol⁻¹. A value of the same order was indicated by a consideration of the temperature of narrowing. The earlier estimate of 21 kcal mol⁻¹ is to be discounted since no account was then taken of the change in line shape. A consistent interpretation of the whole of the resonance data bearing on diffusion in aluminium is thus available.

ACKNOWLEDGMENTS

We wish to thank the Royal Society for a grant which assisted this work. One of us (C. P. F.) wishes to thank the Department of Scientific and Industrial Research for a maintenance allowance.

REFERENCES

- ANDERSON, H. L., 1949, *Phys. Rev.*, **76**, 1460.
BLOEMBERGEN, N., PURCELL, E. M., and POUND, R. V., 1948, *Phys. Rev.*, **73**, 679.
FLYNN, C. P., and SEYMOUR, E. F. W., 1960, *Proc. Phys. Soc.*, **75**, 337.
GUTOWSKY, H. S., 1951, *Phys. Rev.*, **83**, 1073.
HOLCOMB, D. F., and NORBERG, R. E., 1955, *Phys. Rev.*, **98**, 1074.
KUBO, R., and TOMITA, K., 1954, *J. Phys. Soc., Japan*, **9**, 888.
KUPER, A., LETAW, H., SLIFKIN, L., SONDER, E., and TOMIZUKA, C. T., 1954, *Phys. Rev.*, **96**, 1224.
— 1955, *Phys. Rev.*, **98**, 1870.
MASUDA, Y., 1958, *J. Phys. Soc., Japan*, **13**, 597.
NOWICK, A. S., 1951, *J. Appl. Phys.*, **22**, 1182.
REDFIELD, A. G., 1956, *Phys. Rev.*, **101**, 67.
SEYMOUR, E. F. W., 1953, *Proc. Phys. Soc. A*, **66**, 85.
SPOKAS, J. J., and SLICHTER, C. P., 1959, *Phys. Rev.*, **113**, 1462.
ZENER, C., 1951, *J. Appl. Phys.*, **22**, 372.

Stereospecific Polymers and Markoff Chains

By T. B. GRIMLEY

Department of Inorganic and Physical Chemistry, University of Liverpool

MS. received 12th October 1960

Abstract. If the only factors restricting the configurations of a polymer molecule are the constancy of the C-C-C bond angle, and the existence of a potential hindering free rotation about C-C bonds, stereospecific polymers of the type $(\text{CHX})_N$ are simple Markoff chains but the stereospecific vinyl polymers $(\text{CH}_2\text{CHX})_N$ are not. These vinyl polymers are examples of Markoff chains with a periodic transition probability. The eigenvalue theory of such chains is briefly discussed.

§ 1. INTRODUCTION

LET a set of vectors $\mathbf{x}_1 \dots \mathbf{x}_j \dots \mathbf{x}_N$ be so related that the probability distribution of \mathbf{x}_j is uniquely determined by that of the s preceding vectors $\mathbf{x}_{j-1} \dots \mathbf{x}_{j-s}$, and the law of dependence of \mathbf{x}_j on $\mathbf{x}_{j-1} \dots \mathbf{x}_{j-s}$. A chain of variables with these properties is known as a Markoff chain. The chain configurations are determined by $p(\mathbf{x}_s \dots \mathbf{x}_1)$, the probability distribution of the first s vectors, and the transition probability $\tau_j(\mathbf{x}_j, \mathbf{x}_{j-1} \dots \mathbf{x}_{j-s}) d\mathbf{x}_j$, which is the probability that the j th vector lies between \mathbf{x}_j and $\mathbf{x}_j + d\mathbf{x}_j$ when the s previous vectors are $\mathbf{x}_{j-1} \dots \mathbf{x}_{j-s}$; $\tau_j(\mathbf{x}_j, \mathbf{x}_{j-1} \dots \mathbf{x}_{j-s})$, which is the law of dependence of \mathbf{x}_j on $\mathbf{x}_{j-1} \dots \mathbf{x}_{j-s}$, satisfies the equation

$$\int \tau_j(\mathbf{x}_j, \mathbf{x}_{j-1} \dots \mathbf{x}_{j-s}) d\mathbf{x}_j = 1.$$

If τ_j is independent of j , the chain is *simple*, and powerful methods are available for the investigation of such chains.

The relevance of the theory of simple Markoff chains to the problem of the configurations of polymer molecules in solution was first recognised by Montroll (1947, 1950). Consider for example the linear polymer $(\text{CHX})_N$. The vectors $\mathbf{x}_1 \dots \mathbf{x}_N$ specify the directions in space of the N carbon-carbon bonds in the backbone of the polymer. The C-C-C bond angle is fixed so that with completely free rotation about C-C bonds, \mathbf{x}_j depends only on \mathbf{x}_{j-1} with a law of dependence $\tau(\mathbf{x}_j, \mathbf{x}_{j-1})$ which is independent of j . We have therefore a simple Markoff chain. In general however, we have to include a potential hindering free rotation about C-C bonds. This makes \mathbf{x}_j depend on \mathbf{x}_{j-2} as well as on \mathbf{x}_{j-1} . Moreover, the law of dependence, $\tau_j(\mathbf{x}_j, \mathbf{x}_{j-1}, \mathbf{x}_{j-2})$, is not necessarily independent of j because the hindering potential depends on the way in which the remaining bonds to the two carbon atoms linked by \mathbf{x}_j are ordered with respect to \mathbf{x}_j . A consideration of the possibilities leads to the notion of stereospecific polymers (Natta and Corradini 1956a, b). The stereospecific polymers $(\text{CHX})_N$ are simple Markoff chains but the stereospecific vinyl polymers $(\text{CH}_2\text{CHX})_{N/2}$ are not because, here, the transition probability τ_j is periodic in j . The theory of Markoff chains with a periodic transition

probability will be discussed briefly in §3. The eigenvalue theory of such chains can be developed in just the same way as for simple chains, and although the resulting description is incomplete, important conclusions concerning the mean dimensions of the chain, and the occurrence of long range order can be reached.

§ 2. STEREOSPECIFIC POLYMERS

Consider first polymers of the type $(\text{CHX})_N$. Let the carbon atoms be numbered $0, 1, \dots, N$, and the C-C bonds $1, 2, \dots, N$. Let the order in which the three neighbours C, H and X of the j th carbon atom appear, going clockwise about the j th C-C bond when viewed from the $(j-1)$ th carbon atom, be specified. If this order is the same (for example, CHX) on each carbon atom, the polymer is isotactic, if it is alternately CHX and CXH, the polymer is syndiotactic, but if it is CHX and CXH indiscriminately, the polymer is atactic. The first two polymers are stereospecific, the third is not.

The specification of the order of neighbours on each carbon atom also specifies the potentials hindering free rotation about the C-C bonds. For the isotactic polymer, the hindering potential, V_i say, is the same for all C-C bonds. Similarly, for the syndiotactic polymer, the hindering potential is always V_s , but $V_s \neq V_i$. For the atactic polymers (there are 2^N atactic polymers) the hindering potentials V_i and V_s occur randomly along the chain. Thus the stereospecific polymers $(\text{CHX})_N$ are characterized by transition probabilities τ_i (isotactic), and τ_s (syndiotactic) which are the same for all C-C bonds, and they are therefore simple Markoff chains. In the atactic polymers, the transition probabilities τ_i and τ_s occur randomly along the chain. Consequently, these polymers are not simple Markoff chains.

When we turn to the vinyl polymers $(\text{CH}_2\text{CHX})_{N/2}$, the situation becomes a little more complicated. The side group X appears only on alternate carbon atoms, and because of this, there are two different hindering potentials V_1 and V_2 . These occur in the order $V_1V_2V_1V_2\dots$ along the chain in the isotactic polymer, and in the order $V_1V_1V_2V_2V_1V_1\dots$ in the syndiotactic polymer. In the atactic polymers V_1 and V_2 occur randomly along the chain. The stereospecific vinyl polymers are therefore characterized by two transition probabilities τ_1 and τ_2 , occurring in the orders $\tau_1\tau_2\tau_1\tau_2\dots$ (isotactic), and $\tau_1\tau_1\tau_2\tau_2\tau_1\tau_1\dots$ (syndiotactic). Thus we have examples of a Markoff chain in which the transition probability τ_j is periodic in j . The period is 2 for the isotactic polymer, and 4 for the syndiotactic polymer. Another example with period 2 is polyisobutylene. In the next section we examine briefly the generalization of the eigenvalue theory of simple Markoff chains to chains with a periodic transition probability.

§ 3. PERIODIC MARKOFF CHAINS

Let the transition probability $\tau_j(\mathbf{x}_j, \mathbf{x}_{j-1} \dots \mathbf{x}_{j-s})$ in a Markoff chain be periodic in j with period r so that the chain has a repeating unit consisting of r vectors. After the first s vectors, let the chain contain a whole number of such repeating units. Then, if there are N vectors in the chain, $N = s + nr$ with n integral. Define an r -fold transition probability $\tau(\mathbf{x}_{s+mr+r} \dots \mathbf{x}_{1+mr})$

by the equation

$$\tau(\mathbf{x}_{s+mr+r} \dots \mathbf{x}_{1+mr}) = \prod_{j=s-mr-1}^{s+mr+r} \tau_j(\mathbf{x}_j, \mathbf{x}_{j-1} \dots \mathbf{x}_{j-s})$$

then τ , which is the law of dependence of all the r vectors in the m th repeating unit on the last s vectors in the $(m-1)$ th repeating unit, is independent of m , and further satisfies the equation

$$\int \tau(\mathbf{x}_{s+mr+r} \dots \mathbf{x}_{1+mr}) d\mathbf{x}_{s+mr+r} \dots d\mathbf{x}_{s+mr+1} = 1.$$

The chain is not completely specified when τ and $p(\mathbf{x}_s \dots \mathbf{x}_1)$, the probability distribution of the first s vectors, are given. For a complete specification the r different transition probabilities τ_j must be given. However, there are several important chain properties, for example, the mean dimensions, and the occurrence of long range order, which depend directly on the form of the function τ . They can be investigated therefore by developing an eigenvalue theory in much the same way as is done for simple Markoff chains.

Provided that $mr \geq s$, the probability distribution $p(\mathbf{x}_{s+mr} \dots \mathbf{x}_{1+mr})$ of the sequence of s vectors finishing at the end of the m th repeating unit, is given by

$$p(\mathbf{x}_{s+mr} \dots \mathbf{x}_{1+mr}) = \int K_m(\mathbf{x}_{s+mr} \dots \mathbf{x}_{1+mr}, \mathbf{x}_s \dots \mathbf{x}_1) p(\mathbf{x}_s \dots \mathbf{x}_1) d\mathbf{x}_s \dots d\mathbf{x}_1 \quad \dots (1)$$

with

$$K_m(\mathbf{x}_{s+mr} \dots \mathbf{x}_{1+mr}, \mathbf{x}_s \dots \mathbf{x}_1) = \int \tau(\mathbf{x}_{s-mr} \dots \mathbf{x}_{1-mr-r}) \tau(\mathbf{x}_{s+mr-r} \dots \mathbf{x}_{1+mr-2r}) \dots \tau(\mathbf{x}_{s+mr} \dots \mathbf{x}_1) d\mathbf{x}_{mr} \dots d\mathbf{x}_{s+1} \quad \dots (2)$$

The restriction $mr \geq s$ is only imposed for brevity so that the two cases, $r > s$ and $r < s$, can be treated together. Two separate discussions would otherwise be needed. $K_m d\mathbf{x}_{s+mr} \dots d\mathbf{x}_{1+mr}$ is the transition probability over m repeating units, giving the probability that the sequence of s vectors finishing at the end of the m th repeating unit is $\mathbf{x}_{s+mr} \dots \mathbf{x}_{1+mr}$ to within $d\mathbf{x}_{s+mr} \dots d\mathbf{x}_{1+mr}$ when the first s vectors in the chain are $\mathbf{x}_1 \dots \mathbf{x}_s$. The simplest possible Markoff chain has $r=s=1$, and for such chains, important theoretical results follow by introducing the eigenfunctions of the transition probability τ . We now see how these developments follow when r and s are arbitrary.

Define the right and left eigenfunctions ϕ_k and ψ_k , and the eigenvalues λ_k , $k=0, 1, \dots$, of the transition probability τ by the equations

$$\int \tau(\mathbf{x}_{s+r} \dots \mathbf{x}_1) \phi_k(\mathbf{x}_s \dots \mathbf{x}_1) d\mathbf{x}_r \dots d\mathbf{x}_1 = \lambda_k \phi_k(\mathbf{x}_{s+r} \dots \mathbf{x}_{1+r}), \quad \dots (3)$$

$$\int \psi_k(\mathbf{x}_{s-r} \dots \mathbf{x}_{1-r}) \tau(\mathbf{x}_{s+r} \dots \mathbf{x}_1) d\mathbf{x}_{s+r} \dots d\mathbf{x}_{s+1} = \lambda_k \psi_k(\mathbf{x}_s \dots \mathbf{x}_1). \quad \dots (4)$$

The eigenfunctions depend on s (vector) variables, and form a bi-orthogonal set

$$\int \psi_k(\mathbf{x}_s \dots \mathbf{x}_1) \phi_l(\mathbf{x}_s \dots \mathbf{x}_1) d\mathbf{x}_s \dots d\mathbf{x}_1 = \delta_{kl}.$$

Now $\tau \geq 0$, and

$$\int \tau(\mathbf{x}_{s+r} \dots \mathbf{x}_1) d\mathbf{x}_{s+r} \dots d\mathbf{x}_{s+1} = 1.$$

From these properties of τ , the following statements are easily proved.

(i) There is one eigenvalue, λ_0 say, equal to the eigenvalue unity, and

$$c \int \phi_0(\mathbf{x}_s \dots \mathbf{x}_1) d\mathbf{x}_s \dots d\mathbf{x}_1 = 1$$

with c some number.

(ii) For $k=1, 2, \dots$, $|\lambda_k| < 1$, and

$$\int \phi_k(\mathbf{x}_s \dots \mathbf{x}_1) d\mathbf{x}_s \dots d\mathbf{x}_1 = 0.$$

(iii) If λ_0 is non-degenerate, $\psi_0(\mathbf{x}_s \dots \mathbf{x}_1) = c$, but if not, only one of the degenerate set of left eigenfunctions is independent of $\mathbf{x}_s \dots \mathbf{x}_1$.

For the simplest Markoff chain ($r=s=1$), long range order is investigated by expanding K_m in eigenfunctions of τ . A similar procedure is possible when r and s are arbitrary. First we prove from Eqns (2), (3) and (4) that

$$\int K_m(\mathbf{x}_{s+mr} \dots \mathbf{x}_{1+mr}, \mathbf{x}_s \dots \mathbf{x}_1) \phi_k(\mathbf{x}_s \dots \mathbf{x}_1) d\mathbf{x}_s \dots d\mathbf{x}_1 = (\lambda_k)^m \phi_k(\mathbf{x}_{s+mr} \dots \mathbf{x}_{1+mr}).$$

This shows that the ϕ_k are right eigenfunctions of K_m with eigenvalues $(\lambda_k)^m$. Hence if K_m is expanded in terms of the left eigenfunctions ψ_k ,

$$K_m = \sum_k a_k(\mathbf{x}_{s+mr} \dots \mathbf{x}_{1+mr}) \psi_k(\mathbf{x}_s \dots \mathbf{x}_1),$$

the formula for the expansion coefficients is

$$a_k = (\lambda_k)^m \phi_k(\mathbf{x}_{s+mr} \dots \mathbf{x}_{1+mr}).$$

Since $\lambda_0 = 1$, and $|\lambda_k| < 1$ for all other eigenvalues, an important result follows at once. Namely, if the eigenvalue unity is non-degenerate then, as $m \rightarrow \infty$, $K_m \rightarrow c \phi_0(\mathbf{x}_{s+mr} \dots \mathbf{x}_{1+mr})$. Thus, the transition probability over m repeating units is independent of the configuration of the first s vectors in the chain when m is large, and the chain does not show long range order. Long range order is connected with degeneracy in the eigenvalue unity of the transition probability τ . This is exactly the same situation as in the simplest Markoff chain with $r=s=1$.

Consider now the moment generating function. Put

$$\mathbf{L} = \mathbf{x}_1 + \mathbf{x}_2 + \dots + \mathbf{x}_{s+nr},$$

and let κ be a vector with the same number of dimensions as the \mathbf{x}_j . The function $Z(\kappa)$ defined by

$$Z(\kappa) = \int p(\mathbf{x}_{s+nr} \dots \mathbf{x}_1) \exp(\kappa \cdot \mathbf{L}) d\mathbf{x}_{s+nr} \dots d\mathbf{x}_1$$

is the moment generating function because, if X is the projection of \mathbf{L} on κ , and \bar{X}^ν is the mean value of X^ν averaged over all the configurations of the chain, then

$$Z(0) \bar{X}^\nu = \nu! [\text{the coefficient of } \kappa^\nu \text{ in } Z(\kappa)].$$

If $r=s=1$ we would define

$$T(\mathbf{x}_{1+m} \mathbf{x}_m) = \tau(\mathbf{x}_{1+m} \mathbf{x}_m) \exp \left[\frac{1}{2} \kappa \cdot (\mathbf{x}_{1+m} + \mathbf{x}_m) \right], \quad \dots \dots (5)$$

and

$$T_m(\mathbf{x}_{1+m} \mathbf{x}_1) = \int T(\mathbf{x}_{1+m} \mathbf{x}_m) T(\mathbf{x}_m \mathbf{x}_{m-1}) \dots T(\mathbf{x}_2 \mathbf{x}_1) d\mathbf{x} \dots_m d\mathbf{x}_2,$$

so that

$$Z(\kappa) = \int T_n(\mathbf{x}_{1+n}\mathbf{x}_1) p(\mathbf{x}_1) \exp [\tfrac{1}{2}\boldsymbol{\kappa} \cdot (\mathbf{x}_{1+n} + \mathbf{x}_1)] d\mathbf{x}_{1+n} d\mathbf{x}_1.$$

When n is large, we can drop the exponential factor in the integrand, and take

$$Z(\kappa) = \int T_n(\mathbf{x}_{1+n}\mathbf{x}_1) p(\mathbf{x}_1) d\mathbf{x}_{1+n} d\mathbf{x}_1. \quad \dots\dots (6)$$

Important results now follow by introducing left and right eigenfunctions of T .

When r and s are arbitrary, the theory can be developed along the same lines. However, the definition of the function T which generalizes Eqn (5) is tedious, and it is easier to write it down for particular cases which may be of interest than to give a general formula. For example, with $r=2$ and $s=3$ (isotactic vinyl polymers)

$$T(\mathbf{x}_5 \dots \mathbf{x}_1) = \tau(\mathbf{x}_5 \dots \mathbf{x}_1) \exp [\tfrac{1}{6}\boldsymbol{\kappa} \cdot (2\mathbf{x}_5 + 3\mathbf{x}_4 + 2\mathbf{x}_3 + 3\mathbf{x}_2 + 2\mathbf{x}_1)],$$

and with $r=4$ and $s=3$ (syndiotactic vinyl polymers),

$$T(\mathbf{x}_7 \dots \mathbf{x}_1) = \tau(\mathbf{x}_7 \dots \mathbf{x}_1) \exp [\tfrac{1}{2}\boldsymbol{\kappa} \cdot (\mathbf{x}_7 + \mathbf{x}_6 + \mathbf{x}_5 + 2\mathbf{x}_4 + \mathbf{x}_3 + \mathbf{x}_2 + \mathbf{x}_1)].$$

Provided that $nr \geq s$, the generalization of Eqn (6) is

$$Z(\kappa) = \int T_n(\mathbf{x}_{s+nr} \dots \mathbf{x}_{1+nr}, \mathbf{x}_s \dots \mathbf{x}_1) p(\mathbf{x}_s \dots \mathbf{x}_1) d\mathbf{x}_{s+nr} \dots d\mathbf{x}_{1+nr} d\mathbf{x}_s \dots d\mathbf{x}_1,$$

with

$$T_n = \int \prod_{m=1}^n T(\mathbf{x}_{s+mr} \dots \mathbf{x}_{1+mr-r}) d\mathbf{x}_{nr} \dots d\mathbf{x}_{s+1}.$$

Again the restriction $nr \geq s$ is imposed only for brevity so that the two cases, $r > s$ and $r < s$, can be treated together.

We now introduce the right and left eigenfunctions Φ_k and Ψ_k , and the eigenvalues Λ_k , $k=0, 1, 2, \dots$, of the function $T(\mathbf{x}_{s+r} \dots \mathbf{x}_1)$ by definitions similar to those of Eqns (3) and (4). Again these eigenfunctions form a biorthogonal set, and of course $\Phi_k \rightarrow \phi_k$, $\Psi_k \rightarrow \psi_k$, and $\Lambda_k \rightarrow \lambda_k$ as $\kappa \rightarrow 0$. We can now establish the result

$$\int T_n(\mathbf{x}_{s+nr} \dots \mathbf{x}_{1+nr}, \mathbf{x}_s \dots \mathbf{x}_1) \Phi_k(\mathbf{x}_s \dots \mathbf{x}_1) d\mathbf{x}_s \dots d\mathbf{x}_1 = (\Lambda_k)^n \Phi_k(\mathbf{x}_{s+nr} \dots \mathbf{x}_{1+nr}),$$

and the expansion

$$T_n = \sum_k (\Lambda_k)^n \Phi_k(\mathbf{x}_{s+nr} \dots \mathbf{x}_{1+nr}) \Psi_k(\mathbf{x}_s \dots \mathbf{x}_1).$$

Thus, if $p(\mathbf{x}_s \dots \mathbf{x}_1)$ be expanded in terms of the right eigenfunctions Φ_k ,

$$p(\mathbf{x}_s \dots \mathbf{x}_1) = \sum_k c_k \Phi_k(\mathbf{x}_s \dots \mathbf{x}_1), \quad c_k = \int \Psi_k(\mathbf{x}_s \dots \mathbf{x}_1) p(\mathbf{x}_s \dots \mathbf{x}_1) d\mathbf{x}_s \dots d\mathbf{x}_1,$$

the moment generating function can be written

$$Z(\kappa) = \sum_k (\Lambda_k)^n c_k \int \Phi_k(\mathbf{x}_s \dots \mathbf{x}_1) d\mathbf{x}_s \dots d\mathbf{x}_1, \quad \dots\dots (7)$$

which is a straightforward generalization of the corresponding formula for the simplest Markoff chain. The expression for $\overline{\Lambda^2}$, the mean value of the square of the projection of \mathbf{L} on the direction of $\boldsymbol{\kappa}$, follows at once. If the eigenvalue unity of τ is non-degenerate then as $n \rightarrow \infty$,

$$\overline{X^2} \rightarrow 2n\lambda_0^{(2)}, \quad \dots\dots (8)$$

where $\lambda_0^{(2)}$ is the second-order perturbation of the eigenvalue unity of τ , namely, the coefficient of κ^2 in the series

$$\Lambda_0 = 1 + \lambda_0^{(1)}\kappa + \lambda_0^{(2)}\kappa^2 + \dots$$

Eqn (8) expresses the important result that the mean square end-to-end distance of the chain is proportional to n , the number of repeating units, when n is large.

If the eigenvalue unity of τ is ω -fold degenerate, then in general, this degeneracy will not be carried over to the eigenvalues of T . Instead, there will be a set of eigenvalues of T , which we denote by $\Lambda_{0\nu}$, $\nu = 1, 2, \dots, \omega$, each connected to unity by a power series in κ ,

$$\Lambda_{0\nu} = 1 + \lambda_{0\nu}^{(1)}\kappa + \lambda_{0\nu}^{(2)}\kappa^2 + \dots$$

Provided that $\lambda_{0\nu}^{(1)}$ (the first-order perturbation) does not vanish, it follows from Eqn (7) that

$$\overline{X^2} \rightarrow n^2 \sum_{\nu=1}^{\omega} [\lambda_{0\nu}^{(2)}]^2 A_{0\nu} / \sum_{\nu=1}^{\omega} A_{0\nu},$$

where

$$A_{0\nu} = \int \psi_{0\nu}(\mathbf{x}_s \dots \mathbf{x}_1) p(\mathbf{x}_s \dots \mathbf{x}_1) d\mathbf{x}_s \dots d\mathbf{x}_1 \int \phi_{0\nu}(\mathbf{x}_s \dots \mathbf{x}_1) d\mathbf{x}_s \dots d\mathbf{x}_1.$$

Thus the mean square end-to-end distance is proportional to n^2 . This is the expected result for a chain with long range order; a straight walk with no reversing is the simplest example.

§ 4. CONCLUSION

We have seen that, when a potential hindering free rotation about C-C bonds is included, stereospecific polymers provide examples of Markoff chains which are either simple or have a transition probability which is periodic along the chain. Atactic polymers, on the other hand, lead to Markoff chains with two randomly occurring transition probabilities. However, when all factors controlling the configuration are included, a polymer molecule is no longer a Markoff chain. If the backbone has any flexibility at all, and if the molecule is long enough, it can turn back on itself to form a loop with two parts of the molecule seeking to occupy the same region of space. The exclusion of self penetration, which is known as the 'volume effect', means that the transition probability for the j th bond vector depends on the values of all other bond vectors in chain. A chain with this property is not a Markoff chain, and a proper treatment of it has not yet been given. There are theoretical reasons for the belief that, if the osmotic pressure of a polymer solution follows van't Hoff's law (and this can usually be achieved by a suitable choice of the solvent and the temperature), the volume effect must vanish. Only under these conditions therefore is a polymer molecule in solution really a Markoff chain.

REFERENCES

- MONTROLL, E. W., 1947, *Ann. Math. Statist.*, **18**, 18.
 — 1950, *J. Chem. Phys.*, **18**, 734.
 NATTA, G., and CORRADINI, P., 1956 a, *Angew. Chem.*, **68**, 615.
 — 1956 b, *J. Polymer. Sci.*, **20**, 251.

REVIEWS OF BOOKS

Cosmology, 2nd Edn, by H. BONDI. Pp. iii+182. (Cambridge: University Press, 1960.) 30s.

In this monograph the author aims at presenting cosmology as a branch of physics in its own right, and has therefore devoted a substantial part of the book to the observational aspect.

The second edition takes full account of recent developments including, for example, the growing importance of radio-astronomy. The final chapter, surveying the present position in cosmology, has been completely rewritten.

The Design of Physics Research Laboratories (A Symposium held by the London and Home Counties Branch of the Institute of Physics, at the Royal Institution on 27th November 1957). Pp. 108. (London: Chapman and Hall, on behalf of The Institute of Physics, 1959.) 21s.

This report of a symposium held by The Institute of Physics makes useful and interesting reading to anyone who is concerned with laboratory planning. The views of the speakers strongly reflect their personal experiences and tastes, and show clearly how various are the circumstances in which physicists work.

Most of the contributions were largely concerned with the design of service installations. Decisions in this field are particularly difficult to reach; the quantitative requirements are often hard to foresee, even though the general types of facility may be clear. Even when the needs are fully specified, it is often necessary to choose between several systems by which they can be provided (convectors, fan-driven air heaters or floor heating; conduit or trunking for electric circuits; overhead or runabout lifting tackle) and it is always necessary to select the routes along which services will run.

Working within the financial provisions made by the building owner, there are usually two pairs of parties to these decisions: architects and engineering consultants, prospective users and prospective maintainers of the services. The symposium showed from many angles the vital importance of members of each pair working closely together.

Many contributions are profusely illustrated and all show the enthusiasm and originality of the authors.

P.B.M.

The Concepts and Theories of Modern Physics, by J. B. STALLO, edited by P. W. BRIDGMAN. Pp. xxix+325. (Harvard: University Press; London: Oxford University Press, 1960.) 38s.

This book appears to be the first of a series of carefully edited reprints of "significant books and documents from the American past". No more felicitous choice could have been made, to inaugurate such a series, than that of Stallo's unjustly forgotten essay on the fundamental ideas of physics as they presented themselves to his searching criticism about 1880. Certainly, such a book must be primarily regarded as an historical document, pertaining to a stage in the development of physical science which is now almost as antiquated as the speculations of the ancient philosophers. Yet, when we read it now, against the background of our increased insight into the structure of matter, we are

struck by the prophetic tone rung by some of the author's pronouncements. This is not because he had any particularly remarkable foresight in physical problems; far from it, his main shortcoming was precisely an insufficient appreciation of the valuable features of the physical theories whose weaknesses he exposed: but the lasting value of his criticism is due to the fact that alone, or nearly alone, in a very uncritical age he realized the importance of a rigorous epistemological analysis of the physical concepts, and was able, thanks to an unusual independence of judgment and a healthy dose of common sense, to carry out such an analysis much further than any of the contemporary physicists, except perhaps Mach.

As a result, Stallo's book still offers to the modern reader a valid exposition of the insufficiency of any *classical* picture of the atomic structure of matter, and of the epistemological and methodical requirements which physical theories have to fulfil. The presentation of the argument is not free from wordiness and pedantry here and there, and there is even a serious error in the discussion of the kinetic theory of gases; but on the whole it gives such an impression of freshness and vigour that one readily forgives its minor imperfections. In a most readable introduction, Professor Bridgman, besides giving all desirable information on the curious career and personality of the author, presents an interesting assessment of the book in which he very fairly apportions praise and stricture. I am inclined to plead for still more indulgence for its failings, in view of the excellence of its positive contributions to the epistemology and methodology of physics. In particular, I should like to recommend a careful study of it to the younger generation of theoretical physicists, who too often, behind a dazzling screen of formal virtuosity conceal a deplorable tendency to woolly thinking.

L. ROSENFELD.

Quantitative Inorganic Analysis, 2nd Edn, by R. BELCHER and A. J. NUTTEN.
Pp. x+390. (London: Butterworths, 1960.) 35s.

The appearance of the second edition of this book after five years is an indication of its value to technical colleges and other teaching departments. The text has been thoroughly revised and brought up to date. Of particular value to the student in a textbook of this kind is the inclusion of sections on modern balances, including one-pan balances and controlled release balances, a discussion on redox indicators, which is one of the clearest to be found in textbooks of this kind, and considerable discussion of the use of ethylenediaminetetra-acetic acid and appropriate indicators for the determination of calcium, magnesium, and the heavy metals.

Only 32 of the 360 pages are devoted to the use of physical techniques in inorganic analysis. This may reflect the backwardness of many technical colleges and industrial firms. It seems unfortunate, however, that textbooks should perpetuate this, and that one of this calibre which, in the section on colorimetric analysis, finds space to illustrate a stand for holding Nessler tubes, has to relegate mention of 'Spekker'-type absorptiometers to two lines of footnotes. A table of logarithms has been added, but these are not printed on facing pages so that they are very difficult to use.

The price of 35s. should make this book available to a wide range of students of whom it should be of great value.

D. J. FERRETT.

- (1) *A Table of the Incomplete Elliptic Integral of the Third Kind*, by R. G. SELFRIDGE and J. E. MAXFIELD. Pp. xiv+805. (New York: Dover Publications; London: Constable, 1958.) 60s.
- (2) *Tables of the Incomplete Elliptic Integrals of the First and Third Kind*, by F. A. PAXTON and J. E. ROLLIN. Pp. 436. (Quehanna, Pennsylvania: Curtiss-Wright Corporation Research Division, 1959.)

The second of these works has already been listed in the *Proceedings* (1960, 75, 816), and a review of the first by Dr. Alan Fletcher has been given in *Math. Tab., Wash.*, 1960, 14, 209.

They each tabulate the trivariate function of Legendre

$$\Pi(p, k, \phi) = \int_0^\phi \frac{d\psi}{(1-p \sin^2 \psi)(1-k^2 \sin^2 \psi)^{1/2}}.$$

The tables are reproduced from the sheets printed out by an I.B.M. 704 computer; the integrations were performed by Simpson's rule. In neither is there any discussion of the problem of interpolation.

In (1) Π is tabulated to 6D for $p = -1(0.05) - 0.1(0.02) - 0.02$; $0.05(0.05) 0.5(0.02) 0.8(0.01) 0.99$; $\phi = 0(0.01) 1.57$ and $\pi/2$; $\sin^{-1}(k) = 0.1(0.1) 1.5$. A second entry is given for $\phi = \pi/2$, calculated by a Runge-Kutta solution of the third-order differential equation satisfied by $\Pi(p, k)$ (with k as independent variable). This is given as a check on the rest of the table. The printing is clear and the figures should be free from mistakes as they were checked automatically by the machine. The presentation is slightly marred by careless mistakes in the headings: our p is written as x^2 in the introduction but as α in the tables, ϕ is written as Θ in the tables, and the columns for successive moduli are headed not with θ (the modular angle, which increases in steps of 0.1 radian) but with values of k^2 which (contrary to the preface) are labelled κ . The omission of the tables for $p = 0$ on the grounds that the function is then $F(k, \phi)$ will inconvenience those who need to interpolate in p in the neighbourhood of $p = 0$.

In (2) Π is tabulated to 7D for $p = 0(0.02) 1$, $k^2 = 0(0.02) 1$, $\phi = 0(1^\circ) 90^\circ$, but the seventh decimal is purely a rounding figure. Thus $\Pi(0, 0, \pi/2)$ is given as 1.5707957, cf. $\pi/2 = 1.5707963$. The printing is somewhat smaller than that of (1) and on some pages of the copy seen it is faint.

J. C. E. JENNINGS.

Nuclear Reactor Optimisation (*Nuclear Engineering Monographs*), by P. H. MARGEN. Pp. x+81. (London: Temple Press, 1960.) 12s. 6d.

In 80 pages this book sets out to provide an account of what might be termed first-order optimization of nuclear power stations. The way in which various groups of independent parameters optimize is discussed generally, and worked examples are given of a complete transition from an assumed design to a first optimized design. Although the book succeeds in giving an account of the way in which first-order optimization may be carried out, this object might have been achieved with rather less detailed calculation, which somewhat obscures the reasoning. As a result, the reader is given some useful information on reactor design calculations in general, quite apart from the question of optimization, but as such calculations can be satisfactorily carried out in a variety of ways, a fully detailed presentation of one way may prove misleading.

The optimization method described by the author is of the type in which a number of design parameters are regarded as independently variable, for which

initial values are first assumed. Thereafter, each such parameter is varied in turn to give minimum unit cost of electricity generation. The result is a more economical design to which the same processes can be applied for a second time and an even more economical design thereby achieved. To-day, however, this sort of study is coming to be performed with the aid of one of the larger digital computers. With such aid at hand, the detailed account given of a tabular method of calculation is not of very great value as a guide to optimization. Furthermore, even when one has achieved what appears to be an optimum design in this way, that is to say a design such that the variation of any one independent parameter individually results in an increase in unit cost, there are still other equally economic designs to be found by choosing different initial values for the independent parameters.

Whilst the book is a useful compendium of fairly standard design calculations, it is very sketchy, and perhaps inevitably so, on a major contribution to nuclear power costs, viz. capital costs. Although it may be assumed that the user of the book has access to the capital cost breakdown of a design or two, information is still lacking on the way in which the capital cost of any particular component of a power station varies with the independent parameters chosen. Even without quoting subsequent cost figures, one might have expected a book on this subject to derive some useful relationships between the dimensions of the various plant items, which must affect capital costs, and the independent design parameters.

In conclusion, this book may be summarized as a useful collection of design formulae, as giving an indication of one way in which these formulae may be applied to work out a design, and as an introduction to the possibilities of design optimization.

C. E. ILIFFE.

The Theory of Elementary Particles, by P. ROMAN. Pp. xii + 575. (Amsterdam: North Holland Publishing Co., 1960.) 100s.

One cannot but envy the students in the Physics Department of Manchester University for, as the author tells us in his preface, this book was prepared from what must have been a thorough and stimulating lecture course which he delivered in that department. The author to a large extent has developed the theory he requires and only occasionally calls for a knowledge of elementary theory that he has not dealt with rigorously. This is a feature that will commend itself to many students, but one cannot help thinking that in his effort to keep this volume self-contained the author may have gone into more mathematical detail than others would desire. Despite the warning given that all is plain sailing after the first chapter on the four-dimensional orthogonal group has been digested, some will come to grief before they come on to the stimulating subsequent chapters. It is indeed unfortunate that the student of theoretical physics is not prepared at the undergraduate level for this important subject. On the other hand, some will feel that it is an excellent feature to have this subject dealt with in a place where it has been especially adapted to their uses. For the student who is not prepared or considers it unnecessary to go into the ramifications of this first chapter the rest of the book can be read with considerable benefit.

After dealing with the representations of the four-dimensional orthogonal group the author discusses the field equations for particles of various spin and their quantization, including a discussion of the relation between spin and

statistics. The major part of the book is devoted to invariance properties and selection rules. Here parity, charge conjugation and time reversal are dealt with in an exhaustive fashion. The author devotes a section to the parity violating weak interactions and examines the consequences of invariance under C and PC transformations. In the final chapter isobaric spin is introduced, and developed to discuss the $\Delta I = \frac{1}{2}$ decay rule and various classification schemes.

G. R. SCREATON.

Rheology: Theory and Applications, Vol. III, edited by F. R. EIRICH. Pp. xvi+680. (New York: Academic Press, 1960.) \$21.00.

The last of three volumes initially planned on *Rheology: Theory and Applications* consists, for the most part, of chapters by different authors on the rheological behaviour of some materials of special importance in industry. The rheology of latex is presented by S. H. Maron and I. M. Krieger, of Printing inks by A. C. Zettlemoyer and R. R. Myers, of Pastes and paints by R. N. Weltmann, of Inorganic glasses by W. A. Weyl, of Concrete by M. Reiner; the rheology of Lubrication and lubricants by A. Bondi, of Adhesion by J. J. Bikerman, of Moulding by C. E. Beyer and R. S. Spencer and of Spinning by B. R. Roberts. One is reminded in these chapters of the wide variety of non-Newtonian flow properties that are of commercial importance, and also of the all too common practice of measuring some one parameter, most often an apparent viscosity—and the way it varies with temperature, concentration, rate of shear and other relevant conditions—instead of seeking equations of state to represent the rheological behaviour of a material fairly completely when it is known that a single parameter does not suffice to do so.

An admirable survey of the theory and observation of electroviscous effects is given by B. E. Conway and A. Dobry-Duclaux in a chapter on Viscosity of suspensions of electrically charged particles and solutions of polymeric electrolytes. Atomistic approach to the rheology of sand-water and of clay-water mixtures by W. A. Weyl and W. C. Ormsby, The deformation of crystalline and cross-linked polymers by I. L. Hopkins and W. O. Baker, and The viscosity and elasticity of interfaces by D. W. Criddle are further chapters which serve to draw attention to some of the effects of inter-particle and inter-molecular forces on macroscopic rheological behaviour.

Some calculated flow patterns in certain types of apparatus are discussed by W. L. Gore and J. M. McKelvey in Theory of screw extruders, and by S. Oka in a long chapter on The principles of rheometry; the latter includes, for example, the theory of flow in capillaries, between coaxial cylinders and in a cone-and-plate viscometer, and overlaps with the content of earlier volumes more conspicuously than any other chapter. A lecture by B. H. Zimm on The normal-coordinate method for polymer chains in dilute solution is reproduced as the opening chapter, a token demonstration that theoretical rheology has not remained static during the years that have elapsed since the publication of Volume I. One feels that the editor could well have left this subject for a fairly complete treatment in the now contemplated Volume IV—a volume that would fill some of the gaps in the present treatise and add more recent developments in the field in a few years' time.

The present volume, taken in conjunction with the two earlier ones, should become a useful reference book for all who are concerned with deformation and

flow phenomena. Without attempting to co-ordinate the different approaches to the study of rheological behaviour, this work brings together what is known of non-Newtonian flow and non-Hookean elasticity in many different materials. It is inevitable that it will facilitate a healthy interchange of ideas between workers in the field whose lines of thought have hitherto diverged.

J. G. OLDROYD.

L'Essai de Microdureté et ses Applications, par H. BÜCKLE. Pp. 274. (Paris: Publications Scientifiques et Techniques du Ministère de l'Air, No. 90, 1960.) 61.00 n fr.

Dr. Bückle is well known as a specialist in the field of microhardness measurement. In this book he has distilled the essence of his work over the last twenty years and summarized his main conclusions. The book is divided into five parts. In Part I Dr. Bückle suggests that the term microhardness should be limited to loads below about 100 g since it is only in this range that characteristics are observed differing from those observed in macrohardness measurements. In Part II he describes briefly and critically the main types of microhardness apparatus available. In Part III he discusses very fully the experimental procedures and the problems involved in obtaining measurements that are reliable and meaningful. It is clear that Dr. Bückle is himself an extraordinarily skilful worker and his experimental results are extremely satisfying both technically and aesthetically. In Part IV he discusses the laws of microhardness. He suggests that the hardness is independent of load for indentations above a certain size and also for indentations below a certain size but that different values of hardness occur at the two extremes. This is connected with the size of what the author terms the coherent domains. As the load is decreased there is a transition from one régime to the other giving a variation of hardness with load. This is an interesting empirical approach for which the author provides a good deal of experimental evidence. In Part V Dr. Bückle describes the technical and scientific applications of microhardness measurements.

The book is very well produced and, if one is not entirely happy with some of Dr. Bückle's theoretical explanations, one is full of admiration for the beautiful experimental work which he has carried out and which he describes with infectious enthusiasm.

D. TABOR.

Introduction à l'Étude de la Rhéologie, par B. PERSOZ. Pp. xx+251. (Paris: Dunod, 1960.) 44 n fr.

This addition to the literature of rheology is divided formally into two parts. The first part develops systematically the basic concepts of rheology, with particular emphasis on the classification of types of stress-strain-time relations and their mathematical formulation. The second part is concerned with the properties of particular materials and their interpretation, and includes chapters on metals and crystal imperfections, inorganic glasses, high polymers, elastomers, aqueous suspensions, paints and varnishes, emulsions, and petroleum products. The last three chapters discuss applications of rheology to biological problems, the rheology of soils, and rheology in geological phenomena respectively.

The first part of the book is the more satisfactory. The second part contains too many short unrelated individual contributions, some of which are rather superficial. There is no uniformity in presentation, and there is little common

ground between the theoretical treatment in the first part and the practical applications in the second. Some contributions give proper literature references, but many give none, even where data are quoted or illustrated graphically.

It is a pity that the editor did not decide on a more limited range of subjects which could be more satisfactorily co-ordinated. The attempt to interest all rheologists will, it is feared, succeed in interesting very few.

L. R. G. TRELOAR.

Solid State Physics, Vol. X, edited by F. SEITZ and D. TURNBULL. Pp. xv + 516. (New York, London: Academic Press, 1960.) \$14.50.

The tenth volume of *Solid State Physics* maintains in all respects the high standards to which we have become accustomed from the earlier volumes of this series. It contains five articles by experts in their respective fields, which are both readable and instructive. They provide up-to-date accounts of their subjects which should be of value, not only to specialists, but also to those whose interests lie in neighbouring fields and who wish to become acquainted with one or other of these aspects of solid state physics without the labour of searching the literature. There is little or no relationship between the topics of the five articles and therefore this volume by itself is unlikely to be of use in its entirety to any individual. It is, therefore, as one of a series that it is to be recommended and those already possessing the earlier volumes will no doubt wish to add this one to their collection. The prior knowledge necessary to appreciate any of these articles, even that dealing with the modern theory of superconductivity, is not beyond what a good graduate research student should possess.

The titles of the five articles are as follows: Positron annihilation in solids and liquids (45 pages), Diffusion in metals (43 pages), Wave functions for electron-excess color centers in alkali halide crystals (118 pages), The continuum theory of stationary dislocations (42 pages), and Theoretical aspects of superconductivity (193 pages).

H. JONES.

Proceedings of International Symposium on the Theory of Switching, Parts I and II. Part I, pp. xi + 305, part II, pp. vii + 345. (Cambridge Mass.: Harvard University Press; London: Oxford University Press, 1959.) 120s.

These two large handsome volumes contain 39 papers, about six referring to transistors, cores or such elements, the remainder being mathematical. One only deals with telephone switching the others being concerned with the switching problems arising in computers and automata. A number use Boolean matrices and one uses topology for net reduction, another reduces multi-output nets by considering an associated larger single output net. There is a valuable paper on the theory of asynchronous circuits and one on multipurpose logical devices. Unfortunately majority logic has no place.

J. M. LOCK.

Plasma Physics, by J. G. LINHART. Pp. xi + 278. (Amsterdam: North-Holland; New York: Interscience, 1960.) 50s.

The past few years have been a period of intense research activity, both theoretical and experimental in attempts to achieve controlled thermonuclear fusion. From this work has grown the new subject of plasma physics, and Dr. Linhart's is the first textbook to correlate the essential aspects of this rapidly expanding field.

A degree level of mathematics is assumed and the necessary refined techniques built up from this basis. The first two chapters deal with plasma behaviour under the influence of variable fields of force using the single particle and the fluid model modes of representation. In a further three chapters these principles are applied to the problems of equilibrium configurations, waves and instabilities and shock waves in a plasma. Transport mechanisms are considered in the next chapter devoted to collision and relaxation processes. The remaining two chapters apply the foregoing material to topical research problems, particularly to that of controlled fusion. Other applications cited include high-frequency oscillators, particle accelerators and rocket propulsion. A very complete index of current literature is included.

Such a comprehensive list of topics demands concise treatment if the volume is to remain a useful size. The result is a textbook which any workers in plasma physics should add to his library.

C. B. WHEELER.

The Study of Elementary Particles by the Photographic Method, by C. F. POWELL, P. H. FOWLER and D. H. PERKINS. Pp. xvi+669. (London, New York, Paris, Los Angeles: Pergamon Press, 1959.) £12 10s.

As the authors explain, their original intent was to produce an atlas of photomicrographs, but the enterprise grew into a treatise on elementary particles. This process was fortunate in that they have succeeded in producing not only a valuable and useful text, both for the specialist and the beginner, but also a visual document of great aesthetic value. Except for limitations set by the rather high price of the book, it is one which should be owned by all who are interested in this field of physics. The shortcomings which are pointed out in this review are of minor importance and do not significantly detract from a work of such magnitude.

Three hundred and fifty photographic documents assembled in about 185 plates constitute the core of the work. Of these, only one-half were previously available in published form. The rest have been produced expressly in order to introduce and underline each subject of the text with a visual reference. Judicious selection from a great wealth of material has resulted in such an harmonious balance of the text with the image that very few of the photographs could be omitted without upsetting this balance and interfering with the logic of the whole work.

As a text, the book can be considered as falling into three parts, which might well have been bound in three separate volumes, lighter and handier than the single big book.

The first section describes the history of the photographic method, and serves as an introduction to the rest of the book by explaining the various techniques involved in the preparation and handling of the emulsions and in making the measurements on the processed plates. The development of the tool from a simple particle detector to a powerful analytical device is warmly and effectively demonstrated. This section is not meant to be a handbook; the reader will find here neither tables of constants nor detailed recipes. Although these can be found through the bibliography, it is a pity that the authors with their great experience on the subject decided not to give a more complete treatment in a text which covers all the aspects of the art. This section is, however, invaluable as a comprehensive introduction to the method

for the beginner or the layman, and as an up-to-date summary and appraisal of the fundamental points for the specialist. The duality of approach, historic and didactic, in this as in the later sections calls for a clear, complete and accurate index and cross reference; this requirement is not entirely fulfilled. While this will not worry the specialist it may put the less initiated at a disadvantage.

The second section shows how the nuclear emulsion, once the ugly duckling of nuclear physics techniques, rose to the ultimate test of discovery; in the decade following the first major technical break-through in 1945 six of the present fundamental particles were found with its help. In the case of many of the others the method made important, if not decisive, contributions. These achievements are presented as a part of a masterly treatment of the history and the properties of the fundamental particles as they are known today. Since many of the aspects of the problems discussed are by now well understood, this section should become a classic as a textbook for the beginner and reference book for the specialist. In this as in the previous section the great clarity and vigour of the text derives from a presentation which necessarily somewhat simplifies the problems. For example, as an historical account one misses the discussion of the errors and misinterpretations which did occur in the field, and whose clarification often added much to an understanding of the method.

The last section is devoted to the study of high-energy particles, the spectacular cascades, jets and heavy primary particles of the cosmic radiation. Unlike the preceding sections, it deals primarily with problems which are still unsolved and so while it is the least complete part of the work, it is most encouraging, since it shows that there are still new ways of using this technique, and new problems to be investigated. It leaves the reader with the conviction that while it is improbable that emulsion workers will be revisited by the continuous excitement of the discoveries of the great decade, the photographic method still has very important contributions to make. G. P. S. OCCHIALINI.

Principles of Semiconductor Device Operation, by A. K. JONSCHER. Pp. viii + 168. (London: Bell, 1960.) 30s.

This excellent book is intended primarily for those who wish to gain a better understanding of semiconductor devices based on minority carrier injection. In Chapter 1 the essential concepts of electrons and holes on the energy band diagram, mobility, transition processes, the effects due to changes in impurity concentration and the motions of free carriers are laid down. Chapter 2 deals with the concept of generation and recombination of non-equilibrium densities of holes and electrons. The central problem of semiconductor device physics, namely the transport of these carriers in a semiconductor, is covered in Chapter 3 in relatively simple terms by limiting the treatment to homogeneous material, one-dimensional flow, no trapping and limited surface recombination. An extension to inhomogeneous material, including LH junctions, is made in Chapter 6. Chapter 4 gives a detailed analysis of the properties of p-n junctions and actual junction diodes, which is extended in Chapter 5 to cover junction transistors, four-layer devices p-n-p-n and LH(n₊-n-n₊) devices. The book concludes with eight short appendices, including a list of symbols and an index. Basic references and a few related problems are given at the end of each chapter. The text is well illustrated with many good line drawings.

W. BARDSLEY.

Cryophysics, Interscience Tracts on Physics and Astronomy, No. 7, by K. MENDELSSOHN. Pp. viii+183. (New York, London: Interscience, 1960.) 34s.

Low temperature physics has undergone something of a revolution in recent years; from being an esoteric art practised in a very few specialized laboratories it has now changed into a common technique which is beginning to find industrial applications. In fact some people are beginning to deny the existence of low temperature physics as a separate subject. Dr. Mendelssohn stoutly maintains, however, that the region of temperature where the thermal energy is reduced to the same order as the zero point energy is still worthy of separate study; this is the physics of the quantization of energy in aggregate matter, where superfluidity perhaps makes manifest a new state of order and poses a unique problem in the statistical interpretation of entropy.

This book is an up-to-date review, brief but stimulating, of the main topics of traditional low temperature studies. There are chapters on cryogenics in general, specific heats, magnetism, transport phenomena, superconductivity and the helium problem, and an extra chapter dealing with odd offshoots such as trapped free radicals, bubble chambers and masers. The book is written for the final year undergraduate and it is excellently designed to stimulate interest in this important field of physics.

E. MENDOZA.

Heat Transfer, Vol. 2, by M. JAKOB. Pp. xxxiii+652. (London: Chapman and Hall, 1957.) 120s.

This second volume by Jakob, which has been brought to print by Dr. Kezios after Jakob's death in 1955, takes its natural place as one of the treatises on heat transfer which everyone interested in the subject will want to possess. The second volume deals with a rather curious mixture of radiation configuration problems and a number of special applications such as regenerators, cooling towers, high speed gas flows, liquid metals, which at first sight fit into no particular pattern, but which nevertheless includes many of the fields of current importance. The presentation has the clarity and originality of the author's first volume and will be found excellent, among other uses, for advanced lectures in heat transfer. The treatment in many cases includes quite novel calculations worked out by the author. It is inevitable in a book of this kind that some sections, such as that on high speed laminar boundary layers, will become out of date sooner than others, but there is much which will remain authoritative for a long time, such as the chapters on regenerator theory and thermometric devices.

This book, with the first volume, occupies a unique place in heat transfer literature, both for the width of subjects covered and the thoughtful and thorough presentation of the fundamentals.

O. A. SAUNDERS.

Physique des Circuits, par P. GRIYET and R. LEGROS. Pp. vii+553. (Paris: Masson, 1960.) 90 n fr.

In these days, with a steady stream of books appearing in the field of electric circuit theory, so many of which seem to be closely related in content, few with anything new to say, it is refreshing to come across one which is totally

different. Nevertheless it is not clear for whom this book has been written, being a rather strange mixture of theoretical and very practical matters.

It starts with an historical introduction, covering the development of radio, radar, television and other electronic techniques, referring to the main contributions of the great. Then circuit theory is started, from the very beginning, with definitions of resistors, capacitors, inductors. Gradually their differential equations are built up, complex numbers introduced and the well-known properties of single and multimesh circuits developed and illustrated for transient and steady-state conditions. All this is interlarded with practical matters (e.g. including drawings of a transformer and high frequency coaxial connector).

Various devices are described: microphones, bolometers, thermocouples, directive couplers, etc., and used to illustrate fundamental physical principles. There is extensive treatment of single and coupled tuned circuits, skin effect, parasitic elements, together with details of design and construction of practical circuit elements (inductance coils, variable capacitors, etc.).

The book closes with notes on new developments in electrical materials; ferrites, magnetic powder and solid cores of many kinds, their preparation and their properties. The book is entitled *Physics of Circuits* which indeed it is; it is not mathematical 'circuit theory'.

COLIN CHERRY.

Plasma Physics, by S. CHANDRASEKHAR (notes compiled by S. K. TREHAN). Pp. x+217. (Chicago: University Press, 1960.) 14s.

This work is based on lectures given by Chandrasekhar using notes compiled by Trehan. Rather surprisingly we learn from the introduction that Professor Chandrasekhar has not read the book. There are chapters on the basic equations and conservation laws, first-order orbit theory, adiabatic invariants in the motion of charged particles, application of first-order orbit theory, the stability of pinched discharges, plasma oscillations and finally transport phenomena in ionized gases.

The work of Rosenbluth, Spitzer, Kruskal and of Chandrasekhar himself is often referred to, together of course with that of other workers in this field.

There are many interesting sections, especially of course those on stability criteria, and the treatment of the Rayleigh-Taylor instability is particularly good.

J. D. CRAGGS.

Approaches to Thermonuclear Power, by R. F. SAXE. Pp. x+65. (London: Temple Press, 1960.) 12s. 6d.

This monograph in the *Nuclear Engineering* series is concerned with presenting a simple exposition of the basic ideas of high temperature plasma physics. In particular it aims at giving a non-specialist account of the various experimental approaches to thermonuclear power.

The first two chapters briefly discuss the requirements imposed on a thermonuclear power producing device, and the basic theory relating to the experimental devices existing at present. The remainder of the book is devoted to discussions of the linear pinch, the toroidal pinch, the stellarator, and mirror machines. Unfortunately no account is given of the so-called θ or orthogonal pinch.

The accounts presented of each of these experimental devices are extremely limited in extent and are meant to serve as an introduction to some of the problems of plasma physics. The material is well presented and is very readable.

J. A. NATION.

The Many Body Problem, compiled at the UNIVERSITÉ DE GRENOBLE. Pp. xv + 675. (Paris: Dunod, 1959.) 6900 fr.

Les Houches is becoming something of a legend in the world of theoretical physics, the most famous of the Summer Schools. The 1958 School was primarily concerned with the applications of modern perturbation theory to a number of many body problems of current interest. This book contains the principal lectures delivered during the School. It is, unlike many superficially similar collections of lectures, likely to remain of permanent worth. After an introductory article by Hugenholtz setting out the diagrammatic methods of perturbation theory, there follow articles by Brueckner, Thouless, Bloch and de Dominicis, Mottelson, Weisskopf, Stroutinski, Lipkin, Beliaev, Bohm, Pines, Schrieffer, Lynton, and Huang. The subjects treated include nuclear matter, liquid ^3He and ^4He and the electron gas, superconductivity, nuclear structure (and especially the superconductivity-like effects of pairing forces), and plasmas. Nowhere else can one find such a complete and mostly lucid account of the several different aspects of many body theory, and it would be difficult to imagine a better tribute to the genius of those responsible for the creation of Les Houches.

B. H. FLOWERS.

Introduction to Laplace Transforms for Radio and Electronic Engineers, by W. D. DAY. Pp. vii + 183. (London: Iliffe; New York: Interscience, 1960.) 32s. 6d.

Electromagnetic Wave Propagation, edited by M. DÉSIRANT and J. L. MICHIELS. Pp. xiii + 730. (London, New York: Academic Press, 1960.) \$ 22.

Experimental Physics for Colleges, by W. A. SCHNEIDER and L. B. HAM. Pp. xiv + 442. (New York, London: Macmillan, 1960.) 34s. 6d.

Mechanics, 2nd Edn, by K. R. SYMON. Pp. xiv + 557. (London, Reading, Massachusetts: Addison-Wesley, 1960.) 60s.

Nuclear Engineering Abstracts, Vol. 1, No. 1. July, 1960. Pp. 100. (London: Edwards High Vacuum.) £6 6s. per volume.

Beryllium, Metallurgy of the Rarer Metals No. 7, by G. E. DARWIN and J. H. BUDDERY. Pp. ix + 392. (London: Butterworths Scientific Publications, 1960.) 70s.

Flames, their Structure, Radiation and Temperature, by A. G. GAYDON and H. G. WOLFHARD. Pp. xiii + 383. (London: Chapman and Hall, 1960.) 70s.

Landolt-Börnstein, Zahlenwerte und Funktionen aus Physik, Chemie, Astronomie, Geophysik und Technik, Vol. 2, Part 6, 6th Edn. Pp. xvi + 1018. (Berlin, Göttingen, Heidelberg: Springer, 1959.) 448 DM.

Concepts of Thermodynamics, by EDWARD F. OBERT. Pp. xxi + 528. (New York, Toronto, London: McGraw-Hill, 1960.) 85s. 6d.

Special Functions, by EARL D. RAINVILLE. Pp. xii + 365. (New York, London: Macmillan, 1960.) 82s.

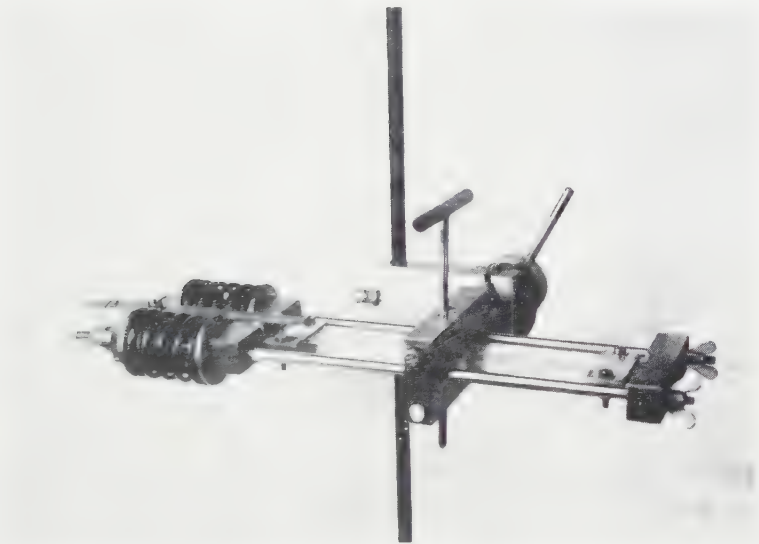


Fig. 2. Straining frame showing specimen under test.



Comparison of Reflection Methods for Measuring Optical Constants without Polarimetric Analysis, and Proposal for New Methods based on the Brewster Angle

BY THE LATE S. P. F. HUMPHREYS-OWEN

Department of Physics, Birkbeck College, University of London

MS. received 8th August 1960

Abstract. The pairs of observations at non-normal incidence which specify the various reflection methods of determining the optical constants n and k are compared as to their arithmetical sensitivity to changes in n and k and hence as to their theoretical suitability. Only the simple methods which do not require polarimetric analysis are considered. The comparison of sensitivity is done by inspection of charts prepared from computed tables and which cover a wide range of n and k . A previously unnoticed property of the Fresnel equations at 45° incidence allows any method, not just one in which a ratio of reflectivities is measured, to be employed without a standard reflector. Experimental factors as well as theoretical sensitivity are considered, and the use of the Brewster angle as one observation is proposed. An exact analysis of the Brewster condition has been made, which leads to explicit equations applicable to two proposed methods. The distinction between the Brewster angle and the principal angle of incidence, which are often confused, is emphasized.

§ 1. INTRODUCTION

THE optical constants of an isotropic medium can in principle be derived from a pair of reflection measurements at non-normal incidence. In this paper attention is confined to the experimentally simple methods which do not require any polarimetric analysis. Linearly polarized incident radiation, with electric vector either in or normal to the plane of incidence is assumed except in one method which uses unpolarized incident radiation. The various reflectivities which can be measured are defined as follows: R_w , incident electric vector in the plane of incidence; R_y , incident electric vector normal to the plane of incidence; R_w/R_y , the ratio of the above two reflectivities; $\frac{1}{2}(R_w + R_y)$, the mean, i.e. the reflectivity for natural incident radiation.

From these reflectivities, together with knowledge of angles of incidence, various pairs of measurements can be chosen. A particular pair of measurements represents a method, and the following is a list of possible methods.

Class 1. Two reflectivity measurements at one angle of incidence, or one reflectivity measurement at each of two angles of incidence, comprising:

Method A: reflectivity at two angles of incidence using natural incident radiation.

Method B: R_w at two angles of incidence.

Method C: R_y at two angles of incidence.

Method D: the ratio R_w/R_y at two angles of incidence.

Method E: R_w and R_y separately at one angle of incidence.

Class 2. One reflectivity measurement at any angle of incidence, and measurement of a special angle of incidence having an optical property which supplies the necessary second condition. There are two special angles, the principal angle of incidence which is not discussed in this paper, except incidentally in § 6, and the Brewster angle which is here defined as that angle for which R_w is a minimum as function of angle. This class comprises:

Method F: Brewster angle and R_w at that angle.

Method G: Brewster angle and R_y at that angle.

Method H: Brewster angle and R_w/R_y at that angle.

Methods J: Brewster angle and either R_w , R_y or R_w/R_y at any other angle.

All these methods have their various experimental aspects, but one aspect is shared, namely the arithmetical sensitivity of the chosen pair of quantities to changes in the optical constants. The equations for reflectivity at non-normal incidence are complicated and because hand computation over a large range of values of the optical constants has been impracticable very little has been published on this aspect of the various reflection methods:

But the computations are rapidly performed by machine, and one purpose of this paper is to show some charts, prepared from machine computed tables, which reveal this sensitivity.

Another purpose is to publish an exact analysis of the Brewster condition, i.e. minimum of R_w , which does not seem to have been done previously; and since two Brewster angle methods seem promising the analysis has been used in order to derive explicit equations which allow these methods to be used without numerical or graphical interpolation from tables.

The Fresnel reflectivity equations have been put into forms which are rather more explicit and simple than those in the few textbooks which contain the equations. A result was the discovery of the property at 45° incidence dealt with in § 3.

§ 2. SYMBOLS, ABBREVIATIONS AND FORMULAE

Angle of incidence $= \theta$, $\cos \theta = x$, $\sin \theta = y$. The optical constants are defined from the equation $N = n - ik$. Abbreviations are

$$\begin{aligned} n^2 + k^2 &= p, & n^2 - k^2 &= q, & q - y^2 &= \lambda, \\ \mu^2 &= \lambda^2 + 4n^2k^2, & \text{or} & & \mu^2 &= p^2 - 2qy^2 + y^4. \end{aligned} \quad \dots (1)$$

The abbreviations μ and λ are related to the more usual a and b by

$$\mu = a^2 + b^2, \quad \mu + \lambda = 2a^2, \quad \mu - \lambda = 2b^2.$$

The formulae for the reflectivities are used in the following forms.

Incident electric vector in plane of incidence:

$$R_w = \frac{\mu + p^2x^2 - x(\mu + y^2)[2(\mu + \lambda)]^{1/2}}{\mu + p^2x^2 + x(\mu + y^2)[2(\mu + \lambda)]^{1/2}}. \quad \dots (2)$$

Incident electric vector normal to plane of incidence:

$$R_y = \frac{\mu + x^2 - x[2(\mu + \lambda)]^{1/2}}{\mu + x^2 + x[2(\mu + \lambda)]^{1/2}}. \quad \dots (3)$$

Ratio of above two reflectivities:

$$\frac{R_w}{R_y} = \frac{\mu + (y^2/x)^2 - (y^2/x)[2(\mu + \lambda)]^{1/2}}{\mu + (y^2/x)^2 + (y^2/x)[2(\mu + \lambda)]^{1/2}}. \quad \dots (4)$$

§ 3. NORMALIZATION OF AN INSTRUMENTAL READING PROPORTIONAL TO REFLECTIVITY

Methods based on the ratio of reflectivities, Eqn (4), are often recommended because, amongst other advantages, they do not necessitate comparison with a standard reflector. For the ratio of two readings, ϕ_w/ϕ_y say, is the same as R_w/R_y as long as the readings are proportional to the reflectivities under all conditions. But it does not appear to have been noticed that reflectivities R_w and R_y can be obtained from readings ϕ_w and ϕ_y by standardizing them at 45° incidence. It is immediately seen from Eqns (3) and (4) that at $\theta = 45^\circ$, $R_y = R_w/R_y$ for all n and k . Thus if, generally, $R_w = \alpha\phi_w$, and $R_y = \alpha\phi_y$, then α is given by

$$\alpha = (\phi_w/\phi_y^2)_{45^\circ} \dots\dots (5)$$

so that the instrumental constant may be determined from two readings at 45° incidence, and no standard reflector is needed. Of course, as in all experiments in which the angle of incidence is changed, care must be taken that the effective aperture remains constant.

§ 4. COMPARISON OF THE METHODS

In the charts of this section the two measured quantities form the axes. Since these two quantities fix n and k a point in the plane of a chart fixes an (n, k) value pair. Through some of these points intersecting curves of constant n and k , at fixed intervals, are drawn. The sensitivity is estimated from the spaces between the curves for a given scale of the axes. Large spacing means high sensitivity and vice versa. Fine details of this sensitivity are not important because experimental factors are over-riding, but one distinguishes between methods of poor sensitivity in which the curves are relatively crowded as in Figs 1 and 5, and methods of good sensitivity such as in Figs 2 and 4. One also notices favourably the methods in which the sensitivity is maintained at high n , for example Figs 2 and 4 in contrast to Fig. 3.

All the methods show an apparent fall in sensitivity at very low k ; but in practice this may not be such a disadvantage as it seems, for the sensitivity with

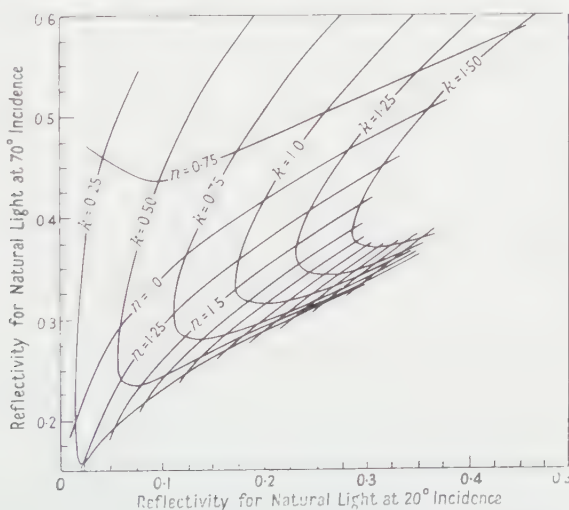


Fig. 1. Sensitivity chart for natural light reflectivity at two angles of incidence, 20° and 70° . Method A of the text.

respect to k^2 is maintained, and k^2 is the important quantity in most physical theories.

In general, methods which use the ratio R_w/R_y are to be preferred, and Avery (1952) discusses the reasons. But other methods can still be considered if some special advantage exists, especially as comparison with a standard reflector is now not necessary. In the following discussion the methods will be denoted by the letters in § 1.

The chart for method A is Fig. 1. The method has been used and is due to Simon (1951). Although the sensitivity is relatively poor, the method can be used at wavelengths at which polarization is difficult. The most important experimental disadvantage is the large change in angle of incidence which is necessary. The figure is for 20° and 70° , the angles chosen by Simon.

The methods B and C, which are variants of D, have not been considered because they have no special advantages to counter the use of the ratio R_w/R_y in method D and its good sensitivity.

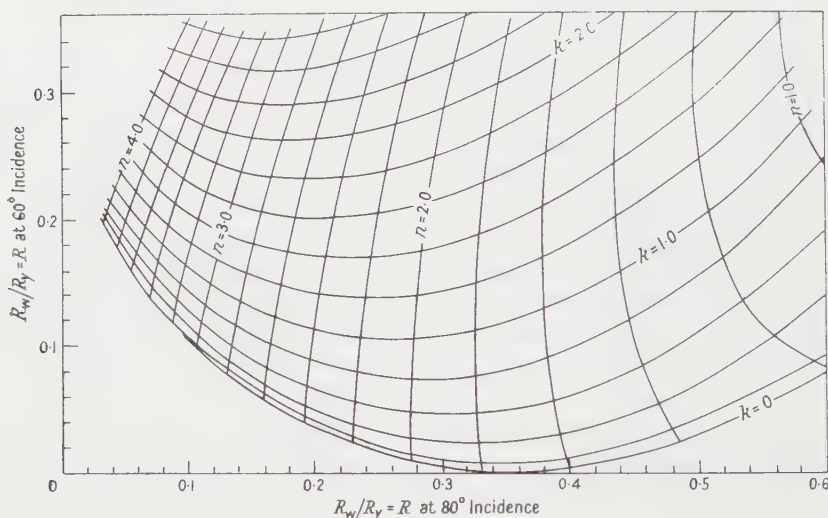


Fig. 2. Sensitivity chart for $R_w/R_y = R$ at two angles of incidence, 60° and 80° . Method D of the text.

The chart for method D is Fig. 2. It has been used in practice and is due to Avery. The angles, 60° and 80° , are those chosen by him. They have to be high, not too far apart because of aperture difficulties, and not too close together because of loss of sensitivity. The disadvantage is the need for one of these angles to be so near grazing. With most materials the reflectivities are changing very rapidly with angle near 80° and a slight error in setting to the angle has important consequences.

The chart for method E is Fig. 3; 70° is about the best value for the angle. There are disadvantages in measuring R_w and R_y separately and having to normalize by the method of § 3, but the method is worth considering because of the use of only one angle, which is not changed, and which is not too close to grazing. There is a good range of n and k for which the sensitivity is satisfactory.

Methods F and H have similar charts and that for H is Fig. 4. H is a promising method; it has a good chart, it measures the ratio, the angle is not changed during a

determination of n and k , and explicit equations are available (see §5). A disadvantage, shared by F, is the fact that R_w and R_y have very low values when k is small, and this raises experimental difficulties. Nothing is gained by considering methods J because of the change of angle, but method G is a possible alternative with materials of low k . Its chart is Fig. 5. The advantage of measuring R_y , which has quite high magnitudes, is set against the poorer sensitivity and the need to normalize. Explicit equations are available (see §5).

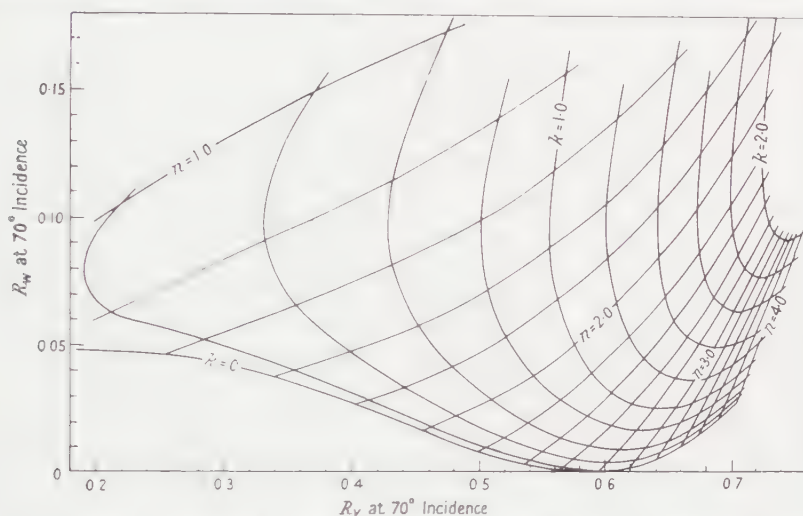


Fig. 3. Sensitivity chart for R_w and R_y separately at 70° incidence. Method E of the text.

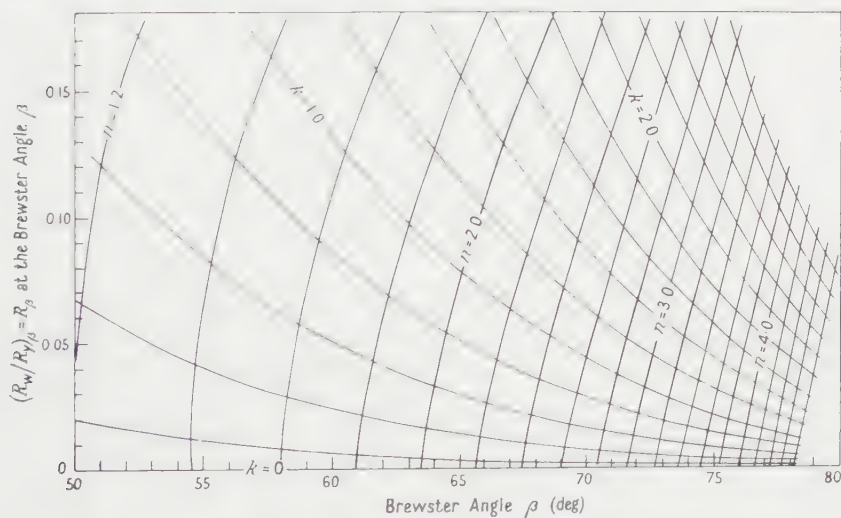


Fig. 4. Sensitivity chart for $(R_w/R_y)_B = R_B$ and the Brewster angle β . Method H of the text.

No one method shows up overwhelmingly above the others. On the whole, method H, with the alternative of G at low k , seems the best, though D and E are not to be excluded. Perhaps the fact that explicit equations are available for H and G tips the balance in their favour. These equations will be derived in the next section.

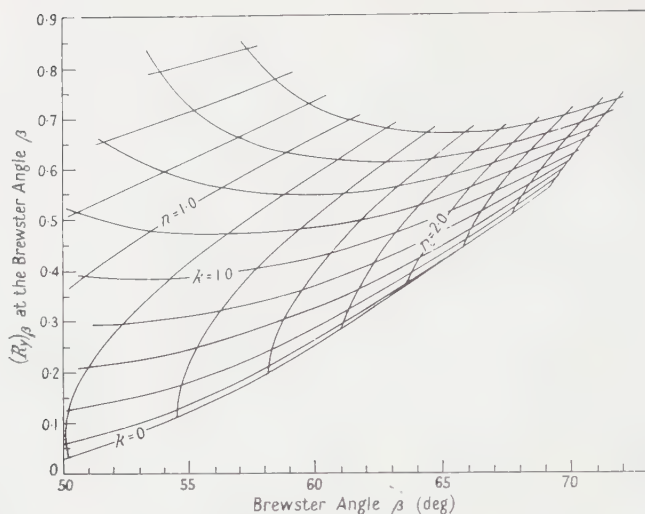


Fig. 5. Sensitivity chart for $(R_y)_\beta$ and the Brewster angle β . Method G of the text.

§ 5. ANALYSIS OF THE BREWSTER ANGLE CONDITION

5.1. The Condition for Minimum R_w

The algebra is very laborious and there may be more elegant routes to the final result. The following is an outline of one procedure.

Write Eqn (2) in the form

$$R_w = \frac{1 + A^2 - 2A \cos \psi}{1 + A^2 + 2A \cos \psi}$$

where

$$A = \frac{\mu^{1/2}}{p x}, \quad \cos \psi = \frac{\mu + y^2}{p} \left(\frac{\mu + \lambda}{2\mu} \right)^{1/2}.$$

Taking x as independent variable, the condition for an extremum is

$$\frac{d(1 + A^2)/dx}{1 + A^2} = \frac{d(A \cos \psi)/dx}{A \cos \psi}, \quad \text{or} \quad \frac{A^2 - 1}{A^2 + 1} \frac{1}{A} \frac{dA}{dx} = \frac{d \cos \psi / dx}{\cos \psi}.$$

The following equalities may be noted in doing the differentiation,

$$\frac{d\lambda}{dx} = 2x, \quad \frac{d\mu}{dx} = \frac{2x\lambda}{\mu}, \quad \frac{1}{A} \frac{dA}{dx} = \frac{\lambda x^2 - \mu^2}{\mu^2 x},$$

$$\frac{d}{dx} (\mu + \lambda)^{1/2} = \frac{x(\mu + \lambda)^{1/2}}{\mu}, \quad \frac{d}{dx} (\mu + y^2) = - \frac{2x(\mu - \lambda)}{\mu}.$$

After differentiation the condition becomes

$$\frac{\mu - p^2 x^2}{\mu + p^2 x^2} = \frac{x^2(\mu - \lambda)(\mu - y^2)}{(\mu^2 - \lambda x^2)(\mu + y^2)}.$$

This equation can be greatly simplified, but the way is easily missed. Expand into the form $\mu E = \mu^2 F$ where

$$E = x^2 (\mu^2 - p^2 x^2 y^2) - (y^2 - p^2 x^2)(\mu^2 - 2\lambda x^2),$$

$$F = \mu^2 - p^2 x^2 y^2 + x^2 (y^2 - p^2 x^2).$$

Put $p^2 - 2q + 1 = c$, say, and Eqn (1) becomes $\mu^2 = c + 2qx^2 - x^2 - x^2y^2$. Substitute this for μ^2 in E and F and put $\lambda = q - y^2$. Remembering that $x^2 + y^2 = 1$, it is found that E simplifies to $c(p^2x^2 - y^4)$ and F simplifies to cy^2 . Then, since $\mu = E/F$, the condition is

$$\mu_\beta = (p^2x^2 - y^4)/y^2 = p^2 \cot^2 \beta - \sin^2 \beta \quad \dots\dots (6)$$

where β is the Brewster angle. After squaring and use of Eqn (1) the condition becomes

$$p^4 \cot^4 \beta - p^2(1 + 2 \cos^2 \beta) + 2q \sin^2 \beta = 0 \quad \dots\dots (7)$$

which is a cubic in $\sin^2 \beta$. It is discussed further in §6.

5.2. Derivation of Explicit Equations

Method H. Eqn (4) is of the form $R = (r - s)/(r + s)$. Let $s/r = P$, and in the expression for P^2 substitute for μ and μ^2 using Eqn (6). Put $\lambda = q - \sin^2 \beta$ and substitute for q using Eqn (7). Solve as a quadratic in p^2 . Near the end, it is slightly simpler to use $Q^2 = 1 - P^2$. The solution is

$$p^2 = \frac{\sin^2 \beta \tan^2 \beta}{2(1 - Q^2 \cos^2 \beta)} \left(2 + \tan^2 \beta - 2Q^2 \cos 2\beta + \tan^2 \beta (1 + 8Q^2 \cos^2 \beta)^{1/2} \right) \quad \dots\dots (8)$$

where $Q^2 = 4R_\beta/(1 + R_\beta)^2$.

The second explicit equation is the rearrangement of Eqn (7):

$$q = \frac{p^2(1 + 2 \cos^2 \beta - p^2 \cot^4 \beta)}{2 \sin^2 \beta} \quad \dots\dots (9)$$

Method G. A similar process, starting with Eqn (3), yields

$$p^2 = \frac{\sin^2 \beta \tan^2 \beta}{2(1 - Q_y^2 \sin^2 \beta)} \times \left(3 + 2Q_y^2 \cos 2\beta + [9 - 4 \operatorname{cosec}^2 \beta + 4Q_y^2 (\operatorname{cosec}^2 \beta - 2 \sin^2 \beta)]^{1/2} \right) \quad \dots\dots (10)$$

where $Q_y^2 = 4(R_y)_\beta/(1 + (R_y)_\beta)^2$.

The second equation is Eqn (9).

An approximation for method H. The approximation $|n^2 + k^2| \gg 1$ introduces error which may be acceptable for certain values of n and k , and since it leads to very simple equations it may be preferred in such cases. Under the approximation Eqn (4) becomes

$$R_\beta \sim \frac{(n - \sin \beta \tan \beta)^2 + k^2}{(n + \sin \beta \tan \beta)^2 + k^2}$$

and Eqn (6) becomes $p \sim \sec^2 \beta$. The resulting explicit equations are

$$n \sim \frac{1 - R_\beta}{1 + R_\beta} \sec \beta \quad \dots\dots (11)$$

$$k \sim \frac{2R_\beta^{1/2}}{1 + R_\beta} \sec \beta. \quad \dots\dots (12)$$

Figure 6 shows the percentage errors produced when n and k are derived from observed R_β and β using Eqns (11) and (12).

§ 6. DISTINCTION BETWEEN THE BREWSTER ANGLE AND THE PRINCIPAL ANGLE OF INCIDENCE

When $k=0$ there exists one special angle, the polarizing angle, which is defined by two features: (i) R_w is a minimum (zero), (ii) the phase difference δ between the vector amplitudes r_w and r_y changes abruptly by 180° .

When $k>0$, these two features become modified and they now belong respectively to two different angles. Zero R_w is modified to merely minimum R_w and belongs to the Brewster angle by definition, and the abrupt 180° phase change is modified to a gradual phase change, and the principal angle is defined such that δ passes through the value 90° .

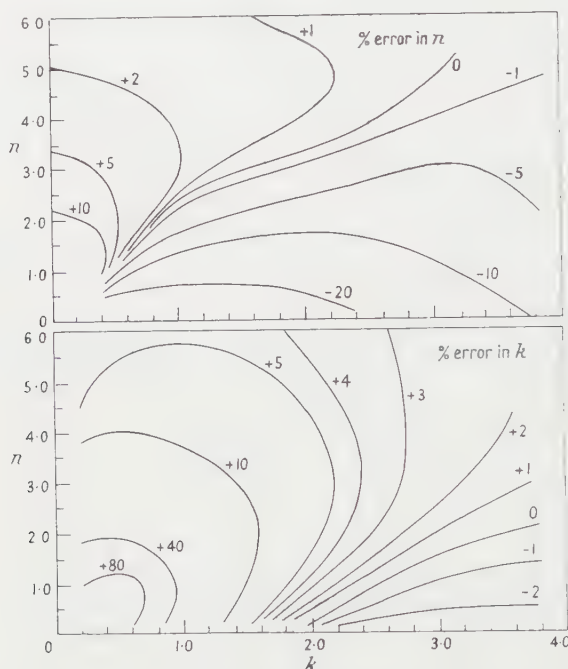


Fig. 6. Charts to show, over an (n, k) range, the errors in n and k produced when using the approximation $|n^2 \pm k^2| \gg 1$ in method H.

The Brewster angle and the principal angle are different from each other and from the polarizing angle. (The polarizing angle is also sometimes called the Brewster angle but it is better to keep a special name for the special case $k=0$.)

The above is not new, but there still exists confusion on the subject. For example, Pfund (1941) describes a method for glasses of measuring n based on the abrupt 180° phase change and using the equation $n = \tan \theta$. But he goes on to claim that the method is applicable to black materials. This may be approximately true if k is small, but strictly it is not correct. When $k>0$, the 180° phase change is no longer abrupt and is no longer associated with one angle. Also the equation $n = \tan \theta$ is no longer valid.

Another example is taken from a recent textbook (Longhurst 1957). In a paragraph concerned with metals one reads: "It is found that δ is always exactly 90° for the angle of incidence for which R_i is a minimum. This angle is called

the principal angle of incidence." This is a straightforward instance of incorrect identification of the Brewster angle and the principal angle where $k > 0$.

Analytically, the Brewster condition can be expressed as the cubic derived from Eqn (7), namely,

$$2(p^2 + q)v^3 + p^2(p^2 - 3)v^2 - 2p^4v + p^4 = 0 \quad \dots\dots (13)$$

where $v = \sin^2 \beta$.

The principal angle condition is well known, and is, in the present notation, $\mu_\gamma = \sin^2 \gamma \tan^2 \gamma$, where γ is the principal angle. The corresponding cubic is

$$2(q + 1)\omega^3 - (p^2 + 4q + 1)\omega^2 + 2(p^2 + q)\omega - p^2 = 0, \quad \dots\dots (14)$$

where $\omega = \sin^2 \gamma$.

When k is put equal to zero in Eqns (13) and (14) they do not become identical: they remain different but have the same physically significant root corresponding to $n = \tan \beta = \tan \gamma$. The other roots remain different.

Regarding the values of β and γ , it turns out that their difference is quite small, of the order of 0.1° for materials approximately of $n=3$ and $k=0.4$. This explains the apparently accurate values of n obtained by Pfund for material such as anthracite.

It is not worth while tabulating the difference; the intention has been merely to clarify the matter.

ACKNOWLEDGMENTS

All the programmes for computing were done by Dr. J. C. E. Jennings, Department of Physics, Birkbeck College. Computing machines used were APEX of Dr. A. D. Booth, Department of Numerical Automation, Birkbeck College, and MERCURY of the University of London Computing Unit.

REFERENCES

- AVERY, D. G., 1952, *Proc. Phys. Soc. B*, **65**, 425.
 LONGHURST, R. S., 1957, *Geometrical and Physical Optics* (London: Longmans Green), p. 441.
 PFUND, A. H., 1941, *J. Opt. Soc. Amer.*, **31**, 679.
 SIMON, I., 1951, *J. Opt. Soc. Amer.*, **41**, 336.

Diffraction of Light by very High Frequency Ultrasonic Waves

BY B. RAMACHANDRA RAO AND J. SATYANARAYANA MURTY

Ultrasonic Laboratories, Andhra University, Waltair, India

MS. received 6th January 1960, in revised form 25th July 1960

Abstract. This paper embodies the results of the investigation on the diffraction of light by very high frequency ultrasonic waves in the range of 50 to 230 Mc/s. Intensity measurements were made by using a highly sensitive photomultiplier photometer. Results of the variation of the intensity of the first order of the diffraction pattern with the tilt angle for weak sound fields agreed equally well with both the theories of David and that of Bhatia and Noble. Measurement of the intensity variation of the first order with length of the sound field at the Bragg incidence angle showed that only the theory of Bhatia and Noble is valid for stronger sound fields.

§ 1. INTRODUCTION

ASYMMETRY in diffraction of light by ultrasonic waves at oblique incidence was first studied experimentally by Bär (1936), Parthasarathy (1936) and Körff (1936). It was later extended to very high frequencies by Bhagavantam and Rao (1948) and Raghupathi Rao (1955), who showed that the theory of David (1937) explains satisfactorily the experimental results. According to David's theory the intensity of the first order of the diffraction pattern $I_{\pm 1}$ on either side of the central order expressed as a fraction of the incident light is given by the relation

$$I_{\pm 1} = I_{\max} \left[\frac{\sin(\pi L \theta / \lambda^*)}{\pi L \theta / \lambda^*} \right]^2 \quad \dots\dots (1)$$

where L is the length of sound field, λ^* the wavelength of the sound wave, θ the angle of deviation from the Bragg angle and I_{\max} the maximum intensity of the diffraction line. I_{\max} is given by the relation

$$I_{\max} = \pi \mu L / \lambda \quad \dots\dots (2)$$

where μ is the maximum change in the refractive index and λ is the wavelength of light. Recently Bhatia and Noble (1953) have worked out a general theory of diffraction of light by ultrasonic waves and obtained the same expressions as those of David for angles of incidence far from the Bragg incidence angle. However, at angles close to the Bragg incidence angle, they obtained the following entirely different expression for the intensity I_{-1} of the first-order diffraction line:

$$I_{-1} = \frac{1}{4} \frac{\delta^2 \alpha^2}{\{(\xi - \frac{1}{2})^2 + \frac{1}{4} \delta^2 \alpha^2\}} \sin^2 [\beta \delta \{(\xi - \frac{1}{2})^2 + \frac{1}{4} \delta^2 \alpha^2\}^{1/2}] \quad \dots\dots (3)$$

where $\delta = 2\mu\mu_0\lambda^{*2}/\lambda\alpha$, $\alpha = (\mu_0^2 + 2)(\mu_0^2 - 1)/3 \simeq 1$ for water, $\xi = (\mu_0\lambda^*/\lambda)\sin\phi$, $\beta = \pi\lambda/\mu_0\lambda^{*2}$, μ_0 is the refractive index of the medium (water) and ϕ the angle of

incidence. At the Bragg incidence angle, this expression may be simplified so that I_{\max} is given by

$$I_{\max} = \sin^2 (\pi \mu L / \lambda) \quad \dots\dots (4)$$

which is different from relation (2) obtained by David, particularly when the term $\pi \mu L / \lambda$ is sufficiently high.

With a view to the understanding of the phenomenon of diffraction of light at very high frequencies and to study the relative validity of the above two theories, the authors have undertaken the problem of setting up ultrasonic waves of frequencies up to 250 Mc/s in water and studying experimentally the intensity variation of the first order of the diffraction pattern, both with tilt angle and also with the length of the sound field.

§ 2. EXPERIMENTAL DETAILS

For the purpose of exciting the quartz crystals, conventional series-fed oscillators were used for frequencies up to 150 Mc/s using an RCA 826 valve which could be used up to a frequency of 250 Mc/s with slightly reduced efficiency. To cover the frequency range of 150 to 300 Mc/s, a twin parallel-line oscillator circuit was constructed using silver plated copper tubes for the parallel resonant lines. The crystal was connected across the parallel line at points corresponding to maximum radio-frequency voltage.

A special type of crystal holder using low loss amphenol polystyrene insulators was designed for use at frequencies above 150 Mc/s. An important point in the design of the crystal holders for observing diffraction at very high frequencies was that the light beam traversing the liquid must be very close to the crystal holder on account of the rapid attenuation of the sound beam at these frequencies. This point will be appreciated if we note that even in the case of a low absorption liquid like water, the intensity of the ultrasonic waves falls to 0.15 of its initial intensity in a distance of 0.5 mm for a frequency of 300 Mc/s. The crystal holder was therefore designed in such a way that the light beam passed almost grazing the bottom surface of the crystal which was in contact with the liquid.

The crystal holder was mounted on the top of a small hollow transparent glass cell containing water. The glass cell together with the crystal holder rested on a horizontal platform attached to the shaft of a slow motion rotating arrangement. This arrangement enabled the tilting of the sound wave front about a horizontal axis, so that the angle of incidence of the light beam could be continuously varied. The vernier and the main scale of the slow motion arrangement was calibrated to give the tilt angle from the readings. An X-cut quartz plate of thickness of 0.5 mm was used for frequencies up to 100 Mc/s and a Z-cut precious red tourmaline crystal of 0.6 mm thickness was used for frequencies up to 300 Mc/s. The usual Debye Sears set-up for recording diffraction spectra was used with a sodium lamp as the light source for frequencies up to 100 Mc/s. A constant voltage transformer served the purpose of stabilizing the intensity of the light source. Above 100 Mc/s a mercury vapour lamp was used as the source, since the greater sensitivity of the photomultiplier tube 1P21 could be used advantageously in the green region for measuring the feeble diffraction orders obtained at these very high frequencies. The instrument used for intensity measurements is a highly sensitive photomultiplier photometer whose highest sensitivity is as high as 0.0001 μ m per division in the highest sensitive range.

§ 3. RESULTS AND DISCUSSION

Using the experimental technique outlined above, the main features of diffraction at very high frequencies have been studied extensively. The intensities of the first-order lines of the diffraction pattern were measured at various angles of incidence for the spot frequencies of 50, 98, 139 and 230 Mc/s and a plot of the variation of the intensity with angle of incidence is shown in Fig. 1.

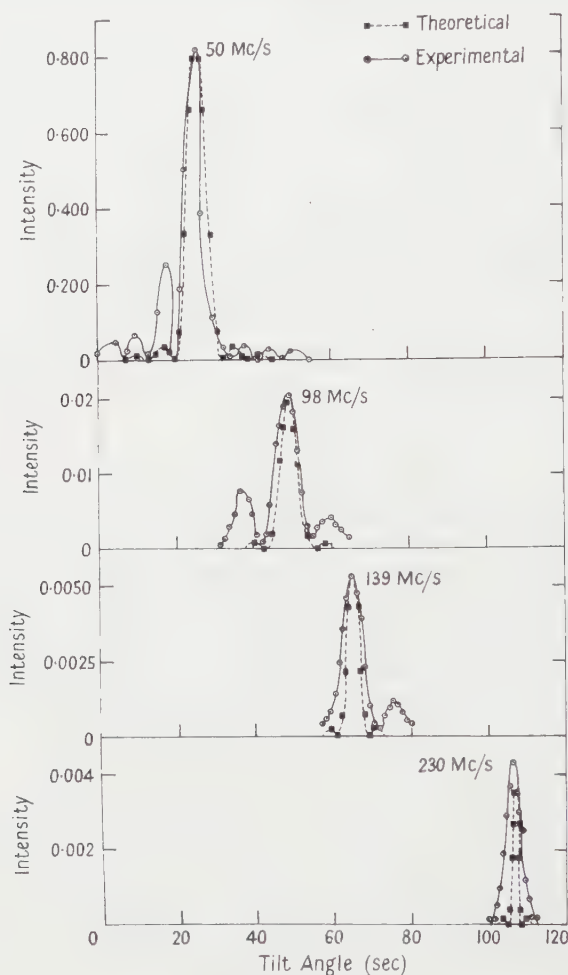


Fig. 1. Intensity variation of first-order diffraction lines with angle of incidence at frequencies 50, 98, 139 and 230 Mc/s. Full curve, experimental; broken curve, theoretical.

The intensities are expressed as fractions of the incident light. The width of the ultrasonic beam, which is about 1.5 cm, is larger than the width of the light beam. The theoretical intensity curves shown as broken lines in Fig. 1 are drawn by using relation (1) in which I_{\max} is taken as the experimental value, as the calculation of this requires a knowledge of μ , which cannot be easily estimated. The length of the sound field is taken to be the same as the geometrical length of the crystal. The following salient features of diffraction at very high frequencies may be noted before discussing the experimental results in the light of the theoretical work.

(i) It may be seen from Fig. 1 that there is a rapid decrease of intensity of the first order with increase of frequency. This progressive decrease of intensity with increase of frequency is attributed to the rapid increase of absorption with frequency and decrease of ultrasonic power due to the crystal being excited at higher and higher harmonics.

(ii) At normal incidence position it is found that no diffraction pattern is seen above 100 Mc/s for moderate intensities.

(iii) The first order appears with maximum brilliancy when the light rays meet the sound wave front at the Bragg incidence angle $\phi = \lambda/2\mu_0\lambda^*$. In this position it is found that only a single diffraction line on the appropriate side appears for frequencies above 100 Mc/s. At lower frequencies the first order on the other side appears but it is very weak up to 50 Mc/s, as more than 80% of the incident light is sometimes thrown into the first order on the appropriate side.

(iv) For frequencies up to 100 Mc/s, the second order on the same side also appears besides the first order, at Bragg incidence. Above 100 Mc/s no higher order other than the first appears.

(v) It is a common feature of observations at low frequencies that the first-order diffraction line appears with fairly good intensity even though the angle of incidence is varied considerably. But, at higher frequencies of 100 Mc/s and above, the setting of the angle of tilt for obtaining first order is considerably sharp, the sharpness being very much higher at higher frequencies. For instance, at 300 Mc/s the intensity falls to zero for a slight deviation of $2'$ which corresponds to a fraction of $1/70$ of the Bragg angle. This extraordinary sharpness of the appearance is responsible for the difficulty in experimentally setting up the position for obtaining the diffraction spectra at these very high frequencies.

3.1. Variation of Intensity of First Order with Angle of Incidence

The nature of the variation of the first-order intensity of the diffraction pattern observed experimentally is in fairly good agreement with the theoretical curves. In the case of diffraction at 50 Mc/s, it may be pointed out that the intensity of the first order at normal incidence is very much higher than the calculated value. Further, it is observed that the secondary maxima are more intense and do not always occur at the angles expected theoretically. This suggests that some of the prominent secondary maxima may not be genuine. The fact that there is only one strong secondary maximum for each order and that they are situated on the same side of the main first-order maximum at the same angle suggests that they may be due to a secondary sound field inclined slightly to the main sound field. In addition there may be less intense sound fields oriented at different angles which are responsible for the intensity of the first order at normal incidence being much higher than that expected theoretically. Secondary maxima similar to the one observed at 50 Mc/s are also noticed at 100 Mc/s.

Figure 1 shows that the width of the theoretical curves is greater than the experimental curves particularly at very high frequencies. It is evident from relation (1) that the width of the theoretical curves increases with decrease of the length of the sound field, resulting in decrease of the sharpness of setting. The observation that the experimental curves are broader than the theoretical ones may be due to the actual length of the sound field being less than the geometrical length of the crystal used in the calculations. Thus the increasing deviation from

theoretical curves at higher frequencies suggests that as we go to higher and higher frequencies the crystal may not be vibrating over its whole area but only in smaller portions.

It has already been pointed out that the expression (3) for the intensity of the first order given by Bhatia and Noble differs from that of David when the intensity of the first order is appreciable. So with a view to test which of the two theories is in agreement with experimental data, the observations at 50 Mc/s are plotted in Fig. 2 and compared with both the theoretical curves. It is very

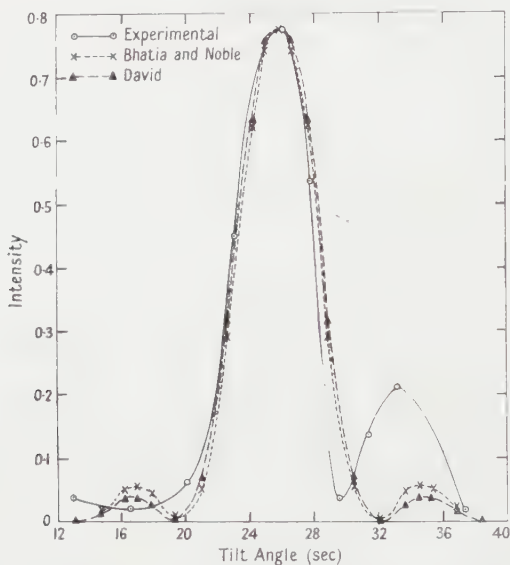


Fig. 2. Theoretical and experimental curves for intensity variation of first-order diffraction line with tilt angle near Bragg incidence.

difficult from these curves to say which of the two theories is in better agreement with experimental results. As far as the main maximum is concerned both the theoretical curves follow it closely. But the single strong secondary maximum of the experimental curve is not in agreement with the secondary maxima expected on both the theories. In view of the small difference between the experimental and theoretical curves and the lack of uniformity in the ultrasonic waves, it has not been possible to test from these observations as to which of the two theories is valid.

3.2. *Effect of Length of Sound Field on the First Order Diffraction*

A real test between two theories could, however, be made by studying the variation in the intensity of the first order at Bragg incidence with the length of the sound field. For this purpose it is essential to use high intensity ultrasonic waves in order that the sinusoidal variation predicted by relation (4) of Bhatia and Noble is observed experimentally. When the first-order intensity at Bragg incidence attains a maximum given by the condition $\pi\mu L/\lambda = \frac{1}{2}\pi$, it can be easily seen from this relation that the central order should completely disappear and all the incident light should be thrown into the first order. This condition could not be realized experimentally, despite our best efforts, although in some cases

it has been possible to obtain as much as 80% of the incident light intensity in the first order.

For the purpose of this study a quartz crystal of about 2 cm length was used and high power ultrasonic waves were generated at 50 Mc s. The length of the sound field was varied by moving a thin air cell, formed between two thin glass plates, beneath the crystal. The experimental curve showing the variation of intensity of the first order with length is presented in Fig. 3 together with the theoretical curves of Bhatia and Noble. It is evident from this figure that the type of intensity variation which is nearly sinusoidal is not in accordance with David's theory which predicts a linear variation, but corresponds closely to that predicted by Bhatia and Noble, even though the maximum intensity observed is about 1/6 of that of the incident light. It may be noted that the amount of the incident light that is actually passing through the sound field and undergoing diffraction effects may be relatively small on account of non-uniformity in the field and may correspond to the observed maximum intensity in the first order.

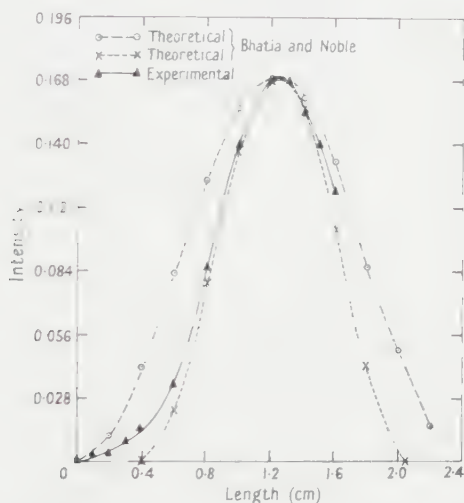


Fig. 3. Experimental and theoretical curves for the variation of intensity of the first order with length of sound field; O O curve A, x x curve B.

Bearing on this argument and assuming that only 1/6 of the incident light corresponds to the maximum intensity undergoing diffraction, the intensity variation with length as predicted by relation (6) is plotted and shown by broken curves in Fig. 3. Of the two theoretical graphs, curve A is drawn by taking the length scale the same as that for the experimental curve. In this case the length of the sound beam is measured from the position of the air film when the first-order intensity is just sufficient to be measurable. It is gratifying to note that the type of variation expected theoretically fits fairly well with the experimental curve. The slight deviation observed for small lengths is due to the inherent limitations in the method of using the air film for cutting the sound beam. At very small lengths of sound field, the diffraction effect of the sound beam at the edge of the cell produces a marked deviation from the linear variation which is normally expected. This can be easily seen from the experimental fact that the first-order diffraction line remains with sufficient intensity even when the air film completely covers

the area of the crystal. Reckoning the length of the sound field from this point and adjusting the value of length L to coincide with the maximum, another theoretical curve B is drawn which shows excellent agreement with almost the entire portion of the experimental curve. It may be noted that although the length of crystal exposed to the liquid is known, this value is not utilized in drawing the theoretical curves as the effective length of the sound beam is usually less than the crystal length exposed on account of the non-uniform nature of vibration. This study has thus strikingly confirmed the validity of the theory given by Bhatia and Noble for diffraction of light by high frequency sound waves.

REFERENCES

- BÄR, R., 1936, *Helv. Phys. Acta*, **9**, 265.
BHAGAVANTAM, S., and RAO, B. R., 1948, *Proc. Ind. Acad. Sci. A*, **28**, 54.
BHATIA, A. B., and NOBLE, W. J., 1953, *Proc. Roy. Soc. A*, **220**, 369.
DAVID, E., 1937, *Phys. Z.*, **38**, 587.
KÖRFF, W., 1936, *Phys. Z.*, **37**, 708.
PARTHASARATHY, S., 1936, *Proc. Ind. Acad. Sci. A*, **3**, 442.
RAGHUPATHI RAO, C., 1955, *Proc. Ind. Acad. Sci. A*, **42**, 158.

Plasma Diffusion in Systems with Particle Losses

By N. J. PHILLIPS

Atomic Weapons Research Establishment, Aldermaston, Berks.

MS. received 7th June 1960, in revised form 19th December 1960

Abstract. In certain experimental fusion devices, plasma is confined by a magnetic field and steadily lost out of the ends of a magnetic bottle. When the scattering rate of particles is high, field diffusion and particle loss can be considered from a macroscopic point of view. The formation of a steady-state sheath into which particles diffuse only to be lost along the lines of force was suggested by Wright and Phillips (1960). The elementary theory is considerably developed here into a state in which the original approximations are evident, though the theory remains essentially phenomenological. It is shown that a steady-state plasma sheath is formed whose thickness depends on the plasma resistivity sound speed and length. The sheath moves into the plasma with a speed which depends on the same parameters.

§ 1. INTRODUCTION

AMONGST the problems of thermonuclear research is that of plasma containment in magnetic bottles. At low particle densities and pressures, the problem is fairly well understood. Binary collisions result in the scattering of particles into trajectories which permit their escape from a region in which they are confined. In this paper, we deal with a situation in which the plasma density and pressure may be large and the electron and ion gasses are separately in thermal equilibrium, but not necessarily at the same temperature.

It is characteristic of experiments using fast plasma compression in axial magnetic fields that, in each, an attempt is made to set up a region of high density plasma surrounded by a thin current sheath. Ions can escape from the magnetic bottle provided that each one takes an electron with it to preserve the electrical neutrality of the plasma. Since the electrons because of their small Larmor radius are only free to move along the lines of force, the ions which are responsible for particle losses have their velocity vectors orientated closely parallel to the lines of force. In an earlier letter (Wright and Phillips 1960) it was suggested that some sort of steady state must be reached in which the radial diffusion of particles into the current sheath is balanced by the loss of particles along the lines of force. In this paper, the problem is set up in a more rigorous fashion, though it must be stressed that the theory is still phenomenological. The result of the theoretical manipulation of the problem is a second-order non-linear differential equation which describes the field distribution in the sheath. The scale factors of the problem reveal that a sheath is formed whose thickness depends on the plasma resistivity sound speed and length.

§ 2. THE STEADY STATE PLASMA SHEATH

We consider here a plasma of high density bounded by a sheath of mixed magnetic field and plasma (Fig. 1).

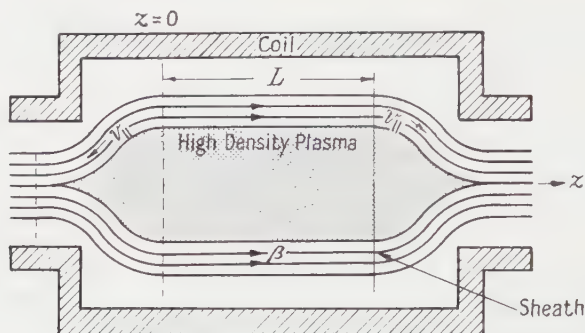


Fig. 1. Section of magnetic bottle.

The magnetic bottle is formed by the rotation of this figure about its axis and the magnetic field is assumed to be bounded by some current carrying conductors which are remote from the plasma. We are not concerned with the hydro-magnetic stability of this configuration, but merely the diffusive loss of particles from the bottle assuming it to be hydromagnetically stable. Plasma diffuses into the sheath radially and flows out along the lines of force. Thus we neglect the possibility of electrons being dragged out perpendicular to the field. In the middle of the plasma (axially) there can be no axial flow by symmetry. Towards the ends of the sheath, the flow will gradually increase until we come to the region bounded by the dotted lines. In this region, there will be approximately steady-state streamline flow. What we shall do here is to consider the radial distribution of magnetic field in the plasma in the planes $z=0$ and $z=L$.

§ 3. MATHEMATICAL FORMULATION OF THE PROBLEM

We consider the sheath to be much thinner than the plasma dimensions so that we can work in plane geometry. The sheath is pictured in cross section as in Fig. 2.

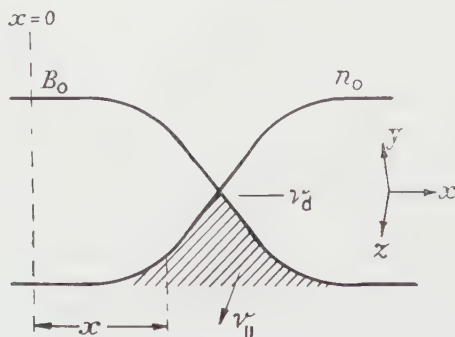


Fig. 2. Section of plasma sheath.

The magnetic field falls from its maximum value B_0 to zero and is in the z direction out of the plane of the paper. The plasma density rises to a maximum value n_0 .

It is assumed the plasma temperature is constant in space and time. The first of these assumptions is justified if there is a high thermal conductivity in the plasma which permits the immediate distribution of heat if it is produced locally. Thermal conduction probably takes place via the ions because the electron thermal conduction across a strong magnetic field may be inhibited. In this model of the plasma we also have the possibility of the removal of the heat produced by field diffusion by convection due to the escape of particles in the sheath. This second mechanism is very important for it suggests that little is to be gained in the heating of such a confined plasma by Joule heating of the electrons. The second assumption is of course consistent with a steady state.

Plasma diffuses into the shaded area from the right and is lost out of the plane of the paper. The shaded region is where the field and plasma are intermixed.

The basic equations are

$$\partial B_z / \partial x = -4\pi j_y \quad \dots\dots (3.1)$$

$$\eta j_y = v_d / B_z \quad \dots\dots (3.2)$$

where v_d is the plasma diffusion speed from right to left, j_y the current density and η the plasma resistivity.

From pressure balance we have

$$B_0^2 / 8\pi = B_z^2 / 8\pi + nk(T_e + T_i) \quad \dots\dots (3.3)$$

where $n = n_i = n_e$ is the particle density of each species (assuming singly charged ions) and T_e and T_i are respectively the electron and ion temperatures.

The equation of continuity representing a balance of radial and axial particle fluxes can be written

$$\hat{c}(nv_z) - \hat{c}z = \hat{c}(nv_d) - \hat{c}x, \quad \dots\dots (3.4)$$

where v_z is the flow speed parallel to the lines of force. We can combine Eqns (3.1), (3.2), (3.3) and (3.4) to give

$$\frac{\partial}{\partial z} \left[v_z \left(1 - \frac{B_z^2}{B_0^2} \right) \right] + \frac{\eta}{4\pi} \frac{\partial}{\partial x} \left[\left(1 - \frac{B_z^2}{B_0^2} \right) \frac{1}{B_z} \frac{\partial B_z}{\partial x} \right] = 0$$

which, upon integration with respect to z between the limits $z=0$ and $z=L$, yields the result

$$2 \left\{ v_z \left(1 - \frac{B_z^2}{B_0^2} \right) \right\}_{z=0} = - \frac{\eta}{4\pi} \int_0^L \frac{\partial}{\partial x} \left[\left(1 - \frac{B_z^2}{B_0^2} \right) \frac{1}{B_z} \frac{\partial B_z}{\partial x} \right] dz, \quad \dots\dots (3.5)$$

assuming symmetry along the z axis.

The variation in the z direction of the integrand is not determinable in our simple model and in the Wright-Phillips letter it was assumed that the integrand is constant with respect to z . If we suppose that the plasma is lost only from the current sheath then v_z must depend on the strength of the magnetic field locally in the planes $z=0$ and $z=L$. This supposition is based on a simple physical picture:

A magnetic bottle is so constructed that the magnetic field increases towards the ends. Thus we assume that the particle transverse pressure is not sufficient to force apart the lines of force in the neck and permit the escape of plasma. Thus plasma escapes in a pressureless fashion by means of particles travelling along the

lines of force with small velocity components in the transverse direction. In the planes $z=0$ and $z=L$, we expect therefore to see most of the plasma pouring from the current sheath and not much loss from the central region near the axis. The picture can be interpreted mathematically by supposing that

$$v_z = v_{it}\phi(B_z/B_0) \quad \dots\dots (3.6)$$

in the planes $z=0$ and L , where v_{it} is the ion thermal speed and ϕ is a function such that $\phi \rightarrow 0$ as $B_z \rightarrow 0$ and $\phi \rightarrow 1$ as $B_z \rightarrow B_0$.

Under the above assumptions, i.e. the constancy of the integrand in (3.5) and using (3.6), we obtain the result

$$\frac{d}{ds} \left\{ \frac{1-\xi^2}{\xi} \frac{d\xi}{ds} \right\} + (1-\xi^2)\phi(\xi) = 0, \quad \dots\dots (3.7)$$

where $s = x/\lambda$, $\xi = B_z/B_0$ and λ is a skin depth defined by

$$\lambda^2 = L\eta/8\pi v_{it}. \quad \dots\dots (3.8)$$

Eqn (3.7) describes the field distribution in the sheath. We now go on to discuss the solution of this equation subject to the boundary conditions $\xi=1$, $s=0$ and $\xi \rightarrow 0$ as $s \rightarrow \infty$.

§ 4. SOLUTION OF THE FIELD EQUATION AND NUMERICAL RESULTS

A first integral of Eqn (3.7) is

$$\left(\frac{1-\xi^2}{\xi} \frac{d\xi}{ds} \right)^2 = 2 \int_{\xi}^1 \phi(p) \frac{(1-p^2)^2}{p} dp. \quad \dots\dots (4.1)$$

This integral enables us to evaluate the total loss rate of particles from the system. Let us suppose that in the planes $z=0$ and L , the plasma is of radius r_0 . The loss rate is then

$$\begin{aligned} Q &= 2(2\pi r_0) \int_0^\infty n v_z dz \\ &= 2n_0 v_{it} \lambda (2\pi r_0) \int_0^\infty (1-\xi^2)\phi(\xi) ds. \end{aligned} \quad \dots\dots (4.2)$$

It follows by integration of (3.7), that

$$\int_0^\infty \phi(\xi)(1-\xi^2)d\xi = - \left[\frac{1-\xi^2}{\xi} \frac{d\xi}{ds} \right]_{s=0}^{s=\infty}$$

or, since we are only interested in the modulus of the right-hand side, we have

$$Q = Q_0 \lim_{s \rightarrow \infty} \left\{ \frac{1-\xi^2}{\xi} \frac{d\xi}{ds} \right\} \quad \dots\dots (4.3)$$

where $Q_0 = 4\pi r_0 n_0 v_{it} \lambda$. Since the limit $s \rightarrow \infty$ is the same as the limit $\xi \rightarrow 0$, we have from Eqn (4.1)

$$Q = Q_0 \left[2 \int_0^1 \frac{(1-p^2)^2}{p} \phi(p) dp \right]^{1/2}. \quad \dots\dots (4.4)$$

Now let us for simplicity choose the function ϕ to be of the form

$$\phi(\xi) = \xi^\alpha, \quad \dots\dots (4.5)$$

then

$$Q = Q_0 \left[\frac{16}{\alpha(\alpha+2)(\alpha+4)} \right]^{1/2}.$$

As α decreases the loss rate increases, but when α drops below about 2, Q is insensitive to α , depending only on the square root. Thus because of the square root dependence of Q on the integral in (4.4), the choice of ϕ need not be very restricted. The case $\alpha = 1$ has been studied in detail and the results are presented below.

The loss rate is $Q = Q_0 [16/15]^{1/2}$, which apart from the factor $[16/15]^{1/2}$ is identical with the result obtained by Wright and Phillips (1960) in which the skin depth λ was treated as a variable. The solution of (3.7) has been obtained numerically in the case $\alpha = 1$ and the results are shown in Fig. 3.

The quantities plotted are $\xi = B_z/B_0$, $\zeta = n/n_0$, $v = v_d/v_0$ and $d\xi/ds$, where $v_0 = \eta/4\pi\lambda$ is a diffusion scale speed. The magnetic field falls off to about 4% of its maximum value in about five characteristic lengths λ . The diffusion velocity v_d vanishes at the outside of the plasma. The quantities v_0 and λ have

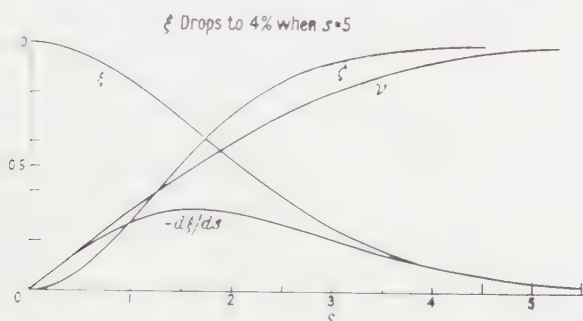


Fig. 3. Graph showing the distribution of the dimensionless quantities ξ , ζ , v , $-d\xi/ds$ as functions of s .

been evaluated numerically taking $L = 10$ cm, equal electron and ion temperatures and the resistivity of a quiescent hydrogen plasma. The results are shown in the Table.

$$v_0 \simeq 10^5 / \sqrt{T} \text{ and } \lambda \simeq 10^5 / T$$

T (°K)	10^5	10^6	10^7	10^8
λ (cm)	1	10^{-1}	10^{-2}	10^{-3}
v_0 (cm sec $^{-1}$)	3×10^5	10^5	3×10^4	10^4

It is more enlightening to write the plasma resistivity in the form

$$\eta = 4\pi\lambda_p^2/\tau_{es}, \quad \dots\dots (4.6)$$

where $\lambda_p = (m_e c^2/4\pi n e^2)^{1/2}$ is the plasma wavelength and τ_{es} is the electron scattering time. The scale length is

$$\lambda = (\eta L/8\pi v_{it})^{1/2} = \lambda_p (\tau_{it}/\tau_{es})^{1/2}, \quad \dots\dots (4.7)$$

where $\tau_{it} = L/2v_{it}$ is an ion transit time from the middle of the plasma to the end of the bottle. The particular significance of λ_p can be seen as follows:

The mean electron Larmor radius in the confining magnetic field is

$$r_{Le} = v_{et}/(eB_0/m_e c) \quad \dots\dots (4.8)$$

where v_{et} is the electron thermal speed. Using the pressure balance relation $B_0^2/8\pi = nm_e v_{et}^2$, we find that

$$r_{Le} = \lambda_p / \sqrt{2}. \quad \dots (4.9)$$

Thus λ_p is just the mean electron Larmor radius in a confined high β plasma. The diffusion speed is

$$v_0 = \eta / 4\pi\lambda = \lambda_p / (\tau_{it}\tau_{et})^{1/2}. \quad \dots (4.10)$$

It is of great importance to realize that in this model of the magnetic bottle particle losses have the effect of maintaining the gradient of the magnetic field. Thus particle losses enhance the ohmic dissipation of the confining current, but because the electrons, once they have diffused into the sheath, are removed along the lines of force, a steady-state sheath is set up.

Microscopic instabilities may be responsible for particle scattering in the 'collision free' limit. Pfirsch and Biermann (1960) have begun to study the problem of micro-instabilities in plasma sheaths. Unlike the study of instabilities in uniform unbounded plasmas, the study of non-uniform bounded plasmas is much in its infancy. This is because of the vastly increased mathematical complexity introduced by the spatial variation of the equilibrium state. Without elaborate theoretical backing, we can however make some general comments on the relevance of micro-instabilities to the subject of this paper.

Unstable electrostatic waves in the electron gas will have the effect of lowering τ_{es} and hence thicken the sheath. Since particle losses will keep the sheath thin we may expect that if instabilities of this type are to be contended with, then the sheath will exist on the verge of electrostatic stability. This conclusion is drawn because micro-instabilities should be more important when the gradient of magnetic field is large because in such a condition there is a great deal of available entropy. Two physical phenomena may thus compete in determining the sheath thickness, the micro-instability tending always to thicken the sheath by electron scattering until it is electrostatically stable, and particle losses tending to keep the sheath thin. Finally these two effects would balance out with the steady-state sheath thickness being the minimum consistent with electrostatic stability. We can thus also conclude that the turbulent state in the sheath in conditions of electrostatic instability would depend on the geometry of the system because the ion transit time determines the rate at which plasma can be removed from the sheath and hence the gradient of magnetic field in the remaining plasma.

§ 5. CONCLUSIONS

Plasma loss and diffusion from a magnetic bottle gives rise to a steady-state plasma sheath. The sheath thickness depends on the ion transit time, the electron scattering time and the particle density.

Particle losses have the effect of maintaining ohmic dissipation in a confined plasma and may play an important role in the generation of unstable plasma waves.

ACKNOWLEDGMENTS

I should like to thank Dr. J. W. Dungey for much helpful discussion and Mr. F. J. Birkin for the numerical solution of (3.7).

REFERENCES

- PFIRSCH, D., and BIERMANN, L., 1960, *Z. Naturf.*, **15a**, 10.
 WRIGHT, J. K., and PHILLIPS, N. J., 1960, *J. Nucl. Energ.*, **1C**, 4.

Oscillations of a Plasma in a Static Magnetic Field

By N. ANDERSON†

Trinity College, Cambridge

MS. received 7th July 1960, in revised form 2nd December 1960

Abstract. We consider the propagation of waves through an infinite homogeneous plasma permeated by a static magnetic field. The Boltzmann equation is linearized by the usual perturbation method and the distribution function obtained in the form of an integral. From the expression for the distribution function we calculate the current density, which on insertion into Maxwell's equations gives the dielectric tensor relating the components of the displacement to those of the electric field. Explicit expressions are given for the components of the dielectric tensor in the particular case when the mean Larmor radius of the particles is considerably less than the wavelength of the oscillation and the wave velocity considerably greater than the mean thermal velocity of the particles. Under these conditions, the change in the wave velocity due to thermal effects is calculated by means of an eigenvalue method which uses the wave velocity in the absence of thermal effects and the dielectric tensor we have calculated.

§ 1. INTRODUCTION

WE shall consider the propagation of small amplitude waves through an infinite homogeneous plasma, composed of particles of a single type, pervaded by a uniform static magnetic field. We assume that the state of the plasma is always close to equilibrium. The currents which flow in the plasma as a result of the wave are regarded as producing an anisotropic behaviour of the dielectric tensor, which relates the components of the displacement to those of the electric field. Under the following assumptions: (i) that the mean Larmor radius of the particles is small compared with the wavelength of the oscillation, (ii) that the ratio of the square of the mean thermal velocity of the particles to the square of the wave velocity is small, we shall give first approximations to the components of the dielectric tensor in terms of rational functions. This differs from other treatments of this problem (see Akhiezer *et al.* 1958), where the components of the tensor are given in the form of integrals.

The corrections that must be added to the solutions that we obtain for the zero temperature problem, the 'cold' solutions, to take into account the thermal motions of the particles, will be obtained, for the general case of an arbitrary angle of propagation to the magnetic field, by an eigenvalue method which uses the 'cold' solutions and the dielectric tensor which we shall calculate. Under the assumptions given, this method of including thermal effects seems more compact than the usual method of taking further terms in the coefficients of the determinant which expresses the dispersion relation between the frequency of the oscillation

† Now at the Atomic Weapons Research Establishment, Aldermaston, Berks.

and the wave number (see Bernstein 1958), or the method adopted by Akhiezer *et al.* (1958) which results in a dispersion relation in the form of a sixth-order equation in the refractive index. The particular case of propagation perpendicular to the magnetic field has been considered for a plasma consisting of two particle types under more general conditions (see Anderson 1960), but the method used is not readily extended to the general direction of propagation.

In the following discussion any motion of the plasma is assumed to be collision-free, and the magnetic interactions of the particles are ignored. The equations for the electromagnetic field will be written in mixed Gaussian units.

§ 2. THE DISTRIBUTION FUNCTION AND CURRENT DENSITY

Suppose we choose a system of rectangular cartesian coordinates such that the magnetic field is in the direction of the positive z axis. We define new coordinates

$$x_1 = (x + iy)/\sqrt{2}, \quad x_{-1} = (x - iy)/\sqrt{2}, \quad x_0 = z,$$

and velocities

$$v_1 = (v_x + iv_y)/\sqrt{2}, \quad v_{-1} = (v_x - iv_y)/\sqrt{2}, \quad v_0 = v_z.$$

With these definitions and using the convention that we sum over any suffix which appears more than once, unless otherwise stated, we have for the scalar product of two vectors

$$\mathbf{x} \cdot \mathbf{v} = x_\nu v_{-\nu} = x_{-\nu} v_\nu.$$

The equations of motion of the particles in the unperturbed state are

$$\ddot{x} = \Omega \dot{y} \quad \ddot{y} = -\Omega \dot{x} \quad \ddot{z} = 0 \quad \Omega = qH/mc$$

where Ω is the gyrofrequency of the particles which have charge q , mass m , and H is the strength of the magnetic field. We may write these equations of motion in the abbreviated form

$$\ddot{x}_\nu = -i\nu\Omega\dot{x}_\nu \quad (\text{no summation})$$

which integrates to give

$$\dot{x}_\nu(t') = \dot{x}_\nu(t) \exp[i\nu\Omega(t-t')] \quad (\text{no summation}). \quad \dots\dots (1)$$

A further integration gives

$$x_\nu(t') = x_\nu(t) + \dot{x}_\nu(t) \{ \exp[i\nu\Omega(t-t')] - 1 \} / (-i\nu\Omega) \quad (\text{no summation})$$

where if any subscript takes the value zero then by division we understand the passage to the limit of the quotient as the subscript tends to zero. Hence we have

$$x_\nu(t) - x_\nu(t') = v_\nu(t) \{ \exp[i\nu\Omega(t-t')] - 1 \} / i\nu\Omega \quad (\text{no summation}). \quad \dots\dots (2)$$

If we write the distribution function characterizing the state of the plasma in the form

$$f = f_0 + f_1,$$

where f_1 is the perturbation due to the wave from the equilibrium distribution f_0 , we can write the collision-free Boltzmann equation in the form

$$\frac{\mathcal{D}f_1}{\mathcal{D}t} = - \frac{d\mathbf{v}}{dt} \cdot \frac{\partial f_0}{\partial \mathbf{v}}, \quad \dots\dots (3)$$

where the derivative of f_1 follows the trajectory of the particle in phase space, and we have assumed that the equilibrium distribution is uniform in configuration space. We write Eqn (3) in this particular form to enable us to adopt the following

approach to the integration with respect to time. The time derivatives in (3) are quantities due to the perturbation which we assume to be first-order small values. The difference between the orbits in the perturbed and unperturbed states is also a first-order small quantity, and hence the difference between integrating the two sides of (3) along perturbed and unperturbed orbits will be a second-order small quantity, which we shall neglect. Hence in the time integration of (3) we use the unperturbed orbits given by (2). First we write (3) in the form

$$\frac{\mathcal{D}f_1}{\mathcal{D}t} = -\frac{d\mathbf{r}_v}{dt} \frac{\partial f_0}{\partial \mathbf{r}_{-v}} = \frac{q}{\mathbf{k}T} E_{-v} \mathbf{v}_v f_0 - \frac{q}{mc} (\mathbf{v} \times \mathbf{H})_v \frac{\partial f_0}{\partial \mathbf{r}_{-v}}. \quad \dots\dots (4)$$

We assume the equilibrium distribution to be Maxwellian, i.e.

$$f_0 = N(m/2\pi\mathbf{k}T)^{3/2} \exp(-mv^2/2\mathbf{k}T)$$

where T is the absolute temperature, \mathbf{k} is Boltzmann's constant and N is the unperturbed particle density.

Suppose we now look for solutions of the system, from which by means of Fourier analysis we can construct an arbitrary waveform. This means that we look for solutions of the equations with the form

$$f_1, \mathbf{E} \propto \exp(-i\mathbf{k} \cdot \mathbf{x}).$$

In this case Eqn (4) gives

$$f_1(t) \exp[-i\mathbf{k} \cdot \mathbf{x}(t)] = f_1(0) \exp[-i\mathbf{k} \cdot \mathbf{x}(0)] + \frac{qf_0}{\mathbf{k}T} \int_0^t E_{-v}(t') v_v(t') \exp[-i\mathbf{k} \cdot \mathbf{x}(t')] dt', \quad \dots\dots (5)$$

and if we combine (2) and (5) to integrate along unperturbed orbits as discussed previously we have

$$f_1(t) = f_1(0) \exp \left\{ ik_{-v} v_v \left[\frac{\exp(i\nu\Omega t) - 1}{i\nu\Omega} \right] \right\} + \frac{qf_0 v_v}{\mathbf{k}T} \int_0^t E_{-v}(t') \exp \left\{ ik_{-v} v_v \left[\frac{\exp[i\lambda\Omega(t-t')] - 1}{i\lambda\Omega} \right] + i\nu\Omega(t-t') \right\} dt'. \quad \dots\dots (6)$$

The last term is a convolution integral which is a type prominent in the theory of Laplace transforms. The particular advantage of using a Maxwellian distribution for the equilibrium state is that the last term in (4) is zero for this case. If a non-isotropic velocity distribution was used then this term would be non-zero and would give considerable difficulty.

If we use mixed Gaussian units we have for the components of the current density

$$j_\mu = \frac{q}{c} \int f_1 v_\mu d\mathbf{v}; \quad \dots\dots (7)$$

hence we wish to consider the first moment of (6). We integrate the last term in (6) over all velocity space and then perform the convolution. The integral over velocity space is

$$N \left(\frac{m}{2\pi\mathbf{k}T} \right)^{3/2} \int v_\mu v_v \exp \left\{ -\frac{mv_\lambda v_{-\lambda}}{2\mathbf{k}T} + ik_{-\lambda} v_\lambda \left[\frac{\exp[i\lambda\Omega(t-t')] - 1}{i\lambda\Omega} \right] + i\nu\Omega(t-t') \right\} d\mathbf{v}, \quad \dots\dots (8)$$

which reduces to

$$\frac{N\mathbf{k}T}{m} \exp \left\{ i\nu\Omega(t-t') - \frac{1}{2} \frac{\mathbf{k}T}{m} k_\lambda k_{-\lambda} \frac{\sin^2[\lambda\Omega(t-t')/2]}{(\lambda\Omega/2)^2} \right\} \\ \times \left\{ \delta_{\mu, -\nu} - \frac{\mathbf{k}T}{m} k_\mu k_\nu \left[\frac{\exp[-i\mu\Omega(t-t')] - 1}{-i\mu\Omega} \right] \left[\frac{\exp[-i\nu\Omega(t-t')] - 1}{-i\nu\Omega} \right] \right\}. \quad \dots\dots(9)$$

Hence, substituting (9) into (6) and using (7) we have the current density as an integral of the convolution type. The Kronecker delta symbol is defined in the usual manner

$$\delta_{m,n} = \begin{cases} 1 & m=n \\ 0 & m \neq n. \end{cases}$$

The expression for the current density finally reduces to

$$j_\mu = \frac{q}{c} \int f_1(0) v_\mu \exp \left\{ ik_{-\nu} v_\nu \left[\frac{\exp(i\nu\Omega t) - 1}{i\nu\Omega} \right] \right\} d\mathbf{v} \\ + \frac{Nq^2}{mc} \int_0^t \left[\exp \left\{ i\nu\Omega(t-t') - \frac{1}{2} \frac{\mathbf{k}T}{m} k_\lambda k_{-\lambda} \frac{\sin^2[\lambda\Omega(t-t')/2]}{(\lambda\Omega/2)^2} \right\} E_{-\nu}(t') \right. \\ \left. \times \left\{ \delta_{\mu, -\nu} - k_\mu k_\nu \frac{\mathbf{k}T}{m} \left(\frac{\exp[-i\mu\Omega(t-t')] - 1}{-i\mu\Omega} \right) \left(\frac{\exp[-i\nu\Omega(t-t')] - 1}{-i\nu\Omega} \right) \right\} \right] dt'.$$

§ 3. THE DISPERSION RELATION

Consider Maxwell's equations for the electromagnetic field in the form

$$\nabla \times (\nabla \times \mathbf{E}) = -\frac{4\pi}{c} \frac{\partial \mathbf{j}}{\partial t} - \frac{1}{c^2} \frac{\partial^2 \mathbf{E}}{\partial t^2},$$

which we may write as

$$\frac{\partial^2 E_\mu}{\partial t^2} + c^2(k_\lambda k_{-\lambda} E_\mu - k_{-\lambda} k_\mu E_\lambda) = -4\pi c \frac{\partial j_\mu}{\partial t}. \quad \dots\dots(10)$$

We define the polarization vector \mathbf{P} , as done by Auer, Hurwitz and Miller (1958) in their treatment of a cold plasma, by the relation

$$\mathbf{P} = c \int \mathbf{j} dt$$

and write

$$c(\nabla \times \mathbf{H}) = \frac{\partial}{\partial t} (\mathbf{E} + 4\pi \mathbf{P}) = \frac{\partial}{\partial t} (\epsilon \mathbf{E}),$$

where we have put

$$\epsilon = 1 + 4\pi K$$

and K is a tensor operator which produces the components of \mathbf{P} from those of \mathbf{E} . We call K the dielectric susceptibility tensor and ϵ the dielectric tensor.

If we now use a Laplace transform, with parameter s , and denote the transform of a function by placing a bar over it, we have

$$\bar{P}_\mu(s) = \bar{K}_{\mu\nu} \bar{E}_{-\nu}$$

where \bar{K} is now a tensor.

We have, letting \mathcal{L} also denote a Laplace transform

$$\bar{P}_\mu(s) = \frac{Nq^2}{m} \frac{1}{s} \mathcal{L} \left\{ \exp \left[i\nu\Omega t - \frac{1}{2} \frac{\mathbf{k}T}{m} k_\lambda k_{-\lambda} \frac{\sin^2(\lambda\Omega t/2)}{(\lambda\Omega/2)^2} \right] \right. \\ \left. \times \left[\delta_{\mu, -\nu} - \frac{\mathbf{k}T}{m} k_\mu k_\nu \left(\frac{\exp(-i\mu\Omega t) - 1}{-i\mu\Omega} \right) \left(\frac{\exp(-i\nu\Omega t) - 1}{-i\nu\Omega} \right) \right] \right\} E_{-\nu} \\ (\mu \text{ not summed}). \quad \dots\dots(11)$$

For the particular case of propagation at zero temperature we obtain, in agreement with Aström (1951), on putting $s = i\omega$

$$K_{\mu\nu} = -\frac{\omega_p^2}{4\pi\omega(\omega - \nu\Omega)}\delta_{\mu,-\nu} \quad (\text{no summation}), \quad \dots\dots (12)$$

where ω_p is the plasma frequency $(4\pi Nq^2/m)^{1/2}$. Now consider the corrections due to thermal effects to first order in χ , where

$$\chi = k^2 kT/m\Omega^2$$

is the ratio of the mean square Larmor radius of the particles to the square of the wavelength of the oscillation, which we shall assume to be considerably less than unity. In this case (11) gives

$$\begin{aligned} \bar{K}_{\mu\nu} = \frac{\omega_p^2}{4\pi s} \mathcal{L} \left\{ \exp(i\nu\Omega t) [1 - \chi + \chi \cos \Omega t] \left[\delta_{\mu,-\nu} + \frac{\chi k_\mu k_\nu}{\mu\nu k^2} \right. \right. \\ \left. \left. \times (\exp(-i\mu\Omega t) - 1)(\exp(-i\nu\Omega t) - 1) \right] \right\} \quad (\text{no summation}). \quad \dots\dots (13) \end{aligned}$$

Let

$$F(s) = \mathcal{L}[1 - \chi + \chi \cos \Omega t] = \frac{(1 - \chi)}{s} + \frac{\chi s}{s^2 + \Omega^2}.$$

Then if $\mu, \nu \neq 0$, we have

$$\begin{aligned} \bar{K}_{\mu\nu} = \frac{\omega_p^2}{4\pi s} \left\{ F(s - i\nu\Omega) \delta_{\mu,-\nu} + \frac{\chi k_\mu k_\nu}{\mu\nu k^2} [F(s + i\mu\Omega) + F(s - i\nu\Omega) \right. \\ \left. - F(s + i\mu\Omega - i\nu\Omega) - F(s)] \right\} \quad (\text{no summation}). \end{aligned}$$

Hence, for propagation in the x direction

$$\begin{aligned} K_{0,0} &= -\frac{\omega_p^2}{4\pi\omega^2} \left\{ 1 - \chi + \frac{\chi\omega^2}{\omega^2 - \Omega^2} \right\} \\ K_{1,-1} &= -\frac{\omega_p^2}{4\pi\omega^2(\omega + \Omega)} \left\{ \omega + \frac{2\chi\Omega^2}{\omega + 2\Omega} \right\} \\ K_{-1,1} &= -\frac{\omega_p^2}{4\pi\omega^2(\omega - \Omega)} \left\{ \omega + \frac{2\chi\Omega^2}{\omega - 2\Omega} \right\} \\ K_{1,1} - K_{-1,-1} &= -\frac{\chi\omega_p^2\Omega^2}{4\pi\omega^2(\omega^2 - \Omega^2)} \\ K_{0,1} &= K_{1,0} = K_{0,-1} = K_{-1,0} = 0. \end{aligned}$$

From (10), by taking Laplace transforms with respect to time, we have

$$\begin{aligned} s^2 \bar{E}_\mu - sE_\mu(0) + c^2(k_\lambda k_{-\lambda} \bar{E}_\mu - k_{-\lambda} k_\mu \bar{E}_\lambda) + c[\nabla \times \mathbf{H}(0)]_\mu \\ = -4\pi qs \mathcal{L} \left\{ \int f_1(0) \exp \left[ik_{-\nu} v_\nu \left(\frac{\exp(i\nu\Omega t) - 1}{i\nu\Omega} \right) \right] v_\mu d\mathbf{v} \right\} + 4\pi s^2 \bar{K}_{\mu,-\lambda} \bar{E}_\lambda. \end{aligned} \quad \dots\dots (14)$$

Equation (14) is a tensor equation of the form

$$\tau_{\lambda\mu} \bar{E}_\lambda + \lambda' \bar{E}_\mu = C_\mu, \quad \dots\dots (15)$$

where

$$\lambda' = c^2 k^2 + s^2$$

$$\begin{aligned} C_\mu = sE_\mu(0) + c[\nabla \times \mathbf{H}(0)]_\mu - 4\pi qs \mathcal{L} \left\{ \int f_1(0) \exp \left[ik_{-\nu} v_\nu \left(\frac{\exp(i\nu\Omega t) - 1}{i\nu\Omega} \right) \right] v_\mu d\mathbf{v} \right\} \\ \tau_{\lambda\mu} = -c^2 k_{-\lambda} k_\mu + 4\pi s^2 \bar{K}_{\mu,-\lambda}. \end{aligned}$$

Suppose now that we look for solutions of the form

$$f_1, \mathbf{E} \propto \exp(i\omega t)$$

for large t . Then \bar{E} has a pole at the point $i\omega$ in the s plane. Hence, by (15), $|\tau_{\lambda\mu} + \lambda'\delta_{\lambda\mu}|$ has a zero for this value of s , giving

$$\Delta = |\tau_{\lambda\mu} + \lambda'\delta_{\lambda\mu}| = 0. \quad \dots\dots (16)$$

The frequencies obtained are the so-called natural frequencies of the system and are due to the dynamical properties of the plasma rather than its initial state. This type of solution excludes all transient effects which can be produced by a careful initial preparation of the plasma. In the following, for the sake of convenience, we shall often retain the symbol s for $i\omega$.

For the special case of propagation in the x direction we obtain the following results:

(i) Zero temperature

$$\omega^2 = \omega_p^2 + \frac{1}{2}(c^2k^2 + \Omega^2) \pm [(c^2k^2 - \Omega^2)^2 + 4\omega_p^2\Omega^2]^{1/2}; \quad \dots\dots (17)$$

(ii) χ small

$$\begin{aligned} \tau_{0,0} &= \omega_p^2 \left\{ 1 - \chi + \frac{\chi\omega^2}{\omega^2 - \Omega^2} \right\} \\ \tau_{1,1} &= -\frac{c^2k^2}{2} + \frac{\omega_p^2}{\omega + \Omega} \left\{ \omega + \frac{2\chi\Omega^2}{\omega + 2\Omega} \right\} \\ \tau_{-1,-1} &= -\frac{c^2k^2}{2} + \frac{\omega_p^2}{\omega - \Omega} \left\{ \omega + \frac{2\chi\Omega^2}{\omega - 2\Omega} \right\} \\ \tau_{1,-1} &= \tau_{-1,1} = -\frac{c^2k^2}{2} + \frac{\chi\omega_p^2\Omega^2}{\omega^2 - \Omega^2} \\ \tau_{1,0} &= \tau_{0,1} = \tau_{-1,0} = \tau_{0,-1} = 0. \end{aligned}$$

If we put $\omega \ll \Omega$ then the dispersion equation becomes, from (16),

$$\Delta = [(1 - \chi)\Omega^2 - \chi\omega^2][\omega^2\omega_p^4 + 2\chi\omega_p^2\Omega^2c^2k^2] = 0, \quad \dots\dots (18)$$

hence there are no real solutions for $\omega \ll \Omega$. This is in agreement with the results of Bernstein (1958).

Now we will consider the more general case with $k_1 = k_{-1}$, $k_0 \neq 0$. Here we have

$$\begin{aligned} \bar{K}_{\mu,\nu} &= \frac{\omega_p^2}{4\pi s} \mathcal{L} \left\{ \exp(i\nu\Omega t) \exp \left[-\frac{4\chi k_1^2 \sin^2(\Omega t/2)}{k^2} - \frac{\chi k_0^2 \Omega^2 t^2}{2k^2} \right] \right. \\ &\times \left[\delta_{\mu,-\nu} - \frac{\chi\Omega^2 k_\mu k_\nu}{k^2} \left(\frac{\exp(-i\mu\Omega t) - 1}{-i\mu\Omega} \right) \left(\frac{\exp(-i\nu\Omega t) - 1}{-i\nu\Omega} \right) \right] \left. \right\} \\ &\quad \text{(no summation).} \quad \dots\dots (19) \end{aligned}$$

Let

$$G(s) = \mathcal{L} \left\{ \exp \left[-\frac{4k_1^2 \chi \sin^2(\Omega t/2)}{k^2} - \frac{\chi k_0^2 \Omega^2 t^2}{2k^2} \right] \right\}.$$

We now make the assumption that the wave velocity is considerably greater than the mean thermal velocity of the particles, i.e.

$$\frac{\omega^2}{k^2} \gg \frac{kT}{m},$$

and expand $G(s)$ to first order in $(k^2 \mathbf{k} T / m s^2)$, giving

$$G(s) = \frac{\Omega^2}{k^2 s} \left\{ \frac{k^2}{\Omega^2} - \frac{\chi(k^2 s^2 + k_0^2 \Omega^2)}{s^2(s^2 + \Omega^2)} \right\}. \quad \dots\dots (20)$$

We must remember that s is retained instead of $i\omega$ for convenience. The result of the exponentials in (19) is merely to shift the argument of the transform if μ, ν are non-zero, and if either μ or ν is zero then the corresponding exponential terms become multiples of t and represent a differentiation of $G(s)$. If we write the components of the displacement D in the form

$$D_\mu = \epsilon_{\mu\nu} E_{-\nu},$$

then

$$\epsilon_{\mu\nu} = \delta_{\mu, -\nu} + 4\pi K_{\mu, \nu}.$$

Hence, if we write

$$\epsilon_{\mu\nu} = \epsilon_{\mu\nu}(\text{cold}) + \epsilon'_{\mu\nu},$$

where the last term includes the contribution due to thermal effects, we have

$$\epsilon_{\mu\nu}(\text{cold}) = \left\{ 1 - \frac{\omega_p^2}{\omega(\omega - \nu\Omega)} \right\} \delta_{\mu, -\nu} \quad (\text{no summation})$$

and

$$\begin{aligned} \epsilon'_{0,0} &= -\frac{\omega_p^2 \mathbf{k} T}{m\omega^4} \left\{ 2k_0^2 + \frac{(k_0^2 \Omega^2 - k^2 \omega^2)}{\Omega^2 - \omega^2} \right\} \\ \epsilon'_{1,-1} &= -\frac{\omega_p^2 \mathbf{k} T}{m\omega} \left\{ \frac{k_0^2}{(\omega + \Omega)^3} + \frac{2(k^2 - k_0^2)}{\omega(\omega + \Omega)(\omega + 2\Omega)} \right\} \\ \epsilon'_{-1,1} &= -\frac{\omega_p^2 \mathbf{k} T}{m\omega} \left\{ \frac{k_0^2}{(\omega - \Omega)^3} + \frac{2(k^2 - k_0^2)}{\omega(\omega - \Omega)(\omega - 2\Omega)} \right\} \\ \epsilon'_{0,-1} = \epsilon'_{1,0} &= \frac{\omega_p^2 \mathbf{k} T k_0 k_1 (2\omega + \Omega)}{m\omega^3 (\omega + \Omega)^2} \\ \epsilon'_{0,1} = \epsilon'_{-1,0} &= \frac{\omega_p^2 \mathbf{k} T k_0 k_1 (2\omega - \Omega)}{m\omega^3 (\omega - \Omega)^2} \\ \epsilon'_{1,1} = \epsilon'_{-1,-1} &= \frac{2\omega_p^2 \mathbf{k} T k_1^2}{m\omega^2 (\Omega^2 - \omega^2)}. \end{aligned}$$

If we carried out the expansion to higher order in χ then we would obtain resonances at the higher multiples of the gyro-frequency which do not occur in the expressions we have just obtained.

§ 4. THERMAL CORRECTIONS TO THE VELOCITY OF PROPAGATION

For the case of a cold plasma we have shown that we have 'principal directions' with dielectric constants given by

$$\epsilon_{\mu\nu} = \left\{ 1 - \frac{\omega_p^2}{\omega(\omega - \nu\Omega)} \right\} \delta_{\mu, -\nu} = \epsilon_{-\mu}, \text{ say} \quad (\text{no summation}). \quad \dots\dots (21)$$

Maxwell's equations give us

$$\epsilon_{\mu\nu} E_{-\nu} = \left(\frac{c^2 k^2}{\omega^2} \right) E_\mu - \left(\frac{c^2 k_\mu k_\nu}{\omega^2} \right) E_{-\nu}, \quad \dots\dots (22)$$

hence

$$E_\nu = \frac{(c^2 / \omega^2) \mathbf{k} \cdot \mathbf{E}}{(c^2 k^2 / \omega^2) - \epsilon_\nu} k_\nu \quad (\text{no summation}). \quad \dots\dots (23)$$

Multiply (23) by k_{-v} and sum over v . Let $\epsilon = c^2 k^2 / \omega^2$, the effective dielectric constant. Then we have

$$\mathbf{k} \cdot \mathbf{E} = \left\{ \frac{1}{2} \left[\frac{\epsilon}{\epsilon - \epsilon_1} + \frac{\epsilon}{\epsilon - \epsilon_{-1}} \right] \sin^2 \theta + \frac{\epsilon}{\epsilon - \epsilon_0} \cos^2 \theta \right\} \mathbf{k} \cdot \mathbf{E}, \quad \dots (24)$$

where θ is the angle between \mathbf{k} and \mathbf{H} . Solutions of (24) with $\mathbf{k} \cdot \mathbf{E} = 0$ give us waves which do not produce charge separation. Such a solution is seen in (22) by putting $\epsilon = \epsilon_0$, with $E_1 = E_{-1} = 0$, $E_0 \neq 0$. This gives us waves with frequencies given by

$$\omega^2 = \omega_p^2 + c^2 k^2$$

and which are transverse. If we now assume that $\mathbf{k} \cdot \mathbf{E} \neq 0$, we have

$$\frac{1}{2} \left\{ \frac{\epsilon_1}{\epsilon - \epsilon_1} + \frac{\epsilon_{-1}}{\epsilon - \epsilon_{-1}} \right\} \sin^2 \theta + \frac{\epsilon_0}{\epsilon - \epsilon_0} \cos^2 \theta = 0$$

and the solutions are waves which produce charge separation. If we let $W_v = c/\sqrt{\epsilon_v}$ be the three 'principal' speeds of propagation we have

$$(W^2 - W_0^2)(W^2 - \frac{1}{2}W_1^2 - \frac{1}{2}W_{-1}^2) \sin^2 \theta + (W^2 - W_1^2)(W^2 - W_{-1}^2) \cos^2 \theta = 0, \quad \dots (25)$$

where we have written $W = \omega/k$ for the wave velocity.

For propagation along the field, $\theta = 0$,

$$W = W_1 \text{ or } W_{-1}, \quad \dots (26)$$

and for propagation perpendicular to the field, $\theta = \pi/2$,

$$W = W_0 \text{ or } W^2 = \frac{1}{2}(W_1^2 + W_{-1}^2). \quad \dots (27)$$

The case $W = W_0$ we have already discussed. The second case gives

$$\frac{E_y}{E_x} = \frac{-i(W_1^2 + W_{-1}^2)}{W_1^2 - W_{-1}^2}$$

and the waves are elliptically polarized, partly longitudinal and partly transverse.

We will now modify these 'cold' solutions to include thermal effects under the same conditions that the components of the dielectric tensor were calculated. In the case of zero temperature we write Maxwell's equations in the form

$$n^2(\delta_{\mu\nu} - k_\mu k_\nu / k^2) E_\nu = \epsilon_\mu E_\mu \quad (\mu \text{ not summed}), \quad \dots (28)$$

where n is the refractive index relating the wave velocity to the velocity of light *in vacuo*, i.e. $n = c/W$. We write the equations when thermal effects are included in the form

$$(n^2 + \delta n^2) \left(\delta_{\mu\nu} - \frac{k_\mu k_\nu}{k^2} \right) (E_\nu + \delta E_\nu) = \epsilon_\mu (E_\mu + \delta E_\mu) + \epsilon'_{\mu, -\nu} (E_\nu + \delta E_\nu) \quad (\mu \text{ not summed}), \quad \dots (29)$$

so that we may utilize the eigenvalues of (28). Put

$$\delta_{\mu\nu} - k_\mu k_\nu / k^2 = A_{\mu\nu}. \quad \dots (30)$$

Then the matrix A is Hermitian, and we may write (26) and (27) as

$$n^2 A_{\mu\nu} E_\nu = \epsilon_\mu E_\mu \quad (\mu \text{ not summed}) \quad \dots (31)$$

$$(n^2 + \delta n^2) A_{\mu\nu} (E_\nu + \delta E_\nu) = \epsilon_\mu (E_\mu + \delta E_\mu) + \epsilon'_{\mu, -\nu} (E_\nu + \delta E_\nu) \quad (\mu \text{ not summed}). \quad \dots (32)$$

If we expand (32) to first order and use (31) we obtain

$$n^2 A_{\mu\nu} \delta E_\nu + \delta n^2 A_{\mu\nu} E_\nu = \epsilon_\mu \delta E_\mu + \epsilon'_{\mu, -\nu} E_\nu \quad (\mu \text{ not summed}).$$

Multiply by E_μ and sum over μ . Using the fact that A is Hermitian ($k_y = 0$ does not represent any loss of generality) and (31), we obtain

$$\frac{\delta n^2}{n^2} = \frac{E_\mu \epsilon'_{\mu\mu} E_\mu}{\epsilon_\lambda E_\lambda E_\lambda}$$

which we can write in terms of the 'cold' wave velocity as

$$\frac{\delta W^2}{W^2} = - \frac{E_\mu \epsilon'_{\mu\mu} E_\mu}{\epsilon_\lambda E_\lambda E_\lambda}.$$

Finally, substitution from (22) gives

$$\frac{\delta W^2}{W^2} = - \frac{k_\mu \epsilon'_{\mu\mu} k_\nu (\epsilon - \epsilon_\lambda)^2}{\epsilon_\lambda (\epsilon - \epsilon_\mu) (\epsilon - \epsilon_\nu) k_\lambda^2} \dots\dots (33)$$

We see that the wave velocity and the thermal correction are real which means that the waves are undamped. The reason for the absence of damping probably lies in the assumption that the wave velocity is considerably greater than the mean thermal velocity of the particles, which means that at the value of the wave velocity the slope of the curve of the distribution function is very small and hence the difference between the number of particles accelerated by the wave, which produce damping, and the number of particles retarded by the wave, which produce growth, is very small.

§ 5. CONCLUSION

We have shown that the effect of currents flowing in a plasma is to introduce a change in the dielectric tensor which is proportional to the square of the plasma frequency. In the particular case when the wave velocity of the disturbance is considerably greater than the mean thermal velocity of the particles, and the mean Larmor radius of the particles considerably less than the wavelength of the oscillation, we have obtained the dielectric tensor. The change due to thermal effects is small except near integral multiples of the gyrofrequency of the particles where it has singularities. Using this dielectric tensor and the solutions to the propagation problem at zero temperature, we have calculated the correction that must be applied to the 'cold' wave velocity to allow for thermal effects. This correction shows the same singularities as the change in the dielectric tensor. The employment of an eigenvalue method for calculating the thermal correction to the wave velocity seems more compact than the usual method of expanding each term in the determinant which usually gives the dispersion relation. However the method used in this paper does not seem to be applicable under assumptions other than those stated.

ACKNOWLEDGMENTS

The author wishes to express his gratitude to Dr. O. Buneman for suggesting this approach to the problem and to Dr. F. Haas for reading the manuscript.

REFERENCES

- AKHIEZER, *et al.*, 1958, *Proc. Second U.N. Conf. Geneva*, **31**, 99.
 ANDERSON, N., 1960, *Proc. Phys. Soc.*, **75**, 905.
 ASTRÖM, E., 1951, *Ark. Fys.*, **2**, 446.
 AUER, P. L., HURWITZ, H., Jr, and MILLER, R., D., 1958, *Phys. Fluids*, **1**, 501.
 BERNSTEIN, I., 1958, *Phys. Rev.*, **109**, 10.

On the Identification of the K_{α} Satellites—I: LS Region†

BY Z. HORÁK

Institute of Technical Physics, Czechoslovakian Academy of Science, Prague

MS. received 14th October 1960

Abstract. The lines α'' , α' , α_3 , α_3' , α_4 in the spectra of neon and a few of its neighbours ($10 \leq Z \leq 14$) are identified as $K^{-1}L^{-1} \rightarrow L^{-2}$ transitions. For this purpose the case $Z=10$ was analysed using earlier self-consistent-field results together with optical term values and intensity considerations. The necessary Z -dependences were developed by means of Layzer's theory.

§ 1. INTRODUCTION

THE origin of certain x-ray satellites was for a long time attributed to transitions in multiply ionized atoms (typical ones are $K^{-1}L^{-1} \rightarrow L^{-2}$, $K^{-1}M^{-1} \rightarrow L^{-1}M^{-1}$, $L^{-1}M^{-1} \rightarrow M^{-2}$, etc.). In many cases, however, detailed correspondence between the theoretically predicted and measured lines has not yet been completely established. Recently some successful work in this direction has been done by Candlin (1955) who tried to identify the predicted $K^{-1}L^{-1} \rightarrow L^{-2}$ lines with observed K_{α} -satellites for elements with atomic number Z lying between 19 and 42.

However, for lower values of Z ($8 \leq Z \leq 18$) these satellites were also observed and their identification would be of interest. The situation for $Z=10$ is investigated in §2. Earlier calculations of Kennard and Ramberg (1934a)‡ are employed together with the fact that the L^{-2} levels are exactly known in this case from the optical spectra. These results and also relative intensity considerations strongly support the hypothesis that the origin of some K_{α} -satellites is really due to the transitions $K^{-1}L^{-1} \rightarrow L^{-2}$; however the methods of §2 are still not sufficient to give a detailed correspondence between the theoretical and experimental lines.

For this purpose it is necessary to study the spectra of the elements immediately neighbouring on neon, with $Z > 10$ (§3). In this region the dependence on Z is calculated by means of Layzer's (1959) theory. The effect of 3s and 3p electrons is considered by means of Slater's (1930) rules and the external screening due to 3s and 3p electrons is neglected throughout. It is also possible to neglect spin-orbit and relativistic contributions if Z is not too high. For these elements our results support the earlier Kennard and Ramberg identifications (KR II, p. 1043). Some consequences and limitations of the latter are briefly discussed.

† Some results obtained in this paper were already briefly reported (Horák 1958, 1960) and they also represent a part of the author's Candidate Thesis.

‡ In the following we shall denote Kennard and Ramberg's (1934 a, b) paper as KR I, II respectively.

§ 2. THE NEON SPECTRUM

We shall first study the lines $K^{-1}L^{-1} \rightarrow L^{-2}$ in the spectrum of neon, $Z=10$. 'Pure' theory developed in KR I for the neighbouring sodium ($Z=11$) spectrum predicts the following five $K^{-1}L^{-1} \rightarrow L^{-2}$ lines:

$$\left. \begin{array}{l} \text{A } 1s2s^1S \rightarrow 2s2p^1P \\ \text{B } 1s2p^1P \rightarrow (2p)^2^1S \\ \text{C } 1s2p^3P \rightarrow (2p)^2^3P \\ \text{D } 1s2s^3S \rightarrow 2s2p^3P \\ \text{E } 1s2p^1P \rightarrow (2p)^2^1D \end{array} \right\} \dots\dots (1)$$

(holes in the complete shells are indicated). The quantities

$$\frac{\Delta\nu}{R} = \frac{\nu_{\text{sat}}}{R} - \frac{r}{R} (K_\alpha)^\dagger$$

were also calculated in KR I (cf. KR II, Table 1) but the results are not sufficiently exact to make a complete identification at the observed lines in terms of the transitions (1) (KR II, p. 1042). It was shown, however, that the wave numbers of the predicted lines (1) definitely fall into the region of the satellites α' , α_3 , α_4 , in the sodium spectrum. In the following a similar prediction is made concerning the spectrum of neon.

To do this we shall obtain the Z -dependence of $\Delta\nu'(Z)/R$ for the transitions (1) in an isoelectronic sequence, i.e. neglecting the presence of the $3s$ and $3p$ electrons for $10 < Z \leq 18$. Generally $\Delta\nu'/R = W(K^{-1}L^{-1}) - W(L^{-2}) - W(K^{-1}) + W(L^{-1})$ where the W 's have the form $W_2Z^2 + W_1Z + W_0 + \sum_{i=1}^{\infty} W_{-i}Z^{-i}$ (neglecting relativistic and spin-orbit contributions). It is possible to evaluate the coefficients W_2 , W_1 by means of a first-order perturbation calculation based on strictly hydrogenic radial wave functions (Layzer 1959). The coefficients W_2 are $W_2(K^{-1}L^{-1}) = -(1+7/4)$, $W_2(L^{-2}) = -(2+6/4)$, $W_2(K^{-1}) = -(1+8/4)$, $W_2(L^{-1}) = -(2+7/4)$ which implies that the coefficient of Z^2 in $\Delta\nu'/R$ is zero. The quantities $W_1(L^{-1})$, $W_1(L^{-2})$ are given in Layzer's paper (1959, Table 1) and $W_1(K^{-1}L^{-1})$, $W_1(K^{-1})$ are calculated in the Appendix to the present paper. Finally the various $\Delta\nu_{\text{iso}}/R = \Delta\nu'/R$ are

$$\left. \begin{array}{l} \frac{\Delta\nu'}{R} (\text{A}) = 0.08084Z + \dots; \quad \frac{\Delta\nu'}{R} (\text{B}) = 0.10094Z + \dots; \quad \frac{\Delta\nu'}{R} (\text{C}) = 0.12334Z + \dots; \\ \frac{\Delta\nu'}{R} (\text{D}) = 0.11024Z + \dots; \quad \frac{\Delta\nu'}{R} (\text{E}) = 0.14943Z + \dots \end{array} \right\} \dots\dots (2)$$

The coefficients of Z^{-r} , $r \geq 0$, are very difficult to determine directly. For the present application we shall assume that they are negligible if $r > 0$.

To find the terms in (2) independent of Z we employ at first the results of KR II (Table 1, column (1)). The values listed there are calculated by means of a first-order perturbation scheme (Condon and Shortley 1953, Chapters VI, VII) using self-consistent-field radial wave functions. However, it is necessary to correct these results in two ways. (i) Reduction to Na^+ , i.e. addition of the quantity $E(K^{-1}L^{-1}) - E(L^{-2}) - E(K^{-1}) + E(L^{-1})$ where the E 's are ionization

† The measured wave number difference between the satellite and the K_α line is expressed in units of $R=109\,737\text{ cm}^{-1}$. The Rydberg unit of energy ($=13.605\text{ eV}$) is used throughout this paper.

potentials of the 3s electron in the corresponding states. It is possible to evaluate the E 's immediately from KRI, Table 1, where the energy parameters of the Hartree equations are listed. (ii) Interaction of the configurations $(2p)^2\ ^1S$ and $(2s)^2\ ^1S$ increases the value of $\Delta\nu'(B)/R$. The magnitude of this correction will be determined as follows. The difference

$$\delta(^1S, ^1D) = W(2p^2\ ^1S) - W(2p^2\ ^1D) = \Delta\nu'(E)/R - \Delta\nu'(B)/R = 0.04849Z + \text{const.}$$

was calculated for $Z=8$ by Hartree, Hartree and Swirles (1939). Using their value $\delta(Z=8)=0.172$ we find $\delta(Z=11)=0.317$ in contrast to the value 0.43 obtained from KR II, Table 1, column (1). This implies the configuration interaction correction to be 0.11 and the correct

$$\Delta\nu'(B)/R = 0.12 + 0.02 + 0.11 = 0.25.$$

The values $\Delta\nu'/R$ corrected in the above approximate manner were used, together with linear dependences (2), to obtain the predicted $\Delta\nu'/R$ values in the neon spectrum. The latter are compared with the experimental results of Moore and Chalklin (1955) in Fig. 1. The comparison shows that in the spectrum

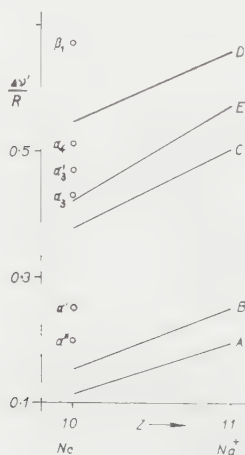


Fig. 1. Linear extrapolation of the self-consistent-field results. Circles, experimental points. The positions of the theoretical lines A–E (2) are determined from the corrected self-consistent values at $Z=11$ (cf. § 2).

of neon probably all the five transitions (1) were resolved (this is not the case for the neighbouring elements). The groupings of theoretical and experimental points suggest the identification

$$(\alpha'', \alpha') \longleftrightarrow (A, B); \quad (\alpha_3, \alpha_3', \alpha_4) \longleftrightarrow (C, D, E). \quad \dots\dots (3)$$

In KR II (p. 1042) the error of the calculated values is assumed to be about ± 0.1 , thus making impossible any more detailed identification in the two groups (3).

However, for this purpose the following property will be useful. Consider the transitions B, E (1). Their wave number difference $\nu(E)/R - \nu(B)/R$ can be evaluated (exactly for $Z=10$ only) by means of the optical term values (Moore 1949): $\nu(E)/R - \nu(B)/R = W(2p^2\ ^1S) - W(2p^2\ ^1D) = \delta(Z=10) = 0.273$ and their predicted intensity ratio is $I(E)/I(B) = 5$ (Condon and Shortley 1953, Table 3^o). Table 1 shows that these predictions are fulfilled within the limits of experiment (Moore and Chalklin 1955) by the two pairs of lines α'', α_3' and α', α_4 .

Table 1. Energy Difference and Intensity Tests

	Lines	Wave number difference	Intensity ratio
Predicted	E, B	$\frac{\nu}{R}(E) - \frac{\nu}{R}(B) = 0.273$	$\frac{I(E)}{I(B)} = 5$
Experimental	α_3', α''	$\frac{\nu}{R}(\alpha_3') - \frac{\nu}{R}(\alpha'') = 0.27 \pm 0.02$	$\frac{I(\alpha_3')}{I(\alpha'')} = 3.3 \dagger$
	α_4, α'	$\frac{\nu}{R}(\alpha_4) - \frac{\nu}{R}(\alpha') = 0.26 \pm 0.02$	$\frac{I(\alpha_4)}{I(\alpha')} = 3.3 \dagger$

† Values indicated by the more probable analysis (i) (cf. Moore and Chalklin 1955, Table 2).

§ 3. THE DEPENDENCE ON Z

To make the final identification in the two groups (3) it is necessary to study the change of the satellite structure with Z . Neglecting the external screening and possible angular momentum splitting due to incomplete 3s and 3p shells we can write $\Delta\nu/R = \Delta\nu'/R + \Delta\nu''/R$, where $\Delta\nu''/R$ is the contribution of the 3s and 3p electrons. It is plausible to assume the latter in the simple form

$$\frac{1}{3^2} \left\{ -(Z - \sigma + x + y)^2 + (Z - \sigma + 2y)^2 + (Z - \sigma + x)^2 - (Z - \sigma + y)^2 \right\} = \frac{2}{9} y(y - x)$$

(per one 3s or 3p electron). Here $Z - \sigma$ is the effective nuclear charge per 3s or 3p electron in the normal (non-excited) state and x, y are contributions to the screening from K, L electrons respectively. According to Slater (1930) $x = 1$, $y = 0.85$ which implies for $10 \leq Z \leq 18$

$$\frac{\Delta\nu''}{R} = - (Z - 10) \frac{2}{9} y(x - y) = - 0.02833(Z - 10). \quad \dots\dots (4)$$

Adding this term and $\Delta\nu'/R$ from (2) we obtain the expected linear dependence still with the absolute terms undetermined. To find the latter we shall assume the identifications

$$x'' \equiv A, \quad \alpha' \equiv B, \quad \alpha_3 \equiv C, \quad \alpha_3' \equiv D, \quad \alpha_4 \equiv E; \quad \dots\dots (5)$$

this will be discussed below. In this way the lines A-E were obtained and compared with experimental results in Fig. 2.

We first discuss possible identifications other than (5). At first, starting from (3) and the 'coupling' property of α'', α_3' and α', α_4 (cf. Table 1) we consider $\alpha' \equiv A$, $\alpha'' \equiv B$, $\alpha_3' \equiv E$. In Fig. 2 $\alpha_3' \equiv E$ is shown by a broken line, which evidently fits the experimental points much worse than the full line, corresponding to $\alpha_4 \equiv E$ (Horák 1960). We shall further reject the other possible identification alternative to (5), namely $\alpha_3 \equiv C$, $\alpha_4 \equiv D$. Let us suppose that α_3 can be identified with C for $Z > 10$. Using the optical term values (Moore 1949) and the wave numbers of α , α_3 , α_4 (Tyron 1940), we are able to find the values of the energy levels $1s2p^3P$, 1P ; cf. Table 2. The level $1s2p^1P$ can be derived either from α' or from α_4 (in Table 2 these values are denoted (α') , (α_4) respectively) and it is very satisfactory that both values agree within the experimental limits.

Table 2. Energy Levels $1s2p^1, ^3P$ deduced from the Measurements of Tyrén (1940)[†]

Z	11		12			13			
Compound	Metal	NaF	Metal	MgO	MgF ₂	Metal	Al ₂ O ₃	AlF ₃	
1s2p ¹ P	(α')	77.423	77.440	93.243	93.242	93.251	110.514	110.565	110.561
	(α ₄)	77.430	77.440	93.249	93.251	93.259	110.524	110.554	110.574
	mean	77.426	77.440	93.246	93.247	93.255	110.519	110.560	110.567
1s2p ³ P	77.039	77.043	92.786	92.796	92.798	109.997	110.034	110.041	
(α')-(α ₄)	-0.007	0.000	-0.006	-0.009	-0.008	-0.010	+0.011	—	
Exptl error	—	—	±0.007 ±0.01		—	—	±0.013		—

[†] Zero level is $[2p^2 \ ^3P_2] + K$ where K is approximately the same for $1s2p^1P$ and $1s2p^3P$. A first-order correction for spin-orbit interaction was applied to derive the energy of $(2p)^2 \ ^3P$.

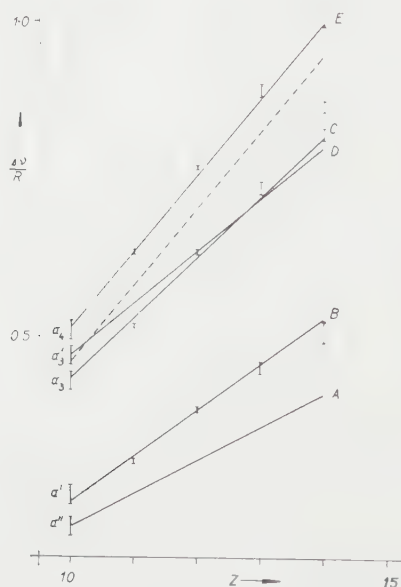


Fig. 2. Predicted and experimental dependence of $\Delta\nu/R$ on Z . Experimental values are taken from the papers of Moore and Chalklin (1955, $Z=10$), Tyrén (1940, $Z=11-13$), Flemberg (1935, $Z=14$); they are marked with small intervals which represent either all values measured in various chemical compounds for $10 < Z \leq 14$, or possible errors for $Z=10$ (± 0.015). The broken line corresponds to $E \equiv \alpha_3'$, the full ones assume (5).

We shall further examine the energy difference $\Delta(^1P, ^3P)$ of the levels $1s2p^1P$ (mean) and $1s2p^3P$ using the theory of Layzer (1959). The latter predicts the slope of the linear dependence,

$$\Delta(^1P, ^3P) = 0.06828Z + \text{const. (cf. Appendix)} \quad \dots\dots (6)$$

which was found to agree with the experimental points $Z=11, 12, 13$ (Fig. 3). Now such a line gives a reasonable value of $\Delta(^1P, ^3P)$ for $Z=10$ if (5) is assumed.

On the other hand, the alternative identification for $Z=10$, namely $\alpha_3' \equiv C$, $\alpha_3 \equiv D$ leads to an unsatisfactory value of $\Delta(^1P, ^3P)$, denoted by the cross in Fig. 3.

In this way the identifications (5) are supported. They predict reasonable values of the relative intensities in the neon spectrum (Horák 1958).

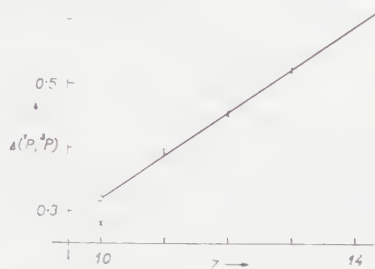


Fig. 3. The dependence of $\Delta(^1P, ^3P)$ on Z . The predicted line (6) has its position fixed by (5). Small intervals for $Z > 10$ represent all values from Table 2. In the case $Z=10$ there are two points: circles corresponding to (5), crosses corresponding to $\alpha_3' \equiv C$, $\alpha_3 \equiv D$.

They also agree with those suggested previously by Kennard and Ramberg (KR II, p. 1043) with the only exception that α' was resolved into two components α' , α'' (Moore and Chalklin 1955, Bačkovský and Drahokoupil 1954). It is surprising, however, that no such resolution was made for $Z > 10$ (Fig. 2). For the explanation of this 'effect' a more detailed study of the excitation and de-excitation would be necessary. The present theory also cannot explain the strong dependence of the relative intensities on the chemical combination of the emitting substance (Nordfors 1956). For $Z < 10$ the whole appearance of the satellite structure also depends on the chemical constitution (Tyrén 1940) and moreover the present theory fails in this region as the terms in (2), containing Z^{-1} , are probably not negligible here.

On the other hand, with increasing Z the relativistic and spin-orbit contributions which were neglected in the present treatment, may become important. Consequently, the triplet transitions C, D will be split and this makes any identification very difficult (cf. $Z=14$, Fig. 2). A more detailed discussion of these splittings forms the subject of a subsequent paper 'On the identification of the K_{α} -satellites II' (Horák, to be published). In that paper we shall also discuss the relation to the work of Candlin (1955).

ACKNOWLEDGMENTS

The author is greatly indebted to Dr. Bačkovský and Dr. Drahokoupil for suggesting this problem and for helpful discussions, and to his wife for her assistance in the numerical work.

APPENDIX

CALCULATION OF THE TERMS CONTAINING Z

In the case of K^{-1} , $K^{-1}L^{-1}$ states the quantities W_1 (Layzer 1959, p. 276 theorem (i)) are simply the diagonal matrix elements of the electrostatic repulsion $V = \sum_{i,j} (2/r_{ij})$ constructed in the LS scheme (Condon and Shortley 1953, Chapter VI) with hydrogenic radial wave functions. Consequently the

W_1 's can be expressed as linear combinations of Slater-Condon parameters $F_i(nl, n'l')G_i(nl, n'l')$ (cf. Condon and Shortley 1953, § 8⁶). In this way we find:

$$\begin{aligned} W_1(1s^2S) &= 2F_0(1s2s) - G_0(1s2s) + 6F_0(1s2p) - 3G_1(1s2p) + F_0(2s2s) \\ &\quad + 12F_0(2s2p) - 6G_1(2s2p) + 15F_0(2p2p) - 30F_2(2p2p), \\ W_1(1s2p^3P) &= W_1(1s^2S) - F_0(1s2p) - 2F_0(2s2p) + G_1(2s2p) - 5F_0(2p2p) \\ &\quad + 10F_2(2p2p), \\ W_1(1s2s^3S) &= W_1(1s^2S) - F_0(1s2s) - F_0(2s2s) - 6F_0(2s2p) + 3G_1(2s2p), \\ W_1(1s2p^1P) &= W_1(1s2p^3P) + 2G_1(1s2p), \quad W_1(1s2s^1S) = W_1(1s2s^3S) + 2G_0(1s2s) \end{aligned}$$

where the F_i 's and G_i 's are

$$\begin{aligned} F_0(1s2s) &= 0.41975, & F_0(1s2p) &= 0.48560, & F_0(2s2p) &= 0.32422, \\ F_0(2s2s) &= 0.30078, & F_2(2p2p) &= 0.36328, & F_2(2p2p) &= 0.00703, \\ G_1(1s2p) &= 0.03414, & G_1(2s2p) &= 0.05859, & G_0(1s2s) &= 0.04389. \end{aligned}$$

$$\begin{aligned} \text{Finally} \quad W_1(1s^2S) &= 12.68489, \\ W_1(1s2p^3P) &= 9.86336 = W_1(1s2p^1P) - 0.06828, \\ W_1(1s2s^3S) &= 10.19483 = W_1(1s2s^1S) - 0.08778. \end{aligned}$$

REFERENCES

- BAČKOVSKÝ, J. M., and DRAHOKOUPIL, J., 1954, *Czech. J. Phys.*, **4**, 4.
 CANDLIN, D. J., 1955, *Proc. Phys. Soc. A*, **68**, 322.
 CONDÓN, E. U., and SHORTLEY, G. H., 1953, *The Theory of Atomic Spectra* (Cambridge: University Press).
 FLEMBERG, K'SON, 1935, *Z. Phys.*, **96**, 167.
 HARTREE, D. R., HARTREE, W., and SWIRLES, B., 1939, *Phil. Trans. R. Soc.*, **238**, 229.
 HORÁK, Z., 1958, *Exp. Tech. Phys.*, **6**, 29.
 ——— 1960, *Bull. Acad. Sci. U.S.S.R., Ser. Phys.*, **24**, 422.
 KENNARD, E. H., and RAMBERG, E. G., 1934 a, *Phys. Rev.*, **46**, 1034.
 ——— 1934 b, *Phys. Rev.*, **46**, 1040.
 LAYZER, D., 1959, *Ann. Phys., Lpz.*, **8**, 271.
 MOORE, C. E., 1949, *Nat. Bur. Standards Circular No. 467 (Atomic Energy Levels)*.
 MOORE, H. R., and CHALKLIN, F. C., 1955, *Proc. Phys. Soc. A*, **68**, 717.
 NORDFORS, B., 1956, *Ark. Fys.*, **10**, 279.
 SLATER, J. C., 1930, *Phys. Rev.*, **36**, 57.
 TYRÉN, F., 1940, *Nova Acta Reg. Soc. Scient. Uppsala. Ser. IV*, **12**, 1.

**(d-d) Reaction Product Velocities in SCEPTRE III
according to a Two-Group Model**

BY R. HERDAN AND T. P. HUGHES

Research Laboratory, Associated Electrical Industries Limited, Aldermaston, Berks.

Communicated by D. R. Chick; MS. received 28th September 1960

Abstract. The relation is given between the drift velocity Δ of a hot group of deuterons, mixing with a cooler stationary group, and the mean centre-of-mass velocity $\langle \mathbf{W} \rangle$ of reacting deuteron pairs. Subject to certain restrictions on temperatures and densities, $\langle W \rangle / \Delta$ can be as high as 3 or more. It is suggested that departures from the Maxwellian distribution may make the ratio large enough to explain results obtained with SCEPTRE III, without invoking any acceleration other than that due to the applied electric field.

§ 1. INTRODUCTION

MEASUREMENTS of the energy spectrum of protons from the (d-d) reaction in the toroidal discharge apparatus SCEPTRE III, using nuclear emulsion techniques (Jones *et al.* 1958), indicate that the reacting deuteron pairs have a mean centre-of-mass velocity of about $4 \times 10^7 \text{ cm sec}^{-1}$ in the direction of the positive ion current. Preliminary observations of the Doppler displacements of spectral lines from highly ionized impurity atoms in the hotter parts of the discharge (Hughes and Kaufman 1959) suggest that the deuterons in this region have drift velocities of the order of $5 \times 10^6 \text{ cm sec}^{-1}$ (Ware 1959). In the present paper a mathematically simple model is set up in an endeavour to relate these two results.

The model requires the mixing of two groups of deuterons which possess a relative drift velocity. Each group has a Maxwellian velocity distribution in its own centre-of-mass coordinate system. Fusion reactions will occur between deuterons belonging to the *same* group at a rate depending on their density and temperature; these reactions constitute the 'self yield' of the group, and the reaction rates have been calculated (Thompson 1957). In addition, however, reactions will occur between deuterons belonging to *different* groups: these constitute the 'cross yield' of the two groups. Observations of the energy spectrum of protons (or neutrons) emitted from the reactions in different directions will indicate the mean value of \mathbf{W} , the centre-of-mass velocity of a reacting deuteron pair, averaged over all pairs. This mean value is called $\langle \mathbf{W} \rangle$. Denoting the self yields of groups 1 and 2 by r_{11} and r_{22} , and the cross yield of the two groups by r_{12} , it is clear that if $r_{11} \gg r_{22} + r_{12}$, $\langle \mathbf{W} \rangle$ will approximately equal the drift velocity of group 1, while if $r_{22} \gg r_{11} + r_{12}$, $\langle \mathbf{W} \rangle$ will approximate to the drift velocity of group 2. If, however, $r_{12} \gg r_{11} + r_{22}$, the value of $\langle \mathbf{W} \rangle$ will depend on the temperatures and drift velocities of the two groups. Supposing one group to be stationary and the other to be moving with drift velocity Δ , it will be shown that in this last case $\langle W \rangle$ can exceed Δ under certain conditions by a factor of 3 or more. As will

be seen, this magnification effect is only predicted if a fundamental asymmetry is introduced by giving the two groups different temperatures. It will also be shown that the condition $r_{12} \gg r_{11} + r_{22}$ requires one group of deuterons to be hot and of low density, while the other must be somewhat cooler and of high density.

The somewhat paradoxical requirement that the two groups should retain their identities and yet interact may be satisfied if a magnetic field is present perpendicular to the temperature gradient. This will tend to inhibit bulk mixing of the two groups while permitting those energetic deuterons of the hot group which contribute most to the reaction rate to penetrate into the cooler region.

§ 2. MATHEMATICAL FORMULATION

If f_1 and f_2 are the velocity distribution functions of two *distinct* populations of deuterons, which we shall call groups 1 and 2, the fusion reaction yield per unit time due to collisions involving a deuteron from each group is given by an integral of the form

$$r_{12} = \int f_1 f_2 \sigma_{12} |\mathbf{v}_1 - \mathbf{v}_2| d\mathbf{v}_1 d\mathbf{v}_2, \quad \dots\dots (1)$$

where \mathbf{v}_1 and \mathbf{v}_2 represent typical velocities of deuterons in the two respective groups and σ_{12} is the appropriate cross section. The integrals are taken over the whole of the sixfold velocity space $(\mathbf{v}_1, \mathbf{v}_2)$; $d\mathbf{v}_1$ and $d\mathbf{v}_2$ denote $dv_{1x} dv_{1y} dv_{1z}$ and $dv_{2x} dv_{2y} dv_{2z}$ in a suitable Cartesian reference frame. In addition to the cross yield r_{12} defined above, we also have similar expressions for the self yields r_{11} and r_{22} . Thus for group 1

$$r_{11} = \frac{1}{2} \int f_1 f_1' \sigma_{11} |\mathbf{v}_1 - \mathbf{v}_1'| d\mathbf{v}_1 d\mathbf{v}_1'. \quad \dots\dots (2)$$

Here \mathbf{v}_1 and \mathbf{v}_1' are the velocities of a typical pair of particles in group 1. The factor $\frac{1}{2}$ appearing in Eqn (2) is necessary because otherwise each pair would be counted twice. It should be noted that, since f_1 and f_2 are in general functions of position, r_{12} etc. are in effect *local* quantities.

We now define the yield-weighted mean centre-of-mass velocities $\langle \mathbf{W} \rangle$, which are in effect the mean centre-of-mass velocities of *reacting* deuteron pairs. In the case of the cross yield we have

$$\langle \mathbf{W}_{12} \rangle = \frac{1}{r_{12}} \int f_1 f_2 \sigma_{12} |\mathbf{v}_1 - \mathbf{v}_2| \cdot \frac{1}{2} (\mathbf{v}_1 + \mathbf{v}_2) d\mathbf{v}_1 d\mathbf{v}_2. \quad \dots\dots (3)$$

Similar expressions for $\langle \mathbf{W}_{11} \rangle$ and $\langle \mathbf{W}_{22} \rangle$ need not be calculated because the mean velocity of reacting pairs within a group having a symmetric velocity distribution in its centre-of-mass system is simply that of the group itself.

Let us now suppose that group 2 is stationary and that group 1 has a centre-of-mass velocity Δ , each group having a Maxwellian distribution about its mean velocity. The appropriate laboratory space distribution functions are then

$$f_1 = n_1 \left(\frac{m}{2\pi k T_1} \right)^{3/2} \exp \left[-\frac{m}{2k T_1} \left\{ (v_{1x} - \Delta)^2 + v_{1y}^2 + v_{1z}^2 \right\} \right], \quad \dots\dots (4)$$

$$f_2 = n_2 \left(\frac{m}{2\pi k T_2} \right)^{3/2} \exp \left[-\frac{m}{2k T_2} \left\{ v_{2x}^2 + v_{2y}^2 + v_{2z}^2 \right\} \right], \quad \dots\dots (5)$$

where n_1 and n_2 , T_1 and T_2 are the number densities and temperatures of groups 1 and 2 respectively, m is the deuteron mass and k Boltzmann's constant. The x axis is taken in the direction of the drift velocity of group 1.

The cross section σ_{12} will be assumed to have the Gamow form,

$$\sigma_{12} = \frac{A \exp [-(B/E^{1/2})]}{E}, \quad \dots\dots (6)$$

and the energy E is understood to be the kinetic energy of either particle of a colliding pair as seen from the other. The reason for this choice of energy parameter in preference to the more symmetrical centre-of-mass energy is that cross section measurements are usually made with stationary target particles and referred to the energy of an incident beam.

§ 3. EVALUATION OF THE INTEGRALS

The multiple integrals of the previous section are unsuitable for computation as they stand, but we show in an Appendix that they may be reduced to single integrals. We define (as in the Appendix)

$$S = \int_0^\infty \exp[-(4sw^2 + G/w)] \sinh(4s\Delta w) dw,$$

$$C = \int_0^\infty \exp[-(4sw^2 + G/w)] w \cosh(4s\Delta w) dw,$$

$$\rho = S/C$$

$$\text{and } F_{12} = \frac{s^{1/2} \exp[-s\Delta^2]}{\Delta} \int_0^\infty \exp[-(4sw^2 + G/w)] \sinh(4s\Delta w) dw$$

where $s = m/2k(T_1 + T_2)$, $G = B/(2m)^{1/2}$ and $w = \frac{1}{2}|\mathbf{v}_1 - \mathbf{v}_2|$.

It is found (see Appendix) that the cross yield r_{12} may be written

$$r_{12} = 8A\pi^{-1/2}n_1n_2F_{12}/m. \quad \dots\dots (7)$$

It is interesting that the temperature enters this expression only as $T_1 + T_2$.

To obtain the self yield r_{ii} of group i , we set $\Delta = 0$, replace n_1n_2 by $n_i^2/2$ and use the appropriate value of $s = m/4kT_i$ to find F_{ii} , so that

$$r_{ii} = 4A\pi^{-1/2}n_i^2F_{ii}/m. \quad \dots\dots (8)$$

The yield-weighted mean centre-of-mass velocity

$$\langle \mathbf{W}_{12} \rangle = \mathbf{i} \left[\frac{\lambda}{\lambda+1} \Delta + \frac{1-\lambda}{1+\lambda} \left(\rho - \frac{1}{4s\Delta} \right) \right], \quad \dots\dots (9)$$

where $\lambda = T_2/T_1$ and \mathbf{i} is the unit vector in the x direction. In the case of equal temperatures ($\lambda = 1$), $\langle \mathbf{W}_{12} \rangle = \mathbf{i}\Delta/2$. When $\Delta = 0$, $\langle \mathbf{W}_{12} \rangle$ must also be zero from obvious symmetry considerations.

The integrals S and C and the function F_{12} were calculated by simple quadrature on a Ferranti PEGASUS computer using Δ and $T_1 + T_2$ as variable parameters. The Gamow constant B was assigned the theoretical value $1.776 \times 10^{-3} \text{ erg}^{1/2}$. Numerical values of ρ and F_{12} are given in the Table for limited ranges of the variables.

Absolute values of the reaction rate for $\Delta = 0$, $T_1 = T_2 = 10^6$ °K and also 10^7 °K have been calculated from these results and are in satisfactory agreement with values given by Thompson (1956).

$T_1 + T_2 (^{\circ}\text{K})$	$\Delta \text{ (cm sec}^{-1}\text{)}$	$F_{12} \text{ (sec cm}^{-1}\text{)}$	$\rho \text{ (cm sec}^{-1}\text{)}$
4×10^6	0	4.08×10^{-22}	—
	2×10^6	4.44×10^{-22}	4.91×10^7
	5×10^6	6.58×10^{-22}	3.33×10^7
	10^7	1.89×10^{-21}	3.27×10^7
6×10^6	0	2.23×10^{-20}	—
	2×10^6	2.34×10^{-20}	6.90×10^7
	5×10^6	2.98×10^{-20}	4.06×10^7
	10^7	5.96×10^{-20}	3.75×10^7
8×10^6	0	2.74×10^{-19}	—
	2×10^6	2.83×10^{-19}	8.91×10^7
	5×10^6	3.34×10^{-19}	4.81×10^7
	10^7	5.54×10^{-19}	4.16×10^7
10^7	0	1.62×10^{-18}	—
	2×10^6	1.66×10^{-18}	1.09×10^8
	5×10^6	1.87×10^{-18}	5.56×10^7
	10^7	2.77×10^{-18}	4.54×10^7
1.2×10^7	0	6.21×10^{-18}	—
	2×10^6	6.33×10^{-18}	1.30×10^8
	5×10^6	6.98×10^{-18}	6.33×10^7
	10^7	9.56×10^{-18}	4.91×10^7

Fig. 1 shows $\log F_{12}$ plotted against $\log(T_1 + T_2)$ for several values of Δ . Figs 2 (a), (b) and (c) show how the ratio $\langle W_{12} \rangle / \Delta$ depends on T_1 and T_2 for three different values of Δ .

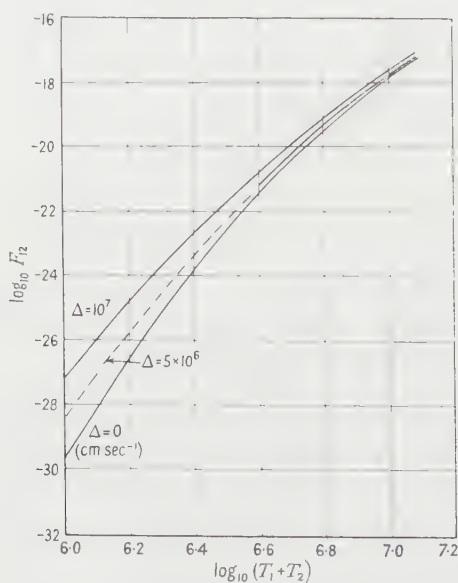


Fig. 1. Variation of F_{12} with $T_1 + T_2$ for various values of Δ .

§ 4. RELATION BETWEEN CROSS YIELD AND SELF YIELDS

The values of yield calculated in §3 will now be used to find the conditions under which the cross yield exceeds the sum of the self yields by a given factor. Denoting the ratio $r_{12}/(r_{11}+r_{22})$ when $\Delta=0$ by R_0 , and n_2/n_1 by b , we have from Eqns (7) and (8)

$$R_0 = \frac{2bF_{12}}{F_{11} + b^2F_{22}}. \quad \dots\dots(10)$$

Clearly the density ratio b may be adjusted for given F_{11} , F_{22} and F_{12} so as to make R_0 a maximum. This occurs when $b=b_{\text{opt}}=(F_{11}/F_{22})^{1/2}$, i.e. when the two self yields are equal. Using this value in Eqn (10), we obtain the maximum value of R_0 , $\hat{R}_0=F_{12}/(F_{11}F_{22})^{1/2}$.

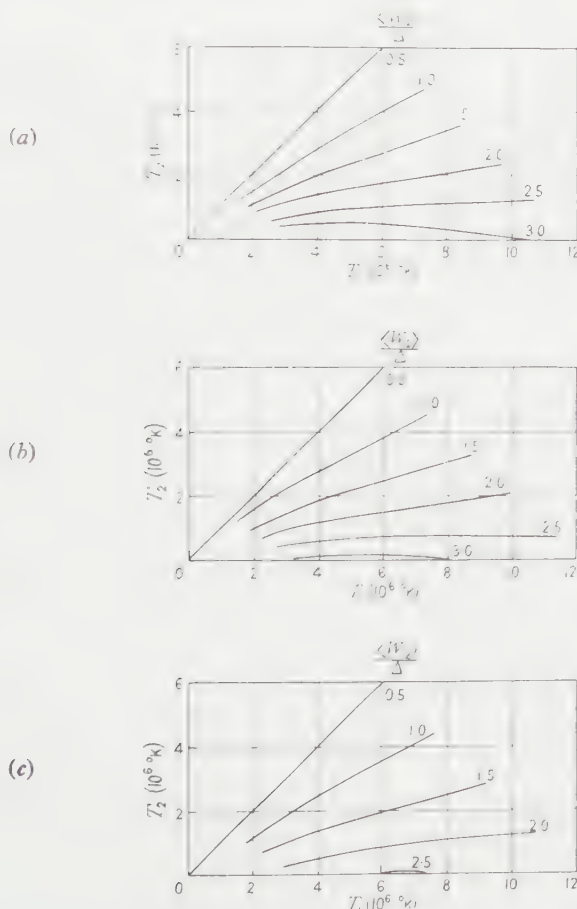


Fig. 2. Dependence of $\langle W_{12} \rangle / \Delta$ on T_1 and T_2 : (a) for $\Delta = 2 \times 10^8$ cm sec $^{-1}$, (b) for $\Delta = 5 \times 10^8$ cm sec $^{-1}$, (c) for $\Delta = 10^7$ cm sec $^{-1}$.

The value of R_0 is not very sensitive to departures from the optimum density ratio b_{opt} . This may readily be seen by putting $b = \epsilon b_{\text{opt}}$ in Eqn (10), so that $R_0 = \{2\epsilon/(\epsilon^2 + 1)\}\hat{R}_0$. It follows that as b varies between $\frac{1}{2}b_{\text{opt}}$ and $2b_{\text{opt}}$, R_0 never falls below $4\hat{R}_0/5$.

Values of $\log \hat{R}_0$ and $\log b_{\text{opt}}$ are plotted in Fig. 3. If $|\Delta| > 0$, R_Δ will always exceed R_0 because F_{12} increases with $|\Delta|$.

The proton energy spectra obtained experimentally so far exclude the possibility of the self yields being much in excess of 10% of the cross yield on the present model (Hunt, private communication) i.e., $\log \hat{R} \geq 1$. To obtain such values of \hat{R} with temperatures consistent with the observed total fusion reaction rate in the discharge, $\log b$ must be about 2.5. More accurate proton energy measurements will provide an interesting test of the theory, because if they should indicate that the self yields are less than, say, 0.1% of the cross yield the density ratio required according to the present model would be excessively large.

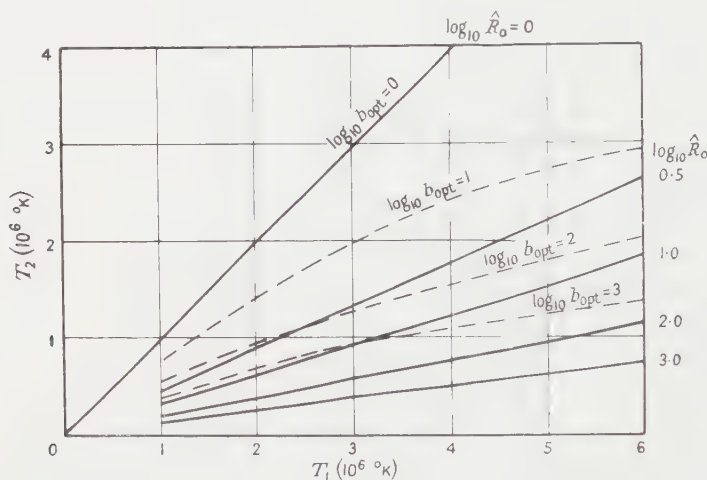


Fig. 3. Dependence of \hat{R}_0 and b_{opt} on T_1 and T_2 .

§ 5. EFFECT OF DEPARTURES FROM MAXWELLIAN DISTRIBUTIONS

For mathematical simplicity we have restricted our detailed discussion to deuteron velocity distributions which are Maxwellian in their centre-of-mass coordinate systems. Departures from the Maxwellian distribution may occur in the plasma as the result of various non-thermal processes (see, for example, Parker and Tidman 1958). The shapes of the tails of the deuteron velocity distributions are bound to have a considerable effect on the ratio $\langle W_{12} \rangle / \Delta$; this will be illustrated by a simple qualitative argument.

We suppose that one of the two mixing groups is cold and stationary while the other is hot. The distribution of relative velocities for pairs of particles of which one comes from each group is then approximately that of the deuteron velocities in the hot group. Next we suppose that the velocity distribution of the hot group when it has no centre-of-mass velocity is isotropic, with a cut-off at a speed which is greater by a small amount δc than the minimum speed c_0 required to produce a detectable cross yield. If now the hot group is given a small centre-of-mass velocity Δ , roughly equal in magnitude to δc , the cross yield due to those members of the hot group moving in the forward direction (i.e. in the direction of Δ) interacting with the cold group will be increased, while the cross yield due to hot deuterons moving in the opposite direction will be greatly reduced. Thus, the mean centre-of-mass velocity $\langle \mathbf{W}_{12} \rangle$ of the

deuteron pairs producing the cross yield will be parallel to Δ and will have a magnitude approaching $\frac{1}{2}c_0$, which will be very much greater than Δ . If on the other hand the hot deuteron distribution is nearly Maxwellian, its tail extends well beyond c_0 , so that giving it a small centre-of-mass velocity will only produce a comparatively small transfer of yield to the forward tail from the backward tail. Thus, if the deuteron distributions have tails steeper than those of Maxwellians, it is to be expected, though it is difficult to prove, that the ratio $\langle W_{12} \rangle / \Delta$ will be greater than the value calculated in §3 above.

§ 6. CONCLUSION

It has been shown that when two groups of deuterons at different temperatures are mixed, one of which has a drift velocity Δ , the protons or neutrons emitted from fusion reactions will come mainly from deuteron pairs having centre-of-mass velocities \mathbf{W} in the same direction as Δ but of considerably greater magnitude for certain temperatures and densities of the two groups. It is suggested that this effect may be enhanced by attenuation of the Maxwellian tail: $\langle \mathbf{W} \rangle$ might then be large enough to explain the observed displacement of the energy spectrum of protons emitted from SCEPTRE III on the basis of deuteron drift velocities deduced from spectroscopic observations of highly ionized impurity atoms, without invoking any accelerating mechanism other than the applied electric field.

ACKNOWLEDGMENTS

The authors are grateful to many members of the Nuclear Sciences Group of this Laboratory, especially Dr. A. A. Ware, Dr. W. M. Jones, Mr. K. M. Young and Dr. J. A. Wesson for helpful discussions. They acknowledge with thanks the assistance of Mr. E. A. Allwright and other members of the Computer Section, Engineering Mathematics Department, Associated Electrical Industries (Rugby) Limited, and of Mr. R. K. Taylor of this Laboratory in computing the integrals. The work was supported in part by a contract from the Atomic Energy Research Establishment, Harwell, and is published with the permission of Dr. T. E. Allibone, Director of the Laboratory.

APPENDIX

REDUCTION OF THE MULTIPLE INTEGRALS OF §2

It will be convenient to introduce the following notation:

$$z_1 = m/2kT_1, \quad z_2 = m/2kT_2,$$

$$s = \frac{\alpha_1\alpha_2}{\alpha_1 + \alpha_2} = \frac{m}{2k(T_1 + T_2)}.$$

Letting \mathbf{i} denote the unit vector along the x axis we change the variables of integration to

$$\mathbf{w} = \frac{1}{2}(\mathbf{v}_1 - \mathbf{v}_2)$$

and

$$\mathbf{Q} = (\alpha_1 + \alpha_2)^{-1/2}(\alpha_1\mathbf{v}_1 + \alpha_2\mathbf{v}_2 - \alpha_1\Delta\mathbf{i}).$$

Then from Eqns (4) and (5) of the text we obtain

$$f_1 f_2 = \pi^{-3} n_1 n_2 (\alpha_1 \alpha_2)^{3/2} e^{-M} \dots\dots (A1)$$

where

$$M = Q^2 + 4szw^2 - 4szw_x\Delta + s\Delta^2$$

and w_x is the x -component of \mathbf{w} .

Expression (6) of the text for the Gamow cross section σ_{12} becomes

$$\sigma_{12} = \frac{A}{2mw^2} \exp[-G/w], \quad \dots\dots (A2)$$

where

$$G = B/(2m)^{1/2}.$$

It is easily verified that

$$\left| \frac{\partial(\mathbf{v}_1, \mathbf{v}_2)}{\partial(\mathbf{Q}, \mathbf{w})} \right| = 8(\alpha_1 + \alpha_2)^{-3/2} \quad \dots\dots (A3)$$

where the positive root is of course understood.

Equations (1) and (3) of the text may now be rewritten

$$r_{12} = \frac{8A\pi^{-3} s^{3/2} \exp[-s\Delta^2] n_1 n_2}{m} \int \exp[-(Q^2 + 4szw^2 - 4s\Delta w_x)] \\ \times \exp[-G/w] \frac{1}{w} d\mathbf{Q} d\mathbf{w}, \quad \dots\dots (A4)$$

$$\langle \mathbf{W}_{12} \rangle =$$

$$\frac{\int \exp[-(Q^2 + 4szw^2 - 4s\Delta w_x)] \exp[-G/w] (1/w) \{(\alpha_1 + \alpha_2)^{-1/2} \mathbf{Q} - \beta \mathbf{w} - \mathbf{i}\gamma\} d\mathbf{Q} d\mathbf{w}}{\int \exp[-(Q^2 + 4szw^2 - 4s\Delta w_x)] \exp[-G/w] (1/w) d\mathbf{Q} d\mathbf{w}}, \quad \dots\dots (A5)$$

where $\beta = (\alpha_1 - \alpha_2)/(\alpha_1 + \alpha_2)$ and $\gamma = -\alpha_1\Delta/(\alpha_1 + \alpha_2)$. The integrals are taken over the whole of the sixfold (\mathbf{Q}, \mathbf{w}) space.

The integral in Eqn (A4) occurs also in the denominator of Eqn (A5); in it the integration over $d\mathbf{Q}$ is immediate, for

$$\int \exp[-Q^2] d\mathbf{Q} = \pi^{3/2}.$$

Thus

$$r_{12} = \frac{8A\pi^{-3/2} s^{3/2} \exp[-s\Delta^2] n_1 n_2}{m} \int \exp[-(4szw^2 - 4s\Delta w_x)] \exp[-G/w] \frac{1}{w} d\mathbf{w}. \quad \dots\dots (A6)$$

The numerator in Eqn (A5) is the sum of three parts, corresponding to the three terms in the curly brackets. On integration over $d\mathbf{Q}$ the first of these vanishes because of symmetry. Thus

$$\langle \mathbf{W}_{12} \rangle = \frac{-\int \exp[-(4szw^2 - 4s\Delta w_x)] \exp[-G/w] (1/w) \{\beta \mathbf{w} + \mathbf{i}\gamma\} d\mathbf{w}}{\int \exp[-(4szw^2 - 4s\Delta w_x)] \exp[-G/w] (1/w) d\mathbf{w}}. \quad \dots\dots (A7)$$

The y and z components in the numerator of Eqn (A7) will also vanish because of symmetry. We introduce a system of spherical polar coordinates (w, θ, ϕ) in velocity space with axis in the x direction, so that $w_x = w \cos \theta$ and $d\mathbf{w} = w^2 \sin \theta d\phi d\theta dw$. Putting $\mu = \cos \theta$, Eqns (A6) and (A7) become on integrating over $d\phi$

$$r_{12} = \frac{16A\pi^{-1/2} s^{3/2} \exp[-s\Delta^2] n_1 n_2}{m} \int_0^\infty \int_{-1}^{+1} \exp[-(4szw^2 - 4s\Delta w\mu)] \\ \times \exp[-G/w] w d\mu dw, \quad \dots\dots (A8)$$

$$\langle \mathbf{W}_{12} \rangle = \frac{-i \int_0^\infty \int_{-1}^{+1} \exp[-(4sw^2 - 4s\Delta w\mu)] \exp[-G/w] w \{\beta w\mu + \gamma\} d\mu dw}{\int_0^\infty \int_{-1}^{+1} \exp[-(4sw^2 - 4s\Delta w\mu)] \exp[-G/w] w d\mu dw} \dots (A9)$$

The integration over $d\mu$ in Eqn (A8) is readily performed, so that

$$r_{12} = \frac{8A\pi^{-1/2}s^{1/2} \exp[-s\Delta^2] n_1 n_2}{m\Delta} \int_0^\infty \exp[-(4sw^2 + G/w)] \sinh(4s\Delta w) dw.$$

Introducing the function

$$F_{12} = \frac{s^{1/2} \exp[-s\Delta^2]}{\Delta} \int_0^\infty \exp[-(4sw^2 + G/w)] \sinh(4s\Delta w) dw,$$

we finally have

$$r_{12} = 8A\pi^{-1/2} n_1 n_2 F_{12}/m, \dots (A10)$$

which is expression (7) of the text.

Turning our attention now to $\langle \mathbf{W}_{12} \rangle$, the integral in the numerator of Eqn (A9) may be written

$$\int_0^\infty \exp[-(4sw^2 + G/w)] w \int_{-1}^{+1} \exp[4s\Delta w\mu] (\beta w\mu + \gamma) d\mu dw.$$

But

$$\begin{aligned} & \int_{-1}^{+1} \exp[4s\Delta w\mu] (\beta w\mu + \gamma) d\mu \\ &= 2\beta \left\{ \frac{\cosh(4s\Delta w)}{4s\Delta} - \frac{\sinh(4s\Delta w)}{16s^2\Delta^2 w} \right\} + \frac{2\gamma}{4s\Delta w} \sinh(4s\Delta w), \end{aligned}$$

so that Eqn (A9) becomes

$$\langle \mathbf{W}_{12} \rangle = i \frac{\left[\left\{ \frac{2\beta}{(4s\Delta)^2} - \frac{2\gamma}{4s\Delta} \right\} S - \frac{2\beta}{4s\Delta} C \right]}{\left(\frac{2}{4s\Delta} \right) S},$$

where

$$S = \int_0^\infty \exp[-(4sw^2 + G/w)] \sinh(4s\Delta w) dw$$

and

$$C = \int_0^\infty \exp[-(4sw^2 + G/w)] w \cosh(4s\Delta w) dw.$$

Putting $\rho = C/S$ and $\lambda = T_2/T_1$, we obtain finally on substituting for β and γ

$$\langle \mathbf{W}_{12} \rangle = i \left\{ \frac{\lambda}{\lambda - 1} \Delta + \frac{1 - \lambda}{1 - \lambda} \left(\rho - \frac{1}{4s\Delta} \right) \right\}, \dots (A11)$$

which is expression (9) of the text.

It will be seen that there is a singularity in this expression at $\Delta = 0$. Obvious considerations demand that $\langle \mathbf{W}_{12} \rangle = 0$ in the limit of small Δ . To verify this, we note that

$$(\partial/\partial\Delta)S = 4sC.$$

Supposing S to be expanded as a power series in Δ , so that $S = c_1\Delta + c_2\Delta^3 + \dots$, we obtain $C = (1/4s)(c_1 + 3c_2\Delta^2 + \dots)$. It follows that

$$C/S - 1/4s\Delta \sim O(\Delta^2)$$

so that

$$\langle \mathbf{W}_{12} \rangle \rightarrow 0 \quad \text{as} \quad \Delta \rightarrow 0.$$

REFERENCES

- HUGHES, T. P., and KAUFMAN, S., 1959, *Nature, Lond.*, **183**, 7.
 JONES, W. M., BARNARD, A. C. L., HUNT, S. E., and CHICK, D. R., 1958, *Nature, Lond.*, **182**, 216.
 PARKER, E. N., and TIDMAN, D. A., 1958, *Phys. Rev.*, **111**, 1206.
 THOMPSON, W. B., 1956, *A.E.R.E. Report T/M138*.
 THOMPSON, W. B., 1957, *Proc. Phys. Soc. B*, **70**, 1.
 WARE, A. A., 1959, *Nature, Lond.*, **183**, 8.

Optical Model Analysis of the Elastic Scattering of 5.5 MeV ^3He by Carbon, Magnesium, Aluminium and Copper

By P. E. HODGSON

Clarendon Laboratory, Oxford

MS. received 18th November 1960

Abstract. Recent measurements of ^3He scattering are analysed using the optical model of the interaction, and the values of the parameters of the potentials giving the best fit to the data are obtained.

§ 1. INTRODUCTION

MEASUREMENTS of the differential cross section for the elastic scattering of 29 MeV helium 3 nuclei by a range of nuclei have been made by the Birmingham Group and analysed using the optical model of the interaction (Aguilar *et al.* 1960, Greenlees and Rowe 1960, Hodgson 1960, Greenlees *et al.* 1961). It is therefore useful to extend the analysis to the recent data of Parry, Scott and Swierszczewski (1961) on the elastic scattering of 5.5 MeV helium 3 by carbon, magnesium, aluminium and copper.

The optical model potential describing the interaction between the incident helium 3 and the target nuclei was assumed to have the form

$$V(r) = V_c(r) + (U + iW)f(r)$$

where $V_c(r)$ is the Coulomb potential due to a uniformly charged sphere, U and W the refracting and absorbing parts of the nuclear potential, and $f(r) = [1 + \exp[(r - R)/a]]^{-1}$ the Saxon Woods form factor, with nuclear diffuseness a and radius $R = r_0 A^{1/3}$. The Schrödinger wave equation with this interaction may be solved to give the observable quantities by the methods described by Buck, Maddison and Hodgson (1960). All the calculations were carried out on the Oxford University computer. Spin-orbit forces were not taken into account, as they have only a small influence on the differential cross section.

§ 2. FITTING PROCEDURE AND RESULTS

The four parameters U , W , r_0 and a were systematically varied to minimize

$$\Delta_N = \sum_N \left(\frac{(d\sigma/d\Omega)_{\text{exp}} - (d\sigma/d\Omega)_{\text{theor}}}{\delta(d\sigma/d\Omega)_{\text{exp}}} \right)^2$$

where the summation extends over all the experimental points except those at less than 35° , as these are subject to uncertainties in the timing of the exposure. The minimization was done using the systematic procedure of Maddison (to be published). The parameters of the potentials giving the best fit to the data are given in the Table, and the corresponding calculated differential cross sections are

Parameters of the Best-fit Potentials, the Calculated Reaction Cross Sections and the Values of Δ_N for the N Measured Points

Nucleus	$-U$ (MeV)	$-W$ (MeV)	r_0 (10^{-13} cm)	a (10^{-13} cm)	σ_R (mbn)	N	Δ_N	A
Carbon	83	56	1.6	0.7	941	25	49	1.25 ± 0.02
Magnesium	33	38	1.6	0.7	401	46	497	1.32 ± 0.02
Aluminium	82	30	1.6	0.7	471	40	264	1.51 ± 0.03
Copper†	—	—	—	—	~ 1	40	1905	1.16 ± 0.02

A is the normalization constant by which the experimental distribution must be multiplied to agree with the theoretical one.

† In the case of copper the scattering is essentially Coulomb, so that the calculated distribution is quite insensitive to the nuclear potential.

compared with experiment in Fig. 1. In this figure the experimental data have been normalized to the theoretical by multiplying by the constant A given in the Table. In each case A is equal to unity within the absolute accuracy of the experimental results.

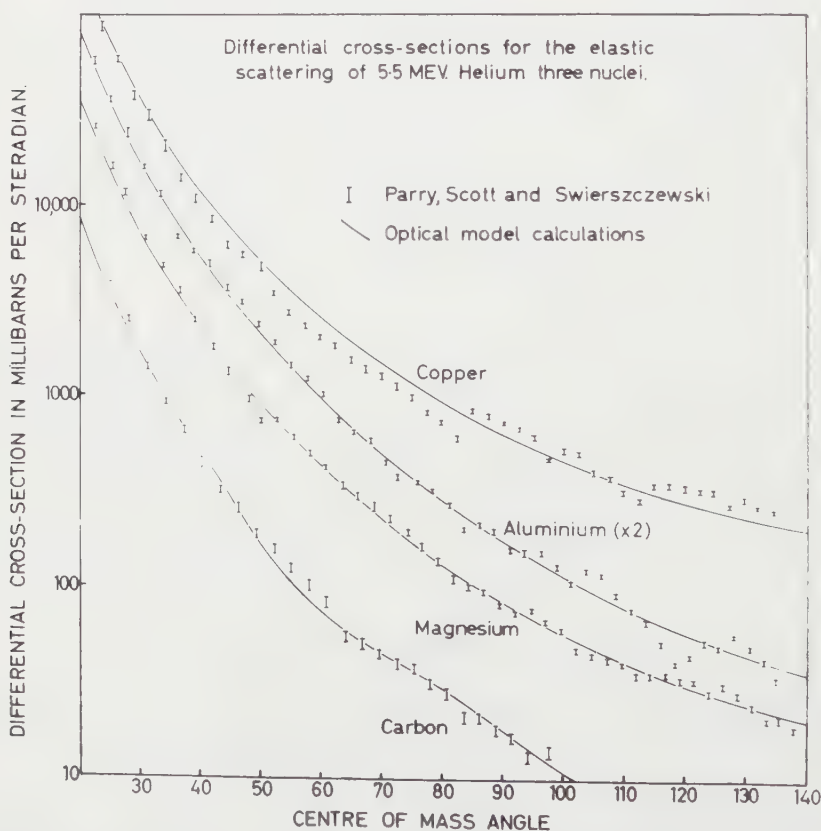


Fig. 1. Differential cross sections for the elastic scattering of 5.5 mev helium 3 by carbon, magnesium, aluminium and copper compared with the best optical model curves, using the parameters given in the Table.

The theoretical curves show no evidence of the diffraction structure noted by Parry *et al.* in the experimental distributions. Physically, the reason for this is that the helium 3 nuclei have insufficient energy to penetrate far enough into the nuclear field for diffraction effects to occur. The structure found by Parry *et al.* cannot therefore be ascribed to bulk diffraction. It would seem, however, that further experimental work is required before the structure is established beyond doubt. Until this is done the potential parameters given in the Table cannot be considered at all reliable, and it would be premature to discuss their variation with energy and from nucleus to nucleus.

In the case of copper, several sets of potential parameters gave essentially the same differential cross section and a very small reaction cross section, showing that the scattering is almost pure Coulomb. This conclusion is confirmed by comparing the classical distance of closest approach for helium 3 scattered by copper through 140° (~ 16.5 f) with the nuclear radius (~ 5.2 f). At this distance from the nucleus the nuclear field is negligible and no diffraction structure is expected. At the much higher energy of 29 MeV the structure is only just visible, and is correctly given by the optical model (Hodgson 1960). If the observed structure at 5.5 MeV is confirmed it must therefore be attributed to an effect due to the outer fringe of the nuclear field that is not accounted for by the optical model.

The variation of the reaction cross section with nuclear charge is shown in Fig. 2. The reaction cross sections for carbon, magnesium and aluminium

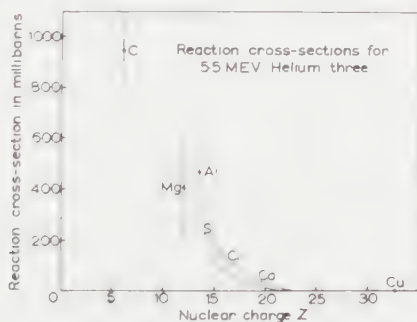


Fig. 2. Reaction cross section as a function of nuclear charge for 5.5 MeV helium 3 nuclei. The values for carbon, magnesium and aluminium are those associated with the best fits of the Table, and the remainder are those calculated using the optical model with the parameters given in the text. The upper curve is calculated with $a=0.7$ f, and the lower with $a=0.6$ f. The error bars on the C, Mg and Al values are qualitative estimates indicating that optical model analyses of elastic scattering do not give accurate reaction cross sections.

associated with the best-fit potentials of the Table are plotted, together with values for other nuclei calculated from the optical model with parameters $U = -20$ MeV, $W = -30$ MeV, $r_0 = 1.6$ f, and $a = 0.6$ and 0.7 f. The reaction cross section falls rapidly as the field of the increasing nuclear charge keeps the helium 3 further away from the nucleus. The sensitivity of the reaction cross section to the fringe of the nuclear field increases with the nuclear charge. A similar effect is found if the reaction cross section is plotted as a function of the energy of the helium 3 for the same nucleus. If these small reaction cross sections could be measured they would provide useful information on the fringe of the nuclear field.

ACKNOWLEDGMENTS

I would like to thank Dr. G. Parry for communicating his results before publication, the Director of the Oxford University Computing Laboratory for the use of the Ferranti Mercury Computer, Dr. B. Buck and Mr. R. N. Maddison for their work on the computer programmes, Miss N. Reynolds, Miss S. Tilley and the staff of the Computing Laboratory for their assistance, and the Department of Scientific and Industrial Research for its support.

REFERENCES

- AGUILAR, J., BURCHAM, W. E., ENGLAND, J. B. A., GARCIA, A., HODGSON, P. E., MARCH, P. V., MCKEE, J. S. C., MOSINGER, E. M., and TONOR, W. T., 1960, *Proc. Roy. Soc. A*, **257**, 13.
- BUCK, B., MADDISON, R. N., and HODGSON, P. E., 1960, *Phil. Mag.*, **5**, 1181.
- GREENLEES, G. W., LILLEY, J. S., ROWE, P. C., and HODGSON, P. E., 1961, *Nucl. Phys.* (in the press).
- GREENLEES, G. W., and ROWE, P. C., 1960, *Nucl. Phys.*, **15**, 687.
- HODGSON, P. E., 1960, *Nucl. Phys.*, **21**, 28.
- PARRY, G., SCOTT, H. D., and SWIERSZCZEWSKI, S., 1961, *Proc. Phys. Soc.*, **77**, 230.

The Hole Theory of Liquids†

By J. GRINDLAY‡

The University of Wisconsin Theoretical Chemistry Laboratory,
Madison, Wisconsin

MS. received 23rd November 1960

Abstract. It is shown that the partition function occurring in the hole theory of liquids may be expressed in closed form by means of the quasi-chemical approximation alone. The thermodynamic properties of this form are described. It is concluded that this theory fails to provide a satisfactory description of the critical point of the liquid state.

§ 1. INTRODUCTION

THE work on the hole theory of liquids, admirably summarized by Rowlinson and Curtiss (1951, to be referred to as RC), presents the difficulty that it would appear necessary to linearize one of the functions occurring in the sum for the partition function, in order to obtain the partition function in closed form. This procedure throws some doubt on the significance of the thermodynamic properties generated by such a partition function. It is the purpose of this note to obtain the partition function in closed form without linearization and to describe the resulting thermodynamic properties.

§ 2. PARTITION FUNCTION

RC show that the configurational partition function corresponding to N atoms distributed over L cells, with co-ordination number z , may be written in the form

$$Z = \sum \exp \left\{ \frac{-zYE(0)}{2kT} \right\} \prod_{i=1}^N j(y_i) \quad \dots\dots(1)$$

where

$$j(y_i) = \int_{\text{cell}} \exp \left\{ \frac{-y_i u_i}{kT} \right\} d\mathbf{r}_i \quad \dots\dots(2)$$

and

$$Y = \sum_{i=1}^N y_i \quad \dots\dots(3)$$

The energies $E(0)$ and u_i are defined by RC and the quantities y_i are numbers such that the i th atom has $y_i z$ nearest neighbours. The sum in Eqn (1) is over all the arrangements of N particles, subject to the geometrical conditions imposed by the lattice of L cells.

† Part of this work was carried out at the University of Wisconsin Theoretical Chemistry Laboratory under contract N7 onr-28511 with the Office of Naval Research.

‡ Now at Physics Department, The University of British Columbia, Vancouver 8, B.C., Canada.

At this point, previous authors have derived a closed form for Eqn (1) in two steps. (a) They assume that the product of the j 's appearing in Eqn (1) is a function of the y_i 's only through the sum Y , Eqn (3); then (b) they apply the quasi-chemical approximation (Fowler and Guggenheim 1939) to calculate the number of arrangements of N atoms corresponding to the set of numbers (y_1, y_2, \dots, y_N) . The present treatment avoids step (a).

In the quasi-chemical approximation, the various nearest neighbour links of each atom are decoupled, in as much as each link is treated as a separate entity. The resulting distribution function G which denotes the number of arrangements in which the i th atom has $y_i z$ nearest neighbours ($i = 1, 2, \dots, N$), accounts for the geometrical properties of the lattice, in so far as they affect the counting problem. Moreover, once these links have been decoupled, the y_i 's may be treated as independent variables subject to the condition $0 \leq y_i \leq 1$.

Thus in the quasi-chemical approximation, Eqn (1) becomes

$$Z = \sum G(L, N, Y) \exp \left\{ \frac{-zYE(0)}{2kT} \right\} \prod_{i=1}^N j(y_i). \quad \dots (4)$$

The sums in Eqn (4) are over the y_i in the range $(0, 1)$ for each y_i .

In the usual way (Fowler and Guggenheim 1939) the sum (4) may be replaced by its maximum term Z_m which is readily shown to be

$$Z_m = G(L, N, Ny) \exp \left\{ \frac{-zNyE(0)}{2kT} \right\} [j(y)]^N \quad \dots (5)$$

where y is determined by the condition

$$\left(\frac{\partial Z_m}{\partial y} \right)_{L, V, T} = 0. \quad \dots (6)$$

Z_m is the partition function for the cell model with holes, evaluated solely by means of the quasi-chemical approximation. The equilibrium value of the number of cells L satisfies the equation

$$\left(\frac{\partial Z_m}{\partial L} \right)_{u, V, T} = 0. \quad \dots (7)$$

Equations (5), (6) and (7) serve to determine the thermodynamic properties of the model.

§ 3. THERMODYNAMIC PROPERTIES

The compressibility resulting from Eqns (5), (6) and (7) may be shown to be

$$\frac{PV}{RT} = 1 + \frac{2zy}{\tau} [q^{-4}A(y/\tau, q) - q^{-2}B(y/\tau, q)] \quad \dots (8)$$

where $A = 1 + \xi$, $B = 1 + \eta$ and ξ, η, q, τ are defined by RC.

What follows is a brief description of some of the properties of Eqn (8).

The second virial coefficient agrees closely with that of RC (see Table).

At the critical point, the equilibrium value of y is in the range $(0.9, 1.0)$, so that in the region about the critical point the compressibility (8) behaves as

$$\frac{PV}{RT} = 1 + \frac{2z}{\tau} [q^{-4}A(1/\tau, q) - q^{-2}B(1/\tau, q)] \quad \dots (9)$$

which is exactly the expression for the compressibility of the cell theory of

	Second virial coefficient B		K_c	ρ_c	Critical point		v_c
	Boyle point	Asymptotic form			τ_c	τ_c	
Lennard-Jones & Devonshire (1937)	3.42(a)	$3.63(N\tau_0^{-1.4})$ (a)	0.293(b)	0.121(b)	3.09(b)	1.28(b)	~ 0.6 (d)
		$B \equiv 0$	0.591(c)	0.434(c)	1.77(c)	1.30(c)	1.0
Cernuschi & Eyring (1939)	12.49	$0.5(N\tau_0)$	0.342	0.469	2.00	2.74	0.544
Ono (1947)	0.96	$5.4(N\tau_0^{-1.4})$	0.342	0.128	2.00	0.75	0.544
Peek & Hill (1950)	2.2		0.719	0.261	3.25	1.18	0.825
Rowlinson & Curtiss (1951)	2.2		—	—	—	—	—
Present calculations	2.4		0.591(c)	0.434(c)	1.77(c)	1.30(c)	~ 1.0

(a), Values based on exact calculations using the Lennard-Jones potential; (b), mean values for Ne, Ar, N₂ (see RC); (c), values from Wentorf, Buehler, Hirschfelder and Curtiss (1950); (d), based on x-ray scattering measurements.

Lennard-Jones and Devonshire (1937) (see in particular RC, Eqn (12)). Moreover Eqn (9) is an excellent approximation to Eqn (8) close to the critical point, as it may be shown that higher order terms contribute less than 5% of the whole, when y lies in the range (0.9, 1.0). As a result, the calculations of Wentorf, Buehler, Hirschfelder and Curtiss (1950) for the critical point values of the cell model have been adopted for the compressibility, Eqn (8). The Table enables a comparison to be made between the various hole theories to date.

The vapour pressure curve and the entropy of evaporation for the cell model are described by RC. Their results apply, for the reason given above, to Eqn (8).

§ 4. DISCUSSION

X-ray scattering measurements show that the average number of nearest neighbours of a molecule in a liquid ranges from about 12 for the dense liquid to about 7 when the liquid is close to its critical point. In the above notation these values correspond to $y=1$ and $y=0.6$ respectively.

Holes were introduced into the cell theory in an attempt to account for both the communal entropy and this variation in the number of nearest neighbours. The former objective is readily obtained (see RC) but the present calculations lead to an equilibrium value of $y \simeq 1$ at the critical point. Thus the hole theory combined with the quasi-chemical approximation fails to provide a satisfactory description of the critical point of the liquid state.

ACKNOWLEDGMENTS

The author gratefully acknowledges the financial assistance from the Office of Naval Research, during his stay in Madison and from the President's Research Committee at the University of British Columbia. The author is also indebted to Dr. Hirschfelder for extending the invitation to work at the Theoretical Chemistry Laboratory and to both Dr. Hirschfelder and Dr. Curtiss for many helpful discussions. Thanks are also due to the staff of the University of British Columbia Computing Centre.

REFERENCES

- CERNUSCHI, F., and EYRING, H., 1939, *J. Chem. Phys.*, **7**, 547.
FOWLER, R. H., and GUGGENHEIM, E. A., 1939, *Statistical Thermodynamics* (London: Cambridge University Press).
LENNARD-JONES, J. E., and DEVONSHIRE, A. F., 1937, *Proc. Roy. Soc. A*, **163**, 53.
ONO, S., 1947, *Memoirs of the Faculty of Engineering*, Kyushu University, Japan, **10**, 190.
PEEK, H. M., and HILL, T. L., 1950, *J. Chem. Phys.*, **18**, 1252.
ROWLINSON, J. S., and CURTISS, C. F., 1951, *J. Chem. Phys.*, **19**, 1519.
WENTORF, R. H., BUEHLER, R. J., HIRSCHFELDER, J. O., and CURTISS, C. F., 1950, *J. Chem. Phys.*, **18**, 1484.

The Law of Wiedemann and Franz

By G. V. CHESTER† AND A. THELLUNG‡

† Department of Mathematical Physics, University of Birmingham

‡ Department of Theoretical Physics, University of Zurich, Switzerland

MS. received 17th November 1960

Abstract. The exact expressions for the transport coefficients of a metal are used to show that the Wiedemann–Franz law is valid provided that (a) the electrons do not interact with each other and form a degenerate Fermi–Dirac assembly, (b) the scattering of the electrons is due to impurities or lattice vibrations and is elastic. The derivation is valid no matter how strong the scattering and it is therefore more general than the usual weak-coupling derivation of the Wiedemann–Franz law.

§ 1. INTRODUCTION

THE purpose of this paper is to present a new derivation of the law of Wiedemann and Franz (Wiedemann and Franz 1853, Wilson 1953). This law states that if K is the thermal conductivity of a metal (neglecting any lattice contribution), σ the electrical conductivity and T the absolute temperature then the ratio $K/\sigma T$ is equal to $\pi^2(k/e)^2/3$. Here k is Boltzmann's constant and e the charge of the electron, consequently this ratio is a universal constant for all metals. This constant is usually referred to as the Lorenz number. The most general derivation of this law is due to Kohler (Kohler 1941) and is based on the following assumptions: (i) the electrons are scattered elastically either by static impurities or by lattice vibrations, (ii) the electrons move independently of one another and form a degenerate Fermi–Dirac assembly, (iii) the conventional Boltzmann equation for the system is valid. This last assumption implies that the scattering is sufficiently weak that the condition that $\hbar/\tau \ll \eta$ (Chester and Thellung 1959) is fulfilled. Here \hbar is Planck's constant divided by 2π , τ is the relaxation time and η is the Fermi energy of the electrons. Our derivation of the Wiedemann–Franz law is based on the expressions for the transport coefficients of a metal derived by Kubo (Kubo, Yokota and Nakajima 1957) and other authors (Mori 1956, Nakano 1956, McLennan 1959). While the method of derivation of these expressions is not in all cases entirely satisfactory we believe that the final formulae are in fact exact and we shall treat them as such for the purpose of this paper.

The essential point of this paper is that by using these exact expressions for the transport coefficients it is possible to show that the Wiedemann–Franz law is valid no matter how strong the scattering by the impurities or lattice waves. We do of course require that assumptions (i) and (ii) are fulfilled. To establish this result we shall consider two ranges of coupling: (a) the intermediate and strong coupling range which we define to be the range of values of the relaxation time τ of the system such that $\hbar/\tau \geq \eta(h/T_0\eta)^{1/2}$ and (b) the weak coupling range for which $\hbar/\tau < \eta(h/T_0\eta)^{1/2}$. Here T_0 is a typical time over which the configuration of the scatterers changes appreciably. In practice it will be of the order of Ω^{-1} where Ω is a typical vibrational frequency of the lattice or of the impurities. That is to say $T_0 \geq 10^{-13}$ sec and hence $(\hbar/T_0\eta)^{1/2} < 10^{-1}$; η is the exact Fermi energy of the system which is a well-defined quantity as long as assumption (ii) is fulfilled.

In case (a) we have

$$\hbar/\tau \geq \eta(\hbar/T_0\eta)^{1/2} = (\eta T_0/\hbar)^{1/2} \hbar/T_0 \gg \hbar/T_0,$$

that is to say $\tau \ll T_0$. Therefore in this range of coupling the scatterers do not change their configuration appreciably during a time interval equal to the relaxation time of the system. This implies that we can calculate the transport coefficients of the system assuming that the scatterers remain in a fixed position. We shall show in §2 that if this is so then we can give a simple and rigorous derivation of the Wiedemann-Franz law. The physically interesting systems to which this derivation would apply are very impure metals or disordered alloys. Elastic scattering by phonons nearly always falls into the weak coupling range. Our strong coupling derivation is therefore of little physical interest for this case (except perhaps at rather high temperatures where τ may become comparatively small).

In the weak coupling range (b) we have

$$\hbar/\tau < \eta(\hbar/T_0\eta)^{1/2} \ll \eta.$$

That is to say τ is sufficiently long that the standard weak coupling theory can be applied to the system. But since τ can now be very long indeed we cannot assume that the scatterers do not change their configuration during the relaxation time of the system. Consequently we must take into account the motion of the scatterers; or in the language of statistical mechanics we must perform an ensemble average over their degrees of freedom. We shall show in §3 that in this case we can derive the Wiedemann-Franz law using Van Hove's methods (Van Hove 1955) in quantum mechanical transport theory. This weak coupling range could of course be treated adequately by the usual Boltzmann equation for the system. Our result is therefore not new. We believe however that our derivation is both simpler and more rigorous than Kohler's.

In the final section we make some remarks about the applicability of our methods to semiconductors and classical plasmas.

§ 2. THE STRONG COUPLING RANGE

In this section we shall derive the Wiedemann-Franz law assuming that the electrons are scattered elastically by impurities or phonons, that assumption (ii) is fulfilled and that $\hbar/\tau \geq \eta(\hbar/\eta T_0)^{1/2}$.

We first express K and σ in terms of the transport coefficients derived by Kubo.

If a uniform electric field \mathbf{E} and temperature gradient ∇T are present in a metal then to first order in these quantities the electric current \mathbf{J} and heat current \mathbf{Q} are given by the equations (Wilson 1953):

$$\mathbf{J} = eS_{11} \left(e\mathbf{E} + T\nabla \frac{\mu}{T} \right) + eS_{12} \frac{1}{T} \nabla T, \quad \dots\dots (1)$$

$$\mathbf{Q} = -S_{21} \left(e\mathbf{E} + T\nabla \frac{\mu}{T} \right) - S_{22} \frac{1}{T} \nabla T. \quad \dots\dots (2)$$

Here the S_{ij} are the transport coefficients of the metal†, e is the electric charge and μ the chemical potential. The electrical conductivity is given by the equation,

† In an anisotropic metal the S_{ij} will be tensors. For simplicity we shall confine our calculations to isotropic metals; the subsequent analysis can be easily generalized to the anisotropic case.

$$\sigma = e^2 S_{11}. \quad \dots\dots (3)$$

Since the heat current is measured when $\mathbf{J}=0$ we have at once that

$$K = \frac{S_{11}S_{22} - S_{12}S_{21}}{TS_{11}}. \quad \dots\dots (4)$$

We can, therefore, define a Lorenz number L by the equation,

$$L = \frac{K}{\sigma T} = \frac{S_{11}S_{22} - S_{12}S_{21}}{(eTS_{11})^2}. \quad \dots\dots (5)$$

Now Kubo and others have shown that the S_{ij} are given by expressions of the form

$$S_{ij} = \int_0^\infty dt \int_0^\beta d\lambda \langle S_i(0)S_j(t+i\lambda) \rangle, \quad (i, j = 1, 2). \quad \dots\dots (6)$$

Here S_1 is a component of the total velocity operator of the system, S_2 is the corresponding component of the total energy current operator and $S_j(t+i\lambda)$ is the appropriate Heisenberg operator at the complex time $t+i\lambda$. The symbol $\langle X \rangle$ stands for the statistical average of the quantity X with the equilibrium density matrix

$$\rho_0 = \exp(-\beta\mathcal{H})/Z,$$

where Z is the partition function, $\beta = 1/kT$ and \mathcal{H} is the total Hamiltonian of the system. From our assumptions it follows that \mathcal{H} can be written as a sum of single-particle Hamiltonians:

$$\mathcal{H} = \sum_x H_x \quad \dots\dots (7)$$

where each H_x contains the kinetic energy of the electron, and the interaction energy of the electron with the periodic crystal potential and with the scattering mechanism. As we have already discussed in detail we can assume the scatterers remain in fixed positions over the time intervals of interest. The Schrödinger equation for the system separates into N one-electron equations, where N is the number of electrons. Consequently there is a well-defined set of one-electron energy levels which at absolute zero will be filled up to a Fermi energy η . At any finite temperature the electrons will be distributed over these levels with the usual Fermi weighting factor $f(E)$ where

$$f(E) = \{\exp[\beta(E - \mu)] + 1\}^{-1}. \quad \dots\dots (8)$$

Here E is the energy of the electron and μ the chemical potential. It is now straightforward to show that if our assumptions are fulfilled then S_{ij} can be written as

$$S_{ij} = -\frac{1}{2} \text{Tr} \left[\frac{df}{dH} \int_{-\infty}^{\infty} \mathcal{J}_i(0)\mathcal{J}_j(t)dt \right], \quad \dots\dots (9)$$

where H is the Hamiltonian of a single electron, \mathcal{J}_i is the appropriate current operator for a single electron and $\mathcal{J}_j(t)$ is the corresponding Heisenberg operator defined in terms of the one-electron Hamiltonian. The symbol Tr stands for a trace over any complete set of one-electron wave functions. The reduction of the many-particle formula given by Eqn (6) to the simpler single-particle form given by Eqn (9) is carried out in the Appendix. Now the energy current operator \mathcal{J}_2 is given in terms of the velocity operator \mathcal{J}_1 by the equation

$$\mathcal{J}_2 = \frac{1}{2}(H\mathcal{J}_1 + \mathcal{J}_1H). \quad \dots\dots (10)$$

The operator \mathcal{J}_2 is defined as the integral over all space of the local operator $\mathcal{J}_2(\mathbf{x})$.

This local operator satisfies the equation of continuity

$$\dot{H}(\mathbf{x}) = (i/\hbar)[H, H(\mathbf{x})] = -\nabla \cdot \mathcal{J}_2(\mathbf{x}).$$

Here $H(\mathbf{x})$ is the local energy operator defined by the equation

$$H(\mathbf{x}) = \frac{1}{2}[H\delta(\mathbf{x}-\mathbf{r}) + \delta(\mathbf{x}-\mathbf{r})H],$$

where \mathbf{r} is the position vector of the electron.

We evaluate the trace in Eqn (9) using the complete set of one-electron states $|n\rangle$ defined as the eigenstates of the single-particle Hamiltonian H , and satisfying periodic boundary conditions,

$$H|n\rangle = E_n|n\rangle. \quad \dots\dots(11)$$

In this representation we find that,

$$S_{ij} = -\pi \sum_{n,m} \frac{df}{dE_n} \langle n|\mathcal{J}_i(0)|m\rangle \langle m|\mathcal{J}_j(0)|n\rangle \delta(E_n - E_m). \quad \dots\dots(12)$$

The delta function in this equation is only a 'genuine' delta function if we let the size of the system tend to infinity. It is only after this limiting process has been performed that one can allow the time integration in the formula for S_{ij} to run over an infinite range. An essential assumption has been made at this point; namely that the current operator S_1 has no diagonal elements in this representation and that the eigenstates $|n\rangle$ are non-degenerate. This condition is necessary in order that the expressions we have given for the transport coefficients should be finite (Greenwood 1958). We now define a generating function $\mathcal{L}(s)$ by the equation,

$$\mathcal{L}(s) = -\sum_n \frac{df}{dE_n} \exp(-sE_n) Q_n, \quad \dots\dots(13)$$

where

$$Q_n = \pi \sum_m |\langle n|\mathcal{J}_1(0)|m\rangle|^2 \delta(E_n - E_m). \quad \dots\dots(14)$$

In terms of this function we find that

$$\begin{aligned} S_{11} &= \mathcal{L}(0), \\ S_{12} &= S_{21} = -\left(\frac{\partial \mathcal{L}(s)}{\partial s}\right)_{s=0} \end{aligned} \quad \dots\dots(15)$$

and

$$S_{22} = \left(\frac{\partial^2 \mathcal{L}(s)}{\partial s^2}\right)_{s=0}.$$

To obtain these results we have used Eqn (10). The Lorenz number can also be conveniently expressed in terms of this generating function,

$$L = \frac{1}{e^2 T^2} \left(\frac{\partial^2 \log \mathcal{L}(s)}{\partial s^2}\right)_{s=0}. \quad \dots\dots(16)$$

If we assume that the sum in Eqn (13) can be replaced by an integral, then

$$\mathcal{L}(s) = -\int_0^\infty G(E) \exp(-sE) \frac{\partial E}{\partial f} dE \quad \dots\dots(17)$$

where

$$G(E) = \rho(E) \bar{Q}(E). \quad \dots\dots(18)$$

Here $\bar{Q}(E)$ is the average of Q_n over all quantum numbers of the electron other than the energy and $\rho(E)$ is the number of states per unit energy range. Since we assume that the electrons form a degenerate Fermi-Dirac assembly we may expand $\mathcal{L}(s)$ in powers of $(kT/\eta)^2$ where η is the exact Fermi energy of the system.

To second order in kT/η we get (Peierls 1955),

$$\mathcal{L}(s) = G(\eta) \exp(-s\eta) + \frac{\pi^2}{6} (kT)^2 \exp(-s\eta) \left[\frac{\partial^2 G(\eta)}{\partial \eta^2} - 2s \frac{\partial G(\eta)}{\partial \eta} + s^2 G(\eta) \right]. \quad \dots\dots (19)$$

As long as $G(E)$ is a smoothly varying function of E the second term on the right-hand side of this equation will be of the order $(kT/\eta)^2$ compared with the first term. We can, therefore, write to the same order of accuracy,

$$\log \mathcal{L}(s) = \log G(\eta) - s\eta + \frac{\pi^2}{6} (kT)^2 G(\eta)^{-1} \left[\frac{\partial^2 G(\eta)}{\partial \eta^2} - 2s \frac{\partial G(\eta)}{\partial \eta} + s^2 G(\eta) \right]. \quad \dots\dots (20)$$

Combining Eqns (16) and (20) we find that

$$L = \frac{1}{3} \pi^2 (k/e)^2.$$

This is the usual expression for the Lorenz number and we have therefore shown that the Wiedemann-Franz law is in fact valid no matter how strongly the electrons are scattered by the impurities or lattice vibrations.

§ 3. THE WEAK COUPLING RANGE

In this section we shall derive the Wiedemann-Franz law using Van Hove's methods (Van Hove 1955) in quantum mechanical transport theory. Our assumptions are now that the electrons are scattered elastically by impurities or lattice vibrations (phonons) that assumption (ii) is valid and that the weak coupling condition that $\hbar/\tau < \eta(\hbar/\eta T_0)^{1/2}$ is fulfilled. This last assumption means that $\hbar/\tau \ll \eta$.

Equation (6) for S_{ij} is of course valid for any system and we can therefore base our analysis on it. It is shown in the Appendix that the assumptions we have just made are sufficient to allow us to reduce S_{ij} to the following form

$$S_{ij} = \text{Tr}^{(s)} \rho_0^{(s)} \left\{ -\frac{1}{2} \text{Tr}^{(\text{el})} \frac{\partial f}{\partial H} \int_{-\infty}^{\infty} \mathcal{J}_i(0) \mathcal{J}_j(t) dt \right\}. \quad \dots\dots (21)$$

In this equation $\rho_0^{(s)}$ is the equilibrium density matrix for the scattering degrees of freedom. The symbol $\text{Tr}^{(s)}$ stands for a trace over these degrees of freedom. The Hamiltonian H is again the single-electron Hamiltonian and includes the interaction of the electron with the scattering mechanism. The other symbols have the same meaning as before. We now use Van Hove's weak coupling approximation to reduce this expression to a more explicit form. If the coupling constant is λ then it follows from Van Hove's analysis that to order λ^{-2} S_{ij} is given by the equation

$$S_{ij} = - \sum_{E, \alpha, \alpha'} \frac{\partial f}{\partial E} \mathcal{J}_i(E\alpha) \mathcal{J}_j(E\alpha') \int_0^{\infty} P_t(E\alpha', E\alpha) dt, \quad \dots\dots (22)$$

where we have labelled the one-electron states by their energy E and any other set of labels α that are sufficient to specify the state. These one-electron states are in the weak coupling approximation the usual Bloch states of an electron moving freely in the potential of the periodic crystal lattice. $S_i(E\alpha)$ stands for the diagonal element of $S_i(0)$ in this representation. The function $P_t(E\alpha, E\alpha')$ is

Van Hove's master function and satisfies the master equation,

$$\begin{aligned} \frac{dP_t(E\alpha', E\alpha)}{dt} = & \sum_{\alpha''} \bar{W}(E\alpha', E\alpha'') P_t(E\alpha'', E\alpha) \\ & - \sum_{\alpha''} \bar{W}(E\alpha'', E\alpha') P_t(E\alpha', E\alpha), \end{aligned} \quad \dots\dots (23)$$

with the initial condition that

$$P_0 = \delta_{\alpha, \alpha'}.$$

The transition probabilities \bar{W} are given by the standard expressions in terms of the matrix elements of the interaction energy of the electron with the scatterers; they include however an explicit ensemble average over the scattering degrees of freedom.

We can now again define a generating function $\mathcal{L}^W(s)$ by the equation,

$$\mathcal{L}^W(s) = - \sum_E \frac{\partial f}{\partial E} \exp(-sE) Q^W(E), \quad \dots\dots (24)$$

where

$$Q^W(E) = \sum_{\alpha, \alpha'} \phi_1(E\alpha) \phi_1(E\alpha') \int_0^\infty P_t(E\alpha', E\alpha) dt. \quad \dots\dots (25)$$

Using Eqn (10) we find

$$L = \frac{1}{e^2 T^2} \left(\frac{\partial^2 \log \mathcal{L}^W(s)}{\partial s^2} \right)_{s=0}. \quad \dots\dots (26)$$

The rest of the proof is now exactly the same as before and we again arrive at the usual statement of the Wiedemann-Franz law, namely that,

$$L = \frac{1}{3} \pi^2 (k/e)^2.$$

The advantage of this derivation is that it follows directly from Van Hove's results on the weak coupling master equation. It therefore does not require the assumptions that are used in the conventional derivation of the Boltzmann equation for the system. The derivation we have given seems to be considerably shorter than that given by Kohler (1941).

§ 4. CONCLUSION

We end by making some comments on the possible extension of our methods to semiconductors and classical plasmas. For our problem the essential difference between a metal and a semiconductor is that the electrons in a semiconductor do not usually form a degenerate Fermi-Dirac assembly. If they are degenerate then all our previous results are at once valid. On the other hand if they obey Boltzmann statistics then all our formulae are valid provided we replace the Fermi function that appears in them with the Boltzmann function

$$\exp[-\beta(E-\mu)].$$

The Lorenz number is now given by the equation,

$$L = \frac{1}{e^2 T^2} \left(\frac{\partial^2 \log \mathcal{L}^B(s)}{\partial s^2} \right)_{s=0} \quad \dots\dots (27)$$

where

$$\begin{aligned} \mathcal{L}^B(s) &= \beta \int_0^\infty \exp[-\beta(E-\mu)] \exp(-sE) G(E) dE \quad \dots\dots (28) \\ &= \beta \exp(\beta\mu) \phi(\beta+s) \end{aligned}$$

where $G(E)$ is given either by Eqn (18) or by $Q^{\text{W}}(E)$ times $\rho(E)$. Now if L is to have the form $\gamma(k/e)^2$ where γ is a universal pure number then it is easily shown that $\phi(\beta)$ must satisfy the equation

$$\frac{\partial^2 \log \phi(\beta)}{\partial \beta^2} = \gamma \beta^{-2}. \quad \dots\dots (29)$$

The most general solution of this is

$$\phi(\beta) = A\beta^{-\gamma} \exp(a\beta), \quad \dots\dots (30)$$

where A and a are arbitrary constants. From Eqn (28) we see that $G(E)$ is the inverse Laplace transform of $\phi(\beta)$ with respect to β . If we assume that the energy spectrum starts at $E = 0$ then we can show that the constant a in Eqn (30) must be zero and that $G(E)$ must have the form $AE^{-\gamma-1}$. That this is impossible in general can be verified by calculating $G(E)$ in the weak coupling approximation.

A very similar argument can be constructed for a classical plasma in which we treat the ions as scattering centres for the electrons. We again conclude that the Wiedemann-Franz law will not be true for such a system.

These remarks might seem to be in conflict with the statement that is sometimes made that the Wiedemann-Franz law is valid for the Drude model of metal or plasma. Since the electrons in the Drude model are assumed to obey Boltzmann statistics this model is, from our point of view, relevant to a semiconductor rather than to a metal. However, the most general form of the law that can be derived for this model states that L is equal to $\gamma'(k/e)^2$ where γ' is *not* a universal constant but depends on the law of force responsible for the scattering of the electrons (Wilson 1953). Consequently the strict form of the Wiedemann-Franz law we have discussed in this paper is not valid for this model.

ACKNOWLEDGMENTS

We wish to express our gratitude to the Swiss National Fonds for financial aid which enabled part of this work to be carried out in Zurich. We also wish to thank Professor R. E. Peierls for some useful comments on the contents of this paper.

This work was also supported in part by the Office of Naval Research while one of us (G. V. C.) was at the Laboratory of Atomic and Solid State Physics, Cornell University, Ithaca, New York.

APPENDIX

In this Appendix we shall show how the many-particle formula (6) can be reduced, using our assumptions, to one of the simpler single-particle forms given by Eqns (9) or (21).

We start from Eqn (6), namely

$$S_{ij} = \text{Tr} \left[\rho_0 \int_0^\beta d\lambda \int_0^\infty dt S_i(0) S_j(t + i\lambda) \right].$$

For the strong coupling range we can at once write the total Hamiltonian \mathcal{H} in the form,

$$\mathcal{H} = \sum_{\alpha} H_{\alpha}$$

where H_{α} is the Hamiltonian for a single electron interacting with the static

scatterers. It is now convenient to use a second quantization representation for our operators. We take as the basic set of functions for this representation the eigenfunctions of the single-particle Hamiltonian H . In this representation we have that,

$$\mathcal{H} = \sum_s E_s a_s^* a_s$$

$$S_i(t + i\lambda) = \sum_{s,s'} (\mathcal{J}_i)_{ss'} a_s^* a_{s'}.$$

Here a_s^* and a_s are the usual creation and annihilation operators and the E_s are the eigenvalues of H . The matrix elements $(\mathcal{J}_i)_{ss'}$ are given by the equation

$$(\mathcal{J}_i)_{ss'} = \langle s | \mathcal{J}_i | s' \rangle$$

$$[\mathcal{J}_i(t + i\lambda)]_{ss'} = \exp [i(t + i\lambda)(E_s - E_{s'})] (\mathcal{J}_i)_{ss'}$$

when $|s\rangle$ is the eigenstate of H corresponding to E_s . Using these equations S_{ij} becomes

$$S_{ij} = \text{Tr} \left[\rho_0 \sum_{ss'} \sum_{rr'} \int_0^\beta d\lambda \int_0^\infty dt (\mathcal{J}_i)_{ss'} [\mathcal{J}_j(t + i\lambda)]_{rr'} \right. \\ \left. \times a_s^* a_{s'}^* a_{r'} a_r \right].$$

If we evaluate the trace with the eigenfunctions of H then ρ_0 is diagonal in this representation and we only require the diagonal part of the product $a_s^* a_{s'}^* a_{r'} a_r$. We can, therefore, write S_{ij} in the form,

$$S_{ij} = \sum_{s \neq r} \text{Tr} \rho_0 \left[n_s (1 - n_r) \int_0^\beta d\lambda \int_0^\infty dt (\mathcal{J}_i)_{sr} [\mathcal{J}_j(t + i\lambda)]_{rs} \right]$$

where $n_s = a_s^* a_s$ and we have used the assumption that in this representation \mathcal{J} has no diagonal elements. This trace can be evaluated at once to give

$$S_{ij} = \sum_{s \neq r} f_s (1 - f_r) \int_0^\beta d\lambda \int_0^\infty dt (\mathcal{J}_i)_{sr} [\mathcal{J}_j(t + i\lambda)]_{rs}$$

where

$$f_s = \bar{n}_s = \text{Tr} (\rho_0 n_s)$$

and we have used the fact that for $r \neq s$, $\overline{n_s(1 - n_r)} = f_s(1 - f_r)$. The function f_s is of course the usual Fermi-Dirac distribution function. We can now perform the λ and t integrations to get,

$$S_{ij} = - \sum_{s \neq r} \frac{f_s - f_r}{E_s - E_r} (\mathcal{J}_i)_{rs} (\mathcal{J}_j)_{sr} \\ \times \left[\pi \delta(E_s - E_r) + iP \frac{1}{E_s - E_r} \right].$$

The principal part gives no contribution because it is antisymmetric in the indices s and r , and all other factors in the sum over these indices are symmetric. The part containing the delta function can easily be reduced to the form,

$$S_{ij} = -\pi \sum_{s \neq r} \frac{\partial f}{\partial E_s} (\mathcal{J}_i)_{sr} (\mathcal{J}_j)_{rs} \delta(E_s - E_r)$$

and now we can write this last expression as a trace, namely,

$$S_{ij} = -\frac{1}{2} \text{Tr} \left[\frac{\partial f}{\partial H} \mathcal{J}_i(0) \int_{-\infty}^{\infty} \mathcal{J}_j(t) dt \right].$$

For the weak coupling range the reduction of the many-particle formula to the form given by Eqn (21) proceeds in a very similar manner. The only difference is that now we must take the scattering degrees of freedom into account explicitly. The Hamiltonian of the metal is now given by the equation,

$$\mathcal{H} = \mathcal{H}_s + \sum_{\alpha} H_{\alpha}$$

where \mathcal{H}_s is the Hamiltonian of the scattering degrees of freedom. If the scattering is elastic then we must assume that each H_{α} commutes with the total Hamiltonian. This of course implies that for phonon scattering $T \gg \theta$. This assumption allows us to write Eqn (6) in the form

$$S_{ij} = \text{Tr} [\rho_0^{(e)} \left[\text{Tr}^{(el)} \rho_0^{(el)} \int_0^{\beta} d\lambda \int_0^{\infty} dt S_i(0) S_j(t + i\lambda) \right]]$$

where $\rho_0^{(e)}$ is the equilibrium density matrix for the electronic degrees of freedom and $\text{Tr}^{(el)}$ stands for the trace over these degrees of freedom. The quantity

$$\text{Tr}^{(el)} \left[\rho_0^{(el)} \int_0^{\beta} d\lambda \int_0^{\infty} dt S_i(0) S_j(t + i\lambda) \right]$$

can now be reduced to the standard single-particle form and we therefore obtain Eqn (21) for S_{ij} .

REFERENCES

- CHESTER, G. V., and THELLUNG, A., 1959, *Proc. Phys. Soc.*, **73**, 745.
 GREENWOOD, D. A., 1958, *Proc. Phys. Soc.*, **71**, 585.
 MCLENNAN, J. A., 1959, *Phys. Rev.*, **115**, 1405.
 KUBO, R., YOKOTA, M., and NAKAJIMA, S., 1957, *J. Phys. Soc. Japan*, **12**, 570, 1203.
 KOHLER, M., 1941, *Ann. Phys., Lpz.*, **40**, 601.
 MORI, H., 1956, *J. Phys. Soc. Japan*, **11**, 1029.
 NAKANO, H., 1956, *Progr. Theor. Phys.*, **15**, 77.
 PEIERLS, R. E., 1955, *Quantum Theory of Solids* (Oxford: Clarendon Press).
 VAN HOVE, L., 1955, *Physica*, **21**, 517.
 WIEDEMANN, G., and FRANZ, R., 1853, *Ann. Phys., Lpz.*, (2), **89**, 497.
 WILSON, A. H., 1953, *The Theory of Metals* (Cambridge: University Press).

Two Channel Five Nucleon Reactions with Central Forces

BY W. LASKAR†, C. TATE†, B. PARDOE† AND P. G. BURKE‡

† University College London

‡ University of London Computer Unit

Communicated by Sir Harrie Massey; MS. received 23rd August 1960

Abstract. The two-channel five-nucleon reaction has been formulated using the resonating group method and including the two groupings $dt, n^4\text{He}$. The central potential used is of Gaussian shape with exchange dependence (Serber and symmetrical exchange have been mainly investigated). The wave functions for the nuclear ground states are Gaussian (double Gaussian for deuteron and single Gaussian for t and ^4He) the parameter being determined by variational methods to fit the binding energies. Coupled integro-differential equations have been derived for each value of the total spin and angular momentum of the corresponding system. Numerical results have been obtained and are given here.

§ 1. INTRODUCTION

THE five-nucleon reaction has been formulated using the resonating group method (Wheeler 1937) and including two channels

$$\begin{pmatrix} dt \rightarrow dt & dt \rightarrow n^4\text{He} \\ n^4\text{He} \rightarrow dt & n^4\text{He} \rightarrow n^4\text{He} \end{pmatrix}.$$

The elastic scattering $n^4\text{He} \rightarrow n^4\text{He}$ has been already studied by Hochberg, Massey and Underhill (1954) and Hochberg, Massey, Robertson and Underhill (1955). The elastic scattering of deuterons by tritons represented by the other diagonal element has been previously studied (Laskar, Tate and Burke 1960) and the results compared with the experimental values at 10.2 Mev given by Allred *et al.* (1952).

These earlier results are compared with the present calculation in which the coupling to the $n^4\text{He}$ channel is included. Since we are not including any tensor interaction, a choice of central potential of larger range than is normal has been chosen. This interaction has been shown by many workers (cf. Bransden 1960) to give results in close accord with experiment for many light nuclei collisions. Three types of exchange forces are considered and the conclusion reached is that a near Serber interaction gives best agreement with experiment both for this work and similar work.

§ 2. THEORY

The notation is that used by Buckingham and Massey (1941). The inter-nucleonic interaction is assumed to be purely central and of the form

$$\mathcal{V}(ij) = (wW_{ij} + mM_{ij} + bB_{ij} + hH_{ij})V(r_{ij}) + \epsilon_{ij} \frac{e^2}{r_{ji}}$$

where W, M, B, H are the usual Wigner, Majorana, Bartlett and Heisenberg

operators. The constants w , m , b , h give the exchange dependence of the interaction and satisfy

$$w + m + b + h = 1$$

$$w + m - b - h = x.$$

$x=0.6$ is the ratio of the singlet to the triplet interaction (Motz and Schwinger 1940).

$$r_{ij} = |\mathbf{r}_i - \mathbf{r}_j|$$

$$\epsilon_{ij} = 1 \text{ if } i \text{ and } j \text{ are protons and zero otherwise.}$$

Denoting protons by even numbers and neutrons by odd numbers, a resonating group wave function of correct symmetry may be written as

$$\begin{aligned} \Psi_s(12345) = & (1 - P_{13} - P_{15})(1 - P_{24})\phi(12)\phi(345)\sigma_s(12, 345)F_s(12, 345) \\ & + (1 - P_{13} - P_{15})\phi(2345)\sigma_s(1, 2345)G_s(1, 2345) \end{aligned}$$

P_{ij} are exchange operators of Heisenberg type, σ_s is the spin function corresponding to the total spin S of the system ($S = \frac{1}{2}, \frac{3}{2}$). The coupled equations are obtained by the variational principle according to Wheeler's method (Wheeler 1937).

The equations have the structure

$$\int \phi_A(H - E)\psi_s d\tau_A = 0$$

and

$$\int \phi_B(H - E)\psi_s d\tau_B = 0$$

when ϕ_A is the product of the d and t bound wave functions and ϕ_B is the ${}^4\text{He}$ wave function, H is the total Hamiltonian, E the energy, $d\tau_A$ includes all variables except the relative d-t coordinate and $d\tau_B$ all variables except the relative $n^4\text{He}$ coordinate. ψ_s is linear in ϕ_A and ϕ_B .

For $S = \frac{1}{2}$ we have two coupled equations. For $S = \frac{3}{2}$ we have only one,

$$\int \phi_A(H - E)\phi_A d\tau_A = 0.$$

Let the nucleons 1, 2, 3, 4, 5 be denoted by the position vectors $\mathbf{r}_1, \mathbf{r}_2, \mathbf{r}_3, \mathbf{r}_4, \mathbf{r}_5$ with respect to the same arbitrary origin. We take (345) as the target triton and (12) as the incident deuteron.

For the first equation the basic intergroup separation variable will be

$$\mathbf{v} = \frac{1}{2}(\mathbf{r}_1 + \mathbf{r}_2) - \frac{1}{3}(\mathbf{r}_3 + \mathbf{r}_4 + \mathbf{r}_5).$$

There will be two types of exchanges:

$$\text{first type of exchange} \quad \mathbf{r}' = \frac{1}{2}(\mathbf{r}_3 + \mathbf{r}_2) - \frac{1}{3}(\mathbf{r}_1 + \mathbf{r}_4 + \mathbf{r}_5)$$

$$\text{second type of exchange} \quad \mathbf{r}'' = \frac{1}{2}(\mathbf{r}_3 + \mathbf{r}_4) - \frac{1}{3}(\mathbf{r}_1 + \mathbf{r}_2 + \mathbf{r}_5).$$

In the equations given below, the terms of the first type of exchange are preceded by the corresponding Jacobian of the transformation J_{AA}^I and similarly for the second type of exchange J_{AA}^{II} ; the Jacobian kept in front of the terms

explains at once their origin. For the off diagonal term, similar considerations are applied.

$$\begin{array}{ll} \text{1st type } \mathbf{r}' = \mathbf{r}_1 - \frac{1}{4}(\mathbf{r}_2 + \mathbf{r}_3 + \mathbf{r}_4 + \mathbf{r}_5) & J_{AB}^I \\ \text{2nd type } \mathbf{r}'' = \mathbf{r}_3 - \frac{1}{4}(\mathbf{r}_1 + \mathbf{r}_2 + \mathbf{r}_4 + \mathbf{r}_5) & J_{AB}^{II} \end{array}$$

For the second equation the basic intergroup separation variable is

$$\mathbf{v} = \mathbf{r}_1 - \frac{1}{4}(\mathbf{r}_2 + \mathbf{r}_3 + \mathbf{r}_4 + \mathbf{r}_5),$$

which becomes after a unique type of exchange (with Jacobian J_{BB})

$$\mathbf{r}' = \mathbf{r}_3 - \frac{1}{4}(\mathbf{r}_2 + \mathbf{r}_1 + \mathbf{r}_4 + \mathbf{r}_5).$$

From conservation of energy we have:

$$\mathcal{E} = E_d + E_t + E(d) = E_\alpha + E(n)$$

where E_d , E_t , E_α are the binding energies for deuteron, triton and ^4He nucleus respectively, $E(d)$ and $E(n)$ being the kinetic energies of the incident deuteron and the outgoing neutron in the centre-of-mass system.

Premultiplying by the appropriate ϕ 's and σ 's, summing over spin variables, integrating over internal variables and using the integral equation satisfied by each nuclear wave function,

$$\text{i.e.} \quad \int \phi(H - E_{\min}) \phi d\tau = 0,$$

to simplify the equations, a set of two coupled three-dimensional integro-differential equations is obtained for $S = \frac{1}{2}$.

$$\begin{aligned} 0 = & - \left[\frac{5}{12} \frac{\hbar^2}{M} \nabla_v^2 + E(d) \right] F_{1/2}(\mathbf{v}) + F_{1/2}(\mathbf{v}) \int \phi^2(12) \phi^2(345) \\ & \times [V_{24}^c + (6w - \frac{1}{2}m + b - 3h)V^{13}] d(12)d(345) \\ & - \frac{1}{2} J_{AA}^I \int \phi(12) \phi(345) \{ T - \mathcal{E} + 2V_{24}^c - V_{13}^c + (zw + m + 4b + 4h)V^{45} \\ & + (zw - 12m + 6b - 2h)V^{13} + (2w + 4m - 2b + 2h)V^{24} + V^{12} + V^{32} \\ & + (2w + 2m - 4b - 4h)[V^{14} + V^{34}] \} \phi(32) \phi(145) F_{1/2}(\mathbf{r}') d\mathbf{r}' \\ & - \frac{1}{2} J_{AA}^{II} \int \phi(12) \phi(345) \{ T - \mathcal{E} + V_{24}^c + 2V^{12} + (4w + 2m + 2b - 2h)V^{13} \\ & + (2w + 2m - b - h)[V^{15} + V^{25}] \} \phi(34) \phi(125) F_{1/2}(\mathbf{r}') d\mathbf{r}' \\ & + \frac{\sqrt{3}}{2} J_{AB}^I \int \phi(12) \phi(345) \{ T - \mathcal{E} + V_{24}^c + V^{12} + (3w - 2m + b - 3h)V^{13} \\ & + 3(w + m)[V^{25} + V^{35}] \} \phi(2345) G_{1/2}(\mathbf{r}') d\mathbf{r}' \\ & + \frac{\sqrt{3}}{2} J_{AB}^{II} \int \phi(12) \phi(345) \{ T - \mathcal{E} + V_{24}^c + V^{12} + (2w - 3m + 3b - h)V^{13} \\ & + 2(2w + 2m - b - h)V^{14} \\ & + (2w + 2m - b - h)V^{34} + V^{45} \} \phi(2145) G_{1/2}(\mathbf{r}') d\mathbf{r}'. \\ 0 = & BA - \left[\frac{5}{8} \frac{\hbar^2}{M} \nabla_v^2 + E(n) \right] G_{1/2}(\mathbf{v}) + (4w + 2b - m - 2h) \int \phi^2(2345) V^{12} d(2345) \\ & + J_{BB} \int \phi(2345) \{ T - \mathcal{E} + V_{24}^c + (4m + 2h - w - 2b)V^{12} - 3(m + w) \\ & \times [V^{23} + V^{13} + V^{45}] \} \phi(2145) G_{1/2}(\mathbf{r}') d\mathbf{r}'. \end{aligned}$$

For $S = \frac{3}{2}$ we have only one equation:

$$\begin{aligned}
 0 = & - \left[\frac{5}{12} \frac{\hbar^2}{M} \nabla_v^2 + E(d) \right] F_{3/2}(\mathbf{v}) + F_{3/2}(\mathbf{v}) \int \phi^2(12) \phi^2(345) \\
 & \times [V_{24}^c + (6w + 4b - 3h - 2m)V^{13}] d(12) d(345) \\
 & + J_{AA}^I \int \phi(12) \phi(345) \{ 2[T - \mathcal{E}] - V_{24}^c - V_{23}^c - 2[V^{12} + V^{32}] \\
 & + (4m + 5h - 2b - 4w)V^{24} + (6m + 4b - 3b - 2w)V^{13} \\
 & - (4w + 4m + b + h)(V^{14} + V^{34}) - (2w + 2m - b - h)V^{45} \} \phi(32) \phi(145) \\
 & \times F_{3/2}(\mathbf{r}') d\mathbf{r}' \\
 & + J_{AA}^{II} \int \phi(12) \phi(345) \{ -T - \mathcal{E} + V_{24}^c + (2w + 2m - b - h)[V^{15} + V^{25}] + 2V^{12} \\
 & + (4w + 5b - 4m - 2h)V^{13} \} \phi(34) \phi(125) F_{3/2}(\mathbf{r}') d\mathbf{r}'.
 \end{aligned}$$

§ 3. THE POTENTIAL SHAPE AND THE NUCLEI WAVE FUNCTIONS

The potential shape is assumed to be the same for all types of exchange, and of Gaussian form: $V(r) = V_0 \exp(-\mu r^2)$. The value of μ ($\mu = 0.2669 \times 10^{26} \text{ cm}^{-2}$) is that used in previous four and five nucleon calculations (Bransden 1960). The value of V_0 ($V_0 = -46.8 \text{ MeV}$) was interpolated from the results obtained by Burke and Robertson (1957).

The wave function for the deuteron is a double Gaussian

$$\phi = \frac{1}{N_d} \{ \exp(-\alpha r^2) + c \exp(-\beta r^2) \}$$

and for any other nuclei, a single Gaussian

$$\phi = \frac{1}{N} \exp \left[-\frac{1}{2} \lambda \Sigma (r_{ij}^2) \right].$$

The values of the parameters are listed below in Table 1, and have been obtained by a variational method. The table also includes E_{\min} , the variational value of the binding energy.

Table 1

	t	⁴ He	d	
$\lambda (10^{+26} \text{ cm}^{-2})$	0.15715	0.15780	$\alpha (10^{+26} \text{ cm}^{-2}) = 0.0299$ $\beta (10^{+26} \text{ cm}^{-2}) = 0.186$	$C = 2.73$
$E_{\min} (\text{MeV})$	-6.744	-27.315	-2.133	
$E_{\exp} (\text{MeV})$	-8.3	-28.2	-2.226	

§ 4. METHOD OF CALCULATION

After integration over the angular variables, the equations become:

$$\left. \begin{aligned}
 \left(\frac{d^2}{dr^2} - \frac{l(l+1)}{r^2} + k_A^2 \right) f_l(r) &= U^{AA}(r) f_l(r) + \int_0^\infty K_l^{AA}(r, r') f_l(r') dr' \\
 &+ \int_0^\infty K_l^{AB}(r, r') g_l(r') dr' \\
 \left(\frac{d^2}{dr^2} - \frac{l(l+1)}{r^2} + k_B^2 \right) g_l(r) &= U^{BB}(r) g_l(r) + \int_0^\infty K_l^{BA}(r, r') f_l(r') dr' \\
 &+ \int_0^\infty K_l^{BB}(r, r') g_l(r') dr'
 \end{aligned} \right\} \dots \dots (4.1)$$

$f_l(r)$ (and $g_l(r)$) and $K_l^{(ij)}(r, r')$ are defined as usual:

$$F(r) = \sum_l \frac{1}{r} f_l(r) P_l(\cos \theta)$$

$$K^{(ij)}(r, r') = \sum_l \frac{(2l+1)}{4\pi r r'} K_l^{(ij)}(r, r') P_l(\cos \Theta),$$

θ is the angle of scattering in the centre-of-mass frame, Θ is the angle between \mathbf{r} and \mathbf{r}' .

All the kernels are symmetric in r and r' because the S matrix is unitary.

The kernels $K^{(ij)}$ include, of course, the Coulomb kernels and are the sums of many terms; they cannot be listed here, but the authors will be pleased to supply their explicit form on request. Most of the kernels are of the form

$$K_l^{(k)}(r, r') = \phi_k(r, r') \exp[-\beta_k r^2 - \gamma_k r'^2] \mathcal{J}_{l+\frac{1}{2}}(K_k r r')$$

where $\phi_k(r, r')$ is a polynomial in r and r' , β_k, γ_k, K_k are algebraic expressions in $\alpha, \beta, c, \lambda$'s,

$$\mathcal{J}_{l+\frac{1}{2}}(x) = i^{l-\frac{1}{2}} \left(\frac{\pi x}{2} \right)^{1/2} \mathcal{J}_{l+\frac{1}{2}}(ix).$$

$\mathcal{J}_{l+\frac{1}{2}}(x)$ is the hyperbolic spherical Bessel function, the first two being

$$\mathcal{J}_{1/2}(x) = \sinh x, \quad \mathcal{J}_{3/2}(x) = \frac{\sinh x}{x} - \cosh x.$$

Equations (4.1) are represented as a set of linear simultaneous equations, the unknowns being the values of $f_l(r)$ and $g_l(r)$ over the range of r required (Robertson 1956). It is necessary to find two independent solutions such that:

$$f_l^{ij}(r) \sim \frac{1}{\sqrt{v_i}} [A_l^{ij} F_l^i(r) + B_l^{ij} G_l^i(r)] \quad i=1, 2 \text{ (2 channels)}$$

$$j=1, 2 \text{ (2 independent solutions)}$$

where $F_l^i(r), G_l^i(r)$ are the regular and irregular wave functions for the corresponding channel.

Then the reactance matrix is

$$R = BA^{-1}$$

and the scattering matrix $S = (1 + iR)/(1 - iR)$.

The scattering amplitude $f_s(\theta)$ corresponding to the total spin S can be written

$$f_{\alpha'\alpha}^s(\theta) = -\frac{1}{2ik_\alpha} \sum_l [\delta_{\alpha'\alpha} - S_{\alpha'\alpha}^l] (2l+1) P_l(\cos \theta).$$

Then the corresponding differential cross section is

$$\sigma_{\alpha'\alpha}^s(\theta) = |f_{\alpha'\alpha}^s(\theta)|^2$$

and the differential cross section for d-t elastic scattering will be

$$\sigma(\theta) = \frac{2}{3} \sigma_{3/2}(\theta) + \frac{1}{3} \sigma_{1/2}(\theta).$$

The differential cross section has been tabulated for $\theta^\circ = 5^\circ(5^\circ) 175^\circ$ taking S, P and D phases only into account.

The calculation was carried out using the Ferranti MERCURY digital computer. A programme prepared by B. Easlea was used to calculate the different regular and irregular wave functions needed.

§ 5. RESULTS AND CONCLUSIONS

The calculation has been carried out for the three following types of exchange forces.

I	MHWB or symmetrical exchange	$m=2b$	$h=2w$
II	Serber	$m=w$	$h=b$
III	Biel's mixture ($\frac{1}{3}$ MHWB + $\frac{2}{3}$ Serber) (Biel 1957).		

The energies considered are given in Table 2.

		Table 2					
		k	0.075	0.12	0.2	0.4	0.6
d-t	c.m. system	E_d (mev)	0.097	0.249	0.691	2.764	6.219
	lab. system	E_d (mev)	0.162	0.415	1.152	4.607	10.366

The following Tables (3 and 4) give the results obtained in the single-channel elastic case dt-dt for the phases δ_l expressed in degrees, modulo 180°, l being the angular momentum quantum number.

Table 3. Phases for $S = \frac{1}{2}$ in degrees (modulo 180°)

k		MHWB	Serber	Biel
0.075	δ_0	-2.150	3.730	-0.395
	δ_1	-0.131	0.001	-0.031
	δ_2	-0.000	0.000	0.000
0.12	δ_0	-7.951	14.093	-1.704
	δ_1	-1.002	0.009	-0.261
	δ_2	-0.003	0.009	0.003
0.2	δ_0	-20.744	24.997	-5.838
	δ_1	-5.278	0.013	-1.621
	δ_2	-0.056	0.176	0.069
0.4	δ_0	-52.443	6.412	-24.418
	δ_1	-23.496	-1.936	-10.126
	δ_2	-1.319	7.036	2.563
0.6	δ_0	-81.703	-24.368	-50.026
	δ_1	-42.026	-10.538	-22.577
	δ_2	-4.768	39.301	13.601

Table 4. Phases for $S = \frac{3}{2}$ in degrees (modulo 180°)

k		MHWB	Serber	Biel
0.075	δ_0	-0.983	2.219	0.571
	δ_1	-0.077	-0.046	-0.058
	δ_2	0.000	0.001	0.001
0.12	δ_0	-3.879	8.103	1.808
	δ_1	-0.636	-0.389	-0.484
	δ_2	0.009	0.019	0.015
0.2	δ_0	-11.142	14.853	1.921
	δ_1	-3.982	-2.540	-3.088
	δ_2	0.173	0.366	0.289
0.4	δ_0	-32.611	2.601	-11.949
	δ_1	-27.839	-18.319	-21.300
	δ_2	5.217	14.563	10.089
0.6	δ_0	-52.185	-15.279	-29.380
	δ_1	-51.336	-35.217	-44.059
	δ_2	24.507	73.032	50.919

§ 6. CONCLUSION

There are two main conclusions to be drawn from the work presented here. The first is that the experimental data are best fitted by the Serber interaction, and the second is that the deuteron-triton elastic scattering is only slightly affected by the inclusion of the coupling to the neutron alpha particle channel.

For deuteron-triton elastic scattering the result given by Allred *et al.* (1952) at 10.5 MeV is the only experimental angular distribution known to the authors at an energy sufficiently high to give a sensitive test of the exchange type. From

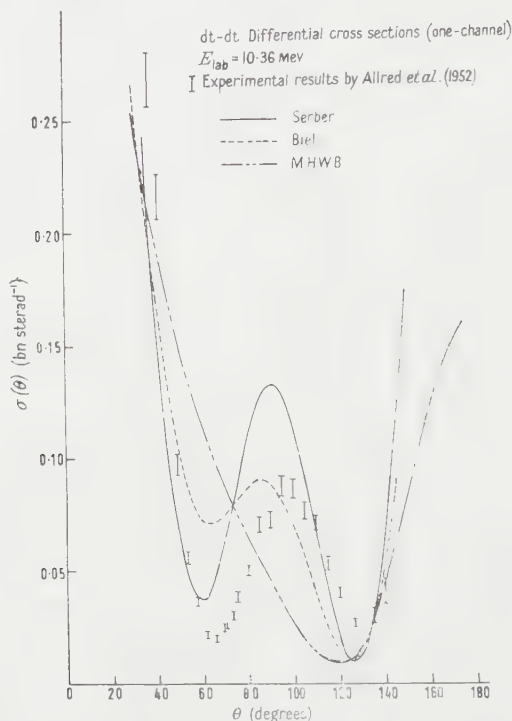


Fig. 1. dt-dt differential cross sections (one-channel) at $E_{lab} = 10.4$ MeV.

Fig. 1 it can be seen that these data are best represented by the Serber force. It would be desirable to have more experimental data, particularly phase shift analyses, with which to compare the results shown in Tables 3 and 4.

There are more data available for the reaction $t(d, n)^4\text{He}$ but in this case the calculations are more difficult to perform, and it has only been possible to investigate two energies. The differential cross section for the reaction $dt \rightarrow n^4\text{He}$, as measured by Brolley, Fowler and Stovall (1951) at 10.4 MeV is shown in Fig. 2. The corresponding theoretical curves are compared with this and it can be seen that, although the agreement is not very good, the Serber force again provides a better fit than the Biel mixture (Biel 1957). Although a calculation was not performed with the MHWB interaction it is safe to assume that this would be even less satisfactory than the Biel force since the last is composed of 70% Serber and 30% MHWB.

A calculation of the reaction cross section was also made at 1.5 MeV but this is not shown as it disagrees badly with the observations of Galonsky and Johnson (1956).

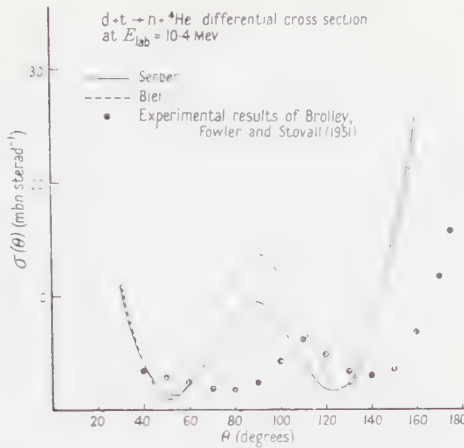


Fig. 2. $dt-dt$ differential cross sections (one-channel and two-channel) at $E_{\text{lab}} = 10.4 \text{ Mev}$.

Figure 3 illustrates the second conclusion. The elastic cross section at 10.4 Mev was calculated, using the Serber force, in the one-channel approximation and also including the pair of coupled equations in the doublet state.

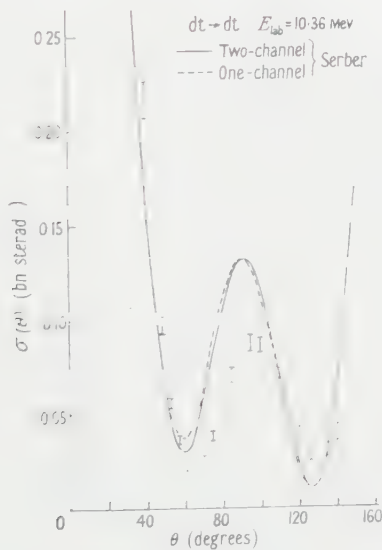


Fig. 3. $dt-n^4\text{He}$ differential cross section at $E_{\text{lab}} = 10.4 \text{ Mev}$.

The effect of the inclusion of the $n^4\text{He}$ channel on the $d-t$ elastic scattering is very small, although it is such as to bring the theoretical curves nearer the experimental. The small rate of the reaction $dt \rightarrow n^4\text{He}$ and consequently the small effect of the $n^4\text{He}$ state on the elastic $d-t$ scattering can probably be understood in terms of the small overlap integrals between the extended deuteron and triton wave functions in the initial state and the deuteron and the compact ${}^4\text{He}$ wave function in the final state.

It is difficult to know to what factors we must ascribe the lack of close agreement between the theoretical and experimental results. The effects of resonance in the five-nucleon system would be to give larger cross sections than those which have been calculated, but these are already larger than the experimental ones. The strongest resonance in ${}^5\text{He}$ is at $E_d = 107$ kev and this would have negligible effect on a cross section at an energy higher than 1 mev.

Another reason for expecting the present calculations of the reaction cross section to be poor at low energies is the following. At energies not much greater than zero in the incident dt channel, the ${}^4\text{S}$ dt channel might be strongly coupled to the ${}^2\text{D}$ n ${}^4\text{He}$ channel, since the reaction is exothermic by about 17.5 mev and, of course, this mode of interaction has not been included as it would require a non-central force. At higher energies, however, the processes conserving spin would be expected to increase in relative importance and to mask the spin-orbit effect just mentioned.

The Gaussian shaped wave functions might be criticized as being too short ranged. This, however, would only be expected to be serious for small angle scattering and, in any case, the elastic cross sections of Figs 1 and 2 are dominated by the Coulomb contribution for angles less than 20° .

The competition of other processes, such as the break up of the deuteron to give three scattered particles, is not expected to be serious (and, in any case, such processes could not be dealt with by the present methods).

The effect of polarization of the deuteron in neutron-deuteron scattering (Burke and Haas 1959) has been shown not to be serious and there is no reason to suspect otherwise here.

As possible explanations of the discrepancies, there remain the other types of internucleonic interaction which have not been discussed here. These are the non-central forces and many body forces. The inclusion of a tensor component would increase enormously the amount of labour involved in the calculation, but it is not until such a thorough calculation has been performed (at least for the three body problem) that the possibility of many body forces can be excluded.

Recently there has been considerable criticism directed against Wheeler's method as a practical means of studying nuclear interactions. There are, however, important uses to which it is well suited, as pointed out by Bransden (1960). First it is a means of correlating the data for the few-nuclear problem with just a few parameters, namely the range and depth of the potential and the exchange type. In this respect the Serber force (or a near Serber force) has been used to calculate approximate values for the scattering of most of the few-nucleon configurations. The method should also have important uses in the future when, with the advent of computers of greater capacity than are at present generally available, it can be hoped to perform calculations with more realistic potentials such as those of Gammel, Christian and Thaler (1957) and Signell and Marshak (1957), at the same time using numerical wave functions for the nuclear clusters.

REFERENCES

- ALLRED, J. C., ARMSTRONG, A. H., HUDSON, A. M., POTTER, R. M., ROBINSON, E. S., ROSEN, L., and STOVALL, E. J., Jr., 1952, *Phys. Rev.*, **88**, 425.
 BIEL, S. J., 1957, *Proc. Phys. Soc. A*, **70**, 866.
 BRANSDEN, B. H., 1960, *The Proceedings of the London Conference on Nuclear Forces and the Few-nucleon Problem*, 1959 (London: Pergamon).

- BROLLEY, J. E., JR., FOWLER, J. L., and STOVALL, E. J., JR., 1951, *Phys. Rev.*, **82**, 502.
- BUCKINGHAM, R. A., and MASSEY, H. S. W., 1941, *Proc. Roy. Soc. A*, **179**, 123.
- BURKE, P. G., and HAAS, F. A., 1959, *Proc. Roy. Soc. A*, **252**, 177.
- BURKE, P. G., and ROBERTSON, H. H., 1957, *Proc. Phys. Soc. A*, **70**, 777.
- GALONSKY, A., and JOHNSON, C. H., 1956, *Phys. Rev.*, **104**, 421.
- GAMMEL, J. L., CHRISTIAN, R. S., and THALER, R. M., 1957, *Phys. Rev.*, **105**, 311.
- HOCHBERG, S., MASSEY, H. S. W., ROBERTSON, H. H., and UNDERHILL, L. H., 1955, *Proc. Phys. Soc. A*, **68**, 746.
- HOCHBERG, S., MASSEY, H. S. W., and UNDERHILL, L. H., 1954, *Proc. Phys. Soc. A*, **67**, 957.
- LASKAR, W., TATE, C., and BURKE, P. G., 1960, *The Proceedings of the London Conference on Nuclear Forces and the Few-nucleon Problem*, 1959 (London: Pergamon).
- MOTZ, L., and SCHWINGER, J., 1940, *Phys. Rev.*, **58**, 26.
- ROBERTSON, H. H., 1956, *Proc. Camb. Phil. Soc.*, **52**, 538.
- SIGNELL, P. S., and MARSHAK, R. E., 1957, *Phys. Rev.*, **106**, 832.
- WHEELER, J. A., 1937, *Phys. Rev.*, **52**, 1107.

The Angular Distributions of Alpha Particle Groups from the Reaction $^{24}\text{Mg}(^3\text{He}, \alpha)^{23}\text{Mg}$

BY G. PARRY, H. D. SCOTT AND S. SWIERSZCZEWSKI

Physics Department, University of Liverpool

MS. received 15th December 1960

Abstract. Angular distributions of two alpha-particle groups from the reaction $^{24}\text{Mg}(^3\text{He}, \alpha)^{23}\text{Mg}$ at 5.5 MeV incident beam energy have been measured by magnetic analysis. For both groups a peak is observed in the forward direction, but for one of the groups an additional peak is observed at large angles of observation. An attempt has been made to explain the results in terms of a direct interaction mechanism.

§ 1. INTRODUCTION

THE angular distributions of $(^3\text{He}, \alpha)$ type reactions have been investigated experimentally by Holmgren, Greer, Johnston and Wolicki (1957) for ^{13}C , by Hinds and Middleton (1959, 1960) for ^{16}O and ^{12}C and by Taylor, Barros, Forsyth, Jaffe and Ramavataram (1960) for ^{10}B , ^{11}B , ^{14}N , ^{16}O and ^{27}Al . Both Hinds and Middleton (1960) and Taylor *et al.* (1960) were successful in describing most of their experimental angular distributions in terms of a direct interaction neutron pick-up mechanism.

In some angular distributions, however, besides the usual forward peak, characteristic for the known direct interaction pick-up process, a second maximum occurs at large angles of observation. The second maximum as observed by Holmgren *et al.* (1957) for the $^{13}\text{C}(^3\text{He}, \alpha)^{12}\text{C}$ ground state reaction was much too large in amplitude to be attributed to a pick-up process. If a compound nucleus model of interaction were devised to produce the observed angular distributions, a strong dependence on energy should be expected. The angular distributions observed by Holmgren *et al.* at 2.0 and 4.5 MeV bombarding energy show some similarity and they considered this ruled out the application of a compound nucleus model.

The concept of 'heavy particle' stripping was introduced by Owen and Madansky (1955) to describe some (d, n) reactions showing large backward maxima in the angular distributions. In this model the target nucleus is considered as core nucleus plus an alpha particle. The incident ^3He particle interacts with the core nucleus forming the final nucleus while the alpha particle is preferentially emitted in a backward direction.

In the present work, the angular distributions of two alpha-particle groups from the $^{24}\text{Mg}(^3\text{He}, \alpha)^{23}\text{Mg}$ reaction are investigated and an attempt is made to analyse the results in terms of a mechanism including pick-up and heavy particle stripping. The $^{24}\text{Mg}(^3\text{He}, \alpha)^{23}\text{Mg}$ reaction has been studied previously by Barros, Forsyth, Jaffe and Taylor (1959) and they have determined the energy levels of ^{23}Mg . The angular distributions of alpha particles from this reaction have not been studied previously.

§ 2. EXPERIMENTAL PROCEDURE

The 5.5 MeV ^3He beam from the 37 in. cyclotron of the University of Liverpool was used to bombard a self-supporting, 0.6 mg cm^{-2} thick magnesium target. The extracted beam of singly charged ^3He ions was collimated by means of three slits, focused by magnetic lenses and passed into the target chamber 14 ft from the cyclotron. The alpha particles from the reaction were magnetically analysed and the spectra were recorded on nuclear plates using the apparatus described by Green and Middleton (1956) and Dalton, Hinds and Parry (1957).

The spectra were measured for angles of observation in the range 10° to 130° . To obtain adequate statistics with the small yield of the reaction the exposures had to be as high as 4000 microcoulombs per spectrum.

§ 3. RESULTS

The angular distribution of the ground-state alpha-particle group (Fig. 1) could not be studied beyond 70° (lab) as at larger angles of observation the group became obscured by a group from carbon impurity present in the target.

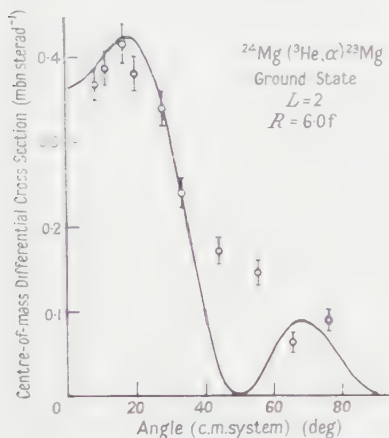


Fig. 1.

Fig. 1. Angular distribution of the ground state group of alpha particles from the reaction $^{24}\text{Mg}(^3\text{He}, \alpha)^{23}\text{Mg}$. The observed differential cross section for the centre-of-mass system as a function of centre-of-mass angle. The curve was calculated from the expression (1).

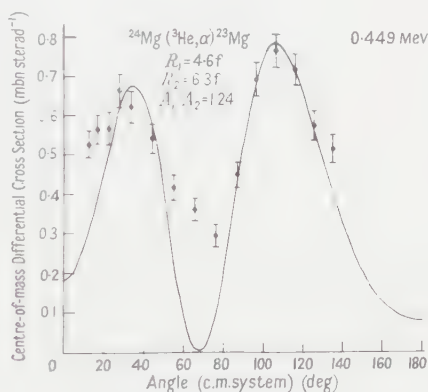


Fig. 2.

Fig. 2. Angular distribution of the first excited state group of alpha particles from the reaction $^{24}\text{Mg}(^3\text{He}, \alpha)^{23}\text{Mg}$. The observed differential cross section for the centre-of-mass system as a function of centre-of-mass angle. The curve was calculated from the expression (1).

The angular distribution of the first excited state group is shown in Fig. 2. The excitation of this level in ^{23}Mg has been measured by Barros *et al.* (1959) to be 0.449 MeV. The curves shown in Figs 1 and 2 were calculated from an approximate expression for a direct process proceeding both via pick-up and heavy-particle stripping:

$$W(\theta) = [A_1 j_l(K_1 R_1) + A_2 j_{l'}(K_2 R_2)]^2 \quad \dots\dots (1)$$

where R_1 and R_2 are the radii of interaction for the pick-up and heavy-particle stripping respectively, and momentum transfer vectors are

$$\mathbf{K}_1 = \mathbf{K}_\alpha - \frac{M_j}{M_f} \mathbf{K}_3, \quad \mathbf{K}_2 = \mathbf{K}_\alpha + \frac{M_\alpha}{M_f} \mathbf{K}_3 \quad \dots\dots (2)$$

where K_α and K_3 are wave numbers for alpha particle and ^3He ; M_α , M_i and M_f are masses of alpha particle and of initial and final nuclei, the j_l is a spherical Bessel function of the order l and the coefficients A_1 and A_2 for the pick-up and heavy-particle stripping terms are chosen empirically.

The selection rule for the pick-up process is

$$J_f = J_i + 1 + \frac{1}{2} \quad \dots\dots (3)$$

and for the heavy-particle stripping in this reaction

$$J_f = J_{\text{CN}} + 1' + \frac{1}{2}. \quad \dots\dots (4)$$

The subscript CN indicates the core nucleus. For both processes the parity changes or not according as l is odd or even.

The radii of interaction for pick-up and heavy-particle stripping R_1 and R_2 , and the ratio A_2/A_1 were chosen to give the best agreement with the results. The ground state reaction seems to proceed mainly by a pick-up process and the second term was neglected in fitting the experimental points. For the first excited state reaction the heavy-particle stripping term is appreciable and the value for the ratio $A_2/A_1 = 0.81$ was used. The shape of the curve is much more sensitive to changes in R_1 and R_2 since K_2 changes slowly with angle. The l -values $l=2$ and $l'=2$ were found adequate to fit the data. The parameters used in the calculations are shown in the Table.

Excitation energy (MeV)	J_f	J_i	J_{CN}	l	l'	R_1 (fermi)	R_2 (fermi)	A_2/A_1
0	$\frac{3}{2}^+, \frac{5}{2}^+$	0^+	0^+	2	—	6.0	—	0
0.449	$\frac{3}{2}^+, \frac{5}{2}^+$	0^+	0^+	2	2	4.6	6.3	0.81

§ 4. DISCUSSION

In view of the approximate nature of the calculation the agreement obtained with the experimental data is rather striking. The positions of the two maxima are determined mainly by the oscillations of $j_l(K_1 R_1)$ and they are sensitive to changes of R_1 , and the relative amplitudes of the maxima are governed by the choice of the ratio A_2/A_1 rather than by adjustments to R_2 , and a good fit can be obtained within reasonable values of R_1 and R_2 .

The l -values used in the fits lead to assignments for the ^{23}Mg ground state and first excited state of $\frac{3}{2}^+$ or $\frac{5}{2}^+$ which are compatible with the known assignments of $\frac{3}{2}^+$ and $\frac{5}{2}^+$ for the corresponding levels in the mirror nucleus ^{23}Na . A total angular momentum of 0^+ is required for the core nucleus ^{20}Ne . In consequence it is most likely that the core nucleus takes part in the reaction in its ground state, unlike the calculations for $^{13}\text{C}(^3\text{He}, \alpha)^{12}\text{C}$ heavy-particle stripping reactions (Owen, Madansky and Edwards 1959, Owen and Madansky 1957), where the total angular momentum assumed for the core is different from the total angular momentum of the nucleus in its ground state.

ACKNOWLEDGMENTS

We wish to thank Dr. H. C. Newns for helpful discussions on the interpretation of the results. One of us (S. S.) thanks the Polish Academy of Sciences for a grant which enabled him to undertake the work.

REFERENCES

- BARROS, F. DE S., FORSYTH, P. D., JAFFE, A. A., and TAYLOR, I. J., 1959, *Proc. Phys. Soc.*, **73**, 513.
- DALTON, A. W., HINDS, S., and PARRY, G., 1957, *Proc. Phys. Soc. A*, **70**, 586.
- GREEN, T. S., and MIDDLETON, R., 1956, *Proc. Phys. Soc. A*, **69**, 16.
- HINDS, S., and MIDDLETON, R., 1959, *Proc. Phys. Soc.*, **74**, 775.
- 1960, *Proc. Phys. Soc.*, **75**, 745.
- HOLMGREN, H. D., GREER, E. H., JOHNSTON, R. L., and WOLICKI, E. A., 1957, *Phys. Rev.*, **106**, 102.
- OWEN, G. E., and MADANSKY, L., 1955, *Phys. Rev.*, **99**, 1608.
- 1957, *Phys. Rev.*, **105**, 1766.
- OWEN, G. E., MADANSKY, L., and EDWARDS, S., JR., 1959, *Phys. Rev.*, **113**, 1575.
- TAYLOR, I. J., BARROS, F. DE S., FORSYTH, P. D., JAFFE, A. A., and RAMAVATARAM, S., 1960, *Proc. Phys. Soc.*, **75**, 772.

The Anisotropy of Young's Modulus in Drawn Polyethylene

By G. RAUMANN AND D. W. SAUNDERS†

British Rayon Research Association, Heald Green Laboratories, Manchester 22

MS. received 25th October 1960

Abstract. The macroscopic physical properties of a partially crystalline polymer become anisotropic when the polymer is 'drawn', i.e. when the polymer undergoes a large permanent deformation from its isotropic state. The anisotropy of refractive index, x-ray scattering etc. has been investigated by many workers. In this paper the anisotropy of Young's modulus in samples of polyethylene, drawn by simple tensile loading so as to have transverse isotropy, is studied experimentally at room temperature, 20°C. According to classical elasticity theory the Young's modulus of a transversely isotropic material can be defined completely in terms of three independent parameters. These have been chosen to be E_0 , E_{45} and E_{90} , the Young's moduli at angles 0°, 45° and 90° to the symmetry axis respectively. It is found that: (a) the polar distribution of Young's modulus in highly drawn polyethylene (draw ratio 4.65) agrees well with the distribution predicted by classical elasticity theory; (b) at draw ratios up to approximately 1.2, E_0 , E_{45} and E_{90} all decrease from the isotropic value and $E_{45} > E_{90} > E_0$; (c) at draw ratios greater than 1.2, E_0 and E_{90} both increase with increasing draw ratio but E_{45} continues to decrease; (d) in the highly drawn material, draw ratio approximately 4.65, $E_0 \simeq 1.5E_{90} \simeq 12E_{45} \simeq 5E_{\text{isotropic}}$.

These results are discussed in terms of the classical theory of elasticity.

§ 1. INTRODUCTION

PARTIALLY crystalline high polymers prepared in the laboratory by simple cooling of a melt or by precipitation from solution are isotropic in their macroscopic physical properties. However, when such an isotropic polymer is subjected to a suitable set of forces it undergoes a large deformation much of which persists when the forces are removed. The polymer is then said to be 'drawn' and many of its physical properties exhibit anisotropy. The precise nature of the anisotropy depends upon the property studied, the nature of the polymer and the geometry of the deformation during drawing.

Drawing (and the accompanying anisotropy) is important in the commercial production of many synthetic polymeric materials because it is accompanied by marked changes in mechanical properties. The strength and Young's modulus of synthetic textile fibres, for instance, are greatly enhanced by drawing. On the other hand articles produced by rolling, pressing or extrusion are frequently inhomogeneously anisotropic and thus have physical properties varying considerably from point to point.

Many workers have investigated the anisotropy of such properties as refractive index (i.e. birefringence) and x-ray scattering in drawn polymers; however,

† Now at Department of Materials, College of Aeronautics, Cranfield, Bletchley, Bucks.

little is known about the anisotropic nature of their elastic properties. Investigations of such properties in drawn materials appear to have been almost exclusively confined to work on simple tension parallel to the direction of drawing and simple torsion about this direction. However, the recent work of Shinohara and Tanzawa (1957) in Japan and of Wilson (1960) in these laboratories, on samples of drawn, regenerated cellulose, has shown that the elastic properties of this material do become markedly anisotropic as drawing increases.

In the work described in this paper polymer samples drawn by simple tensile loading, in a manner designed to produce transverse isotropy (i.e. complete rotational symmetry about the direction of drawing), are assumed to be ideally elastic for sufficiently small strains from the drawn state. A complete specification of the elastic properties of these materials can then be given in terms of five independent material parameters. Three of these independent parameters can be determined from simple tensile measurements on strips cut at various angles to the direction of drawing; such measurements are reported here for samples of polyethylene drawn to various extents.

The results of experiments designed to allow the determination of the two remaining independent parameters, for the same materials, will be reported later.

§ 2. THEORY

The elastic properties of an ideally elastic, anisotropic body, for infinitesimal strains, may be described in terms of a generalized Hooke's law (see Love 1927) expressed as:

$$\begin{aligned} e_{xx} &= s_{11}p_{xx} + s_{12}p_{yy} + s_{13}p_{zz} + s_{14}p_{yz} + s_{15}p_{zx} + s_{16}p_{xy} \\ e_{yy} &= s_{21}p_{xx} + s_{22}p_{yy} + s_{23}p_{zz} + s_{24}p_{yz} + s_{25}p_{zx} + s_{26}p_{xy} \\ e_{zz} &= s_{31}p_{xx} + s_{32}p_{yy} + s_{33}p_{zz} + s_{34}p_{yz} + s_{35}p_{zx} + s_{36}p_{xy} \\ e_{yz} &= s_{41}p_{xx} + s_{42}p_{yy} + s_{43}p_{zz} + s_{44}p_{yz} + s_{45}p_{zx} + s_{46}p_{xy} \\ e_{zx} &= s_{51}p_{xx} + s_{52}p_{yy} + s_{53}p_{zz} + s_{54}p_{yz} + s_{55}p_{zx} + s_{56}p_{xy} \\ e_{xy} &= s_{61}p_{xx} + s_{62}p_{yy} + s_{63}p_{zz} + s_{64}p_{yz} + s_{65}p_{zx} + s_{66}p_{xy} \quad \dots\dots (1) \end{aligned}$$

in which $e_{xx}, e_{yy} \dots e_{yz} \dots$ are the components of strain at a point in the body (referred to the rectangular Cartesian coordinate system $Oxyz$) and $p_{xx}, p_{yy}, \dots p_{yz} \dots$ are the components of stress at the same point. The 36 constants, s_{ik} , $i = 1$ to 6, $k = 1$ to 6, are material parameters with the dimensions of a compliance (e.g. $\text{cm}^2 \text{dyn}^{-1}$). Consideration of elastic energy shows that $s_{ik} = s_{ki}$ so that the number of independent parameters is 21. These can conveniently be written in an array

$$\left\{ \begin{array}{cccccc} s_{11} & s_{12} & s_{13} & s_{14} & s_{15} & s_{16} \\ & s_{22} & s_{23} & s_{24} & s_{25} & s_{26} \\ & & s_{33} & s_{34} & s_{35} & s_{36} \\ & & & s_{44} & s_{45} & s_{46} \\ & & & & s_{55} & s_{56} \\ & & & & & s_{66} \end{array} \right\}. \quad (2)$$

Thus 21 independent compliances are required to specify completely the elastic properties of the most generally anisotropic body. However, this number is further reduced according to the symmetry of the body (Nye 1957, p. 140).

For materials with transverse isotropy about the axis $0z$ the general array (2) reduces to

$$\left\{ \begin{array}{cccccc} s_{11} & s_{12} & s_{13} & 0 & 0 & 0 \\ & s_{11} & s_{13} & 0 & 0 & 0 \\ & & s_{33} & 0 & 0 & 0 \\ & & & s_{44} & 0 & 0 \\ & & & & s_{44} & 0 \\ & & & & & 2(s_{11}-s_{12}) \end{array} \right\} \dots\dots (3)$$

which contains only the five independent elastic compliances s_{11} , s_{33} , s_{44} , s_{12} and s_{13} .

Although the five compliances in (3) are independent quantities certain restrictions can be set upon their relative magnitudes (Nye 1957, p. 142) by the necessary condition that the strain-energy function for the material must always be positive. These restrictions may be written

$$s_{11} > 0, s_{33} > 0, s_{44} > 0, |s_{12}| < s_{11}, 2s_{13}^2 < s_{33}(s_{11} + s_{12}). \dots\dots (4)$$

It follows immediately from (1) and (3) that the Young's modulus E_0 for a transversely isotropic material subjected only to a tensile stress parallel to the symmetry axis $0z$ will be given by $E_0 = p_{zz}/e_{zz} = 1/s_{33}$ whilst the Young's modulus E_{90} for a similar material subjected to a load in any direction perpendicular to $0z$ will be given by $E_{90} = p_{xx}/e_{xx} = 1/s_{11}$.

The general relation for the Young's modulus of the material subjected only to a tensile stress parallel to a direction making an angle θ with $0z$ is given by (Nye 1957, p. 144)

$$1/E_\theta = s_{11} \sin^4 \theta + (2s_{13} + s_{44}) \sin^2 \theta \cos^2 \theta + s_{33} \cos^4 \theta. \dots\dots (5)$$

This relation involves three independent quantities s_{11} , $(2s_{13} + s_{44})$ and s_{33} , which can therefore be determined by measurements of E_θ for any three values of θ , say 0° , 45° and 90° .

It should be noted that the application of a simple tensile stress along any direction other than $\theta = 0^\circ$ or 90° results in a deformation which is a composition of both a tensile strain (i.e. an extension parallel to the applied stress with perpendicular contractions) and a shear strain; the Young's modulus under these conditions is the ratio of the tensile stress to the parallel component of strain.

§ 3. PREPARATION OF SAMPLES

After a number of preliminary experiments, a branched-chain polyethylene ('Alkathene' Grade 7) was chosen as a suitable material. Isotropic sheets, approximately 1 mm thick, were prepared by moulding between stainless steel plates in a press at 135°C and subsequently cooling by quenching in water at room temperature. The sheets had a density of 0.915 g cm^{-3} corresponding to a crystallinity of approximately 47%; they were transparent and had a birefringence of less than 10^{-4} . Visual inspection of x-ray diffraction diagrams taken both perpendicular and parallel to the plane of the sheet confirmed that the crystal orientation, if present at all, was very small. The Young's moduli of strips of the isotropic material cut in various directions were determined and found to be identical within experimental error.

Samples approximately $15\text{ cm} \times 6\text{ cm}$ were cut from the sheets, ruled with a grid of $\frac{1}{2}\text{ cm}$ squares and drawn, at room temperature, at rates of extension between 40 and 400% per minute to various extents. After drawing, the samples were allowed to stand load-free until changes in dimensions and birefringence could no longer be detected (approximately 24 hours). The draw ratio for each sample (i.e. the ratio of the length of a linear element parallel to the direction of drawing in this final load-free state to its length in the isotropic state) was then determined from measured grid dimensions.

As a check on possible deviations from transverse isotropy transverse sections of some of the drawn samples were prepared and inspected by x-ray diffraction and in the polarizing microscope. Visual inspections of the diffraction patterns did not reveal any departures from transverse isotropy, whilst the birefringence in the plane of the sections was found to be less than 10^{-4} . A further check was also obtained by comparing changes in width and thickness during drawing. No systematic deviations from transverse isotropy were encountered.

Specimens for the modulus measurements were cut in the form of parallel-sided strips about 2.5 cm long and 0.1 to 0.3 cm wide. These strips were cut with their long axes at known angles θ , usually 0°, 45° and 90°, to the direction of drawing. The Young's moduli of the strips were measured with loads applied parallel to their length and are designated E_θ , e.g. E_0 , E_{45} and E_{90} . The dimensions of the strips were determined with a travelling microscope and a micrometer thickness gauge. The birefringence of each specimen was also determined from measurements with a Babinet compensator.

Ideally, three specimens were required from each of the drawn samples (i.e. specimens cut at 0°, 45° and 90°) and these would be cut from a single area of uniformly drawn material of adequate size with the draw ratio, estimated as indicated above, therefore identical for all three specimens. In practice, however, particularly at intermediate draw ratios, it was not usually possible to find a sufficiently large area over which the drawing was perfectly uniform. Deviations from uniformity were manifested as distortions of the grid and variations of birefringence from point to point. The draw ratios used are therefore averages, from length measurements parallel to the direction of drawing, over the whole area of the sample from which the specimens were cut.

§ 4. MEASUREMENT OF YOUNG'S MODULI

The Young's moduli of the various specimens were determined at room temperature from the measured load-extension behaviour for total extensions of less than 3% from the drawn state. The load was applied to a clamp, fixed at the lower end of the specimen, and consisted of two parts, a 'steady' load and a superimposed 'cyclic' load; the latter was alternately applied and removed for periods of 12 sec during the measurements. The extension of the specimen was taken to be uniform and was determined by observing the movement of the lower clamp, the upper end of the specimen being held in a fixed clamp. The sensitivity was such that strains as small as 0.002% were readily observed.

Although for the purposes of applying classical elasticity theory to this work it has been assumed that the materials used are ideally elastic, it was found in practice that they exhibit, even at small strains, some departures from ideal elasticity. Accordingly the pattern of loading was chosen so as to give some indication of these effects.

The magnitude of the cyclic load was chosen, for each specimen, so as to produce a reversible extension of between 0.1 and 0.2%. The following loading pattern was then used: a steady load of similar magnitude to the cyclic load was applied and several cycles of loading and unloading superimposed. The steady load was then increased, in steps equal to the cyclic load, up to a maximum of ten times the cyclic load and subsequently decreased in similar steps. The extension was observed during several cycles at each value of the steady load. It was found that at each value of the steady load the extension could be represented as a 'reversible' part, approximately in phase with the cyclic loading, and a steady creep (due to the steady load) which diminished with time, becoming small after about eight cycles. During the whole of the loading pattern the total extension never exceeded 3% from the drawn state.

The Young's moduli were calculated from the ratio of the cyclic load to the reversible part of the observed extension. For all specimens the Young's moduli so calculated were found to vary only slightly with the magnitude of the steady load. For example the isotropic material showed only an 8% decrease of Young's modulus as the steady load was increased over the range described. In the case of the most highly drawn material, as the steady load increased E_0 increased by about 8%, E_{90} decreased by about 12% and E_{45} showed no measurable change. All these changes were reversible.

The values of Young's moduli used later are the mean values over the range of steady loads described.

§ 5. RESULTS AND DISCUSSION

During the course of the measurements room temperature varied between 18° and 22°C. The variation of moduli with temperature was therefore investigated over this range and a small correction (approximately a 10% decrease in modulus for a 3°C increase in temperature) was made to the observed values to give values correct at 20°C.

The modulus of a visco-elastic material such as polyethylene is known to depend upon rate of loading; experiments were therefore carried out to assess the importance of this effect. It was found that when the period of dead loading was increased from a half to twice its normal value the moduli decreased by less than 6%. A sinusoidal loading pattern gave approximately the same moduli as a square loading pattern with a similar load-time integral. In detail, the moduli of the drawn material (draw ratio 3.8) showed some anisotropy of time dependence, but such effects were small enough not to affect the overall pattern of results significantly.

It was also found that the moduli of the specimens increased slightly during the first three weeks after drawing but thereafter remained substantially constant. The values used refer to measurements made three weeks or more after drawing.

The Young's moduli of the various isotropic sheets were measured and found to vary between 13.4 and 14.0×10^8 dyn cm⁻².

In the case of the most highly drawn sample, in addition to E_0 , E_{45} and E_{90} , the Young's moduli E_θ for various other values of θ were determined. In Fig. 1 a plot of E_θ against θ for this sample is presented. The measured values are shown by the points whilst the full curve is obtained by re-writing Eqn (5) in the form

$$\frac{1}{E_\theta} = \frac{\sin^4 \theta}{E_{90}} + \sin^2 \theta \cos^2 \theta \left(\frac{4}{E_{45}} - \frac{1}{E_{90}} - \frac{1}{E_0} \right) + \frac{\cos^4 \theta}{E_0} \quad \dots\dots (6)$$

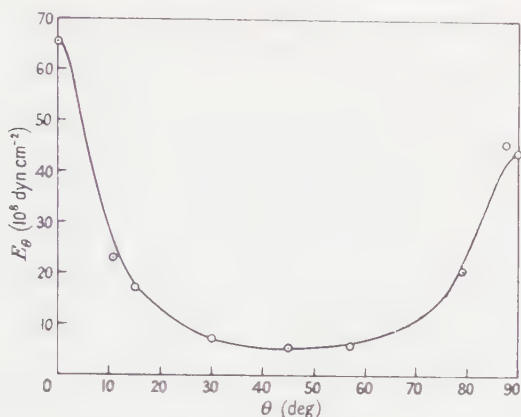


Fig. 1. Comparison of the observed variation of modulus with angle and the theoretical relation (i.e. the full curve) calculated from E_0 , E_{45} and E_{90} , for draw ratio 4.65.

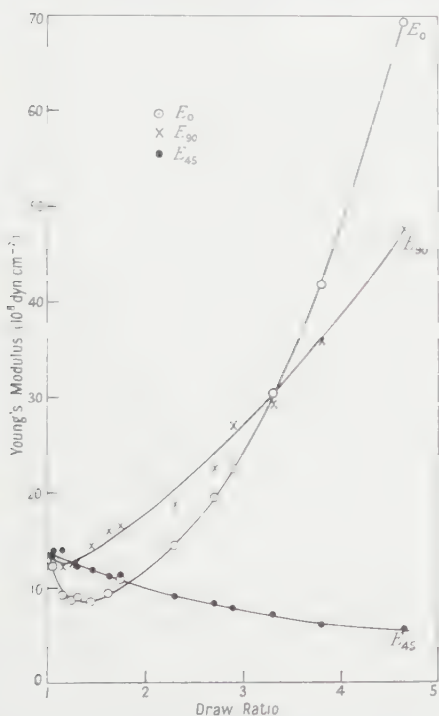


Fig. 2. The variation of E_0 , E_{45} and E_{90} with the draw ratio of the samples from which the specimens were cut. The curves are drawn through the points 'by eye'.

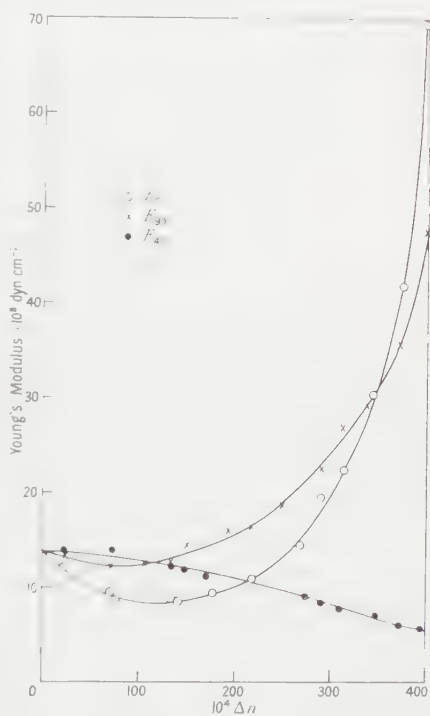


Fig. 3. The variation of E_0 , E_{45} and E_{90} with the birefringence of each specimen. The curves are drawn through the points 'by eye'.

and using the measured values of E_0 , E_{45} and E_{90} in Eqn (6) to compute E_θ for all values of θ . The agreement between the curve so obtained and the measured values of E_θ , other than E_0 , E_{45} , E_{90} , is good and is taken as an indication of the general applicability of the classical theory of elasticity to these results.

The principal set of results is shown in Fig. 2 in which E_0 , E_{45} and E_{90} are plotted against draw ratio for the various samples. The full curves in the figure

are drawn 'by eye' through the points. Although there is some scatter of the points about the smooth curves the overall pattern of the results is well defined.

The accuracy of determination of the moduli from the observed load-extension behaviour and the measured dimensions of the samples is estimated to be about $\pm 4\%$. Some of the points in Fig. 2 lie further from the curves than such an accuracy would allow. However because of the non-uniformity of drawing, particularly in samples of intermediate draw ratios, the actual value of draw ratio most appropriate to a particular specimen may be slightly different from the quoted average value for the sample from which the specimen was cut. This is a further source of scatter of the points from the line. The work of Crawford and Kolsky (1951) and Stein and Norris (1956) on polythene and of other workers (see for example de Vries 1953, Hermans 1949, and Culpin and Kemp 1956) on other polymers suggests that the birefringence of a drawn crystalline polymer increases monotonically with draw ratio and it may well be a better index of molecular orientation than the draw ratio. The observed birefringence-draw ratio relations for our specimens has the same general shape as that found by

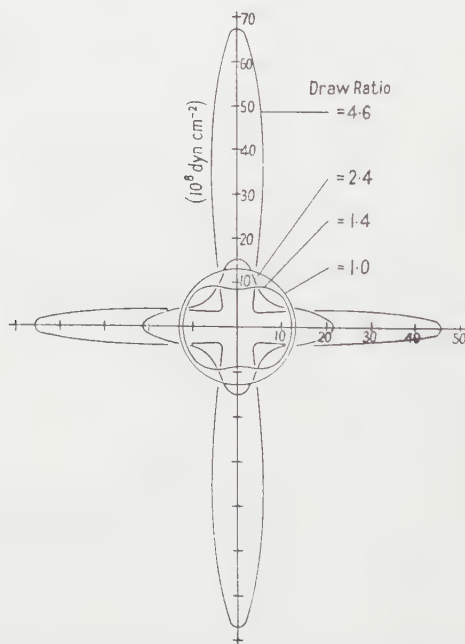


Fig. 4. Polar diagrams of Young's moduli at various draw ratios. The curve for each draw ratio is calculated from values of E_0 , E_{45} and E_{90} taken from the lines in Fig. 2.

earlier workers despite differences in the mode of preparation of the specimens. In Fig. 3 the moduli E_0 , E_{45} and E_{90} are plotted against the birefringence for each individual specimen used for the load-extension measurements. The scatter of the points about the smooth curves drawn 'by eye' through them is slightly less than in Fig. 2 and close inspection shows that none of the points deviate from the line by more than the estimated error of the modulus measurements.

By making use of Eqn (6) the variations of modulus with angle θ can be calculated from the results in Fig. 2 for samples of any draw ratio within the

range covered. In Fig. 4 the polar diagrams of Young's moduli, determined from the ordinates corresponding to the smooth curves in Fig. 2, are presented for draw ratios of 1.0, 1.4, 2.4 and 4.6. It should be noted that if the drawn material has in fact transverse isotropy about the direction of drawing, then these figures are sections of surfaces of revolution about the symmetry axis since the properties in all planes containing that axis are identical.

It should be further noted that the absence of significant birefringence in transverse sections of the drawn samples and also the similarity of the changes in widths and thicknesses of the samples during drawing are not in themselves sufficient conditions to ensure transverse isotropy of such a property as elastic modulus. A precise x-ray investigation would be sufficient to establish this point, but such an investigation was not undertaken, simple x-ray diffraction patterns were obtained but were subjected only to visual inspection. A small measure of uncertainty therefore persists, but subsequent discussion is based on the assumption of transverse isotropy.

There are several features of the results presented here which call for comment:

(a) The initial decrease in all the moduli as the draw ratio increases; in particular the pronounced minimum in the (E_{00} , draw ratio) curve. It is known that fairly small changes in the degree of crystallization of a partially crystalline polymer can be accompanied by large changes in the elastic moduli, see for example the work of Sandiford (1959) on polythene and of Leitner (1955) on isotropic natural rubber. It appeared, therefore, that a reduction in the degree of crystallinity during the early stages of drawing would account for the observed minima. However, measurements of the densities of the samples showed a continuous increase of density with draw ratio, amounting to about 0.3%, over the range of draw ratios 1.0 to 4.65. In isotropic polyethylene such an increase in density would correspond to an increase in crystallinity of only about 1.7%, and it seems likely therefore that changes in crystallinity during drawing are small. It should also be noted that the birefringence (which is an index of amount of molecular orientation), increases continuously with draw ratio. Further, visual inspection of a series of x-ray diffraction patterns, taken at various draw ratios, suggests that crystalline orientation increases monotonically with draw ratio. There appears then to be no correlation between simple structural parameters and modulus in this region. Hillier and Kolsky (1949) have previously reported a minimum in the curve of dynamic modulus (at 3000 c/s) against extension for polythene. The minimum was less pronounced and occurred at a slightly smaller strain than that reported here. A similar observation in cross-linked natural rubber (amorphous) has been reported by Mason (1959).

(b) For draw ratios between 1.0 and 1.85 the smallest modulus is E_{00} , i.e. that parallel to the direction of drawing. E_{00} only becomes greater than E_{90} for draw ratios greater than 3.3 and even in the most highly drawn material the ratio E_{00}/E_{90} is only 1.45. This behaviour is unexpected and is in marked contrast to that shown by drawn, regenerated cellulose as reported by Shinohara and Tanzawa (1957) and Wilson (1960). These authors investigated the variation of E_{00} and E_{90} with draw ratio and found that E_{00} increased markedly with draw ratio whilst E_{90} decreased slightly. Wilson reports values of E_{00}/E_{90} of about 6 and 9 for highly drawn cellulose (draw ratio approximately 3.12) at 65% and 100% relative humidity respectively.

(c) In the most highly drawn material E_{45} is very much smaller than either E_0 or E_{90} ; the ratio E_0/E_{45} is approximately 12. The writer is not aware of previous measurements of this type on drawn polymers but Hearmon (1946, 1956) has quoted results for eight single crystals with hexagonal symmetry (i.e. transversely isotropic elastic properties) and for wood and plywood. The results for the single crystals are such that $0.5 < E_0/E_{45} < 2.5$ in all cases. In the case of wood orthorhombic symmetry is assumed so that different variations of Young's moduli can be observed in three principal symmetry planes. Hearmon (1948) quotes Hörig's results on *Sitka Spruce* which show the polar variation of Young's modulus in the plane perpendicular to the grain direction to have a pronounced lobular form not dissimilar to that shown in Fig. 4 for draw ratio 4.6. For the spruce $E_0/E_{90} \approx 1.3$ and $E_0/E_{45} \approx 6$.

A complete specification of the elastic properties of drawn polythene requires values for all five constants s_{11} , s_{33} , s_{44} , s_{12} and s_{13} . The Young's moduli E_0 , E_{45} and E_{90} are given by $1/E_0 = s_{33}$, $1/E_{90} = s_{11}$, and $4/E_{45} = s_{11} + s_{33} + s_{44} + 2s_{13}$. By making use of these relations, the inequalities (4) and the results in Fig. 2 restrictions can be put on the possible values of s_{44} , s_{12} and s_{13} for any draw ratio in the range covered. It can readily be shown, for example, that in the most highly drawn material s_{44} (i.e. the reciprocal of the rigidity modulus for shear in the yz or xz planes, such as occurs for instance in torsion about the symmetry axis) is approximately 30 times as great as s_{11} or s_{33} . In isotropic materials the ratio of the Young's modulus to the rigidity modulus cannot be greater than three. Because the bulk modulus of many crystalline polymers is much greater than their rigidity modulus it is frequently convenient to regard them as virtually incompressible and to specify their elastic properties, for infinitesimal strains, by a single elastic constant. For polyethylene, for example, Bridgman (1948) and Parks and Richards (1949) quote values of bulk modulus of 2 and 4×10^{10} dyn cm $^{-2}$; these are some 30 times as great as the Young's moduli for our isotropic samples and therefore approximately 100 times as great as their rigidity moduli. In isotropic materials volume changes are always associated with the hydrostatic component of the applied stress, the shearing components resulting in changes of shape without changes of volume. A high value of bulk modulus, relative to rigidity modulus, is therefore a sufficient condition for an assumption that all deformations occur at constant volume.

In the case of anisotropic materials, however, the conditions are more complicated since, in general, volume changes may be associated with both the hydrostatic and shearing components of stress. For an anisotropic material with transverse isotropy an assumption that all deformations occur at constant volume leads to two independent relations between the five elastic constants, thus reducing their number to three. If such an assumption could be made for drawn polyethylene then the measurements reported here would be sufficient to give a complete specification of its elastic properties. However such an assumption cannot be justified, in whole or in part, by the data at present available. Further experiments are therefore required to enable the remaining two independent elastic constants to be measured; such experiments are being undertaken and will be reported later.

In the absence of any accepted quantitative theory relating the mechanical properties and molecular structure of crystalline polymers no comment is offered on the structural implications of these results.

ACKNOWLEDGMENTS

The authors wish to thank Mr. E. W. Wilson for his assistance with the experimental work and Dr. L. Roldan-Gonzalez for the x-ray diffraction work. This work forms part of the fundamental research programme of the British Rayon Research Association.

REFERENCES

- BRIDGMAN, P. W., 1948, *Proc. Amer. Acad. Arts Sci.*, **76**, 71.
- CRAWFORD, S. M., and KOLSKY, H., 1951, *Proc. Phys. Soc. B*, **64**, 119.
- CULPIN, M. F., and KEMP, K. W., 1956, *Proc. Phys. Soc. B*, **69**, 1301.
- HEARMON, R. F. S., 1946, *Rev. Mod. Phys.*, **18**, 409.
- 1948, *Forest Products Research Special Report Number Seven* (London: H.M.S.O.).
- 1956, *Advances in Physics*, **5**, 323.
- HERMANS, P. H., 1949, *Physics and Chemistry of Cellulose Fibres* (Amsterdam: Elsevier).
- HILLIER, K. W., and KOLSKY, H., 1949, *Proc. Phys. Soc. B*, **62**, 111.
- LEITNER, M., 1955, *Trans. Faraday Soc.*, **51**, 1015.
- LOVE, A. E. H., 1927, *The Mathematical Theory of Elasticity* (Cambridge: University Press).
- MASON, P., 1959, *Soc. Chem. Ind. Monograph No. 5*, 262.
- NYE, J. F., 1957, *Physical Properties of Crystals* (Oxford: Clarendon Press).
- PARKS, W., and RICHARDS, R. B., 1949, *Trans. Faraday Soc.*, **45**, 203.
- SANDIFORD, D. J. H., 1959, *Soc. Chem. Ind. Monograph No. 5*, 213.
- SHINOHARA, Y., and TANZAWA, H., 1957, *Chem. High Polym. Japan*, **14**, 488.
- STEIN, R. S., and NORRIS, F. H., 1956, *J. Polym. Sci.*, **21**, 381.
- DE VRIES, H., 1953, *On the Elastic and Optical Properties of Cellulose Fibres*, Thesis, Delft.
- WILSON, N., 1960, *J. Polym. Sci.*, **43**, 259.

Antiferromagnetism of Mixed Crystals of Zinc and Manganese Fluoride

By J. M. BAKER†, J. A. J. LOURENS† AND R. W. H. STEVENSON‡

† Clarendon Laboratory, Oxford

‡ Department of Natural Philosophy, Marischal College, Aberdeen

Communicated by B. Bleaney; MS. received 22nd December 1960

Abstract. An attempt has been made to measure the Néel temperature of mixed crystals of various composition by finding the temperature T_c at which the nuclear magnetic resonance of the fluorine nuclei disappears on cooling from room temperature. The dependence of T_c upon concentration of manganese is compared with theoretical predictions. Measurements of the variation of line-width with temperature above T_c are also discussed.

THE Néel temperature of several materials has been measured by observation of the disappearance of the magnetic resonance of nuclei in the material when antiferromagnetism sets in (e.g. Shulman and Jaccarino 1957). In many materials the disappearance temperature T_c measured in this way has agreed well with that T_N at the peak of the specific heat anomaly; but sometimes the nuclear magnetic resonance disappears at a temperature above T_N (e.g. Robinson and Friedberg 1960, Kim and Sugawara 1958). We have attempted to measure the Néel temperature of mixed crystals of Mn-ZnF₂ by observing the disappearance of the fluorine nuclear resonance.

Current theories of dilute systems suggest that there is a critical concentration below which antiferromagnetism does not occur (e.g. Elcock 1957, Sato, Arrott and Kikuchi 1959, Elliott 1960, Smart 1960, Elliott, Heap, Morgan and Rushbrooke 1960). Measurements to test these theories have been made so far in dilute alloys only (see references 4 and 5 in Sato, Arrott and Kikuchi 1959), and the only work done on mixed crystals is an estimate of the Weiss constant of Mn-ZnF₂ mixtures from susceptibility measurements by Corliss, Delabarre and Elliott (1950) and Robertson (1959).

In our experiments the nuclear magnetic resonance was usually observed at about 30 Mc/s using a Colpitts plate detector which develops a high radio-frequency voltage across the sample coil and hence gives a strong signal. Using a phase-sensitive detector with 1 c/s bandwidth the signal/noise ratio of the derivative of the line at 20°K for a typical case ($c=43\%$) is about 50. Nearest neighbour manganese ions produce a large paramagnetic shift of the fluorine nuclear magnetic resonance line because of appreciable overlap of the magnetic electrons onto the fluorine ions (Shulman and Jaccarino 1956, Tinkham 1956). In the manganese rich samples four resonance lines are observed corresponding to the fluorine ions with respectively three, two, one and none of the three nearest neighbour sites being occupied by a manganese ion. The relative intensities of these four lines are a function of concentration, and only the 'unshifted line' (three zinc neighbours, so little paramagnetic shift) is observed in the zinc-rich crystals. The experiments showed, when more than one line

was observed, that each disappeared at the same temperature, so that all of the detailed measurements were made on the 'unshifted line'. The temperatures were measured using a carbon resistance thermometer and where possible were checked by a measurement of the vapour pressure of the refrigerant.

The samples were prepared by the Stockbarger technique. The speed of growth used ($\sim 10 \text{ mm h}^{-1}$) was considerably higher than the normal in order to avoid segregation. A pressure of $20\text{--}30 \text{ lb in}^{-2}$ of dry nitrogen was used to reduce evaporation so that the initial concentration would be preserved. Some of the crystals were of very good optical quality and showed no colour variation throughout the volume, others were polycrystalline and of more doubtful uniformity. In many of the samples, pieces from two different places in the sample were analysed to see if the concentration varied (only one showed a very large concentration spread and this has been rejected). The concentration c was measured by dissolving the sample in 50% HNO₃ followed by oxidation of Mn²⁺ to MnO₄⁻ with sodium bismuthate and titration with standard solutions of ferrous ammonium sulphate and potassium permanganate.

The fluorine nuclear magnetic resonance line does not remain unchanged down to T_c and then disappear, but broadens as the temperature is lowered towards T_c . The width of the line ΔH is mainly due to interaction with the manganese electronic magnetic moments. At high temperatures the line is narrowed by rapid flipping of these magnetic moments due to exchange interaction between them. As the temperature approaches T_N short range order increases and tends to inhibit the exchange flipping. This lowers the flipping frequency and further broadens the line until at T_N , when long range order sets in, the line becomes very broad. This contribution to ΔH is small at high temperatures but increases very rapidly close to T_N . In addition in diluted specimens one would expect the random arrangement of the manganese neighbours to give rise to a line-width proportional to the specific magnetization of the sample χH , i.e. to the paramagnetic shift. Thus in specimens which remain paramagnetic to very low temperatures ΔH should vary as χH and in specimens which eventually become antiferromagnetic it should vary much more rapidly as T_N is approached. Because the line broadens, the signal/noise ratio decreases and the line eventually disappears at T_c . Thus the closeness of T_c to T_N depends upon the sensitivity of the nuclear magnetic resonance apparatus and may be estimated from the rate of change of ΔH with T when the line disappears.

Figure 1 shows some of our curves of $\Delta H/H$ and χ (χ for some of the specimens was measured by Robertson 1959 and one was measured by Mr. M. Brown†; rough values are also obtained from the paramagnetic shift) against $T - T_c$. At lower concentrations, where T_c is lower, ΔH is larger before the onset of short range order broadening, owing to the larger values of χ , so that the range of signal/noise ratio available for the study of the additional broadening tends to be smaller. Also at higher concentrations the probability of finding an F⁻ with no Mn²⁺ neighbours decreases so that the available signal is smaller. As a result of these effects $T_c - T_N$ is probably smaller at the centre of the range of concentration (about 0.5 K at $c = 40\%$ if T_N is estimated by extrapolating a curve of $1/\Delta H$ against T to $1/\Delta H = 0$), and larger at its ends. The value of T_c for pure MnF₂ ($67.5 \pm 1.0^\circ \text{K}$), where the dilution effects are absent and only short range order broadening occurs, agrees well with the value determined from specific heat

† Clarendon Laboratory, Oxford.

measurements (Stout and Adams 1942). The measured values of T_c , here taken as the temperature at which the signal/noise ratio becomes about unity, are plotted in Fig. 2. The measured spread of c in the specimen and the error in the determination of T_c are indicated by the size of the points on the graph. For the samples where $c=25\%$ and below, T_c has been taken to be zero as ΔH remains proportional to χH down to the lowest temperatures used; 4°K in the 25% sample limited by signal/noise ratio, and 2°K in the others limited by the cryostat.

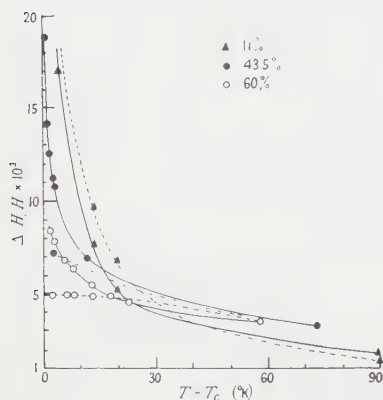


Fig. 1. Reduced line-width $\Delta H/H$ (full curves) as a function of $T - T_c$ compared with the variation of χ (broken curves) with $T - T_c$. The units of χ are normalized to make the curves for χ and $\Delta H/H$ correspond roughly at high temperatures where short range order broadening makes little contribution.

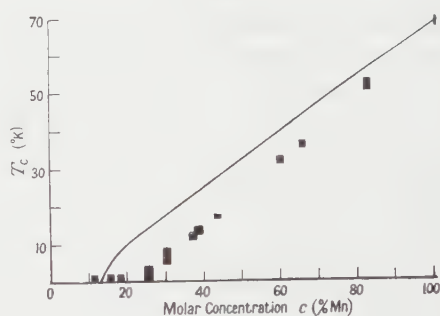


Fig. 2. Disappearance temperature T_c as a function of c , the molar concentration of manganese.

For comparison with our results in Fig. 2 the theoretical curve of Sato, Arrott and Kikuchi has been drawn for eight neighbours, appropriate to the body-centred tetragonal structure of MnF_2 . The results are in qualitative agreement with the theory in giving a critical concentration, and the lack of quantitative agreement is probably due to the fact that each manganese ion interacts with two types of near neighbours. In fact, Mr. B. Heap (unpublished) has obtained fair agreement with the experimental points and critical concentration by including the effect of exchange with two types of neighbour.

Some of the theoretical discussions suggest that the shape of the curve of T_c against c should be different for different values of the effective electronic spin S . We have therefore started a similar series of measurements on Co-ZnF_2 mixed crystals where $S = \frac{1}{2}$ for comparison with Mn-ZnF_2 where $S = \frac{5}{2}$, and where probably the ratio of the exchange interaction with nearest and next nearest neighbours is different. Preliminary results show a more rapid fall-off of T_c with c than for Mn-ZnF_2 .

Concurrent with this investigation the magnetic properties of Mn-ZnF_2 systems are being studied by a number of other methods both in Aberdeen and Oxford, such as susceptibility, anisotropy, specific heat; but it initially appeared

that the nuclear magnetic resonance measurements would be the quickest and perhaps the best way of measuring T_N . Although it is unlikely that T_C and T_N differ by very much, the fact that there is uncertainty makes it valuable to have additional measurements of T_N using another technique, and it is hoped that the experiments now in progress will provide these.

ACKNOWLEDGMENTS

We wish to thank Dr. W. Marshall for pointing out to us the theoretical interest in this problem; Dr. G. Garton for performing many of the tedious chemical analyses of the samples; Professor B. Bleaney and Dr. R. J. Elliott for many helpful discussions; Dr. N. F. Robinson for the gift of the nuclear magnetic resonance oscillator; Mr. W. Mitchell for help in the furnace operation; the Ministry of Supply for providing the crystal growing facilities; and the Board of Admiralty and the U.S. Air Force for support of the nuclear magnetic resonance work.

REFERENCES

- CORLISS, L., DELABARRE, Y., and ELLIOTT, N., 1950, *J. Chem. Phys.*, **18**, 1256.
ELCOCK, E. W., 1957, *Proc. Camb. Phil. Soc.*, **53**, 863.
ELLIOTT, R. J., 1960, *J. Chem. Phys. Solids*, **16**, 165.
ELLIOTT, R. J., HEAP, B. R., MORGAN, D. J., and RUSHBROOKE, G. S., 1960, *Phys. Rev. Letters*, **5**, 366.
KIM, P. H., and SUGAWARA, T., 1958, *J. Phys. Soc. Japan*, **13**, 968.
ROBERTSON, I., 1959, *Thesis*, Aberdeen University.
ROBINSON, W. K., and FRIEDBERG, S. A., 1960, *Phys. Rev.*, **117**, 402.
SATO, H., ARROTT, A., and KIKUCHI, R., 1959, *J. Phys. Chem. Solids*, **10**, 19.
STOUT, J. W., and ADAMS, H. E., 1942, *J. Amer. Chem. Soc.*, **64**, 1535.
SHULMAN, R. G., and JACCARINO, V., 1956, *Phys. Rev.*, **103**, 1126.
——— 1957, *Phys. Rev.*, **108**, 1219.
SMART, J. S., 1960, *J. Chem. Phys. Solids*, **16**, 169.
TINKHAM, M., 1956, *Proc. Roy. Soc. A*, **236**, 535.

Faraday Effect for Direct Magneto-optical Transitions in Germanium

BY M. SUFFCZYNSKI

Institute of Theoretical Physics, University of Warsaw, Poland

MS. received 26th October 1960

Abstract. The Faraday effect due to the interband magneto-optical transitions in germanium is calculated. The direct transitions from the uppermost Landau levels of the two light hole ladders and two heavy hole ladders are considered. The magnitude of the effect depends sensitively on the effective masses of the levels in the presence of the magnetic field.

IN the magneto-optical absorption the positions of the lines have been successfully calculated for germanium (Luttinger 1956, Roth, Lax and Zwerdling 1959). The absolute values of the peaks of the lines are more difficult to calculate. Here we try to estimate the Faraday effect due to the interband magneto-optical transitions in intrinsic germanium, under special circumstances. We consider the direct interband transitions from the uppermost Landau levels in the two light hole ladders and the uppermost levels in the two heavy hole ladders, both to the lowest Landau levels in the conduction band.

For a small wave vector component k_H along the constant magnetic field H the valence band energy levels have the form

$$\epsilon_{a,b}^{\pm}(n, k_H) = \epsilon_{a,b}^{\pm}(n) + \hbar^2 k_H^2 / 2m_{a,b}^{\pm}(n). \quad \dots (1)$$

The valence band levels can be calculated for $k_H = 0$ from Luttinger's formulae (1956) and for $k_H \neq 0$ from the perturbation formulae as suggested by Elliott, McLean and Macfarlane (1958).

Assuming the quadratic dependence of energy on k_H and the momentum matrix element constant one can calculate, in closed form, the contribution of the magneto-optical transitions to the dielectric constant. The contribution to the real part is, for one value of the spin,

$$4\pi\alpha = \frac{e^2 eH}{\hbar c m\omega} \frac{|\langle S | p_z | Z \rangle|^2}{m\hbar\omega} w_{a,b}^{\pm}(n) (m_{a,b}^{\pm}(n)^* / \hbar)^{1/2} \\ \times \left\{ \left[\frac{[(\omega_n - \omega)^2 + \gamma^2]^{1/2} + \omega_n - \omega}{(\omega_n - \omega)^2 + \gamma^2} \right]^{1/2} \right. \\ \left. + \left[\frac{[(\omega_n + \omega)^2 + \gamma^2]^{1/2} + \omega_n + \omega}{(\omega_n + \omega)^2 + \gamma^2} \right]^{1/2} - 2(2/\omega_n)^{1/2} \right\}. \quad \dots (2)$$

Here $\omega = 2\pi c/\lambda$ is the frequency of light, γ is the width of the line. For the line of Landau quantum number n the transition energy is $\hbar\omega_n$, and $m_{a,b}^{\pm}(n)^*$ is the reduced effective mass for the transition

$$m_{a,b}^{\pm}(n)^* = [1/m_c + 1/m_{a,b}^{\pm}(n)]^{-1}, \quad \dots (3)$$

m_c being the effective mass at the bottom of the conduction band. $w_{a,b}^{\pm}(n)$ is a weight factor for the transition. It depends on the light or heavy hole (+ or -) making transition, and on the polarization of radiation or the magnetic quantum numbers of the levels a, b. The value of the momentum matrix element $\langle S | p_z | Z \rangle$ is known from cyclotron resonance experiments (Dresselhaus, Kip and Kittel 1955).

When a constant magnetic field is set along the [100] axis of germanium and light is passed along the same direction, the first direct transitions are from the $\epsilon_a^+(0)$ and $\epsilon_b^-(0)$ light hole levels for the left circularly polarized radiation and from the $\epsilon_a^-(2)$ and $\epsilon_b^-(2)$ heavy hole levels for the right circularly polarized radiation (Elliott, McLean and Macfarlane 1958, Burstein *et al.* 1959). This gives rise to a Faraday effect. The angle θ of the Faraday rotation can be calculated from the formula

$$\theta = 2\pi^2 l (\alpha^{\text{right}} - \alpha^{\text{left}}) / \lambda \tilde{n} \quad \dots\dots (4)$$

if the light is transmitted through a specimen of thickness l , of the mean refractive index \tilde{n} . We take $\tilde{n} \simeq 4$ for germanium. The contribution of the imaginary part of polarizability can be neglected for germanium. Also, in the real part we keep in the computation only the first term of Eqn (2).

The magnitude of the Faraday rotation in the arrangement considered depends essentially on the effective k_H -masses of the light and heavy holes. As a representative example we take $H = 46.6 \times 10^3$ gauss and $l = \lambda$. We use the cyclotron resonance parameters quoted by Roth, Lax and Zwerdling (1959): $\gamma_1 = 13.1$, $\gamma_2 = 4.15$, $\gamma_3 = 5.5$, $\kappa = 3.23$. We also quote here $m/m_e = 27.1$ and $|\langle S | p_z | Z \rangle|^2 / m\epsilon_g = 14$, where ϵ_g is the energy gap at the zone centre.

We have

$$w_{a,b}^{\pm}(n) = |a_1^{\pm}(n)|^2 + \frac{1}{3} |b_1^{\pm}(n)|^2 \quad \dots\dots (5)$$

where $a_1^{\pm}(n)$ and $b_1^{\pm}(n)$ are defined by Luttinger (1956) and Burstein *et al.* (1959). The energy difference between the two components, a and b, of each line and of the two lines corresponding to right and left circularly polarized radiation, are neglected here. They are less than 10^{-3} ev, while $\hbar\gamma = 2 \times 10^{-3}$ ev at room temperature as found in absorption experiments (Burstein *et al.* 1959). The peak in the real part of the dielectric constant occurs at $\omega = \omega_n - \gamma/\sqrt{3}$. The peak of the absorption line occurs at $\omega = \omega_n + \gamma/\sqrt{3}$, that is at about $\hbar\omega = 0.808$ ev for our transitions.

If the valence band k_H -masses were taken as they are for high quantum numbers n ,

$$m/m^+ = 25 \quad m/m^- = 3.33, \quad \dots\dots (6)$$

the resulting θ would be nearly -21° at the peak of the real part of dielectric constant. If the valence band k_H -masses were calculated from the perturbation formulae, which are certainly valid for sufficiently small values of k_H , they would be

$$\begin{aligned} m/m_a^+(0) &= 1.42 & m/m_a^-(2) &= -23.95 \\ m/m_b^+(0) &= 4.8 & m/m_b^-(2) &= 12.45 \end{aligned} \quad \dots\dots (7)$$

and thus $\theta = 279^\circ$. This large figure is mainly due to the large negative value of $m/m_a^-(2)$.

In the absorption experiments the light hole transitions appear more strongly (Burstein *et al.* 1959, Roth, Lax and Zwerdling 1959). Therefore θ should be negative. It is borne in mind that in calculating the interband contribution to the dielectric constant the summation over k_H is to be performed from 0 to values much larger than $(\gamma m^*/\hbar)^{1/2}$. There the perturbation formulae for the k_H -masses are no longer valid. The way to proceed is a direct numerical solution of the secular equation of Luttinger (1956). The matrix of this equation is, following his notation, $D_0 + D_3$, where in D_0 we have to put $s=0$, $c=1$ for our experimental set-up. We neglect Luttinger's D_1 and D_2 in his equation (81) because we do not perform second-order perturbation calculations on $\gamma_3 - \gamma_2$. The part we call D_3 depends on $k = k_H(\hbar c/eH)^{1/2}$.

$$D_3 = \begin{vmatrix} (\frac{1}{2}\gamma_1 - \gamma_2)k^2 & 0 & -k\gamma_3(6(n-1))^{1/2} & 0 \\ 0 & (\frac{1}{2}\gamma_1 + \gamma_2)k^2 & 0 & k\gamma_3(6(n+1))^{1/2} \\ -k\gamma_3(6(n-1))^{1/2} & 0 & (\frac{1}{2}\gamma_1 + \gamma_2)k^2 & 0 \\ 0 & k\gamma_3(6(n+1))^{1/2} & 0 & (\frac{1}{2}\gamma_1 - \gamma_2)k^2 \end{vmatrix}. \quad \dots\dots (8)$$

Eigenvalues obtained by direct numerical solution of the secular equation for $k_H \neq 0$ can be expressed in terms of effective masses which change with k_H . The absolute values $|m/m_{a,b}(2)|$ drop for larger k_H so the above perturbation values, Eqn (7), are not decisive in the summation over k_H .

For k_H^2 as large as $eH/\hbar c$, that is in our example, about $7.3\gamma m_c/\hbar$ we find

$$\begin{aligned} m/m_a^+(0) &= 2.6 & m/m_a^-(2) &= -4.0 \\ m/m_b^+(0) &= 4.8 & m/m_b^-(2) &= 7.4. \quad \dots\dots (9) \end{aligned}$$

With the use of these figures in (2) the value $\theta = -95'$ is obtained. The use of these figures was checked to be permissible by an integration with numerical energy eigenvalues in place of the analytical one which led to (2).

This last value of θ is two orders of magnitude larger than that found experimentally by Walton and Moss (1959) in intrinsic germanium at $H = 8 \times 10^3$ gauss. One possible explanation of the discrepancy may be that at this field the magneto-optical lines are not yet peaked enough over the background. Our theoretical calculation is uncertain because all the background contributions to the dielectric constant have been neglected. These are due to the free carriers and to the tails of the interband lines with higher n 's. It is difficult to estimate these effects and they are certainly there (Stephen and Lidiard 1958). Since their contribution has frequency dependence different from the peaked one of Eqn (2) they may cancel in the Faraday difference of Eqn (4).

The background contributions increase for the lines of higher n 's. It is for this reason that the calculation has been attempted for the lowest levels in the conduction band only. On the other hand, for these levels of lowest n 's the exciton effects (Elliott and Loudon 1959) are most pronounced. In the present calculation the Coulomb interaction between the electron and the hole is neglected. It is difficult to take it into account in the presence of the magnetic field, especially here, where one has to perform the summation over all relevant values of k_H . The error resulting from this neglect is serious, particularly for the levels of lowest n 's. Other errors of the calculation resulting, for instance, from the choice of the set of cyclotron resonance parameters quoted, instead of some other cited in the literature, are minor in comparison with the ones mentioned.

In any case the measurement of the Faraday rotation for the interband magneto-optical transitions seems to offer a sensitive experimental way to investigate the difference between the masses of the light and heavy holes in the presence of the magnetic field. The main experimental difficulty in the measurement is the limitation of the sample thickness. The increase of the thickness quoted above by more than a factor of 3 would cause too great a loss in the transmitted intensity.

ACKNOWLEDGMENTS

My thanks are due to Dr. M. Miasek for help in the calculations, and to her and Mr. J. Mycielski for valuable discussions. The referees' comments have been most useful.

REFERENCES

- BURSTEIN, E., PICUS, G. S., WALLIS, R. F., and BLATT, F., 1959, *Phys. Rev.*, **113**, 15.
DRESSSELHAUS, G., KIP, A. F., and KITTELL, C., 1955, *Phys. Rev.*, **98**, 368.
ELLIOTT, R. J., and LOUDON, R., 1959, *J. Phys. Chem. Solids*, **8**, 382.
ELLIOTT, R. J., McLEAN, T. P., and MACFARLANE, G. G., 1958, *Proc. Phys. Soc.*, **72**, 553.
LUTTINGER, J. M., 1956, *Phys. Rev.*, **102**, 1030.
ROTH, L. M., LAX, B., and ZWERDLING, S., 1959, *Phys. Rev.*, **114**, 90.
STEPHEN, M. J., and LIDIARD, A. B., 1958, *J. Phys. Chem. Solids*, **9**, 43.
WALTON, A. K., and MOSS, T. S., 1959, *J. Appl. Phys.*, **30**, 951.

An X-ray Absorption Process in Ionic Crystals

BY P. E. BEST AND J. L. ROBINS

Department of Physics, University of Western Australia, Nedlands,
Western Australia

Communicated by C. J. B. Clews; MS. received 7th November 1960

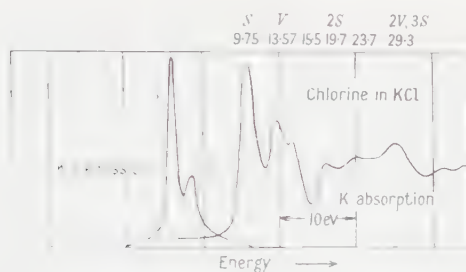
Abstract. Two peaks at 9.8 eV and 13.9 eV, in the observed characteristic electron energy loss spectrum of potassium chloride, have been identified as being due to the excitation of surface and volume plasma oscillations respectively. The first two maxima of the K x-ray absorption spectrum of the chloride ion in potassium chloride are of energy 9.8 eV and 13.6 eV greater than the valence \rightarrow K emission line, and it is proposed that these two peaks are caused by the transition $K \rightarrow$ valence plus excitation of some mode of plasma oscillation. It is suggested that corresponding peaks in the x-ray absorption spectra of other ionic crystals have the same origin.

It has been established that the K x-ray absorption spectra of ionic crystals show a pronounced structure of narrow, well-defined peaks, and Parratt (1959) has recently suggested an explanation for these in terms of excited states. We have observed a striking correlation between this structure and the plasma oscillation energies as observed in characteristic electron energy loss studies.

Peaks due to the excitation of plasma oscillations have now been observed in the characteristic loss spectra of a number of compounds, and there is good agreement between experiment and theory (Pines 1956), also lowered plasma oscillations have been observed for a number of pure elements (Powell 1960). The theoretical plasma oscillation energy is given by the expression $\hbar\omega_p$, where $\omega_p = (4\pi ne^2/m)^{1/2}$ and e and m are the electronic charge and mass respectively and n is the free electron density. The energy associated with the lowered plasma loss, which is a surface effect, is theoretically $\hbar\omega_p/\sqrt{2}$. We shall use the terms volume plasma and surface plasma to refer to these two types of oscillation respectively.

We have recently measured the characteristic electron energy loss spectrum of potassium chloride, using equipment described by Powell and Swan (1959). A 127 electrostatic focusing spectrometer and electrical recording were used in conjunction with the reflection technique, the primary electron energy being 800 eV. In the spectrum we have identified a plasma and a lowered plasma loss peak from energy considerations, and this has led us to attempt an interpretation of the results of earlier workers on the same basis.

In Table 1 the theoretical values of the volume and surface plasma oscillation energies are compared with prominent electron energy loss peaks. The agreement supports the assumption that such collective oscillations do exist in ionic compounds. The free electron density n is here obtained by including all the valence electrons outside the last closed shell (1 electron per atom for K, 7 for Cl, etc.).



The K_1 emission and K absorption spectra of the chloride ion in KCl (Parratt 1959).

Table 1. A Comparison between Experimental and Theoretical Plasma Oscillation Energies for Alkali Halides

Compound	Experiment energy losses (ev)		Theoretical	
			$\hbar\omega_p/\sqrt{2}$	$\hbar\omega_p$
KCl (present work)	9.8 ± 0.3	13.9 ± 0.3	9.4	13.3
NaCl (Leder 1956)	9.3	15.9	11.0	15.6
KBr (Kleinn 1954)	9.7	13.4	8.8	12.4

Table 2. A Comparison between X-ray Absorption and Electron Energy Loss Data in ev

	S	V	2S	2V	3S
KCl Cl ⁻ (a)	9.75	13.57	19.7		29.3
Cl ⁻ (b)	9.4	13.0	19.2		
K ⁺ (a)	9.76	13.32			
K ⁺ (c)	9.4	13.0	20.1		
Plasma theory	9.4	13.3	18.8	26.6	28.2
Characteristic losses (d)	9.8	13.9	19.5		
NaCl Cl ⁻ (b)	11.0	17.4	22.0		
Na ⁺ (e)	13.0	15.9	23.3		32.6
Plasma theory	11.0	15.6	22.0	31.2	33.0
Characteristic losses (f)	9.3	15.9			
NaF Na ⁺ (e)	14.5	22.2	31.7		
Plasma theory	15.1	21.4	30.2		
NaI Na ⁺ (e)	11.3	13.8	18.6		
Plasma theory	9.0	12.7	18.0		
KBr K ⁺ (c)	8.8	11.9	17.3		
Plasma theory	8.8	12.4	17.6		
Characteristic losses (g)	9.7	13.4			

(a) Parratt (1959), (b) Brewington (1943), (c) Kiyono (1952), (d) Present work, (e) Rule (1944), (f) Leder (1956), (g) Kleinn (1954).

In the Figure we have reproduced the $K\beta_1$ emission and K absorption curves of the chloride ion in KCl (Parratt 1959). Above each absorption peak we have indicated its energy separation from the $K\beta_1$ emission line in ev. We propose that in ionic crystals x-rays are absorbed, causing a $K \rightarrow$ valence transition plus a simultaneous excitation of some form of plasma oscillation. The observed absorption peaks are then interpreted in terms of a volume or surface plasma oscillation. The origin of each peak, whether a volume or surface plasma oscillation, is indicated by the letters V or S respectively. Evidence presented in the Figure and Table 2 suggests that excitation of multiples of plasma oscillations may also occur in x-ray absorption. The shape of the absorption curve and the increasing width of the multiple peaks is consistent with this interpretation. The shift of the peaks in the absorption curve with change of temperature (Parratt 1959) also supports our suggestion, as the plasma frequencies will decrease with increasing temperature due to the decrease of the free electron density n with thermal expansion.

The transition $K \rightarrow$ valence should not be possible as the valence band is full, and it is probably significant that such a transition is not observed without the simultaneous excitation of oscillations. For other features of the absorption spectra, notably the peak at 15.5 ev and the background, a different explanation must be sought.

Although correlation of characteristic energy losses with x-ray absorption data has been attempted before both experimentally and theoretically, the only comparison for ionic crystals was made using the position of the absorption maxima as measured from the absorption edge (Leder, Mendlowitz and Marton 1956).

The similarity between the x-ray absorption fine structure for the potassium ion and that of the chloride ion in KCl (Parratt 1959) points to the extension of the above ideas to include the cations of ionic crystals. Parratt measured the separation of the first two maxima in the K^+ absorption curve to be 3.56 ev compared with 3.82 ev for corresponding peaks in the Cl^- absorption curve. If the $K\beta_5$ of the K^+ emission spectra of KCl is considered to be the result of a valence $\rightarrow K$ transition (Valasek 1938), then the separation of the absorption peaks from this line will represent the energies involved in the plasma oscillations. The values of 9.76 and 13.32 ev obtained in this manner from the potassium curve are comparable with the values of 9.75 and 13.57 ev as found from the chloride curve.

In Table 2 we have collected the results of x-ray and characteristic energy loss studies, together with the relevant plasma oscillation energies calculated from the theory. Brewington (1934) and Kiyono (1952) did not record the appropriate emission peaks, so the first value has been assumed equal to the surface plasma energy. The agreement shown in Table 2 for these simple ionic crystals suggests that a correlated theoretical, x-ray and electron energy loss investigation of more complicated compounds should be attempted.

ACKNOWLEDGMENTS

The authors wish to thank Professor C. J. B. Clews for his continued interest and encouragement. One of us (P.E.B.) acknowledges the tenure of a General Motors Holden Postgraduate Research Fellowship, and the other (J.L.R.) a Commonwealth Postgraduate Award.

REFERENCES

- BREWINGTON, G. P., 1934, *Phys. Rev.*, **46**, 861.
FRÖHLICH, H., and PELZER, H., 1955, *Proc. Phys. Soc.*, **68**, 525.
KIYONO, 1952, *Sci. Rep. Res. Insts Tohoku Univ.*, Ser. 1, 36.
KLEINN, W., 1954, *Optik, Stuttgart*, **11**, 226.
LEDER, L. B., 1956, *Phys. Rev.*, **103**, 1721.
LEDER, L. B., MENDLOWITZ, H., and MARTON, L., 1956, *Phys. Rev.*, **101**, 1460.
PARRATT, L. G., 1959, *Rev. Mod. Phys.*, **31**, 616.
PINES, D., 1956, *Rev. Mod. Phys.*, **28**, 184.
POWELL, C. J., 1960, *Proc. Phys. Soc.*, **76**, 593.
POWELL, C. J., and SWAN, J. B., 1959, *Phys. Rev.*, **115**, 869.
RULE, K. C., 1944, *Phys. Rev.*, **66**, 199.
VALASEK, J., 1938, *Phys. Rev.*, **53**, 274.

Note added in proof.—In a subsequent discussion with Dr. J. Collins it became clear that a surface effect should not appear in the x-ray absorption, and that the plasma oscillation which here has been associated with the surface is better identified as an ionic plasma oscillation (Fröhlich and Pelzer 1955).

A Study of the Reaction $^{40}\text{Ca}(\text{d}, \text{n})^{41}\text{Sc}$

BY B. E. F. MACEFIELD, J. H. TOWLE AND W. B. GILBOY

Atomic Weapons Research Establishment, Aldermaston, Berkshire

MS. received 14th November 1960

Abstract. The neutron time-of-flight technique has been used to study the reaction $^{40}\text{Ca}(\text{d}, \text{n})^{41}\text{Sc}$. A ground state Q value of -1.145 ± 0.015 mev was obtained which disagrees with previous measurements. Excited states of ^{41}Sc have been located at 1.709 ± 0.030 mev and 2.476 ± 0.030 mev. Angular distributions of the corresponding neutron groups have been measured. The application of Butler stripping theory enables an assignment of $l=3$ for the captured proton for the ground state and $l=1$ for the 1.71 mev state. An unambiguous assignment is not possible for the 2.48 mev state.

§ 1. INTRODUCTION

PLENDL AND STEIGERT (1959) have studied the reaction $^{40}\text{Ca}(\text{d}, \text{n})^{41}\text{Sc}$ using a cyclotron beam and nuclear emulsions. Q values of -0.57 ± 0.05 , -2.43 , -2.64 and -2.85 mev were obtained for the ground state and three excited states of ^{41}Sc respectively. Their ground state Q value agrees with the value of -0.60 ± 0.08 mev deduced from the β^+ decay end point of ^{41}Sc (Elliot and King 1941) and the ground state Q value for the reaction $^{40}\text{Ca}(\text{d}, \text{p})^{41}\text{Ca}$ (Braams 1956). The large discrepancy between these results and the present measurement, which is in excellent agreement with the Q value obtained for the $^{40}\text{Ca}({}^3\text{He}, \text{d})^{41}\text{Sc}$ reaction by Hinds and Middleton (private communication, 1959) has been briefly reported previously by Macefield and Towle (1960). Hinds and Middleton's value of -4.414 ± 0.010 mev leads to an expected Q value for $^{40}\text{Ca}(\text{d}, \text{n})^{41}\text{Sc}$ of -1.147 ± 0.015 mev.

Further doubt has been cast on the previously accepted mass of ^{41}Sc in a recent paper by Wegner and Hall (1960). These workers report Q values of -1.32 ± 0.07 mev and -4.47 ± 0.10 mev for the (d, n) and $({}^3\text{He}, \text{d})$ reactions on ^{40}Ca respectively. There is a discrepancy of 0.12 mev in the mass of ^{41}Sc as derived from these two Q values but it is within the combined experimental errors. Their $^{40}\text{Ca}(\text{d}, \text{n})^{41}\text{Sc}$ Q value, however, differs by more than twice its quoted error from the present result.

A strong group with a Q value of -2.86 ± 0.02 mev, which was attributed to the first excited state of ^{41}Sc (Macefield and Towle 1960), has also been reported by Wegner and Hall, who obtain -2.85 ± 0.03 mev.

Class *et al.* (1959) have located levels in ^{41}Sc at excitations between 2.4 and 7 mev by a study of the elastic scattering of protons from ^{40}Ca .

In this paper we report Q values and angular distributions for the ground and two excited state groups of the $^{40}\text{Ca}(\text{d}, \text{n})$ reaction. These data were obtained

using a time-of-flight spectrometer, the sensitivity of which has recently been improved by reducing the random background counts.

§ 2. EXPERIMENTAL DETAILS

The time-of-flight spectrometer, used in this investigation has been described previously by Batchelor and Towle (1959) and, with a modified shielding system, by Macefield and Towle (1960). The technique of pulse shape discrimination against γ -rays has been applied to the spectrometer to reduce the background counting rates (Batchelor *et al.* 1960). This utilizes the different decay times of proton and electron pulses in a liquid scintillator (NE 213 supplied by Nuclear Enterprises, Edinburgh).

The detector efficiency was obtained by comparison with a long counter of known efficiency (McTaggart -unpublished data). The time-to-pulse-height converter was adjusted so that each channel of the 100 channel analyser was equivalent to approximately 2 nsec, the time scale being calibrated with a double pulse generator.

Calcium targets were made by evaporation (*in situ*) of pure natural calcium metal. A spectrographic analysis of a sample of the metal revealed the following constituents: Al 0.12%, Mg 0.23%, N_2 0.31% and Ca 99.3%. Target thicknesses were determined by quantitative chemical analysis at the completion of the bombardment. The targets, of thicknesses $200\text{--}300\text{ }\mu\text{g cm}^{-2}$, produced a total energy loss of approximately 25 keV for 4 MeV deuterons. The calcium targets were deposited on a thick platinum backing which was cooled with demineralized water thus maintaining electrical insulation and enabling a current integrator to be used. A cold trap, cooled by liquid nitrogen, was placed close to the target chamber to reduce the build-up of pump oil on the target.

In order to determine the position, in the spectra, of peaks due to carbon and oxygen contamination, targets of these elements were prepared and irradiated. The carbon targets were made by placing 0.005 in. tantalum foil near an arc discharge maintained *in vacuo* between pure graphite electrodes, and the oxygen targets by vacuum evaporation of Nb_2O_5 to a thickness of $200\text{ }\mu\text{g cm}^{-2}$.

Owing to high backgrounds due to radiation from the beam deflection system, and the presence of radiations from target contaminants, it was impossible to monitor the $^{40}\text{Ca}(d, n\gamma)^{41}\text{Sc}$ reaction with neutron or γ -ray counters. As an alternative the total charge arriving at the target was measured with a current integrator, and used to normalize the angular distribution data. A check on the stability of the calcium targets, under bombardment, was made by comparing the angular distribution of neutrons from the $^{16}\text{O}(d, n)^{17}\text{F}$ reaction, arising from contamination of the target by oxygen, with that obtained with a more durable target of Nb_2O_5 . The spectra also showed no increase in the ratio of oxygen to calcium on the calcium targets throughout their use.

The technique of pulse shape discrimination does, of course, remove the γ -ray peak which is normally used to obtain the time zero on the spectra. On all the time spectra, however, contaminant neutron groups from the reaction $^{16}\text{O}(d, n)^{17}\text{F}$ were observed, and since the Q values for this reaction are accurately known (Ajzenberg-Selove and Lauritsen 1959), these groups were used to calibrate the time scale. This method of using nearby peaks to obtain the energy of the unidentified groups mitigates the need for a γ peak and an accurate calibration over a long range of the time analyser.

The analysing magnet of the 6 MV Van de Graaff accelerator was calibrated using the ground state thresholds for the reactions ${}^7\text{Li}(p, n){}^7\text{Be}$ and ${}^6\text{Li}({}^3\text{He}, n){}^8\text{B}$ (Ajzenberg-Selove and Lauritsen 1959).

§ 3. RESULTS

In the time spectra (Figs 1, 2 and 3) the neutron groups have been labelled according to the levels in the residual nucleus. Despite the precautions taken against contaminants, intense groups due to carbon and oxygen were observed.

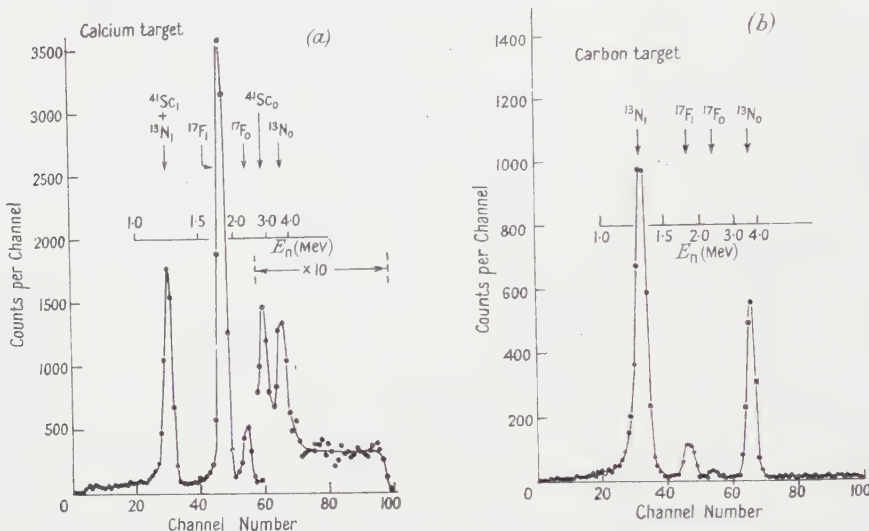


Fig. 1. Time spectrum obtained at (a) 10° and (b) 5° with $E_d = 3.981$ mev and a flight path of 231.2 cm.

This is due to their large (d, n) cross sections relative to calcium at the deuteron energies used. Fig. 1(a) shows a time spectrum measured at 10° with $E_d = 3.981$ mev using a calcium target. The group ${}^{41}\text{Sc}_0$ corresponding to the ground state of ${}^{41}\text{Sc}$, is clearly resolved from the contaminant groups ${}^{17}\text{F}_0$ and ${}^{13}\text{N}_0$. An excited state group ${}^{41}\text{Sc}_1$ is also shown. This peak contains a small contribution from the first excited state group of the reaction ${}^{12}\text{C}(\text{d}, \text{n}){}^{13}\text{N}$. The extent of this contribution, which only occurs at forward angles, was determined experimentally from the spectra of the reaction ${}^{12}\text{C}(\text{d}, \text{n}){}^{13}\text{N}$ obtained with a pure carbon target. Fig. 1(b) shows the spectrum obtained at 5° with a carbon target. From the angular distributions of the groups ${}^{13}\text{N}_0$ and ${}^{13}\text{N}_1$ (Fig. 4 (a), (b)) the contamination of the ${}^{41}\text{Sc}_1$ group is estimated to be $(15 \pm 5)\%$ at 10° . Similar contamination corrections have been applied to all the measurements on the ${}^{41}\text{Sc}$ groups.

Figure 2(a) shows a time spectrum obtained at 90° with a calcium target, also at 3.981 mev. A spectrum obtained with a carbon target is shown in Fig. 2(b) for comparison. Absence on 2(a) of any peak due to a ${}^{13}\text{N}_1$ group indicates that the contamination of ${}^{41}\text{Sc}_0$ by ${}^{13}\text{N}_0$ is negligible. Fig. 3(a) shows a time spectrum obtained at 60° with $E_d = 5.645$ mev using a calcium target. At this energy a further group ${}^{41}\text{Sc}_2$ is observed. Comparison with Fig. 3(b) shows that although the ${}^{13}\text{N}_0$ and ${}^{13}\text{N}_1$ peaks would appear at the same position as ${}^{41}\text{Sc}_0$ and ${}^{41}\text{Sc}_1$ respectively, the contamination of these latter groups is less than 5%.

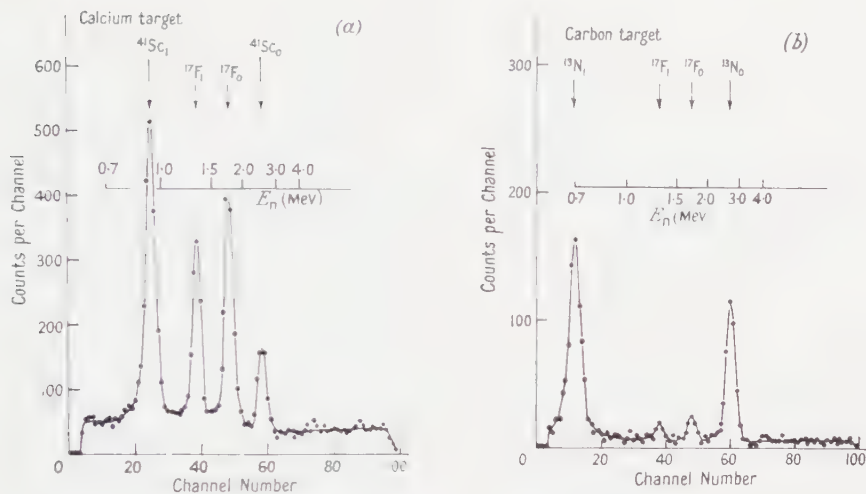


Fig. 2. Time spectra obtained at 90° with $E_d = 3.981$ MeV and a flight path of 231.2 cm.

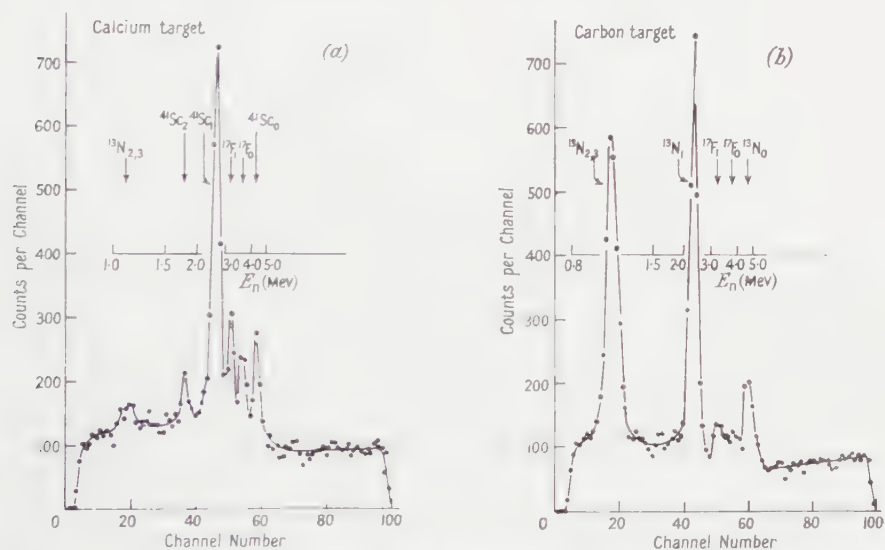


Fig. 3. Time spectra obtained at 60° with $E_d = 5.645$ MeV and a flight path of 231.2 cm.

Table 1 shows the Q values assigned to the reaction $^{40}\text{Ca}(\text{d}, \text{n})^{41}\text{Sc}$ which were obtained at bombarding energies of 3.226, 3.981 and 5.645 MeV. Since the energy spread (ΔE_n) equivalent to the width (6 nsec) of a peak in the time spectra increases proportionally to $E_n^{3/2}$ the highest accuracy was obtained for the more negative Q values and lowest bombarding energy.

In some of the runs at 5.645 MeV deuteron energy broad or unresolved levels were observed in ^{41}Sc at excitations of 2.8, 3.0 and 3.6 MeV. An upper limit in intensity of about 15% of the $^{41}\text{Sc}_0$ group, could be placed on any other group from the reaction $^{40}\text{Ca}(\text{d}, \text{n})^{41}\text{Sc}$, in particular those quoted by Plendl and Steigert.

Table 1. Q Values of Reaction $^{40}\text{Ca}(d, n)^{41}\text{Sc}$

(1)	(2)	(3)	(4)
3.226	-1.142 ± 0.040	1	0
3.981	-1.145 ± 0.015	12	1.709 ± 0.030
3.981	-2.854 ± 0.010	12	
5.645	-2.878 ± 0.040	8	
5.645	-3.621 ± 0.015	8	2.476 ± 0.030

(1) E_d (MeV), (2) mean Q values (MeV), (3) number of different angular readings averaged, (4) excitation in ^{41}Sc (MeV).

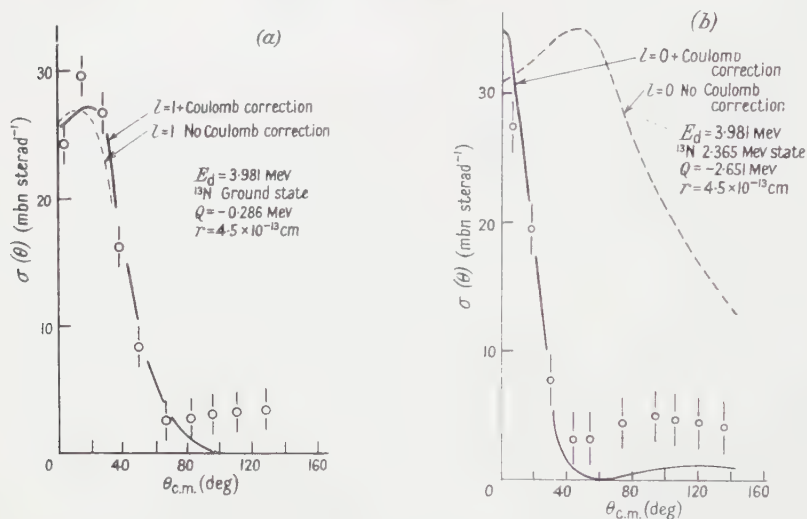


Fig. 4. ^{13}N angular distributions obtained at $E_d = 3.981$ MeV. (See §§ 3 and 4.2 for description of curves in Figs 4, 5, 6, 7 and 8.)

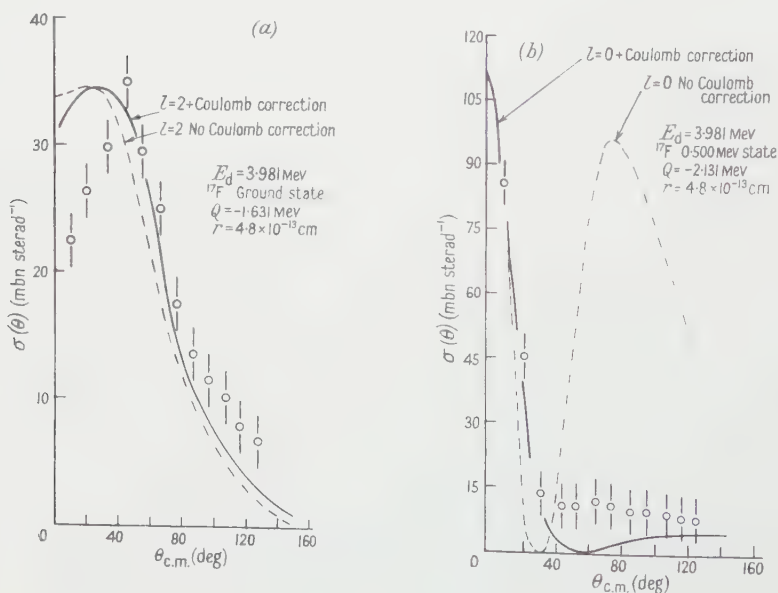


Fig. 5. ^{17}F angular distributions obtained at $E_d = 3.981$ MeV.

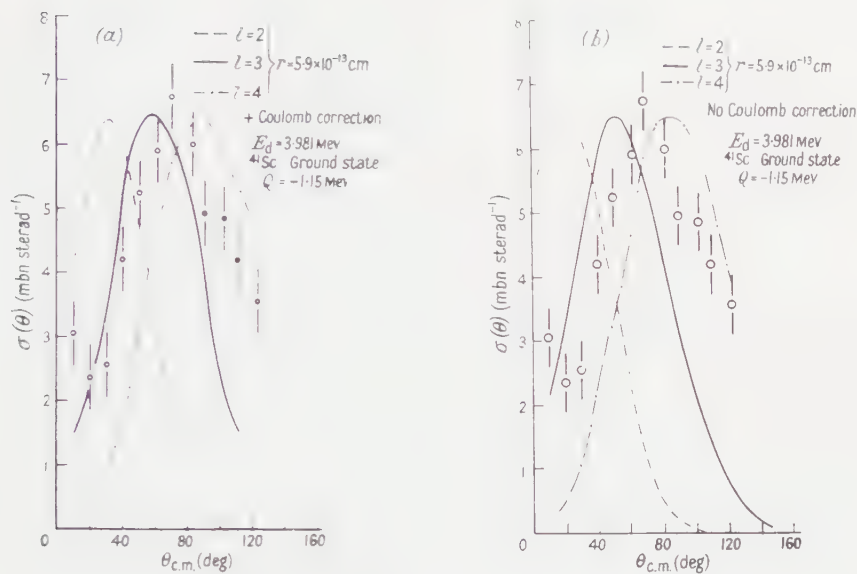


Fig. 6. Angular distribution for ground state group of ^{41}Sc obtained at $E_d = 3.981$ Mev.

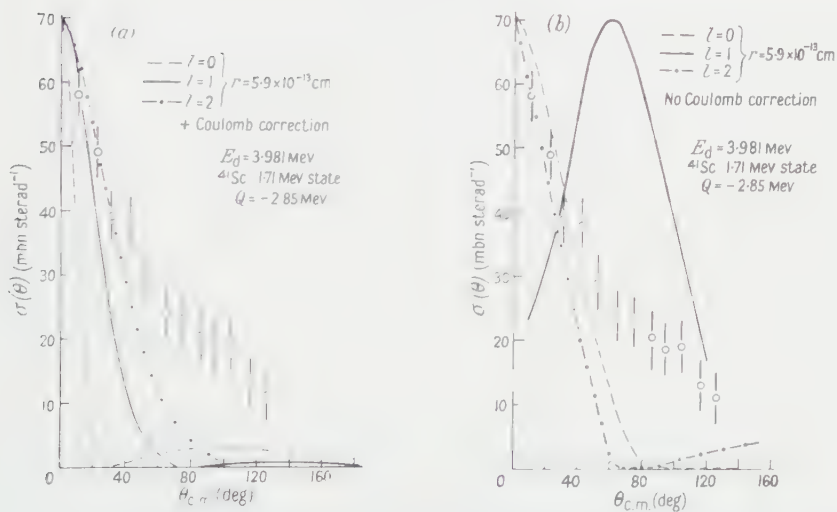


Fig. 7. Angular distribution for 1.71 Mev state group of ^{41}Sc obtained at $E_d = 3.981$ Mev.

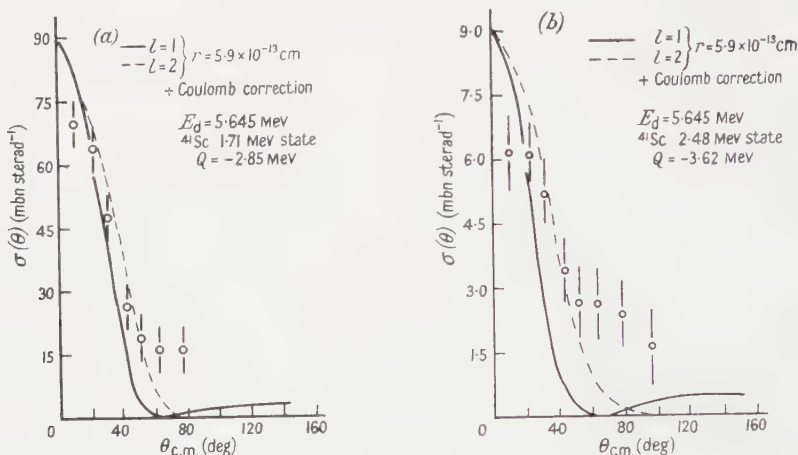


Fig. 8. Angular distribution for (a) 1.71 Mev and (b) 2.48 Mev state group of ^{41}Sc obtained at $E_d = 5.645$ Mev.

The results of the angular distribution measurements are shown in Figs 4 to 8. The error bars represent the sum of the statistical, detector efficiency and background subtraction uncertainties. The absolute values of the cross sections may be in error by as much as 40% due to possible non-uniformity of the target.

The curves in Figs 4 to 8 were obtained from Butler stripping theory using the numerical tables produced by Lubitz (1957). In some cases a Coulomb correction has been made (see discussion).

§ 4. DISCUSSION

4.1. Q Values and Energy Levels

The Q value of -1.145 ± 0.015 Mev has been assigned to the ground state of the reaction $^{40}\text{Ca}(d, n)^{41}\text{Sc}$. This value is in good agreement with that calculated from the measured ground state Q value of the reaction $^{40}\text{Ca}(^3\text{He}, d)^{41}\text{Sc}$ but disagrees with previous measurements of the $^{40}\text{Ca}(d, n)^{41}\text{Sc}$ ground state Q value (Plendl and Steigert 1959, Wegner and Hall 1960) and with the ^{41}Sc β^+ decay end point of 4.94 ± 0.07 Mev given by Elliot and King (1941). This new Q value leads to a value for the mass of ^{41}Sc of $40.982\,256 \pm 0.000\,040$ A.M.U. ($^{16}\text{O} = 16.00$, $^{40}\text{Ca} = 39.975\,272$, Endt and Braams 1957) and to an expected β^+ end point of 5.48 ± 0.04 Mev. Wegner and Hall quote a recent measurement of the end point made by Class, Farmer and Cramer. Their preliminary result, 5.65 ± 0.10 Mev, is in better accord with our prediction than that of Elliot and King.

Fig. 9 shows a plot of the atomic mass difference (in Mev) of mirror pairs ($T_z = \pm \frac{1}{2}$) as a function of mass number. The points up to mass 39 were computed from the mass data of Endt and Braams (1957). The full curve is the energy difference calculated from the difference in Coulomb energy, assuming the protons to be uniformly distributed throughout the nucleus, with $r = 1.40 A^{1/3}$ fermi, and the $(n - ^1\text{H})$ mass difference as 0.783 Mev. The two points for mass 41 were deduced from the $^{40}\text{Ca}(d, n)^{41}\text{Sc}$ ground state Q values obtained by Plendl and Steigert and in the present work. It can be seen that the value reported here is considerably more in accord with the trend of the mass data than that of Plendl and Steigert (1959).

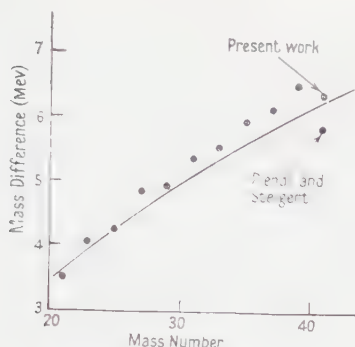


Fig. 9. Atomic mass differences for mirror nuclei ($T_z \pm \frac{1}{2}$) as a function of mass number A . The curve is $E = [0.617 (A-1)A^{-1/3} - 0.783]$ MeV. The errors on the points are approximately ± 0.040 MeV.

Excited states of ^{41}Sc have been found at 1.709 ± 0.030 MeV (in agreement with Macefield and Towle 1960), 2.476 ± 0.030 MeV and possibly at 2.8, 3.0 and 3.6 MeV. Class *et al.* (1959) have observed states at approximately 2.4, 2.7, 3.4 and 3.5 MeV excitation (using the revised mass of ^{41}Sc), while Wegner and Hall report a state at 3.35 MeV from a study of the reaction $^{40}\text{Ca}(^3\text{He}, d)^{41}\text{Sc}$. J. W. Butler (1960, private communication) has observed resonances in the yield of the reaction $^{40}\text{Ca}(p, \gamma)^{41}\text{Sc}$ at proton energies of 0.65 MeV and 1.87 MeV. These correspond to levels in ^{41}Sc at 1.72 MeV and 2.91 MeV, since

$$Q(p, \gamma) = Q(d, n) + 2.225 \text{ MeV.}$$

It now appears that there is considerable doubt as to the level positions in ^{41}Sc as reported by Plendl and Steigert, since their ground and excited state Q values are in disagreement with the present and other recent work. In Fig. 10 we make

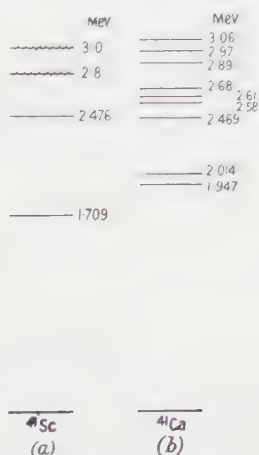


Fig. 10. Energy levels of ^{41}Sc and ^{41}Ca (a) present work, (b) after Bockelman and Buechner (1957).

a comparison of the low-lying excited states of ^{41}Sc obtained in the present work (a) with the low-lying levels of the mirror nucleus ^{41}Ca (Bockelman and Buechner 1957) (b).

It can be seen that the first level in ^{41}Sc is depressed below that in ^{41}Ca . Similar level depressions have been noted in light mirror pairs, e.g. ^{13}C , ^{13}N and ^{17}O , ^{17}F . Thomas (1952) has shown that the effect can be explained, while still retaining the charge independence of nuclear forces, by a difference in the single nucleon wave functions in the region external to the nucleus. It is particularly marked in nuclei having lightly bound particles such as occur near closed shells, and may be expected to be quite large for the ^{41}Sc , ^{41}Ca pair. In the (d, p) reaction on ^{40}Ca all the levels shown in Fig. 10(b) for ^{41}Ca except those at 2.469 and 1.947 MeV excitation were not excited to more than 30% of the ground state group. It thus seems probable that their analogue states escaped detection in the (d, n) reaction due to their low intensity. The level at 2.469 MeV had an intensity twice that of the ground state and the level at 1.947 MeV six times that of the ground state.

Levels in ^{41}Sc above an excitation of 1.08 MeV are unbound to proton emission. Assuming the reduced width of the 1.71 MeV level to be less than the Wigner limit, $(3\hbar^2/2\mu R^2)$ with $R=1.5A^{1/3}$ fermi, and using the penetrabilities given by Sharp *et al.* (1957) one finds the expected upper limit on the width of this level to be 1 eV. The corresponding lower limit on the lifetime for proton emission is about 10^{-16} sec. A limit of 10^{-20} sec for the 2.48 MeV level is similarly obtained. It would be of interest to investigate the decay of these states and to determine the relative proton and γ -ray widths. In the present work one can only obtain an upper limit of 40 keV (the spectrometer resolution) for these level widths.

4.2. Angular Distributions

We have attempted to compare the experimental data (Figs 4 to 8) with Butler stripping theory. The numerical tables of Lubitz (1957) have been used. In fitting the theoretical curves to the experimental points only two variable parameters have been used, i.e. the absolute magnitude and the l value. The interaction radius was put equal to the Gamow radius $r=(1.70+1.22A^{1/3})$ fermi.

In the derivation of a closed form for the angular distribution of a deuteron stripping reaction a number of approximations are made (Butler and Hittmair 1957). The most pertinent as far as this investigation is concerned is that the energy of the incident particle be much greater than the Coulomb barrier of the target. It is evident that the neglect of Coulomb effects is not justified in this reaction study since we have deuterons of energy less than the Coulomb barrier (~ 6 MeV), and the capture of a proton. A further difficulty is that in the Butler theory a singularity occurs when the Q value of the state is about -2.23 MeV, this being the binding energy of the deuteron. This leads to unrealistic angular distributions and cross sections. For positive or large negative Q values there is no singularity.

The main angular dependence of Butler's formula arises in the Wronskian $[J_l(qr), h_l(ikr)]$ where $J_l(qr)$ is a spherical Bessel function of order l , $h_l(ikr)$ is a Hankel function of the first kind, k is the wave number of the captured nucleon, q is the momentum transfer to the target nucleus divided by \hbar and r is the interaction radius (Butler and Hittmair 1957). The Coulomb correction, in the (d, n) case, can be made approximately by replacing $h_l(ikr)$ by a function $h_l(ik^*r)$ (Butler and Hittmair 1957, p. 69).

k^* is defined by

$$k^{*2} = k^2 + 2mZe^2/\hbar^2 r$$

where m is the reduced mass of the captured particle, Z is the atomic number of the target nucleus and r the interaction radius. For this to be a good approximation Butler requires $k^*r > 1$. The smallest value obtained for k^*r in this work was 1.2.

In Lubitz's tables no allowance has been made for Coulomb effects. This correction was calculated using the above expression for k^* .

The inclusion of the Coulomb correction moves the singularity to more negative Q values. The effect of the Coulomb correction is very small on the angular distributions of those groups whose Q values are not within 1 meV of the value -2.226 meV. This can be seen in Figs 4(a) and 5(a) for $^{13}\text{N}_0$ and $^{17}\text{F}_0$.

In the case of the transitions to the 2.365 meV state of ^{13}N and the 0.500 meV state of ^{17}F , which have Q values -2.65 meV and -2.13 meV respectively, and are known to have $l=0$ (Ajzenberg-Selove and Lauritsen 1959), the effect of the Coulomb correction is very large and when applied gives a much better fit to the experimental points (Figs 4(b), 5(b)). Further examples of this correction are given by Macfarlane and French (1959, p. 378).

The ground state group $^{41}\text{Sc}_0$ has a Q value of -1.145 meV and, as for $^{13}\text{N}_0$ and $^{17}\text{F}_0$, the inclusion of the Coulomb correction makes very little difference to the angular distributions (Figs 6(a), (b)). In the case of the 1.71 meV state ($Q = -2.85$ meV) the order of the curves for the different l values is altered by inclusion of the correction, to the normal sequence, i.e. 0, 1, 2 etc. (Figs 7(a) and 7(b)).

For the ground state group $^{41}\text{Sc}_0$ (Fig. 6(a)), to get the $l=3$ curve to peak at the same angle as the experimental points would require $r=4.4$ fermi, and to get the $l=4$ curve to peak at the same position would require $r=6.8$ fermi. The value of 4.4 is unrealistically low while the value of 6.8 fermi is rather larger than the Gamow radius which produced a good fit for the $^{12}\text{C}(d, n)^{13}\text{N}$, $^{16}\text{O}(d, n)^{17}\text{F}$ and $^{40}\text{Ca}(d, p)^{41}\text{Ca}$. The fit of the $l=3$ curve to the experimental points would be improved if the Coulomb correction were arbitrarily increased.

The reduced widths obtained by normalizing the theoretical curves, including the Coulomb correction, to the experimental points, using the Butler and Hittmair (1957) formula for the differential cross section, are shown in Table 2 together with the $^{40}\text{Ca}(d, p)^{41}\text{Ca}$ data (Macfarlane and French 1959). A comparison of the reduced widths of the ground states of ^{41}Sc and ^{41}Ca favours $l=3$ for the transition $^{40}\text{Ca}(d, n)^{41}\text{Sc}_0$.

From these considerations we think that $l=3$ is the most probable assignment for the ground state transition of the reaction $^{40}\text{Ca}(d, n)^{41}\text{Sc}$. The angular distributions of Wegner and Hall for the transition $^{40}\text{Ca}(^3\text{He}, d)^{41}\text{Sc}_0$ are also consistent with $l=3$. The spin of the ground state thus has two possible values $\frac{7}{2}$ or $\frac{5}{2}$ with negative parity. This is consistent with the shell model prediction of $\frac{7}{2}^-$. The angular momentum transfer of the two excited states cannot be determined unambiguously from the stripping curves alone since the half-widths of the curves for different l values are very similar.

The level at 1.71 meV is probably the analogue state of the 1.947 meV level in ^{41}Ca which is similarly prolific in the reaction $^{40}\text{Ca}(d, p)^{41}\text{Ca}$. Good agreement is obtained between the values of $(2J+1)\theta^2$ if $l=1$ is taken for the transition.

The 2.014 meV level in ^{41}Ca was assigned $I_n=2$ and was only weakly excited in the (d, p) reaction at 7 meV. Its analogue state in ^{41}Sc would probably not

Table 2. Comparison of Low-lying Levels of ^{41}Ca and ^{41}Sc

Reaction	Level (mev)	E_d (mev)	$(2J+1)\theta^2$	l	$J\pi$	θ^2
$^{40}\text{Ca}(\text{d}, \text{n})^{41}\text{Sc}$	0	3.981	0.08	2		
			0.09	3	$\frac{7}{2}, \frac{5}{2}-$	0.011 ($\frac{7}{2}-$)
			0.36	4		
	1.709	3.981	3.6	0		
			0.2	1	$\frac{3}{2}, \frac{1}{2}-$	0.05 ($\frac{3}{2}-$)
			0.4	2		
		5.645	2.35	0		
			0.13	1	$\frac{3}{2}, \frac{1}{2}-$	0.03 ($\frac{3}{2}-$)
			0.26	2		
	2.476	5.645	1.0	0		
			0.01	1	—	—
			0.01	2		
$^{40}\text{Ca}(\text{d}, \text{p})^{41}\text{Ca}$	0	7	0.114	3	$\frac{7}{2}-$	0.014
	1.947	7	0.08	1	$\frac{3}{2}-$	0.020
	2.014	7	0.005	2	—	—
	2.469	7	0.27	1	—	—

be observed due to its low intensity which would, perhaps, be accentuated with the lower deuteron energies used in this work.

The 2.476 meV level in ^{41}Sc is only weakly excited in comparison with the 2.469 meV level in ^{41}Ca . An l_p value could not be assigned on the fits of the angular distributions or by comparison of reduced widths.

The l values and reduced widths obtained from the present data on the reactions $^{12}\text{C}(\text{d}, \text{n})^{13}\text{N}$ and $^{16}\text{O}(\text{d}, \text{n})^{17}\text{F}$ are given in Table 3 and are in agreement

Table 3

Reaction	Level (mev)	E_d (mev)	$(2J+1)\theta^2$	l	$J\pi$	θ^2
$^{12}\text{C}(\text{d}, \text{n})^{13}\text{N}$	0	3.981	0.037	1	$\frac{1}{2}-$	0.018
		5.645	0.077	1	$\frac{1}{2}-$	0.088
	2.37	3.981	0.08	0	$\frac{1}{2}+$	0.04
		5.645	0.25	0	$\frac{1}{2}+$	0.12
$^{12}\text{C}(\text{d}, \text{p})^{13}\text{C}$	0	14.8	0.061	1	$\frac{1}{2}-$	0.031
	3.09	14.8	0.30	0	$\frac{1}{2}+$	0.15
$^{16}\text{O}(\text{d}, \text{n})^{17}\text{F}$	0	3.981	0.17	2	$\frac{1}{2}+$	0.03
	0.500	3.981	0.17	0	$\frac{1}{2}+$	0.08
$^{16}\text{O}(\text{d}, \text{p})^{17}\text{O}$	0	9	0.35	2	$\frac{5}{2}+$	0.058
	0.871	9	0.22	0	$\frac{1}{2}+$	0.11

with previous work (Macfarlane and French 1959). Similar data for the reactions $^{12}\text{C}(\text{d}, \text{p})^{13}\text{C}$ and $^{16}\text{O}(\text{d}, \text{p})^{17}\text{O}$ (Macfarlane and French 1959) are also shown in Table 3 for comparison.

ACKNOWLEDGMENTS

We are indebted to Dr. S. Hinds and Dr. R. Middleton for communicating their results prior to publication, and to Mr. R. Batchelor for his helpful comments.

REFERENCES

- AJZENBERG-SELOVE, F., and LAURITSEN, T., 1959, *Nucl. Phys.*, **11**, 1.
- BATCHELOR, R., and TOWLE, J. H., 1959, *Proc. Phys. Soc.*, **73**, 193 and *A.W.R.E. Report* NR/P-12/58 (unclassified).
- BATCHELOR, R., GILBOY, W. B., PURNELL, A., and TOWLE, J. H., 1960, *Nucl. Instrum.*, **8**, 146.
- BOCKELMAN, C. K., and BUECHNER, W. W., 1957, *Phys. Rev.*, **107**, 1366.
- BRAAMS, C. M., 1956, *Phys. Rev.*, **103**, 1310.
- BUTLER, S. T., and HITTMAYER, O. H., 1957, *Nuclear Stripping Reaction* (London: Pitman).
- CLASS, C. M., DAVIS, R. H., and JOHNSON, J. H., 1959, *Phys. Rev. Letters*, **3**, 1, 41.
- ELLIOT, D. R., and KING, L. D., 1941, *Phys. Rev.*, **60**, 489.
- ENDT, P. M., and BRAAMS, C. M., 1957, *Rev. Mod. Phys.*, **29**, 683.
- LUBITZ, C. R., 1957, *Numerical Table of Butler-Born Approximation Stripping Cross Sections* (Ann Arbor: University of Michigan).
- MACEFIELD, B. E. F., and TOWLE, J. H., 1960, *Proc. Phys. Soc.*, **76**, 56.
- MACFARLANE, M. H., and FRENCH, J. B., 1959, *New York University Report*, N.Y.O.—2846.
- PLENDL, H. S., and STEIGERT, R. E., 1959, *Phys. Rev.*, **116**, 1534, and *Bull. Amer. Phys. Soc.*, [II], **4**, 18.
- SHARP, W. T., GOVE, H. E., and PAUL, E. B., 1955, *Graphs of Coulomb Functions*, A.E.C.L. Canada, T.P.I.—70.
- THOMAS, R. G., 1952, *Phys. Rev.*, **88**, 1109.
- WEGNER, H. E., and HALL, W. S., 1960, *Phys. Rev.*, **119**, 1654.

The Nuclear Zeeman Effect, and Quadrupole Splitting in ^{119}Sn

By A. J. F. BOYLE, D. ST. P. BUNBURY AND C. EDWARDS

The Physical Laboratories, University of Manchester

Communicated by B. H. Flowers; MS. received 14th November 1960

Abstract. The recoilless absorption of 24 keV γ -rays from $^{119}\text{Sn}^{\text{m}}$ has been studied with the aid of a velocity spectrometer. Observations with the absorbing nuclei in different environments have enabled a value of 0.83 ± 0.03 n.m. to be given for the magnetic moment of the first excited state in ^{119}Sn , and an upper limit of 3×10^{-8} eV to be put on the interaction energy between the quadrupole moment of this state and the gradient of the electric field in metallic tin.

§ 1. INTRODUCTION

SOON after the discovery of recoilless γ emission and absorption (Mössbauer 1958) it was realized by many workers that a new tool had been found for the direct examination of nuclear fine structure. With quite simple equipment, the interaction of the nuclear moments with magnetic fields and electric field gradients can be studied. Much work has been done on the 14 keV transition in ^{57}Fe , and more recently on the 24 keV transition in ^{119}Sn (Delyagin *et al.* 1960, Picou *et al.* 1960, private communication, Hanna *et al.* 1960). The purpose of the work described here was to determine the magnetic moment of the first excited state of ^{119}Sn .

The general method is to measure the transmission of 24 keV γ -rays through an absorber containing ^{119}Sn . These γ -rays are Doppler shifted by virtue of the relative motion between the source and the absorber, and therefore a plot of the intensity of the transmitted γ -rays against the velocity of the source yields direct information on the energy levels in the emitting and absorbing nuclei.

Metallic tin has a crystal structure with tetragonal symmetry. The gradient of the electric field should therefore interact with the quadrupole moment of the first excited state in ^{119}Sn , splitting it into a close doublet. The results discussed in § 3 indicate that the separation of this doublet is small compared with the width of the absorption line obtained with no quadrupole interaction.

Various observations with the absorber in magnetic fields are described in § 4. To obtain a Zeeman pattern with all six components resolved (see Fig. 3) it was necessary to take advantage of the large magnetic fields existing in ferromagnetic crystals. The magnetic nature of the mechanism causing the splitting was checked by polarization measurements (see § 4).

§ 2. EXPERIMENTAL METHOD

The experimental arrangement was very similar to that used previously (Boyle *et al.* 1961). Approximately $100\mu\text{C}$ of $^{119}\text{Sn}^{\text{m}}$ had been prepared by irradiating separated ^{118}Sn in a flux of about 10^{14} neutrons per $\text{cm}^2 \text{ sec}^{-1}$ for three weeks.

The source, in the form of a thin metallic disk, was placed in a chamber surrounded by liquid air, and was attached to a moving coil vibrator by means of a drinking straw. This chamber was connected to the region containing the vibrator mechanism by a long German silver tube of diameter slightly greater than that of the drinking straw. The thermal isolation between the two regions was sufficient to allow the source temperature to be maintained at 100°K whilst the vibrator could be operated at room temperatures.

The moving plates of a pair of cylindrical trimming condensers were attached to the vibrator, and these condensers formed part of a radio-frequency bridge. The rectified output of this bridge, proportional to the displacement of the source, was continuously compared with a controlling signal, and the difference was used, after amplification, to drive the vibrator. For the measurements described here, the controlling signal was a sine wave of frequency between 1 and 12 c/s. The calibration of the amplitude of vibration, which was stabilized and continuously variable, was performed with a micrometer-eyepiece microscope.

The absorber was mounted in the vacuum space below the liquid air vessel, and was thermally connected to it. A heating coil attached to the absorber enabled its temperature to be maintained anywhere between that of liquid air and room temperature, although, for simplicity, all room temperature measurements were carried out with the absorber mounted externally to the cryostat. Palladium foils were used to absorb the unwanted 25 keV x-rays of Sn that are also produced in the decay of $^{119}\text{Sn}^m$.

The detector was a scintillation counter with a resolution of 25% for the 24 keV γ -rays. Pulses from the counter were fed into a single-channel analyser, the output pulses of which were modulated in amplitude by a saw-tooth waveform whose peaks were made to coincide with the zeros of the controlling sine wave. They were then fed to a 90-channel pulse height analyser which therefore displayed the absorption spectrum directly (with a non-linear velocity scale).

§ 3. ABSORPTION SPECTRA IN ZERO MAGNETIC FIELD

Figures 1 and 2(a) show the velocity spectrum obtained with a white tin absorber. The tin was in the form of a metal foil of thickness 50 mg cm^{-2} and was maintained at room temperature. The small displacement of the absorption dip towards positive velocity is due to the temperature difference between the source and the absorber (Boyle *et al.* 1960). Velocity is reckoned positive when the source is moving towards the absorber.

Figure 1 is in direct contrast to the results of Delyagin *et al.* (1960). These authors obtain a velocity spectrum that exhibits subsidiary peaks at $\pm 1.46\text{ mm sec}^{-1}$ which they attribute to the splitting of the excited level in both the source and the absorber by the interaction of the quadrupole moment with the electric field gradient. It would appear from the present results that a splitting of this magnitude does not exist, although a weak interaction may be contributing towards the width of the absorption dip.

The velocity half-width of the spectrum in Fig. 2(a) is 0.62 mm sec^{-1} , whereas the half-width expected from the measured lifetime (Olsen, Mann and Lindner 1957) is 0.31 mm sec^{-1} . Nearly the whole of this increase in width is accounted for by the resonant self-absorption of the recoilless γ -rays in the source which contained 5% of ^{119}Sn . An accurate calculation of the effect could

not be made because of non-uniformity in the thickness of the source; however, using an average value of 25 mg cm^{-2} and the results of a previous investigation (Boyle *et al.* 1961) it was found that the emitted line-width is almost doubled when the source is at 100°K . This would result in a 50% increase in the width of the absorption dip. A further small increase in width, about 10%, is expected because the absorber is not thin; in this case approximately 40% of the recoilless γ -rays are absorbed. The detailed calculation also showed that despite the increased width, the shape of the absorption line should remain very nearly Lorentzian. This is verified by the curves drawn in Figs 1 and 2.

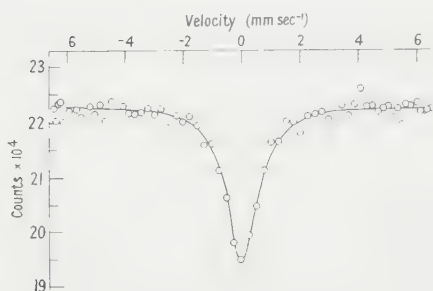


Fig. 1. The absorption spectrum in white tin measured at room temperature with an absorber 50 mg cm^{-2} thick.

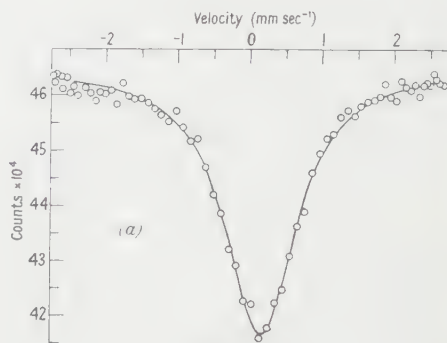


Fig. 2 (a).

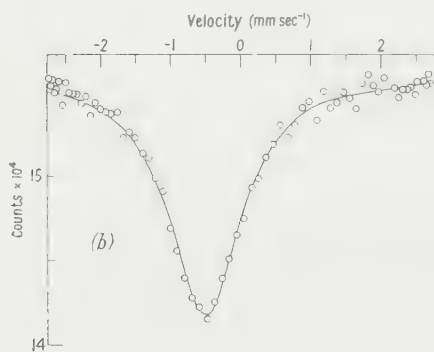


Fig. 2 (b).

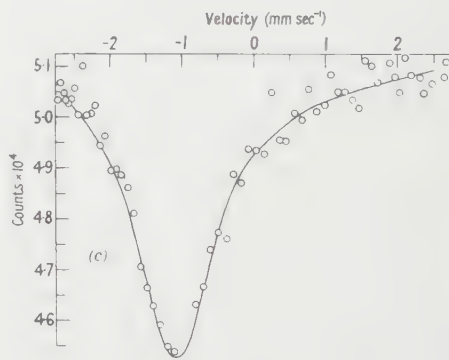


Fig. 2 (c).

Fig. 2. Absorption spectra taken at a temperature of 280°K in (a) white tin, 50 mg cm^{-2} thick, (b) grey tin, 20 mg cm^{-2} thick, and (c) niobium tin (Nb_3Sn), 60 mg cm^{-2} thick. The full curves represent Lorentzian functions fitted to the experimental points.

In order to obtain a better estimate of the magnitude of the quadrupole interaction, the white tin absorber was replaced by grey tin, which has a cubic structure and hence no field gradient. The absorption spectrum is shown in Fig. 2 (b). Apart from a displacement which is mainly due to the effects of chemical binding (Kistner and Sunyar 1960), Figs 2 (a) and (b) are very similar. The Debye Θ of grey tin is greater than that of white tin and since the absorber could not be kept above 15°C , a very thin layer (20 mg cm^{-2}) was necessary to give a total absorption that was comparable with that obtained with 50 mg cm^{-2} .

of white tin. The absorber was prepared by pressing grey tin powder between 0.001 in. palladium foils and as a result of the large grain size the final layer was rather non-uniform over the 3 cm^2 area used in this experiment. (Uniform layers were obtained with the much smaller area absorbers used in the experiments on the Zeeman effect.) This non-uniformity would account for the slightly greater width of the spectrum of Fig. 2(b). Since a quadrupole interaction would result in a greater width with the white tin absorber for the same equivalent thickness, it would seem that the splitting produced by such an interaction is certainly less than 0.5 mm sec^{-1} , corresponding to a 5% difference in the widths of the absorption dips for white and grey tin.

Confirmation of the very small quadrupole splitting in white tin is provided by Fig. 2(c) obtained using an absorber of Nb_3Sn , which has a β -wolfram structure in which the tin nucleus has a very nearly cubic environment. Again this result is in direct contrast to the results of Delyagin *et al.* who find a doublet symmetric about zero velocity with a spacing of 1.46 mm sec^{-1} . The Nb_3Sn was prepared by dissolving powdered niobium metal in molten tin at about 1500°C in an atmosphere of argon. The compound was then crushed into a fine powder and pressed into a shallow depression in a graphite disk.

We can conclude from the foregoing that the quadrupole splitting in white tin is small compared with the observed line width and will not affect the interpretation of the Zeeman spectra obtained in the next section except as a small correction. Quadrupole splitting of about 1 mm sec^{-1} has been observed with an absorber of SnO .

§ 4. THE NUCLEAR ZEEMAN EFFECT IN ^{119}Sn

The ground state of ^{119}Sn has a spin of $\frac{1}{2}^+$ and a magnetic moment $\mu_g = -1.04\text{ n.m.}$ (Kopferman 1956). The first excited state has a spin of $\frac{3}{2}^+$ and if it were a pure d $\frac{3}{2}$ state it would have a magnetic moment μ_e of about $+1.1\text{ n.m.}$ Fig. 3 indicates the level positions in the presence of a magnetic field and the accompanying transitions for M1 radiation.

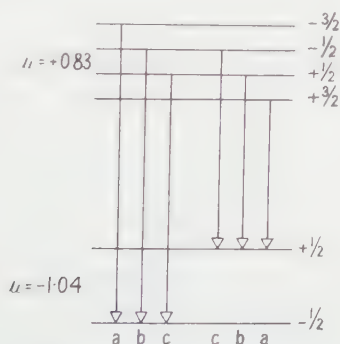


Fig. 3. Energy level diagram of ^{119}Sn in a magnetic field, showing the components of the M1 transition.

Figure 4(b) shows the velocity spectrum obtained with a grey tin absorber placed in a transverse magnetic field of 16 kOe . In this case the intensities of the components labelled a, b and c in Fig. 3 should be in the ratio 3:4:1. The curve

drawn in Fig. 4 was calculated on this basis using a value of $\mu_e = 0.8$ n.m. The shape of the spectrum is not very dependent on the magnitude of μ_e and a value between $+0.7$ and $+0.9$ n.m. would be reasonably consistent with the experimental points.

The velocity spectrum obtained with a white tin absorber in the same magnetic field is shown in Fig. 4(a). Apart from a small asymmetry (and, of course, the displacement due to the chemical shift), Fig. 4(a) is practically identical with Fig. 4(b). The effect of a small quadrupole interaction can be calculated using the term values for a level of spin $\frac{3}{2}$ that have been tabulated by Parker (1956). (Each term value depends on the angle between the magnetic field and the electric field gradient, and since the absorber was polycrystalline, an appropriate average was taken over all angles.)



Fig. 4. Absorption spectra taken with the absorbers at 0°C in a field of 16 kOe. (a) Spectrum of a white tin absorber, 50 mg cm^{-2} thick. The curves were calculated assuming $\mu_e = 0.8$ n.m. and $\frac{1}{2}eQd^2V/dz^2 = 2.4 \times 10^{-8}$ ev, and 4.8×10^{-8} ev for the full and broken curves respectively. (b) Spectrum of a grey tin absorber, 20 mg cm^{-2} thick. The full curve was calculated with $\mu_e = 0.8$ n.m., and zero quadrupole splitting.

The results for a quadrupole splitting in zero magnetic field of 0.3 mm sec^{-1} and 0.6 mm sec^{-1} are shown in Fig. 4(a) by the solid and broken lines respectively. It is apparent that an upper limit of about 0.4 mm sec^{-1} can be put on the value of the quadrupole splitting which is consistent with the results of the previous section. Thus the upper limit to the value of $\frac{1}{2}eQd^2V/dz^2$ in white tin is 3×10^{-8} ev.

In order to obtain a more accurate estimate of μ_e it would be necessary to resolve the six components of the transition and for this purpose a very large field would be required. It is well known that the fields at the nuclei in ferromagnetic substances are indeed very large. The ferromagnetic alloy containing the largest percentage of tin and the highest saturation magnetization is Mn_2Sn . This alloy was prepared by melting together the manganese and tin, and after being finely powdered it was pressed into a depression in a graphite disk. It was found that the resolution obtained in the absorption spectra was greatly improved by annealing the sample for 24 hours at 450°C .

Figure 5(a) shows the absorption spectrum obtained with the Mn_2Sn at a temperature of 120°K . Spectra were also taken at various temperatures up to 300°K ; these showed the dependence of the magnetic field strength on the temperature. Above the Curie point of around 260°K , only a single narrow peak

was observable. The background at zero velocity in Fig. 5 and the slight indication of further structure is attributed to other compounds that are present in the sample (cf. Hanna *et al.* 1960). The poor resolution (each line is approximately three times the expected width) is probably caused by a slight inhomogeneity of the magnetic field strength due to the possible inequivalence of the Sn sites in the lattice. The asymmetrical nature of the spectrum may be accounted for by the presence of an electric field gradient in that the first effect of a small quadrupole perturbation will be to shift both the $m = \frac{3}{2}$ levels in the same direction relative to the $m = \frac{1}{2}$ levels, having the effect of compressing one side of the spectrum and expanding the other. The relative intensities of the three lines in each triplet agree fairly well with the 3:2:1 ratio expected for a random orientation of the magnetic field with respect to the direction of observation. The fact that the negative velocity side of the spectrum is not resolved makes an accurate estimate of μ_e difficult.

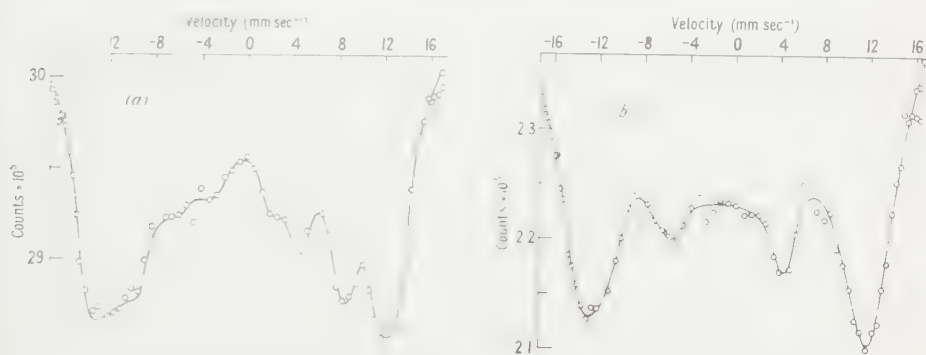


Fig. 5. The absorption spectra measured with an Mn_2Sn absorber, 50 mg cm^{-2} thick, and at a temperature of 100°K : (a) zero applied field, (b) axial field of 7 kOe. The absence of the central components of each triplet in this case confirms the magnetic nature of the splitting.

Figure 5 (b) shows the spectrum obtained when the absorber was placed in a longitudinal field of 7 kOe. Since the saturation value of the induction is 5.9 kG (Potter 1931) all the domains in the disk-shaped specimen should be aligned in the direction of the external field. The central component, the transition for which $\Delta m = 0$, is therefore missing from the absorption spectrum. Using $\mu_g = -1.04 \text{ n.m.}$, the value of μ obtained from the results in Fig. 5 (b) is $0.83 \pm 0.03 \text{ n.m.}$ and the value of the magnetic field at the tin nucleus in Mn_2Sn is $195 \pm 10 \text{ kOe}$. A positive moment of 0.83 is about the average value for nuclei in this region which have ground state spins of $\frac{3}{2}^+$.

ACKNOWLEDGMENTS

We wish to express our thanks to the Chemistry Division and the Isotopes Division respectively of the Atomic Energy Research Establishment, Harwell, for the provision and irradiation of the separated ^{118}Sn ; to the Director of the Tin Research Institute for the supply of grey tin; to the Metallurgy Department of Manchester University for making facilities available for the preparation of the alloys; and to Professor H. E. Hall, Mr. A. Black and Mr. K. Roe for the loan of a magnet and generous assistance during its use. One of us (C.E.) is indebted to the Department of Scientific and Industrial Research for financial support.

REFERENCES

- BOYLE, A. J. F., BUNBURY, D. ST. P., EDWARDS, C., and HALL, H. E., 1960, *Proc. Phys. Soc.*, **76**, 165.
—— 1961, *Proc. Phys. Soc.*, **77**, 129.
DELYAGIN, N. N., SHPINELL, V. S., BRYUKANOV, V. A., ZVENGHINSKY, B., 1960, *J. Exp. Theor. Phys.*, **39**, 220.
HANNA, S. S., MEYER-SCHUTZMEISTER, L., PRESTON, R. S., and VINCENT, D. H., 1960 *Phys. Rev.*, **120**, 2211.
KISTNER, O. C., and SUNYAR, A. W., 1960, *Phys. Rev. Letters*, **4**, 412.
KOPFERMANN, H., 1956, *Kernmomente* (Frankfurt am Main: Akademische).
MÖSSBAUER, R. J., 1958, *Z. Phys.*, **151**, 124.
OLSEN, J. L., MANN, L. G., and LINDNER, M., 1957, *Phys. Rev.*, **106**, 985.
PARKER, P. M., 1956, *J. Chem. Phys.*, **24**, 1096.
POTTER, H. H., 1931, *Phil. Mag.*, **12**, 255.

Emission of Sub-millimetre Electromagnetic Radiation from Hot Plasma in ZETA

By G. N. HARDING[†], M. F. KIMMITT[‡], J. H. LUDLOW[‡],
P. PORTEOUS[‡], A. C. PRIOR[‡] AND V. ROBERTS[‡]

[†] Atomic Energy Research Establishment, Harwell

[‡] Royal Radar Establishment, Malvern

MS. received 1st November 1960

Abstract. The first results are reported of experiments using a technique new to plasma research, namely spectroscopy in the far infra-red region (wavelength 0.1–1.6 mm). The shapes of the spectra obtained from ZETA are consistent with the observed radiation being entirely due to free-free transitions (bremsstrahlung) and become characteristic of black-body emission at the longer wavelengths. The measured absolute values of the surface brightness of the discharge are in agreement (subject to reasonable assumptions) with the predictions of quantum theory.

§ 1. INTRODUCTION

THE spectroscopic study of high-temperature laboratory plasmas has received considerable attention in the last few years, usually with one of two objects: (i) to find out the physical condition of the plasma (temperature, density, etc.), (ii) to throw light on the physical processes involved in the interaction of the radiation and the plasma, and to verify theoretical predictions, a process which in many cases had previously only been possible in the realm of astrophysics. As a result, theoretical studies have also received impetus. One reason why this subject is so interesting is the remarkable richness of the spectrum of radiation emitted by hot plasmas, ranging from hard x-rays to short radio waves. For practical reasons the two parts of the spectrum most studied have been (i) the visible and ultra-violet region, and (ii) the microwave region, in which measurements have been made at spot frequencies, or over very narrow bands, depending on the availability of apparatus.

The present work extends the spectroscopic study of plasmas into a new region, namely, that lying between microwaves and the infra-red.

The reasons why this region is of interest are: (i) it includes the plasma frequency for a range of densities useful in thermonuclear research, (ii) it should be free of line and band spectra arising from transitions between atomic and molecular energy levels, (iii) the optical behaviour of the plasma in this region should be related to its macroscopic properties, e.g. temperature, density, etc.; (iv) the interaction between the plasma and radiation should be of appreciable magnitude, and (v) spectroscopy in this region in the past has been restricted

by the problem of finding suitable sources, which the existence of high-temperature laboratory plasmas should now help to solve.

In the experiments described here, the source used was ZETA (Butt *et al.* 1958) because of its large size, long pulse and reliable cyclic operation over long periods. The measurements were of the emitted spectrum under different conditions of operation.

§ 2. EXPERIMENTAL METHOD

The experimental arrangement is outlined schematically in Fig. 1. The spectrometer used for these studies has already been briefly described (Roberts 1959). It follows the layout of Czerny and Turner (1930) and has three interchangeable metal echelette gratings G, of area $25\text{ cm} \times 20\text{ cm}$. The gratings are blazed at about 9° and have ruling spacings of 0.5, 1.25 and 3.4 mm. Overlapping spectra due to higher orders of diffraction are eliminated by an arrangement of scattering filters F and various absorption filters. No conventional slits are used, the entrance and exit apertures being circles 2 cm in diameter. With these apertures the pass band is about 10% of the wavelength to which the instrument is set, a compromise between adequate resolving power for the experiment and sufficient signal-to-noise ratio to complete measurements in a reasonable time.

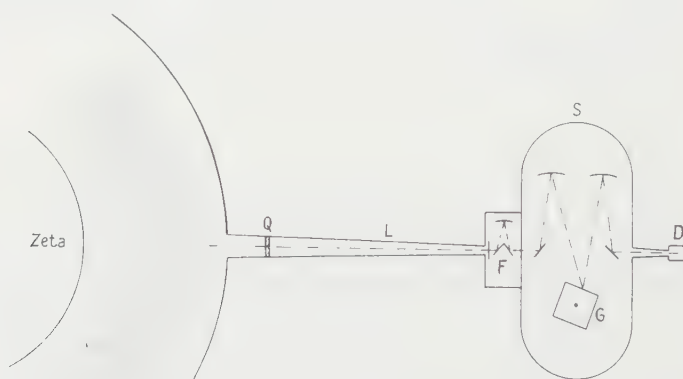


Fig. 1. General experimental arrangement (schematic).

The spectrometer was positioned at some distance from ZETA and radiation falling on a 4 in. diameter aperture in the east window block (Mitchell *et al.* 1959) was guided to the spectrometer by the light pipe L. This consisted of a hollow light-alloy tube about 3.6 m long tapering from an internal diameter of 10 cm at the ZETA end to 2 cm at the spectrometer entrance aperture. The inner surface of L had a finely machined finish, and the geometry was such that the spectrometer aperture $f/2.5$ was filled by radiation collected from the solid angle corresponding to $f/10$ at the ZETA end. The transmission of the light pipe was about 65%. Microphonic noise caused by mechanical shock on firing ZETA was reduced by including a flexible seal and sliding joint in the light pipe. In order to eliminate loss of energy and tedious corrections due to atmospheric water vapour

absorption, the spectrometer and light pipe were evacuated to a pressure below 0.1 torr. The spectrometer was isolated from the closely controlled pressure conditions in ZETA by the vacuum-tight crystal quartz window Q. Calculation shows that the radiation due to heating of this window was negligible.

The detector D was a carbon bolometer similar to that described by Boyle and Rodgers (1959), and operated in liquid helium at 1.7°K. For preliminary exploration a Golay pneumatic detector was used, but was found to be insufficiently sensitive. Radiation was condensed on to the bolometer element by a thin-walled cupro-nickel light pipe. The detector output was amplified and the amplifier output pulse was integrated for a time (10 msec) equal to about twice the bolometer time constant. This integration time was calculated to give optimum signal-to-noise ratio for measurements on ZETA, which operates in pulses of the order of a millisecond in length at intervals of some tens of seconds. The integrated signal was recorded on a pen recorder. The results are thus time-averaged over the duration of the pulse. In addition, the amplifier output signal could be viewed on a cathode-ray tube and photographed. These photographs were used to determine the time for which the radiation was emitted, but the time-resolution was not good enough to enable any further information to be obtained. It is hoped in future experiments to remove this limitation by using photoconductive detectors (Putley 1960).

§ 3. CALIBRATION

The grating orientation was calibrated in terms of wavelength by calculation and by observing known absorption bands in the atmospheric water vapour spectrum. The absolute sensitivity of the complete system was determined throughout the wavelength range by using a black-body source as standard. When using a continuously radiating source for calibration purposes, the radiation was chopped at a convenient frequency and the output rectified by a phase sensitive detector and displayed on a pen recorder.

§ 4. MEASUREMENTS AND RESULTS

Measurements were spaced at wavelength intervals roughly equal to the spectrometer pass band. The average of a suitable number of pulses, usually ten, was taken at each wavelength and the signal readings were interspersed with readings of background noise made with the radiation cut off by a shutter. After a number of trial runs, it was found that the most interesting results were obtained by varying the pressure in ZETA, keeping all other running conditions constant, and recording a complete spectrum at each value of pressure. The lowest pressure which gave a measurable signal was 1.5 mtorr and the upper limit of 7 mtorr was set by operation of ZETA. The discharge was in deuterium, the condenser bank (3 MJ nominal) was charged to 10 kv and the applied axial magnetic field 560 gauss. The gas current was of the order of 300 kA, and the pulse length 2 msec.

The spectra obtained are plotted in Figs 2 and 3. The statistical accuracy of the points is of the order of $\pm 10\%$ at short and medium wavelengths, falling to $\pm 50\%$ at the long-wave end. The absolute values are estimated to be correct within a factor of 2.

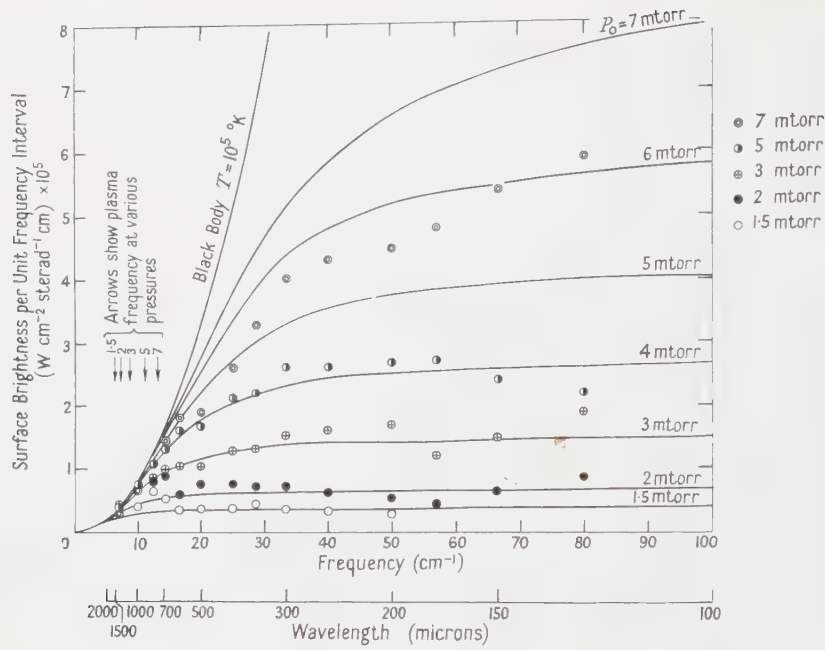


Fig. 2. Experimental (points) and theoretical (curves) values of surface brightness of ZETA discharge plotted against frequency. ZETA conditions; 3MJ (nominal) bank charged to 10 kv; axial magnetic field 560 gauss; deuterium gas, pressure as indicated. The theoretical curves are calculated in accordance with assumptions discussed in the text.

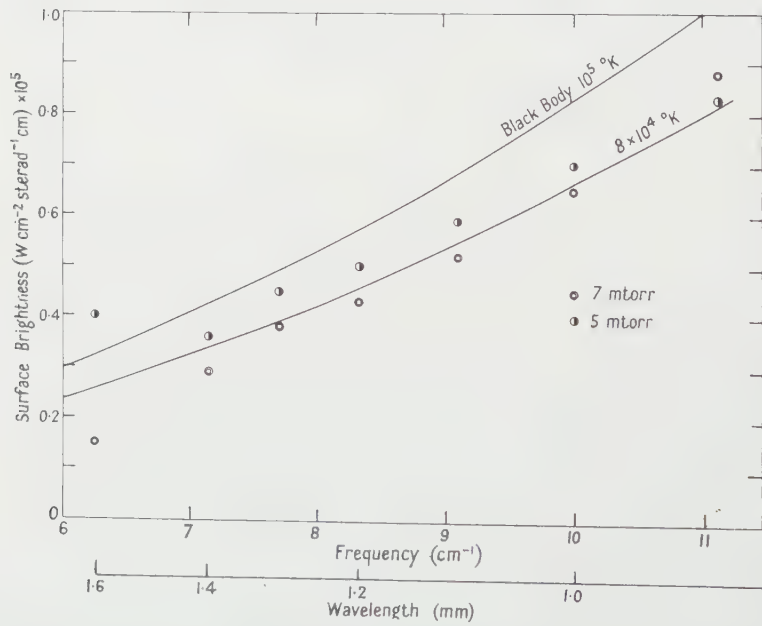


Fig. 3. Part of Fig. 2 on an expanded scale showing experimental points and black-body curves for two temperatures.

§ 5. COMPARISON WITH THEORY

The spectral distributions in the high frequency part of the measured region show an energy emission per unit frequency interval independent of frequency, in agreement with the theoretical prediction for free-free radiation (bremsstrahlung). At the three lowest pressures, the surface brightness is proportional to the square of the pressure, again as expected for free-free radiation. The lack of proportionality at higher pressures is discussed below.

At the low frequency end the emission falls away and approaches a value almost independent of pressure but proportional to the square of the frequency. Our interpretation is that long-wavelength radiation would be completely absorbed in traversing the plasma, which therefore behaves as a black-body. If this interpretation is correct, we can use this part of the curve to obtain a value for the mean electron temperature of the plasma. Fig. 3 shows the low frequency measurements on an expanded scale with calculated black-body curves for 10^5 °K and 8×10^4 °K. Because the overall accuracy is not high, in what follows we have taken the round figure of 10^5 °K as the mean electron temperature for all the measurements. This value is in general agreement with values obtained on ZETA under similar conditions by spectroscopic measurements in the visible and ultra-violet regions (McWhirter 1960, private communication) and from measurements of the electrical resistance of the plasma (Butt 1960, private communication).

Using this value of temperature, we are now able to compare the experimental emission with theoretical predictions. Free-free absorption coefficients have been calculated by Gaunt (1930) and emission by Cillié (1932). The effect of stimulated emission was discussed by Allen and Hindmarsh (1955). The Gaunt correction factor g for the case $h\nu \ll kT$ has been evaluated by Martyn (1948) and Smerd and Westfold (1949). The appropriate expressions have been conveniently assembled by C. W. Allen (1955).

The theoretical surface brightness, per unit solid angle and frequency interval, at the high frequency end of the curves (where absorption is negligible) is

$$Pd\nu = 1.63 \times 10^{-35} Z^2 g T^{-1/2} n_e n_i \frac{d}{1-R} d\nu \text{ W cm}^{-2}. \quad \dots\dots (1)$$

In this expression the Rayleigh Jeans approximation has been used ($h\nu \ll kT$) and in introducing the temperature we have taken for granted that the electrons have a Maxwellian velocity distribution. We make the simplifying assumption that the plasma is an infinite plane slab of thickness d , and let R be the reflectivity of the metal walls of the containing vessel. The other symbols have the usual meanings. Taking values for d in the neighbourhood of 50 cm (not measured in this experiment, but determined in magnetic probe measurements done under similar conditions by Lees and Rusbridge (1960)), and taking the pulse length as 2 msec, as estimated from photographs of the cathode-ray tube traces, we can obtain agreement between the measured and theoretical surface brightness (assuming the gas is fully ionized), by choosing a suitable value for the reflectivity R . The values found are between 0.3 and 0.5. The lack of proportionality between surface brightness and (pressure)² at the two higher pressures could be due to (a) incomplete ionization, (b) shorter time of emission, or (c) different degree of compression of the plasma. Further experiments will be necessary to settle this point.

Considering now the intermediate regions of the curves showing the transition from bremsstrahlung to black-body characteristics, i.e. where absorption is significant but not complete in traversing the plasma, the theoretical expression is in this case

$$Pdv = 1.63 \times 10^{-35} Z^2 g T^{-1/2} n_e n_i \left(\frac{1 - e^{-Kd}}{K} \right) \left(\frac{1}{1 - Re^{-Kd}} \right) dv \text{ W cm}^{-2}. \quad \dots (2)$$

This expression goes over into (1) when the absorption coefficient $K \rightarrow 0$.

The term in the first bracket is obtained by integrating the emission through the finite depth of the plasma. The second bracket represents the sum of a geometrical series due to multiple reflections, combined with absorption.

The absorption coefficient, including stimulated emission, is

$$K = 1.78 \times 10^{-2} Z^2 g \nu^{-2} T^{-3/2} n_e n_i \text{ cm}^{-1}.$$

The surface brightness has been calculated from (2) and is plotted against frequency for conditions relative to this experiment in Fig. 2. For simplicity we have taken $d = 50$ cm and $R = 0.5$. The measured points are seen to fit the calculated curves well for the three lowest pressures, and a reasonable fit for the two higher pressures can be obtained by adjusting one of the parameters mentioned at (a), (b) and (c) above.

§ 6. DISCUSSION

The agreement between the experimental and calculated curves over the whole of the wavelength range investigated supports the interpretation that the observed radiation is pure bremsstrahlung and provides experimental confirmation of the theoretical expressions, hitherto mainly confined to the x-ray region and to astrophysical problems. If separate determinations were made of the thickness of the plasma, the reflectivity of the vessel, and the pulse length, such measurements could be used to determine the mean density.

In the arguments above it has been assumed for simplicity that the refractive index is unity. This assumption is justified for most of the measurements since they are made at a frequency well above the plasma frequency. Furthermore, no increased emission due to change in refractive index would be expected to show up in the present experiments since it happens in each case that in the region where the refractive index departs appreciably from unity the emission is that of a black body. The spectrum in the plasma-frequency region should, however, be of considerable interest; to obtain measurements in this region which are not 'black body limited' we should require a higher plasma temperature and increased detector sensitivity. The fact that radiation is apparently emitted at frequencies below the plasma frequency is probably due to the plasma density falling off continuously towards the outside of the discharge and not being uniform as assumed in the above model.

ACKNOWLEDGMENTS

Much of the early work on the design of this experiment, and in particular of the spectrometer, was done by D. G. Avery and J. C. Gill of the Royal Radar Establishment, Malvern.

REFERENCES

- ALLEN, C. W., 1955, *Astrophysical Quantities* (London: University of London Press).
- ALLEN, J. E., and HINDMARSH, W. R., 1955, *Atomic Energy Research Establishment Report* GP/R 1761.
- BOYLE, W. S., and RODGERS, K. F., 1959, *J. Opt. Soc. Amer.*, **49**, 66.
- BUTT, E. P., CARRUTHERS, R., MITCHELL, J. T. D., PEASE, R. S., THONEMANN, D. C., BIRD, M. A., BLEARS, J., and HARTILL, E. R., 1958, *Proc. 2nd Int. Conf. on Peaceful Uses of Atomic Energy, Geneva* (Geneva: United Nations), **32**, 42.
- CILLIÉ, G., 1932, *Mon. Not. R. Astr. Soc.*, **92**, 820.
- CZERNY, H., and TURNER, A. F., 1930, *Z. Phys.*, **61**, 792.
- GAUNT, J. A., 1930, *Phil. Trans. Roy. Soc. A*, **229**, 163.
- LEES, D. J., and RUSBRIDGE, M. G., 1960, *Proc. 4th Int. Conf. on Ionization Phenomena in Gases, Uppsala* (Amsterdam: North Holland), **2**, 954.
- MARTYN, D. F., 1948, *Proc. Roy. Soc. A*, **193**, 44.
- MITCHELL, J. T. D., WHITTLE, H. R., JACKSON, E. M., and CLARKE, P. B., 1959, *Proc. Instn Elect. Engrs*, **106 A**, Suppl. 2, 74.
- PUTLEY, E. H., 1960, *Proc. Phys. Soc.*, **76**, 802.
- ROBERTS, V., 1959, *Proc. 5th Conf. of Int. Comm. for Optics, Stockholm* (Stockholm: International Commission for Optics).
- SMERD, S. F., and WESTFOLD, K. C., 1949, *Phil. Mag.*, **40**, 831.

On the Indication of Vibration Nodes by Fine Powders†

BY A. F. B. WOOD

Royal Holloway College, University of London‡

MS. received 29th June 1960, in revised form 23rd December 1960

Abstract. A simple theory is used to explain the motion of small particles on a horizontal surface vibrating with any combination of horizontal and vertical displacements. The motion depends on the relative phase of these displacements and causes the powder to collect at some of the nodes of the vertical and some of those of the horizontal displacement, but, except in particularly simple modes, not at all the nodes of either. The use of a powder to indicate vibration nodes can therefore be misleading unless backed up by another method, such as interferometry, which can discriminate between displacements parallel and normal to the vibrating surface.

§ 1. INTRODUCTION

THE use of a fine powder to indicate the nodes of a vibrating body has been widespread since the classic experiments of Chladni (1787) and is known to give reliable indications of the nodal patterns in the case of flexural vibrations. In spite of the antiquity of the method, however, the first quantitative analysis of the movements of the powder particles was that of Andrade and Smith (1931) who tested their conclusions by examining the motion of particles on flexurally vibrating bars and plates.

The use of powder on longitudinally vibrating bars and plates does not give such straightforward results and few papers have been published on the motion of the particles in this case. Savart (1820) examined the longitudinal vibrations of thin, narrow, glass strips held horizontally and noticed that many more nodes were indicated than the solitary, central node which he expected and also that the nodal patterns indicated on one surface were not the same as those indicated when the other surface was uppermost. It seemed that every alternate node was indicated, so that the complete system could be realized only by superposing the two patterns. He supposed that the strip vibrated in a second mode simultaneously with the longitudinal mode. Terquem (1858) repeated these observations and pointed out that, as a result of the longitudinal and transverse displacements, a point on the surface traces out a line which is oblique to the plane of the bar and the particles move in the direction of the part of this line which is above the equilibrium plane. Lissajous (1858) and later Lord Rayleigh (1894) also commented on the phenomenon but Petrzilka was unaware of these results when publishing papers on the longitudinal vibrations of Z-cut disks of tourmaline (1932) and quartz (1935). In commenting on Petrzilka's work, Lonn (1937) referred to the earlier workers and considered that the discrepancies between the

† This work forms part of a Ph.D. thesis (University of London, 1955).

‡ Now at Standard Telephones and Cables Limited, Crystal Division, West Road, Temple Fields, Harlow, Essex.

theoretical nodal patterns and those observed by Petrzilka using lycopodium powder were due to the presence of flexural vibrations coupled to the longitudinal mode of vibration.

Since lycopodium powder is still used for indicating the nodes of vibrating bodies, particularly quartz crystal vibrators, and since the results of this method are not fully trusted, the movements of a particle on a horizontal surface vibrating both vertically and horizontally are considered in the next section. The theoretical conclusions are supported by experiment.

§ 2. THE MOTION OF SMALL PARTICLES ON A VIBRATING HORIZONTAL SURFACE

A full analysis of the motion of a particle on a horizontal surface vibrating both vertically and horizontally would have to take into account the trajectory of the particle after leaving the surface and the bouncing of the particle on returning to it. This would not be possible for the irregularly shaped particles used in practice. In what follows, the simpler case of completely inelastic particles is discussed so that the trajectories and bouncing do not have to be considered at all. As a result the particles move continuously towards certain of the nodes and stay there, whereas in practice the particles take longer to get to the nodes, making some retrograde steps, and may bounce away from the nodes even when they get there, as will be seen later.

Suppose that a particle is on a horizontal surface at a point where the horizontal and vertical displacements are u and w (the positive direction being upwards). As free vibrations in a normal mode are being considered these displacements are in phase:

$$u = U \sin \omega t; \quad w = W \sin \omega t \quad \dots\dots (1)$$

and so are the corresponding accelerations:

$$\ddot{u} = -\omega^2 U \sin \omega t; \quad \ddot{w} = -\omega^2 W \sin \omega t. \quad \dots\dots (2)$$

The thrust of the particle on the surface is $mg - m\omega^2 W \sin \omega t$, so that for no slipping to occur

$$|U\omega^2 \sin \omega t| \leq \mu(g - W\omega^2 \sin \omega t) \quad \dots\dots (3)$$

where μ is the coefficient of friction between a particle and the surface. The particle leaves the surface when the normal reaction falls to zero, that is, when

$$W\omega^2 \sin \omega t = g. \quad \dots\dots (4)$$

This applies irrespective of the value of U and Andrade and Smith give the same relation. In a typical case, for the specimens used in the experiments described in §3 of this paper, U or W may be 1000 Å and ω may be 10^6 sec^{-1} giving an acceleration of 10^7 cm sec^{-2} or about $10\,600g$. This is so great compared with g that for all practical purposes the particle will remain completely at rest relative to the surface only where $U = 0$ and $W = 0$. Where this is not so the particle will leave the surface when w is positive and will slip when w is negative unless $\mu W \geq |U|$ (neglecting the small effect due to gravity). If the particle does not slip when w is negative then it moves horizontally with the surface as the latter moves upwards towards its equilibrium position, $u = 0$, $w = 0$. At the equilibrium position the particle is projected from the surface with horizontal and vertical velocities equal to ωU and ωW respectively. If $\mu W < U$, the horizontal velocity of projection will be less than ωU but the subsequent motion will be qualitatively the same. The particle then describes some sort of trajectory and reaches another part of

the surface where the process is repeated, ultimately reaching a point where conditions are favourable for it to remain.

It is interesting, in passing, to calculate the order of magnitude of the height and range of the trajectory of a particle projected in this manner. For the example quoted above, the peak velocity is only 10 cm sec^{-1} in spite of the large acceleration. This is quite high, however, compared with the terminal velocity of lycopodium particles falling freely in air, which has been found experimentally to be about 5 cm sec^{-1} at room temperature. From this, and assuming the particles to be spherical, with air resistance proportional to velocity, the height of the trajectory for an initial upward velocity of 10 cm sec^{-1} is about 0.22 mm and the time of flight 0.014 sec . If the initial horizontal velocity be equal to the vertical then the horizontal distance travelled in this time is 0.47 mm . These are the values corresponding to starting points near the antinodes but generally the trajectories will not be as large as this. As the method is a sensitive one, good results can be obtained with maximum displacement amplitudes smaller than the 1000 \AA quoted above.

It is generally stated that very light particles are influenced by the air currents above vibrating plates and these drive them to the antinodes, rather than the nodes. Andrade and Smith (1931) found that this effect could be eliminated, as expected, by performing the experiment in a vacuum. In the present work no disturbance by air currents has been encountered, the reason presumably being that the ratio of velocity to acceleration is so low that only feeble air currents are set up at the small amplitudes that nevertheless give good powder patterns.

The particles leave the surface immediately after passing through the equilibrium position in the upward direction and therefore move in the direction of the horizontal displacement corresponding to the upward vertical displacement, as stated by Terquem. The motion of particles at two points close together but on opposite sides of a node of horizontal or vertical displacement must be opposite since either the horizontal or vertical displacement, respectively, changes sign in crossing the node and so the phase relation between the horizontal and vertical components is reversed. If there is a component of the horizontal displacement acting towards a node then it will either collect or strongly disperse the powder depending on the relative phase of horizontal and vertical displacements. Even at a node which collects powder the particles are rarely at rest relative to the surface, for if the node is one of horizontal displacement then particles are continually projected vertically above the surface while if it is one of vertical displacement then slipping occurs during most of the vibration cycle. In practice the second type is usually more clearly defined since at the first type the particles, being elastic and irregularly shaped, can bounce away from the node on landing. In either case, however, the particles encounter strong restoring forces if they stray too far from the favoured node. An exception occurs if a node of the vertical displacement coincides with one of the horizontal displacement, when the direction of motion of the particles would be the same on both sides. If the displacement has a component towards the node the particles will move towards the node on one side and away from it on the other. Such a node would not be very clearly indicated, since, although it is an absolute node and undergoes no displacement whatever, it is a region of unstable equilibrium as far as the particles are concerned. A particle may remain on the node indefinitely but the slightest jostling by any incoming particles will push it just outside the node where it is swept away.

When the displacements are due to vibration in a simple mode a complete nodal pattern may be indicated. For example, in the case of a pure flexural vibration in a horizontal plate there is a small displacement parallel to the surface, due to the tilting of the surface, approximately proportional to the thickness. This has maximum amplitude at the nodes of the vertical (i.e. flexural) displacement and is zero at the antinodes. Near a node of the vertical displacement the horizontal displacement is towards the node when the vertical displacement is upwards and the node will collect powder. Likewise a horizontal lamina vibrating in a pure longitudinal mode, in which the vertical displacement in the direction of the thickness is due solely to the Poisson's ratio contraction, will have all the nodes of the longitudinal displacement indicated.

On the other hand, in the more general case of coupled modes, for which the displacements may, for example, be partially flexural and partially longitudinal, only part of the nodal system of each displacement (i.e. horizontal and vertical) will be indicated. Moreover the same parts will not necessarily be indicated if the specimen is turned over and the powder pattern formed on the other side. In a very thin horizontal lamina the horizontal displacement due to the flexure will be negligibly small compared with that due to the longitudinal vibration while the vertical displacement due to the Poisson's ratio contraction may be negligibly small compared with that due to the flexure. Hence the horizontal displacement is symmetrical about the median plane whereas the vertical displacement is antisymmetrical. This results in a reversal of the relative phases on the two sides of the lamina and so the directions of motion of the powder particles are opposite.

These conclusions have been tested by examining the powder patterns formed on Z-cut quartz disks vibrating in a known manner. When the displacements are known, it is a simple matter to find the direction of motion of the powder over the whole surface as follows: the nodes of the horizontal and vertical displacements are drawn on the upper surface of the body dividing it into regions bounded on all sides by nodes or the periphery of the surface. Arrows are drawn representing the directions of the horizontal displacements in these regions at any instant. A region is chosen in which the relative phases of the vertical and horizontal displacements are such that the powder moves in the direction of the arrows. The direction of motion in any other region is then found by reversing its arrows once for each node of vertical displacement crossed in reaching it from the starting region.

§ 3. EXPERIMENTAL TEST OF THE THEORY

Love (1927) has shown that thin, circular, isotropic disks may vibrate in two series of simple longitudinal modes in which the displacements are primarily parallel to the plane of the disk and depend only on the radial coordinate. In both cases the nodes are a series of circles, concentric with and including the centre, but in the first (type A) the displacements are radial while in the second (type B) they are normal to the radius. Type A modes have also a small lateral displacement normal to the plane of the disk, due to the Poisson's ratio contraction, the nodes of which fall in between those of the longitudinal displacement. Type B modes should give rise to no such displacements since they involve a state of pure shear. In the following discussion the disk is imagined to have its plane horizontal, as it would for obtaining powder patterns, so that the longitudinal

displacements become horizontal ones and the lateral displacements become vertical ones. Z-cut quartz disks behave substantially as though isotropic to the stresses involved in these modes of vibration. An experimental photoelastic study of such disks (Wood 1960) reveals that the longitudinal stresses are what would be expected from the theory of the isotropic disk and from this it may reasonably be inferred that the longitudinal displacements are also in agreement with the theoretical values. An experimental multiple-beam interference examination of the displacements normal to the surface (Tolansky and Wood 1958) reveals a flexural displacement in addition to the Poisson's ratio contraction. This flexure may be accounted for by the presence of the small elastic compliances, $s_{14} = -s_{24} = \frac{1}{2}s_{56}$ which are zero for an isotropic medium. It has three diametral nodes and a number of circular nodes whose radii depend on the frequency; the nearer this is to the frequency of a free flexural mode, the nearer the radii are to those of the circular nodes of the free vibration. Since type B modes have no lateral displacement of their own, the flexural displacement may be observed directly by interferometry. In the case of type A modes the lateral displacements normal to the plane of the disk are symmetrical about the median plane whereas the flexural displacements are antisymmetrical. The combination gives a vertical displacement whose nodal system has trigonal symmetry about the axis of the disk rather than the hexagonal symmetry of the flexural mode. The patterns on the two sides of the disk are complementary so that their superposition gives a pattern of hexagonal symmetry.

The polished Z-cut crystal used was 25.4 mm in diameter and 2 mm in thickness. The orders of the coupled flexural modes are fairly low for such a thick crystal as this and the essential features of the resulting patterns are more clearly defined than those of a thinner crystal. It had previously been found from the photoelastic study that when the thickness is as great as 3 mm the stress patterns depart from the theoretical ones but that they were not significantly distorted for a 2 mm crystal. The nodal patterns shown in the photographs were generally produced by brushing a camel hair brush charged with dry lycopodium powder across a piece of stretched lens tissue held 5–10 cm above the surface of the vibrating crystal. This usually gave good results, but sometimes local applications of powder were necessary to show up the whole pattern because some nodes collect powder from a wider area than others and so would amass a heap of powder before the others had become clearly defined. The vibrations were excited by six electrodes round the periphery of the disk connected alternately in antiphase to a source of suitable frequency and the modes were identified by polarized light observations. The interference patterns were produced by coating the lower surface of the crystal with a dielectric reflecting layer, resting it on a similarly coated reference flat and photographing the patterns observed in transmission, using parallel, monochromatic, mercury green light for illumination. Since the interference patterns were formed on the lower surface of the crystal and the powder patterns on the upper, and since it is necessary to compare the patterns produced by both methods on each surface, some of the photographs shown here (see Plates) have been reversed in the printing process so that all the patterns appear as though they were viewed from the same side of the crystal.

Figures 1 and 2 show the powder patterns on the two sides of the crystal for the type A, $m=1$ mode at a frequency of 369 kc/s while Fig. 3 shows the interference pattern corresponding to Fig. 1. The crystal was unfortunately shattered by

overstressing while attempting to photograph the interference pattern on the other side, but it was complementary to Fig. 3, that is, it was identical but turned through 60° . Fig. 4 shows a superposition of the theoretical nodes of the radial displacement on a diagram of the nodes of the vertical displacement shown by Fig. 3. The m th type A mode has m nodal circles of the radial displacement in addition to the centre, the fundamental, $m=0$, having the central nodal point only; the diameter of the node for $m=1$ is 0.715 of the disk diameter. Since the flexural displacement is zero at the centre, owing to the intersection of the diametral nodes there, the vertical displacement at the centre is due entirely to the Poisson's ratio contraction associated with the longitudinal stress. Thus the vertical displacement of the upper surface near the centre is upwards for a horizontal displacement towards the centre and the powder will collect there. The phase relation is the same on both sides and so if the crystal is turned over the centre will again collect powder. Starting from this fact the direction of motion of the powder elsewhere is then found by the method given at the end of §2 and is indicated in Fig. 4 by arrows. This diagram accounts for all of the nodes indicated by the powder in Fig. 1. It will be noticed that the indicated parts of the circular node of the horizontal displacement are not so well defined as the nodes of the vertical displacement because, as mentioned in §2, the particles are actually projected into the air at the former while they are merely slipping at the latter.

Figures 5 and 6 show the powder patterns on the two sides for the type B, $m=1$ mode at a frequency of 380 kc/s, and Fig. 7 the interference pattern corresponding to Fig. 5. The interference pattern on the other side is identical since it is due entirely to the coupled flexural vibration. Fig. 8 is a superposition of the theoretical nodes of the longitudinal displacement on the observed nodes of the vertical displacement. The m th type B mode has $m+1$ nodal circles in addition to the centre, the fundamental being $m=0$; the nodal diameters of the $m=1$ mode are 0.455 and 0.834 of the disk diameter. To determine the direction of motion of the powder at any point the relative phases of the longitudinal and coupled flexural displacements must be known and this necessitates an analysis of the coupling mechanism and a knowledge of the directions and sign of the X -axes of the crystal disk. Whatever phase relation is assumed, however, the resulting pattern must be that on one side of the crystal or the other and these are the same as each other except for a rotation of 60° about the axis of the disk. An arbitrary phase was therefore chosen and resulted in the arrows shown in Fig. 8. In the powder patterns themselves the circular nodes of the horizontal and vertical displacements are indicated mainly by the discontinuity of the radial nodes because the horizontal displacements are parallel to the circular nodes and there is no movement of powder towards them.

Finally, Figs 9 and 10 show the powder pattern and interference pattern respectively for the free flexural mode at 273 kc/s and Figs 11 and 12 show those for the free flexural mode at 420 kc/s. These patterns are identical on the two sides and every part of the nodal systems shown by the interference patterns is indicated by the lycopodium powder, as discussed in §2. It will be noticed that the radii of the circular nodes of the coupled flexure in Fig. 7 are slightly greater than those of the circular nodes in Fig. 12, this being accounted for by the lower frequency. Some of the circular nodes of the free flexural modes are distorted; this may be because the plate is not ideally thin.

§ 4. CONCLUSIONS

It has been shown that a simple theory can explain the motion of small particles on a horizontal surface vibrating with any combination of horizontal and vertical displacements. The experimental observations are in full agreement with this theory. Regarded as a practical method for finding nodes the use of a powder alone cannot be recommended, because of the incompleteness of the information given. However, if the nodal system of the vertical displacement is determined by interferometry then it should be possible to deduce the nodes of the horizontal displacement by comparing the interferometric nodal pattern with that indicated by lycopodium powder.

ACKNOWLEDGMENTS

The author is grateful to Professor S. Tolansky for his interest and encouragement throughout this work and to the Department of Scientific and Industrial Research for a maintenance grant.

REFERENCES

- ANDRADE, E. N. DA C., and SMITH, D. H., 1931, *Proc. Phys. Soc.*, **43**, 405.
CHLADNI, E. F. F., 1787, *Entdeckungen über die Theorie des Klanges* (Leipzig).
LISSAJOUS, J. A., 1858, *C.R. Acad. Sci., Paris*, **46**, 846.
LONN, E., 1937, *Ann. Phys., Lpz.*, **30**, 420.
LOVE, A. E. H., 1927, *The Mathematical Theory of Elasticity* (Cambridge: University Press).
PETRZILKA, V., 1932, *Ann. Phys., Lpz.*, **15**, 881.
— 1935, *Ann. Phys., Lpz.*, **23**, 156.
RAYLEIGH, LORD, 1894, *The Theory of Sound*, 2nd Ed. (London: Macmillan), § 222.
SAVART, F., 1820, *Ann. Chim. (Phys.)*, **14**, 113.
TERQUEM, A., 1858, *C.R. Acad. Sci., Paris*, **46**, 775.
TOLANSKY, S., and WOOD, A. F. B., 1958, *Physica*, **24**, 508.
WOOD, A. F. B., 1960, *J. Mech. Phys. Solids*, **8**, 26.

Energy Transfer in Organic Systems

II: Solute-Solute Transfer in Liquid Solutions

BY J. B. BIRKS AND K. N. KUCHELA†

The Physical Laboratories, The University, Manchester

MS. received 29th September 1960, in revised form 31st October 1960

Abstract. Solute-solute intermolecular energy transfer has been studied in the ternary solution system toluene-TP (*p*-terphenyl)-TPB (1, 1', 4, 4'-tetraphenylbutadiene) with a TP concentration of 2.17×10^{-2} M, and TPB concentrations from 1.5×10^{-6} M to 6×10^{-3} M, using excitation wavelengths from 285 m μ to 365 m μ .

The behaviour is described quantitatively by competition between radiative transfer, which predominates up to 10^{-4} M, and non-radiative dipole-dipole transfer, which becomes important at higher concentrations. The observed radiative transfer agrees with that predicted from the TPB absorption and TP emission spectra, and depends on the solution thickness. The observed dipole-dipole transfer corresponds to a critical transfer distance $R_0 = 42.2 \text{ \AA}$, compared with a theoretical value of $R_0 = 42.5 \text{ \AA}$, indicating that molecular diffusion and TP excitation migration have a negligible influence on the transfer process, which is single-step.

The bearing of the results on the choice and design of organic scintillator systems is briefly discussed.

§ 1. INTRODUCTION

IN the paper by Birks and Cameron (1958, to be referred to as I) studies of solvent-solute energy transfer in *p*-terphenyl-toluene solutions have been described. Such binary solutions are commonly used for liquid scintillation counting (see, for example, Bell and Hayes 1958) but they have certain limitations. The solute emission spectrum is in the near ultra-violet and does not therefore match optimally the blue-green spectral response of the standard photomultipliers used for detection. High concentrations (5 g l⁻¹) of solute are required to provide maximum scintillation efficiency, and hence, although the overlap of the absorption and emission spectra of *p*-terphenyl is small, self-absorption effects can become appreciable when large volume liquid scintillators are used. Self-absorption causes a decrease in the technical scintillation efficiency, and an increase in the technical scintillation decay time of the system (Birks 1954).

These limitations of binary solutions can be overcome by the introduction of a secondary solute, with an absorption spectrum which strongly overlaps the emission spectrum of the primary solute, and with an emission spectrum which matches closely the photomultiplier spectral response (Hayes 1953, Hayes *et al.* 1955, 1956). The function of such a 'wavelength-shifter' is to accept the

† Now at University of Mysore, India.

excitation energy of the primary solute and to emit it efficiently in the spectral region where the photomultiplier is most sensitive. Relatively low concentrations (up to 0.5 g l^{-1}) of secondary solute are adequate for efficient solute-solute energy transfer, so that self-absorption effects are considerably reduced in such ternary solutions.

Hayes (1953), Hayes *et al.* (1955, 1956), Ott *et al.* (1957) and others have studied the variation of scintillation efficiency with secondary solute concentration for many combinations of organic solvents and solutes, but they did not attempt to discriminate between the alternative processes of radiative and non-radiative energy transfer. Bowen and Brocklehurst (1953) and Bowen and Livingston (1954) have studied solute-solute energy transfer in liquid solutions, of rather different composition from those used as scintillators, and have shown that non-radiative transfer occurs, and is independent of the solvent viscosity, indicating that the process is not diffusion-controlled.

Weinreb (1957) has studied the ternary liquid scintillator system, toluene-PPO (2,5-diphenyloxazole)-DPH (diphenylhexa-1,3,5-triene), by adding varying concentrations of a quenching agent, which competes with the PPO-DPH non-radiative transfer for the PPO excitation energy. He concludes that at a DPH concentration of $5 \times 10^{-5} \text{ M}$ at least 80% of the PPO-DPH transfer is radiative, while at a DPH concentration of $5 \times 10^{-3} \text{ M}$ about 25% is radiative and 75% non-radiative.

In the present work a detailed investigation has been made of solute-solute transfer in the system toluene-TP (*p*-terphenyl)-TPB (1,1',4,4'-tetraphenyl-1,3-butadiene). This was chosen for study as a representative ternary scintillator solution system, because of the clear separation of the TP and TPB emission spectra and the availability of suitable filters for distinguishing the two solute emissions.

§ 2. EXPERIMENTAL

2.1. Apparatus and Calibration

The materials used were of 'scintillation grade' purity and supplied by Nuclear Enterprises (G.B.) Ltd., Edinburgh. All measurements were made at room temperature, and the solutions were not 'deoxygenated'. The presence of oxygen has been shown to have no effect on the energy transfer, though it quenches the solute emission somewhat (I).

A Chance glass filter OX 1 was used to isolate the TP emission, since the filter had negligible luminescence, and did not transmit the TPB emission. Two Chance glass filters OY 18 and OGr 3 were considered to isolate the TPB emission. The OY 18 had excellent transmission characteristics, but was unsuitable because of its luminescence. The OGr 3 had a lower transmittance, but negligible luminescence, and it was therefore adopted. The OGr 3 was found to transmit a small fraction of the TP emission, and an appropriate small correction was made for this where necessary (§ 2.3). The cells used for containing the solutions were of 'Spectrosil' (Thermal Syndicate Ltd., Wallsend) and had a negligible luminescence.

The experimental arrangement was similar to that described in I, as modified by Birks and Kuchela (1959). A Unicam SP 500 spectrophotometer with a hydrogen lamp source was employed as a monochromator, the standard absorption cell holder and photocell detectors being replaced by a light-tight box

containing an EMI 6097B photomultiplier. The photomultiplier could be mounted either along the axis of the monochromator exit beam or normal to it, and its position was adjustable to accommodate different cell geometries. The photomultiplier was operated at a potential of about 1.2 kv from a stabilized 2 kv supply, and the output current was measured with a Scalamp galvanometer. All readings were corrected for the dark current which was steady and usually small compared with the light signal being observed.

To calibrate the monochromator exit beam, its relative quantum intensity was measured as a function of wavelength λ from 220 to 400 m μ (only part of this wavelength region is relevant to this particular investigation), using a fluorescent solution whose quantum yield is constant over this region. Two solutions described by Weber and Teale (1958), namely, A, 1-dimethyl-aminonaphthalene 7-sodium sulphonate in water, and B, 1-dimethyl-aminonaphthalene 5-sulphonic acid in N sodium hydroxide, have been found to give reliable, consistent results. In a preliminary calibration test a 2×10^{-2} M concentration of solution A was prepared, and used to fill a cylindrical 'Spectrosil' cell to a depth of 1 cm. The cell was optically coupled to the photomultiplier, the aperture of the photomultiplier being limited to a diameter of 1 cm to eliminate the detection of light from the sides of the cell. Observations of the photomultiplier current as a function of λ were taken and repeated for different solution depths, different solution concentrations, different exit slit widths, and at different intervals after the solution preparation. It was found that these measurements of relative quantum intensity were consistent and reproducible. In the subsequent experiments, individual calibrations were made using a 2×10^{-2} M solution A, for each of the different specimen geometries employed.

2.2. Study of TP Emission

A series of 13 solutions was prepared, each containing 2.17×10^{-2} M (5 g l $^{-1}$) TP in toluene, and TPB concentrations of 0, and 1.5, 3 and 6 $\times 10^{-x}$ M, where $x=6, 5, 4$ and 3, respectively. In investigating the TP emission, excitation was at $\lambda=290-310$ m μ , in which region toluene is transparent and almost all the incident light is absorbed by TP in a thickness of about 40 μ . The intensity of the TP emission was measured as a function of TPB concentration c and of solution thickness t , for $t=4$ mm, 8 mm and 16 mm. The thickness was introduced as a parameter to distinguish between radiative and non-radiative transfer. The former increases in efficiency with t , while the latter is independent of t .

The experimental arrangement is shown in Fig. 1. The integrating cell had a 'Spectrosil' base and was filled completely with a 2×10^{-2} M solution A. A 'Spectrosil' disk was then slipped over the solution, care being taken to exclude any air bubbles. The function of the integrating cell was to eliminate the effect of changes in the technical emission spectrum of TP due to selective absorption by (i.e. radiative transfer to) TPB. The cell provided the photomultiplier with a constant spectral distribution, whose intensity was proportional to the quantum intensity of the TP emission incident on it.

Measurements were made initially on the binary 2.17×10^{-2} M TP-toluene solution for $\lambda=290-310$ m μ and $t=4$ mm, 8 mm and 16 mm. If I_4 , I_8 and I_{16} represent the intensities of TP emission for the three values of t respectively, then it was found that $I_4/I_8=1.04$ and $I_8/I_{16}=1.11$, at all excitation wavelengths. The increase in the TP emission intensity as t is decreased is due to the increased

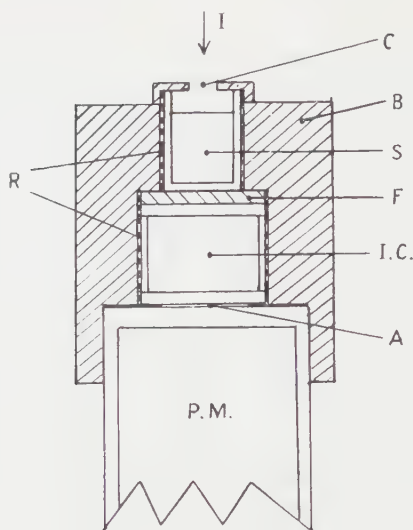


Fig. 1. Experimental arrangement for study of TP emission. I, incident light from monochromator; C, 8 mm diameter aperture; B, ebonite holder; S, cylindrical Spectrosil cell containing specimen solution; F, OX 1 filter and glycerin films; I.C., cylindrical Spectrosil cell containing 2×10^{-2} M integrating solution A; A, 2 cm diameter aperture and glycerin film; P.M., photomultiplier; R, aluminium foil reflector.

solid angle subtended at the photomultiplier, since self-absorption in TP solutions is negligible at these thicknesses. This geometrical effect was corrected for in the measurements on the ternary solutions by normalizing them to correspond to a common $t = 8$ mm, i.e. by using a common scale for $I = I_4/1.04$, I_8 and $1.11I_{16}$ respectively.

Figure 2 shows the normalized results for the variation of intensity of the TP emission with TPB concentration c , for $t = 4$ mm, 8 mm and 16 mm, and $\lambda = 290$ m μ . The results at other excitation wavelengths were similar. It is clear

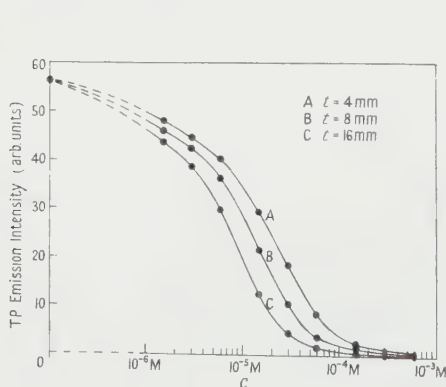


Fig. 2. Intensity of TP emission plotted against TPB concentration c for specimens of thickness t .

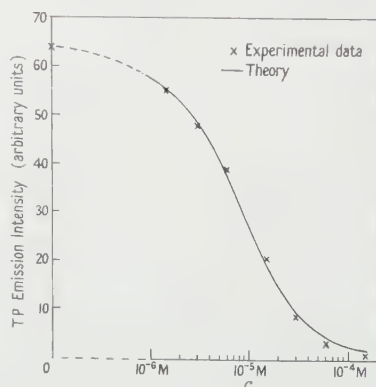


Fig. 3. Intensity of TP emission against TPB concentration c , for specimens of thickness $t = 13$ mm. The theoretical curve, for radiative transfer, is obtained from (2).

the TP emission intensity at a given c increases as t is decreased, even after correcting for the change in solid angle, showing that radiative transfer occurs in this concentration range.

A similar set of measurements, taken for $\lambda = 285\text{--}320\text{ m}\mu$ and $t = 13\text{ mm}$, and normalized to constant incident quantum intensity, are plotted in Fig. 3. Within the experimental error, the TP emission quantum intensity was found to be independent of λ .

2.3. Study of TPB Emission

The experimental arrangement used for studying the TPB emission was similar to that shown in Fig. 1, except that the integrating cell was omitted, and an OGr 3 filter was used at F. The cylindrical 'Spectrosil' cell was filled with the specimen solution to a depth of 13 mm. Measurements were made of the relative quantum intensity of the TPB emission from $\lambda = 285\text{ m}\mu$ to $365\text{ m}\mu$ for each of the 12 solutions containing TPB.

Similar measurements were also made for the binary TP-toluene solution. In conjunction with the observations of the relative quantum intensity of TP emission against c (Fig. 3), these latter measurements enabled the appropriate small corrections to be applied for the leakage of any TP emission through the OGr 3 filter.

The TPB fluorescence excitation spectra, showing the variation of relative quantum intensity with wavelength for the twelve ternary solutions, are plotted in Fig. 4. From $\lambda = 285$ to $305\text{ m}\mu$, practically all the incident radiation is

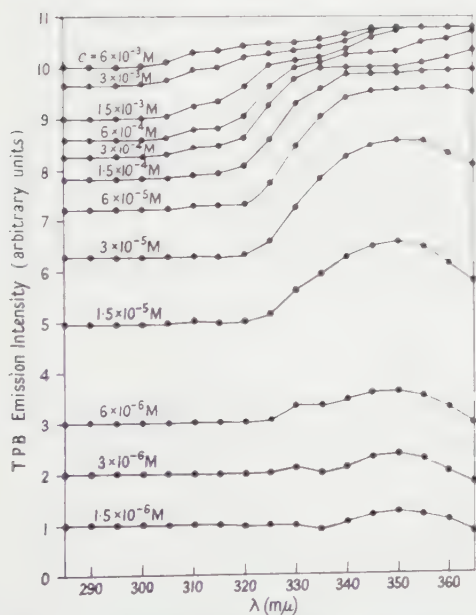


Fig. 4. Excitation spectra of TPB emission. Intensity against wavelength λ , for solutions of different TPB concentration c .

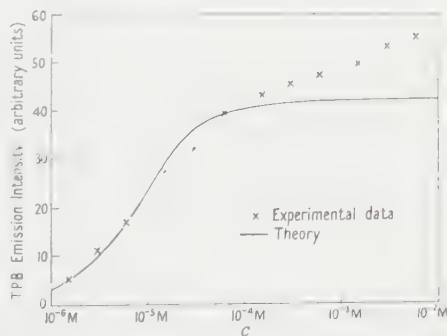


Fig. 5. Intensity of indirectly excited TPB emission against TPB concentration c , for specimens of thickness $t = 13\text{ mm}$. The theoretical curve, for purely radiative transfer, is obtained from (3).

absorbed by TP and the observed TPB emission is that excited by energy transferred from TP to TPB. The variation of the intensity of this indirectly excited TPB emission with concentration is plotted in Fig. 5.

From $\lambda = 325$ to $365 \text{ m}\mu$, TP is transparent and the observed TPB emission is excited directly. At low concentrations only a fraction of the incident radiation is absorbed in the specimen thickness, and the shape of the direct excitation spectrum is related to the TPB absorption spectrum (see Fig. 7). At high concentrations the intensity tends to a constant value independent of c and λ , corresponding to all the incident radiation being absorbed by TPB near the solution surface. In the intermediate wavelength region, $\lambda = 305$ to $325 \text{ m}\mu$, where the TP absorption is decreasing with increasing λ but is still finite, the TP and TPB compete for the absorption of the incident radiation, the TPB absorption becoming more significant as c is increased.

2.4. Influence of Terphenyl Concentration

To investigate the influence of the terphenyl concentration on the energy transfer, four toluene solutions were prepared containing TP concentrations of $2.17 \times 10^{-2} \text{ M}$, $1.09 \times 10^{-2} \text{ M}$, $5.43 \times 10^{-3} \text{ M}$ and $2.71 \times 10^{-3} \text{ M}$ respectively, and each containing $6 \times 10^{-3} \text{ M}$ concentration of TPB. Measurements at $\lambda = 285$ to $310 \text{ m}\mu$ showed that the indirectly excited TPB emission intensity was independent of the TP concentration.

§ 3. THEORY AND ANALYSIS

3.1. Radiative Transfer

We shall denote the primary solute (TP) and the secondary solute (TPB) by Y and Z respectively, the molar concentration of Z (relative to the solvent) by c , the molar decadic extinction coefficient of Z at a wavelength λ by $\epsilon_Z(\lambda)$, and the molecular quantum intensity of the emission of Y at λ by $I_Y(\lambda)$.

In a binary solution of Y ($c = 0$) the total molecular quantum intensity of Y emission is

$$Q_{0Y} = \int I_Y(\lambda) d\lambda. \quad \dots\dots (1)$$

If the effective path length of the Y emission through a solution containing Z is d , then the quantum intensity of Y emission is reduced by absorption to the technical value,

$$Q_{PY} = \int I_Y(\lambda) 10^{-cd\epsilon_Z(\lambda)} d\lambda. \quad \dots\dots (2)$$

The technical quantum intensity of Z emission excited by radiative transfer from Y is given by

$$\begin{aligned} Q_{PZ} &= q_{0Z} \int I_Y(\lambda) [1 - 10^{-cd\epsilon_Z(\lambda)}] d\lambda \\ &= q_{0Z}(Q_{0Y} - Q_{PY}) = q_{0Z}aQ_{0Y} \end{aligned} \quad \dots\dots (3)$$

where q_{0Z} is the fluorescence quantum efficiency of Z, and a , which is a function of c and d , is the fraction of Q_{0Y} absorbed by Z.

The values of $I_Y(\lambda)$ against λ for TP have been taken from Hayes (1953) and of $\epsilon_Z(\lambda)$ against λ for TPB from Birks and Kuchela (1959) (see Fig. 7), and the corresponding values of Q_{PY} and Q_{PZ} against c for $d = 15$ mm have been calculated from (2) and (3). The value of $d = 15$ mm corresponds to the estimated mean optical path length in a solution of thickness $t = 13$ mm. The theoretical values, normalized to the arbitrary experimental intensity scales at $c = 0$ and $c = 6 \times 10^{-6}$ M respectively, are plotted in Figs 3 and 5 and are in excellent agreement with the experimental data.

The agreement between the experimental and theoretical curves of Q_{PY} and Q_{PZ} up to $c \sim 10^{-4}$ M shows conclusively that the solute-solute energy transfer is purely radiative up to these concentrations. The increase in Q_{PZ} which occurs at higher c cannot be accounted for by radiative transfer, which limits when all the TP emission is absorbed, and it is therefore evidence of non-radiative transfer at high c .

3.2. Non-radiative Transfer

The quantum efficiency of solute-solute energy transfer f has been evaluated from the experimental results (Fig. 4), using the expression (part I)

$$f = I_Z/I_{0Z} - \rho c(1 - I_Z/I_{0Z}) \quad \dots\dots (4)$$

where I_Z is the TPB emission intensity excited indirectly ($\lambda = 285 - 310$ m μ), I_{0Z} is the maximum TPB emission intensity excited directly ($\lambda = 345 - 365$ m μ) at high c , where the incident radiation is completely absorbed near the surface, and

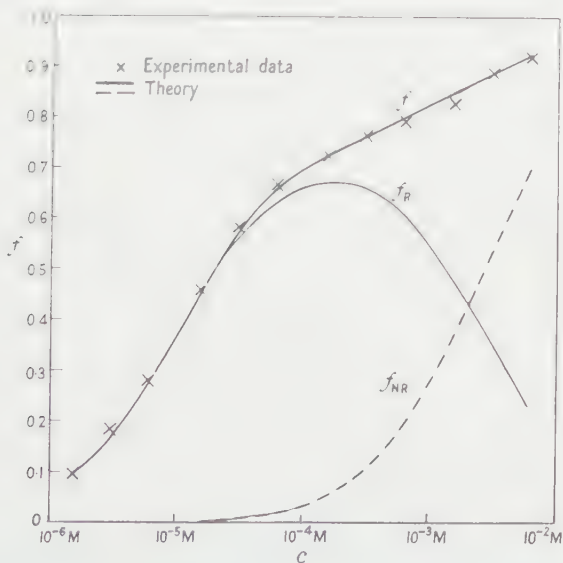


Fig. 6. Quantum efficiency of TP-TPB energy transfer f against TPB concentration c for specimens of thickness $t = 13$ mm. The theoretical curves are obtained from (9): f_R , radiative transfer efficiency; f_{NR} , non-radiative transfer efficiency; f , total transfer efficiency.

$\rho = \epsilon_Z(\lambda)/\epsilon_Y(\lambda)$ is the ratio of the molar extinction coefficients of TPB and TP at a given λ . The second term on the right-hand side of (4) is a correction, negligible except at high c , for the fraction of the incident radiation absorbed directly by TPB. f has been calculated for each of the 12 specimens of $t = 13$ mm at six equally spaced wavelengths from $\lambda = 285$ m μ to 310 m μ . The results are most consistent, deviations from the mean being random and less than $\pm 1\%$ in all cases, showing that f is independent of λ in this wavelength region. The mean values of f against c are plotted in Fig. 6.

The molecular fluorescence quantum efficiency of Y is, when $c = 0$,

$$(q_{0Y})_0 = \frac{k_{fY}}{k_{fY} + k_{iY}} \quad \dots\dots (5)$$

where k_{fY} , k_{iY} are the rate parameters (sec^{-1}) of emission and internal quenching respectively. When $c \neq 0$, and non-radiative transfer occurs, $(q_{0Y})_0$ is reduced to

$$q_{0Y} = \frac{k_{fY}}{k_{fY} + k_{iY} + k_t c} \quad \dots\dots (6)$$

where $k_t c$ is the rate parameter of non-radiative transfer to Z .

The quantum efficiency of radiative transfer to Z is

$$f_R = a q_{0Y} \quad \dots\dots (7)$$

where a is given by (3) and (1).

The quantum efficiency of non-radiative transfer to Z is

$$f_{NR} = \frac{k_t c}{k_{fY} + k_{iY} + k_t c} \quad \dots\dots (8)$$

Thus the total quantum efficiency of energy transfer from Y to Z is

$$\begin{aligned} f &= f_R + f_{NR} \\ &= \frac{a(q_{0Y})_0 + \sigma c}{1 + \sigma c} \quad \dots\dots (9) \end{aligned}$$

where

$$\sigma = \frac{k_t}{k_{fY} + k_{iY}} \quad \dots\dots (10)$$

Two concentration regions can be distinguished (Fig. 6): $c < 10^{-4}$ M, where σc is small, and

$$f = a(q_{0Y})_0 \quad (\text{low } c) \quad \dots\dots (11)$$

and $c > 10^{-4}$ M, where $a \sim 1$, and (9) approximates to

$$f = \frac{(q_{0Y})_0 + \sigma c}{1 + \sigma c} \quad (\text{high } c). \quad \dots\dots (12)$$

Eqn (12) can be written in the form

$$f = (q_{0Y})_0 + \sigma c(1 - f). \quad \dots\dots (13)$$

The experimental data (Fig. 6) for $c > 10^{-4}$ M have been plotted as f against $c(1 - f)$, and a straight line obtained in agreement with (13). From the intercept and slope of this line, values of $(q_{0Y})_0 = 0.75$, $\sigma = 390$ are obtained. These values have been substituted in (9), using the calculated data on a (§ 3.1), to determine f ,

f_R and f_{NR} as a function of c , and these are compared with the experimental results in Fig. 6. It will be noted that non-radiative transfer becomes significant at $c > 10^{-4}$ M, at higher c it competes with the emission of Y^* (and hence reduces f_R), and at high c it tends towards unity.

3.3. Dipole-Dipole Transfer

Förster (1948, 1949) has developed a quantum-mechanical theory of non-radiative dipole-dipole transfer between donor and acceptor molecules. He obtains the following expression for R_0 , the critical intermolecular distance, below which the energy transfer takes place within the donor excitation time :

$$R_0^6 = \frac{3 \times 10^6 (\ln 10)^2 \mathbf{c} \tau_Y}{8 \pi^4 n^2 \mathbf{N}^2 \bar{\nu}_0^2} J(\bar{\nu}) \quad \dots\dots (14)$$

where \mathbf{c} is the velocity of light, τ_Y is the donor fluorescence decay time, n is the refractive index of the solution, \mathbf{N} is Avogadro's number, and $\bar{\nu}_0$ is the mean wave number of the electronic excitation of the donor. $J(\bar{\nu})$ is the overlap integral of the donor emission and acceptor absorption spectra, given by

$$J(\bar{\nu}) = \int_0^\infty \epsilon_Y(2\bar{\nu}_0 - \bar{\nu}) \epsilon_Z(\bar{\nu}) d\bar{\nu} \quad \dots\dots (15)$$

where $\bar{\nu}$ is the wave number and $\epsilon_Z(\bar{\nu})$ is the decadic molar extinction coefficient of the acceptor. $\epsilon_Y(2\bar{\nu}_0 - \bar{\nu})$ is the emission coefficient of the donor, expressed in decadic molar units, and is obtained from the reflection of the donor absorption spectrum $\epsilon_Y(\bar{\nu})$ about $\bar{\nu}_0$. $\bar{\nu}_0$ is the mean of the wave numbers of the maxima in the emission and absorption (1st π -electronic excited singlet state) spectra of the donor.

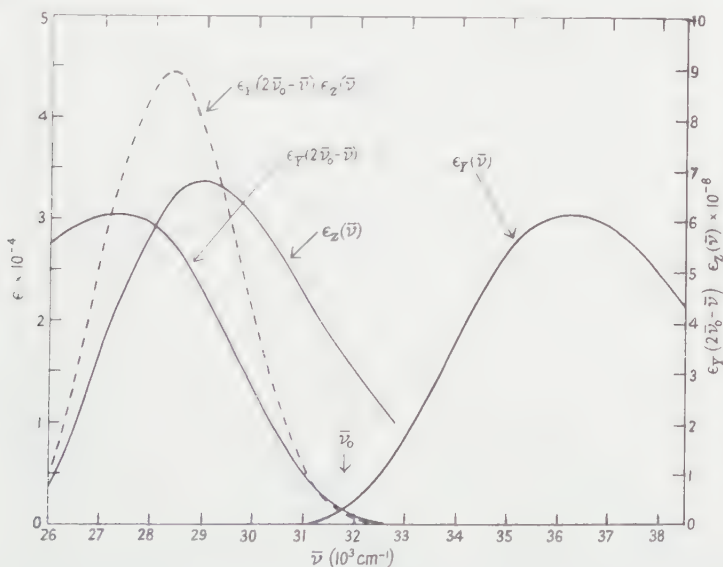


Fig. 7. TP absorption spectrum $\epsilon_Y(\bar{\nu})$, TP emission spectrum $\epsilon_Y(2\bar{\nu}_0 - \bar{\nu})$, TPB absorption spectrum $\epsilon_Z(\bar{\nu})$ (left-hand scale), and TP-TPB overlap spectrum $\epsilon_Y(2\bar{\nu}_0 - \bar{\nu}) \cdot \epsilon_Z(\bar{\nu})$ (right-hand scale), in molar decadic units, against wave number $\bar{\nu}$.

$J(\bar{\nu})$ has been evaluated from (15) for the TP-TPB system. The TPB absorption spectrum $\epsilon_Z(\bar{\nu})$ (Birks and Kuchela 1959), the TP absorption spectrum

$\epsilon_Y(\bar{\nu})$ (1), the TP emission spectrum (Hayes 1953) converted, using $\epsilon_Y(\bar{\nu})$, into decadic molar units $\epsilon_Y(2\bar{\nu}_0 - \bar{\nu})$, and the overlap product $\epsilon_Y(2\bar{\nu}_0 - \bar{\nu}) \cdot \epsilon_Z(\bar{\nu})$ are plotted in Fig. 7. $J(\bar{\nu}) = 3.2 \times 10^{12}$ is obtained from the area under the overlap product curve. Taking $\tau_Y = 2.5$ nsec, $n = 1.5$, $\bar{\nu}_0 = 3.2 \times 10^3 \text{ cm}^{-1}$, a theoretical value of $R_0 = 42.5 \text{ \AA}$ is obtained from (14).

Förster (1959) defines a critical concentration c_0 related to R_0 by

$$c_0 = 3000/4\pi N R_0^3. \quad \dots\dots (16)$$

In terms of σ in the Stern-Volmer type equation (9),

$$c_0 = 2.05/\sigma \quad \dots\dots (17)$$

so that substituting the experimental value of $\sigma = 390$, we obtain $R_0 = 42.2 \text{ \AA}$ from (16). This close quantitative agreement between the theoretical and experimental values of R_0 confirms the dipole-dipole nature of the non-radiative transfer. It indicates that Brownian translational motion (molecular diffusion) has a negligible influence on the transfer process in this system, confirming the conclusions of Bowen and Livingston (1954) that solute-solute transfer is not diffusion controlled.

The observation that f is independent of the TP concentration (§ 2.4) eliminates the possibility of TP-TP excitation migration. Such migration is not to be expected theoretically because of the small overlap of the TP emission and absorption spectra (Fig. 7). The TP-TPB system appears to be a perfect example of single-step energy transfer, with competition occurring between the radiative and the dipole-dipole processes.

§ 4. DISCUSSION

The TP-TPB system is believed to be the first of its kind to have been analysed in such detail, and it is most satisfactory that the theory provides such an accurate quantitative description of the observed behaviour.

There are some conclusions that can be drawn from the results about the design and operation of ternary liquid solution scintillators. TPB is not an ideal secondary solute, since the match of its absorption spectrum with the TP emission spectrum (Fig. 7) is not an optimum, so that f_R and f_{NR} at a given c are rather less than the maxima obtainable. It is probable that the preferred secondary solutes, such as 1,4-bis 2-(5-phenyloxazolyl)-benzene (POPOP), which have been chosen semi-empirically (Hayes *et al.* 1955, 1956, Ott *et al.* 1957), satisfy the spectral overlap criterion more closely. Measurements of the absorption spectrum $\epsilon_Z(\bar{\nu})$ of any secondary solute, in conjunction with the known data on TP, would enable the energy transfer, f_R and f_{NR} , to be predicted for any concentration c or thickness t of a ternary solution scintillator, based on TP-toluene. The only physical data required in choosing a secondary solute are its absorption and emission spectra, its photo-fluorescence quantum efficiency, and its solubility. This approach to scintillator design through simple molecular parameters appears preferable to the more complicated experimental procedures normally used for 'screening' organic compounds as potential scintillators.

At low c ($< 10^{-4} \text{ M}$) where the transfer is purely radiative, $f = f_R$ depends on the solution thickness t , and increases with t towards a maximum of $(q_{0Y})_0$ (11). At higher c ($> 10^{-4} \text{ M}$ for $t = 13 \text{ mm}$) where $a = 1$, f_R and f_{NR} are both independent of the solution thickness, the relative amounts of radiative and non-radiative transfer being determined only by the competition between primary solute

emission and dipole-dipole transfer (12). In this concentration range therefore the behaviour of small and giant scintillators is the same.

$f_R (=0.23)$ is still significant compared with $f_{NR} (=0.7)$ at the highest TPB concentration studied, which is about $\frac{1}{3}$ of the practical TP concentration of 5 g l^{-1} . At $c=0.1$ of the TP concentration, which is that normally used in ternary scintillators, $f_R \sim f_{NR} \sim 0.44$. With POPOP, f_{NR} will be increased slightly relative to f_R , due to the better solute-solute spectral overlap, but f_R will still contribute a substantial component, delayed by τ_T (2.5 nsec), to the secondary solute emission. Hence the technical scintillation decay time of a ternary solution will be longer than that of an equivalent binary solution.

By increasing c beyond 10^{-2} M f_{NR} can be made to tend towards unity, and f_R to tend towards zero. The factors which normally limit the use of such a high c are (a) self-absorption effects, which the secondary solute was originally introduced to eliminate, (b) concentration quenching, (c) the maximum solubility, and (d) the cost of the secondary solute, which is usually high. Moreover at high c , the secondary solute will compete with the primary solute for the solvent excitation energy, and the primary solute becomes redundant.

Since the toluene-TP transfer efficiency = 0.88 for a 5 g l^{-1} TP-toluene solution and $f \sim 0.9$ at $c=0.1$ of this TP concentration, the overall quantum efficiency of transfer from toluene to secondary solute is approximately 0.8. It would appear therefore that, other things being equal, binary solutions with high primary solute concentrations (e.g. 10 g l^{-1} PBD in *p*-xylene) in which solvent-solute transfer efficiencies in excess of 0.9 should be obtainable, are to be preferred to ternary solutions as liquid scintillators, since their scintillation efficiency should be higher.

The high photo-fluorescence quantum efficiency of TP, $q_{0Y}=0.75$, which compares with a technical photo-fluorescence quantum efficiency of only 0.62 for crystalline anthracene, the most efficient organic scintillator known to date, makes a major contribution to the scintillation efficiency of all liquid scintillators containing TP as a major constituent. It partially compensates for the lower inherent energy conversion efficiency of a binary or ternary scintillator, compared with a unitary, single-crystal scintillator (Birks 1960). The ideal primary solute would have an emission matching the photomultiplier response, and an even higher q_{0Y} than TP. Improved solvents, either liquid or plastic, containing larger (i.e. 2- or 3-ring) molecular groups would be needed to utilize such an ideal solute to the best advantage, and hence to rival or exceed the efficiency of crystalline anthracene.

A general theory of the efficiency of crystalline and liquid and plastic binary and ternary solution scintillators, in which the other factors apart from energy transfer which influence the scintillation efficiency are considered, will be described elsewhere†. It is hoped to discuss the applications of this theory to the design of organic scintillators more fully in a subsequent paper.

REFERENCES

- BELL, C. G., and HAYES, F. N., 1958 (Editors), *Liquid Scintillation Counting* (London: Pergamon).
 BIRKS, J. B., 1954, *Phys. Rev.*, **94**, 1567.
 BIRKS, J. B., and CAMERON, A. J. W., 1958, *Proc. Phys. Soc.*, **72**, 53.

† 1960 *Albuquerque Conference on Organic Scintillation Detectors*.

- BIRKS, J. B., and KUCHELA, K. N., 1959, *Disc. Faraday Soc.*, **27**, 57.
BOWEN, E. J., and BROCKLEHURST, B., 1953, *Trans. Faraday Soc.*, **49**, 1131.
BOWEN, E. J., and LIVINGSTON, R., 1954, *J. Amer. Chem. Soc.*, **76**, 6300.
FÖRSTER, T., 1948, *Ann. Phys., Lpz.*, Ser. 6, **2**, 55.
——— 1949, *Z. Naturf.*, **4a**, 321.
——— 1959, *Disc. Faraday Soc.*, **27**, 7.
HAYES, F. N., 1953, *Report LA-1639*, Los Alamos Scientific Laboratory, October.
HAYES, F. N., OTT, D. G., and KERR, V. N., 1956, *Nucleonics*, **14**, No. 1, 42.
HAYES, F. N., OTT, D. G., KERR, V. N., and ROGERS, B. S., 1955, *Nucleonics*, **13**, No. 12, 38.
OTT, D. G., HAYES, F. N., HANSBURY, E., and KERR, V. N., 1957, *J. Amer. Chem. Soc.*, **79**, 5448.
WEBER, G., and TEALE, F. J. W., 1958, *Trans. Faraday Soc.*, **54**, 640.
WEINREB, A., 1957, *J. Chem. Phys.*, **27**, 133.

LETTERS TO THE EDITOR

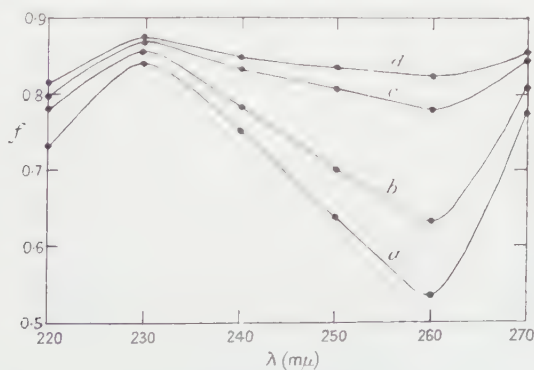
Energy Transfer in Organic Systems
III: Spectral Effects in Liquid Solutions

In part I (Birks and Cameron 1958) an experimental method has been described for the determination of f , the quantum efficiency of π -electronic excitation energy transfer from solvent to solute molecules in organic solutions. f is determined from the solute fluorescence excitation spectrum, by comparing the solute fluorescence intensities excited (a) indirectly by solvent absorption, and (b) directly by solute absorption. Measurements on solutions of *para*-terphenyl in toluene indicated that f depended on the excitation wavelength λ , varying by up to $\pm 25\%$ in the region from $\lambda = 220 \text{ m}\mu$ to $265 \text{ m}\mu$.

Cohen and Weinreb (1956, 1960), on the other hand, reported measurements on similar solutions in which the observed variation of f with λ was only $\pm 5\%$, which they interpreted as showing f to be independent of λ .

A study has been made of the origin of this discrepancy. The main difference between the two experimental arrangements is the distance d between the spectrophotometer exit slit and the illuminated surface of the solution. Cohen and Weinreb placed their solutions near the slit ($d \sim 4 \text{ cm}$) in the normal absorption cell position, while Birks and Cameron placed theirs at $d \sim 10 \text{ cm}$, using a mirror to deflect the beam vertically. Both pairs of investigators viewed the emission from the opposite side of the cell to the incident beam.

Measurements have been made of f as a function of λ (220 to $270 \text{ m}\mu$) for a 5 g l^{-1} ($2.17 \times 10^{-2} \text{ M}$) *para*-terphenyl-toluene solution for different values of d . The results plotted in the Figure (curves a-d) show that the apparent variation of f with λ is reduced considerably as d is decreased. With $d = 4.5 \text{ cm}$ the variation of f with λ is reduced to $\pm 4\%$, and is similar to that observed by Cohen and Weinreb.



Dependence of apparent solvent-solute transfer efficiency f on wavelength λ for 5 g l^{-1} *para*-terphenyl-toluene solution.

a, $d = 10.5 \text{ cm}$; b, $d = 8.8 \text{ cm}$; c, $d = 6.5 \text{ cm}$; d, $d = 4.5 \text{ cm}$.

The curves shown in the Figure resemble closely the transmittance spectra of toluene vapour of different path lengths. Calculations from the vapour absorption spectrum, which is similar to that of the liquid (part I) but shifted slightly to shorter wavelengths, and the vapour density show that the spectral effect can be adequately accounted for by the presence of toluene vapour which attenuates the incident light. This has been confirmed by observations of f using a sealed cell in place of the open cell used in the previous experiments. It is found that f is independent of λ within the experimental error ($\pm 1\%$) over the complete wavelength range, and is equal to that observed at $\lambda = 230 \text{ m}\mu$, $d = 4.5 \text{ cm}$ (curve d). Under these conditions f has been measured for five *para*-terphenyl-toluene solutions of concentration

$$c = 1.36 \times 10^{-3} \text{ M to } 2.17 \times 10^{-2} \text{ M,}$$

and these have been analysed in terms of the relation (part I)

$$f = \frac{k_t c}{k_f + k_i + (k_t + k_e)c} \quad \dots\dots (1)$$

where k_f , k_i , $k_t c$ and $k_e c$ are the rate parameters in sec^{-1} of solvent fluorescence, internal quenching, non-radiative transfer and external quenching respectively. This may be re-written as

$$c/f = (1 + k_e/k_t)c + (k_f + k_i)/k_t. \quad \dots\dots (2)$$

c/f has been plotted against c , and from the slope and intercept of the straight line obtained, it is found that $k_e = 0$, $(k_f + k_i)/k_t = 0.80 \text{ mol l}^{-1}$. This value is in agreement with that of Lipsky and Burton (1959), and corresponds to a critical dipole-dipole transfer distance $R_0 = 38 \text{ \AA}$, in agreement with that obtained by Cohen and Weinreb (1956). This compares with a theoretical value of $R_0 = 20 \text{ \AA}$, computed from the absorption and emission spectra of *para*-terphenyl and toluene, for dipole-dipole transfer between static molecules (Förster 1949). The difference between the experimental and theoretical values is due to Brownian motion and solvent-solvent energy migration.

The toluene fluorescence decay time $\tau = (k_f + k_i)^{-1} = 7.4 \text{ nsec}$ (Swank *et al.* 1958), so that $k_t = 1.69 \times 10^8 (\text{mole/l})^{-1} = 1.59 \times 10^9 (\text{mole/mole})^{-1}$. Many of the better liquid scintillator solutions contain a concentration of 5 g l^{-1} of *para*-terphenyl in toluene, with or without a secondary solute. The present results show that the maximum quantum transfer efficiency from solvent to primary solute in such scintillators is 0.87.

The Physical Laboratories,
The University,
Manchester.

J. B. BIRKS.
K. N. KUCHELA†.
F. H. READ.

7th September 1960, in revised form 27th March 1961.

BIRKS, J. B., 1952, *Phys. Rev.*, **86**, 569.

— 1953, *Phys. Rev.*, **90**, 1131.

BIRKS, J. B., and CAMERON, A. J. W., 1958, *Proc. Phys. Soc.*, **72**, 53.

COHEN, S. G., and WEINREB, A., 1956, *Proc. Phys. Soc. B*, **69**, 593.

— 1960, *Proc. Phys. Soc.*, **75**, 623.

FÖRSTER, T., 1949, *Z. Naturf.*, **4a**, 321.

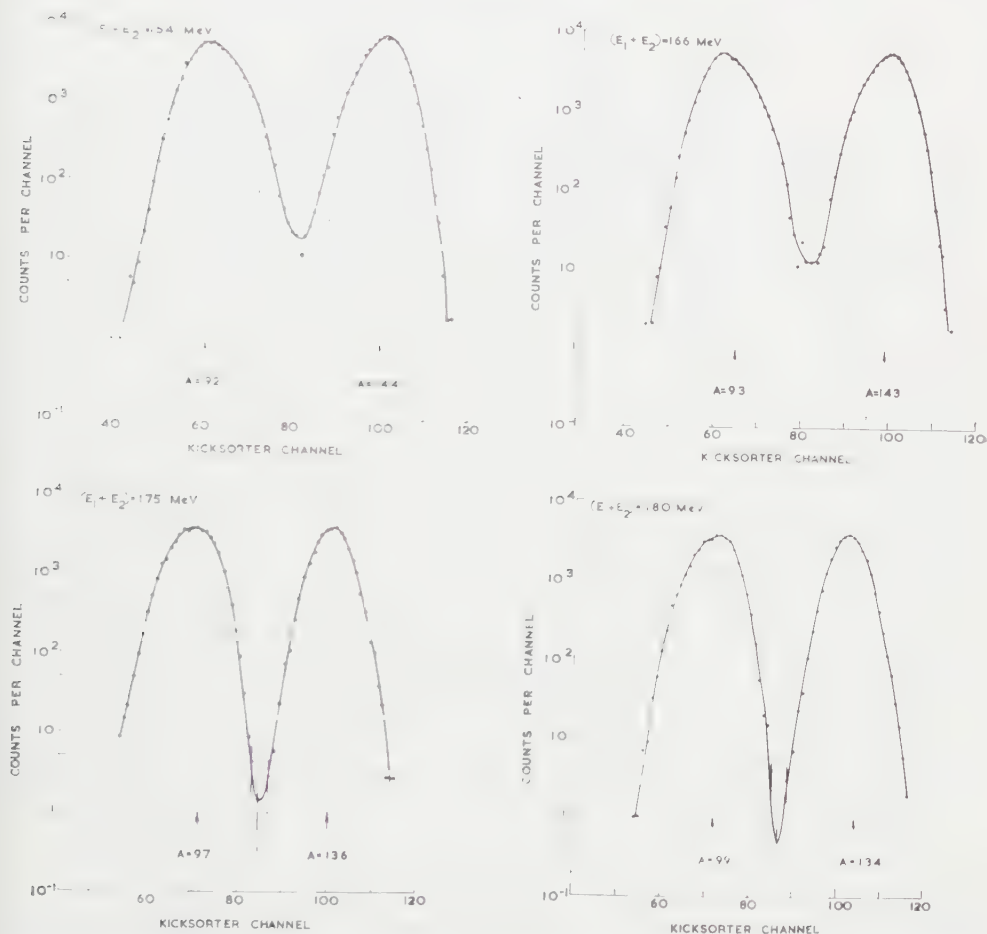
LIPSKY, S., and BURTON, M., 1959, *J. Chem. Phys.*, **31**, 1221.

SWANK, R. K., PHILLIPS, H. B., BUCK, W. L., and BASILE, L. J., 1958, *Instn Radio Engrs Trans. Nucl. Sci.*, **NS-5**, 183.

† Now at the University of Mysore, India.

Kinetic Energy Effects in the Thermal Neutron Fission of ^{235}U

In this letter it is shown that the mass distribution in the thermal neutron fission of ^{235}U is extremely sensitive to the total kinetic energy released. The peak-to-valley ratio of the mass curve, averaged over all kinetic energies is well known to be about 600:1. We have obtained peak-to-valley ratios greater than 3000:1 for selected values of the total kinetic energy. These measurements are preliminary but show clearly that in view of the importance of the mass distribution to the theory of the fission process, detailed investigations of this effect should be made.



Mass distributions for four values of $E_1 + E_2$, the total kinetic energy of the fragments. The arrows indicate the most probable masses. The mass calibration is uncertain to within a few units and the energy calibration to within a few MeV.

The experimental set-up consists of two gold-silicon surface barrier semiconductor counters in a back-to-back arrangement. The construction of the detectors and the details of the experiment are described elsewhere (Dearnaley and Whitehead 1960, Melkonian 1961). $50 \mu\text{g cm}^{-2}$ of 93% enriched ^{235}U was evaporated directly on to one of the detectors, thus eliminating the supporting

film which is necessary in corresponding experiments with ionization chambers, gas scintillators, etc.

The energy spectrum in each detector was used as a measure of its quality. The peak-to-valley ratio of the energy spectrum was 15:1 in one counter which is better than reported in the literature, while in the other it was 12:1. This difference is not understood but it is certainly not due to geometrical or edge effects but is inherent in the detectors themselves. The ratio of the energies for the two peaks was slightly greater than the accepted value and introduces some error in the mass calibration.

Neglecting the loss of energy and momentum due to neutron and γ -ray emission it is easily shown from conservation of momentum that

$$\frac{M_1}{M_1 + M_2} = \frac{E_2}{E_1 + E_2}$$

where M_1 , M_2 , E_1 and E_2 are the masses and kinetic energies of the two fragments. The mass distribution of M_1 may be obtained by measuring E_2 for fixed values of $E_1 + E_2$, provided that $M_1 + M_2$ is known. $M_1 + M_2$ was taken as 233.5, (235 + 1 - 2.5). Pulses from the two detectors were added and passed through a single-channel kicksorter with a window of about 4 Mev to select $E_1 + E_2$ and gate a multi-channel kicksorter displaying E_2 . In this way the mass distribution was obtained for four values of the total kinetic energy.

The results are shown in the Figure. In all cases the areas under the two mass peaks are unequal. This is due to the slight difference in response of the two detectors and will tend to fill in the minimum, giving peak-to-valley ratios somewhat less than the true ones.

As the total kinetic energy of the fragments is increased, the ratio of the most probable masses decreases as previously observed. However, the peak-to-valley ratio increases by more than a factor of ten over this energy range and thus, although the two most probable masses become closer together, the relative probability of symmetric fission decreases. These surprisingly deep minima seem to be related to the formation of fragments with mass near 132, which is near the closure of the $Z = 50$ and $N = 82$ shells.

It is a pleasure to thank Dr. E. Melkonian who realized the suitability of the technique and initiated the experiment, and Drs. G. Dearnaley, H. G. Pugh and E. R. Rae, for helpful comments.

Atomic Energy Research Establishment,
Harwell, Berks.
29th December 1960.

T. J. GOODING†.

DEARNALEY, G., and WHITEHEAD, A. B., 1960, *Atomic Energy Research Establishment Report* No. R-3437.

MELKONIAN, E., 1961, *Atomic Energy Research Establishment Report* No. R-3524.

Gross Structure in the Proton Spectra from the $^{51}\text{V}(\text{d}, \text{p})^{52}\text{V}$ Reaction

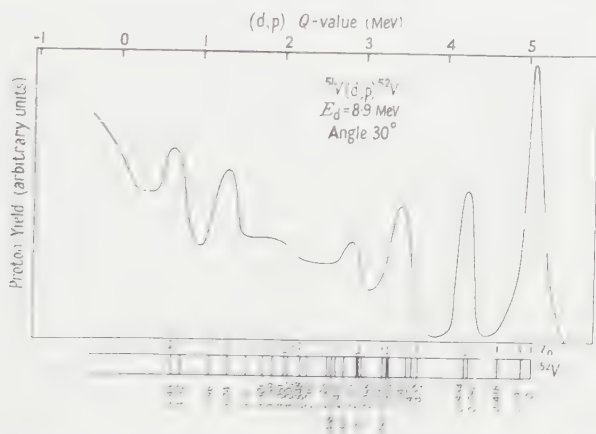
Schiffer, Lee and Zeidman (1959) have recently published data on the gross structure observed in proton spectra from d, p reactions on medium-weight elements using 10 Mev deuterons. We have recently reported the results

† Now at Lawrence Radiation Laboratory, Berkeley, California.

of a study at medium resolution of the $^{51}\text{V}(\text{d}, \text{p})^{52}\text{V}$ reaction (Dalton, Kirk, Parry and Scott 1960) using 8.9 Mev deuterons and we have now re-examined the spectra for comparison with the results of Schiffer *et al.* on gross structure.

Schiffer *et al.* deduce the presence of single particle states $\text{p}_{3/2}$, $\text{p}_{1/2}$, $\text{d}_{5/2}$ and $\text{s}_{1/2}$ corresponding to groups in the spectra with Q -values about 4.8, 3.3, 2.6 and 1.1 Mev respectively. These groups arise from transitions with l -values 1, 1, 2 and 0 for the ingoing neutron. We have constructed spectra to show gross-structure effects by subtracting the impurity groups from the good resolution spectra and adding together points in the resulting distributions. The energy interval over which averaging was performed was about 250 kev. A typical spectrum is shown in the Figure, and while there is some similarity between it and the spectrum shown by Schiffer *et al.* there are some differences.

For $l=1$ groups we find four strong broad groups corresponding to Q -values of 5.07, 4.27, 3.45 and 1.3 Mev. A weak group appears at a Q -value of about 2.8 Mev. The first two of these groups combined could correspond to the group found by Schiffer *et al.* with Q -value 4.8 Mev and the 3.45 Mev group could correspond to the 3.3 Mev group of Schiffer *et al.* Regarding $l=2$ transitions there is one possibility at a Q -value of 2.23 Mev, but a stronger group is seen at a Q -value of 0.64 Mev.



Gross-structure proton spectrum at 30° with impurity groups removed. Below the spectrum are shown individual groups in the spectrum and the l -values of the transitions giving rise to these groups.

The biggest disagreement occurs over the possibility of $l=0$ transitions. Schiffer *et al.* report an $l=0$ group with Q -value about 1.1 Mev. From the figure quoted by them for the reduced width the group should be large, but in our spectra the only $l=0$ group in the region of Q -value 1 Mev is that due to oxygen impurity. When this is subtracted no other $l=0$ group is seen. It might be thought that the oxygen impurity group could be masking a vanadium group, but this seems unlikely for two reasons. First, the oxygen impurity also gives rise to an $l=2$ transition with Q -value 1.918 and from the size of this group it is possible to estimate the size of the oxygen $l=0$ group. All the $l=0$ group in the spectrum is accounted for by oxygen impurity. Second, if an oxygen group and a vanadium group were coincident at one angle of observation then broadening

of the group should appear at other angles of observation due to the relative shift with angle of the two individual groups. No sign of this was observed.

Physics Department,
University of Liverpool.
16th December 1960.

A. W. DALTON,
G. PARRY.
H. D. SCOTT.

DALTON, A. W., KIRK, A., PARRY, G., and SCOTT, H. D., 1960, *Proc. Phys. Soc.*, **75**, 95.
SCHIFFER, J. P., LEE, L. L., and ZEIDMAN, B., 1959, *Phys. Rev.*, **115**, 427.

Modulation of Light by Means of an Electric Field

Filinski (1957) has claimed that it is possible to modulate light reflected from a germanium surface by injecting current carriers from a point contact. Sosnowski (1957) has postulated that the magnitude of the modulation depth observed (of the order of 0.5%) can only be explained in terms of a surface carrier density change.

In theory, the requisite change in carrier density (up to 10^{18} cm^{-3}) can be achieved by means of the field effect (Montgomery and Brown 1956). Consequently, if a transparent material is used as the field plate, it should be possible to modulate the light reflected from the germanium surface, at the frequency of the applied field.

A collimated light beam from a tungsten filament lamp was directed on to the surface of an etched specimen of germanium. The field electrode consisted of a glass plate on to one side of which a transparent film of cadmium oxide had been evaporated. The oxide film was separated from the germanium surface by a sheet of dielectric (approximately 0.001 in. thick) which served to increase both the break-down voltage and the induced charge. The change in intensity of the reflected beam was measured by means of a photomultiplier and either a micro-ammeter or an oscilloscope.

Using field strengths of up to $2 \times 10^5 \text{ v cm}^{-1}$, modulation depths as high as 35% were obtained with mica or 'Mylar' as the dielectric. These results could not be explained in terms of a variation of the surface carrier density. Indeed, similar percentage modulations were observed if the germanium was replaced by a polished metal. In addition, modulation of both the transmitted and reflected beams was obtained, using two glass electrodes separated by a 'Mylar' spacer.

The above experiments and the fact that with the germanium system no modulation was obtained if a window was cut in the dielectric so that there was an air gap between the germanium and the field electrode, suggested that the effect was a function of the dielectric rather than of the reflecting material. The absence of modulation in this case also cast some doubt on the proposed mechanism of the Filinski effect, though it is quite possible that the fields used were too small.

An examination of the frequency response of the germanium-'Mylar' system suggested a frequency cut-off below 100 kc/s. With an a.c. field the signal on the oscilloscope was not very reproducible, while with a d.c. bias changes of photomultiplier current were obtained which depended both on the bias direction and on the previous history of the system.

The shape of the frequency response curve, the lack of reproducibility, and the fact that the system emitted an audible note, all suggested that the effect was connected with mechanical vibration of the dielectric. By means of a suitable lens arrangement, it was possible to observe interference fringes formed at the 'Mylar'-glass interface or at the 'Mylar'-germanium interface. Observations of movement of these fringes on the application of an electric field indicated the probable cause of the light modulation.

In the absence of an applied field, the dielectric spacer will be separated both from the reflecting material and from the conducting glass by a small air gap. Application of an electric field presumably causes the dielectric to move towards one of the adjacent surfaces, thereby reducing the air gap sufficiently for the dielectric to come into optical contact with this surface over a considerable area.

It is possible to estimate the change in reflectivity for normal incidence if it is supposed that the 'Mylar' comes into contact with the germanium over the whole area. In the absence of an applied field, without optical contact, it is necessary to consider reflection at both the 'Mylar'-air interface R_1 and the air-germanium interface R_2 . Hence, neglecting multiple reflections and also reflection at the front surface of the dielectric

$$R = R_1 + (1 - R_1)R_2$$

where
$$R_1 = \frac{(n_1 - n_0)^2}{(n_1 + n_0)^2} \quad \text{and} \quad R_2 = \frac{(n_0 - n_2)^2 + k_0^2}{(n_0 + n_2)^2 + k_0^2}.$$

n_0 , n_1 and n_2 are the refractive indices of air, 'Mylar' and germanium respectively and k_0 is the extinction coefficient of germanium.

$n_2 \simeq 4$ and $k_0 \simeq 2$ at 4200 Å, the sensitivity peak of the photomultiplier tube (Archer 1958), so that with $n_1 = 1.8$, $R_1 \simeq 0.08$, $R_2 \simeq 0.45$ and $R \simeq 0.5$.

With the field applied and optical contact established, only reflection at a 'Mylar'-germanium boundary need be considered so that

$$R = \frac{(n_1 - n_2)^2 + k_0^2}{(n_1 + n_2)^2 + k_0^2} \simeq 0.24.$$

On this basis, it should be possible to obtain changes in reflectivity of the order of 50% if the whole of the illuminated region were involved. A change in reflectivity might likewise occur at the cadmium oxide surface. This would no doubt be smaller in magnitude owing to the relatively low reflectivity of this interface, but it could clearly account for the modulation of both the reflected and transmitted beams when two conducting glass electrodes are used.

To explain the movement of the 'Mylar' under the influence of the applied field, it must be supposed that it carried surface charges, but this is not unlikely in view of its known property of becoming electrified easily by friction.

I would like to thank Standard Telecommunication Laboratories for permission to publish this work and Mr. C. F. Drake for helpful suggestions.

Standard Telecommunication Laboratories Ltd.,
Harlow,

B. H. CLAUSSEN.

Essex.

23rd February 1961.

ARCHER, R. J., 1958, *Phys. Rev.*, **110**, 354.

FILINSKI, I., 1957, *Phys. Rev.*, **107**, 1193.

MONTGOMERY, H. C., and BROWN, W. L., 1956, *Phys. Rev.*, **103**, 865.

SOSNOWSKI, L., 1957, *Phys. Rev.*, **107**, 1193.

Detection of Millimetre and Sub-millimetre Wave Radiation by Free Carrier Absorption in a Semiconductor

If radiation, incident on a semiconductor, is absorbed by free carriers, their energy will be increased above the value corresponding to thermal equilibrium with the lattice. In principle, this change in energy can be observed by the change in mobility and hence, in conductivity. It can be shown that, with a suitable semiconductor, at a low temperature, this effect can be made the basis of a detector for millimetre and sub-millimetre wave radiation of high sensitivity and short time constant.

If E is the mean carrier energy when absorbing power W , we can put

$$dE/dW = \tau_r \quad \dots\dots (1)$$

where τ_r may be described as the time for exchange of energy between the carriers and phonons. It can be shown (Gunn 1957) that τ_r is related to the time τ_p for scattering of carriers by phonons

$$\tau_r \simeq \frac{kT\tau_p}{2m^*u^2} \quad \dots\dots (2)$$

where u is the phonon velocity and m^* the effective mass of the carriers. For scattering by acoustical phonons in a non-polar, non-degenerate semiconductor

$$\tau_p \propto T^{-1}E^{-1/2}(m^*)^{-3/2} \quad \dots\dots (3)$$

and hence

$$\tau_r \propto E^{-1/2}(m^*)^{-5/2}. \quad \dots\dots (4)$$

If the mobility μ is determined mainly by ionized impurity scattering

$$\mu \propto E^{3/2}. \quad \dots\dots (5)$$

From Eqns (1), (4) and (5) it is seen that the sensitivity $\mu^{-1}d\mu/dW$ is proportional to $E^{-3/2}(m^*)^{-5/2}$. For a polar semiconductor in which piezoelectric scattering is the predominant phonon interaction $\tau_p \propto E^{1/2}(m^*)^{-1/2}$ (Harrison 1956) and hence the sensitivity is proportional to $E^{-1/2}(m^*)^{-3/2}$. Optimum conditions are therefore obtained with a semiconductor with low effective mass, cooled to a low temperature. An obvious choice of material is n-type indium antimonide for which $m^* = 0.015m_e$. We shall attempt to estimate the sensitivity which might be obtained at a temperature of about 2°K. The value of τ_p at this temperature has not been directly measured, but τ_p and τ_r can be estimated from experiments on the change in mobility with applied voltage (Putley 1959, Sladek 1960). For a particular specimen of indium antimonide of volume $\Omega = 2 \times 10^{-3} \text{ cm}^3$, carrier density $n = 5 \times 10^{13} \text{ cm}^{-3}$, and resistance $R = 140 \text{ ohms}$ at 2°K, the change of mobility with input power for applied voltage $V = 0.04 \text{ v}$, was found to be (M. A. Kinch, private communication) $\mu^{-1}d\mu/dW = 6 \times 10^4 \text{ w}^{-1}$. Since

$$\frac{1}{\mu} \frac{d\mu}{dW} \simeq \frac{1}{E} \frac{dE}{dW} \simeq \frac{\tau_r}{n\Omega kT}$$

this corresponds to a value of τ_r of about $0.2 \mu\text{sec}$. The sensitivity should be

$$\frac{dV}{dW} = \frac{V}{\mu} \frac{d\mu}{dW} \simeq 2.4 \times 10^3 \text{ v w}^{-1}.$$

If we assume that the minimum detectable change in voltage is determined by Johnson noise

$$(\Delta V^2)_{av} = 4kTR\Delta f \simeq 10^{-20} \Delta f \text{ v}^2,$$

the minimum detectable change in power absorbed by the carriers, for an amplifier of bandwidth Δf is $\Delta W \simeq 4 \times 10^{-14} (\Delta f)^{1/2}$ W.

One cannot, of course, be certain that it will be possible to attain the limit set by Johnson noise and it is necessary to consider the possibility of other sources of noise. Since the carriers do not condense into the impurity states at temperatures above 1°K , there should be no resistance fluctuation due to generation-recombination noise. At the present time, no excess low-frequency noise has been reported for indium antimonide. There may be noise due to fluctuation of the incident photon flux and also temperature fluctuation of the carriers

$$\frac{(\Delta V^2)_{\text{av}}}{V^2} \simeq \frac{(\Delta T^2)_{\text{av}}}{T^2} \simeq \frac{8\tau_r \Delta f}{3n\Omega} \simeq 10^{-17} \Delta f.$$

This gives a voltage fluctuation about equal to Johnson noise. In order to realize the full sensitivity, it is necessary for the radiation to be fully absorbed within the thickness of the specimen, that is the absorption coefficient a should be not less than about 0.1 cm^{-1} . From classical theory

$$a = \frac{4\pi ne^2}{m^* c K^{1/2}} \frac{\tau}{1 + \omega^2 \tau^2}.$$

In this expression it seems reasonable to use the value of τ appropriate to excited carriers with energy $E = \hbar\omega$. When ionized impurity scattering is dominant $\tau \propto (m^*)^{1/2} E^{3/2}$ so, for $\omega\tau \gg 1$, $a \propto (m^*)^{-3/2} \omega^{-7/2}$ in agreement with quantum calculation (Fan 1956). From the measured mobility $\mu = 5 \times 10^4 \text{ cm}^2 \text{ sec}^{-1} \text{ V}^{-1}$ it is concluded that $\tau = 5 \times 10^{-13} \text{ sec}$, and the calculated value of a is about 60 cm^{-1} for wavelength 1000 microns and 0.02 cm^{-1} for 100 microns. It should be possible to increase the absorption of short wavelength radiation by application of a magnetic field H of the correct magnitude for cyclotron resonance, $\omega = eH/m^*c$ (Dingle 1952, Zeiger, Rauch and Behrndt 1959). Another way of increasing the absorption at particular frequencies would be to place the specimen in a resonant cavity. It should also be possible to increase the sensitivity by operating the device as a mixer with difference frequency $\Delta\omega < 1/\tau_r$.

It is a pleasure to acknowledge the assistance received from discussion of this project with D. M. S. Bagguley, B. Bleaney, D. W. Goodwin, E. H. Putley, J. M. Rowell and J. H. Sanders. The specimen of indium antimonide on which measurements are reported was kindly supplied by Dr. E. H. Putley. This research was supported partly by an Admiralty Contract.

The Clarendon Laboratory,
Oxford.

B. V. ROLLIN.

22nd March 1961.

- DINGLE, R. B., 1952, *Proc. Roy. Soc. A*, **212**, 38.
 FAN, H. Y., 1956, *Rep. Progr. Phys.*, **19**, 107 (London: Physical Society).
 GUNN, J. B., 1957, *Progress in Semiconductors*, **2**, 213.
 HARRISON, W. A., 1956, *Phys. Rev.*, **101**, 903.
 PUTLEY, E. H., 1959, *Proc. Phys. Soc.*, **73**, 280.
 SLADEK, R. J., 1960, *Phys. Rev.*, **120**, 1589.
 ZEIGER, H. J., RAUCH, C. J., and BEHRNDT, M. E., 1959, *J. Phys. Chem. Solids*, **8**, 496.

REVIEWS OF BOOKS

Non-relativistic Quantum Mechanics, by R. M. SILLITTO. Pp. x + 230. (Edinburgh: University Press, 1960.) 35s.

This book is intended as an introduction to the subject for honours students in physics. The author very wisely abandons the historical approach and tries from the start to demonstrate the general mathematical structure of the theory. Thus matrix mechanics are combined throughout with wave mechanics; indeed both the harmonic oscillator and angular momentum are dealt with by operator methods before any serious use is made of the Schrödinger representation.

Although we are entirely in favour of this trend in the presentation of quantum mechanics, our impression is that Mr. Sillitto has allowed himself to become rather too mathematical in the early chapters. Thus already on page 8 we have "Now let P be a linear operator in the vector space defined by the π_i ", and the extremely general treatment of the uncertainty principle in Chapter II will not cut much ice with most physics students.

However, once the book gets into its stride it runs much more smoothly, and the choice of material is interesting. In addition to the almost inevitable discussion of the Stern-Gerlach experiment and the Zeeman effect, there is a good chapter on many electron atoms, which leads naturally into a discussion of quantum statistics not usually found in an elementary text. After a brief treatment of scattering, the book ends with chapters on the semi-classical theory of radiation and the quantization of the radiation field.

Even if Mr. Sillitto has not quite pulled off an ambitious beginning, he has put a lot of interesting material into a conveniently small book. P. T. MATTHEWS.

Some Mathematical Methods of Physics, by G. GOERTZEL and N. TRALLI. Pp. xiii + 300. (New York, Toronto, London: McGraw-Hill, 1960.) 66s.

It is a pleasure to review a book on mathematical physics which has not the dimensions of a tombstone. This is a compact work, which does not attempt to be exhaustive, but which none the less covers quite a wide field. Much of the material presented can be found scattered through books on quantum mechanics, but it is useful to have a uniform treatment in one volume.

The first part of the book discusses matrices, vector spaces and linear operators, in relation to systems with a finite number of degrees of freedom, and includes a short account of the Dirac notation, which should appeal to those who may still find this notation puzzling, if not unpleasant. The second part extends the work to continuous systems, and deals with a number of problems involving the Laplacian in one, two and three dimensions. There is also a short but useful chapter on Green's functions. The third and final part is concerned with approximate methods, including perturbation theory, the variational method and various numerical procedures. There are also several appendices.

The book is written in a lively and informative style. While it would prove heavy going for the average physics undergraduate, it is strongly recommended to graduate students, particularly those studying quantum mechanics.

S. RAIMES.

Diffraction. Structure des Images, Vol. 2 of *Traité d'Optique Instrumentale*, by A. MARÉCHAL and M. FRANÇON. Pp. 204. (Paris: Revue d'Optique théorique et instrumentale, 1960.) 32 n fr.

This is a survey of recent developments in the diffraction theory of optical image formation within the domain of small-angle scalar diffraction. The following topics are discussed: the Huygens-Fresnel principle, Fourier series and transforms, modulation of spatial frequencies by transmission through an optical system; the contrast of images of simple non-periodic and periodic objects, image formation in an aberration-free system; coherent illumination, phase contrast, partial coherence, image formation in the microscope; effects of small aberrations with coherent and incoherent illumination; effects of large aberrations on point images and on frequency response; information theory in optics. Topics briefly discussed in a final section on applications include apodization, alignment devices, decentring tolerances and photographic noise. There are extensive but not exhaustive bibliographies for each section and a very detailed table of contents. Some excellent diagrams and photographs of aberrated point images are reproduced, but the utility of the latter is much reduced because the magnitudes of the aberrations are not given. There are two beautiful photographs of pairs of point sources completely resolved and on the limit of resolution; these are stated to be incoherently illuminated but the forms of the images suggest that there is actually a considerable degree of coherence between the two sources in both cases. The mathematical treatment is compact and is usually limited to a statement of general formulae without a study of particular cases, e.g., in the discussion of image formation in the microscope only a few numerical results are given, in graphical form. One might in fact complain that not enough of the recently published data on image quality is reproduced but there is still a very useful collection of ideas and methods concerned with this rapidly evolving subject; the book can thus be recommended to all concerned with optical image formation.

W. T. WELFORD.

High Speed Aerodynamics and Jet Propulsion, Vol. 5, *Turbulent Flows and Heat Transfer*, edited by C. C. LIN. Pp. xv+549. (Princeton: University Press; London: Oxford University Press, 1959.) £5 5s.

This volume of the series of books on high-speed aerodynamics and jet propulsion is entitled *Turbulent Flow and Heat Transfer* but the later chapters deal with other topics such as boiling heat transfer, transpiration cooling, and radiation. The explanation of this lies in the purpose of the series which is to describe the basis of the variety of problems associated with high-speed flight. Thus the book is mainly for specialists in this field for whom it is a valuable gathering together of recent information with full lists of references at the end of each section. The volume will, however, be welcomed by those with less specialist interest as an excellent account of transition and turbulent flows of all kinds in relation to heat transfer. The theoretical treatment is clearly set out along with the experimental evidence and is well suited for advanced students in fluid mechanics and heat transfer. From the general reader's point of view the sections on other subjects are not quite on the same level of comprehensiveness, and it is perhaps a pity that the bulk of the book dealing with the fundamentals of turbulent flow and heat transfer could not have been issued as a separate complete volume.

O. A. SAUNDERS.

The International Encyclopedia of Physical Chemistry and Chemical Physics, Vol. 1, *Elements of the Kinetic Theory of Gases*, by E. A. GUGGENHEIM. Pp. xii + 92. (Oxford, London, New York, Paris: Pergamon Press, 1960.) 17s. 6d.

This slim volume has a double significance, out of all proportion to its size. It is probably the best introduction to kinetic theory yet written, and it is also the first volume to appear in the new *International Encyclopedia of Physical Chemistry and Chemical Physics*, of which Professor Guggenheim, Joseph Mayer and F. C. Tompkins are the three Editors-in-Chief. The *Encyclopedia* is conceived according to the admirable scheme of some twenty topics, each under its own editor, and in each of these sections we are promised some five monographs written by appropriate experts. The present work is volume 1 of section 6 (Kinetic theory of gases), which section is Professor Guggenheim's own special care in the encyclopedia. It certainly augurs well for the future.

Without fully agreeing with the author's statement in his preface, that in view of later work criticism that Maxwell's premises, though admittedly true, are not *a priori* obviously true, may now reasonably be regarded as antiquated, there is certainly a lot to be said for approaching kinetic theory much as Maxwell did. Criticism and justification can come later, and we may hope that later volumes in this same section will help to supply them. No one can hope to appreciate sophisticated kinetic theory who has not some acquaintance with a more naïve approach, and in this present book he will progress past naïve arguments to Chapman's first approximation in the theories of gaseous viscosity, thermal conductivity, and diffusion. There are also short chapters on collision rates, thermal diffusion, and gas imperfections; and the book ends with a synopsis of the recent review by Guggenheim and McGlashan of evidence bearing on the precise form of interaction for argon atoms. Altogether it provides an admirable means whereby a newcomer to kinetic theory can get his bearings. The mathematics is beautifully expounded, and the work is most lucidly written.

There are, unfortunately, some misprints, though less than a score and few of them serious. But pp. 24 and 25, in the chapter on collision rates, should be read with caution. The printing and production are excellent. G.S.R.

Numerical Methods for High Speed Computers, by G. N. LANCE. Pp. x + 166. (London: Iliffe, 1960.) 42s.

Among the many books on numerical analysis now available there are few, indeed very few, which are strongly oriented towards the use of automatic computers. This book by Dr. Lance is perhaps a portent that in the future the subject must be linked closely with the facilities and limitations of these machines. Certainly it is the first known to the reviewer which virtually disregards any other form of computation, and in which the use of finite differences is confined to about two pages. Although this emphasis is extremely welcome, it does carry with it some dangers. It is probably fair to say that Dr. Lance does expect his readers to have had experience of hand computation, but rather more stress on the need for caution in accepting answers produced by the computer, with warning examples, is desirable.

The five main chapters deal with evaluation of functions (with considerable emphasis on the use of Chebyshev polynomials), ordinary differential equations, matrix processes, partial differential equations, and miscellaneous processes including root-finding and the evaluation of continued fractions. The approach is fresh, the explanations concise and clear, and the methods described are

reasonably up-to-date. Some methods and topics it is pleasant to see discussed in a book for the first time. However, numerical illustrations are rather infrequent. The account of programming procedures might also be improved if the differences between autocode assembly and interpretive schemes were clarified, and their relative merits discussed.

A book of this size cannot of course be comprehensive, but in the main the methods are well chosen—at least for one type of computer. There is no question that it will be a valuable aid to many computer users, and anyone using it will find the references to original papers most helpful in following up details of methods.

R. A. BUCKINGHAM.

Translation from Russian for Scientists, by C. R. BUXTON and H. S. JACKSON
Pp. xix + 299. (London, Glasgow: Blackie, 1960.) 30s.

This book is intended to enable scientists to acquire rapidly an adequate reading knowledge of Russian. The first section on grammar is set out in a very clear and logical manner which is particularly convenient for back reference.

There follows then a section of text for translation, annotated to explain the grammar. The second half of the book contains passages in Russian for practice accompanied by a good vocabulary.

Fourier Analysis and Generalized Functions, Students' Edn, by M. J. LIDTHILL.
Pp. 79. (Cambridge: University Press, 1960.) 10s. 6d.

This is a reprint, in an inexpensive series, of the book first published in 1958 by Professor Lighthill.

This new series is of great value to students, making available to them books in the range of their pocket.

University Physics, by F. C. CHAMPION. Pp. 786. (London: Blackie & Son, 1960.) 30s.

This book, first published in 1939 as a series of five parts: General physics, Heat, Light, Wave motion and sound, Electricity and magnetism, is now revised and produced as one complete volume. It is still restricted to these five basic subjects.

Handbuch der Physik, Vol. 12, *Thermodynamik der Gase*, edited by S. FLÜGGE.
Pp. vi + 686. (Berlin, Göttingen, Heidelberg: Springer, 1958.) 154.00 DM.

Volume 12 of the new *Handbuch der Physik* falls within the group (6–15) devoted to the mechanical and thermal properties of matter: a group embracing classical elasticity and fluid mechanics as well as crystal- and low-temperature physics. Entitled 'The Thermodynamics of Gases', it is primarily concerned with theories of the equilibrium properties and of the transport properties of actual, non-perfect gases. There are in fact six articles, but this review will confine attention to the first four. The two remaining ones, on 'General vacuum physics' and 'Production and measurement of ultra-high vacuum', while doubtless excellent, seem rather misplaced. It should also be observed that the whole field of sonics and ultrasonics will eventually be covered in Volume 11, and so is not dealt with in the present work.

The four articles with which we are thus concerned, while integrally connected in content, could hardly be more diverse in character. The first (72 pp.) entitled 'The properties of real gases', by J. S. Rowlinson, is a beautiful

summary of the equilibrium properties of real gases and gas mixtures, written from the standpoint of classical thermodynamics and with an eye always firmly kept on actual experimental behaviour. It could be read comfortably and profitably by most final year undergraduates. The second article (131 pp.) 'The theory of real gases', by J. E. Mayer, is much more formal. It deals with the statistical mechanics of imperfect gases, both classical and quantal. But it is perhaps rather difficult to decide just for whom it is written. It is not a guide to the literature (there are comparatively few references), nor is it entirely suitable for novices (though a mature student could gain a lot from it). There is a lot of information in this article, but comparisons with experimental data are rather minimal.

With the third and fourth articles we turn to transport properties. First 'Principles of the kinetic theory of gases' (89 pp.), by H. Grad, and then 'Transporterscheinungen in Gasen von mittlerem Druck' (220 pp.), by L. Waldmann. Professor Grad presents a masterly critique, parts of it hitherto unpublished, of different methods of solving Boltzmann's equation; and Professor Waldmann gives a most comprehensive account of both theoretical and experimental work on gaseous transport coefficients. There are some 350 references, of which approximately a third are to papers published since 1950. Both these articles are in the best tradition of the *Handbuch der Physik*. G.S.R.

Travaux Pratiques de Physique Nucléaire et de Radiochimie, par M. DUQUESNE, R. GRÉGOIRE and M. LEFORT (with an appendix by R. DEVORET). Pp. 324. (Paris: Masson, 1960.) 39 n fr.

The authors of this book have drawn upon the experiences of many years of teaching at the Faculty of Science in Paris to produce a modern practical survey of nuclear physics. Presumably it was primarily intended for a particular university course where the experimental details of the exercises would be supplemented by laboratory instruction sheets.

The work is divided into three parts. The introduction presents in 55 pages a clear and concise survey of atomic and nuclear structure and the interaction of radiations with matter. The section contains over fifty figures and several tables. Part I of 107 pages deals with the detection of radiation using ion chambers, Geiger and proportional counters, scintillators and nuclear emulsions. The section is copiously illustrated and there are many useful practical calculations. There is an excellent chapter on statistics. Part II occupies nearly half the book and is devoted to the study of nuclear structure. This part includes a very small amount of radiochemistry which is scarcely sufficient to justify the inclusion of this subject in the title of the book. Dr. Devoret's appendix on radiological protection is concise and informative with some useful tables, and the book ends with a collection of physical constants and some problems on nuclear physics.

A striking feature of the book is the large number of figures and tables—over 230 of the former. A serious shortcoming, however, is that there is no subject index and it is therefore difficult to find the information one needs. There is no bibliography beyond a set of references to *Annual Reviews of Nuclear Science* and *Progress in Nuclear Physics*. The general style makes for easy reading and one feels that the book ought to be a mine of useful information. If a further edition could be produced in better binding and with a good index it should sell well.

R. A. FAIRES.



9



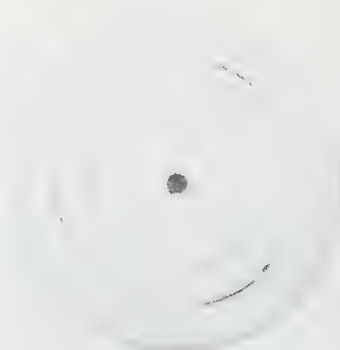
10



5



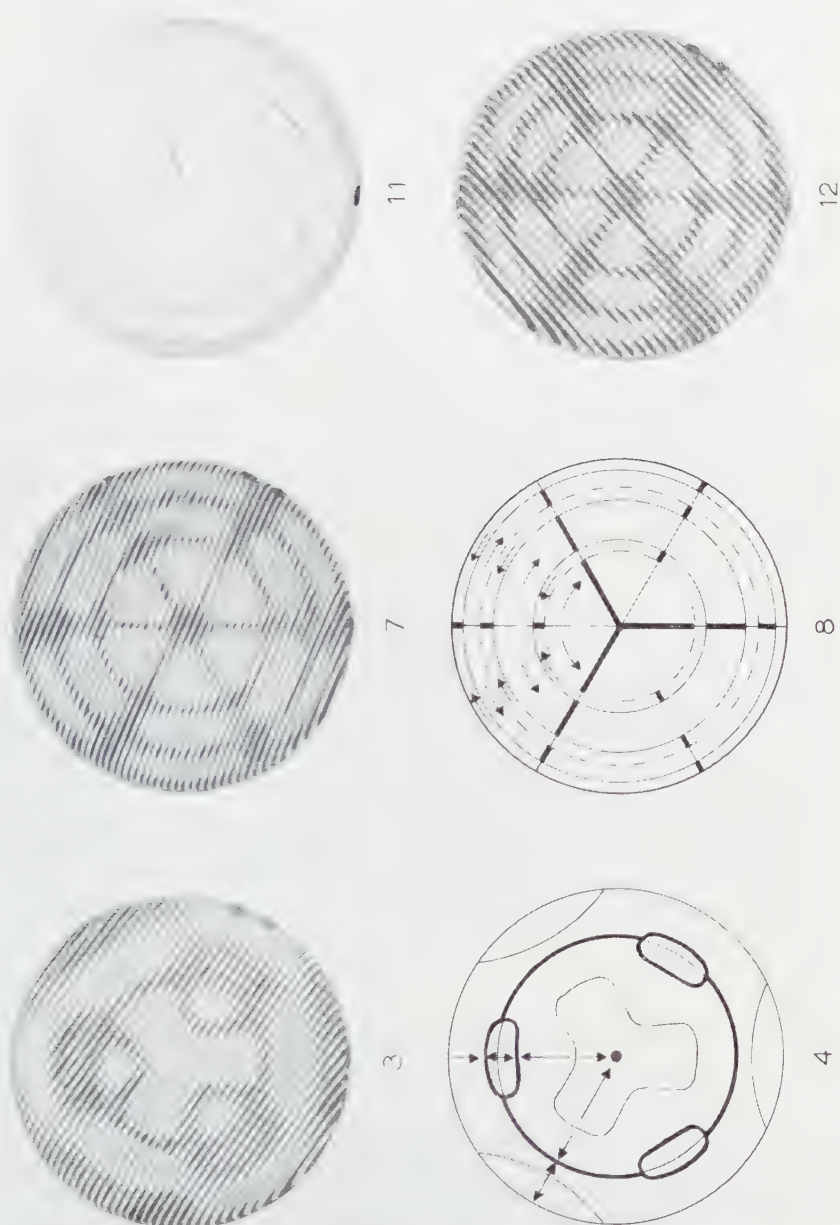
6



1



2



Figs 1-12. Vibration patterns on Z-cut quartz disks. Figs 1-4: type A, $m=1$ mode; diameter of the longitudinal node is $0.715d$ (d is the disk diameter). Figs 5-8: type B, $m=1$ mode; diameters of the longitudinal nodes are $0.455d$ and $0.834d$. Figs 9 and 10: flexural mode with two circular nodes. Figs 11 and 12: flexural mode with three circular nodes.



Radiation by Charged Particles passing through an Electron Plasma in an External Magnetic Field

By S. K. MAJUMDAR

Saha Institute of Nuclear Physics, Calcutta, India

MS. received 27th September 1960, in revised form 5th December 1960

Abstract. The motion of a charged particle through a low density electron plasma in an external magnetic field has been investigated. The interaction of the particle through transverse waves has only been considered, and the consequent energy losses are calculated. It is found that the coupling between the longitudinal plasma wave and the transverse electromagnetic wave modifies the nature of radiation emitted by the particle. The results show that for a velocity greater than that needed for exciting plasma waves in the medium, the particle emits non-Čerenkov type of radiation, in addition to Čerenkov radiation obtained previously by others.

§ 1. INTRODUCTION

IN an earlier paper (Majumdar 1960, to be referred to as I) the interaction of a moving charged particle with the longitudinal plasma wave in an electron plasma without any external magnetic field was investigated. In this paper we shall study the particle interaction with the transverse electromagnetic wave for a non-zero constant magnetic field.

Kolomenskii (1956) has investigated the interaction of the moving particle with the plasma as a result of which the particle emits Čerenkov radiation. The calculation is based on the well-known condition for the appearance of Čerenkov radiation, and the fact that the electromagnetic properties of a plasma in a magnetic field is described by the following dielectric tensor:

$$\epsilon = \begin{bmatrix} \epsilon_1 & -i\epsilon_2 & 0 \\ i\epsilon_2 & \epsilon_1 & 0 \\ 0 & 0 & \epsilon_3 \end{bmatrix}, \quad \dots\dots (1)$$

where

$$\epsilon_1 = \frac{\omega^2 - \omega_p^2 - \omega_c^2}{\omega^2 - \omega_c^2}; \quad \epsilon_2 = \frac{\omega_p^2 \omega_c}{\omega(\omega^2 - \omega_c^2)}; \quad \epsilon_3 = 1 - \frac{\omega_p^2}{\omega^2}; \quad \dots\dots (2)$$

and

$$\left. \begin{aligned} \omega_p &= \left(\frac{4\pi n_0 e^2}{m} \right)^{1/2} \\ \omega_c &= \left(\frac{eH_0}{mc} \right) \end{aligned} \right\}, \quad \dots\dots (3)$$

are the plasma frequency and cyclotron frequency for the electron, and H_0 is the constant external magnetic field. From the method of investigation followed by Kolomenskii we cannot say whether the moving particle, as a result of its

interaction with the transverse field, can excite any radiation in a form other than Čerenkov radiation. The reason for expecting some radiation other than Čerenkov radiation can be seen as follows.

It is known that in a plasma placed in an external magnetic field the transverse electromagnetic wave and the longitudinal plasma wave are intimately coupled (see, for example, Spitzer 1956). Presence of inhomogeneities in the medium also results in coupling between the two waves. In the case of this latter type of coupling, i.e. gradient coupling, it has been shown by Field (1956) and Kritz and Mintzer (1960) that radiation may be generated by the plasma waves themselves. The essential requirement for this to occur is the presence of the coupling and so there is no obvious reason why this should not happen in a magnetic field. Whenever a charged particle moves through the plasma in external magnetic field, it will excite both longitudinal and transverse waves. Due to the effect of coupling, longitudinal wave energy will transform itself to radiation energy which should ultimately be coming from the moving particle exciting them. If this physical picture be correct this does not necessitate that the particle velocity should be greater than the phase velocity of radiation in the medium; on the other hand, the particle velocity should be greater than the sound wave velocity in the medium. This is so, because it has been shown in I that only in the latter case, can the moving particle excite plasma waves in the medium. We thus see that when the particle velocity is not so large as to satisfy the Čerenkov condition, there is still a possibility of radiation emitted by the moving particle.

Secondly, the dielectric tensor represented by Eqns (1) and (2) is derived on the basis that the motion of the individual plasma electron is governed only by the fluctuating electric field in the plasma and the external magnetic field (see, for example, Åström 1951). Presence of longitudinal disturbance in the medium modifies the equation of motion of the electrons by an additional term proportional to the fluctuating pressure gradient. Thus the dielectric tensor (1) takes no account of the longitudinal disturbance, and hence it cannot give rise to any radiation phenomenon which may arise due to the presence of plasma waves.

The aim of the present paper is to investigate the problem of interaction of the moving particle with the transverse field in the light of above discussions. The calculation is done in a phenomenological way, starting from Maxwell's equations and equation of motion of plasma electrons as modified by fluctuating pressure gradient. The loss of energy by the moving particle will be calculated, as has been done in I, from the amount of work done against the transverse disturbance excited by the moving particle itself. Thus, if $\mathbf{E}^\perp(\mathbf{r}, t)$ is the transverse electric field at any point \mathbf{r} within the plasma, then the energy loss per unit length of the path of the particle of charge q , moving with a velocity \mathbf{u} is given by

$$-\left(\frac{dE}{dx}\right)_{\text{rad}} = F = \frac{q}{u} (\mathbf{E}^\perp \cdot \mathbf{u})_{\mathbf{r}=\mathbf{u}t}, \quad \dots\dots (4)$$

evaluated at the position of the particle. The result turns out that for a velocity sufficiently greater than the average thermal velocity of the plasma electron, the particle indeed loses energy, in addition to Čerenkov radiation obtained by Kolomenskii. This extra energy loss will appear in the form of radiation because it is used up to excite transverse waves in the medium. The calculation for this extra loss is not very rigorous, and has been carried out only for the case when the

particle velocity is much less than that needed for exciting Čerenkov radiation. For particle velocity greater than the phase velocity of the radiation in the medium the analysis has been done by neglecting the effect of plasma waves, and yields the result obtained by Kolomenskii.

As an additional point of interest we have thoroughly discussed the analogy of a plasma in magnetic field with a gyrotropic crystal, a fact already known, as it follows automatically from our calculations.

§ 2. BASIC EQUATIONS

We consider an electron plasma of unlimited extent placed in a constant magnetic field \mathbf{H}_0 , through which a particle of charge q (e.s.u.) moves with a uniform velocity \mathbf{u} . The plasma is supposed to be of low density and the ionic motions are neglected as compared with those of electrons. Taking the magnetic field \mathbf{H}_0 along the z direction of rectangular coordinate axes, the state of the electromagnetic field in the plasma is described by the following equations:

$$\nabla \times \mathbf{E} = -\frac{1}{c} \frac{\partial \mathbf{H}}{\partial t}, \quad \dots\dots (5)$$

$$\nabla \times \mathbf{H} = \frac{1}{c} \frac{\partial \mathbf{E}}{\partial t} - \frac{4\pi}{c} n_0 e \mathbf{v} + \frac{4\pi}{c} q \mathbf{u} \delta(\mathbf{r} - \mathbf{ut}), \quad \dots\dots (6)$$

$$\frac{\partial \mathbf{v}}{\partial t} = -\frac{e}{m} \mathbf{E} - \frac{V^2}{n_0} \nabla n - \frac{e}{mc} \mathbf{v} \times \mathbf{H}_0, \quad \dots\dots (7)$$

$$\nabla \cdot \mathbf{E} = -4\pi n e + 4\pi q \delta(\mathbf{r} - \mathbf{ut}), \quad \dots\dots (8)$$

$$\nabla \cdot \mathbf{H} = 0. \quad \dots\dots (9)$$

In the above equations the Gaussian system of units is used. \mathbf{v} and V denote the instantaneous and average thermal velocities of plasma electrons, n and n_0 are the density perturbation and average density of plasma electrons, and $\delta(\mathbf{r} - \mathbf{ut})$ exactly locates the moving particle 'q' at time t . In Eqn (7) it is assumed that the plasma is isothermal and the effect of the a.c. magnetic field on the electrons can be neglected, compared with that of the steady magnetic field.

Equations (5) to (9) are the same as used in I except that in Eqn (7) the effect of the magnetic field is included. From these equations we get the following equation determining the electric field vector at any point within the plasma

$$\begin{aligned} \frac{\partial^3 \mathbf{E}}{\partial t^3} + 4\pi q \mathbf{u} \frac{\partial^2}{\partial t^2} \delta(\mathbf{r} - \mathbf{ut}) + c^2 \left(\nabla \times \nabla \times \frac{\partial \mathbf{E}}{\partial t} \right) \\ = -\omega_p^2 \frac{\partial \mathbf{E}}{\partial t} - V^2 \frac{\partial}{\partial t} [4\pi q \nabla \delta(\mathbf{r} - \mathbf{ut}) - \nabla(\nabla \cdot \mathbf{E})] \\ - \omega_c \left[\frac{\partial^2 \mathbf{E}}{\partial t^2} + 4\pi q \mathbf{u} \frac{\partial}{\partial t} \delta(\mathbf{r} - \mathbf{ut}) + c^2 (\nabla \times \nabla \times \mathbf{E}) \right] \times \mathbf{n}, \quad \dots\dots (10) \end{aligned}$$

where \mathbf{n} is a unit vector along \mathbf{H}_0 , i.e. along the z axis, and ω_p and ω_c are given by Eqns (3).

Taking the Fourier transform of the electric field in an unbounded configuration space, by writing

$$\left. \begin{aligned} \mathbf{E}(\mathbf{r}, t) &= \int \mathbf{E}_k \exp [i\mathbf{k} \cdot (\mathbf{r} - \mathbf{ut})] d\mathbf{k} \\ \delta(\mathbf{r} - \mathbf{ut}) &= \frac{1}{8\pi^3} \int \exp [i\mathbf{k} \cdot (\mathbf{r} - \mathbf{ut})] d\mathbf{k} \end{aligned} \right\}, \quad \dots\dots (11)$$

we get from (10), assuming $\mathbf{u} \parallel \mathbf{n}$,

$$a\mathbf{E}_k + \mathbf{k} \left[i \frac{qV^2}{2\pi^2} - (c^2 - V^2)(\mathbf{k} \cdot \mathbf{E}_k) \right] = i \frac{q\omega}{2\pi^2} \mathbf{u} \\ + ib(\mathbf{E}_k \times \mathbf{n}) + i \frac{\omega_c}{\omega} c^2 (\mathbf{k} \cdot \mathbf{E}_k)(\mathbf{k} \times \mathbf{n}), \quad \dots\dots (12)$$

where

$$\left. \begin{aligned} a &= k^2 c^2 + \omega_p^2 - \omega^2 \\ b &= \omega_c \left(\omega - \frac{c^2 k^2}{\omega} \right) \\ \omega &= \mathbf{k} \cdot \mathbf{u} \end{aligned} \right\}, \quad \dots\dots (13)$$

and

is the frequency of the k th Fourier component of the field. Taking the vector product of Eqn (12) with \mathbf{k} and breaking up the electric field \mathbf{E}_k into its transverse and longitudinal parts, as

$$\left. \begin{aligned} \mathbf{E}_k &= \mathbf{E}_k^\perp + \mathbf{E}_k^\parallel \\ \mathbf{k} \cdot \mathbf{E}_k^\perp &= 0 \\ \mathbf{k} \times \mathbf{E}_k^\parallel &= 0 \end{aligned} \right\}, \quad \dots\dots (14)$$

where

and

we get

$$\mathbf{E}_k^\perp (b^2 \omega^2 - a^2 k^2 u^2) \\ = \mathbf{k} \left[i \frac{q}{2\pi^2} a \omega^2 u^2 - b \omega \omega_c \frac{\omega^2}{k^2} (\mathbf{k} \cdot \mathbf{E}_k) \right] \\ - \mathbf{n} \left[i \frac{q}{2\pi^2} a k^2 u^3 \omega - b \omega^2 \omega_c u (\mathbf{k} \cdot \mathbf{E}_k) \right] \\ - (\mathbf{k} \times \mathbf{n}) \left[\frac{q}{2\pi^2} b \omega^2 u^2 + i a \omega \omega_c u^2 (\mathbf{k} \cdot \mathbf{E}_k) \right]. \quad \dots\dots (15)$$

Equation (15) shows that the transverse waves \mathbf{E}_k^\perp are coupled with the longitudinal waves \mathbf{E}_k^\parallel (contained in $\mathbf{k} \cdot \mathbf{E}_k$) through the term ω_c . If $\omega_c = 0$, i.e. in the absence of the magnetic field, \mathbf{E}_k^\perp is independent of \mathbf{E}_k^\parallel , and the two waves propagate as independent modes. We shall see later in §4, that if we neglect the effect of plasma waves, we can write

$$\mathbf{k} \cdot \mathbf{E}_k = -i \frac{q}{2\pi^2}, \quad \dots\dots (16)$$

giving only the Coulomb field due to a charge q for the longitudinal disturbance. Using (16) and the first equation of (11), we get from Eqn (15) the following expression for the total transverse field in the medium:

$$\mathbf{E}^\perp(\mathbf{r}, t) = -\nabla \phi(\mathbf{r}, t) - \frac{1}{c} \frac{\partial}{\partial t} \mathbf{A}(\mathbf{r}, t) - \nabla \times \mathbf{B}(\mathbf{r}, t), \quad \dots\dots (17)$$

where

$$\phi(\mathbf{r}, t) = \frac{q}{2\pi^2} \int \frac{\omega^2}{k^2} \frac{a k^2 u^2 + b \omega \omega_c}{a^2 k^2 u^2 - b^2 \omega^2} \exp [i \mathbf{k} \cdot (\mathbf{r} - \mathbf{u}t)] d\mathbf{k}, \quad \dots\dots (18)$$

$$\mathbf{A}(\mathbf{r}, t) = \frac{cq\mathbf{u}}{2\pi^2} \int \frac{a k^2 u^2 + b \omega \omega_c}{a^2 k^2 u^2 - b^2 \omega^2} \exp [i \mathbf{k} \cdot (\mathbf{r} - \mathbf{u}t)] d\mathbf{k}, \quad \dots\dots (19)$$

and

$$\mathbf{B}(\mathbf{r}, t) = i\mathbf{n} \frac{qu^2}{2\pi^2} \omega_p^2 \omega_c \int \frac{\omega \exp [i \mathbf{k} \cdot (\mathbf{r} - \mathbf{u}t)]}{a^2 k^2 u^2 - b^2 \omega^2} d\mathbf{k}. \quad \dots\dots (20)$$

Equations (17) to (20) show that in addition to a scalar and a vector potential, \mathbf{E}^\perp contains another term which is expressed as curl of an imaginary vector in the direction of the magnetic field. This additional term is responsible for the crystal-like behaviour of the medium as we shall see in the next section.

§ 3. NATURE OF THE TRANSVERSE FIELD

In a crystalline medium the dielectric displacement can be expressed in terms of a complex quantity, the imaginary part of which is known as the 'gyration vector'. This gyration vector is an axial vector and belongs only to those crystals which are optically active (gyrotropic) and possess no centre of symmetry (Sommerfeld 1954). The imaginary nature of this vector signifies the fact that the electric displacement at any point depends not only on the local electric field, but also on its variation in the neighbourhood of the point. Also, this gyration vector does not change the electrical energy density of the medium.

We now compare the above properties of a gyrotropic crystal with our plasma medium. A plasma in a magnetic field possesses only an axis of symmetry along \mathbf{H}_0 , and as is evident from Eqns (17) to (20) the electric field is given by a complex quantity, the imaginary part of which can be compared with a gyration vector. This is so because Eqn (20) represents an imaginary axial vector along the magnetic field direction, and does not contribute to the transverse wave energy as we shall see in the next section. We can then conclude that a plasma in a magnetic field will behave like a gyrotropic crystal with respect to the propagation of transverse waves.

To complete the analogy we now show that the medium will be doubly refracting. For this, we rearrange Eqn (15) in the following way:

$$\begin{aligned} \mathbf{E}_k = & \frac{\mathbf{k} \cdot \mathbf{E}_k}{b^2\omega^2 - a^2k^2u^2} \left[b\omega^2\omega_c u \left(\mathbf{n} - \mathbf{k} \frac{k_z}{k^2} \right) - ia\omega\omega_c u^2 (\mathbf{k} \times \mathbf{n}) \right] \\ & - i \frac{q}{2\pi^2} \frac{1}{b^2\omega^2 - a^2k^2u^2} \left[ak^2u^3\omega \left(\mathbf{n} - \mathbf{k} \frac{k_z}{k^2} \right) - ib\omega^2u^2 (\mathbf{k} \times \mathbf{n}) \right]. \end{aligned} \quad \dots\dots (21)$$

Here we have divided the vector \mathbf{k} into two parts, one is along and the other is perpendicular to the magnetic field direction

$$\left. \begin{aligned} \mathbf{k} &= \mathbf{k}_\rho + \mathbf{k}_z \\ k^2 &= k_\rho^2 + \frac{\omega^2}{u^2} \end{aligned} \right\}, \quad \dots\dots (22)$$

where $\mathbf{k}_z \parallel \mathbf{n}$ and $\mathbf{k}_\rho \perp \mathbf{n}$.

We define two unit vectors \mathbf{p} and \mathbf{q} as follows

$$\left. \begin{aligned} \mathbf{p} &= \frac{k}{k_\rho} \left(\mathbf{n} - \mathbf{k} \frac{k_z}{k^2} \right) \\ \mathbf{q} &= \frac{\mathbf{k} \times \mathbf{n}}{k_\rho} \end{aligned} \right\}. \quad \dots\dots (23)$$

and

It can be easily verified that \mathbf{p} and \mathbf{q} are unit vectors, perpendicular to each other, and that the vector \mathbf{p} is perpendicular to \mathbf{k} .

Writing

$$\begin{aligned}\frac{1}{b^2\omega^2 - a^2k^2u^2} &= \frac{1}{2b\omega} \left(\frac{1}{b\omega + aku} + \frac{1}{b\omega - aku} \right) \\ &= \frac{1}{2aku} \left(\frac{1}{b\omega - aku} - \frac{1}{b\omega + aku} \right),\end{aligned}$$

and using (23), we at once get from (21) the following expression for \mathbf{E}_k^\perp

$$\begin{aligned}\mathbf{E}_k^\perp &= \frac{\mathbf{p} + i\mathbf{q}}{b\omega + aku} \left[\frac{1}{2}(\mathbf{k} \cdot \mathbf{E}_k) \frac{k_\rho}{k} \omega_c \omega u + i \frac{q}{4\pi^2} k_\rho \omega u^2 \right] \\ &\quad + \frac{\mathbf{p} - i\mathbf{q}}{b\omega - aku} \left[\frac{1}{2}(\mathbf{k} \cdot \mathbf{E}_k) \frac{k_\rho}{k} \omega_c \omega u - i \frac{q}{4\pi^2} k_\rho \omega u^2 \right]. \quad \dots\dots (24)\end{aligned}$$

Eqn (24) shows that the transverse field consists of two circularly polarized waves of opposite polarization. The vector $\mathbf{p} + i\mathbf{q}$ rotates in the same direction as that in which the electron gyrates about the magnetic field, and is known as the 'extraordinary wave'. The other vector $\mathbf{p} - i\mathbf{q}$ rotates in the opposite direction and is known as the 'ordinary wave'. The medium thus behaves like a doubly refracting crystal with respect to the propagation of transverse waves. Again, using Eqns (13) we can write

$$\begin{aligned}b\omega + aku &= \omega^2 \left(\frac{\omega}{\cos \theta} - \omega_c \right) \left[\frac{c^2 k^2}{\omega^2} - \left\{ 1 - \frac{\omega_p^2}{\omega(\omega - \omega_c \cos \theta)} \right\} \right] \\ \text{and} \\ b\omega - aku &= -\omega^2 \left(\frac{\omega}{\cos \theta} + \omega_c \right) \left[\frac{c^2 k^2}{\omega^2} - \left\{ 1 - \frac{\omega_p^2}{\omega(\omega + \omega_c \cos \theta)} \right\} \right] \end{aligned} \quad \dots\dots (25)$$

and we get the dispersion relations for these two waves, given by

$$\frac{\omega^2}{k^2} = c^2 \left/ \left(1 - \frac{\omega_p^2}{\omega(\omega \pm \omega_c \cos \theta)} \right) \right., \quad \dots\dots (26)$$

where the angle θ denotes the direction in which the wave is propagated with respect to the magnetic field, and the positive and negative signs before ω_c refer to ordinary and extraordinary waves respectively.

From (26), we get the indices of refraction for these waves as

$$\eta_0, \epsilon^2(\omega, \omega_c, \omega_p, \theta) = 1 - \frac{\omega_p^2}{\omega(\omega \pm \omega_c \cos \theta)}, \quad \dots\dots (27)$$

η_0 and η_e denoting the ordinary and extraordinary indices of refraction corresponding to the positive and negative signs before ω_c . From (27) we can make the following remarks: for propagation at right angles to the magnetic field ($\theta = \frac{1}{2}\pi$), there is no double refraction and a single electromagnetic wave propagates with a phase velocity given by

$$V_{ph}^2 = \frac{c^2}{1 - \omega_p^2/\omega^2},$$

as in the case of plasma without magnetic field. Further, putting $\theta = 0$ and π , we can see that the roles of ordinary and extraordinary waves are exchanged as the propagation direction changes from \mathbf{n} to $-\mathbf{n}$. The results expressed by (27) are somewhat different from that obtained from the magneto-ionic theory

(Ratcliffe 1959, Åström 1951). For $\theta = \frac{1}{2}\pi$, magneto-ionic theory gives an extra wave in addition to that obtained here, but that extra wave is not purely transverse. As we are considering only the case of a purely transverse wave, our analysis will not yield that additional wave.

Equation (24) also permits us to estimate the amplitude ratios of the longitudinal and transverse waves. All these waves are excited by the moving particle q . If we neglect the particle itself after the appearance of these waves in the medium, i.e. if we put $q=0$, then Eqn (24) at once gives

$$\text{and} \quad \left. \begin{aligned} \frac{E_{ke}^\perp}{E_k^\perp} &= \frac{\omega_c \sin \theta}{\sqrt{2(\omega - \omega_c \cos \theta)[(c^2 k^2/\omega^2) - \eta_e^2]}} \\ \frac{E_{ko}^\perp}{E_k^\parallel} &= \frac{\omega_c \sin \theta}{\sqrt{2(\omega + \omega_c \cos \theta)[(c^2 k^2/\omega^2) - \eta_0^2]}} \end{aligned} \right\} \dots\dots (28)$$

Here we have separated the ordinary and extraordinary part of the wave and have considered only the magnitudes. These equations show that there is no coupling between \mathbf{E}_e and \mathbf{E}_k when the wave propagates along the magnetic field ($\theta=0$), and maximum coupling effect for propagation at right angles to \mathbf{H}_0 ($\theta=\frac{1}{2}\pi$).

§ 4. ENERGY LOSS BY RADIATION

We shall now calculate the loss of energy by the moving particle in exciting transverse waves in the medium. For this we need the expression for $\mathbf{k} \cdot \mathbf{E}_k$ as a function of different frequencies and wave vector. The term $\mathbf{k} \cdot \mathbf{E}_k$ can be directly evaluated from Eqn (12) by a laborious but straightforward calculation, and can be written as follows:

$$\mathbf{k} \cdot \mathbf{E}_k = i \frac{q}{2\pi^2} + i \frac{q}{2\pi^2} N, \quad \dots\dots (29)$$

where N is a function of ω , ω_p , ω_c and \mathbf{k} . Multiplying (29) by $\exp i\mathbf{k} \cdot (\mathbf{r} - \mathbf{u}t)$ and integrating over \mathbf{k} , it can be shown that the first term in (29) represents only the charge q , whereas the second term gives the plasma wave. We shall now consider the effect of these two terms separately.

4.1. Absence of Plasma Waves

As explained above, we shall in this case put $N=0$ in (29), and thus the value of $\mathbf{k} \cdot \mathbf{E}_k$ will be given by (16). Using Eqn (16) for $\mathbf{k} \cdot \mathbf{E}_k$ and the expressions (25) and (27) in Eqn (24), we obtain

$$\mathbf{E}_k^\perp = i \frac{q}{4\pi^2} \frac{k_\rho u}{k\omega} \frac{\mathbf{p} + i\mathbf{q}}{(c^2 k^2/\omega^2) - \eta_e^2} + i \frac{q}{4\pi^2} \frac{k_\rho u}{k\omega} \frac{\mathbf{p} - i\mathbf{q}}{(c^2 k^2/\omega^2) - \eta_0^2}.$$

Use of the first equation of (11) then gives

$$\mathbf{E}^\perp(\mathbf{r}, t) = i \frac{q}{4\pi^2} \int d\mathbf{k} \exp [i\mathbf{k} \cdot (\mathbf{r} - \mathbf{u}t)] \left[\frac{k_\rho u}{k\omega} \left\{ \frac{\mathbf{p} + i\mathbf{q}}{(c^2 k^2/\omega^2) - \eta_e^2} + \frac{\mathbf{p} - i\mathbf{q}}{(c^2 k^2/\omega^2) - \eta_0^2} \right\} \right]. \quad \dots\dots (30)$$

We take the scalar product of (30) with \mathbf{u} and evaluate it at the point $\mathbf{r} = \mathbf{u}t$. The resulting expression when used in Eqn (4) together with Eqn (23), gives

for the amount of energy loss the following expression:

$$F = i \frac{q^2 u}{4\pi^2 c^2} \int \frac{k_p^2}{k^2} \omega \left[\frac{1}{k^2 - (\omega^2/c^2)\eta_e^2} + \frac{1}{k^2 - (\omega^2/c^2)\eta_o^2} \right] dk. \quad \dots\dots (31)$$

We note here that the vector \mathbf{q} which corresponds to the gyration vector discussed in the last section, does not contribute to the energy loss, as \mathbf{u} is parallel to \mathbf{n} .

To integrate Eqn (31), it is convenient to write

$$d\mathbf{k} = k_p dk_p \frac{d\omega}{u} d\varphi$$

where φ is the azimuthal angle of \mathbf{k} . In that case, however, the angle θ appearing in the expressions for $\eta_{o,e}$ is to be expressed in terms of k_p and k_z , which will make the integrand very complicated. To avoid this, we make one simplification. We have already seen in the last section that the roles of η_o and η_e are exchanged for a change of θ from 0 to π . If we then take the value of $\eta_{o,e}$ averaged over $\theta = 0$ and $\theta = \pi$, we get

$$\eta^2 = (\eta_o^2)_{av} = (\eta_e^2)_{av} = 1 + \frac{\omega_p^2}{\omega_c^2 - \omega^2}. \quad \dots\dots (32)$$

Instead of calculating the energy loss through ordinary and extraordinary waves separately, we shall calculate the total energy loss averaged over the two waves, by using η^2 given by (32) in place of η_o^2 and η_e^2 appearing in (31). With this simplification, Eqn (31) gives, after integrating over φ ,

$$F = i \frac{q^2}{\pi c^2} \int_{-\infty}^{+\infty} \omega d\omega \int_0^{k_m} \frac{k_p^3 dk_p}{(k^2 + \omega^2/u^2)[k^2 + (\omega^2/u^2)(1 - \beta^2\eta^2)]}, \quad \dots\dots (33)$$

where $\beta = u/c$. In (33), we have used the upper limit of k_p as k_m in place of infinity. This is because in our basic plasma equation (7) we have neglected the 'collisions' of plasma electrons. This is possible for a low-density plasma, and is justified if the impact parameter for interaction has some minimum value which should be greater than u/ω_p . Thus, as $1/k_p$ corresponds to the impact parameter, the upper limit of k_p instead of being infinity will have some maximum value k_m .

Integrating over k_p Eqn (33) gives

$$F = i \frac{q^2}{2\pi c^2} \int_{-\infty}^{+\infty} \frac{1}{\beta^2 \eta^2} \ln \left(1 + \frac{k_m^2 u^2}{\omega^2} \right) \omega d\omega \\ + i \frac{q^2}{2\pi c^2} \int_{-\infty}^{+\infty} \left(1 - \frac{1}{\beta^2 \eta^2} \right) \ln \left[1 + \frac{k_m^2 u^2}{\omega^2 (1 - \beta^2 \eta^2)} \right] \omega d\omega. \quad \dots\dots (34)$$

We shall consider two different cases:

Case I. $\beta\eta < 1$.

In this case, we can at once apply the theorem of residue to the integrals in (34). The singularities are given by

$$\omega = \pm (\omega_c^2 + \omega_p^2)^{1/2}.$$

As these singularities fall on the real axis we indent the contour about these points to get the principal values of the integrals. The contributions of the two

integrals in (34) will then be equal in magnitude, but opposite in sign, so that we get

$$F = 0, \quad \dots\dots (35)$$

Hence, in the absence of plasma waves, the particle does not emit any radiation for $\beta\eta < 1$.

Case II. $\beta\eta > 1$.

In this case since the argument of the logarithm of the second term on the right-hand side of (34) is negative, we write

$$\ln \left[1 + \frac{k_m^2 u^2}{\omega^2 (1 - \beta^2 \eta^2)} \right] = \ln \left| 1 + \frac{k_m^2 u^2}{\omega^2 (1 - \beta^2 \eta^2)} \right| - i\pi,$$

where the sign of the phase term π is so chosen as to make the energy loss positive. With this, Eqn (34) gives

$$F = \frac{q^2}{c^2} \int_{\beta\eta > 1} \left(1 - \frac{1}{\beta^2 \eta^2} \right) \omega d\omega + i \frac{q^2}{2\pi c^2} \int_{-\infty}^{+\infty} \frac{1}{\beta^2 \eta^2} \ln \left(1 + \frac{k_m^2 u^2}{\omega^2} \right) \omega d\omega \\ + i \frac{q^2}{2\pi c^2} \int_{-\infty}^{+\infty} \left(1 - \frac{1}{\beta^2 \eta^2} \right) \ln \left| 1 + \frac{k_m^2 u^2}{\omega^2 (1 - \beta^2 \eta^2)} \right| \omega d\omega.$$

In the first integral the limits given by $\beta\eta > 1$ take account of both positive and negative part of the frequency and hence the integral is multiplied by 2.

As before, the sum of the last two integrals will give zero value by residue theorem, and we shall obtain

$$F = \frac{q^2}{c^2} \int_{\beta\eta > 1} \left(1 - \frac{1}{\beta^2 \eta^2} \right) \omega d\omega. \quad \dots\dots (36)$$

To evaluate the integral (36) we set $\beta \sim 1$. Also, from (32) we note that the condition $\beta\eta > 1$ requires that ω cannot exceed the value ω_c . Hence, using the limits of ω as 0 and ω_c and taking $\beta \sim 1$, Eqn (36), with the help of Eqn (32), gives after integration

$$F = \frac{q^2 \omega_p^2}{2c^2} \ln \left(\frac{\omega_c^2 + \omega_p^2}{\omega_p^2} \right). \quad \dots\dots (37)$$

Equation (37) is identical with the expression for the loss of energy by Čerenkov radiation as obtained by Kolomenskii from a different consideration. As the condition $\beta\eta > 1$ is necessary for the particle to emit Čerenkov radiation, we can infer from Eqns (35) and (37) that in the absence of plasma waves, the moving particle can emit only Čerenkov radiation.

4.2. Effect of the Plasma Waves on the Emitted Radiation

When plasma waves are present in the longitudinal disturbance, N has a non-zero value in Eqn (29). Instead of using the exact expression for N in presence of magnetic field, we shall use its value for zero magnetic field, as given in I. We make this approximation in order to avoid excessive mathematical difficulties. However, this will permit us to investigate how the nature of radiation changes its character, and to calculate the approximate value of the energy loss. Therefore, we write

$$\mathbf{k} \cdot \mathbf{E}_k = i \frac{q}{2\pi^2 k^2 V^2 + \omega_p^2 - \omega^2}. \quad \dots\dots (38)$$

Equation (38) takes account of the plasma wave only, and neglects the static Coulomb field of the particle. We shall, however, neglect here this static field, as given by the first term of (29), because we have already considered it before in §4.1.

Thus using (38) in (24), we get, with the help of Eqns (25) and (27),

$$\mathbf{E}_k^\perp = -i \frac{q\omega_p^2 u}{4\pi^2} \frac{k_p \omega_c}{k\omega} \frac{1}{k^2 V^2 + \omega_p^2 - \omega^2} \times \left[\frac{\mathbf{p} + i\mathbf{q}}{(\omega_c - ku)(c^2 k^2/\omega^2 - \eta_e^2)} + \frac{\mathbf{p} - i\mathbf{q}}{(\omega_c + ku)(c^2 k^2/\omega^2 - \eta_o^2)} \right]. \quad \dots\dots (39)$$

We shall here consider only those values of particle velocities which are much less than the phase velocity of the waves. Taking a large value of ω_c , i.e. large magnetic field, and assuming u not very large, we can neglect ku in comparison with ω_c in the denominators of (39), and obtain, with the help of the first equation of (11),

$$\mathbf{E}^\perp(\mathbf{r}, t) = -i \frac{q\omega_p^2 u}{4\pi^2} \int d\mathbf{k} \exp[i\mathbf{k} \cdot (\mathbf{r} - \mathbf{u}t)] \frac{k_p}{k\omega} \frac{1}{k^2 V^2 + \omega_p^2 - \omega^2} \times \left[\frac{\mathbf{p} + i\mathbf{q}}{(c^2 k^2/\omega^2) - \eta_e^2} + \frac{\mathbf{p} - i\mathbf{q}}{(c^2 k^2/\omega^2) - \eta_o^2} \right]. \quad \dots\dots (40)$$

Proceeding exactly as in §4.1 we obtain from Eqns (4), (23), (32) and (40) the expression for energy loss as

$$F = i \frac{q^2 \omega_p^2}{2\pi c^2} \int_{-\infty}^{+\infty} \frac{\omega d\omega}{\omega^2 - \omega_p^2} \left[\left(1 - \frac{1}{\beta^2 \eta^2} \right) \ln \left\{ 1 + \frac{k_m^2 u^2}{\omega^2 (1 - \beta^2 \eta^2)} \right\} - \left(\frac{1}{\delta^2 \mu^2} - \frac{1}{\beta^2 \eta^2} \right) \ln \left(1 + \frac{k_m^2 u^2}{\omega^2} \right) - \left(1 - \frac{1}{\delta^2 \mu^2} \right) \ln \left\{ 1 + \frac{k_m^2 u^2}{\omega^2 (1 - \delta^2 \mu^2)} \right\} \right], \quad \dots\dots (41)$$

where

$$\mu^2 = 1 - \frac{\omega_p^2}{\omega^2}, \quad \delta^2 = \frac{u^2}{V^2}. \quad \dots\dots (42)$$

We shall again consider two different cases:

Case I. $u < V$.

In this case we can easily neglect $\delta^2 \mu^2$ and $\beta^2 \eta^2$ in comparison with unity within the logarithm terms, and so Eqn (41) gives

$$F = 0. \quad \dots\dots (43)$$

Case II. $u > V$ such that $\delta^2 \mu^2 > 1$, but $\beta^2 \eta^2 < 1$.

In this case, we can still neglect $\beta^2 \eta^2$ in comparison with unity in the logarithm term. Writing

$$\ln \left[1 + \frac{k_m^2 u^2}{\omega^2 (1 - \delta^2 \mu^2)} \right] = \ln \left| 1 + \frac{k_m^2 u^2}{\omega^2 (1 - \delta^2 \mu^2)} \right| + i\pi,$$

with the positive sign before the phase term to make the energy loss positive, we get from (41) exactly as before

$$F = \frac{q^2 \omega_p^2}{c^2} \int_{\delta\mu > 1} \frac{\omega d\omega}{\omega^2 - \omega_p^2} \left(1 - \frac{1}{\delta^2 \mu^2} \right). \quad \dots\dots (44)$$

From (42), the condition $\delta\mu > 1$ gives a lower limit to ω , such that

$$\omega^2 > \frac{u^2}{u^2 - V^2} \omega_p^2.$$

Hence, using the limits of ω in (44) as $\omega = \{u^2/(u^2 - V^2)\}^{1/2} \omega_p$ and $\omega = \omega_m$, where ω_m is some maximum value of ω , we get after integration

$$F = \frac{q^2 \omega_p^2}{2c^2} \left[\ln \left(\frac{\omega_m^2 u^2}{\omega_p^2 V^2} \right) - \left(1 - \frac{V^2 \omega_p^2}{u^2 \omega_m^2} \right) \right]. \quad \dots\dots (45)$$

Equation (45) gives the radiation energy loss of the particle which will appear in a form different from Čerenkov radiation, because $\beta\eta < 1$. The velocity required for this is such that

$$\delta\mu > 1, \quad \text{i.e.} \quad u > \left(\frac{\omega^2}{\omega^2 - \omega_p^2} \right)^{1/2} V.$$

Using the dispersion relation for plasma waves without magnetic field, viz.

$$\omega^2 = k^2 V^2 + \omega_p^2,$$

and setting the maximum value of k as $2\pi/\lambda_D$, where λ_D is the Debye length (see I), we obtain

$$u > \left(\frac{12\pi^2 + 1}{12\pi^2} \right)^{1/2} V.$$

As shown in I, this is exactly the limit of the particle velocity needed for exciting plasma waves in the medium. Therefore, we get the result that if there is no plasma wave in the medium, there will be no radiation from the particle other than Čerenkov radiation. On the other hand, if plasma waves are present, the particle will emit non-Čerenkov type of radiation, for which the amount of energy loss is given by Eqn (45).

§ 5. DISCUSSION

In Eqn (45) for the energy loss by non-Čerenkov radiation, we have not specified the value of ω_m used as the upper limit of integration in Eqn (44). This limit cannot be greater than that given by $\beta\eta > 1$. If we want to make a comparison of the two energy losses given by Eqns (37) and (45), we can set $\omega_m = \omega_c$. In that case if ω_c is not very large compared to ω_p , and if the kinetic temperature of the plasma is not very small (i.e. V not very small compared with u), we find that the energy loss given by Eqn (45) is small compared with that given by Eqn (37). On the other hand, if ω_c is very large compared with ω_p and the plasma is of sufficiently low temperature, the two losses may be comparable with each other.

Regarding the frequency ranges in which these radiation losses will appear, we cannot make any remark from the calculations done in this paper. For this, actual evaluation of the integrals represented by Eqns (30) and (40) is necessary. The results of these integrations should give the different frequency ranges occupied by both ordinary and extraordinary waves and also their Čerenkov angles for the case $\beta\eta > 1$. This, at present is being carried out by the author.

In conclusion, we mention that all our calculations are based on the plasma equation (7), which only takes account of the local distribution of pressure. For a collisionless gas this approach to the problem is not a very rigorous one. A better

method is to start from the full Boltzmann equation with the collision term put equal to zero. Because this will involve excessive mathematical difficulties, we have limited ourselves to the simpler equation. The qualitative effects which the Boltzmann equation will have on the results, when used in place of Eqn (7), have already been discussed in I in connection with longitudinal waves. The same remarks are valid for the case of transverse waves as discussed in this paper.

ACKNOWLEDGMENT

The author wishes to express his sincere gratitude to the Director, Professor B. D. Nag, for his keen interest and valuable discussions.

REFERENCES

- ÅSTRÖM, E., 1951, *Ark. Fys.*, **2**, 443.
FIELD, G. B., 1956, *Astrophys. J.*, **124**, 555.
KOLOMENSKII, A. A., 1956, *Dokl. Akad. Nauk, SSSR*, **106**, 982.
KRITZ, A. H., and MINTZER, D., 1960, *Phys. Rev.*, **117**, 382.
MAJUMDAR, S. K., 1960, *Proc. Phys. Soc.*, **76**, 657.
RATCLIFFE, J. A., 1959, *The Magneto-ionic Theory and its Applications to the Ionosphere* (Cambridge: University Press), p. 18.
SOMMERFELD, A., 1954, *Optics* (New York: Academic Press), Ch. IV.
SPITZER, L., 1956, *Physics of Fully Ionised Gases* (New York: Interscience).

Some Theoretical Considerations on the Longitudinal Magnetic Field Induced Oscillations in Semiconductors (the Oscillistor) and a Tentative Explanation

By A. C. PRIOR

Royal Radar Establishment, Great Malvern, Worcs.

MS. received 21st November 1960, in revised form 2nd January 1961

Abstract. The conditions under which oscillations have been observed are shown to be such that a system of transient circulating currents can arise. These currents will tend to increase the carrier concentration at one surface of the specimen, and thus modify the surface recombination. Oscillations of a relaxation type could plausibly result. The model suggests variations of frequency and amplitude with magnetic field intensity and direction, and with electric field and temperature similar to that reported, and could account for the occurrence of incoherent oscillations with an accurately aligned magnetic field.

§ 1. INTRODUCTION

SEVERAL authors (Ivanov and Ryvkin 1958, Bok and Veilex 1959) have reported electrical oscillations when current-carrying semiconductor specimens are situated in an approximately longitudinal magnetic field, and Larrabee and Steele (1960) have investigated the conditions necessary for such oscillations. To the writer's knowledge no detailed mechanism which accounts for these oscillations has yet been proposed.

This paper points out that for the conditions under which oscillations have been observed a system of transient circulating currents can arise. A connection between these currents and the occurrence of oscillations seems likely, and with some plausible assumptions a tentative explanation for the oscillations is suggested.

§ 2. ORIGIN OF THE CIRCULATING CURRENTS

Consider a heavily injected bar of semiconductor carrying a longitudinal current in a magnetic field as shown in Fig. 1(a) and (b). The distribution of carriers over any cross section will be influenced by the combined effects of injection from the ends, recombination at the surface and in the bulk, and diffusion. In addition the Lorentz force arising from the current flow and the transverse component H_T of the field will tend to drive the carriers towards the face AB.

Now consider the consequences of the motion of the carriers towards AB in the presence of the longitudinal field H_P . Firstly a motion of the holes and electrons towards the faces AC and BD respectively will occur, and result in charge distributions appearing on these faces. These charge distributions will in turn exert forces on the electrons and holes in the opposite direction to those resulting from H_P . If the latter forces were independent of the distance from AB, the net result would simply be the establishment of uniform charge densities along AC and BD just adequate to cancel the effect of the magnetic field. However, the forces resulting from H_P will not in general be independent of the distance from AB, since

they are proportional to the velocity v_z towards AB. In particular, if there were no surface recombination, v_z would on the average be zero on AB, as the carriers cannot cross this surface. With surface recombination, v_z could still decrease towards AB under appropriate conditions of concentration gradient. To take an extreme example for illustration, suppose that carriers generated on CD crossed the specimen in a uniform flux to recombine on AB; if their density increased towards AB under the action of the transverse field H_T , v_z would correspondingly fall. In general therefore the forces due to the surface charges and those due to H_p will not balance except at particular positions; the electric forces will predominate near AB and those due to H_p will predominate in the interior. The net result will be circulating currents as indicated in Fig. 1 (c).

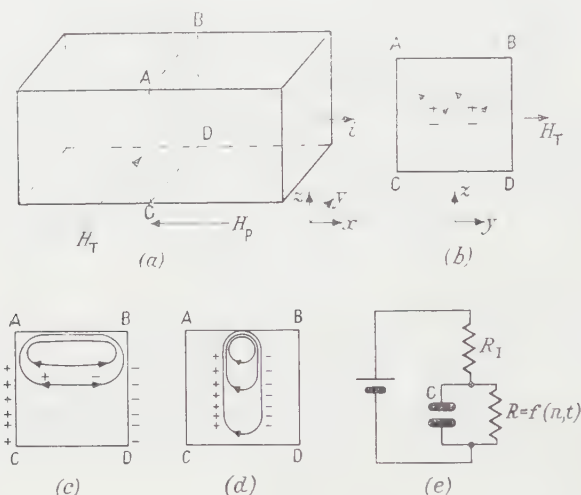


Fig. 1. Development of circulating currents, and (e) analogous oscillating circuit.

Even if the system were in a steady state, circulating currents might result from a flux of carriers moving to recombine on the surface AB; however, the currents occurring under such conditions are unlikely to be important. Changes of carrier distribution are probably necessary to produce circulating currents sufficient to cause major effects. It will be shown in the next section that such currents could, through the mechanism of surface recombination, react back on the system in such a way as to enhance their generation. This could lead to an unstable situation causing the fluctuations in the density distribution necessary to produce substantial circulating currents. However, before proceeding with a discussion of such instabilities it is relevant to compare the conditions necessary for the production of the circulating currents with those necessary for the occurrence of coherent oscillations. For both effects a longitudinal and transverse component of magnetic field are required, as well as the presence of a surface towards which the Lorentz force of the transverse component is tending to drive the carriers. The oscillations appear to be essentially a plasma phenomenon, as are the circulating currents, which will be of substantial magnitude only if the densities of electrons and holes are comparable. These similarities strongly suggest a connection between the two phenomena.

Larrabee and Steele (1960) state that a necessary condition for oscillistor action is that "the ambipolar mobility of the plasma of electrons and holes times the minimal magnetic field be approximately 0.1 dimensionless m.k.s. units". This corresponds to an effective plasma Hall angle $\theta_p = \tan^{-1} 0.1$, and leads to values adequate for the generation of significant circulating currents. Taking room temperature germanium for example with this minimum field (~ 3000 gauss), and with $H_T = 0.1 H_p$, the z component of the carrier velocity would be approximately 0.01 of the longitudinal drift velocity or approximately 3000 cm sec^{-1} for an applied field of 100 v cm^{-1} . This would give a y component for holes of the order of 200 cm sec^{-1} and for electrons of the order of 400 cm sec^{-1} , corresponding to a transverse field of the order of 0.1 v cm^{-1} . For the actual room temperature germanium oscillistor quoted by Larrabee and Steele, the field was $10\,000$ gauss which would give an equivalent field of about 1 v cm^{-1} . If the oscillations are in some way connected with the motion of carriers to the surface, these velocity components across the specimen seem adequate for the observed frequencies of a few kilocycles per second in room temperature germanium and of a few megacycles per second in cooled semiconductors, where the higher mobilities will increase the velocities both directly and through the increased Hall angles achievable.

§ 3. A POSSIBLE MECHANISM FOR OSCILLATION

In view of these arguments it is relevant to consider whether any additional properties of the system could provide an actual mechanism for oscillation, and the following tentative suggestions are put forward as a possibility. The detailed flow of the circulating currents can be further influenced by the field H_p , which will in particular tend to compress the current near AB against the surface, and so raise the surface concentration. This effect seems rather small for the minimum value of the product $\mu_n H$ but would increase rapidly as this product is increased. Intuitively another concentrating effect on the surface AB seems likely owing to the restriction imposed by the surface AB on the volume available for carrying the current; however such a concentrating effect would be opposed by diffusion and no simple way of estimating its magnitude has occurred to the writer. If the circulating current does produce a significant concentration increase near AB the recombination occurring at the surface will be increased. This increased recombination rate will tend to increase the z velocity component and hence the charge-separating y velocity component, and the circulating currents will be enhanced. If, further, the surface recombination velocity increases with density a powerful additional mechanism for positive feed-back is provided. The process will continue until the volume concentration is reduced to such a value that a high concentration near AB can no longer be maintained. The surface recombination velocity will then fall and with it the means whereby the circulating current mechanism was enhanced. The cycle will start again when the bulk concentration has been sufficiently restored by injection.

Figure 1 (*d*) illustrates another possible mode whereby the volume could be extracted by the circulating currents; in this mode the plasma would shrink in the y direction. The actual flow of carriers to the surface is likely to be a complex combination of various possible modes, and would probably be dependent on the relative values of the y and z velocity components.

This model is analogous to the circuit shown in Fig. 1 (*e*) in which the charge on C corresponds to the plasma, and the battery and resistance R_I to the injection

process; R which represents the recombination mechanism, tends to decrease as the plasma density n increases, but is also a complicated function of time through the instantaneous distribution of the plasma.

A detailed quantitative treatment of these ideas would be extremely complicated and has not been attempted. Qualitatively the model appears to account for the observed properties of the oscillistor. The increase in oscillation frequency with the electric and magnetic fields, and with an increase of mobility on cooling, follows either directly from the increase in all the velocities, or through the resulting increase in surface concentration and hence surface recombination rate. The tendency towards white noise when the field is closely aligned with the specimen is reasonable, since the mechanism could operate independently with different characteristic frequencies in small regions of the crystal where a suitable transverse field component exists at the surface. It is conceivable on this model that a transverse field component may be unnecessary for these incoherent oscillations; diffusion flow, arising from suitable local time-varying concentration-gradients, might be adequate to set up circulating currents sufficient to maintain an unstable condition. The increase in frequency with increasing obliquity of the field follows from the increased transverse velocity. The reduction in amplitude as the obliquity increases beyond about 5° could well follow from the necessity for an appropriate relationship between the 'charging' time, which depends on the injection velocity along the specimen, and the 'discharging' time, which depends on the transverse velocities.

Ideally to test these ideas, measurements of plasma density and of current and field distributions are required. Infra-red absorption techniques as developed by Harrick (1956) could be used for density determination, though probably the simplest technique to yield relevant information would be the use of potential probes variously positioned around a cross section.

ACKNOWLEDGMENT

This paper is published by permission of the Controller, H.M. Stationery Office.

REFERENCES

- BOK, J., and VEILEX, R., 1959, *C.R. Acad. Sci., Paris*, **248**, 2300.
HARRICK, N. J., 1956, *Phys. Rev.*, **101**, 491.
IVANOV, I. L., and RYVKIN, S. M., 1958, *Soviet Physics-Tech. Phys.*, **3**, 722.
LARRABEE, R. D., and STEELE, M. C., 1960, *J. Appl. Phys.*, **31**, 1519.

Gamma Ray Spectra in Large Organic Scintillators

By P. R. J. BURCH

Medical Research Council Environmental Radiation Research Unit,
Department of Medical Physics, University of Leeds,
The General Infirmary, Leeds, 1

MS. received 28th March 1961

Abstract. For moderately large organic scintillators, a linear relation is found between the position of the γ -ray 'Compton peak' and the maximum energy transfer in a first Compton collision. Extrapolation yields a positive intercept on the energy axis as a result of the dependence of the specific light output of scintillators on the linear energy transfer of charged particles. The broadening of the Compton peak on the high-energy side has three components: (*a*) statistical, (*b*) intrinsic line broadening arising from multiple interactions of the γ -ray, and (*c*) geometrical, resulting from the variation of light collection efficiency with the position of the event in the scintillator. The dependence of these three components on γ -ray energy is considered and their approximate magnitudes for two plastic scintillator units are calculated from experimental γ -ray spectra.

§ 1. INTRODUCTION

LARGE volume liquid and plastic organic scintillators have found wide application in cosmic ray investigations (see references in the article by Barnaby and Barton 1960), for neutron detection (Reines *et al.* 1954), for neutrino and anti-neutrino detection (Cowan *et al.* 1956, Reines and Cowan 1959), for anticoincidence shields (Roulston and Naqvi 1956, Ellett and Brownell 1960, Parker 1960, Perkins, Nielson and Diebel 1960), and in the assay of low level γ -radioactivity in biological materials, including whole animals (Van Dilla, Schuch and Anderson 1954) and human beings (Anderson 1956, Bird and Burch 1958, Anderson, Newton Hayes and Hiebert 1958). Although this type of detector is used in situations where a high energy-resolution is not of overriding importance, the ability to discriminate between γ -rays of different energy is often an advantage and sometimes essential when investigating radioactivity in biological specimens. An understanding of the spectral characteristics of this kind of scintillator is therefore of practical importance.

Two factors militate against high γ -ray resolution: (*a*) a low specific light output (at most, one-fifth of that from good NaI (Tl) crystals) and (*b*) the general predominance of Compton over photoelectric interactions. An additional factor, which is dependent on the design of the detector, is the variation in photocathode response to a given event with respect to its position in the scintillator (Brini *et al.* 1955, Burch 1961).

In this article consideration will be given to the contributions of these three factors to the γ -ray spectral broadening observed in large organic scintillators.

§ 2. SPECTRAL CHARACTERISTICS

When a moderately large organic scintillator is irradiated with monochromatic γ -rays, a somewhat asymmetric peak is observed (Fig. 1). On plotting the peak

position as a function of the maximum energy transfer in a Compton collision, a linear relationship is obtained (Fig. 2). However the curve extrapolates to yield a positive intercept on the abscissa of about 0.05 meV for NE101† and NE102 plastic scintillators. On plotting peak position against the full γ -ray energy, a slightly non-linear relationship is obtained (Fig. 3), and the intercept on the abscissa is much larger (about 0.22 meV).

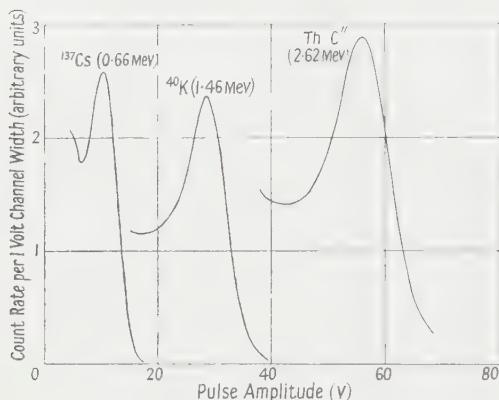


Fig. 1. γ -ray spectra from ^{137}Cs (0.66 meV), ^{40}K (1.46 meV) and ThC'' (2.62 meV), taken with a plastic scintillator (NE101) unit (20 in. \times 10 in. \times 6½ in.) employing two 7 in. diameter Twentieth Century Electronics photomultipliers.



Fig. 3. Relation between observed peak position for ^{137}Cs , ^{40}K and ThC'' (2.62 meV) γ -rays and γ -ray energy. A, B as in Fig. 2.

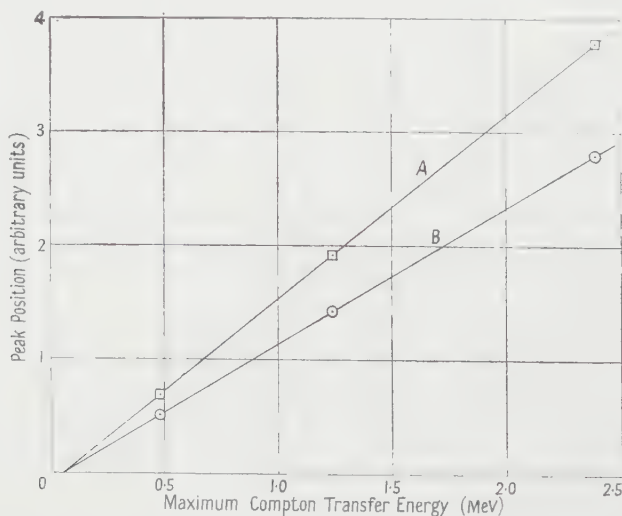


Fig. 2. Relation between observed peak position for ^{137}Cs , ^{40}K and ThC'' (2.62 meV) γ -rays and maximum Compton transfer energy. A, results for 15 in. diameter, 9 in. thick NE102 plastic scintillator unit with four 5 in. diameter E.M.I. photomultipliers; B, results for 20 in. \times 10 in. \times 6½ in. NE101 plastic scintillator unit with two 7 in. diameter Twentieth Century Electronics photomultipliers.

† Obtainable from Nuclear Enterprises (G.B.) Ltd., Edinburgh.

The linearity found in Fig. 2 suggests that the most probable high-energy interaction corresponds to that of the maximum energy transfer in a first Compton collision; absorption of the back-scattered photon does not, in these examples, occur with sufficient frequency appreciably to distort this correspondence. The intercept on the abscissa arises from the dependence of the specific light output on linear energy transfer. Protons (of 0 to 14 mev) for example, give a much lower specific light output in NE102 than high-energy electrons (Evans and Bellamy 1959); it follows that the specific light output from low energy (high linear energy transfer) electrons will also be less than that from high energy (low linear energy transfer) electrons. Low-energy electrons occur not only at the ends of tracks but also as delta rays along the path of a high-energy electron. Consequently, this dependence of specific light output on linear energy transfer will also contribute to statistical fluctuations in the light output, since the number of low-energy delta rays generated will be subject to random fluctuations.

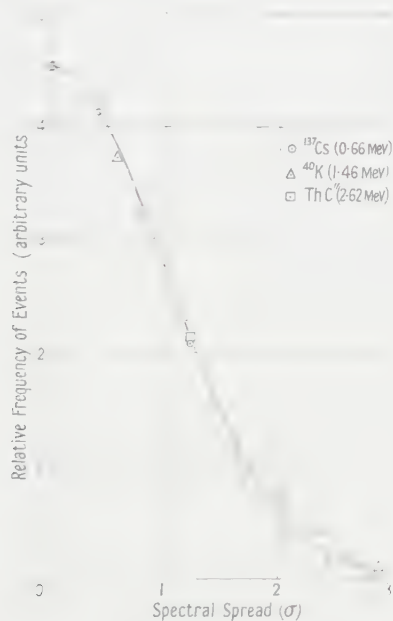


Fig. 4. Comparison of high-energy side of ^{137}Cs , ^{40}K and ThC'' 2.62 mev, spectra in 20 in. \times 10 in. \times 6½ in. NE101 plastic scintillator unit, with Gaussian distribution (solid line). Experimental points are fitted to the Gaussian distribution at peak and at 'half-width' (1.18 σ).

Except in very large ' 4π ' detectors, the peak/trough ratio is low for ^{137}Cs 0.66 mev γ -rays but somewhat larger for ^{40}K 1.46 mev and ThC'' 2.62 mev γ -rays. This is a consequence of the energy distribution of first-collision Compton electrons which is more peaked at the maximum transfer energy for high than for low energy γ -rays. With a very large ' 4π ' detector (Anderson 1961) the probability of multiple Compton interactions is high and there is little variation in the peak/trough ratio with γ -ray energy (from 0.66 to 1.46 mev).

With the detectors investigated in this laboratory, the shape of the Compton peak on the high-energy side is a good approximation to a Gaussian distribution (Fig. 4) and it will be assumed in the following section that each component

contributing to spectral spread has this kind of error distribution, although it is highly unlikely that this assumption will be strictly valid for the non-statistical components. Thus it will be seen from Fig. 4, that although all spectra give a very good fit up to 1.5σ , beyond this point the ^{137}Cs spectrum falls inside, the ^{40}K just outside, and the ThC'' 2.26 mev spectrum further outside, the Gaussian curve. (It is possible that the occasional simultaneous detection of a coincident γ -ray could make a contribution to the spread of the ThC'' 2.62 mev spectrum.)

§ 3. SPECTRAL WIDTH

3.1. Statistical Component

The most obvious, although not necessarily the largest, contribution to spectral broadening is statistical. Thus if the average number of photoelectrons released from the photocathode(s) for a given event is n , this average number will be subject to the $n^{1/2}$ type of standard deviation. However, the whole area of the photocathode(s) is never uniform in sensitivity and area irregularities contribute a further source of random error. As already mentioned, significant random fluctuations occur at an earlier stage of the scintillation process because of the dependence of scintillator efficiency on linear energy transfer together with the statistical fluctuations in δ -track generation. At a later stage, dynode multiplication makes another generally small contribution. With the exception of the δ -track effect, the standard deviation of the photomultiplier signal output from the above causes will be proportional to the square root of the light output for all but small events. Over the γ -ray energy range considered (0.66 to 2.62 mev), this relationship will be nearly true even for the statistical variations in δ -track formation. This can be deduced from the energy dissipation characteristics of high-energy (~ 1 mev) electrons (Burch 1957 a, b); from these it can be seen that the energy dissipated throughout the 'track' in the form of low-energy δ -rays, is nearly proportional to the initial kinetic energy of the parent electron.

3.2. Multiple Compton Collisions

For most γ -ray energies and the low atomic number organic scintillators, photoelectric and pair-production absorption will be unimportant in comparison with the Compton process. The γ -ray emerging from a first collision may undergo further Compton collisions, and in this way the total energy dissipated in the scintillator can easily exceed the maximum transfer energy (the 'Compton peak') for first collisions only. Consequently, these multiple interactions will broaden the spectrum, the degree of broadening being mainly dependent on scintillator size, and source-scintillator geometry. For γ -rays of 0.66, 1.46 and 2.62 mev, giving Compton peaks at 0.48, 1.25 and 2.39 mev respectively, the energies of the 180° back-scattered photons, 0.18, 0.22 and 0.23 mev respectively, are nearly independent of the primary γ -ray energy. Hence the 'intrinsic line broadening' on the high-energy side of the spectrum (in absolute energy terms) will, for these γ -rays and moderately large scintillators, be nearly independent of their primary energy. In very large 4π scintillators we may expect a more marked dependence; thus the higher energy γ -rays will, on the average penetrate a little further into the scintillator before undergoing a first Compton collision and hence the path length available to the slightly more energetic back-scattered photons will be higher. We should expect, therefore, that the 'intrinsic line broadening' for very large 4π

scintillators will increase slightly with increasing γ -ray energy. To evaluate this effect, extensive Monte Carlo case history calculations would be necessary. Some progress in this direction is being made in connection with the Los Alamos 'HUMCO II' large 4π liquid scintillator (Anderson 1961).

3.3. Geometrical Non-uniformity

The efficiency of light collection at the photocathode is always less than unity and thus it will inevitably depend, to some extent, on the geometrical relation between the scintillation event and the photocathode. In some large-volume scintillators this dependence can be very marked (see the survey by Barnaby and Barton 1960) and in our 15 in. diameter by 9 in. thick cylindrical plastic scintillator, the extreme variations in light collection efficiency as a function of geometry must be somewhat greater than $\pm 5\%$ (Burch 1961).

From the point of view of the present analysis, it is important to consider the dependence of this type of spectrum broadening on energy, or more strictly, average light output. In a homogeneous scintillator, the average light emission for a given event will be independent of its position but the average light *collection* at the photocathode from a given position will have a constant *ratio* to the mean for all similar events. Since the scintillation emission is nearly proportional to particle energy, this source of spectral spread will be nearly proportional (in absolute energy terms) to the energy of the event. In most practical arrangements of sources and detectors, the geometrical distribution of scintillation events in the detector will vary slightly with γ -ray energy and markedly with source-detector geometry. In attempting to analyse the magnitude of this factor from experimental results, it is important therefore that comparable source-detector geometries should be used for each source.

§ 4. ANALYSIS

The preceding arguments and assumptions will first be summarized.

4.1.1. The high-energy side of the γ -ray 'Compton peak' is assumed to follow a Gaussian distribution.

4.1.2. The spread in line width on the high-energy side is compounded of three independent factors: (a) Statistical σ_s in which errors are proportional to $A^{1/2}$, where A is the mean amplitude of the Compton peak. (A is nearly proportional to the energy of the Compton peak.) (b) Intrinsic line width σ_i resulting from absorption of scattered photons. For the γ -ray energy range considered here (0.66 to 2.62 MeV) and for moderately large detectors, σ_i is regarded as being independent of γ -ray energy and hence of A . (c) Geometrical σ_g for which, in moderately large detectors and a given source-detector geometry, the spread is proportional to A .

4.1.3. If the half-width of the peak on the high-energy side is W (in the same units as A), the standard deviation σ of the (Gaussian) distribution is given by

$$\sigma = \frac{W}{1.18}. \quad \dots\dots (1)$$

4.2. With the assumptions above, errors can be compounded vectorially, hence

$$\sigma^2 = \sigma_s^2 + \sigma_i^2 + \sigma_g^2. \quad \dots\dots (2)$$

Since, $\sigma_s \propto A^{1/2}$, σ_i is independent of A , and $\sigma_g \propto A$, we may write

$$\sigma^2 = sA + i + gA^2 \quad \dots\dots (3)$$

where s , i and g are constants.

By determining A and W (and hence σ) for three well-separated γ -ray energies under comparable source-detector geometries, we can obtain three simultaneous equations from which s , i and g can be calculated. The ideal γ -ray energies would be such that the 's term', the 'i term' and the 'g term' respectively dominated.

§ 5. EXPERIMENTAL RESULTS

The results for two plastic scintillators are presented and analysed here. The first detector is a cylinder of NE102, 15 in. diameter and 9 in. thick surrounded by a diffuse reflector (packed magnesium carbonate) and with four EMI 9530A 5 in. diameter photomultipliers mounted on one face. The second, NE101, scintillator is 20 in. long, 10 in. wide and $6\frac{1}{2}$ in. thick with hemi-cylindrical ends; two 7 in. diameter Twentieth Century Electronics photomultipliers are mounted on one surface, concentric with the hemi-cylindrical ends. Each detector was irradiated by ^{137}Cs , ^{40}K and ThC'' γ -rays, the sources being placed about 10 in. from the face opposite to the photomultipliers; the results are shown in the Table where the solutions to the three simultaneous equations of type (3) are also given. The value of A for ^{137}Cs is made equal to unity in each case, hence the terms A and gA^2 for ^{137}Cs are equal to s and g respectively.

§ 6. CONCLUSIONS

As would be expected, the value of i (0.042) for the 9 in. thick detector, is somewhat larger than the value (0.032) obtained for the $6\frac{1}{2}$ in. thick detector. Also, the values of g (0.0038 and 0.0024) show that the volume uniformity of the thinner detector is superior to that of the thicker one. The square root of g gives the 'standard deviation' of the geometrical factor: $\pm 6.2\%$ and $\pm 4.9\%$ respectively. The value for the thicker unit is perhaps a little larger than would have been anticipated from the variations in peak position observed with a narrow beam of collimated ^{60}Co γ -rays (Burch 1961).

It should be mentioned that the standard deviation of the geometrical factor for penetrating cosmic-ray particles passing through the entire thickness of the detector should be considerably less than the values of $g^{1/2}$ obtained here for γ -rays. These latter values are derived from the variations in scintillation generation and collection efficiency from rather small volume elements; the average variation from path to path for penetrating cosmic-ray particles will be much smaller. In comparison with the cosmic-ray detectors referred to by Barnaby and Barton (1960) our units would appear to have good geometrical uniformity.

Improvements in efficiency and uniformity of the scintillation and photo-cathode responses would reduce s , but for these units the limit of performance is set by the i and g terms. (With a well-designed detector the g term achieves appreciable significance only at the highest ($>2\text{ MeV}$) γ -ray energies.) Thus even if s could be made negligibly small for the 20 in. \times 10 in. \times $6\frac{1}{2}$ in. unit, the half-resolution for ^{40}K γ -rays would only be reduced from 14.4% to about 9.6%—the ultimate limit for this unit. For ^{137}Cs γ -rays, the dominance of the i term reduces still further the margin of this hypothetical improvement—from

Scintillator	γ -ray source and energy	Peak position (A)	Half-resolution W/A (%)	W (A.u.)	σ ($W/1.18$) (A.u.)	σ^2	σ_{s^2} ($s^2 A$)	σ_1^2 (i)	σ_{g^2} (g, I^2)
Plastic NE102, 15 in. diam., 9 in. thick, Four 5 in. diam. photo- multipliers	^{137}Cs , 0.66 Mev	1	35.7	0.357	0.303	0.092	0.046	0.042	0.004
	^{40}K , 1.46 Mev	2.77	19.0	0.526	0.446	0.199	0.128	0.042	0.029
	$^{232}\text{ThC''}$, 2.62 Mev	5.44	13.7	0.749	0.635	0.403	0.249	0.042	0.112
Plastic NE101, 20 in. \times 10 in. \times 6 $\frac{1}{2}$ in. Two 7 in. diam. photo- multipliers	^{137}Cs	1	28.2	0.282	0.239	0.057	0.023	0.032	0.002
	^{40}K	2.77	14.4	0.399	0.338	0.114	0.064	0.032	0.018
	^{232}ThC	5.44	10.4	0.566	0.479	0.229	0.125	0.032	0.072

28.2% to about 21.8%. The i term depends on the size of the detector and can only be diminished by reducing detector size. However in many applications (such as coincidence or anticoincidence shields, and body γ -ray monitoring) a large size is essential for efficient γ -ray detection. A possible escape from this dilemma would be the incorporation of a high atomic number element in the material of the scintillator, to produce marked photoelectric absorption and the total absorption of the γ -ray. Unfortunately, this expedient invariably produces quenching of the scintillation event, a consequent decrease in light output, and an increase in the s term. Nevertheless further exploration along these lines might reveal a better compromise than any found so far.

REFERENCES

- ANDERSON, E. C., 1956, *Inst. Radio Engrs Transactions of the Professional Group on Nuclear Science*, **NS. 3**, 96.
 — 1961, *Proceedings of University of New Mexico Conference on Organic Scintillation Detectors, August 1960*, in the press and private communication.
 ANDERSON, E. C., NEWTON HAYES, F., and HIEBERT, R. D., 1958, *Nucleonics*, **16**, 106.
 BARNABY, C. F., and BARTON, J. C., 1960, *Proc. Phys. Soc.*, **76**, 745.
 BIRD, P. M., and BURCH, P. R. J., 1958, *Phys. Med. Biol.*, **2**, 217.
 BRINI, D., PELI, L., RIMONDI, O., and VERONESI, P., 1955, *Nuovo Cim., Suppl.* **4**, [10], 2, 1048.
 BURCH, P. R. J., 1957 a, *Radiation Research*, **6**, 289.
 — 1957 b, *Brit. J. Radiol.*, **30**, 524.
 — 1961, *Proceedings of University of New Mexico Conference on Organic Scintillation Detectors, August 1960*, in the press.
 COWAN, C. L., JR., REINES, F., HARRISON, F. B., KRUSE, H. W., and MCGUIRE, A. D., 1956, *Science*, **124**, 103.
 ELLETT, W. H., and BROWNELL, G. L., 1960, *Nucl. Instrum. Methods*, **7**, 56.
 EVANS, H. C., and BELLAMY, E. H., 1959, *Proc. Phys. Soc.*, **74**, 483.
 PARKER, R. P., 1960, *Nucl. Instrum. Methods*, **8**, 339.
 PERKINS, R. W., NIELSON, J. M., and DIEBEL, R. N., 1960, *Rev. Sci. Instrum.*, **31**, 1344.
 REINES, F., and COWAN, C. L., JR., 1959, *Phys. Rev.*, **113**, 273.
 REINES, F., COWAN, C. L., JR., HARRISON, F. B., and CARTER, O. S., 1954, *Rev. Sci. Instrum.*, **25**, 1061.
 ROULSTON, K. I., and NAQVI, S. I. H., 1956, *Rev. Sci. Instrum.*, **27**, 830.
 VAN DILLA, M. A., SCHUCH, R. L., and ANDERSON, E. C., 1954, *Nucleonics*, **12**, 22.

MgH and MgD Bands at 2819 Å and 2702 Å

By M. ASLAM KHAN†

Department of Physics, Imperial College, South Kensington, London, S.W.7

Communicated by R. W. B. Pearse; MS. received 15th December 1958

Abstract. During an investigation of the spectra of metallic hydrides of group II of the periodic table, five new bands of MgH at $\lambda\lambda$ 2819, 2702, 2172, 2100 and 2088, a band system of ZnH at 2426 Å and a band system of CdH at 2483 Å, have been observed and analysed. Also the corresponding deuteride bands, where possible, have been observed. Only the MgH and the corresponding MgD bands at 2819 Å and 2702 Å are dealt with in this paper. They are classified as $E^2\Sigma \rightarrow X^2\Sigma$ and $F^2\Sigma \rightarrow X^2\Sigma$ transitions respectively. The rotational constants are calculated as follows:

MgH

$$E^2\Sigma \rightarrow X^2\Sigma(0,0) \text{ band at } 2819 \text{ Å} \begin{cases} B_r' = 6.08 \text{ cm}^{-1}, & D_v' = 3.31 \times 10^{-4} \text{ cm}^{-1} \\ B_r'' = 5.73 \text{ cm}^{-1}, & D_v'' = 3.43 \times 10^{-4} \text{ cm}^{-1} \\ \nu_0 = 35\,550.61 \text{ cm}^{-1}. \end{cases}$$

$$F^2\Sigma \rightarrow X^2\Sigma(0,0) \text{ band at } 2702 \text{ Å} \begin{cases} B_r' = 5.78 \text{ cm}^{-1}, & D_v' = 4.0 \times 10^{-4} \text{ cm}^{-1} \\ B_r'' = 5.73 \text{ cm}^{-1}, & D_v'' = 3.63 \times 10^{-4} \text{ cm}^{-1} \\ \nu_0 = 36\,995.41 \text{ cm}^{-1}. \end{cases}$$

MgD

$$E^2\Sigma \rightarrow X^2\Sigma(0,0) \text{ band at } 2816 \text{ Å} \begin{cases} B_v' = 3.20 \text{ cm}^{-1} \\ B_v'' = 2.80 \text{ cm}^{-1} \\ \nu_0 = 35\,548.95 \text{ cm}^{-1}. \end{cases}$$

§ 1. INTRODUCTION

THE spectrum of magnesium hydride has been the subject of intense investigation. Many systems of bands in the visible and ultra-violet regions of the spectrum of MgH are now well known. They are the $A^2\Pi \rightarrow X^2\Sigma^+$, $B^2\Sigma^+ \rightarrow X^2\Sigma^+$, $C^2\Pi \rightarrow X^2\Sigma^+$, $C^2\Pi \rightarrow A^2\Pi$ and $D^2\Sigma^- \rightarrow A^2\Pi$ systems. The $A^2\Pi \rightarrow X^2\Sigma$ system emitted by the magnesium arc in hydrogen at low pressures and first observed by Fowler (1909) has been subsequently studied by a number of workers in the light of the quantum theory. The $B^2\Sigma^+ \rightarrow X^2\Sigma^+$, $C^2\Pi \rightarrow A^2\Pi$ and $D^2\Sigma^- \rightarrow A^2\Pi$ systems have been observed and analysed by Guntch (1939) during an overall study of the magnesium hydride spectrum. The system $C^2\Pi \rightarrow X^2\Sigma$ at 2430 Å has been studied by Pearse (1929) who noticed a sudden breaking off of the rotational structure in the P and R branches after a certain J value—a phenomenon now known as pre-dissociation.

† Now at the University of Karachi, Pakistan.

By considering the analogy of molecular states of MgH with atomic states of Mg, it can be easily seen that there were and still are many more atomic states available corresponding to which analogous molecular states can be expected. What was required, of course, was suitable experimental techniques for making the observations. Thus, it was with the intention of taking this analogy a step further that the present investigation was undertaken. Coupled with this was the desire to furnish the astrophysicist with more data on these molecules to enable him to make use of these in his researches of astrophysical phenomena. It was during such an investigation that five new bands of MgH, which are the (0, 0) bands of different systems, at $\lambda\lambda$ 2819, 2702, 2172, 2100 and 2088 were observed and analysed. The first two of these along with their deuteride analogues form the subject of this paper. The latter three and the discussion of the pre-dissociation in the 2430 Å band and the correlation of the molecular states to the atomic states will be published subsequently. The fact that these bands appear in absorption only and not in emission at ordinary pressures may be attributed to pre-dissociation taking place in the upper state of the molecule. A detailed account has already been given by the author (Khan 1958).

§ 2. EXPERIMENTAL

The source for production of the spectrum used was the one described already in the author's thesis (Khan 1958). The source of power supply was a 5000 v, 7 kva transformer. To begin with an attempt was made to get the spectrum in emission. For this purpose photographs were taken under a wide range of conditions of pressure and current. The current was varied from about 0.5 A to about 2 A and pressure from a few millimetres to about 2 cm. The capillaries used were those of quartz and graphite. The photographs were taken when the discharge was quite intense, the green system of MgH appearing with remarkable intensity when viewed through the direct vision spectroscope. Whereas the 2430 Å system (including the (1, 0) and (0, 1) bands) was quite strong, there was no indication whatsoever of any new band in the far ultra-violet region, although the exposure time was extended from a few minutes to about an hour for Ilford Q₁ and for Q₂ plates. Thus it was thought that if new systems occurred in this region at all, either they were too feeble to be perceptible against the background of hydrogen continuum or, alternatively, they might be pre-dissociated. In either case absorption might bring them up.

This was achieved by using a conical capillary in the discharge. This meant that the current density and therefore the temperature varied along the length of the capillary. Thus by placing the metal in the broader part of the bore, the hydride bands thereby excited corresponded to a lower temperature than that of the continuum emitted from the narrow part of the bore. The continuum was therefore absorbed by the metal hydride formed in the broad part of the capillary.

The capillary used was of graphite. The diameter of the bore varied from 2 mm at one end to about 6 mm at the other end. The length of the tube was about 8 cm. It was held between the disks and presented 'end on' with its wider end facing the spectrograph. Magnesium metal, spectroscopically pure, in the form of thin laminae, was placed in the broad end. A discharge current of about 0.8 A was sufficient to produce enough vapour pressure of the metal

to form magnesium hydride. Hydrogen was continuously kept flowing. This led to the observation of the five new bands mentioned above, the former two of which form the subject of this paper. It is interesting to note that this technique was convenient in so far as it disposed of the use of a separate source for the continuum. The photographs which were taken with this arrangement on the large quartz (Littrow type) spectrograph are presented in the Plate, (a). The exposure time ranged from five to ten minutes for all bands except the one at 2088 Å. At this far ultra-violet region of the spectrum the exposure time had to be extended to about 45 minutes for Ilford Q₂ plates.

Later on it was found possible to take photographs with different sources for the background continuum. A high pressure xenon arc run at about 20 A was used in this instance. The capillary made of graphite was of uniform bore of about 6 mm diameter. The exposure time was between 10 and 15 seconds. The photographs are given in the Plate, (b). In addition two more new lines in the R and P branches of the band at 2430 Å were observed in absorption. They did not appear in emission because the levels from which they arise are known to be pre-dissociated.

The next source of continuum used was the flash tube (Garton 1953). The continuum was generated under the conditions of extreme current density resulting from periodic discharge of a condenser, charged to a high potential, through a narrow bore tube of quartz. The absorbing source (the discharge tube) was run continuously and only exposed to the spectrograph when the flash tube was pulsed. This was achieved by using a shutter (Rajaratnam 1958) in front of the slit of the spectrograph which was open only when the flash was operated. The photographs were taken in the first order of a 10' grating (Eagle mounting) spectrograph. They are shown in the Plate, (d) and (e).

For recording the spectrum obtained by using the capillary of conical form in the vacuum region, pictures were taken on the 10' vacuum spectrograph designed by Dr. Garton in this laboratory. Though there seemed to be an indication of a band near 2040 Å, it was so weak that no conclusive decision could be made.

For the production of the spectrum of magnesium deuteride a separate discharge tube was built which was exactly similar to the one used for hydrides. This was done to avoid contamination of the deuteride spectrum with that of the corresponding hydride as far as possible. To further minimize contamination of the spectrograms with MgH band lines, light from the first few minutes of passing discharge through the tube in an atmosphere of deuterium was not used. The gas was then pumped out of the discharge tube and fresh deuterium admitted at a pressure of a few millimetres of mercury. The flow of deuterium was continued during the exposure.

§ 3. 2819 Å SYSTEM, $E^2\Sigma \rightarrow X^2\Sigma$ TRANSITION

3.1. Measurements

As already mentioned, photographs of the band were taken on the large quartz (Littrow type) spectrograph as well as on the 10' grating spectrograph. The dispersion of the quartz spectrograph in this region is about 4.1 Å mm^{-1} and that of the grating is about 5.6 Å mm^{-1} . The measurements of the plate taken on the quartz spectrograph were made by comparison with the iron arc and

those of the plate taken on the grating were made with respect to silicon lines in the spectrum originating from the flash tube. Iron standards were taken from the *Transactions of the International Astronomical Union*. The mean of these two observations was taken for the wavelengths of the lines of the band. The reduction to wave numbers was effected with the help of Kayser's *Tabelle der Schwingungszahlen*. A catalogue of the wavelengths in air and corresponding wave numbers *in vacuo* is given in Table 1.

Table 1

K	P Branch		R Branch	
	λ_{air}	ν_{vac}	λ_{air}	ν_{vac}
0			2811.12	35562.6
1	2812.97	35539.2	2810.09	35575.6
2	2813.83	35528.3	2809.03	35589.0
3	2814.63	35518.2	2807.88	35603.6
4	2815.38	35508.7	2806.71	35618.4
5	2816.04	35500.4	2805.43	35634.6
6	2816.63	35493.0	2804.20	35650.3
7	2817.10	35487.0	2802.88	35667.1
8	2817.70	35479.5	2801.52	35684.4
9	2818.15	35473.8	2800.06	35703.0
10	2818.52	35469.2	2798.54	35722.4
11	2818.84	35465.2	2797.19	35739.6
12	2819.05	35462.5	2795.59†	35760.1
13	2819.25	35459.9	2794.01	35780.3
14			2792.46	35800.2
15			2790.76†	35822.0
16			2789.10	35843.3
17			2787.34	35865.9
18			2785.63	35888.0
19			2783.89	35910.4
20			2782.09	35933.6
21			2780.28†	35957.0
22			2778.40†	35981.4

Unfortunately the R branch lies in the region which is richly populated with Mg and Mg⁺ atomic lines. Therefore many of the lines are obscured. These are marked †.

3.2. Structure of the Band

A photograph of the band with an analysis of its structure into branches is shown in the Plate, (a). The apparent structure is that of P and R branches. The missing line at the band origin suggests that the transition involved is of $^2\Sigma \rightarrow ^2\Sigma$ type, since the presence of the lines R(0) and P(1) can be, without any difficulty, ascertained. In a $^2\Pi \rightarrow ^2\Sigma$ transition two lines P(0) and P(1) are always missing. The levels have been treated as though single in obtaining the rotational term differences, since the doublet structure was not resolved.

In Table 2, the combination differences for the final state (ground state) of this band are compared with the combination differences for the green system (5210 Å) and the ultra-violet (2430 Å) system of MgH having the same final state.

Table 2. Comparison of the Final State Term Differences

K	Band system 5210 Å (0, 0)	Band system 2430 Å (0, 0)	Band system 2819 Å (0, 0)
1	35.02	34.46	34.3
2	57.43	—	57.4
3	80.16	—	80.3
4	{ 102.90 102.64	103.02	103.2
5	{ 125.67 125.73	125.46	125.4
6	{ 147.92 148.27	148.26	147.6
7	{ 170.84 170.83	170.62	170.8
8	{ 193.17 193.22	193.09	193.3
9	{ 215.46 215.49	215.38	215.2
10	{ 237.68 237.56	237.83	237.8
11	{ 259.65 259.65	—	259.9

Examination of these combination differences confirms that the electronic transition involved is of ${}^2\Sigma \rightarrow {}^2\Sigma$ type.

The rotational constants for the upper and the lower states are calculated by using the following relation (cf. Herzberg 1950):

$$\frac{\Delta_2 F(K)}{K + \frac{1}{2}} = 4B_v - 8D_v(K + \frac{1}{2})^2.$$

The band origin is calculated by using the equation,

$$\nu = \nu_0 + (B_v' + B_v'')m + (B_v' - B_v'')m^2$$

where $m = -J$ for the P branch and $m = J + 1$ for the R branch.

The constants thus calculated are listed below:

$$\begin{aligned} B_v' &= 6.08 \text{ cm}^{-1} & D_v' &= 3.31 \times 10^{-4} \text{ cm}^{-1} \\ B_v'' &= 5.73 \text{ cm}^{-1} & D_v'' &= 3.43 \times 10^{-4} \text{ cm}^{-1} \\ \nu_0 &= 35\,550.61 \text{ cm}^{-1}. \end{aligned}$$

No vibrational constants could however be calculated because of the absence of the other vibrational bands.

§ 4. BAND AT 2702 Å, $F^2\Sigma \rightarrow X^2\Sigma$ TRANSITION

The band at 2702 Å (origin) is much weaker than the one studied previously and was only fully developed in absorption when the flash tube was used as the background source. It is a simple band consisting of single P and single R branches. Both the R and P branches could be traced to quite high K values. The intensity maxima occur somewhere near the middle of each branch. The wavelengths and wave-numbers are given in Table 3. The comparison of the term differences for the lower state is shown in Table 4. The first column shows

Table 3. Wavelengths and Wave Numbers

K	P Branch		P Branch		K	P Branch		R Branch	
	λ_{air}	ν_{vac}	λ_{air}	ν_{vac}		λ_{air}	ν_{vac}	λ_{air}	ν_{vac}
0			2701.38	37007.2	21	2717.79	36783.7	2683.81	37249.4
1	2703.09	36983.7	2700.52	37019.9	22	2718.46	36774.7	2683.13	37258.8
2	2703.99	36971.4	2699.68	37030.5	23	2719.17	36765.1	2682.49	37267.7
3	2704.85	36959.7	2698.88	37041.4	24	2719.86	36755.7	2681.93	37275.5
4	2705.62	36949.2	2698.07	37052.6	25	2720.59	36745.9	2681.44	37282.3
5	2706.46	36937.7	2697.07	37066.3	26	2721.37	36735.3	2680.99	37288.6
6	2707.17	36928.0	2696.26	37077.4	27	2722.08	36725.7		
7	2707.89	36918.2	2695.28	37091.0	28	2722.85	36715.4		
8	2708.68	36907.4	2694.41	37102.9	29	2723.55	36705.9		
9	2709.44	36897.1	2693.55	37115.7	30	2724.09	36698.6		
10	2710.19	36886.9	2692.72	37126.2	31	2724.83	36688.7		
11	2710.91	36877.1	2691.76	37139.4	32	2725.40	36681.0		
12	2711.58	36868.0	2690.92	37151.0	33	2726.09	36671.7		
13	2712.32	36857.9	2690.12	37162.1	34	2726.70	36663.5		
14	2713.03	36848.2	2689.19	37174.9	35	2727.34	36654.9		
15	2713.70	36839.2	2688.40	37185.8	36	2727.94	36646.9		
16	2714.41	36829.5	2687.54	37197.7	37	2728.67	36637.1		
17	2715.07	36820.6	2686.74	37208.8	38	2729.50	36625.9		
18	2715.76	36811.2	2685.97	37219.5	39	2730.35	36614.5		
19	2716.43	36802.1	2685.22	37229.9	40	2731.25	36602.4		
20	2717.09	36793.2	2684.48	37240.1					

Table 4. Comparison of the Rotational Term Differences of the Final State

Band system K	2702 Å	$B^2\Sigma \rightarrow X^2\Sigma$	$A^2\Pi \rightarrow X^2\Sigma$	$c^2\Pi \rightarrow X^2\Sigma$
1	35.8	—	34.12	34.46
2	60.2	57.5	57.55	—
3	81.3	83.4	80.21	—
4	103.7	99.5	102.98	103.02
5	124.6	125.2	125.70	125.46
6	148.1	149.5	148.35	148.26
7	170.0	171.0	170.88	170.62
8	193.9	193.7	193.29	193.09
9	216.0	215.6	215.14	215.38
10	238.6	236.0	237.70	237.83
11	258.2	261.4	259.71	—
12	281.5	281.5	281.58	—
13	302.8	304.2	302.61	—
14	322.9	—	324.05	—
15	345.4	—	345.49	—
16	365.2	—	366.27	—
17	386.5	—	386.50	—
18	406.7	—	406.81	—
19	426.3	—	426.81	—
20	446.2	—	446.43	—
21	465.4	—	465.81	—
22	484.3	—	484.84	—
23	503.1	—	503.51	—
24	521.8	520.2	521.90	—
25	540.2	538.9	539.79	—
26	556.6	556.2	557.32	—

the differences for the new band, the second and third give the differences found by Guntch (1939) and the fourth gives those found by Pearse (1929) for the respective systems.

The rotational analysis shows that the transition is of the ${}^2\Sigma \rightarrow {}^2\Sigma$ type, the lower state being the ground state.

The rotational constants are calculated as follows. The values of K used were from $K=5$ to $K=26$:

$$\begin{aligned} B_v' &= 5.78 \text{ cm}^{-1} & D_v' &= 4.0 \times 10^{-4} \text{ cm}^{-1} \\ B_v'' &= 5.73 \text{ cm}^{-1} & D_v'' &= 3.63 \times 10^{-4} \text{ cm}^{-1} \\ \nu_0 &= 36\,995.4 \text{ cm}^{-1}. \end{aligned}$$

§ 5. MgD BAND AT 2816 Å

The photograph of the MgD band at 2816 Å, corresponding to the MgH band at 2819 Å is given in the Plate, (c). The pictures were taken on a large quartz (Littrow type) spectrograph. The source of continuum used was a high pressure xenon arc. The exposure time ranged from 10 to 25 sec for the Ilford Q₂ plates. The catalogue of wavelengths and wave numbers is given in Table 5.

Table 5. Wavelengths and Wave Numbers

K	P Branch		R Branch	
	λ_{air}	ν_{vac}	λ_{air}	ν_{vac}
0			2811.59	35556.6
1			2811.08	35563.1
2	2812.98	35539.1	2810.45	35571.0
3	2813.41	35533.6	2809.83	35578.9
4	2813.74	35529.5	2809.15	35587.5
5	2813.99	35526.3	2808.51	35595.6
6	2814.38	35521.4	2807.82	35604.4
7	2814.72	35517.1	2807.06	35614.0
8			2806.28	35623.9
9			2805.51	35633.7
10			2804.70	35644.0
11			2803.86	35654.6
12			2803.02	35665.3
13			2802.13	35676.7
14			2801.21	35688.4
15			2800.27	35700.3
16			2799.34	35712.2
17			2798.37	35724.6
18			2797.34	35737.7
19			2796.34†	35750.5
20			2795.52	35761.0
21			2794.18†	35778.2

† Obscured by Mg atomic lines.

5.1. Structure and Analysis of the Band

It may be seen from the Figure (Plate) that the band is of simple structure consisting of a single P and a single R branch and is degraded to the violet.

Table 6. Comparison of the Combination Differences for the Final State

K	Band system 2816 Å	Band system 2430 Å	Band system 5210 Å
1	17.5	—	—
2	29.5	—	29.9
3	41.5	—	41.9
4	52.6	—	53.9
5	66.1	65.1	65.8
6	78.5	77.4	77.8

The analysis of the band was carried out in the usual way. The comparison of the combination differences for the final state is made in Table 6. Only a few lines in the P branch could be measured because of low dispersion. The rotational constants are: $B_v' = 3.20 \text{ cm}^{-1}$, $B_v'' = 2.80 \text{ cm}^{-1}$, $\tilde{\nu}_0 = 35\,548.95 \text{ cm}^{-1}$.

§ 6. MgD BAND AT 2702 Å

The MgD band corresponding to the MgH band at 2702 Å is shown in the Plate, (c). The band, as can be seen from the photograph, is so weak that it was not possible to measure the band lines.

ACKNOWLEDGMENTS

The author wishes to express his thanks to Dr. R. W. B. Pearse for his guidance and valuable suggestions.

REFERENCES

- FOWLER, A., 1909, *Phil. Trans. R. Soc. A*, **209**, 447.
 GARTON, W. R. S., 1953, *J. Sci. Instrum.*, **30**, 119.
 GUNTSCHE, A., 1939, *Dissertation*, Stockholm.
 HERZBERG, G., 1950, *Spectra of Diatomic Molecules*, 2nd Edn (New York : Van Nostrand), pp. 169, 182.
 KHAN, M. A., 1958, *Ph.D. Thesis*, London.
 PEARSE, R. W. B., 1929, *Proc. Roy. Soc. A*, **122**, 442.
 RAJARATNAM, N., 1958, *Ph.D. Thesis*, London.

Hyperfine Structure of the Level $5^2P_{1/2}$ of Potassium 39

By W. N. FOX† AND G. W. SERIES

Clarendon Laboratory, Oxford

Communicated by H. G. Kuhn; MS. received 29th December 1960

Abstract. The hyperfine structure of the level $5^2P_{1/2}$ of potassium 39 has been measured by the techniques of optical-radio-frequency double resonance. The magnetic interaction constant $a_{1/2}$ was found to be 8.99 ± 0.15 Mc/s, which leads to the value 4.56 ± 0.3 for the ratio $a_{1/2}/a_{3/2}$. This is significantly lower than the value 5.08 which the Goudsmit Fermi Segrè theory would predict. The measured value of the Landé g -factor is 0.665 ± 0.003 .

§ 1. INTRODUCTION

THE present work is the completion of a study of the hyperfine structure of the term 5^2P in ^{39}K , using the techniques of optical-radio-frequency double resonance (Brossel and Bitter 1952). The structure of the level $5^2P_{3/2}$ was measured by Ritter and Series (1957, to be referred to as I) and values deduced for the nuclear magnetic dipole and electric quadrupole interaction constants $a_{3/2}$ and b , respectively. The preliminary measurements which these authors also made on the structure of the level $5^2P_{1/2}$ have now been refined, and a more precise value obtained for the magnetic interaction constant $a_{1/2}$. It was of particular interest to find the ratio $a_{1/2}/a_{3/2}$, since deviations from the value 5.08, which are to be expected on the Goudsmit Fermi Segrè theory of hyperfine structure (including the relativistic correction) have been observed in the term 5^2P of rubidium (Senitzky and Rabi 1956).

§ 2. EXPERIMENTAL TECHNIQUE

2.1. *The Method*

The experiment was similar in essentials to that described in I. The significant differences lay in the use of a sealed-off absorption cell rather than an atomic beam, and a light source of the radio frequency, rather than of the hollow cathode, type of excitation. Longer time constants were used in recording the resonance curves.

The study of an excited level $P_{1/2}$ is technically more difficult than that of $P_{3/2}$ since it is necessary to discriminate between σ^+ and σ^- light both in the exciting and in the fluorescent beams. The directions of these two beams were arranged at right angles, with the magnetic field bisecting the angle between them. The light was elliptically polarized.

With this arrangement, radio-frequency resonances in the $P_{3/2}$ level are detected in addition to the $P_{1/2}$ signals, but they lie in a different part of the radio-frequency spectrum. At a frequency of about 40 Mc/s, the eight hyperfine

† Now at Atomic Energy Research Establishment, Winfrith Heath, Dorset.

lines of the $P_{3/2}$ spectrum lie within the range of magnetic field 17–27 gauss, while the four more widely spaced $P_{1/2}$ lines lie between 20 and 60 gauss. Three of the four are resolved from the $P_{3/2}$ lines.

2.2. *The Absorption Cell and the Magnetic Fields*

Considerable difficulty was experienced in preparing a sealed-off cell in which resonance fluorescence could be excited. The fluorescence is particularly susceptible to traces of foreign gas. A successful cell was eventually constructed by including a barium getter in a small side-chamber attached to the sealed-off cell. The potassium was introduced by electrolysis from a mixture of fused potassium nitrate and nitrite through potassium glass (Strong 1940), though the cell itself was of Pyrex.

The cell was mounted in an oven and maintained at a temperature of 90°C by a stream of hot air.

A uniform magnetic field of up to 100 gauss could be applied by Helmholtz coils. A radio-frequency field of about one gauss at frequencies in the neighbourhood of 40 Mc/s was applied in a perpendicular plane.

2.3. *The Light Source*

An electrodeless discharge tube, operated by a power oscillator at 15 Mc/s, was found to be more efficient than commercial potassium lamps. The tube contained neon at a pressure of about 0.1 mm Hg, and potassium, whose vapour pressure was controlled independently of the discharge current by adjusting the thermal shielding.

A colour filter and elliptical polarizers were placed between lamp and cell, and between cell and photomultiplier.

2.4. *Detection of the Resonances*

The radio frequency was held constant while the magnetic field was varied uniformly. The photoelectric signal was modulated at 220 c/s by sinusoidal modulation of the magnetic field, of amplitude a small fraction of a resonance line-width. This modulated signal was applied to a phase-sensitive detector and the rectified output displayed on a chart recorder, whose input circuit had a time constant of 15 seconds.

Figure 1 (a) shows the three resolved lines of the $P_{1/2}$ spectrum superimposed on a sloping base-line which is discussed in §2.5. In recordings from which measurements were taken, the resonances were explored separately, using an expanded scale of magnetic field as in Fig. 1 (b), at a number of fixed frequencies in the neighbourhood of 40 Mc/s.

2.5. *Spurious Signals*

In the range of magnetic fields from zero to about 15 gauss a strong signal of a non-resonant character was induced by the radio-frequency field. Above 15 gauss this signal fell sharply at first, then more gradually. The residual signal in the region 30–60 gauss can be seen in the sloping background of Fig. 1 (a). The signal was due to a weak discharge in the absorption cell, presumably to be associated with the electron cyclotron motion, for which the critical field would be about 14 gauss.

In the earlier work (I, p. 273), certain signals were attributed to $\Delta m_J = \pm 2$, $\Delta m_I = \mp 1$ transitions. Re-examination of the recordings suggests that they should rather be associated with the spurious signals described in this section. The authors wish to withdraw the former interpretation.

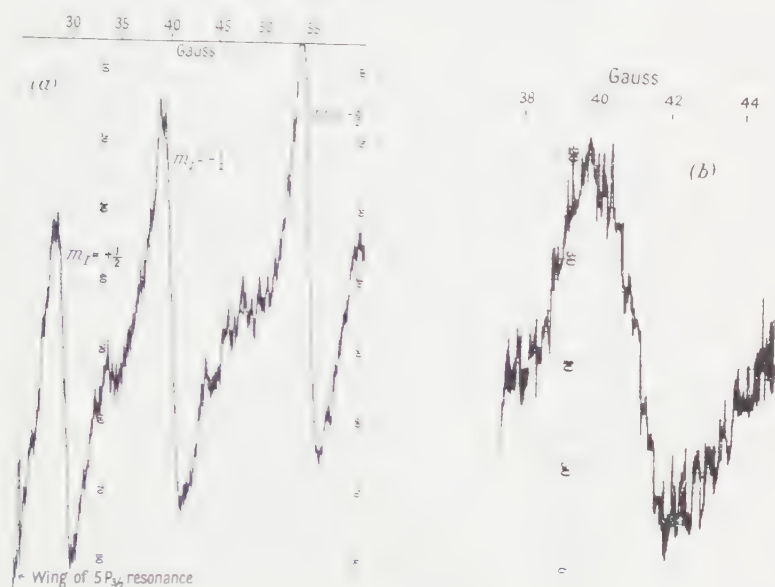


Fig. 1. (a) Three resolved lines of the $P_{1/2}$ spectrum at 40.0 Mc/s. Time constant 15 sec, modulation 0.3 G r.m.s. (b) Typical resonance ($m_I = -\frac{1}{2}$) using an extended scale of magnetic field. Frequency 39.057 Mc/s.

As in the earlier work, the conditions of the experiment were such that resonances in the ground level might, in principle, have been observed. An estimate indicated that their intensity would have been less than one-tenth of the minimum detectable signal. No trace of such effects was found.

§ 3. INTERPRETATION OF OBSERVATIONS

The interaction constant $a_{1/2}$ is defined by the Hamiltonian

$$\mathcal{H} = a_{1/2} \mathbf{I} \cdot \mathbf{J} + g_J \beta \mathbf{J} \cdot \mathbf{H} + g_I \beta (m/M) \mathbf{I} \cdot \mathbf{H},$$

where the other symbols have their usual significance. We shall ignore the small term in g_I .

Figure 2 shows the energy levels, as functions of magnetic field, according to the Breit-Rabi formula. The transitions of interest, $\Delta m_J = \pm 1$, $\Delta m_I = 0$, are also shown. They may be labelled by the values of m_I .

The three resonances which are resolved from the $P_{3/2}$ hyperfine structure are those for which $m_I = +\frac{1}{2}$, $-\frac{1}{2}$ and $-\frac{3}{2}$. The centre of the observed resonances gives a field which, it is assumed, is the value which satisfies the Breit-Rabi formula for that particular frequency. Each observation then yields an equation in which $a_{1/2}$ and g_J are the only unknowns. The set of equations obtained from observations on all three resonances is solved by plotting curves over a small range near the expected values of the two constants (Fig. 3). The

only significant intersections, from which the most probable values of $a_{1/2}$ and g_J are determined, are those between curves of different m_I .

Measurements of the centres of the resonance curves were made with respect to the sloping background discussed in §2.5. Uncertainty in locating the centres was dominated by the noise on the curves, rather than by uncertainty in drawing the baseline.

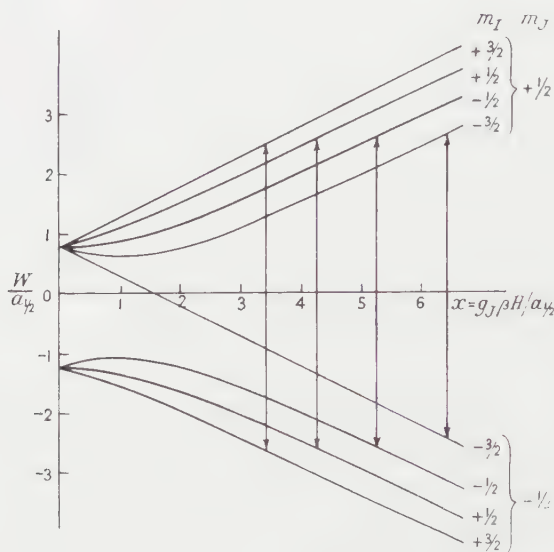


Fig. 2. Energy levels ($W/a_{1/2}$) as a function of $x = g_J \beta H / a_{1/2}$, showing the radio-frequency transitions at 40 Mc/s.

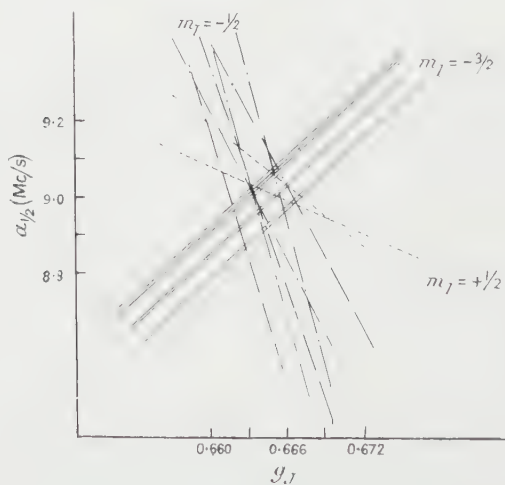


Fig. 3. $a_{1/2}$ as a function of g_J . Each line corresponds to a single determination of the centre of a resonance curve.

The values $a_{1/2} = 8.99 \pm 0.15$ Mc/s, $g_J = 0.665 \pm 0.003$ within the quoted limits embrace all but three of the 76 significant points of intersection in Fig. 3.

The width of the resonance curves at half intensity is approximately 2 gauss (rather less than 2 Mc/s). This is similar to the line-widths observed in I.

§ 4. DISCUSSION OF THE RESULTS

4.1. The g_J Factor

There is no evidence that g_J departs from the value $\frac{2}{3}$ which is to be expected for a pure $P_{1/2}$ state.

4.2. The a Factor

It is of interest to relate the present measurement to other measurements of hyperfine structure in potassium, and to the nuclear moment, for the Goudsmit Fermi Segre theory may be applied in such a way that various uncertain quantities are eliminated; for example, the ratio $a(5P_{1/2})/a(4P_{1/2})$ is simply the ratio of the doublet intervals for the P levels (see, for example, Kopfermann 1958). In the Table the measured value of $a(5P_{1/2})$ is compared with values computed on the basis of the Goudsmit Fermi-Segre theory from these other measurements.

Quantity μ	Authors	Measured value	$a(5P_{1/2})$ (Mc/s) (Computed)
	Kusch, Millman and Rabi (1939)	0.391 (± 0) n.m.	9.76
$a(4S_{1/2})$	Bloom and Carr (1960)	231 (± 0) Mc/s	9.09
$a(4P_{1/2})$	Buck and Rabi (1957)	28.85 ± 0.3 Mc/s	9.38
$a(4P_{3/2})$	Buck and Rabi (1957)	5.70 ± 0.3 Mc/s	9.44
$a(5P_{3/2})$	Ritter and Series (1957)	1.97 ± 0.1 Mc/s	10.0
$a(5P_{1/2})$	Measured in the present work		8.99 ± 0.15 Mc/s

The first and last of the computed values of $a(5P_{1/2})$ are in definite conflict with the measured value.

The value computed from $a(4P_{3/2})$ is included only for completeness. There is no conflict with any other value in the Table when the fractional error of the measurement is taken into account.

The measured values of $a(4S_{1/2})$ and $a(4P_{1/2})$, which are much more precise, yield values of $a(5P_{1/2})$ which agree reasonably well with the measured value. It is noteworthy that this consistency is found between the a -factors of levels of the same J , even though the comparison is between different configurations.

The greatest discrepancy is between the a -factors within the 5P configuration itself. Theoretically, the ratio $R = a(5P_{1/2})/a(5P_{3/2})$ is simply $(2l+3)/(2l-1) = 5$. Relativistic corrections bring the value of R up to 5.08. The experimental value is 4.56 ± 0.3 .

A similar discrepancy in R for the 5P term in rubidium has been discussed on the basis of configuration interaction (Phillips 1956). Similar arguments might be adduced for potassium. More recently, however, calculations have been made for lithium and sodium of the consequences of the exchange interaction between the outer s-electrons and the electrons of the core (Cohen, Goodings and Heine 1959). It was shown that there results polarization of the core, and a very substantial contribution to the hyperfine structure. For a p-electron, the core polarization would make different contributions to the hyperfine structures of the $P_{1/2}$ and $P_{3/2}$ levels, owing to the difference in J (Goodings and Heine, private communication), and might account for the

observed discrepancies in R . If, further, it should turn out that the exchange interaction in different configurations is roughly proportional to the hyperfine interaction, then the corrections to the a -factors would be roughly the same for levels of the same J . This could explain the consistency between the a -factors of the levels $4S_{1/2}$, $4P_{1/2}$ and $5P_{1/2}$.

ACKNOWLEDGMENT

One of us (W. N. F.) expresses his thanks to the Department of Scientific and Industrial Research for a maintenance grant.

REFERENCES

- BLOOM, A. L., and CARR, J. B., 1960, *Phys. Rev.*, **119**, 1946.
BROSSEL, J., and BITTER, F., 1952, *Phys. Rev.*, **86**, 308.
BUCK, P., and RABI, I. I., 1957, *Phys. Rev.*, **107**, 1291.
COHEN, M. H., GOODINGS, D. A., and HEINE, V., 1959, *Proc. Phys. Soc.*, **73**, 811.
KOPFERMANN, H., 1958, *Nuclear Moments* (English version by E. E. SCHNEIDER), (New York: Academic Press).
KUSCH, P., MILLMAN, S., and RABI, I. I., 1939, *Phys. Rev.*, **55**, 1176.
PHILLIPS, M., 1956, *Phys. Rev.*, **103**, 322.
RITTER, J. J., and SERIES, G. W., 1957, *Proc. Roy. Soc. A*, **238**, 473.
SENITZKY, B., and RABI, I. I., 1956, *Phys. Rev.*, **103**, 315.
STRONG, J., 1940, *Modern Physical Laboratory Practice* (London: Blackie).

Determination of the Effective Ionic Charge of Gallium Arsenide from Direct Measurements of the Dielectric Constant

By K. G. HAMBLETON, C. HILSUM AND B. R. HOLEMAN

Services Electronics Research Laboratories, Baldock, Herts.

MS. received 16th January 1961

Abstract. Direct measurements of static and optical dielectric constants have been made on GaAs with a resistivity of 10^9 ohm cm at room temperature. Values obtained were $\epsilon_0 = 12.5(3)$ and $\epsilon_\infty = 10.90$. An effective ionic charge e_s^* of $0.46e$ can be deduced from these values.

SZIGETI (1949) has shown that for ionic crystals with simple cubic structure the effective ionic charge on the atoms e_s^* is given by

$$\epsilon_s^* = \frac{3\omega_0}{\epsilon_\infty + 2} \left(\frac{M(\epsilon_0 - \epsilon_\infty)}{4\pi n_0} \right)^{1/2}$$

where ϵ_s^* is the high frequency (optical) dielectric constant, ϵ_0 the static dielectric constant, $\omega_0/2\pi$ the lattice fundamental transverse optical mode frequency, n_0 the number of ion pairs per unit volume, and M the reduced mass of the ion pairs. Previous estimates of e_s^* for III-V compounds (Picus *et al.* 1959) have been based on infra-red reflection experiments, the analysis involving an indirect calculation of ϵ_∞ by fitting theoretical reflection curves to the experimental results. The uncertainty in the dissipative terms makes it difficult to achieve high accuracy, and a more direct method would be preferable.

Gallium arsenide has now been prepared in this laboratory with a resistivity at room temperature of up to 10^9 ohm cm, and with this material both ϵ_0 and ϵ_∞ have been measured more accurately than has been previously possible. The measurement of ϵ_0 was made by a conventional parallel plate capacitance technique. Most contacts to high-resistance GaAs are non-ohmic, and to avoid effects due to junction capacitance, insulating layers of SiO_2 were evaporated on to the GaAs before the evaporated gold contacts were applied. The capacitance was measured on a radio-frequency bridge at 20 kc/s and 3 Mc/s, and the mean value obtained for ϵ_0 was $12.5(3) \pm 0.26$. The variation with frequency was much less than the experimental error in each result. The main source of error was the determination of the effective contact area, and therefore a second method was used which did not involve this determination. The dielectric constant of GaAs was compared with that of a suitable liquid by completely immersing the sample in the liquid between parallel contact plates of variable spacing. Capacitance readings were taken over a range of plate separation to ensure that end effects due to the size of the sample were negligible. The method is most accurate when the ratio of the dielectric constants is near unity, and amyl alcohol, with $\epsilon = 16$ at 20°C , was chosen for the liquid. The dielectric constant of amyl alcohol was checked in a separate experiment. The comparative measurement was carried out at 1 Mc/s, and ϵ_0 was found to be $12.5(3) \pm 0.10$.

To determine ϵ_{∞} infra-red refraction measurements were used. Observations were made on an accurately figured 15° prism of high resistivity GaAs, and the results are summarized in the Table. Free carrier absorption was, of course, negligible, since the carrier concentration was less than 10^8 per cm^3 .

Values of Refractive Index as a Function of Wavelength				
λ (microns)	1.9	3.0	4.0	5.0
Refractive index (η)	3.347	3.313	3.302	3.298

The refractive index increases at the shorter wavelengths as the absorption edge at 0.9μ is approached. The longer wavelengths are sufficiently far from the lattice absorption at 33μ to give an accurate value for ϵ_{∞} ($=\eta^2$), and this can be taken as 10.90 ± 0.04 . The error in η is estimated as ± 0.007 . Previous determinations of η have given values of 3.4 (Oswald and Schade 1954) and 3.34 (Briggs 1950).

A value for ω_0 of $5.04 \times 10^{13} \text{ sec}^{-1}$ has been deduced by Picus *et al.* (1959) from far infra-red reflectivity measurements. We may obtain an independent estimate of ω_0 from measurements on GaAs tunnel diodes (Hall, Racette and Ehrenreich 1960). These give a value for ω_1 , the lattice fundamental longitudinal optical mode frequency, of $5.47 \times 10^{13} \text{ sec}^{-1}$. The Lyddane-Sachs-Teller relation, $\omega_0 = \omega_1 (\epsilon_{\infty}/\epsilon_0)^{1/2}$ then gives a value for ω_0 of $5.10 \times 10^{13} \text{ sec}^{-1}$.

If we use this latter value, take n_0 as 2.23×10^{22} and M as $6.00 \times 10^{-23} \text{ g}$, we find e_s^* is equal to $0.46e$, a slightly higher value than previously reported.

ACKNOWLEDGMENTS

We are grateful to W. R. Harding for the supply of the GaAs and to R. Broom for assistance in the preparation of the samples. Permission to publish has been given by the Admiralty.

REFERENCES

- BRIGGS, H. B., 1950, *Phys. Rev.*, **77**, 287.
 HALL, R. N., RACETTE, J. H., and EHRENREICH, H., 1960, *Phys. Rev. Letters*, **4**, 456.
 OSWALD, F., and SCHADE, R., 1954, *Z. Naturf.*, **9a**, 611.
 PICUS, G. S., BURSTEIN, E., HENVIS, B. W., and HASS, M., 1959, *J. Phys. Chem. Solids*, **8**, 282.
 SZIGETI, B., 1949, *Trans. Faraday Soc.*, **45**, 155.

The Energy Loss of Singly Charged Heavy Relativistic Particles in an Organic Material†

By C. F. BARNABY

Medical Research Council, Department of Clinical Research, University College Hospital Medical School, London, W.C.1., and Northern Polytechnic, London

MS. received 23rd November 1960

Abstract. An experiment is described in which a large area plastic scintillation counter is used to measure the energy loss of relativistic μ -mesons. The results, which are not dependent on the particular method used to fit them to the Landau distribution, show that the increase in the most probable energy loss is less than 1% for mesons of energies between 500 and at least 10 000 mev. This conclusion is consistent with the Sternheimer density correction to the ionization loss theory of Bethe-Bloch.

§ 1. INTRODUCTION

WHEN a fast charged particle, heavier than an electron, passes through matter it loses energy mainly by inelastic collisions with atomic electrons, causing excitation or ionization. The average amount of energy lost by a singly-charged heavy particle, per g cm⁻², is given by the Bethe Bloch formula

$$E_a = \frac{2Cm_e c^2}{\beta^2} \left[\ln \left(\frac{4m_e^2 c^4 \beta^4}{(1-\beta^2)^2 I^2(Z)} \right) - 2\beta^2 - \delta(\beta) \right]$$

where $C = \pi N Z r_e^2 / A = 0.150 Z / A$ g⁻¹ cm², $\delta(\beta)$ is the correction factor due to the screening effect of polarization in the material, and the other symbols have their usual significance.

Because the energy lost by a particle passing through matter is the result of a large number of independent events the process is a statistical phenomenon. The resultant distribution of energy loss has been shown by Landau (1944) to be a negatively skewed distribution—the high-energy tail being due to those collisions in which a large amount of energy is transferred to the target electron. Experimentally it is the peak of this distribution, or the *most probable energy loss*, that is usually measured. Symon (1948) analysed the energy-loss distribution more completely than Landau and showed that the most probable energy loss of a singly-charged heavy particle traversing an absorber of thickness x is given by

$$E_p = \frac{2Cm_e c^2 x}{\beta^2} \left[\ln \left(\frac{4Cm_e^2 c^4 x}{(1-\beta^2)^2 I^2(Z)} \right) - \beta^2 + j - \delta(\beta) \right].$$

The value of j is related to the function $G = Cx(1-\beta^2)/\beta^4$ and for $G < 0.05$ Symon's formula is the same as that of Landau, in which j is a constant equal to 0.38.

The correction factor $\delta(\beta)$, commonly called the 'density correction', was first estimated by Fermi (1940) and has since been investigated by various authors (see Price 1955) and in greatest detail by Sternheimer (1952, 1953, 1956, 1959). In Sternheimer's treatment it is assumed that the dispersive properties of the

† This work formed part of a Ph.D. thesis which has been accepted by the University of London.

absorber can be described in terms of an appropriate number of dispersion oscillators, rather than the single type of dispersion oscillator assumed by Fermi (1940) and others. $\delta(\beta)$ is evaluated in terms of the oscillator strength of the i th atomic transition and the energy of the transition.

The theoretical value of $\delta(\beta)$ is small for gases, except at very high energies, and at relativistic energies the value of E_p increases logarithmically with the energy of the particle until it finally saturates at some value of the velocity determined by $\delta(\beta)$. The predicted value of $\delta(\beta)$ is, however, of much greater significance for condensed media; and for some materials—in particular, materials of low Z —it may almost eliminate the relativistic logarithmic rise.

The experimental determinations of ionization loss using gaseous detectors (e.g. Ghosh, Jones and Wilson 1952, 1954, Eyeions *et al.* 1955, Lanou and Kraybill 1959) all show the expected relativistic increase of probable energy loss with velocity and the onset of the density effect. Because of the enhanced value of $\delta(\beta)$ in solids the results using condensed media should more clearly show the reduction in ionization loss. Photographic emulsions, solid conduction counters and scintillation counters have been used for this purpose. Unfortunately the photographic plate technique has not proved satisfactory (Price 1955) for the substantiation of small differences of ionization at relativistic energies.

More definite results have been obtained with sodium iodide. Bowen (1954), using μ -mesons in the cosmic radiation, found that the relativistic increase up to 5000 MeV was $10.9 \pm 1.0\%$ which is in good agreement with Sternheimer's predicted value. The ionization loss in organic materials, in which the predicted density effect is very large, was investigated by Bowen and Roser (1952) using an anthracene crystal and μ -mesons. The statistics of the experiment were not good, but the results showed that the relativistic rise up to 3000 MeV was less than 10%. A similar result was obtained by Baskin and Winckler (1953) with a liquid scintillation counter.

The experiment to be described was an attempt to measure the ionization loss of relativistic particles in an organic material with greater accuracy than that obtained previously.

§ 2. THE EXPERIMENTAL ARRANGEMENT

A large area plastic scintillation counter (Barnaby and Barton 1960) was used to measure the energy loss. The plastic phosphor was a polished block, 55 cm \times 17.5 cm \times 3.8 cm, of NE102 by Nuclear Enterprises Ltd. The uniformity of response of the phosphor was shown to be reasonably good throughout its volume. The performance of the counter is discussed in detail in the earlier paper.

Because the incident radiation is more homogeneous underground than at sea level the measurement of the energy loss of cosmic-ray μ -mesons in the plastic scintillator was carried out in the cosmic-ray laboratory at Holborn, at a depth of 60 m water equivalent.

It was decided that the best way of analysing the pulses from the scintillator (the heights of which were proportional to the ionization loss in the plastic) was to lengthen them to about 100 μ sec, display them on a cathode-ray tube, and photograph them on a slowly moving film. A major advantage with this method is that an oscilloscope can be made to have a very stable response over long periods of time.

The μ -mesons accepted for measurement were those in the beam defined by a cosmic-ray telescope consisting of five trays of Geiger counters placed one above the other in the positions shown in Fig. 1. The top three trays operated in coincidence. Each of the bottom trays was connected to an anticoincidence circuit in which the second input was the coincidence pulse from the top three trays.

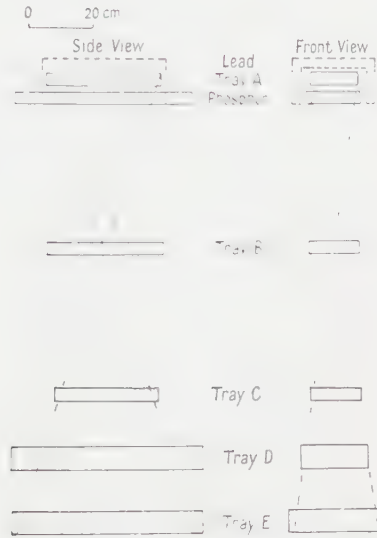


Fig. 1. Counter arrangement.

A simple hodoscope arrangement indicated whether the meson had stopped between trays C and D, had stopped between trays D and E, or had passed through tray E.

The phosphor was positioned immediately beneath tray A. It was necessary to record only those pulses from the photomultiplier due to μ -mesons which had triggered the telescope. This was done by providing a brightening-up circuit for the cathode-ray tube. Under normal working conditions the brightness control on the cathode-ray tube was turned down until the spot was just bright enough to record a thin base line on the moving film. This brightness level was insufficient to record the phosphor pulses on the film, but when a master event occurred the brightening-up pulse increased the brightness and the pulse was photographed.

The long time constant (about one-tenth of a second) required to flash the hodoscope lamps made it necessary to ensure that any master events occurring during this time were not recorded. The brightening-up circuit was therefore triggered by a circuit which provided a paralysis time that was just longer than the time constant of the lamp-flashing circuit (Fig. 2).

The energy of the mesons recorded depended on the thickness of the lead absorbers placed in the telescope. Those passing through the telescope when the maximum amount of lead was in position had a minimum energy of 1550 mev; the energy spectrum at 60 m water equivalent is such that the median energy was 10 000 mev.

Some μ -mesons inevitably 'leaked' through the anticoincidence screen, despite precautions taken to reduce their number to a minimum. The measured rate of leakage was, however, less than 5% of the stopping rate (about 1.5 mesons per hour) associated with the minimum absorber thickness between trays C and D and trays D and E. It was also important that the rates of the various accidental events be small compared with those recorded for measurement. These rates were measured and found to be insignificant in number.

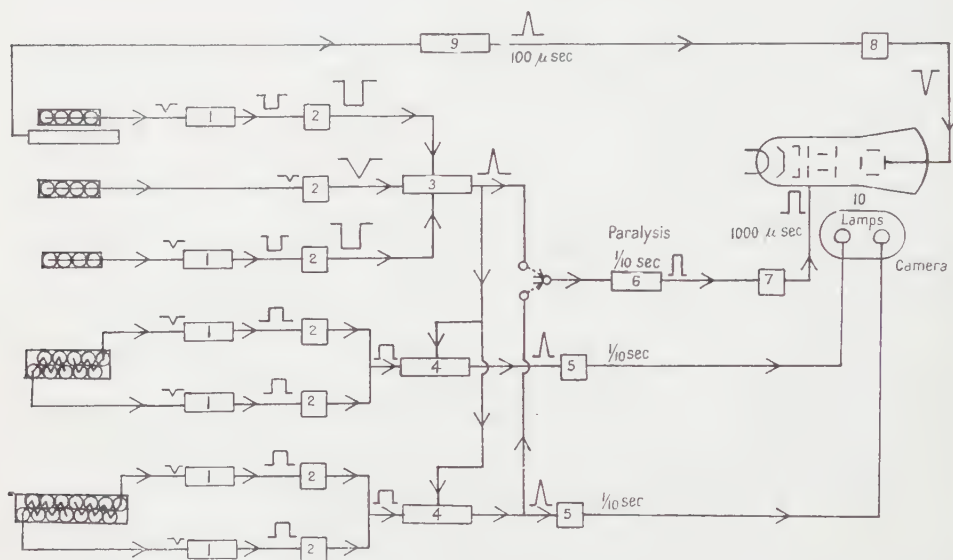


Fig. 2. Block diagram of electronics. 1, Quenching circuit; 2, cathode follower; 3, Rossi circuit; 4, anticoincidence circuit; 5, lamp circuit; 6, paralysis circuit; 7, brightening-up circuit; 8, X plate amplifier; 9, pulse lengthener; 10, cathode-ray oscilloscope.

The heights of the pulses were measured by projecting the film on to a graduated screen. The accuracy of this measurement was about $\pm 0.5\%$. Because of the relatively slow fall-off of the energy loss distribution curve, a small number of events gave pulses from the photomultiplier which were greater than the diameter of the cathode-ray tube, and which were therefore lost to the measurement. The number of off-scale pulses was about 0.3% of the total number of pulses—a figure small enough to have no significant effect on the determination of the position of the peak of the distribution curve. A regular check of the overall linearity of the system was carried out.

At each energy value about 500 pulses were analysed and a histogram constructed of the distribution of pulse heights. The most probable energy loss distribution curve which must fit a given histogram has a shape determined by the Landau effect, the statistical variation in the number of photoelectrons leaving the photocathode of the photomultiplier and the non-uniformity of the phosphor response. Contributions from variations in the angle to the vertical of the μ -meson paths and in the energies of the μ -mesons were comparatively small. The result of adding the various effects was a negatively skewed pulse-height distribution curve with a half-width of about 26%.

§ 3. CALCULATION OF THE PEAK POSITIONS OF THE EXPERIMENTAL HISTOGRAMS

The absolute magnitude of the various factors which determine the shape of the pulse-height distribution curve were not very accurately known. It was not possible, therefore, to obtain this theoretical curve with much confidence. In view of this it was desirable to analyse the results using a number of independent methods.

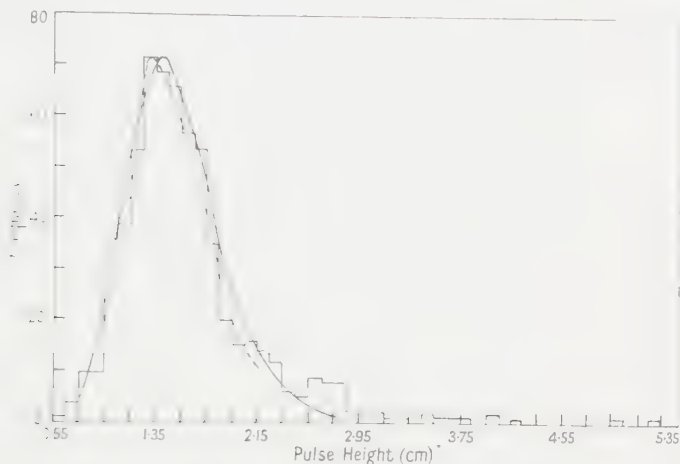


Fig. 3. Typical experimental histogram, together with the logarithmic normal distribution (solid curve) and the distribution obtained by the reciprocal method (broken curve).

Note.—The values of the abscissa scale should all be increased by 1.15 cm to give the actual value of the pulse height.

Because the curves which fit the histograms—a typical histogram is shown in Fig. 3—are negatively skewed it might be thought that a skewed normal distribution function could be made to fit them. It was found, however, that the so-called 'second approximation to the normal function' did not provide a reasonable fit.

However, three methods were found which gave satisfactory results.

3.1. *The Area Method*

The area method of analysing the histograms has been described by Bowen (1954). The tail of the pulse-height distribution curve was artificially cut off at the position which divided the area so that 20% was in the cut-off tail (it was found that the method was insensitive to the position of the cut-off provided the area removed was not more than 20%). The ratio of the areas on each side of the maximum ordinate of the remainder of the assumed theoretical distribution curve was then found. The peak position of an experimental histogram was then calculated by starting with a rough estimate of the peak position. The value of the pulse height whose ordinate divided the remaining area in the above ratio was then found. The procedure was then repeated with the new pulse height and this process of successive approximations continued until no further improvement was obtained.

3.2. *The Reciprocal Method*

The distribution given by plotting the experimentally obtained frequencies against the reciprocals of the corresponding pulse heights of Fig. 3 was found to be

approximately normal. This offered a method of obtaining the peak positions of the histograms; the method implies that the reciprocal of the abscissa corresponding to the maximum point of the distribution of the reciprocal pulse heights gives the value of the pulse height corresponding to the maximum point of the histogram.

The cumulative percentage frequencies were plotted on arithmetical probability paper against the reciprocals of the mid-points of the pulse height intervals (which corresponded to energy intervals of about 0.4 mev). The fact that the points were approximately linear (Fig. 4) for all the histograms confirmed the

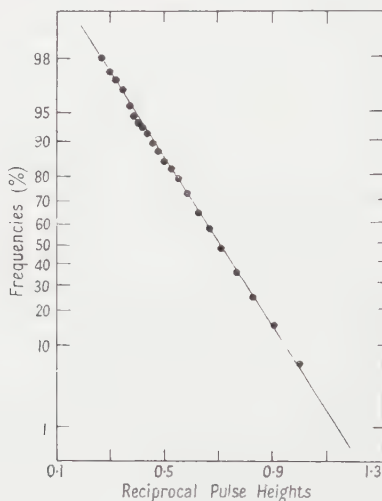


Fig. 4. Straight line obtained by plotting the reciprocal pulse heights against the cumulative percentage frequencies on arithmetical probability paper.

expectation that the distributions of the reciprocal pulse heights were close to normal. The best straight line was calculated for each set of points using the method of least squares. The peaks of the distributions were given by the points on the lines whose ordinates corresponded to 50% on the probability paper. An example of the distribution obtained by this method is shown in Fig. 3.

3.3. The Logarithmic Normal Method

The third method of analysis involved fitting the logarithmic right-skewed normal distribution given by

$$Y = \frac{0.17326Ni}{X\sigma_{\log}} \exp\left(\frac{-x_{\log}^2}{2\sigma_{\log}^2}\right)$$

where N is the total number of pulses, i the histogram interval, σ_{\log} the standard deviation, x_{\log} the difference between the logarithm of the limit of the histogram interval and the arithmetic mean of the logarithms of the X values. The X values represented the pulse heights and the Y values the pulse frequencies.

§ 4. RESULTS

Because of the difficulty of performing an absolute energy calibration of the plastic phosphor the results given by each of the three methods of analysis were expressed relative to the peak position of a calibration histogram obtained

immediately after each reading. Each of the calibration histograms was constructed from the pulse heights of about 1000 pulses produced by μ -mesons with a median energy of 9000 Mev. The theoretically predicted most probable energy loss (Fig. 5) for this energy is 6.79 Mev and the peak positions of the

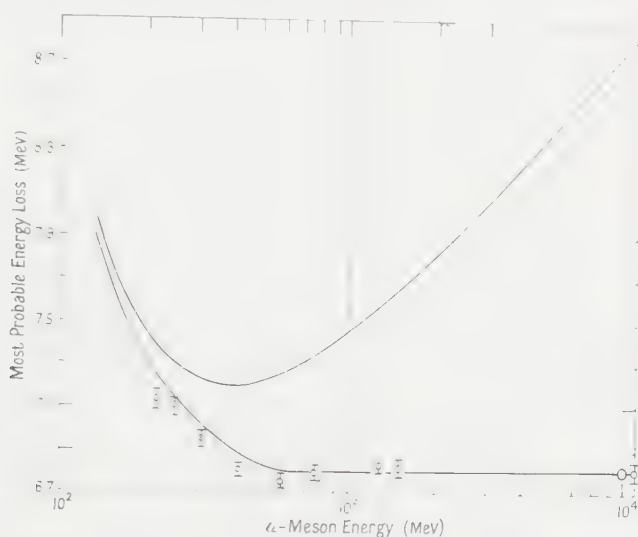


Fig. 5. Experimental results. The upper curve shows the theoretical most probable energy loss distribution for μ -mesons in the plastic phosphor, uncorrected for the density effect. The lower curve shows this distribution after the subtraction of the Sternheimer density correction.

histograms were all normalized to this energy value. The results obtained are shown in the Table.

Results Obtained from the Three Methods of Analysis

μ -meson energy (mev)	Area method	Most probable energy loss (mev)		Mean
		Reciprocal method	Log-normal method	
215	7.13	7.17	7.11	7.14
250	7.09	7.13	7.12	7.11
310	6.98	6.97	6.90	6.95
415	6.87	6.72	6.84	6.81
580	6.77	6.77	6.72	6.75
760	6.78	6.79	6.84	6.80
1285	6.82	6.85	6.82	6.83
1475	6.79	6.82	6.82	6.81
10 000†	6.79	6.79	6.81	6.80

† Because of the shape of the μ -meson spectrum it is not clear whether the median energy or the average energy should be used. Since the median is less than the average the range of energy values is up to at least 10 000 Mev.

The half-width of the distribution curve that fits the histogram is about 26%. The root mean square deviation is therefore about 11%‡. Since each histogram

‡ This is strictly true only for a normal distribution; but although the energy loss distribution is negatively skewed it can be taken as approximately correct.

consists of about 500 events the theoretical error is approximately $\pm 11/\sqrt{500}$ or $\pm 0.5\%$. Reference to the Table will show that the error of the experimental points is of this order.

The logarithmic normal curves did not fit the histograms very well—as could be seen by eye (Fig. 3). The relative peak positions obtained, however, agreed reasonably well with the other two methods and the results are, in fact, almost independent of the method of analysis. Since the histograms were all of the same general shape the relative displacement of the logarithmic normal curve might be expected to be the same in each case.

§ 5. CONCLUSIONS

The experimental results, with the theoretical errors, are shown in Fig. 5 together with the theoretically predicted curve using Sternheimer's density correction. The most probable energy-loss curve for the plastic phosphor, with no correction for the density effect, is also shown. The uncorrected theory predicts a rise of about 23% over the energy range 500 mev to 10 000 mev. The experimental results, however, are not inconsistent with the Sternheimer prediction that the density effect in organic materials is so large that it eliminates the relativistic rise of the most probable energy loss of singly-charged heavy particles. The results show, in fact, that if there is a rise it must be less than 1%.

ACKNOWLEDGMENTS

I wish to thank Dr. P. T. Trent, Birkbeck College, London, and the London Transport Executive for the use of the facilities of the Underground Laboratory at Holborn. I would also like to thank Dr. J. C. Barton, Northern Polytechnic, London, for his invaluable help throughout this work.

REFERENCES

- BARNABY, C. F., and BARTON, J. C., 1960, *Proc. Phys. Soc. A*, **76**, 745.
 BASKIN, R., and WINCKLER, J. R., 1953, *Phys. Rev.*, **92**, 464.
 BOWEN, T., 1954, *Phys. Rev.*, **96**, 754.
 BOWEN, T., and ROSER, F. X., 1952, *Phys. Rev.*, **85**, 992.
 EYEIONS, D. A., OWENS, B. G., PRICE, B. T., and WILSON, J. G., 1955, *Proc. Phys. Soc. A*, **68**, 793.
 FERMI, E., 1940, *Phys. Rev.*, **57**, 485.
 GHOSH, S. K., JONES, G. M. D. B., and WILSON, J. G., 1952, *Proc. Phys. Soc. A*, **65**, 68.
 ——— 1954, *Proc. Phys. Soc. A*, **67**, 331.
 LANDAU, L., 1944, *J. Phys. U.S.S.R.*, **8**, 201.
 LANOU, R. E., and KRAYBILL, H. L., 1959, *Phys. Rev.*, **113**, 657.
 PRICE, B. T., 1955, *Rep. Progr. Phys.*, **18**, 52 (London: Physical Society).
 STERNHEIMER, R. M., 1952, *Phys. Rev.*, **88**, 851.
 ——— 1953, *Phys. Rev.*, **91**, 256.
 ——— 1956, *Phys. Rev.*, **103**, 511.
 ——— 1959, *Phys. Rev.*, **115**, 137.
 SYMON, K. R., 1948, *Ph.D. Thesis*, Harvard (see ROSSI, B., 1952, *High Energy Particles* (New York: Prentice Hall)).

Space Charge Limited Current Flow and Deep Trapping in Selenium

By H. P. D. LANYON AND W. E. SPEAR

Physics Department, University of Leicester

MS. received 5th December 1960

Abstract. Current-voltage characteristics of evaporated specimens of vitreous selenium have been studied. They show an ohmic part at low applied voltages and, with increasing hole injection, a I^2 region which precedes the trap-filled limit as predicted by Lampert's theory. Ohmic contacts of tellurium or platinum were formed on newly prepared specimens by the prolonged application of a moderately high electric field, but this was not found possible with a low work function electrode such as magnesium. The detailed analysis of the results from formed specimens between 2 and 31μ thick indicates the existence of a volume distribution of hole traps of density $9 \times 10^{13} \text{ cm}^{-3}$, 0.79 eV above the valence band. These values agree with independent results from measurements of the transient photoconductivity after saturation of the centres with strong illumination. At room temperature the average trapping time is 50 seconds leading to a capture cross section of $8 \times 10^{-16} \text{ cm}^2$. The presence of the 0.79 eV level offers some explanation for the pronounced difference between the absorption and photoconductive edges in vitreous selenium. It is concluded that the level lies near the upper edge of a comparatively dense distribution of states extending towards the valence band.

§ 1. INTRODUCTION

MUCH progress towards the understanding of the processes of charge transport through insulating materials has been made in recent years. Rose (1951) first pointed out the necessity to interpret the complicated current-voltage characteristics of photoconductors in terms of a few fundamental parameters, and considered the effect of various distributions of traps in the forbidden band on the gain and response time of photoconductors under illumination. Later, Lampert (1956) investigated the effect of a single discrete trapping level upon the dark current-voltage characteristics of an insulator. This analysis was for one sign of carrier only and neglected the diffusive contribution to the current. An idealized 'ohmic' contact was assumed. The theory was extended by Parmenter and Ruppel (1959) and Lampert (1959) to the case of the two mobile carriers in an insulator with shallow traps provided that recombination occurred only between free carriers. As yet no theory has been developed for the case of two mobile carriers in the presence of deep trapping centres.

The experimental studies of current-voltage characteristics in single crystals of CdS (Smith 1958, 1959, Wright 1958) and ZnS (Alfrey and Cooke 1957, Ruppel 1958) have largely verified the predictions of the Rose-Lampert theory. Recently, measurements of space charge limited currents in evaporated specimens of amorphous Se have been reported (Spear and Lanyon 1960). Unlike the

previous work on CdS and ZnS, these experiments refer to a non-crystalline p-type semiconductor. In this paper a more detailed account of the experiments will be given.

The results have been interpreted by using the concepts and nomenclature of the band theory. This requires some justification as vitreous Se possesses no well-defined long-range order. Ioffe and Regel (1960) have discussed this problem and concluded that the band theory possesses a far wider range of applicability than is implied by the assumption of a periodic structure on which it was originally based; long-range order is not a necessary condition for the occurrence of typical semiconducting properties and its absence does not preclude the application of the band model.

§ 2. EXPERIMENTAL DETAILS AND RESULTS

2.1. Specimen Preparation

The specimens, which were produced by vacuum evaporation on to a freshly cleaved mica base, consisted of a layer of amorphous Se sandwiched between two metal electrodes. 'Specpure' Se pellets were used in the evaporation. A technique was developed whereby the complete preparation of a set of specimens could be carried out without breaking the vacuum. This eliminated disturbing effects connected with surface contamination by adsorption of oxygen and moisture. Specimens were prepared with Au, Mg, Te and Pt electrodes. Their thicknesses ranged from 2 to 31μ and the area of overlap of the metal electrodes was about 0.1 cm^2 . All measurements were made with the specimen in high vacuum. Exposure to air between experimental runs did not appear to have any effect.

2.2. Forming of Contacts

One of the main difficulties in the comparison of theory with experiment lies in the preparation of specimens with suitable contacts. The theory, as developed by Rose and Lampert, presupposes an 'ohmic contact' between the insulator and its electrodes. By this, it is meant that at the electrode-insulator interface there exists a reservoir of charge carriers which can be injected into the bulk of the insulator by the application of a field. Such contacts are not normally present on a newly prepared Se specimen. However, with specimens carrying Te or Pt electrodes it was found possible to form ohmic contacts by the prolonged application of a moderately high electric field (5×10^4 – $1 \times 10^5\text{ v cm}^{-1}$), still well below the breakdown value for Se ($\approx 4 \times 10^5\text{ v cm}^{-1}$).

Curve *a* in Fig. 1 illustrates the typical high power law dependence of current density on voltage of a newly prepared specimen carrying Te electrodes. After forming, curve *b* is obtained. The current is now far more stable, particularly at higher *V* and reaches its steady value within a few minutes. The ohmic region at low applied voltages now indicates that the surface barrier no longer controls the current flow through the specimen. The forming is a continuous process, the rate of which depends on the magnitude of the field used. With a comparatively small field it has been possible to stop the forming process at several intermediate stages and observe the development of the ohmic region. Specimens carrying Mg electrodes gave current-voltage characteristics similar to those shown by curve *a*. However, unlike the Te or Pt contacts, these electrodes could not normally be formed even with fields close to the breakdown

value. With the exception of one specimen (Table, specimen 6) the same applied to Au electrodes.

The general features of the forming process are essentially similar to those observed with CdS or ZnS crystals. It is likely that the model suggested by Kröger, Diemer and Klasens (1956) for CdS also applies to Se contacts. In this case, the ohmic contact after forming should be due to a highly conductive p-type accumulation layer close to the electrode. This will act as a reservoir of charge carriers for the bulk and will also reduce the effective thickness of the surface barrier so that replenishment of the reservoir can take place predominantly by tunnelling.

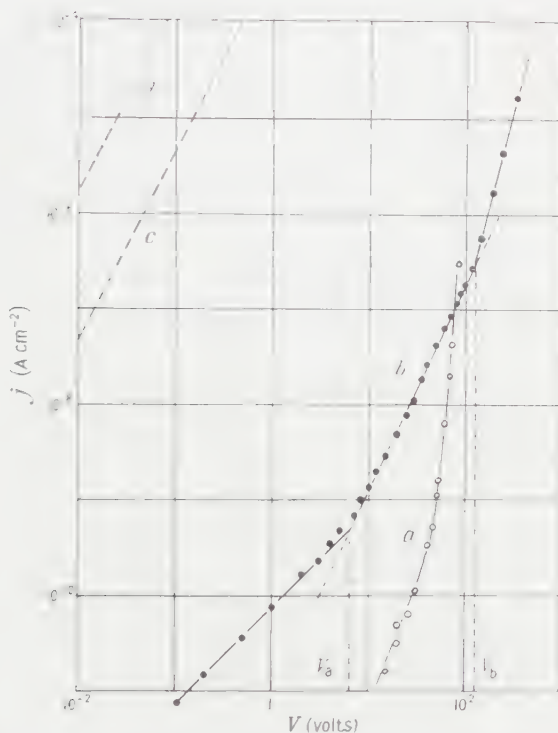


Fig. 1. Current density-voltage curves for a specimen with Te electrodes, $31\ \mu$ thick: *a*, before forming; *b*, after forming; *c*, calculated V^2 curve on saturation of the 0.79 eV level; *d*, calculated V^2 curve in absence of all traps.

The experiments of Alfrey and Cooke on ZnS indicate that the diffusion of the electrode material can play an important part in the forming process. The same might be expected for Se, particularly when Te is used as the electrode material. Se and Te form an alloy in all proportions, and the addition of a few percent of Te to vitreous Se is known to decrease the resistivity by one or two orders of magnitude (Keck 1952). This could explain the formation of the conductive layer in the surface region.

2.3. Experimental Results

The typical current density-voltage curve of a formed specimen is shown in Fig. 1 (curve *b*). It possesses the general characteristics predicted by the Rose-Lampert theory. At low applied voltages there is negligible injection of

(1)	(2)	(3)	(4)	(5)	(6)	(7)	(8)	(9)	(10)	(11)	(12)	(13)
+	—			$\times 10^{-12}$	$\times 10^5$	$\times 10^{13}$	$\times 10^{-9}$	$\times 10^{-9}$	$\times 10^{13}$	$\times 10^6$	$\times 10^6$	
1 Te	Te	6.3	2.0	2.3	2.3	1.1	21	34	3.6	0.96	6.2	0.79
"	"	0.25	1.5	1.7	1.7	0.45	39	56	2.7	1.3	6.2	0.785
"	"	0.21	3.6	0.11	0.11	0.38	3.0	2.1	6.5	0.16	2.6	0.815
2 Te	Te	6.3	2.2	3.8	3.8	0.36	110	120	4.0	4.6	2.8	0.775
"	"	0.6	2.2	6.3	6.3	1.1	59	94	4.0	3.0	2.4	0.785
3 Pt	Te	1.7	6.5	14	14	3.0	37	94	12	7.1	3.6	0.77
4 Te	Te	0.18	2.0	0.44	0.44	2.3	1.9	32	25	1.9	4.7	0.78
5 Te	Te	2.3	5.0	1.6	1.6	1.7	9.4	17	3.6	0.45	0.26	0.835
"	"	1.7	6.5	1.3	1.3	1.2	11	23	4.8	0.76	0.98	0.81
6 Te	Au	1.8	65	1.6	1.6	0.7	23	9.6	24	3.6	3.2	0.78
"	"	5.0	55	8.8	8.8	2.0	44	9.6	20	4.2	4.8	0.77
"	"	3.0	36	4.4	4.4	1.3	34	9.6	14	2.5	2.5	0.785
7 Pt	Au	6.5	130	0.21	0.21	0.5	4.2	1.7	9.8	0.26	0.63	0.83
Mean values												
				3.6	3.6	1.0	36	17	9.0	2.2	2.0	0.79

(1) Specimen and electrodes; (2) $d(\mu)$; (3) V_a ; (4) V_b ; (5) σ ($\Omega^{-1} \text{ cm}^{-1}$); (6) ρ (cm^{-8}); (7) p_t (cm^{-3}); (8) θ_1 ; (9) θ_2 ; (10) N_t (cm^{-3}); (11) $\theta_m N_t$; (12) θN_t ; (13) ϵ_t (ev).

excess carriers into the insulator, and Ohm's law holds. At V_a the injected carrier density becomes comparable with the initially present thermal equilibrium density. The current becomes space-charge limited and between V_a and V_b follows a V^2 law. The excess carrier density increases in proportion to the applied voltage and the steady state Fermi level moves towards the valence band. At $V \simeq V_b$, the trap-filled limit, the Fermi level passes through the level of trapping states of density N_t , ϵ_t ev above the valence band. If, as is assumed in the theory, the occupancy of the trapping level is determined solely by the thermal equilibrium with the valence band, the traps should completely fill under these conditions and any further increase in voltage should lead to a sharp rise in current, which is in fact observed with CdS and ZnS crystals. With the Se specimens, however, the slope of the characteristic in the trap-filled limit is considerably smaller than would be expected from the theory. Also the second V^2 region, predicted for $V > 2V_b$, has not been found in the present experiments. A calculated part of this curve is shown in Fig. 1 (curve c). A possible explanation of these differences will be given in § 5.

The experimental results for a number of specimens are summarized in the Table. Columns (1) and (2) refer to the electrode material and the specimen thickness; in columns (3) and (4) the observed values of V_a and V_b are given. The conductivity (column (5)) is obtained from the ohmic region. Although most specimens led to strictly linear characteristics in this voltage range, the spread in σ values is considerable and the reproducibility of the experimental points in successive runs was often found to be unsatisfactory. It appears that with some specimens the application of higher fields during the experiment leads to further changes in the contact region. However, the uncertainty in the σ values does not greatly affect the final results of the analysis; N_t is independent of σ , and the dependence of ϵ_t on σ is not very sensitive.

The reproducibility of the curves in the V^2 region and beyond is better than in the ohmic range, as can be seen from the V_a and V_b values in the Table referring to the same specimens.

§ 3. EVALUATION OF EXPERIMENTAL RESULTS

The interpretation of the results in terms of the Rose-Lampert theory depends on the choice of the model of the conduction process. Recent measurements of the temperature dependence of the hole mobility in vitreous Se (Spear 1960) have been interpreted in terms of an effective mobility μ_h , which is controlled by a level of shallow centres 0.14 ev above the valence band and in thermal equilibrium with it. μ_h was calculated directly from the measured transit time of the carriers and therefore includes the total time a hole is trapped in the shallow centres during transit. The microscopic mobility μ_0 , on the other hand, refers to a free hole between trapping events. An estimate of the density of these centres led to a value of $\mu_0 \simeq 60 \text{ cm}^2 \text{ v}^{-1} \text{ sec}^{-1}$.

This model has been used in the evaluation of the present results. It is assumed that the trapping in the deep level under investigation can only occur through the valence band; the average free hole density $p = \sigma/\mu_0 e$ is given in column (6). The use of μ_0 takes account of the fact that for every free hole in the valence band μ_0/μ_h ($\simeq 400$) holes are trapped in the shallow centres.

θ , listed in columns (8) and (9), is defined as p/p_t , where p_t is the density of trapped holes in the deep level at ϵ_t and $p_t \gg p$. If this is solely determined by

the thermal equilibrium with the valence band,

$$\theta = (N_v/N_t) \exp(-\epsilon_t/kT).$$

At room temperature $N_v = 9.4 \times 10^{19} \text{ cm}^{-3}$, using $m^* = 2.5m$, a value deduced from the Faraday effect (Moss 1959). The first value θ_1 is obtained from the intercept V_a which according to the theory is given by

$$V_a = \frac{2\pi e d^2}{\kappa} \frac{p}{\theta},$$

where κ denotes the dielectric constant. A second value θ_2 is found by comparing, at a given V , the measured current density in the V^2 region with the calculated value in the absence of all trapping centres in the specimen (curve (d), Fig. 1). The latter is given by

$$j = \frac{9\kappa\mu_0}{32\pi d^3} V^2.$$

The trap density in column (10) is obtained directly from the intercept $V_b = (2\pi e d^2/\kappa) N_t$. For the calculation of ϵ_t the product $\theta_m N_t$ is tabulated in column (11), where $\theta_m = \frac{1}{2}(\theta_1 + \theta_2)$. A check on θN_t is provided by the fact that when the Fermi level passes through ϵ_t , $p = \theta N_t$. From the measured current density at $V = \frac{2}{3}V_b$, p is calculated and the value of θN_t given in column (12). Finally, ϵ_t is obtained from the mean of $\theta_m N_t$ and θN_t .

The mean values of the calculated results are given at the bottom of each column. In the case of p_t , θ , N_t and ϵ_t , which were derived from intercepts on a log-log plot, the mean value has been obtained from the logarithms of the tabulated quantities.

§ 4. FURTHER EXPERIMENTAL EVIDENCE

A number of measurements based on a different experimental method was made as an independent check of the above results. Unformed specimens with thin Au electrodes were used and carriers were generated near the top electrode by steady illumination with an intense blue source or by light pulses from a spark gap. The field was applied from the top to the bottom electrode so as to draw the comparatively large number of holes generated by the steady illumination across the specimen. On the assumption that under these conditions most of the deep centres will trap a hole, a fairly uniform positive space charge of density eN_t should form between the electrodes. A solution of Poisson's equation shows that the resultant field at the top electrode will vanish unless $V/d > 2\pi e N_t d/\kappa$. The limiting value of V/d could be determined approximately by observing the onset of the response to a single light pulse immediately after the steady illumination had been extinguished. From measurements on a number of specimens of varying thicknesses it was found that the onset of response occurred within the ranges of V/d indicated in Fig. 2. This gives a mean value of N_t of $1.1 \times 10^{14} \text{ cm}^{-3}$ in reasonable agreement with the results in the Table.

A similar method was used to determine the average trapping time τ_t of a hole before thermal release. With an applied potential below the limiting value the response to the test pulse was measured at time t after removing the steady illumination. It is reasonable to assume that the transient photocurrent is proportional to the field near the top electrode; at time t this is given by

$$E(t) = \frac{V}{d} - \frac{2\pi e d p_t(t)}{\kappa}.$$

The results for several specimens showed that at room temperature p_t decreases exponentially with a time constant τ_t lying between 40 and 50 sec, which leads to a trapping cross section

$$\sigma = (\tau_t v_{th} N_t \theta)^{-1} \simeq 8 \times 10^{-16} \text{ cm}^2,$$

where v_{th} denotes the thermal velocity. As $\tau_t \propto \exp(\epsilon_t/kT)$, an independent

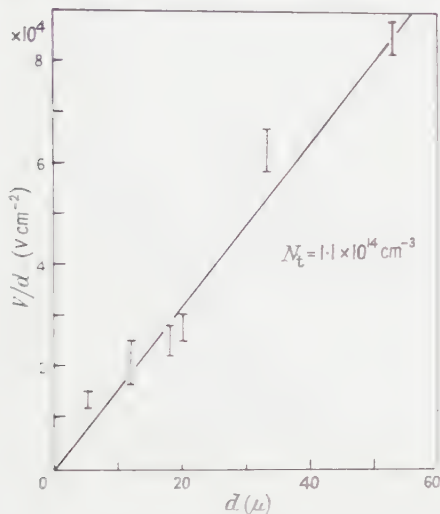


Fig. 2. Values of V/d at the onset of photoresponse for specimens of various thicknesses d .

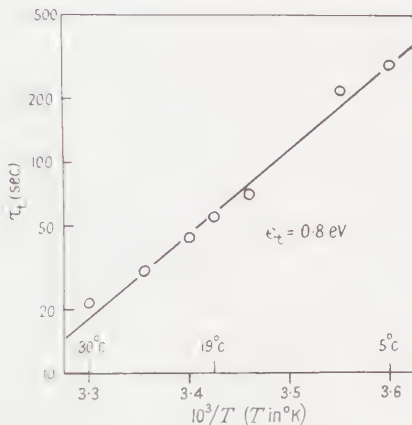


Fig. 3. Temperature dependence of τ_t for a 20μ specimen.

value of ϵ_t should be obtainable from a measurement of the temperature dependence of τ_t . This has been done over a limited range (Fig. 3) and leads to $\epsilon_t \simeq 0.8$ eV.

A similar experiment has recently been carried out by Fotland (1960) who obtained values between 0.75 eV and 0.80 eV for the activation energy.

§ 5. DISCUSSION

The experiments show that with increasing hole injection the steady state Fermi level moves from its equilibrium position at 0.85 eV towards the valence band and enters a level of predominantly filled states at $\epsilon_t \simeq 0.79$ eV. Within the experimental accuracy the measured density N_t is independent of specimen thickness (Table) and one would therefore expect that these centres are distributed uniformly throughout the volume. The experiments on unformed specimens (§4) show further that the trapping states could not have been introduced by the forming process.

As pointed out in §2.3, the slope of the characteristics in the trap-filled limit was found to be considerably smaller than predicted by theory. In our case this slope, as measured on a logarithmic plot, should be about 8. However, experimentally, values as low as 3 have been obtained. It is likely that this may be due to the existence of other states below the 0.79 eV level, about which the present experiments can give no information. The shift of the steady state Fermi level would increase the probability of trapping a hole in these states and if, as might be expected, their density is larger than N_t , at higher V the

number of holes so trapped might well approach that in the 0.79 eV level. This would slow down the rate of increase of current with voltage in the trap-filled limit.

Another reason could be the injection of electrons at the second electrode. Electrons are mobile in amorphous Se, but their effective mobility μ_e is only about 1/30 of that of the holes (Spear 1957). If recombination between holes trapped in the 0.79 eV level and injected electrons takes place, then the level might partially be emptied by a kinetically controlled process. This again would tend to decrease the gradient of the characteristics beyond V_b .

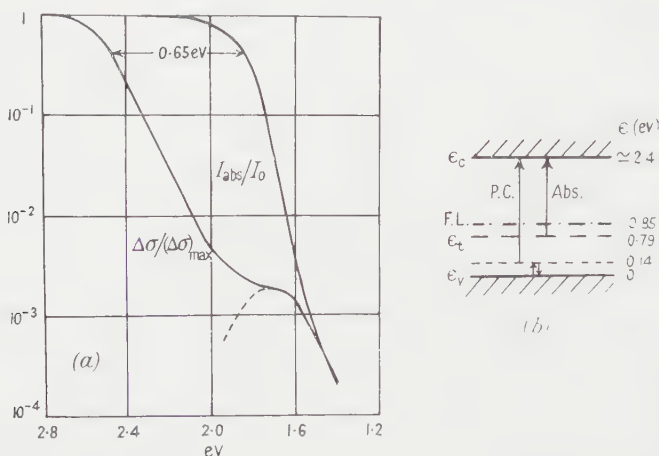


Fig. 4. (a) Photoconductivity (normalized to maximum response) and absorption curves as a function of photon energy. (b) Suggested transitions to explain energy difference between photoconductive and absorption edges.

The existence of the 0.79 eV states offers some explanation for the pronounced energy difference between corresponding levels of optical absorption and photo-response in amorphous Se pointed out by Moss (1959). This is shown in Fig. 4(a) plotted from data given in the literature (see Moss 1952, 1959). It is suggested that the beginning of the absorption is connected with transitions from ϵ_t into the conduction band at photon energies of approximately 1.6 eV (Fig. 4(b)). As $\mu_v \ll \mu_h$ the excited electrons will give rise to only a small photo-response which might explain the shoulder in the $\Delta\sigma$ curve at about 1.7 eV. Appreciable photoconductivity should set in at photon energies of about 2.25 eV; then transitions of electrons from the dense shallow level at 0.14 eV can take place leading to the thermal excitation of a considerable number of free holes. At the higher photon energies one would therefore expect an energy difference of about 0.65 eV between the photoconductivity and absorption curves. This is in fact borne out by the experimental data in Fig. 4.

The difficulty with the above model lies in the fact that the value of N_t determined from the electrical measurements is too small by at least an order of magnitude to account for the optical absorption in the 1.6 eV region. This again points to the conclusion that the 0.79 eV level lies close to the upper edge of a fairly dense distribution of states extending towards the valence band. It is of interest to note that on conversion to the hexagonal form the photo-conductivity associated with transitions from these states seems to increase by

several orders of magnitude, so that the energy difference between the photoconductive and the absorption edge largely disappears.

Experiments are in progress to study in more detail the changes in both the electrical and optical properties of Se at intermediate stages between the amorphous and crystalline forms.

REFERENCES

- ALFREY, G. F., and COOKE, I., 1957, *Proc. Phys. Soc. B*, **70**, 1096.
FOTLAND, R. A., 1960, *J. Appl. Phys.*, **31**, 1558.
IOFFE, A. F., and REGEL, A. R., 1960, *Progress in Semiconductors* 4 (London: Heywood), p. 237.
KECK, P. H., 1952, *J. Opt. Soc. Amer.*, **42**, 221.
KRÖGER, F. A., DIEMER, G., and KLASSENS, H. A., 1956, *Phys. Rev.*, **103**, 279.
LAMPERT, M. A., 1956, *Phys. Rev.*, **103**, 1648.
——— 1959, *R.C.A. Rev.*, **20**, 682.
MOSS, T. S., 1952, *Photoconductivity in the Elements* (London: Butterworth), p. 187.
——— 1959, *Optical Properties of Semiconductors* (London: Butterworth), p. 156.
PARMENTER, R. H., and RUPPEL, W., 1959, *J. Appl. Phys.*, **30**, 1548.
ROSE, A., 1951, *R.C.A. Rev.*, **12**, 362.
RUPPEL, W., 1958, *Helv. Phys. Acta*, **31**, 311.
SMITH, R. W., 1958, *Bull. Amer. Phys. Soc. [II]*, **3**, 129.
——— 1959, *R.C.A. Rev.*, **20**, 69.
SPEAR, W. E., 1957, *Proc. Phys. Soc. B*, **70**, 669.
——— 1960, *Proc. Phys. Soc.*, **76**, 826.
SPEAR, W. E., and LANYON, H. P. D., 1960, *Proc. of the International Conference on Semiconductor Physics, Prague*, in the press.
WRIGHT, G. T., 1958, *Nature, Lond.*, **182**, 1296.

Viscosity and Thermal Conductivity of Binary Gas Mixtures: Krypton-Argon, Krypton-Neon, and Krypton-Helium

By E. THORNTON†

Battersea College of Technology, London

Communicated by L. R. B. Elton; MS. received 12th December 1960

Abstract. The coefficients of viscosity and thermal conductivity of binary mixtures of krypton with argon, neon and helium have been determined over the full range of composition of each mixture at a pressure of 70 cm of mercury and at a temperature in the range 18.0 to 18.3°C. The experimental values are compared with theoretical values based on the Lennard-Jones (6-12) potential of interaction between molecules. Agreement between the experimental and calculated values is generally satisfactory, but there are discrepancies between some of the measurements given here and those of other workers.

§ 1. INTRODUCTION

THE viscosity and thermal conductivity of binary mixtures of krypton with argon, neon and helium, at a pressure of 70 cm Hg and at a temperature in the range 18.0 to 18.3°C, were determined by Mr. W. Gordon at Battersea College of Technology in 1955-6. These results have not previously been published, and the opportunity is being taken to compare them with theoretical values based on the Lennard-Jones (6-12) potential of interaction between molecules.

The details of the experimental work and the calculation of the theoretical values are the same as those given by Thornton (1960).

§ 2. RESULTS

The experimental and calculated values of viscosity and thermal conductivity of the mixtures are given as functions of mixture composition in the Table.

§ 3. DISCUSSION

To facilitate comparison of the results the experimental points and theoretical curves for viscosity and thermal conductivity are shown plotted in the Figure.

3.1. Viscosity

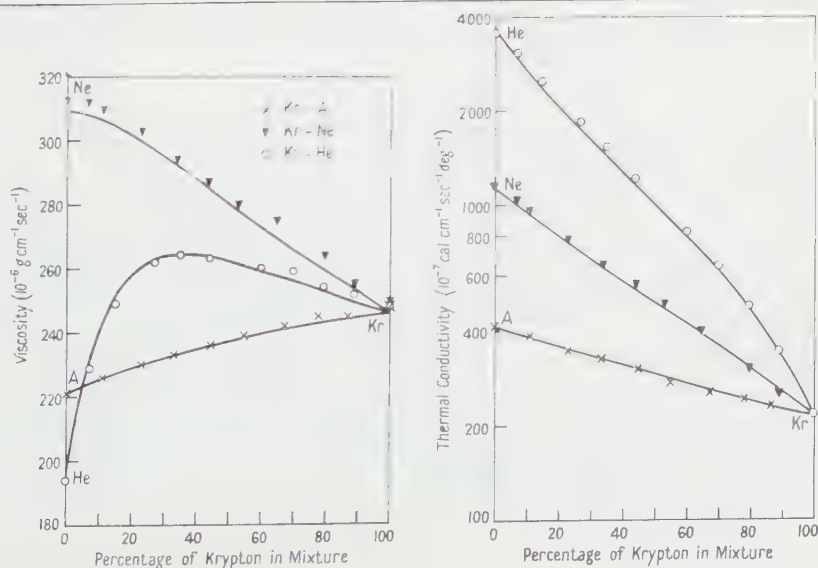
The experimental values for the viscosities of the pure gases given here are within one per cent of the average values for these gases obtained with this apparatus, other results for these gases having been obtained by Heath (1953), Baker (1955), and Thornton (1960). These average values are also within one per cent of the values quoted by other workers—for krypton by Rankine (1910) and by Nasini and Rossi (1928a), and for argon, neon and helium by Trautz and Binkele (1930) and by Johnston and Grilly (1942).

† Now at the Gas Council, London Research Station, Watson House, London, S.W.6.

Viscosity and Thermal Conductivity: Experimental and Calculated Values

Gas mixture	%Kr	Viscosity (10^{-6} g cm sec $^{-1}$)		Thermal conductivity (10^{-7} cal cm $^{-1}$ sec $^{-1}$ deg $^{-1}$)	
		Exp.	Calc.	Exp.	Calc.
Kr-A	100	248	246	220†	218
	86.5	245	244	233	236
	77.7	245	243	242	248
	67.3	242	241	256	264
	54.6	239	239	277	286
	44.3	236	236	302	305
	33.0	233	233	326	328
	22.8	230	230	348	352
	10.9	226	226	387	382
	0	221	221	416†	412
Kr-Ne	100	249	246	220†	218
	88.9	255	253	257	264
	79.7	264	259	305	307
	64.7	275	269	400	391
	53.3	280	278	482	467
	43.8	287	285	568	542
	33.9	294	292	650	635
	22.9	303	300	780	760
	11.1	310	306	960	931
	6.5	312	308	1030	1011
	0	313	309	1160†	1141
Kr-He	100	248	246	220†	218
	89.1	252	249	343	341
	79.7	254	253	480	464
	69.8	259	256	642	615
	60.0	260	259	825	793
	43.9	263	264	1210	1172
	35.3	264	264	1530	1438
	27.2	262	263	1850	1746
	15.1	249	252	2500	2365
	6.9	229	231	3050	2952
	0	194	194	3560†	3614

† Calibration values for katharometer (Kannuliuk and Carman 1952).



The only published results found with which the present experimental values could be compared were those for binary mixtures of krypton and helium, reported by Nasini and Rossi (1928 b). The experimental values quoted by these authors for mixtures at 16°C are less than the corresponding values given here by up to 2.8% for a mixture of 30% krypton; however, their experimental values for temperatures of 27.2, 26.6, 26.4, 26.0 and 23.0°C agree closely with the values given here. This lack of consistency shows that further experimental determinations are required.

There is good general agreement between the experimental and calculated values, despite the fact that the experimental values given here for pure krypton and neon are somewhat higher than those given by other workers. The force constants for krypton resulting from the recent re-determination by Mason (1960) give a calculated value for this gas lower than that obtained here, and the use of these force constants throughout the calculations would probably give less satisfactory agreement with the experimental results. It has been suggested by Madan (1953) and Saxena (1957) that better agreement for the Lennard-Jones (6-12) potential is obtained by the use of force constants for unlike interactions derived from thermal diffusion data rather than from the empirical rules; however, for these mixtures the values given by the empirical rules appear to be satisfactory.

3.2. Thermal Conductivity

Experimental values with which the present results may be compared are those for krypton-argon and krypton-neon at 38°C given by Srivastava and Saxena (1957), and for the three mixtures at 29°C quoted by Mason and von Ubisch (1960) from the work of von Ubisch (1959).

For krypton-argon mixtures the scatter of the actual experimental values given by Srivastava and Saxena precludes any direct comparison, but the smoothed values given by these authors are between 5 to 8% greater than those given here throughout the complete range of composition; this represents quite satisfactory agreement. The values quoted by Mason and von Ubisch are between 6 and 11% greater than the corresponding values given here; again the agreement may be considered satisfactory. However, the fact that the experimental values of von Ubisch are higher than the corresponding smoothed values of Srivastava and Saxena, although measured at a lower temperature, suggests that further experimental work is required.

For krypton-neon mixtures the smoothed values of Srivastava and Saxena are between 2 and 6% greater than those given here; the shapes of the curves showing thermal conductivity against mixture composition are very similar, so agreement between the results may be considered satisfactory. However, the results quoted from the work of von Ubisch do not show agreement; for his mixture of 76.3% neon, the value is approximately 7% less than the corresponding value from the present work, whereas for his mixture of 25.0% neon, the value is approximately 12% greater than the corresponding result from the present work.

For krypton-helium mixtures, the values due to von Ubisch are within $\pm 3\%$ of the results of the present work, except for pure krypton which is approximately 10% greater than the value used here. For the mixtures the agreement between the two sets of results appears satisfactory.

In comparing the experimental and calculated values for the mixtures due allowance must be made for the differences found for the pure gases. For krypton argon and krypton neon mixtures agreement between experimental and calculated values is generally satisfactory and is comparable with that given by Mason and von Ubisch (1960) for these mixtures using the exp-six potential, although not as close as that reported for these mixtures by Srivastava (1958) using the exp-six model. For krypton-helium mixtures, however, the differences between some of the experimental and calculated values are greater than the estimated experimental error; agreement is not as close as that given by Mason and von Ubisch (1960) for the exp-six potential. The results need to be compared with values calculated from the more accurate formula of Mason and Saxena (1959).

§ 4. CONCLUSIONS

The differences between some of the experimental results discussed here indicate the need for further experimental determinations of the viscosities of mixtures and of the thermal conductivities of both pure gases and mixtures. The agreement between experimental results and calculated values based on the Lennard-Jones (6-12) potential is generally satisfactory.

ACKNOWLEDGMENTS

Thanks are due to Mr. W. Gordon for permission to publish his experimental results, to Professor P. E. Liley, Thermophysical Properties Research Center, Purdue University, for pointing out certain relevant publications, and to Dr. L. R. B. Elton and Dr. R. J. Huck, Physics Department, Battersea College of Technology, for helpful discussions and valuable suggestions in preparing the manuscript.

Grateful acknowledgment is made to the North Thames Gas Board for facilities afforded in carrying out the work.

REFERENCES

- BAKER, W. A. D., 1955, *M.Sc. Thesis*, University of London.
HEATH, H. R., 1953, *Proc. Phys. Soc. B*, **66**, 362.
JOHNSTON, H. L., and GRILLY, E. R., 1942, *J. Phys. Chem.*, **46**, 948.
KANNULUIK, W. G., and CARMAN, E. H., 1952, *Proc. Phys. Soc. B*, **65**, 701.
MADAN, M. P., 1953, *Proc. Nat. Inst. Sci. India*, **19**, 713.
MASON, E. A., 1960, *J. Chem. Phys.*, **32**, 1832.
MASON, E. A., and SAXENA, S. C., 1959, *J. Chem. Phys.*, **31**, 511.
MASON, E. A., and VON UBISCH, H., 1960, *Phys. Fluids*, **3**, 355.
NASINI, A. G., and ROSSI, C., 1928 a, *Gazz. Chim. Ital.*, **58**, 433.
— 1928 b, *Gazz. Chim. Ital.*, **58**, 898.
RANKINE, A. O., 1910, *Proc. Roy. Soc. A*, **83**, 265.
SAXENA, S. C., 1957, *Indian J. Phys.*, **31**, 146.
SRIVASTAVA, B. N., and SAXENA, S. C., 1957, *Proc. Phys. Soc. B*, **70**, 369.
SRIVASTAVA, K. P., 1958, *J. Chem. Phys.*, **28**, 543.
THORNTON, E., 1960, *Proc. Phys. Soc.*, **76**, 104.
TRAUTZ, M., and BINKELE, H. E., 1930, *Ann. Phys., Lpz.*, **5**, 561.
VON UBISCH, H., 1959, *Ark. Fys.*, **16**, 93.

A Correction to the Smoluchowski Equation in the Molecular Theory of Liquids

BY A. SUDDABY AND J. R. N. MILES

Department of Physics, Sir John Cass College, London

MS. received 13th December 1960

Abstract. The Smoluchowski equation has been used to obtain the distribution function in coordinate space of pairs of molecules in a non-uniform liquid and hence to calculate the viscosity and flow anisotropy. This equation is the first approximation in an expansion of the Kramers–Chandrasekhar equation in inverse powers of the friction constant. In this paper, the second approximation, which leads to a fourth-order differential equation, is considered. The equation is solved numerically and the contributions to the radial distortion of the pair distribution and to the flow anisotropy are calculated for chloroform. It is found that the friction constant must be at least $4 \times 10^{12} \text{ sec}^{-1}$ for the Smoluchowski equation to be a reasonable approximation.

§ 1. INTRODUCTION

IN the molecular theory of transport processes in liquids (Kirkwood 1946, Eisenschitz 1952, Cole 1952), the distribution of a pair of molecules is determined by a differential equation identical with the Kramers equation (sometimes called the Planck–Fokker equation) of Brownian movement theory. In relative coordinates, this is:

$$\frac{\partial f}{\partial t} + \frac{\mathbf{P}}{m} \cdot \text{grad}_{\mathbf{r}} f + \mathbf{F} \cdot \text{grad}_{\mathbf{p}} f = \gamma m \text{div}_{\mathbf{p}} \frac{\mathbf{P}}{m} f + \nabla_{\mathbf{p}}^2 \gamma m k T f$$

where f is the pair distribution in relative coordinates and momenta. For large values of γ , the friction constant, this equation may be replaced by the Smoluchowski equation, which determines the relative pair distribution in coordinate space (Chandrasekhar 1943, Kirkwood, Buff and Green 1949). This equation represents the process as Markovian in coordinate space and, for Brownian movement theory, appears to be an adequate approximation.

The Smoluchowski equation has been used as an approximation to (1) by Eisenschitz (1949), and Kirkwood, Buff and Green (1949), to obtain the non-equilibrium pair distribution for a non-uniform liquid in the steady state, and hence to provide a method of calculating the transport coefficients. The method leads to a second-order equation for $u(r)$, the radial distortion of the pair distribution, the solution requiring the specification of two boundary conditions for its determination (Eisenschitz 1952, Champion and Suddaby 1960). The first, that $u = du/dr = 0$ at $r = \infty$, was applied by both Eisenschitz and Kirkwood while, for the second, two alternative conditions have been put forward. Kirkwood, Buff and Green, using the ‘weak condition’ that $u = 0$ at $r = 0$, have obtained a value for the coefficient of viscosity η for liquid argon which is in fair agreement with experiment, but depends on a somewhat hypothetical estimate of the value of the friction constant. Eisenschitz has used the ‘strong’ condition, that $r^3 u = 0$ at $r = \infty$, and obtained a solution which leads to a dependence of η on the

temperature of the same sign and the same order of magnitude as that observed experimentally. The 'strong condition' was imposed to keep the integral

$$\int_0^R g_0 u r^2 dr \quad \dots\dots (1)$$

where g_0 is the equilibrium pair distribution, finite for all values of R . This was considered necessary to prevent the anisotropy of the flowing liquid becoming appreciable. To prevent divergence of the integral at the lower limit, the pair potential ψ , given by

$$g_0(r) = \frac{1}{V} \exp(-\psi) \quad \dots\dots (2)$$

was assumed to have a first-order pole at the origin. This causes $u(r)$ to become exponentially infinite at $r=0$. This was justified by the fact that the Smoluchowski equation is a poor approximation at $r=0$. By expanding the Kramers equation in inverse powers of the friction constant, Suddaby (1954, see also Eisenschitz and Suddaby 1953), obtained the Smoluchowski equation as a first approximation to a differential equation in coordinate space. In the second approximation, a fourth-order differential equation was obtained. The expansion process was found to diverge in the region of the origin while, at large distances, the first approximation was adequate. By requiring the solution with zero force to reduce to the solution corresponding to a flowing gas, mathematical arguments were advanced to support the strong condition.

The solution determined by the strong condition has also been used by Cole (1952) to calculate the electro-viscous effect for chloroform, and by Champion (1958) to calculate the flow double refraction, and good agreement with experiment was obtained in both cases. The Smoluchowski equation thus leads to results which are in agreement with experiment, and it is therefore of interest to investigate the range of validity of the approximation more closely. The expansion of the Kramers equation leads to a method of successive approximation to $u(r)$ as higher inverse powers of the friction constant are included. If the correction to the distortion obtained in the next highest approximation is not large, the Smoluchowski equation could be regarded as a satisfactory equation. In this paper, $u(r)$ is calculated to a higher degree of approximation by retaining terms in $1/\gamma^2$.

§ 2. THE FOURTH-ORDER DIFFERENTIAL EQUATION

This has been shown by Suddaby to be

$$\left(F_1 + \frac{1}{2} \frac{kT}{m\gamma^2} F_2\right) u = \frac{a\gamma m}{kT} \left(-r\psi' + \frac{kT}{m\gamma^2} P\right) \quad \dots\dots (3)$$

where

$$\begin{aligned} F_1 &= D^2 + \left(\frac{2}{r} - \psi'\right) - \frac{6}{r^2}, & \left(D = \frac{d}{dr}\right) \\ F_2 &= 3D^4 + \left(\frac{12}{r} - 7\psi'\right)D^3 - \left[\frac{36}{r^2} + \frac{16}{r}\psi' - 5\psi'^2 + 5\psi''\right]D^2 \\ &\quad + \left(\frac{46}{r^2}\psi' + \frac{4}{r}[\psi'^2 - \psi''] + 3\psi'\psi'' - \psi''' - \psi'^3\right)D \\ &\quad + \frac{72}{r^4} - \frac{48}{r^3}\psi' + \frac{6}{r^2}[\psi'^2 - \psi''] \end{aligned}$$

and

$$P = \frac{5\psi'}{r} + \psi'' + \psi'^2 + \frac{1}{2}r(\psi''' + \psi'^3 - 3\psi'\psi'')$$

ψ is the mean pair potential, given by (2), γ the friction constant and $a/2$ the rate of shear.

We now write

$$u = \frac{\gamma m}{kT} \left(q_1 + \frac{kT}{m\gamma^2} q_2 + \text{higher powers of } \frac{1}{\gamma^2} \right)$$

and substitute in (3). Equating powers of γ and neglecting the terms of higher order than $1/\gamma^2$ we obtain

$$F_1(q_1) = -\psi' ar \quad \dots\dots (4)$$

$$\frac{1}{2} F_2(q_1) + F_1(q_2) = aP. \quad \dots\dots (5)$$

Eqn (4) is simply the Smoluchowski equation. $1/a$ and $(1/a)(dq_1/dr)$ have been calculated by means of the Kutta-Runge procedure using a potential curve erected for chloroform (Cole 1952).

By expressing F_2 in terms of F_1 and substituting from (4) into (5), we obtain, after some calculation, the relation

$$F_1(q_2) = a \left\{ 7\psi'' - \frac{\psi'}{r} - 2\psi'^2 + r(2\psi''' - 3\psi''\psi' + \psi'^3) - \left[\psi''' D + \frac{6}{r^2} \left(\psi'^2 - \frac{\psi'}{r} \right) \right] \frac{q_1}{a} \right\} = aR(r, \psi, q_1). \quad \dots\dots (6)$$

Thus an equation similar in form to (4) is obtained.

§ 3. NUMERICAL PROCEDURE

The function R was first computed in the region $3 \text{ \AA} < r < 9 \text{ \AA}$, at intervals of 0.1 \AA , using the values of q_1/a and $(1/a)(dq_1/dr)$ obtained by Cole. The derivatives of ψ were calculated from the mean potential curve constructed by Cole. This relatively crude empirical curve had been designed merely to satisfy the normalization condition, and to give the correct values at the first minimum and the second maximum. It decayed as $1/r^7$ beyond 9 \AA and was linear in the vicinity of the origin. A series of straight lines and ellipses were fitted to this curve and the derivatives calculated analytically, avoiding the 'joins' and the discontinuities which would have arisen from them.

The boundary conditions to be imposed on (6) are the same as those for (4). The form of the solution of (6) at large distances is therefore

$$q_2 = \frac{a}{5} \left[r^2 \int_{\infty}^r \frac{R}{r} dr - \frac{1}{r^3} \int_{\infty}^r r^4 R dr \right] \quad \dots\dots (7)$$

(Suddaby 1954). This was computed at $r = 9 \text{ \AA}$ taking $\psi = A/r^7$. In the same way dq_2/dr at $r = 9 \text{ \AA}$ was found. These values provided the starting point for the Runge-Kutta procedure which was then applied to (6). The result is shown in Fig. 1.

§ 4. THE CONTRIBUTION TO THE ANISOTROPY

The streaming birefringence in a flowing liquid is calculated from an expression involving the integral

$$I_1 = \alpha \int_r^R \exp(-\psi) u(r)/r dr \quad \dots\dots (8)$$

(Champion 1958) where $\alpha = a\gamma m/kT$. In the second approximation a term

$$I_2 = \alpha \int_r^R \frac{kT}{m\gamma^2} \frac{q_2}{a} \frac{1}{r} \exp(-\psi) dr \quad \dots\dots (9)$$

must be added to (8).

The integrand of (9) is shown graphically in Fig. 2. It becomes rapidly large and negative for r less than 5 \AA owing to the divergence of q_2 in this range (Fig. 1). The latter must be regarded as a consequence of the divergence of the expansion procedure at small values of r , magnified by the feed-back procedure of calculating q_2 in terms of q_1 . In the first approximation, despite the divergence of q_1 for small r , the main contribution to the anisotropy arises from the range $r > 5 \text{ \AA}$, but recent calculations (Champion, private communication) show that this is due to a fortuitous choice of the slope of the potential near the origin. It seems reasonable to expect the true distortion to return to zero at $r=0$, and

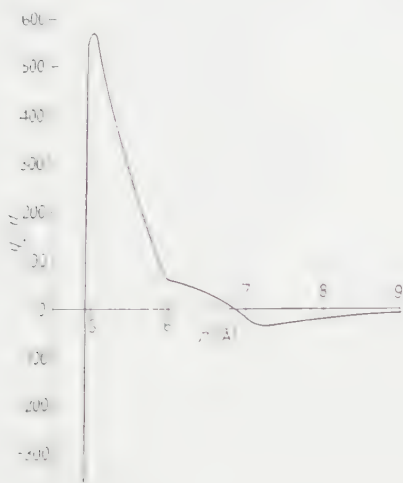


Fig. 1. The correction to the radial distortion.

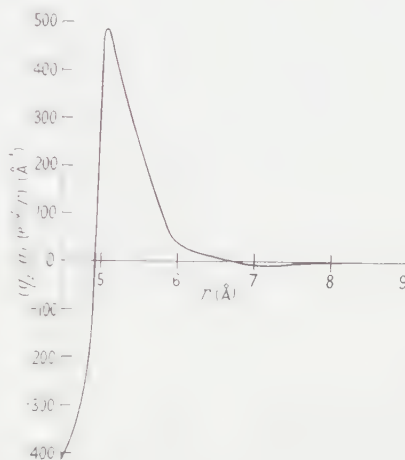


Fig. 2. The correction to the anisotropy integral.

to exclude from the appropriate integrals the region close to the origin in which the divergence of the expansion process has serious consequences. It follows that the large negative values of the integrand of (9) should not be included in I_2 , since the integrand calculated from the true distortion would tend to zero and give a negligible contribution in this region. Although the exact point of the cut-off must be chosen arbitrarily, the effect of the divergence suddenly becomes appreciable over a comparatively narrow range of r . This can be seen in Fig. 1. This divergence begins at $r=5 \text{ \AA}$ so that the lower limit of (9) can be fixed near this value. The value of 4.9 \AA was chosen as giving the maximum positive contribution.

On evaluating the integrals using the value of the friction constant taken by Champion (1958), viz. 10^{11} sec^{-1} , we find that $I_2/I_1=560$. In order that $I_2/I_1=0.3$, as required for a reasonable approximation (see § 5), it is found that γ must have the value $4.2 \times 10^{12} \text{ sec}^{-1}$.

In the table below, $S=q_1/a$ and $Q=(kT/m\gamma^2)(q_2/a)$ are both calculated for $\gamma=10^{11} \text{ sec}^{-1}$ for a series of values of r . γ^* is the value of γ for which $|Q/S|=0.3$.

$r (\text{\AA})$	8.9	8.5	8.0	7.5	7.0	6.5	6.0	5.5	5.0
$S (\text{\AA}^2)$	+22.02	+28.41	+38.14	+49.75	+62.83	+71.81	+76.19	+81.12	+93.82
$Q (10^3 \text{\AA}^2)$	-1.66	-2.62	-4.24	-5.95	-4.19	+6.20	+11.5	+59.2	+86.2
$\gamma^* (10^{12} \text{ sec}^{-1})$	1.5	1.66	1.82	1.90	1.41	1.61	2.13	4.6	5.2

§ 5. EFFECT OF THE FRICTION CONSTANT

The application of the Smoluchowski equation is based on the assumption that, in the expansion for u ,

$$u = \frac{\gamma m}{kT} \left(q_1 + \frac{kT}{m\gamma^2} q_2 + \text{higher powers of } \frac{1}{\gamma^2} \right),$$

the term $(kT/m\gamma^2)q_2$ is substantially smaller than q_1 . In the calculation of the optical anisotropy this means that I_2 should be substantially smaller than I_1 .

This makes it possible to calculate the minimum value of the friction constant for which the Smoluchowski equation is a reasonable approximation. If, for instance, to make the approximation tolerable we demand that $I_2/I_1 < 0.3$ then the friction constant must be at least $4.2 \times 10^{12} \text{ sec}^{-1}$. Kirkwood, Buff and Green (1949) obtained and used a value of 7.2×10^{12} in calculating the viscosity of liquid argon, but this value has been considered by Suddaby (1954) to be too large. Values of 8.56×10^{11} and 5.6×10^{10} have been calculated by Eisenschitz and Turner (1956) and Turner (1958) respectively, for liquid argon, while Champion (1958, 1960) has worked with a value of 10^{11} in the case of chloroform.

The use of the Smoluchowski equation has led to results in agreement with experiment in the case of chloroform as well as liquid argon. The calculation of the electro-viscous effect (Cole 1952, Eisenschitz and Cole 1954) and that of the general form of the temperature dependence of viscosity do not depend on an assumed value for the friction constant. The agreement with experiment obtained in these instances suggests that the approximation involved by the use of the Smoluchowski equation is a reasonable one. This implies that the friction constant in the case of chloroform is sufficiently high to justify the use of the Smoluchowski equation. The present calculations indicate that this requires a minimum value which is higher by at least a factor of 10 than the value which is considered likely on other grounds.

ACKNOWLEDGMENTS

The numerical calculations were carried out on the 'Pegasus' computer, facilities for the use of which were provided by the Northampton College of Advanced Technology. We wish to thank Dr. J. V. Champion for his advice on programming.

REFERENCES

- CHAMPION, J. V., 1958, *Proc. Phys. Soc.*, **72**, 711.
 — 1960, *Proc. Phys. Soc.*, **75**, 421.
 CHAMPION, J. V., and SUDDABY, A., 1960, *Proc. Phys. Soc.*, **75**, 799.
 CHANDRASEKHAR, R., 1943, *Rev. Mod. Phys.*, **15**, 1.
 COLE, G. H., 1952, *Ph.D. Thesis*, University of London.
 EISENSCHITZ, R., 1949, *Proc. Phys. Soc. A*, **62**, 41.
 — 1952, *Proc. Roy. Soc. A*, **215**, 29.
 EISENSCHITZ, R., and COLE, G. H., 1954, *Phil. Mag.*, **45**, 394.
 EISENSCHITZ, R., and SUDDABY, A., 1953, *Proc. 2nd Int. Congress on Rheology* (London: Butterworths), 320.
 EISENSCHITZ, R., and TURNER, R. E., 1956, *Proceedings of the Int. Symposium on Transport Processes, Brussels* (New York: Interscience).
 KIRKWOOD, J. G., 1946, *J. Chem. Phys.*, **14**, 180.
 KIRKWOOD, J. G., BUFF, F. P., and GREEN, M. S., 1949, *J. Chem. Phys.*, **17**, 988.
 SUDDABY, A., 1954, *Ph.D. Thesis*, University of London.
 TURNER, R. E., 1958, *J. Chem. Phys.*, **29**, 856.

Collective Modes in the Theory of Superconductivity

By D. J. THOULESS AND D. R. TILLEY

Department of Mathematical Physics, University of Birmingham

MS. received 8th December 1960

Abstract. Some results which were derived by use of finite temperature perturbation theory are used to investigate the possibility of a low-energy collective mode in a superconductor. It is found that such a mode should exist, and the ratio of its energy to its momentum is calculated. This ratio approaches infinity exponentially as the temperature goes to zero, in agreement with Anderson's result that at zero temperature the collective mode is destroyed by the Coulomb force. The effect of this collective mode on the specific heat is negligible. The relation of this mode to 'second sound' is discussed. A comparison is made between the behaviour of this collective mode in a charged superfluid system (superconductor) and the behaviour of the collective modes in a superfluid system of neutral fermions.

§ 1. INTRODUCTION

IN an earlier paper (Thouless 1960, to be referred to as I), a method of applying perturbation theory to the problem of superconductivity was discussed. This method allows us to go beyond the Bardeen, Cooper and Schrieffer (1957) theory of superconductivity, but all corrections to that theory which were investigated in I are very small. In this paper, a more careful study of the correction to the specific heat is made. The phonon-like collective mode, whose existence was suggested in I, is studied in more detail.

The expression for the correction to the thermodynamic potential which was derived in I is

$$\Omega_L = \frac{1}{2} \sum_{\mathbf{K}} \sum_{\nu=-\infty}^{\infty} \sum_{j=1}^3 \beta^{-1} \{ \ln [1 - \beta \lambda_j(K, \nu)] + \beta \lambda_j(K, \nu) \} \quad \dots\dots (1)$$

where $\lambda_j(K, \nu)$ is one of the three solutions of Eqn (I, 70). The sum over total momentum \mathbf{K} occurs however we try to evaluate Eqn (1), but there is a method of evaluation which avoids the infinite sum over ν . The transformation which we use is given by Eqn (I, 28), and this replaces the sum over ν by a contour integral, while this contour integral is equal to a sum of contributions from the poles and zeros of the argument of the logarithm. Making this transformation and then integrating by parts, we get

$$\begin{aligned} \Omega_L = & (4\pi i)^{-1} \sum_{\mathbf{K}} \sum_{j=1}^3 \int_C \beta \lambda_j \left(K, \frac{\beta z}{2\pi i} \right) \\ & \times \left[\frac{d}{dz} \lambda_j \left(K, \frac{\beta z}{2\pi i} \right) \right] \left[1 + \beta \lambda_j \left(K, \frac{\beta z}{2\pi i} \right) \right]^{-1} \\ & \times \ln [1 - e^{-\beta z}] dz \quad \dots\dots (2) \end{aligned}$$

where the contour C' surrounds all of the real axis, except the origin, in a clockwise direction. Since the function inside the curly bracket is an odd function of z , which has a simple pole of residue $-\beta^{-1}$ whenever λ_j is equal to $-\beta^{-1}$, and a second-order pole of residue β^{-1} whenever λ_j has a simple pole, we can write Eqn (2) as

$$\Omega_L = \sum_K \sum_s \left\{ \frac{1}{2} y_s + \beta^{-1} \ln [1 - \exp(-\beta y_s)] - \frac{1}{2} x_s - \beta^{-1} \ln [1 - \exp(-\beta x_s)] \right\} \dots\dots (3)$$

where y_s is any zero of $1 - \beta^{-1}\lambda$, on the positive real axis, and x_s is any pole of λ on the positive real axis. These points are given by the zeros and poles of

$$\begin{vmatrix} A + \beta^{-1} & B & D \\ B & A + \beta^{-1} & -D \\ D & -D & E + \beta^{-1} \end{vmatrix} = (A + B + \beta^{-1}) \begin{vmatrix} A - B + \beta^{-1} & 2D \\ D & E + \beta^{-1} \end{vmatrix} \dots\dots (4)$$

where A , B , D and E are the functions of K and z obtained by substituting $z = 2\pi i\nu/\beta$ in Eqns (I, 59) and (I, 69). The poles are at $|\Omega_{K+m} \pm \Omega_{K-m}|$ where Ω_m is the quasi-particle energy, and so they are at the uncoupled two quasi-particle energy levels, while the zeros give the coupled two quasi-particle energy levels. Eqn (3) shows that the correction to the thermodynamic potential is equal to the sum of contributions from the coupled two quasi-particle levels minus the contribution from the uncoupled two quasi-particle levels; each level contributes as if it were a vibrational mode.

In I, we used Eqn (1) and estimated the effect of those terms in which the argument of the logarithm is very close to zero; the effect of terms where the argument is close to unity can be estimated by using a power series expansion. These terms are the ones with K close to zero and $\nu = 0$. At very low temperatures, this is not so easy, since many values of ν may contribute. Also, many values of ν must certainly be included if the effects of the Coulomb force are to be evaluated, since the temperatures at which superconductivity occurs are very much smaller than the Coulomb energy divided by the Boltzmann constant. In this paper we use an approximation suggested by Eqn (3).

§ 2. COLLECTIVE MODES

The energies of the coupled two quasi-particle excited states are given by Eqn (4). Most of the roots of this equation lie in the range of possible values of $\pm \Omega_{K+m} \pm \Omega_{K-m}$, and so form a 'continuum' of energy levels. There may be roots which lie outside the continuum, or which persist even when the sums over states which define A , B , D and E are replaced by integrals, and these solutions are called collective modes. One such collective mode is the plasma mode, which, as Anderson (1958) has shown, has the same energy in the superconducting state as in the normal state. Anderson also showed that at zero temperature there is a low-lying collective mode, lying below the energy gap, if the Coulomb force can be neglected, but that this low-lying mode does not exist in the presence of a Coulomb force between the electrons. We show here that the low-lying mode exists at all finite temperatures, and only disappears at zero temperature.

We can put Eqn (4) into the form of Eqn (96) of the paper by Anderson (1958). We get

$$\begin{vmatrix} A-B+\beta^{-1} & 2D \\ D & E+\beta^{-1} \end{vmatrix} = 0 \quad \begin{vmatrix} A-B+\beta^{-1} & 4i\left[\frac{V(2K)}{J}\right]^{1/2} \frac{\Delta D}{z} \\ z\left[\frac{J}{V(2K)}\right]^{1/2} \frac{D}{2i\Delta} - A+B-\beta^{-1} & E-4i\left[\frac{V(2K)}{J}\right]^{1/2} \frac{\Delta D}{z} + \beta^{-1} \end{vmatrix} = 0 \quad \dots\dots (5)$$

It is the quantity

$$\beta E - \left(\frac{4i\beta C_m \{V(2K)\}^{1/2}}{z\sqrt{J}} \right) D$$

in Eqn (5) whose behaviour is different at finite temperatures and zero temperature. If we put z proportional to K and let K tend to zero, this term increases like $1/K^2$ at finite temperatures, but tends to a finite limit at zero temperature. The product of β^2 with the off-diagonal terms in Eqn (5) tends to a constant. This is why the Coulomb force can destroy the mode with energy proportional to K at zero temperatures, but not at finite temperatures.

Let us now find the way in which the velocity of the low-lying mode varies with temperature. That is, we find the zero of Eqn (4) that gives the relation $z = cK$, so that c is the velocity.

From Eqns (I, 59) (I, 52) and (I, 56), the quantities occurring in Eqn (4) are:

$$\begin{aligned} A-B &= -\frac{J}{2\beta} \sum_m \left\{ \frac{[\tanh(\frac{1}{2}\beta\Omega_{K+m}) + \tanh(\frac{1}{2}\beta\Omega_{K-m})]}{(\Omega_{K+m} + \Omega_{K-m})^2 - z^2} \right. \\ &\quad \times \left[\Omega_{K+m} + \Omega_{K-m} - \frac{1}{2}(\epsilon_{K+m} - \epsilon_{K-m}) \left(\frac{\epsilon_{K+m}}{\Omega_{K+m}} - \frac{\epsilon_{K-m}}{\Omega_{K-m}} \right) \right] \\ &\quad - \frac{[\tanh(\frac{1}{2}\beta\Omega_{K+m}) - \tanh(\frac{1}{2}\beta\Omega_{K-m})]}{(\Omega_{K+m} - \Omega_{K-m})^2 - z^2} \\ &\quad \times \frac{(\Omega_{K+m} - \Omega_{K-m})(\epsilon_{K+m} - \epsilon_{K-m})}{2(\Omega_{K+m} + \Omega_{K-m})} \left(\frac{\epsilon_{K+m}}{\Omega_{K+m}} - \frac{\epsilon_{K-m}}{\Omega_{K-m}} \right) \Big\} \\ iD &= \frac{z\Delta}{4\beta} \{JV(2K)\}^{1/2} \sum_m \left\{ \frac{[\tanh(\frac{1}{2}\beta\Omega_{K+m}) + \tanh(\frac{1}{2}\beta\Omega_{K-m})]}{(\Omega_{K+m} + \Omega_{K-m})^2 - z^2} \right. \\ &\quad \times \left(\frac{1}{\Omega_{K+m}} + \frac{1}{\Omega_{K-m}} \right) \\ &\quad + \frac{[\tanh(\frac{1}{2}\beta\Omega_{K+m}) - \tanh(\frac{1}{2}\beta\Omega_{K-m})]}{(\Omega_{K+m} - \Omega_{K-m})^2 - z^2} \left(\frac{1}{\Omega_{K+m}} - \frac{1}{\Omega_{K-m}} \right) \Big\} \\ E &= \frac{V(2K)}{2\beta} \sum_m \left\{ \frac{[\tanh(\frac{1}{2}\beta\Omega_{K+m}) + \tanh(\frac{1}{2}\beta\Omega_{K-m})]}{(\Omega_{K+m} + \Omega_{K-m})^2 - z^2} \right. \\ &\quad \times \frac{(\Omega_{K+m} + \Omega_{K-m})}{\Omega_{K+m}\Omega_{K-m}} (\Omega_{K+m}\Omega_{K-m} + \epsilon_{K+m}\epsilon_{K-m} + \Delta^2) \\ &\quad + \frac{[\tanh(\frac{1}{2}\beta\Omega_{K+m}) - \tanh(\frac{1}{2}\beta\Omega_{K-m})]}{(\Omega_{K+m} - \Omega_{K-m})^2 - z^2} \\ &\quad \times \frac{(\Omega_{K+m} - \Omega_{K-m})}{\Omega_{K+m}\Omega_{K-m}} (\Omega_{K+m}\Omega_{K-m} + \epsilon_{K+m}\epsilon_{K-m} - \Delta^2) \Big\}. \end{aligned} \quad \dots\dots (6)$$

Here β is the inverse temperature, and $V(2K)$ is the matrix element of the Coulomb potential, equal to $\pi e^2/K^2$ divided by the normalization volume. We have taken the Bardeen-Cooper-Schrieffer potential

$$\begin{aligned} V_{mn} &= -J \quad \text{for} \quad -\hbar\omega < \epsilon_m < \hbar\omega \\ &\quad \text{and} \quad -\hbar\omega < \epsilon_n < \hbar\omega \\ &= 0 \quad \text{otherwise,} \end{aligned}$$

and the sums in Eqn (6) run only over wave vectors \mathbf{m} with energies between $-\hbar\omega$ and $\hbar\omega$. Δ is the energy gap, so that $\Omega_m = (\epsilon_m^2 + \Delta^2)^{1/2}$.

We want to find the zeros of Eqn (4) for small values of K and z , so we expand the quantities occurring in Eqn (6) to lowest order in these variables. After this expansion the determinant is homogeneous in z and K , so that we do have a solution $z = cK$. The elements of the determinant have the following structure:

$$\begin{aligned} A - B + \beta^{-1} &= pK^2 - qz^2 \\ D &= ic[r - f(c)] \\ E &= [u + g(c)]/K^2. \end{aligned} \quad \dots\dots (7)$$

Here we have written $z/K = c$. Expanding the determinant, we obtain an implicit equation for c

$$pu + (p - qc^2)g(c) + 2c^2[f(c)]^2 - 4c^2rf(c) = 0 \quad \dots\dots (8)$$

where we have used the relation $qu = 2r^2$ (see Eqn (9)). The quantities occurring in (7) and (8) are:

$$\begin{aligned} p &= (\beta k_F^2/6M^2)NJ(2\mathcal{K} - \mathcal{L}) \\ q &= \frac{1}{4}\beta NJ\mathcal{K} \\ r &= \frac{1}{2}\beta\Delta eNJ^{1/2}\mathcal{K} \\ u &= 2\beta\Delta^2e^2N\mathcal{K} \\ f(c) &= \frac{\beta\Delta eNJ^{1/2}}{16} \left\{ 4\mathcal{L} + v \int_0^{\beta\hbar\omega} dx \frac{\text{sech}^2[\frac{1}{2}(x^2 + x_0^2)^{1/2}]}{x(x^2 + x_0^2)^{1/2}} \ln \left| \frac{x - v(x^2 + x_0^2)^{1/2}}{x + v(x^2 + x_0^2)^{1/2}} \right| \right\} \\ g(c) &= \frac{e^2N}{4\beta} \left\{ 4 \int_0^{\beta\hbar\omega} dx \frac{x^2 \text{sech}^2[\frac{1}{2}(x^2 + x_0^2)^{1/2}]}{x^2 + x_0^2} \right. \\ &\quad \left. + v \int_0^{\beta\hbar\omega} dx \frac{x \text{sech}^2[\frac{1}{2}(x^2 + x_0^2)^{1/2}]}{(x^2 + x_0^2)^{1/2}} \ln \left| \frac{x - v(x^2 + x_0^2)^{1/2}}{x + v(x^2 + x_0^2)^{1/2}} \right| \right\}. \end{aligned} \quad \dots\dots (9)$$

Here \mathcal{K} and \mathcal{L} stand for the integrals

$$\begin{aligned} \mathcal{K} &= \int_0^{\beta\hbar\omega} dx \frac{\tanh[\frac{1}{2}(x^2 + x_0^2)^{1/2}]}{(x^2 + x_0^2)^{3/2}} \\ \mathcal{L} &= \int_0^{\beta\hbar\omega} dx \frac{\text{sech}^2[\frac{1}{2}(x^2 + x_0^2)^{1/2}]}{x^2 + x_0^2}. \end{aligned}$$

N is the density of states per unit energy range at the Fermi surface. We have put $x_0 = \beta\Delta$ and $v = Mc/k_F$, where M is the effective mass of the electrons and k_F their Fermi momentum. The variable v is the ratio of the velocity of the collective mode to the Fermi velocity. The Eqns (7), (8) and (9) are obtained from Eqns (4) and (6) by changing from sums over momentum to integrals over energy, assuming that $\hbar\omega \ll k_F^2/2M$ so that we can treat the density of states N as constant over the range of integration.

Now if we substitute the expressions (9) into Eqn (8), we find that the constants with dimensions are either of the form $N^2 J e^2 k_F^2 / M^2$ or of the form $c^2 N^2 J e^2$. The ratio of the second of these constants to the first is $M^2 c^2 / k_F^2$, that is v^2 , so we can write Eqn (8) entirely in terms of the dimensionless velocity and energy gap, v and x_0 . In fact,

$$(2\mathcal{K} - \mathcal{L})[128x_0^2\mathcal{K} + 16G(v)] - 24v^2\mathcal{K}G(v) + 3x_0^2v^2F(v)[F(v) - 16\mathcal{K}] = 0 \quad \dots\dots (10)$$

where we have put $F(v)$, $G(v)$ for the terms in curly brackets in $f(c)$, $g(c)$ respectively.

§ 3. SOLUTION OF THE EQUATIONS FOR THE VELOCITY

We want to solve Eqns (9) and (10) for v as a function of x_0 , where x_0 varies from ∞ at zero temperature to zero at the critical temperature since $x_0 = \beta\Delta$. The behaviour at $x_0 = 0$ and as $x_0 \rightarrow \infty$ can be found exactly.

For $x_0 \rightarrow 0$, we can see

$$x_0\mathcal{K} \rightarrow \frac{\pi}{2} \quad x_0\mathcal{L} \rightarrow \frac{\pi}{2} \quad G(v) \rightarrow 2v \ln \left| \frac{1-v}{1+v} \right|$$

and v is given by $\ln\{(1+v)/(1-v)\} = 4/v$, with numerical solution $v = 0.97$. Thus at the critical temperature the velocity of the collective mode is nearly equal to the Fermi velocity.

For $x_0 \rightarrow \infty$,

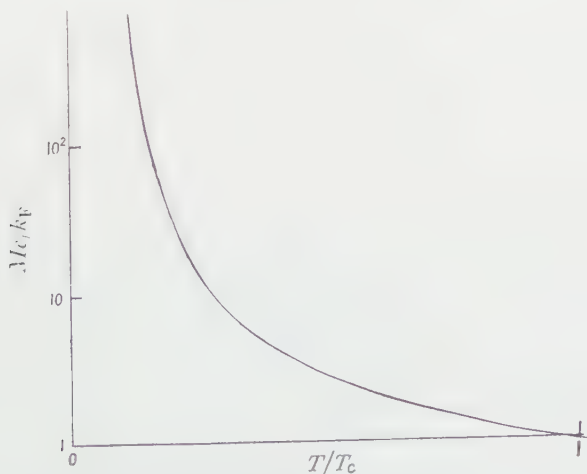
$$\mathcal{K} \sim x_0^{-2} \quad \mathcal{L} \sim 2(2\pi)^{1/2} x_0^{-3/2} \exp(-x_0).$$

If we assume $v \rightarrow \infty$ as $x_0 \rightarrow \infty$, we can expand $F(v)$ and $G(v)$ to first order only in v^{-2} . This expansion leads straightforwardly to asymptotic expressions for $F(v)$ and $G(v)$, and thence to a linear equation for v^2 , with

$$v \sim 0.73x_0^{-1/4} \exp(x_0/2). \quad \dots\dots (11)$$

The velocity tends to infinity exponentially as the temperature tends to zero.

For intermediate values of x_0 we can again try expanding $F(v)$ and $G(v)$ in powers of v^{-2} . We can check a value of v by evaluating $F(v)$ and $G(v)$ exactly for that value, and then treating them as constants in Eqn (10). We were able to get fairly accurate values of v for a good range of temperatures: as the



The velocity c of the collective mode as a function of temperature.

temperature decreases from the critical temperature v increases monotonically. The Figure shows v plotted on a logarithmic scale against T/T_c , where T_c is the critical temperature.

It remains to calculate the specific heat of the mode whose velocity we have found. Since we started from an expansion of the thermodynamic potential, we must use the relation

$$c_v = \frac{d}{dT} \left[kT^2 \frac{d}{dT} \frac{\Omega}{kT} \right]$$

where k is Boltzmann's constant.

The thermodynamic potential for a system of bosons with energy-momentum relation $E = cK$ is given by

$$\Omega = kT \sum_{\mathbf{K}} \ln [1 - \exp(-cK/kT)].$$

Using these two expressions, we find for the specific heat:

$$c_v = \frac{2\pi^2 k^4 T^3}{15c^3} \left[1 - 7 \frac{d \ln c}{d \ln T} + 3 \left(\frac{d \ln c}{d \ln T} \right)^2 - \frac{d^2 \ln c}{d (\ln T)^2} \right]. \quad \dots (12)$$

As $T \rightarrow 0$, the specific heat of the quasi-particle modes is proportional to $(\Delta/kT)^{3/2} \exp(-\Delta/kT)$ (see, for example, Khalatnikov and Abrikosov 1959), whereas the leading term in Eqn (12) is proportional to $(\Delta/kT)^{1/4} \exp(-3\Delta/2kT)$. Thus the quasi-particle term is dominant.

At $T = T_c$, the quasi-particle specific heat per unit volume is $1.2\pi^2 k \rho T/T_F$, where ρ is the density of electrons and T_F their Fermi temperature (see Khalatnikov and Abrikosov 1959). The ratio of the factor before the bracket in Eqn (12) to this specific heat is 1.5×10^{-14} . From a graph of $\ln c$ against $\ln T$ it appears that the term inside the curly brackets is not unusually large at any temperature, so we must conclude that the phonon-like mode always has a very small specific heat compared with that of the electrons. The reason for the small specific heat is the high velocity of the mode: at the critical temperature it is a factor 10^3 times the velocity of the lattice phonons.

§ 4. SECOND SOUND

It was suggested by Anderson (1958) that the correlations which must exist in an electron gas in order to screen the electrons from one another are not compatible with the collective motion which should be possible in a superfluid system of neutral fermions. The reappearance of this collective mode at finite temperatures must be due to the effect of the excited quasi-particles. The unexcited quasi-particles, which are the ones responsible for superconductivity, have this collective motion, but the screening of the Coulomb effects is done by the excited quasi-particles, which should behave almost like free particles. As the temperature goes to zero there are fewer and fewer excited quasi-particles to do the screening, so the Coulomb energy of the collective mode rises rapidly, and the collective mode disappears at zero temperature. This collective mode is like second sound, in that both the normal fluid and the superconducting fluid are needed to propagate it. It is not, however, the second sound discussed by Bardeen and Schrieffer (1961), which has a velocity comparable with the velocity of ordinary sound, many orders of magnitude less than the Fermi velocity. The reason for the difference is that Bardeen and Schrieffer assume that the mean free path of a quasi-particle is sufficiently short that a local thermodynamic

equilibrium can be set up in a distance less than a wavelength, whereas we have neglected the damping of the quasi-particles, and so we have assumed on the contrary that a quasi-particle can travel several wavelengths without suffering an inelastic collision. The difference between the two modes is similar to the difference between sound and zero sound in the theory of a Fermi liquid (Abrikosov and Khalatnikov 1959).

It must be noticed that scattering of a quasi-particle by the lattice inhibits the propagation both of Bardeen and Schrieffer's second sound and of the mode considered here. In both cases the wavelength should be greater than the coherence length; in their case so that a local equilibrium can be set up, in our case because the energy of the mode should be less than the energy of the gap for our approximations to make any sense. The factor that determines which mode is propagated is the distance a quasi-particle with an energy just above the top of the gap travels before it has an inelastic collision with another quasi-particle.

§ 5. NEUTRAL SYSTEMS

We have made no detailed calculations of the collective modes for a superfluid system of neutral fermions at a finite temperature, but some of the general features can be seen by examining Eqns (5) and (6). Above the critical temperature there should be the usual 'zero sound' mode, for which the ratio of energy to momentum is somewhat greater than the Fermi velocity (Abrikosov and Khalatnikov 1959). We can see how this mode behaves below the critical temperature by putting $[V(2K)]^{1/2}$ equal to a fairly small constant in Eqn (6). The quantities $A - B$, D and E are then all small except for special values of z . The zero sound mode comes from a zero of $E + \beta^{-1}$, but this can only have a zero for small z when

$$\tanh(\tfrac{1}{2}\beta\Omega_{K+m}) - \tanh(\tfrac{1}{2}\beta\Omega_{K-m})$$

is non-zero, so this mode disappears at zero temperatures. On the other hand, the collective mode due to the zero of $A - B + \beta^{-1}$ persists at zero temperature, as Anderson (1958) and Bogoliubov, Tolmachev and Shirkov (1959) have shown.

ACKNOWLEDGMENTS

We would like to thank Dr. G. V. Chester and Professor J. R. Schrieffer for some illuminating discussions. One of us (D.R.T.) would like to thank the Department of Scientific and Industrial Research for a maintenance grant.

REFERENCES

- ABRIKOSOV, A. A., and KHALATNIKOV, I. M., 1959, *Rep. Progr. Phys.*, **22**, 329.
 ANDERSON, P. W., 1958, *Phys. Rev.*, **112**, 1900.
 BARDEEN, J., COOPER, L. N., and SCHRIEFFER, J. R., 1957, *Phys. Rev.*, **108**, 1175.
 BARDEEN, J., and SCHRIEFFER, J. R., 1961, "Recent Developments in Superconductivity", *Progress in Low Temperature Physics*, Vol. III (Amsterdam: North Holland), p. 170.
 BOGOLIUBOV, N. N., TOLMACHEV, V. V., and SHIRKOV, D. V., 1959, *A New Method in the Theory of Superconductivity* (New York: Consultants Bureau), p. 31.
 KHALATNIKOV, I. M., and ABRIKOSOV, A. A., 1959, *Advanc. Phys.*, **8**, 45.
 THOULESS, D. J., 1960, *Ann. Phys.*, N.Y., **10**, 553.

Note added in proof.—Since the momentum of the excitations discussed in this paper is $2K$ rather than K , the velocity is $\frac{1}{2}c$ rather than c .

The Collective Treatment of a Fermi Gas: II

By T. GASKELL

Theoretical Physics Department, University of Manchester

Communicated by B. H. Flowers; MS. received 9th December 1960

Abstract. The ground state energy of the free electron gas is calculated using the Rayleigh-Schrödinger variational method with the wave function $\Psi = D \prod_{i < j} f(x_{ij})$ where D is a determinant of plane waves and $f(x_{ij})$ a correlation function. Consideration of the wave function in terms of the collective coordinates $\rho_{\mathbf{k}}$, the Fourier components of the density, suggests an accurate approximation for the energy integral which is then evaluated over the coordinates of the particles so that the use of subsidiary conditions is avoided. Effects omitted in the random phase approximation are included and the final results extend continuously over plasma and particle modes and should be valid in the range of densities encountered in real metals. The results agree closely with those of Nozières and Pines, and of Hubbard obtained by more elaborate methods.

§ 1. INTRODUCTION

THE ground state energy of a free electron gas has been calculated exactly in the limit of very high densities, where the random phase approximation is valid for all wave numbers. As yet, however, no exact procedure has been found for performing a calculation which would be valid within the region of electron densities existing in metals.

This paper discusses a variational approach to the idealized problem of a free electron gas in the presence of a neutralizing background of positive charge, using a wave function

$$\Psi = D \prod_{i < j} f(x_{ij}),$$

D being a determinant of plane waves. The product of binary functions is written in terms of the Fourier components of the density

$$\rho_{\mathbf{k}} = \sum_i \exp(-i\mathbf{k} \cdot \mathbf{x}_i)$$

so that Ψ has the form

$$D \exp \left[- \sum_{\mathbf{k}} c(k) \rho_{\mathbf{k}} \rho_{\mathbf{k}}^* \right],$$

$c(k)$ being treated as a variational parameter. Ideally the integrations should be performed exactly and $c(k)$ determined by minimizing the energy. Unfortunately the integrals are very complicated and have not yet been performed exactly, and a strictly variational approach has not been achieved. However, writing the wave function in terms of the $\rho_{\mathbf{k}}$ suggests a method of evaluation which should agree closely with an exact calculation.

A wave function of the above type is suggested in the Bohm-Pines collective treatment of the problem, though in that theory the explicit introduction of

collective coordinates involves the use of subsidiary conditions to maintain the correct number of degrees of freedom. In this calculation the fact that the $\rho_{\mathbf{k}}$ are good collective coordinates is exploited, though the integrations are finally carried out over the particle coordinates, and the use of subsidiary conditions is avoided.

The paper proceeds by first setting up the calculation; the second section explains the method of evaluating the integrals, while the third section gives details of the results.

Consider then a system consisting of a gas of N electrons enclosed in a box in the presence of a neutralizing background of positive charge, there being periodic boundary conditions. It represents a simplified model of a metal, where the only effect of the ion cores is to produce the neutralizing background.

We thus consider the Hamiltonian

$$H = -\frac{\hbar^2}{2m} \sum_i \nabla_i^2 + \frac{e^2}{2} \sum_{i \neq j} \frac{1}{x_{ij}} + V_1$$

where V_1 , a constant, represents the effect of the positive charge. Expanding the $1/x_{ij}$ as a Fourier series within the box, the $k=0$ term cancelling with V_1 , the required Schrödinger equation is

$$-\frac{\hbar^2}{2m} \sum_i \nabla_i^2 \Psi + \frac{2\pi e^2}{V} \sum_{\mathbf{k} \neq 0} \frac{1}{k^2} (\rho_{\mathbf{k}} \rho_{\mathbf{k}}^* - N) \Psi = E \Psi \quad \dots\dots (1)$$

where

$$\rho_{\mathbf{k}} = \sum_i \exp(-i\mathbf{k} \cdot \mathbf{x}_i).$$

Within the Hartree Fock approximation, a determinant of plane waves, D , represents a self-consistent solution. This wave function, as is well known, only gives correlation between electrons of parallel spin, and that due to the effect of the Pauli exclusion principle. There is no correlation due to the inter-particle forces. It is possible to improve D , however, by modulating it with a function $\prod_{i,j} f(x_{ij})$, where $f(x_{ij})$ is always positive and decreases as x_{ij} decreases. This correlation function can be written in terms of the $\rho_{\mathbf{k}}$, since

$$\prod_{i < j} f(x_{ij}) = \exp \left[\sum_{i < j} \log f(x_{ij}) \right] = \exp \left[\frac{1}{2V} \sum_{\mathbf{k}} c(k) (\rho_{\mathbf{k}} \rho_{\mathbf{k}}^* - N) \right],$$

and we may therefore consider a wave function in the form

$$\Psi = D \exp \left[- \sum_{\mathbf{k} \neq 0} c(k) \rho_{\mathbf{k}} \rho_{\mathbf{k}}^* \right],$$

treating $c(k)$ as a variational parameter. (The term ρ_0 is not a variable and has therefore been omitted.)

The expectation value of the energy is given by

$$E = \frac{\int \Psi^* \left[-\left(\frac{\hbar^2}{2m}\right) \sum_i \nabla_i^2 + (2\pi e^2/V) \sum_{\mathbf{k} \neq 0} \frac{1}{k^2} (\rho_{\mathbf{k}} \rho_{\mathbf{k}}^* - N) \right] \Psi \prod d\mathbf{x}_i}{\int \Psi^* \Psi \prod d\mathbf{x}_i} \quad \dots\dots (2)$$

The kinetic energy includes the terms

$$\begin{aligned} & \int DD^* \exp \left[- \sum_{\mathbf{k} \neq 0} c(k) \rho_{\mathbf{k}} \rho_{\mathbf{k}}^* \right] \nabla_i^2 \exp \left[- \sum_{\mathbf{k} \neq 0} c(k) \rho_{\mathbf{k}} \rho_{\mathbf{k}}^* \right] \prod d\mathbf{x} \\ & + 2 \int D^* \exp \left[- \sum_{\mathbf{k} \neq 0} c(k) \rho_{\mathbf{k}} \rho_{\mathbf{k}}^* \right] \nabla_i D \cdot \nabla_i \exp \left[- \sum_{\mathbf{k} \neq 0} c(k) \rho_{\mathbf{k}} \rho_{\mathbf{k}}^* \right] \prod d\mathbf{x}_i \end{aligned}$$

which on integrating by parts become

$$- \int D^* D \nabla_i \exp \left[- \sum_{k \neq 0} c(k) \rho_k \rho_k^* \right] \cdot \nabla_i \exp \left[- \sum_{k \neq 0} c(k) \rho_k \rho_k^* \right] \Pi d\mathbf{x}_i.$$

Hence

$$E = \frac{\hbar^2}{2m} \sum_{k \leq k_F} k^2$$

$$\int \Psi^* \Psi \left[- \frac{4\hbar^2}{2m} \sum_{\mathbf{k}, \mathbf{n} (\mathbf{k} \neq -\mathbf{n})} c(k) c(n) \rho_{\mathbf{k}} \rho_{\mathbf{n}} \rho_{\mathbf{k}+\mathbf{n}}^* \mathbf{k} \cdot \mathbf{n} + \frac{4\hbar^2}{2m} \sum_{\mathbf{k}} N c^2(k) k^2 \rho_{\mathbf{k}} \rho_{\mathbf{k}}^* \right. \\ \left. + \frac{2\pi e^2}{V} \sum_{\mathbf{k}} \frac{1}{k^2} (\rho_{\mathbf{k}} \rho_{\mathbf{k}}^* - N) \right] \Pi d\mathbf{x}_i$$

$$+ \frac{\int \Psi^* \Psi \Pi d\mathbf{x}_i}{\dots\dots\dots (3)}$$

where k_F denotes the Fermi momentum.

§ 2. EVALUATION OF INTEGRALS

The main integral to perform is

$$I = \frac{\int D^* D \rho_{\mathbf{k}} \rho_{\mathbf{k}}^* \exp \left[- 2 \sum_{n \neq 0} c(n) \rho_{\mathbf{n}} \rho_{\mathbf{n}}^* \right] \Pi d\mathbf{x}_i}{\int D^* D \exp \left[- 2 \sum_{n \neq 0} c(n) \rho_{\mathbf{n}} \rho_{\mathbf{n}}^* \right] \Pi d\mathbf{x}_i}.$$

It was suggested in paper I (Edwards 1958) that for small values of k , D will have a dependence upon the $\rho_{\mathbf{n}}$ like $\exp [-\Sigma b(n) \rho_{\mathbf{n}} \rho_{\mathbf{n}}^*]$. Thus if one neglects the short range effects the integral I may be converted from an integral over the particle coordinates to one over $\rho_{\mathbf{n}}, \rho_{\mathbf{n}}^*$. The Jacobian is approximately

$$\exp \left[\frac{-\sum \rho_{\mathbf{n}} \rho_{\mathbf{n}}^*}{N} \right]$$

and I is replaced by

$$I' = \frac{\int \rho_{\mathbf{k}} \rho_{\mathbf{k}}^* \exp \left[- 2 \sum \{c(n) + b(n) + 1/2N\} \rho_{\mathbf{n}} \rho_{\mathbf{n}}^* \right] \Pi d\rho_{\mathbf{n}}}{\int \exp \left[- 2 \sum \{c(n) + b(n) + 1/2N\} \rho_{\mathbf{n}} \rho_{\mathbf{n}}^* \right] \Pi d\rho_{\mathbf{n}}}$$

$$= \frac{1}{4[c(k) + b(k) + 1/2N]}.$$

The quantity $b(n)$ is chosen from the condition that

$$\frac{\int \rho_{\mathbf{k}} \rho_{\mathbf{k}}^* \exp \left[- 2 \sum \{b(n) + 1/2N\} \rho_{\mathbf{n}} \rho_{\mathbf{n}}^* \right] \Pi d\rho_{\mathbf{n}}}{\int \exp \left[- 2 \sum \{b(n) + 1/2N\} \rho_{\mathbf{n}} \rho_{\mathbf{n}}^* \right] \Pi d\rho_{\mathbf{n}}} = \int D^* D \rho_{\mathbf{k}} \rho_{\mathbf{k}}^* \Pi d\mathbf{x}_i \equiv I(0)$$

i.e.

$$\frac{1}{4[b(k) + 1/2N]} = I(0).$$

Therefore

$$I' = \frac{I(0)}{1 + 4c(k)I(0)}. \dots\dots\dots (4)$$

This suggests expanding the exponentials in the original integral I , in such a way that it has the form of I' , but this time performing the integrations exactly over the particle coordinates.

Let
$$I(\mu) = \frac{\int D^* D \rho_{\mathbf{k}} \rho_{\mathbf{k}}^* \exp [-\mu \sum 2c(n) \rho_{\mathbf{n}} \rho_{\mathbf{n}}^*] \prod d\mathbf{x}_i}{\int D^* D \exp [-\mu \sum 2c(n) \rho_{\mathbf{n}} \rho_{\mathbf{n}}^*] \prod d\mathbf{x}_i}.$$

We will denote the expectation value of the quantity A with the wave function

$$\Psi = D \exp [-\mu \sum 2c(n) \rho_{\mathbf{n}} \rho_{\mathbf{n}}^*] \quad \text{by} \quad \langle \mu | A | \mu \rangle.$$

Then using the identity

$$\frac{1}{I(\mu)} - \frac{1}{I(0)} = \int_0^\mu \frac{\partial}{\partial \mu'} \left[\frac{1}{I(\mu')} \right] d\mu',$$

$I(\mu)$ is given by the equation,

$$I(\mu) = I(0) \left\{ \left[1 - I(0) \int_0^\mu d\mu' \left\{ 4c(k) \frac{\langle \mu' | (\rho_{\mathbf{k}} \rho_{\mathbf{k}}^*)^2 | \mu' \rangle - (\langle \mu' | \rho_{\mathbf{k}} \rho_{\mathbf{k}}^* | \mu' \rangle)^2}{(\langle \mu' | \rho_{\mathbf{k}} \rho_{\mathbf{k}}^* | \mu' \rangle)^2} \right. \right. \right. \\ \left. \left. \left. + 2 \sum_{\mathbf{n} \neq \mathbf{k}} c(n) \frac{\langle \mu' | \rho_{\mathbf{k}} \rho_{\mathbf{k}}^* \rho_{\mathbf{n}} \rho_{\mathbf{n}}^* | \mu' \rangle - \langle \mu' | \rho_{\mathbf{k}} \rho_{\mathbf{k}}^* | \mu' \rangle \langle \mu' | \rho_{\mathbf{n}} \rho_{\mathbf{n}}^* | \mu' \rangle}{(\langle \mu' | \rho_{\mathbf{k}} \rho_{\mathbf{k}}^* | \mu' \rangle)^2} \right\} \right] \right\}. \quad \dots (5)$$

Expanding as a Taylor series in μ , the leading term is

$$4c(k) \frac{\langle 0 | (\rho_{\mathbf{k}} \rho_{\mathbf{k}}^*)^2 | 0 \rangle - (\langle 0 | \rho_{\mathbf{k}} \rho_{\mathbf{k}}^* | 0 \rangle)^2}{(\langle 0 | \rho_{\mathbf{k}} \rho_{\mathbf{k}}^* | 0 \rangle)^2} \\ + 2 \sum_{\mathbf{n} \neq \mathbf{k}} c(n) \frac{\langle 0 | \rho_{\mathbf{k}} \rho_{\mathbf{k}}^* \rho_{\mathbf{n}} \rho_{\mathbf{n}}^* | 0 \rangle - \langle 0 | \rho_{\mathbf{k}} \rho_{\mathbf{k}}^* | 0 \rangle \langle 0 | \rho_{\mathbf{n}} \rho_{\mathbf{n}}^* | 0 \rangle}{(\langle 0 | \rho_{\mathbf{k}} \rho_{\mathbf{k}}^* | 0 \rangle)^2}. \quad \dots (6)$$

The first term in (6), ignoring terms of order $1/N$ is $4c(k)$ and I then has the form of Eqn (4). The second term is a measure of the correlation between the ρ 's, and will make an increasingly important contribution as k increases. If the approximation (4) is an accurate one which is reproduced by the first term in this expansion, then the assumption that this series converges rapidly will be justified. The remainder can in fact be written down in a compact form. The integral $I(\mu)$ is given by

$$I(\mu) = I(0) \left\{ \left(1 + I(0) \int_0^\mu \frac{\partial}{\partial \mu'} \left[\frac{1}{I(\mu')} \right] d\mu' \right) \right. \\ \left. = I(0) \left\{ 1 + \mu I(0) \frac{\partial}{\partial \mu'} \left[\frac{1}{I(\mu')} \right]_{\mu'=0} + I(0) \int_0^\mu (\mu - \mu') \frac{\partial^2}{\partial \mu'^2} \left[\frac{1}{I(\mu')} \right] d\mu' \right\} \right\}.$$

The assumption therefore is that

$$I(0) \int_0^\mu (\mu - \mu') \frac{\partial^2}{\partial \mu'^2} \left[\frac{1}{I(\mu')} \right] d\mu' \quad \text{is small.}$$

The rest of this section is concerned with the evaluation of $I(0)$ and the expression (6).

$$I(0) \equiv \int D^* D \rho_{\mathbf{k}} \rho_{\mathbf{k}}^* \prod d\mathbf{x}_i, \quad \dots (7)$$

D is a determinant of plane waves, where, for the ground state of a metal, the wave vectors \mathbf{k}_α all lie within the Fermi sphere.

$$I(0) = \frac{1}{N!} \frac{1}{V^N} \int \epsilon_{\alpha\beta\gamma} \dots \epsilon_{\alpha'\beta'\gamma'} \dots \exp [i(\mathbf{k}_\alpha - \mathbf{k}_{\alpha'}) \cdot \mathbf{x}_1 + i(\mathbf{k}_\beta - \mathbf{k}_{\beta'}) \cdot \mathbf{x}_2 + \dots] \times \rho_{\mathbf{k}} \rho_{\mathbf{k}}^* \prod d\mathbf{x}_i.$$

Now
$$\rho_{\mathbf{k}} \rho_{\mathbf{k}}^* = N + \sum_{i,j (i \neq j)} \exp [i\mathbf{k} \cdot (\mathbf{x}_i - \mathbf{x}_j)].$$

Therefore

$$\begin{aligned} I(0) &= N + \frac{1}{N!} N(N-1) \frac{1}{V^N} \int \epsilon_{\alpha\beta\gamma} \dots \epsilon_{\alpha'\beta'\gamma'} \dots \exp [i(\mathbf{k}_\alpha - \mathbf{k}_{\alpha'} + \mathbf{k}) \cdot \mathbf{x}_1 \\ &\quad + i(\mathbf{k}_\beta - \mathbf{k}_{\beta'} - \mathbf{k}) \cdot \mathbf{x}_2 + \dots] \prod d\mathbf{x}_i \\ &= N + \frac{1}{V^2} \iint \{\delta_{\alpha\alpha'} \delta_{\beta\beta'} - \delta_{\alpha\beta'} \delta_{\beta\alpha'}\} \exp [i(\mathbf{k}_\alpha - \mathbf{k}_{\alpha'} + \mathbf{k}) \cdot \mathbf{x}_1 \\ &\quad + i(\mathbf{k}_\beta - \mathbf{k}_{\beta'} - \mathbf{k}) \cdot \mathbf{x}_2] d\mathbf{x}_1 d\mathbf{x}_2 \\ &= N - \frac{2}{V^2} \sum_{\alpha, \beta} \iint \exp [i(\mathbf{k}_\alpha - \mathbf{k}_\beta + \mathbf{k}) \cdot \mathbf{x}_1 + i(\mathbf{k}_\beta - \mathbf{k}_{\alpha'} - \mathbf{k}) \cdot \mathbf{x}_2] d\mathbf{x}_1 d\mathbf{x}_2 \\ &= N - \frac{2}{V} \sum_{\alpha, \beta} \int \exp [i(\mathbf{k}_\alpha - \mathbf{k}_\beta + \mathbf{k}) \cdot \mathbf{x}] d\mathbf{x} \end{aligned}$$

where $\mathbf{x} = \mathbf{x}_1 - \mathbf{x}_2$,

the 2 appearing from the summation over spin coordinates. Therefore

$$I(0) = N - \left\{ 2 \sum_{\alpha, \beta} \delta(\mathbf{k}_\alpha - \mathbf{k}_\beta + \mathbf{k}) \right\}.$$

The summation over β may be carried out and yields 1 if $\mathbf{k}_\alpha + \mathbf{k}$ is an occupied state, zero otherwise. The bracketed expression is therefore equal to the number of states \mathbf{k}_α for which $\mathbf{k}_\alpha + \mathbf{k}$ is occupied. This is just

$$\begin{aligned} &2 \frac{V}{(2\pi)^3} \left[\frac{4}{3} \pi k_F^3 - \pi k_F^2 k + \frac{\pi k_F^3}{12} \right] \\ &= N - \frac{3}{4} N \left(\frac{k}{k_F} \right) + \frac{N}{16} \left(\frac{k}{k_F} \right)^3, \end{aligned}$$

where the expression in square brackets is the volume indicated by shading in Fig. 1 below. It becomes zero for $k \geq 2k_F$.

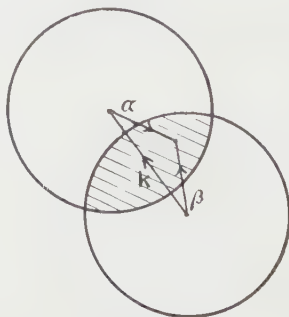


Fig. 1.

Therefore

$$\begin{aligned} I(0) &= \frac{3}{4} N \left(\frac{k}{k_F} \right) - \frac{N}{16} \left(\frac{k}{k_F} \right)^3 & \text{if } k < 2k_F, \\ &= N & \text{if } k \geq 2k_F. \end{aligned}$$

Two other integrals arise in the calculation

$$I \equiv \int D^* D (\rho_{\mathbf{k}} \rho_{\mathbf{k}}^*)^2 \prod d\mathbf{x}_i$$

$$= 2 \left[\int D^* D \rho_{\mathbf{k}} \rho_{\mathbf{k}}^* \prod d\mathbf{x}_i \right]^2 + O(N)$$

which for large N

$$\simeq 2 \left[\frac{3N}{4} \left(\frac{k}{k_F} \right) - \frac{N}{16} \left(\frac{k}{k_F} \right)^3 \right]^2,$$

$$\text{and } I \equiv \int D^* D \rho_{\mathbf{k}} \rho_{\mathbf{k}}^* \rho_{\mathbf{n}} \rho_{\mathbf{n}}^* \prod d\mathbf{x}_i = \int D^* D \rho_{\mathbf{k}} \rho_{\mathbf{k}}^* \prod d\mathbf{x}_i \int D^* D \rho_{\mathbf{n}} \rho_{\mathbf{n}}^* \prod d\mathbf{x}_i + A,$$

where the quantity A consists of three types of integral;

$$I(1) = N(N-1) \int D^* D \exp [i(\mathbf{k} + \mathbf{n}) \cdot (\mathbf{x}_1 - \mathbf{x}_2)] \prod d\mathbf{x}_i$$

$$= - \left[N - \frac{3N}{4} \frac{|\mathbf{k} + \mathbf{n}|}{k_F} + \frac{N}{16} \frac{|\mathbf{k} + \mathbf{n}|^3}{k_F^3} \right] \quad \text{if } |\mathbf{k} + \mathbf{n}| < 2k_F$$

$$= 0 \quad \text{if } |\mathbf{k} + \mathbf{n}| \geq 2k_F \quad \dots\dots (8)$$

$$I(2) = N(N-1)(N-2) \int D^* D \exp [i(\mathbf{k} + \mathbf{n}) \cdot \mathbf{x}_1 - i\mathbf{k} \cdot \mathbf{x}_2 - i\mathbf{n} \cdot \mathbf{x}_3] \prod d\mathbf{x}_i$$

$$= 4 \sum_{\alpha, \beta, \gamma} \delta(\mathbf{k}_\alpha - \mathbf{k}_\gamma + \mathbf{k} + \mathbf{n}) \delta(\mathbf{k}_\beta - \mathbf{k}_\alpha - \mathbf{n}) \delta(\mathbf{k}_\gamma - \mathbf{k}_\beta - \mathbf{k}). \quad \dots\dots (9)$$

This quantity is the common volume of three intersecting spheres, Fig. 2, the centres of two of which are displaced by the vectors \mathbf{k} and \mathbf{n} respectively from that of the third.

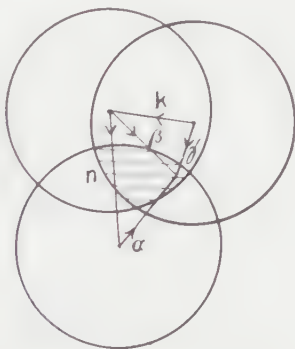


Fig. 2.

Fortunately however this expression appears under a summation over \mathbf{n} . In fact the required expression is

$$4 \sum_{\mathbf{n}, \alpha, \beta, \gamma} c(\mathbf{n}) \delta(\mathbf{k}_\alpha - \mathbf{k}_\gamma + \mathbf{k} + \mathbf{n}) \delta(\mathbf{k}_\beta - \mathbf{k}_\alpha - \mathbf{n}) \delta(\mathbf{k}_\gamma - \mathbf{k}_\beta - \mathbf{k}).$$

Carrying out the summation over \mathbf{n} , this expression becomes

$$4 \sum_{\alpha, \beta, \gamma} c(|\mathbf{k}_\beta - \mathbf{k}_\alpha|) \delta(\mathbf{k}_\gamma - \mathbf{k}_\beta - \mathbf{k})$$

$$= 4 \sum_{\alpha, \beta, |\mathbf{k}_\beta - \mathbf{k}_\alpha| < k_F} c(|\mathbf{k}_\beta - \mathbf{k}_\alpha|).$$

$$I(3) = 2 \sum_{\alpha, \beta, \gamma, \epsilon} \delta(\mathbf{k}_\alpha - \mathbf{k}_\epsilon - \mathbf{k}) \delta(\mathbf{k}_\beta - \mathbf{k}_\alpha + \mathbf{n}) \delta(\mathbf{k}_\gamma - \mathbf{k}_\beta + \mathbf{k}) \delta(\mathbf{k}_\epsilon - \mathbf{k}_\gamma - \mathbf{n}). \dots (10)$$

This expression is the common volume of four intersecting spheres. Fortunately it again appears under a summation over \mathbf{n} . Carrying out this summation, the required expression is

$$2 \sum_{\alpha, \beta, \gamma, \epsilon} c(|\mathbf{k}_\epsilon - \mathbf{k}_\gamma|) \delta(\mathbf{k}_\alpha - \mathbf{k}_\epsilon - \mathbf{k}) \delta(\mathbf{k}_\gamma - \mathbf{k}_\beta + \mathbf{k}).$$

The delta functions impose restrictions on both \mathbf{k}_ϵ and \mathbf{k}_γ , i.e. they are only summed over a fraction

$$\left[1 - \frac{3}{4} \left(\frac{k}{k_F} \right) + \frac{1}{16} \left(\frac{k}{k_F} \right)^3 \right]$$

of the Fermi sphere. This integral has been done approximately by relaxing the restriction on \mathbf{k}_γ , say, and multiplying by the above fraction. Hence the above integral is given approximately by

$$2 \sum_{\epsilon, \gamma, |\mathbf{k}_\epsilon + \mathbf{k}| < k_F} c(|\mathbf{k}_\epsilon - \mathbf{k}_\gamma|) \left[1 - \frac{3}{4} \left(\frac{k}{k_F} \right) + \frac{1}{16} \left(\frac{k}{k_F} \right)^3 \right].$$

An analysis of the expression $\langle \rho_{\mathbf{k}} \rho_{\mathbf{k}}^* \rho_{\mathbf{n}} \rho_{\mathbf{n}}^* \rangle - \langle \rho_{\mathbf{k}} \rho_{\mathbf{k}}^* \rangle \langle \rho_{\mathbf{n}} \rho_{\mathbf{n}}^* \rangle$, using the above geometrical interpretation of the integrals, shows that it is small for small values of $|\mathbf{k}|$ and $|\mathbf{n}|$ as one would expect if the ρ 's are to be interpreted as independent useful coordinates. It is also true that the terms (9) and (10) are zero, when either k or n exceed $2k_F$, but (8) still gives a contribution provided that $|\mathbf{k} + \mathbf{n}| \leq 2k_F$.

It may be mentioned at this stage that the term in the kinetic energy

$$- \sum_{\mathbf{n} \neq -\mathbf{k}} c(n) \langle \rho_{\mathbf{k}+\mathbf{n}}^* \rho_{\mathbf{k}} \rho_{\mathbf{n}} \mathbf{k} \cdot \mathbf{n} \rangle,$$

is of the same order of magnitude as

$$\sum_{\mathbf{n} \neq \mathbf{k}} c(n) \{ \langle \rho_{\mathbf{k}} \rho_{\mathbf{k}}^* \rho_{\mathbf{n}} \rho_{\mathbf{n}}^* \rangle - \langle \rho_{\mathbf{k}} \rho_{\mathbf{k}}^* \rangle \langle \rho_{\mathbf{n}} \rho_{\mathbf{n}}^* \rangle \}$$

and if one includes the latter in the calculation of the expectation value of $\rho_{\mathbf{k}} \rho_{\mathbf{k}}^*$, then one must include the former also in the expression for the energy. For small values of k and n both terms are small and may be ignored, as will be demonstrated in the next section by a calculation of the long-range correlation energy. Therefore to the approximation (4)

$$I = \frac{\int D^* D \rho_{\mathbf{k}} \rho_{\mathbf{k}}^* \exp \left[-2 \sum_{n \neq 0} c(n) \rho_{\mathbf{n}} \rho_{\mathbf{n}}^* \right] \prod d\mathbf{x}_i}{\int D^* D \exp \left[-2 \sum_{n \neq 0} c(n) \rho_{\mathbf{n}} \rho_{\mathbf{n}}^* \right] \prod d\mathbf{x}_i} = \frac{I(0)}{1 + 4c(k)I(0)}. \dots (11)$$

When one includes the remainder of expression (6) one has instead

$$I = \frac{I(0)}{1 + 4c(k)I(0) + A(k) + B(k) + C(k)} \dots (12)$$

where

$$A(k) = -4 \sum_{\mathbf{n}, |\mathbf{k} - \mathbf{n}| < 2k_F} c(n) \left[N - \frac{3}{4} N \frac{|\mathbf{k} - \mathbf{n}|}{k_F} + \frac{N}{16} \frac{|\mathbf{k} - \mathbf{n}|^3}{k_F^3} \right] / I(0)$$

$$B(k) = 16 \sum_{\alpha, \beta, |\mathbf{k}_\beta + \mathbf{k}| < k_F} c(|\mathbf{k}_\alpha - \mathbf{k}_\beta|) / I(0)$$

$$C(k) = -8 \sum_{\alpha, \beta, \mathbf{k}_\alpha + \mathbf{k}_\beta = \mathbf{k}} c(|\mathbf{k}_\alpha - \mathbf{k}_\beta|) \left[1 - \frac{3}{4} \left(\frac{k}{k_F} \right) + \frac{1}{16} \left(\frac{k}{k_F} \right)^3 \right] / I(0)$$

and
$$I(0) = \left[\frac{3N}{4} \left(\frac{k}{k_F} \right) - \frac{N}{16} \left(\frac{k}{k_F} \right)^3 \right].$$

§ 3. RESULTS

3.1. Long-range Correlation Energy

The first approximation, which should be valid for small values of the wave number k , is to neglect the term

$$\sum_{\mathbf{n}, \mathbf{k}, (\mathbf{k} \neq -\mathbf{n})} c(k)c(n)\rho_{\mathbf{k}-\mathbf{n}}^* \rho_{\mathbf{k}} \rho_{\mathbf{n}} \mathbf{k} \cdot \mathbf{n}$$

(random phase approximation) and to evaluate the integrals using Eqn (11). Substituting (11) into (3) and determining the value of $c(k)$ which minimizes the energy, gives

$$Nc(k) = -\frac{1}{4} \left[\frac{3}{4} \left(\frac{k}{k_F} \right) - \frac{1}{16} \left(\frac{k}{k_F} \right)^3 \right]^{-1} - \frac{1}{2} \left\{ \frac{1}{4} \left[\frac{3}{4} \left(\frac{k}{k_F} \right) - \frac{1}{16} \left(\frac{k}{k_F} \right)^3 \right]^{-2} + \frac{16\pi^2 e^4}{k^4} \left(\frac{N}{V} \right)^2 \frac{1}{\hbar^2 w_p^2} \right\}^{1/2}$$

where
$$w_p^2 = 4\pi \left(\frac{N}{V} \right) \frac{e^2}{m}. \quad \dots\dots (13)$$

Then

$$E = \frac{3}{5} \frac{\hbar^2}{2m} N k_F^2 + \frac{\hbar^2}{2m} \sum_{k \neq 0} k^2 \left\{ \frac{1}{4} \left[\frac{3}{4} \left(\frac{k}{k_F} \right) - \frac{1}{16} \left(\frac{k}{k_F} \right)^3 \right]^{-2} + \frac{16\pi^2 e^4}{k^4} \left(\frac{N}{V} \right)^2 \frac{1}{\hbar^2 w_p^2} \right\}^{1/2} \quad \dots\dots (14)$$

$$- \frac{\hbar^2}{2m} \sum_{k \neq 0} \frac{k^2}{2} \left[\frac{3}{4} \left(\frac{k}{k_F} \right) - \frac{1}{16} \left(\frac{k}{k_F} \right)^3 \right]^{-1} - 2\pi e^2 \left(\frac{N}{V} \right) \sum_{k \neq 0} \frac{1}{k^2}.$$

An interesting comparison may be made at this stage with the Bohm Pines collective treatment of this problem. If one neglects the electron-plasma interaction the wave function is approximately $\Psi = \Phi D$, where Φ is a product of harmonic oscillator ground state wave functions and D a determinant of plane waves. In the momentum representation

$$\Phi = \exp \left[- \sum_{k < k_0} P_{\mathbf{k}} P_{\mathbf{k}}^* / 2\hbar w_p \right],$$

$P_{\mathbf{k}}$ being the collective coordinate introduced to describe the plasma oscillations. They must satisfy the subsidiary condition

$$\left[P_{\mathbf{k}} - i \left(\frac{4\pi e^2}{V k^2} \right)^{1/2} \rho_{\mathbf{k}}^* \right] \Psi = 0.$$

This is satisfied if the expression in brackets is identically zero; and in this case

$$\Psi = D \exp \left[- \sum_{k < k_0} \frac{2\pi e^2}{V} \frac{1}{\hbar w_p} \frac{1}{k^2} \rho_{\mathbf{k}} \rho_{\mathbf{k}}^* \right].$$

For small k the wave function used in this calculation is just this. The long range correlation energy calculated by the two methods agrees closely. It is

convenient to introduce the inter-electron spacing r_e defined by $V/N = 4\pi r_e^3/3$, where N is the number of electrons and V the volume of the box, and to use the rydberg as unit of energy and the Bohr unit as unit of length. The correlation energy is defined as usual by the equation

$$E = \left(\frac{2.21}{r_e^2} - \frac{0.916}{r_e} + E_c \right),$$

where E is the ground state energy per electron and $2.21/r_e^2 - 0.916/r_e$ that quantity calculated in the Hartree-Fock approximation.

Using $c(k)$ as given by Eqn (13), then

$$E = \left\{ \frac{2.21}{r_e^2} - \frac{1.22}{r_e} \beta_c + \frac{0.866}{r_e^{3/2}} \beta_c^3 - \frac{0.92}{r_e^2} \beta_c^4 + \frac{0.52 \beta_c^5}{r_e^{5/2}} + \dots \right\} \\ + \left\{ - \frac{0.916}{r_e} + \frac{1.22}{r_e} \beta_c - \frac{0.458}{r_e} \beta_c^2 + \frac{0.019}{r_e} \beta_c^4 \right\}$$

where β_c is the dimensionless quantity (k_c/k_F) . The latter expression is just the exchange energy

$$\frac{2\pi e^2}{V} \int D^* D \sum_{k > k_c} \frac{1}{k^2} [\rho_{\mathbf{k}} \rho_{\mathbf{k}}^* - N] \prod d\mathbf{x}_i \\ = - \frac{2}{\pi} \left(\frac{9\pi}{4} \right)^{1/3} \frac{1}{r_e} \int_{\beta_c}^2 \left[1 - \frac{3}{4} \beta + \frac{1}{16} \beta^3 \right] d\beta.$$

Therefore

$$E_c^{\text{long range}} = - \frac{0.458}{r_e} \beta_c^2 + \frac{0.866}{r_e^{3/2}} \beta_c^3 - \frac{0.92}{r_e^2} \beta_c^4 + \frac{0.52}{r_e^{5/2}} \beta_c^5 + \frac{0.019}{r_e} \beta_c^4.$$

The kinetic and potential energy contribute equally to the term $0.866 \beta_c^3 / r_e^{3/2}$, as one might expect, since it may otherwise be written $\sum_{k < k_c} \hbar w_p / 2$, the ground state energy of the collective oscillations. Nozières and Pines (1958) give for this quantity

$$E_c^{\text{long range}} = - \frac{0.458}{r_e} \beta_c^2 + \frac{0.866}{r_e^{3/2}} \beta_c^3 - \frac{0.98}{r_e^2} \beta_c^4 + \frac{0.706}{r_e^{5/2}} \beta_c^5 + \frac{0.019}{r_e} \beta_c^4.$$

Hiroike (1960) has derived the expression (14) for $E(k)$ from a theory of the collective motion of the system.

3.2. Total Correlation Energy

There is no need in this calculation to restrict the correlation function to values of k less than k_c ; one could sum over all values of the wave number and calculate the total correlation energy. Thus far the $\rho_{\mathbf{k}}$'s have been treated as independent coordinates in the sense that the correlation term

$$\sum_{\mathbf{n} \neq \mathbf{k}} c(n) \{ \langle \rho_{\mathbf{k}} \rho_{\mathbf{k}}^* \rho_{\mathbf{n}} \rho_{\mathbf{n}}^* \rangle - \langle \rho_{\mathbf{k}} \rho_{\mathbf{k}}^* \rangle \langle \rho_{\mathbf{n}} \rho_{\mathbf{n}}^* \rangle \} \quad \dots (15)$$

has been ignored in evaluating the expectation value of $\rho_{\mathbf{k}} \rho_{\mathbf{k}}^*$; and the term

$$- \sum_{\mathbf{k} \neq -\mathbf{n}} c(k) c(n) \langle \rho_{\mathbf{k}} \rho_{\mathbf{n}} \rho_{\mathbf{k}+\mathbf{n}}^* \mathbf{k} \cdot \mathbf{n} \rangle \quad \dots (16)$$

assumed small as implied by the expression 'random phase approximation'. This approximation may be valid for small k as indicated by the calculation of the long-range correlation energy, but it is essential to include the above terms when computing the total correlation energy, since for large values of k , the ρ 's are no longer independent useful coordinates.

Now the previous value of $c(\beta)$ was

$$c(\beta) = -\frac{1}{4} \left[\frac{3}{4} \beta - \frac{1}{16} \beta^3 \right]^{-1} + \frac{1}{2} \left\{ \frac{1}{4} \left[\frac{3}{4} \beta - \frac{1}{16} \beta^3 \right]^{-2} + 4 \frac{\mu^2}{\beta^4} \right\}^{1/2}$$

where

$$\mu^2 = \frac{1}{3\pi} \left(\frac{4}{9\pi} \right)^{1/3} r_e. \quad \dots (17)$$

Unfortunately terms (15) and (16) are difficult to evaluate with this function, and it has been necessary to choose a somewhat simpler form for $c(\beta)$, which will be discussed below.

For small values of β , the leading term in a power series expansion of $c(\beta)$ (as given by (17)) in terms of β , is μ/β^2 . This is a good approximation to the function which minimizes the energy even with the inclusion of the correlation terms, because the latter are small anyway in this limit. For $\beta > 2$ an adequate approximation for (17) is $2\mu^2/\beta^4$, though this form has no particular merit because it was determined by ignoring the now important correlation terms; instead one might use $4\mu^2/\beta^4$ for $\beta > 2$, so that there is no discontinuity at $\beta = 2$. The following choice for $c(\beta)$ has been in fact used:

$$\begin{aligned} c(\beta) &= \mu/\beta^2 & \text{for } \beta < 2 \\ c(\beta) &= 4\mu/\beta^4 & \text{for } \beta > 2. \end{aligned} \quad \dots (18)$$

The choice of $\beta = 2$ for the change in $c(\beta)$ is a convenient one, since in evaluating terms (15) and (16), as discussed in the previous section, it has been necessary to carry out the summation over \mathbf{n} before summing over the state vectors \mathbf{k}_α . Since these expressions vanish for $n > 2k_F$ only the term μ/β^2 is involved.

The results are given in Table 1 below. $E(1)$ is the total correlation energy calculated using the expression (14). $E(2)$ is the energy given by evaluating the integrals to the same approximation as in $E(1)$ but using expression (18) for $c(\beta)$, the parameter μ being determined by minimizing the energy.

Table 1

r_e	2	3	4	5
$E(\text{B.P.})$	-0.094	-0.081	-0.072	-0.065
$E(\text{Hubbard 1958})$	-0.099	-0.086	-0.074	-0.067
$E(1)$	-0.116	-0.100	-0.089	-0.081
$E(2)$	-0.098	-0.088	-0.080	-0.074
$E(3)$	-0.090	-0.078	-0.070	-0.064
μ	0.090	0.125	0.155	0.190

The difference between $E(1)$ and $E(2)$ therefore is entirely due to use of two different expressions for $c(\beta)$. $E(3)$ includes the terms (15) and (16), and uses the function $c(\beta)$ given in (18) throughout the expression for the energy, not just in the terms (15) and (16), with the value of μ which minimized $E(2)$. $E(3)$ agrees well with the Bohm-Pines result, but the difference between $E(1)$ and $E(2)$ suggests that had the expression (17) been used to calculate $E(3)$ the energies would certainly have been lower. Since the difference between $E(2)$ and $E(3)$ is due to the inclusion of the correlation terms, one can estimate what percentage of the energy they represent and subtract this from $E(1)$. Therefore even with the inclusion of the terms (15) and (16), if the expression (17) had been used for $c(\beta)$ the values, $E(4)$, may have been as low as those given in Table 2.

Table 2

r_e $E(4)$	2 -0.106	3 -0.089	4 -0.078	5 -0.070
-----------------	-------------	-------------	-------------	-------------

Hence with the inclusion of the correlation terms it appears that the correlation energy lies between the values $E(3)$ and $E(4)$.

One point perhaps worth making is that Eqn (14), which is an expression for the energy within the random phase approximation, does have the correct behaviour as a function of r_e in the limit of high densities, where exact calculations have been performed. Within the random phase approximation the correlation energy in this limit (i.e. small r_e) is $0.0622 \log r_e - 0.142$ (Nozières and Pines 1958). Eqn (14) gives $0.057 \log r_e - 0.132$.

ACKNOWLEDGMENTS

The author would like to thank Dr. S. F. Edwards for suggesting this problem and for many helpful discussions. He would also like to express his appreciation to Professor B. H. Flowers for consenting to read the manuscript.

REFERENCES

- EDWARDS, S. F., 1958, *Proc. Phys. Soc.*, **72**, 685.
 HIROIKE, K., 1960, *Progr. Theor. Phys.*, **23**, 1, 44.
 HUBBARD, J., 1958, *Proc. Roy. Soc. A*, **243**, 336.
 NOZIÈRES, P., and PINES, D., 1958, *Phys. Rev.*, **111**, 443.

Collision Broadening in the Argon Spectrum

By W. R. HINDMARSH AND K. A. THOMAS†

University Observatory, Oxford

MS. received 16th January 1961

Abstract. High resolution photographs of the near infra-red spectrum of an argon discharge at various pressures revealed that lines whose lower levels are connected by resonance transitions to the ground state suffered markedly greater collision broadening than those whose lower levels are metastable. The excessive broadening of the former group of lines is believed to be due to resonance collision broadening of their lower levels. The collision broadening of one line from each group, namely $1s_2-2p_2$, $\lambda 8264 \text{ \AA}$ and $1s_5-2p_2$, $\lambda 6965 \text{ \AA}$, was measured. The half intensity collision width of $\lambda 8264$ was $14.7 \pm 1.0 \times 10^{-20} \text{ cm}^{-1}$ per atom per cm^3 of argon, while that of $\lambda 6965$ was $2.0 \pm 0.3 \times 10^{-20} \text{ cm}^{-1}$ per atom per cm^3 of argon. The ratio of collision width to collision shift (the latter being taken from Hindmarsh and Thomas 1959) was 3.1 ± 0.8 . This is in agreement with the value 2.75 predicted by the Lindholm theory for interaction due to van der Waals forces between the atoms. The resonance broadening of $\lambda 8264$ is related to the f -value of the argon resonance line $1p_0-1s_2$, $\lambda 1048$, and this is found to be $f = 0.13 \pm 0.03$, in agreement with calculations quoted by Knox in 1958.

§ 1. INTRODUCTION

COLLISION broadening in spectral lines is caused by the interactions between the radiating atoms and other particles present in the emitting gas. Thus for spectral lines of argon excited in a glow discharge in pure argon, collision broadening may be caused either by collisions between neutral argon atoms or by collisions between an argon atom and an electron or ion. Only collisions between neutral argon atoms are important in the experiments described in this paper. The interaction between two argon atoms may be of three types. First, an argon atom in an excited state may exchange its energy with an argon atom in the ground state without involving electromagnetic radiation. This is the so-called 'exchange' interaction and gives rise to 'resonance' or 'self'-broadening of the excited state. Secondly, there are dispersion or van der Waals forces between two argon atoms, and the potential of these forces varies as the inverse sixth power of the distance between the two atoms. Thirdly, short-range, repulsive forces exist between two argon atoms. These are important only when the distance between the two atoms becomes comparable with the diameter of the charge cloud of one atom. For argon, this diameter is about 3 \AA . According to the theory developed by Lindholm (1945) and by Foley (1946) the second and third types of interaction cause shift as well as broadening of the spectral lines. The measurement and interpretation of collision shifts in the argon spectrum have been described in an earlier paper (Hindmarsh and Thomas 1959).

† Now at the Department of Physics, University College, Swansea.

Wavelength (Å)	Pressure (mm Hg)	Length of discharge column (cm)	Gaussian half-width (cm ⁻¹)	Dispersion half-width (cm ⁻¹)
8264	8	5.5	0.031	0.058
	8	12.0	0.033	0.047
	16	5.5	0.028	0.078
	16	12.0	0.021	0.089
6965	8	12.0	0.038	0.017
	16	12.0	0.043	0.024
7147	0.32	12.0	0.036	0.010

The estimated error in each entry of a line width is 15%.

The collision widths 2γ are then found to be given by

$$2\gamma/N = 2.0 \pm 0.3 \times 10^{-20} \text{ cm}^{-1} \text{ cm}^3 \quad \text{for } \lambda 6965 \text{ Å}$$

and

$$2\gamma/N = 14.7 \pm 1.0 \times 10^{-20} \text{ cm}^{-1} \text{ cm}^3 \quad \text{for } \lambda 8264 \text{ Å.}$$

N is the number of argon atoms per cm^3 , and is calculated from the measured argon pressure with the additional assumption that the temperature of the argon in the discharge was 285 K. This was the wall temperature of the discharge tube, and the Doppler width calculated from this temperature agrees with the observed Gaussian width of the lines after allowance has been made for instrumental effects.

§ 3. DISCUSSION OF RESULTS

(a) $\lambda 6965$. The shift β of this line was found in the earlier work to be given by $\beta/N = -0.65 \pm 0.07 \times 10^{-20} \text{ cm}^{-1} \text{ cm}^3$ so that $2\gamma/\beta = -3.1 \pm 0.8$. The Lindholm theory predicts that if the interaction between the atoms is of the van der Waals type, then $2\gamma/|\beta| = 2.75$. Theory and experiment are therefore in agreement within the limits of error. This result is different from that found for two calcium lines broadened by helium (Hindmarsh 1959, 1960), where theory and experiment are in marked disagreement. The cause of that disagreement seems to be that the interaction between helium and calcium atoms is not of a pure van der Waals type, but includes also a component due to the short-range repulsive forces. This hypothesis is supported by the fact that the collision radius for helium and calcium atoms is less than the sum of the radii of the charge clouds of calcium and helium atoms. For two argon atoms, on the other hand, the sum of the radii of the charge clouds is 3.1 Å, while the collision radius calculated from the measured width of $\lambda 6965$ is 4.2 Å. It is thus to be expected that for argon the predominant forces are of the van der Waals type, and the observed ratio of width to shift confirms this hypothesis.

(b) $\lambda 8264$. The broadening in this line is much greater than that of $\lambda 6965$, but the shift is less than $0.5 \times 10^{-20} \text{ cm}^{-1}$ per atom of argon. The broadening is therefore believed to be mainly due to resonance broadening of the lower level of the transition. Some van der Waals broadening must also be present, and this has been assumed to be equal to that of $\lambda 6965$, since the upper level is common to both lines. This leaves a half-intensity width due to resonance broadening whose magnitude is given by $2\gamma/N = 11.6 \pm 1.5 \times 10^{-20} \text{ cm}^{-1} \text{ cm}^3$. Now the resonance broadening of the lower level of the line $\lambda 8264$ is related to the f -value of the argon resonance

§ 2. MEASUREMENT OF THE BROADENING

2.1. *Preliminary Experiments*

Preliminary experiments revealed that the collision broadening of some infra-red lines excited in a glow discharge was markedly larger than that of others. Lang (1957) had previously noticed the same phenomenon in the blue region of the spectrum. It was found that all the strongly broadened lines had for the lower level $1s_2$ or $1s_4$ (in the notation of Moore (1959)), while all the weakly broadened lines had for the lower level $1s_3$ or $1s_5$. The $1s_2$ and $1s_4$ levels are connected to the ground state of the argon atom by resonance transitions, while the $1s_3$ and $1s_5$ states are metastable. We believe that the excessive broadening is due to resonance broadening of the $1s_2$ and $1s_4$ levels. This broadens not only the resonance line itself, but also all lines which involve a transition to this level. This hypothesis was tested qualitatively by observing the argon lines when excited in an atmosphere of helium. As expected, the lines excessively broadened in pure argon appeared quite normal when excited in a helium atmosphere.

2.2. *Quantitative Measurements*

The positive column of a glow discharge in spectroscopically pure argon was viewed end-on, and the light examined by means of a Fabry-Perot interferometer crossed with a prism spectrograph. Spacers of 2 and 3 cm were used to separate the interferometer plates, which were coated with silver films of reflectivity 87%. Interferograms of the lines $\lambda 6965 \text{ \AA}$, $1s_5 - 2p_2$, and $\lambda 8264 \text{ \AA}$, $1s_2 - 2p_2$ were obtained at argon pressures of 8 mm and 16 mm of mercury, while $\lambda 7147 \text{ \AA}$, $1s_5 - 2p_4$ was photographed at a pressure 0.37 mm of mercury in order to estimate the instrumental contribution to the line width. The lines $\lambda 6965 \text{ \AA}$ and $\lambda 8264 \text{ \AA}$ became too weak for satisfactory observation at lower pressures than 8 mm, while $\lambda 7147 \text{ \AA}$ was too weak at pressures higher than 0.4 mm. The profile of the line $\lambda 8264$ was determined for two different lengths of the discharge column as part of the necessary investigation of the possible influence of self-absorption. Microphotometer tracings of the line contours were obtained, and reduced to intensity profiles in the usual way. The intensity profiles were fitted to Voigt profiles with the help of the tables given by van de Hulst and Reesinck (1947), and the half-intensity width of Gaussian and dispersion contributions to the line width calculated. The table shows the results obtained. It is seen that the Gaussian width is, within the limits of error, independent of pressure and discharge column length, and this strongly supports the view that in the conditions of measurement there is no self-absorption broadening of the line, although in other discharge conditions the lines were sometimes self-reversed.

The half-intensity width of the dispersion contribution to the line profile is due partly to collisions between argon atoms and partly to instrumental effects. Measurements made during the determination of the line shifts (Hindmarsh and Thomas 1959) excluded the possibility of broadening due to collisions with electrons or ions. Instrumental effects may be estimated from the known properties of the interferometer, or deduced from the extrapolation of the measured widths of $\lambda 8264$ and $\lambda 6965$ to zero pressure, or equated to the dispersion width of $\lambda 7147$ at very low pressure. All these procedures give results in agreement, and the mean value of the instrumental component of the dispersion width is $0.012 \pm 0.005 \text{ cm}^{-1}$.

line ($\lambda 1048 \text{ \AA}$, $1p_0 - 1s_2$) by the expression

$$\frac{2\gamma}{N} = \frac{\sqrt{3}e^2f}{4\sqrt{2}mc^2\nu}$$

which is taken from Foley (1946), where ν is the wave number of the resonance transition. We may therefore deduce a value for the oscillator strength of the argon line $\lambda 1048 \text{ \AA}$. It is

$$f = 0.13 \pm 0.03.$$

This result agrees as well as can be expected with the value $f = 0.20$ calculated by Knox (1958) with the use of Hartree-Fock wave functions. Knox claims an accuracy to between 10 and 20% for his calculations.

REFERENCES

- FOLEY, H. M., 1946, *Phys. Rev.*, **69**, 616.
 HINDMARSH, W. R., 1959, *Mon. Not. R. Astron. Soc.*, **119**, 11.
 ——— 1960, *Mon. Not. R. Astron. Soc.*, **121**, 48.
 HINDMARSH, W. R., and THOMAS, K. A., 1959, *Mon. Not. R. Astron. Soc.*, **119**, 21.
 VAN DE HULST, H. C., and REESINCK, J. J. M., 1947, *Astrophys. J.*, **106**, 121.
 KNOX, R. S., 1958, *Phys. Rev.*, **110**, 375.
 LANG, K., 1957, *Acta Phys. Austriaca*, **11**, 76.
 LINDHOLM, E., 1945, *Ark. Mat. Astr. Fys.*, **32A**, No. 17.
 MOORE, C. E., 1949, *Atomic Energy Levels*, Vol. 1 (*Nat. Bur. Stand., Wash.*, Circular 467).

Angular Correlations in the Reactions

$^{18}\text{O}(\alpha, n\gamma)^{21}\text{Ne}$ and $^{22}\text{Ne}(\alpha, n\gamma)^{25}\text{Mg}$

By W. M. DEUCHARS AND D. DANDY

Atomic Weapons Research Establishment, Aldermaston, Berks.

Communicated by K. W. Allen; MS. received 10th November 1960

Abstract. The angular correlation of the gamma radiation from the first excited state of ^{21}Ne , in coincidence with neutrons, has been studied using an axially symmetric neutron counter at 0° to the incident beam direction. Our results for ^{21}Ne together with the published lifetime measurement of the first excited state of ^{21}Ne , show that the amplitude of the electric quadrupole radiation divided by the amplitude of the magnetic dipole radiation is $0.004 \leq \delta \leq 0.03$.

The gamma radiation from the first excited state of ^{25}Mg , in coincidence with neutrons, was also observed but no detailed study of the angular correlation was made.

§ 1. INTRODUCTION

RECENT experiments by Litherland and McCallum (1960) have shown that by using an axially symmetric counter to detect the second radiation in a triple angular correlation experiment it is possible to select aligned nuclear states in the reaction. Moreover the magnetic substates which are populated according to this selection are limited by the spins of the incident and emergent particles and the target (Litherland 1959). The example chosen by Litherland and McCallum, viz. the reaction $^{26}\text{Mg}(\alpha, n\gamma)^{29}\text{Si}$, narrowed this selection even further, choosing a target nucleus and bombarding particle both with spin zero and observing the neutrons from the reaction at 0° to the beam, then only the $m = \pm \frac{1}{2}$ substates of the levels in the residual nucleus are populated and the angular correlations of the γ -rays in coincidence with the neutrons are only dependent on the properties of the levels of the residual nucleus.

We have applied this type of angular correlation measurement to a study of the reactions $^{18}\text{O}(\alpha, n\gamma)^{21}\text{Ne}$ and $^{22}\text{Ne}(\alpha, n\gamma)^{25}\text{Mg}$. In both these cases the target nucleus has spin zero and so the same considerations apply as for the reaction $^{26}\text{Mg}(\alpha, n\gamma)^{29}\text{Si}$.

The reaction $^{18}\text{O}(\alpha, n)^{21}\text{Ne}$ has been studied by Bonner *et al.* (1956), Serdiokova, Khabakhpashev and Tsenter (1957), and by Tsenter, Khabakhpashev and Pirkin (1960). Bonner *et al.* observing the neutrons from the reaction, found a number of resonances in the energy region 2–5 mev. Serdiokova, Khabakhpashev and Tsenter, and Tsenter, Khabakhpashev and Pirkin using natural α -sources, observed γ -rays from the decay of excited states in ^{21}Ne .

The reaction $^{22}\text{Ne}(\alpha, n)^{25}\text{Mg}$ has been studied by Ollano and Roy (1951) using a Po- α source. They observed two neutron groups from the reaction.

Both of these reactions have low Q -values (-0.705 MeV for $^{18}\text{O}(\alpha, n)^{21}\text{Ne}$ and -0.483 MeV for $^{22}\text{Ne}(\alpha, n)^{25}\text{Mg}$). Thus by using alpha particles of energy less than 3 MeV we ensure that only the low-lying states in the final nucleus are excited and the angular momentum of the emitted neutrons is low. These features are important for simple interpretation of the angular correlation data, as shown by Litherland and McCallum (1960).

§ 2. THEORY

For a detailed account of the theory of angular correlations as applied to the case where the emergent particle is observed in an axially symmetric counter at 0° or 180° to the incident beam direction, we refer to the paper by Litherland and Ferguson (1960, private communication).

It can be shown that in this case the theoretical expression for the angular correlation of the gamma rays from the reaction is given by

$$W_{LL'}(\theta) = \sum_{k,m} (-1)^{I+m+L+L'+k/2} P(m) (JJm-m/k0) Z_1(LJL'J, Ik) Q_k P_k(\cos \theta), \quad \dots\dots (1)$$

when the angular correlations are expressed in terms of Legendre polynomials.

In Eqn (1), $P(m)$ is the population of the m th substate of the nuclear state of spin J which decays to another state of spin I by emission of a gamma-ray quantum of total angular momentum L . $(JJm-m/k0)$ is a Clebsch-Gordan coefficient and the coefficient $Z_1(LJL'J, Ik)$ has been tabulated by Sharpe (1957). The attenuation coefficients Q_k have been calculated for a cylindrical gamma-ray counter of dimensions 5 in. diameter \times 6 in. long, which is the size used in the present experiments, by Rutledge (1959).

The full expression for the angular correlation must include a sum over the different multipole radiations that may be present. For the dipole-quadrupole case we then have

$$W(\theta) = W_{1,1}(\theta) + 2\delta W_{1,2}(\theta) + \delta^2 W_{2,2}(\theta) \quad \dots\dots (2)$$

where δ is the amplitude of the electric quadrupole radiation divided by the amplitude of the magnetic dipole radiation.

As mentioned above, when one considers only reactions in which the target nucleus and incident particle both have spin zero then the only values of m which contribute to the reaction are $\pm \frac{1}{2}$. Eqns (1) and (2) refer to the ideal case of a point detector set at $\theta_n = 0^\circ$ or 180° with respect to the incident beam direction. The use of a finite size detector introduces additional contributions to $W(\theta)$ from other m substates which can be populated. In the particular case considered the effect is to introduce contributions from the $m = \pm \frac{3}{2}$, and possibly $\pm \frac{5}{2}$, substates. Of course if only s-wave particles are emitted in the reaction we are still limited to $m = \pm \frac{1}{2}$ irrespective of the neutron counter dimensions.

§ 3. APPARATUS

A $2\mu\text{A}$ beam of $^4\text{He}^+$ ions from the 3 MeV Van de Graaff generator at the Atomic Weapons Research Establishment, Aldermaston, was used in these experiments.

The ^{18}O targets were prepared by evaporation of tungsten oxide, enriched in ^{18}O , on to a 0.010 in. aluminium backing. The targets were about 20 keV thick for 2.5 MeV alpha particles.

The ^{22}Ne targets were obtained from the Atomic Energy Research Establishment, Harwell, and were deposited on 0.010 in. copper backings. The target thickness was unknown.

The gamma-ray counter consisted of a 5 in. diameter \times 6 in. long sodium iodide crystal mounted on an E.M.I. photomultiplier. The counter was mounted on a rotating arm whose angular position with respect to the incident beam direction could be varied from 0° to 135° . The distance from the target to the front face of the γ -ray counter could be varied from 12 cm to 30 cm.

The neutrons were detected by a 2 in. diameter \times 2 in. long liquid scintillator† mounted on a RCA 6810A photomultiplier. A pulse shape discriminating circuit of the type first described by Owen (1959) and later developed by Batchelor *et al.* (1960) was used to discriminate between neutrons and γ -rays.

The neutron counter was mounted with its cylindrical axis in line with the direction of the incident beam and the distance from the target to the front face of the neutron counter could be varied from 10 cm to 30 cm. It was also possible to mount the neutron counter at 270° to the incident beam direction. Movement of the counter in the 0° position allowed us to study any effect arising from deviation from axial symmetry in the reactions.

The electronic apparatus consisted of a fast-slow coincidence system in which a fast coincidence output from both counters was put into slow coincidence with an output pulse from the neutron-gamma-ray discriminating circuit and the slow coincidence output opened a linear gate which allowed slow linear pulses from the gamma-ray detector to be transmitted to a 100-channel kicksorter.

The fast coincidence circuit was based on the design of Garg (1960) and had a variable resolving time which was set at 40 nsec in the present experiments.

The coincidence spectrum at each angle was monitored by counting the neutrons corresponding to the ground state transition. This enabled us to normalize the coincidence count at each angle to a given neutron flux.

§ 4. EXPERIMENTAL TECHNIQUE

The operation of the neutron-gamma-ray discriminator was checked using a Pu-Be source of neutrons and gamma rays. Final adjustments were made using mono-energetic neutrons from the reaction $\text{T}(p, n)^3\text{He}$. This enabled us to adjust the discriminating circuit to detect neutrons of energy 0.5 MeV, which was the lower limit of interest in either of the reactions studied.

Satisfactory operation of the neutron-gamma-ray discriminator was checked by observing the lack of coincidences between the neutron and gamma-ray counters when using a ^{60}Co source.

On measuring the angular correlations it was found that when the two counters were close together a 'true' background was observed due to neutrons being scattered from the neutron counter into the γ -ray counter and producing γ -rays inside the sodium iodide crystal by capture and inelastic scattering reactions. This background was measured at each angular position by using neutrons from the reaction $\text{T}(p, n)^3\text{He}$. The measured background was normalized to the coincidence spectrum and then subtracted from it.

Each angular correlation was measured at 15° intervals, the angular positions being chosen at random to allow for any gain variations in the electronic apparatus.

† Type Ne213 supplied by Nuclear Enterprises (G.B.) Ltd., Sighthill, Edinburgh.

§ 5. RESULTS AND DISCUSSION

5.1. $^{18}\text{O}(\alpha, n\gamma)^{21}\text{Ne}$

The excitation functions for the ground state and first excited state of ^{21}Ne at 0.35 mev were measured in the energy region $2.4\text{ mev} < E_\alpha < 3.0\text{ mev}$ and are shown in Fig. 1. Fig. 1(a) was obtained by measurement of the photo-peak intensity of the 0.35 mev gamma ray observed in the coincidence spectrum. This spectrum is shown in Fig. 2. Fig. 1(b) was obtained by measurement of the ground state neutron group intensity. In these measurements the gamma-ray counter was set at 120° to the incident beam direction and the neutron counter at 0° .

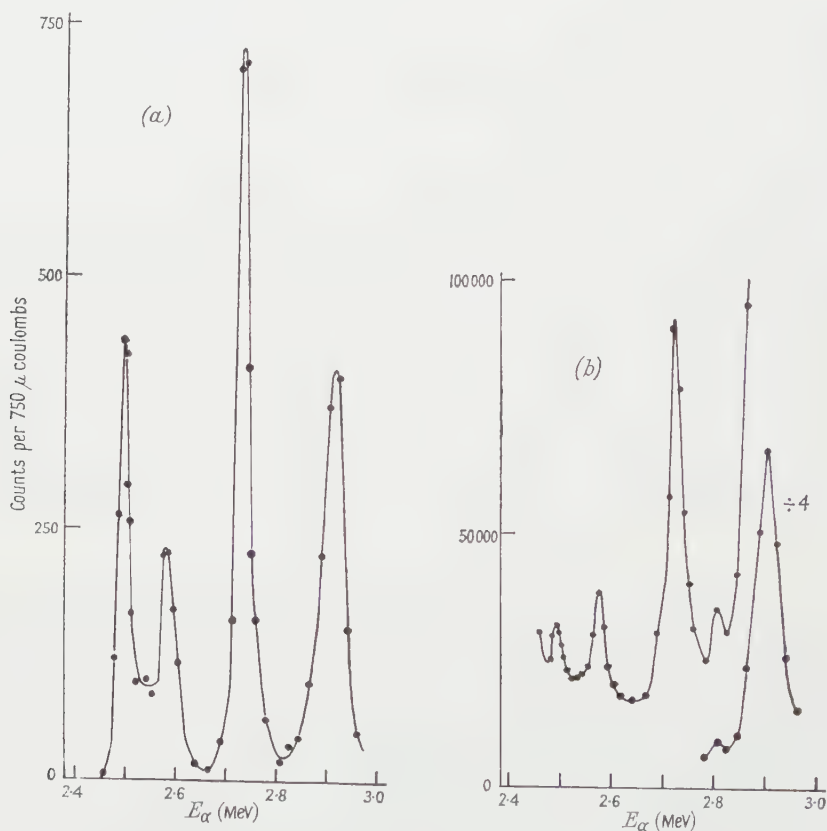


Fig. 1. Excitation function for $^{18}\text{O}(\alpha, n)^{21}\text{Ne}$, (a) 1st excited state, (b) ground state.

The energy of the $^4\text{He}^+$ was measured relative to the 2.605, 2.675 and 2.805 mev resonances in $^{13}\text{C}(\alpha, n)^{16}\text{O}$ (Ajzenberg-Selove and Lauritsen 1959). Resonances were observed at $2.47 \pm 0.03\text{ mev}$, $2.56 \pm 0.03\text{ mev}$, $2.73 \pm 0.03\text{ mev}$ and $2.91 \pm 0.03\text{ mev}$. These results are in good agreement with the results of Bonner *et al.*

The angular correlation of the 0.35 mev gamma ray from the first excited state of ^{21}Ne was measured at the 2.73 mev resonance, with the neutron counter at 0° to the incident beam direction. The correlation was measured with the

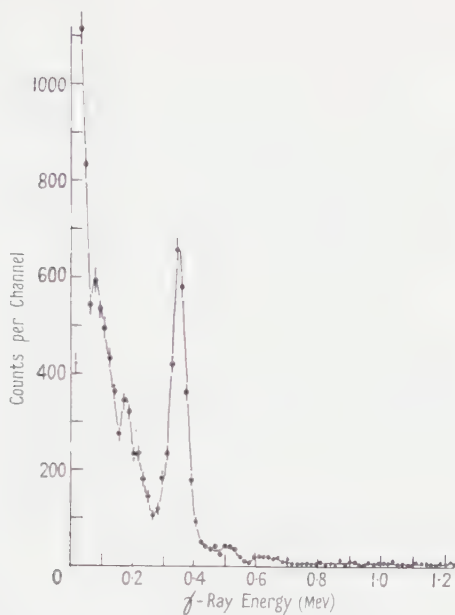


Fig. 2. Coincidence spectrum from reaction $^{18}\text{O}(\alpha, n\gamma)^{21}\text{Ne}$ at $E = 2.73$ MeV.

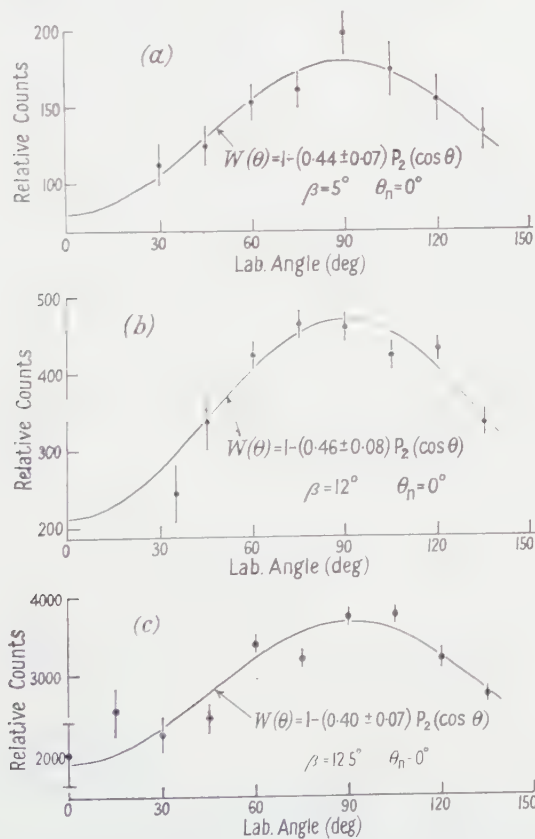


Fig. 3. Angular correlation of 0.35 MeV γ -ray at 2.73 MeV resonance. β is the half-angle subtended by neutron counter at target. Curve (c) was obtained with the neutron counter set with cylindrical axis perpendicular to the incident beam direction.

neutron counter at three distances from the target in the 0° direction. The results for the 2.73 MeV resonance with $\theta_n = 0^\circ$ are shown in Figs 3 (a), (b), (c).

A least squares fit to the measured correlations for $\theta_n = 0^\circ$ was carried out on the IBM 709 computer at the Atomic Weapons Research Establishment assuming a correlation of the form $W(\theta) = 1 + (a_2/a_0)P_2(\cos\theta)$. Table 1 gives the results obtained for the coefficient a_2/a_0 . Also included in Table 1 are the half-angles of acceptance β of the neutron counter.

Table 1

E_α (MeV)	β (deg)	a_2/a_0
2.73	5	-0.44 ± 0.07
2.73	12	-0.46 ± 0.08
2.73	12.5†	-0.40 ± 0.07

† This result was obtained with the neutron counter set so that its cylindrical axis was perpendicular to the incident beam direction. This arrangement did not strictly preserve the axial symmetry of the neutron detector but, as will be seen from Table 1, the effect was not appreciable in this case.

The mean value for the a_2/a_0 coefficient at the 2.73 MeV resonance was -0.43 ± 0.04 .

The results of Litherland and McCallum (1960) show that provided only s-wave neutrons are emitted from the compound state then the angular correlation is independent of the solid angle subtended by the neutron counter and of the properties of the compound state.

The results given in Table 1 show that at the 2.73 MeV resonance the measured correlation is independent of the half-angle β , and hence the emitted neutrons must be predominantly s-wave.

Thus the experimental results can be directly compared with the theoretical predictions for an ideally small neutron counter set at 0° to the incident beam direction.

The results of Middleton and Tai (1951), studying the reaction $^{20}\text{Ne}(d, p)^{21}\text{Ne}$, showed that the spin and parity of the first excited state of ^{21}Ne was either $\frac{5}{2}^+$, or $\frac{3}{2}^+$, with $\frac{5}{2}$ the more probable value.

Using these values for J in Eqn (1) and taking $I = \frac{3}{2}^+$ and δ as defined in Eqn (2) we find that for $a_2/a_0 = -0.43 \pm 0.04$ we obtain the values of δ shown in Table 2.

Table 2

a_2/a_0	J^π	δ
-0.43 ± 0.04	$\frac{5}{2}^+$	$0.004 \leq \delta \leq 0.03$ or $2.70 \leq \delta \leq 3.11$
-0.43 ± 0.04	$\frac{3}{2}^+$	$0.55 \leq \delta \leq 0.65$ $2.34 \leq \delta \leq 3.06$

Khabakhpashev and Tsenter (1959) measured a γ - γ correlation involving the first excited state of ^{21}Ne and in addition they found that the lifetime of this state was $(6.2 \pm 6.2) \times 10^{-11}$ sec. They concluded that the radiation was nearly

pure M1. Interpreting Table 2 in the light of their lifetime measurements we find that for values of $\delta \geq 0.5$ the E2 enhancement is not less than 500, which is larger by a factor of about 20 than that expected in this part of the periodic table. This leads us to the conclusion that the only value of δ from Table 2 which is acceptable is $0.004 \leq \delta \leq 0.03$ and that the spin and parity of the 350 keV level is $\frac{5}{2}^+$.

Using this assumption in conjunction with the fact that the neutrons emitted at the 2.73 MeV resonance must be predominantly s-wave, we are led to the conclusion that the compound state in ^{22}Ne at an excitation energy of 11.89 MeV is nearly all 2^+ .

5.2. $^{22}\text{Ne}(\alpha, n\gamma)^{25}\text{Mg}$

The excitation function for this reaction was measured in the energy region $2.2 < E_\alpha < 3$ MeV and is shown in Fig. 4.

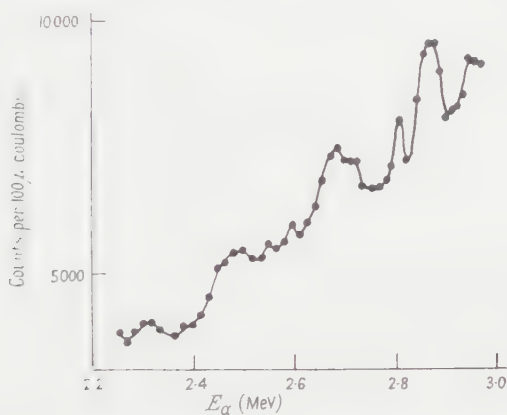


Fig. 4. Excitation function for the reaction $^{22}\text{Ne}(\alpha, n)^{25}\text{Mg}$.

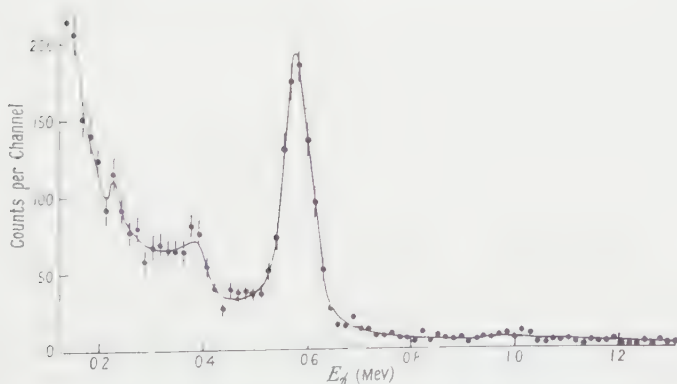


Fig. 5. Coincidence spectrum from the reaction $^{22}\text{Ne}(\alpha, n\gamma)^{25}\text{Mg}$ at $E_\alpha = 2.88$ MeV.

Only one definite resonance, at $E_x = 2.88$ MeV, was observed which could be assigned to the reaction $^{22}\text{Ne}(\alpha, n)^{25}\text{Mg}$ and the coincidence spectrum taken at this energy is shown in Fig. 5. From the fact that only a 0.58 MeV gamma ray is observed we conclude that only the first excited state of ^{25}Mg at 0.58 MeV is excited in this reaction at the α -particle energies used. This level is known to

have spin and parity $\frac{1}{2}^+$ (Endt and Braams 1957), and thus the angular correlation must be isotropic. In view of the poor quality of the ^{22}Ne targets no further measurements were made using this reaction.

§ 6. CONCLUSION

The application of this method of angular correlation measurements has been limited in the present case by the energy of α -particles available. Considerable improvement could be made using α -particles of energy up to 6 MeV. This is particularly true of the reaction $^{22}\text{Ne}(\alpha, n\gamma)^{25}\text{Mg}$ and it is hoped that these experiments will be repeated using the 6 MeV Van de Graaff at the Atomic Weapons Research Establishment.

Since our experiment was carried out, a paper has been published by Lemberg (1960) in which values are quoted for $B(E2)$ and the lifetime of the first excited state in ^{21}Ne . There is agreement between our values for δ and those determined from the $B(E2)$ and lifetime measurement of Lemberg.

ACKNOWLEDGMENTS

We wish to thank Dr. A. E. Litherland for making available his results prior to publication and for his interest and assistance during these experiments. We wish to thank Mr. D. Akers, Mr. G. Garner and Mr. M. Grant for their assistance in carrying out the experiments and to Mr. A. H. F. Muggleton for providing the ^{18}O targets.

Finally we wish to thank Mr. A. Gibbs and Mr. R. Scott for their efficient operation of the Van de Graaff generator during the course of these experiments.

REFERENCES

- AJZENBERG-SELOVE, F., and LAURITSEN, T., 1959, *Nucl. Phys.*, **11**, 1.
 BATCHELOR, R., GILBOY, W., PURNELL, A., and TOWLE, J. H., 1960, *Nucl. Instrum.*, **8**, 146.
 BONNER, T. W., KRAUS, A. A., MARION, J. B., and SCHIFFER, J. P., 1956, *Phys. Rev.*, **102**, 1348.
 ENDT, P. M., and BRAAMS, C. M., 1957, *Rev. Mod. Phys.*, **29**, 683.
 GARG, J. B., 1960, *Nucl. Instrum.*, **6**, 187.
 KHABAKHPASHEV, A. G., and TSENTER, E. M., 1959, *Izv. Akad. Nauk U.S.S.R., Ser. Fiz.*, **23**, 883.
 LEMBERG, I. KH., 1960, *Proceedings of the Second Conference on Reactions between Complex Nuclei, Gatlinburg, Tennessee* (New York: John Wiley)
 LITHERLAND, A. E., 1959, *Bull. Amer. Phys. Soc.*, [II], **4**, 58.
 LITHERLAND, A. E., and MCCALLUM, G. G., 1960, *Canad. J. Phys.*, **38**, 927.
 MIDDLETON, R., and TAI, C. T., 1951, *Proc. Phys. Soc. A*, **64**, 801.
 OLLANO, Z. M. I., and ROY, R. R., 1951, *Nuovo Cim.*, **8**, 77.
 OWEN, R. N., 1959, *Nucleonics*, No. 9, **17**, 92.
 RUTLEDGE, A. R., 1959, *Chalk River Report CRT-831*.
 SERDIOKOVA, I. A., KHABAKHPASHEV, A. G., and TSENTER, E. M., 1957, *Izv. Akad. Nauk, U.S.S.R., Ser. Fiz.*, **21**, 1017.
 SHARPE, W. T., 1957, *Chalk River Report, CRT 556*.
 TSENTER, E. M., KHABAKHPASHEV, A. G., and PIRKIN, I. A., 1960, *Soviet Physics, J.E.T.P.*, **37**, 806.

Orbital Electron Capture Ratio and Beta Spectrum of ^{204}Tl

By B. R. JOSHI

Department of Natural Philosophy, The University, Glasgow

MS. received 9th December 1960

Abstract. A direct measurement of the L/K electron capture ratio has been made for ^{204}Tl . An improved internal source scintillation counter technique was used. A crystal was grown containing ^{204}Tl and this crystal was totally enclosed in a well-type crystal. The experimental value obtained for this unique first forbidden transition ($\Delta J = 2$, yes) is 0.42 ± 0.05 . This value may be compared with the value 0.45 ± 0.05 calculated from the electron capture transition energy.

In addition, information has been obtained on the β^- decay branch. The low energy end of the Fermi-Kurie plot of the β^- spectrum, after applying an exact shape correction factor, deviates slightly downwards from a straight line. This deviation is in the opposite sense from that obtained by previous workers with magnetic spectrometers.

§ 1. INTRODUCTION

EXPERIMENTAL investigation of the L/K capture ratios for high Z nuclei is of considerable importance, since there exists little or no direct experimental evidence to check the validity of the theory in this region. The theoretical treatment of the problem has been given by Marshak (1942), Brysk and Rose (1958) and Odier and Daudel (1956). For allowed and unique forbidden transitions, the capture ratio is independent of the nuclear matrix element and can be calculated from the electron capture transition energy. Moreover, for the unique forbidden transitions, capture from the L_{III} shell is favoured with low transition energy.

The experimental results on capture ratios have been reviewed by Radvanyi (1955), and more recently by Robinson and Fink (1960) and Bouchez and Depommier (1960). It was pointed out that among the few precise experimental measurements—mostly confined to elements of low atomic number—the observed L/K capture ratios were generally found to be some ten per cent greater than the calculated value. Recently, however, possible agreement between calculated and experimental values was obtained by Joshi and Lewis (1960) for the intermediate Z element ^{131}Cs . Before the theory of L/K capture can be used with full confidence, more precise experimental data, particularly on the higher Z elements, seems necessary.

Of the higher Z elements, the isotope ^{204}Tl is of special interest for an L/K capture measurement because the electron capture transition energy has been determined at 376 ± 20 keV from the inner bremsstrahlung work of Jung and Pool (1956). The half-life is 3.78 ± 0.04 years (Fink and Robinson 1959), and hence $\log fT = 8.4$. The electron capture transition is classified as unique first forbidden ($\Delta J = 2$, yes). Evidence for the assignment of 2 for ^{204}Tl is derived

from the unique first forbidden shape of the β^- spectrum as reported by Lidofsky, Macklin and Wu (1952). The decay scheme is shown in Fig. 1 after der Mateosian and Smith (1952).

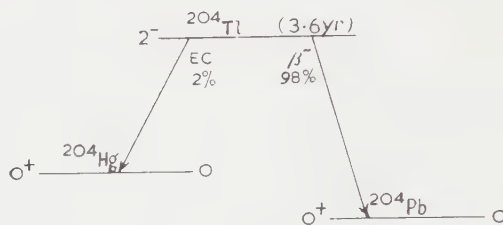


Fig. 1. Decay scheme of ^{204}Tl .

The β^- spectrum, investigated by Lidofsky, Macklin and Wu (1952) with a solenoid spectrometer, gave a value of 765 ± 10 keV for the end point energy. The Fermi-Kurie plot was shown to have an 'S' shape, characteristic of unique first forbidden transitions. After treating the Fermi-Kurie plot with an exact shape correction factor, as given by Konopinski (see Siegbahn 1955, p. 305), a linear plot was obtained down to 100 keV (of Wu (see Siegbahn 1955, p. 331)). Below 100 keV the linear plot was found to deviate upwards and it was suggested that this deviation might be due to the finite source thickness. Recently Grard (1958) has obtained a Fermi plot which, after exact correction, is linear down to 50 keV. Below 50 keV he suggested that the rising curve found by others is due to instrumental error. Further information on the β^- spectrum has been obtained here.

§ 2. EXPERIMENTAL METHOD

^{204}Tl , of high specific activity, was produced by the irradiation of TlNO_3 in the neutron beam at the United Kingdom Atomic Energy Authority, Harwell, by means of the $^{203}\text{Tl}(n, \gamma)^{204}\text{Tl}$ reaction. A preliminary search was made to determine the purity of the sample with an external source of ^{204}Tl and a 2 in. diameter \times 2 in. NaI(Tl) Harshaw scintillator mounted on a Du Mont multiplier with a CDC multichannel pulse height analyser. Aluminium sheet (5 mm thick) was introduced between the source and the detector to remove β^- particles. Except for a very prominent $K\alpha$ peak at about 70 keV, no γ -ray lines were observed between this energy and 1 MeV. The total γ -radiation probability was less than 0.15% of the total disintegration probability.

The technique employed for the measurement of K and L capture events has been discussed in a previous communication (Joshi and Lewis 1960). This method is illustrated in the inset of Fig. 2. The inner crystal was grown from Harshaw NaI(Tl) chippings with a trace of ^{204}Tl source by the Bridgman (1925) method. The crystal was then cut and polished to a size of approximately 6 mm diameter \times 6 mm. This fitted closely into the well-type Harshaw NaI(Tl) crystal. This latter had an external size of 2 cm³ with a central well 6 mm diameter \times 6 mm deep and the whole was fitted with a lid 6 mm thick. The crystal assembly was immersed in liquid paraffin in an aluminium container having a thin mylar window with an aluminized mylar reflector. An E.M.I. 9514S phototube was employed. The L events, which consist of L x-rays and L Auger electrons are completely

absorbed in the inner active crystal. Some of the K x-rays, from K-capture events, or the iodine x-rays associated with the detection process may escape from the surface layers of the inner crystal. As these will be absorbed in the outer crystal and be recorded as simultaneous events, no x-ray escape correction is necessary.

To reduce the effect of cosmic ray background, 2 in. of lead shielding, with a 5 mm copper lining, was used. The pulses were amplified in an NE5202 non-blocking amplifier and displayed on a CDC multichannel pulse height analyser. Sharp peaks due to K- and L-capture events at 84 keV and about 15 keV were observed by comparison with RaD (46.5 keV and approximately 15 keV Pb x-rays). Typical K and L peaks, superimposed on the continuous β^- background, are shown in Fig. 2. Similar runs were made with the outer well-type crystal alone, to assess background effects. Fig. 3 shows the results obtained with a lower gain. The small peak at the lower energy end is due to K capture.

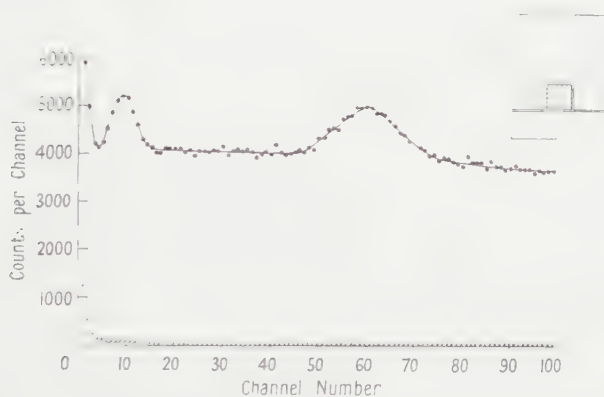


Fig. 2. ^{204}Tl L and K peaks superimposed on the continuous β^- background in a 2-hour run. The background run obtained under similar conditions from the outer well-type crystal, without the inner active crystal, is shown by crosses. The inset diagram shows the well method.

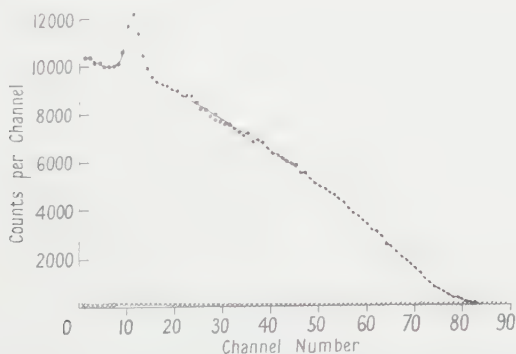


Fig. 3. ^{204}Tl β^- spectrum in a 1-hour run. Crosses show the background of the well-type crystal alone under similar conditions.

To obtain a quantitative measurement of the intensity of the β^- spectrum, the crystal assembly was further mounted in dry air without liquid paraffin. This was done so that the high energy β^- particles liberated at the surface of the inner

crystal could reach the outer crystal without losing any of their energy. The whole assembly was packed in magnesium oxide. The small air gap between the active inner crystal and the well-type crystal was shown, under these conditions, not to impair the light-collection efficiency. This was effected with a ^{204}Tl external source, and the pulse height of the dominant K α line so obtained was compared with the height of the electron capture K peak due to the inner crystal. The ratio of the heights differed only slightly from that obtained with paraffin in the gap.

Figure 4, curve *a*, shows the full Kurie plot of the β^- spectrum down to 10 keV after subtracting the K and L peaks, for the arrangement without paraffin. Some of the points at the low-energy end were obtained from a subsidiary run with a higher gain. After applying the exact shape correction factor (of Konopinski (see Siegbahn 1955, p. 305)) given by the expression

$$\alpha = q^2 L_0(p, -Z) + 9 L_1(p, -Z),$$

the plot of Fig. 4, curve *b*, was obtained. Here q is the neutrino energy and p is the electron momentum, L_0 and L_1 are the tabulated functions of Rose, Perry and Dismuke (see Siegbahn 1955, appendices II and III).

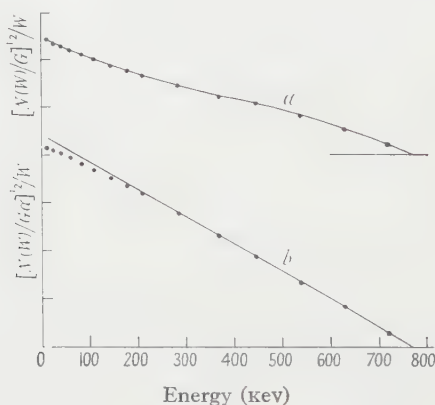


Fig. 4. Curve *a*, S-shaped ^{204}Tl Kurie plot obtained with the crystal assembly in dry air without paraffin, $G = pF/W$; curve *b*, ^{204}Tl Kurie plot of *a* corrected by the exact shape factor α (see text).

§ 3. RESULTS AND DISCUSSION

K and L events were analysed by measuring the relative number of counts under the K and L peaks. The β^- background was assessed by drawing a smooth curve under the K and L peaks. Several runs were taken and a mean value of 0.42 ± 0.05 was obtained for the L/K ratio. The error limits are mainly associated with the assessment of the β^- background.

The Fermi-Kurie plot of the β^- spectrum given in Fig. 4, curve *a*, shows the distinct 'S' shape, characteristic of first forbidden unique transitions. The data corrected by the exact shape factor are linear down to 220 keV, and end at 770 keV. Below 220 keV the corrected plot deviates slightly downwards and not upwards from a straight line. The β^- spectra shown in Fig. 4 are not corrected for the resolution of the instrument as this correction was shown to be negligible in the range considered. The points in the figure are well clear of the L and K peaks, so that the results are not influenced by them.

The K/β^- ratio can be determined fairly accurately. The ratio is 0.0155 ± 0.001 . This lies in the range $(1\frac{1}{2} \pm \frac{1}{2})\%$ obtained by der Mateosian and Smith (1952).

In conclusion, the experimental value of the L/K capture ratio of 0.42 ± 0.05 is just lower than the calculated value at 0.45 ± 0.05 obtained from the electron capture transition energy, 376 ± 20 kev. The transition energy 335 kev reported by der Mateosian and Smith (1952) yields a higher capture ratio. The L/K ratio found here appears to demand the higher value for the transition energy.

ACKNOWLEDGMENTS

I am grateful to Dr. G. M. Lewis for his guidance and suggestions and to Mr. E. Gabathuler for helpful discussions. I would like to thank Professor P. I. Dee for his interest in the work. I am indebted to the Colombo Plan Authorities for the award of a research fellowship and to the Government of Nepal for their sponsorship.

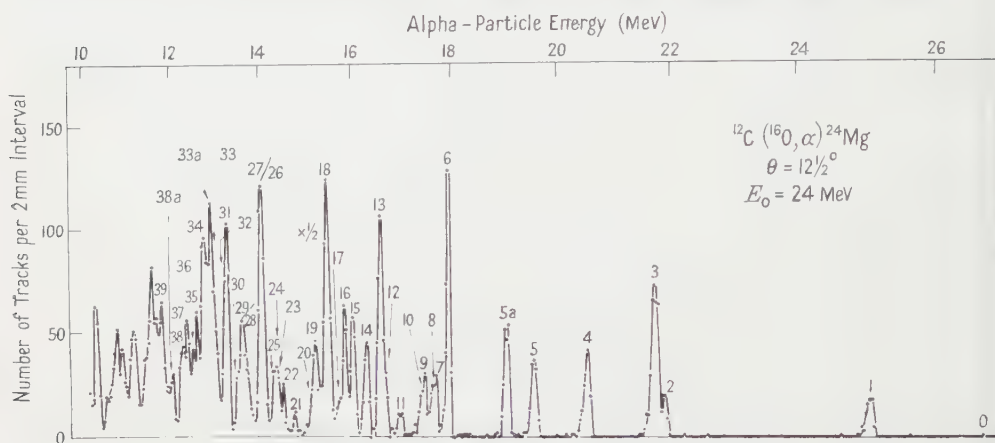
REFERENCES

- BOUCHEZ, R., and DEPOMMIER, P., 1960, *Rep. Progr. Phys.*, **23**, 395 (London: Physical Society).
- BRIDGMAN, P. W., 1925, *Proc. Amer. Acad. Arts Sci.*, **60**, 350.
- BRYSK, H., and ROSE, M. E., 1958, *Rev. Mod. Phys.*, **30**, 1169.
- FINK, R. W., and ROBINSON, B. L., 1959, *Nucl. Phys.*, **10**, 82.
- GRARD, F., 1958, *Physica, 's Grav.*, **24**, 868.
- JOSHI, B. R., and LEWIS, G. M., 1960, *Proc. Phys. Soc.*, **76**, 349.
- JUNG, R. G., and POOL, M. L., 1956, *Bull. Amer. Phys. Soc.*, [11], **1**, 172.
- LIDOFKY, L., MACKLIN, P., and WU, C. S., 1952, *Phys. Rev.*, **87**, 391.
- MARSHAK, R. E., 1942, *Phys. Rev.*, **61**, 431.
- DER MATEOSIAN, E., and SMITH, A., 1952, *Phys. Rev.*, **88**, 1186.
- ODIOT, S., and DAUDEL, R., 1956, *J. Phys. Radium*, **17**, 60.
- RADVANYI, P., 1955, *J. Phys. Radium*, **16**, 509.
- ROBINSON, B. L., and FINK, R. W., 1960, *Rev. Mod. Phys.*, **32**, 117.
- SIEGBAHN, M., (Ed.), 1955, *Beta- and Gamma-Ray Spectroscopy* (Amsterdam: North Holland).

LETTERS TO THE EDITOR

An Energy Level of ^{24}Mg at 6.44 Mev Excitation

In a recent communication (Hinds and Middleton 1960) the energy levels of ^{24}Mg below an excitation energy of 11.9 Mev were reported. These were measured by magnetic analysis of the $^{23}\text{Na}(^3\text{He}, d)^{24}\text{Mg}$ reaction. Since this work was completed α -particles have been observed leading to states of ^{24}Mg from the $^{12}\text{C}(^{16}\text{O}, \alpha)^{24}\text{Mg}$ reaction. In this experiment the Aldermaston Tandem Van de Graaff generator was used to accelerate $^{16}\text{O}^{4+}$ ions to a laboratory energy of 24 Mev. The emitted α -particles were analysed in a multi-channel spectrograph which will be described in a forthcoming paper (Middleton and Hinds, to be published).



A typical α -particle spectrum measured from the bombardment of a thin carbon target with 24 Mev $^{16}\text{O}^{4+}$ ions.

The Figure shows one of the 24 α -particle energy spectra which were simultaneously recorded by the spectrograph, the channel angle being $12\frac{1}{2}^\circ$. Groups arising from the $^{12}\text{C}(^{16}\text{O}, \alpha)^{24}\text{Mg}$ reaction were identified by their characteristic variation of energy with angle and are labelled numerically using the same notation as in a previous communication on ^{24}Mg (Hinds and Middleton 1960). A new level was immediately apparent (group 5a) at an excitation energy of $6.44 \pm 0.02 \text{ Mev}$ which had not been observed previously in the study of the $^{23}\text{Na}(^3\text{He}, d)^{24}\text{Mg}$ reaction.

Due to the large energy loss of the ^{16}O ions in the carbon target, the energy resolution of the spectrograph was limited to about 100 keV. Nevertheless, it was possible to identify almost all the levels observed in the $(^3\text{He}, d)$ reaction except for certain close doublets such as groups 26/27 and 28/29. Evidence was obtained for other new levels at $11.08 \pm 0.03 \text{ Mev}$ (group 33a) and at $11.73 \pm 0.03 \text{ Mev}$ (group 38a). It should be stressed, however, that it is probable that several levels might have been missed above 7.53 Mev in the present and also the $(^3\text{He}, d)$ investigations. This possibility arises in the $(^{16}\text{O}, \alpha)$ reaction because of the inadequate energy resolution. In the $(^3\text{He}, d)$ case the inherent stripping nature of the reaction causes extreme variations in the intensities of individual groups and

it is possible that very weak groups would not be observed. Re-examination of the $^{23}\text{Na}(^3\text{He}, d)^{24}\text{Mg}$ data failed to reveal even a weak deuteron group corresponding to an excitation energy of 6.44 MeV.

It is interesting to note that the new level observed at 11.73 MeV can probably be identified with a state of 11.726 MeV observed by Goldberg, Haerberli, Galonsky and Douglas (1954) from the resonant scattering of α -particles from ^{20}Ne . Also the 6.44 MeV level is almost certainly the same as the 6.4 MeV level tentatively assigned to ^{24}Mg by Broude and Gove (1960) from a study of the $^{24}\text{Mg}(p, p'\gamma)^{24}\text{Mg}$ reaction. Further evidence for this level has recently been obtained by Cohen and Cookson of this laboratory (private communication) who directly observed the inelastically scattered protons as well as accompanying γ -rays.

Atomic Weapons Research Establishment,
Aldermaston,
Berks.

S. HINDS.
R. MIDDLETON.
A. E. LITHERLAND†.

12th December, 1960.

† Seconded from the Atomic Energy of Canada, Chalk River, Ontario, Canada.

BROUDE, C., and GOVE, H. E., 1960, *Proceedings of the Kingston Conference on Nuclear Structure* (Toronto: University Press).

GOLDBERG, N., HAEBERLI, W., GALONSKY, A. I., and DOUGLAS, R. A., 1954, *Phys. Rev.*, **93**, 799.

HINDS, S., and MIDDLETON, R., 1960, *Proc. Phys. Soc.*, **76**, 553.

The Spin of a New Level in ^{24}Mg

During the course of a programme for measuring the total angular momentum of levels in even-even nuclei in the 1d-2s shell, a gamma ray of energy about 5.05 MeV was found in coincidence with one of 1.37 MeV when a natural magnesium target was bombarded with 8.75 MeV protons from the Chalk River tandem accelerator (Broude and Gove 1960). This would correspond to a level in ^{24}Mg at about 6.42 MeV (as discussed below, 6.44 MeV is a better value for this energy) and no such level had previously been reported. In particular, the very careful recent work of Hinds and Middleton (1960) on the reaction $^{23}\text{Na}(^3\text{He}, d)^{24}\text{Mg}$ failed to reveal any levels between 6.005 and 7.350 MeV in ^{24}Mg .

The evidence for this level is shown in Fig. 1. A natural magnesium metal target about 18 mg cm⁻² thick and backed with gold was bombarded with 8.75 MeV protons. The direct spectrum of gamma rays measured in an unshielded 5 inch diameter by 6 inch long NaI(Tl) crystal with its front face located about 6.2 inches from the target centre, is shown in the upper half of Fig. 1. A very intense 1.37 MeV gamma ray is observed corresponding to de-excitation of the first excited state of ^{24}Mg . A weak 1.83 MeV gamma ray, presumably corresponding to the first excited state of ^{26}Mg , is also seen. In addition to these, there is a peak at 2.80 MeV which could arise from de-excitation of the 4.12-4.23 MeV doublet in ^{24}Mg . Higher energy peaks including one of 4.63 and 5.07 MeV are also seen as well as a number of peaks near 4.4 MeV, some of which may be due to inelastic proton scattering from ^{12}C contamination on the target. The energy calibration of the direct spectrum is not very accurate since only the 1.37 MeV peak is well defined. When a narrow voltage gate was set to include only the 1.37 MeV peak in a second NaI(Tl) crystal

(5 inches in diameter and 4 inches long) also located at 6.2 inches from the target centre, the coincidence spectrum shown in the lower half of Fig. 1 is observed in the larger crystal. All the observed gamma-ray peaks can be accounted for as shown in the inset level diagram, if one assumes a new level at 6.44 MeV in ^{24}Mg and if one assumes that the 6.01 MeV level cascades through the 4.23 MeV level as well as through the first excited state at 1.37 MeV. The energies for the 1.76, 2.73, 4.64 and 5.07 MeV gamma rays are obtained directly in this spectrum by comparison

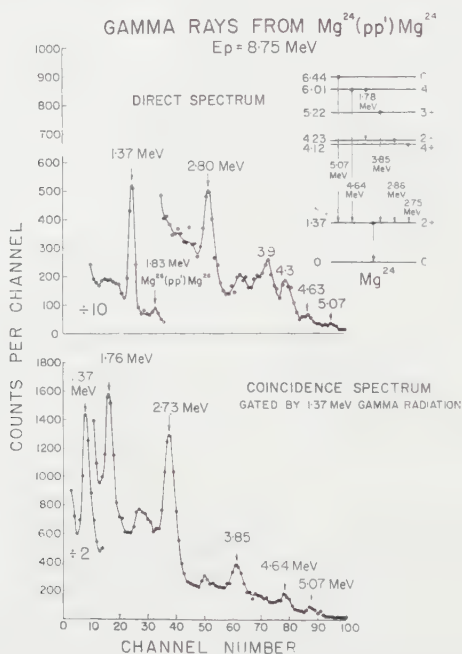


Fig. 1. The upper curve shows the direct spectrum of gamma rays measured in a 5 inch diameter by 6 inch long NaI(Tl) crystal resulting from the bombardment of a natural magnesium target of thickness about 18 mg cm^{-2} with 8.75 MeV protons. The lower curve shows the gamma spectrum measured in the same crystal in coincidence with a gate set on the 1.37 MeV peak measured in a second NaI(Tl) crystal 5 inches in diameter and 4 inches long. The inset decay scheme indicates the gamma transitions observed.

with the peaks at 1.37 and 3.85 MeV, which are almost certainly single peaks. If inelastic protons excited the 4.12 and 4.23 MeV levels equally strongly, the coincidence spectrum would show mainly a 2.75 MeV gamma ray in coincidence with a 1.37 MeV since the 4.23 state de-excites mostly by a direct ground state transition (Batchelor *et al.* 1960) and this may account for the 2.73 MeV peak. The peak at 1.76 MeV is very close in energy to that arising from the de-excitation of the 1.83 MeV level in ^{24}Mg . However, in measuring its energy in several runs an average value of $1.76 \pm 0.01 \text{ MeV}$ was obtained which suggests the possibility that the 6.01 MeV level cascades through the state at 4.23 MeV as well as through the ground state. The average values for the two highest energy gamma rays are $4.62 \pm 0.02 \text{ MeV}$ and $5.07 \pm 0.03 \text{ MeV}$, respectively.

To determine the total angular momentum of this $6.44 \pm 0.03 \text{ MeV}$ level as well as the known level at 6.01 MeV, coincidence correlations between the 4.62 and 5.07 MeV gamma ray and the 1.37 MeV gamma ray were measured in a variety of

geometries at a proton bombarding energy of 8.75 MeV. A detailed description of the technique has been given by Gove (1960) and will not be presented here. The results of these measurements for the 5.07 MeV gamma ray in coincidence with the 1.37 MeV gamma ray, are shown in Fig. 2. In these measurements the 5 inch by 4 inch counter is fixed at 90° on one side of the beam in the horizontal plane while the other is moved along the edges of the upper, forward octant on the other side of the beam. Progressing from left to right on the angle scale the moving counter

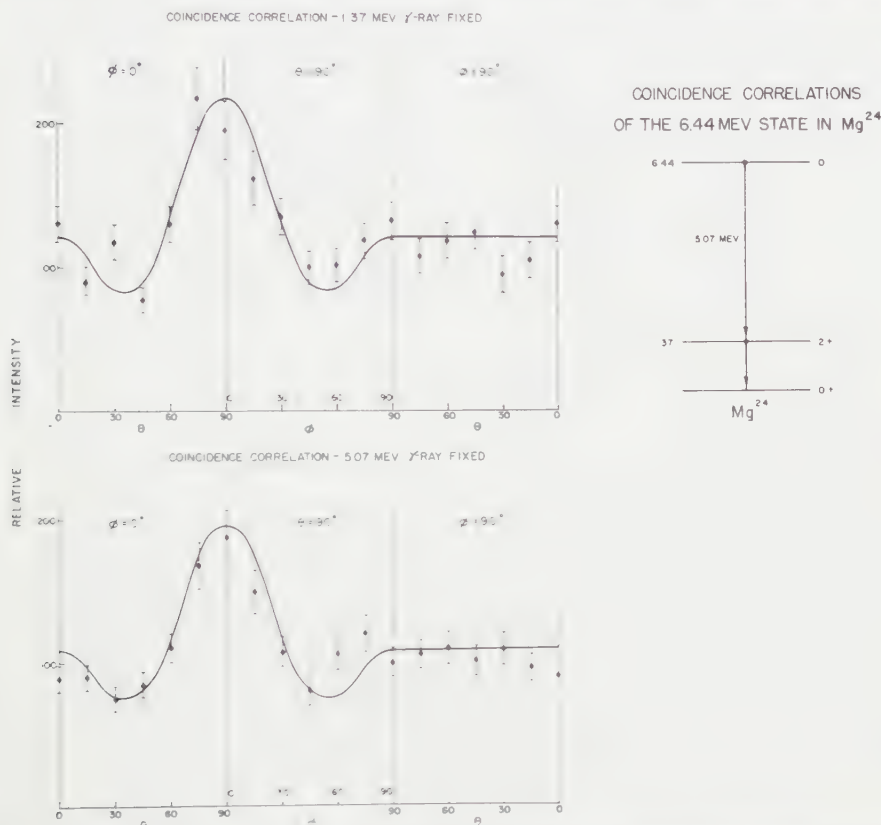


Fig. 2. The upper curve shows the coincidence angular correlations between the 5.07 MeV gamma ray measured in a crystal moving as described in the text and a 1.37 MeV gamma ray measured in a fixed crystal. The lower curve is similar data for the case in which the 5.07 MeV gamma ray is measured in the fixed crystal. The particular cascade involved is shown in the inset level diagram. The curves through the data points are theoretical ones for a $0-2-0$ spin sequence.

starts at $\phi = 0, \theta = 0$ in line with the beam. It moves in the horizontal plane until it is at 90° to the beam ($\phi = 0, \theta = 90^\circ$). It is then moved up in the plane perpendicular to the beam until it is at 90° above the target ($\theta = 90^\circ, \phi = 90^\circ$). It is then moved down towards its starting point in a vertical plane containing the beam until it again reaches the position $\phi = 0, \theta = 0$ (this is equivalent to $\phi = 90^\circ, \theta = 0$). During this motion two correlations are measured simultaneously by setting a gate on the 1.37 MeV gamma-ray peak in both crystals and measuring the corresponding coincidence spectrum from both. A third crystal at a fixed angle measures the spectrum in coincidence with the gate set on the 1.37 MeV peak in

the 5 inch by 4 inch crystal fixed at 90° and thus serves as a monitor. Fig. 2 shows the experimental points and their errors obtained as described above. The solid lines are the theoretical predictions for a 0-2-0 angular correlation (modified to take into account the finite solid angle subtended by each crystal) normalized to give a best fit to the data. A detailed theoretical description of angular correlations measured in this way has been given by Litherland and Ferguson (1961). This fit provides an unambiguous spin sequence assignment and proves that the 5.07 Mev gamma ray is a transition to the first excited state of some even-even nucleus and almost certainly from a state in ^{24}Mg at 6.44 Mev. Similar measurements which show that the 5.22 and 6.01 Mev levels in ^{24}Mg have spins of 3 and 4, respectively, will be reported elsewhere.

Recently the alpha particles from the reaction $^{12}\text{C}(^{16}\text{O}, \alpha)^{24}\text{Mg}$ $Q = 6.76$ Mev have been measured in a high resolution magnetic spectrograph by Hinds, Litherland and Middleton (1960, private communication). In addition to the levels already known in ^{24}Mg (Hinds and Middleton 1960) they find an alpha-particle group corresponding to a new state at about 6.44 Mev. This provides very convincing confirmation of the existence of such a level in ^{24}Mg .

Physics Division,
Atomic Energy of Canada Limited,
Chalk River, Ontario, Canada.

C. BROUDE†.
H. E. GOVE.

9th January 1961.

† Now at the Department of Physics, University of Jerusalem, Jerusalem, Israel.

- BATCHELOR, R., FERGUSON, A. J., GOVE, H. E., and LITHERLAND, A. E., 1960, *Nucl. Phys.*, **16**, 38.
 BROUDE, C., and GOVE, H. E., 1960, *Proceedings of the International Conference on Nuclear Structure, Kingston, Canada* (Eds D. A. BROMLEY and E. W. VOGT) (Toronto: University of Toronto Press; Amsterdam: North-Holland), p. 471.
 GOVE, H. E., 1960, *Proceedings of the Accelerator Conference, Amsterdam, The Netherlands* (1961, *Nuclear Instruments and Methods*, **11**, 63).
 HINDS, S., and MIDDLETON, R., 1960, *Proc. Phys. Soc.*, **76**, 553.
 LITHERLAND, A. E., and FERGUSON, A. S., 1961, *Canad. J. Phys.*, in the press.

The Effective Number of Electrons in the π Band of Graphite

A self-consistent field calculation of the graphite π band (Peacock and McWeeny 1959, Peacock 1960) has been used to calculate the effective number of electrons which contribute to the electrical conductivity of the two-dimensional infinite sheet.

The first Brillouin zone is a regular hexagon and contains two electrons per unit cell. The energy at points in \mathbf{k} space about the corners of the zone is given by

$$E = E_0 \pm 2.108\pi a\beta |\mathbf{k} - \mathbf{k}_c|$$

where β is the resonance integral of a nearest neighbour bond in benzene and has the value -4.79 eV (McWeeny and Peacock 1957); a is the length of the primitive translation vector in the direct lattice (2.46 Å) and \mathbf{k}_c the value of the reciprocal

lattice vector \mathbf{k} at the corners of the zone. The positive sign refers to the first zone and the negative sign to points in the second zone, which at absolute zero is completely empty.

The difference in energy between a point near the zone corner and a corner point is given by

$$E - E_c = 2 \cdot 108 \pi a \beta |\mathbf{k} - \mathbf{k}_c|.$$

At 0°K , the first zone is completely filled and the second empty. At higher temperatures thermal overflow of electrons occurs into the second zone across the zero energy gap. The extent to which this occurs depends upon kT . The energy contour $E = E_c + kT$ is circular about the zone corner with radius $kT/2 \cdot 108 \pi a \beta$. The total length of the contour with this energy is $6 \times 2\pi kT \cdot 3 \times 2 \cdot 108 \pi a \beta$ (there being six corners in the hexagonal zone).

If $N(E)dE$ is the number of electronic states in an interval dE , then

$$N(E) = 2A \int \frac{dS}{|\text{grad}_{\mathbf{k}} E|}$$

where A is the area of the lattice, and the integration is over the whole curve of constant E . The expression for $N(E)$ in the graphite π band is then

$$N(E) = \frac{8A |E - E_c|}{4 \cdot 444 a^2 \beta^2 \pi}.$$

Since the area per atom in the lattice is $\sqrt{3}a^2/4$, the number of available states per atom per unit energy interval is

$$n = \frac{\sqrt{3} |E - E_c|}{2 \cdot 222 \pi \beta^2}.$$

Conduction occurs through exciting electrons into the upper band and through positive holes which are created in the lower band.

At temperatures above absolute zero, the number of free electrons per atom is

$$n' = \int_0^\infty n f(E) dE = \frac{\pi}{8 \cdot 888 \sqrt{3}} \left(\frac{kT}{\beta} \right)^2$$

where $f(E)$ is the Fermi-Dirac distribution function. Since the number of free electrons is equal to the number of holes, the effective number of free electrons will be twice this.

At room temperatures $2n'$ has the value $1 \cdot 1 \times 10^{-5}$.

This compares with the value using the simple theory of $2 \cdot 3 \times 10^{-4}$ (Wallace 1947). The best experimental data appear to be those of McClure (1960). From cyclotron resonance data he gives a value of $4 \cdot 6 \times 10^{-5}$ electrons per atom. The agreement between theory and experiment appears to be very satisfactory.

Chemistry Department,
King's College,
University of London,
Strand, W.C.2.

T. E. PEACOCK.

7th February 1961.

- McCLURE, J. W., 1960, *J. Chim. Phys.*, **57**, 859.
McWEENY, R., and PEACOCK, T. E., 1957, *Proc. Phys. Soc. A*, **70**, 41.
PEACOCK, T. E., 1960, *J. Chim. Phys.*, **57**, 844.
PEACOCK, T. E., and McWEENY, R., 1959, *Proc. Phys. Soc.*, **74**, 385.
WALLACE, P. R., 1947, *Phys. Rev.*, **71**, 622.

Dislocation Relaxation in Zinc at Low Temperatures

Low temperature dislocation relaxation peaks, known as Bordoni (1954) peaks, have been observed in face-centred cubic metals such as Cu, Ag, Al and Pb by various investigators. Recently the attenuation peak of face-centred cubic type has been observed in single crystals of zinc (hexagonal close-packed lattice) by Bordoni and his associates (Bordoni, Nuovo and Verdini 1960). By studying the effect of annealing and pre-strain they have shown that the relaxation peak observed at 210°K is the dislocation relaxation effect.

We suggest the following dissociation reaction is responsible for the relaxation effect:

$$\frac{1}{3}a[11\bar{2}0] = \frac{1}{3}a[10\bar{1}0] + \frac{1}{3}a[01\bar{1}0].$$

In zinc at low and moderate temperatures glide occurs only on the basal plane, the close-packed directions $\langle 1120 \rangle$ in this plane being the possible glide directions. The basal plane corresponds to $\{111\}$ glide plane and glide directions $\langle 11\bar{2}0 \rangle$ to glide directions $\langle 110 \rangle$ in face-centred cubic metals. We believe that Bruner's (1960) mechanism, if it is correct for face-centred cubic systems, should be applicable to zinc also. We have calculated the activation energy W_0 and estimated N_0/l^2 , where N_0 is the total number of dislocation vacancy configurations participating in the relaxation phenomena and l is the distance between the pinning points.

The values of the various parameters used in the calculation are as follows. The lattice spacing in the basal plane $a = 2.66 \times 10^{-8}$ cm, the lattice spacing normal to the basal plane $c = 4.94 \times 10^{-8}$ cm, shear modulus $\mu_E = 3.83 \times 10^{11}$ dyn cm $^{-2}$, Poisson's ratio $\nu = 0.33$, the magnitude of the Burgers vector of the undissociated dislocation $b_0 = \frac{1}{3}a[11\bar{2}0] = 2.66 \times 10^{-8}$ cm, the magnitude of the Burgers vector of a partial $b = \frac{1}{3}a[10\bar{1}0] = 1.54 \times 10^{-8}$ cm, the magnitude of the edge component of the Burgers vector of the partial $b_1 = b \cos 30^\circ = 1.33 \times 10^{-8}$ cm, the stacking fault energy $E_f = 50$ erg cm $^{-2}$ (Suzuki 1957), the angle between the dislocation and the Burgers vector of the undissociated dislocation $\theta = 90^\circ$, the separation between the two partials $\lambda = 25.13 \times 10^{-8}$ cm, the radius of the solvent atom $r = a/2$, Gruneisen constant $\gamma_G = 2.68$ and the distance of the vacancy above the glide plane $R_0 = c/4 = 1.23 \times 10^{-8}$ cm.

The calculated value of the activation energy $W_0 = 0.303$ ev is in good agreement with the experimental value 0.33 ev. We have estimated $N_0/l^2 = 46.08$ cm $^{-1}$, which can be compared with Bruner's estimate $N_0/l^2 = 30$ cm $^{-1}$ in copper. Recently, stacking faults in zinc have been studied by Fourdeux, Berghezan and Webb (1960). They have observed dislocation loops, in zinc foils and vapour grown crystals, of radii 5–50 μ . If we take $l = 10$ –100 μ , then $N_0 = 4.6 \times 10^5$ to 4.6×10^7 cm $^{-3}$.

Physics Department,
University of Allahabad,
India.

BAL KRISHNA AGRAWAL.
G. S. VERMA.

17th January 1961.

BORDONI, P. G., 1954, *J. Acoust. Soc. Amer.*, **26**, 495.

BORDONI, P. G., NUOVO, M., and VERDINI, L., 1960, *Nuovo Cim.*, **16**, 373.

BRUNER, L. J., 1960, *Phys. Rev.*, **118**, 399.

FOURDEUX, A., BERGHEZAN, A., and WEBB, W. W., 1960, *J. Appl. Phys.*, **31**, 918.

SUZUKI, H., 1957, *Dislocation and Mechanical Properties of Crystals* (New York: John Wiley), p. 387.

The Threshold of the $^{12}\text{C}(^3\text{He}, n)^{14}\text{O}$ Reaction

This work was undertaken in order to resolve a discrepancy between measurements reported previously. Bromley *et al.* (1957) reported a value of 1449.6 ± 2.8 kev while Butler (1956), and Bondelid *et al.* (unpublished†) have obtained 1435 ± 5 kev and 1436.2 ± 0.9 kev respectively. Since the present measurement was completed, a further result has been published by Bardin *et al.* (1960). Their value of 1437.0 ± 0.9 kev is in agreement with the results of Butler, and Bondelid *et al.*, and with the present measurement.

The importance of this threshold energy in computing the *ft* value for the $(0^+ \rightarrow 0^+)$ transition in $^{14}\text{O}(\beta^+)^{14}\text{N}^*$ and hence a value for the β -decay coupling constant has already been stressed (Bondelid *et al.*, unpublished, Bardin *et al.* 1960). Further, this threshold is a convenient calibration point for the beam analysers of machines accelerating ^3He particles.

In this experiment, the energy of the beam from the 6 mv Van de Graaff accelerator was defined by three slits used in conjunction with the 90° analysing magnet. Two slits, of 1 mm and 0.7 mm gap width, were placed one radius away from the entrance and exit faces of the magnet respectively, and the third slit, set to 2 mm gap, was located 4.5 m from the exit face. The beam energy spread for this system was not more than 0.1%. The energy was determined from measurements of the magnetic field made with a proton resonance magnetometer, which was calibrated using the threshold of the $^7\text{Li}(p, n)^7\text{Be}$ reaction.

The target was fixed some 36 ft from the magnet, and focusing was achieved with an electrostatic strong focus lens placed midway between them. In order to minimize background, the procedure described in a previous paper (Towle and Macefield 1961) for positioning the beam on target by means of a removable aperture was also employed. The target materials were evaporated *in vacuo* on to thick tantalum backings.

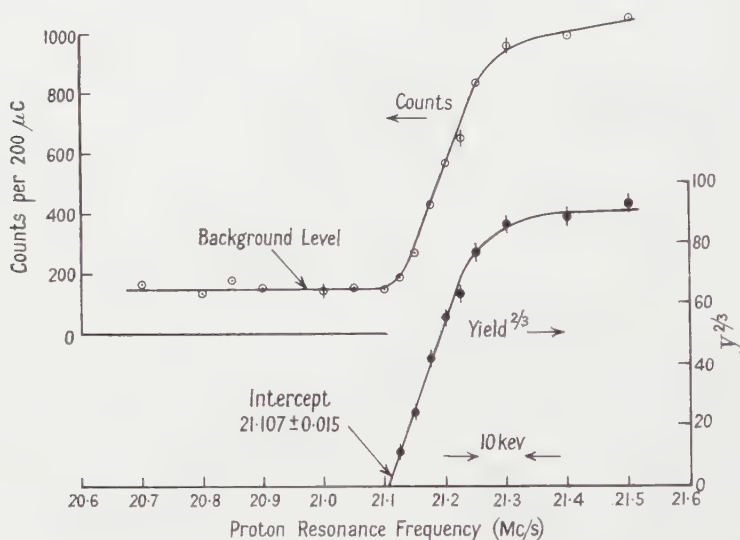
The yield of neutrons at threshold was measured with a long counter placed at 0° to the beam, the sensitive area subtending a cone of half angle about 65° . This cone contains all the neutrons emitted from the $^{12}\text{C}(^3\text{He}, n)^{14}\text{O}$ reaction with ^3He particles of energy up to 20 kev above threshold, and all the neutrons from $^7\text{Li}(p, n)^7\text{Be}$ providing E_p does not exceed threshold by more than 31 kev. The beam current was measured with a current integrator.

Two measurements of the $^7\text{Li}(p, n)$ threshold were made using natural Li_2O targets of thickness 6 and 15 kev to 1.9 mev protons. For a thick target the yield of (S wave) neutrons should increase proportionally to $(\Delta E)^{3/2}$ where ΔE is the amount by which the energy of the bombarding particles exceeds the threshold. Thus a linear extrapolation of a plot of yield^{2/3} against proton energy should be made in order to obtain the threshold (Marion 1960‡). Such extrapolations gave proton resonance frequencies at threshold of 13.975 ± 0.0015 Mc/s and 13.976 ± 0.0015 Mc/s for the 6 kev and 15 kev targets respectively. For calibration purposes we have taken the mean of these two results to correspond to the 'best value' of the threshold energy of 1880.7 ± 0.4 kev (Marion 1960‡).

† Bondelid, R. O., Butler, J. W., Kennedy, C. A., and del Callar, A., 1960, *N.R.L. Quarterly on Nuclear Science and Technology*, January 1960, page 7 (unpublished).

‡ Marion, J. B., 1960, *University of Maryland Physics Dept., Technical Report 184* (unpublished).

In the Figure we show data for the $^{12}\text{C}(^3\text{He}, n)$ threshold obtained with a target 30 kev thick to 1.4 mev ^3He particles. The plot of the neutron counts shows the amount of background observed below threshold. The yield Y was obtained by subtracting the background, assuming this to remain constant through the threshold. The errors shown in the plot of $Y^{2/3}$ include background subtraction errors, and a linear extrapolation of this plot gave a frequency at threshold of 21.107 ± 0.015 Mc/s. A similar measurement with a 90 kev thick target gave a result of 21.120 ± 0.015 Mc/s. The average of these results together with the



Plots of the neutron counts per 200 μC and $\text{yield}^{2/3}$ at the $^{12}\text{C}(^3\text{He}, n)^{14}\text{O}$ threshold.

calibration leads to a threshold energy of 1434.8 ± 1.6 kev for $^{12}\text{C}(^3\text{He}, n)^{14}\text{O}$. This result and the results mentioned above, excluding that of Bromley *et al.*, when weighted as error⁻² give a mean value of 1436.33 ± 0.60 kev, which, using the masses of ^{12}C , ^3He and n given by Everling *et al.* (1960), gives a Q -value of -1147.8 ± 0.5 kev, and a mass excess of 8007.4 ± 0.7 kev for ^{14}O on the ^{12}C scale.

In order to check on any saturation effects which may have been present in the analysing magnet, a measurement of the $^7\text{Li}(p, n)$ threshold was made using the H_2^+ beam. This threshold occurs at a higher magnetic field than that of $^{12}\text{C}(^3\text{He}, n)$. Using a linear extrapolation of a $Y^{2/3}$ plot for the thicker Li_2O target, we obtained a threshold at 3758.8 ± 2.0 kev. The proton energy, 1879.4 ± 1.0 kev, is about 0.07% below the expected value. However, we note that this small discrepancy may possibly be due to effects suggested by Bondelid and Kennedy (1958) and Dahl, Costello and Walters (1960), who have observed that resonances in $^{27}\text{Al}(p, \gamma)^{28}\text{Si}$ obtained from thick target yield curves, appear to be about 0.05% to 0.08% low when measured with H_2^+ ions. Dahl *et al.* have explained the phenomenon on the basis of the Coulomb effects attending the immediate break up of the H_2^+ ion in the target, and Bondelid and Kennedy have suggested in

addition that the effect may be partly due to a slight penetration of the ion prior to break up. We concluded that magnet saturation effects were negligible in the present experiment.

Atomic Weapons Research Establishment,
Aldermaston,
Berkshire.

J. H. TOWLE.
B. E. F. MACEFIELD.

20th February 1961.

- BARDIN, R. K., BARNES, C. A., FOWLER, W. A., and SEEGER, P. A., 1960, *Phys. Rev. Letters*, **5**, 323.
BONDELID, R. O., and KENNEDY, C. A., 1958, *U.S. Naval Research Laboratory Report* 5083.
BROMLEY, D. A., ALMQVIST, E., GOVE, H. E., LITHERLAND, A. E., PAUL, E. B., and FERGUSON, A. J., 1957, *Phys. Rev.*, **105**, 957.
BUTLER, J. W., 1956, *Bull. Amer. Phys. Soc.*, [II], **1**, 94.
DAHL, P. F., COSTELLO, D. G., and WALTERS, W. L., 1960, *Nucl. Phys.*, **21**, 106.
EVERLING, F., KÖNIG, L. A., MATTAUCH, J. H. E., and WAPSTRA, A. H., 1960, *Nucl. Phys.*, **18**, 529.
TOWLE, J. H., and MACEFIELD, B. E. F., 1961, *Proc. Phys. Soc.*, **77**, 399.

The Determination of the Half Life of RaC'

Radium C' is the shortest-lived member of the radium family, and its half-life (approximately $160\mu\text{sec}$) is very much shorter than the other half-lives in the decay chain. It is formed by the β -decay of radium C, and decays by α -emission to radium D. Its half-life is measured by obtaining the time distribution of these α -particles relative to the β -particles which provide the zero time signal. In the measurement, α -particles are also registered which are not related to the β -particles through the birth and death of radium C', and these form a background.

In our measurement, a radium source, two proportional counters and a time analyser were used. The source, a thin coating of radium deposited on a foil, was placed between two proportional counters and by suitable choice of absorber and counter settings, one counter was made sensitive to α -particles only and the other to β -particles. Pulses from the β -counter provided the zero time signals for the analyser, and the time distribution of the pulses from the α -counter was recorded. The time analyser had 9 channels of $50\mu\text{sec}$ width and was controlled by a crystal oscillator through a beam switching tube (Dobrowolski and Walker 1960).

The experiment was carried out in two ways. In the first, a separate determination of the background was made and the results, corrected for background, were analysed by a least squares fit to a pure exponential (Dobrowolski 1960). As the source of radium C' atoms was radium in equilibrium with its daughter products, this background remained constant over the whole series of measurements as long as the proportional counters remained stable. The background was measured by introducing a delay of 1.2msec after the zero time signal. By the introduction of this delay, the dead-time of the analyser for β -triggers was changed, and this had to be corrected for.

In the second way of carrying out the experiment, no separate measurement of the background was made, and the results were analysed by a least squares fit to a pure exponential plus a constant background. The analysis was carried out by a digital computer. In this case, the requirement that the background should remain constant over the whole series of measurements is not necessary.

The results obtained by these two methods were compatible. The weighted mean value and standard deviation of the two results give for the half-life of RaC' $164.3 \pm 1.8 \mu\text{sec}$.

The recently published values known to the authors are:

$$t_{1/2} = 163.7 \pm 0.2 \mu\text{sec} \quad (\text{von Dardel 1951}),$$

$$t_{1/2} = 158 \pm 2 \mu\text{sec} \quad (\text{Ballini 1953}),$$

$$t_{1/2} = 159.5 \pm 3 \mu\text{sec} \quad (\text{Ogilvie 1960}).$$

The authors wish to thank D. Jakeman and J. Walker for many useful discussions during the experiment and J. B. C. Brown and S. A. Scott for preparing the programme for the digital computer.

Department of Physics,
University of Birmingham.
18th April 1961.

T. DOBROWOLSKI†.
J. YOUNG.

BALLINI, R., 1953, *Ann. Phys., Paris*, **8**, 441.

VON DARDEL, G. F., 1951, *Ark. Fys.*, **2**, 337.

DOBROWOLSKI, T., 1960, *Ph.D. Thesis*, Birmingham University.

DOBROWOLSKI, T., and WALKER, J., 1960, *J. Sci. Instrum.*, **37**, 289.

OGILVIE, K. W., 1960, *Proc. Phys. Soc.*, **76**, 299.

Consideration of Exchange in Ionization

Consideration of exchange in ionization of atoms by electron impact differs somewhat from consideration of exchange in the excitation of discrete energy levels.

Let us consider, for instance, the ionization of a hydrogen atom. The differential cross section including exchange can be expressed (Mott and Massey 1949) in atomic units as follows:

$$\sigma(\epsilon, E - \epsilon) = \frac{kc}{q} \iint \left[\frac{1}{4} |f(\mathbf{k}, \mathbf{c}) + g(\mathbf{k}, \mathbf{c})|^2 + \frac{3}{4} |f(\mathbf{k}, \mathbf{c}) - g(\mathbf{k}, \mathbf{c})|^2 \right] d\hat{\mathbf{k}} d\hat{\mathbf{c}},$$

.....(1)

where q is the momentum of the incident electron, $\epsilon = \frac{1}{2}k^2$, $E = \epsilon + \frac{1}{2}c^2$ —the energy of the system, $f(\mathbf{k}, \mathbf{c})$ is the amplitude of transition into the final state in which the momentum of the incident electron is \mathbf{c} but that of the atomic electron is \mathbf{k} . A similar meaning, with interchanged \mathbf{k} and \mathbf{c} , is expressed by $g(\mathbf{k}, \mathbf{c})$. Hence, we have†

$$g(\mathbf{k}, \mathbf{c}) = f(\mathbf{c}, \mathbf{k})$$

.....(2)

and

$$\sigma(\epsilon, E - \epsilon) = \sigma(E - \epsilon, \epsilon).$$

.....(3)

† On leave from the Institute for Nuclear Research, Warsaw.

‡ For stricter deduction of expression (2), taking into account also the long-range character of Coulomb interaction, see Appendix.

Since $\sigma(\epsilon, E - \epsilon) d\epsilon$ is the transition cross section into a state in which the energy of the (no matter which) electron is within the interval $d\epsilon$, we obtain the total ionization cross section with exchange as follows:

$$Q = \int_0^{E/2} \sigma(\epsilon, E - \epsilon) d\epsilon = \frac{1}{2} \int_0^E \sigma(\epsilon, E - \epsilon) d\epsilon. \quad \dots\dots (4)$$

Considering expressions (1) and (2) we obtain

$$Q = \int_0^E \frac{kc}{q} d\epsilon \iint |f(\mathbf{k}, \mathbf{c})|^2 d\mathbf{k} d\mathbf{c} - \int_0^{E/2} \frac{kc}{q} d\epsilon \iint \mathcal{A}[f(\mathbf{k}, \mathbf{c})f^*(\mathbf{c}, \mathbf{k})] d\mathbf{k} d\mathbf{c}. \quad \dots\dots (5)$$

The first term of the right-hand side of (5) gives the cross section without exchange; the second term describes the interference of direct and exchange scattering. Thus, as distinct from exchange effects in the excitation of discrete energy levels, the effect of exchange in the ionization of hydrogen reduces itself to interference. This corresponds with the view of classical mechanics, according to which there is a complete absence of exchange in the process of ionization of hydrogen.

Ionization of multi-electron atoms may involve apart from interference effects also exchange in the classical sense, when the incident electron remains inside the ion in a bound state.

It is easy to generalize formulae (3) and (4) for n -fold ionization. In this case the differential cross section with exchange $\sigma(\epsilon_1, \epsilon_2, \dots, \epsilon_n, E - \epsilon_1 - \dots - \epsilon_n)$ must be invariant with respect to any transposition of arguments. We have then for the total cross section

$$Q = \frac{1}{(n+1)!} \int_0^E d\epsilon_1 \int_0^{E-\epsilon_1} d\epsilon_2 \dots \int_0^{E-\epsilon_1-\dots-\epsilon_{n-1}} d\epsilon_n \sigma(\epsilon_1, \epsilon_2, \dots, \epsilon_n, E - \epsilon_1 - \dots - \epsilon_n). \quad \dots\dots (6)$$

The necessity of introducing the factor $[(n+1)!]^{-1}$ when one integrates over all possible energy values has been disregarded by Geltman (1956, 1960) considering the twofold ionization of He and the onefold ionization of H, H^- , and He. Therefore Geltman (1956) actually obtained the double cross section of ionization for H. Considering the ionization of H^- and He another mistake has been made: in the expression $\sigma = \frac{1}{4}(\sigma_s + 3\sigma_t)$ for the differential cross section, where σ_s and σ_t are the cross sections for excitation of singlet and triplet states of atom (ion) respectively, the factor $\frac{1}{4}$ is redundant because it is necessary to obtain the sum and not the mean value. Thus the result for H^- obtained by Geltman (1960) is half of the correct value and therefore the cross section without exchange was reduced by about half with the inclusion of exchange.

APPENDIX

It is possible to show (Peterkop 1960) that the wave function describing the collision of an electron with a hydrogen atom can be asymptotically expanded within the configuration space in directions corresponding to ionization as follows:

$$\phi(\mathbf{r}_1, \mathbf{r}_2) \sim r^{-5/2} \exp \left[i\kappa r + \frac{i}{\kappa} V(\hat{\mathbf{r}}) \ln r \right] \left[A_{00}(\hat{\mathbf{r}}) + \sum_{n=1}^{\infty} \sum_{p=0}^{2n} I_{np}(\hat{\mathbf{r}}) \frac{(\ln r)^p}{r^n} \right], \quad \dots\dots (7)$$

where $r = (r_1^2 + r_2^2)^{1/2}$, $\mathbf{r} = (\mathbf{r}_1, \mathbf{r}_2, \lambda = \arctan r_2/r_1)$, $\kappa = (2E)^{1/2}$, \mathbf{r}_1 and \mathbf{r}_2 are the radii vectors of the incident and the atomic electron respectively,

and $V(\mathbf{r}) = (\cos \lambda)^{-1} + (\sin \lambda)^{-1} - [1 - \sin 2\lambda \cos(\mathbf{r}_1, \mathbf{r}_2)]^{-1/2}$.

On the other hand, omitting exponentially diminishing terms, we have for the first term of the asymptotic expansion:

$$\phi(\mathbf{r}_1, \mathbf{r}_2) \sim \frac{1}{r_1} \int_0^\kappa k^2 dk \int d\mathbf{k} \psi(\mathbf{k}, \mathbf{r}_2) f(\mathbf{k}, \mathbf{c}) \exp[i\kappa r_1 + i\eta(\mathbf{k}, \mathbf{r}_1)]; \quad (\hat{\mathbf{c}} = \hat{\mathbf{r}}_1), \quad \dots\dots (8)$$

$$\sim \frac{1}{r_2} \int_0^\kappa k^2 dk \int d\mathbf{k} \psi(\mathbf{k}, \mathbf{r}_1) g(\mathbf{k}, \mathbf{c}) \exp[i\kappa r_2 + i\eta(\mathbf{k}, \mathbf{r}_2)]; \quad (\hat{\mathbf{c}} = \hat{\mathbf{r}}_2), \quad \dots\dots (9)$$

where $\psi(\mathbf{k}, \mathbf{r}_i)$ is the function of the continuous spectrum of hydrogen which has the asymptotic form of 'plane' plus ingoing wave and is normalized towards $\delta(\mathbf{k} - \mathbf{k}')$ (see, for example, Landau and Lifschitz 1948). As distinct from Mott and Massey (1949), here η has been introduced to account for phase distortion of the function of the scattered electron.

Comparing (7) with (8, 9), it is possible to find η which can be determined with the accuracy of the \mathbf{k} and \mathbf{c} function. One of the possible choices of phase is

$$\eta(\mathbf{k}, \mathbf{r}_i) = \left(\frac{1}{c} - \frac{1}{|\mathbf{k} - \mathbf{c}|} \right) \ln \frac{\kappa r_i}{c} - \frac{1}{k} \ln \frac{2k^2}{\kappa}; \quad (\hat{\mathbf{c}} = \hat{\mathbf{r}}_i). \quad \dots\dots (10)$$

With this phase we have

$$f(\mathbf{k}, \mathbf{c}) = g(\mathbf{c}, \mathbf{k}) = \left(\frac{i}{\kappa} \right)^{3/2} A_{00}(\mathbf{r}), \quad \dots\dots (11)$$

where $k = \kappa \sin \lambda$, $c = \kappa \cos \lambda$, $\hat{\mathbf{k}} = \hat{\mathbf{r}}_2$, $\hat{\mathbf{c}} = \hat{\mathbf{r}}_1$.

Institute of Physics of the Latvian Academy of Sciences,
Riga,
U.S.S.R.

R. PETERKOP.

24th October 1960.

GELTMAN, S., 1956, *Phys. Rev.*, **102**, 171.

— 1960, *Proc. Phys. Soc.*, **75**, 67.

LANDAU, L., and LIFSCHITZ, E., 1948, *Quantum Mechanics* (Moscow: Gostechizdat).

MOTT, N., and MASSEY, H., 1949, *The Theory of Atomic Collisions* (Oxford: University Press).

PETERKOP, R., 1960, *Izv. Akad. Nauk Latv. S.S.R.*, Riga, **9**, 79.

I agree with the conclusions in the above Letter and would like to thank Dr. Peterkop for finding my errors concerned with the counting of final states in the ionization problem.

Atomic Physics Section,
National Bureau of Standards,
Washington 25, D.C.,
U.S.A.

S. GELTMAN.

24th March 1961.

New Heavy Bosons

In recent publications (Fröhlich 1960 a, b) a new approach to space-time reflections† was used to postulate a wave equation which comprises all known bosons, i.e. π - and K-mesons, and light quanta; from the symmetries involved it followed that four further bosons (denoted as ν -particles) should exist. These ν -particles have spin 1, a mass larger than that of K-mesons, and consist of a positive, a negative and two neutrals. In isospace the properties of the bosons are described in terms of two vector operators with components Q_K and T_K ($K=1, 2, 3$). Here Q_3 is the electric charge operator and, on the usual assignments, T_K is the isospin operator. For both K- and ν -particles T_K consists of two doublets ($T=\frac{1}{2}$) and Q_K of a triplet and a singlet ($Q=1, 0$).

The above results follow simply from the symmetries of the wave equation; interactions have not been considered as yet. It seems of considerable interest, therefore, to note that from a discussion of the empirical properties of weak interaction, Lee and Yang (1960) came to the conclusion that four new bosons should exist with exactly the same properties as have been predicted from my wave equation. Lee and Yang's 'schizoid'‡ isospin behaviour as doublets, or as triplet and singlet, in particular is described in exactly this manner in terms of eigenvectors diagonalizing the operators T_3 and T^2 , or Q_3 and Q^2 , respectively.

Department of Theoretical Physics,
University of Liverpool.
27th March 1961.

H. FRÖHLICH.

FRÖHLICH, H., 1960 a, *Helv. Phys. Acta*, **33**, 803.

— 1960 b, *Proc. Roy. Soc. A*, **257**, 283.

LEE, T. D., and YANG, C. N., 1960, *Phys. Rev.*, **119**, 1410.

CORRIGENDUM

Spin-Lattice Relaxation in Cerium Magnesium Nitrate at Liquid Helium Temperatures: a New Process, by C. B. FINN, R. ORBACH and W. P. WOLF (*Proc. Phys. Soc.*, 1961, **77**, 261).

Note added in proof on page 268:

The line above the equation and the equation itself should read

T_1 varies inversely as the ninth power of temperature, viz.

$$\frac{1}{T_1} = \frac{(9!) G^4 \hbar^2}{\pi^3 \rho^2 v^{10} \Delta^4} \left(\frac{kT}{\hbar} \right)^9.$$

† From a more detailed analysis than given previously, a completely geometrical interpretation of the neutrino has now been obtained; quantization of its field according to the Pauli principle follows as a necessary consequence (*Nuclear Physics*, in the press).

‡ As an alternative to schizon I propose to name the particles $\phi_{\chi\nu\chi\omega\nu}$ (from $\phi\alpha\nu\omega\sigma$ and $\chi\omega\gamma$).

OBITUARY NOTICES

Professor F. J. M. Stratton

Professor Stratton, who died in Cambridge last September, was a man about whom it would be possible to write several biographies, as an astronomer and mathematician, as a soldier, as an organizer of international unions and as a Fellow of his college.

Frederick John Marrian Stratton was born in Birmingham on 16th October 1881, and was educated at King Edward's Grammar School, at the University College (subsequently the University) of Birmingham and at Cambridge, where he took the mathematical tripos in 1904 and was third Wrangler. In 1906 he was elected to a fellowship at Gonville and Caius College, a fellowship which he held for fifty-four years till the day of his death.

His first research work was in planetary motions and in the drift of sunspots, but he soon turned to what became his main interest, the behaviour of novae. He became an expert on their spectroscopic behaviour; he made observations on Nova Aquitae 1918, Nova Cygni 1920, and when in 1934 Nova Herculis appeared he and the staff of the Cambridge Solar Physics Observatory made a remarkable record of the changes in the spectrum of what turned out to be an exceptionally interesting star. With W. H. Manning he published the *Atlas of the Spectrum of Nova Herculis*, still one of the most complete records we have of a nova outburst. His other writings include *Astronomical Physics* in 1925, an article on novae in the *Handbuch der Astrophysik* in 1928 and the *Halley Lecture in Oxford* in 1927. He was appointed assistant director of the Cambridge Solar Physics Observatory in 1913 but relinquished this post in 1919 to become a tutor at Caius. In 1928, however, he succeeded Professor Newall as the second holder of the Chair of Astrophysics and director of the Solar Physics Observatory. He was president of the Royal Astronomical Society from 1933–1935 and was elected to the Fellowship of the Royal Society in 1947.

In addition to his research work in Astronomy, Professor Stratton made very considerable contributions to the organization of science on an international scale. From 1925–35 he was general secretary of the International Astronomical Union, one of the earliest and most successful of these unions which he did much to help. He was also General Secretary of the International Council of Scientific Unions from 1937 until 1952, General Secretary of the British Society from 1930–35 and President of the Royal Astronomical Society from 1933–35. He was Honorary Secretary of that most useful and homely club, the Society for Visiting Scientists, from 1948–55. All this work involved a great deal of travelling and he was a welcome figure wherever he went. As can be imagined he was enthusiastic about the organization of expeditions to view eclipses, and it was believed by his friends that he had never missed one since he became an astronomer, though I can only find records of his attendance at the Crimea, Sumatra, Siam, Calcutta and Japan where he generally had bad luck with the weather.

But science was only a part of his life. Before the war of 1914–18 he took part under the Haldane Scheme for the Territorial Army in the organization of a signals section in the Officers Training Corps of the Universities. The men who worked in this section included many who had very distinguished careers afterwards; three were Nobel Laureates, one an Astronomer Royal, one a Bishop and one an Olympic Gold Medallist. With the outbreak of the war Stratton returned from an eclipse and joined the Army immediately, serving with great distinction, rising to the rank of Lieutenant-Colonel and being awarded the D.S.O. and the Legion d'Honneur.

Finally, something must be said of Stratton's work for and life in Gonville and Caius College, where he was a Tutor from the end of the first war until 1928 and in which he lived as a bachelor Fellow until a few weeks before his death. His affection for the College filled his whole life, and former members could always be sure of a welcome in his room in the corner of Gonville Court and of the opportunity to talk about old times, about the College and about the future. He was a man who did not seem to grow old; if he regretted the disappearance of some of the practices of the former day, he never said so and was always willing with the youngest of his colleagues to plan for the present day. He was "Chubby" to everyone; down to the day before his death he was learning with pleasure about what was going on in the College and it gave him great satisfaction to hear, through the indiscretion of one of his colleagues, that a Caian was likely to be the next President of the Royal Society.

N. F. MOTT.

Robert Kenworthy Schofield, M.A., Ph.D.

One's abiding memory of Schofield is of a happy man who enjoyed life, work, hobbies, and friendship. He had an extraordinary range of skills and interests and a bubbling sense of humour. He was a stimulating friend to whom one turned instinctively for advice on almost any subject, and with his orderly, scientific, and well-stored mind one seldom turned in vain.

Educated at Oundle and Trinity College, Cambridge, he served on the staff at Durham University, 1926–1928, and thence went to Rothamsted Experimental Station, where he became head of the Physics Department in 1946, and then transferred in 1954 to the post of head of the Chemical Department. In 1956 he became Reader in Soil Science at Oxford University, where his somewhat revolutionary ideas made a great impact.

He was a pioneer in the study of the physical and chemical behaviour of soils, and in 1947 he drew attention to the consequences of the fact that cation nutrients in the soil are held by electrostatic attraction to charged surfaces "it is not surprising that investigations with a purely chemical outlook which take no account of the powerful electrical fields close to soil particles, have achieved only a limited success . . . much groundwork is needed before results can be obtained that bear directly on the very complex conditions actually existing in field soil"†—and in the following years made many contributions to the elucidation of the complex situations involved. His enunciation of the Ratio Law in 1947 represented an important advance. Successive papers and the theses of his pupils

† Quoted from Rothamsted report.

represent stages in the gradual elucidation of the form of the relationships between quantity and intensity for the major inorganic plant nutrients. Numerous papers printed at the International Congress of Soil Science at Madison, Wisconsin, in 1960, at which he would have been Chairman of commission I (Soil Physics), indicated the extent to which his ideas were being followed up at centres all over the world.

He was presented with an honorary Doctorate in Agriculture at Lisbon University in 1956 for his outstanding contributions to soil science and was President of the British Soil Science Association from 1959 until his death in June 1960.

His interest in the colour of soils led him to the study of colorimetry, and his paper in the *Journal of Scientific Instruments* (March 1939) entitled 'The Lovibond Tintometer Adapted by Means of the Rothamsted Device to Measure Colours on the C.I.E. System' brought him into close contact with other workers in the field of colour. He was Chairman of the Colour Group of the Physical Society 1945-47, and Chairman of the Committee of the Colour Group which, in 1947, presented the *Report on Colour Terminology* which was published by the Physical Society.

To an entirely different circle of friends he was renowned as one of the great exponents of Morris dancing. He was a member of the Committee of the English Folk Dance and Song Society for 30 years, and Chairman of the executive for the last 12 years, as well as being Senior Squire of the Morris Ring, and in that capacity led many teams to foreign countries to uphold our national honour. He was one of the greatest performers on the pipe and tabor, and frequently broadcast music for folk-dancing.

With all these accomplishments he was humble, very human, and a 'good mixer', at home in any company.

G. J. CHAMBERLIN.

Harry Moore

Emeritus Professor Harry Moore died on 5th August 1960 at the age of 72. He held the Chair of Glass Technology in the University of Sheffield from 1946 to 1955. He was educated at Belle Vue School, Bradford, and the Royal College, of Science, London, where he was subsequently Demonstrator and then was Lecturer in Physics at King's College, London, from 1908 to 1915.

During the war he made use of his considerable talent as a craftsman by acting as co-manager from 1915 to 1918 of the Munitions Training Department at King's College, London. This was followed by a short period as Technical Officer to the Training Department of the Ministry of Labour, but in 1919 he received an invitation from Sir Herbert Jackson to join the newly formed British Scientific Instrument Research Association. It was during this period that he first became interested in glass for he was responsible with Jackson for a programme of research on glasses which had been sponsored by a war-time committee for glass research of the Institute of Chemistry. He followed Sir Herbert Jackson in 1933 as Director of Research of the Association and after holding this post for four years he became the first director of the research laboratories of Pilkington Brothers, Ltd., in St. Helens. During his tenure of this post from 1937 to 1945 he became very active in circles concerned with

glass technology and served as President of the Society of Glass Technology from 1944 to 1946. In 1946 he was appointed to the Chair of Glass Technology. During his time at Sheffield his chief research interest was in coloured glasses and particularly the colours due to iron, but he was also much occupied with problems proposed by the industry for at that time the department was not only a teaching department but was also charged, under a committee known as the Glass Delegacy, to carry out investigations for industry. Moore soon found that this dichotomy of interests prevented the best realization of the two functions, although this unique arrangement did function well during the period in which W. E. S. Turner held the Chair and while the number of university students was small. Moore played an important part in the discussions which led finally to the separation of the department into a University Department and the new British Glass Industry Research Association.

Shortly after Moore retired from the Chair, the Society of Glass Technology found itself without an Editor and he allowed himself to be persuaded to step into the breach. Once having been persuaded he threw himself into the task with characteristic energy and attention to detail for a period of eighteen months. Towards the end of this period, however, he seemed to realize that he was no longer a young man and after a short period in hospital he and Mrs. Moore decided to move South and, as he himself put it, "to rusticate completely". In September 1958 they moved to Arundel where his younger son had been living for a year or so. The move was a success and it is pleasant to think that he and Mrs. Moore had two years of quiet retirement together.

His many friends in the glass industry miss the familiar twinkle in his eye. One of his characteristics was a very highly developed sense of fun, and he could adopt various dialects and accents at will to embellish his stories, but at the same time he was a man of high ideals and with an intense devotion to duty. He had a kindly and generous nature, the full extent of which was only revealed to those fortunate enough to be in close contact with him.

The University and the glass industry will always be conscious of the great debt it owes to Harry Moore for his energetic leadership and wise guidance of the Department of Glass Technology at a critical period of development and decision.

R. W. DOUGLAS.

Abram Feodorovich Ioffe

Professor A. F. Ioffe died in September 1960, not very long after attending the Prague Conference on Semiconductors. On this occasion he had appeared to be in good health and had given one of the invited papers.

Ioffe was born in 1880, and studied in St. Petersburg and later under Röntgen in Munich. He returned to St. Petersburg in 1906 and carried out research work in solid state physics, on both the electrical and the mechanical properties of various types of crystal. He became a Doctor of Science in 1915, and an Academician in 1920. He was elected an Honorary Fellow of the Physical Society in 1944.

He played a leading part in the large-scale growth of physics in the U.S.S.R. between 1920 and 1940, and was already working on semiconductors during that period. Many Russian scientists who later became prominent worked under his direction during those years.

After 1940, Ioffe concentrated mainly on semiconductors, and on the possibility of utilizing them for thermoelectric refrigeration and power generation. He became Director of the Institute for Semiconductors of the U.S.S.R. Academy of Sciences, which specialized on this subject, and has been in the forefront in its development in recent years. In addition to this, his main activity, Ioffe still found time to play a leading part in the continued growth of physics in the U.S.S.R., and was responsible for the foundation and establishment of a large number of Institutes of Physical Research throughout the country.

In his later years, Ioffe paid several visits to the West, in particular to the Rochester Semiconductor Conference in 1958 and to the Transistor Conference in this country in 1959. Western scientists were very fortunate in being able to make his acquaintance during these visits, and all who met him were charmed by his personality and impressed by his vitality. Feelings of affection were soon added to those of veneration resulting from his reputation.

Ioffe is particularly well known in the West for his two books, *The Physics of Semiconductors*, first published in the U.S.S.R. in 1957, and *Semiconductor Thermoelements and Thermoelectric Cooling*, based on books first published in 1949 and 1956. The latter in particular has served as a guide to the very large number of people throughout the world now engaged in research on thermoelectricity.

D. A. WRIGHT.

S. P. F. Humphreys-Owen

Dr. Stephen Patrick Francis Humphreys-Owen, lecturer in physics at Birkbeck College, University of London, died on 21st November 1960 at the age of 52.

He was educated at Eton and Trinity College, Cambridge, where he obtained a B.A. honours degree in Natural Sciences in 1929. After a prolonged stay on the Continent, in order to acquire a good knowledge of French and German, he studied textile technology at Manchester and joined a Merchant Bankers' firm who sent him to India.

In 1935 he decided to take up the study of science again and returned to England after a world tour. He entered Imperial College, London, for a special physics course, and after having obtained his B.Sc. started postgraduate research work on an interferometric study of the growth of crystals from solutions under Sir George Thomson.

The second world war interrupted this work. He was commissioned into the R.A.F. and served with great distinction as Radar Officer in Scotland, the Middle East and Italy.

On demobilization he returned to his scientific work at Imperial College and was awarded the degree of Ph.D. of the University of London in 1948. In his thesis he established, among other things, the existence of a layer of an intermediate adsorbed phase at the crystal surface.

In the same year he became my research assistant at Birkbeck College under a Department of Scientific and Industrial Research grant for the purpose of studying the phenomenon of the scattering of visible and ultra-violet light by single crystals, a subject on the various aspects of which he kept working during

the next ten years, partly in collaboration with myself and Mlle. L. Taurel, but mostly on his own. The results of these investigations were published in the *Proceedings of the Physical Society* between 1955 and 1959.

In 1950 he was appointed to the academic staff of Birkbeck College which was the beginning of a most successful but unfortunately far too short period of teaching physics to special and general students.

In 1958 he published a paper (jointly with A. Klug and the late Rosalind Franklin) on the scattering of light by a virus crystal which established the fact that the particles in this crystal formed a face-centred cubic lattice and that the light scattering was dominated by Bragg's law.

During the last years of his life he became interested in the determination of the refractive index and extinction coefficient of graphite by means of the measurement of the reflection of light from graphite crystals. His last paper, written during his last illness and recently published in the *Proceedings of the Physical Society*†, describes a new and ingenious method of determining optical constants of materials by reflectivity measurements.

Humphreys-Owen was not only a brilliant research worker in his own field but he also had a thorough knowledge of physics as a whole and was an outstanding and devoted teacher, a combination which is not frequently found in our Universities nowadays. He was also deeply interested in problems of the philosophy of science. He was loved and admired by his colleagues and students who will miss him very much. I myself have lost a close collaborator and a dear friend.

R. FÜRTH.

George William Osborn Howe

Dr. G. W. O. Howe died at Glasgow in November 1960 at the age of 84. He was for over 40 years an outstanding university teacher, with an unusually clear grasp and power of exposition of the principles of electromagnetism, and particularly of their application to the problems of radio communication.

George William Osborn Howe was born at Charlton, Kent, on 4th December 1875. He became an apprentice with Messrs. Siemens Brothers, Woolwich, and remained with the firm for seven years while receiving technical education at Woolwich Polytechnic. Later he went to Armstrong College, Durham University, from which he graduated with honours in electrical engineering in 1900. After spending two years with Messrs. Siemens and Halske at Charlottenberg, Germany, he returned to England as a lecturer at Hull Technical College. In 1909 he became Assistant Professor at the City & Guilds Engineering College, which is part of the Imperial College, London. He held this position until 1920, when he was appointed head of the electrical standards and measurements department of the National Physical Laboratory. In 1921 he was elected as the first James Watt Professor of Electrical Engineering at the University of Glasgow, where he remained until he retired in 1946. In the following year he was made an honorary LL.D. of Glasgow University.

† *Proc. Phys. Soc.*, **77**, 949.

At the Imperial College, Professor Howe carried out research on the properties of condensers and on the high-frequency resistance of coils. He also made a notable contribution to the theory of the radiation of electromagnetic waves from wireless (as it was then termed) transmitting aerials. He contributed several papers on these subjects before the Royal Society of Arts, British Association, Physical Society and Institution of Electrical Engineers, of which latter body he was one-time Chairman of the Wireless Section. In 1956 he was awarded the Faraday Medal of the Institution of Electrical Engineers for his pioneering work in the study and analysis of high frequency oscillations, on the theory of radio propagation and for his outstanding contributions to the education of electrical and radio engineers.

In addition to his academic work, Dr. Howe was a critical technical writer of considerable distinction. From 1926 to 1954 he was a consultant, technical editor of the *Wireless Engineer*, published in London. Over this period he wrote a monthly editorial on some topic of electrical, and usually radio, interest. The range of subjects discussed was very great, from specialist studies of radio to discussions on the basic concepts of electrical science. Although on occasions they were touched with humour, these articles were in many cases highly critical of the work of other authors, who sometimes lacked the clarity of mind and grasp of fundamental principles of which Dr. Howe showed himself to be a great master.

All those who trained under him or worked with him—and the writer was privileged to do both—held Dr. Howe in high affectionate regard as a great teacher and adviser. He was one of the small band of pioneers in the field of radio, and the professional engineer of today is greatly indebted to the contributions to our knowledge which Dr. Howe made over a period of nearly half a century.

R. L. SMITH-ROSE.

Sir Arthur Fleming

Arthur Percy Morris Fleming, born in 1881, the younger son of a farming family in the Isle of Wight, was a remarkable example of a man who advanced science and engineering by his breadth of vision and tenacity in organizing what he saw to be needed more than by his individual contribution to knowledge or techniques.

In 1900 he had completed his formal engineering education at Finsbury Technical College, briefly occupied two posts in electrical engineering, and agreed to join the ambitious new factory which the Westinghouse Company had just set up in Britain. After a period of training in U.S.A. he started work in 1902 at the factory in Trafford Park, Manchester, on problems of insulation of electrical equipment.

In 1908 he became responsible for the training of apprentices, his first formal responsibility for the education and training of future engineers, which was to become the most important and influential activity of his life. He was responsible for the adoption of the principle that professional engineers in training should be paid a living wage instead of themselves paying a premium, and began to establish an apprentice system and organization which later became the pattern throughout the industry. Perhaps of equal importance in his mind

then, however, was the promotion of research in industry; and in 1913, as the first head of a new transformer department, he was already pressing his firm to set up a research department. The first World War delayed this project for four years, and meanwhile he and some of his colleagues contributed to methods of submarine detection, work for which he was awarded the C.B.E. in 1920. In this same year buildings for the new research department of Metropolitan-Vickers (as it had now become) began to appear. It was typical of the energy with which he pursued new projects that within two years of the completion of the first of these research buildings a wireless transmitter had been constructed, and, using the department's conference room as a studio, the British Broadcasting Company's Manchester station, 2ZY, began to broadcast programmes from Trafford Park the day after 2LO began from Savoy Hill; it continued there until it was transferred to the centre of Manchester the following year. By 1929 the department had what was then one of the largest high voltage laboratories in the world.

Fleming steadily gathered a team of scientists and engineers, many of whom are now prominent men, and while he worked to ensure that the problems of engineering materials and design received all possible attention, he never restricted the scope of his staff to matters of immediate utility. He insisted that a substantial portion of the resources of this new department would be provided without question as to the problems it was used for, an attitude easy to adopt now but extremely courageous 40 years ago. He inspired a high sense of loyalty among those who worked with him, and reciprocated it; he was always ready to help anyone with whose career he had ever been concerned. He himself remained with the same organization under different ownerships throughout his active working life, serving as Director of Research and Education of Metropolitan-Vickers from 1930 until 1951. Thereafter he remained for some years Director of Research and Education of Associated Electrical Industries, the company which had taken financial control in 1929.

He played an important part in establishing the Department of Scientific and Industrial Research and the Electrical Research Association. On a smaller scale he often contrived to give individual help to men of science and never under-estimated the importance of both fundamental and applied research.

He became a Fellow of the Physical Society in 1925 and a Fellow of the Institute of Physics in 1933; he was a very prominent and active member of the Institution of Electrical Engineers, becoming its President for 1938, Faraday Medallist in 1941 and an Honorary Member in 1952. He was at different times President of the Education and Engineering Sections of the British Association, and he served on a considerable number of government, university and industrial bodies concerned with education and research. After his retirement from executive work he lived in the Isle of Wight until his death on 14th September 1960.

He will be remembered for his influence on industrial research in this country, but still more for his unending work to improve the education, training and reputation of engineers in this country and abroad. For these efforts he was knighted in 1945, and throughout the world many thousands of engineers, and not a few scientists, eminent and humble, will gratefully remember the benefits they derived from systems which he fostered and the spirit which he inspired among his friends and colleagues.

R. W. SILLARS.

Maurice, Duc de Broglie

Maurice, Duc de Broglie, who died on 14th July 1960, was one of that small band of scientists who pursue their researches privately with their own means. In some respects he was unique. Not only did he establish a laboratory for his own research in his Paris home, he also collected around him a group of younger men who worked under his guidance. His brother, Louis de Broglie, joined him shortly before World War I, and much of the initial inspiration of Louis de Broglie's work came from Maurice de Broglie's influence. Louis Leprince-Ringuet, Jean Trillat, Jean Thibaud, Alexandre Dauvillier and Bruno Rossi were amongst those in his research school. It was his achievement to establish a private research centre of world-wide reputation in his hôtel in the Rue Chateaubriand.

Maurice de Broglie was born on 27th April 1875 in Paris. He entered the Ecole Navale in 1893 and served for ten years in the Navy. When he left it in 1904 he established a small laboratory in his house. He was at that time interested in the electrical charges on fine particles suspended in an ionized gas, and studied these movements in an electric field, the method afterwards used by Millikan to measure the electronic charge. In 1913 he was one of the first to study x-ray spectra and x-ray absorption. He developed a spectrometer in which he registered on a photographic plate the reflected rays from the lattice planes of a slowly rotating crystal. I remember that time well because Maurice de Broglie and my father corresponded so regularly and compared their results.

During World War I, he had a naval commission and made a considerable contribution to the underwater detection of submarines and the development of radio.

After the War, de Broglie continued his researches on x-ray absorption discontinuities, and published with his brother Louis *La Physique des Rayons X*, which was a well-known standard work at that time. The laboratory was greatly enlarged and the number of researchers increased. De Broglie's interests turned towards nuclear physics, and some of the devices for observations of high energy particles which have now become classical were first developed by de Broglie's team. He was elected to the Académie Française in 1934. For ten years he was President of the 'Conseil Scientifique de l'Energie Atomique'.

De Broglie won the warm affection of his students and his many friends all over the world, who will retain pleasant memories of their visits to his home and laboratory where he was the kindest and most genial of hosts. W. L. BRAGG.

Thomas Yeomans Baker

Instructor Captain Thomas Yeomans Baker, R.N., B.A., died at Hayling Island on 4th June 1960 at the age of 83. He was a Fellow of the old Optical Society and of the Physical Society from 1909-60—over 50 years—serving on the Council from 1936-41 and Chairman of the Optical Group from 1945-47. A Founder Fellow of the Institute of Physics, from 1920-60, he served on the

Board in the periods 1920–22, 1923–25, and 1926–27. He was also a member of the Technical Optics Advisory Committee for the Imperial College, South Kensington.

He was born at Leicester on 4th January 1877, the son of William Mason Baker and Elizabeth Yeomans Baker—a family which has widespread connections in, and with, Leicester. He was educated at Wyggeston School, Leicester, where he won a senior mathematical scholarship and proceeded to Christ's College, Cambridge (1895–98). In some autobiographical notes (incomplete) which he left among his papers he says “ Maths. Tripos 1898, 16th Wrangler (ought to have been in first 6 but was ill during the examination) ”. In his fourth year at Cambridge he was taking Mechanical Sciences but left during the May Term to join the Royal Navy as Naval Instructor. There he served, from 1899–1905, successively in H.M.S. *Empress of India*, *Royal Oak*, *Victorious*, *Revenge*, *Theseus*, *Duke of Wellington*, *Mars*, and *Formidable*. After this sea service he was transferred to the Royal Naval College, Greenwich, as Lecturer in mathematics. It was there he took up the study of optics and optical instruments. About this time he joined the Optical Society and worked in his spare time with Chalmers at the Northampton Institute, on ‘ The longitudinal spherical aberration of a non-paraxial ray ’. Another of his activities was in connection with air navigation: I quote: “ Creagh-Osborne, who had been Navigator in H.M.S. *Mars*, told me that a friend of his, Commander Porter, was going to have a try for a £10 000 prize offered by the *Daily Mail* for the first man to fly the Atlantic. Porter's difficulty was that he could take sights but wasn't able to work them out while flying. I suggested an idea which later developed into the Navigational Machine, and made the first machine myself. I think that machine is now in the Science Museum, South Kensington.” This instrument was used by Alcock and Brown on their first transatlantic flight and subsequently developed by the R.A.F. in the second world war.

During the first world war he served (1914–17) in the Naval Intelligence Department at the Admiralty, where he became French Interpreter and Liaison with the French Ministry of Marine. For these services he was made Chevalier of the Legion of Honour (London Gazette 25th January 1918), having previously received a bronze statuette, in appreciation, presented to him in 1916 by the French Naval Attaché in London on behalf of the Minister of Marine.

In the late summer of 1917 he was transferred to the Admiralty Compass Observatory at Ditton Park, Slough, where he worked until 1920. In that year he joined the staff of the Admiralty Research Laboratory, at Teddington, where he was head of the new Optics division until his retirement in 1935. Since his sea-going days he was always interested in optical instruments and his work on the Air Sextant, the prismatic astrolobe, crossed-wedges station-keeper, and a photo-theodolite for use at sea are examples of his mathematical and experimental ingenuity.

In his autobiographical notes he says “ About this time, I became interested in Prismatic Astrolobes. Two Frenchmen, Claude and Driencourt, had invented one which could be used to observe stars when they had reached an altitude of 60° above the horizon. I managed to make an improvement on this with an astrolobe of 45° altitude and which could be used to get nine observations on each star. This was tried out at the Observatory, Greenwich, and the Astronomer Royal was very complimentary about it. The great point about it

was that one could get sufficient observations in one night to fix the latitude to 1 second of arc, i.e. about 100 feet on the earth's surface. The Admiralty Survey Service tried it out when surveying the West Coast of Scotland, and the Hydrographer, Admiral Douglas, came to see how they were getting on . . . ”

The crossed-wedges station-keeper which he designed was used by the Officer of Watch for verifying that his ship was keeping station on her next ahead. A pair of optical wedges, with a concentric hole through them, could be rotated relative to each other to bring some prominent feature (e.g. a yard) as seen through the glass wedges, into coincidence with some other reference (e.g. on the quarter deck) as seen through the central hole, making the initial setting when the two ships were ‘in station’. Any error in station-keeping would then be shown up by lack of coincidence.

The photo-theodolite was used in connection with the testing of gyro compasses.

He published many papers on optical theory and instrument design in the *Transactions of the Optical Society*, *Proceedings of the Physical Society*, *Transactions of the Royal Aeronautical Society*, *Philosophical Magazine*, *Proceedings of the Optical Convention*, *Geographical Journal*, etc. Professor L. C. Martin speaks of his mathematical attainments which (apart from the Cambridge School) were not very common in the ‘optical world’—he had the reputation, with one other member of the Optical Society, that they were the only two people who could understand each other's papers ! In the discussion of papers at scientific meetings he spoke with great clarity, accompanied by a sense of humour and a readiness to learn. He gave noteworthy help to the Imperial College, South Kensington, when the Technical Optics Section was seeking (soon after the end of the last war) to stimulate interest in the use of aspheric surfaces in Optical Design, and he co-operated with Professor Martin in giving a course of public lectures on this subject.

In addition to the design of the optical instruments mentioned above, Captain Baker, whilst at the Admiralty Research Laboratory, was closely associated with the adoption by the Admiralty of optical instruments, particularly binoculars and gunsights, of greater light-gathering power than had hitherto been in service.

This notice of T. Y. Baker would be incomplete without reference to his outstanding personal qualities. He was universally liked by all his colleagues whom he was invariably pleased to help when the occasion arose. After his retirement when he was living at Hayling Island, he still took a lively interest in the doings of the Navy and in particular in the work that was going on in Admiralty Research Establishments. It was always a great pleasure to have a chat with him about the happenings of ‘the past’ and the prospects of ‘things to come’. His hobbies at his Hayling Island home after retirement were carpentry and knitting, at both of which he was very proficient. His kindness, good humour and pleasant smile were always an encouragement to those who were privileged to know him.

In 1906 he married E. Winifred Windley who survives him. They had two sons, John the younger son who died some years ago, and Philip who now holds a position of responsibility in the Royal Naval Scientific Service and who was awarded the D.S.C. in 1942 “for outstanding courage, skill and enterprise”.

A. B. WOOD.

Charles Vickery Drysdale

C. V. Drysdale, C.B., O.B.E., D.Sc., M.I.E.E., F.R.S.E., F.Inst.P., who died in retirement on 7th February 1961 was born in 1874 at Barnstaple, Devon, of cultured parents—both his father and mother were medical doctors. After private schooling he studied for two years in the electrical department of Finsbury Technical College, followed by three years in the physical and engineering department of the Central Institution at South Kensington, the forerunner of the City and Guilds College. On completing the course he received Diplomas in Physics and Engineering and the Siemens Medal.



On leaving college Drysdale spent fifteen months as experimental assistant in the works of Nalder Brothers, and then obtained a teaching appointment at the recently established Northampton Institute (London), a post which he held in association with Mullineux Walmsley until 1910.

Having developed a lively interest in the design, making and use of scientific instruments, he then joined H. Tinsley and for six years devoted his time with enthusiasm to the practical side of the industry. Some of the instruments, such

as the a.c. potentiometer and the polyphase wattmeter, gave him scope for work of a fundamental nature as a result of which they have today become high precision instruments. His contribution at this stage was largely the elimination of errors in changing over from direct to alternating current measurement. He later became a partner in the firm.

The evidence of Drysdale's energetic interest at this period is seen in the large number of articles and papers which appeared under his name. During the fifteen years or so from 1900 the pages of the *Electrician* show him leading contemporary thought in this field, and in 1902 he described in a paper before the Institution of Electrical Engineers a permeameter he had devised for testing the magnetic qualities of materials in bulk. This drew warm congratulation from Dr. Walmsley for "his own chief assistant" and from Professor Perry who referred to "the very beautiful instrument" he had produced.

Although well-equipped mathematically himself, Drysdale recognized the difficulties encountered by students and in the preface to a book on fundamental a.c. theory which he published in 1910 he supported Heaviside's dictum that "the best results of mathematics is to be able to do without it" and on the French saying that "the last word on a theory is when it can be explained shortly to a passer-by in the street".

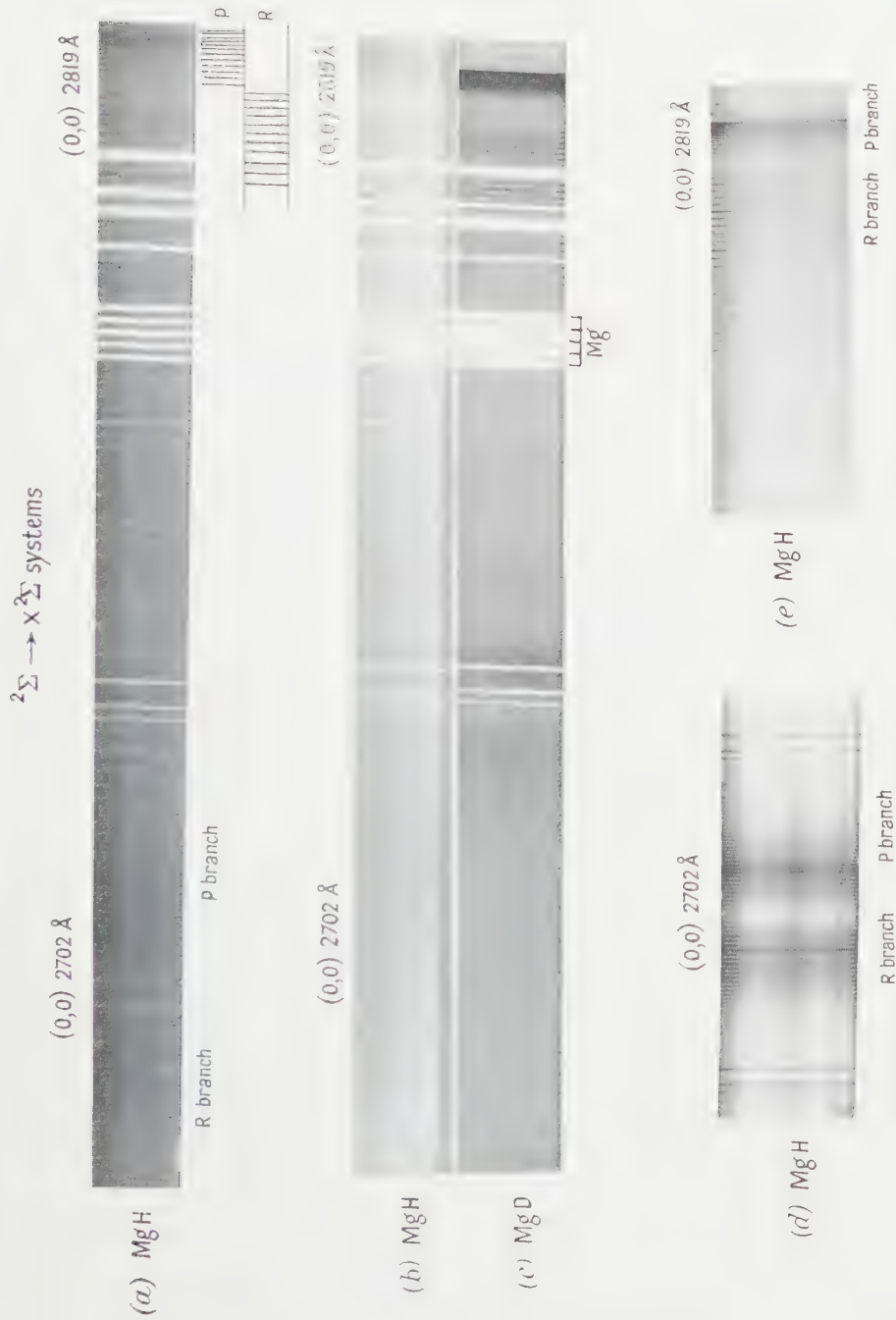
In January 1918, Dr. Drysdale joined the staff of the Admiralty Research Laboratory at Parkston Quay, where his extensive knowledge of alternating current theory and instrument design led him to produce the 'leader' cable system for guiding ships blindfold in crowded estuaries, the story of which is told in the *Philosophical Transactions* for 1924.

From Harwich via Shandon (1919-1921) and Teddington (Superintendent, Admiralty Research Laboratory 1921-1929) Drysdale progressed to the leading position of Director of Scientific Research, Admiralty, which he took over from Sir Frank E. Smith, with whom he had been closely associated for many years. He held this position from 1929 until his retirement in 1934 at the age of 60.

Owing, no doubt, to the confidential nature of his work in the services, Drysdale's output of published papers dried up from about 1930. In 1920 he delivered the Kelvin Lecture at the Institution of Electrical Engineers on "Modern Marine Problems in War and Peace" which contained an account of progress in anti-submarine warfare, and four years later his valuable two-volume work on *Electrical Measuring Instruments*, written in collaboration with A. C. Jolley, appeared. In 1928 and 1931 he wrote two important progress reviews on instrument practice for the Institution of Electrical Engineers journal.

Throughout his working life Drysdale was an enthusiastic supporter of The Physical Society and of The Institution of Electrical Engineers. He was a Founder Fellow of The Institute of Physics and a Fellow of The Royal Statistical Society. He had many interests outside his specialist field. As a young man he took a great interest in student life and technical education, as appears from two revealing addresses which he gave before the Students Section of the Institution of Electrical Engineers in 1914 and 1916. The humanitarian features of his character later developed into a lively enthusiasm for the teachings of Malthus. He was Secretary and President of the Malthusian League for many years and in 1913 published *The Small Family System*. By his will he left a legacy of £2500 to Cambridge University for the erection of a memorial to Malthus in the University precincts.

P. DUNSHEATH.



(a) The absorption spectrum of MgH as obtained by using a 'conical capillary' technique (large quartz); (b) and (c) The absorption spectra of MgH and MgD respectively, obtained by using a high pressure xenon arc (large quartz); (d) and (e) The absorption spectrum of MgH, obtained by using a flash tube as the background source (10' grating, 1st order). All spectrograms are mounted 'red to right'.

PROCEEDINGS OF THE PHYSICAL SOCIETY

1961—VOL. 77

SUBJECT INDEX

	PAGE
Aberrations, symmetrical and asymmetrical in Twyman interferometer, separation	328
Absorption, optical, of GaAs in reststrahlen band (L)	215
Absorption, optical, <i>see also</i> Z-centres	
Absorption, recoilless, of γ -rays from ^{119}Sn	1062
Absorption spectrum of magnesium vapour	797
Absorption spectrum, ultra-violet, of TeS	147
Absorption, <i>see also</i> X-ray absorption	
Activation curve $^{12}\text{C}(\gamma, n)^{11}\text{C}$, fine structure	166
Air bubbles in ice	757
Alkaline earths, u.v. extensions of arc spectra	797
Alloys, Cu-Mn, heat capacities	807
Alloys, GaAs-InAs, electrical and optical properties	700
Alloys, nickel-copper, ferromagnetic resonance in	913
Alloys, U-Mo, stable and metastable, electrical resistivities and magnetic susceptibilities	691
Alpha particle groups, angular distribution from reaction $^{24}\text{Mg}(^3\text{He}, \alpha)^{23}\text{Mg}$	1024
Angular correlations in $^{18}\text{O}(\alpha, n\gamma)^{21}\text{Ne}$ and $^{22}\text{Ne}(\alpha, n\gamma)^{25}\text{Mg}$ reactions	1197
Angular distributions of α -particle groups from reaction $^{24}\text{Mg}(^3\text{He}, \alpha)^{23}\text{Mg}$	1024
Anisotropy of Young's modulus in drawn polyethylene	1028
Anode spots and moving striations in neon	476
Antiferromagnetic behaviour of GdB_6 (L)	213
Antiferromagnetic exchange interactions, estimation	116
Antiferromagnetism of mixed crystals of zinc and manganese fluoride	1038
Argon spectrum, collision broadening in	1193
Atmospheric scale height, application to times and lengths, with geomagnetic and ionospheric illustrations	424
Atomic spectra, <i>see</i> Spectra	
Atomic transitions, optically allowed, produced by electron impact, strong coupling in	174
Atoms, multipole polarizabilities, approximate calculation	447
Atoms, one-dimensional chains, with random spacings	705
Band spectra, MgH and MgD bands at 2819 Å and 2702 Å	1133
Band spectra, relative intensities in triplet system of CO bands (L)	817
Beryllium 9 target, pick-up reactions on	65
Beta spectrum and orbital electron capture ratio of ^{204}Tl	1205
Born approximation for calculation of electron-hydrogen collision cross sections	199
Born partial wave integrals, calculations for transitions in H produced by electron impact	192
Born partial wave integrals evaluation	184
Bosons, new heavy (L)	1223
Central forces and two-channel five-nucleon reactions	1014
Cerium salts, spin-lattice relaxation at liquid He temperatures	261, corr. 1223
Cerium 141, internal conversion	346
Charge independence of nuclear forces and isobaric triplets in nuclear 2p-shell	599
Charged particles, <i>see</i> Particles, charged	
Circuit, tuned, Hamiltonian formalism of damping	515

	PAGE
Collective treatment of Fermi gas: II	1182
Collision broadening in argon spectrum	1193
Collisions, inelastic, of electrons with helium, secondary emission— 2^3S excitation	866
Collisions, inelastic ion-atom, energy transferred	269
Collisions, <i>see also</i> Scattering	
Conductivity, thermal, <i>see</i> Thermal conductivity	
Conversion, internal, of ^{141}Ce	346
Cosmology, observational tests (Guthrie Lecture)	1
Counter coincidences, multiple, from γ -radiation	377
Coupling, strong, in optically allowed atomic transitions produced by electron impact	174
Cracks, in elastomer, stresses at	483
Cross sections, activation, with 14 mev neutrons	508
Cross sections, electron-hydrogen collision, Born approximation for	199
Cross sections, radiative capture, of ^{22}Al and ^{31}P for ^{16}O ions, upper limits	526
Cross sections, scattering, of γ -radiation	593
Cross sections, <i>see also</i> Scattering	
Crystal field splitting, cubic, of Gd^{3+} ion (L)	550
Crystal, zinc, features of elastic wave surface	335
Crystals, alkali halide, angular dependence of nuclear spin-lattice relaxation time	36
Crystals, ionic, x-ray absorption process in	1046
Crystals, luminescent decay for varying ionization density	751
Crystals, mixed, of zinc and manganese fluoride, antiferromagnetism of	1038
Crystals, non-equilibrium elastic constants	885
Crystals, rare gas, reduced equation of state at absolute zero	889
Crystals, single, of NaCl with Ca, Z-centres in	153
Damping in tuned circuit, Hamiltonian formalism	515
Debye characteristic temperatures, calculation (L)	218
Debye characteristic temperatures, determination, and inversion temperature function of first-order scattering	712
Deuteron pairs, drift velocities in SCEPTRE III	987
Diamagnetism of many-fermion systems	136
Diamond, luminescence excitation spectrum near fundamental absorption edge	869
Dielectric constant, measurements, and determination of effective ionic charge of gallium arsenide	1147
Diffraction by finite irregular objects	318
Diffraction by irregular screen of limited extent	305
Diffraction of light, <i>see</i> Light	
Discharge, pinched, linear, effect of electrodes	643
Discharge source, glow, negative oxygen ions from	845
Dislocation relaxation in zinc at low temperatures (L)	1216
Elastic constants, non-equilibrium	885
Elastic wave surface in zinc crystal, features	335
Elasticity, <i>see also</i> Young's modulus	
Elastomers, stresses at a crack	483
Electric field, and light modulation (L)	1100
Electrical and optical properties of GaAs-InAs alloys	700
Electrical resistivities of stable and metastable U-Mo alloys	691
Electron capture ratio, orbital, and β spectrum of ^{204}Tl	1205
Electron collisions with Na atoms	617
Electron impact and atomic transitions, strong coupling in	174
Electron impact and transitions in H, partial wave integrals for	192
Electron interaction, Wiedemann-Franz law	1005
Electron spin resonance of free radical in solution, thermal motion effect	729
Electrons, <i>see also</i> Scattering	
Energy level of ^{24}Mg at 6.44 mev excitation (L)	1210

	PAGE
Energy level, new, in ^{24}Mg , spin (L)	1211
Energy levels, $5^2\text{P}_{1/2}$ of potassium, hyperfine structure	1141
Energy loss of carbon and oxygen ions in solids	97
Energy transfer in organic systems II: solute-solute transfer in liquid solutions	1083
Energy transfer in organic systems III: spectral effects in liquid solutions (L)	1095
Equation of state, reduced, of inert gas solids at absolute zero	889
Exchange interactions, <i>see</i> Interactions	
Exchange in ionization, consideration (L)	1220
Faraday effect for direct magneto-optical transitions in Ge	1042
Fermi gas, collective treatment: II	1182
Ferrites, cobalt, thermomagnetic behaviour	567
Ferrites, 'square loop', irreversible change of magnetization produced by pulsed magnetic fields	576
Ferrites, 'square loop', shape of hysteresis loop	225
Ferromagnetic resonance in Ni-Cu alloys	913
Fluorescence and other yields of L_{II} shell in Pu	657
Fluorine 18, O^+ , $T=1$ level	93
Four-nucleon reactions with central forces	49
Fracture energy of brittle plastics, variation with temperature	876
Frequency response, optical, scanning instrument for measurement	901
Gadolinium hexaboride, antiferromagnetic behaviour (L)	213
Gallium arsenide, effective ionic charge from direct measurements of dielectric constant	1147
Gallium arsenide, optical absorption in reststrahlen band (L)	215
Gamma radiation, multiple Geiger counter coincidences from	377
Gamma radiation, scattering cross sections	593
Gamma-ray source and detector on same orbit, absence of Doppler shift	350
Gamma-ray spectra in large organic scintillators	1125
Gamma rays from excitation of ^{12}C by 150 mev protons	362
Gamma rays, recoilless absorption from ^{119}Sn	1062
Gas, classical hard sphere, lattice model: II.	451
Gas mixtures, binary, viscosity and thermal conductivity: Kr-A, Kr-Ne, Kr-He	1157
Gases, inert, <i>see</i> Inert gases	
Geomagnetic applications of generalized conception of atmospheric scale height.	424
Germanium, direct magneto-optical transitions, Faraday effect	1042
Germanium, p-n junction, variation of photovoltaic response with magnetic field	459
Graphite, π band, effective number of electrons in (L)	1214
Guthrie Lecture: Observational tests in cosmology	1
Half-life of RaC' , determination (L)	1219
Halides, including thallium, polymorphism at low temperatures	471
Hartree energies of helium sequence	165
Hartree-Fock approximation, stationary properties	748
Hartree perturbation method for helium	673
Heat capacities of Cu-Mn alloys	807
Helium, 2^3S excitation	866
Helium, Hartree perturbation method.	673
Helium, liquid, temperatures, <i>see</i> Low temperatures	
Helium, positronium formation in	811
Helium sequence eigenvalues, perturbation-variation calculation	467
Helium sequence, Hartree energies	165
Helium, theories	531
Helium 3, elastic scattering by C, Mg, Al and Cu	230
Helium 3, 5.5 mev, elastic scattering by C, Mg, Al and Cu, optical model analysis	997
Hole theory of liquids	1001
Hydrogen, atomic, excitation of $1\text{s}-2\text{p}$ transition by proton and α -particle impact	59
Hyperfine structure of level $5^2\text{P}_{1/2}$ of potassium 39.	1141
Hysteresis loops, <i>see</i> Ferrites	

	PAGE
Ice, air bubbles in	757
Image recording, photographic, properties	17
Inert gases, in solid phase, reduced equation of state at absolute zero	889
Interaction, quadrupole-quadrupole, in rare earths	113
Interaction, S-wave pion-pion	278
Interactions, antiferromagnetic exchange, estimation	116
Interactions, exchange, in polymorphic forms of MnS	124
Interferometer, Twyman, separation of symmetrical and asymmetrical wave-front aberrations	328
Ionization coefficients and attachment coefficients in oxygen, measurements	385
Ionization, exchange in (L)	1220
Ionization, moving striations and anode spots in neon	476
Ionosphere, effect on signals from satellites	337
Ionospheric applications of generalized conception of atmospheric scale height	424
Ions, positive, ohmic heating in impure plasma	801
 Jump diffusion model for neutron scattering from liquid	 353
 K _α satellites, identification in LS region	 980
 Lattice model of classical hard sphere gas: II	 451
Lattice model of liquid, improvements	630
'Level crossings' in Hg	669
Levels, 0 ⁺ , T=1, in ¹⁸ F	93
Lifetime of 364 kev level in ¹³¹ Xe	610
Light, diffraction by very high frequency ultrasonic waves	958
Light, modulation by means of electric field (L)	1100
Liquid, lattice model, improvements	630
Liquid solutions, solute-solute intermolecular energy transfer	1083
Liquid solutions, spectral effects in energy transfer (L)	1095
Liquids, hole theory	1001
Liquids, molecular theory, correction to Smoluchowski equation	1170
Low temperatures, dislocation relaxation in zinc at (L)	1216
Low temperatures, polymorphism of thallium and other halides	471
Low temperatures, spin-lattice relaxation in Ce salts	261, corr. 1223
Luminescence, decay in crystals for varying ionization density	751
Luminescence excitation spectrum of diamond near fundamental absorption edge	869
 Magnesium 24, energy level at 6.44 mev excitation (L)	 1210
Magnesium 24, spin of new level (L)	1211
Magnetic susceptibilities of stable and metastable U-Mo alloys	691
Magnetization, irreversible change in 'square loop' ferrites by pulsed magnetic fields	576
Magneto-optical transitions, direct, in Ge, Faraday effect	1042
Manganous sulphide, exchange interactions in polymorphic forms	124
Many-fermion systems, diamagnetism	136
Markoff chains and stereospecific polymers	931
Microtron, 29 mev, design and construction	769
Molecular motion in liquid toluene by proton magnetic resonance relaxation	737
Molecular theory of liquids, correction to Smoluchowski equation	1170
Mössbauer absorption for γ-ray source and detector on same orbit	350
Mössbauer effect in tin from 120°K to melting point	129
Mu-mesons, high energy, range-energy relation	587
Mu-mesons, relativistic, energy loss in organic material	1149
 Neutron fission, thermal, of ²³⁵ U, kinetic energy effects (L)	 1097
Neutron scattering, <i>see</i> Scattering	
Nuclear forces, charge independence, and isobaric triplets in nuclear 2p-shell	599
Nuclear magnetic resonance in Al and Cu, diffusion narrowing	922

Nuclear magnetic resonance, measurement of indirect coupling between nuclei by transient method	273
Nuclear and relativistic effects in atomic spectra	786
Nuclei, finite, perturbation theory	81
Obituaries	1224
Optical constants, comparison of reflection methods for measurement without polarimetric analysis	949
Optical constants, measurement method based on Brewster angle	949
Optical and electrical properties of GaAs-InAs alloys	700
Optical frequency response, scanning instrument for measurement	901
Optical model analysis of elastic scattering of 5.5 mev ^3He by C, Mg, Al and Cu	997
Oscillations, induced in semiconductors, oscillator, theoretical considerations and explanation	1121
Oscillator, harmonic, damping in quantum mechanical discussion	515
Oscillator, longitudinal magnetic field induced oscillations in semiconductors	1121
Oxygen ions, negative, from glow discharge source	845
Panofsky ratio for negative pions stopped in hydrogen, redetermination	77
Paramagnetic resonance, 'forbidden' transitions, explanation	103
Paramagnetic resonance spectrometry at zero magnetic field	561
Paramagnetic salts, spin-lattice relaxation, theory	821
Particles, Bose, integrable many-body wave functions for	433
Particles, charged, emission from bombardment of silver with nitrogen ions	833
Particles, charged, passing through electron plasma in magnetic field, radiation from	1109
Particles, relativistic, heavy singly charged, energy loss in organic material	1149
Partition function, quantum mechanical, for imperfect fluid	531
Perturbation method, Hartree, for helium	673
Perturbation theory in finite nuclei	81
Perturbation-variation calculation of eigenvalues	467
Photographic image recording, properties	17
Photovoltaic effect in magnetic field	459
Pinched discharge, <i>see</i> Discharge	
Pion-pion interaction, S-wave	278
Pion-pion resonance, P-wave	917
Pions, negative, stopped in hydrogen, redetermination of Panofsky ratio	77
Plasma containment in magnetic bottles	965
Plasma diffusion in systems with particle losses	965
Plasma, electron, in external magnetic field, radiation by charged particles passing through	1109
Plasma, impure, ohmic heating of positive ions in	801
Plasma oscillations in static magnetic field	971
Plasma research, <i>see also</i> ZETA	
Plastics, brittle, variation of fracture energy with temperature	876
Polarizabilities, multipole, of atoms, approximate calculation	447
Polarization of protons from low resonances in $^{12}\text{C}(\text{d}, \text{p})^{13}\text{C}$	499
Polarization of 9 mev protons elastically scattered from C and Al	830
Polyethylene, drawn, anisotropy of Young's modulus in	1028
Polymers, stereospecific, and Markoff chains	931
Polymers, <i>see also</i> Polyethylene	
Positronium formation in helium	811
Powders, fine, indication of vibration nodes by	1076
Pressure broadening, selective, of Si and F spectral lines	665
Proton magnetic resonance relaxation and molecular motion in liquid toluene	737
Proton spectra from $^{51}\text{V}(\text{d}, \text{p})^{52}\text{V}$ reaction, gross structure (L)	1098
Protons, <i>see also under</i> Scattering	
Quadrupole-quadrupole interaction in rare earths	113
Quantum mechanical discussion of harmonic oscillator, introduction of damping	515

Radiation by charged particles passing through electron plasma in external magnetic field	1109
Radiation, millimetre and submillimetre, detection by free carrier absorption in semi-conductors (L)	1102
Radiation, sub-millimetre electromagnetic, emission from hot plasma in ZETA	1069
Radium C', determination of half-life (L)	1220
Range-energy relation for high energy μ -mesons	587
Range-energy relations for carbon and oxygen passing through solids	97
Rare earths, quadrupole-quadrupole interaction	113
Rare earths, <i>see also</i> Cerium	
Reaction, four-nucleon, with central forces	49
Reaction, photoproduction $^{60}\text{Ni}(\gamma, \pi^-)^{60}\text{Cu}$	293
Reaction, $^{12}\text{C}(\gamma, n)^{11}\text{C}$, fine structure in activation curve	166
Reaction $^{12}\text{C}(\text{d}, \text{p})^{13}\text{C}$, polarization of protons in	499
Reaction $^{12}\text{C}(^3\text{He}, \text{n})^{14}\text{O}$, threshold (L)	1217
Reaction $^{12}\text{C}(\text{p}, \text{p}')\gamma$, γ -rays from	362
Reaction, $^{40}\text{Ca}(\text{d}, \text{n})^{41}\text{Sc}$	1050
Reaction, $^{24}\text{Mg}(^3\text{He}, \alpha)^{23}\text{Mg}$, and angular distributions of α -particle group	1024
Reaction $^{51}\text{V}(\gamma, \alpha)^{47}\text{Sc}$	417
Reaction $^{51}\text{V}(\text{d}, \text{p})^{52}\text{V}$ gross structure in proton spectra (L)	1098
Reactions, pick-up, on ^9Be target	65
Reactions, two-channel five-nucleon, with central forces	1014
Reactions (γ, α)	417
Reactions $^{12}\text{C}(^3\text{He}, \text{n})^{14}\text{O}$ and $^{16}\text{O}(^3\text{He}, \text{n})^{18}\text{Ne}$	399
Reactions $^{58}\text{Ni}(\text{d}, \text{p})^{59}\text{Ni}$ and $^{60}\text{Ni}(\text{d}, \text{p})^{61}\text{Ni}$	682
Reactions $^{18}\text{O}(\alpha, \text{n}\gamma)^{21}\text{Ne}$ and $^{22}\text{Ne}(\alpha, \text{n}\gamma)^{25}\text{Mg}$, angular correlations in	1197
Reactions, (t, d), in light nuclei at 5.5 mev	853
Relativistic and nuclear effects in atomic spectra	786
Relaxation, dislocation, in zinc at low temperatures (L)	1216
Relaxation, spin-lattice, in cerium salts at liquid He temperatures	261, corr. 1223
Relaxation, spin-lattice, in paramagnetic salts, theory	821
Relaxation time, nuclear spin-lattice, angular dependence for alkali halide crystals	36
Relaxation time, rotational-translational, in H_2 calculated from thermal conductivity	677
Relaxation times, spin-lattice, in sapphire and chromium-doped rutile at 34.6 Gc/s	257
Resonance collisions, validity of two conjectures (L)	551
Resonance fluorescence, ' level crossings ' in Hg	669
Resonance, P-wave, pion-pion	917
Resonance, <i>see also</i> Electron spin resonance, Ferromagnetic resonance, Nuclear magnetic resonance, Paramagnetic resonance, Proton magnetic resonance	
Rutile, chromium-doped, spin-lattice relaxation times at 34.6 Gc/s	257
Sapphire, spin-lattice relaxation times at 34.6 Gc/s	257
Satellites, application of ray tracing methods to radio signals	337
Scattering, elastic, of electrons and positrons by hydrogen atoms	724
Scattering, elastic, of ^3He by C, Mg, Al and Cu	230
Scattering, elastic, of 5.5 mev ^3He by C, Mg, Al and Cu, optical model analysis	997
Scattering, elastic, of 9 mev protons from C and Al, polarization	830
Scattering, elastic, of slow electrons by helium atoms	721
Scattering, first-order, inversion temperature function, and Debye characteristic temperatures	712
Scattering, inelastic, of 150 mev protons on ^{12}C , γ -rays from	362
Scattering, neutron, from liquid on jump diffusion model	353
Scattering, p-p, spin correlation measurements at 382 and 320 mev	234
Scattering, zero-energy electron-hydrogen, application of Schwinger variational method	827
Scattering, <i>see also</i> Collisions, Cross sections, Lifetime	
SCEPTRE III, (d, d) reaction product velocities according to two-group model	987
Scintillators, large organic, γ -ray spectra in	1125
Selenium, space charge limited current flow and deep trapping	1157

	PAGE
Self-consistent field theory, calculation of electrons in graphite π band (L)	1214
Semiconductors, detection of millimetre and sub-millimetre radiation by free carrier absorption (L)	1102
Semiconductors, longitudinal magnetic field induced oscillations, theoretical considerations	1121
Semiconductors, <i>see also</i> Gallium arsenide, Germanium, Selenium	
Shell model, isobaric triplets and charge independence	599
Smoluchowski equation in molecular theory of liquids, correction	1170
Sodium chloride, specific heats, revision of Kellermann's calculations	303
Space charge limited current flow and deep trapping in selenium	1157
Specific heats of NaCl, Kellermann's calculations, revision	303
Spectra, arc, of alkaline earths, u.v. extensions	797
Spectra, atomic, nuclear and relativistic effects	786
Spectra, K_{α} satellites, identification in LS region	980
Spectra, selective pressure broadening of Si and F spectral lines	665
Spectra, γ -ray, <i>see</i> Gamma-ray	
Spectra, <i>see also</i> Absorption, Band spectra, Luminescence	
Spectrometry, paramagnetic resonance, at zero magnetic field	561
Spectrum, argon, collision broadening in	1193
Spin correlation measurements in p-p scattering at 382 and 320 mev	234
Spin-lattice relaxation, <i>see</i> Relaxation	
Superconductivity, quasi-particle approximation	299
Superconductivity, theory, collective modes in	1175
Tellurium monosulphide, absorption spectrum in ultra-violet	147
Temperatures, Debye characteristic, calculation (L)	218
Temperatures, Debye characteristic, and inversion temperature function of first-order scattering	712
Thermal conductivity and rotational-translational relaxation time in H_2	677
Thermal conductivity and viscosity of binary gas mixtures: Kr-A, Kr-Ne, Kr-He	1157
Thermomagnetic behaviour of cobalt ferrite	567
Tin, Mössbauer effect in, from 120°K to melting point	129
Tin, nuclear Zeeman effect and quadrupole splitting in ^{119}Sn	1062
Transition, $1s-2p$, of atomic hydrogen, excitation by proton and α -particle impact	59
Transitions, 'forbidden', in paramagnetic resonance	103
Trapping, deep, and space charge limited current flow in selenium	1157
Ultrasonic waves, very high frequency, diffraction of light by	958
Ultra-violet absorption, <i>see</i> Absorption	
Ultra-violet extensions of arc spectra of alkaline earths	797
Uranium 235, thermal neutron fission, kinetic energy effects (L)	1097
Variational method, Schwinger, application to zero-energy electron-hydrogen scattering	827
Vibration nodes, indication by fine powders	1076
Viscosity and thermal conductivity of binary gas mixtures: Kr-A, Kr-Ne, Kr-He	1157
Wave functions, Hartree-Fock, stationary properties	748
Wave functions, integrable many-body, for system of Bose particles	433
Wiedemann-Franz law	1005
X-radiations and yields of L_{II} shell in Pu	657
X-ray absorption process in ionic crystals	1046
Young's modulus, anisotropy in drawn polyethylene	1028
Z-centres in sodium chloride containing calcium	153
ZETA, emission of sub-millimetre electromagnetic radiation from hot plasma	1069
Zinc, dislocation relaxation at low temperatures (L)	1216

INDEX TO AUTHORS (WITH TITLES)

	PAGE
Agrawal, Bal Krishna, and Verma, G. S. : Dislocation relaxation in zinc at low temperatures (L)	1216
Aitken, D. K., Heymann, F. F., Jennings, R. E., and Kalmus, P. I. P. : Design and construction of 29 mev microtron	769
Allaby, J. V., Ashmore, A., Diddens, A. N., Eades, J., Huxtable, G. B., and Skarsvåg, K. : Spin correlation measurements in p-p scattering at 382 and 320 Mev	234
Allcock, G. R., and Kamal, A. N. : S-wave pion-pion interaction	278
Amorós, J. L., with Canut, M. L. : On inversion temperature function of first-order (one phonon) scattering and determination of Debye characteristic temperatures	712
Anderson, N. : Oscillations of plasma in static magnetic field	971
Andrew, E. R., Swanson, K. M., and Williams, B. R. : Angular dependence of nuclear spin-lattice relaxation time for several alkali halide crystals	36
Andrews, E. H. : Stresses at crack in elastomer	483
Armstrong, N. H. K., with Coulter, J. R. M., and Emeleus, K. G. : Moving striations and anode spots in neon	476
Ashmore, A., with Allaby, J. V., Diddens, A. N., Eades, J., Huxtable, G. B., and Skarsvåg, K. : Spin correlation measurements in p-p scattering at 382 and 320 Mev	234
Ashton, F. : Range-energy relation for high energy μ -mesons	587
Aslam Khan, M. : MgH and MgD bands at 2819 Å and 2702 Å	1133
Bagguley, D. M. S., and Heath, M. : Ferromagnetic resonance in nickel-copper alloys	913
Baker, J. M., Lourens, J. A. J., and Stevenson, R. W. H. : Antiferromagnetism of mixed crystals of zinc and manganese fluoride	1038
Barnaby, C. F. : Energy loss of singly charged heavy relativistic particles in organic material	1149
Barnard, R. D., with Bates, L. F. : Electrical resistivities of some stable and metastable uranium-molybdenum alloys	691
Barros, F. de S., Forsyth, P. D., Jaffe, A. A., and Taylor, I. J. : Investigation of some (t, d) reactions in light nuclei at 5.5 mev	853
Barton, J. C., and Michaelis, E. G. : Multiple Geiger counter coincidences due to gamma radiation	377
Barua, A. K., with Srivastava, B. N. : Rotational-translational relaxation time in H ₂ calculated from thermal conductivity	677
Bates, D. R. : Excitation of 1s-2p transition of atomic hydrogen by proton and alpha particle impact	59
Bates, L. F., and Barnard, R. D. : Electrical resistivities and magnetic susceptibilities of some stable and metastable uranium-molybdenum alloys	691
Bates, L. F., and Pacey, A. J. : Thermomagnetic behaviour of cobalt ferrite	567
Best, P. E., and Robins, J. L. : X-ray absorption process in ionic crystals	1046
Birch, K. G. : Scanning instrument for measurement of optical frequency response	901
Birks, J. B., and Kuchela, K. N. : Energy transfer in organic systems. II: Solute-solute transfer in liquid solutions	1083
Birks, J. B., Kuchela, K. N., and Read, F. H. : Energy transfer in organic systems III: spectral effects in liquid solutions (L)	1095
Blackman, M., and Khan, I. H. : Polymorphism of thallium and other halides at low temperatures	471
Bleaney, B. : Quadrupole-quadrupole interaction in rare earths	113
Bleaney, B., and Rubins, R. S. : Explanation of some 'forbidden' transitions in paramagnetic resonance	103
Bogle, G. S., Symmons, H. F., Burgess, V. R., and Sierins, J. V. : Paramagnetic resonance spectrometry at zero magnetic field	561

	PAGE
Borland, R. E. : One-dimensional chains with random spacing between atoms	705
Bounden, J. E., with Whitlock, W. S. : Negative oxygen ions from glow discharge source	845
Boyle, A. J. F., Bunbury, D. St. P., and Edwards, C. : Nuclear Zeeman effect, and quadrupole splitting in ^{119}Sn	1062
Boyle, A. J. F., Bunbury, D. St. P., Edwards, C., and Hall, H. E. : Mössbauer effect in tin from 120°K to melting point	129
Briggs, B. H. : Diffraction by irregular screen of limited extent	305
Broude, C., and Gove, H. E. : Spin of new level in ^{24}Mg (L)	1211
Bunbury, D. St. P., with Boyle, A. J. F., and Edwards, C. : Nuclear Zeeman effect, and quadrupole splitting in ^{119}Sn	1062
Bunbury, D. St. P., with Boyle, A. J. F., Edwards, C., and Hall, H. E. : Mössbauer effect in tin from 120°K to melting point	129
Burch, P. R. J. : Gamma ray spectra in large organic scintillators	1125
Burgess, V. R., with Bogle, G. S., Symmons, H. F., and Sierins, J. V. : Paramagnetic resonance spectrometry at zero magnetic field	561
Burke, P. G., and Laskar, W. : Four nucleon reactions with central forces	49
Burke, P. G., with Laskar, W., Tate, C., and Pardoe, B. : Two channel five nucleon reactions with central forces	1014
Burke, V. M., and Seaton, M. J. : Calculation of electron-hydrogen collision cross sections using Born approximation for reactance matrix	199
Burley, D. M. : Lattice model of classical hard sphere gas : II	451
Caffyn, J. E., and Ridley, B. K. : Z-centres in sodium chloride containing calcium	153
Calvert, J. M., with Read, F. H. : Pick-up reactions on ^9Be target	65
Canut, M. L., and Amorós, J. L. : On inversion temperature function of first-order (one phonon) scattering and determination of Debye characteristic temperatures	712
Capon, I. N. : Application of ray tracing methods to radio signals from satellites	337
Carte, A. E. : Air bubbles in ice	757
Carver, J. H. : Reaction $^{51}\text{V}(\gamma, \alpha)^{47}\text{Sc}$ and some remarks on (γ, α) reactions	417
Champeney, D. C., and Moon, P. B. : Absence of Doppler shift for gamma ray source and detector on same circular orbit	350
Chapman, Sydney : Scale times and scale lengths of variables : with geomagnetic and ionospheric illustrations	424
Chester, G. V., and Thellung, A. : Law of Wiedemann and Franz	1005
Chudley, C. T., and Elliott, R. J. : Neutron scattering from liquid on jump diffusion model	353
Claussen, B. H. : Modulation of light by means of electric field	1100
Codling, K. : Ultra-violet extensions of arc spectra of alkaline earths : absorption spectrum of magnesium vapour	797
Cohen, M., and Dalgarno, A. : Hartree energies of helium sequence	165
Cohen, M., and Dalgarno, A. : Stationary properties of Hartree-Fock approximation	748
Coleman, R. F., Herbert, D. N., and Perkin, J. L. : Upper limits for radiative capture cross sections of ^{27}Al and ^{31}P for ^{16}O ions	526
Coles, B. R., with Griffiths, D. : Antiferromagnetic behaviour of GdB_6 (L)	213
Cook, J. R. : Internal conversion of ^{141}Ce	346
Coulter, J. R. M., Armstrong, N. H. K., and Emeleus, K. G. : Moving striations and anode spots in neon	476
Craggs, J. D., with Prasad, A. N. : Measurement of Townsend's ionization coefficients and attachment coefficients in oxygen	385
Dalgarno, A., with Cohen, M. : Hartree energies of helium sequence	165
Dalgarno, A., with Cohen, M. : Stationary properties of Hartree-Fock approximation	748
Dalgarno, A., and McNamee, J. M. : Hartree perturbation method for helium	673
Dalgarno, A., and Stewart, A. L. : Perturbation-variation calculation of eigenvalues	467
Dalton, A. W., Parry, G., and Scott, H. D. : Gross structure in proton spectra from $^{51}\text{V}(\text{d}, \text{p})^{52}\text{V}$ reaction	1098

	PAGE
Dalton, A. W., Parry, G., Scott, H. D., and Swierszczewski, S. : $^{58}\text{Ni}(\text{d}, \text{p})^{59}\text{Ni}$ and $^{60}\text{Ni}(\text{d}, \text{p})^{61}\text{Ni}$ reactions	682
Dandy, D., with Deuchars, W. M. : Angular correlations in reactions $^{18}\text{O}(\alpha, \text{n}\gamma)^{21}\text{Ne}$ and $^{22}\text{Ne}(\alpha, \text{n}\gamma)^{25}\text{Mg}$	1197
Danielian, A., and Stevens, K. W. H. : Estimation of antiferromagnetic exchange interactions	116
Danielian, A., and Stevens, K. W. H. : Exchange interactions in polymorphic forms of MnS	124
Dayal, B., and Tripathi, B. B. : Revision of Kellermann's calculations of specific heats of sodium chloride	303
Deuchars, W. M., and Dandy, D. : Angular correlations in reactions $^{18}\text{O}(\alpha, \text{n}\gamma)^{21}\text{Ne}$ and $^{22}\text{Ne}(\alpha, \text{n}\gamma)^{25}\text{Mg}$	1197
Diddens, A. N., with Allaby, J. V., Ashmore, A., Eades, J., Huxtable, G. B., and Skarsvåg, K. : Spin correlation measurements in p-p scattering at 382 and 320 mev	234
Dobrowolski, T., and Young, J. : Determination of half-life of $\text{RaC}'(\text{L})$	1219
Dodd, J. N. : 'Level crossing' experiment in mercury	669
Dunstan, W. : Variation of photovoltaic response with magnetic field for germanium p-n junction	459
Eades, J., with Allaby, J. V., Ashmore, A., Diddens, A. N., Huxtable, G. B., and Skarsvåg, K. : Spin correlation measurements in p-p scattering at 382 and 320 mev	234
Eccleshall, D., and Yates, M. J. L. : O^+ , $T=1$ level in ^{18}F	93
Edwards, C., with Boyle, A. J. F., and Bunbury, D. St. P. : Nuclear Zeeman effect, and quadrupole splitting in ^{119}Sn	1062
Edwards, C., with Boyle, A. J. F., Bunbury, D. St. P., and Hall, H. E. : Mössbauer effect in tin from 120°K to melting point	129
Edwards, S. F., and Naqvi, M. A. : Integrable many body wave functions for system of Bose particles	433
Elliott, R. J., with Chudley, C. T. : Neutron scattering from liquid on jump diffusion model	353
Emeleus, K. G., with Coulter, J. R. M., and Armstrong, N. H. K. : Moving striations and anode spots in neon	476
Evans, J. A., with Woolley, J. C., and Gillett, C. M. : Electrical and optical properties of GaAs-InAs alloys	700
Fairbairn, W. M. : Isobaric triplets in nuclear 2p-shell and charge independence of nuclear forces	599
Ferreira, J. G., with Salgueiro, L., Park, J. J. H., and Ross, M. A. S. : Fluorescence and other yields of L_{II} shell in Pu	657
Finn, C. B. P., Orbach, R., and Wolf, W. P. : Spin-lattice relaxation in cerium magnesium nitrate at liquid helium temperatures : new process	261, corr. 1223
Flynn, C. P., and Seymour, E. F. W. : Diffusion narrowing of nuclear magnetic resonance in aluminium and copper	922
Forsyth, P. D., with Barros, F. de S., Jaffe, A. A., and Taylor, I. J. : Investigation of some (t, d) reactions in light nuclei at 5.5 mev	853
Fox, W. N., and Series, G. W. : Hyperfine structure of level $5^2\text{P}_{1/2}$ of potassium 39	1141
Fray, S. J., Johnson, F. A., Quarrington, J. E., and Williams, N. : Optical absorption of gallium arsenide in reststrahlen band (L)	215
Fröhlich, H. : New heavy bosons (L)	1223
Ganguly, A. K., with Mukherjee, S. K., and Majumder, N. K. : Activation cross sections with 14 mev neutrons	508
Gaskell, T. : Collective treatment of Fermi gas : II	1182
Geltman, S. : Consideration of exchange in ionization (L)	1220
Gilbert, N. : Gamma rays corresponding to dipole or high quadrupole excitation of carbon 12 by 150 mev protons	362
Gilboy, W. B., with Towle, J. H., and Macefield, B. E. F. : Study of reaction $^{40}\text{Ca}(\text{d}, \text{n})^{41}\text{Sc}$	1050

	PAGE
Gillett, C. M., with Woolley, J. C., and Evans, J. A. : Electrical and optical properties of GaAs-InAs alloys	700
Gooding, T. J. : Kinetic energy effects in thermal neutron fission of ^{235}U	1097
Gove, H. E., with Broude, C. : Spin of new level in ^{24}Mg (L)	1211
Greenlees, G. W., with Hoare, D., and Robbins, A. B. : Polarization of 9 mev protons elastically scattered from C and Al	830
Gregory, A. G., and Treacy, P. B. : Polarization of protons from low resonances in $^{12}\text{C}(\text{d}, \text{p})^{13}\text{C}$	499
Griffiths, D., and Coles, B. R. : Antiferromagnetic behaviour of GdB_6 (L)	213
Grimley, T. B. : Stereospecific polymers and Markoff chains	931
Grindlay, J. : Hole theory of liquids	1001
Haines, M. G. : Effect of electrodes in linear pinched discharge	643
Hall, H. E., with Boyle, A. J. F., Bunbury, D. St. P., and Edwards, C. : Mössbauer effect in tin from 120°K to melting point	129
Hambleton, K. G., Hilsum, C., and Holeman, B. R. : Determination of effective ionic charge of gallium arsenide from direct measurements of dielectric constant	1147
Hamilton, W. D. : Lifetime of 364 kev level in ^{131}Xe	610
Harding, G. N., Kimmitt, M. F., Ludlow, J. H., Porteous, P., Prior, A. C., and Roberts, V. : Emission of sub-millimetre electromagnetic radiation from hot plasma in ZETA	1069
Hariharan, P., and Sen, D. : Separation of symmetrical and asymmetrical wave-front aberrations in Twyman interferometer	328
Harper, P. G. : Quasiparticle approximation in superconductivity	299
Hartland, A., with Powles, J. G. : Measurement of indirect (J) coupling between nuclei in liquids in magnetic resonance by transient method	273
Hasted, J. B. : Energy transferred in inelastic ion-atom collisions	269
Heath, M., with Bagdasaryan, D. M. S. : Ferromagnetic resonance in nickel-copper alloys	913
Herbert, D. N., with Coleman, R. F., and Perkin, J. L. : Upper limits for radiative capture cross sections of ^{27}Al and ^{31}P for ^{16}O ions	526
Herdan, R., and Hughes, T. P. : (d-d) reaction product velocities in SCEPTRE III according to two-group model	987
Heymann, F. F., with Aitken, D. K., Jennings, R. E., and Kalmus, P. I. P. : Design and construction of 29 mev microtron	769
Higginson, G. S., and Kerr, L. W. : $2\ ^3\text{S}$ excitation in helium	866
Hilsum, C., with Hambleton, K. G., and Holeman, B. R. : Determination of effective ionic charge of gallium arsenide from direct measurements of dielectric constant	1147
Hindmarsh, W. R., and Thomas, K. A. : Collision broadening in argon spectrum	1193
Hinds, S., Middleton, R., and Litherland, A. E. : Energy level of ^{24}Mg at 6.44 mev excitation (L)	1210
Hoare, D., Robbins, A. B., and Greenlees, G. W. : Polarization of 9 mev protons elastically scattered from C and Al	830
Hodgson, P. E. : Optical model analysis of elastic scattering of 5.5 mev ^3He by carbon, magnesium, aluminium and copper	997
Holeman, B. R., with Hambleton, K. G., and Hilsum, C. : Determination of effective ionic charge of gallium arsenide from direct measurements of dielectric constant	1147
Horák, Z. : On identification of K_α satellites I : LS region	980
Hoyle, F. : 44th Guthrie Lecture : Observational tests in cosmology	1
Hughes, T. P., with Herdan, R. : (d-d) reaction product velocities in SCEPTRE III according to two-group model	987
Humphreys-Owen, S. P. F., the Late : Comparison of reflection constants for measuring optical constants without polarimetric analysis, and proposal for new methods based on Brewster angle	949
Huxtable, G. B., with Allaby, J. V., Ashmore, A., Diddens, A. N., Eades, J., and Skarsvåg, K. : Spin correlation measurements in p-p scattering at 382 and 320 mev	234

- Jaffe, A. A., with Barros, F. de S., Forsyth, P. D., and Taylor, I. J. : Investigation of some (t, d) reactions in light nuclei at 5.5 mev 853
- Jain, D. C., with Singh, N. L. : Relative intensities in triplet system of Co bands (L) 817
- Jaswon, M. A., and Shaw, B. J. : Note on non-equilibrium elastic constants 885
- Jennings, R. E., with Aitken, D. K., Heymann, F. F., and Kalmus, P. I. P. : Design and construction of 29 mev microtron 769
- Jnanananda, S., with Lakshminarayana, V. : Scattering cross sections of gamma radiation 593
- Johnson, F. A., with Fray, S. J., Quarrington, J. E., and Williams, N. : Optical absorption of gallium arsenide in reststrahlen band (L) 215
- Jones, D. P., Murphy, P. G., O'Neill, P. L., and Wormald, J. R. : Redetermination of Panofsky ratio for negative pions stopped in hydrogen 77
- Joshi, B. R. : Orbital electron capture ratio and beta spectrum of ^{204}Tl 1205
- Kalmus, P. I. P., with Aitken, D. K., Heymann, F. F., and Jennings, R. E. : Design and construction of 29 mev microtron 769
- Kamal, A. N. : P-wave pion-pion resonance 917
- Kamal, A. N., with Allcock, G. R. : S-wave pion-pion interaction 278
- Katz, L., and Thorson, I. M. : Fine structure in $^{12}\text{C}(\gamma, n)^{11}\text{C}$ activation curve 166
- Kerr, L. W., with Higginson, G. S. : 2^3S excitation in helium 866
- Khan, I. H., with Blackman, M. : Polymorphism of thallium and other halides at low temperatures 471
- Kimmitt, M. F., with Harding, G. N., Ludlow, J. H., Porteous, P., Prior, A. C., and Roberts, V. : Emission of sub-millimetre electromagnetic radiation from hot plasma in ZETA 1069
- Kingston, A. E., and Skinner, B. G. : Elastic scattering of electrons and positrons by hydrogen atoms 724
- Knowles, J. E. : Further explanation of hysteresis loop of 'square loop' ferrites 225
- Knowles, J. E. : Irreversible change of magnetization produced in 'square loop' ferrite by pulsed magnetic fields 576
- Kuchela, K. N., with Birks, J. B. : Energy transfer in organic systems II : solute-solute transfer in liquid solutions 1083
- Kuchela, K. N., with Birks, J. B., and Read, F. H. : Energy transfer in organic systems III : spectral effects in liquid solutions (L) 1095
- Lacroix, R. : Cubic crystal field splitting of Gd^{3+} ion (L) 550
- Lakshminarayana, V., and Jnanananda, S. : Scattering cross sections of gamma radiation 593
- Lanyon, H. P. D., and Spear, W. E. : Space charge limited current flow and deep trapping in selenium 1157
- Laskar, W., with Burke, P. G. : Four nucleon reactions with central forces 49
- Laskar, W., Tate, C., Pardoe, B., and Burke, P. G. : Two channel five nucleon reactions with central forces 1014
- Lawson, J., Lawson, W., and Seaton, M. J. : Calculation of Born partial wave integrals for some transitions in H produced by electron impact 192
- Lawson, W., with Lawson, J., and Seaton, M. J. : Calculation of Born partial wave integrals for some transitions in H produced by electron impact 192
- Lilley, J. S. : Emission of charged particles from bombardment of silver with nitrogen ions 833
- Litherland, A. E., with Hinds, S., and Middleton, R. : Energy level of ^{24}Mg at 6.44 mev excitation (L) 1210
- Lourens, J. A. J., with Baker, J. M., and Stevenson, R. W. H. : Antiferromagnetism of mixed crystals of zinc and manganese fluoride 1038
- Ludlow, J. H., with Harding, G. N., Kimmitt, M. F., Porteous, P., Prior, A. C., and Roberts, V. : Emission of sub-millimetre electromagnetic radiation from hot plasma in ZETA 1069
- Lynch, J. G., with Robertson, J. C. : Luminescent decay of various crystals for particles of different ionization density 751

	PAGE
Macefield, B. E. F., with Towle, J. H. : Study of reactions $^{12}\text{C}(^3\text{He}, n)^{14}\text{O}$ and $^{16}\text{O}(^3\text{He}, n)^{18}\text{Ne}$	399
Macefield, B. E. F., with Towle, J. H. : Threshold of $^{12}\text{C}(^3\text{He}, n)^{14}\text{O}$ reaction (L)	1217
Macefield, B. E. F., Towle, J. H., and Gilboy, W. B. : Study of reaction $^{40}\text{Ca}(d, n)^{41}\text{Sc}$	1050
McNamee, J. M., with Dalgarno, A. : Hartree perturbation method for helium	673
Majumdar, K., with Mohan, H. : Absorption spectrum of tellurium monosulphide in ultra-violet region	147
Majumdar, S. K. : Radiation by charged particles passing through electron plasma in external magnetic field	1109
Majumder, N. K., with Mukherjee, S. K., and Ganguly, A. K. : Activation cross sections with 14 mev neutrons	508
Male, J. C. : Luminescence excitation spectrum of diamond near fundamental absorption edge	869
March, P. V., and Walker, T. G. : Photoproduction reaction $^{60}\text{Ni}(\gamma, \pi^-)^{60}\text{Cu}$	293
Markham, M. F., with Musgrave, M. J. P. : Features of elastic wave surface for zinc crystal	335
Massey, Sir Harrie, and Moussa, A. H. : Positronium formation in helium	811
Mercier, R. P. : Diffraction by finite irregular objects	318
Michaelis, E. G., with Barton, J. C. : Multiple Geiger counter coincidences due to gamma radiation	377
Middleton, R., with Hinds, S., and Litherland, A. E. : Energy level of ^{24}Mg at 6.44 mev excitation (L)	1210
Miles, J. R. N., with Suddaby, A. : Correction to Smoluchowski equation in molecular theory of liquids	1170
Mohan, H., and Majumdar, K. : Absorption spectrum of tellurium monosulphide in ultra-violet region	147
Morsewitsch, B. L. : Elastic scattering of slow electrons by helium atoms	721
Moon, P. B., with Champeney, D. C. : Absence of Doppler shift for gamma ray source and detector on same circular orbit	350
Mosley, M. H., with Powles, J. G. : Thermal motion effect in electron spin resonance of free radical in solution	729
Moussa, A. H., with Massey, Sir Harrie : Positronium formation in helium	811
Mukherjee, S. K., Ganguly, A. K., and Majumder, N. K. : Activation cross sections with 14 mev neutrons	508
Murphy, P. G., with Jones, D. P., O'Neill, P. L., and Wormald, J. R. : Redetermination of Panofsky ratio for negative pions stopped in hydrogen	77
Musgrave, M. J. P., and Markham, M. F. : Features of elastic wave surface for zinc crystal	335
Naqvi, M. A., with Edwards, S. F. : Integrable many-body wave functions for system of Bose particles	433
Neale, D. J., with Powles, J. G. : Molecular motion in liquid toluene by proton magnetic resonance relaxation	737
O'Neill, P. L., with Jones, D. P., Murphy, P. G., and Wormald, J. R. : Redetermination of Panofsky ratio for negative pions stopped in hydrogen	77
Orbach, R. : On theory of spin-lattice relaxation in paramagnetic salts	821
Orbach, R., with Finn, C. B. P., and Wolf, W. P. : Spin-lattice relaxation in cerium magnesium nitrate at liquid helium temperatures : new process	261, corr. 1223
Pace, J. H., Sampson, D. F., and Thorp, J. S. : Spin-lattice relaxation times in sapphire and chromium-doped rutile at 34.6 Gc/s	257
Pacey, A. J., with Bates, L. F. : Thermomagnetic behaviour of cobalt ferrite	567
Pardoe, B., with Laskar, W., Tate, C., and Burke, P. G. : Two-channel five-nucleon reactions with central forces	1014
Park, J. J. H., with Salgueiro, L., Ferreira, J. G., and Ross, M. A. S. : Fluorescence and other yields of L_{II} shell in Pu	657

	PAGE
Parry, G., with Dalton, A. W., and Scott, H. D. : Gross structure in proton spectra from $^{51}\text{V}(\text{d}, \text{p})^{52}\text{V}$ reaction	1098
Parry, G., with Dalton, A. W., Scott, H. D., and Swierszczewski, S. : $^{58}\text{Ni}(\text{d}, \text{p})^{59}\text{Ni}$ and $^{60}\text{Ni}(\text{d}, \text{p})^{61}\text{Ni}$ reactions	682
Parry, G., Scott, H. D., and Swierszczewski, S. : Angular distributions of alpha groups from reaction $^{24}\text{Mg}(\alpha, \alpha)^{23}\text{Mg}$	1024
Parry, G., Scott, H. D., and Swierszczewski, S. : Elastic scattering of ^3He by C, Mg, Al and Cu	230
Peacock, T. E. : Effective number of electrons in π band of graphite (L)	1214
Pearson, F. J. : Some notes on theories of helium	531
Perkin, J. L., with Coleman, R. F., and Herbert, D. N. : Upper limits for radiative capture cross sections of ^{27}Al and ^{31}P for ^{16}O ions	526
Peterkop, R. : Consideration of exchange in ionization (L)	1221
Phillips, N. J. : Plasma diffusion in systems with particle losses	965
Porat, D. I., and Ramavatham, K. : Rate of energy loss and ranges of carbon and oxygen ions in solids	97
Porteous, P., with Harding, G. N., Kimmitt, M. F., Ludlow, J. H., Prior, A. C., and Roberts, V. : Emission of sub-millimetre electromagnetic radiation from hot plasma in ZETA	1069
Powles, J. G., and Hartland, A. : Measurement of indirect (J) coupling between nuclei in liquids in magnetic resonance by transient method	273
Powles, J. G., and Mosley, M. H. : Thermal motion effect in electron spin resonance of free radical in solution	729
Powles, J. G., and Neale, D. J. : Molecular motion in liquid toluene by proton magnetic resonance relaxation	737
Prasad, A. N., and Craggs, J. D. : Measurement of Townsend's ionization coefficients and attachment coefficients in oxygen	385
Prior, A. C. : Some theoretical considerations on longitudinal magnetic field induced oscillations in semiconductors (oscillator) and tentative explanation	1121
Prior, A. C., with Harding, G. N., Kimmitt, M. F., Ludlow, J. H., Porteous, P., and Roberts, V. : Emission of sub-millimetre electromagnetic radiation from hot plasma in ZETA	1069
da Providencia, J. : Perturbation theory in finite nuclei	81
Quarrington, J. E., with Fray, S. J., Johnson, F. A., and Williams, N. : Optical absorption of gallium arsenide in reststrahlen band (L)	215
Ramachandra Rao, B., and Satyanarayana Murty, J. : Diffraction of light by very high frequency ultrasonic waves	958
Ramavatham, K., with Porat, D. I. : Rate of energy loss and ranges of carbon and oxygen ions in solids	97
Raumann, G., and Saunders, D. W. : Anisotropy of Young's modulus in drawn polyethylene	1028
Read, F. H., with Birks, J. B., and Kuchela, K. N. : Energy transfer in organic systems III : spectral effects in liquid solutions	1095
Read, F. H., and Calvert, J. M. : Pick-up reactions on ^9Be target	65
Ridley, B. K., with Caffyn, J. E. : Z-centres in sodium chloride containing calcium	153
Robbins, A. B., with Hoare, D., and Greenlees, G. W. : Polarization of 9 mev protons elastically scattered from C and Al	830
Roberts, V., with Harding, G. N., Kimmitt, M. F., Ludlow, J. H., Porteous, P., and Prior, A. C. : Emission of sub-millimetre electromagnetic radiation from hot plasma in ZETA	1069
Robertson, J. C., and Lynch, J. G. : Luminescent decay of various crystals for particles of different ionization density	751
Robins, J. L., with Best, P. E. : X-ray absorption process in ionic crystals	1046
Rollin, B. V. : Detection of millimetre and sub-millimetre wave radiation by free carrier absorption in semiconductor	1102

Ross, M. A. S., with Salgueiro, L., Ferreira, J. G., and Park J. J. H. : Fluorescence and other yields of L_{II} shell in Pu	657
Rubins, R. S., with Bleaney, B. : Explanation of some 'forbidden' transitions in paramagnetic resonance	103
Salgueiro, L., Ferreira, J. G., Park, J. J. H., and Ross, M. A. S. : Fluorescence and other yields of L_{II} shell in Pu	657
Salmona, A., and Seaton, M. J. : Electron collisions with Na atoms	617
Sampson, D. F., with Pace, J. H., and Thorp, J. S. : Spin-lattice relaxation times in sapphire and chromium-doped rutile at 34.6 Gc/s	257
Saraph, H. E. : Application of Schwinger variational method to zero-energy electron-hydrogen scattering	827
Sarma, M. B. K. : Selective pressure broadening of Si and F spectral lines	665
Satyanarayana Murty, J., with Ramachandra Rao, B. : Diffraction of light by very high frequency ultrasonic waves	958
Saunders, D. W., with Raumann, G. : Anisotropy of Young's modulus in drawn polyethylene	1028
Scott, H. D., with Dalton, A. W., and Parry G. : Gross structure in proton spectra from $^{51}\text{V}(\text{d}, \text{p})^{52}\text{V}$ reaction	1098
Scott, H. D., with Dalton, A. W., Parry, G., and Swierszczewski, S. : $^{58}\text{Ni}(\text{d}, \text{p})^{59}\text{Ni}$ and $^{60}\text{Ni}(\text{d}, \text{p})^{61}\text{Ni}$ reactions	682
Scott, H. D., with Parry, G., and Swierszczewski, S. : Angular distributions of alpha groups from reaction $^{24}\text{Mg}(\text{}^3\text{He}, \alpha)^{23}\text{Mg}$	1024
Scott, H. D., with Parry, G., and Swierszczewski, S. : Elastic scattering of ^3He by C, Mg, Al and Cu	230
Seaton, M. J. : Evaluation of partial wave integrals in Born approximation	184
Seaton, M. J. : Strong coupling in optically allowed atomic transitions produced by electron impact	174
Seaton, M. J., with Burke, V. M. : Calculation of electron-hydrogen collision cross sections using Born approximation for reactance matrix	199
Seaton, M. J., with Lawson, J., and Lawson, W. : Calculation of Born partial wave integrals for some transitions in H produced by electron impact	192
Seaton, M. J., with Salmona, A. : Electron collisions with Na atoms	617
Sen, D., with Hariharan, P. : Separation of symmetrical and asymmetrical wave-front aberrations in Twyman interferometer	328
Series, G. W., with Fox, W. N. : Hyperfine structure of level $5^2\text{P}_{1/2}$ of potassium 39	1141
Sewell, G. L. : Diamagnetism of many-fermion systems	136
Seymour, E. F. W., with Flynn, C. P. : Diffusion narrowing of nuclear magnetic resonance in aluminium and copper	922
Shaw, B. J., with Jaswon, M. A. : Note on non-equilibrium elastic constants	885
Sierins, J. V., with Bogle, G. S., Symmons, H. F., and Burgess, V. R. : Paramagnetic resonance spectrometry at zero magnetic field	561
Singh, N. L., and Jain, D. C. : Relative intensities in triplet system of Co bands (I).	817
Skarsvåg, K., with Allaby, J. V., Ashmore, A., Diddens, A. N., Eades, J., and Huxtable, G. B. : Spin correlation measurements in p p scattering at 382 and 320 mev	234
Skinner, B. G. : On validity of two conjectures relating to resonance collisions (I).	551
Skinner, B. G., with Kingston, A. E. : Elastic scattering of electrons and positrons by hydrogen atoms	724
Spear, W. E., with Lanyon, H. P. D. : Space charge limited current flow and deep trapping in selenium	1157
Srivastava, B. N., and Barua, A. K. : Rotational-translational relaxation time in H_2 calculated from thermal conductivity	677
Stevens, K. W. H. : Hamiltonian formalism of damping in tuned circuit	515
Stevens, K. W. H., with Danielian, A. : Estimation of antiferromagnetic exchange interactions	116
Stevens, K. W. H., with Danielian, A. : Exchange interactions in the polymorphic forms of MnS	124

	PAGE
Stevenson, R. W. H., with Baker, J. M., and Lourens, J. A. J. : Antiferromagnetism of mixed crystals of zinc and manganese fluoride	1038
Stewart, A. L. : Approximate method for calculation of multipole polarizabilities of atoms	447
Stewart, A. L., with Dalgarno, A. : Perturbation-variation calculation of eigenvalues	467
Stone, A. P. : Nuclear and relativistic effects in atomic spectra	786
Suddaby, A., and Miles, J. R. N. : Correction to Smoluchowski equation in molecular theory of liquids	1170
Suffczynski, M. : Faraday effect for direct magneto-optical transitions in germanium	1042
Svensson, N. L. : Variation of fracture energy of brittle plastics with temperature	876
Swanson, K. M., with Andrew, E. R., and Williams, B. R. : Angular dependence of nuclear spin-lattice relaxation time for several alkali halide crystals	36
Swierszczewski, S., with Dalton, A. W., Parry, G., and Scott, H. D. : $^{58}\text{Ni}(d, p)^{59}\text{Ni}$ and $^{60}\text{Ni}(d, p)^{61}\text{Ni}$ reactions	682
Swierszczewski, S., with Parry, G., and Scott, H. D. : Angular distributions of alpha groups from reaction $^{24}\text{Mg}(^3\text{He}, \alpha)^{23}\text{Mg}$	1024
Swierszczewski, S., with Parry, G., and Scott, H. D. : Elastic scattering of ^3He by C, Mg, Al and Cu	230
Symmons, H. F., with Bogle, G. S., Burgess, V. R., and Sierins, J. V. : Paramagnetic resonance spectrometry at zero magnetic field	561
Tate, C., with Laskar, W., Pardoe, B., and Burke, P. G. : Two-channel five-nucleon reactions with central forces	1014
Taylor, I. J., with Barros, F. de S., Forsyth, P. D., and Jaffe, A. A. : Investigation of some (t, d) reactions in light nuclei at 5.5 mev	853
Temperley, H. N. V. : Improvements in lattice model of liquid	630
Thellung, A., with Chester, G. V. : Law of Wiedemann and Franz	1005
Thomas, K. A., with Hindmarsh, W. R. : Collision broadening in argon spectrum	1193
Thornton, E. : Viscosity and thermal conductivity of binary gas mixtures: krypton-argon, krypton-neon, and krypton-helium	1166
Thorp, J. S., with Pace, J. H., and Sampson, D. F. : Spin-lattice relaxation times in sapphire and chromium-doped rutile at 34.6 Gc/s	257
Thorson, I. M., and Katz, L. : Fine structure in $^{12}\text{C}(\gamma, n)^{11}\text{C}$ activation curve	166
Thouless, D. J., and Tilley, D. R. : Collective modes in theory of superconductivity	1175
Tilley, D. R., with Thouless, D. J. : Collective modes in theory of superconductivity	1175
Titman, J. M. : Heat capacities of some copper-manganese alloys	807
Towle, J. H., and Macefield, B. E. F. : Study of reactions $^{12}\text{C}(^3\text{He}, n)^{14}\text{O}$ and $^{16}\text{O}(^3\text{He}, n)^{18}\text{Ne}$	399
Towle, J. H., and Macefield, B. E. F. : Threshold of $^{12}\text{C}(^3\text{He}, n)^{14}\text{O}$ reaction (L)	1217
Towle, J. H., with Macefield, B. E. F., and Gilboy, W. B. : Study of reaction $^{40}\text{Ca}(d, n)^{41}\text{Sc}$	1050
Treacy, P. B., with Gregory, A. G. : Polarization of protons from low resonances in $^{12}\text{C}(d, p)^{13}\text{C}$	499
Tripathi, B. B., with Dayal, B. : Revision of Kellermann's calculations of specific heats of sodium chloride	303
Verma, G. S., with Agrawal, Bal Krishna : Dislocation relaxation in zinc at low temperatures (L)	1216
Walker, T. G., with March, P. V. : Photoproduction reaction $^{60}\text{Ni}(\gamma, \pi^-)^{60}\text{Cu}$	293
Ware, A. A., and Wesson, J. A. : Ohmic heating of positive ions in impure plasma	801
Wesson, J. A., with Ware, A. A. : Ohmic heating of positive ions in impure plasma	801
Whitlock, W. S., and Bounden, J. E. : Negative oxygen ions from glow discharge source	845
Wilczynski, J. S. : Some properties of photographic image recording	17
Williams, B. R., with Andrew, E. R., and Swanson, K. M. : Angular dependence of nuclear spin-lattice relaxation time for several alkali halide crystals	36
Williams, N., with Fray, S. J., Johnson, F. A., and Quarrington, J. E. : Optical absorption of gallium arsenide in reststrahlen band (L)	215

Wolcott, N. M. : Calculation of Debye characteristic temperatures (L)	218
Wolf, W. P., with Finn, C. B. P., and Orbach, R. : Spin-lattice relaxation in cerium magnesium nitrate at liquid helium temperatures: new process.	261, corr. 1223
Wood, A. F. B. : On indication of vibration nodes by fine powders	1076
Woolley, J. C., Gillett, C. M., and Evans, J. A., : Electrical and optical properties of GaAs-InAs alloys	700
Wormald, J. R., with Jones, D. P., Murphy, P. G., and O'Neill, P. L. : Redetermination of Panofsky ratio for negative pions stopped in hydrogen	77
Yates, M. J. L., with Eccleshall, D. : 0^+ , $T=1$ level in ^{18}F	93
Young, J., with Dobrowolski, T. : Determination of half-life of RaC' (L)	1220
Zucker, I. J. : Reduced equation of state of inert gas solids at absolute zero	889

INDEX TO REVIEWS OF BOOKS

	PAGE
Aharoni, J.: <i>The special theory of relativity</i>	221
Batchelor, G. K., (Ed.): <i>The scientific papers of Sir Geoffrey Ingram Taylor</i> , Vol. 2, <i>Meteorology, oceanography and turbulent flow</i>	222
Belcher, R., and Nutten, A. J.: <i>Quantitative inorganic analysis</i> , 2nd Edn	938
Bondi, H.: <i>Cosmology</i> , 2nd Edn	937
Booth, A. D., (Ed.): <i>Progress in automation</i> , Vol. 1	224
Brown, Sanborn C.: <i>Basic data of plasma physics</i>	556
Bückle, H.: <i>L'essai de microdureté et ses applications</i>	942
Burbidge, G. R., Kahn, F. D., Ebert, R., v. Hoernër, S., and Temesváry, St.: <i>Die Entstehung von Sternen durch Kondensation diffuser Materie</i>	220
Buxton, C. R., and Jackson, H. S.: <i>Translation from Russian for scientists</i>	1107
Chace, W. G., and Moore, H. K., (Eds): <i>Exploding wires</i>	221
Champion, F. C.: <i>University physics</i>	1107
Chandrasekhar, S., (notes compiled by S. K. Trehan): <i>Plasma physics</i>	947
Clagett, M.: <i>The science of mechanics in the middle ages</i>	223
Cross, A. D.: <i>Introduction to practical infra-red spectroscopy</i>	219
<i>The design of physics research laboratories. (A symposium held by the London and Home Counties Branch of The Institute of Physics, at the Royal Institution on 27th November 1957)</i>	937
Duquesne, M., Grégoire, R., and Lefort, M.: <i>Travaux pratiques de physique nucléaire et de radiochimie</i>	1108
Eirich, F. R., (Ed.): <i>Rheology: theory and applications</i> , Vol. III	941
Felici, N.: <i>Accélérateurs de particules et progrès scientifique</i>	818
Flügge, S., (Ed.): <i>Handbuch der Physik</i> , Vol. 12, <i>Thermodynamik der Gase</i>	1107
Goertzel, G., and Tralli, N.: <i>Some mathematical methods of physics</i>	1104
Goldsmid, H. J.: <i>Applications of thermoelectricity</i>	819
Grivet, P., and Legros, R.: <i>Physique des circuits</i>	946
Guggenheim, E. A.: <i>The international encyclopedia of physical chemistry and chemical physics</i> , Vol. 1, <i>Elements of the kinetic theory of gases</i>	1106
Herzberger, M.: <i>Modern geometrical optics</i>	554
Hutter, R. G. E.: <i>Beam and wave electronics in microwave tubes</i>	555
<i>Instrument Construction</i> , No. 1, Jan. 1959 (translated from the Russian)	560
Jakob, M.: <i>Heat transfer</i> , Vol. 2	946
de Jong, W. E.: <i>General crystallography. A brief compendium</i>	220
Jonscher, A. K.: <i>Principles of semiconductor device operation</i>	945
Kopal, Zdenek: <i>Figures of equilibrium of celestial bodies</i>	820
Lance, G. N.: <i>Numerical methods for high speed computers</i>	1106
Lawson, D. F.: <i>The technique of photomicrography</i>	560
Lighthill, M. J.: <i>Fourier analysis and generalized functions</i> , Students' Edn	1107

	PAGE
Lin, C. C., (Ed.): <i>High speed aerodynamics and jet propulsion</i> , Vol. 5, <i>Turbulent flows and heat transfer</i>	1105
Linfoot, E. H.: <i>Qualitätsbewertung optischer Bilder</i>	820
Linhart, J. G.: <i>Plasma physics</i>	943
Maréchal, A., and Françon, M.: <i>Diffraction. Structure des images</i> , Vol. 2 of <i>Traité d'optique instrumentale</i>	1105
Margen, P. H.: <i>Nuclear reactor optimisation (Nuclear engineering monographs)</i>	939
Mendelssohn, K.: <i>Cryophysics. Interscience tracts on physics and astronomy</i> , No. 7	946
Messel, H. (Ed.): <i>Selected lectures in modern physics for school science teachers</i>	556
Meyer-Eppler, W., (Ed.): <i>Kommunikation und Kybernetik in Einzeldarstellungen</i> , Vol. I, <i>Grundlagen und Anwendungen der Informationstheorie</i>	819
Olson, Harry F.: <i>Dynamical analogies</i> , 2nd Edn	560
Päsler, M.: <i>Mechanik deformierbarer Körper</i>	219
Paxton, F. A., and Rollin, J. E.: <i>Tables of the incomplete elliptic integrals of the first and third kind</i>	939
Persoz, B.: <i>Introduction à l'étude de la rhéologie</i>	942
Powell, C. F., Fowler, P. H., and Perkins, D. H.: <i>The study of elementary particles by the photographic method</i>	944
Preuss, H.: <i>Integraltafeln zur Quantenchemie</i> , Vol. IV	558
<i>Proceedings of international symposium on the theory of switching</i> , Parts I and II	943
Pugh, E. M., and Pugh, E. W.: <i>Principles of electricity and magnetism</i>	224
Quastler, H., and Morowitz, H. J., (Eds): <i>Proceedings of the first national biophysics conference, Columbus, Ohio, March, 1957</i>	555
Reitz, J. R., and Milford, F. J.: <i>Foundations of electromagnetic theory</i>	559
Roberts, J. K., and Miller, A. R.: <i>Heat and thermodynamics</i> , 5th Edn	557
Roman, P.: <i>The theory of elementary particles</i>	940
Sauer, R., Stiefel, E., Todd, J., and Walther, A., (Eds): <i>Numerische Mathematik</i>	555
Saxe, R. F.: <i>Approaches to thermonuclear power</i>	947
Seitz, F., and Turnbull, D., (Eds): <i>Solid state physics</i> , Vol. X	943
Selfridge, R. G., and Maxfield, J. E.: <i>A table of the incomplete elliptic integral of the third kind</i>	939
Sillitto, R. M.: <i>Non-relativistic quantum mechanics</i>	1104
Stallo, J. B.: <i>The concepts and theories of modern physics</i>	937
Turnbull, H. W., (Ed.): <i>Correspondence of Isaac Newton</i>	559
Université de Grenoble: <i>The many body problem</i>	948
Wilson, J. G., and Wouthuysen, S. A., (Eds): <i>Progress in elementary particle and cosmic ray physics</i> , Vol. V	557
Ziman, J. M.: <i>Electrons and phonons</i>	219

Printed in England
TAYLOR & FRANCIS, LTD., Red Lion Court, Fleet Street, London, E.C.4